

1 Earth Observation History on Technology Introduction

Prior to the space age (conventionally dated from 1957), humankind had never been able to take in the whole of a hemisphere in a single glance. In fact it had never had a global view of the world in which it lived. It was not until the first spacecraft went into orbit that our horizons expanded and we saw our planet as never before. During more than four decades of spaceflight, planet Earth has been rediscovered through the systematic collection and analysis of vast amounts of information. At the turn of the century/millennium, satellite-provided services in many fields of application (environmental monitoring, navigation, weather forecasting, communication, etc) are taken for granted. We've come to depend on the satellites in a way that would have been unimaginable a few decades ago.

Before the space age, remote sensing, although not named as such, was done exclusively with photographic cameras. The so-called aerial photo emerged in the 1850's, a mere dozen years after the invention of photography, with pictures taken from a tethered balloon – the French photographer, Gaspard Félix Tournachon (1820–1910), alias Nadar, obtained the first aerial photographs over Paris (Oct. 23, 1858) from an altitude of about 80 m; Nadar also used his art for mapping the countryside. In 1859, Napoleon III ordered Nadar to obtain reconnaissance photography in preparation of the Battle of Solferino in northern Italy. Thereafter, tethered balloons were used a few times during the US Civil War (1861–1865) by General George McClellan, to study enemy positions using aerial photographs.²⁾ At the beginning of the twentieth century, the aeroplane proved its advantage as a civil and military observation/reconnaissance platform. Aerial photography was extensively employed during both World Wars for military reconnaissance. In 1947, a number of captured V–2 rockets were modified and instrumented by the US military to photograph the clouds from 110–165 km altitudes in New Mexico, USA. [In the same year (Oct. 18, 1947), the Soviet Union launched its first LRBR (Long Range Ballistic Rocket) based on the German rocket A4 (V–2)]. The photographs demonstrated the immense potential of observing weather.³⁾ After the wars and prior to 1960, the development of aerial color and color infrared film gave civilian remote sensing a distinct boost. The color infrared photography allowed some interpretation means for a rough classification of some vegetation types. High-speed cameras, combined with wide-angle lenses, provided greater opportunities to image Earth's surfaces. A more detailed account of the early rocket development history in Germany, in particular before and during WW–II (World War–II), and in USA after WW–II, is provided in the following reference.^{4) 5)}

Earth observation covers a wide field of remote sensing as well as of other sensing methods (in-situ), it encompasses the study of the Earth system (in particular its outer surface) and also Earth's environment, including the study of interactions with the outside. *Earth observation (i.e. remote sensing) is based on the fact that information is available from the electromagnetic energy field arising from the Earth's surface (or atmosphere, or both) and in particular from the spatial, spectral and temporal variations in that field.*⁶⁾ Spaceage Earth observation (although not named as such initially) started with the launch of Russia's first Sputnik satellite on Oct. 4, 1957 on the R–7 launch vehicle from Baikonur (satellite mass = 83.6 kg, diameter = 58 cm, perigee = 228 km, apogee = 947 km, inclination = 65.1°, period = 96 min,

- 2) As early as 1783, when as US ambassador to France, Benjamin Franklin observed the first Montgolfier balloons in flight over Paris and predicted their use in “conveying Intelligence” about “an Enemy's Army,” generals and spies have understood the power of aerial reconnaissance; the high-altitude surveillance possible from satellites promised both a revolution in surveillance and insurance against political embarrassments (see Ref. 54).
- 3) “The conception, growth accomplishments and future of meteorological satellites,” NASA Conference Publication 2257, 1980
- 4) W. K. Dahm, K. Dannenberg, W. Haeussermann, G. Reising, E. Stuhlinger, G. von Tiesenhausen, I. Willhite, “From Peenemünde, Germany, to Fort Bliss, Texas, White Sands, New Mexico, and Huntsville, Alabama, USA: A Classical Case of Technology Transfer – Rocket Propulsion, Missile and Launch Vehicle Technology,” Proceedings of the 54th IAC (International Astronautical Congress), Bremen, Germany, Sept. 29 – Oct. 3, 2003
- 5) Note: The history of rocket development as primary propulsion is not within the scope of this documentation
- 6) D. Landgrebe, “Hyperspectral Image Data Analysis,” IEEE Signal Processing Magazine, Vol. 19, No 1, pp. 17–28, Jan. 2002

RF frequencies: 20.005 MHz and 40.002 MHz). The chief designer and general manager of the Sputnik project was Sergei Pavlovich Korolev (1907–1966, also spelling of: Sergey Pavlovich Korolyov).⁷⁾ Sputnik–1 made measurements that permitted a first estimation of the density of the upper atmosphere. Sputnik–1 reentered the atmosphere on Jan. 4, 1958. In the following period each new spacecraft launch produced new discoveries. The first successful US satellite was Explorer–1 (launch Jan. 31, 1958 with a S/C mass of 5 kg; orbit of 384 km x 1859 km, inclination of 32.2°) of the US Army, built by the Army Ballistic Missile Agency and by JPL. Explorer–1 (instruments included a cosmic ray and micrometeorite package, a micrometeorite impact microphone, micrometeorite erosion gages, and internal and external temperature gages) provided preliminary information on the environment and conditions in space outside Earth’s atmosphere. It resulted in the discovery of the **Van Allen radiation belts** (James Alfred Van Allen, US physicist at the University of Iowa, *Sept. 7, 1914, †Aug. 9, 2006). Explorer–1 reentered the Earth’s atmosphere on March 31, 1970.

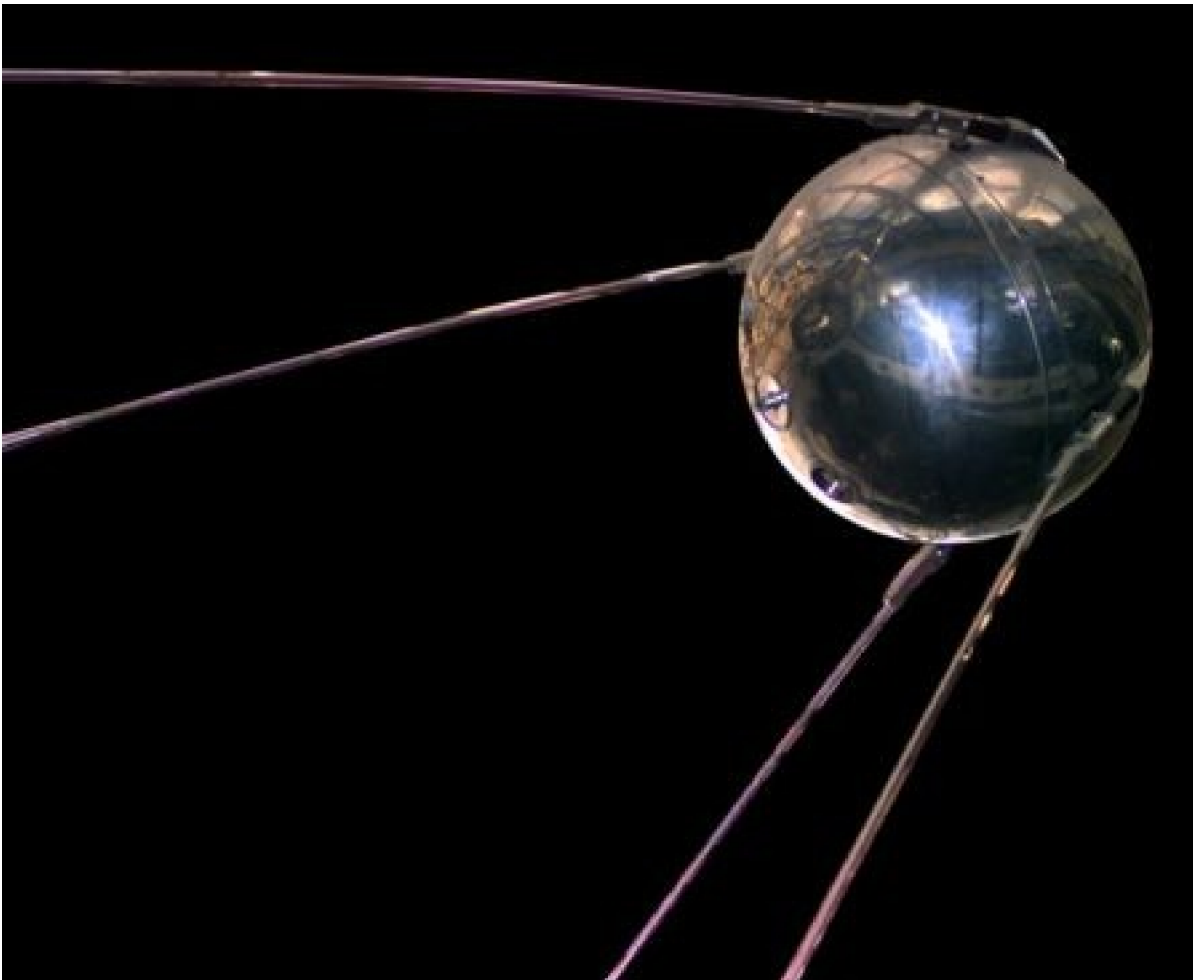


Figure 1: Illustration of Sputnik–1 (image credit: Roscosmos)

Some background on the early space race (this and next paragraph): The IGY (International Geophysical Year) was created May 16, 1952 by the ICSU (International Council of Scientific Unions) plenary meeting in Paris, France as a platform for international cooperation in studying the physics of the Earth. The IGY was planned for 1957/58, a year of expected maximum solar activity. In the preparation phase for IGY, various project scenarios were considered in international meetings; the US introduced information on the evolving

7) Sergei P. Korolev (Jan. 12, 1907 – Jan. 14, 1966), Chief Designer of the Soviet space program and head of Special Design Bureau–1 (Russian acronym OKB–1), ancestor of today’s RKK Energia (until recently, NPO Energia). Korolev is the father of Soviet rocketry, they called him the “Grand Designer.” But more than that, he was the heart and sole of the Soviet space program. In March 1962, Korolev started the Soyuz program, the rocket with the most launches in space history.

potential for launching satellites and their unique capabilities as tools for geophysical research. On Oct. 4, 1954, in an ICSU meeting in Rome, Italy, a resolution to recommend the use of satellites during the IGY was adopted by the international body. The USSR, which only recently had announced IGY participation, had no comment on the subject. – In reflection of the meeting, however, an atmosphere of suspicion and mistrust began to grow in both camps of the world (USA and USSR), each wondering of what the other side was up to with regard to their satellite plans.⁸⁾

Thus, the space race in post WW – II history had somehow started, generating a lot of activity and technology development, binding in turn many resources for the respective IGY satellite programs of each side. On July 29, 1955, President Dwight D. Eisenhower announced publicly the US intention to launch satellites during the upcoming IGY. The NRL (Naval Research Laboratory) was selected to build and launch the first satellite. The world was somehow stunned by the news that space endeavors were in planning and would soon become a reality. The Soviet Union followed with a similar announcement within a few days. Both announcements put even more pressure on the various teams from the East and the West, including the military organizations. The launch of Sputnik – 1 on Oct. 4, 1957 happened to coincide with the plan outlined for IGY. For the Soviet Union, Sputnik – 1 was an impressive technical achievement that caught the world’s attention, but for the US it was a stunning blow to fall behind in the race for space.⁹⁾ – As a consequence, the US Congress passed the National Aeronautics and Space Act in July 1958, legislation that led to the creation of the National Aeronautics and Space Administration (NASA) on October 1, 1958.

The first successful operational flight within the US IGY program was Vanguard – 2 (launch Vanguard vehicle on Feb. 17, 1959 from Cape Canaveral). The objective of Vanguard – 2 was to measure the Earth’s albedo, the amount of sunlight reflected by the Earth’ surface and cloud layers. The spherical S/C of 50 cm diameter had a mass of 9.5 kg and carried two photoelectric detecting units, a data recorder, a transmitter and a receiver. As the satellite spun, its photocells registered variations in albedo intensity.

The first spaceborne imaging sensors flown were the film cameras, looking down toward Earth and providing a “bird’s eye view” from space. Initial efforts concentrated on the most obvious phenomenon to study, namely the weather. However, the major goals of the early US and Russian space programs were set to explore outer space (looking out), and not to look at Earth. Strangely enough, Earth was somehow considered to be sufficiently known at the time. It is interesting to note that planning for a deliberate and systematic approach to Earth observation, i.e. the survey and research of the Earth’s surface (and many other items), did not start before the mid 1960s. The reason for the new interest in Earth was stimulated mainly by the study of some 1100 photographs (film imagery), taken of Earth by astronauts during the manned Mercury (1961 – 1963) and Gemini (March 1965 – Nov. 1966) missions and subsequently being used in preparation for the Apollo program (the objective was the study of possible lunar landing sites as seen from space).¹⁰⁾ In any case, in trying to analyze and to interpret the Earth imagery at hand, it began to dawn upon some people (familiar with the basic physics of the electromagnetic spectrum) that these photographs might contain a wealth of information – worthy of systematic analysis. Quantitative interpretation schemes had to be developed to interpret the data!

-
- 8) Roger D. Launius, “An Unintended Consequence of the IGY: Eisenhower, Sputnik, and the Founding of NASA,” Proceedings of the 59th IAC (International Astronautical Congress), Glasgow, Scotland, UK, Sept. 29 to Oct. 3, 2008, IAC – 08.E4.1.1
- 9) H. K. Ziegler, “A Signal Corps Space Odyssey: Part I – Prelude SCORE,” The Army Communicator, Fall 1981, pp. 17 – 24.. URL page created November 04, 2000 by InfoAge: <http://www.infoage.org/tac-ziegler.html>
- 10) If there were any lingering questions about the promise of space observation, they were dispelled – to everyone’s considerable surprise – by John Glenn, Wally Schirra, and Gordon Cooper. Despite cramped conditions, these astronauts took conventional (Glenn) as well as large – format cameras (70 mm Hasselblad) aboard America’s early space flights and came back with breathtaking photographs of the earth shot through the window of their Mercury and Gemini spacecraft. These were ordinary photos using visible light, not the information – rich spectral images pushed by the remote – sensing crowd, but the surprising amount of clarity and detail excited geologists. More important, the images excited the public (Ref 54). The Gemini photos were taken from flight altitudes of 160 km.

The planning for the first dedicated civil spaceborne Earth–surface imaging project was initiated at a press conference on Sept. 20, 1966 in Washington, DC.¹¹⁾ At this conference, Stewart Udall, Secretary of the Department of the Interior (DOI), and William T. Pecora, Director of USGS (United States Geological Survey), announced plans for a program called **Earth Resources Observation Satellites (EROS)**. “...*the time is now right and urgent to apply space technology towards the solution of many pressing natural resource problems being compounded by population and industrial growth.*” (Steward L. Udall).¹²⁾

Fortunately, President Lyndon Johnson, the US Congress, and the US public supported this idea, there were strong objections voiced by DoD and the State Department. This was indeed a new direction in the US space program at a time, when young NASA’s foremost task was to get a man on the moon (a national goal), in the middle of the Cold War and a hot war (Vietnam). NASA was given the task to plan and build the newly designated ERTS (Earth Resources Technology Satellite) spacecraft (launch of ERTS–1 on July 23, 1972) that was later renamed to Landsat–1.¹³⁾¹⁴⁾¹⁵⁾

In the words of Stephen S. Hall (Ref. 54), the Landsat project was a political stepchild in the 1960s, sought by scientists but shunned by the military, claimed by the Interior Department but coveted by Agriculture, a nuisance to NASA and undermined at almost every step of the way by the Bureau of Budget (later the Office of Management and Budget). The military and the National Security Council didn’t like the idea of the civilian community looking at the Earth at all. – In the long run, the greatest benefits of the space program have come from those satellites that, year in and year out, steadily and unspectacularly help us understand our planet better, improve lives, and, as in a recent program to identify breeding areas of the insect that causes sleeping sickness, even save lives. There is a place for manned flight, but over the long haul it can’t compete with the satellites. Former astronaut Walter Schirra admitted back in 1972, when he said, “We should start looking down instead of up.”

The introduction of new technologies was and is fundamental and indispensable to all aspects of space flight. New types of instruments were developed and flown, many of them capable of detecting and measuring radiation (such as radiometers) in the visible to microwave region of the spectrum.¹⁶⁾ The creativity of the space age generated in effect a revolution and an evolution in sensor technology resulting in a multitude of sensor types as well as in many other innovations. The concepts of these new instruments were based on such diverse fields as optics, solid–state electronics, pattern recognition, signal processing, computer technology, and communications. The history of humankind is in general characterized by an evolution of tools. At the start of the 21st century it can safely be stated that the space age was instrumental of initiating and fostering new and vastly improved measurement technologies, accompanied by the greatest instrument–development spree (tools) in the history of science.

11) <http://academic.emporia.edu/aberjame/remote/landsat/landsat.htm> (Author: J. S. Aber)

12) P. D. Lowman, “Landsat and Apollo: The Forgotten Legacy,” PE&RS, Vol. 65, No 10, Oct. 1999, pp. 1143–1146

13) Ironically, objections of the State Department and DoD against the distribution of civil high–resolution Earth imagery (in the optical and microwave regions) and the proliferation of space technology have been around ever since and continue to be a major issue in US space policy. Special rules (including shutter control) may be imposed in particular conflict situations to restrict US–based commercial remote–sensing firms from unauthorized distribution of their imagery. Special rules apply also to the export of space technology by US companies. However, with space–imaging technology readily available outside the USA, the US–internal control functions became more or less ineffective as of 2000. Note: the US military campaign in Afghanistan, launched in the wake of the terrorist attacks in New York and Washington D. C. (Sept. 11, 2001), led to US government action to purchase every high–resolution satellite image of Afghanistan produced by the Ikonos spacecraft. This was a purely commercial deal that should not be confused with a government–ordered denial of access. Of course, with such a good customer, Space Imaging had no need and desire to sell its Ikonos imagery from Afghanistan to anybody else.

14) The policies on US remote sensing technologies and their restrictions evolved from two primary sources: a) the secret capabilities first developed for the NRO (National Reconnaissance Office), and b) civil systems like the Landsat series instruments MSS and TM. Originally, commercial considerations were not a factor in either of these areas.

15) P. L. Hays, R. F. Houchin, “Commercial Spysats and Shutter Control: The Military Implications of the US Policy,” Proceedings of AIAA Space 2000 Conference and Exposition, Long Beach, CA, Sept. 19–21, 2000

16) Note: The term “radiometer” is a generic label for any instrument that quantitatively measures the EM radiation in some interval of the EM spectrum.

A most important space–age achievement (along with parallel developments in the wide field of electronics) is the ability, to observe the Earth and its environment as well as the universe in **the entire breadth of the electromagnetic spectrum**. This in turn opened a new era in experimentation and discovery in virtually all fields of the Earth and space sciences. For instance, synoptic observations over wide regions of the Earth and the capability to communicate, process and interpret vast amounts of information, practically in real–time, has revolutionized the way we do things and in which scientists study the atmosphere, oceans, land, vegetation, glaciers, sea ice, and other environmental aspects of the Earth’s surface and their interactions. Earth observation has become the prime source of input for the considerable advances in the geosciences and many related disciplines, permitting research into the distant past, the present, and into the future (by assessing environmental impacts). As a consequence, Earth itself assumed a new clarity and gave us a better awareness of its dynamic nature. In the Sun–Earth system, space exploration provided for the first time a perception and understanding of the electromagnetic state of the interplanetary space between the Sun and the Earth. ¹⁷⁾

Beside the research benefits, Earth observation has also evolved to become a technology driver and a mature service provider for a large spectrum of useful applications, ranging from weather forecasting over monitoring and managing of Earth resources (crop surveys, mineral surveys) to navigation–aid systems and monitoring of international treaty compliance. Also, more emphasis is being placed on such fundamental issues as the global environment and its changes (global interconnectivity of weather phenomena, preservation of the bio–environment, etc.). *The goal is to develop predictive environmental, climate, natural disaster, and natural resource models to help ensure sustainable development and improve the quality of life on Earth.* – At the turn of the century/millennium, the new concept of **“formation flying”** [a combination of Earth observation, navigation (onboard propulsion), inter–satellite communication, onboard autonomy, and onboard processing functions] has the potential of revolutionizing the way the space community conducts Earth observation missions. The space community is just beginning to understand the potential and perspectives of satellite formation flying. New distributed observation concepts of spaceborne **bistatic and multistatic systems** are in the planning stage that may eventually permit more affordable spacecraft constellations for interferometric imagery.

The utilization of solar energy from LEO or MEO space power stations and conversion of the electricity into microwave energy for transmission to Earth are other concepts being explored and investigated today (lasers are also under consideration for beaming the energy from space). Space solar power – a dream today – has a good chance of becoming a reality in the decades ahead. ^{18) 19)}

In a long–term perspective, the past forty–five years of space flight at the start of the 21st century can be regarded as the “early or adolescence period” in the field of Earth observation and Earth science. The future requires truly concerted efforts to bring about solutions for such unsolved global problems as biosphere–climate–interactions, and much more. All indications on enabling technology developments lead to the conclusion, that the best is yet to come, leading to a better understanding of the total Earth System. – “Earth functions as a system – a large, complex, and dynamic one, but a system nonetheless. It is affected in

- 17) Note: The “First Symposium on Remote Sensing of Environment” took place in Feb. 1962 – when the Institute of Science and Technology at the University of Michigan, a research organization funded by the US military, invited seventy agronomists, agriculturists, foresters, geologists, hydrologists, land–use experts, photogrammetrists, and of course, cartographers. From that date, civilian remote sensing as a discipline began to come of age. On that same date, the two converging streams (military and civil) began to back up behind a dam of security and secrecy. Scientists complained about how the military scrambled to classify information about remote sensing. William Fischer, a photogeologist at USGS, who attended that first meeting, returned to Washington and suggested to his boss at the Department of the Interior, William T. Pecora, that the time might be right for a remote–sensing satellite. (Ref. 54).
- 18) J. C. Mankins, “A Technical Overview of the SUNTOWER Solar Power Satellite Concept,” *Acta Astronautica*, Vol. 50, No 6, pp. 369–377, 2002
- 19) S. Magnuson, “Japanese Scientists, Politicians Support Space Solar Power,” *Space News*, Mar. 18, 2002, p. 15

measurable ways by external forces such as the sun and its variability, and by the internal forces that are shaped by variations in the atmosphere, oceans, continents, life, and the complex web of interactions among them.

We are the first generation with the ability to observe global—scale changes from the perspective of space and the scientific knowledge to link them with their causes and consequences. This ability to record and understand global change will be among the greatest gifts that we can offer our children and their children after them, for it will put in their hands the power to make informed decisions about the environmental challenges of the future.

The quest for a true predictive capability for Earth system changes requires a flexible and progressive space system architecture. That's why we need to design and establish a smart, autonomous, and flexible constellation of Earth—observing satellites that can be reconfigured based on the contemporary science and specific issues at hand.”²⁰⁾

United Nations statistics in the 1990s reveal that less than half of the Earth's exposed land has been mapped at scales suitable for economic development measures. The need is particularly great for Africa. The answer lies in satellite image maps, which are accurate and can be quickly compiled and systematically updated. Satellite image maps have become the mapmaker's benchmark for small and medium scale mapping. Moreover, Earth observation satellites have become the precious allies of a new type of agriculture managed from the sky, especially in developing countries where agricultural management is still at an early stage. With a single glance they report on crop areas, identify soil types and inventory water resources. All of which can be used to plan future agricultural development. Likewise, as the season changes, they monitor crop changes and enable early detection of diseases. Today, Earth observation satellites are becoming an extremely valuable monitoring and decision—making tool for disasters and environmental hazards (assessment of the extent of destruction, etc.).

The term “**Digital Earth**” was coined by US Vice President Al Gore, presented in a speech at the California Science Center in Los Angeles, on Jan. 31, 1998. His vision of the proposed concept model of “Digital Earth” refers to a multi—resolution, 3—D virtual representation of Earth, into which geo—referenced data can be embedded. A “Digital Earth” (along with Digital Earth Models) offers, for instance, a mechanism for users to navigate and search for geospatial information, etc. The consistent combination of all of this information is only possible if the reference frame is provided by geodesy. — Obviously, such an objective is so vast, that only international standardization bodies can undertake such a project. But it has to happen! The benefits of such a seamless system are apparent to the entire Earth Observation community. Eventually, the data from “Digital Earth” may also contribute to a new genre of virtual reality applications.

Prior to Digital Earth, a number of technical challenges have to be addressed and solved in such areas as graphics, visualization, image processing, spatial data structures, computer cartography, and support of global and regional modeling. Geovisualization and 4—D simulation will require parallel—processing, high—performance (teraflop) computing architectures and advanced (100—plus terabyte) storage systems. Even the most powerful computers and storage devices will require optimization of software functions and maximal data compression. A new class of space/time/entity/process linkage systems must be invented to represent and analyze spatial phenomena across fields as diverse as medicine, biology, engineering and physics.

Regarding to the activities on the research of Digital Earth, the most significant event was the “International Symposium on Digital Earth,” held in Beijing from Nov. 29 to Dec. 2, 1999. The symposium was organized by the Chinese Academy of Sciences (CAS), and at-

20) Daniel S. Goldin, “NASA in the 21st Century,” Millennial Challenges Colloquium series, Oct. 10, 2000, the address was presented at JHU/APL, Laurel, MD

tended by over 500 delegates from 27 countries. The meeting set up an International Steering Committee for ISDE (International Symposium on Digital Earth). ²¹⁾

During the 1990s, industry is gearing up as a commercial total system (space and ground segment owner and operator) service provider. ²²⁾ The global research community is still a very large user of remotely sensed data, but an increasing amount of Earth observation data (information) permeates also into applications for everyday use. This development into a wider base is indeed a good perspective for a maturing service and utility environment.

At the turn of the 21st century, first attempts are being made by space agencies to design and demonstrate optical instruments to permit “remote sensing applications” from GEO (Geostationary Orbit). Earth observation missions (with spatial resolutions in the range of 1–4 km in the optical region of the spectrum) from GEO are rather challenging due to their enormous distance from the Earth’s surface (about 36,000 km, or 45 times further away than from normal LEO altitudes of 800 km). Still, Earth observation missions from GEO are very attractive, offering the advantage of a continuous viewing capability, which so far has only been employed by GEO weather satellites (much better data resolutions). NASA plans to fly GIFTS (Geostationary Imaging Fourier Transform Spectrometer) in 2006.

The intent of this chapter on “Earth Observation Short History” is to **put some events, pertaining to the wide field of Earth observation, into proper (thematic) context** – the past has to be known and understood in order to plan for the future. The emphasis is on sensor technologies, system concepts, observation techniques, operational aspects, and navigation. Of interest is also the introduction/provision of general services and the start of international cooperation. ²³⁾ The select nature of this EO–history overview precludes any claim for completeness. The scope of Earth observation is so immense, I simply do hope that some of the most important achievements are properly covered or even mentioned. It should also be pointed out that there is plenty of room left, as well as considerable needs, for creativity and innovation to continue to change things for the better. – At the beginning of the 21st century, a better understanding is emerging of the relationship between technology development and the ability to do science.

Of all satellite launches on a worldwide scale, 70–75% are commercial communication satellites, the rest are military and civil satellites for such services as surveillance, technology development, Earth observation and navigation. Hence, telecommunication is by far the most widespread application of space technology. ²⁴⁾ The field of Earth observation is in second place when compared by the number of spacecraft launches. Next to telecommunications, remote sensing may be the most significant commercial application in the space industry – one which, like satellite telecommunications, has the potential to fundamentally change the way certain industries operate.

Space programs, in particular high–risk technology demonstration missions, are by nature technology drivers, due to the high demands on their functional capabilities, performances, and services in system hardware and software (service includes operational aspects). The term technology driver implies also technology transfer opportunities. Technology development in virtually any space program of the world is mostly carried out by the space industry of a country (or in a number of member countries like those of ESA) in response to an

- 21) H.–D. Guo, C.–L. Wang, “Digital Earth: Bridging the Scales from Global to Local for Sustainable Development,” 4th ISDE, Tokyo, March 28–31, 2005; URL: <http://www.millenniumassessment.org/documents/bridging/papers/huadong.guo.pdf>
- 22) J. C. Baker, K. M. O’Connell, J. A. Venzor, “Commercial observation satellites: broadening the sources of geospatial data,” *Optical Engineering*, Vol. 41, No 9, Sept. 2002, pp. 2077–2082
- 23) The fields of signal processing, data processing, interpretation and use (applications) are topics outside the scope of this text. The interested reader is given a good survey reference: Celebrating a half Century of Signal Processing, “The Past, Present and Future of Image and Multidimensional Signal Processing,” *IEEE Signal Processing Magazine*, March 1998, pp. 21–58
- 24) Background Paper No 5: “Space Communications and Applications,” UNISPACE–III Conference in Vienna, Austria, July 19–30, 1999, p. 112, A/CONF.184/BP/13 with the title: Space Benefits for Humanity in the Twenty–First Century, ISBN: 92–1–100818–2

agency's need. Over the years, it has become increasingly necessary for the economy of any spacefaring nation to transfer and to share the enabling technologies as well as the knowledge/expertise to the industry in general. Technology transfer means that a technology developed for a particular application, turns out to be conceptually more general in its functionality and in its application range than originally identified, planned, or envisaged.

It is then used as a spin-off in sometimes totally different areas of applications, resulting in a benefit to all involved. Start-up companies are often set up in the wake of newly developed technologies (promising ideas and concepts), usually by the same people/experts involved in the particular development, to exploit them with marketable products. Technology transfer often implies also licensing of a product, and/or a process, and/or a service. Besides totally new technology developments, many space agencies, military establishments, institutions, and space industry, invested (and continue to invest) in particular in raising the available technologies of their programs to new levels of performance and functional capabilities. The range of these advanced applications – of new technologies and of improved (or advanced) technologies – is certainly enormous; hence, many organizations [NASA, ESA, JAXA (formerly NASDA), CNES, etc.] have established special programs to better facilitate technology transfer and commercialization.

It is ideas (unusual and daring ones) and imagination, coupled with a considerable amount of determination and persistence, that bring about innovation and technology development. ²⁵⁾ In 2001, I was somehow quite irritated when I discovered ESA's decision to drop the proposed atmospheric mission CLOUDS (Cloud and Radiation Monitoring Satellite), an excellently defined project study (after all, it represented a real consistent approach, the best definition I had seen so far of any project), conducted by 12 European partners. Considerable investments of time and money had gone into the realization of this study. The main arguments for the non-selection of CLOUDS were that the **payload complement lacked at least to some degree an element of daring concept introduction needed for future observations**. Tight budgets were of course another reason. Eventually, the EarthCARE (Earth Clouds Aerosol and Radiation Explorer) proposal was considered as more advanced to fill the gap. Space research, in particular technology introduction into instrumentation and/or spacecraft, is by its very nature an inherently high-risk and also a high-payoff enterprise. Trying and failing is often far better than not trying at all. High-risk development projects require an aggressive approach; they are a necessary complement to those (conventional service) missions, in which new ideas, approaches and technologies are more or less avoided to maximize the chances of success.

Yuri Gagarin, the first Soviet cosmonaut, the first human in outer space, reported: "Circling the Earth .. I marveled at the beauty of our planet .. Looking at our Earth from space, what strikes me is not only the beauty of the continents .. but their closeness to one another ... their essential unity. The different parts that make up the world all merge into one whole ... How worthwhile life would be on our planet, if the people of all the continents were to really become aware of their closeness .. their common interests .. Let us safeguard and enhance this beauty – not destroy it!" ²⁶⁾ *An American astronaut, Russell Schweickart, lunar module pilot on Apollo 9, had similar feelings. "You look down there and you can't imagine how many borders and boundaries you cross again and again ... and you don't even see them. From where you see it, the thing is a whole and it is so beautiful ... And there you are – hundreds of people killing each other over some imaginary line that you're not even aware of, that you can't even see ... You realize that on that small spot, that little blue – and – white thing is everything that means anything to you – all history, and music, and poetry, and art, and birth, and death, love, tears, joy, games."*

25) P. Brisson, D. Raitt, J. Rootes, "Down to Earth – Everyday Uses for European Space Technology," ESA Bulletin, No. 108, Nov. 2001, pp. 21–31

26) Anatoly Gromyko, Martin Hellman (Editors in Chief), Craig Barnes, Alexander Nikitin (Executive Editors), Olivia Simantob (Online Editor), "Breakthrough, Emerging New Thinking," Soviet and Western Scholars Issue a Challenge to Build a World Beyond War, Walker and Company, New York, 1988 – Online version: www.global-community.org/breakthrough/book/pdfs/breakthrough.pdf

All of humanity now shares that picture of the Earth from space. We are one human species; we live on one tiny, fragile planet suspended in the darkness of space; there is one life–support system that maintains us all. The borders and boundaries that separate us are artificial. Whatever our differences – however emotional they are, however intractable they have become, however inevitable they may seem – they are insignificant compared to what we share.

An Earth observation and scientific research program may answer some of the following questions of profound importance to humankind: ²⁷⁾

- How is the Earth changing and what are the consequences of life on Earth?
- How is the global Earth system *changing*?
- What are the primary *forcings* of the Earth system?
- How does the Earth system *respond* to natural and human–induced changes?
- What are the *consequences* of changes in the Earth system for human civilization?
- How well can we *predict* future changes in the Earth system?

Earth observation gives a new view and perception onto as well as into Earth – providing a new understanding of Earth system processes on a global scale; its information may also serve as a much improved assessment tool for decision support on all levels.

The ultimate challenge of Earth system science is to consolidate all scientific findings (observations) from the different disciplines into an integrated representation of the coupled atmosphere, ocean, ice, land and biosphere system, including the sun–Earth connection. This involves nothing less than the development of high–resolution modeling of the Earth system and a continuous process of re–assessment and improvement of these models. Impressive models already exist within each individual Earth science discipline, the models incorporate many relevant components.

27) G. Asrar, “NASA’s Role, Its Plan and Achievement in Global Climate Research,” Proceedings of the Weikko A. Heiskanen Symposium in Geodesy, Ohio State University, Columbus, OH, USA, Oct. 1–4, 2002

1.1 GEOSS (Global Earth Observation System of Systems)

An important step into the direction of a unified Earth observation approach was done at the **GEO** (Group on Earth Observations) summit in Tokyo, Japan, on April 25, 2004 when GEOSS was created. GEO was actually launched in response to calls for action by the 2002 World Summit on Sustainable Development and by the G8 (Group of Eight) leading industrialized countries. GEO is a voluntary partnership of governments and international organizations. It provides a framework within which these partners can develop new projects and coordinate their strategies and investments. – As of October 2010, the GEO intergovernmental organization includes 84 members and 58 participating organizations with a mandate in Earth observation or related issues have been recognized. ^{28) 29) 30)}

GEOSS is an international framework to develop a 10–year implementation plan (for the period 2005–2015), a comprehensive, coordinated and sustained system that will help to better understand Earth systems, including weather, climate, oceans, water cycle, geology, ecosystems, agriculture and biodiversity, energy, disasters, etc.. Representatives of 47 countries and more than a dozen international organizations [UN (UNEP, FAO, UNESCO), ESA, EUMETSAT, EC, ECMWF, ISCU, WMO, IGOS–P, CEOS, WCRP, etc.] were present at the ad hoc GEO (Group on Earth Observations) summit, signing the document (the finalization of a draft implementation plan). ³¹⁾

Recognizing that the societal benefit of Earth observations cannot be achieved without data sharing, GEOSS aims at reaching a “targeted collective action” and bases on a full and open exchange of data, metadata and products, which will be made available with minimum time delay and at minimum cost.

The plan represents a useful step forward in turning the GEOSS idea into a reality. The aim behind GEOSS is to maximize the effectiveness of Earth Observation by minimizing data gaps, building capacity and exchanging information as fully and quickly as possible. Developed and developing nations alike will have access to all data gathered by the network, following the model of the World Meteorological Organization’s four–decade–old World Weather Watch, which coordinates the globe’s weather satellites along with in–situ climate stations. ^{32) 33)}

Note: The ad hoc intergovernmental Group on Earth Observations (GEO) was created during the first “Earth Observation Summit” in Washington DC (July 31, 2003) and was made responsible for producing a 10–year program to coordinate space– and ground–based global monitoring systems, to be known as GEOSS.

GEOSS will be a distributed system of systems, building step–by–step on current cooperation efforts among existing observing and processing systems within their mandates, while encouraging and accommodating new components. Participating members will determine ways and means of their participation in GEOSS. ³⁴⁾

For the success of GEOSS, interoperability among each system is mandatory.

28) Jose Achache, “GEO Progress and Issues for the Future,” 24th CEOS Plenary, Rio de Janeiro, Brazil, October 12–15, 2010, URL: http://www.dpi.inpe.br/ceos/apresentacoes/Item_07_CEOS_Achache.pdf

29) Russell J. Lefevre, Jay Pearlman, Thomas Freud Wiener, “The Role of Science and Technology in GEOSS,” Proceedings of the 2010 IEEE Aerospace Conference, Big Sky, MT, USA, March 6–13, 2010

30) “The Role of Science and Technology in GEOSS,” Prepared by the GEO Science & Technology Committee, EC, 2008, URL: <http://ec.europa.eu/research/environment/pdf/geoss.pdf>

31) S. Di Ciaccio, G. Rum, “Remote Sensing Data as Global Public Goods – A founding concept for the Global Earth Observation System of Systems,” Proceedings of the 58th IAC (International Astronautical Congress), International Space Expo, Hyderabad, India, Sept. 24–28, 2007, IAC–07–B1.5.01

32) D. Normile, “Summit Pledges Global Data Sharing,” *Science*, Vol. 304, April 30, 2004, p. 661

33) G. Gibbs, B. O’Donnell, B. Smith, H. M. Wood, “Group on Earth Observations (GEO): Toward Comprehensive, Coordinated, and Sustained Global Observations,” Proceedings of IAF/IAC 2004, Vancouver, Canada, Oct. 4–8, 2004, Paper: IAC–04–B.1.05

34) Y. Furuhashi, “GEOSS Challenges and Asia–Pacific Activities,” Proceedings of IGARSS 2004, Anchorage, AK, USA, Sept. 20–24, 2004

- Standards and practices: For each observation type or system, it is essential that standards are being developed, shared and implemented internationally. Otherwise, the value of the Earth observation investments will be significantly reduced.
- Data quality: Data quality is at the heart of every step of data management. Data are processed automatically more and more, the impact of the ingestion of bad data will become more serious and costly.

The 10–year GEOSS program implementation plan was formally approved/adopted by government delegates at the 3rd Earth Observation Summit on February 16, 2005 in Brussels, Belgium. Nearly 60 nations and about 40 international organizations, including ESA, EUMETSAT, and the EC (European Commission), are working to establish the emerging network of Earth observation systems. The participants have also agreed to share their scientific data. The 10–year plan states: “*The vision for GEOSS is to realize a future wherein decisions and actions for the benefit of humankind are informed by coordinated, comprehensive and sustained Earth observations and information.*” The plan sets out a timescale for achieving certain objectives in the fields of improved Earth monitoring, understanding of Earth processes and prediction capabilities for the behavior of Earth systems.

The 10–year implementation plan prescribes a user–driven approach to the creation of GEOSS.³⁵⁾ GEOSS interoperability arrangements are to be based on the view of complex systems as assemblies of components that interoperate primarily by passing structured messages over network communication services. The core in building and operating GEOSS is thus interoperability specifications established and adhered to by all contributing systems. Building on existing systems and initiatives points to the importance of using existing international standards organizations and institutes in the identification and adoption of standards to achieve GEOSS interoperability objectives.

In November 28–29, 2007, another GEO Ministerial Summit convened on Cape Town, South Africa. Some early achievements: The GEO community is benefiting from coordinated planning and improved interoperability of systems, increased collaboration, streamlined communications, more efficient exchange of data and information, improved access to global Earth observation data, and a better understanding of user needs.^{36) 37) 38) 39)}

In particular, a rich menu of topics, “List of Early Achievements – GEOSS Transverse Components”, is described and illustrated. The reader is asked to consult the following reference.⁴⁰⁾

The GEOSS Implementation Plan has identified nine different user communities, called SBA (Societal Benefit Areas), that are responding to the challenges posed by climate and technology change (Figure 2). Each SBA has unique needs and capabilities but can share common services and approaches through a network of community portals.

-
- 35) R. Garello, J. Pearlman, J. J. S. Khalsa, R. Shibasaki, “IEEE Committee on Earth Observation and GEOSS,” Proceedings of IGARSS 2006 and 27th Canadian Symposium on Remote Sensing, Denver CO, USA, July 31–Aug. 4, 2006
- 36) “Report on Progress 2007,” Cape Town Ministerial Summit, GEO, Nov. 30, 2007, URL: http://earthobservation.org/documents/2007_GEO%20Report%20on%20Progress.pdf
- 37) “Cape Town Declaration,” Cape Town Ministerial Summit, GEO, Nov. 30, 2007, URL: http://earthobservation.org/05_Cape%20Town%20Declaration.pdf
- 38) Douglas M. Muchoney, “An Evolving Business Model for Commercial Imagery: How Will GEOSS Help?,” Proceedings of the JACIE 2008 Workshop (Joint Agency Civil–commercial Imagery Evaluation), March 25–27, 2008, Fairfax, VA, USA, URL: http://calval.cr.usgs.gov/JACIE_files/JACIE08/2008_JACIE_DVD/Tuesday_AM/Muchoney_GEO.pdf
- 39) George Percivall, “GEO Architecture and Data Committee, Task AR–07–02, Architecture Implementation Pilot,” Feb. 6, 2008, URL: <http://www.ogcnetwork.net/system/files/080206+ADC–6+Percivall.ppt>
- 40) “The First 100 Steps to GEOSS,” Annex of Early Achievements to the Report on Progress 2007, Cape Town Ministerial Summit, GEO, Nov. 30, 2007, URL: http://earthobservations.org/documents/2007_%20Annex%20of%20Early%20Achievements%20to%20the%20Report%20on%20Progress.pdf

To be developed over ten years: 41) 42) 43)

- GEOSS AIP programs are coordinated by the Open Geospatial Consortium (OGC)
- 2007–08 Phase 1 demonstrated GEO Portal and Clearinghouse solutions. As of Nov. 2007, these are now called: IOC (Initial Operating Capability)
- 2008–09 Phase 2 augments IOC with “persistent” services to support SBAs and GEOSS Infrastructure
- Pilots address data and information architecture interoperability and user support
- Implemented using international standards.

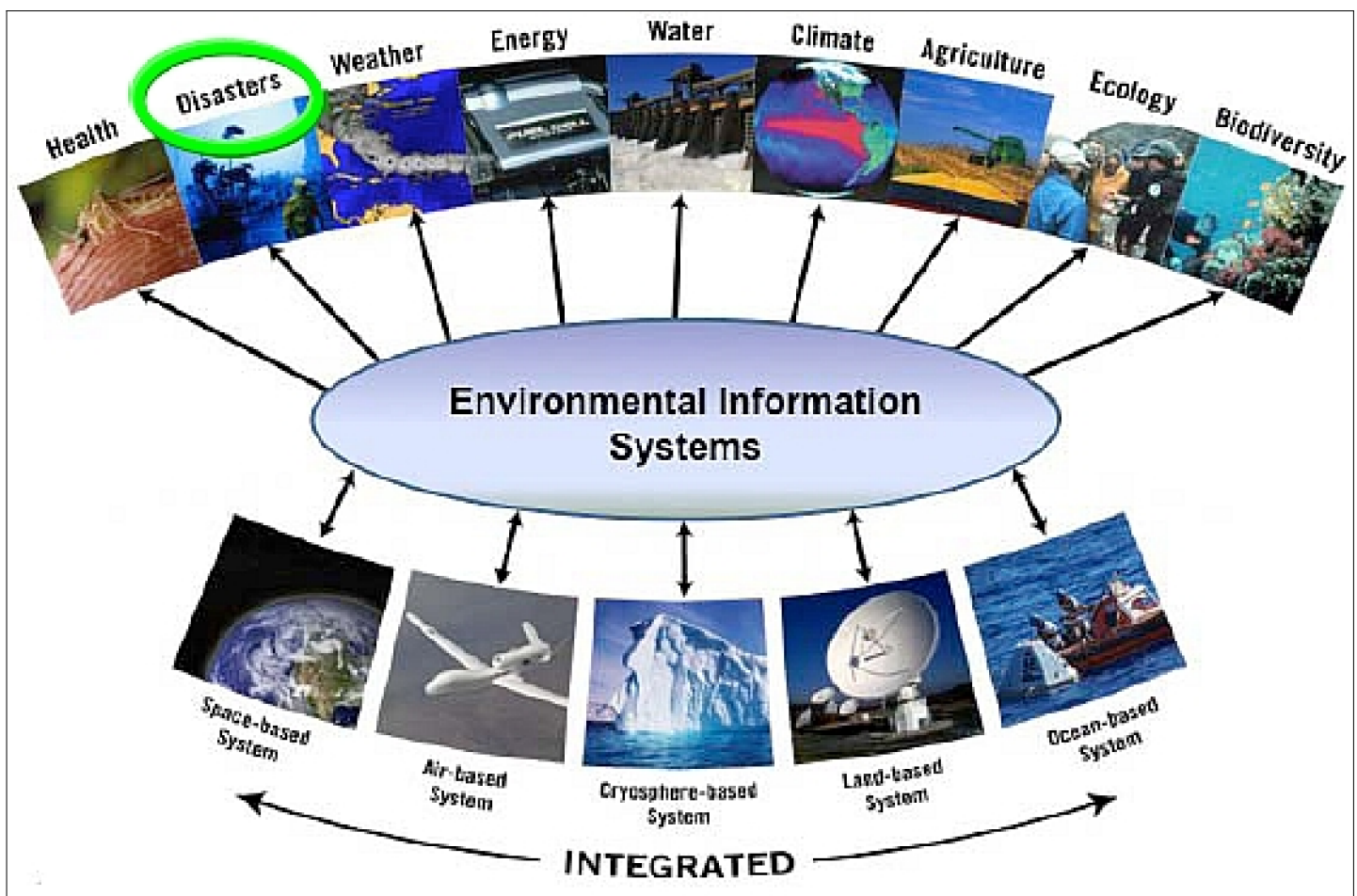


Figure 2: GEOSS AIP (Architecture Implementation Pilot) phase 2 as of June 2008

- 41) Morris Brill Ronald Lowther, “A User–Centric System–of–Systems Approach for Delivery of Actionable Earth Environmental Data,” Proceedings of the Ground System Architectures Workshop (GSAW 2009), Torrance, CA, USA, March 23–26, 2009, URL: <http://sunset.usc.edu/gsaw/gsaw2009/s2/brill.pdf>
- 42) “GEOSS Architecture Implementation Pilot,” URL: <http://www.ogcnetwork.net/AI/pilot>
- 43) “The Space–based Global Observing System in 2010 (GOS–2010),” WMO Space Programme SP–7, WMO/TD–No. 1513, 2010, URL: ftp://ftp.wmo.int/Documents/PublicWeb/sat/SP-7_TD-1513_GOS-2010.pdf

1.2 Decadal Survey:

The Space Program of the United States received a strategic external assessment and a new focusing of its priorities in January 2007 when the NRC (National Research Council) committee of NAS (National Academy of Science) released a report entitled: *“Earth Science and Applications from Space: National Imperatives for the Next Decade and Beyond”* which was requested by NASA, NOAA, and the US Geological Survey (USGS). This “**decadal survey**”, as it is simply referred to, recommended a series of space missions for NASA and NOAA to undertake over the course of the next decade to further humankind’s knowledge of the Earth system. ⁴⁴⁾

Earth observations from satellites and in situ collection sites are considered critical for an ever-increasing number of applications related to the health and well-being of society. The committee found that fundamental improvements are needed in existing observation and information systems because they only loosely connect three key elements:

- The raw observations that produce information
- The analyses, forecasts, and models that provide timely and coherent syntheses of otherwise disparate information
- The decision processes that use those analyses and forecasts to produce actions with direct societal benefits.

The committee offered the following overarching recommendation: *The US government, working in concert with the private sector, academe, the public, and its international partners, should renew its investment in Earth-observing systems and restore its leadership in Earth science and applications.*

Partnerships in the various programs are advocated to obtain improvements that are needed in the structure, connectivity, and effectiveness of Earth-observing capabilities, research, and associated information and application systems—not only to answer profound scientific questions, but also to effectively apply new knowledge in pursuit of societal benefits.

The committee recommended to address in particular the environmental and societal challenges by taking up key scientific questions related to ice sheets and sea-level change, large-scale and persistent shifts in precipitation and water availability, transcontinental air pollution, shifts in ecosystem structure and function in response to climate change, impacts of climate change on human health, and the occurrence of extreme events, such as severe storms, heat waves, earthquakes, and volcanic eruptions.

Specific recommendations were given for long-term programs in development such as NPOESS, GOES-R (Next generation Geostationary Operational Environmental Satellites), GPM (Global Precipitation Measurement mission), and LDCM (Landsat Data Continuity Mission), to retain/restore the original program goals with regard to the sensor complements which are considered vital for a sustainable observation capability – in spite of budgetary shortfalls.

The committee’s recommended Earth observation strategy for the next decade consists of 17 missions (a prioritized set). Along with the missions themselves, the decadal survey provided a notional schedule for implementation of these missions.

- CLARREO (Climate Absolute Radiance and Refractivity Observatory). Monitoring of solar and Earth radiation characteristics for understanding climate forcing. The goals of the CLARREO mission are to provide a benchmark climate record that is global, accurate in perpetuity, tested against independent strategies that reveal systematic errors, and pinned to international standards (SI traceability).

44) Executive Summary: “Earth Science and Applications from Space: National Imperatives for the Next Decade and Beyond,” URL: http://www.nap.edu/nap-cgi/report.cgi?record_id=11820&type=pdfxsum

-
- SMAP (Soil Moisture Active/Passive) mission – to monitor global soil moisture with unprecedented resolution, sensitivity, area coverage, and revisit times. SMAP will use a combined radiometer and high-resolution radar to measure surface soil moisture and freeze–thaw state.
 - ICESat–2 (Ice, Cloud and land Elevation Satellite–2) – to quantify the polar ice sheet mass balance to determine contributions to current and recent sea level change and impacts on ocean circulation.
 - DESDynI (Deformation, Ecosystem Structure, and Dynamics of Ice) – a combined radar/lidar mission to collectively study the solid Earth, the ice masses, and ecosystems systematically and globally.
 - HypsIRI (Hyperspectral Infrared Imager) mission – to detect responses of ecosystems to human, land management, and climate change and variability.
 - ASCENDS (Active Sensing of CO₂ Emissions over Nights, Days, and Seasons) – to enhance understanding of the role of CO₂ in the global carbon cycle with three science objectives: distribution of the atmosphere, distributions of terrestrial and oceanic sources and sinks, and provide a prediction mechanism for CO₂ distributions.
 - SWOT (Surface Water Ocean Topography) mission, formerly called: WATER HM (Water And Terrestrial Elevation Recovery) Hydrosphere Mapper. The goal is to contribute to a fundamental understanding of the Earth system by providing global measurements of continental surface water storage changes and discharge, which are critical for water and climate cycle models.
 - GEO–CAPE (Geostationary Coastal and Air Pollution Events) mission. The objective is to collect data that identifies human versus natural sources of aerosols and ozone precursors, tracks air pollution transport, and studies the dynamics of coastal ecosystems, river plumes and tidal fronts.
 - ACE (Aerosol Cloud Ecosystems) mission – to answer emerging fundamental science questions associated with aerosols, clouds, air quality and global ocean ecosystems.
 - LIST (Lidar Surface Topography) mission – to provide global high resolution topography mapping (5 m spatial, 0.1 m vertical accuracy) to detect active faults, global shifts in vegetation patterns, etc.
 - PATH (Precipitation and All–weather Temperature and Humidity) mission – a microwave array spectrometer was recommended as a suitable payload to monitor hurricanes and severe storms and improve models.
 - GRACE–2 (Gravity Recovery and Climate Experiment–2) – to provide high–temporal–resolution gravity fields for tracking large–scale water movement
 - SCLP (Snow and Cold Land Processes) – to monitor frozen landscapes – cold areas of the land surface where water is frozen either seasonally or permanently. These areas form a major component of the Earth’s hydrological system, and interact significantly with the global weather and climate system, the geosphere, and the biosphere.
 - GACM (Global Atmospheric Composition Mission) – to monitor the atmospheric composition observations, along with cloud ice and water vapor data needed for improvements in climate and weather forecasting models. The mission comprises ultraviolet and infrared nadir and microwave limb viewing instruments observing wide swaths each orbit.
 - 3D–Winds (Three–dimensional Tropospheric Winds) mission – to monitor tropospheric winds for weather forecasting and pollution transport.
 - XOVWM (Extended Ocean Vector Winds Mission) – to provide high–resolution ocean vector winds.

1.3 Some background on policies of commercial high-resolution imagery

In the time frame 1960 to the early 1990s (the so-called Cold War period), spaceborne high-resolution imagery was the exclusive province of the two superpowers, USA and the USSR (Union of Soviet Socialist Republics). Both of them used dedicated military reconnaissance satellite systems to collect strategic intelligence with film-based camera and capsule reentry systems.^{45) 46)} The level of secrecy was extremely high, and the technology was restricted to the military sector (in particular, national interests were of great priority). In the USA, no civil applications were allowed for spaceborne imagery below 30 m GSD (Ground Sample Distance). This corresponded directly to the imagery provided by the Landsat series of NASA. All bands of LS-4/5 had a spatial resolution of 30 m (except band 6 with 120 m). LS-4 was launched July 16, 1982, LS-5 was launched March 1, 1984.⁴⁷⁾

The availability of high-resolution imagery on a commercial basis is a fairly recent event in spaceborne remote sensing history. The government restrictions began to erode in the mid 1980s, with the commercialization of the Landsat program and the response to the development/operation of the SPOT series by CNES (France). Escalating Landsat costs led to its commercialization in 1983, and in July 1984 the “Land Remote Sensing Policy Act” turned over Landsat operation to the Eosat corporation.⁴⁸⁾

Some of the events are enumerated:

- In the fall of 1987, the USSR made the images, taken by the KFA-1000, the MK-4, and the MKF-6 film-based camera systems (flown on the Resurs-F1 and -F2 system series as well as on other spacecraft), commercially available; these were panchromatic (i.e., black and white) as well as color images at spatial resolutions of 5–10 m. Then in 1992, two Russian companies began to sell selected high-resolution imagery acquired by the KVR-1000 camera of the Kometa spacecraft series (film camera, spatial resolution imagery of 2 m). This panchromatic camera was designed for intelligence applications and is still being used by the Russian intelligence community.⁴⁹⁾
- The potential of commercial imagery gained considerable momentum in the late 1980s when the space agencies of several countries announced plans to develop and launch high-resolution commercial imaging systems. For instance, France started its very successful SPOT satellite series in Feb. 1986 with the launch of SPOT-1 providing a spatial resolution of 10 m (first long-term introduction of CCD detector technology). ISRO of India followed closely with its IRS series imaging satellites (launch of IRS-1A in 1988). Realizing these facts and the current practises of high-resolution imagery sales by Russia, the US government removed some of its restrictions in January 1988 to remain commercially competitive (on the international scene).
- In Oct. 1992, the Land Remote Sensing Policy Act (US Congress) was signed into law.⁵⁰⁾ This law reversed the 1984 decision to commercialize the Landsat system and recognized the scientific, national security, economic, and social utility of “land remote sensing from space.” In addition, it streamlined the procedure for considering license applications for commercial imaging satellites, and eliminated many of the legal obstacles that had been imposed in 1972 to prevent approval of most such applications.

45) G. Steinberg, “Dual Use Aspects of Commercial High-Resolution Imaging Satellites,” *Mideast Security and Policy Studies*, No. 37, February 1998, URL: <http://www.biu.ac.il/Besa/books/37pub.html>

46) L. W. Fritz, “High Resolution Commercial Remote Sensing Satellites and Spatial Information Systems,” <http://www.isprs.org/publications/highlights/highlights0402/fritz.html>

47) G. T. Richardson, R. N. Merz, High-resolution Commercial Imagery and Open-Source Information: Implications for Arms Control,” *Intelligence Note*, May 16, 1996, URL: <http://www.fas.org/irp/offdocs/acda.htm>

48) US Congress, 1984. Public Law 98-365: Land Remote-sensing Commercialization Act of 1984, 98th Congress, July 1984, U.S. Government Printing Office, Washington, D.C.

49) Z. Li, “High-Resolution Satellite Images: Past, Present and Future,” *Journal of Geospatial Engineering*, Vol. 2, No.2, 2000, pp. 21–26., URL: http://www.lsgl.polyu.edu.hk/STAFF/zl.li/vol_2_2/03_li_zl_1.pdf

50) US Congress, 1992. Public Law 102-555: Land Remote Sensing Policy Act of 1992, 102nd Congress, October 28, 1992, U.S. Government Printing Office, Washington, D.C.

-
- In 1993, after the commercialization of KVR–1000 imagery by Russia, the US Government implemented a new policy [Presidential Decision Directive (PDD) No 23] that encouraged the commercialization of high–resolution imagery into the international market. As a consequence, the DOC (Department of Commerce) granted the first US license in 1993 to DigitalGlobe’s predecessor, namely WorldView Inc. of Longmont, CO, allowing a private enterprise to build and operate a satellite system and to gather high spatial resolution digital imagery (1 m GSD) of the Earth for commercial sale. Under the new policy, a number of private companies have obtained licences for the operation of private satellite remote sensing systems.
 - In Feb. 1995, the US government declassified over 800,000 images taken between the years 1960 and 1972 – making the imagery available to the civil community (execute order by President Bill Clinton). The second declassification occurred in the fall of 2002 when NIMA (National Imagery and Mapping Agency) cleared imagery for public release from the KH–7 and KH–9 programs.
 - Since 1996, under the national space policy signed by President Bill Clinton (PDD No 49, Sept. 19, 1996), the U.S. government has been committed to using commercial imagery satellites to augment its capabilities, save money and help ensure the health of the domestic industry.
 - Space Imaging Inc. of Thornton, CO, obtained also a license for high–resolution imagery. The first spaceborne 1 m spatial resolution panchromatic **solid–state digital imagery** with an optoelectronic imager (using a CCD detector – i.e., no film) was obtained by the commercial spacecraft Ikonos–2 (launch Sept. 24, 1999) of Space Imaging. This was followed with data at a resolution of 0.62 m delivered by the optical imager of the QuickBird–2 mission (launch Oct. 18, 2001) of DigitalGlobe Inc. – Prior to this time, both companies had suffered severe setbacks with launch failures in their commercial ventures: Worldview/Earthwatch with its EarlyBird (launch Dec. 24, 1997) and QuickBird–1 (launch Nov. 20, 2000) satellites, and Space Imaging with its Ikonos–1 spacecraft (launch April 27, 1999).
 - In a significant shift in policy, the Bush administration has ordered US federal agencies to rely much more heavily on private satellite companies to provide high–resolution imagery from space (April 25, 2003). Obviously, the quality of commercial imagery has improved over the years to an extent that military interest in these commercial products is on the rise. Naturally, there are also hard economic reasons to change the policies toward dual–use by the civil and military communities.
 - NIMA (National Imagery and Mapping Agency), Arlington, VA, a US government agency, was established in Oct. 1996. NIMA incorporates the Defence Mapping Agency (DMA), the Central Imagery Office, and the Defense Dissemination Office as well as CIA’s Photographic Interpretation Center. NIMA is also the principal buyer of commercial imagery for all DoD organizations. In Nov. 2003, **NIMA was renamed to NGA (National Geospatial–Intelligence Agency)**.
 - To assure availability of imagery from the next–generation of commercial, high–resolution imaging satellites, NGA awarded DigitalGlobe with the first “**NextView**” vendor contract in Oct. 2003 – implementing a new level of partnering between the federal government and the US commercial remote sensing industry. It provides NGA and its military customers with greater access to and priority acquisition of high–resolution imagery. It further allows NGA to participate in the development cycle for commercial next–generation imaging capabilities.
 - The next high–resolution imaging satellite of DigitalGlobe (Longmont, CO) is called WorldView–1, a successor of QuickBird–2 (launch Sept. 18, 2007). The NGA requirements, a major sponsor of the system, call for imagery with a spatial resolution of 0.5 m pan-

chromatic and 2 m MS (Multispectral) data. – The GeoEye–1 (formerly OrbView–5, change of name on January 2006) satellite of GeoEye Inc. of Dulles, VA, (formerly OrbImage), was launched on Sept. 6, 2008. GeoEye Inc. The imager of the GeoEye–1 spacecraft provides panchromatic imagery with a resolution of 0.41 m and multispectral imagery with a resolution of 1.64 m on a swath of 15.2 km.

Improvement in imaging technology: In 1999, GeoEye’s Ikonos–2 remote–sensing satellite (formerly of Space Imaging Inc.) represented the “state of the art,” and its panchromatic detectors produced a spatial resolution of 82 cm. Nine years later, GeoEye–1 launched to the same orbital altitude with a camera and electronics that deliver black–and–white imagery at 41 cm spatial resolution, a five–times gain in power efficiency, a 10–times improvement in weight efficiency and a three–times advance in cost efficiency, according to GeoEye.

- Naturally, this doesn’t mean the end of military imaging (reconnaissance) satellites. The military establishments of the USA, Russia, China (ZY–2B), France (Helios–1, Helios–2), Israel (Ofeq series), Germany (SAR–Lupe constellation), Italy (COSMO–SkyMed constellation), Japan (IGS series), Spain, etc. are operating high–resolution imaging systems (in the optical and/or microwave region) or are in the process to do so (Germany). There is no intention in the foreseeable future to offer the classified imagery to commercial users.

Table 3 gives a general chronological overview of spaceborne imaging missions on a global scale. A lot of things have changed since the 1990s on the remote sensing scene. In the meantime, high–resolution commercial imagery is also available by a lot of other nations.

- In October 2008, the USGS (United States Geological Survey) made the entire Landsat archive, over 3 million images, available via the Internet at no cost. In the words of Adam Gerrand, Food and Agriculture Organization of the United Nations: “The opening of the Landsat archive to free, web–based access is like giving a library card for the world’s best library of Earth conditions to everyone in the world.”

The innovative benefits of open availability are: ⁵¹⁾

- Studies indicate societal value exceeds data acquisition and distribution costs
- Encourages development of research applications leading to innovative commercial endeavors.

51) Frank P. Kelly, “EROS – The Next 40 Years,” Proceedings of the 11th Annual JACIE (Joint Agency Commercial Imagery Evaluation) Workshop, Fairfax, Va, USA, April 17–19, 2012, URL: http://calval.cr.usgs.gov/wordpress/wp-content/uploads/Kelly_Frank_EROS-The-Next-40-Years-FINAL-for-JACIE-rev-1.pdf

1.4 Sensor/Technology Development

In the early years of Earth observation (in particular satellite meteorology) attention was focused on those phenomena which could be observed relatively directly in the visible and near–infrared bands of the spectrum. First images were obtained by photographic systems⁵²⁾ such as automated still or movie cameras, followed eventually by vidicon electronic imaging systems [a framing system of TV heritage – the image from the photoconductive surface (detector) is raster scanned by an electron beam; example: RBV (Return Beam Vidicon), AVCS],⁵³⁾ and later by optomechanical scanner systems [examples: M–7 an airborne multispectral mapper of ERIM (first flown in 1971) and MSS on Landsat–1, launch July 23, 1972 from VAFB, CA]. The TV cameras of the TIROS–1 satellite (launch April 1, 1960) provided daily low–resolution black and white pictures in the visible spectrum (panchromatic) of cloud cover and the Earth’s surface where clear. A time sequence of these synoptic coarse–resolution images permitted a visual interpretation by the meteorological community of large weather patterns which moved slowly across a continent (inferring atmospheric motions) – a first application of the emerging field of Earth observation. The TV cameras of the very next TIROS satellites experimented already with the infrared spectrum. The resulting images permitted a first look at the Earth’s heat distribution. In addition to the TV cameras, TIROS–2 and its successors experimented with the infrared spectrum by adding, variously, medium–angle, omni–directional and scanning radiometers.

The first years in Earth observation were dominated by such overall requirements for **repetitive coverage** (frequent observations) and the need of an **operational capability**, in particular for meteorological satellites. But it was also recognized that to create the new remote sensing technology, and to begin its utilization, would require an interdisciplinary effort by all parties involved. The challenges were monumental for research and technology development on all fronts, to create an infrastructure and to come up eventually with operational services.

The success of initial large–scale weather sensing started a planning and development period for better sensor systems, in particular with improved spatial and spectral resolutions, capable of land–surface imaging. Spectral resolution meant parallel sensing and detection in several bands of the visible and near–infrared spectrum. This technique was referred to as multispectral sensing, enhancing considerably the value (interpretability) of imagery.

The MSS (Multispectral Scanner System) instrument of the Landsat series (for land surface imaging) is such an early multispectral instrument (1972), with the visible and near–infrared spectrum almost evenly divided into four bands (band specification for MSS was simply adopted from airborne photographic experience of films).

The imagery of the Landsat–1 MSS instrument was a sensation of the time. Stephen S. Hall of USGS recalls the situation and his feelings of first Landsat imagery availability in the following way (book 1992). *Within days it had stunned geologists, rewritten the textbooks of forestry and land use, and revolutionized cartography.*⁵⁴⁾ *Its earliest transmissions revealed several dozen earthquake faults near Lake Tahoe and Monterey Bay in California, faults that had escaped the notice of geologists who had crawled over that same shifting seismic terrain for decades. Undiscovered lakes winked up at the camera. One early image of Alaska showed a forest fire eating through a forest north of Fairbanks; nothing unusual about that, except people in Fairbanks didn’t know about it. A ship stranded by chance in the Arctic Ocean received Landsat’s satellite maps of the ice pack and picked its way to freedom. Previously unseen terrestrial patterns*

52) Note: A photographic system is also referred to as a framing system. It means that all of the data in an image are acquired simultaneously.

53) RBV was a three–camera video system designed for what was then regarded as high accuracy cartographic mapping data. It was a successful proof–of–concept instrument, but one that was eclipsed in the science community by the more versatile and popular MSS.

54) Stephen S. Hall, “Ground Truth: Landsat Maps and the Remote–Sensing Revolution,” <http://edc.usgs.gov/earthshots/slow/Help–GardenCity/groundtruthtext> – – – Also book by Stephen S. Hall, “Mapping the next millennium; the discovery of new geographies,” New York, Random House, p. 52–70, 1992

took on the beauty of modern art and modern metaphor: there were peeling fragments of landscape around Elephant Butte, Montana, that reminded one of Clyfford Still, Cairo as it might be imagined by Helen Frankenthaler, a network of Russian roads imitating astrocytes in the mammalian brain. From those first heady days, Landsat images have graduated to the level of cultural artifacts with coffee-table status: the posters hang in offices and homes, the maps have generated entire atlases, the images fill year after year of calendars. The satellite taught us, NASA administrator James C. Fletcher said at the time, "a new way to look."

In this context: in the Soviet Union, a parallel development to MSS (on Landsat) took place with the development of the MSS Fragment instrument at IKI (Space Research Institute), an 8-channel imager with a spectral range of 0.4–2.4 μm , flown on Meteor–Priroda–5 (launch June 18, 1980). Fragment operated successfully onboard the spacecraft for four years.

Starting with Landsat–4 in 1982, a more sophisticated multispectral imaging sensor with the name of Thematic Mapper (TM) began its operation. It featured seven spectral bands and a ground resolution of 30 m in the VNIR bands. The TM band-selection process was on the basis of a comprehensive study and analysis of spectral reflection features for a variety of vegetation types. – The rather successful Landsat instruments eventually spawned other spaceborne Earth-surface imaging systems. Some of them are: The MOMS sensor missions on Shuttle (MOMS–01 in 1983), the SPOT satellite series sensors HRV (High Resolution Visible) of CNES (SPOT–1 launch in 1986), the Resurs–O1 series of Russia with MSU–E and MSU–SK (launch of Resurs–O1–1 in 1985), the IRS series of ISRO (launch of IRS–1A in 1988), JERS–1 of NASDA with OPS (launch of JERS–1 in 1992), ADEOS of NASDA with AVNIR (launch Aug. 17, 1996). See Table 3. At the beginning of the 21st century, the data from the Landsat S/C series constitute the longest record of the Earth's continental surfaces as seen from space. It is a record unmatched in quality, detail, coverage, and value.

Most of the instruments placed into orbit for the study of the Earth's atmosphere and surface have been of the type **passive sensors**,⁵⁵⁾ imagers and sounders operating in the visible, infrared and microwave spectral regions. Passive detection can only work, when the naturally occurring energy is available. The sun's energy is either reflected, as it is for visible wavelengths, or absorbed and then re-emitted, as it is for thermal infrared wavelengths. Detection of reflected solar energy, for example, can only proceed when the target is illuminated by the sun, thus limiting visible light sensor observations on satellites from being used during a nighttime pass. Technology developments over the past four decades have allowed the capabilities of the current generation of passive sensors to advance far beyond those of the first instrument on Sputnik–1 and also the TV cameras on TIROS–1. – **Active sensors** are devices providing their own energy source for illumination of the target. They offer the capability to obtain measurements anytime, regardless of the time of day or season. Active sensors need of course a fairly large amount more power to perform their observation application. The first spaceborne active sensors were radar systems on Skylab (the instrument was named S–193, a combination of passive microwave radiometer with an active scatterometer, and a radar altimeter) operated between May 1973 and Feb. 1974. The next radar altimeter was flown on GEOS–3 (launch April 9, 1975, E.7.3) of NASA.

Many items/instances of technology introduction^{56) 57) 58)} (the emphasis is on civil Earth observation programs, military programs are considered only when enough published information is available) are presented below. The scope of description must be limited to

55) Note: A passive instrument is a sensing system that detects and measures incoming radiation emitted by the target. Such sensing systems do not emit any power to the target for purposes of measurement..

56) "Perceiving Earth's Resources from Space," Special issue of Proceedings of the IEEE, Vol. 73, No. 6, June 1985, pp. 947–1128

57) Special Issue on Remote Sensing for Environmental Research, Proceedings of the IEEE, Vol. 82, No. 12, Dec. 1994, pp. 1771–1929

58) Special Issue on Remote Environmental Sensing, Proceedings of the IEEE, Vol. 57, No. 4, April 1969

abstract level detail due to the vast number of topics in the general field of Earth observation. The reader is invited to consult also the survey references of the published literature as well as the bracketed references in the text, referring to descriptions in other chapters of the book..

1.4.1 Concepts in Optical Observations

The principal detection methods used in optical observations are photographic [e.g., (analog) film], photoemissive (photomultipliers), and photoconductive (semiconductor).

- The first low-resolution space photograph of the Earth's full disk was taken and transmitted by the US satellite Explorer-6, a spin-stabilized S/C with a mass of 64 kg (launch Aug. 7, 1959 on a Thor vehicle from Cape Canaveral into a highly eccentric orbit, perigee = 237 km, apogee = 41,900 km, inclination = 47°, period = 765 minutes) in August of 1959. The camera system flown was a TV optical scanner, consisting of an optical unit containing a concave spherical mirror and phototransistor, a video amplifier, timing and logic circuits, and telemetry. The scanner's optical axis was directed 45° away from the S/C spin axis, which was parallel to the orbital plane. The vehicle's spin furnished the line scanning, and the spacecraft's forward motion along its trajectory provided the frame scanning. The first "television" photo, received in Hawaii, took nearly forty minutes to transmit.
- On June 7, 1967 the first color image of the Earth from space was taken by the Molniya-1 spacecraft of the USSR. In the US, the first color picture of the Earth from a near-synchronous orbit was taken on July 25, 1967 by the Dual Vidicon Camera system of the DODGE satellite (see M.10).
- **Spaceborne photographic film imagery** for reconnaissance and mapping (also referred to as "perspective imagery").^{59) 60) 61)} The early US military program, endorsed by President Dwight D. Eisenhower in Feb. 1958, employed traditional camera technology for information gathering (to support SALT treaty verification). On June 25, 1959, the world's first spaceborne ISR (Intelligence, Surveillance and Reconnaissance) satellite was launched on the classified **Corona** program. The US Discoverer-14 satellite [also known as the Corona mission 9009 of NRO (National Reconnaissance Office) was the first full-fledged CORONA mission, launch Aug. 18, 1960 with a Thor vehicle from VAFB, CA; perigee of 250 km].⁶²⁾ – On this first Discoverer-14 mission, Corona and its KH-1 camera provided more photographic coverage of the Soviet Union than all of the previous U2 missions combined. More importantly, though, Corona's 12 m resolution imagery provided hard evidence of the pace and scope of Soviet ballistic missile deployments and allowed analysts to count Soviet heavy bombers.⁶³⁾

A new era in spaceborne photoreconnaissance was opened by successfully returning the film product in a reentry vehicle (capsule) and subsequent **mid-air recovery on Aug. 19, 1960 northwest of Hawaii by a JC-119 aircraft**, representing the first successful aerial recovery of an object returned from orbit.⁶⁴⁾

A total of 95 successful CORONA missions took place over a period of 12 years, ending on May 25, 1972 with mission 1117 (D.10). The high-resolution Earth-surface imagery

59) J. Asker, "US Declassifies More Cold War Recce Satellite Imagery," Aviation Week & Space technology, Nov. 4, 2002, pp. 68–70

60) R. A. McDonald, "CORONA: Success for Space Reconnaissance, A Look into the Cold War, and a Revolution for Intelligence," PE&RS, Vol. 61, No. 6, 1995, pp. 689–719

61) <http://www.fas.org/spp/eprint/mckinley.htm>

62) "First Successful Corona Remote Sensing Satellite Marks 50 Year Anniversary," Space Daily, Aug. 27, 2010, http://www.spacedaily.com/reports/First_Successful_Corona_Remote_Sensing_Satellite_Marks_50_Year_Anniversary_999.html

63) Bruce Carlson, "NRO's Historical, Current, and Potential Future Use of Small Satellites," Aug. 8, 2011, URL: <http://www.nro.gov/news/speeches/2011/2011-01.pdf>

64) J. Terry White, "First Mid-Air RV Retrieval," August 8, 2011, URL: <http://blog.seattlepi.com/american-aerospace/2011/08/08/first-mid-air-rv-retrieval/>

(5–12 m) of the programs CORONA, ARGON (12 missions between Feb. 17, 1961 and Aug. 21, 1964), and LANYARD (single mission in 1963) predated the imagery of the civil program Landsat.

The first declassification (i.e. availability to the civil community) of the imagery of the three programs took place in spring 1995 by the US government [Executive Order 12951, declassifying reconnaissance satellite images from the Corona program and two related subprograms – Argon (KH–5) and Lanyard (KH–6)]. This, in turn, extends the baseline for historical systematic Earth surface coverage backwards by more than a decade [some 866,000 images taken in the period 1960–1972 by KH–1 (Keyhole–1, a code name) through KH–6 were released].

The second declassification occurred in the fall of 2002 when NIMA (National Imagery and Mapping Agency) cleared imagery for public release from the KH–7 and KH–9 programs. At 1.2 m resolution initially and later at 0.6 m, the KH–7 imagery was very fine in its time [KH–7 was operational from July 1963 to June 1967; its imagery had a swath width of about 23.5 km with a scene length anywhere from about 8 km to 750 km in length, the camera could be turned (tilted) in the cross–track direction to extend the field of regard]. A KH–9 scene has a size of 130 km x 260 km at an initial resolution of 10 m and 6 m on follow–up missions. A total of 20 KH–9 satellites were launched from June 1971 until April 1986.

Note: The US military reconnaissance program gave up the concept of high–resolution film imagery (70 mm unperforated film) and film capsule recovery in the mid–seventies in favor of optoelectronic imaging (more practical for routine operations, but lower spatial resolution than film) with the launch of the KH–11 (Keyhole designation) spacecraft series. The KH–11–1 satellite was launched Dec. 19, 1976. The KH–12 (advanced KH–11) series have a spacecraft mass of about 18 tons (up to 7 tons of propellant for extended in–orbit maneuverability) providing observations in moderately elliptical orbits of about 250 km x 1000 km. The moderate elliptic orbit is of interest in a so–called “theater context” when coverage need is limited and concentrated, but revisit and resolution are paramount. KH–12–1 was launched Nov. 28, 1992 from VAFB, CA, on a Titan–4 vehicle. The KH–12–5 spacecraft was launched Oct. 5, 2001.

- The former Soviet Union started its photoreconnaissance satellite program in 1957 (Zenit–2 spacecraft based on the Vostok design). The entire program was launched under the cover of the “Cosmos scientific program” of “DS” satellites to disguise its true intentions. The very first Zenit–2 launch took place Dec. 11, 1961, but the spacecraft didn’t achieve a proper orbit. The first version designed consisted of an equipment section and a re–entry capsule. The equipment section included the camera, ELINT (Electronic Intelligence) receivers, and control systems for orbital flight. The conical re–entry capsule contained the film cassettes to be returned to Earth and the recovery systems. The capsule was deorbited by a separate braking rocket. – The second launch of a Zenit–2 satellite (built by NPO Energia) occurred on April 26, 1962 and was successful.

A film camera of considerable sophistication on this spacecraft was MKF–6 (Multi–Kanal–Fotografie–6) or “multispectral film camera–6”, developed at VEB Carl Zeiss, Jena, German Democratic Republic (former East Germany). The camera employed a battery of six lenses (two rows of 3 lenses in parallel), all looking into the same footprint, each for a different spectral band and furnished with a special filter, in the spectral range of 0.45 – 0.90 μm . Thus, color imagery with a high degree of geometric and radiometric accuracy and resolution was obtained in six spectral bands by using different films for each band. Un–perforated 70 mm films of 120 m length were used (shutter speeds of 7–56 ms, image format of 55 mm x 81 mm). MKF–6 was initially flown on aircraft (Antonov–30). The so–called “data processing” consisted of an opto–analog image analysis using MSP–4 (Multi–spectral Projector–4). This instrument assisted in the human visual inspection process by generating a color–coded synthesis, using multiple negative imagery of a multispectral set (analysis by superposition). A first spaceborne demonstration of MKF–6 took place on

Soyuz–22 (launch Sept. 1976) within the framework of a Kosmos experiment called “Raduga” and within the Intercosmos program. During the 8–day flight of Soyuz–22, Soviet Kosmonauts took over 2,500 Earth images with the hand–held MKF–6 camera. Thereafter, MKF–6 was also utilized on the Salyut–6 and –7 space stations as well as on MIR. ⁶⁵⁾

Note: The latest entry in Russian military surveillance is the Arkon–2 spacecraft with a launch on July 25, 2002 on a Proton vehicle from Baikonur. The satellite, built by Lavochkin (Lavochkina Scientific Production Association) of Khimki, is designed to produce imagery of 1 m resolution in the visible range. The telescope of the imaging instrument was built by LOMO of St. Petersburg; it has a focal length of 27 m (folded optics). Orbit of 1,506 km x 1,774 km, inclination of 63.4°. The Arkon–2 imagery is dual–use, i.e. for military and commercial applications. Prior to this mission, Russia launched its first optoelectronic high–resolution imagery mission (Arkon–1) on Cosmos 2344 on June 6, 1997. ⁶⁶⁾

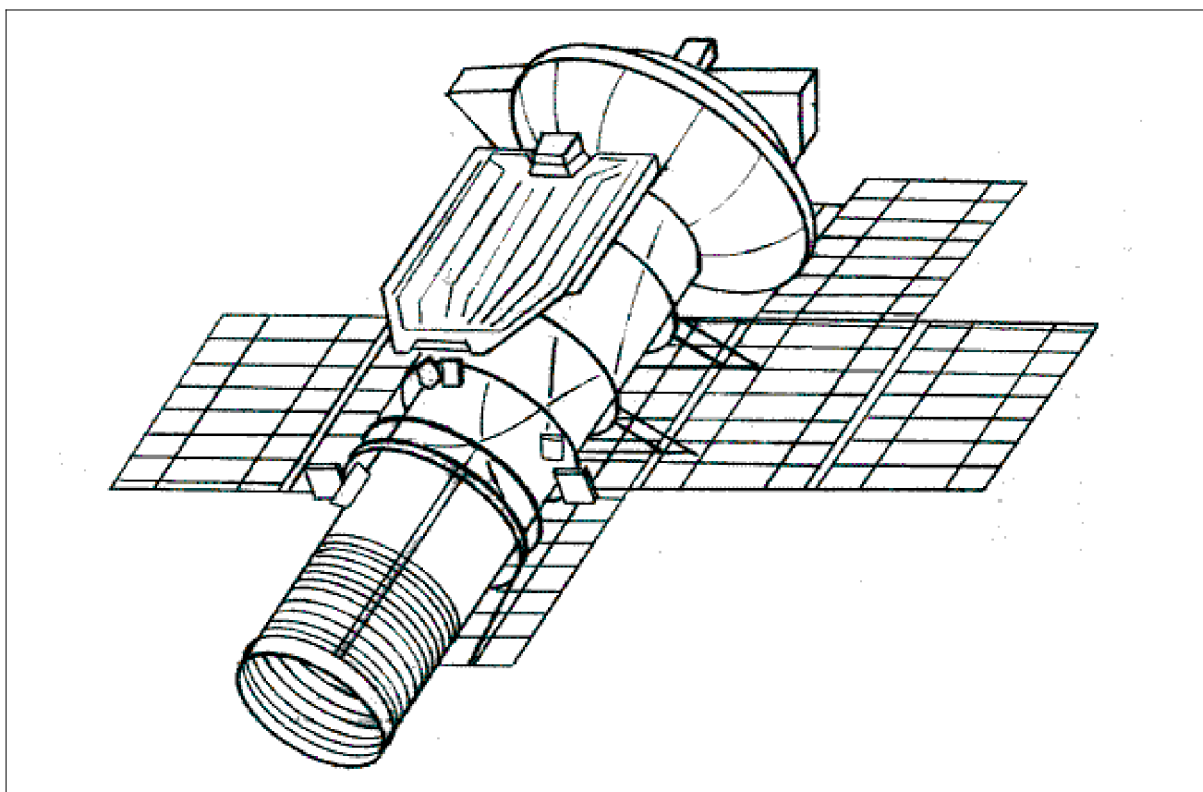


Figure 3: Illustration of the Arkon–2 spacecraft (image credit: Maney Publishing, London, UK)

- TV camera observations. Among the very early imaging sensors in space were shutter–style TV cameras, used to collect meteorological data. These so–called RBV (Return–Beam Vidicon) TV cameras employed a frame–sensor technique (instantaneous scene), where an electron beam scans the image on a photosensitive surface (raster scan of a complete image, ground size of image: 185 km x 185 km, spatial resolution of 80 m). In this concept, the image is exposed by a shutter device and stored on a photosensitive surface within each camera. This surface is then scanned in raster form by an internal electron beam to produce a video signal (the image is focused onto a photoconductor which causes the intensity of the electron beam, discharged from the electron gun, to vary with the intensity of light radiation). The values of the video signal are converted into digital information. Such RBV cameras were flown in several early satellite series such as: TIROS (TIROS–1 launch April 1, 1960), ESSA (launch of ESSA–1 on Feb. 3, 1966), Landsat–1 to –3 (LS–1 launch July

65) “Atlas zur Interpretation Aerodynamischer Spektralaufnahmen – Methodik und Ergebnisse,” Akademie–Verlag, Berlin, 1982

66) G. H. Thomson, “Evaluation of Russian Arkon–2 Earth observation satellite,” *The Imaging Science Journal*, Vol. 53, No. 3, Sept. 2005, pp. 163–171

23, 1972), DMSP (Block IV series started in 1965), and Meteor (Meteor-1-1 launch March 23, 1969). – The pictures obtained in this fashion were relayed to the ground and required substantial signal processing, including oscilloscopes, to recover a satellite image.

- Spaceborne film cameras in civil Earth observations (western world): The **Metric Camera** of DLR, flown on the Spacelab-1 Shuttle mission of NASA and ESA (STS-9, Nov. 28 to Dec. 8, 1983), is considered to be the first civil spaceborne experiment dedicated to photogrammetry. The calibrated Metric Camera was demonstrating high-resolution space photography on a large film format (23 cm x 23 cm) for topographic and thematic mapping applications. The Metric Camera was a slightly modified aerial survey camera of Carl Zeiss, Oberkochen, Germany, of the type RMK A (Reihenmesskammer A) 30/23. It was mounted on the optical-quality window in the ceiling of the Spacelab pressurized module. The results of the analog (film) imagery obtained can be summarized as follows:

- Ground resolution: 10–15 m (pixel equivalent)
- Planimetric accuracy: ± 10 m
- Height accuracy: ± 15 m
- Due to the limited ground resolution the maximum map scale that could be derived was 1:100,000. ^{67) 68)}

The only calibrated mapping film camera which has been flown after the Metric Camera was the **LFC** (Large Format Camera) of NASA, which was operated on Shuttle flight STS-41G, Oct. 5–13, 1984. This camera was equipped with a FMC (Forward Motion Compensation) system and a large image size of 46 cm x 23 cm (with the long size of the film in the flight direction) to improve the stereoscopic effect. It could be shown, that from these images, location accuracies of better than 10 m could be obtained for all three coordinates of a point target, and that compiling and revision of topographic maps at a scale of 1:50,000 and larger was possible.

1.4.1.1 Solid-state (digital) imaging – CCD detector technology

Solid-state imaging – a key technology in optical remote sensing capability – started a new era in quantitative information collection. The technique (introduced in the early 1960s) uses silicon-based photodetectors onto which radiation (photons) can be focused and an electronic readout scheme (scanner) for image capture. The new method, later referred to as an optomechanical system (and a later introduction of the optoelectronics system with CCD technology), converts incident photons directly into electrical current, offering many advantages [true space-point (pixel based) information, high dynamic range, low power dissipation, low voltage operation, no geometric distortions, sampled signal output, rapid response, etc.] over the conventional electron beam scanning vacuum tube technology, such as the vidicons, traditionally used in the RBV TV cameras. The new solid-state-oriented imaging technology provided considerable flexibility; in particular, it is suitable for digital processing, offering a variety of readout schemes [imaging arrays (1-D, 2-D) such as self-scanned photodiodes, CIDs, CCDs], permitting the use of many detector element types. CCDs, CIDs, analog film (silver-halide crystals in photographic emulsions), and even the human eye are “**photon counters**”. ^{69) 70)} While CCDs are regular arrays of receptors of identical size, photographic emulsions consist of a random three-dimensional arrangement of receptors in size significantly smaller than CCD cells. In practical applications, CCD images can be built up one-dimensionally (line scanner) or two-dimensionally; all cells in the lightsensitive part of a CCD are biased in the integrating mode.

67) M. Schroeder, E Suckfüll, G. Todd, P. Lohmann, “Spacelab-1 Metric Camera, User Handbook and Data Catalogue,” of DLR, Oberpfaffenhofen, Dec. 1986

68) M. Schroeder, “Flight Performance of the Spacelab Metric Camera Experiment,” Proceedings of IGARSS '84, Strasbourg, France, Aug. 27–30, 1984, ESA SP-215

69) P. K. Weimer, et al., “Multielement self-scanned mosaic sensors,” IEEE, Spectrum, March 1969, pp. 52–65

70) Special Issue on Solid-State Imaging, IEEE Transactions on Electron Devices, Vol. ED-15, No. 4, April 1968, pp. 190–261

The new solid–state radiation detection concept employs scanner systems (see chapter O.3) permitting the acquisition of imagery within and outside the VNIR spectral region of photographic films, offering also a strategy of separating the received radiation into a number of spectral bands. *This key technology provides the only practical means for obtaining high–accuracy radiometric information.* The early scanners form an image successively on a cell–by–cell basis by the process of scanning. The first scanners employed were optomechanical **whiskbroom** systems where imaging occurs on a cell–by–cell basis in the cross–track direction (later whiskbroom systems are using multiple parallel cells in the along–track direction to offset somewhat the disadvantage of cross–track scanning); these were followed by more efficient parallel line–scanned pushbroom (CCD) systems. Note: pushbroom scanners are also referred to as “along–track scanners” because they use the forward motion of the platform to record successive scan lines and build up a 2–D image perpendicular to the flight direction. However, instead of a mirror, they use a linear array of detectors, located in the focal plane, which are “pushed” in along–track to build up a ground swath; hence, “pushbroom.”^{71) 72) 73) 74)}

The newly available scanner technology (whiskbroom/pushbroom) offered a means of making imagery quantitatively available to computer processing methods; it stimulated in turn the development of new sensor systems with greatly enhanced performance and observation capabilities, it permitted also a better modular design concept of imaging sensors. An imager based on solid–state technology consists of a suitable lens system (the optics subsystem), a scanner subsystem with the detector positioned at the focal plane, and operating electronics.

– Solid–state multispectral imaging in the 1960s. It signifies a great step forward in image interpretation capability, namely from visual or machine–sensed photointerpretation (analysis based on image characteristics) to quantitative interpretation of several bands of imagery (analysis based on spectral characteristics). The new quantitative approach relies on image processing methods of the evolving computer industry of the time.

The pioneering airborne instrument of spatially–registered multispectral scanners is M–5, developed by the Willow Run Laboratories of the University of Michigan. The M–5 whiskbroom scanner is based on solid–state technology, and developed around an optomechanical scanning system called the S–5 (built by HRB Singer for the US Army). The S–5 had two optical channels (not registered) and recorded its data on film.^{75) 76)} From 1963 to 1965, two of these instruments were flown in tandem, each in a DeHavilland Beaver aircraft, to obtain four unregistered bands (selectable from UV through LWIR). From June 1963 through June 1964, around–the–clock (every 4 to 6 hours) imagery was collected once a month over a local fifty mile flight path, selected for natural and cultural diversity. These data were manually analyzed to form the initial basis for an understanding of day–night–seasonal spectral imaging phenomena. The M–5 instrument provided support of

71) Note: The term “whiskbroom scanning” comes from the notion of sweeping a pathway in a side–to–side fashion by a small handheld broom. – Cross–track scanners use a rotating or oscillating mirror to scan contiguous series of narrow ground strips at right angles to the flight path.

72) Conventional photographic films with high resolution imagery were not amenable for direct processing and transmission methods in remote sensing. Film material was not suitable for quantitative radiation measurements, only a small spectral range (VNIR, SWIR) could be covered with film.

73) D. Landgrebe, “The Evolution of Landsat Data Analysis,” PE&RS (Photogrammetric Engineering and Remote Sensing), Vol. 63, No 7, July 1997, pp. 859–867, Special Issue commemorating the 25th anniversary of the launch of Landsat 1, July 1972, URL: <http://dynamo.ecn.purdue.edu/~landgreb/Landsat.paper.pdf>

74) Note: Realizing the value of multispectral data, there were a number of implementations in the early 1960s to obtain multispectral data (i.e. photographs) by special cameras. Spectral separation was accomplished by using photographic filters with multi–objective camera systems, each for a separate spectral range. This left the photo–interpreter with a dozen or so photos of the same scene, each at a different spectral band. The human eye finds it difficult to keep track of tonal variations over 16 or more levels of gray for even a modest number of different scene objects. – The discrimination problem was eventually solved with the availability of data from multispectral scanners and the development of proper algorithms for computer interpretation of imagery.

75) Information provided by B. Horvath of ERIM, who operated the M–5 imager and analyzed the data.

76) Note: In 1973 the Willow Run Laboratories team separated from the University of Michigan and became ERIM (Environmental Research Institute of Michigan). In 2000, ERIM became part of Veridian ERIM International

the developing ERTS (Landsat) program, in particular for the design of MSS (Multispectral Scanner). The M-7 multispectral scanner was a direct successor of M-5, it became operational in 1971, was upgraded several times, and provided a long-term source of remotely-sensed multispectral imagery (P.83.2). A much later descendent of optomechanical whiskbroom technology was AVIRIS (Airborne Visible/Infrared Imaging Spectrometer) of NASA/JPL (P.43). This early airborne hyperspectral imager was introduced in 1987 and became operational in 1989, the first sensor to contiguously cover the 0.4–2.5 μm region with narrow spectral bands. At the start of the 21st century, its data is still very much in demand. – The short dwell-time problem of these cross-track whiskbroom scanners was solved by introducing a parallel coverage arrangement of detector arrays in the along-track direction. In this way, the wide along-track coverage permitted sufficient integration time for all parallel cells in each cross-track scan sweep.

Note: In some instances, preference is given to a whiskbroom imager design (the older imaging technology) because the optics for pushbroom operation must always cover FOV (the total field of view – meaning the full swath width) while the optics for whiskbroom operation deal with IFOV (instantaneous field of view) which is much smaller than FOV. Hence, there are less distortions at the swath edge for whiskbroom systems. ⁷⁷⁾

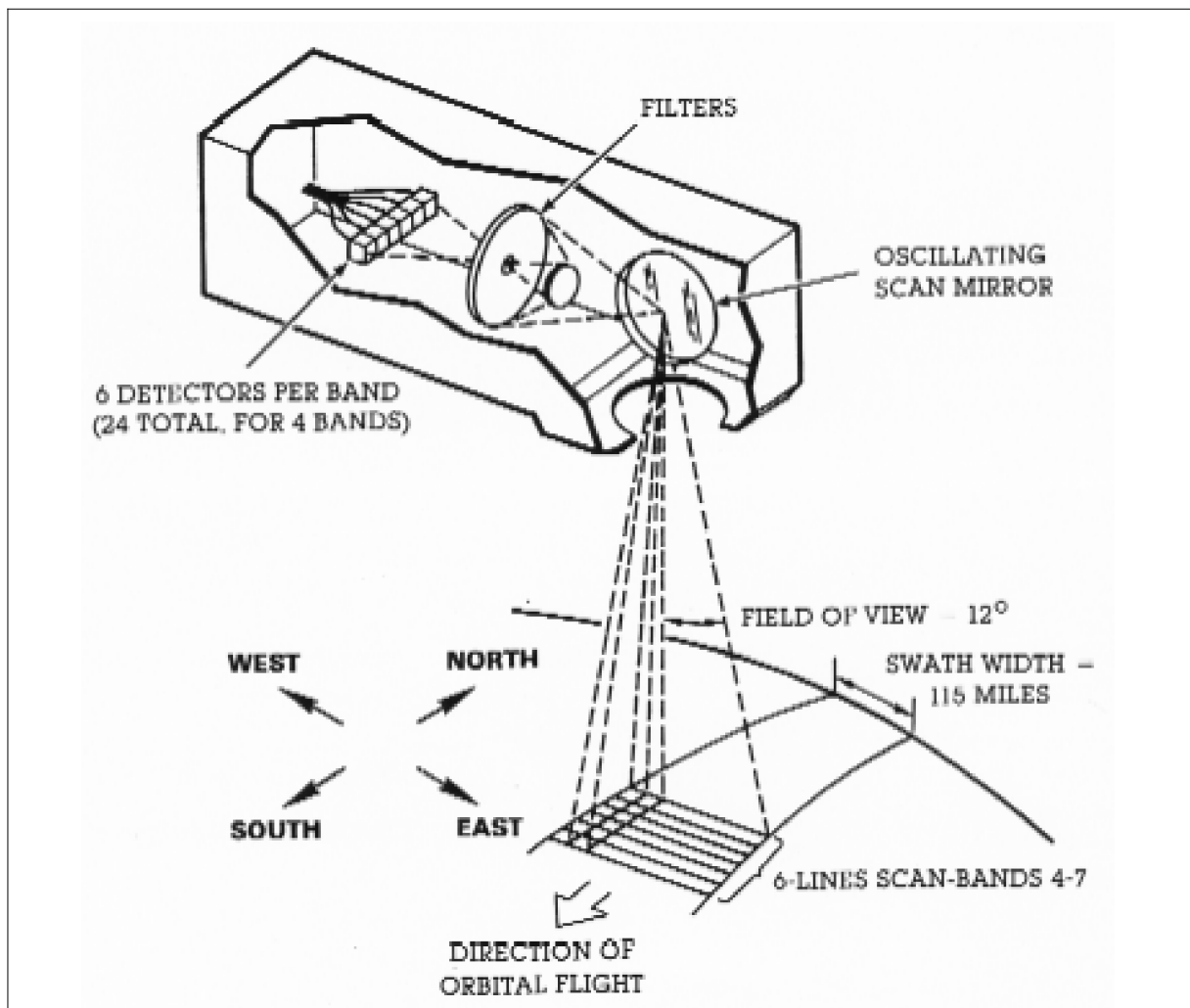


Figure 4: Illustration of the Landsat-1 MSS whiskbroom scanning geometry (image credit: SBRC)

⁷⁷⁾ Note: The requirement of very wide FOVs of CCD instruments is usually being implemented today with a double mount instrument design in cross-track to achieve a high-resolution wide swath observation coverage.

- The electronic imaging concept **converts incident photons** on a silicon–based detector (such as a photodiode, CCD, CID, CMOS.) **directly** into electrical current offering such features as: true space–point (pixel–based) information, high dynamic range, low power dissipation, low voltage operation, little or no geometric distortions, sampled signal output, and rapid response times. These are real advantages over the previous electron beam scanning vacuum tube technology of vidicons.
 - The technology provides a new unit of measurement: the **pixel** (picture element). An image is made up of a series of spatially–fixed pixels providing a unique location reference of the data of each element along with the target radiation measurement. Thus, the technique provides a firm concept of **spatial resolution**.
 - The solid–state radiation detection concept offers a strategy of **separating the received radiation into a number of spectral bands**. This key technology provides the only practical means for obtaining high–accuracy radiometric information by the parallel collection of **multispectral** or of **hyperspectral imagery**. The use of a dense detector array provides the capability of high–resolution spatial and spectral imagery. This offers very extensive interpretation capabilities for many applications.
 - The data is available in **digital form**, quantified at the instrument level – providing a great deal of flexibility by offering all the capabilities of digital processing, storage, and communication.
 - The concept signifies a great step forward in **image interpretation capability**, namely from visual or machine–sensed photo interpretation (analysis based on image characteristics) to **quantitative interpretation** of several bands of imagery (analysis based on spectral characteristics).
 - The electronic imaging concept permits the collection of imagery in a **wide region of the optical spectrum** (from UV, VIS, NIR, SWIR, MWIR, TIR, to FIR). This represents a vast improvement over the (analog) photographic film technology which is basically limited to the VIS and NIR regions of the spectrum.
 - Two solid–state electronic imaging concepts were developed in the 1960s starting a new era in remote sensing – with so–called scanner systems, based on serial and parallel imaging techniques, respectively:
 - 1) **Whiskbroom scanning technique** – an optomechanical design where imaging occurs serially on a cell–by–cell basis in the cross–track direction of the spacecraft orbit using an oscillating mirror for each scan sweep. The first spaceborne whiskbroom imager, MSS (Multispectral Scanner), developed at SBRC (Santa Barbara Research Center of Hughes Aircraft Company (now Raytheon), was flown on Landsat–1 of NASA (launch July 23, 1972). Silicon–based photodiodes became first available in 1961 at Bell Labs.
 - 2) **Pushbroom scanning technique** – an optoelectronic design where imaging occurs in parallel for all line detector cells in the cross–track direction with the use of CCD (Charge–Coupled Devices) detectors. The first spaceborne pushbroom imager (MSU–E) was flown on Meteor–Priroda–5 (launch June 18, 1980) satellite of the former Soviet Union. The CCD technology was invented in 1969 by Bell Labs.
- In remote sensing terminology a line scanner is a (nonphotographic) device that forms instantaneous exposure geometries between a target and a detector, with the sensor optics in between, thus forming an image by the successive addition of picture elements (effectively a 1–D configuration to build up a 2–D image by the S/C forward motion).

Table 1: Basic characteristics of solid–state imaging in the optical spectrum

- Spaceborne scanners. In 1968, SBRC (Santa Barbara Research Center) of Hughes Aircraft Company proposed to NASA to place a new type of imaging device on the planned ERTS spacecraft, namely a “scanner system” in combination with a photodiode detector system. At the time, scanners were viewed with great skepticism by most scientists for two reasons. First of all, the scanner employed a moving part, **an oscillating mirror**, which was considered unreliable. Secondly, the scanner was not a full-frame imaging device; it created images from strips. Cartographers were suspicious of the scanner’s geometric integrity.

Note: Silicon-based photodiodes had become available in 1961 [PIN (Positive Insulator Negative) type], the first high-speed avalanche photodiodes were formed in 1966.⁷⁸⁾ In 1939, Russell S. Ohl, an electrical engineer at Bell Labs, stumbled on the first semiconductor p–n junction.

The scanner did have one important advantage, namely its multispectral capability. Agricultural research had demonstrated the value of multispectral imagery. For example, the 0.63 to 0.68 μm band measures chlorophyll absorption; the 0.79 to 0.9 μm band indicates water content in leaves; and the 1.55 to 1.75 μm band displays soil moisture. SBRC initially designed a six-band scanner for the satellite. However, NASA’s small satellite could not house the large scanner, so a more modest four-band MSS (Multispectral Scanner) was built for ERTS–1. The spectral bands were chosen to simulate false-color infrared photography. NASA put RBV cameras as well as the new scanner system (MSS) onboard the ERTS–1 satellite (in 1975 ERTS–1 was renamed to Landsat–1) to compare imagery from both types of systems. Within hours after launch of ERTS–1 (launch July 23, 1972), the first MSS images created a sensation with their amazing clarity and synoptic views of the landscape. Spatially, both systems (RBV and MSS) provided a resolution of about 80 m. Spectrally, each of the three-camera RBV systems was designed to cover a band: the blue-green, yellow-red, and red/NIR. MSS provided a similar band set along with a fourth band to extend coverage into the infrared region. **The imagery of MSS was in digital form. The scan mirror assembly of MSS was the key to providing wide-field and ‘high-resolution’ coverage.**⁷⁹⁾

The new technique of scanning had the promise of more things to come. Thus, on the spaceborne side, MSS (with a cross-track whiskbroom scanner) ushered in an era of previously unimaginable synoptic knowledge of the Earth. – By seeing the world in electromagnetic increments beyond the normal range of human vision, Landsat revealed whole new worlds hidden within the folds of a familiar world we thought we knew so well. It was no great surprise that Landsat, from an average altitude of 910 km in space, could discern the health of corn plants on a half-acre plot of land in Iowa, could determine which were suffering from corn blight and where a fungal infestation appeared to be gaining a foothold. That is exactly what it was designed to do.

– The TM (Thematic Mapper) sensor on LS–4 (launch July 16, 1982, end of LS–4 mission on June 15, 2001) is a much improved successor in spatial and spectral resolutions to MSS. A good portion of land-surface observation history is intimately connected with this pioneering sensor (TM) and program (Landsat). All TM sensors (including ETM+ of Landsat–7) employed the optomechanical whiskbroom concept with a two-axis gimbaled scan mirror. Other spaceborne optomechanical (whiskbroom or flying spot) instruments of note are:

VIRS flown on TRMM, AVHRR (on the NOAA/POES series, all three generations of instruments, since 1978 starting with TIROS–N, see Table 114), OLS (flown on DMSP series, first introduced in 1976 – OLS uses a flying spot design), ASTER (whiskbroom in TIR, pushbroom in VNIR and SWIR), MODIS (Terra, launch Dec. 18, 1999), and OSMI (Ocean

78) “Timeline” Bell Labs. <http://www.bell-labs.com/org/physicalsciences/timeline/>

79) A. M. Mika, “Three decades of Landsat instruments,” *Photogrammetric Engineering & Remote Sensing*, ASPRS, Vol. 63, No 7, July 1997, pp.839–852

Scanning Multispectral Imager, flown on KOMPSAT – 1, launch Dec. 20, 1999). Note: Instrument designs like AVHRR and MODIS are of the optomechanical type because the extended focal planes, coupled with relatively short focal lengths, lead to unworkable field angles and geometric distortion problems (pushbroom designs are not well suited to moderate – resolution wide – field systems). The whiskbroom optomechanical scanner technology continues its usefulness in such next – generation instruments as JAMI (Japanese Advanced Meteorological Imager) of the MTSAT – 1R mission of Japan (launch Feb. 26, 2005), IASI of the MetOp – A mission of EUMETSAT (launch Oct. 19, 2006), and VIIRS (Visible/Infrared Imager and Radiometer Suite) of the NASA/IPO NPP program (launch Oct. 28, 2011); the instrument was developed by SBRS (Santa Barbara Remote Sensing) of Raytheon Electronic Systems, Goleta, CA.

- Charge – transfer devices (see O.4.2). The CCD (Charge – Coupled Device) detector technology was invented in 1969 by Willard S. Boyle and George E. Smith and first demonstrated (one – line eight pixel detector) by Gil Amelio, Mike Tompsett and George Smith at the Bell Labs (Bell Telephone Laboratories of AT&T, since 1996 of Lucent Technologies, Inc.) in Murray Hill, New Jersey, USA.

The CCD technology makes use of the **photoelectric effect**, as theorized by Albert Einstein and for which he was awarded the 1921 Nobel Prize. By this effect, light is transformed into electric signals. The challenge, when designing an image sensor, was to gather and read out the signals in a large number of image points, pixels, in a short time.

The silicon – based detector invention, along with the development of the planar process for integrated circuits (ICs), eventually led to a revolution in optical imaging capabilities (resulting in the birth of digital photography), providing in addition a wide forum for multi – disciplinary applications. Early industry CCD manufacturers were: TI (Texas Instruments), RCA (Radio Corporation of America), Fairchild Semiconductor, GEC (General Electric Co., UK), and Thomson – CSF (France, since 1978). By 1970, the Bell Labs researchers had built the CCD into the world’s first solid – state video camera. ^{80) 81) 82) 83) 84) 85)}

A CCD ^{86) 87)} is a photosensitive solid – state silicon – based detector, consisting of many cells or pixels that are capable of producing an electrical charge proportional to the amount of light they receive. Typically, the pixels are arranged in either a single line (referred to as linear array or line array) or in a two – dimensional grid (area array CCDs). Each CCD cell is essentially a MOS capacitor, of which there are two types: surface channel and buried channel. The device is typically built on a p – type silicon substrate with an n – type layer formed on the surface. The particular application will, in general, dictate the type of CCD that is being used. One of the fundamental parameters of a CCD is resolution, which is equal to the total number of pixels that makes up the light sensitive area of the device.

At the start of the 21st century, the CCD technology is still having profound effects in the fields of optical imaging, particle tracking, X – ray detection, as well as analog storage de-

80) W. S. Boyle, G. E. Smith, “Charge – Coupled Semiconductor Devices,” Bell System Technical Journal, Vol. 49, April 1970, pp. 587 – 593

81) G. F. Amelio, M. F. Tompsett, G. E. Smith, “Experimental Verification of the Charge Coupled Device Concept,” Bell System Technical Journal, April 1970, pp. 593 – 600

82) G. F. Amelio, W. J. Bertram, M. F. Tompsett, “Charge – Coupled Imaging Devices: Design Considerations,” IEEE Transactions on Electron Devices, Vol. ED – 18, pp. 986 – 992, Nov. 1971

83) S. M. Gruner, M. W. Tate, E. F. Eikenberry, “Charge – coupled device area x – ray detectors,” Review of Scientific Instruments, Vol. 73, No 8, Aug. 2002, pp. 2815 – 2842

84) C. J. S. Damerell, “Charge – coupled devices as particle tracking detectors,” Review of Scientific Instruments, Vol. 69, No. 4, April 1998, pp. 1549 – 1573

85) D. F. Barbe, “Imaging Devices Using the Charge – Coupled Concept,” Proceedings of the IEEE, Vol. 63, No. 1, Jan. 1975, pp. 38 – 67

86) S. A. Taylor, “CCD and CMOS Imaging Array Technologies: Technology Review,” Technical Report EPC – 1998 – 106,

87) J. Janesick et al., “Charge – coupled – device response to electron beam energies of less than 1 keV up to 20 keV,” Optical Engineering, Vol. 26, pp. 686 – 691, August 1987; see also: <http://www.site-inc.com/>

vices. The application spectrum ranges from security monitoring to high–definition television, from endoscopy to desktop videoconferencing, from Earth observation to astronomy.

In remote sensing,⁸⁸⁾ the CCD pushbroom concept permits simultaneous measurements of an entire scan line (detector line array over the full swath width) for each spectral band (and serial shift–register readout), thereby improving the dwell time (or sampling time) over whiskbroom systems. (Note: very short dwell times, in the order of a few microseconds, limit the number of photons that can be detected without using very large optics). Advantages of the digital CCD technology lie in the real–time processing capabilities of the data, the high accuracy potential, the good radiometric characteristics, and the availability of relatively inexpensive system components. – The first astronomical CCD ground observation (of Jupiter, Saturn and Uranus) was done in early 1976 at the Mount Bigelow observatory of the University of Tucson, AZ (CCD detector array built by Texas Instruments).⁸⁹⁾

The first experimental airborne optoelectronic instrument, featuring a pushbroom CCD detector line array, was **EOS** (Electro–Optical Scanner) of DLR (former DFVLR), designed and developed by EADS Astrium GmbH (formerly MBB) of Munich, Germany in 1977, and flown on a DLR aircraft (DO–28) in early 1978 (chapter P.80). MEIS (P.133) of CCRS (Ottawa, Canada) followed in 1978, and TIMS of Daedalus in 1981. ISRO built a single–band CCD camera in the late 1970s and had it flight–tested on an aircraft in 1980.

In the fall of 2009, Willard S. Boyle and George E. Smith have been awarded the Nobel Prize in Physics for their “invention of an imaging semiconductor circuit – the CCD sensor” in 1969 – which revolutionized photography as light could now be captured electronically instead of on film and became an irreplaceable tool in Earth observation and in astronomy, providing new possibilities to visualize the previously unseen. The CCD device also made it possible for amateur astronomers to rival the professionals in terms of quality astrophotography. CCD technology is also used in many medical applications, e.g. imaging the inside of the human body, both for diagnostics and for microsurgery. Sharing the prize with Boyle and Smith is Charles K. Kao of the Standard Telecommunication Laboratories, Harlow, UK, and the Chinese University of Hong Kong, who in 1966 made a discovery that “led to a breakthrough in fiber optics communications.” Both achievements helped shape the foundations of today’s networked societies.

Table 2: Nobel prizes in physics for the invention of fiber optics and CCD technology⁹⁰⁾

Some performance characteristics of CCDs:

- Fill factor. The fill factor is basically the percentage of each pixel that is sensitive to light. Ideally, the fill factor should be 100%; however, in reality, it is often less than this. The net effect of reducing the fill factor is a lowering of the array sensitivity.
- Dark current noise. Dark current can be defined as the unwanted charge that accumulates in the CCD pixels due to natural thermal processes that occur while the device operates at any temperature above absolute zero. At any temperature, electron–hole pairs are randomly generated and recombine within the silicon and at the silicon–silicon dioxide interface. Some of the electrons may be collected in the CCD wells, appearing as unwanted signal charges (e.g, noise) at the output.
- Quantum efficiency (QE). QE is the measure of the efficiency with which incident photons are detected. Some incident photons may not be absorbed due to reflection or may be

88) Note: The terms “optoelectronics” and “photonics” are being used as synonyms throughout the literature. The term optoelectronics is a contraction of ‘optical electronics’ and refers to all types of photon effects (interaction/conversion, transmission) with a medium and vice versa, including magneto–optic phenomena. Optoelectronic or photonic devices are being used in a wide variety of applications in the fields of optical detection and imaging, communications, energy generation, and computing, to name just a few. Examples of optoelectronic or photonic devices include: CCD, CMOS/APS (Active Pixel Sensor), LED (Light Emitting Diode), all types of photodiodes, ILD (Injection Laser Diode), CRT (Cathode Ray Tube), IOC (Integrated Optical Circuit), photovoltaic cells also referred to as solar cells, fiber cables, and photonic links..

89) I. S. McLean, “Electronic Imaging in Astronomy–Detectors and Instrumentation,” John Wiley&Sons, 1997, pp.128

90) “The Nobel Prize in Physics 2009,” Oct. 6, 2009, URL: http://nobelprize.org/nobel_prizes/physics/laur-ates/2009/press.html

absorbed where the electrons cannot be collected. The QE is the ratio of the number of detected electrons divided by the product of the number of incident photons times the number of electrons each photon can be expected to generate. Visible wavelength photons generate one electron–hole pair, thus the QE for visible light is given by the ratio of the number of detected electrons divided by the number of incident photons. Back illumination of a CCD is a technique to improve the QE.

– Blooming is an effect that occurs when, during the integration period, a potential well becomes full of electrons; this is usually caused by the presence of a bright object in the scene being imaged (assuming that the overall exposure is correctly set). When a potential well overflows, the electrons flow into surrounding potential wells, thus creating an area of saturated pixels. If blooming isn't controlled, the resultant image will suffer from large overexposed regions.

• Spaceborne CCD detector technology was introduced with the **MSU–E** (Multispectral Scanning Unit–Electronic) flown on the Meteor–Priroda–5 (launch June 18, 1980) spacecraft of the former Soviet Union. MSU–E was built at ISDE (Russian Institute of Space Device Engineering) in Moscow; it featured a CCD line array of 1024 pixels, three parallel line arrays, each of 1024 elements, provided pushbroom imagery in three spectral bands (visible and near–infrared range); the spatial resolution was 28 m on a swath of 28 km. The CCD line arrays were designed and manufactured in the “Pulsar” plant, Moscow. The results obtained with MSU–E confirmed the potential of CCD technology for use in high–resolution multispectral monitoring. The MSU–E pushbroom instrument was also introduced on the Soviet Resurs series, starting with Resurs–O1–1 (launch Oct. 3, 1985).^{91) 92)}

Further early CCD pushbroom instruments were: **MOMS–01** (Modular Optoelectronic Multispectral Scanner) of DLR, built by EADS Astrium GmbH, and flown on Shuttle flights STS–7 in June 1983 and STS–41B in Feb. 1984), the **HRV** sensors on the SPOT series of CNES (launch of SPOT–1 on Feb. 22, 1986), and **LISS** on the IRS series of ISRO (launch of IRS–1A on March 17, 1988).

The UoSatsat–1 (launch Oct. 6, 1981) and UoSatsat–2 (launch March 1, 1984) microsattellites of the University of Surrey, UK, carried the first experimental 2D CCD Earth imaging snapshot cameras (area array detectors). – Other early spaceborne CCD area–array detector implementations were introduced in the TVS (TV System) instrument, a wide–angle TV camera [TVS, an IKI instrument (Moscow), developed in cooperation with France and Hungary) of the Soviet Vega interplanetary missions to Venus and later to Halley's Comet in 1984 (launched Dec. 15 and Dec. 21, 1984, respectively). On June 9 and 13, 1985, each Vega S/C deployed a Venus capsule. In March 1986, each Vega S/C encountered Halley's Comet. TVS provided color images of Halley's coma and core [~ 500 images from Vega–1, ~ 700 images from Vega–2, each at closest approach (8000–9000 km) to Halley's Comet].⁹³⁾

In the meantime CCDs have evolved to a sophisticated level of performance (high radiometric and spatial resolution). Starting with the 1990s CCDs have become the technology of choice for most imaging applications in remote sensing. The microelectronics industry provides CCD technology (area arrays) on a chip level. A high–resolution VNIR camera can be built around a CCD chip by combining it with a suitable lens system, a cooling method, and operating electronics. CCDs take the place of vacuum–tube based imagers and film in conventional cameras. They provide a wide field of applications in science as well as in the consumer market. An astronomical imaging system with the name of STIS (Space Telescope Imaging Spectrograph) on Shuttle flight STS–82 (launch Feb. 11, 1997) was installed aboard the orbiting Hubble Space Telescope (HST); the key element of STIS is a very sensi-

91) A. S. Selivanov, Y. M. Tuchin, M. K. Naraeva, B. I. Nosov, “Experimental Satellite System for Earth Monitoring,” *Issledovanie Zemli iz Kosmosa*, W 5, 1981

92) Information provided and document translation: courtesy of Boris Zhukov, DLR and Ian Ziman, IKI, Moscow

93) Halley's Comet is named after the 18th century English astronomer Edmond Halley (1656–1742) who first calculated the comet's orbit and predicted that it would reappear at regular intervals.

tive CCD array (developed by SITe) enabling faint radiation measurements of distant stars. Also in 1997 Philips Co. with several partners was testing a CCD area array of 9216 by 7168 detectors (pixels) on a chip. The pixel size is 12 μm x 12 μm , the chip size is 111 mm x 86 mm. The first application of the 7k x 9k area array detector was in astronomy. – Some drawbacks of the CCD technology are: CCD's provide good image quality, but they are expensive, power hungry, and rather bulky with the required accessory chips.⁹⁴⁾

• **Introduction of the ILT (Interline Transfer) CCD architecture in spaceborne instruments.** The technology of the progressive scan ILT CCD image sensor (an area array detector type) was introduced in space with MFEX (Microrover Flight Experiment), also referred to as “Sojourner” (a 6-wheel vehicle of 11 kg), of NASA's Mars Pathfinder Mission (launch Dec. 4, 1996 from KSC; arrival on Mars: July 4, 1997). Two separate Kodak area interline sensors (detectors) were aboard MFEX, the KAI-0371 monochrome sensor and the KAI-037M color sensor. In this imaging concept, separate area arrays for image capture and charge transfer are being utilized, allowing images to be read out while the next image is captured. These sensors perform a progressive three-step process to produce images. The first step converts light from the exposure into an electronic charge at discrete sites, making up pixels. Next, the packets of charge are transferred within the silicon substrate. Finally, the charge-to-voltage conversion and output amplification takes place. This concept enables the detector to detect light and deliver extremely clear and sharp imagery. The ILT technique provides in effect the fastest electronic shuttering performance possible. The progressive-scan technology permitted the sensors to deliver still/video imaging of fast moving objects without breakup. Additionally, the sensors were designed to continually capture images while simultaneously transferring the previous image out of the sensor memory.

Note: The progressive scan ILT technology was actually introduced in the early 1990s, mainly for the purpose of solving some industrial CCD imaging (machine vision, traffic control, and television) applications occurring with fast-moving targets. The time delay between the transmission of odd and even fields – makes the image to appear blurred when an object is moving quickly compared to the CCD refresh rate. The best solution to this problem turned out to be the progressive-scan interline-transfer CCD detector featuring simultaneous integration of all pixels resulting in sharp imagery.

Launch Date	Satellite Platform (Agency or Company)	Earth Imaging Sensors of respective Payload	Comment (ops = operations)
Jul. 23, 1972	Landsat-1 (NASA)	MSS, RBV	MSS whiskbroom imaging End of service Jan. 6, 1978
Jan. 22, 1975	Landsat-2 (NASA)	MSS, RBV	S/C ops until 1983
Mar. 5, 1978	Landsat-3 (NASA)	MSS, RBV	S/C ops until Jan. 7, 1983
June 18, 1980	Meteor-Priroda-5 (Russia) G.6	MSU-E, MSS Fragment	1st long-term use of CCD pushbroom technology
Jul. 16, 1982	Landsat-4 (NOAA)	MSS, TM	Standby since Dec. 1993 End of mission Jun. 15, 2001
Mar. 1, 1984	Landsat-5 (NOAA)	MSS, TM	Operational as of 2003
Nov. 3, 1985	RESURS-O1-1 (Russia)	2 MSU-E, 2 MSU-SK	S/C ops until Nov. 11, 1986 Use of CCD technology
Feb. 22, 1986	SPOT-1 (CNES) ops until Feb. 4, 2002	2 HRV	Use of CCD pushbroom technology, standby as of Feb. 2002
Mar. 17, 1988	IRS-1A (ISRO)	LISS-I, LISS-II A/B	Three CCD imagers S/C ops until 1992
Apr. 20, 1988	RESURS-O1-2 (Russia)	2 MSU-E, 2 MSU-SK	S/C ops until June 1, 1999

94) Note: HST is named after Edwin P. Hubble (1889–1953), an American astronomer. In 1924, he coined the word “galaxy,” referring to a large star system such as the Milky Way and the Andromeda Nebula. He devised the classification scheme for galaxies that is still in use today. In 1929, Hubble analyzed the speed of recession of a number of galaxies and showed that the speed at which a galaxy moves away from us is proportional to its distance (Hubble's Law). This discovery of the expanding Universe marked the birth of the “Big Bang Theory.”

Launch Date	Satellite Platform (Agency or Company)	Earth Imaging Sensors of respective Payload	Comment (ops = operations)
Jan. 22, 1990	SPOT-2 (CNES)	2 HRV	Operational as of 2000
Aug. 29, 1991	IRS-1B (ISRO)	LISS-I, LISS-II A/B	Ops until Aug. 2001 (10 years)
Feb. 11, 1992	JERS-1 (NASDA)	OPS	S/C ops until Oct. 11, 1998
Oct. 5, 1993	Landsat-6 (NOAA)	ETM	Launch failure
Sept. 20, 1993	IRS-P1 (ISRO)	LISS-2, MEOSS (DLR)	Launch failure
Sept. 26, 1993	SPOT-3 (CNES)	2 HRV	S/C ops until Nov. 14, 1997 (loss of Earth lock)
Oct. 15, 1994	IRS-P2 (ISRO)	LISS-II A/B	S/C ops until Sept. 1997
Nov. 4, 1994	RESURS-O-3 (Russia)	2 MSU-E, 2 MSU-SK	Operational as of 2000
Dec. 28, 1995	IRS-1C (ISRO)	PAN, LISS-III, WiFS	Operational as of 2001
Mar. 21, 1996	IRS-P3 (ISRO)	WiFS	Operations ended in 2005
Aug. 17, 1996	ADEOS (NASDA)	AVNIR	S/C operations terminated June 30, 1997 (loss of power)
Apr. 26, 1996	MIR/Priroda (Russia)	MSU-E, MSU-SK, MOMS-2P (DLR)	The Priroda life ended with the de-orbit of MIR on March 23, 2001
Sept. 29, 1997	IRS-1D (ISRO)	PAN, LISS-III, WiFS	Operational as of 2000
Dec. 24, 1997	EarlyBird (EarthWatch)	EBP, EBM, 3 m resolution	The first commercial imaging S/C failed to operate
Mar. 24, 1998	SPOT-4 (CNES)	2 HRVIR, Vegetation	Operational as of 2008
July 10, 1998	RESURS-O-4 (Russia)	2 MSU-E, 2 MSU-SK	Operational as of 2000
April 15, 1999	Landsat-7 (NASA)	ETM+	Optomechanical (whisk-broom) imaging, operational
April 27, 1999	Ikonos-1 (Space Imaging)	OSA (Optical Sensor Assembly)	Launch failure of commercial imaging mission
Sept. 24, 1999	Ikonos-2 (SI) Identical backup satellite and payload to Ikonos-1	OSA built by Kodak	A new era of 1 m spatial resolution imagery began for spaceborne instruments
Oct. 14, 1999	CBERS (China/Brazil)	HRCC, IRMSS, WFI	Ziyuan-1 (Chinese name) Mission end: Aug. 13, 2003
Dec. 18, 1999	Terra of NASA)	ASTER (NASDA)	S/C operational as of 2008
Dec. 20, 1999	KOMPSAT-1 (KARI)	EOC	S/C ops ended in Jan. 2008
Nov. 20, 2000	QuickBird-1 (Earth-Watch of Longmont, CO)	BGIS-2000 (Ball Global Imaging System-2000)	Commercial imagery at 1 m GSD, Launch failure
Nov. 21, 2000	EO-1 (NASA)	ALI (Advanced Land Imager)	The Landsat-7, EO-1, SAC-C and Terra "morning constellation" train started in 2001
Dec. 5, 2000	EROS-A, ImageSat International, Cayman Islands	PIC (Panchromatic Imaging Camera)	Commercial imagery at 1.9 m GSD, swath=14 km
Sept. 21, 2001 Launch failure	OrbView-4 (Orbimage of Dulles, VA)	OHRIS with Pan & 4 MS bands, OHIS, 280 bands	Commercial imagery at 1 m Pan, 4 m MS, swath of 8 km 8 m resol., 5 km swath,
Oct. 18, 2001	QuickBird-2 (DigitalGlobe of Longmont, CO)	BGIS-2000 (Ball Global Imaging System-2000)	Commercial imagery at 0.61 m Pan, 2.5 m MS
Oct. 22, 2001	TES (Technology Experiment Satellite, ISRO)	HRPIC (High Resolution Pan Imaging Camera)	Imagery for defense appl. At ≤ 1 m
May 4, 2002	SPOT-5 (CNES)	2 HRG, HRS, Vegetation	5 m resolution for HRG PAN data, 2.5 m in super-mode
June 26, 2003	OrbView-3 (OrbImage)	OHRIS (OrbView High Resol. Imaging System)	Commercial imagery at 1 m PAN, 4 m MS, 8 km swath
Oct. 17, 2003	IRS-P6 (ISRO), also called: ResourceSat-1	LISS-IV, LISS-III, AWiFS	LISS-IV with 5.8 m GSD from SSO at 820 km altitude
Oct. 21, 2003	CBERS-2 (China/Brazil)	HRCC, IRMSS, WFI	ZY-1B (Chinese name)
May 20, 2004	FormoSat-2 (NSPO), Taiwan	RSI (Remote Sensing Instrument)	2 m GSD, 24 km swath 8 m MS data (5 bands)

Launch Date	Satellite Platform (Agency or Company)	Earth Imaging Sensors of respective Payload	Comment (ops = operations)
May 5, 2005	IRS-P5 (ISRO) CartoSat-1	PAN-F, PAN-A	Along-track stereo imagery 2.5 m GSD, 30 km swath
Oct. 27, 2005	TopSat (QinetiQ, RAL), UK	RALCam1, 3 bands of MS, 1 Pan	Imagery at 2.5 m GSD Pan and 5 m MS, FOV= 15 km
Jan. 24, 2006	ALOS nicknamed Daichi (JAXA, formerly NASDA)	PRISM, (stereo mapping) AVNIR-2	2.5 m GSD, 35 km swath 10 m MS, 70 km swath
Apr. 25, 2006	EROS-B (ImageSat International), Israel	PIC-2 (Pan Imaging Camera) with TDI capability	Commercial imagery at 0.7 m GSD, 13 km swath
June 15, 2006	Resurs-DK1, TsSKB- Progress, Samara (Volga), part of Russia's space program	Geoton-1 imager, PAN+ 7 MS bands	1 m GSD all 8 VNIR bands, swath of 28.3 km (altitude 350 km), FOR = 448 km
July 28, 2006	KOMPSAT-2 (KARI), Korea	MSC (Multi-Spectral Camera) Pan and MS	1 m GSD for Pan, 4 m GSD for MS, 15 km swath
Jan. 10, 2007	CartoSat-2, ISRO	Pan Camera	< 1 m GSD, swath of 9.6 km
Sept. 18, 2007	WorldView-1 (Digital- Globe) Longmont, CO	WV60 camera	Commercial imagery at 0.50 m (nadir) in Pan only
April 28, 2008	CartoSat-2A (ISRO)	Pan Camera	0.8 m GSD, swath of 9.6 km
Aug. 29, 2008 (constellation of 5 S/C)	RapidEye (BlackBridge, Berlin, Germany)	REIS, 5 bands MS	Commercial MS and Pan im- agery at 6.5 m, 78 km swath
Sept. 6, 2008	GeoEye-1 (GeoEye, Dulles, VA)	GIS (GeoEye Imaging System)	Commercial MS and Pan im- agery at 1.64 m, 0.41 m
Oct. 1, 2008	THEOS (GISTDA) Thailand	PAN camera MS Camera	2 m GSD, 22 km swath 15 m GSD, 90 km swath
July 14, 2009	MACSat(RazakSat (ATSB, Malaysia)	MAC (PAN, 4 MS)	2.5 m GSD, 5 m MS, 20 km swath, Near-equatorial orbit
July 29, 2009	Deimos-1 (Deimos Space, Spain)	SLIM6	22 m, swath of > 600 km 3 bands in VIS
July 29, 2009	UK-DMC-2 (SSTL)	SLIM6	22 m, swath of > 600 km 3 bands in VIS
July 29, 2009	DubaiSat-1 (EIAST, Dubai)	DMAC, Pan MS	2.5 m GSD (20 km swath) 5 m GSD (4 bands)
Oct. 08, 2009	WorldView-2 (Digital Globe) Longmont, CO	WV110 camera	Commercial imaging at 0.41 m Pan + 2 m MS (8 bands)
July 12, 2010	CartoSat-2B (ISRO)	Pan Camera	0.8 m GSD, swath of 9.6 km
July 12, 2010	AlSat-2A (CNTS) Algeria	NAOMI (New AstroSat Op- tical Modular Instrument)	Pan: 2.5 m, MS: 10 m, 17.5 km swath
Apr.20, 2011	ResourceSat-2 (ISRO)	LISS-4, LISS-3, AWiFS	LISS-4 with 5.8 m GSD with a swath of 70 km
April 20, 2011	XSat (NTU, Singapore)	IRIS, PAN and 3 MS bands	12 m MS imagery, 50 km swath (technology test)
Aug. 17, 2011	NigeriaSat-2 (NASRDA, Nigeria)	VHRI MRI	2.5 m Pan, 5 m MS, 20 km 32 m, 4 MS bands, 300 km
Aug. 17, 2011	NigeriaSat-X (NASRDA, Nigeria)	SLIM6	22 m, swath of 600 km 3 bands in VIS
Dec. 17, 2011	Pleiades-HR1A (CNES)	OHRI (Optical High- Resolution Imager)	Commercial imagery at 0.7 m Pan, 2.8 m for 4 MS bands
Dec. 17, 2011	SSOT (ACE), Chile	NAOMI (New AstroSat Op- tical Modular Instrument)	Pan: 1.5 m, 4 MS bands: 6 m, 10.15 km swath
Dec. 22, 2011	ZY-1-02C, CNSA, China	HRC (HighResolution C.) PMS (Pan/MS) camera	2.36 m Pan, swath of 57 km 5 m Pan, 10 m MS, 60 km
Jan. 09, 2012	Zy-3A (Zi Yuan-3A), CAST), China	TAC (Three-line Array Camera) MSC (Multispectral Cam)	Pan nadir camera, 2.1 m Forward/backward, 3.5 m 5.8 m
May 17, 2012	KOMPSAT-3 (KARI), Korea	AISS (Advanced Earth Imaging Sensor System)	Pan band: 0.7 m MS (4 bands): 2.8 m

Launch Date	Satellite Platform (Agency or Company)	Earth Imaging Sensors of respective Payload	Comment (ops = operations)
Sept. 09, 2012	SPOT-6 EADS Astrium (commercial imagery)	NAOMI (New AstroSat Optical Modular Instrument)	Pan: 1.5 m, 4 MS bands: 6 m, 10–60 km swath
Sept. 29, 2012	VRSS-1 / Francesco de Miranda, ABAE, Venezuela	PMC (Pan&MS Camera) WMC (Wide-swath MS Camera)	Pan=2.5 m, MS=10 m, Swath=57 km; MS=16 m, Swath= 369 km
Dec. 02, 2012	Pleiades-HR1B (CNES)	OHRI (Optical High-Resolution Imager)	Commercial imagery at 0.7 m Pan, 2.8 m for 4 MS bands
Dec. 18, 2012	Göktürk-2, TUBITAK-UZAY, Turkey	MSI (Multispectral Imager)	Pan=2.5 m, MS=10 m, SWIR=20 m, Swath=20 km
Apr. 26, 2013	GF-1 (Gaofen-1), CNSA, China	PMC, WVC(Wide View Camera)	Pan = 2 m, MS = 8 m and 16 m (800 km swath)
May 7, 2013	VNREDSat-1A, VAST, Vietnam	NAOMI (New AstroSat Optical Modular Instrument)	Pan: 2.5 m, 4 MS bands: 10 m, Swath of 17.5 km
Nov. 21, 2013	DubaiSat-2 (EIAST, Dubai)	HiRAIS (Pan+4 MS)	1 m Pan, 12 km swath, 4 m of 4 MS bands (RGB+NIR)
Apr. 16, 2014	EgyptSat-2 (NARSS)	MSI (Pan + MS)	1 m Pan, 4 m of MS bands
Apr. 30, 2014	KazEOSat-1, Kazcosmos, Kazakhstan	NAOMI (Astrium)	1 m Pan, 4 m MS, swath of 20 km
June, 19, 2014	Deimos-2 (Deimos Imaging, Spain)	EOS-D (Electro Optical Camera-D)	Commercial imagery at 1 m (Pan), 4 m MS, 12 km swath
June 19, 2014	KazEOSat-2, Kazcosmos, Kazakhstan	KEIS (Kazakh Earth Imaging System)	MS imagery (5 bands) at 6.5 m, >70 km swath
June 30, 2014	SPOT-7 Airbus Group (commercial imagery)	NAOMI (New AstroSat Optical Modular Instrument)	Pan: 1.5 m, 4 MS bands: 6 m, 10–60 km swath
2014 (planned)	ASNARO (NEC, USEF), Japan	OPS (Optical Sensor)	Commercial imagery at < 0.5 m Pan, 2 m for 6 MS bands
2014 (planned)	FormoSat-5 (NSPO), Taiwan	RSI (Pan+4 MS)	2 m Pan, 34 km swath, 4 m MS bands (RGB+NIR)
2014 (planned)	VEN μ S, ISA, CNES	VSSC (12 bands in VNIR)	5.3 m, 27.56 km swath
2014 (planned)	DMC-3 constellation 3 S/C, DMCii, Surrey, UK	DMC-3 Imager	1 m Pan, 4 m GSD, swath of 22.6 km
2015 (planned)	SEOSat/Ingenio (CDTI, INTA, Spain)	PP (Primary Payload)	2.5 m Pan, 60 km swath, 10 m of 4 MS bands (RGB+NIR)

Table 3: Chronology of optical Earth-surface satellite imaging missions

With regard to area array CCDs, there are the following basic architectures available:

1) **Full Frame (FF)** CCDs consist of a parallel CCD shift register, a serial CCD shift register, and a signal-sensing output amplifier. In FF operation, the CCD must alternate between exposure and readout. In this support mode, the exposure is controlled by a mechanical shutter or strobe to preserve scene integrity, because the parallel register is used for both scene detection and readout. This arrangement cannot be used for high frame rate requirements (due to serial readout configuration).

2) **Frame Transfer (FT)** CCD. This type of imager has a dedicated (radiation-shielded) storage (readout) area (of at least the same size as the imaging section of the array) separate from the imaging area with the following advantages:

- The collection of radiation is continuous, maximizing the fill-factor in the imaging region; the functions of image readout and radiation collection run in parallel
- This greatly increases the time available for the image integration period
- Better reliability is provided, in particular at higher frame rates that result from sub-imaging or binning
- The concept offers some electronic shuttering (prevention of smearing effects)

– The FT concept can be extended to multiple frames (also referred to as split frame transfer) by masking most of the parallel register and using only a small region as the image array.

A frame transfer CCD is a specialized CCD, often used in astronomy and some professional video cameras, designed for high exposure efficiency and correctness.

3) **Interline Transfer (ILT) CCD.** The ILT has a parallel register which is subdivided so that the masked storage area fits between columns of exposed pixels. The electronic image accumulates in the exposed area of the parallel register, just as it does in the frame transfer CCD. At readout, the entire image is shifted under the interline mask. The masked pixels are read out in a fashion similar to the FT CCD.

The image collection mode of an area array sensor can be either “interlaced” or “progressive scan” (non–interlaced). The interlaced technique is used by the major broadcast standards PAL and NTSC and is done to reduce the bandwidth of the image for transmission. In this mode, the frame is divided into two fields: an odd field consisting of all the odd numbered rows, and the even field consisting of all the even numbered rows. Half of the frame is recorded by the odd field at time T1, and the other half of the frame is recorded by the even field at time T2.

4) **Electron–Multiplying (EMCCD):** EMCCD, also known as an L3Vision CCD, is a charge–coupled device in which a gain register is placed between the shift register and the output amplifier. The gain register is split up into a large number of stages. In each stage the electrons are multiplied by impact ionization in a similar way to an avalanche diode. The gain probability at every stage of the register is small ($P < 2\%$) but as the number of elements is large ($N > 500$), the overall gain can be very high ($g = (1 + P)^N$), with single input electrons giving many thousands of output electrons.

In the first decade of the 21st century, EMCCD technology has had a profound influence on photon starved imaging applications. Advances in chip technology and the ability to optimise the performance of these chips have allowed scientists to see things they have never been able to see before, from live cell microscopy to photon counting astronomy and raman spectroscopy.

EMCCDs were first produced at e2v Technologies Plc (Chelmsford, Essex, UK) in the late 1990s they have found use in many applications where either the signal level is very low or where high frame rate imaging is required. These include surveillance, astronomy and in other scientific imaging applications including very low level bioluminescence for drug discovery and genetic engineering applications.

- **Spatial resolution.** The requirement of high spatial resolution (and with it the ability to discriminate between small objects), in particular to land surface imagery, has been around since the early days of remote sensing. In parallel, there are virtually always the needs for wide–swath coverage and high temporal resolution (i.e., frequent repeat coverage capability). High spatial resolution implies of course high data rates which conflicts in turn the wide–area coverage. An overview of major land–surface imaging missions (Figure 5, Table 4) demonstrates the trends and practical compromises taken with the best available technology of the time. – The first spaceborne 1 m spatial resolution panchromatic image with an optical imager was obtained by the commercial spacecraft Ikonos–2 (launch Sept. 24, 1999) of Space Imaging Inc. This was followed with a resolution of 0.61 m delivered by the optical imager of the QuickBird–2 mission (launch Oct. 18, 2001) of DigitalGlobe Inc.

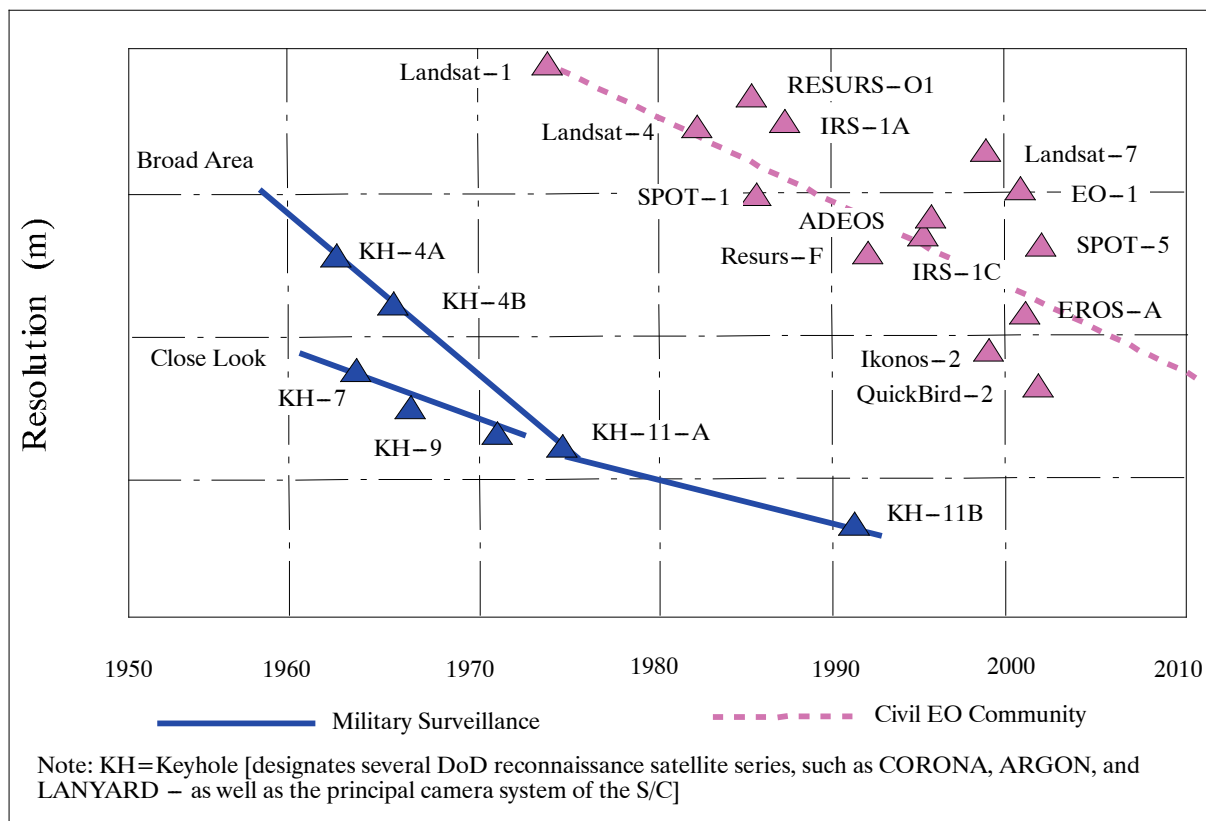


Figure 5: Spaceborne surface imaging resolution trends in the civil & military fields

- The high spatial resolution imagery of commercial satellite platforms led to new applications in cartography such as the fully automatic feature extraction of road networks in urban areas. The analysis method reported has its bases in a vegetation mask derived from coregistered multispectral Ikonos data (4 m resolution) and in texture derived from pan-chromatic Ikonos data (1 m resolution).⁹⁵⁾

Mission/Launch Date	Sensor	Spatial Resolution (best band)	Swath width	Data Rate
Landsat-1 / Jul. 23, 1972	MSS	80 m	185 km	15 Mbit/s
Landsat-4 / Jul. 16, 1982	TM	30 m	185 km	85 Mbit/s
Resurs-O1-1 / Nov. 3, 1985	2 MSU-E	45 m x 33 m	80 km (total)	
SPOT-1 / Feb. 22, 1986	2 HRV	10 m	117 km (total)	50 Mbit/s
IRS-1A / Mar. 17, 1988	2 LISS-II,	36 m	2 x 74 km	2 x 10.4 Mbit/s
Resurs-F / (series)	KFA-1000	6-8 m	70 km	Film
IRS-1C / Dec. 28, 1995	PAN	6 m	70 km	125 Mbit/s
ADEOS / Aug. 17, 1996	AVNIR	8 m	80 km	60 Mbit/s
Landsat-7 / Apr. 15, 1999	ETM+	13 m x 15 m	185 km	150 Mbit/s
EO-1 / Nov. 21, 2000	ALI	10 m	185 km	300 Mbit/s
Ikonos-2 / Sept. 24, 1999	OSA	1 m PAN 4 m MS	11-13 km	320 Mbit/s
QuickBird-2 / Oct. 18, 2001	BGIS 2000	0.61 m PAN 2.5 m MS	16.5 km	320 Mbit/s

95) D. Haverkamp, "Extracting straight road structure in urban environments using Ikonos satellite imagery," Optical Engineering, Vol. 41, No 9, Sept. 2002, pp. 2107-2110

Mission/Launch Date	Sensor	Spatial Resolution (best band)	Swath width	Data Rate
SPOT-5 / May, 4, 2002	2 HRG	5 m Pan (2.5 m in supermode) 10 m MS data	120 km (total)	2 x 50 Mbit/s
Landsat-8 (Feb. 13, 2013)	OLI TIRS	15 m Pan 30 m VIS, SWIR 100 m TIR	185 km	440 Mbit/s

Table 4: Spatial resolutions of major land-surface imagers

- Detector technology extension. The measurement of electromagnetic radiation in the various spectral ranges, in particular in the **infrared region**, is at the heart of the problem. The infrared sensor “Eye in the Sky” was the first successfully flown long wavelength sensor launched in 1967 (Corona military program of DoD). Significant advances in Earth observation capability have come from the development of on-chip detector circuitry (see chapter O.4).^{96) 97) 98)}
- The directional pointing capability of a sensor (on command) in the cross-track direction was introduced in the SPOT series in 1986 with SPOT-1 (for imaging satellites in the civil domain) and continued until SPOT-5 (launch May 4, 2002). The new pointing technique introduced the term “FOR (Field of Regard)”, designating the angular coverage capability beyond (and including) the swath – it allowed the imaging of nearby events of interest that happened to be outside the regular (nadir-centered) swath width. At the start of the 21st century, the capability of tilting – either the imaging instrument by itself or the entire spacecraft with the imager (referred to as body-pointing) – is being practiced by many optical imaging missions, in particular by the commercial imaging data providers. – On the military side, the KH-7 (Keyhole-7) reconnaissance satellite of DoD (launch July 12, 1963, operational until June 1967) featured a film camera (also by the name of Keyhole) with an instrument cross-track tilting capability (very probably the first instance in history on a spacecraft), to extend FOR.

Mission	Instrument	Instrument Mass, Power	Comment
Landsat-5 (launch Mar. 1, 1984), NASA	TM	285 kg, 385 W	Optomechanical instrument
IRS-1C (launch Dec. 28, 1995), ISRO	LISS-III	171 kg, 78 W	Optoelectronic instrument
NEAR/Shoemaker (launch Feb. 17, 1996), NASA	MSI	7.7 kg, 6.9 W	Optoelectronic instrument
DS1 (launch Oct. 24, 1998), NASA	MICAS	12 kg,	CMOS/APS technology
Landsat-7 (launch Apr. 15, '99), NASA	ETM+	425 kg, 590 W	Optomechanical instrument
Ikonos-2 (launch Sept. 24, '99), SI	OSA	171 kg, 350 W	Optoelectronic instrument
Terra (launch Dec. 18, 1999), NASA	ASTER	421 kg, 463 W	Optoelectronic and optomechanical instrument
QuickBird-1 (launch Nov. 20, 2000), Earthwatch	BGIS 2000	380 kg, 430 W	Optoelectronic instrument (launch failure)
EO-1 (launch Nov. 21, 2000), NASA	ALI	106 kg, 100 W	Optoelectronic instrument
PROBA (launch Oct. 22, 2001), ESA	CHRIS	15 kg, 10 W	Optoelectronic instrument
SMART-1 (launch Sept, 27, 2003) ESA	AMIE	2.2 kg, 0.5 W	Optoelectronic instrument
Diamant-1 (launch 2010), OHB-System	MSRS	64 kg, 120 W	Optoelectronic instrument
NPOESS (launch 2014)	VIIRS	160 kg, 134 W	Optomechanical instrument

Table 5: Mass/power reduction trends in typical spaceborne imaging instruments

- 96) Note: In 1800, William Herschel (1738–1822) reported the discovery of light beyond the visible spectrum. He dispersed the solar spectrum with a prism and found thermal effects of invisible radiation beyond the red.
- 97) A good reference is: W.D. Rogatto, “The Infrared and Optical Systems Handbook, Vol. 3 Electro-Optical Components,” Copublished by ERIM and SPIE, 1993, chapter 4.5.2
- 98) A Rogalski, K. Chrzanowski, “Infrared devices and techniques,” Opto-Electronics Review, Vol. 10, No 2, 2002, pp. 111–136

- Size/mass/power/cost reduction of imaging instruments. ⁹⁹⁾ Miniaturization and the introduction of new technologies is the name of the game, in particular in the late 1990s and the early 21st century. The JHU/APL sensor MSI (Multispectral Imager) with a 537 x 244 CCD detector array, a spectral range of 0.4 to 1.1 μm , and a FOV of $2.9^\circ \times 2.25^\circ$ (pixel resolution of 95×161 mrad), was flown on NEAR (Near Earth Asteroid Rendezvous/Shoemaker) of NASA (launch Feb. 17, 1996). A newer MSI design of JHU/APL with a lightweight reflective telescope, high-density solid-state memory and miniaturized on-chip-board electronics has a mass of 0.5 kg and a power of 1 W.

S/C	S/C Launch (End of Service)	Sensor Complement	Data Resolution (m)	Data Communications	Orbital Altitude	S/C Operator(s)	Revisit Time (days)	Data Rate Mbit/s
LS-1 (ERTS)	Jul. 23, 1972 (Jan. 6, 78)	RBV MSS, DCS	80 80	DD (Direct Downlink) 2 WBVTR	907 km	NASA	18	15
LS-2	Jan. 22, 1975 (Feb. 25, 82)	RBV MSS, DCS	80 80	DD with 2 WBVTR	908 km	NASA	18	15
LS-3	Mar. 5, 1978 (Mar. 31, 83)	RBV MSS, DCS	30 80	DD with 2 WBVTR	915 km	NASA	18	15
LS-4	Jul. 16, 1982 (standby Dec. 93)	MSS TM, GPS	80 30	DD TDRSS	705 km	NOAA ('83) Eosat ('85)	16	85
LS-5	Mar. 1, 1984	MSS TM, GPS	80 30	DD TDRSS	705 km	NOAA ('84) Eosat ('85)	16	85
LS-6	Oct. 5, 1993	ETM	15 (PAN) 30 (MS)	DD with recorders	launch failure (contact lost during launch)			85
LS-7	Apr. 15, 1999	ETM+	15 (PAN) 30 (MS)	DD with recorders	705 km	NOAA, USGS	16	150
LS-8	Feb. 11, 2013	OLI, TIRS	15 (PAN) 30 (MS) 100 m	DD with recorders	705 km	USGS	16	440

Table 6: Overview of Landsat S/C series

- In 1993, the US government (Department of Commerce) granted the first US license to DigitalGlobe's predecessor, namely WorldView Inc. of Longmont, CO, allowing a private enterprise to build and operate a satellite system and to gather high spatial resolution digital imagery of the Earth for commercial sale.

1.4.1.2 Solid-state (digital) imaging – CMOS/APS detector technology

CMOS/APS (Complementary Metal–Oxide Semiconductor/Active Pixel Sensor) detector technology. In CMOS image sensors, the photo-voltaic conversion effect of silicon semiconductors, in this case diodes, is being exploited to make optical sensors that are sensitive to visible light. In the CMOS/APS design concept, the individual pixels do not only contain the actual photosensitive element, but also other (analog domain) processing circuitry, ranging from in-pixel buffers and amplifiers up to application-specific computational pixels.

CMOS/APS represents an alternate approach to the proven CCD-imaging concepts, a second generation solid-state imaging sensor technology. The emerging CMOS/APS technology was first proposed at CSMT (Center for Space Microelectronics Technology) of NASA/JPL in 1993. Sabrina Kemeny and Eric R. Fossum were on the CSMT team who developed the

⁹⁹⁾ Binh Q. Le, P. D. Schwartz, Sharon X. Ling, et al., "A Low-Cost Miniaturized Scientific Imager Design with Chip-on-Board Technology for Space Applications," Johns Hopkins APL Technical Digest, Vol. 20, No 2, 1999, pp. 170–179

APS technology. In 1995 JPL licensed the APS technology to Photobit Corporation of La Crescenta, CA, a JPL spin-off company. ^{100) 101) 102) 103) 104) 105) 106)}

The APS method basically provides a current as a function of the irradiance for each pixel. Normally, the output is proportional to the irradiance falling onto the APS detector (there are also APS versions providing a logarithmic output of the irradiance). *The CMOS/APS technology employs an amplifier at each pixel site, thereby eliminating the bus capacitance and resistance problems of CCDs or CIDs (newer APS technology utilizes active transistors in each pixel to buffer the photo-signal).* It was not until sub-micron photolithography became available that APS imagers became useful. CMOS/APS imagers sense radiation (light) in the same way as CCDs. Both technologies convert incident photons into electronic charge (electrons) by the same photo-conversion process. However, in the CMOS/APS technique, the charge packets are not transferred, they are instead being detected by the charge-sensing transistors.

Architecturally, the principal difference between the CCD and the APS is that the CCD is inherently a serial output device, with all pixels in the array being read in series by one (or at most a few parallel) on-chip amplifiers. The APS, in contrast, can have random access capability, and features an output amplifier in each pixel. Moreover, the on-chip circuitry in most APS devices exploits modern CMOS design and fabrication characteristics that allow operation with much less power than is required by CCDs.

The CMOS/APS concepts take advantage of the microprocessor (CMOS) fabrication processes (mature and widely available manufacturing techniques) resulting in reduced manufacturing costs of APS detectors over similar CCD devices (down to 30% of the cost of a comparable CCD). Some performance advantages of the CMOS/APS technology are:

- TTL-compatible operation (0–5V), with low-power requirements (e.g. 10 mW at 1 M pixel/s; includes ADC)
- Only a single power supply is needed (at 3.3 V or at 5 V)
- Electronic shuttering (having on-chip control logic, smart functions such as automatic exposure control can be incorporated)
- Provision of high dynamic range and good functionality like readout windowing (the window-of-interest readout feature may be used to track objects in the image for machine vision; handling of simultaneous multiple windows)
- Variable integration time (timing control)
- On-pixel amplification, x-y addressability, and random access readout
- A single CMOS/APS system-on-chip can integrate image capture of 1 Mpixel
- A/D conversion and digital processing. In particular, APS can integrate analog and digital processing on the same die.

-
- 100) E. R. Fossum, R. K. Bartman, A. Eisenman, "Application of the active pixel sensor concept to guidance and navigation," *Space Guidance, Control and Tracking, Proceedings of SPIE*, Vol. 1949, 1993, pp. 256–265
- 101) S. Mendis, S. Kemeny, E. R. Fossum, "A 128x128 CMOS active pixel image sensor for highly integrated imaging systems," *International Electron Devices Meeting (IEDM) Technical Digest*, pp. 583–586, Washington D. C., December 5–8, 1993.
- 102) E. R. Fossum, "Active Pixel Sensors – Are CCDs Dinosaurs?," *Charge-Coupled Devices and Solid State Optical Sensors III, Proceedings of SPIE*, Vol. 1900, San Jose, CA, Feb. 2–3, 1993, pp. 2–14,
- 103) D. Renshaw, P. Denyer, G. Wang, M. Lu, "ASIC image sensors," *Proceedings of the IEEE International Symposium on Circuits and Systems*, New Orleans, LA, 1990
- 104) S. Kemeny, B. Pain, E. Fossum, L. Matthies, R. Panicacci, "Multiresolution image sensor using switched capacitor circuits," *Proceedings of 1994 International CMOS Camera Workshop*, Holmdel NJ, Oct. 17–18, 1994.
- 105) S. E. Kemeny, R. Panicacci, B. Pain, L. Matthies, E. R. Fossum, "Multiresolution image sensor," *IEEE Transactions on Circuits and Systems for Video Technology*, Vol. 7, No 4, pp. 575–583, 1997
- 106) E. Fossum, "Assessment of Image Sensor Technology for Future NASA Missions," *SPIE Vol. 2172*, 1994

- *APS detectors provide generally a considerably higher radiation hardness over CCD detectors since they can be manufactured with processes such as silicon-on-insulator.*

Initial drawbacks of CMOS/APS with respect to CCD technology are seen in the relatively low pixel sensitivity (low quantum efficiency and non-uniformity), the relatively high noise levels of the small pixel arrays, and in reduced calibration capabilities of the array. Further, with CCDs up to 100% of a pixel's area can be made sensitive to light ("fill factor"), where APS pixels by their very nature devote only a small portion of the total area to the actual photodiode or phototransistor function. The lower fill factors of APS result in longer exposure times for the same scene as compared to CCD concepts.¹⁰⁷⁾ – Note: APS (Active Pixel Sensor) is also being referred to as APA (Active Pixel Array), both terms have the same meaning.

The CMOS/APS imager in silicon technology offers a spectral response in the UV/VNIR spectral regions. The CMOS/APS micro-technology implies low-power micro-instruments (imagers and other devices) for near-future microsattellites. Other fields of CMOS/APS technology applications include:

- In the early the 21st century, replacement of CCD detector technology in AOCS (Attitude and Orbit Control System) pointing applications like in star trackers and in sun sensors (providing high-accuracy pointing performance of star trackers)
 - Commercial camera market
 - Optical communications
 - Multimedia machine vision, and biomedical imaging.

Description	CIF (Common Immediate Format) SOC	VGA (Video Graphics Array) SOC
Pixel array size	352 (H) x 288 (V)	640 (H) x 480 (V)
Frame rate	30 frame/s	30 frame/s
Supply voltage	3.3 V	3.3 V
Power dissipation	55 mW (typical)	<100 mW (typical)
Output format	8-bit/10-bit color digital video (SRGB)	10-bit color digital video (SRGB)
Shutter	Electronic rolling snap	Electronic rolling snap
Common features	<ul style="list-style-type: none"> • On-chip: a) analog signal processing; b) 8/10-bit ADC; c) DACs (Digital-Analog Converter) for bias control; d) gain control (user programmable); e) Pan and zoom (user programmable); f) Timing and clock generator • Standard digital output and control interface (I²C) • Auto exposure control (user programmable) 	

Table 7: Specification of a typical CMOS/APS SOC (System-on-Chip)

At the start of the 21st century, the CMOS/APS imaging concept is regarded a viable and complementary solid-state imaging technology to that of CCDs. However, it should be realized that the CCD technology has experienced three decades of advances and optimizations, specifically for imaging applications. They present today excellent performance and image quality, thanks to extremely low noise, low dark current, high quantum efficiency, and good fill factor efficiency. Due to these characteristics, the CCD concept will remain the technology of choice for high-quality imaging applications (in particular for hyperspectral applications). The general trend is to replace the older CCD technique by the more flexible, cheaper, and less power-hungry CMOS/APS technique. Several programs have been funded by ESA to support the development of APS technology, in particular for such applications as attitude sensors (smart sun sensors, star sensors, etc.) and vision cameras.

107) Note: The APS noise problem is due to the so-called "fixed pattern noise," a noise that results from small differences in the behavior of the individual pixel amplifiers. As of 1998, Bell Labs researchers developed circuits outside the sensor array that detect and cancel this noise – resulting in a patented camera-on-chip technology. The chip of 1 cm² in size contains over 100,000 active pixels. JPL built DICE (Digital Imaging Camera Experiment), a camera-on-chip containing an array of 1024 x 1024 pixels.

In the CMOS/APS image sensor, each pixel contains not only the photodetector element but also active transistor (amplifier) circuitry for readout of the pixel signal. In addition to the APS (Active Pixel Array) that detects photons and produces an analog voltage output, an ADC (Analog–Digital Converter) is an essential element of the CMOS/APS SOC (System–on–Chip) technology. The CMOS/APS SOC also contains an integrated timing generator for sequencing all operations, control registers for setting up the operation of the chip, on–chip generated bias voltages (that can be adjusted), and a rapid serial digital interface for controlling and verifying the operation of the chip. A typical realization (2002) of this architecture in a 0.5 μm standard CMOS technology is defined in Table 7.

Detector arrays can be monolithic or hybrid. Monolithic arrays, which are built from a single chip, are typically CMOS–based and are usually the cheapest alternative at least for large volumes. It is expected that image sensors operating at visible wavelengths will in the long run be almost completely CMOS–based. – When monolithic sensors cannot be made one has to resort to hybrid ones, where several chips are combined into a unit. The reason is usually that detectors cannot be based on silicon or materials compatible with silicon, and that more exotic materials are needed such as GaAs, InSb and MCT for infrared detection, and CdTe or GaAs for X–ray detection. In this hybrid case a chip consisting of the detector pixels is usually flip–chip bonded to a silicon CMOS chip, consisting of a ROIC (Readout Integrated Circuit) where multiplexing and conditioning of the electronic signals take place. An example of this hybrid detector technology is for instance a QWIP (Quantum Well Infrared Photodetector) array.

Parameter (typical values)	CMOS/APS technology	CCD technology
Format	512 x 512 pixels	1024 x 1024 pixels
Pitch	5 – 20 μm	10 – 20 μm
Fill factor	15 – 43%	100%
SNR (Signal–to–Noise Ratio)	50 – 70 dB	75 dB
Non–uniformity	3%	N/A
Dark signal	4000 e^-/s	150 – 400 e^-/s
Pixel rate	1 – 10 MHz	10 MHz
Power consumption	20 – 200 mW	50 mW

Table 8: Comparison of typical CMOS/APS and CCD imagers

- Some early examples of CMOS/APS imaging technology demonstrations/implementations are:
 - The first spaceborne demonstration of a camera with CMOS/APS technology was VTS (Visual Telemetry System), a joint project of: Matra Marconi Space, UK; DSS/OIP (Delft Sensor Systems/Optronics Instruments & Products), and IMEC, both of Belgium, and flown on TEAMSAT (M.52), an ESA low–cost satellite demonstrator mission, launched on Oct. 30, 1997 from Kourou (Ariane–502, 2nd qualification flight of an Ariane–5 vehicle). VTS, with a 512 x 512 pixel array for each of the three camera modules, performed visual post–launch monitoring of structure deployments. VTS used the FUGA15 random–access sensors, these chips were effectively the world’s first CMOS/APS imagers operational in space.
 - The TMSat (renamed to Thai–Paht–1) microsatellite of Thailand, built by SSTL of Surrey, UK (launch July 10, 1998), carries a CMOS Video Camera with APS technology.
 - APS (Active Pixel Sensor) technology is also part of MICAS (Miniature Integrated Camera Spectrometer) flown on DS1 (Deep Space 1, launch Oct. 24, 1998, M.11) of JPL.
 - APS imaging technology is flown on ESA’s XMM–Newton spacecraft (launch Dec. 10, 1999). Two cameras were mounted on the exterior of the spacecraft’s focal plane assembly: a) the VMC (Visual Monitoring Camera), and b) the IRIS–1 (Integrated Radiation–tolerant Imaging System–1) color sensor, developed by FillFactory NV of Mechelen, Belgium

(a spin-off company of IMEC, Belgium). About 5 hours after launch of XMM–Newton by an Ariane 4 launcher, these cameras took pictures of the left and the right solar array assemblies of the S/C.¹⁰⁸⁾ – IRIS–1 characteristics: 640 x 480 pixels, 14 μm pitch; integrating photodiode pixel sensor, double sampling amplifiers; 8 bit digitization on–chip, 10 images/s; photo response of 2.05×10^{12} V/Ws; pixel response non–uniformity 2.27%; readout noise 63 e^- ; SNR (full range) 67 dB; power consumption 80 mA; 20 krad radiation tolerance. – During launch of the ESA Cluster–2 mission (launch Aug. 9, 2000), the IRIS–1 camera provided a color movie of the Cluster–2 satellite separation (a first in space). A follow–up development at FillFactory resulted in the series of STAR–250 radiation–hardened CMOS/APS imagers for star and beam tracking as well as sun tracking purposes, introduced throughout 2001 [ESA funded project called ASCoSS (Attitude Sensor Concepts for Small Satellites)].

In 1999, this exercise produced a miniaturized **CMOS/APS–based star sensor** (detector by FillFactory) for ASCoSS according to Sira Electro–Optics specifications (thus, the first APS star sensor built by Sira included multi–chip module electronics and diffractive optics)]. The **STAR–250** is a line–scan based integrating imager with provisions for versatile readout (windowing, electronic shuttering, etc.). – Note: In 2004, Cypress Semiconductor Corporation with HQ in San Jose, CA (USA) acquired FillFactory NV of Mechelen, Belgium.

– An early spaceborne CMOS/APS technology star sensor implementation is being flown on the SWIFT (Catching Gamma–Ray Bursts on the Fly) satellite, a NASA space science mission (launch Nov. 20, 2004). In this configuration, the FillFactory STAR–250 imager is being used in TAM (Telescope Alignment Monitor) as an alignment sensor in the calibration system of the SWIFT X–ray telescope (provided by Sira Electro–Optics, Chislehurst, UK). The sensor measures 68 mm x 69 mm x 28 mm, weighs 240 g, and consumes just 0.5 W of power.

– The ST–6 (Space Technology–6) “Compass” mission of NASA, is flying an APS star sensor package by the name of **ISC** (Inertial Stellar Compass), developed by CSDL (Charles Stark Draper Laboratory Inc.) of Cambridge, MA.^{109) 110)} The ISC attitude system employs a STAR–250 APS imager of FillFactory NV with a pixel pitch of 25 μm . The ISC has the following key performance features: 0.1° (1σ) pointing accuracy in each axis; high–rate maneuver capability; self–initializing capability; mass of about 2.5 kg; power of about 3.5 W. ISC is composed of a wide FOV APS camera and a MEMS gyro assembly with associated processing and power electronics.

Note: While ISC was initially planned to be launched as a Hitchhiker payload on a Shuttle flight, NASA selected in Sept. 2003 a commercial ride on a solar sail mission, namely Team Encounter Flight One, of Team Encounter LLC, Houston, TX. The Team Encounter Flight One mission is expected to be launched in 2006 ??.

– SSS (Smart Sun Sensor). With ESA funding, Galileo Avionica (of Florence, Italy) has developed SSS (validation phase as of 2002/3) consisting of an attenuation filter with a photoengraved pin hole, a CMOS/APS detector (**STAR–1000** of Cypress/FillFactory, a 1024 x 1024 pixel chip) for sun spot imaging, proximity electronics for data processing (barycenter detection of the incident energy of the sun) and power interfaces. In acquisition mode, the entire FOV ($128^\circ \times 128^\circ$) is searched for sun presence finding (sub–pixel sun position and

108) D. J. Purril, A. Adolph, D. Uwaerts, K. Weible, “A New Technology Attitude Sensor,” 4th ESA International Conference on Spacecraft Guidance, Navigation and Control Systems, Oct. 18–21, 1999, pp. 267–272, ESA/ESTEC, Noordwijk, The Netherlands, (ESA SP–425, Feb. 2000)

109) T. Brady, C. Tillier, R. Brown, A. Jimenez, A. Kourepenis, “The Inertial Stellar Compass:– A New Direction in Spacecraft Attitude Determination,” AIAA/USU Conference on Small Satellites, Logan, UT, Aug. 12–15, 2002, SSC02–II–1

110) T. Brady, S. Buckley, C. J. Dennehy, J. Gambino, A. Maynard, “The Inertial Stellar Compass: A Multifunction, Low Power, Attitude Determination Technology Breakthrough,” 26th Guidance and Control Conference, Breckenridge, CO; AAS (American Astronomical Society), Vol. 113, Feb. 5–9, 2003, ASS–03–003, pp. 39–56

housekeeping digital I/F). The sun angle resolution is 0.005° with a pointing accuracy of 0.02° (2σ).^{111) 112) 113)}

Applications: SSS is to fly onboard the GOCE mission of ESA (launch March 17, 2009). Furthermore, SSS is also part of the SOLAR payload, mounted on the external pallet of the ESA Columbus module of ISS, to keep the supported SOLAR payload instruments pointed toward the sun. SSS will also be flown on the SICRAL–1B military satellite of Italy, developed by Alcatel Alenia Space Italy.

Parameter	Value	Parameter	Value
Device dimensions	110 mm x 108 mm x 45	Device mass	< 330 gram
Operating temperature	–35 to +70 °C	Power consumption	< 1 W with DC/DC
FOV (Field of View)	$128^\circ \times 128^\circ$	Accuracy	< 0.02° (2 sigma)
Resolution	< 0.005°	Radiation hardness	> 100 krad

Table 9: Characteristics of SSS based on APS technology

– The 3CSat (Three Corner Satellite) constellation of UNP (University Nanosatellite Program), consisting of three cooperating S/C – built by CU (University of Colorado) at Boulder, ASU (Arizona State University), and NMSU (New Mexico State University) and sponsored by DoD, NASA and US industry – utilizes CMOS/APA (Active Pixel Array) imaging technology in a distributed observation concept. Note: The cluster launch of 3CSat took place on Dec. 21, 2004; however, the two microsatellites that were launched as secondary payloads, did not reach their proper orbit.

– As of 2005, STAR–250 and STAR–1000 are monochrome,^{114) 115) 116)} radiation hard CMOS/APS image sensors developed and validated under ESA contract. These sensors have a broad range of spaceborne applications, including star tracking, sun sensing and optical inter–satellite link beam tracking. Both sensors are designed using radiation–tolerant design techniques to allow a high tolerance against radiation effects. STAR–250 is a 250 k pixel sensor (512×512 with $25 \mu\text{m}$ pixel pitch), STAR–1000 is a 1 M pixel sensor (1024×1024 with $15 \mu\text{m}$ pixel pitch).

The next generation CMOS/APS star tracker detector design is referred to as **HAS** (High Accuracy Sensor) detector by the Cypress/FillFactory featuring a noise level sensitivity of < 1 arcsecond. The HAS device integrates a 1024×1024 pixel array with a pixel pitch of $18 \mu\text{m}$, providing a dual addressable y shift register for rolling shutter operation, programmable offset and gain amplifier and an on–chip 12 bit pipelined ADC. The qualification work (ESA contract) has shown the feasibility of the HAS sensor technique to compete with front illuminated CCDs in terms of performance for space applications. Hence, the HAS detector might very well become the APS detector of choice for future spaceborne AOCS applications. An essential objective of this HAS technology introduction is that it becomes eventually available as a COTS (Commercial–Of–The–Shelf) device being a space–qualified and low–cost detector. The HAS detector design is providing an accuracy comparable with those achievable so far only with the costlier CCD star trackers. See also chapt. 1.23.2.5.

- 111) F. Boldrini, E. Monnini, D. Procopio, “Applications of APS Detector to GNC Sensors,” 4th IAA Symposium on Small Satellites for Earth Observation, Berlin, Germany, April 4–8, 2005
- 112) F. Boldrini, E. Monnini, D. Procopio, “Applications of APS Detector to GNC Sensors,” 4th IAA Symposium on Small Satellites for Earth Observation, Berlin, Germany, April 7–11, 2003
- 113) F. Boldrini, G. Berrighi, E. Monnini, “The APS Based Smart Sun Sensor,” AAS Guidance and Control Conference, Breckenridge, CO, Feb. 6–10–, 2002, pp. 325–331
- 114) S. Cos, D. Uwaerts, L. Hermans, “Evaluation of STAR250 and STAR1000 CMOS Image Sensors,” Proceedings of the 6th International ESA Conference on Guidance, Navigation and Control Systems, Loutraki, Greece, Oct. 17–20, 2005 (ESA SP–606, Jan. 2006)
- 115) U. Schmidt, C. Kuehl, K. Michel, “Advanced Star Sensors based on Active Pixel Sensor Technology,” Proceedings of the 6th International ESA Conference on Guidance, Navigation and Control Systems, Loutraki, Greece, Oct. 17–20, 2005 (ESA SP–606, Jan. 2006)
- 116) J. Bogaerts, W. Ogiers, T. Cools, W. Diels, “Next Generation CMOS Active Pixel Sensors for Attitude and Orbit Control Systems,” Proceedings of the 6th International ESA Conference on Guidance, Navigation and Control Systems, Loutraki, Greece, Oct. 17–20, 2005 (ESA SP–606, Jan. 2006)

Parameter	HAS (High Accuracy Sensor) detector	STAR–1000 detector
Detector technology	CMOS/APS	
Pixel structure	3–transistor active pixel Radiation–tolerant pixel design	
Photodiode	High fill factor photodiode, using n–well technique	
Technology	0.35 μm CMOS	0.5 μm CMOS
Sensitive area format	1024 x 1024 pixels	
Pixel size	18 x 18 μm^2	15 x 15 μm^2
Pixel output rate	5 MHz (nominal) Speed can be exchanged for power consumption	
Windowing	X– and Y–addressing random programmable	
Electronic shutter	– Electronic rolling shutter. Integration time is variable in time steps equal to the row readout time. – Possibility to have non–destructive readout (NDR)	– Electronic rolling shutter. – Integration time is variable in time steps equal to the row readout time.

Table 10: Comparison of some HAS and STAR–1000 detector specification

– As of 2006, Galileo Avionica of Florence, Italy, is introducing the AA–STR (APS based Autonomous Star Tracker) device using the HAS detector technology. A first test flight is planned on the Sentinel–3 mission of ESA (launch 2012). The AA–STR is planned to be flown on the Alphas series starting in 2012 as well as on EO missions. The HAS (High Accuracy Star) APS detector technology of Cypress/Fillfactory is being used by the HYDRA multiple head Star Tracker of EADS Sodern. ^{117) 118) 119)}

- The “**digital camera**,” a commercial product of the photo industry (e.g., Kodak, Sony, Agfa, Canon, Fuji, Konica, Minolta, Nikon), is a natural application derivative of the CCD and CMOS/APS detector technologies, pioneered by the remote sensing and the electronics industry. The digital camera became a consumer product in the latter part of the 1990s when the detector densities (multi–megapixel detectors – approaching high–resolution quality) and storage capacities for image capture were sufficient and in addition economical for an evolving consumer market. – Since CCD detectors are inherently monochromatic, special filters are needed to separate the RGB radiation reflected by an object. A number of techniques are in use to capture color: a) RGB filter wheel (three exposures), b) tri–linear sensor (use of three linear sensors), c) multi–chip detectors, etc.

- A notable exception of the trend away from photographic film in spaceborne imaging technology was and is the RESURS–F satellite series of State Center Priroda, Moscow, Russia. The Resurs–F1 series (58 satellites in the time frame 1979–1993, Resurs–F2 series since 1995, see chapter D.44) onboard sensors are film cameras whose data (namely the films) are recaptured after the end of each mission. The film camera systems (examples: KFA–1000, TK–350, KVR–1000, KFA–200, MK–4) are returned to the ground in small spherical descent capsules which are reused an average of three times. The films are processed after each mission (average mission life is in the order of 14 to 30 days in orbits of 240 – 275 km altitude).

- At the start of the 21st century, film still holds the edge in spatial resolution over solid–state digital technology (CCD, APS, CID, etc.). However, digital technology can usually de-

117) L. Majewski, L. Blarre, N. Perrimon, Y. Kocher, P.E. Martinez, S. Dussy, “HYDRA multiple head star sensor and its in–flight self–calibration of optical heads alignment,” Proceedings of the 7th ICSO (International Conference on Space Optics) 2008, Toulouse, France, Oct. 14–17, 2008, URL: <http://www.icsconference2008.com/cd/pdf/S8%20-%20Auxillary%20Sensors%20-%20Majewski.pdf>

118) L. Blarre, N. Perrimon, A. Lacroix, L. Majewski, E. Anciant, “New Sodern’s APS based Autonomous Multiple Heads Star Sensor (HYDRA): Three Heads are better than one,” Proceedings of the 6th International ESA Conference on Guidance, Navigation and Control Systems, Loutraki, Greece, Oct. 17–20, 2005 (ESA SP–606, Jan. 2006)

119) L. Blarre, N. Perrimon, L. Majewski, Y. Kocher, “HYRDA multiple heads star tracker based on active pixel sensor and the gyrometer assistance option,” Proceedings of the 57th IAC/IAF/IAA (International Astronautical Congress), Valencia, Spain, Oct. 2–6, 2006, IAC–06–C.1.2.10

liver images much faster while allowing greater flexibility in storage, manipulation and distribution. The real-time aspect of digital imagery is of considerable importance for many applications. In addition, the digital technology offers a much wider spectral coverage than film (for multispectral and hyperspectral applications).

Overview of some detector types for digital imagery applications (as of 2004):

- CCDs have been the dominant solid-state imagers since the 1980s, primarily because CCDs gave far superior images with the fabrication technology available.
 - CCDs offer superior image performance as measured in quantum efficiency (>90%) and noise, and flexibility at the expense of system size. They continue to rule in the applications that demand the highest image quality.
 - CMOS/APS imagers offer more integration (more functions on the chip), lower power dissipation (at the chip level), and smaller system size at the expense of image quality and flexibility.
- ICCD (Intensified Charge Coupled Device). An ICCD is a CCD that is fiber-optically connected to a MCP (Micro-Channel Plate) to increase the sensitivity. In ICCD cameras, a photo-cathode in front of the MCP converts photons to electrons which are multiplied by the MCP. In general, ICCDs are used in low-light (night-vision) environments. Besides the gain in sensitivity the possibility of gating the MCP also offers the possibility to gate ICCD cameras very fast. Therefore ICCD cameras are also used for range-gated imaging.
 - An example of a spaceborne ICCD detector implementation is SWUIS (Southwest Ultraviolet Imaging System), a payload (telescope) developed at Southwest Research Institute, San Antonio, TX, and flown on Shuttle flights STS-85 (Aug. 7-19, 1997) and on STS-93 (July 23-28, 1999). SWUIS was used to observe objects in the inner solar system, using a FOV of 0.3-0.6° (30 times that of Hubble).
- EMCCD (Electron Multiplying Charge Coupled Device), the on-chip multiplication technology was initially introduced in 2001/2 by Andor Technology, Belfast, Northern Ireland. An EMCCD is a CCD in which a gain register is placed between the shift register and the output amplifier. The electron multiplication register (provides gain) multiplies the electrons before they pass the output amplifier. With this gain the detected signal reaches an order of magnitude improvement so that the noise in the output amplifier is negligible. At a gain of about 100 single photon counting is possible.
 - The EMCCD can use several detection channels on the same device, reducing the amount of front end electronics. The device is immune against the ground echo saturation.
 - The EMCCD technique (or on-chip multiplication) offers single photon detection capability. When combined with back-illuminated sensor quantum efficiency for maximum photon conversion, it provides unequalled sensitivity for ultra low light imaging conditions.
 - First imagers (commercial cameras) with EMCCD technology were introduced in 2003. The WALES (Water Vapor Lidar Experiment in Space) mission of ESA, under definition as of 2004, is considering the use of EMCCD detector technology instead of the APD (Avalanche Photo Diode) technique of previous lidar implementations.

1.4.1.3 Solid-state (digital) imaging – STJ detector technology

- **STJ (Superconducting Tunnel Junction)** is a new type of optical radiation detector technology, first developments/demonstrations started in the 1990s. Initially, the STJ technology was only considered for X-ray detection, it is now also being used as single pho-

ton (or particle) detectors in the visible spectrum as well. A niobium–based STJ detector is capable to detect radiation in the spectral range of 200 – 1000 nm with a spectral resolution of 45 nm. Unlike a silicon–based CCD detector, the STJ arrays record not only the position of incoming photons, but also their energy (one photon, depending on its energy, can generate thousands of electrons). This property eliminates the need for filters or diffraction gratings that lower the overall efficiency. The multispectral detection of colors of photons is of particular interest to astronomers and biomedical researchers alike. ^{120) 121) 122) 123) 124)}

An STJ device is a Josephson–type junction, consisting of two thin films of a superconducting metal such as niobium, tantalum or hafnium, separated by a thin insulating layer. When operated at temperatures well below the superconductor’s critical temperature (typically below 1 K), the equilibrium state of the junction is easily perturbed by any photon striking it. By applying a small bias voltage across the junction and a suitable parallel magnetic field to suppress the Josephson current, an electrical charge proportional to the energy of the perturbing photon, can be extracted from the device. Future STJ implementations will excel in particular in low–resolution spectroscopy applications. The STJ technology has the potential of offering “all–in–one” detectors, providing spectroscopy, imaging, photon timing, and high quantum efficiency in the spectral ranges from the γ –rays to the infrared. Some STJ characteristics are:

- STJ detectors combine the high energy resolution of wavelength dispersive spectrometers with the high count rate of energy dispersive spectrometers
- X–rays absorbed in a superconductor excite excess charge carriers across the superconducting gap in proportion to their energy.
- The small superconducting gap (\sim meV) translates into a large number of charge carriers and consequently high energy resolution (\sim 2 eV at 1 keV). Fast pulse decay times (\sim μ s) allow high count rates (\sim 10 kHz).
- Energy–discriminate photon counting with tantalum has been demonstrated over a full decade in wavelength: 200 nm – 2000 nm (or 2 μ m)
- By arranging a number of STJ detectors into a 2–D array, a true “3–D” detector can be constructed, whose output is not just the number of photons registered in each pixel of the image, but their distribution in energy throughout the UV, VIS and NIR spectral ranges. However, detector operation at cryogenic temperatures is required (typically below 1 K), to exploit the STJ–unique ability, namely to discriminate photons in wavelength without the use of filters or dispersive elements.

A first prototype STJ Camera (S–Cam) was developed at ESA/ESTEC and installed into a ground–based astronomical telescope (William Herschel Telescope, located on La Palma in the Canary Islands). The initial successful operation (first light) of S–Cam took place on Feb. 2, 1999. S–Cam employs a 6 x 6 array of tantalum devices (25 μ m x 25 μ m) and covers the 300–700 nm spectral range. As a photon counting system, STJ provides position and arrival time of each detected photon, along with the photon energy. Space–based instruments with STJ detectors are considered at the start of the 21st century for astronomical applications; Earth observation applications might follow soon.

120) Brian D. Josephson, a British physicist, predicted and discovered the phenomenon of superconductivity in 1962.

121) T. Peacock, P. Verhoeve, N. Rando, et al., “Superconducting tunnel junctions as detectors for ultraviolet, optical, and near infrared astronomy,” *Astronomy and Astrophysics Supplement Series*, Vol. 123, June 2, 1997, pp. 581–587

122) A. Peacock et al, “Single optical photon detection with a superconducting tunnel junction”, *Nature*, Vol.381, pp.135–137, 1996.

123) P. Verhoeve, S. Kraft, N. Rando, A. Peacock, et al., “The Soft X–Ray Performance of Superconducting Tunnel Junction Arrays,” *Journal of Applied Physics*, Vol. 83, 6118, 1998

124) N. E. Booth, D. J. Goldie, “Superconducting particle detectors,” *Superconducting Science and Technology*, Vol. 9, 1996, pp. 493–516

1.4.1.4 Introduction of airborne digital frame cameras (photogrammetry)

- On the airborne side, conventional film–based (analog) photogrammetry is a mature process developed for nearly a century. These camera systems are still very much in use by commercial service providers at the start of the 21st century. The aerial analog systems provide discrete frame–type images with a very high geometric resolution. They are mostly being used for mapping applications with high–resolution photo scales between 1:5,000 and 1:15,000. Typical high–resolution aerial film camera examples are the RMK cameras of Carl Zeiss, Oberkochen (see P.183) and the Wild RC10, RC20 and RC30 systems of Leica AG, Heerbrugg, Switzerland (P.122).

In contrast, there are digital CCD mapping systems in spaceborne and also in some airborne applications, linear arrays with pushbroom technology, providing continuous strips of linescan imagery having a much lower geometric resolution than the discrete frame–type film imagery. The production of linear CCDs is straightforward and these detectors offer excellent features, such as defect–free linear arrays, electronic exposure control and multispectral sensing. – *However, from a photogrammetric data processing point–of–view, the use of linear imaging CCD arrays in aerial mapping applications has been difficult, since the orientation of every image line requires robust modeling of the data acquisition trajectory. In contrast, area array CCD imagers, completely analogous to the film–based imaging system in function, work with a standard frame camera model, which easily suits the current map–production practice.* ^{125) 126)}

Manufacturer	CCD model	Array size (pixel)	Pixel size (µm)	Data rate (MHz)
Kodak	DCS–460	3,072 x 2,048	9	10
Lockheed Martin Fairchild	BigShot™	4,096 x 4096	15	5
Kodak	MegaPlus 16.8i	4,096 x 4096	9	10
Philips	Icam28	7,168 x 4,096	12	18
Reco/Optical/Dalsa	CA–260/50	10,080 x 5,040	10	48/64
Lockheed Martin	F–979F	9,216 x 9,216	8.75	160
Philips	FTF3020–C	3,072 x 2,048	12	

Table 11: Some high–resolution CCD area arrays in the 1999 time frame

One of the major limitations in the introduction of the new aerial digital frame cameras has been the low spatial resolution or the availability of only fairly small pixel sizes of the CCD area arrays. ^{127) 128)} In the mid–1990s, advances in semiconductor technology enabled the manufacturing of larger CCD area array detectors, the 4k x 4k (= 16 Mpixel) arrays were the largest sizes used in experimental airborne digital cameras; examples are those instruments developed by IGN (Institut Geographique National), France; or AIMS™ (Airborne Integrated Mapping System) of CFM (Center for Mapping) at OSU (Ohio State University) built in 1996/8 with NASA support. In addition, a GPS/INS comes along with AIMS. In 1998 Philips Electronics N. V. produced a 7k x 9k (= 63 Mpixel) array and Lockheed Martin an 8k x 8k array.

A performance comparison of the digital and analog imaging technologies with respect to spatial resolution shows that even the larger CCD arrays (start of the 21st century) fall way

125) Note: The linescan (pushbroom) technique was initially confined largely to spaceborne systems due to the fact that atmospheric turbulence caused some gaps and double imaging. However, the use of modern fast–acting gyro–controlled mounts limits these effects. In addition, the development of integrated DGPS/INS systems provide location and attitude information needed to correct the imagery geometrically and to provide a photogrammetric solution on a line–by–line basis. An example of this solution is the ADS40 camera of LH Systems (P.3).

126) C. Toth, “Experiences with frame CCD arrays and direct georeferencing,” Photogrammetric Week 99, pp. 95–107, Fritsch and Spiller (editors), Wichmann Verlag, also: www.ifp.uni-stuttgart.de/publications/phowo99/toth.pdf

127) C. Thom, J.–P. Souchon, “The IGN digital camera system in progress,” Photogrammetric Week ’97, pp. 75–82, Fritsch/Hobbie Eds. URL: <http://www.ifp.uni-stuttgart.de/publications/phowo99/thom.pdf>

128) C. K. Toth, “Direct Sensor Platform Orientation: Airborne Integrated Mapping System (AIMS),” International Archives of Photogrammetry and Remote Sensing, ISPRS Comm. III, Vol. XXXII, part 3–2W3, pp. 148–155, 1997

short with the 25k x 25k (= 625 Mpixel) imagery that can be produced by digitizing the (analog) film image of a standard 23 cm x 23 cm aerial film camera at the same pixel size.^{129) 130)} Aerial analog film cameras with 23 cm x 23 cm film format have been the mapping and reconnaissance instruments around the world for decades. Obviously, the digital area array CCD detector technology falls short in size, offering no more than 1/4 the imaging size (i.e. number of pixels per image) of the analog film technology. However, in spite of the smaller detector size, frame or area CCD arrays have other properties quite different or simply non-existent for analog film. Some of these special area array features include:

- CCDs with more than 10 million pixels usually cannot be manufactured without faults; hence, they come with a large number of inactive more malfunctioning pixels. However, the location of these bad pixels can be traced. Note: the manufacture of such large arrays lies at the very edge of current chip fabrication technology.
- The read-out rate of all the pixels from a CCD array can be substantial and is measured in seconds. Newer designs work with multiple output gates making this limitation less severe.
- The radiometric sensitivity of CCDs is around 100–200 ASA (American Standards Association) or higher (better than that analog film).
- In contrast to analog film, CCDs have a linear characteristic and thus are much more subject to saturation, in which case the charge from the saturated pixel map spill over to neighboring pixels (this phenomenon is called blooming).
- CCDs, especially cooled ones, can exhibit very good SNRs and can therefore typically produce pixel intensities with 10–12 bit resolution. This is much better than the currently realized 6–7 bit intensity resolution of scanned analog imagery.
- Unfortunately, electronic shutters, while easily incorporated into linear arrays, are not a feasible solution for large CCDs due to manufacturing complexities.
- CCDs provide immediate availability of the image data.

At the start of the 21st century,^{131) 132) 133) 134)} developments in storage and compression technology have reached the point where large-format digital imagery can quite effectively compete with analog, film-based techniques in airborne applications. *In particular, the fully digital workflow of CCD (digital) imagery offers numerous advantages, such as improved triggering, low noise level, no signal corruption during storage, and requirements for digitization. Also, several real-time processing tasks are possible while using digital imagery.* These include:^{135) 136)}

- Signal conditioning (gain and offset control, color corrections)

129) A raster scan of the aerial film image of 23 cm x 23 cm with a pixel size of 9 µm amounts to about 625 Mpixel; while a state-of-the-art photogrammetric scanner with a pixel size of 7 µm produces an image of 32k x 32k = 1 Gpixel.

130) H. Heier, A. Hinz, "A Digital Airborne Camera System for Photogrammetry and Thematic Applications," Proceedings of ACRS 1999, Hong Kong, China, Nov. 22–25, 1999

131) D. A. Grejner-Brzezinska, "Direct Sensor Orientation in Airborne and Land-based Mapping Applications," Report Nr. 461, Geodetic GeoInformation Science, OSU, Columbus, OH, June 2001

132) C. Toth, "A Conceptual Approach to Imaging for Mobile Mapping," Proceedings of Mobile Mapping Symposium, OSU, 1995, pp. 19–27

133) A. Hinz, C. Dörstel, H. Heier, "Digital Modular Camera: System Concept and Data Processing Workflow, Proc. IAPRS Vol. XXXIII, Amsterdam, July 16–23, 2000

134) W. Zeitler, C. Dörstel, K. Jacobsen, "Geometric Calibration of the DMC: Method and Results," Pecora 15/Land Satellite Information IV Conference, ISPRS Commission I Mid-term Symposium/FIEOS (Future Intelligent Earth Observing Satellites), Nov. 10–14, 2002, Denver, CO

135) S. Diener, M. Kiefner, C. Dörstel, "Radiometric Normalization and Color Composite Generation of the DMC," International Archives of Photogrammetry and Remote Sensing (ISPRS Congress), Vol. XXXIII, Part B1, Amsterdam, The Netherlands, July 16–23, 2000

136) G. Ferrano, Ch. Feix, "The Z/I Imaging DMC – Digital Mapping Camera System: Status, Configuration & Calibration," ASPRS 2003, Anchorage, AK, May 5–9, 2003

- Image enhancements (real–time histogram collection and correction)
- Imprinting
- Image compression

The following examples illustrate the introduction of state–of–the–art ultra–high–resolution digital technology of large–format framing camera systems in aerial photogrammetry applications – resulting eventually in the replacement of the existing base of aerial film cameras (no film, no photo lab, no scanning, no noise from film grain and no cost of duplication).

1) **DMC** (Digital Modular Camera)¹³⁷⁾, an airborne digital photogrammetric camera of Z/I (Zeiss Imaging, Oberkochen, Germany). Note: As of Oct. 2002, Intergraph Corporation of Huntsville, ALA, acquired ownership of Z/I Imaging. Some of the instrument features/technologies are:

- DMC employs the CCD area array detector technology (i.e., a 2–D system consisting of a frame or matrix detector) for wide area coverage. The observed imagery has a known and precise geometry in x and y due the two dimensional area sensor. With regard to geometric accuracy, the CCD array (frame technology) has a clear advantage over the CCD line sensor (pushbroom technology).
- The modular instrument concept employs an optics frame, referred to as CBU (Camera Base Unit), which consists of 8 cameras: 4 high–resolution panchromatic cameras (using a 7 k x 4 k CCD array), and 4 multispectral cameras (using a 3 k x 2 k CCD array), thus providing a reduced spatial resolution. The multi–camera configuration (four parallel cameras can generate multispectral (MS) imagery for the acquisition of color composites; four panchromatic images from converging cameras are mosaicked digitally to form a single high resolution image) resulting in a large FOV (Field of View). The MS cameras are collecting imagery in the red, green, blue and near infrared bands. A post–processing procedure (mosaicking) is used to transform four individual PAN images into one virtual image considered as normal central projection.
- DMC is integrated into ASMS (Airborne Sensor Management System) to achieve the highest possible level of data flow during observations. The operator driven ASMS covers DMC and all auxiliary devices such as GPS, stabilization mount, IMU, FMC, etc.
- Electronic FMC (Forward Motion Compensation) is used for acquiring a blur–free imagery under large–scale mapping conditions (wide FOV of 74°)
- DMC is equipped with four 7k x 4k large area CCDs (PAN cameras), the resulting ground resolution of the system is 14,000 pixels in cross–track and approximately 8,000 pixel in along–track.
- The electronics of the CCD matrix sensors can be operated in TDI (Time–Delay Integration) mode. This allows fully electronic FMC of the imagery (blur compensation). Note: FMC is not possible for pushbroom cameras, using the three–line sensor principle.
- Each single camera module of the DMC is calibrated with regard to geometry and radiometry.
- The imagery of such an advanced technology CCD digital aerial camera turns out to be of a higher quality and very cost effective compared to that based on analog film and scanning techniques. The reason is not only the higher radiometric sensitivity of CCD devices (as well as the potential of a larger spectral range), **but in particular the elimination of film development and film scanning**. These two steps of the film workflow are very sensitive and have to

137) K. J. Neumann, “The Z/I Imaging DMC – Digital Mapping Camera, Photogrammetric Results,” ASPRS 2003, Anchorage, AK, May 5–9, 2003

be maintained very carefully to avoid product degradation. The direct availability of digital imagery for all types of processing is also a great advantage for the user. ¹³⁸⁾

2) **UltraCam–D** (Digital) of Vexcel Imaging GmbH, ¹³⁹⁾ ¹⁴⁰⁾ Graz, Austria (a unit of Vexcel Corporation, Boulder, CO), along with partners Wild Austria and GIP (Gesellschaft für Industriephotoграмmetrie mbH), Aalen, Germany. A prototype system is available as of 2002/3. In addition to the sensor unit, there is SCU (Controller, Storage and Processing Unit) with a storage capacity of >1 TByte.

3) **BAE Systems** (formerly Fairchild) of Greenlawn, NY (with support from NRL) is developing a new digital framing camera incorporating an ultra high resolution CCD detector array comprised of 9,216 x 9,216 pixels which measures 8 cm x 8 cm and is fabricated on one silicon wafer. The new all–digital camera allows a very high framing rate (1 frame/s, later 2 frame/s) and differential image motion compensation for use with oblique imaging. ¹⁴¹⁾

4) **Leica Geosystems** of Heerbrugg, Switzerland, introduced the first commercial digital airborne camera to the market in 2001, namely the **ADS40** (Aerial Digital Sensor 40). The ADS40 is a **pushbroom imager** capable of acquiring color and false color strip images at the same high resolution as the black and white stereo images. This high resolution of 12,000 pixels across the swath combined with 100% forward overlap in the three to six black/white image strips results in high–quality DSMs (Digital Surface Models). The ADS40 is capable of recording pan images of 5 cm GSD and larger and RGB images of 15 cm GSD and larger under normal lighting conditions. ¹⁴²⁾

Panchromatic image size (2–D detector)	11,500 x 7,500 pixels
Panchromatic physical pixel size	9 μ m
Panchromatic lens focal distance (alternative exchangeable lenses)	100 mm (75 mm, 125 mm)
Lens aperture	f = 1/5.6
FOV (Field of View), cross track (along–track),	55° (37°)
Color (multi–spectral capability) 4 channels – – Color image size Color physical pixel size Color lens system focal distance Color lens aperture Color field of view from vertical, cross track (along track)	RGB & NIR 4,008 x 2,672 pixels 9 μ m 28 mm f = 1/4.0 65° (46°)
FMC (Forward Motion Compensation),	TDI controlled
Smallest pixels on the ground at flying height of 500 m (at 300 m)	5 cm (3 cm)
Frame rate per second (minimum inter–image interval)	1.3 frames (0.75 seconds)
Analog–to–digital conversion Radiometric resolution in each color channel	14 bit >12 bit
Physical dimensions of the camera unit Weight , Power consumption at full performance	45 cm x 45 cm x 60 cm < 30 kg, 150 W

Table 12: Specification of the UltraCam–D sensor unit

138) K. J. Neumann, “Aerial Mapping Cameras – Digital Versus Film, The Benefits of a New Technology,” Proceedings of ASPRS 2003, Anchorage, AK, May 5–9, 2003

139) F. Leberl, M. Gruber, M. Ponticelli, S. Bernoegger, R. Perko, “The UltraCam Large Format Aerial Digital Camera System,” Proceedings of ASPRS 2003, Anchorage, AK, May 5–9, 2003

140) M. J. Smith, K. S. Qtaishat, D. W. G. Park, A. Jamieson, “Initial Results from the Vexcel UltraCAM–D Digital Aerial Camera,” Proceedings of the ISPRS Hannover Workshop, Hannover, Germany, May 17–20, 2005

141) B. A. Gorin, “Application of the 9 k x 9 k Digital Framing Camera for Real–time Orthophotography,” Proceedings of ASPRS 2003, Anchorage, AK, May 5–9, 2003

142) P. Fricker, A. Rohrbach, “Pushbroom scanners provide highest Resolution Earth Imaging Information in Multi-spectral Bands,” Proceedings of the ISPRS Hannover Workshop, Hannover, Germany, May 17–20, 2005

Panchromatic image	3 Pan CCD lines, each 2 x 12,000 pixels, staggered by 3.25 μm to generate stereo imagery (forward, nadir, back) with 3 line scanners
Multispectral image	4 MS CCD lines, each 12,000 pixels (4 RGB+NIR line scanners)
Pixel size	6.5 μm x 6.5 μm
Spectral bands (nm)	Pan = 465–680, blue=430–490, green=535–585, red=610–660, NIR=835–885
FOV (Field of View)	64° (cross track)
Focal length of camera	62.77 mm
Stereo angles	16°, 26°, 42°
Sensor Head SH40	Comes with digital optics (DO64) and with IMU
Control Unit CU40	Comes with POS (Position & attitude computer)

Table 13: Specification of the ADS40 of Leica Geosystems

- At the start of the 21st century, there are three different data sources available in photogrammetry, resulting from: a) high–resolution analog airborne mapping cameras, b) digital airborne cameras, and c) high–resolution (digital) spaceborne instruments.
- Automation of the map–making process is the ultimate goal of digital photogrammetry. The fundamental step of any data integration process is georeferencing or geometric fusion of data (time–space registration), most commonly provided by GPS/INS (see also **photogrammetry** in Glossary).

As of 2005/6¹⁴³ it looks like the high–resolution pushbroom digital airborne camera systems (DMC, ADS40, etc.) are outperforming their sister film (analog) frame cameras in many respects. In particular, the geometric quality of airborne digital pushbroom systems is excellent and fulfils all demands of the classical and modern photogrammetric work. Hence, the traditional distinction of airborne (film–based) and spaceborne (digital) remote sensing is slowly disappearing.



Figure 6: Illustration of the DMC imager (image credit: Z/I Imaging)

143) H. Weichelt, B. Wagner, H.–G. Klaedtke, “Remote Sensing Approach for Digital Aerial Imagery,” Proceedings of the ISPRS Hannover Workshop, Hannover, Germany, May 17–20, 2005

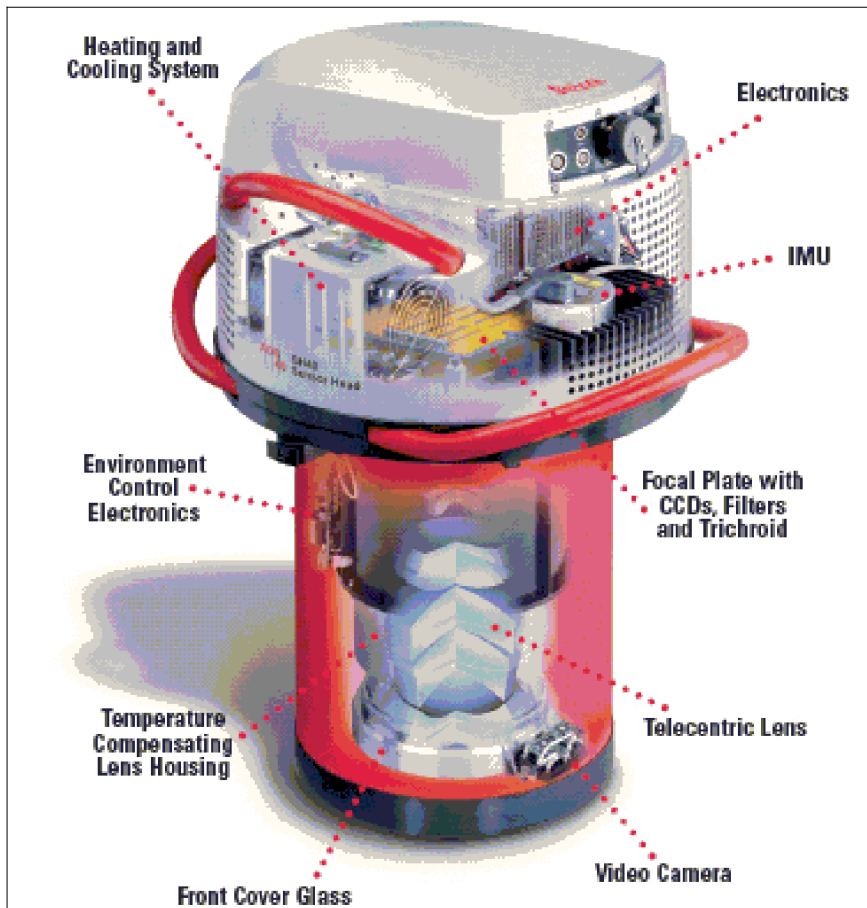


Figure 7: Illustration of the ADS40 imager (image credit: DLR)

Solid–state imaging is based on the physical principle of converting incident light (photons) into a measurable quantity (electrical voltage, electrical current, density for photographic emulsions). The link between the photons at the input of an imager and the output of the device (voltages, metallic silver or color dyes) are the electrons. The collection and transport of those electrons is of great importance in this chain.

[It should be noted that the actual sensor is an analog device. It sends out a voltage or a current which is proportional to the intensity of the light that falls on it. This analog signal is converted into a digital signal by an analog–to–digital converter, also known as an A/D converter.]

When comparing film–based and solid–state (CCD) imagery, it should be remembered that film (as well as the human eye) respond to incident brightness levels nearly logarithmically. This is conveniently expressed in terms of densities (D), where $D = \log(1/\tau)$ and where τ is the transmittance of the detecting surface. Density ranges of about 0–3 (max) can be obtained. – CCDs, on the other hand, respond nearly linearly to incident energy, i.e. digital values obtained from initially measured analog values of the detector are actually transmittance (or reflectance) values. But the intensity of the reflected or transmitted light (radiation) in the image is proportional to the logarithmic density of the image.

- In an analog recording medium, the response of film is a continuum over its range of photographic density/exposure. The level of quantization possible with an image on film is subject to limitations due to resolving power, the MTF (Modulation Transfer Function), granularity and such considerations as the Wiener spectrum (after Norbert Wiener, 1894–1964) of the grain structure and wavelength of illumination used in scanning. All these characteristics being unique to a particular combination of camera, film and processing, as well as the scanner performance.
- Due to the logarithmic response relationship of film – – – a film negative can easily adopt to very large exposure ranges to obtain the desired density range for the image. By comparison, CCDs with their "linear range response" to brightness levels are much more susceptible to saturation in which case the charge from the saturated pixel map spill over to neighboring pixels (this phenomenon is called **blooming**).

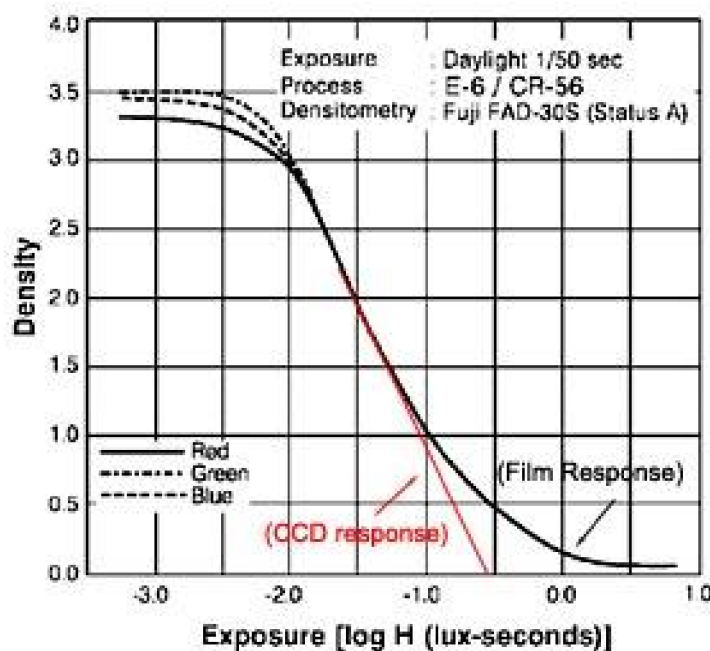


Figure 8: Qualitative performance characteristics of film–based and solid–state imagery

1.4.1.5 Advanced CCD technology in astrometry missions

An example of today's large-format CCD area array state-of-the-art technology is provided by ESA's Gaia mission with 1 Gpixel in the focal plane, representing the largest digital camera built so far for any spaceborne mission.

The Gaia mission (launch Dec. 19, 2013) involves the operation of a spacecraft from the Lagrangian L2 position located in space 1.5 million km beyond the Earth where it will keep pace with the orbit of the Earth around the sun. From this position, where the Earth will help to shield the spacecraft from the sun's radiation, it is intended that principally the instruments on-board the spacecraft will map the objects lying within our own galaxy (the Milky Way).^{144) 145)}

Gaia's star measurement principle relies on the repeated observation of star positions in two fields of view. The spacecraft rotates slowly at a constant angular rate of $1^\circ/\text{min}$ around the spin axis, completing four great circles on the sky in one day. In addition, the orientation of the spin axis is modulated by a slow precession around the Sun-to-Earth line with a period of 63.12 days that enables the observation of about 70 transits of the same celestial object over the five-year mission duration.

Gaia's observation technique is 'wide-angle' astrometry, which allows direct measurement of the absolute parallax. This technique is based on continuous star detections in two fields of view separated by a large angle which needs to be known and maintained at a very high accuracy over the entire mission lifetime. This technique was successfully demonstrated on Hipparcos, ESA's first astrometry mission, launched in 1989.

One of the enabling technologies to reach the required Gaia measurement accuracy is a long signal integration time and the detection of a large number of stars at the same time. This led to a focal plane of almost half a square meter, and hence the large-sized CCD area arrays.

The Gaia payload module consists of two telescopes separated by a 'basic angle' of 106.5° sharing the same focal plane. The ultimate astrometric accuracy is determined by the size of the telescope aperture and the total number of photons detected. Therefore, the fundamental design criteria are:

- The mirrors M1 and M1' as large as possible but still compatible with the size of fairing of the Soyuz launcher.
- Maximum transmittance of the optics and 'quantum efficiency' (i.e. the conversion efficiency of photons into electrons) of the CCD detectors
- Large focal plane to simultaneously maximize signal integration time and number of stars detection.

The detection of these photons is performed with CCDs, and the focal plane assembly consists of 106 CCDs and individual front-end electronics. The CCDs are arranged in seven rows, and the signals from each row are collected by an Interconnection Module that handles power, data and clock distribution. The thermal dissipation is purely passive. The mass of the focal plane assembly is 190 kg and the power consumption is 430 W.

Focal detection plane: Out of the 106 CCDs, 102 are dedicated to star detections and they are grouped into four fields: Star Mapper CCDs, Astrometric Field CCDs, Photometric Field (Blue and Red) CCDs and Spectroscopic Field CCDs (radial velocity measurement).

144) Philippe Gare, Giuseppe Sarri, Rudolf Schmidt, "ESA's 'Billion-Pixel' Camera – The challenges of the Gaia mission," ESA Bulletin No 137, February 2009, pp. 50–59, URL: http://www.esa.int/esapub/bulletin/bulletin137/bul137g_sarri.pdf

145) "Billion pixel Gaia camera starts to take shape," ESA, July 6, 2011, URL: <http://sci.esa.int/science-e/www/object/index.cfm?fobjectid=48901>

A further four CCDs are used for monitoring the stability of the basic angle between the two telescopes and the quality of the optical performances.

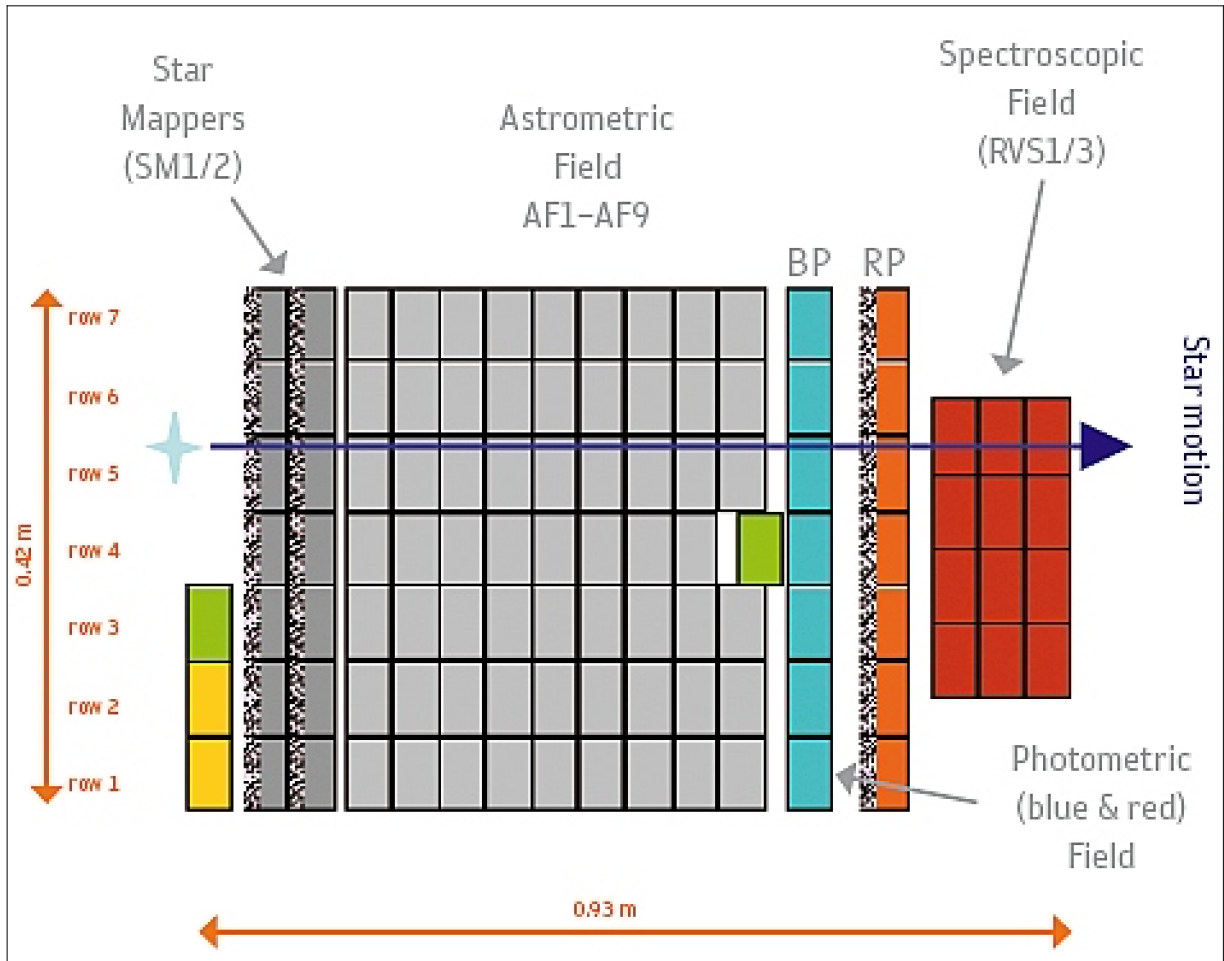


Figure 9: The focal plane mosaic of CCD area arrays (image credit: ESA)

Legend to Figure 9: The strips SM1 and SM2 are used for initial star acquisition. The strips AF1 to AF9 constitute the astrometric field for precision position measurement. The strips BP and RP allow spectral measurement in the range 330–680 nm and 640–1000 nm. The strips RVS1 to RVS3 allow fine spectroscopy in the range 847–874 nm.

CCD operating modes and geometric characteristics: The optical image of a star on the Gaia focal plane, the PSF (Point Spread Function), corresponds to a ‘charge cloud’ that extends over a few pixels on a CCD array. Unlike a normal digital camera that takes pictures as a full frame, the Gaia ‘camera’ tracks the movement of a PSF across the CCDs. In short, not one single image of a star is taken but a continuous sampling of the image is made as it moves across the focal plane.

Star design density for sizing of the focal–plane control electronics and scientific software resources	750 000 stars/deg ²
Maximum number of simultaneous star detections which can be followed per CCD at any time	5400 stars
Maximum number of simultaneous star detections which can be processed by the CCD and control electronics per CCD per second	1200 stars
Maximum number of simultaneous star detections which can be followed in the astrometric focal plane at any time	334 000 stars
Maximum number of simultaneous star detections which can be processed by the focal plane per second	8400 stars

Table 14: Basic detection and processing capabilities of the Gaia focal plane

The CCDs operate in a TDI (Time Delayed Integration) mode, where the photo–electrons generated by the star image are clocked across a CCD together with the moving star image. The amount of collected charge at the output of the CCD is proportional to the brightness of the star image and the time it needs to cross a detector. A star similar to our Sun, with a magnitude of 15, accumulates a total charge of about 90 000 electrons during the crossing of a CCD. The moving star image, i.e. at the spin rate of the satellite, has to match the clocking speed of the charge cloud across the focal plane. To this end the Gaia spacecraft is equipped with a novel ‘cold gas’ micropropulsion system.

The physical size of the CCDs has been chosen to match today’s wafer technologies (5 inch/127 mm wafers) and to be in line with realistic production yields of the manufacturing company. The Gaia CCD features 4500 pixels in the along–scan direction and 1966 pixels in across–scan. Each CCD array has a size of 9 Mpixel; hence the tiled focal plane with a total of 106 CCD area arrays has a size of close to **1 Gpixel**). The packaging of the CCDs is selected for maximum packing density and best thermomechanical properties, since the focal plane operates at about -110°C .

The CCDs for the Gaia mission are being manufactured by **e2v technologies plc** of Chelmsford, UK. All CCDs populating the focal plane have the same format and, in principle, the same function. Some differences exist due to the wavelength range for which they are optimized. Three different CCD types were developed: the astrometric, the ‘red–enhanced’ and the ‘blue–enhanced’. The only difference between the astrometric CCD and the ‘blue’ CCD is the additional anti–reflection coating optimized for maximum quantum efficiency at the chosen wavelength. The ‘red’ CCDs are manufactured from high–resistivity silicon. The thickness of this detector is $40\ \mu\text{m}$ for enhanced quantum efficiency instead of the $16\ \mu\text{m}$ used for the other two CCD types.

1.4.1.6 Stereoscopic imaging in the optical region

Stereoscopic imaging from a single S/C instrument in its orbital path requires a parallel observation geometry from at least two different angular positions of the same target area. A few seconds of time delay in the imaging sequence of multiple image viewing directions is of no consequence to the stereo concept (superposition of imagery). The technique is particularly suitable for topographic mapping applications (photogrammetry), it is also used for event coverage. Several observation schemes are in use:

- Along–track multidirectional target observation (successive viewing in one pass). A single imaging instrument provides two or three or more images of the same ground path (stereo line scanner implementation where each scan line is pointing into another along–track direction of the swath, like forward, nadir, backward). This technique provides continuous and contiguous long–term stereo observations.
- The imaging device has a cross–track tilting mechanism (thereby increasing its FOR (Field of Regard). This technique requires either a quick pointing capability (introducing possibly S/C vibrations), or two parallel instruments to perform stereo imaging.
- Body pointing of an agile spacecraft with a single imager to obtain along–track or cross–track imagery from different positions (body–pointing implies the imager is pointed along with its platform (satellite) into the desired direction). This technique is more suitable for short event coverage applications, a function mostly provided in commercial imaging missions. Only small–mass spacecraft can provide sufficient agility.
- Examples of spaceborne stereoscopic missions with **along–track multi–line** imaging instruments are:
 - MOMS–02 (Modular Optoelectronic Multispectral Scanner), a **three–line** camera system of DLR on Shuttle flight STS–55 in April/May 1993, followed by a MOMS–02 re-

flight on MIR/Priroda (launch of Priroda April 23, 1996). The MOMS-02 payload has a total of five optical systems: three are used for stereoscopic imagery, two are employed for multispectral imagery, one is used for high-resolution data. ¹⁴⁶⁾

- OPS (Optical Sensor) of the JERS-1 mission of NASDA (launch Feb. 11, 1992, end of mission in October 1998). OPS offered a **two-line** stereoscopic along-track imaging capability in two spectral bands, both of the same wavelengths (760–860 nm). Band 4 is for off-nadir viewing (15.33° forward in flight direction); bands 3 (nadir) and 4 make a stereo pair.

- The Terra mission of NASA (launch Dec. 18, 1999) with the NASDA/NASA cooperative instrument ASTER (Advanced Spaceborne Thermal Emission and Reflection Radiometer). ASTER is an along-track **two-line** system in the VNIR subsystem. VNIR features two telescopes, one nadir-looking with a three-spectral-band detector, and the other backward-looking with a single-band detector. The backward-looking telescope provides a second view of the target area in band 3B (0.76–0.86 μm) for stereo observations. The resolution is 15 m on a 60 km swath.

In addition, the NASA/JPL instrument MISR (Multi-angle Imaging SpectroRadiometer) is flown on Terra. MISR is an along-track **nine-line** camera system, offering multidirectional observations of each ground (or target) scene within a time scale of minutes. MISR uses nine CCD pushbroom cameras to observe the Earth at nine discrete viewing angles: one at nadir (0°), plus eight other symmetrical views at 26.1°, 45.6°, 60.0°, and 70.5° forward and aft of nadir. Images at each angle are obtained in four spectral bands centered at 0.446, 0.558, 0.672, and 0.866 μm. Each camera employs four independent line arrays (one per filter), 1504 active pixels per line. The swath width is 360 km. Ground sampling resolutions of 275 m, 550 m, or 1100 m are provided. MISR provides global maps of planetary and surface albedo (brightness temperature), and aerosols and vegetation properties. – MISR provides new types of information for scientists studying Earth's climate, such as the partitioning of energy and carbon between the land surface and the atmosphere, and the regional and global impacts of different types of atmospheric particles and clouds on climate. ¹⁴⁷⁾

- The BIRD (Bi-Spectral Infrared Detection) mission of DLR (launch Oct. 22, 2001) with the WAOSS-B (Wide-Angle Optoelectronic Stereo Scanner, BIRD version). The along-track stereo imaging system of WAOSS-B is based on **3 CCD lines** (single optics and focal plate), operating in pushbroom mode, and taking images simultaneously in the forward-, nadir- and backward-pointing direction of the orbital ground track (spatial resolution of 183 m, swath of 527 km).

- SPOT-5 of CNES with HRS (High Resolution Stereoscopic) instrument, an along-track **two-line** camera system) with a launch May 4, 2002. HRS provides parallel forward and aft swaths (120 km width) in the along-track direction at fixed pointing angles of ±20°. A pixel size of 5 m (along-track) by 10 m (cross-track) is provided. The stereo acquisition mode can be sustained for scene lengths of up to 600 km. The panchromatic band (0.51–0.73 μm) of SPOT-1, -2, -3 is being reintroduced.

- The ALOS mission of JAXA (Japan Aerospace Exploration Agency, formerly NASDA, launch Jan. 24, 2006) flies PRISM (Panchromatic Remote-sensing Instrument for Stereo Mapping), a **three-line sensor** with three independent catadioptric systems for nadir, forward and backward-looking (along-track stereoscopy). Each of the three telescopes employs a three-mirror type optics design (30 cm aperture diameter and 2 m focal length) and several CCD detectors for pushbroom scanning. Eight silicon CCDs (5000 pixels each) are physically aligned at each telescope's focal plane. The nadir-looking tele-

146) Note: The three-line observation concept results in forward, nadir and aft views of the CCD pushbroom array. The imagery from each scan line is assembled into strips. Relief displacement in the line perspective geometry of the strip approach differs from conventional nadir perspective geometry. Every object appears on all three strips. In contrast, on film imagery only about 60% of the area of any one photograph is in a triple overlap.

147) <http://www-misr.jpl.nasa.gov/>

scope provides a swath of 70 km width (28,000 pixels per band), each of the fore and aft-looking telescopes provides a swath of 35 km (14,000 pixels per band).

– IRS–P5 (CartoSat–1, launch May 5, 2005) of ISRO flies a **two–line camera** assembly. PAN–F (Panchromatic Forward–pointing Camera) is tilted at 26° forward from nadir. PAN–A (Panchromatic Aft–pointing Camera) is tilted 10° aft. Each camera provides a spectral range of 500–750 nm, a spatial resolution of 2.5 m is provided on a swath of 30 km.

On the airborne side, DLR developed **HRSC** (High–Resolution Stereo Camera) which features three–line stereo imaging in color. The instrument is flown since Feb. 1997 (heritage of the HRSC instrument flown on the Russian Mars–96 mission with a launch Nov. 16, 1996 on a Proton vehicle from Baikonur – a malfunction of the third stage of the launch vehicle ended the mission prematurely). A completely automatic photogrammetric and cartographic processing procedure including digital image matching, digital terrain model (DTM) and ortho–image (orthophoto)¹⁴⁸⁾ generation, mosaicking and merging of multi-spectral data has been developed at DLR (P.106). A further *HRSC instrument is flown on the Mars Express spacecraft of ESA (launch June 2, 2003, Mars insertion on Dec. 25, 2003), orbiting planet Mars and providing spectacular stereo imagery at 10 m resolution (and at 2 m super–resolution) of the Martian terrain.*

Another airborne example of a three–line stereo pushbroom camera is DPA (Digital Photogrammetric Assembly) of DASA/MBB Ottobrunn (P.72). DPA has been operational since the end of 1992 and is a parallel development to MOMS–02. – JPL’s “AirMISR” is flown since 1997 on NASA’s ER–2 aircraft. Unlike the spaceborne MISR instrument, which has nine cameras oriented at various angles, AirMISR utilizes a single camera in a pivoting gimbal mount. A data run by the ER–2 aircraft is divided into nine segments, each with the camera slewed to a different MISR look angle. The gimbal rotates aft between successive segments, such that each segment acquires data over the same area on the ground as the previous segment. This process is repeated until all nine look–angles of the target area are collected.

- Example of a tilting camera scheme. The parallel HRV sensors of the SPOT series satellites (all SPOT missions, including HRG of SPOT–5) provide some degree of stereo capability with their individual side–viewing feature (up to 27° cross–track pointing capability).

- Examples of **body–pointing spacecraft** with an imager (boresight configuration of S/C and imager) to obtain along–track or cross–track imagery (pointing on a cyclic basis, slewing capability) collecting stereo pairs of imagery.

- Ikonos–2 S/C of Space Imaging (launch Sept. 24, 1999) with the OSA sensor (along–track slewing capability of up to $\pm 30^\circ$)

- QuickBird–2 of DigitalGlobe Inc., with a launch Oct. 18, 2001 (orbital altitude of 450 km) is flying BHRC 60 (Ball High Resolution Camera 60). The instrument provides along–track stereo imagery (by S/C slewing).

- The EROS–B satellite of ImageSat International, Israel (launch April 25, 2006) provides stereo scenes by S/C slewing. The instrument is PIC–2 (Panchromatic Imaging Camera–2).¹⁴⁹⁾

- MSRS (Multi–Spectral high Resolution System), built by ELOP (El–Op Electro–Optics Industries of Rehovot, Israel) in cooperation with OHB–System, Bremen, Germany. MSRS is planned to fly on on Diamant of OHB–System with a planned launch in 2007. The spacecraft has an along–track slewing capability for stereo imaging.

148) Note: Digital orthophotos are scale correct aerial photographs.

149) Fred Ortenberg, “Israel in Space – Twenty Years of Exploration (1988–2008),” book, 2009, printed at Technion Press, Haifa, Israel, ISBN: 987–965–555–457–1

– The Pleiades spacecraft of CNES (launch of Pleiades–HR1A on Dec. 17, 2011 and Pleiades–HR1B on Dec. 02, 2012, 2 operational satellites in one orbital plane with a phase shift of 180°) permit a body–pointing capability with roll and pitch maneuvers, each up to 60° , within a period of 25 s. OHRI (Optical High–Resolution Imager) will be used for along–track stereo imagery and other support modes.

- DEM (Digital Elevation Model): DEMs from optical satellite data. Since spaceborne stereo imagery is very suitable for topographic applications, there is a great demand for DEM or DTM (Digital Terrain Model) generation, in particular from along–track stereoscopy [a DTM or DEM forms the basic building block for combining other data for analysis; for instance, digitized spatial data (images) can be draped onto a DEM and analyzed using a GIS.]. Simultaneous along–track multidirectional imagery is not affected by the changes in radiometric variations that may occur in cross–track stereo image pairs collected on different satellite passes (possibly also over long time periods). On the other hand, cross–track stereo data has the advantage of more symmetrical view angles to the target area of interest as compared to along–track data collections (the stereo pairs are always at different angles). In the past 15 years, the long–term SPOT series imagery has been a frequently used source for stereoscopy and DEM extraction applications [superposition of multitemporal data in this analysis approach; a disadvantage is the multi–date imagery available reflecting the target changes during a growing season, etc.].¹⁵⁰⁾ Alternative solutions are available at the start of the 21st century.

The Terra mission of NASA is flying ASTER (launch Dec. 19, 1999). The stereo data is available to the public, it can be downloaded freely (<http://asterweb.jpl.nasa.gov>). This makes the ASTER data very attractive for the user community interested in DEM applications. SPOT–5 (launch May, 4, 2002) is also flying an along–track instrument HRS (High Resolution Stereoscopic); this capability adds to the normal cross–track capability of the SPOT series. In this scenario, PRISM of ALOS mission (launch Jan. 24, 2006) and PAN–F of the IRS–P5 mission (launch May 5, 2005) are further major entries for stereoscopic imagery applications, beside a number of commercial imaging missions. Naturally, DEMs (or DTMs) may also be generated from spaceborne stereo imagery in the microwave region, better known as SAR interferometry.

150) T. Toutin, P. Cheng, “Comparison of automated digital elevation model extraction results using along–track ASTER and across–track SPOT stereo images,” *Optical Engineering*, Vol. 41, No 9, 2002, pp. 2102–2106

1.4.2 Spectrometry, imaging spectrometry, and hyperspectral imaging

In remote sensing “spectrometry” or “spectroscopy”¹⁵¹⁾ refers to the detection and measurement of radiation spectra of a target (area or volume) in many bands of the medium (generally the atmosphere). In Earth observation, the measurement arrangement is that of a **sounding instrument**, i.e., measuring the medium of the incoming atmospheric spectra with a spaceborne (or airborne) instrument along the instantaneous field of view (IFOV), basically a straight line.¹⁵²⁾ From a historic perspective, the information obtained by the first spaceborne sounders was that of “total column content,” i.e., only the entire spectrum measurement along the line-of-sight yielded a value (or a set of values). Later improved sounder versions [in particular with better radiometric performance (SNR)] permitted a more detailed analysis of the measured spectra, resulting eventually in the interpretation capability of pinpointing many measurements along an IFOV path in the atmosphere, and ending as a small area on the ground for the case of nadir observations. These improved results were referred to as **profile measurements** of various state parameters/constituents of the atmosphere that could be determined/extrapolated for various heights.

The data analysis approach of such a process is by its very nature iterative, requiring a comparison of intermediate results with atmospheric models until a suitable fit is reached. Also, it took a while to understand all the physics and various methods of interpretation, to develop the proper diagnostic tools for data analysis, and to develop suitable models. On hindsight, today’s (start of 21st century) arsenal of analysis tools and interpretation methods have reached a considerable level of sophistication, permitting also the extraction of “profiles” from the data sets of early space-age sounders (that provided only “total column content” at the time of first interpretation). This example demonstrates that improved interpretation capabilities (better algorithms, models, etc.) may eventually lead to a greater harvest (more parameters and/or better results) from observation data analysis without the added introduction of an improved instrument (measurement) technology.

The performance of early atmospheric sounders hinged in particular on the available detector technology of opto-mechanical systems. Practically all early instruments featured the following components: foreoptics, a grating, prism spectrometer, or filter spectrometer, a single detector element, and readout electronics. A mirror assembly was used in combination with the detector element to resolve the various components of the spectrum sequentially. In this fashion, a one-dimensional multi-spectral image was formed by the forward motion of the spacecraft (i.e., a sequence of measurement points, spectrally resolved, along the flight path for a nadir-viewing sounder).

Historically, the first spectrometers (e.g., sounders) on spacecraft were used to measure the atmospheres of the sun’s planetary system. The IRS (Infrared Spectrometer) instrument, developed at UCB (University of California at Berkeley), was flown on Mariner-6 (launch Feb. 24, 1969, Mars flyby mission) to measure the atmosphere of Mars. IRS (using a variable filter spectrometer) measured the infrared region 1.8–14.4 μm in approximately 1400 discrete measurements with a spectral resolution of 1%. IRS was also flown on Mariner-7 (launch Mar. 27, 1969). The Mars atmosphere showed hints of dust suspended in the atmosphere as well as: carbon dioxide ice, water ice clouds, carbon monoxide, ionized hydrogen, and ionized oxygen. Surface temperatures of 280–290 K were recorded near the equator.¹⁵³⁾

In Earth observation, BUV (Backscatter UV Spectrometer) is an early spectrometer instrument flown on the NASA missions Nimbus-4 (launch April 8, 1970, see M.29.4) and AE-

151) Note: Both terms are used in the literature with the same meaning. Spectroscopy is the science of measuring the spectral distribution of photon energies (as wavelengths or frequencies) associated with radiation that may be transmitted, reflected, emitted, or absorbed upon passing from one medium (vacuum or air) to another (material objects).

152) The technical information of this chapter was obtained in discussions with Peter Haschberger of DLR, Oberpfaffenhofen, Germany

153) L. Kirkland, J. Pimentel, P. Forney, K. Herr, R. R. Brattain, “Design and Flight of the Mariner Mars 1969 Infrared Spectrometers,” URL: <http://www.lpi.usra.edu/science/kirkland/IRS/History1/>

E (Atmosphere Explorer–E, Explorer 55) with a launch Nov. 20, 1975. UV monitored the vertical distribution and total amount of atmospheric ozone by measuring the intensity of UV radiation backscattered by the Earth/atmosphere system during day and night in the spectral band of 250 – 340 nm. An improved version, SBUV/TOMS (Solar Backscatter Ultraviolet/Total Ozone Mapping Spectrometer), was later flown on Nimbus–7 (launch Oct. 24, 1978). The SAM (Stratospheric Aerosol Measurement) was flown on ASTP (Apollo–Soyuz Test Project), July 15–24, 1975, to perform the first successful solar occultation measurement of stratospheric aerosol. SAM was a single spectral instrument (sounder) measuring the aerosol extinction near the 1000 nm wavelength region.

At the start of the 21st century, Earth observation based on imaging spectroscopy has been transformed in less than 30 years from a sparsely available research tool into a commodity product available to a broad user community. Currently, imaging spectrometer data are widespread and they prove for example, that distributed models of biosphere processes can assimilate these observations to improve estimates of Net Primary Production, and that in combination with data assimilation methods, access complex variables such as soil respiration, at various spatial scales. ¹⁵⁴⁾

Today, technological advances in the domain of focal plane development, readout electronics, storage devices and optical designs, are leading to a significantly better sensing of the Earth’s surface. Improvements in signal–to–noise, finer bandwidths and spectral sampling combined with the goal of better understanding the modeled interaction of photons with matter will allow for more quantitative, direct and indirect identification of surface materials based on spectral properties from ground, air, and space. Advances in sensor technology, electronics, and (pre–) processing have led to the development of a suite of new applications.

The future: Imaging spectrometer instrument technology will profit from true spectroscopy focal plane arrays, with improved quantum efficiency, several readout ports, a rectangular design and consistent readout in the spectral domain, eventually also being expanded to the emissive part of the spectrum. To achieve high spectral–spatial uniformity and high precision measurements advanced optical designs are required combined with enabling components (curved, high–efficiency dispersive elements and ultra–straight slits). Optomechanical designs must focus on spectral and radiometric stability. With stability, spectral, radiometric and spatial calibration can be readily established from the spectral features of the atmosphere as well as uniform/measured calibration targets on the Earth.

1.4.2.1 Imaging spectrometry

In literature, the terms “imaging spectroscopy”, “imaging spectrometry” and “hyperspectral imaging” are often used interchangeably in remote sensing. Even though semantic differences might exist, a common definition is: *simultaneous acquisition of spatially coregistered images, in many, spectrally contiguous bands, measured in calibrated radiance units, from a remotely operated platform.*

Imaging spectrometry is a scheme of combining the spatial and spectral information capture techniques into a common technique to obtain the best of both worlds, namely spatial information matched (or coregistered) with the corresponding multi–band spectral information. See also “spectrometer” in Glossary and in chapter O.6. In general, there are three “image capture” technologies of imaging spectrometers in use (two are scanning types, one employs framing):

¹⁵⁴⁾ M. E. Schaepman, R. O. Green, S. G. Ungar, B. Curtiss, J. Boardman, A. J. Plaza, Bo–Cai Gao, S. Ustin, R. Kokaly, J. R. Miller, S. Jacquemoud, E. Ben–Dor, R. Clark, C. Davis, J. Dozier, D. G. Goodenough, D. Roberts, G. Swayze, E. J. Milton, A. F. H. Goetz, “The Future of Imaging Spectroscopy – Prospective Technologies and Applications,” Proceedings of IGARSS 2006 and 27th Canadian Symposium on Remote Sensing, Denver CO, USA, July 31–Aug. 4, 2006

1) **Whiskbroom line array** (bandinterleafed by pixel). Optical filtering of the incoming radiation into multiple bands can be provided by the following means:

- Grating: an example instrument is AVIRIS (see Table 15)
- Prism: an example instrument is HyMap

2) **Pushbroom area array** (bandinterleafed by line). Optical filtering of the incoming radiation into multiple bands can be implemented by:

- Grating: an example instrument is AIS (see Table 15)
- Prism: an example instrument is HYDICE
- FTS (Fourier Transform Spectrometer): an example instrument is SMIFTS
- Wedge–type variable filter spectrometers: an example instrument is WIS (Wedge Imaging Spectrometer)

3) **Framing camera** (band sequential). Optical filtering of the incoming radiation into multiple bands can be implemented by the following techniques: ¹⁵⁵⁾

- AOTF (Acousto–Optic Tunable Filter)
- LCTF (Liquid Crystal Tunable Filter)
- FPI (Fabry–Perot Interferometer)

The availability of *line–array detector* and of *area–array detector* technology in the 1980s and 1990s changed the capabilities of Earth observation profoundly, offering new dimensions in the fields of imagery and spectrometry (i.e. in the spatial and spectral domains). The pushbroom imaging concept was introduced as a result of available **line–array** detector technology, permitting the simultaneous (parallel) observation of a cross–track line of spatial resolution cells (i.e., a large number of pixels providing a swath width). The 2–D image is formed by the forward motion of the spacecraft.

The pushbroom imaging concept had immediate consequences for the spectral data domain as well. It meant the introduction of “imaging spectrometry.” The straight–line measuring constraint of sounding could now be considerably enhanced over an extended area or scene (i.e., giving the spectral sounding data also the spatial dimensions of x and y). In comparison with the one–element detector sounding technology of 1–D observations, pushbrooming in combination with a rotating mirror (for sequential spectral sampling) offered now the capability of multiple–line (2–D) spectroscopy (all parallel in the cross–track direction) for nadir sounding observations. This resulted in a fairly close–gridded observation pattern, contiguous in the cross–track, but discrete in the along–track direction due to the sequential sampling of the spectral domain.

The introduction of the area array detector technology provided finally the so–called contiguous “image cube” with two spatial dimensions and one spectral dimension. In this concept, the instantaneous spatial information is resolved in cross–track, while the corresponding spectral information for each spatial element is resolved by the along–track elements of the detector array. The second spatial dimension is obtained by pushbrooming, i.e., by the along–track motion of the spacecraft. Naturally, a fast area array readout tech-

155) Note: A photographic system is an example of a “framing system” using either the conventional analog film or a digital 2D detector array system for instantaneous image format capture (referred to as “staring imagers”); it means that all of the data of an image are acquired simultaneously in a snapshot. A TV system employs also the framing technique with a rapid refreshment rate. However,, motion compensation is generally needed with a staring imager (2D detector array) to correct for smearing effects on a moving platform. – In scanning systems (like whiskbroom or pushbroom type imagers) an image is acquired sequentially. A pushbroom imager with a 2D detector array is generally being used to collect spectral information in the second dimension (in parallel to the spatial information) such as in multispectral, hyperspectral or TDI support applications.

nique is needed in this concept to free the array for the next detection/integration/read–out cycle.

Imaging spectrometry means that for every position in an observed target field, a spectrum is being obtained. The information content is a 3–dimensional “image or data cube” which contains radiometric information spatially and spectrally resolved.

Two techniques (instrument types) have been mainly applied in imaging spectrometry: the dispersive spectrometer and the interferometer. Both methods can only acquire two of the three dimensions of the data cube at any time. The third dimension has to be obtained sequentially: In the dispersive spectrometer case it is the second spatial dimension; in the case of the interferometer it is the wavelength dimension.

1) Dispersive spectrometer instrument technique: This involves stepping the long slit of a dispersive (grating or prism) spectrometer across the target field. The basic system passes the incoming target radiation through a slit and onto a grating (or a prism) before illuminating a 2–D detector array. In this manner, one axis of the array corresponds to the spatial dimension and the other to the spectral. The second spatial dimension of the image is obtained by the forward motion of the spacecraft, thus producing an “image cube” with two spatial dimensions and one spectral dimension.

2) Interferometer instrument technique: Traditional FTS (Fourier Transform Spectrometer) imagers possess two major advantages over grating, prism, and circular variable filter (CVF) spectrometers. These are:

- Timemultiplexing. An interferometer’s (Michelson, etc.) single detector views all the wavelengths (within the sensor bandpass) simultaneously throughout the entire measurement period. This effectively lets the detector collect data on each wavelength for the entire integration time while staring at the target, measuring more photons and therefore, results in higher SNR (Signal–to–Noise Ratio) values, at best for situations where the source is stable.
- Throughput advantage, because the FTS does not need spatial filters (e.g. slit) in the optical light path.

The FTS (Fourier Transform Spectrometer) method generates an **interference pattern** as detector output (an intermediate product), also called the **interferogram**, which requires a Fourier transformation to obtain the measured radiance spectrum. The optical and detector system of the instrument can be devised in such a fashion that at any given OPD (Optical Path Difference) of the FTS, the image of the target is modulated spatially by the interferometer fringe pattern, which encodes the spectral information. Scanning the OPD generates the interferogram, representing the sum of all modulated waves. These interferograms are Fourier transformed individually yielding a spectral image data cube composed of the same spatial elements as the image.

However, a disadvantage of the conventional FTS imager concept is their optical delay by physically translating one or more optical components (the instrument has to go through all OPD positions to complete the measurement cycle of strokes). Such a mechanical translation mechanism reduces of course the performance of interferometer instruments. Over the course of a multi–year mission, millions of strokes are needed resulting in instrument wear or fatigue. Also, the moving optical elements may result in alignment problems.

The enormous information content provided by the technique of imaging spectrometry is of course very advantageous for analysis in many applications of Earth observation. In the past, imaging spectrometry had to overcome the technical challenges of available detector technology, computing power, and very large data volumes. These problems are somewhat alleviated with the available technology at the start of the 21st century. – In the 1980s, the potential of new and improved imaging spectrometer concepts lead eventually into the for-

mulation of the term “**hyperspectral imaging**,” referring to a considerable number of spectral bands that could be observed by a single instrument.

- Hyperspectral imaging is an optical sensing technique breaking up the incoming radiation into numerous contiguous (i.e., adjacent and not overlapping) spectral bands (normally >20 – 200 narrow bands or many more). The technology was introduced with such pioneering airborne instruments as AIS (1982, 128 spectral bands) and AVIRIS (1989, 224 spectral bands), both of JPL. Another early airborne hyperspectral imaging spectrometer was FLI (Fluorescence Line Imager), developed by Moniteq Ltd and Itres Ltd for the Canadian Department of Fisheries and Oceans. It was first flown in 1984, using pushbroom technology and 288 spectral bands (see P.95). Early hyperspectral imagery with airborne instruments demonstrated also the technique for mineral mapping applications.^{156) 157)}
- The first spaceborne hyperspectral imagers launched were:
 - **UVISI** (Ultraviolet/Visible Imaging and Spectrographic Imaging) instrument suite on MSX (Midcourse Space Experiment) of DoD (launch Apr. 24, 1996)
 - HSI and LEISA, both on the Lewis spacecraft (launch Aug. 23, 1997; however, Lewis never became operational and reentered the Earth’s atmosphere on Sept. 28, 1997)
 - FTTHSI on MightySat II.1 of AFRL (Air Force Research Laboratory) with a launch July 19, 2000. FTTHSI demonstrated the advantage of Fourier systems over dispersive hyperspectral imagers. FTTHSI is the first spaceborne hyperspectral imager to record the full spectra without any time delay using the **spatially modulated technique** (decoupling the spatial and spectral signatures).
 - The Hyperion and LAC (LEISA Atmospheric Corrector) instruments on EO–1 (NASA/GSFC), of HSI and LEISA heritage, respectively, were launched Nov. 21, 2000.¹⁵⁸⁾ Hyperion is an imaging dispersive grating spectrometer in VNIR and SWIR (in this context, the ALI instrument on EO–1 is also an imaging dispersive–type grating spectrometer, but in the multispectral class). Hyperion has a GSD of 30 m, a spectral range of 357–2576 nm on a swath of 7.65 km.
 - The PROBA–1 mission of ESA (launch Oct. 22, 2001) is flying **CHRIS** (Compact High Resolution Imaging Spectrometer), a hyperspectral imager of the UK, funded by BNSC. The spectral range is 400–1050 nm (18, 37, 6 bands), GSD of 17 or 34 m. The nominal swath is 13 km.
 - The IMS–1 (Indian Microsatellite –1) of ISRO (launch April 28, 2008) is flying HySI (Hyperspectral Imager) providing 64 contiguous bands in the region 0.45–0.95 μm . The swath is 128 km with a spatial resolution of 550 m.
 - The HJ–1A mission of CAST, China (launch Sept. 5, 2008) is carrying HSI (Hyperspectral Imager) to observe in the spectral range of 450 –950 nm (115 bands). The spatial resolution is 100 m on a swath of 50 km.
 - The TacSat–3 mission of AFRL (launch May 19, 2009) carries ARTEMIS with a spectral range of 400–2500 nm (5 nm sampling, > 200 bands), a GSD of 5 m on a swath of 20 km). On April 30, 2012, TacSat–3 reentered Earth’s atmosphere due to its low orbital altitude.
 - The HICO (Hyperspectral Imager for the Coastal Ocean) instrument of ONR/NRL was launched on Sept. 19, 2009 on the inaugural flight of the Japanese H–II Transfer Ve-

156) R. B. Gomez, “Hyperspectral imaging: a useful technology for transportation analysis,” *Optical Engineering*, Vol. 41, No 9, Sept. 2002, pp. 2137–2143

157) G. Vane, A. F. H. Goetz, “Terrestrial Imaging Spectrometry: Current Status, Future Trends,” *Remote Sensing of Environment*, Vol. 44, 1993, pp. 117–126

158) D. R. Hearn, “Characterization of instrument spectral resolution by the spectral modulation transfer function,” *Proceedings of SPIE Vol. 3439, Earth Observing Systems III, San Diego, July 1998*, pp. 400–407

hicle (HTV–1) to the ISS (as part of HREP (HICO–RAIDS Experiment Payload). HICO observes in the range of 353–1081 nm in 128 bands. The spatial resolution is 100 m on a swath of 42 km.

- The YouthSat mission of ISRO (launch April 20, 2011) is carrying **LiVHySI** (Limb Viewing Hyperspectral Imager) for observations of the altitude profile of neutral and ionized species of the upper atmosphere (altitude range of 100 to 1100 km). Observations in the spectral range of 450 – 950 nm with a spatial resolution of 4 km and a spectral resolution of 8 nm.

Note: The hyperspectral imagers are also known by the term of “imaging spectrometers.”

- Planned spaceborne missions with hyperspectral imagers are:
 - ZASat–003, a microsatellite mission of SunSpace and Stellenbosch University, South Africa. A launch is planned for 2014. The instrument is MSMI (Multi–Sensor Microsatellite Imager) with over 200 bands in the spectral range of 400–2350 nm, GSD=14.5 m on a swath of 14.9 km.
 - PRISMA (Hyperspectral Precursor and Application Mission) of ASI, Italy is a minisatellite mission (400 kg) under development with a planned launch for 2015. Observations will be conducted in VNIR (400–1010 nm), 92 bands, and in SWIR (920–2505 nm) in 157 bands. The GSD = 30 m on a swath of 30 km.
 - HypIRI (Hyperspectral InfraRed Imager) is a planned NASA/JPL mission to be launched in the timeframe 2015/16. The spectral range is 400–2500 nm, spectral resolution = 10 nm, > 200 bands, GSD= 60 m, swath = 145 km.
 - HISUI (Hyperspectral Imager Suite) is a pushbroom imager to be launched on the ALOS–3 mission of JAXA in 2016. HISUI observes in the spectral range of 400–2500 nm in 185 bands. The GSD is 30 m on a swath of 15 km.
 - EnMAP (Environmental Monitoring and Analysis Program): A German spacecraft with a launch planned for 2017. The HSI sensor has a spectral range of 420–2450 nm with 96 bands in VNIR and 126 bands in SWIR. A swath of 30 km is provided with a GSD of 30 m.

Typical examples of hyperspectral filter techniques include dispersive gratings or prisms, multi–order (mode) etalons, interference filters, Michelson interferometers, acousto–optic tunable filters (AOTF), and wedge–type variable filter spectrometers [an example is WIS (Wedge Imaging Spectrometer). The other key feature is focal plane detector array technology which allows multiple spatial and/or spectral samples through 1–D or 2–D arrays. ¹⁵⁹⁾

Sensor (Agency/Company)	No. of Bands	Spectral Range (nm)	Bandwidth at FWHM (nm)	IFOV (mrad)	FOV (°)	Data Product	Period of Operation
AAS (ASTER) (DAIS–2815) (GER)	1 3 20	760–850 3000–5000 8000–12000	90 600–700 200	1.0, 2.5, or 5.0	28.8, 65, or 104	Image cube	since 1991
AHS, Daedalus	48	440–12700	20–1500	2.5	86	Image cube	1994
AIS–1	128	990–2100 1200–2400	9.3	1.91	3.7	Image cube	1982–85
AIS–2 (NASA/JPL)	128	800–1600 1200–2400	10.6	2.05	7.3	Image cube	1986–87
AISA (Karelsilva Oy)	1–286	450–900	1.56–9.36	1	21	Image cube	since 1993

¹⁵⁹⁾ Note: The Michelson interferometer is named after the US physicist Albert Abraham Michelson (1852–1931) who is regarded the father of interferometry providing the first successful measurements in interferometry (see O.9). Also first successful measurements of the diameters of Jupiter’s moons in 1891. Michelson is the first American who received the Nobel Prize in physics in 1907.

Sensor (Agency/Com- pany)	No. of Bands	Spectral Range (nm)	Bandwidth at FWHM (nm)	IFOV (mrad)	FOV (°)	Data Product	Period of Operation
AMSS (GEOSCAN)	32 8 6	490–1090 2020–2370 8500–12000	170–240 430–440 550–590	2.1 x 3.0	92	Image cube	since 1985
ARES (AIP) (Lockheed)	75	2000–6300	25–70	1.17	3 x 3	Image cube	since 1985
ASAS upgraded ASAS (NASA/GSFC)	29 62	455–873 400–1060	15 11.5	0.80 0.80	25 25	Image cube Image cube	1987–91 since 1992
AVIRIS (JPL)	224	380–2500	9.7–12.0	1	30	Image cube	since 1989
CASI (Itres Research)	288 19	400–1000 (nominal)	650	1.3, 1.6	37.8 44.7	Profile image	since 1990
CIS (China)	64 24 1 2	400–1040 2000–2480 3530–3940 10500–12500	10 20 410 1000	1.2 x 3.6 1.2 x 1.8 1.2 x 1.2 1.2 x 1.2	80°	Image cube	since 1993
CHRIS, SAIC AAHIS, (SAIC)	40 288	430–860 440–880	11 3	0.05 1.0	10 11.5	Image cube Image cube	1992 1994
DAIS–7915 (GER/DLR)	32 8 32 1 6	400–1010 1500–1788 1970–2450 3000–5000 8700–12700	10–16 36 36 2000 600	3.3, 2.5, or 5.0	64–78	Image cube	since 1994
DAIS–16115 (GER)	76 32 32 6 12 2	400–1000 1000–1800 2000–2500 3000–5000 8000–12000 400–1000	8 25 16 333 333 stereo	3	78	Image cube	since spring 1994
DAIS–3715 (GER)	32 1 2 1 1	360–1000 1000–2000 2175–2350 3000–5000 8000–12000	20 1000 50 2000 4000	5	±45	Image cube	since 1994
FLI/PMI (Moniteq)	≥ 288	430–805	2.5	1.3	70	Profile image	1984–90
FTVHSI (Kestrel)	256	440–1150	67 cm ⁻¹	0.8	15	Image cube	1996
GER–63 Chan- nel Scanner (GER)	24 4 29 6	400–1000 1500–2000 2000–2500 8000–12500	25 125 17.2 750	2.5, 3.3, or 4.5	90	Image cube	since 1986
HYDICE (NRL/ERIM)	206	400–2500	7.6 – 14.9	0.5	8.94	Image cube	since 1994
ISM (DESPA/ IAS/OPS)	64 64	800–1600 1600–3200	12.5 25.0	3.3 x 11.7	40 (select.)	Image cube	since 1991
MAS (Daedalus)	50	547–14521	31–517	2.5	85.92	Image cube	since 1992
MISI (RIT)	60	400–1000	10	2	±45	Image cube	from 1996
MIVIS (Daedalus)	20 8 64 10	433–833 1150–1550 2000–2500 8200–12700	20 50 8 400–500	2.0	70	Image cube	1993
MUSIC (Lockheed)	90 90	2500–7000 6000–14500	25–70 60–1400	0.5	1.3	Image cube	1989

Sensor (Agency/Company)	No. of Bands	Spectral Range (nm)	Bandwidth at FWHM (nm)	IFOV (mrad)	FOV (°)	Data Product	Period of Operation
ROSIS-03 (DLR/GKSS)	115	430–830	4	0.56	16	Image cube	since 1993 ROSIS-03 since 1998
SFSI (CCRS)	115	1200–2400	10.4	0.4	9.4	Image cube	since 1994
SMIFTS (U. of Hawaii)	75 35	1000–5200 3200–5200	100 cm ⁻¹ 50 cm ⁻¹	0.6	6.0	Image cube	since 1993
TRWIS-A	128	430–850	3.3	1.0	15	Image cube	1990
TRWIS-B	90	460–880	4.8	1.0	15	Image cube	1991
TRWIS-II	80	1500–2500	12	0.5/1.0	7.5/15	Image cube	1992
TRWIS-III (TRW)	384	400–2450	5/6.25	0.9	15	Image cube	1996
Hybrid VIFIS (U. of Dundee)	30 30	440–640 620–890	10–14 14–18	1 1	31.5 31.5	Image cube	Test phase 1994
WIS-FDU	64	400–1030	10.3	1.36	10 & 15	Image cube	Test 1992
WIS-VNIR	129,265	400–1000	12.5 & 6	0.66	19.1	Image cube	1995
WIS-SWIR (Hughes SBRC)	81+90	1000–2500	30 & 23	0.66	12.0	Image cube	1995

Table 15: Summary of some early hyperspectral airborne imaging spectrometers

The passive remote sensing technique of hyperspectral imaging offers an unparalleled spectral interpretation capability of the data (quantitative monitoring) for many applications, including land, water and atmospheric parameters [detection/discrimination of spectral fingerprints of matter (solids, liquids, gaseous or particulate matter) that cannot be derived from coarser multispectral imagers]. Land applications include vegetation studies (species identification, plant stress, leaf water content), soil science (erosion), geology (mineral identification and mapping, detection of underground/camouflaged structures), and hydrology (liquid/solid water differentiation, snow/grain size). Water applications include monitoring of water quality, bathymetry, etc. Atmospheric applications include the measurement of water vapor, trace gases, aerosols, and cloud characteristics. – A disadvantage of the technique is the generation, communication, processing, interpretation and storage of immense data volumes.

1.4.2.2 Spectral dispersion methods

There are three mainstream instrumental dispersion approaches to spectral imaging (SI): a) filter/interferometer (FSI), b) wavelength/dispersive (WDSI), and c) a hybrid of FSI and WDSI (hybrid). The main properties of the three dispersion techniques are given in Table 16.

- The FSI (Filter/Interferometer Spectral Imaging) method images a fixed FOV sequentially through a series of filters, each of which has a certain bandpass and center wavelength. The filtered image is then focused onto a CCD camera. Electronic methods used to generate the filters include LCTF (Liquid Crystal Tunable Filters), AOTF (Acousto-Optic Tunable Filters), and interferometry. Overall, the spectral acquisition process is slow in hyperspectral applications due to the sequential acquisition approach of many channels.

Parameter/instrument technique	Filter/interferometer (FSI)	Wavelength/dispersive prism/diffraction grating	Hybrid/PMT (Photomultiplier Tube)
Wavelength acquisition	Sequential	Simultaneous	Limited simultaneous
FOV (Field of View)	Simultaneous over a fixed FOV	Sequential over an unlimited FOV	Point-by-point confocal over a fixed FOV
Spectral acquisition	Bandpass	All contiguous wavelengths	Bandpass

Parameter/instrument technique	Filter/interferometer (FSI)	Wavelength/dispersive prism/diffraction grating	Hybrid/PMT (Photomultiplier Tube)
Spectral discrimination	Moderate	High	Low
Relative spectral acquisition time	Slow	Fast	Fast
Sensitivity	Good	Good	Excellent
Time-resolved fluorescence with the lanthanide series	No	Yes	Yes

Table 16: Comparison of performance characteristics of FSI, WDSI, and hybrid systems

- The WDSI (Wavelength/Dispersive Spectral Imaging) technique (the most common in imaging) uses an imaging spectrometer that incorporates a diffraction grating or prism as the dispersive device to split the radiation into all its component wavelengths. The CCD detector is positioned to intercept focused diffracted light at all contiguous wavelengths simultaneously. The design of the spectrometer enables the user to know the location on the sample that emits a particular spectrum. The CCD presents one spectrum per row of pixels. If there are 240 rows of pixels, then a slice of the sample will be characterized by 240 spectra. Software automatically classifies the spectra obtained, so that all spectra that are the same can be similarly pseudo-color-coded. – Because each CCD row of pixels acquires a complete spectrum in one shot, data processing can begin immediately after one acquisition. This is in direct contrast to the FSI approach, where it is necessary to wait until a FOV has been acquired through a series of filters and each pixel has accumulated a full spectrum. All wavelength/dispersive imaging spectrometers abide by the following rules:

- 1) Light must pass through an entrance aperture (ES) that is almost always a slit.
- 2) An image of the slit is focused at different locations in space as a function of wavelength and the dispersive properties of the spectrometer. Hence, the term “spectral lines” is derived from the slit image produced at various wavelengths. A detector array or CCD is in focus when it records spectral lines at their narrowest. Each row of pixels provides a spectrum associated with a particular point in the slice.
- 3) The width of the detector determines the wavelength dispersion; for example, spectral range: 360–800 nm; wavelength range: 440 nm (800–360 nm); detector: 8 mm active length; and pixel size: 8.5 μm . Therefore, the average wavelength dispersion is 55 nm/mm (440 nm/8 mm). A prism presents nonlinear wavelength dispersion, with significantly greater dispersion in the blue compared to the red.
- 4) The spectral bandpass is a function of dispersion of the spectrometer, the entrance slit width, and the detector size, so that: Bandpass = FWHM = (effective slit width x dispersion) where the effective slit width is the greater of the width of the detector elements or the image of the slit. In this case, the detector elements are the pixel dimensions of the CCD.
- 5) The spectral resolution of a spectrometer is defined as the limiting bandpass for an emission source of infinitely narrow natural line width, such as a single-mode laser, the narrowest possible slit width, and the finite dimensions of the detector elements.
- 6) A slice of the FOV is defined by the projected width of the ES on the sample following the microscope objective (MO). For example, if the magnification of the MO = 10x, and ES = 0.025 x 5.0 mm, then the slice will be 0.0025 x 0.5 mm at the sample.
- 7) Spatial resolution is determined either by the projected width of the slit through the microscope objective or by the projected image of the object, whichever is smaller.

- Hybrid spectral imaging. One of the most sensitive detectors is the photomultiplier tube (PMT). This device contributes very low noise and a high dynamic range (10^6),

compared to 10^3 with a CCD, with good efficiency (from 185 to 700 nm). A PMT is the detector of choice with almost all laser confocal imaging systems. New developments in PMT technology include the IPMT (Imaging PMT) of Hamamatsu. Unlike a typical PMT that has only one detector element, the IPMT has a linear array of detector elements on 1 mm centers and an active area of 800 μm .

1.4.2.3 ETF (Electronically Tunable Filter) systems and technologies

The capture of reflectance information (i.e., reflective solar radiation observation from the Earth's surface using imaging devices, extraction of color–light interactions in computer vision, etc.) in spectrally higher dimensions (multispectral or hyperspectral imagery) generally improves image analysis. To acquire spectrally and spatially high–dimensional images, one has to employ specialized image acquisition devices [a spaceborne hyperspectral imager builds an image cube (x, y, λ dimensions) in a pushbroom fashion, by capturing typically one spatial and all spectral dimensions simultaneously in each camera frame, while the second spatial dimension is captured displaced in time]. Electronically tunable filters offer the fastest, most accurate and flexible color filtering techniques that are currently available.

Background on reflective optical instruments: ¹⁶⁰⁾ Reflective optical systems for imaging spectrometry have a number of advantages for use in spaceborne applications. They operate over a broader wavelength band than refractive systems. In particular, a single foreoptic and (sometimes) spectrometer optic can be made to work over the full wavelength band (400 to 2500 nm) of interest for remote sensing of solar reflected radiation. The optics can be aligned using visible light, and the result will hold at all wavelengths. Reflecting systems are inherently more radiation hard than refractive ones, and reflective systems can be designed and built to have a stable optical performance over a wider temperature range than refractive systems.

An ETF is a filter device whose spectral transmission can be electronically controlled through the application of voltage or acoustic signal, etc. There are no moving parts and no discontinuity in the spectral transmission range, thus a fine spectral sampling is provided as well as rapid and random switching between the various spectral bands. ¹⁶¹⁾

There are three prominent classes of ETFs to achieve wavelength selectivity in imaging applications (generation of hyperspectral imaging cubes) in combination with framing cameras for sequential wavelength scanning:

- 1) AOTF (Acousto–Optical Tunable Filter)
- 2) LCTF (Liquid Crystal Tunable Filter)
- 3) FPI (Fabry–Perot Interferometer) tunable filter.

The ETF technology is sensitive to polarization so that the **imagery can be used to discern polarization information about a scene in addition to spectral information**. The light transmission through an AOTF, LCTF, or an interferometer is always wavelength dependent and typically polarization dependent. It is difficult to reach even 50% transmission efficiency, especially as most biological samples present randomly polarized light.

Attributes/System	LCTF (Liquid Crystal Tunable Filter)	AOTF (Acousto–Optical Tunable Filter)	FPI tunable filter
Tunability time	~ 50 ms	~ 15 ms, ~ 30 ms	~ 40 ms FPI ~ 4 ms DE–FPI
Operating spectral range	0.4 – 1.7 μm	0.2 – 5 μm	0.4 – 1.55 μm

160) P. Mouroulis, D. A. Thomas, T. G. Chrien, V. Duval, R. O. Green, J. J. Simmonds, A. H. Vaughan, “Trade Studies in Multi/hyperspectral Imaging Systems – Final Report,” Oct. 29, 1998, URL: <http://esto.gsfc.nasa.gov/files/1999/Mouroulis.pdf>

161) S. Poger, E. Angelopoulou, “Selecting Components for Building Multispectral Sensors,” <http://www.cs.stevens-tech.edu/~elli/cvpr01.sketch.pdf>

Attributes/System	LCTF (Liquid Crystal Tunable Filter)	AOTF (Acousto-Optical Tunable Filter)	FPI tunable filter
Max width of tunable range	450 nm (VNIR) 950 nm (SWIR)	700 nm (VNIR) 3900 nm (SWIR, MWIR)	100 nm
Min output bandwidth	5 nm	0.4 nm	0.05 nm
Max output bandwidth	30 nm multispectral 100 nm trichromatic	50 nm	10 nm
Mean error in central wavelength	0.5 nm	1 nm (varies with λ)	1 nm (varies with λ)
Average transmission rate	20–50%	98%	20–50%
Transmission rate over wavelength	increases with wavelength	constant	increases with wavelength
Out of band transmission	0.01–0.05%	0.05–0.1%	0.5–1%
Range of aperture sizes	20–35 mm	3–10 mm	15–76 mm
Incident light limitations	None	Requires collimated light	None
Power consumption	Low	Low	Low (FPI) High (DTFPI)

Table 17: Typical tunable filter characteristics

1.4.2.4 Acousto-Optic Tunable Filters (AOTF)

Acousto-Optic Tunable Filters (AOTF) in acousto-optic imaging systems (O.4.5). The AOTF technique is based on diffraction of an acoustic wave of electromagnetic radiation traversing a transparent medium. An AOTF consists of a crystal in which radio frequencies (RF) acoustic waves are used to separate a single wavelength of light from a broadband source. The wavelength of light selected is a function of the frequency of the RF applied to the crystal. An acousto-optic cell is a transparent birefringent crystal excited by a radio frequency transducer. Propagating acoustic waves inside the crystal create regular spatial variations of the refractive index. Under phase-matching conditions, light of a particular linear polarization and wavelength, incident on the crystal at a very specific angle, is diffracted by the moving grating produced by the acoustic wave. ^{162) 163) 164)}

In the 1990s AOTF devices are based on solid-state technology, they are RF-tunable and random access devices, offering the important capability of spectral agility. When combined with a 2-D CCD array, the complete spectral, spatial, and polarimetric characterization of a scene can be measured with an imaging system that has no moving parts. An AOTF device, can switch from one spectral range to another in the time that it takes an acoustic wave to traverse the crystal, (typically in the μ s range). By making the AOTF part of an imaging system [i.e. an AOS (Acousto-Optic Spectrometer)], and projecting the diffracted light onto a 2-D array, it is possible to form an image extracted from the particular spectral component of the incident radiation. CCD arrays have been utilized for this purpose.

Because the crystal is birefringent, the polarization of the light incident on the device affects the angle to which the light is diffracted. Diffraction changes the polarization of the incident radiation so that some of the initially ordinary polarization emerges from the device with extraordinary polarization, and some of the initially extraordinary polarization emerges from the device with ordinary polarization. The result of this sensitivity to polarization is that an AOTF imager can be used to discern polarization information about a scene in addition to spectral information. Because the two polarizations of incident light are diffracted

162) P. Katzka. "AOTF overview: Past, present, and future," *Acousto-Optic, Electro-Optic, and Magneto-Optic Devices and Applications*, Vol. 753, pp. 22–28. Society of Photo-optical Instrumentation Engineers, 1987

163) L. J. Cheng, T. H. Chao, M. Dowdy et al., "Multispectral imaging systems using acousto-optic tunable filters," *Infrared and Millimeter-Wave Engineering*, Vol. 1874, pp. 224–231, 1993. Society of Photo-optical Instrumentation Engineers

164) D. A. Glenar et al., "Acousto-optic imaging spectropolarimetry for remote sensing," *Applied Optics*, Vol. 33, No. 31, Nov. 1, 1994, pp. 7412–7424

differently, it is possible to use two CCD arrays in order to capture separately the image generated by each polarization. The birefringent material of TeO₂ (Tellurium dioxide) is frequently used due to its high acousto–optic figure of merit, and good transmission in the UV, visible and infrared (range of application 0.25–4.5 μm).

- Some airborne precursor instruments with AOS (Acousto–Optic Spectrometer) technology, leading toward AOTF capabilities are: POLAS (Polarization–sensitive Acousto–optic Spectrometer) of Russia introduced in 1989, AHSTRA (Airborne Heterodyne Spectrometer THz Astronomy) of the Max–Planck–Institute for Radio Astronomy, Bonn; AMSOS (Airborne Millimeter & Submillimeter–wave Observing System) since winter 1997/98, Univ. of Bern, Switzerland; SUMAS/ASUR (Submillimeter Atmospheric Sounder/Airborne Submillimeter SIS Radiometer), Institute of Environmental Physics at the University of Bremen, Germany; THOMAS (THz OH Measurement Airborne Sounder), DLR (Institute of Optoelectronics, Oberpfaffenhofen, Germany).
- In the field of spaceborne Earth observation, the Russian instrument Trasser with AOTF technology was first flown on Okean–O1–N2 (or Cosmos 1869) with a launch on July 16, 1987. The instrument was operational until 1990. Another Trasser–O instrument was flown on Okean–O–1 (launch July 16, 1999, end of mission fall 2000). All Trasser instruments were designed and built by STCUI (Scientific Technological Center of Unique Instruments), Moscow. The Swedish SMR (Submillimeterwave Radiometer) instrument on ODIN (launch Feb. 20, 2001) features an AOS detector provided by France. The Japanese instrument SMILES (Superconducting Submillimeter–wave Limb–Emission Sounder) employs two acousto–optical spectrometers (AOS) with the objective to observe submillimeter–wave radiation (monitoring of trace gas distribution in the atmosphere). SMILES is an ISS payload planned to be launched in 2009 (L.2.15).
- In spaceborne science, the NASA SMEX mission SWAS (Submillimeter Wave Astronomy Satellite) with a launch on Dec. 5, 1998 carries the instrument AOS (Acousto Optical Spectrometer), provided by the University of Cologne, Germany, to investigate the composition of dense interstellar clouds. AOS on SWAS is used as a backend in combination with a heterodyne receiver to analyze the intermediate frequency signal. Inside AOS, the RF signals are converted to acoustic waves within a crystal causing pressure waves to travel through the crystal. When illuminated by laser light, the alternating patterns of compression and expansion within the crystal act like the finely spaced lines of a grating causing the laser light to be dispersed along one dimension with intensity variations along this direction that are proportional to the intensities within the input 1.4 to 2.8 GHz band.

1.4.2.5 LCTF (Liquid Crystal Tunable Filter)

A liquid crystal tunable filter is a bandpass filter technique¹⁶⁵⁾ that allows selection of the wavelength of the transmitted light by varying an electrical input voltage, and also functions as a linear polarizer. LCTFs use electrically controlled liquid crystal elements to select a specific visible wavelength of light for transmission through the filter at the exclusion of all others. The method relies on constructive and destructive interference effects in a multi–layer stack of quarter–wave reflective layers and half–wave spacer layers. This type of filter is ideal for use with electronic imaging devices, such as CCDs (Charge Coupled Devices), because it offers excellent imaging quality with a simple linear optical pathway.

In simple terms, an LCTF is something like an optical filter wheel – featuring a large aperture, large field of view, and good optical quality. But being electronic, there are no moving parts and no distortion of the image between wavelengths; therefore, it is ideal for automation. Being continuously tunable, a wider range of colors (bands) is available, beyond the

165) Note: The term “bandpass” is defined as the FWHM (Full Width Half Maximum) spectral response measured from the peak maximum if the line shape is Gaussian. The half–power width of a response is easier to describe than true resolution because the concept does not involve the contrast of the target.

conventional three fixed colors (RGB). A typical wavelength–selective liquid crystal tunable filter is constructed from a stack of fixed filters consisting of interwoven birefringent crystal/liquid–crystal combinations and linear polarizers (Lyot–type birefringent design consisting of multiple cells of increasing retardance). A single Lyot stage of the LCTF system is a “sandwich” of birefringent liquid crystal, glass, quartz, and sheet polarizers. The spectral region passed by LCTFs is dependent upon the choice of polarizers, and the liquid crystal characteristics (nematic, cholesteric, smectic, etc.). In general, visible–wavelength (VIS) devices of this type usually perform quite well in the 400 to 700 nm region. To achieve monochromatic throughput in the LCTF, a series of these “sandwiches” are stacked horizontally in order of increasing retardance. The bandwidth of the LCTF is constant in frequency space.

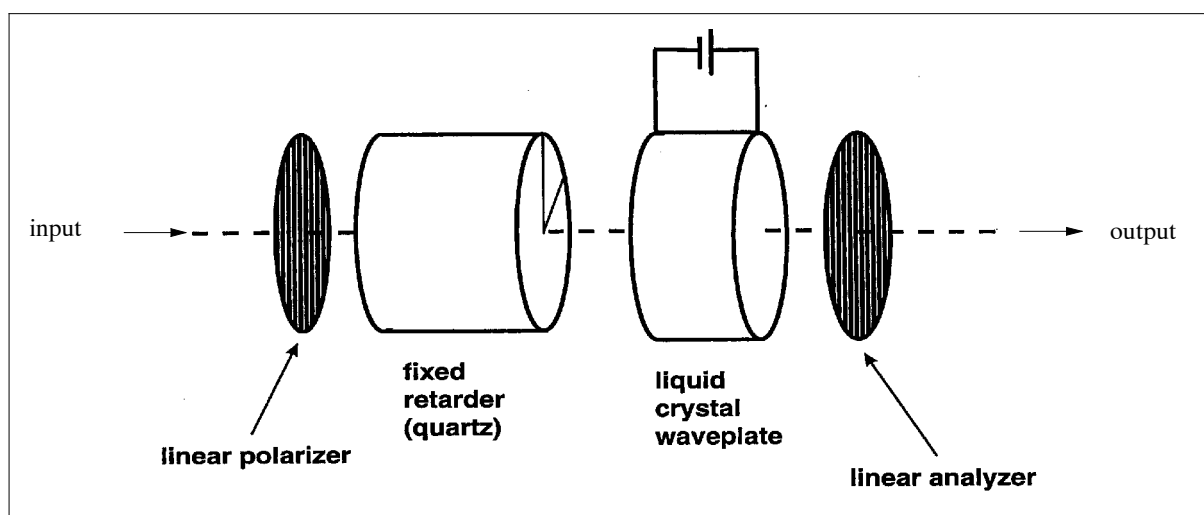


Figure 10: Schematic principle of an LCTF cell

An LCTF is based on two principles: **birefringence** and **polarization**. Birefringence is the phenomenon exhibited by some crystalline substances which display two different indexes of refraction. Polarization is related to the geometry of light wave propagation. It is associated with the plane of oscillation of the electric field of a light wave. Light waves can have no preferred oscillation plane (unpolarized light) or have all rays oscillate on a single plane (polarized light). The process of converting from unpolarized to polarized light is called polarization and the optical device that achieves this is a polarizer. Once light is polarized, its plane of vibration can be rotated through a process called retardation. The corresponding optical device is called a retarder. Some birefringent materials (e.g. calcite, quartz) can be used as retarders.

Background: The working principle of the AOTF technique, namely the diffraction of an acoustic wave of electromagnetic radiation traversing a transparent medium, was first recognized and discovered by L. Brillouin in 1921.¹⁶⁶⁾ In the 1990s the LCTF technology was first introduced in the medical field. Things not visible to the human eye can often be imaged using the LCTF and multispectral techniques. Separate images are prepared at different parts of the visible or infrared spectrum, and the images of their differences and contrasts are combined to prepare a new image. This technique has been applied to fingerprint recovery and for the detection of forgeries in altered documents. – JPL illustrated the power of multispectral imaging techniques using an LCTF when legible images of the Dead Sea Scrolls were obtained. Little contrast existed between the ancient papyrus and the ink, making it unreadable to the unaided eye. However, in the spectrum’s near–infrared band, the parchment becomes more reflective while the carbon–based ink remains dark. An LCTF made it possible to quickly scan the spectrum for the best imaging frequency.

166) L. Brillouin, *Ann. de Physique*, Vol.17, p. 103, 1921

At the start of the 21st century, the LCTF technology is being used in airborne applications and is also considered a viable and potential technique for spaceborne imaging applications. Example: ¹⁶⁷⁾

- NASA/JPL is using the LCTF technology in the design of an EOIFTS (Electrooptical Imaging Fourier Transform Spectrometer), a new type of interferometer, for hyperspectral measurements in the infrared region (1–2.5 μm), but without any moving parts as experienced in traditional Michelson interferometers. This approach takes advantage of fast switching ferroelectric or dual–frequency nematic LC modulators to quickly vary the time delay in order to implement fast–acquisition of the time–series data. This project addresses also the need by reducing the weight, size and power consumption of FTS (Fourier Transform Spectrometers) by eliminating all moving parts. The mechanical scanning mechanism of conventional FTS technology is being replaced with a solid–state time delay design using optoelectronic components. EOIFTS is a low–mass instrument to permit hyperspectral imaging of atmospheric constituents and many other applications. ¹⁶⁸⁾

1.4.2.6 FPI (Fabry–Perot Interferometer) tunable filter

The FPI (etalon) functions like a tunable interference filter by varying the gap between the two reflective plates, changing the wavelengths that undergo constructive interference. Some of the most important properties of an FPI filter are the in–band transmittance at the design wavelength, its bandwidth or its full width half maximum (FWHM) and the tunable spectral range. The concept may be used for a number of applications such as in imaging spectroscopy (to disperse the frequency components), Doppler wind measurements, and in optical communications for WDM (Wavelength Division Multiplexing). Prototype implementations are:

- Physical Sciences Inc. (PSI) of Andover, MA, developed AIRIS (Adaptive Infrared Imaging Spectroradiometer) for DoD. The operation of AIRIS from an airborne platform was demonstrated in 2002. In contrast to other approaches to multispectral and hyperspectral infrared imaging, e.g., pushbroom spectrometers and FTIR (Fourier Transform Infrared) spectrometers, AIRIS may be commanded to collect data at only those wavelengths which facilitate target detection. This capability can reduce data volume and data processing requirements for many multispectral imaging applications. The patented AIRIS concept employs an FPA (Focal Plane Array) which views the far field through a tunable Fabry–Perot interferometer (etalon). The tunable etalon is the critical enabling technology. Some features of AIRIS are: ¹⁶⁹⁾
 - Continuous coverage of MWIR ($\lambda \sim 3 - 5 \mu\text{m}$) or TIR ($\lambda \sim 8 - 12 \mu\text{m}$) atmospheric transmission windows
 - High spectral resolution ($\lambda/\Delta\lambda > 100$) imagery
 - Random wavelength access
 - Etalon tuning time is 10 to 20 ms
 - Etalon easily integrated with commercial IR cameras or operated as a stand–alone device
 - Tunable bandpass filter for differential absorption LIDAR receivers

167) C–Y. Mao, T. A. Gress, “A Hyperspectral Imaging Sensor Implemented with a Liquid Crystal Tunable Filter,” Proceedings of 1st International Conference on Geospatial Information in Agriculture and Forestry, Lake Buena Vista, FL, USA, 1998

168) T.–H. Chao, H. Zhou, X. Xia, S. Serati, “Electro–Optic Imaging Fourier Transform Spectrometer,” Proceedings of ESTC (Earth Science Technology Conference), Palo Alto, CA, June 22–24, 2004, <http://esto.gsfc.nasa.gov/conferences/estc2004/papers/b5p1.pdf>

169) <http://www.psicorp.com/products/airis.shtml>

Note: FTIRs as well as FPI instruments involve moving parts which must be accelerated and decelerated (linear mechanical motion is required), which dramatically limits the speed of acquiring a spectrum, typically to a maximum of ~ 1 frame/s. Real-time spectroscopic imaging (30 frames/s) cannot be done with the FTIR technology.

- NASA/LaRC is developing the TTSS–FPI (Tropospheric Trace Species Sensing Fabry–Perot Interferometer) instrument within IIP (Instrument Incubator Program).¹⁷⁰⁾ The TTSS–FPI instrument concept employs a double–etalon FPI (DE–FPI) to achieve the necessary high–resolution (0.068 cm^{-1}), narrow–band infrared emission measurements within the strong $9.6\text{ }\mu\text{m}$ ozone band. The technology will first be demonstrated on an airborne instrument while the intended implementation for future science missions is a geostationary–based measurement of tropospheric ozone and other trace gas species (application considered for the post–Aura time period). The goal is to provide a new measurement capability intended for geostationary Earth orbit (GEO)–based observation of tropospheric ozone.

170) A. M. Larar, W. B. Cook, C. S. Mills, M. A. Flood, J. J. Puschell, W. R. Skinner, “Tropospheric Trace Species Sensing FPI – Airborne System Development,” Proceedings of ESTC (Earth Science Technology Conference), Palo Alto, CA, June 22–24, 2004, URL: <http://esto.gsfc.nasa.gov/conferences/estc2004/papers/b4p2.pdf>

1.4.3 Microwave Region, Active Observations (Radars)

The term RADAR (Radio Detection and Ranging) was probably first suggested by S. M. Taylor and F. R. Furth of the U.S. Navy and became in November 1940 the official acronym of equipment built for radio detecting and ranging of objects. The acronym was by agreement adopted in 1943 by the Allied Forces of World War II and thereafter received general international acceptance. The term “radio” refers to the use of electromagnetic waves with wavelengths in the so-called radio wave portion of the spectrum, which covers a wide range from 10^4 km to 1 cm in wavelength (ELF to SHF). The microwave region with wavelengths generally considered from 1 m to 1 mm, happens to be the most frequently used spectrum range for radar instruments within the radio spectrum; this is the reason why “radar” is mostly equated with “microwave.”

The theoretical work of microwave technology is certainly based on the electromagnetic wave theory of James Clerk Maxwell (1831–1879) a Scottish physicist, followed by the experimental work of Heinrich Rudolf Hertz (1857–1894), a German physicist who demonstrated the existence of electromagnetic waves by building an apparatus to produce and detect VHF or UHF radio waves.

The following list provides some background on the early history of radar developments. Most of the chronology was compiled by BBC of London, UK. It should be said that all countries involved in an aspect of radar technology invention state somewhat different claims as to their contributions (examples: a) there are several claims to the coining of word “radar”, b) there is a claim that SAR and a chirp radar existed in 1945).¹⁷¹⁾

- In 1904, the German engineer Christian Hülsmeyer (1881–1957) of Eydelstedt in Lower Saxonia received a German patent (patent Nr. 165 546, plus others in the UK, the USA and some more countries) for the so-called “Telemobiloskop” or Remote Object Viewing Device. The device achieved ranges of up to 3000 m against ships, even before amplifier tubes were invented. It was offered for an application to prevent ship collisions, but didn’t find the interest of any customer and fell into oblivion.¹⁷²⁾

- R. C. Newhouse of Bell Labs received a patent in 1920, and his experiments performed throughout the decade eventually led to the radio altimeter which became operational in 1937.

- In 1922, the Italian inventor/physicist Guglielmo Marconi ((1874–1937)) held a speech which showed that he had a clear idea of detecting remote objects by radio signals. But it was not before 1933 that he was able to show a first working device. The principle of radio navigation, referred to as RDF (Radio Direction Finder), is based on the use of a radio source to guide the navigation of a mobile means (airplane or ship) through the use of a directional antenna.

In July 1934, Marconi steered his ship by wireless control (radio waves were used to aid navigation). He used a beacon operating on the 60 cm wavelength (500 MHz), installed along the coast of Sestri Levante (located in the Ligurian Sea of Italy) at a height of 100 m above sea level, to direct the navigation of the boat through a route marked out by buoys. This demonstration was conducted in the presence of technicians, Italian and British Navy officials and numerous representatives of the press.

- In 1924/26, the American physicists Gregory Breit (1899–1981) and Merle A. Tuve (1901–1982) as well as the British researchers Edward V. Appleton (1892–1965) and Samuel Barnett performed measurements of the Earth’s ionosphere, using a pulse-modulated (or simply pulsed) radio transmitter which could be called a radar. Appleton received the 1947 Nobel Prize in physics for his discovery of the F layer of the ionosphere in 1924.

171) “The History of Radar,” <http://www.bbc.co.uk/dna/h2g2/A591545>

172) Hermann Rohling, “Milestones in Radar and the Success Story of Automotive Radar Systems,” Proceeding of the 4th Microwave & Radar Week, MRW-2010, Vilnius, Lithuania, June 14–18, 2010

- It was 1928 when H. M. Signal School of the UK received the first patent on Radio Location, credited to L. S. Alder.
- In 1930, a team of engineers from the US Naval Research Lab performed measurements of a radio antenna, and more or less by serendipity – they independently discovered radar. Their radio link happened to stretch across an aircraft landing strip, and the signal quality changed significantly when an aircraft crossed the beam.
- In 1933 when Hitler took over power in Germany, the German Kriegsmarine (Navy) started research into what they called “Funkmesstechnik,” or remote radio measuring technology.
- Research in USSR/Russia began in 1934, but was somewhat hindered by quarrels between different authorities. However, one of the earlier radar devices was a success, with 70 km detection range against aircraft. RUS–1 (Radio Ulavlivatel Samoletov – Radio Catcher of Aircraft), a bistatic CW (Continuous Wave) radar, was introduced by the Red Army in 1939.¹⁷³⁾ Transmitting and receiving stations were separated by 35 km, the wavelength was 4 m (VHF). The first pulse–modulated radar, Redut (in production RUS–2), was adopted by the Red Army in 1940. It was bistatic as well, though with a shorter baseline (up to 1000 m). It provided not only aircraft detection (as CW radars) but range and angle coordinate measurement. First Soviet aircraft VHF radars (1.5 m wavelength) were introduced in 1943.
- In the fall of 1934, the German company GEMA [of Hans Erich Hollmann (born in 1899 in Solingen, Germany)¹⁷⁴⁾¹⁷⁵⁾ and his partner Hans–Karl von Willisen] built the first commercial radar system for detecting ships. Operating in the 50 cm wavelength range, it could detect ships up to 10 km away. In the summer of 1935, a pulse–modulated radar was developed with which they could spot the ship, the Königsberg, 8 km away, with an accuracy of up to 50 m. The same system could also detect an aircraft at 500 m altitude at a distance of 28 km.
- In 1935, the British physicist Robert A. Watson–Watt (1892–1973) successfully demonstrated the detection of an aircraft by a radio device, during the so–called Daventry Experiment. An order for full scale development of radar was issued later that year, after it was realized that sound locators (which at the time were the only means of detecting inbound bombers) could not provide adequate reaction time. This was the starting point of the world’s first operative radar network, called “Chain Home” or CH in short. The Chain Home became operational in 1937, well before the war broke out. Bombers could be detected at ranges of 150 km and more. Sir Watson Watt is often being addressed as the ‘father’ and ‘inventor’ of radar, the latter of which must now be debated. He was elected a Fellow of the Royal Society in 1941 and Knighted in 1942 for his role in the development of radar.
- Also in 1935, a French ship was equipped with a collision avoidance device of local fabrication. A landbased device, the “barrage electronique” was tested in 1936 and found application in the early days of World War II.
- By 1939, the following countries had more or less rudimentary, but operational radars in their inventories: Britain, France, Germany, Hungary, Italy, Japan, the Netherlands, Russia, Switzerland, and the USA. To some extent the technology behind these devices can be described in terms of today’s buzzwords, such as continuous wave Doppler, conical scan, bistatic, and spread spectrum radars.
- On Dec. 7, 1941, radar missed a chance to significantly change history. There was a first system deployed on a hill on the Pacific island of Hawaii, close to Pearl Harbor. The opera-

173) V. S. Chernyak, I. Y. Immoreev, B. M. Vovshin, “Radar in Soviet Union and Russia – A Brief Historical Outline,” International Radar Symposium (IRS 2003), Dresden, Germany, Sept. 30 – Oct. 2, 2003

174) In 1935, H. E. Hollmann wrote the first comprehensive two–volume books on microwaves entitled: “Physik und Technik der ultrakurzen Wellen,” (Physics and Technique of Ultrashort Waves), published in Berlin, 1936. Hollmann is considered as one of the “Fathers of Modern Radar and Microwave Technology.”

175) <http://www.radarworld.org/hollmann.html>

tors actually detected the Japanese attack squadrons and reported their observation, but none of their superiors believed them because they were deemed unexperienced.¹⁷⁶⁾ Had the reports been acted upon, then the whole attack could have been turned into a failure.

- During the war, higher and higher frequencies of the electromagnetic spectrum were put to use. Researchers started with the first experiments at some 10 MHz, the Chain Home operated around 20 MHz (with later extensions up to 70 MHz), and the bulk of air surveillance and tracking radars worked between 200–800 MHz. The cavity magnetron transmitter device was invented by A. W. Hull of the General Electric Co. in 1921,¹⁷⁷⁾ no practical use was found for it at that time (the practical and efficient magnetron tube gathered world interest only after Kinjiro Okabe proposed the divided anode – type magnetron in 1928). In 1939/40 the British physicists John T. Randall and Henry A. H. Boot invented the resonant – cavity magnetron; the new technology represented a significant breakthrough. This new efficient high – power (10 kW) multi – cavity pulsed magnetron (oscillator), referred to as H2S¹⁷⁸⁾ and invented/developed at the University of Birmingham, became quickly the heart of the American H2S bombing radar which operated at 3 GHz (10 cm wavelength).¹⁷⁹⁾ 180) In September 1940 the British military decided to share its radar technology with the United States. The Americans moved quickly and opened the Radiation Laboratory at MIT under the leadership of Lee DuBridge. – The H2S plan position indicator (PPI) screen showed a map of the underlying terrain with a resolution that was hitherto unheard of. This type of magnetron wasn't known in Germany, and 3 GHz was far beyond the frequency range of Germany's intercept and warning devices. – But then in the spring of 1943, an American bomber was shot down near Rotterdam and the H2S radar with its magnetron was a big surprise for the German military. Significant effort went into repair, study and reproduction of the device, but only a few examples became operational by the end of 1944.
- At the end of the war, most of today's technologies had already been put to use, although they relied on contemporary technical means. There was a chirp radar in production, the monopulse principle was invented and even a Synthetic Aperture Radar (SAR) already existed. The Chain Home was used to detect the V2 rockets after they left their launch sites, hence it can also be called the world's first Anti Ballistic Missile (ABM) radar system. Among the few ideas which were born later than 1945 are the phased array antenna technology and the concept of multistatic radar.
- The radar technology was kept highly secret throughout World War II, and only in 1946 was it published that an American device had successfully measured the distance to the moon, which is a round trip of some 770,000 km. Much later it became known that a Hungarian device had already done the same measurement in 1944.
- Most early radar applications involved simply echo measurements of a pulsed signal that bounced back from a target to the receiver. By the end of WW – II, radar was able to pick up the placement of naval shells being fired from ships, and gave the navy the ability to correct their fire.

176) Note: Other sources state that the blips were misinterpreted as a weather front or an American squadron.

177) A. W. Hull, "The effect of a uniform magnetic field on the motion of electrons between coaxial cylinders," *Phys. Rev.*, Vol. 18, p. 31, Jan. 1921.

178) Note: The acronym H2S (or H₂S) stands for Hydrogen Sulfide (meaning Stink bombs!)

179) H. A. H. Boot, J. T. Randall, "The cavity magnetron," *IEEE Proceedings, Radiolocation Conference*, 1946, p. 928.

180) H. A. H. Boot, J. T. Randall, "Historical Notes on the Cavity Magnetron," *IEEE Transactions on Electron Devices*, Vol. ED – 23, No. 7, pp. 724 – 729, July, 1976

1.4.3.1 SAR (Synthetic Aperture Radar) concepts

Active microwave instruments (providing their own illumination) of the type SLAR (Side-Looking Airborne Radar), **RAR** (Real Aperture Radar)¹⁸¹⁾, and **SAR** (Synthetic Aperture Radar) were developed and flown. In the SAR imaging scheme, a microwave signal at known frequency is sent out from a SAR transmitter on a platform located above the target zone. That signal travels through the atmosphere, reflects off a target (generally the surface of the Earth), and returns back to the receiving antenna (receiver). The resultant signal is measured as a combination of phase and amplitude data that, after processing, form a single-look complex radar image of the ground surface (the information content of a radar system originates at the target and requires interpretation). Originally discovered in the 1950s, SAR uses high-range resolution waveforms and synthetic aperture techniques to produce images of objects. Rather than depending on a large physical (real) aperture, a SAR forms a large virtual aperture in the processor when operating on an ensemble of received signals. In this way, an antenna only about 10 m in length on the S/C leads to image resolutions comparable to those of very large real antennas (several km in length). First radar systems for range measurements (tracking of aircraft, ships, etc.) were developed during World War II.

In the USA, the first RAR instrument, developed initially for military use in the early 1960s, became available for civilian use in 1965 with the airborne instrument **AN/APQ-97**, developed by the Westinghouse Corp. (Baltimore, MD). The multi-polarized Ka-band (35 GHz) RAR provided imagery with a resolution of 7.5 m in cross-track (range resolution) and 1.1 R m along-track (azimuth resolution), where R is the range (distance in km) from the radar instrument to the target. Thus, at a range of 10 km, the airborne RAR instrument produced imagery with a resolution of 7.5 m x 11 m. The AN/APQ-97 instrument is the best-known dual-polarized side-looking RAR imaging radar. In this radar, image data seen through the like-polarized and the cross-polarized channels were recorded directly onto photographic film. Hence, extensive, unclassified SLAR coverage of the United States was acquired under the NASA radar program.^{182) 183)}

Aperture synthesis is a processing technique of generating high spatial resolution imagery by dividing the collection area of an antenna [(in the microwave region), or of a telescope (in the optical region)] into smaller subapertures spread out in a pattern covering several baselines. An active microwave antenna is restricted to wavelength ranges in which reasonable intensities of radiation must be generated and transmitted by the remote sensing device in order to obtain a measurable return echo radiation. Conceptually, each SAR instrument is by definition an aperture synthesis device. A real (but relatively long) SAR antenna system, pointed into the cross-track direction of a flight path, **is synthesized through the motion of the antenna relative to the target** with either the antenna, or the target, or both moving. A synthesized antenna can be thought of as a number of independently radiating elements (i.e., the real aperture), whose separation is established by the pulse repetition frequency (PRF) and the platform velocity. The change of the phase with respect to time is the Doppler angular frequency. The azimuth resolution is determined by the Doppler bandwidth of the received signal. – In LEO spaceborne SAR missions or with aircraft-mounted SAR antennas, this relative motion to the target area is provided simply by the forward mo-

181) Note: RAR systems are usually much simpler than SAR systems in design and data processing. RAR-pulse-modulated signals, based on the range-Doppler principle, are not required to be coherent (only the signal amplitude information is recovered and processed), representing and displaying backscatter characteristics from the surface sweep.

182) K. Raney, "On Dual-Polarized SARs and the Stokes Parameters," Proceedings of EUSAR 2006, Dresden, Germany, May 16-18, 2006

183) Note: The side-viewing orientation from spacecraft of conventional flat antenna screens turned out to be the most simple and efficient way to obtain a well-defined observation swath. Conventional imaging SARs use a series of pulses instead of a continuous signal. Each transmitted wave front hits the target surface at near range and sweeps across the swath to far range. Successive sweeps are produced to form a continuous observation coverage in the long-track direction. The pulse bandwidth determines the cross-track or range resolution. The echos are sensed coherently.

tion of each system in its flight path. The signal (echo) received by the antenna is processed coherently over an integration time. The synthesized antenna length is given by the trajectory traversed by the antenna relative to the target during the coherent integration time.

An active microwave antenna system measures not only the **intensity** (phase and amplitude) of received radiation, but also:

- The time taken for the emitted pulse of radiation to travel from the satellite to the ground and back. Conceptually, in a pulsed–modulated radar system, the radar platform is assumed to be stationary during the transmission and reception of a pulse.
- The Doppler shift in the frequency of the radiation echo as a result of **relative motion** of the satellite orbit with respect to the target area
- The polarization of the radiation (note: polarization can also be measured by passive devices)
- The nature of the information content of an observation in the microwave region differs from that in the visible and infrared region (optical region) of the electromagnetic spectrum. Scattering in the optical region depends very much on the molecular properties of the surface layer of the vegetation or soil, while microwave scattering depends on the largescale surface roughness (roughness in the cm range) and volume scattering (e.g. within a forest canopy).

The range resolution (in the direction normal to flight path)¹⁸⁴⁾ of a pulse–modulated radar system is limited fundamentally by the bandwidth of the transmitted pulse (the wider the bandwidth, the better the range resolution). A wide bandwidth can be achieved by a short duration pulse. However, the shorter the pulse, the lower the transmitted energy (for a fixed–peak power limitation), and the poorer the SNR, resulting in a lower radiometric resolution.

The azimuth resolution (oriented into the flight direction) of a real aperture radar system is a function of the antenna length (the larger the antenna, the better the azimuth resolution). It can be shown that a spaceborne real aperture radar, giving a useful azimuth resolution for points on the Earth’s surface, would require an impractically large antenna. Aperture synthesis, therefore, offers a means of greatly improving the azimuth resolution.

The first ever Earth–orbiting civilian spaceborne imaging radar instrument (SAR) was flown on SeaSat (NASA/JPL, L–band SAR, launch June 27, 1978, see D.52).^{185) 186) 187)} Unfortunately, SeaSat suffered a malfunction 106 days later (ending the mission abruptly); still, during its brief life, SeaSat, conred to be the first oceanography mission, collected more information about the oceans than had been acquired in the previous 100 years of shipboard research. It pioneered satellite oceanography and proved the viability of imaging radar for studying our planet. The SAR instrument provided a wealth of information on such diverse ocean phenomena as surface waves, internal waves, currents, upwelling, shoals, sea ice, wind, and rainfall (first global view of ocean circulation).

Beyond the oceans, SeaSat’s synthetic aperture radar instrument provided spectacular images of Earth’s land surfaces. The antenna of the planar antenna array (passive microstrip based array type) had a size of 11 m x 1.2 m. LMSS (Lockheed Missiles and Space Systems), of Sunnyvale, CA, was the prime contractor of the mission. The SAR instrument provided an analog source data stream of 20 MHz requiring a special downlink and ground station design (implemented by JHU/APL). The received radar echoes were downlinked in S–

184) <http://envisat.esa.int/instruments/asar/descr/concept.html>

185) S. W. McCandless, Jr. “The Origin, Evolution and Legacy of SeaSat,” IEEE/IGARSS 2003, Toulouse, France, July 21–25, 2003

186) F. Monaldo, “Seasat Sees the Winds with SAR,” IEEE/IGARSS 2003, Toulouse, France, July 21–25, 2003

187) W. Alpers, “Ocean Surface Wave Imaging from Seasat to Envisat,” IEEE/IGARSS 2003, Toulouse, France, July 21–25, 2003

band (analog data link at 2.265 GHz) to a total of five ground receiving stations in real-time (no onboard high-rate recording capability was possible at the time) located at: Goldstone, CA, Fairbanks, AK, Merrit Island, FL, Shoe Cove, Newfoundland (provided by CCRS), and Oakhanger, UK (provided by ESA).

A side-looking spaceborne RAR instrument with the name of RLSBO was first flown on the Cosmos-1500 satellite (launch Sept. 28, 1983), later also on the Okean series of the former Soviet Union (launch of Okean-O1-1, July 5, 1988).

The standard or conventional architecture of a spaceborne SAR instrument features a SAR antenna (analogous to a telescope of an optical instrument), mounted in a side-looking configuration (see O.8.2 and Glossary) and tilted at a look angle, usually between 15–60°, into the swath. As the platform moves in its orbit, a continuous strip of swath width is mapped in the along-track direction of the satellite ground path.

SAR instruments provide high-resolution imagery (typically 1–30 m spatial resolution) of selected polarization and frequency in the microwave region (typical wavelengths from a few cm to about 1m). The active SAR observation technique is transparent to cloud coverage and rain, and does not need any sun illumination.

Sensor Name	Sensor Provider	Introduction	Microwave Band
E-SLAR	DFVLR (DLR), Germany	1976	X-band
NIT	IKI RAN, Soviet Union	early 1980s	Ku-band
SLAR (part of MSS)	SSC, Sweden	1985	X-band
R-SLAR	RRL (CRL), Japan	1986	X-band
HUTSLAR	HUT, Finland	1988	X-band
SLAR	TNO/NLR, The Netherlands		X-band

Table 18: Some early SLAR (Side-Looking Airborne Radar) instruments

Some background on early SAR developments: The earliest statement that Doppler frequency analysis could be used to obtain fine cross-range resolution is attributed to Carl Wiley (USA) of the Goodyear Aircraft Corporation in June 1951. Wiley observed that a one-to-one correspondence exists between the along-track coordinate of a reflecting object (being linearly traversed by a radar beam) and the instantaneous Doppler shift of the signal reflected to the radar by that object. – In 1953, the Doppler-frequency technique was studied by the US Army in the Project Wolverine at the University of Michigan, resulting in an Army project to further develop the range-Doppler radar principle (the **pulsed Doppler radar** is an example of an extension of the basic pulsed radar system). Part of the program was to develop a practical data processor which could accept wideband signals and carry out the required Doppler-frequency analysis at each resolvable range interval.

A group at the Willow Run Laboratories at the University of Michigan (ERIM since 1973) was assigned the problem of developing an optical computer for the purpose. – In the summer of 1957, the Willow Run researchers constructed an X-band radar and built an optical computer. The first fully focused SAR map was produced in August 1957. Soon afterwards, the Willow Run group, in cooperation with Texas Instruments, constructed the first demonstration system, AN/UPD-1, on Army request. Five radar systems were built and various demonstration flights on aircraft were conducted in early 1961. ^{188) 189) 190)}

The first fielded phased-array radar, called ESAR (Electronically Scanned Array Radar), was designed by MIT/LL and built by Bendix Corp., completed in 1960 for the DoD. ESAR

188) D. A. Ausherman, A. Kozma, J. L. Walker, H. M. Jones, E. C. Poggio, “Developments in Radar Imaging,” IEEE Transactions on Aerospace and Electronic Systems, Vol. AES-20, No 4, July 1984, pp. 363–400

189) W. M. Brown, L. J. Porcello, “An introduction to synthetic-aperture radar,” IEEE Spectrum, Vol. 6, No 9, Sept. 1969, pp. 52–60

190) C. A. Wiley, “Synthetic Aperture Radars – A Paradigm for Technology Evolution,” IEEE Transactions on Aerospace and Electronic Systems, AES Vol. 21, 1885, pp. 440–443

had IF analog phase shifters and an IF beamformer. This beamforming technique was bulky and required good temperature control. ¹⁹¹⁾

On the civilian side, a three-wavelength SAR instrument was developed and flown by NASA on the Apollo-17 lunar mission (launch Dec. 7, 1972, moon landing on Dec. 11, return to Earth on Dec. 19, 1972). The objectives of ALSE (Apollo Lunar Sounder Experiment) were to detect subsurface geologic structures (“sounding”), to generate a continuous lunar profile, and to image the moon at radar wavelengths. The ALSE instrument, aboard the Apollo-17 CSM (Command and Service Module), operated at the wavelengths of 60 m, 20 m, and 2 m (corresponding to 5, 15, and 150 MHz). The instrument consisted of two distinct coherent radar subsystems, one operating at two frequencies in the HF-band and the second at a single VHF frequency. The combined HF/VHF radar had a mass of 49 kg and required 103 W of power. The radar data were recorded on 70 mm photographic film (optical recorder – CRT film type) in a conventional SAR format, and returned to Earth for processing. The HF-1 system (5 MHz) was capable of the deepest exploration. The HF-2 system (15 MHz) was operated simultaneously with the HF-1 system to provide partial overlap in the depth of exploration, trading off for improved resolution. The VHF system (150 MHz) was designed for shallow sounding and for surface imaging. All three frequencies were capable of surface profiling. Separate transmit/receive antenna systems were provided for the HF and VHF ranges. The returned data were optically processed and provided good profiles of the lunar surface/subsurface. ¹⁹²⁾

The first high-quality images (from a ground-based instrument) of near-Earth space objects were obtained in the early 1970s with ALCOR (ARPA, Lincoln Laboratory, C-band, Observables Radar). The data of ALCOR were processed by Lincoln Laboratory of MIT (MIT/LL) and Syracuse Research Corporation. Successful results were made possible by the range resolution of 50 cm, by the coherent recording, and by sufficient sensitivity to image low-altitude satellites. In the late 1970s, LRIR (Long-Range Imaging Radar), an X-band instrument, was an ALCOR successor system, built at MIT/LL. The objective: imaging of satellites at geosynchronous range. In particular, significant image processing developments were achieved with LRIR such as ECP (Extended Coherent Processing).

NASA/JPL started its coherent radar test program in 1968, resulting in the development of an airborne L-band SAR instrument, flown on the CV-990 aircraft of NASA/ARC since 1971. ¹⁹³⁾ The objective was to observe ocean surface patterns and to study the relationships between the image and the surface effects by using synthetic aperture techniques. The L-band SAR (1.215 GHz, bandwidth of 10 MHz) featured a **phased array antenna** with HH and HV polarization. This airborne instrument was a predecessor to the L-band SAR on SeaSat. – Star-1 (of Intera, Canada, developed by ERIM) was another early civilian airborne SAR instrument in 1983.

Mission	Launch Date	Spatial Resolution (m)	Swath Width (km)	Freq. GHz (Band)	Polarization	Look Angle	Data Rate Mbit/s	Altitude, Inclina. (km, °)	Instrument, Remarks
SeaSat	27.6.78	25	100	1.28 (L)	HH	20°	110	800, 108°	SAR
SIR-A	12.11.81	40	50	1.28 (L)	HH	47°	N/A	260, 38°	SAR, Shuttle
SIR-B	5.10.84	25	30	1.28 (L)	HH	15-60°	34	225, 57°	SAR, Shuttle
Kosmos 1870	25.7.87	25-30	20-35	3.125(S)	HH	25-60°		270, 72°	EKOR
Almaz-1	31.3.91	13-20	2 x 172	3.125(S)	HH	25-60°	100	350, 72°	EKOR-A
ERS-1	17.7.91	30	100	5.3 (C)	VV	23°	105	785, 98.5°	AMI, 3 modes

191) A. J. Fenn, D. H. Temme, W. P. Delaney, W. E. Courtney, “The Development of Phased-Array Radar Technology,” Lincoln Laboratory Journal, Vol. 12, No 2, 2000, pp. 321–340; see also URL: www.ll.mit.edu/news/journal/pdf/vol12_no2/12_2devphasedarray.pdf

192) L. J. Porcello, et al., “The Apollo lunar sounder radar system,” Proceedings of the IEEE, June 1974, pp. 768–783

193) W. E. Brown, C. Elachi, T. W. Thomson, “Radar Imaging of Ocean Surface Patterns,” Journal of Geophysical Research, Vol. 81, No 15, May 20, 1976, pp. 2657–2667

Mission	Launch Date	Spatial Resolution (m)	Swath Width (km)	Freq. GHz (Band)	Polarization	Look Angle	Data Rate Mbit/s	Altitude, Inclina. (km, °)	Instrument, Remarks
JERS-1	11.2.92	18	75	1.27 (L)	HH	35.21°	60	568, 97°	SAR
ERS-2	21.4.94	30	100	5.3 (C)	VV	23°	105	785, 98.5°	AMI, 3 modes
SIR-C/X-SAR	9.4.94 30.9.94	15-25	30-100	1.28, (L) 5.3, (C) 9.6 (X)	VV,HH VV,HH HH	15-55°	46/Ch.	225, 57°	L-SAR, Scan X-SAR, Scan X-SAR, Scan
RADAR-SAT-1	4.11.95	25-100 (12x9)	100-170	5.3 (C)	HH	20-60°	110	800, 98.6°	SAR, Scan-SAR
Priroda	23.4.96	50	50	1.28, (L) 3.28 (S)	HH, VV	35°	16	400, 52°	SAR Travers
SRTM (NASA)	11. - 22. 2. 2000	30 30	225 50	5.3 (C) 9.6 (X)	VV,HH HH	45° 52°	180 90	225, 57°	C-RADAR X-RADAR Interferometry
Envisat (ESA)	1.3. 2002	<30	100	5.33 (C)	Polarimetric	15-45°	100	800, 98.5°	ASAR, ScanSAR
ALOS (JAXA)	24.01. 2006	10	70	1.27 (L)	HH or VV	9-60°	240	700, 98°	PALSAR, ScanSAR
SAR-Lupe (5 S/C)	19.12.20 06	<1 -5	5.5 x 5.5 60 x 8	9.6 (X)					SAR (spotlight and stripmap)
TerraSAR-X	15.06.20 07	1 - 6	15 - 30 (100 km)	9.6 (X)	Polarimetric	20-60°	300	515, 97.44°	TSX-SAR
COSMO-SkyMed	2007-10	1, 3-15, 30, 100	10, 40 100-200	9.6 (X)	HH, VV,	20-60°	2 x 150	620	SAR-2000
RADAR-SAT-2	14.12.20 07	3-100	10 - 500	5.3 (C)	Polarimetric	10-50°	105	800, 98.6°	SAR, Scan-SAR
TecSAR (israel)	21.01.20 08	<1 - 20	100 km	9.59 (X)	Polarimetric	20-45°		550; 41°	XSAR
RISAT-2 (ISRO)	20.04.20 09	<1 - 20	100 km	9.59 (X)	Polarimetric	20-45°	620	550; 41°	XSAR
TanDEM-X	21.06.20 10	1 - 6	15 - 30 (100 km)	9.6 (X)	Polarimetric	20-60°	300	515, 97.44°	TSX-SAR
RISAT-1 (ISRO)	26.04.20 12	3-50	10-240	5.3 (C)	multi-polariz.			609, 98°	SAR, Scan-SAR, spotlight
HJ-1C (CNSA)	18.11.20 12	20	100	3.13 (S)	HH or VV	25-47°	2 x 160	500, 97.3°	
KOMP-SAT-5 (Korea)	22.08.20 13	1-20	5-100	9.6 (X)	HH,H V, VH, VV	20-55°	310	550, 97.6°	COSI
Sentinel-1 (ESA)	03.04.20 14	5-100	20-400	5.3 (C)	HH,H V, VH, VV	20-45°	600	693, 98.18°	C-SAR
ALOS-2 (JAXA)	24.05.20 14	3-100	25-350	1.256 (C)	single, full	8-70°	800	628, 97.9°	ePALSAR
PAZ (Spain)	2014	1-6	15 - 30 (100 km)	9.6 (X)	Polarimetric	15-60°	300	515, 97.44°	PAZ-SAR
NovaSAR (SSTL)	2015	6-30	15-20 100, 750	3.2 (S)	HH, VV	16-34 48-73	500	580	S-SAR
RCM (Canada)	2016-18	5-50 m	20-350	5.4 (C)	HH, or HH,VV			593; 97.74°	SAR

Table 19: Chronological survey of spaceborne imaging radars (SAR instruments)

- Tilting capability of a SAR antenna. The SIR-B Shuttle mission (launch: Oct. 5, 1984) provided for the first time the ability to mechanically tilt the antenna over a range (15° – 55°) so that radar imagery from multiple angles of incidence could be obtained.
- First onboard recording of high-rate SAR data. The USSR missions Kosmos-1870 (launch July 25, 1987) and Almaz-1 (launch March 31, 1991) were the first to record and

dump SAR data during station passes, followed by JERS-1 (launch Feb. 11, 1992).¹⁹⁴ JERS-1 is regarded the first long-term mission which provided an onboard SAR-recording capability for its user community on a regular basis. This enabled extended observations beyond the limits of available ground stations. JERS-1 is also the first S/C carrying two types of imaging instruments, namely a microwave imager (SAR) and an optical imager (OPS).

- Until 1978, SAR images were formed using analog techniques, incorporating optical lenses and photographic film (initially, over 95% of the SeaSat data was processed in a survey mode using optical laser techniques). – Also in 1978, the first reconstruction of a SAR image was formed on a digital computer (a slow process at the time with the available computer power, but good quality imagery was generated with this technique). This SAR processor was developed by MDA (MacDonald Dettwiler and Associates Ltd.) of Richmond, BC, Canada, for the purpose to manage SeaSat SAR data. These early digital SAR processors required all the processing power available of a system; they were installed on main-frame computers or on large dedicated hardware. – On the other hand, today's SAR images (since the late 1990s) can be formed on relatively inexpensive equipment like a workstation or a PC.¹⁹⁵ ¹⁹⁶

Figure 11 demonstrates the concept behind optical SAR processing that was the original method employed until the 1980s. At that time, the signal film was used for recording the history in the first stage, light from the CRT (Cathode Ray Tube), was used as an input for the processor. The reconstructed SAR image is recorded on another film.¹⁹⁷

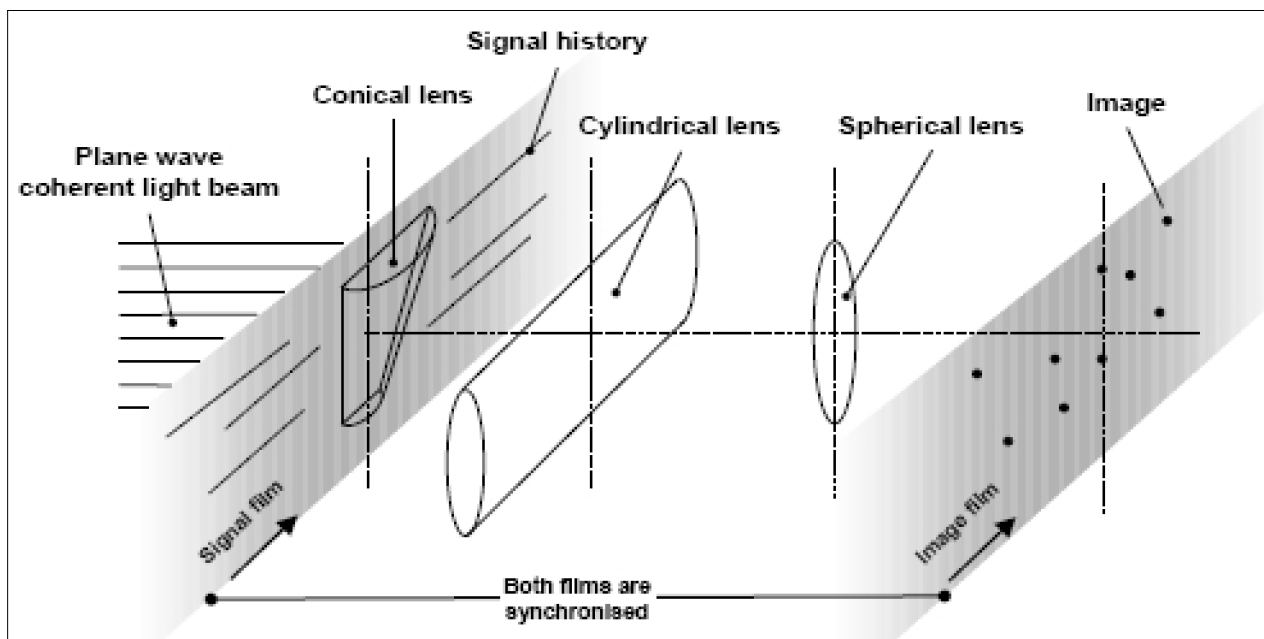


Figure 11: Original optical SAR processing concept (image credit: INO, MDA)

- 194) Note: The two Shuttle imaging radars, SIR-A and SIR-B, had recorders, but data was collected only for select sites due to the short mission duration of one week each.
- 195) J. R. Bennett, I. G. Cumming, R. A. Deane, "The Digital Processing of SeaSat Synthetic Aperture Radar Data," Proceedings of the IEEE International Radar Conference, pp. 168–174, 1980.
- 196) Note: The SeaSat SAR analog radar echo data were downlinked in S-band (analog data link at 2.265 GHz) and recorded at the receiving stations on film using a cathode ray tube. The data were then processed to pictures using analog Fourier Optical techniques in what is known as an "Optical SAR Processor." – SAR echo data is effectively a microwave hologram of the illuminated area, so by recording this data on film, optical processing becomes the natural approach to forming an image of the ground.
- 197) Alain Bergeron, Michel Doucet, Bernd Harnisch, Martin Suess, "Satellite On-Board Real-Time SAR Processor Prototype," ICSSO 2010 (International Conference on Space Optics), Rhodes Island, Greece, Oct. 4–8, 2010, URL: http://congrex.nl/ICSSO/Papers/Session%2014a/FCXNL-10A02-1977297-1-BERGERON_ICSSO_PAPER%20.pdf

Hybrid solution of SAR data processing in the 21st century. ¹⁹⁸⁾ For the future, SAR processing technology may come full circle. Important breakthroughs in acousto–optic and piezoelectric modulators, and very large format image collection planes make it possible to consider designs using the benefits of compact, power efficient, fast optical computers. Considering the continuing improvements of both the digital and optical technologies, it is not unreasonable to expect that a high performance onboard SAR processor, capable of providing a direct–downlink compressed data stream to operational users, will become a reality within the next decade.

In 2010, the availability of high resolution spatial light modulators (SLM) gives to the optronic processor advantages, such as reprogrammability, that were not available when photographic film was used as the recording medium. An SLM is basically a two–dimensional transmissive electronically addressable display on which images or data can be imaged. The SLMs are used as input devices for the SAR raw data (Ref. 197).

- A limitation and drawback in the analysis of SAR data ¹⁹⁹⁾ from conventional (single–frequency or single wavelength) SAR instruments is of course the availability of data at only one frequency (or single wavelength) with a fixed polarization. It means that only one component of the total surface scattering matrix is being measured, while any additional information contained within the reflected radar signal is being lost.

Instrument – Agency	Frequencies/Band (GHz)	Polarizations	Comment
AIRSAR – NASA/JPL	0.45/(P), 1.26/(L), 5.31/(C)	H, V, full polarimetric	since 1987
TOPSAR – NASA/JPL	5.288/(C)	VV	AIRSAR configuration
CARABAS – FOA Sweden	20–90 MHz UWB, (VHF center frequency)	H	foliage/ground penetration
CASSAR – CAS/ISRA China	9.375/(X)	HH, VV, HV, VH,	
C/X–SAR – CCRS Canada	5.3/(C) 9.25/(X)	C–band polarimetric X–band V or H	C–band interferometry
DCS, ERIM	9.66/(X) 14.96/(Ku)	full polarimetric VV only	SAR single–pass interferometer
DO–SAR (Dornier, Germany)	3.2/(S) 5.3/(C) 9.6/(X) 35/(Ka)	VV, VH, HH, HV VV, VH, HH, HV VV, VH, HH, HV VV	polarimetric
DRA–SAR – DRA/UK	5.7/(C) 9.65/(X)	full HH	
EMISAR – EMI/TUD Denmark	5.3/(C) 1.4/(L)	full, polarimetric full, polarimetric	since 1993 since 1994
E–SAR – DLR, Germany	1.3/(L) 5.3/(C) 9.6/(X) 0.450/(P)	full polarimetric VV or HH V or H full polarimetric	E–SAR since 1989 added in 1994
FOLPEN – SRI, CA	100–500 MHz/(VHF/UHF)	HH	foliage/ground penetration
IFSARE, ERIM	9.5 (X)	HH	interferometric mapping SAR
INGARA, Australia	9.375 (X)	HH	
MMW–SAR – MIT	33.56/(Ka)	V, H, full polarimetric	
NASAR (NASDA/EORC)	1.291 (L–band)	full polarimetric	operation starting in fall 1996
NEC–SAR – NEC Jap.	9.53/(X)	HH	Interferometric mode

198) http://southport.jpl.nasa.gov/reports/iwgsar/4_SAR_Data_Processors.html

199) H. A. Zebker, J. J. Van Zyl, “Imaging radar polarimetry: a review.” Proceedings of the IEEE, Vol. 79, 1991, pp. 1581–1606.

Instrument – Agency	Frequencies/Band (GHz)	Polarizations	Comment
P-3/SAR – ERIM, Navy	0.350/(UWB) 1.25/(L) 5.30/(C) 9.35/(X)	VV, VH, HH, HV VV, VH, HH, HV VV, VH, HH, HV VV, VH, HH, HV	UBW added in 1994 existing, polarimetric
PHARUS – TNO – FEL Delft, The Netherlands	5.25/(C)	full, polarimetric	
PI-SAR, CRL, NAS-DA	9.55 (X), 1.27 (L)	full polarimetric in X,L Interferometric in X	since 1996, initially also called CLR-SAR
SAR Travers – Vega, Moscow	3.0/(S)	VV or HH	
SASAR U. of Cape Town, South Africa	5.3/(C), 0.141 (VHF)	VV or HH	under construction, July 1996 first flight
RAMSES – ONERA France	1.6/(L), 3.0/(S), 6.2/(C) 9.5/(X), 14.5/(Ku), 35/(Ka) 95/(W)	VV, HH, VH, HV full polarimetric	
STAR-1,2 – INTERA	9.375/(X)	HH	since 1983
IMARC – Vega Moscow	118 MHz/(VHF) 0.44/(L), 1.28/(L), 7.7/(X)	HH, VV, HV, VH full polarimetric	
Sandia SAR (SNL)	14.850 (Ku)	VV	
IFSAR (SNL)	15 (Ku)		interferometric

Table 20: Overview of some early airborne SAR systems

- SAR observations from ocean surfaces (see Ref. 7479). Initial applications of ocean surface SAR observations were already reported in 1980. Ocean backscatter has increasing sensitivity with increasing frequency, particularly in the relation of backscatter to wind speed. In general, C-band is preferred over L-band for most SAR ocean applications. In terms of power, lower-frequency SARs have lower power requirements. For a given signal-to-noise ratio, for example, L-band is easier to accommodate on a satellite than C- or X-bands. Next, ocean backscatter falls off rapidly with increasing viewing angle as compared with backscatter from other surfaces. This results in a comparatively narrow range of viable SAR viewing angles over which the ocean produces backscatter sufficiently above a reasonable noise floor to be detected as signal. Thus, simply increasing the swath width by viewing at higher angles is not feasible for ocean sensing unless the orbital altitude is raised. On the positive side, however, viewing at angles beyond this narrow range improves the detection of ships and icebergs, because the ocean clutter becomes significantly lower than the target returns. ²⁰⁰⁾
- Introduction of multifrequency SAR instruments. On the airborne side multifrequency SAR instruments/observations were introduced with AIRSAR (C, L, and P-band) of JPL in 1987. AIRSAR was also the first SAR instrument that introduced the concept of quadrature polarization (or full polarization). ²⁰¹⁾ The Russian IMARC SAR instrument used two frequencies (X and VHF-band) since 1990, three frequencies (X, VHF, and P-band) were available since 1993, and four frequencies (X, VHF, P, and L-band) since 1994. More information of other instruments is given in Table 20. – Spaceborne multifrequency SAR instruments (L, C, and X-band) were introduced with the two SIR-C/X-SAR Shuttle mission in April and October of 1994. The SIR-C/X-SAR missions featured in addition to multifrequency (3) the polarimetric observation capability (meaning the availability of full scattering matrix) to extent the data analysis into such fields as geology, hydrology, ecology, oceanography and other applications.
- **ScanSAR** refers to a radar imaging technique permitting extended observation coverage (e.g. wider swath). In ScanSAR mode, the scene size in range is extended by scanning

200) C. Elachi, "Spaceborne imaging radar: Geologic and oceanographic applications," *Science*, Vol. 209, No 4461, Sept. 5, 1980, pp. 1073–1082

201) J. J. van Zyl, H. A. Zwebker, C. Elachi, "Imaging radar polarization signatures – Theory and observation," *Radio Science*, (ISSN 0048–6604), Vol. 22, July–Aug. 1987, pp. 529–543

the antenna in elevation and alternating illumination of several subswaths. Like in stripmap SAR, the scene extension in azimuth is principally only determined by the length of the observation period. The ScanSAR mode requires rapid electronic steering of the elevation beam pattern of the antenna (phased array antenna with analog beamforming).^{202) 203)} The principle of ScanSAR is to share radar operational time between two or more separate subswaths in such a way, as to obtain full image coverage of each. However, scanning in elevation implies that the synthetic aperture length is reduced to the burst length (the burst length or burst duration is defined as the time interval for each target illumination in a ScanSAR cross-track sequence). A consequence of the shorter burst length (as compared to stripmap SAR) is that each target has a different Doppler history (depending on its azimuth position) resulting in a reduced ScanSAR azimuth resolution. The basic differences between ScanSAR and stripmap SAR processing are:

- The azimuth consists of several bursts, each of them corresponding to a fraction of the full synthetic aperture
- The azimuth resolution is limited by the burst duration and is no longer determined by the synthetic aperture length
- The Doppler history of each target within a burst has a different frequency offset depending on its azimuth location
- The azimuth multilook technique is constrained more by the scanning strategy than by the processing strategy
- The radiometric correction due to the azimuth antenna pattern is much more critical than in stripmap SAR since each target is illuminated by different parts of the azimuth antenna diagram
- For SAR data processing, an additional mosaic operation is needed in azimuth and range directions to join the azimuth bursts and the range subswaths, respectively.

The ScanSAR technique was initially developed by JPL and first flown on two Shuttle missions with the SIR-C/X-SAR payload in 1994, SRL-1 (STS-59, April 9 – 20, 1994) and SRL-2 (STS-68, Sept. 30 – Oct. 11, 1994). Further implementations of ScanSAR are on RADARSAT-1 (Canada, launch Nov. 4, 1995), SRTM/C-RADAR (NASA/JPL, launch Feb. 11–22, 2000), Envisat/ASAR (ESA, launch Mar. 1 2002), and ALOS/PALSAR (Japan, launch Jan. 24, 2006). Until RADARSAT-1, the maximum swath width of any previously orbiting SAR instrument had been 100 km, a parameter tightly constrained by the need to: a) “fill the aperture” and b) receive all the returned energy between transmitter pulses. RADARSAT-1 achieved with ScanSAR swaths up to 510 km with 100 m resolution, from an 800 km orbit, through the use of multiple electronically steered antenna beams and carefully synchronized transmitter pulse timing.

The advantage of wider ScanSAR observation coverage is crucial in obtaining global repeat SAR imagery in several days, eventually on a daily basis (enhanced sampling capability) irrespective of cloudcover or sunlight conditions. [The narrow-swath high-resolution (< 10 m) SAR imagery yields exciting periodic snapshot views of the 2-D ocean surface to study a number of applications (interactions with the atmosphere, long waves, and current)]. The wide-swath ScanSAR capability of RADARSAT (up to 510 km), Envisat (up to 400 km) and ALOS (up to 350 km) permit for the first time the study of larger-scale phenomena (mesoscale wind fields and circulation features, atmospheric boundary-layer processes,

202) J. Mittermayer, A. Moreira, “A Generic Formulation of the Extended Chirp Scaling Algorithm (ECS) for Phase Preserving ScanSAR and Spot SAR Processing,” Proceedings of the IEEE IGARSS 2000 Conference, Honolulu, HI, July 24–28, 2000

203) A. Moreira, J. Mittermayer, R. Scheiber, “Extended Chirp Scaling Algorithm for Air- and Spaceborne SAR Data Processing in Stripmap and ScanSAR Imaging Modes,” IEEE Transactions on Geoscience and Remote Sensing, Vol. 34, No. 5, Sept. 1996, pp. 1123–1136

study of storm dynamics, etc.), thus providing a better monitoring capability that may eventually lead to operational SAR missions. The potential of SAR imagery wind–field monitoring alone is much higher than is possible with spaceborne scatterometers. A future operational SAR mission service can of course also provide several other services for land surface monitoring besides ocean surface monitoring, such as monitoring of natural hazards in a wide variety of applications: flooding, earthquakes, wildfires, severe weather events, etc. (204) 205) 206) 207) 208) 209) 210) 211)

- In **SpotSAR** (or spotlight) mode (see O.8.3 for definition of SAR imaging modes), the antenna is steered in the azimuth direction (usually with electronic beam–steering capability). During the formation of the synthetic aperture, the antenna is constantly looking into the scene center direction. The available synthetic aperture is in this case much longer than in stripmap mode and is denoted by spotlight aperture. The long spotlight aperture provides azimuth signals with a large Doppler bandwidth and therefore provides a high geometric resolution in azimuth. The operation in spotlight mode allows for improved azimuth resolution by decreasing the ground speed. This has to be paid with along track gaps between consecutive scenes.

- Phased array microwave technology of SAR antennas (see also O.8.4). The observation requirements of wide swaths for global coverage led eventually to the introduction of a new scanning concept referred to as ‘phased array technology,’ making use of electronic beam steering in the elevation domain (the use of electronic scanning allows flexibility in beam pointing and beam shape control for swath coverage). Naturally, the technology requires a lot of computer power to handle such complex radar functions as: beam switching, signal detection, frequency management, ranging, etc. The technique was first tested on active sensors (SARs) in the microwave region of the spectrum and later on laser radars. The SAR instrument of SeaSat (launch June 27, 1978) pioneered the phased array / beam–pointing method for spaceborne instruments (see chapter 1.4.3.3).²¹²⁾

Other instruments with phased array technology followed or are being planned, such as: PR on TRMM (launch Nov. 27, 1997), C–RADAR on SRTM (launch Feb. 11–22, 2000), ASAR on Envisat (launch Mar. 1, 2002), and PALSAR on ALOS (launch Jan. 24, 2006). The following instruments are operational on the airborne side: FOLPEN (SRI International), PHARUS (TNO), CRL–SAR (CRL), and Sandia SAR (SNL). In the 1990s the phased array has become a key component in the design of advanced antenna systems, taking advantage of the considerable advances in microelectronics, transmitter/receiver architectures, miniaturized device (module) integration methods, and signal processing techniques.

Phased arrays are random–access devices (active antennas) whose basic architecture consists of two building blocks, namely radiating elements and a beamforming network. They

204) K. B. Katsaros, et al., “Wind Fields from SAR: Could They Improve Our Understanding of Storm Dynamics?” JHU/APL Technical Digest, Vol. 21, No. 1, 2000, pp. 86–93

205) S. Wu, A. Liu, et al., “Ocean Feature Monitoring with Wide Swath Synthetic Aperture Radar,” JHU/APL Technical Digest, Vol. 21, No. 1, 2000, pp. 122–129

206) G. S. Young, “SAR Signatures of the Marine Atmospheric Boundary Layer: Implications for Numerical Forecasting,” JHU/APL Technical Digest, Vol. 21, No. 1, 2000, pp. 27–32

207) R. C. Beal, “Toward an International Storm Watch Using Wide Swath SAR,” JHU/APL Technical Digest, Vol. 21, No. 1, 2000, pp. 12–20

208) B. Holt, J. Hilland, “Rapid–Repeat SAR Imaging of the Ocean Surface: Are Daily Observations Possible?” JHU/APL Technical Digest, Vol. 21, No. 1, 2000, pp. 162–169

209) J. Horstmann, S. Lehner, W. Koch, R. Tonboe., “Computation of Wind Vectors over the Ocean Using Spaceborne Synthetic Aperture Radar,” JHU/APL Technical Digest, Vol. 21, No. 1, 2000, pp. 100–107

210) J. Schulz–Stellenfleth, S. Lehner, J. Horstmann, R. Bamler, “Global wind and ocean wave measurements using reprocessed ERS–2 wave mode data,” Proceedings of CEOS Workshop, Tokyo, Apr. 2–5, 2001, CEOS–SAR01–027

211) J. Horstmann, W. Koch, S. Lehner, R. Tonboe, R. Bamler, “High Resolution Wind Fields Retrieved from RADAR–SAT–1 ScanSAR,” Proceedings of CEOS Workshop, Tokyo, April 2–5, 2001, CEOS–SAR01–041

212) Note: JHU/APL was instrumental in developing the phased array radar technology for the US Navy whose construction began in 1959. A first prototype was installed on a Navy ship in 1961. See: A. Kossiakoff, “APL – Expanding the Limits,” Johns Hopkins APL Technical Digest, Vol. 13, No. 1, 1992, pp. 8–27

are employed for electronic beam–steering applications in the microwave and/or optical regions of the spectrum (see Glossary). The phased array antenna concept offers several striking performance advantages over other concepts (like conventional horn antennas).

- The most fundamental advantage of sampling the wavefront with nearly omnidirectional antenna elements is that it allows multi–beam operation at wide angle separation and with full sensitivity
- This opens up the possibility to run several independent observational programs simultaneously (multi–target tracking and imaging), each with full aperture sensitivity. The independent beam agility is important when the radar has multiple functions to be performed simultaneously.
- The benefits of random–access and rapid beam–pointing with no moving parts have made phased arrays the technology of choice. Sub–array units provide the capability of re-configuration.
- Phased arrays can be used for spatial power combining techniques that are considered to be very effective for generating high power microwaves and millimeter–waves
- Phased antenna arrays find increasingly wider application in mobile communications; the concepts of spatial signal processing and of space–division multiple access (SDMA) based upon the utilization of antenna arrays are introduced and extensively used.
- **Multi–beam systems:** Systems that operate with multiple beams in parallel require the operation with separate signal paths for multiple beams or multiple phase centers. These systems already have been realized on single instruments like on SRTM with the two antennas for across–track interferometry and TerraSAR–X with the DRA (Dual Receive Antenna) implemented. A further extension is the TanDEM–X mission acquiring signals of up to four phase centres in parallel within a close formation.
- **Digital chirp generator.** The radar chirp concept of pulse frequency modulation was developed at the Bell Telephone Laboratories (at Whippany and Murray Hill, NJ) by J. R. Klauder et al. in the 1950s and first reported in the literature in 1960 (declassification of work supported by the US military). Early experimental work on radar signal design used the chirp, a linearly frequency–modulated (FM) pulse with a frequency range set by the required angular resolution, and with a pulse duration set for the required range resolution performance. By transmitting a modulated pulse, it was possible to obtain range resolutions that were smaller than the transmitted pulse length by very large factors. The reported technique employed the so–called “pulse compression technique” (covering a frequency range many times the inherent bandwidth of the envelope), permitting radars to transmit a pulse with about 100 times the energy of a short pulse with equivalent range resolution and peak power. The cost of the chirp radar technique is that the pulse compression processing in the receiver section is numerically intensive.^{213) 214)}

Modern spaceborne SAR instruments are equipped with a **digital chirp generator**; this technique allows to generate pulses with a programmable slope and bandwidth. The resulting flexibility in terms of pulse duration and frequency–tuning capability allows the operation of the SAR system in different modes like a high–resolution narrow–swath mode, and a wide–swath low–resolution mode. Also, within one mode of operation, it is useful to adjust the chirp bandwidth according to the incidence angle in order to maintain a more constant ground–range resolution and a more homogeneous signal–to–noise ratio over the access region (the number of independent looks within a cell can be increased by modulating the chirp over the bandwidth). This method is used for example in the ASAR instru-

213) J. R. Klauder, A. C. Price, S. Darlington, W. J. Albersheim, “The Theory and Design of Chirp Radars,” *The Bell System Technical Journal*, Vol. 39, No 4, July 1960, pp. 745–808

214) The term “chirp” was coined at the Bell Telephone Laboratories in the 1950s to designate a new and more effective radar signal generation method.

ment of Envisat for the global monitoring and the wide-swath mode with its 5 different swaths. The chirp waveform (linear FM) is also used for better onboard processing of the radar signals including compression schemes. ^{215) 216)}

- SAR instrument design constraints. General well-known major design constraints of spaceborne SAR missions are the antenna size and the availability of SAR instrument power. Both factors limit the swath/resolution ratio, a key performance criteria. The lack of continuous sufficient transmission power is usually handled with the introduction of a so-called **duty cycle**, representing the fraction of the orbital period (i.e. instrument observation time), in which a power-hungry instrument can be operated. Some examples: ESA introduced duty cycles for the AMI instrument of its ERS-1/2 missions (10%–12%) and for ASAR (30%) of the Envisat mission (launch Mar. 1, 2002). The SAR instrument of RADARSAT-1 (launch Nov. 4, 1995) of CSA has a duty cycle of up to 28%. The PALSAR instrument of JAXA's (Japan Aerospace Exploration Agency, formerly NASDA) ALOS (launch Jan. 24, 2006) features a duty cycle of about 70%.
- Some design considerations of conventional (planar array) SAR antennas. SAR antennas, like those of RadarSat-1, and -2, of ASAR (on Envisat), or of PALSAR (on ALOS), are rather heavy and bulky elements of a SAR instrument, their mass is in the range of 500–800 kg (representing about 90% of the total instrument mass). A typical size for a spaceborne L-band SAR antenna is 10 m x 2 m. Hence, the antenna design will remain a key technological challenge in SAR systems. Naturally, the features of large mass and volume translate directly into launch costs; hence, they are important design drivers, restricting the available choices for the satellite and its launcher. ^{217) 218) 219)} At the start of the 21st century, there are some emerging alternatives on the horizon offering large light-weight deployable antenna designs using membrane technology in combination with the inflatable structure technology. Both can serve as the basis for large antenna applications on spacecraft.

SAR Mission (launch)	System description	Antenna mass (approx. value)	SAR instrument electronics mass (kg)
SeaSat (1978)	L-band (passive microstrip based arrays)	103 kg	120 kg
SIR-A (1981)	L-band (passive microstrip based arrays)	181 kg	136 kg
SIR-B (1984)	L-band (passive microstrip based arrays)	190 kg	
ERS-1 (1991)	C-band	325.8 kg (total)	AMI shared with SCAT
JERS (1992)	L-band	130 kg	90 kg
SIR-C/X-SAR (1994) shuttle payload	L/C-band, distributed phased array X-band, using a conventional waveguide array antenna (12 m x 0.4 m)	3300 kg 50 kg	450 kg (4 radar channels)
Radarsat-1 (1995)	C-band, electronic beam steering	680 kg	240 kg
Envisat (2002)	C-band, electronic beam steering	832 kg (total ASAR mass)	
ALOS (2006)	L-band, electronic beam steering	500 kg	100 kg
TerraSAR-X (2007)	X-band, electronic beam steering	394 kg (total TSX-SAR instrument mass)	
Radarsat-2 (2007)	C-band, electronic beam steering	850 kg (total SAR instrument mass)	
TecSAR (2008)	X-band, electronic beam steering	100 kg (total SAR instrument mass)	

- 215) M. Suess, C. Schaefer, R. Zahn, "Discussion of the Introduction of Onboard SAR Data Processing in Spaceborne Instruments," Proceedings of IEEE/IGARSS 2000, Honolulu, HI, July 24–28, 2000
- 216) Note: "Chirping" a signal or a wave means stretching it in time. In chirped pulse amplification, the first step is to produce a short pulse and stretch it. The stretched pulse has low intensity, allowing it to be amplified again; thus, boosting the peak intensity. A "chirped pulse" is frequency modulated.
- 217) SAR System Technology, NASA/JPL (1995), <http://southport.jpl.nasa.gov/nrc/chapter7.html>
- 218) P. Wood, G. Seguin, "SAR Antenna for a Small Satellite," CEOS SAR Workshop 2001, Tokyo, Japan, April 2–5, 2001, CEOS-SAR01-012
- 219) A. Baylis, M. M. Gavrilovic, R. Girard, D. Kefallinos, Guy Séguin, "Progress in Large Membrane Antennas for SAR Applications," Proceedings of EUSAR 2004, Ulm, Germany, May 25–27, 2004

SAR Mission (launch)	System description	Antenna mass (approx. value)	SAR instrument electronics mass (kg)
RISAT-2 (2009)	X-band, electronic beam steering	100 kg (total SAR instrument mass)	
TanDEM-X (2010)	X-band, electronic beam steering	394 kg (total TDX-SAR instrument mass)	
RISAT-1 (2012)	C-band, electronic beam steering	850 kg (total SAR instrument mass)	
Sentinel-1 (2014)	C-band, electronic beam steering	800 kg, antenna size of 12.3 m x 0.84 m	

Table 21: Overview of approximate masses of some spaceborne imaging radar systems

- SAR data archive. ESA operates and maintains a long-term and continuous archive of spaceborne SAR data from every continent (since 1991). It is probably the largest civilian SAR data archive in the world. This archive represents a unique source of reference imagery and can for instance be used to generate interferograms to identify and locate damage in the wake of a disaster.
- **Introduction of spaceborne SAR reflector antenna designs (curved apertures).** These antenna designs are relatively new in SAR observations compared to conventional flat panel antennas (also referred to as planar arrays) with electronic beam steering. Reflector antennas can provide observation support in the conventional support modes of: Stripmap, Spotlight and ScanSAR. Use of reflector antennas is seen in such applications as: surface mapping, rain radar, [soil moisture and ocean salinity radiometers], hazards monitoring, etc. Possible scanning technologies for such reflector designs are: a) spin-scanned reflector, b) spin-scanned feed, or c) pushbroom. The large reflector designs are generally of the deployable type; the conventional mechanical designs feature mostly a surface mesh (or dish) structure, while future inflatable structures may select the lighter membrane structure. The smoothness of the deployed reflector surface and its accuracy to required shape are of considerable importance in these antenna designs for high-quality observation performance.²²⁰⁾

Some SAR reflector antenna implementations are:

- The Condor-E commercial SAR mission, under construction at NPO Machinostroyenia (Reutov, Moscow region, with a planned launch in 2004), employs an antenna design concept using a large space-deployed **SAR reflector antenna** (parabolic configuration of 6 m diameter) with a cross-track pointing capability (see also chapter B.1 and Figure 284 for Condor-E).²²¹⁾ The parabolic reflector antenna is mounted in the along-track direction of the S/C with an antenna look direction toward nadir. The reflector antenna configuration permits the SAR observing pattern to be dynamically redirected in the cross-track direction (the ground target observation capability is symmetrical to either side of the spacecraft). The concept employs a central electronically steerable phased array feed system at the focal point of the antenna (including a master oscillator and phase modulator linked to the S/C), using the antenna reflector to direct the outgoing radar signals and measuring the incoming echo (both signal streams, forward and return, are being reflected by the antenna; the antenna itself is only partially illuminated). Thus, a FOR (Field of Regard) within the incidence-angle range of 20–55° to either side of the spacecraft ground path may be observed. [Note: A sidelobe suppression problem might arise within this elegant SAR reflection configuration due to the curvature of the parabolic antenna].
- A similar large-diameter parabolic reflector (SAR antenna) design concept is also being employed on the US DoD Lacrosse/Onyx satellite series (X-band radar imaging reconnaissance program of NRO; manufacturer of spacecraft: Lockheed Martin). The prototype program and spacecraft of the series, referred to as Indigo, was launched in January 1982 (built by Martin Marietta Company). The first operational satellite, Lacrosse-1, was

220) C. G. M. van 't Klooster, "On Space-based Synthetic Aperture Radar Antennas," Proceedings of EUSAR 2008, 7th European Conference on Synthetic Aperture Radar, June 2–5, 2008, Friedrichshafen, Germany

221) Note: In 2003, the realization of project Condor-E became questionable.

launched Dec. 2, 1988 from Shuttle flight STS–27. Lacrosse–2 was launched from VAFB on March 8, 1991; the launch of Lacrosse–3 took place on Oct. 24, 1997. while Lacrosse–4 was launched on a Titan–4 vehicle from VAFB on Aug. 17, 2000 into a 680 km orbit at 68° inclination. Generally, two Lacrosse missions are kept operational for high–resolution SAR image recovery. The classified nature of the military program doesn't permit any specifics. ²²²⁾

- The Cassini–Huygens deep space mission to Saturn and its moons, a joint venture of ESA, NASA/JPL, and ASI (Italian Space Agency), launch Oct. 15, 1997, employs a single high–gain 4 m diameter parabolic Cassegrain reflector. The radar instrument (five–beam Ku–band antenna feed assembly, 13.78 GHz) can operate in three ways: imaging, altimetry, and radiometry. ²²³⁾ The Huygens probe of ESA landed on Titan, a moon of Saturn, on Jan. 14, 2005.
- The USSR SAR missions Venera–15 (launch June 2, 1983) ²²⁴⁾ and Venera–16 (launch June 7, 1983) were flown to Venus with the objective to study the surface properties of the planet. Both S/C were identical, each carried an S–band SAR instrument with a parabolic dish antenna of 6 m diameter, permitting observations to either side of the ground track.. In SAR mode, the antenna transmitted a code sequence of 127 pulses, each of duration 1.54 μ s. After transmission, the antenna was switched to the receiver, which recorded the reflection of the radar pulses from the surface over a period of 3.9 ms.
- The satellite constellation SAR–Lupe, a German military mission with a spacecraft and SAR instrument design of OHB Bremen (launch of first S/C in constellation of 5 on Dec. 19, 2006, launch of SAR–Lupe–5 on July 22, 2008), features also a parabolic SAR reflector antenna of 3 m diameter. The fixed parabolic SAR antenna (used either for SAR observations or for RF communications of payload data) is integrated into the S/C design in such a fashion as to permit agile maneuvers of each satellite. This in turn implies a large FOR coverage capability into either the right or left cross–track direction for event observations (an important mission objective). Within this FOR, the spotlight (5 km x 5 km) or the stripmap (8 km x 60 km) observation modes can be conducted freely. In spotlight mode, the entire spacecraft (with a fixed antenna) is rotated to increase the integration time of the scene (increase of resolution in flight direction).
- The TecSAR mission of Israel (MOD, IAI/MBT, launch Jan. 21, 2008) features a paraboloid mesh antenna with electronic beam steering (antenna dish system) which permits greatly increased viewing capabilities from the spacecraft.
- At the start of the 21st century, the SAR technology can provide measurements that are key to the following applications:
 - Water cycle (e.g. soil moisture and water level)
 - Global ecosystem (biomass estimation, land cover change)
 - Ocean circulation and ice motion
 - InSAR techniques can provide very accurate and systematic measurements of surface deformation and surface strain accumulation due to seismic and volcanic activity.

²²²⁾ Note: The US imaging radar reconnaissance program assumed various code names during the past two decades. It was first known as Indigo, then Lacrosse, and most recently as Vega. The name Onyx is associated with Lacrosse–4

²²³⁾ <http://saturn.jpl.nasa.gov/spacecraft/instruments–cassini–radar.cfm>

²²⁴⁾ <http://www.solarviews.com/eng/venera16.htm>

1.4.3.2 Radar (microwave) instrument classes in Earth observation

Radar systems for SAR applications may be classified by the signal measurement technique employed – there is the **pulse–modulated radar** class and the **FMCW** (Frequency Modulated Continuous Wave) radar class, the latter is also referred to as **FM–CW** or **LFM–CW** (Linear Frequency Modulated – Continuous Wave). Each of these classes employs different principles with respect to the signal measurement technique. In a pulse–modulated radar system, the radar platform is considered to be stationary during the signal run time (transmission and reception of a pulse sequence). This stop–and–go approximation is valid because pulse–modulated radar systems employ very short pulses (the phase of the reflected signal changes).

On the other hand, FMCW radars transmit relatively long sweeps (the frequency spread is typically made by means of a linear sweep of a signal having constant amplitude); the stop–and–go approximation may not be valid. Hence, the additional phase change due to the platform motion must be accounted for. Pulse–modulated radars measure range in the time domain; FMCW radars measure range in the frequency domain. For both measurement techniques (pulse–modulated and FMCW radar) the generation of SAR images requires the coherent combination of the echoes recorded. The orbital movement of the SAR platform with a certain constant speed introduces a Doppler effect, which is implicitly exploited in enhancing the image resolution in the direction of the movement.

- The pulse–modulated radar is the most widely used type of monostatic radar systems. It is so called because the transmitter sends out pulses of microwave energy with relatively long intervals (listening periods) between pulses. The actual pulse duration (pulse width) in the energy transmission sequence is in the order of ns to ms. The receiver picks up the echoes of the returned signals; the elapsed time (or run time) is a measure of the distance travelled. Basic characteristics of pulse–modulated systems are:

- The peak power is generally many times greater than the average power
- The range resolution of a pulsed radar system is limited fundamentally by the bandwidth of the transmitted pulse (the wider the bandwidth, the better the range resolution).

- The CW (Continuous Wave) radar system transmits continuous microwave energy at a known frequency. The return signals from the target area are shifted away from this base frequency via the Doppler effect. By measuring this change of the Doppler Shift, caused by motion of the transmitter, target or both, the speed of the object can be determined. However, this measurement configuration requires a separate receiving antenna in addition to the transmission antenna (i.e. bistatic), otherwise there is no basis for the measurement of the time delay (the resultant continuous echo cannot be associated with a specific part of the transmitted signal) in this arrangement. A disadvantage of conventional CW systems is that they cannot measure range (distance).

More recent and more sophisticated **FMCW** instrument designs, known as: 1) **LFM** (Linear Frequency–Modulated), and 2) **FSK** (Frequency Shift Keying) CW waveform radar, are also able to measure **range** (and of course the range rate). The range measurement is being done by tagging each part of the transmitted microwave signal (by continuously changing the frequency), rendering it recognizable upon reception. With the rate of frequency change known, the difference in frequency can be interpreted as a range measurement. **Both configurations, CW and FMCW, are by nature bistatic systems**, see chapter 1.4.3.6.

At the start of the 21st century, the capabilities of an emerging FMCW SAR imaging technology experience a new interest by the Earth observation community; the technique has the following advantages as compared to the classical pulse–modulated waveform procedure:

- A considerably lower transmission power can be used due to the better efficiency of the continuous wave concept (the peak power is the same as the average power). The FMCW method can provide peak performance in both accuracy and sensitivity

- A higher bandwidth of the microwave signal can be used – resulting in a better reflection separation and a reduction of noise
- A smaller antenna size can be used for the same measuring range geometry
- The FMCW technology results in simpler and more compact (cost effective) instrument designs
- Lower data rates (resulting in smaller data volumes) are inherent with the use of the FMCW technique.

The state-of-the-art FMCW radar technology experiences already an introductory or operational status in such fields as ground-based industrial precision measurement applications (level gauge), multi-mode automotive radar sensors [ACC (Adaptive Cruise Control)], obstacle detection and warning systems in civil aviation, etc. In Earth observation, first FMCW SAR imaging instruments are being developed for airborne technology demonstrations.²²⁵⁾ Ground-based FMCW instruments are being used in meteorological applications such as cloud radar systems and in boundary layer research (ultra-fine-resolution vertical profiling of clear-air turbulence).^{226) 227) 228)}

On the spaceborne side, the Japanese (JAXA) lunar mission SELENE (SELenological and ENgineering Explorer, launch Sept. 14, 2007) carries **LRS** (Lunar Radar Sounder), an FMCW radar in HF-band with a transmission power of 800 W, the PRF is linearly swept from 4–6 MHz in 200 μ s. The objective is to monitor subsurface structures (stratification and tectonic features) of the moon. Penetration depths of several km are anticipated.

1.4.3.3 Electronic beam steering

Electronic beam steering is a technique that applies the radar signal with a different phase shift to different parts (elements or panels) of the antenna. In this approach the SAR antenna design consists of several separate radiating parts. The method requires to apply the correct relative phase shift to each element and to maintain synchronization. This action causes the beam to point into the desired direction (the choice of the phase difference between two radiators defines the direction in which the phase front will propagate). Naturally, the antenna elements have to send a signal in that direction as well as to obtain the return information (echoes).

The conventional technique of electronic beam steering (or electronic scanning) with analog (i.e. RF) beamforming technology is based on the constructive/destructive interference concept (by stimulating individual elements or groups of elements within the array). The electromagnetic energy received at a point in space from two or more closely spaced radiating elements is a maximum when the energy from each radiating element arrives at a point in phase. Positioning the antenna beam to a specific angle off the antenna boresight axis is accomplished by applying a **phase shift to the specific set of array elements** which shift the angle of constructive interference.

The method of electronic beam steering of a phased array SAR antenna permits for some current operational systems the extension of the swath width with the use of the ScanSAR technique (instantaneous positioning of the radar beam), an important criteria in global coverage requirements. In particular, increased operational flexibility and functionality of

225) J. J. M. de Wit, P. Hoogeboom, "Performance Analysis of a High Resolution Airborne FM-CW Synthetic Aperture Radar," International Radar Symposium (IRS 2003), Dresden, Germany, Sept. 30 – Oct. 2, 2003

226) A. Meta, P. Hoogeboom, "Time analysis and processing of FM-CW SAR signals," International Radar Symposium (IRS 2003), Sept. 30 – Oct. 2, 2003

227) R. Mende, M. Behrens, M. – M. Meinecke, A. Bartels, T. – B. To, "The UMRR – S: A High-Performance 24 GHz Multi Mode Automotive Radar Sensor for Comfort and Safety Applications," IRS 2003, Sept. 30 – Oct. 2, 2003

228) K. Yamamoto, K. Yamada, N. Yonemoto, H. Yasui, et al., "94 GHz FMCW Radar for Obstacle Detection," International Radar Symposium (IRS 2003), Dresden, Germany, Sept. 30 – Oct. 2, 2003

the SAR instrument is provided in multi-mode operations support and in multi-target tracking capabilities.

Several techniques exist to apply the phase shift to the signal.

1) Time delay scanning. By making the feed line to a certain antenna element longer or shorter, a time delay and thus a phase delay is introduced. This is mostly obtained by switching line sections in and out of the feed line, using diodes or using MEMS (Micro Electro Mechanical Switches).

- Use of time delay to achieve the desired phase relationship
- Time delay networks installed in front of each radiating element
- Expensive, complex and heavy

2) Frequency scanning. By designing the feed lines to each of the radiating elements all with a different length, the phase shift to each element will change as the frequency of the signal that is sent is changed, for the line lengths are fixed but the wavelength changes.

- Simpler method
- The physical length of the wave guide is utilized to delay the frequency interval
- Vary the frequency about a base frequency. The receiver has to demodulate with the varying carrier frequency, that is the reason why the method is seldom used.

3) Phase scanning. By changing the properties of the medium in which the signal propagates, a phase shift can be obtained. This is mostly done by changing the permittivity (ϵ) or the permeability (μ) of the medium. This changes the speed and the wavelength of the propagating wave in the medium and thus the phase at the end of the line.

- The radiating elements are fed by phase-shifting networks (phasers)
- The phasers are adjustable over a range of 0 to 2π radians
- More expensive than frequency scanning but cheaper than time delay
- The method is widely used.

Some spaceborne examples of system implementations with electronic beam steering are given. However, these systems provide **analog beamforming** (i.e. RF beam forming) which limits their beam steering capability to 1-D applications (see 1.4.3.8).

– Two Shuttle missions with the SIR-C/X-SAR payload in 1994, namely SRL-1 (STS-59, April 9 – 20, 1994) and SRL-2 (STS-68, Sept. 30 – Oct. 11, 1994), demonstrated phased arrays with electronic beam steering. The distributed C- and L-band SIR-C radars of JPL allowed electronic beam steering in range direction (elevation plane) permitting the acquisition of multi-incidence angle data.

– The SAR instrument of RADARSAT-1 of CSA (launch Nov 4, 1995) employs an electronically steerable active remote sensing radar antenna. A slotted waveguide array (and not a phased array) of 15 m x 1.5 m is used as the active microwave sensor. The azimuth beam pattern is fixed but the elevation angle of the main beam can be varied (the SAR instrument has seven beam modes to obtain different incidence angles from 10–60°) by the use of 32 variable phase shifters. Because the ferrite phase shifters are not reciprocal, they have to switch back and forth each time the antenna is switched between transmit and receive mode.

– ASAR (Advanced SAR) on Envisat of ESA (launch March 1, 2002) is an active phased array of size 1.3 m x 10 m with distributed T/R (transmit/receive) modules arranged across

the antenna, such that by adjusting individual module phase and gain, the transmit and receive beams may be steered and configured (independent control of the phase and amplitude of the transmitted radiators from different regions of the antenna surface). The antenna array contains 20 tiles (each 1 m x 0.65 m in size) with 16 T/R modules each. Use of MMIC (Monolithic Microwave Integrated Circuit) technology, based on field effect transistors (FETs), for amplifiers, switches, attenuators, and phase shifters. ASAR also provides independent weighting of the received signal to each of these regions. Support of 37 different and mutually exclusive high-rate operating modes. In general, the use of digital technologies for signal generation and processing is implemented. These permit chirp versatility in terms of pulse duration and bandwidth required for the operational modes and various swaths of the instrument. Electronic beam steering is in elevation only, a phase-scanning implementation allowing observations at different incidence angles and alternating polarization modes providing simultaneous dual-polarized images.

– Background: Although the concept of spaceborne **phased array technology** was initially demonstrated on the SeaSat SAR instrument of NASA/JPL (launch June 27, 1978), it took a while before the concept of electronic beam steering found more applications in the 1990s. The early spaceborne SAR instruments such as SAR on SeaSat, or the AMI instruments on ESA's ERS-1/2 missions, employed a conventional passive phased array antenna. On the other hand, an active phased array antenna design employs T/R modules to steer the beam in one direction (in elevation), thereby performing cross-track scanning. Active phased array technology is also being introduced in the communication satellite industry as well as in general communication downlinks from spacecraft. Examples: The Iridium constellation of nominally 66 satellites (Iridium Satellite LLC) was deployed (completed) in 1998. Each S/C carries three phased array panels. These allow each satellite to produce 48 fixed downlink beams. The EO-1 mission of NASA (launch Nov. 21, 2000) is flying XPAA (X-band Phased Array Antenna) as a communications experiment with the objective to demonstrate link-pointing capability with the use of a body-fixed low-mass and low-cost phased array antenna (see M.12).

The following advantages of electronic beam steering are expected, in particular for future spaceborne phased array systems, namely with the introduction of **digital beamforming (DBF) techniques** permitting instantaneous two-dimensional beam steering in elevation as well as in azimuth settings: ²²⁹⁾

- Electronic beam steering permits an antenna beam stabilization to compensate for roll and yaw angles of the platform. In addition, it enables true spotlight mode support to image a confined target area in high resolution, from varying aspect angles, and permits operation of different tasks in multiplex.
- Partitioning of the phased array antenna into multiple receiving subgroups in along-track substantially improves moving-target detection and estimation of motion and position parameters in the scene by exploiting the phase differences extracted from the different subgroups.
- Connecting the channels to antennas or subapertures in cross-track permits to extract height information of the imaged area using interferometric techniques. In contrast to conventional digital maps which show the height of the ground, this new method includes analysis of height information of vegetation canopy as well as of man-made structures/targets. In fact, the high-accuracy height measurement potential will eventually permit the detection of objects their mere elevation over ground level.
- Adaptive interference suppression. Steps against signal jamming can be taken by means of spatial jammer suppression. The distorted part of the SAR image is drastically reduced.

²²⁹⁾ http://www.fhr.fgan.de/fhr/el/el_rsrch_sar00_e.html

- For each pixel the polarimetric scattering matrix can be measured by assigning the channels to different transmit/receive polarizations. Hence, separation of target and clutter can be improved and target structures in SAR imaging can be supported.
- Real-time and near-real-time event recognition and subsequent event tracking in SAR scenes are rather desirable goals for spaceborne SAR systems, in parallel to conventional SAR imaging functions. These features are of importance in general surveying (monitoring of fires, volcanoes, floods, etc.) and in surveillance [MTI (Moving Target Indication)] applications. These operational support goals require in particular a high degree of onboard system processing capability and flexibility.

1.4.3.4 SAR interferometry (InSAR techniques in the microwave region)

Interferometric Synthetic Aperture Radar (IFSAR or InSAR) refers to active microwave fringe visibility phase measurements which are being used for moderate resolution imaging, polarimetry, and elevation mapping of planetary surfaces. Radar interferometers operate by independently detecting signals from two antennas (or from a single antenna in a repeat pass configuration) and combining them a posteriori for indirect fringe generation. This method involves heterodyne receivers which experience shot noise from their local oscillators – about 1 photon per Hz of bandwidth. However, this noise level is acceptable at microwave wavelengths.

- SAR interferometry (see also O.9.1). Two interferometric observation concepts are in use: ‘**single-pass**’ and ‘**two-pass**’ (or multi-pass) interferometry. The InSAR principle relies on phase differences between repeat radar images and provides measurements of surface deformation in the satellite line-of-sight direction with sensitivities of a small fraction of the radar wavelength (sub cm level). The interferometric phase (or phase of the interferogram), i.e. the phase difference between the two images acquired with slightly different sensor positions, contains geometric information allowing the derivation of the 3-D position of the scattering element. The phase difference can be exploited to provide topographic height information, as well as changes on the Earth’s surface at cm scales. SAR interferometry techniques promise to produce global topography maps in a similar fashion as stereo photogrammetry. The InSAR technique is well suited to studying deformation associated with all phases of the seismic cycle, volcanic activity, and glacier flow. ^{230) 231) 232)}
 - Simultaneous observation of the same footprint by two antennas in parallel (single-pass cross-track interferometry) separated at a distance (baseline) on the same spacecraft. Two separate images are received of the same ground track by two spatially-separated antenna systems (the interferometric baseline) to produce phase differences from slightly different viewing angles. DCS (Data Collection System of ERIM) is probably the first single-pass airborne InSAR instrument with first flights in 1987. TOPSAR (JPL) started its observations in 1991.

On the spaceborne side, the SRTM (Shuttle Radar Topography Mission, J.27) mission of NASA represents worldwide the **first fixed baseline single-pass spaceborne InSAR** (Interferometric SAR) system with simultaneous dual-polarization wide-swath scanning SAR and dual-frequency (C-band and X-band) coverage (Shuttle mission STS-99, Feb. 11–22, 2000). SRTM featured a fixed cross-track baseline which was achieved with separate receive antennas (X- and C-band) mounted on the tip of a 60 m long boom. The SRTM digital topographic map production objective (referred to as C-RADAR) calls for a

- 230) S. N. Madsen, H. A. Zebker, “Imaging Radar Interferometry” (pp. 359–380), Chapter 6 in “Principles and Applications of Imaging Radar,” (F. Henderson and A. J. Lewis, eds.), Manual of Remote Sensing, 3rd Edition, Volume 2 (R.A. Ryerson, ed-in-chief), John Wiley & Sons, 1998
- 231) R. Burgmann, P. A. Rosen, E. J. Fielding, “Synthetic aperture radar interferometry to measure Earth’s surface topography and its deformation,” Annual Review of Earth and Planetary Sciences, Vol. 28, pp. 169–209, 2000.
- 232) M. Simons, “Constraints on Crustal Deformation from Imaging Geodesy,” Proceedings of the Weikko A. Heiskanen Symposium in Geodesy, Ohio State University, Columbus, OH, USA, Oct. 1–4, 2002

spatial pixel (30 m x 30 m) posting with a 16 m absolute vertical linear accuracy and 20 m absolute horizontal radial accuracy at 90%. High-quality DEM mosaics of entire continents have been generated with the SRTM data from the JPL C-band radar and the DLR/ASI X-band radar, both systems operated in parallel. ²³³⁾

- Two-pass (multi-pass) measurements of a single-antenna SAR platform. **The measurement of ground deformations from space** (a historic perspective on two-pass SAR interferometry). Spaceborne SAR instruments can indeed detect barely perceptible movements of the Earth's surface (after analysis and comparison of the data). In the 1990s, the value of SAR imagery experienced a considerable boost with the correct processing and interpretation of the **phase and amplitude information** in the SAR data. Superimposing SAR imagery obtained from different epoches (possibly from nearly identical observation positions of a single satellite) of the same surface area results in the ability to detect very small (centimeter-scale) movement of land surface features on the Earth (slipping faults, surging glaciers, bulging volcanos, etc.). In general, the single-antenna SAR repeat-pass technique is limited to observations to regions of low vegetation cover due to surface changes (such as vegetation growth) between passes. In addition, differences in atmospheric water vapor between passes may cause errors in the elevation models.

Some early examples of the technique of “repeat-pass interferometry” are:

- In 1974, L. C. Graham of Goodyear Aerospace ²³⁴⁾ first demonstrated that it was possible to take advantage of the phase measured by an airborne radar (he took phase measurements and the conventional amplitude measurements of SAR images). He was the first to report experiments to determine terrain elevation of the Earth's surface by repeat-pass interferometry.

- In the early 1980s, scientists at NASA/JPL showed that they could extract similar results from the phase measured by SeaSat, the first civilian radar satellite, which was launched in 1978 (but worked for only three months). They did so by comparing two radar images taken from roughly the same position but at different times. **In a sense, that exercise was akin to taking two widely separated frames of time-lapse photography.** Although the phase itself appeared random every time, the phase differences between corresponding pixels in the two radar images produced a relatively straightforward interference pattern. ²³⁵⁾

- **Derivation of the first interferometric maps of the co-seismic displacement of the 1992 Landers earthquake.** Didier Massonnet of CNES and his colleagues produced a striking image of ground displacements caused by the magnitude 7.3 Landers earthquake, which struck south-eastern California (about 150 km east of Los Angeles) on 28 June 1992. For their demonstration, they assembled all the radar images of the area available from the ERS-1 satellite and formed several interferograms by combining one image taken before the earthquake with another one taken afterward from approximately the same position. ²³⁶⁾ ²³⁷⁾ Because the satellite tracks were never identical, the rugged relief in the region affected these interferograms markedly. Yet with the help of a digitized map of elevations, they were able to calculate the topographic contribution and remove it. Doing so unveiled a tantalizingly rich picture of interference fringes. But were these colored bands truly showing what the earthquake had done to the surface of California's Mojave Desert? – Massonnet and his colleagues tested their representation of tiny ground movements by calculating an idealized interferogram based on measurements that geologists had made for the motion

233) <http://www.jpl.nasa.gov/srtm/>

234) L. C. Graham, “Synthetic interferometer radar for topographic mapping,” *Proceedings of IEEE*, Vol. 62 (6), 1974, pp.763–768

235) A. K. Gabriel, R. M. Goldstein and H. A. Zebker, “Mapping Small Elevation Changes over Large Areas: Differential Radar Interferometry,” *Journal of Geophysical Research: Solid Earth and Planets*, Vol. 94, No B7, pp. 9183–9191; July 10, 1989

236) D. Massonnet, “Satellite Radar Interferometry,” *Scientific American*, Vol. 276, pp. 46–53 February 1997.

237) D. Massonnet, D., K. Feigl “Radar interferometry and its application to changes in the Earth's surface,” *Review of Geophysics*, Vol. 36:, 1998, pp. 441–500.

along the main fault. The model interferogram showed a striking resemblance to the radar pattern obtained by analysis. Geodesists around the world were struck by the remarkable detail visible in the image, which resembled the displacement pattern predicted by theoretical models of such an earthquake. ²³⁸⁾

– Also in 1992, Richard M. Goldstein of the JPL and his co-workers used radar interferometry to track the movement of glacial ice in Antarctica. They took advantage of an exceptional opportunity presented by the ERS-1 satellite when it passed within a few meters of the path it had followed six days previously. Because the satellite had taken “before” and “after-the-event” radar images from virtually the same position, the topography of the glacier did not influence the pattern of fringes, and the resulting picture directly indicated the motion of the ice. That image displayed movement of an ice stream (where flow is relatively rapid) in superb detail. ²³⁹⁾

– In 1993, Massonnet and his colleagues conducted a further demonstration of small deformation detection by radar interferometry. They experimented with a set of radar imagery of the Mount Etna volcano in Sicily. At the time, the volcano was nearing the end of an eruptive cycle during an 18-month period in 1992 and 1993 when the ERS-1 satellite passed over it 30 times. ²⁴⁰⁾ With those many radar images and an elevation map of the area, they were able to produce dozens of interferograms that were free from topographic effects. Some of the results were clearly degraded by changes in vegetation on the flanks of the volcano (certain pairs of images used in constructing these interferograms spanned many months; others encompassed more than a year). Nevertheless, they were able to follow the deflation of Mount Etna, as the last of the magma erupted and the pressure within the mountain declined. The radar images showed that Mount Etna subsided by 2 cm/month during the final seven months of eruption. This deformation extended for a large distance around the volcano, suggesting that the subterranean magma chamber was much deeper than geologists had previously thought. The great interest in SAR interferometry is due in large part to the quantity and quality of interferometric products made available from the ERS-1 mission.

– ESA’s ERS-1/2 tandem mission (start in Aug. 1995, end in May 1996) is considered the first SAR interferometry formation flight. The prime objectives were focused on the collection of SAR data pairs for exploitation in interferometry, together with the synergistic use of instruments on the two platforms. ^{241) 242)} The configuration was that of two-pass measurements of a single-antenna SAR platform (the same SAR instrument on both satellites observing the same area on the ground), permitting the superposition technique of imagery (in data processing) of fairly close repeat tracks. The ERS-1/2 tandem mission was flown with a one day delay of a coinciding ground track of the second S/C, providing good interferometric results. About 110,000 ERS SAR scene pairs have been acquired during the nine months period, covering nearly the total global land surface. The data of the tandem mission permitted the generation of DEMs (Digital Elevation Models), also over vegetated land surfaces. Over forests, however, many data sets had to be averaged to gain a DEM of acceptable quality. – The SRL-1/2 missions of NASA in 1994 (April 9–20 for SRL-1, Sept. 30 – Oct. 11 for SRL-2) employed two-pass (and repeat pass) interferometry for topographic mapping (detection of topographic surface change in SRL-1 and SRL-2). The C-band SAR instruments of the ERS-1/2 and RADARSAT-1 (launch Nov 4, 1995)

238) D. Massonnet, M. Rossi, C. Carmona, F. Adragna, G. Peltzer, K. Feigl, T. Rabaute, “The Displacement Field of the Landers Earthquake Mapped by Radar Interferometry,” *Nature*, Vol. 364, 1993, pp. 138–142

239) C. L. Werner, S. Hensley, R. M. Goldstein, P. A. Rosen, H. A. Zebker, “Techniques and Applications of SAR Interferometry for ERS-1, Topographic Mapping Change Detection and Slope Measurement,” *Proceedings of the First ERS-1 Symposium, 1992, Cannes, France*, pp. 205–210

240) D. Massonnet, “Validation of ERS-1 Interferometry at CNES,” *Proceedings of the second ERS-1 Symposium, October 11–14, 1993, Hamburg, Germany Vol.2*, pp. 703–709

241) G. Duchossois, P. Martin, “ERS-1 and ERS-2 Tandem Operations,” *ESA Bulletin*, No.83, 1995, pp. 54–60

242) G. Duchossois, G. Kohlhammer, P. Martin, “Completion of the ERS Tandem Mission,” *ESA Earth Observation Quarterly*, No 52, June 1996, pp. 1–2, also: <http://esapub.esrin.esa.it/eoq/eoq52/duch52.htm>

missions demonstrated the ability to detect cm-scale surface strain over large contiguous areas. The L-band SAR of JERS-1 (launch Feb. 11, 1992) demonstrated also two-pass SAR-interferometry for change detection.

– ERS-1/2 InSAR data were also used by USGS to study magma body systems by mapping the surface deformation and modeling the observed deformation (same technique as employed by Massonnet).²⁴³⁾ InSAR measures the corresponding phase difference resulting from the difference in the round trip path length to the same ground point between two synthetic aperture radar (SAR) images. The phase difference is due mainly to five effects: 1) differences in the satellite orbits in the two passes, 2) topography, 3) ground deformation, 4) atmospheric propagation delays, and 5) systematic and environmental noise. Knowledge of the position and attitude of satellites is required to remove the effect caused by the differences in the satellite orbits of the two passes. The topographic effects in the interferogram can be removed by producing a synthetic interferogram based on an accurate DEM and subtracting it from the interferogram to be studied. This results in a deformation interferogram. The component of ground deformation along the satellite's look direction can potentially be measured with a precision of from sub-centimeters to centimeters using the C-band ERS-1/2 SARs. InSAR studies at six Alaska volcanoes were conducted, including New Trident, Okmok, Akutan, Kiska, Augustine, Westdahl, Peulik, Shishaldin, and Se-guam.

The ERS-1/2 Tandem Mission was particularly interesting for **POD (Precise Orbit Determination)**: a unique occasion of having two altimetric satellites flying the same orbit. With ERS-2 enjoying an abundance of tracking through SLR and PRARE (operational on ERS-2 only), these inputs were used to improve the ERS-1 orbits in simultaneous orbit determinations. Dual-satellite altimeter crossover height differences were used as a kind of satellite-to-satellite tracking data type, linking the two orbits. See also 1.23.3.9 for POD description.

– MAMM (Modified Antarctic Mapping Mission), a joint CSA/NASA interferometric mapping mission of Antarctica in the period Sept. 3 – Nov. 14, 2000, using RADARSAT. The overall objective of MAMM was to acquire repeat-pass interferometry to estimate ice surface velocity of the outer regions of the continent, north of 81° S. The science objectives called for SAR mapping of the Antarctic continent over three consecutive 24-day repeat cycles. See D.42.3

• **AT-InSAR (Along-track Interferometric SAR) or ATI-motion sensing.**^{244) 245) 246)} An along-track InSAR refers to a synthetic aperture radar instrumentation of two antennas, separated by a fixed distance, observing along-track, i.e. in the flight direction (a single-pass along-track interferometry configuration). Both antennas image the same footprint simultaneously, but with a short time lag in the acquisition of the two images, due to the baseline difference, results in a phase difference, which is proportional to the Doppler shift of the backscattered signal, and thus to the line-of-sight velocity of the scatterers. The phase difference image can thus be converted into a velocity map. Hence, the ATI technique offers beside other observations also direct velocity measurements [not available from the conventional cross-track InSAR (CT-InSAR) intensity image].

A number of experiments/campaigns, employing the AT-InSAR measurement technique, have shown a potential for oceanic and coastal applications, offering the promise of synop-

243) Z. Lu, T. Masterlark, Ch. Wicks, W. Thatcher, D. Dzurisin, J. Power, "Interferometric Synthetic Aperture Radar Studies of Alaska Volcanoes," Pecora 15/Land Satellite Information IV Conference, ISPRS Commission I Mid-term Symposium/FIEOS (Future Intelligent Earth Observing Satellites), Nov. 10-14, 2002, Denver, CO

244) R. Romeiser, O. Hirsch, "Possibilities and Limitations of Current Measurements by Airborne and Spaceborne Along-Track Interferometric SAR," Proceedings of IGARSS/IEEE 2001, Sydney, Australia, July 9-13, 2001

245) D. R. Thompson, "The Potential of SAR Interferometry for Oceanographic Measurements: A Review," Proceedings of IGARSS/IEEE 2001, Sydney, Australia, July 9-13, 2001

246) M. Bao, C. Bruening, W. Alpers, "Simulation of ocean wave imaging by an along-track interferometric synthetic aperture radar," IEEE Transactions on Geoscience and Remote Sensing, Vol. 35, No 3, pp. 618-631, 1997.

tic current measurements. AT – InSAR measurements have also been found to be useful for estimating bathymetry variations in shallow coastal waters, and for estimating surface wave spectra. ²⁴⁷⁾ ²⁴⁸⁾ ²⁴⁹⁾ ²⁵⁰⁾ ²⁵¹⁾ ²⁵²⁾ ²⁵³⁾

The principle of AT – InSAR ocean current measurements was first demonstrated with the airborne AirSAR system of NASA/JPL in the late 1980s and early 1990s. However, the data processing and interpretation at the time was not properly understood. In the meantime, further AT – InSAR (as well as CT – InSAR) projects were conducted or are underway to test more performance aspects in the field. ²⁵⁴⁾ Examples are:

- Spaceborne ATI has successfully been demonstrated on the SRTM mission (STS – 99 in 2000) of NASA/DLR/ASI. The along – track separation of the two SAR antennas of the SRTM was about 7 m (60 m in cross – track). ²⁵⁵⁾

- The TerraSAR – X mission of DLR/EADS – Astrium (launch June 15, 2007). For ATI (Along Track Interferometry) support, the SAR antenna can be grouped into two segments, each of 2.4 m. The antenna transmits at full aperture and is capable to receive in two along – track half apertures. Ideal ATI time lags for oceanic current measurements at X – band should be on the order of a few milliseconds, i.e. about 20 times longer than this; thus, the sensitivity of TerraSAR – X to small ocean current variations will be quite low.

A completely different approach is proposed/planned in the spaceborne ICW (Interferometric Cartwheel) mission of CNES. ²⁵⁶⁾ The ICW concept employs a bistatic constellation of three passive microsatellites, each equipped with a receiver dish antenna (a slave receiver), to co – orbit with a conventional SAR mission (Envisat, RADARSAT – 3) as “illuminator.” Such a co – planar constellation offers InSAR by definition (same footprint observation of all S/C), providing AT – InSAR as well as CT – InSAR measurements [see Ref. 305) and 306)].

Complex data processing: ²⁵⁷⁾ The processing of ATI data requires accurate knowledge of the location of the phase centers of the antennas, motion compensation, correction for cross – track baseline components, etc.. At the start of the 21st century, there is an improved understanding of the complex signature mechanisms/factors involved making interpretation of the data more reliable. According to model results, high radar frequencies, such as X – band, VV polarization, and incidence angles of $\geq 45^\circ$ are preferable for ATI current

247) G. Zilman, L. Shemer, “An exact analytic representation of a regular or interferometric SAR image of ocean swell,” IEEE Trans. Geoscience and Remote Sensing, vol. 65 no. 3, 1999.

248) R. M. Goldstein, H. A. Zebker, “Interferometric radar measurements of ocean surface currents,” Nature, Vol. 328, pp. 707 – 709, 1987

249) J. Schulz – Stellenfleth, S. Lehner, R. Bamler, J. Horstmann, “A model for ocean wave imaging by a single pass cross track interferometric SAR (INSAR) – The SINEWAVE experiment,” IGARSS’98, Vol. II, 98CH36174, Seattle, WA, July, 6 – 10, 1998, pp. 962 – 964

250) H. C. Graber, D. R. Thompson, R. E. Carande, “Ocean surface features and currents measured with synthetic aperture radar and HF radar,” J. Geophys. Res., vol. 101 C11, pp. 25, 813 – 25,832, 1996.

251) F. Bordoni, F. Gini, F. Lombardini, L. Verrazzani, “A Class of Algorithms for Multibaseline ATI Oceanic Surface Velocity Estimation in Presence of Bimodal Doppler Spectrum,” Proceedings of EUSAR 2002, Cologne, Germany, June 4 – 6, 2002

252) Note: ATI is not based on a certain interferometric baseline but on the time lag between two moving SAR instruments separated in along – track direction and imaging the same terrain. A severe limitation of single – satellite ATI is caused by the physical dimensions of the spacecraft bus. The shorter the time lag, the coarser the resolution of velocity measurement.

253) R. Romeiser, H. Breit, M. Eineder, H. Runge, P. Flament, K. de Jong, J. Vogelzang, “On the Potential of Spaceborne Along – Track InSAR for High – Resolution Current Measurements,” SAR Workshop on Coastal and Marine Applications, Svalbard (Spitzbergen), Norway, Sept. 8 – 12, 2003

254) D. R. Thompson and J. R. Jensen, “Synthetic aperture radar applied to ship – generated internal waves in the 1989 Loch Linnhe experiment,” Journal of Geophysical Research, Vol. 98 C6, pp. 10,259 – 10,269, 1993.

255) H. Breit, M. Eineder, J. Holzner, H. Runge, R. Bamler, “Traffic Monitoring using SRTM Along – Track Interferometry,” IEEE/IGARSS 2003, Toulouse, France, July 21 – 25, 2003,

256) D. Massonnet et al., “A wheel of passive radar microsats for upgrading existing SAR projects,” in Digests IGARSS 2000, pp. 1000 – 1003, IEEE, Piscataway, N.J., USA, 2000

257) R. Romeiser, D. R. Thompson, “Numerical study on the along – track interferometric radar imaging mechanism of oceanic surface currents,” IEEE Transactions on Geoscience and Remote Sensing, Vol. 38 – II, pp. 446 – 458, 2000

measurements. The ATI time lag must be shorter than the coherence time of the backscattered signal, but long enough to obtain significant, detectable phase differences.

1.4.3.5 Scatterometry – the microwave measurement of wind fields

Surface wind fields (speed and direction) are an important observable in a wide variety of atmospheric and oceanic processes. They are required, for instance, to drive ocean models and to validate coupled ocean–atmosphere global models. Operational prediction of ocean circulation relies heavily on accurate knowledge of wind forcing. As the largest source of momentum for the ocean surface (input of momentum via surface stress), winds affect the full range of ocean movement – from individual surface waves to complete current systems. Winds over the ocean modulate air–sea exchanges of heat, moisture, gases, and particulates. This modulation regulates the interaction between the atmosphere and the ocean, which establishes and maintains both global and regional climates. One of the important applications of surface wind observations is to increase the accuracy of weather analysis and forecasts and to improve NWP (Numerical Weather Prediction).^{258) 259) 260)}

Conventional wind field measurements over the ocean are performed by a set of radar cross–section measurements at different azimuth view angles over the resolution cell, and by inverting the backscatter model, a so–called GMF (Geophysical Model Function), to extract the wind information, using the azimuth anisotropy of the radar backscatter of the sea–surface in the presence of wind.

Background: Scatterometry has its origin in early radar applications in World War II. These radar (microwave) measurements over oceans were corrupted by sea surface clutter (noise). It was not known at that time that the clutter was the radar response to the winds over the oceans. The radar response was first related to wind in the late 1960’s – by realizing that the sea surface roughened by the wind modifies the surface backscatter (reflected signal or echo) properties. Initial experiments of marine wind measurements began with a scatterometer [S–193, also referred to as RADSCAT (Radiometer/Scatterometer)] on Skylab of NASA in 1973 and in 1974. This was followed by SASS (SeaSat–A Satellite Scatterometer) on SeaSat (1978), the first S/C to measure sea surface wind vectors on two simultaneous swaths of 500 km (with a nadir gap of 350 km). SASS had two stick dual–polarization antennas on each side of the S/C. Typically, the SASS instrument achieved a wind speed accuracy of 1.6 m/s with respect to buoy measurements. Today’s scatterometers are flown on such missions as ERS–2, QuikSCAT and ADEOS–II, providing global wind fields.

Note: Communications with the **ADEOS–II** spacecraft stopped on Oct. 24, 2003, just after 7 months of Earth observation activities. A power failure is cited for the termination of the mission (due to very high solar flare activities).²⁶¹⁾ The satellite’s planned lifetime was three years. Japanese experts analyzed the possible causes of the failure. The most probable cause is that a short– or open–circuit failure occurred on the solar array paddle. Also, a space environment analysis demonstrated that the > 30 keV electron flux was two orders of magnitude higher than normal. In any case, the anomaly caused a permanent power outage when ADEOS–II was orbiting over the North Pole region – an end of the mission.

Scatterometers are **active** microwave instruments (radars that measure the target reflectivity or backscatter over a wide range of incidence angles; values are reported in terms of the normalized radar cross section, σ^0) offering a capability of wind speed and direction deter-

258) A. Bentamy, Y. Quilfen, P. Flament, “Scatterometer wind fields: A new release over the decade 1991–2001,” *Canadian Journal of Remote Sensing*, Vol. 28, No. 3, 2002, pp. 431–449

259) Special Issue: Remote Sensing of Marine Winds, *Canadian Journal of Remote Sensing*, Vol. 28, No. 3, 2002

260) R. Atlas, R. N. Hoffman, S. M. Leidner, J. Sienkiewicz, T.–W. Yu, S. C. Bloom, et al., “The Effects of Marine Winds from Scatterometer Data on Weather Analysis and Forecasting,” *BAMS*, Vol. 82, No 9, Sept. 2001, pp. 1965–1990

261) T. Goya, H. Matsumoto, K. Koga, Y. Kimoto, “Space Environment Effects on two Satellite Anomalies in Oct. 2003 Storm;” *Proceedings of IAC 2004, Vancouver, Canada, Oct. 4–8, 2004, IAC–04–IAA.4.9.3.U.6.01*

mination. Scatterometers operate by acquiring multiple spatially and temporally co-located measurements of backscattered power from different viewing geometries. The known relationship between cross-section, wind velocity, and viewing geometry is then used to estimate wind speed and direction. ²⁶²⁾

Newer data analysis reveals that **passive** microwave instruments (i.e., radiometers) with V/H polarization capability, in operation or under development, like SMM/I and SSMIS (successor of SSM/I) on DMSP ²⁶³⁾, Windsat on Coriolis and MIS (Microwave Imager/Sounder) on NPOESS, also have the ability to sense ocean surface wind speed and direction, among other parameters (like SST). The microwave radiation that is emitted by the wind-roughened ocean surface and measured by passive radiometer sensors shows a distinct signature with respect to the wind vector (the satellite brightness temperature measurements are space and time collocated with the wind vectors). ²⁶⁴⁾

An overview of operational and emerging and complementary techniques for wind retrieval measurements are:

- Scatterometers (can be regarded as quasi-operational instruments at the start of the 21st century, their windfield measurements are used in global-scale meteorological models). The spatial resolution of today's scatterometer windfields turn out to be rather coarse, in the order of 15 to 25 km, quite suitable for open ocean observations, but not as suitable for coastal regions with more variability of wind patterns.
- Polarimetric radiometers (emerging wind retrieval applications)
- SAR instruments (SAR meteorology ²⁶⁵⁾ ²⁶⁶⁾ ²⁶⁷⁾ is an emerging field with the potential of providing high-resolution wind fields). In addition, the SAR observation technique provides a means to image ocean waves. Unlike other techniques – wavebuoys, altimetry – SAR provides more complete information on the wave field, the spectrum, rather than some data at a view discrete points. Like polarizations (HH or VV) are needed to map and model ocean waves.
- Altimeter data. The altimeters of the missions: TOPEX/Poseidon, ERS-2 and GFO provide routinely along-track measurements of wind speed (no direction) and significant wave height (SWH) since 1992, 1995 and 1999, respectively.
- GPS reflection data from ocean surfaces (see chapter 1.20.6)
- The GIFTS (Geostationary Imaging Fourier Transform Spectrometer) wind system uses the retrieved moisture fields on constant altitude surfaces to identify gradients for motion vector calculation. ²⁶⁸⁾ This represents a novel approach to wind tracking, since it eliminates the vector height assignment issue (often the largest source of error).

262) F. M. Naderi, M. H. Freilich, D. G. Long, "Spaceborne radar measurements of wind velocity over the ocean – an overview of the NSCAT scatterometer system," *Proceedings of the IEEE*, 79, pp. 850–866, 1991.

263) Note: Wind retrievals are also available from SSM/I, flown since 1987 on the DMSP series. However, the design of SSM/I, a microwave radiometer, only permits the retrieval of the speed component of the wind vector.

264) T. Meissner, F. Wentz, "The Ocean Surface Wind Direction Signal in Passive Microwave Brightness Temperatures," *Proceedings of IGARSS 2002*, Toronto, Canada, June 24–28, 2002

265) W. Alpers, "Ocean Surface Wave Imaging from Seasat to Envisat," *IEEE/IGARSS 2003*, Toulouse, France, July 21–25–2003

266) D. G. Flett, K. J. Wilson, P. W. Vachon, J. F. Hopper, "Wind information for marine weather forecasting from RADARSAT-1 synthetic aperture radar data: Initial results from the "Marine winds from SAR" demonstration project," *Canadian Journal of Remote Sensing*, Vol. 28, No 3, 2002, pp. 490–497

267) N. Fichaux, T. Ranchin, "Combined extraction of high spatial resolution wind speed and wind direction from SAR images: A new approach using wavelet transform," *Canadian Journal of Remote Sensing*, Vol. 28, No3, 3, 2002, pp. 510–516

268) C. Velden, G. Dengel, R. Dengel, A. Huang, D. Stettner, H. Revercomb, R. Knuteson, "Determination of Wind Vectors by Tracking Features on Sequential Moisture Analysis Derived from Hyperspectral IR Satellite Soundings," 20th International Conference on Interactive Information and Processing Systems (IIPS) for Meteorology, Oceanography, and Hydrology, Seattle, WA, Jan. 11–15, 2004

The ocean surface wind vector is a key parameter in understanding the weather due to its dominant role in the energy exchange at the air–sea interface. Winds over the ocean modulate air–sea exchanges in heat, moisture, and gases regulating much of the global weather.

The data analysis of the PR (Precipitation Radar) sensor on TRMM, designed for the measurement of the precipitation profile in the atmosphere, has shown that wind speed and direction can also be obtained from other instruments than scatterometers. The reason is that PR also measures the normalized radar cross section (σ^0) of the Earth's surface. The small incidence angles of the PR beam and the single look capability of its cross–track scan geometry may act to limit its wind retrieval potential using traditional scatterometer techniques. Nonetheless, the small horizontal footprint and vertical range gate of the PR offer other advantages over the conventional scatterometer systems presently in use. More important, the potential addition of wind sensing capability to the TRMM PR complements in fact its rain profiling skills in providing coincident wind and rain observations at the same high spatial resolution, which represents a significant improvement in science value over the individually generated wind and rain measurements using separated sensors at different spatial resolutions. ²⁶⁹⁾

Background: For a given wind speed and direction and radar geometry, the NRCS [NRCS (Normalized Radar Cross–Section), an aspect of ocean surface reflectivity, also referred to as σ^0] can be predicted using empirically–derived geophysical model functions. Unfortunately, the inverse is not true. A given NRCS does not correspond to a unique wind speed and direction pair. Many different wind speed and direction pairs could produce a particular NRCS. – Measuring the sea surface NRCS from a number of different aspect and incident angles limits the number of potential solutions and alleviates this inversion difficulty. This multi–measurement approach to inversion is the basis of conventional spaceborne radar scatterometer measurements of the wind vector (Ref. 186). ²⁷⁰⁾

Mission	Launch Date	Spatial Resolution (km)	Swath Width (km)	Frequency GHz (Band)	Polarization	Data Rate (kb/s)	Altitude, Inclination (km/°)	Sensor, Remarks
Skylab	14.5.73	16	180	13.9 (Ku)		5.33	435, 50°	S-193
SeaSat	27.6.78	50	500 x 2	14.6 (Ku)	VV,HH		800/108° ^a	SASS
Spacelab-1	28.11.83							MRSE, Shuttle
ERS-1 (Fanbeam)	17.7.91 to May 1996	50	500	5.3 (C)	LV		785, 98.5° ^a	AMI in Scat. mode
ERS-2 (Fanbeam)	21.4.95	50	500	5.3 (C)	LV		785/98.5	AMI in Scat. mode
ADEOS	17.8.96	25,50	600 x 2	13.99 (Ku)	VV,HH	2.9	797/98.6° ^b	NSCAT
QuikSCAT	19.6.99	50	1800	13.4 (Ku)		40	803/98.6° ^b	SeaWinds
Envisat	1.3.2002	28 m x 30 m	5 km vignette, 7 subswath	5.331 (C)	VV or HH	900	800/98.6° ^b	ASAR in wave mode
ADEOS-II	14.12.02	50	1800	13.4 (Ku)		20	803, 98.6° ^b	SeaWinds
Coriolis	6.1.2003	25	1400	6.8, 10.7, 18.7, 23.8, 37.0 GHz	Circular	5000	830,98.7° ^b	Windsat
MetOp-A	19.10.2006	50	2 x 550	5.255 (C)	VV	60	825, 98.7° ^b	ASCAT (Fanbeam)
MetOp-B	17.09.2012	50	2 x 550	5.255 (C)	VV	60	825, 98.7° ^b	ASCAT (Fanbeam)

Table 22: Survey of spaceborne radar/microwave scatterometers (wind measurements)

269) L. Li, E. Im, “Detecting Ocean Surface Winds Using TRMM Precipitation Radar,” Proceedings of IGARSS 2002, Toronto, Canada, June 24–28, 2002

270) A. Stoffelen, D. L. T. Anderson, “Scatterometer data interpretation: Measurement space and inversion,” Journal of Atmospheric and Oceanic Technology, Vol. 14, 1997, pp. 1298–1313

Wind vector retrievals by today's operational scatterometers (like AMI and SeaWinds) are based on indirect measurements, where the wind vector is inferred through a relationship between the backscattered power (NRCS), the small-scale ocean surface roughness, and the local wind vector at the ocean surface. This relationship is empirical, based primarily on matches between sensor measurements, buoy wind measurements and analysis from numerical weather prediction models.²⁷¹⁾

- The first spaceborne scatterometers were S-193 on Skylab (launch 1973) and SASS on SeaSat (launch June 28, 1978), followed by MRSE on Spacelab-1 and the AMI-SCAT (wind scatterometer mode) instrument on ERS-1 (launch July 17, 1991).²⁷²⁾ See Tables 22 and 23. The newer (since 1999) spaceborne wind vector measurement instruments can be put into three classes:

- Broad-swath, dual-pencil beam active Ku-band scatterometers (e.g. SeaWinds)
- Dual swath, 3-look active C-band scatterometers (e.g., ASCAT)
- Dual- and single-look passive polarimetric radiometers (e.g., Windsat, CMIS)

With the launch of ADEOS-II (Dec. 14, 2002), there is the first opportunity since SeaSat to obtain collocated active microwave radar with SeaWinds-II and passive microwave radiometer data of AMSR (Advanced Microwave Scanning Radiometer), from the same platform. Note: Contact with ADEOS-II was lost on Oct. 25, 2003.

Traditional **fanbeam** scatterometer designs such as SASS, AMI-SCAT, and NSCAT require significant power and mass and have antenna systems which are difficult to accommodate aboard any spacecraft. The fanbeam systems employ multiple fixed antennas to cast broad fan-shaped beams on the Earth's surface at multiple azimuth angles needed to measure wind. These designs have degraded wind performance limitations in particular in the near-nadir region of the measurement swath. The reason: the backscatter measurements in the region ± 200 km to either side of the nadir track are at small incidence angles and are insensitive to wind direction, thus, creating a large "nadir gap" in their coverage.

Sensor	Sensor Provider	Frequency Band	Flown since
CRL Radar/Radiometer	CRL Japan NASA/GSFC/WFF	X-band, Ka-Band	1981 since 1985
Delta-K Spectrometer	IKI RAN, Moscow	X-band	1981
DUTSCAT	DUT/NLR, Holland	1.2–17.2 GHz (6 bands)	1983
ERASME	CNRS/CETP, France	C-band, X-band	1983
RACS	U. of Hamburg	C-band	1987
HELISCAT	U. of Hamburg	L, S, C, X, Ku	1989, 1990
HUTSCAT	HUT, Helsinki	C-band, X-band	1988
MINISCAT	HUT, Helsinki	C-band	1990
C-SCAT	NASA/MIRSL	C-band	1990
RESSAC	CRPE, France	C-band	1990 (rebuilt ERASME)
NUSCAT	NASA/JPL	Ku-band	1991
RENE	CNRS/CETP, France	X-band	1992

Table 23: Overview of some airborne radar scatterometers

Newer scatterometer designs employ the **conical-beam scanning technique** (with dual-beams). SeaWinds (of NASA/JPL on QuikSCAT, launch June, 19, 1999) introduced a scanning pencil-beam scatterometer with a dual-beam conical scan, provided by a 1 m diameter reflector (rotating dish) antenna. Although the pencil-beam approach adopted by Sea-

271) P. S. Chang, L. N. Connor, J. R. Carswell, R. S. Dunbar, "Operational Scatterometry: High Wind Speed Retrievals," Proceedings of IEEE/IGARSS Conference, Honolulu, HI, July 24–28, 2000

272) R. F. Millief, M. H. Freilich, et al., "Global Ocean Surface Vector Wind Observations from Space," Proceedings of OCEANOBS 99, Oct. 18–22, 1999, Saint-Raphael, France

Winds significantly lessens the nadir gap problem by making measurements at suitably high incidence angles, the problem is not completely eliminated. Measurements in the extreme inner and outer swath still suffer some degradation because the relative azimuth angles of backscatter measurements are too close together (approaching 0° for the outer swath), or are too far apart (approaching 180° for the inner swath) to determine the wind speed direction accurately. – A performance improvement is also introduced with the ASCAT instrument of ESA on MetOp – A of EUMETSAT, it employs a solid – state design and the use of a double – beam scanning technique. Scatterometer antenna and radar electronic concepts remain key technology issues in the design of efficient and low – cost instruments. 273) 274) 275)

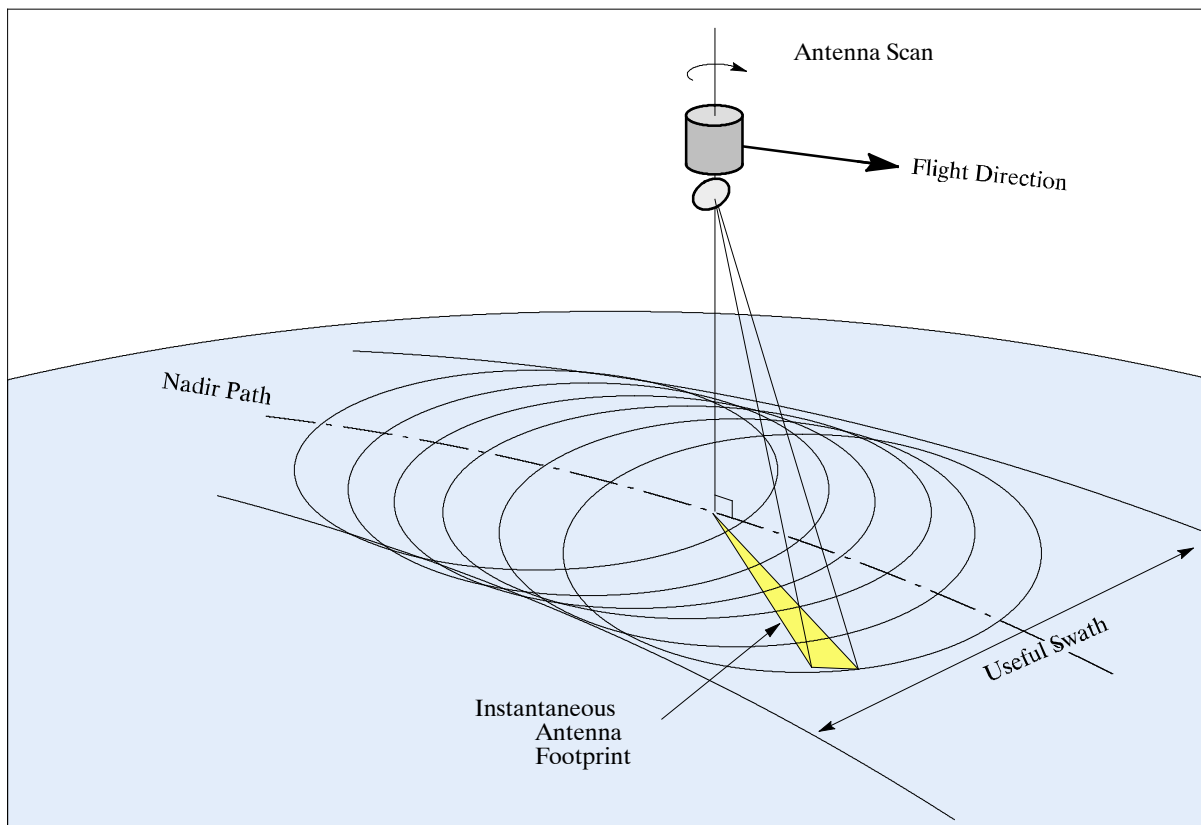


Figure 12: Rotating fanbeam scatterometer concept (RFSCAT)

Beyond the original mission of spaceborne scatterometers to provide measurements of wind velocity over the ocean, a large number of applications of the radar data have emerged in such areas as: a) land applications, b) polar snow and ice, c) oceans and NWP (Numerical Weather Prediction), and d) polarimetric scatterometry.

The capabilities of the next – generation polarimetric scatterometers are of particular interest (RFSCAT). They will be able to simultaneously measure the conventional co – polarized backscatter as well as the polarimetric correlation of the co – and cross – polarized radar returns from the ocean surface. The technique promises potential performance gains by improving in particular the ambiguity resolution. Combined with the spacecraft motion of about 7 km/s of ground speed, large overlaps are produced by the successive sweeps. A pixel

273) M. R. Drinkwater, C. C. Lin, "Introduction to the Special Section on Emerging Scatterometer Applications," IEEE Transactions on Geoscience and Remote Sensing, Vol. 38, No 4, July 2000, pp. 1763 – 1764

274) W – Y. Tsai, S. V. Nghiem, J. N. Huddleston, et al., "Polarimetric Scatterometry: A Promising Technique for Improving Ocean Surface Wind Measurements," IEEE Transactions on Geoscience and Remote Sensing, Vol. 38, No 4, July 2000, pp. 1903 – 1921

275) V. Wismann, "Monitoring the Earth with Spaceborne Scatterometers," Proceedings of 32nd ESLAB Symposium on 'Remote Sensing Methodology for Earth Observation and Planetary Exploration,' ESA/ESTEC, Sept. 15 – 18, 1998 (SP – 423 Dec. 1998), pp.189 – 199

within the total swath, depending on its cross-track position, may be intercepted several times (up to 10 times) by the antenna footprint, first in the forward beam and later in the backward beam. The radar operates in a pulsed mode, so that each point of the echo profile can be attributed to a unique pixel position within the antenna footprint along the radial direction. The pixels in the radial direction are resolved by range-gating the radar echo. The following advantages of the fanbeam, multiple-beam concept and the conically scanning spot beam concept are provided: ^{276) 277)}

- A large continuous swath can be achieved (order of >1500 km)
 - A large number of azimuth views per pixel can be generated depending on the rotation speed and swath position
 - The rotation speed of the antenna can be greatly reduced as compared to the conically scanning spot beam concept due to the large coverage of the fanbeam antenna
 - A single, rotating fanbeam antenna is required (no switching is needed between different antennas)
 - Simple data processing is required (scan position and range dependent Doppler compensation, pulse compression, and look summations).
- **Estimation of the wind field from SAR NRCS (Normalized Radar Cross Section) imagery** poses a different challenge (Ref. 186). A SAR instrument measures NRCS at only one aspect angle and a unique wind vector solution is not possible. However, if the wind direction is known a priori, then wind speed can be determined. There are at least three ways to estimate wind direction: 1) determine wind direction from features in the SAR image, 2) use numerical weather forecast models, and 3) obtain wind direction from other spaceborne instruments. What differentiates the various approaches are the NRCS model used and the manner to estimate wind direction. – The ability to retrieve wind fields from SAR imagery, with the high resolution (< 1 km) and wide coverage (500 km), represents an important improvement for applications where knowledge of the wind field at fine spatial scales is crucial. ^{278) 279)} SAR-derived wind fields can contribute to the usefulness of other SAR applications as well. For example, SAR winds can aid wave field retrieval by providing a first guess wind-wave spectrum. Algorithms for automated detection of oil spills and ships as well as ice identification can be improved with knowledge of the local wind field.

Examples of missions with wind retrieval from SAR data:

- For the ERS-1/2 SAR sensors (AMI in scatterometer mode) of ESA, which operate in VV polarization, the NRCS geophysical model function (GMF) comes from validated SCAT models.
- For the Canadian RADARSAT-1 SAR sensor, which operates in HH polarization, no such validated GMF models existed. A work-around for wind speed retrievals was found by combing SAR (RADARSAT-1) and SeaWinds scatterometer data (QuikSCAT). This involved comparison of SAR-derived wind speeds with SeaWinds wind speeds. When wind

276) C. C. Lin, B. Rommen, J. J. W. Wilson, F. Impagnatiello, P. S. Park, "An Analysis of a Rotating, Range-Gated, Fan-beam Spaceborne Scatterometer Concept," *IEEE Transaction on Geoscience and Remote Sensing*, Vol. 38, No 5, Sept. 2000, pp. 2114–2121

277) C.-C. Lin, A. Stoffelen, J. de Kloe, V. Wismann, S. Bartha, H. Schulte, "Wind retrieval capability of rotating, range-gated, fanbeam spaceborne scatterometer," *Proceedings of SPIE*, Vol. 4881, 9th International Symposium on Remote Sensing, Aghia Pelagia, Crete, Greece, Sept. 23–27, 2002

278) Note: SAR imagery is not as extensive or complete as data from scatterometer or passive radiometric measurements, but offers the prospect of wind speed measurements in coastal areas where more conventional instruments fail.

279) F. Monaldo, V. Kerbaol, "The SAR Measurement of Ocean Surface Winds: An Overview for the 2nd Workshop on Coastal and Marine Applications for SAR," *SAR Workshop on Coastal and Marine Applications*, Svalbard (Spitzbergen), Norway, Sept. 8–12, 2003, URL: http://fermi.jhuapl.edu/meetings/svalbard_2003/

speed retrieval from SAR imagery is initialized with SeaWinds scatterometer wind directions, SAR wind speed retrievals are significantly improved. ²⁸⁰⁾ ²⁸¹⁾ ²⁸²⁾ ²⁸³⁾

– An investigation on the polarization effects on the SAR wind algorithms is being conducted with ASAR polarimetric data of Envisat (ESA, launch March 1, 2002). ²⁸⁴⁾ SAR imagery permits also the study of mesoscale circulation systems such as polar low storms and hurricanes. In particular, SAR offers an effective way of centering the location of these systems at the ocean surface. SAR imaging of storm systems may also include patterns of convective cell activity, precipitation, cloud ice, and even storm-induced ocean swell. Other ocean features readily imaged by SAR and under active research include ocean fronts and mesoscale circulation, river plume outflow and coastal interaction, oceanic internal gravity waves, upwelling, biological activity, and near shore bathymetric features.

- Microwave rain measurement instruments. First radiometer data evaluations with regard to rainfall started around 1975 using ESMR data of Nimbus-5 (launch Dec. 11, 1972) and later SMMR data of SeaSat (launch June 27, 1978). The SSM/I radiometer on the DMSP series is flown since 1987, rainfall is determined for sea surface regions. The airborne radiometer AMR (NASDA, since 1995) is to confirm AMSR on ADEOS-II (launch Dec. 14, 2002). Active microwave instruments: CRL Radar/Radiometer (CRL Tokyo, since 1981), ARMAR (NASA/JPL, since 1992) is an airborne rain radar in support of the spaceborne PR (Precipitation Radar) instrument on TRMM (launch Nov. 27, 1997). The TRMM mission represents the first concerted effort (NASA/NASDA) to tackle the complex nature of rainfall with a complement of passive and active sensors. ²⁸⁵⁾ – GPM (Global Precipitation Measurement), a follow-on mission to TRMM with a reference constellation of six to eight microsatellites and advanced rain-measuring instruments (passive microwave imaging radiometers), is in the design phase as of 2002/3 (NASA/JAXA). The goal of GPM is to provide precipitation rate on ground accurately and frequently from space with global coverage. A major objective of GPM is to ensure the delivery of global precipitation fields 8 times per day. The GPM concept of JAXA (former NASDA) employs DPR (Dual-frequency Precipitation Radar) at 13.6 and 35 GHz with phased array antennas that scan in cross-track with beam widths matched at the two frequencies. DPR should provide more detailed information on the drop size distribution and other parameters (rain rates, liquid and ice water contents).

- Active microwave medium-penetrating instruments, in particular with regard to soil and foliage penetration (see also: ‘microwave signal penetration’ in Glossary), were first introduced with airborne instruments (Table 24). Microwave observations of active and passive sensors in L-band, P-band, UHF, VHF and UWB (Ultra-Wide Bandwidth) are of great interest. ²⁸⁶⁾

280) C. Wackerman, W. G. Pichel, P. Clemente-Colón, “A Projection Method For Automatic Estimation Of Wind Vectors With RADARSAT SAR Imagery,” SAR Workshop on Coastal and Marine Applications, Svalbard (Spitzbergen), Norway, Sept. 8–12, 2003

281) F. Monaldo, D. Thompson, N. Winstead, “Combining SAR and Scatterometer Data to Improve High Resolution Wind Speed Retrievals,” Proceedings of IEEE/IGARSS 2003, Toulouse, France, July 21–25, 2003

282) J. Horstmann, W. Koch, N. Winstead, F. Monaldo, D. Thompson, P. Clemente-Colón, W. Pichel, “Comparison of RADARSAT-1 SAR Retrieved Wind Fields to Numerical Models,” IEEE/IGARSS 2003, Toulouse, France, July 21–25, 2003

283) F. M. Monaldo, D. R. Thompson, W. G. Pichel, P. Clemente-Colon, “A Systematic Comparison of QuikSCAT and SAR Ocean Surface Wind Speeds,” IEEE Transactions on Geoscience and Remote Sensing, Vol. 42, No 2, Feb. 2004, pp. 283–291

284) P. Clemente-Colón, W. G. Pichel, D. Lamb, M. van Woert, F. M. Monaldo, D. R. Thompson, C. C. Wackerman, “Operational Use of SAR-Derived Ocean Products: Are we there yet?” The 2003 EUMETSAT Meteorological Satellite Conference, Weimar, Germany, Sept. 29 – Oct. 3, 2003

285) L. J. Allison, et. al., “Tropical cyclone rainfall as measured by the Number 5 EMSR,” BAMS, Vol. 55, pp. 1074–1089, 1975

286) L. Peters, J. J. Daniels, J. D. Young, “Ground Penetrating Radar as a Subsurface Environmental Sensing Tool,” Proceedings of the IEEE, Vol. 82, No. 12, Dec. 1994, pp. 1802–1821

– The L–band is an attractive complement to the X–band in particular for biomass and land use applications. Fully polarimetric sensors provide valuable additional information for classification.

– The P–band (435 MHz) is attractive not only for biomass estimates, but also for sounding of the thickness and internal layers of the Antarctic and Greenland ice sheets.

The dielectric properties of the underground are of fundamental importance for the system concept. The microwave permittivity of water is an order of magnitude higher than that of any natural dry material.^{287) 288)} Radar penetration and resolution tend to be reduced by the EM attenuation, with a range that goes from a few meters in conductive media, to 50 m at most for low–conductivity (below 1 ms/m) materials such as sand, gravel, rock and fresh water. High–power pulses are essential in order to increase the ratio between signal and clutter (or noise). For this reason, instead of using a pulsed radar, one may use swept–FM or step–frequency continuous wave transmitters (SFCW). The frequency synthesizer technique seems to overcome some of the limitations of pulse–modulated radars which makes them interesting for future developments.

System	Description
GPR (Ground Penetrating Radar) SRI, P.96.1	First airborne tests/studies (ice penetration) were conducted in 1974, GPR first flown in 1993
FOLPEN, SRI, since 1990, P.96	FOLPEN–I and–II are VHF impulse SAR systems with foliage penetration capability
CARABAS, FOA, Sweden, P.50	Penetration of vegetation/foilage and to some extent of the ground surface, since 1992
TOPSAR, JPL (upgrade 1994), P.13.1	Calculation of the differential penetration characteristics of the dual–frequency radar waves for different Earth terrain types
P3/SAR, ERIM/Navy (upgrade 1994), P.83.3	Support of foliage and ground penetration experiments/applications
LARSEN, CCRS, since 1985, P.116	A lidar for the measurement of shallow water depths
LFS, University of Oldenburg, P.121	Lidar for the analysis of the upper sea surface layers, since '93
SHOALS, USACE, 1994, P.191	A lidar for the measurement of shallow water depths
SASAR, U. of Cape Town, since 1996, P.188	The VHF–band of SASAR offers a surface/foilage penetrating capability
Passive Instruments	
PBMR, GSFC/WFF, since 1983, P.167	L–band radiometer for the measurement of soil moisture, etc.
RADIUS, NPO Vega, since 1986, P.178	Microwave radiometer for the measurement of soil moisture, etc.
ESTAR, MIRSL/GSFC, 1988, P.88	L–band radiometer for the measurement of soil moisture and ocean salinity
AIMR, AES, Canada, since 1989, P.8	Microwave radiometer for the measurement of soil moisture and snow depth
PORTOS, CNES, since 1992, P.174	Microwave radiometer for the measurement of soil moisture
MIRAS, ESA, since 1996, P.138	L–band radiometer (2–D aperture synthesis) for the measurement of soil moisture and ocean salinity
STAR–Light (U. of Michigan), since 2002	L–band radiometer (10 element 1.4 GHz 2–D aperture synthesis using 3–bit correlation), measurement of soil moisture

Table 24: Overview of medium–penetrating airborne microwave instruments

Spaceborne L–band SAR instruments were flown on SIR–A (NASA/JPL, Shuttle, Nov. 12, 1981), SIR–B (Shuttle, Oct. 5, 1984), and SIR–C/X–SAR (Shuttle, SRL–1 April 1994, SRL–2 Sept. 1994), and on JERS (NASDA/MITI, launch Feb. 11, 1992).

In the late 1990s, the applications of medium–penetrating radars (a non–destructive monitoring technique), are becoming rather diverse. The technique is employed in civil engineer-

287)) Note: In ground penetrating applications the frequency range is determined by ground losses which in general are increasing with the frequency range selected.

288)) Note: In general, the medium–penetrating SAR instruments are also referred to as GPR (Ground Penetrating Radar). The GPR technology is one of the most promising concepts for land mine detection.

ing for void detection, prediction of concrete deterioration from variations of its permittivity by the presence of moisture and chloride, pavement profiling for programmed road and bridge deck maintenance, reinforcing bar location, subgrade deterioration in railroad and airport runways. Object detection and classification by extent and permittivity contrast with the overburden, it is crucial in environmental engineering. Furthermore, the technique is useful for mapping hazardous wastes and buried contaminant containers, imaging and monitoring subsurface contaminants (e.g., gasoline and other hydrocarbon fuels). Stratigraphic and bedrock mapping are essential in geotectonic, archaeologic, and hydrogeologic applications, in site characterization, in mining planning (e.g., borehole profiling), in tunnel excavations, ice thickness profiling, permafrost mapping, etc.

1.4.3.6 Bistatic and Multistatic Systems in Remote Sensing

The bistatic remote – sensing concept refers to a measurement geometry in which the transmitter and receiver of an active system [Doppler radar, SAR, lidar (altimeter), radionavigation systems (GPS, GLONASS, Galileo), all broadcasting systems, etc.] are separate units (i.e. physically different antennas), either collocated on the same platform but separated by some distance, or they (transmitter and receiver) are positioned on different platforms. ²⁸⁹⁾ 290) 291) 292)

Bistatic, or for that matter “**multistatic**” observation concepts that may be divided into fully active and semi – active configurations.

- In a fully active configuration, each radar has both transmit and receive capabilities where all radars look into a common footprint (different views of the observed target area). The TechSat – 21 constellation design of three satellites in formation flight (the project was cancelled in 2003 due to the technical challenges involved) is an example of a fully active system.
- Semi – active systems combine an active illuminator (one transmitting system) with one or more passive receivers. All systems look into a common footprint (multiangle observations as in the fully active configuration). An example design is the ICW (Interferometric Carthwheel) configuration. The passive members in such a system require obviously reduced power budgets; when in addition deployable antennas (receivers) are used, the payload may be accommodated on microsattellites. The use of a single illuminator in a semi – active configuration represents a significant reduction in constellation investment cost.

Both of these distributed arrangements, can improve system flexibility and reliability, offering some advantages such as stereoscopic views, different target signatures, and in particular shorter revisit times. – In fact, the flexibility of the multistatic observation concept is such as to permit the positioning of the transmitter and receiver satellites into different orbits; configurations of LEO – MEO and/or LEO – GEO constellations are possible. The ultimate goal is a highly reconfigurable and scalable satellite constellation for a broad spectrum of remote sensing applications. – Bistatic/multistatic SAR observations may require accurate time synchronization; antenna pointing between transmitter and receiver may also be involved.

The distributed nature and functionality in bistatic and multistatic SAR systems allows for a natural separation of the radar payloads, providing the potential to support the use of small, low – cost satellites in the future. A constellation of multiple radar satellites, recording the

- 289) G. Krieger, H. Fiedler, M. Rodriguez – Cassola, D. Hounam, A. Moreira, “System Concepts for Bi – and Multi – Static SAR Missions,” International Radar Symposium (IRS 2003), Dresden, Germany, Sept. 30 – Oct. 2, 2003
- 290) A. Moccia, N. Chiacchio, A. Capone, “Spaceborne bistatic Synthetic Aperture Radar for remote Sensing applications,” International Journal of Remote Sensing, Vol. 21, No 18, 2000, pp. 3395 – 3414
- 291) N. J. Willis, “Bistatic Radar,” Artech House, Boston, 1991, ISBN: 0 – 89006 – 427 – X
- 292) G. Krieger, H. Fiedler, A. Moreira, “Bi – and Multistatic SAR: Potentials and Challenges,” Proceedings of EUSAR 2004, Ulm, Germany, May 25 – 27, 2004

signals from a common illuminated footprint, is regarded as a **large aperture system with sparsely distributed subaperture elements**. [Within this context, a multichannel instrument (i.e. a distributed system configuration) can be obtained of a single SAR antenna by splitting the active phased array antenna electrically into multiple subapertures for multiple beam support]. This fact opens a number of new potential applications:

- The linear combination of multiple receiver signals can be treated in the framework of array processing.
- Sparse aperture systems enable highly accurate velocity measurements of moving objects on the ground and may also overcome the problem of blindness against certain directions of target motion.
- Precise target location capability.
- A coherent combination of multiple SAR images acquired from slightly different view angles can also improve the geometric resolution (super-resolution technique).
- A further promising application is SAR tomography which enables e.g. a real 3D imaging of the vegetation structure for biomass estimation on a global scale.
- Another very promising application for future bistatic and multistatic SAR systems is digital beamforming on receive. Multiple independent beams in elevation allow for the simultaneous and unambiguous mapping of several distinct subswaths with full azimuth resolution and high antenna gain. Multiple subswaths can then be combined to form a wide image swath.

In contrast, a **monostatic system** refers to a measurement arrangement, in which both transmitter and receiver functions are collocated on the same platform, the same antenna unit is being used for both functions (transmitter and receiver have also the same viewing geometries). The reasons for the selection of a monostatic system are mostly mission simplicity and autonomy. The monostatic geometry is understood, specifically with regard to the imaging mechanisms and to the data processing. The great majority of all radars (SAR instruments, Doppler radars, lidars, etc.) in use today (and flown on spaceborne missions) are of the monostatic type, providing their own illumination and measuring the echo at the same location. The dual monostatic or repeat-pass approach (for interferometric operation) has been demonstrated by the ERS-1/2 tandem mission (Aug. 1995 to May 1996) of ESA. In a tandem mission in monostatic mode, the two spacecraft have equal status, there is no direct link between them. In the bistatic semi-active concept, one satellite (the master or illuminator) generates the radar pulses, and the reception of the echoes by both master and slave must be synchronized.

Background. It is interesting to note here that all early radar experiments, conducted by experimenters in various countries like in France, Germany, Italy, Japan, Russia, UK, and USA (from about 1904 on until after World War II), were of the bistatic type. In the USA, for instance, an observation of the radar effect was made in 1922 at the U.S. Naval Research Laboratory (NRL) in Washington, D.C. NRL researchers conducted an experiment by positioning a radio transmitter on one shore of the Potomac River and a receiver on the other. A ship sailing on the river caused fluctuations in the intensity of the received signals when it passed between the transmitter and receiver. Today, such a configuration is called a **bistatic radar system**. In spite of the promising results of this experiment, U.S. Navy officials were unwilling to support further work at the time. Practically all early military radar systems until the end of World War II were of the bistatic type. – In the space age era, bistatic radar systems employing an orbiting transmitter and an Earth-based receiver have been used for lunar and planetary exploration.

Bistatic or multistatic radar systems offer some advantages:

– A significant cost reduction can be achieved in the design and operation of a bistatic system (passive radiometers are significantly less expensive than active SAR instruments). Microsatellites may be used to accommodate the passive receiver antennas.

– The physical separation of the transmitter and receiver function permits for instance designs, in which the number of participating receivers can be any number in an observation system; thus, the receiver function is of a **parasitic or opportunistic nature**, simply passively participating in an observation environment/arrangement, it is in a sense “independent” of the transmitter function (not in the time domain for SAR applications). Systems with two or more receiving sites are also referred to as multistatic systems. They employ overlapping coverage of the illumination footprint and combine target data coherently and noncoherently at a central location.

– Bistatic systems offer the potential of upgrading existing monostatic missions. For instance, an existing SAR mission may be complemented with a constellation of passive receiver spacecraft in its neighborhood. This improvement results in added value to the master mission offering bistatic SAR data. Interferometric processing of the bistatic data may be unrealistic, due to rather large antenna separations; however, cross-track and along-track interferometry may be achieved. See also the Cartwheel mission below.

There may be also some disadvantages in upgrading an existing monostatic system: a) the transmitting antenna and satellite are non-cooperative; i.e., they are unaware of the new satellite with its receiver; in this case, time-synchronization of the receiving-only antenna may pose added complexities on the data processing side. Hence, long-term plans are needed for upgrading options.

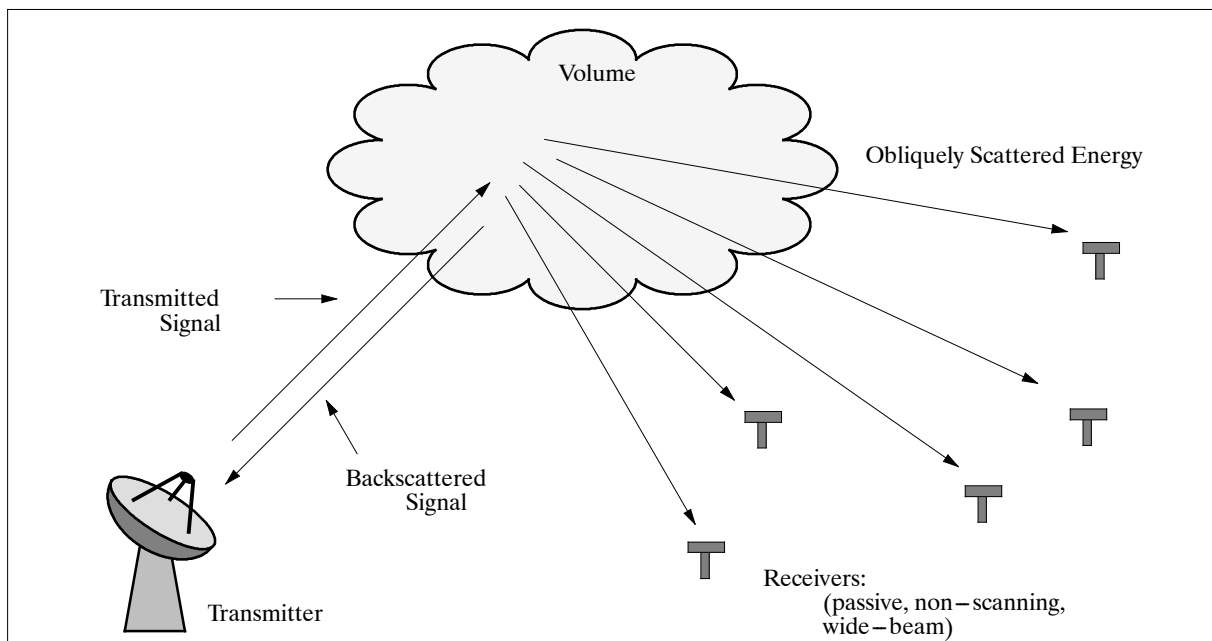


Figure 13: Schematic illustration of a ground-based bistatic multiple Doppler network

Since the 1990s, bistatic systems are also finding ever increasing applications in the wide field of Earth observation. A typical example is atmospheric research where ground-based bistatic multiple-Doppler radar networks have significant scientific and economic advantages accruing from the use of only single sources of illumination. The NEXRAD (Next-Generation Weather Radar), a bistatic ground-based Doppler radar network of NMS/NOAA (distributed over the entire USA) with the name of WSR-88D (Weather Surveillance Radar-1988 Doppler), is an example. Individual spatial volumes are viewed simultaneously from multiple look angles, minimizing storm evolution induced errors. The passive

receivers in a bistatic network do not require expensive transmitters, moving antenna hardware, or operators. Thus they require only a small percentage of the investment needed to field traditional transmitting radars.

Some examples of bistatic system designs are:

- PoldiRad (Polarimetric Doppler Radar) is a C–band bistatic Doppler ground–based radar system installed in 1988 at DLR in Oberpfaffenhofen, Germany. This system is a bistatic installation for a C–band weather radar system using a magnetron transmitter. The remote receiver is located at the DLR Weilheim tracking site at a distance of 27 km from the radar. The bistatic hub of the system receives the Doppler velocity and reflectivity from both receivers. The data from each ray are merged into a common data file and the horizontal wind vectors are estimated in real time. – Two more bistatic receivers were installed in 1999 into the PoldiRad network. ²⁹³⁾
- In 1993, NCAR (National Center of Atmospheric Research) developed a ground–based dual–Doppler weather radar network at its facilities in Boulder, CO, referred to as BINET (Bistatic Radar Network). The network provides three–dimensional fields of full vector winds, including directly measured vertical precipitation particle velocities for numerous applications in meteorological research, aviation, forecasting, media, and education. ^{294) 295) 296)}
- The GPS and GLONASS spaceborne navigation constellations are also examples of multistatic systems. By its very nature, each navigation constellation provides the transmitter function while the “signal user community” at its numerous instant locations plays the role of the receiver function. The direct reception of GNSS signals can be used a) as navigation function, b) as timing reference, and/or c) as remote sensing function (for refractive sounding, etc.). Manuel Martin–Neira of ESA/ESTEC was one of the earliest advocates of bistatic/multistatic altimetry using GPS signals. See also chapter 1.20.6 (GPS Signal Applications – Bistatic Reflection Measurements).
- Lately, indirect or reflected GNSS signals are also being used as information of opportunity (bistatic or multi–static scattering is at the heart of this phenomenon). In radar remote–sensing nomenclature, GPS reflection data (of the ocean surface or of any ground surface) can be characterized as a “bistatic radar scatterometer.” Upon impinging on the ocean surface, the GPS signal is reflected primarily in the specular (forward) direction, in an amount dependent on surface roughness and angle of incidence. An airborne or spaceborne GPS receiver, connected to a down–looking antenna, is able to collect such scattered signals. By analogy to traditional altimetry, the bistatic GPS reflected signals are analyzed to derive the important descriptors of the ocean surface: i.e., sea surface height and sea surface wind vector (an augmentation to existing spaceborne altimetry; the GPS coverage is dense and rapid; sea surface heights are obtained not only along the altimetry tracks but at many points in between). ²⁹⁷⁾ An entire new spectrum of remote sensing applications is beginning to unfold with the measurement of this new source of reflection data. Initial experiments with airborne GPS receivers were conducted in the early 1990s (see also “ocean reflection measurements of GNSS signals” in 1.20.6).

293) M. Hagen, P. Meischner, J. Wurman, M. Randall, C. Burghart, “A C–Band Bistatic Doppler Radar System at DLR Oberpfaffenhofen,” Proceedings of the 29th International Conference on Radar Meteorology, July 12–16, 1999, Montreal, Canada

294) J. Wurman, “Vector Winds from a Single Transmitter Bistatic Dual–Doppler Radar Network,” Bulletin of the American Meteorological Society, July 1994

295) J. Wurman, M. Randall, C. Frush, E. Loew, C. Holloway, “Design of a Bistatic Dual–Doppler Radar for Retrieving Vector Winds using One Transmitter and a Remote Low–Gain Passive Receiver,” Proceedings of IEEE, Dec. 1994

296) J. Wurman, S. Heckman, D. Boccippio, “A Bistatic Multiple–Doppler Radar Network: Part 1, Theory,” Journal of Applied Meteorology, Dec. 1993

297) A. Komjathy, J. L. Garrison, V. Zavorotny, “GPS: A New Tool for Ocean Science,” GPS World, April 1999, pp. 50–56

- Reflected ocean wave spectra,²⁹⁸⁾ caused by Bragg scattering, were already performed with LORAN–A (Long–Range Navigation) radionavigation systems in the 1960s. The LORAN–A bistatic experiments demonstrated that the Doppler shift of the radar echo is exactly equal to the wave frequency; it is also related to the bistatic angle. See LORAN background in chapter 1.27.1.
- The D2P (Delay–Doppler Phase–monopulse Radar) payload is an airborne bistatic Ku–band radar altimeter system of JHU/APL, sponsored by NASA. D2P is a proof–of–concept instrument featuring the new altimetric concepts of: a) pulse–to–pulse coherence and full Doppler processing to allow for the measurement of the along–track position of the range measurement, and b) use of two antennas and two receiver channels that allow for measurement of the across–track angle of the range measurement (bistatic configuration). Measurement campaigns were conducted in April 2000 and May 2002 (see P.63).^{299) 300)}
- **Bistatic and multistatic SAR systems.** SRTM (Shuttle Radar Topography Mission), a cooperative project of NASA, DLR and ASI on STS–99 (Feb. 11–22, 2000, see J.27), was the first spaceborne bistatic SAR mission (single–pass InSAR) where both SAR systems operated with the main antenna of each instrument located in the open cargo bay of the Shuttle, and a second receive antenna mounted on a deployable outboard mast, respectively (a single–pass interferometer on a 60 m baseline in cross–track and 7 m along–track).
- The SIRAL (SAR Interferometer Radar Altimeter) instrument of ESA’s CryoSat mission (launch on Oct. 8, 2005 – but launch failure) is a bistatic radar Ku–band altimeter using two Cassegrain antennas, mounted side–by–side and forming the interferometric cross–track. Both antennas are identical; one is used to transmit and receive, whereas the other antenna is used to receive echoes (bistatic configuration, see E.2). Note: The SIRAL instrument has two major heritage lines. 1) The hardware is essentially that of Poseidon. Alcatel’s nickname for SIRAL is Poseidon 3 (Alcatel is the manufacturer of SIRAL). 2) The SIRAL design concept is essentially that of the D2P radar, with delay–Doppler as the driving theme along–track, and the cross–track interferometer proven by D2P campaigns.

Bistatic interferometric systems such as the SRTM, D2P and SIRAL are referred to as short–baseline systems. Examples of long–baseline systems are: the Cartwheel constellation of CNES, the BINET approach of NCAR, and the TechSat–21 constellation of AFRL. The short–baseline interferometers are “bistatic” only in a narrow sense; they do not enjoy the major advantages of long–baseline systems.

Interferometric capabilities are becoming a key requirement at the start of the 21st century to obtain topographic performance. A number of projects under development are planning to test the bistatic concepts in the spaceborne arena of close formation–flying satellite missions. A viable option in such a distributed concept is for example a master–slave implementation. A single so–called master spacecraft is equipped with an active radar (i. e., a transmitter and receiver function), while the rest of the constellation (slave spacecraft) is outfitted with just a radiometer (receiver). All observation instruments of the constellation are directed to look into the same footprint. Thus, all passive instruments in the constellation are also able to detect coherently the bistatic responses from the single active radar of the master spacecraft as well.³⁰¹⁾ The multi–location (or nodal) spacecraft data collected in this fashion provides automatically interferometric imagery after ground processing. The distributed apertures improve also the performance of the system with regard to detection

298) A. M. Peterson, C. C. Teague, G. C. Tyler, “Bistatic–radar observation of long–period, directional ocean–wave spectra with LORAN–A,” *Science*, Vol. 170, 1970, pp. 158–161

299) R. K. Raney, D. L. Porter, “WITTEX: An innovative three–satellite radar altimeter concept,” *IEEE Transactions on Geoscience and Remote Sensing*, Vol. 39 No11, 2001, pp. 2387–2391.

300) M. Martin–Neira, C. Mavrocordatos, E. Colzi, “Study of a Constellation of Bistatic Radar Altimeters for Mesoscale Ocean Applications,” *IEEE Transactions on Geoscience and Remote Sensing*, Vol. 36(6), 1998, pp. 1898–1904

301) Note: Coherent detection requires synchronization between master and slaves. The synchronization may either be achieved using a crosslink from master to slaves, or by accurate synchronization of all involved to the same source.

and resolution capabilities. A wealth of independently sampled angle-of-arrival data can be collected, the constellation forms a large but sparse coherent array. By virtue of its sparseness, the independent apertures look through different parts of the ionosphere, thus temporal and spatial variations on the scale of their separation could adversely affect their operation. This innovative bistatic observation concept has the potential to reduce the mass, power and cost of the constellation as a whole.

Examples of the first collaborating constellations demonstrating the new bistatic and multi-static SAR observation technologies (for along-track and cross-track interferometry) are under intensive study at the start of the 21st century.

- In Europe, CNES (in cooperation with ESA and DLR) is proposing/planning a so-called **Interferometric Cartwheel (ICW)** mission constellation of three passive microsatellites, each equipped with a receiver dish antenna (a slave receiver), to co-orbit with a soon-to-come conventional SAR mission (as host or “illuminator” or master satellite). The candidate conventional SAR missions considered for Cartwheel are: Envisat, Radar-Sat-2, TerraSAR-X and -L, and ALOS (in fact, any radar satellite mission provides a suitable context for a cartwheel mission). An “interferometric cartwheel orbit” of the passive constellation is employed. In such a cartwheel concept, the locations of the passive satellites are planned to be ahead or behind of the transmitter satellite at a fairly constant angle. Their orbits are the same as the transmitter spacecraft orbit, but with an eccentricity slightly different from that of the transmitter spacecraft orbit (the three passive satellites are moving relatively to a common reference point, in motion and coplanar with the transmitter S/C; the common reference is either lagging or preceding the transmitter S/C orbit at a constant angle). The new orbital concept is considered to offer a good geometric stability of the baselines, both vertically and horizontally, essential for interferometric processing (see O.10.8 for a definition of the Cartwheel orbit). The Cartwheel configuration is a single-pass InSAR implementation (a multi-static configuration); it offers increased geometric resolution of SAR images by: ^{302) 303) 304) 305) 306) 307) 308)}

- The along-track displacement of the receiving (parasitic) satellites
- Different Doppler centroids
- Super-resolution in azimuth by coherent combination of shifted Doppler spectra
- Cross-track displacement of the receiving satellites
- Different incidence angles
- Super-resolution in range by coherent combination of images with different range spectra
- A potential for moving analysis in the SAR imagery.

302) H. Runge, R. Bamler, J. Mittermayer, F. Jochim, D. Massonnet, E. Thouvenot, “The Interferometric Cartwheel for Envisat,” 3rd International Symposium of IAA, Berlin, April 2–6, 2001, pp.187–190

303) S. Ramongassie, L. Phalippou, E. Thouvenot, D. Massonnet, “Preliminary design of the payload for the interferometric Cartwheel,” Proceedings of EUSAR 2000, Munich, Germany May 2000, pp. 29–32

304) The term “cartwheel orbit” was initially coined by D. Massonnet of CNES in 1997

305) D. Massonnet, “Capabilities and Limitations of the Interferometric Cartwheel,” CNES paper presented at the CEOS Workshop in Toulouse, October 1999

306) J. Mittermayer, G. Krieger, M. Wendler, A. Moreira, E. Thouvenot, T. Amoit, R. Bamler, “Preliminary Interferometric Performance Estimation for the Interferometric Cartwheel in Combination with ENVISAT ASAR,” CEOS Workshop, Tokyo, Japan, April 2–5, 2001

307) D. Massonnet, “Capabilities and Limitations of the Interferometric Cartwheel,” IEEE Transactions on Geoscience and Remote Sensing, Vol. 39, No. 3, 2001, pp.506–520.

308) G. Krieger, M. Wendler, H. Fiedler, J. Mittermayer, A. Moreira, “Performance Analysis for Bistatic Interferometric SAR Configurations,” Proceedings of IGARSS 2002, Toronto, Canada, June 24–28, 2002

A SAR campaign, BASE (Bistatic Airborne SAR Experiment),³⁰⁹⁾ took place Feb. 11–14, 2003 as an ICW (Interferometric Cartwheel) preparatory project in the vicinity of Nimes, France. The campaign was conducted with an X–band SAR instrument on each aircraft, namely E–SAR of DLR on the Do–228 (Germany), and RAMSES of ONERA on a Transall (France) aircraft. One of the two systems served as transmitter and receiver while the other was operated in a passive receive–only mode. The main objective was to simulate the following footprint geometries:

- Along–track configuration. This geometry is very suitable in support of bistatic interferometric data acquisition; also, the synchronization strategies were tested.
- Cross–track configuration. This geometry is suitable for improved scene and target classification support by evaluating bistatic scattering coefficients.

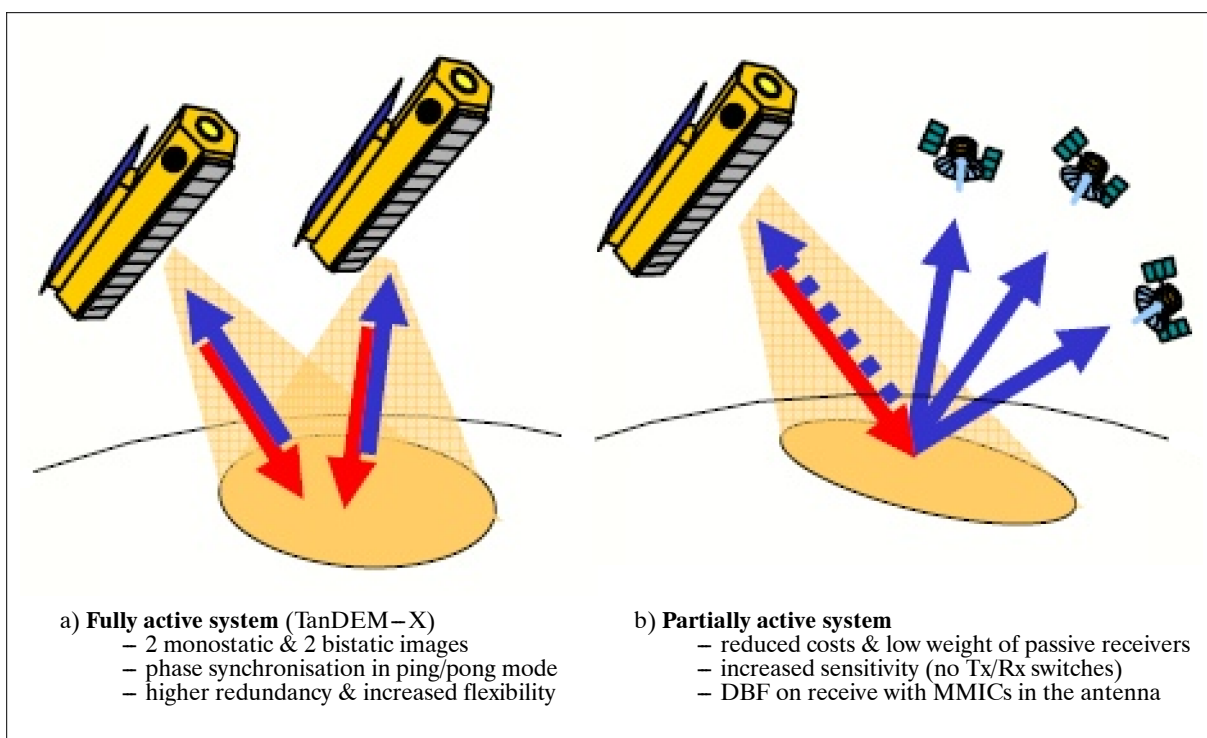


Figure 14: Bistatic and multistatic SAR systems (image credit: DLR)³¹⁰⁾

- The TanDEM–X mission concept of DLR (launch June 21, 2010) is based on an extension the TerraSAR–X mission (launch June 15, 2007) by a second TerraSAR–X–like satellite, namely TanDEM–X. A close orbit formation flight is planned for both satellites – thereby providing a flexible single–pass SAR interferometer configuration, where the baseline can be selected according to the specific needs of the application. In the TanDEM–X and TerraSAR–X spacecraft mission design, the SAR (Synthetic Aperture Radar) instruments of each spacecraft are fully compatible, both offer transmit and receive capabilities along with polarimetry. Availability of the following support modes: a) monostatic, b) bistatic, and c) alternating bistatic mode.³¹¹⁾

309) M. Wendler, G. Krieger, R. Horn, B. Gabler, P. Dubois–Fernandez, B. Vaizan, O. Ruault du Plessis, H. Cantaloube, “Results of a Bistatic Airborne SAR Experiment,” IRS (International Radar Conference) 2003, Dresden, Germany, Sept. 30. – Oct. 2, 2003

310) H. Fiedler, G. Krieger, M. Zink, “Constellation & Formation Flying Concepts for Radar Remote Sensing,” Proceedings of the Advanced RF Sensors for Earth Observation 2006 (ASRI), Workshop on RF and Microwave Systems, Instruments & Sub–Systems, ESA7ESTEC, Noordwijk, The Netherlands, Dec. 5–6, 2006

311) G. Krieger, A. Moreira, H. Fiedler, I. Hajnsek, M. Zink, M. Werner, M. Eineder, “TanDEM–X: Mission Concept, Product Definition and Performance Prediction,” Proceedings of EUSAR 2006, Dresden, Germany, May 16–18, 2006

1.4.3.7 SAR imaging and detection of moving targets (motion sensing)

The conventional cross-track SAR imaging technology is based on the assumption that an imaged target (i.e., a scene) is **motionless**, thus allowing the computation of the variation of the range during the observation (integration time) required for the in-phase (coherent) synchronization of the successive pulse returns. If an object is moving through the scene during its illumination by the radar, the range, and hence the relative phase of successive echoes, varies significantly (different rates), causing localization errors and out-of-focus blur. The latter may even lead to the invisibility for a vehicle of large radar cross section on the synthesized images.

Motion sensing and subsequent event recognition, however, is a very desirable goal in SAR imagery for many applications in the civil as well as in the military domains. Since the motion of moving objects interacts with the conventional image forming process in the SAR scene, resulting in both location errors and blurring, other concepts with considerably more functional capability had to be devised to solve the problem.

Today's motion sensing synthetic aperture radar concept, referred to as SAR/MTI (Synthetic Aperture Radar/Moving Target Indication/), uses two or more physical antenna phase centers aligned with the platform flight vector (i.e. in the along-track direction) in order to provide a means of detecting and/or measuring the radial component of object velocities within the observed scene (cross-track direction). This scheme permits time and azimuth position to be partly decoupled, which allows radial velocity of a scatterer to be distinguished from an offset in azimuth position of that scatterer.

In general, the measurement of object motion using SAR requires two operations. Firstly, detection of motion in the SAR scene, and secondly, parameter estimation such as location, speed and trajectory. Target detection and estimation can either be performed incoherently with a single SAR sensor, or coherently, with much higher fidelity, using two or more apertures.^{312) 313)}

Background: The pulsed Doppler radar technology was developed during World War II to better detect aircraft and other moving objects in the presence of echoes from sea and land that are illuminated by microwave emissions through sidelobes of the antenna's radiation pattern. Although pulsed Doppler radar was developed in the early 1940s, Doppler effects were observed in radio receivers when echoes from moving objects were received simultaneously with direct radiation from the transmitter or scattered from fixed objects. The earliest pulsed Doppler radars were called **MTI (Moving Target Indication)** radars in which a coherent CW (Continuous-Wave) oscillator, phase-locked to the random phase of the sinusoid in each transmitted pulse, is mixed (i.e., beat) with the echoes associated with that pulse. The mixing of the two signals produces a beat or fluctuation of the echo intensity at a frequency equal to the Doppler shift.

The first application of pulsed Doppler radar principles to meteorological measurements was made by Ian C. Browne and Peter Barratt of the Cavendish Laboratories at Cambridge University in England in the spring of 1953. Barratt and Brown showed that the shape of the Doppler spectrum agreed with the spectrum expected from raindrops of different sizes falling with different speeds.

The MTI technology has also its roots in post World-War-II political developments in the 1950s with regard to North American air defense/surveillance requirements [a) threat of manned bombers carrying nuclear weapons across the arctic region was of paramount concern in continental defense, b) some time later the threat of intercontinental ballistic missiles]. For the first threat, MIT/LL (Massachusetts Institute of Technology/Lincoln Labora-

312) J. H. G. Ender, "Detection and estimation of moving target signals by multi-channel SAR," Proceedings of EU-SAR'96 Conference, Königswinter, Germany, March 1996, pp. 411-417.

313) E. F. Stockburger, D. N. Held, "Interferometric moving ground target imaging," Proceedings of the IEEE International Radar Conference, May 8-15, 1995, Alexandria, VA, pp. 438-443.

tory) developed the so-called DPCA (Displaced Phase Center Antenna) technique which was used to improve the detection performance of airborne MTI radars that are subject to clutter. In the second case, MIT/LL formulated a concept of what became later known as BMEWS (Ballistic Missile Early Warning System), this ground radar warning system was eventually built and installed by industry in Greenland, the UK, and in Alaska. In the 1970s several innovative waveform and signal processing techniques were synergistically combined to significantly improve the detection of moving targets in the presence of large clutter echoes. An early advanced MTI system of MIT/LL is referred to as MTD (Moving Target Detection), a concept that is currently being used extensively in airport-surveillance radars.^{314) 315)}

Pulsed Doppler radars (or simply “pulse Doppler radar”) are very useful radar systems as they combine their ability to determine target velocity with the other functionality of a standard pulse-modulated radar. A pulsed Doppler radar can, therefore, determine range, angle and velocity of a target. This makes the pulsed Doppler radar extremely valuable in situations involving many small moving targets hidden by heavily cluttered environments.

- Today’s MTI (Moving Target Indication) measurement concept utilizes the pulsed Doppler radar technique, mostly in combination with a high-resolution SAR imaging capability (due to its all-weather and day/night observation capability) to detect and locate the motion of moving targets (cars, trucks, etc.) in the ground segment, as well as airborne or spaceborne vehicles within the SAR image. In general, MTI systems have the capability to provide location and tracks of moving space/air/ground vehicles, but not to identify them. Of course, the SAR/MTI concept may also be complemented with other imaging sensors (IR, VIS, etc.) for possible identification enhancement. Potential future motion sensing capabilities may also be provided by polarimetric SAR systems and along-track interferometric SAR systems (used for single-pass extraction of topographical information). Some SAR/MTI basics are:

- MTI discriminates moving targets from background by the Doppler frequency shift induced by radial motion
- MTI employs a narrow beam which a large antenna
- The S/C motion complicates MTI: fast-moving platforms require additional clutter suppression using multiple antennas or an antenna divided into subapertures.
- MTI target tracking can be accomplished by repeated beam scans
- Advanced MTI systems employ STAP (Space-Time Adaptive Processing) techniques to cancel the background clutter (conventional STAP implementations require a very high computational load, see also Glossary on STAP). STAP offers a means of detecting targets that compete with clutter located within the skirts of the mainlobe. The introduction of STAP allows antenna apertures to be reduced by perhaps as much as 50 to 75 percent.
- A promising solution to detect moving targets with a SAR/MTI system is the use of a multi-channel system with phase centers separated in along-track direction and the exploitation of the data via algorithms like along-track interferometry or STAP.

A SAR image is formed by processing many radar pulse echoes from a target. Each pulse provides information as to the range to the target, and the pulse-to-pulse variations at a given range provides the necessary information to extract the azimuth target position. A moving target may pass through many range resolution cells during this data collection process (which may be in the order of many seconds) producing a blurred image using conventional ground focused SAR image formation techniques.

314) M. I. Skolnik, “Radar and MIT Lincoln Laboratory: A View from a Distance,” Lincoln Laboratory Journal, Vol. 12, No 2, 2000, pp. 143–145

315) W. P. Delaney, W. W. Ward, “Radar Development at Lincoln Laboratory: An Overview of the First Fifty Years,” Lincoln Laboratory Journal, Vol. 12, No 2, 2000, pp. 147–166

Obviously, the MTI technology is of great interest in reconnaissance/surveillance applications, in the military as well as in the civil communities. Potential MTI applications include: environmental monitoring, change detection, oceanography, analysis of meteorological features, marine traffic monitoring, monitoring of vehicles on land, air traffic monitoring, treaty verification, etc.). At the start of the 21st century, most existing MTI systems were developed for military peace-keeping reconnaissance applications and are flown on aircraft or on UAVs (Unmanned Aerial Vehicles). Some AGS (Airborne Ground Surveillance) implementations are:

- JSTARS (Joint Surveillance and Target Attack Radar System) is a joint development of the US Air Force and Army. Since 1996, the system has been installed in 13 aircraft (Boeing 707-300 aircraft series E-8C – the aircraft employs a canoe-shaped radome of 12 m in length).³¹⁶⁾³¹⁷⁾ JSTARS was first deployed in Operation Desert Storm in 1991 when still in development (2 aircraft were used in Desert Storm with a JSTARS demonstrator). JSTARS was designed and built at Northrop Grumman Norden Systems in Norwalk, CT (delivery of the 13th aircraft in April 2002). – The new next-generation JSTARS will be an electronically scanned 2-D X-band active aperture radar which features a helicopter detection mode with an ISAR (Inverse Synthetic Aperture Radar) imaging capability, as well as an MTI mode, allowing realtime imaging of moving objects.
- TESAR (Tactical Endurance Synthetic Aperture Radar) of Northrop Grumman, operational since 1996. The radar payload operates in both synthetic aperture radar (SAR) and moving target indication (MTI) modes. In SAR mode, continuous, fully focused, high-resolution (0.3 m), near real-time stripmap imagery is formed on either side of the aircraft. The radar provides two SAR stripmap modes and a spot map mode. In MTI mode, the radar provides target reports overlaid on a digital map.
- The EL/M-2055 is a high performance SAR and MTI tactical airborne reconnaissance system, developed by ELTA Electronics Industries Ltd., a subsidiary of Israel Aircraft Industries Ltd. The system is available as of 1999. It provides real-time SAR image generation offering strip mode, spot mode and MTI mode operations support.
- HISAR (Hughes Integrated Synthetic Aperture Radar) is an airborne reconnaissance/surveillance system (of Raytheon) designed to provide high-resolution SAR imagery in real-time displayed on a workstation onboard an aircraft (support of military and civil applications). Baseline HISAR modes include wide-area search to provide a rapid overview of a large area. An operator can map land areas as large as 110 km x 70 km in seconds with resolutions of 15–50 m depending on range to the target. Baseline HISAR modes also include stripmap for border or coastline surveillance or environmental monitoring. In this mode, HISAR maps a continuous swath at an aircraft's speed up to 37km wide and 110km away from the ground track. The resolution of the pixels is 6m x 6m. MTI is also available in this mode. HISAR is available as of 2000.
- AER-II (Airborne Experimental Radar-II) designed and developed by FGAN (German Defense Research Facility for Applied Science), Wachtberg near Bonn, Germany.³¹⁸⁾³¹⁹⁾ This X-band SAR system (10 GHz) possesses a fully polarimetric phased array with variable subaperture partitioning. A vertical displaced auxiliary antenna of identical geometry allows the use of the interferometric mode. Four receive channels may be used

316) <http://www.airforce-technology.com/projects/jstars/>

317) Note: ISAR is a well-established technique to identify the reflectivity centers of the target with high spatial resolution. A fine 2-D reflectivity map of the target is generated by using large bandwidth transmitted signal, to have high range resolution, and by coherently processing the echoes received from different aspect angles of the target, to achieve fine cross-range resolution. An ISAR image is a 2-D representation of the target, with the resolution in the horizontal dimension determined by the short pulse characteristic of the radar and the vertical dimension by the Doppler of the radar returns. The result is a recognizable image at long range under all weather conditions.

318) J. H. G. Ender, "The airborne experimental multi-channel SAR-system AER-II," Proceedings of EUSAR'96 Conference, Koenigswinter, Germany, March 1996, pp.49–52

319) http://www.fhr.fgan.de/fhr/el/c_el_facil_aer00_e.html

simultaneously with four subapertures for an improved moving target indication (MTI), in addition four polarimetric channels are provided in parallel. By exploiting the electronic steering in azimuthal direction, operational modes are possible which cannot be employed with conventional SAR systems with fixed look directions. AER–II comes with four parallel receive channels in the analog and digital domain. Thus, it is possible to create four complex coherent SAR images of the same scene within one acquisition. AER–II is operational since 1998 installed on a Transall C–160 aircraft (it was preceded by AER since 1996). The AER–II instrument provided the first spotlight demonstration in Europe with its electronic beamsteering capability.

A further FGAN instrument with improved capabilities is PAMIR (Phased Array Multifunctional Imaging Radar). Since 2003, a new SCAN/MTI mode has been implemented and experimentally tested. This mode provides a significant improvement to the usual MTI mode with fixed beam, since the antenna is regularly steered to different azimuth angles, allowing to scan much larger scenes (see P.166).³²⁰⁾

- MiniSAR (Miniature, Lightweight, Scalable SAR System) is being developed by TNO–FEL (Netherlands Organization for Applied Scientific Research – Physics and Electronics Laboratory), The Hague, The Netherlands (and a consortium of industrial partners). The demonstrator system will be integrated in a two–seater motor glider platform. MiniSAR operates in X–band with a center frequency of about 9.75 GHz. The design aims at achieving a bandwidth of 500 MHz for the first demonstrator system. The system covers a swath of at least 1 km in high resolution mode and a swath of about 4 km in stripmap mode. MiniSAR features also an MTI mode capable of operating simultaneously with the typical SAR modes.

- ASTOR (Airborne Stand Off Radar) is a joint program of the British Army and Royal Air Force (RAF). ASTOR is similar in concept to JSTARS, its objective is to develop a surveillance capability (SAR/MTI on aircraft). Raytheon Systems Ltd. UK was awarded the prime contract in 1999 to build the system (five ASTOR systems along with two portable ground sites and six tactical ground stations), funded by MoD (Ministry of Defence), London, UK. The ASTOR system features a low–resolution wide–swath mode, and a spot mode for high resolution imaging of specific targets. Initial flights are expected in 2004 on a “Global Express” business jet of Bombardier.³²¹⁾

- SOSTAR (Stand–Off Surveillance and Target Acquisition Radar) is a European SAR/MTI system under development for airborne ground surveillance support functions in the context of NATO. SOSTAR is to provide detection and tracking of slow–moving targets, high–resolution imaging and target classification. A group of five companies from Germany, France, Italy, Spain and The Netherlands have developed a plan, in close cooperation with their governments and Ministries of Defence, for the realization of a ground surveillance system, SOSTAR. In Feb. 2001, a new joint venture company was established called SOSTAR GmbH, Friedrichshafen, Germany. The consortium consists of the following companies: EADS/Dornier (Germany), Thales Airborne Systems (Elancourt, France), FIAR (Milan, Italy), INDRA (Madrid, Spain), and Fokker Space (Leiden, The Netherlands). The SOSTAR contract was awarded by BWB (Bundesamt für Wehrtechnik und Beschaffung – German Federal Office of Defence Technology and Procurement, Koblenz), acting on behalf of all governments. Initial activities of the program started in 1999. The first demonstrator system, SOSTAR–X, is expected to be available in 2005.³²²⁾ The demonstrator will perform all the required functions of the full scale model, including the simultaneous interleaved operation of SAR and MTI, but has a smaller antenna size (than the final version) to reduce costs. SOSTAR–X will be installed on a Fokker–100 aircraft for evaluation and demonstration purposes.

320) D. Cerutti–Maori, U. Skupin, “First Experimental SCAN/MTI Results Achieved With the Multi–Channel SAR–System PAMIR,” Proceedings of EUSAR 2004, Ulm, Germany, May 25–27, 2004

321) <http://www.airforce-technology.com/projects/astor/>

322) M. Kirscht, “Core Electronics for SOSTAR–X,” Proceedings of EUSAR 2004, Ulm, Germany, May 25–27, 2004

At the start of the 21st century, there is an increasing interest in spaceborne MTI applications such as LEO satellite constellations for global coverage. These SAR/MTI systems could of course provide an unobstructed view of any area of interest along with real-time information availability. However, there are considerable technical challenges for a spaceborne SAR/MTI system implementation. Very large antenna sizes would be needed for a single spacecraft for an acceptable performance of MTI as well as for azimuth estimation in an X-band SAR system. A multi-satellite system (in formation flight) with a sparsely distributed antenna array would be able to measure up to such a task.³²³⁾

- A spaceborne MTI project under development was the DoD Discoverer-II space-based radar technology demonstration program of DARPA, USAF and NRO which started in 1998, the design featured also a SAR/MTI capability. However, the US Congress cancelled the two-spacecraft program in 2000 due to fear of large cost overruns.
- TechSat-21 (Technology Satellite of the 21st Century) was a DoD initiative under AFRL management with the objective to exploit new paradigms (formation flight of a three microsatellite constellation) and enabling technologies such as SAR/MTI. Demonstration of sparse-aperture sensing to combine InSAR and GMTI (Ground Moving Target Indication) using innovative waveforms and signal-processing technologies. A launch was projected for 2006; **however, the TechSat-21 program was cancelled in early 2003** due to cost overruns and the technical challenges involved.

1.4.3.8 Digital Beam Forming (DBF)

Digital beamforming (DBF) is an enabling technology for modern SAR system functions such as MTI (Moving Target Indication) and many other applications in remote sensing. Beam steering in DBF systems can be achieved using signal processing techniques in the digital domain. The DBF scheme represents an advanced technology in avoiding tolerance problems and temperature effects – thus reducing significantly the time-consuming procedures in very complex RF calibration tests still needed today (2007) for phased array sub-units such as T/R modules, radiators, etc.

SAR beamforming techniques: Today's conventional multiple-mode SAR systems, like ScanSAR, employ an electronically steered phased array antenna using T/R (transmit/receive) modules and enabling **analog beamforming (ABF) with the T/R modules**. The analog techniques previously developed for the electronic steering of phased arrays relied on components such as line stretchers, phase shifters, time delay lines, and attenuators. Such a system design offers the advantage of distributed power radiation and hardware redundancy. However, the overall efficiency of the system is still low and the complexity is rather high. A major disadvantage of the analog beamforming system is the inherent loss of information during the beamforming process.^{324) 325)}

The general tendency is to move the digital interface further towards the antenna (i.e. very early in the receive chain, at the array element level), replacing, whenever possible, analog RF hardware. Instead of analog beam forming future SAR instruments will utilize DBF on **receive where the receiving antenna is split into multiple sub-apertures**. In this concept, one transmit antenna is fed through a high power amplifier. On receive, the signals from each of the sub-arrays are separately amplified, down-converted and digitized for processing. The footprint of all receive sub-arrays is identical (coverage of the entire transmit target area); hence, each antenna covers the same spatial target area both in azimuth and

323) J. H. G. Ender, "Space-based SAR/MTI using Multistatic Satellite Configurations," Proceedings of EUSAR 2002, Cologne, Germany, June 4–6, 2002; also Proceedings of IGARSS 2002, Toronto, Canada, June 24–28, 2002

324) M. Younis, C. Fischer, W. Wiesbeck, "An Evaluation of Performance Parameters of Reconfigurable SAR Systems," Proceedings of IGARSS 2002, Toronto, Canada, June 24–28, 2002

325) M. Younis, C. Fischer, W. Wiesbeck, "An Evaluation of Performance Parameters of Reconfigurable SAR Systems," Proceedings of EUSAR 2002, Cologne, Germany, June 4–6, 2002

elevation. This scheme enables an a–posteriori combination of the recorded sub–aperture signals to form multiple beams with adaptive shapes. The additional information about the direction of the scattered radar echoes can then be used to: 1) suppress spatially ambiguous signal returns from the ground in range and/or azimuth direction, 2) to increase the receiving antenna gain without a reduction of the imaged area, 3) to suppress spatially localized interferences, and 4) to gain additional information about the dynamic behavior of the scatterers and their surroundings. By this, it becomes possible to overcome the fundamental limitations of conventional SAR systems. ^{326) 327)}

The introduction of DBF technology will widen the application of next generation spaceborne SAR systems significantly. Physical limitations of today’s conventional SAR systems – e.g. the seeming contradiction between high geometric along–track resolution and continuous wide swath coverage – will be overcome along with improved performance provision.

Scan–on–receive technique: An attractive and promising instrument concept is the so–called **HRWS** (High Resolution Wide Swath) SAR instrument, a multi–channel bistatic SAR system which uses in its architecture separate antenna subsystems (T/R modules) for transmit and receive (bistatic radar refers to separate transmit and receive elements). This DBF concept allows a separate optimization scheme of the antenna electrical design in its subsystems. A wide beam transmit antenna (wide–area illuminator) is used to illuminate a large target area. The receive antenna uses DBF elements offering a **SCORE** (Scanning On Receive in Elevation) capability and features multiple phase centers in azimuth (along–track), hence permitting for a low PRF (Pulse Repetition Frequency) level and wide swaths. The acquisition of multiple phase centers in azimuth uses the concept of **DPCA** (Displaced Phase Center Antenna) allowing the imaging of a wider swath without rising azimuth ambiguities. ^{328) 329) 330) 331) 332)}

HRWS technology development has been conducted in particular at Astrium GmbH since 2005 in the frame of closely linked ESA and DLR projects. Reference requirements and related strawman instruments in X– and C–band have been defined as basis for the breadboarding activities (Ref. 328).

– Under ESA contract, an active frontend for the receive antenna has been designed. In the current project phase, a subassembly consisting of five RF units and a five channel Digital Beamforming Unit is being breadboarded. Manufacturing of the units will be finalized in the summer 2008, followed by the overall integration of the breadboard and its evaluation in the anechoic chamber.

– Under DLR contract, a HRWS demonstrator, i.e. an integrated, pre–qualified receive X–band antenna panel, will be realized in 2012 (TRL–5). The reference HRWS instrument uses a monostatic, T/R–module based antenna, with several panels (phase centers) in flight direction for on–ground beamforming in the Doppler domain. Each panel comprises several receive channels in elevation, which are combined by on–board DBF in realtime in

326) A. Moreira, “Spaceborne Radar Technologies for Earth Remote Sensing,” Proceedings of the International Radar Symposium 2007 (IRS 2007), Cologne, Germany, Sept. 5–7, 2007

327) M. Younis, Y. Venot, W. Wiesbeck, “A Simulator for Digital Beam Forming SAR,” International Radar Symposium (IRS 2003), Dresden, Germany, Sept. 30 – Oct. 2, 2003

328) C. Fischer, C. Schaefer, C. Heer, “Frontend Development for the High Resolution Wide Swath SAR,” Proceedings of EUSAR 2008, 7th European Conference on Synthetic Aperture Radar, June 2–5, 2008, Friedrichshafen, Germany

329) G. Krieger, N. Gebert, M. Younis, F. Bordoni, A. Patyuchenko, A. Moreira, “Advanced Concepts for Ultra–Wide–Swath SAR Imaging,” Proceedings of EUSAR 2008, 7th European Conference on Synthetic Aperture Radar, June 2–5, 2008, Friedrichshafen, Germany

330) C. Fischer, C. Heer, G. Krieger, R. Werninghaus, “A high resolution wide swath SAR,” Proceedings of EUSAR (European Conference on Synthetic Aperture Radar), Dresden, Germany, May 15–18, 2006.

331) N. Gebert, G. Krieger, A. Moreira, “Digital Beamforming for High Resolution Wide Swath SAR Imaging,” GeMIC 2005 (German Microwave Conference), Ulm Germany, April 5–7, 2005

332) C. Heer, F. Soualle, R. Zahn, R. Reber, “Investigations on a new high resolution wide swath SAR concept,” Proceedings of IGARSS’03, Toulouse, France, July 21–25, 2003

order to realize the "scan-on-receive" function. Each receive channel consists of an RRDCU (RF Down-Conversion Unit) for amplification, filtering and down-mixing the receive signals, and a DBFU (Digital Beamforming Unit (DBFU) for IF signal digitization and signal processing. ³³³⁾

In a further stage of the HRWS demonstrator, the digital beamforming elements will be integrated in a representative panel structure, together with radiating elements and RF front-ends, ready for tests in an anechoic chamber and pre-qualification activities (Ref. 333).

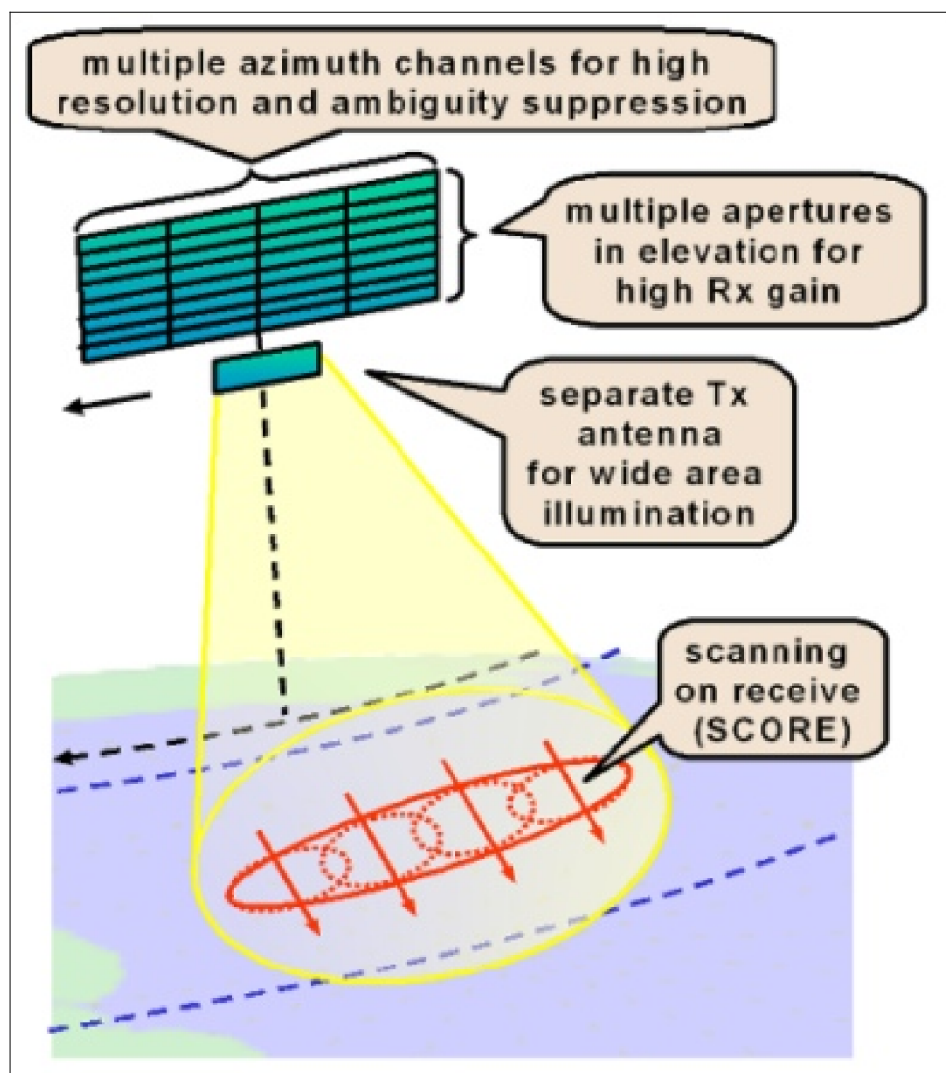


Figure 15: Conceptual view of a HRWS (High Resolution Wide Swath) system with separate transmit antenna and scanning on receive by means of digital beamforming (image credit: DLR, EADS Astrium)

Digital beamforming on transmit allows furthermore a flexible distribution of the RF signal energy on the ground. This enables not only a switching between different SAR modes like spotlight, ScanSAR and HRWS stripmap, but it allows also for the simultaneous combination of multiple imaging modes in one and the same data acquisition.

AESA (Active Electronically Scanned Array): AESA is a novel radar antenna concept with considerably improved performance permitting very flexible support modes. The AESA concept offers full flexibility on spatial and time performance management. AESA based radars with very thin antenna arrangements have the highest power-aperture product of any radar system, allowing the detection of very small objects at large ranges. AESA offers

333) Christian Fischer, Christoph Heer, Rolf Werninghaus, "X-Band HRWS Demonstrator: Digital Beamforming Test Results," Proceedings of EUSAR 2012 (9th European Conference on Synthetic Aperture Radar), Nuremberg, Germany, April 23-26, 2012

several GHz bandwidths, quasi instantaneous beam steering and adaptive beamforming with deterministic nulling capabilities. The availability of future broadband RF modules with GaN high power amplifier circuits and the rapidly growing availability of Rx A/D circuits enables the realisation of very broadband aperture functionalities in the long term.³³⁴⁾

AESA principle: By controlling the relative phase of the transmitted/received signals, the beam direction can be changed without any moving parts. An AESA radar consists of an array of T/R modules linked by high-speed processors (space-time processing). The various T/R modules in the array can be configured and assigned to different tasks (ranging, mapping, multi-target tracking, etc.) with more modules allocated to tasks that require greater power or sensitivity. The concept permits also the simultaneous support for several tasks. – The availability of today's high-speed digital processing acts as an enabler for digital beamforming, enhancing radar functionality and instantaneous coverage in bistatic applications. A DBF radar or SAR (i.e. an AESA) uses multiple receive channels simultaneously, each corresponding to an elemental radar whose data are digitized and processed to be digitally combined for final output. This is why DBF radars are so flexible. The number of beams is virtually unlimited and their characteristics can be optimized for each mission, type of target and environment.

The major difference of DBF to conventional T/R module systems is that the beamforming is performed during the digital processing. *The DBF configuration is a bistatic configuration since separate antennas are used for transmit and receive functions.* The two antennas can be mounted on one carrier or placed on two platforms. A further advantage is the possibility of separate optimization of transmitter and receiver subsystems. For example a high-efficiency high-power amplifier can be used on the transmit side, whereas low noise amplifiers can be integrated into the receive sub-arrays. The DBF concept includes the advantages of T/R module based systems while increasing the coverage. It is adaptable to various requirement sets and the system can be reconfigured by software. Digital beamforming provides superior performance over traditional analog sub-array beamforming. It allows the radar to maintain its performance in the presence of a strong clutter environment (as well as in severe electronic countermeasures). The digital beamforming technique offers the potential of virtually an infinite number of independent beams, all with different shapes.

DBF concepts provide several advantages like fast beamscanning, adaptive beamforming, and multiple beam generation on a software basis.^{335) 336) 337)} At the start of the 21st century, the design of a DBF phased array system poses great challenges with respect to antenna array design, the electronic circuitry, the general modular construction architecture, and the processing hardware and software for the DBF part. This is due to the complex nature of the integration and packaging tasks involved; each antenna element in a DBF array must be equipped with dedicated transmitter/receiver circuitry, great demands are put on the selection of materials, components and technologies that allow a cost-efficient implementation. In particular, high frequency implementations (Ka-band) require a high degree of packaging densities involving component miniaturization (i.e. MEMS technology). In spite of all complexities involved, DBF demonstrator systems are of great interest in many spaceborne applications, in remote sensing, in surveillance, as well as in communications.

- The UAVSAR (Unmanned Aerial Vehicle Synthetic Aperture Radar) of NASA, an L-band SAR instrument, mounted in an underbelly pod and flown on a Gulfstream-III

334) H. Brugger, M. Böck, "Technology Trends for Future Radar Applications," Proceedings of the International Radar Symposium 2007 (IRS 2007), Cologne, Germany, Sept. 5–7, 2007

335) R. Gehring, E. Sommer, H. Wolf, A. Wolfram, P. Rinous, "A combined Transmit/Receive Feed System for Personal Mobile Communications in L/S-band in Consideration of Increased Power Applications," 25th Antenna Workshop on Satellite Antenna Technology, Sept. 18–20, 2002, ESA/ESTEC, Noordwijk, The Netherlands

336) A. Dreher, D. Heberling, S. Holzwarth, C. Hunscher, A. F. Jacob, et al., "Ka-band DBF terminal concepts for broadband satellite communications," 25th Antenna Workshop on Satellite Antenna Technology, Sept. 18–20, 2002, ESA/ESTEC, Noordwijk, The Netherlands

337) C. Kuhnert, K. Schuler, W. Wiesbeck, "Overview of Beamforming Principles," Proceedings of EUSAR 2006, Dresden, Germany, May 15–18, 2006

research aircraft at NASA/DRFC (first test flights in Sept. 2007), represents the first civilian implementation of the AESA concept. The antenna is electronically steered along-track to assure that the antenna beam can be directed independently, regardless of speed and wind direction.

- An early implementation of the DBF concept, using the AESA technology of Northrop Grumman, is the USAF F-35 aircraft, under development by Lockheed Martin (the F-35 is expected to enter service in 2008).³³⁸⁾

1.4.4 SAR technology roadmap

The history of SAR technology, also projected into the future, shows an implementation scenario based on the various orbital observation levels: each level with increasing system complexity, new technology introduction (also new measurement methods), more advanced and enabling capabilities and potentials, and also with a considerably greater harvest of information and derived knowledge.³³⁹⁾

1) Demonstration of new SAR technology in ground-based and airborne systems (an ongoing activity that started in the 1950s)

2) LEO SAR satellite systems. The considerably higher altitudes of spaceborne SAR mission orbits provided the capability of much wider swaths (coverage).

- Starting in 1978 with the launch of the NASA demonstration mission SeaSat. Later (1990s) long-term SAR observations evolved into a well-established technology and service infrastructure due in particular to the ERS-1/2 missions of ESA, the JERS mission of NASDA, and the RADARSAT-1 mission of Canada.

- The SIR-A (Shuttle Imaging Radar) mission of NASA/JPL (STS-2, Nov. 12, 1981, 3-day mission) was the first SAR mission with a side-looking SAR antenna (fixed angle look angle configuration).

– The SIR-B mission of NASA/JPL (STS-41-G, Oct. 5, 1984, 1 week mission) provided **for the first time the ability to mechanically tilt the SAR antenna over a range of 15 – 55°** so that radar imagery from multiple angles of incidence could be obtained.

– Introduction of a distributed analog T/R (Transmit/Receive) module **phased array antenna architecture** on the SIR-C/X-SAR on flight STS-59, Apr. 9–20, 1994). In the multiple T/R module approach, the total peak transmit power is shared among all the modules, and each one only needs to transmit at a relatively low peak power. – Note: The first long-term mission using T/R technology in an active phased array configuration is Envisat of ESA (launch March 1, 2002).

– The distributed C- and L-band SIR-C radars allowed **electronic beam steering in the range direction** (123°) from a fixed antenna position of 38° (look angle), thus making it possible to acquire multi-incidence angle data without tilting the entire antenna. First demonstration of **ScanSAR** operating mode for wide swath data acquisition.

– The SIR-C/X-SAR mission represents also the first spaceborne **multi-frequency** and **multipolarization** SAR observations from the same platform.

- Introduction of configurations with interferometric capabilities [ERS-1/2 with repeat pass interferometry, SRTM with single-pass short-baseline interferometry (on Shuttle

338) <http://www.fags.org/docs/air/avf35.html>

339) M. Ludwig, C. H. Buck, C. Mangenot, M. Suess, "Impact of New Technologies on Future Spaceborne Radar Design," Proceedings of IEEE/IGARSS 2003, July 21–25, 2003

flight STS–99, Feb. 11–22, 2000)]. Interferometric SAR (InSAR) advanced SAR data processing techniques through analysis of phase differences between SAR images of the same scene – thus, obtaining terrain elevations [generation of DEMs (Digital Elevation Models)].

- Introduction of ScanSAR technology in long–term missions like RADARSAT–1 of Canada (launch Nov. 4, 1995). ScanSAR provided a much greater flexibility in observation support (subswaths) and swath widths of up to 500 km.
- The **TRM** (T/R Module) is a key component of SAR phased array antenna modularity and performance.³⁴⁰ Its efficiency has direct implications on the power dissipation and power generation requirements of the system.

In 2001/2, NASA started an ACT (Advanced Component Technology) program to improve the overall performance and architecture of L–band T/R modules. The goals are: integration of power amplifiers into T/R modules, reduction of power consumption (30 W of peak transmit power), miniaturization of T/R modules (<100 g of mass, size of 10 cm x 2 cm x 0.1 cm), large bandwidth (80 MHz), and overall module efficiency of 70% or better.

EADS Astrium GmbH in Ulm, Germany, started the SMTR (Standardized Modular Transmit/Receive) module development, along with the FEU (Frontend Electronics Unit) and CE (Control Electronics) subassemblies, all assembled into a common housing, and firstly installed in the TSX–SAR antenna of the TerraSAR–X spacecraft (launch June 15, 2007, see Figure 16). The development work was funded by DLR and Astrium. The most important requirements for SMTR were:³⁴¹

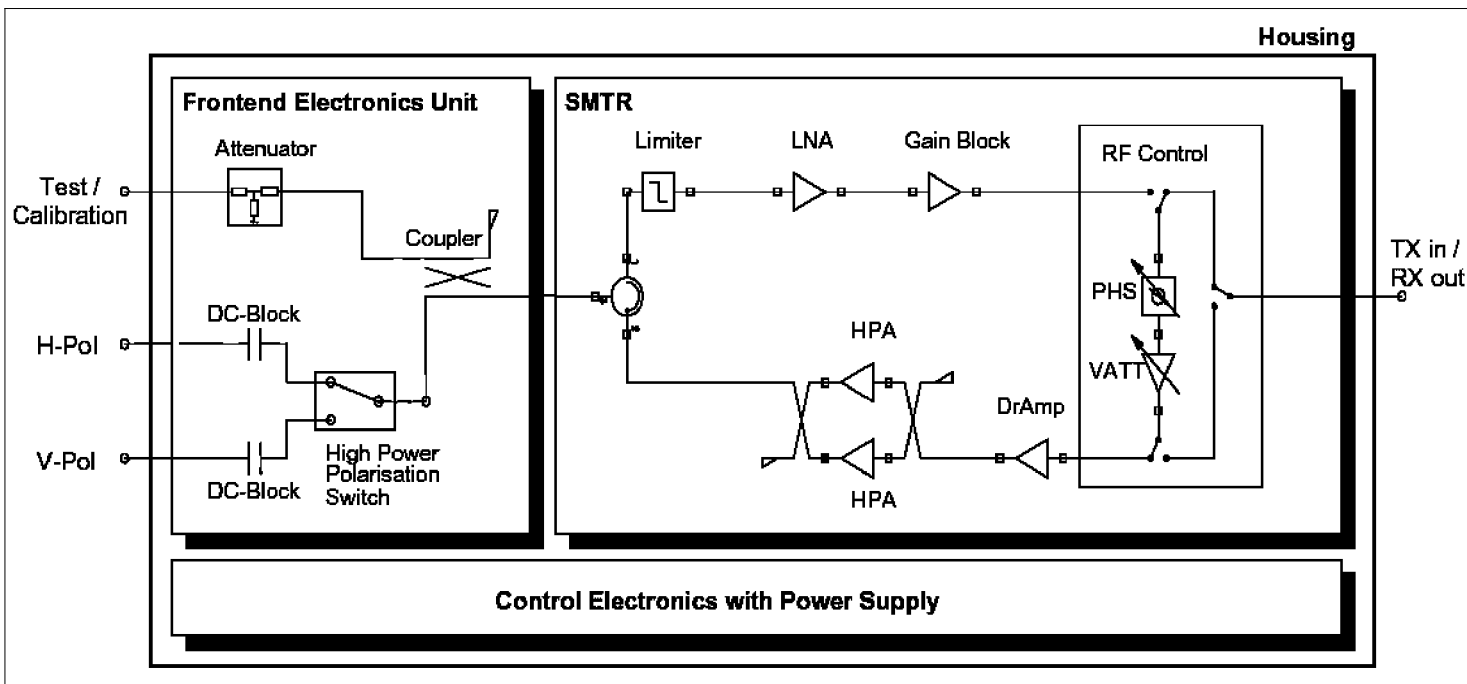


Figure 16: T/R module RF architecture for the TerraSAR antenna (image credit: EADS)

- High precision of amplitude and phase adjustment over the temperature range -20°C to $+60^{\circ}\text{C}$.
- Full polarimetry of operation (HH, VV, HV, VH) and switching capability of polarization from pulse to pulse

340) W.N. Edelstein, C. Andricos, S. Madsen, F. Wang, D. B. Rutledge, “Current Status of the High–Efficiency L–band Transmit/Receive Module Development for SAR Systems,” Proceedings of ESTC (Earth Science Technology Conference, College Park, MD, June 24–26, 2003

341) M. Wahl, M. Adolph, K. Biller, U. Hackenberg, R. Rieger, B. Schweizer, B. Adelseck, H. Brugger, M. Loercher, “High Precision T/R Module for SAR Earth Observations,” Proceedings of EUSAR 2006, Dresden, Germany, May 15–18, 2006

- High overall efficiency
- High reliability of the mission lifetime
- Low mass
- Affordable cost
- Uniform T/R module performance.

The key features of this new T/R development are polarization agility with excellent channel isolation, high gain and phase accuracy, low noise amplification during receive operation and internal temperature drift compensation over a wide temperature range.

- As of 2008, **WiSARTM** (Wireless Synthetic Aperture Radar) is a new SAR payload design and architecture of MDA (MacDonald Dettwiler and Associates, Ltd.), Richmond, BC, Canada. The objective is to provide a leading-edge performance in both X- and C-band SAR imagery at a significantly lower cost than the conventional state of the art. The key technology breakthrough is a modular, low mass phased array antenna technology that enables high performance multi-mode SAR imaging from a smallsat platform.

A number of key architectural elements make WiSAR possible, including the use of space feed, distributed power, reduced mass and thickness of the SAR antenna panels, and a means for maintaining the SAR antenna patterns within requirements. In particular, this unique approach includes the following innovations:³⁴²⁾

- A self-contained active antenna node known as a **WiNode**, that incorporates the RF circuitry of a TRM (Transmit Receive Module) with a solar power source, Lithium-ion cells, and control and monitoring functions. This eliminates power distribution cables and harnesses and the requirement for separate bus-mounted solar array panels and bus-mounted batteries to provide power for the SAR antenna.
- A wireless “**space feed**” as a means of eliminating the azimuth and elevation RF power distribution networks, including all the associated cables and harnesses on a typical SAR antenna. Within the WiSAR payload, the antenna subsystem consists of the active WiNodes and RF radiators mounted on deployable RF antenna panels with the space feed antennas mounted on a boom.
- Deployment of the SAR Antenna using low cost solar array deployment mechanisms to stow and deploy the WiSAR active phased array antenna. This is enabled by the antenna panel thickness and mass reduction that results from the elimination of the APDNs and the EPDNs. This eliminates the need for special purpose deployment and stowing mechanisms for the antenna, further reducing the overall mass.
- An active, dynamic antenna distortion measurement and compensation system is used for measuring the antenna geometry and dynamically computing the necessary phase corrections required to maintain the desired beam shape. This eliminates the need for heavy thermoelastically stable and stiff antenna panels and the associated complex ESS (Extendable Support Structure) required to keep the antenna rigid and flat.

The individual innovations combine to impact all aspects of the spacecraft: the payload, the bus, their interface and the launch. These architecture and technology innovations enable WiSAR to achieve significant cost and mass reductions over traditional SAR payloads. A demonstration mission of this new technology can be expected in a few years.

- Introduction of **UWB** (Ultra-Wideband) SAR imaging technology. The UWB SAR technology has the potential to make high-resolution but low-frequency band (P-band,

342) Peter A. Fox, Kenneth V. James, Alan Thompson, “WiSARTM: A New Solution for High-Performance, Smallsat-Based Synthetic Aperture Radar Missions,” Proceedings of the 22nd Annual AIAA/USU Conference on Small Satellites, Logan, UT, USA, Aug. 11–14, 2008, SSC08-VI-1

VHF, UHF) SAR imaging applications feasible. Conventional SAR instruments use a frequency band (say, C–band, X–band, Ku–band) with a signal bandwidth generally $< 10\%$ of the center frequency (also referred to as narrowband SAR signal). An UWB SAR system (a UWB system uses RF signals with a bandwidth $> 25\%$ of the center frequency) could be the answer in terms of resolution requirements and other features such as range measurement accuracy, ground penetration capability, etc. The UWB technology permits topographic as well as tomographic imaging applications. ^{343) 344) 345)}

Using (UWB radar signals appears to be the most promising future approach to building radar systems with new and better capabilities and direct applications to civil uses and environmental monitoring. The classical radar approaches usually employ RF–sounding signals of comparably low fractional bandwidth. These waves have a short wavelength but their envelope is spread over a large distance. Since typical dimensions of single targets are much smaller than the spatial extension of the signal envelope (more precisely: the envelope of their auto–correlation function), the captured radar signal represents a mixture of signal components from the individual scattering centers of the target. ³⁴⁶⁾

The situation is inverted for UWB sensing. Here, the spatial extension of the sounding signal is in the same order as the objects to be observed. Even if narrowband and ultrawideband radar are working on the same physical basis, they partially require different thinking on how to interpret scattering effects. Furthermore, due to the large bandwidth occupation of UWB–sensors much lower power emission than in the narrowband case is allowed. Consequently, in exploring new fields of radar applications, one should mainly look for new device conceptions using weak sounding signals for short range sensing tasks which profit from cm– and mm–resolutions as well as penetration of opaque objects.

An introduction of UWB technology in SAR systems (with very short duration pulses resulting in a high RF bandwidth) has only been done in airborne SAR instruments so far. The introduction of UWB technology on spaceborne SAR instruments has to overcome the following obstacles: 1) the power requirements are very large for spaceborne UWB instruments, and 2) regulatory issues of the ITU might refuse licensing of a UWB spectrum allocation for spaceborne applications.

Examples of early airborne UWB SAR instruments are:

– CARABAS (Coherent All Radio Band Sensing). ^{347) 348)} CARABAS (see P.50) is a Swedish airborne experimental SAR instrument designed and built at FOA (National Defense Research Establishment, Linköping, Sweden), which operates in the lower part of the VHF–band. The objective is good penetration of vegetation/foilage and to some extent of the ground surface. The frequency band was chosen: 1) to reduce the image speckle level without sacrificing resolution, and 2) to obtain a system with diffraction–limited resolution (i.e. a system with a dimension of the resolution cell comparable to those of the wavelengths employed, to minimize the influence of speckle). CARABAS–I was first flown in a SAR campaign in Oct. 1992. An upgraded CARABAS–II version is flown since 1996. CARABAS–II operates in the frequency range of 22–80 MHz (HF/VHF–band) with a center frequency of 51.25 MHz and a bandwidth of 58 MHz. The bandwidth is provided by stepped frequency generation.

343) J. D. Taylor, “Ultra–Wideband Radar Technology,” CRC Press LLC, 2001, ISBN: 0–8493–4267–8

344) Note: Bandwidth refers to the difference between the highest and lowest frequencies of interest, containing about 95% of the signal power.

345) A. Alvarez, J.–L. Garcia, M. Lobeira, “UWB techniques in Radar,” Proceedings of IRSI (International Radar Symposium India), Bangalore, India, Dec. 20–22, 2005

346) J. Sachs, “Ultra–Wideband Sensing: The Road to new Radar Applications,” Proceeding of the 4th Microwave & Radar Week, MRW–2010, Vilnius, Lithuania, June 14–18, 2010

347) A. Barmettler, E. Meier, D. Nüesch, “Development of an Ultra Wideband SAR Processor,” CEOS SAR Workshop 2001, April 2–5, 2001, Tokyo, Japan, URL: <http://www.geo.unizh.ch/rsl/research/SARlab/uwb/ceos2001.Tokyo.Barmettler-et-al.pdf>

348) W. Pierson, P. Follo, A. Gustavsson, M. Lundberg, L. M. H. Ulander, “A Ground Target Change Detection Experiment Based on VHF SAR Data,” ISR 2003, Dresden, Germany, Sept. 30 – Oct. 2, 2003

– P-3/SAR (ERIM/Navy Sensor) is operational since 1988. The P-3/SAR system (see P.83.3) is jointly owned and operated by ERIM and NAWC/AD, and is installed on a US Navy P-3A Orion aircraft. The sensor is a multimode SAR operating at X-, C-, and L-band. A polarimetric UWB mode (200–900 MHz) was added in 1994 (foliage and ground penetration experiments).

- SAR Earth surface imagery with resolutions < 1 m can only be provided with X-band (or higher frequency, i.e. Ku-band) instruments. The L-band is an attractive complement to X-band in particular for such applications as: biomass and land use as well as for ocean salinity mappings. Fully polarimetric SAR instruments provide valuable additional information for such applications as classification, geological investigations, and in particular for lithological mapping. The PALSAR instrument of JAXA's ALOS mission (launch Jan. 24, 2006) provides L-band polarimetric imagery in a support mode with duty cycle.

- The RADARSAT-2 mission of CSA/MDA, Canada (launch Dec. 14, 2007) features a C-band dual-receive phased array antenna capability (two subapertures in along-track may be used independently with two separate receivers) in combination with a DPCA (Displaced Phase Center Antenna) scheme [two channels, where the second channel views the same scene as the first, but one pulse repetition interval (PRI) later].³⁴⁹ The AT-interferometric technique is being used for very high resolution imagery as well as for SAR-GMTI (Ground Moving Target Indication) demonstrations. In addition, RADARSAT-2 is the first mission **offering the choice of right- or left-looking observations from the subsatellite track on an operational basis** (see D.42.4). This left- or right-look direction capability of the SAR antenna doubles the instrument FOR (Field of Regard) coverage for event monitoring and other tasks. The provision of multi-polarization as well as polarimetric imagery is another enabling feature of RADARSAT-2.

- Among the SAR satellite missions only RADARSAT-2, TerraSAR-X, COSMO-SkyMed, TanDEM-X, KOMPSAT-5 (launch Aug. 22, 2013), and Sentinel-1 (launch April 3, 2014) of the ESA Copernicus (formerly GMES) program feature a **right or left side observation capability**.

- The TerraSAR-X (TSX-1) mission of DLR/EADS Astrium GmbH (launch June 15, 2007) introduces also the concept of split along-track antenna design providing full-transmit and dual-channel receive apertures for AT-interferometry applications (increased resolution and demonstration of ocean current motion sensing). The DPC (Displaced Phase Center) antenna technique is used on a single platform.³⁵⁰ In receive, time-frequency variant digital beam forming is applied to focus the receive gain on the transmitted pulse as it observes on the Earth's surface. – While nominal observations of TSX-1 are taken on the right of the subsatellite track, there is also a capability for left-side observations for limited periods only. This support mode limitation is due to the fact that power generation is interrupted (the S/C performs a roll maneuver turning the solar array away from the sun).

- The Sentinel-1 SAR mission within the EU-ESA Copernicus (formerly GMES) program (launch 2014) will introduce a new type of ScanSAR mode called **TOPS** (Terrain Observation with Progressive Scan) SAR operations support mode (note: the terms TOPS and SAR is simply contracted to **TOPSAR**). TOPSAR is an ESA-proposed acquisition mode (Evert Attema, Fabio Rocca) for wide swath imaging which aims at reducing the drawbacks of the ScanSAR mode (namely the ScanSAR performance variation along azimuth as well as scalloping). The basic principle of TOPSAR is the shrinking of the azimuth antenna pattern (along-track direction) as seen by a spot target on ground. This is obtained by steering

349) P. D. Beaulne, C. H. Gierull, C. E. Livinstone, I. C. Sikaneta, S. Chiu, S. Gong, M. Quinton, "Preliminary design of a SAR-GMTI processing system for RADARSAT-2 MODEX data," IEEE/IGARSS 2003, Toulouse France, July 21–25, 2003

350) A. Currie, M. A. Brown, "Wide-Swath SAR," IEE Proceedings – Radar Sonar and Navigation Vol. 139 No 2, pp 122–135, 1992.

the antenna in the opposite direction as for Spotlight support. The TOPSAR signal includes particularities of both ScanSAR and Spotlights modes, but existing processing algorithms do not provide an efficient processing of TOPSAR data.

The TOPSAR mode is intended to replace the conventional ScanSAR mode. The technique aims at achieving the same coverage and resolution as ScanSAR, but with a nearly uniform SNR (Signal-to-Noise Ratio) and DTAR (Distributed Target Ambiguity Ratio).^{351) 352)}

The TOPSAR mode has been implemented on the Sentinel-1 mission due to the performance advantages compared to ScanSAR. The TOPSAR technique has already been demonstrated on the TerraSAR-X spacecraft during its commissioning phase (fall 2007) and showed very promising results. The measured values of the intensity variation of the analyzed images corresponded very well with the expected theoretical values. Scalping in the TOPSAR image is 0.3 dB against 1.2 dB in the ScanSAR image. Additionally, fewer bursts are required in TOPSAR, which also positively affects the image quality.^{353) 354) 355) 356)}

- **Hybrid-polarity SAR architecture:** A dual-polarized radar is one that transmits on one polarization, and the resulting backscatter is observed through a two-channel antenna and receiver, designed to match a given pair of orthogonal polarizations.³⁵⁷⁾ – Full characterization of a SAR scene implies coherent dual-polarization to support the four Stokes parameters. Evaluation of the Stokes parameters requires knowledge of the (complex) cross-correlation between the two orthogonal receive channels of a dual-polarized SAR. Most so-called dual-polarized SAR systems so far provide only the like- and cross-product images, ignoring the complex cross-product, thus discarding potentially valuable information.

It turns out that the Stokes parameters are rotationally invariant with respect to backscatterer orientation – if and only if – the transmission is circularly polarized. Thus, if a given SAR is to be deployed against a variety of scenes in which there may be arbitrary orientation of geometrical backscattering elements, the only suitable choice of transmit polarization is **circular**.^{358) 359) 360)}

The hybrid-polarity radar concept, proposed and developed by R Keith Raney of JHU/APL, is finding its way into ever more new SAR missions in the first decade of the 21st century. The hybrid-polarity architecture consists of transmitting *circular polarization*, and re-

- 351) F. De Zan, A. M. Monti Guarnieri, "TOPSAR: Terrain Observation by Progressive Scans," IEEE Transactions on Geoscience and Remote Sensing, Vol. 44, Issue 9, Sept. 2006, pp. 2352–2360
- 352) D. D'Aria, F. De Zan, D. Giudici, A. Monti Guarnieri, F. Rocca, "Burst-mode SARs for wide-swath surveys," Canadian Journal of Remote Sensing, Vol. 33, No 1, 2007, pp. 27–38, URL: <http://home.dei.polimi.it/monti/papers/tucan.pdf>
- 353) A. Meta, P. Prats, U. Steinbrecher, J. Mittermayer, R. Scheiber, "TerraSAR-X TOPSAR and ScanSAR comparison," Proceedings of EUSAR 2008, 7th European Conference on Synthetic Aperture Radar, June 2–5, 2008, Friedrichshafen, Germany
- 354) P. Prats, A. Meta, R. Scheiber, J. Mittermayer, A. Moreira, J. Sanz-Marcos, "A TOPSAR Processing Algorithm Based on Extended Chirp Scaling: Evaluation with TerraSAR-X Data," Proceedings of EUSAR 2008, 7th European Conference on Synthetic Aperture Radar, June 2–5, 2008, Friedrichshafen, Germany
- 355) Rolf Scheiber, Steffen Wollstadt, Stefan Sauer, Elke Malz, Josef Mittermayer, Pau Prats, Paul Snoeij, Evert Attema, "Sentinel-1 Imaging Performance Verification with TerraSAR-X," Proceedings of EUSAR 2010, 8th European Conference on Synthetic Aperture Radar, June 7–10, 2010, Aachen, Germany
- 356) Josef Mittermayer, Pau Prats, Davide D'Aria, Riccardo Piantanida, S. Sauer, Andrea Monti Guarnieri, Evert Attema, Paul Snoeij, "TOPS Sentinel-1 and TerraSAR-X Processor Comparison based on Simulated Data," Proceedings of EUSAR 2010, 8th European Conference on Synthetic Aperture Radar, June 7–10, 2010, Aachen, Germany
- 357) R. K. Raney, "On dual-polarized SARs and the Stokes parameters," Proceedings of EUSAR 2006. Dresden, Germany, May 16–18, 2006.
- 358) R. Keith Raney, "Hybrid-polarity SAR architecture," IEEE Transactions on Geoscience and Remote Sensing, Vol. 45, No 11, 2007, pp. 3397–3404, DOI: 10.1109/TGRS.2007.895883
- 359) R. K. Raney, "Decomposition of Hybrid Polarity SAR Data," POLInSAR 2007 Workshop, Frascati, Italy, Jan. 22–26, 2007, URL: http://earth.esa.int/workshops/polinsar2007/papers/30_raney.pdf
- 360) R. Keith Raney, Anthony Freeman, "Hybrid-Polarity SAR Architecture," POLInSAR Workshop, Frascati, Italy, Jan. 26–30, 2009, URL: http://earth.esa.int/workshops/polinsar2009/participants/141/pres_1_Raney_141.pdf

ceiving two orthogonal *linear polarizations* (such as H and V) and also their relative phase. These data are sufficient to calculate the four Stokes parameters which contain all of the information available in the backscattered field. As long as the relative phase between the received polarizations is retained, the specific choice of linear orientation does not matter (Figure 17).

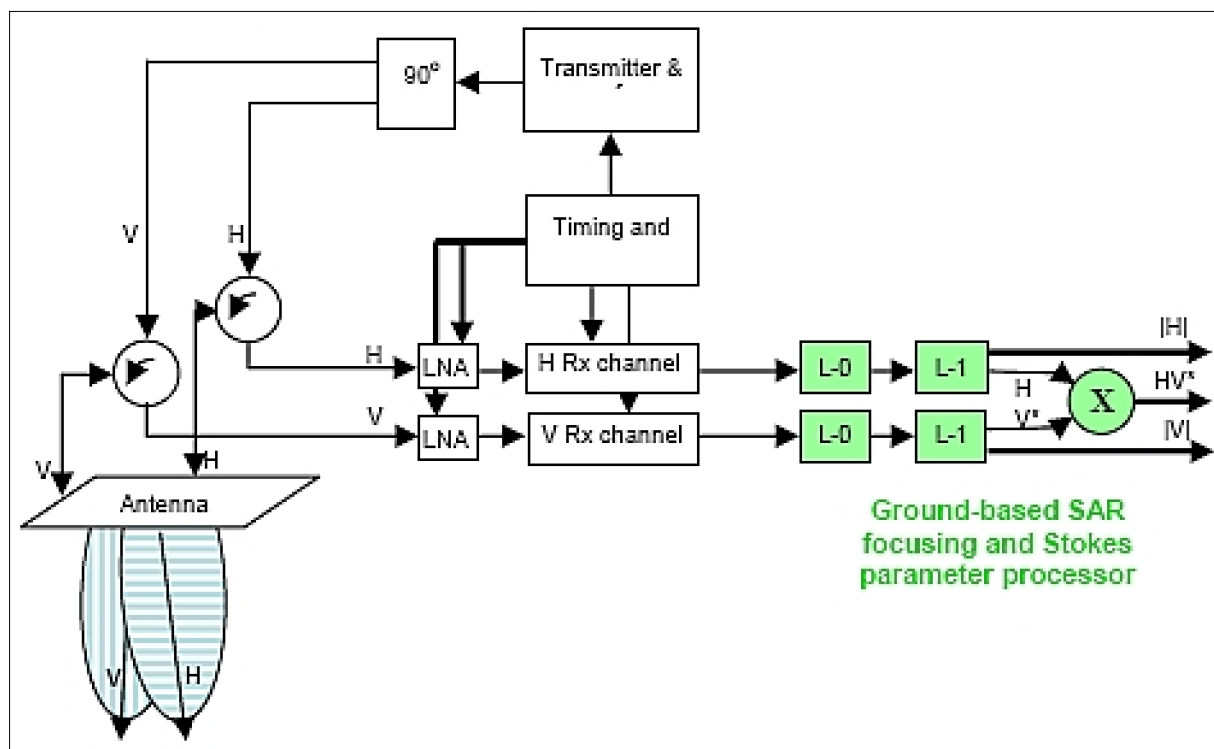


Figure 17: Generic hybrid polarity architecture in which the transmitted field is circularly polarized (right or left), and the receive polarization basis is linear (image credit: R. Keith Raney)

In contrast to alternative compact polarimetric concepts, the hybrid–polarity architecture provides unique advantages for system calibration, including relative gain and phase characterization without an imaged ideal point target.

Outlook of hybrid polarity architecture implementations:

- A low mass Mini–SAR S–band instrument package (< 9 kg, 150 m baseline resolution), a technology demonstration of NASA, is installed on the lunar mission Chandrayaan–1 of ISRO (launch Oct. 22, 2008, end of mission in Aug. 2009).

A more advanced low mass Mini–RF instrument package is flying on the LRO (Lunar Reconnaissance Orbiter) mission of NASA (launch June 18, 2009). Mini–RF features SAR observations in S–band and X–band and two resolutions (150 m baseline and 30 m zoom capability in both bands) with interferometric and communications functionality in one lightweight (< 14 kg) package. ^{361) 362)}

- An X–band active phased–array Earth–viewing SAR is flown on RISAT–2 of ISRO (launch April 20, 2009). The instrument includes a hybrid dual–polarity mode.

- In 2009, India (ISRO) has concluded Phase A studies for an Earth–viewing L–band SAR based on hybrid polarity

361) Paul Spudis, Stewart Nozette, Ben Bussey, Keith Raney, Helene Winters, Christopher L. Lichtenberg, William Marinelli, Jason C. Crusan, Michele M. Gates, “Mini–SAR: an imaging radar experiment for the Chandrayaan–1 mission to the Moon,” *Current Science*, Vol. 96, No 4, Feb. 25, 2009, pp. 533–539 URL: <http://www.ias.ac.in/currsci/feb252009/533.pdf>

362) Stewart Nozette, Paul Spudis, Ben Bussey, Robert Jensen, Keith Raney, Helene Winters, Christopher L. Lichtenberg, William Marinelli, Jason Crusan, Michele Gates, Mark Robinson, “The Lunar Reconnaissance Orbiter Miniature Radio Frequency (Mini–RF) Technology Demonstration,” *Space Science Review*, Vol. 150, 2010, pp. 285–302, DOI 10.1007/s11214–009–9607–5

- Canada is studying hybrid–polarity dual–pol as a mode on the future RCM (RADAR-SAT Constellation Mission), a successor to RADARSAT–2
- The DESDynI (Deformation, Ecosystem Structure, and Dynamics of Ice) mission in the definition phase at NASA/JPL as of 2009, is hosting a lidar/SAR dual payload; the SAR quad–pol mode will be hybrid–polarity.³⁶³⁾
- Initial plans for the future ALOS–2 mission include hybrid–polarity modes.
- Bistatic configurations (see 1.4.3.6) offer the potential of upgrading existing monostatic missions (Interferometric Cartwheel proposed mission of CNES). In this concept, a single SAR instrument on a spacecraft in LEO serves as illuminator – with receiving–only instruments on other nearby spacecraft, participating in the signal recovery from the illuminator (providing in parallel an interferometric configuration). The Cartwheel configuration employs a number of comparatively inexpensive receive antennas mounted on simple platforms arranged such that they can make parasitic (bistatic) use of the signals from a classical SAR instrument (a transmitter) flying in the same orbit and maintaining an optimal interferometric baseline.
- Most spaceborne LEO SAR observations so far (civil missions) were from orbital altitudes between 500 and about 800 km on free–flying spacecraft. Exceptions to this rule were: 1) Almaz–1 with an S–band SAR of the Soviet Union operated at altitudes of 270–380 km (launch March 31, 1991, end of mission Oct. 17, 1992); and 2) The Shuttle missions operated SAR instruments at altitudes between 225 – 300 km.
- Introduction of long–term multiband (multifrequency and multipolarization) SAR systems on a single platform. An instrument with L–band, C–band, and X–band capabilities could greatly enhance the observation return.
- Introduction of the AESA (Active Electronically Scanned Array) 2–D digital beam steering capability, an enabling technology into next–generation civil spaceborne projects (beyond 2010). The AESA technology is providing a spectrum of new applications, including MTI (Moving Target Indication) observations (into otherwise static conventional SAR imagery).³⁶⁴⁾ – The functional potential of a phased array antenna with 2–D digital beam steering is greatly increased offering such features as: a) introduction of a multichannel system by splitting the beamforming network of the radar antenna and the addition of simultaneous receiving channels, b) simultaneous beam steering in elevation and azimuth (the steering capability in elevation allows the acquisition of images in each point of the access region; the steering capability in azimuth allows the implementation of spotlight–SAR modes that yield high resolution imagery), c) the presence of an active antenna, together with control in both amplitude and phase of each individual T/R module independently in transmission and reception mode, allows optimization of the antenna beam for each individual operational mode.
- The introduction of an onboard information extraction capability (in particular for event monitoring) will be a logical consequence of the image processing capability as the information is the final objective of SAR observations. Naturally, this real–time function requires considerable onboard processing capabilities. The onboard SAR processing capability reduces also considerably the downlink data transmission needs in support of high–resolution imagery.
- The goal of an ESA study in 2013, conducted by Astrium GmbH, is to demonstrate DBF (Digital Beamforming) antenna technology with a combined analog/digital beam forming unit called **TRIM** (TRM Interface Module), required for a follow–on Sentinel–1

363) R. Keith Raney, “DESDynI Adopts Hybrid Polarity SAR Architecture,” Proceedings of the 2009 IEEE Radar Conference, Pasadena, CA, USA, May 4–8, 2009

364) P. Lombardo, “A Multichannel Spaceborne Radar for the COSMO/SkyMed Satellite Constellation,” Proceedings of 2004 IEEE Aerospace Conference, Big Sky, MT, March 6–13, 2004

SAR instrument. – Functionally, the TRIM is a combined RF and digital unit inserted into the receive chain of the antenna. Any DBF phased array antenna will need a significant number of high–speed digital processors. An important function of the TRIM is on–line, continuous internal tile calibration. During instrument data take operation, the central electronics successively inject calibration pulses into the antenna, and these are routed by setting of switches in adequate sequence. The returning signals pass through the digital processor (ASIC) of each TRIM, and the associated transfer functions are immediately computed. The comparison of nominal transfer functions with the ones obtained from calibration procedure, exposes the instantaneous gain and phase drifts of all active RF components on the antenna. ³⁶⁵⁾

The approach for a DBF frontend demonstrator is to utilize these inevitable parts not just for beam forming, but also for TRM (Transmit/Receive Module) and TCU (Tile Control Unit) control functions, thereby simplifying the TRMs and avoiding the TCUs altogether. At the same time, an effort is made to minimize the number of processors needed per tile, by incorporating both polarization channels into one device. The digital processors can be utilized in a synergetic manner to support dynamic tile calibration during instrument operation. The proposed calibration concept measures and corrects the signal drifts of active parts directly, thereby avoiding on–ground calibration campaigns and temperature tabulation.

- **WorldDEM™ introduction on April 2014:** WorldDEM is a global DEM (Digital Elevation Model) of unprecedented quality, accuracy, and coverage. WorldDEM was made available by Airbus Defence and Space (former EADS Astrium GEO–Information Services) starting in mid–April 2014. WorldDEM is based on data acquired by the German high–resolution radar satellites TerraSAR–X and TanDEM–X (TSX/TDX). The combined processing of these various data takes ensure the global consistency and quality of the final WorldDEM product.

WorldDEM is based on the a global DEM at HRTE–3 (High Resolution Terrain Elevation, level–3), representing a significant jump forward in accuracy. In terms of resolution, it is setting new standards by providing 12 m grid spacing globally, compared to 90 m grid spacing on the existing global dataset from SRTM (Shuttle Radar Topography Mission). ³⁶⁶⁾

The 12 m posting product meets a vertical accuracy of 2 m relative and better than 10 m absolute and guarantee full homogeneity and seamlessness. These specifications exceed any other global satellite–based elevation model available today. WorldDEM will improve the performance of worldwide operating systems and cross–border mission planning.

365) Christoph Schaefer, Friedhelm Rostan, Christoph Heer, Grzegorz Adamiuk, Martin Suess, Michael Ludwig, “Digital Beam Forming Frontend Demonstrator for Sentinel–1 Follow–on Mission,” Proceedings of IGARSS (IEEE International Geoscience and Remote Sensing Symposium), Melbourne, Australia, July 21–26, 2013

366) “Airbus Defense and Space Sets New Accuracy and Quality Standards for Global Elevation Models with WorldDEM™ Launch,” Airbus Defence and Space, April 16, 2014, URL: <http://www.astrium-geo.com/en/5734-airbus-defense-and-space-sets-new-accuracy-and-quality-standards-for-global-elevation-models-with-worlddem-launch>

1.4.4.1 Advanced concepts for high–resolution wide–swath SAR imaging

Wide unambiguous swath coverage and high azimuth resolution pose contradicting requirements on the design of spaceborne SAR (Synthetic Aperture Radar) systems.^{367) 368)} This motivated the development of advanced SAR imaging modes with different trade–offs between spatial coverage and azimuth resolution. Examples are the ScanSAR (or TOPS) mode which enables a wide swath at the cost of an impaired azimuth resolution and the Spotlight mode which allows for an improved azimuth resolution at the cost of a non–contiguous imaging along the satellite track. Up to the early 21st century, it is not possible to combine both operational modes simultaneously in one and the same data take. This dilemma motivated further research towards the development of new radar techniques for spaceborne high–resolution wide–swath SAR imaging.

System architectures: Several proposals resolve the azimuth resolution vs. wide–swath coverage dilemma by combining a multi–channel radar receiver with a small aperture transmitter illuminating a wide area on the ground. Example SAR configurations are: Figure 18)

- Squinted multiple beam SAR (Multi–Beam)
- DCPA (Displaced Phase Center Antenna)
- Quad–array SAR
- HRWS (High–Resolution Wide–Swath)
- Radiating Reflector Array.

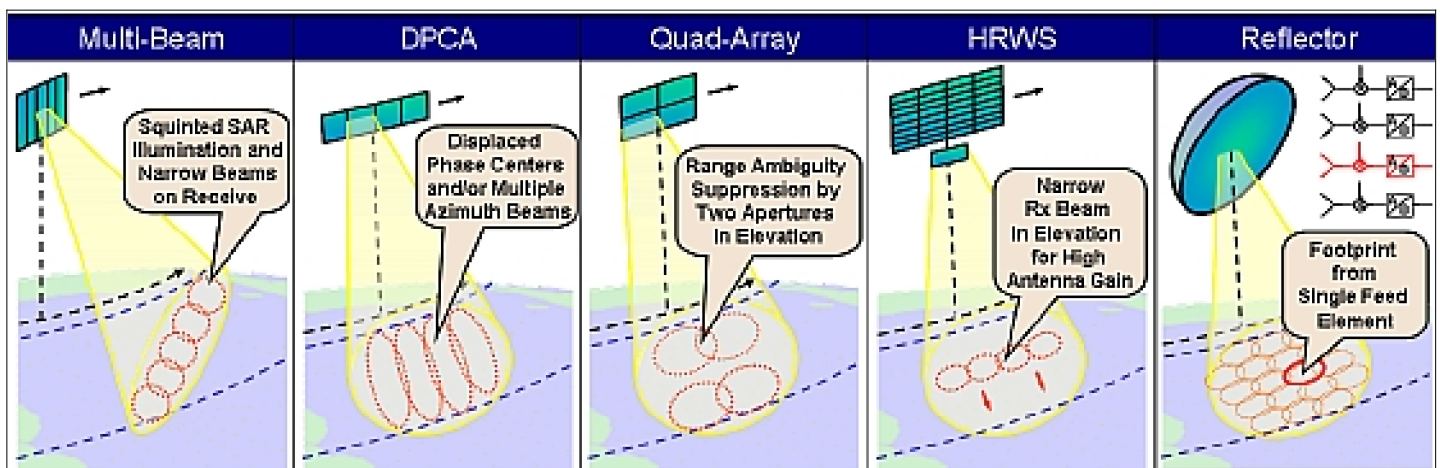


Figure 18: SAR system solutions for high–resolution wide–swath SAR imaging (image credit: DLR)³⁶⁹⁾

An interesting alternative^{370) 371)} to a direct radiating array is the **combination of a reflector with a digital feed array** as shown on the right–hand side of Figure 18. This architecture combines the capabilities of digital beamforming with the high gain provided by a large reflector aperture. A reflector antenna offers moreover the potential to use one and the same aperture for multiple frequency bands simultaneously, thereby paving the way for future

367) G. Krieger, M. Younis, N. Gebert, S. Huber, F. Bordoni, A. Patyuchenko, A. Moreira, “Advanced Concepts for High–Resolution Wide–Swath SAR Imaging,” Proceedings of EUSAR 2010, 8th European Conference on Synthetic Aperture Radar, June 7–10, 2010, Aachen, Germany, URL: <http://elib.dlr.de/61910/1/KrYoGe-HuBoPaMo09.pdf>

368) G. Krieger, M. Younis, N. Gebert, S. Huber, F. Bordoni, A. Patyuchenko, A. Moreira, “Advanced Digital Beamforming Concepts for Future SAR Systems,” Proceedings of IGARSS (IEEE International Geoscience and Remote Sensing Symposium) 2010, Honolulu, HI, USA, July 25–30, 2010

369) G. Krieger, M. Younis, N. Gebert, S. Huber, F. Bordoni, A. Patyuchenko, A. Moreira, “Advanced Concepts for High–Resolution Wide–Swath SAR Imaging,” Proceedings of EUSAR 2010, 8th European Conference on Synthetic Aperture Radar, June 7–10, 2010, Aachen, Germany, URL: <http://elib.dlr.de/64963/1/KrYoGe10.pdf>

370) M. Spencer, S. Chan, L. Veilleux, K. Wheeler, “The Soil Moisture Active/Passive (SMAP) Mission Radar: a Novel Conically Scanning SAR”, Proceedings of the IEEE Radar Conference, Pasadena, USA, May 4–8, 2009.

multi–frequency SAR systems. To lower launch volume and weight, the reflector could be deployable as already suggested for several L–band radar missions. ^{372) 373) 374) 375)}

The reflector based digital beamforming architecture offers several attractive features for the design of high performance spaceborne SAR systems. For example, the simultaneous activation of all feed elements generates a broad transmit beam for wide swath illumination. The opportunity to use all feed elements simultaneously for the generation of a wide transmit beam avoids the necessity of a separate transmit antenna as suggested for the HRWS system and/or the use of sophisticated illumination strategies in case of using a combined Tx/Rx array. – On the other hand, radar echoes arriving as plane waves from a given direction activate typically only one or a small number of feed elements if the feed array is located close to the focal plane.

The systematic correspondence between beam direction and activated feed array element(s) is well suited to significantly enhance the imaging performance of future side–looking radar sensors where the scattered radar echoes arrive at each instant of time only from a rather narrow angular range. The angle of arrival migrates in synchrony with range time as the radar echoes arrive in successive order from near to far range. By using this correspondence, a significant improvement in the sensitivity (NESZ) and range ambiguity suppression can be achieved via a dynamic routing of those feed signal(s) that exceed a given threshold level. The gain of the narrow Rx pattern is about 10 dB higher than that of the broad Tx pattern, thereby compensating the inevitable gain loss from the illumination of a wide image swath.

Operational modes: The new digital architectures will also provide new SAR imaging modes. To compare these modes, a design example considers a system which shall be able to map a swath width of ~ 400 km with an azimuth resolution of 5 m from an orbital altitude of 700 km. Such a system exceeds by far the capabilities of current spaceborne SAR sensors.

- Multi–aperture mapping in standard stripmap mode (Ref. 367)
- Multi–channel ScanSAR mode
- Multiple beam SAR modes
- Hybrid SAR modes

The innovative concepts rely on the combination of advanced multi–channel radar front–end architectures with novel operational modes. The deployable reflector antennas represent an interesting alternative to direct radiating arrays and a low number of receiver channels are already sufficient to enhance the imaging capabilities far beyond those of current spaceborne SAR systems. Moreover, the implementation of digital radar systems will benefit from rapid developments in integrated microwaves and semiconductor technologies (Ref. 367).

- 371) A. Freeman, A. Donnellan, P. Rosen, D. Evans, J. Graf, A. Loverro, R. Treuhaft, R. Oberto, W. T. K. Johnson, M. Simard, T. Farr, E. Rignot, R. Kwok, Xiaoqing Pi, “Deformation, Ecosystem Structure, and Dynamics of Ice (DESDynI),” Proceedings of EUSAR 2008, June 2–5, 2008, Friedrichshafen, Germany
- 372) G. Krieger, N. Gebert, M. Younis, F. Bordoni, A. Patyuchenko, A. Moreira. “Advanced Concepts for Ultra–Wide–Swath SAR Imaging.” Proceedings of EUSAR 2008, pp. 31–34, Friedrichshafen, Germany, June 2–5, 2008, URL: http://elib.dlr.de/54455/1/eusar08_ultrawideswath_final.pdf
- 373) M. Younis, S. Huber, A. Patyuchenko, F. Bordoni, G. Krieger, “Performance Comparison of Reflector– and Planar–Antenna Based Digital Beam–Forming SAR”, IJAP (International Journal of Antennas and Propagation), Article ID 614931, 2009, doi:10.1155/2009/614931
- 374) A. Freeman, G. Krieger, P. Rosen, M. Younis, W. Johnson, S. Huber, R. Jordan, A. Moreira. “SweepSAR: Beam–forming on Receive using a Reflector–Phased Array Feed Combination for Spaceborne SAR.” Proceedings of the IEEE Radar Conference, Pasadena, USA, May 4–8, 2009
- 375) G. Krieger, I. Hajnsek, et al., “The Tandem–L Mission Proposal: Monitoring Earth’s Dynamics with High Resolution SAR Interferometry,” Proceedings of the IEEE Radar Conference, Pasadena, USA, May 4–8, 2009., URL: <http://elib.dlr.de/58480/1/PID841883.pdf>

1.4.4.2 LEO SAR satellite constellations and formations

At the start of the 21st century, the technology frontier (and the challenges) in high-resolution Earth observation involves LEO constellations/formations as well as eventually observations from MEO and/or GEO.

- The space segment of the COSMO/SkyMed program of ASI, Italy (the launch of the first satellite took place on June 8, 2007, COSMO-SkyMed-2 was launched on Dec. 9, 2007, COSMO-SkyMed-3 was launched on Oct. 25, 2008), COSMO-SkyMed-4 was launched on Nov. 6, 2010 (UTC), represents the first constellation of SAR satellites (4 S/C, each equipped with an X-band SAR instrument), all S/C are phased in the same orbital plane). Nominal observations are taken on the right of the subsatellite track; however, there is also a capability for left-side observations for limited periods only. Provision of commercial SAR imagery for civil and military use. Frequent global coverage capability.
- SAR-Lupe, a German military mission, consists of a constellation of 5 S/C in three orbital planes (launch of first S/C in constellation of 5 on Dec. 19, 2006, the SAR-Lupe-2 launch took place on July 2, 2007, SAR-Lupe-3 launch on Nov. 1, 2007, SAR-Lupe-4 launch on March 27, 2008, SAR-Lupe-5 launch on July 22, 2008). Orbital plane 1 contains 2 S/C; orbital plane 2 contains 1 S/C, orbital plane 3 contains 2 S/C. The angle between orbital plane 1/2 is 64° ; the angle between orbital planes 2/3 is 65.6° . The phase angles of the S/C are: Orbital plane 1 = $0^\circ + 69^\circ$; orbital plane 2 = 34.5° ; orbital plane 3 = $0^\circ + 69^\circ$. The five spacecraft constellation offers very short response times and a high system redundancy.

- Introduction of bistatic and multistatic SAR system configurations (starting with the TechSat-21 mission, a three spacecraft SAR formation of DoD/AFRL.

Note: **The TechSat-21 program was cancelled in early 2003.**

- Starting on June 21, 2010 with the launch of the TanDEM-X spacecraft, a close-orbit X-band SAR constellation will be formed with the TerraSAR-X spacecraft (launch June 15, 2007). Both spacecraft, owned and operated by DLR, will provide high-resolution interferometric observations in monostatic, bistatic, and alternating bistatic modes.
- NovaSAR-S is a joint technology demonstration initiative in of SSTL (Surrey Satellite Technology Ltd.), UK, EADS Astrium Ltd (Stevenage, UK), and the UKSA. The overall objective is to make SAR (Synthetic Aperture Radar) observation missions more affordable to a customer base and to open up new application-oriented in the microwave region of the spectrum. NovaSAR-S, with a S-band SAR instrument on a minisatellite of < 400 kg, is planned for launch in 2014. ³⁷⁶⁾

1.4.4.3 GEO SAR /Radar satellites – in study phase as of 2002/8.

The GEO location provides a continuous observation capability (and much larger target areas, i.e. footprints, to be observed than from LEO); ^{377) 378) 379)} for instance, large weather systems can be sampled in intervals of minutes to an hour or so (depending on the application – rather than days as is normally provided by LEO spacecraft – this is because SAR interferograms may only be formed from identical viewing geometries, so the temporal sampling of an InSAR system is determined by the time required for the spacecraft to repeat its flight track).

376) NovaSAR-S the small satellite approach to Synthetic Aperture Radar, SSTL brochure, URL: <http://www.sstl.co.uk/Downloads/SSTL-Brochure-pdfs/1904-SSTL-NovaSAR-Brochure>

377) S. N. Madsen, C. Chen, W. Edelstein, "Radar Options for Global Earthquake Monitoring," Proceedings of IGARSS 2002, Toronto, Canada, June 24–28, 2002

378) S. N. Madsen, W. Edelstein, L. D. DiDomenico, J. LaBrecque, "A geosynchronous synthetic aperture radar; for tectonic mapping, disaster management and measurements of vegetation and soil moisture," IEEE Symposium on Geoscience and Remote Sensing, IGARSS, Sydney, Australia, pp. 447–449, 2001.

379) D. Bruno, S. E. Hobbs, G. Ottavianelli, "Geosynchronous Synthetic Aperture Radar: Concept Design, Properties and Possible Applications," Proceedings of the 56th IAC 2005, Fukuoda, Japan, Oct. 17–21, 2005, IAC-05-B1.2.08

Generally, SAR observations from geostationary orbit require larger apertures (GEO S/C are 45 higher in orbit than LEO S/C) and additional power to achieve sufficient SNR as compared to LEO missions; also a relative motion to the target area is needed to form a synthetic aperture. An inclined GSO (Geosynchronous Orbit) provides a relative motion to the target area. The advantages of GSO apply, i.e. the observation coverage time of a region of interest is greatly increased, the overall FOR (Field of Regard) is dramatically increased at this altitude. With a $\pm 8^\circ$ beam–steering capability in cross–track as well as in along–track, it is possible to cover out to 6800 km on either side of the nadir point and the beam can be squinted forward and backward as desired. A key characteristic of a geosynchronous SAR is that it is very flexible in terms of operational modes (stripmap, ScanSAR, spotlight).

- RELOSS (Regional Earth –Locked Observation SAR System) is an ESA study (completed in 2003) for a possible future mission, to assess the feasibility of a SAR observation concept from a GSO platform.
- NIS (NEXRAD–In–Space), is a challenging mm–wave technology development concept in NASA’s ESE (Earth Science Enterprise) program. The objective is to fly a Doppler radar instrument on a GEO spacecraft, permitting detailed tracking and monitoring of the life cycle of severe storm systems like hurricanes and cyclones. A Doppler radar has the ability to penetrate precipitating and non–precipitating clouds to support the study of: a) the dynamics of mesoscale structures, b) vertical profiling of precipitation and c) input data for NWP models. The requirements call for the use of a Ka–band (35 GHz) Doppler radar for high spatial resolution and the use of a very large scanning reflector antenna (30 m diameter, deployable system). The instrument is designed to measure rainfall rate at 13 km horizontal resolution and 300 m vertical resolution, and the line–of–sight Doppler velocity at 0.3 m/s precision, of the 3–D hurricane structure once per hour throughout its life cycle. A spirally scanning radar with a maximum off–nadir look angle of 4° results in a 28° incidence angle from GEO providing a coverage of 5,300 km diameter on Earth’s surface. ^{380) 381)}
- SAR observations from GEO require the introduction of new technologies to make the concept affordable. In particular, lightweight, large–aperture, and electronically–steerable phased array antennas are required to address the measurement needs. ³⁸²⁾ Current LEO systems are designed using modular architectures where electronic components are individually packaged and integrated onto rigid manifolds or panels (the phased array structure of the SRTM mission had an aerial density of 20 kg/m^2). One method to dramatically reduce the weight, volume and associated cost of space–based SAR is to replace the conventional rigid manifold antenna architecture with a flexible thin–film membrane. NASA/JPL designed a new membrane antenna with an aerial density of $< 2 \text{ kg/m}^2$ providing an antenna bandwidth of 80 MHz at L–band. This concept requires nothing less than the development of “T/R membrane,” analogous to the TRM system of LEO missions.

Parameter	LEO	Low MEO	High MEO	GEO
Altitude	800 km	3000 km	14,000 km	35,800 km
Capability enabled	– Improved modeling of fault dynamics	– Local earthquake forecasting – Limited disaster response	– Earthquake forecasting – Disaster response	– Earthquake forecasting – Disaster response
Usuable swath	350 km	3900 km	6200 km	7000 km
Repeat time	8 day	2 day	1 day	1 day

380) E. Im, E. A. Smith, S. L. Durden, S. Tanelli, J. Huang, Y. Rahmat–Samii, M. Lou, “Conceptual Design of a Geostationary Radar for Hurricane Studies,” Proceedings of ISRSE, Honolulu, HI, Nov. 10–14, 2003

381) Simone Tanelli, Houfei Fang, Stephen L. Durden, Eastwood Im, Yahya Rahmat–Samii, “Prospects for Geostationary Doppler Weather Radar,” Proceedings of the 2009 IEEE Radar Conference, Pasadena, CA, USA, May 4–8, 2009, paper: 3294

382) A. Moussessian, L. Del Castillo, W. N. Edelstein, T. Hatake, J. Huang, S. Madsen, A. D. Paris, G. Sadowy, A. Shapiro, “Transmit/Receive Membranes for Large Aperture Scanning Phase Arrays,” Proceedings of ESTC (Earth Science Technology Conference), College Park, June 24–26, 2003

Parameter	LEO	Low MEO	High MEO	GEO
Spatial resolution	30 m	30 m	30 m	30 m
3-D displacement acc	Good	Very good	Excellent	Excellent
Radiation environment	Moderate	High	Severe	High to severe
Antenna area	50 m ²	400 m ²	500 m ²	700 m ²
Transmit power	5 kW	30 kW	45 kW	60 kW
Beam scan	±30° (elevation)	±15° (az/ele)	±8° (az/ele)	±6° (az/ele)
No of T/R modules	400	14,000	17,000	24,000
T/R module efficiency	30%	40%	50%	60%
DC power	1667 W	7500 W	9000 W	10,000 W

Table 25: Summary of InSAR L-band characteristics for LEO, MEO, and GEO observations ³⁸³⁾

1.4.4.4 GEO or GEO/LEO SAR satellite constellations

This field of multistatic SAR applications (see chapter 1.4.3.6) is in the study phase by several institutions. Such concepts may of course drastically increase the capabilities of future SAR remote sensing applications.

- Geostationary illuminator – LEO echo data reception, i.e., the transmitter and receiver are in different orbits (concept feasibility study phase of DLR as of 2002/3). Such a multistatic SAR imaging concept consists of an illuminator S/C in GEO, using a high-power FMCW (Frequency Modulated Continuous Wave) transmitter and a steerable antenna that can be pointed to an observation region of interest (CW operation implies higher average power or lower peak power of the transmitter). In parallel, a cluster of microsatellites is flown in LEO, with a receive antenna on each S/C. Such a configuration may be optimized for a broad range of applications like frequent monitoring, wide swath imaging, single-pass cross-track interferometry, along-track interferometry, resolution enhancement or radar tomography (the SAR tomographic information is obtained from a wideband pulse that provides multiple illuminating wavelengths). – This concept offers a number of implementation solutions to suit project constraints/requirements. An example is the installation of the transmitter payload on a commercial communications satellite in GEO (a low-cost flight of opportunity), this would save the cost of a separate GEO spacecraft for the illumination function. ^{384) 385)}

The coverage region of a SAR instrument in GEO is restricted to approximately ±55° latitude due to the shallow incident angle with respect to the illuminator. This restriction may be avoided by use of illuminators in GEO or in MEO.

A SAR constellation in GEO (illuminator) and in LEO (multiple receiver platforms) offers an interesting feature by the fact that the transmit path exceeds by far the distance from the target to the receiver (the ratio is about 45:1). As a result of the long transmit path, the antenna footprint of the geostationary illuminator will have an extension of more than 100 km in both azimuth and range. ³⁸⁶⁾

383) W. N. Edelstein, S. N. Madsen, A. Moussessian, C. Chen, "Concepts and technologies for synthetic aperture radar from MEO and geosynchronous orbits," Proceedings of SPIE, Vol. 5659, 'Enabling Sensor and Platform Technologies for Spaceborne Remote Sensing,' G. J. Komar, J. Wang, T. Kimura, Editors, Jan. 2005, pp. 195–203, Conference location: Honolulu, HI, USA, Nov. 9, 2004

384) Note: Pulse radar systems measure range in the time domain, whereas FMCW radars measure range in the frequency domain. An advantage of the FMCW technology may lead to smaller instruments.

385) G. Krieger, H. Fiedler, D. Hounam, A. Moreira, "Analysis of System Concepts for Bi- and Multi-Static SAR Missions," IEEE/IGARSS 2003, Toulouse, France, July 21–25, 2003

386) G. Krieger, A. Moreira, "Potentials of Digital Beamforming in Bi- and Multistatic SAR," IEEE/IGARSS 2003, Toulouse, France, July 21–25, 2003

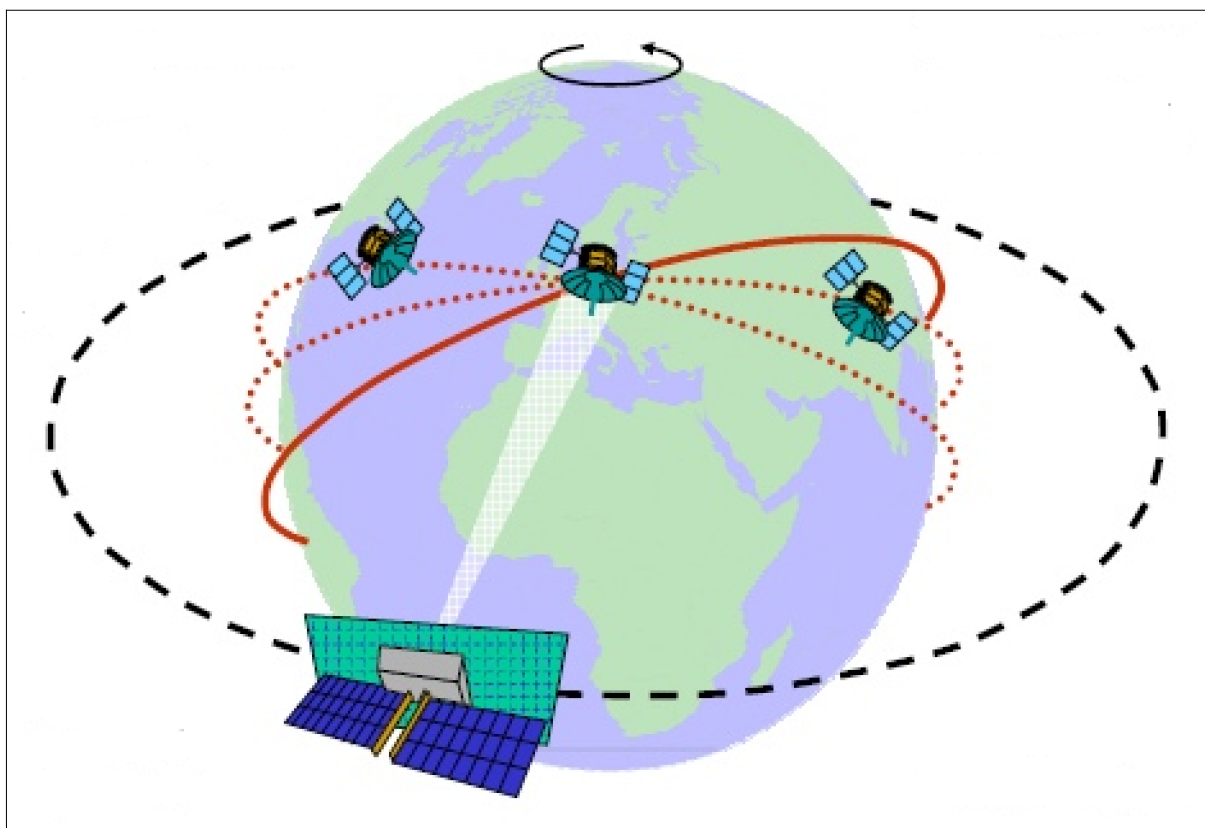


Figure 19: Schematic of a possible GEO illuminator configuration with LEO receivers ³⁸⁷⁾

This is in fundamental contrast to the small footprints of the LEO receivers for which we will have a typical diameter in the order of 6 km, assuming a downward-looking parabolic antenna with a radius of 1.25 m. Thus, the simultaneously accessible region with a fixed aperture receiver is very limited from LEO. Such a limitation may be avoided by DBF (Digital Beamforming) on receive, where the receiver antenna is split into multiple subapertures and each subaperture signal is separately amplified, down-converted, and digitized. The digital signals can then be combined in a dedicated signal processor to form multiple antenna beams with arbitrary shapes. This makes effective use of the total signal energy within the large illuminated footprint and will introduce a high flexibility in operating the bistatic SAR constellation (see Ref. 289).

- DBF in elevation: The formation of multiple independent beams in elevation allows for the simultaneous mapping of several distinct subswaths with full azimuth resolution and high antenna gain. By combining multiple subswaths, it is also possible to map a wide image swath (>100 km). Furthermore, the use of a frequency modulated continuous wave (FMCW) illumination source with low chirp rate will allow for a sub-sampling of the recorded signals, thereby reducing the data rate substantially. This is due to the fact, that at any instant of time the bandwidth within a sufficiently narrow elevation beam will only be a small fraction of the total bandwidth of the transmitted chirp. The digital beamforming corresponds therefore to a bandpass filter bank which divides the recorded range spectrum in multiple sub-spectra.

- DBF in azimuth: The formation of multiple beams in azimuth will allow for the division of a broad Doppler spectrum into multiple sub-spectra with different Doppler centroids. The bandwidth in each subchannel corresponds to the total length of the receiver antenna, which determines the minimum allowable PRF. A coherent combination of the sub-spectra will then yield a broad Doppler bandwidth for high azimuth resolution. This technique is

³⁸⁷⁾ The image was provided by Gerhard Krieger of DLR, Oberpfaffenhofen, Germany

especially attractive for high resolution imaging with SAR systems that require long antenna structures for the unambiguous imaging of a wide swath.

- GLORIA (Geostationary/Low–Earth Orbiting Radar Image Acquisition System), a study proposal by the University of Michigan. The proposal is based on a constellation of few (4) geostationary, radar transmitter satellites in L–band (as illuminators), and a constellation of LEO receiver satellites in various orbits. Tandem LEO satellites with sufficient spatial separation, are envisioned to form a high–resolution single–pass bistatic interferometric SAR. ³⁸⁸⁾

1.4.4.5 Planetary ground–penetrating radar:

MARSIS (Mars Advanced Radar for Subsurface and Ionospheric Sounding) is a low–frequency nadir–looking pulse–limited radar sounder and altimeter on ESA’s Mars Express mission (launch June 2, 2003) designed to search beneath Mars’s surface for liquid water, ice, or permafrost layers. MARSIS employs SAR techniques and a secondary receiving antenna (monopole) to isolate subsurface reflections. The primary goal is to map the composition of the top 5 km of the planet’s crust; secondary goals are surface characterization and ionospheric sounding. The instrument broadcasts very long wavelength radio waves (in the VF and VLF range) and observes the time of the reflections, an observation technique called ground–penetrating radar. RF waves in the range 1.3 – 5.5 MHz (corresponding to a wavelength range of 230 m to 55 m) are being transmitted from a 40 m long deployed antenna (high–efficiency dipole antenna). A significant portion of the VF/VLF waves are capable of penetrating the planets surface to depths of 2 to 5 km, thereby encountering various layers of different material. For boundaries between materials of different types – like ice and rock, or sand dunes and bedrock – there should be a detectable radar echo. The time delay between the surface reflection and any subsurface reflections permits to determine the depth to the boundary. The time differences involved are tiny, measured in nanoseconds. The multi frequency observation allows the estimation of the material attenuation in the crust, providing significant indications on the dielectric properties of the detected interfaces. The best ground penetrating studies are being made during night when the Martian ionosphere is least active and when the spacecraft is less than 800 km from the Martian surface, a condition that occurs for 26 minutes during each 6.75 hour orbit of Mars Express. ³⁸⁹⁾ ³⁹⁰⁾ ³⁹¹⁾

In its standard operating mode, the instrument is capable of making parallel measurements in 4 bands centered at 1.8, 3.0, 4.0 and 5.0 MHz. MARSIS functions by transmitting a linear frequency modulated chirp using a nadir–looking dipole antenna. The return signal is received on both the dipole antenna and a secondary monopole antenna oriented along the nadir axis. The secondary antenna has a null in the nadir direction and receives primarily the off–nadir surface reflections. The main transmit and receive antenna is a deployable dipole with two 20 meter elements, arranged so that its peak gain is in the spacecraft nadir direction. The entire instrument, including antenna and data processing unit, weighs about 12 kg. The PI of MARSIS is Giovanni Picardi, “La Sapienza” University of Rome, Rome, Italy.

388) K. Sarabandi, J. Kelndorfer, L. Pierce, “GLORIA: Geostationary/Low–Earth Orbiting Radar Image Acquisition System: A Multi–Static GEO/LEO Synthetic Aperture Radar Satellite Constellation for Earth Observation,” IEEE/IGARSS 2003, Toulouse, France, July 21–25, 2003

389) G. Picardi, D. Biccari, R. Seu, J. Plaut, W. T. K. Johnson, R. L. Jordan, R. Huff, O. Bombaci, et al., “The Synthetic Aperture and Monopole in MARSIS,” Proceedings of EUSAR 2004, Ulm, Germany, May 25–27, 2004

390) <http://sci.esa.int/science–e/www/object/index.cfm?fobjectid=31033&fbodylongid=658>

391) http://www.marsis.com/index.php3?page=instrument_description.php3

Center frequency	1.8 MHz	3 MHz	4 MHz	5 MHz
Bandwidth	1 MHz	1 MHz	1 MHz	1 MHz
Radiated power	1.5 W	5 W	5 W	5 W
Transmit pulse width	250 or 30 μ s			
PRF (Pulse Repetition Rate)	130 s^{-1}			
Science data rate, max (min)	75 (18) kbit/s			

Table 26: Characteristics of the MARSIS instrument

The typical spatial resolution of the MARSIS data is 5 km x 10 km in the along track and cross track directions, respectively. The ground resolution requirements for the subsurface and surface sounding experiments indicate the maximum footprint dimensions at the surface. The along-track requirement of 10 km width and spacing means that the system is required to obtain data uniquely associated with a 10 km wide along-track footprint, every 10 km. The cross-track footprint shall be no larger than 32 km in a pulse-limited sense; for most smooth regions, the surface area responsible for echoes in cross-track dimension is expected to be much smaller. The range resolution requirement of 150 m in free space is intended to result in a subsurface depth resolution better than 100 m.

The MARSIS instrument was developed within the framework of a Memorandum of Understanding between the Italian Space Agency (ASI) and NASA. It was developed by Alenia Spazio under ASI management and the scientific supervision of the University of Rome, La Sapienza, in partnership with the Jet Propulsion Laboratory (JPL) in Pasadena, California, and the University of Iowa. JPL provided the antenna manufactured by Astro Aerospace. It is the first instrument designed to actually look below the surface of Mars. – Note: MARSIS started its science operations on July 4, 2005, after the first phase of its commissioning was concluded. ³⁹²⁾

³⁹²⁾ http://www.esa.int/esaCP/SEMQAN808BE_index_0.html

1.4.5 Microwave Region, Passive Observations

Radiometry is the science of radiation measurement in any portion of the electromagnetic spectrum, i.e. the study of creation, transport, and absorption of electromagnetic energy, and the wavelength–dependent properties of these processes (see O.7). The term radiometry is also often used to include the detection of the quantity, quality, and effects of such radiation. Microwave radiometry is the measurement microwave radiation, generally considered to be in the wavelength region from about 1 mm to 1 m. A passive system is restricted to measuring the incoming radiation intensity of a wave spectrum in question. – The term **photometry** describes these phenomena for the optical region of the spectrum, generally considered to be in the wavelength region from about 0.1 μm to 1000 μm (the latter value corresponds to 1 mm).

Some background in radiative history: It was Johann H. Lambert (1728–1777) who noted that the amount of radiated energy in a solid angle is proportional to the cosine of the angle between the emitter and the receiver. Gustav Kirchhoff (1824–1887) discovered that the emissivity of a radiating surface is equal to its absorptivity and that the total of reflection, absorption and transmission of a material was always equal to 1. The Austrian physicist Josef Stefan (1835–1893) determined the total radiant emittance from a source for all spectral wavelengths to be equal to the emissivity multiplied by a constant (the Stefan–Boltzmann constant) times its temperature raised to the fourth power. In 1866, Samuel P. Langley (1834–1906) used a crude bolometer to study the radiation of carbon at different temperatures. The main architect of modern radiometry was Max Planck (1858–1947, Humboldt University, Berlin). In 1900, Max Planck presented his blackbody radiation law, representing a great achievement in all of physics (in 1918, Max Planck received the Nobel prize in physics for his work).³⁹³⁾

Quantity	Unit	Comment
Radiant energy	Joule (J)	Energy leaving or reaching a surface or a point
Radiant flux	Watt (W)	Energy per unit of time (also referred to as “power”)
Radiant emittance	Watt/meter ² (W/m ²)	Radiative energy leaving a point on a surface as measured on the hemisphere centered on that point
Irradiance	Watt/meter ² (W/m ²)	Radiative flux incident on a surface
Radiant intensity	Watt/steradian (W/sr)	Radiative energy per unit time measured per unit solid angle
Radiance	Watt/meter ² /steradian (W/m ² /sr)	Radiative flux emitted from a single point per unit solid angle

Table 27: Radiometric terms and abbreviations (quick reference)

Passive microwave radiometry is of fundamental importance in Earth observation yielding a wealth of information, in particular in such applications as meteorology, climate, and hydrology (water cycle).³⁹⁴⁾ A microwave radiometer is a highly sensitive receiver system capable of detecting and **measuring the rather low energy levels of microwave radiation** whose nature is generally incoherent (i.e. noise–like source). Note: If there is mentioning of “coherent” microwave radiation in the literature, it usually refers to the “sampling method at Nyquist frequency or better.” – When a scene is observed by a microwave radiometer, the radiation received by the antenna is partly due to the self–emission by the scene and partly due to the reflective radiation originating from the surroundings. For sounding applications (i.e. measuring the atmosphere), microwave radiometers are relatively unaffected by cloud cover, this is considered a great advantage when compared to observations in the infrared region, making the microwave region particularly suitable for future NWP (Numerical Weather Prediction) applications.

393) Edward Friedman, John Lester Miller, “Photonics Rules of Thumb – Optics, Electro–Optics, Fiber Optics, and Lasers,” Second Edition, McGraw–Hill, ISBN: 0–07–138519–3, Chapter 14, “Radiometry”

394) U. Klein, C.–C. Lin, J. Charlton, J.–M. Goutoulec, N. Atkinson, L. Eymard, “Future Microwave Instruments for Numerical Weather Prediction and Climate Research,” Proceedings of SPIE, Vol. 4881, 9th International Symposium on Remote Sensing, Aghia Pelagia, Crete, Greece, Sept. 23–27, 2002

1.4.5.1 Microwave radiometers

The spectral range of remotely-sensed data was considerably enlarged by the use of radiometers in the microwave region [the overall microwave region is considered for wavelengths from about 1 mm (300 GHz) to 1 m (300 MHz); remote sensing is being conducted in the MMW (millimeter-wave) region (i.e., 1–10 mm or 300 GHz to 30 GHz); the frequency range from 1–20 GHz is mostly used for surface radiometry due to atmospheric attenuation].³⁹⁵⁾ Passive microwave (MW and MMW) Earth observation radiometry introduced such applications as temperature sounding for meteorological and climate applications, sea-ice mapping for navigation in polar regions, measurements of ocean surface temperature and ocean surface wind speeds. Eventually the applications of radiometers included also observations of land surface features and the measurement of atmospheric constituents (trace gases for atmospheric chemistry applications). – Imaging in the MMW region is known to provide reasonable penetration of poor weather and dielectrics. This attribute has always been of interest to the civil and military communities with such applications as surveillance mapping.

Atmosphere	Ocean Surface	Land Surface
Temperature, moisture soundings	Sea Surface Temperature (SST)	Vegetation condition monitoring
Winds, Clouds, Aerosols	Surface winds	Soil moisture, Snow cover
Precipitation monitoring	Ocean color	Albedo, insolation
Earth radiation budget	Ice cover	Fire location, plume smokes
Trace gases (ozone, CO ₂ , etc.)	Sea level	Land Surface Temperature (LST)

Table 28: Typical application spectrum of radiometric instruments

Two generic types of radiometers have evolved, **profiling instruments** (or sounders, also referred to as broadband radiometers), and **surface imaging instruments** (multichannel radiometers). The respective measurement techniques employed by these radiometer types involve in general multi-channel observations:

1) Measurement of microwave emissions (brightness temperatures) near known molecular “**absorption/emission lines**” are used for profile retrievals.³⁹⁶⁾ The retrieval water vapor profiles (and inferred temperature) involve measurements of brightness temperatures near known absorption lines of oxygen and water vapor molecules (oxygen lines near 50–57 GHz and near 118 GHz; water vapor absorption lines are for instance near 22.3 GHz, 183 GHz, 383 GHz, 425 GHz, 625 GHz). Note: Other atmospheric trace gases exhibit absorption lines different from those of oxygen or water vapor. See also chapter 1.4.7.

2) Atmospheric “**window frequencies**” refer to those wavelength regions of the spectrum, where absorption for the whole atmosphere is very low; hence, these “transparent” frequencies are mostly used to study surface phenomena (ocean, ice, land, etc.). The most common window frequencies from LEO are near: 6 GHz, 10 GHz, 19 GHz, 23 GHz, 37 GHz, 90 GHz, and 150 GHz. Typical “**sounding channels**” are at: 23 (water vapor), 50–60 (oxygen), 118, 166–183 (water vapor), 380, 425 GHz, etc. – the concept exploits more the absorption bands. Hence, the profiles observed at the different frequencies exhibit also different sensitivities to the various items being observed.

3) Dual polarization for roughness effects (over the sea) and scattering from ice (over land).

- Spaceborne microwave observations started September 23, 1968 with the launch of Cosmos 243 satellite (in sun-synchronous LEO) which carried a non-scanning, nadir-

395) L. Phalippou, E. Gerard, “Study report to the European Space Agency on the use of precise microwave imagery in numerical weather prediction,” ECMWF, 1996.

396) Note: The absorption/emission principle is based on energy exchanges between the gas molecules and the electromagnetic field occurring at characteristic frequencies.

viewing 4-channel radiometer [wavelengths: 8.5 cm (3.5 GHz), 3.4 cm (8.8 GHz), 1.35 cm (22.2 GHz), and 0.8 cm (37.5 GHz)] with the objective to estimate atmospheric water vapor, liquid water, ice cover, and sea temperature. The same radiometer was also flown on Cosmos 384 with a launch in 1970. Nimbus-5 (launch Dec. 11, 1972) of NASA carried a radiometer with the name of NEMS (Nimbus-E Microwave Spectrometer). This represented the first step in the application of the microwave spectrum to global sensing of the atmospheric temperature structure. Another radiometer on Nimbus-5 was ESMR (Electrically Scanning Microwave Radiometer). The Skylab (launch of Skylab-1 May 14, 1973) space station flew two radiometers, S-193 and S-194. The NEMS instrument on Nimbus-5 was followed by SCAMS (Scanning Microwave Spectrometer), flown on Nimbus-6 (launch June 12, 1975), which led to the first MSU (Microwave Sounding Unit), flown on TIROS-N (launch Oct. 13, 1978). The SMMR sensor was flown on SeaSat (launch June 27, 1978) and on Nimbus-7 (launch Oct. 24, 1978). See also chapter O.7 and Table 930.^{397) 398)}

- Passive spaceborne radiometers have been primarily frequency-tuned to vertically sound and map specific constituents (gases and dust in atmospheres, and bulk properties on planetary surfaces). The first systems implemented were sounders (profiling systems). These were followed by the new type of surface imaging radiometers with the availability of focal plane antennas and better processing capabilities. The 1980s and 1990s mark a shift away from Dicke-switched superheterodyne radiometers to **total-power** systems, facilitating radiometer configuration simplification and sensitivity improvements (example: the SSM/I instrument, flown on the DMSP series since 1987, is the first mission which employs a total-power radiometer configuration). In the 1990s, superheterodyne receivers with mixers directly coupled to feedhorns and feeding low-noise IF amplifiers continue to dominate MMW radiometry. The mixers in superheterodyne radiometers remain the critical element for sensitivity. Mixers with whiskerless diodes yield significant improvements in reliability relative to mixers with whisker-contacted diodes.

- Future radiometer instruments are expected to include more receiver channels in a wider spectral range (MW, MMW, and sub-MMW), offering the ability for interpretation of a wider range of geophysical parameters. To reduce mass and volume, multichannel sounding instruments generally employ a single reflector antenna, along with FSS (Frequency Selective Surface) technology in the quasi-optical feed train to provide spatial demultiplexing. Improvements are likely to come from solid-state technologies based on MMIC (Microwave Monolithic Integrated Circuit) receiver chip development, providing direct amplification and detection in combination with FPA (Focal Plane Array) imaging. In addition, the aperture synthesis method seems to be a promising development, providing a capability of 2-D radiometer imagery generation. Some required technologies in radiometry are:

- Improvements to the front-end quasi-optical components, particularly the beam splitters, are required to satisfy the demanding radiometric performance which has been specified for future mm-wave instruments.³⁹⁹⁾

- The MMIC technology is gradually replacing the older MIC (Microwave Integrated Circuit) and TWTA (Traveling Wave Tube Amplifier) technology in RF electronics. MMIC-based receivers are capable of observing the stronger atmospheric signals

- SIS (Superconductor-Insulator-Superconductor). SIS-based receivers provide the lowest noise level environment in the frequency range of 200–300 GHz

397) A. E. Basharinow, et al., "Some Results of Microwave Sounding of the Atmosphere and Ocean from the Satellite Cosmos 243," in COSPAR Space Research XI, Proceedings of Open Meetings of Working Groups of the Thirteenth Plenary Meeting of COSPAR, Leningrad May 20–29, 1970, Akademie-Verlag, Berlin, 1971, pp. 593–600

398) E. G. Njoku, "Passive Microwave Remote Sensing of the Earth from Space—A Review," Proceedings of the IEEE, Vol. 70, No. 7, July 1982, pp. 728–750

399) R. Dickie, R. Cahill, H. S. Gamble, V. F. Fusco, et al., "Micromachined 300GHz High Q Resonant Slot Frequency Selective Surface Filter," Proceedings of the 54th IAC, Bremen, Germany, Sept. 29 – Oct. 3, 2003

- The HEB (Hot Electron Bolometer) technology provides best noise performance in the frequency range > 1000 GHz
- An effective low–power cooling system is essential for all microwave measurements.
- Submillimeter–wave radiometers [300 GHz (1 mm) $<$ frequency range > 3000 GHz (0.1 mm)]. At the end of the 1990s, new generations of microwave limb sounders (profilers) and imaging radiometers (or spectroradiometers) are emerging with advances in microwave detector technology, extending their measuring capability into the sub–mm wavelength region. The technology for these high–frequency ranges requires radiometers with superconducting heterodyne receivers or with FTS–based systems (the FTS technique provides a means to measure atmospheric radiance). The cooling to superconducting temperatures of the detection system represents always a major investment in instrument design. The problem of past LTS (Low–Temperature Superconductivity) cooling seems to be gradually replaced by HTS (High–Temperature Superconductivity) cooling systems. The interest in the short wavelengths is due to the fact that many molecules of importance in photochemistry exhibit emission lines in these wavelengths (e.g. HCl, OH). Submillimeter remote sensing has in addition advantages that complement visible and infrared techniques. Since the wavelength of submillimeter radiation is comparable to the size of ice particles in cirrus clouds, observed brightness temperature changes from cirrus are correlated to ice mass. Some early airborne instruments in this class are: MIR (Millimeter–wave Imaging Radiometer) of NASA/GSFC flown on ER–2 which was upgraded in 1994 with three 325 GHz channels. THOMAS (THz OH Measurement Airborne Sounder, since 1994) of DLR, and ASUR (Airborne Submillimeter SIS Radiometer, since 1994) a cooperative sensor of SRON (Groningen, Netherlands) and the Institute of Environmental Physics at the University of Bremen. The NASA–sponsored FIRSC (Far Infrared Sensor for Cirrus) FTS instrument is flown on a T–39 (Sabreliner) aircraft since April 1998. ^{400) 401) 402) 403) 404)}

The first spaceborne sub–mmw instruments for the measurement of trace gases are: SMR (Submillimeterwave Radiometer) flown on the Swedish satellite ODIN (launch Feb. 20, 2001). There are sub–mm channels and one lower frequency channel on SMR. SMILES (Superconducting Submillimeter–wave Limb Emission Sounder) of JAXA (Japan Aerospace Exploration Agency), formerly NASDA, is planned to fly on ISS/JEM in 2009. ESA/ESTEC has the following limb–sounding sensors (in the sub–mm region) under development: MASTER (Millimeter–wave Acquisition for Stratosphere Troposphere Exchange Research), SOPRANO (Sub–millimeter Observation of Processes in the Absorption Noteworthy for Ozone) and PIRAMHYD (Passive InfraRed Atmospheric Measurements of HYDroxyl). NASA developed MLS (Microwave Limb Sounder), with three channels in the mm–range and two double sideband sub–mm channels, flying on Aura (former EOS–CHEM) in 2004 (launch July 15, 2004). MLS is a high background microwave sounder with room temperature detection capability. The new MLS instrument (frequencies of > 600 GHz) is a further development of MLS flown on UARS [Note: MLS on UARS has observed atmospheric thermal emissions from chlorine monoxide (ClO), ozone (O₃), water vapor

400) K. F. Evans, S. J. Walter, et al., “Modeling of Submillimeter Passive Remote Sensing of Cirrus Clouds,” *Journal of Applied Meteorology*, Vol. 37, 1998, pp. 184–205

401) K. F. Künzi, “Microwave Limb Sounders,” *Proceedings of 32nd ESLAB Symposium on Remote Sensing Methodology for Earth Observation and Planetary Exploration*, ESA/ESTEC, Sept. 15–18, 1998 (SP–423 Dec. 1998), pp.17–22

402) J. Mees, S. Crewell, et al., “ASUR – An Airborne SIS Receiver for Atmospheric Measurements of Trace Gases at 625 to 760 GHz,” *IEEE Transactions on Microwave Theory and Techniques*, Vol. 43, No 11, Nov. 1995, pp. 2543–2548

403) G. W. Schwaab, “Heterodyne spectrometers,” *Infrared Physics & Technology*, Vol. 40, 1999, pp. 207–218

404) Note: The heterodyning technology is particularly suitable for the detection of very weak infrared and microwave radiation sources; heterodyning instruments (microwave limb sounders) play a crucial role for the monitoring performance of the Earth’s atmosphere (chemical composition of the atmosphere, monitoring/deduction of the fine structure of the spectra) as well as in the study of astronomical objects. The heterodyning technique is applicable in the spectral range from about $10\ \mu\text{m}$ (TIR) to the microwave region of about 10 mm wavelength.

(H₂O), sulfur dioxide (SO₂), and molecular oxygen (O₂), at frequencies of 63, 183 and 205 GHz].

Instrument	Launch (mission)	Comment (observation bands)
MLS (Microwave Limb Sounder), NASA/JPL, RAL	12.09.1991, (UARS)	63 GHz (1 band), 183 GHz (2 bands) and 205 GHz (3 bands)
MAS (Millimeter-wave Atmospheric Sounder), MPAe Lindau	March 1992, STS-45 (shuttle) Aug. 1993, STS-56 Nov. 1994, STS-66	61 GHz, 62 GHz, 63 GHz, 183 GHz, 184 GHz and 204 GHz
SMR (Submillimeterwave Radiometer), Sweden, Finland	20.02.2001, (Odin)	119 GHz, 495 GHz, 561 GHz
MLS (Microwave Limb Sounder), NASA	15.07.2004 (Aura)	118 GHz, 190 GHz, 240 GHz, 640 GHz, 2.5 THz
SMILES (Superconducting Submillimeter-wave Limb Emission Sounder), JAXA	2009 (JEM/EF on ISS)	624.32 – 626.32 GHz 649.12 – 650.32 GHz

Table 29: Overview of limb-sounding millimeterwave and sub-mm instruments flown

- Radiometric imaging and the introduction of **sea ice observation**. The NOAA-2 S/C (launch Oct. 15, 1972) was the first operational weather satellite to rely solely upon radiometric imaging to obtain cloudcover data and some sea ice information using VHRR. Prior to 1972, sea ice observations were generally obtained from coastal stations, transiting ships, and aircraft patrol. Nimbus-5 of NASA followed shortly thereafter (launch Dec. 11, 1972) with a payload of 4 radiometers, in particular EMSR (Electrically Scanning Microwave Radiometer). Nimbus-5 made it possible for the first time to routinely observe sea ice covered regions of the globe from space. The sea ice observing capability was greatly enhanced in 1978 with SeaSat (launch June 28, 1978), TIROS-N (launch Oct. 13, 1978) the first AVHRR sensor is flown, and Nimbus-7 (launch Oct. 24, 1978). SeaSat and Nimbus-7 were flying SMMR (Scanning Multichannel Microwave Radiometer), permitting sea ice observations among other geophysical parameters. The DMSP series of DoD is providing sea ice observation data with OLS (since 1979) and in particular since the launch of the first SSM/I in 1987.⁴⁰⁵⁾

The polar orbiting weather satellites of today continue to provide information on sea ice (surveillance function). The extent of sea ice is of importance to the all seafaring nations (forecasts for operation of commercial marine, navy, etc.). In addition, the extent and topography of sea ice is an important variable in connection with both ocean heat budget and Earth's radiation balance [in the context of climate research (global change, cryosphere and its effect on sea level, etc.)], using such radiometers as MODIS, MERIS, ASTER, AMSR, AMSR-E and WindSat (Wind Microwave Radiometer).

- Conventional radiometers offer bandwidths in the order of about 20 MHz at a particular center frequency (say, at L-band of 1.4 GHz). For increased sensitivity in radiometry, bandwidths in the order of 100 MHz are desirable.⁴⁰⁶⁾ However, RFI (Radio Frequency Interference) impairs considerably the operation of microwave radiometry, in particular at L-band, to improve sensitivity in applications such as soil moisture and ocean salinity sensing. Much of the RFI in this band originates from radars with pulse lengths of microseconds. Conventional total-power radiometers, which integrate over intervals in milliseconds or greater, are affected by the interference; hence, they are poorly suited to this task. A mitigation technique, using FPGAs, has been demonstrated in a number of field tests and flights (in 2002) conducted by the Electro Science Laboratory at OSU (Ohio State University) with NASA and NSF funding. The results indicate that appropriate choices of the parameters of

405) M. L. Van Woert, "US Navy Operational Sea Ice Remote Sensing," Proceedings of IGARSS 2002, Toronto, Canada, June 24-28, 2002

406) S. W. Ellingson, G. A. Hampson, J. T. Johnson, "Design of an L-Band Microwave Radiometer with Active Mitigation of Interference," Proceedings of ESTC (Earth Science Technology Conference), College Park, MD, June 24-26, 2003

the RFI mitigation algorithms can significantly reduce the impact of the interference on the microwave brightness measurements. Obviously, these findings are of considerable value in future radiometer designs. ⁴⁰⁷⁾

As of 2003/4, NASA/GSFC is developing CoSSIR (Conical Scanning Submillimeter – wave Imaging Radiometer), an airborne total – power broadband microwave radiometer that is designed to measure cirrus cloud parameters: IWP (Ice Water Path), Dme (Median Mass Diameter of Ice Crystals), and WV (Water Vapor) profiles (between 0–12 km altitudes). The instrument has fifteen channels; nine of them at the frequencies of 183.3 ± 1 , 183.3 ± 3 , 183.3 ± 6.6 , 220 , 380 ± 0.8 , 380 ± 1.8 , 380 ± 3.3 , 380 ± 6.2 , and 640 GHz are horizontally polarized, and the remaining six are dual – polarized at three frequencies of 487 ± 0.7 , 487 ± 1.2 , and 487 ± 3.3 GHz. The goal of this radiometer development is a receiver centered at 874 GHz with a 75 GHz LO input, an RF horn antenna and an output connector for the IF amplifier. The system will be useful for a broad frequency range without tuning, and the resulting receiver will also be readily scaled to other frequencies in THz band. ⁴⁰⁸⁾

1.4.5.2 Soil moisture in passive microwave radiometry

The microwave portion of the electromagnetic spectrum offers a large contrast between water and dry soil sensing, offering the greatest potential for monitoring soil moisture. Soil moisture is a fundamental parameter of the terrestrial environment. Its spatial distribution and temporal variation are crucial ingredients of hydrologic, ecologic, and climatic models, on regional and global scales. ⁴⁰⁹⁾

These measurements are based on relatively low frequency thermal microwave emission [at L – band (1.4 GHz) for soil moisture and SSS (Sea Surface Salinity), 10 GHz and up for precipitation monitoring, and 19 and 37 GHz for snow]. Passive microwave sensing of soil moisture [< 6 GHz (i.e., C – band, L – band, UHF, VHF)] in particular offers a very large contrast between dry and wet soils, little absorption by the atmosphere, and low scattering by vegetation canopy, resulting in analysis over large areas with little or no contamination of the signal. – However, the long wavelengths at these frequencies (microwave range), coupled with the high spatial and radiometric resolutions required by the various global hydrology communities, necessitate the use of very large apertures (e.g., > 20 m at 1.4 GHz) and highly integrated stable RF electronics on orbit. – At the start of the 21st century, technology developments point into the direction of distributed instrument architectures using *microwave interferometric techniques such as “synthetic thinned array radiometry” to reduce the mass of large area antenna structures.*

Background on synthetic aperture radiometry. Aperture synthesis is a relatively new technique for microwave remote sensing of the environment (monitoring of “microwave brightness temperature” which is analogous to brightness temperature monitoring in the optical range of the spectrum). The technique (pioneered in radio astronomy) generates high spatial resolution images by dividing the collection area of a telescope (or antenna) into smaller apertures spread out in a pattern covering several baselines. In microwave radiometry the concept employs an interferometric technique, in which the product from antenna pairs is sampled as a function of pair spacing. Substantial reductions in the antenna aperture needed for a given spatial resolution can be achieved with this technique. However, the advantages gained from aperture synthesis comes at the expense of reduced sensitivity resulting from the corresponding reduction in physical aperture. Detection sensitivity is an especially

407) G. A. Hampson, S. W. Ellingson, J. T. Johnson, “Design and Demonstration of an Interference Suppressing Microwave Radiometer,” Proceedings IEEE Aerospace Conference, Big Sky, MT, March 6–13, 2004

408) J. L. Hesler, D. W. Porterfield, W. L. Bishop, T. W. Crowe, P. Racette, “Development of Compact Broadband Receivers at Submillimeter Wavelengths,” Proceedings of the IEEE Aerospace Conference, Big Sky, MT, March 6–13, 2004

409) V. Lakshmi, J. Bolten, et al., “Estimation of Soil Moisture Using Data from Advanced Microwave Scanning Radiometer,” IEEE/IGARSS 2003, Toulouse, France, July 21–25, 2003

critical issue for measurements in LEO orbits (with orbital speeds of about 7 km/s) because of very limited instrument integration time availability per scene.

ESTAR [of NASA/GSFC and MIRSL (Univ. of MA, Amherst), P.88, first flown in 1988], a hybrid real–and–synthetic aperture combination, was the first radiometer built to test the concept of aperture synthesis. The experiences with the airborne ESTAR and MIRAS (ESA, P.138) instruments have demonstrated in particular the potential of aperture synthesis for remote sensing of soil moisture. While ESTAR is based on a 1–D (across–track) interferometer approach, MIRAS employed the 2–D synthetic aperture alternative. The new technology may eventually lead to a new generation of spaceborne passive microwave sensors by helping to overcome limitations set by antenna aperture size. The advantage of aperture synthesis is that it can achieve spatial resolutions equivalent to a total power radiometer with a large effective collecting area using relatively small antennas. The reduction in sensitivity that this entails can be restored because the synthetic aperture system does not need to scan and collect energy from many independent antenna pairs simultaneously.

Satellite; Instrument	Coverage	Frequency (GHz)	Polarization	Ground resolution	Repeat period
Passive Microwave Instruments (radiometers)					
Nimbus–7, SMMR SeaSat, SMMR	1978–1988 1978–1988	6.6, 10.69, 18, 21, 37 6.6, 10.69, 18, 21, 37	H, V H, V	0.25° 0.25°	
DMSP; SMM/I	since 1987	19.4, 22.2, 37.0, 85.5	H, V	70 km x 5 km	1–2 days
TRMM; TMI	since 1997	10.7, 19.4, 21.3, 37.0, 85.5	H, V	60 km x 6 km	1 day
IRS–P4; MSMR	since 1999	6.6, 10.65, 18, 21	V&H, V&H, VH, VH	50 km x 36 km	2 days
Aqua, AMSR–E	since 2002	6.9, 10.7, 18.7, 23.8, 36.5, 89.0	H, V	75 km x 7 km	2–3 days
ADEOS–II, AMSR	since 2002	6.9, 10.7, 18.7, 23.8, 36.5, 89.0	H, V	70 km x 6 km	2–3 days
Coriolis, WindSat	since 2003	6.8, 10.7, 18.7, 23.8, 37	H, V	50 km x 10 km	2–3 days
DMSP; SSMIS	since 2003	24 channels: 19.35–183.31	H, V, and H+V	70 km x 42 km 14 km x 13 km	1–2 days
SMOS; MIRAS	since 2009	1.4 (L–band)	H, V	< 50 km	3 days
NPOESS, MIS + VIIRS	2014	24 channels: 6 – 183.31 3 channels			
SMAP,	2015				
Active Microwave Instruments (SARs)					
ERS–1/2, AMI	since 1991	5.3 (C–band)	VV	30 m	35 days
Radarsat–1, SAR	since 1995	5.3 (C–band)	HH	7–100 m	24 days
Envisat, ASAR	since 2002	5.3 (C–band)	VV or HH, VV/ HH or VV/VH	30–1000 m	35 days
ALOS, PALSAR	since 2006	5.3 (C–band)	HH/HV or VV/ VH; HH or VV	10–100 m	46 days
Radarsat–2, SAR	since 2007	5.3 (C–band)	HH, VV, HV and VH	3–100 m	24 days

Table 30: Overview of LEO instruments for passive and active soil moisture retrieval

[Note: Spaceborne soil–moisture sensing may already get a start with two active instruments, namely ASAR (Advanced SAR) on Envisat (launch Mar. 1, 2002), and with PALSAR (Phased Array L–band Synthetic Aperture Radar) on ALOS (launch Jan. 24, 2006). Each of these SAR instruments is dual–polarized, permitting the retrieval of soil moisture for bare soil surfaces and for surfaces with short vegetation cover.]

Examples of passive microwave radiometry (sounding instruments) from LEO satellites for soil moisture retrieval (among other parameters) are:

- ESMR (Electrically Scanning Microwave Radiometer) of the Nimbus–5 mission (launch Dec. 11, 1972) and Nimbus–6 (launch June, 12, 1975) provided first tests of soil moisture retrieval.
- SMMR (Scanning Multichannel Microwave Radiometer) on Nimbus–7 (launch Oct. 28, 1978) and on SeaSat (launch June 28, 1978) provided data for soil moisture retrieval. The instrument provided data until July 1988.⁴¹⁰⁾
- SSM/I (Special Sensor Microwave Imager) of DMSP series.⁴¹¹⁾ Soil moisture retrieval is provided with spatial resolutions of 50 km on a 1400 km swath. SSM/I is flown since 1987. SSMIS (Special Sensor Microwave Imager Sounder) is the SSM/I successor instrument on DMSP with soil moisture retrieval capabilities. The first mission of SSMIS is flown on F–16 (launch Oct. 18, 2003). See G.1.1.
- MSMR (Multifrequency Scanning Microwave Radiometer) of ISRO’s IRS–P4 mission (launch May 26, 1999) demonstrates soil moisture retrievals. MSMR is a dual–polarized four–frequency radiometer (see D.24.7).
- MWR (Microwave Radiometer) on ESA’s Envisat mission (launch Mar. 1, 2002). Measurement of atmospheric humidity and of soil moisture.
- AMSR–E (Advanced Microwave Scanning Radiometer–EOS) of AMSR heritage on NASA’s Aqua S/C (launch May 4, 2002) retrieves land surface wetness.⁴¹²⁾
- AMSR (Advanced Microwave Scanning Radiometer) of JAXA’s ADEOS–II mission (launch Dec. 14, 2002) retrieves soil water content.
- WindSat (NRL/IPO) is flown on the Coriolis mission (launch Jan. 6, 2003). The WindSat instrument is considered a technology validation of CMIS (Conical–scanning Microwave Imager/Sounder) a prime instrument on the NPOESS series.
- VIIRS (Visible/Infrared Imager and Radiometer Suite) of the US NPOESS series (first launch on Oct. 28, 2011 on NPP) provides for soil moisture retrieval in 3 channels.⁴¹³⁾ In addition, MIS, also flown on NPOESS, providing estimates soil moisture at coarse spatial resolution. A data fusion solution of coarse MIS and fine VIIRS imagery will provide excellent soil moisture retrievals.
- A first spaceborne demonstration project,⁴¹⁴⁾⁴¹⁵⁾ employing “synthetic thinned aperture radiometry” (i.e. passive microwave remote sensing) with a sparsely filled 2–D antenna design, is **MIRAS** (Microwave Imaging Radiometer using Aperture Synthesis) of ESA’s **SMOS** (Soil Moisture and Ocean Salinity) mission, an approved science–driven demonstration mission in the ESA Explorer program – the objective is to obtain multi–incidence observations with sufficient spatial resolution and revisit time. The SMOS spacecraft with a microwave imaging radiometer (the interferometric design employs aperture synthesis) was launched on Nov. 2, 2009.

410) W. Ni–Meister, J. Walker, P. Houser, “Soil Moisture Initialization for Climate Prediction Through Data Assimilation,” Proceedings of ISRSE (International Symposium of Remote Sensing of Environment), Honolulu, HI, Nov. 10–14, 2003

411) S. Paloscia, G. Macelloni, E. Santi, T. Koike, “A Multifrequency Algorithm for the Retrieval of Soil Moisture on a Large Scale Using Microwave Data from SMMR and SSM/I Satellites,” IEEE Transactions on Geoscience and Remote Sensing, Vol. 39, No 8, Aug. 2001, pp. 1655–1661

412) W. T. Crow, M. Drusch, E. F. Wood, “An Observation System Simulation Experiment for the Impact of Land Surface Heterogeneity on AMSR–E Soil Moisture Retrieval,” IEEE Transactions on Geoscience and Remote Sensing, Vol. 39, No 8, Aug. 2001, pp. 1622–1631 (Note: Special issue on large–scale passive microwave remote sensing of soil moisture)

413) P. Ardanuy, C. Schueler, S. Miller, K. Jensen, W. Emery, Use of CAIV Techniques to Build Advanced VIIRS Approaches for NPOESS Key EDRs,” SPIE Annual Meeting 2002: Remote Sensing and Space Technology, Seattle, WA, July 7–11, 2002, SPIE Vol. 4814

414) Y. H. Kerr, P. Waldteufel, J. – P. Wigneron, et al., “Soil Moisture Retrieval from Space: The Soil Moisture and Ocean Salinity (SMOS) Mission,” IEEE Transactions on Geoscience and Remote Sensing, Vol. 39, No 8, Aug. 2001, pp. 1729–1735

415) M. A. Fischman, A. W. England, “Sensitivity of a Direct Sampling Digital Correlation Receiver for Aperture Synthesis Radiometry,” Proceedings of the IEEE IGARSS 2000 Conference, Honolulu, HI, July 24–28, 2000

In this concept, the required spatial resolution of <50 km for global microwave brightness temperature retrieval (3 day revisit time) in (L–band, 1.4 GHz), demands in turn a large number of aperture synthesis radiometer elements – each having an independent receiver. Measuring the microwave brightness temperature over the oceans enables a determination of sea surface salinity (SSS). At best (open ocean with high salinity) the brightness sensitivity to salinity is $\Delta TB/\Delta S = 1K/\text{psu}$ (practical salinity unit), and salinity determination to a 0.1 psu level thus requires radiometric measurements to better than 0.1 K. – The swath width of the radiometer is 934 km at an orbital altitude of 755 km, sufficient for a 3–day equatorial revisit time. The microwave brightness temperature is observed in H and V polarization (standard operating mode) with the option to acquire full polarimetric data. The quest for still higher resolutions (in the order of 10 km x 10 km) of future missions will certainly increase the number of receivers in their designs. – On the applications side such data is very much needed for the implementation of hydrologic models of large basins.

A key issue in comparing passive and active microwave spaceborne methods is the tradeoff between the high spatial resolution of SAR (Synthetic Aperture Radar) methods and the robust retrieval and frequent temporal coverage provided by passive methods (Table 30).⁴¹⁶⁾

- SAC–D/Aquarius is a cooperative mission of NASA and CONAE (Argentina, provider of S/C, launch June 10, 2011). The goal is to observe SSS (Sea Surface Salinity) and its variations to climate changes, to study the hydrospheric cycle and variations in the general ocean circulation. The L–band pushbroom radiometer employs a fixed offset system with three beams to scan the ocean surface. It employs a parabolic reflector (3 m diameter pushbroom antenna) illuminated by three feedhorns. On each of the feedhorns is an L–band radiometer (1.413 GHz) to measure ocean microwave emissions. An L–band (1.26 GHz) real–aperture scatterometer (correction for ocean surface roughness) shares the antenna with the radiometer system. The radiometer is of polarimetric design with four separate channels and four noise diode calibration sources. A launch of Aquarius is planned for 2008 (SSO at 600 km altitude with a revisit time of 8 days). The resolution (footprint size) of the data varies between 62 and 100 km. Monthly 100 km resolution maps of SSS will be provided for a mission life of 3 years.^{417) 418)}

- The NASA technology development program **STAR** (Synthetic Thinned Aperture Radiometry) is focused on achieving a 10 km spatial resolution global soil moisture mission towards the end of the decade (study phase as of 2002/4) from LEO.^{419) 420)} The L–band STAR microwave sounding technology promises higher spatial resolutions comparably sized mechanical scanners as well as antenna software–based antenna beam–forming to match the geometry and size of other sensors’ footprints (use of low–power digital correlators and ADC ASICs). Digital correlators are a key hardware component of the new STAR radiometer designs. Combinations of antenna signals are correlated and the resulting spatial coefficients are processed by image reconstruction algorithms. Also development of CULPRiT (CMOS Ultra–Low Power Radiation Tolerant) IC chip design. – This involves a 2–D L–band radiometer with light–weight components, namely LRR (Lightweight Rainfall Radiometer). – The STAR technology concept is also a prime candidate in the GPM (Global Precipitation Measurement) mission of NASA and JAXA (launch Feb. 27,

416) T. J. Jackson, “Current Potential and Outlook for Satellite Remote Sensing of Soil Water Content,” Proceedings of ISRSE (International Symposium of Remote Sensing of Environment), Honolulu, HI, Nov. 10–14, 2003

417) <http://aquarius.gsfc.nasa.gov/>

418) S. H. Yueh, W. J. Wilson, E. Njoku, D. Hunter, K. S. Kona, K. Bahadori, Y. Rahmat–Samii, “Compact, Lightweight Dual–Frequency Microstrip Antenna Feed for Future Soil Moisture and Sea Surface Salinity Missions,” Proceedings of ESTC (Earth Science Technology Conference), College Park, MD, June 24–26, 2003

419) C. M. Principe, J. R. Piepmeier, C. S. Ruf, “Low–Power Digital Microwave Radiometer Technologies,” Proceedings of ESTC (Earth Science Technology Conference), College Park, MD, June 24–26, 2003

420) J. R. Piepmeier, F. A. Pellerano, P. O’Neill, D. LeVine, E. Kim, T. Doiron, “Synthetic Thinned Aperture Radiometry (STAR) Technologies Enabling 10 km Soil Moisture Remote Sensing from Space,” Proceedings of 2nd Annual Earth Science Technology Conference, NASA/JPL, Pasadena, CA, June 11–13, 2002. URL: [http://esto.nasa.gov/conferences/estc-2002/Papers/B2P7\(Piepmeier\).pdf](http://esto.nasa.gov/conferences/estc-2002/Papers/B2P7(Piepmeier).pdf)

2014) at a center frequency of 10.7 GHz (X–band) to permit high–frequency sampling of rainfall. The technology provides wide swath pushbroom imaging with no moving parts, which significantly reduces spacecraft accommodation requirements. The LRR–X prototype aircraft radiometer is functionally equivalent to the candidate spaceborne sensor design. ⁴²¹⁾ ⁴²²⁾ ⁴²³⁾

1.4.5.3 Viewing geometries of microwave radiometers in LEO missions

There are two fundamental types of scanning that can be used in passive microwave radiometry: cross–track and conical scanning (Figure 20). ⁴²⁴⁾

1) **Cross–track scanners:** Traditionally, these scanners have been used for sounding applications. This type of scan generates a wide swath width with modest apertures, allowing an end to end instrument calibration that includes the main aperture. Equally important, it allows longer dwell times per pixel. Integration times are of the order 14–18 ms. The disadvantages are that the spatial resolution and polarization varies across the swath width. In general, the spatial resolution is defined as the nadir point.

2) **Conically–scanning microwave radiometers:** This scan mode provides constant pixel resolution across the swath with a constant polarization angle. It does inherently produce a narrow swath and this will impact on the daily repeat cycle for a given latitude. Larger antenna apertures are required for a given spatial resolution due to the observing geometry and calibration cannot include the primary reflector. This leads to poorer radiometric calibration accuracy. Indeed to date the radiometric accuracy of in–orbit conically scanning radiometers has been universally poor. Furthermore the integration times per pixel are short (5–10 ms), which degrades temperature sensitivity. So although sounding can be used with this scan geometry, there are many reasons for avoiding this approach given the more demanding requirements for sounding especially calibration accuracy. Further compromises arise if polarimetry is introduced as the feed–horn cluster becomes more congested resulting in more bands located away from the focal point resulting in degraded beam efficiency.

Introduction of conical–scanning multi–frequency microwave sounding/imaging radiometers: The general design of such a radiometer features a mechanical scanning mechanism in which a parabolic antenna reflector is physically rotated around an axis. ⁴²⁵⁾ For Earth surface sensing this is normally a vertical axis, and a conical scan with constant incidence angle on the ground results. The antenna reflector can provide a range of frequencies, and the result is often a compact and efficient system. The technology provides a common FOV (Field of View) combining imaging and sounding channels in a wide–swath observation geometry. For each frequency channel, a constant–size resolution cell pattern is maintained along the continuous rotating observation scene using a constant incident angle observation scheme. Ground resolution sizes may range from about 5 km to about 80 km, the higher the frequency channel the finer the resolution. The passive microwave technology has the advantage of cloud penetration observations, it also has the potential to provide such observations as rain rate, wind speed and direction over oceans, as well as the conventional temperature and humidity profiles.

421) E. A. Smith, W. J. Adams, C. Kummerow, C. Principe, C. S. Ruf, T. T. Wilheit, “Potential Applications of LRR–STAR Technology for GPM Mission,” Proceedings of 2nd Annual Earth Science Technology Conference, NASA/JPL, Pasadena, CA, June 2002. URL: [http://esto.nasa.gov/conferences/estc–2002/Papers/B2P2\(Smith\).pdf](http://esto.nasa.gov/conferences/estc–2002/Papers/B2P2(Smith).pdf)

422) C. Ruf, C. Principe, T. Dod, B. Monosmith, S. Musko, et al., “Synthetic Thinned Aperture Radiometer Technology Developments Enabling a GPM Lightweight Rainfall Radiometer,” Proceedings of 2nd Annual Earth Science Technology Conference, NASA/JPL, Pasadena, CA, June 11–13, 2002

423) R. D. De Roo, A. W. England, J. Munn, “Circular Polarization for L–band Radiometric Soil Moisture Retrieval,” Proceedings of the IEEE Aerospace Conference, Big Sky, MT, March 6–13, 2004

424) J. E. Charlton, U. Klein, “Next Generation Microwave Radiometry Missions for Meteorology in Low Earth Orbits,” Proceedings of the Advanced RF Sensors for Earth Observation 2006 (ASRI), Workshop on RF and Microwave Systems, Instruments & Sub–Systems, ESA7ESTEC, Noordwijk, The Netherlands, Dec. 5–6, 2006

425) N. Skou, “Spaceborne L–band Radiometers: Push–broom or Synthetic Aperture?” Proceedings of IGARSS 2004, Anchorage, AK, USA, Sept. 20–24, 2004

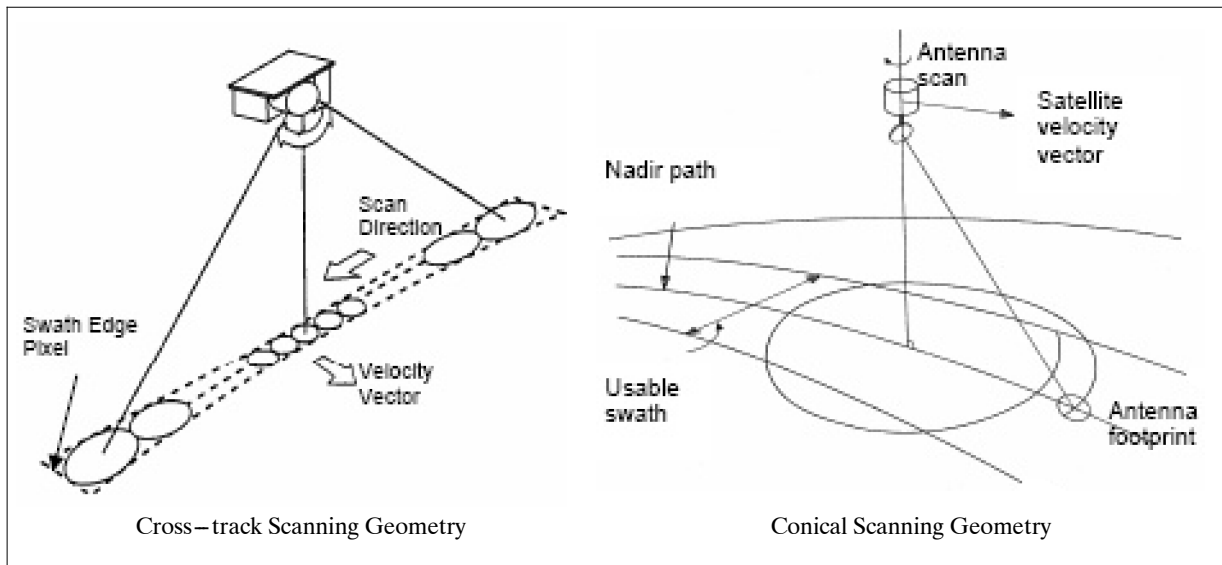


Figure 20: Observation geometries for passive microwave radiometers (image credit: ESA)

The following list provides an overview of conical-scanning microwave radiometers:

- SMMR (Scanning Multichannel Microwave Radiometer), a conical-scanning dual-polarization Dicke type instrument (6.6 – 37 GHz) flown on SeaSat (launch June 27, 1978) and on Nimbus-7 (launch Oct. 28, 1978) of NASA. Measurement of SST and wind speed in a 600 km swath.
- SSM/I (Special Sensor Microwave Imager), a conical scanning microwave radiometer with 7 channels, 4 vertical and 3 horizontal. SSM/I of DoD is flown since 1987 on the DMSP series. However, the design of SSM/I, a microwave radiometer, only permits the retrieval of the speed component of the wind vector. The follow-up of SSM/I is SSMIS (Special Sensor Microwave Imager Sounder), first flown on DMSP-F-16 (launch Oct. 18, 2003). SSMIS, a 24-channel instrument, provides a conical scan with a swath width of 1700 km. It is also capable of retrieving soil moisture.
- MSR (Microwave Scanning Radiometer), a conical-scanning instrument flown on the MOS-1 (Marine Observation Satellite-1; launch Feb. 19, 1987) and MOS-1B (launch Feb. 7, 1990) of NASDA, Japan. MSR is composed of two Dicke-type radiometers at 23.8 and at 31.4 GHz.
- ATSR (Along-Track Scanning Radiometer and Microwave Sounder), a conical scanning infrared radiometer (IRR) flown on ERS-1 (launch July 17, 1991), ERS-2 (Apr. 21, 1995), and as AATSR on Envisat (launch March 1, 2002).
- TMI (TRMM Microwave Imager) is a dual-polarization conical-scanning radiometer (10–85 GHz) on the TRMM mission of NASA (launch Nov. 27, 1997). The 9 channels on TMI allow for simultaneous retrieval of SST, wind speed, columnar water vapor, cloud liquid water, and rain rate. Accurate through-cloud SST retrievals were first provided by TMI at a resolution of 10 km.
- IKAR-P is a 3-channel conical-scanning microwave radiometer that was flown on the Priroda module (launch Apr. 23, 1996) of the MIR station. Measurement of SST.
- MSMR (Multifrequency Scanning Microwave Radiometer) is a dual-polarized four-frequency conical-scanning radiometer flown on IRS-P4 (OceanSat-1) of ISRO (launch May 26, 1999). The eight-channel MSMR employs six independent receivers at 6.6, 10.6, 18, 21 GHz. MSMR provides SST, sea surface wind speed, atmospheric water vapor and cloud liquid content in a swath of 1360 km.

-
- MTVZA (Microwave Imaging/Sounding Radiometer) flown on Meteor–3M–1 spacecraft of Russia (launch Dec. 10, 2001); a 26–channel instrument with a swath of 2200 km. A follow–up instrument, MTVZA–OK (Combined Microwave–Optical Imaging/Sounding Radiometer), a 22–channel instrument, is flown on (launch Dec. 24, 2004) of Ukraine (NSAU) and Russia (Rosaviakosmos). Swath of 2000 km. Monitoring of SST, sea surface wind speed, precipitation, ocean color, and atmospheric temperature and humidity profiles.
 - AMSR–E (Advanced Microwave Scanning Radiometer–EOS) is a JAXA instrument flown on NASA’s Aqua mission (launch May 4, 2002). The AMSR–E instrument is a conically scanning total power passive microwave radiometer sensing microwave radiation (brightness temperatures, 40 rpm, 1.6 m parabolic reflector) in 12 channels and 6 frequencies ranging from 6.9 to 89.0 GHz. Horizontally and vertically polarized radiation are measured separately at each frequency. At an altitude of 705 km, it measures the upwelling scene brightness temperatures over an angular sector of $\pm 61^\circ$ about the subsatellite track, resulting in a swath width of 1445 km. AMSR–E is of AMSR heritage.
 - AMSR (Advanced Microwave Scanning Radiometer) is flown on ADEOS–II (launch Dec. 4, 2002) of JAXA. AMSR is an eight–frequency, total–power microwave radiometer with dual polarization (2 m aperture). Conical scanning at 40 rpm is employed to observe the Earth’s surface with a constant incidence angle of approximately 55° . A swath of 1600 km is provided for the measurement of SST, soil moisture, sea wind speed, water equivalent of snow cover, precipitation intensity, sea ice distribution, precipitable water, etc.
 - The WindSat (Wind Microwave Radiometer) instrument on the Coriolis mission (launch Jan. 6, 2003) of NRL uses a conically scanned 1.83 m parabolic offset reflector with multiple feeds.
 - The MADRAS (Microwave Analysis and Detection of Rain and Atmosphere Systems) radiometer of ISRO is planned to be flown on the cooperative mission of ISRO and CNES, called Megha–Tropiques (launch Oct. 12, 2011). MADRAS is a five–frequency (9 channel) mechanical conical–scanning passive microwave radiometer providing brightness temperature measurements (18.7 to 157 GHz). The LEO S/C orbit will only cover the equatorial regions (inclination of 20°), see A.22.
 - The AMSR–2 (Advanced Microwave Scanning Radiometer–2) of AMSR heritage is flown on the GCOM–W1 (Global Change Observation Mission– Water 1) mission of JAXA (successor to ADEOS, ADEOS–II). Launch of GCOM–W1 on May 17, 2012.
 - The MIS (Microwave Imager/Sounder) instrument of the IPO NPOESS program (first launch in 2016) employs a single–rotating reflector with an aperture of 1.8 m in diameter to make “all–weather” measurements across a large frequency range of 6–183 GHz and use of an FFT implementation. Polarizations for selected imaging channels are being used to derive ocean surface wind vectors similar to what has previously been achieved with active scatterometers. Measurement of soil moisture, cloud base height, etc. MIS is considered to be the next–generation conical–scanning microwave radiometer (with regard to capabilities); it is the largest and also the most complex payload of the NPOESS satellites.
 - As of 2003/4, NASA is defining HYDROS (Hydrosphere State Mission) within ESSP. The objective is to provide a global view of the Earth’s changing soil moisture and land surface freeze/thaw state. The HYDROS measurement approach employs a **combined passive/active low–frequency (L–band) microwave instrument** to measure the land hydrosphere state globally from space. The scatterometer (1.26 GHz) and radiometer (1.41 GHz) share a common 6 m diameter antenna pointing at 39.3° (incidence angle) with respect to nadir. The antenna is rotated at 14.6 rpm to provide a scanned swath of 1000 km (conical scan). Polarization of the scatterometer in VV, HH, and HV with a resolution of 3 km. The

radiometer is polarized in H, V, and U with resolutions of 40 km. An expected launch of HYDROS is in 2009/10 (SSO of 670 km altitude). The revisit time is 3 days. ⁴²⁶⁾

Note: In Dec. 2005, NASA stopped funding the HYDROS project in the definition phase due to budgetary problems. ⁴²⁷⁾

1.4.5.4 Pushbroom versus synthetic aperture concept in radiometry

The provision of adequate spatial data resolution on the ground (i.e., to obtain a small footprint size for brightness temperature observations) has been an inherent requirement (and problem area) for all LEO spaceborne missions carrying a radiometer payload, in particular of the type L–band microwave radiometer (spectral window of 1.4 GHz, wavelength of about 22.5 cm), needed for the derivation of such geophysical parameters as soil moisture and ocean salinity.

A conventional microwave radiometer (such as a conically scanning instrument) creates imagery by mechanically scanning the antenna in such a way that the footprint covers a certain swath consecutively. Apart from mechanical complications, this observing method (of a single radiometer) leads to relatively short dwell times for each footprint, resulting in a short integration time and in poor instrument sensitivity.

In most microwave radiometer implementations, the antenna is generally the dominant instrument subsystem that determines the ultimate measurement performance and governs the spacecraft accommodation (dictated by resolution requirements). Of course, higher spatial resolutions of radiometers can be achieved by providing larger real–aperture antennas (and using the pushbroom imaging concept) or by the application of synthetic aperture (i.e., thinned array) techniques. So far, antennas of substantial size (10 m aperture or more) have not been employed in spaceborne microwave applications because of the substantial penalty in associated physical weight and launch packaging volume required.

The two configuration concepts for parallel (simultaneous) radiometric observations may be characterized by: ⁴²⁸⁾

- Thinned arrays remove much of the bulk of the antenna by using elements at carefully selected positions (related to a wavelength) and “filling in the antenna pattern” with computer processing techniques. They are attractive for single frequency remote–sensing applications, such as soil moisture, but increase in complexity with added frequencies and polarizations.
- In the pushbroom concept, a special antenna having many simultaneous beams each associated with its individual feed and receiver, is employed (analogy to a pushbroom CCD line array). When the satellite moves forwards the beams sweep the Earth’s surface like a broom and make an image without scanning. The many receivers ensure the ultimate in radiometric sensitivity. The price to pay is: many receivers as well as a complicated and large antenna. However, at the start of the 21st century, receivers made as MMICs (Microwave Monolithic Integrated Circuit) are small and low power units, and a foldable reflector structure, that works well at L–band, is possible using proven technology.

The radiometer technology that is employed in real–aperture pushbroom radiometer systems utilizes significantly less complex electronic circuitry as compared with the electronic

426) E. Njoku, M. Spencer, K. McDonald, J. Smith, P. Houser, T. Doiron, P. O’Neill, >R. Girard, D. Entekhabi, “The HYDROS Mission: Requirements and System Design,” Proceedings of the IEEE Aerospace Conference, Big Sky, MT, March 6–13, 2004

427) <http://hydros.gsfc.nasa.gov/index.php>

428) N. Skou, “Spaceborne L–band Radiometers: Push–broom or Synthetic Aperture?” Proceedings of IGARSS 2004, Anchorage, AK, USA, Sept. 20–24, 2004

subsystems required for synthetic aperture radiometers. The traditional real–aperture system design utilizes a more mature technology.^{429) 430)}

The synthetic aperture radiometer works as a radio camera and acquires a two–dimensional image of the ground by interferometric means. As the satellite moves forwards a swath is imaged. Again, many receivers (and antenna elements) are needed. The big advantage is that a relatively slim structure – the antennas can for example be positioned along 3 arms arranged in a Y shape – can be used, and the structure is easily foldable. A drawback is substantial data processing requirements and less straight–forward calibration issues.

The main virtues of the pushbroom radiometer system are that it gives superior radiometric resolution and very likely also superior accuracy and stability.

The main virtues of the synthetic aperture system is that it measures the brightness temperature as a function of incidence angle, and that it is relatively straight forward to fold the Y–shape structure for launch.

The advantages of a pushbroom system might point towards use in cases with extreme requirements to radiometric resolution and accuracy, like in the case of ocean salinity. The advantages of the synthetic aperture system, on the other hand, point towards use in cases with complicated targets like vegetation covered soil, where it is possible to retrieve soil moisture, cleaned for the vegetation influence, due to the multi–incidence angle imaging.

Spaceborne missions under development with implementations of the two techniques:

- The SMOS (Soil Moisture and Ocean Salinity) mission in LEO (Low Earth Orbit) of ESA (launch Nov. 2, 2009) employs the **synthetic aperture radiometer concept** with MIRAS (Microwave Imaging Radiometer using Aperture Synthesis). MIRAS is a 1.415 GHz system with 69 antenna elements and radiometers mounted on three 4.3 m long arms as well as on a central hub, that also holds the many correlators – one for each possible pair of antennas (Y shape, providing a 2–D interferometric radiometer configuration). The corresponding interferometer measurements, also called complex visibilities, are obtained by cross–correlating the signals collected by every pair of antennae; a regularized reconstruction process provides a band–limited brightness temperature map in the reference frame of the instrument. The spatial resolution of the data is < 50 km on a swath of 934 km at an orbital altitude of 754 km. SMOS, although a dual–purpose mission, has its largest focus on soil moisture.
- The SAC–D/Aquarius spaceborne mission, a cooperative project of NASA and CONAE (launch June 10, 2011), employs the **pushbroom radiometer concept**. The objective of the radiometer is to demonstrate the measurement of microwave brightness temperatures of the ocean surface with sufficient accuracy and resolution, which are sensitive to salinity and surface roughness. In parallel, the scatterometer measures the surface roughness for correcting the radiometric brightness temperature. The radiometer implementation provides only a small and simple pushbroom demonstration system with 3 beams. The footprint sizes of the beams are: 62 km x 68 km, 68 km x 82 km, and 75 km x 100 km, respectively. The SAC–D/ Aquarius mission concept builds on experiences gathered by the airborne instrument PALS (Passive–Active L– and S–band Radar and Radiometer), a pushbroom radiometer of NASA/JPL. The PALS instrument was installed on the NCAR C–130 aircraft and first soil moisture measurements were made in support of the SGP’99 (Southern Great Plains) campaign in Oklahoma from July 8–14, 1999. Other campaigns with PALS participation were SMEX02 (Soil Moisture Experiment) in Iowa in 2002, and SMEX03 conducted in Oklahoma, Georgia, and Alabama (USA) during the summer of 2003 and in Brazil during December 2003.

429) L. C. Schroeder, M. C. Bailey, R. F. Harrington, B. M. Kendall, T. G. Campbell, “Design Studies of Large Aperture, High–Resolution Earth Science Microwave Radiometers Compatible With Small Launch Vehicles,” NASA Technical Paper 3469, Sept. 1994

430) “Soil Moisture Research Mission (EX–4),” http://www.cesbio.ups–tlse.fr/data_all/SMOS_WS/smm3.htm

Background: The idea of a pushbroom radiometer was initially proposed in the late 1970s to improve the spatial resolution of radiometers. This concept places many identical microwave receivers (a line array) in the focal plane of the reflector antenna, such that each receiver observes at a specific pixel cross-track to the orbital motion of the large reflector antenna. An image is thus developed through the forward motion of the spacecraft. The swath width can be increased by adding identical receivers. This can add up to 50 or more for a modest footprint size across a wide swath.

The pushbroom microwave radiometer concept was initially demonstrated with airborne instruments, developed in parallel by NASA/LaRC and the Technical University of Denmark. Initial flights of TUDRAD (Technical University of Denmark. Radiometer), a 3 receiver 21 channel frequency-scanned pushbroom system, were conducted in Nov. 1990 using a C-130 aircraft of the Royal Danish Air Force. A parabolic antenna of 1 m aperture was used scanning vertically. TUDRAD was designed to give a contiguous coverage over a swath of 2000 m at a flying altitude of 2000 m. This resulted in a minimum dwell time per footprint of 34 ms (at 15.4 GHz). – However, the difficulty with the pushbroom concept at the time was the continued growth in antenna size that was required in order to accommodate a large number of receivers. A 10 km ground resolution with a 1000 km swath would have required an antenna aperture with dimensions of 25 m x 50 m. ^{431) 432)}

1.4.5.5 Microwave sounding from GEO (Geostationary Earth Orbit) satellites

The idea of microwave sounding from GEO is of great interest because such a concept offers some unique observation capabilities of great value for the meteorological community (temperature and humidity sounding as well as the precipitation rate). The attraction of GEO observations is based on the capability to continuously view the same portion of the Earth (an area of interest which can be of considerable size, a continent), during day and night and at all weather conditions. Hence, observations from GEO provide very high temporal resolutions suitable not only for NWP (Numerical Weather Prediction), but in particular for nowcasting and very short range weather forecasts. ⁴³³⁾ The full viewable Earth disk from GEO subtends an angle of 17.4°, representing 42% of the Earth's surface area. However, with the GEO radial distance 45 times larger than the average LEO distance of 800 km, **the GEO concept requires a considerably larger aperture (antenna structure)** to achieve a sufficiently high spatial resolution for applications in the microwave region. The large aperture requirement is the only reason why microwave sounders and radiometers haven't been flown in GEO so far. Another disadvantage of GEO observations is the limited coverage of the high latitudes. An alternative to GEO are MEO (Medium Earth Orbit) observations. The MEO might offer a compromise on antenna size and as well as a less dramatic degradation of the spatial resolution at the swath edges. The concept has even the potential of covering the poles.

Microwave soundings from GEO or MEO are highly desirable for short-interval observation of rapidly evolving meteorological phenomena such as convective systems, precipitation and cloud patterns, providing the required high temporal resolution from a geostationary or medium Earth orbit. Some potential observation parameters to be obtained are: 1) the precipitation rate from convective clouds; 2) the cloud liquid and ice water column content; 3) atmospheric temperature and humidity profiles; and 4) atmospheric motion vectors (winds). – At the start of the 21st century, the technology is available to extend radiometry

431) R. W. Lawrence, M. C. Bailey, R. F. Harrington, C. P. Hearn, J. Wells, W. D. Stanley, "Design and Development of a Multibeam 1.4 GHz Pushbroom Microwave Radiometer. NASA TM-89005, 1986

432) N. Skou, S. S. Kristensen, "Comparison of Imagery from a Scanning and a Pushbroom Radiometer," Proceedings of IGARSS'91, June 1991, pp. 2107-2110

433) U. Klein, C.-C. Lin, N. Atkinson, J. Charlton, C. Philpot, "Future Microwave Radiometers in Geostationary and Medium Earth Orbit," IEEE/IGARSS 2003, Toulouse, France, July 21-25, 2003

to the submillimeter–wavelength range, which enables corresponding reductions in antenna size or, alternatively, improvements in resolution for a given antenna size. ^{434) 435)}

The principle of precipitation measurement from geostationary orbit is based on the use of absorption bands of O₂ for atmospheric temperature profiling and H₂O for water vapor profiling. Profiles retrieved by bands at different frequencies are differently affected by liquid water, ice water, drop size and shape, and hence precipitation.

Background: So far, infrared/microwave (IR/MW) sounder instrument combinations, [like the TOVS (TIROS Operational Vertical Sounder) instrument series with HIRS, SSU and MSU flown since TIROS–N (launch 1978), and the ATOVS (Advanced TOVS) HIRS/AMSU–A and AMSU–B (Advanced Microwave Sounding Unit) combination, first flown on NOAA–15 (launch May 13, 1998)], have only been flown on operational weather satellites in polar orbits [i.e., LEO (Low Earth Orbit)]. The Aqua LEO mission of NASA (launch May 4, 2002) flies two microwave sounders (AMSU, HSB) in combination with AIRS (Atmospheric Infrared Sounder). Together, the three sensors constitute the advanced operational sounding system. These combined IR/MW observations have the advantage to provide more nearly all–weather soundings (recovery of vertical distribution of temperature and humidity soundings). Such S/C observations have had a significant impact on weather forecasting accuracy, especially in regions where in–situ observations are sparse. Infrared sounders alone do not have adequate cloud–penetration ability to satisfy most forecast requirements, while microwave sounders alone do not satisfy observations in the infrared region.

The following initial concept studies on the topic of GEO MW (Microwave) sounding give an overview of converging activities in the field, leading eventually to a solid mission with international cooperation.

- Two early US studies on GEO MW sounding ⁴³⁶⁾ were conducted for NASA in 1978. The essential conclusions of both studies were that placing a large aperture antenna to realize reasonable spatial resolution and developing reliable low–noise receivers sensitive enough for GEO sounding measurements were of greatest challenge.
- In Europe, ^{437) 438) 439) 440)} GEO MW sounding was placed in 1984 as a requirement for the MSG (Meteosat Second Generation) mission of ESA/EUMETSAT. However, the technology prerequisites were not available at this time. The current post–MSG activities involve studies for future MW sounders in GEO or MEO. Main drivers for the GEO concepts are the large main reflector of about 3.5 m diameter, the scan mechanism and the combination of radiometric accuracy, geographical coverage and repeat cycle.
- In the USA, a “Geosynchronous Microwave Sounder Working Group” ⁴⁴¹⁾ reported to the NOAA/NESDIS GOES Program Office in 1997 (first time). This led in 1998 to the **GMS** (Geostationary Microwave Sounder) proposal [also referred to as GEM (GEostationary Microwave Sounder/Imager)]. The intent is to demonstrate the GMS observation concept on future NOAA GOES platforms starting with GOES–R, the next–generation

434) B. Bizzarri, A. Gasiewski, D. Staelin, “Initiatives for Millimeter/Submillimeter–Wave Sounding from Geostationary Orbit,” Proceedings of IGARSS 2002, Toronto, Canada, June 24–28, 2002

435) A. J. Gasiewski, “Numerical Sensitivity Analysis of Passive EHF and SMMW Channels to Tropospheric Water Vapor, Clouds and Precipitation,” IEEE Transactions on Geoscience and Remote Sensing, Vol. 30, No. 5, pp. 859–870., 1992

436) D. H. Staelin, P. W. Rosenkranz, (editors): “Applications Review Panel: High resolution passive microwave satellites”. Report for NASA Contract NAS5–23677, MIT Research Laboratory of Electronics, April 1978

437) F. E. Goodwin, R. E. Graves, M. S. Hersman, M. Luming, “Geosynchronous Microwave Atmospheric Sounding Radiometer (MASR) Feasibility Study,” Final Report, Hughes Ref. No. D8647 SCG 80039R, January 1978.

438) L. Hilliard, D. Jenstrom, D. Chesters, P. Racette, “Geosynchronous Technology Infusion Studies,” at URL: rsd.gsfc.nasa.gov/pub/goes/AGS.IGARSS97.pdf

439) A. Chedin, D. Pick, R. Rizzi, 1985: “Definition study and impact analysis of a microwave radiometer on a geostationary spacecraft,” ESA Report, March 1985, pp.58

440) U. Klein, J. Guijarro, B. Rommen, P. Vogel, P. de Maagt, C.C. Lin, “Microwave Instruments Development in ESA’s Earth Observation Future Programs,” IEEE/IGARSS 2003, Toulouse, France, July 21–25, 2003

satellite (launch 2014).⁴⁴²⁾ The GMS instrument is considered along with the HES (Hyperspectral Environmental Suite) infrared sounder (see also 1.20.3).

– NASA/HQ released in Sept. 1998 a research announcement for new measurement concepts of the planned EO–3 (Earth Observing–3) mission.^{443) 444)} Four concepts were selected in March 1999, these were: a) active large aperture optical systems to provide high resolution thermal imaging from GEO (referred to as HORIZON), b) GEO/SAMS (Geostationary Synthetic Aperture Microwave Sounder), c) GIFTS (Geostationary Imaging Fourier Transform Spectrometer), and d) GEO–TRACE (Geostationary Tropospheric Trace–gas imager). Regarding GEO/SAMS, the proposed concept employs the synthetic aperture radiometer technique (a sparsely populated antenna array is substituted for a filled array). However, in 2000 the GEO/SAMS proposal was not accepted.

– In January 2003,^{445) 446)} a new proposal was selected/awarded (within IIP) to NASA/JPL, namely **GeoSTAR** (Geostationary Synthetic Thinned Aperture Radiometer), an interferometric system for **geostationary microwave sounding** applications using aperture synthesis. The development effort under way at JPL, with important contributions from the Goddard Space Flight Center and the University of Michigan, is intended to demonstrate the measurement concept and retire much of the technology risk.^{447) 448) 449) 450)}

GeoSTAR is an atmospheric sounder with rain mapping capabilities. It operates primarily in two millimeter–wave bands. For tropospheric temperature sounding it will have a small number of channels positioned near 50 GHz. For water vapor sounding it will use a set of channels positioned near 183 GHz, which are also used for rain mapping. In addition, there is also an intermediate “window” channel near 90 GHz (same approach as implemented with AMSU–A/B on the current POES series). GeoSTAR will also use the 183 GHz water vapor sounding channels for precipitation measurements. The GeoSTAR approach is primarily based on measuring the scattering effects associated with precipitation. The GeoSTAR scattering approach derives from observations made in recent years with 183 GHz radiometers operated on high altitude aircraft. When passing over rain cells, a pronounced apparent cooling due to scattering is observed. This cooling can exceed 100 K over intense convective cells, a very large signal that can be used to detect and track hurricanes and other severe storms without the need for high radiometric sensitivity (i.e. dwell time).

441) D. H. Staelin, A. J. Gasiewski, J. P. Kerekes, M. W. Shields, F. J. Solman III, “Concept proposal for a Geostationary Microwave (GEM) Observatory”. Prepared for the NASA/NOAA Advanced Geostationary Sensor (AGS) Program, MIT, Lexington MA., 1998 pp.23

442) Note: Accommodation issues on the spacecraft are most severe for microwave sounding instruments due to large antenna size requirements

443) J. Gurka, J. Heil, “The US National Weather Service Operational Requirements for the Evolution of future NOAA Operational Geostationary Satellites,” Proceedings of the EUMETSAT Meteorological Satellite Data User’s Conference, Copenhagen, Denmark, Sept. 6–10, 1999, pp. 69–76

444) W. C. Bonyck, W. J. Wilson, B. H. Lambrigtsen, “The Enabling Technologies of the Geostationary Synthetic Aperture Microwave Sounder (GEO/SAMS),” Proceedings of IGARSS Conference, Honolulu, HI, July 24–28, 2000

445) B. H. Lambrigtsen, W. J. Wilson, A. Tanner, P. Kangaslahti, “Progress in developing GeoSTAR: a microwave sounder for GOES–R,” Proceedings of the SPIE Conference Optics & Photonics 2005, Vol. 5882–23, San Diego, CA, USA, July 31–Aug. 4, 2005

446) B. Lambrigtsen, W. Wilson, A. Tanner, T. Gaier, C. Ruf, J. Piepmeier, “GeoSTAR – A Microwave Sounder for Geostationary Satellites,” Proceedings of IGARSS 2004, Anchorage, AK, USA, Sept. 20–24, 2004

447) A. B. Tanner, W. J. Wilson, P. P. Kangaslahti, B. H. Lambrigtsen, S. J. Dinardo, J. R. Piepmeier, C. S. Ruf, S. Rogacki, S. M. Gross, S. Musko, “Prototype development of a Geostationary Synthetic Thinned Aperture Radiometer, GeoSTAR,” Proceedings of NASA’s ESTC 2004, Palo Alto, CA, June 22–24, 2004; URL: <http://www.estc.nasa.gov/conferences/estc2004/papers/b6p1.pdf>

448) B. Lambrigtsen, W. Wilson, A. Tanner, T. Gaier, “GeoSTAR – A Synthetic Aperture Approach for a Geostationary Microwave Sounder,” Proceedings of the IEEE Aerospace Conference, Big Sky, MT, March 6–13, 2004

449) B. Lambrigtsen, “GeoSTAR – A New Approach for a Geostationary Microwave Sounder,” 13th ITSC (International TOVS Study Conference), Sainte. Adèle, Quebec, Canada, Oct 28 – Nov. 4, 2003, http://cimss.ssec.wisc.edu/itwg/itsc/itsc13/session10/10_1_lambrigtsen.pdf

450) B. H. Lambrigtsen, W. J. Wilson, A. B. Tanner, P. Kangaslahti, “GeoSTAR: a synthetic aperture microwave sounder for geostationary missions,” Proceedings of SPIE, Vol. 5659, ‘Enabling Sensor and Platform Technologies for Spaceborne Remote Sensing,’ G. J. Komar, J. Wang, T. Kimura, Editors, Jan. 2005, pp. 185–194, Conference location: Honolulu, HI, USA, Nov. 9, 2004

The goals are to complement LEO microwave soundings of the POES series from GEO (on future GOES satellites, considered for GOES–R and thereafter) and to provide full hemispheric observations at resolutions of $\leq 50/25$ km (temperature/moisture) every 1/2 to 1 hour on a continuous basis. The GeoSTAR project foresees a first step in ground testing to demonstrate the feasibility of the synthetic aperture approach – in the form of a small ground–based prototype. The GeoSTAR design concept employs a 2–D spatial interferometric system (synthetic aperture imaging approach) of horn antennas and receivers, which measures the complex cross–correlations between the output signals of all receiver pairs that can be formed from a large number of millimeter wave radiometers arrayed in a “Y–shaped” configuration.

For GEO where the required field of regard is about 17.5° – the size of the Earth disk as seen from GEO, the receiver spacing is therefore approximately 3.5 wavelengths (about 2 cm at 50 GHz and about 6 mm at 183 GHz). The longest baseline determines the smallest spatial scale that can be resolved. To achieve a 50 km spatial resolution at 50 GHz, an aperture diameter in excess of 4 meters is required. That corresponds to approximately 100 receiving elements per array arm, or a total of about 300 elements. This in turn results in 45,000 unique baselines and 90,000 uv sampling points.

As of 2007, the GeoSTAR concept is also considered for a possible selection on the future **PATH** (Precipitation and All–weather Temperature and Humidity) mission of NASA and/or NOAA. PATH is one of the 17 mission concepts which was recommended in the “decadal survey” report of NRC (National Research Council) released in January 2007. The primary objective of the PATH mission is to fly a microwave array spectrometer to monitor hurricanes and severe storms and improve existing models. The GeoSTAR concept happens to be the only sensor that can meet the PATH mission objectives.⁴⁵¹⁾

– Within NASA’s IIP (Instrument Incubator Program), BATC (Ball Aerospace and Technologies Corporation) was awarded the **SIRAS–G** (Spaceborne Infrared Atmospheric Sounder for Geostationary Orbit) technology study in Jan. 2003. SIRAS–G is an instrument concept for infrared sounding at a moderate spectral resolution $\lambda/\Delta\lambda$ of 1400, using 2048 channels in the spectral range 3.4 – 15.4 μm . The concept (laboratory demonstration instrument) utilizes the grating spectrometer technology of AIRS (Atmospheric Infrared Sounder) heritage flown on NASA’s Aqua mission.^{452) 453) 454) 455) 456)}

SIRAS–G employs a WFOV hyperspectral infrared optical system that splits the incoming radiation into four separate grating spectrometer channels. This allows for slow scanning of the scene, increased dwell time, and improved radiometric sensitivity. The ability of SIRAS–G to provide simultaneous observations of the Earth’s atmospheric temperature, ocean surface temperature, and land surface temperature, as well as humidity, clouds, and the distribution of atmospheric trace gases enables SIRAS–G to provide a single data set

451) Bjorn Lambrigtsen, Alan Tanner, Todd Gaier, Pekka Kangaslahti, Shannon Brown, “Prototyping GeoSTAR for the PATH Mission,” NSTC2007 (NASA Science and Technology Conference 2007), June 19–20, 2007, College Park, MD, USA, URL: http://esto.nasa.gov/conferences/nstc2007/papers/Lambrigtsen_Bjorn_B1P4_NSTC-07-0020.pdf

452) Thomas U. Kampe, Holden Chase, Vincent Kotsubo, Paul Hendershott, Gary Mills, John Wassmer, “The Spaceborne Infrared Atmospheric Sounder for Geosynchronous Earth Orbit (SIRAS–G) – Pathfinder IR Imaging Spectrometer for Space Missions,” NSTC2007 (NASA Science Technology Conference), June 19–21, 2007, College Park, MD, USA, URL: http://esto.nasa.gov/conferences/nstc2007/papers/Kampe_Thomas_B6P2_NSTC-07-0045.pdf

453) T. Kampe, H. H. Aumann, “SIRAS–G, The Spaceborne Infrared Atmospheric Sounder: The potential for high–resolution infrared imaging spectrometry from geosynchronous orbit,” 13th ITSC, Sainte. Adèle, Quebec, Canada, Oct 28 – Nov. 4, 2003, http://cimss.ssec.wisc.edu/itwg/itsc/itsc13/session10/10_8_aumann.pdf

454) T. U. Kampe, “SIRAS–G: The Space–based Infrared Atmospheric Sounder from Geosynchronous Orbit,” Proceedings of ESTC (Earth Science Technology Conference), Palo Alto, CA, June 22–24, 2004, <http://esto.gsfc.nasa.gov/conferences/estc2004/papers/b7p3.pdf>

455) T. U. Kampe, T. S. Pagano, J. W. Bergstrom, “SIRAS, The Spaceborne Infrared Atmospheric Sounder: an approach to next–generation infrared spectrometers for Earth remote sensing,” Proceedings of SPIE, Vol. 4485, 2002

456) T. U. Kampe, “SIRAS–G: the spaceborne infrared atmospheric sounder: laboratory instrument development,” Proceedings of SPIE, Volume 5523, pp. 39–50, 2004

that can be used to understand the horizontal and temporal changes in column abundances of important minor atmospheric gases such as CO₂, CO, CH₄, and N₂O.

Background: The SIRAS–G program builds on an earlier IIP effort (referred to as SIRAS–1999) in which one of the SIRAS spectrometers was demonstrated. Initially, the SIRAS grating spectrometer instrument architecture was primarily seen as a potential option for the next–generation IR sounder (like AIRS–Light). AIRS on Aqua has a mass of 150 kg, an average power consumption of about 250 W, and a volume of about 0.8 m³. Both SIRAS and AIRS–Light enable large reductions in mass (> 2x), power (> 2x), and size (> 5x) through 2 different strategies of technology introduction. SIRAS uses a strategy of combining wide–field refractive optics with high dispersion gratings to miniaturize the instrument. AIRS–Light introduced a newly–developed photovoltaic detector, namely an HgCdTe long–wave infrared FPA for the 14.5–15.5 μm band and a pulse–tube cryocooler technology.^{457) 458) 459)}

Subsequently, it has been shown that this instrument architecture is also well suited to a large variety of Earth science missions including geosynchronous deployment. SIRAS–G will provide measurements similar to those currently being made by AIRS (AIRS is in LEO on Aqua), but from GEO. Again, SIRAS–G is primarily a laboratory instrument; the objective of the program is to develop innovative conceptual designs and to test these for future missions. SIRAS–G potentially serves as a technology pathfinder for the Hyperspectral Environmental Suite (HES), planned to be flown on the GOES–R (NOAA 3rd generation geostationary satellite, launch 2014) mission.

– In Europe, a new analysis was prepared for EUMETSAT in 2000.⁴⁶⁰⁾ And in January 2002, a proposal by the name of GOMAS (Geostationary Observatory for Microwave Atmospheric Sounding) was submitted to ESA in the framework of the Earth Explorer Opportunity Missions. GOMAS includes all GMS (GEM) heritages.

– The **GMS (USA) / GOMAS (Europe)** observation principle is based on the use of absorption bands of oxygen (54, 118 and 425 GHz) and of water vapor (183, 380 and 424 GHz). The design considers narrow–bandwidth channels (for a total of about 40 in the six bands) so as to observe the full profiles of temperature and water vapor. The GMS (Geostationary Microwave Sounder) concept employs a scanning Cassegrain reflector antenna of 2 m diameter in a dual stage scanning system. The dual–stage system consists of a slow momentum–compensated azimuth mechanism and fast scanning subreflector scanning system to provide both wide–area synoptic coverage and fast regional coverage with adaptive scan capabilities. The 2 m antenna will provide ~ 16 km horizontal subsatellite resolution at the highest GMS frequency. As of 2003, GMS is candidate instrument on GOES–R (2014).

– A GOMAS antenna of about 3 to 3.5 m diameter can provide spatial resolutions ranging from 10 km (for precipitation) to 20 km (for water vapor and cloud liquid/ice water) and 30 km (for temperature). A GOMAS demonstration mission is proposed for the timeframe 2007–2009.^{461) 462)}

457) K. Marschhoff, “AIRS–Light Instrument Concept and Critical Technology Development,” Earth Science Technology Conference,” College Park, MD, Aug. 28–31, 2001

458) T. Pagano, “The Spaceborne Infrared Atmospheric Sounder (SIRAS) IIP Demonstration,” Earth Science Technology Conference,” College Park, MD, Aug. 28–31, 2001

459) J. Hartley, G. Komar, L. Lemmerman, A. Gerber, “Advanced Instruments and their Impact on Earth Science Missions (I),” Proceedings of 5th Symposium on Small Satellites for Earth Observation, Berlin, Germany, April 4–8, 2005

460) B. Bizzarri, “MW/Sub–mm sounding from geostationary orbit,” Report to EUMETSAT Science W. G., EUM/STG/SWG/9/00/DOC/11, pp.11., 2000

461) A. J. Gasiewski, A. Voronovich, B. L. Weber, B. Stankov, M. Klein, R. J. Hill, J. W. Bao, “Geosynchronous Microwave (GEM) Sounder/Imager Observation System Simulation,” IGARSS 2003, Toulouse, France, July 21–25, 2003

462) A. J. Gasiewski, A. Voronovich, B. L. Weber, B. Stankov, M. Klein, R. J. Hill, J. W. Bao, “Prospects for All–Weather Microwave Radiance Assimilation,” 13th ITSC (International TOVS Study Conference), Sainte. Adèle, Quebec, Canada, Oct 28 – Nov. 4, 2003

An airborne campaign in Europe is to verify the concepts of GOMAS [use of the M-55 Geophysica of Russia in the timeframe Oct. 2003 to April 2004; and PSR (Polarimetric Scanning Radiometer) of NOAA].

– AMIGO (Advanced Microwave Interferometer from GEO),⁴⁶³ an ESA/EADS study which transposes the concepts of the LEO SMOS mission, namely the Y-shape MIRAS (sparse array instrument), into GEO. The aim is at sounding the Oxygen line in the 54/57 GHz region. Some key features of the GEO orbit favor the concept: a 4λ antenna covers the Earth disk, and the integration time goes up to 30 min. Such a radiometer becomes realistic because of progress in MMIC (Millimeter-wave Monolithic Integrated Circuit) technology for the receiver and because of the next generation of low power space qualified ASIC's for the correlator.

463) J.-M. Goutoule, C. Bredin, "Advanced Microwave Interferometer from Geo Orbit," Proceedings of IGARSS 2004, Anchorage, AK, USA, Sept. 20-24, 2004

1.4.6 Optical Region, Active Observations (LIDARs)

Laser radars (active instruments), or LIDARs (Light Detection and Ranging), combine the principles of submillimeterwave radar and optics. A lidar instrument consists of the following basic elements:

- Laser transmitter. By far the most effective approach in all forms of active lidar systems is the use of laser energy in high intensity pulsed form, although range information can also be derived from continuous wave (CW) transmissions.
- Collector (receiving telescope). The telescope acts as an optical antenna (analogous to radar) with a corresponding detector system (heterodyne, etc.) in the focal plane.
- Electronics and data processing resources.

In this measurement technique, a sequence of monochromatic laser pulses are being generated and transmitted outward into a medium [this may for instance be the atmosphere, or a celestial body (the moon), or the surface of Earth from a spaceborne lidar] – an analysis of the return signals (echoes) provides information about the laser pulse interaction with the backscattering medium. A number of parameters may be derived from the analysis, such as: distance (range), physical state, or chemical composition (LIDAR spectroscopy).

The LIDAR concept is generally applied in the optical (and IR) regions of the electromagnetic spectrum, specifically to the spectral range of 0.3 μm to about 10 μm , or the equivalent frequency range of 1000 – 30 THz. This wave spectrum (shorter wavelengths than the microwave spectrum) implies and promises to be the next level of observation technology and of information interpretation (in the number of phenomena as well as in detail and accuracy, the targets can be much smaller), due to the use of a much finer scale of measurement.

In Earth observation, the LIDAR measurement technique provides the capability to study the following fine – scale phenomena of the atmosphere [with respect to structure, dynamics (transport and mixing), models and climatology], the Earth’s surface (texture, terrain profiling, shallow water depth sounding, etc.), as well as ocean surfaces.

Space LIDAR applications started with the ruby laser, but the Nd:YAG laser has become the light source of choice, especially since its fundamental doubled and tripled frequencies can sense aerosol particles as well as macroscopic surfaces. In meteorology, geology, and even forestry, lidar systems flying on airplanes and spacecraft complement each other in terms of ground – coverage, time, and field of view. – LIDAR performance decreases as the inverse square of the distance between the instrument and its target surface. Hence, spaceborne lidar systems must have 10^3 to 10^5 times better performance than their airborne counterparts. Thus, to fly in space, lidars need more powerful laser transmitters and/or bigger receiver telescopes.⁴⁶⁴⁾

- For atmospheric profiling, a lidar detects the laser energies backscattered from the atmospheric aerosols and molecules. The backscattered laser energies may be used to analyze the geophysical parameters such as aerosol concentrations and spatial distribution profiles, atmosphere wind profiles and trace gas profiles.
- For terrain profiling, lidar systems derive the terrain surface ranges and vegetation density/height profiles using surface backscattered laser signals. In addition to these range derived terrain profiles, the backscattered laser signal amplitudes can be used to derive the surface reflectivity profiles for classification of different surface types.
- For the ocean profiling, the lidar profiles the water surfaces by detecting laser backscattered energies from the ocean surface as a function of laser energy flight time and backscat-

⁴⁶⁴⁾ Patricia Daukantas, “Lidar in SPACE: From Apollo to the 21st Century,” OPN (Optics & Photonics News), June 2009, Vol. 20, No. 6, pp. 30–35

tered laser signal amplitudes. For this ocean surface application, a lidar functions similar to a microwave altimeter. However, in this altimeter mode, the laser footprints on the water surface are orders of magnitudes smaller than a typical microwave altimeter.⁴⁶⁵⁾

- The highly accurate ranging capability of the lidar technique was initially introduced in the 1960s in ground-based lidar systems, referred to as SLR (Satellite Laser Ranging), to measure the distance to retroreflectors mounted on spacecraft (see chapter 1.23.3.6). The precise analysis of the orbit (measured by the lidar technique), permitted in turn the study of crustal dynamics and plate tectonics.
- The last three Apollo missions of NASA in the early 1970s [Apollo-15 launch July 26, 1971, Apollo-16 launch April 16, 1972, Apollo-17 launch Dec. 7, 1972] carried each a lidar altimeter to map the terrain elevations around prospective landing sites of the moon.
- The ICESat (Ice Cloud and Land Elevation Satellite) mission of NASA is often regarded as the first true LIDAR mission (launch Jan. 13, 2003) carrying the GLAS (Geoscience Laser Altimeter System). Mission operations were terminated in Feb. 2010.
- The ADM-Aeolus mission of ESA (launch 2014) has ALADIN (Atmospheric Laser Doppler Instrument), a DWL (Doppler Wind Lidar) as its payload. The instrument fires laser pulses towards the atmosphere and measures the resulting Doppler shift of the return signal, backscattered at different levels in the atmosphere.
- The ICESat-2 mission of NASA is scheduled for launch in 2016. The payload is ATLAS (Advanced Topographic Laser Altimeter System), a multi-beam micropulse laser altimeter.
- JAXA (Japan Aerospace Exploration Agency) is studying a GLS (Global Laser Scanner) mission in 2012 to obtain high-accuracy 3D information on the global land surface.⁴⁶⁶⁾

Some lidar detection / ranging techniques employed are:

- CDL (Coherent Doppler Lidar) for wind observations [also referred to as DWL (Doppler Wind Lidar)]. CDL measures wind by determining the Doppler shift of backscattered radiation (light backscattered from aerosol particles transported by the wind) that has been originally transmitted (by the primary laser). The collected, backscattered light is mixed with that from another laser, called the local oscillator (LO) onto a light-sensitive detector (this mixing technique is referred to as heterodyning). CDL heterodyne systems combine the weak (observed) optical signal at nominal frequency f_1 with a strong optical reference beam, the frequency-stable LO at frequency f_2 , on a wideband square-law detector, thereby producing radio frequency beats at the frequency difference $f_1 - f_2$. The resultant beat-frequency signal is analyzed in a post-detection step to provide the Doppler frequency.
- IBL (Incoherent Backscatter Lidar). Incoherent-detection heterodyning refers to direct detection of an optical signal on an optical detector, with no LO present. The backscattered optical signal field is analyzed and dispersed in an interferometric filter (or in diffraction grating) prior to detection. The measurement accuracy of a direct-detection interferometric system depends only on the total scattered signal, it is not dependent on the energy of individual pulses, but on the total laser energy. The IBL detection scheme of the wind speed Doppler shift, using optical interferometry, is an emerging and alternate approach to obtain global wind measurements.

465) C. S. Lin, "Ocean lidar instrument and measurements," Proceedings of SPIE, Vol. 4881, 9th International Symposium on Remote Sensing, Aghia Pelagia, Crete, Greece, Sept. 23-27, 2002

466) Takashi Kobayashia, Yohei Sato, Shiro Yamakawa, "Conceptual Study of Earth Observation Missions with a Space-Borne Laser Scanner," Proceedings of the ICSO (International Conference on Space Optics), Ajaccio, Corse, France, Oct. 9-12, 2012, paper: ICSO-043

– DIAL (Differential Absorption Lidar). The objective is generally to measure the distribution/concentration of atmospheric constituents (such as ozone or aerosols). DIAL is a path absorption technique (by exploiting the fact that a gas will absorb light emitted at a certain laser wavelength while transmitting light at most others); information is derived relating to the path along which energy is transmitted or received by comparing the lidar echoes in a tuneable multiwavelength laser system (measurement of the differential ratios of the lidar returns with those of the transmitted ratios by tuning the laser wavelength to the specific absorption features of atmospheric trace constituents). The technique offers the capability to determine the densities of specific atmospheric constituents as well as water vapor and temperature profiles at better accuracies than obtainable with passive sounders. DIAL measurements are made at two different wavelengths. One wavelength, f_{on} (for the DIAL on-line laser beam), is chosen in a region of high absorption cross-section of the gaseous constituent under study, whereas at the second wavelength, f_{off} (for the DIAL off-line wavelength), the gaseous absorption should be minimal.

– Laser altimetry [the time-of-flight (TOF) of an echoed pulse determines the range of a surface (point) being detected; a sequence of pulses provides a point-wise sampling scheme]. Laser ranging and altimetry can provide accurate measurements of the distance from a reference height (i.e. the satellite orbital height) to precise locations on the Earth's surface. The technique is being used to study many processes and phenomena in such solid Earth Sciences such as geodesy, geodynamics, ice dynamics, land topography, and Earth resources. Most laser altimeters provide exact height measurements over oceans, land, and ice.

Airborne lidars are flown since about 1977 [AOL (1977), CALS 1979), ALEX (1979), ALPHA-1 (1979), etc.], most instruments were developed during the latter 1980s and the 1990s. MACAWS of NASA/MSFC (since 1995) is the first airborne 'coherent atmospheric wind lidar' measuring 2-D, 3-D or vertical wind fields.

On the spaceborne side, the first lidars were introduced in 1994 for atmospheric applications (detection of stratospheric and tropospheric aerosols; measurement of the planetary boundary layer, cloud top heights, atmospheric temperature and density); these were followed by lidar altimeters, mainly used for ocean surface or terrestrial surface monitoring.

- Atmospheric lidars: LITE (Lidar In-Space Technology Experiment) of NASA/LaRC, a triple wavelength lidar, was test-flown on Shuttle (STS-64) in Sept. 1994. LITE operated for more than 220 hours and gathered the first global measurements of the height of the planetary boundary layer. LITE also measured the directional reflectance of the sea surface and its dependence on the speed of surface winds, which in turn drive the ocean's waves. – Balkan-1 of Atmospheric Optics, Tomsk (Russia), was flown on the MIR/Spektr module (launch May 20, 1995). ALISSA, a CNES-developed lidar was flown on MIR/Priroda (launch April 23, 1996).

The collaborative CALIPSO mission of NASA/CNES (launch Apr. 28, 2006) includes CALIOP (Cloud-Aerosol Lidar with Orthogonal Polarization), providing vertical profiles of aerosol backscatter. – In 2002, NASA started to define a mission called OCO (Orbiting Carbon Observatory). The OCO objective was to provide global measurements of atmospheric carbon dioxide (CO_2) needed to describe the geographic distribution and variability of carbon dioxide sources and sinks.⁴⁶⁷⁾

OCO was launched on Feb. 02, 2009; unfortunately, a launch failure was experienced, ending the mission.

In Europe, the instruments **ATLID** (Atmospheric Lidar) of the EarthCARE (Earth Clouds Aerosol and Radiation Explorer) S/C and **ALADIN** (Atmospheric Laser and Doppler In-

⁴⁶⁷⁾ F. Einaudi, G. K. Schwemmer, B. M. Gentry, J. B. Abshire, "LIDAR Past, Present, and Future in NASA's Earth and Space Science," Proceedings of 22nd ILRC (International Laser Radar Conference), Matera, Italy, July 12-16, 2004, ESA SP-561, Vol. I, pp. 7-10

strument) of ADM–Aeolus (Atmospheric Dynamics Mission) are part of ESA’s spaceborne lidar program (launch of ADM–Aeolus in 2013). Of the latter two sensors, ALADIN will be the first spaceborne instrument in a sustained mission using the **incoherent DWL (Doppler Wind Lidar) technique** of direct detection of wind profiles on an optical detector (with no LO). In this measurement scheme the backscattered optical signal field is analyzed and dispersed in a Rayleigh receiver consisting of a dual filter (double–edge Fabry–Perot interferometer) prior to detection (a combined Mie and Rayleigh backscattering fringe–imaging receiver is employed to analyze aerosol and cloud backscatter). – The EarthCARE mission of ESA and JAXA is scheduled for launch in 2015. From an altitude of 450 km, the ATLID instrument will use its high spectral resolution at 355 nm to discriminate between Rayleigh scattering from molecules and Mie scattering from aerosols and cloud particles in the lower 20 km range of the atmosphere.

Note: Mie scattering is named after Gustav Mie (German physicist, 1868–1957). In 1908 Mie presented a description of light scattering from particles that are not small compared to the wavelength of light, taking account of particle shape and the difference in refractive index between the particles and the supporting medium. Gustav Mie was the first to use the Maxwell equations to compute the scattering properties of small spheres suspended in a medium of another index of refraction. Gustav Mie’s work, along with the work of Peter Debye (Dutch physicist, 1884–1966), is now generally referred to as the “Mie theory.”

Instrument name	LITE	Balkan–1	ALISSA	ALADIN	ATLID (ESA)
Platform/Mission	Shuttle STS–64	MIR/Spektr	MIR/Priroda	ADM (ESA)	EarthCARE
Orbit altitude (km)	260	350–400	350–400	400	400
Laser type	Nd:YAG	Nd:YAG	Nd:YAG	Nd:YAG	Nd:YAG
Wavelength (nm)	1064,532,355	532	532	355	1064
PRF (Hz)	10	0.18	50	100	100
Telescope diameter	100 cm	27 cm	40 cm	150 cm	60 cm
Range resolution	35 m	3 m	150 m	100–2000	15 m
Scanning					$\pm 20^\circ$
Instrument mass	990 kg	150 kg		263 kg	240 kg
Instrument power	2000 W	250 W	3000 W	304 W	520 W

Table 31: System performance parameters of spaceborne atmospheric lidars

- Altimeter lidars: ⁴⁶⁸⁾ ⁴⁶⁹⁾ ⁴⁷⁰⁾ SLA–1 (Shuttle Laser Altimeter), was flown on STS–72 (Jan. 11–20, 1996), SLA–2 was flown on STS–85 (Aug. 7–19, 1997) to acquire altimetric samples of land topography (see J.19). The SLA experiments showed scientists how to analyze on–orbit laser ranging measurements of the Earth’s surface and to perform laser–pulse waveform analysis to assess overall surface roughness and tree height in forested regions.

GLAS (Geoscience Laser Altimeter System) has been built by NASA/GSFC and is flown on the ICESat mission (launch Jan. 13 2003, see D.23) to determine the mass balance of the polar ice sheets and their contributions to global sea level change. ICESat is considered to be the first free–flying and long–term lidar mission. GLAS is intended as a laser sensor filling complementary requirements for both surface and atmospheric measurements. In addition to a high–resolution altimetry channel, GLAS contains both 1064 and 532 nm backscatter lidar channels for atmospheric profiling. – Advantages of the laser technology include small footprint size, individual pulse processing of surface elevations, and dense ground sample spacing. The early EOS (Earth Observing System) program of NASA considered the development of LAWS (Lidar Atmospheric Wind Sounder), a coherent

468) Special Issue on Laser Radar, Proceedings of the IEEE, Vol. 84, No. 2, February 1996, pp. 99–298

469) J. A. McKay, D. Rees, “Space–based Doppler Wind Lidar: Modeling of Edge Detection and Fringe Imaging Doppler Analyzers,” *Advances in Space research*, Vol. 26, No. 6, 2000, pp. 883–891

470) Courtesy of A. Ginati of OHB–System, Bremen

Doppler wind lidar with a carbon dioxide laser. However, the project was cancelled in 1994 due to severe budget cuts in the EOS program.

The **LOLA** (Lunar Orbiter Laser Altimeter) of NASA's LRO (Lunar Reconnaissance Orbiter) mission (launch on June 18, 2009) will make a new multiple-spot pattern on the lunar surface, thanks to a diffractive optical element that splits the single laser beam into multiple beams which are directed toward the lunar surface. This paves the way for surface lidar to start imaging topography, instead of profiling topography and reconstructing it later from the one-dimensional scans.

1.4.7 Sounding of the Atmosphere

The Earth's atmosphere can conceptually be regarded as an optical filter for observational purposes. Such a filter attenuates and modulates the resolution and contrast of the measured radiation sources caused by such effects as gases, aerosols, fogs and precipitation, refractive turbulence, and background radiation. Everyday language and thinking uses atmospheric filter analogies. For example: spectral regions of high transmittance are referred to as "atmospheric windows;" the seeing conditions often use such terms as "visibility" and "visual range."⁴⁷¹⁾

Each of the gases that comprise the atmosphere has a different ability to absorb the radiation, or let it through, which varies with the radiation wavelength. Wavelength regions where absorption for the whole atmosphere is very low are called **window regions** and are obviously suitable for Earth–surface observation (such as the spectral regions: VNIR, SWIR, MWIR, TIR). Wavelength (or frequency) regions where a significant absorption of solar radiation occurs for some gas (or constituent) are called **absorption bands** for that particular gas and may be used to get information about it.

The general techniques for remote sensing (sounding) of the atmosphere include active instruments (such as millimeter–wave radars, SAR, lidars), passive absorption spectroscopy (e.g. solar occultation soundings) and passive emission spectroscopy. Among these techniques, **emission spectroscopy**, based on spontaneous thermal emissions of the gas, has important advantages.⁴⁷²⁾ The technique can be applied continuously (day and night) and in all directions without depending on external sources as is the case of absorption spectroscopy. Naturally, emission measurements are only possible within those spectral regions, in which the atmosphere provides emission radiation of detectable intensity, which is generally the optical region of the spectrum (0.1–1000 μm or from the UV to the millimeter region), in particular the infrared region of the optical spectrum, and beyond in the microwave region. It is worth noticing that the wide infrared domain (of the optical region) is particularly suited to retrieve the concentration profiles of a large number of species. – Passive emission instruments for atmospheric sounding include such devices as spectrometers, FTS (Fourier Transform Spectrometers), heterodyning instruments, radiometers, etc. Atmospheric sounders generally make **passive measurements of the distribution of IR or microwave radiation** emitted by the atmosphere, from which vertical profiles of temperature and humidity through the atmosphere may be obtained. An overview of some spaceborne instruments (alphabetic order) is given in Table 34.

The optical properties of the Earth's atmosphere and its emission spectrum depend on both the temperature and the composition of the atmosphere. Each molecular species present in the atmosphere has characteristic transitions due to its rotational and vibrational spectrum. Good information is obtained from measurements made in a broad spectral range, so that numerous features are present, at a high spectral resolution and individually resolved. The FTS (Fourier Transform Spectrometer) technology combines these capabilities best among the various sounding instrument types. FTS instruments have the important capability of broadband measurements. The property permits observations of the full blackbody distribution of thermal emissions of the atmosphere and the measurement of the Earth's radiation budget. In comparison to radiometers (which do not resolve the atmospheric windows), FTS instruments can resolve the signal made inside and outside the atmospheric windows and determine the contributions of the different altitudes to the outgoing radiation flux.

- Sounding (see also: Limb/occultation sounding in Glossary). Airborne and spaceborne Earth observation adapted fairly early the ancient technique of sounding ('to find bottom'

471) W. M. Farmer, "The Atmospheric Filter, Volume I Sources, JDC Publishing, 2001, ISBN: 0–9640000–8–3

472) B. Carli, U. Cortesi, L. Palchetti, "Infrared Emission Spectroscopy," J. Demaison et al. (editors), Spectroscopy from Space, NATO Science Series, II Mathematics, Physics and Chemistry, Vol. 20, Kluwer Academic Publishers, 2001, pp. 171–186

– originally used for the measurement of shallow water depths) into the development of suitable sensors (sounders) to measure conditions of the medium ‘atmosphere.’ Sounders provide profiles of state parameters (a series of measurements of temperature, pressure, moisture, trace gases, etc.) in a particular plane of observation (nadir or limb configuration) at various heights. The early sounder measurements were obtained from filter radiometers with a spectral resolving power ($\lambda/\Delta\lambda$) typically in the order of 100. At the start of the 21st century the spectral resolving power of typical radiometers is more in the range of 1000.

Later applications included also the sounding of aerosols, trace gas constituents (“absorptive” or “extinctive” occultation monitoring), and of wind components with a variety of instruments, employing such techniques as FTS (Fourier Transform Spectrometry) and Doppler. The technique of sounding has also been extended far beyond the Earth’s atmosphere to measure plasma densities of the solar wind. Active airborne sounders (namely lidars) are also used to fathom the depths of shallow waters (FLASH since 1989, SHOALS since 1994), to detect sea surface pollution, and to measure surface emissions. Naturally, the entire spectrum may be used for sounding measurements, but the microwave region is the traditional and dominant arena for sounders.

The presence of clouds in the field of view of sounders has a detrimental effect on the quality of a retrieval. The absorption properties of cloud droplets and ice particles at infrared sounding wavelengths are so strong that even thin clouds contaminate the measurement of radiances. As a result, a number of post–processing techniques have been developed to minimize the effects of clouds on soundings. These usually require some way of identifying cloudy scenes to arrive at an equivalent clear–sky radiance quantity. Methods accounting for the effects of clouds on the data are generally based on higher–resolution visible and infrared imaging data that are required to supplement the sounding channels.

- The first airborne devices used were self–registering instruments (referred to as sondes) on balloons to record meteorological data. The MTS (Microwave Temperature Sounder of GSFC) instrument was first flown on aircraft in 1976.

- There are two basic types of sounding instruments depending on the observation geometry, namely vertical and/or horizontal measurement concepts. Each technique requires different retrieval algorithms.

- 1) Vertical sounding observations. The instrument faces to nadir and senses the radiation coming both from the Earth’s surface as well as from the atmosphere. The BUV (Backscatter Ultraviolet) technique is mostly applied to vertical sounding observations (nadir viewing). In BUV, measurements are made of solar UV radiation entering the atmosphere (referred to as the irradiance) at a particular wavelength and of the solar UV that is either reflected from the surface or scattered back from the atmosphere (referred to as the radiance) at the same wavelength. Examples of BUV instruments are: SBUV (Solar Backscatter Ultraviolet) first flown on Nimbus–7 (later SBUV/2 flown on the POES series of NOAA), TOMS (Total Ozone Mapping Spectrometer), and GOME (Global Ozone Monitoring Experiment) flown on ERS–2 (launch Apr. 21, 1995).

- 2) Limb–viewing and occultation sounding systems (observations in horizontal direction). In these measurements the sounder (spectrometer) is carried on a spaceborne platform and probes the Earth’s limb at various depths in the atmosphere. Each observation is characterized by the altitude and the geolocation of the tangent point (that is, the point where the line of sight reaches the lowest altitude). A full set of measurements that covers the altitude interval of interest is usually referred to as a limb–scanning sequence. Limb–sounding measurements provide in effect a sampling grid of vertical profiles. The tangent altitudes of the measured spectra are generally in the 10 – 50 km range. Fine observation grids provide a high number of vertical layers within a sequence. A limb sounder may be oriented in a side–viewing direction, in a forward–viewing direction, or in a backward–viewing direction. The sounder measures in general the infrared emission based on temper-

ature and trace gas concentrations in the mesosphere, stratosphere and the upper troposphere. For species which absorb in the solar spectrum (for example ozone, water vapor and nitrogen dioxide, as well as aerosols) solar occultation instruments can be used to measure the extinction of sunlight through the atmospheric limb during satellite sunrise and sunset. Note: All limb-viewing remote sensing measurements are sensitive to errors in pointing. Pointing errors result from spacecraft attitude errors, errors in correcting for the oblateness of the Earth, and errors in correcting for the time varying thermal expansion within the instrument or spacecraft.

Mission and launch date	Limb-viewing sounders	Spectral Region
AE-C, NASA (Dec. 16, 1973)	UVNO (Ultraviolet Nitric-Oxide) Experiment	UV
Nimbus-7, NASA (Oct. 24, 1978)	LIMS (Limb Infrared Monitor of the Stratosphere) SAMS (Stratospheric and Mesospheric Sounder)	Infrared Infrared
ERBS, NASA (Oct. 5, 1984)	SAMS-II (Stratospheric and Mesospheric Sounder)	Infrared
UARS, NASA (Sept. 12, 1991)	CLAES (Cryogenic Limb Array Etalon Spectrometer) ISAMS (Improved Stratospheric & Mesospheric Sounder) HALOE (Halogen Occultation Experiment) MLS (Microwave Limb Sounder) WINDII (Wind Doppler Imaging Interferometer)	Infrared Infrared Infrared Micro-wave VIS, NIR
SPOT-3, CNES (Sept, 26, 93)	POAM-II (Polar Ozone and Aerosol Measurement), NRL	UV, NIR
STS-66, NASA (Nov. 3-14, 94) STS-85, NASA (Aug. 7-19, 97)	CRISTA (Cryogenic Infrared Spectrometers and Telescopes for Atmosphere) of DARA	Infrared
ADEOS, NASDA (Aug. 17,96)	ILAS (Improved Limb Atmospheric Spectrometer)	VIS, IR
SPOT-4, CNES (Mar. 24, 1998)	POAM-III (Polar Ozone and Aerosol Measurement) NRL	UV, NIR
Terra, NASA, (Dec. 18, 1999)	CERES (Clouds and the Earth's Radiant Energy System)	VIS, IR
ODIN, Sweden, (Feb. 20, 2001)	SMR (Submillimeterwave Radiometer) OSIRIS (Optical Spectrograph & Infrared Imaging System)	Sub-mm Infrared
TIMED, NASA (Dec. 7, 2001)	SABER (Sounding of the Atmosphere using Broadband Emission Radiometry) TIDI (TIMED Doppler Interferometer) GUVI (Global Ultraviolet Imager)	Infrared Infrared UV
Meteor-3M-1, Russia (Dec. 10, 2001)	SAGE III (Stratospheric Aerosol and Gas Experiment III) NASA/LaRC	UV, VNIR
Envisat, ESA (Mar. 1, 2002)	MIPAS (Michelson Interferometer for Passive Atmospheric Sounding); GOMOS (Global Ozone Monitoring by Occultation of Stars); SCIAMACHY (Scanning Imaging Absorption Spectrometer for Atmospheric Cartography) Note: SCIAMACHY performs limb or nadir observations	Infrared UV,VIS, NIR UV,VIS, IR
ADEOS-II, (Dec. 14, 2002)	ILAS-II (Improved Limb Atmospheric Spectrometer-II)	VIS, IR
SciSat-1/ACE (Aug. 13, 2003)	ACE-FTS (ACE-Fourier Transform Spectrometer), CSA	Infrared
Aura, NASA (July 15, 2004)	MLS (Microwave Limb Sounder), mm and sub-mm range HIRDLS (High-Resolution Dynamics Limb Sounder) TES (Tropospheric Emission Spectrometer), limb or nadir	Sub-mm Infrared Infrared
NPP, NASA/IPO (Oct. 28, 2011) NPOESS, IPO (2014)	OMPS (Ozone Mapping and Profile Suite) limb and nadir OMPS (Ozone Mapping and Profile Suite) limb and nadir	UV, VNIR UV, VNIR

Table 32: Overview of limb-viewing spaceborne sounders

- A large number of daily atmospheric profiles from spaceborne sounders [SSH on the DMSP series, launch of F-1 Sept. 11, 1976; TOVS (TIROS Operational Vertical Sounder), on TIROS-N consisting of HIRS/2, SSU and MSU, launch Oct. 13, 1978; SBUV/TOMS on Nimbus-7, launch Oct. 24, 1978], ILAS and IMG on ADEOS (launch Aug. 17, 1996) and ILAS-II on ADEOS-II (launch Dec. 14, 2002) began to find their way into global forecasting models.

Today's sounders like AMSU (Advanced Microwave Sounding Unit), first flown on NOAA-15 (launch May 13, 1998), provide atmospheric temperature profiles with a sensitivity of about 1 K and a vertical resolution of about 2 km in the troposphere. SSMIS (Special Sensor Microwave Imager Sounder) of the DMSP series, first flown on F-16 (launch Oct. 18, 2003), features a similar performance as AMSU. Current generation sounder performance (AMSU, SSMIS) still falls short of the requirements for NWP (Numerical Weather Prediction). – Some examples of next-generation sounders are: AIRS (Atmospheric Infrared Sounder) on Aqua (launch May 4, 2002), IASI (Improved Atmospheric Sounder Interferometer) on MetOp-A (launch Oct. 19, 2006), ATMS (Advanced Technology Microwave Sounder) and CrIS (Cross-track Infrared Sounder) on NPP (launch on Oct. 28, 2011). Their data is planned to be used in NWP models and in many other applications. – AIRS is in fact the first spaceborne instrument that employs hyperspectral sounding to give global coverage of temperature, water and ozone on a daily basis.

- Measurement of global cloud profiles. Clouds play an important role in climate modeling. The CPR (Cloud Profiling Radar) instrument of the NASA/CSA CloudSat mission (launch Apr. 28, 2006, see A.10) measures the vertical profiles of cloud structures [CloudSat formation flight with CALIPSO (Cloud-Aerosol Lidar and Infrared Pathfinder Satellite Observations), to augment the data of CloudSat]. The quantitative evaluation/representation of clouds and cloud processes in global atmospheric circulation models is a major objective. *At 94 GHz (3 mm wavelength) the CPR instrument of CloudSat represents the first spaceborne millimeter-wave radar system.*

- As of 2002/3, a further CPR (Cloud Profiling Radar) instrument at 94.05 GHz is under joint development by JAXA (formerly NASDA) and CRL of Tokyo. The CPR is considered a core instrument of EarthCARE (Earth Clouds, Aerosol and Radiation Explorer), a joint ESA/JAXA candidate mission in ESA's Earth Explorer Program with a planned launch in the time frame 2015. The entire sensor complement [ATLID (Atmospheric Lidar), CPR, MSI (Multispectral Imager), BBR (broadband Radiometer), and FTS (Fourier Transform Spectrometer)] of EarthCARE is dedicated to the study of clouds, aerosols and radiation parameters (determination of the global distribution of vertical profiles of cloud and aerosol field characteristics) to provide basic, essential input data for numerical modelling.

Parameter	IASI (IASI pixel)	AMSU-A	MHS	AVHRR/3	HIRS/3 (4)
Mission (s) of instrument flown	MetOp-A, etc.	MetOp-A, NOAA-15, etc.	MetOp-A, NOAA-N	NOAA-15, etc. MetOp-A, etc.	NOAA-15, etc. MetOp-A, etc.
Scan type	Step and dwell	Step and dwell	Continuous	Continuous	Step and dwell
Scan rate	8 s (8 s)	8 s	2.667 s	0.167 s	6.4 s
Sampling interval	216 ms (216 ms)	200 ms	19 ms	0.025 ms	100 ms
Scan separation	52.69 km (23.81)	52.69 km	17.56 km	1.1 km	42.15 km
Pixels/scan	–, (120)	30	90	2048	56
IFOV	3.33° (0.84° circular)	3.3° circular	1.1° circular	0.0745° square	0.69° circular
IFOV at nadir	47.63 km, (12 km)	47.63 km	15.88 km	1.1 km	10.0 km
IFOV edge cross-track (km) along-track (km)	146.89, (39.14) 78.79, (20.31)	146.89 78.79	52.83 27.10	6.15 2.27	33.27 17.03

Parameter	IASI (IASI pixel)	AMSU–A	MHS	AVHRR/3	HIRS/3 (4)
FOV	$\pm 48.33^\circ$ (49.16°)	$\pm 48.33^\circ$	$\pm 49.44^\circ$	$\pm 55.37^\circ$	$\pm 49.5^\circ$
Swath (km)	2052, (1228)	2052	2134	2900	2160

Table 33: FOV and scan parameter comparison of major sounding instruments

- Monitoring of atmospheric constituents (trace gases)⁴⁷³ in support of atmospheric chemistry and other environmental applications. The first spaceborne instrument of this genre, namely SAM (Stratospheric Aerosol Measurement) of NASA/LaRC, was flown on the US/Soviet mission ASTP (Apollo–Soyuz Test Project), July 15–24, 1975, to perform the first successful solar occultation measurement of stratospheric aerosol. This was followed by SAM–II on Nimbus–7 (launch Oct. 24, 1978). Since then considerable progress has been made in the design of new instruments and in the interpretation of the retrieved data.

- Aerosol monitoring plays an important role in global climate change. Spaceborne monitoring of aerosols started with SAM of NASA/LaRC [SAM (Stratospheric Aerosol Measurement) was flown on ASTP (Apollo–Soyuz Test Project), July 15–24, 1975, to perform the first successful solar occultation measurement of stratospheric aerosol], SAM II (launch Oct. 24, 1978 on Nimbus–7, see M.29.7), SAGE I, SAGE II). Both SAM and SAM–II were single spectral instruments measuring the aerosol extinction near the 1000 nm wavelength region. Multiple spectral measurements began with SAGE–I, with a launch on the AEM–2 (Application Explorer Mission–2) satellite, Feb. 18, 1979 (see A.5). SAGE–II is an advanced version of SAGE–I with 7 channels at 385, 448, 453, 525, 600, 940, and at 1020 nm. SAGE–II was flown on ERBS with a launch on Oct. 5, 1984 (see A.16). The measurements of SAM–II, SAGE–I and SAGE–II have provided long–term observations of aerosol and ozone for over 20 years. Note: The SAGE–II instrument continues to operate as of early 2004; its data were made available to the public as of Oct. 28, 2003.

SAGE–III is an Earth limb–scanning grating spectrometer (part of NASA’s EOS mission) which is flown on Meteor–3M–1 (Russia) with a launch on Dec. 10, 2001. An important objective of SAGE–III is to characterize tropospheric and stratospheric aerosols and upper tropospheric and stratospheric clouds, and investigate their effects on the Earth’s environment, including radiative, microphysical, and chemical interactions. SAGE–III is also scheduled to fly on ISS in 2005. – Note: There is an inherent coverage weakness in the solar occultation technique by offering only two measurement opportunities per orbit. It has been estimated that six spaceborne SAGE–III instruments on various orbits would be needed to achieve a weekly coverage of the Earth.

- **SHS (Spatial Heterodyne Spectroscopy)**, see O.6.3 and J.18. The SHS technique provides the first practical approach to extend interference spectroscopy into the FUV (Far Ultraviolet, 1200–2000 Å) spectral range. SHS is a relative of the FTS (Fourier Transform Spectroscopy) concept, but has fundamental advantages over FTS in certain applications. In the SHS instrument, diffraction gratings replace the flat mirrors used in each arm of a conventional Michelson, and an imaging detector is used at the output to record a spatially heterodyned interferogram without any scanning elements. The mechanical simplicity of a diffraction grating is combined with the high light–gathering power of interference spectrometers.

In the basic SHS design, Fizeau fringes of wavenumber–dependent spatial frequency are produced by a modified Michelson interferometer in which the return mirrors are replaced by conventional blazed diffraction gratings (see Figure 21 part a). The fringes are recorded on a position sensitive detector and Fourier–transformed to recover the spectral content of the source. Zero spatial frequency corresponds to the Littrow wavenumber of the gratings,

473) P. Borrell, J. P. Burrows, U. Platt C. Zehner, “Determining Tropospheric Concentrations of Trace Gases from Space,” ESA Bulletin No 107, Aug. 2001, pp.72–81

which can be chosen by adjustment of the interferometer. Since zero spatial frequency corresponds to a finite wavenumber, SHS measures differences between the source and alignment wavelengths, and high resolution spectra over a limited spectral range can be recovered with modest requirements on the spatial resolution of the detector. In this process, no element is mechanically scanned.

The resolving power of an SHS design is equal to the theoretical resolving power of the dispersive (i.e. grating) system while the field of view of the system is characteristic of interferometric spectrometers (conventional Michelson and Fabry–Perot). The interferometric field of view gives SHS systems a 100–fold gain in sensitivity for diffuse source spectroscopy over diffraction grating spectrometers of the same size and resolving power. Furthermore, field widening techniques can be applied to SHS systems which enable SHS to view even larger fields of view. Gains associated with field widening are typically two orders of magnitude in solid angle over conventional interferometers (10^4 larger than diffraction grating spectrometers).

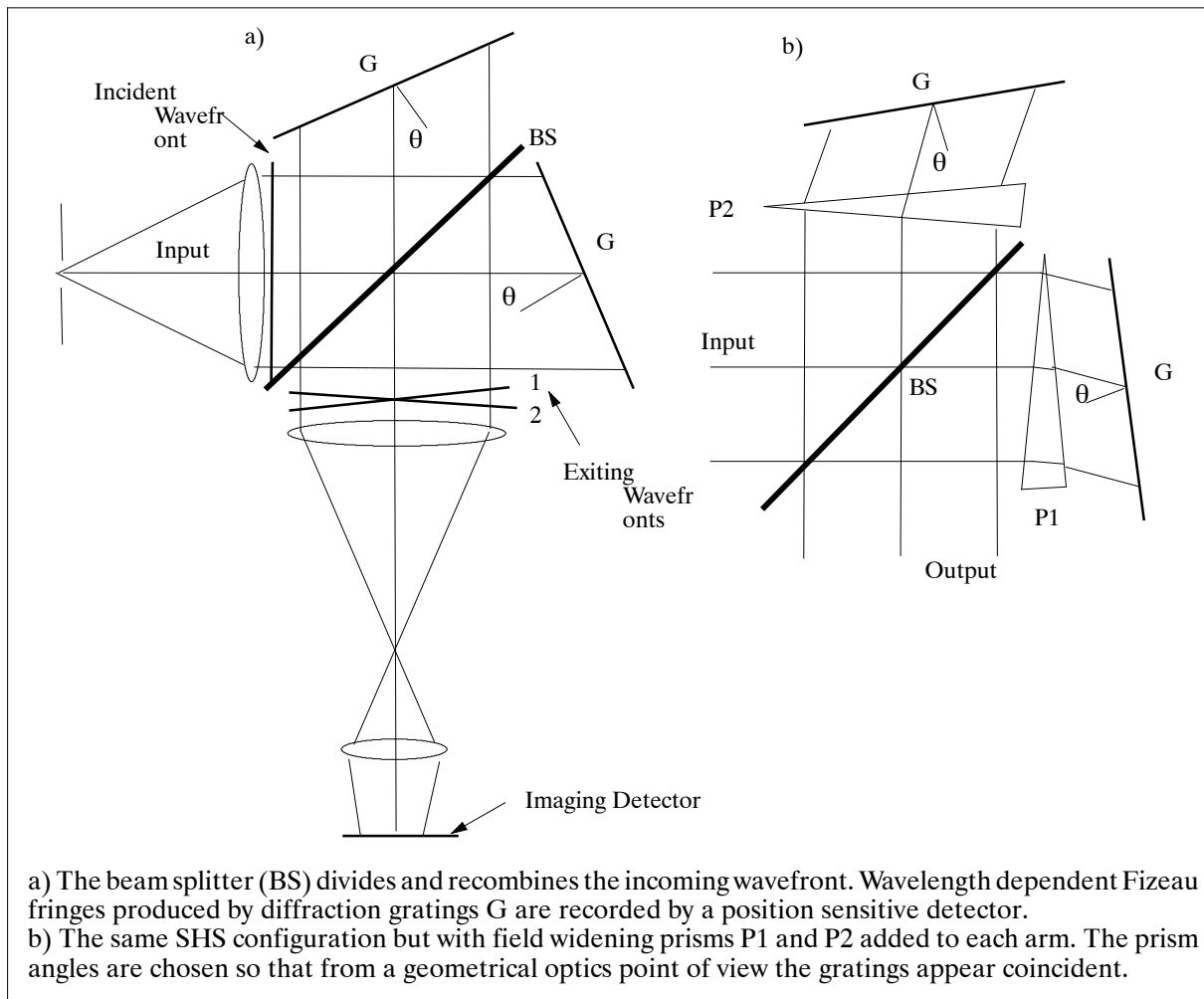


Figure 21: Schematic diagram of the SHS configuration

The SHS technique appears to be offering high–resolution spaceborne spectroscopy applications in astronomy (detection of faint interstellar emission lines, study of the dynamics of hot interstellar gases) as well as in Earth observation. A first example in this field include the measurement of vertical density profiles of the hydroxyl (OH) radical in the middle atmosphere (30–100 km), study of the distribution of aerosols in the mesosphere, and to investigate the role of OH in the photochemistry of water vapor and ozone in the presence of aerosols in the mesosphere.

The SHS concept was first described in 1971 by Dohi and Susuki (they used holographic film as detectors).⁴⁷⁴⁾ H. Butcher et al. (1989) developed SHS for astronomical telescopes. John Harlander and Fred Roesler (1990) developed practical SHS designs using CCD detectors.

NRL (Naval Research Laboratory) in Washington, DC has been cooperating with J. M. Harlander at UWM (University of Wisconsin–Madison) for the last years to develop an instrument. A first implementation of the SHS concept is realized in **SHIMMER** (Spatial Heterodyne Imager for Mesospheric Radicals). The instrument was flown on Shuttle flight STS–112 (Middeck), Oct.7–18, 2002. – Additional plans call for SHIMMER flights (improved sensor versions) on STPSat–1 (Space Test Program Satellite–1), a USAF/AFRL mission with a launch on March 9, 2007.⁴⁷⁵⁾

Instrument/Agency	Mission/Platform, Coverage period	Species observed	Orbit
ACE–FTS (Atmospheric Chemistry Experiment – Fourier Transform Spectrometer)/CSA	SciSat–1/ACE of CSA (Aug. 13, 2003)	O ₃ , N ₂ O, CH ₄ , HNO ₃ , H ₂ O, HCl, Hf, NO, NO ₂ , ClONO ₂ , CO, CO ₂ , CCl ₃ F, CCl ₂ F ₂ , and N ₂ O ₅	Inclined orbit
ATMOS (Atmospheric Trace Molecule Spectrometer)/JPL	STS–51–B (1985), ATLAS–1, 2, 3 (1992, 93, 94)	O ₃ , NO _x , N ₂ O ₅ , ClONO ₂ , HCl, HF, CH ₄ , CFCs	Inclined orbits
ATSR (Along–Track Scanning Radiometer and Microwave Sounder)/ESA	ERS–1/2 (1991 to present)	Aerosols, clouds, SST (Sea Surface Temperature)	Polar sun–synchronous
AVHRR (Advanced Very–High Resolution Radiometer (chan. 4/5)/NOAA	TIROS–N, NOAA–6 to –16 (1978 to present)	Smoke, fire, clouds, aerosols, vegetation	Polar sun–synchronous
BUV (Backscatter UV)/NASA	Nimbus–4 (1970–1974)	O ₃ profiles	Polar sun–synchronous
GOME (Global Ozone Monitoring Experiment)/ESA	ERS–2 (1995–present) MetOp–A (2006) of EUMETSAT	O ₂ , NO ₂ , H ₂ O BrO, OClO, SO ₂ , HCHO, clouds, aerosols,	Polar sun–synchronous
GOMOS (Global Ozone Monitoring by Occultation of Stars)/ESA	Envisat (2002 –)	O ₃ , NO ₂ , upper troposphere	Polar sun–synchronous
HIRDLS (High–Resolution Dynamics Limb Sounder)/U. of CO and Oxford University	Aura of NASA (July 15, 2004)	O ₃ , H ₂ O, CH ₄ , N ₂ O, NO ₂ , N ₂ O ₅ , HNO ₃ , CFC ₁₁ , CFC ₁₂ , ClONO ₂ , and aerosols	Polar sun–synchronous
IASI (Imaging Atmospheric Sounding Instrument)/CNES	MetOp–A (Oct. 19, 2006) of EUMETSAT	O ₃ , CO, CO ₂ , CH ₄ , N ₂ O, SO ₂	Polar sun–synchronous
ILAS–II (Improved Limb Atmospheric Spectrometer–II)/EA	ADEOS–II of JAXA (2002, formerly NASDA)	O ₃ , HNO ₃ , NO ₂ , N ₂ O, CH ₄ , H ₂ O, CFC–11, CFC–12, ClONO ₂ , etc., aerosols, temp. pressure	Polar sun–synchronous
IMG (Interferometric Monitor of GreenHouse Gases)/MITI	ADEOS of NASDA (1996–1997)	O ₃ , N ₂ O, H ₂ O, CH ₄ , CO, CO ₂	Polar sun–synchronous
LORAAS (Low Resolution Airglow/Aurora Spectrograph)	ARGOS of DoD (1999), see M.3	O ⁺ , O, O ₂ , N ₂ , T	Polar sun–synchronous
MERIS (Medium–Resolution Imaging Spectrometer for Passive Atmospheric Sounding) MIPAS (Michelson Interferometer for Passive Atmospheric Sounding)/ESA	Envisat of ESA (2002 –)	H ₂ O, clouds, aerosols O ₃ , NO _x , N ₂ O ₅ , ClONO ₂ , CH ₄ , CFCs, etc., temperature,	Polar sun–synchronous

474) J. Harlander, R. Reynolds, F. Roesler, “Spatial Heterodyne Spectroscopy for the Exploration of Diffuse Interstellar Emission Lines at Far–ultraviolet Wavelengths,” *Astrophysics Journal*, Vol. 396, 1992, pp. 730–740

475) J. M. Harlander, F. L. Roesler, J. G. Cardon, C. R. Englert, R. R. Conway, “SHIMMER: A spatial heterodyne spectrometer for remote sensing of the Earth’s middle atmosphere,” *Applied Optics*, Vol. 41, pp.1343–1352, 2002

Instrument/Agency	Mission/Platform, Coverage period	Species observed	Orbit
MLS (Microwave Limb Sounder)/JPL CLAES (Cryogenic Limb Array Etalon Spectrometer)/NASA ISAMS (Improved Stratospheric and Mesospheric Sounder)/UK HALOE (Halogen Occultation Experiment)/LaRC	UARS of NASA (1991 to present) (1991–1993) (1991–1992) (1991– ?)	O ₃ , ClO, H ₂ O ₂ , H ₂ O and pressure N ₂ O, NO, NO ₂ , HNO ₃ , CF ₄ , CF ₂ Cl ₂ , CFC1 ₃ , HCl, O ₃ , ClONO ₂ , CO ₂ , H ₂ O, ClO, CH ₄ , temperature CO, H ₂ O, CH ₄ , N ₂ O ₅ , NO, N ₂ O, O ₃ , HNO ₃ and aerosols HF, HCl, CH ₄ , NO, H ₂ O, O ₃ , NO ₂ and pressure	Inclined orbit
MLS (Microwave Limb Sounder)/JPL	Aura of NASA (2004)	H ₂ O, O ₃ , ClO, BrO, HCl, OH, HO ₂ , HNO ₃ , HCN, N ₂ O,	Polar sun– synchronous
MODIS (Moderate–Resolution Imaging Spectroradiometer)/NASA	Terra of NASA (1999 – present) Aqua of NASA (2002 –)	O ₃ , clouds, aerosols, SST,	Polar sun– synchronous
MOPITT ((Measurement of Pollution in the Troposphere)/CSA	Terra of NASA (1999 – present)	Vertical profile of CO and total column of CH ₄	Polar sun– synchronous
OMI (Ozone Monitoring Instrument) of NIVR and FMI	Aura of NASA (2004)	NO ₂ , SO ₂ , BrO, OClO, and aerosol	Polar sun– synchronous
OMPS (Ozone Mapping and Profiler Suite)	NPOESS of NOAA (2014)	Nadir and limb soundings of O ₃ (ozone)	Polar sun– synchronous
POLDER (Polarization and Directionality of the Earth's Radiance)/CNES	ADEOS of NASDA (1996–1997)	Polarization, aerosols, clouds	Polar sun– synchronous
SABER (Sounding of the Atmosphere using Broadband Emission Radiometer)/NASA	TIMED of NASA (2001)	O ₂ , O ₃ , H ₂ O, NO, NO ₂ CO, CO ₂ , OH,	Inclined orbit
SAGE–I/–II (Stratospheric Aerosol and Gas Experiment)/LaRC	AEM–2 of NASA (1979) ERBS of NASA (1984)	O ₃ , NO ₂ , (H ₂ O), aerosols	Inclined orbit Inclined orbit
SAGE–III (Stratospheric Aerosol and Gas Experiment)/LaRC	Meteor–3M–1 of Rosaviakosmos (Dec. 10, 2001), ISS (2005)	O ₃ , NO ₂ , NO ₃ , OClO, aerosols,	Polar sun– synchronous, Inclined 51.6°
SAM (Stratospheric Aerosol Measurement)/NASA SAM–II (Stratospheric Aerosol Measurement–II)/NASA	ASTP (Apollo–Soyuz Test Project), 1975, SAM–II on Nimbus–7, NASA (1978)	stratospheric aerosols stratospheric aerosols	Inclined Polar sun– synchronous
SAMS (Stratospheric and Mesospheric Sounder) LIMS (Limb Infrared Monitor of the Stratosphere) SBUV (Solar Backscatter UV) / TOMS (Total Ozone Mapping Spectrometer)	Nimbus–7 of NASA (1978–1985) (1978–1990) (1978–1993)	Profiles of H ₂ O, CH ₄ , CO and NO O ₃ , H ₂ O, NO ₂ , HNO ₃ Vertical O ₃ profiles and total column amount	Polar sun– synchronous
SBUV/2 (Solar Backscatter UV/2)/ NASA/NOAA	NOAA–9 (1984), NOAA–11 (1988), NOAA–14 (1994), NOAA–16 (2000) all PM missions from K to N' and late AM missions	O ₃ (ozone profiles, nadir pointing instrument)	Polar sun– synchronous
SCIAMACHY (Scanning Imaging Absorption Spectrometer for Atmospheric Cartography)/ESA	Envisat of ESA (2002)	O ₂ , O ₃ , O ₄ , NO, NO ₂ , N ₂ O, BrO, OClO, H ₂ CO, CO, CO ₂ , CH ₄ , H ₂ O, SO ₂ , HCHO, clouds, aerosols, pressure temperature,	Polar sun– synchronous
SSULI (Special Sensor UV Limb Imager)/NRL	DMSP/F–16 of DoD (2003)	O ⁺ , O, O ₂ , N ₂ , T (in ionosphere)	Polar sun– synchronous

Instrument/Agency	Mission/Platform, Coverage period	Species observed	Orbit
TES (Tropospheric Emission Spectrometer)/JPL	Aura of NASA (2004)	NO _y , CO, O ₃ , H ₂ O, SO ₂ ,	Polar sun-synchronous
TOMS (Total Ozone Mapping Spectrometer)/NASA	Meteor-3-6 (1992-94) ADEOS, of NASDA (1996/97) TOMS-EP (1996 to present) QuikTOMS (launch failure, Sept. 21, 2001)	O ₃	Inclined orbit Polar sun-synchronous Polar sun-synchronous

Table 34: Overview of some major spaceborne trace gas instruments

Instrument	Mission	Comment
ISAMS, HALOE	UARS (launch Sept. 13, 1991), NASA	ISAMS failure in July 1992
ORA	EURECA-1 (1992 - 1993), ESA	Retrievable carrier platform
LITE	STS-64 (Sept. 9-20, 1994), NASA	Technology experiment
GOME	ERS-2 (launch Apr. 21, 1995), ESA	Spectral range of 240-790 nm for ozone, aerosols, etc.
SPIRIT-III	MSX of DoD (launch Apr. 24, 1996)	S/C built and operated by JHU/APL
POLDER, CNES and ILAS of JEA	ADEOS (launch Aug. 17, 1996), NASDA	S/C failure June 30, 1997
MOS of DLR	IRS-P3 (launch Mar. 21, 1996), ISRO	also MOS-P on Priroda
SLA of NASA	SLA-1 (Jan. 11-20, 1996 on STS-72) SLA-2 (Aug. 7-19, 1997 on STS-85)	Shuttle missions
POAM-II of NRL	SPOT-3 (launch Sep. 26, 1993), CNES	S/C operations until Nov. 16, 1996
POAM-III of NRL	SPOT-4 (launch Mar. 24, 1998), CNES	Aerosols in altitudes of 10-30 km
AVHRR/3 of NOAA	NOAA-15 (launch May, 13, 1998)	First flight of AVHRR/3 instrument
MODIS, MISR MODIS	Terra (launch Dec. 18, 1999), NASA Aqua (launch May 4, 2002), NASA	EOS (Earth Observing System) program
OSIRIS of CSA	ODIN (launch Feb. 20, 2001), Sweden	UV/VIS/IR limb sounder
CHRIS	PROBA (launch Oct. 22, 2001), ESA	Aerosol studies
MERIS, MIPAS, GOMOS, SCIAMACHY	Envisat (launch Mar. 1, 2002), ESA	
GLAS	ICESat (launch Jan. 13, 2003), NASA	Nadir-viewing lidar
ILAS-II of JEA	ADEOS-II (launch Dec. 14, 2002), JAXA	Contact with ADEOS-II was lost on Oct. 25, 2003
ACE-VNIRI	SciSat-1/ACE (launch Aug. 13, 2003), CSA	
HIRDLS	Aura (launch July 15, 2004), NASA	EOS program
EPIC	Triana (NASA cancelled the mission in early 2006)	Measurement of aerosol amounts from Lagrangian point L1
GOME-2	MetOP-1 (launch Oct. 19, 2006), EUMETSAT	
ALADIN (ESA)	ADM-Aeolus (launch 2014)	Incoherent direct detection lidar

Table 35: Some aerosol-monitoring instruments of spaceborne missions

Instrument	Mission	Swath (km)	Spatial resolution, nadir (km)	Spectral range (nm)	Global coverage	Polarization detection
ATSR-2	ERS-2	500	1 x 1	VNIR+TIR	3 days	No
AVHRR/3	NOAA-POES	>2400	1.1 x 1.1	VNIR+TIR	1 day	No
GOME	ERS-2	960	320 x 40	240 – 790	3 days	Partial
GOME-2	MetOp-A	960	40 x 40 (40x5)	240 – 790	3 days	Yes
MERIS	Envisat	1150 km	0.26 x 0.3	390 – 1040	3 days	No
MISR	Terra	360	0.275 x 0.275	VIS+IR	9 days	No
MODIS	Terra	2330	0.25 x 0.25	400 – 14,500	1–2 days	No
OMI	Aura	2600	13 x 24	270 – 500	1 day	No
POLDER-1	ADEOS	1140 x 2200	7 x 6	443 – 920	1 day	Yes
POLDER-2	ADEOS-II	1140 x 2200	7 x 6	443 – 920	1 day	Yes
POLDER-P	PARASOL	1160 x 2200	5.3 x 6.2	443 – 1030	1 day	Yes
SCIAMACHY	Envisat	960	32 x 16	240 – 2380	3 day	Yes
TOMS	ADEOS	2795	50 x 50	UV	1 day	No

Table 36: Observation characteristics of some aerosol instruments

1.4.7.1 Monitoring of ozone in the atmosphere

Monitoring of ozone (global coverage). Detection of short-term and long-term (seasonal) changes in ozone (UV radiation) with measurements of total column amounts and stratospheric and tropospheric profiles of ozone. See also Table 730 for a survey of Shuttle flights with the SSBUV payload.

Atmospheric ozone has several environmental implications, it can be classified according to atmospheric layers (or altitude). Long-term trend measurements are of great importance. Ozone depletion leads to an increase in the intensity of UV radiation reaching the Earth surface in some regions of the world.

- Stratosphere. About 90% of the atmospheric ozone is contained in the stratosphere. Ozone plays a critical role in absorbing UV radiation and preventing it from reaching Earth's surface. The so-called "ozone hole" is a consequence of stratospheric ozone depletion over the poles of the Earth.
- Troposphere. In the upper and middle troposphere, ozone is a major greenhouse gas, causing inhomogeneous radiative forcing.
- Troposphere. Ozone is an oxidizing power in the lower and middle troposphere.
- Surface air. Ozone is a pollutant, toxic to humans and to vegetation.
- Airborne cloud investigations (properties, interactions, phases, droplets, microphysics, etc.) with radiometers, lidars, radars, hyperspectral imagers, etc. have been performed since the mid 1970s (with most observations in the 1990s) on various scales with a number of instruments, such as: ARES (NASA/JSC), AWSR (NOAA), AMMS, CALS and CAR (NASA/GSFC), CVI (MISU), Deimos and MARSS (UKMO), ALEX, OLEX, H₂O-DIAL and Microlidar (DLR), MPIR (SNL), CDL (LLNL), ELDORA/ASTRAIA (NCAR/CRPE), LASAL (GSFC), LEANDRE (CNRS/CNES), MCR and MIR (GSFC), MTP (JPL), NAILS (NCAR), OVID (MPIfM Hamburg), RAMS (NASA/NOAA), MAKREL-2 and M2M (Tomsk), APDOR-95 (MIRSL).
- The first project⁴⁷⁶ to use in-service aircraft for trace-constituent data collection took place in 1968 with carbon monoxide (CO) measurements made from Lufthansa B-707 aircraft. A vertical CO gradient was observed in the tropopause, this resulted in an

estimation of the size of the stratospheric CO sink. (The same group of researchers employed a manned laboratory inside a container on 10 German cargo service flights between 1981 and 1987 to measure CO).

– The meridional distribution of tropospheric ozone concentrations was studied by MPAe (Max–Planck–Institut für Aeronomie, Katlenburg–Lindau, Germany) on 37 commercial flights between Northern Europe (Frankfurt) and South Africa (Cape Town) during the period 1970–1974. ⁴⁷⁷⁾ ⁴⁷⁸⁾

– GASP (Global Atmospheric Sampling Program) ⁴⁷⁹⁾ was introduced by NASA in 1975 to measure trace gases on commercial airliners. Four B–747 (two Pan American, one United, and one Qantas) aircraft were equipped with instruments to routinely measure ozone, carbon monoxide, water vapor, aerosols, temperature, and horizontal winds. GASP was over the period 1975–1979 with over 6900 flights.

– The Japanese ASE (Automatic Air–Sampling Equipment) program with instrumentation on a Boeing 747 aircraft between Japan and Australia was introduced in 1993. It lasted until 1996. ⁴⁸⁰⁾

– Also in 1993, the EU started its MOZAIC (Measurement of Ozone by Airbus In–Service Aircraft) program. During MOZAIC–I (1993– Sept. 1996), fully automated devices, developed by CNRS (France) and Forschungszentrum Jülich (Germany), were flown on five Airbus aircraft in normal airline serve (Air France, Qantas, Lufthansa, Sabena). MOZAIC–II started in Oct. 1996 with the aim to continue the ozone and water vapor measurements, several new instruments were added to measure CO and NO_y. Between Sept. 1994 and Dec. 1997, 7500 flights (54,00 flight hours) were made in the MOZAIC program over the continents (Europe, North America, Asia, South America, and Africa) and the Atlantic Ocean. A MOZAIC–III program is currently being carried out in the Fifth Framework Program of the EU. ⁴⁸¹⁾ ⁴⁸²⁾

Instrument (Agency)	Platform	Launch Date	Comment
BUV (NASA)	Nimbus–4 (NASA) AE–E (NASA)	Apr. 8, 1970 Nov. 20, 1975	2 Ebert–Fastie–type monochromators AE–E reentered on June 10, 1981
SSH, SSH–2 (DoD)	DMSP (DoD) series	Sep. 11, 1976	Starting with F1 satellite
SBUV/TOMS (NASA)	Nimbus–7	Oct. 24, 1978	Nadir–viewing Ebert–Fastie spectrometer of TOMS. Swath width of 2700 km (scanning). TOMS failed in May 1993. SBUV failed in 1990
SAGE–I (NASA)	AEM–2 (NASA)	Feb. 18, 1979	
UVSP (NASA/MSFC)	SMM (NASA)	Feb. 14, 1980	
UV Ozone Experiment Airglow Instrument Solar UV Monitor	SME (NASA)	Oct. 6, 1981	
UV Spectrometer	EXOS–C (ISAS)	Feb. 14, 1984	
SBUV/2 (NASA)	NOAA–9 (NOAA) NOAA–11 (NOAA)	Dec. 12, 1984 Sep. 24, 1988	S/C service ended Aug. 3, 1995 S/C service ended Sep. 9, 1994

476) W. Seiler, C. Junge, “Carbon Monoxide in the Atmosphere,” *Journal of Geophysical Research*, Vol. 75, No. 20, April 20, 1970, pp. 2217–2226

477) P. Fabian, P. G. Pruchniewicz, “Meridional Distribution of Ozone in the Troposphere and its Seasonal Variations,” *Journal of Geophysical Research*, Vol. 82, No 15, May 20, 1977, pp. 2063–2073

478) H. K. Tiefenau, P. G. Pruchniewicz, P. Fabian, “Meridional Distribution of Tropospheric Ozone from Measurements Aboard Commercial Airliners,” *Pure and Applied Geophysics*, Vol. 106–108, 1973, pp. 1036–1040

479) G. D. Nastrom, “Ozone in the Upper Troposphere From GASP Measurements,” *Journal of Geophysical Research*, Vol. 84, No C7, July 20, 1979, pp. 3683–3688

480) H. Matsueda, et al., “Carbon Monoxide in the upper troposphere over the western Pacific between 1993 and 1996,” *Journal of Geophysical Research*, Vol. 103, 1998, pp. 19,093–19,110

481) A. Marengo, et al., “Measurement of ozone and water vapor by Airbus in–service aircraft: The MOZAIC airborne program, An overview,” *Journal of Geophysical Research*, Vol. 103, No D19, Oct. 20, 1998, pp. 25,631–25,642. The same volume, D19, contains a special section, pp. 25,631–25,737

482) J. Y. N. Cho, et al., “Trace Gas Study Accumulates Forty Million Frequent–Flyer Miles for Science,” *EOS Transactions of AGU*, Vol. 80, No. 34, Aug. 24, 1999, pp. 377–384

Instrument (Agency)	Platform	Launch Date	Comment
SSBUV (NASA)	STS-34 (NASA)	Oct. 19, 1989	Coincident observations with SBUV/2 on NOAA-9 and NOAA-11
TOMS (NASA)	Meteor-3-6 (Russia)	Aug. 15, 1991	TOMS operation until Dec. 1994
HALOE, MLS, CLAES, ISAMS	UARS (NASA)	Sep. 13, 1991	Sun occultation method (HALOE) Heterodyne limb sounder (MLS)
POAM-II (NRL)	SPOT-3 (CNES)	Sep. 26, 1993	SPOT-3 entered safehold Nov. 14, '97; Solar occultation through the Earth's atmospheric limb
GOME (ESA) a scanning optical double spectrometer	ERS-2 (ESA)	Apr. 21, 1995	DOAS (Differential Optical Absorption Spectroscopy) measurement concept
Ozon-M	Priroda (Russia)	Apr. 23, 1996	Priroda, a module of the MIR station
TOMS (NASA)	TOMS-EP	July 2, 1996	Operational as of 2000
TOMS (NASA), RIS	ADEOS (NASDA)	Aug. 17, 1996	ADEOS failed on June 30, 1997
MAHRSI (NRL)	CRISTA-SPAS-2	Aug. 7-19, 97	STS-85 Shuttle, OH interaction with ozone and other trace gases
POAM-III (NRL)	SPOT-4 (CNES)	Mar. 24, '98	Operational
OLME (FACH)	FASat-Bravo (Chile)	July 10, 1998	Total column ozone measurements
OM-2	TechSat/Gurwin-II	July 10, 1998	Technion (Israel Institute of Techn.)
OSIRIS (CSA)	ODIN (Sweden)	Feb. 20, 2001	Detection of aerosols and trace gases
TOMS-5 (NASA)	QuikTOMS	Sep. 21, 2001	Failure of Taurus launch vehicle
SAGE-III (NASA)	Meteor-3M-1 (Russia)	Dec. 10, 2001	Self-calibrating solar and lunar occultations (9 spectral channels)
GLI, ILAS-II	ADEOS-II (JAXA)	Dec. 14, 2002	Swath width of 1600 km
GOMOS, SCIAMACHY (ESA)	Envisat (ESA)	Mar. 1, 2002	Star occultation measurement method, DOAS and UV in parallel
ACE-FTS (CSA)	SciSat-1/ACE (CSA)	Aug. 13, 2003	FTS instrument for trace gases
HIRDLS, MLS, TES (NASA), OMI (NIVR)	Aura (EOS/CHEM) (NASA)	July 15, 2004	Limb sounder (HiRDLS), FTS (TES), Hyperspectral capabilities of OMI
GOME-2, IASI (ESA/Eumetsat)	MetOp-A (Eumetsat)	Oct. 19, 2006	DOAS measurements
TANSO-FTS	GOSAT (JAXA)	Jan. 23, 2009	FTS instrument
OMPS NOAA	Suomi NPP (NASA)	Oct. 28, 2011	Limb-viewing sensor suite

Table 37: Major spaceborne instruments for the global measurement of ozone

- NOXAR (Nitrogen Oxides and ozone measurements along Air Routes)⁴⁸³ was conducted aboard 540 flights of Swissair B-747 aircraft in the period from May 1995 to May 1996. The instruments recorded data at a temporal resolution of 3s.
- Another German program, CARIBIC (Civil Aircraft for Remote-Sensing and In-Situ-Measurements in Troposphere and Lower Stratosphere Based on the Instrumentation Container Concept), started in 1996.

1.4.7.2 Occultation measurements

The history of occultation observations must be as old as astronomy itself, ancient. An occultation occurs whenever a celestial object passes in front of another one, whereby the more distant object is hidden (eclipsed); occultation refers literally to the “obscuring-of-light event” of an astronomical body to an observer. One type of such an event is the occultation of stars by the moon or by any other object within the solar system. An eclipse of the sun takes place when the moon comes between the Earth and the sun so that the moon's shadow sweeps over the face of the Earth. – The phenomenon of occultation helped ancient astronomers to determine the periods and motions of the sun and the moon. Historically, the eclipses of Jupiter's moons Io, Europa, Ganymede, and Callisto (discovered by Galileo

483) D. Brunner, et al., “Large-scale nitrogen oxide plumes in the tropopause region and implications for ozone,” *Science*, Vol. 282, 1998, pp. 1305–1309

Galilei in 1610) are important, for they provided one of the earliest proofs of the finite speed of light. In 1675, the Danish astronomer Ole Rømer noticed discrepancies between the observed and calculated times of such eclipses, which he correctly explained as being due to the difference in the travel time of light when the Earth is nearest to Jupiter or farther away from it. Today's astronomers use occultation measurements to determine for instance the variations in the length of the mean solar day or to estimate the diameter and size of a distant planet, even those of tiny asteroids.

Conceptually, occultations may also be observed by an instrument on a spacecraft in orbit and/or by a radio communication path interference between the spacecraft and the Earth. During the beginning and the end of such an occultation, signals sent out by the spacecraft's communication system and received on Earth have penetrated the planet's atmosphere. Occultation measurements employ generally the technique of passive absorption spectroscopy. In the early 1960s, this occultation technique was first employed by NASA/JPL in its planetary exploration program to Venus and Mars; the analysis of the data yielded information about atmospheric density and composition of Venus and Mars, respectively.

At the start of the 21st century, use of the occultation measurement principle for observing the Earth's atmosphere and climate has become so broad as to exploit natural radiation sources such as the sun, the moon, and the stars, as well as man-made radio signals from the GNSS (Global Navigation Satellite System) constellations and other satellite constellations (crosslink signals), to employ the whole electromagnetic spectrum (from EUV/UV to VIS/IR to MW and radio waves), and to utilize all kinds of atmosphere-radiation interaction such as refraction, absorption, and scattering (see also Glossary and chapter O.2.1; there are also many occultation and limb/occultation sounding instances within the "history" itself). In general, good occultation monitoring coverage is obtained with a sufficient density of occultation sources. – *The occultation measurement methods share the unique properties of self-calibration* (via normalized intensities or time-standard reference), *high accuracy and vertical resolution, global coverage, and an all-weather capability* (due to the use of long wavelengths in the microwave region). The self-calibration property is particularly crucial for climate research and climate change monitoring applications, as it enables unique long-term stability in climatological datasets. Occultation measurements bear a great potential for such applications as operational meteorology, climate research, and many other fields. Some examples are: ⁴⁸⁴⁾

- The occultation sounding of aerosols, trace gas constituents including ozone ("absorptive" or "extinctive" occultation monitoring), and of wind components with a variety of instruments (see 1.4.7).
- Refractive (or radio) occultation sounding of the GPS constellation. Earth-observation applications of navigation systems and use of GPS receivers as science instruments (in experimental state as of 2002). The goal is to use the meteorological occultation data to augment the data from other meteorological data sources (see 1.20.4)
- Bistatic ocean reflection measurements (see 1.20.6)
- Measurement of plasma densities of the solar wind.

484) <http://www.uni-graz.at/OPAC1Workshop-Sep2002/>

1.4.8 Sounding of the Ionosphere

The ionosphere is a layer of the Earth's atmosphere, between approximately 60 and 1000 km in altitude (a highly variable and complex physical system), that is partially ionized by solar X-rays, ultraviolet radiation, and energetic particles from space. The parameters of the ionospheric plasma are primarily controlled by the solar activity. Their sporadic perturbations usually appear as a response to perturbations in the solar wind and the magnetosphere. The interaction between the solar wind, the magnetosphere and the ionosphere is of great interest in solar-terrestrial physics studies. Spaceage observations reveal that the ionosphere locally reflects tropospheric phenomena (storms, upward shooting lightning, large cyclones and atmospheric fronts), anthropogenic factors (rocket launches, especially powerful ones, descent of spacecrafts, explosions, radio transmitter operations, etc.) and lithospheric processes (seismic activity, earthquakes, active fractures). The possibility to use these data for the prediction of earthquakes and monitoring of the anthropogenic and natural hazards is a new area of current research. ⁴⁸⁵⁾ ⁴⁸⁶⁾

Ground-based echo sounding of the ionosphere has been conducted since about 1924/25 to obtain information about the upper atmosphere and the effects of solar emissions. By 1947, an instrument known as the "ionosonde" was routinely used to measure automatically the characteristics of the ionosphere. During the International Geophysical Year (IGY) of 1957/58, an international cooperative effort created a worldwide network of ionosondes to record vertical incidence measurements for the 1957/59 period of maximum solar activity. Since the IGY, a loosely coordinated worldwide network of vertical incidence ionosondes, varying between 100 and 200 sites, has been operated continuously. ⁴⁸⁷⁾

- Modern "bottomside" digital sounders ⁴⁸⁸⁾ measure the frequency, time delay, amplitude, phase shift, Doppler shift and spread, polarization, and the return direction of echoes reflected off the underside of the earth's ionosphere. These measurements are typically shown as **ionograms** and are regularly inverted to give plasma density, velocity, and even turbulence versus altitude. However, ionograms represent only a fraction of the information available to a modern sounder, but they do display the echoes from ionospheric structures in a clear and graphical format. Many of the advantages of modern sounders over earlier devices are due to increased use of digital signal processing and flexible software controlled designs. Radio sounding offers a way to simultaneously measure the largest and some of the smallest scales in the magnetosphere, plasmasphere, and boundary layers.

The ionosphere is divided into four broad regions called D, E, F, and topside. These regions may be further divided into several regularly occurring layers, such as F1 or F2. ⁴⁸⁹⁾

– D-region: The region between about 75 – 95 km above the Earth in which the (relatively weak) ionization is mainly responsible for absorption of high-frequency radio waves.

485) Note: No single physical process can be made responsible for the diverse phenomena claimed to be associated with or indicators of impending earthquake activity. Transient thermal anomalies and short-term ionospheric variations have different possibilities as pre-earthquake activity indicators.

486) D. Ouzounov, P. Taylor, N. Bryant, S. Pulnits, J.-Y. Liu, K.-S. Yang, "Near Space Tracking of EM Phenomena Associated with the main Earthquakes," Proceedings of IAC 2004, Vancouver, Canada, Oct. 4-8, 2004, IAC-04-IAF-C.1.06

487) P. H. Reiff, C. B. Boyle, J. L. Green, S. F. Fung, et al., "Radio Sounding of Multiscale Plasmas," 1995, URL: http://image.gsfc.nasa.gov/publication/document/1995_reiff_etal/

488) Note: Ionograms are recorded tracings of reflected high frequency radio pulses generated by an ionosonde. Unique relationships exist between the sounding frequency and the ionization densities which can reflect it. As the sounder sweeps from lower to higher frequencies, the signal rises above the noise of commercial radio sources and records the return signal reflected from the different layers of the ionosphere. These echoes form characteristic patterns or "traces" that comprise the ionogram. Radio pulses travel more slowly within the ionosphere than in free space, therefore, the apparent or "virtual" height is recorded instead of a true height. For frequencies approaching the level of maximum plasma frequency in a layer, the virtual height tends to infinity, because the pulse must travel a finite distance at effectively zero speed. The frequencies at which this occurs are called critical frequencies. Characteristic values of virtual heights (designated h'E, h'F, and h'F2, etc.) and critical frequencies (designated foE, foF1, and foF2, etc.) of each layer are scaled, manually or by computer, from these ionograms.

489) <http://www.ngdc.noaa.gov/stp/IONO/ionogram.html>

- E–region: The region between about 95 – 150 km above the Earth that marks the height of the regular daytime E layer. Other subdivisions isolating separate layers of irregular occurrence within this region are also labeled with an E prefix, such as the thick layer, E2, and a highly variable thin layer, sporadic E. Ions in this region are mainly O_2^+ .
- F–region: The region above about 150 km in which the important reflecting layer, F2, is found. Other layers within this region are also described using the prefix F, such as a temperate–latitude regular stratification, F1, and a low–latitude, semi–regular stratification, F1.5. Ions in the lower part of the F layer are mainly NO^+ and are predominantly O^+ in the upper part. The F layer is the region of primary interest for radio communications.
- Topside region: This part of the ionosphere starts at the height of the maximum density of the F2 layer of the ionosphere and extends upward with decreasing density to a transition height where O^+ ions become less numerous than H^+ and He^+ ions. The transition height varies but seldom drops below 500 km at night or 800 km in the daytime, although it may lie above 1000 km. Above the transition height, the weak ionization has little influence on transionospheric radio signals.
- Spaceborne soundings of the ionosphere started with the launch of Alouette–1 in 1962 (see below). A radio plasma sounder operates by emitting a series of pulses over a range of frequencies, and listening for returned echoes. The properties of the dielectric, the surrounding plasma in this case, dictate the wave modes which propagate and their dependence on the dielectric (plasma) parameters.

Topside sounding of the ionosphere:

The term refers to RF (Radio Frequency) sounders looking from a LEO spacecraft into the nadir direction for ionospheric electron density observations. Other ionospheric parameters such as TEC (Total Electron Content), critical frequency (f_oF2) and F2–layer peak height, plasma temperature, and ion composition may be derived from the topside ionograms. The ionosphere below the peak electron concentration is referred to as bottomside ionosphere, while the outer part of the ionosphere, extending to about 2000 km and further, is referred to as the **topside ionosphere**. A sounder, installed onboard a LEO satellite (generally in the 800–1500 km range) and practically immersed in the medium it is measuring, is able to see only the uppermost portion of the ionosphere down to about the peak electron height, i.e., the topside ionosphere; hence, such a sounder is referred to as a “**topside sounder**.”^{490) 491) 492)}

An ionospheric topside sounder is a high frequency radar system that is located above the ionosphere, ideally onboard a polar orbiting satellite to provide global coverage. The sounder sweeps in frequency from around 0.3 to 15 MHz approximately every 32 seconds – its signals reflecting vertically off the upper F2 region of the ionosphere. The lowest frequency at which the signal passes through the ionosphere is called the critical frequency (f_oF2). Electrons are also stimulated at various lower frequencies causing resonances. The results from topside sounding are generally displayed as an ionogram, which is a display of reflections and resonances of the swept frequency against apparent range.⁴⁹³⁾

Following is a list in the early era of spaceflight of countries or agencies with various techniques of topside sounding implementations:

- The Canadian spacecraft **Alouette–1** (launch Sept. 29, 1962 from VAFB) can be regarded as the first satellite (with a circular orbit of 1000 km altitude and an inclination of

490) S. A. Pulinets, “Prospects of Topside Sounding,” Chap. 3 of ‘World Ionosphere/Thermosphere Study,’ WITS Handbook, Vol. 2, edited by C. H. Liu, Dec. 1989

491) Proceedings of the IEEE, Special Issue on Topside Sounding and the Ionosphere, Vol. 57, June 1969, pp. 859–1240

492) S. A. Pulinets, R. F. Benson, “Radio–Frequency Sounders in Space,” Review of Radio Science, ed. by W. Ross. Stone, Oxford University Press, Chapter 28, 1999, p. 711–733.

493) D. J. Palmer, M. Sweeting, “Ionospheric Sounding on a Microsatellite,” International Journal of Small Satellite Engineering, Vol. 1, Issue 1, Dec. 1995, URL: <http://www.ee.surrey.ac.uk/SSC/CSER/UOSAT/IJSSE/issue1/palmer/palmer.html>

80.5°) carrying a topside sounder to investigate the ionosphere (Canada/USA cooperative venture). The primary purpose of the Alouette–1 mission was to investigate the geographic, seasonal, and diurnal properties of the topside ionosphere up to 1000 km in altitude. Designed for a one–year life span, the satellite lasted 10 years producing more than 1 million images of the ionosphere. The Alouette–1 swept–frequency revealed that an equatorial anomaly extends high into the topside ionosphere; it also demonstrated its usefulness in observing HF electron resonances. The Alouette–1 ionospheric sounder had the following parameters: Frequency range of 1–12 MHz, transmitter power of 100 W, pulse width of 100 μ s, pulse repetition frequency of 62 Hz, and a frequency sweep rate of 1 MHz/s. In a supporting experiment, an untuned VLF receiver operated in the range of 400 Hz to 10 kHz. The VLF receiver permitted the measurement of relative ion abundances in conjunction with the sounder. A worldwide network of 22 ground receiving stations collected the sounding data of Alouette–1 and –2. Alouette–2 followed in 1965, also with a topside sounder. Each Alouette S/C produced topside ionograms for 10 years. ^{494) 495) 496)}

- Explorer–20 of NASA (launch Aug. 25, 1964), the basic sounder instrumentation comprised a two–frequency transceiver coupled to an electrically short dipole antenna (three transceivers were used for sounding at six fixed frequencies between 1.5–7.22 MHz)
- Explorer–22 of NASA (launch Oct. 10, 1964)
- ISIS–1 (International Satellite for Ionospheric Studies–1) ^{497) 498)} of NASA with a launch in 1969 (the ISIS program was actually an extension of the Alouette program), ISIS also demonstrated the ability to remotely sound the magnetospheric cusp.
- ISIS–2 of NASA (launch April 1, 1971). The ISIS satellites collected several million topside ionograms in the 1960s and 1970s (ISIS–1 and ISIS–2 collected for 21 and 19 years, respectively) with a multinational network of ground stations providing good global coverage. – – Note: ISIS–1 and –2 are considered second generation topside sounder missions because they provided an onboard data storage capability and limited experimental control capability. These two topside sounders contained 4 track tape recorders with 550 m of tape to record telemetry, sounder and VLF information, along with reference tone & clock.
- SJ–2A (launch Sept. 20, 1970) of CAST, China, used two frequencies: 162 MHz and 40.5 MHz
- Cosmos–381 (launch in 1970) of the Soviet Union;
- ISS–A (Ionospheric Sounding Satellite–A) of NASDA with a launch in 1976; ISS–B of NASDA (launch Feb. 16, 1978). The missions were also referred to as Ume–1 and Ume–2. The ISS–B spacecraft had only memory for about 4 orbits (6 hours); hence, much of the available data was lost. It took nearly 4 months to build up one local time (LT) map of the Earth.

494) C. A. Franklin, M. A. Maclean, “The Design of Swept–Frequency Topside Sounders,” *Proceedings of the IEEE*, Vol. 57, No 6, June 1969, pp. 897–929

495) C. D. Florida, “The Development of a Series of Ionospheric Satellites,” *Proceedings of the IEEE*, Vol. 57, No 6, June 1969, pp. 867–875

496) Note: Swept–frequency sounding is a technique in which a measurement is made of the frequency shift, phase shift, or time delay between the transmitted signal and its echo). Because of the Earth’s magnetic field, the ionosphere is birefringent with the result that a transmitted electromagnetic wave normally splits into two characteristic waves which travel independently at different velocities and different polarizations. These are called the ordinary (O) and the extraordinary (X) waves and are typically elliptically polarized. As the sounding frequency is increased, the electron number density required to reflect the transmitted signal increases until reflection occurs at a region or height of maximum ionization. Above the critical frequency corresponding to the electron number density at the peak of the F2–layer, reflection can no longer take place and the ionosphere becomes transparent to the sounding signal.

497) D. Bilitza, X. Huang, B. W. Reinisch, R. F. Benson, H. K. Hills, W. B. Schar, “Topside Ionogram Scaler With True height Algorithm (TOPIST): Automated processing of ISIS topside ionograms,” *Radio Science*, Vol. 39, RS1S27, DOI: 10.1029/2002RS002840, 2004, pp. 1–7

498) R. F. Benson, “Application of ionospheric topside–sounding results to magnetospheric physics and astrophysics,” *Radio Science*, Vol. 39, RS1S18, DOI: 10.1029/2002RS002834, 2004, pp. 1–6

- EXOS–B (Exospheric Satellite–B or Jikiken) of NASDA (launch Sept. 16, 1978)
- ISEE–1/–2 of NASA/ESA (launch Oct. 22, 1977)
- Intercosmos–19 spacecraft of the Soviet Union (launch Feb. 27, 1979). A digital topside sounder, IS–338, developed by IZMIRAN (Russian Institute of Terrestrial Magnetism, Ionosphere and Radiowave propagation) of Moscow, was flown. The spacecraft carried a computer to process data, having enough memory to record information from about 10 orbits (16 hours) of soundings recorded every 64 seconds.
- EXOS–C (Ohzora, launch Fe. 14, 1984) of NASDA
- Cosmos–1809 (launch Dec. 1986) of the Soviet Union. The spacecraft carried also the digital topside sounder IS–338.
- Coronas–I of Russia (launch March 2, 1994 from Plesetsk), and the orbital MIR Space Station (the topside sounder was installed on the Priroda module in 1998).

Topside sounding from a satellite reveals the response of the ionosphere to disturbances such as a geomagnetic storm. The pulses emitted by the sounder on consecutive frequencies are reflected on different heights depending on electron density height distribution. The time delay dependence of emitted pulses on the frequency is called the height–frequency characteristic of the ionosphere, referred to as the ionogram. With the help of a special algorithm, which takes into account the propagation characteristics of electromagnetic waves in magnetized plasma, the measurements are transformed into density height distributions from the satellite altitude down to the maximum F2–layer density distribution, which is usually located at altitudes of 250 to 350 km. In equatorial regions, especially in geomagnetically disturbed conditions, the F2–layer peak height may extend to altitudes of 500 km and even more.⁴⁹⁹⁾

Direct observations of ionospheric features are crucial for various applications in the fields of communications, navigation, early earthquake warning, radar, etc. – In spite of the numerous early missions, topside global sounding of the ionosphere has not become an operational service at the turn of the 21 century, rather it can still be put into the experimental category of missions.

An overview of the history of seismo–ionospheric effects is provided in the following reference.^{500) 501) 502) 503)} A disturbance of ionospheric electromagnetic radiation in the range of 10 Hz – 1 kHz was for the first time observed by Gokhberg,⁵⁰⁴⁾ when the NASA satellite OGO–6 (Orbiting Geophysical Observatory–6; launch June 5, 1969 from VAFB, end of mission Oct. 12, 1979) had gone over the sources of strong earthquakes ($M > 5.5$). An ion density trough (about 20%) over the earthquake source was also observed when the data from the NASA satellites ISIS–2 (International Satellite for Ionospheric Studies–2, launch April 1, 1971) and AE–C (Atmospheric Explorer–C; launch Dec. 16, 1973) were analyzed. Additional disturbance effects were found from statistical data of the Intercosmos–19 mission (launch Feb. 27, 1979), and reported for the first time.

499) S. A. Pulnits, “Seismic activity as a source of the ionospheric variability,” *Advances in Space Research*, Vol. 22, 1998, No 6, pp. 903–906

500) M. Gousheva, P. Hristov, P. Angelov, B. Kirov, K. Georgieva, et al., “New Technologies for Earthquake Ionosphere Precursor Monitoring,” *Proceedings of 54th IAC, Bremen, Germany, Sept. 29 – Oct. 3, 2003*

501) V. I. Larkina, A. V. Nalivayko, N. I. Gershenzon, M. B. Gokhberg, V. A. Liperovsky, S. L. Shalimov, “VLF emission related with seismic activity on the Intercosmos–19 satellite,” *International Journal of Geomagnetism and Aeronomy*, Vol. 23, 1983, pp. 684–687, 1983. (English translation)

502) V. I. Larkina, V. V. Migulin, O. A. Molchanov, et al., “Some statistical results on very low frequency radiowave emissions in the upper ionosphere over earthquake zones,” *Physics of the Earth and Planetary Interiors*, Vol. 57, 1989, pp. 100–109

503) M. B. Gokhberg, V. A. Pilipenko, O. A. Pokhotelov, “Seismic precursors in the ionosphere, *Izv. Acad. Nauk SSSR, Fiz. Zemli*, Vol. 10, pp. 17–21, 1983. (in Russian)

504) M. B. Gokhberg, V. A. Pilipenko, O. A. Pokhotelov, “Observation from a satellite of electromagnetic radiation above the region of an earthquake in preparation,” *Doklady AN SSSR (Reports to the USSR Acad Sc.)*, Vol. 268, 1, pp. 56–58, 1983. (in Russian)

The phenomenon of ionospheric perturbations prior to strong earthquakes has been known for some time. But the problem is how to distinguish the perturbations caused by solar flares and magnetic storms from those that are genuinely due to seismic activity. The idea of using satellites to predict earthquakes is based on the fact that Earth's crust emits characteristic electromagnetic signals a few hours before an impending quake.

The observed seismo–activity influence on the ionosphere is rather weak and is usually masked by the solar activity effects.⁵⁰⁵⁾ The seismogenic disturbances are typically detected in the ionosphere under low solar activity conditions ($Kp < 4$). Nevertheless, making use of modern signal processing methods there is a hope to extract them if the structural peculiarities of seismogenic “signals” can be reliably determined. This approach, however, requires a huge amount of experimental data as well as appropriate theoretical modeling.

Mission	Time frame	Mission	Time frame
Alouette–1 (Canada)	1964	Cosmos–274 (USSR)	1969
OGO–6 (NASA)	1969	OVI–17	1969
ISIS–2 (NASA)	1971	AE–C (NASA)	1973
GEOS–2 (NASA)	1978	Intercosmos–19 (USSR)	1979
Aureol–3 (CESR, France)	1981	Intercosmos–Bulgaria 1300	1982
Salyut–7 (USSR)	1985	Meteor–3 (USSR)	1986
Cosmos–1809 (USSR)	1987	ACTIVE (Intercosmos–24)	1987
TOPEX/Poseidon (NASA/CNES)	1996	MIR Space Station (Russia)	1994–1999

Table 38: Overview of seismo–ionospheric effects registered in missions (some a posteriori)

The ionograms of the Intercosmos–19 mission^{506) 507) 508)} (launch 1979) of the former Soviet Union (orbit of 502 km x 995 km, inclination of 74°; it produced topside ionograms every 64 seconds along its orbital path) have been analyzed extensively to model the electron density distribution above and below the F2 peak layer.

- Possible future applications of topside ionospheric monitoring may involve the capability to diagnose the effect of anomalous atmospheric electric fields that penetrate into the ionosphere.^{509) 510)} The data analysis from the topside sounder on the Intercosmos–19 (1979) spacecraft showed strong variations in the vertical structure of the ionosphere over regions of impending earthquakes. The ionosphere rises over a seismic active region forming a dome of density depletion. One of the main sources of atmosphere–ionosphere modification over the regions of preparing earthquakes is the emanation of various gases (radon, hydrogen and helium) from the ground as well as sub–micron aerosols. These may lead to the changes in the electrodynamic properties of the atmosphere–ionosphere that can be observed by the topside sounder.
- Seismo–ionospheric studies make use of atmospheric electricity distributions.^{511) 512)} The large–scale vertical electric field of high intensity (in the order of 1000 V/m), appearing over seismically active regions a few days prior to a strong earthquake, is due to the ani-

505) M. Parrot, “Electromagnetic Noise Due to Earthquakes,” Handbook of Atmospheric Electrodynamics, II, pp. 95–116, CRC Press, 1995

506) B. Nava, S. M. Radicella, S. Pulnits, V. Depuev, “Modelling Bottom and Topside Electron Density and TEC with Profile Data from Topside Ionograms,” Advances in Space Research, Vol. 27, No. 1, pp. 31–34, 2001

507) S. A. Pulnits, V. H. Depuev, A. T. Karpachev, S. M. Radicella N. P. Danilkin, “Recent Advances in Topside Profile Modeling,” Advances in Space Research, Res. Vol. 29, No. 6, 2002, pp. XIX–X23

508) G. F. Daminova, “Asymmetry of the Longitudinal Effect in the Low–Latitude Ionosphere,” Advances in Space Research, Vol. 29, No. 6, 2002, pp. 911–915

509) S. A. Pulnits, A. D. Legen'ka, “Spatial–Temporal Characteristics of Large Scale Disturbances of Electron Density Observed in the Ionospheric F–Region before Strong Earthquakes,” Cosmic Research, Vol. 41, No. 3, 2003, pp. 221–229

510) S. A. Pulnits, “Strong Earthquake Prediction Possibility with the help of Topside Sounding from Satellites,” Advances in Space Research, Vol. 21, No. 3, 1998, pp. 455–458

511) S. A. Pulnits, K. A. Boyarchuk, V. V. Hegai, V. P. Kim, A. M. Lomonosov, “Quasielectrostatic Model of Atmosphere–Thermosphere–Ionosphere Coupling,” Advanced Space Research, Vol. 25, No 8, 2000, pp. 1209–1218

sotropy of atmospheric conductivity at heights > 60 km. It normally penetrates into the ionosphere thereby creating the specific irregularities of electron concentrations. The resulting seismogenic variations in the ionospheric plasma represent a modification of the so-called magnetic-force-tube which is leaning into the direction of a developing earthquake region. The monitoring of the following parameters is of particular relevance in connection with corresponding models.

- F-layer maximum density (critical frequency)
 - Measurements of the height of the F-layer maximum
 - Vertical ionization profiles (both for topside and bottomside ionosphere)
 - TEC (Total Electron Content)
 - Measurement of ion composition
 - Measurement of electron temperature.
- The COMPASS-1 microsatellite (launch Dec. 10, 2001) of IZMIRAN is a new topside sounding mission dedicated to the study of the structure of the geodynamic processes (in particular above deep tectonic faults and earthquake regions). The sensor complement of the mission employs ionospheric tomography (monitoring of electromagnetic fields of various intensities and frequencies as well as heat distributions). The combined measurements are processed and analyzed in search of possible earthquake indicators. Note: The satellite experienced uncontrolled behavior ending in a loss of the mission shortly after deployment.
 - The COMPASS-2 microsatellite (launch May 26, 2006) of IZMIRAN is a topside sounding mission.
 - Hyperspectral imaging of the global ionosphere is provided by the HIRAAS (High-Resolution Airglow/Aurora Spectroscopy) instrument package of NRL flown on the ARGOS satellite of DoD (launch Feb. 23, 1999, see M.3). The imagery of the ionosphere obtained is “hyperspectral” at wavelengths from 50 to 310 nm. The HIRAAS, GIMI (Global Imaging Monitor of the Ionosphere) and EUVIP (Extreme Ultraviolet Imaging Photometer) instruments on the ARGOS S/C provide a powerful remote sensing exploration of the global ionosphere. This unusual combination of hyperspectral imagers and imagers provides a unique database of global structure and variability of ionospheric structure.
 - QuakeSat (launch June 30, 2003) is a research nanosatellite of the QuakeFinder Team and SSDL (Space Systems Development Laboratory) at Stanford University, Stanford, CA, with the objective of earthquake signature detection. QuakeSat’s primary scientific mission is to detect, record, and downlink ELF (Extremely Low Frequency) magnetic signal data, which may lead to groundbreaking techniques to predict earthquake activity. QuakeSat flies a very sensitive magnetometer. As of July 2004, a total of nearly 2000 magnetometer collections were made of all modes, primarily in the mode 2 configuration (10 to 150 Hz), roughly 500 MB raw binary uncompressed data.
 - The DEMETER microsatellite mission of CNES (see M.28.1), with a launch June 29, 2004, has the objective to: a) study the ionospheric disturbances in relation to the seismic activity, b) estimate the ionospheric disturbances in relation to the human activity, c) study the post-seismic effects in the ionosphere.
 - The Russian/Ukrainian multi-purpose Sich-1M spacecraft (launch Dec. 24, 2004) carries the instrument package Variant (“version”) to investigate the coupling of the lithosphere-atmosphere-ionosphere-magnetosphere, and to study space weather and fine seismogenic effects in the ionosphere. Variant is an international joint scientific project of

512) S. Jason, S. Pulnits, A. da Silva Curiel, Sir M. Sweeting, “Earthquake Forecast Science Research with a Small Satellite,” 53rd IAC, Oct. 10–19, 2002, Houston, TX, IAF-02-B.P.02

Great Britain, Poland, France, Russia, and Ukraine. The Variant scientific payload includes three instruments for registration of space current density: a split Langmuir probe, a Rogovskiy coil and a Faraday cup. The first two of these instruments are dedicated to measure current density variations and the last the particle fluxes. The equipment also includes sensors for measurements of the electric and magnetic field fluctuations in the frequency range from 0.1 Hz to 40 kHz.

- Project Vulkan (Volcano) is being funded by Rosaviakosmos for a launch of the minisatellite constellation in 2006. The satellites are being built by NIIEM of Istra; the scientific package is being developed by IZMIRAN of Troitsk and IKI of Moscow. The Vulkan orbital constellation will comprise two types of spacecraft (each of about 300 kg) built around the same multipurpose satellite bus: a) Vulkan–N at altitudes of 500–550 km, b) Vulkan–V at altitudes of 900–950 km. Monitoring of the following ionospheric phenomena/characteristics: ^{513) 514)}
 - Waveform of electromagnetic oscillations by electric and magnetic components within the 0.1 Hz to 5 kHz frequency band
 - Spectral density of electromagnetic oscillations within the 1 Hz to 15 kHz band
 - Electromagnetic field oscillation spectrum within the 15 kHz to 15 MHz band
 - Quasi–constant electric field within the 0–1 Hz band
 - Magnetic flux density within the band: $-60 \mu\text{T}$ to $+60 \mu\text{T}$
 - Parameters of the ionospheric plasma
 - The satellites will also measure characteristics of the underlying terrain and vertical profiles of aerosols.
- Ionospheric sounding from GEO (Geostationary Orbit). The IMAGER (Ionospheric Mapping and Geocoronal Experiment) instrument of NRL is planned to fly on the EO–3 (Earth Observing–3) mission in 2006 (of NASA, US Navy and NOAA). The overall objective is to demonstrate real–time tracking of ionospheric irregularities and scintillation storms. The tracking of these storms provides advanced warnings of navigation and satellite communication outages.

513) A. Fournier–Sicre, T. Suslova, A. Krasnov, “Project Vulkan – monitoring of the Earth seismic activity for earthquake and volcano eruption control,” ESA “News from Moscow,” Special Issue No 9, July 7, 2003, pp. 21–23

514) V. N. Oraevsky, K. A. Boyarchuk, S. A. Pulinetz, “The Problems of Satellite Monitoring of Earthquake Precursors and Russian Satellite Constellation ”Vulkan”, URL: <http://www.ss.ncu.edu.tw/~istep/word/F6.doc>

1.5 Some Instrument/Observation Techniques

- DOAS (Differential Optical Absorption Spectroscopy). A measurement technique that identifies and quantifies trace gas abundances with narrow band absorption structures in the near UV and visible region of the spectrum. The atmospheric spectra technique was first developed by Dieter Perner at KfA Jülich (now Forschungszentrum Jülich, Germany) in the early 1970s for the analysis of spectral windows. The distinguishing feature of DOAS (as compared to other spectrometers measuring atmospheric constituents) is that it aims to measure differential rather than absolute spectra. This means that broadband absorption or scattering effects arising from aerosols or gases can be separated (in ground analysis) from differential features which are characteristic of the trace gases absorbing in a given window. The distinguishing feature of a DOAS instrument is that it records simultaneously the entire spectrum of a selected spectral window. ^{515) 516) 517)}

The DOAS technique was first applied to long–path tropospheric investigations by D. Perner, U. Platt and co–workers. This resulted in an experimental ground–based DOAS–UV and VIS spectrograph installation at KfA Jülich in 1978, Germany (measurement of atmospheric CH₂O, O₃, and NO₂). Further ground–based DOAS instruments were built. Two airborne instruments, DOAS–VIS, developed by the Institute of Environmental Physics at the University of Heidelberg, and DOAS–UV of MPI for Chemistry (MPICH), Mainz, are flown since Jan. 1991 on a C160 Transall aircraft. A DOAS–type experiment by the name of “Mapping Atmospheric Pollution” was first proposed to ESA in March 1985 by J. P. Burrows, D. Perner, and P. J. Crutzen to fly on the EURECA free–flyer platform (EURECA was launched on STS–46 on July 31, 1992 and retrieved with STS–57 on July 1, 1993). – First spaceborne DOAS instruments are GOME (Global Ozone Monitoring Experiment) flown on ERS–2 (launch April 21, 1995), OSIRIS (Optical Spectrograph and Infrared Imaging System) flown on Odin (launch Feb 20, 2001), SCIAMACHY (Scanning Imaging Absorption Spectrometer for Atmospheric Cartography) flown on Envisat of ESA (launch Mar. 1, 2002), OMI (Ozone Monitoring Instrument), a Dutch–Finish nadir–pointing instrument on the Aura mission of NASA (launch July 15, 2004), and GOME–2 on MetOp–A of EUMETSAT (launch Oct. 19, 2006). Since the launch of ERS–2, there are also several ground–based DOAS stations in Europe providing ground truth measurements for GOME and SCIAMACHY.

- TDLAS (Tunable Diode Laser Absorption Spectrometer) is an open path spectroscopic technique that utilizes a diode laser as its light source [also referred to simply as TDL (Tunable Diode Laser) technique]. TDLAS is an alternate technique (to DOAS) of measuring atmospheric trace gases. The in–situ measurement technique makes use of the existence of rotational–vibrational molecule transitions in the mid IR spectrum and monitors a single absorption line. TDLAS has an advantage over other spectroscopic methods in that the diode laser can be operated in a relatively high–frequency modulation regime, where its noise contribution is very low. The airborne instrument FAST (Frequency–modulated Absorption Spectroscopy by TDLAS) of MPICH (Max–Planck–Institut für Chemie) of Mainz, Germany, flown since 1992, is an example of the TDLAS instrument technique. NASA utilized the TDL technique in particular to improve water vapor measurements in the upper atmosphere. The ALIAS (Aircraft Laser Infrared Absorption Spectrometer) instrument, developed in the 1980s, was flown on the ER–2 aircraft with over 50 flights completed by the end of 1993. At the start of the 21st century, TDL instrument technology is

515) J. P. Burrows, K. V. Chance, A. P. H. Goede, R. Guzzi, B. J. Kerridge, C. Muller, D. Perner, U. Platt, J. – P. PommerEAU, W. Schneider, R. J. Spurr, H. van der Woerd, “Global Ozone Monitoring Experiment: Interim Science Report”, *ESA SP–1151 Edited by T. D. Guyenne and C. J. Readings ISBN 92–9092–041–6 European Space Agency 1993*

516) H. Edner, P. Ragnarson, S. Spannere, S. Svanberg, “Differential optical absorption spectroscopy (DOAS) system for urban atmospheric pollution monitoring,” *Applied Optics*, Jan. 20, 1993, Vol. 32, No. 3, pp. 327–333

517) J. Frerick, H. Bovensmann, S. Noel, J. P. Burrows, M. R. Dobber, “SCIAMACHY on–ground/in–flight calibration, performance verification, and monitoring concepts,” *Proceedings of SPIE*, Vol. 3117, pp. 176–187, *Earth Observing Systems II*, William L. Barnes; Ed. Publication Date: 09/1997

being used for a wide range of applications, such as monitoring the exchange of CO₂ between specific ecosystems. In 2000, NASA/JPL licensed its TDL technology to SpectraSensors Inc. of Altadena, CA, for commercial exploitation (air pollution emissions, etc.).

- Wedge Imaging Spectrometer (WIS) technology. WIS is a spectral separation technique in which the spectral separation filters are mated to the detector array to achieve two-dimensional sampling of the combined spatial/spectral information passed by the filter. The technique obviates the need for a complex aft-optics assembly; it was developed by Hughes SBRC and sponsored by ARPA (introduced in 1992, see chapter P.215). The technology (hyperspectral imaging in the VNIR and SWIR regions) was initially flown on airborne sensors (WIS). It is also employed for the spaceborne sensor AC (Atmospheric Corrector) of the EO-1 mission (launch Nov. 21, 2000).
- Supermode acquisition of imagery. The term “supermode” refers to an acquisition process, introduced by CNES for the HRG (High Resolution Geometric) instrument of SPOT-5 (launch May 4, 2002), through which an image, sampled at 2.5 m, may be obtained from two 5 m resolution panchromatic images acquired simultaneously, keeping within the same borders as the two 5 m resolution images. See chapter D.55.3.

The new sampling concept of imagery, technically referred to as **quincunx sampling pattern** (an arrangement of five things with one at each corner and one in the middle of an area), employs a linear dual-array CCD detector in the focal plane, offset by one half pixel in one direction and 3.5 pixels in the other to avoid overlapping. This configuration is sufficient to improve the sampling grid without doubling each array's acquisition rate. The new sampling concept is based on Claude E. Shannon's theory of information which states that “*the sampling frequency must be equal to or greater than twice the maximum signal frequency*” to obtain clean images.⁵¹⁸ A specific image processing software, developed by CNES, is used to reconstruct the final image after three processing steps: interleaving, interpolation and restoration (involving de-noising and de-convolution). The quincunx sampling mode is also referred to as THR (Très Haute Résolution) or very high resolution mode.⁵¹⁹ CNES intends to implement the THR ground processing mode also within the framework of its Pleiades program delivering panchromatic data at 70 cm and MS data at 2.8 m resolution. Note: In Oct. 2003, the French government gave its final approval and go-ahead to the Pleiades program.

1.5.1 QWIP (Quantum-Well Infrared Photodetector)

QWIP^{520) 521) 522) 523) 524) 525)} represents a new passive infrared photoconductive solid-state detection technology (using 2-D focal plane arrays), holding great promise for a variety of infrared imaging applications in the spectral region of 6–20 μm which includes TIR [Thermal Infrared = 6–14 μm (an atmospheric window) – great efforts are being made to extent the QWIP observation coverage in the infrared range beyond the 25 μm range). Op-

518) C. E. Shannon, W. Weaver, “The Mathematical Theory of Communication,” University of Illinois Press, 1963.

519) “The Secrets of SPOT-5 Supermode,” SPOT Magazine, No 31, 2000, pp. 21–23

520) J. P. Burrows, 1994 “GOME and SCIAMACHY,” in Ozone Layer Observation by Satellite Sensors - *Proceedings of the International Workshop on Global Environment and Earth Observing Satellite Sensors Tokyo, Dec. 8-9, 1993* pp 67-74

521) J. P. Burrows, M. Buchwitz, M. Eisinger, V. Rozanov, M. Weber, A. Richter, A. Ladstätter-Weissenmayer 1998, “The Global Ozone Monitoring Experiment (GOME), Mission, Instrument Concept, and first scientific results”, *Proceedings of the third ERS Symposium Florence, Italy, March 18-23, 1997. Space at the service of our Environment, 1997.* ISBN 92-9092-656-2, ESA SP 414, pp. 585-590

522) U. Platt, D. Perner, H. W. Pätz, “Simultaneous measurements of atmospheric CH₂O, O₃, and NO₂ by differential optical absorption,” *Journal of Geophysical Research*, Vol. 84, 1979, pp. 6329–6335

523) J. F. Noxon, “Nitrogen dioxide in the stratosphere and Troposphere. Measurement by ground-based absorption spectroscopy,” *Science*, 189, 1975, p. 547

524) S. Gunapala, M. Sundaram, S. Bandara, “Quantum Wells stare at long-wave IR scenes,” *Laser Focus World*, June 1996 p. 233

525) S. Gunapala, S. Bandara, J. Bock, M. Ressler, et al., “GaAs/AlGaAs Based Multi-Quantum Well Infrared Detector Arrays for Low-Background Applications,” *Proceedings of SPIE Annual Meeting 2002: Remote Sensing and Space Technology*, July 7–11, 2002, Seattle, WA, Vol. 4823

erating principle: QWIPs operate by photoexcitation of electrons between ground and first excited state subbands of multi-quantum wells which are artificially fabricated by placing thin layers of two different high-bandgap semiconductor materials alternatively. The bandgap discontinuity of two materials creates quantized subbands in the potential wells, associated with conduction bands or valence bands. The structure parameters are designed so that the photo-excited carriers can escape from the potential wells and be collected as photocurrent. ^{526) 527)}

The QWIP technology employs large-bandgap III-V compound semiconductor materials such as GaAs (Gallium Arsenide) and AlGaAs (Aluminum Gallium Arsenide) with different aluminum compositions. The potential advantages of QWIP manufacturing (GaAs and AlGaAs) include the use of standard manufacturing methods based on GaAs growth and processing techniques. Some QWIP technology applications require low-temperature cooling for good spectral performance (higher sensitivity and speed). Note: Infrared detection may also be implemented on QWIP structures operated in photovoltaic mode (as opposed to photoconductive mode). QWIPs are ideal due to their tunable, narrowband response, obtained in point detectors and focal plane arrays. – QWIP structures are intrinsically very fast photodetectors since the re-capture time of optically excited carriers is very short, in the order of a few picoseconds (ps). Besides infrared imaging applications, QWIP structures are also interesting for heterodyne applications, where the high electrical bandwidth results in an improved spectral range of a heterodyne spectrometer.

Background: Initial work on QWIP technology started in the early 1980s at AT&T Bell Laboratories in Murray Hill, NJ (funded by BMDO, NASA and the US Army). The project goals were to produce a highly sensitive infrared photodetector addressing such issues as cost, fabrication technique, wavelength response, and large array size [the QWIP technology is actually a product/result out of Ronald Reagan's SDI (Strategic Defense Initiative) program to remotely detect the "signature" (i.e. slight changes in heat) of a ballistic missile launch, allowing for better tracking of a projectile]. The first experimental demonstration of a staring 2-D QWIP imaging array took place in 1985. The first demonstration model of a QWIP FPA camera with a 128 x 128 pixel array was developed by B. F. Levine and his colleagues at Bell Labs in 1991. This included the successful demonstration of the first bound-to-continuum GaAs/Al_xGa_{1-x}As indirect bandgap QWIP, operating at a cutoff wavelength of 4.2 μm. Semiconductor nanostructures, especially quantum wells and dots made of GaAs and InP related compounds, have enabled several unique infrared devices. Two prime examples are: QWIP devices and the QCL (Quantum Cascade Laser). ^{528) 529)}

With the advent of QWIP technology, large format and high uniformity single- and two-color QWIP FPAs have been developed for IR imaging applications. ^{530) 531)} The first multicolor FPAs are being developed at the start of the 21st century by a number of manufacturers, capable to detect three and four color ranges of the spectrum simultaneously, thereby offering more detailed views of the spectrum resulting in a wider range of applications [Earth observation (infrared imaging, hot spots), medicine, astronomy, atmospheric studies (IR spectroscopy for chemical sensing, pollution monitoring, smog detection), surveillance,

- 526) B. F. Levine, C. G. Bethea, K. G. Glogovsky, et al., "Long-wavelength 128 x 128 GaAs quantum well infrared photodetector arrays," *Semiconductor Science Technology*, Vol. 6, pp. C114–C119, 1991, IOP Publishing Ltd., UK
- 527) B. F. Levine, "Quantum-well infrared photodetectors," *Journal of Applied Physics*, Vol. 74, No. 8, Oct. 15, 1993, pp. R1 – R81, part of the series: *Applied Physics Reviews*; it includes an extensive review of the QWIP literature.
- 528) S. D. Gunapala, S. V. Bandara, "Quantum well infrared photodetectors (qwip) focal plane arrays," in H.C. Liu and F. Capasso, editors, "Intersubband Transitions in Quantum Well: Physics and Device Applications I," Academic Press, San Diego, 2000.
- 529) Note: The SDI program implementation was stopped in the 1980s because of technological shortfalls.
- 530) M. Walther, F. Fuchs, et al., "III-V Semiconductor Quantum Well and Superlattice Detectors," *Infrared Technology and Applications XXIV*, B. F. Andresen, M. Strojnik, Editors, *Proceedings of SPIE*, Vol. 3436, 1998, pp. 348–358
- 531) M. Walther, F. Fuchs, et al., "Electrical and optical properties of 8–12 μm GaAs/AlGaAs quantum well infrared photodiodes in 256x256 focal plane arrays," in 'Intersubband transitions in quantum wells: physics and devices,' ed. by S. Li and Y. K. Su, pp. 207 – 212, Kluwer Academic Publishers, Boston, 1998

navigation aids for pilots (night vision), commercial and industrial applications, traffic safety, etc.].

Some early imaging instruments of the QWIP technology are:

- In 1994, CSMT (Center for Space Microelectronics Technology) of NASA/JPL demonstrated a QWIP prototype camera with a detector array of 128 x 128 pixels (size of 38 μm x 38 μm), a cutoff wavelength of 14.9 μm (spectral bandwidth of 2 μm), and a frame rate of 5–210 Hz.

- In 1996, NASA/JPL and Amber (of Raytheon) demonstrated the QWIP technology with the development of a hand-held infrared camera (256 x 256 pixel FPA of QWIPs to detect radiation at 8.5 μm , frame rate of 60 Hz, camera mass of 4.5 kg).

- In 1997, FhG/IAF (Fraunhofer Gesellschaft / Institut für Angewandte Festkörperphysik) of Freiburg, Germany, in partnership with AIM (AEG Infrarot Module) GmbH of Heilbronn, Germany, demonstrated also a QWIP-based camera system (256 x 256 pixel FPA with a peak wavelength of 8.1 μm , the FPA is cooled to 65 K. – (Note: Objects at room temperature glow brightest in the wavelength range of 8–10 μm). The camera exhibits extremely low noise levels corresponding to NEDT (Noise Equivalent Differential Temperature) of 9.5 mK over the entire array. The research was supported by the German Ministry of Defence. The same camera, with the name of AIM-640Q, is also commercially available.⁵³²⁾

- Another QWIP FPA camera with 640 x 512 pixels and 20 mK NEDT was developed by AIM in 1999/2000. The GaAs/AlGaAs QWIP FPA was fabricated at IAF. Detector size of 16.3 mm x 13.3 mm, frame rate of 50 Hz. The QWIP detector chips are hybridized to a silicon-based ROIC (Readout Integrated Circuit) by flip-chip bonding with In-bumps. A peak wavelength of 8.8 μm and a cutoff wavelength of 9.3 μm are chosen to match the dark current of the detector to the charge handling capacity of the readout circuit.

- In 1997, JPL licensed its QWIP technology patent to OCT (OmniCorder Technologies Inc.), a Delaware corporation located in Stony Brook, NY. OCT developed in turn its “BioScanIR System,” a device to detect minute changes in blood distribution found in tissues surrounding a cancerous lesion.

- A spaceborne QWIP camera, funded by BMDO and built/managed by JPL, is flown on the STRV-1d (launch Nov. 16, 2000) microsatellite of DERA (Defence Evaluation Research Agency, Farnborough, UK) (M.47.2.2). STRV-1d is flown in GTO (Geosynchronous Transfer Orbit) of 600 km x 36,000 km. – The QWIP demonstration/performance on STRV-1d is considered essential for the development of the SBIRS (Space-Based Infrared System) Low program payload of DoD. – Note: Only the first two weeks of the mission were successful. Then, the telemetry from both spacecraft (STRV-1c and -1d) indicated a serious problem. The unrecoverable problem with the spacecraft receivers caused the end of the mission.

Another QWIP sub-experiment on STRV-1d is sponsored by NRC (National Research Council) of Canada and developed by DREO (Defence Research and Development) Ottawa, Canada. The objective is to explore the radiation effects on a new QWIP detector design (radiation detection performance within the 11–17 μm spectral region). The sub-experiment employs a passive radiator to cool the detector to 150 K. Measurements of the I–V curves of representative QWIP detector elements are gathered over the STRV-1d mission life under DHS (Data Handling System) control for post analysis by Canadian researchers.

⁵³²⁾ W. A. Cabanski, R. Koch, W. Rode, J. Ziegler, K. Eberhardt, R. Oelmaier, “High-resolution QWIP and MCT FPAs at AIM,” Proceedings of SPIE, Vol. 3698, Apr. 5–9, 1999, Orlando, FLA, Infrared Technology and Applications

1.5.2 TDI (Time Delay Integration)

TDI is an observation concept of increasing the effective dwell time of CCD detector arrays, usually in a pushbroom imaging mode configuration, by accumulating multiple exposures of the same (moving) target line. In scanned infrared imaging systems, TDI is one of the most important functions performed by CCDs. It was developed along with the early CCD technology at several places in the US industry and at NRL (DoD) in the later 1970s as well as at RSRE (Royal Signal and Radar Establishment, Malvern, UK) in 1982. RSRE introduced TDI into an infrared detector system by the name of SPRITE (Signal Processing In The Element). The TDI technique refers to a cumulative exposure concept of each ground image line by a CCD detector array (or any equivalent array). In TDI operation, signals generated by a moving scene – segment in successive detector lines are sequentially added in a delayed fashion. In this arrangement, the object motion must be synchronized with the exposures to ensure a crisp image. The main TDI objective is to improve the SNR (signal-to-noise ratio) value which is one of the most important issues for high resolution imaging. [Since the total detector noise is given by the root mean summation while the total signal is given by a simple sum, an increase in SNR equal to the square root of the number of detector rows is obtained].^{533) 534) 535)}

Some spaceborne instruments with TDI implementations are: The SeaWiFS instrument of SeaStar (the renamed OrbView–2 mission, launched Aug. 1, 1997), the ISIR sensor of NASA/GSFC flown on Shuttle flight STS–85 (Aug. 7–19, 1997), the OSA instrument of the Ikonos–2 satellite (launch Sept. 24, 1999), BGIS 2000 of QuickBird–1 (launch Nov. 20, 2000 – launch failure), PIC–2 of the EROS–B satellite program of ImageSat International, Cayman Islands – launch of EROS–B on April 25, 2006), and MSRS (Multi–Spectral high Resolution System) of the Diamant satellite of OHB–System, Bremen (launch 2010) – are examples of more recent TDI implementations in 2–D CCD line–array technology in the visible range of the spectrum. Note: For extrinsic detector arrays (such as silicon detectors in the visible range) there are two possible observation approaches: TDI or “staring array.” (see also O.3.6).

An unconventional TDI implementation is provided with RALCam1 (Rutherford Appleton Laboratory Camera 1) on the TopSat (launch Oct. 27, 2005) spacecraft of the UK (QinetiQ, SSTL, RAL, Infoterra Ltd.). The S/C platform is capable of supporting TDI, an attitude mode where the S/C maneuvers to allow the camera to “look” at its target for a longer period of time – equivalent to increasing the exposure time on a camera. scanning effect. During TDI observations the pitch of the S/C is manipulated such that it stares at the target for a longer period.

1.5.3 Polarimetric radiometry, imaging polarimeters, SAR polarimeters

Polarimetry deals with the vector nature of polarized electromagnetic radiation throughout the frequency spectrum. The electromagnetic field is a traveling wave (at the velocity of light) with electric and magnetic vector fields (scattering matrix) perpendicular to each other and to the direction of wave travel. A change in the index of refraction (or permittivity, magnetic permeability, and conductivity) causes the polarization state of a single frequency wave to be transformed, i.e. to be repolarized. Hence, a reflected (scattered) polarized wave from an object such as a radar target must contain some innate information about the object. The interpretation of the behavior of these complex signatures (in particular the direction of the electric field vector of the reflected polarized radiation) is in effect a major objective in polarimetry. By its very nature, the “full polarimetric imaging” technique pro-

533) D. F. Barbe, “Charge–Coupled Devices,” Topics in Applied Physics, Vol. 38, Springer–Verlag, Berlin, 1980

534) J. A. Cox, “Signal–to–noise ratio dependence on frame time, time delay and integration (TDI), and pulse shaping,” Optical Engineering, May/June 1982, Vol. 21, No. 3, pp. 528–536

535) W. L. Wolfe, G. L. Zissis, “Time Delay and Integration in CCD Signal Processing,” The Infrared Handbook, prepared by the Environmental Research Institute of Michigan for ONR (US Navy), 1978, pp. 12–66 and 12–28

vides the total information content of a scene, far more than the conventional “intensity imaging” scheme can do, since it retrieves the full scattering matrix (without the loss of spatial or spectral resolution). Hence, polarimetry has the potential to improve the harvest of remotely sensed data considerably.

Polarimetric radiometry refers to microwave and optical observations (imagery) and interpretation of polarized microwave/optical emission from natural surfaces. Polarimetry can be used to identify materials and to distinguish samples from a cluttered background. – The polarimetric imaging technique represents an extension of the measurement of vertically and horizontally polarized microwave/optical brightness temperatures by considering, in addition, the third and fourth of Stokes parameters [Sir George Gabriel Stokes (1819–1903), British mathematician, Stokes’s theorem]. Collectively, the four Stokes parameters provide a complete characterization of the Gaussian–random electromagnetic field (scattering matrix).

The development of a full polarimetric optical imaging instrument technology is still in an early stage (complex and costly) at the start of the 21st century. It requires in particular substantial research efforts in high–speed and high–sensitivity detector technology. Examples of early instrument implementations are:

Airborne instruments: 1) PSR (Polarimetric Scanning Radiometer), a multi–channel conical–scanning instrument of NOAA/ETL (Boulder, CO) and Georgia Tech, flown since 1997, providing fully polarimetric imagery in the microwave and optical regions (see P.176). PSR is being used for post–launch satellite calibration and validation (underflights) of a variety of current/future spaceborne passive microwave sensors (like WindSat on Coriolis, AMSR–E on Aqua, SSMIS on DMSP, MIS and ATMS on NPOESS). 2) APMIR (Airborne Polarimetric Microwave Imaging Radiometer) of NRL provides four polarimetric channels. The first flight of APMIR took place in Dec. 2001.

Early examples of instruments with polarization capability on spaceborne platforms.

– POLDER (Polarization and Directionality of the Earth’s Reflectances) of CNES is flown on ADEOS (launch Aug. 17, 1996) and ADEOS–II (launch Dec. 14, 2002). POLDER is an example of a passive spaceborne multi–band polarimetric imaging radiometer in the optical region (use of telecentric lens, a rotating wheel supporting filters and polarizers, and a matrix CCD sensor). It measures the bidirectionality and polarization of the solar radiation reflected by the atmosphere: tropospheric aerosols (inversion of the physical properties); ocean color (accurate determination of sea surface reflectances); land surfaces (determination of surface BRDF and improvement in the correction of the surface bidirectional and atmospheric effects on vegetation indices).

– NICMOS (Near–Infrared Camera and Multi–Object Spectrometer) was installed on HST (Hubble Space Telescope) in 1997. It contains optical elements which enable high spatial resolution, high sensitivity observations of linearly polarized light in the spectral range of 0.8 – 2.1 μm . The filter wheels for Camera 1 (NIC1) and Camera 2 (NIC2) each contain three polarizing elements sandwiched with bandpass filters. NICMOS is capable to retrieve three Stokes parameters, to derive the polarization intensity, the degree of polarization, and the position angle at each pixel.

– WindSat (Wind Microwave Radiometer) flown on the Coriolis mission (launch Jan. 6, 2003) of NRL, is a 22 channel fully polarimetric microwave instrument retrieving all four Stokes parameters by measuring the six principal polarizations (see A.12). WindSat is also considered a precursor instrument to MIS (Conical–scanning Microwave Imager/Sounder), a radiometric polarimeter to be flown on NPOESS (first launch in 2014).

– APS (Aerosol Polarimeter Sensor) is also flown on NPOESS to retrieve aerosol and cloud parameters (operational products) for climate research using multispectral photopolarimetry.

- Introduction of polarimetric measurements in the microwave (radar) region of the spectrum (retrieval of full scattering matrix).

SAR polarimetry (microwave region): In addition to measuring the amplitude of the radar return from a target, **a polarimetric radar measures the relative phase difference between the four linear polarizations**. This allows calculation of the target scattering matrix that can be used to optimize the polarization combination of radar for various applications. In fact, the new interpretation technique of **POLinSAR** (SAR Polarimetry and Polarimetric Interferometry) shows great potential for Earth surface analysis in such applications as forests canopies (biomass estimates), agriculture, ice, and other terrain types. The POLinSAR approach combines the analysis of polarization of SAR signals (polarimetry) with those for the analysis of phase differences between signals and to measure differential range (interferometry) using two or more images captured by SAR instruments. Taken together, polarimetry and interferometry offer the potential to summarize Earth surface characteristics in three dimensions with color. ^{536) 537) 538) 539)}

First airborne radar (SAR) polarimeters started to be flown in the time frame 1988 to 1990 with such instruments as C/X–SAR (CCRS), ARMAR (NASA/JPL), DO–SAR (Dornier), HUTSCAT (HUT), MMW–SAR (MIT/LL), NUSCAT (NASA/JPL), P–3/SAR (ERIM), IMARC (NPO Vega), and RAMSES (ONERA).

Spaceborne polarimetric data were obtained from the L/C–band SAR (NASA/JPL) of the SIR–C/X–SAR Shuttle missions (SRL–1 in April 1994, SRL–2 in Sept/Oct. 1994). Further spaceborne missions with polarimetric SAR instruments are: Envisat with ASAR, ALOS with PALSAR (launch Jan. 24, 2006, polarimetric mode on an experimental basis), RADARSAT–2 with SAR (launch Dec. 14, 2007), TerraSAR–X with TSX–SAR (launch June 15, 2007). See also Table 19.

1.5.4 FTS (Fourier Transform Spectrometer) instruments

FTS is a powerful observation technique which can be applied to the entire optical region extending from 0.01 – 1000 μm , i.e., from the UV to the FIR region inclusively, providing high spectral resolution and sensitivity for remote–sensing applications [conceptually, the FTS observation technique may of course also be applied to the microwave region]. FTS offers a very high throughput, or *étendue*, which is largely independent of the wavelength of the incident radiation. FTS at long wavelengths has obvious utility in two domains which are beyond the reach of standard heterodyne receivers: a) spectral measurements over very wide wavelength intervals, and b) observations of very broad individual spectral lines. Early FTS implementations suffered from the available detector technology. However, at the start of the 21st century, the FTS technology is very attractive for many remote–sensing applications due to the availability of a vastly improved detection technology, and onboard computational power.

The FTS method measures the interference pattern (i.e., the interferogram) as detector output (an intermediate product) which requires a Fourier transformation to obtain the measured radiance spectrum. The spectral resolution is governed by the OPD (Optical Path

- 536) Y. Kim, J. van Zyl, “On the Relationship between Polarimetric Parameters,” Proceedings of the IEEE/IGARSS 2000 Conference, Honolulu, HI, July 24–28, 2000
- 537) POLinSAR 2003 Workshop on Application of SAR Polarimetry and Polarimetric Interferometry,” ESA Earth Observation Quarterly, June 2003, pp. 16–18
- 538) W.–M. Boerner, A. Moreira, K. Papathanassiou, I. Hajnsek, E. Pottier, L. Ferro–Famil, A. Reigber, S. Cloude, M. Sato, Y. Yamaguchi, H. Yamada, J.–S. Lee, T. Ainsworth, D. Schuler, R. Touzi and T. Lukowski, “Need for Developing Multi–Band Single and Multiple Pass POLinSAR Monitoring Platforms in Air and Space,” Proceedings of IGARSS 2003, Toulouse, France, July 21–25, 2003
- 539) G. Krieger, K. Papathanassiou, S. Cloude, A. Moreira, H. Fiedler, M. Völker, “Spaceborne Polarimetric SAR Interferometry: Performance Analysis and Mission Concepts,” POLinSAR Workshop 2005, Jan. 17–21, 2005, ESA/ESRIN, Frascati, Italy, http://earth.esa.int/workshops/polinsar2005/participants/182/paper_PolInSAR_frascati_2005_15Feb05.pdf

Difference). A comparison of FTS instrument technology with that of a conventional dispersive spectrometer brings out the following points:

- The throughput of an FTS instrument can be orders of magnitude greater than that of a dispersive spectrometer. Both methods have the capability to provide “hyperspectral data”
- The spectral resolution of an FTS instrument is usually much better than that of a dispersive spectrometer; it is in fact constant across the spectrum
- The frequency coverage of an FTS can be very large, 10:1 is routine. Dispersive spectrometers rarely cover more than 2:1
- FTS instruments generate the interferogram (a frame as an intermediate product). Split spectrometers offer the image cube (spatial/spectral) directly
- A high SNR occurs in the FTS concept due to the simultaneous observation of a wide spectral range. There is an increase in the accuracy of interferometry over dispersive spectrometry by a factor of square root ($N/2$), where N is the number of samples taken. The SNR advantage is particularly noticeable for low-energy conditions or where scale expansion is required to bring out very weak signals.

A disadvantage of traditional spaceborne FTIR (Fourier Transform Infrared) spectrometers is that they obtain their optical delay by physically translating one or more optical components – the instrument has to go through all OPD positions to complete the measurement cycle of strokes (as discussed in chapter 1.4.2.1). This so-called translation mechanism usually dominates the risk, cost, power consumption, and performance of such FTS instruments

- Introduction of FTS (Fourier Transform Spectrometer) technology⁵⁴⁰⁾ in sensor development, usually in combination with an interferometer (Michelson, Sagnac, Fabry–Perot, Fizeau, etc.) for the measurement of the composition of the atmosphere (trace gases, air pollution monitoring, monitoring of accidental releases of toxic gases at industrial plants, etc.). See Tables 39 and 40 as well as chapter O.6.

The first spaceborne FTS instrument [sometimes also referred to as FTIR (Fourier Transform Infrared) spectrometer, due to the fact that most observation occurs in the IR region observing the Earth’s thermal emissions] flown in Earth observation was **IRIS** (Infrared Interferometer Spectrometer), a Michelson interferometer on Nimbus–3 (launch April 14, 1969) and on Nimbus–4 (launch April 8, 1970), followed by SI–1 (also referred to as SI–GDR) and SI–2 aboard the USSR satellites Meteor 25 (also referred to as Meteor–Priroda–2, launch May 15, 1976) and Meteor 28 (also referred to as Meteor–Priroda–3, launch June 29, 1976). **ATMOS** of NASA/JPL was an FTS sensor flown on the Shuttle (STS–17) in 1985. **Mark–IV** of JPL collected first ground-based spectra in April 1985, in 1987 the sensor was flown on a balloon and in aircraft campaigns.^{541) 542)}

- In Table 40, **FTHSI** (Fourier Transform Hyperspectral Imager) of AFRL represents the first spaceborne instrument using a **spatially modulated scheme**. to obtain an instantaneous spatial and spectral interferogram. The optical instrument design concept overcomes the complexities of conventional interferometers (of sequential OPD generation) by splitting the input beam of the target into two mutually coherent beams that interfere and generate a spatially modulated (instantaneous) interference pattern that is recorded as an interferogram by a detector array (the amplitude of the interference pattern depends on the path difference). An image cube is formed by assembling the contiguous pushbroom stripes (in

540) M. J. Persky, “A review of spaceborne infrared Fourier transform spectrometers for remote sensing,” *Review of Scientific Instruments*, Vol. 66, No. 10, October 1995, pp. 4763–4797

541) V. Kempe, D. Oertel, R. Schuster, H. Becker–Ross, H. Jahn, “Absolute IR–spectra from the measurement of Fourier spectrometers aboard Meteor 25 and 28,” *Acta Astronautica*, Vol. 7, 1980, pp. 1403–1416

542) H. Buijs, “History of Fourier Transform Spectrometer Technology Development,” *Proceedings of the 26th ISTS (International Symposium on Space Technology and Science)*, Hamamatsu City, Japan, June 1–8, 2008

the cross-track) produced by the forward motion of the spacecraft to create the second spatial dimensions of data. Hence, each pixel element of a single pushbroom imaging action contains the spatial as well as the complete spectral information, collected simultaneously (i.e. within the dwell time of each stripe) across the entire imaging stripe. – The method of a spatially modulated interferometer (of simultaneous interferogram availability at the detector plane) is directly analogous to the imaging of the spectrum onto the detector array in a dispersive spectrometer. See also M.24.2 and O.6.2.

Some historical background on spatially modulated interferometers. The first spatially modulated interferometer was the one made in 1801/2 by Thomas Young (see O.9). However, the first “modern form” of Young’s interferometer was the one developed in 1965 by G. W. Stroke and A. T. Funkhouser. They replaced Young’s double slit with a beam splitter and they generated a spatially varying OPD (Optical Path Difference) by tilting the two mirrors in the arms of a Michelson interferometer. The two tilted wavefronts were focused onto a photographic plate to record the interference pattern. Another practical spatially modulated Sagnac interferometer design was developed by K. Yoshihara and A. Kitade of Japan in 1967. They were the first to generate static fringes at a pupil plane by using the triangle-path Sagnac interferometer. In 1984, T. Okamoto, S. Kawata and S. Minami were the first to use a digital detector array to scan the static interferogram. Since that time there have been many groups building static interferometers, all using variations of conventional interferometer layouts (Michelson, Sagnac, Mach–Zehnder, Wollaston Prisms, etc.).^{543) 544) 545) 546)}

A fairly early modern spatially modulated interferometer is SMIFTS (Spatially Modulated Imaging Fourier Transform Spectrometer), an airborne instrument developed at the Hawaii Institute of Geophysics and Planetology of the University of Hawaii at Manoa, and sponsored by the Office of Naval Research (ONR) and by DARPA. (see P.194). SMIFTS was first flown on a helicopter in March 1994.

Sensor	Aircraft, Platform	Spectral Range	Observation Direction	Start of Operation Comments
HIS (U. of Wisconsin)	ER-2	3.6–4.63 μm 5.1–9.6 μm 9.3–16.4 μm	Nadir viewing	1986
FIRS-2 (SAO)	Balloon	14–25 μm 48–125 μm	Limb viewing	1987
MkIV (JPL)	Balloon, DC-8	1.8 – 16 μm	Limb and zenith	1987
MIPAS-FT (KfK)	Transall	7.4 – 8.7 μm 10.0 – 13.2 μm	Limb viewing	1991
MIPAS-B (KfK)	Balloon	7.25–8.45 μm 10.3–13 μm	Limb viewing	1992
SMIFTS (U. of Hawaii)	Helicopter	1.0–5.2 μm	Nadir	1994
AES (JPL)	DC-8, P-3	2.4–15.4 μm	Nadir viewing	1994
FTS (NPL)	BAe Jetstream	3–13 μm		1994
FTVHSI (Kestrel)	Cessna TU-206	0.44–1.15 μm	Nadir viewing	1995
MIPAS-B2 (FZK)	Balloon	5.25–5.48 μm 6.0–6.36 μm 7.4–8.8 μm 10.2–13.2 μm	Limb viewing	1995

543) K. Yoshihara, A. Kitade, “Holographic spectra using a triangle path interferometer,” Japan. Journal of Applied Physics, Vol. 6, 1967, p.116

544) T. Okamoto, S. Kawata, S. Minami, “Fourier Transform Spectrometer With a Self-Scanning Photodiode Array,” Applied Optics, Vol. 23, Jan. 1984, pp. 269–273.

545) Information provided by Francis M. Reininger of NASA/JPL, Pasadena, CA

546) G. W. Stroke, A. T. Funkhouser, “Fourier-Transform Spectroscopy Using Holographic Imaging Without Computing and with Stationary Interferometers,” Phys. Letters, Vol 16, 1965, pp. 272–274

Sensor	Aircraft, Platform	Spectral Range	Observation Direction	Start of Operation Comments
MIPAS-STR (FZK)	Strato-2C	5.15 – 5.42 μm 6.08 – 6.31 μm 7.30 – 8.33 μm 10.0 – 13.0 μm	Limb viewing	1996
MIROR (DLR)	VFW 614	2–18 μm	Aircraft jet engine	1995 (trace gas emissions)
SAFIRE-A (CNR/IROE)	Balloon, M-55 Geophysika	62.5–125 μm 20–350 μm future	Limb viewing	1996, polarizing FTS
UAV-AERI (U. of Wisconsin)	Perseus-A	3–25 μm	Nadir viewing	1996

Table 39: Survey of airborne Fourier Transform Spectrometer (FTS) instruments

- In 2000, NASA/JPL developed a new type of imaging interferometer featuring double the efficiency of conventional interferometers and only a fraction of the mass and volume; the instrument is referred to as SMPI (Spatially Modulated Prism Interferometer). SMPI overcomes the complexities of traditional interferometers and the inherent limitations of diffraction gratings, dispersion prisms, and spectral selection filters. The design employs a prism triplet (a single-crystal material to maintain the same optical path length for both beams) providing 100% throughput of radiation. Applications include atmospheric sounding, geologic mapping, in-situ mineralogy, oceanography, pollution monitoring, poisonous gas detection, medical spectroscopic imaging, and industrial inspection. See O.6.2.

- **The first FTS instrument to be flown in geostationary orbit is GIFTS (Geostationary Imaging Fourier Transform Spectrometer) on EO-3 (Earth Observing-3), a NASA/NOAA/DoD technology demonstration mission within NASA's NMP with a planned launch in 2006 (see M.13). GIFTS is in effect an infrared hyperspectral sounder and imager (spectral resolution: 0.6 cm^{-1} ; spectral range: MWIR = $4.4\text{--}6.06 \mu\text{m}$, TIR = $8.85\text{--}14.6 \mu\text{m}$). In parallel, a low visible light sensitive boresighted camera, using 512×512 active pixel detector arrays (APS), provides quasi-continuous imaging of clouds at 1 km spatial resolution. The GIFTS infrared measurement concept combines a number of advanced technologies, including LFPA [Large-area format Focal Plane detector Arrays (128×128)] and a compact, light-weight Fourier Transform Spectrometer (FTS) enabling atmospheric radiance spectra to be observed simultaneously for all LFPA detector elements, thereby providing high vertical resolution temperature and moisture sounding information.^{547) 548)} The GIFTS design offers high sounding resolutions, about 1–2 km in vertical resolution (for temperature and water vapor profiles) using rapid profile retrieval algorithms. The profiles are obtained on a 4 km grid over an instantaneous target area of $512 \text{ km} \times 512 \text{ km}$ within a 10 s time interval (representing a single frame). Extended Earth coverage is achieved by step scanning the instrument FOV (Field of View) in a contiguous fashion across any desired portion of the visible Earth disk from GEO (the full disk or a regional map can be constructed from individual data frames; the seamless coverage of the Earth's disk is made up of a frame matrix of 25×25). A star tracker provides real-time pointing information for GIFTS. The FOR (Field of Regard, $24^\circ \times 24^\circ$) dwell period of GIFTS will range between 0.125 and 11.0 s per frame, depending on the observation application (i.e., imaging or sounding).**

The FTS approach for GEO satellite applications allows spectral resolution to be easily traded for greater area coverage or higher temporal resolution. – Dynamic observations of temperature, water vapor, wind profiles (with accuracies of 1 K, 15%, and 3 m/s, respective-

547) W. L. Smith, H. E. Revercomb, G. Bingham, H.-L. Huang, D. K. Zhou, C. S. Velden, J. B. Miller, G. D. Emmitt, "GIFTS – Hyperspectral Imaging and Sounding from Geostationary Orbit," 20th International Conference on Interactive Information and Processing Systems (IIPS) for Meteorology, Oceanography, and Hydrology, Seattle, WA, Jan. 11–15, 2004

548) S. S. Limaye, T. Smith, R. O. Knuteson, H. E. Revercomb, "Geolocation of the Geosynchronous Imaging Fourier Transform Spectrometer (GIFTS) Data," 20th International Conference on Interactive Information and Processing Systems (IIPS) for Meteorology, Oceanography, and Hydrology, Seattle, WA, Jan. 11–15, 2004

ly), SST (Sea Surface Temperature) and emissivity, LST (Land Surface Temperature) and emissivity, enable a better understanding of climate physics, hydrology and the water cycle, the transport of chemical species, and weather processes. The GIFTS data have the potential to offer considerable advancement in meteorological observation capability which is expected to have dramatic impacts on weather forecasting capability. For example, the ability to observe water vapor flux and convergence and divergence patterns should enable meteorologists to view the formation of storm systems before clouds and rainfall are produced. – The GIFTS instrument will serve as the prototype of sounding systems to fly on future operational GEO satellites of NOAA. – Infrared hyperspectral sounding instruments with broad spectral coverage have the potential to provide unprecedented atmospheric profiling, surface characterization, cloud property and trace gas information.

Note: as of 2004 the launch of the GIFTS mission became uncertain due to DoD funding problems (Navy).

Sensor	S/C or Platform	Spectral Range	Observation Direction	Start of Operation Comments
IRIS, (NASA/GSFC)	Nimbus-3 Nimbus-4	5 – 20 μm 6.25 – 25 μm	Nadir viewing	launch, Apr. 14, 1969 launch, Apr. 8, 1970
SI-GDR (IKF)	Meteor-P-2 Meteor-P-3 Meteor-P-4	6.25 – 25 μm	Nadir viewing	launch, May 15, 1976 launch, Jun. 29, 1977 launch, Jan. 25, 1979
ATMOS (NASA/JPL)	Spacelab-2, -3, ATLAS-1, -2, -3	2.2–16.0 μm	Limb viewing	1985, (2) 92, 93, 94
CIRRIS (DoD/USAF)	STS-39 Shuttle Discovery	2.5–25 μm	Limb viewing	Apr. 28 – May 6, 1991
IMG (NASDA, JAROS)	ADEOS	3.3–16.7 μm	Nadir viewing	launch, Aug. 17, 1996
MIRIAM (Free U. of Berlin)	MIR/Priroda	2.5–20 μm	Limb viewing	1996
SPIRIT-III (BMDO, USU)	MSX	2.5–28 μm	Limb viewing	launch, Apr. 24, 1996 FTS+scanning radiometer
FTHSI (AFRL, Kestrel Corp.)	Mightysat II.1	0.475–1.05 μm	Nadir viewing	launch July 19, 2000.
MIPAS (ESA,FZK)	Envisat	4.15–14.6 μm	Limb viewing rear-wards & sideways	launch Mar. 1, 2002
ACE-FTS (CSA) ACE-VNIR (CSA)	SciSat-1/ACE	2–14 μm 0.5–1 μm	Limb viewing	launch Aug. 13, 2003
TES (JPL)	Aura (EOS/ Chem-1)	2.3–15.4 μm	Limb or nadir viewing	launch July 15, 2004
IASI (CNES/ASI)	MetOp-A	3.62–15.5 μm	Nadir viewing	launch Oct. 19, 2006
TANSO-FTS (JAXA)	GOSAT	0.75–14.3 μm	Nadir viewing	launch Jan. 23, 2009
CrIS (IPO)	NPP (NASA) NPOESS	4.63–15.3 μm SWIR-TIR	Nadir viewing	Launch Oct. 28, 2011 launch 2014
GIFTS (NASA/LaRC)	EO-3	IR (4–14.6 μm)	Nadir viewing (directional)	launch in ??? (observation from GEO)

Table 40: Survey of spaceborne Fourier Transform Spectrometer (FTS) instruments

1.5.5 Onboard radiometric sensor calibration

The goal of any calibration procedure is to determine a functional relationship between the target source flux and the sensor output signal. Instrument calibration provides a means for consistent long-term data set interpretation by reducing the assumptions to be made (see O.2 and Glossary). All instrument calibration involves generally extensive pre-flight calibration as well as repeated in-flight (or onboard) calibration in various time intervals. The

discussion here is limited to onboard calibration. Most successful onboard calibration approaches employ a number of various targets including onboard calibrators, space targets (views to deep space, the sun, the moon, the stars, etc.), and/or ground targets (the reflectance-based approach relies on surface reflectance measurements of a selected site). All of these targets or calibrators have the objective to provide the instrument with a known reference. Many of these onboard calibration techniques are described with the sensor documentation of the various projects in the book.

The very early spaceborne instruments (cameras) didn't provide a calibration capability. But the need for onboard calibration became evident from the very start of regular observations. Today's sensor calibration involves usually comparing the detector of a particular spectral range against a known reference. For the VNIR region, a calibration source may be internal lamps or the sun (external source). In the infrared region, a suitable calibration reference may be an internal black body or an external source like deep (cold) space that may be viewed periodically. A calibration 'period' may be a scan sequence, each orbital eclipse period, the pass over a **dedicated ground calibration site**, or it may be a month or more, depending on need or opportunity. Some sensors employ several calibration techniques (for instance: GOME on ERS-2 retrieves ozone distributions by exploiting the traditional backscatter calibration approach, as well as by differential optical absorption spectroscopy). The ETM+ sensor on Landsat-7 uses three independent onboard calibration systems [the two new systems are: FAC (Full Aperture Calibrator), and PAC (Partial Aperture Calibrator), the ETM+ calibration system is a diffuser], representing a significant step forward in absolute radiometric calibration accuracy. The radiometric calibration of these systems not only helps characterize the operation of the sensors, but, more importantly, this calibration allows the full Landsat data set (the Landsat project has the longest data set of imagery anywhere since 1972) to be used in a quantitative sense for such applications as land use and land cover change.⁵⁴⁹⁾

Long-term studies such as those needed for documenting and understanding global climate change require not only that a remote sensing instrument be accurately characterized and calibrated, but also that its characteristics and calibration be stable over the life of the mission.

A major (ideal) objective of the calibration of a sensor type (imager, radiometer) is to make the measurements independent of the instrument. This means that when a particular physical entity is to be measured at different times and places or with different instruments, the results should always be the same. It also means that attributes inferred by the measurements are target attributes and not instrument attributes.

- Another (rather costly) method of data calibration occasionally employed is that of airborne underflights of spaceborne missions. Many spaceborne sensors (in particular since the 1980s) have their airborne predecessors, which makes underflight calibrations a natural extension for independent parameter checks. Very important observations of a mission (proving a concept, etc.) are usually verified with parallel campaigns to compare spaceborne, airborne and ground-based observations. An example of such a scenario are the SRL-1/2 (Space Radar Laboratory) missions in 1994 (see SRL Campaigns). ESA's ERS-1 and Envisat missions are further examples of extensive underflight campaigns in the commissioning phase (prior to mission operations). A very special instrument among the airborne underflight sensors is NASIC (P.154), operated by NASA/GSFC since 1988 (built in 1980), capable of providing independent calibration data for several long-term satellite sensors, such as: AVHRR (on several NOAA satellites), TM (Landsat), VAS (GOES satellites), and CZCS (Nimbus-7).

⁵⁴⁹⁾ K. J. Thome, "Ground-Look Radiometric Calibration Approaches for Remote Sensing Imagers in the Solar Reflective," Pecora 15/Land Satellite Information IV Conference, ISPRS Commission I Mid-term Symposium/FIEOS (Future Intelligent Earth Observing Satellites), Nov. 10-14, 2002, Denver, CO

- **MOBY (Marine Optical Buoy)** see P.145. MOBY is an important ocean–based remote sensing calibration station of NOAA, funded by NASA and NOAA, and deployed off the coast of Lanai, Hawaii, in 1994. Its primary objective is to function as a calibration standard in support of spaceborne ocean color instruments. Typically, these instruments measure the received radiance in selected wavelength intervals from 410 to 870 nm to derive ocean color products such as the phytoplankton distribution of the ocean surface. However, the path of the radiance arriving at the spacecraft is very much dominated by atmospheric contributions. As it turns out, these ocean color sensors cannot be calibrated with sufficient accuracy before launch to meet the requirements for climate quality data products. Consequently, the calibration of ocean color instruments is performed during the mission with in situ spectral measurements of water–leaving radiance. MOBY is a 14 m long buoy system instrumented to measure upwelling radiance and downwelling irradiance at the sea surface and at three deeper depths. Examples of the MOBY instrument calibration services are: SeaWiFS, MODIS, OCTS, POLDER, MOS, GLI, etc. The MOBY calibration reference is a key element in the international effort to develop a global, multi–year time series of consistently calibrated ocean color products using data from a wide variety of independent satellite sensors. ^{550) 551) 552) 553)}
- **Microwave radiometer calibration (absolute calibration).** The SSM/I instrument, flown on the DMSP series since 1987, introduced a so–called “external calibration scheme” a total–power radiometer configuration, each scan consists of a cold reading, a warm load reading, and the scene stations. ⁵⁵⁴⁾ The cold reading utilizes a view to deep space (3 K black body radiation), the warm load temperature is variable over an orbit. Some other radiometer implementations employing the same technique are: SSM/T–2 (Special Sensor Microwave Water Vapor Profiler–2) first flown on DMSP F–11 (launch Nov. 28, 1991) and thereafter; TMI (TRMM Microwave Imager) on TRMM (launch Nov. 27, 1997); MTVZA (Microwave Imaging/Sounding Radiometer), a 26 channel conical–scanning microwave imager/sounder in the range of 10.6–183.3 GHz on Meteor–3M–1 (launch Dec. 10, 2001); AMSR–E (Advanced Microwave Scanning Radiometer–EOS) on Aqua (launch May 4, 2002); AMSR on ADEOS–II (launch Dec. 14, 2002); and SSMIS (Special Sensor Microwave Imager Sounder), first flown on F–16 of the DMSP series (launch Oct. 18, 2003).
- **Silicon photodiode self–calibrating technique.** This technique became common in the 1980s permitting the development of 100% quantum–efficient silicon radiometers. In the 1990s, absolute cryogenic radiometers have become common in many national laboratories. ⁵⁵⁵⁾
- The use of ground test sites for post launch calibration has continued to expand over the years – calling for the provision of an **online ground test site catalog**. As of 2007, the USGS (United States Geological Survey) is working with partner organizations around the world to accumulate an online catalog of ground test sites on a global scale – in support of post–launch characterization and calibration of spaceborne optical imaging sensors. This service is considered vital to achieve an integrated Global Earth Observation System of Sys-

550) B. C. Johnson, S. W. Brown, N. Souaidia, M. E. Feinholz, M. Yarbrough, S. Flora, D. C. Clark, “New Technologies for Radiometry: Impact on Ocean Color Research,” Proceedings of ISRSE, Nov. 10–14, 2003, Honolulu, HI

551) D. Herring, “MODIS/SeaWiFS Team Deploys Marine Optical Buoy, Continues Marine Optical Characterization Experiment,” The Earth Observer, NASA, Vol. 6, No. 1, January/February 1994, pp. 17–22

552) <http://physics.nist.gov/Divisions/Div844/news/mgcc.html>

553) H. R. Gordon, “In–orbit calibration strategy for ocean color sensors,” Remote Sensing of the Environment, Vol. 63, 1998, pp. 265–278.

554) Note: The total–power observation/calibration scheme compares the atmospheric signal to the cold and hot loads.

555) Y. Ohno, “Recent Developments in Detector–Based Photometry and Future Needs in Photometry,” Proceedings of CIE Symposium ’99 – 75 Years of CIE Photometry, Budapest, 1999; also at URL: physics.nist.gov/Divisions/Div844/facilities/photo/Publications/CIE_Sympo99.pdf

tems (GEOSS) for coordinated and sustained observations of Earth. The online catalog can be accessed at: http://calval.cr.usgs.gov/sites_catalog_map.php⁵⁵⁶⁾

– The test site catalog provides a comprehensive list of prime candidate terrestrial targets for consideration as benchmark sites for the postlaunch radiometric calibration of space-based optical sensors. The online test site catalog provides easy public Web site access to this vital information for the global community. – The incompleteness of available information on even these prime test sites is an indication that much more coordination and documentation are still needed to facilitate the wider use of calibration test sites in remote sensing.⁵⁵⁷⁾

– For ten months of the year Tuz Golu (Lake Tuz) in southern Turkey appears to be like any other lake. However, during July and August it dries to become a bright, pristine, white surface, which is ideal for calibrating Earth observation satellites. – Tuz Golu is one of eight sites recently (2010) endorsed by the Committee on Earth Observation Satellites (CEOS) to become an international reference standard to evaluate satellites' sensor-to-sensor biases, and also to calibrate/validate their radiometric performance.⁵⁵⁸⁾

For the CEOS reference standards sites to be of use, their radiometric characteristics (as measured by ground teams) must be consistently evaluated and, of course, traceable to SI Units. The National Physical Laboratory (NPL) of the UK, with funding from both the European Space Agency (ESA) and the National Measurement Office, has led international efforts to achieve this (Ref. 558).

Consistent data quality implies the adherence of data to appropriate standards of fidelity to the underlying physical quantities that they measure. These well-calibrated data then assure the accuracy and enhance the intercomparability that enables the development of advanced Earth observation technologies beneficial to user communities.

1.5.6 Lightning detection instruments (event-based monitoring)

Lightning in the atmosphere is a transient, high-current carrying electric discharge event. It occurs when some region of the atmosphere reaches an electric charge sufficiently large so that the electric fields associated with the charge cause an electric breakdown in the air.^{559) 560)} The optical detection of lightning events is based on the imaging of a specific spectral oxygen multiplet, which is excited during the lightning event. The lines are a triplet located at 777.4 nm, consisting of lines at 777.19 nm, 777.42 nm and, 777.54 nm.

• Early detections of optical emissions^{561) 562)} by a spaceborne satellite of terrestrial lightning were first made by NASA's OSO-2 (Orbiting Solar Observatory) with a launch Feb. 3, 1965. Since that time, additional optical observations of lightning have been made by the OSO, Vela, the spacecraft of the DMSP (Defense Meteorological Satellite Program) series, and the GPS satellite series. The Vela (detection of super bolts on Sept. 22, 1979), DMSP and GPS observations provided a time history of optical pulses produced by light-

556) G. Chander, J. B. Christopherson, G. L. Stensaas, P. M. Teillet, "Online Catalog of World-Wide Test Sites for the Post-Launch Characterization and Calibration of Optical Sensors," Proceedings of the 58th IAC (International Astronautical Congress), International Space Expo, Hyderabad, India, Sept. 24-28, 2007, IAC-07-B1.1.08

557) Gyanesh Chander, "Catalog of Worldwide Test Sites for Sensor Characterization Catalog Characterization," March 18, 2009, URL: <http://calval.cr.usgs.gov/PDF/sites.pdf>

558) "Measuring Salt Shine To Improve Climate Understanding," Space Daily, Aug. 17, 2010, URL: http://www.space-daily.com/reports/Measuring_Salt_Shine_To_Improve_Climate_Understanding_999.html

559) S. K. Jain, V. P. Singh, "Lightning Paths in Sky Share Similarities with Channel Networks on Earth," EOS Transactions, AGU, Vol. 85, No 26, June 29, 2004

560) NIST Atomic Spectra Database Lines, Data, http://physics.nist.gov/cgi-bin/AtData/main_asd

561) http://www.agu.org/pubs/sample_articles/ae/2000JD000190/1.html

562) B. N. Turman,, "Analysis of lightning data from the DMSP satellite," Journal of Geophysical Research, Vol. 83, 1978., p. 5019

ning.⁵⁶³⁾

- Systematic spaceborne lightning studies were initiated by NASA/MSFC in the 1980s by using cameras aboard the Space Shuttle to make striking images of lightning from above the cloud tops. Later instruments on spaceborne missions with event–based monitoring capabilities revealed the extent of global lightning activities. *Typically, more than 2,000 thunderstorms are active throughout the world at any given moment, producing on the order of 100 flashes per second (or > 8 million strikes/day).* The length and duration of each lightning stroke vary, but typically average about 30 ms. The average peak power per stroke is about 10^{12} W. An average bolt carries 20,000 A (ampere) of current, while the most powerful lightning bolts carry > 300,000 A. The most common types of lightning are: a) cloud–to–ground lightning, b) intra–cloud lightning, c) inter–cloud lightning.^{564) 565)}

The GHRC (Global Hydrology and Climate Center) in Huntsville, ALA, serves as the operational data processing and archive center for two satellite–based lightning instruments (OTD and LIS). Both instruments detect lightning in day and night conditions. Using the lightning detection software, the GHRC produces global daily, monthly, seasonal, and annual summaries of lightning strikes, providing the first truly global distribution maps of lightning. Lightning sensors in space and on the ground are showing the value of having a space–based network of sensors that could spot and track storms which are likely to spawn tornadoes.

- In the early 1980s, the NOSL (Night–time and daytime Optical Survey of Lightning) instrument of NASA/MSFC was flown in the Space Shuttle program on flights STS–2 (Nov. 12–14, 1981), STS–4 (Jun. 27–July 4, 1982) and STS–6 (Apr. 4–9, 1983).

- This was followed by MLE (Mesoscale Lightning Experiment) on Shuttle flights in the late 1980s (STS–26, Sept. 29– Oct. 3, 1988; STS–30, May 4–8, 1989; STS–34, Oct. 18–23, 1989; STS–32, Jan. 9–20, 1990). MLE used the Shuttle’s sensitive payload bay monochrome video cameras to record the Earth’s nighttime lightning activity from space. An analysis of the MLE video tapes positively identified two or three “upward lightning” events (i.e., **sprites**) in the stratosphere. The discovery of the phenomenon, now known as a sprite, was first documented on a video tape recorded the night of July 6, 1989 at the University of Minnesota (ground observations). The appearance of bright high–altitude flashes above thunderstorms have been reported by pilots for nearly a century.^{566) 567)}

- OLS (Operational Linescan System) of the DMSP weather satellite series of DoD is also able to detect lightning activity (data sets exist starting from 1973, see G.1.1).

- An airborne sensor with a capability for lightning detection is LIP (NASA/MSFC, an upgraded instrument as of 1990).⁵⁶⁸⁾

- Another spaceborne sensor with a capability for lightning detection/distribution is Blackbeard (an RF experiment), flown on ALEXIS of LANL and SNL (launch of ALEXIS April 25, 1993).

- The OTD (Optical Transient Detector) of NASA/MSFC has been flown on Orb–View–1/Microlab–1 (launch April 3, 1995, B.11). The instrument is capable to gather lightning data under daytime conditions as well as at night. OTD collected a five–year record of lightning observations between April 1995 and April 2000.

563) B. N. Turman, “Detection of Lightning Superbolts,” *Journal of Geophysical Research*, Vol, 82, 1977, p.:2566

564) Note: Benjamin Franklin performed the first systematic, scientific study of lightning during the second half of the 18th century.

565) A. F. Rivera, H. C. Koons, R. L. Walterscheid, R. Briet, “Protecting Space Systems from Lightning,” URL: <http://www.aero.org/publications/crosslink/summer2001/05.html>

566) W. L. Boeck, “The Role of the Space Shuttle Videotapes in the Discovery of Sprites, Jets and ELVES,” <http://thunder.msfc.nasa.gov/bookshelf/pubs/sprites.html>

567) <http://www.knology.net/~skeetv/myobs.htm>

568) <http://thunder.msfc.nasa.gov/ols/>

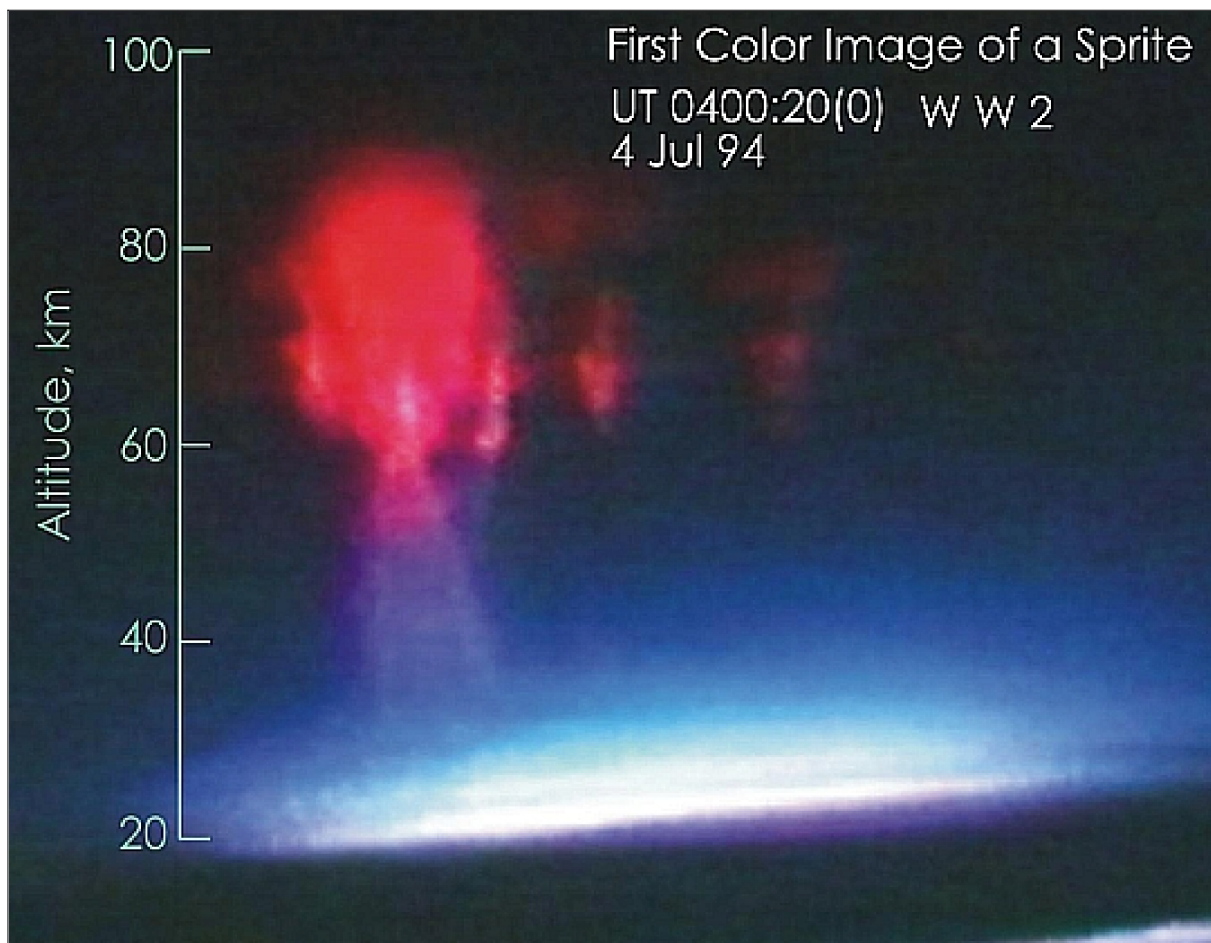


Figure 22: First color image sprite observed on July 4, 1994 (image credit: University of Fairbanks) ⁵⁶⁹⁾

- LIS (Lightning Imaging Sensor, NASA/MSFC) is flown on TRMM (launch Nov. 27, 1997, A.34). LIS is designed to study the distribution and variability of total lightning on a global basis. The staring imager which is optimized to locate and detect lightning with storm-scale resolution of 5–10 km over a large region (600 km x 600 km) of the Earth’s surface.
- FORTE: Simultaneous observations of optical and RF emissions (in the VHF spectrum) of lightning activity was observed with the instruments: OLS (Optical Lightning Subsystem) and the RF-System (an advanced RF impulse-detection system), and an event classifier, all flown on the FORTE spacecraft of LANL/SNL (launch Aug. 29, 1997, A.18). OLS detects, locates, and characterizes lightning flashes. The event classifier consists of a set of adaptive processors that can distinguish lightning from man-made electromagnetic signals. It is a key technology in detecting secret nuclear weapons tests. The FORTE instruments provided a long-term assessment (> 3 years) of several million lightning events. One of the major observations performed by FORTE are the so-called TIPP (Trans-Ionospheric Pulse Pairs) events, which are pairs of intense VHF electromagnetic energy pulses, the second one being the reflection of the first from the Earth’s surface. TIPPs are frequently associated with upper atmospheric discharges called “Sprites”, “Jets” and “Elves”, and with intense X-ray and gamma-ray energy bursts.
- The Andromède mission of CNES to ISS with a launch on Oct. 21, 2001 (on a Russian Soyuz-TM-33 flight) delivered LSO (Lightning and Sprite Observations) of CEA (Commissariat à l’Energie Atomique) with the objective to study emissions generated by light-

⁵⁶⁹⁾ Jason Major, “On the Hunt for High-Speed Sprites,” Universe Today, Aug. 23, 2012, URL: <http://www.universetoday.com/96984/on-the-hunt-for-high-speed-sprites/>

ning, sprites (very large luminous displays) and elves (rapidly moving optical flashes, <1 ms).

– The ROCSat–2/FormoSat–2 mission of NSPO (Taiwan, launch May 20, 2004) flies the instrument ISUAL (Imager of Sprite Upper Atmospheric Lightning) with the objective to observe the natural upward lightning discharge phenomena toward the ionosphere on top of the troposphere.

– The SpriteSat mission (45 kg) of Tohoku University (Japan) was launched on Jan. 23, 2009. The objective is to monitor transient luminous emissions (TLEs) in the upper atmosphere, called sprites. The payload consists of: LSI–1, –2 (Lightning Spectrum Imager–1, 2), WFC (Wide Field–of–view Camera), TGC (Terrestrial Gamma–ray Counter), Star Tracker (camera), and a VLF receiver.

– The Tatiana–2 mission (also spelling of Tatyana–2) is a cooperative international microsatellite science mission of the D. V. Skobel'syn Institute of Nuclear Physics (SINP) at the Lomonosov Moscow State University (MSU), Moscow, Russia (launch Sept. 17, 2009). Tatiana–2 is carrying the MTEL (MEMS Telescope for Extreme Lightning) instrument, designed and developed at the Ewha Womans University (EWU), Seoul, Korea. MTEL is equipped with a fast tilting MEMS micromirror array and MAPMT (Multi–Anode Photomultiplier Tube) photodetectors. The rapid tilting of the MEMS micromirror array and the fast response of the photo detectors to lights make the telescope capable of observing the space–time development of TLEs with a time resolution of 1,000 times better than CCD cameras.

– V–GLASS (VHF Global Lightning and Severe Storm) monitor is a proposed system of LANL (Los Alamos National Laboratory) to be flown on the upcoming Block–IIF/III GPS system in MEO. – The conceptual design of VGLASS is based on a similar VHF receiver of LANL flown on the GPS satellite SVN 54 (launch Feb. 15, 2001).⁵⁷⁰⁾

– A demonstration instrument, LMS (Lightning Mapper Sensor) of NASA/MSFC is planned to be flown on the next–generation GOES–R spacecraft (launch 2014) of NOAA. The LMS on GOES represents the first lightning instrument to monitor lightning from GEO, permitting the continuous observation of the electrosphere over dimensions ranging from the Earth's radius down to individual thunderstorms.⁵⁷¹⁾

– ASIM (Atmosphere–Space Interactions Monitor) is an instrument proposal of ESA (in Phase B as of 2006) to be flown on the Columbus External Platform Facility (CEPF) of the ISS (International Space Station). The objective is to observe TLEs (Transient Luminous Emissions) that occur in the Earth's upper atmosphere accompanied by thunderstorms in the lower atmosphere. These events are known as blue jets, sprites and elves, the phenomena were first observed in 1989 [MLE (Mesoscale Lightning Experiment) of NASA/MSFC on Shuttle flights]. Plans are to launch ASIM in the timeframe 2014 on the HTV vehicle of JAXA.^{572) 573)}

– EUMETSAT and ESA are developing the instrument LI (Lightning Imager)⁵⁷⁴⁾ designated to fly on the MTG–I (Meteosat Third Generation–I) series spacecraft in GEO (a launch is planned for 2018).

570) D. M. Suszcynsky, A. R. Jacobson, J. Linford, M. B. Pongratz, T. E. Light, X. Shao, "Global Lightning and Severe Storm Monitoring from GPS Orbit," URL: <http://ams.confex.com/ams/pdfpapers/81285.pdf>

571) <http://thunder.msfc.nasa.gov/>

572) Rosario Nasca, "The Columbus External Payload Facility (CEPF) and the ESA observation Payloads (SOLAR and ASIM)," Dec. 7, 2009, URL: http://esamultimedia.esa.int/docs/hsf_research/Climate_change_ISS_presentations/CEPF_Nasca.pdf

573) T. Neubert, I. Kuvvetli, C. Budtz–Jørgensen, N. Østgaard, V. Reglero, N. Arnold, "The Atmosphere–Space Interactions Monitor (ASIM) for the International Space Station," ILWS (International Living With a Star) Workshop 2006, Goa, India, Feb. 19–20, 2006

1.5.7 Some telescopes for optical instruments

TMA (Three Mirror Anastigmatic) telescope off-axis design method in optical instruments. The term ‘anastigmatic’ refers to lenses that are able to form approximately point images of target (object) points. The TMA concept provides within a slit-like wide FOV (Field of View) a **diffraction-limited performance** (this property is especially useful for pushbroom imaging spectrometers in remote sensing applications). TMA is normally the preferred optical design with emphasis on precise imaging applications. It also serves to provide flat image projections, free of first order aberrations. Normally, two of the mirrors are off-axis sections resulting in an obstruction-free aperture system.

Background: The first modern three-mirror telescope concept by M. Paul dates back to 1935. Paul recognized that a Mersenne telescope, a concave and convex paraboloid pair, was corrected for spherical aberration, coma and astigmatism. Knowledge of basic aberration theory led to a three-mirror design, corrected for these three aberrations, in which both the secondary and tertiary mirrors are spherical. J. G. Baker and R. V. Willstrop refined the Paul design in 1969 and 1984, respectively, to create telescopes with larger fields of view. ^{575) 576)}

Since 1980, an optimized optical telescope configuration is increasingly being used from a family of TMAs discovered by Dietrich G. Korsch of Korsch Optics, Inc., Huntsville, AL. ^{577) 578) 579)} The design uses a tertiary mirror to correct and relay a real Cassegrain image onto the final focal surface. Korsch designs a three-mirror telescope by applying aplanatic conditions (constant optical path length and the Abbé Sine condition) to two mirrors of his three-mirror system. The shape of the third mirror is then optimized to minimize all other aberrations. – Korsch telescopes are increasingly being introduced in various high-performance astronomical as well as in Earth observation instruments. Some examples of Korsch-type TMA instruments flown or considered in spaceborne EO missions are:

- OSA (Optical Sensor Assembly) is flown on Ikonos-2 of Space Imaging Inc. of Thornton, CO (launch Sept. 24, 1999). The TMA concept in combination with a Korsch-Cassegrain type telescope design.
- Hyperion and ALI (Advanced Land Imager) of the EO-1 (Earth Observing-1) mission of NASA (launch Nov. 21, 2000)
- The BHRC 60 (Ball High Resolution Camera 60) instrument of Ball Aerospace is flown on QuickBird-1 (launch Nov. 20, 2000)
- The MTI mission of DOE (LANL, SNL) with a launch March 12, 2000 is flying the MTI (Multispectral Thermal Imager) instrument
- OHRIS (OrbView High Resolution Imaging System) of ORBIMAGE is flown on OrbView-3 (launch June 26, 2003)
- JAMI (Japanese Advanced Meteorological Imager) of the MTSAT-1R mission mission of Japan (launch Feb. 26, 2005). JAMI features an off-axis TMA telescope.
- The RALCam1 (Rutherford Appleton Laboratory Camera 1) of the UK TopSat mission (launch Oct. 27, 2005). While the camera optics are capable of a 25 km FOV at 600 km altitude, a 15 km FOV was selected as a result of CCD and data throughput limits.

574) “Work proceeds on MTG,” EUMETSAT Image, Issue 34, May 2011, URL: http://www.eumetsat.int/Home/Main/AboutEUMETSAT/Publications/IMAGENewsletter/groups/cps/documents/document/pdf_image34_en.pdf

575) M. Paul, “Système Correcteurs pour Réflecteurs Astronomiques,” Rev. d’Optique, Vol. 14, 1935, pp. 169–202

576) R. N. Wilson, “Reflecting Telescope Optics I,” 1996, pp. 215–229, A&A Library, Springer-Verlag

577) D. Korsch, “Anastigmatic three-mirror telescope,” Applied Optics, Vol. 16, no 8, 1977, pp. 2074–2077

578) D. Korsch, “Design and optimization technique for three-mirror telescopes,” Applied Optics, Vol. 19, No 21, Nov. 1980, pp. 3640–3645

579) D. Korsch, “Comparison of large aperture telescopes with parabolic and spherical primaries,” Optical Engineering, Vol. 25, No 9, Sept. 1986

- The RSI (Remote Sensing Instrument), built by EADS Astrium SAS, France is flown on the FormoSat–2 mission of NSPO, Taiwan (launch May 20, 2004). RSI uses a TMA optics design with an all–reflective Korsch telescope of 600 mm aperture. The Pan camera of the THEOS spacecraft of GISTDA, Thailand (launch Oct. 1, 2008), built by EADS Astrium, uses a Korsch telescope of 600 mm aperture. The NAOMI imager of the AlSat–2A mission of CNTS, Algeria (launch July 12, 2010), built by EADS Astrium, uses a Korsch telescope of 200 mm diameter.
- The imager of the CNES Pleiades spacecraft, referred to as OHRI (Optical High–Resolution Imager), employs TMA concepts (launch in 2011) in combination with a Korsch telescope. The primary mirror has a diameter of 650 mm.

1.5.8 Adaptive optics (AO)

AO is a technology referring to the physical modification of components of an optical system for the purpose of compensating for the distortion of electromagnetic radiation (refractive index variations) as it passes through the turbulent atmosphere and the optical system.^{580) 581) 582)} In particular, infrared radiation is degraded by atmospheric turbulence to resolve fine detail by at least a factor of 10. Although the problem of aberration was long recognized in the field of optics (in particular in astronomy), two initial solutions were proposed by Horace W. Babcock (1953, USA) and by Vladimir P. Linnik (1957, USSR). They independently published papers with the conjecture that the aberrations caused by atmospheric turbulence could be corrected in real–time by (what became later known as) an “adaptive optical system.”^{583) 584)}

Principle: Adaptive optics is a technique which measures the wavefront phase errors generated by the variations in the index of refraction in the atmosphere and corrects the resulting image in real–time to achieve an angular resolution close to the diffraction limit of the telescope. For unresolved sources, adaptive optics attempts to put as many photons in as small an image area as possible, thus enhancing the image against the background, improving the resolution of spectroscopy, and allowing better interferometric imaging with a telescope array. For resolved sources, the improved resolution extends imaging to fainter and more complex objects.⁵⁸⁵⁾

AO systems unite several advanced technologies to remove noise from optical signals: precision optics, wavefront sensors, deformable mirrors, and lasers, tied together by high–speed control systems. Light entering an AO system is reflected off a special adaptive optical element called a deformable mirror that applies anti–noise to the beam, canceling aberrations on the incoming beam.

580) H. W. Babcock, “The possibility of Compensating Astronomical Seeing,” Publications of the Astronomical Society of the Pacific, Vol. 65, 1953, pp. 229–236

581) V. P. Linnik, “About a basic opportunity of reduction of influence of an atmosphere on the star image,” Optics and Spectroscopy, Vol. 25, No. 4, 1957, pp. 401–402

582) M. C. Roggemann, V. P. Lukin, V. E. Zuev, “Adaptive optics: introduction to the feature issue,” Applied Optics, July 20, 1998, Vol. 37, No. 21

583) P. M. Hinz, et al., “Imaging circumstellar environments with a nulling interferometer,” Nature Vol. 395, Sep. 17, 1998, pp. 251–253

584) G. Stix, “Shading the Twinkle,” Scientific American, Dec. 1998, p. 20

585) <http://www.pha.jhu.edu/~jlotz/aoptics/node4.html>

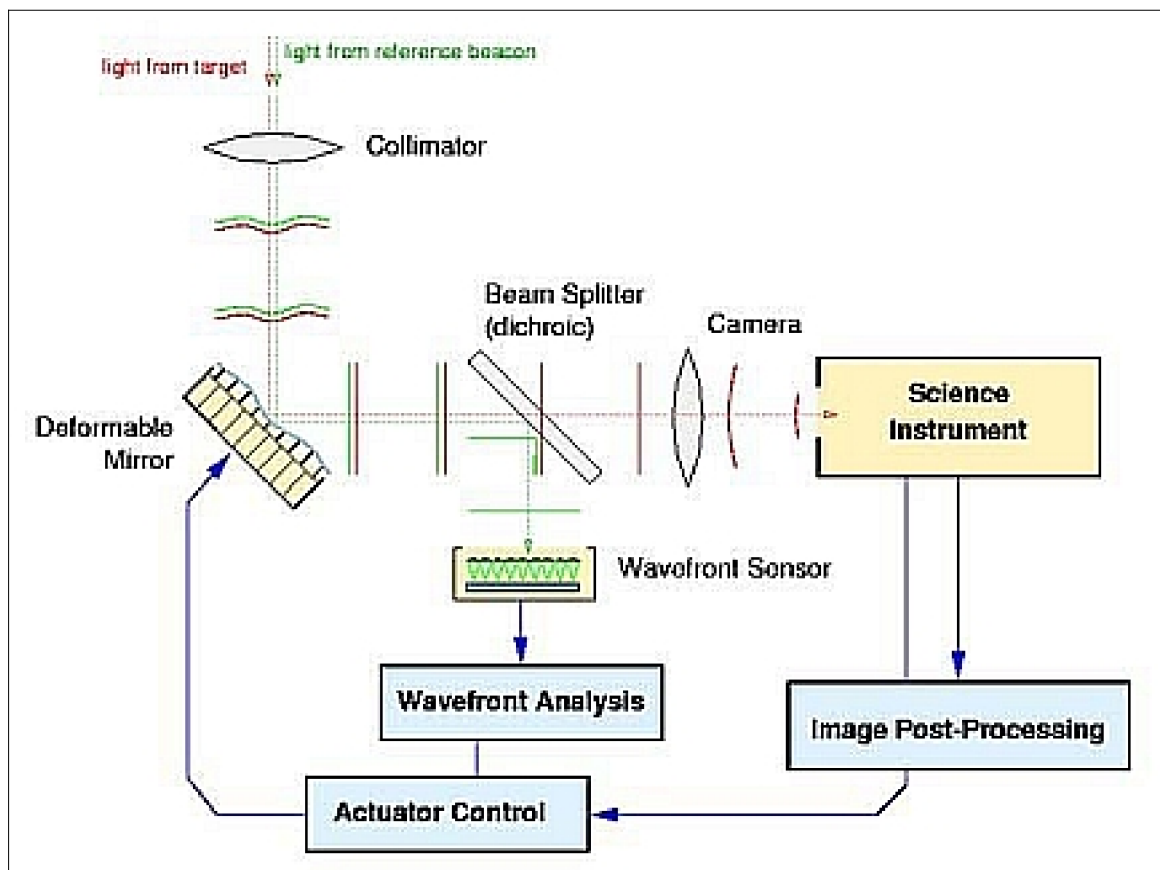


Figure 23: A typical adaptive optics system used in ground telescopes to correct image aberration due to atmospheric turbulence

Essential elements of an AO system are: a high-speed wavefront sensor (sensing the turbulence-induced aberrations), a thin flexible mirror whose surface can be electronically controlled to correct for aberrations, and a computer controller that converts the wavefront measurements into deformable mirror commands. The mirror is physically deformed in real-time by a large number of actuators (piezoelectric devices, liquid crystal devices, etc.). The device that measures the distortions in the incoming wavefront of light is called a “wavefront sensor” (analysis of wavefront, estimation of the shape of the original wavefront, derivation of the correction signals for the deformable mirror). High update rates are an essential ingredient for distortion removal. The MEMS technology is enabling the production of low-cost deformable mirrors. In addition, the APS/CMOS imaging technology permits the production of low-cost high-speed wavefront sensors. ^{586) 587) 588)}

Background: In the field of astronomy there exists already extensive experience in building large segmented actively controlled mirrors for ground-based telescopes. Astronomical imagery taken from ground-based Earth observatories equipped with AO rival the quality of those taken by the Hubble Space Telescope (HST) from outside the Earth’s atmosphere. This use of AO is the most revolutionary development in astronomy since Galileo Galilei invented the telescope in 1609–1611. These new ground-based astronomy telescopes have led the way in showing how to use adaptive optics to maintain figure (shape) at low temporal bandwidth in the presence of wind, gravity, and structural disturbances. Additionally, most ground-based systems also use these technologies to correct higher frequency

586) J. D. Mansell, “Commercialization of Adaptive Optics,” SPIE Annual Meeting 2002: Remote Sensing and Space Technology, Seattle, WA, July 7–11, 2002, SPIE Vol. 4825

587) R. K. Tyson, B. W. Frazier, M. Smith, “Robust control system for a compact modular adaptive optics system,” SPIE Annual Meeting 2002: Remote Sensing and Space Technology, Seattle, WA, July 7–11, 2002, SPIE Vol. 4825

588) S. R. Restaino, T. Martinez, J. R. Andrews, S. W. Teare, “On the characterization of Large Format LC devices for adaptive and active optics,” SPIE Annual Meeting 2002: Remote Sensing and Space Technology, Seattle, WA, July 7–11, 2002, SPIE Vol. 4825

effects from atmospheric turbulence. However, adaptive astronomical telescopes have a relatively narrow FOV (Field-of-View) of about 1 arcmin when compared with high-resolution Earth observing telescopes ($\sim 2^\circ$).

Some examples of installations using AO technology in the field of ground-based astronomy are:

- In the 1980's ESO (European Southern Observatory) developed a 1 m diameter, 20 mm thick active mirror which served as demonstration model for the 3.5 m diameter mirror of the NTT (New Technology Telescope) in operation in Chile since 1989.
- The SOR (Starfire Optical Range) at Kirtland AFB, Albuquerque, NM, houses two telescopes with adaptive optics systems: ⁵⁸⁹⁾ 1) the 1.5 m telescope was installed in 1991 (first operational AO system anywhere). 2) a 3.5 meter telescope equipped with adaptive optics. Both telescopes are of Cassegrain design, they are being used to develop methods for atmospheric compensation using adaptive optics and laser guide stars (they are also being used for satellite tracking). The first light on the 3.5 m telescope with the adaptive optics installed was achieved in September of 1997.
- In 1997, a 3.5 m telescope by the name of ALFA (Adaptive optics with a Laser For Astronomy system), a cooperative project of MPIA Heidelberg and MPE Garching, was installed at the Calar Alto Observatory in Almería (Southern Spain). The AO system of ALFA was developed by Adaptive Optics Associates, Inc. of Cambridge, MA, USA.
- In 1997/8, some demonstrations of the adaptive optics ⁵⁹⁰⁾ ⁵⁹¹⁾ technique were conducted in the field of astronomy with MMT (Multiple Mirror Telescope) Observatory on Mount Hopkins (AZ), a joint facility of the University of Arizona and the Smithsonian Institution (the MMT consisted of six 1.83 m telescopes in a common mount, a circle of 5.04 m diameter). – In Nov. 2002 and in Jan. 2003, astronomers were very successful in demonstrating the removal of atmospheric blurring with a new and integrated adaptive optics system in a flexible secondary mirror (2 mm thick) telescope of 6.5 m diameter (the adaptive optics system is part of the telescope).
- An adaptive optics system was introduced on the segmented 10 m primary mirror of the Keck Observatory on Mount Kea, Hawaii, in operation since 1999.
- The ground-based VLT (Very Large Telescope) interferometer of ESO uses four 8.2 m diameter, 175 mm thick segmented primary mirrors, controlled by 150 actuators. First light for the MACAO (Multi Application Curvature Adaptive Optics) of VLT at the Paranal Observatory, Chile, occurred on April 18, 2003. VLTI consists of four MACAO units. MACAO in turn consists of a 60 element curvature system (vibrating membrane, radial geometry microlenses, bimorph deformable mirror and Tip-Tilt mount). The wavefront sensor employs an APD (Avalanche Photodiode) detector. At present, just one of the four telescopes is equipped with AO, but plans call for the eventual addition of AO for all four telescopes. – Nothing less than a revolution in VLT interferometry is expected. An enormous gain in efficiency will result, because of the associated 100-fold gain in sensitivity of the VLT.
- The ground-based BBSO (Big Bear Solar Observatory), located in Big Bear Lake, California, high in the San Bernardino Mountains, features an adaptive optics off-axis telescope with a clear aperture of 1.6 m, referred to as NST (New Solar Telescope). First light of NST was achieved in the summer 2010 when sunspot images were taken with the atmospheric distortion corrected by its 97 actuator deformable mirror array. The BBSO facility is being owned and operated by NJIT (New Jersey Institute of Technology), the NST is providing a resolution of ~ 80 km on the sun's surface.

589) <http://www.de.af.mil/sor/>

590) G. Schilling, "Technique for Unblurring The Stars Comes of Age," Science, Vol. 286, Nov. 19, 1999, pp. 1504–1506

591) <http://www.spaceref.com/news/viewpr.html?pid=10649>

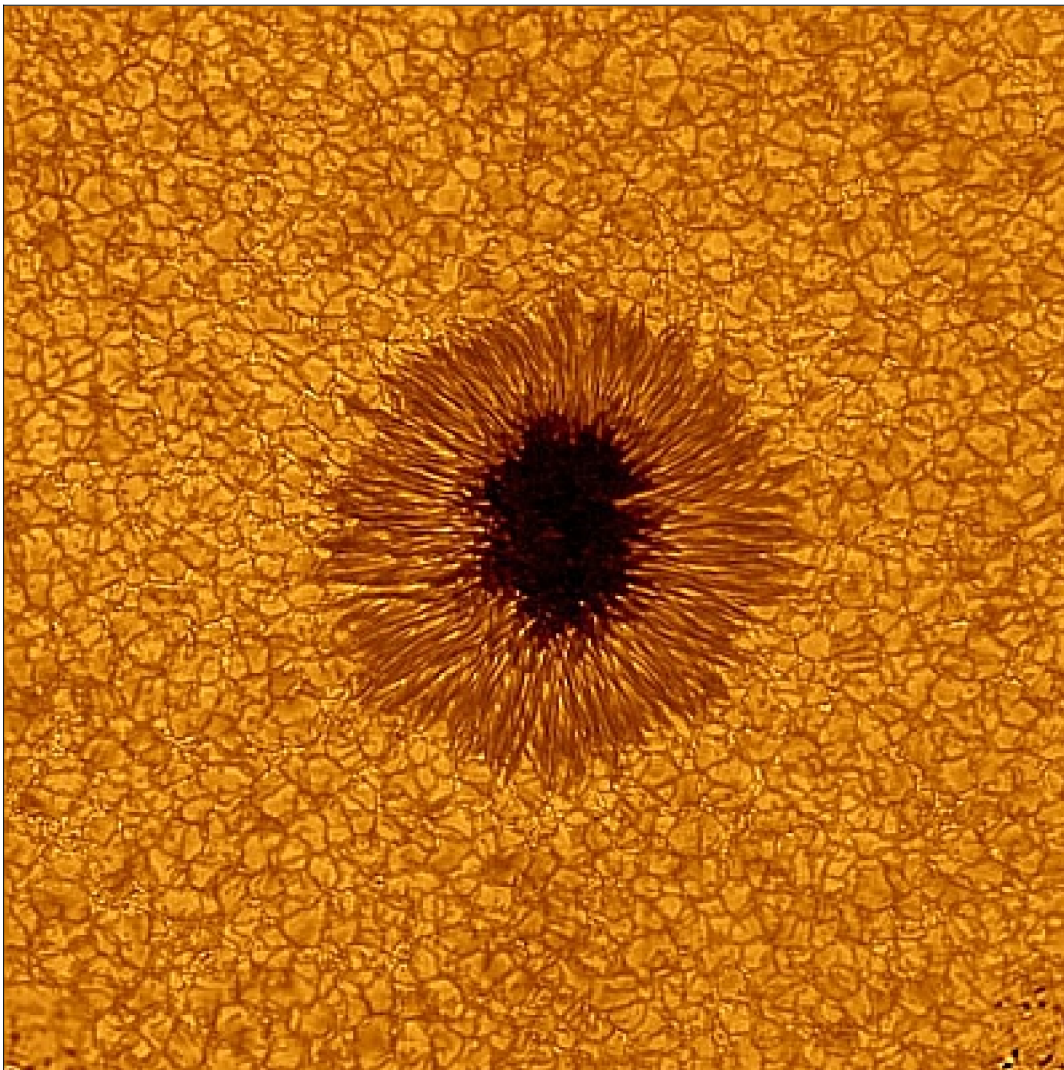


Figure 24: The most detailed sunspot so far obtained in visible light in July 2010 (image credit: NJIT)

The NST first light image of Figure 24 represents ⁵⁹²⁾ ⁵⁹³⁾ the most detailed sunspot captured so far of solar phenomena. It will help researchers understand the complexities of solar weather and its impact on the space climate in our neighborhood of the solar system. By the summer of 2011, in collaboration with the National Solar Observatory, BBSO will have upgraded the current adaptive optics system to one utilizing a 349 actuator deformable mirror array.

– The deployment of space telescopes, such as Hubble Space Telescope (HST) has been very challenging in terms of cost, schedule, and performance. Initial, poor wavefront quality for HST was corrected by an enormously costly in-orbit astronaut servicing mission. The first Hubble repair mission was launched Dec. 2, 1993 on STS–61. Installation of **COSTAR** (Corrective Optics Space Telescope Axial Replacement) which employed an adaptive optics technology. After the mission, Hubble became operational transmitting stupefying images of supernovas, gigantic explosions that marked the death of a star and revealed mysterious black holes in the center of virtually all galaxies.

592) “Amazing New Sun Images From NJIT’s Big Bear Solar Observatory,” Space Daily, Aug. 26, 2010, URL: http://www.spacedaily.com/reports/Amazing_New_Sun_Images_From_NJIT_Big_Bear_Solar_Observatory_999.html

593) “See Amazing New Sun Images From NJIT’s Big Bear Solar Observatory,” BBSO News, Aug. 24, 2010, URL: <http://www.bbsso.njit.edu/>

– The space telescope of the Deep Impact mission of NASA (launch on Jan. 12, 2005) was severely defocused after launch. However, no repairs could be made due to absence of adaptive optics on-board.

In the early 21st century, the technology of lightweight adaptive optics is also being **considered for Earth observation (EO) instruments** (looking from space toward Earth). However, for EO instruments, the required response times are much shorter than those of astronomical instruments. The latter have long exposure times while EO instruments have dwell times in the order of microseconds. In particular, an adaptive optical system, designed for narrow-field applications (as in astronomy), is not sufficient for WFOV systems needed in EO applications. To address these needs, a new WFOV adaptive optics theory and a new error function were developed. Modeling and experimental results demonstrate the validity of the WFOV adaptive optics theory and new error function. This new error function, which is an extension of conventional adaptive optics, lead to the development of three new types of imaging systems: WFOV, selectable FOV, and steerable FOV. These new systems can have nearly diffraction-limited performance across the entire FOV or a narrow movable region of high-resolution imaging.⁵⁹⁴⁾

A first attempt to develop an EO imager based on the AO technique (a deformable mirror design to correct for residual wavefront errors in a large segmented aperture optical system) was proposed by NASA in the late 1990s. This was the so-called **RedEye** (Regional Environmental Dynamics Active-aperture Infrared Imager) instrument, considered to be flown on the EO-3 mission (Earth Observing-3, launch planned for 2006) in geostationary orbit. However, as of spring 2000 the RedEye proposal was not accepted by NASA management for realization. – In the meantime, many advancements occurred [such as: high-resolution wavefront control with optically addressed liquid crystal (LC) spatial light modulators], making the AO technique a key enabling technology for a great variety of future imaging applications.

Not all adaptive optics implementations are used to correct for atmospheric turbulence. The technique is also being used to compensate in general for optical aberrations in the design of very small and light-weight optical systems to improve the optical characteristics (including focal length, aberrations, removal of misalignments, improvement of wider FOV, etc.) of a system subjected to space environment variations. Not all adaptive optics implementations use piezoelectric actuators in combination with computers for mirror control.

Adaptive optics⁵⁹⁵⁾ must also be seen in the context of FSO (Free-Space Optics) communications, in reducing the bit error rate of a transmission. FSO is considered a valuable technology for many applications such as short-distance fiber-optic links, for mobile high-bandwidth data transfer as needed in military and industrial applications, or for long-range ground-to-satellite communication and vice versa.

Newer adaptive optics instrument designs (21st century) employ so-called **MOEMS** (Micro-Opto-Electro-Mechanical System) devices, microchips, able to physically react to a non-normal situation. In adaptive optics applications, **MMAs** (Micro Mirror Arrays) are a MOEMS sub-type, permitting the correction of distorted wavefronts and/or to compensate for optical imperfections in the micro mirrors themselves. MMAs are arrays of individually controllable micro mirrors, where each mirror can be adjusted to alter either the phase or direction of the light reflected back from that pixel (a light beam may also be spectrally

594) B. K. McComas, E. J. Friedman, R. B. Hooker, M. A. Cermak, "Configurable Adaptive Optical System for Imaging of Ground-Based Targets from Space," Proceedings of SPIE, Vol. 4884, 9th International Symposium on Remote Sensing, Aghia Pelagia, Crete, Greece, Sept. 23–27, 2002

595) T. Weyrauch, M. A. Vorontsov, J. W. Gowens II, "Adaptive compensation of atmospheric effects with a high-resolution micro-machined deformable mirror," SPIE Annual Meeting 2002: Remote Sensing and Space Technology, Seattle, WA, July 7–11, 2002, SPIE Vol. 4825

modified).⁵⁹⁶⁾⁵⁹⁷⁾ MMAs are fabricated by means of semiconductor process technology, they can form arrays with a large number of independent mirror elements, providing high spatial resolution. The technology is already being commercially exploited in such applications as high–definition TV sets, video devices, and in digital cinema projection systems. MMAs work on a pixel basis, they are rugged and compact devices with relatively low power requirements, providing update rates in the order of 1 kHz.. The technology can be used to correct distortion and step errors on wavefronts. These devices look rather promising to allow future large telescopes to fly large lightweight apertures. – The **MSA** (Micro Shutter Array) device is another variant of MOEMS technology, permitting a redirection of light by individually controllable structures (MSAs may for instance be used as a programmable aperture mask for object selection devices in multi–object spectrometers).

A prominent candidate for these new technologies is the **JWST** (James Webb Space Telescope) mission (launch 2015 to Lagrangian point L2), a NASA/ESA collaboration – to succeed HST (Hubble Space Telescope). JWST features the following science instruments: NIRCam (Near Infrared Camera) provided by NASA, NIRSpec (Near Infrared Spectrograph) in the 0.6–5 μm range provided by ESA, and MIRI (Mid Infrared Instrument), comprising an imager and a spectrometer in the 5–27 μm range, provided by ESA and NASA, and FGS (Fine Guidance Sensor) provided by CSA.

ESA research into MMA technology examines two required MMA actuator functions for simultaneous support services:⁵⁹⁸⁾

- 1) Binary operated tilt mirrors – permitting some manipulation of the incident light (for instance discarding of those parts of the incoming wavefront causing interference). This is done by turning a mirror element optically “on” or “off” when below or above a threshold.
- 2) Analog–operated piston mirrors to be used for continuous phase–shifting operations. The principle of analog MMA wavefront correction is to compensate the local wavefront deviation averaged across the one micro mirror by appropriate height adjustment of that element.

- In June 2007, the **LGS** (Laser Guide Star) system started regular operations on the VLT (Very Large Telescope) of ESO at Paranal, Chile (one of the world’s most advanced large ground–based telescopes). The LGS system provides assistance for the adaptive optics instruments on the VLT and so allows astronomers to obtain images free from the blurring effect of the atmosphere, regardless of the brightness and the location on the sky of the observed target. – Two of the Adaptive Optics (AO) science instruments at the Paranal observatory, NACO and SINFONI, have been upgraded to work with the recently installed LGS and have delivered their first scientific results.⁵⁹⁹⁾⁶⁰⁰⁾

The LGS system installed at Paranal uses the PARSEC dye laser developed by MPE Garching and MPIA Heidelberg, while the launch telescope and the laser laboratory was developed by ESO. The first objects that were observed are interacting galaxies. The images obtained reveal exquisite details, and have a resolution comparable to that of the Hubble Space Telescope. In one case, it was possible to derive for the first time the motion of the stars in two merging galaxies, showing that there are two counter–rotating discs of stars.

The VLT Laser Guide Star system is the result of a collaborative work by a team of scientists and engineers from ESO and the Max Planck Institutes for Extraterrestrial Physics in

596) A. Gehner, W. Doleschal, et al., “Active–matrix addressed micromirror array for wavefront correction in adaptive optics,” Proceedings of SPIE, Vol. 4561, MOEMS and Miniaturized Systems II, pp. 265–275, 2001

597) N. Clark, P. Furth, S. Horan, “Intelligent Star Tracker,” Proceedings of the 14th Annual AIAA/USU Conference on Small Satellites, Logan, UT, Aug. 21–24, 2000, SSC00–III–1

598) W. Hupfer, A. Gehner, H. Schenk, H. Lakner, J. Liesener, K. Wallace, “Micro–Mirror Arrays for Adaptive Wavefront Correction,” Proceedings of 54th IAC, Bremen, Germany, Sept. 29 – Oct. 3, 2003

599) http://www.innovations–report.de/html/berichte/physik_astronomie/bericht–85769.html

600) http://www.spacedaily.com/reports/Laser_Guide_Star_System_On_ESO_VLT_Starts_Regular_Science_Operations_999.html

Garching and for Astronomy in Heidelberg, Germany. NACO was built by a Consortium of French and German institutes and ESO. SINFONI was built by a consortium of German and Dutch Institutes and ESO.

- **GeMS** (Gemini Multi–conjugate adaptive optics System): In 2013, GeMS is a unique new instrument, installed at the Gemini South telescope in La Serena, Chile, which takes the removal of atmospheric distortions (using adaptive optics technology) to a new level.

GeMS is the first of its kind to use laser guide stars and the MCAO (Multi–Conjugate Adaptive Optics) technology to image the sky. The technology behind MCAO involves the use of multiple laser guide stars (five in the GeMS system) and several deformable mirrors (three in all) to sample atmospheric distortions and cancel them out in real–time as imaging data is collected. Using algorithms similar to those developed for medical tomographic imaging the GeMS MCAO system creates a three–dimensional snapshot of atmospheric turbulence about 500 to 1000 times per second. The result is about a 16–fold increase in the patch of sky observed, while providing uniform corrections over the entire field.⁶⁰¹⁾

Adaptive optics allows ground–based telescopes to take full advantage of their large mirrors. The laser, a solid–state sodium (yellow/orange) laser, was developed with significant supplemental funding through the U.S. National Science Foundation (NSF) and from the entire Gemini Observatory partnership.

The Gemini Observatory is an international collaboration with two identical 8.1 m telescopes. The Frederick C. Gillett Gemini Telescope is located on Mauna Kea, Hawai'i (Gemini North) and the other telescope on Cerro Pachón in central Chile (Gemini South); together the twin telescopes provide full coverage over both hemispheres of the sky. The telescopes incorporate technologies that allow large, relatively thin mirrors, under active control, to collect and focus both visible and infrared radiation from space.⁶⁰²⁾

The ground–based Gemini Observatory consists of twin 8.1 m diameter optical/infrared telescopes located on two of the best observing sites on the planet. From their locations on mountains in Hawaii and Chile, Gemini Observatory's telescopes can collectively access the entire sky.

Gemini was built and is operated by a partnership of seven countries including the United States, United Kingdom, Canada, Chile, Australia, Brazil and Argentina.

On December 16, 2011, a decade of hard work culminated at the Gemini South telescope in Chile when a new generation of **AO** (Adaptive Optics) produced its first ultra–sharp, wide–field image. The target, a dense globular cluster of stars called NGC 288, reveals details at nearly the theoretical resolution limit of Gemini's large 8 m mirror.

Called the Gemini Multi–conjugate adaptive optics System (**GeMS**), it uses five artificial guide stars made by a laser to provide extreme clarity over the largest area of night sky ever captured in a single AO observation — an area of the night sky which is 10 times larger than that covered by any other existing AO system in the world.

Gemini's new system overcomes two limitations that have plagued the previous generation of AO systems: (1) a limited number of stars bright enough to guide on; and (2) a small field–of–view (the size of the patch of sky observed in a single observation).

601) Peter Michaud, Antonieta Garcia, Peter Peshev, Benoit Neichel, "Next–Generation Adaptive Optics Brings Remarkable Details to Light in Stellar Nursery," Gemini Observatory Press/Image Release, Jan. 9, 2013, URL: <http://www.gemini.edu/node/11925>

602) Peter Michaud, Rodrigo Carrasco, Benoit Neichel, "Revolutionary Instrument Delivers a Sharper Universe to Astronomers," Gemini Observatory, July 2, 2013, URL: <http://www.gemini.edu/node/12028> , and URL: <http://www.gemini.edu/node/12020>

While not a new solution, lasers have proved to be an effective solution to the first problem. When no "natural" guide star is available, an artificial one is created using a powerful laser emitting the well-known orange color used in some streetlights. This laser guide star technology is currently being used by observatories around the world, including both Gemini telescopes in Chile and Hawaii.

Gemini solved the FOV (Field-of-View) problem with MCAO (Multi-Conjugate Adaptive Optics) technique. By using five laser guide stars (rather than a single one as in other systems), tomographic atmospheric modeling techniques borrowed from medical imaging, and several deformable mirrors, MCAO extends the FOV of AO systems by 10 times or more; it also produces images with exquisitely uniform image quality across the entire FOV. GeMS is the first of its kind to combine laser guide stars with MCAO, which opens up more of the nighttime sky for detailed study.

GeMS development started at Gemini in the early 2000s. The system was assembled in the Gemini instrumentation laboratories over the past four years and uses an infrared imager, called the Gemini South AO Imager (GSAOI), built at the Australian National University. The GeMS team field-tested it on the telescope during several commissioning periods in 2011, and performed the final tests in mid-December.

The smallest detail that can be resolved by GeMS measures about 0.04 to 0.06 arcsec over a FOV of 85 x 85 arcsecs – which is very close to the diffraction limit of 0.043 at this wavelength of 1.65 μm. The new record significantly beats the typical resolution in "seeing" limited (non-AO) conditions of 0.5 arcsec at good astronomical sites.

As many astronomers and AO scientists have already commented or acknowledged, GeMS has turned a page in the history of adaptive optics and raised the bar for the rest of the AO world.

Table 41: Revolutionary AO system propels astronomical imaging to new extremes ⁶⁰³⁾ ⁶⁰⁴⁾

- **MagAO** (Magellan Adaptive Optics system). In the summer of 2013, the Magellan II 6.5 m telescope in the high Atacama Desert of Chile was upgraded with the new MagAO system. The 'first light' images captured with MagAO provided for the first time long-exposure images that resolve objects just **0.02 arcsec** across — the equivalent of a dime (1.7 cm) viewed from a distance of more than a hundred miles away.

Astronomers at the University of Arizona, the Arcetri Observatory near Florence, Italy, and at the Carnegie Observatory (HQ in Pasadena, CA) have developed a new type of camera that allows higher resolution (sharper) images to be taken than ever before. The team has been developing this technology for over 20 years at observatories in Arizona and has now deployed the latest version of these cameras in the high desert of Chile at the Magellan 6.5 m telescope. ⁶⁰⁵⁾

Background: Since its beginnings, diffraction-limited ground-based AO (Adaptive Optics) imaging has been limited to wavelengths in the near IR ($\lambda > 1\mu\text{m}$) and longer. Visible AO ($\lambda < 1\mu\text{m}$) has proven to be difficult because shorter wavelengths require wavefront correction on very short spatial and temporal scales. The pupil must be sampled very finely, which requires dense actuator spacing and fine wavefront sampling with large dynamic range. In addition, atmospheric dispersion is much more significant in the visible than in the near-IR. Imaging over a broad visible band requires a very good ADC (Atmospheric Dispersion Corrector).

The Magellan Clay telescope is a 6.5m Gregorian telescope located at the Las Campanas Observatory (LCO) in Chile at an altitude of 2400 m, it is operated by the Carnegie Obser-

603) <http://www.gemini.edu/node/11715>

604) "Revolutionary Adaptive Optics System Propels Astronomical Imaging to New Extremes," URL: <http://www.gemini.edu/node/11718>

605) Jared Males, "Magellan AO – Scientists Make Highest Resolution Photos Ever of the Night Sky," University of Arizona, Aug. 21, 2013, URL: <https://visao.as.arizona.edu/>

vatory. The Gregorian design allows for a concave F/16 ASM (Adaptive Secondary Mirror) that can be tested off-sky with a retroreflecting optic at the far ellipsoidal conjugate. The ASM has a diameter of 85 cm that uses 585 actuators with <1 ms response times. In this manner the "blurring" effects of the atmosphere can be removed, and thanks to the high density of actuators on this mirror, astronomers can see the visible sky more clearly than ever before. ⁶⁰⁶⁾

The reason for the factor of 2 improvement over past efforts is that, for the first time, a large 6.5m telescope is being used for digital photography at its theoretical resolution limit in wavelengths of visible light. The new MagAO along with its VisAO (Visible-light camera) corrects the atmospheric turbulence by using a magnetic field to float a thin (1.6 mm) curved glass mirror (85 cm across) on a magnetic field 9.2 m above the big primary mirror of the telescope.

The MagAO has already made some important scientific discoveries. As the system was being tested, the team tried to resolve the famous star that gives the Great Orion Nebulae most of its UV light. This star (~ 1 million years old) is called Theta 1 Ori C and it is about 44 times the mass of the Sun. It was already known to be a binary star system (two stars, C_1 and C_2 rotating around each other); however, the separation between them is so small that this famous pair has never been resolved into two stars in a direct telescope photo. Once MagAO and the VisAO CCD camera were pointed towards Theta Ori 1 C, the results were exciting and immediate. The first light photo displayed clearly the 2 stars just 0.32 arcsec apart. ⁶⁰⁷⁾

606) Derek Kopon, Jared Males, Laird M. Close, Victor Gasho, "Enabling Technologies for Visible Adaptive Optics: The Magellan Adaptive Secondary VisAO Camera," 2010, URL: <http://arxiv.org/ftp/arxiv/papers/1008/1008.0146.pdf>

607) L. M. Close, J. R. Males, K. Morzinski, D. Kopon, K. Follette, T. J. Rodigas, P. Hinz, Y-L. Wu, A. Puglisi, S. Esposito, A. Riccardi, E. Pinna, M. Xompero, R. Briguglio, A. Uomoto, T. Hare, "Diffraction-limited Visible Light Images of Orion Trapezium Cluster With the Magellan Adaptive Secondary AO System (MagAO)," *The Astrophysical Journal*, Sept. 10, 2013, arXiv:1308.4155 [astro-ph.SR]

1.5.9 Optical phased array (OPA) technology

At the start of the 21st century, OPA is an emerging and an enabling technology for rapid and accurate redirection (beam steering in 2-D) of the wavefront FOV (field of view) of an optical sensor. These non-mechanical beam steering devices operate in an analogous fashion to microwave frequency phased array radar antennas. ^{608) 609) 610) 611)}

Optical phased arrays (imaging or tracking systems with a potentially large effective telescope/antenna area) provide an elegant means for an inertialess, high-speed, high-resolution and random-access electronic beam steering capability, required by numerous applications, including laser radar (laser radars may be used for such applications as target detection and wind profiling), laser communication (including high-speed and high bandwidth switching, intersatellite links), and laser projection display. For such applications, a phase profile is imposed on an optical beam as it is either transmitted through or reflected from the phase shifter array. The OPA technique is actually a promising approach for both sensing and transmitting functions. Current optical arrays are basically monolithic structures with no discrete elements, consisting of an array of phase shifters rather than individual transmit/receive modules; they are designed to use low-cost addressing electronics. **Passive** optical arrays consist solely of phase shifters, they are operated as space-fed arrays, meaning that an already formed beam is fed to the array of phase shifters, which then effects the steering of the beam. This contrasts to an **active** phased array, in which individual transmit modules form a beam as it exits a large array of transmitters (such as a laser phased array antenna).

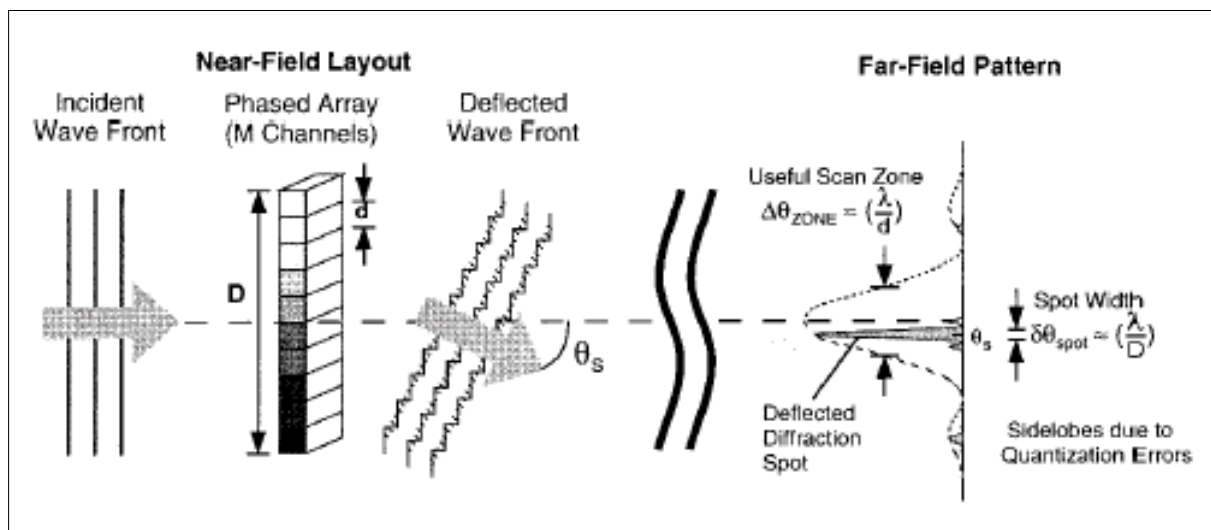


Figure 25: Schematic concept of a 1-D phased-array deflector arrangement

The early generation (1990s) of optical device implementations are 1-D, space-fed, passive, phase-only, apertures (Note: the 1-D approach is selected to reduce the possible number of interconnections). An already formed beam is fed to the array of phase shifters,

- 608) P. F. McManamon, T. A. Dorschner, D. L. Corkum, L. J. Friedman, D. S. Hobbs, et al., "Optical Phased Array Technology," *Proceedings of the IEEE*, Vol. 84, No.2, Feb. 1996, pp. 268–298
- 609) J. A. Thomas, Y. Fainman, "Optimal cascade operation of optical phased-array beam deflectors," *Applied Optics*, Vol. 37, No. 26, Sept 10, 1998, pp. 6196–6212
- 610) J. D. Perkins, C. W. Teplin, M. van Hest, "Optimization of Transparent Conducting Oxides for Liquid Crystal Based Optical Phased Arrays," *Proceedings of IEEE Aerospace Conference, Big Sky, MT, March 8–15, 2003*
- 611) Note: An OPA system can be composed of multiple liquid crystal or micro-mirror elements that modify the optical phase of an incident optical signal in transmission or reflection. These phase modifications can be used in beam steering and/or aberration correction. The liquid crystal elements, also referred to as "writable gratings," are solid state devices that are manufactured using semiconductor fabrication techniques. The dynamically-variable grating modifies the phase of an incident optical signal via a voltage-controlled index of refraction. Creation of a linear gradient in the optical path delay tilts the phase front and steers the optical beam. The realized linear gradient is actually folded, similar to a blazed grating. An OPA system can be flood illuminated by a single high power laser source or, alternatively, each element of the array can be fed by an individual laser. See URL: [http://www.fbodaily.com/cbd/archive/2001/01\(January\)/18-Jan-2001/spmsc001.htm](http://www.fbodaily.com/cbd/archive/2001/01(January)/18-Jan-2001/spmsc001.htm)

which then affects steering of the beam (analog beamforming of phased arrays). The imposed phase profile steers, focuses, fans out, or corrects phase aberrations on the beam. High efficiency large-angle steering with phased arrays requires phase shifter spacing on the order of a wavelength or less; hence, addressing issues make 1-D optical arrays more practical than 2-D arrays. Generally, requirements call for a large number of addressable points, which in turn requires at least an equal number of independently controlled phase modulators in the array. Numerous line-management techniques have been explored to reduce the number of control lines required to regulate fully such a phased-array deflector while still providing continuous scan-angle control.

The optical phased array concepts are the direct functional analogs of the microwave phased array technology (that make possible agile and inertialess steering of microwave beams). However, due to the orders-of-magnitude difference in wavelengths between the microwave and the optical worlds, a different implementation approach is used for optical arrays. Future OPA implementations for airborne/spaceborne applications are distributed architectures providing a means for graceful degradation.

LC (Liquid Crystal) optical phased array concept: A promising implementation of an optical phased array is provided by the nematic-phase LC technology. A prism inserted into the aperture of an optical system introduces a linear gradient of OPD (Optical Path Delay) across the aperture, tilting the phase front and thereby steering the optical beam. For a given wavelength, a phase shift of 2π (OPD of one wavelength) can be subtracted periodically from the phase front without influencing the far-field pattern produced by the phase front. The “folded” phase profile represents a blazed grating. The phase ramp can be approximated by a series of small discrete phase steps.⁶¹²⁾

The application of a relatively low voltage (1–10 V) reorients the LC molecules and changes the effective index of refraction. The maximum phase shift available is proportional to the thickness of the LC layer. By using a cascaded course/fine beam steering architecture, full angular addressing flexibility is recovered.

LC optical phased array applications are also attractive optoelectronic components for simple, light weight and low-cost optical sensors. They have the potential to replace rotating or moving mirrors and prisms in many scanning devices. Liquid crystal phased arrays offer the following advantages over mechanical systems:

- Random access, rapid beam pointing
- Precise pointing stabilization
- Programmable multiple beams
- Potential for large aperture
- High optical damage threshold
- Low power consumption
- The use of optical phased arrays is a promising technology for laser radars
- Optoelectronic applications include a) laser free-space communications, b) 1- or 2-D photonic deflecting switches can be designed for optical interconnects to route optical signals from one fiber (or source) to another, c) optical phased arrays can be used as receivers for focal plane array detectors, d) optical wavefront correction and beam shaping (potential use in adaptive optics), (see Ref. 588).

Besides optical phased arrays (on LC technology) there are alternative options that realize rapid beam steering without the use of conventional mechanical systems. An example is:

612) U. Krishnamoorthy, K. Li, K. Yu, et al., “Dual-Mode micromirrors for Optical Phased Array Applications,” The 11th International Conference on Solid-State Sensors and Actuators, Munich, Germany, June 10–14, 2001

Cascaded microlens arrays consisting generally of a closely packed periodic array of miniature lenses. In this setup, beam steering is affected by translating one microlens array with respect to the other.

Some background on OPA: ⁶¹³⁾ ⁶¹⁴⁾ ⁶¹⁵⁾ In 1971, R. A. Meyer demonstrated a multichannel array of bulk lithium tantalate modulators for optical beam deflection. The deflector consisted of 46 phase shifters in a 1-D geometry; independent control lines were provided for each channel to obtain continuous scan control. ⁶¹⁶⁾ Several fundamental concepts of optical phased-array deflection were verified by this simple single-stage device. In 1973, Y. Ninomiya demonstrated a phased array of bulkprism deflecting elements made with lithium niobate. This device exploited an array concept primarily to enhance the deflector resolution beyond that of a single deflecting element. Ninomiya also introduced a two-stage phased array arrangement that included offset phase electrodes set in front of each prismlike deflecting element. Later efforts (1979) led to the design of fast, high-performance 1-D phased-array beam deflectors that use integrated-optics AlGaAs channel waveguides. An optical solid-state phased array designed for potentially high-speed operation with PLZT (Lead Lanthanum Zirconium Titanate) technology was demonstrated in 1995. An optimal arrangement for cascading 1-D phased array deflectors is presented in reference 609). Cascading is required by high-resolution scanning systems to reduce the number of control lines significantly and can be achieved with phased arrays while still allowing for continuous deflection-angle control, restricted voltage requirements, and compensation for non-ideal optoelectronic behavior and aging effects.

-
- 613) C. H. Bulmer, W. K. Burns, T. G. Giallorenzi, "Performance criteria and limitations of electro-optic waveguide array deflectors," *Applied Optics*, Vol. 18, 1979, pp. 3282–3295
- 614) J. A. Thomas and Y. Fainman, "Programmable diffractive optical element using a multichannel lanthanum-modified lead zirconate titanate phase modulator," *Optical Letters*, Vol. 20, 1995, pp. 1510–1512
- 615) Y. Ninomiya, "Ultrahigh resolving electrooptic prism array light deflectors," *IEEE Journal on Quantum Electronics*, Vol. 9, No 8, Aug. 1973, pp. 791–795
- 616) R. A. Meyer, "Optical beam steering using a multichannel lithium tantalate crystal," *Applied Optics*, Vol. 11, 1972, pp. 613–616

1.5.10 Advanced telescope design – lightweighted optics and structures

At the start of the 21st century, the prevailing observation technology in LEO and GEO provides global data sets to study seasonal and long-term changes of the Earth's environment. The problem: LEO missions can provide only periodic high-resolution snapshots of the Earth's environment at any given location. On the other hand, GEO missions (weather satellites) provide contiguous coverage over its viewing geometry, but only at moderate spatial resolutions (generally in the order of 1–2 km for VIS and 4–5 km for the TIR range). Hence, none of these current systems is sufficient, in temporal and spatial resolution, to monitor the development of dynamic environmental processes. While a single GEO observatory cannot provide global coverage, a high-resolution sensing capability from such a vantage point (GEO) can better reveal short term forcing processes on complex Earth ecosystems.

Conventional high-resolution and wide-FOV imagers in the optical region ($0.1 < \lambda < 1000 \mu\text{m}$) employ generally fairly heavy instrumentation, even with moderate aperture size (about 0.3 – 0.5 m) telescopes.⁶¹⁷⁾ The mass of these monolithic telescopes is mainly due to the optical components with solid glass lenses and mirrors (and aluminum coatings). Examples of conventional imagers are: ETM+ of Landsat–7 with a mass of 428 kg, ASTER of Terra with a mass of 421 kg, HRG of SPOT–5 with a mass of 356 kg, BGIS 2000 of the QuickBird–2 mission with a mass of 380 kg (telescope of 138 kg).

The performance requirements of future EO missions, in particular for higher-resolution imagery from GEO (or further out at L1), will lead to much larger aperture sizes. In order to obtain high-resolution VIS/TIR imagery from GEO, equivalent to that of conventional instruments in LEO (say, 30 m in VIS and 300 m in TIR), requires a telescope aperture of 4 m in diameter (see Airy diffraction limit in chapter 1.7). Hence, today's challenge is to produce such a large-aperture and low-mass telescope at affordable costs. Possible design solutions for such systems may require concepts of deployed, semi-rigid segments with actively controlled mirrors.⁶¹⁸⁾

In the field of space science and astronomy, future large-aperture telescopes will have apertures of 3–5 m diameter or much more. This will eventually require a segmented telescope design for the launch phase and a subsequent space deployment of the telescope instrument due to launcher fairing limitations. Obviously, a new design concept approach in lightweight manufacturing technology of optical systems (use of composite materials) is needed to reduce the instrument mass to tolerable levels. The advantages of large-aperture space telescopes are obvious – the sensitivity increases (and observation time decreases) proportionately to aperture area; spatial resolution improves proportionately with aperture diameter; the orbital environment is generally stable and quiet.⁶¹⁹⁾

- **Lightweighted structures.** SiC (Silicon Carbide) is an important composite material for precision applications in reflecting optics components, in semiconductor electronics technology, as well as in many other fields.^{620) 621)} SiC-type ceramic mirrors and structures are becoming state-of-the-art technology components in lightweight optomechanical systems (telescopes). Silicon carbide has several advantages as a primary mirror substrate material: SiC is isotropic, homogeneous, dimensionally stable when subjected to re-

617) Note: An exception to this rule are the telescopes of lidar instruments. Examples are: a) the CALIPSO mission of NASA/CNES (launch Apr. 28, 2006) carries a lidar instrument with a telescope aperture diameter of 1 m; b) ALADIN (Atmospheric Laser Doppler Instrument), a lidar on ESA's ADM–Aeolus mission (launch 2011) has a telescope diameter of 1.5 m.

618) F. Peri, M. Hagopian, M. Lake, "Lightweight Deployable UV/Visible/IR Telescopes," Proceedings of IGARSS 2002, Toronto, Canada, June 24–28, 2002

619) P. A. Warren, "Lightweight, Precision, Deployable Structures," <http://origins.jpl.nasa.gov/meetings/ulsoc/papers/warren.pdf>

620) B. Harnisch, B. Kunkel, M. Deyerler, S. Bauereisen, U. Papenburg, "Ultra-lightweight C/SiC Mirrors and Structures," ESA Bulletin, No 95, August 1998

621) M. Gedig, "XLT Large Telescope – Design Development of a 20 Meter Segmented Mirror with Lightweighted Silicon Carbide Segments," Feb. 2002, <http://www.hia-ija.nrc-cnrc.gc.ca/XLT/Reports/xltmirc0.pdf>

peated temperature variations. SiC has a relatively high strength-to-weight ratio compared to other viable mirror materials. A major advantage of SiC is that it can be formed into complex shapes, allowing for optimal material usage. SiC is also useful as a mirror substrate because some forms of SiC can be polished to a high quality mirror finish using diamond grit.

There are several different manufacturing processes for producing SiC. The processes include CVD (Chemical Vapor Deposition), Reaction-bonded SiC, S-SiC (Sintered SiC), Hot Pressed SiC, Foamed SiC, and C/SiC (Carbon fiber-reinforced/Silicon Carbide); the latter material is part of the CMC (Ceramic Matrix Composite) family, which replaces the previous organic, resin-carbon matrix family with a more stable, oxidation-resistant ceramic matrix, such as SiC.^{622) 623)} The use of CMCs is highly desirable in a number of critical space components (telescopes, nozzles, thrust chambers, control surfaces, leading edges, sensors for combustion monitoring, wear-resistant brakes, etc.) to save weight, improve reuse capability, and increase performance (high temperature resistance).

Of major interest to high-temperature applications are carbon/carbon (C/C), carbon-silicon carbide (C/SiC) and silicon carbide-silicon carbide (SiC/SiC) composites. Examples: a) the Space Shuttle has been demonstrating the maturity of carbon/carbon (C/C) nosecones and leading edges for more than 20 years, b) CMCs have been developed by an ESA/NASA team for integration and flight demonstration on the X-38 Vehicle 201 (Jan. 2001), the prototype for the ISS (International Space Station) CRV (Crew Return Vehicle).

- A special form of SiC, namely C/SiC (Carbon fiber-reinforced Silicon Carbide), is composed of coated C-fibers and a SiC matrix. C/SiC materials benefit from the high-temperature capability of carbon fibers and high modulus and oxidation resistance of the SiC matrix. As a fiber-reinforced composite, the mechanical and thermal properties can be tailored by adjusting fiber volume and placement (i.e., fiber architecture) to meet the needs of many applications. The C/SiC technology is based on infiltration processing (without any shrinkage) of porous C/C-structures with molten silicon by capillary forces. Common C/SiC infiltration processes are: CVI (Chemical Vapor Infiltration), MI (Melt Infiltration), and PIP (Polymer Infiltration and Pyrolysis). The following list represents some of the C/SiC ceramic material characteristics:

- Very broad operating temperature range (4 to 1570 K)
- Low specific density (2.6–2.7 g/cm³) approximately the same as aluminum
- High stiffness (tunable stiffness 240–260 GPa) and strength (140–210 MPa)
- Low CTE (Coefficient of Thermal Expansion), CTE = $1.8 \times 10^{-6} \text{ K}^{-1}$ at room temperature, and near zero below 150 K, (CTE about $4.1 \times 10^{-6} \text{ K}^{-1}$ at 1000 °C)
- High thermal conductivity (125–135 W/mK), approaches that of aluminum
- Low electrical resistance ($2 \times 10^{-4} \text{ Ohm} \times \text{m}$)
- Isotropic characteristics of CTE, thermal conductivity, mechanical properties, etc.
- Very high chemical and corrosion resistance
- No ageing or creep deformation under stress (stability of shape)
- No porosity, non-magnetic
- High quality optical surface layers (e.g. SiC, glass and Si, roughness: < 5 Å)

622) P. C. Chen, T. T. Saha, A. M. Smith, R. Romeo, "Progress in very lightweight optics using graphite fiber composite materials," *Optical Engineering*, Vol. 37, No 2, 1998, pp. 666–676

623) M. Giegerich, "Crossing the Threshold – Applying CMCs to Space Vehicles," <http://esapub.esrin.esa.it/onstation/onstation4/os4x38.pdf>

- Fast and low–cost machining (no special tools required)
- Short manufacturing times
- Considerable flexibility in structural design (including large structure scaling)
- Ultra–lightweight capability (small wall thickness and complex stiffeners)
- Composition of C/SiC material: SiC : Si : C = 50–60% : 20–30% : 10–20% (typical value)
- High hardness (>1500 N/mm) harder and stronger than most other optical materials.

CESIC[®] (Carbon–fiber reinforced Silicon Carbide) is a ceramic matrix composite material (made of SiC, Si and C) of high stiffness, high thermal conductivity, and low thermal expansion from room to cryogenic temperatures. This material is obtained from the transformation of the Carbon in SiC, due to the reaction at high temperature between C/C greenbody and liquid silicon. The use of C/C greenbody manufacturing is one of the key technologies of the CESIC process. CESIC is a product of ECM Ingenieur–Unternehmen, Munich, Germany (ESA provided funding for CESIC technology development). – CESIC is an ideal material to produce lightweight, stable structures and a range of high–precision opto-mechanical components, such as lightweight mirrors, focal planes, telescopes, instrument structures, and optical benches for both land– and space–based applications. ⁶²⁴⁾

Background: Classic materials in telescope design technology include fused silica, Zerodur, ULE, titanium, Invar, Pyrex, etc. However, at the start of the 21st century, carbon fiber composite materials (such as carbon/carbon or graphite cyanide ester) offer significant advantages over the classic materials in terms of: density, low thermal expansion, and high stiffness. Essential technology elements for lightweight and dimensionally stable telescopes are composite materials based on graphite and carbon fibers. Also, replication with fiber composite materials yields areal densities that approach the minimum possible for a free-standing optical surface. ⁶²⁵⁾

– Schott Glas of Mainz, Germany, developed an essentially zero–expansion glass ceramic by the name of Zerodur^{RM} in 1968. The material is machinable and is suitable for telescope mirrors, ring laser gyroscopes and other applications that demand high precision. A technique to fuse Zerodur allows to fabricate large lightweight mirrors that cannot be produced by traditional machining methods. Examples of Zerodur implementations: In 1991/93, the VLT (Very Large Telescope) of ESO (European Southern Observatory), a glass monolith produced in a centrifugal casting process, was built by Schott Glas consisting of a Zerodur mirror substrate with a diameter of 8.2 m. In fact, VLT has four main Zerodur mirrors, each of 8.2 m in diameter for the visible and near–infrared spectrum. When coupled together, they form a giant telescope with an effective diameter of 16 m.

The telescope of **SOFIA** (Stratospheric Observatory For Infrared Astronomy), a NASA/DLR long–term airborne observatory on a Boeing 747 aircraft (start of first flight in May 2010), employs a Zerodur mirror substrate (a milled honeycomb structure on the backside; 2.7 m diameter, the primary mirror employs a rigid CFRP structure) thereby reducing the instrument mass from originally 4 tons to about 890 kg.

– The ULETM (Ultra–Low Expansion) glass, face sheets bonded to a honeycomb core, achieves about 85–90% lightweight. ULE of Corning Inc., Corning, NY, is a titanium silicate glass (consisting of 92.5% SiO₂ and 7.5% TiO₂). The material is characterized by supe-

624) C. Devilliers, M. R. Krödel, “CESIC – A new Technology for Lightweight and Cost Effective Space Instrument Structures and Mirrors,” Proceedings of the IAC 2005, Fukuoda, Japan, Oct. 17–21, 2005, IAC–05–B1.3.03

625) Note: Invar is a nickel–steel alloy invented in the early 1900s by the Frenchman Charles Edouard Guillaume. Invar (derived from “invariable” due to its particular characteristics) was the ideal material for balances as its coefficient of expansion is 15 times lower than that of steel.

rior dimensional stability, which results from the essentially zero expansion at room temperature. The HST (Hubble Space Telescope) of NASA (launch Apr. 24, 1990 on STS–31) features a ULE primary mirror of 2.4 m diameter (f/24 Ritchey–Chretien) and a 0.3 m Zerodur secondary mirror. The HST primary mirror was a lightweighted monolithic design (824 kg) by Perkin–Elmer (now Goodrich Inc.), Danbury, CN, using a lightweight, thick egg crate core sandwiched between two plates and fused together. – The Subaru infrared telescope of NAOJ (National Astronomical Observatory of Japan), atop Hawaii’s Mauna Kea, contains a primary mirror of 8.2 m, created from Corning’s ULE precision glass (telescope operation since 1999). Subaru employs also the monolithic mirror technology.

– Pyrex is a borosilicate glass (originally cookware and dishware consumer products) developed by Corning Glass Works between 1911 and 1914. Among other things, borosilicate glass resists thermal shock and expansion (changes in temperature make Pyrex expand and contract much less than ordinary glass). The first telescope of Mount Palomar, CA, ordered by George E. Hale (1868–1938), is a 5 m diameter Pyrex mirror, casted by Corning in 1934. Pyrex is being used today as a low–cost substrate material in moderate–size telescopes due to its outstanding thermal characteristics. ⁶²⁶⁾

– The AMSD (Advanced Mirror Systems Demonstrator) program is a jointly funded effort by the USAF, NASA/MSFC, and NRO (started in the late 1990s). ⁶²⁷⁾ The main objective of AMSD is to effect order of magnitude improvements for the JWST (James Web Space Telescope) as compared to HST. In this program, Eastman Kodak demonstrated the AWJ (Abrasive Water Jet) milling technique to fabricate thin walled, open–ended, honeycomb core structure out of bulk ULE glass. A honeycomb sandwich–type results by a fusion bonding process attaching the front and back faceplates. Mirror areal densities of about 15 kg/m² are being achieved using monolithic glass mirror designs.

– At the start of the 21st century, new concepts in mirror design are being introduced with the so–called “**active optics**” technology by combining the elements of: a lightweight meniscus facesheet, figure control actuators, and computer technology, with mirror shape control. ⁶²⁸⁾ The integrated “meniscus mirror design” approach (pioneered by Xinetics Inc., Devens, MA in 1995) provides a mirror construction, in which a maximum amount of weight can be removed without affecting the optical figure properties and the dimensional stability of the mirror surface. A thin meniscus facesheet is made from SiC (Silicon Carbide) or C/SiC (Carbon fiber–reinforced Silicon Carbide), using a near net shape casting process. In the implementation of Xinetics, the facesheet has a reflective front surface and a back surface, which contains an integral stiffening structure that mitigates the dimensional stability problems often associated with thin, flimsy mirrors. Formed directly within the web support ribs are cutouts, which enable the integration of high strain, solid–state electroceramic actuators.

Some application examples of lightweight telescope mirror technology in spaceborne instruments (Earth observation and astrophysics missions):

- The SEVIRI (Spinning Enhanced Visible and Infrared Imager) radiometer on EU-METSAT’s MSG–1 mission (launch Aug. 28, 2002 into GEO) is employing a TMA (Three Mirror Anastigmatic) telescope design (5367 mm focal length) with Zerodur ceramic mirrors on a substructure. The primary elliptical plane mirror (M1) measures 830 mm x 530 mm. The secondary mirror is 500 mm in diameter; the tertiary mirror has a diameter of 60 mm. The mirror assembly has a total mass of 15.6 kg (mass reduction of 70% by milling honeycomb–shaped holes in the back of each mirror). The mirror micro–roughness is < 10 Å. Note: MSG–1 became Meteosat–8 on Jan. 29, 2004 when the mission was declared “op-

⁶²⁶⁾ <http://www.rfroyce.com/pyrex.htm>

⁶²⁷⁾ L. E. Matson, D. Mollenhauer, “Advanced Materials and Processes for Large, Lightweight, Space–Based Mirrors,” Proceedings of IEEE Aerospace Conference, Big Sky, MT, March 8–15, 2003

⁶²⁸⁾ M. A. Ealey, “Large Optics in the 21st Century: A Transition from Discrete Manufacturing to Highly Integrated Techniques,” Proceedings of IEEE Aerospace Conference, Big Sky, MT, March 8–15, 2003

erational” (commencement of routine operations). MSG–2 was launched on Dec. 22, 2005.

Product/Material (manufacturer)	Specific Density (ρ) (g/cm^3)	Young’s Modulus of Elasticity (E) (GPa)	Coefficient of Thermal Expansion (α), ($10^{-6}/\text{K}$)	Thermal conductivity (k), (W/mK)	Specific Heat (c) J/(kg·K)
ULE, (Corning)	2.20	68	<0.03	1.31	776
Pyrex (Corning)	2.23	64	3.2	1.3	726
Zerodur, (Schott)	2.53	92	<0.05	1.46	821
SiC (many)	3.05	466	2.37	240	660
Silica (many)	2.20	73	0.52	1.38	703
Borofloat (Schott)	2.23	63	3.2	1.1	830
C/SiC	2.65	250	1.8	130	700

Table 42: Overview of some optical material properties

- The Japanese astronomical space mission IRIS (Infrared Imaging Surveyor) of JAXA was launched on Feb. 21, 2006. IRIS, also known by the names ASTRO–F and Akari, is also the name of the telescope on this mission with a lightweight primary mirror of 685 mm diameter.⁶²⁹ It has a mass of 8.2 kg and is made of a sandwich–type SiC material, consisting of light porous SiC core and dense CVD (Chemical Vapor Deposition) SiC coat. The mirror is polished to high precision, it has an areal density of 20.7 kg/m².
- ATLID (Atmospheric Lidar) is an instrument technology development program of ESA since 1998. The instrument is being developed for EarthCARE (Earth Clouds, Aerosol and Radiation Explorer), a future cooperative mission of ESA/JAXA in planning. ATLID features a lightweight C/SiC telescope design of a lidar instrument (mirror diameter of 630 mm, mass = 6 kg including coating and mounting provision).
- The Herschel telescope of the ESA, flown on the HSO (Herschel Space Observatory) mission, uses a Ritchey–Chrétien type telescope with a primary mirror diameter of 3.5 m (the largest mirror built so far for a spaceborne infrared observatory). The HSO was launched on May 14, 2009 into a halo orbit at Lagrangian point L2.⁶³⁰⁶³¹ The telescope design employs a lightweight mirror (300 kg) consisting of silicon carbide (SiC) segments that are “brazed” together to form a monolithic mirror that can be polished to “any” required accuracy. Requirements call for a total WFE (Wave Front Error) of < 6 μm corresponding to diffraction–limited operation at 90 μm during operations, and a very low emissivity. Since the accuracy of the manufacturing of the primary mirror is the driver in the overall telescope WFE budget, the control of this parameter is important. The Herschel telescope is passively cooled to < 90 K and feeds three payload instruments inside a dewar (a helium tank of about 2560 l, the helium cools the instrument detectors to 4 K):
 - SPIRE (Spectral & Photometric Imaging REceiver). SPIRE consists of a 3–band imaging photometer (wavelengths at 250, 350 and 500 μm) and a Mach–Zender FTS (Fourier Transform Spectrometer) in the spectral range of 200–670 μm , providing simultaneous imaging of the entire infrared band.
 - PACS (Photoconductor Array Camera & Spectrometer), 57–210 μm spectral range. The PACS FPU (Focal Plane Unit) employs two Ge:Ga photoconductor arrays (spectroscopy mode) and two bolometer arrays (photometry mode). PACS features an accurate positioning cryogenic mechanism for positioning control (4 arcsec within 40° of arc). The detec-

629) T. Onaka, H. Kaneda, H. Okuda, H. Murakami, T. Kohno, S. Miura, et al., “Development of Lightweight Silicon Carbide Mirror at Cryogenic Temperatures for Infrared Imaging Surveyor (IRIS),” <http://origins.jpl.nasa.gov/meetings/ulsoc/papers/onaka.pdf>

630) <http://sci.esa.int/home/first/index.cfm>

631) Note: ESA’s HSO was formerly called FIRST (Far Infrared and Submillimeter Telescope), renaming in 2002 in honor of William Herschel (1738–1822)

tors are cooled to liquid helium temperatures (4.2 K). PACS built by the MPE Garching in cooperation with partners from six European countries. ⁶³²⁾

– HIFI (Heterodyne Instrument for Far Infrared). A high-resolution heterodyne spectrometer providing continuous coverage over the frequency range of 480 to 1250 GHz in five bands and 1410 to 1910 GHz in two additional bands.

Herschel is the only space observatory to cover a spectral range from the far infrared to sub-millimeter, so there's a wide range of objects and topics covered, including star formation, galaxy evolution, and cosmology.

- The JWST (James Webb Space Telescope, formerly NGST) of NASA has a planned launch in 2015 to L2. ⁶³³⁾ The JWST telescope design will feature a figure-controlled (flexible) segmented lightweight primary mirror structure of about 6–8 m diameter controlled by an array of surface-mounted actuators (TMA design, and use of C/SiC technology). Requirements call for observations in the spectral region of 0.5 – 30 μm (VIS to FIR) and a telescope mass of < 600 kg with an areal density of < 15 kg/m^2 . – The primary mirror architecture of Northrop Grumman Space Technologies (formerly TRW) features a 36-segment configuration with semi-rigid segments, each actuated in tilt, piston, and radius-of-curvature degrees of freedom.

- A further entry into the ring is SPICA ⁶³⁴⁾ (Space Infrared Telescope for Cosmology and Astrophysics), a JAXA-led mission to L2 with a planned launch in the timeframe 2017/18. The telescope aperture will have a diameter of 3.5 m with a monolithic C/SiC mirror design. The ESA contribution to the SPICA mission is the provision of the cryogenic telescope assembly. The SPICA requirements call for a spectral coverage of 5 – 200 μm with a diffraction limit at 5 μm . The telescope is cooled to 5 K. The core wavelength range of SPICA will be covered with two focal plane instruments: Mid Infrared Camera and Spectrometer, and the Far Infrared Camera and Spectrometer. ⁶³⁵⁾

- A completely new approach, away from the traditional polished glass technique, may eventually be realized in the future with deployable thin-film mirror technology. The lightweight thin film can be folded during the launch phase. The film mirror is subsequently being shaped into its correct form by an electron gun – resulting in an ultralight space telescope. The new mirror, which is composed of a piezoelectric material that expands and changes shape when an electric field is applied, uses a whole new technique of mirror fabrication. ⁶³⁶⁾

1.5.11 AHM (Actuated Hybrid Mirror) Segments

Future optics programs will require a new paradigm for manufacturing largeaperture space telescopes. The technology development of meter-class AHMs (Active Hybrid Mirrors) specifically addresses the problem of how to provide tens of square meters of high-quality, lightweight space-qualified optics at reduced costs and within a shorter manufacturing schedule. The AHM replaces passive mass with actuators and controls to provide low-scatter, diffraction-limited imaging in the space environment.

632) E. Renotte, E. Callut, P. Delvaux, J. – M. Gillis, et al., “The Herschel – PACS Grating Drive and its Controller,” Proceedings of 54th IAC (International Astronautical Congress), Bremen, Germany, Sept. 29 – Oct. 3, 2003

633) D. C. Redding, F. Shi, S. A. Basinger, D. Cohen, J. Green, A. E. Lowman, C. M. Ohara, “Wavefront Sensing and Control for Large Space Optics,” Proceedings of IEEE Aerospace Conference, Big Sky, MT, March 8 – 15, 2003

634) <http://www.ir.isas.ac.jp/SPICA/>

635) <http://esamultimedia.esa.int/docs/gsp/completed/C21781ExS.PDF>

636) C. Burroughs, “New deployable thin-film, ultralight mirror may be future of space telescopes and surveillance satellites, ‘Smart’ material promises whole new approach to space mirrors,” Sandia Lab News, Vol. 52, No 9, May 5, 2000, http://www.sandia.gov/LabNews/LN05-05-00/mirror_story.html

State-of-the-Art technology (2009). Two 75-cm AHMs have been fabricated and optically tested, both in air and in vacuum to a controlled parabolic shape. The AHMs developed for this instance are the combination of three distinct technologies: ⁶³⁷⁾ ⁶³⁸⁾

- 1) a metallic nanolaminate facesheet that provides a high optic quality reflective surface
- 2) a SiC (Silicon Carbide) facesheet that provides structural support and houses actuators to provide an adaptive surface figure
- 3) wavefront sensing that provides active figure control. Reported measurements exclude gravity sag around mounts.

The AHM concept was first developed early in 21st century by a merger of two technologies: the actuated 'Integrated Meniscus Mirror' and 'magnetron sputtering of thick, metallic nanolaminate optical facesheets.' This development occurred through collaboration between LLNL (Lawrence Livermore National Laboratory) and Xinetics, Inc. Over the past several years, these Actuated Hybrid Mirrors have evolved through a range of sizes, establishing the ability to scale their manufacture up to the 1.5 m diameter class. AHMs have been fabricated as flat, spherical, and aspherical (both on- and off-axis) mirrors and mirror segments. The substrate employed has been reaction bonded silicon carbide fabricated by what is now Northrop Grumman Xinetics (NGX) in Devens, MA. NASA/JPL is also in the development cycle. ⁶³⁹⁾

The AHM technology under development is a hybrid structure integrating a precision nanolaminate foil facesheet and SiC substrate embedded with electroactive ceramic actuators. Wavefront sensors are used to determine wavefront errors created by mirror surface errors. A control system is used to determine voltage for actuators based on the wavefront errors. The concept is similar to adaptive optics. ⁶⁴⁰⁾

AHM performance: Actuated hybrid mirrors of less than 15 kg/m² have demonstrated 40 nm total WFE (Wave Front Error), gravity effect included, limited by mandrel polishing residual errors. Active mirrors at cold temperatures for IR astronomy offer the potential to reduce or eliminate "cryo figuring," by using actuators to correct WFE induced by cooling mirrors to cryogenic temperatures.

The next generation telescope in planning (as of 2010) is **ATLAST** (Advanced Technology Large-Aperture Space Telescope), a highly versatile UVOIR (UV-Optical-Near IR) observatory in space, larger and more capable than either HST or its IR-optimized successor, the JWST. ATLAST will use the AHM technology resulting in a primary aperture diameter in the 8-16 m range that will allow the project to perform some of the most challenging observations to answer some of our most compelling questions, including "Is there life elsewhere in the Galaxy?" A launch of ATLAST could be in the timeframe 2025 if the development resources are made available. ⁶⁴¹⁾

637) Gregory Hickey, "Actuated Hybrid Mirror (AHM) Segments," Feb. 23, 2009, in 'Technology Development Plan for the Advanced Technology Large Aperture Space Telescope (ATLAST),' April 24, 2009, URL: http://www.stsci.edu/institute/atlast/documents/ATLAST_Tech_Dev_Plan.pdf

638) Stephen C. Unwin, G.S. Hickey, R.A. Laskin, D.C. Redding, W.A. Traub, M.W. Werner, "Active Space Telescope Systems: A New Paradigm," 2010, URL: http://www.stsci.edu/institute/atlast/documents/active_STSystems_Unwin2010.pdf

639) Howard A. MacEwen, "Actuated Hybrid Mirror Technology," 2010, URL: <http://www8.nationalacademies.org/astro2010/DetailFileDisplay.aspx?id=566>

640) Brij N. Agrawal, Jae Jun Kim, "Surface Control of Actuated Hybrid Space Mirrors," Proceedings of the 61st IAC (International Astronautical Congress), Prague, Czech Republic, Sept. 27-Oct. 1, 2010, IAC-10.C2.5.8

641) Marc Postman, Vic Argabright, Bill Arnold, David Aronstein, Paul Atcheson, Morley Blouke, Tom Brown, Daniela Calzetti, Webster Cash, Mark Clampin, Dave Content, Dean Dailey, et al., "Advanced Technology - Large-Aperture Space Telescope (ATLAST): A Technology Roadmap for the Next Decade," NRC (National Research Council) ASTRO-2010 (Astronomy and Astrophysics Decadal Survey), URL: http://www.stsci.edu/~marel/decadal/rfi/ATLAST_Astro2010_PPP_REFI_FINAL.pdf

1.5.12 Deployable space structures

Deployable space structures (antennas, solar panels, booms, trusses, etc.) are structures capable of large configuration changes when deployed in an autonomous way (generally on orbital insertion after launch). Obvious advantages of deployable structures are savings in mass and launch volume. Also, a compact and tightly packaged configuration offers considerable stiffness to withstand the launch loads. In its deployed configuration, the spacecraft structure is only subjected to the orbital loads, which are considerably lower than those on Earth. An important issue in the design of quite a few deployable space structures is the true attainment of its deployed configuration with regard to shape and size, alignment, precision, and stiffness requirements in the deployed state (the variable on-orbit thermal and vibration environments must also be considered). These aspects are usually critical to the measurement performance of the mission.

Deployable space structures play an important part in the realization of practically all space missions, since the limited envelopes of the existing launchers constrain the payloads geometrically. From a historic point of view, deployable structures have been used since the very beginning of the spaceage. Eventually, an arsenal of lightweight space-deployable structures evolved for a variety of applications that include spacecraft stabilization, mobile communications, radiometry, active microwave sensing (deployable space frames like the apertures of SAR antennas, scatterometer fans), robotic manipulators, etc. Considerable research has been invested to study the dynamics and control of such deployable structures and to validate these concepts in space.

At the start of the 21st century, increasing demands, for example for energy supply, require more and more very large appendages on spacecraft.⁶⁴²⁾ Power generation of the International Space Station (ISS) is provided by eight deployable solar arrays, each spreading an area of approximately 32.6 m x 11.6 m. The 60 m long boom which was deployed and retracted in 2000 onboard of the Space Shuttle Endeavour during the Shuttle Radar Topography Mission (SRTM) is another prominent example. Presently, a clear trend for an increasing need can be identified for a number of future space structure applications like instrument booms, antennas and mesh reflectors, solar sails, deployable mirrors for large telescopes, and eventually huge solar space power systems.

642) C. Sickinger, L. Herbeck, T. Ströhlein, J. Torrez-Torres, "Lightweight Deployable Booms: Design, Manufacture, Verification, and Smart Materials Application," Proceedings of IAC 2004, Vancouver, Canada, Oct. 4-8, 2004, IAC-04-I.4.10

1.5.13 Inflatable Space Structures

Large and low-mass in-orbit deployable structures, in particular effective apertures, are enabling elements for a wide spectrum of applications, ranging from remote sensing (radars, radiometers, interferometers, telescopes, etc.) to radio astronomy, communications, and wireless power transmissions (WPT). Large antenna reflectors for the next-generation space applications are characterized by a diameter in excess of 12–15 m which can be packed in a limited fairing envelope of the available launch systems. The challenge is to design antennas with a reliable deployment mechanism and with high contour accuracy and stiffness after deployment. The mass reduction potential of these advanced antennas enables an increasing payload instrumentation to be integrated on a mission (or the use of a smaller S/C). The principal design of available deployable structures can generally be divided into mechanically deployable structures as well as into inflatable structures.

Background: At the start of the 21st century, the space inflatable structure technology is one of the emerging/enabling technologies that can potentially revolutionize the designs and applications of large space structural systems. Concepts of inflatable deployable space structures have been under development since the early 1960s when the ECHO balloon satellites of NASA were successfully sent into orbit. The inflatables were chosen because the launch capabilities of the early US space program were rather limited. Major advantages of using inflatable elements in space are their high packaging efficiency, extremely light weight, high deployment reliability, and low cost. ⁶⁴³⁾ ⁶⁴⁴⁾ ⁶⁴⁵⁾

Flexible inflatable composite materials are utilized in many applications today but perhaps may find their greatest benefit in space structures. The automobile tire is the best known example of a flexible inflatable composite structure. In this case, the flexible matrix material is reinforced with woven materials such as steel or Kevlar. The reinforcement materials aid in supporting the structural loads due to inflation and also increase the composite material's puncture resistance. Inflatable structures for space use similar principles to achieve the same or better performance as rigid structures. As is the case with automotive tires, space inflatable structures have become more durable and robust with the advent of new materials. Advanced flexible polymers and high strength fibers such as Kevlar, Vectran, and Spectra, have enabled the fabrication of very low mass structures that are deployable from a densely packed state.

Inflatable structures minimize mass and volume of a spacecraft, they are far less expensive and will become increasingly important in future space missions. The inflatable technology fulfils best the requirements of large-diameter space structures (antennas, etc.), followed by the mesh technology with straight or foldable ribs. Inflatable structures are classified into three categories, depending upon the type of inflation they require. The categories are:

- CI (Continuously Inflated) structures
- RI (Rigidized Inflatable) structures
- SI (Single-Inflation) devices

CI structures such as balloons, data collection antennas, rover tires and habitats require continuous inflation (pressurization) throughout a mission. Hence, leakage (attributable to

643) D. P. Cadogan, S. E. Scarborough, "Rigidizable Materials for use in Gossamer Space Inflatable Structures," AIAA Gossamer Spacecraft Forum, April 16–19, 2001, Seattle, WA

644) R. E. Freeland, G. D. Bilyeu, G. R. Veal, M. M. Mikulas, "Inflatable Deployable Space Structures Technology Summary," 49th IAF Congress, Melbourne, Australia, Sept. 28 to Oct. 2., 1998, IAF-98-1.5.01

645) Note: Large mechanically deployable antennas have been in great demand over the past two decades for a variety of space applications, such as satellite/mobile communications, radiometry, SAR (Synthetic Aperture Radar), and VLBI (Very-Long-Baseline Interferometry). – In the summer 2000, NASA started a Gossamer Spacecraft Initiative. The overarching goal is to achieve breakthrough enhancements in mission capability and reductions in mission cost, primarily through revolutionary advances in structures, materials, optics, and adaptive and multifunctional systems. The enabling technology is in particular envisioned for such applications as: very large aperture telescopes, large inflatable antennas, solar sails, and large solar power collection. The field of Earth observation will also profit from this initiative.

flaws in materials and holes from micrometeorites) is a major disadvantage of these structures. Pure inflatable CI structures are used only for missions with short operational life and where the supply of make-up gas does not pose a problem. RI structures, including antennas, solar arrays, light sails and solar shields, are made of materials that harden when they are inflated and exposed to sunlight. RI structures provide long-term structural integrity (mission life of 10–15 years); today, they are being considered for a variety of space applications. SI and RI devices are only inflated once. SI devices, such as landing bags, are then discarded.

RI structures are fabricated from flexible composite laminates. The material can be folded and packaged; once in orbit, it is being rigidized in situ via some external influence (thermal heating is a proven rigidization method by exposure to sunlight). Typical shapes or building blocks of the material are: toroids, spheres, dish structures, tubes, etc., which can be assembled into the required final structures. Naturally, process control is a major issue in the deployment/inflation/rigidization procedure.

The use of inflatable technology in a deceleration system offers some great advantages because of its low storage volume, mass and cost. Due to these advantages inflatable deceleration technology can successfully be used for planetary exploration or to return a small payload from ISS (International Space Station).

- Inflatable spaceborne structures have been used since 1960 with the launch NASA's ECHO series experimental communication and geodesy satellites. These balloon satellites of 30 m diameter (ECHO-1A launch Aug. 12, 1960 available until 1968, ECHO-2 launch Jan. 25, 1964 available until 1969) were deployed from a packing container 0.67 m in diameter using inflation gas.⁶⁴⁶ The deployment event of the balloon satellites was uncontrolled and depended only on the packing method used. The ECHO satellites were large metalized balloons (manufactured from a laminate of 1100-0 aluminum foil and polyester film) that served as passive reflectors of radio signals (unfortunately the reflected signal was rather weak, hence not attractive for commercial use). ECHO-2 remained in orbit for several years.

- The follow-up Explorer IX and XIX inflatable spacecraft of NASA were used for high altitude atmospheric studies. Explorer IX (launch Feb. 16, 1961 from Wallops Island, VA) was a 3.5 m diameter sphere after inflation at orbital altitude (966/2157 km) with a mass of 17 kg. Explorer XIX was launched on Dec. 19, 1963. The PAGEOS (Passive Geodetic Earth Orbiting Satellite) spacecraft of NASA (launch June 24, 1966 from VAFB) was an aluminum-coated Mylar balloon of 30 m diameter with a mass of 55 kg (2953 km perigee, 5207 km apogee). Over 30 launches of inflatable spheres occurred during the period from 1960 to 1971 with some remaining in orbit for over 11 years. Several of the early balloon satellites failed during the inflation event. Some of these failures were attributed to lack of control of the inflation process. Modifications were made to the packing and inflation procedure which lead to success with subsequent flights. Most of the early research on space inflatables centered on methods of making the structure rigid.

- **Inflatable antenna structures.** Inflatable structures have the advantages of low mass, low stored volume, and of low cost. They also have the potential to deploy much more reliably than the conventional mechanical systems used for deploying rigid structures. However, the deployment of high-performance antennas needs some supervision in form of antenna surface shape control to satisfy the requirements of surface accuracy. Inflatable structures have been analyzed and developed in the US by NASA/JPL and AFRL in cooperation with L'Garde, ILC Dover, etc.; in Europe by ESA in cooperation with Contraves, Switzerland, with EADS Astrium, etc. – Inflatable antennas may be used in various frequency ranges (in particular VHF, UHF, MW) for such diverse applications as measuring soil mois-

⁶⁴⁶) D. P. Cadogan, M. S. Grahn, "Deployment Control Mechanisms for Inflatable Space Structures," 33 rd Aerospace Mechanisms Symposium, Pasadena, CA, May 19–21, 1999

ture and ocean salinity or communications and power generation for satellites. Following are some demonstrations of inflatable and of mechanically deployable structures. ⁶⁴⁷⁾ ⁶⁴⁸⁾

– In 1996, the spaceborne NASA **IAE** (Inflatable Antenna Experiment) was flown on SPARTAN–207 of the Shuttle mission STS–77 (May 19 – 29, 1996), a small free–flying satellite, made up of four major components: lens, torus, struts, and body. The experiment was conceived to verify the accuracy of an inflatable off–axis parabolic lenticular antenna structure deployed in space and to demonstrate its performance. NASA and L’Garde Inc. of Tustin, CA, worked together in the IN–STEP (In–Space Technology Experiments Program) to conduct the experiment. ⁶⁴⁹⁾ The inflated antenna (successfully deployed on May 20) consisted of a 14 m lenticular, supported around its perimeter by an inflatable torus. The antenna assembly was attached to the parent spacecraft, SPARTAN–207, by three 28 m inflatable struts. The entire deployment system had a mass of 60 kg. Antennas of this type have the potential to be used for such applications as for space and mobile communications, Earth observations, astronomical observations, and space–based radar.

– The Russian/Georgian EGS “**Reflector**” experiment at the MIR Space Station (successful deployments in the period, July 23–28, 1999). ⁶⁵⁰⁾ ⁶⁵¹⁾ The objective was to demonstrate and validate the mechanical deployment (form creation process in the space environment) of a large deployable high–precision offset (mesh) antenna. The reflector construction included many novelties which make it different from all other presently known reflectors. The reflector structure is of parabolic design. The stowed transport package had dimensions of 620 mm x 1060 mm. Together with electrical and mechanical systems the reflector mass is 38 kg, while together with the interface and container its weight is 46.5 kg. The stowed pack was delivered by the cargo ship “Progress M–42” to MIR on July 18, 1999. At the end of the experiment, the cosmonauts turned the reflector mounting ring around of the SOFORA mast (a 14 m mast structure on the Kvant–1 module) on MIR and jettisoned the antenna away from the orbital station.

Parameter	Value	Parameter	Value
Optics	Offset parabolic	Antenna rim geometry	6420 mm x 5500 mm
Projected aperture	5500 mm diameter	Length closed	1060 mm
Focal length	4200 mm	Diameter closed	620 mm
Offset	1950 mm	Deployment time	7 minutes

Table 43: Characteristics of Reflector

– The US AFRL at Kirtland AFB, NM, launched an inflatable sphere, named OCSE (Optical Calibration Sphere Experiment, built by L’Garde), on the JAWSAT mission (launch Jan. 27, 2000 on a Minotaur launcher into LEO, see N.12) of Weber State University, Ogden, UT. The objective was to refine and support spacecraft SLR tracking from the ground. The balloon had a diameter of 3.5 m. After successfully completing its one year mission, OSCE reentered the Earth’s atmosphere on March 5, 2001.

– The ISAR (Inflatable SAR) antenna under development at NASA/JPL is an L–band radar that has an aperture size of 10 m x 3 m, an operating frequency of 1.25 GHz, dual–lin-

647) C. E. Willey, R. S. Bokulic, W. E. Skullney, R. C. Schulze, “Ka–band Hybrid Inflatable Dish Antenna,” JHU/APL Technical Digest, Vol. 22, No 2, 2001, pp. 110–111

648) H. Tanaka, M. C. Natori, “Shape Control of Inflatable Antennas Based on Radiation Pattern Analysis,” 25th Antenna Workshop on Satellite Antenna Technology, Sept. 18–20, 2002, ESA/ESTEC

649) J. A. Lewis, “Finite Element Modeling and Active Control of an Inflated Torus Using Piezoelectric Devices,” Thesis submitted at Virginia Polytechnic Institute and State University, Blacksburg, VA, Dec. 2000

650) E. Medzmarishvili, G. Kinteraya, L. Datashvili, et al., “Space Experiment ‘Reflector’ on Testing the Large–Scale Deployable High–Precision Offset Antenna Reflector of a New Generation at the Orbital Station Mir,” Proceedings of the AP2000 Millennium Conference on Antennas & Propagation, Davos, Switzerland, April 9–14, 2000

651) A. Cherniavsky, M. Djanikashvili, Yu. Kravchenko, C. Catallo, et al., “The Large Deployable Reflector Program at S. P. A. EGS and Alenia Spazio,” 25th Antenna Workshop on Satellite Antenna Technology, Sept. 18–20, 2000, ESA/ESTEC

ear (vertical and horizontal) polarization, 80 MHz bandwidth, and electronic beam scanning. The antenna aperture consists of three layers of thin-film membranes that form the radiating plane, the ground plane, and the transmission line plane. The ISAR designs are lightweight (11–12 kg).

- **IRDT (Inflatable Reentry and Descent Technology).** IRDT is an inflatable reentry vehicle (cone-shaped shield) project, co-sponsored by ESA, EC and EADS Astrium GmbH, designed/developed by NPO Lavochkin in Moscow, and EADS Astrium GmbH (sensor package) in Bremen, Germany, and launched by Starsem (Russian/European launch company). The first demonstration flight was conducted Feb. 9, 2000 when IRDT successfully returned the Fregat upper stage of the Soyuz launch vehicle; a second one returned a small 15 kg ESA payload called “Mission 2000.” The reentry packages were returned to Earth about eight hours later, with the inflatable shields also doubling as drag devices and soft-landing “airbags” instead of using parachutes. The Mission 2000 payload used a 95 kg two-stage IRDT shield. The first stage was inflated to envelop the payload upon separation from the Fregat stage; the second was inflated at an altitude of about 20 km, after entering the atmosphere, to serve as an airbrake for landing. The second stage apparently malfunctioned, allowing the payload to land at 60 m/s instead of the planned 13 m/s. The payload was not damaged, however. — IRDT makes use of technologies originally developed by NPO Lavochkin within the Russian Mars program in 1996. The IRDT system presents a potential lightweight, economical method to return payloads to Earth. A goal of the demonstration is to use the IRDT system in future autonomous small payload return flights (samples) from ISS (international Space Station).

- In the late 1990s, NASA was engaged in the development of **TransHab**, a large inflatable habitat in space whose multi-layer shell was based on Kevlar high-strength fibers (TransHab requirements called for an inflated volume of 340 m³, 11 m in length and 4.3 m in diameter, and a launch mass of 13,200 kg) for protection from orbital and meteoroid debris. TransHab was intended as a replacement for the already existing rigid International Space Station crew habitation module. However, the US Congress (and NASA) cancelled the TransHab project in 2000 due to budgetary constraints.

- In 2002, Bigelow Aerospace of Las Vegas, NV, bought the TransHab license from NASA and started to pursue a development scheme for a civilian space complex. This resulted in the launch of two technology demonstration missions, Genesis–1 and Genesis–2 with launches on July 12, 2006 and June 28, 2007, respectively, to evaluate inflatable/expandable space module technology. The privately built and financed habitable structures are intended to be available for research, manufacturing and other uses, including lodging for future space tourists.

Each Genesis spacecraft has a launch mass of about 1,360 kg and a size of 4.6 m in length and 1.6 m in diameter at launch. The spacecraft architecture features an expandable outer surface that is wrapped around a central core at launch and expanded through air inflation in orbit. The skin is made of several layers that include proprietary impact-resistant materials. The flexible structure is designed to double in diameter once in orbit. The one-third scale hardware is to produce important data regarding multiple features of a full-scale spacecraft. The goal/commitment is to develop and operate a privately-owned inflatable space complex commercially and to be of service to a community of customers interested in space exploration and space habitats.

- **ARISE (Advanced Radio Interferometry between Space and Earth).** A NASA/JPL astronomy satellite mission in planning consisting of a 25 m diameter radio telescope (an inflatable structure with a very thin reflecting surface that does all the work in collecting light from the cosmos) in a highly elliptical Earth orbit (HEO). The new lightweight telescope architecture is called DART (Dual Anamorphic Reflector Telescope). The DART concept makes use of two parabolic, cylindrical trough-shaped reflectors oriented with respect to each other to produce a point focus. Since each reflector contains only a single simple curve,

the mirrors can be formed by tensioning a reflective foil over a frame that has a parabolic contour along one axis. The use of an extremely low-mass membrane for the reflective surfaces reduces the mass of the telescope.

The orbiting telescope (inflatable antenna with a size of the 25 m diameter) is used in a SVLBI configuration with arrays of ground-based telescopes to image radio sources in the universe with a resolution of 10–20 microarcseconds. Lowering the cost and maximizing the antenna performance are the two primary goals of the mission. The ARISE design is an upscale version of the IN-STEP structure IAE (Inflatable Antenna Experiment).

- **STR (Spring-Tape-Reinforced) booms.** Besides antennas, inflatable structures may also be employed for other components of space structures such as: solar arrays, sunshades, solar concentrators, and telescope reflectors.⁶⁵²⁾ The STR technology, invented at JPL, represents another enabling element of inflatable structures, including self-rigidizable booms made of stretched aluminum laminates. A typical boom consists of a tube, formed of aluminum laminate sheet, and seamed by a Kapton tape and two end caps. A number of distinct advantages of the STR booms have been identified and demonstrated during the development process. These include: simplicity of the design, self-rigidizable in space, high-load carrying capability, high packing efficiency, and low inflation deployment pressure.

- **HIA (Hybrid Inflatable Antenna) for Ka-band applications.** JHU/APL and ILC Dover Inc. developed a hybrid antenna concept combining a fixed parabolic dish with an inflatable reflector annulus that greatly increases antenna area. The objective is to provide a credible backup capability with the high-gain parabolic dish in the event of an inflation failure. In this scenario, the inflated annulus enhances the science return above the minimum level already provided by the existing rigid dish. The rigid reflector provides a guaranteed high-gain capability, and the inflated annulus provides a “bonus” science return. For instance, a 1 m diameter rigid dish acquires a 16 times greater data rate capability when the annulus is inflated to a 4 m diameter.^{653) 654)}

- **MOIRE (Membrane Optical Imager for Realtime Exploitation)**

MOIRE is a DARPA (Defense Advanced Research Projects Agency) technology demonstration program of the U.S. DoD which started in 2010. The overall goal of the program is to incrementally demonstrate technologies needed to develop a large lightweight spaceborne telescope for GEO (Geosynchronous Orbit) using advanced diffractive membrane optics.

MOIRE plans to demonstrate the manufacturability of large collection area telescopes (up to 20 m in aperture), large structures to hold the optics tight and flat, and also demonstrate the additional optical elements needed to turn a diffraction-based optic into a wide bandwidth imaging device.⁶⁵⁵⁾

Size and cost constraints have so far prevented placing large-scale imaging satellites in GEO, so MOIRE is developing technologies that would make orbital telescopes much lighter, more transportable and more cost-effective.

Note: The French word “moiré” refers to an interference pattern, such as one used during the fabrication of diffractive optics. It is an appropriate name for a project where diffractive optics are central to success.

652) M. Lou, H. Fang, L. M. Hsia, “Development of Space Inflatable/Rigidizable STR Aluminum Laminate Booms,” Proceedings of the AIAA Space Conference and Exhibition, Long Beach, CA, Sept. 19–21, 2000

653) C. E. Willey, R. C. Schulze, R. S. Bokulic, W. E. Skullney, “A Hybrid Inflatable Dish Antenna System for Spacecraft,” 42nd AIAA/ASME/ASCE/AHS/ASC Conference & Exhibit, AIAA Gossamer Spacecraft Forum, Apr. 16–19, 2001, Seattle, WA

654) B. G. Boone, “Materials and Structures Research and Development at APL,” Johns Hopkins Technical Digest, Vol. 24, No 1, 2003, pp. 102–111

655) “Membrane Optic Imager Real-Time Exploitation (MOIRE),” URL: http://www.darpa.mil/Our_Work/TTO/Programs/Membrane_Optic_Imager_Real-Time_Exploitation_%28MOIRE%29.aspx

BATC (Ball Aerospace & Technologies Corporation) is the prime contractor for the MOIRE program. During the summer of 2011, BATC successfully demonstrated in the first phase of the program the ability to create a diffracted optical element on a membrane. ⁶⁵⁶⁾

In 2013, the MOIRE program is in its 2nd and final phase; the program recently successfully demonstrated a ground-based prototype that incorporated several critical technologies, including new lightweight polymer membrane optics to replace glass mirrors. Membrane optics traditionally have been too inefficient to use in telescope optics. MOIRE has achieved a technological first for membrane optics by nearly doubling their efficiency, from 30 percent to 55 percent. The improved efficiency enabled MOIRE to take the first images ever with membrane optics. ^{657) 658)}

While the membrane is less efficient than glass, which is nearly 90% efficient, its much lighter mass enables creating larger lenses that more than make up the difference. The membrane is also substantially lighter than glass. Based on the performance of the prototype, a new system incorporating MOIRE optics would come in at roughly one-seventh the mass of a traditional system of the same resolution and size. As a proof of concept, the MOIRE prototype validates membrane optics as a viable technology for orbital telescopes.

Instead of reflecting light with mirrors or refracting it with lenses, MOIRE's membrane optics diffract light. Roughly the thickness of household plastic wrap, each membrane serves as a Fresnel lens — it is etched with circular concentric grooves like microscopically thin tree rings, with the grooves hundreds of microns across at the center down to only 4 μm at the outside edge. The diffractive pattern focuses light on a sensor that the satellite translates into an image.

MOIRE technology houses the membranes in thin metal “petals” that would launch in a tightly packed configuration roughly 6 m in diameter. Upon reaching its destination orbit, a satellite would then unfold the petals to create the full-size multi-lens optics. The envisioned diameter of 20 m would be the largest telescope optics ever made and dwarf the glass mirrors contained in the world's most famous telescopes.

From GEO, it is estimated, a satellite using MOIRE optics could see approximately 40 % of the Earth's surface at once. The satellite would be able to focus on a target area of 10 km x 10 km area at 1 m resolution, and provide real-time video at 1 frame per second.

The MOIRE program plans to perform an on-orbit experiment of optical membrane imaging technologies through the FalconSAT-7 program of the USAFA (United States Air Force Academy) in 2015.

1.5.14 MEMS (Micro-Electro-Mechanical System) technology

MEMS – also known as “microsystems” in Europe or “micromachines” in Japan. MEMS technology first emerged in the late 1960s and early 1970s. MEMS devices, tiny machines virtually invisible to the naked eye (they range in size from a few μm to mm), fashioned largely from silicon with techniques adapted from the microchip industry, are able to **“touch” the physical world and act upon it**. There is a trend toward complete microsystems – merging sensing, actuating, computing and communications. Microtechnology represents essentially a synergetic combination between thin film technology, semiconductor technology, silicon micromechanics, ultra precision engineering, LIGA technique, laser li-

656) <http://www.ballaerospace.com/page.jsp?page=259>

657) “First Folding Space Telescope Aims to ‘Break the Glass Ceiling’ of Traditional Designs, DARPA, Dec. 05, 2013, URL: <http://www.darpa.mil/NewsEvents/Releases/2013/12/05.aspx>

658) Rose Hansen, “Developing Lightweight Optics for Space,” S&TR (Science & Technology Review) January/February 2013, URL: <https://str.llnl.gov/content/pages/january-2013/pdf/01.13.4.pdf>

thography, and several technologies for packaging and assembly.^{659) 660) 661)} The new microsystems offer enhanced levels of perception, control, and performance (nanoscale design, low power quantum electronics, high bandwidth photonic devices, etc.). The evolving list of MEMS features includes: provision of inputs and outputs for information systems, permitting multiple and mixed technology integration (CMOS/MEMS integration, integrated trench technology, etc.); in particular, there is the ability **to sense and measure changes of physical parameters on the micro–scale (atomic) level**, orders of magnitude better, than traditional techniques. At the end of the 1990s, the technology of miniaturization experiences a tremendous growth. It is destined to become a natural pick for a diverse number of applications in all fields, in particular for the design of new instruments in the space industry. The potential of MEMS as an enabling technology has a definite impact on new designs, similar to the impact of integrated circuits for the electronics industry during the 1960s and 1970s.

At the start of the 21 century, RF and microwave frequency MEMS have indeed potentially enormous and widespread applications in the electronics and telecommunications industry.^{662) 663)} The MEMS technology is in particular an enabler for high–frequency switches (GHz range). Components based on MEMS technology such as switches, varactors, and phase shifters exhibit virtually no power consumption or loss. There are always two distinct functions to a MEMS switch or varactor, namely: 1) the actuation (or mechanical) function, and 2) the electrical function. The forces required for the mechanical movement can be obtained using electrostatic, magnetostatic, piezoelectric, or thermal designs.

Some examples of MEMS space applications are:

- MEMS technology is being applied to a variety of optical applications, ranging from adaptive mirrors to integrated optical benches, grating spectrometers, optical scanners, fluid pumps, etc.
- MEMS technology is making possible the development of many different types of thermal sensors for spaceborne instruments and operational hardware. At the start of the 21st century, these are becoming available with high performances and in the case of arrays (linear or matrix) make possible a new class of imaging and spectrographic instruments.
- Integrated microaccelerometers and gyros
- Uncooled infrared detectors
- MEMS technology is used to form miniature antennas for millimeter–wave applications
- MEMS technology is being applied to micropropulsion systems.
- MEMS technology is applied for distributed sensors and actuators (closed–loop control is a viable option)
- MEMS is being used for electromechanical signal processing
- In the early 1980s, the Institute of Microstructure Technology of KfK (Kernforschungszentrum Karlsruhe (Nuclear Research Center, Karlsruhe, Germany) initiated/developed a micromachining technology by the name of LIGA [Lithographie, Galvanoformung und Abformung (lithography, electroplating and moulding)]. LIGA is widely used throughout in-

659) M. Lacher, W. Ehrfeld, “Microproducts for Space Applications,” Proceedings of the 2nd International Conference on MicroNanotechnology for Space Applications, Apr. 11–15, 1999, Pasadena, CA, Vol. 1, pp. 4–25

660) J. Mueller, I. Chakraborty, et al., “MEMS–Micropropulsion Activities at JPL,” Proceedings 2nd Int. Conference on MicroNanotechnology for Space Applications, Apr. 11–15, 1999, Pasadena, CA, Vol. 1, pp. 175–200

661) I. Amato, “Fomenting a Revolution in Miniature,” *Science*, Vol. 282, Oct. 16, 1998, pp. 402–405

662) Note: A varactor is a special semiconductor diode that exhibits change in capacitance with a change in applied voltage; used as a voltage–variable capacitor.

663) Gabriel M. Rebeiz, “RF MEMS, Theory, Design, and Technology,” John Wiley & Sons, Inc. 2003, chapter 1

dustry and the research community for advanced MEMS applications. LIGA is a three-stage process which can be used for the manufacture of high aspect ratio, 3-D microstructures in a wide variety of materials (e.g. metals, polymers, ceramics and glasses). By using the penetrating power of X-rays from a synchrotron, LIGA allows the fabrication of structures which have vertical dimensions from hundreds of microns to millimeters and horizontal dimensions which can be as small as microns. SUMMiT (Sandia Ultra-planar Multi-level MEMS Technology) is another fabrication process developed by SNL (Sandia National Laboratories).

- In 1993 the **nanosatellite** concept experienced more definition by Siegfried W. Janson, Henry Helvajian, and Ernest Y. Robinson of the Center for Microtechnology at The Aerospace Corporation, El Segundo, CA. In this paper, the proposed nanosatellite architecture employs MEMS and ASIMs (Application Specific Integrated Microinstruments).⁶⁶⁴ ⁶⁶⁵ The integration of MEMS with microelectronics for data processing, memory, signal conditioning, power conditioning and communications results in stand-alone ASIMs (chip-to-chip wireless integration). ASIMs with silicon or other semiconductor substrate can be applied to S/C systems, i.e. tiny instruments, for such functions as guidance, navigation and control, attitude sensing, attitude control, thermal control primary propulsion, power and communication. In this concept, the nanosatellite denotes a S/C built almost entirely of ASIMs. The silicon satellites are spacecraft that utilize single-crystal silicon wafers for electronic substrates, mechanical structure, thermal control system, and radiation shield.

1.5.15 Cryogenic cooling techniques of observation instruments

The accurate measurement of incoming radiation, a principle used in all passive observation sensors, requires thermal and structural (vibration) instrument stability, and in various applications cryogenic cooling (simply referred to as “cryocooling”), to obtain reproducible results. Cryocooling is needed to provide the required detector response, reduce preamplifier noise, and/or reduce background radiation. Cryogenic operation has been required for a number of spaceborne instruments, including infrared sensors (focal plane imaging arrays, filters, occasionally optics), x- and gamma-ray detectors, and a number of emerging superconducting technologies. The objective of cryocooling is always to improve the sensitivity of the sensing device by suppressing unwanted noise. Typical cooling temperatures in space systems range from the boiling point of liquid Nitrogen at 77.36 K, down to near the boiling point of liquid Helium at 4 K (Note: the boiling point of Helium 4 is a bit above 4 K while that of Helium 3 is 3.2 K).

All infrared radiation generates heat on detection requiring generally a cooling method of the detector system for accurate signal measurements. This unwanted side effect of infrared heating involves rather costly implementations of cryocooling to circumvent this nuisance. In general, a cryogenic cooler (cryocooler) increases the mass, volume, and power consumption of the detector assembly by about an order of magnitude. A high price to pay for accuracy.

A number of technical approaches to meeting this need are possible and have been developed over the years.

- **Passive coolers** have been used for many years in space science applications due to their relatively high reliability and low vibration levels. These passive radiator systems have taken advantage of the inherent cold of deep space (however, they generally require large large

664) Siegfried W. Janson, Henry Helvajian, Ernest Y. Robinson, “The Concept of “Nanosatellite” for Revolutionary Low Cost Space Systems,” Proceedings of the 44th Congress of the International Astronautics Federation, Oct. 16–22, 1993, Graz, Austria, IAF–93–U.5.573

665) S. W. Janson, “Silicon Satellites for 21 st Century Missions,” Proceedings of the 2nd International Conference on MicroNanotechnology for Space Applications, Apr. 11–15, 1999, Pasadena, CA, Vol. 1, pp. 535–544

radiator areas and shading from heat sources such as the sun and IR emission from the spacecraft and planetary surface).

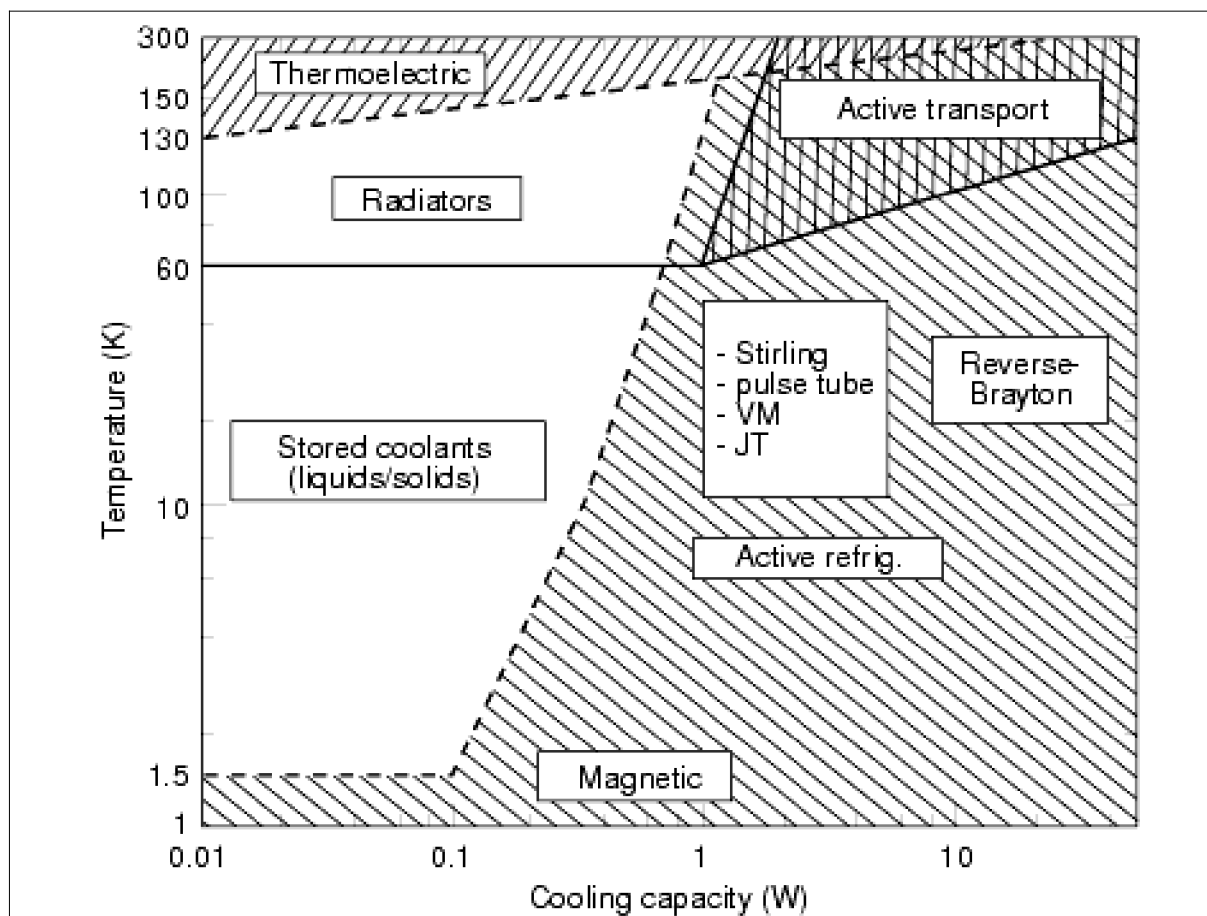


Figure 26: Cryogenic cooling methods in space (image credit: M. Donabedian, Vol. II: Cryogenics) ⁶⁶⁶

On spacecraft, focal planes are sometimes cooled with passive radiators, the performance of which is highly dependent on mission parameters and spacecraft configuration. Passive radiative coolers are well developed and provide exceptional reliability for detector arrays. The size of these coolers is, however, governed by the first-order physics of Planck's radiation law. The required minimum area for the radiative surface is governed by the relationship $W = A\epsilon sT^4$, where W is the radiated power, A is the area of the radiator, ϵ is the effective emissivity of the radiator's surface, s is the Stefan-Boltzmann constant, and T is absolute temperature. This relationship can be expressed as $A = W/(\epsilon sT^4)$. Thus, the area of the radiator needed to achieve a given cryogenic temperature depends directly upon the amount of cooling power required and upon the inverse fourth power of temperature. This is a highly nonlinear relationship; for example, it takes four times as much radiator area to reach 60 K as to reach 85 K. ⁶⁶⁷ Consequently, application of this comparatively straightforward technology is limited to relatively modest levels of cooling power at temperatures of about 65 K or warmer. This is more than adequate for sensors such as MODIS, but passive cooling would be a challenge for a high-resolution pushbroom longwave infrared imager, for example.

Some examples of passive radiative cooling are:

- 1) The HgCdTe detectors of the MVIRI (Meteosat Visible and Infrared Imager) on the first-generation Meteosat series are radiatively cooled to 90 K by a passive system (launch of Meteosat-1 Nov. 23, 1977, launch of Meteosat-7 Sept. 3, 1997).

⁶⁶⁶) <http://www.aero.org/publications/donabedian/donabedian-1.html>

⁶⁶⁷) <http://www.nationalacademies.org/ssb/smallsatappendb.htm>

2) The ETM+ (Enhanced Thematic Mapper Plus) of Landsat-7 (launch Apr. 15, 1999) is radiatively cooled. The second focal plane is the cold focal plane which includes the optical filters, infrared detectors, and input stages for ETM+ spectral bands 5,6, and 7. The temperature of the cold focal plane is maintained at 91 K using a radiative cooler.

3) The MODIS instrument of the Terra mission (launch Dec. 19, 1999) uses a high-performance passive radiative cooler to cool the infrared FPA to 83 K.

- **Dewars** [named after Sir James Dewar (1842–1923) who first liquefied hydrogen in the 1890s] containing liquid cryogen (stored coolants) have been flown. Typically, containment dewars are used for space systems that require cooling below 80 K. These open systems employ the latent heat of vaporization or sublimation for cooling. Although this technique has several advantages, such as the absence of exported vibration, the systems are massive, inconvenient to accommodate, and have limited lifetimes. The main applications are in infrared astronomy. Some examples:

- The joint IRAS (Infrared Astronomical Satellite) mission of NASA, The Netherlands, and the UK (launch Jan. 25, 1983) employed a dewar for infrared observations (wavelengths of 8.5–15, 19–30, 40–80, and 83–119 μm) of the universe. The telescope of 0.57 m diameter was housed in the dewar, filled with 480 liter of liquid helium and contained a plane array of 62 detectors. The entire telescope was cooled to a temperature of about 4 K. IRAS operated for 10 months until the cryogen was depleted. In addition, there was a spectrometer in the range 7.4–23 μm , and a photometer in the range 4.1–8 μm .

- SHOOT (Superfluid Helium On-Orbit Transfer), a NASA/GSFC cooling demonstration experiment, was part of the space shuttle STS-57 mission in June, 1993. The experiment objectives included: transfer of superfluid between two dewars connected by a tube in a low gravity environment at different flow rates; operation of two different liquid acquisition devices within the dewars; liquid/vapor phase separation for normal liquid helium as well as superfluid at varying venting rates; accurate mass gauging and flow metering; and autonomous control of the transfer process by an expert system aboard a computer on the Shuttle. ⁶⁶⁸⁾

- The NICMOS (Near Infrared Camera and Multi-Object Spectrometer) instrument of NASA, built by BATC, was flown to the HST (Hubble Space Telescope) on mission SM-2 [the second Hubble service flight on STS-82 (Feb. 11–21, 1997)]. NICMOS was designed to fit inside a cryogenic dewar, cooling the NICMOS detector with a block of solid nitrogen (104 kg). However, due to unforeseen design problems, the dewar ran out of nitrogen coolant after less than two years, and had to stop operation (see NICMOS under item 5 below, “Reverse Brayton cycle cooler”).

- The Spitzer Space Telescope mission of NASA/JPL (formerly SIRTF, launch Aug. 25, 2003) employs a dewar of 335 liter of super-cold liquid helium. The cryogen is used to cool the FPA (Focal Plane Array) of IRAC (Infrared Array Camera), IRS (Infrared Spectrograph), and MIPS (Multiband Infrared Photometer for Spitzer) to a temperature near absolute zero for highest-level sensitivity (the mission is to last until 2008/9). Observations are made in the range 3–160 μm .

Note: On May, 15, 2009, after more than 5 1/2 years of operations, Spitzer’s prime mission ran out of coolant (liquid helium). Since then, the telescope has warmed to ~ 30 K. On July 27, 2009, NASA started the so-called “warm” science mission of Spitzer using two of its infrared channels. ⁶⁶⁹⁾

- The payload of the GP-B (Gravity Probe-B) mission of NASA (launch April 20, 2004) is in effect a large ‘thermos bottle’ in space. The objective is to cool the science instru-

668) J. G. Tuttle, M. J. DiPirro, P. J. Shirron, “Liquid/gas phase separators for the Superfluid Helium On-Orbit Transfer (SHOOT) project,” *Advances in Cryogenic Engineering*, 39,1994, p. 121

669) http://www.nasa.gov/mission_pages/spitzer/news/spitzer-20090727.html

ment constantly to 1.8 K to test Einstein's relativity principle. The science payload consists of a superfluid helium dewar (2,440 l), within which a high-vacuum probe is installed, containing the SIA (Science Instrument Assembly), made up of a Quartz Block Assembly (QBA), which is optically contacted to a fused quartz Cassegrainian telescope. The SIA is maintained at a stable temperature of 1.8 K (over a period of 1–2 years) which provides the necessary stability of the precision alignment between the gyroscopes and the telescope.⁶⁷⁰⁾

- **Active coolers** (referred to as cryocoolers, they are refrigerators used to reach cryogenic temperatures).^{671) 672) 673) 674)} Active coolers use closed thermodynamic cycles to transport heat up a temperature gradient to achieve lower cold-end temperatures at the cost of electrical input power. – Active cryogenic refrigerators offer an alternative to passive radiators. Active coolers offer greater capacity and provide additional freedom in packaging and locating the sensor on the spacecraft, since there are no preferred orientations or constraints on view factors. These benefits are provided at the expense of fairly high power consumption, added mass, and diminished reliability. Indeed, there is a crossover point in size/mass efficiency: Passive coolers tend to be the better choice for modest heat loads (< 1 W) at temperatures above approximately 80 K; active coolers are more attractive for higher heat loads (>2 W) at temperatures of 65 K or colder.

Depending on the temperatures required, several cooling schemes are commonly used to actively cool focal planes of optical detectors or other components. The general reliability requirement associated with the development of cryocoolers for space applications leads to the rule that a reliable cooler shall be simple, have no friction, or better have no moving parts. – At the start of the 21st century, cryocoolers represent an important enabling technology for many Earth and space science instruments. As a consequence, NASA started ACTDP (Advanced Cryocooler Technology Development Program) directed towards 6 K/180 K two-stage cooling with remote cold heads. The idea is to be able to commit to missions in the 2007–2015 timeframe.

The following list gives short-descriptions of some cryocooler types and applications. In particular, the mechanical cryocoolers represent a significant enabling technology for Earth observation and science missions.^{675) 676)}

1) Stirling cycle engines, named after the Scottish brothers, Robert and James Stirling.⁶⁷⁷⁾ They invented the Stirling engine in 1816 (the original Stirling cycle was developed as a closed-cycle steam engine – and reversed for application to refrigeration by Kirk in 1874). – Stirling cycle coolers are based on causing a working gas to undergo a Stirling cycle which consists of 2 constant volume processes and two isothermal processes. Devices consist of a compressor pump and a displacer unit with a regenerative heat exchanger, known as a 'regenerator'. Stirling cycle coolers were the first active cooler to be used successfully in space and have proved to be reliable and efficient. – Recent years have seen the development of two-stage devices (minimization of losses) which extend the lower temperature range from 60–80 K to 10 K (with a practical load). EADS Astrium and RAL, in fact, built such a

670) http://einstein.stanford.edu/content/lithos/VIP_Lithos-9.pdf

671) B. C. Edwards, J. E. Anderson, R. I. Epstein, "Solid State Optical Cooler Developments, Proceedings of the International Cryocooler Conference, Keystone, CO, June 2000, Paper No 76

672) G. L. Mills, A. J. Mord, P. A. Slaymaker, "Design and Predicted Performance of an Optical Cryocooler for a Focal Plane Application," Proceedings of the International Cryocooler Conference, Keystone, CO, June 2000

673) G. Mills, J. Fleming, Z. Wei, J. Turner-Valle, "Optical Cryocooling and the Effects of Dielectric Mirror Leakage," Earth Science Technology Conference, Pasadena, CA, June 11–13, 2002

674) T. R. Gosnell, "Laser Cooling of a Solid by 65 K Starting from Room Temperature," Optical Letters, Vol. 24, No. 15, 1999, pp. 1041–1043

675) "Cryocoolers for space applications," URL: <http://www.eng.ox.ac.uk/cryogenics/spacecoolers.html>

676) R. G. Ross, Jr., R. F. Boyle, "An Overview of NASA Space Cryocooler Programs – 2006," 14th International Cryocooler Conference, (ICC-14), June 14–16, 2006, Annapolis MD, USA, URL: <http://conferences.library.wisc.edu/index.php/icc14/article/download/2/2>

677) G. Baker, D. Feger, A. Little, A. H. Orłowska, T. W. Bradshaw, M. Crook, B. J. Tomlinson, A. Sargeant, "The development of a 10 K closed cycle Stirling cooler for space use," Cryocoolers, Vol. 11. 2001. pp 55–61.

machine in the late 1990s. A flight qualified model is expected in 2006 to reach around 6 K with no load.

Examples of first-generation Stirling cycle cryocoolers are:

- The first long-life active cooler system (> 1 year in service) successfully operated in space was a cluster of four Stirling cycle machines launched Feb. 24, 1979 aboard the P-78-1 spacecraft of the USAF.⁶⁷⁸⁾ P-78-1, also referred to as “Solwind”, was the first satellite to carry a gamma-ray spectrometer and an X-ray monitor that were cooled by mechanical refrigerators (the X-ray monitor, referred to as NRL-606 or XMON, was a collaboration between the Naval Research Laboratory and Los Alamos National Laboratory). In addition, the payload consisted of a white-light spectrograph, an EUV (Extreme Ultraviolet) spectrometer, a high-latitude particle spectrometer, and an aerosol monitor.

The four Stirling cycle engines were developed by North American Philips Laboratories and by JHU/APL, Laurel, MD (the Stirling coolers were actually a development of an on-going technology program developed by Philips Co. of Eindhoven, The Netherlands, since World War II). Each pair of coolers nominally consumed 30–35 W, produced 0.3 W of cooling at 75 K, and had a mass of 7.2 kg (including electronics). Although the cooler systems showed significant performance degradation on orbit, they operated sufficiently well to keep the payload operating until it was deliberately destroyed by the USAF during a successful test of an anti-satellite interceptor on Sept. 13, 1985. At least one cooler was still in operation when the spacecraft was destroyed in 1985.^{679) 680) 681)}

NASA considered the single-stage Stirling cryocooler of the North American Philips Laboratories in the most mature stage of development.^{682) 683)} This cooler incorporated linear motors and magnetically levitated moving parts (piston, displacer and counterbalancer) with clearance seals.

- Actually, the very first spaceborne Stirling cryocooler (and a Vuilleumier cooler) were flown on the Skylab missions in 1973. However, these were only fairly short-duration refrigerators (i.e. low duty cycles) during each Skylab occupancy by the astronauts. They were used to cool the S-191 (Visible-Infrared Spectrometer) and S-192 (Multispectral Optomechanical Scanner) instruments onboard Skylab.

- The *Oxford cryocooler*, designed and built by the University of Oxford, UK, was first flown on the NASA UARS mission (Upper Atmosphere Research Satellite, launch Sept. 12, 1991) to provide cooling for the ISAMS (Improved Stratospheric and Mesospheric Sounder) instrument, a limb-sounding radiometer of Oxford University, Oxford, UK. Its design cooling power was 0.8 W at 80 K and its mass was about 4.3 kg. Two coolers were installed for vibrational balance. [Note: the ISAMS cryocooler was a joint development by groups in the Physics and Engineering Departments at Oxford University and at the Rutherford Appleton Laboratory (RAL), UK].⁶⁸⁴⁾

678) <http://heasarc.gsfc.nasa.gov/docs/heasarc/missions/p78-1.html>

679) http://www-atm.physics.ox.ac.uk/main/capabilities/mechanical_coolers.html

680) Information provided by Jaime Reed of EADS Astrium in Stevenage, UK (formerly of Cryogenics Group at the University of Oxford, UK)

681) C. M. Hargreaves, “The Philips Stirling Engine, Elsevier,” New York, 1991. Details the Stirling developments at Philips which led to the modern Stirling engine

682) O. C. Ledford Jr., “Mechanical cryorefrigerators for spacecraft,” presented at the 1987 Cryogenic Engineering Conference, St. Charles, IL (1987)

683) S. H. Charles, “Current Developments in NASA cryogenic technology,” pp. 799–807, in ‘Advances in Cryogenic Engineering, Vol. 33, Proceedings of the Cryogenic Engineering Conference, June 1987, Plenum Press, New York, 1988

684) Oxford cryocooler information provided by Manny Tward of TRW, Redondo Beach, CA

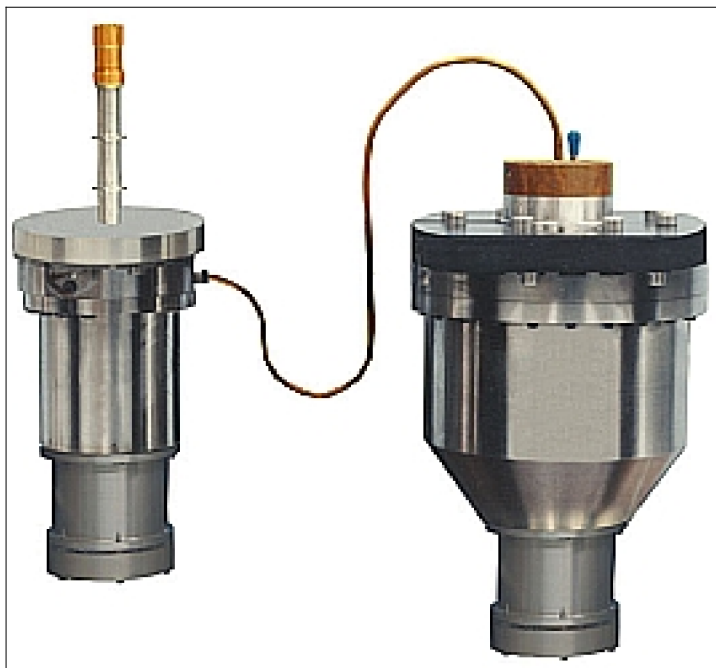


Figure 27: Oxford University ISAMS 80 K Stirling cooler (image credit: NASA)

The use of mechanical coolers in space was pioneered by this program. Already in 1990, BATC (Ball Aerospace & Technologies Corp.) of Boulder, CO, licensed the Oxford University/Rutherford Appleton Laboratory cryocooler technology. In addition, the Oxford cryocooler technology was licensed by British Aerospace, now EADS Astrium Ltd., for use in Europe. A derivative of an Oxford cryocooler was part of the NRL HTSSE–II instrument flown on the ARGOS mission of DoD (launch Feb. 23, 1999). The MOPITT instrument coolers, flown on the Terra mission of NASA (launch Dec. 18, 1999), were built by British Aerospace/EADS Astrium Ltd.

- The CSE (Cryo System Experiment), a hybrid cryogenic cooling system within NASA's IN–STEP (In–Space Technology Experiments Program), built by Hughes Aircraft Co., first flown on STS–63 (Feb. 3–11, 1995), provides 1.2 W of cooling at 65 K [it is the first US–built long life (1.5 years of continuous operation) Stirling cooler to operate in space]. In addition, there was an experimental diode oxygen heat pipe. The heat pipe enables large physical separation between the cryocooler and its thermal load, and provides on–off switching to limit reverse heat flow when the cooler is turned off. CSE achieved all of its objectives. ⁶⁸⁵⁾

- The MIDAS (Materials in Devices as Superconductors) experiment was a NASA cryogenic facility for the characterization of high temperature superconductors during extended flights. It was based on a Stirling cooler capable of 1 W cooling at 80 K, with a power consumption of 60 W max. Launched on STS–79 (Sept. 16–26, 1996) it was installed on board the Russian space station MIR where it operated for about 3 months before returning to Earth.

- The Terra mission of NASA (launch Dec. 19, 1999) ⁶⁸⁶⁾ is flying several Stirling coolers. The SWIR and TIR subsystems of the ASTER instrument of Japan are each cooled to 80 K (continuous operation of the cryocoolers, nominal cooling capacity of 1.2 W, design life of 50,000 h of operational service). The MOPITT instrument of Terra, build by the University of Toronto, provides thermal control by an 80 K Stirling cycle cooler, capillary–pumped cold plate, and passive radiation.

⁶⁸⁵⁾ <http://www.infobloom.se/cesk/cryo.htm>

⁶⁸⁶⁾ M. Kawada, H. Akao, M. Kobayashi, et al., “Performance evaluation of ASTER cryocooler in orbit,” Proceedings of SPIE, Vol. 4881, 9th International Symposium on Remote Sensing, Aghia Pelagia, Crete, Greece, Sept. 23–27, 2002

– The Gamma Ray Spectrometer of NASA's RHESSI mission (launch Feb. 5, 2002) uses an array of nine large germanium gamma-ray detectors to observe solar flares from 3 keV to 25 GeV. The detector array is cooled to 75 K by a Sunpower M77B Stirling cooler at 65 K. This mission represents the first application of a low-cost commercial cooler to achieve multi-year operation in space. Additionally, the cooler uses a heat intercept strap clamped to the Stirling coldfinger to provide simultaneous cooling to the instrument's higher temperature radiation shields at 155 K.

– HIRDLS (High Resolution Dynamics Limb Sounder) instrument, flown on the Aura mission of NASA (launch July 15, 2004), was an international joint development between the USA and UK. It uses a single-stage Stirling cryocooler manufactured by Ball Aerospace under contract to Lockheed Martin. The HIRDLS detectors are cooled to 65 K.

– The ASTRO-F / Akari mission of JAXA, the first Japanese infrared astronomical satellite of Japan, was launched on Feb. 21, 2006. ESA is also collaborating in the mission.⁶⁸⁷⁾ The design of this cryocooler is based on a small two-stage Stirling-cycle cryocooler developed in 1991 for space applications with temperatures below 20 K. AKARI uses the FPI (Focal Plane Instrument), the IRC (Infrared Camera), and the FIS (Far-Infrared Surveyor) to survey the entire sky over infrared wavelengths from 2–200 μm . These optical devices and primary mirror of 68.5 cm diameter are refrigerated to below 7 K by a hybrid cooling system consisting of 170 l (25 kg) of super-fluid liquid helium (He-II) cryogen plus two sets of two-stage cryocoolers for redundancy. During nominal operations, each two-stage cryocooler is driven with 50 W of input power to achieve 0.1 W of cooling at 20 K. The compressor mass is 7 kg, the cold head mass is 2 kg. – Akari surveyed the whole sky in six infrared bands from May 2006 to August 2007. In March 2010, ESA released two Akari all-sky survey catalogs to the astronomers' community. The new catalogs contain more than one million celestial sources and will be a major tool for astronomers, after having to rely on the IRAS atlas for more than 25 years.

2) Pulse tube systems. Pulse tube coolers are similar to the Stirling cycle coolers although the thermodynamic processes are quite different. They consist of a compressor and a fixed regenerator. Since there are no moving parts at the cold-end reliability is theoretically higher than Stirling cycle machines. Efficiencies approaching Stirling cycle coolers can be achieved and several recent missions have demonstrated their usefulness in space.

Pulse tube coolers are capable of achieving cryogenic temperatures of <20 K in the 0.5–3.5 W cooling capacity range. The principal benefits of a pulse tube cooler are greater reliability and lower cost compared to the Stirling cooler and an order of magnitude lower mass, lower cost, and longer life than the current state-of-the-art coolers. A pulse tube cooler is also more efficient than a TEC-type instrument, however, as a mechanical cooler, it is much larger than a TEC. In addition, mechanical coolers can produce vibrations that must be canceled or isolated. Examples:

– The Lewis satellite of NASA (launch Aug. 23, 1997 – however, the S/C was lost and reentered the atmosphere Sept. 28, 1997) was the first spacecraft in civil Earth observation featuring pulse tube cryocooler technology (built by TRW) in its HSI (Hyper-Spectral Imager) for low-noise SWIR cooling. Already in 1994, TRW delivered its first pulse tube instrument, built under contract to the Air Force's Phillips Laboratory.

– The MTI (Multispectral Thermal Imager) mission of DOE (LANL/SNL), launch March 12, 2000, employs a dual-load pulse tube cryocooler of the MTI instrument, built by TRW, now NGST (Northrop Grumman Space Technologies). This technique permits FPA cooling for MWIR (60 K) and TIR (35 K) observations with a total input < 125 W.

⁶⁸⁷⁾ Y. Sato, H. Sugita, K. Komatsu, R. Shimizu, H. Uchida, T. Nakagawa, H. Murakami, K. Mitsuda, M. Murakami, I. Iwata, S. Tsuneta, S. Tsunematsu, K. Kanao, K. Ootsuka, M. Hirabayashi, "Development of Advanced Two-Stage Stirling Cryocooler for Next Space Missions," Proceedings of the 15th International Cryocooler Conference (ICC-15), June 9–12, 2008, Long Beach, CA, USA, URL: <http://conferences.library.wisc.edu/index.php/icc15/article/download/182/182>

Manufacturer	Cooler type	Agency (mission)	Instrument (mission)	Launch date
NGST (TRW), Oxford Plc.	Mini Stirling	NRL (ARGOS)	HTSSE-II (ARGOS)	Feb. 23, 1999
NGST (TRW)	Mid-size pulse tube	SNL/LANL, (MTI)	MTI (Multispectral Thermal Imager),	Mar. 12, 2000
NGST (TRW)	Mini pulse tube	NASA/GSFC (EO-1)	Hyperion (EO-1)	Nov. 21, 2000
NGST (TRW)	Mini pulse tube	NASA/LaRC	SABER (TIMED)	Dec. 7, 2001
Creare	Reverse Brayton	NASA/GSFC, Hubble	NICMOS (HST)	Mar. 2002 (STS-109)
NGST (TRW)	Mid-size pulse tube	NASA/JPL	AIRS (Aqua), 2 units	May 4, 2002

Table 44: Some spaceborne cryocoolers with DoD/MDA (Missile Defense Agency) research funding

- Other instruments with pulse tube cooling technology are AIRS (Atmospheric Infrared Sounder) of NASA's Aqua satellite (launch May 4, 2002) and TES (Tropospheric Emission Spectrometer) on the Aura mission (launch July 15, 2004).⁶⁸⁸⁾
- JAMI (Japanese Advanced Meteorological Imager) flown on the Japanese MTSAT (Multi-functional Transport Satellite) mission (launch Feb. 26, 2005) features a pair of Northrop Grumman pulse tube cryocoolers (derived from Raytheon expertise in DoD programs). JAMI provides high quality multispectral imagery for weather forecasters in Japan, East Asia and Australia.
- The GOSAT (Greenhouse gas Observing Satellite) / Ibuki mission of JAXA (launch Jan. 23, 2009) carries TANSO-FTS (Thermal And Near infrared Sensor for carbon Observation – Fourier Transform Spectrometer) and TANSO-CAI (Thermal And Near infrared Sensor for carbon Observation – Cloud and Aerosol Imager). The focal planes of TANSO-FTS are cooled to 65 K using a cryocooler built by Northrop Grumman under contract to BAE. The flight assembly consists of a single-stage HEC (High Efficiency Cryocooler) pulse tube cooler that utilizes high-pressure helium gas, and cryocooler control electronics.⁶⁸⁹⁾
- The OCO mission of NASA (launch Feb. 2, 2009, experienced a launch failure). The OCO instrument FPAs are being cooled by a pulse tube cryocooler of NGST (Northrop Grumman Space Technologies, formerly TRW) to 120 K. The cryocooler is of TES heritage.
- The NPOESS mission of NOAA (launch 2015) includes a new ABI (Advanced Baseline Imager) developed by ITT for NASA. ABI will have significantly better spatial, spectral, and temporal resolution than the current imager, partly due to the use of colder detectors in the focal planes. A two-stage split pulse tube cooler manufactured by NGAS (Northrop Grumman Aerospace Systems) will cool the MWIR focal plane to 60 K, and the VNIR focal plane to 200 K. The low-temperature cryocooler stage is a standard NGAS HEC (High Efficiency Cryocooler), tuned for 45 K. A transfer line from the HEC compressor drives a remote stage, operating at 183 K.⁶⁹⁰⁾

3) Joule–Thompson (JT) coolers. These coolers work using the well known Joule–Thomson (or Joule–Kelvin), effect. A gas is forced through a thermally isolated porous plug or throttle valve by a mechanical compressor unit leading to isenthalpic cooling. Although this is an irreversible process, with correspondingly low efficiency, JT coolers are simple, reliable, and have low electrical and mechanical noise levels. Note: the JT cooler is actually an open–cycle expansion device. Examples:

688) J. Raab, et al., "TES FPC Flight Pulse Tube Cooler System,". Cryocoolers II, Kluwer Academic/Plenum Publishers, New York, 2001, pp. 131–138

689) "Northrop Grumman–Built Cryocooler Operational On Ibuki," Space Mart, March 31, 2009, URL: http://www.spacemart.com/reports/Northrop_Grumman_Built_Cryocooler_Operational_On_Ibuki_999.html

690) R. Colbert, G. Pruitt, T. Nguyen, J. Raab, S. Clark, P. Ramsey, "ABI Cooler System Protoflight Performance," Proceedings of the 15th International Cryocooler Conference, June 9–12, 2008, Long Beach, CA, USA, URL: <http://conferences.library.wisc.edu/index.php/icc15/article/download/186/186>

– A JT cryocooler experiment of BATC (Ball Aerospace & Technologies Corp.) was successfully demonstrated on Shuttle flight STS–85 in Aug. 1997.

– A 4 K JT stage driven by a valved linear compressor (designed by RAL and EADS Astrium), similar to those used for Stirling cycle and Pulse Tube coolers, was flown on the Herschel/Planck telescope missions of ESA (launch May 14, 2009).

– The SMILES (Superconducting Submillimeter–wave Limb–Emission Sounder) instrument of JAXA and NICT (National Institute of Information and Communications Technology) was delivered to the EF (Exposed Facility of JEM (Japanese Experiment Module) of the ISS (International Space Station) on the maiden flight of the HTV–1 (H–II Transfer Vehicle–1) of JAXA (launch Sept. 10, 2009).

SMILES, with a total mass of 475 kg, uses two SIS (Superconductor–Insulator–Superconductor) mixers for submillimeter–wave atmospheric observations.⁶⁹¹⁾ The SIS mixers are cooled to 4 K levels by a cryogenic system with a two–stage Stirling cooler, a Joule–Thomson (JT) cycle cooler and a cryostat composed of three stages. The cooling capacity is designed to provide ~ 20 mW at 4.5 K, 200 mW at 20 K and 1 W at 100 K with the total input power of approximately 140 W.

– MIRI (Mid–Infrared Camera–Spectrograph) imager on the JWST (James Webb Space Telescope) mission. In 2002, NASA initiated the ACTDP (Advanced Cryocooler Technology Development Program) as a strategic technology investment within the Terrestrial Planet Finder project, to develop long–life cryocoolers for cooling remote space–observatory instruments to 6–18 K.⁶⁹²⁾ The resulting successful demonstrations of 6–18 K cryocooler technology led to the decision in the spring of 2005 to use an ACTDP cryocooler to cool the MIRI to 6 K on the JWST (launch in 2015). After a competitive selection process in winter 2006, the Northrop Grumman ACTDP concept was selected for the flight MIRI cooler. The active cooling is provided by a dedicated three stage Stirling–cycle PT (Pulse–Tube) to precool a circulating helium flow loop, with a Joule–Thomson (JT) expansion stage to provide continuous cooling to 6.2 K to a single point on the MIRI optical bench (Ref. 676).

– The SPICA (Space Infrared Telescope for Cosmology and Astrophysics) mission of JAXA (planned launch in 2017) features a 3.5 m aperture telescope which is maintained at 4.5 K to observe in the spectral FIR region of up to $100 \mu\text{m}$ at L2 (Lagrange Point 2). The cooling system concept does not use any cryogenics; instead, the telescope and FPI (Focal Plane Instrument) are cooled by a hybrid method of radiant and mechanical cooling system to achieve a mission life of 5 years. The required temperature is obtained by the JT (Joule Thompson) circuit, combined with an advanced two–stage Stirling cryocooler for precooling to 15–20 K. The cooling capacity @ 20 K is 0.2 W (Ref. 687). International collaboration is provided by NASA and ESA.⁶⁹³⁾

4) Peltier effect coolers. Solid–state Peltier coolers, or TEC (Thermo–Electric Converter) devices, are routinely used in space to achieve temperatures above 170 K (e.g. the freezers aboard the International Space Station). These devices work on the same principle as the Seebeck effect, but in reverse: the creation of a temperature difference between two dissimilar metals by application of a current.

691) K. Narasaki, S. Tsunematsu, S. Yajima, A. Okabayashi, J. Inatani, K. Kikuchi, R. Satoh, T. Manabe, M. Seta, “Development of Cryogenic System for Smiles,” AIP (American Institute of Physics) Conference, June 23, 2004, Vol. 710, pp. 1785–1796

692) D. Durand, R. Colbert, C. Jaco, M. Michaelian, T. Nguyen, M. Petach, E. Tward, “NGST Advanced Cryocooler Technology Development Program (ACTDP) Cooler System,” 14th International Cryocooler Conference (ICC–14), June 14–16, 2006, Annapolis MD, USA URL: <http://conferences.library.wisc.edu/index.php/icc14/article/download/4/4>

693) C. M. Bradford, Lee Asmus, Dominic Benford, James Bock, Peter Day, George Helou, Warren Holmes, Matthew Kenyon, Hideo Matsuhara, Takao Nakagawa, Hiroshi Shibai, Gordon Stacey, Michael Werner, “U.S. Participation in the JAXA–led SPICA Mission: The Background–Limited Infrared Submillimeter Spectrograph (BLISS), April 1, 2009, URL: http://www.ipac.caltech.edu/DecadalSurvey/BLISS_decadal_final.pdf

The TEC scheme is capable of cooling focal planes to 180 K starting from an ambient temperature of 300 K. TEC instruments are small, lightweight, and, being solid-state, have no vibration. TECs have the main disadvantage of having an efficiency that drops off rapidly with decreasing temperature and tending towards zero around 180 K. Traditionally, TECs are limited to cooling a small detectors; they provide high reliability with slow and low-efficiency cooling.

Examples of thermoelectric cooler implementations are: 1) The RBV (Return Beam Vidicon Camera) flown on early Landsat spacecraft (launch of LS-1 July 23, 1972); 2) GERB (Geostationary Earth Radiation Budget) flown on MSG (Meteosat Second Generation) satellites of EUMETSAT (launch of MSG-1 on Aug. 28, 2002); 3) SHIMMER (Spatial Heterodyne Imager for Mesospheric Radicals) flown on Shuttle flight STS-112, Oct. 7-18, 2002, and on STPSat-1 (launch March 9, 2006).

5) Reverse Brayton cycle cooler. Reverse/Turbo Brayton coolers have high efficiencies and are practically vibration free. Coolers consist of a rotary compressor, a rotary turbo-alternator (expander), and a counterflow heat exchanger (as opposed to the regenerator found in Stirling or Pulse Tube coolers). The compressor and expander use high-speed miniature turbines on gas bearings and small machines are thus very difficult to build. They are primarily useful for low temperature experiments (less than 10 K), where a large machine is inevitable, or for large capacity devices at higher temperatures (although these requirements are quite rare). – Note: a thermodynamic concept of a combustion engine was initially developed by George R. Brayton (an engineer of Boston, MA, 1830-1892) in the 1870s. He invented the continuous ignition combustion engine that later became the basis for the turbine engine. The operation of these combustion turbines is referred to as the “Brayton-cycle” engine. Example applications: ⁶⁹⁴⁾

– A recent application of this class of cooler was the replacement of the old dewar for the NICMOS (Near Infrared Camera and Multi-Object Spectrometer) instrument, flown on the HST (Hubble Space Telescope) mission (installation in March 2002 on HST servicing mission SM-3B) on STS-109. Originally, NICMOS had a solid nitrogen dewar for cooling (the nitrogen depleted in Jan. 1999). The new reverse Brayton cryocooler was developed by Creare Engineering & Development of Hanover, NH, USA. The Creare instrument returned the NICMOS detectors to operational temperatures of 75 K. The NICMOS cooling system maintains the detector temperature by circulating refrigerated neon gas through existing liquid helium freeze lines via bayonet couplings. – The new cooling system technology was first tested aboard Shuttle flight STS-95 in 1998.

– This was preceded by SSRB (Single Stage Reverse Brayton in 1992, a demonstration project of the USAF Phillips Laboratory and NASA/GSFC to maintain a cooling temperature of 65 K (using a combination of centrifugal compressor, recuperative heat exchanger, expansion turbine, and thermal interfaces to the load and heat rejection devices). SSRB was also developed by Creare Engineering & Development.

6) Adsorption cooling. Adsorption (or **sorption**) is the physical mechanism upon which a gas can be trapped onto a material surface: when a gas is brought into contact with a solid surface, some of the molecules striking the surface will be retained for a finite period of time, resulting in a significantly higher molecular concentration at the surface than in the gas phase. Adsorption coolers are essentially JT coolers which use a thermo-chemical process to provide gas compression with no moving parts. Powdered adsorbent materials (e.g. metal hydrides), are electrically heated and cooled to pressurize, circulate, and adsorb a working fluid such as hydrogen. Efficiency is low but may be increased by the use of mixed working gases.

⁶⁹⁴⁾ G. Nellis, F. Dolan, W. Swift, H. Sixsmith, S. Castles, J. Gibbon, “Reverse Brayton Cooler for NICMOS,” *Cryocoolers 10*, ed. by R. G. Ross, Jr., Kluwer Academic/Plenum Publishers, New York, NY, 1999, pp. 431-438

Demonstration models have already been flown and they are expected to be useful in long-life missions where very low vibration levels are required, such as the planned Darwin mission of ESA to image the atmospheres of extra-solar planets.

- In May 1996 the BETSCE (Brilliant Eyes Ten–Kelvin Sorption Cryocooler Experiment) flew on board STS–77. Jointly funded by the DoD and NASA, this JPL sorption cooler experiment demonstrated the capability to cool a 100 mW load to ~ 11 K in less than two minutes and maintain the load at temperature for 10–20 minutes. After this period, the sorption cryocooler recycled in preparation for another cooling cycle. The periodic nature of the cooler allowed the required input power to be averaged over the four-hour recycle time, thus providing a fast-cooldown 150 mW 10 K cooler for a relatively low average power. This was the first flight demonstration of hydride sorption cooler technology (Ref. 676).

- The Planck Space Observatory of ESA (launch May 14, 2009) uses a hydrogen sorption cooler of JPL to cool the HEMT (High Electron Mobility Transistor) receivers to 18–20 K of the LFI (Low Frequency Instrument). In addition, the sorption cooler is used to precool the 4 K helium JT cooler of RAL, which cools the 0.1 K dilution refrigerators in the HFI (High Frequency Instrument) cooling system.

7) Optical cooling. Optical cooling using fluorescence in solids and liquids is an alternate and new concept in refrigeration that represents possible applications in small cryocooler technology, in particular for infrared devices and spectrometers (O.5.4).^{695) 696)} The method uses anti–Stokes fluorescence to remove heat from a glass or crystal that is pumped with laser light. The basic principle of cooling using anti–Stokes fluorescence was suggested by Peter Pringsheim, Berlin, in 1929, but it was not until 1995 that the actual cooling of a solid was first demonstrated at LANL (Los Alamos National Laboratory) using Ytterbium–doped Zirconium Fluoride (Yb:ZBLAN) glass.

- A first demonstration instrument by the name of LASSOR (Los Alamos Solid–State Optical Refrigerator) was developed at LANL (Los Alamos National Laboratory) in 1995 using Yb doped Zirconium Fluoride (Yb:ZBLAN) glass.

- In Oct. 2000, NASA/LaRC awarded to BATC (Ball Aerospace & Technologies Corporation) a contract to develop an optical cryocooler (infrared focal plane demonstrator). In 2003, BATC demonstrated their first optical refrigerator. It cooled an attached load, simulating an infrared detector, to 11.8°C below its surroundings.⁶⁹⁷⁾

Optical cryocooling is a feasible method for cooling focal planes and has a distinct niche in extended solid–state cooling to those temperatures that cannot be achieved efficiently (or at all) by TEC methods. Optical cryocoolers have a clear advantage over mechanical coolers in vibration (because a solid–state diode is used as the pump laser, there are no moving parts and therefore no vibration), ruggedness, EMI (Electromagnetic Interference) and magnetic field, and cooler mass. Nevertheless, they are at a disadvantage to mechanical coolers based on efficiency. Optical cryocoolers have an advantage over TECs in minimum operating temperature, magnetic field, and ruggedness. They are at a disadvantage to TECs in cooler mass, however.

8) ADR (Adiabatic Demagnetization Refrigerator) for cooling applications below 1 K. The basic principle of adiabatic demagnetization of paramagnetic salts (the removal of a magnetic field from certain materials serves to lower their temperature) was initially sug-

695) P. Pringsheim, “Zwei Bemerkungen über den Unterschied von Lumineszenz– und Temperaturstrahlung,” *Zeitschrift für Physik*, Vol. 57, 1929, pp. 739–746

696) R. I. Epstein, M. I. Buchwald, B. C. Edwards, T. R. Gosnell, C. E. Mungan, “Observations of Laser–Induced Fluorescent Cooling of a Solid,” *Nature* 377, p. 500, Oct. 12, 1995

697) G. Mills, W. S. Good, A. J. Mord, “The Performance of the First Optical Refrigerator,” Proceedings of NASA’s ESTC (Earth Science Technology Conference), Palo Alto, CA, June 22–24, 2004, <http://esto.gsfc.nasa.gov/conferences/estc2004/papers/b7p1.pdf>

gested independently by Peter J. W. Debye in 1926 and by William F. Giauque in 1927. The ADR technique was the first method developed for cooling below ~ 0.3 K, and has been used in laboratories on the ground for many years; it is a well-established technology reaching cooling temperatures of about 2 mK.

The ADR heat pump technology was developed at NASA/GSFC (started in 1979) for use on spaceborne instruments; it operates between liquid helium temperature (~ 4 K as reservoir or coolant temperature) and very low temperatures – below 0.1 K to maximize the detector sensitivity (i.e., operation near the quantum limit). ADR is a cyclic superconducting cooling system; it alternates between two states (or stages):

- In the operating state, it cools down and absorbs heat
- In the recycling state, the ADR warms up and dumps heat into a heat sink.

The refrigeration cycle of an ADR utilizes the magneto–caloric effect by exploiting the interaction between the atomic magnetic moments in a paramagnetic material (often a salt) and an externally applied magnetic field. The main components of an ADR are : a) a paramagnetic salt, and its thermal link, b) a magnet and its shielding, and c) the heat switch.

The first spaceborne ADR was realized for the high–resolution XRS (X–Ray Spectrometer) of JAXA (manufactured and integrated by Sumitomo Heavy Industries, Niihama, Japan) to cool the detectors at the focal plane to 0.065 K (or 65 mK). An ADR was chosen for space instead of a dilution refrigerator because it does not require gravity and because it is exceedingly efficient. The ADR for the X–Ray Spectrometer has an efficiency of approximately 50% of Carnot. This efficiency is necessary for spaceborne systems to allow the liquid helium dewar to operate for extended periods of time on orbit.

– This XRS instrument (also called XRS–2) with ADR cooling of NASA/GSFC is flown on the Astro–E2/Suzaku mission of JAXA/ISAS (launch July 10, 2005, orbit of 550 km, inclination = 31°). XRS–2 uses an array of X–ray micro–calorimeters and foil mirrors to achieve an unprecedented combination of high resolution and large collecting area. – Prior to this mission, the newly developed XRS experienced a launch failure on the Astro–E spacecraft of ISAS (launch Feb. 10, 2000) from the Kagoshima launch site in Japan.

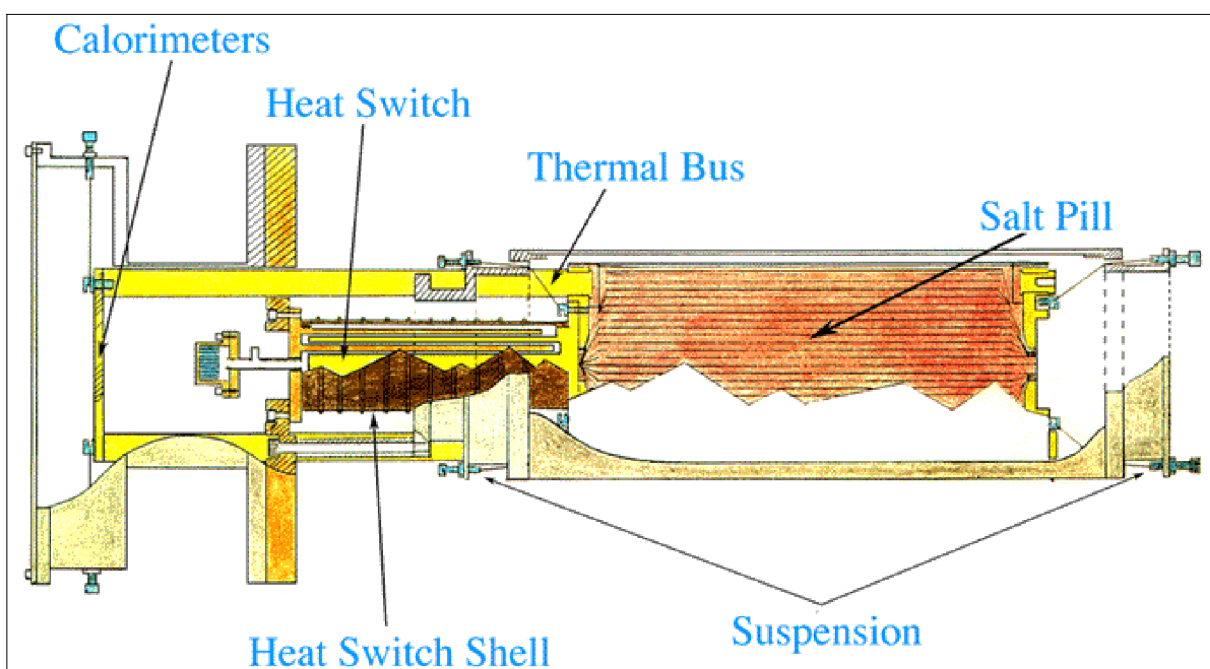


Figure 28: Cutaway drawing of the ADR cooling system (image credit: NASA)

– NASA is utilizing the ADR technology also on **SAFIRE** (Submillimeter And Far Infrared Experiment), an instrument on the airborne mission of SOFIA (Stratospheric Observatory for Infrared Astronomy) with first flights started in May 2010. The first science flights of SOFIA started on November 30, 2010 using FORCAST (Faint Object Infrared Camera for the SOFIA Telescope) which observes in the spectral range of 5–40 μm .

– The Mullard Space Science Laboratory at the University College London, UK (along with EADS Astrium Ltd.), is developing a 10 mK ADR stage. This cooling system is to be flown on the XEUS mission of ESA (launch planned for 2015), a spaceborne X-ray observatory.

1.5.16 Uncooled infrared detectors and HTS (High-Temperature Superconductivity)

- **Use of uncooled infrared detector arrays** in the spectral region of TIR (Thermal Infrared) for surface imaging. The technology employs silicon micromachined microbolometer focal plane arrays. The NASA/GSFC instrument ISIR (Infrared Spectral Imaging Radiometer) demonstrated the potential of the concept on Shuttle flight STS-85 (Aug. 7–19, 1997, see J.8). – [A bolometer is a detector type making use of the change in electrical resistance of certain materials (with small thermal capacity) when their temperature is changed.⁶⁹⁸) The resistance of most conductors varies with temperature, this change in resistance is measured by the bolometer. Bolometers are suitable detectors for the infrared and microwave regions. The main advantage of a bolometer detector system is the absence of a cryogenic cooler system.]

The first micromachined MBAs (Microbolometer Array) were probably developed in the USA in the late 1980's and early 1990's under DARPA's HIDAD (High Density Array Development) program and built by the Honeywell Sensor and System Development Center. This early MBA had about 80,000 pixels (336 x 240) with an average room-temperature sensitivity ($NE\Delta T$) of less than 50 mK, measured at a 30 Hz frame rate, with $f/1.0$ optics and a broadband (8–14 μm) filter.

- HTS (High-Temperature Superconductivity), see also “superconductivity” in the Glossary. The characteristics/performance of superconductive electronic devices have exceptionally low loss, high speed, high dynamic range, and low noise. Superconducting materials (in hybrid components, hybrid digital circuits, semiconductors, sensors) are promising to reduce loss by several orders of magnitude at RF frequencies, increasing the sensitivity and precision of signal discrimination in advanced electronic systems. A new detector type, based on SQUID (Superconducting Quantum Interference Device) technology, offers promising results in such applications as absolute magnetic field measurements.⁶⁹⁹)

– The first program to demonstrate the operation and survivability of simple HTS electronic components in space was initiated by NRL (Naval Research Laboratory) in 1988 within the framework of HTSSE-I (High Temperature Superconducting Space Experiment I).

– The DoD ARGOS satellite (launch Feb. 23, 1999), operated by SMC, carries HTSSE-II (High Temperature Superconducting Space Experiment II) of NRL to demonstrate the performance of superconducting (semiconductors and RF) components at cryogenic temperatures of 70–80 K (see M.3). Reductions in power by several orders of magnitude as well as signal speed increases of an order of magnitude are expected with this technology. HTSSE-I of NRL, with relatively simple HTS devices, the majority being passive components made from a single HTS film, were to be placed in orbit to investigate the durability of HTS in space. However, the DoD satellite with HTSSE-I aboard experienced a launch

⁶⁹⁸) R. A. Wood, N. A. Foss, “Micromachined Bolometer Arrays,” *Laser Focus World*, 30, pp.101–106, 1994

⁶⁹⁹) J. C. Ritter, M. Nisenoff, G. Price, S. A. Wolf, *IEEE Transactions on Magnetics*, Vol. 27, 1991, p. 2533

failure in 1993. Despite the unfortunate loss of on-orbit data from HTSSE-I, the program did conclusively demonstrate that viable and robust HTS microwave devices could be fabricated, packaged and space-qualified. – Note: The HTSSE project started at NRL in December 1988 as a long-term joint venture with other labs/industry [which in turn started CSE (Consortium on Superconducting Electronics) in 1989].

- Another HTS demonstration, namely SUPEX (Superconductivity Experiment), based on thin-film technology is flown on TechSat/Gurwin-II (launch July 10, 1998), a satellite built by the Haifa-based Technion Israel Institute of Technology. N.30

- A magnetometer based on SQUID (Superconducting Quantum Interference Device) technology is flown on Gravity Probe-B (launch April 20, 2004).

- SMILES (Superconducting Submillimeter-wave Limb Emission Sounder) of JAXA/CRL is planned to fly on ISS/JEM in 2006. The superconductive technique enables 3-D global observation of trace gases in the stratosphere in the frequency band of 640 GHz. A heterodyne receiver detects very low level signals in the submillimeter-wave band radiated from trace gases using a sensitive SIS (Superconductor-Insulator-Superconductor) mixer method to perform high-resolution spectral analysis.

- A European consortium led by SRON (Groningen, The Netherlands), is designing HIFI (Heterodyne Instrument for Far Infrared), flown on ESA's HSO (Herschel/Planck Space Observatory, launch May 14, 2009). HIFI takes very high-resolution spectra of astronomical objects in thousands of frequencies simultaneously. HIFI features a large telescope (> 3 m diameter), a large dewar for liquid Helium, and SIS mixers covering the frequency range of 500–1200 GHz continuously, and possibly a Hot Electron Bolometer (HEB) mixer operating at about 1.8 THz.

- SRON is also developing the ESA instrument PIRAMHYD (Passive InfraRed Atmospheric Measurements of HYDroxyl) which features an HTS transition edge bolometer to measure the signal from a spectrally isolated emission line of the OH molecule in the far infrared spectrum of wavelength 84.420 μm .

1.5.17 Observations in the FIR (Far Infrared) region, FIR detectors

The FIR region of the EMS (Electromagnetic Spectrum) is generally considered from about 30 μm to 1000 μm (equivalent to 10 – 0.3 THz in the frequency spectrum), covering by far the largest portion of the optical spectrum. FIR radiation exhibits rather low energy levels (much lower than UV, VIS, VNIR) corresponding to photon energies from 35 to 1 meV. FIR observations require detector cooling to liquid helium temperatures (<4 K) in order to eliminate thermal noise interference (i.e. self-emission) of the observing instrument (detection by thermal emission).⁷⁰⁰ – The FIR spectrum is of particular interest in such fields as astronomy [most galaxies are found to emit strongly in the infrared; the interstellar medium (background radiation) emits energy mostly in the FIR and microwave spectral regions; approximately one half of the total luminosity and 98% of the photons emitted since the Big Bang fall into the FIR region], biomedical imaging, mineral detection, and Earth observation. – The general topic of infrared radiation and detection is covered in O.4.3.

In general, FIR radiation (downwelling and upwelling) is being absorbed by the atmosphere, in particular by the water vapor of the Earth's lower atmosphere (troposphere). It turns out that the spectral range between 30–300 μm is almost completely obscured by the troposphere. This makes ground-based observations in FIR simply obsolete. Early efforts in infrared astronomy included mountain-top observatories; however, with little success (Earth itself as heat source represents already a great noise problem). Hence, airborne (instruments in high-flying aircraft) or spaceborne solutions must be sought to observe in FIR.

700) Note: The FIR region is also referred to as the “sub-millimeter” region

Until the early 1980s FIR detectors have been limited to single pixels. Then, for the first infrared satellites, small manually assembled mosaics of individual photoconductor crystals have been developed. At the start of the 21st century, there is a great need for large-format FIR detector arrays. Some examples in airborne and spaceborne infrared astronomy and some EO projects are: ⁷⁰¹⁾

- A 5 x 5 element detector array of stressed and unstressed GeGa and arrays of up to 60 bolometers, cooled to liquid helium temperature (4 K), were employed onboard KAO (Kuiper Airborne Observatory), flown and operated on a modified Lockheed C-141A aircraft of NASA/ARC. It's main payload was an infrared telescope (1 m aperture Cassegrain reflecting mirror design) for astronomy observations. KAO was flown in the time period 1974–1995 at cruising altitudes of 12 km and higher (i.e., above 85% of the Earth's atmosphere and more than 99% of the Earth's water vapor). KAO opened the MIR (Mid Infrared) and FIR (Far Infrared) window to the universe. – On a historical note: A U.S. aircraft mounted astronomy program began in 1969 with a 30 cm telescope onboard a Lear Jet.
- IRAS (InfraRed Astronomical Satellite) was an international cooperative astronomy mission of the USA (NASA), the Netherlands (NIVR), and the UK (SERC); launch of IRAS on Jan. 25, 1983 (the mission lasted for 10 months because the coolant was depleted). The IRAS mission conducted an all-sky infrared survey in the spectral range of 8–120 μm in four broadband photometric channels centered at 12, 25, 60, and 100 μm . IRAS used an infrared detector of 62 photoconductors (individually wired pixels) of the FPA, and 3 x 3 elements of Ge:Ga (40 to 110 μm).
- ISOPHOT (ISO Photo-Polarimeter) was flown on ISO (Infrared Space Observatory), an ESA space science mission (4 instruments) with a launch Nov. 19, 1995, S/C operation until May, 16, 1998 (no more coolant available). ISOPHOT infrared observations employed three single pixel detectors (Si:Ga, Si:B and Ge:Ga) covering the spectral range of 3.3–120 μm , with two FIR photometric cameras working between 60 and 240 μm (3 x 3 elements of Ge:Ga, and 2 x 2 elements of stressed Ge:Ga), and a spectrometer (two 64 element linear Si:Ga arrays, 2.5–5 μm and 6–12 μm). However, ISOPHOT observations with a grating spectrometer were not able to resolve all the spectra.

A new generation of **large-format FIR detector arrays** were developed for the SIRTf (Space Infrared Telescope Facility) mission of NASA/JPL (launch Aug. 25, 2003). On Dec. 18, 2003, NASA renamed SIRTf to “**Spitzer Space Telescope**” to honor the late astrophysicist Lyman Spitzer Jr. (1914–1997) for outstanding accomplishments during his lifetime (as early as 1946, Spitzer proposed to place an observatory into space where it would be able to detect a wide range of wavelengths and not have to deal with the blurring effects of our atmosphere). The objectives of SIRTf are mostly in astronomy/space science, but it also offers the capability to explore and characterize aspects of the solar system. The SIRTf payload consists of a telescope (0.85 m aperture) and three cryogenically-cooled science instruments which perform imaging and spectroscopy in the 3–180 μm spectral range. MIPS (Multiband Imaging Photometer for SIRTf) is one of the three instruments providing FIR imaging with photometry and total power measurement in broad spectral bands centered at 24, 70, and 160 μm , and low-resolution spectroscopy between 50 and 95 μm . – A MIC (Multiple Instrument Chamber), cooled to < 5 K, contains the cold detectors of the three science instruments as well as the cold parts of the telescope. SIRTf employs also a light-weighted optics technology (beryllium mirrors), resulting in a total telescope mass of < 50 kg. The spacecraft is shielded with a solar panel facing the sun, leaving the rest of the spacecraft facing cold space. ⁷⁰²⁾ – SIRTf (launch mass of 950 kg) was deployed into an Earth-trailing heliocentric orbit (drift rate of about 0.1 AU/year), providing a deep space ambient temperature environment of about 30–40 K (a cryogen-conserving orbit). Naturally, this

701) J. Wolf, A. W. Hoffman, J. W. Beeman, J. Farhoomand, “Design Considerations for Large Format Far-Infrared Array Detectors,” http://www.sofia.usra.edu/det_workshop/papers/session2/3-14wolf_cr_edjw020606.pdf

702) T. S. Glenn, G. B. Heim, J. Troeltzsch, et al., “Multiband Imaging Photometer for SIRTf: An Overview of the Verification and Validation Effort,” Proceedings of IEEE Aerospace Conference, Big Sky, MT, Mar. 8–15, 2003

configuration helps greatly in passively cooling the payload of the spacecraft. SIRTf is the first spacecraft employing the innovative “warm–launch” cryogenic architecture – made possible by the choice of the orbit. The term “warm launch” refers to the fact that the spacecraft was launched at room temperature, and then using the coolness of space to reach a low–temperature equilibrium after a certain period. The 360 liter tank of liquid helium is expected to provide a mission life of five years for active instrument cooling services.⁷⁰³⁾

- IRAC (Infrared Array Camera) is a four–channel camera that provides simultaneous 5.12 x 5.12 arcmin images at 3.6, 4.5, 5.8, and 8 μm . Each of the four detector arrays in the camera are 256 x 256 pixels in size. IRAC uses two sets of detector arrays. The two infrared channels of 5.8 and 8 μm are imaged by composite detectors made from indium and antimony (InSb). The 3.6 and 4.5 μm channels use silicon detectors that have been specially treated with arsenic.
- IRS (Infrared Spectrograph) provides both high– and low–resolution spectroscopy at midwave–infrared wavelengths (MWIR). There are four modules covering the various spectral ranges, each with a detector array of 128 x 128 pixels.
 - 5.3 – 14 μm for low–resolution imagery
 - 10 – 19.5 μm
 - 14 – 40 μm
 - 19 – 37 μm for high–resolution imagery

The shorter–wavelength silicon detectors are treated with arsenic; the longer–wavelength silicon detectors are treated with antimony.

- MIPS (Multiband Imaging Photometer for SIRTf). MIPS has three detector arrays. A 128 x 128 array for imaging at 24 μm is composed of silicon, specially treated with arsenic. A 32 x 32 element hybrid array for imaging at 70 μm , and a 2 x 20 array for imaging at 160 μm , both use germanium, treated with gallium (Ge:Ga). The 32 x 32 array consists of 8 bars of 4 x 32 elements arranged in a stacked format; it takes also spectra from 50 – 100 μm . The FOV (Field of View) varies from about 5 x 5 arcmin at the shortest wavelength to about 0.5 x 5 arcmin at the longest wavelength.
- **SOFIA** (Stratospheric Observatory for Infrared Astronomy) is a next–generation cooperative NASA and DLR (German Aerospace Center) airborne astronomy observatory (after KAO), using a modified Boeing 747–SP aircraft platform. The overall objective is to provide a long–term (20 years) high–resolution observation platform/capability in the infrared spectrum, in particular in FIR. The first phase of flight tests were completed in early 2008. NASA plans to spend most of 2008 installing the remaining elements of the observatory before conducting the first open door test flights toward the end of the year.⁷⁰⁴⁾

The science flights of SOFIA started in May 2010. DLR is providing the SOFIA telescope [Cassegrain design, 2.7 m parabolic primary mirror with 2.5 m effective aperture (light-weighted Zerodur structure) and a hyperbolic secondary mirror, FOV=8 arcmin; total instrument mass of 20,000 kg]. Observations in the spectral range of 0.3 μm to 1,600 μm (diffraction limited wavelengths $\geq 15 \mu\text{m}$) covering the entire optical range (0.3–1000 μm) + a portion in the mm–wave range. A spatial resolution of 1–3 arcsec for 0.3 $\mu\text{m} < \lambda < 15 \mu\text{m}$ and $\lambda/10$ arcsec for $\lambda > 15 \mu\text{m}$ is provided. SOFIA serves also as a platform for detection technology experiments. Some FIR instruments of SOFIA are:

- CASIMIR (Caltech Submillimeter Interstellar Medium Investigations Receiver) of the California Institute of Technology, Pasadena, CA. CASIMIR is a FIR heterodyne in-

703) <http://sirtf.caltech.edu/about/techdev.shtml>

704) “SOFIA Aircraft Completes 1st Round of Flight Tests,” Space News, January 21, 2008, p. 3

strument (0.5 – 2 THz or about 140–600 μm) to achieve very high spectral resolutions ($\nu/\Delta\nu = 10^6$) and very high detection sensitivities using SIS (Superconductor–Insulator–Superconductor) tunnel junction and HEB (Hot Electron Bolometer) mixer receiver detection technology. The goal is to cover the frequency range in seven bands, SIS mixers in four bands up to 1.2 THz, and HEB mixers in three bands covering 1.2–2.1 THz.

- FIFILS (Field Imaging Far–Infrared Line Spectrometer) provided by MPE Garching. FIFILS observes in the spectral range of 40–220 μm . The instrument consists of two medium resolution liquid helium cooled grating spectrometers with common fore–optics feeding two large GeGa detector arrays (16 x 25 pixels each). Capability of simultaneous observations of an object in two spectral bands (45–110 μm and 110–210 μm), respectively.

- SAFIRE (Submillimeter And Far InfraRed Experiment) of NASA/GSFC. SAFIRE is an imaging Fabry–Perot bolometer array spectrometer in the spectral range of 145–655 μm with a spectral resolving power ranging from 5 to 10^4 . The instrument uses two 6 x 32 arrays of bolometers to provide background–limited performance for critical science applications. SAFIRE specifications identify “quantum–noise limited heterodyne spectrometers” as one of four critical detector technologies needed before the goals of the SAFIRE instrument may be realized.

- GREAT (German Receiver for Astronomy at Terahertz Frequencies) of the Max Planck Institute for Radio Astronomy in Bonn, Germany. GREAT is a high–resolution far–infrared spectrometer. SOFIA completed the first science flight with the GREAT instrument on April 6, 2011. Rolf Guesten, the PI of GREAT and his team conducted observations high above the central and western United States beginning the night of April 5 with their instrument installed on SOFIA’s telescope. ⁷⁰⁵⁾ ⁷⁰⁶⁾

- The JWST (James Webb Space Telescope) of NASA (launch 2015) plans on a FIR detector array mosaic of 4096 x 4096 pixels (with a goal of 8 k x 8 k mosaic), rivaling the largest CCD arrays in the visible spectrum.

In the field of Earth observation (EO), the FIR region represents one of the richest areas for spectroscopic research and one of the most difficult areas for obtaining data (emission measurements). ⁷⁰⁷⁾ The FIR region contains the rotational spectra of atoms and molecules and the vibrational spectra of solids, liquids, and gases. Water vapor is the principal greenhouse gas, absorbing a significant fraction of the upwelling radiation and providing much of the downwelling longwave flux that warms the Earth’s surface (i.e., the greenhouse effect). FIR spectroscopy (or THz spectroscopy with an active FIR laser system) may be used for a wide range of climate research studies such as Earth’s energy balance (radiation budget), and measurement of trace gases in the atmosphere (environmental monitoring). Despite their fundamental importance, *spectrally resolved FIR measurements in EO have virtually not been conducted so far*, mostly due to rather expensive detector technology and the high demands on cooling. See also chapter 1.22.2 for broadband measurements of Earth’s radiation budget and the solar constant.

Some early examples of EO FIR instruments are:

- TAFTS (Tropospheric Airborne Fourier Transform Spectrometer), built by ICSTM (Imperial College of Science and Technology & Medicine), London, and funded by NERC, UK. TAFTS is designed to address some scientific problems connected with global warming; the objective is to provide well calibrated, high resolution radiance spectra for both

705) “German instrument GREAT begins its scientific observations on board SOFIA,” April 7, 2011, URL: http://www.dlr.de/en/desktopdefault.aspx/tabid-1/86_read-30074/

706) “German Instrument GREAT Begins Its Scientific Observations On Board SOFIA,” Space Daily, April 8, 2011, URL: http://www.spacedaily.com/reports/German_Instrument_GREAT_Begins_Its_Scientific_Observations_On_Board_SOFIA_999.html

707) Note: Emissivity is an intrinsic property of a material, independent of sample temperature, spectrometer characteristics, and environmental conditions. It is defined as the ratio of the emittance of a sample relative to that of a black-body at the same temperature.

up–welling and down–welling radiation in the upper troposphere/lower stratosphere (study of the impact of water vapor in the radiative transfer process). TAFTS is a Martin–Puplett–type FTS providing in–situ measurements in the upper troposphere in the spectral range 14–120 μm with a spectral resolution of 0.1 cm^{-1} . TAFTS was first flown in Sept. 1999, and participated in the airborne campaign EMERALD–2 (Egrett Microphysics Experiment with Radiation, Lidar and Dynamics), in Nov.–Dec. 2002. The objective was the study cirrus clouds that form as a direct result of deep convection. The detectors used by TAFTS were two pairs of photoconductors cooled to 4 K: (a) silicon BIB (Blocked Impurity Band), and (b) GeGa detectors. ^{708) 709)}

– REFIR (Radiation Explorer in the Far Infrared). REFIR is a FTS (Fourier Transform Spectrometer) as part of a proposed small satellite mission of ASI (Italy) in the field of climate and global change with the objective to measure the Earth’s FIR (100–1000 wavenumber, or 10–100 μm) spectral radiance (in– and outgoing) in the context of ERB (Earth Radiation Budget) estimation.

– MLS (Microwave Limb Sounder) instrument flown on NASA’s Aura mission (launch July 15, 2004). MLS measures, among many other atmospheric constituents, also the concentration and distribution the hydroxyl radical (OH^-) in the stratosphere, a critical component in the ozone cycle. MLS employs a 2.5 THz laser system (84 μm) to sense the hydroxyl. The CW laser source employed is of the type OPTL (Optically Pumped Terahertz Laser) using the TDS (Time Domain Spectroscopy) measurement scheme which relies on a broadband short–pulse Terahertz source. ⁷¹⁰⁾

– FIRST (Far Infrared Spectroscopy of the Troposphere) project of NASA within IIP (Instrument Incubator Program). ⁷¹¹⁾ The design features a nadir–viewing Michelson FTS (of GIFTS heritage) in the spectral range **10–100 μm** with a spectral resolution at 0.6 cm^{-1} (unapodized), a FOV of 100 km x 100 km, and an IFOV of 10 km. The FIRST interferometer is being designed and built by SDL (Space Dynamics Laboratory) at USU (Utah State University), Logan, UT (in partnership with NASA/LARC and SAO). An objective of FIRST is to take advantage of state–of–the–art technologies (bilayer beamsplitters, pyroelectric detectors, and high throughput FTS) to reach the thermal noise limit at ambient temperature of about 180 K in a passively cooled space environment. – A successful balloon–borne technology demonstration flight was conducted in June 2005 (33 km altitude, campaign site: Fort Sumner, New Mexico). A second flight of FIRST took place in Sept. 2006. Eventually, the FIRST instrument will be flown on a spaceborne mission. ⁷¹²⁾

As of 2008, NASA is in the definition phase of the mission **CLARREO** (Climate Absolute Radiance and Refractivity Observatory), a mission and a program within the “decadal survey” recommendation of the NRC (National Research Council). Some version of the FIRST prototype instrument will certainly be selected as a payload sensor of the CLARREO mission – due to the excellent results obtained in the FIRST campaigns. *The FIRST instrument is regarded the first imager capable of observing atmospheric emissions in essentially the entire FIR spectrum.*

708) <http://www.sp.ph.ic.ac.uk/~jon/Tafts/>

709) G. Straine, J. Murray, P. Green, et al., “TAFTS clear sky far infrared radiance observations during EMERALD2,” Proceedings of RMS Conference 2003, Norwich, UK, Sept. 1–5, 2003

710) Eric R. Mueller, “Terahertz Radiation: Applications and Sources,” The Industrial Physicist, Aug./Sept, 2003.

711) M. G. Mlynczak, D. G. Johnson, J. I. Applin, “The Far–Infrared Spectroscopy of the Troposphere (FIRST) Project,” NASA Earth Science Technology Conference 2002, Pasadena, CA, June 11–13, 2003; URL: [http://es-to.gsfc.nasa.gov/conferences/estc-2002/Papers/B4P2\(Mlynczak\).pdf](http://es-to.gsfc.nasa.gov/conferences/estc-2002/Papers/B4P2(Mlynczak).pdf)

712) B. Jannotta, “NASA Tests Global Warming Sensor for Use on Future Satellite,” Space News, June 20, 2005, p.18

1.5.18 Vegetation fluorescence in passive remote sensing

The ability to observe vegetation fluorescence remotely is of great importance to the science community, because such a capability could reveal unique information about the photosynthetic activity of vegetation.⁷¹³⁾ Unlike conventional solar induced reflectance measurements which are affected by numerous surface and atmospheric processes, fluorescence represents an observable whose process originates within plant life itself and whose complex signal is emitted by the plant's surface. The primary regulatory mechanism of natural vegetation fluorescence is considered to occur through photosynthesis. This direct link of photosynthesis to vegetation fluorescence can serve as the prime indicator and quantifier of biomass production (also role of fluorescence in bio-chemical cycles, surface-atmosphere interactions, CO₂ flux, etc.).

In 2002, an ESA-funded feasibility study, FLEX (Fluorescence Explorer), investigated the measurement aspects and challenges of the weak fluorescence signal (detectability assessment). Under natural sunlight illumination, the amount of chlorophyll fluorescence emitted by vegetation represents a very small fraction of the reflected light in the visible part of the spectrum (less than 2% in most cases).⁷¹⁴⁾ ⁷¹⁵⁾ However, at certain wavelengths where the solar spectrum is attenuated (Fraunhofer lines), the fluorescence signal can be quantified (detection in very narrow spectral bands). The fluorescence emission of a leaf as derived from laboratory measurements exhibits peaks at 440, 520, 690 and 740 nm. Chlorophyll pigments exhibit red fluorescence, with a maximum at 690 and 740 nm. In addition to chlorophyll fluorescence emission, the ultraviolet part of the solar spectrum also excites a blue-green fluorescence (BGF) of plants. However, BGF is not directly linked to chlorophyll or to photosynthesis. The study also addressed the need for an integrated canopy fluorescence model (from leaf to canopy) and possible interpretation methods of the signal.

In addition, an ESA field campaign SIFLEX (Solar Induced Fluorescence Experiment) was conducted (June-July 2002) in northern Finland [tower measurements of boreal pine canopy fluorescence at different scales (needle, shoot and crown)]. For the first time, it was possible to observe the chlorophyll fluorescence signal in the natural environment over extended periods of time (passive observation methods). As a result, more realistic simulations can be made of the performance requirements of future spaceborne instruments. The results of the campaign indicate that in principle the chlorophyll fluorescence signal is detectable by a spaceborne instrument, even under low-light conditions (corrections for atmospheric effects arising from molecular and aerosol scattering may be needed, modeling of atmospheric oxygen absorption). The ability of photosynthetic activity monitoring should significantly improve estimates on CO₂ (carbon dioxide) uptake and provide a means for screening and monitoring vegetation vigor over large regions.⁷¹⁶⁾ ⁷¹⁷⁾

An important result of the various ESA study engagements is the recognition that natural fluorescence is now identified as a necessary specific observable complementary to conventional observations in the framework of land surface processes missions that must be included in the overall observation strategy.

Background: Proposals to measure plant fluorescence were already voiced in 1975 when the required detection technology (sensitivity) was not available. Of the passive fluores-

713) M. Davidson, M. Berger, I. Moya, J. Moreno, T. Laurilla, M.-P. Stoll, J. Miller, "Mapping Photosynthesis from Space - a new vegetation-fluorescence technique," ESA Bulletin, 116, Nov. 2003, pp. 34-37

714) J. R. Miller, M. Berger, L. Alonso, Z. Cerovic, et al., "Progress on the Development of an Integrated Canopy Fluorescence Model," IEEE/IGARSS 2003, Toulouse, France, July 21-25, 2003

715) I. Moya, A. Cartelat, Z. G. Cerovic, et al., "Possible Approaches to Remote Sensing of Photosynthetic Activity," IEEE/IGARSS 2003, Toulouse, France, July 21-25, 2003

716) Note: While active fluorescence methods (lidars) have greatly benefited from progress in optoelectronics and laser sources, they are not considered suitable for large-scale and long-range applications in remote sensing.

717) Note: In this context "uptake" refers to the ocean's ability to take up a large fraction of the perturbation CO₂ entering the atmosphere by human activity.

cence measurement techniques, there are three basic vegetation photosynthetic activity indicators: ⁷¹⁸⁾ ⁷¹⁹⁾ ⁷²⁰⁾

- Oxygen absorption technique with spectral lines at 687 and at 760 nm
- PRI (Photochemical Reflectance Index) technique by using reflectances at 531 and at 570 nm
- Derivative technique of high spectral resolution reflectance in the red–edge band (680–750 nm)

So far, no operational system has been developed for remote sensing of fluorescence. Some examples of demonstration instruments or measurement concepts are:

- An early airborne instrument implementation was FLI (Fluorescence Line Imager), a hyperspectral sensor developed by Moniteq Ltd and Itres Ltd for the Canadian Department of Fisheries and Oceans. It was first flown in 1984, using pushbroom technology and 288 spectral bands.
- The spaceborne ocean color instruments provide already the capability of monitoring the chlorophyll and gelbstoff concentrations in the surface layer of the ocean to estimate the phytoplankton production. The spectral band set of MERIS (Medium – Resolution Imaging Spectrometer for Passive Atmospheric Sounding) on Envisat (launch March 1, 2002) already includes a band around 681.25 nm optimized for the retrieval of water chlorophyll fluorescence. However, fluorescence emission from land vegetation chlorophyll cannot be detected in the same way as for water chlorophyll, because over land the background reflectance dominates the signal, and fluorescence spectral features are masked by the dominant reflectance signatures. Another method that has been demonstrated successfully in retrieving vegetation fluorescence over land is by using the atmospheric oxygen absorption band around 760 nm, in particular with two MERIS bands at 753 nm (oxygen absorption reference) and at 760 nm (oxygen absorption R–branch). ⁷²¹⁾ The measurements in these two bands allow to get land vegetation fluorescence provided some assumptions (same reflectance and fluorescence emission in the two spectral bands), and provided also a proper atmospheric correction of the data, or using in–scene non–fluorescent targets as reference.
- A FLEX (Fluorescence Explorer) ⁷²²⁾ spaceborne mission was proposed to ESA in Dec. 1998 (by a European consortium of institutions) with the objective to explore the possible use of the Fraunhofer lines in the spectrum for passive measurements of natural sunlight–induced fluorescence. ⁷²³⁾
- The PMFD (Passive Multi–wavelength Fluorescence Detector) instrument was developed at LURE/CNRS, University of Paris, France. ⁷²⁴⁾ Objective: continuous measurement of chlorophyll fluorescence based on the Fraunhofer line principle, applied in the at-

718) W. R. Hemphill, R. D. Watson, R. C. Bigelow, T. D. Hessin, “Measurement of luminescence of geochemically stressed trees and other materials,” US Geological Survey Professional Paper 1015:93–112, 1975.

719) J. A. Plascyck: “The MKII Fraunhofer Line Discriminator (FLD–II) for airborne and orbital remote sensing of solar–stimulated luminescence,” *Optical Engineering*, Vol. 14, No 4, 1975, pp.:339–346

720) L. Alonso, J. Moreno, I. Moya, J. R. Miller, “A Comparison of Different Techniques for Passive Measurement of Vegetation Photosynthetic Activity: Solar–Induced Fluorescence, Red–Edge Reflectance Structure and Photochemical Reflectance Indices,” *IEEE/IGARSS 2003*, Toulouse, France, July 21–25, 2003

721) J. Moreno, “On the possibility to retrieve land vegetation fluorescence from MERIS,” <http://envisat.esa.int/cgi-bin/confmeris.pl?abstract=232>

722) M.–P. Stoll, A. Court, K. Smorenburg, H. Visser, L. Crocco, J. Heilimo, A. Honig, “FLEX – Fluorescence Explorer: a space mission for screening vegetated areas in the Fraunhofer lines,” *Europto Conference on Remote Sensing for Earth Science Applications*, Florence, Italy, SPIE Vol. 3868, pp.108–119, 1999

723) M.–P. Stoll, T. Laurila, C. Buschmann, J. Moreno, A. Court, I. Moya, “The FLEX–Fluorescence Explorer mission project: motivations and present status of preparatory activities,” *IEEE/IGARSS*, Toulouse, France, Jul. 21–25, 2003

724) S. Evain, L. Camenen, I. Moya, “Three channels detector for remote sensing of chlorophyll fluorescence and reflectance from vegetation,” *8th International Symposium: Physical Measurements and Signatures in Remote Sensing*, Ed. M. Leroy, Aussois, France, 2001, pp. 395–400.

ospheric oxygen absorption A and B bands (760 and 687 nm, respectively). PMFD and a spectroradiometer (ASD FR/FS for the upwelling radiance measurements in the range 350 – 2500 nm) were used in the ESA SIFLEX (Solar Induced Fluorescence Experiment) campaign in 2002. For the duration of the campaign, the vegetation passed from a dormant state, with very low activity, to a fully active state.

- The hyperspectral instrument CASI⁷²⁵⁾ (Compact Airborne Spectrographic Imager) of Itres Ltd., Canada, is capable of acquiring imagery of vegetation for fluorescence retrieval. The instrument has been used in various campaigns.
- AIRFLEX (Airborne Fluorescence Experiment) campaign of ESA. The objective is to measure the fluorescence signal from an airborne platform over a variety of land cover types (information about the fluorescence signal sensitivity, spatial variability and scaling effects, fluorescence dependence on solar irradiance). The campaign took place in Barrax, Spain in June–July 2005.

1.5.19 Sparse aperture imaging concepts

The requirements for high–resolution observation data, along with the constraints of minimum mass/volume (launch phase), and maximum aperture telescope/antenna size of spaceborne instruments, have eventually lead to such design concepts as “sparse aperture telescope” for optical systems and “sparse aperture array”⁷²⁶⁾ for microwave antennas/receivers. Such systems provide improved observation capabilities in the following fields: optical imaging (visible and infrared region), radiometric sounding/imaging (visible to microwave region), and communication applications.

A sparse aperture system refers to a non–filled multiple aperture configuration, with holes or gaps in between the individual elements (subapertures) of the system to obtain a large aperture – and to reduce mass. Conceptually, any sparse aperture is a distributed system of various cooperating elements (an array of receiving dipoles), arranged in a definite (symmetric) pattern or configuration, forming in effect a multi–aperture interferometer system.

Generally, the sparse aperture concept is applicable to all wavelengths of the spectrum as well as to all concepts of interferometry, starting with a two–element interferometer (Fizeau, Michelson, etc.), a multi–aperture interferometer system, up to the highest–resolution VLBI (Very Long Baseline Interferometry) and SVLBI (Space VLBI) techniques.

Sparse–aperture interferometry concepts are currently being used (or are being planned) in remote sensing and in astronomy applications, in the spectral domains of **optical** interferometry and in **microwave** interferometry with radio/radiometry (passive) and radar (active) applications. The distinctions of optical vs microwave are primarily due to the physics involved at the different wavelength regimes (visible wavelengths result in a 10,000–fold improved spatial resolution over that available in the microwave regime).⁷²⁷⁾

– Optical interferometers (Michelson, etc.) employ **direct detection** – in which the two beams are combined using a beam–splitter with the resulting fringe sampled by a single detector. This approach results in a system whose accuracy is properly limited by the source shot noise and detector noise as opposed to the shot noise of some optical local oscillator.

725) P.–J. Zarco–Tejada, J. R. Miller, D. Haboudane, N. Tremblay, S. Apostol, “Detection of Chlorophyll Fluorescence in Vegetation from Airborne Hyperspectral CASI Imagery in the Red Edge Spectral Region,” IEEE/IGARSS 2003, Toulouse, France, July 21–25, 2003

726) Note: The angular resolution of an aperture (telescope or antenna) is primarily determined by the overall diameter of the aperture. The angular resolution is proportional to the diameter of the aperture and inversely proportional to the observing wavelength. The sensitivity of an aperture is determined by both the area of its aperture, and the sensitivity of the sensor.

727) R. M. Duren, “System Engineering for Spaceborne Optical Interferometers,” Proceedings of the IEEE Aerospace Conference, Big Sky, MT, March 6–13, 2004

– Radio and radar interferometers operate by independently detecting signals from two antennas and combining them a posteriori for **indirect fringe generation**. This method involves heterodyne receivers which experience shot noise from their local oscillators – about 1 photon per Hz of bandwidth. While this is acceptable at microwave wavelengths, the local shot noise grows with frequency such that it dominates the source shot noise and detector noise at visible and IR wavelengths (0.4 to 30 μm).

The sparse aperture observation concept is based on “**aperture synthesis**,” an interferometric technique which recombines the radiation (interference fringes) of the various subapertures in a sparse array configuration – thus achieving higher resolutions. Fourier synthesis techniques play a key role in aperture synthesis analysis [the brightness distribution of the incoming target (or object) radiation is actually the Fourier Transform of the set of phase and amplitude measurements from the interferometer]. The high angular resolution of radio telescopes (in astronomy) is achieved by synthesizing a very large effective aperture from a number of small subapertures. In a simple two–element radio interferometer, the signals from an unresolved, or “point” source alternately arrive in–phase and out–of–phase as the Earth rotates and causes a change in the difference in path from the radio source to the two elements of the interferometer. – An important advantage of the aperture synthesis concept is the provision of diffraction–limited observations. A disadvantage is the reduced MTF (Modulation Transfer Function) level causing significant blurring and loss of contrast in the collected imagery. However, image reconstruction algorithms can correct the blurring completely with a sufficiently high SNR (Signal–to–Noise) ratio.

Obviously, a distributed system can be thought of:

– As a coupled system (a monolithic structure, where all discrete elements maintain a fixed arrangement to each other) on a single spacecraft. The distances between the various subapertures represent short baselines. A telescope incorporating a sparse–aperture mirror can be folded in a compact fashion to make a small and lightweight payload, which can be placed into orbit by a relatively inexpensive launch vehicle.

– A loosely–coupled system such as a close spacecraft formation (each spacecraft with a single aperture). This arrangement permits larger sparse apertures, providing larger but only relatively stable baselines.

- Radiometry: A sparse array in the microwave region uses an array of receivers (as discrete elements) that span the imaging aperture. Typically the array is two–dimensional (Y shaped) and does not have optically focusing elements in front of the receivers. The receivers are said to be in the “pupil plane.” To form an image the detectors must record both amplitude and phase of the incoming radiation wave front. The image is formed in the electronics (typically in software) by taking spatial Fourier Transforms across the two axis of the array. A complete image can be formed as long as all of the spatial Fourier components are collected. The sparseness of the array reduces the amount of the collected radiation and reduces the SNR by the ratio of the area of the receivers to the area of the complete aperture. In a conventional sparse array the FOV is fixed and fairly large to avoid having to physically steer the entire array to view different objects of interest. The FOV of the array is determined by the antenna pattern of the individual receivers in the array.⁷²⁸⁾

Background: While the invention of interferometry dates back to the 19th century [Fizeau (first proposal in 1868), Michelson (first measurements in 1890), etc.], it was in the late 1940s when Australian radio astronomers realized that each interferometer pair measurement was in effect one “Fourier component” of the brightness distribution of the radio source. Further developments during the 1950s by Martin Ryle and his colleagues at Cambridge University, Cambridge, UK, involved initially the use of movable–element inter-

728) R. T. Snider, T. L. Rhodes, “Steerable, Millimeter Wave, Sparse Array for Satellite Observations under Cloudy Conditions on Haleakala,” General Atomics Report GA–A24110, Sept. 2002, <http://web.gat.com/pubs-ext/MIS-CONF02/A24110.pdf>

ferometers in the laboratory and the realization that Earth rotation provided already relative motion (of elements A and B as seen from the source), required for the sampling of interferometry observations. All experimentation was done in the microwave region of the spectrum (at wavelengths of 1 m and more) to minimize the alignment problems of instrumentation. The lack of available computer power at the time was the greatest handicap for handling the great amount of Fourier transformations. Nevertheless, radio astronomy observations began in 1964 on the “One Mile Array” at Cambridge, a microwave sparse aperture system consisting of three 18 m dishes in a line 1 mile long array. – The world’s first optical aperture synthesis telescope, COAST (Cambridge Optical Aperture Synthesis Telescope), was built in 1988 (VIS, NIR). The configuration of COAST consists of five apertures (40 cm diameter) arranged in a ‘Y’ configuration, with a maximum element separation of about 22 m. In 1974, Martin Ryle and Anthony Hewish received the Nobel Prize in Physics in recognition of their contributions to the development of the Fourier synthesis technique, also as **aperture synthesis**.⁷²⁹⁾

In 2003, the radioastronomy community started to develop concepts to build a ground-based radiotelescope with a sensitivity two orders of magnitude larger than present-day telescopes. The ground-based project is called **SKA** (Square Kilometer Array), referring to a **sparse aperture synthesis telescope** design with a receiving area $> 1 \text{ km}^2$ and distributed over an area 50 to 300 km in diameter. The sparse array at each participating site would have a diameter of about 300 m in order to achieve the required collecting area.

SKA is an international project and a collaboration of various institutions of the following member countries: Australia, Canada, China, Germany, Italy, The Netherlands, New Zealand, South Africa, Sweden, and the United Kingdom. – As of Jan. 2006, European funding (Framework 6 R&D program of the European Commission) was secured to support a 4-year SKADS (Square Kilometer Array Design Study). By the end of this decade, the design will be complete and astronomers anticipate building SKA in stages, leading to completion and full operation in 2024.^{730) 731) 732)}

In May 2012, a dual-site implementation of the SKA, in Australia and South Africa, was agreed to by the SPDO (SKA Program Development Office).⁷³³⁾ Construction of phase one of the SKA is scheduled to start in 2016.

Some examples of early sparse-aperture implementations or projects in the field of Earth observation are:

- ESTAR (Electronically Steered Thinned Array Radiometer)⁷³⁴⁾ a passive airborne instrument developed by NASA/GSFC and the Microwave Remote Sensing Laboratory of the University of Massachusetts at Amherst (P.88).
- SMOS (Soil Moisture and Ocean Salinity Mission) of ESA (launch Nov. 2, 2009) demonstrates spaceborne synthetic aperture imaging radiometry with MIRAS (Microwave Imaging Radiometer using Aperture Synthesis), a Y-shaped sparse array or a “synthetic aperture radiometer.”⁷³⁵⁾
- STAR (Synthetic Thinned Aperture Radiometry) is a microwave sounder/imager under development at NASA. The objective is to achieve a 10 km spatial resolution global soil moisture mission towards the end of the decade (LEO mission).

729) <http://www.crystalinks.com/telescopes4.html>

730) <http://www.astron.nl/ska/technical/>

731) http://www.skatelescope.org/PDF/SKA_Booklet.pdf

732) <http://www.pparc.ac.uk/Nw/SKA.asp>

733) “Dual site agreed for Square Kilometre Array telescope,” May 25, 2012, URL: <http://www.skatelescope.org/news/dual-site-agreed-square-kilometre-array-telescope/>

734) C. S. Ruf, C. T. Swift, A. B. Tanner, D. M. LeVine, “Interferometric synthetic aperture microwave radiometry for the remote sensing of the Earth,” IEEE Transaction on Geoscience and Remote Sensing, Vol. 26, pp. 597 611, September, 1998.

735) A. Lannes, E. Anterrieu, “Image reconstruction methods for remote sensing by aperture synthesis,” Proceedings of IGARSS Conference, Pasadena, CA, Aug. 8–12, 1994, pp. 1323–1325

- **Conceptually, each SAR instrument is by definition an aperture synthesis device.** The resolution is limited by the synthetic aperture length, and so is the effective received power. Of course, a SAR instrument’s antenna is “real.”
- The ARGOS (Adaptive Reconnaissance Golay–3 Optical Satellite) project of MIT,⁷³⁶⁾ a ground–based testbed, exploits wide–angle Fizeau interferometer technology with an emphasis on modularity in the optics and spacecraft subsystems. The objective of the ARGOS project is to demonstrate the practicality of a modular architecture for spaceborne optical systems.

1.5.20 Astronaut–acquired photography and movies

The spaceage has also provided a wealth of spaceborne photography acquired by hand–held cameras of manned missions. An online database of over 450,000 astronaut photos of Earth, dating back to the early 1960s, is maintained by NASA/JSC. This archive covers the majority of the Earth’s surface and offers imagery taken by a variety of camera configurations, including film (analog) and digital imagery, various lenses, different look angles, and changing solar illuminance.^{737) 738) 739)}

Background: In the US space program, the Mercury project was the first attempt at launching a human being into space. It consisted of six manned flights in the period 1961 to 1963. Astronaut John Glenn, on the first US orbital manned flight (Feb. 20, 1962) in history, was using a conventional camera. Those amateur photographs turned out to be the first Earth observation photographs taken by an astronaut in history. Note: Some additional instrument descriptions of Shuttle EO Imaging Cameras is provided in chapter J.26.

- In subsequent Mercury flights, first experiments were conducted in hand–held photography, recording properties of Earth’s limb, observing the Earth illumination at night, and use of filters to acquire weather photographs. – At about the same time, the first TIROS (Television Infrared Observation Satellite) series meteorological satellites of NASA (unmanned spacecraft, launch of TIROS–1 on Apr. 1, 1960) were making their first attempts of gathering weather information with such instruments as TV–WA (Television Wide Angle), TV–NA (Television Narrow Angle), and a Scanning Radiometer, a five–channel instrument which measured the emitted and reflected radiation of the Earth and its atmosphere.
- The US Gemini program consisted of 12 manned (plus 2 unmanned) missions in the timeframe March 1965– Nov. 1966. Most of the hand–held photography was organized through two science experiments, a) synoptic terrain photography and b) synoptic weather photography.⁷⁴⁰⁾ The objective of the first experiment was to obtain high–quality pictures of significant land areas that had been previously well mapped by aerial photography and to serve as a standard for interpretation of photographs of unknown areas of Earth, the Moon, and other planets. For synoptic terrain photography, a modified Hasselblad camera was used with a mass of 0.45 kg, model 500 C (70 mm camera with black and white film and a special filter mosaic to allow each picture to be taken partly through a red and partly through a blue filter).

736) S.–J. Chung, D. W. Miller, O. L. de Weck, “Design and Implementation of Sparse Aperture Imaging Systems,” SPIE Conference on Highly Innovative Space Telescope Concepts, Waikoloa, HI, USA, Aug. 22–23, 2002, SPIE Vol. 4849–25

737) J. Gebelein, “Astronaut–Acquired Photography of Earth: Its History and Continued Applicability in Quantitative Analysis,” URL: <http://satjournal.tcom.ohiou.edu/pdf/gebelein.pdf>

738) <http://eol.jsc.nasa.gov/sseop/clickmap/>

739) “The Gateway to Astronaut Photography of Earth,” NASA/JSC, URL: <http://eol.jsc.nasa.gov/>

740) S. Garber, “Gemini – Experiments by Flight,” NASA SP–4203, 2001, URL: <http://www.hq.nasa.gov/office/pao/History/SP–4203/appd1.htm>

- The KATE–140 (Multispectral Camera) is an example of a prominent cosmonaut–operated camera system of the Soviet space program. The objectives were the provision of topographic imagery of the Earth’s surface. KATE–140 employed an objective lens with a focal length of 140 mm. The frame format of 18 cm x 18 cm could acquire photographs in the spectral range 500–700 nm (three bands) with a footprint of about 440 km x 440 km (resolution of about 50 m) from an orbital altitude of about 350 km. KATE was mostly being used as a stationary camera, porthole fixed. A further development was the KATE–200 camera with a focal length of 200 mm. The KATE model used frame film cassettes of 600 images. KATE–140 was flown on Salyut–4 (Dec. 26 1974 to Feb. 2, 1977), Salyut–6 (launch Sept. 29, 1977, crew occupation for a total of 676 days, reentry July 28, 1982) and Salyut–7 (launch Apr. 19, 1982 crew occupation for a total of 812 days, reentry 1989).⁷⁴¹ KATE–140 was also flown on the following manned missions: Soyuz–T–9 (launch June 27, 1983), Progress–18 (launch Oct. 20, 1983), Soyuz–T–10B (launch Feb. 8, 1984), Soyuz–T–11 (launch Apr. 3, 1984), Progress–22 (launch May, 28, 1984), Kosmos–1669 (launch July 19, 1985), and on the MIR station from 1987 onwards.⁷⁴²
- **IMAX** video camera (“Image Maximum” –a large screen motion picture camera/format used by the NASA/Smithsonian project to document significant space activities). The IMAX camera was created by the Canadian company IMAX Corporation (inventors: Graeme Ferguson, Roman Kroitor, Robert Kerr, and William C. Shaw), first demonstrated at the Expo ’70 in Osaka, Japan. IMAX has the capacity to record and display images of far greater size and resolution than conventional film systems. The cameras, which captured the scenes for six IMAX movies (on MIR, and ISS), were carried aboard 17 shuttle missions between 1984 and 1998. The National Air and Space Museum partnered with IMAX and Lockheed Martin in 1983 to create early space films such as ‘The Dream Is Alive’ to increase public understanding of spaceflight through large–format films. The spaceborne IMAX system consisted of an in–cabin camera that the astronaut crews operated by hand and the payload bay camera, referred to as ICBC (IMAX Cargo Bay Camera), that was operated by the astronauts remotely. It was always situated in the payload bay of the shuttle.

There is a long tradition of stereoscopic still and video imaging on the International Space Station. Audiences were taken on the first cinematic journey to the orbital outpost in 2002 with a 3D IMAX film. Space Station 3D used two IMAX 3D cameras specifically designed and built for operation in microgravity. These cameras filmed the Station as it grew from a tiny outpost into a permanently inhabited scientific research station. Life in zero gravity got closer to the audiences.

741) Part 2: Almaz, Salyut, and Mir; <http://spaceflight.nasa.gov/history/shuttle-mir/references/documents/mirhh-part2.pdf>

742) <http://home.comcast.net/~rusaerog/aosmsf/ch5.html>



Figure 29: NASA astronaut Bill Shepherd, Expedition 1 Commander, uses an IMAX camera on the ISS in February 2001 (image credit: NASA)

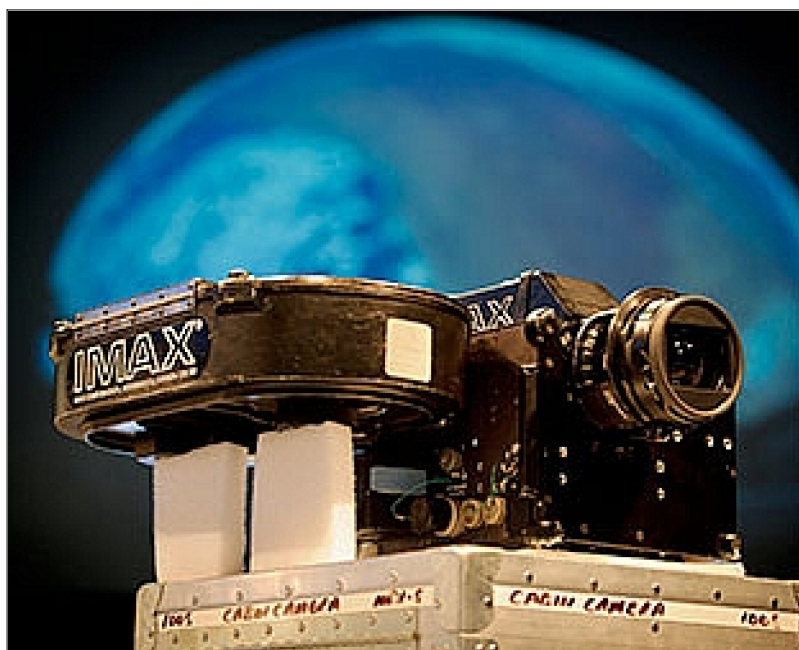


Figure 30: Photo of the IMAX camera that flew aboard the Space Shuttle (image credit: IMAX) ⁷⁴³⁾

Legend to Figure 30: In April 2012, IMAX Corp. donated its two space–flown two–dimensional cameras to the National Air and Space Museum in Washington, DC. In May 2009, the a 3D IMAX camera (of about 315 kg) was used on the Hubble repair mission (STS–125) to chronicle the effort of 7 astronauts.

⁷⁴³⁾ “IMAX space cameras given to Smithsonian,” April 4, 2012, collectSpace, URL: <http://www.collectspace.com/news/news-040412c.html>

- **ESTER** (Earth Science Toward Exploration Research). ESTER is a digital handheld camera of NASA/JSC. ESTER features a 400 mm lens (and a 160 mm and a 50 mm lens). The objective is to use ESTER onboard ISS to document global phenomena (significant events like hurricanes, plankton blooms, and volcano eruptions) in both an automated and hand-held mode in combination with WORF (Window Observational Research Facility). Since delivery of the WORF has been postponed (until 2010), ESTER is using EarthKAM hardware, an educational payload of ISS, mounted in the Destiny Laboratory.⁷⁴⁴⁾
- **ERB-1** (Erasmus Recording Binocular-1): The Erasmus Centre of ESA/ESTEC conceived the ERB-1 3D camera (developed by Cosine BV, The Netherlands) which was flown to the ISS in 2006. The ERB-1 was used extensively during the Astrolab mission of 2006 with ESA astronaut Thomas Reiter. ERB-1 was the first fully digital stereo camera to be used on the ISS. The ERB-1 digital camera was designed for mapping the Station's complex interior at 25 frames/s.⁷⁴⁵⁾



Figure 31: Photo of the ERB-1 camera (image credit: ESA)

- **ERB-2** is the latest ESA camera, a technology demonstration experiment, developed by Cosine Research BV, Leiden, The Netherlands and TSD (Techno System Development), Naples, Italy. The ERB-2 has been launched on February 3, 2010 from Baikonur on the unmanned Progress-36 space ferry. It was first commissioned on June 9, 2010 by NASA astronaut Tracy Caldwell-Dyson.

ERB-2 is a digital stereoscopic camera taking advantage of high-definition optics and advanced electronics to provide a vastly improved 3D video effect for mapping the Station. An improved resolution is provided: 1280 x 720 pixel (HD 720p), thereby achieving a compatible resolution with current commercial HDTV standards. With the ability to perform live broadcast of stereo films and downlink files of recorded video sessions using the HRDL (High Rate Data Link) available onboard the ISS via the EDR (European Drawer Rack). The ERB-2 instrument features 2 high-definition cameras with motorized objectives; it has a mass of 6.82 kg, a size of 397 mm x 186 mm x 269 mm, and a power consumption of 42 W (max).⁷⁴⁶⁾

— On August 18, 2011, the ERB-2 camera produced live-streaming 3D images for the first time in the history of space travel — showing the International Space Station like nev-

744) http://www.nasa.gov/mission_pages/station/science/experiments/Summary.html

745) Nadjeda Vicente, Pantelis Poulakis, Massimo Sabbatini, "Space in 3D, ESA's quest for a three-dimensional - and extraterrestrial - experience," ESA Bulletin, No 150, May 2012, pp. 12-29

746) http://www.esa.int/esaMI/magistra/SEM8M7OOHEG_0.html

er before. On the ground at ESA/ESTEC, viewers wore polarized glasses similar to those used in cinemas and were amazed by the quality of the images. ⁷⁴⁷⁾

- **NightPOD – long–exposure camera system:** In December 2011, Dutch astronaut André Kuipers took Cosine’s NightPOD camera on board to the International Space Station. Cosine’s camera enables him to take photographs of the night side of the earth, a challenge which took Cosine 6 months to build. Earlier in 2011 Cosine Research also developed a 3D camera (ERB) for the ISS. ⁷⁴⁸⁾

NightPOD is an intelligent tripod head that is used to accurately track a SLR (Single Lens Reflex) camera, potentially with a large SLR, to track objects. Extremely sturdy and user friendly, it can be used to take long exposure photographs or eliminate motion blur under demanding conditions. It can be used for accurate tracking of moving objects or track stationary objects from a moving platform, such as boats, airplanes and cars.



Figure 32: NightPOD installed on a mock–up of the European Cupola observatory during testing (image credit: ESA)

NightPOD is a one–of–a–kind product for mounting and accurately tracking a camcorder (or single–lens reflex camera) in the Node–3/Cupola of the ISS. ESA astronaut André Kuipers has installed ‘NightPOD’ on the ISS, an aid for taking night–time pictures of Earth. NightPOD compensates for the motion of the Space Station by tracking single points on Earth automatically. The subject stays centered in frame during a long exposure time so the final image is in focus. ⁷⁴⁹⁾ – The NightPOD project was funded by the Netherlands Space Office and the German government.

At the start of the 21st century, astronaut–acquired photography is considered valuable complementary data to remote sensing data, in particular with regard to unexpected or unplanned event monitoring applications.

747) “First 3D video transmission live from space,” ESA, Aug. 18, 2011, URL: http://www.esa.int/esaCP/SEM-WLEOT9RG_index_0.html

748) “André Kuipers launch Wednesday 21 December 2011 with cosine NightPOD camera,” Cosine, Dec. 20, 2011, URL: <http://cosine.nl/?id=newsitem&code=20111220>

749) “Tracking cities at night from the Space Station,” ESA, April 5, 2012, URL: http://www.esa.int/SPECIALS/PromISSe/SEM3HNEWF0H_0.html

1.5.21 SensorWeb environments in spaceflight

The term “SensorWeb” (also written as Sensor Web) refers to a distributed sensing system in which information is globally shared and used by all networked platforms. The SensorWeb describes a specific type of sensor network: an amorphous network of spatially distributed sensor platforms (**Pods**) that wirelessly communicate with each other. This amorphous architecture is unique since it is both synchronous and router-free, making it distinct from the more typical TCP/IP-like network schemes. The architecture allows every pod to know what is going on with every other pod throughout the SensorWeb at each measurement cycle.

From an application point of view, the SensorWeb concept enables a spatio-temporal understanding of an environment through coordinated efforts between multiple numbers and types of sensing platforms, both orbital and terrestrial, both fixed and mobile. Each of these platforms, communicates with its local neighborhood of sensors and thus distributes information to the instrument as a whole. *The SensorWeb concept is to sensors what the Internet is to computers, with different platforms and operating systems communicating by way of a set of robust protocols.*

It is the sharing of information among the pods that gives the SensorWeb concept its characteristic nature in providing a “macro-intelligence” to the user community. The SensorWeb can be viewed as an online service provider, where greater functionality is derived from a parallel-type architecture as sensor measurements (including pod location) are passed, and collectively interpreted, from pod to pod. This global sharing of information will lead to pod synergism (the whole of their activity being greater than the sum of their parts) by permitting intelligent resource (power, bandwidth, consumables) management by the web, and allowing for self-modifying behavior based on environmental factors and internal web diagnostics. 750) 751) 752) 753) 754) 755)

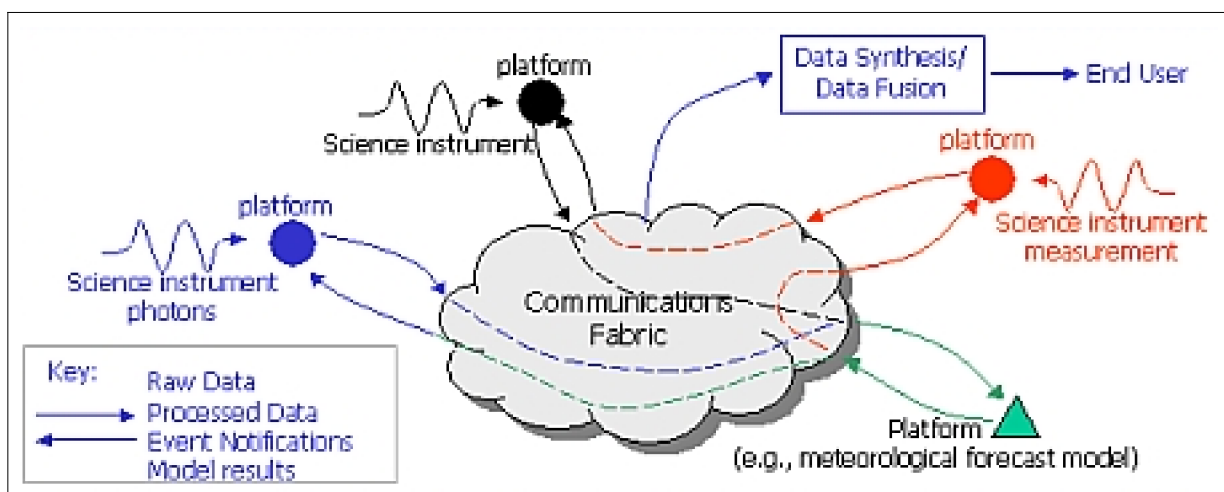


Figure 33: Each sensor platform, or pod, communicates with its “neighborhood” and thus distributes information to the system as a whole (image credit: NASA/JPL)

- 750) K. A. Delin, “The Sensor Web: A Macro-Instrument for Coordinated Sensing,” First IEEE International Conference on Sensors 2002, Vol. 2, pp. 270–285, Orlando, FLA, USA, June 12–14, 2002, URL: <http://www.mdpi.org/sensors/papers/s20700270.pdf>
- 751) http://en.wikipedia.org/wiki/Sensor_Web
- 752) <http://sensorwebs.jpl.nasa.gov/>
- 753) K. A. Delin, S. P. Jackson, R. R. Some, “Sensor Webs,” NASA Tech Briefs, Oct. 1, 1999, Vol. 23, URL: <http://www.techbriefs.com/content/view/2227/32/1/0/>
- 754) <http://esto.nasa.gov/sensorwebmeeting/>
- 755) Report from the Earth Science Technology Office (ESTO) Advanced Information Systems Technology (AIST) Sensor Web Technology Meeting, February 13–14, 2007, San Diego, CA, URL: http://esto.nasa.gov/sensorwebmeeting/files/AIST_Sensor_Web_Meeting_Report_2007.pdf

A SensorWeb pod is merely a physical platform for a sensor which can be orbital or terrestrial, fixed or mobile and might even have real-time accessibility via the Internet. Pod-to-pod communication is both omni-directional and bi-directional where each pod sends out collected data to every other pod in the network. As a result, on-the-fly data fusion, such as false positive identification and plume tracking, can occur within the SensorWeb itself and the system subsequently reacts as a coordinated, collective whole to the incoming data stream. For example, instead of having uncoordinated smoke detectors, a SensorWeb can react as a single, spatially-dispersed, fire locator.

An in situ SensorWeb provides a different type of measurement capability than that associated with remote techniques made by orbital or airborne platforms. By definition, remote measurements require a high degree of knowledge of the physics of the measurement to infer value from the collected data (interpreting ocean currents or a vegetation index, for example). In contrast, a SensorWeb can provide direct, proximity measurements over a large spatial scale whose value is much more immediate. Moreover, unlike remote measurements made by orbital or airborne platforms, a SensorWeb provides a continued, virtual presence in an area. This is particularly important when investigating phenomena of a transient nature where there is no guarantee that an orbiting instrument will be in position to record the event.⁷⁵⁶⁾

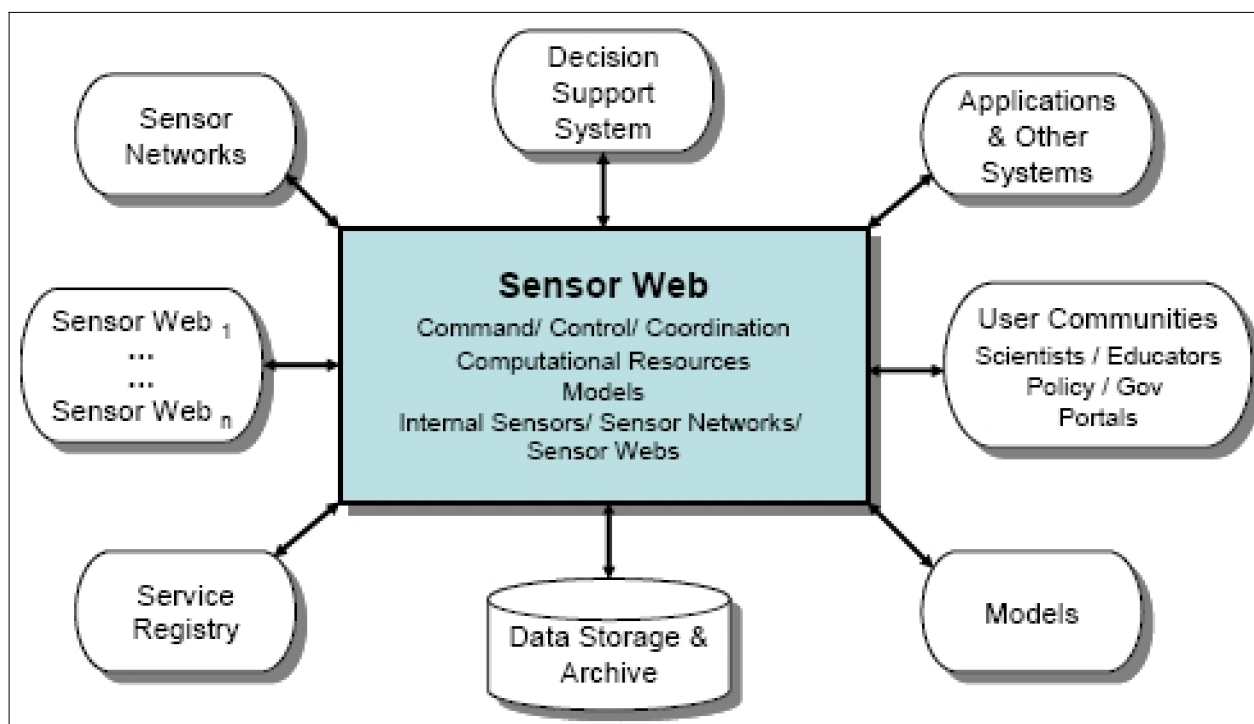


Figure 34: Conceptual view of the SensorWeb architecture (image credit: NASA)

The key elements of the sensor web include autonomous detection of events,^{757) 758)} autonomous monitoring of detection notifications, autonomous generation of observation requests, and autonomous rescheduling of observations to acquire data of higher temporal, spatial, and spectral resolution. An example sensor web might be one satellite observing a target event and triggering another satellite autonomously.

756) D. Mandl, S. Grosvenor, S. Frye, R. Sherwood, S. Chien, A. Davies, B. Cichy, M. A. Ingram, J. Langley, F. Miranda, R. Q. Lee, R. Romanofsky, A. Zaman, "Sensor webs: Autonomous Rapid Response to Monitor Transient Science Events," http://eo1.gsfc.nasa.gov/new/SensorWebs/EO-1_AMS%20Sensor%20Web%201-6-051.pdf

757) R. Sherwood, S. Chien, "SensorWebs for Science: New Directions for the Future," IEEE Infotech@Aerospace Conference, Rohnert Park, CA, May 2007, URL: http://sensorwebs.jpl.nasa.gov/public/papers/sherwood_ieeein-foero07_sensorweb.pdf

758) Pat G. Cappelaere, Stuart W. Frye, Daniel Mandl, "Flow-Enablement of the NASA SensorWeb using RESTful (and Secure) Workflows," Proceedings of the 2009 IEEE Aerospace Conference, Big Sky, MT, USA, March 7-14, 2009

Background: In the timeframe 2009/10, the SensorWeb concept constitutes a revolution in the discovery and assessment of live data sources and archived data produced by sensors.

Sensor networking and interoperability can only obtain meaningful results by generally agreed on standards involving such items as formats, protocols, interfaces, encodings and many more things.^{759) 760)}

The beginnings of an emerging SensorWeb idea can be traced back to CEOS (Committee on Earth Observation Satellites) activities in the latter part of the 1990s as well as to the OGC (Open Geospatial Consortium Inc.), founded in 1994 (government, industrial, academic and private members). In 2004, OGC organized OGCI (OGC–Interoperability Institute) to create academic partnerships in support of the interoperability objectives of the research community, as well as to provide better definition and support for the evolving science of Spatial Analysis.⁷⁶¹⁾

- In April 1998 (Bernried meeting in Germany), the CEOS Global Mapping Task Team recommended the provision for interoperability of multiple space agency sensor data – based on the realization by Earth observation scientists that data from spaceborne sensors were not adequately nor easily georeferenced to meet their requirements. The consequence of this deficiency was evident in the fact that to combine data from different spaceborne sensors or ground–based data was extremely difficult or simply impossible.
- In September 1998 (Boulder, CO meeting), the CEOS Global Mapping Task Team presented a proposal for a Sensor Description Format and recommended also the XML (eXtensible Markup Language), a document markup language for the creation of hierarchical information structures.
- In Sept. 1999 (Charlottesville, VA meeting), CEOS presented a first SensorML concept.

Note: **SensorML** (Sensor Model Language)⁷⁶²⁾ uses the XML markup scheme, which has become a standard in the description of sensor systems. SensorML describes the geometric, dynamic, and observational features of sensors of all kinds. SensorML is a key component for enabling autonomous and intelligent SensorWebs; it provides the information needed for discovery of sensors, including sensor’s capabilities, geolocation and task–ability rather than a detailed description of the sensor hardware. In short: SensorML is the means by which sensors and processes make themselves and their capabilities known.

• In 1999, ESTO (Earth Science Technology Office) of NASA initiated its AIST (Advanced Information Systems Technology) program with the objective to identify, develop and (where appropriate) demonstrate advanced information system technologies. The goal of NASA’s **SensorWeb** approach is to employ new data acquisition strategies and systems for integrated Earth sensing that are responsive to environmental events for both application and scientific purposes. SensorWebs can achieve science objectives beyond the abilities of a single platform by:

- 1) Reducing response time (where events unfold rapidly or where time is otherwise constrained)
- 2) Increasing the scientific value, quantity, or quality of the observation (where unique science criteria are met, or when co–incident observations are possible) by enabling collaboration among sensing and analysis assets.

759) M. Botts, “SensorML and Sensor Web Enablement,” May 2002, URL: http://ceos.esrin.esa.it/ceos_wgiss_grid/wgiss/sensorml_ceos_0502_botts.ppt

760) <http://www.opengeospatial.org/ogc/history>

761) http://www.ceos.org/index.php?option=com_content&view=category&layout=blog&id=152&Itemid=217

762) X. Chu, R. Buyya, “Service Oriented Sensor Web,” URL: <http://www.buyya.com/papers/SensorWebChapter.pdf>

- In 2000, ESTO of NASA sponsored a technology projection workshop that assessed emerging information technology for space and ground use that resulted in the AIST Key Space and Ground Investment Roadmaps.
- In March 2001, the OpenGIS military pilot project was initiated.
- In Sept. 2001, the OpenGIS Web Services project was initiated by OGC.
- In May 2002, Continuation of SensorML development and incorporation into SWE (SensorWeb Enablement) with emphasis on dynamic, remote sensing (sponsored by NGA, formerly NIMA).
- At the start of the 21st century, the SensorWeb is an emerging trend with the potential to improve interoperability between the sensor data providers and the data analyzers.
- The SensorWeb presents a paradigm in which the Internet is evolving into an active sensing macro instrument. Based on internationally adopted standards, the SensorWeb accomplishes the necessary requirements to ensure interoperability among its various components.

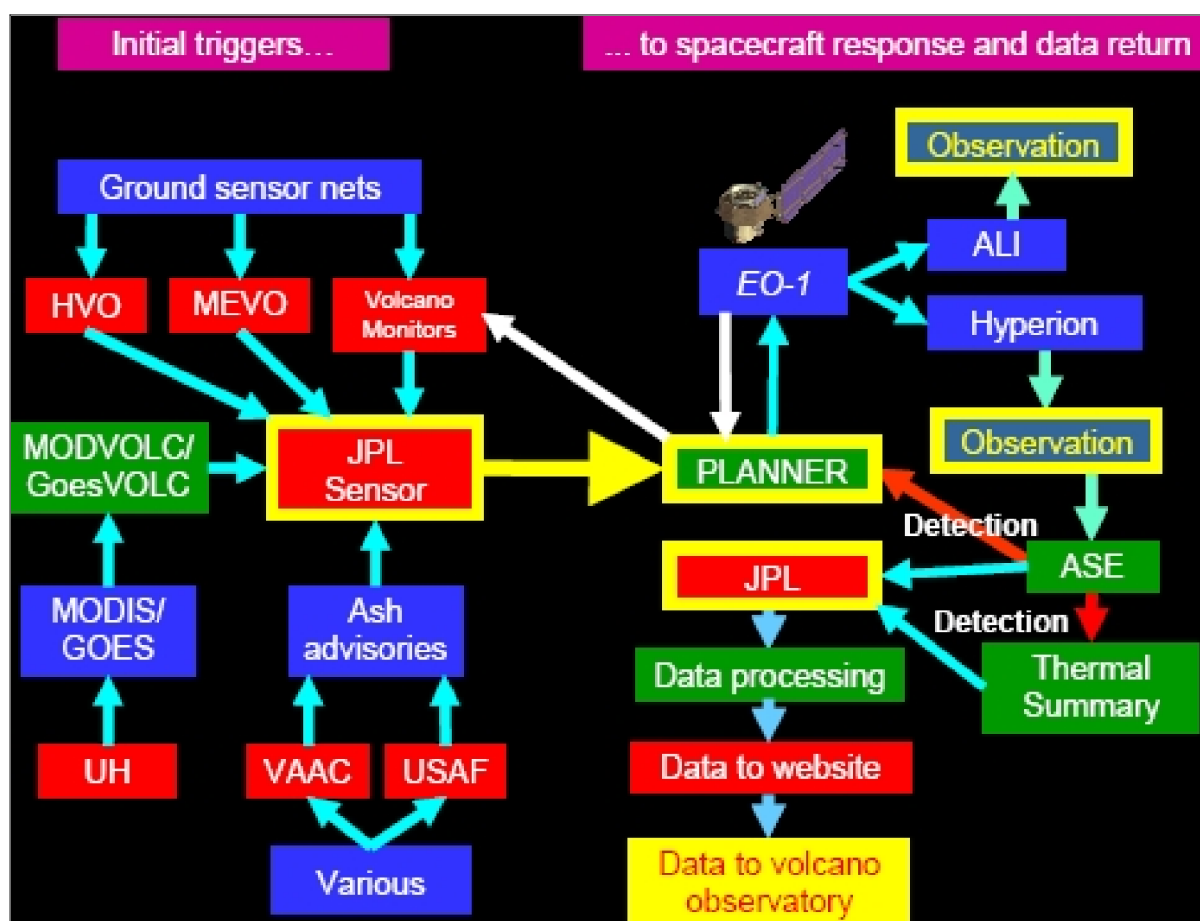


Figure 35: The Volcano Sensor Web at the end of 2007, including two-way triggering between spacecraft and in situ sensors (image credit: NASA/JPL)

Some SensorWeb implementations:

Sensor webs are large-scale, networked systems often made up of heterogeneous computing platforms that include commodity servers and DRE (Distributed Real-time Embed-

ded) systems. Sensor Webs have been demonstrated successfully in variety of environmental sensing applications. ^{763) 764)}

- **VSW** (Volcano SensorWeb). In the timeframe 2004–5, NASA/JPL started to implement VSW in which data from ground–based and spaceborne sensors that detect current volcanic activity are used to automatically trigger the NASA EO–1 (Earth Observing 1) spacecraft to make high spatial–resolution observations of these volcanoes. Several implementation versions of VSW are in existence:

- 1) **MODVOLC** (MODIS Volcano system): The MODVOLC system processes MODIS instrument data from the Terra and Aqua spacecraft that cover every spot on the Earth at least four times per day (two daylight and two night). This instrument data is processed using the MODVOLC algorithms] producing a set of event records indicating the time, location, and magnitude of the thermal detections. ⁷⁶⁵⁾

- 2) **OASIS** (Optimized Autonomous Space In–situ Sensorweb): The fully–automated process allows for rapid acquisition and transmission – typically within 48 hours, though theoretically possible within 2–3 hours – of data products containing the most useful data content, namely the numbers, locations, and spectra of hot pixels. This information allows scientists to evaluate the instantaneous eruption extent and intensity. Prior to VSW, this process took weeks. ^{766) 767) 768) 769)}

The **OASIS** project consists of two main components: ⁷⁷⁰⁾

- the hardware, physical sensor network, and software running on the spiders
- the software for interpretation, command and control of the integrated network.

As part of the OASIS project, the Cascade Volcano Observatory (CVO) of the USGS (United States Geological Survey) designed a network of “**spider**” sensors including data acquisition, sensors, and communication. The spiders carry several COTS sensors including an L1 GPS receiver for timing and deformation monitoring, seismic accelerometer, microphone or microbarograph for infrasonic detection of explosions and emissions, and lighting detector for ash cloud detection. Telemetry between nodes uses IEEE 802.15.4 ISM spread spectrum communication.

At the end of 2009, a self–configuring, self–healing in–situ wireless sensor network has been deployed on Mount St. Helens and linked to the command and control of the EO–1

-
- 763) Philippe M. Teillet, Robert P. Gauthier, Gunar Fedosejevs, Matthew Maloley, Alexander Chichagov, Gino Ainsley, “A soil moisture monitoring sensorweb demonstration in the context of integrated Earth sensing,” Proceedings of the SPIE, Volume 5151, 2003, pp. 63–73, DOI: 10.1117/12.504569
- 764) Costas Tsatsoulis, Heather Amthauer, “Sensor Web Coalition Formation via Argumentation–Based Negotiation,” Proceedings of the 2009 IEEE Aerospace Conference, Big Sky, MT, USA, March 7–14, 2009
- 765) R. Wright, I. P. Flynn, H. Garbeil, A. J. L. Harris, E. Pilger, “MODVOLC: Near–real–time thermal monitoring of global volcanism,” Journal of Volcanology and Geothermal Research, Vol. 135, 2004, pp. 29–49
- 766) Ashley Davies, Daniel Tran, Lukas Mandrake, Kate Boudreau, Johanna Cecava, Andres Mora Vargas, Alberto Behar, Steve Chien, Rebecca Castano, Stuart Frye, Dan Mandl, Lawrence Ong, Philip Kyle, Robert Wright, “The Model–Driven Autonomous Volcano Sensor Web: Progress in 2007,” NASA ESTC–08 (Earth Science Technology Conference), June 24–26, 2008, College Park, MD, USA, URL: <http://esto.nasa.gov/conferences/estc2008/presentations/DaviesA7P3.pdf>
- 767) A. G. Davies, S. Chien, R. Wright, A. Miklius, P. R. Kyle, M. Welsh, J. B. Johnson, D. Tran, S. R. Schaffer, R. Sherwood, “Sensor Web Enables Rapid Response to Volcanic Activity,” EOS (AGU), Vol. 87, No. 1, 3, January 2006, pp.1, 5, URL: http://eol.gsfc.nasa.gov/new/sensorWebExp/Sensor%20Web%20Enables%20Rapid%20Response_Eos.pdf
- 768) Stuart Frye, “Sensor Webs – Experiments in Autonomous Science Discovery using Local and Remote Sensing Platforms,” March 9, 2007, URL: <http://biz.loudoun.gov/Portals/0/BusinessCommunity/Partnerships/ScienceTechCabinet/frye.pdf>
- 769) WenZhan Song, Behrooz Shirazi, Sharon Kedar, Steve Chien, Frank Webb, Danny Tran, Ashley Davis, David Pieri, Rick LaHusen, John Pallister, Dan Dzurisin, Seth Moran, Mike Lisowski, “Optimized Autonomous Space In–situ Sensor–Web for Volcano Monitoring,” Proceedings of the 2008 IEEE Aerospace Conference, Big Sky, MT, USA, March 1–8, 2008
- 770) Steve A. Chien, Joshua Doubleday, Sharon Kedar, Ashley G. Davies, Frank Webb, Richard Lahusen, Wenzhan Song, Behrooz Shirazi, Daniel Mandl, Stuart Frye, “Autonomous Sensorweb Operations for Integrated Space, In–situ monitoring of Volcanic Activity,” Proceedings of the SpaceOps 2010 Conference, Huntsville, ALA, USA, April 25–30, 2010, paper: AIAA 2010–2202

satellite. The ground sensor–web element uses observations data (seismic, gas, and ground deformation) to trigger high–resolution data takes by EO–1. The data are being down-linked back to the ground sensorweb control center, where they are being ingested into a dynamic and scalable communication bandwidth allocation scheme to optimize communication and power usage. NASA/JPL has demonstrated in OASIS the feedback between ground and space operations.

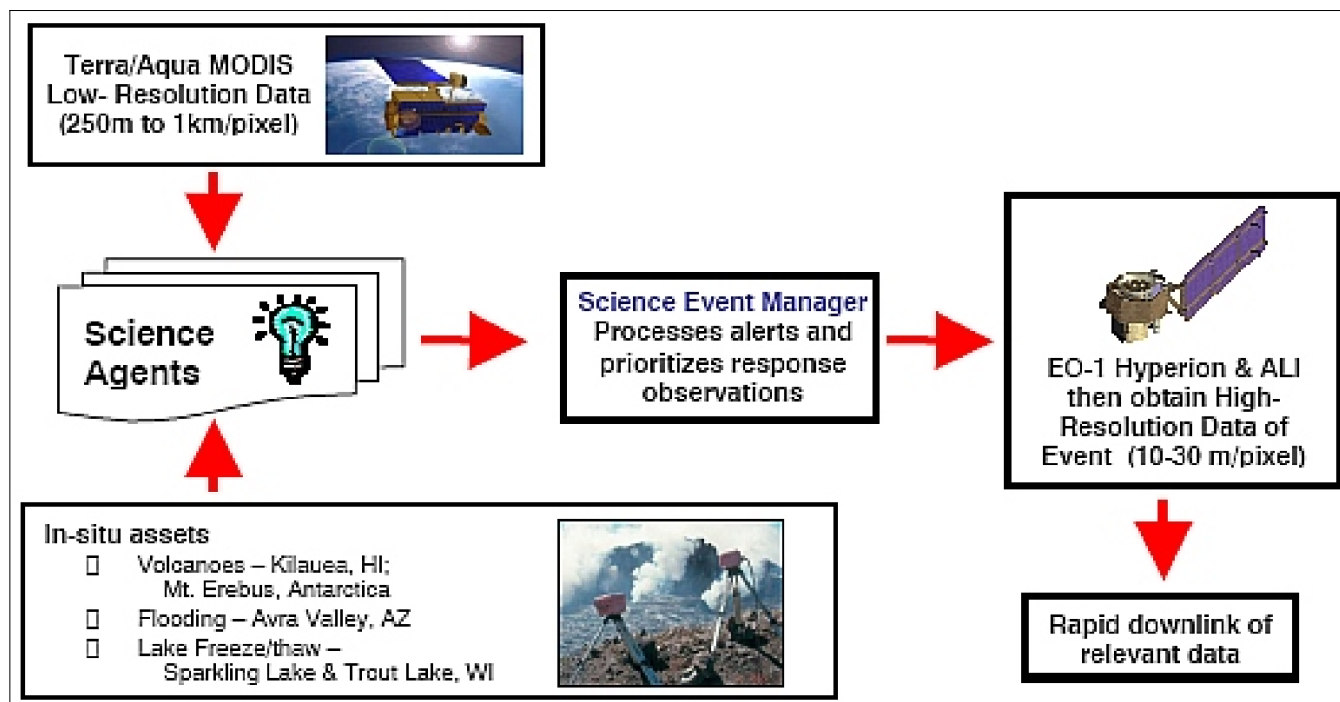


Figure 36: Sensor–web detection and response architecture (image credit: NASA/JPL)

- NYHOPS (New York Harbor Observing and Prediction System)⁷⁷¹⁾ is a real–time, web–based estuarine and coastal ocean observing and modeling system for the waters of NY, NJ and CT currently operated as one of National Oceanic and Atmospheric Administration’s (NOAA) Integrated Ocean Observing System (IOOS) regional ocean forecasting systems. The data includes oceanographic parameters collected using onshore and offshore sensors and from mobile platforms such as unmanned underwater vehicles and passing surface ships.
- SEAMONSTER (South East Alaska MONitoring Network for Science, Telecommunications, Education, and Research). SEAMONSTER is a glacier and watershed sensor web at the University of Alaska Southeast (UAS) in Alaska. This sensor web monitors and collects data regarding glacier dynamics and mass balance, watershed hydrology, coastal marine ecology, and human impact/hazards in and around the Lemon Creek watershed and Lemon Glacier. The collected data is used to study the correlations between glacier velocity, glacial lake formation and drainage, watershed hydrology, and temperature variation.⁷⁷²⁾

The NASA SensorWeb toolbox, developed at NASA/GSFC in collaboration with NASA/JPL, NASA/Ames and other partners, is a set of software and standards that:

- 1) Enables users to create virtual private networks of sensors over open networks

771) Ashit Talukder, Anand Panangadan, “Online Visualization of Adaptive Distributed Sensor Webs,” Proceedings of the 2009 IEEE Aerospace Conference, Big Sky, MT, USA, March 7–14, 2009

772) William R. Otte, John S. Kinnebrew, Douglas C. Schmidt, Gautam Biswas, “A Flexible Infrastructure for Distributed Deployment in Adaptive Sensor Webs,” Proceedings of the 2009 IEEE Aerospace Conference, Big Sky, MT, USA, March 7–14, 2009

- 2) Provides the capability to orchestrate their actions
- 3) Provides the capability to customize the output data products
- 4) Enables automated delivery of the data products to the users' desktop.

In the timeframe 2010/11, a new user interface was added to the SensorWeb toolbox. The web service along with the user interface follows the OGC (Open Geospatial Consortium) standard called WCPS (Web Coverage Processing Service). The WCPS concept increases user access and provides more flexibility for creating data products for sensor data. ⁷⁷³⁾

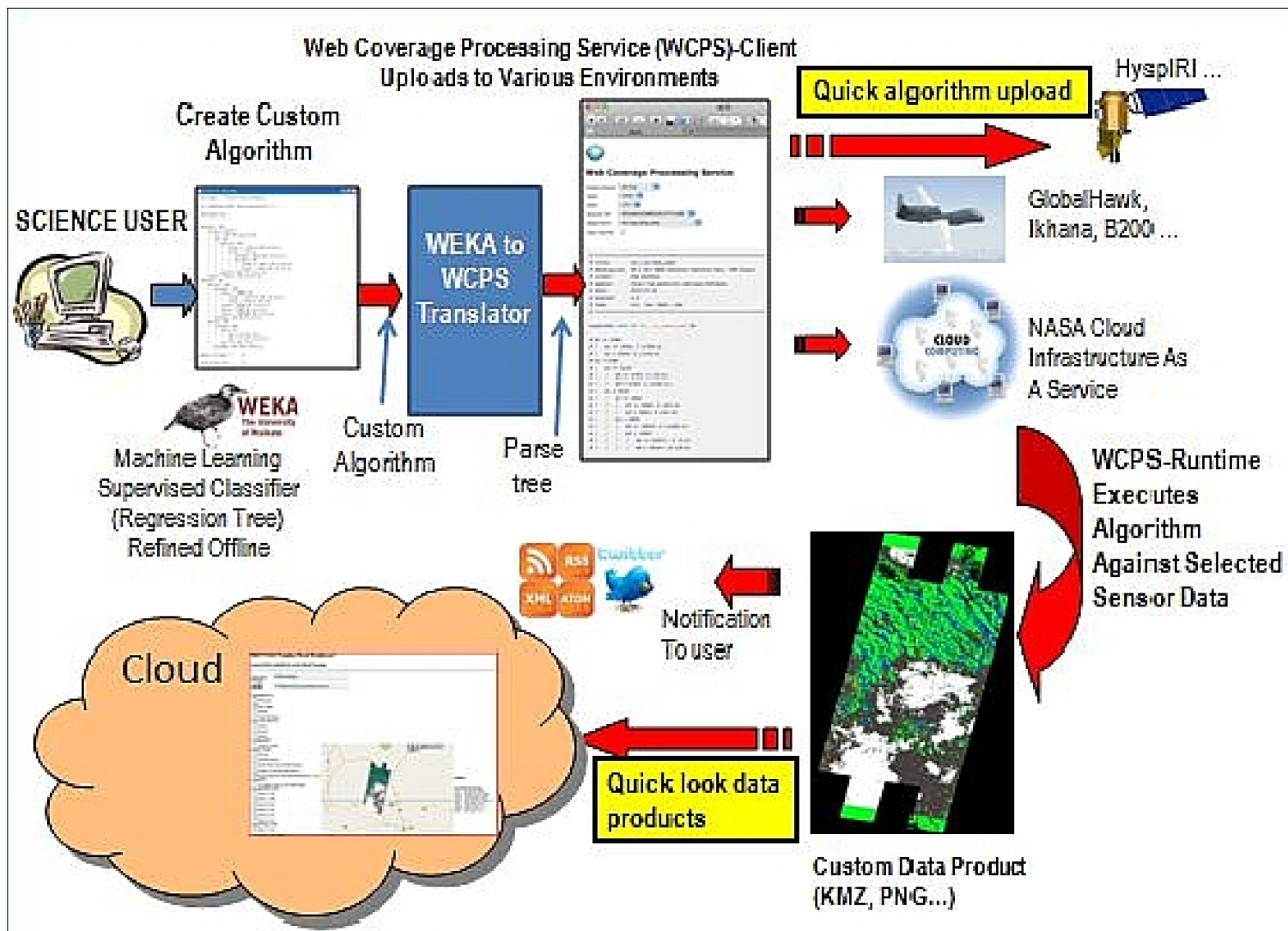


Figure 37: Typical data flow for the use of a WCPS (image credit: NASA)

Legend to Figure 37: Top level operations concepts for WCPS in which a ground based WCPS client is used to design an algorithm and then the algorithm is uploaded to one of three environments. The user selects one of the created algorithms to run via the WCPS–R (Runtime) which causes the quick look data product to be produced and sent to the elastic compute cloud.

Space–based monitoring of flooding:

A number of satellites have been used to track flooding at a global or regional scale: most notably QuikSCAT (Quick Scatterometer), the AMSR–E (Advanced Microwave Scan-

⁷⁷³⁾ Daniel Mandl, Pat Cappelaere, Stuart Frye, Rob Sohlberg, Vuong Ly, Steve Chien, Don Sullivan, "A New User Interface for On–Demand Customizable Data Products for Sensors in a SensorWeb," ESTF 2011 (Earth Science Technology Forum 2011), Pasadena, CA, USA, June 21–23, 2011, URL: http://esto.nasa.gov/conferences/estf2011/papers/Mandl_ESTF2011.pdf

ning Radiometer for Earth Observing System), and MODIS (Moderate Resolution Imaging Spectrometer). The AMSR–E and the TRMM (Tropical Rainfall Measurement Mission) enable measurement of rainfall and therefore can be used as indicators of flooding. (774)

Radars such as the SAR instrument of RADARSAT–2, ASAR (Advanced Synthetic Aperture Radar) of Envisat, and PALSAR (Phased Array type L–band Synthetic Aperture Radar) of ALOS have been used to detect surface water extent from flooding. Radar has the advantage of being able to gather accurate data even in the presence of cloud cover.

Optical imagery of Landsat–7 and the ALI (Advanced Land Imager) instrument of the EO–1 (Earth Observing One) can all be used to detect surface water using spectral methods. While these sensors provide higher resolution data (30 m/pixel) their infrequent revisit rate and challenge with clouds limit their utility for global flood mapping.

In the NASA SensorWeb concept, the SensorWeb constantly assimilates available data from any and all available sources to track flooding. This may be as easy as downloading the available data. Or it may mean active querying to determine if potentially contributing satellites are acquiring data and acquiring the data from relevant servers when available. Data acquisition may also involve downloading in situ data from the web. This data is used to constantly update the model of the flood state. All of these data can then be combined with hydrological models to perform hindcasting (estimation of flood parameters in the past to fill in missing times or areas), nowcasting (estimating the current flood state by using the model to fill in spatial gaps), and forecasting (using the model to predict which areas are at risk for future flooding).

The Thailand Flood Sensorweb – A Pilot Operational Sensorweb: NASA/JPL has operated a sensorweb to monitor flooding in Thailand for the 2010 and 2011 flooding seasons (roughly beginning in May and ending as late as spring the following year). The core of this system uses the MODIS and EO–1/ALI sensors and leverages the unique automated tasking capability of EO–1. Other sensors including Worldview–2, Geo–Eye–1, Ikonos, Landsat–7, and Radarsat–2 have been integrated in a less automated fashion. These sensors and assets are combined with automated workflows to deliver satellite imagery, surface water extent products, and surface water volume products to relevant entities in Thailand.

The success of this core system has led to ongoing work to add additional sensors and data products such as TRMM, river basin and sub–basin hydrological models, and data from in–situ sensor networks.

The primary sensorweb flood alert mechanism is triggering via analysis of MODIS imagery. MODIS provides excellent temporal coverage (at least 2 x per day daylight overflights). The project draws the subsetted FAS Indochina MODIS data in geotiff format from the MODIS rapid response site (originally rapidfire and now LANCE–MODIS). This imagery is then analyzed and surface water pixels compared to baseline dry season levels to detect flooding.

The EO–1 spacecraft is the core of the SensorWeb because of its automated tasking capability. EO–1 is automatically tasked from each MODIS flood detection. The Thailand flood SensorWeb MODIS alerts comprise a SensorWeb campaign within the EO–1 tasking system and therefore each alert can cause an observation request with an assigned mission priority (Ref. 774).

All of the SensorWeb software runs at servers located at JPL (Jet Propulsion Laboratory).

774) Steve Chien, David McLaren, Joshua Doubleday, Daniel Tran, Veerachai Tanpipat, Royol Chitradon, Surajate Boonya–aroonnet, Porraanee Thanapakpawin, Daniel Mandl, “Integrating high–resolution taskable imagery into a SensorWeb for automatic space–based monitoring of flooding in Thailand,” Proceedings of i–SAIRAS (International Symposium on Artificial Intelligence, Robotics and Automation in Space), Turin, Italy, Sept. 4–6, 2012, URL: http://robotics.estec.esa.int/i-SAIRAS/isairas2012/Papers/Session%202C/02C_02_chien.pdf

The Namibia Flood Sensor Web Pilot is an international collaboration under the auspices of CEOS (Committee on Earth Observation Satellite) Disasters team. In each of the past three years (2010–2013), a team from NASA has traveled to Namibia to work with local counterparts towards the infusion of satellite and ground sensors into a sensor web to assess flood damage and provide early flood warnings. — The focus of the team’s most recent trip, in January 2013, was integration of the sensor web with the OpenStreetMap (OSM) standard and corresponding ground data to validate satellite data in an automated and efficient manner. OSM is a collaborative international project to create free, editable maps of the world. Thus, it enables groups to share mapping information in a low cost interoperable manner. The team is combining Sensor Web and OSM functionality to create a shared database for water based information in which water contours are tagged with data source, normal vs. flood water, ground GPS contour, low and high seasonal water levels, and other tags. Thanks to these tags, users will be able to query the database for water contour information based on selected criteria. ⁷⁷⁵⁾

775) Stuart Frye, Karen Moe, Dan Mandl, Matt Handy, George Percivall, John Evans, “Towards a Sensor Web Architecture for Disaster Management: Insights from the Namibia Flood Pilot,” Proceedings of IGARSS (IEEE International Geoscience and Remote Sensing Symposium), Melbourne, Australia, July 21–26, 2013

1.5.22 International Charter Space and Major Disasters

The International Charter "Space and Major Disasters" was initiated by ESA (European Space Agency) and CNES (French Space Agency), following the UNISPACE III conference held in Vienna, Austria in July 1999. Both agencies proposed during the conference to set up an international organization for the support and coordination of major disasters on a global scale. "The Charter", as it is simply called, aims to provide a unified system of space data acquisition and delivery of value-added products free of charge, through authorized users, to those affected by major disasters. ^{776) 777) 778)}

- ESA and CNES as founding members
- On October 20, 2000, CSA (Canadian Space Agency) signed the Charter as the third member of The Charter.
- **The International Charter was declared formally operational on November 1, 2000**
- NOAA (National Oceanic and Atmospheric Administration) of USA and ISRO (Indian Space Research Organization) of India joined in September 2001
- ISRO (Indian Space Research Organisation) joined in January 2002
- CONAE (Space Agency of Argentina) joined in July 2003
- JAXA (Japan Aerospace Exploration Agency) joined in February 2005
- USGS (United States Geological Survey) joined in 2005 as part of the US team
- UKSA (United Kingdom Space Agency), former BNSC (British National Space Center) and DMCii (Disaster Monitoring Constellation International Imaging Ltd.) of the United Kingdom joined in November 2005
- CNSA (China National Space Administration) joined in May 2007
- DLR (German Space Agency) joined in October 2010
- KARI (Korean Aerospace Research Institute) joined in July 2011
- INPE (National Institute for Space Research) of Brazil – formally became a member of the International Charter 'Space and Major Disasters' on November 8, 2011. ⁷⁷⁹⁾
- ROSCOSMOS (Russian Federal Space Agency) formally became a member on August 28, 2013. ⁷⁸⁰⁾
- CMA (China Meteorological Administration) joined the International Charter "Space and Major Disasters", which was recognized by the 31st session of the Charter in Beijing on April 14–17, 2014.

Table 45: Overview of The Charter Members ^{779) 780) 781)}

In 2003 the UN Office for Outer Space Affairs (UNOOSA) was accepted as the cooperating body to the Charter. Beginning on July 1, 2003, the Office set up a 24/7 hotline through

776) http://www.oosa.unvienna.org/oosa/SAP/stdm/stdm_charter.html

777) <http://www.disasterscharter.org/home>

778) "Brochure of The Charter," URL: http://www.disasterscharter.org/c/document_library/get_file?folderId=33636&name=DLFE-2502.pdf

779) "Brazil joins the International Charter 'Space and Major Disasters'," ESA, Nov. 10, 2011, URL: http://www.esa.int/esaEO/SEMFYDTWLUG_index_0.html

780) "The Charter integrates its 15th member ROSCOSMOS," International Charter Newsletter, Oct. 9, 2013, Issue 7, URL: http://www.disasterscharter.org/c/document_library/get_file?p_1_id=23109&folderId=112934&name=DLFE-4703.pdf

781) "CMA's FY-03 satellite joined the International Charter." CMA, April 21, 2014, URL: http://www.cma.gov.cn/en/NewsReleases/News/201404/t20140421_243998.html

which United Nations agencies can request data through the Charter to respond to emergency situations.

Via the Charter mechanism, all of these agencies have committed to provide free and unrestricted access to their space assets to support relief efforts in the immediate aftermath of a major disaster. – Fortunately, many other organizations (commercial and institutional) that are flying imaging satellites or provide space system services (telecommunications, meteorology and positioning data), join into the act as well in providing their imagery and services free of charge when a major disaster strikes.

The most important aspect of the International Charter are the entities that are entitled to request the Charter data. Unlike the historical use of satellite remote sensing data, either by commercial or R&D groups, the Charter data is available to those who are actually engaged in crisis management. They are called Associated Bodies and, for the purpose of the Charter, are the institutions or services responsible for rescue and civil protection, defense and security under the authority of a State whose jurisdiction covers an agency or an operator that is a member of the Charter. The member States of the European Space Agency are included, as are those of any other international organization that is party to the Charter, such as the Disaster Monitoring Constellation (DMC).⁷⁸²⁾

The crisis situation is identified by the authorities of the country affected by the disaster and by at least one Associated Body, which alerts the Charter Executive Secretariat as soon as possible following the advent of the disaster having the potential of creating a crisis situation. In response, the Charter authorities pool their resources together in terms of coordinated spacecraft tasking, data archive searches, data mergers, value adding, and data deliveries.

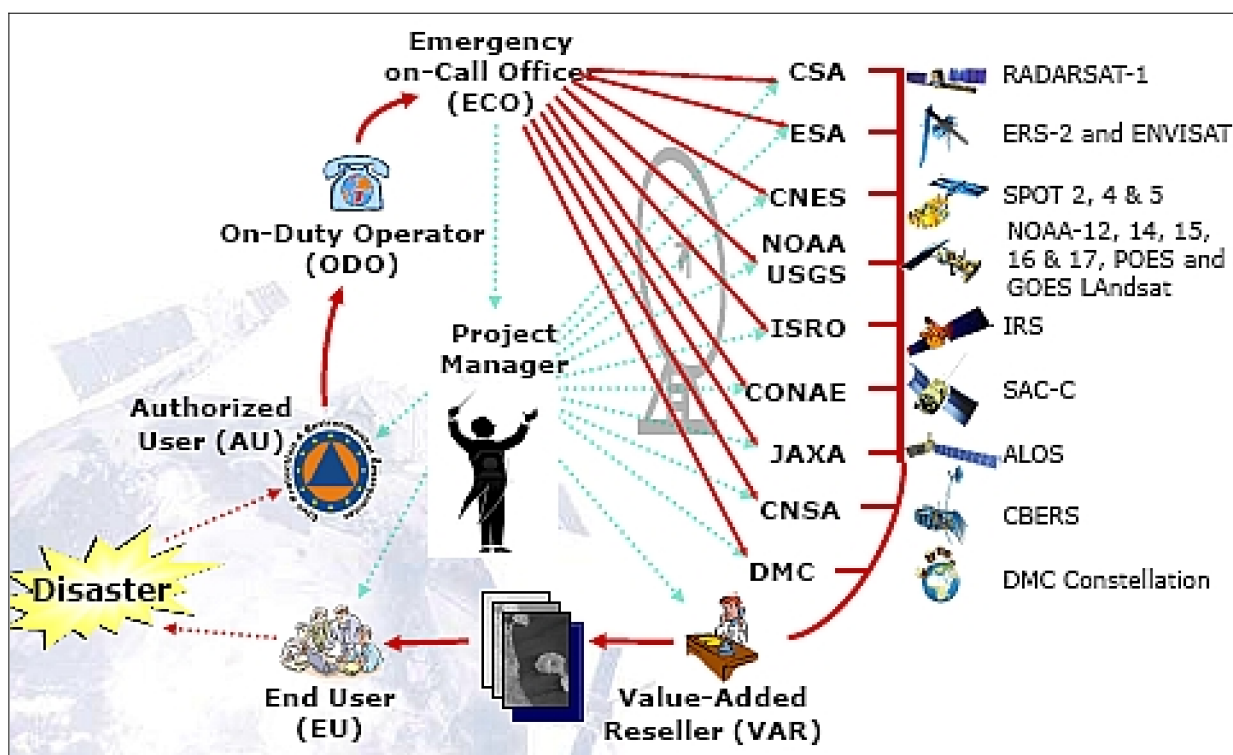


Figure 38: The Charter operational loop (image credit: Charter members)

Celebrating ten years of services in the fall of 2010, the Charter has been activated more than 270 times in around 90 countries (Ref. 782). The success of the Charter is seen through

782) André Husson, Ahmed Mahmood, Philippe Bally, Catherine Proy, Surendra Parashar, Stephen Briggs, "International Charter 'Space and Major Disasters' Ten years of operational services," Proceedings of the 61st IAC (International Astronautical Congress), Prague, Czech Republic, Sept. 27–Oct. 1, 2010, IAC–B.1.1.10

the appraisals of an increasing number of user civil protection, rescue or security organizations and member agencies, which consider the Charter as a credible instrument for applying space technologies to global disaster management. ⁷⁸³⁾

- The International Charter: Space and Major Disasters was activated on March 11, 2014 following a request from the China Meteorological Administration for satellite imagery to assist in the search for the missing Malaysian airliner MH370.

Flight MH370, a Boeing–777, along with its 239 passengers and crew, disappeared in the early hours of March 8, 2014 (local time) after departing Kuala Lumpur in Malaysia (destination Beijing) and has not yet been found. There is a great deal of speculation over the mystery of the plane's disappearance. Air traffic control lost contact with the craft an hour after take off, but recent investigations have indicated that the plane last made automated contact with an orbiting satellite almost seven hours later. While the plane was due to fly to Beijing, Malaysian radar tracked the craft turning back and flying over Malaysia toward the north west instead. The reasons for the plane's change in course and disappearance remain unknown, and have left many wondering if changes should be made to the way aircraft are tracked in the future. ⁷⁸⁴⁾

Over 20 countries are now assisting in the search with aircraft and naval vessels searching the areas where investigators believe the plane may be. Satellite imagery is also being employed to search for the missing aircraft, with multiple satellites from different nations imaging the area in an attempt to locate any signs of the craft or a potential crash site. The International Charter is now contributing towards this search effort, with Charter member space agencies tasking satellites to obtain imagery of the search areas.

783) 10th Anniversary of the International Charter "Space and Major Disasters", ESA, Oct. 12, 2010, URL: http://www.esa.int/esaCP/SEMDOVO1FG_index_0.html

784) "International Charter activated for missing Malaysian airliner," March 17, 2014, URL: http://www.disaster-scharter.org/web/charter/news?p_p_id=NiPortlet_WAR_DisasterCharter&p_p_lifecycle=0&p_p_state=normal&_NiPortlet_WAR_DisasterCharter_articleId=189605

1.6 Hosted Payloads on Commercial Satellites

The term “hosted payload” refers generally to a government payload that is launched to orbit as a secondary payload on a commercial host spacecraft. The host spacecraft provides resources to the payload such as structure, pointing, power, and communications.

The idea of hosted payloads is not new and has been explored and implemented in the past mostly for experimental purposes. The hosted payloads can be technology demonstrations, research equipment, flight qualification units, or fully operational sensors or systems.

In 2011, there are less than 10 hosted payloads on commercial satellites for use by various government agencies around the globe. However, as the capability gap grows and as budgets and schedules tighten, discussions and contractual decisions are being undertaken currently to seriously plan for a more permanent and sustainable arrangement as the next generation of satellites for replacements and new programs begin to be built. ^{785) 786) 787) 788)}

Dual–use programs for use by both commercial and government clients have been in existence for governments and international organizations such as Australia, the European Union, Japan, South Korea and the United States. In the global market for government and military demand, the United States has and continues to account for the vast majority of commercial leases and other satellite–related services. ⁷⁸⁹⁾

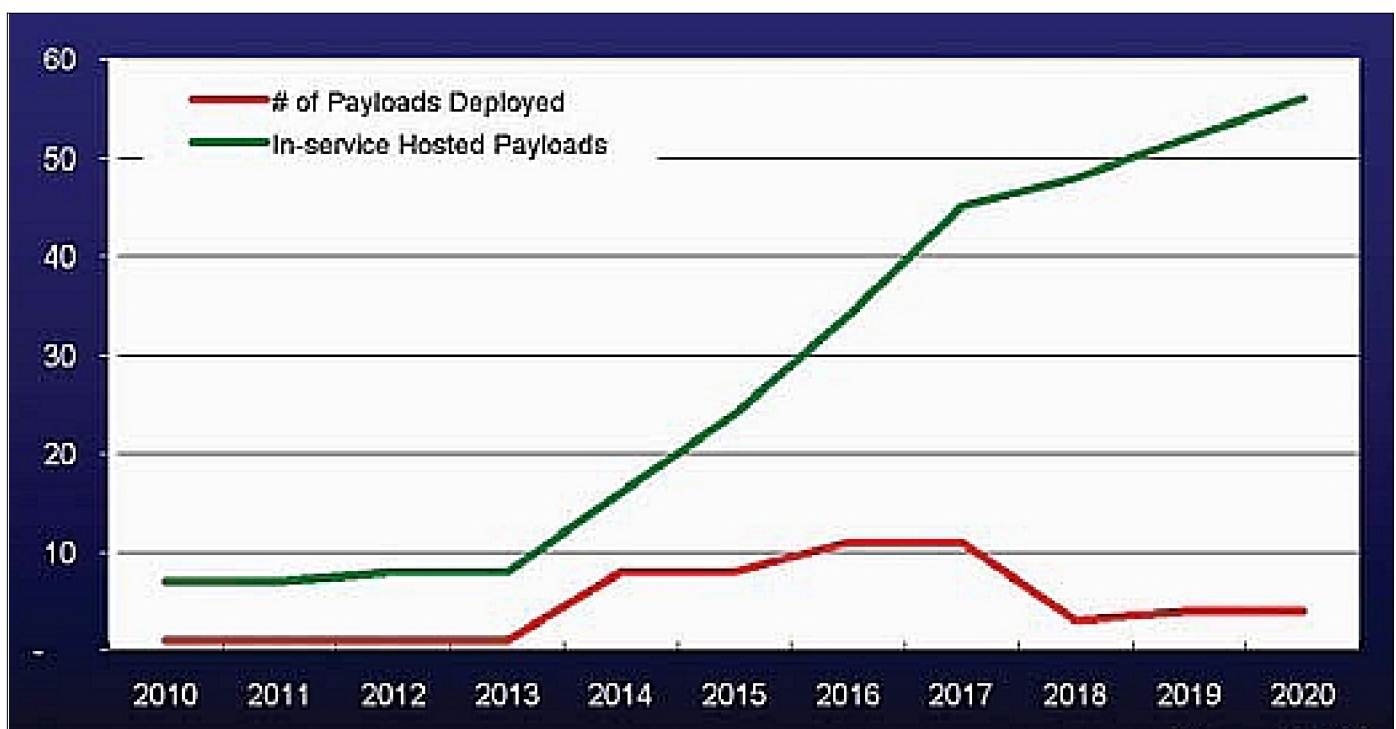


Figure 39: Deployments & in–service hosted payloads on commercial satellites (image credit: NSR)

In the emerging area of hosted payloads, a major demand driver is likely to come from the U.S. Government once again. This will likely change the hosted payload market in terms of

785) “Hosted Payloads On Commercial Satellites,” Milsat Magazine, May 2010, URL: http://www.milsatmagazine.com/cgi-bin/display_article.cgi?number=1593901906

786) Brinton Turner, “U.S. Military Wants To Streamline Hosted Payload Process,” Space News, Sept. 24, 2010, URL: <http://www.spacenews.com/military/100924-military-hosted-payload-process.html>

787) <http://www.intelsat.com/files/resources/knowledge/datasheets/ds-hosted-payload.pdf>

788) J. Del Rosario, C. Rousseau, “An Analysis of Hosted Payloads and Dual–use Satellites as Middle Ground between Commercial Outsourcing and Internal Asset Deployment,” URL: http://www.isunet.edu/index2.php?option=com_docman&task=doc_view&gid=762&Itemid=26

789) “2011 Commercial Space Transportation Forecasts,” FAA, May 2011, URL: http://www.faa.gov/about/office_org/headquarters_offices/ast/media/2011%20Forecast%20Report.pdf

its place in the overall value chain within the industry. More importantly, the growing role of the United States should likewise lead to changes in the entire process of how commercial satellites are to be built and how military and civil government programs will be planned.⁷⁹⁰⁾

It is important to note that hosted payloads will not replace dedicated programs but act as complementary assets to achieve mission–critical goals. Hosted payloads provide an inexpensive and practical option for technology test beds. Before operational payloads are launched, prototypes that are tested and deemed functional in its permanent environment, provide invaluable benefits to the government agency.⁷⁹¹⁾

In 2010, a real problem of hosted payloads still seems to be a general lack of clear policy directions on the topic by governments – resulting in missed flight opportunities. Placing national security and intelligence payloads aboard commercial satellites raises unique issues. Concerns of security and reliability are among the issues generally cited when discussing the expanded use of hosted payloads.^{792) 793) 794)}

The “dual–use” approach today is realized in three ways: a) hosted payloads; b) long–term leased capacity that is pre–specified; c) or having commercial suppliers deploy satellites in governmental and defense–related spectrum bands and then lease this capacity to agencies on demand.⁷⁹⁵⁾

– In the first approach, governments arrange for their payloads to be carried on board commercial satellites. Such an arrangement involves the commercial operator hosting a government payload.

– The second method is used commonly in Europe. The trend there has been to define defense or governmental requirements and then allow a designated commercial manufacturer and service provider to design a satellite or satellite series to carry out the mission under a long–term lease that may span 10 years, or longer.

– The third model is exemplified by XTAR LLC of Rockville, MD, the first U.S. commercial satellite operator to provide communications services in X–band. XTAR, a joint venture between Loral Space & Communications and Spain’s HISDESAT, built satellites that operate in frequency bands assigned for governmental and defense–related uses. These services then are leased to U.S. and Spanish military and governmental agencies on a transponder–by–transponder basis.

1.6.1 Examples of hosted payloads in GEO:⁷⁹⁶⁾

- In the early 1970s, the US Navy contacted Comsat, a commercial U.S. Signatory to Intelsat, with a request to provide an UHF (Ultra High Frequency) satellite. At the time, the Navy could not afford any more than a two year commitment for service on board the new satellites. Comsat responded with a fleet satellites that would fit both commercial and government requirements (dual–use arrangement). Thus, MARISAT (Maritime Telecommunication Satellite) was born. The three–satellite Marisat system, launched in 1976, served as the initial Inmarsat constellation.

790) Mark Andraschko, Jeffrey Antol, Stephen Horan, Doreen Neil, “Commercially Hosted Government Payloads: Lessons from Recent Programs,” 2011 IEEE Aerospace Conference, Big Sky, MT, USA, March 5–12, 2011

791) Jose Del Rosario, “Hosted Payloads for Asia,” APSCC (Asia–Pacific Satellite Communications Council) Quarterly Newsletter, July 2010, URL: http://www.nsr.com/images/download/2010_jul_nsr.pdf

792) Turner Brinton, “U.S. Military Wants To Streamline Hosted Payload Process,” Space News, Sept. 24, 2010, URL: <http://www.spacenews.com/military/100924–military–hosted–payload–process.html>

793) Peter B. de Selding, “U.S. Government Missing Hosted Payload Opportunities,” Space News, March 26, 2010, URL: <http://www.spacenews.com/civil/100326–govt–missing–hosted–payload–opportunities.html>

794) Hosted Payload Guidebook, NASA, authored by Futron Corporation, August 2010, URL: http://science.larc.nasa.gov/hostedpayload/HostedPayloadGuidebook_final_with_acknowledgment.pdf

795) Paul Dykewicz, “Dual–Use Satellites Offer Efficiency and Controversy,” June 14, 2011, URL: <http://www.hosted-payload.com/blog/dual–use–satellites–offer–efficiency–and–controversy>

796) <http://www.space.commerce.gov/general/commercialpurchase/hostedpayloads.shtml>

MARISAT proved to be so much of a success that the LEASAT (Leased Satellite) program followed. Built and operated by the commercial industry, it was provided exclusively for government communication services. The first LEASAT satellite was launched into orbit in 1984. From there, it was no secret that having the commercial industry provide their satellites to the government has indeed benefits. In fact, the LEASAT F5, which was built as a spare, continues its service with the U.S. DoD and Australian Defence Forces today (2011) for Intelsat. The Navy's lease ended in 1997.⁷⁹⁷⁾

- On Dec. 15, 1978, Telesat Canada launched its Anik–B satellite into GEO which carried a governmental Ku–band (hosted) payload used to test DTH and transportable services.
- In the 1990s, the US Navy put the EHF (Extremely High Frequency) hosted payloads on the UFO (UHF Follow-On) constellation, that today (2012) still provide secure communications for government missions. First launch of the UFO (a 9 satellite constellation) took place on 25 March 1993.⁷⁹⁸⁾
- Through the ARTES (Advanced Research in Telecommunications Systems) program, ESA has supported a number of hosted payloads over the years. These include:
 - The Skyplex payload (the world's first on–board DVB multiplexing facility) on the Hot Bird 4 satellite of Eutelsat (launch Feb. 27, 1998 into GEO).⁷⁹⁹⁾
 - This was followed by the AmerHis payload on Amazonas 1 (AmerHis is the first operational regenerative, onboard processing, satellite switching system in the world, launch August 5, 2004, location 61° W). AmerHis has enabled Hispasat (Spanish telecommunications satellite service provider) to provide high–performance interactive multimedia services on its four Ku–band coverage zones: North America, South America, Brazil and Europe. The AmerHis system is an innovative solution of satellite broadband mesh communication based on a regenerative DVB–S/DVB–RCS processor.
- The Australian Defense Force (ADF) launched its first hosted payload in 2003 on the Optus–C1 and Defense satellite into GEO (launch on June 11, 2003, location at 156° E). The hosted payload is accommodated on the FS–1300 platform of Space Systems/Loral (SS/L) with Japan's MELCO (Mitsubishi Electric Company) as prime contractor. The satellite operates in four frequency bands:⁸⁰⁰⁾
 - Commercial services in Ku–band (24 transponders) for the commercial operator SingTel Optus Pty Ltd., Australia (a subsidiary of SingTel (Singapore Telecommunications)).
 - The hosted military communications payload operates at UHF, X–band and Ka–band for ADF. The Ka–band payload provides high–data rate broadcast coverage for video, voice and data communications. The satellite's X–band provides medium–to–high data rate voice and data for land and maritime applications. And finally, the UHF payload provides secure low–rate voice and data communications to mobile platforms.

The ADF payload features military frequencies that are not available in commercial satellites, except for the XTAR LLC commercial service provider (XTAR–EUR and XTAR–LANT satellites), which is a commercial entity (US company, Rockville, MD) licensed to provide X–band to government customers. XTAR–EUR was launched on Feb. 12, 2005 and is located at 29° E. XTAR–LANT was launched on March 16, 2006 and is located at 30° W.

797) Kate Hudson, "Navy's Relationship with Hosted Payloads," Jan. 26, 2011, URL: <http://www.hostedpayload.com/blog/navy%E2%80%99s-relationship-with-hosted-payloads>

798) Jim Mitchell, "Governments Turn to Hosted Payloads for Cost Savings & Risk Sharing," Reinventing Space Conference, May 7–10, 2012, Los Angeles, CA, paper: RS–2012–6006, URL: http://www.responsivespace.com/Papers/RS2012/SESSIONS/Session%20I/6006_Mitchell/6006P.pdf

799) <http://www.geo-orbit.org/easthemipgs/hb4pr.html>

800) http://australianspace.info/sat_optusC.html

- The Anik F2 communications satellite of Telesat Canada was launched on July 14, 2004 (GEO, 111.1°W longitude). Anik F2 is carrying the Telesat hosted commercial WildBlue broadband communications payload that is successfully providing much-needed broadband connectivity to geographically remote U.S. Consumers (Ref. 798).
- MTSat–1R (Multifunction Transport Satellite –Himawari–6) of Japan (launched on Feb. 26, 2005) is a dual–function GEO mission with a primary aeronautical payload and a hosted meteorological payload of JMA called JAMI (Japanese Advanced Meteorological Imager). On July 1, 2010, JMA switched the meteorological observation services from MTSAT–1R to the MTSAT–2 spacecraft. This action put the MTSAT–1R spacecraft into meteorological standby. MTSAT–2 (launch Feb. 18, 2006) is the follow–on spacecraft of MTSat–1R carrying also the host payload JAMI.
- OSC (Orbital Sciences Corporation) of Dulles, VA is offering “hosted secondary payload opportunities” on its StarBus communications platform in GEO. This program takes advantage of the high frequency of commercial satellite launches and the excess resources that typically exist on a commercial communications satellite to provide frequent and low–cost access to space.⁸⁰¹⁾

– OSC integrated the L–band **GCCS** (Geostationary Communication and Control Segment) assembly, built by Lockheed Martin, as hosted payload onto Intelsat’s Galaxy 15 spacecraft (a STAR 2.2 bus) for FAA’s (Federal Aviation Administration’s) **WAAS** (Wide Area Augmentation System) initiative. The purpose of the GCCS–1 is to generate and transmit the WAAS L–band signal in space (SIS).

Galaxy 15, an all C–band communications satellite, was launched on the Ariane 5GS on October 13, 2005 (location: 133° W) and continued successful operations until April 5, 2010 (when Galaxy 15 ceased responding to commands sent to it by controllers on the ground). – FAA has employed a hosted payload approach to place its own GCCS payloads (60 kg, 300 W) on four commercial geosynchronous satellites to date.

– The GCCS–2 payload is hosted on the Anik F1R spacecraft of the Canadian operator Telesat. The S/C was built by EADS Astrium on an Eurostar 3000 bus and launched on Sept. 8, 2005 (location at 107.3° W). Since Sept. 23, 2008, Galaxy 15 and Anik F1R have been sending “precision approach” information to aircraft.

Prior to the launch of the two hosted payloads in 2005, WAAS was operated through leased L–band payload services on existing commercial satellites (Intelsat, Telesat).

– In 2009, FAA signed a contract adding a third commercial GEO (Inmarsat 4F3) to WAAS. It features a leased L–band transponder that the commercial provider installed at their own expense.

- The Republic of Korea launched its first civil–military communications satellite, KoreaSat–5, on August 22, 2006 (location at 113° E). The spacecraft uses the Spacebus–4000–C1 platform of Alcatel Space. The dual–use satellite carries 12 military X–band transponders and 24 commercial Ku– and C–band transponders, whereby the 12 military relays are capable of covering troop communications from the Malacca Strait to the Central Pacific sea areas.

- The hosted demonstration payload **CHIRP** (Commercially Hosted Infrared Payload) was developed for the U.S. Air Force’s Third Generation Infrared Surveillance (3GIRS) program. CHIRP is a WFOV (Wide Field of View) sensor, built by SAIC (Science Applications International Corporation) which was integrated onto an OSC–built, SES World Skies (SES–2, Note: SES World Skies was formerly SES Americom), commercial geosynchronous communications satellite to validate missile warning technologies from geo-

801) “STARBus Hosted Payloads,” URL: <http://www.orbital.com/newsinfo/publications/HostedPayloadFactsheet.pdf>

synchronous orbit in a fast and cost-effective manner. The SES-2 spacecraft, built on a GEOStar™ bus of OSC, was launched on Sept. 21, 2011 on Ariane 5 from Kourou (location at 87° W to provide coverage of North America and the Caribbean).^{802) 803) 804)}

The CHIRP sensor is equipped with a 4 Mpixel FPA (Focal Plane Array) detector manufactured by Teledyne that is sensitive in both short wave and medium wave infrared (SWIR and MWIR). CHIRP features a telescope that can view a quarter of the Earth from GEO. The CHIRP instrument has a mass of 115 kg, a power demand of 275 W, and a customer data rate of 70 Mbit/s.

CHIRP collects data on infrared phenomenology of Earth backgrounds, clutter and missile launch events to demonstrate system performance and evaluate sensor operations concepts. Of equal importance is data collection to evaluate the robust ground system implemented to process the large amount of data produced from a wide field-of-view sensor.

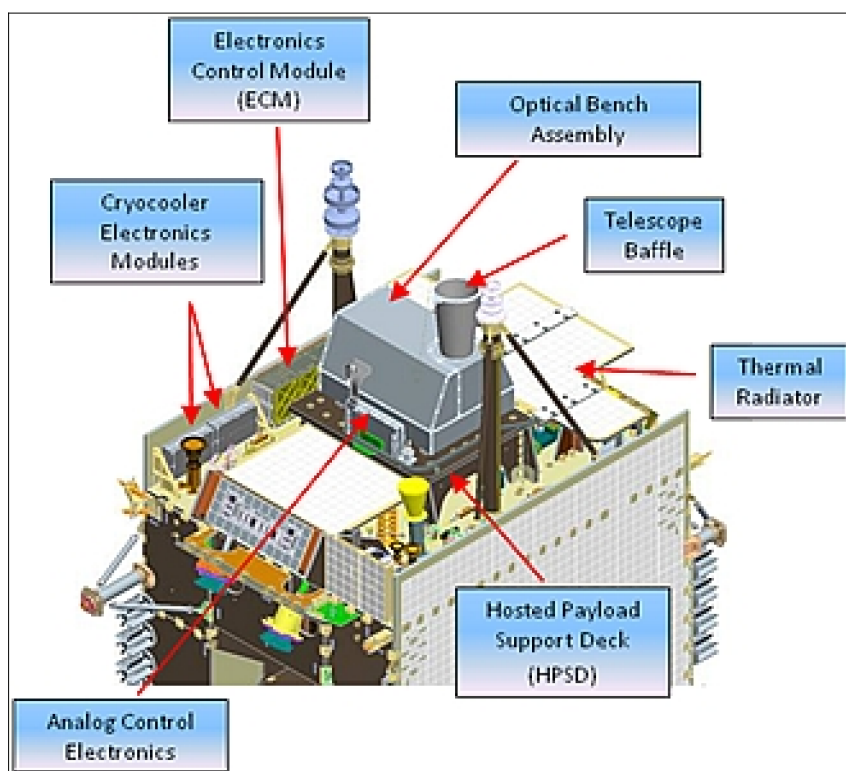


Figure 40: View of the CHIRP wide field of view (WFOV) imager flown on SES-2

The objective of CHIRP will perform risk reduction and evaluation of WFOV infrared staring and data processing technology to potentially evolve future SBIRS (Space-Based Infrared System) staring sensors and processing algorithms.^{805) 806)} An on-orbit demonstration will quantify performance levels of the WFOV sensor in an operational environment. The testing of the CHIRP sensor will also provide FPA performance/calibration characteristics, validate the WFOV staring algorithm performance in an operational environment,

802) Adam Baddeley, Integrating military assets on commercial spacecraft is seen as cutting costs and speeding launches," MIT (Military Information Technology), C4 March 2010, Volume 14, Issue 2, pp. 6-10, URL: http://www.kmimedialogroup.com/files/MIT%2014-2_SMALL.pdf

803) <http://www.ses-usg.com/wp-content/uploads/2010/08/Via-Satellite-Hosted-Payload-TechFocus-Report.pdf>

804) "STAR™ Bus Hosted Payloads," Orbital Fact Sheet, URL: http://www.orbital.com/newsinfo/publications/HostedPayload_Factsheet.pdf

805) Rich Pang, Vickie Kennedy, Brent Armand, Larry Mauch, John D. Fleming, "CHIRP Program Lessons Learned From the Contractor Program Management Team Perspective," Proceedings of the 2012 IEEE Aerospace Conference, Big Sky, Montana, USA, March 3-10, 2012

806) Joseph Simonds, George Sullivan, "CHIRP's Potential to Introduce a New USAF Space Acquisition Paradigm," Proceedings of the 2012 IEEE Aerospace Conference, Big Sky, Montana, USA, March 3-10, 2012

and investigate compatibility with current OPIR (Overhead Persistent Infrared) ground systems for missile warning, missile defense, and other mission areas.

- **IRIS – NGGS (Internet Routing in Space – Next Generation Global Services)** is a spaceborne architecture utilizing the first IP based routing node in geostationary orbit (GEO) and associated ground–based terminals and network operations center. The IRIS NGGS payload is commercially hosted on the Intelsat–14 (IS–14) GEO satellite (launch Nov. 23, 2009) flown on the SS/L 1300 bus. IS–14 covers Europe, Africa and the Americas. IRIS–NGGS has been developed as a Joint Capability Technology Demonstration (JCTD) for the US Department of Defense (DoD) by Cisco Systems.

The IRIS technology demonstrator payload includes a Cisco–sourced router which interconnects one C–band and two Ku–band coverage areas. Its architecture and design allows for flexible IP packet (layer 3) routing, cross–band and crossbeam connectivity within and between coverage areas, and multicast distribution that can be reconfigured on demand (IRIS IP routing for U.S. Military operations). The IRIS payload has a mass of 90 kg, a power demand of 450 W and a customer data rate of 60 Mbit/s.^{807) 808) 809)}

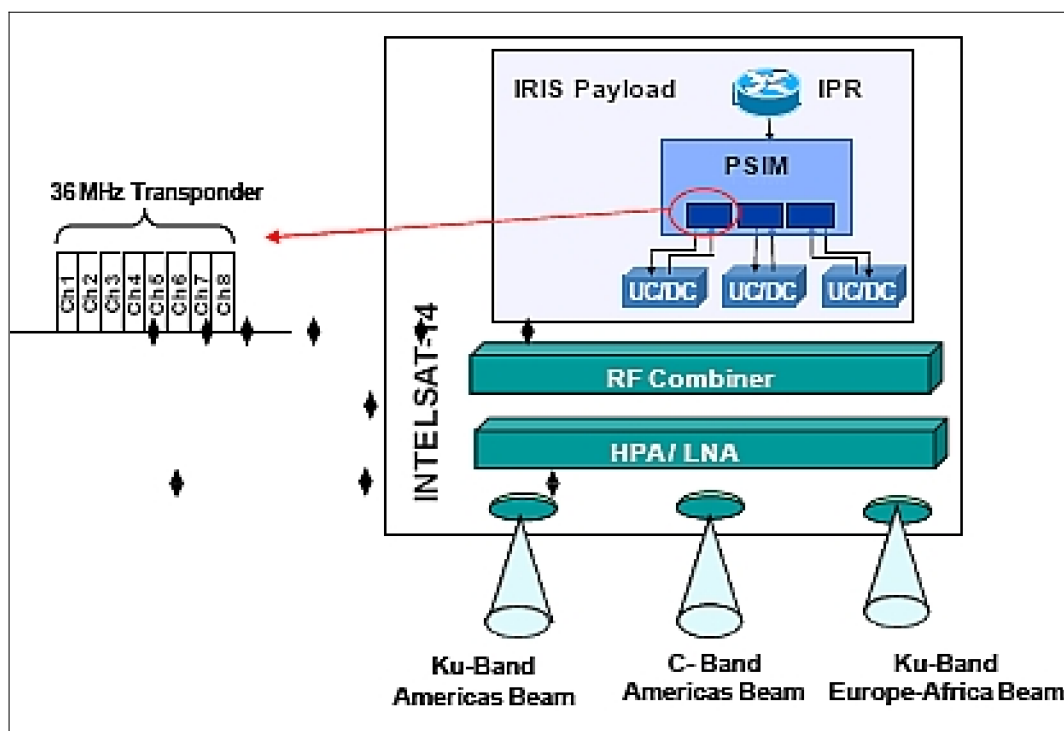


Figure 41: The IRIS payload on Intelsat–14 (image credit: JHU/APL)⁸¹⁰⁾

A preliminary assessment showed that the IRIS network capabilities available for the on–orbit demonstration performed adequately, according to the intended design (Ref. 810).

Highlighting the potential of hosted payloads to demonstrate emerging technology options, in late 2010 Cisco used this system to complete the first–ever VoIP (Voice over Internet Protocol) exchange that did not rely on a ground–based system to connect the call. This marked a significant departure from current satellite communications technology, which

807) “Hosted Payload – IRIS,” Intelsat, URL: <http://www.intelsatgeneral.com/services/hp/iris.aspx>

808) <http://www.intelsat.com/files/resources/knowledge/datasheets/ds-hosted-payload.pdf>

809) Enrique G. Cuevas, Hadi A. Esiely–Barrera, H. Warren Kim, Zhuangbo Tang, “Assessment of the Internet Protocol Routing in Space—Joint Capability Technology Demonstration,” JHU/APL Technical Digest, Vol. 30, No 2, August 2011, pp. 89–102, URL: <http://techdigest.jhuapl.edu/TD/td3002/Cuevas.pdf>

810) Enrique G. Cuevas, Zhuangbo Tang, “Preliminary Results of a Technology Demonstration of the Internet Routing in Space Capability over a Geostationary Communications Satellite,” The 2010 Military Communications Conference (MILCOM), San Jose, CA, USA, Oct. 31–Nov. 3, 2010, URL: <http://202.194.20.8/proc/MILCOM2010/papers/p1499-cuevas.pdf>

requires ground-based hubs to route calls between the users and the satellites that carry the calls.

- On July 9, 2012, the SES-5 ASTRA-4B communication satellite (mass of 6008 kg) of SES S. A., developed by SS/L, was launched from Baikonur, Kazakhstan (SES-5 location at 5° E). The spacecraft carries a spectrum of commercial payloads in Ku-, Ka- and C-band. — SES-5 also features the hosted L-band EGNOS (European Geostationary Navigation Overlay Service) payload of the EC. This represents the EGS-1 (EGNOS GEO Transponder Service-1) service of EGNOS augmenting the signals of the GPS and Galileo series spacecraft for Europe. ^{811) 812)}
- In January 2010, SES ASTRA SA signed a further contract with the EC for a second EGNOS hosted payload. The **EGS-2 (EGNOS GEO Transponder Service-2)** assembly will be onboard the ASTRA-5B spacecraft which is being built by EADS Astrium. The ASTRA-5B spacecraft was launched on March 22, 2014 (location at 31.5° E). In addition to the hosted payload, SES ASTRA will also provide the related ground infrastructure needed to operate the awarded payload. ⁸¹³⁾
- In June 2008, NASA selected the payload **GOLD** (Global-scale Observations of the Limb and Disk) as a mission of opportunity to fly as its first hosted payload experiment on a GEO commercial communications satellite, a STAR-2 bus satellite of OSC, owned and operated by SES Americom. GOLD is an ultraviolet imaging spectrograph that will fly on a geostationary satellite to measure densities and temperatures in the thermosphere and ionosphere. The goal of the mission, led by Richard Eastes (PI) of UCF (University of Central Florida), is to provide answers to key elements of an overarching question for Heliophysics science: what is the global-scale response of the thermosphere and ionosphere to forcing in the integrated Sun-Earth system? ^{814) 815) 816) 817)}

Note, according to reference 790), a number of USG (United States Government) proposed hosted payloads were initially started, but later on not selected. Among them are the following payloads: GOLD (2008), GeoTROPISAT (1996), GeoExpress (1998), VOLCAM (1998), SEI-1 (1999), ESEI (2001), LMI (2001), GeoTrace-2 (2001), GIFTS (2003), MISTI (2005), TIGRIS (2005), GeoDBSim (2007), EAGLES (2007), TIGRIS-2 (2008).

– In April 2013, NASA awarded a contract to UCF (University of Central Florida) and to LASP (Laboratory for Atmospheric and Space Physics) at the University of Colorado to design and develop **GOLD** (Global-scale Observations of the Limb and Disk), an imaging spectrograph with a mass of ~ 30 kg, to be flown as a hosted payload into GEO on one of the SES Government Solutions commercial communication satellites in 2017.

The information collected by the GOLD mission will have a direct impact on understanding space weather and its impact on communication and navigation satellites, which we've

811) "SES-5 to Provide Fresh Satellite Capacity in Multiple Frequency Bands to Europe, Africa and the Middle East," July 10, 2012, URL: <http://www.businesswire.com/news/home/20120709006854/en/SES-5-Provide-Fresh-Satellite-Capacity-Multiple-Frequency>

812) "SES-5 successfully launched," SES, July 10, 2012, URL: <http://www.ses.com/11724498/2012-15-06-ses-5>

813) Markus Payer, "SES ASTRA Awarded Second Navigation Payload for EGNOS," SES ASTRA, Jan. 12, 2010, URL: <http://www.ses-astra.com/business/en/news-events/news-latest/index.php?pressRelease=/pressReleases/pressReleaseList/10-01-12/index.php>

814) W. McClintock, M. Lankton, R. Eastes, A. Aksnes, D. Anderson, L. Andersson, A. Burns, M. Codrescu, R. Daniell, F. Eparvier, J. Harvey, T. Immel, A. Krywonos, J. Lumpe, G. Pröls, A. Richmond, D. Rusch, S. Solomon, D. Strickland, T. Woods, "Global-scale Observations of the Limb and Disk (GOLD): Mission Implementation," American Geophysical Union, Fall Meeting 2006, Abstract No SA41B-1413, URL: http://fsi.ucf.edu/GOLD/DL/GOLD_AGU_poster_McClintock.ppt

815) Eliot F. Young, Cathy B. Olkin, Phillip M. Kalmanson, Russell Mellon, Malcolm Young, "Planetary science experiments flying as hosted payloads on commercial satellites," Proceedings of SPIE 'Instruments and Methods for Astrobiology and Planetary Missions XII,' Vol. 7441, 74410X (2009), San Diego, CA, USA, Sept. 2009

816) http://fsi.ucf.edu/GOLD/GOLD_SMEX_FACT_SHEET.htm

817) Richard Eastes & the GOLD Team, "GOLD (Global-scale Observations of the Limb and Disk)," ITMR Meeting, February 11, 2009, URL: http://www.aero.org/conferences/itmr/pdf/22_Eastes.pdf

come to rely on for everything from television programming to cell phone coverage and GPS in our vehicles. ⁸¹⁸⁾

- Intelsat-22 (IS-22), the first of the four Boeing-built Intelsat satellites on the 702 MP platform, carries 24 C-band and 18 Ku-band transponders for commercial use. In addition a hosted **UHF** (Ultra-High Frequency) payload is onboard the spacecraft to provide service to ADF (Australian Defence Force). The payload design is based on an existing US DoD communications payload that the ADF currently uses as part of a sharing agreement. The ADF awarded the contract to Intelsat in April, 2009. The UHF payload has a mass of 450 kg (representing ~ 20% of the total payload capacity of the Intelsat spacecraft), and a power demand of 2 kW. IS-22 was launched on March 25, 2012 on an ILS Proton-M vehicle from Baikonur. It operates in a 72° E orbital slot over the Indian Ocean. ⁸¹⁹⁾

- The Intelsat-27 (IS-27) satellite is being built by Boeing on the 702 MP platform and features a hybrid C- and Ku-band design (39 transponders) for media and network customers. The commercial payload and will be augmented with a 20 x 25 kHz channel **UHF hosted payload** for use in U.S. government applications. The UHF payload is designed to support the existing UFO (UHF Follow-On) and future MUOS (Multi-User Objective System) satellites. ⁸²⁰⁾ Boeing received the UHF hosted payload contract from Intelsat in August 2010. The payload also supports DAMA (Demand Assigned. Multiple Access) and IW (Integrated Waveform) operations, and is digitally tuneable and completely interoperable with existing terminals. The IS-27 UHF hosted payload will be functionally equivalent to the Navy's UFO-11 satellite. A launch of IS-27 is planned for 2013 (location at 304.5° E).

Note: Intelsat-27 was launched on a Zenit-3SL vehicle of Sea Launch (Odyssey launch platform at 154° W in the Pacific) on Feb. 1, 2013. However, a **launch failure** was experienced about 40 seconds after liftoff. ⁸²¹⁾ ⁸²²⁾

- Alphasat I-XL [also known as Inmarsat I-XL (Extended L-band)] is a joint project of Inmarsat, ESA and CNES. ⁸²³⁾ In Nov. 2007, the commercial operator Inmarsat awarded a contract to EADS Astrium to build the spacecraft on the next-generation European Alphasat platform (protoflight model) to augment its BGAN (Broadband Global Area Network) service. The spacecraft has a launch mass of 6600 kg providing a power of 12 kW (design life of 15 years). Alphasat incorporates innovative on-board processing technology and user services. AlphaSat was launched on July 25, 2013 on an Ariane-5 ECA vehicle (location at 25° E).

In addition to the commercial geosynchronous communication payload of Inmarsat, the spacecraft features four hosted TDPs (Technology Demonstration Payloads) of ESA. The following payloads were selected: ⁸²⁴⁾

- LCT (Laser Communication Terminal) of Tesat-Spacecom (of TerraSAR-X, TanDEM-X and NFIRE heritage) to demonstrate GEO to LEO high-rate link services. The payload is supported by DLR (German Space Agency) funding.

818) Dwayne Brown, "NASA Selects Explorer Projects To Probe Earth's Upper Atmosphere," Contract Release: C13-100, April 12, 2013, URL: http://www.nasa.gov/home/hqnews/2013/apr/HQ_C13-100_Helio_Explorer-s.html

819) <http://www.boeing.com/defense-space/space/bss/factsheets/702/intelsat/intelsat.html>

820) "Intelsat Starts Construction of Intelsat 27 Satellite - The satellite will include UHF Payload for Government Users," Sept. 10, 2010, URL: <http://www.seek4sat.com/intelsat-starts-construction-of-intelsat-27-satellite-the-satellite-will-include-uhf-payload-for-government-users/>

821) "Sea Launch provides initial Details about Zenit 3SL Mishap," Spaceflight 101, Feb. 2, 2013, URL: <http://www.spaceflight101.com/intelsat-27-launch-updates.html>

822) "Intelsat 27 Launch Unsuccessful," Space Travel, Feb. 4, 2013, URL: <http://www.space-travel.com/reports/Intelsat-27-Launch-Unsuccessful-999.html>

823) "Alphasat Technology Demonstration Payloads," ESA, Aug. 2, 2010, URL: http://www.esa.int/SPECIALS/Technology/SEMOTY1O9CG_0.html

824) Andreas Mauroschat, Stephane Lascar, Rudolf Halm, Francois Garat, Kevin Goodey, Xavier Lobao, Fabrice Joly, "Hitching a ride to orbit: The 'hosted payloads' concept," ESA Bulletin, No 148, November 2011, pp. 33-41

- Q–V band communications experiment to assess the feasibility of these unexploited bands for future commercial applications, overseen by Space Engineering S.p.A., Rome, Italy. The Q–V band domains are in the frequency range of 35–50 GHz and 50–75 GHz, respectively.
- An advanced star tracker with APS (Active Pixel Sensor) technology, offering enhanced radiation tolerance and dynamic range, developed by Jena Optronik, Germany. ⁸²⁵⁾
- AEEF (Alphasat Environment and Effects Facility) to monitor the geostationary radiation environment and its effects on electronic components and sensors. The AEEF payload is the work of a consortium led by RUAG Space, Switzerland. ⁸²⁶⁾
- LCRD (Laser Communications Relay Demonstration): In April 2012, NASA/GSFC selected a platform of SS/L (Space Systems/Loral) for a hosted technology demonstration on a commercial satellite with a planned launch in 2016. LCRD is an optical technology demonstration mission; the payload has a mass of 175 kg. LCRD is a joint project between NASA/GSFC, NASA/JPL (Jet Propulsion Laboratory) and MIT/LL (Massachusetts Institute of Technology / Lincoln Laboratory). ^{827) 828)}
- GCPM (Geostationary Carbon Process Mapper) is a NASA Earth science mission to measure key atmospheric trace gases and process tracers related to climate change and human activity. The measurement strategy delivers a process based understanding of the carbon cycle that is accurate and extensible from city to regional and continental scales. This understanding comes from contiguous maps of CO₂, CH₄, CO, and CF collected up to 10 times per day at high spatial resolution (~ 4 km x 4 km) from GEO. GCPM uses a single instrument, the **GeoFTS** (Geostationary Fourier Transform Spectrometer) to make measurements in the near infrared spectral region at high spectral resolution. The GeoFTS is a half meter cube size instrument designed to be a secondary “hosted payload” on a commercial GEO satellite. ⁸²⁹⁾
- The EutelSat–9B communication spacecraft of Eutelsat Communications, intended to be launched in 2014, will carry the hosted relay payload **EDRS–A** (European Data Relay Satellite System – A) in addition to its broadcast mission. The EDRS–A payload will in turn be accommodated with another LCT (Laser Communication Terminal) of Tesat Spacecom, Backnang, Germany. ⁸³⁰⁾

825) “Active Pixel Sensor ASTRO APS,” URL: http://www.maks.german-pavilion.com/gp/maks11/exhibitors/dateien/JOP-MAKS2011_Data%20Sheets_Zuarbeit%2001%20Datenerfassungsbogen%20Punkt%2011.pdf

826) “ARTES 8 Alphasat/Alphasat,” ESA, Feb. 3, 2010, URL: <http://telecom.esa.int/telecom/www/object/index.cfm?fobjectid=251&fcategorid=52>

827) “NASA Selects Loral Platform to Help Enable Next Era of Space Communications,” Space Daily, April 11, 2012, URL: http://www.spacedaily.com/reports/NASA_Selects_Loral_Platform_to_Help_Enable_Next_Era_of_Space_Communications_999.html

828) “Laser Communications Relay Demonstration (LCRD),” URL: http://www.nasa.gov/mission_pages/tdm/lcrd/lcrd_overview.html

829) Richard Key, Stanley Sander, Annmarie Eldering, David Rider, Jean–Francois Blavier, Dmitriy Bekker, Yen–Hung Wu, Ken Manatt, “The Geostationary Fourier Transform Spectrometer,” Proceedings of the 2012 IEEE Aerospace Conference, Big Sky Montana, USA, March 3–10, 2012

830) “Astrium to build EUTELSAT 9B communications satellite,” EADS, Oct. 4, 2011, URL: http://www.eads.com/eads/int/en/investor-relations/investor-news/press.20111004_astrium_eutelsat.html

1.6.2 Examples of hosted payloads in LEO:

The concept of hosted payloads on commercial satellites in LEO (Low Earth Orbit) is not new.

- The OrbView–2 spacecraft, owned and operated by GeoEye Inc. (formerly Orb-Image) of Dulles VA, was launched on August 1, 1997. The commercial OrbView–2 satellite is carrying the SeaWiFS (Sea Viewing Wide Field of View Sensor) hosted payload of NASA. As part of the contract between NASA and OSC, NASA retains all rights to data for research purposes, and ORBIMAGE retains all rights for commercial and operational purposes. Note: The OrbView–2 spacecraft and its payload stopped communicating with ground stations in December 2010 (the mission ended officially in February 2011).
- On June 19, 2008, a CDS–3 (Concept Demonstration Satellite–3) of OrbComm was launched which carries a hosted AIS payload of the USCG (US Coast Guard). The satellite and the AIS payload were designed and developed at OHB–System AG of Bremen, Germany. The objective of the US NAIS (Nationwide Automatic Identification System) is to test the feasibility and effectiveness of AIS message reception and reporting from space for ship tracking and other navigational activities. The CDS–3 spacecraft has a mass 80 kg. Its orbit is at an altitude of 665 km. – However, in August 2009, the NAIS payload failed on-board of CDS–3.⁸³¹⁾
- Government support is a major factor in commercial remote sensing systems development. Companies often depend on governments as anchor tenants. The U.S. NGA (National Geospatial–Intelligence Agency) partially funded the development of the current generation of GeoEye (Dulles, VA) and DigitalGlobe (Longmont, CO) commercial satellites, through NextView contracts awarded in 2008 and purchases of imagery from both of those operators. – In August 2010, both companies won NGA contracts, extending NGA’s ability to tap imagery from the private sector and virtually guaranteeing that GeoEye and DigitalGlobe will provide remote sensing products well into the current decade. – These NGA arrangements, although involving complete missions (satellite and payload plus operations), may also be regarded as “hosted payloads.”
- **HPA (Hosted Payload Alliance):** In March 2011, seven U.S. satellite industry companies agreed to form an industry alliance to increase awareness of the benefits of hosted government payloads on commercial satellites. The objective of HPA is to serve as a bridge between government and private industry to foster open communication between potential users and providers of hosted payload capabilities.^{832) 833) 834) 835)}

The inaugural meeting of the HPA took place on April 11, 2011 at the National Space Symposium in Colorado Springs, CO, USA. The HPA Steering Committee members are: Boeing Space and Intelligence Systems, Intelsat General Corporation, Iridium Communications Inc., Lockheed Martin Space Systems, Orbital Sciences Corporation, SES World Skies U.S. Government Solutions, and Space Systems/Loral.

- **Iridium NEXT constellation initiative:**

In 2007, Iridium Satellite LLC announced its plans to develop its Iridium NEXT constellation and start deployment in 2015. With the announced came the offer of hosted payloads for government and scientific organizations.

831) <http://www.uscg.mil/nais/>

832) “Hosted Payload Alliance Announced to Promote Use on Commercial Satellites,” Space News, March 30, 2011, URL: <http://www.hostedpayload.com/blog/hosted-payload-alliance-announced-to-promote-use-on-commercial-satellites>

833) “Industry alliance to advance the use of hosted payloads on commercial satellites,” URL: <http://hostedpayloadalliance.org/releases/03302011>

834) “Hosted Payload Alliance Inaugural Meeting – April 11, 2011,” URL: <http://hostedpayloadalliance.org/>

835) “Focus On The Hosted Payload Alliance,” SatMagazine, July 2011, URL: http://www.satmagazine.com/cgi-bin/display_article.cgi?number=1562944998

The Iridium NEXT constellation will consist of 66 operational cross–linked LEO satellites in six orbital planes intersecting over the North and South Poles. Iridium NEXT will have extensive built–in redundancy in the space and ground segment, with multiple backup spare satellites in orbit, and backup gateway and command and control facilities, ensuring a high degree of network survivability and resiliency. ^{836) 837) 838) 839) 840) 841)}

Iridium likes to describe its NEXT project as the biggest private space venture in the world today. Certainly, if a lot of these hosted payload opportunities are taken up, then NEXT would also become the largest privately operated Earth observation program as well.

Iridium NEXT constellation	66 operational satellites in 6 planes of 11 spacecraft each
Orbit	Polar at an altitude of 780 km
Inclination	86.4°
Period	101 minutes per orbit
Launch period	2015 – 2017
Mission life	15 years to beyond 2030
Risk mitigation	6 in–orbit spares + 6 hanger spares
Hosted Payload	
Missions	<ul style="list-style-type: none"> – GPSRO (GPS Radio Occultation) for measuring atmospheric humidity, temperature and space weather data – Altimeters for monitoring height of sea surface, waves and ice – Broadband Radiometers for measuring the Earth’s radiation budget – Multispectral Imagers for ocean color and land imaging – Other potential mission areas including cloud motion vector sensors, forest fire detection and polar wind observations
Payload mass limit	50 kg
Payload size	30 cm x 40 cm x 70 cm
Payload power	50 W average (200 W peak)
Payload data rate	< 1 Mbit/s

Table 46: Hosted payload specifications of the Iridium NEXT Constellation

- 836) Howard James, “Cutting Earth Observation Costs with Hosted Payloads,” EIJ (Earth Imaging Journal), URL: http://www.eijournal.com/Hosted_Payloads.asp
- 837) “Hosted Payloads: Iridium NEXT;” URL: <http://www.iridium.com/DownloadAttachment.aspx?attachmentID=921>
- 838) Don Thoma, Om Gupta, “Iridium NEXT GPS Radio Occultation Hosted Payload Opportunity,” GNSS Radio Occultation Workshop, Pasadena, CA, USA, April 7–9, 2009, URL: http://www.cosmic.ucar.edu/gnssro/presentations/26_ThomaGPSRO_Workshop_April-09_rev4.pdf
- 839) “Iridium Reports Progress on ‘Iridium NEXT’ Hosted Payloads Initiative,” Nov. 19, 2009, URL: <http://finance.yahoo.com/news/Iridium-Reports-Progress-on-pz-3639396453.html?x=0&v=1>
- 840) Mike Guest, Chris Chaloner, “Long Term Measurement of the Earth’s Radiation Budget using a constellation of Broadband Radiometers hosted on Iridium NEXT,” Proceedings of the 61st IAC (International Astronautical Congress), Prague, Czech Republic, Sept. 27–Oct. 1, 2010, IAC–10.B1.2.4
- 841) “GEOScan Program Background,” URL: <http://geoscan.jhuapl.edu/>

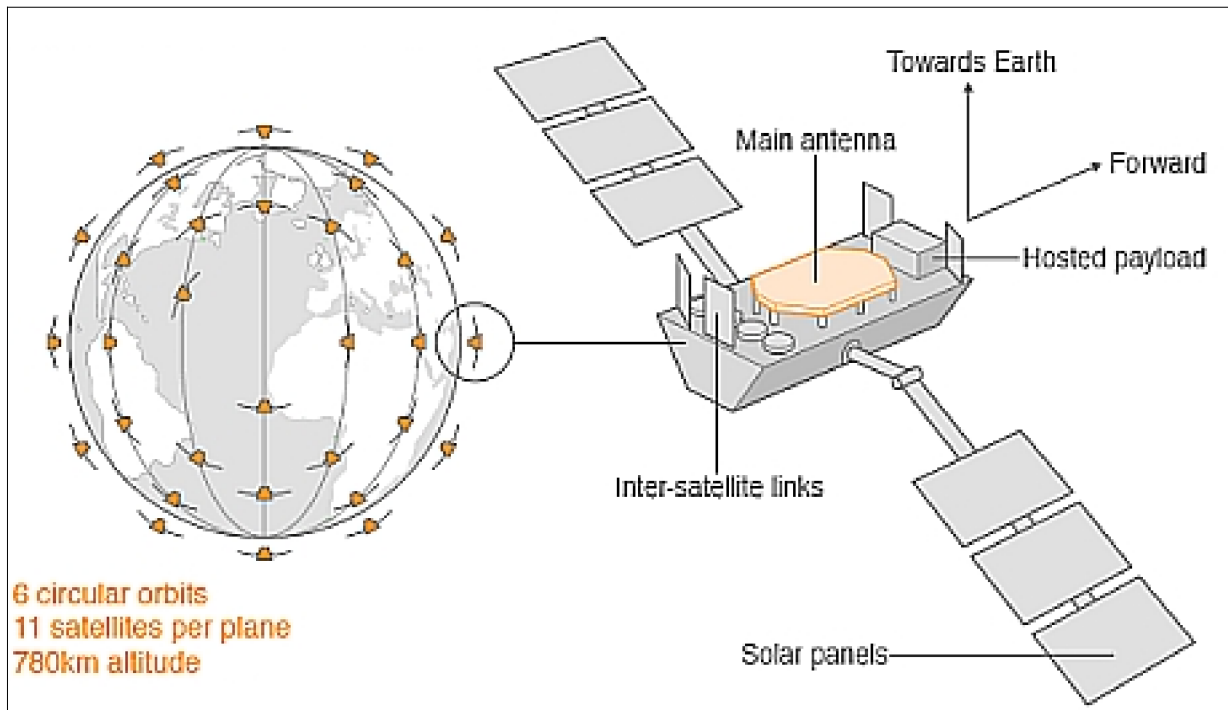


Figure 42: Schematic view of the Iridium NEXT satellite constellation concept (image credit: TAS)

Orbital has been selected by TAS (Thales Alenia Space)⁸⁴²⁾ to assemble, integrate and test 81 spacecraft for the Iridium NEXT program including 66 operational spacecraft.

⁸⁴²⁾ Hosted Payloads,” Orbital, URL: <http://www.orbital.com/HostedPayloads/>

1.7 Fundamental Science Limits in Space Flight and Earth Observation

All system design is subject to the fundamental limits imposed by the laws of physics, especially those formulated by Kepler, Newton, Maxwell, Airy, Nyquist and Planck.⁸⁴³⁾

Background: Prior to their time, the Polish astronomer Nicolas Copernicus (1473–1543 – the name was latinized from Niclas Kopernik) hypothesized his radical new view of a heliocentric system, based on extensive observations. In 1530, Copernicus finished his theory “De Revolutionibus Orbium Coelestium” (on the Revolutions of the Celestial Bodies, the book was published in Nuremberg, Germany, in 1543), which asserted that the Earth rotated on its axis once daily and traveled around the sun once yearly. Up to the time of Copernicus, the thinkers of the western world believed in the cosmology of Aristotle and Ptolemy (Claudius Ptolemy of Alexandria, Egypt, about 150 BC) that the universe was an Earth-centered closed space bounded by spherical envelopes carrying the planets and fixed stars. Copernicus is considered the founder of the modern “Weltanschauung” (world view).

1) Kepler’s laws of planetary motion (his first two laws were announced in 1609, the third law in 1619), after Johannes Kepler (1571–1630)^{844) 845)} a German astronomer, who discovered that the Earth and planets travel about the sun in elliptical orbits. Kepler’s laws, based on extraordinarily accurate observations of the 16th century Danish astronomer Tycho Brahe (1546–1601), describe the motion of a body subject to gravitational forces – and thus describe a satellite in orbit about Earth, the sun or the moon. Kepler’s deduction of the three fundamental planetary laws (which he solved geometrically) were key elements that later enabled Isaac Newton to formulate his theory of gravitational force.

- Kepler’s 1st law: A planet orbits the sun in an ellipse with the sun at one focus
- Kepler’s 2nd law: A ray directed from the sun to a planet sweeps out equal areas in equal times
- Kepler’s 3rd law: The square of the period of a planet’s orbit is proportional to the cube of that planet’s semimajor axis; the constant of proportionality is the same for all planets.

For a satellite in Earth orbit, the time required to complete one revolution is determined primarily by its mean radial distance. LEO spacecraft with typical altitudes of 700–800 km require about 100 minutes for one orbit. Many Earth observation missions require global coverage (see also chapters 1.24 and O.10.1). The laws of orbital mechanics, in combination with the daily Earth rotation, demand a space–time trade–off: a shorter revisit interval implies less dense spatial coverage. Under such constraints, it may not be possible with only one spacecraft to achieve the simultaneity required for fine spatial coverage and short revisit intervals. In this case, a constellation may be the only solution.

2) Newton’s laws of motion (first published in the Principia in 1687), named after Isaac Newton (1642–1727), English physicist and mathematician. Newton’s three laws of motion (two of them were already discovered experimentally by Galileo Galilei) describe the response of a body to its own inertia and to forces applied from internal or external sources – relative to an inertial reference frame (Figure 43). Both sorts of forces impact all spacecraft. Examples of internally applied forces are:⁸⁴⁶⁾

- S/C pointing by the attitude control subsystem. Observation requirements might call for a particular orientation of the S/C along its orbital path.

843) Excerpts are reprinted with permission from “Assessment of Mission Size Trade–offs for NASA’s Earth and Space Science Missions,” pp. 6–12, National Academy Press, 2000, Copyright (2000) by the National Academy of Sciences. Courtesy of the National Academy Press, Washington, D. C.

844) Kepler is considered a founder of modern astronomy, he formulated the famous three laws of planetary motion. They comprise a quantitative formulation of Copernicus’s theory (1530) that the planets revolve around the sun.

845) Kepler’s laws of planetary motion were first published in 1619 in his: “Harmonices Mundi Libri V,” Lincium Austriae, 1619 (Five books on the Harmony of the World)

846) Isaac Newton, “Philosophiae Naturalis Principia Mathematica,” 3rd edition (1726), with variant readings, assembled by A. Koyré, I. B. Cohen, and A. Whitman, 2 Volumes, Cambridge: Harvard University Press, 1972

– In addition to S/C pointing, there may be a requirement for subsystem pointing. This is for instance the case when the solar panels are rotated to keep them facing into the sun for maximum power generation.

In general, instruments that must provide very fine angular resolution require in turn that their host S/C satisfy very stringent angular stability requirements. The unwanted reactive movements generated by these subsystems are in turn offset by reaction wheels or torque rods. – Examples of externally generated forces are:

– All S/C must be launched from Earth. Newton's laws and the characteristics of the available propulsion system impose strict limits on the payload mass that can be lofted into Earth orbit or beyond. These limits are expressed in Newton's second law of motion.

– The solar radiation pressure (a surface force) changes the S/C orbit over long periods of time, depending on S/C mass. The drag in LEO orbits is also a surface force. Both, radiation pressure and drag, represent non-gravitational orbit perturbations.

Newton introduced his three laws of motion in book I of his Principia (1687):

- 1) Every body continues in its state of rest, or of uniform motion in a right (straight) line, unless it is compelled to change that state by forces impressed upon it.
- 2) The change of motion is proportional to the motive force impressed and is made in the direction of the right line in which that force is impressed.
- 3) The every action there is always opposed an equal reaction: or, the mutual actions of two bodies upon each other are always equal and directed to contrary parts.

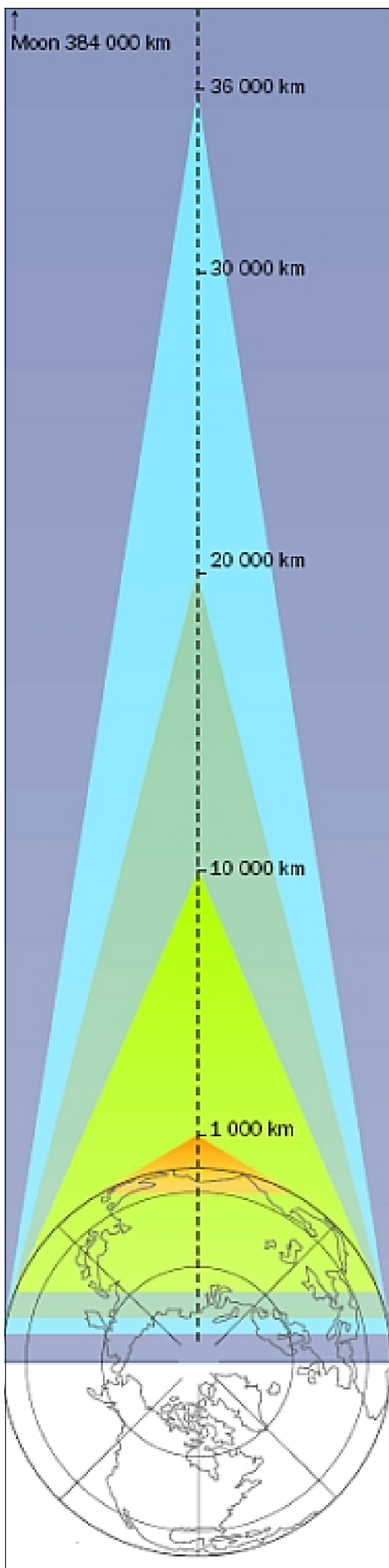
Figure 43: Newton's three laws of motion

– Orbital maneuvers. A S/C propulsion subsystem might change the orbital altitude.

4) Maxwell equations (publication of Treatise on Electricity and Magnetism in 1873), named after James Clerk Maxwell (1831–1879) a Scottish physicist. Maxwell's equations describe the behavior of the electromagnetic waves as they propagate in space. Portions of the electromagnetic spectrum are used by all space missions. Observation instruments as well as the communication subsystems for the transfer of data through space must be designed within the constraints of the Maxwell equations. The first and most obvious constraint is that radio waves travel at the speed of light (c , the speed of light in vacuum, is 299,792,458 m/s). Even at this speed, light travel time imposes substantial delays on all communication between Earth and satellites. This is already quite noticeable for two-way GEO communications, it is in particular apparent for deep-space probes. A further consequence of the Maxwell equations is that all radiation gets weaker in proportion to the square of the distance between the radiation source and the observer. Hence, very distant radiation sources become very faint and therefore require much larger viewing apertures. The system design takes the signal weakening into account through the link budget of the communication system (with corresponding antenna designs and sizes).⁸⁴⁷⁾ – The same physical principles as discussed above apply of course also to a satellite's electrical power generating capability.

5) Airy diffraction (ca. 1835), named after George Biddell Airy (1801–1892), a British Astronomer Royal from 1835 to 1881. The problem: Observed imagery can never be perfect in the geometrical sense. It is either degraded by geometrical aberrations, which are a function of the lens parameters, and/or by diffraction, which is a physical optics effect.

847) Note: The "signal weakening" effect is due to the widening cross-sectional area of the light ray as it propagates through space – resulting of course in ever fewer photons per unit area of cross-section, hence, of measurable energy.



The diffraction degradation is due to the wave nature of light. Diffraction limits the resolution of a telescope to the size of the Airy disk. If the optics of a system is capable of producing an image that diameter or less then it is said to be **diffraction limited**.

The Airy diffraction limit enforces a lower limit on the resolution (or beam width) of any device that radiates or receives electromagnetic energy. The principle applies of course also to all S/C imaging instruments (**the resolution of an imaging system depends on the size of the collecting aperture**). *The diffraction limit requires that the optical aperture diameter must be directly proportional to the satellite's distance from the observed surface.* – The phenomenon of far-field diffraction of a light beam simply limits the distance at which a focused (resolved) image can still be taken. Due to its wave nature (delocalization), light can only be focused to a point as small as half its wavelength by traditional methods. The diffraction limit for an optical system (telescope) is defined as the sharpest possible point image obtainable by far-field beam divergence. According to Airy, the resolving power of a diffraction-limited telescope is solely dependent on its aperture.

As an illustration, the monolithic optics system on a spacecraft at GEO altitude (of about 36,000 km) must have an aperture 45 times larger than a similar instrument on a spacecraft at typical LEO altitudes (of about 800 km) to obtain the same surface resolution (example: an aperture diameter of 4 m in GEO is needed to obtain spatial resolutions of 30 m in VNIR and 300 m in FIR on Earth's surface). In addition, the GEO sensor's internal optical path length also has to grow in proportion to the aperture diameter if similar performance to the LEO instrument is to be obtained. As a consequence, instruments at GEO tend to be considerably larger than their LEO counterparts. – The launch costs of such a monolithic optics system would simply be prohibitive! The adjacent Figure provides a good illustration of scale involved in LEO and GEO missions in relation to Earth's diameter. – From an angular point of view, a 20 m resolution from GEO is equivalent to a 0.4 m resolution from a 720 km orbit. The main challenges are thus the on-board stability of the line of sight (i.e. spacecraft attitude) and the knowledge of the realized line of sight used for image products.

While observations from GEO offer great advantages/relationships of fixed-position, continuous-signal, continuous-coverage, and large-area coverage – the GEO missions remain rather challenging candidates for high-resolution Earth observation missions in the optical and microwave ranges due to the above mentioned diffraction limit constraints.

Some remarks to the Airy diffraction limit:⁸⁴⁸⁾ The defining ability of any optical imaging system is not merely a property of that system's aperture, it is also governed by the Modulation Transfer Function (MTF), the ratio of the object contrast to the contrast of that object in the image plane. Thus, the MTF provides the response of an optical sensor as a function of object scene contrast and spatial frequency. MTF is also a measure of how accurately the actual radiance from a pixel (IFOV) is measured (a lower MTF indicates contributions from other pixels to the pixel of observation). The higher the MTF the greater the resolving power of that system. A radiometrically accurate IFOV is one for which $MTF > 0.95$. Generally, the MTF of a practical optical imaging system is much lower than 1. EIFOV (Effective Instantaneous Field of View) is defined as the resolution corresponding to a spatial frequency (ground resolution) for which the system MTF is 50%. Note: The value of MTF is not only reduced by the aberrations within the optical system, but also by the Earth's atmosphere. Haze, turbulence and differential refraction will each contribute to a reduction in MTF, i.e. in the reduction of total telescope performance.

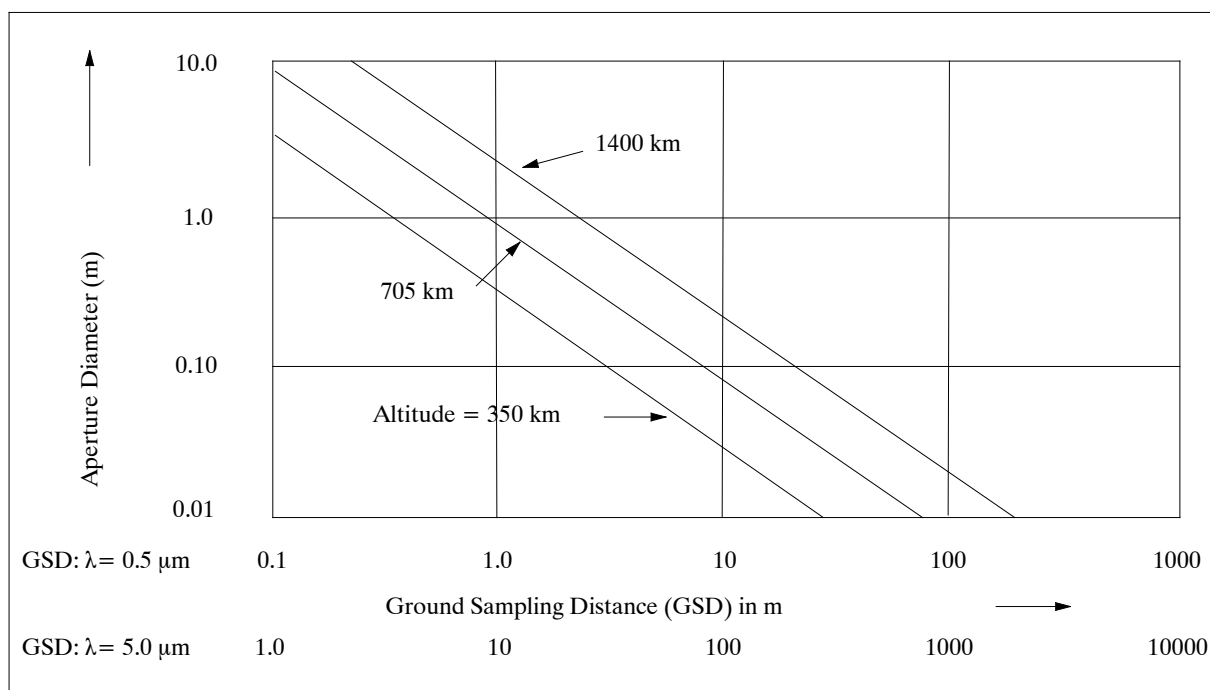


Figure 44: Airy diffraction limit as a function of aperture diameter, GSD and altitude

The physical diffraction limit on aperture size has deeper implications as well. **The laws of physics dictate that the best (highest) angular resolution that any remote sensing system (telescope or antenna) can achieve (i.e. its diffraction limit) is proportional to λ/D , where λ (lambda) is the observing wavelength, and D is the telescope or antenna aperture diameter.** The resolution with which the system can image the scene is therefore $R \times \lambda/D$, where R is the range to the scene. For a satellite-based system in orbit around a planet, the range to the scene is at least a few hundred kilometers. — Hence, for any imaging device that sends or receives energy, the size of the aperture must be proportional to the wavelength it uses. The so-called optical spectrum extends from $0.01 \mu\text{m}$ to $1000 \mu\text{m}$ (or 1 mm), i.e., from the UV to the FIR region inclusively. The microwave region (radar) of the electromagnetic spectrum is generally considered from 1 mm to 1m wavelengths. In general, there are at least three orders of magnitude in wavelength between the optical and microwave instruments. *Hence, the diffraction limit for active radar systems or passive microwave radiometers implies apertures in the order of a thousand times larger than their optical counterparts.* For example, L-band

848) Note: Early pioneers of the diffraction theory were such man as: Christian Huygens (1629–1695) of Holland, William Herschel (1738–1822) of England (born as Friedrich Wilhelm Herschel in Hannover, Germany), Thomas Young (1773–1829) of England, Joseph von Fraunhofer (1787–1826) of Germany, Dominique Arago (1786–1853) and Augustin Jean Fresnel (1788–1827) of France, and George B. Airy (1801–1892) of England.

radiometry (i.e. radiometry in the microwave region) faces the challenge of flying very large apertures to achieve a spatial resolution suitable for scientific applications.

*To meet a given level of performance, an instrument's minimum aperture size is dictated by wavelength and observable distance, it cannot be reduced by technology.*⁸⁴⁹⁾ Thus, even when a major SAR design goal is smallness, the SAR antenna size cannot be reduced to fit that objective. Any mission that relies on SAR to conduct science observations will continue to require a medium-sized or large S/C platform. – Future distributed (complex) apertures in special circumstances may to some extent circumvent this limit using the interferometric technique of aperture synthesis.

Enhanced imaging performance (finer angular resolution) can be obtained under favorable conditions. For example, a thinned array (also referred to as a **sparse array** or a sparse aperture consisting of many distributed but discrete subapertures) may substitute for a filled array if the viewing objective is relatively sparse. An optimal imaging concept of afocal interferometric telescopes, designed for sparsely filled arrays was first proposed by Marcel J. E. Golay in 1971 [Golay 1902–1989, a Swiss-born US information theorist (Golay codes, Golay cell, etc.); Golay used mask designs in which 3-fold symmetric spaces were searched for non-redundant array solutions].⁸⁵⁰⁾ The thinned array technique is a very promising technology to enable these very large (but lightweight) apertures in space (not requiring rotation to form an image). In this concept, the coherent product (correlation) of the signal from pairs of antennas is measured at different antenna-pair spacings (baselines). By correlating the signals received by many identical radiometer receivers each with a very small antenna (and therefore wide beamwidth), the interference pattern of the imaged scene can be measured. A key feature of a thinned array is that all the required baselines are obtained with fewer antennas than there are spacings. The angular resolution of such a thinned array, however, is governed by the Airy diffraction limit, and by the radiometric sensitivity of the array (proportional to the areas summed of all contributing subapertures). Spherical primary elements could also be used in the sparse aperture design with aberration correction by a deformable tertiary or quaternary mirror (Korsch three and four mirror aplanats).⁸⁵¹⁾

Sparse aperture concepts: The use of a large aperture on a spaceborne instrument improves the remote sensing performance considerably, offering in particular increased sensitivities to sensor noise and higher spatial resolutions. This principle applies to passive as well as to active remote sensing instruments (for instance: telescopes or radiometer receivers for passive remote sensing in the optical and the microwave regions, and SAR antennas for active remote sensing in the microwave region). By their very nature, large conventional monolithic aperture structures are rather heavy (requiring stiffness and structural stability, and requiring large launch fairing diameters), These monolithic structures are expensive to build and to launch (the cost of monolithic optics increases faster than the aperture diameter squared).

The approach of “**sparse aperture imaging**,” on the other hand, offers a potential solution, providing the means for large distributed arrays of small (discrete) elements – at a much lower structure mass and a more compact packing volume for the launch phase. After deployment, such a distributed multi-element system (with baselines in between) represents in effect an interferometric measurement arrangement. A receiver of this type can produce images comparable to those generated by a filled aperture of the same diameter, provided that an average SNR on the order of 100 can be maintained over the entire image.

Conceptually, the measurement arrangement of a sparse aperture remains the same, whether it is

849) Note: An example to this challenge of distributed apertures is “two-dimensional aperture synthesis.” In microwave radiometry the concept employs an interferometric technique in which the product from antenna pairs is sampled as a function of pair spacing. Substantial reductions in the antenna aperture needed for a given spatial resolution can be achieved with this technique. However, the performance leap in resolution must be paid for with higher requirements for instrument precision sensing and stabilization.

850) M. J. E. Golay, “Point Arrays Having Compact Non-redundant Autocorrelations”, Journal of the Optical Society of America., Vol. 61, pp 272–273, 1971.

851) Advanced Interferometric Space Telescope (AIST), URL: <http://optics.nasa.gov/concept/aist.html>

being applied to an aperture structure of discrete elements on a single spacecraft (with relatively small baselines), or to a close formation of several spacecraft with a single relatively small aperture to each spacecraft (and with relatively stable but considerably larger baselines).

Although the raw imagery produced by a sparse – aperture system will show significant distortions, near – diffraction – limited images can be recovered by using appropriate data processing techniques. The correction of point – spread – function distortions induced by sparse – aperture receivers is an example of an application for which Fourier deconvolution is particularly well suited.

6) Nyquist frequency (1929), after Harry Nyquist, a US physicist of Swedish descent and a pioneer in the field of communication theory (1889 – 1976). – The Nyquist frequency dictates the minimum number of samples per second, required to transport a given amount of data over a communication channel of certain bandwidth (analog – to – digital conversion begins with sampling, or measuring the amplitude of the analog waveform at equally spaced discrete instants of time). The sample frequency is also determined by how often a point on the surface must be sampled to resolve the variations in the physical processes over time. In general, more information implies more detail but also more data. If those data have to be transferred rapidly, then the data rate must increase in proportion. The Nyquist sampling theorem in its simplest form states that a signal can be uniquely represented by periodic discrete samples whose period is no larger than 1/2 of the signal’s inverse bandwidth.

To resolve an image there is a minimum signal requirement; the number of photons that need to be collected (photon count) by an imaging system. There is an absolute minimum of two photons per ground pixel, determined, by the **Nyquist criterion**. However, to actually determine some type of gray scale information, and to overcome noise in the system, the actual sample size will more realistically be on the order of 10^4 or more photons per ground pixel. – Optical systems in general are limited in their ability to resolve an image by the Rayleigh criterion, and by the number of photons that can be collected (Nyquist criterion).

The **Rayleigh criterion** [John W. S. Rayleigh, English physicist (1842 – 1919) in the fields of acoustics and optics] is important in this context. *It refers to the resolving power of an optical system and its consequences on aperture size. It states that the resolution of a system is directly proportional to the wavelength.* Thus, with perfect optics, an imaging system working at 50 nm (EUV wavelengths) would have an order of magnitude better resolution than one working with visible light (about 500 nm wavelength). *The Rayleigh criterion determines the aperture diameter of an imaging system needed to achieve a spatial resolution (i.e., minimum diameter needed to resolve an image).* While the Rayleigh criterion determines the aperture size, no matter what type of optical system is used, its total area must be greater than or equal to that of a filled aperture system that will collect enough photons to resolve the image. See also the Glossary on the Rayleigh criterion.

Hence, a practicable and economical solution for a larger **effective aperture** can only be achieved with the introduction of **interferometry** and/or the use of **phased arrays**. Phased arrays get around the beamwidth limit (i.e., Rayleigh criterion) by using several small apertures (linked together) to achieve the same result as one large aperture. Phased arrays synthesize larger apertures from an array of elements.

7) Planck’s radiation law, named after Max Planck (1858 – 1947), a German physicist who originated quantum theory. In 1900, Planck formulated an equation to explain the spectral energy distribution of thermal radiation from a perfect absorber (blackbody) and showed that the formulation required a discontinuous process of emission or absorption involving discrete quantities of energy. Planck’s radiation law relates the energy of radiation to its frequency ($E = h \times \nu$). The energy E of each quantum, or of each photon, equals Planck’s constant h multiplied by its radiation frequency ν .

Within the electromagnetic spectrum the spectral radiance (i.e. energy per unit time, area, solid angle, and wavelength) varies considerably and with it the ability to detect (measure)

radiation. In general, photons are considerably more energetic at shorter wavelengths than at longer wavelengths.

All instrument observation techniques based on radiation measurements (there are indeed many instruments in this category) are constrained to Planck's radiation law. Chapter O.4.4 provides some information as to the radiation detection limits in the various spectral ranges. To illustrate the spectral energy distribution, let us consider three imaging instruments on the same spacecraft, all looking into the same footprint, with each instrument observing incoming radiation in a different spectral range, namely:

- The VIS range (0.4 – 0.7 μm) with photon energy levels of 3.1 – 1.8 eV
- The FIR range (30 – 1000 μm) with photon energy levels of 35 – 1 meV
- The MW range (1 mm – 1 m) with photon energy levels of 1 meV – 1 μeV

The photon energy levels for each spectral range decrease practically by three orders of magnitude from VIS to FIR and again from FIR to MW. This vast photonic energy range of 10^6 puts in particular great demands on the detector technology in the microwave range to measure such minute energy levels and to discriminate between signal differences.

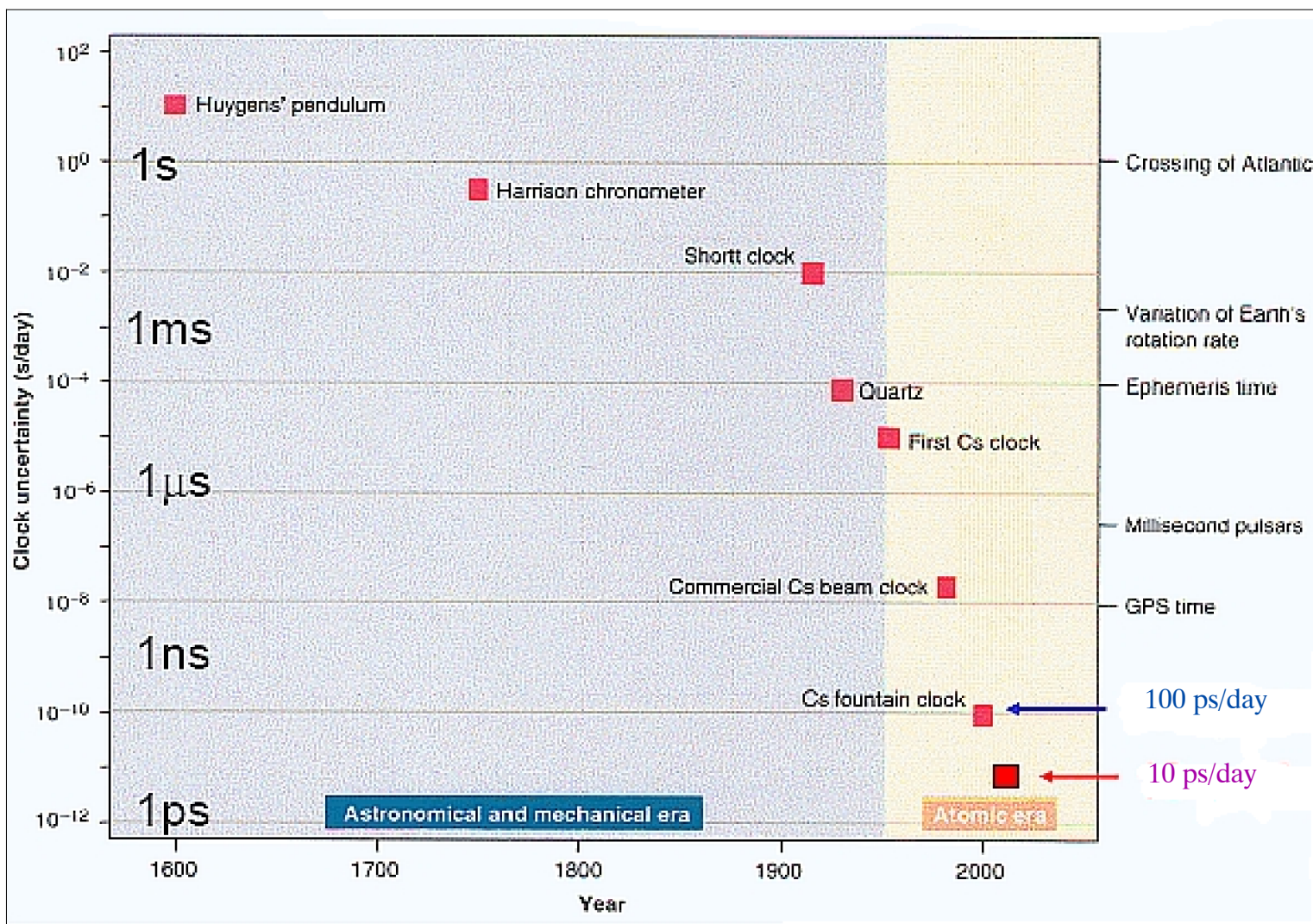


Figure 45: Time precision measurement capabilities reflected on certain events in the modern history of humankind (image credit: C. Salomon, LKB, Paris) ⁸⁵²

⁸⁵²) C. Salomon, "Fundamental Tests with Ultrastable Clocks," March 29, 2008, URL: <http://www.astro.up.pt/investigacao/conferencias/esf2008/files/C.Salomon.pdf>

1.8 Spacecraft Systems

A bouquet of topics is presented in this chapter of spacecraft systems, from system design issues to operations and inflatable structures. At the start of the 21st century considerable change can again be expected in all aspects of space systems due to the introduction of still further innovations. In particular, spacecraft component technologies are becoming important for future mission/observation capabilities. All these changes will introduce more functional flexibility, leading also to more system complexity.

1.8.1 Spacecraft platform stabilization concepts

Spacecraft stabilization is a prerequisite for any observation from space. There are a number of techniques in use to stabilize and orient a spacecraft (also referred to as momentum stabilization). The orbital motion of a spacecraft experiences various disturbance forces that, if they do not act on the center of mass, produce a torque applied to the vehicle. Principal external sources of disturbance on a spacecraft are: a) aerodynamic torque, b) gravity–gradient torque, c) solar radiation pressure torque, d) magnetic torque, e) other disturbance torques. In addition, there may be internal torques of consequence in the control of attitude of the spacecraft, resulting from the exchange of momentum between internal mobile elements. Typical internal torques are generated by the movement of antennas, solar panels, pointing instruments, etc. In addition to the stabilization problem, there may be an independent direction requirement, generally a problem of active control, in which the space vehicle or a part of the equipment of the space vehicle must point into a specific direction (spacecraft body pointing). In general, there are two broad classes of stabilization concepts in use: (see also chapter 1.23.2)

1) **Passive attitude control techniques:** These take advantage of basic physical principles and of forces that are produced spontaneously to design the space vehicle, reinforcing the effect of a force while reducing other. An advantage of the passive control is the capacity to achieve a very long life of the satellite, not limited by onboard consumable or, possibly, even by the wear and mobile pieces breaks. The typical disadvantages of the passive control are the relatively poor total accuracy and response something inflexible to changing conditions. Some passive techniques employed are:

- Spin stabilization
- Gravity–gradient stabilization
- Aerodynamic stabilization
- Solar pressure stabilization (solar sail)
- Permanent magnet

2) **Active attitude control techniques:** The underlying concept of active attitude control is cyclic in nature, involving the continuous sensing of the attitude and comparison of the actual attitude to the required attitude. A corrective actuation is provided in the case of a prescribed deviation. Actuation⁸⁵³⁾ may be provided by each the following devices or combinations thereof: reactions wheels, momentum wheels, control moment gyroscopes, magnetic torquers, thrusters, etc. Obviously, consumables are being required for the maintenance of the actuation process. Some consumables, like electric power, are replenishable while others (fuel) are finite. Some sensor options are: magnetometer, gyro, star tracker, horizon and sun sensors. In general, active attitude control techniques are providing improved pointing accuracies and response times over the passive attitude techniques.

The following list represents some examples of platform stabilization concepts:

⁸⁵³⁾ Note: An actuator is a device able to modify the orientation of a spacecraft.

- Single spin stabilized spacecraft: Early spacecraft relied heavily on pure spin stabilization for gyroscopic stiffness. In such a system, inertial orientation is provided by the spin of the entire spacecraft (generally about its axis of maximum moment of inertia or “major axis”). A nutation damper is used to damp the nutation (precession still exists). In such a configuration, the sensor collection is limited to scanning by the spin motion. This method continues to be used on many of today’s satellites. Examples: The world’s first weather satellite, TIROS–1 (launch April 1, 1960) and the follow–up TIROS and ESSA series S/C (up to ESSA–9, launch Feb. 26, 1969) were all spin–stabilized. Also, the advanced Vela satellite series of USAF (launch of Vela–7 on April 28, 1967; six S/C, Vela–7 to –12 were launched from 1967 to 1970) and SAS–1 (launch Dec. 12, 1970)] followed the single–spin concept.⁸⁵⁴⁾
- Dual–spin stabilization systems were quickly recognized as a superior stabilization concept for satellites (two bodies rotating at different rates about a common axis). The dual–spin concept was developed by Vernon Landon at RCA and Anthony Iorillo at Hughes.^{855) 856)} The term “dual–spin” was coined by Peter Likins in 1967.⁸⁵⁷⁾ With a dual–spin satellite the payload (i.e. the antenna, sensors) is despun while the other portion of the spacecraft spins to provide gyroscopic stability (the system requires torquers such as thrusters or magnets for momentum control and nutation dampers for stability). In general a dual–spin satellite features a relatively fast–spinning rotor and a slowly spinning platform. The de–spun platform portion allows an Earth–pointing payload. – Following is a short history of early dual–spin configurations:⁸⁵⁸⁾
 - The OSO–1 (Orbiting Solar Observatory–1) of NASA, launched on March 7, 1962, demonstrated the dual–spin concept successfully by spinning about its principle axis. The objective of the LEO spacecraft was to study ultraviolet, X–ray and gamma radiation from the sun. OSO–1 was followed by six more OSO S/C launched between 1962 and 1975, all of the same dual–spin design.^{859) 860) 861)}
 - Communication satellites introduced the concept in the late 1960s. The TACSAT–1 (Tactical Communication Satellite–1, launch Feb. 9, 1969) of DoD, built by Hughes Aircraft Company, was the first minor–axis dual–spin–stabilized S/C by the Hughes–developed “Gyrostat” system.
 - The first EO (Earth Observation) missions using the dual–spin Earth–pointing concept were METEOSAT–1 of ESA (launch Nov. 23, 1977) and MAGSAT of APL/NASA/USGS with a launch on Oct. 30, 1979.
 - The Galileo spacecraft of NASA/JPL (launch Oct. 18, 1989) is the first dual–spin interplanetary satellite implementation. A spinning section rotates at 3 rpm, and a despun section is counter–rotated to provide a fixed orientation for cameras and other remote sensors.
- Gravity–gradient stabilization (a passive technique): The concept employs the change in gravity with altitude to create a torque when the principal axes are not aligned with the

854) Note: The Vela (meaning “watchman” in Spanish) spacecraft series of DoD was designed to monitor worldwide compliance with the 1963 nuclear test ban treaty. Vela–1 was launched Oct. 17, 1963; Vela–6 was launched July 20, 1965

855) V. D. Landon, B. Stewart,, “Nutationl Stability of an Axisymmetric Body Containing a Rotor,” *Journal of Spacecraft and Rockets*, Vol. 1, No. 6, 1964, pp. 682–684

856) A. J. Iorillo, “Hughes Gyrostat System,” *Proceedings of the Symposium on Attitude Stabilization and Control of Dual–Spin Spacecraft*, El Segundo, CA, 1967, Air Force Systems Command and Aerospace Corporation, pp. 256–266

857) P. W. Likins, “Attitude Stability Criteria for Dual Spin Spacecraft,” *Journal of Spacecraft and Rockets*, Vol. 4, No. 12, 1967, pp. 1638–1643

858) R. A. Sandfry, “Equilibria of a Gyrostat with a Discrete Damper,” *Dissertation Virginia Tech*, July 9, 2001, pp. 229, URL: <http://scholar.lib.vt.edu/theses/available/etd-07202001-122347/unrestricted/dissert.pdf>

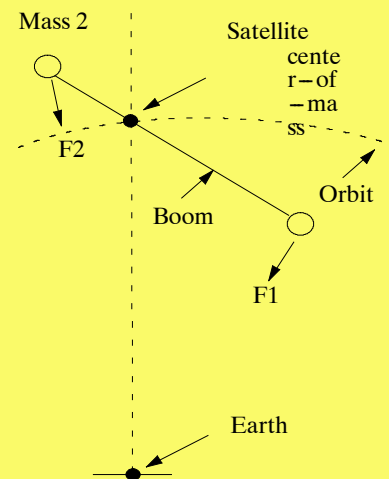
859) R. L. Huston, “Gyroscopic Stabilization of Space Vehicles,” *AIAA Journal*, Vol. 1, No. 7, 1963, pp. 1694–1696.

860) T. W. Flatley, “Equilibrium States for a Class of Dual–Spin Spacecraft,” *Technical Report R–362*, NASA, March 1971.

861) <http://www.nasm.si.edu/research/dsh/artifacts/SS-OSO1.htm>

orbital reference frame. Long booms with an end mass are usually extended to create the torque. The concept is simple and reliable, but pointing accuracies are poor, generally in the order of $< 5^\circ$. – The gravity–gradient boom technique, particularly suitable for microsattellites, was first introduced by the LEO Transit navigation satellite series of the US Navy (starting with the launch of Transit–5A–3 on June 16, 1963), followed by other missions: the GGSE (Gravity Gradient Stabilization Experiment) satellite series of DoD started on Jan. 11, 1964 with GGSE–1, GGSE–4 and –5 were launched May 31, 1967 along with Timation–1 (NRL, launch May 31, 1967); ATS–2 (Application Technology Satellite–2), a NASA GEO stallite prior to GOES, launch April 6, 1967. GGTS–1 (Gravity Gradient Test Satellite–1 with a mass of 47 kg) of the USAF was launched June 16, 1966 from Cape Canaveral. The UoSAT microsattellite series of SSTL, UK (launch of UoSAT–1 on Oct. 6, 1981) is using the gravity–gradient concept (in LEO) extensively. The DODGE S/C (launch July 1, 1967, see M.10) was the first to study a number of advanced biaxial and triaxial gravity–gradient stabilization techniques at near–synchronous altitudes.

Gravity–gradient boom. A deployable extension of a spacecraft (a rod fixed to the S/C with a small mass at its other end) intended to give the spacecraft elongated mass properties to contribute to gravity–gradient stability (the concept was first successfully demonstrated by JHU/APL on the Transit 5A–3 satellite with a launch on June 16, 1963). The principle: The attractive force F_1 of mass 1 (satellite) about the common center of mass exceeds the attractive force F_2 of mass 2. Hence, a torque arises to align the satellite to the vertical. An elongated dumbbellshaped spacecraft is the most gravity gradient stable configuration with the long axis oriented vertically in orbit, i.e. (usually) the smaller mass is always pointing toward the center of the Earth. The gravity–gradient torque, small even for LEO S/C, decreases with the cube of the orbital radius. In GEO, gravity–gradient stabilization can barely be achieved.



- Magnetic field stabilization: The first passive magnetic field stabilization system of a satellite was introduced at JHU/APL on the US Navy's Transit–1A (launch Sept. 17, 1959), Transit–1B (Apr. 13, 1960, see H.7) and DME–A (Direct Measurement Explorer – A) with a launch on Nov. 29, 1965. The principle of operation: If three mutually orthogonal electromagnets are placed in a S/C, a magnetic dipole \mathbf{M} can be created in any direction. The satellite can determine the Earth's magnetic field \mathbf{H} by means of a vector magnetometer. By activating the electromagnets appropriately in response to the magnetometer measurements, a torque $\mathbf{T} = \mathbf{M} \times \mathbf{H}$ in any direction can be obtained. This torque can be used for S/C attitude control (including spin/despin). Essentially, the satellite acts like the rotor of an electric motor, with the Earth's magnetic field being the stator. The method has been used many times since (see also Table 143). Examples:

- The ESRO satellites ESRO–1/Aurora (launch Oct. 3, 1968) and ESRO–1/Boreas (launch Oct. 1, 1969) as well as the German Azur–1 (launch Nov. 11, 1969)

- The Magion–1, –2, and –3 subsatellites of the Czech Republic (launch of Magion–1 on Oct. 24, 1978) all employed the technique of magnetic field stabilization (the Magion–4 and –5 S/C were spin–stabilized). The Magion S/C were part of the USSR mission ACTIVE (K.2)

- The AMSAT OSCAR (Orbiting Satellites Carrying Amateur Radio) microsattellite series [OSCAR 5 (launch Jan. 23, 1970), 16, 17, 18, 19, 26, and 30, for example] employ magnetic field stabilization with its SAPPHIRE ACS (Attitude Control Subsystem)

- The Munin nanosatellite of IRF (Sweden, launch Nov. 21, 2000).
- Momentum–bias S/C.^{862) 863)} Over the years, spin stabilization systems gradually gave way to momentum–bias spacecraft employing internal momentum [a momentum wheel is a flywheel designed to operate at non–zero (i.e. “biased”) angular momentum and providing momentum storage capacity about its rotation axis] or reaction wheels. In concept gyroscopic stiffness is provided by a rapidly spinning momentum wheel rather than the satellite bus itself. The momentum wheel provides control about the spin (pitch) axis; in addition, a combination of nutation damper, magnetic torquing, or propellant provide control about the roll and yaw axis. The advantages of such a system are: better pointing accuracy, better power efficiency due to the despun solar arrays. The momentum–bias approach with magnetic torquers is the dominant ACS (Attitude Control Subsystem) solution in LEO S/C.
- Three–axis stabilization: In this concept all three axes of a S/C are independently controlled either by reaction wheels (RW), or by thrusters, or by CMGs (Control Moment Gyros). The advantages of this technique are: good pointing accuracy, maneuverability and adaptability to changing mission requirements. Usually, RWs or CMGs are used for control and propellant (sometimes magnetic torquing) is used for momentum dumping. The three–axis stabilization concept offers better size and space options, in particular with the mounting of deployable solar panels. Solar arrays may be large and inertially pointed, i.e. independently steered, to maintain normal incidence to the sun, thus optimizing power generation. However, full active control is required. Early examples of three–axis stabilization are:
 - Discoverer–2 (launch Apr. 13, 1959), a US military reconnaissance satellite, was the first satellite to be stabilized in orbit in all three axes, to be maneuvered on command from Earth.
 - The Nimbus–1 satellite (launch Aug. 28, 1964) was the first civil three–axis stabilized spacecraft (followed by the Nimbus series).
 - The Improved TIROS Operational Satellite, ITOS–1 (launch Dec. 11, 1970, the NOAA–1 satellite that followed it (launch Dec. 11, 1970), and all follow–up satellites of the series) featured also three–axis stabilization. The three–axis control concept is still the most applied stabilization method in space flight.
- Yaw spinner: A yaw spinner is a three–axis controlled satellite. The payload/sensor is spun about the yaw axis to provide Earth scanning. A counterspun momentum wheel is used to cancel the angular momentum of the spinning sensor. Reaction wheels are normally used for attitude control. The advantages are: precision pointing and good maneuverability.

1.8.2 Spacecraft/Component Design Topics

Practically all satellites of the first two decades of the spaceage featured **custom designs** (in shape, size, etc.)⁸⁶⁴⁾ to suit the requirements of a particular mission. It meant continued change for the spacecraft builders to incorporate general support functions over and over again along with specific mission instruments. The availability of a standard S/C bus (for a particular observation capability) was practically unknown until the end of the 1970s.

862) Note: A reaction wheel is a flywheel designed to operate at zero bias – i.e. nominally non–rotating. Like a momentum wheel, the reaction wheel is also used for storage and transfer of angular momentum. The term “momentum dumping” refers to the despinning of a reaction wheel.

863) J. Rodden, L. McGovern, J. Higham, X. Price, “Momentum Bias For Spacecraft Attitude,” AAS Guidance and Control Conference, Breckenridge, CO, Feb. 6–10, 2002, pp. 35–44

864) H. J. Kramer, “An Overview of Small Satellites in Remote Sensing,” Proceedings of the International Workshop on Earth Observation Small Satellites for Remote Sensing Applications (EOSS 2007), Kuala Lumpur, Malaysia, Nov. 20–23, 2007

These custom designs of spacecraft had rather long lead times for requirements and definition prior to any implementation. *The general approach of the space industry was to design the technology based on the mission requirements.* After defining the requirements and constraints of the mission, each satellite subsystem – power, propulsion, attitude determination & control, thermal control, communications, command & data handling, and the structure – was designed separately and iteratively. Even after a heritage developed, the increasing complexity of ever unique missions made it difficult to carry a subsystem design from one satellite to another without significant modifications. All of NASA's scientific spacecraft through the late 1980's used this method of design. This methodology of satellite design has unique advantages and disadvantages. On the positive side, the final spacecraft is extremely capable of accomplishing its mission. On the negative side, such spacecraft are extremely expensive to develop due to the large amounts of manpower needed to design each subsystem separately, often leading to considerable cost overruns.

After a number of early spacecraft or subsystem failures were experienced, the reliability issue became a big hurdle for spacecraft designers due to the requirement of space-qualified components. Electronic devices had to be radiation-hardened to sustain the hostile environment of space. This was another cost driver as well as a performance killer, since the so-called COTS (Commercial Off-The-Shelf) products of newer designs provided much better processing power over the much older space-qualified products. In addition, the critical subsystems of a spacecraft had to be designed in a redundant or dual-redundant configuration (alternate path selection capability) to guarantee operational service in case of a single-point failure.

The MagSat mission (launch Oct. 1978), a dual-spin satellite, demonstrated to NASA in particular the usefulness of a general-purpose bus for science applications. The bus could support a variety of bolt-on experiments. However, this was still far away from the so-called “**modular bus**” as is known today.

Spacecraft instrument mounting. A cartwheel mounting configuration was realized in TIROS-9 (launch Jan. 22, 1965). For the first time, the two TV-WA cameras were mounted into the sidewalls of the S/C cylinder, 180° opposite to each other. This cartwheel concept allowed each camera to observe the same ground target during each cycle of rotation. Prior to this time, instruments were generally mounted axially into spin-stabilized S/C.

Integration of flight hardware and subsystems has become an important aspect of modular design. Introduction of such items/concepts as: GaAs solar cells, light-weight composite materials, multi-purpose platforms. Satellite design lives have improved considerably they are now approaching seven to ten years (depending on applications), mini- and microsatellites. In the 1990s, onboard processing is becoming a service introduction.

Spacecraft design (for Earth observation) has experienced interesting trends. Early space-age satellites were small due to the limitations of launch capabilities. The current classes of microsatellites (10 – 100 kg) and minisatellites (100 – 1000 kg) are a fitting description for these early space-age satellites (only with regard to mass). As the space age progressed into the 1970s and 1980s, the capabilities of launch vehicles increased constantly. Hence, satellites became much larger and much more complex. In parallel, electronics became much more dense, many subsystems could be combined into a single instrument on a satellite. The new complexity, along with its demands for reliability and quality assurance, had to be managed, generating bureaucracy and large organizations.

As a consequence, overall creativity suffered considerably while costs increased rapidly. It meant a reduction in launches with longer in-between periods. Large and complex projects of NASA and ESA encountered planning and re-planning phases alone that came close to a decade or longer. Some examples are:

- The planning for HST (Hubble Space Telescope) started in the early 1970s (launch 1990). After launch, the spacecraft required a repair mission to start operations (the

primary mirror had a flaw called “spherical aberration”). This was followed by several servicing missions requiring Space Shuttle flights.

- The ISS program started in 1984. The ISS station build-up began in 1998 until 2010; this is to be followed by regular operations.
- The EOS (Earth Observing System) program planning of NASA started in the early 1980s, rescoping of EOS in 1992. Finally Terra was launched in 1999, Aqua in 2002, and Aura in 2004.
- The planning for the NPOESS (National Polar-orbiting Operational Environmental Satellite System) program started in 1993 with the intention to “converge” the US civil and military operational meteorological satellite programs (POES of NOAA and DMSP of DoD), to reduce duplication of effort and to generate cost savings. A new generation of instruments and spacecraft are under development creating substantial cost overruns and program delays. The program was restructured in 2006/7. The launch of the first NPOESS spacecraft is now expected in 2014.
- The planning for Envisat of ESA started in the early 1980s, the launch was in 2002 (with over 8,000 kg of spacecraft mass, Envisat is the heaviest civil Earth observation mission of all time).

For the experimenter, it meant a reduction in flight opportunities for observations as well as a reduction in technology advances. “Gone are the days when novel ideas, new components or a neat scientific idea can be evaluated in orbit quickly and relatively cheaply – and gone are the invaluable opportunities for young engineers and scientists to gain first-hand experience of space before moving to larger projects.”⁸⁶⁵⁾

The situation in the time period 1980–1990 was simply overdue for a new approach to spacecraft design and development. And it started with the introduction of a new genre of satellites, namely the “microsatellites.” However, over the years this topic has become so extensive and increasingly important that a new chapter is being dedicated to smallsats – starting in 2008 (see chapter 1.19).

1.8.2.1 Spacecraft buses:

Standard spacecraft buses (as listed in Table 47)⁸⁶⁶⁾ come in all shapes and sizes. Again, standards with a “common bus” design approach are important to lower manufacturing costs. The weather satellites of NASA in LEO and GEO were the first to adopt a common design (TIROS series), followed by the commercial communication satellites in GEO (since the 1970s). This is due to the commonality of mission requirements and orbit geometry. In 1997, NASA introduced an online spacecraft catalog to apply the COTS (Commercial Off-The-Shelf) concept approach also to its science missions. RSDO (Rapid Spacecraft Development Office) at NASA/GSFC.

865) M. N. Sweeting, “Why Satellites are Scaling Down,” *Space Technology International*, 1991, pp. 55–59 (the journal was generally referred to as “Space Technology” which has since been discontinued)

866) <http://rsdo.gsfc.nasa.gov/>

Organiza- tion	S/C Bus	Mission
NASA	TIROS/POES series spacecraft (built by LMMS) Nimbus series spacecraft (built by GE Astro Space) Landsat series spacecraft (built by LMMS) GOES D–H series spacecraft (built by Boeing) GOES I–M series spacecraft (built by SS/L) GOES N–Q series spacecraft (BSS, 601 platform) GOES–R next generation MMS (Multimission Modular Satellite), Fairchild SMEX (Small Explorer Program) S/C bus SMEX–Lite	TIROS–1 (launch Apr. 1, 1960) Nimbus–1 launch Aug. 28, 1964 Landsat–1 launch July 23, 1972 GOES–4 to 7, launches 1980–1987 GOES–8 to 12, launch:1994–2001 GOES–N (launch May 24, 2006) GOES–O (launch June 27, 2009) GOES–R, launches in 2015–2030 SMM, launch Feb. 14, 1980 Landsat–4 (launch July 16, 1982) Landsat–5 (launch March 1, 1984) SAMPEX, launch July 3, 1992
DoD	DMSP weather series spacecraft (built by LMMS) More than 30 DMSP S/C have been launched so far	Block–4A series started in 1965 Block–5D3 series started in 2003
ESA	Meteosat series (built by Alcatel)) PPF (Polar Platform) bus, based on an enlarged version of the SPOT Mk2 bus AMM (Advanced Microsatellite Mission) platform PROBA minibus (Verhaert)	Meteosat–1 launch Nov. 23, 1977 Envisat, launch Mar. 1, 2002 MetOp–A, launch Oct. 19, 2006 PROBA (launch Oct. 22, 2001)
CNES Alcatel	Spot Mk1; Mk2; and Mk3 bus; Proteus (Alcatel Space), mass of 100–500 kg Spacebus–3000 (Alcatel Space), mass 2000–3400 kg, power 5–7 kW, 3–40 transponders, 15 year life Spacebus–4000 provides Hall–effect thrusters for north–south stationkeeping (NSSK)	SPOT–1–3, ERS–1/2; SPOT–4/5 Jason–1/2, CALIPSO, SMOS, CoRoT, Telecommunications (Sirius–2, Eutelsat W, Atlantic Bird–2, etc.)
SSTL (UK)	MicroBus since UoSAT–3 and –4 (launch Jan. 22, 1990); MiniBus since UoSAT–12	UoSAT–1, launch Oct. 6, 1981 UoSAT–12, launch, Apr. 21, 1999
LMMS	LM900 (Lockheed Martin Missile & Space)	Ikonos–1, l. Apr. 27, 1999 (failure) Ikonos–2, Launch Sept. 24, 1999
Spectrum Astro, Inc. USA	SA–series platforms SA–200 HP (Spectrum Astro–200 High Performance)	MSTI–1 to –3, (1992 to 1996) DS1 (launch Oct. 24, 1998) Coriolis (launch Jan. 6, 2003) Swift (launch Nov. 20, 2004)
OSC (Orbital Space Cor- poration)	MicroStar platform (payloads up to 68 kg), mission life between 3–5 years LeoStar (payloads up to 360 kg) LeoStar–2 (payloads up to 210 kg)	OrbView–1 (Microlab), Apr. 3, 1995 QuikTOMS (failure of Taurus launcher Sept. 21, 2001) TSX–5 (Jun. 6, 2000), Orbview–3 (Jun. 26, 2003), 5 STEP missions OrbView–4, SORCE (Jan. 25, 2003)
Astrium GmbH Germany	1) Flexbus (minisatellite bus); S/C mass of 100–1000 kg, power of 150–1000 W average 2) MiniFlex bus, S/C mass of 80–250 kg	CHAMP, launch July 15, 2000 GRACE, launch Mar. 17, 2002
EADS As- trium SAS France	Eurostar 2000; S/C mass of 1200–1900 kg, GEO LEOSTAR–200 and –500 bus for LEO orbits Eurostar 3000: S/C mass of 4000–6000 kg, GEO	Nilesat, Asiasat, Ameristar, etc. ROCSat–2 (launch May 20, 2004) Pleiades of CNES (launch 2011) W3A of Eutelsat (launch Mar.16. 2004) is first in this series
EADS Astrium	AstroBus (successor of Flexbus and LEOSTAR due to industrial merger) AstroSat–100, a microsat bus of Myriade heritage AstroSat–500, a minisat bus AstroSat–1000,	TerraSAR–X (launch June 15, 2007) AlSat–2A (launch July 12, 2010) THEOS (launch Oct. 1, 2008)
TRW	T–300 bus series (graphite epoxy bus). The bus provides a low–jitter, precision–pointing and long–term perspective	GeoLITE (T–310), launch May 18, 01 Aqua (T–330), launch May 4, 2002 Aura (T–330), launch July 15, 2004

Organization	S/C Bus	Mission
ASI	1) PRIMA (Reconfigurable Italian Platform for Multiple Applications) of Alenia Aerospazio. Support of payload masses up to 1000 kg 2) MITA (Minisatellite for Advanced Technology) of Carlo Gavazzi Space.	RADARSAT-2, launch Dec. 14, 2007 COSMO/SkyMed (1: June 8, 2007) MITA S/C launch Jul. 15, 2000 AGILE (launch Apr. 23, 2007)
Stanford University	SQUIRT (Satellite Quick Research Testbed)	ORION, planned launch in 2001
CNES	Myriade microsatellite bus for missions of <120 kg, built by Latécoère of Toulouse, mission life of 3 years	DEMETER (launch Jun. 29, 2004), PARASOL (launch Dec. 18, 2004) Picard (launch June 15, 2010), and Microscope (launch in 2012/13)
BATC Ball Boulder, CO	BCP (Ball Commercial Platform) 2000 bus; average power supply of 730 W	QuikSCAT (launch Jun. 19, 1999) QuickBird-2 (launch Oct. 18, 2001) ICESat (launch Jan. 13, 2003) CloudSat (launch Apr. 28, 2006) NPP (launch Oct. 28, 2010)
SSC Sweden	Astrid-microbus; mass of 10-100 kg,	Astrid-1 (launch Jan. 24, 1995) Astrid-2 (launch Dec. 10, 1998)
DERA/ QinetiQ, UK	STRV (Space Technology Research Vehicle) microbus,	STRV-1a/b (launch Jun. 17, 1994) STRV-1c/d (launch Nov. 16, 2000)
EADS+ Thales Alenia Space	AlphaBus a new generation European multi-purpose bus for large communication satellites (15-18 kW, 5.5-8.8 tons); up to 190 transponders; the Alphabus program is supported by ESA and CNES	AlphaSat of Inmarsat is the S/C using the Alphabus proto-flight platform (launch July 25, 2013) with the advanced L-band payload and ESA technology demonstration payloads
SSTL, Surrey, UK	MicroSat-70 bus Utilized for missions between 50-70 kg total mass	UoSAT-3/-4 (launch Jan. 22, 1990) UoSAT-5 (launch July 17, 1991) S89/T, KitSat-1 (1. Aug. 10, 1992) KitSat-2, PoSat-1, HealthSat-2 (1. Sept. 26, 1993) CERISE (launch July 7, 1995) FASat (launch Aug. 31, 1995) Clementine (launch Dec. 3, 1999) PICOSat (launch Jan. 27, 2000) Tsinghua-1 (launch June 28, 2000) TiungSat-1 (launch Sept. 26, 2000)
SSTL Surrey, UK	MicroSat-100 bus (enhanced microsatellite bus) Utilized for missions between 70-130 kg total mass	AlSat-1 (launch Nov. 28, 2002) BilSat-1, NigeriaSat-1, UK-DMC (launch Sept. 27, 2003)
	MicroSat-150 bus (enhanced microsatellite bus)	TopSat (launch Oct. 27, 2005) Beijing-1 (launch Oct. 27, 2005) CFESat (launch March 9, 2007) RapidEye (launch Aug. 29, 2008)
SSTL Surrey, UK	MiniSat-400 bus Utilized for missions up to 400 kg total mass	UoSAT-12 (launch April 21, 1999)
SSTL Surrey, UK	GMP (Geo Minisatellite Platform) bus (400-500 kg), deployable solar arrays, up to 1 kW power, and up to 110 kg payload mass. Utilized for GEO (and MEO) missions	GIOVE-A (launch Dec. 28 2005), EarthSHINE (UK, 2009)
SpaceDev	MMB-100 (Modular Microsat Bus), up to 100 kg	

Organization	S/C Bus	Mission
CAST, Beijing built by DFH (a spin-off company of CAST)	CAST968 (China Academy of Space Technology) minisatellite bus (payload capacity of 200–300 kg)	SJ–5 (launch May 10, 1999) HY–1A (launch May 15, 2002) DSP (launches in 2003 and 2004) HY–1B (launch (April 11, 2007))
	CAST2000, second generation minisatellite bus for payload capacity of 200–400 kg	TS–2 (launch Nov. 18, 2004) HJ–1 Constellation (launch Sept. 5, 2008 of HJ–1A and –1B)
	CAST minibus for payloads of 50–120 kg	
	DFH–3, a 2nd generation bus for communication satellites in GEO	DFH–3 FM1 (launch Nov. 29, 1994) DFH–3 ChinaSat–22 (launch Jan. 26, 2000) DFH–3 bus for Chang’e lunar mission in 2007
ISRO	SSB (Small Satellite Bus), 2 versions are introduced – SSB for a microsatellite (max mass of 100 kg) – SSB for a minisatellite (max mass of 450 kg)	IMS–1 (launch April 28, 2008) SARAL (Launch Fe. 25, 2013)

Table 47: Introduction of some spacecraft bus/platform designs

A very special AstroBus configuration is the so-called **Snapdragon**, a deployable bus of EADS Astrium Ltd., Portsmouth, UK, developed under ESA contract. The design of Snapdragon resulted from the requirement to fly rather large structures, like an L–band SAR antenna, and to accommodate this payload structure elegantly into the available space of a launch vehicle fairing (the smaller the launch vehicle, the lower the launch cost).⁸⁶⁷⁾ In Snapdragon, the accommodation problem was approached from the payload’s point of view. It resulted in a series of “diametric” SAR accommodations, meaning that the SAR antenna is stowed (two hinged halves) across the diameter of the launcher fairing. The basic snapdragon configuration features two similar structural assemblies to either side of the diameter of the launcher payload fairing. A single central deployment mechanism is placed at the foldline between the two halves of the spacecraft, with the rotation axis in the separation plane of the launcher–satellite interface. A series of HRMs (Hold–down and Release Mechanism) up each side of the S/C ensures structural integrity during launch. Thus, the Snapdragon concept represents essentially a re–packaging of existing hardware into a new structure. Several design variations make the Snapdragon concept very attractive for a number of potential applications with a range of options (not only for large structures) in Earth observation as well as in communication payloads. For instance, the Snapdragon concept is capable to support other missions than SAR. It can carry a large optical telescope simultaneously with radar, multi–frequency radars; and when fitted with fixed arrays and a control–moment gyro it can be very agile having a deployed S/C stiffness > 10 Hz. Snapdragon configurations may also be used for large communication antennas as well as antenna farms. A hinge removal provides the option of flying two similar spacecraft.

Platform	Mission	Comments
SPAS–1 (Shuttle Pallet Satellite)	STS–7, June 18–24, 1983 STS–41B, Feb. 3–11, 1984	MOMS–01 imaging instrument of DLR (MOMS–01 and SPAS–1 built by MBB, Munich)
LDEF (Long Duration Exposure Facility)	STS–41–C, Apr. 6, 1984	NASA/LaRC free–flying S/C. Retrieval of LDEF on STS–32, Jan. 12, 1990
SPARTAN–1 (Shuttle Pointed Autonomous Research Tool for Astronomy)	STS–51G, Jun. 17–24, 1985	NASA free–flyer platform
SPARTAN–Halley	STS–51–L, Jan. 28, 1986	Challenger accident
SPAS–II	STS–39, Ap. 28 – May 6, ’91	DoD payload

867) D. M. Simpson, “The Snapdragon Family,” Proceedings of the European Conference on Spacecraft Structure, Materials & Mechanical Testing, ESA/ESTEC, Noordwijk, The Netherlands, Nov. 29 – Dec. 1, 2000, pp.337–344

Platform	Mission	Comments
EURECA-1 (European Retrievable Carrier)	STS-46, Jul. 31, 1992	ESA platform. Retrieval during STS-57 mission, June 21-July 1, 1993
SPARTAN-201-1	STS-56, Apr. 8-17, 1993	Solar physics mission
ORFEUS-SPAS-1	STS-51, Sept. 12-22, 1993	ORFEUS-1 is a DARA/NASA science mission
SPARTAN-201-2	STS-64, Sept. 9-20, 1994	Solar physics mission coordinated with Ulysses south polar pass
CRISTA-SPAS-1	STS-66, Nov. 3-14, 1994	Joint flight of CRISTA-1 and ATLAS-3 mission
SPARTAN-204	STS-63, Feb. 3-11, 1995	
SPARTAN-201-3	STS-69, Sept. 7-18, 1995	Solar physics mission coordinated with Ulysses north polar pass
SPARTAN-206	STS-72, Jan. 11-20, 1996	Also retrieval of SFU (Space Flyer Unit)
SPARTAN-207	STS-77, May 19-29, 1996	Inflatable Antenna Experiment (IAE)
ORFEUS-SPAS-2	STS-80, Nov. 19, Dec. 7, 96	ORFEUS-2 is a DARA/NASA science mission
CRISTA-SPAS-2	STS-85, Aug. 7-19, 1997	Reflight of CRISTA-1 mission
SPARTAN-201-4	STS-87, Nov. 19-Dec. 7, 97	Solar physics mission coordinated with SOHO
SPARTAN-201--5	STS-95, Oct. 29 Nov. , 98	Solar physics mission coordinated with SOHO

Table 48: Chronology of retrievable free-flyer structures on Shuttle missions

- Reusable space platforms. Flown on Shuttle flights as free-flyer structures for experiments/payloads with special requirements, and offering a number of service functions for operational autonomy. SPAS-1 (Shuttle Pallet Satellite) on STS-7 initiated the free-flyer scenario.
- Large-diameter antenna deployment mechanism for GEO communication satellites. The new technology features a springback antenna design, developed by Hughes Space & Communications Company, now BSS (Boeing Satellite Systems) of El Segundo, CA. The springback design employs flexible graphite mesh antenna reflectors. The unique design not only provides a lightweight antenna, it also takes advantage of normally unused space in the top of the rocket fairing – instead of being folded against the spacecraft body for launch as conventional antennas are.
 - The communication satellite MSAT-1 (Mobile Satellite System) of TMI Communications & Company Ltd. of Ottawa and of AMSC (American Mobile Satellite Corporation), with an antenna pair of 6.8 m by 5.25 m (elliptical shape), was the first spacecraft to demonstrate this technology (launch of MSAT-1 on Apr. 20, 1996).
 - The TDRS-H, -I, and -J spacecraft of NASA with a pair of 4.8 m diameter flexible mesh antennas employ the same technology (since 1983). The reflectors fold up for launch, then spring back into their original cupped circular shape on orbit. The springback antennas are equipped with a mechanism to allow for on-orbit contour adjustments. It's a cheaper, lighter (mass of 20 kg), better design and costs 1/10 as much as a conventional large antenna. TDRS-H was launched June 30, 2000; TDRS-I was launched March 8, 2002. Note: The successful demonstration of the springback antenna technology was so convincing to NASA to cause a switch in the TDRS (Tracking and Data Relay Satellite System) spacecraft series contract award from TRW to BSS.
 - In March 2004, a **12 m diameter furlable mesh antenna** (lightweight deployable reflector) with a mass of only 85 kg was successfully deployed in space on Japan's MBSAT (Mobile Broadcasting Corporation Satellite).⁸⁶⁸ The communication satellite in GEO, built by SS/L (1300 S/C bus), was launched on March 13, 2004 from Cape Canaveral, FLA. The reflector, referred to as AstroMeshTM reflector and developed by Northrop Grumman's As-

⁸⁶⁸) <http://www.st.northropgrumman.com/astro-aerospace/SiteFiles/docs/news/news2004-0329.pdf>

tro Aerospace unit in Carpinteria, CA, is a very large aperture antenna of its kind. AstroMesh reflectors, which come in 6 m and 12 m designs, are made of a graphite composite tube truss structure that unfolds from a cylindrical stowed shape. The Thuraya-1 communication satellite of UAE (United Arab Emirates), built by BSS and launched in Oct. 2000, features also a 12 m AstroMesh antenna in L-band.⁸⁶⁹⁾

MBSAT enables MBCO (Mobile Broadcasting Corp. of Japan) and SKT (SK Telecom of Korea) to provide pioneering digital multimedia broadcasting information services such as high CD-quality audio, MPEG-4 video and data to mobile users throughout Japan and Korea who are equipped with receivers in cars, ships, trains, handheld terminals, cellular phones and home portables. The AstroMesh reflector is a key component of the MBSAT's antenna systems, reflecting S-band radio frequency energy and focusing it into a pattern on the ground. — *Obviously, the same large-aperture technology concept (with accurate surfaces and shape) may also be used in future EO missions in support of L-band radiometry, featuring for instance an array of MMIC (Microwave Monolithic Integrated Circuit) receivers in a push-broom configuration.*⁸⁷⁰⁾

- In the USA, new procurement strategies were introduced in the late 1990s with the projects GFO (GEOSAT Follow-On), NPOESS (National Polar-orbiting Operational Environmental Satellite System), LDCM (Landsat Data Continuity Mission), GOES-R, etc. The approach for these projects specifies performance objectives and goals, and requires a data specification of the parameters in the end products (their quality and quantity), rather than a traditional system (i.e., satellite and payload) specification. In this concept, the design of the system is left to the contractor (fostering of creativity and reduction of costs).

- MFS (Multifunctional Structures) technology reduces spaceborne electronics size and mass with improved packing techniques. In the mid-1990s, an MFS development program initiative was launched by AFRL (Air Force Research Laboratory) and by BMDO (Ballistic Missile Defense Office) to reduce spacecraft mass and volume (to reduce launch costs). Lockheed Martin Astronautics Corp. (LMA) of Denver, CO, was given a contract to provide an innovative and enabling MFS design approach (eliminating “black boxes”, lots of cabling, harness, bulky connectors, etc.) by integrating spacecraft electronics, structural, and thermal control functions into a single structure. The MFS concept involved embedding passive-electronic components within the actual volume of composite materials, new approaches to attaching active-electronic components directly to mechanical surfaces, using surface areas for mounting sensors and transducers. This new packaging technology development reduced spacecraft mass and volume considerably.

The first MFS technology demonstration was flown on the STEX (Space Technology Experiment) mission of NRO (launch Oct. 3, 1998). Other missions followed like: DS1 (Deep Space 1, launch Oct. 24, 1998) of NASA, EO-1 (Earth Observing, launch Nov. 21, 2000) of NASA, and the STRV-1d (Space Technology Research Vehicle-1d, launch Nov. 16, 2000) mission of DERA, UK. MFS is now a proven and accepted technology used in virtually all space missions.⁸⁷¹⁾

1.8.2.2 Introduction of COTS parts in spacecraft

Introduction of COTS (Commercial Off-The-Shelf) and PEMs (Plastic Encapsulated Microcircuits) electronic products as well as software products into spacecraft subsystems. For instance, in 1979 a group of radio amateurs and academics at the University of Surrey (4 staff and 8 part-time academics) designed and built a 50 kg satellite using COTS microprocessors (i.e. consumer products). With this implementation the concept of the modern mi-

869) M. Suenaga, R. J. Prevaux, “MBSAT – A Direct Broadcast Satellite for Mobile Users in Japan and Korea,” Proceedings of IAC 2004, Vancouver, Canada, Oct. 4–8, 2004, IAF-04–M.1.01

870) N. Skou, “Spaceborne L-band Radiometers: Push-broom or Synthetic Aperture?” Proceedings of IGARSS 2004, Anchorage, AK, USA, Sept. 20–24, 2004

871) D. M. Barnett, S. Rawal, K. Rummel, “Multifunctional Structures for Advanced Spacecraft,” Journal of Spacecraft and Rockets, Vol. 38, No 2, March–April, 2001, pp. 226–230

cosatellite was born. UoSAT-1 was launched Oct. 6, 1981 pioneering the way for a highly successful series of microsattellites. Since then SSTL (Surrey Satellite Technology Ltd) and the University of Surrey (Surrey, UK) has pioneered the use of COTS products like the commercial GPS technology for spaceborne applications. The PoSAT-1 mission, launched Sept. 26, 1993, was the first microsattellite to make use of a commercial GPS receiver in orbit (Trimble TANS-II receiver). COTS products are normally part of technology-class (and university) missions with emphasis on technology demonstrations, and not on the provision of long-duration support services. At the start of the 21st century, an ever increasing proportion of COTS and PEM products are being integrated into all types of spacecraft, including some military service (communications) missions.

Examples of EO missions: a) Jason-1 (launch Dec. 7, 2001) employs as much as possible electronic parts of commercial or military standard as opposed to the usual space standard; b) the GRACE twin S/C mission of 1.8.7NASA/DLR (launch March 17, 2002) contains about 80% of COTS products. About 5-6 years ago, a similar mission would have used only about 10% of COTS products. The demand of cheaper and affordable missions is the main reason for COTS products in S/C. Space-qualified products are extremely expensive due to the relatively small electronics space market and the long waiting periods for test opportunities (space products account only about 0.5% of the semiconductor market).^{872) 873)}

COTS hardware products are generally not specifically radiation-hardened, or they may lack stiffness for the launch phase, or they do not provide a suitable temperature range for proper operation in a hostile space environment. The performance of COTS products with regard to processing power, etc., is generally always superior to space-qualified products, due to the availability to most recent developments in the electronics field. However, when reliability and long-term provision of service is the decisive mission criteria, then the space-qualified option might turn out to be the best choice. The amount of risk a mission can take on and the available budget dictate generally the percentage of COTS parts.

- Comparison of two computer systems on a spacecraft with regard to radiation hardness performance. The ARGOS (Advanced Research and Global Observation Satellite) mission of DoD (launch Feb. 23. 1999, see M.3) provides the first direct on-orbit comparison of a modern radiation hardened 32 bit processor (RH3000 of Harris) with a similar COTS processor (IDT-3081, a single chip implementation of the MIPS RISC architecture). An ECC (Error Correction Code) software technique was implemented with the IDT-3081 processor for autonomously correcting errant bit patterns for mass storage and communication devices.^{874) 875)} The investigation was motivated by the continuing need for higher capability computers for spaceflight use than can be met with currently available radiation hardened components. The comparison test was conducted within the USA (Unconventional Stellar Aspect) experiment of NRL and ASCAT (Advanced Space Computing and Autonomy Testbed), both part of the ARGOS payload. Both systems featured a package, referred to as SIHFT (Software-Implemented Hardware Fault Tolerance), providing corrections for radiation-induced SEUs (Single Event Upset) and for the purpose of performance analysis. The comparison test demonstrated that even though the RH3000 board uses radiation-hardened technology, the test applications showed a small non-vanishing number of errors occurring over time. The memory test collected 7 errors over 543 days of

872) M. Unwin, R. Myatt, S. Gleason, "The Use of Commercial GPS Technology in Space," NAVITEC 2001, 1st Workshop on Satellite Navigation User Equipment Technologies, Dec. 10-12, 2001, ESA/ESTEC, Noordwijk, The Netherlands

873) S. Magnuson, "Satellite Builders Face Shortage of Proven Electronics," Space News, Mar. 4, 2002, p. 22 (Magnuson is reporting from the 6th Annual International CMSE Conference: Commercialization of Military and Space Electronics Conference & Exhibition, Feb. 11-14, 2002, Los Angeles, CA)

874) M. N. Lovellette, K. S. Wood, D. L. Wood, J. H. Beall, P. P. Shirvani, N. Oh, E. J. McCluskey, "Strategies for Fault-Tolerant, Space-Based Computing: Lessons Learned from the ARGOS Testbed," Proceedings of IEEE Aerospace Conference, Big Sky, MT, March 9-16, 2002

875) M. N. Lovellette, A. Campbell, K. Clark, K. S. Wood, D. L. Wood, A. Ross, J. H. Beall, G. Clifford, "Implications of the Different Classes of Exceptions Experienced During the COTS Processor Test Flight on the ARGOS Satellite," Proceedings of IEEE Aerospace Conference, Big Sky, MT, March 8-15, 2003

actual run time, resulting in an error rate of 3.1×10^{-9} errors/bit–day. While this low rate reflects the memory technology in use, it is higher than the $< 1 \times 10^{-10}$ rate expected for the board.

During the same time period the various IDT–3081 tests of the COTS board produced a total of more than 2000 SEUs detected and more than 50 task exceptions and reboots. The overall error rate is 6.4×10^{-7} errors/bit–day. The performance of the IDT–3081 demonstrates that it is possible to increase the reliability of a COTS system operating in the space environment. This is illustrated by the improvement in the reliability provided by the ECC routines. The error detection and correction software techniques are not able to correct all errors on the IDT–3081 board, resulting in more crashes than the RH3000 board experienced.

- MDS–1 (Mission Demonstration Satellite–1, referred to as Tsubasa) of JAXA (formerly NASDA) in GTO (Geosynchronous Transfer Orbit) with a launch Feb. 4, 2002. The objectives were to verify the use of commercial parts in orbit (COTS components), to verify minimization technology for components, and to collect space environment data (e.g., radiation on equipment, etc.).⁸⁷⁶⁾ One of the onboard COTS devices was SSR (Solid State Recorder) of NEC Toshiba Space Systems Ltd., a high–density semiconductor device (32 Gbit capacity for mission data, 64 Mbit DRAM, EDAC, etc.). An analysis was performed after one year of spacecraft operations on a number of parameters, including SEU (Single Event Upsets) and TID (Total Ionizing Dose). The SSR operational performance was trouble–free (no minor/major failure on stack memory module of SSR). EDAC performance was confirmed (all SEU bit errors were corrected). Operations of MDS–1 were terminated on Sept. 27, 2003 by JAXA.
- SERVIS–1 (Space Environment Reliability Verification Integrated System–1) is a Japanese mission (launch Oct. 30, 2003) with the objective to develop technologies for the use of COTS parts under space environment conditions (establishment of COTS evaluation guidelines and equipment design guidelines to utilize COTS).⁸⁷⁷⁾ The goal is to find solutions for cheaper spacecraft design and development. The SERVIS program of METI (formerly MITI) started in 1999 and is project until 2007. It includes two technology verification spacecraft with launches in 2003 and 2005.

It should be understood, however, that new and more capable onboard components can only be developed and introduced (cost–effectively) by using commercial standards in a **open architecture environment**, all of which are COTS products. This approach is for instance being taken by the selection of new onboard data bus systems (see 1.8.7). New bus examples are: CAN (Controller Area Network); FireWire (IEEE 1394a–2000), and SpaceWire (IEEE 1355–1995). See 1.8.7.

1.8.2.3 Satellite structure vibration/jitter damping

The operation of cryocoolers, needed for the cooling of detectors in the infrared region (to lower the thermal noise threshold), as well as attitude actuators (momentum wheels, power thrusters, etc.) introduce unwanted **micro–vibrations** into the satellite structure which in turn degrade the quality of instrument measurements. – Examples of experiments involving vibration damping are:

- The STRV–1b satellite of DERA (launch June 17, 1994, see M.47.1.2) is flying CVSE (Cryocooler Vibration Suppression Experiment), provided by BMDO and JPL, to demonstrate a new vibration suppression design by employing piezoelectric actuators.

876) T. Sasada, S. Ichikawa, “Application of Solid State Recorders to Spacecraft,” Proceedings of IAC, Bremen, Germany, Sept. 29 – Oct. 3, 2003

877) http://www.usef.or.jp/english/f3_project/servis/f3_servis.html

- The NASA/JPL CSE (Cryo System Experiment) demonstrated vibration suppression on Shuttle flight STS–63 (Feb. 3–11, 1995) in the launch phase and on–orbit by using the Hughes–built ISSC (Improved Standard Spacecraft Cryocooler) Stirling cooler and an experimental diode oxygen heat pipe.
- The TSX–5 mission of AFRL (launch June 6, 2000) carries VISS (Vibration, Isolation, Suppression and Steering System), a self–contained precision vibration control device designed to provide an ultra–quiet environment for sensitive optical sensors, laser transmitters, and other detection and measurement devices (M.55).
- SAMS–II (Space Acceleration Measurement System II) of NASA/GRC was delivered to ISS by STS–100 (Apr. 19– May 1, 2001). The objective is to detect the vibration environment present while the space station is in operation (crew and equipment). SAMS–II has a distributed architecture with multiple locations throughout the US Laboratory Module Destiny. SAMS–II uses small remote triaxial sensor systems that are placed directly next to experiments in various locations throughout the module. MAMS–II (Microgravity Acceleration Measurement System) is complementary to SAMS–II measuring accelerations caused by aerodynamic drag and by ISS roll movements (MAMS–II was also delivered on STS–100).
- SUITE (Satellite Ultraquiet Isolation Technology Experiment), a hybrid vibration isolation system of AFRL is flown on PICOSat (launch Sept. 30, 2001), a microsatellite of the USAF Space Test Program (STP). SUITE employs piezoelectric rather than electromagnetic actuators. The active portion of the system reduces vibration transmission at low frequencies and the passive portion attenuates high frequency inputs.
- ARIS (Active Rack Isolation System) of NASA/MSFC/JSC, developed by the Boeing Co., Seattle, WA. ARIS was installed in EXPRESS (EXpedite the PROcessing of Experiments to the Space Station) Rack No. 2, a standardized payload rack on ISS. Objective: monitoring of on–orbit vibration reduction during a variety of station activities, including crew sleep/wake periods, operation of SSRMS (Space Station Remote Manipulator System), etc. – the goal is to attenuate external vibration disturbances at selected payload locations. ARIS uses a combination of sensors and actuators to achieve vibration damping. Among these are accelerometer assemblies that measure vibration disturbances and send data to the ARIS electronic unit; pushrods that apply force against the framework of ISS; and a microgravity rack barrier that prevents accidental disturbance of the active ARIS rack. – ARIS–ICE (ARIS–ISS Characterization Experiment) is a separate payload created to characterize the on–orbit performance of ARIS. ARIS–ICE works in concert with SAMS–II and MAMS–II to characterize the range of vibrations onboard the Station. ARIS was flown to ISS on STS–100 (Apr. 19–May 1, 2001) and set up during the week of May 25, 2001. ICE was activated on June 12, 2001. The ARIS system became “operational” on ISS in April 2002. ICE was returned to Earth on STS 111 (June 5 – 15, 2002). A prototype of the ARIS system was already tested during the Shuttle STS–79 mission (Sept. 16–26, 1996) during which the Shuttle docked with the Russian space station MIR.
- The JAXA spacecraft OICETS (Optical Inter–orbit Communications Engineering Test Satellite) with a launch on Aug. 23, 2005 is carrying MVE (Micro–Vibration Measurement Equipment) to sense the vibration environment of the spacecraft.
- Control–Structure Interaction (CSI) in space vehicles. Structural vibration (jitter) and structural dynamics issues are the cause of many difficulties in spaceborne structures. CSI occurs when control detrimentally interacts with flexibility in the system. The space programs of the USA and Russia have a history of problems related to CSI, which have ranged from degrading spacecraft performance to causing catastrophic loss of the system. The US MACE program (long–term collaboration effort of AFRL and NASA) explores CSI as a means for controlling rather than avoiding flexibility in space systems (in particular with regard to ISS), thereby penetrating this artificial performance barrier. The MACE (Middeck

Active Control Experiment) program and its predecessor, MODE (Middeck 0–Gravity Dynamics Experiment), were designed to investigate the modeling and control issues related to high–precision pointing and vibration control of future space systems.

- MODE (Middeck 0–Gravity Dynamics Experiment), of the DoD STP program developed by MIT/SSL (Space Systems Laboratory); the MODE experiments were conducted on three Shuttle flights [STS–40 (Jun. 5–14, 1991), STS–48 (Sept. 12–18, 1991), and STS–62 (Mar. 4–18, 1994), respectively]. The objectives of MODE were to study suspension and gravity influences on the structural dynamics of a modular truss system by comparing the measured response in ground and orbital tests and to quantify the suspension and gravity induced perturbations using analytical models of the suspension and nonlinear effects (characterize fluid slosh, Space Station structure behavior, and crew motion dynamics in zero gravity).

- MACE (Middeck Active Control Experiment) flown on Shuttle (STS–67, March 2–18, 1995) for AFRL (developed by MIT). MACE consisted of three components: a multibody platform, experiment support module, and the handheld terminal. MACE, on STS–67, reduced vibration up to 19 dB and achieved a 25 Hz bandwidth of control (using a 50 Hz bandwidth disturbance).

- MACE–II (Middeck Active Control Experiment) is a follow–up experiment to the original MACE flight (MACE–II is sponsored and managed by AFRL and supported by two science teams, led by MIT and by the University of Michigan). The overall objective is use adaptive control algorithms for precision structural control. MACE–II is a significant step **toward spacecraft autonomy**; it consists of a hardware/software package that independently learns to **control motion–dampening technologies and suppress unwanted vibrations**. The first on–orbit demonstration of MACE–II took place on ISS (MACE–II was carried on STS–106 (Atlantis, Sept. 8 – 20, 2000) to ISS. ⁸⁷⁸⁾ ⁸⁷⁹⁾

The MACE–II unit was returned to Earth on STS–105 Aug. 10–22, 2001), successfully completing all its experiment objectives while on Station (adaptive vibration control). MACE II relies on algorithms that enable it to adapt to changing conditions and correct problems without using a ground controller to exchange messages with the space shuttle. This technology, known as frequency domain expert control, is an advancement beyond MACE I, which was able to test and fix gained controls but unable to adapt to unforeseen changes or detect faults and failures in the hardware and technology. The MACE–II is a device of 1.5 m in length that floats free in a pressurized compartment. The unit has gimbals at each end and reaction wheels in the middle. One gimbal creates vibrations, which are detected and counteracted through complex computer algorithms, keeping the other end steady. Most important, these algorithms can modify themselves or “adapt” when they sense changes in the characteristics of the system – without human intervention.

- European scientific space missions (e.g. GOCE, Swarm, Herschel, and Microscope) require the absence of micro–vibrations to a challenging extent, since the experiments on–board include highly sensitive accelerometers to probe gravitational effects or cutting edge optical instruments delivering observations in an unprecedented accuracy. – The stringent micro–vibration requirement leads to a specific spacecraft design which is reducing any potential source of vibration perturbation and is shifting the spacecraft’s eigenmodes to higher frequency compared to previously used designs. Accordingly, the design process and the qu-

878) Note: The essence of MACE–II is that it creates the necessary control instructions “on the fly” to counteract unwanted disturbances without any input from a human being. These vibration control algorithms use embedded sensors and actuators to identify and counteract movement, all without requiring extensive modeling or ground testing. The algorithms can also adapt to changes in a structure caused by temperature fluctuations, moving parts, or the normal degradation of mechanical subsystems. Such autonomy is precisely the requirement aerospace engineers have in mind for spacecraft of the future.

879) R. R. Ninneman, “Middeck Active Control Experiment Reflight (MACE–II) Program: Lessons Learned,” Proceedings of AIAA Space 2000 Conference and Exposition, Long Beach, CA, Sept. 19–21, 2000

alification of such spacecrafts and their subsystems require adopted analysis and onground experiments. ⁸⁸⁰⁾

In the GOCE project, the investigation on the optimal multi-layer insulation design with respect to micro-vibration resulted in the initiative to set-up a specific test bench for the characterization of this potential cause of micro-vibrations. To measure gravity effects precisely, the spacecraft was built without any moving parts such that the entire satellite is actually one extremely sensitive measuring device.

1.8.3 Fractionated satellite systems – the dawn of distributed space architectures

The traditional approach for designing a spacecraft relies on a monolithic architecture requiring mass and cost minimization. In general, a mission is defined and the technology selected several years before the satellite is operational. Once launched, the flexibility will stay in the design margin, on-board redundancies and software uploading. – The conventional approach of space system development is the key to escalating costs and program delays. As complexity grows, so does the system size, cost, and schedule. A radical change is needed.

In the timeframe 2005/6, Owen Brown and Paul Eremenko were investigating for the US DARPA (Defense Advanced Research Projects Agency) the deeper meaning and the nature of “*responsive space*”, a buzzword that had been used in DOD for several years – implying an ability to quickly develop and launch orbital payloads. However, they disagreed with this view and provided the following definition: ^{881) 882)}

Responsive space is the capability of space systems to respond rapidly to uncertainty.

This broadens the solution space; it permits us to consider alternate – and undoubtedly complementary – means of enabling responsiveness across a wide range of systems, large and small.

As a consequence of this broader notion of responsiveness to uncertainties, a new concept of a satellite architecture was introduced, termed “**fractionated spacecraft.**” This approach to spacecraft design promises to affect responsiveness not just by shrinking spacecraft development timelines and enabling launch with smaller, more tactical vehicles, but also by making the spacecraft architecture fundamentally flexible and robust.

In their first paper to formally define the concept (Ref. 881), the fractionated spacecraft is described as: “*The decomposition of the system into distinct free flying modules, which once ‘assembled’ in orbit deliver the capability of the original monolithic system.*” Wireless connections are used to link the modules or nodes, instead of physical ones. The types of connections could include data connections (including those exchanging attitude and position information), the transmission of power and even the sharing of forces and torques.

The main driver for fractionating a system is flexibility of the system; to increase its ability to deal with both technical and programmatic uncertainty, from the initial concept design phases through to the end of the functional life of the satellite. – Unlike constellations or formations, the generalized concept of it is to break a large monolithic spacecraft into smal-

880) Anton Grillenbeck, Georg Deutsch, Aleander Klier, “Micro-Vibration Measurements on Thermally Loaded Multi-Layer Insulation,” Proceedings of the 61st IAC (International Astronautical Congress), Prague, Czech Republic, Sept. 27–Oct. 1, 2010, IAC–10.C2.3.2

881) Owen Brown, Paul. Eremenko, “Fractionated Space Architectures: A Vision for Responsive Space,” AIAA 4th Responsive Space Conference, Los Angeles, CA, USA, April 24–27., 2006, paper: RS4–2006–1002, URL: http://www.responsivespace.com/Papers/RS4/Papers/RS4_1002P_Eremenko.pdf

882) Owen Brown, Paul. Eremenko, “The Value Proposition for Fractionated Space Architectures,” Space 2006, San Jose, Ca, USA, Sept. 19–21, 2006, paper: AIAA–2006–7506, URL: <http://www.darpa.mil/tto/programs/systemf6/Papers/AIAA–2006–7506.pdf>

ler heterogeneous modules, which perform distinct functions and interact through wireless communication links.

In 2007, DARPA began the study of the “fractionated architecture” concept in an initiative entitled: **System F6** (Future Fast, Flexible, Fractionated, Free—Flying Spacecraft united by Information eXchange).⁸⁸³⁾

The System F6 program will demonstrate the feasibility and benefits of a satellite architecture wherein the functionality of a traditional “monolithic” spacecraft is delivered by a cluster of wirelessly—interconnected modules capable of sharing their resources and utilizing resources found elsewhere in the cluster. Such an architecture enhances the adaptability and survivability of space systems, while shortening development timelines and reducing the barrier—to—entry for participation in the national security space industry. The program is predicated on the development of open interface standards—from the physical wireless link layer through the network protocol stack, including the real—time resource sharing middleware and cluster flight logic—to enable the emergence of a space “global commons” which would enhance the mutual security posture of all participants through interdependence. A key program goal is the industry—wide promulgation of these open interface standards for the sustainment and development of future fractionated systems.

In July 2007, DARPA issued a broad agency announcement soliciting proposals for the development of System F6. In 2008, DARPA announced that contracts for the preliminary development phase of the System F6 program were issued to teams headed by Boeing, Lockheed Martin, Northrop Grumman, and Orbital Sciences. The second phase of the program was awarded to Orbital Sciences, along with IBM and JPL, in December 2009.⁸⁸⁴⁾

The goal of the program is to have an on—orbit demonstration in 2014–2015 of the key functional attributes of fractionated architectures. The technology objectives and program plan are driven by a small set of functional on—orbit demonstrations. Program success will be measured by the successful completion of these demonstrations, designed to prove the highest—risk elements of the architecture to potential transition partners and early adopters. The demonstrations will take place in LEO, and will be approximately six months in duration with a potential subsequent residual capability demonstration lasting up to 18 months. The functional demonstrations are as follows:

- Capability for semi—autonomous long—duration maintenance of a cluster and cluster network, and the addition and removal of spacecraft modules to/from the cluster and cluster network
- Capability to securely share resources across the cluster network with real time guarantees and among payloads or users in multiple security domains
- Capability to securely share resources across the cluster network with real time guarantees and among payloads or users in multiple security domains
- Capability to perform a semi—autonomous defensive cluster scatter and re—gather maneuver to rapidly evade a debris—like threat.

The general philosophy that underlies the technical approach and structure of the System F6 program is to arrive at the on—orbit functional demonstrations enumerated above through a disaggregated series of efforts.

By allowing the various functions of a spacecraft to be developed and launched separately, this type of “fractionated” system reduces overall program risk, provides budgetary and

883) “System F6,” URL: <http://www.darpa.mil/tto/programs/systemf6/index.html>

884) David M. LoBosco, Glen E. Cameron, Richard A. Golding, Theodore M. Wong, “The Pleiades fractionated space system architecture and the future of national security space,” AIAA SPACE 2008 Conference & Exposition, Sept. 9–11, 2008, San Diego, CA, USA, paper: AIAA 2008–7687, URL: <http://www.tmwong.org/doc/LoBosco2008–SPACE.pdf>

planning flexibility, speeds initial deployment, offers greater survivability – and allows future technologies to build on existing efforts, in order to create something totally new. ⁸⁸⁵⁾ 886) 887)

Indeed, there are many great challenges on the road to the new paradigm of distributed space architectures. – In the meantime, the concept of fractionated satellite architecture has also caught the attention of the civil space agencies, institutions, and the academic world. ⁸⁸⁸⁾ 889)

-
- 885) Jian Guo, Daan Maessen, Eberhard Gill, “Fractionated Spacecraft: The New Sprout in Distributed Space Systems,” Proceedings of the 60th International Astronautical Congress (IAC), Daejeon, Korea, October 12–16, 2009, IAC–09.D1.1.4, URL: <http://www.tudelft.nl/live/ServeBinary?id=903e0fe5–9d7b–4883–bfd8–b25b8f6174bd&binary=/doc/IAC–09%20D1%20I%20I%20I%20Fractionated%20Spacecraft%20JIAN.pdf>
- 886) Rui Sun, Jian Guo, Eberhard Gill, “Opportunities and Challenges of Wireless Sensor Networks in Space,” Proceedings of the 61st IAC (International Astronautical Congress), Prague, Czech Republic, Sept. 27–Oct. 1, 2010, IAC–10.D1.4.8
- 887) Benjamin Schwarz, Adrian R.L. Tatnall, Hugh G. Lewis, “A Fractionated Satellite Approach to Coastal Salinity Measurement,” Proceedings of the 61st IAC (International Astronautical Congress), Prague, Czech Republic, Sept. 27–Oct. 1, 2010, IAC–10.B1.2.3
- 888) Claude Cournet, Jean François Dufour, Bernard Gerber, “Fractionated Satellites: a step towards flexibility and responsiveness,” Proceedings of the 61st IAC (International Astronautical Congress), Prague, Czech Republic, Sept. 27–Oct. 1, 2010, IAC–10.D1.4.1
- 889) Shashank Tamaskar, Daniel Delaurentis, “Modular Spacecraft Architecture, a new paradigm in spacecraft design,” Proceedings of the 61st IAC (International Astronautical Congress), Prague, Czech Republic, Sept. 27–Oct. 1, 2010, IAC–10.D1.4.9

1.8.4 Some comments on launch deployment capabilities

- Launch vehicles with an upper stage re-ignition capability for payload deployment. This technology represents a cost-efficient solution providing operational/maneuverable freedom in the launch and deployment phase of satellites; a very desirable function is the deployment of multiple satellites into LEO or MEO orbits (release of S/C into various orbits). At the start of the 21st century, solutions with a re-ignition capability are increasingly being offered by the launch service providers. Some examples are:

- The Soyuz-Fregat launch vehicle of STARSEM and its Russian partners employs the Fregat upper stage with its re-ignition capability. The Cluster-2 missions of ESA [July 16, 2000 (1st launch of 2 S/C), Aug. 9, 2000 (2nd launch of 2 S/C)] were the first flights using the re-ignition capability. Once separated from the Soyuz third stage, Fregat injected the payload into a circular parking orbit with its first burn. This was followed by a coast phase in three-axis stabilized mode. The second burn of Fregat injected the payload into a highly elliptical separation orbit. – The ESA Mars Express mission (launch June 2, 2003) employed also the Soyuz-Fregat launcher configuration.

- Eurockot Launch Services (a joint venture company between Russia's Khrunichev Space Center in Moscow and Germany's EADS Astrium GmbH, Bremen) provides a multiple re-ignition capability of its Breeze-KM upper stage. The first successful multiple orbit mission took place on June 30, 2003 from Plesetsk, Russia.⁸⁹⁰ The launch involved a total of eight spacecraft from different agencies and institutions by deploying the various payloads into an elliptical as well as into a sun-synchronous orbit. Additionally a mock-up of the Russian Monitor-E satellite was mounted on Breeze (the Monitor-Experimental bus remained on the upper stage and deorbited with it according to plan). Multiple re-ignitions permitted precise sequential deployment into various orbits. The Czech Mimosa microsatellite was first deployed into an elliptical orbit (323 km x 823 km, inclination of 86.5°), while the other satellites [MOST of CSA and six CubeSats (picosatellites) of various universities] were delivered into sun-synchronous orbits at predetermined intervals.

- As of 2002, the Ariane-5V launch program offers multiple re-ignition of the current storable-propellant upper stage.

- Japan's H-II launch vehicle features a second stage with a re-ignition capability.

- The STP-1 mission of DoD (launch March 9, 2007 from Cape Canaveral, FLA) demonstrated for the first time **the deployment of multiple spacecraft (6) into two different orbital inclinations and at two different altitudes (both in LEO)**. This required a total of 3 burns for the upper stage of the Atlas-V launch vehicle. Also first time use of the ESPA (EELV Secondary Payload Adapter) ring, a low-cost concept to launch multiple secondary satellites. The introduction of these new features represents indeed new capabilities for future missions.

⁸⁹⁰ Russia (Rosaviakosmos, Khrunichev) is developing the Monitor small-size satellite family (650 – 750 kg) within the project SERSS (Space-based Earth Remote Sensing System) based on the Yakhta standardized space platform. The objective is high-resolution imagery in the optical region and eventually also in the microwave region (SAR). The Monitor-E mission (VNIR coverage) is planned for launch in 2005, followed later by the Monitor-I-1 and I-2 missions (each with VIS and TIR coverage). Monitor-S (Stereo Imaging) is planned thereafter.

1.8.5 Spacecraft power generation – solar cells, batteries, etc.

Electrical power is the prime resource for the provision of all spacecraft operations. Practically all spacecraft use the sun as a source of electrical power produced by solar arrays. Photovoltaic (PV) solar cells are the prime devices of conventional long-term electrical power provision for all Earth-orbiting satellites in LEO, GEO, HEO, MEO, etc. They convert solar radiation into electricity directly at the atomic level (by transforming photon energy into electrical energy). Their principle of operation is the same as that for photodiode light detectors. The solar energy, arriving at the top of the atmosphere, amounts to about 1.3–1.4 kW/m². This energy can be tapped by direct conversion into electricity through the use of solar cells.

Background: The energy supply from the sun is truly enormous; on average the Earth's surface receives about 1.2×10^{17} W of solar flux (representing only the tiny fraction of the sun's energy that can be intercepted by the Earth). It amounts to a specific flux of about 1366 W/m² (generally accepted value) at the top of the atmosphere (or for a S/C in LEO). This means that in less than one hour enough energy is supplied to the Earth to satisfy the entire energy demand of the human population over an entire year. Indeed, it is the energy of sunlight, assimilated by biological organisms over millions of years, that has made possible the industrial growth as we know it today. Most of the other renewable means of power generation also depend on the sun as the primary source: hydroelectric, wind and wave power all have the same origin.

Historically, solar energy generation dates back to 1839, when Alexandre Edmond Becquerel, a French physicist (1820–1891), first observed the phenomenon of the **photoelectric effect** while experimenting with an electrolytic cell containing two metal electrodes exposed to sunlight (see Glossary). The photoelectric effect or better, the “photovoltaic effect,” is the basic physical process through which a PV cell converts sunlight into electricity. In 1904, Albert Einstein published his paper on the photoelectric effect (or the release of electrons from metal when light shines on it), in 1921 he received the Nobel Prize for this theory of the photoelectric effect.

However, the process of producing electric current in a solid material using sunlight wasn't truly understood until the arrival of semiconductor technology in the 1940s. The space age, in particular, has played an important role in the development of photovoltaics – requesting ever increased power to accommodate its science instrumentation, housekeeping, communication, and attitude subsystems. Over the years, the main effort has been to increase the conversion efficiency of silicon-based semiconductor technology; another important aspect was to extend their life times (improved radiation hardness response), the end-of-life (EOL) power generation capability per unit mass (W/kg). Photovoltaic power generation is reliable, it involves no moving parts, the operation and maintenance costs are very low. The operation of a photovoltaic system is silent creating no pollution. Photovoltaic systems are modular and can be quickly installed.

The following list represents some development stations in the history of PV technology related to the topic of space applications (naturally, there are many other fields of PV applications today, including many government programs, in many countries, to foster the use of alternative energies):

- In 1883, the American inventor Charles Fritts was probably the first to build a solar cell. He used junctions formed by coating selenium (a semiconductor) with an extremely thin layer of gold – exposed to sunlight. He achieved an energy conversion efficiency of < 1%.
- In 1927, the first solar cells were made from copper and copper oxide
- In the 1930s, both the selenium cell and the copper oxide cell were being employed in light-sensitive devices, such as photometers, for use in photography. They also had conversion efficiencies of < 1%.

– 1930–1940. Neville F. Mott (British physicist, 1905–1996, Nobel Prize in Physics in 1977) and Walter H. Schottky (German physicist, 1886–1976) developed the theory of a solid–state rectifier (diode). Later referred to as “Schottky diode.”

– **In 1954, G. L. Pearson, Daryl M. Chapin, and Calvin S. Fuller of the AT&T Bell Telephone Laboratories, Murray Hill, N.J., USA were the first to demonstrate a crystalline silicon photovoltaic (PV) cell with an efficiency of about 4% (a few months later of 6%).** A patent, “Solar Energy Converting Apparatus,” was submitted in March 1954 (and officially issued in 1957). This was the first practical silicon PV cell available.⁸⁹¹⁾

– In 1957 (at the start of the space age), the Hoffman Electronics Corp. (of El Monte, CA, and Evanston, IL) achieved 8% efficiency on its PV cells. In 1960, 14% efficiency was obtained by the same company. Crystalline silicon was the original materials technology used by the PV industry.



Figure 46: Illustration of the Vanguard–1 spacecraft (image credit: NASA)

– March 17, 1958, successful launch of Vanguard–1 **with the first PV–powered solar cell system in space.** The solar cell was the backup power system of this S/C (< 1 W, approx. 100 cm², powering a 5 mW backup transmitter) and was used to power its radio, referred to as “Minitrack transmitter” which operated at frequencies of 108.0 and 108.3 MHz (VHF). Vanguard–1 was a small satellite, a magnesium sphere of 16.3 cm in diameter, < 2 kg mass; it contained two power systems for the two Minitrack transmitters: 1) a short–life battery as prime (seven mercury cell batteries in a hermetically sealed container), and 2) the solar cell system as backup consisting of six clusters of 16 silicon solar cells each. The solar cells were mounted on the surface of the sphere. Solar power, it turned out, functioned perfectly and kept Minitrack on the air for more than six years (until 1965).⁸⁹²⁾

The battery–powered prime transmitter gave up after the short battery life of a few days. The PV technology has been developing ever since. The solar cells were manufactured by the Bell Laboratories, the solar cell technology was introduced/managed on Vanguard by SRDL (Signal Research and Development Laboratory), Fort Monmouth, NJ (of the US Army Signal Corps). The Vanguard project, the first US satellite program, was managed by

891) D. M. Chapin, C. S. Fuller, G. L. Pearson, “A New Silicon p–n Junction Photocell for Converting Solar Radiation into Electrical Power,” *Journal of Applied Physics*, Vol. 25, 1954, pp. 676–677

892) <http://www.infoage.org/tac-zig23.html>

the US Navy, the S/C was built at NRL (Naval Research Laboratory), Washington DC. The orbit of Vanguard–1 was elliptical at about 750 km x 3900 km, inclination of 34.2°. The orbital life of Vanguard–1 is estimated to be 240 years.

At the 50th anniversary of its launch (March 17, 2008), Vanguard–1 happens to be the oldest surviving artificial Earth satellite. The current orbit is: 653 km x 3,839 km).⁸⁹³⁾

Background:⁸⁹⁴⁾ The first artificial satellite, Sputnik–1, carried a chemical battery (a silver–zinc accumulator – which accounted for some 38% of the spacecraft’s total mass of 83.6 kg) that provided just one watt of power. Since then, the sophistication of spacecraft has increased power demands by many orders of magnitude. Moreover, the lifespan of spacecraft power systems is a determinant of the lifespan of the spacecraft. Sputnik–1 lasted just three weeks; the International Space Station (ISS), with replaceable batteries and long–lived solar arrays, is designed to last decades.

- May 15, 1958, launch of Sputnik–3 from Baikonur. The satellite carried the first Russian–developed solar power PV cell system (according to Ref. 892). Further cell details are not available. Sputnik–3 had a mass of 1,327 kg, its orbit was elliptical (217 km x 1,864 km), inclination of 65.2°. Sputnik–3 was a geophysical laboratory, performing experiments on the Earth’s magnetic field, radiation belt, and ionosphere. Data was transmitted until Apr. 6, 1960.

- OSCAR–1, the first Amateur radio satellite (launch Dec. 12, 1961), carried a small battery–powered pack only. The S/C transmitted continuously the Morse code identifier to amateur receivers on Earth until its battery ran down.

- The Apollo–11 mission (launch July 16, 1969) placed the first solar panel on the moon. Apollo–11 was the first US lunar landing mission with Neil A. Armstrong, Michael Collins and Edwin E. Aldrin.

- In 1976, the amorphous silicon (a–Si) cell was developed by David Carlson and Christopher Wronski at the RCA Laboratories, Princeton, NJ.

- In the late 1970’s, the photovoltaic industry attracted the interest of large energy companies and government agencies. With their investment of capital, a tremendous acceleration in module development took place.

- In 1977, Hideki Shirakawa, Alan J. Heeger, Alan G. MacDiarmid and co–workers at the University of Pennsylvania demonstrated that halogen–doped polyacetylene had a conductivity 10^9 times greater than the undoped material (at the time, plastics were considered nonconductors). Since their discovery (all three received the Nobel Prize in Chemistry in 2000), conducting polymers have found applications in electronic components, also into solar cells.⁸⁹⁵⁾

- In the early 1980s, the Boeing Co. (Seattle, WA) pioneered a new kind of thin–film PV cell technology based on copper indium diselenide (CuInSe_2), later simply referred to as CIS (even when gallium and sulfur are added). The CIS compound displayed some very attractive qualities: sunlight absorption was the strongest of any PV material (absorbing over 90% of available light within 0.2 microns), and the capability of producing high–efficiency cells. In 1981, a CIS conversion efficiency of 10% was obtained. The CIS thin–film solar cell technology is vapor–deposited on a flexible substrate which is substantially lighter than cells bonded to a rigid panel.

- In the 1980s, silicon cells offered EOL efficiencies ranging from 13–16%, while the costlier GaAs cells delivered efficiencies of 16–19%.

893) J. Olberg, “Satellite turns 50 years old ... in orbit!,” March 17, 2008, URL: <http://www.msnbc.msn.com/id/23639980/>

894) M. K. Macauley, J. F. Davis, “An Economic Assessment of Space Solar Power as a Source of Electricity for Space–Based Activities,” Oct. 2001, www.rff.org/disc_papers/PDF_files/0146.pdf

895) C. K. Chiang, C. R. Fincher, Jr., Y. W. Park, A. J. Heeger, H. Shirakawa, E. J. Louis, S. C. Gau, Alan G. MacDiarmid, “Electrical Conductivity in Doped Polyacetylene,” *Physical Review Letters*, Vol 39, Oct. 24, 1977, p. 1098

– June 1986. ARCO Solar of Camarillo, CA, released the G-4000 – the world’s first commercial thin-film “power module.” Note: As of 1990, Siemens AG of Germany bought ARCO Solar from the Atlantic Richfield Company. The new company is called Siemens Solar Industries (the world’s largest producer of PV cells).

– In the 1990s the silicon cell efficiency improved to 17–18%.⁸⁹⁶⁾⁸⁹⁷⁾ Still better cells were made from GaAs (Gallium Arsenide) and GaAs/Ge with efficiencies of 19–21%. Silicon (Si), Gallium Arsenide on Germanium (GaAs/Ge), and multijunction solar cells are technologies that involve crystal growth on a fragile wafer. The CIS thin-film efficiency reached 17.7% in 1996.

Also in the 1990s, the first polymer photocells were produced. Polymer PV cells are cheaper and easier to make than inorganic cells; they permit the fabrication of flexible photodetector arrays (fabrication process identical to that of LEDs).

– In Jan. 1994, a joint US/Russian program MCSA (MIR Cooperative Solar Array) was created between NASA/LeRC and RKK Energia with the objective to construct and test a jointly made solar array. On Nov. 12 1995, the MCSA was launched on Shuttle Atlantis (STS-74) and installed on MIR, supporting experiments conducted on MIR by visiting NASA astronauts during the Phase I Shuttle/MIR program. Successful MCSA operation also served as early validated of the ISS solar arrays. In-orbit measurements made by the MIR crew of the MCSA’s electrical output were used to validate predictions made with a NASA solar array electrical performance computer model. The MCSA consisted of 42 hinged panels with two PPMs (Photovoltaic Panel Module) to each panel. Size: 18 m x 2.7 m; mass = 476 kg; power = 6 kW at 29–33 V. There are 6,720 solar silicon cells in the entire solar array. A PPM is a collection of 80 large-area silicon solar cells in a 5 cell x 16 cell matrix (PPM size: 0.44 m x 1.30 m, average power = 88.5 W, mass = 0.75 kg without frame).

– In 1997, AEC-Able Engineering Co., of Goleta, CA (in cooperation with Entech Inc. and Spectrolab Inc., the program was sponsored by BMDO and NASA/GRC), developed and introduced a new variant of solar cells, referred to as SCARLET (Solar Concentrator Array with Refractive Linear Element Technology).⁸⁹⁸⁾ The method employs curved, glass-composite optics to concentrate the solar energy on a strip of photovoltaic cells (use of cylindrical silicone Fresnel lenses to concentrate sunlight onto GaInP₂/GaAs/Ge cells). Efficiencies of 22% were obtained. Some inherent benefits of concentrator arrays are: a) high array efficiency, b) protection from space radiation effects, and c) minimized plasma interactions. – A disadvantage of this technique is that the solar panels have to be pointed and stabilized (e. g., articulated toward the sun) for maximum output. SCARLET-II is flown on Deep Space 1 (launch Oct. 24, 1998), it uses dual-junction solar cells.

Note: Key components of concentrator arrays were already successfully tested in space on an USAF experiment called PASP-plus (Photovoltaic Array Space Power-Plus Diagnostics) that was launched on APEX (Advanced Power Experiment) Aug. 3, 1994. PASP-plus flew a panel of mini-dome concentrators and proved that their performance was steady and that degradation was much less than with planar arrays. SCARLET was developed and qualified for flight on NASA’s METEOR-1 (Multiple Experiment Transporter to Earth Orbit and Return) spacecraft. However, a launch failure occurred on the first Conestoga 1620 launch from Wallops Island (Oct. 23, 1995).⁸⁹⁹⁾

– DS1 (Deep Space 1, launch Oct. 24, 1998) of NASA is the first S/C to rely exclusively on refractive concentrator arrays, it is among the first to use only multi-bandgap cells. The

896) M. Williamson, “Advancing Satellite Technology,” Space & Communications, March–April 1998, pp. 3–7

897) “NREL World Record Thin-Film Cell Efficiency,” URL: www.nrel.gov/ncpv/pdfs/tf_nrel2.pdf

898) Note: Solar concentrators reflect radiation so as to expose the cells to more radiation, together with multijunction devices that capture a larger slice of the spectrum (UV, VNIR, and IR). Efficiencies of about 30% and more are expected to be achieved in the early years of the next decade.

899) H. W. Brandhorst, J. A. Rodiek, M. J. O’Neill, “From Imagination toward Reality: the Stretched Lens Array’s Journey to Mission Success,” Proceedings of the 59th IAC (International Astronautical Congress), Glasgow, Scotland, UK, Sept. 29 to Oct. 3, 2008, IAC-08.D1.5.2

first dual–junction cells were introduced in 1997 (Spectrolab of Hughes Electronics Corporation and HSC, who built PAS–5) with an efficiency of about 21%. Spectrolab Inc. produced also triple–junction solar cells in 1998 (efficiency of 27%). Spectrolab HQ is in Sylmar, CA (near Los Angeles).

- Nov. 1998. Early versions of the FTFPV (Flexible Thin–Film Photovoltaic) blanket modules, developed by United Solar Power Corp. (United Solar) of Troy, MI (Uni–Solar as of 2000), were installed and tested on the MIR space station for a period of 19 months (with Energia support).⁹⁰⁰⁾ Cells based on FTFPV technology are low–cost because they can be grown on just about any surface, whereas conventional solar cells are produced on crystal wafers. The solar modules are the subject of a new joint development and testing program between United Solar, Kvant GNPP, the leading Russian enterprise in space PV technology, RSC Energia (Energia), the operator/manager of the MIR Space Station, and Sovlux, a Russian–American joint venture owned by United Solar, Kvant of Moscow and the Russian Ministry of Atomic Energy.

- 2002. Hybrid solar cells in a semiconductor–polymer photovoltaic device were demonstrated by researches at LBL (Lawrence Berkeley Laboratory) of UCB. The new generation of solar cells combines nanotechnology with plastic electronics. Ever since the discovery in 1977 of conducting plastics (polymers which feature conjugated double chemical bonds, that enable electrons to move through them), there has been interest in using these materials in the fabrication of solar cells. Plastic solar cells can be made in bulk quantities for a few cents each. So far, the conversion efficiency of the Berkeley hybrid cells was only 1.5% at AM1.5 (which corresponds to a sun–zenith angle of 48°). See Glossary for Air–mass definition.

- AFRL (Air Force Research Laboratory) at Kirtland AFB, NM, is funding a program called LFSA (Lightweight Flexible Solar Array) to demonstrate key array technologies on four space flights.

- The first space opportunity⁹⁰¹⁾ consisted of a successful flight experiment of a Shape Memory Alloy (SMA) deployment hinge experiment that was demonstrated on Shuttle flight STS–93, July 23–28, 1999 (hinges are the primary mechanism used to deploy solar arrays that are folded at launch). The hinge operations for the experiment were reported by the crew as nominal (six SMA hinges were tested).

- The second flight opportunity consisted of a sub–scale two–panel solar array that was demonstrated on NASA's Earth Observing–1 (EO–1) spacecraft (launch Nov. 21, 2000). The new solar array technology is referred to as LFSA (Lightweight Flexible Solar Array) experiment, sponsored by AFRL, managed by GSFC, and built by Lockheed–Martin Astronautics, Denver, CO). EO–1 has two solar panels, the wide wing–like extension employs conventional PV technology with GeAs/Ge cells, and an experimental LFSA panel on the underside of the S/C. LFSA consists of very lightweight composite, window frame–like structures that contain the thin–film CIS solar cells (with polyimide substrate), and SMA (Shape Memory Alloy) technology for the hinge and deployment systems (shape memory alloys are novel materials that have the ability to return to a predetermined shape when heated). The LFSA solar cell modules are 10 cm x 10 cm in size, each module consist of 15 monolithically–interconnected cells in series.^{902) 903)} The AM0 (Air–Mass–Zero) module efficiency achieved for this size was about 2%. The hinges were deployed by means of heaters powered by the S/C bus (28 V). SMAs undergo a reversible crystalline phase trans-

900) J. Tringe, J. Merrill, K. Reinhart, "Developments in Thin–Film Photovoltaics for Space," Proceedings of the 28th IEEE Photovoltaic Specialists Conference, Anchorage, AK, Sept. 15–22, 2000, pp. 1242–1245

901) E. Fosness, J. Guerrero, C. Mayberry, B. Carpenter, D. Goldstein, "Next Generation Solar Array Technologies for Small Satellites," AIAA/USU Conference on Small Satellites, Logan, UT, Aug. 12–15, 2002, SSC02–II–2

902) B. Carpenter, J. Lyons, "EO–1 Technology Validation Report: Lightweight Flexible Solar Array Experiment," eo1.gsfc.nasa.gov/miscPages/TechForumReports/LFSA.pdf

903) W. U. Huynh, J. J. Dittmer, A. P. Alivisatos, "Hybrid Nanorod–Polymer Solar Cells," Science, Vol. 295, 29 March 2002, pp. 2425–2427

formation that is the basis of the “shape memory effect.” – The deployment demonstration turned out to be successful. The new alloys offer a “shockless” solar array deployment technique, a much safer method than conventional solar array systems that use explosives for deployment. In addition, LFSA aboard EO–1 offered an unprecedented specific power–to–weight ratio of 100 W/kg, compared to the 40 W/Kg supplied by conventional solar arrays on satellites today.

– Another demonstration of LFSA technology is planned for the Encounter spacecraft (a commercially funded mission), being developed by Team Encounter LLC of Houston, TX.^{904) 905)} The LFSA array will be the primary power source for the Encounter solar sailcraft, called **Earthview**, for a secondary launch in 2005 on Ariane–V. The S/C bus of Earthview is being built by Microsat Systems of Littleton, CO, the inflatable boom and solar sail (400 m² sail area) are being developed by L’Garde of Tustin, CA, and the High Definition TV Camera will be built by Ecliptic Enterprises Corp. of Pasadena, CA. NASA and NOAA have considerable interest in the Earthview mission and its technology providing some assistance to Team Encounter.

• **Global solar energy production.** About 90 MW of photovoltaic power modules were produced worldwide in 1996 (for Earth–bound applications such as solar roof installations), the figure was 135 MW for 1997 and 360 MW for 2001. Of the global demand for solar photovoltaics (PV), approximately 30% is accounted for by Japan, 20% by European countries and less than 10% by the USA. All indications are that direct conversion of light into electricity, or photovoltaics, is becoming accepted as an important form of power generation in the future. Still, at this stage photovoltaics remains the costliest among the renewable energy sources.

– In 2007, 55% of the PV capacity worldwide is installed in Germany. The main reason for Germany’s leading position in PV energy is the Renewable Energies Act. The law requires power companies to buy electricity from the owners of PV installations at a set price.⁹⁰⁶⁾

– In 2008, the world solar photovoltaic market installations reached a record high of 5.95 GW, an increase of 110% over 2007. Europe amounts for about 82% of the demand (Germany is producing half of the world’s solar power). The United States has lagged behind other countries during the years of the Bush Administration. In 2009, the US Congress passed an economic stimulus bill which contains key items favorable to solar energy.⁹⁰⁷⁾

Conventional solar arrays of the late 1990s provide power/mass ratios of <40 W/kg. Silicon solar cells are made using either single crystal wafers, polycrystalline wafers, or thin films. Amorphous silicon, one of the thin–film technologies, is made by depositing silicon onto a glass substrate from a reactive gas such as silane (SiH₄). Since single PV cells have a working voltage of about 0.5 V, they are usually connected together in series (positive to negative) to provide larger voltages.

At the start of the 21th century, the state of the art in solar array technology provides **specific power levels of 45–80 W/kg and packing efficiencies of about 8 kgW/m³**. These systems represent a power generation cost of approximately \$1000–2000/W. Some examples of large power installations in space are:

– ISS (International Space Station). The STS–97 assembly flight of Endeavour (Nov. 30 to Dec. 11, 2000) brought the P6 Integrated Truss Segment to ISS. The P6 consists of two identical PVAAs (Photovoltaic Array Assembly), each of which is made up of an SAA (Solar

904) B. Berger, “Earthview Satellite to Demonstrate Solar Sail Technology,” Spacenews, Oct. 28, 2002, p. 19

905) B. Berger, “NASA Offers Expertise for Solar Sail Spacecraft Project,” Space News April 28, 2003, p. 10

906) http://www.solardaily.com/reports/Germany_Leading_The_International_PV_Market_999.html

907) Alexandre Y. Fong, “Solar Energy: A Global Perspective,” OPN (Optics & Photonics News, June 2009, Vol. 20, No 6, pp.8–9

Array Assembly) and a SAW (Solar Array Wing). The two SAWs have a power generation capability of about 64 kW each. The ISS electrical bus system uses 120 V of DC power. Since March 2009 and the STS 119 mission, integrating the fourth and last SAW pair, the ISS BOL power generated by the 8 SAWs is about 264 kW, (208 kW 15 years EOL]), delivering 84–120 kW of usable continuous electrical power. ⁹⁰⁸⁾

- EnviSat of ESA (launch March 1, 2002), the EO (Earth Observation) satellite with a record mass of 8140 kg, provides an onboard electrical power of 6.5 kW (EOL).
- The commercial platform HS–702 of BSS (Boeing Satellite Systems) provides power levels of 10–15 kW. The first communications satellite with this platform is Galaxy–11 of PanAmSat Corp., launched Dec. 21, 1999. HS–702 bus has a design life of 15 years.
- A successor communications satellite on the HS–702 platform, Galaxy–IIC (launch June 15, 2002 into GEO) of PanAmSat Corp., provides a power level of 15 kW (EOL). The solar power array consists of 2 wings each with six panels of improved triple–junction gallium arsenide (ITJ GaAs) solar cells of Spectrolab with a minimum average efficiency of 26.5%, and a battery pack of NiH cells at 328 Ah capacity. Galaxy–IIC is the highest capacity S/C in orbit at the start of its service life.
- The Astra–1K (launch Nov. 25, 2002) commercial communications satellite of SES Societe Europeenne des Satellites) Luxembourg, built by ASI (Alcatel Space Industries) of France, provides 13 kW of solar power (S/C mass of 5250 kg, wingspan of 36 m). The S/C is outfitted with 10 reflector antennas and 52 active active Ku–band transponders to provide coverage for Europe. Note: A launch failure occurred due an upper stage malfunction (Proton K/DM3 launch vehicle from Baikonur) leaving Astra–1K in a useless orbit.

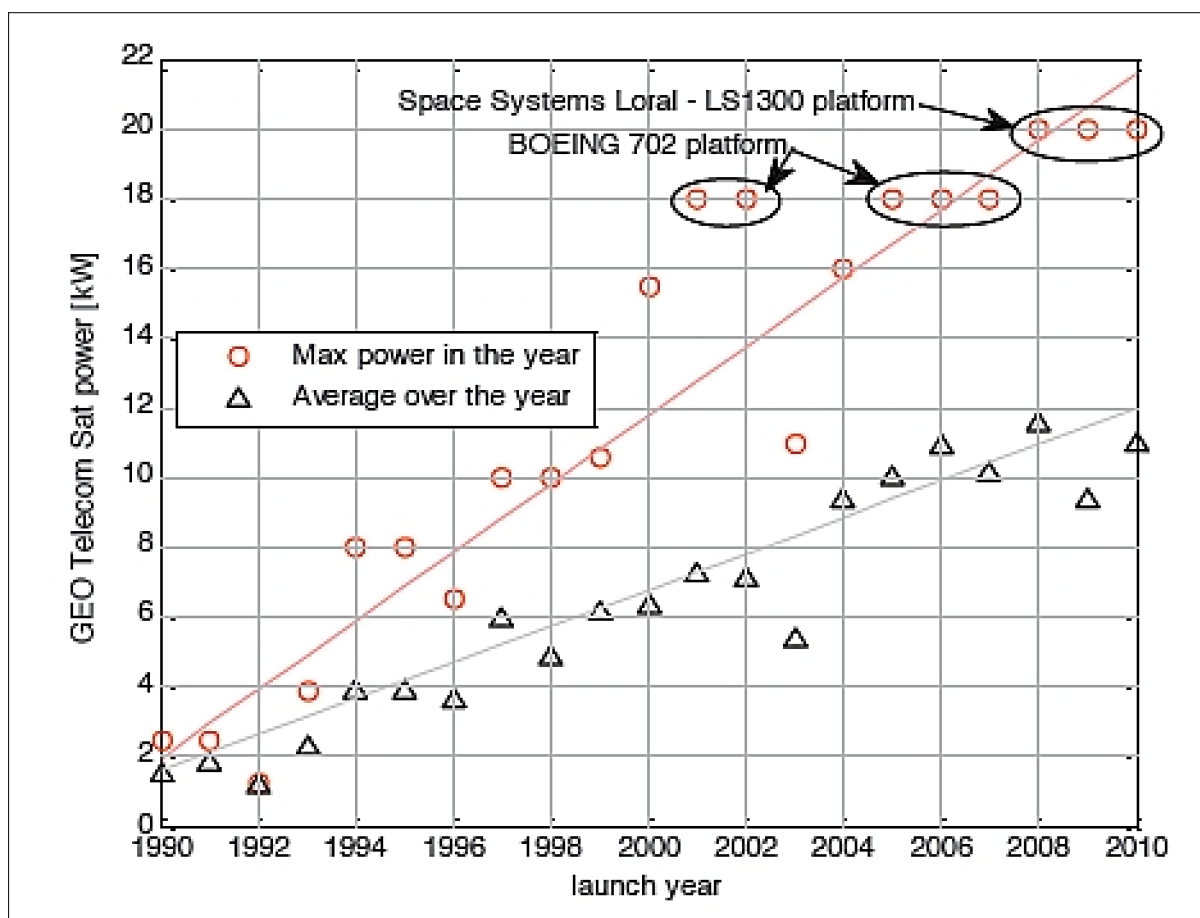


Figure 47: Evolution of telecommunication satellites power over the last two decades, based on the satellite database from May 2011

908) http://www.nasa.gov/pdf/304681main_STS-119_Press_Kit.pdf

- In comparison to the large spacecraft, a typical microsatellite generates an average power of 30–70 W across an orbit of around 100 minutes in LEO, and typically, an energy of 15–50 Wh/orbit is available to the payload.

S/C class	S/C mass (kg)	OAP (Orbit Average Power)	Payload energy(Wh/orbit)	Max payload power	Bus voltage (V)
Picosatellite (1U CubeSat)	~ 1	~ 5 W	~ 0.1	~ 5 W	3.3, 5
Nanosatellite	1–10	5–15 W	0.1~ 5	5–15 W	5, 14
Microsatellite	10–100	30–70 W (~ 100 deployed)	~ 5–50 (~ 100)	15–150 W	28
Minisatellite	100–1000	70–1000 W	50–1000	0.1–1.5 kW	28, 50

Table 49: Typical power performances of smallsats

- The TFSC (Thin–Film Solar Cell) technology⁹⁰⁹⁾⁹¹⁰⁾ offers large reductions in power cost and in weight over traditional cells. However, due to their relatively low efficiency the needed thin–film arrays turn out to be quite large. At the start of the 21st century the US military (AFRL) is developing a new PowerSail (PS) program to meet the power requirements of future missions (Space Based Radar, Space Based Lidar, etc.). The goal of the PS initiative is to develop a scalable solar power generation array technology with performance levels of up to 100 kW; the specific power increases with the new technology are estimated to be 3–5 times higher than conventional systems, there is also a reduction in packing volume and cost. The PS concept replaces the thin polyimide blanket with an FTFPV (Flexible Thin–Film Photovoltaic) solar cell blanket; the technology is also referred to as **FITS** (Foldable Integrated Thin–Film Stiffened) array.

An FTFPV blanket consists of a thin–layer deposition of amorphous or polycrystalline semiconductors onto a lightweight polymer or steel substrate. This configuration permits the FTFPV structure to be pointed (directed into the sun) and to be used in a similar fashion as the Kapton sail. Four key technologies are targeted to support this program: large deployable/inflatable structures, FTFPV blankets, advanced GNC (Guidance Navigation and Control), and electric propulsion. The PowerSail flight demonstration is based on a 50 kg system package and is expected to be flown in the time frame of 2007.

The FTFPV blanket technology shows great potential for use in future space solar array designs. This is due to its increased specific power (W/kg), lower cost and enhanced radiation–resistance compared to conventional single–crystal solar cell technologies such as silicon and gallium arsenide multijunction cells. The high specific power of FTFPV blankets derive from the deposition of ultra–thin (<10 μm) layers of semiconductor absorber material on flexible thin (25–75 μm) polymer or steel substrate blankets. The semiconductor layers are typically deposited onto large polymer or steel sheets using low–cost evaporation, sputtering, or plasma–enhanced techniques. The leading FTFPV candidates under development are amorphous silicon (a–Si) and polycrystalline copper indium gallium diselenide (CIGS) and its alloys. Current solar–to–electric conversion efficiencies are about 8–9% (AM0, space spectrum) for large area (500 – 1000 cm^2) a–Si and 6–8% (20 cm^2) for CIGS on stainless steel. The goal is 10–12% by 2002.⁹¹¹⁾⁹¹²⁾

909) C. Clark, J. Wood, W. Zuckerman, "Self Deploying, Thin–Film PV Solar Array Structure," Proceedings of AIAA/USU Conference on Small Satellites, Logan, UT, Aug. 12–15, 2002, SSC02–VIII–5

910) T. Meink, K. Reinhardt, K. Luu, R. Blankinship, S. Huybrechts, A. Das, "PowerSail – A High Power Solution," Proceedings of the AIAA Space 2000 Conference and Exposition, Long Beach, CA, Sept. 19–21, 2000

911) Ch. F. Hoerber, D. J. Kim, "The Continued Evolution of Communication Satellites," Acta Astronautica, Vol. 47, No 2–9, July–November 2000, pp. 65–89, Special issue: Space an Integral Part of the Information Age

912) V. Venugopalan, "Lithium–Ion Cells for Space Applications," Journal of Spacecraft Technology, Vol. 11, No 1, Jan. 2001, pp. 1–73

PV solar cell type	Description
Crystalline silicon (c-Si)	C-Si is the leading commercial material for photovoltaic cells, and is used in several forms: single-crystalline or monocrystalline silicon, multicrystalline or polycrystalline silicon, ribbon and sheet silicon and thin-layer silicon.
Thin-film photovoltaic cells	They use layers of semiconductor materials only a few micrometers thick, attached to an inexpensive backing such as glass, flexible plastic, or stainless steel. Semiconductor materials for use in thin films include amorphous silicon (a-Si), copper indium diselenide (CIS), and cadmium telluride (CdTe). Amorphous silicon has no crystal structure and is gradually degraded by exposure to light. Because the quantity of semiconductor material required for thin films is far smaller than for traditional PV cells, the cost of thin film manufacturing is far less than for crystalline silicon solar cells.
Group-II-IV technologies	They are based on Group III and V elements in the Periodic Table. The PV technologies display very high conversion efficiencies under either normal sunlight. Single-crystal cells of this type are usually made of gallium arsenide (GaAs). Gallium arsenide can be alloyed with elements such as indium, phosphorus, and aluminum to create semiconductors that respond to different energies of sunlight.
Multijunction devices	Multijunction devices stack individual solar cells on top of each other to maximize the capture and conversion of solar energy. The top layer (or junction) captures the highest-energy light and passes the rest on to be absorbed by the lower layers. Much of the work in this area uses gallium arsenide and its alloys, as well as using amorphous silicon, copper indium diselenide, and gallium indium phosphide. Although two-junction cells have been built, most research is focusing on three-junction (thyristor) and four-junction devices, using materials such as germanium (Ge) to capture the lowest-energy light in the lowest layer.

Table 50: Overview of photovoltaic (PV) solar cell technologies

System/Technology	Comment
Thin GaAs/Ge solar cells	Mass saving, flown on many S/C such as UoSat series (since UoSat-5, launch: July 17, 1991)
Multijunction solar cells	MightySat-I (launch of STS-88, Dec. 4, 98) uses InP (Indium Phosphide) dual-junction solar cells; STEX (launch Oct. 3, 1998) uses dual-junction solar cells PAS-5 (launch July 30, 1997) is the first commercial S/C to use dual-junction GaAs solar cells STARSHINE-3 (launch Sept. 31, 2001) uses triple-junction cells, namely GaInP/GaAs/Ge cells of Emcore Corporation (experiment) Pleiades series of CNES (launch Dec. 17, 2011 of Pleiades-HR1) uses triple-junction cells (RWE-3G, 27%) of RWE Space Solar Power GmbH, Heilbronn
Concentrators for solar cells	DS1 (launch Oct. 24, 1998) employs refractive concentrator arrays (SCARLET-II) in combination with cylindrical lenses and dual-junction GaInP ₂ /GaAs/Ge solar cells
Lightweight solar arrays	Cells on flexible Kapton substrate and inflatable Torus solar array. LFSA (Lightweight Flexible Solar Array) is a technology demonstration on EO-1 (launch Nov. 21, 2000)
Micromachined blue-red reflective cover glasses	Increase of solar cell efficiency

Table 51: Emerging solar cell technologies at the start of the 21st century

- Combing energy generation and communication functions into one structure: SOLANT (Solar Antenna Concept), an ESA-funded project in the time frame Oct. 1998 to March 2000 (the follow-up project "ASOLANT" started in June 2000). SOLANT refers to a new antenna design which combines the functions of solar cells (energy) and printed antenna patches (communication) into one structure.^{913) 914)} The idea is to use thin-film solar panels, which generally occupy large surface areas of a satellite structure, for antenna mounts or prints, provided the system is in itself compatible. Printed antennas, commonly

913) S. Vaccaro, P. Torres, J.R. Mosig, A. Shah, J.-F. Zürcher, A. K. Skrivervik, F. Gardiol, P. de Maagt, L. Gerlach, "Integrated solar panel antennas," IEEE Electronics Letters, Vol. 36, No. 5, March 2, 2000, pp. 390-391

914) J. Kuendig, M. Goetz, J. Meier, et al., "Effect of Proton Irradiation on the Characteristics of different Types of Thin-Film Solar Cells," Proceedings of the 16th EU Photovoltaic Solar Energy Conference, Glasgow, UK, May 1.-5., 2000

used in microwave communications, are naturally suited for this combination, in particular when their radiating patches can be isolated from the feed circuits. Amorphous silicon (a-Si) solar cell technology has been found to be suitable for realizing the solar antennas.⁹¹⁵⁾

The SOLANT concept was demonstrated in the MITA platform (MITA S/C launch Jul. 15, 2000) of ASI, Italy, using the combination of specially designed slot antennas with high efficiency GaAs solar cells.⁹¹⁶⁾ The entire antenna is composed of a low-gain half-omni-directional antenna and of a 2 cm x 2 cm element high-gain array. The low-gain antenna has a bandwidth allowing the coverage of the uplink and downlink bands (2025 MHz–2290 MHz) based on the low-gain antenna.

- The Rosetta deep space mission of ESA (launch March 2, 2004) represents a rather **special case of solar cell technology use**. At its destination in 2014 [rendezvous with Comet 67P/Churyumov–Gerasimenko, (discovered in 1969), followed by an orbital period around the tiny comet of 4 km diameter, etc.], the spacecraft is at a distance of about 675 million km from Earth, corresponding to 4.5 AU, a distance almost as far out as Jupiter. In Earth orbit, Rosetta is the most powerful S/C that ESA ever built, at 12 kW of installed solar power generation provided by two solar arrays, each of 14 m length and each of 32 m² in area. But at the deep space distance of Comet 67P/Churyumov–Gerasimenko, the total solar power available is only 400 W. – *Rosetta is the first deep space mission ever to rely entirely on solar power generation beyond the main asteroid belt (with sunlight levels of only 3–4% as those in LEO) – without the use of RTG (Radioisotope Thermoelectric Generator) technology (as is being done by all other deep space satellites).*^{917) 918) 919)}

- The planetary Dawn spacecraft of NASA on its way to the Asteroid Belt – an 8 year mission to the asteroids Vesta and Ceres (launch Sept. 28, 2007, launch mass = 1210 kg, dry mass of 740 kg) is another entry into the category of deep space missions which is using the **solar cell technology** as its main means of power generation (instead of the commonly used RTG concepts for deep space missions). The two solar arrays of Dawn span 20 m from tip-to-tip. The electric power of the solar arrays is mainly being used during its long journey to the Asteroid Belt to provide power for its ion engines.

The solar–electric ion propulsion system is using three gimballed NSTAR ion engines (of Deep Space 1 heritage) and monopropellant reaction control system. The GaAs triple junction solar arrays are providing 10 kW at Earth (equivalent to LEO) and 1.4 kW at Ceres. Dawn uses also its ion engines to spiral to lower altitudes on Vesta, to leave Vesta and cruise to Ceres and to spiral to a low altitude orbit at Ceres. Dawn’s ion engines have a specific impulse of 3100 s and a thrust of 90 mN. Over their lifetime, Dawn’s three ion propulsion engines will fire cumulatively for about 50,000 hours (over five years) — a record for any spacecraft.⁹²⁰⁾

Dawn’s primary scientific objective is to advance the understanding of the origin and evolution of the solar system by studying two of the largest asteroids, Vesta and Ceres, which appear to have remained intact since their formation 4.6 billion years ago. The Asteroid Belt is a ring of thousands of large rocks, located between Mars and Jupiter, about 440–450 million km from the sun (~ 3 AU). The mission timeline is:

- Mars gravity assist in March 2009
- Vesta arrival on July 16, 2011. With this encounter, the Dawn spacecraft became the first probe ever to enter orbit around an object in the main asteroid belt between Mars and

915) M. Tanaka, Y. Suzuki, K. Araki R. Suzuki, “Microstrip antenna with solar cells for microsattellites,” IEE Electronic Letters, 1995, Vol. 31, No 1, pp. 5–6

916) S. Vaccaro, J. R. Mosig, P. de Maagt, “Application of the solar antenna “SOLANT” concept to a satellite platform,” 25th Antenna Workshop on Satellite Antenna Technology, Sept. 18–20, 2000, ESA/ESTEC

917) P. B. de Selding, “Rosetta Mission to push Envelope of Solar Cell Technology,” Space News, Mar. 8, 2004, p. 9

918) http://www.esa.int/export/SPECIALS/Rosetta/ESAS7E7708D_1.html

919) Rosetta – Europe’s Comet Chaser, ESA brochure, Dec. 2003, BR215, URL: <http://www.esa.int/esapub/br/br215/br215.pdf>

920) <http://dawn.jpl.nasa.gov/>

Jupiter. Vesta has a diameter of 530 km and is the 2nd most massive object in the asteroid belt. ⁹²¹⁾

- Vesta departure in July 2012
- Ceres arrival in February 2015
- End of primary mission in July 2015.
- Juno is a NASA/JPL New Frontiers deep space science mission, ^{922) 923)} the first **solar-powered** spacecraft to the planet Jupiter with a launch on Aug. 5, 2011 – to reach Jupiter in 2016. Juno will orbit Jupiter in an elliptical polar orbit, the objectives are to study the planet's composition, gravity field, magnetic field, and polar magnetosphere. The three JEDI (Jupiter Energetic-particle Detector Instrument) sensors, built at JHU/APL, will measure energetic particles that flow through and are trapped within Jupiter's space environment. – Juno's trajectory will use a gravity assist speed boost from Earth, accomplished through an Earth flyby two years after its launch on Aug.5, 2011. ⁹²⁴⁾

For electric power generation, Juno is using solar panels instead of the RTGs (Radioisotope Thermoelectric Generators). The 3 solar arrays of Juno have a combined area of 60 m² generating 12 kW in Earth orbit – and 400 W when orbiting Jupiter at a distance of > 5 AU from the sun. To study Jupiter's atmosphere, Juno will use MWR (Microwave Radiometer) of JPL and JIRAM (Jovian InfraRed Auroral Mapper) designed by ASI (Italian Space Agency). NASA/GSFC is providing FGM (Fuxgate Magnetometer) while SwRI provides the SHM (Scalar Helium Magnetometer). In addition, an ASC (Advanced Stellar Compass) is built by DTU (Danish Technical University) of Lyngby, Denmark.

1.8.5.1 Electric power subsystem (EPS) on spacecraft

- An EPS of a conventional spacecraft normally consists of the following elements: a solar array for power generation, a power conditioning electronics unit providing a regulated or unregulated bus voltage, and a battery for energy provision to all required satellite functions during eclipse phases of the orbit. The EPS mass is generally dominated by the solar array and battery mass portions (the electronics unit represents the smallest portion of the mass).
- JHU/APL offers an innovative architecture in EPS design for small spacecraft systems (micro and nanosatellites). The patented system is called IPS (Integrated Power Source). IPS includes highly integrated electronics technologies as well as the integration of functions (normally implemented in separate elements) which combines energy storage (a matrix of LI battery cells), solar array electronics (dual-junction solar cells), and processor-based charge control electronics into a single structural element. ⁹²⁵⁾ The final IPS product is a multipurpose panel that may even be used as a S/C side panel.
- A new stand-alone power/storage package, named IMPS (Integrated Microelectronic Power Supply), was also developed at NASA/GRC. It provides the capability of power generation and power storage for microelectronic applications – by combining a thin-film photovoltaic array with a thin-film lithium-ion battery. The first version of IMPS is being flown on STARSHINE-3 (launch Sept. 30, 2001, reentry Jan. 21, 2003; see N.25.3).

921) Tony Phillips, "Dawn spacecraft snaps close-up image of asteroid Vesta," NASA, July 18, 2011, URL: http://science.nasa.gov/science-news/science-at-nasa/2011/18jul_dawn4/

922) Amy Klamper, "Assembly Begins on NASA's First Solar-powered Mission to Jupiter," Space News, April 12, 2010

923) "Juno – NASA's New Frontiers Mission to Jupiter," Nov. 8, 2008, URL: <http://juno.wisc.edu/>

924) Rick Nybakken, "The Juno Mission to Jupiter – Launch Campaign and Early Cruise Report," Proceedings of the 2012 IEEE Aerospace Conference, Big Sky Montana, USA, March 3–10, 2012

925) P. D. Schwartz, A. F. Hepp, et al., "Spacecraft Miniaturization: Integrated Power Source," JHU/APL Technical Digest, Vol. 22, No. 2, 2001, pp. 106–109

Satellites with large power demands normally employ sun tracking with the solar array (also referred to as “sun articulation”) to maximize their power generation capability. This requires usually a drive mechanism (gimbals, control, etc.) to adjust the array(s), generally normal to the sun direction, during the spacecraft’s orbit, for peak power generation results. There are still cases left in satellite operations when the power subsystem of a S/C can’t meet the power demands of its payload. This situation occurs usually with satellites carrying an active payload (SAR and/or lidar instruments) in addition to a passive payload (example: ERS–1/2). These cases are operationally handled with the introduction of a “duty cycle,” representing the fraction of the orbital period, in which a power–hungry instrument can be operated. Hopefully, these observational limitations may soon become a relict of the past with the introduction of power–efficient instrumentation as well as with more efficient power generation capabilities.

- Satellite batteries. Batteries have been in use for spaceflight applications since the flight of Sputnik–1. Since that time, batteries have matured from non–rechargeable one–use power systems to rechargeable multi–use backup power systems. In the early years of spaceflight, relatively short flight times encouraged the use of batteries as a primary source of power. As the mission durations grew longer, solar and nuclear energy took as the primary sources. This development sparked the need for batteries as secondary power sources – for operations support during ecliptic orbit phases as well as for support during peak power demand periods. Batteries, therefore, remain an essential component of spaceflight. Some essential characteristics of a battery are: required power, mission lifetime, system mass, and cost. Non–rechargeable primary batteries are still being used today on short demonstration flights of nanosatellites and picosatellites. Example: The PICOSAT1.0 mission of the USAF (launch Jan. 27, 2000, see N.18.3), flown on OPAL and deployed as a separate S/C, employed only batteries to test low–power communications. ⁹²⁶⁾

A battery consists of several subunits called cells. Early batteries on satellites were silver–zinc (AgZn) non–rechargeable (primary) batteries. These provided the best compromise among several characteristics such as lifetime, energy density, and mass. Later, in the early 1960s, rechargeable AgZn batteries were used for the first time on the Ranger missions. The rechargeable Nickel Cadmium (NiCd) batteries were introduced in the mid–1970s, they remained the battery standard for most missions practically up to the start of the 21st century. NiCd batteries have demonstrated long–term performances, with more 17 years life time on both MARECS B2 (launch Nov. 10, 1984) and SPOT–1 (launch Feb. 22, 1986, decommissioned in Nov. 2003) missions which were initially planned for 3 year duration. – A disadvantage of the NiCd battery is the memory effect that causes them to lose their capacity for full recharging if they are discharged repeatedly. The effect was first noticed in aerospace applications.

Higher efficiency Nickel Hydrogen (NiH₂) cells were first introduced on the NTS–2 (Navigation Technology Satellite–2) with a launch on June 23, 1977 (NiH₂ batteries have the advantage of a high number of charge–discharge cycles; the NiH₂ battery was developed by Comsat). ⁹²⁷⁾ NTS–2 is considered the first NAVSTAR GPS satellite series, built by the NRL (Naval Research Laboratory), Washington, DC, to provide near–instantaneous navigation and time–synchronization service on a worldwide, continuous basis. – There are several designs of NiH₂ batteries available: Individual pressure vessel (IPV), Single Pressure vessel (SPV) and dependent pressure vessel (DPV). The performance varies according to the design used, ranging from 50–75 Wh/kg.

926) “Spacecraft Power Generation,” a document prepared by graduate students at The University of Texas at Austin, Department of Aerospace Engineering and Engineering Mechanics, 1992, www.tsgc.utexas.edu/archive/subsystems/power.pdf

927) J. A. Buisson, R. L. Easton, T. B. McCaskill, “Initial Results of the NAVSTAR GPS NTS–2 Satellite,” <http://www.leapsecond.com/history/1978-PTTI-v9-NTS-2.pdf>

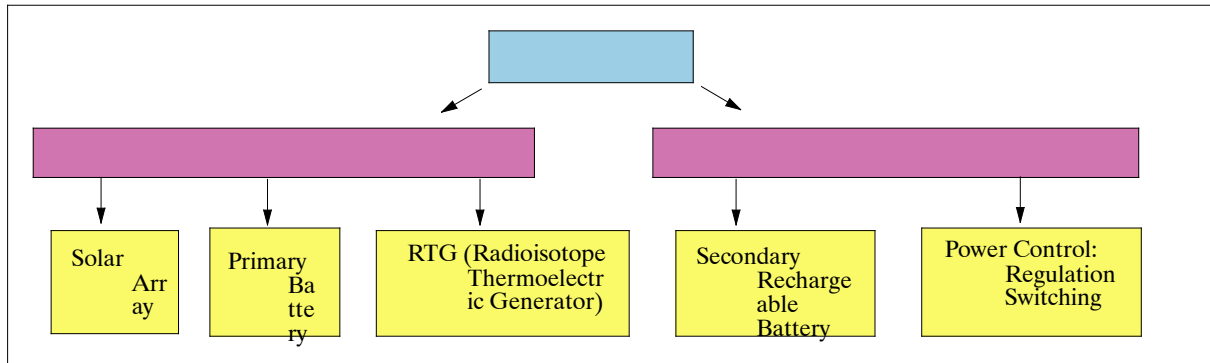


Figure 48: Overview of EPS elements in a spacecraft

The Nickel–Hydrogen technology had been discovered and patented in the 1950’s in Russia, but real developments were initiated in the USA by Comsat/Intelsat only in the early 1970s. A lot of team work was provided by various US laboratories and companies in the development of efficient NiH₂ cells – such as: Comsat, Intelsat, US Air Force, Hughes Aircraft, Eagle Picher Industries, Naval Research Center, TRW, Bell Labs, and Lockheed Missiles and Space Company. Intelsat–V (launch 1983) was the first commercial communication satellite to use NiH₂ batteries. Since then more than 300 GEO satellites have been launched with NiH₂.⁹²⁸⁾

Battery type	Time frame of introduction	Energy density (Energy/unit mass)
AgZn (Silver Zinc)	Since the 1950s (first as non–rechargeable battery). The cell is reliable and inexpensive. It has a low life-time.	50–100 Wh/kg
NiCd (Nickel Cadmium)	Since the mid–1960s (and the 1970s).	20–30 Wh/kg
NiH ₂ (Nickel Hydrogen)	In the early 1980s. Improved energy density and cycle lifetime	36–40 Wh/kg
NiH ₂ (Nickel Hydrogen)	At the end of the 1990s	50–55 Wh/kg
NiMH (Nickel Metal Hydride)	First use probably on Falcon Gold of USAF Academy and UCCS (launch Oct. 24, 1997), SEDSAT–1 (launch Oct. 24, 1998), UniSat–1 (launch Sept 26, 2000)	50–60 Wh/kg
Li–ion (Lithium–Ion)	Introduction at turn of the 21st century. STRV–1d of QinetiQ (launch Nov. 16, 2000) uses the first Li–ion battery developed by ABSL of Abingdon, Oxfordshire, UK. – PROBA of ESA (launch Oct. 22, 2001) uses a 36–cell Li–ion battery of 9 Ah capacity. PROBA is still operational as of 2009.	60–120 Wh/kg (potential up to 170 Wh/kg)
Li–Po (Lithium–Polymer)	In 2009, Clyde Space (UK) is providing a Li–Po battery of 150 Wh/kg	120–200 Wh/kg
SPE (Solid Polymer Electrolyte) fuel cell	Introduction on PICOSat (launch Sept. 30, 2001). SPE is a fully regenerative fuel cell	20–90 Wh/kg
Fuel cell (alkaline)	Rechargeable fuel cells is the emerging technology of the 21st century. So far the Shuttle Orbiter uses fuel cells to generate electricity through the combination of oxygen and hydrogen (about 7 kW at 28 V).	about 90 Wh/kg

Table 52: Overview of the rechargeable battery evolution for spacecraft

The Lithium–Ion (Li–ion) battery still holds greater promises in efficiency at the turn of the 21st century. Li–ion batteries are already common devices in such appliances as cell phones and laptop computers. They have no memory effect and do not use poisonous metals, such as lead, mercury or cadmium.

⁹²⁸⁾ Y. Borthomieu, B. Lagattu, S. Rémy, J.–P. Sémerie, “40 Years Space Battery Lessons Learned,” Proceedings of the 8th European Space Power Conference, Constance, Germany, Sept. 14–19, 2008, ESA SP–661, Sept. 2008

The Lithium–Polymer (Li–Po) technology⁹²⁹⁾ evolved from the Li–ion concept and is a mission enabler for miniature spacecraft (CubeSats). The key advantage of the Li–Po cell is its lightweight, high energy density and slim, volume efficient geometry. The cell uses a polymer electrolyte and is packaged in a foil bag, which provides both mass and magnetic signature advantages.

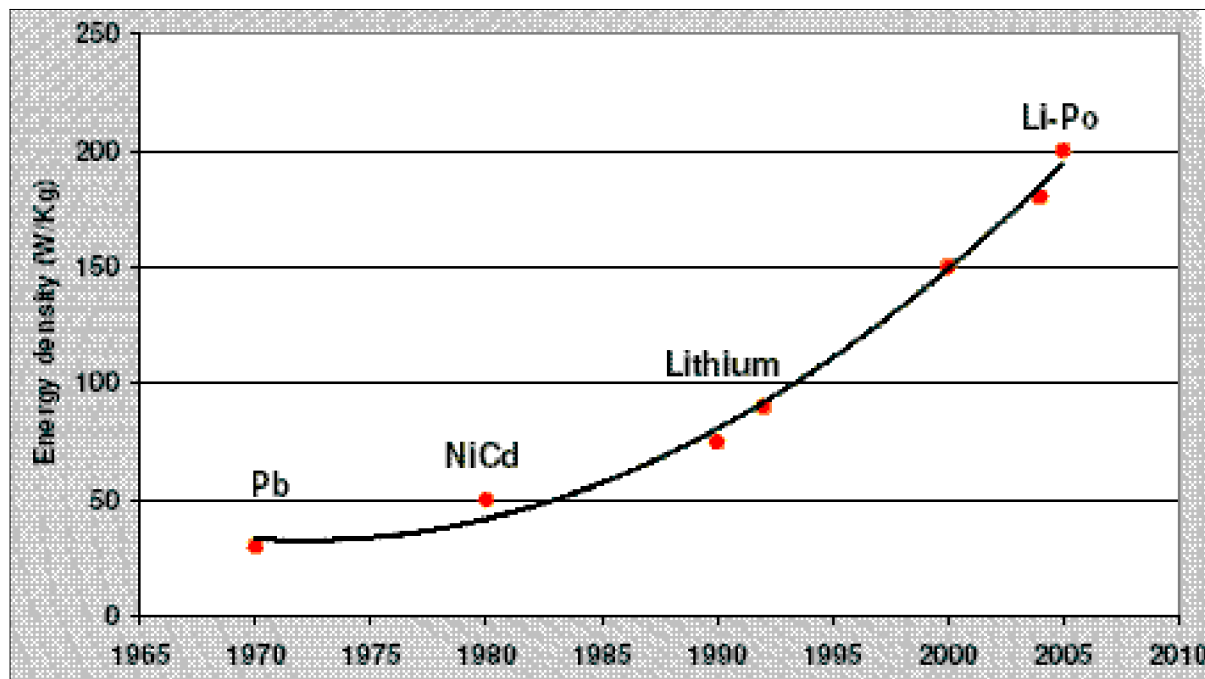


Figure 49: Battery technology development trends (image credit: EADS Astrium SAS)⁹³⁰⁾

- The orbit of ISS (International Space Station) is such that it spends 36 minutes of each orbital period (92 minutes) in eclipse of the sun. During the shadow phase, ISS relies on banks of NiH₂ rechargeable batteries to provide a continuous power source. Each battery consists of 38 cells in series. The batteries, which are recharged during the sunlit phase of each orbit, have a design life of > 5 years. A total of > 110 kW of solar power is available for all uses, 46 kW of continuous electric power is left for research work (experiments). Excess electric storage energy of the ISS power system is being dissipated using liquid ammonia radiators.
- In the 21st century, Li–ion batteries are dominating the field of advanced power sources and have replaced many other types of batteries in different areas and more specifically in space applications. Li–ion is the main technology now for satellite usage following the NiCd technology in the 1960's and NiH₂ in the 1990's. Li–ion batteries that are currently (2011) used for space applications are driven by terrestrial technologies (mainly by the automotive industry) and can reach up to 155 Wh/kg.⁹³¹⁾

Since the commercialization of Li–ion batteries by Sony in 1991, intensive research on electrode material and cell design has led to increased energy densities, (doubled energy density), based though on the initial concept by Sony consisting of the LiCoO₂ cathode and carbon anode in carbonate electrolytes. – The potential improvement in performance and safety of Li–ion batteries is still feasible though, mainly by the use of pioneering electrode materials.

929) <http://cubesat.wdfiles.com/local--files/psu/PLM-PSU-BattDataSheet-301-1.pdf>

930) P. Pelissou, C. Carron, "How the Intra-Satellite Wireless System could be Self-Powered?," Wireless for Space Applications Workshop, 10–13 July 2006, ESA/ESTEC, Noordwijk, The Netherlands

931) M. Nestoridi, E. Simon, L. Daniel, S. Patoux, L. Simonin, W. Porcher, S. Jouanneau, V. Gineste, O. Mourra, "Further Advanced Lithium Cell Development," Proceedings of the 9th European Space Power Conference, Saint Raphael, France, June 6–10, 2011, ESA SP-690

- In March/April 2014, it was 60 years ago that the first practical solar (or ‘photovoltaic’ cell) was demonstrated at Bell Labs in New Jersey, USA. This new invention’s very first practical use was in powering early satellites, and solar cells remain pivotal to the space industry to this day. The design of Figure 50 is a thin version of the European 3G30 triple-junction gallium arsenide solar cell. Produced by Azur Space Solar Power, it is one of the most efficient in the world.⁹³²⁾

But photovoltaic electricity generation is also on the way to becoming a major terrestrial energy source, projected to supply close to 3% of global electricity demand by 2020.

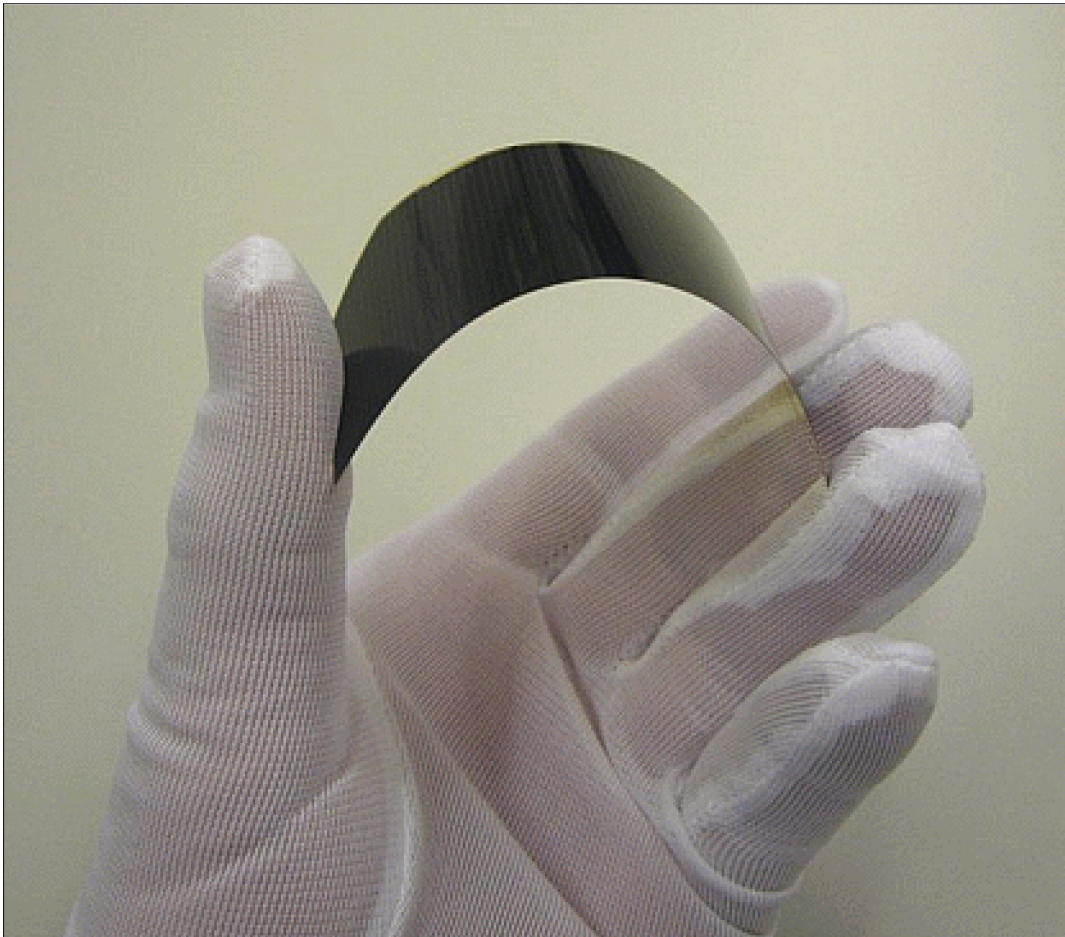


Figure 50: Photo of a 30% efficient multi-junction solar cell of Azur Space (Azur Space and Power)

1.8.5.2 Fuel cell power systems on spacecraft

A fuel cell converts directly the chemical energy of reactants (a fuel and an oxidant) into low-voltage electricity, via electrochemical reactions.^{933) 934) 935)} A fuel cell (FC) is thus similar to a conventional chemical battery. The main difference is that in the ordinary bat-

932) “30% efficient multi-junction solar cell, ESA, April 8, 2014, URL: http://www.esa.int/spaceinimages/Images/2014/04/30_efficient_multi-junction_solar_cell

933) Note: The fuel cell principle was discovered in 1839 by William R. Grove (1811–1896), an English lawyer turned physicist. Grove utilized four large cells, each containing hydrogen and oxygen, to produce electric power which was then used to split the water in the smaller upper cell into hydrogen and oxygen. It took another 120 years until fuel cells were considered for space applications. The fuel cell technology turns out to be two to three times more efficient than an internal combustion engine in converting fuel to power.

934) S. Thomas, M. Zalowitz, “Fuel Cells – Green Power,” www.lanl.gov/energy/est/transportation/trans/pdfs/fuel-cells/fc.pdf

935) G. Gave, J. B. Lévy, “State-of-the-Art of Common Polymer Electrolyte Fuel Cell Technology and Adaptations Needed for Space Applications,” 53rd IAC and World Space Congress, Oct. 10–19, 2002, Houston, TX, IAC-02-R.4.07

tery, the “fuel” is the built–in expendable electrode (representing a fixed amount energy). When this electrode is depleted, the battery is either “dead” or requires recharging in order to restore the chemical state of the electrode. A fuel cell is an electro–chemical converter only, using an external fuel supply. Hydrogen has become the fuel of choice in space applications (due to its high energy density when stored as a cryogenic liquid). Energy is released when two hydrogen molecules (2H_2) exothermally combine with an oxygen molecule (O_2). The fuel is oxidized electrochemically at the anode, i.e., it loses electrons, to produce positively–charged intermediates or protons, H^+ , in the case of hydrogen fuel. At the cathode, oxygen is reduced, accepting electrons to make oxide anions, O^{2-} .

In the late 1950s about 200 research contracts were funded by the US space program to come up with a solution to generate electricity for space missions. The answer was fuel cells. Fuel cells were introduced in the US space program in the 1960s when NASA selected them as the power source for the Gemini (acid type FC) and Apollo (alkaline type FC) programs. NASA first used fuel cells aboard the Gemini V mission in August 1965. The Gemini spacecraft used a PEM (Proton Exchange Membrane) fuel cell stack of GE capable of providing 1 kW of power. The Apollo program spacecraft (1968–1972) used a Pratt and Whitney alkali fuel cell plant providing peak power capability of 2.3 kW.⁹³⁶⁾

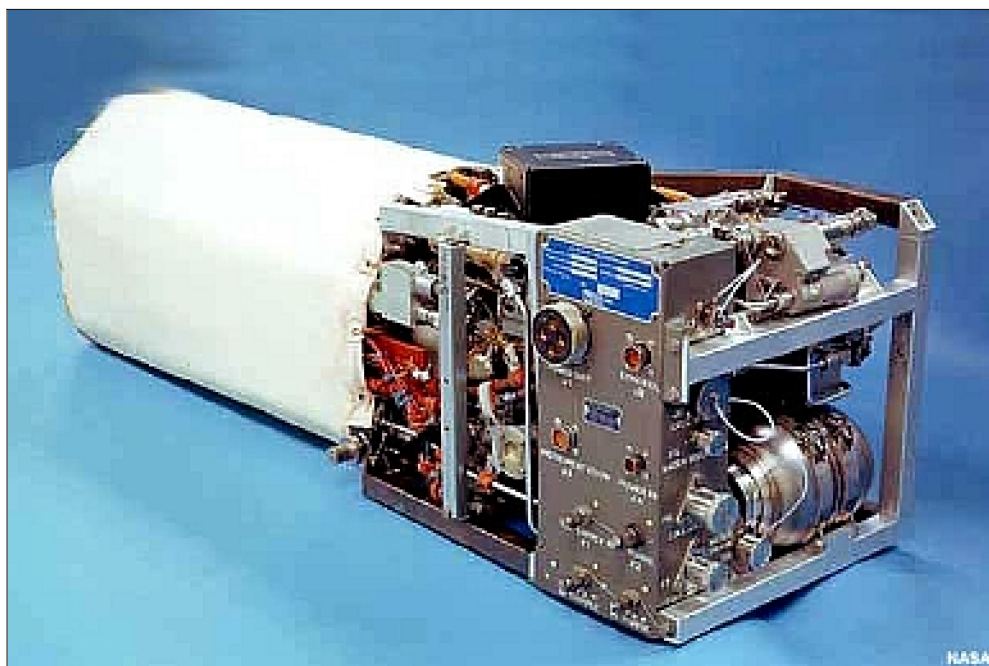


Figure 51: Photo of one Space Shuttle Orbiter fuel cell (image credit: NASA)

All Orbiter electric power of the Space Shuttle missions comes from its three fuel cell stacks (alkaline type) developed by the United Technologies Corporation. Each fuel cell has an average power of 7 kW, 12 kW peak, volume = 154 liter, and a mass of 118 kg. There are no backup batteries, and a single fuel cell is sufficient to insure safe vehicle return. In addition, the water produced by the electrochemical reaction is used for crew drinking and spacecraft cooling. In 7 days the fuel cells consume 680 kg of H_2 and produce 864 liter of drinking water. The Orbiter’s fuel cells can operate for 2000 hours.

In a regenerative fuel cell (RFC) system, the water by–product is broken down into hydrogen and oxygen through electrolysis and reused in the fuel cell. Basic fuel cell types are:

- Alkaline (or Alkali) electrolyte fuel cells (AFC). AFCs operate on compressed hydrogen and oxygen and generally use a solution of potassium hydroxide in water as their elec-

936) Kenneth A. Burke, “Fuel Cells For Space Science Applications,” NASA/TM—2003–212730, AIAA–2003–5938, November 2003, URL: <http://gltrs.grc.nasa.gov/reports/2003/TM–2003–212730.pdf>

trolyte. Operating temperatures inside alkali cells are around 150° to 200° C. In these cells, hydroxyl ions (OH⁻) migrate from the cathode to the anode. At the anode, hydrogen gas reacts with the OH⁻ ions to produce water and release electrons. AFCs operate with efficiencies of up to 70%, and like other fuel cells, create little pollution. Because they produce potable water in addition to electricity, they have been a logical choice for spacecraft. – AFCs are suitable for short mission support. Aqueous alkaline electrolyte systems have a low activation energy for the cell reactions. They therefore have high power output even at below ambient temperatures. This type of fuel cell, however, is not suited for use as a truly regenerative cell (i.e. without an electrolyzer) due to material problems. The alkaline fuel cell system with a separate electrolyzer appears to be best for shorter missions (<5000 hours).

AFCs, with a performance of 1.5 kW, were developed by Pratt & Whitney and used in NASA's Apollo missions from 1968–1972. – AFC history: Francis T. Bacon (1904–1992), UK, began experimenting with alkali electrolytes in the 1930s; he developed the first successful AFC device in 1932.

– SPE (Solid Polymer Electrolyte) fuel cells are fully regenerative and suitable for longer missions. They use NafionTM –type plastics (produced by DuPont), known as ionomer, or its family of compounds [SPE compounds are derivatives of poly(ethylene oxide) or PEO]. General Electric worked on the development of the SPE fuel cell technology (trademark name SPFC) from 1960–1984 and applied it during the Gemini and BioSatellite space programs (BioSatellite–I launch in Dec. 1966; BioSatellite–II launch Sept. 7, 1967), when it was referred to as the IEM (Ion Exchange Membrane) fuel cell. In the period 1962–1965, the IEM (1 kW fuel cells) of GE were used for seven flights in the Gemini Earth–orbiting program. The SPE technology is also referred to as the **PEM** (Polymer Electrolyte Membrane) technology.

In the early 21st century, SPE is considered to be the forerunner of the PEMFC (Polymer Electrolyte Membrane Fuel Cell).

PEM fuel cells work with a polymer electrolyte in the form of a thin, permeable sheet (proton conductive solid polymer technology).^{937) 938)} They work by passing a fuel, such as hydrogen, across the membrane, which is only permeable to protons. The hydrogen's electron must go around the membrane, generating the electrical current. On the other side of the membrane, the hydrogen bonds with atmospheric oxygen, so the only byproduct is water. The solid electrolyte in PEMs reduces corrosion and management problems.

Since the 1990s, the PEMFC technology is under consideration by the automobile industry around the world as an alternative to the internal combustion engine. – NASA considers to replace the current alkaline fuel cells of the Space Shuttle with a PEMFC system. A recent demonstration of the PEM technology in space was realized with PBEX (Polymer Battery Experiment), developed at JHU/APL and flown on **PICOSat** of the USAF (launch Sept. 30 2001, see M.31) STP (Space Technology Program). In PBEX, both electrodes and the electrolyte are made of polymers. The objective is to validate the charging and discharging characteristics of polymer batteries in the space environment. PBEX has a mass of 0.4 kg.⁹³⁹⁾

– SOFC (Solid Oxide Fuel Cell), a high operating temperature device. An SOFC uses a hard ceramic electrolyte instead of a liquid and operates at temperatures up to 1,000° C. The semi–permeable ceramics has the ability to conduct an electric current by the passage of oxygen ions through the crystal lattice at sufficiently high temperatures. The electrolyte material mostly used is zirconium oxide and calcium oxide. SOFCs are fully reversible with

937) http://www.technologyreview.com/articles/wo_jeo041901.asp

938) G. Gave, J. B. Lévy, "State-of-the-art of common Polymer Electrolyte Fuel Cell Technology and Adaptations needed for Space Applications," 53rd IAC/World Space Congress, Oct. 10–19, 2002, Houston, TX, IAC–02–R.4.07

939) L. D. Burns, J. B. McCormick, C. E. Borroni–Bird, "Vehicle of Change," Scientific American, Oct. 2002, pp. 40–49

a potential to provide specific a energy of $> 1\text{ kW/kg}$. Emil Baur and H. Preis of Switzerland experimented with solid oxide electrolytes in the late 1930s, using such materials as zirconium, yttrium, cerium, lanthanum, and tungsten.

At the start of the 21st century, fuel cell power generation is an emerging and enabling technology with potentials in many fields with characteristics of high energy–conversion efficiency and extremely low environmental emissions. The current spaceborne applications are dwarfed by the multitude of fuel cell uses in Earth–based applications, providing an ever increasing functional autonomy, in particular in support of mobile services. The fuel cell market promises also inroads into the distributed–power–generation technology.⁹⁴⁰⁾

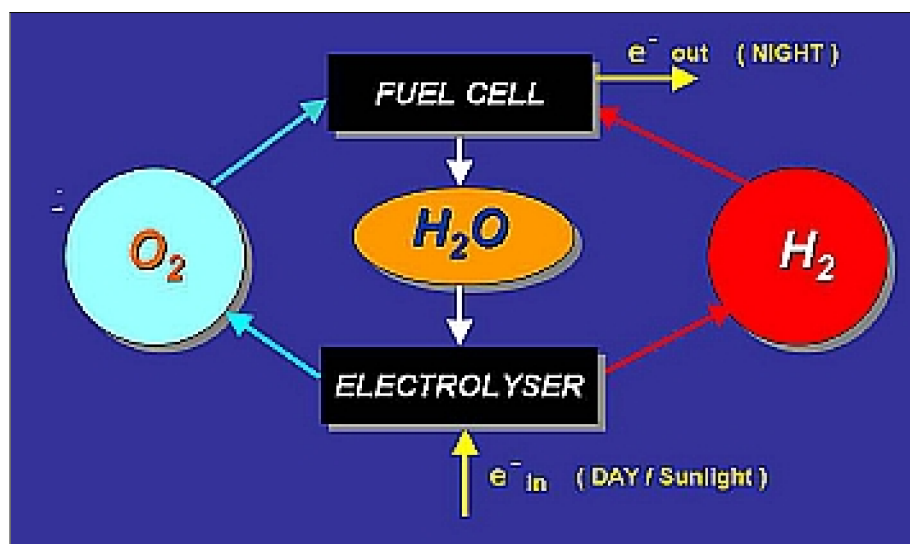


Figure 52: Schematic of a regenerative fuel cell system (image credit: ESA)

Longer space missions, however, clearly require regenerative energy storage; batteries are recharged by solar arrays directly, in fuel cells the reactants hydrogen and oxygen are recharged by electrolyzing the product water from the fuel cell operation whenever solar array power is available. This adds a lot of complexity.⁹⁴¹⁾ Nevertheless the significantly higher energy density provided by regenerative fuel cells (fuel cell + electrolyzer) compared to batteries would be technically speaking a clear choice. A mass saving of 2 to 3 in power system weight vs. the most advanced space battery system is achievable and looks also in terms of launch cost very promising. Additionally a fuel cell can clearly separate power requirements from energy requirements, the power is sized by the electrode stack (the reactor), the energy is defined by the size of the reactant storage. In batteries this option is not available, the reactants are contained in the electrodes – it has to be sized for the worst case.

It seems that the circle might be coming to a full closure after all; first employed in space missions, fuel cells have recently found their mass market application in the automotive sector. Starting with prototype tests in the 1990s, fuel cells form now an integral part of the hydrogen economy and are expected to see their market roll–out by 2015, with the next generation commercial fuel cell electric vehicles. Space in contrary has retired its fuel cells in the summer of 2011, when the last Space Shuttle mission came to a successful end. The high power/energy requirements remain, however, and so we are likely to the spin–in of terrestrial fuel cell technology into space in the years to come (Ref. 941).

940) “DoD Report to Congressional Defense Committees on the Utilization and Demonstration of Fuel Cells,” Aug. 1998

941) Norbert Frischauf, Beatriz Acosta–Iborra, Frederik Harskamp, Pietro Moretto, Thomas Malkow, Michel Honseelaar, Marc Steen, Scott Hovland, Bernhard Hufenbach, Max Schautz, Manfred Wittig, Alexander Soucek, “The hydrogen value chain: Applying the automotive role model of the Hydrogen Economy in the aerospace sector to increase performance and reduce costs,” Proceedings of IAC 2011 (62nd International Astronautical Congress), Cape Town, South Africa, Oct. 3–7, 2011, paper: IAC–11–D.1.2.4

1.8.5.3 RPS (Radioisotope Power Systems) in the US space program

Radioisotope Power Systems (RPS) have been a workhorse for deep space exploration since their first use in 1961. The first decade of RPS use (1961 to 1971) concentrated on missions in LEO and on the Moon. Starting in the early 1970s, RPS began to be used for deep space missions, starting with the Pioneer spacecraft series and ending with the most recent RPS-powered mission, New Horizons, launched in 2006.⁹⁴²⁾

Figure 53 illustrates the relatively simple operation of an RPS. A fuel form containing the Pu-238 fuel steadily generates heat, which is converted in some type of power converter into electrical power. There is always waste heat produced by the conversion process, and this must be discarded. Ordinarily, this is ejected directly to space via radiators, although for some missions, it is used to provide low-temperature heating of payload instruments and equipment.

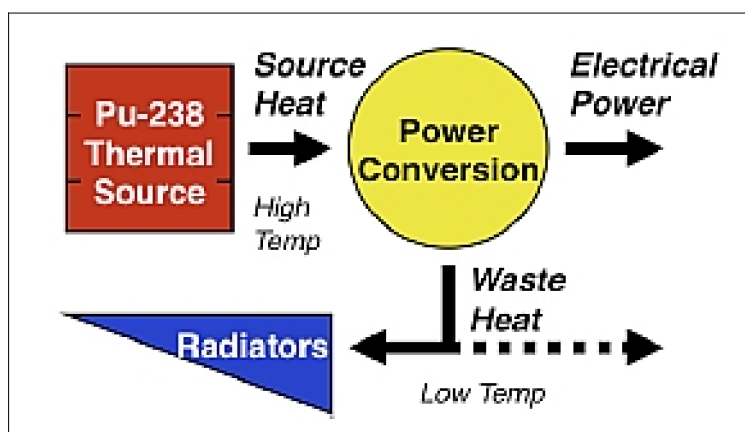


Figure 53: RPS functional schematic (image credit: NASA)

Many different type of energy conversion systems have been considered for RPS. The one used on all missions to date is thermoelectrics, a static process that utilizes the Seebeck Effect to generate a voltage potential via temperature differences. These systems achieve energy conversion efficiencies of about 6%, although values above 10% appear feasible with more advanced materials. Dynamic systems, such as Stirling and Brayton, are capable of higher efficiencies (25–35% and perhaps above), and point to the new direction of converter systems, motivated primarily to conserve the limited inventory of Pu-238 fuel.

Some background on RPS: The first RPS ever built, which was referred to as a **RTG** (Radioisotope Thermoelectric Generator), was developed in the 1950s to demonstrate full operation of a “nuclear battery.” Called **SNAP-3** (Systems for Nuclear Auxilliary Power), it was developed by the AEC (Atomic Energy Commission). The device was fueled using Polonium-210 (Po-210), a very energetic alpha particle generator.

The SNAP-3 never flew in space, but it became an invaluable showpiece for RPS and the SNAP program. After SNAP-3, the AEC completed work on the **SNAP-3B**, which was similar to the original unit but used the preferred Pu-238 fuel. The unit was used as an auxilliary power source on the Transit 4A and 4B satellites of the US Navy in 1961. The RTG on Transit-4A generated electricity from thermoelectric junctions in the RTG module. The two Transit 4 S/C were dual-powered, allowing switching between the solar cells and the radioisotope-derived power. The drum-shaped S/C were covered with solar cells providing 35 W (BOL).

The same metallic Pu-238 fuel form and thermoelectric thermocouples were used in the larger SNAP-9A, which was used as the main power source for the Transit 5BN series of

942) George R. Schmidt, “Nuclear Systems for Space Power and Propulsion,” Proceedings of IAC 2011 (62nd International Astronautical Congress), Cape Town, South Africa, Oct. 3–7, 2011, paper: IAC-11.C4.7–C3.5.2

satellites. The unit produced 25.9 We, and achieved a system specific power almost two times that of the SNAP–3B.

RTG (Radioisotope Thermoelectric Generator): The RTG technology represents an alternate power source to solar radiation energy. Radioisotope power systems convert the heat energy of decaying radioactive material into electricity (use of Plutonium–238). Unlike a nuclear reactor, an RTG uses decay that is not accelerated by controlled chain reaction, so the power density is limited, but so is shielding weight.

The RTG power conversion method employs the thermoelectric effect, where a pair of electrodes, typically SiGe (Silicon–Germanium) held at different temperatures, develop a potential difference due to the Seebeck effect (RTGs use heat from the alpha–particle decay of plutonium 238 (^{238}Pu) to power thermoelectric generators via the Seebeck effect). This can drive a current and hence generate power. Efficiency is low, typically around 4–5%. Note: RTG is also referred to as REP (Radioisotope Electric Propulsion) in the literature. 943)

The major advantage of RTGs is the availability of a constant power source – whatever the distance to the sun. Hence, RTGs are being used in environments (in particular in deep space missions) where the solar radiation becomes ineffective for a spacecraft power subsystem, namely at vast distances from the sun.

The launch failure of Transit 5BN–3 and designed disintegration of the SNAP–9A in the upper atmosphere led to the incorporation of new safety and design features on subsequent RTGs. The next RTG, **SNAP–19B**, employed a PuO_2 fuel form which was designed to remain intact in the event of failures and accidents. Apart from this, the SNAP–19B was very similar to the SNAP–9A. It was also the first RTG to be used on a NASA mission, which interestingly occurred in Earth orbit aboard the Nimbus B–1 and B–2 satellites. Although Nimbus B–1 failed during launch, the RTG was recovered and the fuel was used on a subsequent mission. Most importantly, NASA remained interested in using RTGs for future missions. The Nimbus–3 research weather satellite (launch Apr. 14, 1969) of NASA in LEO was launched successfully with the SNAP–19B.

The next RTG development was the **SNAP–27**, which was built to provide long duration power to Apollo science experiments left on the lunar surface. The SNAP–27 employed much of the same technology as SNAP–19B, however, it had a much higher power and achieved a specific power of 3.2 We/kg, about 50% greater than the SNAP–19B. The SNAP–27 performed flawlessly on five Apollo missions, and far exceeded its design requirements.

Spacecraft	S/C Designation	Launch Date	RTG Mass (kg)	Power Sytem (W)	Ops life of RTG
Transit 4–A	1961 o1	June 29, 1961	78.8	SNAP–3B7, (3)	operated 15 years
Transit 4–B	1961 αη1	Nov. 15, 1961	89.5	SNAP–3B8, (3)	operated 9 years
Transit 5BN–1	1963–38B	Sept. 28, 1963	69.3	SNAP–9A (30)	operated 9 months
Transit 5BN–2	1963–49B	Dec. 5, 1963	74.7	SNAP–9A (30)	operated 6 years
Transit 5BN–3	–	Apr. 21, 1964	75.1	SNAP–9A (30)	Launch failure
TRIAD	1972–69A	Sept. 2, 1972	93.9	RPS (30)	operating in 2007
New Horizons	2006–001A	Jan. 19, 2006	351	GPHS–RTG (295)	Pluto flyby in July 2015

943) Emma S. Hinds, Deaglan McNamara, Micah Walter–Range, “The Future of Radioisotope Power Systems for American Space Exploration,” Proceedings of the 59th IAC (International Astronautical Congress), Glasgow, Scotland, UK, Sept. 29 to Oct. 3, 2008, IAC–08–C4.7.–C3.5.2

Table 53: Radioisotope-powered source for spacecraft built by JHU/APL ⁹⁴⁴⁾

The LES [Lincoln (Laboratory) Experimental Satellite] communication S/C of DoD used the first RTG demonstration called **MHW** (Multihundred Watt) in an inclined GSO (Geosynchronous Orbit), launch of LES-8/9 March 15, 1976. NASA also used the MHW-RTG for its two Voyager probes, each of which carried three of the units. The MHW-RTG was notable for its significant improvement in specific power, 4.2 We/kg versus the ~ 3.0 We/kg common to previous Pb-Te systems. ⁹⁴⁵⁾

Up to 2000, the US had launched a total of 44 spacecraft with an onboard RTG system, among them Pioneer-10 (launch Mar. 2, 1972), Pioneer-11 (launch April 5, 1973), Viking-1 (launch Aug. 20, 1975) Viking-2 (launch Sep. 9, 1975), Voyager-1 (launch Sep. 5, 1977), Voyager-2 (launch Aug. 20, 1977), Galileo (launch Oct. 18, 1989) ⁹⁴⁶⁾, Ulysses (S/C mass of 370 kg, launch Oct. 6, 1990 on STS-41), and Cassini (launch Oct. 1997 on a mission to Saturn, Cassini is powered by 32,8 kg of plutonium fuel).

Spacecraft	Power source	No of RTGs	Mission type	Launch date	Status
Transit 4A	SNAP-3	1	Navigation	29.06.1961	Currently in orbit
Transit 4B	SNAP-3	1	Navigation	15.11.1961	Currently in orbit
Transit 5 BN-1	SNAP-9A	1	Navigation	28.09.1963	Currently in orbit
Transit 5 BN-2	SNAP-9A	1	Navigation	05.12.1963	Currently in orbit
Transit 5 BN-3	SNAP-9A	1	Navigation	12.04.1964	Aborted, burned up
Nimbus B-1	SNAP-19	2	Meteorology	18.05.1968	Aborted, retrieved
Nimbus-3	SNAP-19	2	Meteorology	14.04.1969	Currently in orbit
Apollo 11	ALRHU	Heater	Lunar	16.07.1969	On Lunar surface
Apollo 12	SNAP-27	1	Lunar/ALSEP	14.11.1969	On Lunar surface
Apollo 13	SNAP-27	1	Lunar/ALSEP	14.11.1970	Aborted in Pacific
Apollo 14	SNAP-27	1	Lunar/ALSEP	31.01.1971	On Lunar surface
Apollo 15	SNAP-27	1	Lunar/ALSEP	26.07.1971	On Lunar surface
Pioneer 10	SNAP-19	4	Planetary	02.03.1972	Heliopause
Apollo 16	SNAP-27	1	Lunar/ALSEP	16.04.1972	On Lunar surface
Triad-01-1X	Transit-RTG	1	Navigation	02.09.1972	Currently in orbit
Apollo 17	SNAP-27	1	Lunar/ALSEP	07.12.1972	On Lunar surface
Pioneer 11	SNAP-19	4	Planetary	05.04.1973	Heliopause
Viking 1	SNAP-19	2	Mars Lander	20.08.1975	On Marian surface
Viking 2	SNAP-19	2	Mars Lander	09.09.1975	On Martian surface
LES 8, 9	MHW-RTG	2, 2	Communication	14.03.1976	Currently in orbit
Voyager 2	MHW-RTG	3	Planetary	20.08.1977	Heliopause
Voyager 1	MHW-RTG	3	Planetary	05.09.1977	Heliopause
Galileo	GPHS-RTG	2	Planetary	18.10.1989	Intentionally deorbited to Jupiter
Ulysses	GPHS-RTG	1	Planetary	06.10.1990	Sun's polar regions
Mars Pathfinder	LWRHU	Heater	Mars Lander	04.12.1996	Operated on Mars
Cassini	GPHS-RTG	3	Planetary	15.10.1997	Operating at Saturn

944) J. Dassoulas, R. L. McNutt, Jr., "RTGs on Transit," STAIF (Space Technology & Applications International Forum) 2007, Feb. 11-15, 2007, Albuquerque, NM, USA

945) W. R. Determan, "Systems for Nuclear Auxiliary Power (SNAP) Program: A Review of Space Reactor Power Systems SNAP 2/10A, SNAP 8, and the Adv. UZrH Reactor Programs," STAIF (Space Technology & Applications International Forum) 2007, Feb. 11-15, 2007, Albuquerque, NM, USA

946) The Galileo spacecraft ended its mission with a final intended plunge into Jupiter's atmosphere on Sept. 21, 2003

Spacecraft	Power source	No of RTGs	Mission type	Launch date	Status
New Horizons	GPHS–RTG	1	Planetary	19.01.2006	Enroute to Pluto
MSL rover	MMTRG		Mars lander	26.11.2011	Enroute to Mars

Table 54: US spacecraft using Radioisotope power systems ^{947) 948)}

Legend to Table 54: ALSEP (Apollo Lunar Surface Experiments Package); MHW–RTG (Multi–Hundred Watt–Radioisotopic Thermoelectric Generator); LWRHU (Lightweight Radioisotope Heater Unit); GPHS (General Purpose Heat Source).

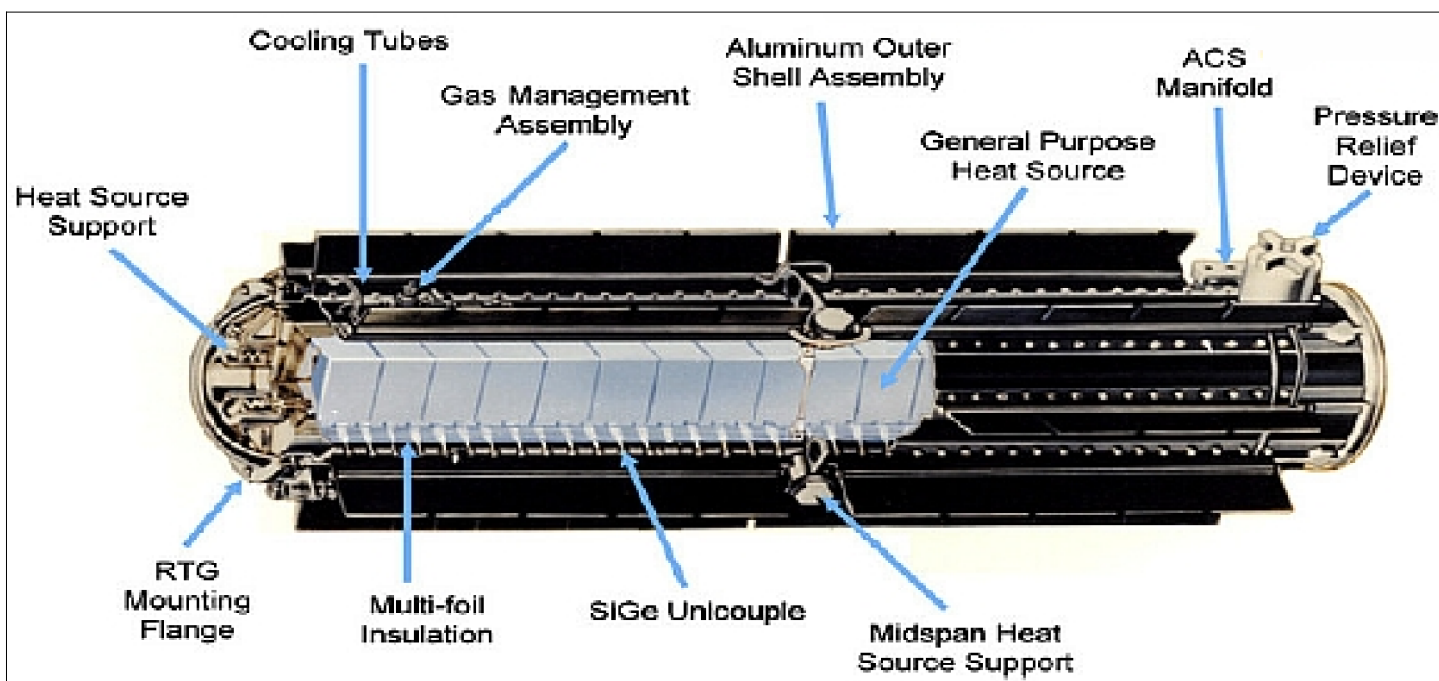


Figure 54: Schematic view of a RTG system (image credit: NASA, ESA) ⁹⁴⁹⁾

The RTGs, all < 500 W, provided a specific power of about 3–8 W/kg. LANL (Los Alamos National Laboratory) developed the MHW (Multihundred Watt) RTG system for the Voyager missions. ^{950) 951) 952)} In MHW, 24 heat sources were contained within a RTG; heat was converted to electrical power by 312 silicon–germanium thermoelectric couples. Each RTG provided about 157 W at BOL. LANL also developed the GPHS (General Purpose Heat Source) RTG for the Galileo, Ulysses, Cassini, and Pluto–New Horizons missions. The GPHS RTG system contains 572 SiGe thermoelectric couples inside a thermoelectric converter, generating of 285 W (BOL). There are 18 GPHS modules to the RTG. A GPHS–RTG has a mass of 54 kg. The GPHS has a specific power of 5.2 We/kg, this was far greater than any other RTG before, along with its substantial power level of ~ 300 We.

The GPHS–RTG system (246 W BOL, 200 W EOL, mass of 56 kg) is also flown on NASA's New Horizons spacecraft (launch of New Horizons on Jan. 19, 2006) to Pluto (the S/C will

947) Roger D. Launius, "Powering Space Exploration in the United States: a History of RTGs, Nuclear Reactors, and outer Planetary Probes," Proceedings of the 59th IAC (International Astronautical Congress), Glasgow, Scotland, UK, Sept. 29 to Oct. 3, 2008, IAC–08.C4.7.–C3.5.1

948) "The Role of Nuclear Power and Nuclear Propulsion in the Peaceful Exploration of Space," IAEA (International Atomic Energy Agency, 2005 URL: http://www-pub.iaea.org/MTCD/publications/PDF/Pub1197_web.pdf

949) Major S. Chahal, "European Space Nuclear Power Programme: UK Activities," Proceedings of the 49 Session of UN COPUOS (Committee on the Peaceful Uses of Outer Space), STSC (Scientific and Technological Subcommittee), Vienna, Austria, Feb. 6–17, 2012, URL: <http://www.oosa.unvienna.org/pdf/pres/stsc2012/tech-18E.pdf>

950) <http://en.wikipedia.org/wiki/SNAP-10A>

951) <http://fti.neep.wisc.edu/neep602/SPRING00/lecture3.pdf>

952) G. L. Bennett, "Space Nuclear Power: Opening the Final Frontier," <http://www.fas.org/nuke/space/bennett0706.pdf>

reach Pluto and its largest moon, Charon, on July 14, 2015). Following this primary mission, the requirements call for a continuation of the mission – exploring objects beyond Pluto in the expanse of the Kuiper Belt.^{953) 954)}

Note: The US has flown one space nuclear fission reactor (SNAP–10A) on the experimental DoD spacecraft SNAPSHOT (launch Apr. 3, 1965). It provided 500 W of electrical power. SNAP–10A was a liquid–metal–cooled nuclear reactor with thermoelectric conversion. The SNAP–10A operated for 43 days.

Of course, the energy generated by an RTG could also be used for electric propulsion, referred to as **NEP** (Nuclear Electric Propulsion) or **REP** (Radioisotope Electric Propulsion), to speed up a mission’s cruise phase. The NEP technology, or the use of nuclear reactors to generate heat, which is converted into electrical power for high–performance electric thrusters, can add significant benefits to space missions:

- NEP will enable much faster and more frequent planetary investigations with greater science capabilities “anywhere, all the time” mission design

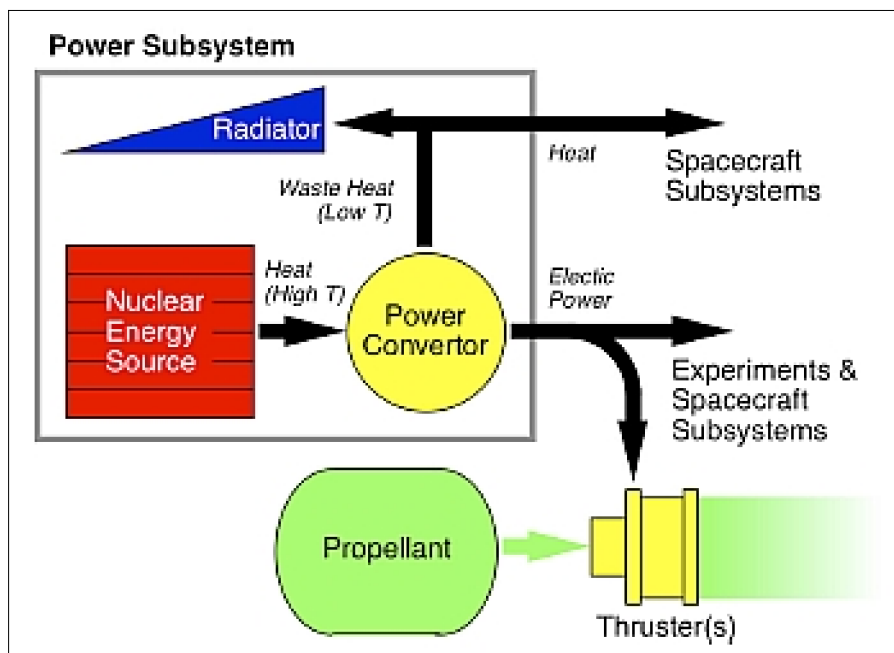


Figure 55: Schematic of the NEP configuration (image credit: NASA)

- NEP enables a revolutionary change in approach to outer solar system exploration
- Drive spacecraft directly to the planets in ways not possible today, and perform complex orbital maneuvers once there
- Provide ample electrical power to operate advanced scientific instruments and transmit the resulting data to Earth at a very high bit rate.
- **Project Prometheus** (formerly known as Nuclear Systems Initiative) is a NASA and DOE program initiative (start in 2002) to develop a next–generation long–term on–orbit propulsion system technology. The objective is to define and to develop an improved performance **ARPS** (Advanced Radioisotope Power System) for the support of future deep

953) C. B. Hersman, D. Y. Kusnierkiewicz, “Optimization of the New Horizons Spacecraft Power Demand for a Single Radioisotope Thermoelectric Generator,” Proceedings of the 57th IAC/IAF/IAA (International Astronautical Congress), Valencia, Spain, Oct. 2–6, 2006, IAC–06–C3.4.–D3.4.05

954) Note: After over 30 years of operation, it appears that Pioneer–10 has sent its last signal to Earth. Pioneer’s last, very weak signal was received on Jan. 23, 2003. The last time a Pioneer 10 contact returned telemetry data was on April 27, 2002. Launched in March 1972, Pioneer–10 was the first spacecraft to travel to an outer planet, providing data and images of Jupiter.

space science missions (starting launches beyond 2012) for solar system exploration. In the past, the availability of sufficient electrical power has always been a very limiting and critical design factor in deep-space missions, in particular for power-hungry active instrument applications like SAR observations of planets. Such SAR missions require the support of high communication links in addition to the power for the SAR instrument. ^{955) 956)}

Note: Project Prometheus was officially **discontinued in October 2005**. In August 2005, NASA re-evaluated its priorities in light of available funding and established “Return to Flight”, the International Space Station, and the Crew Exploration Vehicle as the highest priority tasks for the Agency. Consequently, the Prometheus Project was directed to not proceed into Phase B.

Background: Past/current sample deep-space radar missions with RTG power implementations are: NASA’s Magellan orbiter to Venus (launch of Magellan on STS-30, May 4, 1989, arrival at Venus in Aug. 1990, the mission lasted for 4 years) employed a SAR instrument to be able to observe the surface of Venus through a dense cloud layer [a lot of SAR data collected by Magellan had to be discarded onboard because of the lack of a sufficiently high-rate downlink communication to Earth]. NASA’s Cassini probe, to reach Saturn in July 2004 after a nearly seven-year journey, is also equipped with a SAR instrument. Cassini will use it to map Titan, Saturn’s largest and most mysterious moon. The objective of NASA’s Mars Reconnaissance Orbiter (launch Aug. 12, 2005) is to penetrate the surface of the planet to search for water. Again, this requires a SAR instrument, called SHARAD (Shallow Subsurface Radar), to obtain high-resolution data to surface depths up to 1 km.

In the overall Prometheus program there are two basic types of technologies under consideration: 1) radioisotope-based systems (managed by NASA), and 2) nuclear fission-based systems (managed by DOE). The new ARPS technology focus is on two technologies: ^{957) 958) 959), 960)}

- a) **MMRTG** (Multi-Mission Radioisotope Thermoelectric Generator)
- b) **SRG** (Stirling Radioisotope Generator).

NASA/GRC and its industrial partners are working on the definition of SRG. The efficiency of the new SRG system, referred to as **ASRG** (Advanced Stirling Radioisotope Generator), is expected to be four times higher than that of the conventional RTG technology. The design requirements call for an operational life of $> 10^5$ hr (11.4 years) with an energy provision of > 100 W DC to the S/C. The **ASC** (Stirling Stirling Converter) consists of two free-piston Stirling engines coupled to a linear alternator (two engines are needed to suppress vibration), all of which is contained in a hermetically sealed pressure vessel (first use of a dynamic power conversion technology for space application). Due to the reduced envelope and lighter mass of the ASC compared to the previous Stirling converter, the specific power of the flight generator is projected to increase from 3.5 W_e/kg to 7 W_e/kg, along with a 25% reduction in generator length. As of 2007, tests are being planned and conducted on the

955) B. Berger, “Project Prometheus May Bring Wider Use of Radar Imaging,” Space News, May 3, 2004, p. 3

956) D. H. Lehman, K. B. Clark, B. A. Cook, S. A. Gavit, S. A. Kayali, J. C. McKinney, D. A. Milkovich, K. R. Reh, R. L. Taylor, J. R. Casani, “Experiences in Managing the Prometheus Project,” Proceedings of the 2006 IEEE/AIAA Aerospace Conference, Big Sky, MT, USA, March 4–11, 2006

957) J. G. Schreiber, “Capabilities and Technical Issues Regarding the Stirling Radioisotope Generator,” Proceedings of the IEEE Aerospace Conference, Big Sky, MT, March 9–16, 2002

958) J. Bates, “NASA Science Chief Lays Out Need for New Propulsion System,” Space News, June 9, 2003, p. 8

959) A. M. Baker, V. Lappas, M. Sweeting, “Small Spacecraft to the Limits: Power and Propulsion Technology Drivers for a Robotic Precursor Mission to the Outer Planets and beyond the Solar System,” Proceedings of IAC 2004, Vancouver, Canada, Oct. 4–8, 2004, IAC-04-IAF-U.4.07

960) D. J. Anderson, J. Sankovic, D. Wilt, R. D. Abelson, J. –P. Fleurial, “NASA’s Advanced Radioisotope Power Conversion Technology Development Status,” Proceedings of the 2007 IEEE Aerospace Conference, Big Sky, MT, March 3–10, 2007

ASC prototype to demonstrate the capability for long life, high reliability, and flight qualification needed for use in future missions. ^{961) 962) 963) 964)}

The ASRG is a key technology for NASA's planetary science community. The advantages include higher power and lower mass than the incumbent RTG technologies. The system is comprised of two primary subsystems: the paired ASCs and the control avionics. The ASRG project has sufficient margin to meet the power (130 W) and mass (32 kg) required. In 2012, the qualification test generator is under production, and planned for testing in 2013. The testing is expected to have two phases, both electrically heated and fuelled. The test strategy is based upon the traditional pyramid approach. Two flight generators are planned for completion in 2016. ⁹⁶⁵⁾

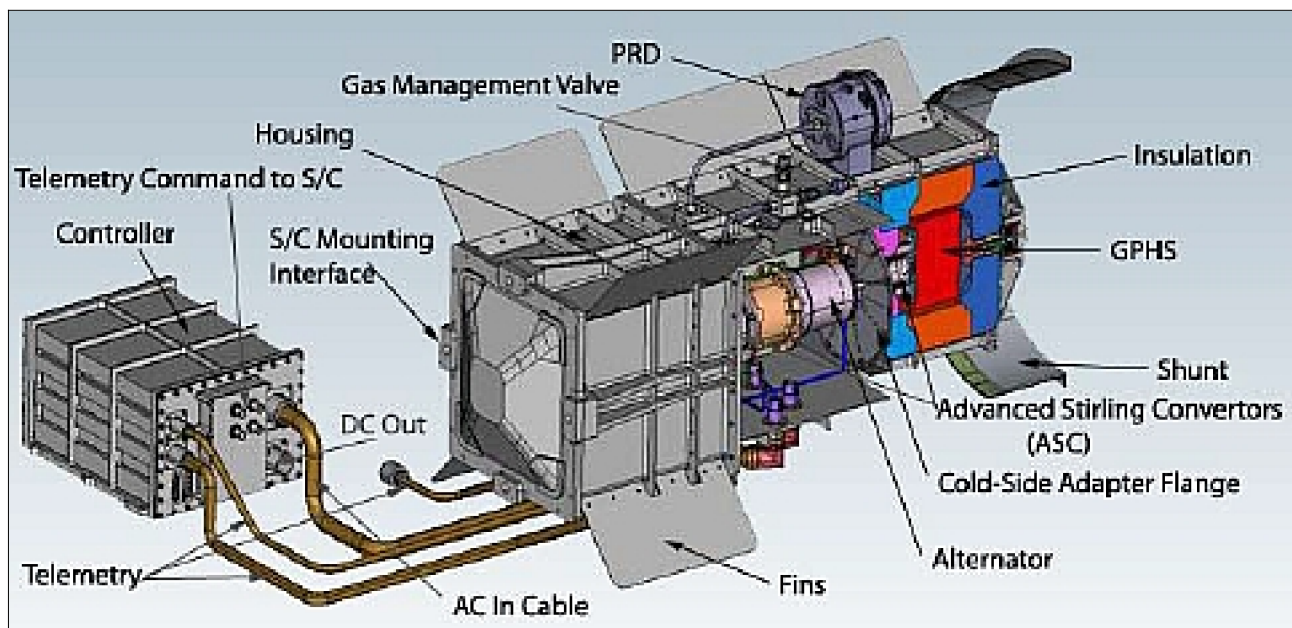


Figure 56: ASRG cutaway image and major subsystems (image credit: NASA/GRC)

– In November 2013, James Green, NASA Director of PSD (Planetary Science Division) announced, that due to the current budget – constrained environment, NASA has decided to **discontinue the procurement of ASRG flight hardware**. NASA has given directions to DOE (Department of Energy) to end work on the flight units. ^{966) 967)}

In June 2003, DOE awarded the MMRTG system design, development, test and integration contract to a team led by the Boeing Company's Rocketdyne Propulsion and Power Divi-

- 961) J. Chan, J. G. Wood, J. G. Schreiber, "Development of Advanced Stirling Radioisotope Generator for Space Exploration," STAIF (Space Technology & Applications International Forum) 2007, Feb. 11–15, 2007, Albuquerque, NM, USA
- 962) R. Richardson, J. Chan, "Advanced Stirling Radioisotope Generator Development," NSTC2007 (NASA Science and Technology Conference 2007), College Park, MD, USA, June 19–21, 2007, URL: http://esto.nasa.gov/conferences/nstc2007/papers/Richardson_Rebecca_D2P2_NSTC-07-0155.pdf
- 963) Richard K. Shaltens, Wayne A. Wong, "Advanced Stirling Technology Development at NASA Glenn Research Center," NSTC2007 (NASA Science and Technology Conference 2007), College Park, MD, USA, June 19–21, 2007, URL: http://esto.nasa.gov/conferences/nstc2007/papers/Shaltens_Richard_D2P1_NSTC-07-0138.pdf
- 964) G. R. Schmidt, D. H. Manzella, H. Kamhawi, T. Kremic, L. A. Dudzinski, "Radioisotope Electric Propulsion (REP): A Near-term Approach to Nuclear Propulsion," Proceedings of the 59th IAC (International Astronautical Congress), Glasgow, Scotland, UK, Sept. 29 to Oct. 3, 2008, IAC-08.C4.7.-C3.5.3
- 965) Thomas Hartline, Glen Horvat, Chris Steffen, "Advanced Stirling Radioisotope Generator Development Status and Potential Near-term Mission Applications," Proceedings of the 63rd IAC (International Astronautical Congress), Naples, Italy, Oct. 1–5, 2012, paper: IAC-12-C4.7-C3.5.2
- 966) "Important Changes in the NASA Planetary Science Division's (PSD) Radioisotope Program," Planetary News, Nov. 2013, URL: http://www.lpi.usra.edu/planetary_news/2013/11/15/important-changes-in-the-nasa-planetary-science-divisions-psd-radioisotope-program/
- 967) Ralph L. McNutt, Jr., "Radioisotope Power Systems: Pu-238 and ASRG status and the way forward," 10th Meeting of the NASA Small Bodies Assessment Group, Jan. 8, 2014, URL: http://www.lpi.usra.edu/sbag/meetings/jan2014/presentations/08_1545_McNutt_Pu238_SBAG.pdf

sion. Top level requirements for the MMRTG design have been established.⁹⁶⁸⁾ The heat source for the MMRTG design will consist of eight (8) enhanced GPHS (General Purpose Heat Source) modules. These modules are similar to those used in the GPHS – RTG that powered the Galileo, Ulysses, and Cassini/Huygens spacecraft. At the beginning of the mission, the MMRTG is designed to generate a minimum of 110 W of power at 28 volt DC, and to have a design life of at least 14 years.

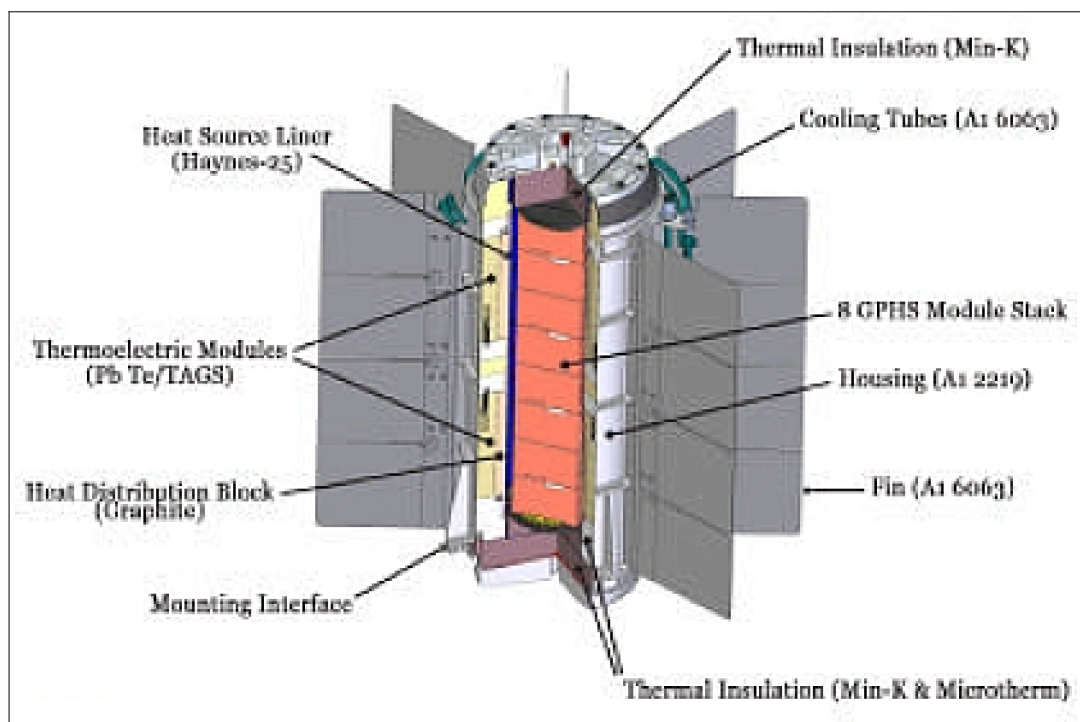


Figure 57: Illustration of the MMRTG instrumentation on Curiosity (image credit: NASA/JPL)

First use of the MMRTG technology is for the **MSL** (Mars Science Laboratory) rover (nicknamed **Curiosity**) of NASA/JPL with a launch on Nov. 26, 2011. The MMRTG power system provides ~ 110 W and is capable of continuous operation for several years. The MMRTG contains 4.8 kg of plutonium dioxide as the source of the steady supply of heat used to produce the onboard electricity and to warm the rover's systems during the frigid Martian night. The MMRTG provides initially ~ 2 kW of thermal power and 120 W of electrical power. The MMRTG carries 8 individually shielded GPHS (General Purpose Heat Source) modules (compared to 18 modules in the previous generation). The thickness of the protective graphite material in the center of the modules and between the shells of each module in the MMRTG has been increased by 20 percent over previous modules. The MMRTG generator is about 64 cm in diameter (fin tip to fin tip) by 66 cm in length and has a mass of ~ 45 kg. – Curiosity landed on Mars on August 5, 2012 to carry out its mission over 23 months.^{969) 970) 971) 972)}

968) F. Ritz, C. E. Peterson, "Multi-Mission Radioisotope Thermoelectric Generator (MMRTG) Program Overview," Proceedings of the IEEE Aerospace Conference, Big Sky, MT, March 6–13, 2004

969) "Mars Science Laboratory Launch Nuclear Safety," NASA/JPL: http://mars.jpl.nasa.gov/msl/files/msl/APP_MSL_Launch_Nuclear_Safety_FS_3-2-11.pdf

970) Space Radioisotope Power Systems – Multi-Mission Radioisotope Thermoelectric Generator, NASA, Jan. 2008, URL: http://www.ne.doe.gov/pdfFiles/MMRTG_Jan2008.pdf

971) <http://mars.jpl.nasa.gov/msl/>

972) "Mars Science Laboratory Landing," NASA Press Kit, July 2012, URL: http://www.jpl.nasa.gov/news/press_kits/MSLLanding.pdf

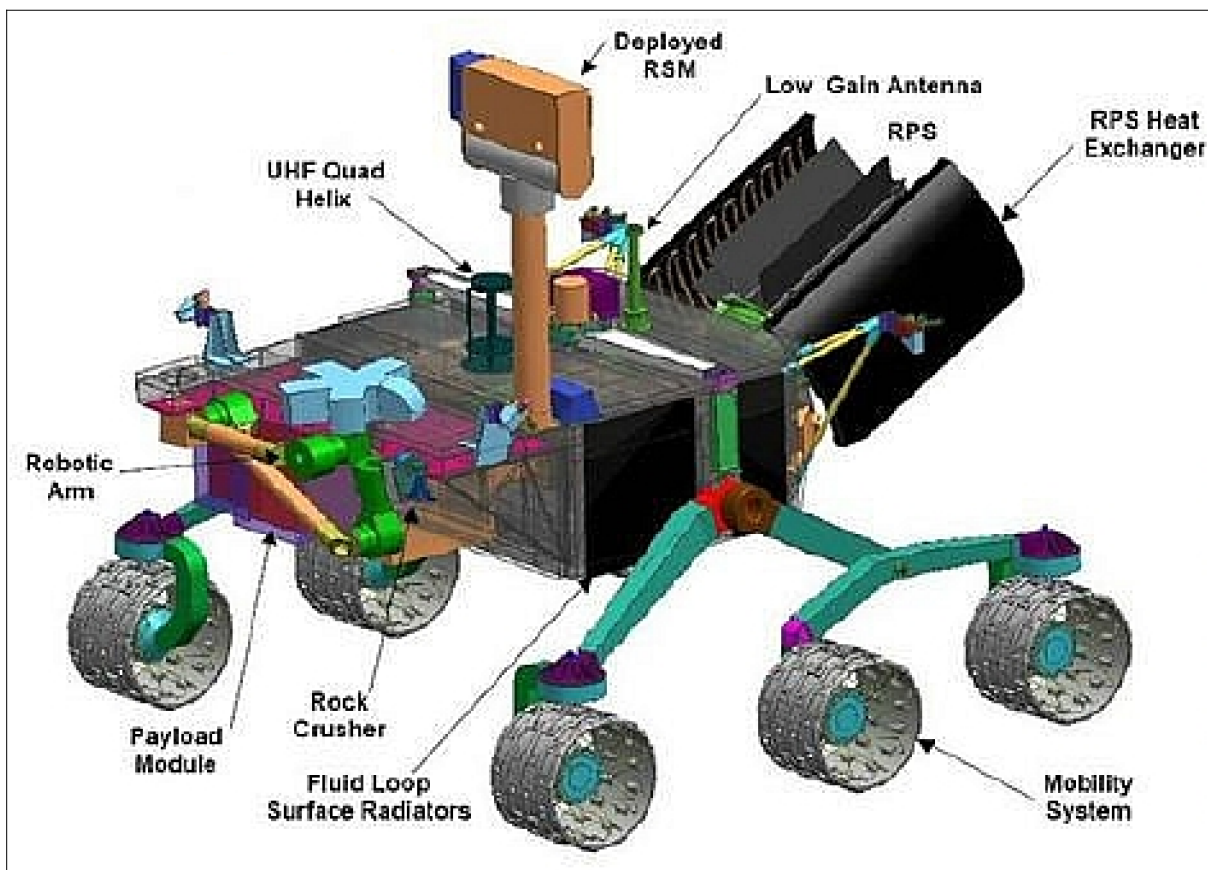


Figure 58: Mars Science Laboratory (Curiosity rover), powered by a Pu-238 fuelled radioisotope (image credit: NASA/JPL)

A first candidate in the nuclear fission–based scenario, a technology with considerably improved power generation capability, is NASA’s proposed **JIMO** (Jupiter Icy Moons Orbiter) demonstration mission to observe three planet–sized moons of Jupiter – Callisto, Ganymede and Europa – which may harbor vast oceans beneath their icy surfaces (planned launch of JIMO in 2015 time frame). The JIMO mission also may raise the capability for deep space exploration to a revolutionary new level by pioneering such features as: a) the use of electric propulsion powered by a nuclear fission reactor, b) use of much higher data rates (> 10 Mbit/s) from deep space, c) more power availability for science instruments, etc.

Note: The JIMO project was cancelled in 2005 and was replaced by a set of missions, as documented in NASA’s 2006 Solar System Exploration (SSE) Roadmap. Potential missions to be selected are in two categories:

- Flagship class missions (Europa Explorer, Titan Explorer, etc.)
- New Frontiers class missions (New Horizons–Pluto Kuiper Belt Explorer, Juno–Jupiter Polar Orbiter, Saturn Flyby, etc.)

As part of this effort^{973) 974)}, the 2006 SSE Roadmap identified RPS (Radioisotope Power System) as high priority technologies, which are necessary to enable future missions. Currently (2007), ARPS systems are under development by NASA, DOE, and industry, with additional input from academia on researching and testing component technologies.

973) T. S. Balint, “Design Reference Mission Set for RPS Enabled Missions in Support of NASA’s SSE Roadmap,” Proceedings of the 2007 IEEE Aerospace Conference, Big Sky, MT, March 3–10, 2007

974) J. A. Cutts, T. S. Balint, A. P. Belz, C. E. Peterson, “Overview of NASA’s 2006 SSE Strategic Roadmap,” Proceedings of the 2007 IEEE Aerospace Conference, Big Sky, MT, March 3–10, 2007

1.8.5.4 NPS (Nuclear Power System) in the Soviet/Russian space program

In the early 1960s, the former USSR initiated a thermal–to electric energy conversion program that received the name ROMASHKA (the program was based on nuclear fission reactors to generate onboard electricity).⁹⁷⁵⁾ The **ROMASHKA** reactor–converter was designed and developed at KIAE (Kurchatov Institute of Atomic Energy) in cooperation with other institutes. The ground testing of the ROMASHKA converter–reactor was conducted with the reactor integrated and operated with a pulsed plasma thruster – for the first time in 1964. ROMASHKA generated electric power of 0.5 kW, thermal power of 28 kW, use of 49 kg of U235, and had a total mass of 450 kg.

– Concurrently, the so–called **BUK** (Space Nuclear Thermoelectric System) propulsion concept was developed (at the Institute of Physics and Power Engineering, as well as at other institutes in the USSR) around a fast reactor and an out–of–core thermoelectric converter. The BUK NPS used 37 fuel rods in the core and a liquid metal cooling system. A lifetime of 4400 hours of operating time was demonstrated. BUK provided electric power of up to 3 kW, thermal power of 100 kW, use of 30 kg of U235, total instrument mass of 900 kg.

– In the period 1967–1988, the USSR launched as many as 36 low–power BUK reactors on the so–called **RORSAT** (Radar Ocean Reconnaissance Satellite) series into LEO (Low Earth Orbit). Note: the RORSAT S/C were part of the Cosmos series. The first RORSAT mission was launched Dec. 27, 1967. The RORSATs operated at an altitude of 255 km, and used NaK–cooled reactor cores and thermoelectrics. Two RORSAT satellites with nuclear–powered generators caused world–wide alerts during their breakup and reentries to Earth in 1978 (Cosmos–954) and in early 1983, respectively.⁹⁷⁶⁾

– In parallel, efforts were initiated in Russia to develop SNPS (Space Nuclear Power Systems) based on in–core thermionic energy converters. Two thermionic system designs were used. The development of the SNPS technology led to first system power tests in 1970 and 1973, using a multi–cell TFE (Thermionic Fuel Cell) system design. In 1987, two experimental **TOPAZ** NPS units were flight–tested as part of the Plasma–A experimental spacecraft (Cosmos–1818 and Cosmos–1867), and demonstrated the lifetime of the SNPS of 142 days during the first test, and 342 days during the second test. – Note: Launch of the Plasma–A spacecraft on flight Cosmos–1818, Feb. 1, 1987 from Baikonur on a Tsyklon–2 vehicle. Launch of the Plasma–B spacecraft on flight Cosmos–1867, July 10, 1987 from Baikonur. The TOPAZ system provided electric power of up to 5 kW, thermal power of 150 kW, use of 11.5 kg of U235, total instrument mass of 980 kg.

– The **TOPAZ–2** project development (referred to as ENISEY in the USSR, and developed by the Krasnoyarsk Design Bureau of Applied Mechanics) employed the thermionic SNPS design based on single–cell TFEs. The TOPAZ–2 system consisted of the following main subsystems: the reactor subsystem, the radiation shield, the primary coolant loop, the cesium supply system, the gas systems, the thermal cover, the primary power system structure, and the instrumentation and control subsystem. – Full cycle ground tests were conducted confirming an operational lifetime of 1.5 years (post flight analysis predicted a lifetime of at least 3 years). Two full–scale system unit ground tests were conducted and completed in 1988 – but project funding cuts stopped all further system work and prevented any flight tests.

– In 1991 (at the end of the Cold War), a cooperative Russian–American space research program was started with the objective to perform demonstration tests with the TOPAZ–2 SNPS units. Two systems without fuel were delivered to the USA under a contract between

975) N. N. Ponomarev–Stepnoi, V. A. Pavshuk, V. A. Usov, “Russian Experience in Development and Testing of Nuclear Power Systems and Nuclear Thermal Propulsion Systems of the First Generation as the Basis for Development of Advanced Power and Propulsion Complexes for Peaceful Exploration of Near and Deep Space,” Proceedings of the 56th IAC 2005, Fukuoda, Japan, Oct. 17–21, 2005, IAC–05–C3.5–C4.7.09

976) G. F. Polansky, G. L. Schmidt, S. S. Voss, E. L. Reynolds, “Issues in the flight qualification of a space power reactor,” URL: <http://www.osti.gov/bridge/servlets/purl/10189746–JqctnU/webviewable/10189746.pdf>

INTERTEK (International Energy Technologies) of Moscow and ISP (International Scientific Products) of San Jose, CA, for ground tests (the systems were electrically heated). The first stage of the TOPAZ program culminated in power tests of two SNPS experimental units (V-71 and Ya-21U) and tests of single-cell TFEs performed in 1992–1993 by a team of specialists from Russia, USA, UK, and France (international inspection !!) at electrically heated test facilities newly built at the University of New Mexico, Albuquerque, NM. The successful tests of the TOPAZ-2 units resulted in plans for flight tests, using a spacecraft called **NEPSTP** (Nuclear Electric Propulsion Program). This resulted in a transfer of 4 more TOPAZ-2 units to the USA. Although the NEPSTP flight tests were never realized, the TOPAZ program remains an outstanding example of cooperation between Russia and USA. ^{977) 978)}

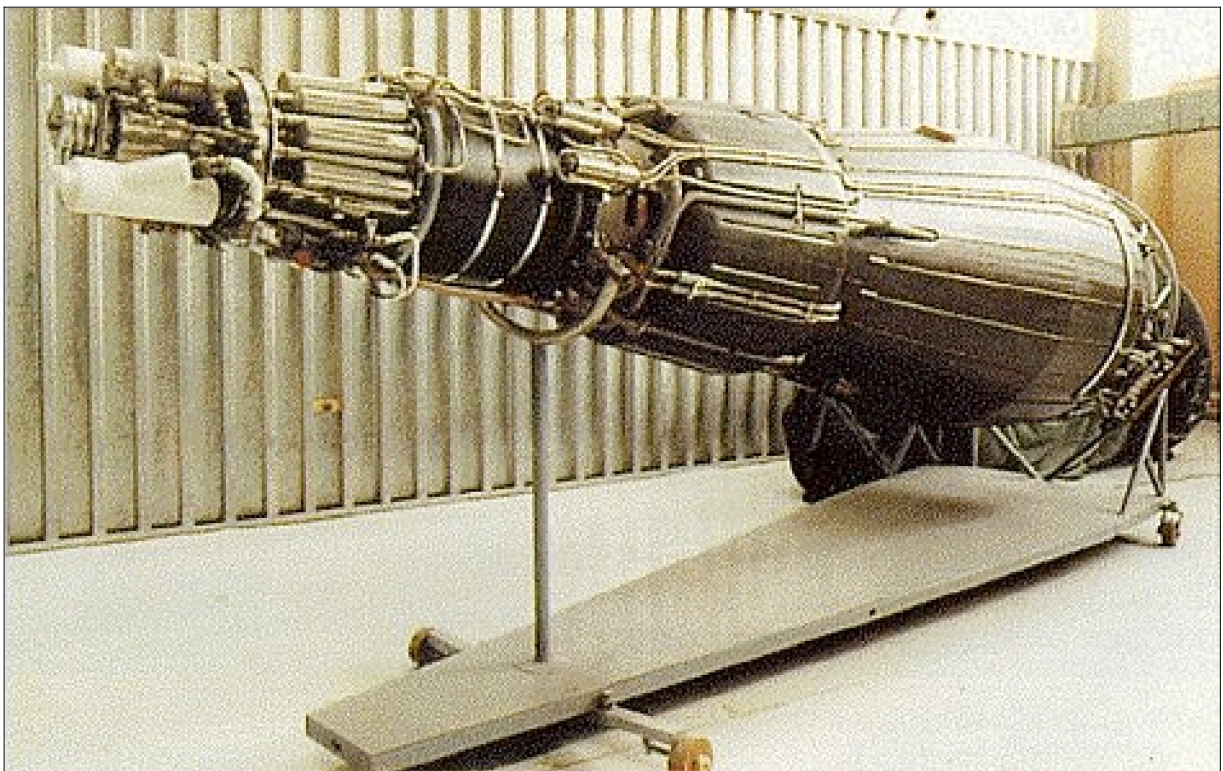


Figure 59: Illustration of a 5 kW TOPAZ thermionic reactor power system (credit: NASA, Ref. 942)

– Also, so-called RHUs (Radioisotope Heater Units) were used in the Soviet/Russian space program. The moon mission Luna-17 (launch Nov. 10, 1970) and Luna-20 (launch Feb. 14, 1973) used Polonium-210 isotopic heat sources to keep the Lunokhod rovers warm during the lunar nights. The MIR Space Station in LEO (1986–2001) used an RHU onboard (controlled reentry into the Pacific Ocean on March 23, 2001).

977) B. H. Mauk, P. F. Bythrow, N. A. Gatsonis, R. L. McNutt, “Science Plan for the Nuclear Electric Propulsion Space Test Program (NEPSTP),” AIAA, SAE, ASME, and ASEE, Joint Propulsion Conference and Exhibit, 29th, Monterey, CA, June 28–30, 1993, 25 p.

978) S. S. Voss, E. L. Reynolds, “An overview of the Nuclear Electric Propulsion Space Test Program (NEPSTP) satellite,” AIAA Intersociety Energy Conversion Engineering Conference, 29th, Monterey, CA, Aug. 7–11, 1994, Technical Papers. Pt. 1 (A94-31838 10-44), Washington, DC, AIAA, 1994, pp. 394–402

Project	Romashka	BUK	Topaz–1	Topaz–2
Development status	Prototype	32 flights	2 flights	Ground test
Time scale	1961–66	1970–78	1987	1992
Reactor type	Fast	Fast	Thermal	Thermal
Fuel	UC ₂	UC ₂	UC ₂	UC ₂
Conversion type	Thermoelectric	Thermoelectric	Thermoemission	Thermoemission
Thermal power (kW)	40	100	150	135
Electric power (kWe)	0.5–0.8	3.5	6	5.5
Mass (kg)	–	930	980	1061
Specific mass (kg/kW _e)	–	266	163	193
Operation (years, design)	0.5	1	1	1
Operation (years, actual)	0.17	0.5	0.96	1.5

Table 55: Summary of Russian nuclear fission power generator projects ⁹⁷⁹⁾

TPM (Transport Power Module):

In 2010, Russia initiated the TPM program with the goal to develop a MW (Mega-Watt)–class NPPS (Nuclear Power Propulsion System). Use of reactor nuclear power in outer space on the basis of the latest technologies, together with the creation of NPPS, are essential in order to meet current and future challenges in near and deep space and to develop space exploration in the twenty–first century. The main objectives of TPM are: ⁹⁸⁰⁾

- Technical and technological space nuclear power groundwork development
- Providing a basis for the realization of advanced programs aimed at deep space exploration and exploitation
- Creation of a new generation of space vehicles with high power availability
- Implementation of new technologies and innovative products creation.

The main project stages are:

- 2012: TPM and NPPS draft design development
- 2018: Ground testing and TPM flight test preparation.

The Russian Federation has established a system for the safe use of space vehicles with NPS that meets international requirements. The project to create TPM is being implemented in accordance with all technical safety measures recommended by the United Nations and prescribed by the relevant regulations of the Russian Federation.

979) Richard Blott, Anthony Donaldson, Dahmane Mazed, “High Power Nuclear Electric Propulsion Next Steps,” Proceedings of Space Propulsion 2010, San Sebastian, Spain, May 3–6, 2010

980) Alexander Solodukhin, “Implementation of the Safety Framework for Nuclear Power Source Applications in Outer Space: Modern and Planned Applications and Challenges,” Proceedings of the 49 Session of UN COPUOS (Committee on the Peaceful Uses of Outer Space), STSC (Scientific and Technological Subcommittee), Vienna, Austria, Feb. 6–17, 2012, URL: <http://www.oosa.unvienna.org/pdf/pres/stsc2012/2012nps-02E.pdf>

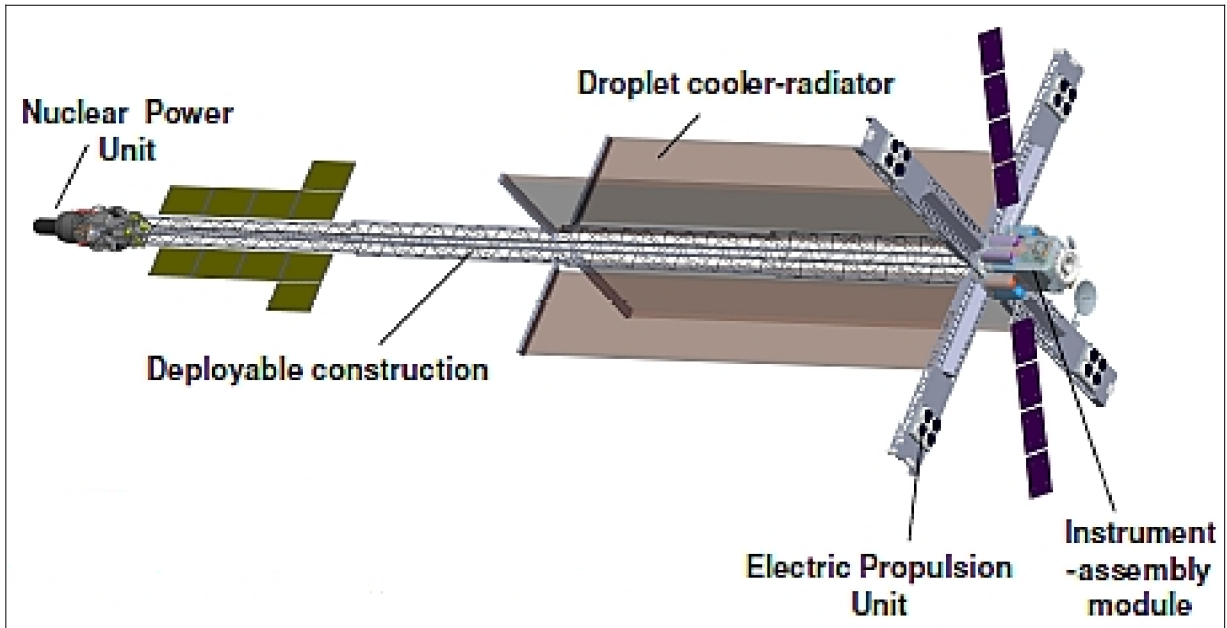


Figure 60: Illustration of the deployed TPM (image credit: Russian Federation)

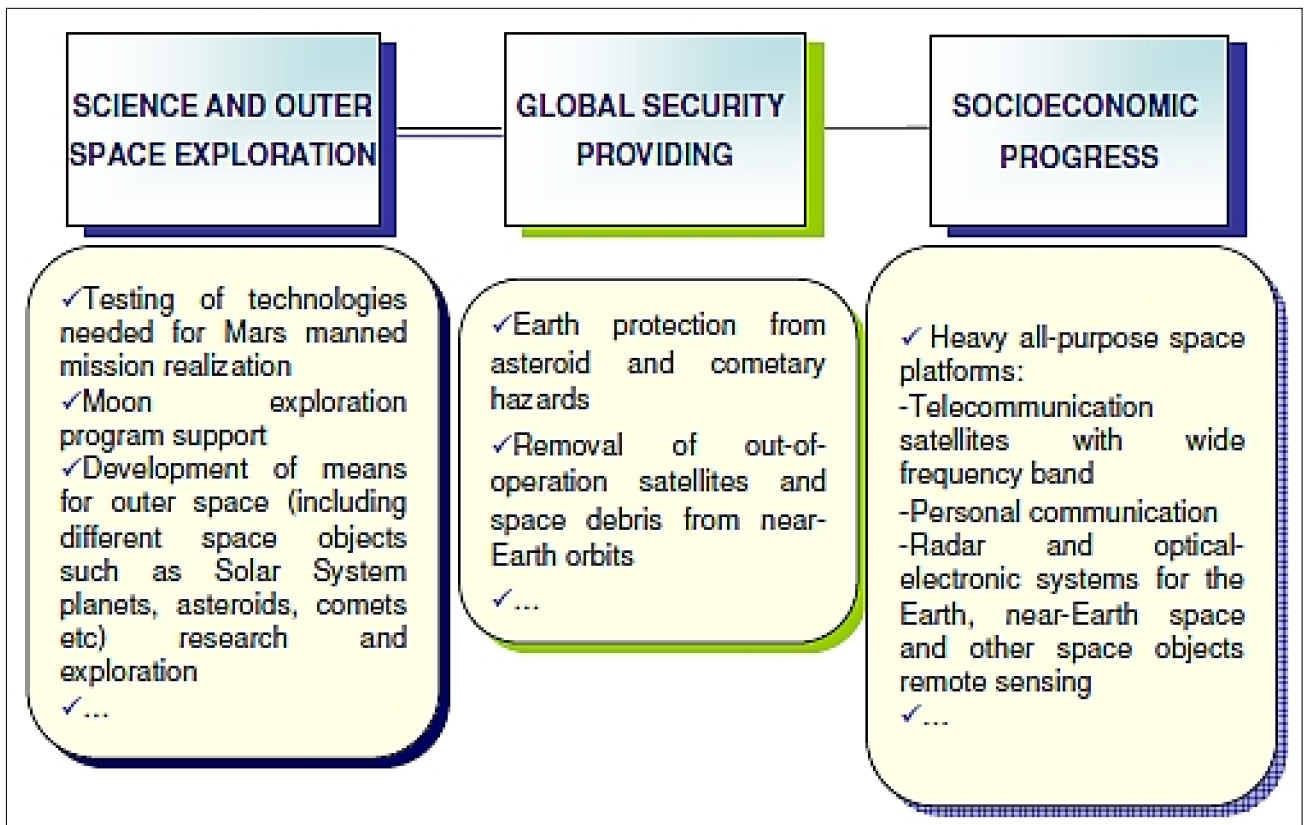


Figure 61: Possible applications of TPM with MW–class NPPS (image credit: Russian Federation)

1.8.6 SPS (Solar Power Satellites): PowerSats

Background: At the start of the 21st century the primary world power consumption is at a level of about 12 TW (12×10^{12} W); the share of electric power generation amounts to about 1.7 TW, while the fossil fuel (oil, gas, coal, nuclear – all non-renewable energies) portion of energy is at a level of > 10 TW. It means that about 85% of the primary world power is fossil-fueled with significant CO₂ emissions into the atmosphere. Obviously, regenerative solutions must be taken into account and installed with higher priority. Significant terrestrial energy options are: solar, wind, hydro, biomass, geothermal (the last one being not strictly regenerative but practically inexhaustible). In addition, power from space may also contribute to the global power supply. Major questions are: Is the “import” of solar energy from space an alternative to its terrestrial use? Is it technically and economically feasible and safe? How does it compete with other terrestrial regenerative alternatives? What could be a reasonable and affordable solution to the energy problem (e.g. a mix of several different options)?^{981) 982) 983)}

The solar irradiation power (the solar energy, arriving at the top of the atmosphere, amounts to about 1.368 kW/m² – or about 1kW/m² arriving on Earth’s surface) is Earth’s prime renewable energy source capable to meet the world’s growing energy needs. When multiplying the above specific solar flux with the Earth’s cross-section (disk projection), leads to a global incoming solar power of 1.7×10^5 TW at the top of the atmosphere, or about 1.3×10^5 TW on the ground. Indeed a great reservoir of renewable energy!

The considerable advances in the field of photovoltaic technologies over the past decades lead logically to consideration of continuous solar power generation from space. Considerable experience is available from large ground-based solar power installations to plan for future space-based generation concepts. Most proposed space designs are based on photovoltaic energy collection/conversion to electricity and wireless (microwave or laser-based concepts) power transmission to Earth, using large high-power antennas – directly or via orbital redirectors – to Earth-based receivers or rectennas (= antennas + electric rectifiers).

The major motivation for pursuing SPS concepts is that in space the sun’s irradiation can be utilized more efficiently than on Earth. A spacecraft in GEO is not eclipsed by the Earth but is in sunlight continuously, 24 hours a day, due to its high orbit of about 36,000 km altitude. The only exceptions are several days around the seasonal equinoxes, March 21 and September 22, when the satellite will be eclipsed briefly around midnight, for up to an hour and 12 minutes. This virtually permanent available power source from GEO implies a factor of almost 5 in favor of an orbital SPS (1366 W/m² average) compared to the best ground solar power plants (300 W/m² average at best due to the atmosphere, weather conditions, day-night cycle, etc.). – A disadvantage in GEO is of course the requirement of fairly large antenna structures (S/C and ground) to transmit the power to Earth. Also, due to safety considerations, only a restricted flux can be allowed on ground for the microwave power transmission.⁹⁸⁴⁾

Studies: Many assessment studies have been made on the topic in the past decades (in fact since the 1960s) looking at new concepts and the feasibility of space-based solar power – – orbiting satellites, so-called “PowerSats,” in GEO (optimal location with nearly continuous irradiation by the sun) that would serve as high-tech space dams, generating power for

981) W. Seboldt, The Peter Glaser Lecture for 2003, “Space and Earth Based Solar Power for the Growing Energy Needs of Future Generations,” 54th IAC, Bremen, Germany, Sept. 29 – Oct. 3, 2003

982) W. Seboldt, M. Reichert, N. Hanowski, M. Novara, “A Review of the Long-Term Options for Space Exploration and Utilization,” ESA Bulletin 101, Feb. 2000

983) International Energy Agency (IEA), World Energy Outlook 2002, OECD/IEA, 2002

984) Note: A spacecraft in GEO is not eclipsed by the Earth but is in sunlight continuously, 24 hours a day, due to its high orbit of 36,000 km. The only exceptions are several days around the seasonal equinoxes, March 21 and September 22, when the satellite will be eclipsed briefly around midnight, for up to an hour and 12 minutes. A disadvantage in GEO is the requirement of large antenna systems (S/C and ground) to transmit the power to Earth.

Earth-bound and space-based applications. However, so far, the considerable economic investment into the development of such a space solar power generation plant is the main barrier that has kept governments away from potential resource commitments into the future. ^{985) 986)}

The past and current SPS concepts are all on a study level. Still, on a long-term perspective, solar power systems from space may eventually turn out to be a promising energy option for the 21st century. On a global and long-term scale, there are three major parameters that have to be considered in connection with the energy system for the 21st century and beyond. The main projections of the IEA (International Energy Agency) for 2030 are as follows: ⁹⁸⁷⁾

- 1) According to current projections and past experience, the global energy need will continue to rise in close connection with the increasing world population
- 2) The availability and use of energy is closely connected to living standards and development levels in the world. Currently, the average primary energy consumption per capita worldwide is about 17,000 kWh/year. It is more than 5 times higher in North America (100,000 kWh/year) but only 4 and 10 kWh/year for the worldwide most numerous and fastest increasing populations, in Africa and Southeast Asia, respectively.
- 3) A significant part of the global emission of greenhouse gases (GHG) stems from the production of electricity (40%) and from transport (21%). Despite the continuous decrease of carbon intensity over the last 30 years, the decrease has not been and will probably not be sufficient to stabilize or reduce the total CO₂ emissions due to the stronger increase of the total power consumption. The IEA estimates that worldwide carbon-dioxide (CO₂) emissions will rise to 38 billion tons per year from currently 16 billion tons (increase of 70%).

System concepts: The overall analysis of solar power generation from space considers two main categories of applications:

- 1) Space-to-Earth energy generation systems, i.e. classic SPS (Solar Power Satellite) concepts.
- 2) Space-to-Space energy generation systems (for space exploration and utilization).

For the space-to-Earth category, the classic application of SPS concepts was first suggested in 1968 by Peter E. Glaser, a Czech-American of Arthur D. Little (consulting company). The basic SPS design requires: ⁹⁸⁸⁾

- a) Very large and light-weight structures in space to collect the solar energy efficiently (solar cells, concentrators or other)
- b) A power transmission system to the ground (based on wireless power transmission) including the conversion of electrical energy and the generation of the transmission beam. Both laser and microwave transmission systems have been considered.
- c) A power receiver system on the ground – closely linked to the laser or microwave technology.

The following items deal with SPS concept studies (energy generation in space) as well as with energy transmission from space to Earth.

-
- 985) F. E. Little, "Solar Power Satellites: Recent Developments," URSI (International Union of Radio Science), Maastricht, The Netherlands, Aug. 17–24, 2002
- 986) L. Summerer, F. Ongaro, "Solar Power from Space – Validation of Options for Europe," Proceedings of the 4th International Conference on Solar Power from Space. SPS'04," June 30 – July 2, 2004, Granada, Spain
- 987) IEA/OECD, "World Energy Outlook 2002," Technical report, International Energy Agency (IEA), Sept. 2002.
- 988) P. E. Glaser, "Power from the Sun: Its Future," Science, Vol. 162, No 3856, Nov. 22, 1968, pp. 857–861

- A NASA/DOE concept of **SSP** (Space Solar Power) was already extensively developed in the 1977–1980 system study.⁹⁸⁹⁾⁹⁹⁰⁾ The overall SSP study goal was to define a reference system and to determine if a space–based solar collection system can produce power for customers on Earth at competitive rates. The purpose of the reference system was also to serve as a basis for evaluating the SPS (Solar Power Satellite) concept for environmental and societal impacts and as an alternative energy source. The power output of one derived SPS reference system (a space structure of 10 km x 5 km x 0.5 km in size and 50,000,000 kg of mass) is 8 GWe, the ground rectenna (~ 10 km diameter) output is 5 GWe. However, negative assessments of the state–of–technology and plans for nearer–term development by the US Congress and NRC (National Research Council) resulted in a termination of SSP activities in the early 1980s.
- Japanese interest in Space Solar Power followed closely in 1981 by the establishment of ISAS (Institute of Space and Astronautical Science) at the University of Tokyo (ISAS became part of JAXA as of Oct. 2003). Japan recognized the enormous cost and technical difficulty of building the NASA/DOE system and decided to concentrate on the development of a ground receiving system, which led to an offshore, floating rectenna design.⁹⁹¹⁾
- In the 1995–1997 “Fresh–Look” study, NASA considered a number of innovative concepts and technologies aimed at reducing the required upfront investment. In this so–called ‘Sun Tower’ concept, NASA employs inflatable, gossamer–like structures for the realization of concentrators which direct the solar radiation onto PV receivers. The Sun Tower, with dimensions of 15 km x 0.2 km x 0.1 km, and a total mass of about 1,000,000 kg, would be in sun–synchronous low Earth orbit (LEO). About 100 inflatable concentrators would be mounted on a central truss structure, and a 5.8 GHz antenna would transmit the power to the surface (ground output of several hundred MWe).⁹⁹²⁾⁹⁹³⁾
- In 1999–2000, NASA started another initiative called SERT (SSP Exploratory Research and Technology) due to significant progress in space technology (e.g. lightweight structures, PV, etc.).⁹⁹⁴⁾⁹⁹⁵⁾ The objective in SERT was to conduct preliminary strategic technology research and development to enable large SSP systems and **WPT** (Wireless Power Transmission) systems for future missions. The designs of the SERT study were the so–called POP (Perpendicular–to–Orbit Plane) configuration and the ISC (Integrated Symmetric Concentrator) configuration. The latter is a modified sandwich concept, in which the photovoltaic array is moved from the back of the two photovoltaic arrays and placed at the focus of the concentrator array.⁹⁹⁶⁾

The following enabling technologies are considered challenging and of great importance to all involved:

– **WPT** methods. Transmission of energy using microwave or laser concepts. The WPT concept has been demonstrated by various research groups in many locations over many years. There is a need for high–power generators (magnetrons, klystrons) and large space

989) DOE 1978 “Satellite power system (SPS) concept development and evaluation program (CDEP) Reference System Report,” DOE/ER–0023, October 1978

990) “The Final Proceedings of the Solar Power Satellite Program Review,” 1980, NASA–TM–84183.

991) M. Nagatomo, S. Sasaki, Y. Naruo, V. A. Vanke, “Solar Power Systems (SPS) – investigations at the Institute of Space and Astronautical Science of Japan,” *Physics – Uspekhi* Vol. 37, No 6, pp. 589–599, 1994, Translated by V. L. Savvin, revised by S. P. Harrop from *Uspekhi Fizicheskikh Nauk* Vol. 164 No 6, pp. 631–641, 1994

992) J. C. Mankins, “A Fresh Look at Space Solar Power: New Architectures, Concepts and Technologies,” IAF–97–R.2.03. URL: http://www.spacefuture.com/archive/a_fresh_look_at_space_solar_power_new_architectures_concepts_and_technologies.shtml

993) NASA: “Space Solar Power – A fresh look at the feasibility of generating solar power in space for the use on Earth,” NASA Report No SAIC–97/1005, 1997

994) <http://www.permanent.com/p-sps-ps.htm>

995) NASA–NSF–EPRI Joint Investigation of Enabling Technologies for SSP (JIETSSP), May 2002, <http://www.nsf.gov/pubs/2002/nsf02098/nsf02098.pdf>

996) J. C. Mankins, “New Directions for Space Solar Power,” Proceedings of the 57th IAC/IAF/IAA (International Astronautical Congress), Valencia, Spain, Oct. 2–6, 2006, IAC–06–C3.1.3

antennas with excellent mechanical properties and exact and safe phase steering. There is also a need for light-weight, high-efficiency, and high-power IR lasers (current laser efficiencies are generally < 5%; however, there are already some diode lasers available with efficiencies of about 30%).

- Intelligent robotics to permit the assembly, inspection and maintenance of large structures in space
- Improved PMAD (Power Management, Distribution and Control) techniques with special emphasis on mass reduction
- Availability of energy conversion levels from solar cells of 170 W/kg specific power and better
- Availability of cheaper and re-usable space transportation (heavy-lift launch vehicles). The attractiveness of SPS is strongly dependent on future launch costs.

Some background on WPT (Wireless Power Transmission). In 1873 Maxwell predicted that power could be transmitted from one point to another in free space. WPT dates back to the early work of Heinrich Rudolf Hertz (1857–1894, German physicist), who demonstrated electromagnetic wave propagation in free space in 1888 using a parabolic reflector. The idea of radio power transmission was first conceived and experimented on in 1899 by Nikola Tesla (1856–1843, Austro-Hungarian/American inventor and scientist).

On 28 Oct. 1964, William C. Brown (1916–1999), an American wireless power transmission pioneer, demonstrated publicly a wireless microwave power transmission experiment to a tethered helicopter at the Spencer Laboratory of the Raytheon Company, sponsored by the USAF. In 1975, a JPL demonstration took place where beamed microwave power (30 kW) was transmitted over a distance of 1.54 km using a transmitting antenna and a microwave receiver referred to as “rectenna” (a rectenna absorbs the microwave beam and simultaneously converts it to DC power). In 1987, Canadian researchers flew a microwave-powered aircraft and concluded that a microwave beam could power it indefinitely. The University of Kyoto, Japan, (cooperation with CRL and Texas A&M University) conducted several experiments demonstrating MPT (Microwave Power Transmission) technology: 997) 998) 999)

- The MINIX (Microwave Ionosphere Nonlinear Interaction eXperiment) rocket experiment was carried out in 1983. The objectives were to verify MPT in space and to investigate the nonlinear plasma effects caused by the microwave energy beam through the space plasma as well as the counter effects onto the microwave beam.
- ISY–METS (International Space Year – Microwave Energy Transmission in Space) rocket experiment carried out on Feb. 18, 1993. ISY–METS also demonstrated that one spacecraft could supply power to another in space using wireless power transmission. ¹⁰⁰⁰⁾ 1001)
- SPS 2000 (Solar Power Satellite 2000) is a Japanese WPT study project. The objective is to demonstrate energy delivery from space to Earth. ¹⁰⁰²⁾ The design calls for a gravity stabilized satellite capable of delivering 10 MW of electricity from a circular 1100 km east–to–

997) W. C. Brown, “Experiments Involving a Microwave Beam to Power and Position a Helicopter,” IEEE Transactions on Aerospace Electronic Systems, Vol. AES–5, No. 5, Sept. 1969, pp. 692–702

998) W. C. Brown, “The History of Power Transmission by Radio Waves,” IEEE Transactions on Microwave Theory and Techniques, Vol. 32, No 9, 1984 pp. 1230–1242

999) Note: The MPT technology is also known under the term “microwave power beaming.” The technology of power beaming is still in the research state, in spite of all the experiments conducted.

1000) <http://www.kurasc.kyoto-u.ac.jp/plasma-group/sps-e.html>

1001) <http://www.kurasc.kyoto-u.ac.jp/plasma-group/sps/mets-e.html>

1002) S. Sasaki, Y. Naruo, M. Nagatomo, “Engineering Research for Solar Power Satellite SPS 2000,” Proceedings, SPS–97 Conference, Montréal, Canada, August 24–28, 1997, pp. 73–77

west equatorial orbit. The phased array antenna will be capable of steering $\pm 30^\circ$ along the orbital path (E–W) and $\pm 16.7^\circ$ perpendicular to the orbital path (N–S). Initial designs studies have been completed and a scale model mock-up of the satellite has been made.

In 2001, a study was provided by the US NRC (National Research Council), entitled: “Laying the Foundation for Space Solar Power: An Assessment of NASA’s Space Solar Power Investment Strategy.” In this study, NASA’s SERT was evaluated in the context of the “plan’s likely effectiveness to meet the objectives of the program.” The outcome: There is considerable interest in solar energy generation by all parties involved (institutional, governmental, industry, and academia).¹⁰⁰³⁾

A first small-scale demonstration of SSP, in the order of 100 kW from GEO, may become a reality in the time frame 2010. Many experts expect large-scale SSP to become technically achievable by about 2020. In the long run, SSP may indeed represent an alternative or at least a needed supplementary energy source to conventional power generation, thus contributing to resource conservation on Earth.

Japan’s METI (Ministry of Economy, Trade and Industry), the former MITI (Ministry of International Trade and Industry), has plans in 2002 to launch a solar power station by 2040. JAXA considers to launch a power satellite demonstration by 2010 and a practical version of a space-based solar-power generation system as early as 2020. In 1992, Japan demonstrated the flight of a small model airplane powered by microwaves beamed up from the ground. – In 2006, JAXA/ISAS is proposing a tethered SPS configuration (without a concentrator) in GEO as a practicable solution.^{1004) 1005) 1006) 1007) 1008) 1009) 1010)}

- An ESA study of 1998–1999 under the lead of DLR came up with a new concept for SPS called “European Sail Tower SPS,” whose design was inspired by the Sun Tower concept of NASA, and the use of innovative solar sail technologies. The dimensions of such a Sail Tower in GEO are 15 km x 0.35 km x 0.05 km (except for the antenna which is 1 km in diameter), the total mass is about 2,000,000 kg. The structure consists of a 15 km long central tether with 120 power generating sun-tracking “sail modules” attached in pairs. Deployable carbon fiber booms (CFRP) spread Kapton film segments coated with thin-film solar cells (TFSC), each sail of 150 m x 150 m in size and a mass of 1100 kg (including all add-ons).¹⁰¹¹⁾

- In 2002, ESA created the “European Network on Solar Power Satellites,” a framework to focus all research activities on SPS (Solar Power Satellite) technology, following an ESA study initiative on advanced SPS concepts.¹⁰¹²⁾

Prohibitive launch costs, limited launcher capabilities, enormous launch mass requirements as well as large frontend investments are among the most prominent reasons – why most proposed

1003) <http://books.nap.edu/books/0309075971/html/12.html#pagetop>

1004) T. Saito, Y. Kobayashi, H. Kanai, “Concept Study of Space Solar Power Systems in USEF,” Proceedings of IAC 2004, Vancouver, Canada, Oct. 4–8, 2004, IAC–04–R.1.02

1005) <http://www.spacedaily.com/news/ssp-01a.html>

1006) M. Oda, M. Mori, “Conceptual Design of Microwave-based SPS and Laser-based SPS,” Proceedings of IAC 2004, Vancouver, Canada, Oct. 4–8, 2004, IAC–04–R.1.05

1007) Y. Fujino, K. Ogimura, “A Rectangular Parabola Rectenna with Elliptical beam for SPS Test Satellite Experiment, Proceedings of IAC 2004, Vancouver, Canada, Oct. 4–8, IAC–04–R.2.02

1008) Y. Saito, T. Fujita, M. Mori, “Summary of Studies on Space Solar Power Systems of Japan Aerospace Exploration Agency (JAXA),” Proceedings of the 57th IAC/IAF/IAA (International Astronautical Congress), Valencia, Spain, Oct. 2–6, 2006, IAC–06–C3.1.04

1009) S. Sasaki, K. Tanaka, K. Higuchi, N. Okuizumi, S. Kawasaki, M. Shinohara, K. Ishimura, “Construction Scenario for Tethered Solar Power Satellite,” Proceedings of the 57th IAC/IAF/IAA (International Astronautical Congress), Valencia, Spain, Oct. 2–6, 2006, IAC–06–C3.1.06

1010) S. Mihara, T. Saito, Y. Kobayashi, H. Kanai, “Activity Results of Experiments for Space Solar Power Systems at USEF,” Proceedings of the 57th IAC/IAF/IAA (International Astronautical Congress), Valencia, Spain, Oct. 2–6, 2006, IAC–06–C3.3.2

1011) W. Seboldt, M. Klimke, M. Leipold, N. Hanowski, “European sail tower SPS concept,” Acta Astronautica, Vol. 48, No 5–12, 2001, pp. 785–792

1012) L. Summerer, M. Vasile, R. Biesbroek, F. Ongaro, “Space and Ground Based Large Scale Solar Power Plants – A European Perspective,” Proceedings of 54th IAC, Bremen, Germany, Sept. 29 – Oct. 3, 2003

WPT systems rely on microwave power transmission instead of laser power transmission (laser WPT is less mature). The following sample calculation, (stated by Leopold Summerer et al. in Ref. 1012), gives an overview of the dimensions involved: A GEO **laser-based** SPS system, using PV solar arrays (GaInP/GaAs/Ge with concentrators operating at 32% efficiency and a mass of 1.6 kg/m²), employing an advanced GaAs laser diode transmission system emitting to the ground at 840–890 nm wavelength with an assumed 70% generation efficiency and only 0.02 kg/W for the laser system — — — lead to a satellite mass of about 384,000,000 kg to deliver 5 GWe to a ground-based PV receiver system (such a gigantic mass is appalling). This configuration, although optimistic, would still be about six times more massive than the 5 GW Sail Tower option using microwave power transmission. Important progress remains to be done in laser generation specific mass kg/kW and efficiency to profit from its advantages. ¹⁰¹³⁾

- NASA conducted already a series of studies testing the environmental impact of microwave energy transmissions from space to ground on plant life, using a tower-mounted microwave transmitter in the experimental setup. An experiment was done that exposed alfalfa to continuous microwave energy at 2.45 GHz with intensities of 0.5–1.2 mW/cm². ¹⁰¹⁴⁾ A tray of growing plants was illuminated with microwaves while control plants were grown behind a microwave-opaque shield. Statistical analysis indicated no difference in chlorophyll content of the leaves between the control and test plant populations throughout the test period. — A set of further experiments will be performed to test if the offspring from plants grown under microwave radiation at 2.45 and 5.8 GHz, the F1 generation, will show any deleterious characteristics as a result the parent plants being exposed to microwave radiation. This experiment will be important for understanding the generational effects of microwave exposure.

1013) L. Summerer, F. Ongaro, M. Vasile, A. Galvez, “Prospects for space power work in Europe,” *Acta Astronautica*, Vol. 53, 2003, pp. 571–575

1014) J. W. Skiles, “Plant Response to Microwaves at 2.45 GHz,” *Proceedings the 54th IAC*, Bremen, Germany, Sept. 29 – Oct. 3, 2003

1.8.7 Spacecraft Avionics and Onboard Data Handling (bus systems)

The early history of spaceflight (all of spaceflight, not only Earth observation) has seen a lot of project–developed (i.e. custom–built, and/or proprietary) “electronic interconnect solutions” (using lots of wiring and cables) with regard to onboard data management systems (interprocessor communication and control functions for the onboard subsystems, the payload instruments, and RF communications), and flight control functions. This was mainly due to the lack of available standards, the multitude of subsystems to be integrated, each with a wide spectrum of operational requirements, performance needs, interfaces on many levels, protocols, data transmissions, distributions and data recordings to be handled (in all directions, various types of data, etc.), and with a fast–changing and evolving field of (often non–compatible) computer technology.

It took a while, even within each space agency, to get a certain “degree of structure and modularity” with standardized building blocks and interface connectivity into the avionics system architecture of satellites along with the general functional service spectrum and procedures. The ever increasing functional demands by the operational side of the spacecraft as well as the science side of the project were probably the main drivers for all these developments. Interface standards are the key to maximizing the benefits of modular systems (decrease of complexity, reduction in integration time and costs, and increase the reuse of a system). Standard interfaces are the technical specifications that ensure interoperability between different products or modules. Standard interfaces enable the independent development of modules and complementary products and services (including flight systems, test/validation systems, simulators, etc.).

In the 1960s and 1970s there was also a great interest among space agencies in international cooperative activities. This gradually led to requirements in cross–support between the respective communications and space data systems of the agencies. The absence of standards led to many costly interface conversions, all were handled by the introduction of so–called “black boxes” to establish compatibility.

Conventionally, space segments are separated into two main functional classes, namely the **platform** and the **payload** subsystems and/or instruments.¹⁰¹⁵⁾

- Conventional tasks of the platform are: maintaining communication with the ground segment, guiding the satellite on the appropriate trajectory, controlling the attitude and performing an overall management of the parts constituting the system. If some autonomy is required the platform has to make decisions with respect to particular situations.
- The payload, being intimately related to the objective of the mission, often consists of multiple instruments, very different in terms of generated data rate and from a command and control viewpoint. In the past, because of technological limits, all data were transmitted to the ground segment where the selection, elaboration and analyses were performed. At the start of the 21st century, payload systems requirements are becoming more and more demanding in order to comply with the project needs to elaborate (select, compress, format, encrypt, etc.) data in real–time or near real–time onboard and only downlink the useful part of the information. Moreover, payload systems are endowed with a certain level of autonomy and are asked to be reconfigurable, reliable and robust. In other words, they frequently drive advances in space data systems.

Some common onboard interface and data–system standards:

The first onboard data buses on the scene were the **MIL–STD–1553** (Military Standard–1553) bus of DoD/USAF and the **OBDH** (On–Board Data Handling) bus of ESA, permitting a frequent system reuse and functional resource sharing. These two buses are

¹⁰¹⁵⁾ L. Tunesi, P. Armbruster, “On–board hierarchical network,” Proceedings of SPIE, Vol. 5234–60, Sensing Technologies II, Sept. 8–12, 2003, Barcelona, Spain

based on well proven technology, commonly used between spacecraft components. Conventional interfaces between spacecraft components are usually provided by **point-to-point** connections (such as RS-422/23), or a master-slave bus architecture (MIL-STD-1553, -1553B, or OBDH). These point-to-point configurations have proven to be extremely limited in flexibility and expendability. In spite of the wide use of MIL-STD-1553 and OBDH, the prevailing situation at the start of the 21st century is that there are still too many different (customized) interface types and “standards” around to interconnect onboard components and subsystems. Note: In this context the reader should also consult chapter O.13.

In contrast to conventional -1553 and OBDH bus systems, newer standardized onboard network architecture concepts (candidates are: CAN, SpaceWire, TCP/IP, FireWire, Ethernet, etc.) employ routers which take care of delivering packets to the appropriate address without processor supervision.¹⁰¹⁶⁾

Bus designation	Main Characterization
MIL STD-1553B (its optical derivative is MIL-STD-1773)	<ul style="list-style-type: none"> - Introduced by USAF in 1973 (1773B released in 1978) - Used in thousands of military and commercial aircraft and in many spacecraft - Multi-drop bus (master-slave architecture) - Mainly for control / configuration purposes - The raw data rate is 1 Mbit/s - The 1553B is transformer-coupled and dual-redundant, providing a level of failure protection - For point-to-point connections that do not require the complexity of a 1553/1773 connection, a synchronous serial connection such as RS-422/23 with a bit rate around 1 Mbit/s is typically used.
OBDH (On-Board Data Handling) data bus	<ul style="list-style-type: none"> - ESA standard onboard data bus (was defined the mid-1970s) - First onboard introduction on Giotto (launch July 2, 1985) - Multi-drop bus (master-slave architecture) - Mainly for control / configuration purposes - The raw data rate is 1 Mbit/s - The bus features a synchronous serial data exchange and time-management - RBI (Remote Bus Interface) ASIC introduction with Envisat (launch 2000)
CAN (Controller Area Network)	<ul style="list-style-type: none"> - CAN was originally developed for automobiles and industrial use - CAN uses a two-wire differential bus - The CAN interface is a 2-wire asynchronous transmission scheme controlled by start and stop bits at the beginning and end of each character - Information is passed from transmitters to receivers in a data frame - CAN employs a serial protocol, with data rates up to 1 Mbit/s - It implements distributed real time control and multiplexing - The CAN specification defines the data link layer, ISI 11898 defines the physical layer of the ISO (International Organization for Standards) networking model - CAN was initially introduced onboard the satellite FaSat-Alfa (Aug. 31, 1995) and UoSat-12 (launch Apr. 21, 1999) of SSTL, UK. It is also being flown on SNAP-1 and Tsinghua-1 (both launched Jun. 28, 2000), TiungSat (launch Sep. 26, 2000), all S/C were developed by SSTL. The TOPSAT mission of QinetiQ (UK, built by SSTL) with a launch Oct. 27, 2005, uses CAN as well as SMART-1 of ESA (launch Sept. 27, 2003, built by SSC). CAN is also being used by many microsatellite missions.
I ² C (Inter-Integrated Circuit) data and control bus	<ul style="list-style-type: none"> - A low-cost commercial data bus (in consumer, telecommunication and industrial electronics appliances) - I²C (also I2C) employs a master-slave architecture - CNES selected the I²C bus for its microsatellite family of Myriade [DEMETER (launch June 29, 2004) PARASOI (launch Dec. 18, 2004), Picard, etc.]; at the start of the 21st century, there are several I²C space-based applications in development. Stanford University is using I²C on Emerald, Orion, etc. - I²C is compatible with the following OSI layers: physical layer, data-link layer (medium access control), and data-link layer (logical link control) - Only two bus lines are required; a serial data line and a serial clock line - I²C is a multi-master bus including collision detection and arbitration - Serial, 8-bit oriented, bidirectional data transfers can be made at up to 100 kbit/s in standard mode or up to 400 kbit/s in the fast mode

1016) R. T. Caffrey, T. W. Simpson, R. Herderson, E. Crawley, “The Strategic Issues with Implementing Open Avionics Platforms for Spacecraft,” Proceedings of the IEEE Aerospace Conference, Big Sky, MT, March 9-16, 2002

Bus designation	Main Characterization
IEEE1394 bus, also referred to as FireWire	<ul style="list-style-type: none"> – An industry/commercial high–speed and low–power serial bus for data communications among multiple nodes (introduced in 1999). – Communication speeds of up to 400 Mbit/s – It supports a transmission mode which guarantees bandwidth – The supported chipsets are Texas Instruments PCILynx/PCILynx2 and OHCI (Open Host Controller Interface) compliant chips (produced by various companies) – It's a thin twisted cord with a 6–pin connector up to 4.5 in length – The bus connects CPUs, telecommunications equipment, and instruments – The bus allows for multiple masters and provides an isochronous channel that gives developers the means to schedule regular and synchronous activities. – A key concept of the bus architecture is the symmetry between flight and ground software.
SpaceWire	<ul style="list-style-type: none"> – A European–born initiative in 1998 (ESA, industry, academia, etc.) and US cooperation on CCSDS–SOIF (Spacecraft Onboard Interfaces) – First onboard introduction on Rosetta and Mars Express mission of ESA – Point–to–point serial links (an onboard network with routers) – Mainly intended for the transfer of data; remote configuration tasks are possible because links are bi–directional. – 1.25 Mbit/s < data rate < 400 Mbit/s (on one point–to–point link). The performance is scalable if the number of links increases. – Key principles of SpaceWire are: modularity, scalability, and reconfigurability
Onboard LAN	<ul style="list-style-type: none"> – NASA plans the introduction of an onboard LAN with TCP/IP protocols in the time frame 2006.

Table 56: Overview of some common onboard buses/networks

At the start of the 21st century, the use of onboard LAN systems is emerging; the non–selection of LANs in the past was mostly due to non availability of space–qualified components. However, the data communication requirements of many advanced space missions involve seamless, transparent connectivity between space–based instruments, investigators, ground–based instruments and other S/C.

1.8.7.1 MIL–STD–1553B

MIL–STD–1553 is a military standard communications bus that defines the electrical, mechanical and timing specifications for a dual–redundant communication network that interconnects cooperating digital units in a system.

The digital communications bus MIL–STD–1553B has become an established global spacecraft data bus standard (a deterministic, command–and–response protocol)) with roots in military aircraft avionics. The serial bus protocol was first introduced by the USAF in Aug. 1973 as MIL–STD–1553 and experienced a number of revisions. The tri–service approved version MIL–STD–1553A was released on April 30, 1975. The F–16 aircraft program of the USAF was the first user of the “A” version. The early Space Shuttle program adopted a preliminary version of the not–yet–released MIL–STD–1553 bus standard already in 1974. All previous onboard systems (in the US) had used bundles of wires, each one dedicated to a specific signal – for system interconnection. The sheer weight of the wiring became simply intolerable. ^{1017) 1018)}

The latest version of the standard, 1553B, was released on Sept. 21, 1978. The 1553B bus is a redundant bus for which compact and reasonably priced (compared to other space qualified solutions) interface circuits are available. At the start of the 21st century the standard is still at the “B” level. Changes to the standard were made in 1980 with Notice 1, and in 1986 with Notice 2 (common set of operational characteristics). The military standard was converted to its commercial equivalent as **SAE AS–15531** (part of the US government’s effort to in-

1017) Ch. deLong, “AS 15531/MIL–STD–1553B Digital Time Division Command/Response Multiplex Data Bus,” Chapter 1 of The Avionics Handbook, edited by Cary R. Spitzer, CRC Press LLC, ISBN 0–8493–8348–X, 2001

1018) R. Killough M. McLelland, “Designing Command and Telemetry Systems Using MIL–STD–1553 and CCSDS,” Proceedings of the 14th AIAA/USU Conference on Small Satellites, SSC00–XI–4, Aug. 21–24, 2000, Logan, UT

crease the use of commercial products). Practically all spacecraft of NASA employ the 1553B bus standard, this applies also to JAXA (formerly NASDA) spacecraft.

The ISS implementation of the 1553B bus system includes multiple redundant buses, each with dual channels and controllers, and multiple redundant MDM (Multiplexer/Demultiplexer) at each level of hierarchy. The ISS 1553B bus architecture consists of a 3 tier C&DH (Command and Data Handling) system composed of a number of specialized computers called MDMs (Multiplexer/Demultiplexer) interconnected by MIL–STD–1553B buses. The reason for its use on ISS: the 1553B is well–proven in space; additionally, it has significant built–in redundancy capabilities that make it a good choice for space applications. However, as the ISS grows in size, functionality and complexity, new solutions must be developed to overcome the low transmission rate (1 Mbit/s) of the 1553B bus. ^{1019) 1020)}

The Chinese technology demonstration satellite SJ–5 (Shi Jian–5, launch May 10, 1999) employs also the 1553B bus. Another example of a 1553B bus implementation (onboard communication via discrete point–to–point lines as well as via a 1553B bus) is the SMOS mission of ESA (launch Nov. 2, 2009) flown on a Proteus platform of Alcatel Space.

The MIL–STD–1553B is a common hardware selection for custom C&DH interfaces; it defines TDM (Time Division Multiplexing) as “the transmission of information from several signal sources through one common system with different signal samples staggered in time to form a composite train.” The standard defines four hardware elements: transmission media, remote terminals, bus controllers, and bus monitors. The structure of the bus consists of a single bus controller connected to remote terminals (up to 31 max can be used). The use of the MIL–STD–1553B communications bus in combination with CCSDS protocols is increasingly being used in the design of small satellite command and data handling systems. In this way, they function as standard spacecraft–to–payload interfaces and protocols. ¹⁰²¹⁾

MIL–STD–1773B (up to 10 Mbit/s fiber optic bus). Optical interconnects have long promised significant advantages over their electrical counterparts. Specific advantages include increased bandwidths at long (10 m or more) interconnection distances, immunity to EMI (Electromagnetic Interference) effects, negligible crosstalk, reduced size, and lower weight. Optical interconnects have some heritage in a range of ground based and aircraft applications, however they are only beginning to gain acceptance in spaceborne systems (in 1990s). Examples: ^{1022) 1023)}

- The SAMPEX mission of NASA (launch July 3, 1992) employs a fiber–optic data bus based on MIL–STD–1773.
- The HST (Hubble Space Telescope) mission was launched April 24, 1990 on Shuttle flight STS–31; it uses the MIL–STD–1773 data bus.
- The Lewis S/C of NASA (launch Aug. 23, 1997 – but no S/C operations could be initiated) was also equipped with a fiber–optic data bus.
- The EO–1 mission of NASA (launch Nov. 21, 2000) was initially planning to use the IEEE 1393 SFODB (Spaceborne Fiber Optic Data Bus), instead of MIL–STD–1773. However, due to technical and budgetary problems, SFODB had to be removed from

1019) D. P. Fletcher, R. Alena, “A Scalable, Out–of–Band Diagnostics Architecture for International Space Station Systems Support,” Proceedings of IEEE Aerospace Conference, Big Sky, MT, USA, March 8–15, 2003

1020) S. Deba, C. Domagalaa, S. Ghoshala, A. Patterson–Hineb, R. Alenab, “Remote Diagnosis of the International Space Station utilizing Telemetry Data,” Proceedings of the SPIE Aerosense Conference, Orlando, FLA, April 16–20, 2001, <http://www.teamqsi.com/doc/spie-iss-2001.pdf>

1021) R. Killough, “Integrating CCSDS and MIL–STD–1553: What You Should Know,” Proceedings of the IEEE Aerospace Conference, Big, Sky, MT, March 9–16, 2002

1022) [7] “MIL–STD–1553 & MIL–STD–1773,” URL: <https://ewhdbks.mugu.navy.mil/1553-bus.htm>.

1023) L. Benussi, S. Berardis, M. Bertani, et al., “Fiber Optic Sensors for Space Missions,” Proceedings of IEEE Aerospace Conference, Big Sky, MT, March 8–15, 2003

EO–1 (hence, there was no fiber optic bus on EO–1). EO–1 ended up using the conventional MIL–STD–1553B data bus.

- The CryoSat mission of ESA (launch Oct. 8, 2005 – but launch failure) uses the MIL–STD–1553B bus for the low rate data channels (handling of onboard communications) and high–speed serial links (IEEE 1355) for payload interfaces. The LISA Pathfinder mission of ESA (formerly SMART–2, launch 2014) is also planning of using the 1553B data bus.
- The next–generation high–resolution imaging satellite series of CNES, Pleiades, is using the MIL–STD–1553 bus. Launch of Pleiades–HR1A on Dec. 17, 2011. Launch of Pleiades–HR1B on Dec. 02, 2012.

Parameter	Description
Data rate	up to 1 Mbit/s
Word length; data bit per word	20 bit; 16 bit
Message length	32 data words maximum
Transmission technique	Half–duplex
Operation	Asynchronous
Encoding	Manchester II Bi–phase
Protocol	Command–response
Bus control	Single or multiple
Message formats	BC–RT (Controller–to–Terminal) RT–BC (Terminal–to–Controller) RT–RT (Terminal–to–Terminal)
Number of remote terminals or interfaces	31 (max)
Terminal types	RT (Remote Terminal), BC (Bus Controller) BM (Bus Monitor)
Transmission media	Twisted shielded pair of cable
Coupling	Transformer or direct

Table 57: Summary of the MIL–STD–1553B data bus characteristics

1.8.7.2 OBDH (On–Board Data Handling)

The OBDH bus was developed by ESA in the 1970s as a standard spacecraft data bus (ESA–STD–OBDH). Its high reliability and performance has been demonstrated through applications to missions such as Giotto (1985), Olympus (1989), HIPPARCOS (1989), ERS–1 (1991), ERS–2 (1994), Cluster (Cluster–I in 1996, Cluster–2 in 2000), Envisat (2002), all SPOT series satellites of CNES, the STRV missions of DERA, UK, as well as many other European missions (SSTL satellites, TUBSAT series, etc.). The ESA standard OBDH data bus is a synchronous serial data exchange and time–management network used onboard ESA spacecraft. ^{1024) 1025) 1026)}

The OBDH bus of Envisat employs for the first time RBI (Remote Bus Interface), an ASIC (Application–Specific Integrated Circuit) which implements the OBDH high–level protocol and which allows direct transfers of data packets into the memory of the payload computer memory without involving its software. The RBI is implanted in each computer in the payload, where it provides a command and control interface to the platform. The RBI is also implemented/considered for all ESA missions [XMM–Newton (launch Dec. 10, 1999), MSG series (MSG–1 launch Aug. 28, 2002), Integral (launch Oct. 17, 2002 from Baikonur),

1024) <http://esapub.esrin.esa.it/pff/pffv6n4/polv6n4.htm>

1025) ESA TTC–B–01, Spacecraft Data Handling Interface Standards.

1026) Note: Development of a standard and modular interface ASIC was started in 1993. The RBI design and development, a common module for onboard computers, was funded by the Envisat program. The device is fabricated using MITEL's (ABB–Hafo, Sweden) radiation–hardened silicon–on–sapphire process and encapsulated in a 132–pin package.

MetOp series (MetOp–A launch Oct. 19, 2006), etc.]. The main benefits accruing from using a standard bus coupler on–a–chip are:

- Reduced cost: one common development can be applied to all payloads whose data interfaces exhibit the same behavior
- Easy accommodation, small size and low power consumption
- Easy to use since the user need not know the protocol involved.

The OBDH bus standard (is not an international standard) includes such features as: a) broadcast distribution of synchronous pulses, b) memory access (load/dump), c) a large number of remote terminals (up to 62) can be supported in a distributed environment. The FLEXBUS design of Astrium is using the OBDH bus on such missions as CHAMP and GRACE. The OBDH bus is also being used on a number of commercial satellites (Eurostar–2000 platform series, Spacebus–3000 platform series, etc.).

1.8.7.3 CAN (Controller Area Network)

CAN is a field bus, a COTS (Commercial–off–the–Shelf) lightweight product. CAN is a commercial standard, a fault–tolerant multipoint field bus suitable for a distributed data–handling architecture, originally developed for industrial process control and automotive use in 1983 by the German company Robert Bosch GmbH of Stuttgart in cooperation with Intel Corporation. In particular, CAN was spawned by the needs of the automotive industry to handle the increasing connectivity requirements of modular electronic systems (the objective was to create a faster and more interference–resistant data network).

In February of 1986, Bosch proposed the serial CAN bus system at the SAE (Society of Automotive Engineers) Congress in Detroit, MI. It was the hour of birth for one of the most successful network protocols ever. It was based on a non–destructive arbitration mechanism, which would grant bus access to the message with the highest priority without any delays. There was no central bus master. Bosch published the CAN 2.0 specification in 1991. The first CAN bus installation in a car (Mercedes 600 series) was realized in 1992.¹⁰²⁷⁾

A CAN bus system usually consists of a bus wire, bus terminations and a bus station. The bus station includes a microcontroller, the bus controller and the bus driver. Twisted cable or coaxial cable are usually used as the cable composing the bus, but the cable specifications are not included in the standard. There is no bus controller for CAN system. Whenever a unit wins the bus and starts the communication, the other units automatically become receiver

In the meantime, the CAN bus is ubiquitous in the auto industry; it is also being used in medical equipment, marine electronics, consumer products, building automation, and in many other application fields. The serial CAN bus consists essentially of a pair of twisted wires connecting a number of CAN nodes. The CAN protocol and physical layer, as defined in ISO–11898 (for high–speed applications) and in ISO 11519 (for lower–speed applications), provides reliable data transmission, error detection, message identification, and excellent immunity to EMI (Electromagnetic Interference).¹⁰²⁸⁾

There is also considerable interest by the space community to use this affordable COTS solution, but there are also concerns with regard to the required radiation hardness of CAN components for support in long–term space missions. A typical industrial component will

1027) G. Leen, M. Porciani, F. Granata, L. Di Marsico, “Controller Area Network in Space – background and lesson learned from practical experience,” Proceedings of the 56th IAC 2005, Fukuoda, Japan, Oct. 17–21, 2005, IAC–05–D1.2.03

1028) M. Khurram, S. M. Y. Zaidi, “CAN as a Spacecraft Communication Bus In LEO Satellite Mission,” Proceedings of the 2nd International Conference on Recent Advances in Space Technology (RAST), Istanbul, Turkey, June 9–11, 2005

survive a radiation dose in the order of 8–40 krad. Many spacecraft have survived using industrial electronics alone. So far, no CAN node failures in spacecraft have been observed.

As of 2005, “CANopy” is a VHDL [VHSIC (Very High Speed Integrated Circuit) Hardware Description Language] IP (Intellectual Property) Core developed at ESA/ESTEC which implements in hardware the basic features of the higher layer protocol for CAN bus on board spacecraft applications.

CANopen is a standardized application for distributed automation systems based on CAN. This includes the basic CANopen features as well as several add-ons that are result of the efforts realised to date by the ESA–Industry Working Group on CAN bus. CANopy implements the basic features of CANopen protocol and the extra features defined in the CAN Working Group draft recommendation. Its main intention is to serve as the higher layer protocol engine in CPU-less nodes like in μ RTUs (Remote Terminal Unit). CANopy can be useful for Space projects using CAN bus allowing simple remote terminals to run the higher layer protocol without any software, and reducing the processor load for handling communications when integrated in a system-on-chips. ¹⁰²⁹⁾

Some examples of CAN implementations in spaceborne missions are:

- SSTL of Surrey, UK, pioneered the implementation of CAN data handling technology on its spacecraft platforms starting with FASat–Alfa (launch Aug. 31, 1995; note, the launch was successful but the S/C failed to separate – making operations of FASat impossible). The CAN bus was also flown on UoSAT–12 with a launch Apr. 21, 1999 as well as on SNAP–1 (launch June 28, 2000), a nanosatellite. In addition, the SGR (Space GPS Receiver), an ESA–funded device of SSTL missions, supports the CAN bus interface. A CAN bus of SSTL is also part of the DMC microsatellite constellation, the UK TopSat mission (launch Oct. 27, 2005) and of FalconSat–2 of USAFA (launch March 24, 2006, but launch failure). In short, the CAN bus has become a standard for SSTL missions.
- The SMART–1 satellite of ESA (launch Sept. 27, 2003) features two CAN buses: the spacecraft platform units are connected to the system CAN bus, and the payload (scientific instruments) are connected to the payload CAN bus.
- With the production of a space-worthy (i.e. a radiation-tolerant) CAN ASIC, EADS Astrium Ltd. has implemented the CAN configuration successfully within radar instruments such as the sensor electronics of the Radarsat–2 mission (launch Dec. 14, 2007). ¹⁰³⁰⁾
- IHI Aerospace of Japan (formerly Nissan), in partnership with AeroAstro Inc. of Herndon, VA, have developed OBCA (On–Board Computer using Automotive electronics), an example of bringing high-reliability high-production automotive technology to the high-reliability low-production market of space systems. ¹⁰³¹⁾ OBCA is an embedded processing system designed for use in spacecraft and other high-reliability environments. Much of its electronics, particularly the central microprocessor, are taken from an automotive screening process. A CAN bus is being used to interconnect the onboard components for vehicle control and data exchange. AeroAstro developed an OBCA/Bitsy–DX computer board.

CANopen standard for space by ECSS (European Cooperation for Space Standardization) for space applications: The standard, **ECSS–E–ST–50–15C**, will be completed in 2011

1029) F. Tortosa López, P. Roos, “A VHDL Implementation of CANopen Protocol for CAN Bus onboard Spacecraft,” Proceedings of DASIA 2005 (Data Systems in Aerospace), Edinburgh, Scotland, May 30–June 2, 2005

1030) B. Barnes, “CAN Bus for Space Instrument Control,” Proceedings of EUSAR 2002, Cologne, June 4–6, 2002

1031) S. A. McDermott, A. Jacobovits, H. Yashiro, “Automotive Electronics in Space: Combining the Advantages of High Reliability Components with High Production Volume,” Proceedings of the IEEE Aerospace Conference, Big Sky, MT, March 9–16, 2002

to be applicable for all ESA missions. This standard will contain all services and recommendations covering the peculiarities and requirements of space specific applications.¹⁰³²⁾

1.8.7.4 I²C (Inter–IC or Inter–Integrated Circuit)

The I²C (also I2C spelling) bus is generically a fieldbus. The I²C name literally explains its purpose, namely to provide a communication link between ICs. The small bus concept was developed in the early 1980s by the Philips Laboratories in Eindhoven (The Netherlands) with the objective to provide an easy way to connect a CPU to peripheral devices in a TV–set. I²C performs chip–to–chip communications using only two wires in a serial interface. The data rate can be 100 kbit/s, 400 kbit/s or 3.4 Mbit/s. The bus may be about 3 m long at most.

In the 1990s, the bus was generally accepted as a de–facto industry standard (by its widespread use as a small diagnostic and control network for chip–to–chip interfacing). The I²C bus design employs a master–slave architecture; it maximizes hardware efficiency and circuit simplicity with a bi–directional two–wire design (a serial data line and a serial clock line). Although this bus standard is very popular in industry, it is not inherently providing a means of error detection.¹⁰³³⁾

The trend in spacecraft design toward micro– nano– and picosatellite platforms has also lead to the selection of a small and low–cost bus, like I²C, into onboard spacecraft applications, often in combination with other buses such as IEEE 1394 and/or MIL–STD–1533B. The I²C bus is mostly used for such tasks as low–speed engineering data collection because of its simplicity and reliability. In 1999, Stanford University and Santa Clara University selected a I²C bus variation (as one of the onboard buses) for the Emerald and Orion spacecraft design. In 2001, CNES selected the I²C bus for its Myriade microsatellite family [DE–METER (launch June 29, 2004) PARASOL (launch Dec. 18, 2004), Picard (launch June 15, 2010), etc.]. The I²C bus is often being used in CubeSat projects.

1.8.7.5 FireWire / IEEE 1394

The IEEE 1394 (FireWire) high–speed and low–power serial bus standard is gaining acceptance in spacecraft design (its roots are in Apple personal computing and in Sony consumer electronics). The standard is well matured and developed. IEEE 1394 defines techniques for serial digital data communications up to 400 Mbit/s among multiple nodes (up to 63 devices). The FireWire harness consists of two conductor pairs for signals and one pair for power and ground (six wires). Two modes of data transfer are available asynchronous and isochronous. The asynchronous mode provides guaranteed delivery of the data via receiver acknowledgement and isochronous provides guaranteed bandwidth and latency where data accuracy is less important than assuring the sender’s data buffers do not overflow from large quantities of data.

There are two revisions to the FireWire standard. In IEEE 1394a, the number of wires is reduced to 4 (power and ground wires are removed). In IEEE 1394b released in 2002, higher data rate (up to 1600Mbps) and a longer cable length (up to 100 m with glass optical fiber) are supported.

FireWire implementation are also being used in combination with MIL–STD–1553B. Example of IEEE 1394 interfaces:

1032) Aitor Viana Sanchez, Alberto V. Carretero, Gianluca Furano, Maurizio Caramia, Luca Bolognino, Mario Montagna, Oliver Notebaert, S. Gunes–Lasnet, et al. “CAN Bus for Modern Spacecraft Control Systems,” Proceedings of the DASIA (DATA Systems In Aerospace) 2011 Conference, San Anton, Malta, May 17–20, 2011, ESA SP–694, August 2011

1033) B. Palmintier, Ch. Kitts, P. Stang, M. Swartwout, “A Distributed Computing Architecture for Small Satellite and Multi–Spacecraft Missions,” Proceedings of AIAA/USU Conference on Small Satellites, Logan, UT, Aug. 12–15, 2002, SSC02–IV–6

The VIIRS (Visible/Infrared Imager and Radiometer Suite)^{1034) 1035) 1036)} instrument of NPOESS (see G.10.5) utilizes an IEEE 1394 cable. The NPP (NPOESS Preparatory Project), a NASA/IPO spacecraft with a launch on Oct. 28, 2011, employs the IEEE 1394a–2000 (FireWire) data bus for communications with CrIS and VIIRS (first use of the 1394 data bus in a satellite).

The **IEEE P1393–1999** standard SFODB (Spaceborne Fiber Optic Data Bus), developed jointly by DoD and NASA, specifies a wide bandwidth (1 Gbit/s), low–power, highly reliable, fault–tolerant fiber–optic network compatible with the harsh thermal, mechanical, and radiation environments of space missions. The SFODB high–speed architecture is based upon the commercial ATM (Asynchronous Transfer Mode) communications standard which implements a redundant, cross strapped, ring–based configuration; it includes one controller node and up to 127 transmit/receive nodes.

1.8.7.6 X2000 bus

The X2000 bus is of NASA/JPL. In 1997/8, NASA/JPL began the development of its X2000 bus, a generic multi–mission avionics system, based on the **IEM (Integrated Electronics Module)** architecture design, intended to support NASA's future planetary exploration program such as the Europa Orbiter and Mars Missions. Both JPL and JHU/APL, as well as several commercial enterprises, are using similar IEM architectures for their new spacecraft. The IEM contains most of the major spacecraft subsystems, including command and data handling, guidance and control, RF communications, and, when applicable, GPS navigation (a transceiver system, consisting of uplink and downlink cards, is used for RF communications instead of a coherent transponder).^{1037) 1038) 1039) 1040) 1041) 1042) 1043) 1044) 1045)}

The communication of the various subsystems in the X2000 bus architecture is based on two redundant, industry standard, buses: namely the scalable high–speed **IEEE 1394 (FireWire)**, and the low–power, low–speed **I²C** of Philips Laboratories. In both cases the serial approach essentially eliminates miles of harnessing compared to the conventional box approach [Note: the harness refers to the cabling and connectors between flight units, accounting for as much as 10% of the dry mass of a modern spacecraft. The conventional harness comprises the cabling and connectors for power distribution, exchange of data between

1034) M. E. Fraeman, "Advanced Spacecraft Architectures: 1394 Serial Bus," JHU/APL Technical Digest, Vol. 22, No 2, 2001, pp. 114–115

1035) D. J. Andrucyk, F. J. Orlando, C. H. Chalfant, "IEEE 1393 Spaceborne Fiber Optic Data Bus – A Standard Approach to Onboard Payload Data Handling Networks," AIAA paper 99–4507, Sept 15, 1999

1036) K. D. Wolfram, H. J. Bloom, "New Radiation–Hardened High–Speed Serial Data Bus For Satellite Onboard Communication," Proceedings of IEEE/IGARSS, Anchorage, AK, USA, Sept. 20–24, 2004

1037) R. C. Blue, G. S. Bolotin, "X2000 Advanced Avionics Project Development of a New Generation of Avionics for Space Applications," Proceedings of IEEE Aerospace Conference, Big Sky, MT, March 8–15, 2003

1038) D. F. Woerner, "Revolutionary Systems and Technology for Missions to the Outer Planets," Second IAA Symposium on Realistic Near–Term Advanced Scientific Space Missions June 26–July 1, 1998, Aosta, Italy; URL: <http://klabs.org/DEI/Processor/X2000/Aostapaper.pdf>

1039) N. P. Paschalidis, "Advanced System on a Chip Microelectronics for Spacecraft and Science Instruments," Proceedings of the IEEE Aerospace Conference, Big, Sky, MT, March 9–16, 2002

1040) Note: The X2000 label is actually a "deep space systems technology program," the objective is to invent and test new technologies in particular for multiple space exploration missions. The spacecraft X2000 bus is simply one item in the program dealing with the design of a new spacecraft avionics package, including flight and ground software.

1041) S. N. Chau, L. Alkalai, A. T. Tai, "The Design of a Fault–Tolerant COTS–Based Bus Architecture," Proceedings of IEEE Transactions on Reliability, Vol. 48, pp. 351–359, Dec. 1999, :<http://www.ece.uci.edu/~impacct/papers/chau.pdf>

1042) M. E. Fraeman, et al., "A Fault Tolerant Integrated Electronics Module for Small Satellites," Proceedings of the 11th Annual AIAA/USU Conference on Small Satellites, Logan UT, Sep. 15–18, 1997, SSC97–I–3

1043) B. Jackson, J. Campbell, "The Subsystemless Satellite – A New Design Paradigm for Next Generation of Small Satellites," Proceedings of the AIAA/USU Conference on Small Satellites, Aug. 31 – Sept. 3 1998, SSC98–V–5

1044) N. P. Paschalidis, "Microelectronics Technologies Enabling New Generation Spacecraft and Instrumentation," AGU Fall Meeting, San Francisco, CA, Dec. 1997, AGU EOS Transactions, Vol. 78, No 46, 1997

1045) N. Paschalidis, "Advanced System on a Chip Enabling Technologies for Spacecraft and Instrumentation," Proceedings of IAC, Bremen, Germany, Sept. 29 – Oct. 3, 2003

onboard units, acquisition of data from sensors and the control of actuators. Typically, the power cabling accounts for about 25% of the harness mass, while data cabling to sensors and actuators and between on-board units account for around 55% of the harness mass. The remaining 20% is made up of mechanical fasteners and additional shielding.].^{1046) 1047) 1048) 1049) 1050)}

The enabling technologies for this onboard system design approach are the 1394 bus interface chip and the generic RIO (Remote Input Output) chip of JHU/APL. This generic RIO chip is a mixed-signal ASIC with the objective to enable distributed spacecraft and instrument health data collection through the low-speed I²C bus, as well as local data collection through a standard parallel bus. A first tested version of the RIO, with a focus on temperatures and voltages, is TRIO (Temperature Remote Input/Output). The TRIO chip is part of the X2000 bus. In addition to temperatures, TRIOs are used with pressure sensors in the propulsion system, and for radiation dose profile measurements throughout the S/C. TRIO is a low-power device (chip), that greatly enhances the present capabilities of sensor data acquisition in spacecraft applications.

The X2000 bus architecture is a distributed, symmetric system of multiple computing nodes and device drivers that share a common redundant bus architecture. Most notably, all interfaces used in this distributed architecture are based on COTS (Commercial-Of-The-Shelf) components. That is, the local computer bus is the PCI (Peripheral Component Interface) bus (handling of high-speed C&DH functions); the “system” buses are the IEEE 1394 bus and the I²C bus (both are COTS products). Within each node, there is also a separate “subsystem” I²C bus for sensors and instruments control. A multi-level fault protection methodology is employed to achieve high reliability. The X2000 bus provides data rates of 100 Mbit/s permitting multiple computers and scientific instruments to connect into a single local area network. The total dose requirement for the X2000 avionics at the part level is 1 Mrad (radiation hardness).¹⁰⁵¹⁾

In Oct. 2000, JPL selected the FlexWire™ (Link and Digital PHY Layer cores)¹⁰⁵²⁾ implementation of Innovative Semiconductors (Cupertino, CA), based on the IEEE 1394 standard, for use in the X2000 bus. As of 2004, a standard is being developed for the use of TCP/IP over FireWire.

Spaceborne implementation examples are: The NPP satellite (launch Oct. 28, 2011) and the NPOESS satellite series (starting launches in 2014) are using the IEEE 1394 standard as their high-speed data bus.

1046) N. P. Paschalidis, “A Remote I/O (RIO) Smart Sensor Analog-Digital Chip for Next Generation Spacecraft,” Proceedings of AIAA/USU Conference on Small Satellites, Logan, UT, Aug. 31–Sept. 3 1998, SSC98-I-4

1047) D. J. Hunter, “Integrated Avionics System (IAS), Integrating 3-D Technology on a Spacecraft Panel,” Proceedings of the IEEE Aerospace Conference, Big Sky, MT, March 9–16, 2002

1048) G. A. Carr, G. Wester, J. Sauers, et al., “X2000 Power System Electronics Development,” Proceedings of the IEEE Aerospace Conference, Big Sky, MT, March 9–16, 2002

1049) L. J. Deutsch, C. Salvo, D. Woerner, “NASA’s X2000 Program – an Institutional Approach to Enabling Smaller Spacecraft,” <http://klabs.org/DEI/Processor/X2000/99-0049.pdf>

1050) G. Kottaras, N. Paschalidis, V. Paschalidis, E. Sarris, N. Stamatopoulos, K. Karadamoglou, “The TRIO Smart Sensor Data Acquisition System On a Chip For Space Applications,” Proceedings of the IEEE Aerospace Conference, Big Sky, MT, March 6–13, 2004

1051) Note: The IEEE 1394-b standard of 2002 upgrades the prior standards by allowing for gigabit signaling and by extending signaling distance to 100 m (vs. 4.5 m in IEEE 1394 of 1995)

1052) Note: The IEEE 1394 standard is a low cost serial interface intended for transferring high speed data, especially video, between and among computing and consumer devices. An implementation of IEEE 1394 is FlexWire™ of Innovative Semiconductors (Cupertino, CA), offering a series of application-specific IEEE 1394 Link Layer controller cores.

1.8.7.7 SpaceWire

SpaceWire is an enabling packet-switched network standard for onboard space applications, composed of nodes and routers, interconnected through bi-directional high-speed digital serial links, operating at 2–200 Mbit/s (high-speed data-handling network for connecting together sensors, processing elements, mass-memory units, downlink telemetry subsystems and EGSE equipment). SpaceWire introduces specifications for packet-switching, and therefore aims at providing the full potential of the concept SpaceWire (i.e. Network capabilities are based on point-to-point serial links).^{1053) 1054) 1055) 1056) 1057) 1058)}

SpaceWire is regarded a lightweight network (simple, low gate count implementation) that provides low-latency communication, throughput scalability and fault tolerance capability. One of the principal aims of SpaceWire is the support of equipment compatibility and re-use at both the component and subsystem levels. The concept provides an infrastructure for connecting together sensors (e.g. optical or radar instruments), processing elements (e.g. Digital Signal Processors), MMUs (Memory Management Units), and downlink telemetry subsystems.¹⁰⁵⁹⁾

The SpaceWire standard is based on two existing commercial standards, which have been combined and adapted for onboard use: **IEEE 1355–1995** standard and **LVDS** (Low Voltage Differential Signaling) device interfaces. Furthermore, the SpaceWire framework provides capabilities for integration and test of complex onboard systems, with EGSEs (Electrical Ground Support Equipment), plugging directly into the onboard network.^{1060) 1061) 1062)}

Pre-launch monitoring and testing can be carried out with a seamless interface into the onboard data-handling system. SpaceWire aims also at SMCS (Scalable Multi-channel Communication Subsystem) back compatibility. Special advantages of the SpaceWire concept are:

- the protocol is the most versatile with respect to network topology of the buses considered (it permits loops in the network)
- it provides high bandwidth, compact logic design (low power), simple user interface, very small buffer sizes (because of wormhole routing), very quick recovery from errors (20 µs), deterministic time distribution and protocol flexibility (send any packet structure across it). However, SpaceWire does not define a mechanism for reliable transport across the network, i.e., an acknowledgement/retry scheme (transport layer).

Background: The SpaceWire concept, initiated in 1998 in Europe (first discussions started in 1995 at ESTEC in an “open interface data link” round table), is the result of the efforts of many individuals within ESA, the European space industry and in academia. Also, in 1999 a

1053) IEEE Computer Society, “IEEE Standard for Heterogeneous Interconnect (HIC) (Low-Cost, Low-Latency Scalable Serial Interconnect for Parallel System Construction),” IEEE Standard 1355–1995, IEEE, June 1996.

1054) IEEE Computer Society, “IEEE Standard for Low-Voltage Differential Signals (LVDS) for Scalable Coherent Interface (SCI),” IEEE Standard 1596.3–1996, IEEE, July 1996.

1055) Telecommunications Industry Association, “Electrical Characteristics of Low Voltage Differential Signaling (LVDS) Interface Circuits,” ANSI/TIA/EIA–644–1995, March 1996.

1056) <http://spacewire.esa.int/content/Home/HomeIntro.php>

1057) S. M. Parkes, “SpaceWire: a satellite on-board data-handling network, Aircraft Engineering and Aerospace Technology,” An International Journal Vol. 73 No 4, 2001, pp.374–379

1058) S. M. Parkes, “DICE – Digital Interface Circuit Evaluation Study,” Final Report, March 19, 2001

1059) P. Walker, B. Cook, “SpaceWire: Key principles brought out from 40 year history,” Proceedings of the 20th Annual AIAA/USU Conference on Small Satellites, Logan, UT, Aug. 14–17, 2006, paper: SSC06–III–4

1060) S. M. Parkes, “SpaceWire: The Standard,” Proceedings of DASIA (Data Systems In Aerospace)’99 Conference, Lisbon, Portugal, May 1999

1061) J. R. Guasch, S. M. Parkes, A. Christen, “From IEEE 1355 High-Speed Serial Links to SpaceWire (Programmatic aspects and applications),” Proceedings of DASIA’99, Lisbon, Portugal, May 1999

1062) Note: A SpaceWire router ASIC is being funded/developed by ESA, it is expected to be available by 2004. It is likely that many future missions may select SpaceWire and the ECSS standard because of its potential router function.

new panel (P1K) of CCSDS (Consultative Committee for Space Data Standards) was set up to address satellite onboard communication. In addition, there is ECSS (European Cooperation for Space Standardization), an initiative established to develop a coherent, single set of user–friendly standards for use in all European space activities.

SpaceWire is also an ECSS standard (**ECSS–E–ST–50–12C**), SpaceWire, Links, Routers and Networks) as of Jan. 2003.¹⁰⁶³ The aim of the initiative is to provide a common set of protocols to sit on top of existing onboard data buses and networks. A unified data–handling architecture is considered essential for future cost–effective missions. SpaceWire technology is based on the > 10 years of legacy of transputers and the serial links to communicate them (SpaceWire is a derivative of the INMOS transputer link architecture).¹⁰⁶⁴ Those links are derived in the IEEE 1355 standard.

The SpaceWire standard is an open standard developed for anyone to use. It was authored by Steve Parkes, of the University of Dundee, with contributions from many individuals within the SpaceWire Working Group and from the international space agencies and space industry (Ref. 1074).

The SpaceWire standard covers the following protocol levels:¹⁰⁶⁵ ¹⁰⁶⁶

- Physical level: Defines connectors, cables and EMC (Electro–Magnetic Compatibility) specifications.
- Signal level: Defines signal encoding, voltage levels, noise margins and data rates. DS (Data–Strobe) encoding is used. This is a coding scheme which encodes the transmission clock with the data into data and strobe so that the clock can be recovered by simply XORing (XOR stands for eXclusive OR) the data and strobe lines together.
- Character level: Defines the data and control characters used to manage the flow of data across a link
- Exchange level: Defines the protocol for link initialization, flow control, fault detection and link restart
- Packet level: Defines how a message is delivered from a source node to a destination node.
- Network level: Wormhole routing, path addressing, logical addressing, header deletion, group adaptive routing, how to do broadcast or multicast, network errors and recovery.

The physical level is completely different to IEEE–1355, the signal and exchange levels are largely different, and the character and packet levels have some significant changes. Although SpaceWire is extensively different to IEEE–1355 it was designed to be interoperable at the character, exchange and packet levels with IEEE–1355 devices.

The main features of the SpaceWire specifications (“DS–DE” part of the IEEE–1355 standard, up to 200 Mbit/s per link) are already implemented in a set of TEMIC chips (TSC 21020) SpaceWire interface controllers SMCS–332 (3 DS links) and SMCS–lite or SCMS–132 (1 DS–link with up to 200 Mbit/s transfer rate per direction). These controllers are manufactured in accordance with space equipment requirements. A SpaceWire PCI (Peripheral Connection Interconnect) board, prototype developed by the University of Dundee and 4Links Ltd. (UK) under ESA funding, serves in support of links and networks

1063) S. M. Parkes, et al., “SpaceWire: Links, Nodes, Routers and Networks,” Standard No. ECSS–E–50–12A, Issue 1, January 2003

1064) Note: The INMOS transputer was a pioneering concurrent computing microprocessor design of the 1980s from INMOS, a British semiconductor company based in Bristol, UK

1065) S. Parkes, J. Rosello, “SpaceWire ECSS–E50–12A,” Proceedings of the International SpaceWire Seminar 2003, ESA/ESTEC, Noordwijk, The Netherlands, Nov. 4–5, 2003, pp. 106–113

1066) Steve Parkes, Philippe Armbruster, “SpaceWire: Spacecraftonboarddata–handlingnetwork,” Acta Astronautica, Vol. 66, 2010, pp. 88–95

using the SMCS–332 chip developed by Astrium GmbH. Software drivers for Windows, Linux and VxWorks are available. A TCP/IP driver (as well as other network protocols like Ethernet) is also available, providing Internet services over a SpaceWire network. TCP/IP can be used to provide Network and Transport Layer functionality over SpaceWire. ¹⁰⁶⁷⁾ 1068) 1069) 1070) 1071) 1072) 1073) 1074)

Note: A TEMIC DSP (Data Signal Processor) with a TSC 21020 device is flown in the CHRIS (Compact High Resolution Imaging Spectrometer) instrument on ESA's PROBA mission (launch Oct. 22, 2001). The PROBA spacecraft is also using using the SMCS devices.

The MCM (Multi–Chip Module) DSP (Digital Signal Processor) is an integrated and cost effective solution providing a DSP subsystem in a radiation–tolerant technology qualified for space applications.

The MCM can suit any embedded application thanks to its powerful computation unit based on the TSC21020E floating point DSP, the DPC co–processor, 128 kwords on–module SRAM memory for both program and data, and the various microcontroller type peripherals like cascadable timers, full duplex UARTs, input/output serial links, watchdog timers and PWM (Pulse Width Modulator) channels.

An embedded flow–through EDAC protection on both program and data memory paths enhances the MCM's SEU tolerance. The module's total dose radiation tolerance level is better than 50 krad.

Subsystem integration into a larger system is achieved thanks to the MCM DSP open architecture. It is possible to exchange data with the module via the FIFO memory interface, the optimized user interface or the standards IEEE–1355 high speed serial links. Both data and program memory signals are brought off–module for interfacing with expansion memory or other peripherals.

The ESA–led SpaceWire Working Group is also defining higher–level protocols for SpaceWire, in particular the **RMAP** (Remote Memory Access Protocol), with wide international participation from NASA, JAXA and Roskosmos, as well as universities and industry. The development of several SpaceWire–based ASICs also made significant progress. They will be made available to project users via the ASIC manufacturer Atmel (Nantes, France).

1067) Note: SMCS–332 / SMCS–Lite are chips from the same family called SMCS. SMCS (Scalable Multi–ch@@@@annel Communication Subsystem), designed by EADS Astrium GmbH and manufactured by ATMEL in radiation tolerant technology since 1998.

1068) S. Sampson, P. Duggan, R. Burnell, S. McEndree, et al., "Foreign Comparative Test of Space Qualified Digital Signal Processors," Big Sky Montana, March 9–16, 2002

1069) J. Joseph, J. Lazbin, "TCP/IP Router for Space Applications," Proceedings of NASA's ESTC (Earth Science Technology Conference), Palo Alto, CA, June.. 22–24, 2004, <http://esto.nasa.gov/conferences/estc2004/papers/a9p2.pdf>

1070) S. Parkes, S. Mills, "TCP/IP over SpaceWire," Proceedings of DASIA, Prague, Czech Republic, June 2–6, 2003

1071) S. Fischer, P. Rastetter, U. Liebstückel, T. Pike, S. Parkes, "The New SMCS332 / SMCSlite SpaceWire ASIC," Proceedings of International SpaceWire Seminar, ESA/ESTEC, Noordwijk, NL, Nov. 4–5, 2003

1072) S. Mills, S. Parkes, "The SpaceWire Transport Protocol," Proceedings of International SpaceWire Seminar, ESA/ESTEC, Noordwijk, NL, Nov. 4–5, 2003

1073) S. Parks, P. Armbruster, "SpaceWire: Spacecraft Onboard Data Handling Network," Proceedings of the 59th IAC (International Astronautical Congress), Glasgow, Scotland, UK, Sept. 29 to Oct. 3, 2008, IAC–08–B2.4.1

1074) Steve Parkes, Philippe Armbruster, Martin Suess, "Well Connected — The SpaceWire on–board data–handling network," ESA Bulletin No 145, February 2011, pp. 35–45
URL: <http://spacewire.esa.int/content/Home/documents/SpW%20article.pdf>

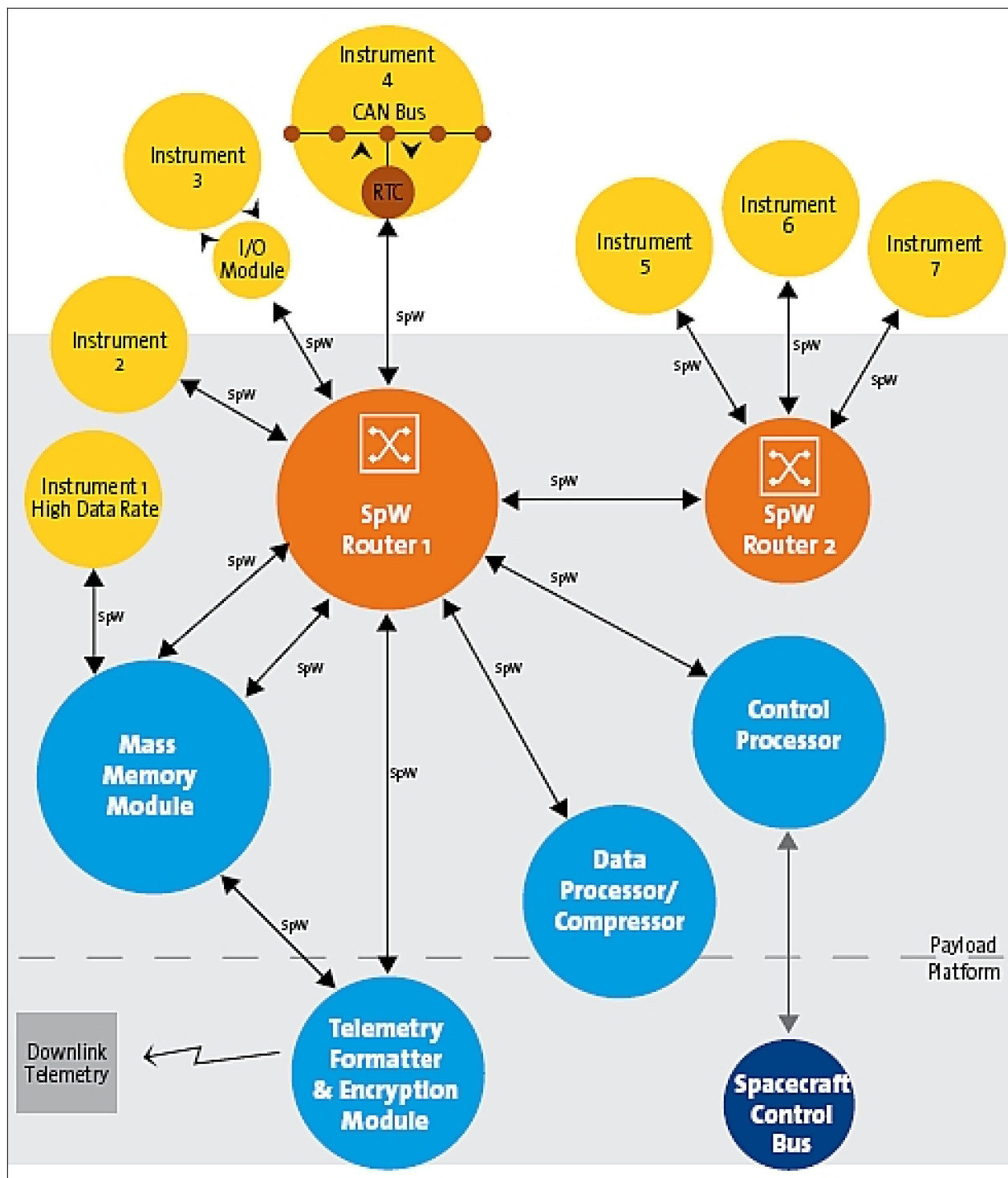


Figure 62: Example of SpaceWire architecture (without redundancy), image credit: ESA (Ref. 1074)

ATMEL is regularly working with most of its key space customers to make their ASIC designs available as standard ASICs when they correspond to commonly used functions on the market. The four ASIC designs of Table 58 are made under ESA contracts. ¹⁰⁷⁵⁾

1075) N. Renaud, Y. Bricard, "ATMEL SpaceWire Products Family," First International SpaceWire Conference 2007, Sept. 17–19, 2007, Dundee, Scotland, UK <http://spacewire.computing.dundee.ac.uk/proceedings/Papers/Components%20202/renaud.pdf>

- The AT7910E SpaceWire Router (SpW–10X) provides eight SpaceWire ports, two external parallel ports and an internal configuration port. It can be used as a standalone router or as a node interface using the external parallel ports. ¹⁰⁷⁶⁾
- The AT7911E, or SMCS332SpW for "Scalable Multi–channel Communication Subsystem for SpaceWire", provides an interface between three SpaceWire links compliant with the SpaceWire standard ECSS–E–50–12A specification and a data processing node consisting of a Control Processing Unit and a communication data memory.
- The AT7912E, or SMCS116SpW, provides an interface between a SpaceWire link compliant with the SpaceWire Standard ECSS–E–50–12A specification and several different interfaces such as ADC/DAC, RAM, FIFO, GPIOs and UARTs.
- The AT7913E SpaceWire Remote Terminal Controller (SpW–RTC) provides a bridge between a SpaceWire network and a CAN bus, and includes a LEON2–FT processor with additional interfaces to ADC/DAC, RAM, FIFO, GPIOs and UARTs. This chip allows the interfacing of high speed serial SpaceWire network and low–speed spacecraft control bus based on CAN. The possible use of the embedded LEON2–FT processor also allows the SpaceWire RTC to contribute to instrument controller processing tasks. ¹⁰⁷⁷⁾

Atmel ASIC name	SpaceWire device name	Designer of ASIC
AT7910E	SpaceWire Router	Austrian Aerospace, University of Dundee, Scotland
AT7911E	SMCS332 (Scalable Multi–channel Communication Subsystem) SpaceWire	EADS Astrium GmbH
AT7912E	SMCS116 SpaceWire	EADS Astrium GmbH
AT7913E	SpaceWire–RTC (Remote Terminal Controller)	Saab Space, Sweden

Table 58: Overview of the Atmel SpaceWire family ASIC products

Some early SpaceWire implementation examples are: ^{1078) 1079) 1080)}

- The Rosetta comet–chasing mission of ESA features the first SpaceWire implementation. [Note: Rosetta, a fully developed spacecraft, was set for a fixed launch date at the end of Jan. 2003. But due to persisting problems with the Ariane 5 rocket and the expiring launch window, the project has been postponed. Rosetta was originally intended to rendezvous with Comet Wirtanen in 2011 (to study both its nucleus and coma through an orbiting spacecraft and a landed platform)]. – A new destination for Rosetta was found in May 2003. Rosetta will now set its sights on Comet 67P/Churyumov–Gerasimenko. The spacecraft was launched March 2, 2004 from Kourou, using an Ariane–5 G+ launcher. The rendezvous with the new target comet is expected in the summer of 2014.
- The Mars Express science mission of ESA employs SpaceWire (as implemented on Rosetta). A launch of the satellite (439 kg S/C bus, 60 kg lander, 116 kg payload, 427 kg propellant) took place on June 2, 2003 on a four–stage Soyuz Fregat launch vehicle from Baiko-

1076) S. Parkes, C. McClements, G. Kempf, S. Fischer, P. Fabry, A. Leon, "SpaceWire Router ASIC," First International SpaceWire Conference 2007, Sept. 17–19, 2007, Dundee, Scotland, UK, URL: <http://spacewire.computing.dundee.ac.uk/proceedings/Papers/Components%202020parkes.pdf>

1077) J. Ilstad, W. Gasti, P. Sinander, S. Habinc, "SpaceWire Remote Terminal Controller," First International SpaceWire Conference 2007, Sept. 17–19, 2007, Dundee, Scotland, UK, URL: <http://spacewire.computing.dundee.ac.uk/proceedings/Papers/Components%202020ilstad.pdf>

1078) S. Parkes, C. McClements, I. Martin, S. Mills, R. Manston, M. Dunstan, "SpaceWire Satellite Onboard Data–Handling Networks," 16th IFAC Symposium on Automatic Control in Aerospace, June 14–18, 2004, St. Petersburg, Russia

1079) C. P. H. Walker, B. M. Cook, "SpaceWire: What, Why, Where," Proceedings of the 57th IAC/IAF/IAA (International Astronautical Congress), Valencia, Spain, Oct. 2–6, 2006, IAC–06–D1.P.1.08

1080) Doug Roberts, Steve Parkes, "SpaceWire Missions and Applications," Proceedings of the International SpaceWire Conference 2010, St. Petersburg, Russia, June 22–24, 2010, URL: <http://2010.spacewire-conference.org/proceedings/Papers/MissionsApplications/Roberts.pdf>

nur. The cruise phase to Mars lasts some six months. ¹⁰⁸¹⁾

- A SpaceWire has also been implemented on the SWIFT (Catching Gamma–Ray Bursts on the Fly) satellite, a NASA space science mission in the MIDEX class with international partners in Europe [ASI; Leicester University; Mullard Space Science Laboratory of the University College, London; CESR, Toulouse; MPE, etc.]. The launch of SWIFT took place on Nov. 20, 2004. – The GSFC SpaceWire implementation on the SWIFT mission is using the SpaceWire protocols and physical layer, but only as a collection of point–to–point links, and is not really a “network” in the classical sense. It is used from the instrument to the instrument electronics only, and the rest of the onboard system uses the MIL–STD–1553 bus as the network for commanding, telemetry collection, etc.
- The InmarSat–IV spacecraft series are using SpaceWire (launch of InmarSat–IV–F1 on March 11, 2005; launch of InmarSat–IV–F2 on Nov. 8, 2005). The two operational spacecraft (a total of 3 spacecraft are planned) are providing instant broadband Internet access.
- The CoRoT (Convection Rotation and planetary Transits) mission of CNES and international partners (ESA, Austria, Belgium, Germany, Spain and Brazil.), launch Dec. 27, 2006, is using SpaceWire.
- The GOCE (Gravity field and steady–state Ocean Circulation Explorer) mission of ESA (launch March 17, 2009) is using SpaceWire.
- EDR (European Drawer Rack) of ESA, part of the Columbus Laboratory of ISS (International Space Station), uses the early version of SpaceWire (data rate of 32 Mbit/s).
- The TacSat–3 demonstration mission of DoD (USA), with a launch on May 19, 2009, is using a SpaceWire implementation for the ARTEMIS (hyperspectral imager) processor. The follow–up mission of TacSat–4 will also use the SpaceWire bus. ¹⁰⁸²⁾
- HSO (Herschel Space Observatory) of ESA (launch May 14, 2009) has been designed with a SpaceWire bus.
- The LRO (Lunar Reconnaissance Orbiter) mission of NASA (launch June 18, 2009) is using SpaceWire along with a SpaceWire ASIC.
- The CryoSat satellite of ESA (launch on Oct. 8, 2005 – but launch failure) employs two fast IEEE 1355 standard links (for the two high–rate interferometric data channels) of the SIRAL instrument and the MIL–STD–1553 bus for the low rate data channels. CryoSat–2 (launch April 8, 2010).
- GLAST (Gamma–ray Large Area Space Telescope, launch June 11, 2008), an astrophysics mission of NASA, uses SpaceWire. – Note: NASA renamed the GLAST mission to Fermi Gamma–ray Space Telescope as of August 26, 2008.
- The future GOES program (NASA/NOAA) selected to use SpaceWire (IEEE–1355) for the next–generation spacecraft starting with GOES–R (launch planned in 2012). ¹⁰⁸³⁾ So are the future NASA missions JWST (James Webb Space Telescope), and SDO (Solar Dynamics Observatory, launch Feb. 11, 2010). The GOES–R SpaceWire test card was designed to use the BAE ASIC providing a platform validating this approach to satisfying GOES–R requirements.

1081) Information provided by Josep Resollo and by Pierre Fabry of ESA/ESTEC, <http://sci.esa.int/science–e/www/area/index.cfm?fareaid=9>

1082) P. Jaffe, G. Clifford, J. Summers, “SpaceWire for Operationally Responsive Space,” Proceedings of the 2008 IEEE Aerospace Conference, Big Sky, MT, USA, March 1–8, 2008

1083) W. H. Anderson, “The Geostationary Operational Satellite R Series (GOES–R) – SpaceWire Implementation,” International SpaceWire Conference, Dundee, UK, Sept. 17–19, 2007, URL: <http://spacewire.computing.dundee.ac.uk/proceedings/Papers/Missions%20and%20Applications%201/anderson.pdf>

- The EarthCARE mission of ESA, JAXA and NICT, is using a SpaceWire implementation (a launch is planned in 2015).
- JWST (James Webb Space Telescope) of NASA/ESA/CSA (launch 2015).¹⁰⁸⁴⁾ The avionics design of JWST employs the FPE (Focal Plane Electronics) onboard network which uses the SpaceWire specification and a transport layer (not part of SpaceWire). SpaceWire is used to provide point-to-point links to ISIM (Integrated Science Instrument Module). A MIL-STD-1553 data bus is being used to communicate with ICEs (Instrument Control Electronics) of each instrument, and FGS (Fine Guidance Sensor).
- The following commercial imaging missions are using the IEEE-1355 SpaceWire standard: a) the TerraSAR-X spacecraft of DLR/EADS Astrium GmbH (launch June 15, 2007), b) RADARSAT-2 (launch Dec. 14, 2007) of CSA and MDA; c) the COSMO-SkyMed constellation of ASI (launch of the first S/C on June 8, 2007, COSMO-SkyMed-2 was launched on Dec. 9, 2007), COSMO-SkyMed-3 was launched on Oct. 25, 2008, COSMO-SkyMed-4 was launched on Nov. 6, 2010; d) TanDEM-X of DLR/EADS Astrium (launch June 21, 2010).
- The DoD is using SpaceWire on the GPS-III spacecraft generation as well as on ORS (Operationally Responsive Space) initiative.
- The SAC-D/Aquarius project of CONAE (Argentina) and NASA is using SpaceWire (launch June 10, 2011).
- JAXA is collaborating with ESA on Bepi-Colombo, using SpaceWire, and developing several chips including a large routing switch.

The First International SpaceWire Conference 2007, held on 17–19 September 2007 in Dundee, Scotland (UK), gave an impressive overview of the current SpaceWire system capabilities and performance spectrum. **The proceedings can be found under the following reference.**¹⁰⁸⁵⁾

The SpaceWire standard is providing many benefits. It helps to facilitate the construction of high-performance onboard data handling systems, reduces system integration costs, increases compatibility between data handling equipment and subsystems, and encourages re-use of data handling equipment across several different missions.

Parameter / Protocol	CAN	I ² C	SpaceWire	MIL-STD-1553
Speed (Mbit/s)	1	up to 3.4	400	1
Topology	Bus	Bus	Point to Point	Bus
No of nodes – No repeaters – Repeaters	30 2048	1024 (10 bit addressing)	Not limited	31
Max length: – @ min speed – @ max speed	10 km 40 m	3–4 m 3–4 m	10 m	122 m ---
Access to medium	CSMA+AMP	start/stop condition	Time windows for real-time	Bus controller
No of master	30	---	Not limited	1 per cycle
Node to node communication	Yes	Yes	yes	---
Broadcasting	Yes	Yes	---	Only master
Error detection	Yes	No	No	No

Table 59: Comparison of some bus characteristics

1084) G. Rakow, R. Schnurr, C. Dailey, K. Shakoorzadeh, “Reliable Transport over SpaceWire for James Webb Space Telescope,” Proceedings of IEEE Aerospace Conference, Big Sky, MT, March 8–15, 2003

1085) <http://spacewire.computing.dundee.ac.uk/proceedings/>

SpaceWire (SpW) standard evolution:

During the past years a number of suggestions have been made to modify the specification of the physical level. These changes involve the following items: cables, connectors, cable assembly, backplane, character level, exchange level, and network level. ¹⁰⁸⁶⁾

SpaceWire–RT (SpaceWire Reliable Timely), or **SpaceWire–D** (deterministic), aims to provide a consistent QoS (Quality of Service) mechanism for SpaceWire that gives SpaceWire reliability and timeliness properties. ¹⁰⁸⁷⁾ ¹⁰⁸⁸⁾ In addition, SpaceWire–RT supports the proposed CCSDS SOIS (Spacecraft Onboard Interface Services) sub–network services. SpaceWire–RT forms the quality of service layer of a complete SpaceWire protocol stack which incorporates the **RMAP** (Remote Memory Access Protocol) and other related protocols currently under development.

SpaceWire–RT adds QoS to the SpaceWire paradigm by providing a stream service over virtual point–to–point links. Any SpaceWire packet can be sent over a SpaceWire–RT virtual point–to–point link (channel) receiving the QoS of that channel.

SpaceWire–RT is part of the layered protocol stack for SpaceWire which is illustrated in Figure 63.

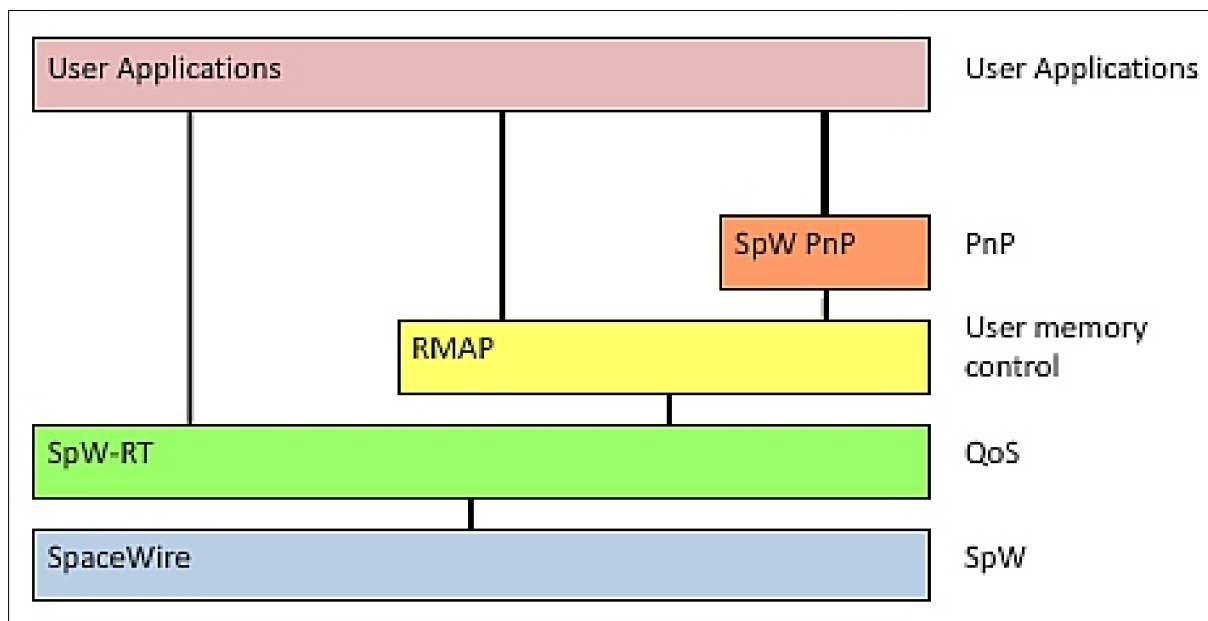


Figure 63: SpaceWire layered protocol stack (image credit: University of Dundee)

SpaceWire is at the bottom of the protocol stack sending SpaceWire packets across the SpaceWire network from source to destination. Immediately on top of SpaceWire is SpaceWire–RT providing quality of service. All traffic has to pass through SpaceWire–RT otherwise the reliability and timeliness QoS cannot be ensured. User applications can talk directly to SpaceWire–RT. RMAP provides a mechanism for reading from and writing to memory in a remote node.

1086) Martin Suess, Steve Parkes, “Mixed SpaceWire – SpaceFibre Networks,” Proceedings of the International SpaceWire Conference 2008, Nov.4–6, 2008, Nara, Japan, URL: <http://2008.spacewire-conference.org/downloads/Papers/Standardisation%201/Suess%202.pdf>

1087) Steve Parkes, Albert Ferrer, “SpaceWire–RT,” Proceedings of the International SpaceWire Conference 2008, Nov.4–6, 2008, Nara, Japan, URL: <http://2008.spacewire-conference.org/downloads/Papers/Standardisation%201/Parkes%202.pdf>

1088) Robert A. Klar, Allison R. Bertrand, “The Evolution of SpaceWire: A Comparison to Established and Emerging Technologies,” Proceedings of the International SpaceWire Conference 2010, St. Petersburg, Russia, June 22–24, 2010, URL: <http://2010.spacewire-conference.org/proceedings/Papers/Posters/Klar.pdf>

SpaceWire–PnP (plug and play) uses RMAP for configuration and management of nodes on the SpaceWire network. User applications can use the services provided by RMAP or SpaceWire–PnP as well as talking directly to SpaceWire–RT. ¹⁰⁸⁹⁾

RMAP and SpaceWire–PnP provide the Memory Access Service and Device Discovery Services. The SOIS Packet Service is provided by a SpaceWire Packet Transfer Protocol (SpaceWire–PTP) that sends packets across the SpaceWire network, providing buffer management and flow control.

The CCSDS SOIS working group has defined a set of common communication services for use onboard a spacecraft. The SOIS subnetwork layer and three of the services provided are shown in Figure 64. The SOIS Packet Service provides for delivery of packets across a sub-network, the Memory Access Service for the access of memory devices on the subnetwork, and the Device Discovery Service supports plug–and–play capability with notification services. ¹⁰⁹⁰⁾

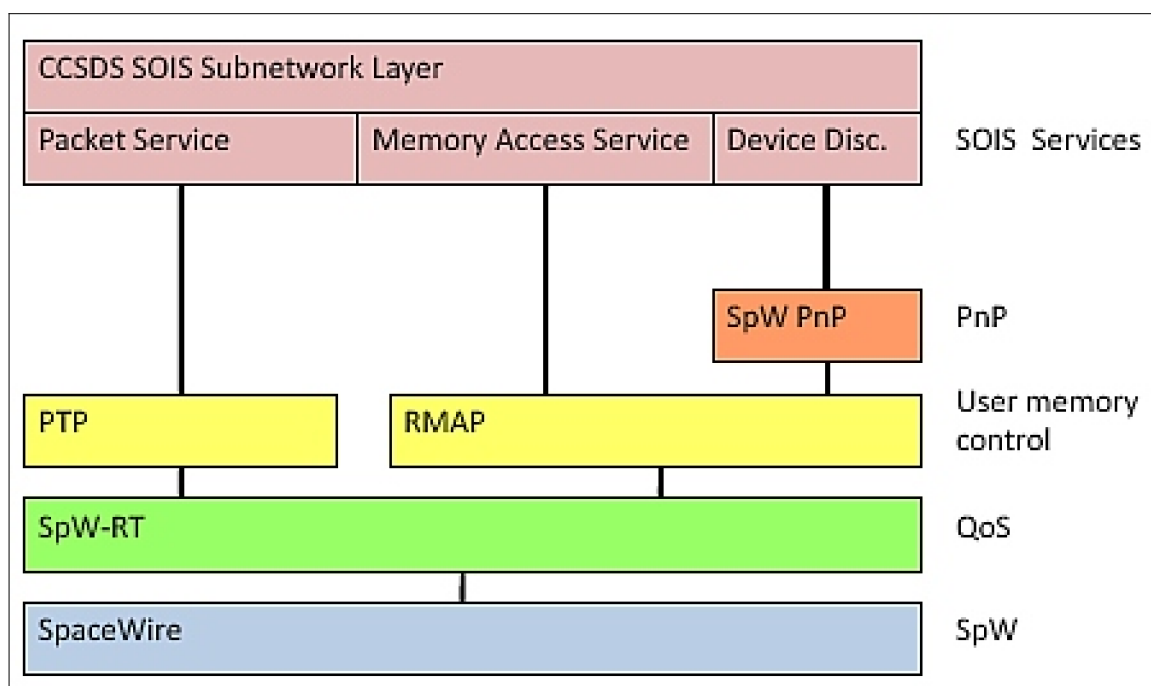


Figure 64: SOIS to SpaceWire layered protocol stack (image credit: University of Dundee)

Network discovery and device configuration: STAR–Launch is a new software tool that can be used to launch applications and modules to interact with STAR–Dundee SpaceWire devices. It will provide the ability to discover devices on a SpaceWire network and display these graphically. ¹⁰⁹¹⁾ – Once the PnP services have been added to the STAR–Dundee Ltd. API, they will be incorporated into example virtual devices provided with the API. It will then be possible to discover these virtual devices if they are connected in a virtual network. If the virtual network is also connected to a physical SpaceWire network, it will be possible to detect the virtual network from any point on the physical SpaceWire network. The virtual network will appear as just another section of the SpaceWire network, and the active node discovering the network will treat the virtual devices in the same way as the physical devices.

1089) Peter Mendham, Albert Ferrer Florit, Steve Parkes, “Standardized Sensor and Actuator Interfaces with SpaceWire–PnP,” Proceedings of the 60th IAC (International Astronautical Congress), Daejeon, Korea, Oct. 12–16, 2009, IAC–09.B4.7.2

1090) Peter Mendham, Stuart Fowell, Chris Taylor, “The SpaceWire–PnP Protocol in the SOIS Plug–and–Play Architecture,” Proceedings of the International SpaceWire Conference 2010, St. Petersburg, Russia, June 22–24, 2010, URL: <http://2010.spacewire-conference.org/proceedings/Papers/NetworksProtocols/Mendham1.pdf>

1091) Stuart Mills, Chris McClements, Steve Parkes, “STAR–Launch and Network Discovery,” Proceedings of the International SpaceWire Conference 2010, St. Petersburg, Russia, June 22–24, 2010, URL: <http://2010.spacewire-conference.org/proceedings/Papers/NetworksProtocols/Mills2.pdf>

SpaceWire–RT is defined in substantial detail in the SpaceWire–RT Initial Protocol Definition.^{1092) 1093)}

SpaceWire–10X router: The router, designed by the University of Dundee and Austrian Aerospace, has eight SpaceWire ports each capable of operating at up to 200 Mb/s and two parallel ports. It includes extensive capabilities making it an extremely versatile SpaceWire routing device.

1.8.7.8 SpaceFibre:

SpaceFibre is a very high–speed serial data–link concept, a next generation SpaceWire, being developed by ESA which is intended for use in data–handling networks for high data–rate payloads. SpaceFibre is able to operate over fibre optic and copper cable and support data rates of 2 Gbit/s in the near future and up to 5 Gbit/s long–term. The objective is to complement the capabilities of the widely used SpaceWire onboard networking standard: improving the data rate by a factor of 10, reducing the cable mass by a factor of four and providing galvanic isolation.^{1094) 1095) 1096)}

SpaceFibre will support high data–rate payloads, for example SAR (Synthetic Aperture Radar) and hyperspectral optical instruments.

As of 2009, a prototype SpaceFibre interface has been designed by the Space Technology Centre at the University of Dundee, a demonstration system built and an initial draft of a standard document written. A prototype has also been built by NASA/GSFC and will shortly fly on a test vehicle.^{1097) 1098)}

The principal requirements for SpaceFibre are:

- Symmetrical, bi–directional, point–to–point link connection
- High speed (1–10 Gb/s) with a target of at least 2.5 Gb/s
- Fibre cable lengths of up to 100 m; copper cable over shorter length of 2 m (target)
- Fibre optic cable mass of less than 20 g/m for a full–duplex link
- Galvanic isolation
- Quality of service support; support of arbitrary network architectures
- Support mixed SpaceWire–SpaceFibre networks using a SpaceWire–SpaceFibre multiplexer/de–multiplexer.

SpaceFibre 2010: The lower levels of SpaceFibre have been specified by the University of Dundee and a prototype SpaceFibre interface developed and tested. NASA have develo-

1092) S. M. Parkes, A. Ferrer–Florit, “SpaceWire–RT Initial Protocol Definition”, Draft 2.1, SpaceNet Report No. SpW–RT WP3–200.1, ESA Contract No. 220774–07–NL/LvH, October 2008.

1093) Paul B. Wood, Sue A. Baldor, “A Software Adaptation Layer for Increased Plug–and–Play Compatibility,” Re-inventing Space Conference, May 7–10, 2012, Los Angeles, CA, USA, paper: AIAA–RS–2012–4002, URL: http://www.responsivespace.com/Papers/RS2012/SESSIONS/Session%20IV/4002_Wood/4002P.pdf

1094) Steve Parkes, Yuriy Sheynin, Masaharu Nomachi, “SpaceWire Missions and Architectures,” Proceedings of the 60th IAC (International Astronautical Congress), Daejeon, Korea, Oct. 12–16, 2009, IAC–09.B2.6.2

1095) Steve Parkes, Chris McClements, Martin Suess, “SpaceFibre,” International SpaceWire Conference 2007, Dundee, UK, Sept. 17–19, 2007, URL: <http://spacewire.computing.dundee.ac.uk/proceedings/Papers/Standardisation/parkes.pdf>

1096) Clifford Kimmery, “SpaceFibre Virtual Channels and Flow–Control,” International SpaceWire Conference 2008, Nara Japan, Nov. 4–6, 2008, URL: <http://2008.spacewire-conference.org/downloads/Papers/Standardisation%20I/Kimmery.pdf>

1097) Steve Parkes, Chris McClements, Martin Dunstan, Martin Suess, “SpaceFibre: Gbit/s Links for use On Board Spacecraft,” Proceedings of the 60th IAC (International Astronautical Congress), Daejeon, Korea, Oct. 12–16, 2009, IAC–09.B2.5.8

1098) Steve Parkes, “Never mind the quality, feel the bandwidth: quality of service drivers for future onboard communication networks,” Proceedings of the 61st IAC (International Astronautical Congress), Prague, Czech Republic, Sept. 27–Oct. 1, 2010, IAC–10.B2.6.6

ped a prototype SpaceFibre system to this specification and tested it on the MAX Launch Abort System (MLAS) test vehicle. JAXA have also developed a prototype SpaceFibre system. QoS mechanisms for SpaceFibre are currently being defined and prototyped to provide a comprehensive capability set for future space missions. SpaceFibre is now being defined for use in several onboard applications including mass memory devices and DSP processors. SpaceFibre fills a growing gap in onboard communications links for spacecraft, which is being widened by the high data-rate demands of new instruments.¹⁰⁹⁹⁾

SpaceFibre in 2013: The University of Dundee and STAR–Dundee Ltd. are working together on a SpaceFibre interface design funded by ESA, the EC (European Commission) and STAR–Dundee Ltd. SpaceFibre is a multi-Gbit/s network technology ideal for spaceflight applications, which is galvanically isolated, which does provide comprehensive quality of service, which includes robust FDIR (Failure Detection, Isolation and Recovery) support, and which extends the time-codes of SpaceWire into a much more versatile Broadcast Message service. Furthermore SpaceFibre uses the same packet format and routing concepts as SpaceWire making it very easy to bridge between existing SpaceWire devices and networks and SpaceFibre. SpaceFibre is planned for ECSS (European Cooperation for Space Standards) standardization in 2014.¹¹⁰⁰⁾

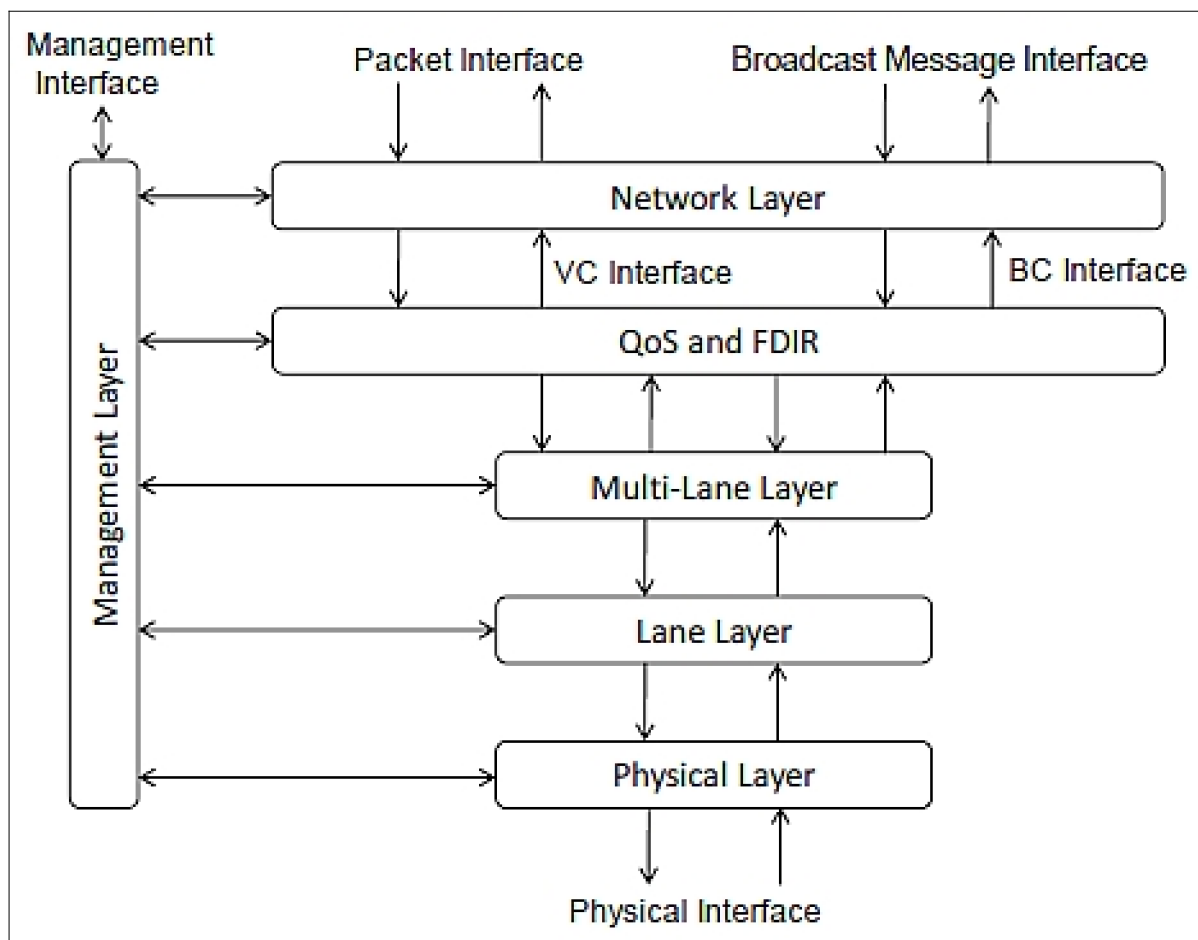


Figure 65: The protocol stack of SpaceFibre (image credit: University of Dundee)

VHiSSI (Very High Speed Serial Interface) is an EC Framework 7 project led by the University of Dundee and including partners from the UK (STAR–Dundee), Germany (As-

1099) Steve Parkes, Chris McClements, Martin Suess, "SpaceFibre," Proceedings of the International SpaceWire Conference 2010, St. Petersburg, Russia, June 22–24, 2010, URL: <http://2010.spacewire-conference.org/proceedings/Papers/Standardisation/Parkes2.pdf>

1100) Steve Parkes, Chris McClements, Albert Ferrer, Alberto Gonzalez, "SpaceFibre: Multi-Gbit/s Network for Spaceflight Applications," Proceedings of the 64th International Astronautical Congress (IAC 2013), Beijing, China, Sept. 23–27, 2013, paper: IAC–13–B2.3.1

trium, IHP), Israel (Ramon Chips, ACE–IC) and Italy (SCI). It aims to design and evaluate technology suitable for implementation of SpaceFibre very high–speed serial interfaces for spaceflight applications. There are six main functions within the VHiSSI chip:

- SpaceWire Bridge
- FIFO, DMA, Memory and Transaction interface
- SpaceFibre Interface
- SerDes (Serializer–Deserializer)
- IO Switch Matrix
- Mode Switch Matrix.

1.8.7.9 SpaceLAN (Spacecraft Local Area Network)

SpaceLAN^{1101) 1102) 1103)} is a further entry into the ring of onboard networks (to give designers a choice for different networking solutions). The networking efforts of NASA/GSFC concentrate on the development of SpaceLAN, an Ethernet (IEEE 802.3) implementation (along with a new space–qualified physical layer) with associated standard switching components as well as a standard package of interfaces and services on a spacecraft. The intent is to replace the MIL–STD–1553/1773 bus implementations of past decades (with custom interfaces, etc.) with a more capable network in particular with regard to communications performance.

The first NASA mission candidates considered for a SpaceLAN Ethernet implementation are SDO (Solar Dynamics Observer) in 2008 and GPM (Global Precipitation Mission) in 2009. A significant effort is underway at NASA to produce a network switch that will tie together multiple nodes on the network.

1.8.7.10 Wireless interfacing on spacecraft (proximity networks)

In the early 21st century, the wireless commercial technologies have reached a considerable state–of–the–art level and are advancing at a rapid pace. The **wireless architecture** – eliminating the cables and reducing the harness from the data bus – has also significant implications in the context of future intra–spacecraft data handling, inter–instrument communications, as well as communications outside the spacecraft (inspection services, extra–vehicular activities, etc.).^{1104) 1105) 1106)} In addition, the wireless link technology of a “proximity network,” a “WSN (Wireless Sensor Network),” or a WLAN (Wireless Local Area Network)” domain offers mobility and flexibility for man or machine. Depending on the distributed nature of a WSN concept, the term “wireless” may also imply the need for self–powered sensor units within the network. There is considerable interest in spaceborne

1101) E. Webb, “Ethernet for Space Flight Applications,” Proceedings of the 2002 IEEE Aerospace Conference, Big Sky Montana, March 9–16, 2002

1102) E. J. Knoblock, V. K. Konangi, K. B. Bhasin, “Local Area Network for Space–Based Instrument Control,” Proceedings of the 2002 IEEE Aerospace Conference, Big Sky Montana, March 9–16, 2002

1103) C. Del Vecchio Blanco, M. D’Errico, “Exploiting the CAN bus as a potential interface for future aerospace vehicles based on modular, intelligent, and autonomous architecture,” Proceedings of the 57th IAC/IAF/IAA (International Astronautical Congress), Valencia, Spain, Oct. 2–6, 2006, IAC–06–B5.7.4

1104) R. Amini, G. Aalbers, R. Hamann, W. Jongkind, P. G. Beethuizen, “New Generations of Spacecraft Data Handling Systems: Less Harness, more Reliability,” Proceedings of the 57th IAC/IAF/IAA (International Astronautical Congress), Valencia, Spain, Oct. 2–6, 2006, IAC–06–D1.4.09

1105) Overview of Space related Wireless Activities, Workshop on Spacecraft Data Systems, May 5–7, 2003, ESA/ESTEC, URL: <http://conferences.esa.int/03C20/s2b–03.ppt>

1106) Wireless for Space Applications Workshop, ESA/ESTEC, July 10–13, 2006,

WSN/WLAN implementations due to the potential of mass, power and cost reductions as well as a number of other benefits. 1107) 1108) 1109)

A wireless bus architecture may be based on various communication techniques, among them may be implementations in **optical** or **RF** (Radio Frequency) link technology.

1) Optical wireless technique: Optical wireless interfaces can be divided into two classes: line-of-sight and diffuse. The line-of-sight technique is a point-to-point data transmission method which requires a clear line of sight between the communication parties, is less flexible for monitoring the data; however, its data rate can be very high and can be very long range. Careful aiming of the receiver and transmitter is also required. – The diffuse technique is more flexible; however, its range of operation is shorter and transmission is not guided. Thus, this method is a point-to-multipoint communication technique.

2) RF technique: RF wireless interfaces use omni-directional, short-range radio links between units. The major benefits of a RF wireless interfaces over an optical interface are that all data traffic on the links can be monitored very easily during the integration and test, and integration is greatly simplified because the units need only be within range of the RF links to operate. The spacecraft units can therefore be operated on the bench during check-out and then progressively integrated into the spacecraft without the need for any special harness. One disadvantage with RF wireless interfaces is that they may be susceptible to RF interference, and may also interfere with other equipment.

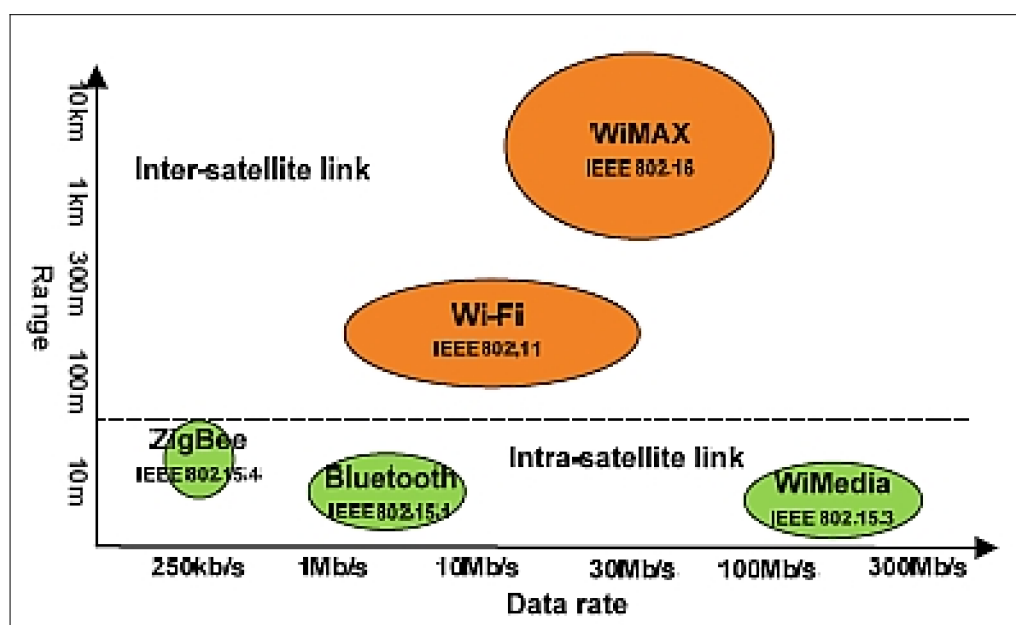


Figure 66: Overview of several potential COTS standards for spaceborne WSNs (Ref. 1109)

Among the different developed wireless communication standards, developments based on the IEEE 802.15.4 and Bluetooth for limited distances and low speed are generally the preferred options. Moreover, the IEEE 802.15.4 standard, which is ultra low power with sleep mode, has attracted more attention. Also the family of IEEE 802.15.3 (WiMedia) standard seems to be very promising for high data rate and short range intra-spacecraft communications. For longer range communication (i.e. inter-spacecraft communication), the IEEE

1107) Position paper “Wireless Interfaces Services” as support to the proposal for a Working Group within the SOIS Area of CCSDS, Atlanta, Sept. 15, 2005

1108) R. Magness, P. Plancke, ESA TEC-E Wireless Technology Dossier, Annex A,” Proceedings of the 9th ESA Workshop on Advanced Space Technologies for Robotics and Automation (ASTRA 2006), Noordwijk, The Netherlands, Nov. 28–30, 2006

1109) Rui Sun, Jian Guo, Eberhard Gill, “Opportunities and Challenges of Wireless Sensor Networks in Space,” Proceedings of the 61st IAC (International Astronautical Congress), Prague, Czech Republic, Sept. 27–Oct. 1, 2010, IAC–10.D1.4.8

802.11 family of standards (specially revision “n”) suits the application. Network topology, bandwidth, power consumption, EMC (Electromagnetic Compatibility) requirements, intrinsic robustness and implementation complexity are the factors to be considered before using any of the wireless standards in the applications.

The main motivations and benefits for developing a wireless data communication system onboard spacecraft can be summarized as:

- Reducing the time and cost of the AIT (Assembly, Integration and Test) process
- Inherently providing galvanic isolation
- Simplifying integration tests and verifications
- Reducing the harness and the complexity of connections
- Reducing the harness of cable connectors
- Removing the risk of happening a mechanical damage to interfaces during the tests
- Possibility of monitoring the data communication without adding new units and cables to the data bus
- Flexibility in upgrading and replacing the units
- Flexibility in designing deployable parts and moving subsystems
- Possibility of integration with new power scavenging techniques for designing totally wireless and autonomous modules
- Possibility of reusing the same hardware design and interface for other missions
- A WSN may consist of tiny energy efficient, battery–powered sensor nodes, with built–in wireless transceivers. The nodes are able to do much more than simple sampling and transmission of data. A WSN is able to setup multi–hop wireless ad–hoc networks automatically.

On the other hand, there are some drawbacks concerning the security and EMC issues of wireless interfaces. Almost all of the available wireless interfacing standards are designed to operate in open environment, and not a close environment such as the area within a spacecraft. It is important to make sure that the wireless interfaces are not sensitive to disturbances made by other on–board electronics, and also are not interfering with other equipments.

Wireless spaceborne implementations: Several types of wireless devices and sensors have already flown on space missions, others are awaiting launch:

- WNE (Mir Wireless Network Experiment), a portion of a joint US/Russian program with Yuri Gawdiak and Richard Alena (both of NASA/ARC) as PI and Co–PI. The third Space Shuttle – Mir Station Docking Mission was flown on STS–76, (March 22–31, 1996). The WNE, a client–server network using a spread spectrum RF technology in the frequency range of 2.400–2.483 GHz, was conducted for the first time in a space environment (close proximity operations and docking) aboard Shuttle and MIR. The WNE system for the MIR station was already launched and installed on the previous STS–74 flight (Nov. 12–20, 1995). ^{1110) 1111) 1112)}

The WNE consisted of three computers: a ruggedized Pentium–based portable computer functioning as WNS (Wireless Network Server); the other two components were a HP Om-

1110) R. Lofton, C. Conley, “International Space Station Phase 1 Risk Mitigation and Technology Demonstration Experiments, 48th International Astronautical Congress, Turin, Italy, Oct. 6–10, 1997

1111) <http://www.hq.nasa.gov/osf/station/issphase1sci.pdf>

1112) “Mir Wireless Network Experiment (MWNE),” URL: <http://spaceflight.nasa.gov/history/shuttle-mir/science/iss/sc-iss-mwne.htm>

nibook Subnotebook computer (SNB), and a NORAND Pen*Key Personal Digital Assistant (PDA).

The objective of this demonstration was to: a) evaluate the function of this system as part of remote communication planning for ISS, b) to test commercial radio frequency wireless data links and mobile computer equipment to determine effective ranges and data throughput rates, c) to investigate the effects of radiation on advanced computer systems, and d) to investigate human/computer interaction factors in the microgravity environment. The experiment (WNE) was performed aboard STS–76 and MIR–Spektr in March 1996. Results:

- Sustainable network throughput of 200–400 kbit/s
- Operating range: within two adjacent station modules
- Passed flight qualification, electromagnetic compatibility and safety review
- No computer failures during operation after 4 months of stowage aboard MIR Spektr
- Reduced power radios will work, but coverage and range is affected
- Radio had mechanical capacitor adjustment drift due to launch vibration resulting in 10% decreased throughput.
- The μ WIS (Micro Wireless Instrumentation System) of NASA consists of autonomous, tiny sensors for data acquisition. The instrument was flown on several missions:
 - STS–96 (May 27–June 6, 1999); the objective was to demonstrate the micro WIS transmitter and recorder
 - STS–101 (May 19–29, 2000); the objective was to demonstrate the operational utility and functionality of μ WIS on–orbit, initially in the crew cabin of the Shuttle Orbiter and then in the ISS.
 - STS–106 (Sept. 8–20, 2000); objective same as on STS–101
 - STS–104 (July 12–24, 2001); objective same as on STS–101
- The ISS (International Space Station) has two wireless RF systems in operation, developed by Invocon Inc., Conroe, TX, USA. ¹¹¹³⁾
 - IWIS (Internal Wireless Instrumentation System)
 - EWIS (External Wireless Instrumentation System)

IWIS was deployed by astronauts [launched on assembly flight 4A, STS–97 flight of Endeavour (Nov. 30 – Dec. 11, 2000)] inside the partially completed ISS to collect data on the impulse response of the structure (strain gauges and temperature sensors are placed at various locations of the ISS structure). This data is used to verify the structural integrity of the ISS on orbit. It is also be used to update models predicting the modal response of the ISS. Complete understanding of the resonant modes of the structure will allow effective planning of the re–boost and Reaction Control System (RCS) firing sequences when the Shuttle is docked with the Station. Since this data will change as the Station is assembled, it is important to keep this data current with each addition to the Station. The wireless nature of the data acquisition network minimizes the time necessary for deployment and recovery of the system.

The first element of **EWIS** was deployed by the STS–115 crew (flight 12A of Atlantis, Sept. 9–21, 2006) as part of the installation of the P3/P4 truss. EWIS was developed as a system for acquiring vibration data from the truss structure to monitor the health of the truss com-

¹¹¹³⁾ http://www.invocon.com/IVC_on_ISS.html

ponents. The single EWIS Remote Sensor Unit (RSU) attached to the truss is currently collecting vibration data. This vibration data will be downloaded when the EWIS Network Control Unit (NCU) is installed during a future mission. Note: the P5 Truss on STS-116 flight (Dec. 10–22, 2006) contains a remote sensor box, two tri-axial accelerometers, and two antenna assemblies as part of its EWIS assembly.

- The experimental microsatellite (20 kg) of INTA (Instituto Nacional de Técnica Aeroespacial), the Space Agency of Spain, called NanoSat-01 (launch Dec. 18, 2004), features two OWLS (Optical Wireless Links for intra-Satellite) communication demonstration experiments, representing the first OWLS in-orbit application. NanoSat-01 is operating nominally as of 2008.
- The Delfi-C3 nanosatellite of TU Delft (Delft University of Technology, Delft), The Netherlands, with a launch on April 28, 2008, has an experiment AWSS (Autonomous Wireless Sun Sensor) of TNO, Delft. The tiny prototype sensor is self-powered and demonstrates a wireless data link to the CDHS (Command & Data Handling Subsystem) of the spacecraft. ¹¹¹⁴⁾
- A further OWLS experiment of INTA was flown on the Foton-M3 mission of Russia (Roskosmos spacecraft), with a launch on Sept. 14, 2007 (12 day mission). The objective of OWLS is:
 - Assessment and validation of the Optical Wireless technology for a future data-harnessing substitution in the Foton capsule
 - To implement the CAN protocol (Controller Area Network) using an optical wireless physical layer. The wireless Foton experience will be the first OWL-CAN inside an spacecraft. ¹¹¹⁵⁾

1.8.7.11 Plug-and-play systems

The term “plug-n-play” (PnP) refers to hardware and software devices in a computer (PC) that, after being installed (“plugged in”), can immediately be used (“played with”) without requiring a system reconfiguration or manual installation of device drivers by the user. Obviously, this kind of self-configuration and interoperability between applications represent important service features in a distributed system environment.

The computer industry (Intel, Microsoft, Phillips, Compaq, and NEC) came out with a PnP standard for the ISA (Industry Standard Architecture) bus in the time frame of 1995 (starting with the Windows 95 operating system) to ease the integration of standard components (peripherals). This first PnP standard was called the USB (Universal Serial Bus), a serial bus supporting a master-slave architecture where peripherals can only talk when spoken to. USB supports swapping and PnP. Since that time, PnP has evolved dramatically.

From the perspective of a user of commercial equipment, application of the term “plug-and-play” indicates that it should be possible to interface two or more arbitrary devices without the need for reconfiguration. ¹¹¹⁶⁾ With many existing interfacing technologies, such as the USB, interfacing may be carried out while power is applied, permitting the plug-and-play aspects of the standard to accommodate changes in configuration while the system is running.

1114) R. Amini, E. Gill, G. Gaydadjiev, “The Challenges of Intra-Spacecraft Wireless Data Interfacing,” 58th IAC (International Astronautical Congress), International Space Expo, Hyderabad, India, Sept. 24–28, 2007, IAC-07-B4.7.08

1115) S. Rodríguez, A. Martín Ortega, J. R. De Mingo, I. Arruego, “Optical Wireless FOTON-M3 experiment,” Wireless for Space Applications Workshop, ESA/ESTEC, July 10–13, 2006, URL: ftp://ftp.estec.esa.nl/pub/ws/wireless2006/Session%202/S2_1_Foton_Experiment.pdf

1116) David Jameux, “Towards SpaceWire Plug-And-Play ECSS Standard,” Proceedings of the International SpaceWire Conference 2011, San Antonio, TX, USA, Nov. 8–10, 2011, URL: <http://2011.spacewire-conference.org/proceedings/Presentations/Networks/Jameux.pdf>

The ultimate effect of these configuration changes is in the services that are available to the system. To this end, a system may also permit the discovery of the services a device provides, for example using the DHCP (Dynamic Host Configuration Protocol) for TCP/IP or the built-in service identification mechanisms of wireless standards such as Bluetooth and ZigBee (IEEE802.15.4). Plug-and-play therefore generally involves two key aspects:

- Automatic discovery and configuration of hardware and software systems in response to changes in hardware interfacing or availability including while the system is running ('hot plugging'); in other words, the capability to detect any connection or disconnection of Plug-and-Play enabled devices.
- Detection registration, and configuration of the services that a plug-and-play enabled device provides; as well as detection and de-registration of the services that a newly disconnected Plug-and-Play enabled device was providing.

PnP concepts in space applications: The space domain offers significant challenges: both computing power and storage space are at a premium and the complexity of a PnP technology could have implications in terms of both mass and power consumption. And reliability is a key requirement in space systems. It is common for a spacecraft to have different operational configurations, corresponding to different phases of the mission, often known as modes. ^{1117) 1118)}

For example, a spacecraft that has just been deployed into orbit by its launch vehicle, may enter a sun acquisition mode, in an attempt to establish coarse pointing. In this initial mode the solar panels are not properly oriented with respect to the sun and the spacecraft may be running from the internal battery. To conserve power, many spacecraft systems will be powered down. As the spacecraft leaves the sun acquisition mode, more instruments may be required which, on powering up, will change the topology of the network. – In such cases, the PnP network discovery facilities could be used to detect this change in topology and modify the routing tables. Furthermore, by considering unexpected changes in onboard network configuration, PnP could be used to provide a degree of tolerance to faults. The feature of network discovery can be used to reconfigure routers to adapt to changes in topology but, perhaps more importantly, service discovery can be used to find alternative services to those that have been lost due to failure.

In view of these potentials, there is considerable interest to extend the PnP technology also into spacecraft onboard information systems. In 2004 AFRL (Air Force Research Laboratory) initiated the collaborative development of a new set of spacecraft standards to bring the same plug-and-play capability enjoyed by the computer industry across to the space industry.

In 2007 the first new open space plug-and-play avionics standards are going to publication, with several additional protocol adaptations set to follow. ^{1119) 1120)} The standards were (and are) being developed by CCSDS (Collaborative Committee for Space Data Systems) and by AIAA (American Institute for Aeronautics and Astronautics). The committee on standards (CoS), formed by AIAA, included representatives from government, industry, and academia. The PnP features have the potential to accelerate in particular the design and development time of space systems.

1117) L. Thienel, G. Robinson, D. Stottleyer, R. Burgess, S. Clough, "Plug and Play – Small Satellite Solutions with Large Satellite Implications," Proceedings of the 22nd AIAA/USU Small Satellite Conference, Logan, UT, USA, Aug. 11–14, 2008, SSC08–III–8

1118) Don Fronterhouse, "Plug and Play Spacecraft Evolution," Proceedings of the 23rd Annual AIAA/USU Conference on Small Satellites, Logan, UT, USA, Aug. 10–13, 2009, SSC09–VI–4

1119) F. A. Slane, A. J. Hooke, "Space Plug and Play Avionics Standards: Progress, Problems and a View of the Future," AIAA 2007 Conference and Exhibit, May 7–10, 2007, Rohnert Park, CA, USA, AIAA 2007–2912

1120) P. Graven, R. Van Allen, L. J. Hansen, J. M. Pollack, "Achieving Responsive Space: The Viability of Plug-and-Play in Spacecraft Development," Proceedings of the 29th AAS Guidance and Control Conference, Breckenridge, CO, USA, Feb. 4–8, 2006, AAS 06–034, URL: http://www.smad.com/analysis/78–Breckenridge_06%20FINAL.pdf

The ORS (Operationally Responsive Space) initiative of DoD (US Department of Defense) is in the process to adopt PnP techniques into the TacSat series for on-orbit demonstrations. Some early (prototype) implementations of the PnP technology in space are:

- The TacSat-3 mission of AFRL (launch May 19, 2009) is introducing the SPA (Spacecraft Plug-and-play Avionics) package to demonstrate and validate common plug-and-play electrical and software interfaces between bus components and between the bus and payload. These concepts include self-forming networks, machine-negotiated interfaces, encapsulation of complexity, and test bypass. ASIM (Appliqué Sensor Interface Module) is a device as well as an enabling technology for SPA systems. One of the challenges faced by the commercial computer electronics industry in designing PnP devices was (and is) the sheer complexity of the interfaces. ^{1121) 1122) 1123) 1124) 1125)}

The ASIM is currently a small printed wiring board (PWB), employing an FPGA-based design serving as a “soft testbed” for further refinement. The standards have initially focussed on interface definitions for low-data-rate components, “SPA-U” which is based on the USB 1.1 standard, and high-data-rate components “SPA-S” (based on the SpaceWire standard).

- The SpaceWire network provides considerable potential for PnP support services. ^{1126) 1127)} SpaceWire offers very few restrictions on network topology, permitting theoretically unlimited chains of routers between devices. Two addressing modes are possible in a SpaceWire network: a) path addressing, and b) logic addressing. For a SpaceWire network to operate correctly using logical addressing, the logical address table in each router must be correctly configured. The configuration of each table is directly related to the current topology of the network. ^{1128) 1129)}

The discovery facilities of a plug-and-play technology offer a management computer to configure routing tables. Changes in the network topology can be detected and routing tables can be reconfigured. Changes in topology can be detected either at the site of the change, for example by a router informing a network manager that a link is no longer available, or by a network manager explicitly probing for topology changes. Service detection and configuration can be used to identify the services that are available on each device and permit suitable management software to match data sources and sinks.

- ¹¹²¹⁾ Denise Lanza, Jim Lyke, Don Fronterhouse, Scott Cannon, Wheaton Byers, “Space Plug-and-Play Avionics, URL: <http://www.responsivespace.com/Papers/RS3%5CSESSION%20PAPERS%5CSESSION%205%5C5001-LYKE%20&%20FRONTERHOUSE%5C5001C.pdf>
- ¹¹²²⁾ P. M. Wegner, R. R. Kiziah, “Pulling the Pieces Together at AFRL,” 4th Responsive Space Conference, Los Angeles, CA, April 24–27, 2006, AIAA-RS4-2006-4002, URL: http://www.responsivespace.com/Papers/RS4%5CPapers%5CRS4_4002P_Wegner.pdf
- ¹¹²³⁾ J. Scott, J. Lyke, P. McGuirk, M. Shaw, D. Fronterhouse, “Appliqué Sensor Interface Module: An Enabling Technology for Space Plug-and-Play Systems,” Proceedings of the 21st Annual AIAA/USU Conference on Small Satellites, Logan, UT, USA, Aug. 13–16, 2007, SSC07-X-1
- ¹¹²⁴⁾ J. Lyke, S. Cannon, D. Fronterhouse, D. Lanza, T. Byers, “A Plug-and-play System for Spacecraft Components Based on the USB Standard,” Proceedings of the 19th Annual AIAA/USU Conference on Small Satellites, Logan, UT, USA, Aug. 8–11, 2005, SSC05-II-1, URL: <http://public.ccsds.org/sites/cwe/cesg/Public/Meetings%20Info/2007%20Winter/Plug-Play-Lunchtalk-19Jan07.pdf>
- ¹¹²⁵⁾ L. J. Hansen, P. Graven, D. Fogle, J. Lyke, “The Feasibility of Applying Plug-and-Play Concepts to Spacecraft Guidance, Navigation, and Control Systems to Meet the Challenges of Future Responsive Missions,” Proceedings of the 7th International ESA Conference on Guidance, Navigation & Control Systems (GNC 2008), June 2–5, 2008, Tralee, County Kerry, Ireland, URL: <http://microcosminc.com/analysis/ESA%20GNC.pdf>
- ¹¹²⁶⁾ P. Mendham, S. Parkes, S. Mills, C. McClements, “Plug and Play Technology for Space Wire: Drivers and Alternatives,” 58th IAC (International Astronautical Congress), International Space Expo, Hyderabad, India, Sept. 24–28, 2007, IAC-07-B4.7.06
- ¹¹²⁷⁾ G. Rakow, P. McGuirk, C. Kimmery, P. Jaffe, “SpaceWire Plug ‘n’ Play,” Proceedings of the 2007 IEEE Aerospace Conference, Big Sky, MT, March 3–10, 2007
- ¹¹²⁸⁾ S. D. Fowell, C. Taylor, “Proposed SOIS Plug-and-Play Architecture and Resulting Requirements on SpaceWire Mapping,” First International SpaceWire Conference 2007, Dundee, Scotland, UK, Sept. 17–19, 2007, URL: <http://spacewire.computing.dundee.ac.uk/proceedings/Papers/Networks%20and%20Protocols%201/fowell.pdf>
- ¹¹²⁹⁾ C. Kimmery, P. McGuirk, G. Rakow, P. Jaffe, “Application of the SpaceWire Plug-and-Play Protocol,” First International SpaceWire Conference 2007, Dundee, Scotland, UK, Sept. 17–19, 2007, URL: <http://spacewire.computing.dundee.ac.uk/proceedings/Papers/Networks%20and%20Protocols%201/kimmery.pdf>

- **PnPSat** (Plug-and-play Satellite).¹¹³⁰ In the timeframe 2005/7, AFRL (Air Force Research Laboratory), Albuquerque, NM, has initiated a program to create the first satellite-based laboratory testbed entirely on the principles of plug-and-play as represented by the Space Plug-and-play (PnP) Avionics – or simply the SPA (Space Plug-and-play Avionics) approach. The PnPSat design implies a modular satellite with open standards and interfaces, self describing components, and an auto-configuring system.

PnPSat represents an extension of the ideas of small, tactical satellites and modular design approaches, with an infusion of technology concepts that aim to simplify and accelerate the construction of spacecraft.^{1131) 1132)}

Building upon the issues uncovered and lessons learned during PnPSat, the PnPSat-2 effort is a follow-on technology demonstrator. Whereas PnPSat leveraged laboratory hardware and software components, PnPSat-2 will demonstrate full space qualified hardware components and mission qualified software components with roots in traditional space flight processes and direct applicability to tactical (or ORS) 1-3 year missions in LEO, HEO, and GEO.¹¹³³⁾

The SPA Component Testbed of PnPSat is designed to allow components that have been developed to the SPA-S (SPA SpaceWire based) standards to be tested and formally accepted for testing on PnPSat-2. It is the gateway through which all components must pass before they can be considered for testing on the PnPSat-2 system.

The PnPSat-2 testbed (2010) is designed to test flight and flight like SPA-S components in as realistic conditions as possible. There are many interactions that may not manifest themselves prior to integration on a spacecraft structure. The baseline PnPSat-2 structure is a hexagonal prism 106 cm across the flat with a 63 cm height and incorporates the standard 5 cm mounting grid on all surfaces. The structural panels are clamshells that contain the Gen2 (2nd generation) SPA-S avionics (SpaceWire Router and combined PowerHub and Test Bypass Router) with the harnessing necessary to support the 10 SPA-S endpoints per panel (Ref. 1133).

A promising principle of rapid satellite integration and incorporation of new technology is the notion of PnP (Plug-and-Play). As envisioned for satellites, PNP explicitly includes both the “plug” and the “play” aspects of rapid integration. To “plug” the architecture requires common physical interfaces, and to “play,” the architecture requires common communications protocols and data ontology, with self-recognition and publication of unit capabilities and services. To truly realize a PNP architecture there would need to be industry-wide adoption of standards, a strong supplier base delivering compatible products, and an architecture that supports both heritage interfaces as well as the new plug and play standards.

Development and broad adoption of standards takes industry-wide agreement on what standards to use, plus timely adoption and incentives that drive down cost, schedule or SWaP (Size, Weight and Power) that facilitate adoption. The state of the industry today (2011) exhibits minimal adoption of PNP standards by component suppliers; nonetheless, the AFRL (Air Force Research Laboratory) has worked extensively to develop standards and promote an adoption program for component suppliers.¹¹³⁵⁾ An architectural approach to phased adoption of PNP on existing satellite products must be established to facilitate wide adoption of standards.

The advantages of implementing the SPA philosophy arise from the fact that it inherently leads to an integrated software and hardware approach. As the industry evolves to include more SPA compliant components, it is critical that a right-size adoption strategy of PNP is developed if we are to leverage this trend and the architectures must be flexible enough to accommodate both new SPA compliant components and legacy systems or components.¹¹³²⁾

1130) D. Fronterhouse, J. Lyke, “Plug-and-Play Satellite (PnPSat),” International SpaceWire Conference, Dundee, UK, September 19, 2007, <http://spacewire.computing.dundee.ac.uk/proceedings/Papers/INT-SPA%20and%20programmable%20FPGA%20critical.pdf>

1131) P. Graven, Y. Plam, L. J. Hansen, S. Harvey, “Implementing Plug-and-Play ADCS to Support Operationally Responsive Space,” Proceedings of the 2008 IEEE Aerospace Conference, Big Sky, MT, USA, March 1-8, 2008

1132) Donald C. Fronterhouse, Ken Center, Bob Strunce, Tom Mann, John Divalma, “Pnpsat-2 SPA Technology Testbed Initial Results and Development Status,” Proceedings of the 2010 IEEE Aerospace Conference, Big Sky, MT, USA, March 6-13, 2010

Background: AFRL at Kirtland Air Force Base, New Mexico, has been studying and developing international standards for PnP technologies in space. These PnP standards provide a set of “discovery principles” that find and join various components in a satellite based on common descriptions of the components. These descriptions are contained in an Extensible Markup Language (XML) data sheet maintained in a data registry called xTED (eXtended Transducer Electronic Datasheets). Standard descriptions are developed for a suite of spacecraft effectors and sensors, published in an ontology that describes the total physical system. This ontology and the standards for physical and electrical interfaces have been documented in Space Plug–and–Play Architecture (SPA) standards, released in draft form in February of 2011 for industry review.^{1136) 1137)}

For simple legacy components that do not have adequate computing capability, the Appliqué Sensor Interface Module (ASIM) provides interfaces to the legacy hardware. The ASIM combines Input/Output (I/O functions), a physical spacewire port, and a simple “edge CPU”, capable of hosting the middleware and physical system abstraction services. The ASIM provides a bridge that connects the component to the system architecture with minimum impact to the main processing computer, providing an “on–ramp” for legacy components to interface with other spacecraft subsystems and services.¹¹³⁸⁾

The SPA networking approach has been implemented as part of the core SPA services in the SSM (SPA Services Manager), developed by SDL (SpaceDynamics Laboratory) at USU (Utah State University). The current (2012) SSM implementation supports SPA Local (SPA–L) and SpaceWire (SPA–S) subnets. Efforts are currently underway to incorporate SPA–1 (I²C), SPA–U (USB), SPA–O (optical), and SPA–C (CAN) subnets as well. – The engineering feasibility of this approach has been demonstrated in multiple laboratory prototype implementations. These include a SPA SSM development testbed located at SDL, a PnPSat–2 satellite structure at the AFRL RST (Responsive Space testbed), and an APT (Advanced PnP Technology) contractor satellite structure. Both the PnPSat–2 and the APT contractor satellite structures represent full–scale, realistic prototype platforms on which the SPA networking approach has been integrated and tested. The APT contractor prototype structure was specifically designed to characterize and evaluate the performance of a desired PnP configuration, including physical, logical, and data function.¹¹³⁹⁾

Table 60: Overview and some background on PnP for small satellites ^{1134) 1135) 1136) 1137) 1138) 1139)}

- **WiFi** (Wireless Fidelity – also written as **Wi–Fi**) is considered an enabling network technology in future PnP space applications. The Wireless Working Group (WWG) of the Consultative Committee for Space Data Services (CCSDS) is a group of engineers that coordinates wireless research among global space agencies and promotes interoperability of spacecraft data systems.

WiFi is in fact a standardized WLAN (Wireless Local Aerea Network) set of RF protocols, a trademark of the Wi–Fi Alliance for certified products based on the IEEE 802.11 stand-

1134) Bruce C. Chesley, Erik S. Daehler, Bonnie Triezenberg, “Modular Architectures for Satellite Product Lines: Implementing plug–and–play technologies for cross–platform innovation,” Proceedings of IAC 2011 (62nd International Astronautical Congress), Cape Town, South Africa, Oct. 3–7, 2011,

1135) F. A. Slane, A. J. Hooke, “Space Plug and Play Avionics Standards: Progress, Problems and a View of the Future,” AIAA Infotech@Aerospace 2007 Conference and Exhibit, May 7–10, 2007, Rohnert Park, CA, USA, AIAA 2007–2912.

1136) “Space Plug–and–Play Architecture (SPA) Standard, Test Bypass Extension, AIAA S–133–8–201X, Draft February 2011, URL: http://aiaa.kavi.com/public/pub_rev/SPA_S-133-8-201X_PR.pdf

1137) “Space Plug–and–Play Architecture (SPA) Standard (DRAFT), Physical interface Standard,” AIAA S–133–4–201X, URL: http://aiaa.kavi.com/public/pub_rev/SPA_S-133-4-201X_PR.pdf

1138) W. L. Walker, W. J. Manning, C. D. McFarland, J. Lyke, “Performance Characterization of a Space Plug–and–Play Avionics Appliqué Sensor Interface Module,” Infotech@Aerospace 2011, March 29–31, 2011, St. Louis, Missouri, USA, AIAA 2011–1502.

1139) Jacob H. Christensen, David B. Anderson, March E. Greenman, “Scalable Network Approach for the Space Plug–and–play Architecture,” Proceedings of the 2012 IEEE Aerospace Conference, Big Sky, Montana, USA, March 3–10, 2012

ards. This certification warrants interoperability between different wireless devices. The underlying WiFi earthbound technologies are already with us (and growing rapidly), in the protocols delivering wireless connectivity to homes, offices, consumer electronics, and public places (airports, trade shows, railway stations, conference centers, hotels, etc.). A WiFi enabled device such as a PC, mobile phone, MP3 player or PDA can connect to the Internet when within range of a wireless network connected to the Internet. ¹¹⁴⁰⁾

Starting in 2005, the WWG of CCSDS began evaluating technologies on solutions (commercial wireless protocols such as the IEEE 802.11 family of standards for computer WiFi or sensor networking standards such as IEEE 802.15.4) *to establish 'plug and play' wireless networking between multiple spacecraft to enable the seamless transfer of data and commands.* This would work for formation–flying satellite constellations and orbiter–lander–rover combinations, but proximity networks could be set up by any spacecraft within signal range as easily as a laptop plugs into a WiFi network.. –However, it will take some time before the first WiFi applications are being tested in space.

- TechEdSat is a 1U CubeSat technology demonstration mission built by students of SJSU (San Jose State University), San Jose, CA, in partnership with NASA/ARC (Ames Research Center), the Swedish National Space Board (SNSB) via ÅAC Microtec, Uppsala, Sweden, and JAXA (Japan Aerospace Exploration Agency). The overall objective of the mission is to evaluate SPA (Space Plug–and–play Avionics) technology designed by ÅAC Microtec, and to perform a communications experiment utilizing the Iridium and Orbcomm satellite phone network. ¹¹⁴¹⁾

TechEdSat was launched to the ISS (International Space Station) aboard the HTV–3 module of JAXA on 21 July, 2012 from Tanegashima, Japan. On October 4, 2012, TechEdSat was deployed from the new J–SSOD (JEM–Small Satellite Orbital Deployer) aboard the ISS. ¹¹⁴²⁾

The TechEdSat CubeSat reentered and decayed in Earth's atmosphere on May 5, 2013. ¹¹⁴³⁾ A short mission life of 7–8 months was expected due to the relatively low deployment altitude of < 400 km from the ISS. *In summary, the TechEdSat–1 mission has been very successful. The project has verified the error correcting code of the fault tolerant avionics on orbit. SPA has been demonstrated and the project has also demonstrated the rapid integration possibilities using the avionics concept.* ¹¹⁴⁴⁾

1140) “Wireless networks spread from Earth to space,” ESA, July 2, 2009, URL: http://www.esa.int/esaMI/Technology/SEMGI1G1P0WF_0.html

1141) “Technology Education Satellite (TechEdSat),” NASA, July 31, 2012, URL: http://www.nasa.gov/mission_pages/station/research/experiments/TechEdSat.html#description

1142) “Swedish breakthrough in space on NASA satellite with electronics from ÅAC Microtec,” ÅAC Microtec, Oct. 11, 2012, URL: http://www.aacmicrotec.com/index.php?option=com_content&view=article&id=105&Itemid=225

1143) http://www.dk3wn.info/sat/afu/sat_techedsat.shtml

1144) Henrik Löfgren, Jan Schulte, Per Selin, Johan Bäckström, Jorge Freyer, Fredrik Bruhn, “TechEdSat – A minimal and robust 1U cubesat architecture using plug–and–play avionics,” Proceedings of the 9th IAA Symposium on Small Satellites for Earth Observation, Berlin, Germany, April 8–12, 2013, paper: IAA–B9–0511

1.8.8 Onboard data compression techniques

Vast amounts of source data, generated by satellite high-resolution data instruments, such as hyperspectral imagery or SAR imagery, require data reduction algorithms to alleviate high-volume data handling and processing problems. These problems are severe (a limiting operational factor) in particular for the functions of onboard storage and high-volume data transmissions to the ground segment. They also permeate throughout the ground segment in communications, data processing (memory), archiving and dissemination. ¹¹⁴⁵⁾ ¹¹⁴⁶⁾ ¹¹⁴⁷⁾

The development of compression algorithms requires a complete understanding of the characteristics and the use of the data. ¹¹⁴⁸⁾ ¹¹⁴⁹⁾ In particular, data compression techniques require internal redundancy in the data sequence if compression is to work. Streamlined approaches of compression are in use by various reversible (lossless) as well as irreversible (lossy) methods for reduction of data. Statistical codes (e.g. Huffman, Shannon-Fano, etc.), statistical methods (e.g. runlength and arithmetic coding), vector quantization (e.g. block truncation coding, JPEG) encoding by transformations [e.g. FFT (Fast Fourier Transformation) and wavelet transformations] and fractal approaches (e.g. contracting mappings) depict some examples of the first, second and third generation approaches for data compression. ¹¹⁵⁰⁾ ¹¹⁵¹⁾ ¹¹⁵²⁾

As of 1999, JPEG-LS (JPEG lossless) is the new lossless/near-lossless compression standard (predictor based) for continuous-tone images, ISO-14495-1/ITU-T.87. The standard is based on the LOCO-I algorithm (LOW COMPLEXITY LOSSLESS COMPRESSION for Images) developed at Hewlett-Packard Laboratories. – Speed is the overriding issue for all real-time compression applications. The compression of video or still image data is widely known in the commercial world. The JPEG and MPEG standards compete with new methods based on DWT (Discrete Wavelet Transform). These techniques can cover the whole range from lossless compression with a factor of 1.5–2 to compression factors 50 or higher.

The Canadian Space Agency (CSA) developed a new algorithm for hyperspectral imagery compression, called SAMVQ (Successive Approximation Multi-stage Vector Quantization). Evaluation and comparison with JPEG-2000 resulted in superior performance. ¹¹⁵³⁾

The JPEG-2000 standard ¹¹⁵⁴⁾ ¹¹⁵⁵⁾ makes use of several recent advances in compression technology in order to achieve certain features, such as improved compression efficiency, lossy to lossless compression, embedded bit-stream, multiple resolution representation, region-of-interest coding, error resilience, and random codestream access. It is based on

- ¹¹⁴⁵⁾ P. Hou, M. Petrou, C. Underwood, "Advanced Onboard Image Compression in Conjunction with Cloud Detection for Microsatellite Optical Imaging," Proceedings of the 13th AIAA/USU Conference for Small Satellites, Aug. 23–26, 1999, Logan UT, SSC99-IV-5
- ¹¹⁴⁶⁾ P. Trinadh, R. Seshiah, U. N. Das, V. Nalanda, "Effect of Transmission Channel Errors on ADPCM and JPEG Compression," Journal of Spacecraft Technology, Vol. 9, No 1, 1999, pp. 23–36
- ¹¹⁴⁷⁾ G. P. Ablousleman, M. W. Marcellin, B. R. Hunt, "Compression of hyperspectral imagery using 3D DCT and hybrid DPCM/DCT," IEEE Transactions on Geosciences and Remote Sensing, Vol. 33, pp. 26–34, 1995
- ¹¹⁴⁸⁾ ISO/IEC, International Standard IS 15444-1, Information Technology – JPEG2000 Imaging Coding System, FDC version 1.0, March 2000
- ¹¹⁴⁹⁾ H. S. Lee, N. H. Younan, R. L. King, "Hyperspectral Image Cube Compression Combining JPEG-2000 and Spectral Decorrelation," Proceedings of IGARSS 2002, Toronto, Canada, June 24–28, 2002
- ¹¹⁵⁰⁾ Note: In "lossy compression" information is thrown away during compression, so that the original data cannot be recovered by decompression. The decompression produces an approximation to the original data, with the level of approximation dependent on the compression ratio. In "lossless compression" the original data is reproduced exactly by decompressing the compressed stream.
- ¹¹⁵¹⁾ B. V. Brower, A. Lan, J. M. McCabe, "Hyperspectral lossless compression," Proceedings of SPIE, Imaging Spectroscopy V, Vol 3753, Denver, CO, July 19–21, 1999, pp. 247–257
- ¹¹⁵²⁾ A. F. H. Goetz, "Imaging spectrometry for earth remote sensing," Science, Vol. 228, pp. 1147–1153, 1985.
- ¹¹⁵³⁾ Shen-En Qian, M. Bergeron, C. Serele, I. Cunningham, A. Hollinger, "Evaluation and Comparison of JPEG 2000 and Vector Quantization Based Onboard Data Compression Algorithm for Hyperspectral Imagery," Proceedings of IGARSS 2003, Toulouse, France, July 21–25, 2003
- ¹¹⁵⁴⁾ <http://www.jpeg.org/>
- ¹¹⁵⁵⁾ P.-S. Yeh, J. Venbrux, "A High Performance Image Data Compression Technique for Space Applications," Proceedings of ESTC (Earth Science Technology Conference), College Park, MD, June 24–26, 2003

replacing the DCT by the DWT, where integer DWT filters are mainly used to provide both lossless and lossy compression within a single compressed bit-stream. Furthermore, JPEG-2000 offers a choice of either the (9,7), or the (5,3) filter-bank for lossy compression.

Some examples of data compression implementations in past, current, and planned spaceborne systems are:

- The SPOT series satellites of CNES employ DPCM (Differential Pulse Code Modulation) on the PAN data stream of the HRV instruments on SPOT-1, -2 and -3 (launch SPOT-1 on Feb. 22, 1986) and on the PAN and MS data streams of HRVIR on SPOT-4 (launch March 24, 1998). SPOT-5 (launch May 4, 2002) uses DCT (Discrete Cosine Transform). The Pleiades spacecraft, the successor series of SPOT, employ a wavelet compression algorithm with compression ratios of 4-7.
- The MOMS-02 (Modular Optoelectronic Multispectral Scanner), a stereoscopic along-track imaging system of DLR – flown on Shuttle flight STS-55 in April/May 1993, followed by a MOMS-02 reflight on MIR/Priroda (launch of Priroda April 23, 1996) – employed DPCM to compress its data from 8 bit to 6 bit.
- PoSAT-1 (launch Sept. 26, 1993), UoSAT-12 (launch April 21, 1999), Tsinghua-1 (launch June 28, 2000) of Tsinghua University in Beijing, China – all S/C built by SSTL, use a compression algorithm by the name of AMPBTC (Adaptive Moment-Preserving Block Truncation Coding), achieving compression ratios of 2.5:1 and 4:1.
- TRACE of NASA/GSFC (launch April 2, 1998) uses a data compression scheme.
- KITSAT-3 of KAIST/SaTReC, Korea (launch May 26, 1999) uses onboard image data compression in JPEG, GIF and DPCM.
- The MTI (Multispectral Thermal Imager) mission of DOE (launch March 12, 2000) employs image data compression with the USES (Universal Source Encoder for Science data) chip for lossless compression (Rice coding algorithm, developed at JPL); the compression ratio is 2.5:1.^{1156) 1157)}
- Kodak developed an algorithm by the name of ADPCM (Adaptive Differential Pulse Code Modulation) for imagery compression. It is applied to Ikonos-2 (launch Sept. 24, 1999) and QuickBird-1 (launch Nov. 20, 2000 – launch failure) imagery. The real-time technique compresses 11-bit digital imagery to average values of 2.6 bit/pixel (reduction of 4.25:1) with little detectable loss in image quality. The compression rate enables more efficient onboard storage and downlink transmission of the data.
- The EO-1 satellite of NASA (launch Nov. 21, 2000) carries WARP (Wideband Advanced Recorder Processor) to demonstrate a number of high density electronic board advanced packaging techniques. Besides storage functions, it provides also a data compression of imagery.
- SPIHT (Set Partitioning in Hierarchical Trees) is a wavelet-based image compression method introduced in 1995 by Rensselaer Polytechnic Institute, Troy, NY. SPIHT is a method of coding and decoding the wavelet transform of an image.¹¹⁵⁸⁾ By coding and transmitting information about the wavelet coefficients, it is possible for a decoder to perform an inverse transformation on the wavelet and reconstruct the original image. The entire wave-

1156) Note: "Rice" is an adaptive variable-length compression scheme on images, an algorithm developed by Robert F. Rice of JPL and implemented by Frank Rabe of the Technical University in Braunschweig, Germany for the Mars Pathfinder Lander IMP imaging system.

1157) Robert F. Rice, "Some Practical Universal Noiseless Coding Techniques, Part III, Module PSI14,K+," JPL Publication 91-3, November 15, 1991.

1158) A. Said, W. A. Pearlman, "SPIHT Image Compression: Properties of the Method," <http://www.cipr.rpi.edu/research/SPIHT/spiht1.html>

let does not need to be transmitted in order to recover the image. Instead, as the decoder receives more information about the wavelet, the inverse—transformation will yield a better quality reconstruction of the original image. As of 2002, a NASA—sponsored project is implementing an optimized SPIHT compression routine into adaptive hardware using FPGA (Field Programmable Gate Array) technology. ¹¹⁵⁹⁾ ¹¹⁶⁰⁾

- WPEB (Wavelet Packet Embedded Block Coding) is an evolutionary method based on SPIHT. ¹¹⁶¹⁾

- The APCA (Adaptive Principal Components Analysis) algorithm is a slightly lossy compression algorithm that uses the noise statistics of the data to preserve information content while maximizing compression ratios. APCA is particularly effective for the compression of hyperspectral imagery providing compression ratios of about 10 to one. The effectiveness of the algorithm has been tested on data sets of airborne hyperspectral imagers like AVIRIS, HYDICE, and HyMap. ¹¹⁶²⁾

- The MSG—1 (Meteosat Second Generation —1) satellite (i.e., Meteosat—8) of EU-METSAT (launch Aug. 28, 2002) uses encryption and JPEG compression on the HRIT (High Rate Information Transmission) data stream.

- IRS—P5 (CartoSat—1) of ISRO (launch May 5, 2005) uses an onboard ADPCM/JPEG compression algorithm of 3.2 : 1 to reduce the source data rate of 338 Mbit/s to 105 Mbit/s in the downlink.

- ESA sponsored the development of a quasi—lossless data compressor ASIC (Application Specific Integrated Circuit) which exploits the advantages of a wavelet—based data compression. The ASIC, developed by Saab Ericsson of Sweden, employs the Rice algorithm defined by CCSDS (with some additional features improving the functionality but maintaining the compatibility with the standard). The ASIC, referred to as TSC21020F, is installed in the PDU (Payload Processing Unit) of the PROBA satellite (launch Oct. 22, 2001). The PDU provides all data handling and processing of payload data including the data compression of the camera images (CHRIS).

- NASA/GSFC is developing a high—performance lossy data compression technique to support high—speed pushbroom frame—based imaging applications. ¹¹⁶³⁾ The algorithm is based on MLT (Modulated Lapped Transform) and DCT techniques combined with bit—plane encoding. Flight qualified hardware implementations are in development. A functional chip set is expected by the end of 2001. The chip set is being designed to compress data in excess of 20 Msamples/s and support quantizations from 2—16 bit.

- As of 2002, NASA and industry (LMSS, ASIT) are developing a real—time onboard processing system to compress hyperspectral imagery. The goal is to reduce the downlink by a factor > 100 while retaining the necessary spectral fidelity of the sensor data. The approach taken integrates state—of—the—art DSP and FPGA technologies. ¹¹⁶⁴⁾

- The ALOS satellite of JAXA (launch Jan. 24, 2006) compression of optical data. It uses a lossy data compression technique DCT (Discrete Cosine Transformation) and Huffman coding on PRISM (Panchromatic Remote—sensing Instrument for Stereo Mapping) to re-

¹¹⁵⁹⁾ T. W. Fry, S. Hauck, “Hyperspectral Image Compression on Reconfigurable Platforms,” Earth Science Technology Conference, Pasadena, CA, June 11—13, 2002

¹¹⁶⁰⁾ A. Said, W. A. Pearlman, “A New Fast and Efficient Image Codec Based on Set Partitioning in Hierarchical Trees,” IEEE Transactions on Circuits and Systems for Video Technology, Vol. 6, pp 243—250, June 1996

¹¹⁶¹⁾ I. Cumming, J. Wang, “Polarimetric SAR Data Compression Using Wavelet Packets in a Block Coding Scheme,” Proceedings of IGARSS 2002, Toronto, Canada, June 24—28, 2002

¹¹⁶²⁾ M. H. Sharp, “Noise—constrained hyperspectral data compression,” Optical Engineering, Vol. 41, No 9, Sept. 2002, pp. 2098—2101

¹¹⁶³⁾ P. Yeh, J. Venbrux, P. Bhatia, W. H. Miller, “A Real—Time High Performance Data Compression Technique for Space Applications,” Proceedings of IEEE/IGARSS Conference, Honolulu, HI, July 24—28, 2000

¹¹⁶⁴⁾ S. Cook, J. Harsanyi, “Real—Time Data Processing Onboard Remote Sensor Platforms,” Proceedings of ESTC (Earth Science Technology Conference), Pasadena, CA, June 11—13, 2002

duce the source data rate (1 Gbit/s) to about 240 Mbit/s in the downlink. DPCM is used on AVNIR–2 data (reduction from 160 Mbit/s to 120 Mbit/s in the downlink).

– JPEG 2000 is a fairly new international standard for image data compression, defined by the International Standards Organization (ISO). Part 1 of the standard, ISO/IEC 15444–1, is the Core Coding System containing the features that all decoders must support, in order to be called JPEG 2000 compliant. JPEG 2000 Part 2, ISO/IEC 15444–2, includes many optional features that are useful for special applications, including the downlink and archiving of Earth science data. – As of 2002, SAIC (Science Applications International Corporation) is developing a low–memory version of JPEG 2000, sponsored by NASA, including both Part 1 and Part 2 features, for use in future ESE (Earth Science Enterprise) missions. ¹¹⁶⁵⁾

1.8.8.1 Onboard SAR data compression

The output of a conventional as well as a state–of–the–art SAR instrument delivers essentially raw data (block format), consisting of a vast number of echo measurements, there is actually no image as in optical sensor outputs. Digitization and compression of the raw data is normally the next processing step prior to onboard storage and/or downlink transmission, followed by an offline ground–based processing of the reconstructed SAR signal into image data. An onboard real–time generation of SAR imagery hasn’t been attempted so far due to the current processing power limitations. But spaceborne capabilities (with corresponding ASIC implementations and more) can certainly be anticipated for the SAR image generation function in the not–so–distant future.

The BAQ (Block Adaptive Quantization) compression technique is most suitable (and a de–facto standard) for raw SAR data compression. The BAQ algorithm allows in general to reduce the data volume to a rate of 8 bits per complex sample without introducing significant distortion. The method is based on the estimation of the standard deviation value and on the coding of the real and imaginary component value of the elements (a data procedure exploiting the statistical behavior of source data, for direct onboard data compression). Also, quasi–logarithmic data coding of raw data can be implemented as BAQ in typical SAR systems; the achievable data reduction is about 2–4. ^{1166) 1167) 1168) 1169) 1170) 1171) 1172) 1173)}

– The BAQ compression technique was probably first introduced and tested in spaceborne applications by the radar instrument (Venus Radar Mapper, operating in 3 modes:

- 1165) J. C. Rountree, B. N. Webb, M. W. Marcellin, “Testing JPEG 2000 Compression for Earth Science Data,” Earth Science Technology Conference, Pasadena, CA, June 11–13, 2002
- 1166) U. Benz, K. Strodl, A. Moreira, “A comparison of several algorithms for SAR raw data compression,” IEEE Transactions on Geoscience and Remote Sensing, Vol.33, No 5, pp. 1266–1276, Sept. 1995
- 1167) B. Botero, N. Hifdi, “Parallelism Exploitation in SAR Data Compression Methods,” <http://www.cert.fr/fr/dprs/publications/eusar.pdf>
- 1168) F. Pittermann, A. Henrichs, Ch. Schaefer, “Data Compression – A key Element of Onboard Data Handling,” Onboard Payload Data Processing Workshop, ESA/ESTEC, Sept. 19–20, 2001
- 1169) G. Poggi, A. R. P. Ragozini, L. Verdoliva, “Compression of SAR Data Through Range Focusing and Variable–Rate Vector Quantization,” IEEE Transactions on Geoscience and Remote Sensing, Vol. 38, No 3, May 2000, pp. 1282–1289
- 1170) Note: The image formation from the radar echo of the SAR instrument involves a highly sophisticated processing effort. In the early history of SAR imaging, processing was done by analog optical focussing of the SAR raw data. Digital processing of SAR data was introduced in the early 1970’s. The method forms the basis of today’s highly flexible, accurate and error compensating SAR image formation. So far, all SAR image generation takes place offline in a ground based facility. The SAR raw data are stored on the satellite, transmitted to the ground station with only low or no compression and are then transferred to the processing facility.
- 1171) T. Algra, “Data compression for operational SAR missions using Entropy–Constrained Block Adaptive Quantization,” Proceedings of IGARSS 2002, Toronto, Canada, June 24–28, 2002
- 1172) E. Magli, G. Olmo, B. Penna, “Wavelet–based compression of SAR raw data,” Proceedings of IGARSS 2002, Toronto, Canada, June 24–28, 2002
- 1173) T. Alegra, “Data compression for operational SAR missions using Entropy–Constrained Block Adaptive Quantization,” Proceedings of IGARSS 2002, Toronto, Canada, June 24–28, 2002

SAR, altimeter, and radiometer) of the NASA/JPL Magellan mission to Venus [Launch of Magellan on STS–30, May 4, 1989, arrival at Venus in Aug. 1990. Magellan orbited Venus for 4 years; at the end of its mission, it was commanded to plunge into the atmosphere of Venus on Oct. 11, 1994]. The objective of the mission was to map the surface of Venus through thick atmospheric clouds. ¹¹⁷⁴⁾ ¹¹⁷⁵⁾

- The ASAR instrument of ESA’s Envisat (launch Mar. 1, 2002) mission employs FBAQ (Flexible Block Adaptive Quantization) implemented in space qualified ASIC technology of Saab–Ericsson. The algorithm compresses the ASAR raw data from 8 bits to either 2, 3, or 4 bits (sign and magnitude are selectable). ¹¹⁷⁶⁾

- The TerraSAR–X satellite of DLR/EADS Astrium (launch June 15, 2007) employs the BAQ algorithm. The BAQ compression is applied to blocks of 128 consecutive samples with a selectable compression rate of 8 to 4, 3, 2 bits per sample.

- At the start of the 21st century, more advanced techniques (BAQ scheme variants) have been proposed for improved compression performance at the expense of higher processing effort. Among them are:

- FBAQ (Flexible Block Adaptive Quantization)

- ECBAQ (Entropy–Constrained Block Adaptive Quantization) ¹¹⁷⁷⁾ ¹¹⁷⁸⁾

- FFTBAQ (Frequency Domain Block Adaptive Quantization) ¹¹⁷⁹⁾

- FFT–BABC (Frequency Domain Block Adaptive Bit–rate Control) ¹¹⁸⁰⁾

- First wavelet algorithms for SAR data compression are being proposed as of 2003. ¹¹⁸¹⁾ ¹¹⁸²⁾

¹¹⁷⁴⁾ R. Kwok, W. T. K. Johnson, “Block Adaptive Quantization of Magellan SAR Data,” *IEEE Transaction. on Geoscience and Remote Sensing*, Vol. 27, No 4, July 1989, pp. 375–383.

¹¹⁷⁵⁾ The mission was named on honor of Ferdinand Magellan (1480–521) of Portugal. He led the first mission to circumnavigate the globe in the services of King Charles V of Spain. He died during his voyage of discovery on the Island of Mactan in the Philippines, 27 April 1521.

¹¹⁷⁶⁾ W. Wijmans, Ph. Armbruster, “Data Compression Techniques for Space Applications,” *DASIA’96*, May 20–23, 1996, Rome, Italy

¹¹⁷⁷⁾ T. Algra, L. Bierens, “Advanced on–board SAR data compressor,” *Proceedings of IGARSS 2006 and 27th Canadian Symposium on Remote Sensing*, Denver CO, USA, July 31–Aug. 4, 2006

¹¹⁷⁸⁾ T. Algra, “Data compression for operational SAR missions using Entropy–Constrained Block Adaptive Quantization,” *Proceedings of IGARSS 2002*, Toronto, Canada, June 24–28, 2002

¹¹⁷⁹⁾ U. Benz, K. Strodl, A. Moreira, “A comparison of several algorithms for SAR raw data compression,” *IEEE Transactions of Geoscience and Remote Sensing*, Vol. 27, No 4, 1989, pp. 375–383

¹¹⁸⁰⁾ C. Schäfer, M. Süß, M. Gottwald, “Compression of SAR Raw Data Using the Method of BABC,” *Frequenz*, Vol. 55, March/April 2001, pp. 91–98, ISSN 0016–1136

¹¹⁸¹⁾ A. El–Boustani, K. Brunham, W. Kinsner, “Investigation of Wavelets for Raw SAR Data Compression,” *Proceedings of IGARSS 2003*, Toulouse, France, July 21–25, 2003

¹¹⁸²⁾ Xingsong Hou, Guizhong Liu, YiYang Zou, “Wavelet Packet Remote–Sensing Images Coding Algorithm Based on Quadtree Classification and UTCQ,” *Proceedings of IGARSS 2003*, Toulouse, France, July 21–25, 2003

1.9 Spacecraft communications

Background: The telecommunication technology itself predates the space age by over a century. The discovery of electromagnetism in 1820 by the Danish physicist Hans Christian Ørsted (1777–1851) allowed for the development of the electrical telegraph, the first practical application of electricity. The first electromagnetic telegraph messages in history were relayed in May 1844 between Washington and Baltimore using a telegraph system invented by the American Samuel F. B. Morse (1791–1872). The revolutionary invention of the electromagnetic telegraph and the demonstration of a successful message relay resulted in the installation of the first electric message network.^{1183) 1184)}

Within ten years after the first telegraph line opened, 38,000 km of wire crisscrossed the USA, affecting profoundly the development of the West. The messages transmitted by telegraph consisted of the so-called “Morse Code” – sputtering dots and dashes that trained radio operators could decode into a message. In 1853, the Austrian physicist Julius Wilhelm Gintl (1804–1883) invented two-way communication. He realized his idea with two batteries. Gintl’s method was called the method of compensation. In 1855, the German inventors Werner Siemens (1816–1892) and Johann Georg Halske (1814–1890), founders of the Siemens & Halske company, improved on this compensation method using only one battery. The first transatlantic telegraph message was relayed in 1866. In 1853, a national authority to deal with the telegraph was created, namely “The Royal Electrical Telegraph Administration,” in Sweden.

The first workable telephone was designed in America in 1876 by the inventor Alexander Graham Bell (1847–1939, born in Edinburgh, Scotland) a pioneer in the field of telecommunications. By 1878, Bell had set up the first telephone exchange in New Haven, Connecticut. – The wireless radio transmission technology required many inventions, based on work of Faraday, Maxwell, Hertz, Lodge, Righi and Tesla, and others. The first successful attempt to transmit by wireless over the Atlantic was carried out from a radio station in England in 1901. The demonstration was done by the Italian inventor/physicist Guglielmo Marconi (1874–1937). Marconi was the first with a workable radio transmitter and receiver. Marconi is credited with the invention of “wireless telegraphy” in 1896. The early radio became possible in 1906 with the invention of the amplifying valve. In 1905, the Canadian Reginald A. Fessenden (1866–1932) invented a continuous-wave voice transmitter, using a high-frequency alternator developed by Charles Steinmetz at GE (General Electric, Schenectady, NY) in 1903. On Christmas eve 1906, Fessenden made the first voice broadcast from USA over the North Atlantic, paving the way for both radio broadcasting and radiotelephony. Fessenden sold to Westinghouse in 1910 the patent for a heterodyne receiver that used the joint operation of two AC currents for a third frequency. In 1913, the invention of the amplifying vacuum tube by the physicist Harold D. Arnold of Western Electric (by then an AT&T subsidiary, later the organization eventually became Bell Labs) permitted the first coast-to-coast (USA) telephony and the first transatlantic radio transmission in 1915.

In 1937, the English scientist Alec H. Reeves (1902–1971) received a patent on the topic of PCM (Pulse Code Modulation) while working at the ITT (International Telephone and Telegraph) laboratories in Paris. Reeves proposed a radical alternate method of signal transmission to Alexander Bell’s “voice-shaped current” (i.e. the valve-based technology of the time). His solution was that the sound be sampled at regular intervals. The values of these samples would be represented by binary numbers and transmitted as unequivocal on-off pulses. However, sending recognizable speech by this method meant networks would have to carry millions of pulses a second. It implied that PCM transmissions could not

1183) Note: The electromagnetic telegraph was predated by the optical telegraph (referred to as semaphore), invented by the Frenchman Claude Chappe in 1793, and a few months later by the Swede Abraham N. Edclcrantz. In 1794, Edclcrantz relayed successfully optical messages in Sweden.

1184) Note: The words telegraph and semaphore first entered the human vocabulary in the late 18th century. They are of Greek origin, though they are not part of the original language. Tele means “at a distance,” graphos means “writer” or “signaler.” Sema means “sign” or “symbol,” and phoros means “bearer” or “carrier.”

be done economically until the discovery of the **transistor effect** and the development of the first device in 1947 at Bell Labs by John Bardeen, Walter H. Brattain and William Shockley (the three received the Nobel Prize in physics in 1956).¹¹⁸⁵⁾ Today, PCM is a digital transmission method with built-in mathematical redundancy and error checking of the received signal offering a high degree of noise rejection and response speed. The modulation may vary the amplitude (PAM or pulse amplitude modulation), the duration (PDM or pulse duration modulation), or the presence of the pulses (PCM or pulse code modulation). For space data transmissions, PCM is the most important modulation type because it can be used to transmit information over long distances with hardly any interference or distortion. Although PCM transmits digital instead of analog signals, the modulating wave is continuous. Digital modulation begins with a digital modulating signal. The two most common digital modulating techniques are PSK (Phase-Shift Keying) and FSK (Frequency-Shift Keying). Without PCM, there would be no Internet, no digital radio or television, no digital land-line or mobile telephones, no CDs, DVDs or CD-ROMs.

1.9.1 Spacecraft RF (Radiofrequency) communications

Telecommunication is the basic means of (wireless) message transfer between a satellite and the ground. All satellite links are based on wireless communication technology [the fundamental distinction of wireless communication is its ability to “communicate on the move” with changing geometry (and signal) characteristics between the communication participants]. Different streams of data [TTC (Telemetry, Tracking & Command) are being mainly used for S/C operations; in parallel there is the user signal or the observed instrument] are being transmitted in various directions at different data rates. In general, the downlink data rate is much higher than the uplink (command, etc.) data rate for an EO satellite.

The early-history of satellite operations used frequencies in the bands HF ($3 < 30$ MHz) or VHF ($30 < 300$ MHz) for low-rate communications [Sputnik-1 (launch Oct. 4, 1957) and Sputnik-2 frequency of 20/40 MHz; Explorer-1 (launch Jan. 31, 1958) frequency of 108 MHz]. UHF transmissions ($300 < 3000$ MHz) followed soon, in particular S-band (2000–4000 MHz), as the communication demands increased with higher instrument rates. Eventually, the S-band became the standard support for all “low-rate” TT&C services of S/C operations. On the user side, however, the transmission demands kept steadily climbing for the EO missions requiring first S-band support, later C-, X-, Ku-, K- and Ka-band to get the instrument data to the ground during the short contact periods with a ground station. The switch to a higher transmission band involved always a considerable investment for each agency, in particular for the upgrading of the ground segment.

Note: Only a few highlights of telecommunication history are provided, otherwise the scope of the documentation would be unduly expanded.

- **Spacecraft onboard recorders.** There was a need for onboard data recording from the very beginning of the space age. TIROS-1 with a launch on April 1, 1960, had already a tape recorder. The first satellite electronic memory in space (384 bits of magnetic core register – required to store its own orbit ephemeris) was flown on Transit-3B (Feb. 21, 1961).
 - Science data storage into solid-state memory followed much later this trend. Some S/C with the provision of solid-state memory are: SAMPEX (NASA, launch July 3, 1992), ALEXIS (LANL, launch Apr. 25, 1993), TEMISAT (Telespazio, launch Au. 31, 1993), PoSAT-1 (SSTL, launch Sept. 26, 1993), FASat (SSTL, launch, Aug. 31, 1995).
 - The ERS-1 spacecraft (launch July 17, 1991) featured an onboard storage volume of 6.5 Gbit, yet the system was only used for low rate data storage; it was not capable to store real-time SAR source data at 105 Mbit/s.

¹¹⁸⁵⁾ David Robertson, “Alec Reeves 1902–1971,” <http://www.privateline.com/TelephoneHistory2/reeves.html>

- An onboard storage capacity of 1 Gbit was first realized with FAST (NASA, launch Aug. 21, 1996), followed by ACE (NASA, launch Aug. 25, 1997) with 2 Gbit, and Equator–S (MPE, launch Dec. 2, 1997) with 1.5 Gbit. EarlyBird (Earthwatch, launch Dec. 24, 1997) had a storage capacity of 16 Gbit.
- The STEX (Space Technology Experiment) mission of NRO (launch Oct. 3, 1998) has a 51 Gbit solid–state recorder (a new storage level in S/C data) and features 64 Mbit DRAM technology.
- ARGOS of DoD (launch Feb. 23, 1999) provides a storage volume of 64 Gbit as well as Ikonos–2 (Space Imaging, launch Sept. 24, 1999).
- The Landsat–7 storage capacity (NASA, launch April 15, 1999) is 378 Gbit.
- The EO–1 (Earth Observing–1 of NASA, launch Nov. 21, 2000) demonstrates with WARP (Wideband Advanced Recorder Processor) a number of high density electronic board advanced packaging techniques. WARP utilizes advanced integrated circuit packaging (3–D stacked memory devices) and “chip–onboard” bonding techniques to obtain very high density memory storage per board (24 Gbit/memory card). It also includes a Mongoose V processor which can perform on–orbit data collection, compression and processing of land image scenes. WARP consists of a high–rate (up to 840 Mbit/s capability), high–density (48 Gbit storage), low weight (< 25 kg) solid–state recorder/processor with X–band modulation capability.
- ALOS of JAXA (launch Jan. 24, 2006) provides a storage capacity of 768 Gbit for its high–resolution optical and SAR imagery. The CNES Pleiades S/C series (launch of Pleiades–HR1 on Dec. 17, 2011) has 600 Gbit of image storage capacity.
- Store & Forward (S&F) satellite communication. The UoSAT–2 S/C (SSTL, launch March 1, 1984) carried the first digital S&F payload in orbit using a protocol suite by the name of PACSAT.
- Satellite crosslink communication refers to intersatellite links (i.e. communication from satellite to satellite without the use of an intermediate ground relay station). The first such crosslink communication demonstration took place in Dec. 1995 between two Milstar communication satellites of DoD (USA) in GSO.¹¹⁸⁶ All Milstar satellites incorporate two crosslink dish antennas located at opposite ends of each spacecraft. Security is assured by conducting crosslink operations exclusively in a high gain, narrow beamwidth mode at or near frequencies that are absorbed by the Earth’s atmosphere (SHF, EHF). Hence, these types of crosslink transmissions cannot be received on Earth. The crosslink communication concept represents in effect a “switchboard–in–the–sky” monitoring and control capability of all satellites in a constellation from a single ground location (a cost–saving feature for constellation operations support). Milstar–2 is a four–satellite communication constellation with the MDR (Medium Data Rate) payload; MDR has 32 channels with data rates up to 1.5 Mbit/s: Block–I satellites (first generation), DFS–1 (Development Flight Satellite–1) and DFS–2, were launched into GEO Feb. 7, 1994 and Nov. 6, 1995, respectively. The last Milstar–2 spacecraft of the series, DFS–4, was launched Apr. 7, 2003.

Features that support the system’s robustness include frequency–hopping, extensive on-board processing, and crosslinks. Features that support flexibility include multiple uplink and downlink channels operating at various rates; multiple uplink and downlink beams, including agile beams; and routing of individual signals among uplinks, downlinks, and crosslinks. Milstar is the first satellite communications system of any kind that uses signal processing algorithms onboard the satellites, allowing an authorized user to establish customized networks within minutes, using his mobile terminal (the terminals are compatible among all US military services). For the Block–II series, data rates up to 1.544 Mbit/s are

1186) <http://www.aero.org/publications/crosslink/winter2002/01.html>

provided (on-demand availability of interactive voice, video, and data links). The onboard digital processing subsystem, combined with the RF subsystem, is called MDR (Medium Data Rate) payload electronics package. For the Block-II series, every MDR payload has eight antennas, each independently steerable and operating in the EHF (Extremely High Frequency) range. Terminal users may communicate with other users within the same antenna beam or with users located in other MDR antenna beams from any of the Block-II satellites. The on-orbit digital router establishes and maintains links within and among beams and responds to users' changing and differing bandwidth requirements. The crosslink communication feature can be regarded as a new and capable networking and distributing resource for future satellite generations in support of a wide field of applications – including formation flying services.¹¹⁸⁷⁾

- ETS-VIII (Engineering Test Satellite – VIII), a GEO technology spacecraft of JAXA (planned launch in 2006, launch delay of 2 years due to H-2A launcher problems). The objective is to demonstrate mobile satellite communications and broadcasting system technologies (in S-band) with small-scale ground terminals such as hand-held terminals. ETS-VIII features two LDAR (Large-scale Deployable Antenna Reflector), each approximately 19 m x 17 m in size, to support the experiments to mobile users. The light-weight reflector features a new structural concept: a combination of module structures, cable/metallic mesh tensile structure and deployable frame structures.

- Communication downlink experiment. XPAA (X-band Phased Array Antenna) is a communication experiment on EO-1 (launch Nov. 21, 2000) of NASA/GSFC with the objective to demonstrate link-pointing capability with the use of a body-fixed low-mass and low-cost phased array antenna (data rate of 105 Mbit/s). XPAA is composed of a flat grid of 64 radiating elements whose transmitted signals are combined spatially to produce the desired antenna directivity. An inherent advantage of the body-fixed design (mass of 5.5 kg) is to permit simultaneous capture and transmission of data, avoiding perturbations to instrument measurements.

Introduction of Ka-band (30 GHz uplink/ 20 GHz downlink) RF communications in GEO satellite systems to allow for high data rate transmissions.^{1188) 1189) 1190)} The demand for increased bandwidth necessitates the move to higher frequency bands such as Ka-band at the start of the 21 century. The use of Ka-band frequencies in satellite communications enables a significant reduction in the size and cost of tracking terminal antenna reflectors for comparable data rates in systems operating at X-band frequencies. An electrically steered Ka-band reflectarray based on low-loss ferroelectric materials offers the low cost and high efficiency of a gimbaled parabolic dish, and fast, vibration-free beam steering of a direct radiating phased array. – It should also be pointed out that most RF propagation effects are considerably more severe at Ka-band frequencies than at X-band.

- In Japan, the actual development of satellite communication technology started with CS-1 (Communications Satellite-1), a spin-stabilized S/C of 676 kg of TSCJ (Telecommunications Satellite Corporation of Japan), which was launched Dec. 15, 1977 on a US Delta 2914 launch vehicle from Cape Canaveral. The objective of CS-1 was to establish fixed satellite communication using Ka-band frequency technology. This represented in fact the first demonstration of Ka-band communications in the world. The technology has since been introduced to successive GEO satellites in Japan such as the CS-2 (1983), CS-3 (1988), etc.

1187) <http://spaceflightnow.com/titan/b38/020110digital.html>

1188) D. Powell, J. Arlat, L. Beus-Dukic, A. Bondavalli, P. Coppola, A. Fantechi, E. Jenn, C. Rabéjac, A. Wellings, "GUARDS: A Generic Upgradable Architecture for Real-time Dependable Systems," IEEE Transactions, Parallel and Distributed Systems, Vol. 10, No. 6, June 1999, pp. 580–599

1189) A. T. Tai, K. S. Tso, L. Alkalai, et al., "Low-Cost Error Containment and Recovery for Onboard Guarded Software Upgrading and Beyond," IEEE Transactions on Computers, Vol. 51, No 2, Feb. 2002, pp. 121–137

1190) R. A. Bauer, R. C. Reinhart, D. R. Hilderman, P. E. Paulsen, "Space Communications and Data Systems Technologies for Next Generation Earth Science Measurements," Earth Science Technology Conference, Pasadena, CA, June 11–13, 2002

- Italsat-1 (launch Jan. 15, 1991 from Kourou) Italy's first pre-operational communications satellite (built by Alenia Spazio) in GEO at 13.2° E (also first use of Ka-band in space). Italsat-1 carried 3 Ka-band transponders (30/20 GHz) for national coverage, and 6 multi-beam Ka-band transponders (2 in 30/20 GHz, 4 in 60/20 GHz). National/global coverage multibeam telephone and TV services; TDMA, onboard regeneration; six spot-beams generated by two 2 m antennas; three transparent transponders, 40 MHz bandwidth. The Ka-band transponders provided onboard switching of signals using a baseband switch matrix. The Italsat program was sponsored by ASI as a national space system for advanced telecommunications. Italsat-2 (launched in Aug. 8, 1996) of ASI featured in addition to the Ka-band payload EMS (European Mobile Services) of ESA.
- ACTS (Advanced Communications Technology Satellite), an experimental NASA S/C (built by Lockheed Martin) in GEO (at 100° W) with a launch on Shuttle mission STS-51 (Sept. 12-22, 1993). The objective of ACTS was to test new communication technologies: a) Ka-band (30/20 with 2.5 GHz bandwidth) operation, b) demonstration of onboard switching, and the use of "hopping" spot beams, c) testing of ATM (Asynchronous Transfer Mode) technology offering networked connectivity. By the mid-1990s, ATM had established itself as the network infrastructure of the Internet Age. In Nov. 1997 a record data rate of 520 Mbit/s TCP/IP (Transmission Control Protocol/Internet Protocol) was achieved using ATM via ACTS and several ground stations. The transmission experiment involved government agencies and commercial partners (the ACTS 118 consortium of researchers) to test their COTS products, all were interested in testing the ability of ATM technology to transfer data at high rates over satellite. ACTS communication capabilities continued to be used by industry, universities, and government to develop new satellite services, including real-time TV transmission to airliners. The ACTS program was managed at NASA/GRC; on May 31, 2000 the ACTS experiments program officially came to a close. Experiments were continuously supported for 78 months of operations. However, NASA extended ACTS availability for education and research purposes to an education-based consortium in Ohio. The deactivation of ACTS occurred on April 28, 2004 when funding was stopped. 1191)
- The new TDRS generation of NASA started with TDRS-H (TDRS-8 in orbit, launch of TDRS-H on June 30, 2000. It features also Ka-band transmissions of up to 800 Mbit/s.
- ARTEMIS (launch Jul. 12, 2001) of ESA (built by Alenia Spazio) uses Ka-band feeder links at 30/20 GHz. ARTEMIS is providing communications support for Envisat as of March 2003.
- HYLAS (Highly Adaptable Satellite) is a small geostationary communications satellite within a PPP (Public Private Partnership) project of ESA with the UK operator Avanti Communications Plc of London (launch Nov. 26, 2010). This is a multi-spot beam Ka-band satellite with very sophisticated flexible transponder technology developed in ESA projects. The overall objective is to develop and demonstrate a series of innovative payload technologies and to provide broadband data services for end users in Europe. HYLAS targets the high demand for broadband services in Europe that cannot be met by terrestrial networks. It will provide capacity to serve hundreds of thousands of Internet users and broadcast up to 30 standard or 15 high-definition TV channels. Astrium UK is the prime contractor leading the design and manufacture of HYLAS and is responsible for developing the advanced Ku- and Ka-band payload.

Introduction of EHF-band [$30 < 300$ GHz, EHF (Extremely-High Frequency)] RF communication in satellite systems. EHF communication satellites have the potential to provide protected, jam-resistant, low probability of intercept, and survivable (anti-scintillation) communication services. EHF communication can experience significant signal fad-

1191) B. Berger, "Lack of Funding Leads to Shutdown of ACTS Satellite," Space News, May 3, 2004, p. 3

ing resulting from cloud penetration and moist atmospheric layers. At the start of the 21st century, all EHF communication is still on a demonstration level. Some projects:

- The US Navy has been upgrading its UFO (Ultra-High Frequency Follow-On) program and GEO network in the 1990s. The first EHF payload was launched with the EHF-F4 satellite on Jan. 28, 1995 (launch on Atlas-II vehicle from Cape Canaveral on a commercial satellite). The launch of the EHF-F-5 followed on May 31, 1995. Both S/C were built by HSC (Hughes Space and Communications, El Segundo, CA) on the HS-601 platform. The satellites F1 through F3 carry UHF and SHF (Super-High Frequency) payloads. In F4, F5 and F6 (launch Oct. 1, 1995), there is an additional EHF payload. A GBS (Global Broadcast Service) package is part of F8 (launch March 16, 1998) through F10 (launch Nov. 23, 1999) spacecraft providing limited capabilities with a Ka-Band package. The EHF payload includes 11 EHF channels distributed between an Earth coverage beam and a steerable 5° spot beam (multiple uplinks distributed between the Earth-coverage antenna and the deployed steerable spot-beam antenna). Each uplink is time-shared by multiple users. The downlink (at 20 GHz) is a combination of all the uplinks (at 44 GHz). Both links are frequency-hopped. The EHF subsystem provides enhanced anti-jam telemetry, command, broadcast, and fleet interconnectivity communications using advanced processing techniques. The UFO-F11 satellite (launch Dec. 18, 2003) on a BSS-601 platform, is equipped with a UHF and EHF payload and an advanced tunable digital receiver (41 channels).
- In 2001, the USAF awarded a contract for the development of an Advanced EHF satellite program (2 demonstration satellites) to Lockheed Martin and TRW. Each AEHF satellite employs more than 50 communications channels via multiple, simultaneous downlinks. For global communications, the Advanced EHF system uses intersatellite crosslinks, eliminating the need to route messages via terrestrial systems. The first spacecraft, AEHF-1, was launched on Aug. 14, 2010. Shortly after launch, AEHF-1 experienced a failure in its bi-propellant propulsion system, which was intended to place the spacecraft near its operational orbit. Over 14 months, a joint team (The Aerospace Corporation, the Air Force, Lockheed Martin, and Aerojet) executed a sophisticated campaign of approximately 500 burns using the hydrazine thrusters and the HCTs (Hall Current Thrusters). The revised orbit-raising plan safely delivered AEHF-1 to its intended orbit on Oct. 24, 2011 while maintaining its required 14 years of mission life. – The AEHF-2 spacecraft was launched on May 4, 2012.
- SECOMS (Satellite EHF Communications for Mobile Multimedia Services) was a 3-year EU project until the end of 1998 [in the framework of the ACTS (Advanced Communications and Technologies) program]. A series of demonstrations were conducted in the 20/30 GHz band using ItalSat-1 in GEO.

ITU Band Name	Old radar band name, IEEE standard (GHz)	Name of Frequency Band (ITU)	Frequency Band (ITU)	Wavelength (λ) range	Comments/Use
HF		High Frequency (Decametric waves)	3 < 30 MHz	100 – 10 m	Radiotelephony, radio navigation,
VHF		Very-High Frequency (Metric waves)	30 < 300 MHz	10 – 1 m	Radio, TV, radio navigation, FM radio, etc.
UHF	L (1–2) S (2–4)	Ultra-High Frequency (Decimetric waves)	300 < 3000 MHz	1 m – 0.1 m	TV, radio beacon, satellite control
SHF	C (4–8) X (8–12) Ku (12–18) K (18–27) Ka (27–40)	Super-High Frequency (Centimetric waves)	3 < 30 GHz	10 – 1 cm	Most radar bands, general satellite communications, etc.

ITU Band Name	Old radar band name, IEEE standard (GHz)	Name of Frequency Band (ITU)	Frequency Band (ITU)	Wavelength (λ) range	Comments/Use
EHF	V (40–75) W (75–110)	Extremely–High Frequency (Millimetric waves)	30 < 300 GHz	10 – 1 mm	New field of telecommunications (mobile multimedia), radar
	mm–band		110 < 300 GHz	2.75–1.0 mm	Radiometry in remote sensing, Lidar,
	Sub–mm band		300 < 3000 GHz	1.0 – 0.1 mm	

Table 61: Some ITU frequency band allocations of the EMS (Electromagnetic Spectrum)

- SICRAL (Italian Satellite System for Military Communications), Italy's first military satellite in GEO (16.2° E, design life of 10 years) with a launch on Feb. 7, 2001 on Ariane–4 from Kourou. The objective is to provide communications (EHF, SHF, and UHF) to fixed and mobile terminals operated by Italy's military. SICRAL has been designed and built as a transmitter able to operate on three frequency bands (multi–payload and multi–transmission) – EHF, UHF and SHF – with a repeater for each band. Onboard processing functions do not include demodulation and remodulation for EHF.

DVB (Digital Video Broadcast). DVB is an open standard initiative for TV broadcast services introduced by European industry and institutions in 1992/3, and managed/published by ETSI (European Telecommunications Standards Institute), CENELEC (Center for Electrotechnical Standards) and EBU (European Broadcasting Union). In the broadcasting market, DVB has been used since the mid 1990s by such companies as SES Astra of Luxembourg. The DVB project quickly expanded to include multimedia applications as well as television. DVB provides in effect unprecedented flexibility in combining digital data (video, audio, Internet content, databases, file transfer, multimedia, etc.) into a multiplexed transport stream. Introduction of DVB–IP (Internet Protocol) in 1997/8. The DVB–IP technology permits a service distributor to maximize the bandwidth (many support options are available). ¹¹⁹²⁾

At the start of the 21st century, DVB has become an integral part of global broadcasting (over 200 organizations in over 30 countries), setting the global standard for satellite, cable and terrestrial transmissions and equipment. The main transmission standards of DVB are: DVB–S (satellite), DVB–C (cable) and DVB–T (terrestrial). While DVB was primarily designed for one–way (forward) broadcast of digital data, DVB–RCS (DVB–Return Channel via Satellite) provides a two–way broadband Internet access solution with its multicast capability. In 2000, DVB–RCS became an ETSI standard (EN 301 790) for GEO satellite interactive networks with fixed RCST (Return Channel Satellite Terminal) support (use for regenerative satellite multimedia systems). DVB–RCS offers satellite based Internet service providers the opportunity to use a common service architecture to deliver a wide range of support options at reasonable costs. – Another ETSI standard under definition is DVB–MHP (DVB–Multimedia Home Platform), a framework for developing iTV (interactive TV) applications. DVB applications use mostly frame format MPEG–2 encoding/compression at data rates between 2–10 Mbit/s. The DVB–IP technology is increasingly being considered in support for such applications as Earth observation satellite missions. Examples:

- The Envisat (launch March 1, 2002) mission of ESA uses DVB–IP services of commercial satellite service providers to distribute its data products to the user community.
- AmerHIS (the first DVB–RCS access and switching node in space) is an advanced communication payload of ESA, a regenerative multimedia system onboard Hispasat's

¹¹⁹²⁾ <http://www.dvb.org/>

Amazonas satellite (built by CDTI, a Spanish subsidiary of Alcatel Espacio), which was launched into GEO (61° W) on Aug. 5, 2004. AmerHIS operations are based on Alcatel's 9343 DVB OnBoard Processor. This processor has the demodulation, decoding, switching encoding and modulation capabilities needed for the 4 transponders on Amazonas. Each transponder covers one of the four geographical regions served by the satellite – namely Europe, Brazil, North and South America. The AmerHIS concept puts the hub onboard the satellite, saving the delay of 250 ms caused by the additional second hop. The regenerative payload thereby enables realtime broadband connections between small user terminals. The complete AmerHIS system consists of: ¹¹⁹³⁾

- The regenerative payload onboard Amazonas
- A network management system, containing the NCC (Network Control Center) and associated management control, responsible for managing the onboard resources and the user terminals
- User terminals using RCST (Return Channel Satellite Terminal) technology oriented towards the commercial demonstration of new services
- Use of RSGW (RCST Satellite Gateways) that provide the system with access to terrestrial networks.

Amateur radio communications via satellite. ¹¹⁹⁴⁾ The amateur X.25 radio communication protocol, referred to as AX.25, is a modified version of the commercial communication X.25 protocol standard. It was developed in the early 1980s. Digital “packet radio” was initially authorized by Canada in 1979 and used by Canadian hams (amateur radio operators). In 1978, Doug Lockhart of Vancouver, British Columbia, developed a device that he called TNC (Terminal Node Controller). It worked with a modem to convert ASCII to modulated tones and convert the demodulated tones back to ASCII. “Packet radio” is a system that uses TNCs and amateur radio transmitters and receivers to send information in AX.25 from place to place (for instance via Internet). It can be used for electronic mail, message transmission, emergency communications, or just plain tinkering in the world of digital communications.

A TNC is a “little black box” permitting a radio to be plugged into any computer that supports the standard RS–232 protocol/port and to communicate ASCII text. The TNC handles all the hardware aspects of data communication automatically, such as modulating [AFSK (Amplitude Frequency Shift Keying)] and demodulating of the digital signals and audible tones for broadcast as well as the software aspects such as forming data packets.

TNCs are increasingly being installed on AMSAT microsats in support for amateur radio satellite communications, they are also being used for many university/student–built satellites. The concepts are being considered by some space agencies as well. The communication data rates supported by TNC are normally at 1200 baud or at 9.6 kbaud at VHF frequencies of 145.825 MHz. The application spectrum of a TNC device onboard a nano– or microsatellite may not only be used to provide the dedicated up– and downlinks and command/control channels, but may also serve as a generic relay for other applications on a secondary basis. Some examples of TNC satellite uses are:

- An early TNC installation on a spacecraft was provided for the Russian MIR station in 1990 by MIREX (Mir International amateur Radio Experiment), an amateur radio group formed to assist with MIREX. Other examples are:
- The DOVE (Digital Orbiting Voice Encoder) spacecraft, designed and built by AMSAT–Brazil (launch Feb. 22, 1990), uses an onboard TNC for all communications.

¹¹⁹³⁾ M. Wittig, F. Petz, F. Zeppenfeldt, S. Pirio, I. Davis, J.–P. Balley, J. M. Casas, “AmerHIS: The First Switchboard in Space,” ESA Bulletin No 121, Feb. 2005, pp. 21–27

¹¹⁹⁴⁾ Larry Kenney, “Introduction to Packet Radio – Part 1,” <http://www.choisser.com/packet/part01.html>

- SPRE (SPARTAN Packet Radio Experiment), a payload on Shuttle flight STS–72 in Jan. 1996; SAREX–II (Shuttle Amateur Radio Experiment II) was flown on STS–93 (July 23–28, 1999) which included a TNC.
- PCSat (Prototype Communications Satellite), a student demonstration nanosatellite of the US Naval Academy, Annapolis, MD (launch Sept. 30, 2001), uses a TNC (Terminal Node Control) device as its onboard computer and employs the APRS (Automatic Position Reporting System) protocols (with generic digipeating capabilities) of AMSAT to permit hundreds of users per pass to access the spacecraft (via AX.25 protocol). **PCSat is the first satellite to use the TNC function as the complete spacecraft system controller with no other CPUs onboard** (see N.20). An advantage of the AX25 protocol is that any node in the system can be used for relaying data between any other nodes. Thus, the TNC can not only provide the dedicated up and downlinks and command/control channels, but also serve as a generic relay for other applications on a secondary basis. Further examples of TNCs on orbit are: SAREX, ISS, OPAL, SAPPHIRE, and STARSHINE–3. ^{1195) 1196)}
- During the last decades of the space age, both scientific knowledge and instrument technology have advanced considerably. Consequently, the transmission rates and daily volumes of data collected by **EO (Earth Observation) missions** have correspondingly increased by several orders of magnitude. As the science data downlink rates have increased, so, too, have the signal bandwidths required to support these transmissions. Hence, the downlink designs have evolved over the decades from S–band to X–band, and near–term future needs compel advancing further to Ka–band. Ka–band offers a factor–of–four improvement (on average) in performance over X–band. Equally important, the current spectrum allocation of the ITU for Ka–band is ~ 10 times that of X–band (1.5 GHz vs 375 MHz); hence, for missions that have sufficient onboard transmitter power, data rates in the several hundreds of Mbit/s to > 1 Gbit/s are feasible.

In the early 21st century, space agencies are starting to consider the introduction of wide-band RF communications in Ka–band, an enabling technology, for need of high–volume (1–10 Gbit/s range) transmission rates in their future EO (Earth Observation) missions. Some examples of operational and planned missions are:

- The SDO (Solar Dynamics Observatory) mission of NASA (launch Fe. 11, 2010) use the Ka–band (26.5 GHz) for the science data downlink at 150 Mbit/s from GSO. In parallel, the TT&C operations are performed in S–band.
- The aeronautical payload of the MTSAT (Multifunction Transport Satellite) of Japan (launch Feb. 26, 2005) is supporting 3 spot beams in Ka–band.
- The Kepler spacecraft of NASA (launch March 6, 2009) features X–band (uplink and downlink) and Ka–band communication links to downlink stored data. Kepler is not in an Earth orbit but in an Earth–trailing solar orbit.
- Within the decadal survey missions of NASA, there are three missions, namely HypsIRI, DESDynI, and SWOT, having significant data volume requirements. The estimated daily data volumes of the missions to be downlinked are: HypsIRI (~ 0.5 TB), DESDynI (~ 5 TB), SWOT (~ 1 TB). Plans are to use the Ka–band. These missions will not be launched prior to 2015. ¹¹⁹⁷⁾
- **Introduction of the 26 GHz band for direct LEO downlink:** Current state–of–the art downlink technology allows LEO (Low Earth Orbit) satellites for Earth observation (EO)

1195) B. Bruninga, C. Otero, H. Evans, T. Kolwicz, M. Silver, E. Henry, D Jones, “PCSat2: Synergy in the Amateur Satellite Service,” AIAA/USU Conference on Small Satellites, Logan, UT, USA, Aug. 11–14, 2003

1196) <http://web.usna.navy.mil/~bruninga/pcsat2.html>

1197) Kevin P. McCarthy, Frank J. Stocklin, Barry J. Geldzahler, Daniel E. Friedman, Peter B. Celeste, “NASA’s Evolution to Ka–Band Space Communications for Near–Earth Spacecraft,” Proceedings of the SpaceOps 2010 Conference, Huntsville, ALA, USA, April 25–30, 2010, paper: AIAA 2010–2176

to downlink just above 500 Mbit/s in the X–band due to bandwidth limitations. The X–band is also becoming very congested. The ITU (International Telecommunication Union) allocates four times more bandwidth in the 26 GHz band (i.e. 25.5 to 27 GHz) for the EESS (Earth Exploration Satellite Service) downlink. However, the 26 GHz band is particularly challenging in terms of atmospheric propagation effects, especially at very low elevation angles. Table 62 shows that the ITU bandwidth allocation in the 26 GHz band is four times greater (i.e. 1.5 GHz) than in the X–band.^{1198) 1199)}

Band	Frequency range (GHz)	Bandwidth (MHz)	Typical use
S–band	2.2–2.29	90	Small missions with low data rate
X–band	7.75–7.9	150	Meteorological, e.g. EPS (Eumetsat Polar System)
X–band	8.025–8.4	375	Earth Explorers, Copernicus Sentinel(s)
26 GHz (K–band)	25.5–27	1,500	All EO (including Envisat, Artemis, MTG, EPS–SG, JPSS); Many other missions: ADEOS–2, ALOS, JEM, SCaN Test Bed, SDO, LRO, ALOS–2, EDRS, JWST, DESDynI, SWOT, HypSIIRI, etc.

Table 62: ITU RF allocations for Earth and space science services

The main reasons for using the 26 GHz band for direct data downlink from LEO to ground are:

- 1) **Increased system performance:** the expanded spectrum availability (by a factor of 4) leads to higher data rates, and as the data volume increases, it becomes a major enabler of missions equipped with information–intensive (> 1 Gbit/s) sensors. When assuming the same data rate, and given that at higher frequencies the antenna beamwidth is narrower, it is also possible to reduce other system aspects such as for example the required spacecraft power amplification or the antenna size on–board and on–ground.
- 2) **Uncluttered spectrum access:** LEO missions generally use stations in high latitudes and do not have to compete with GEO missions. The data downlink concept uses steerable antennas, which at 26 GHz as compared to lower frequencies with the same antenna size, implies a smaller footprint on–ground and therefore less interference. In addition, at present there are fewer satellites using this spectrum.

The future multi–Gbit/s direct LEO to ground RF links at 26 GHz are considered:

- complementary, and not in competition, with LEO to ground links via GEO Data Relay Satellites (DRS). Actually, it is a good thing that both links have similar speed in terms of system reliability
- mature enough and the only possible option for direct LEO to ground communications, since optical links cannot operate under cloud cover conditions, specially in high latitudes where contact time is fundamental.

The IOAG (Inter–Agency Operations Advisory Group) formed a LEO 26 GHz Study Group (LEO26SG) in 2012 with the objectives to:

- Facilitate the utilization of 26 GHz K–band (i.e. (25.5–27.0 GHz) direct space to Earth data downlink for future LEO missions, in the context of cross–supports.
- Develop high level concepts of operations and preliminary architecture inputs for a 26 GHz K–band ground system for LEO.

¹¹⁹⁸⁾J. Rosello, M. Bertinelli, A. Martellucci, P. Rinous, L. Huertas, G. Parzianello, R. Abelló, G. Dauron, “26–GHz Data Downlink for Low Earth Orbit Satellites in ESA,” Proceedings of TTC 2013, 6th International Workshop on Tracking Telemetry and Command Systems for Space Applications, Darmstadt, Germany, Sept. 10–13, 2013

¹¹⁹⁹⁾Kevin P. McCarthy, Frank J. Stocklin, Barry J. Geldzahler, Daniel E. Friedman, Peter B. Celeste, “NASA’s Evolution to Ka–band Space Communications for Near–Earth Spacecraft,” 2010, URL: http://www.ntrs.nasa.gov/archive/nasa/casi.ntrs.nasa.gov/20100015515_2010016112.pdf

- Determine the business case for cross support at 26 GHz for LEO applications.

In 2013, the LEO26SG came up with the following business case (Ref. 1198):

- 1) All the basic technology has already been demonstrated (e.g. for space–to–space, like in Envisat), and therefore it represents a low risk to reuse or slightly adapt this technology for direct LEO–to–ground.
- 2) EPS–SG (ESA/Eumetsat) and JPSS (NASA/NOAA) will use direct LEO–to–ground this decade. This will pave the way for the following satellites (e.g. next generation of Copernicus) requiring multi Gbit/s.
- 3) Cross support will accelerate expansion of the number of stations providing support in the 26 GHz K–band for LEO missions and increased data return to Earth. It will also bring higher reliability, more operational flexibility with higher availability of sites and better knowledge of propagation effects.
- 4) For future missions, there is room for improvement with aspects such as faster data rate. Higher bandwidth components and more efficient schemes like VCM/ACM (Variable Coding and Modulation/Adaptive Coding and Modulation) are needed. Lower cost will come with the use of the 26 GHz by a larger number of satellites and ground stations.

The IOP–3 (Inter–Operability Plenary) recommends that new missions of the member agencies consider the use of the 26 GHz band for its LEO to ground communications, especially: ¹²⁰⁰⁾

- Missions requiring very high data rates, and
- Missions concerned with the use of congested bands.

The IOP recommends that the paths for further improvement of the technology and standards are exercised to fully exploit the capabilities offered by the 26 GHz K–band.

¹²⁰⁰⁾“Interoperability Plenary,” Meeting of IOP–3 at CNES, Toulouse, France, June 25–26, 2013, URL: <https://www.io-ag.org/Public%20Documents/FINAL%20COMMUNIQUE%20IOP3.pdf>

1.9.2 Introduction of CCSDS protocols

Spacecraft data transmission (telemetry and telecommand) using CCSDS protocols. The first **recommendations** for a CCSDS (Consultative Committee for Space Data Systems) standard were released in 1987, allowing information from different parts of a satellite to be placed into packets and to be sent to a ground station (or to be uplinked as telecommand data). By using a standard method of processing and distributing satellite data, one ground station can handle data from different satellites.¹²⁰¹⁾ – The SAMPEX mission was the first in USA to implement the CCSDS communication standards. TEAMSAT (launch Oct. 30, 1997) is the first ESA spacecraft flown with telemetry and telecommand systems both fully compatible with CCSDS standards; it is also the first spacecraft to exploit the self–adaptive asynchronous telemetry capabilities successfully that the CCSDS recommendations support. [The communication system excepts user data as randomly occurring squirts of various sizes or as fully asynchronous individual bytes. The bandwidth on the link is shared among the users according to allocation ratios. Any bandwidth not taken up by one user is offered to the other users in the proportionate ratios].

The CCSDS standard offers a number of significant advantages over the more traditional ‘mission–specific’, fixed–format data frames, such as:

- Very reliable uplink, with automatic retransmission capability
- Cost reducing, commercial off–the–shelf onboard components
- Potential for inter–operability with other ground stations/segments
- A CCSDS protocol design in combination with a MIL–STD–1553B communications bus can provide substantial advantages in terms of spacecraft/payload decoupling. Such a design is for instance implemented in the IMAGE satellite of NASA.¹²⁰²⁾
- As of 2001/2 SSTL (Surrey, UK) was implementing a CCSDS project (single–chip CCSDS–based development) in which a simplified version of the CCSDS protocol has been adapted for small satellite communications.^{1203) 1204)}

As commercial satellite manufacturers adopt the CCSDS recommendations, the scope for international inter–operability will offer significant opportunities for collaborative programs resulting in a reduction in ground control facility costs.

- Encrypted CCSDS protocol demonstration. The STRV–1d mission of QinetiQ (former DERA, UK) with a launch on Nov. 16 2000 (see M.47.2.2), carries ECSE (Encrypted CCSDS Space Experiment). The objective is to test a prototype secure CCSDS packet TM/TC system in an operational environment. a) Demonstration of ESA Packet Telecommand encrypt/decrypt, authentication, validation and anti–replay attack functionality; b) ESA Packet Telemetry encrypt/decrypt functionality, c) Extraction of security management functions onboard the spacecraft and simplified processing of these security management functions.

Satellite (Agency)	Launch Date
ERS–1 (ESA)	July 17, 1991
SAMPEX (NASA in SMEX program)	July 3, 1992
EURECA (ESA)	July 31, 1992, retrieval June 21–July 1, 1993
MSTI–1 (DoD), MSTI–2, MSTI–3	November 21, 1992, May 9, 1994, May 16, 1996

1201) P. Shaki, “Industry, Agencies Adopt Data Collection Standard,” Space News, Oct. 26 – Nov. 1, 1998, p. 6

1202) M. E. Epperly, B. J. Walls, M. Wasiewicz, “FPGA CCSDS Command Decoder with BCH EDAC and Level–0 Command Execution,” Proceedings of the IEEE Aerospace Conference, Big Sky, MT, March 9–16, 2002

1203) D. Zheng, T. Vladimirova, M. Sweeting, “A CCSDS–based Communication System for a Single–Chip On–board Computer,” 5th MAPLD International Conference, JHU/APL, Laurel, MD, Sept. 10–12, 2002

1204) I. Rutter, T. Vladimirova, H. Tiggeler, “A CCSDS Software System for a Single–Chip On–Board Computer of a Small Satellite,” AIAA/USU Conference on Small Satellites, Logan UT, Aug.13–16, 2001, SSC01–VI–4

Satellite (Agency)	Launch Date
Spacelab–D2 (DLR/ESA)	April 26 – May 6, 1993
STRV–1a and –1b (DERA, UK)	July 17, 1994
ERS–2 (ESA)	April 21, 1995
RADARSAT–1 (CSA)	November 4, 1995
SOHO (ESA/NASA)	December, 2 1995
Cluster–I (ESA)	June 4, 1996
TEAMSAT/YES (Young Engineers' Satellite) (ESA)	October 30, 1997
TRMM (NASDA/NASA)	November 27, 1997
ETS–VII (NASDA)	November 27, 1997
SNOE (University of Colorado, Boulder)	February 26, 1998 (reentry Dec. 13, 2003)
DS1 (NASA/JPL)	October 24, 1998
ROCSAT–1 (NSPO, Taiwan)	January 26, 1999
Ørsted (DRSI, Denmark)	February 23, 1999
Landsat–7 (NASA)	April 15, 1999
SJ–5 (Shi Jian – 5) of CAST and CSSAR, China	May 10, 1999
QuikSCAT (NASA)	June 19, 1999
MTSAT (NASDA/JMA, Japan)	November 15, 1999
Terra (EOS/AM–1 of NASA)	December 18, 1999
KOMPSAT–1 (KARI, Korea)	December 20, 1999
MTI (DOE)	March 12, 2000
IMAGE (NASA)	March 25, 2000
MITA (ASI)	July 15, 2000
CHAMP (GFZ/DLR)	July 15, 2000
Cluster–2 (ESA)	July 16, (1st launch), Aug. 9, 2000 (2nd launch)
QuickBird–1 (EarthWatch)	November, 20, 2000
STRV–1c and –1d (DERA, UK)	November 16, 2000
EO–1 (NASA)	November 21, 2000
QuickBird–2 (DigitalGlobe, former EarthWatch)	October 18, 2001
PROBA (ESA), BIRD (DLR)	October 22, 2001
TIMED (NASA), Jason–1 (CNES)	December 7, 2001
GRACE (NASA/DLR/GFZ)	March 17, 2002
Aqua – formerly EOS/PM1 (NASA)	May 4, 2002
ADEOS–II (JAXA)	Dec. 14, 2002 (mission ended Oct. 25, 2003)
ICESat (NASA),	Jan. 13, 2003
SciSat–1/ACE (CSA)	Aug. 13, 2003
DSP (Double Star Project) of CNSA, China and ESA	Dec. 29, 2003 (DSP–1) July 25, 2004 (DSP–2)
GP–B (Gravity Probe–B), NASA/Stanford	April 20, 2004
Myriade (CNES Microsatellite Program) with DEMETER, PARASOL, Microscope, and Picard	start in 2004 with DEMETER (launch June 29)
MTSAT–1R (JAXA/JMA, Japan)	Feb. 26, 2005
ALOS (JAXA), Japan	Jan. 24, 2006
MTSAT–2 (JAXA/JMA, Japan)	Feb. 18, 2006
MetOp–A (EUMETSAT)	Oct. 19, 2006
COSMO–SkyMed (ASI, ESA)	June 8, 2007 (launch of first S/C in a 4 S/C constellation)
TerraSAR–X (DLR/EADS Astrium GmbH)	June 15, 2007
COSMO–SkyMed–2 (ASI)	Dec. 09, 2007
COSMO–SkyMed–3 (ASI)	Oct. 25, 2008
COSMO–SkyMed–4 (ASI)	Nov. 06, 2010
X–Sat (NTU, Singapore)	April 20, 2011
Pleiades (CNES, ESA)	Dec. 17, 2011 (launch of first S/C in a series of 2)
etc.	

Table 63: Some CCSDS protocol implementations on satellite missions

Background: The Consultative Committee for Space Data Systems (CCSDS) represents the ISO Technical Committee 20 (Aircraft and Space Vehicles) Subcommittee 13 (Space Data & Info Transfer Systems), and has the objective of increasing space agency/operator interoperability. ^{1205) 1206) 1207)}

- As of January 2009, 416 missions use CCSDS standards in some way.
- CCSDS has 6 technical Areas; sub-divided into ~ 30 Working Groups that develop recommendations within specific technical domains.
- Four recommendations are part of the Navigation WG Technical Program:
 - ODM (Orbit Data Messages), CCSDS 502.0–B–1
 - TDM (Tracking Data Message), CCSDS 503.0–B–1
 - ADM (Attitude Data Messages), CCSDS 504.0–B–1
 - Navigation Data Messages/XML Specification, CCSDS 505.0–R–2
- The TDM was the 2nd standard developed by the Nav WG (began late in 2003, and was completed in November 2007.
 - The TDM specifies a standard ASCII-based message format for exchanging spacecraft tracking data, in order to facilitate interagency cross-support
 - Standardization of tracking data formats facilitates allocation of tracking sessions to a more diverse set of tracking resources
 - Data Types: Doppler, transmit/received frequencies, range, angles, Delta-DOR, clock offsets, media corrections, weather
 - One primary goal for TDM was to make format and definition of data as independent as possible from tracking equipment
 - Generator of the message converts raw measurements into navigation observables in metric units, so user does not need to know how equipment operates in order to use the data.
- **CFDP** (CCSDS File Transfer Protocol): The CFDP is a standardized file transfer protocol for space, encompassing protocols and procedures for transferring files between ground and spacecraft, including via waypoints such as data relay satellites.

CFDP was initially proposed by ESA in 1988; it was first published as a CCSDS standard in 2002. CFDP files can be transmitted with a unidirectional link, a half-duplex link, or a full-duplex link, with near-Earth and deep space delays. Files can be transferred reliably, where it is guaranteed that all data will be delivered without error, or unreliably, where a 'best effort' delivery capability is provided.

The **DTN** (Delay/disruption Tolerant Networking) ¹²⁰⁸⁾ represents an evolution from CFDP and its store-and-forward capabilities through the introduction of a dedicated bundle protocol layer and, LTP (Licklider Transmission Protocol), at the network layer, that

1205) David S. Berry, Tomas J. Martin-Mur, Neil A. Mottinger, "CCSDS Tracking Data Message Early Implementation Experiences," Proceedings of the Ground System Architectures Workshop (GSAW 2009), Torrance, CA, USA, March 23–26, 2009, URL: <http://sunset.usc.edu/gsaw/gsaw2009/s6/berry.pdf>

1206) David S. Berry, David Finkleman, "The CCSDS Orbit Data Messages – Blue Book Version 2: Status, Applications, Issues," Proceedings of the SpaceOps 2010 Conference, Huntsville, ALA, USA, April 25–30, 2010, paper: AIAA 2010–2282

1207) "Reference Architecture for Space Data Systems," Recommended Practice, CCSDS 311.0–M–1, Magenta Book, September 2008, URL: <http://public.ccsds.org/publications/archive/311x0m1.pdf>

1208) Stuart D. Fowell, Oliver Page, Dai Stanton, Stephen Farrell, Nestor Peccia, Felix Flentge, "Study into the Use of CFDP and DTN for Future ESA Missions," Proceedings of the SpaceOps 2010 Conference, Huntsville, ALA, USA, April 25–30, 2010, paper: AIAA 2010–2204

is tuned for long–delay and disrupted communication links. ¹²⁰⁹⁾

In protocol terms DTN consists of two parts, BP (Bundle Protocol and LTP. LTP is an extraction of the reliability mechanisms of CFDP and is intended to operate over individual long propagation delay links. In some senses BP is analogous to IP (intended as it is to be the “thin waist” of the network) but provides the capability to operate over multiple disjoint data links to provide an end–to–end store and forward networking service.

Both CFDP and DTN based architectures provide solutions to the provision of both message and file oriented services over noisy, long–delay, disrupted channels as found in typical ESA missions. – DTN has some advantages over CFDP with regard to added value features, in particular:

- Consideration of security aspects such as authentication, confidentiality and data integrity
- Dynamic and static routing capabilities for rapidly reconfiguring networks
- Reactive fragmentation to use alternative onward relaying paths as they become available
- Integrated universal addressing applicable to all data types
- Common store and forward networking mechanism for all data types.
- **SCCS–SM** (Space Communication Cross Support–Service Management): The CCSDS SCCS–SM was approved in 2009 as the first (and currently only) international standard for the exchange of data associated with the negotiation, configuration, scheduling, and execution of TT&C (Telemetry Tracking & Command) and SLE (Space Link Extension) services between TT&C networks and spaceflight missions. ¹²¹⁰⁾

JAXA, ESA, and NASA have developed prototype implementations of the SCCS–SM Service Specification that were used to validate the operability and interoperability of the SCSS–SM services.

- **SOA** (Service Oriented Architecture): Since about 2004, there are efforts in CCSDS on the definition of MO (Mission Operations) services between functions resident on–board a spacecraft or based on the ground. These services, if properly orchestrated, will allow for a more internationally–standardized set of mission operations services to be provided. A key challenge for the future will be showing how the MO Service framework can coexist with emerging industry standard service frameworks, such as SCA (Service Component Architecture). ¹²¹¹⁾

1209) Stuart D. Fowell, Simon Wheeler, Dai Stanton, Stephen Farrell, Chris Taylor, Aitor Viana Sanchez, “Space Inter-networking and DTN Prototyping: Evolutions in the Space Communications Architecture,” Proceedings of the DASIA (DAta Systems In Aerospace) 2011 Conference, San Anton, Malta, May 17–20, 2011, ESA SP–694, August 2011

1210) John V. Pietras, Erik J. Barkley, Anthony Crowson, “CCSDS Space Communication Cross Support Service Management,” Proceedings of the SpaceOps 2010 Conference, Huntsville, ALA, USA, April 25–30, 2010, paper: AIAA 2010–2283

1211) Mario Merri & the CCSDS SM&C WG, “CCSDS SM&C: where do we stand today,” Proceedings of the SpaceOps 2010 Conference, Huntsville, ALA, USA, April 25–30, 2010, paper: AIAA 2010–2337

CCSDS overview:

- CCSDS for international collaboration in spaceflight, the most critical enabling technology is communications and data systems.
- The domain of CCSDS is interoperability for comm/data systems
- Interoperability translates to:
 - Operations – flexibility, capability and access to additional resources
 - Development – reduced risk, development time and project costs
 - For government, industry, agencies, vendors, programs and projects
- The CCSDS focus is on multi–agency missions, but standards bring the same benefit comes to single–agency with multiple contractors
- CCSDS started in 1982 developing at the lower layers of the protocol stack. The CCSDS scope has grown to cover standards throughout the ISO communications stack, plus other Data Systems areas (architecture, archive, security, XML exchange formats, etc.

CCSDS composition:

- Produces International Voluntary Consensus Standards
- Agency–led international committee
 - Currently (2013) 11 Member agencies: ASI/Italy, CNES/France, CNSA/China, CSA/Canada, DLR/Germany, ESA/Europe, FSA/Russia, INPE/Brazil, JAXA/Japan, NASA/USA, UKSA/UK.
 - Currently 28 Observer Agencies
 - Agencies represent 26 nations
 - Currently 141 Commercial Associates
 - ~ 160–180 attendees at Spring/Fall meetings
- Also functions as an ISO Committee
 - TC20/SC13 – Space Data & Info Transfer Systems

Some Organizational Interrelationships:

- **OMG** (Object Management Group): Industry standards for exchange of application information among vendor products. CCSDS/OMG have some common standards and periodic joint meetings
- **IETF** (Internet Engineering Task Force) and **IRTF** (Internet Research Task Force). Open international standards for IP suite and DTN. CCSDS uses such industry standards as a basis, whenever possible.
- **ECSS** (European Consortium for Space Standards). European regional standards for space mission support. CCSDS/ECSS coordinate on compatible standards.
- **AIAA** (American Institute of Aeronautics and Astronautics). North American regional standards for space mission support. Regional Standards coordination, and AIAA provides Secretariat support for CCSDS, ISO TC20/SC13 and SC14.

CCSDS Strategic Plan for the Future:

- 1) Systems Engineering: Cross–cutting functions and architecture–wide integration
- 2) Towards standardized Mission Operations Services at Application Level on Ground and On–Board
- 3) Towards a complete Navigation Message Standardization
- 4) Towards an extensible Space Communications Cross Support Service Management and Transfer Services (Cross Support of Communications Assets)
- 5) Towards an unified Space Data Link Protocol, optical links, new sync and channel coding schemes and compression
- 6) Towards standardized Space System Internetworking Services and the Solar System Internet (SSI).

Cross-Cutting Functions and Architecture Integration:

- 1) The System Engineering View, multiple Reference Architectures
 - Space / Ground Interoperability Architecture
 - Security Architecture (application and link layer) — for protecting system elements and information as it flows through the E2E space mission system
 - Information Architecture
 - Timeline Service Architecture
- 2) Distributable Mission Operations Functions
 - M&C (Status, Control), Automation (Procedures, Timelines), Planning (Tasks, Goals), Navigation (Orbit, Attitude), On–Board Software.
- 3) The Navigation Roadmap
- 4) Framework for extensible Space Communications Cross Support Service
- 5) Space Link Services Layered approach
- 6) Top Level Space Communications & Navigation Architecture – The Solar System Internet

CCSDS Summary:

- Enabling interoperability between international agencies for future space missions – from Earth–Orbital to Deep Space
- Long–range vision – automated routing and delay tolerant networking for deep space crosslinks between spacecraft and surface systems
- Near–term need – evolutionary approach to sustain cross–support agreements with other agencies.

Table 64: Overview of CCSDS (Consultative Committee for Space Data Systems) functions ¹²¹²⁾

1212) Adrian Hooke, Nestor Peccia, “A Brief Story of a Success: The CCSDS,” GSAW (Ground System Architectures Workshop) 2013, March 18–21, 2013, Los Angeles, CA, USA, URL: <http://sunset.usc.edu/GSAW/gsaw2013/s4/peccia.pdf>

1.9.3 DTN (Delay/disruption Tolerant Networking)

At the start of the 21st century, DTN is an emerging research area in the end-to-end store-and-forward architectures, which takes a different approach to conventional (inter)networking and allows to work in stressed as well as in highly heterogeneous environments. DTN refers to TCP/IP networks where traditional instant packet forwarding mechanisms fail due to, e.g., high delays, intermittent connectivity, or non-existing end-to-end paths. Unlike Internet routers, which forward packets instantaneously (or discard them if no route is found), DTN nodes may store packets for an extended period of time until the next suitable forwarding opportunity, called contact, becomes available. ^{1213) 1214) 1215)}

These **store-and-forward concepts** are of particular interest to space communications in general where delays and/or disruptions in communication links cause loss of data due to fragmentation and/or the ability to command a spacecraft. Other fields of DTN applications are sparse sensor networks, and opportunistic mobile ad-hoc networks. – Also, considerable interest exists in the space community for an **IPN** (Interplanetary Internet) to serve all future missions (in LEO, GEO, or in deep space). However, a considerable amount of research is needed before IPN becomes a reality. ^{1216) 1217) 1218)}

To provide the DTN store-and-forward service, a **bundle protocol (BP)** sits at the application layer of some number of constituent internets, forming a store-and-forward overlay network. Key capabilities of the BP include:

- Custody-based retransmission – the ability to take responsibility for a bundle reaching its final destination
- Ability to cope with intermittent connectivity
- Ability to cope with long propagation delays
- Ability to take advantage of scheduled, predicted, and opportunistic connectivity (in addition to continuous connectivity)
- Late binding of overlay network endpoint identifiers to constituent internet addresses.

The DTNRG (Delay Tolerant Networking Research Group) was formed in 2002 as a result of the observation that a non-interactive, asynchronous form of messaging service, able to operate over diverse types of networks, would be useful for several networks currently in use or being contemplated. – In 2007, standards for acquisition, DTN architecture and BP specifications achieved RFC (Request for Comments) status (RFC 4838, RFC 5050).

In 2009, some problems with the BP (integrity of checksum) need to be addressed for proper DTN service delivery. ¹²¹⁹⁾

- On January 28, 2008, first **DTN** (Delay/Disruption Tolerant Networking) spaceborne demonstrations were conducted between the partners SSTL (UK) and NASA/GRC (USA). A DTN bundling configuration was implemented onboard the UK–DMC spacecraft and in

1213) Delay Tolerant Networking Research Group, URL: <http://www.dtnrg.org/wiki>

1214) <http://www.netlab.hut.fi/~jo/dtn/index.html>

1215) http://www.nasa.gov/mission_pages/station/science/experiments/DTN.html

1216) I. O'Neill, "Google and NASA are Working on an Interplanetary Internet," Universe Today, Oct. 28, 2008, URL: <http://www.universetoday.com/2008/10/28/google-and-nasa-are-working-on-an-interplanetary-inter-net/>

1217) M. Boucher, "The InterPlanetary Internet (IPN)," SpaceRef, Oct. 29, 2008, URL: <http://www.spaceref.com/focuson/ipn/>

1218) Will Ivancic, Wesley M. Eddy, Lloyd Wood, Dave Stewart, Chris Jackson, James Northam, Alex da Silva Curiel, "Delay/Disruption-Tolerant Network Testing Using a LEO Satellite," NASA Earth Science Technology Conference (ESTC 2008), College Park, MD, USA, June 24–26, 2008, URL: <http://personal.ee.surrey.ac.uk/Personal/L.Wood/publications/uk-dmc-dtn-saratoga-testing-estc-2008.pdf>

1219) Lloyd Wood, Wesley M. Eddy, Peter Holliday, "A Bundle of Problems," Proceedings of the 2009 IEEE Aerospace Conference, Big Sky, MT, USA, March 7–14, 2009

the ground infrastructure of the mission. The communication experiments involved the transmission of image files from the spacecraft to the ground via the 'bundle protocol' which simulated fragments of an observed scene in several passes and the subsequent ground restoration of the image fragments to a complete scene again. – With the addition of the Saratoga Delay Tolerant Networking protocol over IP to provide robustness, UK–DMC was able to act like an internet node in space. ^{1220) 1221)}

- In October 2008, engineers at NASA/JPL conducted a month–long series of DTN demonstrations. Data were transmitted using NASA's Deep Space Network (DSN) in demonstrations between NASA's Deep Impact/EPOXI spacecraft serving as a Mars data–relay orbiter (Epoxi is on a mission to encounter Comet Hartley 2 in November 2010 – an encounter took place on Nov. 4, 2010). The “interplanetary network” consisted of 10 nodes, one was the EPOXI spacecraft itself (32 million km away from Earth) and the other nine nodes were on the ground at JPL. This month–long experiment was used to qualify the technology for use on a variety of upcoming space missions. ^{1222) 1223)}

Note: The **EPOXI** (Extrasolar Planet Observation and Characterization) spacecraft of NASA is the renamed Deep Impact mission of NASA (launch on Jan. 12, 2005). After Deep Impact completed its primary mission on July 4, 2005, when the flyby mother spacecraft slammed an impactor of 370 kg into the comet Tempel 1, the spacecraft was given a new mission and a new name (EPOXI) to encounter another comet, namely Hartley 2.

Also – in the summer of 2008, NASA engineers used the telescope of the EPOXI spacecraft to create a video of the moon transiting (passing in front of) Earth as seen from the spacecraft's point of view 50 million km away. ^{1224) 1225)} Scientists are using the video to develop techniques to study alien worlds. Making a video of Earth from so far away helps the search for other life–bearing planets in the universe by giving insights into how a distant, Earth–like alien world would appear. As a result, a method was developed to indicate the presence of oceans by analyzing how Earth's light changes as the planet rotates. This method can be used to identify extrasolar ocean–bearing Earths.

The encounter of EPOXI with comet 103P Hartley 2 occurred on Nov. 4, 2010. The flyby at a distance of ~ 700 km provided new information about the comet's volume and material spewing from its surface. ^{1226) 1227)}

- DTN on the ISS (International Space Station). In May 2009, the DTN communications protocols were installed on a BioServe payload of ISS known as the CGBA (Commercial Generic Bioprocessing Apparatus). The DTN tests involve sending bundles of data from the ISS to its operations and control facility at Marshall Space Flight Center (MSFC) in

1220) W. Ivancic, W. M. Eddy, L. Wood, D. Stewart, C. Jackson, J. Northam, A. da Silva Curiel, “Delay/Disruption–Tolerant Network Testing Using a LEO Satellite,” ESTC2008 (Earth Science Technology Conference 2008), June 24–26, 2008, College Park, MD, USA, URL: http://esto.nasa.gov/conferences/estc2008/papers/Ivancic_William_A4P2.pdf

1221) Lloyd Wood, Will Ivancic Wesley M. Eddy, Dave Stewart, James Northam, Chris Jackson, Alex da Silva Curiel, “Use of the Delay–Tolerant Networking Bundle Protocol from Space,” Proceedings of the 59th IAC (International Astronautical Congress), Glasgow, Scotland, UK, Sept. 29 to Oct. 3, 2008, IAC–08–B2.3.10

1222) “NASA Tests First Deep–Space Internet,” NASA/JPL, Nov. 18, 2008, URL: <http://www.jpl.nasa.gov/news/news.cfm?release=2008–216>

1223) Vint Cerf, Scott Burleigh, Ross Jones, Jay Wyatt, Adrian J. Hooke, “First Deep Space Node on the Interplanetary Internet: the Deep Impact Networking Experiment (DINET),” Proceedings of the Ground System Architectures Workshop (GSAW 2009), Torrance, CA, USA, March 23–26, 2009, URL: <http://sunset.usc.edu/gsaw/gsaw2009/s6/burleigh.pdf>

1224) Nancy Atkinson, “An Alien View of the Moon Transiting Earth,” Universe Today, July 17, 2008, URL: <http://www.universetoday.com/2008/07/17/an-alien-view-of-the-moon-transiting-earth/>

1225) Nancy Atkinson, “New Technique Could Find Another 'Pale Blue Dot',” Universe Today, May 26, 2009, URL: <http://www.universetoday.com/2009/05/26/new-technique-could-find-another-pale-blue-dot/>

1226) http://www.nasa.gov/mission_pages/epoxi/index.html

1227) “EPOXI Comet Encounter Fact Sheet,” Nov. 2, 2010, URL: http://www.nasa.gov/pdf/494786main_EPOXI–FlybyFactSheet.pdf

Huntsville, AL, then on to a POC (Payload Operations Center) at CU–Boulder’s BioServe.¹²²⁸⁾¹²²⁹⁾

The DTN capability is in parallel with and designed to augment current capabilities. The architecture consists of DTN endpoint nodes on the ISS and at the Boulder POC, and a DTN node at the HOSC (Huntsville Operations Support Center). The DTN network is composed of two implementations: the Interplanetary Overlay Network (ION) of JPL and the open source DTN2 implementation. DTN has proven to be an effective technology that can simplify the current operations concept involved with payload commanding and telemetry receipt. The results clearly indicated that the DTN technology reduced the number of retransmissions, allowing the project to start changing their operations concept to allow for autonomous operations.¹²³⁰⁾

- Although DTN was originally conceived with a space focus, as the technology underpinning an InterPlanetary Network (IPN), the intermittent connectivity DTN has found increasingly broad application to military networks, wireless sensor networks, village networks, “pocket switched” networks, and peer–to–peer networks.¹²³¹⁾

In 2010, DTN technologies are being employed in a wide variety of challenging environments such as deep space communication, military networks and sensor networks. These types of networks exhibit long delays, intermittent connectivity and do not ensure contemporaneous end–to–end paths between nodes. In such environments special protocols for communication must be developed (BP) where traditional Internet communication protocols will fail. DTN protocols are specifically designed to operate efficiently and effectively in adverse network conditions while bringing Internet–like services to the network.

- The SmartSSR is a solid–state recorder (SSR) that is being developed under an Independent Research and Development program by JHU/APL specifically for space applications. This component combines a large NAND (Negated AND) flash array with a general–purpose processor in order to host several closely related functions in a way that efficiently provides their services to the other components of the spacecraft. It is based on the LEON3FT processor and uses SpaceWire interfaces to communicate with other spacecraft components.¹²³²⁾

The SmartSSR manages the spacecraft data through SpaceFFS (Space Flash File System). The SpaceFFS is APL’s adaptation of a commonly available flash file system to the special requirements of the space operational environment. The DTN router capability, as well as several other capabilities, is provided by JPL’s ION (Interplanetary Overlay Network) implementation of the standard DTN protocols. Combined, the SmartSSR DTN router is capable of providing the following:

- A high–capacity, high–performance, solid–state data recorder that serves as a local area (spacecraft) network file system server
- Delay–tolerant routing that is based on the ION implementation of the DTN BP
- CFDP (CCSDS File Delivery Protocol) file transfers and file management using the ION CFDP

1228) “New ‘Space Internet’ Protocols On ISS Tested,” Space Mart, July 7, 2009, URL: http://www.spacemart.com/reports/New_Space_Internet_Protocols_On_ISS_Testing_999.html

1229) Andrew Jenkins, Sebastian Kuzminsky, Kevin K. Gifford, Robert L. Pitts, Kelvin Nichols, “Delay/Disruption–Tolerant Networking: Flight Test Results from the International Space Station,” Proceedings of the 2010 IEEE Aerospace Conference, Big Sky, MT, USA, March 6–13, 2010

1230) Kelvin Nichols, Mark Holbrook, R. Lee Pitts, Kevin K. Gifford, Andrew Jenkins, Sebastian Kuzminsky, “DTN Implementation and Utilization Options on the International Space Station,” Proceedings of the SpaceOps 2010 Conference, Huntsville, ALA, USA, April 25–30, 2010, paper: AIAA 2010–2173

1231) Loren Clare, Scott Burleigh, Keith Scott, “Endpoint Naming for Space Delay / Disruption Tolerant Networking,” Proceedings of the 2010 IEEE Aerospace Conference, Big Sky, MT, USA, March 6–13, 2010

1232) Christopher J. Krupiarz, Edward J. Birrane, Benjamin W. Ballard, Lotfi Benmohamed, Alan A. Mick, Katherine A. Stambaugh, Edward W. Tunstel, “Enabling the Interplanetary Internet,” JHU/APL Technical Digest, Vol. 30, No 2, August 2011, pp. 122–134, URL: <http://techdigest.jhuapl.edu/TD/td3002/Krupiarz.pdf>

- A remote gateway for publish/subscribe distributed computing using the ION asynchronous message service protocol.

The ION software is implemented using a layered approach that exploits standard software interfaces. The interplanetary communication infrastructure layer provides common functionality to other ION packages through general-purpose libraries. A key component is the “zero copy objects” capability, which, in turn, is used to build linked lists of data objects representing the data and tasks that need to be performed. Subsets of these are included in the “traffic database,” which is built on the simple data recorder (SDR) component.

- DTNMP (Delay-Tolerant Network Management Protocol): The DTNMP is designed around four desirable properties: (1) the intelligent push of information through the network, (2) low messaging overhead, (3) detailed data identification, and (4) compatibility with existing terrestrial management protocols. The DTNMP has been designed to operate in any DTN environment and is naturally suited for implementation in flight software systems. A reference implementation of DTNMP has been implemented to work with the NASA ION (Interplanetary Overlay Network) flight software suite of DTN protocols and utilities.¹²³³⁾
- The Packet Service will provide a crucial transitional step toward SI (Space Internetworking). Not only are the underlying PS (Packet Service) functions required for SI, early infusion of PS capabilities and operational experience will be highly valuable in making both users and providers accustomed to basic packet-oriented operations. This incremental step heavily leverages existing capabilities, facilitating its implementation. For example, NASA’s DSN (Deep Space Network) currently offers the **CFDP** (CCSDS File Delivery Protocol) service to missions, within which all the processing capabilities required for Packet Service already exist for both uplink and downlink. The next step is to expose these processing capabilities as external interfaces accessible to missions.¹²³⁴⁾

1.9.4 FSO (Free-Space Optics) communications with satellites

FSO is an emerging wireless communications technology at the start of the 21st century that transports data from point-to-point and multipoint via **laser technology**. Commercial FSO systems became available in the 1990s, primarily to interconnect buildings and campus LANs (short-distance interconnections). The technology is based on connectivity between FSO units, each consisting of an optical transceiver with a laser transmitter and a receiver to provide full duplex (bi-directional) communications. The interest here is focused on FSO links between a satellite and the ground as well as on optical **ISLs** (Intersatellite Links) or **IOLs** (Inter-Orbit Links).^{1235) 1236) 1237)}

- Laser links have the potential to offer much higher transmission rates (up to 10 Gbit/s) for LEO-to-ground communications than conventional TT&C radio frequency (i.e., RF-based) links which are limited to rates of about 300 Mbit/s to 1 Gbit/s maximum. The

1233) Edward J. Birrane, III, Vignesh Ramachandran, “Configuration and Monitoring Across Delay-Tolerant Links: Robust Management of Space Internetworks,” Proceedings of the 63rd IAC (International Astronautical Congress), Naples, Italy, Oct. 1–5, 2012, paper: IAC-12-B2.1.1

1234) Jay L. Gao, Loren P. Clare, David J. Israel, “The Benefits of Packet Service in Evolving Space Communications Provider Networks,” SpaceOps 2014, 13th International Conference on Space Operations, Pasadena, CA, USA, May 5–9, 2014, paper: AIAA 2014-1687, URL: <http://arc.aiaa.org/doi/pdf/10.2514/6.2014-1687>

1235) H. P. Lutz, “Optical Communications in Space – Twenty Years of ESA Effort,” ESA Bulletin No 91, Aug. 1997, <http://esapub.esrin.esa.it/bulletin/bullet91/b91lutz.htm>

1236) Davide M. Forin, G. Incerti, G. M. Tosi Beleffi, A. L. J. Teixeira, L. N. Costa, P. S. De Brito Andrè, B. Geiger, E. Leitgeb, F. Nadeem, “Free Space Optical Technologies,” URL: http://www.intechopen.com/download/pdf/pdfs_id/9705

1237) Nikos Karafolas, Zoran Sodnik, Josep Perdigues, Iain McKenzie, “Optical Communications in Space,” 2009, URL: <http://www.ida.ing.tu-bs.de/noncms/ondm2009/schedule/invited/karafolas.pdf>

optical information bandwidth of a signal is only a fraction of the RF carrier frequency, typically 0.1 that of RF systems. Extremely high ‘antenna’ gains with relatively modest apertures are obtained in optical communication systems, resulting in very low carrier power (for instance 60 mW in SILEX (Semiconductor Intersatellite Link Experiment) data transmissions of 50 Mbit/s over a distance of 42,000 km). The optical spectrum for TT&C applications may range in bandwidth from about 532 nm (563 THz) to about 1550 nm (194 THz), providing for many GHz of information transfer on optical carriers. Space laser optical communications benefit from the intrinsic high operating frequency (200 to 400 THz) leading to very high optical antenna gains (> 110 dB). This intrinsic advantage comes with a beam divergence of a few μrad , requiring accurate antenna pointing.

One of the main advantages of laser links – apart from the intrinsic benefits of low power consumption and the potential of very high data rates – is that by their very nature, there can be no interference between optical and radio transmissions.¹²³⁸⁾¹²³⁹⁾¹²⁴⁰⁾ Hence, FSO systems offer the perfect answer to some of the main requirements for secure communications, in particular with respect to counter–measures. It is very difficult to detect optical transmissions (unless being exactly within the transmission path), it is very difficult to locate such a communication, and to jam it. Naturally, such security aspects are of great interest for a variety of applications in the military, commercial and to some extent also in the Earth observation fields.

The technical challenge of the technology demonstration involves in particular alignment and stabilizing issues, it requires pointing errors of $< 10 \mu\text{rad}$ (or $< 0.0005^\circ$). This pointing accuracy is several orders of magnitude lower (better) than open–loop pointing of a typical platform. Also, platform jitter caused by the operation of other payload instruments, must be mitigated. Other constraints to be considered deal with eye–safety issues and with weather and atmospheric effects. The optical signals can be greatly attenuated by the weather and the atmosphere. Numerous applications of optical communication links are envisioned, such as: Space–to–ground, interorbit (LEO–GEO), intersatellite (LEO–LEO or GEO–GEO), or deep space to ground. The laser technologies used for space optical communications are inherited from commercial terrestrial applications:

- 0.8 μm technology, commercially used in printer and CD applications
- 1.06 μm technology, commercially used in scientific and lidar applications
- 1.55 μm technology, commercially used in terrestrial telecommunications (fiber optic networks). A fairly large number of component manufacturers exists.

Although some functions are common to all technologies, the laser wavelength drives key optical terminal elements such as the transmitter, the receiver, the acquisition and tracking sensors.

Some early demonstrations in space are:

- **LCE** (Laser Communication Equipment),¹²⁴¹⁾ a CRL (Japan) payload flown on ETS–6 (Experimental Test Satellite–6) of NASDA and NTT. Launch of ETS–6 on Aug. 28, 1994. Note: ETS–6 attained a highly elliptical orbit (instead of a planned GEO) due to a failure in the launch vehicle propulsion system. In spite of this misfortune, some LCE experiments were conducted with ground stations in Japan and at JPL (low data rate transmis-

1238) B. Laurent, G. Planche, C. Michel, “Inter–Satellite Optical Communications: From SILEX to Next Generation Systems,” Proceedings of the 5th International Conference on Space Optics, March 30–April 2, 2004, Toulouse, France, ESA SP–554

1239) M. Shikatani, et al., “Ground system development for the ETS–6/LCE laser communication experiment,” Proceedings of SPIE, 20–21 Jan. 1993, Los Angeles, Vol. 1866, pp. 21–29

1240) Y. Arimoto, et al., “Preliminary Results on Laser Communication Experiment using ETS–6,” Proceedings of SPIE, Vol. 2381, 1995

1241) W. T. Brandon, V. W. S. Chan, R. K. Kwan, “Japanese Research Satellite Projects,” URL: http://www.wtec.org/lovo-la/satcom/c6_s1.htm

sions of 1 Mbit/s were conducted, mostly due to the use of a small optical antenna and non-diffraction-limited optics on the spacecraft).

- **SILEX** (Semiconductor Intersatellite Link Experiment), an ESA technology demonstration of an optical link system, ^{1242) 1243) 1244)} built by EADS Astrium SAS (formerly MMS). SILEX consists of two optical terminals, a LEO and a GEO terminal, namely **PAS-TEL** (PAssager SPOT de Télécommunication Laser, mass of 162 kg), a LEO terminal on-board SPOT-4 (launch March 22, 1998) on the anti-Earth side of the SPOT platform, and **OPALE** (Optical Payload for Intersatellite Link Experiment) a GEO terminal mounted on ESA's geostationary satellite ARTEMIS. ARTEMIS was launched on July 12, 2001. The ARTEMIS downlink to the ground segment at CNES Toulouse uses a conventional radio transmission (Ka-band). See also SILEX under D.55.2. The SILEX experiment has a two-fold objective: validation of the laser transmission concept and operational transmission of SPOT 4 imagery to the ground.

The SILEX technology was selected in early 1990s. Since this time, several technological improvements have come about. These improvements allow today simplified and more powerful optical terminals with the following technologies:

- More powerful laser diodes: 0.4 W output power compared to 60 mW used on SILEX LEO terminal
- Full communication chain (transmit and receive chains) completely validated and performance correlated up to 600 Mbit/s
- CMOS detector availability: CMOS detector (750 x 750 pixels) sampled at 8 MHz with windowing capability permits to only a single detector for acquisition and tracking. This simplification reduces the optical path and increases the available power for tracking and communication
- SiC technology qualification: this technology, now mature and implemented on several optical payloads, allows simplifying telescope and focal plane design and increases stiffness, mass and stability performances.

Parameter	Description
Link range	45,000 km to SPOT-4/ARTEMIS (worst case configuration)
Link capacity	Forward link (GEO --> LEO): 2 Mbit/s capability Return link (LEO --> GEO): 50 Mbit/s of SPOT-4 useful data rate
Wavelength range	800 – 852 nm
Key components	Laser diodes, CCD detectors, APD (Avalanche Photodiode) sensor
Telescope diameter	250 mm
Optical power	Communication laser diodes power set-point: 60 mW (LEO), 40 mW (GEO) Beacon laser diodes power: 9.5 W (19 diodes x 500 mW)
Beam divergence	Communication beam: 4 µrad (LEO) and 8 µrad (GEO) Beacon beam (GEO): 750 µrad
Link performances	Acquisition: 240 s duration (worst case) with 0.95 probability of success achievable down to 13° sun aspect angle Data transmission: average BER better than 10 ⁻⁸ (return link); limited occurrence of errors (short term quality), achievable down to 1° sun aspect angle
Availability	better than 92.5% of the LEO-GEO annual visibility

1242) G. Griseri, "SILEX Pointing Acquisition and Tracking: ground tests and flight performances," 5th ESA Conference on Guidance Navigation and Control Systems, Oct. 22-25, 2002, Frascati, Italy, ESA SP-516, pp. 385-391

1243) G. Griseri, "SILEX Pointing Acquisition and Tracking: ground tests and flight performances," 4th ESA International Conference on Spacecraft Guidance, Navigation and Control Systems, Oct. 18-21, 1999, pp. 467-472, ESA/ESTEC,

1244) G. Planche, V. Chorvalli, "SILEX In-Orbit Performances," Proceedings of the 5th International Conference on Space Optics, March 30-April 2, 2004, Toulouse, France, ESA SP-554

Parameter	Description
Operations	Autonomy w.r.t. ground : 24 hours operation without ground command Autonomy w.r.t. satellite: Onboard processor and software, integrated thermal control, safe configuration GEO multi-user capability (operation of 2 LEOs in an interleaved way)
Typical terminal data	Pointing accuracy : about 2 μ rad Optical quality : better than $\lambda/10$ on each optical path Isolation between paths : better than 10^{-10} Defocus : better than 10 μ m

Table 65: Overview of SILEX optical link characteristics ¹²⁴⁵⁾

- **LUCE** (Laser Utilizing Communications Equipment), a Japanese payload (built by NEC) flown on OICETS (Optical Interorbit Communications and Engineering Test Satellite) of JAXA (launch Aug. 23, 2005). OICETS in LEO conducts interorbit communications experiments with ARTEMIS of ESA in GEO (50 Mbit/s using a 25 cm telescope on both ends of the link). – From Sept. 9–14, 2003, JAXA conducted successfully communication experiments (link tests) between the ground-based LUCE engineering model via ARTEMIS and OGS (Optical Ground Station) on Tenerife, operated by IAC (Instituto de Astrifísica de Canarias), Spain.

- **Lasercom** (Laser Communication Experiment), an experiment on the AFRL mission TSX–5 and its payload STRV–2 (launch on June 6, 2000), see M.55.

- **A first optical data transmission test, using the laser link between ARTEMIS (ESA) and SPOT–4 (CNES), was realized on Nov. 21, 2001** on four consecutive SPOT–4 orbits for contact periods between four and 20 minutes each. The SILEX terminal onboard ARTEMIS, in a parking orbit of 31,000 km, activated its optical beacon to scan the area where SPOT was expected to be (LEO at 830 km). ^{1246) 1247)} When contact was made, SPOT–4 responded by sending its own laser beam to ARTEMIS. On receiving the SPOT–4 beam, ARTEMIS stopped scanning and the optical link was maintained for a pre-programmed period lasting from 4 to 20 minutes. Data rates of 50 Mbit/s were reached transmitting test data from SPOT–4 via ARTEMIS to the ground. An extremely low bit error rate of the data stream was confirmed at at ESA’s test station in Redu (Belgium) and the SPOT 4 receive station in Toulouse, France. On Nov. 30, 2001, the first-ever civil transmission of an image by laser link took place from one S/C to another. – In the meantime, many operational validation tests have been conducted with optical transmissions of the SILEX system. It turns out that the SILEX configuration via ARTEMIS offers significant observation coverage and transmission advantages, practically in real-time.

PASTEL operation period on SPOT–4: The PASTEL mission really started just after the beginning of functionality of the European relay satellite ARTEMIS on 1 April 2003. Since that time until the apparition of anomaly on January 9, 2008 (slightly less than 5 years), there were a total of 2018 laser communication links requested and 1862 effectively done (156 canceled communications). A total of 1789 transmissions were properly conducted, bringing to 96.08% the success rate. The duration of all transmissions was around 378 hours for all communication sessions. ¹²⁴⁸⁾

1245) G. Griseri, “SILEX Mission Overview,” AAS/IFAC/AIAA International Workshop on Control of Optical Systems, Breckenridge, CO, Feb. 2–5, 2003

1246) “ARTEMIS and SPOT–4 chat with laser light,” ESA Bulletin, No 108, Nov. 2001, p. 114

1247) I. Gaudel, L. Moliner, B. Romeo, S. Teodomante, “Operational Use of PASTEL Passenger on SPOT–4 Satellite,” Proceedings of 54th IAC (International Astronautical Congress), Bremen, Germany, Sept. 29 – Oct. 3, 2003

1248) Information provided by Frédéric Tavera, SPOT Mission Exploitation Manager of CNES, Toulouse, France

1960: laser invention	
1970: first continuous wave semiconductor laser	
21st century FSO technology:	
Minimum diffraction losses:	greatly reduced apertures
Abundant optical bandwidths:	no regulation required
Secure communications:	narrow spatial diversity
Optical communications show high potential for high-speed, long distance free space links	

Figure 67: Optical communications potential

- On December 5, 2006, ARTEMIS successfully relayed optical laser links from an aircraft.^{1249) 1250) 1251)} These airborne laser links, established over a distance of 40 000 km during two flights at altitudes of 6000 m and 10 000 m, represent a world first. The relay was set up through six two-way optical links between a French Mystère 20 equipped with the airborne laser optical link **LOLA** (Liaison Optique Laser Aéroportée – Airborne Optical Laser Link) and the **SILEX** laser link payload on board ARTEMIS in its geostationary orbital position at 36 000 km altitude. These tests were made by Astrium SAS (France), the prime contractor for both LOLA and SILEX, as part of the airborne laser optical link program funded by the DGA (Délégation Générale pour l'Armement – the French Arms Procurement Agency).

- Internet fiber-based communication using OEIC (Optoelectronic Integrated Circuit) technology. The monolithic integration of high-speed electronic and optoelectronic devices into (OEICs) is very attractive for use as optical receivers (photoreceiver) and transmitters in fiber-optic communication systems. The OEIC scheme utilizes an on-chip technology containing light sources, photodetectors, modulators, and VLSI-density electronic circuitry. The OEIC technique offers a higher bandwidth and an improved functionality at a reduced cost, as compared with hybrid solutions, making it possible to utilize the potential of optical fibers for high-speed communication. Photoreceivers for several bit rates ranging from 10 to 40 Gb/s have been fabricated in the late 1990s and installed for internet applications. Demands for greater bandwidths have driven the telecommunication research communities to realize complex OEICs such as transceivers, switching systems, low chirp optical sources and multichannel optical distribution systems.

The next logical step to optical fiber-based Internet communications are **FSO** (Free Space Optics) network applications of OEIC technology (support of mobile communications with ubiquitous connectivity). The photoreceiver array employs unique optical amplifier and conversion technologies that provide the ultra-sensitivity required for free space optical communications networks. This sensitivity is achieved by monolithically integrating a VCSEL (Vertical Cavity Surface Emitting Laser–diode) optical preamplifier with a photodiode receiver and related amplifiers and filters on the same chip, resulting in sensitivities as low as -47 dBm (62 photons/bit at 2.5 Gb/s).¹²⁵²⁾

Parameter	OPALE on ARTEMIS	PASTEL on SPOT-4
Instrument mass	158 kg	158 kg
Power	185 W (acquisition) 154 W (communication)	143 W (max EOL)
Angular mobility (optical tracking range)	-11° to $+12^\circ$ (elevation) -11° to $+89^\circ$ (azimuth)	Quasi hemispherical

1249) http://www.esa.int/esaCP/SEMN6HQJNVE_index_0.html

1250) L. Vaillon, G. Planche, V. Chorvalli, L. Le Hors, "Optical Communications between an aircraft and a GEO Relay Satellite: Design & flight results of the LOLA demonstrator," Proceedings of the 7th ICSO (International Conference on Space Optics) 2008, Toulouse, France, Oct. 14–17, 2008, URL: <http://www.icsconference2008.com/cd/pdf/S13%20-%20Fiber-Free%20Space%20Optic%20-%20Vaillon.pdf>

1251) V. Cazaubiel, G. Planche, V. Chorvalli, L. Le Hors, B. Roy, E. Giraud, L. Vaillon, F. Carré, E. Decourbey, "LOLA: a 40,000 km optical link between an aircraft and a geostationary satellite," Proceedings of the 6th International Conference on Space Optics (ICSO), ESA/ESTEC, The Netherlands, June 27–30, 2006, ESA SP-621

1252) L. Aina, A. Fathimulla, H. Hier, J. Foshee, J. Arnold, "Monolithic Photoreceiver Technology For Free Space Optical Networks," Proceedings of IEEE Aerospace Conference, Big Sky, MT, March 8–15, 2003

Parameter	OPALE on ARTEMIS	PASTEL on SPOT-4
FOV	$\pm 4000 \mu\text{rad}$	$\pm 4000 \mu\text{rad}$
Isolation	better than 10^{-10}	better than 10^{-10}
Pointing accuracy	$2.3 \mu\text{rad} (3\sigma)$	$2.2 \mu\text{rad} (3\sigma)$

Table 66: Instrument and view parameters of the two optical terminals

- **LCT** (Laser Communication Terminal) is a regenerative system (homodyne BPSK) designed and developed by Tesat–Spacecom of Backnang, Germany. LCT provides either a high data rate, bidirectional communications link for binary digital data transfer between two satellites, or between one satellite and an optical ground station. ^{1253) 1254)}

- The TerraSAR–X mission of DLR and EADS Astrium GmbH (launch June 15, 2007) is flying LCT as a secondary experimental payload – this represents the on–orbit verification of the first coherent optical communication system on a satellite.

LCTSX (LCT on TerraSAR–X) FSO (Free Space Optics) communication demonstrations: – In a series of ISL (Intersatellite Link) tests that began in February 2008 (continued for several months), the LCT (Laser Communication Terminal) on TerraSAR–X as well as the one flown on the DoD **NFIRE** (Near Field Infrared Experiment, launch Apr. 24, 2007) spacecraft, have exchanged data simultaneously at rates of 5.625 Gbit/s. According to Tesat–Spacecom GmbH, it has taken < 25 seconds, on average, for the terminals to lock onto each other and begin transmissions. A key feature of the system is its ability to establish and maintain a link, even when the sun is directly behind the target spacecraft. ¹²⁵⁵⁾

Continuous free–space optical transmissions were maintained for as long as the two spacecraft were within line–of–sight position of each other (both spacecraft in LEO) amounting to about 20 minutes on an average pass. On these free–space transmissions, the measured BER (Bit Error Rate) was < 10^{-9} . Since the NFIRE spacecraft is not producing its own imagery, a closed–loop link was configured where the data from TerraSAR–X was directly re–transmitted from NFIRE to establish “duplex operations” at 5.625 Gbit/s. Further tests are planned with transmissions to ground stations in Germany and in Spain. ¹²⁵⁶⁾

- The TanDEM–X of DLR and EADS Astrium GmbH (launch June 21, 2010) is also flying the LCT instrument of Tesat–Spacecom. The objective is to demonstrate and verify the performance of a 2 Gbit/s optical LEO–to–GEO link as part of an experimental broadband data relay transmitting a 300 Mbit/s user data stream from TanDEM–X to ground.

- The AlphaSat mobile communications spacecraft in GEO (launch on July 25, 2013), on order for Inmarsat Plc. of London and referred to as Inmarsat 1–XL, uses the first next–generation European Alphabus platform and carries in addition to the commercial Inmarsat payloads four hosted TDPs (Technology Demonstration Payloads) of ESA. The LCT is

1253) Note: LCT is considered the first laser communication system in space that will operate on a **coherent** basis. In a coherent system the receiver operates by optically adding a locally generated field to the receiver field prior to photodetection. The prime objective is to use the added local field to improve the detection of the weaker received field in the presence of the receiver thermal noise. – In contrast, the SILEX concept employs a direct–detection system in which the desired information is intensity modulated onto an optical source and transmitted to the receiver terminal. In this concept, the photodetector at the receiver side provides basically the function of a power detection device.

1254) Note: Coherency in optical communication implies to add electromagnetic fields (for instance: two wavelengths) in such a fashion that the receiver obtains in effect a single field. The spatial addition of the fields (i.e., the receiving light and the light of the local oscillator in the receiver) require an identical frequency as well as a fixed phase shift. In the end, the modulation difference is practically all that is left; or in other words, the intermediate frequency is equal to zero.

1255) P. B. de Selding, “US–German Laser Intersatellite Link Performs Well on 2 Spacecraft,” Space News, March 17, 2008, pp. 1+4

1256) M. Gregory, F. Heine, H. Kämpfner, R. Meyer, R. Fields, C. Lunde, “Tesat Laser Communication Terminal Performance results on 5.6 Gbit Coherent Inter Satellite and Satellite to Ground Links,” ICSO 2010 (International Conference on Space Optics), Rhodes Island, Greece, Oct. 4–8, 2010, URL: http://congrex.nl/ICSO/Papers/Session%208a/FCXNL-10A02-2012697-1-GREGORY_ICSO_PAPER.pdf

one of the TDPs, representing a further development of already existing flight hardware on TerraSAR–X and NFIRE, to provide the capability of high data rate transmissions.

– The Copernicus (GMES) Sentinel–1A and Sentinel–2A missions of ESA (planned launches in 2014) carry the LCT instrument of Tesat–Spacecom – providing an optical LEO–GEO communications link to EDRS–1 (in parallel to the RF communications).

– The EDRS (European Data Relay Satellite) constellation of ESA (planned launch of EDRS–A in 2014, EDRS–A is a hosted payload on EutelSat–9B) will fly the LCT instrument of Tesat–Spacecom. EDRS–C is a dedicated satellite on the SmallGEO platform of OHB with a launch in 2015.

With constantly increasing communication rates, optical systems (ISLs) are also being considered for small satellites. Apart from governmental/institutional research in the area, a significant driver for the development of advanced TT&C systems is the prospect of commercial LEO communication systems, such as the Teledesic/Celestri constellations which include laser communication intersatellite crosslinks (ISLs) as part of their baseline design. Note: The planned Teledesic constellation, with up to 840 satellites to provide “Internet in the Sky”, was never realized.¹²⁵⁷⁾

- Optical links have high throughput, transparent, bidirectional links with 5.6 Gbit/s for LEO–LEO transmissions and 1.8 Gbit/s for LEO –GEO
- Capacity is good for next generation systems, and expandable
- Beam diameter is ~ 10 m at 1000 km distance
- Eve must be on board of S/C for eavesdropping
- Beacon–less acquisition saves SWAP
- Localization of COT is unlikely for others
- First demonstration of B–L acquisition in worst case (LEO – LEO) scenario
- Spatial acquisition < 10 s, frequency acquisition < 5 s
- 1 W of Tx power for LEO–LEO, 5 W for LEO–GEO transmissions
- Recurring design limits cost and schedule risks

Table 67: Some performance facts of the Tesat LCT (Laser Communication Terminal)

¹²⁵⁷⁾ M. Enoch, S. Herrin, et al., “Optical Tracking Telemetry and Commanding (TT&C) for Small Satellites,” Proceedings of the 13th AIAA/USU Conference on Small Satellites, Aug. 23–26, 1999, Logan, Utah, SSC99–IIb–4

Mission	Launch
SILEX: Europe / Japan, 45,000 km, 2 Mbit/s / 50 Mbit/s, 800 nm	
ARTEMIS (GEO, ESA)	July 12, 2001
SPOT-4 (LEO, CNES)	March 24, 1998
OICETS (LEO, JAXA)	August 23, 2005
LOLA Aircraft to/from GEO S/C (DGA / France)	Dec. 2006
Tesat-Spacecom, Germany - 45,000 km at ~ 2 Gbit/s, 1064 nm	
NFIRE (LEO, MDA / USA)	April 24, 2007
TerraSAR-X (LEO, DLR / Germany)	June 15, 2007
LEO-LEO ISL demonstrated 5.6 Gbit/s over ~ 5000 km, Feb. 2008 between TerraSAR-X & NFIRE	
TanDEM-X (LEO, DLR)	June 21, 2010
AlphaSat (GEO, ESA)	July 25, 2013
Copernicus (GMES) Sentinel-1A (LEO, ESA)	April 03, 2014
SOCRATES microsatellite of NICT, Japan, SOTA	2014
Copernicus (GMES) Sentinel-2A (LEO, ESA)	2014
EDRS (European Data Relay Satellite) System	EDRS-A in 2014 (GEO, ESA)
BIROS microsatellite of DLR, OSIRIS	2015

Table 68: Overview of near-Earth space Lasercom systems in use and planned

Direct optical satellite downlinks for Earth observation telemetry data have been tested with experimental and prototype systems (NICT tested first LUCE downlinks from OICETS of JAXA in 2006 to optical ground stations in Tokyo). This technology has the potential of boosting downlink throughput by several orders of magnitude compared to current RF-links by increasing the data rate of the downlink signal to multi-Gbit/s. At the same time, power consumption and mass and volume of the optical transmit terminal on board the satellite can be dimensioned very beneficially. This is done by making use of the asymmetric link scenario, where a larger ground receive telescope of the OGS (Optical Ground Station) can make up a large fraction of the link budget, allowing small and lightweight transmit telescopes on the satellite side.

OGSL (Optical Satellite-to-Ground Link) is a high-directivity point-to-point link technology and bears characteristics which are completely different from those known from the RF channel:

- Atmospheric attenuation of laser signals increases at low elevations, causing a high overall link dynamic of mean received power
- Link-blockage by clouds has to be regarded:
 - long-term (complete blockage of an OGS by cloud cover during an over-flight)
 - short-term (transitional blocking by small clouds during one downlink).
- Scintillation of Rx-power: in contrast to RF-links, optical downlinks feature very small scale amplitude scintillation patterns (cm to dm size) caused by atmospheric IRT (Index-of-Refractive Turbulence). This leads to fast fades and surges (in the range of ms) of the received optical power of typical up to ± 6 dB in the downlink and more in the uplink
- With the extremely narrow optical beam, residual pointing errors from the space terminal can cause an additional source of fading
- Depending on the modulation format and the applied receiver technology, further impacts onto the signal stability due to IRT have to be regarded.

Table 69: OSGL (Optical Satellite-to-Ground Links) ¹²⁵⁸⁾

- **LLCD (Lunar Laser Communications Demonstration):** The NASA minisatellite mission LADEE (Lunar Atmosphere and Dust Environment Explorer) was launched on Sept. 7, 2013. It carries LLCD with the objective to demonstrate and validate duplex optical communications from a lunar orbiting spacecraft to an Earth-based ground receiver. The requirements call for data rates of up to 620 Mbit/s in downlink and up to 20 Mbit/s in uplink. In addition, two-way time-of-flight measurements are needed with the potential to perform ranging with sub-centimeter accuracy. ¹²⁵⁹⁾

This represents a first step to introduce optical communications into deep space missions. NASA has identified optical communications as an important technology for the future of deep space communications. The LLCD technology demonstration on LADEE is intended to be a first step toward developing an operational optical communications capability for future manned and robotic missions.

– On Oct. 18, 2013, the LLCD transmitted data lunar orbit to Earth at a record-breaking download rate of 622 Mbit/s. It also has demonstrated an error-free data upload rate of 20 Mbit/s transmitted from the primary ground station in New Mexico to the spacecraft currently orbiting the moon. ¹²⁶⁰⁾

- Starting in the timeframe 2012, Tesat Spacecom is planning to introduce the LCT (Laser Communication Terminal) concept of FSO (Free-Space Optics) communications from **spaceborne systems to airborne platforms**. A near future demand for increased bandwidth to ground communication is anticipated for UAVs (Unmanned Aerial Vehicles), exceeding currently installed RF communication capabilities. A high bandwidth optical link between an above-the-weather UAV and a GEO spacecraft offers a secure, jamming resistant, non-ITU regulated alternative to RF links. ¹²⁶¹⁾

While the spaceborne LCT has already reached the highest Technical Readiness Level TRL 9, the airborne remote station for aeronautical applications will have to be developed. The design of the airborne LCT will significantly differ from the design of the spaceborne LCT. The development goal is a PnP (Plug and Play) airborne LCT. For this purpose, the previous TerraSAR-X and NFIRE verification program is extended by the realization of coherent optical links from space to a DLR research airborne platform Falcon 20-E. Hence, an OGS (Optical Ground System) is integrated into the Falcon aircraft and operated at altitudes of ~ 11 km. The experimental program for the verification of SAL (Space-to-Aircraft Links) will be completed in early 2013. AlphaSat was launched on July 25, 2013 into GEO and consequently, a GEO-LCT testbed will exist. And with EDRS (European Data Relay System) services starting in 2014 (equipped with GEO-LCT), a space infrastructure will exist in the near future to bridge the communication chain UAS-to-ground. The LCT Space-to-Aircraft Link R&D project is commissioned by the German Space Agency (DLR).

1258) Dirk Giggenbach, Florian Moll, Christian Fuchs, Tomaso de Cola, Ramon Mata-Calvo, "Space Communications Protocols for Future Optical Satellite-Downlinks," Proceedings of IAC 2011 (62nd International Astronautical Congress), Cape Town, South Africa, Oct. 3-7, 2011, paper: IAC-11.B2.2.8

1259) Bryan S. Robinson, Don M. Boroson, Dennis A. Burianek, Daniel V. Murphy, "Overview of the lunar laser communications demonstration," Proceedings of SPIE, Vol. 7993, "Free-Space Laser Communication Technologies XXIII," San Francisco, CA, USA, Jan. 26, 2011, doi:10.1117/12.878313

1260) Joshua Buck, Dewayne Washington, "NASA Laser Communication System Sets Record with Data Transmissions to and from Moon," NASA, Release 13-309, Oct. 22, 2013, URL: <http://www.nasa.gov/press/2013/october/nasa-laser-communication-system-sets-record-with-data-transmissions-to-and-from/#.UmdTWFOzLWI>

1261) Wolfgang Griethe, Frank Heine, Stefan Seel, Thomas Alberty, "Optical Communication for Coping the UAS Data Deluge," Proceedings of the DASIA (DATA Systems In Aerospace) 2012 Conference, Dubrovnic, Croatia, May 14-16, 2012

1.9.5 Internet access for future spacecraft LAN services

The Internet embodies a key underlying technical idea, namely that of **open architecture networking**. It provides a good example of a scalable, robust, efficient, and adaptive network architecture that could support future orbiting sensor webs.^{1262) 1263) 1264)} The use of Internet Protocols in the space segment (i.e. for onboard LAN use as well as for data transmission services) is attractive because it provides for easy interconnection with the terrestrial Internet. IP (Internet Protocol) enables advanced mission concepts (e.g., collaborative science) and allows better alignment with industry standards and products (end-to-end network solutions). IP supports a simpler, yet more capable, overall mission design and enables a simpler operations solution. The SBI (Space-Based Internet), also referred to as **NGSI** (Next Generation Space Internet), is a satellite network system in which each satellite is capable of originating traffic, terminating traffic, and switching traffic traveling between other satellites and the ground.

At the start of the 21st century, developments in the TCP/IP protocol to handle mobility of Internet hosts for mobile data communications (proposed standards), are being carried out under the auspices of the IETF (Internet Engineering Task Force). IETF has designed the so-called **MIP (Mobile Internet Protocol) architecture** to support mobility on the Internet. The MIP concept features a routing protocol that allows hosts (and networks) to seamlessly "roam" among various IP subnetworks (an essential in wireless networks). The basic idea of the MIP concept is a multi-technology architecture mainly independent of the underlying physical layers, where all functions, either related with end-to-end communications or with internal network management and control, are performed at the IP level. Some examples of emerging MIP services and applications are:¹²⁶⁵⁾

- MIP does not have any restrictions related to geographical regions or service providers
- MIP works in conjunction with the standard IP protocol, maintaining transparency with the higher layer protocols
- MIP is not tied to any specific access technology. It can work with wireline and wireless technologies.
- The IP protocol allows the use of MDP (Multicast Dissemination Protocol), which only requires a one-way link. This is an advantage in the event of a temporary receiver failure on a satellite, because the satellite will be able to send data to the ground station without being commanded.
- Using IP also allows secure communications via applications like SSH (Secure Shell), SCP (Secure Copy), and NTP (Network Time Protocol) techniques.
- At the transport layer, TCP (Transmission Control Protocol) or UDP (User Datagram Protocol) may be used to package the application layer data. This package communication contains the data and the necessary error protection sections to ensure a safe data transmission within the overall network.
- MIP (Mobile IP) is a mechanism for maintaining transparent network connectivity to mobile hosts. The MIP protocol enables a mobile host to be addressed by the IP address it uses in its home network (home IP address), regardless of the network to which it is current-

1262) G. Minden, J. Evans, S. Baliga, S. Rallapalli, L. Searl, "Routing in Space Based Internets," Earth Science Technology Conference, Pasadena, CA, June 11–13, 2002

1263) J. Noles, K. Scott, M.–J. Zukoski, H. Weiss, "Next-Generation Space Internet: Standardization and Implementation," Proceedings of ESTC (Earth Science Technology Conference), College Park, MD, June 24–26, 2003

1264) Note: The sensor web concept refers to a group of sensors (distributed), whether spaceborne, ground-based or airborne which act in a collaborative autonomous manner to produce more value than would otherwise result from the individual observations.

1265) Note: IETF is a large open international community of network designers, operators, vendors, and researchers concerned with the evolution of the Internet architecture and the smooth operation of the Internet. The first meeting of IETF was held in January 1986 in San Diego, CA.

ly physically attached. Therefore, ongoing network connections to a mobile host can be maintained even as the mobile host is moving from one subnet to the other.

Some background on Internet: The first proposal for a “global hypertext system” based on TCP/IP, was made at CERN (European Organization for Nuclear Research, Geneva, Switzerland) by Tim Berners–Lee in 1989, and further refined by him and Robert Cailliau in 1990. At the time, the science community world was yearning for interconnection services in the midst of proprietary and incompatible networks by various computer companies. By the end of 1989, prototype software for a basic system was already being demonstrated at CERN. The early Internet included a WWW browser that could be run on any system. ¹²⁶⁶⁾

At the beginning of 1993 there were about 50 known information servers. An International World–Wide Web Consortium, “W3C”, was set up in Oct. 1994 comprising a body of institutes and companies from all over the world. The W3C is run jointly by INRIA, the Institut National pour la Recherche en Informatique et en Automatique (for Europe), MIT, the Massachusetts Institute of Technology (for the USA) and Keio University (for Asia). Today, the overall architecture of the Web consists of three levels: the physical connections (the cables or infrastructure), the common behavior (the Internet, i.e., the communication protocols) and the services provided (electronic mail, file transfer, remote log–in, bulletin boards, information access, directory services, and multimedia streaming). Tomorrows Internet will include the services of multicast and telephony.

Basic Internet ideas (of a connected set of networks, specifically those using TCP/IP) were already realized with the packet–switching ARPANET, BITnet, NSFNET, etc., developed in the 1970s and 1980s on a regional scale (first node of ARPANET in 1969 at UCLA; by 1983 every machine connected to ARPANET had to use TCP/IP). In 1990, the ARPANET simply grew into the Internet. – The development of capable browsers and the provision of Internet servers by many organizations throughout the world made the newly created Internet rather useful and successful to an ever increasing user community. By the end of 1994, the Web had 10,000 servers, 2,000 of which were commercial, and 10 million users. In 1997, there were more than 650,000 servers registered in Internet (1000 new ones added every day) – making Internet with its communication services a truly global utility. Most Internet traffic of today is carried by backbone networks of independent ISPs (Internet Service Providers), including MCI, AT&T, Sprint, UUnet, BBN planet, and many more.

- The first Internet broadcasts appear to have started in 1993 when the IMS (Internet Multicasting Service) was set up in Washington, D.C., as a non–profit experiment.. At the start of the 21st century, literally thousands of radio broadcasting stations are on the Internet, broadcasting from all over the world. In all of these services, the satellite functions only as a reflector for point–to–point or point–to–multipoint. transmissions (various topologies for interconnecting segments of a network). However, this is different from a satellite onboard LAN providing communication services to its payload.

- The STRV–1b (Space Technology Research Vehicle–1b) of DERA (UK) with a launch on June 17, 1994: its sensor complement featured an experiment called SCPS (Space Communications Protocol Standards), provided by the USAF, NASA/JPL, MoD, and DERA. In 1996, a new software was uploaded to STRV–1b with the assistance of an operating system (kernel), developed by the Mitre Corporation to provide the interface to the onboard computer, taking up 120 kByte of the available RAM.

The SCPS software ¹²⁶⁷⁾ runs as an application on the SCPS workstation. It receives instructions from the Internet and forwards them, using the SCPS protocols, to a telecommand workstation which transmits them as STRV CCSDS packets to the spacecraft. Software in the spacecraft monitors the received instructions and provides performance feedback

1266) <http://public.web.cern.ch/Public/ACHIEVEMENTS/WEB/history.html>

1267) R. Blott, N. Wells, “ The Space Technology Research Vehicles: STRV–1A,B,C&D,” Proceedings of the AIAA/USU Conference on Small Satellites, Sept. 16–19, 1996, Logan, UT, http://klabs.org/DEI/References/avionics/small_sat_conference/1996/strv.pdf

through the telemetry downlink. As a part of this experiment, STRV-1b was given by NASA/JPL its own Internet Protocol (IP) address. In 1996, this represents in fact the first spacecraft to do so, and to demonstrate that instructions could be sent by Internet from remote sites to an operational spacecraft.

- Demonstrations of the TCP/IP (Transmission Control Protocol/Internet Protocol) suite occurred through space (ground-to-space-to-ground)¹²⁶⁸ utilizing mostly bent-pipe configurations on GEO satellites such as ACTS (Nov. 1997), TDRS relay service [installed on TDRS-1 in Dec. 1997 to give the US South Pole Station an Internet connection to White Sands, NM (two-way IP and one-way file transfer)], and commercial platforms (for future multimedia broadband services). – In wireless channels, packet losses can occur due to transmission errors. TCP interprets these losses as congestion and initiates its congestion control algorithms (slow start, congestion avoidance), resulting in a performance degradation.
- The routing of commercial Internet service links (so-called bend-pipe systems) via GEO satellite transponder started with the availability of wideband ATM (Asynchronous Transfer Protocol) services in the time frame 1997–1998. One to the commercial Internet access providers is Hughes Network Systems of Hughes Electronics Corp. In 1997, Hughes started offering such services as DirectPC and DirecTV to its customers (requiring the installation of VSATs). Its Spaceway project is a next-generation Ka-band satellite system with service introduction in 2004. SPACEWAY employs high-performance, onboard digital processing, packet switching and spot-beam technology to offer single-hop broadband connectivity, regardless of location. The Spaceway mesh architecture permits customers to communicate directly via satellite, without connecting through a central retransmission service or hub.

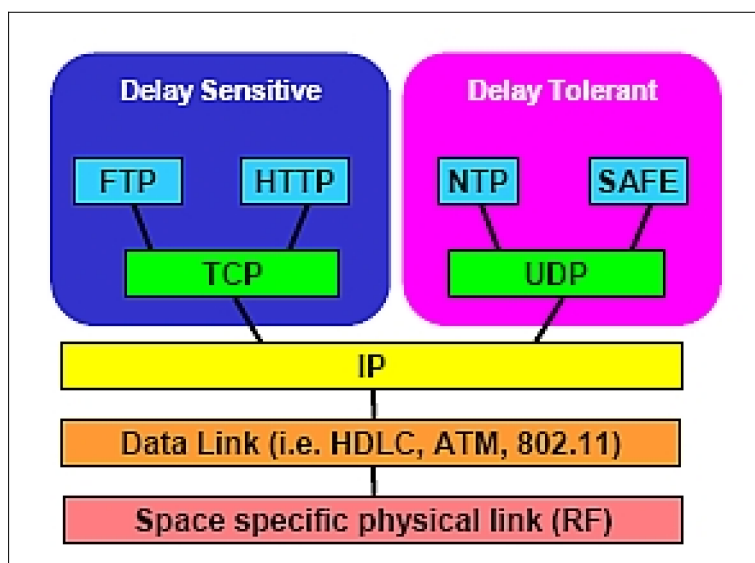


Figure 68: IP protocol based on OSI model

- A demonstration of Internet access to flying LEO spacecraft was performed by SSTL (Surrey Satellite Technology Ltd) using its UoSAT-12 (launch April 21, 1999)¹²⁶⁹¹²⁷⁰ minisatellite. The demonstrations consisted of uploading an IP (Internet Protocol) software stack to the UoSAT-12, including simple modifications to the SSTL ground station, and a series of tests to measure the performance of various Internet applications (Uo-

1268) A. Anzaloni, M. Listanti, A. F. C. Ferreira, A. Durante, "TCP Performance over Satellite Networks," Proceedings of IEEE Aerospace Conference, Big Sky, MT, March 8–15, 2003

1269) J. Rash, R. Parise, K. Hogie, E. Criscuolo, J. Langston, C. Jackson, H. Price, "Internet Access to Spacecraft," Proceedings of the 14th AIAA/USU Conference on Small Satellites, Logan UT, Aug. 21–24, 2000, SSC00-IX-4

1270) <http://ipinspace.gsfc.nasa.gov/general/>

SAT-12 was assigned an IP address). The UoSAT-12 S/C was reconfigured on-orbit. The initial tests included basic network connectivity (PING), automated clock synchronization with NTP (Network Time Protocol), and FTP (File Transfer Protocol) transfers.

- The UoSAT-12 (SSTL) Internet demonstration was carried out in the time frame April–June 2000 within the OMNI (Operating Missions as Nodes on the Internet) project of NASA/GSFC. The UoSAT-12 spacecraft was selected because of its ability to support the HDLC (High-Level Data Link Control) framing in hardware for link-level protocol on space-to-ground links. This allowed simple and straightforward interfacing with existing commercial routers. UoSAT-12 was an ideal test platform because it already used HDLC framing for its AX.25 (Amateur radio X.25) protocol. – Follow-on work is to demonstrate the following functions and additional protocols: http file delivery, mobile IP, security, store-and-forward commanding, data delivery using SMTP (Simple Mail Transfer Protocol), and VPN (Virtual Private Network) to enable automated, operational S/C communication. The use of IP communications over a satellite link is also referred to as “**IP in Space.**” On January 25, 2001, **the UoSAT-12 spacecraft became the world’s first web server in space** (HTTP was used to transfer real-time telemetry and stored image data directly to the user). The demonstration was carried out by the OMNI Lab of NASA/GSFC. ¹²⁷¹⁾

- The DMC (Disaster Monitoring Constellation) microsattellites, built by SSTL, are using IP-based protocols for all routine operations, as pioneered on UoSAT-12. The payload downlink also implements the new CCSDS File Delivery Protocol over IP on the 8 Mbit/s payload downlink. AlSat-1 (Algeria Satellite-1) was launched Nov. 28, 2002 (Cosmos-3M launch vehicle from Plesetsk, Russia). ^{1272) 1273)} – A further DMC launch from Plesetsk took place Sept. 27, 2003, consisting of BilSat-1 (Turkey), NigeriaSat-1 and UK-DMC. The UK-DMC spacecraft flies a COTS internet router referred to as **CLEO** (Cisco router in Low Earth Orbit), provided by Cisco Systems Inc., as a test bed for a range of mobile Internet Protocol (IP) applications.

CLEO was configured for IPv6 (Internet Protocol version 6) and IPsec (Internet Protocol security) use in March 2007, and successfully tested with both features on 29 March 2007. IPv6 is intended to eventually replace IPv4 terrestrially, as the larger address space and simpler routing tables of IPv6 ameliorate the most pressing problems with the scalability of IPv4, namely: ¹²⁷⁴⁾

- Exhaustion of availability of unused address space, requiring workarounds such as Network Address Translation (NAT) that become unneeded in IPv6
- Size of backbone routing tables needed to keep the Internet fully interconnected.

In 2007, the successful demonstration of CLEO has now led to follow-on work taking the concept further, with the announcement of the **IRIS** (Internet Routing in Space) project to place a router as a payload on a geostationary Intelsat satellite. This router will interconnect C- and Ku-band transponders, allowing communication between different frequencies without having to switch between them on the ground, and this use of onboard switching can later lead to the use of onboard routing functionality with intersatellite links.

- **IRIS – NGGS** (Internet Routing in Space – Next Generation Global Services) is a spaceborne architecture utilizing the first IP based routing node in geostationary orbit

1271) J. Rash, R. Parise, K. Hogie, E. Criscuolo, J. Langston, “Internet Technology on Spacecraft,” Proceedings of the AIAA Space Conference and Exhibition, Long Beach, CA, Sept. 19–21, 2000

1272) J. Cooksley, A. da Silva Curiel, P. Stephens, L. Boland, S. Jason, W. Sun, M. Sweeting, “AlSat-1 First Year in Orbit,” Proceedings of AIAA/USU Conference on Small Satellites, Logan, UT, Aug. 11–14, 2003

1273) L. Wood, A. da Silva Curiel, W. Ivancic, D. Hodgson, D. Shell, C. Jackson, D. H. Stewart, “Operating a terrestrial Internet router onboard and alongside a small satellite,” Proceedings of the 56 IAC 2005, Fukuoda, Japan, Oct. 17–21, 2005, IAC-05–B5.3./B5.5.03

1274) L. Wood, W. Ivancic, D. Stewart, J. Northam, C. Jackson, A. da Silva Curiel, “IPv6 and IPsec on a satellite in space,” 58th IAC (International Astronautical Congress), International Space Expo, Hyderabad, India, Sept. 24–28, 2007, IAC-07–B2.6.06

(GEO) and associated ground-based terminals and network operations center. The IRIS NGGS payload is commercially hosted on the Intelsat-14 (IS-14) GEO satellite (launch Nov. 23, 2009). IRIS-NGGS has been developed as a Joint Capability Technology Demonstration (JCTD) for the US Department of Defense (DoD) by Cisco Systems.

IRIS-NGGS introduces an advanced QoS (Quality of Service) architecture¹²⁷⁵⁾ ¹²⁷⁶⁾ in support of providing a SLA (Service Level Agreement) based managed service, through use of the first Internet Routing IPR (In-space Payload Router) at GEO, based on the Cisco IOS (Internet Operating System) and a PSIM (Programmable Satellite IP Modem) based around ViaSat's Linkway design. The multi-frequency TDMA, sophisticated BoD (Broadcast on Demand) and IP-based per terminal virtual circuits (ground terminal to payload) with QoS on both the uplinks and downlinks provides an architecture for converged voice, video and data applications. The GEO location of IS-14 is at 45° W, the spacecraft payload consists of 40 C-band and 22 Ku-band transponders + IRIS.¹²⁷⁷⁾

*Satellite architectures for providing IP services are evolving from transponded satellites to sophisticated on-board regenerative systems. IRIS-NGGS will be the **first on-board regenerative system** to demodulate, decode and extract to the IP packet level, thus providing for more sophisticated routing and QoS architectures.*

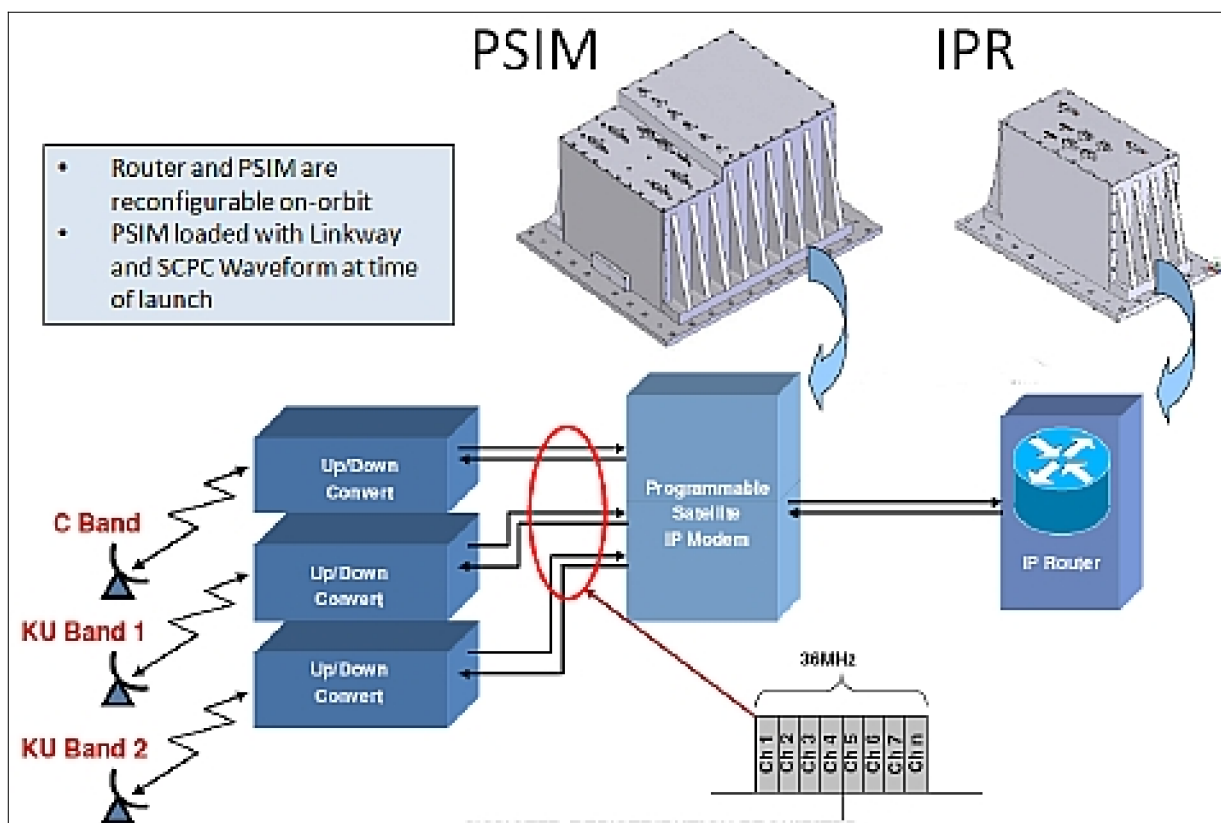


Figure 69: Illustration of the IRIS satellite payload devices (image credit: Cisco Systems)

1275) Julie Ann Connary, Paul Donner, Joe Johnson, Jeff Thompson, "Internet Routing in Space: Architectures for Quality of Service," Proceedings of the 2009 IEEE Aerospace Conference, Big Sky, MT, USA, March 7-14, 2009

1276) "Hosted Payload - IRIS," Intelsat, URL: <http://www.intelsatgeneral.com/services/hp/iris.aspx>

1277) Joe D. Johnson, Julie Ann Connary, Jeff Thompson, Paul Donner, "Internet Routing in Space NMS Architecture," Proceedings of the 2009 IEEE Aerospace Conference, Big Sky, MT, USA, March 7-14, 2009

The IRIS internet router functionality test was completed by Cisco Systems in late December 2009 – followed by a three–month utility demonstration for the DoD. Cisco plans to use the IRIS technology also in the commercial market. ^{1278) 1279)}

- The Rubin–2 microsatellite of OHB–System, Bremen (launch Dec. 20, 2002) uses the commercial Orbcomm constellation of 30 LEO satellites for a demonstration of near real–time spacecraft monitoring and control functions via the Internet (demonstration mission). The performance tests of message delivery show that 90% of the messages, whose length is at most 229 bytes, reach the user within 10 minutes, and 30% within 1 minute.
- The CHIPSat microsatellite of UCB (University of California, Berkeley; launch Jan. 13, 2003 from VAFB), within NASA’s UNEX (University–class Explorer) program, employs **the TCP/IP and UDP/IP (User Datagram Protocol/Internet Protocol) protocol suite to communicate all data between the S/C and the ground user directly** (see N.8). The interface between the S/C and the ground segment consists of an HDLC point–to–point link layer. Layered within the HDLC frames is a standard TCP/UDP/IP protocol stack that, combined with VPN (Virtual Private Network) and firewall–protected use of the commercial Internet, utilizes end–to–end TCP/IP–based connectivity up to each S/C subsystem and down to the ground station router and the ground segment centers. ¹²⁸⁰⁾
- The commercial satellite e–Bird™ of Eutelsat (launch Sept. 27, 2003, located at 33° E, GEO, servicing Europe and the Middle East, 10 year design life) is the first satellite worldwide specifically designed for 2–way broadband communications dedicated to Internet applications. Built by BSS, e–Bird is spin–stabilized (376 platform), it carries 20 active Ku–band transponders, each powered by a 33 W TWTA (Traveling Wave Tube Amplifier).
- As of 2003, EMS Technologies Ltd. of Canada developed SpaceMux™, an onboard processor architecture specifically designed for Internet services (support of single hop interconnectivity between small low–cost terminals). The onboard processing approach (mesh network configuration) of SpaceMux achieves the following advantages compared to a star configuration which would require a double hop: 1) minimizes the latency by reducing the roundtrip delay in half; 2) halves the capacity utilized; and, 3) provides signal regeneration, additional coding gain and switching. SpaceMux will be flown as a demonstration payload of Anik–F2, a GEO commercial service satellite (on a BSS 702 platform, 38 Ka–band transponders, 32 Ku–band transponders and 24 C–band transponders) of Telesat Canada (launch July 18, 2004). Provision of single hop interconnectivity between user terminals and regeneration and format conversion from the DVB–RCS MF–TDMA (Multifrequency–Time Division Multiple Access) uplink to the DVB–S downlink.
- Internet hardware on spacecraft (next generation communication architecture for a “Space Internet”). As of 2001, a NASA/GRC project objective is to develop prototype network hardware in cooperation with industry partners (Cisco, Ball Aerospace, etc.) enabling the use of the TCP/IP protocol for satellite onboard communication services to/from its payload. The four main element requirements of the Space Internet architecture are: ^{1281) 1282)}

1) Security (access control, authentication, and encryption). Under joint DoD/NASA sponsorship, a set of Internet protocols were specified for use in bandwidth–constrained

1278) Laurence Cruz, “Cisco Puts an Internet Router in Space,” January 19, 2010, URL: http://newsroom.cisco.com/dlls/2010/ts_011910.html?POSITION=LINK&COUNTRY_SITE=us&CAMPAIGN=NewsAtCiscoLatestNewsfromCDCHP&CREATIVE=LINK1&REFERRING_SITE=CISCO.COMHOMEPAGE

1279) “Cisco Completes Test of Orbiting Internet Router,” Space News, Jan. 18, 2010, p. 9

1280) E. Taylor, M. Hurwitz, W. Marchant, M. Sholl, S. Dawson, J. Janicik, J. Wolff, “CHIPS: A NASA University Explorer Astronomy Mission,” Proceedings of the AIAA/USU Conference on Small Satellites, Logan, UT, Aug. 11–14, 2003, SSC03–V–3

1281) J. Noles, K. Scott, M–J. Jo Zukoski, H. Weiss, “Next–Generation Space Internet: Prototype Implementation,” Earth Science Technology Conference, Pasadena, CA, June 11–13, 2002

1282) R. A. Slywczak, “Conceptual Design of an IP–based Satellite Bus Using Internet Technologies,” Proceedings of the AIAA/USU Conference on Small Satellites, Logan, UT, Aug. 11–14, 2003, SSC03–X–5

environments. This work, known collectively as SCPS (Space Communications Protocol Suite) includes a Security Protocol, known as SCPS–SP. SCPS–SP provides the same security services as its Internet counterpart, IPSec (IP Security), but with significantly less overhead.

2) A Mobile IP (Internet Protocol) implementation that takes advantage of scheduled contacts to reduce the overhead involved in setting up Mobile IP tunnels. An orbiting S/C, connecting first to one ground station and then to another, fits the definition of a “mobile agent.”

3) Resource reservation mechanisms that allow applications to ensure that data are not lost and/or are delivered in a timely manner (subsequent retransmission is of great concern). This is particularly difficult in the case where multiple semi–autonomous spacecraft need to share communications resources in a controlled manner and in an automated fashion. The RSVP (Resource Reservation Protocol), an end–to–end protocol for resource reservation used in Internet, can prevent data loss.

4) A link–layer driver that allows to easily connect ground and space networks. Conventional CCSDS links transport relatively statically scheduled streams of CCSDS data units encapsulated in virtual channels that may be transferred over several physical links to a control or processing center. In an internetworking environment, however, the virtual channels will transport dynamically changing streams of Internet Protocol packets that are extracted and routed at each spacecraft in a network before being routed to the ground. An efficient driver (for packing, transporting, and extracting IP packets for each space link) implements the CCSDS protocol suite.

The onboard LAN hardware includes a switch and a NIC (Network Interface Card).¹²⁸³⁾ Future plans include utilizing these components as building blocks for a space–based router. The idea behind SND (Space Network Devices) is to take concepts and technologies developed for the Internet and use them to communicate onboard a spacecraft. This technology is considered a first step in transitioning to a space communications paradigm where seamless interoperability is possible using TCP/IP onboard a spacecraft, between a spacecraft and the ground, and from spacecraft to spacecraft.

- **CANDOS** (Communications and Network Demonstrations on Shuttle) is a NASA Hitchhiker payload (one of six payloads called FREESTAR, namely: MEIDEX, SOLSE–2, CVX–2, SOLCON–3, SEM–14, and CANDOS), flown on Shuttle flight STS–107 (Jan. 16– Feb. 1 2003) which ended tragically on its reentry. The CANDOS experiment consisted of the **LPT** (Low Power Transceiver), three S–band antennas, and one L–band antenna; the end–to–end data flow architecture is based entirely on standard IP protocols and HDLC data framing.^{1284) 1285) 1286) 1287)} All data routing was accomplished via IP source/destination addresses over NASA’s existing closed IONet, an operational IP network which is physically isolated from the open Internet. – The LPT (developed by ITT Industries, is a multi–channel, software programmable transceiver, capable of transmitting and receiving SN mode (Space Network) or GN mode (Ground Network) S–band signals while simultaneously receiving L–band GPS signals. The objective was to test ground networking techniques in cooperation with CANDOS. Demonstration of autonomous net-

1283) G. Minden, J. Evans, S. Baliga, S. Rallapalli, L. Searl, “Routing in Space Based Internets,” Earth Science Technology Conference, Pasadena, CA, June 11–13, 2002

1284) D. J. Israel, “CANDOS IP Mission Support Demonstration,” Proceedings of RCSGSO (Reducing the Cost of Spacecraft Ground Systems Operations), Pasadena, CA, July 8–11, 2003, <http://descanso.jpl.nasa.gov/RCSGSO/Proceedings/Paper/A0037Paper.pdf>

1285) D. Israel, K. Hogie, R. Parise, E. Criscuolo, “Space Communications Demonstration Using Internet Technology,” ITC/USA (International Telemetering Conference) 2002, San Diego CA, October 21–24, 2002

1286) <http://ipinspace.gsfc.nasa.gov/CANDOS/>

1287) Scott Pace, Marc Harlacher, Lin Haas, “Test Results From The Communications And Navigation Demonstration On Shuttle (CANDOS) Experiment,” International Symposium on GPS/GNSS in Tokyo, Japan, Nov. 15–18, 2003, URL: <http://www.aes.itt.com/docs/tech%20publication%207.pdf>

work scheduling, prioritization, handoffs, and resource allocation management (including link optimization through autonomous spacecraft acquisition and antenna pointing) using the MDP (Multicast Dissemination Protocol).¹²⁸⁸⁾

The LPT of CANDOS was used to directly contact either ground stations or TDRS, independent of the Shuttle communications system. During all events, payload (LPT) telemetry was being transmitted in UDP (User Datagram Protocol) packets continuously, providing a real-time housekeeping data stream. The use of MIP (Mobile IP) aided the use of the TCP/IP protocols; it reconfigured the data paths between the control center and the payload automatically as the link switched between ground stations (allowing the LPT address to remain static). The CANDOS flight represented the first practical demonstration of the MIP technique. All experiments were a complete success, throughout the course of the mission, CANDOS had almost 60 hours of total contact time via its own communication system. The CANDOS operation on STS-107 represents the second web server implementation in space (the first web server demonstration was being conducted on UoSAT-12 of SSTL on Jan. 25, 2001 – HTTP was used to transfer real-time telemetry and stored instrument data directly from UoSAT-12 to an end user).

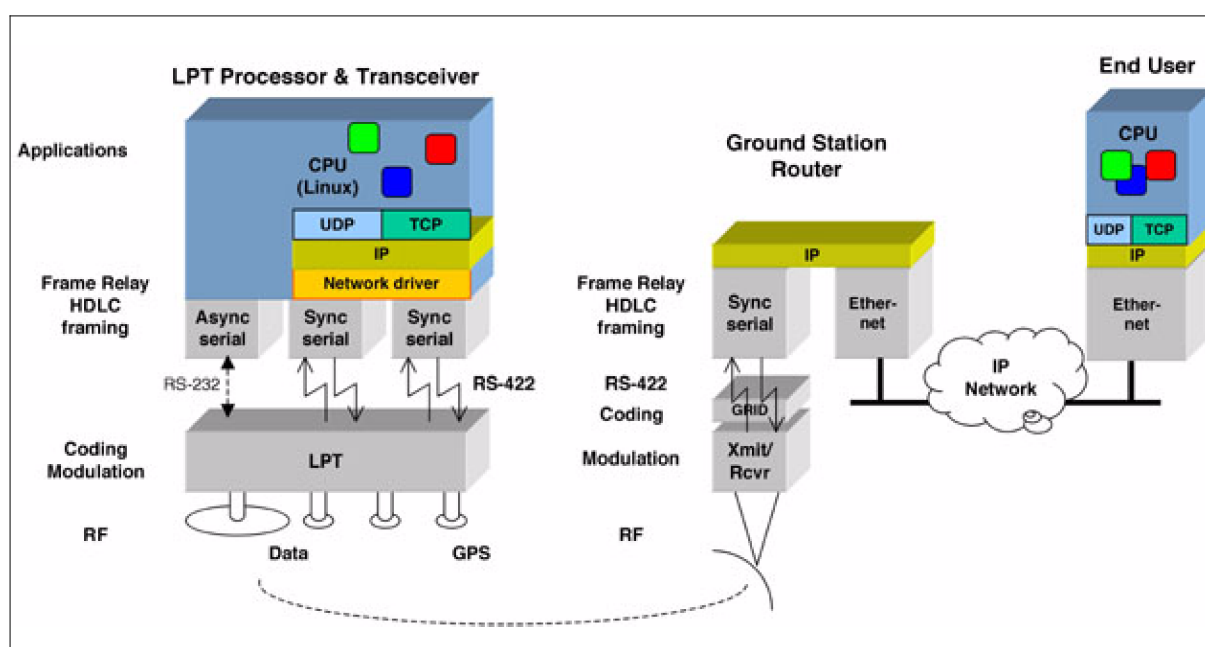


Figure 70: Overview of the CANDOS architecture (image credit: NASA)

- The OMNI (Operating Missions as Nodes on the Internet) project of NASA/GSFC conducted a testbed demonstration of the IP mission concept in the lab in 2003.¹²⁸⁹⁾ The representative mission employed unmodified off-the-shelf Internet protocols and technologies for end-to-end communications between the spacecraft/instruments and the ground system/users. The elements used in the test consisted of: Triana mission flight software, a web-enabled camera (as onboard instrument) connected to the S/C computer via an Ethernet LAN, the HDLC link layer, UDP/TCP transport layer protocols, and MDP file delivery protocol. This activity demonstrated end-to-end satellite data flow concepts in a realistic space and ground system hardware/software environment.
- The requirements of the GPM (Global Precipitation Mission) constellation of NASA and JAXA (launch Feb. 27, 2014) call for the full use of an IP implementation. The GPM

1288) Dave Israel, Ron Parise, Keith Hogue, Ed Criscuolo, "Demonstration of Internet Technologies for Space Communication," 2002, URL: <http://www.aiaa.org/spaceops2002archive/papers/SpaceOps02-P-T5-18.pdf>

1289) J. Rash, A. B. Ferrer, N. Goodman, Samira Ghazi-Tehrani, Joe Polk, L. Johnson, G. Menke, B. Miller, E. Criscuolo, K. Hogue, R. Parise, "Demonstrating a Realistic IP Mission Prototype," Proceedings of ESTC (Earth Science Technology Conference), College Park, MD, June 24-26, 2003

onboard data handling architecture approach employs fault-tolerant concepts with dual Ethernet Local Area Networks (LANs), dual OBCs (On-Board Computer), and dual up/down cards that also perform more routing functions. The particular design features are: 1290) 1291)

- Substitution of the conventional onboard storage concept with a file management system of a modern operating system. All source science data will be stored as files. This replaces the conventional technique of storing the data as a stream onto a recorder. A file system has two advantages: automatic storage management and random playback. Hence, a COTS package can be used. By organizing the data into files, each file can be downlinked using a generic file transfer application, such as MDP, that assures data quality by automatically performing error correction and/or retransmission as needed.
- The onboard Ethernet LANs (redundant) support data transfer between the science instruments (using UDP/IP on Ethernet), the OBCs, and the up/down cards using UDP/IP (User Datagram Protocol/Internet Protocol) packets to transport the data. However, a MIL-STD 1553 data bus is still being used as the data transport mechanism among other S/C subsystems using the current data packet concepts (e.g., between the attitude control subsystem and the OBC).
- HDLC (High-Level Data Link Control) framing for the link layer (as compared to CCSDS framing) of the space-ground RF transmissions is considered
- The use of a standard internet router at the ground station is considered with the corresponding IP mobility and security protocols enabled
- Data downlink, including the real-time S/C housekeeping data (in UDP/IP packets) and science data file transfer using the multicast dissemination protocol (MDP) application
- TCP/IP for reliable real-time commanding and ack/nack confirmations
- UDP/IP for commanding in the blind.
- MidSTAR-1 (Midshipmen Space Technology Applications Research-1), a microsatellite of the USNA (US Naval Academy), was launched on March 8, 2007. It flies ICSat (Internet Communications Satellite) to demonstrate TCP/IP communications on the RF link providing transmission rates of 1 Mbit/s in the downlink and uplink.. The link design employs COTS (Commercial Off-The-Shelf) components.
- VSAT (Very Small Aperture Terminal) satellite communication systems: VSATs are suitable for both point to point networks and mesh networks. Possible VSAT applications include: point of sale, Internet access, file distribution, database access, environmental monitoring, police, customs and excise offices.

September 2007 marked the beginning of a remarkable evolution in maritime satellite communications as KVH Industries together with its partner, ViaSat Inc launched the mini-VSAT BroadbandSM service. Relying on KVH's breakthrough 60 cm TracPhone V7 satellite communications antenna and ViaSat's ArcLight spread spectrum technology, mini-VSAT Broadband represented a radical reduction in the size and cost for maritime communications as well as the first fully integrated VSAT hardware and service solution for mariners.

Service is now (2010) online in the Indian Ocean, Guam, and the waters north of Australia via the JCSAT-85 satellite, the mini-VSAT Broadband network now encircles the globe

1290) J. Rash, R. Casasanta, K. Hogue, "Internet Data Delivery for Future Space Missions," Earth Science Technology Conference, Pasadena, CA, June 11-13, 2002

1291) J. Rash, E. Criscuolo, K. Hogue, R. Parise, "MDP: Reliable File Transfer for Space Missions," Earth Science Technology Conference, Pasadena, CA, June 11-13, 2002

and provides uninterrupted service and coverage for vessels as well as network coverage to the ViaSat Yonder in-flight broadband network for business and commercial aircraft.¹²⁹²⁾

The mini-VSAT Broadband service, along with the KVH TracPhone V7 antenna, comprise the first FCC-approved 60 cm VSAT antenna, service, and support package available for maritime communications. The network's ArcLight technology is delivered via ten satellite transponders providing service on a global basis. The seamless network offers voice service and Internet access as fast as 512 kbit/s (upload) and 2 Mbit/s (download).

- In January 2010, astronauts aboard the ISS (International Space Station) received a special software update permitting them to access to the Internet and the World Wide Web via the ultimate wireless connection. This personal Web access, called the Crew Support LAN, takes advantage of existing communication links to and from the station and gives astronauts the ability to browse and use the Web. The system will provide astronauts with direct private communications to enhance their quality of life during long-duration missions by helping to ease the isolation associated with life in a closed environment.¹²⁹³⁾

During periods when the station is actively communicating with the ground using high-speed Ku-band communications, the crew will have remote access to the Internet via a ground computer. The crew will view the desktop of the ground computer using an onboard laptop and interact remotely with their keyboard touchpad.

1.9.6 Relay satellites of Space Agencies

Relay satellites for data communication from Earth observation and space exploration S/C. The introduction of space agency relay satellite constellations (in GEO) opened up entirely new coverage capabilities in data communication. Operationally, it represents a definite advantage (although more expensive) over the conventional distributed ground-station concept in combination with S/C recorders. Relay stations in space permit extended or continuous (three satellites) coverage between a S/C in LEO and the ground. This can be a decisive advantage to some missions (for instance to Shuttle missions, space station operations, etc.). Extended contact periods permit also the transfer of vast amounts of data.¹²⁹⁴⁾

- The TDRS (Tracking and Data Relay Satellite) series of NASA (built by TRW for TDRS-1 to -7) pioneered this relay technology. The communication services provided by TDRS include such items as: a) simultaneous tracking of multiple satellites, b) multiple access schemes of S-band and Ku-band, etc. The TDRS antenna module consists of seven antennas: two single-access antennas that support both Ku-band and S-band user S/C communications (each 4.9 m diameter); a multiple access S-band phased array consisting of 30 helix-antenna elements; a 2 m diameter space-ground link antenna in K-band; an S-band omnidirectional antenna for TT&C support; a C-band antenna for commercial communications, and a K-band commercial communications antenna.

- TDRS-1 became operational shortly after the first relay satellite was launched in April 1983. The Landsat-4 mission became TDRS's first customer in August 1983.

1292) "KVH Mini-VSAT Network Live In Indian Ocean," SpaceDaily, April 21, 2010, URL: http://www.spacedaily.com/reports/KVH_Mini_VSAT_Network_Live_In_Indian_Ocean_999.html

1293) John Yembrick, Kelly Humphries, "NASA Extends the World Wide Web Out Into Space," NASA, Jan. 22, 2010, URL: http://www.nasa.gov/home/hqnews/2010/jan/HO_M10-011_Hawaii221169.html

1294) <http://esc.gsfc.nasa.gov/space-communications/tdrs.html>

Satellite	Comment
TDRS-1 (NASA), launch Apr. 15, 1983 (STS-6), TDRS-1 is also referred to as TDRSE	Position at 41° W, also support of first SVLBI experiment tests carried out on Aug. 2, 1986 On Apr. 4, 2008 TDRS-1 completed 25 years of successful on-orbit operations. TDRS-1 was decommissioned on Oct. 28, 2009 after 26 years of service. ¹²⁹⁵⁾
Luch-1 (NPO PM) Russia, launch Oct. 25, 1985	Position at 95° E
TDRS-B (NASA), launch Jan. 28, 1986 (STS-51L)	Lost in Challenger accident !!
TDRS-3 (NASA), launch Sept. 29, 1988 (STS-26)	Position at 84.75° E (as of 2003), in 2013 located off the Northeast Coast of Brazil
TDRS-4 (NASA), launch March 13, 1989 (STS-29)	Position at 41° W, replaced TDRS-1. Introduction of commercial C-band services. TDRS-4 completed its mission in 2011 after > 22 years of service. Disposal of TDRS-4 in April 2012.
TDRS-5 (NASA), launch Aug. 2, 1991 (STS-43)	Position at 174° W, replaced TDRS-3
TDRS-6 (NASA), launch Jan. 13, 1993 (STS-54)	Position at 46° W
TDRS-7 (NASA), launch Jul. 13, 1995 (STS-70)	Position at 150° W (deletion of K- and C-band packages). Replacement for TDRS-B.
COMETS (NASDA), launch Feb 21, 1998, H-II launch vehicle	Position at 121° E, a prototype data relay and tracking satellite (DRTS) system with S-band and Ka-band services
TDRS-8 (NASA) launch June 30, 2000 (TDRS-H)	Position at 47° W, S-band, Ku-band, and Ka-band
ARTEMIS-1 (ESA), launch July 12, 2001	Position at 21.5° E, a prototype DRS with S-band, Ka-band, and optical communication tests. Note: ARTEMIS reached its GEO location at the end of Jan. 2003 (18 months after launch) – with an ion engine providing the last 5000 km of orbit raising
TDRS-9 (NASA), launch Mar. 8, 2002 (TDRS-I)	Initial problems to get from GTO into GEO. Final GEO position was reached Sept. 30, 2002
DRTS (JAXA), launch Sept. 10, 2002 (Kodama)	Position at 90.77° E (DRTS), S-band and Ka-band
TDRS-10 (NASA) launch Dec. 5, 2002 (TDRS-J)	Position at 150.5° W,
TDRS-11 (NASA) launch Jan. 31, 2013 (UTC), former TDRS-K), design life of 15 years	TDRS-11 is the first of the third generation S/C built by Boeing. S/C mass of 3454 kg.
TDRS-12 (NASA) launch Jan. 24, 2014 (UTC), former TDRS-L	TDRS-12 is the second of the third generation S/C built by Boeing. S/C mass of 3454 kg.
EDRS-A (ESA) launch planned for 2015	Hosted payload on EutelSat-9B
TDRS-M (NASA), launch scheduled for 2015	

Table 70: Overview of relay satellites operated by space agencies ¹²⁹⁵⁾ ¹²⁹⁶⁾

¹²⁹⁵⁾ Roland Zaleski, Walter Mirczak, Stephen Staich, Richard Caverly, Eric Smith, Nicholas Teti, W. Lynn Vaught, Dave Olney, "Innovative Approach Enabled the Retirement of TDRS-1 Compliant with NASA Orbital Debris Requirements," 2011 IEEE Aerospace Conference, Big Sky, MT, USA, March 5-12, 2011

¹²⁹⁶⁾ Joshua Buck, Dewayne Washington, George Diller, "NASA Launches Third Generation Communications Satellite," NASA, Release 14-027, Jan. 23, 2014, URL: <http://www.nasa.gov/press/2014/january/nasa-launches-third-generation-communications-satellite/#.UuIvsvswdR4>



Figure 71: Artist's view of the TDRS-4 spacecraft in orbit (image credit: NASA)

- A new TDRS generation started with TDRS-H (TDRS-8 in orbit, launch of TDRS-H on June 30, 2000), built by BSS (Boeing Space Systems) at El Segundo, CA. A Boeing 601HP S/C platform structure is used (dry mass = 2910 kg). A new feature of the spacecraft is its innovative springback antenna design. A pair of 5 m diameter, flexible mesh antenna reflectors fold up for launch, then spring back into their original cupped circular shape on orbit. These steerable, single-access antennas (for Ku- and Ka-band) can simultaneously transmit and receive at S-band and either Ku- or Ka-band (additional capability), supporting dual independent two-way communications. The selection of Ku- or Ka-band communications is done on the ground. The receive (return link) data rates are 300 Mbit/s for Ku-band (at 13.7–15.0 GHz), up to 800 Mbit/s for Ka-band (22.5–27.5 GHz), and 6 Mbit/s for S-band (at 2.0–2.3 GHz). Transmit (forward link) data rates are 25 Mbit/s for Ku- and Ka-band, and 300 kbit/s for S-band. In addition, the phased-array antenna in S-band can receive signals from five different S/C simultaneously, while transmitting to one of them. A major payload feature of the TDRS-H, -I, -J series, not available on the previous satellites, is the use of onboard beam forming for the multiple access (MA) system. Advanced multi-mode RF feed systems are used for the Ku and Ka services via the single-access antennas. TDRS-H, I, J S/C use microstrip patch radiating elements for the multiple access antennas. The TDRS-I (TDRS-9 in orbit) launch took place on Mar. 8, 2002 on an Atlas-2A vehicle from Cape Canaveral, FL (launch mass of 3,192 kg).

The list of TDRS users is long, but one can cite for instance such missions as: Landsat-7, HST (Hubble Space Telescope), Space Shuttle, TOPEX/Poseidon (Ocean Topography Experiment), EOS missions like: Terra, Aqua, Aura, XTE (X-ray Timing Explorer), TRMM (Tropical Rainfall Measuring Mission), ISS (International Space Station) and the Space Shuttle. – However, the most bandwidth of the TDRS constellation is devoted to the Pentagon, which covers the lion's share of TDRS operations costs and is driving many of the system's requirements, some of them classified.

- Russia established also a relay satellite network, similar to NASA's TDRS system. The first satellite in the series, Luch-1 (Kosmos-1700), was launched Oct. 25, 1985. It was used to relay communication to the new MIR station (launched in 1986). A controlled reentry of MIR occurred on March 23, 2001 over the Pacific Ocean.

- Japan (JAXA, CRL, JST, etc.) started its geostationary DRTS (Data Relay and Tracking Satellite) system with two test satellites: 1) ETS–VI (launch 1994) equipped with the intersatellite communication device with data rates of up to 10 Mbit/s (only a portion of the tests could be conducted because ETS–VI did not make it to GEO); and 2) the launch of a prototype satellite, called COMETS (Communications and Broadcasting Engineering Test Satellite), on Feb. 21, 1998. COMETS provides S–band and Ka–band communication services. In addition, the satellite is used to test the following technologies: a) Inter–orbit communications for relay of communications between observation satellites or space stations in low–altitude circular orbits (LEO) and Earth stations; b) Advanced satellite broadcast technology for broadband region–specific broadcasts and high definition television (HDTV) broadcasts using Ka–band frequency bands. Note: a second–stage problem failed to put COMETS into GEO.

The DRTS S/C (wet mass of 2800 kg, power of 2.1 kW, design life of 7 years) was launched on Sept. 10, 2002 (positioned at 90.75° E), to complement the system (Japan refers to DRTS as “Kodama”). The objectives are to test and verify advanced receivers, an advanced intersatellite communications antenna (Ka–band, max data rate of 240 Mbit/s, and S–band for TT&C), and a high–performance tracking and acquisition system, to improve data relay speed and performance. Demonstration of intersatellite communications to relay data between a LEO S/C (ALOS, JEM, OICETS) and ground stations. ¹²⁹⁷⁾

- ARTEMIS (Advanced Relay and Technology Mission Satellite) of ESA has been developed for testing and operating new telecommunications techniques in GEO environment, a prototype data relay system for the planned DRS (Data Relay Satellite) system. ARTEMIS features S–band and Ka–band communication services. In addition, ARTEMIS is used to test the following technologies: a) an L–band land mobile payload allows two–way communications, via satellite, between fixed Earth stations and land mobiles – trucks, trains or cars – anywhere in Europe and North Africa; b) a laser–optical payload with a relay terminal called SILEX (Semiconductor Intersatellite Link Experiment), see M.4. – Some users of the ARTEMIS’ communication services are: SPOT–4 (CNES), OICETS (JAXA), Envisat (ESA), ISS, etc.

- Tianlian (Space–Link) Data Relay Constellation of China. The global data relay constellation is used to improve the coverage for China’s manned spacecraft as well as the planned construction of future space labs and space stations.

- Tianlian I–01 was launched on April 25, 2008 into GEO, 77°E

- Tianlian I–02 was launched on July 12, 2011 into GEO, 176.77°E

- Tianlian I–03 was launched on July 25, 2012 in to GEO,

The constellation spacecraft, based on the DFH–3 (Dongfanghong–3) bus, were designed and developed by CAST (China Academy of Space Technology) under the China Aerospace Science and Technology Corporation. The launch of Tianlian I–03 completed China’s first data relay satellite system. ^{1298) 1299)}

1297) Y. Fujiwara, Y. Sudo, H. Nagano, Y. Kanamori, “Japan’s First Data Relay Test Satellite (DRTS),” Proceedings of 54th IAC, Bremen, Germany, Sept. 29 – Oct. 3, 2003

1298) “LM–3C launches China’s third Tianlian data relay satellite,” China Military News, July 26, 2012, URL: <http://www.china-defense-mashup.com/lm-3c-launches-china%E2%80%99s-third-tianlian-data-relay-satellite.html>

1299) “China completes its 1st data relay satellite system,” China Daily, July 26, 2012, URL: http://www.chinadaily.com.cn/china/2012-07/26/content_15618182.htm

1.9.7 Commercial communication service provision for LEO spacecraft, etc.

Conventional LEO satellites rely on dedicated ground stations to receive download data (both Payload and TT&C). This requires the implementation of a specific ground station and/or the lease of additional ground facilities for a ground station network.. These services represent significant program costs in the operation of a satellite mission. In addition, many design aspects (regulatory, availability, coverage, etc.) have to be considered in a space–to–ground communications architecture. Traditional architectures that rely on Earth stations alone have limitations such as limited access duration, long access gaps, and difficulties related to placement in hard–to–reach locations.

BGAN (Broadband Global Area Network). ^{1300) 1301)} BGAN is the world’s first commercial mobile communication service to deliver voice and broadband data simultaneously. Initial service introduction at the end of 2005 with the Inmarsat–4F series to deliver Internet and intranet content and solutions, video on demand, LAN services, e–mail, phone, etc.). BGAN is part of the satellite component of the Third Generation (3G) IMT–2000/ Universal Mobile Telecommunications System (UMTS).

The BGAN program of Inmarsat is supported by the ARTES (Advanced Research in Telecommunications Systems) Program of ESA. BGAN is designed to provide a portfolio of packet–mode and circuit–mode based services, offering speech telephony, ISDN calls and ‘always–on’ Internet/Intranet IP–based mobile data communications at up to 492 kbit/s for Internet access, mobile multimedia and other advanced applications. Future extensions of the multi–service and multi–user detection capability can build on the complementary role of mobile satellite by seamlessly extending GSM (Global System for Mobiles), UMTS and WLAN services to users of terrestrial mobile networks when operating out of reach of cellular coverage.

In 2008, Inmarsat Plc. of London, UK, completed its I–4 (Inmarsat 4th generation) constellation of 3 satellites (phased 120° in GEO) offering constant, near–global and real–time commercial communication services from LEO to the ground using its I–4 constellation as a communications relay. – While a similar service has been available via NASA’s TDRS system for years, this new Inmarsat data service will be available globally and commercially, and dramatically reduce data latency in retrieving payload and TT&C data from LEO spacecraft. ^{1302) 1303)}

The architecture of the Inmarsat **BGAN** (Broadband Global Area Network) system for LEO operations consists of three key elements:

- 1) the Inmarsat I–4 constellation of GEO satellites
- 2) the BGAN network and service infrastructure
- 3) the SB–SAT terminal hardware and software that is deployed on the LEO asset.

In this configuration, the LEO asset hosts the **SB–SAT** (SwiftBroadband Terminal for Satellite) system which communicates with the I–4 satellite constellation. The SB–SAT terminal installed on the LEO S/C utilizes the existing Inmarsat I–4 constellation and the BGAN ground network capabilities, similar to how a ground terminal would function. The SB–SAT system relies on the terminal to adjust its transmit and receive characteristics to fit

1300) <http://broadband.inmarsat.com/>

1301) J. J. Rivera, E. Trachtman, M. Richharia, “The BGAN Extension Program,” ESA Bulletin, No 124, Nov. 2005, pp. 62–68

1302) R. Goldsmith, E. Trachtman, C. Lenz, C. McCormick, “24/7 Access to Leo Spacecraft TTC and Payload Data Using the INMARSAT BGAN Service,” Proceedings of the Symposium on Small Satellite Systems and Services (4S), Funchal, Madeira, Portugal, May 31–June 4, 2010

1303) Christian Lenz, Chris McCormick, Rob Goldsmith, Eyal Trachtman, “Real–time, near global, low earth orbit communications using geostationary Inmarsat BGAN system as a relay,” Proceedings of the 24th Annual AIAA/USU Conference on Small Satellites, Logan, UT, USA, Aug. 9–12, 2010, SSC10–X–4

seamlessly into the existing and operating BGAN system in order to minimize the impacts and changes required at the Inmarsat ground network.

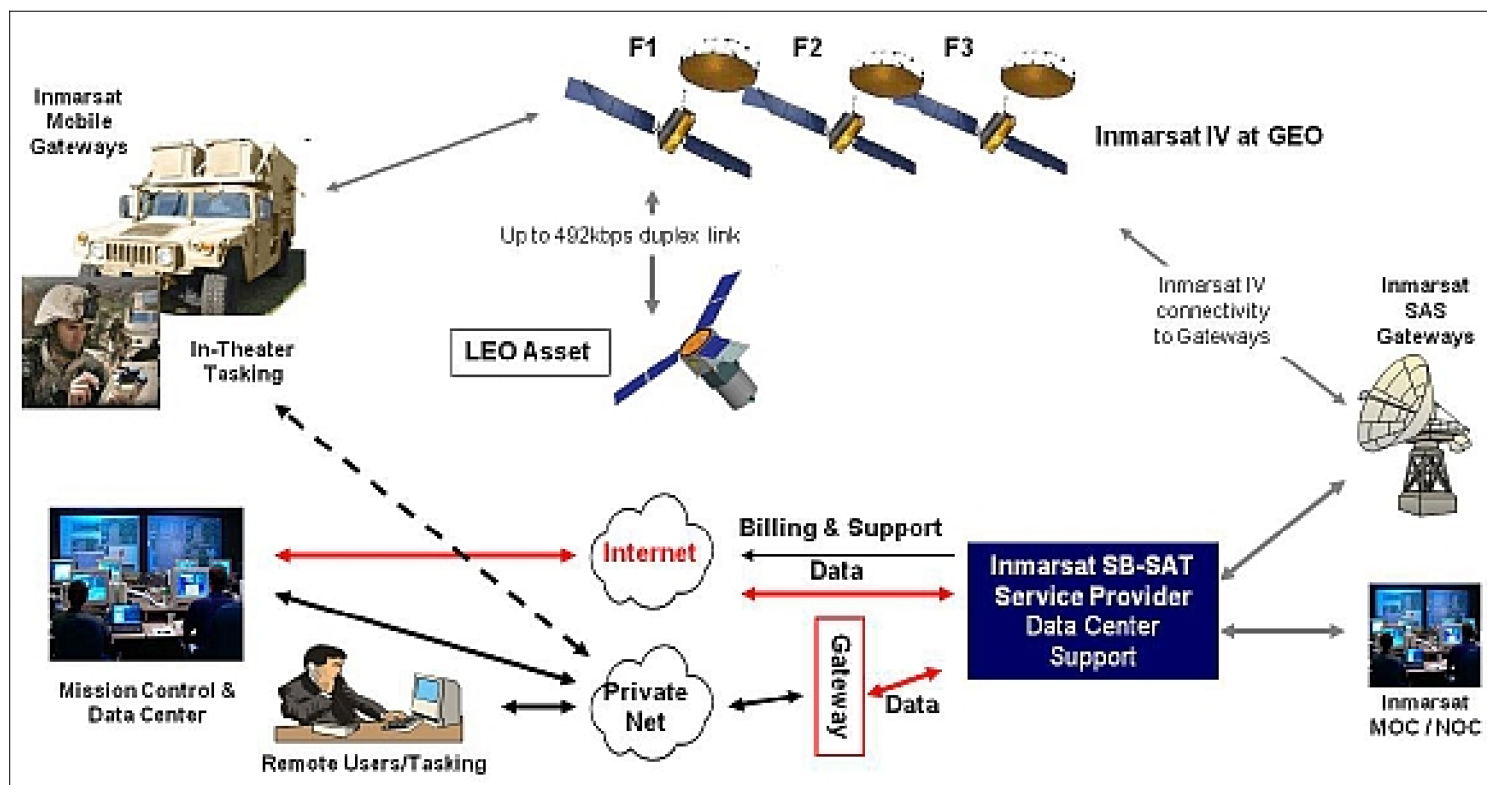


Figure 72: Schematic view of the SB-SAT network architecture (image credit: Inmarsat)

There are many BGAN terminal types in use on the ground from a number of manufacturers.¹³⁰⁴⁾ For the SB-SAT transceiver unit, those technologies are being evolved and adapted for the LEO application through custom development and licensing of existing core BGAN terminal technology by a team led by BRE (Broad Reach Engineering) USA, and COM DEV Europe, UK.

Service coverage: The Inmarsat I-4 constellation is composed of 3 state-of-the-art telecommunications GEO satellites, located at 98° W, 25° E and 143.5° E. Each of the Inmarsat I-4 satellites supports 192 narrow spot beams for traffic channels, plus 19 wide spot beams and a global beam for system and signalling channels. The satellite generates 67 dBW of transmission power, and supports 600 channels of 200 kHz in the forward and return direction. Inmarsat launched the AlphaSat spacecraft in GEO (July 25, 2013), it was added to the Inmarsat I-4 constellation and will provide a significant enhancement in terms of added capacity, service coverage and availability.

SB-SAT terminal: A nominal SB-SAT terminal system consists of the transceiver, L-band antennas, GPS subsystem, and antenna pointing mechanism. Fundamentally SB-SAT can be operated in different configurations, ranging from a transceiver only option with fixed low gain antenna to a system that includes a mechanically steered antenna, the related control electronics, and an internal GPS unit. At the core of all options is the BGAN Core Module which comprises the RF front-end, physical layer implementation (modem) and radio software (protocols, terminal control, and I/O). Since SB-SAT requires position and velocity information, an internal GPS unit is to be included unless a reliable external GPS source can be tightly coupled into the Core module, using the same interface definition of the internal GPS. The SB-SAT terminal design accommodates this configuration through a modular architecture that can be easily extended and modified to accommodate specific mission requirements while maintaining the integrity of the Core Module.

1304) <http://www.broadreachengineering.com/products/inmarsat-swift-broadband-terminal-for-spacecraft/>

The SB–SAT terminal is a box of size 23 cm x 19 cm x 12 cm with a mass of < 4 kg and a power consumption of 40W (including GPS when transmitting).

Several Types of Service offerings are being considered, including:

- Low Data volume, high latency LEOs: This class may be TT&C only and/or provide limited mission data collection. Affordability is the driving constraint. Latency is not considered to be a driving issue.
- High Data volume, low latency LEOs: This class is dominated by time critical TT&C and/or mission data, Latency, of course, is important.
- TT&C only, low latency LEOs: This class is a subset of the High DATA, low latency class, with same assumptions on their drivers and cost base, however mission data is not latency critical and delivered via commercial ground based data relay (at S–band). SB–SAT is used to achieve real–time, always–on, on–demand, low latency TT&C.

The introduction of the SB–SAT terminal for potential customers is scheduled to be available in mid–2012. The novel service may revolutionize the way in which LEO spacecraft are operated as well as enable novel new applications that become possible from having practically a “24/7” access service to spacecraft data and telemetry.

- **GX (Global Xpress®).** Global Xpress of Inmarsat Plc is the world’s first globally available high–speed broadband commercial service delivered via a Ka–band satellite network. The spacecraft are developed by Boeing Satellite Systems on the 702HP platform. The first Global Xpress satellite, Inmarsat–5F1, was successfully launched on December 8, 2013. On March 11, 2014, Inmarsat–5F1 successfully completed on–orbit testing and was handed over to Inmarsat. Boeing is under contract to build four Inmarsat–5 satellites, with two more scheduled for completion and launch by the close of 2014. The Inmarsat–5 satellites carry a secondary payload that Boeing Commercial Satellite Services will lease to potential government customers through a reseller agreement with Inmarsat. Global Xpress is on schedule to achieve full global coverage by the end of 2014 with 3 spacecraft in GEO. The satellite network will deliver consistent high–performance download speeds of up to 50 Mbit/s and up to 5 Mbit/s over the uplink. ^{1305) 1306)}

The three Inmarsat–5 satellites needed for global coverage are being launched on Proton rockets by ILS (International Launch Services) from the Baikonur Cosmodrome in Kazakhstan. Each I–5 satellite is expected to have a commercial life of 15 years.

The spacecraft operate with a combination of fixed narrow spot beams that enable us to deliver higher speeds through more compact terminals, plus steerable beams so additional capacity can be directed in real–time to where it’s needed.

- On December 19, 2013, Astrium Services and Inmarsat signed a strategic distribution partnership agreement for the game–changing Global Xpress service. ¹³⁰⁷⁾

Astrium Services will deliver Global Xpress high–speed broadband services through its worldwide distribution channels. The strategic agreement will cover key vertical markets, including the maritime as well as the government and defense sector, initially in Europe. In due course the Astrium Services Global Xpress offering will encompass all service types – packaged services, bandwidth capacity, as well as commercial and military Ka–band.

1305) “Global Xpress® Another giant leap for mankind,” Inmarsat, URL: <http://www.inmarsat.com/service/global-xpress-2/>

1306) “1st Boeing Built Inmarsat–5 Satellite Successfully Completes On–Orbit Testing,” Boeing News, March 11, 2014, URL: <https://navigator.gmx.net/navigator/show?sid=4db1e8de4b63565e41ae873597dc7f4386e56bd6c1724fa765e0a8dd87567e07b08166ec2d6b8e6db96caae4229c5aae#mail>

1307) “Astrium and Inmarsat sign strategic agreement on Global Xpress®,” Astrium Services, Dec. 19, 2013, URL: http://www.astrium.eads.net/en/press_centre/astrium-and-inmarsat-sign-strategic-agreement-on-global-xpress.html

1.9.8 DAB (Digital Audio Broadcasting)

At the start of the 21st century, DAB is a new and emerging technology to transmit sound (and data) efficiently, it is designed to remedy the weaknesses of conventional analog broadcasting systems. DAB introduces a completely new concept into the world of radio broadcasting, namely to share a unique network of transmitters among several programs. DAB represents in effect the most fundamental advance in radio technology since the introduction of FM stereo radio. Within the context of DAB, a transmitter network can be shared by a group of service providers delivering their contents to an ensemble operator, who assembles the DAB multiplex function. Moreover, the ensemble multiplex function is, by its very essence, a dynamic structure.¹³⁰⁸⁾

The DAB digital sound is far superior to AM or FM in audio quality, bandwidth, and dynamic range. Digital transmission techniques, which, when suitably applied, can lead to a more “effective and more efficient” utilization of the frequency spectrum, providing a means of reducing future spectrum needs, while satisfying increasing program requirements.

The DAB system concept was developed by the Eureka 147 project (founded in 1986 and originally only European), an international consortium of broadcasters, network operators, consumer electronic industries, and research institutes. In January 2000, the Eureka 147 consortium merged into the World DAB forum.

The DAB concept works by combining essentially two digital technologies, namely **data compression** and **data coding**.

- MUSICAM (Masking–pattern, Universal Subband Integrated Coded And Multiplexing) is a compression system that discards sounds that cannot be perceived by the listener, thereby reducing the vast amount of digital information required for broadcasting. MUSICAM allows a data rate of 1411 kbit/s, necessary to deliver a stereo signal on a compact disc, to be reduced to as low as 192 kbit/s (i.e. a reduction by a factor > 7), for delivery of a stereo broadcast program, the quality of which is indistinguishable from that of the original source. MUSICAM was developed at IRT (Institut für Rundfunktechnik) in Munich, Germany (at IRT DAB development started in 1981). The standardized ISO–MPEG layer–2 audio compression algorithm (MUSICAM) is used in DAB to broadcast up to six stereo channels with a “crystal clear” CD quality.

- COFDM (Coded Orthogonal Frequency Division Multiplexing) is applied to shape the DAB signal. By using a precise mathematical relationship, the MUSICAM signal is split across many different carrier frequencies (e.g. for mode I transmission, the number of carrier frequencies is 1,536) and also across time. This process ensures that even if some of the carrier frequencies are affected by interference, or if the signal is disturbed for a short period of time, the receiver is still able to recover the original sound. The signal is then transposed to the appropriate radio frequency band, amplified and transmitted. The COFDM technique was originally developed in the 1980s at the French research laboratory CCETT (Centre Commun d’ Etudes de Télécommunications et de Télédiffusion), Rennes, France. One of the main assets of DAB is its spread–spectrum modulation technique (COFDM) which, among others, allows several transmitters to operate in the same radio frequency channel [SFN (Single Frequency Network)]. Further, the modulation scheme COFDM is well suited for overcoming the problems with multipath that FM suffers from. This allows a far better reception quality especially for mobile users; it also improves the situation for home listeners as well because stationary listeners are not immune from the problems of multipath.

The DAB standard (ETS 300 401) was first published in Feb. 1995, second edition in May 1997. This ETS (European Telecommunication Standard) on DAB (Digital Audio Broadcasting) is based on the overall system and service requirements adopted by the ITU–R

¹³⁰⁸⁾ <http://www.worlddab.org/>

(International Telecommunication Union – Radiocommunication). DAB is intended to supersede eventually the existing analog AM (Amplitude Modulation) and FM (Frequency Modulation) techniques.¹³⁰⁹ The DAB interface standards include:

- STI (Service Transport Interface) standard ETS 300 799 (1997). It defines the way for service providers to deliver their contents to the ensemble provider
- ETI (Ensemble Transport Interface) standard ETS 300 797 (1997). It defines the link used to distribute the DAB Ensemble multiplex to the transmitter sites
- DAB radio broadcasting systems standard ETS 300 401 (1997). It defines the on–air signal as it has to be processed by the DAB receivers.

Digital techniques allow continuous (analog) sound signals to be converted into discrete (digital) signals. The discrete nature of these signals means that they are well–defined to within a large margin of error, and thus do not lose their identity along the transmission path (under normal circumstances). Error correction methods are also available which can further increase the “fidelity” of the transmission. This is the “secret” of the compact disk.

The various advantages offered by a common distributed network infrastructure to broadcast radios on different RF media have been early detected by the French operators Globecast and TDF (TéléDiffusion de France) of France Telecom. In the period 1997/9, they started with the deployment of such collect & distribution networks to feed, on the French territory, the FM, AM and DAB transmitters. After a few months of operation in France, both the network operators and the radio broadcasters have experienced the following advantages of such a network infrastructure:

- The service provides a “universal & professional system” which completely fits the radio and operators expectations
- It provides a high–quality audio signal over several networks and offers sufficient additional data to face the various operational situations in regions
- It is fully DAB compliant, allowing to smoothly increase the DAB coverage in France with additional investments limited to the transmitters themselves
- The new service saves operational costs permitting to share the costly satellite link between several programs and services (AM, FM, DAB).

DAB services can be ground based, referred to as T–DAB (Terrestrial DAB), as is the case with Eureka 147. This system, which is on its way to becoming the de facto world standard, operates in the L–band in France, Canada, Germany (and most of Europe), it is in total operation in the UK, using the higher frequencies of VHF. In 1992, WARC (World Administrative Radio Conference) allocated the L–band frequency range to digital broadcasting, both terrestrial and satellite. Initial T–DAB services (pilot projects) started in 1998. Commercial DAB receivers have been on the market since the summer 1998. The DAB service spectrum will eventually lead into “multimedia broadcasting” in which all forms of information can be conveyed via the common transmission medium DAB.

In 2002, several commercial S–DAB (Satellite Digital Audio Broadcasting) projects (payloads of commercial communication satellites) are in the planning stage.

¹³⁰⁹ <http://portal.etsi.org/broadcast/dab.asp>

1.9.9 SDR (Software Defined Radio):

SDR is a radio communication system, an enabling technology, where components that have been typically implemented in hardware (e.g. mixers, filters, amplifiers, modulators/demodulators, detectors, etc.) are instead implemented by means of software on a personal computer or on embedded computing devices. The SDR method utilizes a minimum amount of RF analog electronics before digitizing the signal. Upon digitization, all other functions are performed in software or firmware. — The SDRF (Software Defined Radio Forum) defines the SDR as a radio in which some or all of the physical layer functions are software defined. In other words, the software is used to determine the specification of the radio and what it does. If the software within the radio is changed, its performance and function may change.

Over the years, the digital domain was pushed further and further toward the front end of the receiver, until eventually the all–digital receiver was born in the 1990s. This receiver converts the intermediate frequency signal directly to digital samples, with all processing thereafter accomplished digitally.

SDR payloads on small satellite platforms are an innovation of the 21st century. The SDR approach provides a reconfiguration capability for functional flexibility and upgrade during the mission lifetime under the operational and resource constraints of the micro–space environment. In other words, the radio is implemented on a software–based reconfigurable platform and can be used to support various functions and signal schemes. Such software based solutions have several very promising advantages. A reconfigurable system allows multiple missions to use the same hardware by loading different application software. The software for each system can be stored in memory and can even co–exist or execute concurrently if desired. In addition, software defined communications systems can be remotely configured or updated, allowing for inexpensive bug fixes, upgrades or optimizations. This is extremely important for a spaceborne system. ^{1310) 1311)}

The growth of SDR technology is empowered by the evolution of microelectronics and the growth of DSP (Digital Signal Processing) technology. The dramatic improvement in DSP performance and cost is the key to enabling the evolution and development of SDR–based designs in future satellite systems, starting primarily in satellites with smaller platforms, especially in nano, micro, and small satellites in LEO orbits.

The applications supported by SDR are equally diverse and include maritime AIS (Automated Identification System) signal reception, amateur radio communications, GPS reception, and surface–to–space and inter–spacecraft relay. It is expected that the utilization of SDR technology will continue to grow across spacecraft platforms and areas of application.

In 2005, NASA has initiated the SDR architecture team ^{1312) 1313)} to evaluate the suitability of SDR technology for their manned and unmanned space flight missions and to develop a standard architecture for NASA space radios of the future. This team is defining the STRS (Space Telecommunications Radio System) architecture; the standards bodies are evaluating STRS as a potential standard architecture for space radios.

The so–called “Frontier radio”, a highly–capable yet low–power and low–mass SDR architecture for high–bit rate communications and two–way coherent radio navigation, has

1310) W. Chen, T. Jones, A. Macikunas, P. Thomas, E. Choi, “Software Defined Radio (SDR) Payloads for Microsatellite Missions,” Proceedings of ASTRO 2010, 15th CASI (Canadian Aeronautics and Space Institute) Conference, Toronto, Canada, May 4–6, 2010, URL: ftp://casi:ASTRO2010@astroconference.ca/./Papers/150_Cheng_etal_ASTRO2010.pdf

1311) Fabrizio Massaro, Jens Elsner, Florio Dalla Vedova, Friedrich K. Jondral, “Components for Software Radio Wideband Receivers: A space segment survey,” URL: http://www.cel.kit.edu/download/WINN_TC_10_Massaro.pdf

1312) “SDRF Comments on NASA Space Telecommunications Radio System (STRS), Open Architecture Specification,” Nov. 2007, URL: http://www.sdrforum.org/pages/documentLibrary/documents/SDRF-07-R-0013-V1_0_0.pdf

1313) Richard C. Reinhart, Sandra K. Johnson, “SDR/STRS Flight Experiment and the Role of SDR–Based Communication and Navigation Systems,” 6th Annual Software Radio Summit February 25 – 28, 2008, URL: http://ntrs.nasa.gov/archive/nasa/casi.ntrs.nasa.gov/20090004687_2009001249.pdf

been developed by JHU/APL, for the NASA and military user communities. Applications include terrestrial, airborne, and near–Earth RF links, with a deep space implementation currently in development. The first inflight use of this radio platform will be on NASA’s RB-SP (Radiation Belt Storm Probes) program, which is preparing to produce two S–band flight units in early 2010 (launch Aug. 30, 2012). – The S/Ka–band implementation of the Frontier radio provides an important milestone in the development of advanced radios for NASA. It provides a highly–capable and reconfigurable radio platform with high bit rate return in a low–power and low–mass implementation. ¹³¹⁴⁾ ¹³¹⁵⁾

CoNNeCT (Communication Navigation and Networking Reconfigurable Testbed) is a NASA–sponsored demonstration mission to ISS which will investigate the usage of SDRs as a multi–function communication system for space missions. The CoNNeCT project is a collaboration between industrial radio providers and NASA. The industrial radio providers are providing the SDRs and NASA is designing, building and testing the entire flight system. ¹³¹⁶⁾

The CoNNeCT system will be called the **SCaN (Space Communications and Navigation) Testbed** when on–orbit. The SCaN Testbed will consist of reconfigurable and reprogrammable SDR (Software Defined Radio) transceivers/transponders operating at S–band, Ka–band, and L–band, along with the required RF/antenna systems necessary for communications. Designed to operate for a minimum of two years, the three SDRs will provide S–band duplex RF (Radio Frequency) links directly with the ground, [also referred to as the Near Earth Network (NEN)], S–band duplex RF links with the TDRSS (Tracking and Data Relay Satellite System), [also referred to as the Space Network (SN)], Ka–band duplex with TDRSS, and L–band receive–only with the GPSS (Global Positioning Satellite System). ¹³¹⁷⁾

Mission	Spacecraft	Organization	Comments on SDR payload
CHAMP	Minisatellite, 522 kg	GFZ, DLR, NASA/JPL	SDR–based Blackjack GPS receiver, launch July 15, 2000
GRACE	Minisatellite, 432 kg	DLR, NASA/JPL	SDR–based Blackjack GPS receiver, launch March 17, 2002
CANDOS	STS–107	NASA/GSFC, ITT Industries	SDR–based LPT (Low Power Transceiver), launch Jan. 16, 2003
MRO (Mars Reconnaissance Orbiter)	Deep Space Probe, 2180 kg	NASA/JPL, Lockheed Martin, CMC Electronics Cincinnati	Electra UHF SDR for communications relay with other Mars orbiters and landed vehicles, launch March 10, 2006
TacSat–2	Minisatellite, 370 kg	AFRL, ITT Industries	SDR–based LPT, launch Dec. 16, 2006
Aprize-Sat–3, –4	Nanosatellite, 12 kg each	SpaceQuest	SDR–based AIS receivers, launch July 29, 2009
Sumbandila-Sat	Microsatellite, 82 kg	SunSpace, University of Stellenbosch, South Africa	SDR–based amateur radio payload, launch Sept. 17, 2009
AISSat–1	Nanosatellite, 6.5 kg	Norwegian Space Center, Kongsberg Seatex AS	SDR–based AIS receiver, launch July 12, 2010

1314) Christopher B. Haskins, Wesley P. Millard, “Multi–Band Software Defined Radio for Spaceborne Communications, Navigation, Radio Science, and Sensors,” Proceedings of the 2010 IEEE Aerospace Conference, Big Sky, MT, USA, March 6–13, 2010

1315) “The Frontier Radio,” JHU/APL, 2010, URL: <http://www.jhuapl.edu/ott/Technologies/featuredTech/2620/>

1316) “CoNNeCT Operations Project–SCaN Testbed Flight & Ground System Description,” GRC–CONN–DOC–5022, June 23, 2011, URL: <http://spaceflight systems.grc.nasa.gov/SpaceOps/CoNNeCT/documents/GRC-CONN-DOC-5022%20Base%20-%20SCAN%20Testbed%20Flight%20and%20Ground%20System%20Description.pdf>

1317) “Space Communications and Navigation Testbed (SCaN_Testbed),” NASA Fact Sheet, Sept. 23, 2011, URL: http://www.nasa.gov/mission_pages/station/research/experiments/SCAN_Testbed.html

Mission	Spacecraft	Organization	Comments on SDR payload
ARISSat-1	Microsatellite, < 100 kg	Radio Amateur Satellite Corp. (AMSAT)	Odyssey SDR, ¹³¹⁸⁾ deployment of ARISSat in Feb. 2011, launch Jan. 2011 on Progress No 41, deployed from ISS on Aug. 3, 2011, the S/C reentered Earth atmosphere on Jan. 4, 2012 (5 month mission) ¹³¹⁸⁾
DICE	2 1.5U Cube-Sats of 4 kg total mass	Collaborative mission of NSF, USU/SDL, ASRA LLC, Embry-Riddle, etc.	Cadet SDR S-band radio of L-3 Communications with a downlink rate of 3 Mbit/s ¹³¹⁹⁾ Launch Oct. 28, 2011.
SCaN/CoN-NeCT	ISS/ExPA (total payload of 365 kg)	NASA	CoNNeCT testbed features 3 SDRs: - S-band SDR by General Dynamics - Ka-band SDR by Harris Corp. - S/L-band SDR by NASA/JPL Launch on July 21, 2012 on HTV-3 of JAXA
exactView-1	Microsatellite, 100 kg	exactEarth, COM DEV	exactView-1 (formerly known as ADS-1B), launch July 22, 2012
Van Allen Probe (RBSP)	2 minisatellites, < 1500 kg	NASA, JHU/APL ¹³¹⁴⁾	Frontier radio (SDR) in S-band, launch August 30, 2012
PULSAR	SDRpayload on HEREOS balloon flight	NASA/MSFC, launch in the fall 2013 from Fort Sumner, N.M.	PULSAR (Programmable Ultra Lightweight System Adaptable Radio) in S- and X-band.

Table 71: List of some spaceborne SDR implementations (Ref. 1310) ¹³¹⁸⁾ ¹³¹⁹⁾

¹³¹⁸⁾ "ARISSat-1/KEDR Amateur Radio Satellite Deorbits," Space Daily, Jan. 6, 2012, URL: http://www.spacedaily.com/reports/ARISSat_1_KEDR_Amateur_Radio_Satellite_Deorbits_999.html

¹³¹⁹⁾ Edward W. Kneller, Kevin L. Hyer, Todd McIntyre, David K. Jones, Charles Swenson, "Cadet: A High Data Rate Software Defined Radio for SmallSat Applications," Proceedings of the 26th Annual AIAA/USU Conference on Small Satellites, Logan, Utah, USA, August 13-16, 2012, paper: SSC12-X-4, URL: <http://digitalcommons.usu.edu/cgi/viewcontent.cgi?article=1083&context=smallsat>

1.9.10 AIS (Automated Identification System) – spaceborne maritime traffic monitoring

AIS is a shipboard broadcast transponder system in which ships continually transmit their ID, position, course, speed and other data to all other nearby ships and to shoreside authorities on a common VHF radio channel. The concept is derived from the pioneering work of a Swedish inventor named Håkan Lans, who developed in the mid 1980s an ingenious technique for spontaneous, masterless communication, which permits a large number of transmitters to send data bursts over a single narrowband radio channel by synchronizing their data transmissions to a very precise timing standard.¹³²⁰⁾

AIS is designed to operate in one of the following modes:

- In a ship–to–ship mode for collision avoidance
- As a means for coastal states to obtain information about a ship and its cargo
- As a traffic management tool when integrated with a VTS (Vessel Traffic System).

AIS will have a far–reaching impact on safety at sea. In 2000, the IMO (International Maritime Organization) adopted a mandatory requirement for all ships to carry an AIS transponder. The regulation requires AIS to be fitted aboard all ships of 300 gross tonnage and upwards engaged on international voyages, cargo ships of 500 gross tonnage and upwards not engaged on international voyages, and all passenger ships irrespective of size. The requirement became effective for all ships by 31 December 2004. – Ships fitted with AIS shall maintain AIS in operation at all times except where international agreements, rules or standards provide for the protection of navigational information.^{1321) 1322)}

AIS for maritime vessels introduced by the IMO is a navigation aid and basically an anti collision system for vessels at sea. Vessels are broadcasting messages (position reports and short messages with information about the ship and the voyage) on two channels in the maritime VHF band on a regular basis to neighboring vessels for collision avoidance, and to shore stations for VTS (Vessel Traffic Services). Updated AIS messages are transmitted every few seconds, to keep the information up to date.

An AIS transponder combines the functions of a GNSS (GPS) receiver and a VHF radio transceiver operating within the band assigned to AIS systems and compliant with the ITU–RM.1371 recommendation. The system can forward up to 2000 messages/minute and update them every 2 seconds; the SOTDMA (Self–Organizing Time Division Multiple Access) transmission technique is used to allow high data exchange rate and ensure ship–to–ship operation.

The broadcast messages of AIS transponders can also be received by a VHF receiver on a **satellite** for wide area observation of maritime activity. This line–of–sight information is of great interest for countries with long shorelines to improve maritime domain awareness. Coastal authorities realized quickly that significant ship tracking capabilities could be accomplished far out to sea if a receiver were placed on a spacecraft. Indeed, the spaceborne collection of AIS data has the potential to provide great cost and performance advantages over existing methods of monitoring marine traffic.

Terrestrial AIS concept:

Terrestrial AIS is a signalling system between ships and ships and shore–stations that uses two VHF narrow band (25 kHz) channels at 161.975 MHz (channel 87) and 162.025 MHz

1320) The Complete Guide to Automatic Identification Systems, Leica Geosystems Inc., 2001, http://www.mx-marine.com/downloads/publications/AIS_Booklet.pdf

1321) http://www.imo.org/Safety/mainframe.asp?topic_id=754

1322) “Technical characteristics for an automatic identification system using time division multiple access in the VHF maritime mobile band,” ITU–R M.1371–3, January 1, 2007

(channel 88). The signal transmitted is a GMSK (Gaussian Minimum Shift Keying) modulated carrier and the use of a SOTDMA (Self-Organized Time Division Multiple Access) protocol. The protocol makes use of short time slots that partition a one-minute 'frame' that allows for up to 4500 time slots per frame to be sent. Figure 73 shows a schematic of the time division of the two AIS channels, each with 2250 slots of 26.7 ms each. ^{1323) 1324)}

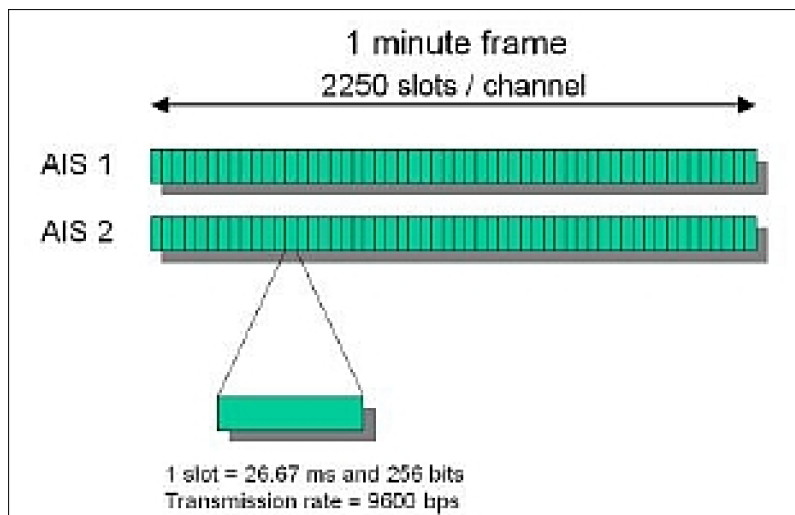


Figure 73: A one minute SOTDMA time frame of AIS messages from the two AIS channels make up a total of 4500 available slots (image credit: COM DEV)

Ships alternatively transmit on AIS channel 1 and 2, and the TDMA protocol ensures that no signal transmissions 'collide' for the local 'cell' of ships. In theory, a large number of ships can be accommodated using this scheme without congestion. The signal transmission range is typically about 50 nautical miles and this characterizes the size of a cell of ships that are self-organized.

Ships at distances greater than 50 NM from other ships need not be coordinated using this TDMA protocol, because the time slots can be re-used due to low signal strength from far away ships. Typical information transmitted on AIS channels includes the ship's identification, latitude, longitude, speed, heading, course over ground, rate of turn etc. Certain AIS messages include other information such as destination, crew information or cargo. The AIS standard calls up to 26 different AIS message types that contain varied information.

1323) Ian D'Souza, David Martin, "Nanosatellite Demonstration Mission: The Detection of Maritime AIS Signals from Low Earth Orbit," Proceedings of the Symposium on Small Satellite Systems and Services (4S), Funchal, Madeira, Portugal, May 31 – June 4, 2010

1324) Jochen Harms, Ghislain Ruy, Bart Van Schie, "Pathfinder to SatAIS Experience and Way Forward," Proceedings of the Symposium on Small Satellite Systems and Services (4S), Funchal, Madeira, Portugal, May 31 – June 4, 2010

The following parameters summarize/characterize AIS signals as transmitted and received on the surface of the Earth:

- Center Frequency: 161.975 MHz (AIS channel 1), 162.025 MHz (AIS channel 2)
- Bandwidth: 25 kHz per channel
- Power: 12.5 W (Class A), 2.5 W (Class B)
- Transmission Range: 50 nautical miles radius (i.e. to the horizon)
- Modulation: Frequency modulation, GMSK at 9.6 kbit/s
- TDMA Frame and Slot: 1 minute frame timing extracted from GPS signals, 26.7 ms slot (256 bit)
- Typical Antenna Mounting: Vertically polarized monopole or dipole antenna mounted at some height above the ship's deck, typically to a mast.
- Propagating Energy of Transmission: Primarily line of sight and along the surface of the Earth (i.e. perpendicular to the antenna)
- Carrier to Co-channel Interference Ratio Threshold C/I : 10 dB
- Typical Maritime AIS Receiver Sensitivity: –108 dBm for 20% packet error rate.

As can be seen from the signal propagation characteristics and ship antenna mounting, because AIS was designed to be a terrestrial system, the radiated energy from the mast-mounted shipboard antennas will propagate primarily along the surface of the Earth to other ships and shore stations and not upwards towards satellites in Earth orbit.

Table 72: Overview of AIS signals transmitted and received by ships

Space-based AIS:

By receiving AIS messages (designed for terrestrial transmissions) in orbit, a wide-area maritime surveillance would be possible. Even a single satellite receiving AIS could eventually map the world's shipping traffic over time, obtaining new statistical knowledge of the world's shipping traffic as clearly demonstrated by a number of AIS missions.

However, while the demonstration of the utility of AIS has proceeded quite quickly and smoothly, with AIS being used for maritime traffic awareness, collision avoidance and vessel traffic management, the terrestrial AIS network was never designed for signal reception from Earth orbit. This has posed some interesting challenges. Any space based AIS receiving system will have some degree of latency due to the orbits of satellites and locations of ground stations at which satellites download the received data. Thus, AIS signals received in orbit are never intended to provide realtime navigational information, but they are still able to provide excellent situational awareness. A LEO satellite will fly over any given area in a time measured in minutes, thus continued monitoring of any particular area is also not possible. These effects must not be seen as short-comings of the system, because as few as 6 satellites can cover every area of the globe with refresh rates of 2 hours typically (in equatorial regions), and much lower rates at the higher latitudes.

An additional complication arises because the self-organized nature of the TDMA signals between ships is lost when viewed from the vantage point of LEO (Low Earth Orbit). The very large IFOV (Instantaneous Field of View) of the satellite allows signals from a vast array of SOTDMA (Self-Organized Time Division Multiple Access) 'cells' to be received at the satellite receiver, Figure 74.



Figure 74: The circles show the typical IFOVs of a LEO satellite (image credit: COM DEV Ltd.)

Hence, the AIS signals that arrive at the satellite consist of multiply collided (overlapped) TDMA time slots from multiple cells. The problem that is faced by space-based AIS systems is how to deal with these overlapping AIS signals. Solution possibilities include narrowing the field of view (requires very large antenna arrays), waiting for statistically random signal messages that do not have overlaps (long observation time required) or attempting to unravel the overlapping messages (difficult algorithms).

Early AIS technology demonstration instruments on a spaceborne platform:

The following list provides an overview of early AIS technology demonstration instruments flown or projected on a spaceborne platform.

- NCube-2 (Norwegian CubeSat-2) was developed by students from several universities in Norway and was coordinated by Andøya Rocket Range and the Norwegian Space Center. The satellite's payloads included an AIS unit and attitude determination and control. NCube-2 was launched on SSETI Express on Oct. 27, 2005, but it is unclear if NCube-2 was ever ejected from SSETI. Unfortunately, no contact could be established with NCube-2. Although no AIS demonstration could be obtained, NCube-2 must still be regarded as the first satellite carrying an AIS payload.
- The TacSat-2 technology demonstration mission (USA) of AFRL (Air Force Research Laboratory) was launched on Dec. 16, 2006 and lasted until Dec. 2007. The TIE/AIS (Target Indicator Experiment/Automated Identification System) receiver system onboard TacSat-2 was provided by NRL. **TIE/AIS, a software-defined radio, was in fact the first implementation to collect AIS signals from space successfully.**
- Rubin-7-AIS of OHB-System, Bremen, Germany was launched on Nov. 1, 2007 on a Cosmos-3M vehicle from Plesetsk, Russia. Rubin-7-AIS consisted of three redundant

units with fixed solar cells. The AIS payload remained attached to the upper stage of the Cosmos–3M launch vehicle. The objective was to demonstrate the functionality of AIS signal receivers in orbit.

- An AIS instrument of ComDev International Ltd. of Cambridge, Ontario, Canada is flown on the CanX–6/NTS (Nanosatellite Tracking Ships) mission. The nanosatellite (6.5 kg) was built by UTIAS/SFL of Toronto, Canada. The launch took place on April 28, 2008 (PSLV, ISRO with CartoSat–2A as primary payload). According to ComDev, the AIS demonstration has validated the predicted performance levels over large coverage areas. – The Canadian Department of National Defense (DND), Project Polar Epsilon, has signed a contract with ComDev to obtain data which it will use to evaluate the results of the trials to assess the suitability of the advanced AIS system for operational requirements.
- Rubin–8–AIS, a demonstration nanosatellite (7 kg) of OHB–System, Bremen was launched on April 28, 2008 on a PSLV launcher of ISRO (along with CanX–6/NTS–1 of ComDev and CartoSat–2A). The NTS–1 of ComDev nanosatellite of 6.5 kg is also equipped with an AIS payload.



Background on NAIS: The USCG (United States Coast Guard) is implementing an AIS system in response to the Maritime Transportation Security Act of 2002. The goal of NAIS is to enhance Maritime Domain Awareness (MDA), with particular focus on improving maritime security, marine and navigational safety, search and rescue, and environmental protection services. AIS data (e.g., vessel location, course and speed) is combined with other government intelligence and surveillance information to form a holistic, overarching view of maritime traffic within or near U.S. and territorial waters.

The CDS–3 spacecraft has a mass 80 kg. Its orbit is at an altitude of 665 km.

Figure 75: Illustration of the CDS–3 microsatellite (image credit: OrbComm) ^{1325) 1326)}

- On June 19, 2008, six communication microsatellites (a Coast Guard Concept Demonstration satellite and five Quick Launch satellites) of OrbComm Inc., Fort Lee, NJ were launched into LEO on a Cosmos–3M vehicle from the Kapustin Yar launch site in South–West Russia. Objective: constellation replenishment; in addition, these satellites are equipped with AIS payloads which will enable them to receive and report AIS transmissions to be used for ship tracking and other navigational activities. One of the S/C launched was OrbComm CDS–3 (Concept Demonstration Satellite–3) which carries a hosted AIS payload of the USCG (US Cost Guard). The satellites and the AIS payloads were designed and developed at OHB–System AG of Bremen, Germany. The objective of the US NAIS (Nationwide Automatic Identification System) is to test the feasibility and effectiveness of AIS

1325) <http://www.uscg.mil/ACQUISITION/programs/pdf/NAIS.pdf>

1326) http://www.gmsa.gov/twiki/pub/Main/TexasIII/ORBCOMM_Worldwide_AIS_from_Space_TexasIII.pdf

message reception and reporting from space for ship tracking and other navigational activities. ¹³²⁷⁾

- On Sept. 23, 2009, the PSLV launch vehicle of ISRO launched a total of 7 satellites, OceanSat–2 (960 kg) being the primary payload. Among the secondary payloads were 2 nanosatellites (Rubin–9.1 and Rubin–9.2) of OHB Bremen with AIS receivers.
- AISSat–1, a nanosatellite (6.5 kg) developed by UTIAS/SFL for the government of Norway, was launched on July 12, 2010. The AIS sensor onboard is a software defined radio (SDR) system developed by Kongsberg Seatex (KSX) of Trondheim, Norway. The project management is with FFI (Norwegian Defense Research Establishment). ^{1328) 1329) 1330)}
- AAUSat–3 (a nanosatellite of Aalborg University, Denmark) is under development as of 2008. An AIS device is the primary payload.
- AprizeSat–3 and –4, two microsatellites (each 12 kg, 25 cm cubes) of Aprize Satellite Inc. of Fairfax, VA, built by SpaceQuest Ltd. of Fairfax, VA, were launched as secondary payloads on July 29, 2009 from Baikonur, Kazakhstan. Both microsatellites carried an AIS payload. AprizeSat–3 and 4 were commissioned 1 hour after separation. ¹³³¹⁾
- In 2008, OrbComm Inc. awarded a contract to SNC (Sierra Nevada Corporation) to build 18 new ORBCOMM Generation 2 (OG2) satellites. All OG2 satellites will be designed with AIS payloads (in addition to their enhanced communication payloads) to receive and report transmissions from AIS–equipped maritime vessels. ORBCOMM intends to market this AIS data to U.S. and international coast guards and government agencies, as well as companies engaged in security or logistics businesses for tracking shipping activities or for other navigational purposes. The various launches of the constellation (Falcon–1e of SpaceX) are planned in the timeframe from late 2010 to 2014.
- In June 2008, COM DEV International Ltd. was awarded the prime contract of the M3MSat (Maritime Monitoring and Messaging Microsatellite) mission, funded by DRDC (Defense Research and Development Canada), an agency of the Canadian Department of Defense, and by CSA (Canadian Space Agency). The overall objective is to demonstrate a complex AIS receiver for maritime surveillance. A launch of M3MSat is planned for 2011.
- The Max Valier nanosatellite (12 kg) of the technical high school of Bozen, Italy will carry an AIS receiver provided by LuxSpace of Luxembourg. A launch is planned in 2011.
- The RCM (RADARSAT Constellation Mission) of Canada, in the design phase as of 2008, is planning to fly an AIS device of CSA and DND, next to the regular SAR equipment on the three spacecraft constellation. A launch is planned for 2014.

1.9.11 History of ISLs (Intersatellite Links)

Intersatellite links or crosslinks provide direct connectivity between two or more satellites, thus eliminating the need for intermediate ground stations when sending data. ¹³³²⁾ Intersatellite links have been considered for satellite constellation missions involving Earth observation and communications.

¹³²⁷⁾ <http://www.uscg.mil/nais/>

¹³²⁸⁾ <http://www.spacecentre.no/?module=Articles;action=Article;publicShow:ID=51125>

¹³²⁹⁾ Bjorn T. Narheim, Oystein Olsen, Oystein Hellenen, Richard Olsen, Alexander M Beattie, Robert E. Zee, “A Norwegian Satellite for Space–based Observations of AIS in the High North,” Proceedings of the 22nd Annual AIAA/USU Conference on Small Satellites, Logan, UT, USA, Aug. 11–14, 2008,

¹³³⁰⁾ G. K. Høyve, T. Eriksen, B. J. Meland, B. T. Narheim, “Space–based AIS for global maritime traffic monitoring,” *Acta Astronautica*, Vol. 62, Issues 2–3, January–February 2008, pp. 240–245

¹³³¹⁾ Dino Lorenzini, Mark Kanawati, “TEXAS III Presentation,” Aug. 19, 2009, URL: <http://www.spacequest.com/Articles/SpaceQuest-TEXAS-III-Presentation.pdf>

¹³³²⁾ Paul Muri, Janise McNair, “A Survey of Communication Subsystems for Intersatellite Linked Systems and CubeSat Missions,” *Journal of Communications*, Vol. 7, No 4, April 2012, doi:10.4304/jcm.7.4.290–308

These ISLs can be between all the various orbits that one might consider: LEO (Low Earth Orbit), MEO (Medium Earth Orbit), HEO (Highly Elliptical Orbit), GEO (Geostationary Earth Orbit) and IGSO (Inclined Geosynchronous Earth Orbit). The older systems, like TDRSS and Iridium, are using RF (Radio Frequency) links for their ISL services as well as for their space-to-Earth links.

The newer relay satellites, like ESA's ARTEMIS, use RF and optical ISLs. In general, the RF links are being used for Space-Earth links, because clouds and/or bad weather in the ground segment, as well as atmosphere disturbances, might interfere with an optical link. The optical ISLs are used for very high-speed (Gbit range) in space-to-space links.

Launch year	Satellite(s)	ISL frequency (band)
1972–1978	OSCARs 6, 7, 8, (Orbiting Satellite Carrying Amateur Radio). The first link was between OSCAR-7 and OSCAT-6 in January 1975 ¹³³⁴	VHF/UHF
1969 (ATS6) 1975	In April 1975, NASA established a link from GEOS-3 (LEO) to ATS-6 (GEO) ¹³³⁴	S-band, C-band to a ground station
1975	In July 1975, ISLs were established, as part of the Apollo-Soyuz Test Project between the Apollo Service Module and ATS-6.	
1976	LES-8 and LES-9 [Lincoln (Laboratory) Experimental Satellite], in IGSO, DoD (USAF, Navy).	36, 38 GHz
1983–2013	TDRSS constellation, NASA	C-, Ku-, Ka-band
1985–1995	Luch (Data Relay Satellites), Soviet Union/Russia	UHF, Ka-band
1994	ETS-6 (Engineering Test Satellite-6), JAXA, LCE optical terminal, tests were conducted with JAXA and JPL ground stations	2, 23, 32 GHz, Optical
1997	Navstar Block IIR, DoD	UHF
1997	Iridium Constellation, Motorola (Iridium Satellite LLC)	23 GHz (Ka-band)
1998	ETS-7, JAXA	2 GHz
1994–2003	MilSTaR I/II, DoD	60 GHz
1998	SPOT-4, CNES, PASTEL optical terminal on LEO satellite	Optical
2001	ARTEMIS, ESA, (OPALE optical terminal)	S-, Ka-band, Optical
2002	Envisat, ESA	S-band
2002	DRTS (Data Relay Test Satellite, Kodama), JAXA	S-band, Ka-band
2002	ADEOS-II (Advanced Earth Observing Satellite-II), JAXA	2 GHz, 26 GHz
2005	OICETS (Optical Interorbit Communications Engineering Test Satellite, Kirari) of JAXA in LEO, LUCE optical terminal. Tests of LUCE with OPALE on ARTEMIS in 2003.	Optical
2006	ALOS (Advanced Land Observing Satellite, Daichi), JAXA	S-band, Ka-band
2007	TerraSAR-X, DLR, use of LCT (Laser Communication Terminal) of Tesat; tests between TerraSAR-X and NFIRE of DoD in 2008	Optical
2010, 2012	AEHF [Advanced EHF (Extremely-High Frequency)], USAF	60 GHz (W-band)
2010	TanDEM-X, DLR, use of LCT, ISL between TSX and TDX	Optical
2014 2014	Copernicus: Sentinel-1A of ESA, use of LCT Copernicus: Sentinel-2A of ESA, use of LCT	Ka-band, Optical Ka-band, Optical
2014 2016	EDRS-A (European Data Relay Satellite-A), payload is hosted on Eutelsat-EB9B EDRS-B, payload is hosted on Hylas-3 of Avanti Communications	Ka-band, Optical Ka-band, Optical
2015–2017	Iridium Next constellation (66+satellites), Iridium Communications Inc.	23 GHz (Ka-band)

Table 73: Overview of Intersatellite Linking Systems ^{1333) 1334)}

1333) Jeng-Shing Chern, Zuu-Chang Hong, Tsai-Lun Chien, Tzu-You Chen, Ji-Chien Dai, "Design and Application of Inter-Satellite Link in Weather Observation Constellation," Journal of Marine Science and Technology, Vol. 20, No. 4, pp. 472–477 (2012), URL: <http://jmst.ntou.edu.tw/marine/20-4/472-477.pdf>

1334) Richard S. Fuhrmann, "Intersatellite Link Design Issues," Thesis, University of Colorado, 1985, URL: <http://www.dtic.mil/cgi-bin/GetTRDoc?Location=U2&doc=GetTRDoc.pdf&AD=ADA166761>

1.10 Spacecraft Operations

There are very many aspects to the wide field of “spacecraft operations” dealing with operation centers, the RF communications to and from the spacecraft, and the onboard spacecraft operations. Only a few topics have been selected to give the reader a better idea of technology introduction in some representative aspects of spacecraft operations and services.

1.10.1 Introduction of computers into space missions

By today's (21st century) technical standards of virtually omnipresent computers, programmable logic devices, and Internet availability – one would expect that computers were part of every spacecraft since the very beginning of the space age. However, this was not the case because the “computer age” was in its infancy at the launch of Sputnik–1 in Oct. 1957 – just 11 years after ENIAC (Electronic Numerical Integrator and Calculator), commonly thought of as the first electronic computer in USA. In fact, the very idea of a computer on a spacecraft was rather farfetched at the time. The transistor was invented in 1947/8 at Bell Labs by John Bardeen, Walter Brattain and William Shockley, who discovered the transistor effect and developed the first device. The Integrated Circuit (IC) was invented in 1958 by Robert Noyce of Fairchild and by Jack Kilby of Texas Instruments; the first microprocessor was introduced in 1971 (Intel 4004; 4 bit, 2,300 transistors).¹³³⁵⁾

The early manned spaceflights (of the USSR as well as of NASA) were guided by navigational computers on the ground; onboard computation was simply non-existent.^{1336) 1337) 1338)}

Prior to ISS, NASA conducted five manned spaceflight programs: Mercury, Gemini, Apollo, Skylab, and Shuttle. There was no onboard computing capability on any Mercury mission at all (six manned flights in the period 1961–1963). The latter four programs produced spacecraft that had onboard digital computers. The Gemini computer was a single unit dedicated to guidance and navigation functions. It is considered the **first computer in orbit** with a launch in 1965 (Gemini–3). In the Apollo program, proprietary processors and subsystems were designed from scratch.

- 1962 – IBM received a contract from NASA to build the first guidance computer for the Gemini spacecraft series. [Note: Gemini–1 was launched Apr. 8, 1964 with no crew aboard; **Gemini–3** (launch March 23, 1965) was the first crewed Earth-orbiting spacecraft of the Gemini series. Gemini–12 (launch Nov. 11, 1966) was the last spacecraft of the series.] The Gemini computer's memory was a random-access, nondestructive readout design with flexible instruction and data storage organization. The custom-built computer had a mass of 27 kg and performed more than 7,000 calculations/s. Onboard computing power enabled Gemini to carry out eventually tasks such as rendezvous and docking even though the computer was underpowered by today's standards:

- Its nominal capacity was 4,096 words (39 bit/word) of core memory
- Its operational capacity was 12,288 13-bit word instructions, 26 bit data
- The computer was programmed in octal by hand

- 1961 – Start of the **AGC** (Apollo Guidance Computer) development program. NASA contracted with the MIT Instrumentation Laboratory for the design, development, and

¹³³⁵⁾ http://www-users.mat.uni.torun.pl/~bala/wyklad_arch/History.pdf

¹³³⁶⁾ J. E. Tomayko, “Computers in Spaceflight: The NASA Experience,” NASA Contractor Report 182505, March 1988, From Sequencers to Computers: Exploring the Moon and the Inner Planets, <http://www.hq.nasa.gov/office/pao/History/computers/Ch5-1.html>

¹³³⁷⁾ P. Norwig, “The Uses of Computers in Spaceflight,” <http://www.norvig.com/spacecycv.html>

¹³³⁸⁾ Note: Unfortunately, I wasn't able to find any documentation on the introduction of computer technology in spacecraft of the former USSR

construction of the Apollo guidance and navigation system, including software (a challenging undertaking at the time). The AGC hardware is considered the first recognizably modern “embedded system” and the first flight computer using ICs (Integrated Circuits), launched in 1968. AGC consisted of:

- Memory: 256 words total of 16 bit erasable memory; 4,000 words of non-erasable memory (core ropes)
- Later upgraded to 2k erasable and 36k non-erasable memory
- Timing: AGC was controlled by a 2.048 MHz crystal clock
- Central register: the AGC had four 16 bit registers for general computational use.

Note: In the early 1960s the so-called minicomputer had not emerged yet and there was no commercial computer suitable for use in the Apollo mission. Most of the technologies that were eventually used in the Apollo computer were just emerging from research and development efforts. The design was mainly a task of fitting the components together in order to meet the mission requirements for computational capacity and miniaturization. ¹³³⁹⁾

Apollo-7 was launched from Cape Kennedy, FLA, on Oct. 11, 1968 (first flight of the Apollo program – the Apollo-1 crew (Edward H. White, Virgil I. Grissom, Roger B. Chaffee) was lost in a tragic fire accident during prelaunch tests on Jan. 27, 1967). The last Apollo flight in the program was Apollo-17 (launch Dec. 17, 1972).

Each Apollo mission carried two AGCs, one in the command module and one in the lunar module. The AGC system served well on the Earth-orbital missions, the six lunar landing missions, the three Skylab missions, and the Apollo-Soyuz test project. Even though plans existed to expand the computer to 16k of erasable memory and 65k of fixed memory, including making direct memory addressing possible for the erasable portion, no expansion occurred. The Apollo computer that controlled the first lunar landing (Apollo-11, July 20, 1969) had only 32,000 words of memory.

- 1970 – Apollo astronauts carry portable programmable calculators as backup to the navigation computer, i.e., the AGC (Apollo Guidance Computer).
- 1973 – Skylab (total of 3 manned missions in 1973/4) had a dual computer system for attitude control of the laboratory and pointing of the solar telescope. The primary objectives of the Skylab missions were to establish a manned workshop in Earth orbit, and to develop orbital operation techniques. Skylab and, later, the Shuttle, used “off-the-shelf” IBM 4Pi series processors (Note: the Gemini and Apollo computer systems were custom-built processors). The 4Pi descended directly from the System 360 architecture of IBM developed in the early 1960s. The 4Pi model chosen for Skylab was the TC-1 (16-bit word length), adapted for use on Skylab by the addition of a custom input/output assembly to communicate with the unique sensors and equipment aboard the laboratory. A TC-1 processor, an interface controller, an I/O assembly, and a power supply made up an ATMDC (Apollo Telescope Mount Digital Computer). Each TC-1 (there 2 on Skylab) had a memory of 16,384 words. ¹³⁴⁰⁾
- 1981 – Space Shuttle (launch of STS-1 on Apr. 12, 1981), the reusable Space Transportation System (STS) of NASA, used closely coupled computers for digital flight, and a multithreaded parallel computer configuration for I/O. The onboard computers were part of IBM’s Advanced System/4 Pi, avionics computer series (also referred to as AP-101). The Shuttle’s general purpose computer was one of five computers – four of which were arranged in a redundant configuration, with a fifth computer acting as a backup unit – allowing early Shuttle missions to continue even if multiple failures were experienced.

1339) E. C. Hall, “The Apollo Guidance Computer – A Designer’s View,” 1982, http://klabs.org/history/history_docs/mit_docs/agc.htm

1340) A. E. Cooper, W. T. Chow, “Development of On-board Space Computer Systems,” IBM Journal of Research Developments, Jan. 1976, <http://www.research.ibm.com/journal/rd/201/ibmrd2001D.pdf>

1.10.1.1 Unmanned space missions:

There were no onboard computers in the early spaceage (the technology didn't exist). Onboard operations (enacting decisions) evolved with automatic sequencing devices (lots of relays and timers) to activate and command experiments (i.e. mission events) according to the logic of predefined schedules. These onboard operations of event sequences applied also to the launch phase of a spacecraft, triggered by onboard sequencers or by ground command.

- The early Earth-orbiting spacecraft of NASA, like TIROS-1 (launch Apr. 1, 1960) and follow-up weather satellites of the series, employed sequencers to facilitate onboard operations.
- The early Pioneer spacecraft series [launch of Pioneer-1 in 1958, launch of Pioneer-13 (last of the series) in 1978] as well as the Lunar Orbiters of NASA used to map the moon in the early 1960s – they did not carry onboard computers. Like their Earth-orbiting cousins and the first JPL probes, they used sequencing devices to activate and command experiments.
- The Ranger spacecraft series of NASA (9 missions, 1961–1965) carried a "Central Computer and Sequencer" to back up the direct command system. Activated before lift-off, it counted the hours, minutes, and seconds until a specified mission event was to occur and then executed a set of commands that performed the required functions. If the uplink radio channel failed, the mission would proceed according to a prepared plan.

At the same time that the Rangers were being built, JPL designed and flew the first Mariners. Mariner's initial mission was a Venus flyby launched in 1962. In the case of this spacecraft and its later brethren, the Central Computer and Sequencer was the prime source of commands, at least for cruise and encounter portions of the mission. The time delay for commands to travel to Venus and Mars defeats real-time control from the ground.

- The Mariner-2 spacecraft to Venus (1962), Mariner-4 to Mars (1964), and Mariner-5 to Venus (1967) carried the same Central Computer and Sequencer.
- The Mariner-6 and -7 missions to Mars (1969) carried a **programmable** Central Computer and Sequencer (12 kg) designed at JPL and built by Motorola. The Sequencer commanded all spacecraft systems, including the Attitude and Pointing System and Flight Data System, each of which evolved to include their own computers by the time JPL designed the outer planets Voyager in the 1970s. – Original requirements for Mariner Mars 1969 called for 20 words of memory, making the 128-word version more than enough. Yet the memory was quickly exceeded, necessitating the use of "creative" programming techniques for the duration of the mission.
- 1971 – Mariner Mars spacecraft computer – upgraded to 512 words
- 1972 – The Pioneer 10 spacecraft, an interplanetary probe of NASA/JPL (launch March 2, 1972), is considered to have **introduced the first microprocessor into a spaceborne mission in history, the Intel 4004 with a 4-bit instruction set.** – Intel introduced the world's first microprocessor, the Intel 4004, on Nov. 15, 1971 commercially. A few months after market introduction, the tiny 4004 chip provided already the computing power for the Pioneer 10 mission. ^{1341) 1342) 1343)}
- NSSC-1 (NASA Standard Spacecraft Computer-1): NSSC-1, developed at NASA/GSFC, has evolved from the on-board processor that was flown as an experiment on the OAO-3 (Orbiting Astronomical Observatory-3) launched on Aug. 21, 1972. This first

¹³⁴¹⁾ <http://www.geocities.com/thestarman3/epc/4004.html>

¹³⁴²⁾ http://en.wikipedia.org/wiki/Intel_4004

¹³⁴³⁾ <http://micro.magnet.fsu.edu/micro/gallery/computers/computer2.html>

computer was referred to as OBP (On–Board Processor). As the computer was applied to other missions, implementation improvements were made. Even before the launch of OAO–3, a program was initiated to improve reliability and reduce size and mass. The result of the program was that the AOP (Advanced On–board Processor) was flown on the Landsat–2 (launch Jan. 22, 1975) and LandSat–3 (launch March 5, 1978) missions, where it was used to augment the stored command capability and perform onboard telemetry limit checking.¹³⁴⁴⁾

On the IUE (International Ultraviolet Explorer) mission (launch Jan. 26, 1978), the AOP performed attitude control computations; on the OSS–1 (Office of Space Science–1), mission, launched on STS–3 on March 22, 1982, the AOP provided the stored commands necessary for efficient instrument control. In 1974, the computer became a NASA standard spacecraft component. The NSSC–1 has flown on two further missions: the SMM (Solar Maximum Mission), launched on Feb. 14, 1980 (however, several instruments on SMM were already controlled by imbedded microprocessors), and Landsat–4, launched on July 16, 1982. Its functions included stored command processing, attitude control, limit checking and corrective action, and backup telemetry.

- 1976 – Beginning with the Viking missions to Mars, reprogrammable digital computers showed up on NASA interplanetary spacecraft.
- The following NASA missions used the 8–bit RCA 1802 microprocessor, a radiation–hardened 8–bit microprocessor in space.

– The Voyager–1 mission, launched Sept. 5, 1977; and Voyager–2 launched Aug. 20, 1977. Both are interplanetary missions.

Note: In early May 2010, the 33 year old Voyager–2 spacecraft experienced an anomaly where the data it returned to Earth was unreadable. Engineers diagnosed the problem as a flip of a bit in the memory in the flight data system that packages data to transmit back to Earth, and were able to successfully reset the data system. In addition, the clock had to be reset in the spacecraft’s data system that lost time while the memory bit was in the wrong state. On May 23, 2010 Voyager 2 sent back data that was again formatted properly. At the time of repair, Voyager–2 was about 13.8 billion km from Earth requiring about 26 hours for a round–trip of the signals.¹³⁴⁵⁾

– The MagSat mission of NASA (launch Oct. 30, 1979). The spacecraft was designed, built and integrated by JHU/APL (Laurel, MD) for NASA.¹³⁴⁶⁾

Note: The RCA 1802 microprocessor was introduced by the company in 1976. The CDP 1802 was used because it could be run at very low power, and because its production process (silicon on sapphire) ensured much better protection against cosmic radiation and electrostatic discharges than that of any other processor of the era.

- *The first spaceborne microprocessor (Intel 8080)¹³⁴⁷⁾¹³⁴⁸⁾ on an Earth observation mission, introduced by JHU/APL, was flown on the SeaSat–A mission of NASA/JPL (launch June 27, 1978). The microprocessor was used for the altimeter instrument onboard SeaSat–A. The*

1344) Paul Schneck, Charles E. Trevathan, Thomas D. Taylor, Raymond G. Hartenstein, Ann C. Merwarth, William N. Stewart, “Development and Application of NASA’s First Standard Spacecraft Computer,” Communications of the ACM, Sept. 1984, Vol. 27, No 9, pp. 902–913, Feb. 3, 2010, URL: <http://klabs.org/DEI/Processor/nssc1/p902-trevathan.pdf>

1345) Nancy Atkinson, “Voyager 2 Update from Dr. Ed Stone,” June 2, 2010, URL: <http://www.universetoday.com/2010/06/02/voyager-2-update-from-dr-ed-stone/>

1346) H. K. Charles Jr., “Electronics Technology at APL,” Johns Hopkins APL Technical Digest, Vol. 24, No 1, 2003, pp. 112–124

1347) E. J. Hoffman, “Spacecraft Design Innovations in the APL Space Department,” Johns Hopkins APL Technical Digest, Vol. 13, No 1, 1992, pp. 167–181

1348) J. MacArthur, “Design of the SeaSat–A Radar Altimeter,” Oceans, Vol. 8, Issue Sep. 1976, pp. 222–229

*microcomputer utilized the 8080 microprocessor with 4096 bytes of program memory and 2048 bytes of scratch pad memory.*¹³⁴⁹⁾

- The Intel 80386 microprocessor, also referred to as i386, (a general purpose 32-bit microprocessor with a multitasking operating system) was first flown on the HST (Hubble Space Telescope) mission of NASA (launch April 24, 1990). Note: Intel introduced the 80386 to the market in 1986. The SAMPEX (Solar Anomalous Magnetospheric Particle Explorer) mission of NASA followed with a launch July 3, 1992. The distinct advantage of the 80386 microprocessor represented a considerable cost reduction for a space mission. However, the use of these commercial parts in spaceflight raises the issue of vulnerability to single event effects (SEE). – Other missions with the 80386 microprocessor are: RXTE (Rossi X-ray Timing Explorer) of NASA (launch Dec. 30, 1995); TRACE mission of NASA's SMEX program (launch April 2, 1998); UoSAT-12 minisatellite of SSTL (launch April 21, 1999).
- 2000 – The SNAP-1 nanosatellite mission of SSTL (Surrey, UK, launch June 28, 2000), with a total mass of 6.5 kg, used a StrongARM onboard computer (4 MB EDAC memory), a CAN bus for data handling, three-axis attitude determination and control, a GPS receiver (SRG-05), power subsystem (4W/9W average/peak, 6-cell NiCd battery), a CMOS camera that served as its primary payload, and a microthruster of 30 μ N with a Δv capacity of 3 m/s (the micro-propulsion system had the size of a pencil).
- An automobile of today¹³⁵⁰⁾ (2004, with cell phones, appliances, radio frequency ID tags, etc.) has more computing power than the Apollo 13 spacecraft (launch Apr. 11, 1970).

The computers used in spaceflight have always been a mixture of leading and lagging technology (unfortunately mostly lagging) introduction. On one hand, space programs like Apollo gave a strong boost to advanced small and rugged computer technology; on the other hand, the introduction of onboard state-of-the-art computer technology was always delayed due to such requirements as “space qualification” (radiation hardened components, etc.) or due long waiting periods caused by long project planning and development times, and/or by waits for a launch opportunity. For large and complex space missions, in particular for new-generation missions involving the specification and development of new observation instruments, the lead times are so enormous (a decade for the EOS missions of Terra, Aqua and Aura, a decade for Envisat and MSG-2, a decade and more for NPOESS and GOES-R) that meanwhile up to 2 new computer generations have already been introduced on the market. And the selection of a computer system has to be made fairly early in the project. In addition, monitoring missions like MSG-2, MetOp, NPOESS, and GOES-R consist of a series of spacecraft (put into storage), each with operational lifetimes of at least 7 years, which are being launched successively, ending with at least 2 decades of operational service. No wonder, technology is outdated after such long periods of service.

Updates of onboard computer software has been practised for a long time (uploads of new and improved algorithms, etc). On the hardware side, updates of computer configurations can now be made with the introduction of FPGA (Field Programmable Gate Array) technology (see chapter 1.8.7 on FPGAs). An FPGA controller provides the capability to directly generate the logical configuration of FPGA gates from a C-like high level language without producing the machine code for a processor.

When development times are fairly short (1–2 years from planning to launch), like in micro-, nano-, or picosatellite projects, and COTS (Commercial-Off-The-Shelf) components can be used, then the chances for state-of-the-art computer technology introduction become much better.

1349) J. A. Perschy, “The SeaSat – A satellite radar altimeter spaceborne microcomputer,” British Interplanetary Society, Journal (Space Technology), Vol. 32, Jan. 1979, pp. 9–14.

1350) A. Schutzberg, “The Future of Sensors: A Conversation with David Rejeski,” EOM (Earth Observation Magazine), Vol. 13, No 6, Oct. 2004

• The RAD6000 computer is the world's first radiation-hardened single board 32-bit microprocessor, containing more than one million transistors. The RAD6000 computer, based on the IBM RISC single chip CPU (Power Architecture), was manufactured by IBM for BAE Systems and is mainly known as the onboard computer of numerous NASA spacecraft [the RAD6000 development came out of a space electronics program, the ASCM (Advanced Spaceborne Computer Module), funded by BMDO, the Air Force, and Phillips Laboratory]. The 1997 34th Space Congress' panel of experts considered the radiation hardened RAD6000 microprocessor chip the most significant technical contribution to space of the last decade. The computer has a maximum clock rate of 33 MHz and a processing speed of about 35 MIPS. In addition to the CPU itself, the RAD6000 has 128 MB of ECC RAM. ^{1351) 1352)}

Examples of US missions with the RAD6000 computer onboard are:

- Mars Pathfinder (lander) mission of NASA with a launch on Dec. 4, 1996
- DS1 (Deep Space 1) probe of NASA with a launch on Oct. 24, 1998
- IMAGE spacecraft (Explorer 78) of NASA with a launch on March 25, 1999
- Genesis spacecraft of NASA with a launch on Aug. 8, 2001
- RHESSI (Reuven Ramaty High-Energy Solar Spectroscopic Imager) mission of NASA with a launch on Feb. 5, 2002
- Coriolis/WindSat of NLR with a launch on Jan. 6, 2003
- MER-A (Mars Exploration Rover) of NASA with a launch on June 10, 2003, and MER-B with a launch on July 7, 2003
- Spitzer Infrared Telescope Facility of NASA with a launch on Aug. 25, 2003
- GB-B (Gravity Probe B) of NASA with a launch on April 20, 2004
- SWIFT mission of NASA with a launch on Nov. 20, 2004
- MESSENGER (Mercury Surface, Space Environment, Geochemistry and Ranging) of NASA with a launch on Aug. 3, 2004. The Messenger spacecraft started orbiting planet Mercury on March 18, 2011 (UTC). This marks the first time that a spacecraft is orbiting the solar system's innermost planet. – The spacecraft carries scientific instruments designed to map Mercury and analyse the structure and composition of its surface. MESSENGER will have to withstand extreme differences in temperature as well as very high levels of radiation. The entire mission will be an endurance test for the spacecraft and the experiments. ¹³⁵³⁾
- STEREO (Solar Terrestrial Relations Observatory) of NASA with a launch on Oct. 26, 2006
- Phoenix Mars polar lander of NASA with a launch on Aug. 4, 2007
- DAWN mission of NASA/JPL with a launch on Sept. 27, 2007 to the asteroid belt of the solar system. DAWN arrived at Vesta in July 2011. DAWN left asteroid Vesta on Sept. 5, 2012 and will reach Ceres in early 2015. These two members of the asteroid belt have been witness to much of our solar system's history.

The RAD6000 processor technology has been implemented on many commercial, DoD as well as other missions. Several variations of the computer board were developed and a set of support ASICs and FPGAs exists for the processor.

1351) <http://www.mdatechnology.net/techprofile.aspx?id=429>

1352) The CPUs of Spacecraft Computers in Space," URL: <http://www.cpushack.net/space-craft-cpu.html>

1353) Tony Phillips, "Historic First: A spacecraft orbits Mercury," NASA, March 18, 2011, URL: http://science.nasa.gov/science-news/science-at-nasa/2011/18mar_orbitmercury/

As of 2008, the RAD6000MC will be manufactured at BAE Systems in the 150 nm radiation hardened CMOS technology called “RH15”. The TID (Total Ionizing Dose) radiation hardness is rated at 1 Mrad (Si), having been tested out to 2 Mrad(Si) without degradation. The RAD6000MC (Microcontroller) is an excellent match for use with the emerging Space PnP (Plug–and–Play) Avionics for the SpaceWire (SPA–S) standard. The Appliqué Sensor Interface Module (ASIM) requires both a SpaceWire interface and analog interfaces to sensors. The inclusion of both 1553 and PCI (Peripheral Connection Interconnect) interfaces provides for connection to legacy peripherals as well as those that support the SpaceWire interface. The RAD6000MC is suitable for many applications, from very small robotic vehicles and satellites to large spacecraft with a distributed processing architecture. 1354) 1355)

- The RAD750 is a radiation–hardened single board computer, based on IBM’s PowerPC 750 architecture. As successor of the RAD6000, the RAD750 is manufactured by BAE Systems. A total of 36 MB of radiation hardened SRAM is available to the RAD750, along with 4 MB of EEPROM and 64 KB of start–up ROM, all provided with additional bits for error correction code (ECC). The RAD750 processor was introduced in 2001 and had its first flight in January 2005 on the Deep Impact mission.

Examples of missions with redundant RAD750 computer systems onboard are: 1356)

- Deep Impact mission of NASA with a launch on Jan. 12, 2005
- XSS–11 (Experimental Spacecraft System–11) of AFRL, launch on April 11, 2005
- MRO (Mars Reconnaissance Orbiter) of NASA with a launch on Aug. 12, 2005
- NFIRE (Near Field Infrared Experiment) of MDA (Missile Defense Agency) and USAF, with a launch on April 24, 2007
- WorldView–1 of DigitalGlobe with a launch on Sept. 18, 2007
- GLAST (Gamma–ray Large Area Space Telescope) of NASA, launch June 11, 2008. Note: NASA renamed the GLAST mission to Fermi Gamma–ray Space Telescope as of August 26, 2008.
- LRO (Lunar Reconnaissance Orbiter) of NASA with a launch on June 18, 2009
- WISE (Wide–Field Infrared Survey Explorer) of NASA with a launch on Dec. 14, 2009
- The SDO (Solar Dynamics Observer) of NASA with a launch on Feb. 11, 2010.
- GPM Core Observatory of NASA/JAXA with a launch on February 27, 2014.

- **SpaceCube:** SpaceCube is a family of high–performance FPGA based on–board science data processing systems developed at the NASA/GSFC. The goal of the project is to provide 10x to 100x improvements in on–board computing power while lowering relative power consumption and cost. The SpaceCube design strategy incorporates commercial rad–tolerant FPGA technology and couples it with an upset mitigation software architecture to provide “order of magnitude” improvements in computing power over traditional

1354) R. Berger, L. Burcin, D. Hutcheson, J. Koehler, M. Lassa, M. Milliser, D. Moser, D. Stanley, R. Zeger, B. Blalock, M. Hale, “The RAD6000MC™ System–on–Chip Microcontroller for Spacecraft Avionics and Instrument Control,” Proceedings of the 2008 IEEE Aerospace Conference, Big Sky, MT, USA, March 1–8, 2008, paper: 7.0101

1355) Joseph R Marshall, Neil Wood, Myrna Milliser, Richard Ferguson, Ed Maher, “Higher Performance BAE Systems Processors and Interconnects Enabling Spacecraft Applications,” Proceedings of the 2009 IEEE Aerospace Conference, Big Sky, MT, USA, March 7–14, 2009

1356) R. Berger, A. Dennis, D. Eckhardt, S. Miller, J. Robertson, D. Saridakis, D. Stanley, M. Vancampen, Q Nguyen, “RAD750™ SpaceWire–Enabled Flight Computer for Lunar Reconnaissance Orbiter,” International SpaceWire Conference 2007, Dundee, Scotland, UK, Sept. 17–19, 2007

rad-hardened flight systems. ¹³⁵⁷⁾

On-board system	MIPS	Power	MIPS/W
MIL-SDT-170A	3	15 W	0.2
RAD6000	35	10–20 W	2.33 ¹⁾
RAD750	300	10–20 W	20 ²⁾
SPARC V8	86	1 W ³⁾	86 ³⁾
LEON 3FT	60	3–5 W ³⁾	15 ³⁾
SpaceCube 1.0	3000	5–15 W	400 ⁴⁾
SpaceCube 2.0	5000	10–20 W	500 ⁵⁾
1) typical, 35 MIPS at 15 W		4) 3000 MIPS at 7.5 W (measured)	
2) typical, 300 MIPS at 15 W		5) 5000 MIPS at 10 W (calculated)	
3) processor device only, total board power TBD			

Table 74: Performance comparison of various on-board processors

SpaceCube is based on the Xilinx Virtex family of FPGA processors, which include CPU, FPGA and DSP resources. These processing elements are leveraged to produce a hybrid science data processing platform that accelerates the execution of science data processing algorithms by distributing computational functions among the elements, allowing each type of processor to do “what it’s good at”. This approach enables the implementation of complex on-board functions that were previously limited to ground based systems, such as on-board product generation, data reduction, calibration, classification, event/feature detection and real-time autonomous operations. The system also is fully reconfigurable in flight, through either ground commanding or autonomously in response to detected events/features in the instrument data stream.

– The SpaceCube 1.0 system is based on the Xilinx Virtex 4 (FX60) FPGA technology and first flew as part of the RNS (Relative Navigation Sensors) experiment during the Hubble Servicing Mission 4 in May 2009, where it proved its ability to provide realtime pose estimation while the shuttle was docking with the Hubble Space Telescope. The Hubble unit (SpaceCube 1.0a) interfaced with three cameras and ran autonomous rendezvous and docking algorithms to simulate a robotic servicing capture and release configuration. The system operated on-orbit for approximately 60 hours, and met all RNS experiment goals.

– The second SpaceCube experiment (SpaceCube 1.0b) flew as part of the NRL (Naval Research Laboratory) MISSE-7 (Materials on the International Space Station Experiment 7) payload and was installed on the Space Station in November 2009 (on STS-129, Nov. 16–27, 2009). The purpose of the MISSE-7 SpaceCube 1.0 experiment is to test and validate the RHBS (Radiation Hardened by Software) mitigation techniques. The RHBS strategy involves a combination of traditional “memory scrubber” functions and a “program execution error detection and correction” software architecture that runs in the background to find and fix single and multi-bit radiation induced upsets. The goal of RHBS is to enable the reliable use of commercial rad-tolerant processing elements in space and to “asymptotically approach” the reliability of true rad-hard systems while providing more computing power for less cost. The MISSE-7 SpaceCube 1.0 experiment will remain on the Station for the next 2–5 years and will serve as an on-orbit testbed for current and future RHBS technology development efforts.

The A-OPSS (Autonomous On-board Processing for Sensor Systems) project uploaded its A-OPSS software onto a SpaceCube 1.0 processor card on board the International Space Station as part of the MISSE-7 experiment. This resulted in an enhanced high performance and low overhead fault strategy on the SpaceCube 1.0 platform. An initial study of representative hyperspectral applications also proves promising due to high levels of data

¹³⁵⁷⁾ Tom Flatley, “Advanced Hybrid On-Board Science Data Processor – SpaceCube 2.0,” Proceedings of the ESTF 2010 (Earth Science Technology Forum), Arlington, VA, USA, June 22–24, 2010, URL: http://esto.nasa.gov/conferences/estf2010/papers/Flatley_ESTF2010.pdf

parallelism and fine grained parallelism achievable within FPGA System on a Chip architectures enabled by A-OPSS RHBS techniques. ¹³⁵⁸⁾

– SpaceCube 1.5, an intermediate version, is being designed to support a quick-turn-around sounding rocket flight and serves as a stepping stone to the next generation SpaceCube 2.0 system currently being developed under funding from ESTO (Earth Science Technology Office). SpaceCube 1.5 moves from the Virtex 4 to the Virtex 5 family of FPGAs and adds several industry standard plug-and-play interfaces such as Gigabit Ethernet and SATA-II (Serial Advanced Technology Attachment-II) interfaces. ^{1359) 1360) 1361)}

The first SpaceCube 1.5 system is flown on the **ORS-1** (Operationally Responsive Space-1) minisatellite of DoD with a launch on June 29, 2011. The ORS-1 satellite, built by ATK, grew out of the success of TacSat-3. ATK used the TacSat-3 bus to build the ORS-1 satellite with the addition of a propulsion module. The ORS-1 spacecraft has a mass of 450 kg (orbit of 400 km, 40° inclination); it carries SYERS-2 (Senior Year Electro-Optical Reconnaissance System-2), a pushbroom VIS/SWIR/MWIR high-resolution camera (7 bands) developed at Goodrich, Danbury, CT. The SYERS-2 instrument is of U-2 aircraft heritage.

ORS-1 proved its operational utility almost immediately, providing timely coverage and responsive fulfillment of theater taskings. ¹³⁶²⁾

– In 2010, NASA's ESTO is funding the development of the SpaceCube 2.0 system under their AIST (Advanced Information Systems Technology) program, to provide advanced on-board science data processing capabilities to the upcoming series of ESDS (Earth Science Decadal Survey) missions. – The SpaceCube 2.0 system is based on Xilinx Virtex 5 technology and adds Spacewire and cPCI interfaces, in addition to the Gigabit Ethernet and SATA-II interfaces developed for the SpaceCube 1.5 system. SpaceCube 2.0 also moves from custom packaging that was used on SpaceCube 1.0 and 1.5 to an industry standard 3U form factor, and is fully scalable to support a wide variety of mission requirements. ¹³⁶³⁾

The SpaceCube 2.0 breadboard will be flown as an experiment on the ISS through a collaboration with the U.S. Air Force as part of their Space Test Payload-H4 (STP-H4) payload. The ISS SpaceCube Experiment 2.0 (ISE 2.0) will couple the SpaceCube 2.0 breadboard with a camera system, gamma ray detector, photometer, antenna and thermal plate experiment, with the primary goals of extending SpaceCube RHBS research, developing Earth Science “event detection” algorithms and studying gamma ray bursts from terrestrial lightning/thunderstorms. ISE 2.0 is scheduled for delivery to the Air Force in 2012, with a launch to the ISS in 2013.

A SpaceCube 2M (SpaceCube 2.0 Mini) system is also being developed to support CubeSat, UAV (Unmanned Aerial Vehicle), in-situ/embedded sensor and robotic/rover applications, and will incorporate a significant subset of the full SpaceCube 2.0 features and functions in a small package. The first SpaceCube Mini will fly as part of the IPEX (Intelligent Payload Experiment) 3U CubeSat that will demonstrate advanced on-board processing capabilities for missions such as HypIRI.

1358) Matthew French, John Paul Walters, Kenneth Zick, “Autonomous On-board Processing for Sensor Systems: Initial Fault Tolerance and Autonomy Results,” ESTF 2011 (Earth Science Technology Forum 2011), Pasadena, CA, USA, June 21–23, 2011, URL: http://esto.nasa.gov/conferences/estf2011/papers/French_ESTF2011.pdf

1359) Turner Brinton, “Pentagon’s ORS-1 Imaging Satellite Carried to Orbit,” Space News, June 30, 2011, p. 7, URL: <http://www.spacenews.com/launch/110630-ors1-sat-orbit.html>

1360) “ATK Spacecraft Bus Contributes to Significant ORS-1 Milestone,” Space Daily, Sept. 23, 2011, URL: http://www.spacedaily.com/reports/ATK_Spacecraft_Bus_Contributes_to_Significant_ORS_1_Milestone_999.html

1361) Scott Prater, “ORS-1, ground system gain final ops acceptance,” Feb. 3, 2012, URL: http://www.afspc.af.mil/news1/story_print.asp?id=123288487

1362) Thomas M. Davis, James C. Barlow, “Operationally Responsive Space-1 (ORS-1),” Proceedings of the 4S (Small Satellites Systems and Services) Symposium, Portoroz, Slovenia, June 4–8, 2012

1363) Tom Flatley, “Advanced Hybrid On-Board Science Data Processor – SpaceCube 2.0,” ESTF 2011 (Earth Science Technology Forum 2011), Pasadena, CA, USA, June 21–23, 2011, URL: http://esto.nasa.gov/conferences/estf2011/papers/Flatley_ESTF2011.pdf

1.10.2 Onboard operating systems

- **Introduction of onboard resource brokering systems.** DoD/AFRL developed DHS (Data Handling System), a package with the objective to establish a plug-and play space experiment **brokering system**. The ETB (Electronics Testbed)/DHS is flown on two satellites: (see M.55.1).¹³⁶⁴⁾

- STRV-2 (Space Technology Research Vehicle-2) which is part of the TSX-5 (Tri-Service Experiments Mission 5) mission of AFRL. TSX-5 was launched June 7, 2000. This interface was developed so that it can be used on other space missions (STRV-1d, etc).

- STRV-1d (Space Test Research Vehicle-1d) of DERA, UK (launch of STRV-1d on Nov. 16, 2000). The AFRL science payload on STRV-1d consists of ETB, nine sub-experiments (5 NASA, 3 DoD, 1 DREO, Canada), and DHS, which in turn interfaces with OBC (On-Board Computer) of TRV-1d (this is an advanced version of the DHS flown on STRV-2).

The DHS improves on-orbit use of individual sub-experiment resources by recording experimental results, storing them locally, and communicating the results to the S/C for down-link transmission. The intent of DHS is to reduce the risk to the mission by providing a degree of separation between the spacecraft and less-proven new technologies contained in each experiment, and by providing a similar degree of separation between the experiments.

- New DHS concepts may eventually lead to tiny, embeddable processors that contain the ability to self-organize fault-tolerant networks of experiments that can be arbitrarily distributed in a S/C.

- **Onboard payload data processing systems.** At the start of the 21st century there is an increasing demand for advanced concepts of onboard payload processing, data handling, and data storage functions. The technologies needed most focus on functional support for: data compression, event recognition and response, hyperspectral and radar data onboard processing, autonomous event detection and response, and situation-based data compression and processing.¹³⁶⁵⁾

- The first **Linux operating system** in space was flown on Shuttle flight STS-83 (Apr. 4-8, 1997). The MLS (Microgravity Science Laboratory) on STS-83 carried an experiment in hydroponics, the growth of plants without soil was being tested (that could eventually provide oxygen and food to astronauts).¹³⁶⁶⁾

- The computer controlling the experiment was a specially-modified PC/104 running Linux. – As of 2002, NASA introduced FlightLinux, a concept that uses a real-time variation of the open source Linux Operating System (GNU license) for onboard spacecraft use. Generally, Linux requires a MMU (Memory Management Unit) for page-level protection, as well as dynamic memory allocation. The advantages of a Linux operating system in space applications are seen in a number of functions provided: reliability, performance, portability (support of a heterogeneous environment and vendor independence), affordability, a number of new onboard capabilities are becoming available such as web serving and file transfer (Linux makes the support for onboard LAN services relatively easy due to its networking and multiprocessing features). The CANDOS (Communications and Net-

1364) J. Lyke, P. Brezna, K. Avery, "BMDO/AFRL Partnership: Advances In Data Handling Systems For Space Experiment Control," Proceedings of AIAA-98-09-06, St. Louis Missouri, also at: http://klabs.org/richcontent/MAPLIDCon00/Abstracts/lyke3_a.pdf

1365) F. Lansing, L. Lemmerman, A. Walton, G. Bothwell, K. Bhasin, G. Prescott, "Needs for Communications and Onboard Processing in the Vision Era," Proceedings of IGARSS 2002, Toronto, Canada, June 24-28, 2002

1366) <http://flightlinux.gsfc.nasa.gov/>

work Demonstrations on Shuttle) payload processor on STS–107 (Jan. 16, Feb. 1, 2003) was flying a Linux operating system (see CANDOS description below).^{1367) 1368) 1369)}

– ESA has selected Linux as the operating system for two software products which controls the rendezvous and docking operations for a servicing spacecraft called ATV (Automated Transfer Vehicle) of ESA. ATV is a cargo resupply vehicle for ISS – the launch of the first flight of ATV (also referred to as Jules Verne) took place on March 9, 2008 with a successful automated docking at the ISS on April 3, 2008.

As of 2003, a number of space agencies are considering the use of Linux operating systems along with TCP/IP for the future communication and distributed processing architectures of their satellite missions (space segment and ground segment).

– The CubeSat UWE–1 (launch Oct. 27, 2005) of the University of Würzburg, Germany, used a micro Linux operating system (μ CLinux) in a low–power H8S–2674R microprocessor (Hitachi) to provide the capability of testing the communication protocols and to increase the potential for applications, such as ftp–server, http–server, or mission–specific applications.

– On the commercial side, a Linux–compatible OS/COMET Satellite Network Control Software is being provided by Harris Corporation of Melbourne, FLA, as of 2004. OS/COMET is an advanced software tool set featuring commercial off–the–shelf (COTS) design and high levels of flexibility. The software package supports both single–satellite missions and the largest and most complex satellite networks.

• **Reconfigurable computing systems in space** are a relatively new but rapidly evolving technology at the start of the 21st century to cope with vastly increased processing demands and to provide a re–allocation capability of system level functions to maximize the efficient use of mission resources. Reconfigurable computing systems are a combination of hardware/software data processing platforms that implement computationally intensive algorithm elements in **FPGA (Field Programmable Gate Array) technology**, yielding eventually a 10–to–1000 time improvement in processing speed over traditional CPU based “software only” systems. FPGAs use fusible links to provide custom interconnections between standard devices and building block elements already fabricated on an IC. This programming burns in a custom pattern of interconnects and hence circuitry to meet the design need. Although the FPGA manufacturer has predetermined which devices and functional building blocks exist on a chip, it is possible to support a high percentage of custom needs using this technology.^{1370) 1371)}

FPGAs are flexible programmable devices that are used in a wide variety of applications such as network routing, signal processing, digital filtering, pattern recognition and rapid prototyping. As such FPGAs provide an alternative to both functions, general purpose processor and to ASIC implementations. With FPGAs, logic can be configured to realize different applications in hardware. The driving force and technological base of reconfigurable computing are reprogrammable logic chips with gate densities exceeding millions of gates and capable of supporting run–time–reconfiguration. The use of run–time–reconfiguration in space will allow to modify onboard hardware by replacing faulty/outdated designs at different stages of a mission. *Hardware reconfigurability and software upgradability are in-*

1367) P. H. Stakem, “FlightLinux: a Viable Option for Spacecraft Embedded Computers,” Proceedings of Earth Science Technology Conference, Pasadena, CA, June 11–13, 2002, [http://esto.gsfc.nasa.gov/conferences/estc–2002/Papers/B7P1\(Stakem\).pdf](http://esto.gsfc.nasa.gov/conferences/estc–2002/Papers/B7P1(Stakem).pdf)

1368) P. H. Stakem, “FlightLinux Project, Onboard LAN, Technical Report,” May 30, 2001, http://flightlinux.gsfc.nasa.gov/docs/onboard_LAN.html

1369) P. H. Stakem, “FlightLinux Project Target Architecture Technical Report,” Oct. 6, 2000, http://flightlinux.gsfc.nasa.gov/docs/Target_Arch_Report.pdf

1370) T. P. Flatley, “Developing Reconfigurable Computing Systems for Space Flight Applications,” Proceedings of the MAPLD (Military and Aerospace Applications of Programmable Devices and Technologies) International Conference, Sept. 28–29, 1999, at JHU/APL, <http://klabs.org/richcontent/MAPLDCon99/Abstracts/flatley.pdf>

1371) S. Habinc, “Suitability of reprogrammable FPGAs in space applications,” Feasibility Report of Geissler Research for ESA, Sept. 2002

creasingly being viewed by the space community as attributes crucial to the survival of a spacecraft in long-life missions, requiring the availability of flexible onboard avionics architectures.

Reconfigurable computing involves manipulation of the logic within the FPGA at run-time. In other words, the design of the hardware may change in response to the demands placed upon the system while it is running. Here, the FPGA acts as an execution engine for a variety of different hardware functions – some executing in parallel, others in serial – much as a CPU acts as an execution engine for a variety of software threads. We might even go so far as to call the FPGA a reconfigurable processing unit (RPU).

During the past decade, FPGA devices have been used in a number of satellite developments, ranging from breadboards to flight equipments. Some implementations of spaceborne reconfigurable systems are:

- The SAMPEX (Solar Anomalous and Magnetospheric Particle Explorer) mission in NASA's SMEX program (launch July 3, 1992) makes extensive use of Actel FPGAs. **SAMPEX is considered the earliest application of FPGAs flown in space.** Twelve FPGAs were installed in the DPU (Data Processing Unit).^{1372) 1373)}
- The WIRE (Wide Field Infrared Explorer) mission of NASA (launch March 4, 1999) failed soon after launch (detection of a spinning problem on second pass). The WIRE mishap investigation found the root cause of the mission loss to be a digital logic error in the instrument control electronics. The turn-on transient characteristics of the FPGA used in the pyro control circuitry were not adequately considered in the electronics design. WIRE is an example of an early FPGA implementation resulting in the loss of the mission.
- The SNAP-1 nanosatellite mission of SSTL (Surrey Satellite Technology Ltd), UK, with a launch on June 28, 2000, employs Intel's StrongARM SA-1100 OBC with 4 MByte of 32 bit wide EDAC protected SRAM. The synchronous communications channel is full duplex (configured for 9.6 kbit/s to receive and 38.4 kbit/s to transmit) and is implemented in an FPGA of Xilinx for logical data interfacing and clock multiplexing.
- The Australian FedSat-1 mission (launch Dec. 14, 2002) carries a technology demonstration experiment called AIM (Adaptive Instrument Module), designed and developed at JHU/APL in cooperation with NASA (GSFC, LaRC), Queensland University of Technology (QUT), and CRCSS (see M.15).^{1374) 1375)} AIM contains a SRAM-based FPGA technology (Xilinx XQR4062XL of Xilinx Inc., San Jose, CA), providing a system capability to evolve or adapt to changing requirements (the functions implemented in the FPGA can be dynamically reconfigured). AIM demonstrates the practicalities of using reconfigurable computing hardware devices by conducting a series of designed experiments. Initial experiments include the demonstration of implementing data compression, data filtering, and communication message processing and inter-experiment data computation.
- SAFER (Simplified Aid for EVA Rescue) is a NASA propulsive crew self-rescue device (a mini-maneuvering unit), worn by astronauts when conducting an extravehicular activity on ISS. The SAFER device (built by QuickFlex Inc., Austin, TX and Titan Corp., Houston, TX) is an upgradable system which employs SRAM-based FPGA technology. An early test of SAFER occurred on STS-88 (Dec. 4-15, 1998, first ISS assembly flight). A full rescue simulation was conducted by the astronauts onboard STS-92 (Oct. 11-24, 2000, ISS-05-3A assembly flight) using SAFER.

1372) http://klabs.org/home_page/first_fpga/index.htm

1373) D. J. Mabry, S. J. Hansel, J. B. Blake, "The SAMPEX Data Processing Unit (DPU)," August 1992, URL: http://www.srl.caltech.edu/sampex/DataCenter/docs/DPU_description.pdf

1374) J. Lyke, "Reconfigurable Systems: A Generalization of Reconfigurable Computational Strategies for Space Systems," Proceedings of the IEEE Aerospace Conference, Big Sky, MT, March 9-16, 2002

1375) Note: FPGA technologies can be defined in two broad classes: one-time programmable and reconfigurable. One-time programmable FPGAs are commonly based on an antifuse approach in which normally open paths in interconnections can be irreversibly shorted. – Reconfigurable FPGAs are differentiated by ASICs in that otherwise fixed logic functions and interconnection patterns are replaced by programmable logic cells and programmable routing networks.

– BAE Systems (Manassas, VA) has developed (2003) a true reconfigurable spaceborne processing system in the MPN (Multi–Processor Network). Reconfigurability is based on a module that can be reprogrammed on orbit using three Xilinx Virtex FPGAs. A non–volatile C–RAM (Chalcogenide RAM) memory FPGA technology is employed to provide reconfigurability. The general onboard MPN architecture consists of four modules: a) a general purpose processor, b) GM (Global Memory), c) ODI (Other Data I/O), d) RCC (Reconfigurable Computer).^{1376)1377) 1378)}

– NPSat1, a student–built microsatellite of NPS (Naval Postgraduate School), Monterey, CA, with a launch in 2010 ?, will demonstrate fault–tolerant onboard operations with CPE (Configurable Processor Experiment), based on an FPGA design to support any application (a Linux distributed processing architecture is used).¹³⁷⁹⁾ In one scenario, the board is configured to act as a TMR (Triple–Modular Redundant) computer such that within FPGA, the three core processors operate in–step. In another application, the FPGA will be configured to act as a data compression engine.

– Flying Laptop is a microsatellite of the Institute of Space Systems (Institut für Raumfahrtssysteme, IRS) at the University of Stuttgart, Stuttgart, Germany. A launch is planned for late 2013 (the original launch date was 2008). The Flying Laptop will probably be the first microsatellite using a fully processor–less primary OBC (Onboard Computer) consisting of field programmable gate arrays (FPGAs). A user–programmable EEPROM (Electrically Erasable Programmable Read–Only Memory) on board can be reconfigured from the ground station via modem. In case of failure, the original FPGA configuration is restored from a PROM.

• **The introduction of the CMOS SOI (Silicon on Insulator) transistor technology** represents an advanced manufacturing process for processors and microchips, developed by IBM. SOI differs from CMOS by placing the transistor’s silicon junction area on top of an electrical insulator. The most common insulators employed with this technique are glass and silicon oxide. With the SOI technique, the gate area can be assured of minimal capacitance, which is a measure of ability to store an electrical charge. Any medium that can conduct electricity has some degree of capacitance. Technically, a MOS transistor is regarded as a capacitive circuit. This implies that the MOS circuit must completely charge to full capacitance to activate its switching capability. The process of discharging and recharging the transistor requires a relatively long amount of time in contrast to the time it requires to actually switch the voltage state of the transistor’s metal layer. SOI attempts to eliminate this capacitance, as a low capacitance circuit will allow faster transistor operation. As transistor latency drops, the ability to process more instructions in a given time rises.

Background: Over the last three decades, SOI CMOS had been identified as one possible method for increasing the performance of CMOS over that offered by simple scaling. Prior to the 1990s, SOI had not been suitable as a substrate for mainstream applications. The barriers to its widespread use were many, the main ones being SOI material quality, device design, and the steady progress in bulk CMOS performance through scaling. In early 1989, the IBM Research Division initiated activity in SOI CMOS with a program focusing on device design and materials research. Major development progress was made in the early 1990s with a technique called SIMOX (Separation by Implantation of Oxygen) to create an insulating layer of silicon oxide on top of the silicon wafer. By injecting oxygen at high pressure onto the silicon wafer at high temperature, the silicon reacts with the oxygen to form a layer

1376) J. R. Marshall, R. W. Berger, “Advancing Reconfigurable Processing Subsystems in Spaceborne Applications,” Proceedings of IEEE Aerospace Conference, Big Sky, MT, March 8–15, 2003

1377) J. Maimon, K. Hunt, J. Rodgers, L. Burcin, K. Knowles, “Circuit Demonstration of Radiation Hardened Chalcogenide Non–Volatile Memory,” Proceedings of IEEE Aerospace Conference, Big Sky, MT, March 8–15, 2003

1378) Note: The term “chalcogen” refers to the Group VI elements of the periodic table. “Chalcogenide” refers to alloys containing at least one of these elements such as the alloy of germanium, antimony, and tellurium.

1379) TMR is a straight forward approach to SEU protection. TMR refers to triple voting, a register implementation technique in which each register is implemented by three flip–flops or latches such that their vote determine the state of the register.

of silicon oxide – bonded to the silicon layer. In 1997, IBM server group designers selected 0.22 μm CMOS SOI for their next-generation microprocessors. That effort resulted in the first mainstream application of SOI CMOS, significant circuit learning, and its fabrication in a CMOS manufacturing line. The first commercial SOI product, a 64-bit IBM PowerPC microprocessor, was shipped in the summer of 1998. In 2002, the SOI technology moves to the 0.13 μm generation, offering an ever-increasing field of implementations/applications, such as in high-end microprocessors, in low-power RF (Radio Frequency) CMOS devices, EDRAMs (Embedded DRAMs), etc. At the start of the 21st century, the SOI technology is being introduced by many companies. IBM expects SOI to eventually replace bulk CMOS as the most commonly used substrate for advanced CMOS in mainstream microprocessors and other emerging wireless electronic devices requiring low power.¹³⁸⁰⁾

Some SOI technology advantages are:

- A marked advantage of SOI technology is its low-power behavior, opening a number of opportunities in the low-power arena.
- SOI offers the opportunity for the use of very-high-resistivity substrates to achieve low-loss passive elements. This capability, along with SOI n-FETs with an f_T of >150 GHz, opens exciting opportunities for low-power RF circuits.
- A lowering of the time taken to open and close bridges means that a processor built on this technology could be as much as 30% faster clock for clock than traditional MOS/CMOS processors. SOI designed microprocessors offer first order benefits of lower power operation, reduced junction capacitance, and higher device densities (miniaturization); all combining in significant improvements in device performance and faster circuit level speeds.
- Performance gains are averaging 25–35% when SOI is employed.
- SOI offers a reduction in soft error rates (SER). Soft errors refer to data corruption caused by cosmic rays and natural radioactive background signals. SER will be an important issue as CPUs scale to smaller die sizes and lower voltages. SOI chips indicate a significant reduction in SER related issues, even with current large die chips.
- SOI is the technology of choice for radiation-critical applications (immunity to single-event latch-up from high-energy particles).

In 2002, the CMOS SOI (Silicon on Insulator) technology is poised to take over from bulk CMOS special microelectronics market niches like: low power, high-speed digital, radiation hardened, and/or high-temperature analog, and even optoelectronic and microwave ASICs reaching into GHz frequencies. Silicon on insulator technology is becoming the process of choice for high performance consumer electronics. First IBM servers with SOI microchip performance came onto the market in 2000. In 2002, Honeywell came out with products of the CMOS SOI RF switch family, a line of highly integrated, low-cost switches with integrated digital, mixed signal (analog and digital circuits on the same chip) and RF functions.¹³⁸¹⁾

1.10.3 Satellite onboard autonomy

Autonomy refers to the migration of intelligence and decision capability from the ground station to the spacecraft. Autonomous instrument and spacecraft control as well as autonomous processing and understanding of data will add flexibility to future satellite missions. An important objective in satellite onboard autonomy is also seen in the context of unat-

1380) G. G. Shahidi, “SOI technology for the GHz era,” IBM Journal of Research and Development, Vol. 46, No 2/3, 2002, <http://www.research.ibm.com/journal/rd/462/shahidi.html>

1381) A. Peczalski, J. Kriz, B. Ohme, “RF/Analog/Digital SOI Technology for GPS Receivers and Other Systems on a Chip,” Proceedings of the IEEE Aerospace Conference, Big Sky, MT, March 9–16, 2002

tended operations; the intent is to reduce operating costs, in particular to free resources of routine operations for long-term follow-up missions, with minimum ground involvement. Other key objectives are: a) to take good advantage of science opportunities, and b) to handle uncertainty – including robust operations in the presence of faults. ^{1382) 1383)}

The provision of enhanced functional autonomy demonstrations has been a goal of a number of technology missions by various agencies/institutions and satellite integrators. Most solutions require a considerable effort in software development and of course an architecture and infrastructure that supports the basic functions required for intelligent autonomous operations. The emerging spacecraft onboard autonomy turns out to be of strategic importance because it may support such functions as:

- Migrate routine functions to the spacecraft level
- Decouple the spacecraft from the ground
- Create a direct link between the PI and his experiment on the spacecraft
- Close planning and control loops onboard.

The nature of “autonomy provision” turns out to be rather complex, in the end it requires nothing less but fault-tolerant systems on all levels. Obviously, various levels of autonomy can be recognized in terms of safety requirements. For instance, the aspect of safety may be 100 times higher for a certain support function of a manned mission than for the same or similar scenario of an unmanned mission. – One aspect of autonomy is the automatic performance of routine operations over a limited period of time, requiring onboard monitoring, analysis and self-correcting measures for each functional aspect on the instrument level, prior to updates from ground control. The other aspect of autonomy is the provision of realistic backup scenarios to handle failure situations. – It has long been realized by all parties involved that so-called “cheapsats” are not really cheapsats, if overall costs (all operations + S/C costs + launch) cannot be reduced. And operations happen to be an important and persistent long-term item in the overall bill. The requirement for an autonomous onboard navigation function seems to be on the agenda of many missions (see also autonomy under Navigation in chapter 1.27.5). ¹³⁸⁴⁾ The reason: onboard knowledge of satellite position in ground coordinates is needed for many operational functions such as: activation (start/stop) of Earth observation instruments, data transmission, satellite attitude control (this includes autonomy of all attitude sensing devices such as star trackers, sun sensors, etc.). The latter devices have to solve the “lost-in-space problem,” overcome start-up operations and re-acquisition sequences, be able to handle anomaly detection and isolation and failure trapping and recovery, be reliable and accurate – to qualify as a fully “autonomous” instrument. Autonomy means to be able to operate safely without any external intervention.

Some examples of partial autonomy demonstrations are being provided. So far, they represent generally small steps in semi-autonomous control provision implemented in an onboard subsystem or in several interrelated subsystems.

At the start of the 21st century, onboard intelligence and autonomy functions and services on a wide front are in fact becoming more and more mandatory, for all types of missions. The reason is to be able of handling the vast information flood and to provide intelligent

¹³⁸²⁾ J. Dungan, J. Frank, A. Jonsson, R. Morris, D. E. Smith, “Advances in Planning and Scheduling of Remote Sensing Instruments for Fleets of Earth Observing Satellites,” Pecora 15/Land Satellite Information IV Conference, ISPRS Commission I Mid-term Symposium/FIEOS (Future Intelligent Earth Observing Satellites), Nov. 10–14, 2002, Denver, CO

¹³⁸³⁾ J. Frank, A. Jonsson, R. Morris, D. Smith, “Planning and scheduling for fleets of earth observing satellites,” Proceedings of the 6th International Symposium on Artificial Intelligence, Robotics and Automation in Space, Montreal, Canada, June 18–22, 2001

¹³⁸⁴⁾ S. Chien, G. Rabideau, R. Knight, R. Sherwood, et al., “ASPEN – Automated Planning and Scheduling for Space Mission Operations,” SpaceOps 2000, Toulouse, France, June 19–23, 2000

tools for spacecraft operators in particular in the fields of: a) bus instrumentation, in particular AOCS, TM/TC and onboard data handling, and amongst these, a significant interest has been in highly autonomous and accurate star sensors, and b) instrument observation coordination (scheduling) and resource planning. Planning and scheduling spacecraft operations involves generating a sequence of low-level spacecraft commands from a set of high-level science and engineering goals. It is a safe prediction that further potential applications of autonomy will eventually lead to onboard processing of science data (including the interpretation of all types of imagery) to achieve a real-time analysis capability for rapid response systems, associated with a reduction in data volumes along with the provision of many new services (change detection will be a major field of applications in this scenario). The challenge is in the development and introduction of suitable hardware and software technology and concepts. ¹³⁸⁵⁾ ¹³⁸⁶⁾

- Redundancy design. Satellite reliability is an important consideration for continued provision of operational services. In Transit-3-A (launch in 1960), a US Navy navigation satellite, JHU/APL integrated for the first time a passively redundant battery system that could automatically switch to a backup battery. – Further redundant designs followed for such subsystems as RF and telecommand.
- Enhancements on the various generations of GPS satellites. The block I S/C series (with launches from Feb. 1978 to Oct. 1985) was able to sustain unattended operations for up to 3.5 days between navigation message uploads from the ground. The latest block IIR S/C series features autonomous satellite operations for a period of up to six months without ground control corrections (first launch of a block IIR S/C on July 23, 1997).
- The PoSAT-1 microsatellite mission of SSTL (launch, Sept. 26, 1993) reached a certain degree of operational autonomy through its onboard orbit determination capability (first orbital elements).
- For NASA's Clark satellite (launch in 1998), a GPS receiver with the name of GADFLY was used to demonstrate autonomous orbit determination and to use GADFLY also for coarse attitude knowledge. Note: At the end of Feb. 1998, NASA cancelled the Clark mission due to severe cost overruns and launch delays.
- The DS1 (Deep Space 1) technology mission of NASA/JPL (launch Oct. 24, 1998) introduced the concept of a single autonomous **Remote Agent Experiment (RAX)**, a technology demonstration package which includes an onboard mission manager with a mission plan expressed in terms of high-level goals [RAX is also referred to as ARAX (Autonomous Remote Agent Experiment), see M.11]. A planning and scheduling engine uses the goals, along with a comprehensive knowledge of the S/C status, and constraints on S/C operations – to generate a set of time-based or event-based activities. The autonomous Remote Agent concept was successfully tested on May 17, 1999 when the primary S/C command was given over to Remote Agent for three days of S/C operations. In this period (several days), Remote Agent successfully planned DS1 activities onboard and then carried out the plan without ground intervention. The software detected, diagnosed and fixed simulated problems, showing that it can make decisions to keep the mission on track.. RAX on DS1 represented the first time that an artificially intelligent agent controlled a NASA spacecraft. ¹³⁸⁷⁾

1385) M. Kafatos, R. Yang, C. Yang, R. Gomez, Z. Boybeyi, "Utilizing Remote Sensed Data in a Quick Response System," Pecora 15/Land Satellite Information IV Conference, ISPRS Commission I Mid-term Symposium/FIEOS (Future Intelligent Earth Observing Satellites), Nov. 10–14, 2002, Denver, CO

1386) D. J. Zimpfer, "Autonomous Mission Manager for Rendezvous, Inspection and Mating," Proceedings of the 26th AAS Conference on Guidance and Control, Breckenridge, CO, Feb. 5–9, 2003, Vol. 113 Advances in the Astronautical Sciences, Edited by I. J. Gravseth and R. D. Culp, AAS 03–016, pp. 207–218

1387) D. Bernard, G. Dorais, E. Gamble, et al., "Spacecraft Autonomy Flight Experience: The DS1 Remote Agent Experiment," Proceedings of the Space Technology Conference and Exposition, Albuquerque, NM. September, 1999., AIAA–99–4512

- The ARGOS technology mission (M.3, launch Feb. 23, 1999) of DoD employs an onboard automated mission planning system to optimize onboard data handling and power.
- The UoSAT-12 minisatellite of SSTL (launch April 21, 1999) in Surrey, UK, carries a closed-loop autonomous control system that enables orbit operations to be performed without the need of any ground segment. The autonomous control system consists of a GPS receiver, an onboard propulsion system EPS (Electric Propulsion System), and an orbit maintenance software package of Microcosm Inc., El Segundo, CA, referred to as OCK (Orbit Control Kit).¹³⁸⁸⁾ ¹³⁸⁹⁾ The objective of the control part of the software is to ensure that the orbital altitude of the satellite never falls outside of a prescribed window due to drag. The orbit is described using a set of epicycle parameters which provide an analytic model of LEO orbits. The parameters in this model are estimated onboard the satellite using a Kalman filter. In addition, the software provides control, and an estimation of the orbit parameters by including drag in the model. The satellite was maneuvered into an exact 7-day repeat (ground track) pass orbit for the technology demonstration. The new orbit maintenance software then maintained the satellite mean radius in its resonant orbit for a test period of 27 days within an error band of ± 5 m (3 sigma), and slowly maneuvered the S/C into a frozen orbit.
- Autonomous navigation on DS1 (Deep Space 1, launch Oct. 24, 1998, see M.11.1). This onboard system enables a S/C to determine its location in the Solar System as well as its flight path without help from controllers on Earth. With the knowledge of onboard time, **AutoNav** computes the position of the asteroids. By measuring where the asteroids appear relative to the stars, it computes where the S/C must be. It then can project its path to its destination and use its propulsion system to make any course changes that are required. On July 29, 1999, DS1 successfully performed a close flyby of asteroid 9969 Braille using the AutoNav system.

The AutoNav system was also flown on the DI (Deep Impact) mission of NASA/JPL (launch Jan. 12, 2005). The DS1 and DI AutoNav systems used nearly identical file-based data management systems.

- The first-ever NASA autonomous orbit navigational maneuver by a satellite was conducted in December 1998 by JPL engineers. The experiment involved an orbit adjustment maneuver of the TOPEX/Poseidon satellite. The technology validation required flight controllers to uplink software to the spacecraft that subsequently autonomously planned the satellite's actions and generated a series of commands to steer it.¹³⁹⁰⁾ The software required minimal input from ground controllers, consisting only of changes in velocity and the time to execute the maneuver. The software then computed the changes in satellite orientation and the amount and timing of satellite thruster burns with no further input from ground controllers.
- The EO-1 mission of NASA/GSFC (launch Nov. 21, 2000, see M.12.2) demonstrated autonomous navigation/instrument operation with an onboard software package referred to as **AutoCon**TM (GSFC teamed with a.i. - solutions Inc.).¹³⁹¹⁾ ¹³⁹²⁾ AutoCon is capable of autonomously planning, executing, and calibrating routine spacecraft maneuvers to maintain satellites in their respective constellations and formations. The AutoCon features include an innovative use of fuzzy logic decision making capabilities and natural language to

1388) G. Gurevich, R. Bell, J. R. Wertz, "Autonomous On-Board Orbit Control: Flight Results and Applications," Proceedings of AIAA Space 2000 Conference and Exposition, Long Beach, CA, Sept. 19-21, 2000

1389) M. Aorpimai, Y. Hashida, P. Palmer, "Autonomous Control System for Precise Orbit Maintenance," Proceedings of the 14th AIAA/USU Conference on Small Satellites, Logan, UT, Aug. 21-24, 2000, SSC00-IX-6

1390) <http://www.jpl.nasa.gov/releases/98/topexnav.html>

1391) D. Folta, J. Bristow, A. Hawkins, G. Dell, "NASA's Autonomous Formation Flying Technology Demonstration, Earth Observing-1 (EO-1)," Proceedings of International Symposium Formation Flying Mission & Technologies, Oct. 29-31, 2002, Toulouse, France

1392) J. Bauer, J. Bristow, D. Folta, K. Hartman, D. Quinn, "Satellite Formation Flying using an Innovative Autonomous Control System (AutoCon) Environment," AIAA Guidance, Navigation and Control Conference, Aug. 1997

resolve multiple conflicting constraints. The EO–1 formation flying experiment validated a fully non–linear autonomous system for formation flying. The AutoCon system is also being considered to fly on follow–up missions such as GPM (Global Precipitation Mission).

- NASA's TIMED mission (launch Dec. 7, 2001), designed and operated by JHU/APL, introduces operational autonomy by separating payload/instrument operations from all S/C system operations activities. In this way, the instrument teams are able to control all of the instrument modes, operations and science data return at their own choice without explicit interactions or approvals by the S/C project team. A combination of onboard GPS processing and the use of the Internet move the data from the APL ground station to each investigator's home site. In addition, the Internet is used by each investigator to control his instrument directly (the packetized messages are integrated into the uplink command structure in an automated fashion). The ultimate goal for TIMED is to develop a "lights–out" concept of operations as the missions progresses.
- ESA's PROBA minisatellite mission (launch Oct. 22, 2001, M.33).¹³⁹³ The attitude control and avionics subsystems accommodate the core technologies for S/C autonomy. Demonstration of autonomous operations for orbit and attitude determination with a GPS receiver (SGR–20). The other autonomous subsystem is ASC (Advanced Stellar Compass) of DTU, Denmark. ASC is capable to reconstruct autonomously the S/C inertial attitude starting from the condition "lost in space." The mission operations concept provides considerable flexibility in the allocation of onboard resources and in scheduling of operations.
- The Block IIR satellites of the GPS constellation [launch of SVN 43 (Block IIR–2 first of series) on July 23, 1997] feature the AutoNav concept, providing the ability of the constellation to self–navigate and to maintain overall accuracy by optimally filtering ranging data and ensembling the clock data from all the GPS satellites. The filters are processed and updated using the crosslink measured range to each viewable satellite along with that remote satellite's crosslinked filter parameters. At the end of 2003, there are 9 Block IIR satellites in orbit. With AutoNav, the specification for the GPS IIR system requires a rms URE (User Range Error) of < 6 m in the survivable mode at the end of 180 days without Ground Segment corrections.
- A NASA/GSFC technology initiative is developing (1998) a concept referred to as IA/GNC (Image–Aided/Guidance, Navigation and Control) to support S/C autonomy and to reduce operating costs. The IA/GNC scheme uses 2–D images from the S/C science instrument or a secondary low–cost camera and generates attitude control and image stabilization information that enhances pointing performance and ultimately permits autonomous onboard geo–referencing and geometric rendering of data. IA/GNC relies heavily on image correlation tracking (ICT) techniques which compute the translational offset between an instantaneous image and a stored reference image derived from a previous image or a model.
- The MSG (METEOSAT Second Generation) spacecraft series of EUMETSAT (launch of MSG–1 on Aug. 28, 2002) provide an onboard software design called FDIR (Failure Detection, Isolation and Recovery), allowing to detect any malfunction and to perform the necessary recovery/reconfiguration action autonomously. This implies recovery after a single onboard failure during 24 hours without ground intervention.
- The SMART–1 moon mission of ESA (launch Sept. 27, 2003, M.38) introduces a software package by the name of **OBAN** (On–Board Autonomous Navigation). OBAN validates navigation algorithms by planetary body tracking. It makes use of the S/C star trackers and of AMIE images. The overall objective is to test navigation algorithms with respect to

¹³⁹³ Note: SGR–20 (Space GNSS Receiver–20) was developed under ESA's ARTES–5 program in the UK (SSTL). First use of SGR–20 on UoSAT–12 (launch Apr. 21, 1999). The receiver has 24 L1 C/A code channels and can operate with four antennas simultaneously. In addition, the SGR–20 features 1 MByte of memory, a 20 MHz processor, EDAC (Error Detection and Correction) and a noncoherent architecture, i.e. the Delay Lock Loop and Phase Lock Loop are decoupled.

their workability in a real–mission environment. The OBAN experiment is designed to function in what is termed an ‘open loop’, obtaining all the data an autonomous navigation system would require, but instead of being processed onboard, this information is down-linked to be processed on Earth.

- The STEREO (Solar Terrestrial Relations Observatory) mission of NASA (launch Oct. 26, 2006, K.30) will demonstrate the feasibility of autonomous solar navigation (the sun is used as a reference). The technique employs a dual–mode imaging system (2 S/C designed by JHU/APL) for measuring the direction of the sun using a CCD camera which captures the image of the sun against a star background (the stars serve as a direction reference). The two–mode design, based on the JHU/APL DSAD (Digital Solar Attitude Detector) imaging system, permits the control of the vast brightness contrast differences. The S/C state vector is determined by onboard processing the solar observation data. ¹³⁹⁴⁾

- Autonomous station keeping of S/C. Up to the late 1990s, the station keeping of satellites (in GEO and LEO) has primarily been ground–based, involving the Control Center personnel in all phases of operations, including orbit maintenance and station keeping. Current GEO satellite operations have evolved so as to take advantage of the stationary nature of the satellite position relative to the ground stations. The favorable geometry provides a continuous window for ranging, tracking, and commanding, thereby minimizing the computational burden on the onboard processors. The LEO satellites (with intermittent ground contacts), on the other hand, always required an onboard processing capability to provide some limited autonomy in navigation. Functional capabilities in the direction of autonomy improved considerably with the availability of onboard GPS systems and advanced feedback control techniques. New orbit control designs are based on the concept of continually minimizing the position and velocity error between a satellite and its target orbital position.

- NASA/JPL developed ASE (Autonomous Sciencecraft Experiment), ¹³⁹⁵⁾ an onboard software package within NMP. The main science objective of ASE is to demonstrate that **process–related change and feature identification can be made during space flight**. ASE is a software suite providing onboard science analysis and replanning to radically increase science return by enabling intelligent downlink selection and autonomous retargeting. The onboard processing package consists of three autonomy software components:

- Onboard science algorithms to analyze the image data, generate derived science products, and detect trigger conditions such as terrain boundaries and change relative to previous observations

- Execution management software using the SCL (Spacecraft Command Language) package to enable event–driven processing and low–level autonomy

- A low–latency continuous planner, **CASPER** (Continuous Activity Scheduling Planning Execution and Replanning), to replan activities, including downlink, based on science observations in the previous orbit cycles. CASPER scheduled activities are inputs to the SCL system, which generates generates the detailed sequence commands.

CASPER is a critical subset of the ASE software package. ^{1396) 1397) 1398) 1399)} It uses iterative repair to support **continuous modification and updating of a current working plan** from goals in light of a changing operating context. The ASE software package of JPL was

¹³⁹⁴⁾ Y. Guo, “Autonomous Solar Navigation System,” JHU/APL Technical Digest, Vol. 22, No 2, 2001, pp. 119–121

¹³⁹⁵⁾ R. Sherwood, S. Chien, R. Castano, G. Rabideau, “Spacecraft Autonomy Using Onboard Processing for a SAR Constellation Mission,” Pecora 15/Land Satellite Information IV Conference, ISPRS Commission I Mid–term Symposium/FIEOS (Future Intelligent Earth Observing Satellites), Nov. 10–14, 2002, Denver, CO

¹³⁹⁶⁾ S. Chien, R. Sherwood, D. Tran, et al., “Proceedings of International Symposium on Artificial Intelligence Robotics and Automation in Space, Nara, Japan, May 19–23, 2003

¹³⁹⁷⁾ R. Knight, G. Rabideau, S. Chien, B. Engelhardt, R. Sherwood, “Casper: Space Exploration through Continuous Planning,” IEEE Intelligent Systems, Sept/Oct 2001, pp. 70–75

¹³⁹⁸⁾ B. Berger, “NASA’s Earth Observing–1 to Play Key Role in Sensor Web Demo,” Space News, May 5, 2003, p. 8

uplinked to the EO-1 spacecraft in the summer and fall of 2003 to realize an autonomy demonstration and validation experiment on the extended EO-1 mission (the spacecraft is in its extended mission phase). The ASE Science Team has developed scene classifiers to detect thermal emission in both day and nighttime Hyperion data. The objective is to extract static features of the imagery and to detect changes relative to previous observations. Also, automatic identification of regions of interest including regions of change (such as flooding, ice melt, and lava flows). – While RAX (Remote Agent Experiment) on DS1 demonstrated a batch onboard planning capability, CASPER on EO-1 verifies a continuous planning capability along with onboard science processing and feature recognition (monitoring of surface change, etc.).^{1400) 1401)}

The objective of ASE is to demonstrate several integrated autonomy technologies to enable autonomous science applications. Several science algorithms including: onboard event detection, feature detection, change detection, and unusualness detection are being used to analyze science data, in particular those of Hyperion. The instrument images a 7.5 km by 42 km land area per image and provides detailed spectral mapping across all 220 channels with high radiometric accuracy.

On May 7, 2004, the ASE package of EO-1¹⁴⁰²⁾ observed/analyzed an eruption of the Mount Erebus volcano in Antarctica autonomously (without human interaction). The software detected an unusual area of heat within an image of Hyperion, it then directed EO-1 to capture more imagery on a pass about 7 hours later. The satellite was able to repeat the experiment on May 14, 2004.

ASE on EO-1 is demonstrating an integrated autonomous mission using onboard science analysis, replanning, and robust execution. The ASE performs intelligent science data selection that leads to a reduction in data downlink. In addition, the ASE increases the science return through autonomous retargeting.¹⁴⁰³⁾

The ASE feature recognition package (i.e. event monitoring) is also being planned for a number of future NASA missions such as GEC (Geospace Electrodynamic Connections) and MMS (Magnetospheric MultiScale).

- The Livingstone software package version 2 (LV2) is being used in EO-1 on-orbit testbed demonstrations. The AI (Artificial Intelligence) software package “Livingstone” was developed by a team at NASA/Ames Research Center (S. Hayden) and uplinked to EO-1 in the summer of 2004. The LV2 automatically detects and diagnoses simulated failures in the EO-1 payload instruments. The software package has the ability to find and analyze errors in the spacecraft’s systems. A key feature of the software is its “reasoner” function, which enables it to compare the predicted performance of a system based on readings from onboard monitors. Contradictions between the predicted and actual performance are used to identify the failures. The autonomous diagnostic tool of LV2 can help controllers in identifying and detecting a potential problem in sufficient time to make repairs or to find a work-around solution.^{1404) 1405)}
- Autonomous onboard control offers several operational capabilities not available to missions without this feature (according to reference 1388):

1399) R. Sherwood, S. Chien, D. Tran, B. Cichy, R. Castano, A. Davies, G. Rabideau, “Preliminary Results of the Autonomous Sciencecraft Experiment,” Proceedings of the IEEE Aerospace Conference, Big Sky, MT, March 6–13, 2004

1400) R. Sherwood, S. Chien, D. Tran, B. Cichy, R. Castano, A. Davies, G. Rabideau, “Preliminary Results of the Autonomous Sciencecraft Experiment,” Proceedings of the IEEE Aerospace Conference, Big Sky, MT, Mar. 6–13, 2004

1401) S. Chien, R. Sherwood, D. Tran, B. Cichy, et al., “The EO-1 Autonomous Science Agent,” Proceedings of NASA ESTC (Earth Science Technology Conference) 2004, Palo Alto, CA, June 22–24, 2004

1402) J. Bates, “Software Lets Satellite Make Its Own Decisions – NASA’s EO-1 Satellite Observed Volcanic Eruption Without Human Help,” Space News, July 5, 2004, p. 16

1403) <http://eo1.gsfc.nasa.gov/new/validationReport/>

1404) J. Bluck, “NASA Software Enables Satellite Self-Service in Space,” Oct. 7, 2004, http://www.nasa.gov/home/hqnews/2004/oct/HO_04339_self_service.html

1405) B. Iannotta, “Diagnostic Software Shows Promise in Testing Aboard EO-1,” Space News, Oct. 18, 2004, p. 20

- The position of the spacecraft at all future times is known as far in advance as desirable
- The ground track (or inertial track) of the spacecraft can be made to follow a predefined pattern which may be changed at user request
- The process for computing future positions is simple and can be included in any ground-based equipment that uses a general-purpose microprocessor
- There is a longer planning horizon dealing with the potential problems of RF or physical interference with other spacecraft or debris
- Disturbance torques are much lower than with more traditional orbit control processes, such that the size and responsiveness of control actuators can be lessened and restrictions on the timing of stationkeeping maneuvers can be reduced or eliminated.

In summary, autonomous onboard orbit control can fundamentally change the way space missions operate. It is a key component in extending the philosophy of “faster, better, cheaper” to 21st century ground operations.

Today’s requirements of future space–system functionality call for nothing less but **system intelligence** (error–tolerant systems) with the following characteristics: (see reference 20)

- Autonomy to think for themselves
- Self–reliance to identify, diagnose, and correct internal problems and failures
- Self–repair to overcome damage
- Self–assembly and evolvability to adapt to and explore new and unknown environments
- Extreme efficiency to operate with very limited resources and without input from mission control.

1.10.4 Autonomous ground stations and systems

- The first ground stations that could be operated autonomously were probably the APT (Automatic Picture Transmission) stations for NOAA satellite data reception. The APT broadcast service was first introduced with TIROS–8 (launch Dec. 21, 1963). Simple APT ground stations could soon be purchased to support autonomous data acquisition.
- The broadcast of HRPT data started with TIROS–N (launch Oct. 13, 1978). Along with this service came simple HRPT stations supporting autonomous data acquisition.
- Autonomy is also invading the mission control room. Traditionally, satellite operations have been performed from a fixed set–up of computers in a dedicated control room at the space agency’s or satellite owner’s premises. The control room was staffed around the clock in order to continuously monitor and operate the spacecraft. This 24 hour staffing approach, however, was very expensive. For small scientific satellites on a constrained budget, this type of support may only be justified during the initial commissioning phase (typically a few weeks) and in case of contingencies or special campaigns. – Future missions of satellites will increasingly rely on autonomy for routine operations and automatic downlinking of housekeeping and instrument data. Both the onboard computer and computers at the ground station or a dedicated control facility will continuously monitor the health of the spacecraft and alert the operator–on–call in case of anomalies.
- Increased use of Internet services in S/C (or mission) operations, in particular for small S/C to save costs over the conventional leased–line communications approach. Furthermore, with the first LEO commercial telephone networks in operation, S/C operators (in

particular student developed satellites) are designing their prime communications needs for uplink and downlink data transmissions entirely on the service provision of these distributed cellular telephone networks. This eliminates the conventional dedicated ground segment to space segment communication links for a space mission.

- Munin (N.16), a Swedish nanosatellite of IRF (Swedish Institute of Space Physics), students at Umeå University (RYP), and students at Luth (Luleå University of Technology) with a launch as a secondary payload on NASA's EO-1 mission (launch Nov. 21, 2000), feeds its science data (space weather parameters) directly into the Internet at reception, available to anyone.
- The ION-F (Ionospheric Observation Nanosatellite-Formation, three satellite constellation of USU (Utah State University), UW (University of Washington, and VT (Virginia Polytechnic Institute) with a launch in 2004, employs also commercial cellular phone communications in all links.

1.10.5 Spaceborne data collection systems (DCS)

Satellite data collection, in particular of environmental data from autonomous remote stations in the ground segment, is an established long-term service provision which started operationally in the 1970s with the introduction of ARGOS (see C.2) on NOAA weather satellites. An overview of DCS (Data Collection Systems) can be found in Table 279 (Part C).

- True and continuous autonomous ground station operations has probably first been realized with the introduction of systematic spaceborne data collection services (DCS) from the ground segment. Each remote ground station (on land, on water, or in the air) had to be operationally autonomous to participate in such a venture. The first such system in LEO (polar orbit) was IRLS (Interrogation, Recording, and Location System), employing a range-only platform location technique and flown on Nimbus-3 (launch April 14, 1969, see M.29.3). The French-US Eole experiment measured ambient air temperature and pressure and determined 200 mb winds over the Southern Hemisphere by tracking constant-density balloons, employing a range and range-rate location technique (launch Aug. 16, 1971). A simplified approach, using only random-access range-rate data, was employed in the TWERLE (Tropical Wind Energy conversion and Reference Level Experiment) flown on Nimbus-6 (launch June 12, 1975, see M.29.6). These systems led eventually to the French-developed **Argos** Data Collection and Location System, first flown on TIROS-N (launch Oct. 13, 1978, see C.2). The Argos system is being managed and operated by CLS (Collecte Localisation Satellites), a CNES subsidiary based in Toulouse, France.
- A similar system to Argos, namely COSPAS, was developed by the Soviet Union and first launched on June 29, 1982 (the name of the satellite was Cosmos-1383 or COSPAS-1).
- In 1982, the USA, Canada, France, and the Soviet Union banded together to form **COSPAS-S&RSAT** (Search and Rescue Satellite Aided Tracking System), an international humanitarian search and rescue system that became fully operational in 1984 (see I.11). As of 2002, over 13,000 persons have been rescued by COSPAS-S&RSAT services since its inception in 1982. For example, in the year 2000, 1520 people were rescued after COSPAS-S&RSAT distress signals were sent out from aircraft, ships, and land vehicles. Since 1982, the four founding countries of COSPAS-S&RSAT have been joined by 32 further countries – a humanitarian program on a global scale.
- The first DCS (Data Collection System) in GEO orbit was flown on SMS-1 (Synchronous Meteorological Satellite-1, launch May 17, 1974). See chapter 1.28.

- INPE of Brazil launched its SCD–1 satellite in 1993 and its SCD–2 spacecraft in 1998 to perform data collection services in the southern hemisphere.
- There are also commercial data collection services available such as: FAISAT (FAISAT–1 launch Jan. 24, 1995, see C.3); Orbcomm satellite constellation (see C.5) initial service started in 1995; the SAFIR system of OHB–System (see C.6) started services with SAFIR–1 in Nov. 1994, and with SAFIR–2 in 1998; TEMISAT of Telespazio (Rome) was launched in 1993 to provide data collection services.
- Starting with NOAA–15 (launch May 13, 1998)¹⁴⁰⁶, the NOAA POES series satellites are equipped with the Argos–2 instrument system featuring a number of improvements such as: a) updated Argos receiver with better sensitivity [an increase of 3 dBm, higher number of Data Processing Units (8 vs. 4 for Argos–1) and larger receiver bandwidth (80 kHz instead of 24)], and b) capability of increased reception in the number of messages with better quality.
- The first Argos–Next instrument [a third–generation system also referred to as ADCS (Argos Data Collection System)] is being flown on ADEOS–II of JAXA (launch Dec. 14, 2002) providing **two–way messaging services** [demonstration and checkout for ADCS until April 2003, then full operation] in the framework of a French–Japanese cooperative project. This service allows users to send messages to fixed and mobile terminals anywhere in the ground segment. The two–way messaging capability paves also the way for more sophisticated terminals, called PPTs (Platform Transmitter Terminal) in the ground segment. The Argos–Next downlink gives users the possibility of sending short messages (up to 128 bit) to their PTTs. – Argos–Next instruments are also being planned to fly on the MetOp series satellites of EUMETSAT (launch of MetOp–A, Oct. 19, 2006) and on the NOAA POES series starting with NOAA–N' (launch Feb. 6, 2009) as well as on the NPOESS series.
- A new DCS by the name of **ADAM** (Advanced Data Acquisition and Messaging System) was developed for FedSat–1 (Australia, launch Dec. 4, 2002, see M.15) and STSat–1 (Science and Technology Satellite–1) of KAIST/SaTReC, Korea (launch Sept. 27, 2003, see M.45). ADAM has been developed in a cooperative effort between SaTReC and ITR (Institute for Telecommunications Research) of the University of South Australia in Adelaide and CRCSS. ADAM provides bi–directional communication between the on–board DCS and the ground segment, consisting of many DCPs (Data Collection Platforms). The DCPs are also referred to as MTs (Mobile Terminals). A TDMA (Time Division Multiple Access) protocol is being used in the uplink to collect the data from various DCPs simultaneously. ADAM, providing the functionality of two–way packet communications for remote environmental monitoring and forward messaging, is primarily used to collect data from Argo.
- **Argo (Data Collection in the Global Oceans)**. Argo is an internationally coordinated program directed at deploying a global array of temperature/salinity profiling floats. The buildup phase was from 1999 to the end of 2007 when the Argo network consisted of an array of about 3,000 free–drifting (Lagrangian) profiling floats, capable of surveying the upper 2000 m of the world's oceans.

The Argo international ocean program is part of GCOS/GOOS (Global Climate Observing System/Global Ocean Observing System), part of CLIVAR (Climate Variability and Predictability Experiment), and part of GODAE (Global Ocean Data Assimilation Experiment).

In 2009, ten years since OceanObs'99, autonomous technologies have brought about a revolution in observational capability that lets us view the subsurface oceans in ways that are comparable to global satellite measurements of the sea surface. The next decade will see

¹⁴⁰⁶ http://www.cls.fr/html/argos/documents/flash/flash01/flash01_avantages_en.html

equally important advances through expanded coverage and a multi-disciplinary approach. These are not expected to come from radically new technologies, but from the use and enhancement of technologies that are now maturing and from developments in existing systems. 1407) 1408) 1409)

Argo would not be possible without extensive international cooperation. 1410) 1411) A group of 45 nations, territories, unions, federations, and freely associated states worldwide participate in different aspects of Argo. Argo has helped to transform traditional methods of data collection and distribution by making oceanographic data available in real time to the physical oceanography research and operational communities.

1.10.6 Hibernation modes in spacecraft operations

- Spacecraft operation system designs may be implemented in various ways to suit a particular operations support scheme. While most observation satellites employ continuous operation schemes of the spacecraft (with intermittent periods of data gathering), there has also been a trend toward event-driven spacecraft operations schemes. In general, the event-driven schemes are of the hibernation/activity type; they react to preset stimuli, come out of hibernation, observe an event for a certain period, and return to hibernation again. Other spacecraft are simply put into a hibernation mode (i.e. standby mode) during particular mission phases of inactivity. In any case, hibernation always implies that resources are being conserved for other planned periods of activity. Hibernation thus extends the general life time of a mission – by reducing cycle times of vital instruments, to save energy, etc. The hibernation periods help also to reduce mission operation costs [ground support of manpower and resources (like antennas, etc.)]. Most hibernation recovery schemes rely to a considerable degree on onboard autonomy systems and capabilities. The following missions are examples of hibernation mode experiments or operations:

- GEOS-2 (GEOstationary Satellite) of ESA (launch July 14, 1978). GEOS-2 provided two years of data, was placed in hibernation for eight months, then revived for eight months in 1981 to support the EISCAT program of upper atmosphere motion measurements. GEOS-2 remained in use until the end of 1983. Periodic monitoring support (1984) of the chemical releases of the AMPTE mission.

- ERS-1 mission of ESA (launch July 17, 1991). The satellite was in hibernation since June 1996. Operations were limited to the monitoring of the platform vital elements, the battery maintenance and the periodic checkout of the entire system every 70 days. – To maintain the ERS-1 batteries performance, the SAR image mode was activated once or twice a day. This was used to perform limited ERS-1/2 SAR interferometry acquisitions. The ERS-1 mission ended on March 10, 2000 by a failure of the onboard attitude control system.

- The GOES-10 spacecraft of NOAA (launch April 25, 1997) was put in standby mode (hibernation) after launch to await its turn of active operations support. GOES-10 was activated on July 21, 1998 to replace the GOES-9 spacecraft.

1407) Dean Roemmich, Lars Boehme, Hervé Claustre, Howard Freeland, Masao Fukasawa, Gustavo Goni6, W. John Gould, Niki Gruber, Maria Hood, Elizabeth Kent, Rick Lumpkin, Shawn Smith, Pierre Testor, “Integrating the ocean observing system: mobile platforms,” Proceedings of OceanObs’09, Venice, Italy, Sept. 21 – 25, 2009, URL: http://www.oceanobs09.net/plenary/files/Roemmich_mobile_platforms_PLENARY_Paper_v2.pdf

1408) http://www.oco.noaa.gov/index.jsp?show_page=page_status_reports.jsp&nav=observing

1409) M. Belbeoch, “Argo Status,” URL: http://www.godae.org/~godae-data/GOVST/meetings/GOVST-1/presentations/7.2_Argo-GOVST.ppt

1410) Coriolis Newsletter, n° 5, January 2009, URL: <http://www.coriolis.eu.org/english/news/CoriolisNewsLetter-Issue-5.pdf>

1411) M. Balmaseda, D. Anderson, A. Vidard, “Impact of Argo on analyses of the global ocean,” Geophysical Research Letters, Vol. 34, 2007, L16605, doi:10.1029/2007GL030452, URL: http://www.oco.noaa.gov/news/pdf/Balmaseda_et_al-GRL2007.pdf

– The SNOE (Student Nitric Oxide Explorer) mission of the University of Colorado at Boulder, CO (launch Feb. 26, 1998) employed a hibernation mode on a GPS receiver, BGSR, provided by JPL. The GPS orbit is determined about three times per orbit for short time intervals, otherwise the receiver is in hibernation. The information is used for post-factum ground orbit determination.

– The TUBSAT (Technical University of Berlin Satellite) series satellites introduced hibernation mode operations with DLR–TUBSAT (launch May 26, 1999) and the subsequent S/C, MAROC–TUBSAT (launch Dec. 10, 2001, see N.31.5). The ACS (Attitude Control Subsystem) design supports hibernation mode operations as a way of life in regular S/C operations. Most of the time (certainly over 95%) the satellite is orbiting in standby mode, slowly tumbling (a few rotations per orbit); all onboard systems are in hibernation (including ACS) to save power; only the UHF receiver is listening for potential commands. In case of an event, the S/C attitude may be restituted within a few minutes. Event recognition or a command from a ground station cause the spacecraft to return to observation mode.

– Hibernation modes are of particular interest in deep space missions with long periods of low activity between major event periods (long-term cruise phases). The Giotto extended mission of ESA is an example.¹⁴¹²⁾ In its extended mission, Giotto hibernated twice – the first hibernation began in March 1986 and lasted for 1,402 days. The second hibernation period began in July 1990 and lasted for 670 days (however, the Giotto S/C was not specifically designed for hibernation). The Giotto hibernation recovery scheme relied on a directional antenna strategy. The NASA CONTOUR (Comet Nucleus Tour) Discovery mission (launch July 3, 2002) is using hibernation modes for the in-between periods of comet encounters. Objective: visit and study of at least two comets. Note: mission failure on Aug. 15, 2002 – An objective of the long-duration deep space mission Rosetta of ESA (launch March 2, 2004) is to rendezvous with comet 67P/Churyumov–Gerasimenko (10 year journey to the comet, reaching it in 2014). To reduce mission operation costs – and also because of trajectory constraints – a good portion of the cruise phase is allocated into unattended hibernations.

– Rosetta was placed into hibernation in June 2011, with only the computer and several heaters remaining active as the spacecraft cruised out to nearly 800 million km from the warmth of the Sun, beyond the orbit of Jupiter.

On Jan. 20, 2014, as Rosetta’s orbit came back to within 673 million km from the Sun, there was enough solar energy to power the spacecraft fully again and **Rosetta’s pre-programmed internal ‘alarm clock’ woke up the spacecraft after a record 957 days of hibernation.** After warming up its key navigation instruments, coming out of a stabilizing spin, and aiming its main radio antenna at Earth, Rosetta sent a signal to let mission operators know it had survived the most distant part of its journey.¹⁴¹³⁾

– Unlike Rosetta, which awoke in January via a pre-programmed signal, the Philae lander received a “personal wake-up call” from Earth, 655 million km away on March 28, 2014. A confirmation signal from the lander was received by ESA 5 1/2 hours later. – After over a decade of traveling across the inner Solar System, Rosetta and Philae are now in the home stretch of their ultimate mission: to orbit and achieve a soft landing on the inbound comet 67/P Churyumov–Gerasimenko.¹⁴¹⁴⁾

• **Disaster monitoring.** Although a spaceborne (LEO) service of disaster monitoring is of great interest to a global community of civil protection authorities, there has been no satel-

1412) E. Reynolds, P. Panneton, M. Reinhart, et al., “The Use of Hibernation Modes for Deep Space Missions as a Method to Lower Mission Operations Costs,” AIAA/USU Conference on Small Satellites, Logan UT, Aug. 13–16, 2001, SSC01–VIIIa–5

1413) ESA’s ‘sleeping beauty’ wakes up from deep space hibernation,” ESA, Jan. 20, 2014, URL: http://www.esa.int/Our_Activities/Space_Science/Rosetta/ESA_s_sleeping_beauty_wakes_up_from_deep_space_hibernation

1414) Jason Major, “ESA Awakens Rosetta’s Comet Lander,” Universe Today, March 28, 2014, URL: <http://www.universetoday.com/110822/esa-awakens-rosettas-comet-lander/>

lite so far dedicated to the task of service provision during periods of natural disasters (volcano eruptions, floods, etc.). However, there have been imagery services, in particular for flood events, from a number of instruments on various satellites of existing space missions. Examples are: ERS-1/2 (AMI), JERS-1 (SAR, OPS), RADARSAT-1 (SAR), IRS-1C and -1D (LISS-3, PAN), Landsat-5 (TM), NOAA (AVHRR) series, and the SPOT (HRV) series, BIRD a demonstration mission of DLR (launch Oct. 22, 2001).

As of 2003, the **DMC (Disaster Monitoring Constellation)** of microsattellites (SSTL, Surrey, UK) is in the build-up phase; the following launches took place: AlSat-1 (Nov. 28, 2002), while a common launch was provided on Sept. 27, 2003 for BilSat-1 (Turkey), NigeriaSat-1 and UK-DMC. – As of March 2004, AlSAT-1, BILSAT-1, NigeriaSat-1 and UK-DMC achieved their target orbits in the constellation with nominal phase slots of 0°, 90°, 180°, and 270° around the DMC orbit (altitude = 686 km, inclination = 98.8°). *With the coordinated constellation systems tested and commissioned, this enables the DMC consortium to provide imaging coverage anywhere on the surface of the Earth with a 24-hour revisit period.* Another microsattellite, Beijing-1 (China-DMC+4), was launched on Oct. 27, 2005 joining the DMC constellation.

A future mission is: FOC/FUEGO (Fire Observation Constellation), in the definition phase by ESA and the EU, is planned to deal in particular with forest fire observations.

1.10.7 Special S/C maneuvers and/or rescue/repair operations

On-orbit equipment malfunctions or failures are a fact of life for all space missions. This section lists some examples of special spacecraft maneuvers and deals in particular with significant repair and/or maintenance accomplishments performed on malfunctioning spacecraft subsystems to salvage/extend the mission. Reported are some in-flight success stories. It should be pointed out, however, that most malfunctions in spaceflight are attributed to the critical launch and deployment phases of a spacecraft. To become “spaceborne in the intended orbit and fully functional” after launch and deployment is certainly a prerequisite of high quality, all further spacecraft operations depend on this requirement.

Some examples of rescue or repair missions are:

- On the night of April 13, 1970, an oxygen tank of the command module of Apollo 13 exploded (after nearly 56 hours into the flight) – with a crew of three astronauts (James A. Lovell, Fred W. Haise and John L. Swigert) onboard on the way to the moon. This mishap crippled the command/service module engines of Apollo 13 some 321,860 km from Earth. Naturally, the scheduled lunar landing was aborted. The crew circled the moon in a dramatic rescue plan devised by Mission Control in Houston. The most immediate problem of the crew was the loss of the oxygen supply to the command module (fortunately, the environmental control system of the lunar module functioned as a backup). A four-day rescue mission followed in which Mission Control in Houston tried to devise a plan for a safe return to Earth. The firing of the lunar module engine provided the means to steer the powerless spacecraft safely back home. Reentry required the unusual step of undocking the lunar module, which had been retained for the flight back to Earth, in addition to the separation of the damaged service module. The lunar module had remained attached to the spacecraft to preserve the maximum electrical power in the command module for entry. All three men returned safely in this breathtaking rescue mission.¹⁴¹⁵⁾
- HST (Hubble Space Telescope). See the Hubble repair missions in chapter 1.26 (on-orbit servicing).
- S/C rotation maneuver of RADARSAT-1 (see D.42.2). During AMM (Antarctic Mapping Mission), in the time period of September to November 1997, the RADAR-

¹⁴¹⁵⁾ <http://nssdc.gsfc.nasa.gov/planetary/lunar/ap13acc.html>

SAT-1 spacecraft underwent a successful maneuver to rotate its normally right-looking radar array into a left-looking attitude. The shift involved rotating the satellite by 180° in yaw. Although other missions do regular yaw maneuvers to reorient S/C, RADARSAT-1 was the first satellite in remote sensing history to perform this maneuver twice (back to nominal right-looking configuration at the end of AMM). The left-looking configuration allowed to map the entire Antarctic continent for the first time (24 day exact repeat observations for interferometric studies). A complete high-resolution mosaic of Antarctica was created, it is available for use by the science community.

- Recovery of momentum wheel (MW) failure in the ACS (Attitude Control Subsystem) of RADARSAT-1 (launch Nov. 4, 1995). The S/C encountered twice the problem in satellite pitch stabilization accuracy degradation: the first occurrence in August 1999 and the second in November 2002.¹⁴¹⁶ Both events were caused by a gradual deterioration (wear) of “pitch momentum wheel” bearings resulting in an increase and destabilization of their friction torque. The first failure was resolved simply by swapping the prime wheel to the redundant one. The second failure, however, required the development of an appropriate ACS configuration to maintain the satellite attitude within the required pointing accuracy. The solution developed involves a switch of attitude control in the pitch channel from the MW to the MTR (Magnetic Torque Rod) actuators by uploading to the satellite ACS processor a new set of control tables. The new ACS configuration developed (an asymmetric control scheme provided by two MW and three MTR) allows the satellite to continue its mission, practically without any performance degradation. The problem solution (and extended mission life) was made possible due to the double-string cold redundancy architecture of the ACS and the upload capability to the onboard ACS processor.
- S/C rescue operations – GOES-10. In May 1997, the solar array mechanism of NOAA’s newly launched GOES-10 (launch April 25, 1997 as an orbit backup) satellite, designed to rotate once each day to keep itself pointed normally at the sun, slowed down and shortly thereafter stopped working entirely.¹⁴¹⁷ The subsequent rescue work by NOAA and NASA engineers led to an unusual solution by turning the spacecraft into an upside down orientation (a yaw-flip maneuver). This maneuver turned out to be highly successful in saving the spacecraft for regular operations, because it permitted the solar array to work in a backwards-rotating orientation. As a consequence, the onboard software was changed so that data from the instruments are provided to users as if the spacecraft were in the normal upright position. GOES-10 was activated on July 21, 1998 to replace the GOES-9 spacecraft.
- MIR station accident. In the summer 1997 (June), an emergency occurred that had considerable impact on MIR’s fate. While docking with the MIR space station, an automated Progress cargo ship, filled with garbage, failed to respond to commands and rammed the Spektr module of MIR. As a result of this first collision between operating spacecraft, the Spektr module was punctured and leaked oxygen (causing a loss of air pressure in the Spektr module). The international crew aboard MIR (two Russian cosmonauts and a US astronaut) retreated to a docked Soyuz spacecraft to prepare for emergency evacuation. However, the situation was brought under control. The punctured module’s hatch was closed and the oxygen leak was stopped. The crash also damaged one of MIR’s solar panels, shutting off much of its electrical power system. The station drifted, starved for power, until the crew could bring it back to life.¹⁴¹⁸ – For the next two years, MIR crews did extensive maintenance and brought the space station back into full working order. By the time MIR was abandoned in the summer of 1999 – after more than 13 years of operations –

1416) Y. V. Kim, G. Deraspe, “Resolving RADARSAT-1 Momentum Wheels Failure Problem,” Proceedings of the 54th IAC, Bremen, Germany, Sept. 29 – Oct. 3, 2003

1417) G. J. Dittberner, “NOAA’s Geostationary Operational Environmental Satellite (GOES) Systems and Plans,” Proceedings of the EUMETSAT Meteorological Satellite Data User’s Conference, Copenhagen, Denmark, Sept. 6–10, 1999, pp. 33–38

1418) <http://www.cnn.com/TECH/9706/25/mir.accident/>

the Russians had shown that humans could face daunting, even terrifying problems in space, and succeed.

- Rescue operations of the ESA/NASA spacecraft SOHO (Solar and Heliospheric Observatory), with a launch of SOHO on Dec. 2, 1995. Operational control of the SOHO S/C was lost on June 25, 1998 (when SOHO spun out of control and communication was lost). Subsequent investigations by a joint NASA/ESA/MMS team showed that the loss of contact with SOHO had been preceded by a routine calibration of the spacecraft's three roll-control gyros. – On July 23, first S/C recovery operations were performed with the Arecibo radio telescope in Puerto Rico. The 305 m diameter dish antenna was used to transmit S-band signals to SOHO, while NASA's DSN at Goldstone functioned as receiver, thereby locating the spacecraft's echo. On Aug. 3, contact with SOHO was re-established and reception of the carrier signal by DSN. Attitude recovery was established on Sept. 16, 1998, resulting in a SOHO lock to the sun. SOHO was finally brought back to normal operating mode on Sept. 25. The only equipment failures at S/C level were in two of the three gyros. Instrument re-commissioning started on Oct. 5 with SUMER and ended with CELIAS on Oct. 24, 1998. – On Dec. 21, 1998, the last onboard gyro failed during the preparation of a routine orbit-correction and wheel management maneuver. ¹⁴¹⁹⁾

In January 1999, a **gyroless mode of operation** was devised and installed with a new software patch for a modification of the AOCS (Attitude and Orbit Control Subsystem), making SOHO the first three-axis-stabilized S/C of ESA to be operated without a gyro. ¹⁴²⁰⁾ The software patch was developed by MMS (Matra Marconi Space), now EADS Astrium SAS of France (an ESA patent is pending). The software allows to determine SOHO's drift by measuring the changes in the speed of the spacecraft's momentum wheels (the software triggers the momentum wheels instead of the faulty gyroscopes). Final recovery from ESR (Emergency Sun Re-acquisition mode) and full S/C operation of SOHO was regained Feb. 1, 1999. A joint ESA/NASA investigation board came to the conclusion that the loss of the SOHO S/C was a direct result of operational errors, a failure to adequately monitor S/C status, and an erroneous decision which disabled part of the onboard autonomous failure detection.

- The ERS-2 satellite of ESA started its mission on April 21, 1995 with six operational gyroscopes (S/C design life of 2 years), three of which were required for its three-axis pointing control, and a further gyro for the back-up safe mode. ^{1421) 1422) 1423)} In 1997, the S/C lost gyro #2 and in 1998 a pointing anomaly on gyro #3 made it unreliable. The measures implemented in Feb. 2000 to protect the satellite against further gyroscope failures have allowed the continuation of the ERS-2 operations, despite two major anomalies that took place in Jan. 2001. Under normal conditions these would have meant the end of the ERS-2 mission, but the measures implemented meant that the effects were limited to the interruption of service for about one month and temporary degradation of data quality.

Close collaboration between ESA and EADS Astrium has resulted in the successful implementation of a **gyroless or ZGM (Zero-Gyro Mode) of operation**. The ZGM software was loaded on June 6, 2001 and activated onboard. The first period of recommissioning lasted until the end of July 2001. In Nov. 2001, the tuning was improved to cover all data products. The ZGM represents a re-design of AOCS, making extended use of the platform's sensors and actuators to compensate for the lack of gyroscopes. The goal is to extend the ERS-2 mission until MetOp-A becomes operational in 2006. – However, one consequence of re-

1419) F. C. Vandenburg, "SOHO's Recovery – An Unprecedented Success Story," ESA Bulletin, Nr. 97, March 1999, pp. 39–47

1420) J. Bates, "Software Extends Satellite Missions When Gyroscopes Fail," Space News, Feb. 5, 2001, p. 8

1421) Project News, ERS, ESA Earth Observation Quarterly No 69, p.4, June 2001

1422) Project News, ERS, ESA Earth Observation Quarterly No 70, p.4, January 2002

1423) X. Neyt, P. Pettiaux, M. Acheroy, "Scatterometer Ground Processing Review for Gyro-Less Operations," Proceedings of SPIE, Vol. 4881, 9th International Symposium on Remote Sensing, Aghia Pelagia, Crete, Greece, Sept. 23–27, 2002

newed ERS–2 operations is that ATSR–2 high–rate operations are suspended since the Wind/Wave mode is used for S/C attitude control (only within narrow limits can the ATSR–2 HR mode be operated).

- PseudoGyro – is a software package of The Aerospace Corporation (El Segundo, CA) to save satellites from failure (US patent as of Feb. 1, 2000). The PseudoGyro package emulates a hardware gyro through software processes.¹⁴²⁴⁾ The technique was successfully demonstrated in 1999 on a classified satellite of NRO (National Reconnaissance Office) which had experienced failures of its primary and secondary hardware gyros. PseudoGyro works in conjunction with orbital–attitude–estimation filtering techniques and takes advantage of all available sensors, including the vehicle itself, in determining attitude. It uses the principle of conservation of momentum to accurately determine the angular velocity of a spacecraft. It can be applied to virtually all types of space vehicles that are controlled by any type of momentum storage device. The technology can be integrated before or after a satellite is in orbit. In general, gyroscope–mimicking software might not replace the real thing, but it can reduce the workload on gyros, thereby extending their lives. PseudoGyro addresses also the need to reduce the risks and costs associated with new technology gyros.
- S/C rescue operations – DS1 extended mission. In November 1999, two months after the end of its extremely successful primary mission and early in its extended bonus mission, the star tracker of DS1, responsible for the spacecraft’s orientation, ceased operating. Rather than abandon the project, NASA engineers managed a deep–space rescue. They sent new software to DS1 (at a distance of 321 million km from Earth), turning an onboard camera (MICAS) into a navigation instrument. The challenging task was completed in June 2000 to resume thrusting in time to give DS1 a chance to encounter comet Borrelly in September 2001 (the encounter took place on Sept. 22, 2001).
- The Italian–Dutch X–ray orbiting observatory, BeppoSAX, was launched Ap. 30, 1996. The original AOCS software design, relying on three gyroscopes and three rate gyros (for continuous rate measurements), has been changed in flight following failures of several of these units (up to 4 out of 6 rate integrating gyros). In Feb. 1997, the original safe mode was replaced by a totally gyroless one, referred to as GSM (Gyroless Safe Mode). Then a fine pointing mode, relying on a single gyroscope, was developed/uploaded in Aug. 1997, allowing the continuation of the scientific mission. In 1999, a fully gyroless scientific pointing mode (ESM2) was designed and developed as a precautionary measure; this software package was uploaded in Oct. 2001, allowing continuation of the SAX observations until April 30, 2002, when the S/C was deactivated on ASI decision.^{1425) 1426)}
- A most unusual salvage of a so–called lost commercial communication satellite has been achieved with the HGS–1 (Hughes Global Services–1) S/C. Hughes Global Services Inc. of HSC (Hughes Space Communication Company) of El Segundo, CA, rescued a stranded communications satellite (intended to be AsiaSat–3) by sending it on a sequence of lunar passes. HGS–1 was launched Dec. 25, 1997. Because of a malfunctioning launch vehicle, it was left in an unusable, highly elliptical orbit. Hughes orbital engineers devised a novel mission to salvage the satellite, using lunar gravity to improve the resulting orbit once the satellite returned to Earth. That flyby, in mid–May 1998, was the first commercial mission to the moon. In a second lunar flyby, the satellite controllers fired the onboard motor for 12 minutes, which slowed the spacecraft enough to enter a circular orbit 36,000 km

1424) <http://www.aero.org/news/newsitems/pseudogyro-012901.html>

1425) M. Montagna, A. Tramutola, P. Martella, L. Salotti, “BeppoSAX Scientific Gyroless Mode in Flight Behavior,” 5th ESA Conference on Guidance Navigation and Control Systems, Oct. 22–25, 2002, Frascati, Italy, ESA SP–516

1426) A. Tramutola, M. Montagna, P. Martella, A. Bacchetta, “BeppoSAX Scientific Gyroless Modes,” 4th ESA International Conference on Spacecraft Guidance, Navigation and Control Systems, Oct. 18–21, 1999, pp. 443–450, ESA/ESTEC

above the equator. As of June 17, 1998 HGS–1 is in GEO (Geostationary Earth Orbit).¹⁴²⁷⁾ 1428)

- The ARTEMIS (Advanced Relay and Technology Mission) rescue mission of ESA (launch July 12, 2001) experienced an extensive reprogramming of its onboard software when it was realized that the launch failure had left ARTEMIS in an elliptical orbit much lower than intended. Before the orbit–raising operations could get underway, a huge reprogramming effort was required. In all, about 20% of the original spacecraft control software had to be modified in order to accomplish the new mission scenario. Thanks, however, to the re-programmable onboard control concept, these modifications could be made by uplinking ‘software patches’ to the satellite. These software patches amounted to a total of 15,000 words, making it the largest reprogramming of flight software ever attempted for a telecommunications satellite. In fact, the new attitude–control strategy developed for the satellite’s recovery has been retained as the best option for normal–mode operation in an inclined orbit. Moreover, an extension of this mode has been devised for station–keeping operations, which could be of great value for future telecommunications missions, as it provides for smooth attitude control during stationkeeping without mode transitions, and with minimal operator involvement.¹⁴²⁹⁾

The unusual route taken by ARTEMIS to get to geostationary orbit was long and hard, and beset with unfamiliar problems. But the mission was saved by the skills of a dedicated team of engineers and other specialists from ESA and its contractor companies (Alenia Spazio, Telespazio, Astrium, etc.).

- The solar array onboard EchoStar–4, a commercial communications satellite in GEO of EchoStar, that had remained stuck in its stowed position since its launch (May 7, 1998), suddenly opened (i.e. deployed) the weekend of Sept. 4, 2004, according to EchoStar (the owner and operator of EchoStar–4). This is a most unusual event in deployment history – after six years! The solar array simply deployed without any warning during routine operations (it probably deployed on its own due to a long–term exposure to the sun).¹⁴³⁰⁾

- The Landsat–7 project de–powered one of its gyros on May 5, 2004, due to indications of anomalous behavior. The spacecraft has three two–degrees–of–freedom gyros and needs two at any time to maintain attitude control. A risk assessment reported a 40% likelihood of another gyro failure by July 2005. A team was assembled to modify the software on board the spacecraft to operate in what is being termed **Virtual Gyro** (V–Gyro) mode. In this mode, if another gyro fails, the attitude control system would use the remaining gyro, along with existing onboard instrumentation and new control logic, to maintain attitude control.

As of February 1, 2006, the Landsat–7 team developed and uploaded flight software that can act like a “virtual” gyro – ready to use if another gyro fails. The enhanced capability was designed, developed, tested, and implemented with no interference to ongoing Landsat–7 operations.¹⁴³¹⁾

- Switch maneuver of the GRACE satellites in Dec. 2005 (joint US–German mission). Since launch (March 17, 2002), the trailing satellite (GRACE–2) of the co–orbiting twin GRACE spacecraft (separated by nominally by 200 km in along–track) has been flying “forward” with its K–band antenna horn exposed to the impacting atomic oxygen.¹⁴³²⁾

1427) <http://www.spacetoday.org/Satellites/SatBytes/MoonCommsat.html>

1428) <http://www.xs4all.nl/~carlkop/asiasat.html>

1429) http://www.esa.int/export/esaCP/SEMVCVY1A6BD_index_0.html

1430) W. Ferster, “Solar Array on EchoStar–4 Deploys after Six Years,” Space News, Sept. 13, 2004, p. 4

1431) “Landsat 7 Maintains Safety of Spacecraft with Gyro Software,” http://landsat7.usgs.gov/project_facts/project_news/February_2006.php#topic_335

1432) “Switch Maneuver Of GRACE Satellites,” URL: http://www.csr.utexas.edu/grace/operations/switch_manuever.html

1433) 1434) There is some risk that overexposure to atomic oxygen could lead to a loss of thermal control over the K–band horn, which would affect the accuracy of the KBR (K–band Ranging system) signal. – To ensure uniform aging and exposure for the K–band antennas on each of the satellites, the GRACE team performed a switch maneuver to exchange the leading and trailing spacecraft of the GRACE formation. For this purpose, an inclination/eccentricity separation has been used for a fuel and operational effort optimized switch maneuver. The switch was accomplished with only three OTMs (Orbit Thrust Maneuvers). OTM–1 took place on December 3, 2005, and the two subsequent maneuvers (OTM–2 and OTM–3) occurred respectively on December 12, 2005, and January 11, 2006. The maneuver was a success and GRACE–2 is now the leading satellite (Jan. 2006).

ISS (International Space Station) computer outage: On June 14, 2007, mysterious problems with the computers in the Russian segment of ISS arose that control the positioning (attitude) of the station. All six redundant control computers went offline at once and could not be rebooted (they were all of the same design, having the same strengths and weaknesses – they were all plugged in at the same time exposed to the same systemic problems: a point of vulnerability in the design). This left the ISS attitude dependent on NASA’s segment as well as on the thrusters of the visiting Shuttle Atlantis (STS–117, June 8–22, 2007). The computers shut down right after astronauts from the Atlantis installed new trusses to the ISS via a spacewalk to give the space station more power. The cause of the computer shutdown turned out to be a faulty secondary power supply switch. After the repair (bypassing the switch with a jumper cable) the computers were restarted in a self–test mode. – The round–the–clock work of the engineers in the partner countries along with the crew on the ISS to solve the problem also shows the resilience and creativity that has been developed in the teams involved. A lesson to be learned is to simply have spares on board that are not plugged in and hence not exposed to what might have been a one–time event. 1435) 1436) 1437)

1433) P. A. M. Abusali, S. Bettadpur, “Switch Maneuver of GRACE Satellites,” *The Earth Observer* (NASA/GSFC), March–April 2006, Vol. 18, Issue 2, pp. 4–5

1434) M. Kirschner, O. Montenbruck, S. D’Amico, “Safe Switching of the GRACE Formation using Eccentricity/Inclination Vector Separation,” 18th International Symposium on Space Flight Dynamics, Oct. 11–15, 2004, Munich, Germany, ESA SP–548

1435) <http://www.nasaspacespaceflight.com/content/?cid=5138>

1436) E. R. Hedman, “The fragility and resilience of NASA,” *The Space Review*, Aug. 6, 2007, URL: <http://www.-thespacereview.com/article/924/1>

1437) T. Malik, “Engineers Close in on Cause of ISS Computer Glitch,” *Space News*, July 23, 2007, p. 13

1.11 Cooperative Distributed Space Systems – Satellite Formations

Distributed space systems (DSS) are multi–satellite systems that work together to perform a unified mission. Such systems are an alternative to monolithic satellite missions in which all on–orbit activities are performed on a single platform. Distributed space systems can range from global constellations offering extended service coverage to clusters of highly coordinated vehicles in formation flight (FF) that perform distributed sensing (FF is a subset of DSS).

Flying several spacecraft in formation enables spaceborne interferometry at a very high angular resolution, distributing the sensor over a collection of optical elements on individual spacecraft, and eliminating the restrictions imposed by the use of physical structures to establish, maintain, and control instrument separation and stability. Global constellations of communication and navigation satellites are considered “loosely coupled” systems, they are in existence for many years. On the other hand, the use of spacecraft formations for remote–sensing applications represents a new and rather unexplored type of constellation, namely “**tightly coupled**” systems with a new quality of service and support capabilities. ^{1438) 1439) 1440) 1441) 1442)}

In general, the presence of multiple satellites leads to multi–point observations at different times and/or locations. This is the key to resolving the spatial–temporal ambiguity, which in turn enables a significant step forward in our understanding of the large–scale system dynamics (such as Earth’s magnetosphere). ^{1443) 1444)}

The logical sequence toward full FF implementations requires a number of technological steps from autonomous navigation and constellation control to one and two–way formation flying, and finally to virtual platforms, defined as collective, coordinated operations of multiple spacecraft oriented and positioned to achieve a set of predefined mission objectives. The entire concept of DSS, leading eventually toward **virtual payloads and/or virtual satellites** [referring to a collective guidance, navigation & control (GN&C) function for multiple spacecraft], represents in fact a **new paradigm for remote sensing in general**.

Formation Flying (FF) is critical to enable an order of magnitude (and greater) improvements in resolution and coverage achievable from scientific remote sensing platforms. Size limitations on launch vehicle fairings leave formation flying as the only option to assimilate coherent large apertures or large sample collection areas in space. The FF concept opens a completely new chapter in all observations from space. ¹⁴⁴⁵⁾

DSS spacecraft architectures offer the following basic benefits and capabilities. ¹⁴⁴⁶⁾

1) Multiple spacecraft can be separated to large baselines thereby improving angular resolution for such missions as Earth imaging, astrometry, and planet detection.

1438) J. Bistrow, D. Folta, K. Hartman, “A Formation Flying Technology Vision,” Proceedings of AIAA 2000 Space Conference and Exposition, Long Beach, CA, Sept. 19–21, 2000

1439) G. H. Fountain, et al., “A Technology Path to Distributed Remote Sensing,” IAA 2nd International Symposium on Small Satellites for Earth Observation, Berlin, April 12–16, 1999, pp. 189–193

1440) J. Esper, P. V. Panetta, et al., “NASA/GSFC Nano–Satellite Technology for Earth Science Missions,” IAA 2nd International Symposium on Small Satellites for Earth Observation, Berlin, April 12–16, 1999, pp. 219–225

1441) F. H. Bauer, K. Hartman, J. P. How, et al., “Enabling Spacecraft Formation Flying through Spaceborne GPS and Enhanced Automation Technologies,” Proceedings of the ION–GPS Conference, Nashville TN, Sept. 15, 1999

1442) J. Leitner, F. Bauer, D. Folta, M. Moreau, R. Carpenter, J. How, “Formation Flight in Space,” GPS World, Feb. 2002, pp. 22–31

1443) M. Martin, M. J. Stallard, “Distributed Satellite Missions and Technologies, The TechSat 21 Program,” Proceedings of the AIAA Space Technology Conference and Exposition, Sept. 28–30, 1999, Albuquerque, NM, Sept. 1999, AIAA 99–4479

1444) N. A. Goodman, J. M. Stiles, “Synthetic Aperture Characterization of Radar Satellite Constellations,” Proceedings of IGARSS 2002, Toronto, Canada, June 24–28, 2002

1445) J. Leitner, “Formation Flying – The Future of Remote Sensing From Space,” 18th International Symposium on Space Flight Dynamics, Munich, Germany, Oct. 11–15, 2004

1446) D. W. Miller, R. J. Sedwick, E. M. C. Kong, S. Schweighart, “Electromagnetic Formation Flight For Sparse Aperture Telescopes,” Proceedings of the IEEE Aerospace Conference, Big Sky, MT, March 9–16, 2002

- 2) Each spacecraft in a formation can be smaller than a single spacecraft designed to perform the same mission and thereby provide easier packaging, launch, and deployment.
- 3) Since interspacecraft interfaces are soft (e.g., communications, optics, control, metrology), if a spacecraft fails, it can easily be removed from the formation and replaced with a functioning spacecraft.
- 4) As technology improves, replacement spacecraft can be launched and integrated into the array thereby evolving the formation's capabilities without the costly "block changes" typical of past programs.

The drawbacks of these architectures are on-orbit FF geometry maintenance requiring energy (a consumable, normally a propellant) as well as a considerable amount of FF control.

The idea of the FF mission concept demonstrations is to use clustered small spacecraft (minisatellites, microsatellites and/or nanosatellites) missions, capable to cooperate and to share resources and functions (processing, communications, payload, and/or observation/mission functions) with each other, in order to perform the functions of a large single satellite. Sensors on satellites, flying in formation, may function as a single large sensor (large aperture), offering entirely new observation capabilities such as:

- More frequent coverage through wider swaths, stereoscopic observations of imaging instruments (multifold coverage of common target regions), parallel provision of similar measurements at higher time-and-space sample rates (altimetry applications), virtual large aperture radar, etc.
- The entire field of spaceborne interferometry is offering new dimensions and observation capabilities with the introduction of DSS.
- An FF configuration offers very large baselines to **synthesize a large sparsely distributed aperture** that cannot be achieved by monolithic apertures. This feature is beneficial for such missions as spaceborne SAR or large apertures for the detection of ground-based moving targets in the cluster, the latter is also referred to as MTI (Moving Target Indication).
- Flexibility of FF architectures: ¹⁴⁴⁷⁾ The ability to reconfigure a cluster's geometry for instance allows modifying the revisit time requirement. This is one particular instance of flexibility – an ability to respond to changes in the requirements occurring after the system has been fielded – it is characteristic of FF and is not feasible with a monolithic design. Furthermore, the ability to modify the revisit time on-orbit implies that it needn't be specified prior to launch or further up front in the development phase of the system. – The idea that critical system requirements need not be narrowly specified prior to launch, because changes can be accommodated afterwards, is one particular advantage of the property of flexibility in design.

An FF experimental testbed by the name of **SPHERES** (Synchronized Position Hold Engage and Reorient Experimental Satellites) ¹⁴⁴⁸⁾ ¹⁴⁴⁹⁾ ¹⁴⁵⁰⁾ is being developed and installed at the Space Systems Laboratory of MIT (Massachusetts Institute of Technology) to provide the USAF and NASA with long-term, replenishable, and upgradable test capabilities for the validation of high risk metrology, control, and autonomy technologies [support of Tech-

1447) J. H. Saleh, D. E. Hastings, D. J. Newman, "Extracting the Essence of Flexibility in System Design," MIT paper ESD-WP-2001-04, Aug. 2001 URL: <http://esd.mit.edu/WPS/esd-wp-2001-04.pdf>

1448) A. Saenz-Otero, D. Miller, "The SPHERES ISS Laboratory for Rendezvous and Formation Flight," 5th International ESA Conference on Guidance Navigation and Control Systems, Frascati, Italy, Oct. 22–25, 2002, SP-516

1449) D. W. Miller, E. M. C. Kong, A. Saenz-Otero, "Overview of the SPHERES Rendezvous and Docking Laboratory on the International Space Station," Proceedings of the 26th AAS Conference on Guidance and Control, Breckenridge, CO, Feb. 5–9, 2003, Vol. 113 Advances in the Astronautical Sciences, Edited by I. J. Gravseth and R. D. Culp, AAS-03-013, pp. 155–169

1450) <http://ssl.mit.edu/spheres/index.html>

Sat–21, TPF (Terrestrial Planet Finder) programs, etc.]. Some flight test experiments, evaluating both testbed and control algorithm performance, have already been conducted (in 2000) onboard NASA’s KC–135 aircraft. DARPA (Defense Advanced Research Projects Agency) is a major sponsor of the SPHERES program.

Another aspect of the SPHERES program is to take a SPHERES payload, an ISS–internal testbed in the US Laboratory, to ISS [Note: a launch of SPHERES took place on April 24, 2006 on a Soyuz–U launch vehicle with the Progress M–56 payload (ISS service flight) from Baikonur, Kazakhstan]. The system consists of: ¹⁴⁵¹⁾

- Three experimental self–contained 20 cm diameter free–floating nanosatellites (each of 3.56 kg) which perform the various algorithms
- A laptop computer
- Five small beacons (metrology beacon system).

The objective is to achieve a mature autonomous satellite formation flight capability (allow for the interchange of control algorithms; demonstrate key close proximity formation flight and docking maneuvers; test autonomous fault diagnosis and recovery; ensure the adaptability of control algorithms). The nanosatellites were designed by MIT students (under a program funded by MIT, DARPA and NASA), and built by Payload Systems Inc. of Cambridge, MA. The ISS testbed provides a risk–tolerant environment capable of testing unknown algorithms and recovering from failures at low costs compared to that of a full mission. The program provides human observability and manipulation by both, the guest scientists in a ground station, and operators in the ISS. ¹⁴⁵²⁾

The ESA FAMOS (Formation Flying Analysis and Missions Operations Simulator) was developed by GMV S. A. of Madrid. ¹⁴⁵³⁾ ¹⁴⁵⁴⁾ FAMOS provides detailed analysis of satellite formations using highly coupled GNC algorithms, which integrate attitude, navigation and maneuvers. FAMOS is a generic, six degrees–of–freedom simulator for 2 satellites flying in LEO formation. It is a powerful tool implementing a wide range of sensors which are integrated into highly coupled GNC.

Distributed S/C control architectures are characterized by interactions between S/C, cooperation between S/C, and collective behavior among S/C within a constellation or formation. The introduction of concepts such as decision making, hierarchical control, decentralized control, etc., within the management of the formation enables spacecraft to cooperate with one another. Autonomy is a critical technology in this scenario that impacts every level of the design, from the subsystem, to the instrument, the platform, as well as the entire formation. If a cooperative formation includes a variety of basic, versatile instruments, for example UV, VIS and IR spectrometers, then “virtual platforms” for different applications can be formed in space, on the fly, and “disassembled” (or reconfigured) later for other uses – flexibility to adapt to the evolving science needs and to implement the newest technologies during the course of an on–going mission are the basic requirements. In this new observation concept of **formation flying**, GPS navigation, i.e. orbit and attitude sensing and vehicle orbit (relative and absolute positioning) and attitude control, plays a key role as a navigation instrument in the maintenance and control of the formation (measurement of formation states, i.e., the relative orientations, positions and velocities of the vehicles).

1451) “Mini Satellites Rocketing To Space Station,” http://www.spacedaily.com/reports/Mini_Satellites_Rocketing_To_Space_Station.html

1452) J. Enright, M. Hilstad, A. Saenz–Otero, D. Miller, “The SPHERES Guest Scientist Program: Collaborative Science on the ISS,” Proceedings of 2004 IEEE Aerospace Conference, Big Sky, MT, March 6–13, 2004

1453) T. W. Beech, G. Bengoa–Endemano, et al., “FAMOS: A Formation Flying Analysis and Missions Operations Simulator,” Proceedings of International Symposium Formation Flying Mission & Technologies, Oct. 29–31, 2002, Toulouse, France

1454) T. W. Beech, G. Bengoa–Endemano, et al. “Close Formation Flying using the FAMOS SW Tool,” Third International Workshop on Satellite Constellations and Formation Flying, Pisa, Italy, Feb. 24–26, 2003, pp. 117–124

- **Definition of general DSS (Distributed Space System) characteristics:** A collection of spacecraft may be categorized as a constellation, a cluster, or a formation, depending on how closely the spacecraft are coupled in time and space.

1) A constellation of spacecraft, such as the 24 GPS satellites orbiting in six orbital planes around Earth, are discrete spacecraft that are partially organized in time and space and controlled separately from Earth.

2) Another type of DSS is the concept of a local cluster, where satellites are intentionally placed close together in the same orbit to train on a common target. Optionally, this cluster of satellites may have a more complex instantiation, namely a formation.

3) **Definition of FF (Formation Flying) architecture.** There are four elements that are unique to the formation flying problem: formation design, relative navigation, intersatellite communication, and formation control. – The new technology of spacecraft formation–flying includes a set of more than one spacecraft in a tightly–controlled spatial configuration (formation), whose operations are closely synchronized, with a collective control system distributed among the spacecraft so that the individual spacecraft are not controlled from Earth (active, real–time, closed–loop control is involved). The relative location (distance) between the satellites in the formation is of prime concern for operational control/maintenance to achieve the distributed observation configuration.

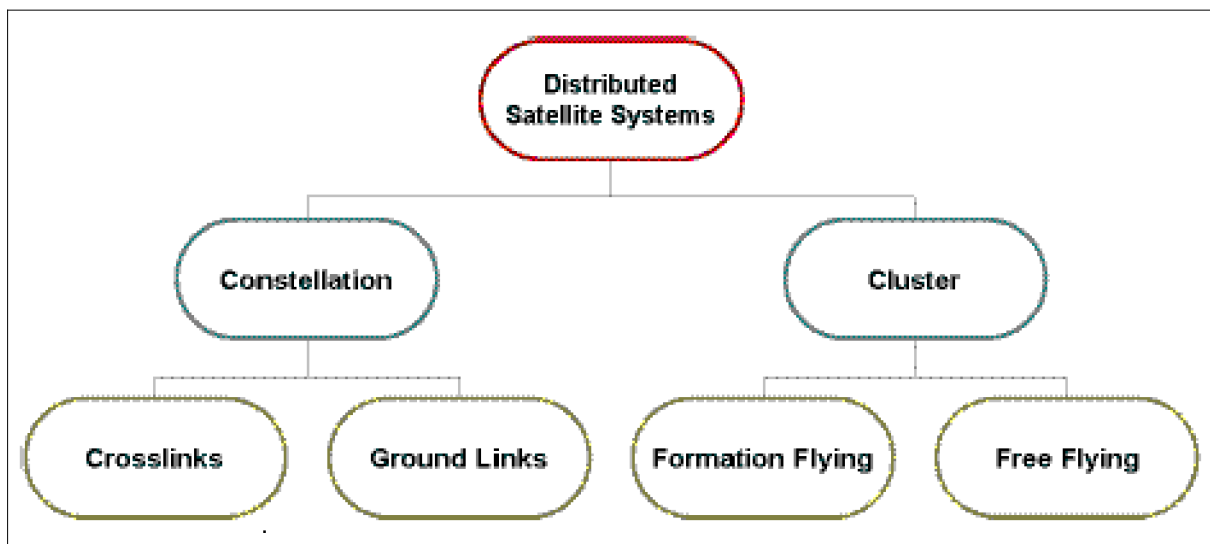


Figure 76: Various views of DSS (Distributed Satellite Systems)

Flying two or more spacecraft in a precise formation for **cooperative observations** (i.e., to obtain **contemporaneous spatial sampling** by a group of separated spacecraft) presents a number of complex challenges:

- Each spacecraft must have a sensory and control system enabling it to attain and maintain a precise relative position.
- Each spacecraft must have a sensory and control system enabling it to attain a specified attitude, with all spacecraft targeting the desired object.
- Each spacecraft must be able to communicate with each other in the formation.

A number of critical FF technologies¹⁴⁵⁵⁾ are required to enable and maintain separated spacecraft FF–based mission architectures. These include:

- Robust, fault tolerant and scalable formation architectures for distributed spacecraft communication, control, and sensing. A key feature in this scenario is the ability to dynami-

cally reconfigure the sensing, information flow and control connectivity across each spacecraft in the formation. Also provision of graceful degradation of performance and functionality within the given onboard hardware redundancy. The formation flying architecture must allow for stand-alone operation in case of inter-spacecraft communication and/or formation sensor faults.

- Formation autonomy. The onboard software needs to autonomously provide formation as well as individual spacecraft guidance, estimation, and control functions within the framework of high level reasoning and commanding to achieve the desired science goals in a resource-efficient manner.
- A new class of formation guidance, estimation and control algorithms. This includes such functions as:
 - The capability of robust lost-in-space acquisition, i.e. the ability to obtain lock of the relative sensors to initialize the formation after initial deployment or after reset/recovery events
 - Collision-free operation
 - Consumable resource balancing across all spacecraft
 - Path planning in both attitude and translation under multiple constraints (e.g. solar, thermal, glint, H/W capability)
 - Precision hierarchical control coordinated across multiple spacecraft
 - Observation-on-the-fly capability to enable continuous science measurements during formation maneuvers.
- Relative sensor technology to provide the inter-spacecraft range and bearing measurement. The knowledge of range and bearing (range vector) between each pair of spacecraft is essential in configuring the overall formation to achieve a desired baseline, and maintaining the baseline within a prescribed tolerance during the course of the science observation. Collision avoidance is another key formation flying requirement enabled by formation sensor based relative range vector knowledge.
- Precision actuator technology to enable fine motion (both inertial and relative) control of each spacecraft in the formation (in particular for interferometry missions). Most missions will require coarse actuation (for retargeting maneuvers) and precision actuation to enable stable and accurate science pointing and tracking.
- Ground and flight demonstration testbeds to integrate and bring these technology elements to a level of maturity for infusion into future missions. See SPHERES above in this chapter.
- The implementation, maintenance and operation of formation flying poses further challenges:¹⁴⁵⁶⁾
 - The performance requirements and disturbance/operating environments vary substantially between Earth-orbiting and deep space missions. For EO missions, orbital and environmental dynamics (J_2 , drag, ground track coverage requirements, etc.) affect each spacecraft in a formation differently. These variations affect the formation stability. Solar radiation pressure is the chief disturbance source for deep space formation flying missions which typically require much tighter formation capabilities (DARWIN, LISA).

1455) F. Y. Hadaegh, A. Ahmed, J. Shields, "Precision Guidance and Control for Formation Flying Spacecraft," Proceedings of International Symposium Formation Flying Mission & Technologies, Oct. 29–31, 2002, Toulouse, France

1456) W. D. Deininger, J. Bladt, B. Carpenter, W. Davis, K. Epstein, et al., "Formation Flying Activities and Capabilities at Ball Aerospace," Proceedings of IEEE Aerospace Conference, Big Sky, MT, March 8–15, 2003

– There are several major formation flying maneuver types: a) formation acquisition and initialization, b) formation maintenance, c) formation resizing (change of interferometer baselines), d) formation rotation (move to new baseline orientations around the line of sight), e) formation retargeting slews, f) stationkeeping, g) rendezvous and docking, and other close proximity maneuvers.

- Orbits in formation flying (FF) configurations. Formation flying guidance (FFG) is defined as the generation of any reference trajectories used as an input for a formation member's relative state tracking control law. This FFG definition includes open-loop control design (i.e., an optimal control profile that only depends on time and initial conditions). In general there are two regions of FFG: POE (Planetary Orbital Environment) and DS (Deep Space). – The POE FFG is of particular interest in the context of Earth observation, where spacecraft in a formation have significant orbital dynamics (LEO missions). General POE FFG mission requirements consider reconfigurations of the formation and on finding passive apertures. – The most common linear passive apertures are thrust-free, periodic solutions to the Hill–Clohessy–Wiltshire (HCW) equations, referred to as FETs (Free Elliptical Trajectories). Example: The ICW (Interferometric Cartwheel) FET is useful for synthetic aperture radar (CNES mission). The FETs rotate with the local-vertical, local-horizontal frame and are useful for looking at the Earth. ^{1457) 1458) 1459) 1460)}

The observation concept from any formation-flying cluster is **regarded as multistatic** where two or more platforms, each furnished with an active instrument, can be used with different views of the same observed area, permitting such applications as stereoscopy and interferometry.

- **DSS as seen from the perspective of mission resolution requirements.** *Distributed spaceborne observing systems offer an attractive architecture for achieving high spatial and temporal resolution.* However, multiple architectural configurations and system sizes should be considered for an optimal observing system design to suit best all functional requirements. Various phenomena which may be observed from space have different temporal and spatial scale requirements. For example, severe storms evolve quickly, and observations every 15 minutes or less may be required. On the other hand, ice sheets evolve slowly and thus may be observed less continuously. Similar arguments can be made for spatial requirements. Thus it is important to consider various vantage points – ice sheet observations could be made from LEO (Low Earth Orbit) while severe storm observations should probably be made from GEO (Geostationary Orbit) or HEO (Highly Elliptical Orbit) to meet the revisit requirement. Surface deformation occurs on a variety of temporal scales ranging from long-term volcanic inflation to seasonal hydrologic variations to earthquakes. ^{1461) 1462) 1463)}

Within this context four major classes of distributed spacecraft systems can be identified where each successive class represents an evolutionary step in DSS formations:

1) Virtual observing systems: Refer to multiple space platforms with limited-to-no interspacecraft communication. Currently meteorological observations from a variety of

1457) D. P. Scharf, F. Y. Hadaegh, B. H. Kang, "A Survey of Spacecraft Formation Flying Guidance," Proceedings of International Symposium Formation Flying Mission & Technologies, Oct. 29–31, 2002, Toulouse, France

1458) W. H. Clohessy, R. S. Wiltshire, "Terminal Guidance System for Satellite Rendezvous," Journal of the Aerospace Sciences, Vol. 27, No 9, Sept. 1960

1459) E. M. C Kong, D. W. Miller, R. J. Sedwick, "Exploiting orbital dynamics for aperture synthesis using distributed satellite systems: Applications to a visible earth imager system," Journal of Astronautical Sciences, Vol.47, No. 1, pp.:53–75, 1999

1460) Note: In this context, the term "guidance" refers to path planning (i.e., reference trajectory generation) and optimal, open loop control design.

1461) C. A. Raymond, J. O. Bistrow, M. R. Schoeberl, "Needs for an Intelligent Distributed Spacecraft Infrastructure," IGARSS/IEEE 2002, Toronto, Canada, June 24–28, 2002

1462) L. Lemmerman, C. Raymond, R. Shotwell, J. Chase, K. Bhasin, R. Connerton, "Advanced Platform Technologies Enabling Efficient Distributed Sensing System for Earth Science," 4th IAA Symposium on Small Satellites for Earth Observation, Berlin, Germany, April 7–11, 2003

1463) E. Torres-Martinez, M. Schoeberl, M. Kalb "A Web of Sensors: Enabling the Earth Science Vision Hazards," IGARSS/IEEE 2002, Toronto, Canada, June 24–28, 2002

sources are brought together as part of the data assimilation process. The platforms that are making the observations are not coordinated nor commanded to alter their observing strategy. The data is simply gathered from wherever it is supplied. Nonetheless, when considered as a whole, the current meteorological observing system constitutes a virtual single observing system with multiple components.

2) Simple formations (a degree of coordination is required): The observing assets are distributed across several spacecraft, replacing the functions of very large spacecraft. The advantage of the formation compared to a single large spacecraft is flexibility, redundancy and lower systems engineering costs. NASA's "A-train" of several spacecraft can be regarded a simple formation, taking advantage of existing assets.

Each mission in the A-train has its own objectives and to study different aspects of the Earth's atmosphere. However the great advantage of formation flying is the possibility to combine observations and gain a better understanding of important parameters related to climate change. In fact the A-Train formation allows for synergistic measurements where data from several different satellites can be used together to obtain comprehensive information about various key atmospheric components or processes. Combining the information from several sources gives a more complete answer to many questions than would be possible from any single satellite taken by itself.

3) Virtual instruments: This refers to a multiple satellite configuration which together provide a single observation configuration. Example missions in this category are: The GRACE mission of two minisatellites, ST5, etc.

4) SensorWeb: Refers to future systems/architectures (a networked collection of heterogeneous space and surface assets organized into a "SensorWeb") in which every element of the deployed system has awareness of all other elements and can coordinate and share duties on a real-time basis with neighboring elements. A SensorWeb may include virtual instruments and simple formations.^{1464) 1465)}

1.11.1 Survey of early formation-flying (EO) demonstrations

The problems yet to be solved associated with formation flying are numerous and each very challenging. Examples of S/C formation-flying demonstration missions (with correlated measurements) or early proximity operations missions (rendezvous and docking applications) are:

- The first ever rendezvous and FF took place with Gemini-6 and -7 spacecraft on Dec. 15, 1965 (5 hours of close FF). The rendezvous of two spacecraft was an important step in preparation for a future moon landing mission.
- The first manually controlled rendezvous and docking between the Gemini capsule and the unmanned Agena vehicle took place in March 1966.
- The first automatic docking of Kosmos 186 & 188 (USSR) took place on Oct. 28, 1967 (on the basis of radar tracking).
- In 1969, data from various US, USSR, and of ESRO (European Space Research Organization) satellites were correlated to study how large solar flares interacted with the Earth's magnetosphere and ionosphere – thereby achieving the **first contemporaneous**

1464) S. Habib, P. Hildebrand, "Sensor Web Architectural Concepts and Implementation Challenges – An Heuristic Approach," Proceedings of SPIE, Vol. 4881, 9th International Symposium on Remote Sensing, Aghia Pelagia, Crete, Greece, Sept. 23–27, 2002

1465) <http://sensorwebs.jpl.nasa.gov/>

spatial sampling by a group of separated spacecraft (although, this was no formation flight configuration). The S/C involved in the measurement campaign were: ¹⁴⁶⁶⁾ ¹⁴⁶⁷⁾ ¹⁴⁶⁸⁾

- US spacecraft: OGO–5 (Orbiting Geophysical Observatory, launch Mar. 4, 1968), Pioneer–8 (launch Dec. 13, 1967), Vela–4B (launch Apr. 28, 1967).
- USSR spacecraft: Venera–4 (launch June 12, 1967) and Venera–5 (launch Jan. 5, 1969)
- ESRO spacecraft: ESRO–1/Aurorae (launch Oct. 3, 1968), ESRO–IIB (launch May 17, 1968) also referred to as IRIS (International Radiation Investigation Satellite), and HEOS–A1 (Highly Eccentric Orbit Satellite), also referred to as HEOS–1, launch Dec. 5, 1968. The objectives of HEOS–1A were to study interplanetary magnetic fields, cosmic rays, the solar wind, and the magnetosheath. HEOS–1 operated for 7 years providing scientists with continuous observations of interplanetary conditions over most of a solar cycle.
- ASTP (Apollo–Soyuz Test Project), launch of both S/C on July 15, 1975. This flight marked the culmination of the Apollo–Soyuz Test Project, a post–moon race ‘goodwill’ flight to test a common docking system for space rescue (also near–proximity operations).
- The ORFEUS–SPAS–2 Shuttle mission of NASA/ESA/DLR on STS–80 (Nov. 19 – Dec. 7, 1996), a free–flyer platform, demonstrated for the first time relative navigation using a code–based DGPS system, ARP (ATV Rendezvous Predevelopment) of ESA, consisting of a GPS receiver on ORFEUS/SPAS deployed from the Shuttle, and a second GPS receiver on the Shuttle (see J.1.3). Raw GPS phase measurements were collected by the two receivers, providing 10–50 m relative positioning accuracy and m/s level relative velocity data in post–processing. ¹⁴⁶⁹⁾
- The SNAP–1 and Tsinghua–1 missions of SSTL, UK (launch June 28, 2000). Each S/C carried a GPS receiver (SGR–05), demonstrating meter–level positioning capabilities using pseudorange (see D.62.17 and D.62.18). However, the two S/C computed their absolute positions independently, the relative positioning capability using DGPS was not demonstrated.
- The ETS–VII (Engineering Test Satellite VII) of NASDA with a launch on Nov. 27, 1997 conducted an autonomous rendezvous and docking experiment using a code–based DGPS navigation receiver. The instrument RGR (Relative GPS Receiver) was used successfully in the docking demonstrations (see M.14.1). Relative position and velocity errors of <10 m and <1 cm/s were achieved. However, the GPS receiver was only used in the coarse approach phase due to its relatively poor accuracy. A laser radar and a proximity image sensor were used in the final approach and docking phase.
- GRACE (Gravity Recovery and Climate Recovery), a cooperative US–German dual–minisatellite mission with a launch March 17, 2002 (see E.13). The mission concept makes use of measurements of the inter–satellite range and its derivatives between two co–planar satellites (in low–altitude and polar orbits), using a K–band microwave tracking system (with ultrastable quartz oscillators) and a GPS receiver system (BlackJack) for precision orbit determination to enable accurate orbit determination. The oscillators’ precise and stable signals continuously measure satellite–to–satellite distance, and thus their relative velocity, with unprecedented accuracy. In addition, each S/C carries a high–accur-

1466) Note: ESRO (created in 1962) was one of the predecessor organizations of ESA (since 1975), the other was ELDO (European Launcher Development Organization)

1467) V. Manno, D. E. Page (eds), “Intercorrelated Satellite Observations related to Solar Events,” Proceedings of the Third ESLAB/ESRIN Symposium, Noordwijk, The Netherlands, Sept. 16–19, 1969, Astrophysics and Space Science Library, Vol. 19, Jul. 1970, Springer Verlag, New York, Hardbound pp. 643., ISBN 90–277–0128–8, and D. Reidel Publishing Company, Dordrecht, Holland

1468) Information was provided by Daniel P. Scharf of NASA/JPL, Pasadena, CA

1469) F. Gottifredi, L. Marradi, G. Adami, “Results from the ARP–GPS receiver flight on ORFEUS–SPAS,” Proceedings of the ION–GPS Conference, Sept. 1999

acy accelerometer (SuperSTAR) and a star camera (SCA) for attitude sensing. It should be noted, however, that the GRACE tandem mission is **not a tightly controlled system** with regard to relative distance between the two spacecraft. The inter-satellite range variations of the freely drifting tandem orbits is in fact the prime observation parameter – inferring variations in the Earth’s gravity field. Note: The varying gravity field is mostly due to variations in water content as it cycles between the atmosphere, oceans, continents, glaciers, and polar ice caps. ¹⁴⁷⁰⁾

- The Orion – Emerald (Electromagnetic Radiation and Lightning Detection) mission, a two-satellite project of Stanford University, Santa Clara University, and NASA). A launch on a Shuttle mission was planned for 2003. The objective was to demonstrate the use of CDGPS as a sensing system for precise relative navigation and formation flying control in real-time. Somehow, the mission Orion–Emerald concept was cancelled after the tragic Columbia accident (Feb. 1. 2003) due to other priorities of the Shuttle program.

- A program initiative, TechSat–21 (Technology Satellite of the 21st Century), was started in 1998 by various US DoD departments/directorates, namely AFRL (Air Force Research Laboratory), AFOSR (Air Force Office of Scientific Research), and DARPA (Defense Advanced Research Projects), with the objective to exploit the new paradigm and enabling technologies, such as MEMS (Micro–Electro–Mechanical Systems) and overall component miniaturization and function integration – that “involves satellites flying in tight formation that operate cooperatively to perform a surveillance mission.” Under this effort, a variety of application missions are being considered including surveillance, passive radiometry, terrain mapping, and communications. Launch of TechSat–21 is planned for 2006 with one year of on-orbit operations. Note: **The TechSat–21 program was cancelled in early 2003.** In spite of this unfortunate mission end, the concept studies have amply highlighted the extreme system-level challenges involved in FF.

- In addition, a University Nanosatellite Program (UNP) ¹⁴⁷¹⁾ was set up for this purpose by AFSOR/DARPA/NASA to fund ten university ‘research projects centered on the design and demonstration of nanosatellites.’ The partially funded projects within TechSat–21 / UNP are:

- 3CSat (3 Corner Sat), a constellation of three microsattellites in formation. 3CSat is a joint project of the University of Colorado at Boulder, ASU (Arizona State University), and NMSU (New Mexico State University). A multiple launch took place on Dec. 21, 2004; however, the two microsattellites that were launched did not reach the proper orbit.

- ION–F (Ionospheric Observation Nanosatellite–Formation), a three-satellite project of USU (Utah State University), Logan, UT; UW (University of Washington), Seattle, WA; and VT (Virginia Polytechnic Institute), Blacksburg, VA. Formation flying is a primary objective. Introduction of new technologies including micro-thrusters, magnetic gimbaled attitude control, and an Internet-based operations center. A Shuttle launch is proposed for 2004.

- Constellation Pathfinder, a one to three satellite mission of Boston University.

- Solar Blade Heliogyro Nanosatellite, a mission of CMU (Carnegie Mellon University), Pittsburgh, PA to demonstrate the solar sail concept.

- ST5 (Space Technology 5), formerly called Trailblazer, is a NASA demonstration mission in the NMP (New Millennium Program) of three microsattellites (each < 25 kg, orbit = GTO), flying in formation, a launch took place on March 22, 2006. The objective is to validate new technologies in space associated with microsattellite design and demonstration of functional capabilities (provision of autonomy and virtual control). Also use of an auto-

1470) A. Ward, “Earth’s Hidden Waters Tracked by GRACE,” *The Earth Observer*, May/June 2003, Vol. 15, No 3, pp. 25–29

1471) W. Ferster, “Tiny Satellite Fleet May Function as One Craft,” *Space News*, Aug. 17–23, 1998, p. 7

mous network scheduling tool to manage ground contacts with multiple satellites. The science objective is the collection of the magnetic field data from a constellation. – Note: The ST5 mission team concluded all mission operations on June 30, 2006, completing all major demonstration objectives within the planned mission life of three months. ¹⁴⁷²⁾ ¹⁴⁷³⁾ ¹⁴⁷⁴⁾

Further projects of flown/planned cluster missions and formation flying are:

- The TanDEM–X mission concept of DLR (launch June 21, 2010) is based on an extension the TerraSAR–X mission (launch June 15, 2007) by a second TerraSAR–X–like satellite, namely TanDEM–X. A close orbit formation flight is planned for both satellites – thereby providing a flexible single–pass SAR interferometer configuration, where the baseline can be selected according to the specific needs of the application. In the TanDEM–X and TerraSAR–X spacecraft mission design, the SAR (Synthetic Aperture Radar) instruments of each spacecraft are fully compatible, both offer transmit and receive capabilities along with polarimetry. Availability of the following support modes: a) monostatic, b) bistatic, and c) alternating bistatic mode.
- The PRISMA mission is a Swedish–led technology mission to demonstrate formation flying and rendezvous technologies (in–orbit servicing). The mission consists of two spacecraft, one advanced and highly maneuverable one, called **MAIN**, and a smaller S/C without a maneuvering capability, called **TARGET**. PRISMA was launched on June 15, 2010. The experiments encompass a) autonomous formation flying, b) homing and rendezvous experiment, and c) proximity operations.
- NASA/GSFC is defining MagCon (Magnetospheric Constellation), a mission of about 50 nanosatellites (deployed from a single mother ship) to acquire vector images of the magnetic and plasma flow fields in highly elliptical orbits (from 3 to 40 R_E). Simultaneous, multi–point observations of the Earth’s magnetospheric environment. The overall science objectives are to a) determine the equilibria of the magnetotail, b) understand the responses of the magnetotail to the solar wind, c) reveal the instabilities of the magnetotail.
Note: Due to budget constraints in NASA’s Solar Terrestrial Program, the planned launch of MagCon has been postponed. ¹⁴⁷⁵⁾

Examples of constellations are:

- GPS (Global Positioning System) constellation of the USAF (United States Air Force). The constellation is composed of 24 satellites in semi–synchronous orbits, placed evenly in six planes designed to provide position and timing information to users on land, sea, air, and in space.
- The GLONASS constellation of Russia (nominally of 24 S/C) is utilizing 12–14 satellites in two orbital planes.
- The Iridium LEO constellation of nominally 66 communications satellites is an example of an early commercial communication constellation (provision of global mobile phone communications). The launches took place in the timeframe 1997–2000/2. Iridium is the only commercial system to date that employs RF crosslinks. Iridium is also one of the first constellations with some degree of autonomy.
- The Cluster mission (Cluster–II) of ESA is a four spacecraft constellation which was launched on July 16, 2000 and on Aug. 9, 2000 (each launch of two identical S/C). The objective of Cluster is to gather scientific data on the magnetosphere in three dimensions (highly elliptical orbits). Cluster has the ability to take simultaneous measurements of phenomena

¹⁴⁷²⁾ K. Blahut, I. Bibyk, “The Space Technology 5 (ST5) Mission Constellation Control System & Operations Approach,” Proceedings of IEEE Aerospace Conference, Big Sky, MT, USA, March 8–15, 2003

¹⁴⁷³⁾ <http://nmp.jpl.nasa.gov/st5/>

¹⁴⁷⁴⁾ C. C. Carlisle, E. J. Finnegan, “Space Technology 5: Pathfinder for Future Micro–Sat Constellations,” Proceedings of the IEEE Aerospace Conference, Big Sky, MT, March 6–13, 2004

¹⁴⁷⁵⁾ <http://stp.gsfc.nasa.gov/missions/mc/mc.htm>

over a large volume. Cluster does not employ controlled formation flight, but rather falls into the free flying category, where only stationkeeping propulsion is required.

- **DMC** (Disaster Monitoring Constellation), a five-microsatellite constellation (international partners), has been developed and built at SSTL (Surrey Satellite Technology Ltd), Surrey, UK. The overall objective is to provide global daily imagery at 32 – 36 m spatial resolution (swath of 600 km) for the monitoring and mitigation of natural and man-made disasters and dynamic Earth observation. The successful launch of AISat-1, the first S/C in the series, occurred on Nov. 28, 2002. Another multiple launch occurred Sept. 27, 2003 with the following DMC spacecraft: BilSat-1 (Turkey), NigeriaSat-1 (Nigeria), and UK-DMC (UK). The Beijing-1 S/C was launched on Oct. 27, 2005. **DMC is in fact the first operational Earth imaging constellation.** All DMC spacecraft are flown in a single orbital plane providing a cumulative swath.
- FormoSat-3/ROCSat-3/COSMIC (Constellation Observing System for Meteorology, Ionosphere and Climate), is a collaborative US/Taiwanese (led by UCAR and NSPO) microsatellite constellation, a launch took place on April 14, 2006. In the scenario, a LEO constellation of six spacecraft in three orbital planes collects atmospheric remote sensing data for operational weather prediction, climate, ionospheric (space weather monitoring), and gravity research (refractive GPS radio occultation measurements).
- RapidEye is a commercial Earth imaging mission of BlackBridge, Berlin, Germany (former RapidEye AG of Brandenburg, Germany), that includes a constellation of five minisatellites (launch Aug. 29, 2008). Multispectral imagery of 6.5 m spatial resolution will be obtained. The constellation approach in a single orbital plane permits a cumulative swath to be built up (the spacecraft view adjacent regions of the ground, with image capture times separated by only a few minutes). A revisit time of one day can be obtained anywhere in the world ($\pm 70^\circ$ latitude) with body pointing techniques.
- The COSMO-SkyMed mission of ASI and the Italian Ministry of Defense, Rome, Italy, is a 4-spacecraft constellation (launch of first S/C on June 8, 2007, launch of COSMO-SkyMed-2 on Dec. 9, 2007), COSMO-SkyMed-3 on Oct. 25, 2008, COSMO-SkyMed-4 on Nov. 6, 2010. Each satellite is equipped with a SAR (Synthetic Aperture Radar) instrument and is capable of operating in all visibility conditions at high resolution and in real time. All spacecraft of the SAR constellation will be positioned in the same orbital plane.
- Swarm is a minisatellite constellation mission of ESA (launch on Nov. 22, 2013). The overall objective is to provide the best ever survey of the geomagnetic field (multi-point measurements) and its temporal evolution (accurate determination and separation of the large-scale magnetospheric field). The three satellites of the constellation are being flown in 3 orbital planes with 2 different near-polar inclinations to provide a mutual orbital drift over time.
- The MMS (Magnetospheric MultiScale) mission is part of NASA's Solar Terrestrial Physics Probe line.^{1476) 1477)} Its goal is to understand the fundamental physics which underlies the solar terrestrial environment and which drives space weather. MMS is composed of four identical spacecraft, each having a complete set of particles and fields instruments to study the ambient plasma. A launch of the constellation is planned for 2014. The spacecraft fly in a tetrahedral array with inter-spacecraft separations ranging for 10 to 1000's of km in four distinct highly eccentric orbital phases. Note: In this formation flying mission, it is only important to control the geometry of the formation (in this case to form a tetrahedron) at the apogee point of the orbit.

1476) S. A. Curtis, C. Petruzzo, P. E. Clark, A. Peterson, "The Magnetospheric Multi-Scale Mission: An Electronically Tethered Constellation of Four Spacecraft," Third International Workshop on Satellite Constellation and Formation Flying, Pisa, Italy, Feb. 24-26, 2003

1477) <http://stp.gsfc.nasa.gov/missions/mms/mms.htm>

1.11.2 Intersatellite communication and navigation

A prerequisite to formation flying is intersatellite communication (also referred to as cross-communication or simply crosslink) for the control and monitoring functions of the spacecraft cluster. Such a service may be provided by the GPS constellation offering a range of sensing options for a formation including such functions as: absolute positioning, relative vehicle positioning, attitude estimation, and precise timing. This approach is based on a combination of CDGPS (Carrier-phase Differential GPS) and GPS-like transceivers (the challenge of using CDGPS is in estimating the cycle ambiguity to sufficient accuracy). The transceivers are RF-based cross-communication devices that can also be used as local ranging systems. In CDGPS, the measured phase of the GPS carrier is compared to the carrier phase measured at the other spacecraft.

Relative navigation: Within a constellation or formation of satellites, the relative position between the spacecraft in the formation is often needed with a higher accuracy than the absolute position of the satellites. — Relative navigation of two or more spacecraft in a formation is done by differencing the measured pseudoranges and carrier-phase measurements of the GPS constellation. In the differencing process, errors common to all spacecraft, such as GPS ephemeris errors or ionospheric delay errors can practically be eliminated (since all S/C in the formation are affected in the same measure). In addition, the carrier phase measurements require to resolve the ambiguity (integer number of whole wavelengths) to obtain utilizable data. Two solutions are available for relative navigation processing: a) an onboard software/hardware package to perform these functions in real-time along with the crosslink communication service. In this setup, requirements for autonomous onboard control of the formation (in position and/or attitude) are becoming a must (essential technology); and b) a ground processing option by a control station or center. However, for the general LEO formation, the latter option does generally not offer a continuous link between the formation and the ground to exercise the control function (actuation).^{1478) 1479) 1480) 1481)}

Examples of GPS-like transceivers for relative navigation include:

- CLT (Cross Link Transceiver) of NASA designed and developed by JHU/APL. CLT is an integrated navigation and communication system for multiple distributed spacecraft flying in formation. The design of CLT provides three core functions: processing/memory, GPS reception, and crosslink communications. The processor supports signal acquisition and tracking, navigation, communications, and distributed command and control for space assets.¹⁴⁸²⁾ The CLT provides both an absolute and relative navigation solution (position and velocity) as well as precision time recovery and a steered one pulse-per-second output. Autonomous orbit determination is provided by the reception of GPS signals and processing by an extended Kalman filter. The crosslink communications module consists of a crosslink transmitter and a multi-channel crosslink receiver. In addition, crosslink signals support relative navigation, with the potential for both, direct solutions as well as relative GPS solutions which rely upon the computation of double differences of GPS data in a paired manner among spacecraft. The mass of the CLT device is 0.86 kg, its size is a cube of 10 cm side length.

- ¹⁴⁷⁸⁾ C. – W. Park, J. P. How, L. Capots, “Sensing Technologies for Formation Flying Spacecraft in LEO using CDGPS and Inter-Spacecraft Communication System,” ION GPS 2000, Sept. 19–22, 2000, Salt Lake City, UT, pp. 1595–1607
- ¹⁴⁷⁹⁾ E. A. Olsen, P. A. Stadter, M. S. Asher, “Long-Baseline Differential GPS based Relative Navigation for Spacecraft with Ranging Measurements,” ION GPS 2000, Sept. 19–22, 2000, Salt Lake City, UT, pp. 1612–1621
- ¹⁴⁸⁰⁾ A. A. Chacos, P. A. Stadter, W. S. Devereux, “Autonomous Navigation and Crosslink Communication Systems for Space Applications,” JHU/APL Technical Digest, Vol. 22, No 2, 2001, pp. 135–143
- ¹⁴⁸¹⁾ E. Imre, P. Palmer, Y. Hashida, “Precise Relative Orbit Determination of Low Earth Orbit Formation Flights Using GPS Pseudorange and Carrier-Phase Measurements,” Proceedings of AIAA/USU Conference on Small Satellites, Logan, UT, Aug. 12–15, 2002, SSC02-IV-1
- ¹⁴⁸²⁾ P. A. Stadter, G. R. Barrett, D. P. Watson, T. C. Esposito, J. O. Bristow, “Autonomous Command and Control for Distributed Spacecraft System Operations,” Proceedings of IEEE Aerospace Conference, Big Sky, MT, March 8–15, 2003

- SPTC (Stanford Pseudolite Transceiver), a relative navigation and crosslink system for formation–flying spacecraft. SPTC uses COTS devices: modems, L1 pseudolites, and an attitude–capable GPS receiver. CDGPS measurements provide precise relative positioning and an attitude determination to within 0.25° .
- Star Ranger of AeroAstro Inc. of Herndon, VA. The system combines CDGPS and an inter–satellite communications link between clustered co–orbiting satellites. Star Ranger is considered for AFRL's TechSat–21 formation–flying mission.
- LPT (Low Power Transceiver) of NASA/GSFC in cooperation with ITT Industries [ITT–AES (Advanced Engineering and Sciences Division) in Reston, VA]. The LPT is a compact, flexible device consisting of multiple PC/104 modules that can be configured to perform custom communications and navigation functions in terrestrial, airborne, and space applications; in addition, rLPT (radiation–tolerant LPT) can withstand radiation environments. The LPT performs signal–processing functions with reprogrammable FPGA and DSP devices. Additionally, the industry standard modules used in the LPT allow it to host application–specific and COTS modules that contain processors and interfaces. The device integrates TDRS S–band two–way communications and Ground Networks (STDN) for TT&C and science data relay, and GPS navigation in a compact package. LPT employs GEONS (GPS Enhanced Orbit and Navigation System) a software package of GSFC. 1483) 1484) 1485)

The first demonstration flight of LPT has been conducted aboard Shuttle flight STS–107 (Jan. 16 – Feb. 1, 2003, see J.6) in the experiment CANDOS (Communications and Network Demonstrations on Shuttle). The LPT navigation software provides several integrated functions, including the absolute navigation, relative navigation, and attitude determination. The most recent generation of the LPT includes a “Dial–a–Channel” feature that dynamically optimizes the LPT's signal processing capability by allowing the user to increase the nominal maximum data rate when the total number of receive channels is reduced.

The vision of NASA's Earth Science Enterprise (ESE) involves the interconnection of future space instruments into a vast network, with each space instrument working individually yet in a collaborative way to achieve new levels of performance. This future network, referred to as the **SensorWeb**, allows multiple vantage points (e.g., LEO, MEO, and GEO) to provide data diversity. Within the Sensorweb, formations of micro– and nanosatellites perform autonomously while achieving reliability through redundancy. In addition, reconfigurable payloads reduce risk by allowing for context switching and instrument/algorithm upgrades and adaptations after deployment. 1486)

- NCLT (Nanosatellite Cross Link Transceiver) of CLT heritage 1487) 1488) is under development at APL. The UNP (University Nanosatellite Program) satellites (of DoD/NASA) employ this device and NASA's ST5 (Space Technology 5, launch March 22, 2006) constellation. NCLT is a multichannel, stand–alone system that implements three fundamental func-

1483) L. Haas, C. Massey, D. Baraban, “Navigation Flight Test Results From The Low Power Transceiver Communications and Navigation Demonstration On Shuttle (CANDOS) Experiment,” ION–GPS/GNSS 2003, Portland, OR, Sept. 9–12, 2003

1484) D. Weigand, M. Harlacher, “A Radiation–Tolerant Low–Power Transceiver Design for Reconfigurable Communications and Navigation Applications,” Proceedings of ESTC, College Park, MD, June 24–26, 2003

1485) S. Draganov, B. Veytsman, L. Haas, “Space Applications Algorithms and Initial Simulation Results for the ITT Low–Power Transceiver,” ION–GPS 2002, Portland, OR, Sept. 24–27, 2002

1486) Rob Sherwood, Steve Chien, “SensorWeb Technologies: A new Paradigm for Operations,” Proceedings of the 7th International Symposium RCGSO (Reducing the Costs of Spacecraft Ground Systems and Operations), Moscow, Russia, June 11–15, 2007, ESA SP–648

1487) P. A. Stadter, A. A. Chacos, R. J. Heins, M. S. Asher, J. O. Bristow, J. A. Leitner, “Enabling Distributed Spacecraft System Operations with the Crosslink Transceiver,” Proceedings of the IEEE Aerospace Conference, Big Sky, MT, March 9–16, 2002

1488) NanoSat Crosslink Transceiver (NCLT) Interface Control Document (ICD), Sept. 30, 2002, http://www.aoe.vt.edu/~hokiesat/subs/gps-crosslink/Final%20APL%20documentation/NCLT_ICD_Del.pdf

tions: onboard processing, GPS receiver, and crosslink communications. NCLT supports multiple-access communications architectures (FDMA/CDMA/TDMA).

- CCNT (Constellation Communication & Navigation Transceiver), developed at JPL. CCNT was flown on the ST5 (Space Technology 5), a three spacecraft microsatellite mission (launch March 22, 2006). CCNT was used for inter-constellation ranging, communications, and GPS-based absolute positioning. Additional requirements called for transfer of event messages between the spacecraft.

- Other distributed observation strategies of constellation flying. This category considers so-called “trains of satellites performing similar observation objectives with their payloads in closely spaced sequences.” Their orbits are optimized to coincide (within a few minutes) with those of other satellites. Examples are:

- The Landsat-7, EO-1, SAC-C and Terra “**morning constellation**” train (in formation as of March 2001). There is 1 minute separation between Landsat-7 and EO-1, a 15 minute separation between EO-1 and SAC-C, and a 1 minute separation between SAC-C and Terra. The objective is to compare coincident imagery from the ETM+ and ALI instruments. The “paired scene” images are used to evaluate the performance of ALI. – Note: The morning train represents the loosest, and least collaborative form of formation flying, implemented through the ground (not through a crosslink); the S/C separations are being controlled. ¹⁴⁸⁹⁾

- As of Jan. 2002, the TOPEX/Poseidon and Jason-1 spacecraft are flying as a tandem mission (Jason was launched Dec. 7, 2001) on the same ground track with a one minute separation time. ¹⁴⁹⁰⁾ This orbital configuration permits cross-calibration to be performed. It also provides ocean topography data with unprecedented accuracy (better than either S/C could attain by itself). After the checkout/verification phase (Sept. 2002), the tandem mission is flying in an interleaved orbit (i.e., the TOPEX/Poseidon orbit has been moved to an orbit that produces interleaved groundtracks with a 1.4° longitude spacing from the Jason-1 tracks). The intent is to address the following topics: a) double the spatial sampling to enhance the resolution of the **Rosby waves** and eddies; b) quadruple the crossover points for the estimation of the current velocity vector; c) enhanced coastal tide models; and d) obtain improved global change detection. ^{1491) 1492)}

- The Aqua, CloudSat, CALIPSO, PARASOL, and Aura spacecraft will successively form the so-called “**A-train**” (Aqua in the lead and Aura at the tail, the nominal separation between Aqua and Aura is about 15 minutes) or “afternoon constellation” (formation flight starting sometime after the Aura launch July 15, 2004). ¹⁴⁹³⁾ The objective is to coordinate observations and to provide a coincident set of data on aerosol and cloud properties, radiative fluxes and atmospheric state essential for accurate quantification of aerosol and cloud radiative effects. The orbits of Aqua and CALIPSO are tied to WRS (Worldwide Reference System) and have error boxes associated with their orbits. The overall mission requirements are written such that CALIPSO is required to be no greater than 2 minutes behind Aqua. – The OCO mission of NASA is a late entry into the A-train sequence. The satellites are required to control their along-track motions and remain within designated

1489) C. Filici, M. Suarez, “SAC-C Positioning in the Earth Morning Constellation,” Third International Workshop on Satellite Constellations and Formation Flying, Pisa, Italy, Feb. 24–26, 2003, pp. 57–62

1490) “Good News from Jason-1,” CNES Magazine, No 15, April, 2002, p. 13

1491) L. L. Fu, Y. Menard, “Summary of the Third Joint TOPEX/Poseidon and Jason-1 Science Working Team Meeting,” The Earth Observer, Jan/Feb. 2001, Vol. 13, No 1, pp. 17–18

1492) C. Scaldeo, “Jason Orbit Acquisition and first Results of Station Keeping,” Proceedings of International Symposium Formation Flying Mission & Technologies, Oct. 29–31, 2002, Toulouse, France

1493) A. C. Kelly, “The A-Train: NASA’s Earth Observing System (EOS) Satellites and other Earth Observation Satellites,” Proceedings of ISRSE (International Symposium of Remote Sensing of Environment), Nov. 10–14, 2003, Honolulu, HI

”control boxes.” Member satellites will exchange orbital position information to maintain their orbital separations. ¹⁴⁹⁴⁾ ¹⁴⁹⁵⁾ ¹⁴⁹⁶⁾

Spacecraft	Primary mission objective	Launch date	Responsibility
Aqua	Water/energy cycle	May 4, 2002	NASA/GSFC
Aura	Atmospheric chemistry	July 15, 2004	NASA/GSFC
PARASOL (Polarization and Anisotropy of Reflectances for Atmospheric Sciences coupled with Observations from a Lidar)	Aerosols and clouds	Dec. 18, 2004	CNES
CloudSat	Clouds	Apr. 28, 2006	NASA/GSFC/JPL
CALIPSO (Cloud–Aerosol Lidar and Infrared Pathfinder Satellite Observations)	Aerosols and clouds	Apr. 28, 2006	NASA/GSFC/ LaRC, CNES
OCO (Orbiting Carbon Observatory) OCO is planned to fly ahead of Aqua	Carbon cycle	Feb. 02, 2009 launch failure	NASA/GSFC/JPL
GCOM–W1 (Global Change Observation Mission–Water 1)	Observations related to global water and energy circulation	May 17, 2012	JAXA
OCO–2 (Orbiting Carbon Observatory– 2)	Carbon cycle	July 02, 2014	NASA/GSFC/JPL

Table 75: Overview of the A–train science mission chronological build–up

The PARASOL spacecraft left the A–train constellation on Dec. 2, 2009 due to fuel shortage.

1.11.3 Operational architecture concepts of DSS networks

Background: The very nature of “conventional” space mission operation concepts is that of a point–to–point architecture, also referred to as stove–pipe operation (i.e., there are only islands of joint situational relations and awareness – maintaining an intermittent operational support). Stove–pipe solutions are built such that different technology parts are bolted on as needed with whatever tools are available. There is generally not a high level of coordination and conceptualization; however, such systems become more difficult to manage with increasing complexity.

Most traditional LEO missions employ direct station communications (to one or several stations) in the ground segment requiring scheduling and some coordination. This support concept requires an onboard S&F (Store & Forward) technique to collect the observational data during the non–contact periods of the orbit. Long spacecraft isolation periods lead of course to greater storage volumes and in turn to higher downlink rates for the relatively short acquisition periods. In a number of early SAR missions (SeaSat, ERS–1, ERS–2, JERS–1, RADARSAT, Envisat), the science source data were simply not recorded onboard (or only very small portions of it), leaving instrument observational support modes only to regions of a direct–downlink contact. Eventually, this lead ESA and others to the installation of SAR receiving ground stations into remote regions of our globe [O’Higgins Station (DLR), and Syowa Station (Japan), both located in Antarctica; Libreville, Gabon (DLR); Ulan Bator, Mongolia (DLR); etc.] to be able to obtain repetitive observational

1494) G. L. Stephens, D. G. Vane, R. J. Boain, G. G. Mace, K. Sassen, Z. Wang, et al., “The CloudSat Mission and the A–Train,” BAMS, Dec. 2002, pp. 1771–1790

1495) M. R. Schoeberl, “The Afternoon Constellation: A Formation of Earth Observing Systems for the Atmosphere and Hydrosphere,” Proceedings of IGARSS 2002, Toronto, Canada, June 24–28, 2002

1496) A. C. Kelly, E. J. Macie, “The A–Train: NASA’s Earth Observing System (EOS) Satellites and other Earth Observation Satellites,” 4th IAA Symposium on Small Satellites for Earth Observation, Berlin, Apr. 7–11, 2003

data of the region of interest. The hyperspectral imaging instruments of today represent another class of very high–volume science source data.

The notion of networks in space (i.e., formation–flying satellites acting as a unit) is a drastic shift in thinking and requires entirely new architectures, radio systems (antennas, modems, and media access) and possibly new protocols. Interoperability is the nature and trademark of DSS (Distributed Space Systems) to provide a flexible service architecture.

Conceptually, a number of standards will be needed for the support of the communication infrastructure. The key issues that need to be addressed regarding communications in a formation–flying constellation include: ¹⁴⁹⁷⁾

- The overall architecture and distribution of processing
- The type of communication that needs to take place among the sensor spacecraft
- Timing and synchronization issues

¹⁴⁹⁷⁾ W. D. Ivancic, “Architecture Study of Space–Based Satellite Networks for NASA Missions,” Proceedings of IEEE Aerospace Conference, Big Sky, MT, USA, March 8–15, 2003

1.12 Space Environment Experiments

All spacecraft inevitably interact with their environments. Besides the interactions one immediately thinks of in space (zero-g, solar heating, atmospheric drag, expansion into vacuum conditions, etc.) other interactions are also important. Those of interest to spacecraft designers so far may be grouped under several headings:

- Plasma interactions and spacecraft charging ¹⁴⁹⁸⁾
- Debris and micrometeoroids impact
- Chemical reaction with neutral species
- Radiation degradation
- Satellite surface charging experiments (see also Glossary). The ionizing radiation environment in space represents one of the most severe environment loads to space hardware and can cause a large number of problems such as spurious errors or permanent damage to electronics, erroneous signals in detectors, electrostatic charging of spacecraft or health damage to astronauts. ^{1499) 1500)} In particular, the electrostatic charge on satellite surfaces can pose a hazard, when differential charging is leading to potential gradients. In some cases this potential build-up causes discharge arcing. Electrostatic charging by the natural space radiation environment is regarded as the most serious source of anomalies of S/C electronics. Hence, in-situ measurement of the space radiation environment is an important prerequisite for the enhancement of the static radiation environment models towards dynamic models which are required for the optimized design of future advanced systems. Examples of missions and experiments are:

– GEOS-1/-2 (Geostationary Satellite) missions of ESA, two reference S/C for IMS (International Magnetosphere Study). Launch of GEOS-1 on April 20, 1977; launch of GEOS-2 on July 14, 1978. The GEOS-1/-2 were the first S/C anywhere to carry a totally conductive coating – even over their solar panels. An electron beam experiment and a pair of probes, 40 m apart, provided independent measurements of the electric field surrounding the S/C. The S/C surface-treatment technology was confirmed. E.6

– SCATHA (Spacecraft Charging at High Altitude), the S/C is also referred to as P78-2. A NASA/JPL mission (launch Jan. 30, 1979; orbit: 28000 km x 42000 km, 8.3° inclination, S/C mass = 360 kg). Experiment SC1 (Engineering+ VLF and HF Receivers) measured surface potentials (RF waves between 0–300 kHz and 2–30 MHz) of various S/C materials. SC2 (Spacecraft Sheath Fields + Energetic Ions) measured low energy electrons and ions, energetic protons, and electrons. SC3 (High Energy Particle Spectrometer) measured high energy electrons and protons. SC4 (Satellite Electron and Positive Ion Beam System) used ion and electron beam guns to control spacecraft surface potential. SC5 (Rapid Scan Particle Detector) measured electrons and ions. SC11 (Magnetic Field Monitor) measured DC and ELF magnetic fields. ML12 (Spacecraft Contamination + Thermal Control Materials Monitoring) measured contamination rates and property changes of several thermal control material samples.

– GEOTAIL

– STRV-1a and -1b (Space Technology Research Vehicle, of DERA, UK, see M.47), launch June 17, 1994. Both S/C flew CAE (Charge Alleviation Experiment) to demonstrate

1498) Note: Spacecraft surfaces exposed to a charged particle or ultraviolet radiation environment are prone to accumulation of static charge buildup. This set of S/C environment interactions is collectively known as spacecraft charging. Differential surface charging results when charge builds up on a surface dielectric, resulting in a potential that is significantly different from the spacecraft's frame or other components on the spacecraft's surface.

1499) D. C. Wilkinson, M. A. Shea, D. F. Smart, "A Case History of Solar and Galactic Space Weather Effects on the Geosynchronous Communication Satellite TDRS-1," *Advances in Space Research*, Vol. 26, No. 1, 2000, pp. 27–30

1500) V. I. Degtjarev, G. V. Popov, A. D. Johnstone, "Solar Wind Control of Spacecraft Charging Conditions in Geostationary Orbit during Magnetic Storms," *Advances in Space Research*, Vol. 26, No 1, 2000, pp. 37–40

an active S/C surface charge alleviation system. Other space environment instruments flown on STRV-1a are: SCDE (Surface Charge Detector Experiment), CID (Cold Ion Detector), LPI (Langmuir Probe Experiment), CREDO-II (Cosmic Radiation Environment and Dosimetry Experiment), and RDRS (Radiation Dose Rate Sensor). Other space environment instruments flown on STRV-1b are: SEE (Space Environmental Effects), and REM (Radiation Environment Monitor). Note: The REM instrument was also flown on the MIR space station starting in Nov. '94 until Nov. '96.

- STRV-1c and -1d (launch Nov. 16, 2000) are follow-up missions of DERA, UK with the environment objectives focused on emerging technology hardware. The ESA device SREM (Standard Radiation Environment Monitor) is flown on STRV-1c. SREM is of REM heritage flown on STRV-1b. - SREM is also being flown on PROBA (launch Oct. 22, 2001, see M.33) and Integral (launch Oct. 17, 2002), both are ESA spacecraft. In addition, SREM is planned to be flown on GIOVE-B (launch April 27, 2008).

- Equator-S (launch Dec. 2, 1997, see K.11) carried PCD (Potential Control Device) to reduce the potential caused by the ambient plasma charging of the outer surfaces.

- SPOT-4 (launch March 24, 1998, see D.55.2) carried SILLAGE to measure electrostatic potentials on the outside of the SPOT satellite which are due to the "wake" effect.

- TSX-5 (Tri-Service Experiments Mission 5) of AFRL (launch June 6, 2000) flies two payloads: a) STRV-2 (Space Technology Research Vehicle) of DERA and AFRL with SAMMES (Space Active Modular Materials Experiment System), and b) CEASE (Compact Environmental Anomaly Sensor) of AFRL.

- Cluster-2 (launch July 16, 2000 of first pair of S/C; on Aug. 9, 2000 the second pair was launched, K.7). The four identical Cluster S/C feature conductive outer surfaces. An extremely low S/C-generated electromagnetic background noise is mandatory for accurate electric field and cold plasma measurements. The solar arrays consist of BSR (Back-Surface-Reflection) cells, arranged in self-compensating formations to minimize the generation of DC magnetic fields. The conductive coating on the cell cover glass minimizes the build-up of differential charge potentials.

- Radiation-hardened components. The adverse effect of the 'space weather' (solar wind acting against the Earth's magnetic field, energetic particle flux, etc.) on space hardware, (in particular electronic components, sensors, power and communication systems) increases with radial distance of the S/C orbit. It implies that the long-term performance and reliability of hardware in GEO is much more subjected to a severe environment than a spacecraft in MEO or LEO orbits. - As a consequence, radiation-hardened components (CMOS chips, solar cells, etc.) were developed to account for the space weather and to improve hardware life times. The introduction of radiation-hardened components was first realized in GEO satellites.

- Space environment experiments - collection of cosmic dust, particles and debris from platforms. Dust is ubiquitous in the solar system, with dust particles abundant in regions as diverse as interplanetary space, the terrestrial and martian atmospheres, comets, asteroids, satellite surfaces, and planetary rings. The dynamics of these short-lived particles are particularly sensitive to their environment, so they serve as probes of a variety of processes and are strongly effected by electromagnetic forces. - Since the early 1980s several programs were initiated with the aim of systematic collection and analysis/curation of cosmic dust. Also study of radiation degradation effects on some types of materials. Initial airborne dust collections (since 1981) were made with instruments mounted underneath a wing using NASA WB-57F aircraft from NASA/JSC. Several space agencies (NASA, ESA, JAXA, CNES, etc.) maintain special laboratories to analyze impact damage, instruments are being developed and flown to measure orbital micro-debris sources. Long-term data on the space environment and its effects on space systems and operations is a constant need of

spacecraft and instrument designers. In addition, the study of recovered long–duration space structures like LDEF and EURECA, and other recovered hardware (solar array from Hubble, etc.), is of major interest. In particular, large surface structures such as solar arrays, can serve as passive detectors for the study of debris impacts. The evidence of hardware brought back from space shows clearly that the risk faced by spacecraft from meteoroids is real. The heavily pitted surfaces of Eureka and the shattered solar cells of the Hubble Space Telescope bear witness to the harsh meteoroid environment in Earth orbit. 1501) 1502) 1503) 1504)

Mission or Instrument	Description
LAC (Large Area Collector), NASA/JSC	LAC is flown on NASA ER–2 aircraft since 1989, P.115
EURECA–1 launched on STS–46 July 31, 1992 and retrieved on STS–57 July 1, 1993	ESA mission. The experiment TICCE on EURECA–1 collected debris, meteoroids, and cosmic dust. See J.5.1
LDEF (Long Duration Exposure Facility) see J.9	NASA/LaRC S/C deployed from Shuttle on April 7, 1984 (STS–41–C) and recovered on STS–32 Jan. 12, 1990 Exposure of many systems to cosmic radiation and collection of cosmic dust by Exp. A0138–2 of CERT/ONERA, and by Exp. A0201, S001, etc. of NASA/LaRC
MIR Space Station	On three occasions (1988, 1995, 1997) dust collection detectors were used on the outside of MIR.
Ulysses mission (ESA/NASA), launch Oct. 6. 1990	DUST experiment of MPIK (Heidelberg, Germany), see K.32
APEX (Advanced Photovoltaic & Electronics Experiment), S/C of DoD, launch Aug. 3, 1994 (no particle collection on APEX)	Study of long–term radiation effects in an orbit of 361 km x 2528 km, inclination = 70°. Experiments included: PASP (Photovoltaic Array Space Power Diagnostics), CRUX (Cosmic Ray Upset Experiment), and FERRO (Thin–film Ferro–electric Experiment)
MEEP (MIR Environmental Effects Payload) deployed on STS–76 (Mar. 22, 96) and retrieved on STS–86 (Oct. 1, 1997)	NASA/LaRC/MSFC conducted a series of experiments such as POSA–I & –II (Passive Optical Sample Assembly), PEC (Passive Experiment Carrier), PPMD (Polished Plate Meteoroid Detector), ODC (Orbital Debris Collector)
CDCE (Cosmic Dust Collection Experiment) and AOE (Atomic Oxygen Experiment), both on STS–85 (Aug. 7–19, 1997)	NASA/LaRC experiments in ESEM program. CDCE: Use of aerogel to capture cosmic dust. AOE: candidate materials for ISS (lubricants, paints, thermal coatings, etc.)
MightySat–1 of AFRL, launch Dec. 4, 1998, see M.24.1	MPID (Micro–Particle Impact Detector)
Stardust (NASA minisatellite in Discovery program), launch Feb. 7, 1999	Rendezvous with a comet and return of comet tail samples to Earth (encounter with comet Wild–2 on Jan.2, 2004). On Jan. 15, 2006, return of interstellar dust grains in a re-entry capsule to Earth
ARGOS (DoD, launch Feb. 23, 1999)	SPADUS (Space Dust Experiment)
SUNSAT–1 of Stellenbosch University, South Africa, launch Feb. 23, 1999	MIS (Meteoroid Impact Sensor) of NASA/LaRC
STRV–1c and –1d, DERA, launch Nov. 16, 2000	CDMS (Compact Debris and Micrometeoroid Sensor) characterizes of the debris and micrometeoroid environment in GTO
STRV–2 of AFRL and DERA (launch June 6, 2000) on TSX–5 mission of AFRL	MDIM (Meteoroid and Debris Impact Monitor) of NASA/LaRC.

Table 76: Overview of some cosmic dust/particle collection platforms

1501) <http://setas-www.larc.nasa.gov/>

1502) N. L. Johnson, “Monitoring and Controlling Debris in Space,” Scientific American, Aug. 1998, pp. 42–47

1503) M. Landgraf, R. Jehn, W. Flury, V. Dikarev, E. Grün, “Meteoroids – A Potential Hazard for Interplanetary and Earth–Orbiting Spacecraft,” ESA Bulletin No 113, Feb. 2003, pp. 58–61

1504) T. Encrenaz, “The stars of cometary science in the 20th century,” CNES Magazine No 18, Feb. 2003, pp. 27–29

In 1995, NASA started its SEE (Space Environments Effects) program ¹⁵⁰⁵ with the objective to collect, develop and to disseminate the technologies required to design, manufacture and operate more reliable, cost-effective spacecraft for the government and commercial sectors. In partnership with industry, academia, and other government agencies, the SEE program defines the space environments and advocates technology development to accommodate or mitigate these harmful environments on spacecraft. The ESEM (Evaluation of Space Environment and Effects on Materials) payload of STS-85, in cooperation with NASDA, is one of many experiments in SEE.

- Measurement of atomic oxygen (see also Glossary). Atomic oxygen is the most abundant atmospheric species in the altitude range of about 100–600 km; it can affect a spacecraft's operational capability. Adverse influences include material degradation (erosion). Of particular concern are the following effects: impact of particulate matter (debris), of high-energy UV radiation and of X-ray radiation, both of which are predominantly of solar origin. – Early missions of atomic oxygen measurements started within the NASA program AE (Atmosphere Explorer). In this series, the AE-A mission (also known as Explorer 17, see A.4.1) flew the Neutral Mass Spectrometer (launch April 3, 1963). The AE-B mission (launch May 25, 1966) carried two instruments to measure atomic oxygen. The San Marco D spacecraft of the University of Rome and NASA/GSFC measured airglow which infers atomic oxygen. The NASA DE-2 (Dynamics Explorer) mission (launch Aug. 3, 1981) carried NACS (Neutral Atmosphere Composition Spectrometer) to measure abundances of neutral species over an altitude range of at least 100 km to 300 km, and FPI (Fabry-Perot Interferometer) to measure ionic atomic oxygen. The HRDI (High Resolution Doppler Imager) of UARS (launch Sept. 12, 1991) observes emission lines of neutral and ionized atomic oxygen in the visible and near-infrared regions. In addition, several Shuttle missions (STS-4, STS-46, STS-85) flew mass spectrometers to measure atomic oxygen.

¹⁵⁰⁵) <http://see.msfc.nasa.gov/>

1.13 Orbital debris

Like any human activity, the conquest of space has generated its share of waste that must now be managed if we are to ensure a sustainable space environment. Orbital debris generally refers to material that is on orbit as the result of human space activities/initiatives, but is no longer serving any function. The use of outer space presents a number of hazards to S/C owners and operators. Temperature extremes, radiation, solar flares, and micrometeoroids have long been essential elements to consider in spacecraft and mission design. Increasing use of space has brought a new source of risk collisions with manmade objects. The proliferation of debris in space generated by spacecraft and launchers is likely to become a serious issue in the near future. Such debris, originating from S/C, upper stage explosions and from the rising number of non-operational and abandoned satellites, represent a hazard for all operational missions (manned and unmanned). The GEO and LEO orbits are in particular littered with debris. 1506) 1507) 1508) 1509) 1510) 1511) 1512) 1513)

Some examples of space debris observations/incidents are:

- During the US Gemini manned space program (March 1965 – Nov. 1966) the TV audience of the world could see as one astronaut “walked” in space while a glove floated up and out of the capsule in full view – a first documented incidence of space debris (Ref. 1539).
- Early satellite experiments, such as those aboard NASA’s Explorer–7 (launch Oct. 13, 1959) and Explorer–16 (launch Dec. 16, 1962), tried to detect the impact of micrometeoroids. In 1964, NASA/JSC developed a project called “Micro–Meteoroid Measurement Capsule” which was renamed the “Pegasus” project. These capsules (Pegasus–A, –B and –C) were intended to determine the level of hazard to which astronauts would be exposed.
- The Explorer–46 mission of NASA (launch Aug. 13, 1972) flew an experiment called the Meteoroid Bumper Experiment for the characterization of the background environment. The objectives were to measure the meteoroid penetration rates in the bumper-protected target, and to obtain data on meteoroid velocity and flux distribution.
- Micro–debris originating from objects launched from Earth were first encountered in 1976 on the US Skylab Space Station, where aluminum oxide exhaust from apogee kick motors was identified.
- In 1986, the spent third stage of the Ariane–4 launcher, used to place SPOT–1 into orbit (launch Feb. 22, 1986), exploded after nine months in orbit (LEO). The explosion generated over 700 fist–sized fragments. In addition, thousands of micro–particles of all sizes were released.
- Meteoroid impact on a satellite. In 1993 a Perseid meteoroid (tiny grains of dust) hit a solar panel on the European Olympus communications satellite. The project management is convinced the hit caused a pulse that sent false signals to the control system of the S/C. As a consequence, the satellite went into the wrong automated sequencing causing the loss of the spacecraft (it took all the remaining propellant to regain control, resulting in the end of the mission).
- On July 24, 1996, the French microsatellite CERISE collided with a piece of debris (a suitcase–sized piece of the old Ariane rocket of 1986 – the first official collision between

1506) “Dossier: Orbital debris,” CNES Magazine No 4, Jan. 1999, pp. 11–28

1507) “Dossier: Comets – Remnants of the early solar system,” CNES Magazine, No 18, Feb. 2003, pp. 17–39

1508) F. Alby, “Regulating orbital debris,” CNES Magazine No 19, May 2003, p. 26

1509) M. J. Meshishnek, “Overview of the Space Debris Environment,” The Aerospace Corporation Report No. TR–95(5231)–3, SMC Report No. SMC–TR–95–9, March 15, 1995

1510) W. Flury, “Space Debris: An Overview,” Earth Space Review, Vol. 9, No 4, 2000, pp. 40–47

1511) M. L. Fudge, “The Effect of Orbital Debris on Commercial Satellites,” Earth Space Review, Vol. 9, No 4, 2000, pp. 48–56

1512) N. L. Johnson, “Man–Made Debris In And From Lunar Orbit,” Earth Space Review, Vol. 9, No 4, 2000, pp. 57–65

1513) B. Reijnen, “Space Debris: A Responsibility of States,” Earth Space Review, Vol. 9, No 4, 2000, pp. 66–70

two catalogued objects), cutting in half the 6 m long stabilizing boom of CERISE. Fortunately, the French ground controllers regained control over the satellite following the collision.

- On Oct. 26, 1999 ISS (International Space Station) made a maneuver to avoid a potentially dangerous piece of orbital debris (the US Space Command and NORAD had reported that a spent Pegasus upper stage would pass ISS to within 1.4 km). Hence, thrusters of ISS were fired to increase the stations altitude by about 1.5 km. Another collision – avoidance maneuver of ISS took place on Dec. 15, 2001, when the Shuttle Endeavour increased the altitude of ISS by 1 km to avoid a collision with a Russian SL–8 upper stage launched 1971.
- A major contributor to the orbital debris background have been breakups of rocket upper stages and satellites. More than 150 breakups have been verified, and more are believed to have occurred. Breakups generally are caused by explosions and collisions. Explosions can occur when propellant and oxidizer inadvertently mix, residual propellant becomes overpressurized due to heating, or batteries become overpressurized.
- In 2008, a disintegrating former Russian military satellite sent some 500 pieces of debris into space during 3 explosions between March and June 2008 (end of life explosions). Shortly thereafter, Shuttle astronauts observed space debris damage to the airlock handrail and tool that are used during spacewalks outside the ISS. – While there is no way to determine where the debris that impacted the ISS, originated, NASA officials were closely tracking pieces falling off the Russian EORSat (Electronic Ocean Reconnaissance Satellite) to make sure it did not pose a risk to the ISS. EORSat (Cosmos 2421), the 50th S/C of a Russian satellite series whose launches started in 1974 (EORSat with a mass of 3150 kg was launched on June 25, 2006), happens to be in an orbit not too far above the ISS. NORAD observations showed that over the lifespan of this Russian series, 22 of the 50 satellites have exploded at least once. The ISS performed a collision avoidance maneuver on Aug. 27, 2008 when a fragment from the Cosmos 2421 spacecraft was projected to pose a collision risk. 1514)
- In the first 4.5 years of ISS operations, ISS collision avoidance maneuvers were executed on seven occasions, three times by a visiting Space Shuttle. However, in the next 5.5 years only a single collision avoidance maneuver was necessary (Aug. 2008). This dramatic reduction in collision avoidance maneuver frequency can be attributed primarily to improved conjunction assessment processes, not an improved orbital debris environment. 1515)

The ISS has well withstood the hazardous space debris environment during its first decade in space. This has been possible by concerted efforts in both the design and the operation of the large orbital complex.

- On Feb. 10, 2009, an inactive Russian military communications satellite (Cosmos 2251, 900 kg, launch June 16, 1993) ¹⁵¹⁶⁾ ¹⁵¹⁷⁾ collided with an active US communications satellite owned by the Iridium company (Iridium 33, 680 kg, launch Sept. 14, 1997). The incidence occurred at an altitude of ~ 780 km, a rather frequented orbit of many LEO spacecraft. The Iridium satellite, which was operational at the time of the collision, was destroyed, as was Cosmos–2251. The resulting debris field adds to the already vast quantity of space junk in LEO (Low Earth Orbit). NASA reported that a large amount of debris was produced by the collision.

1514) B. Ionnotta, “More Orbital Debris Added as Russian Satellite Explodes,” Space News, June 21, 2008, p. 14

1515) Nicholas Johnson, “The International Space Station and the Space Debris Environment: 10 Years On,” Proceedings of the Fifth European Conference on Space Debris, Darmstadt, Germany, March 30 to April 2, 2009, SP–672, July 2009

1516) “Satellite collision threatens space assets,” Spacemart, Feb. 12, 2009, URL: http://www.spacemart.com/reports/Satellite_collision_threatens_space_assets_999.html

1517) N. Atkinson, “Images, Video, Interactive Tools Provide Insight into Satellite Collision Universe Today,” Feb. 12, 2009, URL: <http://www.universetoday.com/2009/02/12/images-video-interactive-tools-provides-insight-into-satellite-collision/>

- On March 12, 2009, the crew of the ISS (International Space Station) was ordered by NASA to seek refuge in the attached Soyuz space capsule due to a close encounter of space debris. A scare arose when the three member crew learned rather late to take evasive action of an approaching a cloud of debris that exposed the space station to the risk of a potentially catastrophic collision. NASA appeared most concerned about a piece of a satellite motor that was close enough to ordinarily have forced the space station to undertake an evasive maneuver. – The US Strategic Command had notified NASA of the debris field late on March 11, but NASA said it was too late for flight controllers to coordinate a "debris avoidance" maneuver. Experts estimate that there are more than 300,000 orbital objects measuring between 1 and 10 cm in diameter and "billions" of smaller pieces. Traveling at speeds of up to thousands of km/hr they pose a risk of catastrophic damage to spacecraft. 1518) 1519)
- During 2012, three ISS collision avoidance maneuvers were executed, the most in any year: 1520)
 - 13 January to evade fragmentation debris from Iridium 33
 - 28 January to evade fragmentation debris from Fengyun–1C
 - 31 October to evade fragmentation debris from Iridium 33
 - On 24 March 2012, the crew of the ISS was forced to retreat to the Soyuz spacecraft when a fragment from Cosmos 2251 was predicted to pass too close and insufficient time was available to perform a collision avoidance maneuver.

These incidents show that all aspects of debris–related issues, including some regulation standards, have to be dealt with in the future. The SSN (Space Surveillance Network) of the US Space Command and NORAD (North American Aerospace Defense Command) in Colorado Springs, CO, maintains orbital element sets of some 8764 objects (of 10 cm diameter or larger) – still many more are too small or in too eccentric orbits to be cataloged. The estimates of objects in size 1–10 cm is in the order of 200,000; in addition, there are more than 35 million objects below 1 cm. Of the 8764 objects being tracked (as of Oct. 20, 1999), there are 2634 satellites (any payload operational or non–operational currently in Earth orbit – meaning LEO, GEO, GTO, MEO, HEO, or any other Earth orbit), 6040 objects are termed "debris" (meaning all man–made objects in Earth orbit), and 90 objects are termed "space probes" (referring to payloads that are not in Earth orbit – such as deep space missions). The historical catalog status of the US Space Command lists on Oct. 20, 1999: payloads decayed = 2,501, debris decayed = 14,680, total = 17,181 objects. – In this context, it is also of interest to look at the estimated distribution of orbital debris in the following scheme: Operating satellites = 6%, spent satellites = 22%, upper stages = 17%, operational debris = 13%, and fragments (of rocket upper stages, etc.) = 42%. Consequently, about 94% of the catalogued objects no longer serve any useful purpose and are collectively referred to as "space debris."

The debris in orbit totals an estimated 4000 tons in 1999, with 175 tons added every year. Complications will arise from the ever–increasing use of space. The operational networks of major commercial satellite constellations (initial launches started in 1998) increases the crowding of space in LEO very rapidly. The Iridium constellation has 77 in orbit (nominal of 66 operational), Orbcomm has 35 (constellation completed in Dec. 1999), Globalstar 48, and Skybridge 64, when fully deployed. These are only a few of the commercial entries. In

1518) "Space junk sparks crew scare on ISS," March 12, 2009, Space Travel, URL: http://www.space-travel.com/reports/Space_junk_sparks_crew_scare_on_ISS_999.html

1519) "ISS Crew May Need to Evacuate: Possible Debris Hit," Universe Today, March 12, 2009, URL: <http://www.universetoday.com/2009/03/12/iss-crew-may-need-to-evacuate-possible-debris-hit/>

1520) N. Johnson, "USA Space Debris Environment, Operations, and Modeling Updates," Proceedings of the 50th Session of Scientific & Technical Subcommittee of UNCOPOUS, Vienna, Austria, Feb. 11–22, 2013, URL: <http://www.oosa.unvienna.org/pdf/pres/stsc2013/tech-17E.pdf>

Earth observation the picture is pretty much the same. Constellations or clusters of small satellites are planned by a number of agencies to enter a new dimension of formation flight observations. ¹⁵²¹⁾ ¹⁵²²⁾

Debris in the geostationary ring. ¹⁵²³⁾ Since the launch of Syncom–1 in Feb. 1963, more than 800 satellites and rocket upper stages have been inserted into GEO or its vicinity. As of 2000, only about 250–270 of these satellites are used operationally. GEO satellites are therefore increasingly at risk of colliding with uncontrolled objects. Contrary to the situation with LEO satellites, there are no effective natural removal mechanisms for GEO objects. [In order to preserve the GEO for future satellite operations users have been encouraged over the years to re-orbit their satellites at the end of their lives. This mitigation measure involves boosting the satellite to a graveyard region above the GEO ring (sometimes referred to as “super-geostationary” orbit). Unfortunately, this practice is not fully embraced by all satellite operators.] Routine surveillance with ground-based radars of SSN (Colorado Springs, CO) is able to catalog objects of 1 m in size or larger in GEO. Observations with ESA’s Zeiss telescope at the Teide Observatory in Tenerife, with an optimized debris-detection system, have shown that there is a significant population of about 1600 small-debris objects (10–100 cm size) in the geostationary ring.

Collision risk monitoring. Starting in about 1995, space agencies (CNES, ESA, NASA, etc.) are beginning to monitor close encounters of catalogued objects with their own S/C. For instance, the flight path of ESA’s ERS–2 satellite is being checked for potential close encounters or collisions several times per week. ESA performed two evasive maneuvers with ERS–1 in June 1997 and in March 1998. CNES experienced in this process, for instance, that on average, an object passes within less than 1500 m of a S/C every two weeks. Even closer approaches (under 800 m) were observed on 19 occasions.

An important tool in characterizing a small-size debris population are so-called “beam-park” experiments. In this operating mode, the radar beam is maintained in a fixed direction with respect to the Earth and all objects that traverse the beam are registered. ¹⁵²⁴⁾ In the course of a day, the Earth’s rotation scans the beam through 360° in inertial space. From the backscattering of the radar signal, the size of the object and some of its orbital parameters can be determined. Example radar systems used in space-debris tracking are:

- US radars are carrying out beam-park experiments from Haystack, MA, Goldstone, CA, and Kwajalein (TRADEX radar) in the Pacific Ocean. Between 1990 and 1994, space debris was observed for more than 3000 hours.
- The first European beam-park campaign was carried out in 1993 at the TIRA (Tracking and Imaging Radar) facility of FGAN (Defense Research Facility for Applied Science, Wachtberg near Bonn, Germany). TIRA consists of a 34 m parabolic antenna, a narrow-band monopulse L-band tracking radar, and a high-resolution Ku-band imaging radar. A second data-collection system was installed by ESA at the 100 m steerable parabolic antenna at Effelsberg in Germany.
- The largest rapid increase in the number of tracked objects occurred starting in March, 2003. This timing correlates to the resumption of full power/full time operation of the AN/FPS–108 Cobra Dane ground-based radar located on Shemya Island, AK, USA (52.7° N latitude, 174.1° E longitude). In contrast to the 1994 debris campaign where the gains were the result of temporary operating procedures, the addition of Cobra Dane to the SSN will

¹⁵²¹⁾ N. L. Johnson, J. P. Loftus, “Reducing Orbital Debris: Standards and Practices,” *Launchspace*, March/April 1999, p. 24

¹⁵²²⁾ M. Bille, D. Dickey, “A Microsatellite ‘Space Guard’ Force,” *Proceedings of the 13th AIAA/USU Conference on Small Satellites*, Aug. 23–26, 1999, Logan UT, SSC99–II–6

¹⁵²³⁾ W. Flury, A. Massart, T. Schildknecht, U. Hugentobler, J. Kuusela, Z. Sodnik, “Searching for Small Debris in the Geostationary Ring,” *ESA Bulletin*, No 104, Nov. 2000, pp. 92–100

¹⁵²⁴⁾ D. Mehrholz, L. Leushacke, W. Flury, R. Jehn, H. Klinkrad, M. Landgraf, “Detecting, Tracking and Imaging Space Debris,” *ESA Bulletin* No 109, Feb. 2002, pp. 128 – 134

provide long-term improvement to the total tracked population. Cobra Dane is an L-band (23 cm wavelength) phased array radar which first became operational in 1977. The radar generates approximately 15.4 MW of peak RF power (0.92 MW average) from 96 TWT (Traveling Wave Tube) amplifiers arranged in 12 groups of 8. This power is radiated through 15,360 active array elements. ¹⁵²⁵⁾

As a result, approximately 2000 orbiting objects have been added to the “Analyst list” of tracked objects.

Debris, reentering the atmosphere, presents a further problem, in particular to population safety. In 1999, it is estimated that about 17,000 objects of debris have reentered the atmosphere since Sputnik – virtually all of them disintegrated in the reentry process, very few actually hit Earth, although some particularly large or well-shielded objects have been known to get through. Controlled deorbiting and reentry procedures over oceans or sparsely populated regions are the rule for larger returning S/C that can still be steered. At the Skylab uncontrolled reentry in 1979, with a mass of 82 metric tons (the size of the structure was 36 m x 6.7 m diameter), fragments fell into the Indian Ocean and the western region of Australia. This uncontrolled reentry definitely caused many alerts throughout the world.

The MIR space station of Russia (with 140,000 kg of mass) was deorbited in a controlled manner in March 2001 with a final reentry into the Pacific Ocean on March 23, 2001. Many governments had their national control centers working for several weeks. An atmosphere of “we are doing something, and everything is under control” was portrayed publicly to keep the people calm. Fortunately, the Russian Control Center did an excellent job to bring MIR to the intended splashdown region. [Russia had asked NASA (incl. radars of the US Space Surveillance Network) and ESA (incl. the radar facilities of FGAN near Bonn, Germany) for support, which was granted. ESOC was the center of a data exchange network among technical centers [TsUP (Moscow Region), NASA/JSC, FGAN (Germany), and other space centers in Europe]].

Category	Definition	Estimated population	Potential risk to satellites
Trackable	≥ 10 cm in diameter	19,000+	Complete destruction
Potentially trackable	≥ 1 cm in diameter	Several hundred thousand	Complete to partial destruction
Untrackable	< 1 cm in diameter	Many millions to billions	Degradation, loss of certain sensors or subsystems

Table 77: Population sizes of artificial objects in Earth orbit ¹⁵²⁶⁾

ISON (International Scientific Optical Network) is an open international non-government project mainly aimed at being a free source of information on space objects for scientific analysis and other applications. It was initiated in framework of the program of the GEO objects investigations started by KIAM (Keldysh Institute of Applied Mathematics) of the Russian Academy of Sciences in 2001. – ISON started routine observations of the GEO objects in 2005 with support of the International Association for the promotion of co-operation with scientists from the New Independent States of the former Soviet Union and the Russian Ministry of education and science grants. In 2009, ISON collaborates with 25 observatories in 9 countries. More than 700 earlier unknown objects were so far discovered. ¹⁵²⁷⁾

1525) E. G. Stansbery, “Growth in the Number of SSN Tracked Orbital objects,” Proceedings of IAC 2004, Vancouver, Canada, Oct. 4–8, 2004, IAC–04–IAA.5.12.1.03

1526) Brian Weeden, “The numbers game – What’s in Earth orbit and how do we know?,” The Space Review, July 13, 2009, URL: <http://www.thespaceview.com/article/1417/1>

1527) I. Molotov, V. Agapov, V. Kouprianov, V. Titenko, V. Rummyantsev, V. Biryukov, G. Borisov, Yu. Burtsev, Z. Khutorovskiy, G. Kornienko, et al., “ISON Worldwide Scientific Optical Network,” Proceedings of the Fifth European Conference on Space Debris, Darmstadt, Germany, March 30 to April 2, 2009, SP–672, July 2009

In 2011, the ISON network collected on a routine basis astrometric and brightness measurements for more than 1700 objects in the GEO region and more than 600 objects in HEO. 1528)

SSA (Space Situational Awareness) is the understanding and maintained awareness of a) the Earth Orbital Population (EOP), b) the space environment, and c) threats to/by the orbit population”. SSA is an upper–set of space surveillance which is itself defined as “the routine, operational service of timely detection, correlation, characterization, and orbit determination of space objects”.

Approximately 95% of the LEO objects in Figure 77 are orbital debris, i.e., not functional satellites. The dots represent the current location of each item. The orbital debris dots are scaled according to the image size of the graphic to optimize their visibility and are not scaled to Earth. These images provide a good visualization of where the greatest orbital debris populations exist. 1529)

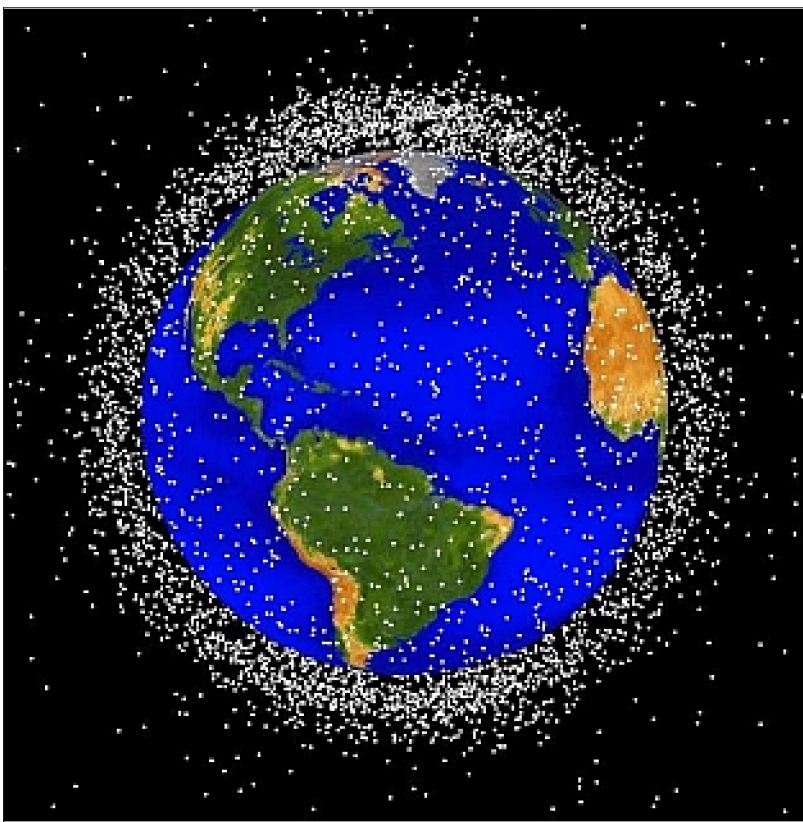


Figure 77: Computer generated image of LEO objects that are currently (2011) being tracked (image credit: NASA/JSC)

- On Sept. 26, 2010, The US AFSPC (Air Force Space Command) launched **SBSS–1** (Space–Based Surveillance System), the first spacecraft (pathfinder) with the goal of tracking space objects (debris) in orbit, and to accomplish SSA for space control operations. SBSS–1 is equipped with a SBV (Space Based Visible) instrument mounted on a two–axis gimbal assembly to give the telescope a very wide FOV without a spacecraft attitude maneuver. SBSS–1 is in LEO (630 km altitude) to track in particular objects in MEO and GEO. SBSS–1 will operate in conjunction with the SSN (Space Surveillance Network) to support spaceflight safety, ensure space catalog completeness, warn of on–orbit separations and

1528) V. Agapov, “Results of GEO and HEO space debris population research within the framework of ISON international project in 2011,” Proceedings of the 49 Session of UN COPUOS (Committee on the Peaceful Uses of Outer Space), STSC (Scientific and Technological Subcommittee), Vienna, Austria, Feb. 6–17, 2012, URL: <http://www.oosa.unvienna.org/pdf/pres/stsc2012/tech-25E.pdf>

1529) NASA Orbital Debris Program Office, URL: http://www.orbitaldebris.jsc.nasa.gov/photogallery/bee_hives.html#leo

maneuvers, and provide indications and warnings of potentially hostile space events. ¹⁵³⁰⁾
1531)

- January 2014: The Air Force declared SBSS fully operational in April 2013. The service’s data show that during the system’s first year of operation, it collected more than 3.8 million observations of objects in deep space. SBSS has a unique ability to swiftly move its onboard sensor, enabling it to observe multiple deep space objects across a broad range, in contrast to the narrow range used by ground–based sensors. ¹⁵³²⁾
- In 2009, Europe (ESA) is in the process to define the baseline architecture of a future ESSAS (European SSA System) able to provide to the user community verifiable, dependable, accurate and timely information in order to: ¹⁵³³⁾
 - Identify non–compliance with relevant international treaties and recommendations
 - Enable the assumption of responsibility (e.g. as launching state, owner, or operator), and support confidence building measures
 - Support safe and secured operation of space assets and related services
 - Support risk management (on orbit and during reentry) and liability assessment
 - Assess the functional status and capabilities of space systems.

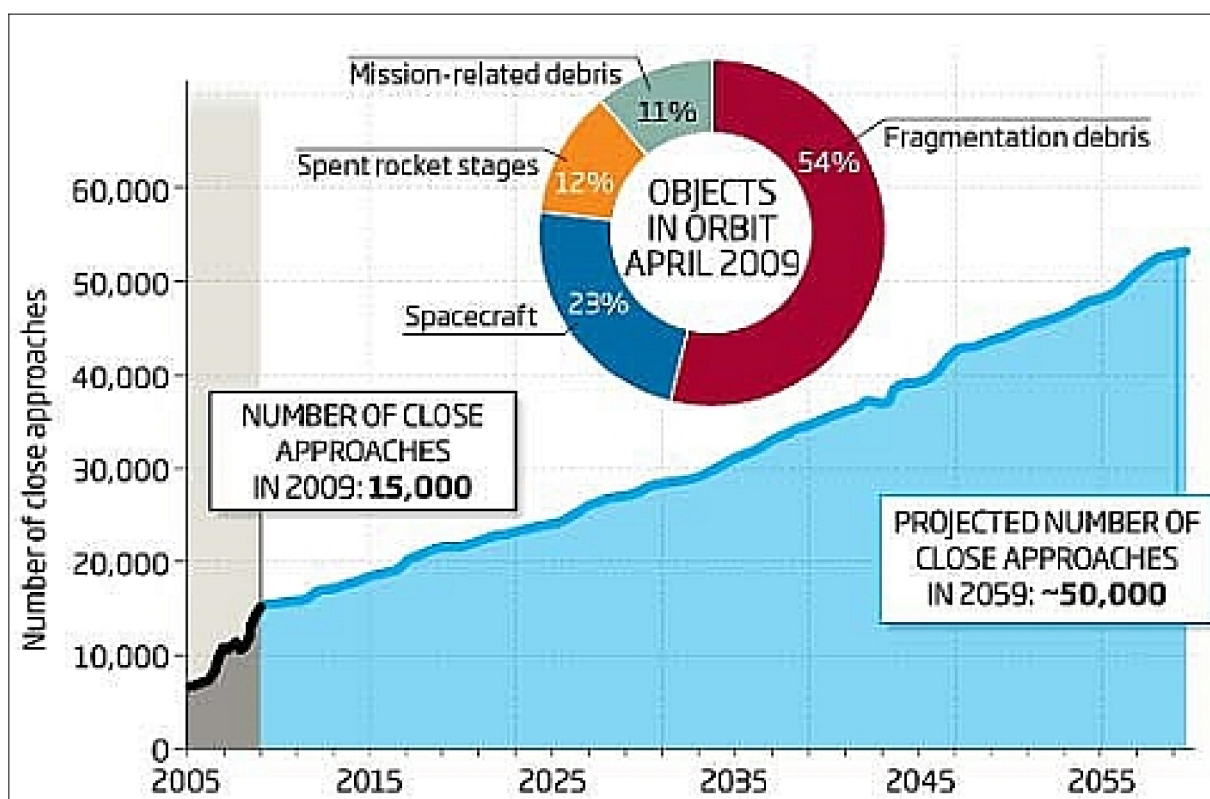


Figure 78: The rising volume of space debris increases the likelihood that satellites will need to be moved to avoid collisions in the future (image credit: NASA)

- In 2009, the SAR–Lupe constellation experienced more than **800 close encounters** with orbital junk or other operating satellites, including 32 passes at less than 1 km from

1530) William Graham, “Minotaur IV launches first Space Based Space Surveillance satellite,” Sept. 25, 2010, URL: <http://www.nasaspacelight.com/2010/09/live-minotaur-first-space-based-space-surveillance-satellite/>

1531) “Space Based Space Surveillance (SBSS),” URL: <http://www.globalsecurity.org/space/systems/sbss.htm>

1532) “Boeing Space Surveillance System Reduces Risk of Satellite Loss by 66 Percent,” Boeing New Release, Jan. 14, 2014, URL: <http://boeing.mediaroom.com/index.php?s=20295&item=128939>

1533) Th. Donath, C. Saunders, V. Martinot, E. Elluin, J. Rey Benayas, “Architectures Analysis for the Future European SSA System,” Proceedings of the Fifth European Conference on Space Debris, Darmstadt, Germany, March 30 to April 2, 2009, SP-672, July 2009

another SAR—Lupe spacecraft, and one that required a collision—avoidance maneuver. Due to these collision concerns, Germany inaugurated in 2009 the **GSSAC** (German Space Situational Awareness Center), located in Uedem near Kleve in North Rhine—Westphalia, Germany. — In addition, Germany’s defense forces, in a rare move, have invested cash in an ESA—led program to design a European space surveillance system starting with ground—based radars already existing in Germany and France. ¹⁵³⁴⁾

Country	Mission	Sensor, Comments
USA	MSX (Midcourse Space Experiment), 1996–2008	SBV (Space Based Visible) sensor of US SSN (Space Surveillance Network) of US Space Command, CO
	STSS (Space Tracking and Surveillance System), experienced a launch failure in 2009 of 2 spacecraft	ATRR (Advanced Technology Risk Reduction), primary mission missile defence, also SSA (Space Situational Awareness)
	SBSS (Space—Based Surveillance System), launch in 2010, ops in 2013	SBV follow—on imager, US SSN
	ANGELS (Autonomous Nanosatellite Guardian for Evaluating Local Space), AFRL,	Planned to launch as a hosted payload into GEO (in 2014 ?) for SAA observations
	SODDAT (Small Orbital Debris Detection, Acquisition, and Tracking), NASA	NASA/MSFC, small LEO debris
Canada	MOST (Microvariability and Oscillations of Stars), CSA, launch in 2003, operational in 2013, spacecraft mass=60 kg	Telescope with an aperture of 15 cm; provides also some SSA observations
	Sapphire (Space Surveillance Mission of Canada), DND, launch Feb. 25, 2013 (148 kg)	OIS (Optical Imaging Subsystem), provide SSA for CSSS (Canadian Space Surveillance System) and for US SSN (Space Surveillance System)
	NEOSSat (Near—Earth Object Surveillance Satellite), CSA, launch Fe. 25, 2013 (74 kg)	NESSI (Near Earth Space Surveillance Imager), also SSA demonstrations
Germany	Asteroid Finder mission in LEO, DLR, planned for launch in 2014	Telescope with 30 cm aperture; used for NEO (Near Earth Object) detection & space debris mission

Table 78: Space—based surveillance missions ¹⁵³⁵⁾

1.13.1 MELVOs – a proposed long—term solution to Orbital Debris

Long—term orbital debris is a continually growing problem that has proven challenging to overcome. A straightforward solution to the problem is to put the majority of future LEO spacecraft into **MELVOs** (Moderately Elliptical Very Low Orbits) with perigees below approximately 300 km, apogees below approximately 500 km, and eccentricities in the range of 0.015 to 0.030. Orbital debris clouds cannot be sustained in this altitude regime and will decay and re—enter in times ranging from a few weeks to at most the time until the next solar maximum. This means that the debris population at this altitude is, and will remain, much lower than at higher altitudes and, of course, any satellites which explode or otherwise die in this region will not be a part of a long—term debris problem. ¹⁵³⁶⁾

The advantage of the elliptical orbit is that if a temporary failure causes the spacecraft to stop doing orbit maintenance burns for a moderate period of time, apogee will decay, perigee will change very little, and the orbit can be recovered with essentially no loss of total

¹⁵³⁴⁾ Peter B. de Selding, “Europe Keeping Increasingly Capable Eye on Orbital Debris,” Space News, April 26, 2010, URL: <http://www.spacenews.com/civil/100421—europe—eye—orbital—debris.html>

¹⁵³⁵⁾ Jens Utzmann, Axel Wagner, “Space—Based Space Surveillance as Complementary Element in an SSA Architecture,” 2011, URL: <http://www.congex.nl/11c01proceedings/Papers/2226204%20Utzmann.pdf>

¹⁵³⁶⁾ James R. Wertz, Nicola Sarzi—Amade, Anthony Shao, Christianna Taylor, Richard E. Van Allen, “Moderately Elliptical Very Low Orbits (MEVLOs) as a Long—Term Solution to Orbital Debris,” Proceedings of the 26th Annual AIAA/USU Conference on Small Satellites, Logan, Utah, USA, August 13–16, 2012, paper: SSC12—IV—6

delta V. Of course, if the loss of orbit maintenance delta V is permanent, then the spacecraft will decay and re-enter, as is desirable.

As space becomes more populated, the orbital debris problem becomes worse and has led to a great many attempts to find ways to monitor and/or remove orbital debris. While some of these may ultimately be successful, it has become clear that removing large amounts of orbital debris or preventing it from accumulating is, at best, a very expensive and challenging task. However, it is possible to mitigate the problem by the correct orbit selection for future space missions.

The orbital debris distribution at LEO altitudes is shown in Figure 79. At altitudes below approximately 500 km, the debris density is about an order of magnitude lower than at altitudes of 700 to 1000 km. At altitudes below approximately 500 km, the atmospheric density is high and, because of that, the debris density is low. The objects in this altitude regime decay and reenter the atmosphere in a short period of time. While the debris from the Iridium 33/Cosmos 2251 collision, which occurred at 790 km, may last for 1000 years or so, a similar collision at 300 to 400 km would create a debris cloud that would last for only a few months. At these altitudes, the atmosphere becomes a natural vacuum cleaner and removes orbital debris effectively and quickly.

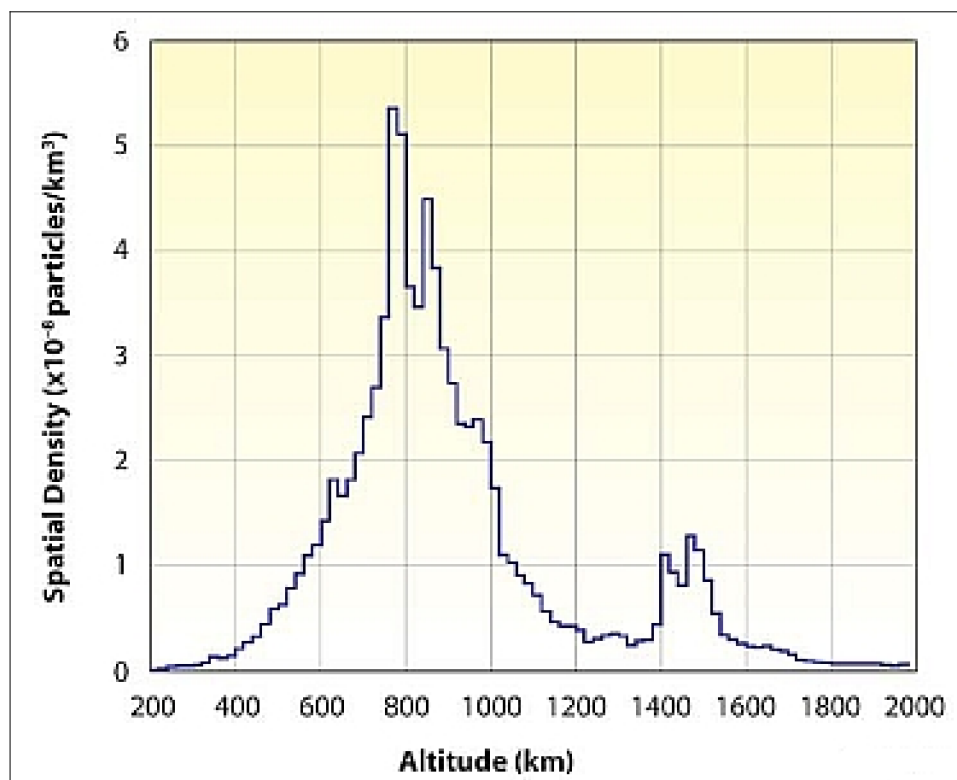


Figure 79: Orbital debris population in LEO as of January, 2011 (image credit: Microcosm Inc.)

The implication of the interaction of the debris population with the atmosphere is that irrespective of the level of future space activity, the debris density below about 500 km will not change greatly. Whatever debris is created will rapidly be removed by the atmosphere.

Spacecraft at low altitudes experience relatively high levels of aerodynamic drag (and also aerodynamic As shown in Figure 80, if no orbit maintenance burns were done, a typical spacecraft would decay and reenter the atmosphere from an initial 300 km circular orbit in about 23 days at solar maximum and 70 days at solar minimum. As shown in Fig. 4, a similar satellite in a 200 km x 500 km elliptical orbit will reenter in about 21 days at solar maximum and in about 45 days at solar minimum.

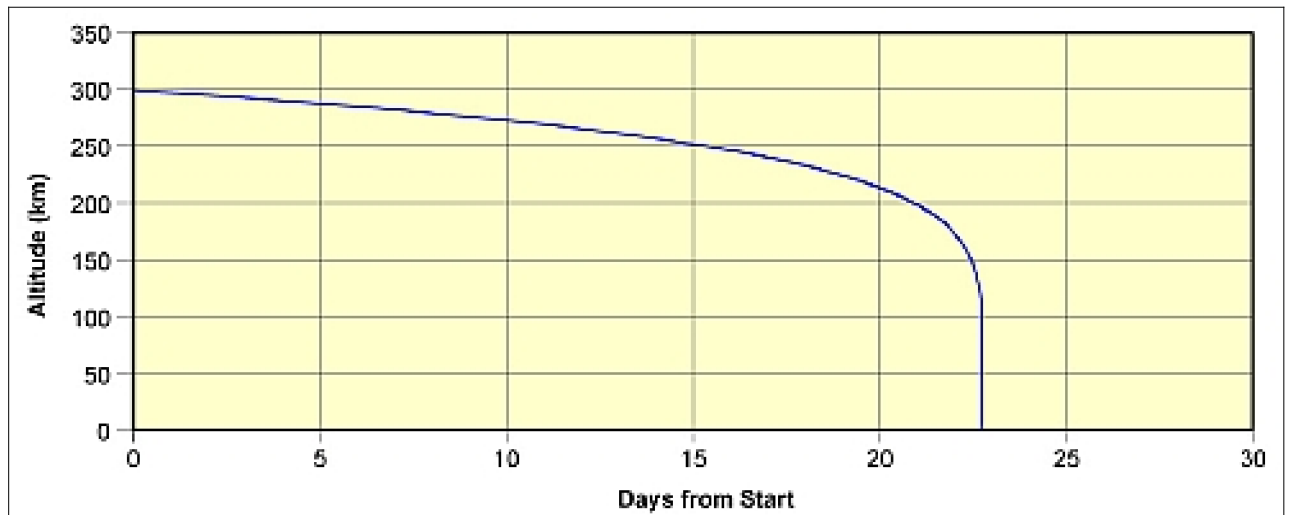


Figure 80: Typical spacecraft orbit decay at solar max with no orbit maintenance from an initial 300 km circular orbit (image credit: Microcosm Inc.)

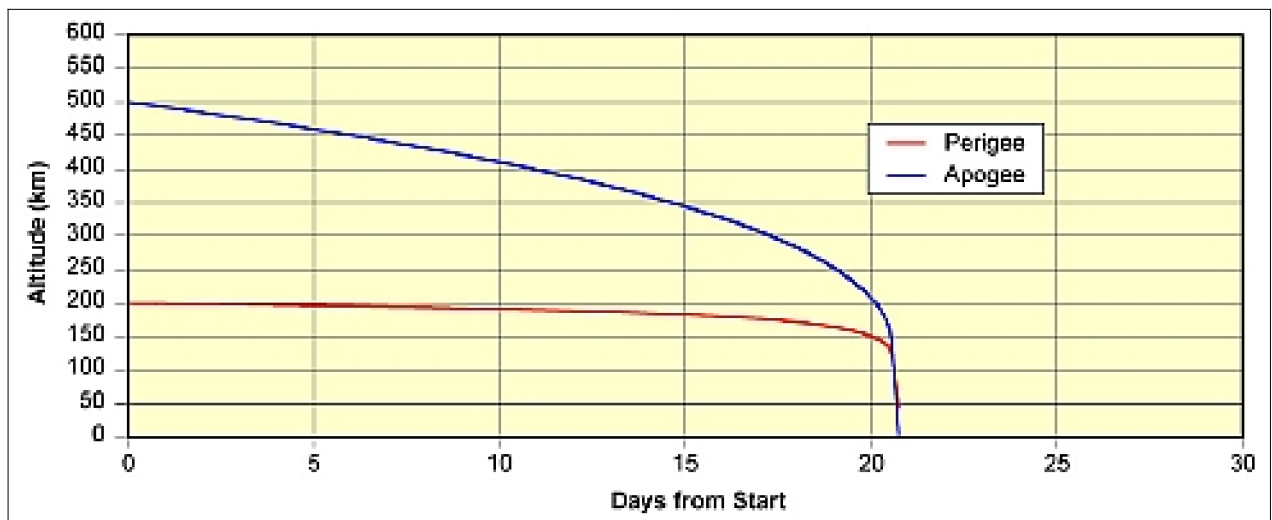


Figure 81: Typical spacecraft orbit decay at solar max with no orbit maintenance from an initial 200 km x 500 km elliptical orbit (image credit: Microcosm Inc.)

Figures 80 and 81 show the principal differences between orbital decay from circular and elliptical orbits. In the circular orbit case, decay begins immediately when orbit maintenance stops. As the orbit decay progresses, the satellite gets deeper and deeper into the atmosphere and the decay rate accelerates.

Several things are different in the elliptical orbit case. Because the atmospheric density is decreasing exponentially as we go up in altitude, essentially all of the orbit decay will occur at perigee, which means that perigee will not change and apogee will decrease. This creates basically a two-step process for elliptical orbit decay as can be seen in Figure 81. In the first step, the perigee remains nearly constant while the apogee decays. When the orbit becomes circular, the spacecraft quickly spirals down and reenters. Notice also that because perigee remains nearly constant, the rate of decay of the apogee is nearly constant over most of the range, then increases sharply prior to reentry.

What this means in practical terms is that there is relatively little harm in orbit maintenance outages, so long as recovery occurs before reentry. The perigee remains nearly fixed, so all that has to happen after recovery is to raise the apogee to its previous value. Because the decay rate has changed very little, there is no added penalty due to excessive decay. One simply has to replace the delta V that wasn't applied during the period that orbit maintenance wasn't working.

In this respect the MEVLO is a fail – safe orbit. In the event of an orbit maintenance failure, nothing bad happens for a period of time until relatively near the time that the satellite reenters. Recoverable failures do indeed occur in space systems and, for example, happened on UoSat–12 during the testing of autonomous orbit maintenance.

There are other significant advantages to MEVLOs. As can be seen from Figures 80 and 81, the 300 km circular orbit has about the same lifetime due to orbit decay as the 200 km x 500 km elliptical orbit. However, the elliptical orbit has a much lower perigee and, therefore, much resolution on the Earth when at perigee. As shown in Figure 82, a given resolution at nadir can be achieved with a smaller, and therefore lighter and much lower cost, telescope at low altitude. A 0.5 m aperture telescope at 200 km has the same ground resolution at nadir as a 2 m aperture telescope at a more traditional altitude of 800 km, but at a much lower cost.

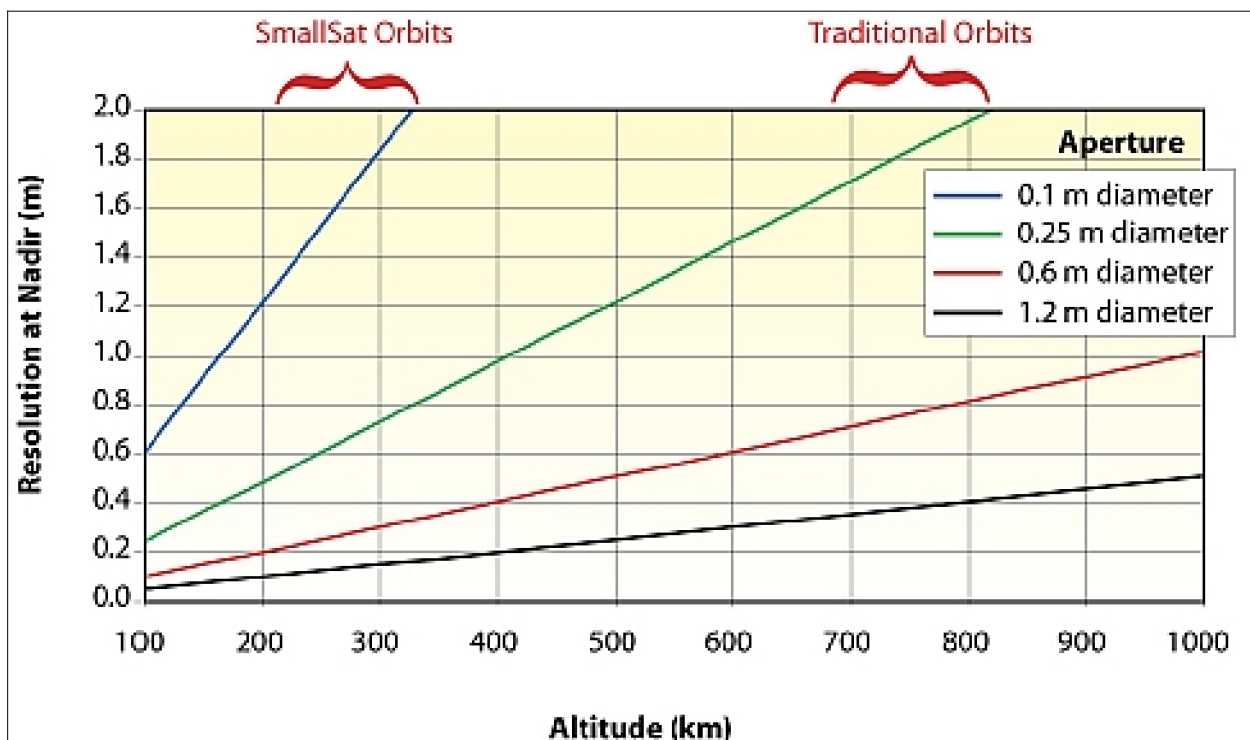


Figure 82: Resolution vs. altitude for low–altitude and higher altitude orbits used in more traditional systems (image credit: Microcosm Inc.)

This advantage is substantially increased with active Earth observation payloads, such as SAR or lidar. For active payloads the power required goes as the 4th power of the distance. This relationship means that an active payload at 200 km would require 256 times less power than a similar payload at 800 km. This, of course, can have a dramatic impact on the size and cost of the payload and the spacecraft that must support it.

MEVLO orbit selection: Traditionally, most LEO spacecraft fly at altitudes above 500 km in order to maximize lifetime and minimize the propellant required for drag make–up. Typically, this has meant flying in the range of 700–900 km, an altitude range that maximizes the potential problem with orbital debris. In addition, if the satellite fails at any point or runs out of propellant (or doesn't have a de–orbit propulsion system), it contributes to the orbital debris problem.

An example of a spacecraft flying successfully at very low altitudes is the GOCE mission of ESA which is flying in the regime of ~ 250–260 km altitude. It is using very–low–thrust electric propulsion to continuously overcome drag so as to create a “drag–free” orbit. In March 2012, the GOCE spacecraft completed 3 years on orbit.

The principal disadvantage of flying at very low altitude is the delta V, and therefore propellant mass, required for drag make-up. Typical values of the total delta V per year required for drag make-up for a spacecraft with a ballistic coefficient of 100 kg/m^2 are shown in Figure 83 for MEVLOs. Note that in Figure 83, the horizontal coordinate is the perigee altitude. The semimajor axis or mean altitude will be just the average of the perigee and apogee altitudes.

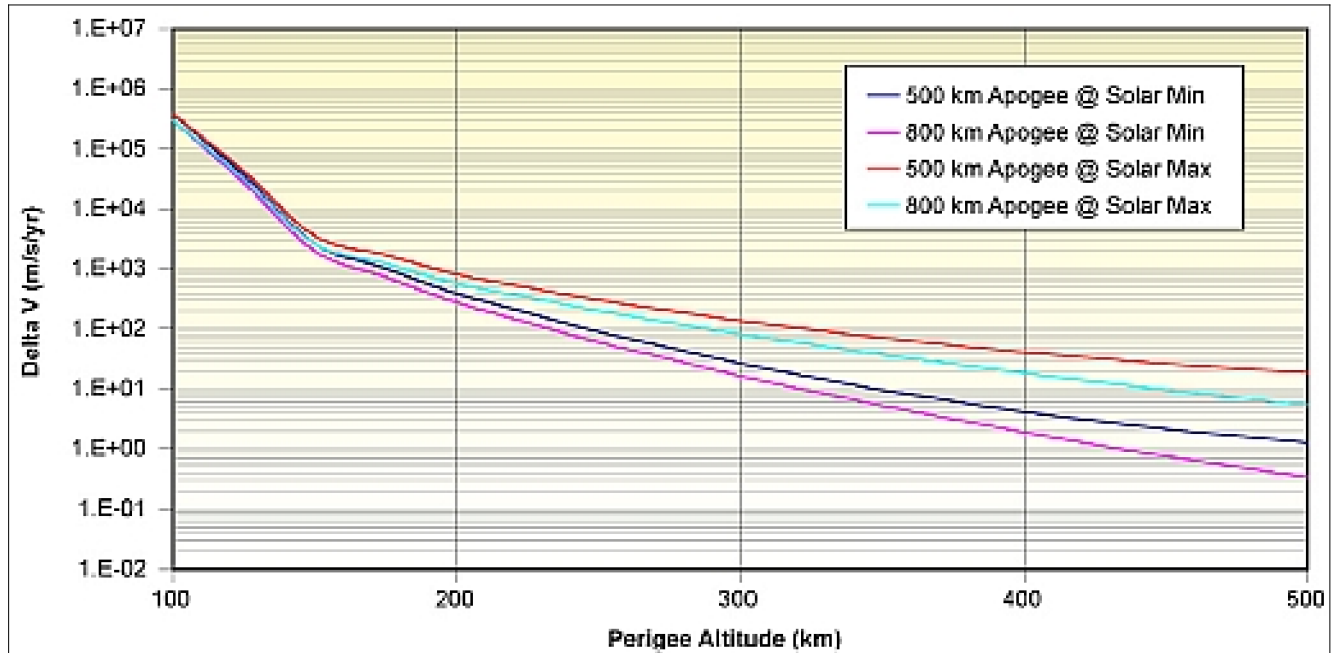


Figure 83: Altitude maintenance delta V for elliptical orbits at various altitudes and a ballistic coefficient of 100 kg/m^2 (image credit: Microcosm Inc.)

Orbit selection for MEVLOs comes down to balancing good resolution, reduced instrument (and, therefore, spacecraft) size and cost, and reduced orbital debris issues (both in terms of collision probability and contribution to the long term debris problem) against the delta V required and reduced coverage. Higher altitude satellites will generally have a longer design life and, therefore, potentially lower cost per year, but in more modern spacecraft this may be more than offset by the increased debris risk and the historically dramatically high cost of trying to design spacecraft for very long life (Ref. 1536).

1.13.2 Debris policies and spacecraft removal from orbit at end-of-life

A principal forum for debating orbital debris issues and new practices (including debris mitigation measures) is the **IADC** (Inter-Agency Space Debris Coordination Committee), created in 1993 by government representatives from USA (NASA), Europe (ESA, ASI, BNSC (now UKSA), CNES, DLR), Russia (Roskosmos), Japan (JAXA), India (ISRO, since 1995), China (CNSA, since 1995), and the Ukraine (NSAU, since 2000), Canada (CSA, since 2010).^{1537) 1538)}

In 2002, IADC completed a set of debris mitigation guidelines agreed to by the agencies. In Feb. 2003, these guidelines were presented to UNCOUOS (United Nations Committee on Peaceful Uses of Outer Space) for review and approval.

Artificial space debris has been with us since the very first satellites, and concerns about the potential hazards of space debris are equally old. However, in spite of continuing concerns

¹⁵³⁷⁾ <http://www.iadc-online.org/>

¹⁵³⁸⁾ J. Yan, "20 Years of IADC," Proceedings of the 51st Session of Scientific & Technical Subcommittee of UNCOUOS, Vienna, Austria, Feb. 11–22, 2014, URL: <http://www.unoosa.org/pdf/pres/stsc2014/tech-32E.pdf>

about the increasing population of artificial debris, the space agencies of the world didn't react to the situation. The humble beginnings of a United States policy on space debris were presented in 1986, with a focus on the space debris situation and its potential hazard to space flight, the urgent need for a space debris classification, and an appeal to avoid further man-made space debris (the military establishment tried to avoid any regulations because these would imply further costs to their programs).¹⁵³⁹⁾ ¹⁵⁴⁰⁾

In 1993, NASA adopted a new policy, a "NASA Management Instruction" (NMI 1700.8) with regard to spacecraft development (concerning debris prevention and end-of-life disposition). A so-called "debris assessment" is needed to determine if requirements are met for waiving the controlled reentry at the end of mission life. Because of lack of global regulations, waivers are likely to be issued for expensive measures that effect the projects of the own agency. But this is not special for the US: most spacefaring nations behave in the same way. Sometimes the US government insists on the strict application of its standard (NASA Management Instruction) as in the case of the Iridium constellation (condition for obtaining the license). In 1997, NASA issued NPD (NASA Policy Directive 8710.3 with regard to space debris. – The NPP (NPOESS Preparatory Project) spacecraft and the follow-up JPSS (Joint Polar Satellite System) series, for instance, are expected to have sufficient debris that survives reentry; hence, they feature the capability of a controlled reentry (propulsive maneuvers) to place the debris in a pre-determined location in the ocean.

The NASA "policy for limiting orbital debris generation" was revised as NPD (NASA Policy Directive) 8710.3A in Jan. 2003. The document introduces for instance the general guideline for limiting the lifetimes of such debris in LEO to 25 years.

ESA came out with an "ESA Space Debris Mitigation Handbook," Release 1, April 7, 1999, and a draft of the "European Space Debris Safety and Mitigation Standard" in 2000 (Sept. 27, 2000, Issue 1, Rev. 0), which discusses the issues of in-orbit debris and gives various scenarios for end-of-life (EOL) disposal. – The two TerraSAR spacecraft of EADS Astrium (TSX and TSL mission with a planned launch in 2006), within the framework of ESA Earth Watch missions, are planning thruster firings at EOL (using budgeted fuel) to obtain an elliptical orbit with a perigee of about 300 km or lower. This generates sufficient atmospheric drag to bring the S/C eventually into a reentry trajectory.

Further references on space debris are: "Position Paper on Orbital Debris," of IAA (International Academy of Astronautics), Paris, 2001, and "Technical Report on Space Debris," UN, New York, 1999. The problem with debris policies is that the standard in its entirety will only be applied when everybody in space will abide by the rules. Since no international regulation concerning space debris exists, this will take some time. Such a regulation must necessarily be issued by the UN, where the deliberations in the UN Committee on the Peaceful Uses of Outer Space (UNCOPUOS) on debris are ongoing since 1994. All agreements must be reached by unanimity. It took several years to reach agreement to have space debris on the agenda.¹⁵⁴¹⁾

In 2007, UNCOPUOS adopted a set of Space Debris Mitigation Guidelines. Subsequently, in 2008, France adopted a national space law, the European Union drafted a code of conduct for outer space activities, and ESA adopted a binding set of requirements on space debris mitigation for their space projects.

In 2003, ISO (International Organization for Standardization) commenced development of a series of spacecraft engineering standards aimed specifically at space debris mitigation. The first of these is due to be published within the next few months (end of 2009). The standards prescribe debris mitigation requirements that have been derived in large part from in-

1539) L. Parker Temple III, "Origin of the US Policy on Space Debris," Proceedings of 54th IAC (International Astronautical Congress), Bremen, Germany, Sept. 29 – Oct. 3, 2003

1540) L. Parker Temple, "The Impact of Space Debris on Manned Space Operations," Proceedings of the 37th Congress of the International Astronautical Federation, Innsbruck, Austria, October 4–11, 1986, IAA–86–420

1541) Information provided by Walter Flury of ESA/ESOC, Darmstadt, Germany

ternationally—agreed guidelines such as those published by the IADC. They also capture industry best practice and specify definite actions to be taken by satellite manufacturers and operators to achieve compliance. The highest level requirements are contained in a top—level standard designated **ISO 24113** “Space Systems – Space Debris Mitigation”. Their purpose is to avoid the intentional release of debris into Earth orbit during normal operations, avoid break—ups in Earth orbit, and remove spacecraft and launch vehicle orbital stages from highvalue orbital regions after end of mission. ¹⁵⁴²⁾

The introduction of space traffic management is a logical consequence of ever—increasing spacecraft and space debris populations. The first steps toward management of space traffic have already been taken in an uncoordinated fashion. Space traffic management is defined in reference 1544). “Space traffic management encompasses all the phases of a space object’s life, from launch to disposal. It consists of activities intended to prevent damage in the near term (such as collision avoidance and coordination of reentry), as well as actions that must be taken to reduce the long—term potential for future damage (such as deorbiting or moving satellites into disposal orbits).” So far, only ITU (International Telecommunications Union) administers a form of space traffic regulation for communication satellites in GEO. However, the management deals only with frequencies used by satellites, not physical locations of satellites. As a result, satellites broadcasting in different frequencies can occupy essentially the same physical space (i.e., in GEO). ^{1543) 1544) 1545)}

Among the space agencies there is practically a consensus that S/C and rocket upper stages in Low Earth Orbit (LEO – orbits <2000 km) should be removed from orbit within 25 – 50 years after mission completion. This is simply to avoid further proliferation and generation of debris (through collision). A regulation is however needed to force everybody, including commercial users/operators to apply the same rules.

In principle two categories of measures to reduce orbital debris growth can be distinguished:

- 1) Debris avoidance ¹⁵⁴⁶⁾
- 2) Debris removal. The natural cleaning of the Earth environment by the trajectory disturbances will no longer be sufficient in the future to keep the Earth environment in an acceptable status for the operation of manned and unmanned spacecraft. The only effective way to limit the growth of the orbiting debris is to systematically remove satellites and rocket upper stages at the end of their mission life from the near Earth space. There is already now international space law, the Liability Agreement, which clearly stipulates the liability of the owner in case of damage on ground or in air—space.

In general, the post—mission disposal options are:

- Option 1 (uncontrolled deorbiting): Maneuver to an orbit (by propulsion or other means, tether) in which atmospheric drag will eventually remove the structure within a given time frame, e.g. 25 years. With relatively small spacecraft masses (destruction and burn—up in the atmosphere), this will probably be the option favored by most satellite operators in the future.

1542) J. R. Davey, P. H. Stokes, “Status of the ISO Standards on Space Debris Mitigation,” Proceedings of the Fifth European Conference on Space Debris, Darmstadt, Germany, March 30 to April 2, 2009, SP—672, July 2009

1543) W. A. Ailor, “Space Traffic Management: Implementations and Implications,” Proceedings of the 54th IAC, Bremen, Germany, Sept. 29 – Oct. 3, 2003

1544) H. Brennan (Editor), “International Space Cooperation: Addressing Challenges of the New Millennium,” Report of an AIAA, UN/OOSA, CEAS, CASI Workshop, March 2001

1545) M. Gerard, J. Carrodegua (Editors), “International Space Cooperation: Solving Global Problems,” Report of an AIAA, UN/OOSA, CEAS, CASI Workshop, Bermuda, April 19–21, 1999.

1546) R. Janovsky, M. Kassebom, H. Lübberstedt, H. Burkhardt, et al., “End—Of—Life De—Orbiting Strategies For Satellites,” Proceedings of 54th IAC, Bremen, Germany, Sept. 29 – Oct. 3, 2003

- Option 2 (controlled deorbiting):¹⁵⁴⁷⁾ Direct retrieval and deorbiting. Examples are: 1) MIR Space Station of Rosaviakosmos (March 2001), 2) Compton Gamma Ray Observatory (CGRO) of NASA (June 4, 2000); 3) The Astra–1K (launch Nov. 25, 2002) commercial communications satellite of SES (Societe Europeenne des Satellites) Luxembourg, built by ASI (Alcatel Space Industries) of France, experienced a launch failure due an upper stage malfunction (Proton K/DM3 launch vehicle from Baikonur) leaving Astra–1K in a useless orbit (very low GTO). CNES and ASI put the satellite into a controlled atmospheric reentry trajectory. As a consequence, Astra–1K was safely de–orbited on Dec. 10, 2002.
- Options 3: Maneuver to one of a set of disposal regions in which the structures will not interfere with future space operations.

Examples of spacecraft removal from orbit (uncontrolled deorbiting category):

- Landsat–4 removal from space. On June 15, 2001, NASA shut down Landsat–4, (launch in 1982) whose instruments were no longer functioning, and initiated an atmosphere reentry maneuver which will result in destruction of the satellite in 5–10 years.
- The SPOT–1 satellite of CNES (1800 kg mass), launched into a sun–synchronous orbit at 830 km altitude in Feb. 1986 for a planned three year imaging mission, was retired in mid–2002 following the launch of SPOT–5. In 2003, CNES decided to de–orbit SPOT–1 to assure a destructive reentry and disintegration in a time period of about 15 years. In Nov. 2003, SPOT–1 was commanded into an elliptical orbit with a perigee of about 550 km (using the remaining fuel in its tanks).^{1548) 1549)}
- As of April 2004, PanAmSat announced that it has decided to deorbit one of its in–orbit international spares, PAS–6, due to a failure in the satellite’s power system. The GEO spacecraft is located at 43° west longitude; PAS–6 was one of two backup satellites supporting PanAmSat’s international fleet. PAS–6 was launched Aug. 8, 1997, a Loral Space Systems model FS–1300 spacecraft.

Removal of commercial satellites operating in GEO (Geostationary Earth Orbit).¹⁵⁵⁰⁾ In June 2004, the US FCC (Federal Communications Commission) stepped into a years–long debate on orbital debris by ordering tough new measures governing how satellites are to be disposed of by their commercial owners. The FCC ruled that all US–licensed satellites launched after March 18, 2002, will have to be placed into a graveyard orbit at EOL (End of Life), 200 to 300 km above GEO, where most commercial satellites operate. The FCC ruling sets a regulatory standard – that will be difficult for other nations to avoid.

In–orbit satellite destruction incidents by interceptor vehicles launched from the ground segment:

- On Jan. 11, 2007, China destroyed its own FY–1C inactive weather satellite (retired as of January 2004), and orbiting in a sun–synchronous polar orbit at an altitude of 850 km, in an interception test causing an explosion and a lot of **debris** in a wide LEO corridor. The incident caused a considerable accidental debris impact risk to other spacecraft – since the sun–synchronous orbit happens to be the predominant orbit of choice for all types of Earth observation missions. Some 40 pieces of debris have been tracked and cataloged by NORAD. Some of these pieces have apogees as high as 3,500 km. As more and more debris is “discovered” it will be clear that more and more of space is threatened. However, even the debris already tracked will start to spread out with time and threaten more and more satellites.

1547) F. Alby, J. P. Berthias, G. Campan, “Astra–1K De–Orbiting Operations,” 54th International Astronautical Congress (IAC), Bremen, Germany, Sept. 29 – Oct. 3, 2003

1548) P. de Selding, “CNES Begins Deorbiting SPOT–1 Earth Observation Satellite, Space News, Nov. 24, 2003, p. 6

1549) “SPOT–1 signs off gracefully,” CNES Magazine, No 21, Jan. 2004, p. 8

1550) P. B. de Selding, “FCC Imposes Strict New Rules for Disposing of Commercial Satellites,” Space News, June 28, 2004, pp. 1 and 3

According to press reports, the interceptor is believed to have been carried by a DF–21 IRBM (known as in the West as the CSS–5), a solid propellant, two stage missile of the Chinese Armed Forces. This test makes China the third country, after the USA and Russia, to have tested ASAT (Anti Satellite) weapons.^{1551) 1552) 1553)} For China, the interception test was a successful military technology demonstration. However, for the rest of the world, the interception test caused many concerns with regard to space debris spreading in the densely populated LEO environment; the test generated a lot of protest from all spacefaring nations.

- On Feb. 20, 2008, the US Navy destroyed a defunct spy satellite with the code name “USA 193” of the USNRO (National Reconnaissance Office) by launching an SM–3 interceptor missile from the ship “USS Lake Erie” in the Pacific Ocean positioned in the region northwest of Hawaii. The missile intercepted the 3 ton spacecraft orbiting at the low altitude of 247 km destroying the satellite through sheer kinetic energy. The satellite apparently disintegrated into many small pieces of debris. The USA 193 satellite malfunctioned shortly after deployment (launch Dec. 14, 2006), and was intentionally destroyed 14 months later (an impact prediction was forecast for March 6, 2008). In the aftermath of the spacecraft destruction, the task of tracking the debris is under way, and the fallout from the January fireworks are impacting the scheduled launch of other space missions. The US government had notified the world only a week in advance about its intentions to shoot down a decaying satellite with a ballistic missile – to avoid greater safety risks to mankind on the soon–to–be impact on reentry. Of particular concern was the large amount of fuel (450 kg of hydrazine) onboard the USA 193 which could be rather harmful on an accidental impact in a populated region.¹⁵⁵⁴⁾

The shoot–down of the spacecraft caused considerable irritation and controversy by the international community. The Russian government claimed that this exercise was a test of the U.S. missile defense program (a cover for a test on an ASAT). Several independent analysts argued that in the last five years more than 300 objects had deorbited – controlled and uncontrolled – without causing havoc. The likelihood of any of them hitting persons or buildings seems to be very small. Uncontrolled reentry to Earth of space vehicles has been a repeated occurrence. Many countries use toxic fuel components. But on no occasion has this called for any extraordinary measures. Even the breakup of the Space Shuttle Columbia over Texas on January 31, 2003 resulted in no damage to human life or property.¹⁵⁵⁵⁾

- NASA deactivated the TDRS–1 (Tracking and Data Relay Satellite–1) on June 27, 2010, following more than 26 years of operation.¹⁵⁵⁶⁾ The EOM (End–of Mission) operations were developed to address the stringent requirements of NPR 8715.6 (NASA Procedural Requirements for Limiting Orbital Debris) which consists of three key items:
 - removal from the geosynchronous arc
 - depletion of the remaining propellant
 - passivation of all sources of energy storage or generation.

The EOM approach minimized risks while accomplishing these goals. Raising TDRS–1 over 350 km above geosynchronous was accomplished via proven station change opera-

1551) G. Forden, “A Preliminary Analysis of the Chinese ASAT Test,” URL: <http://web.mit.edu/stgs/pdfs/A%20Preliminary%20Analysis%20of%20the%20Chinese%20ASAT%20Test%20handout.pdf>

1552) J. Oberg, “The dozen space weapons myths,” March 12, 2007, URL: <http://www.thespacereview.com/article/826/1>

1553) D. Anderson, “Space preservation or space destruction?,” March 12, 2007, URL: <http://www.thespacereview.com/article/825/1>

1554) T. Brinton, “US Satellite Smashed to Pieces by SM–3 Interceptor,” Space News Feb. 25, 2008, p. 4

1555) J. Olberg, “Sense, nonsense, and pretense about the destruction of USA 193,” The Space Review, March 3, 2008, URL: <http://www.thespacereview.com/article/1073/1>

1556) Ronald Zaleski, Walter Mirczak, Stephen Staich, Richard Caverly, Eric Smith, Nicholas Teti, W. Lynn Vaught, Dave Olney, “Innovative Approach Enabled the Retirement of TDRS–1 Compliant with NASA Orbital Debris Requirements,” 2011 IEEE Aerospace Conference, Big Sky, MT, USA, March 5–12, 2011

tions. Depleting propellant was the most challenging task, requiring over 20 hours of thruster on–time accumulated within schedule, orbit, and spacecraft subsystem constraints. The complete EOM campaign lasted 21 days. The TDRS–1 EOM campaign demonstrated that pre–NPR 8715.6 satellite designs can be made to comply and that lessons learned could be applied to other satellite designs.

- A total of 80 space launches reached Earth orbit or beyond during 2011, the most since the year 2000.

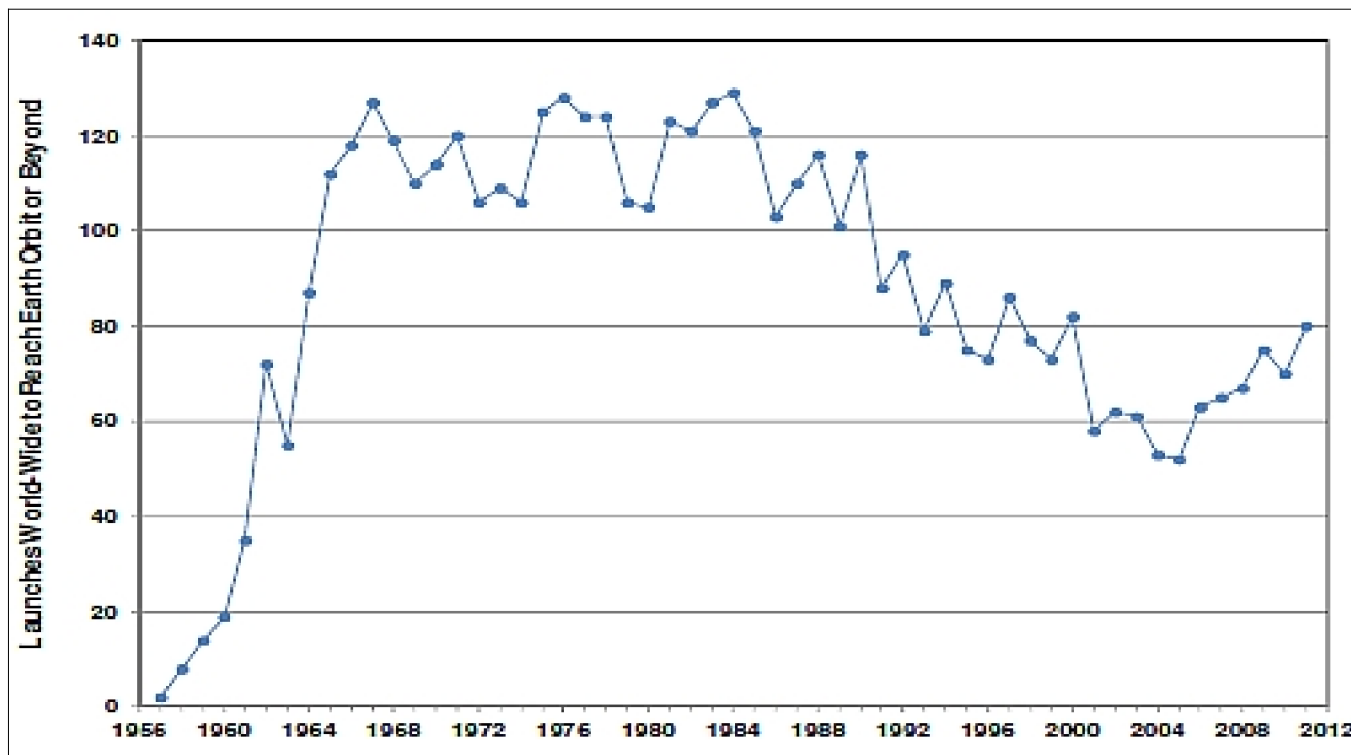


Figure 84: Global space mission launches by year (image credit: NASA) ¹⁵⁵⁷⁾

- ISS 2010: Two debris shields from the USA airlock on ISS were returned to Earth in 2010 after an exposure of nearly nine years. A detailed analysis at the NASA /JSC (Johnson Space Center) in 2011 found 58 craters with a diameter of 0.3 mm or more. The largest crater had a diameter of 1.8 mm and nearly penetrated the shield. Six of the larger craters, including the largest one, contained residue of silica, Teflon, or both. Some of the panel craters might be evidence of secondary debris from initial impacts on ISS solar arrays (Ref. 1557).
- On Nov. 28, 2011, the TDRS–4 spacecraft conducted two maneuvers to reach an initial disposal orbit of approximately 300 km by 500 km above GEO, in accordance with USA and UN guidelines. TDRS–4 completed > 22 years of communication services. A series of additional maneuvers were then conducted to deplete all residual propellants for the purpose of preventing a future, accidental explosion. This was achieved on Dec. 9, 2011, leaving TDRS 4 in an orbit of 460 km x 560 km above GEO (Ref. 1557).
- NOAA’s GOES–11 satellite was replaced on Dec. 6, 2011 by GOES–15. ¹⁵⁵⁸⁾ Two maneuvers were conducted 10 days later to transfer the spacecraft to a disposal orbit 350 km above GEO. Additional small maneuvers were then conducted to deplete all remaining propellants.

¹⁵⁵⁷⁾N. Johnson, “USA Space Debris Environment, Operations, and Policy Updates,” Proceedings of the 49th Session of UNCOPUOS–STSC (UN Committee on the Peaceful Uses of Outer Space–Scientific and Technical Subcommittee), Vienna, Austria, Feb. 6–17, 2012, URL: <http://www.oosa.unvienna.org/pdf/pres/stsc2012/tech-26E.pdf>

¹⁵⁵⁸⁾ “TDRS and GOES Spacecraft Sent to Graveyard Orbits,” Orbital Debris Quarterly News, NASA, Vol. 16, Issue 1, January 2012, p. 3, URL: <http://orbitaldebris.jsc.nasa.gov/newsletter/pdfs/ODONv16i1.pdf>

- The GOES–10 spacecraft of NOAA was de–commissioned on December 2, 2009. – Nearly two years after the GOES–10 spacecraft had been decommissioned and placed in a compliant disposal orbit above GEO, on Sept. 5, 2011 the orbit of the vehicle was abruptly perturbed: the perigee decreased by 20 km. – The cause of this incident is still unknown, but a collision with a small object is a possibility (Ref. 1557).

Spacecraft	Maneuver date	Object avoided
Aqua	January 2, 2011	Cosmos 2251 Debris
Aqua	February 8, 2011	Iridium 33 Debris
Calipso	February 18, 2011	OV2–1
Aqua	March 1, 2011	Agna D Debris
CloudSat	June 18, 2011	Aqua
TDRS–7	October 18, 2011	Ekran 4
CloudSat	November 6, 2011	Terra
Landsat–7	November 29, 2011	Cosmos 374 Debris
CloudSat	December 14, 2011	Fengyun–1C Debris

Table 79: During 2011 NASA robotic satellites conducted 9 collision avoidance maneuvers (Ref. 1557)

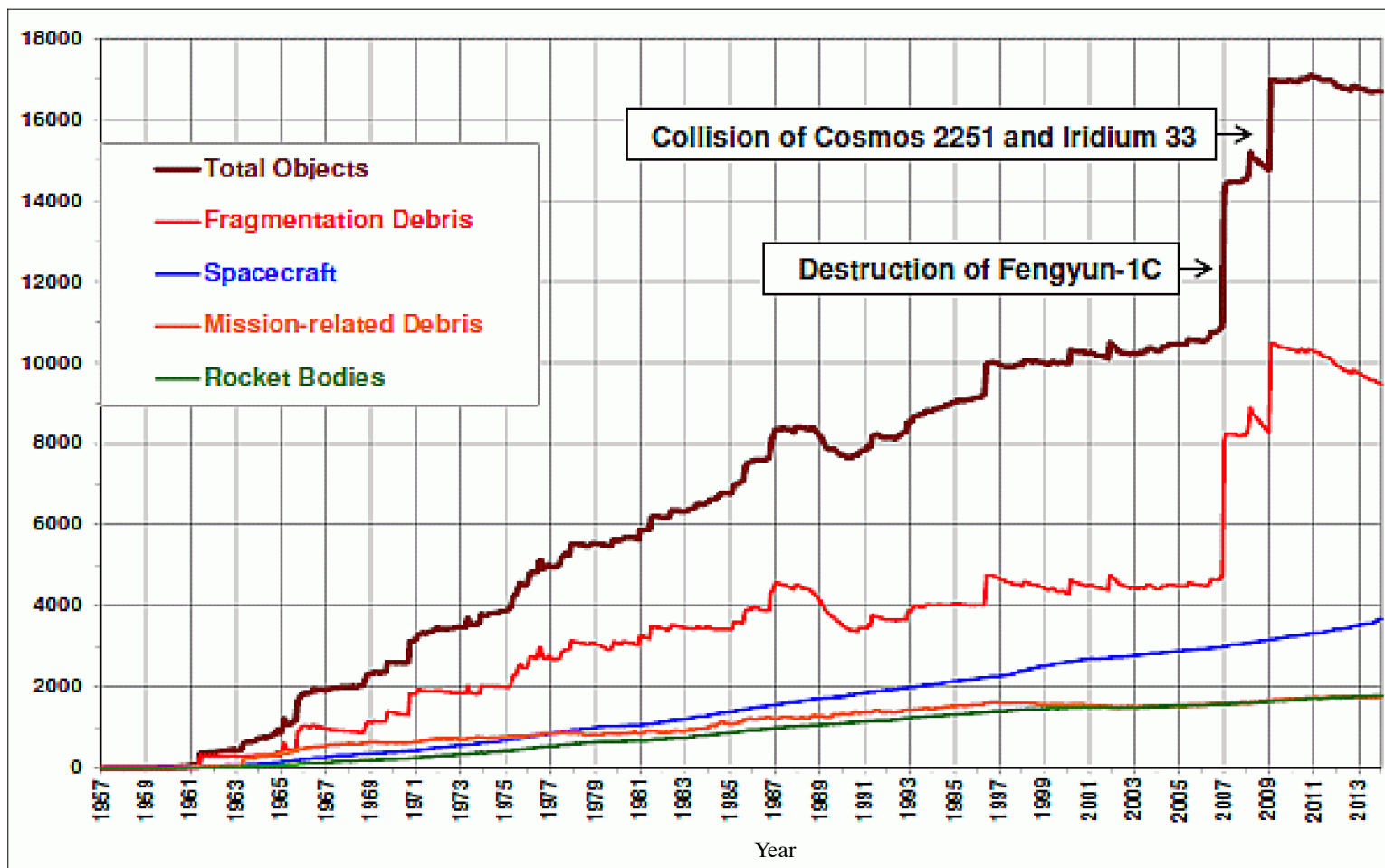


Figure 85: Number of cataloged objects (≥ 10 cm) in Earth orbit by object type (image credit: NASA) ¹⁵⁵⁹⁾

Satellite reentries in 2013:

- More than 400 spacecraft, launch vehicle stage, and other debris reentries were recorded by the U.S. Space Surveillance Network during 2013.

¹⁵⁵⁹⁾ M. Matney, "USA Space Debris Environment, Operations, and Modeling Updates," Proceedings of the 51st Session of Scientific & Technical Subcommittee of UNCOUOS, Vienna, Austria, Feb. 11–22, 2014, URL: <http://www.unoosa.org/pdf/pres/stsc2014/tech-27E.pdf>

- Uncontrolled reentries accounted for a total mass of >100 metric tons from 66 payloads and launch vehicle stages.
- An additional 19 spacecraft and stages executed controlled reentries.

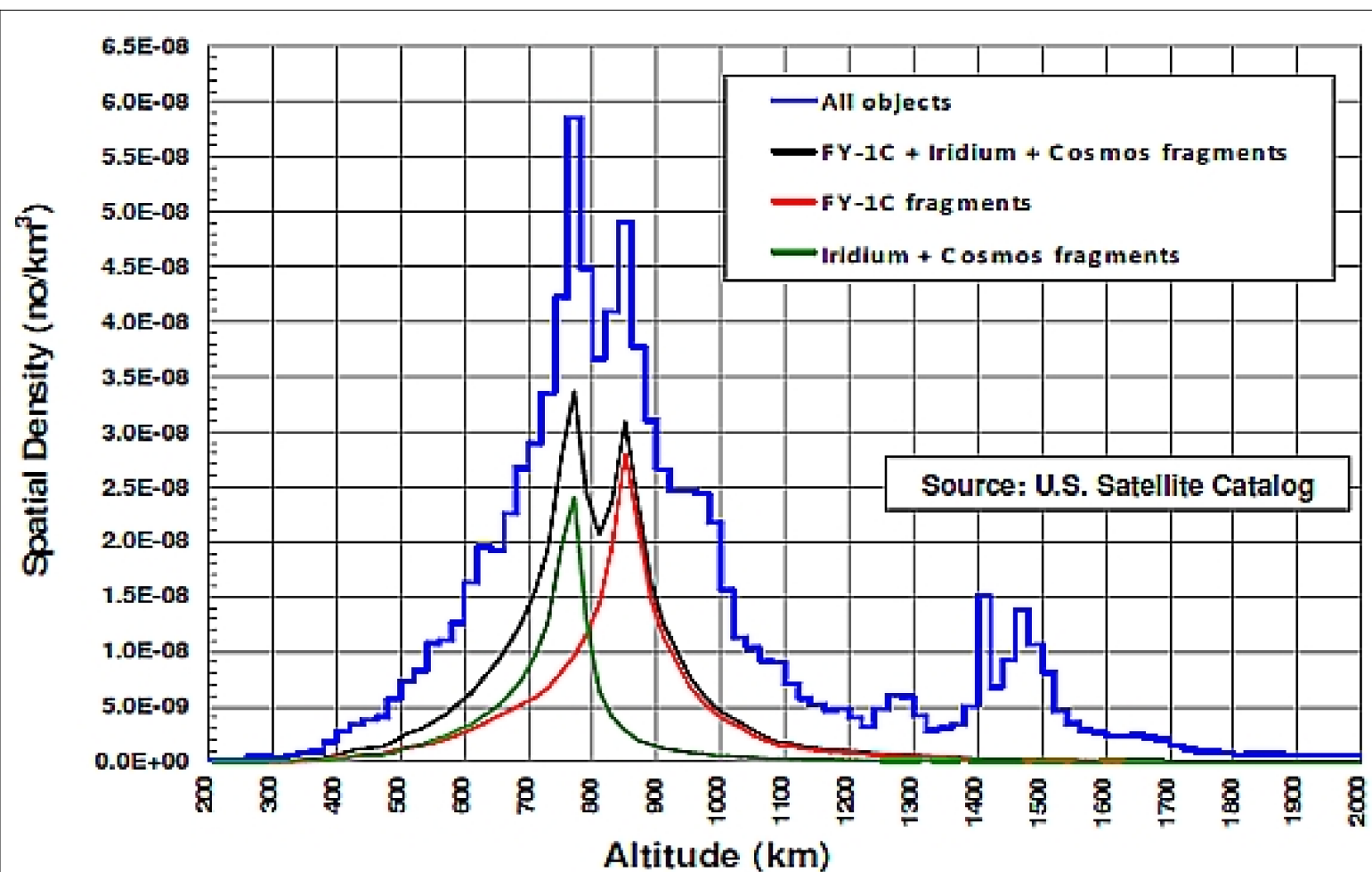


Figure 86: Distribution of objects in LEO (image credit: NASA, Ref. 1520)

Legend to Figure 86: The most congested region in low Earth orbit is between 760 km and 860 km.

Mean altitude	Spacecraft	Object avoided	Maneuver date
550 km	GLAST (2008–029A)	Cosmos 1805	April 3, 2012
700 km	Aura (2004–026A)	Cosmos 2251 Debris	May 17, 2012
	Calipso (2006–016B)	Cosmos 2251 Debris	October 2, 2012
	CloudSat (2006–016A)	Sinah 1	September 8, 2012
	Landsat–5 (1984–021A)	Agenda D stage Debris	July 1, 2012
	Landsat–7 (1999–020A)	Fengyun–1C Debris Meteor 1–10 Debris	March 9, 2012 April 17, 2012
825 km	Suomi–NPP (2011–061A)	Agenda D stage Debris	February 1, 2012

Table 80: During 2012 NASA supported 8 collision avoidance maneuvers for U.S. robotic satellites (Ref. 1520)

Earth satellite population:

In its Space Debris Mitigation Guidelines, the IADC has defined two protected regions about the Earth (Figure 87). The first region is the low Earth orbit (LEO) protected region which extends from the lowest maintainable orbital altitude up to a height of 2,000 km

above the surface of the Earth. The second region is the geosynchronous orbit (GEO) protected region, which includes the volume of space bounded in altitude by ± 200 km of the geosynchronous altitude (35,786 km) and in inclination by $\pm 15^\circ$. Note that the GEO protected region represents only a portion of the entire GEO region. ¹⁵⁶⁰⁾

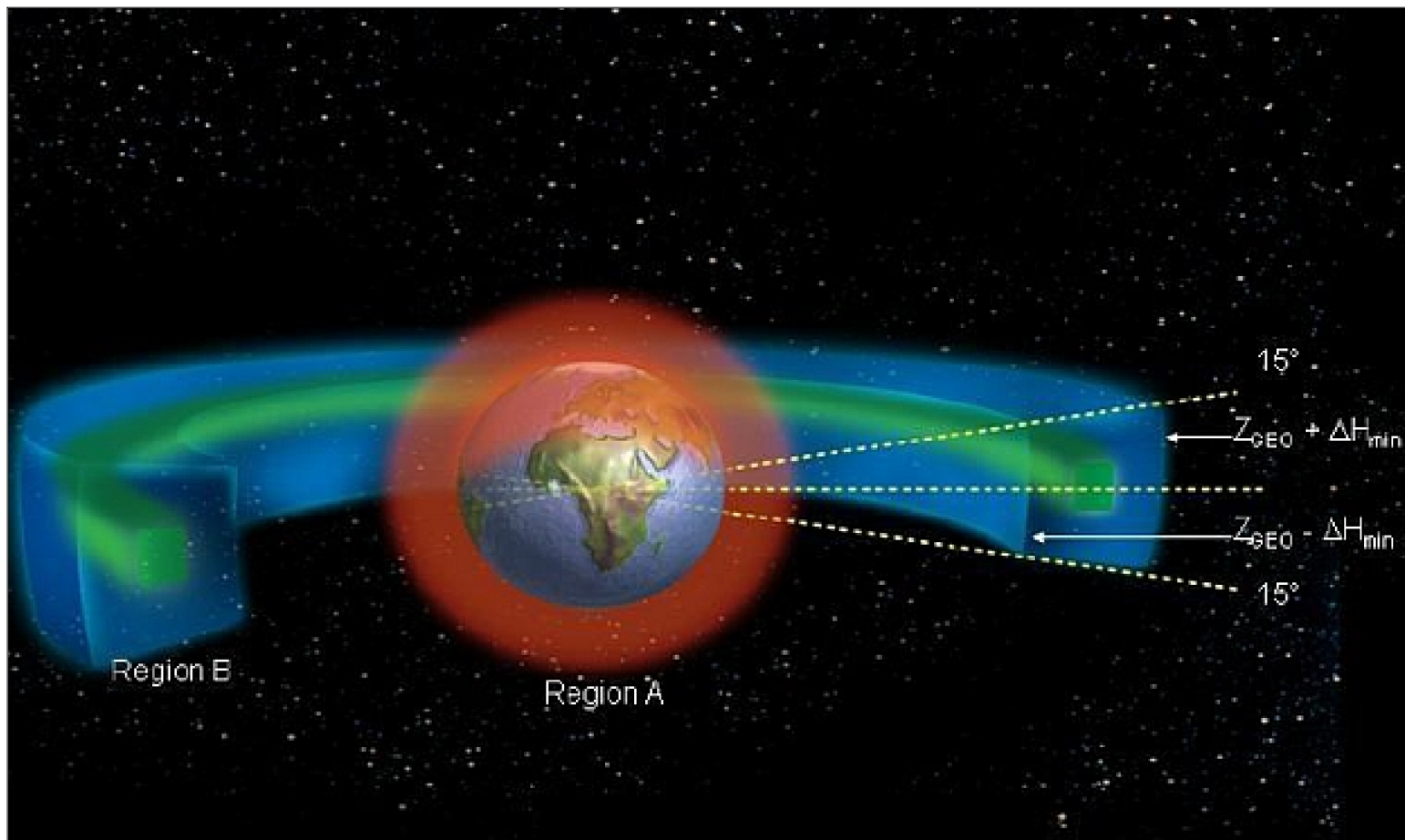


Figure 87: Protected Regions A and B, as defined by the IADC and adopted by the United Nations in 2004.

After more than 50 years of space activities, after about 5 000 launches since 1957 and 240 satellite explosions in orbit, the number of debris larger than 10 cm is estimated at more than 20,000, between 1–10 cm at up to 600,000, and between 1–10 mm at more than 300 million. Overall the current mass which is now in orbit is estimated to be > 6000 tons.

Objects in space larger than ~ 10 cm in LEO and larger than ~ 1 m in GEO, which include intact spacecraft, launch vehicle stages, mission-related debris, and fragmentation and other debris, are tracked by established space surveillance systems, comprised primarily of terrestrially-based radar and electrooptical sensors, such as the U.S. Space Surveillance Network and the Russian Space Surveillance System. The majority of these objects have been identified and officially cataloged and are monitored on a frequent basis.

The objects in the GEO region are much less numerous than in LEO and reside in about seven times the volume of LEO, but this unique regime is the home to more than 400 operational communications and other spacecraft which serve vital purposes for all countries of the world. The total number of cataloged objects in or near the GEO region is in excess of 1,100. The current number of estimated objects as small as 10 cm in or near the GEO region is on the order of 3,000. Only rough estimates are available for debris smaller than 10 cm at these high altitudes. Debris in GEO will orbit the Earth for many centuries, as the stabilizing effect of atmospheric drag is absent.

¹⁵⁶⁰⁾ "Space Debris, IADC Assessment Report for 2011," IADC-12-06, April 2013, URL: <http://www.iadc-online.org/Documents/IADC-2012-06.%20IADC%20Annual%20Report%20for%202011.pdf>

About 90% of the roughly 1300 operational satellites in orbit (2013 time frame) are either in LEO or in GEO. LEO is the most highly congested region in near–Earth space, containing approximately 75% of all cataloged objects. However, in LEO, the satellites and the orbital debris are quite widely scattered in terms of altitude, inclination and ascending node. This, in combination with the fact that orbital speeds are considerably higher than in the GEO case, makes both the amount of crossings and the relative velocities of the bodies during these crossings very high on average.¹⁵⁶¹⁾

Another critical issue is that ISS (International Space Station) operations are performed at low LEO altitudes ($\sim 350\text{--}400$ km), making it essential that the risk of collision is minimized to the greatest possible extent in this area for safety of human spaceflight.

1.13.3 Protecting space assets against small space debris

The number of debris in space is continuously increasing, especially as a result of the collisions that have occurred in the past few years. Thus the presence of debris could become an increasing risk for the survivability of space assets. Indeed, the probability for a satellite to collide with orbital debris, although very low, could become non negligible.

A European FP7 project, entitled **ReVuS** (Reducing the Vulnerability of Space Systems), aims to define design solutions that will reduce the vulnerability of future LEO satellites to small– and medium–sized debris (typically 1mm to 5 cm). Indeed, these debris cannot be tracked, but remain a significant threat.

The ReVuS project started in March 2011 and is funded by the European Union. The project is carried out by a consortium, led by Astrium SAS and gathering the expertise of 9 partners from Universities, SME (Small and Medium sized manufacturing Enterprises) and large enterprises in Europe.¹⁵⁶²⁾

The vulnerability analysis is based on the use of the impact risk assessment SHIELD tool:

- To evaluate the probabilities of penetration of small debris particles in the satellite and in the equipment
- To determine the failure probability for all equipment parts considered.

Two reference satellites, an EO optical satellite and an EO radar satellite, have been taken into account. They have different configurations and different orbit altitude (the optical satellite has a deployed solar array and is located at 820 km altitude while the radar satellite has a rigid body mounted solar array and is located at 515 km altitude).

An evaluation of the flux of debris impacting, and of the flux of debris penetrating the reference satellites on their different faces has been done for successive ranges of particles diameter. It appears that:

- Debris below 1 mm diameter has a high probability of impact, but only few penetrate the satellite, so that the effects on equipment are very low.
- Debris particles with a diameter in the range (1–10 mm) impact and penetrate the satellites 100 times more often than debris particles in the range (10–50 mm).
- The risk of being impacted or penetrated by small debris is much higher at 800 km than at 500 km.

1561) Matteo Emanuelli, Tiffany Chow, Deva Prasad, Giulia Frederico, Joshua Loughmann, “Conceptualizing an Economically, Legally, and Politically Viable Active Debris Removal Option,” Proceedings of the 64th International Astronautical Congress (IAC 2013), Beijing, China, Sept. 23–27, 2013, paper: IAC–13–A6.8.1

1562) Claude Cournet, Laure Brooker, Matthieu David, Bernard Gergonne, Robin Putzar, Hedley Stokes, Paul Bourke, “Protecting the LEO space systems against small debris particles,” Proceedings of the 64th International Astronautical Congress (IAC 2013), Beijing, China, Sept. 23–27, 2013, paper: IAC–13–A6.4.7

Potential solutions: Based on the results of the vulnerability analysis, two main categories of solutions have been defined: solutions at system level, and solutions at satellite architecture level, which includes the shielding solutions.

Shielding concepts: The shielding solution will have a significant impact on the mass and on the layout of the satellite.

The required objective of the shielding is to reduce the probability of failure of the satellite (due to debris) by half. From the vulnerability analysis, it appears that this objective could be achieved at satellite level when all items (taking into account redundancy scheme) are protected against debris in the size range of 3 to 4 mm.

More than twenty shielding concepts have been defined. They are based on the use of shielding technological bricks: reinforced MLI, reinforced structural panels (Al or CFRP), reinforced equipment box and intermediate layers. These bricks can be mixed to define an efficient shielding solution, such as for instance reinforced MLI plus reinforced panel.

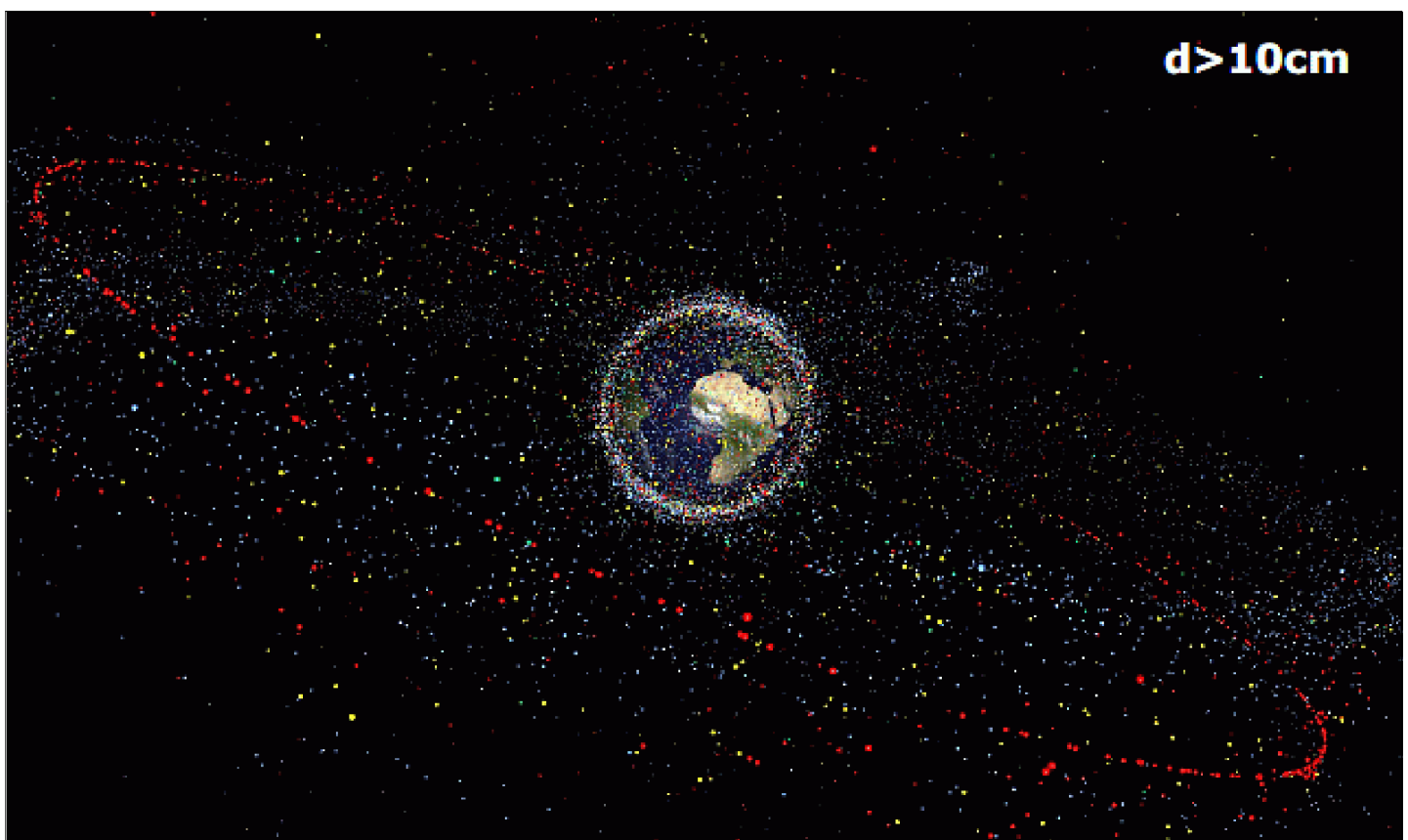


Figure 88: Snapshot of cataloged space debris in 2013 (image credit: ESA) ¹⁵⁶³

Testing of shielding concepts: The aim of the first test campaign was to evaluate promising shielding components identified during the study. The shielding components are placed within a set-up that is representative for their occurrence within a spacecraft: MLI (Multi-Layer Insulation) and sandwich panel samples are placed at the outermost location and impacted directly, whereas intermediate layer samples are placed with some spacing behind a bumper. The targets are impacted with nominally identical impact conditions above their ballistic limit. Behind each target, witness plates are placed. The first witness plate behind the target (WP1) is considered somewhat representative for module walls.

The shielding of critical satellite elements appears to be one of the most promising solutions. The vulnerability analysis of two reference satellites has shown that the particles indu-

¹⁵⁶³ Heiner Klinkrad, "Space Debris Mitigation Activities at ESA in 2013," Proceedings of the 51st Session of Scientific & Technical Subcommittee of UNCOUOS, Vienna, Austria, Feb. 11–22, 2014, URL: <http://www.unoosa.org/pdf/pres/stsc2014/tech-29E.pdf>

cing the highest probability of failure of the satellite have sizes in the range of 2–4 mm. This is mainly due to their high fluxes as compared to particle with size above 1 cm. The shielding of the equipment will be sized against this size of particles. Solutions at architecture and system levels will take into account the larger size of debris up to 5 cm.

- Orbit control status of GEO objects in 2013: Total count: 1396 objects in GEO (Ref. 1563)
 - 305 (21%) \Rightarrow E–W/N–S control
 - 131 (9%) \Rightarrow only E–W control
 - 9 (<1%) \Rightarrow highly inclined
 - 79 (5%) \Rightarrow uncontrolled
 - 12 (1%) \Rightarrow undetermined
 - 18 (1%) \Rightarrow L1+L2 libration
 - 46 (3%) \Rightarrow L2 libration
 - 114 (8%) \Rightarrow L1 libration
 - 114 (8%) \Rightarrow L1 libration
 - 1,142 TLE catalog objects met „near GEO“ criteria ($e < 0.2$, $0.9 < n < 1.1$ rev/d, $i < 70^\circ$); 254 more objects are known to be in this area
 - controlled \Rightarrow 436 (305 thereof E–W/N–S); uncontrolled \Rightarrow 960 orbit
 - 26 new GEO objects were injected in 2013 (25 payloads + 1 rocket body)
 - typical operational lifetimes of GEO satellites are about 15 years; the share of abandoned satellites keeps decreasing since the late 1990s.

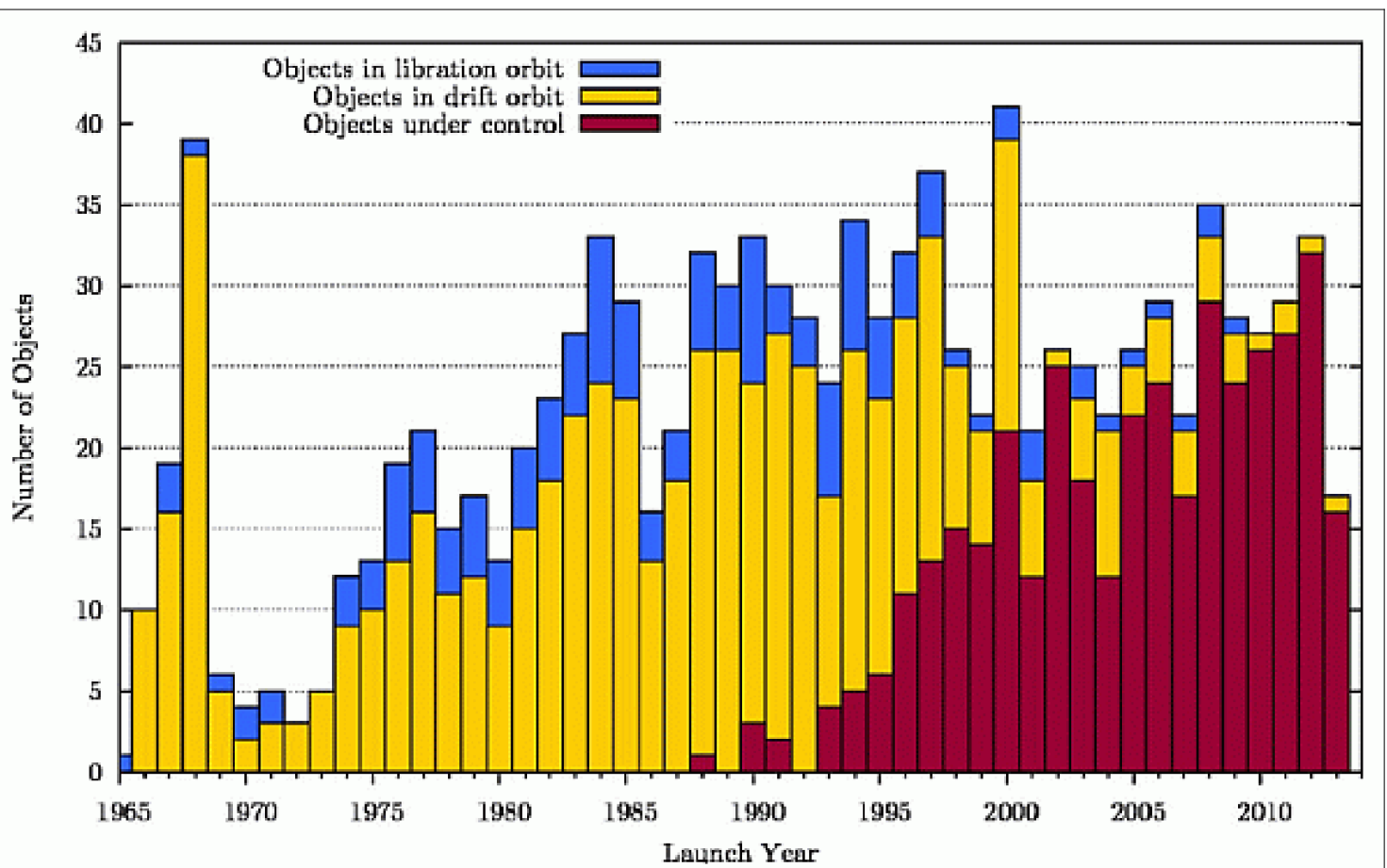


Figure 89: Status of GEO objects versus launch year (image credit: ESA)

1.14 On-orbit Propulsion

On-orbit (or in-space) propulsion has been a basic need and challenge of spaceborne missions from the early days of space flight – offering an extended application range and enhanced mission capabilities. However, it took a while to develop the concepts of maneuvering capabilities of such actuators/dispensers as apogee kick motors and AVCS (Attitude and Velocity Control System) with the available and evolving technologies. Some typical on-orbit propulsion functions are:

- Insertion into a higher operational orbit. Example: from GTO (Geosynchronous Transfer Orbit) into GEO (Geostationary Earth Orbit).
- Other kick stages to non-GEO orbits (including Earth escape trajectories). Some of the more recent upper-stage systems provide multiple restart capabilities for precise LEO or MEO injection and flexible deployment maneuvers.
- Spacecraft onboard control propulsion (such as station keeping, orbit corrections, reboost services, relocation/station changes, survivability/evasive maneuvers, attitude control, acceleration for deployed appendices, autonomous teleoperations, retrieval/rescue operations, repair/resupply, etc.)
- Demonstrations of alternative propulsion means. The evolution of on-orbit electric propulsion and the demand for low-cost space missions have raised interest in small satellites and in their potential use as parts of satellite formations as well as building units of satellite constellations. Formation flying of small satellites can be used to bring in-orbit spares for failed payloads on larger satellites as well as to replace large satellites by flying the mission on more small satellites, each carrying a single payload. The complexity of formation flying requires also a considerable degree of spacecraft autonomy.
- On-orbit chemical propulsion systems are “energy limited systems” because the chemical reactants have a fixed amount of energy per unit mass, which limits the achievable exhaust velocity or specific impulse. However, because the propellants constitute their own energy source, the rate at which energy can be supplied to the propellant (which is ultimately limited by reaction kinetics) is independent of the mass of the propellant, so very high powers and thrust levels can be achieved.

Traditionally, low-thrust propulsion tasks are accomplished with cold gas or hot gas thrusters (bi-propellant technology). These thrusters, which are quite simple in principle, are perfectly suited to most of the applications (attitude control, etc.). There are some drawbacks to the system. Of course, all gases need to be stored in pressurized tanks. This means that extra weight is added to the spacecraft due to the heavy structure, hermetic seals, piping etc. The specific impulse (Isp) of cold gas thrusters is very low (in the order of two orders of magnitude lower than in electric propulsion systems). Low specific impulse means a relatively large amount of propellant to deliver a given total impulse. The total amount of propellant that can be carried poses a limit to the mission lifetime.

- Some chemical thruster types are: cold gas thrusters, monopropellant thrusters, bipropellant thrusters, solid propellant thrusters.

Note: The scope of this text does not consider the history of the numerous on-orbit or Earth-to-orbit chemical propulsion systems.

1.14.1 On-orbit solar electric propulsion (SEP or simply EP) systems

These systems use electrical power provided by the spacecraft's solar panels to accelerate a propellant to high velocity creating a reaction which causes the movement of the spacecraft. Electric systems generate thrust by using electric and magnetic processes to heat and/or accelerate a propellant or plasma (charged particles). Electric thrusters have an exhaust velocity normally 2 to 10 times higher than chemical thrusters, which means their efficiency with respect to propellant usage is greater.

Although the thrust generated in this fashion is rather small, electric propulsion systems are not "energy limited" – they provide nonetheless the capability of raising a satellite's orbit and/or to maintain platform attitude – thereby offering the potential for considerably extended mission life times. Of course, the operational response of an electric propulsion system is constrained by the available electrical power provided the spacecraft's solar panels (a typical microsatellite might only be able to provide electrical power of < 100 W). The **high specific impulse of an electric propulsion system allows a much higher total Δv than a chemical propulsion system.** A further advantage of electric propulsion is spacecraft mass reduction: the fuel load on conventional propulsion systems is considerable for long-term missions; the consumable "fuel" of an electric propulsion system is rather small in comparison. The electric propulsion technology can also be used for missions requiring drag compensation.¹⁵⁶⁴ Several thruster technologies have been demonstrated or are being developed for demonstration.

A new era in space (secondary and/or primary) propulsion is evolving, gaining momentum in the late 1990s. Particular interest in electric propulsion comes from formation flight projects as well as from conventional satellite projects covering the entire breadth of satellite classes for enhanced support services. Only the very high specific impulse of electric ion propulsion will allow future commercial satellites to use more than 50% of their launch mass for payload, to put meaningful scientific payloads into orbit around distant planets like Mercury or the outer planets beyond the asteroid belt, and enable humans to remain in space for long periods of time and ultimately fly to our neighboring planet Mars.

1.14.1.1 Types of electric propulsion systems

In general, solar electric propulsion (SEP) involves the conversion of electrical energy into kinetic energy of the exhaust gases. The various thruster technologies are classified into three categories based on the method of accelerating the propellant – **electrothermal, electrostatic, and electromagnetic.** Of these, the electrostatic and electromagnetic concepts have the potential of being very propellant efficient, expressed by a high value of specific impulse (Isp).¹⁵⁶⁵

1) Electrothermal propulsion systems: arcjets, resistojets (simplest form of electric propulsion). In these systems, electromagnetic fields are used to generate a plasma to increase the heat of the bulk propellant. The propellant gas is heated to a higher temperature than can be obtained through combustion processes resulting in higher exhaust velocities and better propellant efficiency (acceleration is provided by electric propellant heating and thermodynamic gas expansion through a nozzle). Typical arcjet propellants are hydrazine (Isp = 5000 – 7000 m/s), hydrogen (Isp = 10,000 – 20,000 m/s), or ammonia. Resistojets operate by direct ohmic heating of the propellant. In arcjet systems, the methods of propellant heating are: DC current heating, AC current heating, RF heating, as well as laser-thermal heating. Arcjets have also been designed using either alternating or direct current. Pulsed arcjets, or PETs (Pulsed Electrothermal Thrusters), are similar to DC arcjets, except

¹⁵⁶⁴) I. J. E. Jordan, "Electric Propulsion: Which One For My Spacecraft?," http://www-int.stsci.edu/~jordan/other/electric_propulsion_3.pdf

¹⁵⁶⁵) M. LaPointe, "Solar Electric Propulsion," Proceedings of the Sixth Annual NASA Earth Science Technology Conference (ESTC 2006), College Park, MD, USA, June 27–29, 2006

that instead of a steady current, it pulses resulting from charge and discharge of the input capacitance.

2) EIP (Electrostatic ion propulsion): A device is considered “electrostatic” if the acceleration is caused mainly by the Coulomb Force, i.e application of a static electric field in the direction of the acceleration. EIP (electron bombardment ion, radiofrequency ion, field emission electric propulsion/colloid ion, and electron cyclotron resonance/microwave discharge ion thrusters). The EIP concept uses a high voltage electrostatic field to accelerate positively charged particles (or ions) to large exhaust velocities (acceleration is created by the force on charged particles in the electric field). Many electrostatic systems rely on a *gridded system* at the exhaust port for containing and producing the high electric field needed to accelerate the ions. Several types of ion thrusters have been developed: ¹⁵⁶⁶⁾ ¹⁵⁶⁷⁾

- Ion engine or **IPS (Ion Propulsion System)**. Positive ions are produced by bombarding neutral propellant atoms in a discharge chamber with thermionically excited electrons. Traditional ion engines use three closely separated perforated grids containing thousands of millimeter–sized holes attached to a chamber containing a reservoir of the charged particles. The first grid has thousands of volts applied, and the second grid operates at low voltage. The voltage difference over the gap between the two grids creates an electric field that acts to simultaneously extract and accelerate the ions out of the chamber and into space in a single step. The higher the voltage difference, the faster the ions are expelled and the greater the fuel efficiency of the thruster.

- **RIT (Radiofrequency Ion Thruster)**– or **gridded ion engine** (a metallic coil around the outside of the vessel is used to induce a radio frequency field inside the chamber). The RIT technique relies on ion creation by pumping a cavity with radio frequency radiation, usually in an insulated discharge chamber. The ions are then extracted through the exhaust port by an accelerator grid. Thrust levels in the range of tens of mN (milli Newton) have been demonstrated with the RIT–10, developed by the Institute of Physics at the University of Giessen and at EADS Astrium GmbH (Germany, formerly MBB). ¹⁵⁶⁸⁾

- The RF–ion thruster research started at Giessen University in 1962, focussing on a 10 cm diameter ionizer model technology. This RIT–10 type model went into industry (MBB at the time) in 1970. It’s first flight occurred in 1992 on the EURECA mission of ESA. This was followed by scaled–up versions of thrusters with ionizer diameters of: 15, 20, 22, 26, and 35 cm. – RIT advantages: Within the class of gas–discharge electric thrusters, the RF–type seems to be the most suitable for variable thrust levels (scaling–down), because it works without any discharge electrodes, magnetic pole shoes, etc. inside the ionizer. Newer RIT versions provide thrust levels of $\ll 1$ mN for minute thrust–level applications. The complete absence of discharge electrodes guarantees in effect a long life time of the thruster. ¹⁵⁶⁹⁾ ¹⁵⁷⁰⁾ ¹⁵⁷¹⁾

Since 2006, EADS Astrium and Giessen University (Germany) ¹⁵⁷²⁾ have been working on the development of a miniaturized ion engine system, called **RIT– μ X**, supported by ESA’s GST program and also by DLR. The system is especially designed for the demands of high

¹⁵⁶⁶⁾ D. G. Fearn, “Ion Thrusters: Future Technology Trends and Missions,” Proceedings of 54th IAC, Bremen, Germany, Sept. 29 – Oct. 3, 2003

¹⁵⁶⁷⁾ D. G. Fearn, “The Application of Gridded Ion Thrusters to High Thrust, High Specific Impulse Nuclear–Electric Missions,” Proceedings of IAC 2004, Vancouver, Canada, Oct. 4–8, 2004, IAC–04–R.4–S.7.09

¹⁵⁶⁸⁾ <http://nathanderweise.physik.uni-giessen.de/~dhasselk/Diverses/Loeb-Tab.html>

¹⁵⁶⁹⁾ H. W. Loeb, K.–H. Schartner, St. Weis, D. Feili, B. K. Meyer, “Development of RIT–Microthrusters,” Proceedings of IAC 2004, Vancouver, Canada, Oct. 4–8, 2004, IAC–04–S.4.04

¹⁵⁷⁰⁾ H. W. Loeb, J. Freisinger, K.–H. Groh, A. Scharmann; “State–of–the–Art of the RIT–Ion Thrusters and Their Spin–Offs”, IAF–88–258, 39th Congress, Bangalore, India, Oct. 8–15, 1988.

¹⁵⁷¹⁾ H. W. Löb; “Ein elektrostatisches Raketentriebwerk mit Hochfrequenzionenquelle”, *Astronautica Acta* VIII, 1.49, 1962

precision formation flying missions and the needs of fine and ultra-fine drag control. The projected flight date of the RIT- μ X system is 2014. ¹⁵⁷³⁾

- **Electrostatic colloid thruster.** With an electrostatic colloid thruster, droplets of a conductive liquid such as glycerol or sodium iodine are pumped through a needle at a high potential ($\sim 5-10$ kV).
- **FEEP (Field Emission Electric Propulsion).** The FEEP technique relies on a strong electric field, typically 8–15 kV (up to 10^9 V/m), to directly ionize the surface of a working fluid, typically a liquid metal (e.g. Caesium or Indium). The FEEP technology is the only existing thruster capable of accurate thrust modulation in the $1 \mu\text{N} - 1$ mN thrust level range. Typical thrust ranges from $1-100 \mu\text{N}$ are used for drag-free control while thrust levels up to 1 mN are used for small spacecraft AOCS, respectively.

The FEEP working principle is given in figure 3, where an additional external source of electrons (called neutralizer) needs to be included to maintain a balanced overall electrical charge of the system ($\text{ions}^+ = e^-$).

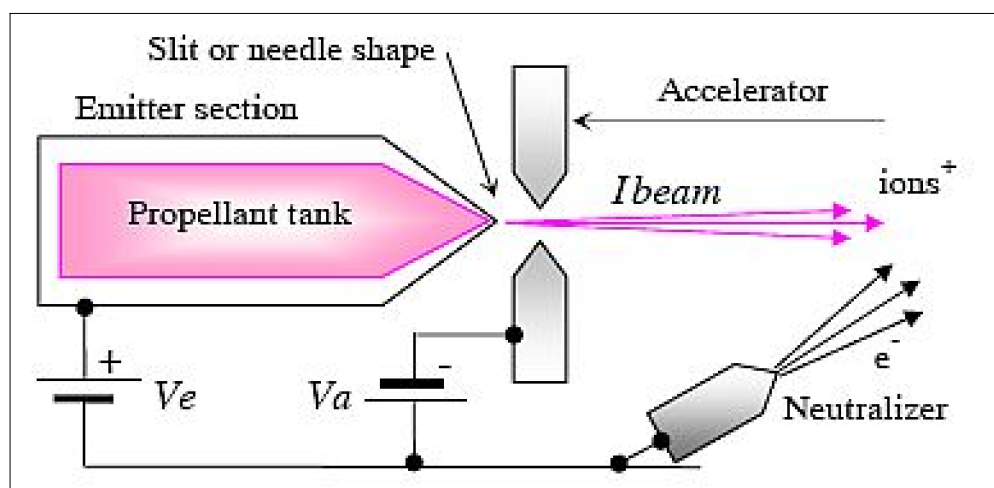


Figure 90: Schematic view of the FEEP propulsion concept (image credit: Galileo Avionica)

3) Electromagnetic propulsion systems (Hall effect, pulsed plasma, and magnetoplasma-dynamic thrusters). The propellant is ionized and accelerated by the combined interaction of electric and magnetic field forces on the resultant propellant plasma. – All electromagnetic techniques rely upon the production of plasma which is then accelerated to its exhaust velocity by an electromagnetic field to generate the desired thrust. A principle advantage of electromagnetic techniques over electrostatic ones is that plasmas with higher temperature and density (typically by several orders of magnitude) can be confined and directed. This results in higher exhaust velocities and therefore more efficient use of propellant mass. Major thruster types are:

- **HET (Hall-Effect Thruster).** ¹⁵⁷⁴⁾ The so-called **Hall effect** was discovered by the American physicist **Edwin H. Hall** in 1879 (1855–1938), then a graduate student at Johns Hopkins University in Baltimore, MD. In Hall effect thrusters, an axial electrical field and a radial magnetic field are established in the discharge chamber. All Hall thrusters are gridded accelerators which use the body forces on charges in crossed electric and magnetic

1572) Hans J. Leiter, Davar Feili, Benjamin Lotz, Davina Di Cara, Clive Edwards, “Development and Qualification of a Miniaturized Ion Engine System RIT- μ X for High Precision Orbital Maneuvers,” Proceedings of Space Propulsion 2010, San Sebastian, Spain, May 3–6, 2010

1573) Hans Leiter, Hartwig Ellerbrock, Davar Feili, Benjamin Lotz, “RIT- μ X – A New Advanced Miniaturized Ion Thruster System for Small Satellites,” 8th IAA (International Academy of Astronautics) Symposium on Small Satellites for Earth Observation, Berlin, Germany, April 4–8, 2011

1574) Hall discovered that a magnetic field would skew equipotential lines in a current-carrying conductor. This effect is observed as a voltage (Hall voltage) perpendicular to the direction of current in the conductor.

fields. The most common configurations in use have an axisymmetric cavity in which a radial magnetic field is generated by electromagnets with the field pointing to (or from) the surrounding coil/chamber body from (or to) an inner magnetic pole. Russia has been a long-time leader in the field of Hall thrusters. Typical usage is for orbit raising and station keeping maneuvers. Two types of HETs are in use: **SPT** (Stationary Plasma Thruster), the technique was mainly developed at the Design Bureau Fakel, and **TAL** (Thruster with Anode Layer), developed mainly at the Central Research Institute for Machine Building (TsNIIM-ASH).¹⁵⁷⁵⁾

In an SPT device, an electric field is established along the axis of the device with the anode located at the non-exhaust end of the ionization chamber and with the cathode located externally or at the exhaust end of the chamber. The applied electrostatic field accelerates the ions into the exhaust flow.

In a TAL thruster the ion production region is positioned more externally than in SPT units. Russia has been using SPT and TAL thrusters for decades (SPT-50, SPT-70, SPT-100, etc.) in such applications as NSSK (North South Stationkeeping), EWSK (East West Stationkeeping), attitude control, orbit injection, and repositioning of spacecraft.

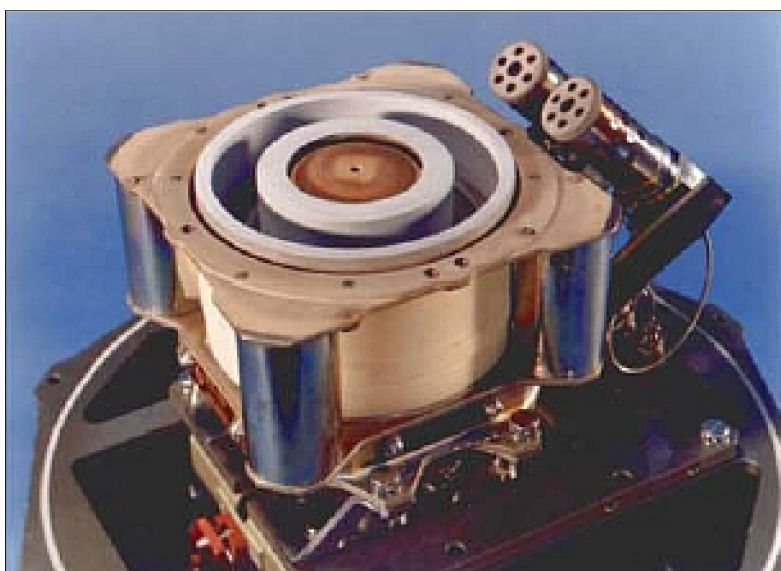


Figure 91: Photo of the SPT-100 thruster (image credit: Design Bureau Fakel)

Parameter	Resistojet	Arcjet	SPT (Stationary Plasma Thruster)	Ion Thruster
Propellant	N ₂ H ₄	N ₂ H ₄	Xenon	Xenon
Input electric power (kW)	0.2 – 0.8	0.5 – 2.0	0.15 – 1.5	0.4 – 2.0
Thrust (mN)	200 – 800	200 – 250	40 – 200	15 – 40
Specific Impulse, Isp (m/s)	2,700 – 3,000	4,500 – 6,000	16,000	28,000 – 35,000
Efficiency	0.9	0.33	0.48	0.75
Mission life (hours)	>390	>830	>4000	>8000

Table 81: Typical performance values of some electric propulsion systems

- **PPT** (Pulsed Plasma Thruster). The plasma is created by an arc discharge from a capacitor across a pair of electrodes. The ions in the plasma are then accelerated by the Lorentz force in the induced magnetic field. The PPT technique generates plasma by ablating a solid

¹⁵⁷⁵⁾ V. Kim, M. K. Konstantinov, V. A. Obukhov, G. A. Popov, I. P. Nazarenko, V. M. Murashko, A. V. Semenko, “Modern State and Problems of the Russian Electric Propulsion Development for the Future Missions,” Proceedings of the 60th IAC (International Astronautical Congress), Daejeon, Korea, Oct. 12–16, 2009, IAC-09.C4.4.3

block of spring–fed Teflon. PPTs are of particular interest for space exploration and exploitation since they essentially combine the advantage of continuously operated high–power MPD (Magneto Plasma Dynamic) thrusters with low average electric power consumption and manageable heat generation. Example: NASA’s EO–1 mission uses the PPT technique.

PPTs are considered an attractive propulsion option for stationkeeping and drag makeup purposes for mass– and power–limited satellites that require an impulse in the range of micro–Newton second (μNs) to milli–Newton second (mNs). The μPPT can deliver an impulse bit in the $10\ \mu\text{Ns}$ range to provide attitude control and stationkeeping for microsattelites. ¹⁵⁷⁶⁾

- **MPD** (Magneto Plasma Dynamic) thrusters. The MPD arcjet evolved from electrothermal arcjets and magnetogasdynamic technology and is sometimes referred to as a Lorentz Force Accelerator. The potential difference between electrodes ionizes the inflowing neutral gas. Once ionized, the plasma is accelerated by both Joule heating and electrodynamic forces. The current carrying plasma interacts with a magnetic field resulting in a Lorentz acceleration which expels the plasma. The Lorentz force provides the dominant acceleration mechanism.
- **ECR** (Electron Cyclotron Resonance) thruster. ECR is an electrode–less technique using a microwave waveguide to deliver the energy for ionizing a gas. Circularly polarized transverse–electric mode radiation is absorbed by the small population of free electrons constrained to move in cyclotronic paths within the plasma chamber in a magnetic field produced by an external surrounding solenoid.
- **HPT** (Helicon Plasma Thruster): A plasma propulsion engine is a type of electric propulsion that generates thrust from a quasi–neutral plasma. The new concept (early 21st century) for electrodeless plasma thruster is called HPT (Helicon Plasma Thruster). The helicon plasma discharge can be operated over wide ranges of external parameters (RF power, RF frequency in the range of MHz, operating gas pressures, magnetic field) and can yield high plasma densities in the $10^{12}–10^{13}\ \text{cm}^{-3}$ range. The system simply consists of an insulator source tube surrounded by a radiofrequency antenna and a magnetic nozzle, which can be produced by solenoids and/or permanent magnets. The recent experiment using a cylindrical source verified the enhancement of the thrust by the magnetic nozzle, due to a Lorentz force originating from an azimuthal plasma current in the applied radial magnetic field. The physics relating to the thruster performance, which is arising from the physical boundaries and the magnetic nozzle, have not been fully understood yet. ^{1577) 1578)}

The HPT is composed of the following parts (Figure 92). A cylindrical chamber, where plasma is produced, typically slender and made of dielectric material, i.e., Pyrex glass. A radio–frequency (RF) antenna wrapped around the chamber, that emits within the range 1–27 MHz, with a wide assortment of topologies: annular, Nagoya–III type, helical. The HPT presents some advantages when compared to other plasma thrusters (Hall effect thrusters, gridded ion thrusters...), such as the lack of electrodes, grids or neutralizers, which suggests the HPT concept to be reliable, simple and robust. ¹⁵⁷⁹⁾

So far, only prototypes of the HPT propulsion technique exist. But the HPT technology is increasingly being researched by the electric propulsion (EP) community due to their pro-

1576) M. Keidar, I. D. Boyd, E. L. Antonsen, R. L. Burton, G. G. Spanjers, “Optimization Issues for a Micropulsed Plasma Thruster,” *Journal of Propulsion and Power*, Vol. 22, No. 1, January–February 2006

1577) K. Takahashi, C. Charles, R. W. Boswell, A. Ando, “Helicon Plasma Thruster Experiment Controlling Cross–Field Diffusion within a Magnetic Nozzle,” *Proceedings of the 33rd International Electric Propulsion Conference (IEPC)*, Washington D.C., USA, Oct. 6–10, 2013, paper: IEPC–2013–163, URL: <http://www.iepc2013.org/get?id=163>

1578) Justin M. Little, Edgar Y. Choueiri, “Plasma transport in a converging magnetic field with applications to helicon plasma thrusters,” *Proceedings of the 33rd International Electric Propulsion Conference (IEPC)*, Washington D.C., USA, Oct. 6–10, 2013, paper: IEPC–2013–125, URL: <http://www.iepc2013.org/get?id=125>

1579) Jaume Navarro–Cavallé, Eduardo Ahedoy, Mario Merino, Victor Gómez, Mercedes Ruiz, José Antonio Gonzalez del Amo, “Helicon Plasma Thrusters: prototypes and advances on modeling,” *Proceedings of the 33rd International Electric Propulsion Conference (IEPC)*, Washington D.C., USA, Oct. 6–10, 2013, paper: IEPC–2013–285, URL: <http://www.iepc2013.org/get?id=285>

duction of high–density plasmas using moderate magnetic fields. Eventually, the HPT technique of electrodeless acceleration of plasma generated by RF waves may provide the foundation for a new class of high–efficiency, long–lifetime electric propulsion systems.

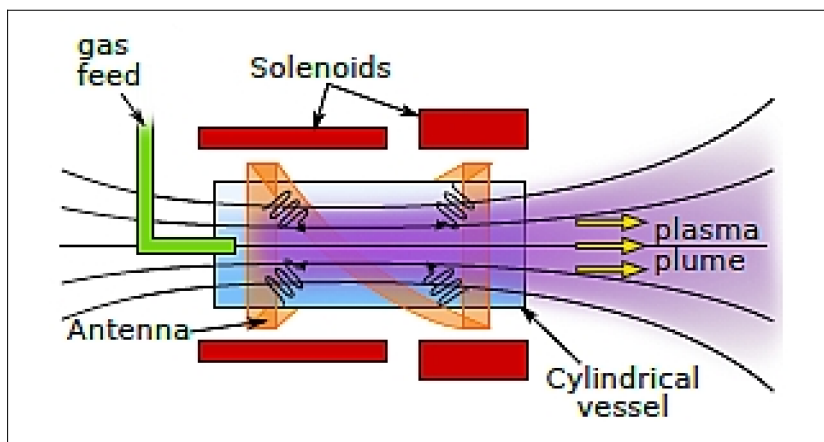


Figure 92: Sketch of the HPT with the main parts (image credit:

- **VASIMR** (Variable Specific Impulse Magnetoplasma Rocket). VASIMR is a high power, radio frequency–driven magnetoplasma rocket, capable of Isp/thrust modulation at constant power. The physics and engineering of this device have been under study since 1980. The plasma is produced in an integrated plasma injector by a helicon discharge. The system features a magnetic nozzle, which accelerates the plasma particles by converting their azimuthal energy into directed momentum. ¹⁵⁸⁰⁾

In a VASIMR® engine, gas such as argon, xenon, or hydrogen is injected into a tube surrounded by a magnet and a series of two radio wave (RF) couplers. The couplers turn cold gas into superheated plasma and the rocket’s magnetic nozzle converts the plasma thermal motion into a directed jet. ¹⁵⁸¹⁾

– NASA and AARC (Ad Astra Rocket Company) of Webster, TX signed the first Space Act Agreement in 2005 to privatize the VASIMR Technology. On March 2, 2011, Ad Astra and NASA/JSC (Johnson Space Center) have signed a Support Agreement to collaborate on research, analysis and development tasks on space–based cryogenic magnet operations and electric propulsion systems currently under development by Ad Astra. ¹⁵⁸²⁾

– First flight unit: The VF–200™ engine is the first flight unit of the VASIMR® engine. It will be tested on the ISS (International Space Station) where the thrust and performance can be measured without the limitations of ground–based space simulation chambers. The VF–200 will consist of two 100 kW thruster units side–by–side. As of June 2012, its launch is anticipated to be in 2015.

Some remarks on the units of the specific impulse:

In the International System of Units [SI], the unit of **specific impulse (Isp)** is **newton–seconds per kilogram or Ns/kg**. Hence, Isp is the impulse (a force applied for a second) exerted with 1 kg of propellant. It follows that the higher the specific impulse, the greater the performance of the engine and the less propellant required. The numerical value of the specific impulse also corresponds to the effective exhaust velocity (**m/s**) of the gas exiting the thruster in a vacuum. However, in the literature the Isp is widely expressed in units of

¹⁵⁸⁰⁾ Franklin R. Chang Díaz, Jared P. Squire, Roger D. Bengtson, Boris N. Breizman, F. Wally Baity, Mark D. Carter, “The physics and engineering of the VASIMR engine,” 36th AIAA/ASME/SAE/ASEE Joint Propulsion Conference, 17–19 July 2000, Huntsville, Alabama, USA, paper: AIAA 2000–3756, URL: http://spaceflight.nasa.gov/shuttle/support/researching/aspl/reference/2000_3756.pdf

¹⁵⁸¹⁾ <http://www.adastrarocket.com/aarc/VASIMR>

¹⁵⁸²⁾ “Variable Specific Impulse Magnetoplasma Rocket,” Wikipedia, URL: http://en.wikipedia.org/wiki/Variable_Specific_Impulse_Magnetoplasma_Rocket

pound–thrust per pound–weight per second, with a remaining unit of “seconds” for Isp. When comparing these “Isp second” values with those of the SI system, then the “Isp second” values have to be multiplied by the factor 9.81 m/s^2 to account for the pound–force to pound–mass ratio and to obtain the unit m/s of the SI system. In this documentation all Isp values are given in the SI system.

Type of electric engine	Input Power (W)	Isp (m/s)	Thrust (mN)	Manufacturer
Arcjet	750	4,700	115	IRS, University of Stuttgart, Germany
Resistojet	500	2,900	372	Primex, USA
Resistojet	600	2,150	270	SSTL, UK
Ion	740	29,000	28	MELCO, Japan
Ion	600	31,500	18	MMS, France
Hall	100	8,700	5.7	KeRC (Keldysh Research Center) Russia
Hall	200	13,700	11.7	KeRC, Russia
Hall	300	15,600	18.5	KeRC, Russia
Hall	600	14,500	36	Busek, USA
Hall	207	12,600	12.4	Busek, USA

Table 82: Performance parameters of some low–power electric propulsion systems ¹⁵⁸³⁾

The future of EP: At the start of the 21st century, electric propulsion is being considered/introduced in ever more space applications (mission types: EO, science, defense, commercial, etc.), and in all types of orbits from LEO, MEO, GEO, HEO, to deep space missions. Still, there is plenty of room left for new technology introduction. The goal is also to use electric propulsion systems in formation flight applications of constellations [a most demanding application is sparse aperture interferometry as used for the JWST (James Webb Space Telescope) spacecraft of NASA with ESA and CSA cooperation; and the LISA (Laser Interferometry Space Antenna) mission of ESA/NASA] requiring a considerable degree of position control. Furthermore, micropropulsion systems are being needed for a variety of applications from drag control to microsattellites. ¹⁵⁸⁴⁾ – The increasing use of EP on modern S/C introduces different operational requirements on the launcher than for conventional spacecraft. These requirements involve issues such as:

- Injection strategies
- Ground operation and control
- Relaxation of launch windows.

1.14.1.2 Introduction of HET technology

Research on **HET** (Hall–effect Thruster) technology started in the early 1960s notably in the Soviet Union. Research and development of an ablative PPT (Pulsed Plasma Thruster) technology had been started in the 1950s. ¹⁵⁸⁵⁾ ¹⁵⁸⁶⁾ ¹⁵⁸⁷⁾ The first spaceborne PPT system was flown on the Soviet satellite Zond–2 (launch Nov. 30, 1964). The Zond–2 S/C, on its

¹⁵⁸³⁾ K. Geelen, “A Trade Study Between Propulsion Methods for a Small Satellite Orbital Transfer Vehicle,” Proceedings of IAC 2004, Vancouver, Canada, Oct. 4–8, 2004, IAC–04–IAA.4.11.5.07

¹⁵⁸⁴⁾ G. Saccoccia, “Introduction to the European Activities in Electric Propulsion,” 28th International Electric Propulsion Conference (IEPC), Toulouse, France, March 17–21, 2003

¹⁵⁸⁵⁾ P. B. de Selding, “Sneema Wants 2004 Breakthrough for Plasma Propulsion Engine,” Space News Apr. 12, 2004, p. 6

¹⁵⁸⁶⁾ R. L. Burton, P. J. Turchi, “Pulsed PLasma Truster,” Journal of Propulsion and Power, Vol. 14, No 5, Sept. 1998

¹⁵⁸⁷⁾ V. Murashko, A. Korjakin, A. Narjatin, V. Kim, A. Romashko, O. Gorshkov, V. Garkusha, et al., “State–of–the–Art and Prospects of Electric Propulsion in Russia,” 28th International Electric Propulsion Conference, Toulouse, France, Mar. 17–21, 2003, paper IEPC–2003–340

way to Mars, was equipped with secondary electric thrusters. The Yantar–1 satellite (launch Oct. 1, 1966 from Kapustin Yar into a 400 km orbit), a Soviet military surveillance S/C built by TsKB, flew the first argon ion engine. In Feb. 1972, the Soviet Meteor–1–10 S/C (launch Dec. 29, 1971) was the first satellite to correct its orbit with an SPT engine. Since 1971, Soviet/Russian spacecraft (more than 20 missions) have been using low–power xenon plasma thrusters, referred to as SPT (Stationary Plasma Thrusters), for station–keeping and on–orbit maneuvering functions on the Express communication satellite series. The early SPT family engines (SPT–60 and SPT–70) were manufactured by EDB (Experimental Design Bureau) Fakel Company of Kaliningrad, Russia. 1588) 1589) 1590) 1591)

EDB is also a partner in the International Space Technology, Inc. (ISTI) joint venture (formed in 1993) that includes the Aerojet division of GenCorp of Sacramento, CA, SS/L (Space Systems/Loral) of Palo Alto, CA, and the SEP division of SNECMA, France. The objective of ISTI is to adapt Fakel thruster to Western–built satellites, in particular communication satellites. Fakel–based technology is even finding its way aboard US military satellites. LMSS (Lockheed Martin Space Systems) Co. of Sunnyvale, CA, has selected Fakel electric thrusters, provided by Aerojet, for use on the USAF AEHF (Advanced Extremely High Frequency) communication satellites.

A list of early Russian electric propulsion systems, used for NNSS stationkeeping, is given in Table 83. The design lifetime of M–70 (or SPT–70) is no less than 5,000 hours. So far, no thruster failure was reported. Since 1994 the SPT–100 are exploited in space with a nominal power of 83 mN and a specific impulse 1600 s.

Further SPT–100 thrusters are being used on the following GEO spacecraft: Telstar–8 (launch June 23, 2005), Intelsat–10–2 (launch June 17, 2004), Inmarsat–4 (launch June 25, 2001), GE Americom, iPSTAR–1 (launch Aug. 11, 2005), and MBSAT (launch March 12, 2004) of Japan’s Mobile Broadcasting Corporation.

Spacecraft	Orbit	Thruster type (quantity)	Launch date
Kosmos–1366 (Potok–1)	GEO	M–70 (4)	18.05.1982
Kosmos–1540 (Potok–2)	GEO	M–70 (4)	02.03.1984
Kosmos–1700 (Luch–1)	GEO	M–70 (4)	25.10.1985
Kosmos–1738 (Potok–3)	GEO	M–70 (4)	04.04.1986
Kosmos–1888 (Potok–5)	GEO	M–70 (4)	01.10.1987
Kosmos–1897 (Luch–2)	GEO	M–70 (4)	26.11.1987
Kosmos–1961 (Potok–6)	GEO	M–70 (4)	02.08.1988
Kosmos–2054 (Luch–4)	GEO	M–70 (4)	27.12.1989
Kosmos2085 (Potok–7)	GEO	M–70 (4)	19.07.1990
Kosmos–2172 (Potok–8)	GEO	M–70 (4)	22.11.1991
GALS–1	GEO	M–100 (8)	20.01.1994
Kosmos–2291 (Potok–9)	GEO	M–70 (4)	21.09.1994
Express–1	GEO	M–100 (8)	13.10.1994
Luch–3	GEO	M–70 (4)	16.12.1994
GALS–2	GEO	M–100 (8)	17.11.1995

1588) S. O. Tverdokhlebov, G. A. Popov, V. P. Kim, V. A. Obukhov, et al., “Overview of the Russian Electric Propulsion Activities,” 38th AIAA/ASME/SAE/ASEE Joint Propulsion Conference & Exhibit, Indianapolis, Indiana, USA, July 7–10, 2002, paper No AIAA–2002–3562

1589) Note: The original thruster series designation of Fakel Company was M–70, M–100, etc. The SPT (Stationary Plasma Thruster) designation came about in the 1990s to make the name and technology more understandable for western engineers involved in electric propulsion thrusters. While the M–70 and SPT–70 are the same product, the SPT–100 represents a modification of the M–100 thruster.

1590) O. Gorshkov, A. Shagayda, V. Muravlev, “The Experience of Hall Thruster Research and Development,” Proceedings of the 57th IAC/IAF/IAA (International Astronautical Congress), Valencia, Spain, Oct. 2–6, 2006, IAC–06–C4.4.08

1591) A. V. Semenkin (editor), N. A. Testoedov., E. N. Yakimov, Yu. M. Ermoshkin, D. V. Volkov, S. V. Yukseev, N. N. Sevast’yanov, V. I. Verkhoturov, S. Yu. Romano, R. M. Samitov, A. A. Borisenko, V. G. Ostrovsky, L. A. Makridenko, S. N. Volkova, B. P. Khodnenko, et al., “Overview of electric propulsion activity in Russia,” The 30th International Electric Propulsion Conference, Florence, Italy, September 17–20, 2007, URL: http://sgc.engin.umich.edu/erps/IEPC_2007/PAPERS/IEPC–2007–275.pdf

Spacecraft	Orbit	Thruster type (quantity)	Launch date
Kosmos–2319 (Potok–10)	GEO	M–70 (4)	30.08.1995
Luch–1	GEO	M–70 (4)	11.10.1995
Express–2	GEO	M–100 (8)	26.09.1996
Express–A–2	GEO	M–100 (8)	12.03.2000
SESAT (Eutelsat consortium)	GEO	SPT–100 (8)	18.04.2000
Potok–11	GEO	M–70 (4)	05.07.2000
Express–A–3	GEO	M–100 (8)	24.06.2000
Express–A–4	GEO	M–100 (8), T–120 (1)	10.06.2002

Table 83: Communication S/C of NPO PM, Russia, with SPT electric propulsion systems

- The **HET** (Hall–effect Thruster) technology has been under intensive [governmental and industrial (TsNIIMASH)] investigation in Russia since the early 1990s (see Table 83).
 - The first US spacecraft with a Hall thruster is the STEX (Space Technology Experiment) mission of NRO (launch Oct. 3. 1998, end of mission in June 2000). STEX was flying **EPDM** (Electric Propulsion Demonstrator Module), developed by NASA/GRC, to provide orbit–raising and station–keeping functions (see O.12.2). The TAL–D55 (Thruster with Anode Layer) Hall–effect thruster used in EPDM was developed by the Russian Central Research Institute of Machine Building (TsNIIMASH).
 - The ESA mission SMART–1 (Small Mission for Advanced Research in Technology) to the moon with a launch Sept. 27, 2003, employs the HET/STS (Hall–Effect Thruster/Stationary Plasma Thruster) concept, referred to as PPS–1350–G, **to use electric propulsion as the primary engine of the S/C on an interplanetary mission**. The thruster assembly can be throttled for variable thrust generation: input power of 462 – 1190 W; variable thrust range of 30–90 mN, Isp of 10,000–16,000 m/s. The PPS–1350–G constitutes the primary propulsion of SMART–1 (370 kg minisatellite) to escape Earth’s gravity for its 16–month cruise to the moon and to stay in lunar orbit for six months. As of Sept. 17, 2005, the PPS–1350–G was shut down (in moon orbit) thus ending all electric propulsion operations of the mission. It had accumulated 4958.3 hours of active firing using a total of 82.5 kg of Xenon fuel.
 - The PPS–1350 electric propulsion engine ^{1592) 1593) 1594) 1595)} (a model with a lower thrust than the PPS–1350–G version) of SNECMA Moteurs (Paris, France) along with a SPT–100 thruster of Fakel, Kaliningrad, Russia, had also been installed on France’s Stentor communication technology demonstration satellite. Unfortunately, a launch failure of Ariane–5ECA occurred on Dec. 11, 2002 with Stentor as payload (fault of Vulcain 2 exhaust nozzle).
- HiPER (High Power Electric propulsion: a Roadmap for the future) is a project co–funded by the European Union (EU) under the space theme of the 7th Framework Program. Its objectives are to assess several innovative Electric Space Propulsion technologies to fulfill future space transportation and space exploration needs. ¹⁵⁹⁶⁾ Three different EP concepts are considered as the candidates with the highest application potential: Hall Effect Thruster (HET), Gridded Ion Engines (GIE) and Magneto Plasma Dynamic Thrusters (MPDT). – Among the possible options, high power HETs are addressed and a 20 kW HET prototype is to be designed, manufactured and tested in the frame of the HiPER project. The 20 kW prototype will be manufactured and tested in 2011.

1592) G. Racca, B. Foing, “The SMART–1 Mission,” ESA Bulletin 113, Feb. 2003, pp. 14–21

1593) C. R. Koppel, D. Estublier, “SMART–1 Primary Electric Propulsion Sub–System, The Flight Model,” 28th IEPC, Toulouse, France, March 17–21, 2003, paper No 205

1594) D. Estublier, C. Koppel, “SMART–1 EPS End–to–End Test: Final Results & Lessons Learnt,” 28th International Electric Propulsion Conference (IEPC), Toulouse, France, March 17–21, 2003

1595) P. Dumazert, S. Lagardère–Verdier, F. Marchandise, et al., “PPS®–1350–G Qualification Status, March 2003, IEPC 2003, Toulouse, France, March 17–21, 2003

1596) S. Zurbach, J. L. Pattyn, N. Cornu, P. Lasgorceix, “HiPER: A High Power 20 kW Hall Effect Thruster for Exploration,” Proceedings of Space Propulsion 2010, San Sebastian, Spain, May 3–6, 2010

1.14.1.3 Examples of electrothermal propulsion systems (arcjets, resistojets)

Electrothermal (arcjet) engines and thrusters have been around since the mid 1960s. However, only since about the 1990s have these devices gained some popularity due to the decrease in mass of the power conditioning systems and improved performance of the thrusters.

- ARGOS of DoD (SMC/TE at Kirtland AFB, NM), launch Feb. 23, 1999. The spacecraft uses arcjet propulsion technology for orbit transfer, maneuvering capability, and attitude adjustment. The electric propulsion system is ESEX (Electric Propulsion Space Experiment), built by TRW. Demonstration of the largest electric propulsion system (26 kW of power input) so far (orbit raising). The ESEX system employs an ammonia arcjet.
- UoSAT-12, the first minisatellite of Surrey (launch April 21, 1999), employs a resistojet electric propulsion system. The thruster can impart velocity changes of up to 10 m/s to the spacecraft.
- SNAP-1 (launch Jun. 28, 2000),¹⁵⁹⁷⁾ ¹⁵⁹⁸⁾ an SSTL nanosatellite of 8.3 kg total mass using a microthruster of 30 μ N with a Δv capacity of 3 m/s. The SNAP-1 micro-propulsion system, the size of a pencil, is also using butane as a cold gas system (note: butane and xenon are considered “green” propellants). The propulsion system is used to maneuver SNAP-1 to rendezvous with Tsinghua-1 of the University of Beijing (see D.62.17 and D.62.18).
- The AMSAT-P-3D [Amateur Satellite-Phase-3D, now called AMSAT-Oscar 40 (AO-40), launch Nov. 15, 2000 from Kourou into HEO (Molniya-type orbit)] spacecraft employs a low-power arcjet thruster by the name of ATOS (Arcjet Thruster on OSCAR Satellite) for on-orbit fine control of the S/C (also for orbit-raising and inclination control.). ATOS was developed at IRS (Institut für Raumfahrtsysteme) of the University of Stuttgart, Germany and funded by DLR. ATOS is a 750 W ammonia arcjet with a specific impulse Isp of 4600 m/s. Orbit maneuvers are achieved by a separate 400 N chemical thruster.
- AlSat-1 (Algeria Satellite-1) is a microsatellite of CNTS (Centre National des Techniques Spatiales), Arzew, Algeria. The S/C was developed and built at SSTL (launch Nov. 28, 2002) and is the first S/C in the DMC (Disaster Monitoring Constellation) of SSTL, Surrey, UK. AlSat-1 carries a resistojet microthruster using 15 W redundant heaters and using butane as propellant. Naturally, the follow-up S/C of DMC, namely BilSat-1 (Turkey), NigeriaSat-1 (Nigeria), and UK-DMC (UK), with a common launch Sept. 27, 2003, feature also resistojet propulsion. In addition, there is a resistojet on Beijing-1 (China DMC+4) with a launch on Oct. 27, 2005.¹⁵⁹⁹⁾ ¹⁶⁰⁰⁾
- The DRTS (Data Relay Test Satellite) of JAXA, Japan, was launched on Sept. 12, 2002 into GTO. A hydrazine AKE (Apogee Kick Engine) brought the S/C into GEO. The dual-mode UPS (Unified Propulsion Subsystem) of DRTS consists of the AKE (20 N thrusters, 1 N thrusters) and a pair of DC arcjet thruster systems for north-south stationkeeping tasks. The DC arcjet system (GenCorp/Aerojet, USA, model: MR-509A/509B) consists of thrusters, PPU (Power Processing Unit), and power cables. Electric power (1.88 kW) is supplied by solar panels through the NiH₂ battery. The system has a specific impulse of 5,000 m/s (4,500 m/s average). The DC arcjet system has a mass of 30.7 kg (see Ref. 1611). The Japanese name of DRTS is “Kodama” (“echo”).

¹⁵⁹⁷⁾ D. M. Gibbon, J. Ward, N. Kay, “The Design, Development and Testing of a Propulsion System for the SNAP-1 Nanosatellite,” 14th AIAA/USU Conference on Small Satellites, Logan, UT, Aug. 21–24, 2000

¹⁵⁹⁸⁾ A. M. Baker, A. da Silva Curiel, J. Schaffner, M. Sweeting, “Advanced Low Cost Propulsion Concepts for Small Satellites Beyond LEO,” Proceedings of IAC 2004, Vancouver, Canada, Oct. 4–8, 2004, IAC-04-IAF-S.1.08

¹⁵⁹⁹⁾ D. Gibbon A. Baker, I. Coxhill, M. Sweeting, “The Development of a Family of Resistojet Thruster Propulsion Systems for Small Spacecraft,” AIAA/USU Conference on Small Satellites, Logan, UT, Aug. 11–14, 2003

¹⁶⁰⁰⁾ D. Nicolini, D. Robertson, E. Chesta, G. Saccoccia, D. Gibbon, A. Baker, “Xenon Resistojets as Secondary Propulsion on EP Spacecrafts and Performance Results of Resistojets using Xenon,” 28th IEPC Conference, Toulouse, France, March 17–21, 2003

- PPT (Pulsed Plasma Thruster) systems:
 - The LES–6 (Lincoln Experimental Satellite–6), designed and built by MIT/LL in Lexington, MA, was launched from Cape Canaveral on Sept. 26, 1968. The DoD spacecraft with a mass of 163 kg flew a PPT propulsion system (positioned in GEO). A further demonstration of PPT technology took place on LES–9 with a launch on March 15, 1976.
 - The navigation satellites of the US Navy (designed and built by JHU/APL), ¹⁶⁰¹⁾ ¹⁶⁰²⁾ namely Triad–2 (also referred to as TIP–2, launched Oct. 11, 1975) and Triad–3 (TIP–3, launched Sept. 1, 1976), were each equipped with a redundant pulsed–plasma thruster (PPT) electric propulsion system, used for drag compensation (drag–free satellite). Three more NOVA satellites, nearly identical to the TIP design, used a PPT propulsion system to compensate for drag. NOVA–1 launch May 15, 1981; NOVA–3 launch Oct. 12, 1984; NOVA–2 launch June 16, 1988.
 - EO–1 (Earth Observing–1) of NASA/GSFC (launch Nov. 21, 2000). A PPT (Pulsed Plasma Thruster) from Aerojet of General Dynamics/OTS (Ordinance and Tactical Systems) Aerospace Operations [formerly Primex Aerospace (formerly Olin (formerly Rocket)] is used to demonstrate on–orbit electromagnetic propulsion technology and to provide a spacecraft precision–pointing capability (complete pitch axis control of the S/C). This is the first flight demonstration of an operations support with PPT throttling capability (see M.12.2).

1.14.1.4 Some background on ion propulsion history:

Although the first viable and practical applications of ion propulsion systems on spacecraft were introduced fairly late in the 20th century (around 1980), the ideas on the topic of ion propulsion go back to 1906 when the US student at Worcester Polytechnic Institute (and later rocket pioneer), Robert H. Goddard (1882–1945), first suggested the possibility of accelerating electrically charged particles to very high velocities without the need for high temperatures. The first experiments with ion thrusters were carried out by Robert Goddard at Clark College from 1916–1917. ¹⁶⁰³⁾

- In 1929, the German physicist, Hermann J. Oberth (1894–1989), had published “Wege zur Raumschiffahrt” (Ways to Spaceflight) where he explained his thoughts on the mass savings of electric propulsion, predicted its use in spacecraft propulsion and attitude control, and advocated electrostatic acceleration of charged gases. Oberth was the first to define EP as a serious and worthy pursuit in astronautics – bringing his ideas into the minds of science fiction writers and scientists. ¹⁶⁰⁴⁾ ¹⁶⁰⁵⁾
- The Russian engineer Valentin P. Glushko (1908–1989) was a pioneer of electric propulsion. ¹⁶⁰⁶⁾ ¹⁶⁰⁷⁾ While attending the St. Petersburg State University (1925–1929) he had the idea of designing an interplanetary spacecraft powered with electric engines. However, in 1929 he started his career at the St. Petersburg GDL (Gas Dynamics Laboratory), who

¹⁶⁰¹⁾ W. L. Ebert, S. J. Kowal, R. F. Sloan, “Operational Nova Spacecraft Teflon Pulsed Plasma Thruster System,” AIAA 89–2497, July 1989

¹⁶⁰²⁾ W. D. Deininger, W. A. Hoskins, R. L. Burton, et al., “Pulsed Plasma Thruster System for Precision Formation Flying,” Proceedings of International Symposium Formation Flying Mission & Technologies, Oct. 29–31, 2002, Toulouse, France

¹⁶⁰³⁾ E. Y. Coueiri, “A Critical History of Electric Propulsion: The First 50 Years (1906–1956),” Journal of Propulsion and Power, Vol. 20, No 2, March–April 2004, URL: <http://alfven.princeton.edu/papers/choueiriJPP04a.pdf>

¹⁶⁰⁴⁾ “Ion Propulsion – Over 50 years in the Making,” NASA, 1999, URL: http://science.nasa.gov/newhome/headlines/prop06apr99_2.htm

¹⁶⁰⁵⁾ http://en.wikipedia.org/wiki/Ion_thruster

¹⁶⁰⁶⁾ <http://www.astronautix.com/astros/glushko.htm>

¹⁶⁰⁷⁾ V. S. Sudakov, V. K. Chvanov, “Academician Glushko – pioneer and creator of soviet rocket engineering,” Proceedings of the 59th IAC (International Astronautical Congress), Glasgow, Scotland, UK, Sept. 29 to Oct. 3, 2008, IAC–08.E4.2.7

were the builders of the earliest Russian liquid rocket engines. From 1974–1989, Glushko was the chief designer of NPO Energia.

- Ernst Stuhlinger (1913–2008), a German rocket scientist who immigrated after WW–II to the United States as part of the 'Operation Paperclip', developed guidance systems in Wernher von Braun's team. Stuhlinger had published several papers on ion propulsion starting in 1954. In particular, he authored the classic textbook "Ion Propulsion for Space Flight", McGraw–Hill, New York, 1964 – when he served as the first director of the space science lab at NASA's Marshall Space Flight Center in Huntsville, ALA. Stuhlinger's work laid the foundation for using EP to send probes into deep space decades later.

Edgar Coueiri of Princeton University (Ref. 1603) labels the various thematic eras of electric propulsion history in the following way:

- 1) The Era of Visionaries: 1906–1945
- 2) The Era of Pioneers: 1946–1956
- 3) The Era of Diversification and Development: 1957–1979
- 4) The Era of Acceptance: 1980–1992
- 5) The Era of Application: 1993–present

Early studies of **EIP** (Electrostatic Ion Propulsion) systems began in the 1950s at LeRC (Lewis Research Center, now NASA/GRC) and the first ion engine was built in 1959 by Harold Kaufman. The first demonstrations in this thruster class were flown on early NASA missions: SERT–1 (Space Electric Rocket Test–1) from Wallops Island on a Scout rocket (launch of SERT–1 July 20, 1964, a suborbital flight); and with SERT–2 (launch Feb. 4, 1970) from VAFB, CA on a Thor Agena vehicle. SERT 2 carried two ion thrusters, one operating for more than five months and the other for nearly three months. Extended ion thruster restarts from 1973 to 1981 were conducted, in addition to cross–neutralization tests. SERT 1 carried one mercury and one cesium engine, while SERT 2 had two mercury engines. ¹⁶⁰⁸⁾ ¹⁶⁰⁹⁾

However, the EIP technology only reached full operational status in the 1990s. The NSTAR development for the DS1 mission (see below) is a prominent example of the use of EIP techniques in space.

- SCATHA (Spacecraft Charging at High Altitude) S/C of the USAF (launch Jan. 30, 1979) flew the first xenon ion engine, built by Hughes Research Laboratories, Malibu, CA. Hughes started development work on ion engines already in the 1960s.
- The ETS–III (Engineering Test Satellite–III; also referred to as Kiku–4) of JAXA (formerly NASDA) demonstrated the first on–orbit operation of a Japanese–developed IES (Ion Engine System) in 1983 (launch of ETS–III on Sept. 3, 1982 from Tanegashima Space Center, Japan). IES, with two electron bombardment mercury ion thrusters of 5 cm anode diameter, was flight tested during the extended mission period from Sept. 1983 to March 1985. ¹⁶¹⁰⁾
- ETS–VI (Engineering Test Satellite –VI; launch Aug. 24, 1994) ¹⁶¹¹⁾ and COMETS (Communications and Broadcasting Engineering Test Satellite; launch 1998) of NASDA, Japan. Both S/C carried an IES (Ion Engine System) for north–south stationkeeping tasks. However, both satellites failed to reach a geostationary orbit because of a malfunctioning

¹⁶⁰⁸⁾ <http://www.nasa.gov/centers/glenn/about/history/sert.html>

¹⁶⁰⁹⁾ J. S. Sovey, V. K. Rawlin, M. J. Patterson, "Ion Propulsion Development Projects in U. S.: Space Electric Rocket Test 1 to Deep Space 1," *Journal of Propulsion and Power*, Vol. 17, No. 3, May–June 2001, pp. 517–526.

¹⁶¹⁰⁾ S. Kitamura, H. Nagano, Y. Nakamura, I. Kudo, K. Machida, "ETS–III Ion Engine Flight Operations in the Extended Mission Period," *Journal of Propulsion and Power*, Vol. 2, No. 6, 1986, pp. 513–520.

apogee kick engine and/or launch vehicle failure. Therefore, both ion engine systems were operated as an experiment.

- DS1 (Deep Space 1) mission of NASA/JPL (launch Oct. 24, 1998) employs IPS (Ion Propulsion System), designed and built by the NSTAR team [the IPS is also referred to as NSTAR (NASA SEP Technology Application Readiness)]. NSTAR was built by Boeing ETI (Electron Technologies Inc.) for NASA/GRC and NASA/JPL. It is the first time that IPS technology was demonstrated as the **spacecraft's primary engine** (smooth and continuous IPS operation from Nov. 24, 1998 for over 200 days) throughout the prime mission which ended in Sept. 1999 (total IPS operation time of about 3000 hours). This was followed by the Extended Mission in which IPS accumulated a total of 16,265 hours of operation and processed approximately 72 kg of xenon. At the end of the Extended Mission for DS1, which successfully flew by the comet Borrelly (flyby on Sept. 22, 2001), NASA executed the Hyper-Extended Mission that was designed to evaluate the wear on the ion engine after extended operation in space.

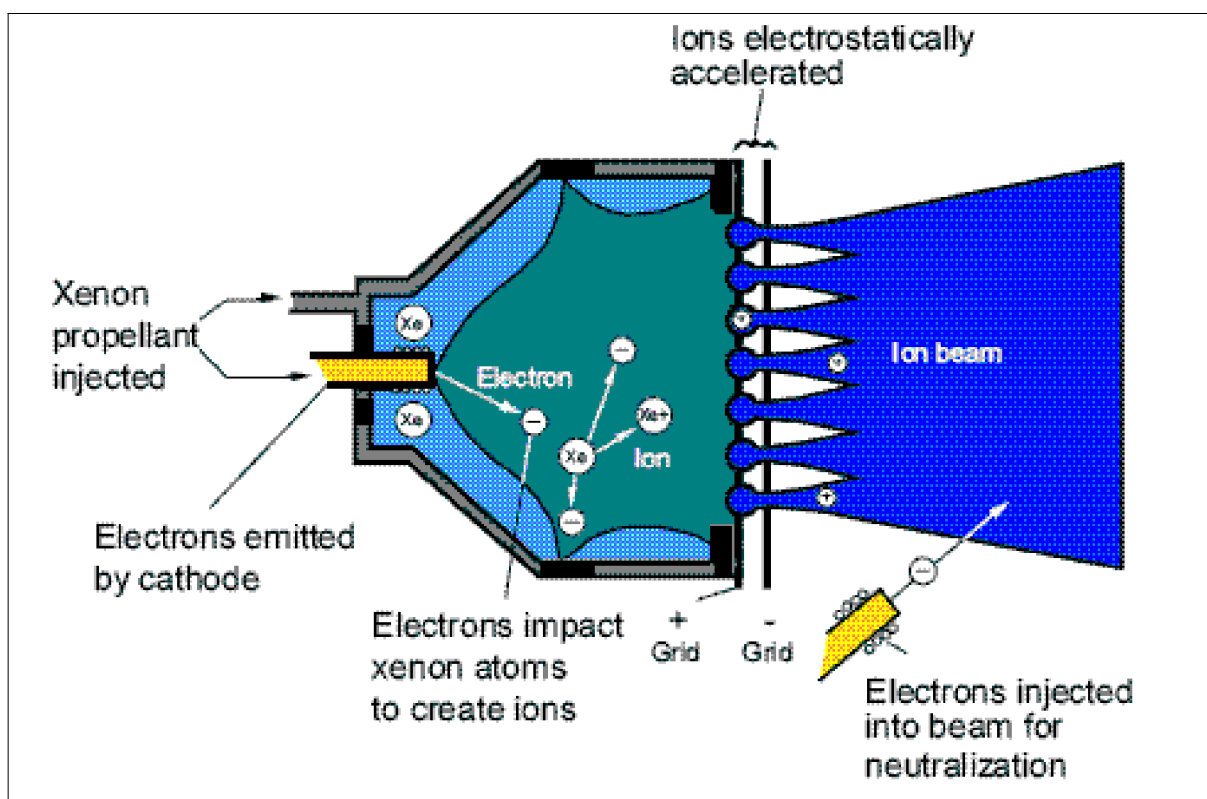


Figure 93: Schematic illustration of the NSTAR/IPS engine on DS1 (image credit: NASA)

- The Dawn spacecraft in NASA's Discovery Program was launched on Sept. 28, 2007 with NSTAR electric propulsion onboard to explore the asteroid Vesta and the dwarf planet Ceres. The dramatic success of Dawn in achieving, supporting, and then departing from its 2012 rendezvous with the asteroid Vesta, demonstrated the unique value that SEP (Solar Electric Propulsion) has for NASA planetary science, by enabling missions that are too challenging and too expensive to conduct using other methods. Dawn will reach its second rendezvous target Ceres in February 2015, fourteen years after it was first proposed.

- The NEXT (NASA's Evolutionary Xenon Thruster) is an evolutionary design/development program of an ion propulsion system (based on NSTAR) by NASA/GRC which started

in 2001.¹⁶¹²⁾ ¹⁶¹³⁾ The NEXT system consists of a high performance, 7 kW ion thruster; a high-efficiency, a power processor unit (PPU); a flexible xenon propellant management system (PMS); a lightweight engine gimbal; and key elements of a digital control interface unit (DCIU) including software algorithms. The NEXT ion propulsion system is a throttleable gridded ion thruster propulsion system (0.6–7 kW) suitable for future Discovery, New Frontiers, and Flagship missions.¹⁶¹⁴⁾ ¹⁶¹⁵⁾

Characteristic	NSTAR	NEXT	Benefit
Max thruster power Max thrust	2.3 kW 91 mN	6.9 kW 236 mN	Enables high power missions (outer planet) with fewer thruster strings
Throttling Range (Max/ Min Thrust)	4.9	13.8	Allows use over broader range of distances from sun
Max Isp (Specific Impulse)	3120 s	4190 s	Reduces propellant mass, thus enabling more payload and/or lighter spacecraft
Total impulse (10 ⁶ Ns) Propellant throughput	4.6 150 kg	> 18 450 kg	Enables low power, high ΔV Discovery–class missions with a single thruster
Max thrust efficiency	> 61 %	> 70%	Reduces power & thermal management requirements
Max PPU efficiency	92%	95%	Reduces mass & thermal management requirements.

Table 84: Performance characteristics of NSTAR vs NEXT

In 2008, the NEXT project is completing one of the final milestones of the effort, that is operation of an integrated NEXT Ion Propulsion System (IPS) in a simulated space environment. At this point, NEXT is ready for flight development.

– In 2010, the NEXT project has brought next-generation ion propulsion technology to a mature state (complete technology validation by the end of 2011).¹⁶¹⁶⁾

The NEXT PM Prototype Model) thruster completed a short duration test in which overall ion-engine performance was steady with no indication of performance degradation. A NEXT PM thruster has also passed qualification level environmental testing. As of Sept. 30, 2010 the LDT (Long Duration Test) of the NEXT engineering model (EM) thruster achieved over 525 kg xenon throughput, 1.95×10^7 Ns of total impulse, and > 31,800 hours at multiple throttle conditions. The NEXT LDT wear test demonstrates the largest total impulse ever achieved by a gridded-ion thruster. The ISPT funding for the thruster life test continues through FY12 with the aim of demonstrating up to 750 kg of xenon throughput.¹⁶¹⁷⁾

– *In June 2013, the NEXT ion propulsion engine* ¹⁶¹⁸⁾ ¹⁶¹⁹⁾ *has successfully operated for more than 48,000 hours, or 5 1/2 years, making it the longest test duration of any type of space propulsion system demonstration project ever. NASA/GRC manufactured the test engine's core ionization chamber. During the endurance test performed in a high vacuum test chamber at*

¹⁶¹²⁾ E. J. Pencil, "An Overview of Recent Developments in Electric Propulsion for NASA Science Missions," Proceedings of the 2008 IEEE Aerospace Conference, Big Sky, MT, USA, March 1–8, 2008, paper: 8.1503

¹⁶¹³⁾ S. W. Benson, M. J. Patterson, "Development Status of NEXT: NASA's Evolutionary Xenon Thruster," 28th IEPC (International Electric Propulsion Conference), Toulouse, France, March 17–23, 2003

¹⁶¹⁴⁾ G. R. Schmidt, M. J. Patterson, S. W. Benson, "The NASA Evolutionary Xenon Thruster (NEXT): The NEXT Step for U.S. Deep Space Propulsion," Proceedings of the 59th IAC (International Astronautical Congress), Glasgow, Scotland, UK, Sept. 29 to Oct. 3, 2008, IAC-08.C4.4.2

¹⁶¹⁵⁾ D. A. Herman, G. C. Soulas, M. J. Patterson, "NEXT Long-Duration Test after 11,570 h and 237 kg of Xenon Processed," 30th International Electric Propulsion Conference, Florence (IEPC 2007), Italy Sept. 17–20, 2007, URL: http://sgc.engin.umich.edu/erps/IEPC_2007/PAPERS/IEPC-2007-033.pdf

¹⁶¹⁶⁾ George R. Schmidt, Michael J. Patterson, Scott W. Benson, "NASA's Evolutionary Xenon Thruster (NEXT): Development Status and Future Mission Applications," Proceedings of Space Propulsion 2010, San Sebastian, Spain, May 3–6, 2010

¹⁶¹⁷⁾ David J. Anderson, Eric Pencil, Todd Peterson, John Dankanich, Michelle M. Munk, "In-Space Propulsion Technology Products for NASA's Future Science and Exploration Missions," 2011 IEEE Aerospace Conference, Big Sky, MT, USA, March 5–12, 2011

¹⁶¹⁸⁾ Dwayne Brown, Katherine K. Martin, Glenn Mahone, "NASA Thruster Achieves World-Record 5+ Years of Operation," NASA Release 13–193, URL: <http://mabsi2.blogspot.de/2013/06/nasa-thruster-achieves-world-record-5.html>

Glenn, the engine consumed ~ 870 kg of xenon propellant, providing an amount of total impulse that would take more than 10,000 kg of conventional rocket propellant for comparable applications. Aerojet Rocketdyne of Sacramento, CA, designed and built the ion acceleration assembly. — The test run will be terminated voluntarily by the end of June with the thruster fully operational. Life and performance have exceeded the requirements for any anticipated science mission.

– October 2013: The NEXT LDT (Long Duration Test) was initiated in June 2005 to demonstrate throughput capability and validate thruster service life modeling. The NEXT LDT exceeded its original qualification throughput requirement of 450 kg in December 2009. To date, the NEXT LDT has set records for electric propulsion lifetime and has demonstrated 50,170 hours of operation, processed 902 kg of propellant, and delivered 34.9 MNs of total impulse. ¹⁶²⁰⁾

• The ARTEMIS data relay satellite of ESA in GEO ¹⁶²¹⁾ (launch July 12, 2001), built by Alenia Spazio of Rome, Italy, includes also a xenon electric propulsion thruster system (redundant systems: RITA (Radio–frequency Ion Thruster Assembly) built by EADS Astrium GmbH, Ottobrunn, Germany, and EITA (Electron–bombardment Ion Thruster Assembly) built by QinetiQ, UK. The RIT–10 system, a predecessor of RITA, was already test–flown on the EURECA–1 mission (launch July 31, 1992 – retrieval of EURECA, July 1, 1993). ¹⁶²²⁾

ARTEMIS rescue mission: ARTEMIS is the first spacecraft in history whose mission was salvaged by the availability of electric propulsion (flexible propulsion architecture using bi–propellant and ion propulsion). ¹⁶²³⁾ ¹⁶²⁴⁾ An upper stage malfunction of Ariane–5 resulted in a useless orbit with a perigee of 592 km, an apogee of 17,518 km, and an inclination close to 3° (the nominal GTO called for a perigee of 857 km, an apogee of 35,837 km, and an inclination of about 2°). The failure orbit represented a shortfall of about 500 m/s in injection velocity. — The liquid apogee kick motor then raised the orbit into a 31,000 km circular parking orbit (5 near–perigee and 3 apogee maneuvers were performed, with sufficient fuel left for S/C east–west stationkeeping and attitude control using a 10 N RCS over the design life), and still about 5000 km short in altitude to GEO. The parking orbit was achieved on Aug. 24, 2001.

The final orbit raising maneuver employed an IPP (Ion Propulsion Package), carried on board for north–south stationkeeping and maintenance functions and not for any orbit boost functions of the S/C. In stationkeeping configuration, the thrust direction of the ion engines is perpendicular to the orbital plane. The rescue operation, however, required thrust to be generated in the orbital plane. This could only be realized by rotating the satellite in the orbital plane by 90° with respect to its nominal orientation. The actual ion–propulsion phase started on April 4, 2002 using a single functional ion thruster (RITA) and gaining between 12–14 km of altitude every day; the final geostationary orbit at about 36 000 km was reached by the end of January, 2003. This is a remarkable accomplishment of ion propulsion considering the S/C launch mass of 3,100 kg (550 kg payload, and 1,538 kg of bi–propellant).

All orbit raising maneuvers were performed by a dedicated team of ESA, Alenia Spazio S. p. A., and EADS Astrium GmbH at the Telespazio center in Fucino, Italy. The deorbiting maneuvers

1619) Dwayne Brown, Katherine K. Martin, Glenn Mahone, “NASA Thruster Achieves World–Record 5+ Years of Operation,” NASA, Aerojet Rocketdyne, June 24, 2013, URL: <http://www.rocket.com/article/nasa–thruster–achieves–world–record–5–years–operation>

1620) Rohit Shastry, Daniel A. Herman, George C. Soulas, Michael J. Patterson, “Status of NASA’s Evolutionary Xenon Thruster (NEXT) Long–Duration Test as of 50,000 h and 900 kg Throughput,” Proceedings of the 33rd International Electric Propulsion Conference (IEPC), Washington D.C., USA, Oct. 6–10, 2013, paper: IEPC–2013–121, URL: <http://www.iepc2013.org/get?id=121>

1621) L. Mazzini, V. Tamilia, “The ARTEMIS Unexpected Trip to GEO Orbit,” 5th International ESA Conference on Guidance Navigation and Control Systems, Frascati, Italy, Oct. 22–25, 2002, ESA SP–516

1622) “ARTEMIS,” ESA brochure BR–220, Feb. 2004, <http://www.esa.int/esapub/br/br220/br220.pdf>

1623) R. Killinger, H. Gray, R. Kukies, M. Surauer, G. Saccoccia, A. Tomasetto, R. Dunster, “ARTEMIS Orbit Raising In–Flight Experience with Ion Propulsion,” 28th International Electric Propulsion Conference (IEPC), Toulouse, France, March 17–21, 2003

1624) G. Oppenhäuser, A. G. Bird, “ARTEMIS Finally Gets to Work,” ESA Bulletin 114, May 2003, pp. 50–53

of the S/C after mission end (a design life time of 10 operational years) will make use of the ion propulsion thruster with the remaining 25 kg of xenon. Since April 2003, ARTEMIS has been routinely providing high–data–rate links to France’s SPOT–4 and ESA’s Envisat missions. Both the optical and Ka–band links are providing very–high–quality image transmission.

- ETS–VIII (Engineering Test Satellite – VIII), a GEO technology spacecraft of JAXA (launch Dec. 18, 2006). The S/C carries an IES (Ion Engine System; Kaufman–type system) for north–south stationkeeping tasks.
- MUSES–C (Mu Space Engineering Satellite; launch May 9, 2003), a deep space asteroid sample return mission of JAXA (formerly ISAS), Japan (Note: MUSES–C is also referred to by its nickname **Hayabusa**). The target asteroid is **Itokawa** (1998SF36). MUSES–C carries an IES (Ion Engine System) in combination with a microwave ECR (Electron Cyclotron Resonance) discharge system. ECR generates plasma which is introduced into a discharge chamber with permanent magnets to take advantage of electrode–less plasma production. In this design, a single microwave source feeds power to a neutralizer which features a small microwave antenna as well as an ion source.^{1625) 1626)} The new IES [system thrust of 5.2 – 23.6 mN; system input power of 0.31 – 1.1 kW; specific impulse of about 30,000 m/s; system mass = 61.8 kg; lifetime > 16,000 hours; xenon mass of < 73 kg; the 4 ion thrusters provide a Δv of about 3.7 km/s] is being used as the **primary propulsion system** to propel MUSES–C from a sun–synchronous orbit into a deep space orbit, asteroid orbiting, sample gathering, and return flight to Earth (see Ref. 1611). The overall mission scenario calls for an Earth swing–by one year after launch (the gravity assist maneuver took place May 19, 2004), spacecraft arrival at the target in Oct. 2005, two months of close target observations and sampling after landing. The rover MINERVA (Micro/Nano Experimental Robot Vehicle for Asteroid) was intended to be deployed onto the surface when the spacecraft touches the asteroid.

In Nov. 2005, the spacecraft performed five descents, among which two touch–down flights were included. Actually Hayabusa made three touch–downs and one long landing on the surface of Itokawa during those two flights.

In the aftermath of the various touch–downs, JAXA was not able to reconstruct the events any more. In early March 2006, JAXA officials said they had re–established communications with the Hayabusa spacecraft, and they managed to estimate the probe’s trajectory for the first time in three months. Hayabusa veered off–course on Dec. 8, 2005 due to some unknown event that JAXA described as a ”strong attitude disturbance.” The operations team continues its efforts to have Hayabusa back to Earth by June 2010. – Originally, a S/C landing on Earth was planned for 2007.¹⁶²⁷⁾

According to JAXA analysis, Hayabusa lost two reaction wheels among three aboard and the chemical propulsion.^{1628) 1629)} The only means left for Hayabusa are the ion engines and xenon gas reserved for them as well as a single reaction wheel. Hayabusa project team devised the use of xenon gas for cold gas propulsion, and also developed the new attitude

1625) J. Kawaguchi, A. Fujiwara, T. K. Uesugi, “The Ion Engines Cruise Operation and the Earth Swingby of Hayabusa (MUSES–C),” Proceedings of IAC 2004, Vancouver, Canada, Oct. 4–8, 2004, IAC–04–Q.5.02

1626) K. Toki, H. Kuninaka, K. Nishiyama, Y. Shimizu, “Flight Readiness of the Microwave Ion Engine System for MUSES–C Mission,” 28th International Electric Propulsion Conference (IEPC), Toulouse, France, March 17–21, 2003, paper: IEPC 03–0098

1627) J. Kawaguchi, A. Fujiwara, T. Uesugi, “Hayabusa – Its Technology and Science Accomplishment Summary and Hayabusa–2,” Proceedings of the 57th IAC/IAF/IAA (International Astronautical Congress), Valencia, Spain, Oct. 2–6, 2006, IAC–06–A3.5.2

1628) Hitoshi Kuninaka, Kazutaka Nishiyama, Jun’ichiro Kawaguchi, Ken’ichi Shirakawa, Masatoshi Matsuoka, “Hayabusa – On Its Return Voyage Back Home,” Proceedings of the 60th IAC (International Astronautical Congress), Daejeon, Korea, Oct. 12–16, 2009, IAC–09.A3.5.4

1629) K. Nishiyama, S. Hosoda, H. Koizumi, Y. Shimizu, H. Kuninaka, J. Kawaguchi, “Summary of the 25000 Hour Round–Trip Ion Drive of Hayabusa,” Proceedings of the 61st IAC (International Astronautical Congress), Prague, Czech Republic, Sept. 27–Oct. 1, 2010, IAC–10.C4.4.3

control strategy taking the advantage of solar radiation pressure. The spacecraft started the ΔV maneuver using the ion engines from 2007 and will continue it until Feb. 2010. Hayabusa is scheduled to reenter into the atmosphere and land in middle of Australia in June of 2010.

After overcoming multiple serious glitches, and a three–year delay in its round–trip journey of over 5 billion km (or 5×10^9 km), JAXA's Hayabusa sample return canister landed in South Australia (Woomera) on June 13, 2010. The canister separated from the spacecraft about three hours before reaching Earth, and returned to Earth via parachute. The canister has been recovered by JAXA engineers, and will be taken to Japan where scientists will open it to find out if there is anything inside. ^{1630) 1631) 1632) 1633)}



Figure 94: Photo of Hayabusa's sample return canister and parachute on the ground in the Australian outback (image credit: JAXA) ¹⁶³⁴⁾

On Nov. 16, 2010, JAXA confirmed that the tiny particles inside the Hayabusa spacecraft's sample return container are in fact from the asteroid Itokawa. ¹⁶³⁵⁾ Based on the results of the scanning electron microscope (SEM) observations and analyses of samples that were collected with a special spatula from sample catcher compartment "A", about 1,500 grains were identified as rocky particles, and most of them were judged to be of extraterrestrial origin, and definitely from Asteroid Itokawa. Their size is mostly less than $10 \mu\text{m}$, and handling these grains requires very special skills and techniques. – These are the first samples from an asteroid ever returned to Earth.

1630) "Welcome back HAYABUSA to Earth after overcoming various difficulties!," JAXA, June 14, 2010, URL: http://www.jaxa.jp/projects/sat/muses_c/index_e.html

1631) Nancy Atkinson, "Hayabusa Returns," Universe Today, June 13, 2010, URL: <http://www.universetoday.com/2010/06/13/hayabusa-returns/>

1632) Louis D. Friedman, "The Hayabusa Adventure," Space Daily, June 18, 2010, URL: http://www.spacedaily.com/reports/The_Hayabusa_Adventure_999.html

1633) "Spacecraft Recovered After 7–Year Journey," Space Daily, June 17, 2010, URL: http://www.spacedaily.com/reports/Spacecraft_Recovered_After_7_Year_Journey_999.html

1634) "Retrieval of the Hayabusa capsule was completed, Heat shield was found in WPA," JAXA, June 14, 2010, URL: http://www.isas.jaxa.jp/e/topics/2010/06/14_3.shtml

1635) "Identification of origin of particles brought back by Hayabusa," Jaxa, Nov. 16, 2010, URL: http://www.jaxa.jp/press/2010/11/20101116_hayabusa_e.html

- The planetary Dawn science spacecraft of NASA's Discovery Program on its way to the Asteroid Belt – an 8 year mission to the asteroids Vesta and Ceres (launch Sept. 28, 2007, launch mass = 1210 kg, dry mass of 740 kg) is another entry into the category of deep space missions which is using the **SEP** (Solar Electric Propulsion) technology as its main means of power generation (instead of the commonly used RTG concepts for deep space missions). – In addition, Dawn uses **ion propulsion** (3 gimbaled NSTAR ion engines) to get the additional velocity needed to reach Vesta once it leaves the Delta rocket. It also uses ion propulsion to spiral to lower altitudes on Vesta, to leave Vesta and cruise to Ceres and to spiral to a low altitude orbit at Ceres. ^{1636) 1637) 1638)}

1.14.1.5 FEED (Field Emission Electric Propulsion):

Initial demonstrations of the FEED technology [indium ion emitter type referred to as LMIS (Liquid Metal Ion Source), provided by ARCS (Austrian Research Centers Seibersdorf) for ESA] have been conducted in space on several occasions: the Russian MIR station in 1991; ^{1639) 1640) 1641)} the GEOTAIL mission with a launch on July 24, 1992; on Equator – S with a launch Dec. 2, 1997, and on the Cluster – 2 mission in July/Aug. 2000. However, in all of these missions the FEED technology was utilized for spacecraft potential control or as a mass spectrometer experiment and not for thruster functions.

The FEED thruster technology offers the advantage of a **highly controllable μN thrust level** (1 – 100 μN range/thruster) as well as a very low thrust noise. The technology is being considered/introduced by a number of missions in planning/preparation such as:

- GOCE (Gravity Field and Steady–State Ocean Circulation Experiment) of ESA (launch March 17, 2009). Electric propulsion in GOCE is being used for drag force compensation in a LEO (240–270 km altitude) gravity mission configuration. FEED technology is used for drag compensation. Propulsion requirements call for a total impulse of 6045 Ns, a total operating time of 14,000 hours, a max. thrust level of 650 μN . ¹⁶⁴²⁾
- Microscope (MICROSatellite à traînée Compensée pour l'Observation du Principe d'Equivalence) is an approved CNES/ESA physics research microsatellite mission for a test of the weak Equivalence Principle (launch 2015). FEED propulsion is being used for drag compensation and for high–accuracy attitude control. Four clusters of thrusters are being implemented on Microscope. The instrument performance requirements call for a max. thrust level of 0–150 μN for each thruster, power needs of 80 W (8 thrusters on) and 120 W (12 thrusters on), and a total mass limit of 40 kg. ^{1643) 1644)}

Note: The initial design of Microscope featured a FEED DFACS (Drag–Free Attitude Control System). However, in 2009, the FEED system was replaced by CGPS (Cold Gas Propulsion System).

¹⁶³⁶⁾ <http://www.aerospaceguide.net/spacecraft/dawn.html>

¹⁶³⁷⁾ http://www.orbital.com/NewsInfo/Publications/Dawn_fact.pdf

¹⁶³⁸⁾ http://dawn.jpl.nasa.gov/mission/ion_prop.asp

¹⁶³⁹⁾ M. Fehring, et al., "Space–Proven Indium Liquid Metal Field Ion Emitters For Ion Microthruster Applications," Proceedings of 33rd AIAA Joint Propulsion Conference, Seattle, WA, July 1997

¹⁶⁴⁰⁾ M. Fehring, F. Ruedenauer, W. Steiger, "Indium Liquid–Metal Ion Sources as Micronewton Thrusters," 1999

¹⁶⁴¹⁾ R. Schmidt, et al., "Results from the Active Spacecraft Potential Control on GEOTAIL", Journal of Geophysical Research, Vol. 100, No A9, 17, pp. 253–17, 259, Sept. 1995

¹⁶⁴²⁾ A. Genovese, N. Buldrini, M. Tajmar, W. Steiger, "2000 Hour Endurance Test of an Indium FEED Cluster," 28th International Electric Propulsion Conference (IEPC), Toulouse, France, March 17–21, 2003

¹⁶⁴³⁾ Information kindly provided by Olivier Vandermarcq of CNES (project manager of Microscope)

¹⁶⁴⁴⁾ S. Marcuccio, L. Serafini, D. Nicolini, L. Jolivet, O. Vandermarcq, P. Touboul, "FEED System for the Microscope Mission," 28th International Electric Propulsion Conference (IEPC), Toulouse, France, March 17–21, 2003

- ST7 (Space Technology 7) mission of NASA within NMP. ¹⁶⁴⁵⁾ ¹⁶⁴⁶⁾ ¹⁶⁴⁷⁾ The objective is the on-orbit system-level validation of the DRS (Disturbance Reduction System) technology. DRS incorporates a set of μN colloid thrusters, provided by Busek Company. The DRS instrument package consists of two sets of 4 μN thrusters each for position and attitude control, DFACS (Drag-Free and Attitude Control System), and a microprocessor. The descoped DRS will now use the LTP (LISA Test Package) inertial sensors as its drag-free sensors. The ST7 DRS, scheduled to fly on the **LISA Pathfinder** mission (formerly SMART-2) of ESA in late 2012, is designed to maintain the S/C position with respect to GRS (Gravity Reference Sensor) to $< 10 \text{ nm}/(\text{Hz}^{1/2})$ over the measurement range of 1–30 mHz.
- LPF (LISA Pathfinder) of ESA. ¹⁶⁴⁸⁾ Aside from the DRS system of NASA, LPF will fly its own MPS (Micro-thrust Propulsion System) consisting of the FCA (FEED Cluster Assembly), one PCU (Power Control Unit), and one NA (Neutralizer Assembly). Two different FEED thrusters technologies are being used. One slit-shaped emitter with Cesium as propellant, and a needle-shaped emitter with Indium as propellant.
- LISA (Laser Interferometry Space Antenna) mission of ESA/NASA with a planned launch in 2018. The LISA formation will consist of three satellites (265 kg minisatellite) each containing two optical benches. They will be deployed with one launch vehicle at each of the vertices of a slowly rotating equilateral triangle (the LISA arm lengths are $5 \times 10^6 \text{ km}$) in a heliocentric orbit. Thus the satellites will form a giant Michelson interferometer. The orbital deployment is designed to maintain the triangular formation, with the triangle appearing to rotate about the center once per year. The center of the triangular formation will be located in the ecliptic plane 1 AU ($150 \times 10^6 \text{ km}$) from the sun and about 20° behind the Earth (Earth trailing orbit). *The objective is to detect gravitational waves from binary galactic systems through very long baseline laser interferometry.* The control system for LISA is DRS (Disturbance Reduction System) providing five control functions: a) attitude control, b) DFC (Drag Free Control), c) proof mass suspension control, d) telescope articulation control, and e) point ahead and acquisition control. ¹⁶⁴⁹⁾ ¹⁶⁵⁰⁾ ¹⁶⁵¹⁾
- DARWIN (Detection and Analysis of Remote Worlds by Interferometric Nulling) of ESA (launch 2015).

¹⁶⁴⁵⁾ P. G. Maghami, F. L. Markley, M. B. Houghton, C. J. Dennehy, "Design and Analysis of the ST7 Disturbance Reduction System (DRS) Spacecraft Controller," Proceedings of the 26th AAS Conference on Guidance and Control, Breckenridge, CO, Feb. 5–9, 2003, Vol. 113 Advances in the Astronautical Sciences, Edited by I. J. Gravseth and R. D. Culp, AAS 03–065, pp. 485–495

¹⁶⁴⁶⁾ V. Hruba, M. Gamero-Castaño, P. Falkos, S. Shenoy, "Micro Newton Colloid Thruster System Development," Proceedings of IEPC 2001, Pasadena, CA, Oct. 2001

¹⁶⁴⁷⁾ V. Hruba, M. Gamero-Castaño, D. Spence, C. Gasdaska, N. Demmons, R. McCormick, P. Falkos, J. Young, W. Connolly, "Colloid Thrusters for the New Millennium, ST7 DRS Mission," Proceedings of the IEEE Aerospace Conference, Big Sky, MT, March 6–13, 2004

¹⁶⁴⁸⁾ Davide Nicolini, Luca Ceruti, Fabio Ceccanti, Christophe Figus, Peter Flueeli, Andrea Novi, Carsten Scharlemann, Rainer Killinger, Marco Capacci, Lorenzo Serafini, Davina Di Cara, Denis Estublier, "LISA Pathfinder FEED Systems Development Achievements," Proceedings of Space Propulsion 2010, San Sebastian, Spain, May 3–6, 2010

¹⁶⁴⁹⁾ M. Tajmar, W. Steiger, A. Genovese, "Experimental Characterization of Indium FEED Microthrusters," NASA/MSFC Workshop on Advanced Propulsion Systems, April 2001

¹⁶⁵⁰⁾ R. Leach, K. L. Neal, "Discussion of Micro-Newton Thruster Requirements for a Drag-Free Control System," Proceedings of AIAA/USU Conference on Small Satellites, Logan, UT, Aug. 12–15, 2002, SSC02–VIII–1

¹⁶⁵¹⁾ T. T. Hyde, P. G. Maghami, "Precision Pointing for the Laser Interferometry Space Antenna Mission," Proceedings of the 26th AAS Conference on Guidance and Control, Breckenridge, CO, Feb. 5–9, 2003, Vol. 113 Advances in the Astronautical Sciences, Edited by I. J. Gravseth and R. D. Culp, AAS 03–066, pp. 497–508

1.14.1.6 Electric propulsion on commercial satellites

Starting with the first flight in 1983, the EHT (Electrothermal Hydrazine Thruster) resisto-jets of Aerojet Rocketdyne became the standard NSSK (North–South Station–Keeping) propulsion for the RCA (now part of Lockheed Martin) Series 3000 and Series 5000 spacecraft buses, as well as some Series 4000 GEO buses. This led to a steady increase in the number of spacecraft flying with EP throughout the 1980's and into the early 1990's. Also at this time, Russian communications and data–relay spacecraft were beginning to fly EP operationally. Both the Luch (Altair) and the Luch (Gelios) flew Fakel SPT–70 Hall effect thrusters in the mid–1980's to early 1990's. ¹⁶⁵²⁾

The US Telstar 401 communications satellite of AT&T (launch Dec. 16, 1993 into GEO) employed the first arcjet system flown (also first use of S7000 bus platform of Martin Marietta Astro Space). The arcjet provided over 500 s mission average specific impulse at 1.6 kW per thruster for NSSK of the Telstar 401 spacecraft. – Later, the Lockheed Martin S7000 platform series communication satellites, such as Intelsat–8, TelStar–IV, and Echostar, continued to use hydrazine arcjets for NSSK functions. Hughes is supplying xenon ion engines as an option on high–powered versions of the HS–601 platform.

- PanAmSat–5 (PAS–5) of PanAmSat Corp., a telecommunications satellite launched July 30, 1997 (and launch of PanAmSat–1R launch Nov. 15, 2000), use **XIPS** (Xenon Ion Propulsion System), a gridded ion engine built by HSC of Hughes Electronics Corp., Los Angeles, CA) on the HS–702 platform for station keeping and attitude maintenance. In the latter case, XIPS is the spacecraft's sole means of station keeping. By the end of 2000, 12 communication satellites were using XIPS and variations thereof. On the 702 platform, XIPS has an active grid diameter of 25 cm, Isp = 37,000 m/s (3,800 s), thrust = 165 mN (max), input power of 4.5 kW. The mass of XIPS is 35 kg.

- Note: ¹⁶⁵³⁾ In 2005, L–3 ETI (L–3 Communications Electron Technologies Inc.) is a new company (formerly Hughes/Boeing EDD) which is building the XIPS instrument assembly.

- In Oct. 2000, The Boeing Company acquired three units within Hughes Electronics Corporation: Hughes Space and Communications Company, Hughes Electron Dynamics, and Spectrolab, Inc., in addition to Hughes Electronics' interest in HRL, the company's primary research laboratory. The four are now part of Boeing's newest subsidiary, Boeing Satellite Development Center. ¹⁶⁵⁴⁾ ¹⁶⁵⁵⁾

- More recent launches of the BSS 702 platform, like the Anik–F2 communications satellite of Telesat (launch July 17, 2004), Canada, employ the XIPS also to augment final orbit insertion, thus conserving even more mass as compared to using only an onboard liquid apogee engine. – SSL (Space Systems/Loral) and ASI (Alcatel Space Industries) are manufacturing communication satellites (Telstar–8 and Astra–1K, respectively) which use SPT (Stationary Plasma Thrusters) type electric propulsion systems to support such functions as stationkeeping.

- In the timeframe 2010, NASA is interested in using a commercially available Electric Propulsion (EP) thruster from an active product line. The demands, however, for Deep

¹⁶⁵²⁾ W. Andrew Hoskins, R. Joseph Cassady, Olwen Morgan, Roger M. Myers, Fred Wilson, David Q. King, Kristi de-Grys, “30 Years of Electric Propulsion Flight Experience at Aerojet Rocketdyne,” Proceedings of the 33rd International Electric Propulsion Conference (IEPC), Washington D.C., USA, Oct. 6–10, 2013, paper: IEPC–2013–439, URL: <http://www.iepc2013.org/get?id=439>

¹⁶⁵³⁾ Kuei–Ru Chien, Stephen L Hart, William G. Tighe, Michael K De Pano, Thomas A Bond, Rafael Spears, “L–3 Communications ETI Electric Propulsion Overview,” 29th International Electric Propulsion Conference (IEPC), Princeton University, Princeton, NJ, USA, paper: IEPC–2005–315, URL: http://sgc.engin.umich.edu/erps/IEPC_2005/pdf/files/papers/315.pdf

¹⁶⁵⁴⁾ J. E. Pollard and K. D. Diamant, “Ion Flux, Energy, and Charge–State Measurement for the BPT–4000 Hall Thruster,” 37th AIAA/ASME/SAE/ASEE Joint Propulsion Conference and Exhibit, Salt Lake City, UT, July 8–11, 2001, AIAA Paper 2001–3351

¹⁶⁵⁵⁾ <http://www.boeing.com/defense-space/space/bss/factsheets/xips/xips.html>

Space missions are far more stringent, particularly in terms of the required life. A 25 cm XIPS® DCA (Discharge Cathode Assembly) was life tested at JPL (Jet Propulsion Laboratory) to verify that the unit can meet these requirements. The JPL–DCA life test was voluntarily terminated at 16,200 hours after successfully demonstrating over 5000 hours each at high, medium and low power levels. The Post–Test analysis did not identify any imminent points of failure. ¹⁶⁵⁶⁾

- The Russian company Fakel Design Bureau in Kaliningrad produces the SPT–100 electric propulsion system for many applications in the commercial satellite market. SNECMA of Paris, adapting technology developed by Fakel Design Bureau, has provided the SPT–100 system for Astra–1K, owned by SES of Luxembourg (provision of NSSK for Astra–1k). EADS Astrium SAS is using the SPT–100 system of SNECMA on three Inmarsat–4 mobile communication satellites, owned by Inmarsat Ventures, London (operational availability in 2005, Inmarsat–4F2 was launched on Nov. 8, 2005). – The function of electric orbit raising is also being considered for large communication satellites. An arcjet electric propulsion system of General Dynamics (Primex) had its first flight in 1994.



Figure 95: Illustration of the BPT–4000 thruster

- As of January 2001, there were over 100 Primex arcjets in orbit (160 as of 2006). As of 2002, General Dynamics Space Propulsion Division (Aerojet) in Redmond, WA, and Lockheed Martin Space Systems of Sunnyvale, CA, are jointly developing an electric propulsion system called **BPT–4000** (Busek Primex Thruster) – a xenon Hall effect thruster with 4.5 kW power input (max). The qualification of HTPS (Hall Thruster Propulsion System), as it is referred to at Aerojet, was completed in 2006. The first flight of the BPT–4000 system is scheduled for mid–2008. The HTPS consists of the following Aerojet–supplied products: a) the 4.5 kW BPT–4000 Hall thruster; b) the PPU (Power Processing Unit); c) and the XFC (Xenon Flow Controller). The BPT–4000 will be used for orbit insertion, orbit maintenance, and repositioning of geosynchronous satellites. ¹⁶⁵⁷⁾

Parameter	3 kW version	4.5 kW version
Thrust (300 V)	195 mN	290 mN
Thrust (400 V)	170 mN	254 mN
Specific impulse, Isp (300 V)	1750 s (17,000 m/s)	1850 s (18,000 m/s)
Specific impulse, Isp (400 V)	1920 s (18,800 m/s)	2020 s (19,800 m/s)
Life capability	> 10,000 hr	
Total impulse	> 5.8 x 10 ⁶ Ns	

1656) William G. Tighe, Kuei–Ru Chien, Rafael Spears, James E. Polk, Dan M. Goebel, “Post Wear Test Evaluation of a 25–cm XIPS® Discharge Cathode Assembly,” Proceedings of Space Propulsion 2010, San Sebastian, Spain, May 3–6, 2010

1657) F. Wilson, Bill Smith, “Hall Thruster System Qualification Provides Major Satellite Benefits,” Proceedings of the 57th IAC/IAF/IAA (International Astronautical Congress), Valencia, Spain, Oct. 2–6, 2006, IAC–06–C4.4.09

Parameter	3 kW version	4.5 kW version
On–off cycles	6,800	
Instrument mass, size	< 12.3 kg, 14 cm x 25 cm x 28 cm	
Input power, input voltage	1 to 4.5 kW, 200 or 400 V	

Table 85: Characteristics of the BPT–4000 thruster performance

- For large telecommunication satellites (EuroStar–3000 of Astrium and Spacebus–4000 platforms of Alcatel)¹⁶⁵⁸⁾ a new version of the Hall–effect thruster, called PPS–1350–G, has been designed and developed by SNECMA Moteurs (Paris) with the objective for GEO NSSK (North–South Stationkeeping) and to reduce the manufacturing cost of the thruster. The lifetime of this thruster is about 11000 hours [thrust of 85 mN, Isp = 16,000 m/s, power input of 1.5 kW]. PPS–1350–G is an upgrade of the standard model PPS–1350. The PPS–1350–G is foreseen for late 2004.

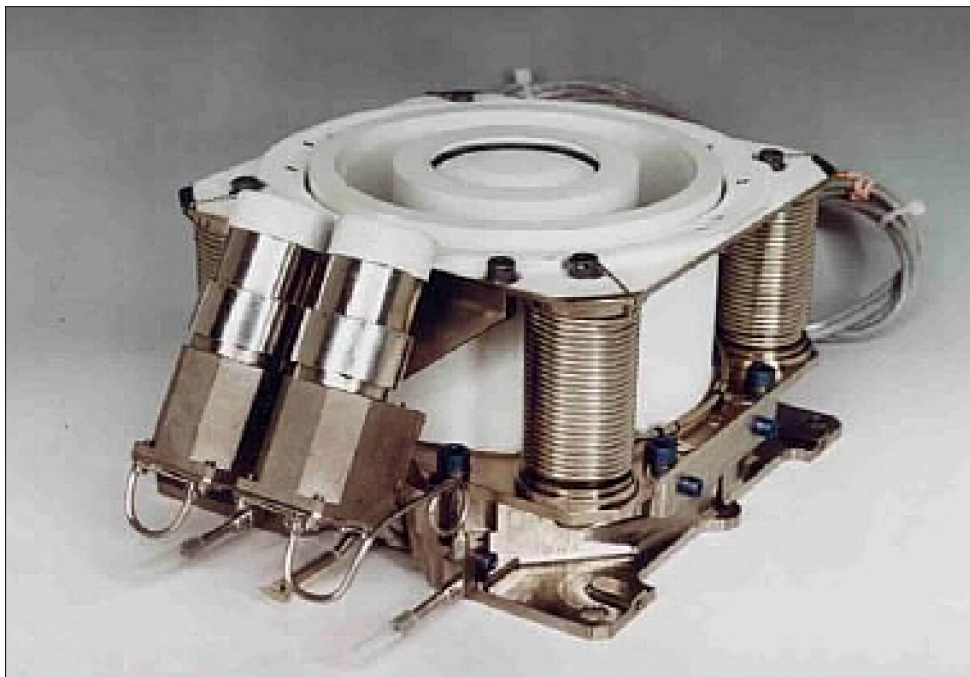


Figure 96: Illustration of the PPS–1350 thruster (image credit: Snecma)

- QinetiQ (UK) along with partners is developing the T6 gridded ion engine, a heavy duty electric propulsion system to propel the BepiColombo mission (2 spacecraft) of ESA and JAXA to Mercury; the system is referred to as **SEPS** (Solar Electric Propulsion System). Electric propulsion will be used for the transfer phase to Mercury. SEPS is based on four T6 thrusters each capable of delivering up to 145 mN thrust.

A variant version of the T6 gridded ion engine, referred to as **HPEPS** (High Power Electric Propulsion System), will be used to provide on–orbit propulsion for the future AlphaBus spacecraft in GEO. The HPEPS functions involve station–keeping, orbit–topping, and end–of–life de–orbit services. Successful technology demonstrations were completed in 2010. Some performance characteristics:^{1659) 1660)}

- HPEPS mass of 8 kg, dimensions of 300 mm length, 300 mm diameter

1658) P. Dumazert, S. Lagardère–Verdier, F. Marchandise, C. R. Koppel, P. Garnero, F. Balme, “PPS®–1350–G Qualification Status March 2003,” 28th IEPC, Toulouse, France, March 17–21, 2003

1659) M. S. Hutchins, N. C. Wallace, J. Palencia Jiménez; “Overview and Status of the T6 Gridded Ion Engine Electric Propulsion Systems for Interplanetary and Geostationary Spacecraft Applications,” Proceedings of the Space Propulsion Conference 2010, San Sebastian, Spain, May 3–6, 2010

1660) H. L. Gray, S. Buchnell, “Propulsion Systems for the BepiColombo Mission,” Proceedings of the Space Propulsion Conference 2010, San Sebastian, Spain, May 3–6, 2010

- High power, thrust and SI figures (throttleable from 30 to 210 mN, based on actual thrust measurements)
- Total impulse > 10×10^6 Ns @ 200 mN, 4700 s
- Cycle life > 8500 On/Off cycles
- Cyclic & continuous operation (station-keeping and primary propulsion).

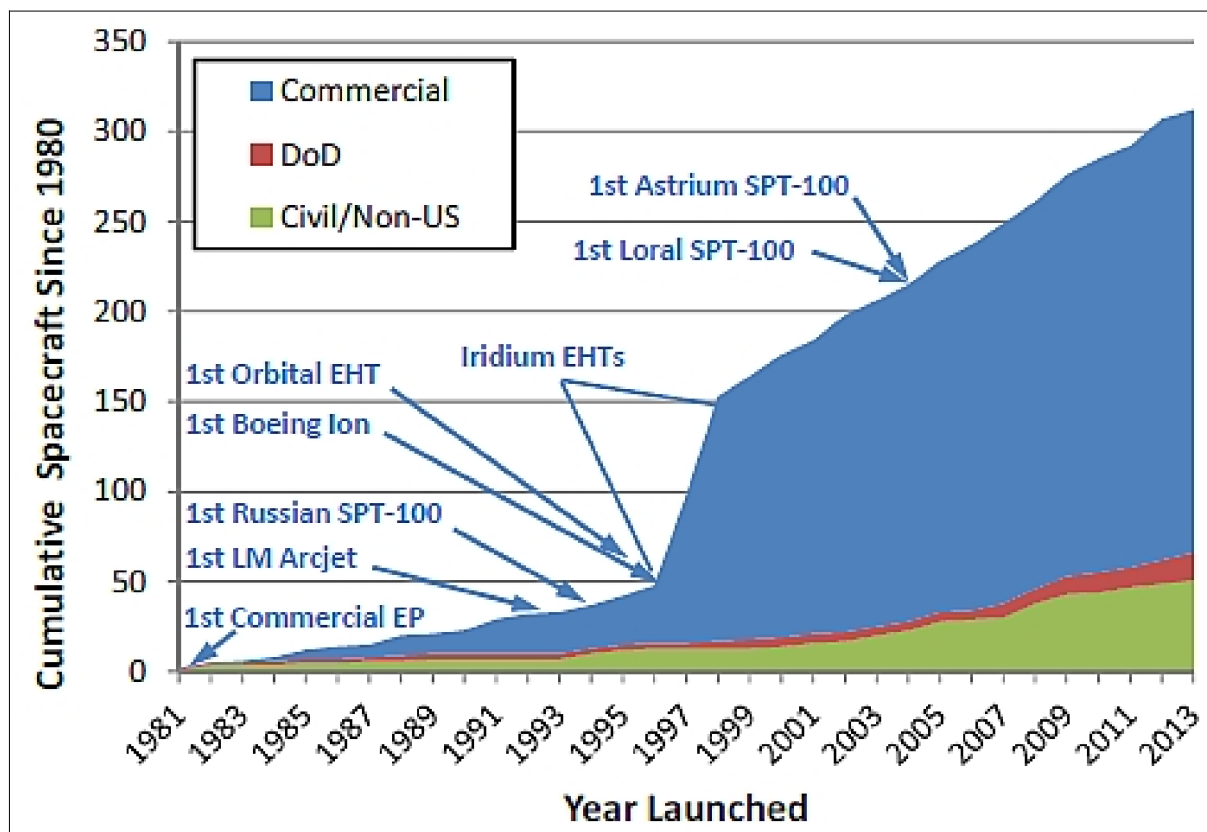


Figure 97: Cumulative number of spacecraft using EP (image credit: Aerojet Rocketdyne, Ref. 1652)

Legend to Figure 97: The major discontinuity in Figure 97 at about that time results from the 86 LM-700 spacecraft launched in the 2 years from 1997 to 1998 for the Iridium LEO satellite constellation. In all, 95 spacecraft were launched by 2002. Each spacecraft flew a single EHT resistojet for orbit trim and deorbit maneuvers.

1.14.1.7 Introduction of all-electric propulsion for satellite orbit raising

In the early 21st century, the SEP (Solar Electric Propulsion) technology is generally being considered mature enough with a potential for game-changing future missions. Commercial companies including Boeing, Lockheed Martin, Aerojet Rocketdyne, and Thales Electronic Systems have achieved notable progress with all-electric propulsion technology which has long proved itself a viable option for keeping a satellite on station or in its position in orbit, but not for orbit raising (from GTO to GEO). Traditionally, more powerful chemical propulsion engines are used to quickly move satellites through Earth's hazardous radiation belt.

All-electric propulsion, which dispenses with heavy chemical propulsion systems, provides a significant reduction in satellite mass, but requires considerably more transit time to reach final orbit. Hence, a lower launch cost must be weighed against a longer transit period. — For the first time, orders were placed for all-electric propulsion of commercial GEO communications satellites in 2012.

Background:

- The DS1 (Deep Space 1) mission of NASA (launch October 24, 1998) demonstrated SEP primary propulsion with its IPS (Ion Propulsion System), provided by the project NSTAR [(NASA SEP Technology Application Readiness). At the end of the primary mission in Sept. 1999, IPS had operated for about 3000 hours. By August 31, 2000, IPS had accumulated > 5200 hours of operations in its extended mission, a longer time period than any propulsion system on any S/C so far. The NSTAR/IPS system components like the ion thrusters and the PPU (Power Processing Unit) were manufactured for NASA/GRC by the Hughes Electron Dynamics Division, Torrance, CA. The total mass of NSTAR/IPS was about 30 kg; in addition, 82 kg of xenon was stored onboard.
 - On July 29, 1999, DS1 successfully performed a close flyby of asteroid 9969 Braille using the AutoNav system.
 - On Sept. 22, 2001, DS1 flew by the comet 19P/Borelli. The DS1 spacecraft was retired on December 18, 2001. ¹⁶⁶¹⁾
- SMART–1 was the first European lunar mission. The spacecraft was launched on September 27, 2003 from Kourou as an auxiliary payload on an Ariane–5 launcher. Using a single Xenon ion thruster (PPS–1350) providing 70 mN of thrust, SMART–1 traveled 82 million km in a spiral trajectory to the Moon. On November 15, 2005, after a journey taking 13½ months, SMART–1 was captured precisely into the intended polar lunar orbit.
 - OHB Sweden (formerly the Space division of the Swedish Space Corporation – SSC) was the prime contractor for the SMART–1 spacecraft and was also responsible for the development of several of its subsystems including the attitude control system and the data handling system. The SMART–1 EP (Electric Propulsion) subsystem was provided by Snecma of France. The trajectory planning and spacecraft operations were performed by ESOC (European Space Operations Center) in Darmstadt, Germany. The overall management and funding of the project was provided by ESA (European Space Agency). ¹⁶⁶²⁾
- Small GEO (or SGEO for short) is a general purpose small geostationary satellite platform that is currently being developed by a consortium led by OHB System AG of Bremen, Germany. OHB Sweden, part of the OHB AG group, is responsible for the provision of both the EP and AOCS (Attitude and Orbit Control Subsystem). The Small GEO platform supports up to 400 kg payload mass, a payload power of up to 3.5 kW and with a lifetime of up to 15 years. The first launch is scheduled for 2015, with Hispasat as the main customer.
 - SGEO has a CPS (Chemical Propulsion System) to perform the transfer from GTO to GEO after which the CPS will be passivated. Thereafter, SGEO will be the first European telecom platform to rely entirely on electric propulsion for all remaining on–orbit tasks, including station acquisition, station–keeping, orbit repositioning and the final graveyard transfer maneuver.
 - At the start of the SGEO project in 2006, OHB Sweden had proposed the use of EP (Electric Propulsion) also for the SGEO GTO–GEO transfer phase. However, at that time it was concluded, that the commercial satellite operators would not accept the associated transfer times of 6–7 months. The general consensus in the space industry was that the maximum allowed transfer duration was in the order of 90 days, which was also what had been applied several times on missions based on Boeing 702HP satellites.

The following events took place, which rapidly changed the feasibility of an “all–EP” telecom scenario.

¹⁶⁶¹⁾ Marc D. Rayman, “The Deep Space 1 Extended Mission: Challenges in Preparing for an Encounter with Comet Borrelly,” *Acta Astronautica*, Vol. 51, No 1–9, 2002, pp. 507–516, also at URL: http://nmp.nasa.gov/ds1/DS1_Challenges.pdf

¹⁶⁶²⁾ Peter Rathsmann, Alain Demaire, Ekaterina Rezugina, Hendrik Lübberstedt, Marco De Tata, “Electra – the implementation of all–electric propulsion on a geostationary satellite,” Proceedings of the 64th International Astronautical Congress (IAC 2013), Beijing, China, Sept. 23–27, 2013, paper: IAC–13–C1.7.4

1) On October 7, 2013, Aerojet Rocketdyne announced, that its Zero-Erosion™ XR-5 (formerly BPT-4000) 4.5 kW Hall thrusters had initiated orbit raising operations on the AEHF (Advanced Extremely High Frequency) Space Vehicle 3 (SV-3) that launched Sept. 18, 2013 aboard a United Launch Alliance Atlas V rocket. ¹⁶⁶³⁾

Each AEHF Space Vehicle includes four of Aerojet Rocketdyne's 4.5 kW XR-5 Hall subsystems, with each subsystem consisting of an XR-5 Hall thruster, power processing unit, and xenon flow controller. During orbit raising (GTO to GEO), two XR-5 thrusters are fired simultaneously for a total operating input power of 10 kW. Like the SV-1 and SV-2 satellites already on orbit (launched on Aug. 14, 2010 and May 04, 2012, respectively), the Aerojet Rocketdyne XR-5 Hall system provides orbit raising as well as on-orbit station keeping propulsion during the vehicle's 14 year mission life.

The use of the zero-erosion XR-5 Hall system on AEHF reduces the launch mass of the space vehicle by ~ 1000 kg, compared to an all-chemical propulsion approach, resulting in greatly reduced mission launch costs for the U.S. Air Force. In addition to the 4.5 kW XR-5 Hall system, Aerojet Rocketdyne also has 12 kW XR-12 and 20 kW XR-20 Hall systems in development. ¹⁶⁶⁴⁾

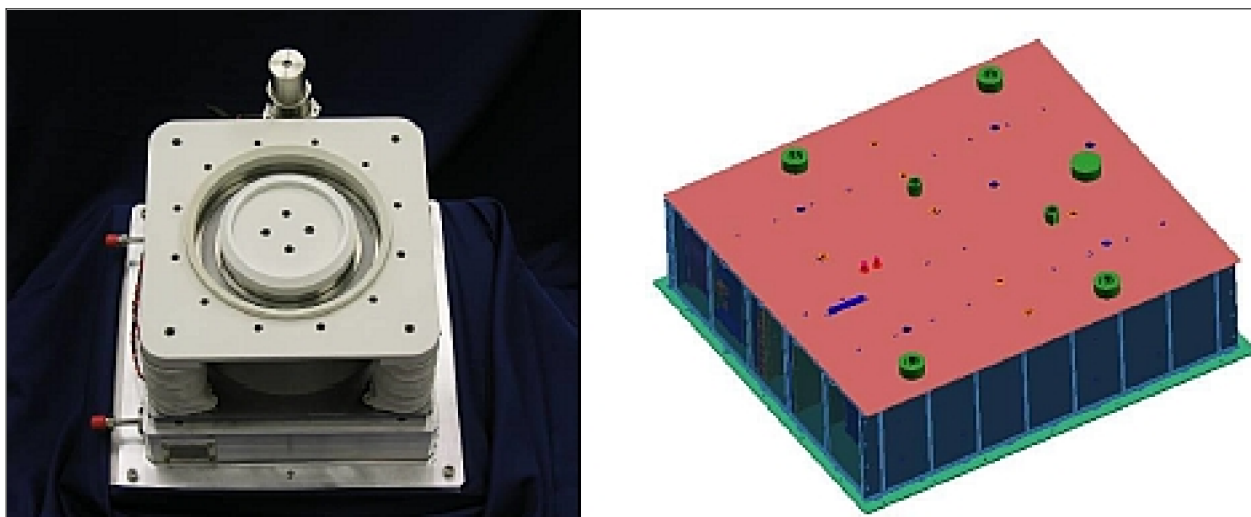


Figure 98: Photo of the XR-12 (left) and model of the high power PPU (right), image credit: Aerojet Rocketdyne

2) In late 2011, SES-Astra, one of the world's major satellite operators, presented a paper where they explored the possibility of integrated end-to-end optimisation for mission cost and orbital life by combining launcher and spacecraft performance models into a single set. The paper discussed the use of smaller launchers and lower injection orbits, where instead a larger ΔV to GEO could be provided by an on-board EP system. This meant that the concept of significantly longer transfer times to GEO was now being proposed by one of the main telecom satellite operators. ¹⁶⁶⁵⁾

3) In March 2012, Boeing announced contracts with two commercial operators: Asia Broadcast Satellite (ABS) and Satelites Mexicanos (Satmex) for four satellites. The satellites were of the 2 ton-class, and were to be launched pairwise on Falcon-9 launchers. The satellite platforms were to be based on a new platform, referred to as BSS-702SP (Small

¹⁶⁶³⁾“Aerojet Rocketdyne High-Power Solar Electric Propulsion System: Providing Orbit Raising Propulsion for the Air Force Advanced Extremely High Frequency SV-3 Satellite,” Oct. 7, 2013, URL: <http://www.rocket.com/article/aerojet-rocketdyne-high-power-solar-electric-propulsion-system-providing-orbit-raising>

¹⁶⁶⁴⁾Benjamin Welander, Jeff Monheiser, Nicole Meckel, Kristi de Grys, Peter Peterson, “Demonstration of the XR-12 Hall Current Thruster,” Proceedings of the 33rd International Electric Propulsion Conference (IEPC), Washington D.C., USA, Oct. 6–10, 2013, paper: IEPC-2013-451, URL: <http://www.iepc2013.org/get?id=451>

¹⁶⁶⁵⁾J. Gonner, M. Franci, P. Francken, O. Lebrethon, “SES, Improving satellite lifecycle cost through more efficient space access – an operator's perspective,” SpaceAccess 2011–61

Platform), using the same XIPS–25 (Xenon Ion Propulsion System, a thruster system with an active grid of 25 cm diameter) as the larger BSS–702HP satellites. What was new was that this platform did not include any chemical propulsion system. **For the first time, commercial satellite operators had procured satellites relying solely on EP for GTO–GEO transfer durations in the order of 6 months.**¹⁶⁶⁶⁾

In August 2013, the BSS–702SP passed the CDR (Critical Design Review). Boeing is on schedule to conduct a dual launch of the first two 702SP satellites in the first quarter of 2015 on a Falcon 9 rocket.¹⁶⁶⁷⁾

4) On November 30, 2012, SES announced its participation to the ARTES–33 program “Electra” of ESA (European Space Agency). SES and ESA announced a PPP (Public–Private Partnership) under the Electra program aimed at developing a full–electric propulsion small/medium sized satellite platform manufactured in Europe.

SES will lead the **Electra** project and in particular the satellite design definition phase. SES will work in close cooperation with OHB System AG of Bremen, who will act as the prime contractor to SES. OHB Sweden, as subsystem providers to OHB System, will provide the EP and AOCS subsystems for Electra. The first Electra satellite will have a launch mass in the range 2000–3000 kg including a payload up to 700 kg and 8 kW of electric propulsion for orbit raising. A launch of Electra is planned for 2018–19 (Ref. 1662).

All–EP is still a hot topic in 2013 with special panel discussions at the IEPC (International Electric Propulsion Conference) in Washington D.C. (Oct. 6–10, 2013).¹⁶⁶⁸⁾

The all–EP technology provides the flexibility required for multiple mission objectives. The concept is also being considered in studies for deep space missions.

1666) “In 2012 Boeing introduced the newest satellite design in its product portfolio,” Boeing, March 2012, URL: <http://www.boeing.com/boeing/defense-space/space/bss/factsheets/702/702SP.page>

1667) Paula Shawa, “Boeing All–Electric Satellite Passes Critical Design Review,” Aug. 6, 2013, URL: <http://boeing.mediaroom.com/2013-08-06-Boeing-All-Electric-Satellite-Passes-Critical-Design-Review>

1668) “Satellite Operators Discuss ‘Why is Electric Propulsion Game Changing?’,” Oct. 25, 2013, URL: <http://www.ae.gatech.edu/node/1254>

1.14.2 Solar sails

Solar sailing is an alternate form of spacecraft propulsion. Rather than carrying propellant, solar sails refer to spacecraft propulsion concepts, which utilize the momentum transfer of photons (solar radiation pressure) on very large, highly reflecting sails in space for passive propulsion and orbit transfer functions.^{1669) 1670) 1671)} The combination of ultra-light weight solar sail structures with micro/nano technologies opens a wide field of space applications. Since solar sails are not limited by a reaction mass, they can provide continual acceleration, limited only by the lifetime of the sail film in the space environment. On a long-term perspective, the solar sail technology offers the potential, to expand the envelope of possible missions (within the solar system), enabling new high-energy mission concepts that couldn't be done with conventional reaction propulsion. The design of a solar sail assembly poses a number of technology challenges, some are listed:

- Rather large surface areas of solar sail are needed to intercept a large flux of photons (the solar radiation pressure is very small – yielding only a small momentum)
- The fabric of solar sails must be extremely light ($< 20 \text{ g/m}^2$) to be able to generate as high an acceleration as possible from the momentum transported
- The mass per unit area of the entire S/C, the so-called sail loading, may be of the order of $20\text{--}30 \text{ g/m}^2$
- The sail assembly loading is a key measure of technology, in addition to the sail loading. The sail assembly loading is defined as the ratio between the mass of the sail structure plus reflective film (excluding the payload and the bus), and the sail area.
- Solar sails must be near-perfect reflectors to maximize the momentum. By adding the forces due to incident and reflected photons, the total force exerted on the sail is directed almost normal to its surface.
- By controlling the orientation of the sail relative to the sun-line, the sail can gain or lose orbital angular momentum. – Achieving a useful characteristic acceleration in the order of $0.1\text{--}1 \text{ mm/s}^2$ (at 1 au) from solar radiation pressure poses great challenges in terms of innovative technology demonstration of low-mass deployable structures, thin-film sails, and also of payload miniaturization.
- In-orbit deployment. The successful functioning of the solar sail structure deployment procedure and mechanism (after orbit attainment of the solar S/C) represents currently the greatest technical challenge in the solar sailing concept.

The solutions to these challenges must be demonstrated in space before solar sail propulsion is considered to be viable for any mission.

A systematic study of solar sail material (fabric) characteristics was conducted by NASA/MSFC evaluating the thermo-optical and mechanical properties after exposure to a simulated GTO radiation environment.¹⁶⁷²⁾ Testing of four materials: aluminized Mylar (DuPont), aluminized Mylar with chromium backing, aluminized Kapton (DuPont), and aluminized CP1 (Colorless Polyamide 1) of SRS Technologies. As of 2003, the thinnest commercially available Kapton films are $7.6 \mu\text{m}$ in thickness with an area density of 11 g/m^2 .

1669) P. Groepper, F. Burger, S. Lascar, T. Niederstadt, C. Sickinger, M. Leipold, et al., "Solar Sails – An Innovative and Enabling Technology for Gossamer Space Structures," Proceedings of 54th IAC, Bremen, Germany, Sept. 29 – Oct. 3, 2003

1670) C. R. McInnes, M. Eiden, P. Groepper, T. Peacock, "Solar Sailing – Mission Opportunities and Innovative Technology Demonstration," ESA Bulletin, No 108, Nov. 2001, pp. 58–65

1671) R. Young, "Solar Sails," Proceedings of the Sixth Annual NASA Earth Science Technology Conference (ESTC 2006), College Park, MD, USA, June 27–29, 2006, URL: <http://www.esto.nasa.gov/conferences/ESTC2006/presentations/C8P3.pdf>

1672) D. Edwards, W. Hubbs, T. Stanaland, A. Hollerman, R. Altstatt, "Characterization of Space Environmental Effects on Candidate Solar Sail Material," SPIE Annual Meeting 2002: Remote Sensing and Space Technology, Seattle, WA, July 7–11, 2002, Vol.. 4823

Background: The concept of solar sailing appears to have been first conceived by Russian space enthusiasts Konstantin Tsiolkovsky (1857–1935) and Friedrich Zander (Fridrikh Tsander, 1887–1933) in the early 1920s. A solar sail works by photon pressure from sunlight, a radial force from the sun into the direction of the universe (*Note: the amount of pressure from the solar wind is negligible in comparison to the photon pressure*). When light reflects from the surface of a body, the momentum of the light is reversed in direction. As a result, the body experiences a force proportional to the power in the light divided by the speed of light: $\mathbf{F} = 2\mathbf{P}/c$ where the factor 2 assumes normal incidence for the light on the reflective surface.¹⁶⁷³⁾

Since the solar energy, arriving at the top of the atmosphere, amounts to about 1.366 kW/m², the SRP (Solar Radiation Pressure) or force, per unit area is about 9.3 N/km² or: $\mathbf{F} = 9.3 \times 10^{-6} \text{ N/m}^2$ (the force or solar radiation pressure on 1 m² of sail surface normal to the sun). A solar sail can be steered by tilting the sail to vary the direction of the resulting force vector (see also solar sail in Glossary).

Although the basic idea behind solar sailing is simple, challenging engineering problems have to be solved. Hence, practical experience with “solar sail missions” is rather limited so far. The following list provides an overview of some solar sailing attempts (demonstrations) by various organizations. In spite of the meager progress made so far in solar sail technology development (the deployment problem must be conquered), it can safely be stated that there is a definite future (beyond 2010) for a great variety of solar sail applications in space.

- The first spaceborne application of solar radiation pressure has been used for passive attitude control of spacecraft. The Mariner–10 interplanetary mission of NASA/JPL (launch March 11, 1973) was the **first spacecraft using the sun–sail concept for maneuvering** by using the pressure of sunlight reflecting off of the solar panels for attitude control. This technique permitted the project to extend the mission life.¹⁶⁷⁴⁾ Since then, many spacecraft in Earth orbit have employed some form of small sun–sail attitude control. In 1974, when Mariner–10 passed by Venus to reach Mercury, the **gravity assist maneuver** was used for the first time by an interplanetary spacecraft.

- Interest in solar sailing was first generated, when a NASA/JPL study proposed a rendezvous mission with Comet Halley, employing the solar sailing concept, in the mid–1970s. Unfortunately, the project could not attain flight readiness for an encounter in 1986.

- In 1990 RSC Energia of Korolev (Moscow region), Russia, as the lead sponsor, formed SRC (Space Regatta Consortium – an association of 15 enterprises) with the objective to promote, develop and demonstrate satellite–based solar sails, so–called solarcraft (large deployable structures based on thin–film sails).

The first practical step toward this end was Znamya–2 (Banner), a demonstration experiment conducted on Feb. 4, 1993, when a segmented spinning disk a “shade” outside of Mir (20 m in diameter, about 22 g/m² area density) was deployed by centrifugal forces from the Progress M–15 spacecraft, docked at the MIR space station (the experiment included verification of the system concept, stability and control of the structure, etc.). The Znamya–2 experiment represents the first solar “shade” deployment experiment in space (but not a solar sail). It consisted of eight pie–shaped panels fabricated from 5 mm thick aluminized PETF film (a Russian version of Mylar) with no supporting structure.

- In parallel to the Znamya–2 deployment, a further experiment, “Novoy Svet” (New Light) was conducted on the same solar sail structure with the objective to illuminate Earth from space. The first illumination from space took place in the early morning hours before sunrise over Western Europe. A reflected spot of light of about 5 km in diameter travelled from southern France through Switzerland, Germany, Czech Republic, and Poland, it then disappeared in the early sunlight of Belarus.

¹⁶⁷³⁾ L. R. Forward: http://www.transorbital.net/Library/D001_S03.html

¹⁶⁷⁴⁾ <http://solarsails.jpl.nasa.gov/introduction/mission-scenarios.html>

- A second Znamya experiment, called Znamya–2.5, from MIR (actually the departing service vehicle Progress M–40) took place on Feb. 4, 1999 with a 25 m diameter sail (solar reflector) structure. The objective of Znamya–2.5 was to demonstrate beaming of solar power (reflected sunlight) from space to Earth for artificial target illumination (spot light of 5–7 km in diameter) under controlled conditions; also test of film structure and test of prolonged illumination. However, a problem in the deployment mechanism resulted in an abort of the demonstration.
- The Cosmos–1 Solar Sail Project, a privately funded venture of The Planetary Society, Pasadena, CA (sponsor: Cosmos Studios). The objective is to conduct a solar sail demonstration flight.
 - In a first step, a sub–orbital test flight of an inflatable tube sail deployment system (600 m² of Mylar sail) on a Volna launch vehicle (a converted SS–N 18 ICBM) took place on July 23, 2001 (submarine launch from Barents Sea).

The Russian Babakin Space Center is the prime contractor and spacecraft integrator for the Planetary Society. The projected sub–orbital flight of the 40 kg S/C was from the Barents Sea to the Kamchatka peninsula (solar sail deployment at 400 km altitude). Initial flight analysis revealed a capsule separation failure (neither the solar sail deployment test nor the re–entry capsule inflation sequence that were planned for this sub–orbital test flight were carried out). The Cosmos–1 test craft was to separate from its capsule and unfurl its two 15 m long, wing–like blades before making a soft landing on Kamchatka.

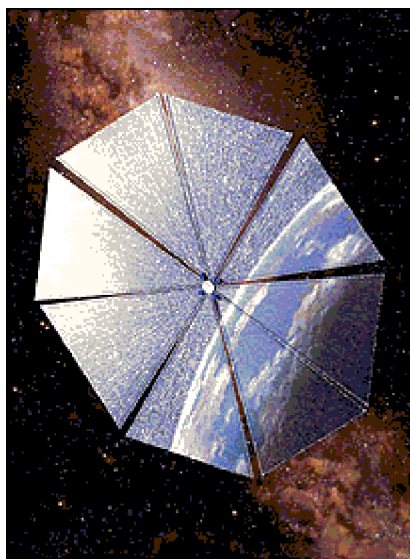


Figure 99: Artist's view of the Cosmos–1 spacecraft

- In a second attempt, a launch of **Cosmos–1** (Solnechny Parus) took place on June 21, 2005 from the submerged Russian Submarine Borisoglebsk in the Barents Sea. This project was of Cosmos Studios and The Planetary Society (Pasadena). However, a launch vehicle failure occurred (Volna rocket) after about 2 minutes into the flight. Hence, flight controllers were unable to confirm any orbit injection of the spacecraft.

This time around, a spacecraft of 103 kg was to be injected into a near circular 800 km orbit with an inclination of 78°. The basic deployment and structural technology relied on an inflatable tube system to which the sail material was being attached. The 600 m² sail was configured in eight roughly triangular blades. The nominal sail material consisted of 5 μm aluminized, reinforced Mylar. Mission success was defined as flying long enough to measurably

increase the orbital energy (or period) from sunlight pressure in controlled flight.¹⁶⁷⁵⁾

On July 21, 2005, the 'Volna Failure Review Board' concluded that the telemetry data from the launch vehicle was sufficient to determine that the launch failed due to an premature shut-down of the first-stage engine caused by a "critical degradation in operational capability of the engine turbo-pump." The engine shut down after firing for 82.86 seconds, instead of the expected burn of approximately 100 seconds. The Failure Review Board concluded also that the first and second stages never separated and, as a result, the spacecraft propulsion system did not fire, and the spacecraft did not separate from the third stage.¹⁶⁷⁶⁾ The review board included members from the Makeev Rocket Design Bureau (manufacturers of the Volna launch vehicle), the Lavochkin Association (which built Cosmos-1) and Tsniimash, a lead engineering center of the Russian Space Agency, Roskosmos.

- In 2003, a DLR-ESA technology demonstration sailcraft design is based on a previous ODISSEE (Orbital Demonstration on an Innovative Solar Sail driven Expandable structure Experiment) proposal.^{1677) 1678)} The sailcraft comprises a central deployment module for the sail and four CFRP booms that diagonally support the four sail segments, a microsatellite, and a deployable control mast (connecting the microsatellite to the sail structure via a gimbal mechanism). In this rigging concept, the center of mass can be offset from the center of pressure – thus, using photon pressure as an external force, a torque can be generated to control the attitude of the sailcraft.

In preparation for this mission, a solar sail ground deployment demonstration with a breadboard model (35 kg), conducted by a DLR-ESA-INVENT GmbH project team at DLR Cologne on Dec. 17, 1999, was highly successful.^{1679) 1680)} During the on-ground solar sail deployment in a time frame of approx. 30 minutes, four CFRP booms as well as four triangular aluminium-coated thin Kapton films were deployed under simulated 0-g and ambient environmental conditions. This deployment experiment finalized the development of a 20 m x 20 m solar sail. In this program, advanced deployable CFRP (Carbon Fiber Reinforced Plastic) booms were developed by DLR. These booms consist of two laminated flexible Ω -shaped sheets which are bonded at the edges to form a tubular shape. Once free of the Solar Sail Boom Deployment Module (BDM), the booms resume their original shape supported by a spontaneous self-deployment.^{1681) 1682)}

As of 2004,¹⁶⁸³⁾ a first ESA mission of a small sailcraft configuration (sail area of 20 m x 20 m) is expected to be launched in 2006 (Kayser-Threde as prime contractor). The mission profile comprises the following mission phases:

- Volna launch (Russia) from submarine and orbit insertion
- Pre-deployment phase including attitude stabilization

1675) L. Herbeck, C. Sickinger, M. Eiden, M. Leipold, "Review on Present Solar Sail Hardware Developments," Proceedings of 54th IAC, Bremen, Germany, Sept. 29 – Oct. 3, 2003

1676) L. Friedman, "Volna Failure Review Board Reports On Loss Of Cosmos 1," SpaceDaily, July 21, 2005
<http://www.spacedaily.com/news/solarsails-05k.html>

1677) W. Seboldt, B. Dachwald, "Solar Sailcraft of the first Generation – Technology Development," Proceedings of 54th IAC, Bremen, Germany, Sept. 29 – Oct. 3, 2003

1678) B. Dachwald, W. Seboldt, "Solar Sailcraft of the first Generation – Mission Applications to Near-Earth Asteroids," Proceedings of 54th IAC, Bremen, Germany, Sept. 29 – Oct. 3, 2003

1679) W. F. Unckenbold, M. J. Eiden, L. Herbeck, M. Leipold, C. Schöppinger, C. Sickinger, "Boom Deployment Mechanism for Large deployable Antennas," 25th Antenna Workshop on Satellite Technology, Sept. 18–20, 2002, ESA/ESTEC

1680) M. Leipold, C. E. Garner, et al., "ODISSEE – A Proposal for Demonstration of a Solar Sail in Earth Orbit," Proceedings of Third IAA Conference on Low-Cost Planetary Missions, Pasadena, CA, April 27 – May 1, 1998

1681) M. Leipold, C. E. Garner, "Solar Sails – Exploiting the Space Resource of the Solar Radiation Pressure," ESA Conference on 'Engineering and Economic Aspects into the 21st Century,' 20–22, Oct. 1998, Cagliari, Italy

1682) M. Leipold, M. Eiden, C. E. Garner, et al., "Solar Sail Technology Development and Demonstration," Proceedings of the 4th IAA International Conference on Low-Cost Planetary Missions, JHU/APL, Laurel, MD, May 2–5, 2000

1683) E. Wulf, M. Leipold, K. Lattner, S. Müncheberg, C. Widani, "Solar Sail Technology Development for Innovative Deep Space Exploration," Proceedings of IAC 2004, Vancouver, Canada, Oct. 4–8, 2004, IAC-04-Q.4.02

- Deployment phase consisting of boom deployment and sail deployment
- Post–deployment phase until reentry into Earth’s atmosphere.

The baseline orbit is defined by an altitude of 400 – 450 km, with an orbital inclination of 78°. The sailcraft is fixed to the fourth stage of the VOLNA rocket which will perform the orbit insertion burn.

- Solar sail deployment experiment with a sounding rocket. On Aug. 9, 2004, JAXA/ISAS (Japan) deployed two types of membrane structures, made of thin polyimide film (7 μm), near apogee (122 km) on a sounding rocket flight. During the ballistic flight, two types of membranes (solar sails) were deployed: a “cloverleaf type sail” and a “fan type sail.” The deployment scenario, using centrifugal force mechanisms, was documented with rocket–mounted cameras and transmitted to ground via telemetry. The cloverleaf sail deployment (10 m diameter) was successful – the first ever successful deployment of a good–sized sail in space, while the fan–type sail deployed only partially. ^{1684) 1685)}

- Team Encounter. The commercial company Team Encounter LLC of Houston, TX, is developing two solar sail missions:

- A mission called Earthview to demonstrate the deployment and control of a small solar sail, 20 m x 20 m in size. A launch of Earthview on Ariane–5 (ASAP) is planned for 2005 into GTO (Geosynchronous Transfer Orbit). The spacecraft is being built by MicroSat Systems of Littleton, CO, the sailcraft with the inflatable boom and solar sail (400 m² sail area) are being developed by L’Garde of Tustin, CA. – In Sept. 2003, NASA selected a commercial ride for the demonstration package ISC (Inertial Stellar Compass), namely Team Encounter.

- A second mission on Ariane–5 with a larger solar sail (4900 m² sail area) ¹⁶⁸⁶⁾ is planned for 2007. The objective is to transport a 3 kg payload out of the solar system by solar sail propulsion. The spacecraft consists of a rocket–powered “carrier” to boost the spacecraft out of Earth orbit, and a “sailcraft.”

- Solar Blade – a mission of CMU (Carnegie Mellon University), Pittsburgh, PA is called “Solar Blade Heliogyro Nanosatellite” (launch in 2005 ???). The objective is to demonstrate the solar sail concept for attitude precession, spin rate management, and orbital adjustments. The mission is supported within UNP (University Nanosatellite Program) of DoD and NASA. The S/C design concept (total mass of 5 kg) employs four solar reflecting blades, each 30 m x 1 m, constructed from ultrathin polyimide film. The blades are attached to a central spacecraft bus and are pitched along their radial axis. Embedded Kevlar and battens provide added stiffness and resistance to tears.

- NanoSail–D (NanoSail–Demonstration) is a small solar sail payload, a nanosatellite, designed and developed at NASA/MSFC in partnership with NASA/ARC (Ames Research Center) and several industry and academic partners. – A launch took place on Aug. 2, 2008 (test flight 003 of the Falcon–1 launch vehicle of SpaceX). **Unfortunately, the mission ended in failure about two minutes after launch**, when the SpaceX Falcon–1 launch vehicle experienced a problem during stage separation and was unable to achieve an Earth orbit. The objective was to demonstrate a successful sail deployment of 10 m² in space under proper attitude control to be followed with some “sailing” capability by using only the solar radiation pressure onto the sail as a propulsion means. ¹⁶⁸⁷⁾

- Fortunately, two units of the NanoSail–D satellites have been built. NASA/MSFC plans to launch the backup NanoSail–D payload from a 3U CubeSat (nanosatellite) of

1684) Y. Nishimura, Y. Tsuda, O. Mori, J. Kawaguchi, “The Deployment Experiment of Solar Sail with a Sounding Rocket,” Proceedings of IAC 2004, Vancouver, Canada, Oct. 4–8, 2004, IAC–04–IAF–A.5.10

1685) <http://www.isas.jaxa.jp/e/snews/2004/0809.shtml>

1686) J. Rogan, P. Gloyer, J. Pedlikin, G. Veal, B. Derbes, “Encounter 2001: Sailing to the Stars,” AIAA/USU Small Satellite Conference, Aug. 13–16, 2001, Logan, UT, SSC01–II–2

1687) http://www.nasa.gov/mission_pages/smallsats/nanosaild.html

ARC on the FASTSat–HSV mission. FASTSat is required to launch the nanosatellite before the NanoSail–D payload can be launched and deployed from the nanosatellite. – FASTSat–HSV is in turn a secondary payload on the STP–S26 mission of DoD. – A launch of STP–S26 took place on Nov. 20, 2010 from Kodiak Island, Alaska, on a Minotaur–4–HAPS (Hydrazine Auxiliary Propulsion System) expandable launch vehicle of OSC.

- **IKAROS** (Interplanetary Kite–craft Accelerated by Radiation Of the Sun) is a small–sized solar sail spacecraft technology demonstration mission of JAXA. IKAROS was launched on May 20, 2010 as a secondary payload to the primary mission of VCO (Venus Climate Orbiter), also referred to as Planet–C (~ 500 kg). The launch site was TNSC [(Tanegashima Space Center), Japan (Yoshinobu Launch Complex)]. The IKAROS spacecraft almost follows the trajectory of Planet–C, but will not actually be flown to Venus.

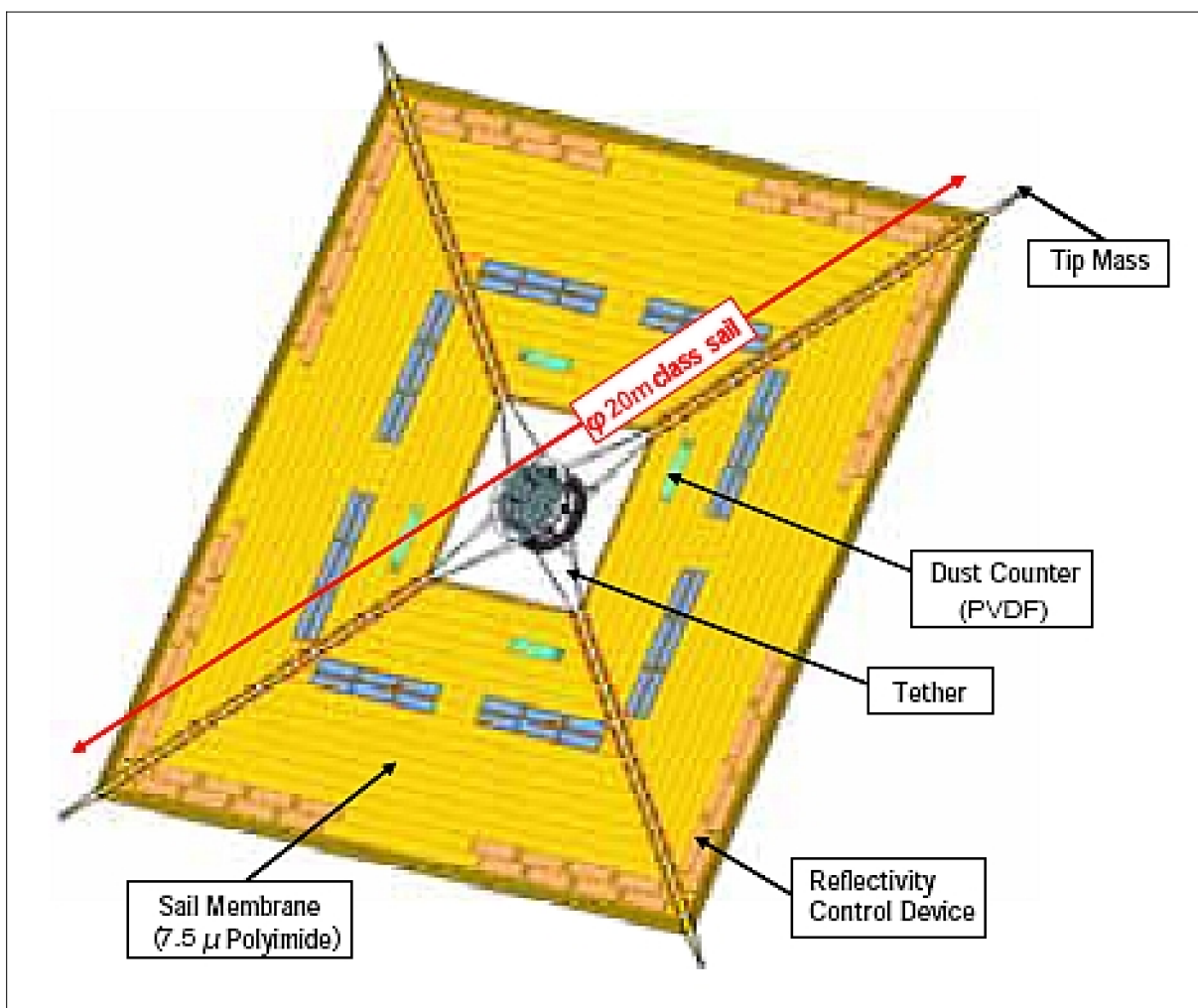


Figure 100: Illustration of the IKAROS satellite configuration (image credit: JAXA)

The deployed sail configuration is shown in Figure 100. The diagonal of the membrane is 20 m in length. The membrane fabric consists of polyimide with a thickness of $7.5 \mu\text{m}$ and covered with a 80 nm evaporated aluminum layer. The polyimide fabric features high thermal, mechanical and chemical resistance properties, along with a very light mass.

The membrane consists of four trapezoid petals. Thin–film Si solar cells are attached to certain areas of the membrane. They are capable of generating almost 500 W of power. The area covered by the thin–film solar cells covers only 5% of the total membrane surface area. The multilayer structure of the film prevents the solar cells from curling because of the symmetric mechanism. It also shields the solar cells from radiation.

In the sail deployment scheme, the membrane is deployed and kept flat by the spinning motion. Four masses are attached to the four tips of the membrane in order to support the deployment. Deployment consists of two stages. In the folded configuration, each petal is line-shaped and rolled up around the satellite. In the first stage, the rolled petals are extracted like a Yo-Yo despinner, and form a cross shape. The shape is maintained by stoppers.

JAXA engineers started the deployment of the solar sail of IKAROS on June 3, 2010 in two stages. Confirmation of a successful sail deployment was arrived at on June 10, when the sail was generating power through its thin film solar cells at about 7.7 million km from the Earth. (1688) (1689)

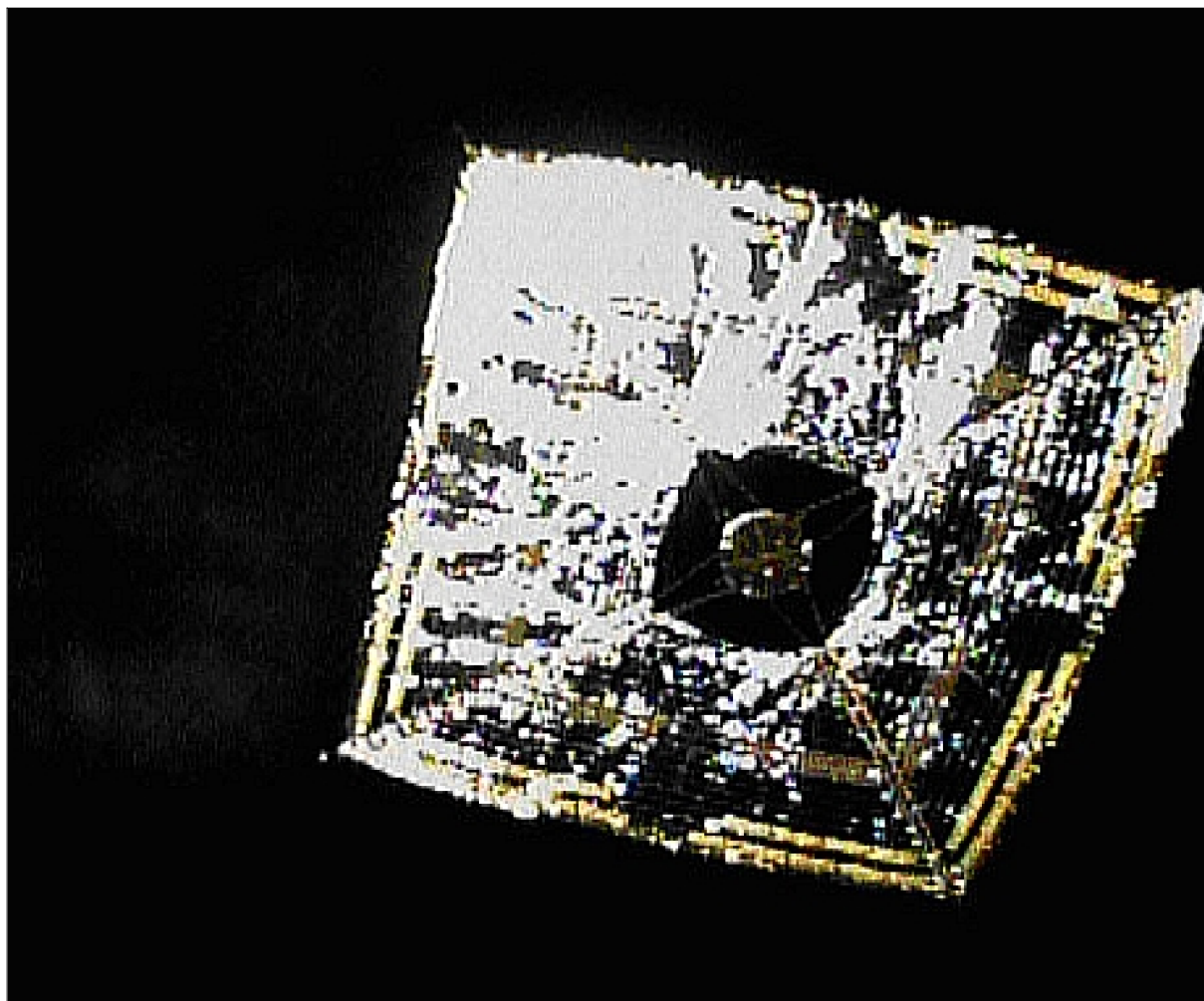


Figure 101: Image of the fully deployed IKAROS sail by the separation cameras (image credit: JAXA)

This achievement represents the first successful solar sail deployment in history – the most difficult step in solar sail unfolding technology and subsequent sailing activities. The solar sail of IKAROS employs both – photon propulsion and thin film solar power generation – during its interplanetary cruise. (1690)

- NanoSail–D2: In 2010, NanoSail–D2 is a NASA demonstration payload on the FASTSat–HSV minisatellite of DoD and NASA. FASTSat–HSV is in turn a secondary payload within the DoD STP–S26 multiple spacecraft mission (launch from Kodiak Island,

1688) “Small Solar Power Sail Demonstrator ‘IKAROS’ Successful Solar Sail Deployment,” JAXA, June 11, 2010, URL: http://www.jaxa.jp/press/2010/06/20100611_ikaros_e.html

1689) “Small Solar Power Sail Demonstrator ‘IKAROS’ Successful Image Shooting by Separation Camera,” JAXA, June 16, 2010, URL: http://www.jaxa.jp/press/2010/06/20100616_ikaros_e.html

1690) “Successful image shooting of solar sail by IKAROS separation camera,” JAXA, June 16, 2010, URL: http://www.jaxa.jp/projects/sat/ikaros/index_e.html

Alaska on Nov. 20, 2010). This time around, NanoSail–D2 is a 3U CubeSat to be deployed from FastSat–HSV. The solar sail subsystem occupies the lower 2/3 volume of the nanosatellite.

– For about 1½ months (Dec. 2010 and Jan. 2011), the NanoSail–D2 nanosatellite was actually stuck in its mothership, FASTSAT. Team members began to give up hope as weeks went by and NanoSail–D2 remained stubbornly and inexplicably onboard. The mission seemed to be over before it even began. *And then came Jan. 17, 2011. For reasons engineers still don't fully understand, NanoSail–D2 spontaneously ejected itself.* ¹⁶⁹¹⁾

– *In an unexpected reversal of fortune, NASA's NanoSail–D spacecraft has unfurled its sail (of size 9.2 m²) in LEO (Low–Earth Orbit) on January 20, 2011.* ^{1692) 1693)}

- LightSail–1 is a nanosatellite (a triple CubeSat configuration with a mass of ~ 5 kg and a deployed sail size of 32 m²) project of The Planetary Society (Pasadena, CA, USA) with the objective to demonstrate solar sail technology in a spaceborne mission (test of sail deployment and controlled flight). A launch of LightSail–1 is planned for 2014.

LightSail–1 is technically more ambitious than NanoSail–D, both because of its lower mass/area ratio (140 versus 300 grams per square meter), and because it has attitude control equipment that will allow it to maintain a commanded orientation relative to the sun, and hence will be able to produce a deliberately–directed solar sailing thrust force.

- Sunjammer: A NASA/GRC (Glenn Research Center) technology demonstration mission. The goal is to deploy and operate a sail of ~ 38 m on a side, with a sail area of ~ 1200 m² and a mass of ~ 32 kg. The TDM (Technology Demonstration Mission) aims to boost the TRL (Technology Readiness Level) of the L'Garde solar sail from ~ 6 to ~ 9.

The Sunjammer mission is co–manifested as a secondary payload with the DSCOVER mission of NASA. The launch is planned for late 2014 on a vehicle sponsored by the USAF. In December 2012, the USAF awarded a contract to SpaceX to launch DSCOVER aboard a Falcon 9 vehicle. ¹⁶⁹⁴⁾

1.14.3 Tether Experiments

Tether experiments in space (see M.53). A space tether is a long cable used to couple a spacecraft with an end mass (conceptually a link between two objects in space). Tethers are usually made of thin strands of high–strength fibers or conducting wires. Although the idea of using space tethers goes back to the 1960s, it was the launch of TSS (Tethered Satellite System) in 1993 on Shuttle mission STS–46, which gave a decisive impetus to tether technology development and projects, by realizing the potential of tethers to meet a broad range of applications in various fields. Tether deployment techniques and stable operations were the dominant themes of the early years including the 1990s. Potential tether applications include: propulsion (orbit changes), payload capture and release, power generation, atmospheric studies [a) reaching otherwise inaccessible flight regions with downward deployed tethers; b) active experimentation with the surrounding plasma], and gravity experiments. First detailed studies of space tether technology were carried out in the 1970s

1691) Tony Phillips, “Solar Sail Stunner,” NASA, January 24, 2011, URL: http://science.nasa.gov/science–news/science–at–nasa/2011/24/jan_solarsail/

1692) Steve Cole, Kim Newton, “NASA Partners On Nanosail–D Amateur Astronomy Image Contest,” NASA release: 11–027, Jan. 24, 2011, URL: http://www.nasa.gov/home/hqnews/2011/jan/HQ_11–027_NanoSail.html

1693) “NanoSail–D Flies Free,” Space Travel, Jan. 28, 2011, URL: http://www.space–travel.com/reports/NanoSail_D_Flies_Free_999.html

1694) “SpaceX Awarded Two EELV Class Missions From The USAF,” Space Travel, Dec. 07, 2012, URL: http://www.space–travel.com/reports/SPACEX_Awarded_Two_EELV_Class_Missions_From_The_USAF_999.html

and early 1980s by Guiseppe Colombo (1920–1984) of the University of Padua, Italy. Colombo envisioned that tethers could be used for transferring payloads to higher orbits, building space structures, and generating power for space platforms. This led eventually to the definition of project TSS (Tethered Satellite System).^{1695) 1696)}

Since the space tether makes it possible to transfer energy and momentum from one object to another, it can legitimately be called a form of space propulsion. There are two general categories of tethers:¹⁶⁹⁷⁾

- **Momentum–exchange tethers** (MET, nonconductive tethers representing passive propulsion). These tethers permit momentum and energy to be transferred between objects in space, enabling a tether system to toss spacecraft from one orbit to another.
- **Electrodynamic tethers** (EDT, conductive tethers representing active propulsion and power generation). These tethers interact with the Earth’s magnetosphere to generate power or propulsion without consuming propellant. There are two subclasses:
 - Electrodynamic power or tether drag system.
 - Electrodynamic thrust tether system.

As of the late 1990s spaceborne tethers are indeed an experimental reality (there are numerous projects) and their potential is far from being fully appreciated. The future of tether space technology looks rather bright providing capabilities and low–cost services for many applications. A very active company in this field is TUI (Tethers Unlimited Inc.) of Lynnwood, WA, USA, offering their expertise and a number of solutions such as:^{1698) 1699)}

- Terminator, a spacecraft deorbiting system.¹⁷⁰⁰⁾ The Terminator Tether™ is a small device that uses electrodynamic tether drag to deorbit a spacecraft. Because it uses passive electromagnetic interactions with the Earth’s magnetic field to lower the orbit of the spacecraft, it requires neither propellant nor power.
- μ PET™ (Microsatellite Propellantless Electrodynamic Tether) propulsion system that will provide propulsive capabilities to microsatellites and other small spacecraft without consuming propellant.
- The so–called Hoytether™ represents a fail–safe tether solution (resistant to impact damage) using synthetic fibers in a weblike arrangement.

Mission (Agency)	Launch (Timeframe)	Orbit	Tether Length	Comment
Gemini–11(NASA)	Sep. 11–15,'66	LEO	30 m	Spin–stabilized, 0.15 rpm
Gemini–12(NASA)	Nov. 11–15,'66	LEO	30 m	Local vertical, stable swing
H–9M–69	1980	Suborbital	500 m	Partial deployment
S–520–2	1981	Suborbital	500 m	Partial deployment
Charge–1	1983	Suborbital	500 m	Full deployment

1695) <http://infinity.msfc.nasa.gov/Public/ps01/ps02/table1.html>

1696) Note: The objective of the Gemini tether missions was to see if tethers could be used for rendezvous and docking in preparation for the future moon missions. A parachute cable was used as the tether, which was attached to the Agena by a spacewalking astronaut. The other mission (Gemini–11) experimented with rotation about the CM (Center of Mass) to see if it was stable – it was. The Gemini missions were not electrodynamic in nature, nor were they performed for scientific purposes – as were the TSS missions.

1697) C. Murakami, “On Orbit Control Using Gravity Gradient Effect,” Acta Astronautica, Vol.8, No.7, 1981, pp. 733–747

1698) <http://www.tethers.com/index.html>

1699) R. P. Hoyt, “The μ Torque Momentum–Exchange Tether Experiment,” STAIF 2002 (Space Technology and Applications International Forum), Albuquerque, New Mexico, Feb. 3–7, 2002

1700) R. Hoyt, R. Forward, “The Terminator Tether™: Autonomous Deorbit of LEO Spacecraft for Space Debris Mitigation,” AIAA 38th Aerospace Sciences Meeting & Exhibit, Jan. 10–13, 2000, Reno, Nevada, USA, AIAA 00–0329

Mission (Agency)	Launch (Timeframe)	Orbit	Tether Length	Comment
Charge-2	1984	Suborbital	500 m	Full deployment
ECHO-7	1988	Suborbital		Magnetic field aligned
Oedipus-A (NRC/NASA, CRC, CSA)	Jan. 30, 1989	Suborbital	958 m	Spin-stabilized, 0.7 rpm (Canada/USA)
Charge-2B	1992	Suborbital	500 m	Full deployment
TSS-1 (STS-46) (ASI/NASA)	Jul. 31 - Aug. 8, 1992,	LEO	< 270 m	Electrodynamic tether, partial upward deployment and retrieval of tether
SEDS-1 (NASA)	Mar. 29, 1993	LEO	20 km	Nonconducting tether, downward deployment, swing and cut
PMG (DoD) Plasma Motor Generator	June 26, 1993	LEO	500 m	Electrodynamic tether, upward deployment, tether current in both directions. Demonstration of hollow cathode plasma contactors for current collection and emission
SEDS-2 (NASA)	Mar. 9, 1994	LEO	20 km	Local vertical stable, downward deployment
Oedipus-C (NRC/NASA, CRC, CSA)	Nov. 6, 1995	Suborbital	1 km	Spin-stabilized, 0.7 rpm (Canada/USA)
TSS-1R (STS-75) (ASI/NASA)	Feb. 22 - Mar. 9, 1996	LEO	19.6 km	Electrodynamic tether, severed prior to full deployment
TIPS (NRO/NRL)	May 12, 1996 Jun. 20, 1996 deployment	LEO	4 km	Long life tether of 2.5 mm diameter (tracking of one year). The tether was still in orbit as of 2000.
YES (ESA, Delta-Utec, students)	Oct. 30, 1997	GTO	35 km	YES (of TEAMSAT) was deployed; but tether could not be deployed
STEX/ATEX (NRO/NRL)	Oct. 3, 1998 Jan. 16 1999 deployment	LEO	6 km	Nonconductive tether, planned demonstration of tether system stability and control. However, a deployment malfunction caused an experiment failure
PICOSAT1.0 (The Aerospace Corporation)	Jan. 27, 2000 on OPAL of Stanford	LEO	30 m	PICOSAT1.0 was ejected OPAL on Feb 6, 2000. The system of two S/C operated for 3 days when battery power decayed.
PICOSAT1.1 (The Aerospace Corporation)	July 19, 2000 on MightySat II.1 of AFRL	LEO	30 m	PICOSAT1.1 was ejected successfully from Mightysat II.1 13 months after launch (Sept. 2001) to test storage effects on the system and to demonstrate ideas on on-board and on-call operations.
METS (MIR Electrodynamic Tether System)	2001	LEO	5 km	Considered to be the first practical application of non-rocket propulsion in space. - However, However, METS was never realized but remained in the proposal stage.
ProSEDS (NASA)	2006	LEO	15 km	Upward deployment (producing drag and electrical power). The tether consists of 5 km bare wire plus 10 km of Spectra tether.
MAST (TUI, Stanford)	April 17, 2007	LEO	1 km	Deployment of 3 CubeSats. However, only a few meters of deployment could be achieved.
YES2 (ESA, Delta-Utec, students)	Sept. 14, 2007 YES2 deployment/reentry Sep7. 25, 2007	LEO	31.7 km	Deployment from Foton-M3 satellite of Russia. Demonstration of SpaceMail technology, i.e. delivery of a small payload in a tethered reentry capsule

Table 86: Chronology of tether missions

1.15 ISS (International Space Station) Build–up Phase

The ISS (International Space Station) build–up era in LEO began in 1998. – The program of an international space station was first announced/initiated by President Reagan in his ‘State of the Union’ address on Jan. 25, 1984. A total of 45 US/Russian missions are planned up to 2005 to assemble more than 100 elements that will complete the International Space Station (total mass of 460 tons of structures and equipment). Other nations, participating in the ISS project (besides the USA and Russia), include: Brazil, Belgium, Canada, Denmark, France, Germany, Italy, Japan, the Netherlands, Norway, Spain, Sweden, Switzerland and the United Kingdom (all of Europe is represented through ESA). ISS is the largest space structure ever built and represents also the largest cooperative space research program in the history of space flight (with the participation of 15 countries, for about 25 years).

When assembled ISS will have dimension of: 108 m in length and 74 m in width. The total mass will be more than 460 tons, representing the largest man–made object in Earth orbit. Three of the four operational Shuttles – Discovery, Atlantis and Endeavour – have been modified for increased lift capability (16,000 kg max payload into orbits of 51.6° inclination) to meet the projected needs of ISS. See chapter L.1 for some ISS payload descriptions relating to Earth observation.

- **ISS orbit:** The ISS target orbit altitude is 360 – 460 km, orbit inclination is 51.6°. The increased inclination (from normally 28° for Shuttle flights from KSC) has two advantages: 1) it permits servicing of the ISS from the Russian launch site at Baikonur, and 2) the increased inclination of 51.6° offers a considerably larger observation coverage of the Earth. About 75% of the Earth’s land area and approximately 95% of the Earth’s population is covered with ISS overflights.

The ISS orbit varies in altitude from approximately 460 km to 360 km, based on the paradigm that the Station vehicle is being boosted to it’s maximum altitude every 90 days and allowed to drift down to it’s minimum altitude. This 90–day drift allows for a significant increase in the microgravity period available in comparison to the Space Shuttle. Due to the westward precession of orbit tracks, the ISS overflies the same location every three days, with the identical lighting conditions being repeated every three months.

- The ISS will be a multi–module vehicle when completed, providing research laboratories, stowage for scientific and logistics items, an external truss that accommodates unpresurized payloads, and living quarters for up to seven crew members. Of the four research laboratories, two are supplied by the United States, one by ESA, namely COF (Columbus Orbital Facility), and one by JAXA, the JEM (Japanese Experiment Module). – Each of these laboratories provides for the installation of ISPRs (International Standard Payload Racks), a large commercial structure (size of a refrigerator) that provides a mounting place for a variety of equipment. The United States Laboratory, called Destiny, has 24 locations for ISPRs, of which 13 will be devoted to research capabilities and the remaining 11 to systems functions such as environmental control. In addition, there will be the MLM (Multipurpose Laboratory Module), the RM (Research Module) of Rosaviakosmos, Russia. MLM is the modified (yet unlaunched) backup FGB–2 (Functional Cargo Block–2); it will eventually be docked to the nadir port of FGB “Zarya”. MLM will provide ISS roll control maintenance; it will also serve as a docking port for “Soyuz” and “Progress” vehicles. ¹⁷⁰¹⁾

– The first component of ISS, namely **FGB** (Functional Cargo Block), also referred to as **Zarya** (meaning ‘sunrise’), was launched Nov. 20, 1998 on a Proton vehicle from the Baikonur Cosmodrome in Kazakhstan. Zarya serves as the cornerstone of ISS, it is a 20,040 kg pressurized module. Zarya was built for NASA by KhSC ((Khrunichev State Research and

1701) S. K. Shaevich, “Multipurpose Laboratory Module on the Base of the FGB–2, FGB “Zarya” Module Backup – A Step of the ISS Further Development,” Proceedings of IAC 2004, Vancouver, Canada, Oct. 4–8, 2004, IAC–04–T.1.08

Production Space Center) of Moscow in cooperation with Russian space industry, under contract with the US Boeing Company.

- The second component of ISS, Unity (11,800 kg, 11 m in total length), referred to as Node 1, with six berthing ports, was launched Dec. 4, 1998 on Shuttle (STS–88, Endeavour) and mated to Zarya three days later.

- The STS–96 Shuttle flight on Discovery (May 27 – June 6, 1999) carried a) internal logistics and resupply cargo for station outfitting, and b) an external Russian cargo crane that was mounted to the exterior of the Russian station segment and used to perform space-walking maintenance activities.

- The STS–101 flight on Atlantis (May 19 – 29, 2000, assembly mission 2A.2a) services were: a) prepared the station for the arrival of the Zvezda Service Module, b) installed four new batteries, 10 new smoke detectors and four new cooling fans on the Zarya module, c) installed the final parts of the Strela crane on Pressurized Mating Adapter 1, d) removed and replaced the early communications system antenna, and e) installed handrails on the Unity module.

- The Russian–built Zvezda (meaning “star”) Service Module (SM) was launched on July 12, 2000 by a Proton–K vehicle from Baikonur (ISS assembly mission 1R). Zvezda was docked to ISS on July 26, 2000. The Zvezda Service Module provided a) the first primary living quarters for three–person crews, b) primary docking port for Progress–type cargo resupply vehicles, c) power and steering (propulsive attitude control and reboost) capability to keep ISS in a safe orbit.

- Aug. 6, 2000 launch of Russian Soyuz–2 from Baikonur on ISS flight 1P with the Progress M1–3 resupply ship for ISS. Progress docked with ISS on Aug. 9, 2000.

- The STS–106 flight of Atlantis (Sept 8–20, 2000) provided a) internal logistics and re-supply cargo for station outfitting, b) a space walk was conducted to perform maintenance on the station.

- STS–92 flight of Discovery (Oct. 11–24, 2000, ISS–05–3A assembly flight) provided: ITS (Integrated Truss Structure) Z1, PMA–3 (Pressurized Mating Adapter–3), a Ku–band communications system, and CMGs (Control Moment Gyroscopes) for non–propulsive attitude control (see also 1.23.2.6). ITS–Z1 is an early exterior framework to allow first U.S. solar arrays on flight 4A to be temporarily installed on Unity for early power. The Z1 truss is the first permanent lattice–work structure for ISS.

- A Russian Soyuz rocket (launch Oct. 31, 2000) lifted the first expedition crew to ISS from Baikonur, referred to as ISS–2R. Objectives: a) to establish the first station manning with a three–person crew (Commander Bill Shepherd; Soyuz Commander Yuri Gidzenko, Flight Engineer Sergei Krikalev), b) provides Russian assured crew return capability without the Shuttle present, c) **the “permanent” habitation of ISS has begun.**¹⁷⁰²⁾

- STS–97 flight of Endeavour (Nov. 30 – Dec. 11, 2000). The ISS assembly flight 4A provided the P6 Integrated Truss Segment, a 7700 kg package containing the PV (Photovoltaic) Module, plus S4 and S5 radiators. The US–provided power system increases the available electrical power of ISS by a factor of five. The P6 consists of two identical PVAAs (Photovoltaic Array Assembly), each of which is made up of an SAA (Solar Array Assembly) and a SAW (Solar Array Wing). The two SAWs have a total power generation capability of about 64 kW. Each SAW has a structure size of 35 m x 11.58 m and a mass of 1087 kg. Each SAW contains 33,000 solar arrays, each of size 8 cm x 8 cm with 4,100 diodes. The entire assembly represents the largest structure deployed in space so far (73 m from tip to tip) as well as the largest space–installed power supply.

¹⁷⁰²⁾ <http://spaceflight.nasa.gov/station/assembly/flights/2000/2r.html>

- STS–98 flight of Atlantis (Feb. 7 – 20, 2001). The ISS assembly flight 5A carried the Destiny Laboratory Module, an aluminum structure of 8.5 m in length and 4.3 m in diameter. The module provides an initial US user capability in the field of near–zero gravity research. The Destiny module features also a nadir–looking **window** (50 cm in diameter) of the best optical quality ever flown on a crewed spacecraft.¹⁷⁰³⁾

Use of the window for future Earth science research will begin in earnest sometime after the research infrastructure, called **WORF** (Window Observational Research Facility), is brought to the space station and installed behind the Laboratory (Destiny) window. WORF will enable researchers to mount cameras, sensors and telescopes behind the window, and to hook up with power, thermal control, and other systems. WORF was launched on STS–131 in April 2010.

- STS–102 flight of Discovery (March 8–21, 2001). The ISS logistics and resupply flight 5A.1 provided the Leonardo MPLM (Multi–Purpose Logistics Module). The module is about 6.4 m long and 4.6 m in diameter containing equipment racks. Exchange of first crew by a new crew.

- STS–100 flight of Endeavour (April 19 – May 1, 2001). The assembly flight 6A provided the Raffaello MPLM (lab outfitting) for the US Lab, the UHF antenna (for EVA support), and delivery/installation of the Canadian SSRMS (Space Station Remote Manipulator System), the cornerstone of ISS’s Mobile Servicing System (MMS), also referred to as **Canadarm2**. SSRMS, has been attached to the Destiny module and used as “construction crane” of ISS, lifting payloads and performing maintenance work. With the installation of Canada’s Mobile Base System (MBS) in June 2002 (STS–111), SSRMS is able to slide along the main truss of the station (lateral mobility), providing an additional functional capability with four Power Data Grapple Fixtures.^{1704) 1705)}

A further upgrade of Canadarm2 is planned for 2008 with SPDM (Special Purpose Dexterous Manipulator). This smaller two–armed robot has the capability to perform even more delicate tasks at ISS. SSRMS is 17.6 m long when fully extended and has seven motorized joints. This arm is capable of handling large payloads and assisting with docking the Shuttle.

- A Russian Soyuz spacecraft arrived at ISS on April 30, 2001 with the **first space tourist ever onboard, namely Dennis Tito**, a well–to–do US citizen who paid \$20 Million to Rosaviakosmos, the Russian Space Agency (one week stay at ISS). There was considerable criticism and protest from NASA officials prior to the launch, but Rosaviakosmos insisted on Tito’s mission. The agency wanted and needed the cash badly due to the abysmal lack of governmental funding for its space programs. Further space tourists are waiting in the wings for a flight to ISS.

- STS–104 flight of Atlantis (July 12–24, 2001, assembly mission 7A). Installation of an ISS Joint Quest Airlock. The airlock is the primary path for ISS space walk activity (entry and departure of astronauts or cosmonauts) without the presence of a Shuttle or a Soyuz. The airlock is a pressurized flight element consisting of two cylindrical chambers attached end–to–end by a connecting bulkhead and hatch. The airlock structure, built at MSFC, is 6 m in length and 4 m in diameter with a mass of about 6500 kg. There are two main components to the airlock: a crew airlock and an equipment airlock for storing EVA gear and EVA preflight preparations. STS–104 also carried a spacelab pallet with four High Pressure Gas Assembly containers that were attached to the exterior of the airlock.

1703) K. Scott, S. Biggar, D. Eppler, E. Zalewski, L. Brownlow, K. Lulla, “International Space Station Destiny Module Science Window Optical Characterization,” Proceedings of ISRSE (International Symposium of Remote Sensing of Environment), Honolulu, HI, Nov. 10–14, 2003

1704) M. Stieber, S. Sachdev, J. Lymer, “Robotics architecture of the mobile servicing system for the International Space Station,” Proceedings of the 31st International Symposium on Robotics, Montreal, Canada, May 2000, pp. 416–421

1705) Note: Canadarm1 is the standard payload handling system on Shuttle flights since STS–2 (Nov. 12–14, 1981) with a first deployment of Canadarm1 out of the cargo bay of Space Shuttle Columbia, on November 13, 1981

- STS–105 flight of Discovery (Aug. 10–22, 2001, assembly mission 7A.1). The STS–105 attached the Leonardo MPLM (Multi–Purpose Logistics Module), provided by ASI, containing US stowage racks and ISPRs (International Standard Payload Racks).
- A Russian Soyuz/TsSKB–Progress, launched from the Baikonur Cosmodrome in Kazakhstan on Sept. 21, 2001, delivered Docking Compartment–1 (DC–1) and a Strela boom of Rosaviakosmos to ISS. Also delivery of a portion (70 kg) of the CNES Andromède payload. DC–1 provides additional egress and ingress location for Russian–based space walks and a Soyuz docking port.
- A Russian Soyuz/TsSKB–Progress launch vehicle, launched on Oct. 21, 2001 from Baikonur, delivered a three–person crew to ISS for a 8–10 day mission (Oct. 21–31, 2001).¹⁷⁰⁶ The payload is TM–33 of Rosaviakosmos. The Soyuz vehicle was left at the station as a crew return vehicle. CNES of France is using this taxi flight for its Andromède technology mission (85 kg total mass) with investigations covering the fields of Earth observation, life sciences, and material sciences. The Earth observation payload consists of IMEDIAS (film and digital camera), designed to collect images of global change phenomena. In addition, the instrument LSO (Lightning and Sprite Observations) of CEA (Commissariat à l’Energie Atomique – the French Atomic Energy Agency) is used on ISS to measure emissions generated by lightning, sprites and elves. The measured data are needed to define parameters of a future CNES microsatellite mission instrument in France’s Myriade program.
- STS–108 UF–1 (Utilization Flight–1) of Endeavour (Dec. 5–16, 2001). The main element of this flight was the payload Raffaello MPLM (Multi–Purpose Logistics Module) with experiment racks for the US module Destiny.¹⁷⁰⁷
- STS–110 flight 8A of Atlantis (Apr. 8–19, 2002). The primary objective is to deliver and assemble the first segment of the ISS external truss, the S0 (S–Zero) truss of ITS (Integrated Truss Structure). Equipment installed on the truss includes MT (Mobile Transporter) and its associated power and data umbilical reels. MT (built by Boeing) creates a movable base for the station’s Canadian mechanical arm (Canadarm2), allowing it to travel along the station truss after delivery of the MBS (Mobile Base System). ITS has a length of 91 m and is attached to the US Lab.¹⁷⁰⁸
- STS–111 UF–2 (Utilization Flight–2) of Endeavour (June 5 – 19, 2002). The objectives are: 1) To deliver the Expedition Five crew to the ISS and return the Expedition Four crew to Earth. 2) MPLM (Multi–Purpose Logistics Module) carries experiment racks and three stowage and resupply racks to the station. 3) The US provided MBS (Mobile Base System) is installed on the Mobile Transporter to complete the MSS (Mobile Servicing System) of Canada. The MSS is used to perform ISS assembly operations as well as routine maintenance and video inspection tasks. At this stage, the MSS space segment includes several major elements: 1) Canadarm2 (SSRMS), 2) the MBS (Mobile Remote Servicer Base System) installed on the US–provided Mobile Transporter, 3) SPDM (Special Purpose Dexterous Manipulator), 4) the OCS (Operations Control Software), and 5) the AVU (Artificial Vision Unit). The MSS Operations Complex (MOC), supporting the unique operations of the sophisticated space robotics system, is the MSS ground segment.¹⁷⁰⁹ – The mechanical arm of Canadarm2 has now the capability to “inchworm” from the U.S. Lab fixture to the MSS and travel along the truss to work sites.
- STS–112 flight 9A of Atlantis (Oct. 7–18, 2002).¹⁷¹⁰ The main objective was the delivery and assembly of the right–side ISS truss segment (ITS S1) with a mass of 12,572 kg. The truss contains a new external cooling system for the station, a second S–band commu-

1706) “Andromède – A taxi flight devoted to science and technology,” CNES Magazine No 13, Sept. 2001, pp.5–6

1707) http://www.shuttlepresskit.com/sts-108/108_SPK.pdf

1708) <http://www.shuttlepresskit.com/STS-110/spk-110.pdf>

1709) G. Gibbs, S. Sachdev, B. Marcotte, R. Colley, M. Vachon, “Canada and the International Space Station Program: Overview and Status,” Proceedings of IAC, Bremen, Germany, Sept. 29 – Oct. 3, 2003

nications system to provide enhanced and extended voice and data capability, a cart CETA (Crew and Equipment Translation Aid) which serves as a mobile work platform for future spacewalkers, two new external television cameras and the first Thermal Radiator Rotary Joint (TRRJ).

- STS–113 flight ISS–11A of Endeavour (Nov. 24 to Dec. 7, 2002). Delivery of the Port–side (left–side) ISS truss segment (ITS–P1), assembly to S0. ITS–P1 has a mass of 12,572 kg. Both P1 and S1 trusses provide structural support for ATCS (Active Thermal Control Sys tem), the Mobile Transporter, a CETA (Crew and Equipment Translation Aid) cart, and antennas. ¹⁷¹¹⁾
- The Shuttle research mission STS–107, Columbia (not a flight to ISS), with a launch Jan. 16 and a scheduled return on Feb. 1, 2003, **experienced a reentry catastrophe on Feb. 1, disintegrating over Texas and resulting in the tragic loss of the crew of seven astronauts. Their names are: Rick Husband, William McCool, Kalpana Chawla, David Brown, Mike Anderson, Laurel Clark, and Ilan Ramon.** The accident resulted into the largest investigation ever by NASA, with help from many other institutions, finding clues (proof) as to the most possible causes of the accident. The Columbia tragedy has also entailed an examination of the US space program in addition to the accident investigation. ^{1712) 1713)}

As consequence of the investigation, the ISS build–up phase came to a complete halt. NASA is planning to resume Shuttle flights to ISS in 2005. The three remaining Shuttles are undergoing extensive tail repairs prior to being cleared for flight again.

During the long vacant period in Space Shuttle flights after the accident, Russia provided significant services to ISS through the provision of crew transportation and with unmanned Progress resupply flight capabilities, to safely maintain a human presence on–orbit. Indeed, a most appreciated and cooperative service by all involved.

- STS–114, ISS–LF1 (Logistics Flight 1) of Discovery (July 26–Aug. 9, 2005). **Return to flight test mission (after 2 1/2 years of Shuttle grounding).** The payload elements are: a) Raffaello MPLM (Multi–Purpose Logistics Module), b) delivery of the ESP–2 (External Stowage Platform) to ISS, c) removal and replacement of the CMG–1 (Control Moment Gyro–1). ¹⁷¹⁴⁾

During the mission, the astronauts Soichi Noguchi and Stephen Robinson performed a number of repair and maintenance jobs on the ISS and on shuttle during three spacewalks. The most important tasks to be done were:

- 1) They inspected the underside of the Shuttle and tested some new techniques for replacing or repairing damaged tiles on the Shuttle.
- 2) They removed and replaced one of the four CMGs used to orient the ISS (a CMG has a mass of 227 kg). The broken CMG–1 failed on June 8, 2002, leaving ISS with two primary CMGs and one spare for momentum management. That spare shut down in 2004 when a circuit breaker failed. Though subsequently repaired, it failed again in March 2005. The astronauts were also able to fix the faulty circuit breaker of the spare CMG. Hence, the ISS attitude control system is complete again after a successful repair during the EVA on Aug. 1, 2005.
- 3) During the third spacewalk, Noguchi and Robinson installed and activated an External Stowage Platform on the Station’s Quest Airlock. Noguchi also installed another MISSE

1710) <http://www.shuttlepresskit.com/STS-112/spk-112.pdf>

1711) http://www.shuttlepresskit.com/STS-113/SPK_sts-113.pdf

1712) “Columbia Crew Survival Investigation Report,” NASA/SP–2008–565, URL: http://www.nasa.gov/pdf/298870main_SP-2008-565.pdf

1713) http://www.shuttlepresskit.com/STS-107/STS-107_SPK.pdf

1714) http://www.shuttlepresskit.com/STS-114/Presskit_RTF_STS114.pdf

(Materials International Space Station Experiment). Finally, Robinson rode the end of the Station's Canadarm2 to the underside of Shuttle Discovery to **remove gap fillers from between the orbiter's heat shielding tiles**. The latter task was critical for a safe return flight of the Discovery and its crew.

- STS-121, ULF1.1 (Utility and Logistics Flight 1.1) of Discovery, July 4–17, 2006 (13 day mission). The payload elements are: a) MPLM-7 (Leonardo), b) ICC (Integrated Cargo Carrier), and c) LMC (Lightweight Multi-Purpose Experiment Support Structure Carrier), AstroLab (EC-13). Other payloads are: MEPSI-2A (MEMS-based PicoSat Inspector) and MEPSI-2B of AFRL (DARPA-funded) and the 2nd "ball" of **SPHERES**. The mission was critical for the US space program's recovery from the disaster. Like last year's first post-Columbia flight, the latest shuttle mission was largely aimed at improving safety before NASA resumes regular launches to finish constructing the International Space Station by 2010. ¹⁷¹⁵⁾
- STS-115, flight 12A of Atlantis, Sept. 9–21, 2006 (12 day mission, resumption of ISS construction work, the last assembly flight was in 2002). The primary payload of this assembly flight is the Port 3/4 truss segment (mass of 15,700 kg, each truss has a length of 13.8 m and a width of 4.9 m), the next major addition to the 11-segment integrated truss structure. The P3/P4 integrated truss structure contains several discrete elements: two Solar Array Wings (SAW), Integrated Equipment Assembly (IEA), Solar Alpha Rotary Joint (SARJ), two Beta Gimbal Assemblies (BGA) and the Photovoltaic Thermal Control Subsystem. P3 consists of the SARJ, which continuously rotates to keep the solar array wings on P4 and P6 oriented towards the sun as the station orbits the Earth. ¹⁷¹⁶⁾

Following its installation utilizing both the Shuttle and the station robotic arms, a series of three space walks will complete the final connections and prepare for the deployment of the station's second set of solar arrays. The P3/P4 truss, with its two large solar arrays (73 m in length with a new set of photovoltaic solar arrays), will provide one-fourth of the total power generation capability of the completed station in 2010 (110 kW). The truss also contains a device called SARJ (Solar Alpha Rotary Joint), capable to rotate 360° either clockwise or counterclockwise to position the P4 and P6 solar arrays to track the sun for electrical power generation. ¹⁷¹⁷⁾

Other payloads are: MEPSI-3A (MEMS-based PicoSat Inspector) and MEPSI-3B of AFRL (DARPA-funded).

- STS-116, flight 12.A.1 of Discovery, Dec. 10–22, 2006 (13 day mission). Delivery of three primary payloads: a) the third port truss segment, b) the Spacehab single logistics module (transfer of supplies, hardware and experiments to and from ISS), and c) the ICC (Integrated Cargo Carrier) with the service module debris panels and the DOD space transportation program deployable experiments. ¹⁷¹⁸⁾

The P5 Truss connects the power and cooling lines and serves as a spacer between the P4 photovoltaic module (PVM), or solar battery, and P6 PVM, which will be joined during a later assembly mission. The P5 Truss has a mass of 1864 kg and a size of 3.37 m x 4.55 m x 4.24 m. The Truss element is installed robotically with a crew assist. P5 also contains a remote sensor box, two tri-axial accelerometers and two antenna assemblies as part of the EWIS (External Wireless Instrumentation System). ICC contains the following payloads: SMDP (Service Module Debris Panels), STP-H2 (Space Test Program-H2), 15 AMPs (Adjustable Mass Plates), and ISS-PFRAM (Passive Flight Releasable Attachment Mechanism).

¹⁷¹⁵⁾ http://www.nasa.gov/pdf/149873main_sts121_press_kit.pdf

¹⁷¹⁶⁾ <http://www.nasaspaceflight.com/content/?cid=4667>

¹⁷¹⁷⁾ http://www.nasa.gov/pdf/154433main_sts115_press_kit3.pdf

¹⁷¹⁸⁾ http://www.shuttlepresskit.com/STS-116/Presskit_STS116.pdf

The ISS control system is composed of Russian and US segments that maintain attitude control (a fixed attitude relative to the surface of the Earth). When the Russian segment is in control, it uses **thrusters**, which consume a propellant. When the US segment is in control, the **CMGs** (Control Moment Gyroscopes) are used which consume replenishable electric power from the ISS solar array structure. The 4 CMGs are mounted on the Z1 truss initially installed in October 2000 (STS–92 flight, Oct. 11–24, 2000).

To maintain the station in the desired attitude, referred to as TEA (Torque Equilibrium Attitude), the CMG system must cancel or absorb the momentum generated by the disturbance torques acting on the station (contribution of gravity gradient, atmospheric drag, solar pressure, and geomagnetic interactions).

A CMG consists of a large flywheel (100 kg) that rotates at a constant speed of 6,600 rpm and provides an angular momentum of 4,880 Nms (newton meter second) about its spin axis. Each CMG has diameter of 1.22 m, a mass of 227 kg, and is capable of producing a torque of up to 257 Nm. The rotating wheel is mounted in a two–degree–of–freedom gimbal system capable of pointing the spin axis of the wheel into any direction. Control motors on the CMG gimbals change the orientation of the spinning rotors to produce a torque on the station to balance the effects of gravity and aerodynamics, maintaining the station at an equilibrium attitude without using a propellant.

At least two CMGs are needed to provide attitude control; they are the minimum necessary to steer and steady the station in its orbital path. The energy of CGMs is provided by the solar arrays of the Station, a replenishable resource.

Up to mid–2007, the ISS had three CMGs operating nominally. The 4th one had been shut down due to a high vibration behavior in late 2006. This CMG was replaced by astronauts of the STS–118 Shuttle flight.

On Nov. 5, 2006, a new method of performing large angles of ISS rotations was flight tested using the CMGs. The ISS was maneuvered through a pre–planned trajectory, referred to as **ZPM** (Zero Propellant Maneuver), a method developed at Draper Laboratory of Houston, TX. – The ZPM is accomplished using the current Station controllers and effectors without modification to flight software. This flight demonstration of the ZPM method successfully completed a 90° rotation of ISS using only three CMGs. The maneuver used 80 combined attitude and rate commands spaced 90 seconds apart, taking a total time of approximately 2 hours. An equivalent maneuver using the Station thrusters would have taken less time but would have consumed costly propellant (Ref. 1719).

On March 3, 2007, the ISS was rotated by 180° using the ZPM method (Ref. 1720). The maneuver was completed in 2 hours and 47 minutes and reached 76% of the CMG momentum capacity. The same 180° maneuver was performed with thrusters on Jan. 2, 2007 and consumed 50.8 kg of propellant. At an estimated \$ 20,000/kg, the 180° ZPM maneuver saved in fact \$1,120,000. – The impact of this new technology is to substantially reduce ISS lifetime propellant use, and avoid solar array contamination and loads (due to considerably reduced propellant exhausts).

Figure 102: Overview of the ISS Motion Control Subsystem 1719) 1720) 1721)

In addition, the third (and last) “ball”, a nanosatellite of the **SPHERES** (Synchronized Position Hold Engage and Reorient Experimental Satellites) system of MIT (sponsored by DoD) was delivered to ISS (Note: the first ball of SPHERES, 20 cm in diameter, was deliv-

1719) “Draper–Developed Trajectory Maneuvers ISS Without Using Propellant,” Jan. 4, 2007,, URL: http://www.space-daily.com/reports/Draper_Developed_Trajectory_Maneuvers_ISS_Without_Using_Propellant_999.html

1720) International Space Station Zero–Propellant Maneuver (ZPM) Demonstration (ZPM),” NASA, June 27, 2008, URL: http://www.nasa.gov/mission_pages/station/science/experiments/ZPM.html

1721) N. Bedrossian, S. Bhatt, M. Lammers, L. Nguyen, Y. Zhang, “First Ever Flight Demonstration of Zero Propellant Maneuver™ Attitude Control Concept,” URL: http://www.elissar.biz/uploads/LSR_ZPM.pdf

ered to ISS on April 24, 2006 on a Soyuz–U launch vehicle with the Progress M–56 payload). SPHERES consists of 3 free–flying satellites inside the ISS. They’re equipped with a cold gas propulsion system for maneuverability; they communicate with each other using radio and ultrasonic frequencies. The satellites will test autonomous formation flying, rendezvous and docking techniques (see description of SPHERES on eoPortal).

The STP–H2 of DoD is a payload which deployed the following satellites after the Shuttle undocked from ISS (Dec. 21, 2006) using the newly developed CAPE (Canister for All Payload Ejections) system: ¹⁷²²⁾ ¹⁷²³⁾ ¹⁷²⁴⁾

– a) Two microsatellites called **ANDE** (Atmospheric Neutral Density Experiment); the objective is to measure the density and composition of Earth’s thermosphere (see ANDE description on eoPortal).

– b) **MEPSI** (MEMS–based PicoSat Inspector) of AFRL to demonstrate the use of picosats for inspection services;

– c) **RAFT** (Radar Fence Transponder), student experimental satellites, two CubeSats, of the USNA (US Naval Academy), Annapolis, MD. The objective of RAFT is to calibrate the US Space Surveillance Network’s (SSN) radar fence. As one RAFT picosat flies through the radar fence, it will transmit its location. When the second picosat flies through the radar fence, it exercises the radar fence’s locating capability. This effort will improve the SSN’s ability to track small Resident Space Objects. RAFT also contains an amateur radio onboard to train midshipmen at Annapolis in communications.

- STS–117, flight 13A of Atlantis June 8–22, 2007 (14 day mission). Delivery and addition of ITS (Integrated Truss Segment) Starboard–3/Starboard–4 (S3/S4), the primary payload for power generation (dimension 13.66 m x 4.6 m and a mass of 16,200 kg). The S3/S4 segments were attached to the S1 segment by the robotic arm. ¹⁷²⁵⁾

- STS–118, flight 13A.1 of Endeavour Aug. 8–21, 2007 (13 day mission). Delivery of the Starboard 5 (S5) segment as prime payload. S5 is part of the 11 segment ITS (Integrated Truss Structure) and the third starboard truss element to be delivered. S5 has a size of 3.37 m x 4.55 m x 4.24 m and a mass of 1810 kg. S5, providing about 1/4 of the stations total power, is used primarily to connect power cooling lines and serve as a spacer between the S4 PVM (Photovoltaic Module) and the S6 PVM (to be joined in another assembly mission). Further payloads are: ESP–3 (External Stowage Platform–3), an external pallet that can securely hold up to seven critical spare parts or ORUs (Orbital Replacement Units) for the station. It was attached to the Port 3 truss element. The parts flown on ESP–3 include a CMG (Control Moment Gyroscope), the NTA (Nitrogen Tank Assembly) and the BCDU (Battery Charge/Discharge Unit). ¹⁷²⁶⁾

- STS–120, assembly flight 10A of Discovery, Oct. 23–Nov. 7, 2007 (16 day mission). Delivery and integration of Node 2, referred to as the connecting module “**Harmony**”. ¹⁷²⁷⁾ The addition of Harmony to the ISS sets the stage for the arrival of new research laboratories in upcoming Shuttle missions such as the “Columbus” module from ESA and JEM (Japanese Experiment Module), referred to as “Kibo”, from JAXA.

Harmony has dimensions of 7.3 m in length and 4.5 m in diameter, the mass is 14,200 kg. The module is being used as a utility hub, providing air, electrical power, water and other sys-

¹⁷²²⁾ A. F. Meza, “DoD Experiments Launch Aboard Space Shuttle Discovery,” *Horizons*, Vol. 32, Issue 1, Winter 2006/7, pp. 21–22, URL: <http://www.aiaa-houston.org/newsletter/jan07/jan07.pdf>

¹⁷²³⁾ N. Bedrossian, S. Bhatt, A. Alaniz, E. Mc Cants, L. Nguyen, Greg Chamitoff, “ISS Contingency Attitude Control Recovery Method for Loss of Automatic Thruster Control,” Proceedings of the AAS Guidance and Control Conference, Breckenridge, CO, USA, Feb. 1–6, 2008, paper: AAS 08–001

¹⁷²⁴⁾ G. W. Vajdos, “International Space Station GN&C: 2006 Year in Review,” Proceedings of the 30th Annual AAS GNC 2007 (Guidance & Navigation Conference), Breckenridge, CO, USA, Feb. 3–7, 2007, AAS 07–094

¹⁷²⁵⁾ http://www.nasa.gov/pdf/169469main_STS-117_Press_Kit_final.pdf

¹⁷²⁶⁾ http://www.nasa.gov/pdf/182728main_STS-118_Press_Kit.pdf

¹⁷²⁷⁾ http://www.nasa.gov/pdf/192719main_STS120_Shuttle_Press_Kit.pdf

tems essential to support life on the station. Harmony will distribute resources from the station's truss to the Destiny laboratory, to the Columbus module of ESA, and to the Kibo module of JAXA. Harmony will act as an international connecting port and passageway to additional science labs and cargo spacecraft. The exterior of Harmony will serve as a work platform for the station's robotic arm, Canadarm2.

Harmony was designed and built for NASA by TAS (Thales Alenia Space) of Torino, Italy as part of an agreement between NASA and ESA. The Boeing Company provided many sub-systems of Harmony and installed five ACBMs (Active Common Berthing Mechanisms). The mechanisms enable on-orbit mating and airtight seals between the station and its pressurized elements. The ACBMs consist of powered, computer-controlled components that align capture and are secured to the passive CBMs (Common Berthing Mechanisms). The Boeing-built PMA (Pressurized Mating Adapter) permit pressurized spacecraft to dock with one-another despite differences in the diameters of the spacecraft adapters.

As part of assembling the Harmony module, the astronauts will relocate the Port 6 (P6) truss elements and solar arrays to a permanent position (reattachment to the P5 truss).

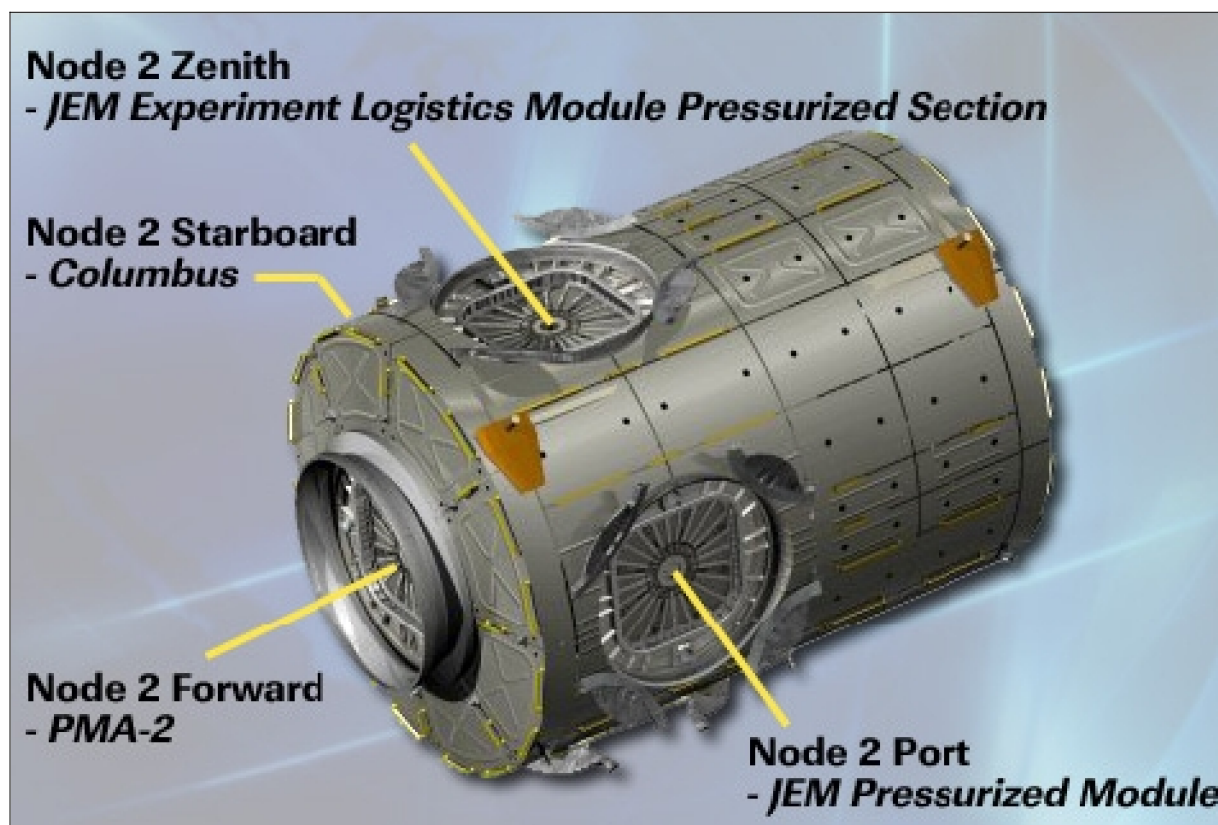


Figure 103: Illustration of Harmony's future port utilization at the ISS (image credit: NASA)

- STS-122, assembly flight 1E of Atlantis, Feb. 7-20, 2008 (13 day mission). The prime objective is the delivery and installation of ESA's (European Space Agency's) **Columbus Laboratory** - ESA's biggest contribution to the ISS (built by EADS Space Transportation). Three EVAs are needed to install the Columbus Laboratory at the US Node 2 of ISS, called Harmony. The addition of Columbus will expand the research facilities of the station and provide scientists around the world with the ability to conduct a variety of life, physical and materials science experiments. ^{1728) 1729)}

The 7 m long laboratory consists of a pressurized cylindrical hull 4.5 m in diameter, closed with welded end cones, providing a volume of 75 m³. The primary and internal secondary

1728) http://www.nasa.gov/pdf/203212main_sts122_presskit3.pdf

1729) http://www.esa.int/esaCP/SEMTO73R8F_index_1.html#subhead2

structures of Columbus are constructed from aluminum alloys. The mass of the Columbus Laboratory is 10,300 kg. It can accommodate 16 standard racks arranged around the circumference of the cylindrical section in four sets of four racks. When fully outfitted, Columbus will provide a shirt sleeve environment of 25 m³ in volume in which up to three astronauts can work. The laboratory is provided from the station with a nominal power supply of 25 kW of which 13.5 kW can be used for experimental facilities.

At launch, the laboratory is already outfitted with 2,500 kg of experiment facilities and additional hardware. This includes the ESA–developed experiment facilities such as: Biolab, Fluid Science Lab, and the European Physiology Modules Facility. The CSA (Canadian Space Agency) is flying MVIS (Microgravity Vibration Isolation System) in the Columbus Laboratory. MVIS uses a sophisticated system to control large gap Lorentz force actuators mounted on the Functional Core Element of the Fluid Sciences Laboratory (FSL) to damp out the ISS on–board vibrations during materials science experiments.

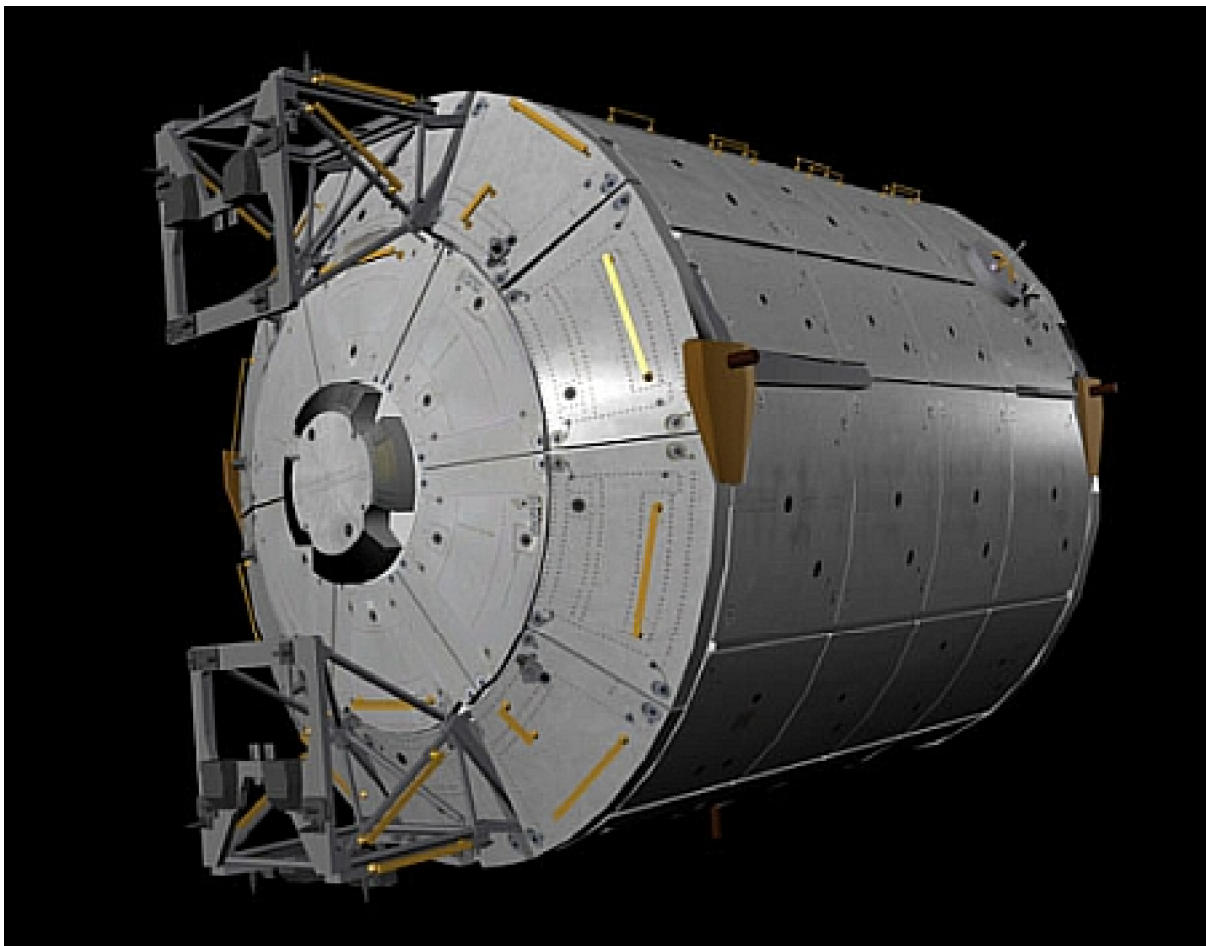


Figure 104: External view of the Columbus laboratory (image credit: ESA, NASA)

Outside its pressurized hull, Columbus has four mounting points for external payloads related to applications in the field of space science, Earth observation, technology and innovative sciences from space. Two external payloads will be installed after the Columbus is attached to the ISS: the **EuTEF** (European Technology Exposure Facility) carries a range of experiments, which need exposure to space, and the **SOLAR** observatory, with the objective to carry out a spectral study of the sun with unprecedented accuracy for a minimum of 18 months. The SOLAR payload consists of three instruments complementing each other. These are: SOVIM, SOLSPEC, and SolACES.

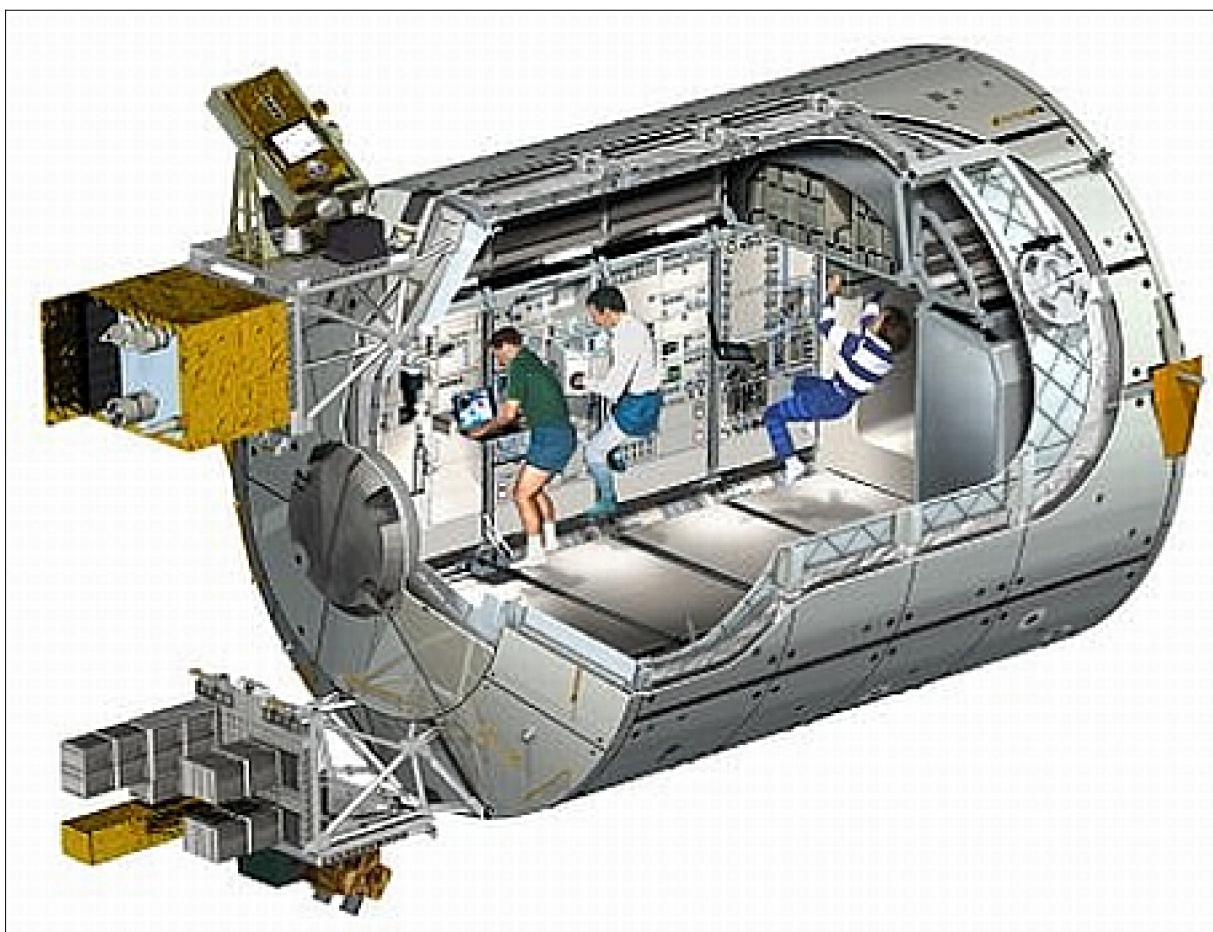


Figure 105: Cut-away view of the Columbus laboratory (image credit: ESA)

Future external facilities of the Columbus Lab will be:

- ACES (Atomic Clock Ensemble in Space). The objective of ACES is to test a new generation of microgravity cold-atom clock in space. The two clocks: PHARAO (Project d'Horloge Atomique par Refroidissement d'Atomes en Orbit) developed by CNES (France), and SHM (Space Hydrogen Maser) developed in Switzerland, will be characterized and their output signals compared with each other and with national frequency standards worldwide using a dedicated microwave link.
- ASIM (Atmosphere Space Interactions Monitor). The objective is to study the interaction of thunderstorms with the upper regions of the atmosphere, reaching into the ionosphere and magnetosphere and energetic particle radiation effects on the mesosphere and thermosphere.

The Columbus laboratory payloads are being controlled, monitored and coordinated by the Col-CC (Columbus Control Center) at DLR in Oberpfaffenhofen, Germany on behalf of ESA. All data of the European payloads/experiments is being transferred to the Col-CC directly via the ISS data transfer system. The Col-CC is responsible for distributing the data to the various USOCs (User Science Operation Centers) in Europe and receiving information from them such as requests for resources and reconfiguration of Columbus systems in support of experiments and payload facility operations. Col-CC is also in close contact with the Mission Control Center in Houston, which has overall responsibility for the ISS, together with the Mission Control Center in Moscow. In addition, Col-CC coordinates operations with the ISS POIC (Payload Operations and Integration Center) at NASA/MSFC in Huntsville, ALA.

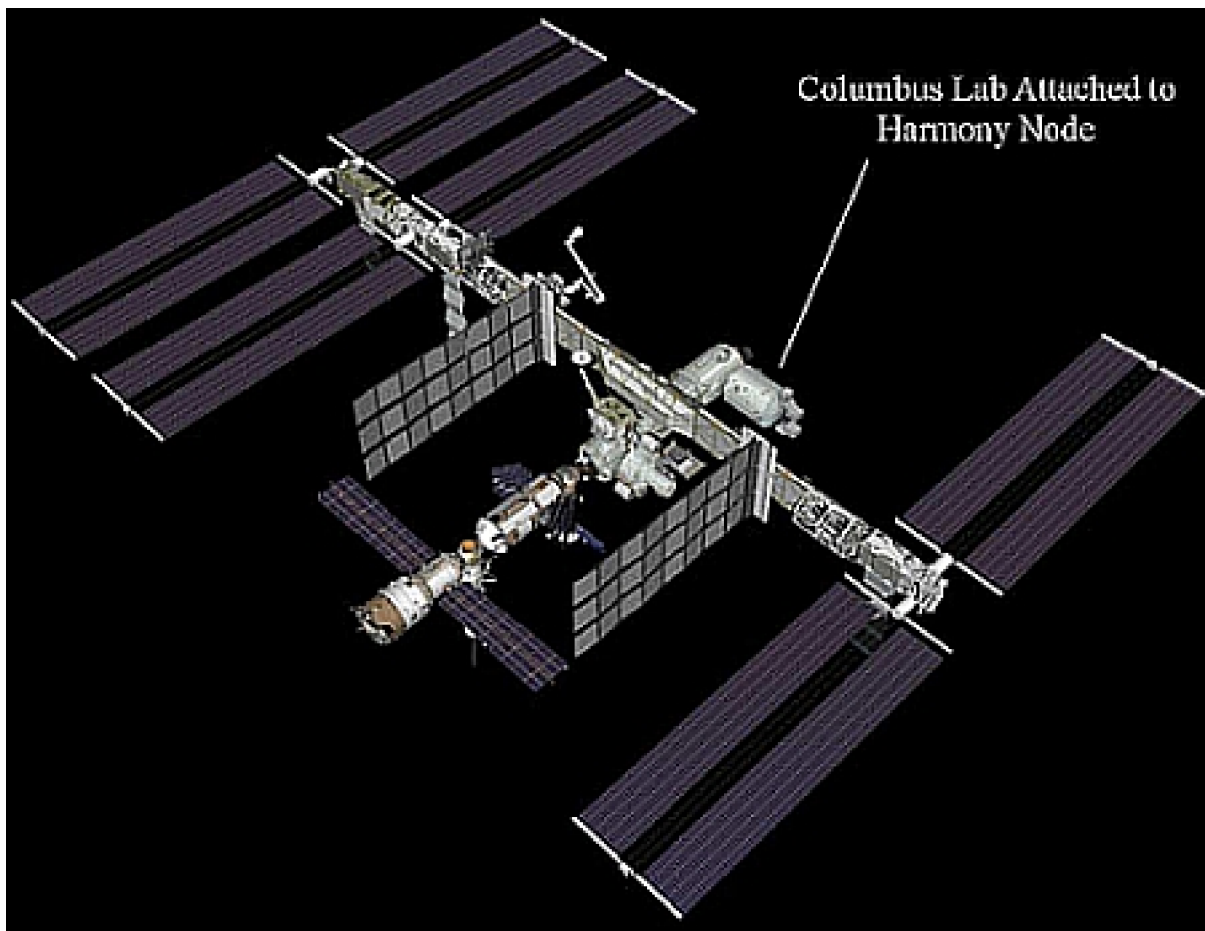


Figure 106: Space station configuration after the STS-122 flight (image credit: NASA)

- **STS-123**, assembly flight 1J/A of Endeavour, March 11–26, 2008 (16 day mission). The objective is the delivery and installation of **ELM-PS** (Experiment Logistics Module – Pressurized Section) of JAXA to the ISS. ELM-PS is the first element of JEM (Japanese Experiment Module), also referred to as Kibo (hope). The ELM-PS is a Kibo storage facility that provides stowage space for experiment payloads, samples, and spare items. The pressurized interior of the ELM-PS is maintained at one atmosphere, thus providing a shirt-sleeve working environment. ELM-PS is a short cylinder that will be attached to the top of the PM (Pressurized Module) that can hold eight experiment racks. The ELM-PS measures 4.4 m in diameter and is 3.9 m long. ^{1730) 1731)}

In total Kibo consists of: PM (Pressurized Module), EF (Exposed Facility), a logistics module attached to both the PM and EF, and a remote manipulator system, the JEM-RMS (Japanese Experiment Module – Remote Manipulator System).

NASA plans to launch the entire JEM complex in three Shuttle flights:

- 1) JEM/Kibo-ELM-PS (Experiment Logistics Module-Pressurized Section). Launch: March 11, 2008 on STS-123
- 2) STS-124 (1J) delivered the PM (Pressurized Module), System Racks, and JEM-RMS. A launch took place on May 31, 2008.
- 3) STS-127 (2J/A) will deliver the EF (Exposed Facility) and the ELM-ES (Experiment Logistics Module-Exposed Section). A launch of STS-127 took place on July 15, 2009.

¹⁷³⁰⁾ http://www.nasa.gov/pdf/216132main_sts123_press_kit_b.pdf

¹⁷³¹⁾ http://www.nasa.gov/pdf/216157main_sts123_factsheet.pdf

Once in orbit, the Kibo facilities will be used to perform collaborative experiments by all the station partners.

Element Parameter	Pressurized Module (PM)	Experiment Logistics Module		EF (Exposed Facility)	RMS (Remote Manipulator System)
		ELM-PS (Pressurized Section)	ELM-ES (Exposed Section)		
Structure type	Cylindrical	Cylindrical	Frame	Box	Main/small fine arm type
Outer diameter	4.4 m	4.4 m	–	–	Main arm = 9.9 m
Inner diameter	4.2 m	4.2 m	–	–	
Width	–	–	4.9 m	5.0 m	Small arm = 1.7 m
Height	–	–	2.0 m	4.0 m	
Length	11.2 m	3.9 m	4.2 m	5.2 m	
Dry mass	15,900 kg	4,200 kg	800 kg	3,800 kg	780 kg
Payload/experiment equipment	23 racks (total) including 10 experiment racks	8 racks	3 payloads	10 payloads	Max. handling capability = 7,000 kg
Electric power	25 kW (max), 120 VDC (max)				
Data management	32-bit computer system, high-rate data link of 100 Mbit/s (max)				
Crew	Two persons for normal operation, max. 4 with time limitation				
Design life	Over 10 years				

Table 87: Overview of the JEM/Kibo configuration

Kibo operations will be jointly monitored and controlled from the JAXA Space Station Integration and Promotion Center at Tsukuba, in Japan, and the Mission Control Center at NASA's JSC in Houston, where the overall operations of the space station are controlled.



Figure 107: Artist's view of the Dextre manipulator arm in orbit (image credit: CSA, NASA)

In addition to the Kibo payload on STS-123, there is the **SPDM** (Special Purpose Dexterous Manipulator) payload, known simply as "**Dextre**", a two-armed robotic device, provided by CSA (Canadian Space Agency). It was installed on ISS a few days after its arrival. Dextre can be carried by two elements, the MBS (Mobile Base System) and Cana-

darm2, or move independently. Dextre adds robotic tools and a range of fine manipulation abilities to construction and maintenance operations on the Space Station, which is now much larger than in 2001 when Canadarm2 was installed. Dextre has a mass of ~ 1560 kg and dimensions of: 3.67 m (height), 2.37 m (width), and an arm length of 3.35 m. It can lift payloads of up to 600 kg to an incremental positioning accuracy of 2 mm. The average operating power is 1.4 kW.

Dextre was designed and developed at MD Robotics of Brampton, Ontario, a subsidiary of MDA (MacDonald Dettwiler Associates), Canada. Dextre is an advanced two-armed robotic system consisting of a central body with a grapple fixture at one end and a latching end-effector at the other. Each of its two arms is identical, has seven joints, and is equipped with a tool change-out mechanism at the end. The mechanism can remotely change-out orbit-replaceable units and can also pick up and use special tools stored on the body of Dextre.

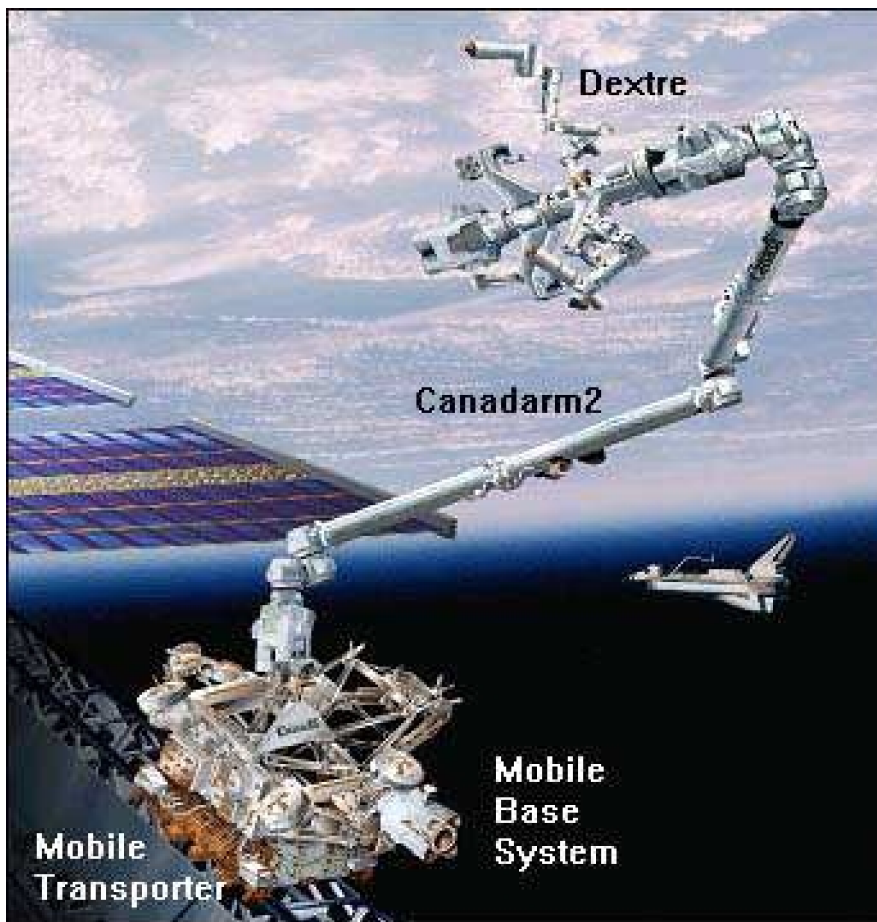


Figure 108: The complete MSS (Mobile Servicing System) of ISS (image credit: NASA, CSA) ¹⁷³²

Technology demonstration: The STS-123 flight took also a new transistor design experiment to the ISS, developed by the research group of Tobin Marks and Vladimir N. Ipatieff of Northwestern University in Evanston, IL, USA. The new transistors use a new type of gate dielectric material called SAND (Self-Assembled Nanodielectric). Initial tests of the new transistors in nuclear reactors indicated a high resistance to a radiation environment. The SAND technology has an added benefit – the transistors can be printed and they are flexible. This has obvious applications for flat-screen technology and condensing vastly complex circuitry into a very small space. As this is a departure from the traditional silicon dioxide technique, these transistors appear to be very robust when faced with a high-radiation environment here on Earth.

¹⁷³²) “ISS Elements: Mobile Servicing System (MSS),” URL: <http://www.spaceref.com/iss/elements/mss.html>

The new transistors were attached to the outside of the International Space Station for radiation testing (spacewalk on March 22, 2008). The ISS experiments are expected to take a year to complete, so the space computing world will be waiting to see if this new technology can revolutionize space-based instrumentation, protecting valuable spacecraft from the ravages of energetic particles. ¹⁷³³⁾ ¹⁷³⁴⁾

- Launch of the ESA **ATV-1** (Automated Transfer Vehicle-1) on an Ariane-5 launch vehicle from Kourou on March 9, 2008. **ATV-1 is a new service vehicle for the ISS.** The first ATV is named in honor of the French visionary and science fiction author Jules Verne (1828-1905). Four additional ATV flights are planned for launches in 2009, 2011, 2012 and 2013.

The objective of the ATV servicing vehicle is to deliver cargo (i.e. resupplies, including food and clothing for the astronauts, and equipment of up to 6500 kg of net payload mass) to the ISS. All ATV transporters use the berthing port of the Russian Zvezda Service Module where they can remain docked for nominally up to six months. Similar to the Russian transporter Progress, the ATV can lift the ISS to a higher orbit by using its main rocket motors. During its visiting period at the ISS, the ATV can be loaded with up to 6.5 tons of waste from the ISS. On its return flight from the ISS, the ATV will reenter Earth's atmosphere under supervision and finally burn up high over the Pacific Ocean. ¹⁷³⁵⁾ ¹⁷³⁶⁾

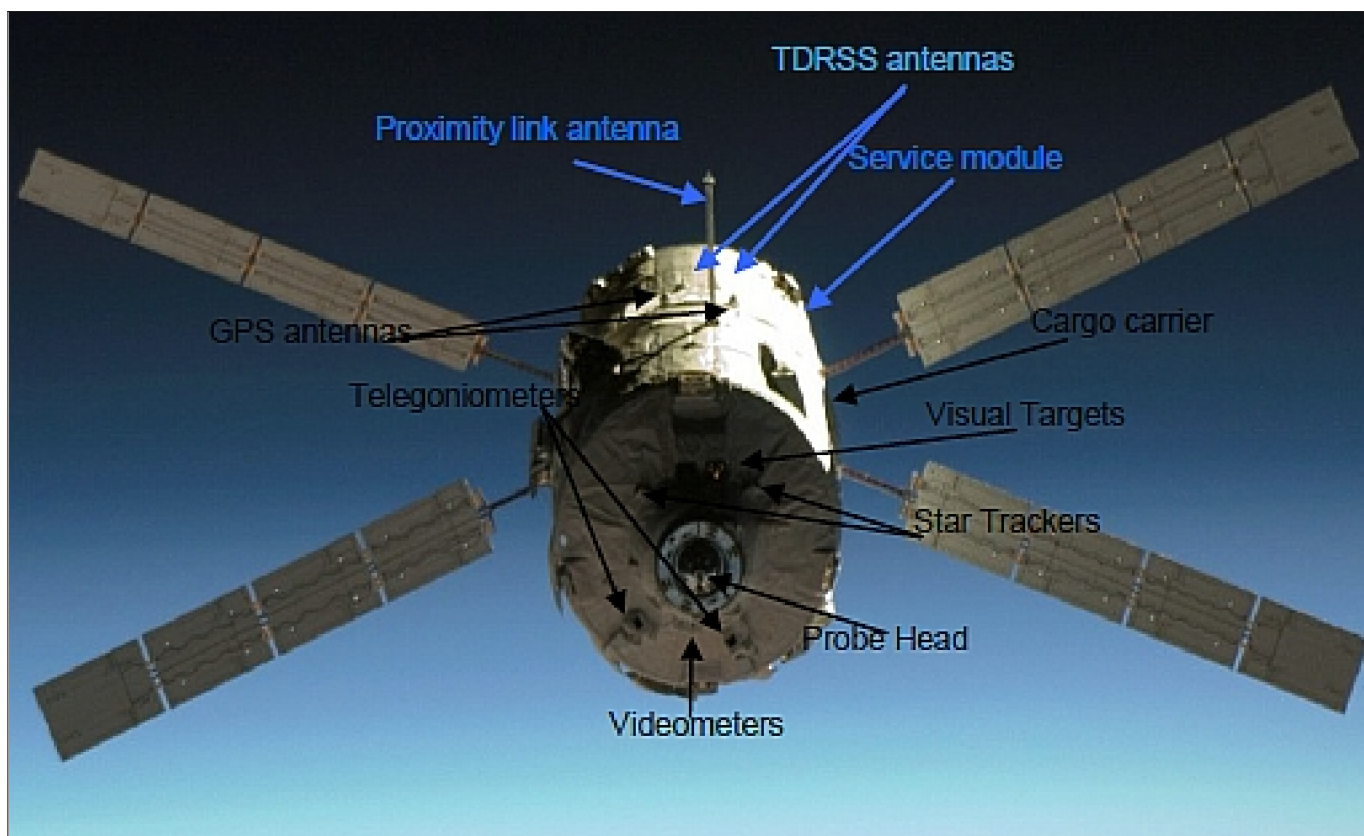


Figure 109: Photo of ATV-1 taken from ISS during rendezvous (image credit: NASA, ESA)

The ATV transporter has a length of ~ 10 m and a diameter of 4.5 m – with a maximum launch mass of over 19 tons. The vehicle consists of one section for the drive and the avionics

1733) “Northwestern Transistors Blast Off Into Space, Hang Out At International Space Station,” June 10, 2008, URL: <http://www.mccormick.northwestern.edu/news/articles/388>

1734) I. O’Neill, “New Transistor Could Side-Step Space Radiation Problem,” Universe Today, June 12, 2008, URL: <http://www.universetoday.com/2008/06/12/new-transistor-could-side-step-space-radiation-problem/>

1735) http://esamultimedia.esa.int/docs/ATV/newspaper/ESA_ATV_newspaper_ENG.pdf

1736) “Europe launches its first re-supply ship – Jules Verne ATV – to the ISS,” March 9, 2008, URL: http://www.esa.int/esaCP/SEMDYOK26DF_index_0.html

– the electronic steering devices. In addition it has a load-bearing pressurized segment (of 45 m³ in volume, referred to as the “Integrated Cargo Carrier”), in which dry cargo is transported. The freight is packed into racks, called ISPR (International Standard Payload Racks). This concept permits easy handling and storage of goods. Although people will not be carried by ATV, astronauts dressed in normal clothing will be able to access the cargo and systems compartments during the period it is docked to the ISS. ATV’s structure also incorporates several storage tanks for drinking water (270 kg), refuelling propellant (860 kg) for the Space Station’s own propulsion system, and air (oxygen and nitrogen, 21 kg) for the crew.

ATV’s docking to the ISS is fully automatic and, in the event of any last minute problems, either the ATV’s computers or the ISS crew can trigger a preprogrammed sequence of anti-collision maneuvers, fully independent of the main navigation system. ¹⁷³⁷⁾

On April 3, 2008, Jules Verne docked successfully to the aft port of the Space Station’s Zvezda Service Module. Contact was confirmed at 14:45 GMT. ¹⁷³⁸⁾ Docking was complete 7 minutes later when the hooks were closed. Following nearly a month of on orbit operations – including two successful rehearsal days, controllers in France, the United States and Russia carefully monitored the unmanned vehicle, along with its five tons of cargo, as it arrived for docking with the Station for the first time. This is indeed a great achievement for Europe and its partners. ¹⁷³⁹⁾

On April 25, 2008 the ATV–1 (Jules Verne) gave for the first time an orbit re-boost to the ISS by carrying out a 12 minute and 20 second burn of its main engines. As a result, the 280 ton station was lifted ~ 4.7 km in its orbit to a new altitude of 342 km. This event validated one of the major tasks of the ATV’s inaugural flight, demonstrating the ability to lift the ISS back into the correct orbit. About half of the payload onboard Jules Verne ATV is re-boost propellant, which will be used by its own propulsion system for periodic maneuvers to increase the altitude of the ISS to compensate its natural decay caused by atmospheric drag.

On June 19, 2008, ATV–1 boosted the 300 ton ISS 7 km higher to an orbit of 345 km altitude. In addition, it has refuelled the station with 856 kg of propellant. Although these were essential tasks, the ATV has provided an invaluable service to the crew. The roomy temporary supply vessel has provided a great area for the crew to sleep and wash, plus one of its empty tanks has been used to store 110 litres of condensation water from the ISS. ATV’s mission has been mission has been extended for a month, allowing the crew to enjoy the ATV for a little while longer. ¹⁷⁴⁰⁾

The undocking of ATV from the ISS took place Sept. 5, 2008. This was followed by a successful controlled and destructive reentry into the Pacific Ocean on Sept. 29, 2008. ¹⁷⁴¹⁾

- **STS–124**, assembly flight 1J/B of Discovery, May 31–June 11, 2008 (10 day building mission, landing on June 14, 2008). The objective was the delivery and installation of Kibo components, the **JEM–PM** (Japanese Experiment Module–Pressurized Module) – also referred to as JPM (Japanese Pressurized Module), and JEM–RMS (Japanese Remote Manipulator System) to the ISS.

The RMS consists of two robotic arms that support operations outside of Kibo. ¹⁷⁴²⁾ The lab’s logistics module, which was installed in a temporary location during STS–123 in March 2008, will be attached to the new lab. With a diameter of 4.4 m and 11.2 m in length,

1737) E. de Pasquale, “ATV Jules Verne: a Step by Step Approach for In–Orbit Demonstration of New Rendezvous Technologies,” Proceedings of SpaceOps 2012, The 12th International Conference on Space Operations, Stockholm, Sweden, June 11–15, 2012

1738) <http://www.nasaspaceflight.com/content/?cid=5395>

1739) “Europe’s automated ship docks to the ISS,” ESA, April 3, 2008, URL: http://www.esa.int/esaCP/SEMORO5QGEF_index_0.html

1740) http://www.esa.int/esaCP/SEM61ZUG3HF_index_0.html

1741) “Successful re-entry marks bright future for ATV,” Sept. 29, 2008, URL: http://www.esa.int/SPECIALS/ATV/SEME556EJLF_0.html

1742) “STS–124 Mission Summary,” NASA, http://www.nasa.gov/pdf/221164main_sts124_Fact_Sheet.pdf

Kibo is the largest habitable module on the space station and is equipped with its own airlock and robotic arm for external experiments. Kibo's experiments and systems are being operated from the JAXA's control center, the SSIPC (Space Station Integration and Promotion Center) in Ibaraki Prefecture, Japan, just north of Tokyo.

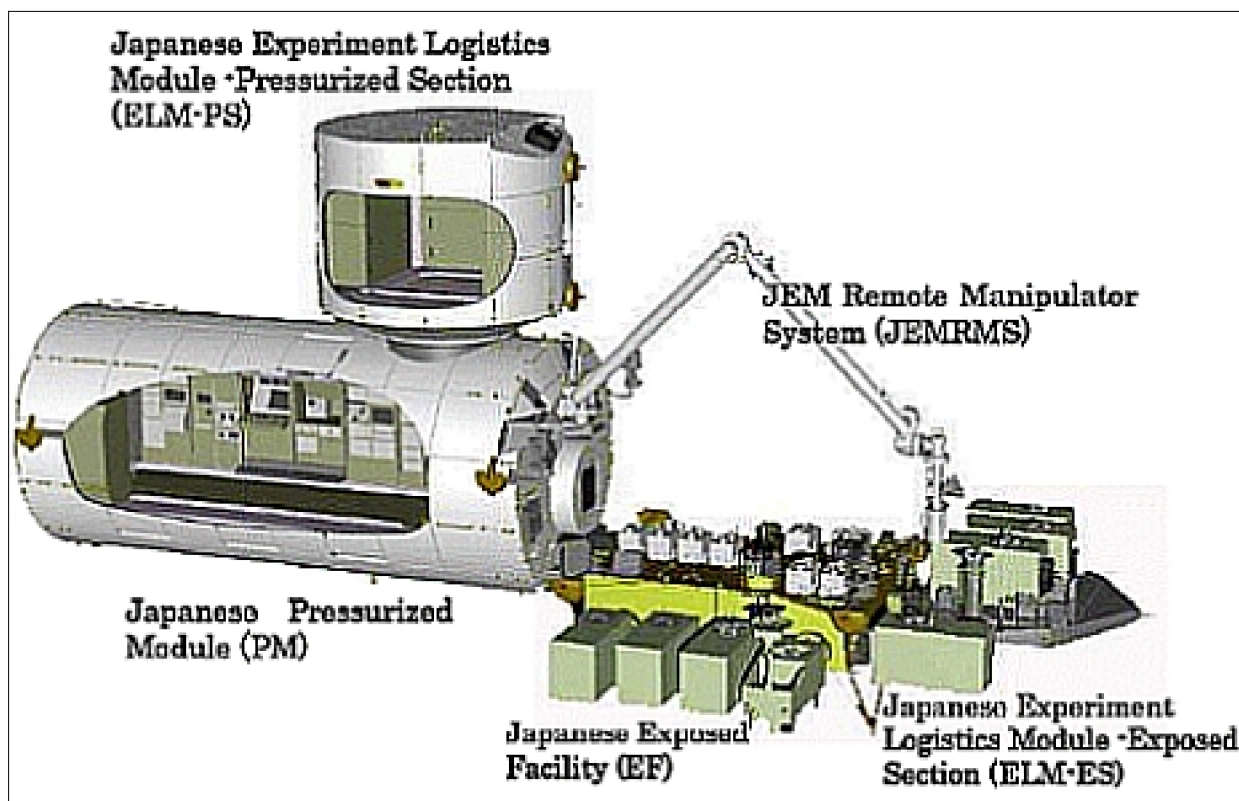


Figure 110: Overview of Kibo and its components (image credit: JAXA,NASA)

- **Debris avoidance maneuver:** On Aug. 27, 2008, the ISS had to perform an evasive maneuver to dodge space debris from a Russian satellite that disintegrated earlier in 2008. ESA's ATV (Automated Transfer Vehicle) was used to perform the avoidance maneuver, the first time it had been used for such a maneuver. Information on a possible collision was received from Russian and American services.¹⁷⁴³⁾

Some items of the maneuver are of general interest:¹⁷⁴⁴⁾

- This is the first time in five years that the ISS has had to perform a debris avoidance maneuver.
- The maneuver was unusual in that it was a retrograde maneuver, which slows the ISS and brings it to a lower orbit instead of a higher one. The last time a retrograde maneuver was performed was eight years ago. This time around, the ISS orbit was lowered by 1.7 km to an altitude of 353.7 km.
- While the Russian side denied that the debris was from their broken-up spacecraft, the Mission Control Center in Moscow carried out the maneuver.
- **STS-126, ULF2 (Utility and Logistics Flight 2)** of Endeavour, Nov. 14 – 30, 2008. The objective is to provide additional capability for the ISS to house astronauts and to increase

1743) "ISS Orbit Adjusted To Dodge Space Junk," Spacedaily, Aug. 29, 2008, URL: http://www.space-travel.com/reports/ISS_Orbit_Adjusted_To_Dodge_Space_Junk_999.html

1744) Nancy Atkinson, "Space Station Evades Space Debris," Universe Today, Aug. 28, 2008, URL: <http://www.universetoday.com/2008/08/28/space-station-evades-space-debris/>

the station crew size from three to the desired six crew members by spring 2009.¹⁷⁴⁵⁾ Delivery of supplies in the MPLM (Multi-Purpose Logistics Module), called Leonardo. In addition to Leonardo, Endeavour carries the Lightweight Multi-Purpose Experiment Support Structure Carrier and a spare Flex Hose Rotary Coupler Unit (FHRC) for a future replacement spare.

The cargo of flight STS–126 included also a nanosatellite, PSSCT (Pico Satellite Solar Cell Testbed) of the DoD STP (Space Test Program) with a mass of 6.5 kg and a size of 12.5 cm x 12.5 cm x 25 cm. The objective is to provide space flight data on radiation degradation of multijunction solar cells. PSSCT was deployed from the shuttle on Nov. 29, 2008.¹⁷⁴⁶⁾

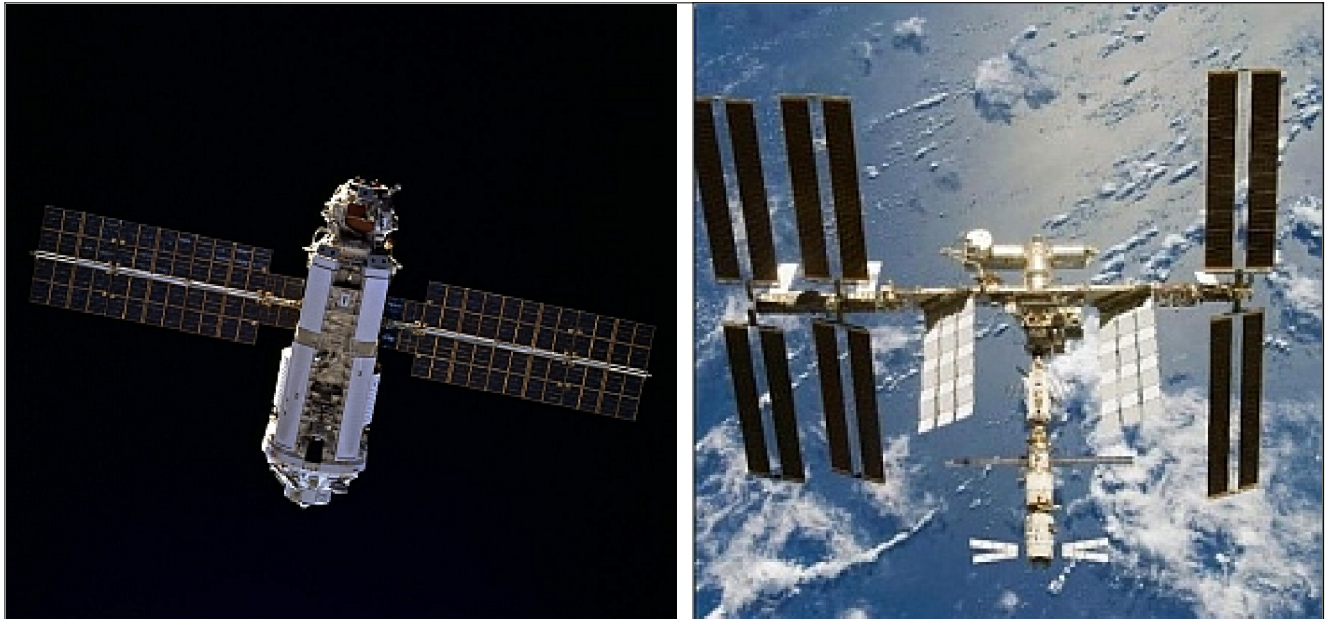


Figure 111: The ISS configuration in 1998 (left) and at 10 years in Nov. 2008 (right), image credit: NASA

- **ISS ten years in space on Nov. 20, 2008:** – The first module of the ISS, Zarya (Russian for “Dawn”) also known as FGB (Functional Cargo Block), was launched by a Proton rocket from the Baikonur Cosmodrome on Nov. 20, 1998. This represented a new era in space exploration and in particular in a long–term space cooperation between Russia, the US, Europe, Canada, and Japan.¹⁷⁴⁷⁾
- **STS–119, ISS assembly flight 15A of Discovery (March 15–28, 2009).** The objective is to deliver and assemble the fourth (and last) Starboard Integrated Truss Segment (S6), and the fourth set of solar arrays and batteries to the station. The S6 PVM (Photovoltaic Module) includes all equipment outboard Truss Segment S5, namely the two PVAA (Photovoltaic Array Assemblies) and the IEA (Integrated Equipment Assembly). S6 was manufactured by the Boeing Company. It has a size of 5 m (wide) x 13.8 m (length) x 4.5 m (high), the total mass is 14,000 kg.¹⁷⁴⁸⁾

With the addition of the S6, the total SAA (Solar Array Assembly) area of the ISS amounts to 3000 m² (the masts are subtracted). There are 8 SAWS, each wing has a size of ~ 400 m².

1745) http://www.nasa.gov/pdf/287211main_STS-126_Press_Kit.pdf

1746) Siegfried W. Janson, David A. Hinkley, “Spin Dynamics of the Pico Satellite Solar Cell Testbed Spacecraft,” Proceedings of the 23rd Annual AIAA/USU Conference on Small Satellites, Logan, UT, USA, Aug. 10–13, 2009, SSC09–IV–5

1747) “Ten Years In Space: The International Space Station,” Space Travel, Nov. 19, 2008, URL: http://www.space-travel.com/reports/Ten_Years_In_Space_The_International_Space_Station_999.html

1748) http://www.nasa.gov/pdf/304681main_STS-119_Press_Kit.pdf

Parameter	Current 3 PVMs	Starboard 6 (S6)	Total (post STS–119)
Power generation capability	198 kW	66 kW	264 kW
Usable power capability*	63–90 kW	21–30 kW	84–120 kW
Power for science experiments**	15 kW	15 kW	30 kW

Table 88: Overview of ISS power

* The amount of usable power varies depending on the time of year and the orientation of the station relative to the Earth and sun.

** A greater fraction of power from the first three photovoltaic modules (PVMs) currently installed is needed to support day–to–day station systems operation.

With the STS–119 mission, the ISS was made ready to accommodate from now on up to 6 astronauts/specialists on a permanent basis.



Figure 112: The symmetrical ISS, the image was taken from Discovery return flight on March 25, 2009 of STS–119 (image credit: NASA)

- *A new era for ISS began when the crew size doubled on a permanent basis with the arrival of three new crew members of the Soyuz TMA–15 spacecraft to the ISS on May 29, 2009. Also, for the first time in its 11–year history, all the ISS partner agencies are being represented on board the station at once as astronauts from NASA, CSA, ESA, JAXA and Roskosmos are part of the first six–person crew. The increased number of ISS crew members will improve considerably the ISS research capabilities.*

- **STS–127**, ISS assembly flight 2J/A of Endeavour (July 15 –31, 2009, 16 day mission). The primary objective is to deliver and install the final three components (MAXI, SEDA–AP, and ICS) of the JEM/Kibo (Japanese Experiment Module): the Exposed Facility (JEM EF), and the Exposed Section of the Experiment Logistics Module (ELM–ES). The ICS (Inter–orbit Communication System) is used to communicate between JEM/Kibo and the

MCC (Mission Control Center) at Tsukuba of JAXA via DRTS (Data Relay Test Satellite).¹⁷⁴⁹⁾

Also, delivery of the ICC–VLD (Integrated Cargo Carrier – Vertical Light Deployable). The ICC–VLD contains a) 6 new batteries for installation on the P6 truss, b) LDU (Linear Drive Unit), PM–2 (Pump Module–2), and the SGANT (Space to Ground Antennas).

– DragonSat (Dual RF Astrodynamic GPS Orbital Navigator Satellite) payload – NASA GPS Demonstrator – consisting of a pair of student–built nanosatellites, namely **AggieSat–2** built by Texas A&M University (TAMU) and **Paradigm** (nicknamed Bevo–1) of the University of Texas (UT). Deployment of the DragonSat payload (i.e., AggieSat–2 and Bevo–1) on July 30, 2009 at 14:31.20 UTC from the Space Shuttle Bay using SSPL (Space Shuttle Picosatellite Launcher).

– ANDE–2 (Atmospheric Neutral Density Experiment) payload of NRL to measure density and composition of atmosphere. Deployment of ANDE–2 on July 30, 2009 at 19:19:52 UTC, from the Space Shuttle Bay using the CAPE (Canister for All Payload Ejections) deployment system.

• **STS–128.** ISS assembly flight 17A of Discovery (August 29– Sept. 11, 2009, 14 day mission). The primary objective is to deliver the reusable Multi–Purpose Logistics Module (MPLM), Leonardo. MPLM will be temporarily docked with the ESA–delivered Harmony Node–2 module. Leonardo provides a pressurized environment for three life–support and three science racks to be transferred into the Station. The science racks include MELFI–2 (Minus Eighty Laboratory Freezer for ISS) supplied by ESA, which provides very low temperature storage for samples, as well as the first ISS research laboratory fully dedicated to Material Sciences: ESA’s Material Science Laboratory. MELFI–2 will be installed inside Japan’s JEM–Kibo laboratory. It will double the capacity provided by MELFI–1, which has been in operation onboard the US Destiny laboratory since 2006.¹⁷⁵⁰⁾

Leonardo’s payload also includes food, clothes, water and astronaut sleeping quarters. Both MELFI–2 and the sleeping quarters will be placed temporarily in Japan’s Kibo research module (and later in Node 3).

Aside from the MPLM, the shuttle payload includes LMC (Lightweight Multi–Purpose Experiment Support Structure Carrier). The total payload mass (MPLM+LMC but not counting the middeck) is 14,300 kg.

– The MISSE–6 (Materials on International Space Station Experiments–6) of NASA will be removed from the Columbus module and transferred into the MPLM for return to Earth. MISSE–6a and –6b were launched by space shuttle Endeavour during mission STS–123 on March 13, 2008, and contained more than 400 specimens of various materials (measurement of long–term exposure effects of materials to the environment).

– The EuTEF (European Technology Exposure Facility), currently mounted on an external payload facility outside ESA’s Columbus laboratory module, has been placed into Discovery’s cargo bay and returned to Earth. The STS–122 mission (Feb. 2008) brought EuTEF into space. The science package includes nine experiments designed to expose samples to the harsh conditions of space, test materials, analyze the near Earth orbit environment and take pictures of the Earth.¹⁷⁵¹⁾

• Launch of the **HTV–1** (H–II Transfer Vehicle), a resupply vehicle of JAXA on Sept. 10, 2009 (UTC) from the TNSC (Tanegashima Space Center) in Japan, representing the maiden flight of HTV to the ISS. JAXA launched the HTV demonstration flight aboard the

¹⁷⁴⁹⁾ STS–127, Prees Kit, NASA, June 2009, URL: http://www.nasa.gov/pdf/358018main_sts127_press_kit.pdf

¹⁷⁵⁰⁾ http://www.nasa.gov/pdf/379392main_STS-128_Press_Kit.pdf

¹⁷⁵¹⁾ http://www.esa.int/esaCP/SEMVGVH7KYF_index_0.html

newly developed H–IIB launch vehicle. About 2 hours later, the HTV–1 reached its target orbit. The JAXA nickname of HTV–1 is Kounotori. ^{1752) 1753)}

The flight profile had the HTV taking seven days to reach the ISS so controllers could run various tests and demonstrations on its maiden voyage before rendezvousing with the space station. Unlike previous re–supply ships that dock directly to the station, the HTV approached to within 10 m from the ISS on September 17 – from where it was grappled using the **Canadarm2** robotic arm of the space station. Then, astronaut Robert Thirsk (Canada) used Canadarm2 and moved the HTV spacecraft to the nadir port of the Harmony module. Shortly after 22:00 hours UTC on Sept. 17, 2009, the HTV–1 was mated to the ISS. ¹⁷⁵⁴⁾

HTV–1 delivered about 4500 kg of cargo and resupplies (propellant and batteries) to the ISS. The payload instruments on this flight are: SMILES (Superconducting Submillimeter–Wave Limb–Emission Sounder) of Japan and HREP (HICO–RAIDS Experiment Payload) which are two payloads of the USA. Both of these payloads will be mounted onto JEM/Kibo–EF (External Facility). – In addition, the HTV–1 delivered two experimental instruments: NorAIS (Norwegian Automatic Identification System) and LuxAIS (LuxSpace AIS) of ESA; they will be mounted internally to the Columbus module and are intended to track the AIS signals of the maritime ship traffic.

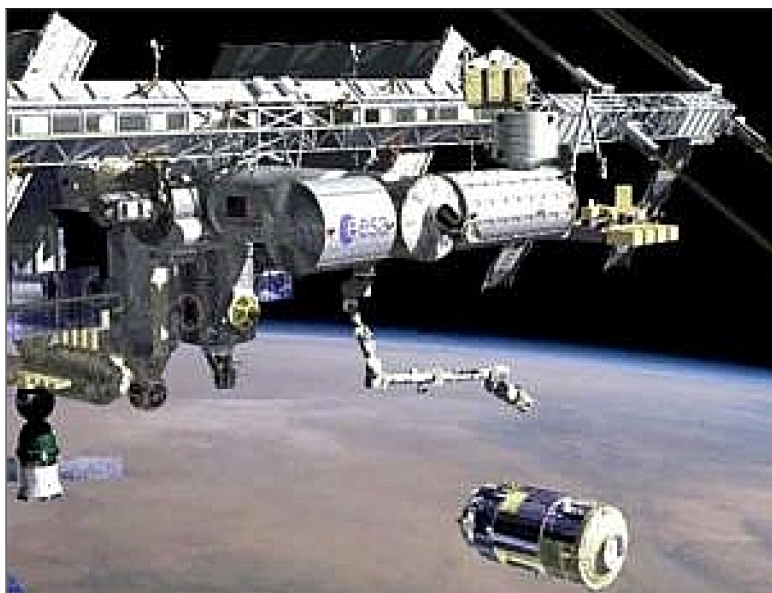


Figure 113: Artist's view of the HTV–1 approach and capture by Canadarm2 (image credit: JAXA)

- **STS–129.** ISS ULF–3 (Utilization and Logistics Flight–3) mission of Atlantis (Nov. 16–27, 2009, 11–day flight). The payload consists of 2 ELCs (ExPRESS Logistics Carriers), delivery of ~ 14,000 kg of important spare parts for its electrical, plumbing, air conditioning, communications and robotics systems. A new MISSE–7 (Materials on International Space Station Experiment) carrier, the SASA (S–Band Antenna Sub–Assembly) package of 116 kg, plus additional equipment, supplies and scientific experiments that will be used by the continuing crew of six aboard the station. Prepare for Node 3 (Tranquility) arrival. ¹⁷⁵⁵⁾

ELC is a platform designed to support external payloads mounted to the ISS starboard and port trusses with either deep space or Earthward views. Each pallet spans the entire width of the shuttle's payload bay, carries science experiments, and serves as a parking place for

1752) <http://iss.jaxa.jp/en/htv/mission/htv-1/>

1753) Nancy Atkinson, "Japan Launches New Era of ISS Resupply Ships," Sept. 10, 2009, URL: <http://www.universetoday.com/2009/09/10/japan-launches-new-era-of-iss-resupply-ships/>

1754) "Historic Cosmic Catch," CSA, URL: <http://www.asc-csa.gc.ca/eng/iss/canadarm2/htv.asp>

1755) NASA Press Kit: URL: http://www.nasa.gov/pdf/397216main_sts129_presskit.pdf

spare hardware that can be replaced robotically once on-orbit. ELC-1 (~ 6300 kg) is mounted on the Port 3 truss element UCCAS (Unpressurized Cargo Carriers Attachment System), while ELC-2 (~ 6100 kg) is placed on the Starboard 3 truss upper outboard PAS. The UCCAS and PAS (Payload Adapter System) were deployed during the STS-128 mission.

Each ELC can accommodate 12 FRAM (Flight Releasable Attachment Mechanism)-based cargos that includes two payload attached sites with full avionics accommodation. The mass capacity for an ELC is 4,445 kg with a volume of 30 m³. The ISS provides power to the ELCs through two 3 kW, 120 V direct current (V dc) feeds at the ISS to ELC interface.

A total of 14 large ORUs (Orbital Replacement Units) are being carried on ELC-1 and -2. The ORUs include the ATA (Ammonia Tank Assembly), BCDU (Battery Charger Discharge Unit), CTC (Cargo Transportation Container), two CMGs (Control Moment Gyroscopes), HPGT (High-Pressure Gas Tank), Canadarm2 Latching End Effector (LEE), MISSE-7 (Materials International Space Station Experiment 7), two NTA (Nitrogen Tank Assemblies), PCU (Plasma Contactor Unit), two PMA (Pump Module Assemblies), and a TUS-RA (Trailing Umbilical System-Reel Assembly).

On Nov. 23, 2009 astronauts manually deployed the MISSE-7 containers on the exterior of the ISS. SNL (Sandia National Laboratories) has been receiving data from this research payload ever since. FPGAs are at the heart of these new computing architectures from Xilinx. Sandia, in a partnership with Xilinx, Inc., designed the S¹⁷⁵⁶ EU Xilinx-Sandia Experiment (SEUXSE) for this opportunity to fly on MISSE-7.

- **STS-130.** ISS assembly flight 20A of Endeavour (Feb. 8 – 22, 2010, 14-day mission). The primary payload consists of the Tranquility module and the Cupola (Italian for 'dome'), a robotic control station with six windows around its sides and another in the center that provides a 360° view around the station. **Tranquility, formerly known as Node-3**, is the last element of a barter agreement by which ESA supplied NASA with ISS hardware, including the Cupola and two Node modules (Node 2 and 3). All elements were designed and built by TAS-I (Thales Alenia Space-Italia). In return, NASA ferried the European Columbus laboratory to the ISS in February 2008. ^{1757) 1758) 1759)}

The Tranquility module connects to the port side of the Unity Node and provides room for eight refrigerator-sized racks, two of the locations being used for the avionics racks controlling Node 3. Node 3 consists of a pressurized cylindrical hull 4.5 m in diameter with a shallow conical section enclosing each end. It is almost 7 m long with a mass of 13,500 kg (Node 3 + Cupola) at launch. ¹⁷⁶⁰⁾

The Tranquility node differs significantly from the others. It is state-of-the-art, the most complex pressurized element of the ISS, offering many more capabilities than originally planned. It will accommodate sophisticated crew and life-support equipment, some relocated from the US Destiny laboratory module, leaving more room there for science racks.

The Cupola is an aluminum structure of 2.95 m (max) in diameter, 1.5 m high with a mass of ~ 1600 kg. The Cupola is a "shirtsleeve" module with six trapezoidal side windows and a circular top window of 80 cm in diameter, making it the largest window ever flown in space (providing a panoramic view of Earth). Each window is built using very advanced technolo-

¹⁷⁵⁶⁾ "Breaking the logjam: improving data download from outer space," May 18, 2010, URL: https://share.sandia.gov/news/resources/news_releases/space_download/

¹⁷⁵⁷⁾ http://www.nasa.gov/pdf/420302main_sts130_press_kit.pdf

¹⁷⁵⁸⁾ Philippe Deloo, Sara Pastor, "ISS Hardware Handover, Transferring ownership of Node-3 (with Cupola attached)," ESA Bulletin Nr 141, Feb. 2010, pp. 38-45

¹⁷⁵⁹⁾ "Cupola: a window over the Earth," TAS-I, URL: <http://www.thalesaleniaspace-issmodules.com/index.php/cupola>

¹⁷⁶⁰⁾ "Node-3 and Cupola: European technology to complete the ISS," ESA, Feb. 8, 2010, URL: http://www.esa.int/es-ACP/SEMY29XJB5G_index_0.html

gies to defend the sensitive fused silica glass panes from years of exposure to solar radiation and debris impacts.

The Cupola will operate as more than a workstation. With a clear view of Earth and celestial bodies, the Cupola will have scientific applications in the areas of Earth observation and space science as well as holding psychological benefits for the crew.

The windows are protected by special external shutters, which can be opened by the crew inside the Cupola with the simple turn of a wrist. At the end of their tasks, the window shutters are closed to protect the glass from micrometeoroids and orbital debris and to prevent solar radiation from heating up the Cupola or to avoid losing heat to space. – The 10–year in–orbit lifetime calls for user–friendly replacement of the windows while in orbit. The entire window or the individual scratch and debris panes can be replaced in space.

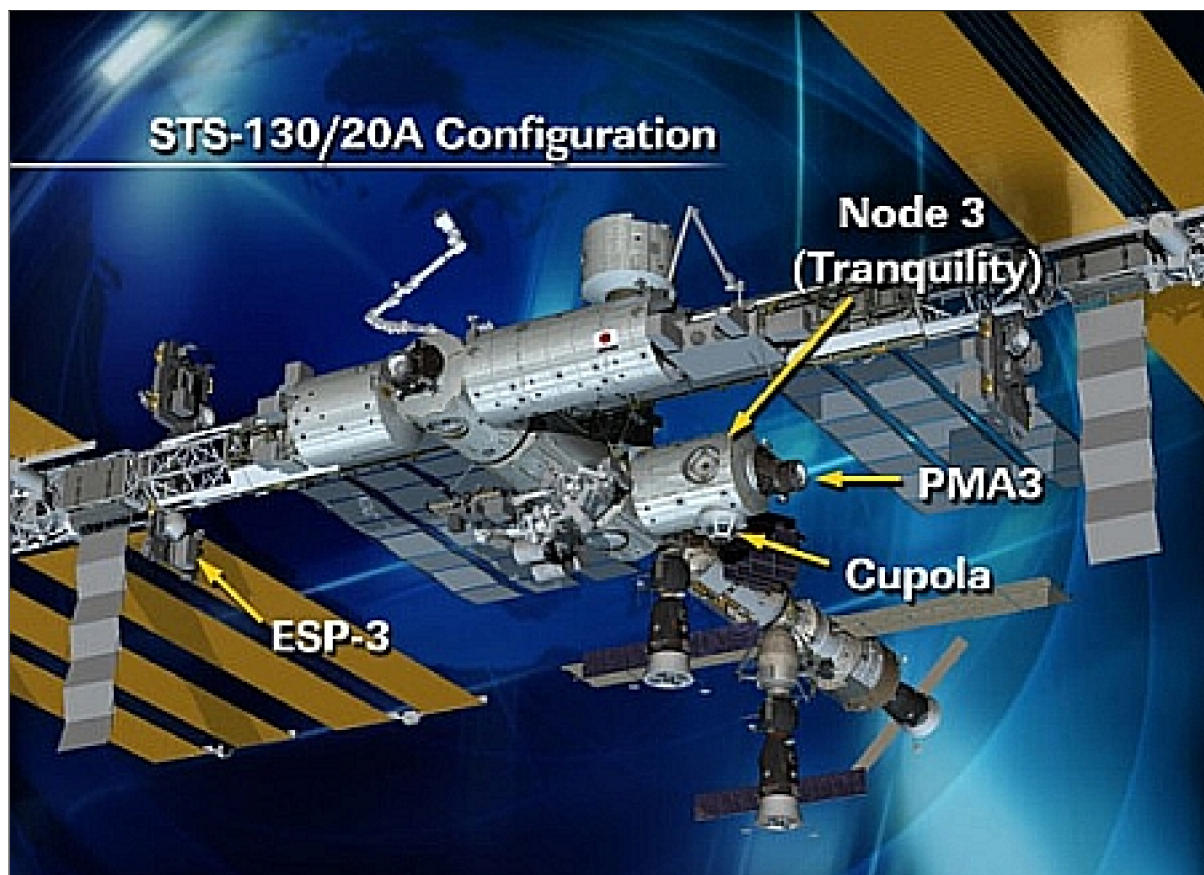


Figure 114: Artist's rendition of ISS configuration after shuttle flight STS–130 (image credit: NASA)

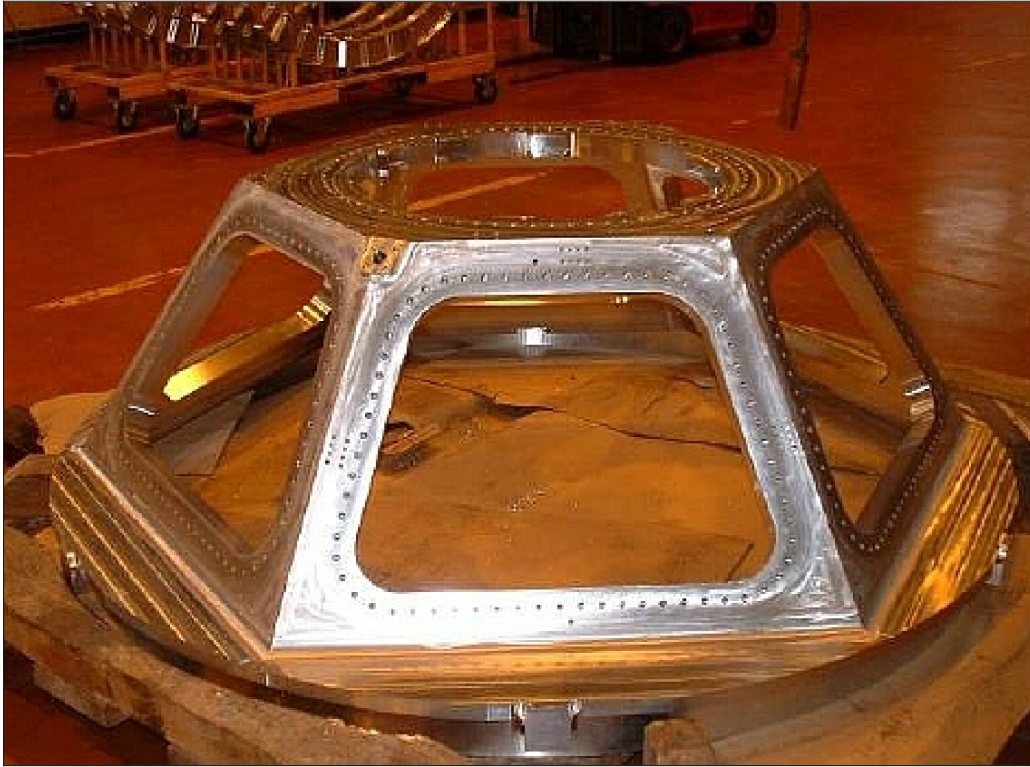


Figure 115: Illustration of the Cupola dome (image credit: TAS-I)



Figure 116: Astronaut Tracy Caldwell Dyson reflects on the view from the ISS's Cupola (image credit: NASA)

- *On March 11, 2010, the heads of the national space agencies, NASA, Roskosmos, ESA, JAXA, and CSA met in Tokyo, Japan to review ISS cooperation. With the assembly of the ISS nearing completion (in 2011) and the capability to support a full-time crew of six established, they noted the outstanding opportunities now offered by the ISS for on-orbit research and for discovery including the operation and management of the world's largest international space complex.*

*The heads of agency emphasized their strong mutual interest in extending the ISS operations to 2020 and beyond. **The five partners are currently working to certify on-orbit elements through 2028.** The ISS operations extension to 2020 and beyond enables a comprehensive research and sustainable utilization of a microgravity platform 400 km above Earth's surface.* ¹⁷⁶¹⁾

The previous planning horizon called for a retirement and deorbit of the station around 2015–2016. ^{1762) 1763) 1764)}

- **STS–131.** ISS flight 19A of Discovery (April 5–20, 2010, 14-day mission). ¹⁷⁶⁵⁾ The payload includes the Leonardo MPLM (Multi-Purpose Logistics Module) and the LMC (Lightweight Multipurpose Experiment). The total payload mass, not counting the middeck, is 14,000 kg. The GLACIER payload is stowed on the middeck, which is a freezer designed to provide cryogenic transportation and preservation capability for samples. Further middeck payloads are: MERLIN, Mouse Immunology, Space Tissue Loss, NLP-Vaccine-8, BRIC-16, APEX Cambium, ESA ECCO with WAICO2, JAXA 2D Nano Template, JAXA Myo Lab, JAXA Neuro Rad, Sleep.

The four experiment racks carried in Leonardo are: Express Rack 7, MARES (Muscle Atrophy Research Exercise System), MELFI–3 (Minus Eighty Laboratory Freezer–3) and **WORF** (Window Observational Research Facility). The station system rack is Crew Quarters 4 (CQ–4).

WORF provides a new capability for scientific and commercial payloads and will be a resource for public outreach and educational opportunities for Earth sciences (e.g., the EarthKAM, etc.). The WORF is located on the Earth-facing side of the US Destiny laboratory module. The Lab window, which features the highest quality optics, allows viewing of 39.5° forward along the axis of the station, 32.2° aft, and 79.1° from the port to starboard.

The flight will include three spacewalks to switch out a gyroscope on the station's truss, or backbone, install a spare ammonia storage tank, and retrieve a Japanese experiment from the station's exterior. ¹⁷⁶⁶⁾

1761) Michael Braukus, "Heads of Agency International Space Station Joint Statement," NASA, March 11, 2010, Release: 10–063, URL: http://www.nasa.gov/home/hqnews/2010/mar/HO_10-063_HOA_statement.html

1762) "Impacts of Shuttle Extension," NASA, April 2009, URL: http://www.wired.com/images_blogs/wiredscience/2010/03/finalstsextend.pdf

1763) Peter B. de Selding, "Germany is First ESA Member To Commit to Station Extension," Space News, Sept. 30, 2010, URL: <http://www.spacenews.com/civil/100930-germany-commit-iss-extension.html>

1764) Matthew J. Hart, Robert J. Kinsey, Austin S. Lee, Justin S. Yoshida, "International Space Station Life Extension," Proceedings of the 2010 IEEE Aerospace Conference, Big Sky, MT, USA, March 6–13, 2010

1765) http://www.nasa.gov/pdf/435885main_sts131_press_kit.pdf

1766) J. Yembrick, C. Thomas, "NASA's Shuttle Discovery Heads to Station after predawn launch," April 5, 2010, URL: <https://service.gmx.net/de/cgi/g.fcgi/application/navigator?CUSTOM-ERNO=11673889&t=uk844426059.1270440378.95a1230e>

The **SRS** (Sabatier Reactor System) is a reaction–based carbon dioxide reduction system, a new hardware package that was installed and integrated into the Water Recovery System of the ISS in mid–October 2010. On Oct. 26, 2010, NASA announced the successful activation of the Sabatier hardware that supports water production services aboard the International Space Station. ¹⁷⁶⁷⁾

The Sabatier reactor system can create up to 2000 liter of water per year from byproducts of the station’s Oxygen Generation System and Carbon Dioxide Removal Assembly. The process is named for Paul Sabatier (1854–1941), a French Chemist and a 1912 Nobel Prize winner in chemistry. The Sabatier process involves the reaction of hydrogen with carbon dioxide at elevated temperatures and pressures in the presence of a nickel catalyst to produce methane and water.

Prior to adding the Sabatier system, hydrogen produced while generating station oxygen was considered a waste gas and vented overboard. Carbon dioxide generated by crew metabolism also was vented overboard. With the Sabatier system, these two former waste gases will generate a valuable product for the space station: **water**.

Under contract to NASA, Hamilton Sundstrand, Space, Land & Sea of Windsor Locks, CT, (a subsidiary of United Technology Corp.) supplied the flight hardware and operational support for a Sabatier–reaction–based system that operates as part of the station’s ECLSS (Environmental Control and Life Support System). This contract is unique because NASA did not participate in design reviews or impose any specifications on the design, except for those defined in the safety, interface and acceptance requirements met by Hamilton Sundstrand.

ECLSSS provides or controls atmospheric pressure, fire detection and suppression, oxygen levels, waste management and water supply. The highest priority for the ECLSS is the ISS atmosphere, but the system also collects, processes, and stores waste and water produced and used by the crew—a process that recycles fluid from the sink, shower, toilet, and condensation from the air. – The Elektron system aboard Zvezda and a similar system in Destiny generate oxygen aboard the station. ^{1768) 1769) 1770)}

After the retirement of the Shuttle fleet in 2011, there will be an additional need for water on the ISS. Hence, the installation and operation of the SRS technology is a creative way to support environmental conditions on the ISS and to generate in addition an essential resource for the station crew, water.

Table 89: The SRS payload was delivered to the ISS on the STS–131 flight of Discovery ^{1767) 1768) 1769) 1770)}

- **STS–132.** ISS ULF–4 flight of Atlantis (May 14– 26, 2010, 12 day mission). The objective is to deliver the Russian–built **MRM1** (Mini–Research Module–1), also known as the **Rassvet** module (“dawn” in Russian). Rassvet has a dry mass of ~ 4,700 kg (launch mass of 5075 kg), a length of 6.0 m, diameter = 2.35 m, and an internal volume of 17.4 m³ (5.5 m³ for cargo storage). Rassvet was developed and built by RSC Energy of Korolev for Roskosmos. MRM1 provides a fourth docking port on on the Russian operation segment. On its shell, MRM1 carries the first equipment portion of **ERA** (European Robotic Arm) of ESA. ERA will be the second ‘intelligent’ robot arm for the ISS. The complete operational ERA

¹⁷⁶⁷⁾ Michael Curie, “International Space Station Water System Successfully Activated,” NASA, Oct. 26, 2010, URL: http://www.nasa.gov/home/hqnews/2010/oct/HQ_10-275_Sabatier.html

¹⁷⁶⁸⁾ “International Space Station, Environmental Control and Life Support System,” URL: http://www.nasa.gov/centers/marshall/pdf/104840main_eclss.pdf

¹⁷⁶⁹⁾ ISS ECLSS, URL: http://en.wikipedia.org/wiki/ISS_ECLSS

¹⁷⁷⁰⁾ Russell C. Burkey, Steven T. Green, Shane P. Siebenaler, J. Christopher Buckingham, “From CO₂ to H₂O: SwRI compressor technology helps NASA to produce water in space,” Summer 2010, URL: <http://www.swri.org/3pubs/today/Summer10/PDFs/From-CO2-to-H2O.pdf>

will be launched in 2012 by a Proton rocket, attached to the MLM (Multipurpose Laboratory Module) of Russia. ^{1771) 1772)}

In parallel, the STS-132 mission ICC-VLD-2 (Integrated Cargo Carrier-Vertical Lightweight Deployable-2) carries replacement components and spare parts for the space station (total mass of 3800 kg). There are 6 battery ORUs (Orbital Replacement Units) for Port 6 IEA (Integrated Equipment Assembly). Further components are: SGANT (Space-to-Ground Antenna), one SGANT boom and one EOTP (Enhanced Orbital Replacement Unit Temporary Platform). SGANT provides Ku-band communication between the ISS and the TDRS.

ERA will be used to service the Russian segment of the ISS and to transfer small payloads directly to space via MLM's special airlock, liberating astronauts from time-consuming, fatiguing and potentially hazardous tasks outside the Station.

- January 22, 2011, launch of the **HTV-2** (H-II Transfer Vehicle 2) of JAXA, nicknamed Kounotori 2 (White Stork). HTV-2 has a size of 4 m Ø x 10 m in length. This is the second Japanese service flight to the ISS with a payload (a mixture of pressurized and unpressurized cargo), the total cargo mass is ~ 5,300 kg (16,061 kg of HTV-2 liftoff mass). The launcher is the H-IIB F2 vehicle, manufactured by MHI and JAXA; the launch site is TNSC (Tanegashima Space Center), Japan. Cargo in PLC (Pressurized Logistics Carrier) consists of spare system components (51% of cargo mass), foods (24%), science experiment materials (10%), crew commodities (8%), and water (7%). It includes the Kobairo (Gradient Heating Furnace) rack and the MSPR (Multipurpose Small Payload Rack). ¹⁷⁷³⁾

The ULC (Unpressurized Logistics Carrier) contains an EP (Exposed Pallet) with two US ORUs (Orbital Replacement Units) attached: a FHRC (Flex Hose Rotary Coupler) and CTC-4 (Cargo Transportation Container-4).

On Jan. 27, 2011, Kounotori 2 arrived at the ISS (automatic rendezvous) ¹⁷⁷⁴⁾ and was successfully grappled by the ISS crew via the SSRMS (Space Station Remote Manipulator System), or Canadarm2, ahead of berthing to Node-2 Nadir. Both the FHRC and CTC-4 were transferred from Kounotori 2's EP to the space station's ELC-4 using the ISS's SPDM "Dextre". The operations marked Dextre's first scheduled task since the robot was commissioned in December 2010.

1771) STS-132 Press Kit, May 2010, URL: http://www.nasa.gov/pdf/451029main_sts132_press_kit.pdf

1772) "ESA Giving A Spare Arm To Space Station," May 13, 2010, URL: http://www.space-travel.com/reports/ESA_Giving_A_Spare_Arm_To_Space_Station_999.html

1773) "Launch Result of H-IIB Launch Vehicle No. 2 with Kounotori 2 (HTV2) Onboard," JAXA, Jan. 22, 2011, URL: http://www.jaxa.jp/press/2011/01/20110122_h2bf2_e.html

1774) Ken Kremer, "Japans White Stork Kounotori Grappled and Nested at Space Station: Video, Photo Album," Universe Today, Jan. 27, 2010, URL: <http://www.universetoday.com/82884/japans-white-stork-kounotori-grappled-and-nested-at-space-station-videophoto-album/>

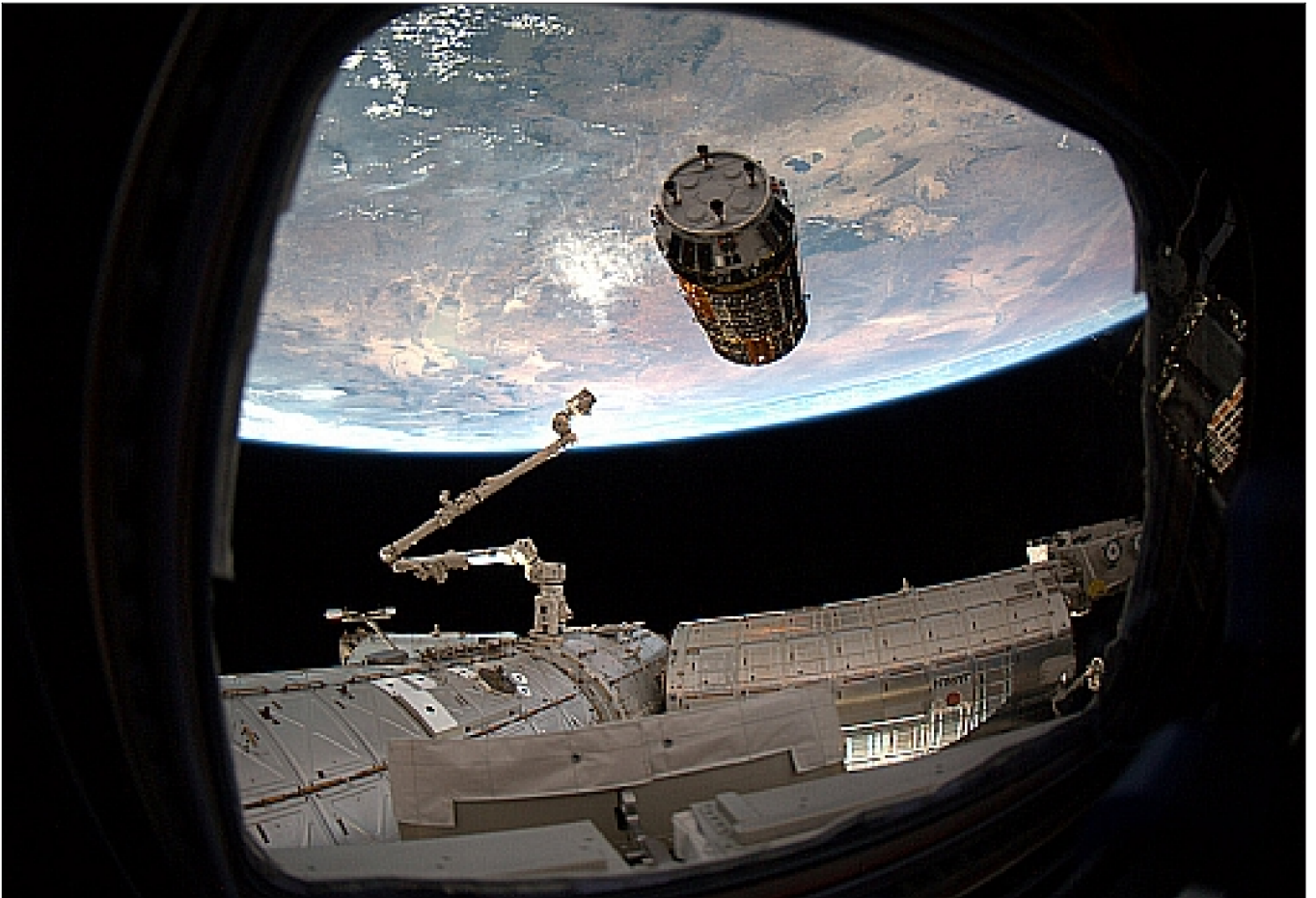


Figure 117: Photo of the HTV-2 arrival at the ISS with the extended Canadarm2 (image credit: NASA)

On March 28, 2011 HTV-2 was undocked from the ISS for reentry into the Pacific Ocean. Onboard of HTV-2 was the REBR (Reentry Breakup Recorder), an instrument designed and constructed by engineers at The Aerospace Corporation (El Segundo, CA). It successfully collected data during the breakup of the HTV2 vehicle and "phoned home" that data as it fell into the ocean on March 30, 2011. The REBR is a small autonomous device that is designed to record temperature, acceleration, rotation rate, and other data as a spacecraft reenters Earth's atmosphere. The REBR test was coordinated by the U.S. STP (Space Test Program) of DoD. ¹⁷⁷⁵⁾

- Feb. 16, 2011, launch of the **ATV-2** (Automated Transfer Vehicle-2, named 'Johannes Kepler') ^{1776) 1777) 1778) 1779)} service flight to the ISS from Europe's Spaceport, Kourou, on the Ariane-5ES vehicle (ATV-2 launch mass of ~ 20,000 kg, size ~ 10 m x 4.5 m Ø). ATV-2 will navigate, fly and dock to the Station automatically, but it will be monitored and commanded via ARTEMIS (ESA's GEO data relay satellite) and TDRSS of NASA from the ATV Control Center (ATV-CC) in Toulouse, France. Several upgrades permit ATV-2 to ferry a full propellant load of almost 5 tons. All the cargo – liquid, gas and dry

¹⁷⁷⁵⁾ "First REBR Reentry a Success," The Aerospace Corporation, March 30, 2011, URL: <http://www.aero.org/news/newsitems/032911-REBRsuccess.html>

¹⁷⁷⁶⁾ "Europe's ATV space ferry ready for launch," ESA, Feb. 3m 2011, URL: http://www.esa.int/esaCP/SEM5ZFY1LJG_index_0.html

¹⁷⁷⁷⁾ "ATV @@@@Johannes Kepler operating flawlessly," ESA, Feb. 17, 2011, URL: http://www.esa.int/esaCP/SEMBVAPT1KG_index_0.html

¹⁷⁷⁸⁾ "ATV Johannes Kepler on its way to the ISS," Feb. 16, 2011, URL: http://www.dlr.de/en/desktopdefault.aspx/tabid-6221/10233_read-29140/

¹⁷⁷⁹⁾ "ATV2 – preparing to be space-bound!," EADS Astrium, Dec. 14, 2010, URL: <http://www.astrium.eads.net/en/news2/atv2-%E2%80%93-preparing-to-be-space-bound.html>

goods – totals 7.5 tons. Arrival at the ISS on Feb. 24, 2011 (flawless rendezvous and docking with the ISS).

– At the Station, ATV–2 provided storage and help in adjusting the orbit, performing regular orbit reboosts and avoiding space debris. – On June 20, 2011, after staying for four months at the Station, ATV–2 undocked, after being commanded by the ATV–CC; it burned up in the atmosphere over an uninhabited area of the southern Pacific Ocean on June 21, 2011. On board was a Re–entry Break–up Recorder, a special flight data recorder designed to log the mechanical stresses on the ATV–2 during break–up and radio the data to the ground station via satellite. ¹⁷⁸⁰⁾

• **STS–133** ISS ULF5 flight of Discovery (Feb. 24– March 9, 2011, 13 day mission at ISS). The objective is to deliver the PPM (Permanent Multipurpose Module), the converted version of the multi–purpose logistics module Leonardo. The PPM provides additional storage for the station crew and serves as an experiment module. — Note: The Leonardo module was originally built to ferry cargo to and from the Station in the Shuttle cargo bay, Leonardo’s modifications include improved debris shielding and easier access by the crew to its internal equipment. Leonardo flew into space for the first time in 2001, as the first of three Multipurpose Logistics Modules built by the Italian space agency, ASI, under an agreement with NASA.

In addition, Discovery carried critical spare components and the Express Logistics Carrier 4 (ELC4) to the station. Express (Expedite the Processing of Experiments to the Space Station) is an external platform that holds large equipment that can only be transported using the unique capability of the shuttle. **R2** (Robonaut 2), the first humanoid robot in space, is part of the PPM payload, and became the permanent resident of the station, in the US Destiny laboratory. ¹⁷⁸¹⁾



Figure 118: Photo of the Robonaut 2 torso (image credit: NASA)

Robonaut 2, the next generation of dexterous humanoid robots, was designed through a joint venture between NASA and General Motors. R2 is a robotic torso with movable hands and arms plus two high image cameras for eyes. ^{1782) 1783)} This dexterous robot is designed to perform tasks that assist the human crew members. For the initial testing in the Destiny laboratory, Robonaut 2 will manipulate switches, remove dust covers and install handrails. Once the technology is demonstrated, more difficult tasks will be scheduled. – The torso of R2 has a mass of ~ 135 kg. On arrival at the Station, R2 joined the crew of six human residents as an official member of the ISS crew.

1780) “ATV–2: re–entry over the south Pacific,” DLR, June 22, 2011, URL: http://www.dlr.de/en/desktopdefault.aspx/tabid-6221/10233_read-31259/

1781) http://www.nasa.gov/pdf/491387main_STS-133%20Press%20Kit.pdf

1782) <http://robonaut.jsc.nasa.gov/default.asp>

1783) Dauna Coulter, Tony Phillips, “Robonaut 2 set to launch in February,” January 31, 2011, URL: http://science.nasa.gov/science-news/science-at-nasa/2011/31jan_r2/

NPBX (Nucleate Pool Boiling Experiment) is a NASA science experiment. It may seem illogical, but boiling is a very efficient way to cool engineering components and systems used in the extreme environments of space. The objective is to gain a basic understanding of this phenomena. NPBX is one of two experiments in the BXF (Boiling eXperiment Facility).¹⁷⁸⁴⁾

Nucleate boiling is bubble growth from a heated surface and the subsequent detachment of the bubble to a cooler surrounding liquid. As a result, these bubbles can efficiently transfer energy from the boiling surface into the surrounding fluid. This investigation provides an understanding of heat transfer and vapor removal processes that happen during nucleate boiling in microgravity.

The LMM (Light Microscope Module) is part of the STS–133 payload and will be used as a remotely controllable on–orbit microscope subrack facility, allowing flexible scheduling and control of physical science and biological science experiments within the GRC Fluids Integrated Rack (FIR) on the ISS (International Space Station).¹⁷⁸⁵⁾

- **STS–134** ISS ULF6 flight of Endeavour (May 16–June 1, 2011, 12 day mission at ISS). The primary objective is to deliver the **AMS–02** (Alpha Magnetic Spectrometer–2). The AMS–02 instrument assembly is a cube–shaped structure with a total mass of 6,917 kg. The spectrometer consists of a huge superconducting magnet and six specialized detectors, and requires 2.4 kW of power @ 28 V. The downlink data rate is 6 Mbit/s.¹⁷⁸⁶⁾

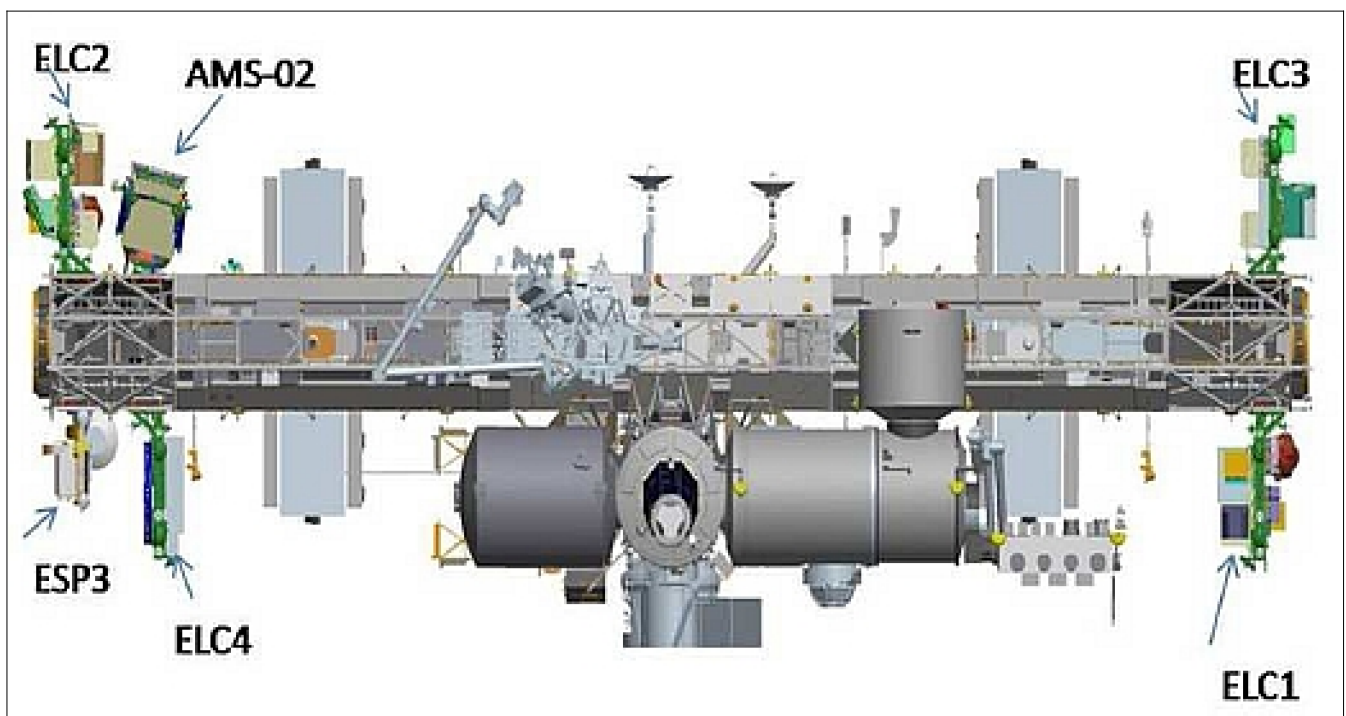


Figure 119: ISS truss configuration with ELC–3 and AMS–02 (image credit: NASA)

– Endeavour also will fly the ExPRESS (Expedite the Processing of Experiment to Space Station) Logistics Carrier 3 (ELC–3), a platform that carries spare parts that will sustain space station operations once the shuttles are retired from service. The mission will feature four spacewalks to do maintenance work and install new components. These are the last

¹⁷⁸⁴⁾ “Boiling Bubbles are Cool in Space,” NASA, Feb. 28, 2011, URL: http://www.nasa.gov/mission_pages/station/research/news/npbx.html

¹⁷⁸⁵⁾ <http://issresearchproject.grc.nasa.gov/Investigations/LMM/>

¹⁷⁸⁶⁾ STS–134 Press Kit, NASA, April 2011, URL: http://www.nasa.gov/pdf/538352main_sts134_presskit_508.pdf

scheduled spacewalks by shuttle crew members. Shuttle mission STS–134 is the final flight for Endeavour and the second to last flight for the Space Shuttle Program. ¹⁷⁸⁷⁾

– MHTEX (Massive Heat Transfer Experiment) is a collaborative development of Northrop Grumman and AFRL (Air Force Research Laboratory) within the STP (Space Test Program) of DoD. The new payload uses an advanced capillary pump loop that moves heat generated by electronic systems so it can be safely expelled from the spacecraft. The objective is to demonstrate how satellite systems can be cooled eight times more efficiently than today's systems (flight qualification of instrument). This will allow new cooling systems to be developed that support more complex hardware on military spacecraft. ¹⁷⁸⁸⁾

– The second STP experiment is VADER (Variable emissivity device Aerogel insulation blanket Dual zone thermal control Experiment suite for Responsive space), also sponsored by AFRL. VADER is a reconfigurable thermal control system. It will also test a new form of MLI (Multi–Layer Insulation) protection using Aerogel material as the thermal isolator.

– The 3rd STP experiment is DISC (Digital Imaging Star Camera) of NRL. It is a low size, mass and power sensor used for pointing knowledge of 0.02° or greater.

– Canary is a highly sensitive and extremely compact instrument for plasma monitoring built by JHU/APL. The objective is to investigate the interaction of approaching spacecraft with the background plasma environment around the ISS and disturbances in the ionosphere caused by space vehicles. The device will also provide a better understanding of the origin and impact of plasma irregularities in the Earth's ionosphere, and demonstrate low–cost techniques for monitoring those conditions. ¹⁷⁸⁹⁾

– STS–134 will deliver a spare arm for Dextre to the station. The spare is 3.53 m long with seven joints and a load–carrying capability of 600 kg.

The AMS–02 will be able to detect high–energy particles that would not make it to the surface. Cosmic rays will pass through the AMS–02 and be bent by its magnetic field, generated by a permanent magnet 4,000 times stronger than the Earth's own magnetic field. In a real sense, the International Space Station will transform into a high–energy physics laboratory, with access to the most powerful accelerator in the universe, which is the universe itself. – Most of our understanding of the cosmos up to now comes from measuring light. Besides the light rays, there are charged particles –and the observation of charged particles have not been done nearly as much as light to understand the universe. Hence, the operation of AMS–02 on the ISS will open a door into a new area.

After the Space Shuttle Endeavour undocked from the ISS on May 30, 2011, it performed a re–approach maneuver to the station. ^{1790) 1791)} The objective was to demonstrate advanced navigation sensor technologies known as **STORRM** (Sensor Test for Orion Relative Navigation Risk Mitigation). In particular, the requirement called for the performance characterization of the flash Lidar of VNS (Vision Navigation Sensor), the primary navigation instrument used by the future Orion vehicle. For the test, the VNS and Docking Camera was mounted on the existing unused TCS (Trajectory Control System) on the ODS (Or-

1787) “STS–134 Mission Summary,” March 2011, URL: http://www.nasa.gov/pdf/531933main_STS134_MissionSummary.pdf

1788) “Northrop Grumman To Test Heat Management System On ISS,” Space Travel, April 13, 2011, URL: http://www.space-travel.com/reports/Northrop_Grumman_To_Test_Heat_Management_System_On_ISS_999.html

1789) “APL–Built Plasma Detector Launches on Space Shuttle Endeavour,” Space Travel, May 19, 2011, URL: http://www.space-travel.com/reports/APL_Built_Plasma_Detector_Launches_on_Space_Shuttle_Endavour_999.html

1790) John A. Christian, Heather Hinkel, “The Sensor Test for Orion RelNav Risk Mitigation Development Test Objective,” URL: http://ntrs.nasa.gov/archive/nasa/casi.ntrs.nasa.gov/20110005446_2011004705.pdf

1791) “On–Orbit Orion MPCV Navigation System Tested During STS–134 Shuttle Mission,” Space Travel, May 31, 2011, URL: http://www.space-travel.com/reports/On_Orbit_Orion_MPCV_Navigation_System_Testing_During_STS_134_Shuttle_Mission_999.html

biter Docking System) Truss. The Star Tracker and data interface controller were mounted on an Orbiter sidewall carrier in the orbiter Payload.

The flight test represented the first and only opportunity for in-flight collaboration of NASA's three human spaceflight programs – space shuttle, International Space Station and Orion MPCV (Multi-Purpose Crew Vehicle).



Figure 120: Photo of the Space Shuttle Endeavour docked to the ISS (image credit: NASA, Paolo Nespoli)

Legend to Figure 120: This image of the ISS and the Space Shuttle (STS–134) was taken by Expedition 27 crew member Paolo Nespoli from the Soyuz TMA–20 following its undocking on May 23, 2011. It is the first–ever image of a Space Shuttle docked to the International Space Station. The Endeavour is at left while the European ATV–2 (Automated Transfer Vehicle–2) cargo carrier is at the far right.^{1792) 1793)}

- **STS–135** ISS ULF7 flight of Atlantis (July 8–21, 2011, 13 day mission), representing the final Shuttle mission. The primary objective is to deliver cargo and supplies to the ISS; among them the Raffaello MPLM (Multi-Purpose Logistics Module) and the LMC (Lightweight Multi-Purpose Carrier). The MPLM will carry supplies, logistics and spare parts to the ISS. The LMC will be used to return a failed Ammonia Pump for troubleshooting and analysis to help NASA better understand the failure mechanism and improve pump

¹⁷⁹²⁾ http://www.nasa.gov/mission_pages/station/multimedia/e27depart.html

¹⁷⁹³⁾ Ken Kremer, “NASA Releases Spectacular Portrait Photos of Endeavour Docked at the ISS from Soyuz and Paolo Nespoli,” Universe Today, June 7, 2011, URL: <http://www.universetoday.com/86369/nasa-releases-spectacular-portrait-photos-of-endeavour-docked-at-the-iss-from-soyuz-and-paolo-nespoli/>

designs for future systems. The total payload launch mass is 13,900 kg (not counting the mid-deck payload).¹⁷⁹⁴⁾

STS–135 is a late—and final—addition to the shuttle manifest. It is carrying out a key mission to help support the continued operations of the ISS and testing technology that can support satellite servicing.

Some payload short descriptions are:

- GLACIER is a freezer designed to provide cryogenic transportation and preservation capability for samples. The unit is a double locker equivalent unit capable of transport and operation in the middeck and in–orbit operation in the ExPRESS (Expedite the Processing of Experiments to the Space Station) rack.

- First iPhone Flying on Last Shuttle: NanoRacks Smartphone–1 will test Apple’s gyroscope–equipped iPhone 4 and an application as a potential space navigation tool. The experiment will use the phone’s camera and an Earth limb tracker to test its capabilities to estimate altitude, calibrate spacecraft instruments and update navigation state vectors. The experiment also will characterize the effects of radiation on the device.

- ARFTA (Advanced Recycle Filter Tank Assembly), consisting of a tank, three types of filter assemblies, a Compressor Adapter, a Rodnik/ATV adapter and several hose assemblies. The ARFTA replaces the RFTA (Recycle Filter Tank Assembly). The function of the RFTA is to collect the residue left over from extracting water from the astronaut urine.

- **RRM** (Robotic Refueling Mission) payload, a joint NASA–CSA project: RRM is an experiment designed to demonstrate and test the tools, technologies and techniques needed to robotically refuel satellites in space, even satellites not designed to be serviced. RRM is an external ISS experiment that will use Dextre, a space robot of CSA, to demonstrate and test the tools, technologies and techniques engineers on Earth would need to robotically refuel satellites in space—even satellites not designed to be serviced. The test is expected to take place approximately six months after STS–135.¹⁷⁹⁵⁾

- TriDAR (Triangulation and LIDAR Automated Rendezvous and Docking system): The TriDAR technology will undergo further testing on board the Space Shuttle. TriDAR provides critical guidance information that can be used to position a vehicle during rendezvous and docking operations. Unlike current technologies, TriDAR does not rely on any reference markers, such as reflectors, positioned on the target spacecraft. It counts on a laser–based 3D sensor and a thermal imager. The TriDAR technology is developed by Neptec Design Group of Kanata, Ontario, Canada with funding from CSA and NASA.¹⁷⁹⁶⁾

The TriDAR system’s capabilities were successfully demonstrated on previous test flights (STS–128 and). The third flight of the system is set to continue demonstration of the system’s capabilities.

- The **PSSCT–2** (Pico–Satellite Solar Cell Testbed–2) testbed, also referred to as “PicoSat”, is a nanosatellite of The Aerospace Corporation (El Segundo, CA) with a size of 12.7 cm x 12.7 cm x 25.4 cm and a mass of 3.7 kg.

PicoSat was ejected on June 20, 2011, shortly before shuttle re–entry into a low (< 360 km altitude) orbit with an expected orbital lifetime of three to nine months, depending on solar activity. Multiple on–board megapixel cameras imaged Atlantis as the satellite departed,

1794) “STS–135 Press Kit: The Final Mission,” NASA, July 2011, URL: http://www.nasa.gov/pdf/566071main_STS-135_Press_Kit.pdf

1795) Ken Kremer, “Revolutionary Robotic Refueling Experiment Opens New Research Avenues at Space Station,” Universe Today, July 16, 2011, URL: <http://www.universetoday.com/87419/revolutionary-robotic-refueling-experiment-opens-new-research-avenues-at-space-station/>

1796) “Canada’s contribution to final shuttle flight,” Space Travel, June 30, 2011, URL: http://www.space-travel.com/reports/Canada_contribution_to_final_shuttle_flight_999.html

thus supplying the last in-orbit photos of NASA's workhorse human space transportation system for the last few decades.

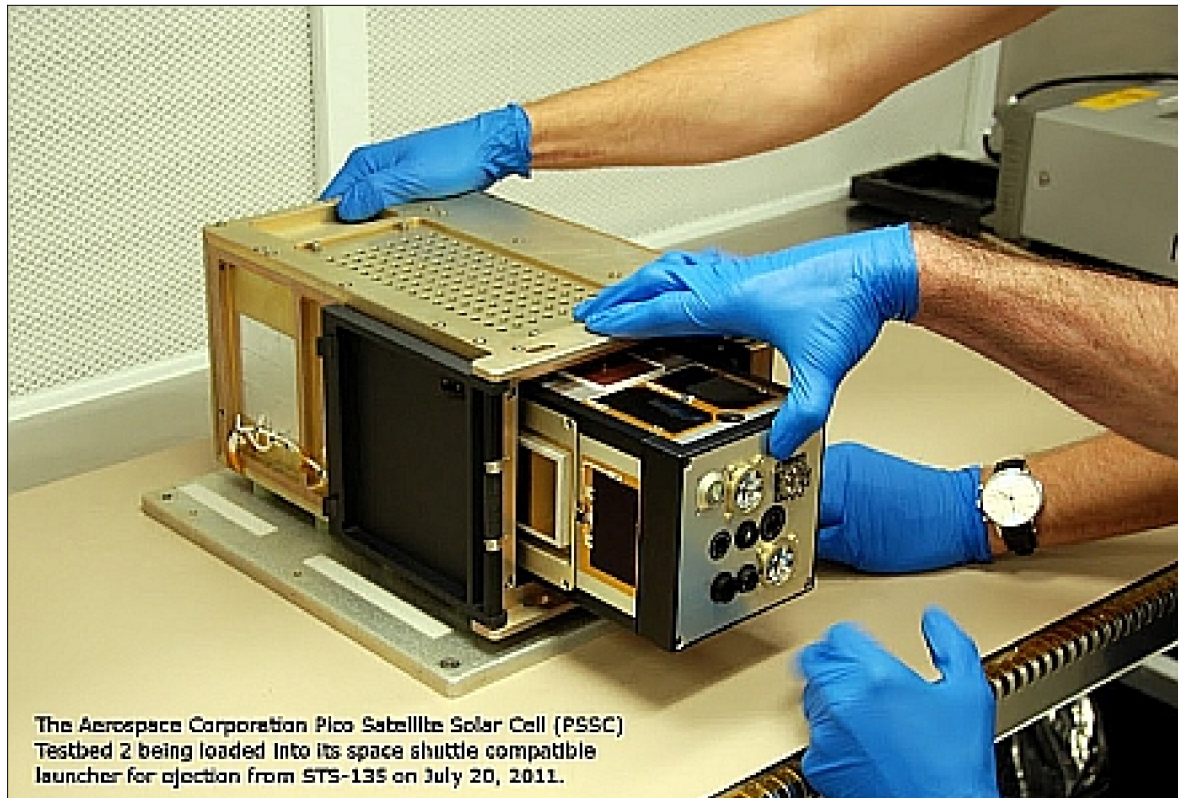


Figure 121: Photo of the PSSC-2 testbed (image credit: The Aerospace Corporation)

PicoSat will perform two DoD experiments during its in-orbit lifetime: ¹⁷⁹⁷⁾

1) First, the MTV (Miniature Tracking Vehicle) experiment goal is to demonstrate the capability of a nano-satellite to serve as an orbiting reference for ground tracking systems while demonstrating 3-axis attitude control, solid rocket propulsion for orbit modification, adaptive communications and active solar cell performance monitoring in a nanosatellite platform. An on-board GPS receiver will provide accurate time and position information to facilitate tracking error analyses.

2) The second experiment, CTECS (Compact Total Electron Content Sensor), will demonstrate a CubeSat form factor space weather sensor with the capability to detect ionospheric density. It uses a modified commercial GPS receiver to detect differences in radio signals generated by occulting GPS satellites.

After PicoSat's orbit lowers for approximately one month, four ammonium perchlorate solid rocket motors will provide 40 Ns of impulse each and could extend orbital lifetime by an additional two months or alternatively, actively deorbit the satellite. – The PSSC-2 bus, MTV and CTECS experiments will be controlled by a primary ground station at The Aerospace Corporation in El Segundo, CA, and secondary stations that comprise the Aerospace Corporation Internet-based Picosatellite Ground Station Network. – The PSSC-2 operated until its reentry into Earth's atmosphere on Dec. 7, 2011.

The return flight of STS-135 and the landing at Cape Canaveral on July 21, 2011 ended the 30 year era of Shuttle flights in the U.S. Space program.

- A Russian Soyuz capsule carrying the first crew of humans to fly to space in the post Space Shuttle Era docked successfully at the ISS on Nov. 16, 2011. After an 11 year stretch

¹⁷⁹⁷⁾ "Final Nanosatellite Launched from Space Shuttle Atlantis," Space Daily, July 25, 2011, URL: http://www.space-daily.com/reports/Final_Nanosatellite_Launched_from_Space_Shuttle_Atlantis_999.html

of continuous human occupation, the future residency of humans aboard the ISS swung in the balance in the wake of a Russian Soyuz rocket failure in August 2011 (carrying an unmanned Progress cargo resupply vessel.) that temporarily grounded all Soyuz launches – manned and unmanned – until the root cause was determined and satisfactorily rectified with NASA’s consent.

The very survival of the ISS hinged on the successful launch of a trio of Russian and American space flyers from the Baikonur Cosmodrome in Kazakhstan aboard the Soyuz TMA–22 capsule, which took place amidst an unprecedented blizzard and white out conditions with near zero visibility. – A full complement of 6 crew members was thus restored to the ISS.

Space Shuttle of NASA, USA	<p>The reusable Space Shuttle provides provides a number of services to the ISS. It carries payloads and supplies for the crew and provides crew rotation for ISS. The Shuttle may also return large payloads from the ISS to Earth.</p> <ul style="list-style-type: none"> – The first Shuttle flight to the ISS took place on STS–88 (Endeavour, launch Dec. 4, 1998) delivering the Unity (11,800 kg, 11 m in total length), referred to as Node 1. Unity was mated to Zarya. – STS–117 (Atlantis, launch June 8, 2007) was a flight with the largest payload of a Space Shuttle (S3/S4 Truss of 16,183 kg) – Up to May 31, 2008 there were 20 Shuttle assembly flights to the ISS. – NASA plans call for 9 additional Shuttle flights to the ISS until mid–2010.
ISS logistics	<p>ISS logistics has been accomplished with STS pallets/lockers and available pressurized modules (SPACEHAB and MPLM)</p> <ul style="list-style-type: none"> • SPACEHAB is a commercial logistics module of Astrotech Corp., formerly SPACEHAB, Inc., developed for the Space Shuttle in the mid–1980s (derived from ESA’s Spacelab). The 3 m long SPACEHAB module is carried inside the Shuttle cargo bay providing ~ 28 m³ of space for experiments and logistics transport. • MPLM (Multi–Purpose Logistics Module). Three MPLMs were provided by ASI (Italian Space Agency) to NASA (independent of Italy’s role as a member state of ESA). The three MPLMs are named: Leonardo, Raffaello, and Donatello. These are pressurized modules that serve as the International Space Station’s ”moving vans,” carrying equipment, experiments and supplies to and from the ISS aboard the cargo bay of the Space Shuttle. Each MPLM has an empty mass of 4500 kg and can carry a payload mass of up to 10,000 kg. <p>Construction of the Leonardo module began in April 1996 at TAS (Thales Alenia Space) in Turin, Italy (formerly Alenia Aerospazio). Leonardo was delivered to Kennedy Space Center from Italy in August 1998 by a special Beluga cargo aircraft. Raffaello arrived at Kennedy in August 1999. The third module, named Donatello, was delivered to Kennedy on Feb. 1, 2001</p>
Proton spacecraft of RKK Energia, Russia	<p>Proton is the largest Russian launch vehicle in regular use (since 1965). Proton heavy–lift vehicles were used to ferry the Salyut and Mir space stations to orbit, as well as large mass elements to the ISS.</p> <ul style="list-style-type: none"> – The first component of ISS, namely FGB (Functional Cargo Block), also referred to as Zarya (meaning ‘sunrise’), was launched Nov. 20, 1998 on a Proton–K vehicle from the Baikonur Cosmodrome in Kazakhstan. Zarya had a launch mass of 20,040 kg. – The Russian–built Zvezda (meaning “star”) Service Module (SM) was launched on July 12, 2000 by a Proton–K vehicle from Baikonur. Zvezda had a launch mass of 20,295 kg.
Soyuz spacecraft of RKK Energia, Russia	<p>The Soyuz vehicle has a long history in the Russian Space Program dating back to the 1960s. It consists of an Orbital Module, a Descent Module and an Instrumentation/Propulsion Module. The Soyuz–TM was used to from May 1986 to take cosmonauts and astronauts to the Russian MIR Station.</p> <ul style="list-style-type: none"> – Soyuz–TMA vehicles (an upgrade of the TM version) deliver crews, equipment and supplies to the ISS (Ref. 1808). – <i>A Soyuz vehicle flew the first crew to the ISS in Nov. 2000 (launch on Oct. 31, 2000).</i> Since that time, at least one Soyuz has always been at the Station, generally to serve as a lifeboat should the crew have to return to Earth unexpectedly. – Up to three crew members can launch and return to Earth from the Station aboard a Soyuz TMA spacecraft. – A new Soyuz capsule is normally delivered to the station by a Soyuz taxi crew every six months – the taxi crew then returns to Earth in the older Soyuz capsule. – A Soyuz spacecraft generally takes two days after launch to reach the space station. The rendezvous and docking are both automated. The Russian Mission Control Center monitors the close approach maneuvers to the ISS.

Progress spacecraft of RKK Energia, Russia	<ul style="list-style-type: none"> – Progress is an automated, uncrewed version of the Soyuz spacecraft that is used to bring supplies, equipment and fuel to the ISS. – Progress also has the ability to raise the Station's altitude and control the orientation of the Station using the vehicle's thrusters – Progress has a pressurized Cargo Module to carry supplies, a Refueling Module that holds fuel tanks containing propellant and pressurized gases, and an Instrumentation/Propulsion Module where the Progress systems equipment and thrusters are located. – The Cargo Module can carry up to 1700 kg of supplies to the ISS in a pressurized volume of $\sim 6 \text{ m}^3$ – Prior to its return flight from the ISS, Progress is loaded with trash, unneeded equipment and waste water, which will burn up with the spacecraft when it reenters the Earth's atmosphere. – The launch of the first Progress service flight to ISS took place on Feb. 26, 2001 (Progress M-44). Permanent habitation of the ISS had started with the first expedition crew launched on Oct. 31, 2000 on a Soyuz vehicle.
ATV (Advanced Transfer Vehicle) of ESA, Europe	<p>ATV is an automated and uncrewed service vehicle of ESA capable of delivering net payloads of up to 7,667 kg (equipment) plus resupplies, fuel and water. The large amount of fuel provides a very good reboost capability for the ISS.</p> <ul style="list-style-type: none"> – The launch first ATV flight took place on March 9, 2008 from Kourou on an Ariane-5 launch vehicle (max launch mass of 19 tons) – The ICC (Integrated Cargo Carrier) of ATV is a pressurized module with a volume of 48 m^3 representing 60% of the total ATV volume. Astronauts may use the ICC as a recreational facility during its docking period. – Each ATV will remain docked to the Station for about 6 months providing occasional reboosts to the ISS. ATV will be loaded with the trash that accumulates in the Station which will burn up with the spacecraft when it reenters the Earth's atmosphere. – The ESA program foresees 4 additional service flights of the ATV to the ISS
HTV (H-II Transfer Vehicle) of JAXA, Japan	<p>HTV is the Japanese entry of ISS robotic resupply vehicles to the ISS (unmanned cargo transfer and waste disposal vehicle on reentry).</p> <ul style="list-style-type: none"> – The first HTV service flight to the ISS occurred on Sept. 10, 2009 (launch from TNSC, Japan on the H-II B launch vehicle – HTV approached the ISS automatically; it was captured and berthed by Canadarm2. – HTV has 2 types of logistics carriers. One is a mixed (pressurized & unpressurized) carrier and the other is a pressurized carrier. – The total mass of HTV 16,500 kg (max) – Net cargo of the pressurized carrier is up to 7,000 kg – In the mix version (pressurized/unpressurized) the max cargo may be $\leq 6,000 \text{ kg}$
Dragon spacecraft (SpaceX)	<p>Dragon is a free-flying, reusable S/C developed by SpaceX for NASA's COTS (Commercial Orbital Transportation Services) program. Dragon is made up of a pressurized capsule and an unpressurized trunk used for Earth to LEO transport of cargo and/or crew members.</p> <p>In Dec. 2008, NASA selected the Falcon-9 launch vehicle and the Dragon S/C to resupply the ISS after the Space Shuttle retires (starting in 2011).</p>
Cygnus (OSC)	<p>Cygnus is an unmanned resupply spacecraft developed by OSC (Orbital Sciences Corp.) for NASA's COTS program. The objective is to resupply the ISS after the retirement of the Space Shuttle. Cygnus consists of a service module and a cargo module. Cygnus can deliver up to 2,700 kg of cargo/flight to the ISS and to return up to 1200 kg of cargo from the ISS to Earth.</p>

Table 90: Overview of service vehicles and their functions between the ground segment and ISS ^{1798) 1799) 1800) 1801) 1802) 1803) 1804) 1805)}

1798) Russian Soyuz TMA Spacecraft, http://www.nasa.gov/mission_pages/station/structure/elements/soyuz/index.html

1799) Russian Progress Spacecraft, http://www.nasa.gov/mission_pages/station/structure/elements/progress.html

1800) <http://seds.org/~spider/shuttle/iss.html>

1801) http://www.nasa.gov/mission_pages/station/structure/iss_assembly.html

1802) <http://www.spaceflight.esa.int/projects/index.cfm?act=default.page&level=11&page=779>

1803) http://www.jaxa.jp/projects/rockets/htv/index_e.html

1804) <http://www.spacex.com/dragon.php>

1805) <http://www.orbital.com/HumanSpaceExplorationSystems/COTS/>

ISS Element	Launch Date	Description
Zarya (Sunrise)	Nov. 20, 1998	Functional Cargo Block (FGB), 20,040 kg pressurized module
Unity	Dec. 4, 1998	Node 1 (11,800 kg, 11 m in total length)
Zvezda	July 12, 2000	Service Module
Z1 truss	Oct. 2000	Zenith truss segment, first permanent lattice–work structure for ISS
P6 arrays	Nov. 30, 2000	First US arrays, a package of 7,700 kg containing the PV module
Destiny	Feb. 7, 2001	US laboratory module, structure of 8.5 m in length and 4.3 m diameter
Canadarm2	Apr. 19, 2001	SSRMS (Space Station Remote Manipulator System)
Quest	July 12, 2001	Joint airlock, primary path for ISS space walk activity
Pirs	Sep. 21, 2001	DC–1 (Docking Compartment 1), Russian–based space walks
S0 truss	April 8, 2002	Center truss segment
S1 truss	Oct. 7, 2002	First starboard truss segment
P1 truss	Nov. 24, 2002	First port truss segment
There were no Space Shuttle flights for 2 1/2 years due to Columbia accident in Feb. 2003		
MPLM	July 26, 2005	Raffaello Multi–Purpose Logistics Module ESP–2 (External Stowage Platform), Removal/replacement of CMGs
P3, P4 truss	Sept. 9, 2006	Second port ITS (Integrated Truss Structure), ITS P3/P4 (15,700 kg)
P5 truss	Dec. 10, 2006	Third port truss segment (ITS P5)
S3, S4	June 8, 2007	ITS (Integrated Truss Segment) Starboard–3/–4 (16,200 kg)
S5	Aug. 8, 2007	Third starboard truss segment (ITS S5), CMG replacement
Harmony	Oct. 23, 2007	Node 2 (14,200 kg, 7.3 m in length)
Columbus Lab	Feb. 7, 2008	Columbus Orbital Facility (COF) of ESA (10,300 kg)
JEM–PS (Kibo)	Mar. 11, 2008	ELM–PS (Experiment Logistics Module–Pressurized Section), JAXA SPDM (Special Purpose Dexterous Manipulator), Canada, “Dextre”
JEM–PM (Kibo)	May 31, 2008	JPM (Japanese Pressurized Module) of JAXA (15,900 kg) JEM–RMS (Japanese Remote Manipulator System), 1700 kg
Poisk (MRM2)	Nov. 10, 2009 Poisk docked on Nov. 12, 2009 at the ISS.	Poisk (“explore” or “search” in Russian) also known as the MRM2 (Mini–Research Module 2), is one of the two new Russian modules to the ISS. During launch, it was inside a Progress M–MRM2 spacecraft and powered into space from a Soyuz–U rocket. Poisk had a launch mass of ~ 3760 kg, the module has a diameter of 2.6 m and a length of 4.6 m (delivery of 820 kg of cargo/supplies). The module is being used as an additional docking port for Russian vehicles, as an airlock for Russian–based spacewalks and as a platform for external science experiments (Ref. 1809).
Tranquility Node	Feb. 08, 2010 on STS–130	The Tranquility module was funded by ESA and ASI and built by TAS (Thales Alenia Space) of Turin for NASA. Tranquility was built within the ESA–NASA ISS bartering system. ESA committed to build both Node 2 and Node 3 as well as the ATV in order to use the NASA ISS facilities, fly astronauts on the Shuttle and for other ISS services. – A formal handover ceremony of Node 3 ownership from ESA to NASA took place on Nov. 20, 2009 at KSC, Cape Canaveral, FLA.
MRM1 Rassvet	May 14, 2010 on STS–132	Russian (Roskosmos) MRM1 (Mini–Research Module 1)

ISS Element	Launch Date	Description
PMM	Feb. 24. 2011 on STS–133	The MPLM (Multi Purpose Logistics Module) of ASI, known as Leonardo, is being transformed into PMM (Permanent Multipurpose Module) for the ISS. The supply–laden PMM was flown aboard shuttle Discovery during the STS–133 mission.
Nauka (Science) (MLM)	planned for 2014	Russian (Roskosmos) MLM (Multipurpose Laboratory Module). MLM is Russia’s primary research module as part of the ISS. It has a length of 13 m, diameter = 4.11 m, mass = 20,300 kg The MLM will accommodate both service systems for the Russian segment of the ISS and scientific payloads. MLM will be launched on a Russian rocket. – The launch of the Nauka was initially slated for the first half of 2011, but has since been repeatedly delayed. The module is being constructed by Khrunichev and RKK Energia. ¹⁸⁰⁷⁾

Table 91: Overview of major ISS element buildup phase ^{1806) 1807)}

Crew transportation to and from the ISS: ¹⁸⁰⁸⁾ For manned missions to/from the ISS, the US Space Shuttle and the Russian service vehicle Soyuz–TMA are being used (built by Rocket Space Corporation Energia, Korolev, Russia). As a rule, an autonomous flight before docking with ISS require about two days (this applies to the Shuttle as well as to the Soyuz–TMA spacecraft).

The Soyuz–TMA has a mass of ~ 7000 kg. Obviously, for such small volume available, it is difficult to provide comfortable crew accommodations in the descent capsule. The crew has to be in the descent capsule during all or most of the essential flight events: insertion, maneuvering, docking and landing. The free volume in capsule for one member of a three–cosmonaut crew is 0.5 m³, and by using the habitation module it is 1.2 m³.

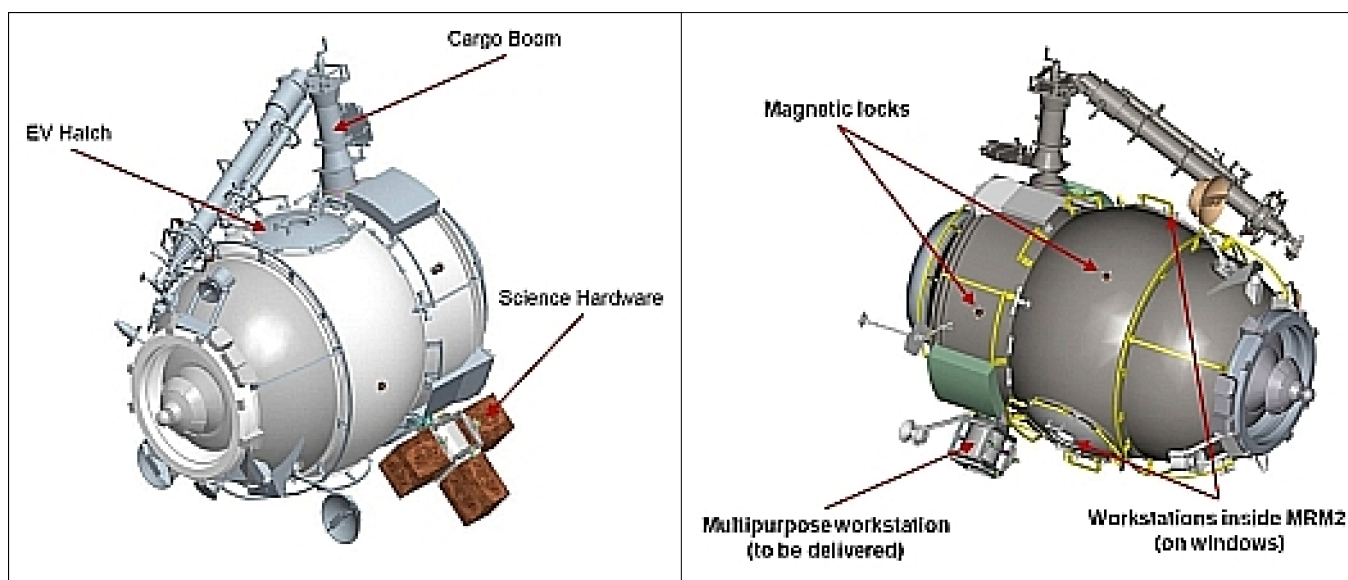


Figure 122: Two views of the Poisk module (image credit: NASA) ¹⁸⁰⁹⁾

¹⁸⁰⁶⁾ NASA and Italian Space Agency Find New Use for Module,” Feb. 26, 2010, URL: <https://service.gmx.net/de/cgi/g.fcgi/application/navigator?CUSTOMERNO=11673889&t=uk805074888.1267154284.8809bf8d>

¹⁸⁰⁷⁾ “Russian Space Lab Launch Delayed Again,” Space Travel, July 18, 2012, URL: http://www.space-travel.com/reports/Russian_Space_Lab_Launch_Delayed_Again_999.html

¹⁸⁰⁸⁾ Rafail Murtazin, Sergey Budylov, “Short rendezvous missions for advanced Russian human spacecraft,” Proceedings of the 60th IAC (International Astronautical Congress), Daejeon, Korea, Oct. 12–16, 2009, IAC–09.B3.3.8

¹⁸⁰⁹⁾ “Poisk module adds room to International Space Station,” Nov. 12, 2009, Spaceflight Now, URL: <http://spaceflight-now.com/station/exp21/091112poisk/>

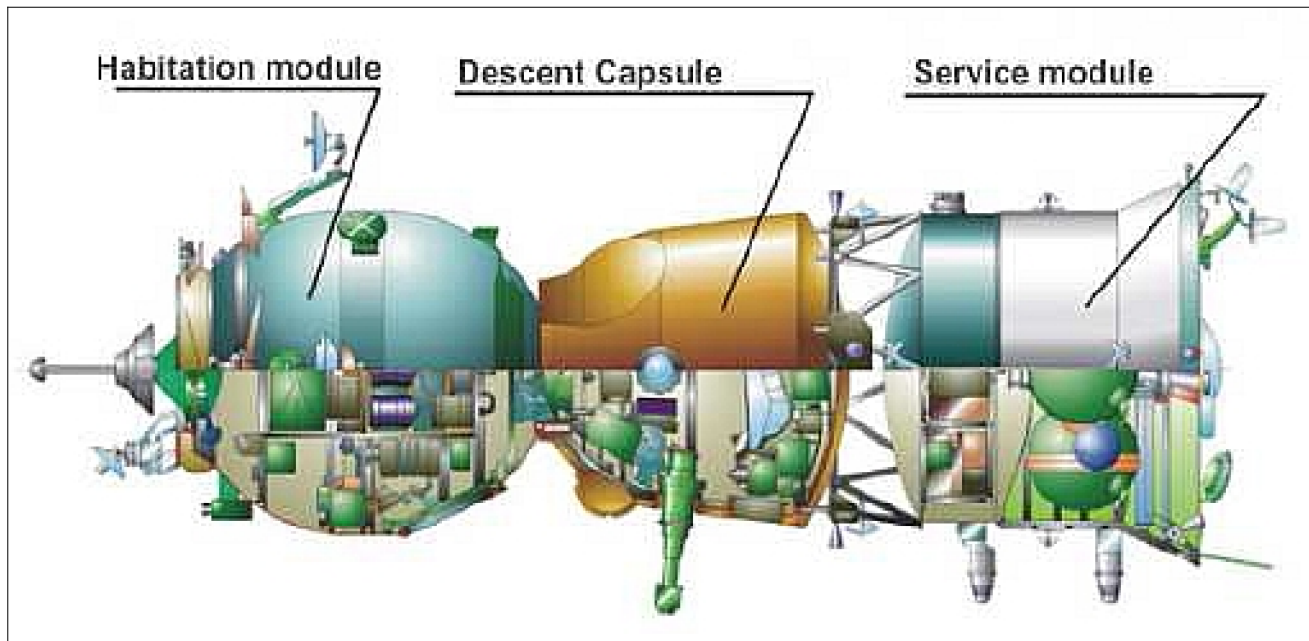


Figure 123: Illustration of the Soyuz–TMA service vehicle (image credit: Rocket Space Corp. Energia)

The two–day stay of the crew in the rather limited habitable volume of the “Soyuz–TMA” until docking at the ISS is regarded as one of the most stressful parts of space flight. Russia is working on new strategies to reduce the phasing time considerably during a rendezvous with ISS

The Soyuz–TMA service vehicle is vital to ISS operations (short–term availability). In particular, the very practical interest is to use it as a crew rescue vehicle in case of an emergency.

1.16 ISS–RS (ISS– Russian Segment)

As of April 2011, the Russian Segment (RS) of the ISS consists of 5 modules: SM Zvezda DC1 (Docking Compartment 1), Pirs, MRM2 Poisk, and MRM1 Rassvet (including FGB Zarya as a functional part of the ISS–RS), with a total mass ~ 67 tons and an internal volume of its pressurized compartments of more than 200 m³.

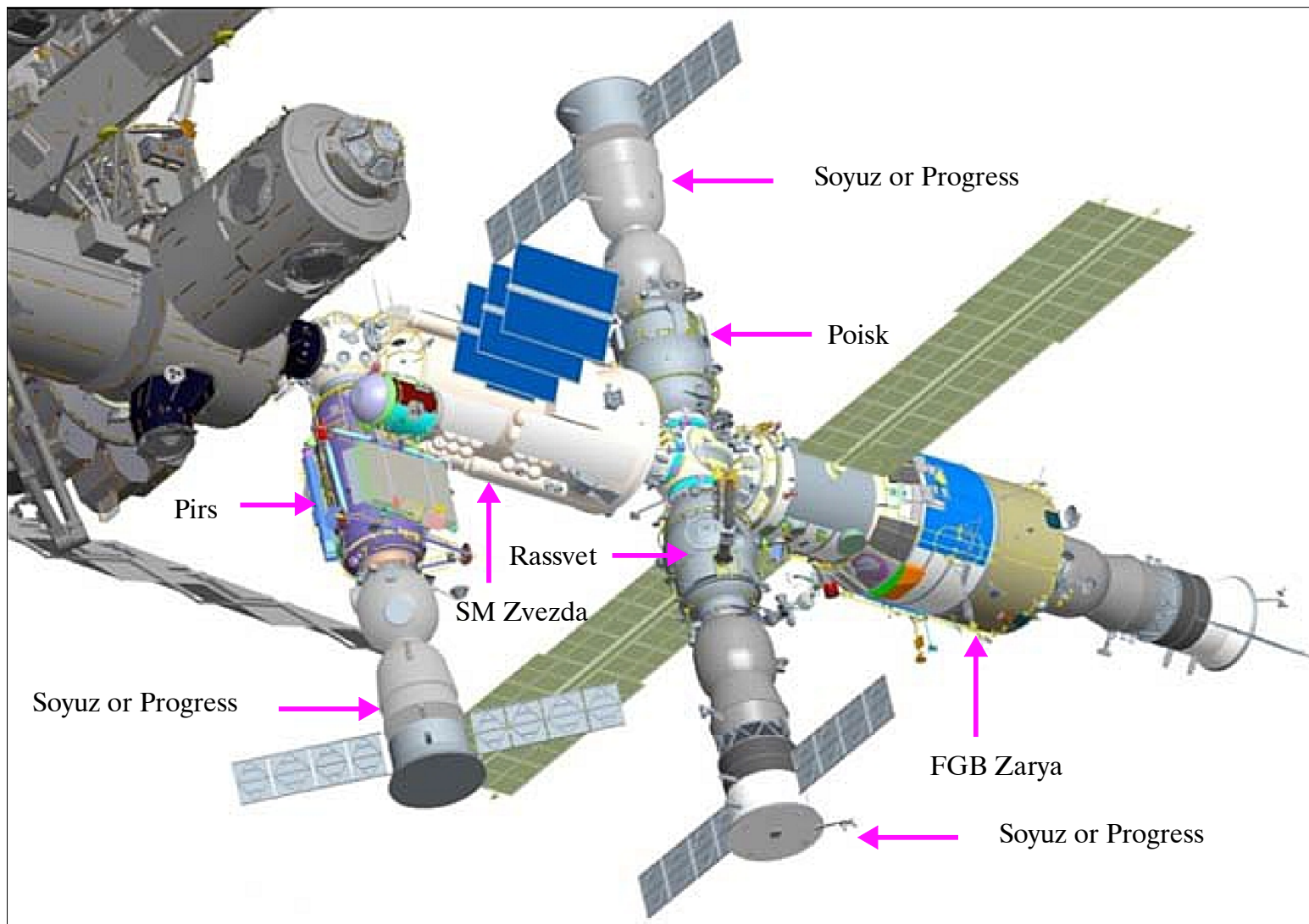


Figure 124: External view of the RS (Russian Section) of the ISS in 2011 (image credit: RSC Energia) ¹⁸¹⁰⁾

The newest modules MRM2 and MRM1 (Mini Research Modules), also known as SRM2 and SRM1, Poisk and Rassvet respectively, have become integral parts of the ISS in 2009–2010. The MLM (Multipurpose Laboratory Module) is targeted for the station in early 2014. After that, the Scientific–Power Modules (SPM) 1 and 2, will be integrated. All of them provide new capabilities for accommodation of research facilities. On the Service Module (SM Zvezda), the distributed payloads service principle is utilized: payloads are provided with onboard resources directly by means of universal interfaces. ¹⁸¹¹⁾

The first phase of the ISS–RS new configuration assembly will be completed when MLM (Nauka) will be mated to the ISS (Figure 126). The MLM will replace the DC1 on the nadir

¹⁸¹⁰⁾ Igor V. Sorokin, “Evolution of Payloads Integration Principles on the ISS Russian Segment – from SM to MLM,” Proceedings of the 28th ISTS (International Symposium on Space Technology and Science), Okinawa, Japan, June 5–12, 2011, paper: 2011–h–19

¹⁸¹¹⁾ S. V. Avdeev, B. V. Zagreev, G. F. Karabadzhak, E. G. Lavrenko, I. Yu. Repin, E. I. Rossiyskaya, V. N. Chikirev, “Scientific and applied experiments onboard the ISS Russian Segment,” Proceedings of the 64th International Astronautical Congress (IAC 2013), Beijing, China, Sept. 23–27, 2013, paper: IAC–13–B3.3.5

docking port of SM. The MLM will provide new capabilities for accommodation of existing and next-generation research facilities (multipurpose payload workstations inside and outside the module) and goal-oriented applications of advanced robotic systems (ERA robotic arm, automated lock-chamber).

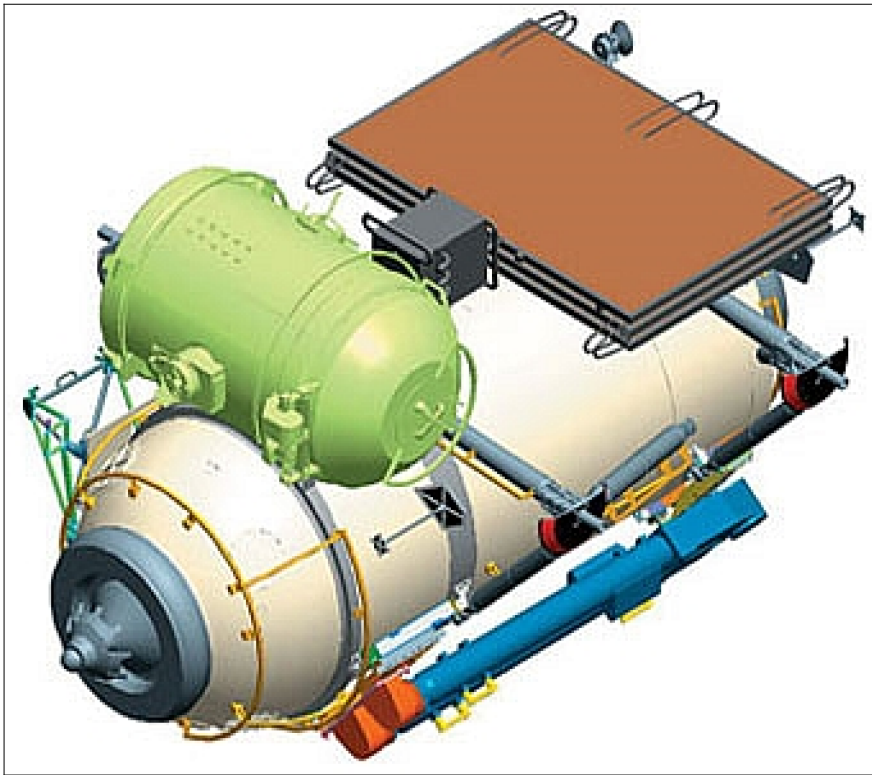


Figure 125: Illustration of the MRM1/Rassvet research module (image credit: RSC Energia)

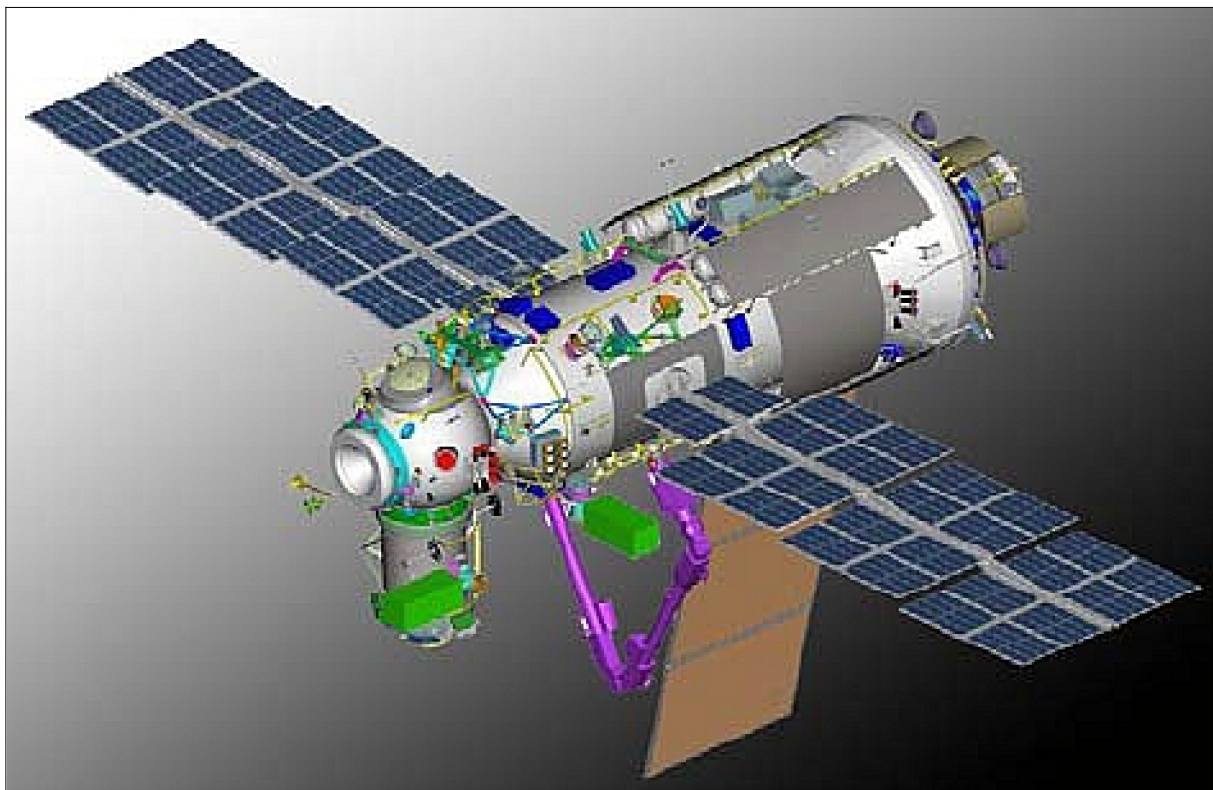


Figure 126: Illustration of the MLM (Multipurpose Laboratory Module, Nauka) of the ISS-RS, Image credit: RSC Energia)

The second phase of ISS–RS utilization provides for launching and attaching to the ISS of the NM (Node Module) in 2014, and two Scientific–Power Modules (SPM1) and (SPM2) in 2017. ^{1812) 1813)}

The NM (Node Module), having six docking ports, is targeted for the station in 2014 and will be attached to the nadir port of MLM, serving as a multipurpose adaptor for the next generation modules of the ISS RS. The module represents a spherical hull 3.3 m in diameter equipped with active and adaptive docking nodes, having 19.0 m³ of pressurized volume and an advanced thermal control system.

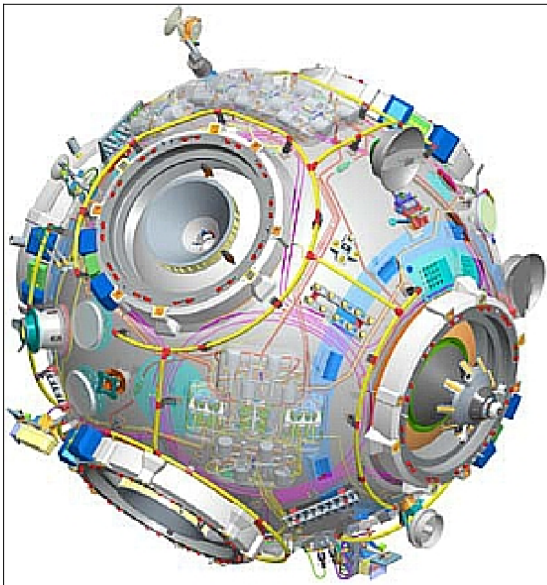


Figure 127: Illustration of the NM (Node Module), image credit: RSC Energia

The pair of SPMs (Scientific–Power Modules) are state–of–the–art elements of the ISS–RS, having launch mass 21 tons each, and a pressurized volume 94 m³, being attached to the NM they will complete the ISS RS assembly in 2017. The SPMs will be equipped with efficient solar arrays using two–degree–of–freedom suspension and providing up to 24 kW power in total.

The main purpose of utilization of the newest modules will be technology development and demonstrations for the benefit of future human space missions. Among them are:

- regenerative life support systems
- fault–tolerant computers
- improved power generation and distribution systems
- electrical rocket engines
- robotic tools, systems and operations
- advanced communication/navigation systems, etc.

After the ISS–RS assembly is completed in 2017 it will consist of 8 modules with total mass more than 132 tons and total volume of the segment’s pressurized compartments of 470 m³ (Figure 128).

1812) Igor V. Sorokin, “Further utilization of the ISS Russian Segment: research accomplishments and plans for the next decade,” Proceedings of the 63rd IAC (International Astronautical Congress), Naples, Italy, Oct. 1–5, 2012, paper: IAC–12.B3.3.4

1813) A. Markov, A. Kaleri, “Development of the ISS Russian Segment in 2010–2020,” RSC Energia, May 2011, URL: <ftp://130.206.92.88/Espacio/Mesa%20Redonda%205%20-%20R4%20-%20ENER-GIA%20-%20A%20MARKOV%20-%20A%20KALERI.pdf>

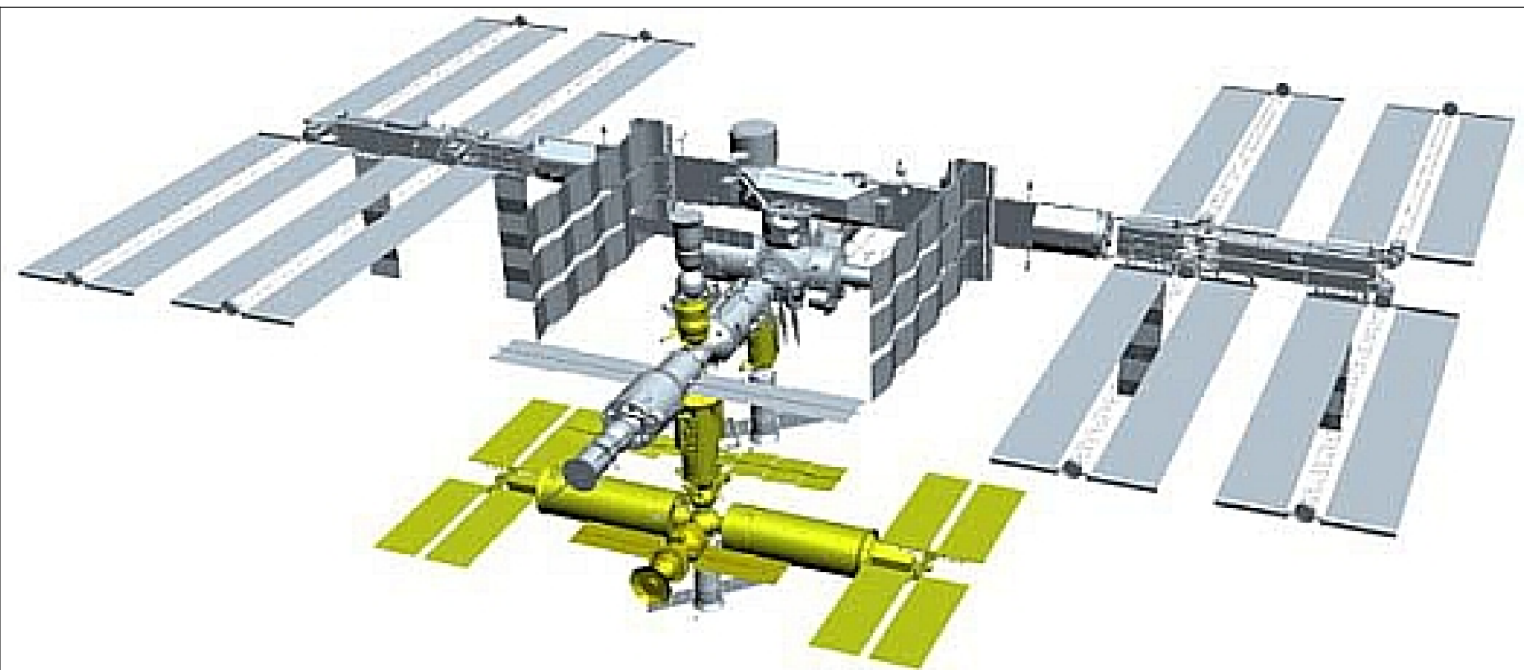


Figure 128: Modules of the ISS–RS (green) after its assembly completion in 2017 (image: RSC Energia)

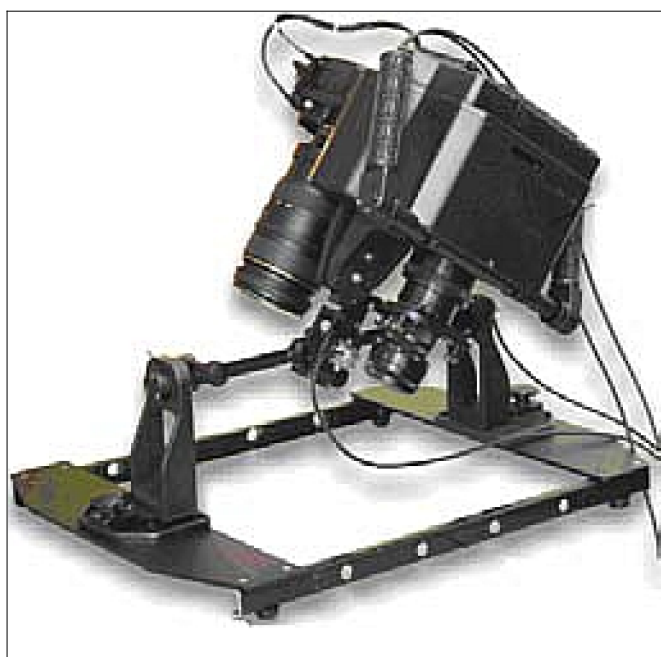


Figure 129: Photo of the Uragan – FSS photospectrometric system (image credit: RSC Energia, Ref. 1812)

Astronaut photography from ISS–RS: The Uragan program aboard the ISS–RS uses digital photography to study Earth’s natural resources by monitoring catastrophes, both natural and human made. Uragan, which means “hurricane” in Russian, began during the first days of habitation on the station and continues to be an important Earth observation program, with the primary goal of defining requirements for a ground–space system for disaster warning and damage mitigation. The program is a logical continuation of the Earth Visual–Instrumental Observations Program (in other words, a crew Earth observation program) started in the Soviet Union/Russia in the early 1970s as part of the Salyut series of space stations and followed by the Mir orbiting complex.¹⁸¹⁴⁾

1814) “Investigation of Earth Catastrophes From the International Space Station: Uragan Program,” NASA, URL: http://www.nasa.gov/mission_pages/station/research/benefits/uragan_program_prt.htm

1.17 Research on the ISS:

The ISS partnership (CSA, ESA, JAXA, NASA, Roskosmos) reached a significant milestone in May 2011 with the completion of the vehicle assembly phase of the ISS. Focus for the ISS is now on the full and continuous use of the orbiting laboratory for research, technology development and education/outreach activities. ¹⁸¹⁵⁾

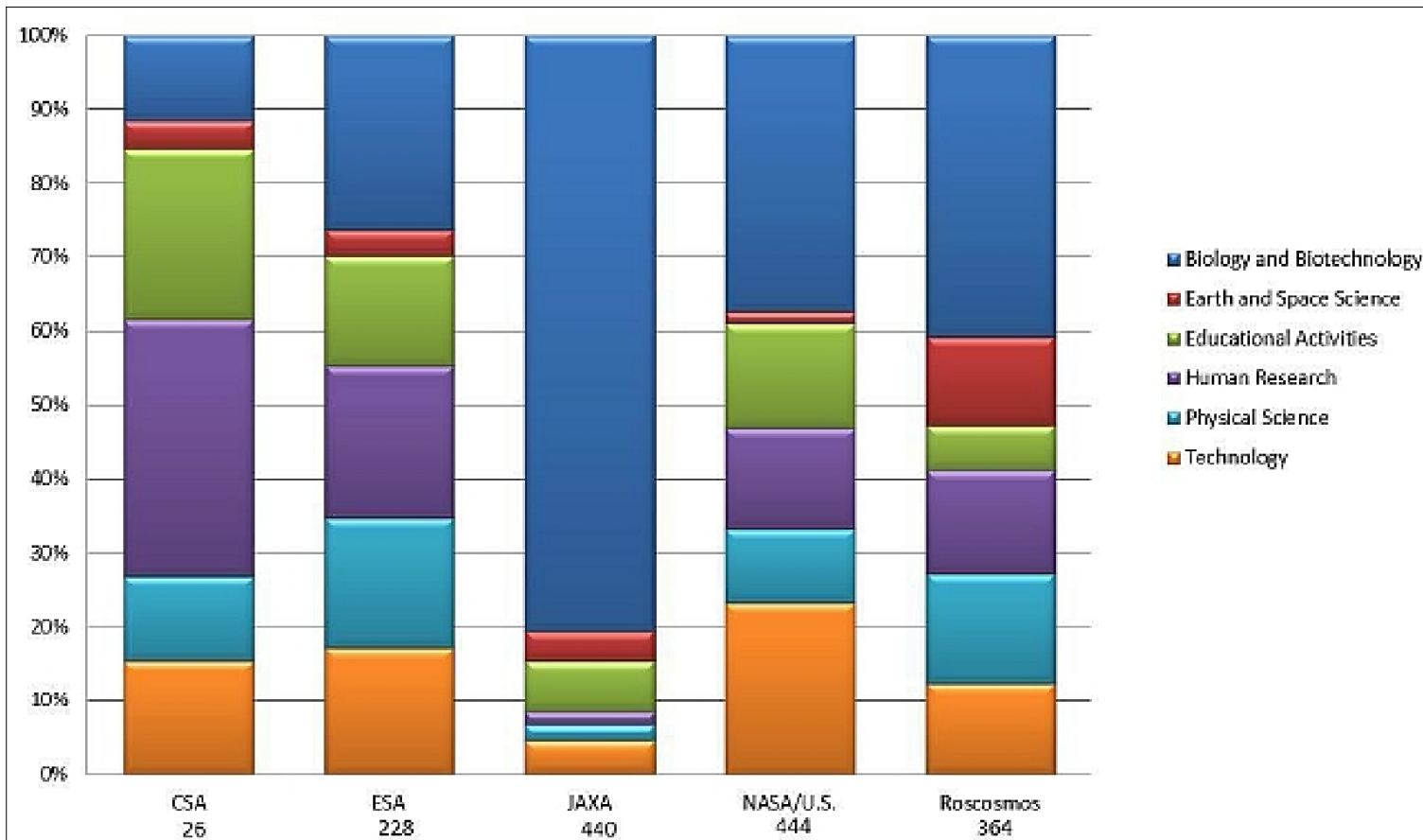


Figure 130: Research disciplines of ISS investigations by partner agency: Dec. 1998–March 2013 (image credit: NASA)

Even before the first permanent crew inhabited the ISS, scientific investigations were conducted. The first investigations began in December 1998 – almost two years before the Expedition 1 crew arrived. From December 1998 through March 2013, over 1500 investigations have been conducted and of these, approximately 87% of the investigations have been completed or considered permanent installations (Figure 130).

The ISS offers a unique environment for scientists from around the world to conduct investigations. To date, researchers from 69 countries have participated in ISS research (producing over 700 publications). The environment of microgravity and other space conditions provides a unique lab environment for experiments that cannot be reproduced on Earth—experiments where the effect of gravity is controlled as an experimental variable. The breadth of research this enables is unique among research platforms.

- **RRM (Robotic Refueling Mission) experiment on ISS:** RRM is an external ISS (International Space Station) experiment that paves the way for future robotic refueling missions by demonstrating robotic refueling tasks and servicing technologies in a zero-g environ-

¹⁸¹⁵⁾ Tracy Thumm, Julie A. Robinson, Camille Alleyne, Pete Hasbrook, Susan Mayo, Perry Johnson–Green, Nicole Buckley, George Karabadzhak, Shigeki Kamigaichi, Sayaka Umemura, Igor V. Sorokin, Martin Zell, Eric Istasse, Jean Sabbagh, Salvatore Pignataro, “International Space Station Accomplishments Update: Scientific Discovery, Advancing Future Exploration, and Benefits Brought Home to Earth,” Proceedings of the 64th International Astronautical Congress (IAC 2013), Beijing, China, Sept. 23–27, 2013, paper: IAC–13–B3.3.4

ment. RRM, a joint technology demonstration of NASA and CSA (Canadian Space Agency), uses the ISS's Special Purpose Dexterous Manipulator (Dextre), "representative satellite fueling interfaces" and four unique RRM tools to validate the tasks, tools, and techniques needed to repair "legacy" satellites, spacecraft not designed to be refueled in orbit. During operations, RRM validated in-orbit the same tasks that were demonstrated on the ground by NASA/GSFC's Satellite Servicing Capabilities Office Robotic Team during RRM preparations. ^{1816) 1817) 1818) 1819)}

The first RRM experiment was conducted very successfully on March 7–9, 2012, marking important milestones in satellite-servicing technology and the use of the space station robotic capabilities. During the three-day RRM Gas Fittings Removal task, Dextre performed the most intricate task ever attempted by a space robot: cutting two separate "lock wires" of 0.5 mm in diameter using the RRM WCT (Wire Cutter Tool). Deftly maneuvered by ground-based mission operators and Dextre, the WCT smoothly slid its hook under the individual wires and severed them with only a few mm of clearance. This wire-cutting activity is a prerequisite to removing and servicing various satellite parts during any future in-orbit missions.

Tests to prepare for on-orbit RRM operations were conducted at Goddard and at MDA in Brampton, Ontario (formerly SPAR Aerospace, the prime contractor for the Canadarm as well as the CSA's Mobile Servicing System on board the station).

RRM operations are scheduled to resume in May 2012 with the completion of the gas fittings removal task. The RRM Refueling task is scheduled for later this summer.

- March 23, 2012, launch of **ATV-3 (Automated Transfer Vehicle-3)**, service flight to ISS: ESA's third Automated Transfer Vehicle cargo ferry, named **Edoardo Amaldi** (Italian physicist and space flight pioneer), was launched on an Ariane-5ES from Europe's Spaceport in French Guiana. The ATV-3 has a launch mass of slightly more than 20 tons, a diameter of 4.5 m, and a length of 10 m. The deployed solar panels have a span of > 22 m.

The launch of ATV-3 was part of the internationally coordinated servicing effort to support the International Space Station (total mass of supplies = 7,200 kg; ~ 2 000 kg of dry cargo, 285 kg of water, and 3150 kg of propellant). ^{1820) 1821)} ATV-3 will automatically dock with the Station's Russian Zvezda module on ISS during the night of March 28–29, 2012. Edoardo Amaldi is expected to remain at the ISS through early September, when it will undock and be commanded to deorbit and burn up upon reentry into Earth's atmosphere over the Pacific Ocean.

1816) Adrienne Alessandro/Dewayne, "Robotic Refueling Mission Begins With Space Station Robotics," NASA, March 7, 2012, URL: http://www.nasa.gov/mission_pages/station/research/news/RoboticRefuelingMission.html

1817) Ken Kremer, "Robotics Refueling Research Scores Huge Leap at Space Station," Universe Today, March 24, 2012, URL: <http://www.universetoday.com/94122/robotics-refueling-research-scores-huge-leap-at-space-station/>

1818) "Robotic Refueling Mission: Fueling up in Space," Space Daily, March 30, 2012, URL: http://www.spacedaily.com/reports/Robotic_Refueling_Mission_Fueling_up_in_Space_999.html

1819) http://ssco.gsfc.nasa.gov/robotic_refueling_mission.html

1820) "Europe's smart supply ship on its way to Space Station," ESA, March 23, 2012, URL: http://www.esa.int/esaCP/SEM3AR2T00H_index_0.html

1821) "Europe's smart supply ship on its way to Space Station," Space Travel, March 26, 2012, URL: http://www.space-travel.com/reports/Europes_smart_supply_ship_on_its_way_to_Space_Station_999.html

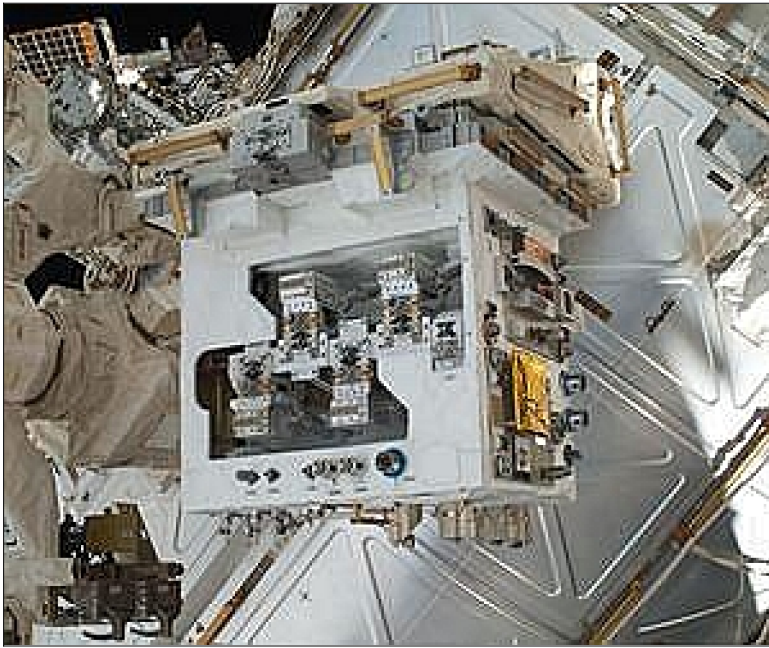


Figure 131: Dextre (left) with the Robotic Refueling Mission module (center), image credit: NASA



Figure 132: ATV Edoardo Amaldi seen before docking with the ISS on 28 March (image credit: NASA/ESA)

ESA's ARTEMIS communications satellite was dedicated to ATV-3 throughout the vessel's free-flying phase up to the docking with the Station. ARTEMIS was handling communications between Edoardo Amaldi and the ATV Control Centre in Toulouse, France.¹⁸²²⁾

¹⁸²²⁾ "Artemis: the ATV whisperer," ESA, March 26, 2012, URL: http://www.esa.int/esaCP/SEMAFBGY50H_index_0.html

On March 29, 2012, the ATV–3 vehicle docked with the Russian Zvezda module of the International Space Station. ¹⁸²³⁾

On August 22, 2012, the ATV–3 spacecraft raised the ISS orbit to an average altitude of 420 km.

On September 28, 2012, ATV–3 departed from the ISS in a flawless undocking under control of the ATV Control Centre in Toulouse, France and in close cooperation with control centres in Moscow, Russia and Houston, USA. – On October 3, 2012, ATV–3 completed the final part of its highly successful six–month servicing mission to the International Space Station by reentering the atmosphere and burning up as planned over an uninhabited area of the southern Pacific ocean. ¹⁸²⁴⁾

Item	ATV–1 Jules Verne	ATV–2 Johannes Kepler	ATV–3 Edoardo Amaldi
Launch date	March 9, 2008	February 16, 2011	March 23, 2012
Demo flight	Yes	1st production flight	2 nd production flight
Docking date	April 3, 2008	February 24, 2011	March 28, 2012
Undocking (attached phase duration)	September 5, 2008 (155 days)	June 20, 2011 (116 days)	September 25, 2012 (182 days)
Dry cargo to ISS	1200 kg	1605 kg	2200 kg
Refueling propellant	825 kg	850 kg	860 kg
Re–boost/DAM propellant	2400 kg	4535 kg	3150 kg
Water	265 kg	None	285 kg
Gas	O ₂ 20 kg	O ₂ 77 kg	O ₂ 66.7 kg, Air 33.3 kg

Table 92: Summary of ATV missions ¹⁸²⁵⁾

- July 21, 2012, launch of **HTV–3** (H–II Transfer Vehicle–3) of JAXA, nicknamed Kounotori 3 (White Stork). This represents the second operational flight to the ISS. Delivery of about 4600 kg of cargo to the International Space Station. This included internal supplies as well as unpressurized cargo delivered via the ULC (Unpressurized Logistics Carrier). The PLC (Pressurized Logistics Carrier) cargo is comprised of system equipment (61%), science hardware (20%), crew food (15%) and personal crew items (4%). HTV–3 carries eight HTV Resupply Racks that are filled with CTBs (Cargo Transfer Bags). Two spare parts for the Kibo Laboratory of the Space Station are part of HTV’s cargo: one Catalytic Reactor needed for the Japanese Experiment Module Water Processing System and a Kibo Coolant Water Circulation Pump. Both of these units are needed for Kibo Laboratory Maintenance. ^{1826) 1827)}

Several major ISS Utilization Payloads are part of HTV’s cargo: The Aquatic Habitat will house small fresh water fish. They will be monitored for several generations as they grow and adept to the space environment to understand the changes that occur in these small, model vertebrates. The Payload includes two transparent aquariums that have been specially designed for the Microgravity Environment. It includes environmental control systems as well as camera equipment to monitor the fish. The camera equipment consists of standard still cameras and infrared imagers. Aquatic Habitat will start actual science operations in 2013 with a study looking at skeletal changes of fish grown in microgravity.

1823) “Europe’s third cargo vehicle docks with the Space Station,” ESA, March 29, 2012, URL: http://www.esa.int/esaCP/SEMUASGY50H_index_0.html

1824) “Mission accomplished for ATV Edoardo Amaldi,” ESA, Oct. 3, 2012, URL: http://www.esa.int/esaCP/SEMZM-NERI7H_index_0.html

1825) Regina Mosenkis, Massimo Cislighi, Victor Blagov, “ATV Missions – 15 Years of International Cooperation,” Proceedings of the 63rd IAC (International Astronautical Congress), Naples, Italy, Oct. 1–5, 2012, paper: IAC–12–B3.4–B6.5.3

1826) “HTV–3 Cargo Manifest,” Spaceflight 101, URL: <http://www.spaceflight101.com/htv-3-cargo-manifest.html>

1827) “Kounotori3 (HTV3) Mission,” JAXA, URL: <http://iss.jaxa.jp/en/htv/mission/htv-3/>

A new Earth observation payload for the US Segment is also aboard HTV–3. The ISERV (ISS SERVIR Environmental Research and Visualization) payload will further improve Earth observation techniques in support of environmental management, humanitarian assistance and disaster assessment. The project is managed by NASA and USAID (U.S. Agency for International Development). It will operate from the WORF (Window Observation Facility) in the Destiny Laboratory.

The HTV–3 carried a J–SSOD (JEM Small–Satellite Orbital Deployer) along with five CubeSats that are planned to be deployed by the Japanese Robotic Arm later in 2012. The CubeSats are: RAIKO, FITSAT–1, WE WISH, F–1 and TechEdSat.

Note: The five CubeSats were deployed successfully on Oct. 4, 2012.



Figure 133: Photo of the CubeSats flown to the ISS on HTV–3 (image credit: Koumei Shibata)

The Unpressurized Cargo Carrier of HTV–3 carried two external ISS payloads accounting for 1,100 kg.

- The SCaN (Space Communications and Navigation) testbed, designed and developed at NASA/GRC, is planned to be active aboard the ISS for about a year. The three SCaN devices provide a testbed for the development of SDR (Software Defined Radio) technology. The functions performed by the three radios include communication with the TDRS (Tracking and Data Relay Satellite) system in both S–band and Ka–band, receive GPS (Global Positioning Satellite) signals, and enable proximity communications between the ISS and approaching vehicles.

- The MCE (Multi–mission Consolidated Equipment) system consists of five small mission payloads dedicated to science and technology demonstrations. These investigation payloads include two atmospheric observation investigations that study lightning and resonant scattering from plasma and airglow.

- The REBR (Reentry Breakup Recorder) and the iBall, which is also a reentry recorder. REBR records data regarding the thermal, acceleration, rotational and other stresses the vehicle experiences during its destructive re–entry process. This data is used to improve reentry simulation models that show inaccuracies for the peak heating environment of reentry. REBR has a mass of about 4 kg and is 31 cm in diameter.

iBall is a reentry data recorder. The device is spherical in shape, has a diameter of 40 cm and includes two cameras that are expected to acquire footage of HTV’S fiery return to Earth and give insight in the destructive reentry environment. The data recorder was developed by IHI Aerospace Co. Ltd.; it has a total mass of 15.5 kg.

On July 27, 2012, the HTV–3 Japanese cargo spacecraft was successfully captured with the International Space Station’s Canadarm 2 robotic arm, and then installed to a docking port. JAXA astronaut Aki Hoshide berthed the HTV–3 (Kounotori–3) supply ship to the Earth–facing side of the Harmony node on the ISS. ¹⁸²⁸⁾ ¹⁸²⁹⁾

- May 2013: The latest round of NASA’s RRM (Robotic Refueling Mission) satellite–servicing tasks was completed on May 10, 2013. Five days of operations were held aboard the ISS, during which the Canadian–built Dextre robot with RRM tools demonstrated how tiny caps can be retrieved and stowed in space. This task, along with slicing through satellite blanket tape were performed on the RRM module affixed outside the space station. ¹⁸³⁰⁾

The conclusion of the May operations wraps up the first phase of tasks for RRM, a modular activity box with tools that launched to the space station aboard the final space shuttle flight. New task boards and tools are slated for launch this summer and again in early 2014, along with another set of activities for this groundbreaking operation. – NASA developed RRM to demonstrate how remotely–operated robot mechanics could extend the lives of the hundreds of satellites residing in GEO (Geosynchronous Earth Orbit). RRM is a joint effort with the Canadian Space Agency (CSA). It uses the space station as a test bed for technology research and development.

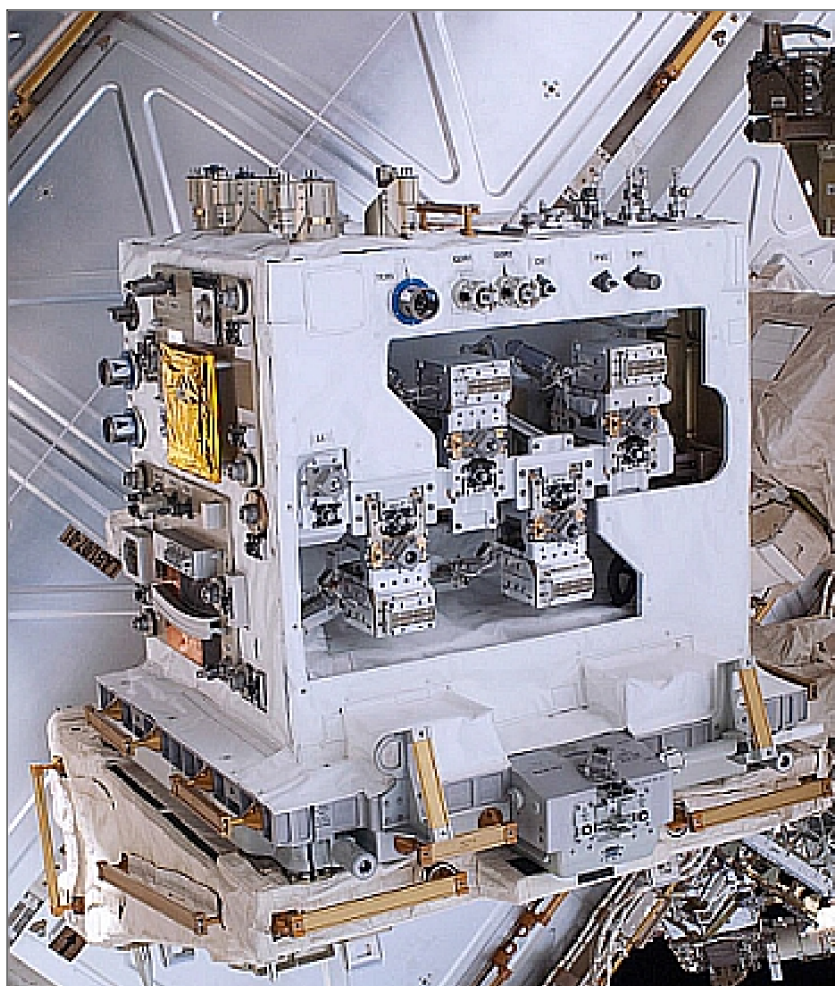


Figure 134: Illustration of the NASA designed RRM module (image credit: NASA)

1828) “Successful berthing of the H–II Transfer Vehicle ”KOUNOTORI 3” (HTV3) to the International Space Station (ISS),” JAXA, July 28, 2012, URL: http://www.jaxa.jp/press/2012/07/20120728_kounotori3_e.html

1829) “Japanese Cargo Spacecraft Berthed to Station,” NASA, July 27, 2012, URL: http://www.nasa.gov/mission_pages/station/expeditions/expedition32/htv3_berth.html

1830) Adrienne Alessandro, “NASA’s Robotic Refueling Mission Practices New Satellite–Servicing Tasks,” NASA May 10, 2013, URL: http://www.nasa.gov/mission_pages/station/research/news/rrm_practice.html

- May 2013: Spacewalk repairing ammonia leak. Astronauts Chris Cassidy and Tom Marshburn ventured into space on May 11, 2013 and replaced a pump unit on the outside of the International Space Station that was leaking ammonia. After more than five hours working outside, the astronauts reentered the Station. Liquid ammonia is used to keep the Space Station at the right temperature by being pumped through external radiators to lose excess heat. ¹⁸³¹⁾

- June 2013: The ESA space freighter **ATV-4** (Automated Transfer Vehicle-4), named **Albert Einstein**, was launched on June 5, 2013 onboard an Ariane 5 ES launcher from Europe's Spaceport in Kourou, delivering 2480 kg of dry cargo to the International Space Station. It will also haul fuel, water, and oxygen to space, as well as carrying its own fuel to reboost the Station's orbit. ATVs can deliver up to 7000 kg of total cargo mass to the ISS.

The total mass of ATV Albert Einstein with all its cargo is 20 190 kg, making this spacecraft the heaviest ever lofted into orbit by an Ariane rocket, beating the previous Ariane launch record by over 500 kg set last year by its predecessor ATV Edoardo Amaldi. ¹⁸³²⁾

This time around, a special payload was also included: the DLR-developed SterEx (Stereo Experiment), which has four cameras attached to the Ariane 5ES rocket providing a continuous 3D view of the mission, from liftoff to separation to orbit and docking to the Station at an altitude of about 400 km. ¹⁸³³⁾

ATV-4 completed a flawless rendezvous with the International Space Station on June 15, 2013 when it docked smoothly with orbital outpost at 14:07 GMT. Like its predecessors, ATV-4 is much more than a simple supply vessel: it is a space tug, a tanker, a freighter and a temporary habitation module. ^{1834) 1835) 1836)}

ATV-4 spent over 4 months docked to the Zvezda module, during this time the module provided extra storage room and a quiet rest area for the astronauts. It also offered a powerful maneuvering capability to raise the Station's altitude to combat natural orbital decay and, if required, to steer it out of the way of dangerous space debris.

On October 28, 2013, the ATV-4 was undocked from the ISS, controlled by the joint ESA/CNES mission operations team at the ATV Control Centre, Toulouse, France. A controlled, destructive reentry is planned for 2 November. Prior to reentry, a few maneuvers are planned with ATV-4 over the course of five days to position itself directly below the Station. Controllers will start the reentry procedure on Nov. 2 when the ATV-4 is 120 km below the Station – so astronauts will observe the craft from above as it disintegrates over the Pacific Ocean. This procedure will provide valuable information to calibrate future spacecraft reentries. ¹⁸³⁷⁾

On Nov. 2, 2013, ¹⁸³⁸⁾ ESA's ATV-4 cargo ferry, Albert Einstein, completed its five-month mission to the ISS by reentering the atmosphere today and burning up safely over an uninhabited area of the southern Pacific Ocean.

- August 2013: The **HTV-4** (H-II Transfer Vehicle-4) of JAXA, nicknamed Kounotori 4 (White Stork), was launched on August 3, 2013 (19:48 hr UTC) on the H-IIB 304 vehicle

1831) "Astronauts Complete Spacewalk to Repair Ammonia Leak, Station Changes Command," NASA, May 12, 2013, URL: http://www.nasa.gov/mission_pages/station/expeditions/expedition35/e35_051113_eva.html

1832) "Europe's heaviest cargo ship launched to Space Station," ESA, June 6, 2013, URL: http://www.esa.int/Our_Activities/Human_Spaceflight/ATV/Europe_s_heaviest_cargo_ship_launched_to_Space_Station

1833) "Successful premiere – SterEx video shows ATV-4 in orbit," DLR, June 6, 2013, URL: http://www.dlr.de/dlr/en/desktopdefault.aspx/tabid-10081/151_read-7278/year-all/#gallery/11092

1834) "Europe's largest spaceship reaches its orbital port," ESA, June 15, 2013, URL: http://www.esa.int/Our_Activities/Human_Spaceflight/ATV/Europe_s_largest_spaceship_reaches_its_orbital_port

1835) "Amazing ATV," ESA, June 18, 2013, URL: http://www.esa.int/Our_Activities/Human_Spaceflight/ATV/Amazing_ATV

1836) Alberto Novelli, "From ATV Jules Verne to Albert Einstein – Europeans Mastering of Space Rendezvous Operations," Proceedings of the 64th International Astronautical Congress (IAC 2013), Beijing, China, Sept. 23–27, 2013, paper: IAC-13-B3.4-B6.5.5

1837) "ATV-4: All good missions must come to an end," ESA, Oct. 26, 2013, URL: http://www.esa.int/Our_Activities/Human_Spaceflight/ATV/ATV-4_all_good_missions_must_come_to_an_end

of Mitsubishi Heavy Industries from TNSC (Tanegashima Space Center), Japan. HTV-4 is the fourth cargo transfer vehicle of JAXA to the ISS (International Space Station). After about 15 minutes into the flight, the separation of the HTV-4 vehicle was confirmed.¹⁸³⁹⁾

The secondary payloads on this flight are:

- TechEdSat-3, a 3U CubeSat of NASA/ARC (Ames Research Center), it was developed by SJSU (San Jose State University) and the University of Idaho.
- Pico Dragon, a 1U CubeSat of VNESC (Vietnam National Center)
- ArduSat-1, a 1U CubeSat of NanoSatisfi Inc., San Francisco, CA, USA
- ArduSat-X, a 1U CubeSat of NanoSatisfi Inc.

Note: Arduino refers to an open-source electronics platform or board and the software used to program it. Arduino is designed to make electronics more accessible to users and anyone interested in creating interactive objects or environments.

– On Aug. 9, 2013, HTV-4 was captured by the Canadarm2 and berthed to the Harmony module. The HTV-4 (Kounotori 4) delivered a total of ~ 5400 kg of cargo/supplies (water, experiments and spare parts) to the ISS (International Space Station).

– The four CubeSats onboard HTV-4 will be deployed from the ISS by the J-SSOD (JEM Small Satellite Orbital Deployer) on Kibo between October 2013 and March 2014.

– On Sept. 5, 2013, the HTV-4/Kounotori-4 left the ISS and reentered the atmosphere on Sept. 7 at an altitude of 120 km – completing its cargo resupply mission (destructive reentry into the Pacific Ocean).¹⁸⁴⁰⁾

- On November 20, 2013, the ISS was celebrating 15 years on orbit. On Nov. 20, 1998 a Russian Proton rocket lifted off from the Baikonur space center in Kazakhstan carrying Zarya, the Station's first component. – The Space Station is the largest cooperative project ever carried out in science, involving NASA, ESA, Roscosmos, the Canadian Space Agency and the Japan Aerospace Exploration Agency.¹⁸⁴¹⁾

- **January 2014: Extension of ISS operations until at least 2024.** Representatives of nations from around the globe met in Washington, DC, on January 9, 2014, at the International Space Exploration Forum (ISEF) to further advance the exploration and utilization of space and to highlight their direct benefit to humankind. This ISEF meeting continued the dialog initiated by the European Commission and the European Space Agency, and most recently held in Italy in November 2011, which underscored the importance of space exploration, and its benefit to all citizens of the world.

The extension of ISS operation will allow NASA and the international space community to accomplish a number of important goals.^{1842) 1843)}

– First, it will allow NASA to complete necessary research activities aboard the ISS in support of planned long-duration human missions beyond low-Earth orbit.

1838) “A fiery end to a perfect mission: ATV Albert Einstein,” ESA, Nov. 2, 2013, URL: http://www.esa.int/Our_Activities/Human_Spaceflight/ATV/A_fiery_end_to_a_perfect_mission_ATV_Albert_Einstein

1839) “Launch Result of H-II Transfer Vehicle “KOUNOTORI4” (HTV4) by H-IIB Launch Vehicle No. 4,” JAXA Press Release, Aug. 4, 2013, URL: http://www.jaxa.jp/press/2013/08/20130804_h2bf4_e.html

1840) “Successful re-entry of H-II Transfer Vehicle “KOUNOTORI4” (HTV4),” JAXA Press release, Sept. 7, 2013, URL: http://www.jaxa.jp/press/2013/09/20130907_kounotori4_e.html

1841) “Happy Birthday, Space Station,” ESA, Nov. 20, 2013, URL: http://www.esa.int/Our_Activities/Human_Spaceflight/International_Space_Station/Happy_birthday_Space_Station

1842) John P. Holdren, Charles Bolden, “Obama Administration Extends International Space Station until at Least 2024,” White House Office of Science and Technology Policy, Jan. 08, 2014, URL: <http://www.whitehouse.gov/blog/2014/01/08/obama-administration-extends-international-space-station-until-at-least-2024>

1843) Lauren B. Worley, Michael Braukus, “NASA, Obama Administration Highlight International Space Station Extension at Global Forum,” NASA Release 14-012, Jan. 09, 2014, URL: http://www.nasa.gov/press/2014/january/nasa-obama-administration-highlight-international-space-station-extension-at/#.Us-AtfuFf_p

– Second, ISS extension will extend the broader flow of societal benefits from research on the Station. A further benefit of ISS extension is it will give NASA and its private–sector partners time to more fully transition to the commercial space industry the transportation of cargo and crew to low–Earth–orbit, allowing NASA to continue to increase its focus on developing the next–generation heavy–lift rocket and crew capsule necessary for deep–space exploration.

– The ISS is also playing an increasingly important role in the study of the Earth and its changing climate.

– Finally, extending the ISS will help cement continuing U.S. leadership in human spaceflight going forward. The ISS is the most complex and challenging engineering endeavor in history. The key to its success has been the combination of NASA ingenuity and international cooperation.¹⁸⁴⁴⁾

• **March 2014 – Crimian Crisis :** Virtually every aspect of the manned and unmanned US space program – including NASA, other government agencies, private aerospace company’s and crucially important US national security payloads – are highly dependent on Russian & Ukrainian rocketry and are therefore potentially at risk amidst the current Crimea crisis as tensions flared up dangerously in recent days between Ukraine and Russia with global repercussions.¹⁸⁴⁵⁾

– The International Space Station (ISS), astronaut rides to space and back, the Atlas V and Antares rockets and even critical U.S. spy satellites providing vital, real time intelligence gathering are among the examples of programs that may be in peril if events deteriorate or worse yet, spin out of control.

– The Crimean confrontation and all the threats and counter threats of armed conflicts and economic sanctions shines a spotlight on US vulnerabilities regarding space exploration, private industry and US national security programs, missions, satellites and rockets. The consequences could be catastrophic for all sides.

Some future ISS instruments (Ref. 1815):

• CATS (Cloud–Aerosol Transport System): CATS is a NASA sponsored instrument, using LiDAR (Light Detection and Ranging) for remote detection of atmospheric aerosols and clouds. This high repetition rate laser operates at three wavelengths — 1064, 532 and 355 nm — to determine the layer height, layer thickness, optical depth, extinction and particle type in clouds. The data obtained from this investigation will give researchers a better understanding of cloud and aerosol particulates which may lead to improved Earth system models associated with climate feedback. Operations are expected to begin in late 2014/early 2015.

• The ASIM (Atmosphere–Space Interaction Monitor) project is led by ESA. ASIM will use camera and X–ray– and γ –ray detectors on the ISS. It will observe the upper atmosphere, looking for sprites, jets and elves in connection with thunderstorms. It is hoped that measurements of these phenomena from space will contribute to our understanding of the upper atmosphere. Its launch is scheduled for 2016.

• RapidSCAT of NASA is set to launch to the ISS in 2014. This radar scatterometer will measure the ocean surface wind speed and direction filling a gap in the global constellation

1844) Tony Phillips, “10 more years for the ISS,” NASA, Feb. 14, 2014, URL: http://science.nasa.gov/science–news/science–at–nasa/2014/14feb_10years/

1845) Ken Kremer, “ISS, NASA and US National Security dependent on Russian & Ukrainian Rocketry Amidst Crimean Crisis,” Universe Today, March 5, 2014, URL: <http://www.universetoday.com/110006/iss–nasa–and–us–national–security–dependent–on–russian–ukrainian–rocketry–amidst–crimean–crisis/>

of wind scatterometers. The orbit of the ISS gives researchers data coverage over multiple orbits per day where the current scatterometers are in a polar sun–synchronous orbit where the instrument passes over the same point at the same time every day. The advantage of multiple passes per day at lower inclination is greater coverage and calibration that will improve the scatterometer constellation as a whole. Scatterometer data is used operationally in the predictions of eyewall regeneration of hurricanes.

- SAGE–III–ISS (Stratospheric Aerosol and Gas Experiment–III–ISS) of NASA will collect high resolution spectral data using light from the sun or the moon, depending on the location in the ISS orbit, to determine the distribution of aerosol and ozone in the upper troposphere through the stratosphere. SAGE–III–ISS will also provide temperature and trace gases profiles in the stratosphere and mesosphere. This instrument is scheduled to launch to the ISS in the 2014–2015 timeframe.
- ACES (Atomic Clock Ensemble in Space) is a fascinating new ESA mission developed in cooperation with the French Space Agency (CNES) that will expand the range of research on the ISS. The atomic clocks frequency reference generated on–board the ISS will be used by a worldwide network of ground terminals to perform comparisons with the best available atomic clocks on the ground. The most precise measurement of time yet – in space – will be used to probe our knowledge of the fundamental laws of physics ruling the Universe. ACES will test Einstein’s general relativity and alternative theories of gravitation. Taking full advantage of the microgravity environment and worldwide coverage provided by the ISS, ACES will establish a stable and accurate onboard timescale which will be used to perform space–to–ground and ground–to–ground comparisons of best available atomic frequency standards. This is why measuring time as accurately as possible in space is of extreme interest. The ACES launch is currently foreseen in 2016.

1.18 NASA's COTS (Commercial Orbital Transportation Services) Program

COTS is a NASA program to coordinate the delivery of crew and cargo to the International Space Station by private companies (partnership agreements with U.S. Industry). The program was announced on January 18, 2006.

NASA signed agreements with SpaceX and Rocketplane Kistler (RpK) in 2006, but later terminated the agreement with RpK due to insufficient private funding. NASA then signed an agreement with Orbital Sciences in 2008. Independently, NASA awarded contracts for cargo delivery to the International Space Station in December 2008, to OSC (Orbital Sciences Corporation) and SpaceX to utilize their COTS cargo vehicles.

COTS must be distinguished from the related CRS (Commercial Resupply Services) program. COTS relates to the development of the vehicles, CRS to the actual deliveries. COTS involves a number of Space Act Agreements, with NASA providing milestone-based payments.

1.18.1 Dragon program of SpaceX and NASA

The Dragon capsule of SpaceX (Space Exploration Technologies Inc.), a commercial company of Hawthorne, CA, is a free-flying, reusable spacecraft capable of hosting pressurized and unpressurized payloads. The subsystems include propulsion, power, thermal control, environmental control, avionics, communications, thermal protection, flight software, guidance, navigation & control, entry, descent & landing, and recovery. ¹⁸⁴⁶⁾ ¹⁸⁴⁷⁾

The Dragon spacecraft is comprised of 3 main elements: the Nosecone, which protects the vessel and the docking adaptor during ascent; the Spacecraft, which houses the crew and/or pressurized cargo as well as the service section containing avionics, the RCS system, parachutes, and other support infrastructure; and the Trunk, which provides for the stowage of unpressurized cargo; it supports Dragon's solar arrays and thermal radiators.

In December 2008, NASA announced the selection of SpaceX's Falcon 9 launch vehicle and Dragon spacecraft to resupply the ISS (International Space Station) when the Space Shuttle retires. Though designed to address cargo and crew requirements for the ISS, as a free-flying spacecraft Dragon also provides an excellent platform for in-space technology demonstrations and scientific instrument testing.

Launch: The Dragon C2 capsule was launched successfully on May 22, 2012 (7:44 UTC) with the SpaceX Falcon-9 vehicle from the Cape Canaveral Air Force Station, Florida.

The demonstration flight, called COTS 2/3 (Commercial Orbital Transportation Services-2/3), was the premiere test flight in NASA's new strategy to resupply the ISS with privately developed rockets and cargo carriers under the COTS initiative. *The launch of the SpaceX Dragon capsule to the ISS started a new era in NASA's ISS program.*

- During the flight, SpaceX's Dragon capsule was commanded to conduct a series of check-out procedures to test and prove its systems, including rendezvous and berthing with the ISS.
- The primary objectives for the flight demonstration included a flyby of the ISS at a distance of approximately 2.5 km to validate the operation of sensors and flight systems necessary for a safe rendezvous and approach. The spacecraft also demonstrated the ability to abort the rendezvous. – At this point, the COTS-2 objectives were completed — and immediately followed by the COTS-3 goals (involving the vehicle approach and attachment

¹⁸⁴⁶⁾ "DragonLab Data sheet," SpaceX, URL: <http://www.spacex.com/dragon.php>

¹⁸⁴⁷⁾ "SpaceX Demonstration Mission," URL: http://www.nasa.gov/pdf/641019main_pk_overview.pdf

operations to the station).¹⁸⁴⁸⁾

- After these capabilities were successfully proven, the Dragon spacecraft was cleared to berth with the ISS. Dragon was commanded by the SpaceX flight control team based in Hawthorne, CA.



Figure 135: Artist's rendition of the Dragon spaceship with solar panels deployed (image credit: SpaceX)

- On May 25, 2012, Dragon was berthed at the ISS, after being captured by the astronaut crew using the station's robotic arm (Canadarm2) and maneuvered it carefully into the Harmony module docking port.
- The Dragon capsule delivered 460 kg of supplies to the station, which included non-critical experiments, food, clothing and technology.
- On May 31, 2012, Dragon was detached from the Harmony module, after being loaded with 620 kg of hardware and cargo no longer needed aboard the station.
- The Dragon capsule, featuring a heat shield, deorbited ~ 4 hours after leaving the station, taking about 30 minutes to re-enter Earth's atmosphere. It landed on a parachute assembly in the Pacific Ocean about 500 km west of Baja California.¹⁸⁴⁹⁾

The flight of the SpaceX Dragon, the first private spaceship ever to connect to the International Space Station, was a major achievement for the company and for NASA, demonstrating its ability to safely deliver cargo to the station.

¹⁸⁴⁸⁾“SpaceX Demonstration Mission,” NASA, URL: http://www.nasa.gov/pdf/641018main_pk_objectives.pdf

¹⁸⁴⁹⁾http://www.nasa.gov/exploration/commercial/cargo/spacex_rss_feed_collection_archive_1.html



Figure 136: NASA TV snapshot of the Dragon capsule after it was captured by the robotic arm (image credit: NASA)

- In August 2012, NASA Administrator Charles Bolden announced new milestones in the nation's commercial space initiatives. The latest advances made by NASA's commercial space partners pave the way for the first contracted flight of cargo to the International Space Station (ISS) this fall and mark progress toward a launch of astronauts from U.S. soil in the next 5 years.

SpaceX (Space Exploration Technologies) has completed its Space Act Agreement with NASA for COTS (Commercial Orbital Transportation Services). SpaceX is scheduled to launch the first of its 12 contracted cargo flights to the space station from Cape Canaveral in October 2012, under NASA's Commercial Resupply Services Program. ¹⁸⁵⁰⁾

- On October 8, 2012 (UTC) Dragon launched atop a Falcon 9 rocket from the Cape Canaveral Air Force Station in Florida, beginning NASA's first contracted cargo delivery flight, designated SpaceX **CRS-1 (Cargo Resupply Services-1)** mission, to the station. ¹⁸⁵¹⁾
 - On Oct. 10, 2012, Dragon was securely in the grasp of Canadarm2, ground controllers remotely operated the arm to guide the capsule to the Earth-facing side of the Harmony module. Dragon is scheduled to spend 18 days attached to the station. It will be loaded with ~ 720 kg of cargo for return to Earth. ^{1852) 1853)}
 - The OG2-1 (OrbComm Second Generation-1) prototype satellite, flying as a secondary payload on this mission, was separated from the Falcon 9 launch vehicle at approximately 9:00 pm EST. However, due to an anomaly on one of the Falcon 9's first stage engines, the rocket did not comply with a pre-planned ISS safety gate to allow it to execute the

1850) "NASA Administrator Announces New Commercial Crew And Cargo Milestones," NASA, Aug. 23, 2012, URL: <http://www.nasa.gov/exploration/commercial/crew-cargo-milestones.html>

1851) "SpaceX CRS-1 Mission," NASA Press Kit/October 2012, URL: http://www.nasa.gov/pdf/694074main_SpaceX-CRS-1PressKit.pdf

1852) "Station Welcomes First Commercial Resupply Mission," NASA, Oct. 10, 2012, URL: http://www.nasa.gov/mission_pages/station/expeditions/expedition33/dragon_arrives.html

1853) Trent J. Perrotto, Josh Byerly, "SpaceX's Dragon Carrying NASA Cargo Resupplies Space Station," Oct. 10, 2012, URL: <https://service.gmx.net/de/cgi/g.fcgi/application/navigator?CUSTOM-ERNO=11673889&t=uk645295985.1350143387.9a83a734>

second burn. For this reason, the OG2–1 prototype satellite was deployed into an orbit that was lower than intended. ORBComm and Sierra Nevada Corporation engineers have been in contact with the satellite and are working to determine if and the extent to which the orbit can be raised to an operational orbit using the satellite’s on–board propulsion system. ¹⁸⁵⁴⁾

Although OG2–1 reentered the atmosphere on October 10, 2012, the engineering teams made significant strides in testing various hardware components. After telemetry and command capability was established, several critical system verifications were performed. ¹⁸⁵⁵⁾

– On Oct. 28, 2012, the Dragon capsule of SpaceX left the ISS and splashed down in the Pacific Ocean west of Baja California, Mexico. The splashdown successfully ended the first NASA contracted cargo delivery flight to resupply the ISS. The capsule delivered 450 kg of cargo to the space station and is taking home 758 kg of supplies, hardware and scientific tests and results. The ability to return frozen samples is a first for this flight and will be tremendously beneficial to the station’s research community. ¹⁸⁵⁶⁾

• **CRS–2 (Cargo Resupply Services–2) mission:** On March 1, 2013, SpaceX launched its second CRS mission for NASA to the ISS (International Space Station). The Dragon spacecraft was launched on the Falcon 9 rocket from the Cape Canaveral Air Force Station in Florida, carrying ~ 575 kg of supplies, including critical materials to support the 160 investigations – 50 of which are new – planned for the station’s Expedition 34 crew. ^{1857) 1858)}

After Dragon separated from Falcon 9’s second stage approximately nine minutes after launch and achieved orbit, a malfunction occurred with some of Dragon’s thruster pods. The Dragon lost three of its four thruster pods. Solar array deployment was delayed while SpaceX engineers worked to purge blocked valves and get the pods back online. Ninety minutes after launch, Dragon’s solar arrays were deployed. A few hours later, all four thruster pods were online and attitude control was regained. Following a series of tests to ensure the spacecraft could safely approach the space station, Dragon was approved to approach the orbiting laboratory on March 3, one day after its originally planned arrival.

The Dragon spacecraft was berthed to the ISS on March 3, 2013 using the station’s robotic arm (Canadarm 2). The capture came one day, 19 hours and 22 minutes after the mission’s launch. Following its capture, the spacecraft was installed onto the Earth–facing port of the Harmony module through ground commands issued by mission control at NASA/JSC in Houston. ¹⁸⁵⁹⁾

Height, diameter	6.1 m, 3.7 m
Volume	10 m ³ pressurized, 14 m ³ unpressurized, 34 m ³ unpressurized with extended trunk
Dry mass	4200 kg
Payload capability	3310 kg pressurized+ 3310 kg unpressurized
Payload return	2500 kg
Endurance	1 week to 2 years

Table 93: Some parameters of the Dragon spacecraft

After Dragon’s mission at the station is completed, the crew will use Canadarm2 to detach Dragon from Harmony on March 25 and release it for a parachute–assisted splashdown in

1854) “ORBCOMM Launches Prototype Satellite – OG2 satellite’s insertion orbit lower than planned,” Space Ref, Oct. 8, 2012, URL: <http://spaceref.com/news/viewpr.html?pid=38833>

1855) “OG2 Prototype Hardware Functionality Verified Prior to Deorbit,” Space Daily, Oct. 15, 2012, URL: http://www.spacedaily.com/reports/OG2_Prototype_Hardware_Functionality_Verified_Prior_to_Deorbit_999.html

1856) Trent J. Perrotto, Josh Byerly, “SpaceX Dragon Returns from Space Station with NASA Cargo,” NASA, Oct. 28, 2012, URL: http://www.nasa.gov/home/hqnews/2012/oct/HQ_12-381_SpaceX_CRS-1_Splashdown.html

1857) “SpaceX CRS–2 Mission Press Kit,” SpaceX, NASA, URL: <http://www.spacex.com/downloads/crs2-press-kit.pdf>

1858) “SpaceX 2 Cargo Manifest,” NASA, URL: http://www.nasa.gov/pdf/729030main_spacex_2_cargo_manifest.pdf

1859) “Dragon Arrives With Treasure Trove of Science,” NASA, March 3, 2013, URL: http://www.nasa.gov/mision_pages/station/expeditions/expedition34/dragon_arrives.html

the Pacific Ocean about 500 km west of the coast of Baja California. Dragon is the only cargo craft capable of returning a significant amount of supplies from station to Earth, including experiments.

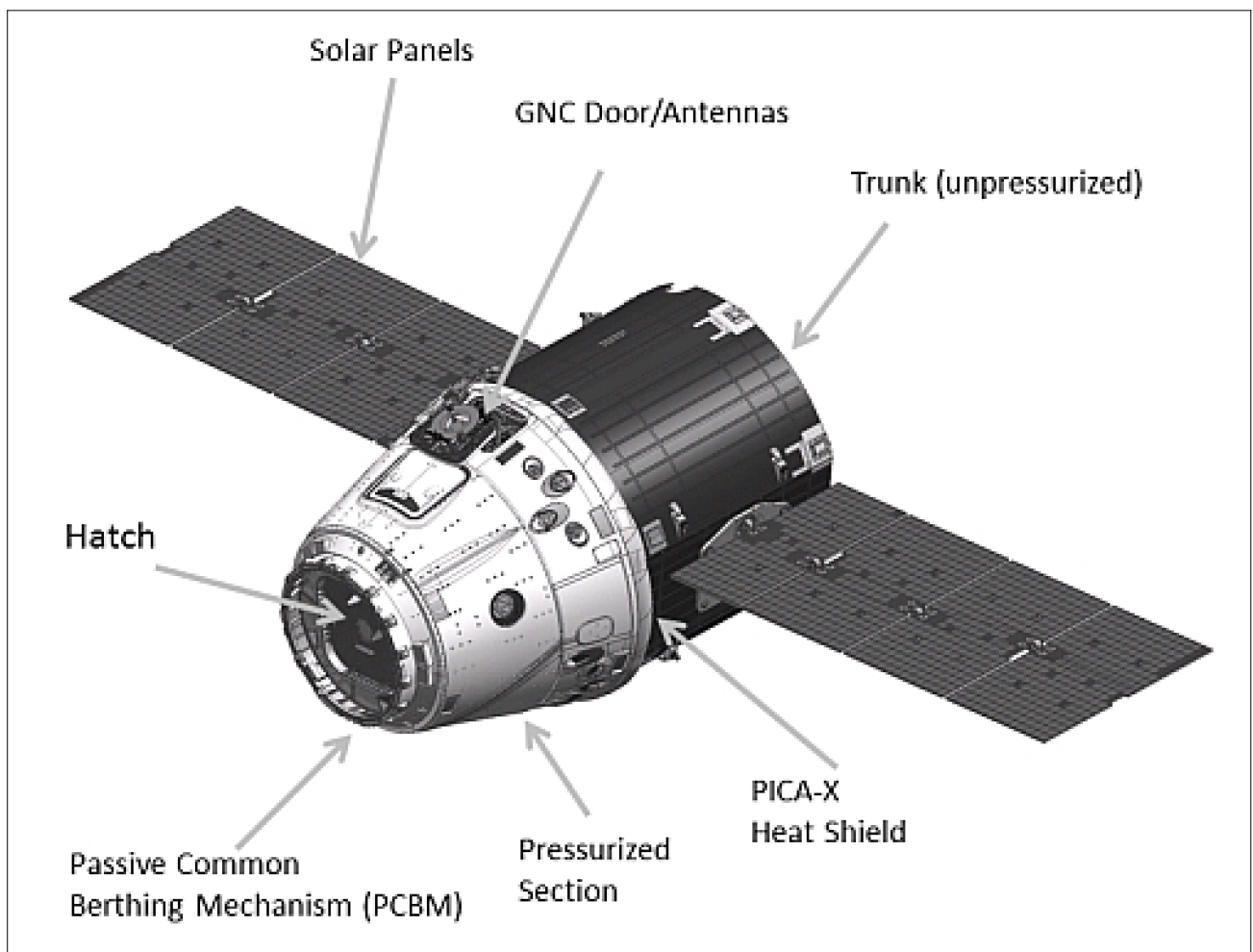


Figure 137: Illustration of the Dragon capsule (image credit: SpaceX)

On March 26, 2013, the Dragon spacecraft of SpaceX completed the company's second cargo flight to the ISS with a splashdown in the Pacific Ocean off the coast of Baja California, Mexico. Dragon returned returned ~ 1210 kg of science samples, equipment and education activities. Among the returned investigations was the CSLM-3 (Coarsening in Solid-Liquid Mixtures) experiment, which also launched to space aboard this Dragon. CLSM-3 studies how crystals known as dendrites form as a metal alloy becomes solid. The research could help engineers develop stronger materials for use in automobile, aircraft and spacecraft parts. Dragon also returned several human research samples that will help scientists continue to examine how the human body reacts to long-term spaceflight. ¹⁸⁶⁰⁾

- **CRS-3 (Cargo Resupply Services-3) mission:** On April 18, 2014, SpaceX launched its third CRS mission for NASA to the ISS on a Falcon-9v.1.1 vehicle of SpaceX from Space Launch Complex 40 at Cape Canaveral Air Force Station in Florida. ¹⁸⁶¹⁾

Dragon carried ~ 2090 kg of supplies and payloads, including critical materials to support more than 150 investigations that will occur during Expeditions 39 and 40. On May 18, 2014,

¹⁸⁶⁰⁾ Trent J. Perotto, Josh Byerly, "SpaceX Dragon Spacecraft Returns Critical NASA Science to Earth," NASA Release: 13-085, March 26, 2013, URL: http://www.nasa.gov/home/hqnews/2013/mar/HO_13-085_SpaceX_Splashdown.html

¹⁸⁶¹⁾ "NASA Cargo Headed for ISS Aboard Dragon Spacecraft," NASA, April 18, 2014, URL: http://www.nasa.gov/mision_pages/station/structure/launch/index.html#.U1Hj5KKegkA

the Dragon capsule splashed down in the Pacific Ocean, off the coast of Baja California. It returned with about 1630 kg of cargo, which includes crew supplies, hardware and computer resources, science experiments, biotechnology, and space station hardware. ¹⁸⁶²⁾

The external payloads included:

- **OPALS** (Optical Payload for Lasercomm Science). The external OPALS payload will test the use of laser optics to transfer information to Earth from space.
- **HDEV** (High Definition Earth Viewing). The HDEF external investigation includes four high–definition cameras to be placed on the space station’s exterior for use in streaming live video of Earth for online viewing.

The science payloads include: ¹⁸⁶³⁾ ¹⁸⁶⁴⁾

- **VEGGIE** (Vegetable Production System), a unit capable of producing salad–type vegetables in space. ¹⁸⁶⁵⁾
- **Micro–7** (MicroRNA Expression Profiles in Cultured Human Fibroblasts in Space) . Micro–7 is the first spaceflight study of gene and microRNA expression in non–dividing cells. The study also will investigate how spaceflight affects the response of non–dividing cells to DNA damage. ¹⁸⁶⁶⁾
- **T–Cell Act in Aging** (T–Cell Activation in Aging) experiment that seeks the cause of a depression in the human immune system while astronauts are in microgravity. ¹⁸⁶⁷⁾
- **HEART FLIES** (Heart Effect Analysis Research Team conducting FLY Investigations and Experiments in Spaceflight). HEART FLIES is the first investigation to use the fruit fly, *Drosophila melanogaster*, to study the effects of spaceflight on the structure and function of the heart. ¹⁸⁶⁸⁾
- **Project MERCCURI** (Microbial Ecology Research Combining Citizen and University Researchers on the ISS). A crowdsourced mission to send the litany of microbes to the space station for research. The goal of this project was to be a citizen science project and to engage the public as much as possible. ¹⁸⁶⁹⁾

Some hardware deliveries of the CRS–3 flight:

- **Legs for Robonaut**: After spending three years aboard the Space Station without a set of legs, Robonaut is finally set to receive its high–tech legs built by NASA. Delivered by the SpaceX Dragon, the legs will be installed on Robonaut to enable it to move around aboard the space station. Each leg has seven joints and an End Effector acting as foot used by Robonaut to hold on to handrails and sockets inside and outside ISS. ¹⁸⁷⁰⁾
- **EMU** (Extravehicular Mobility Unit). The CRS–3 mission will also involve the delivery of a replacement EMU, allowing for the return of a faulty suit on the same vehicle when it returns to Earth.

1862) Rachel Kraft, Dan Huot, “SpaceX Dragon Spacecraft Returns Critical NASA Science from Space Station,” NASA Release 14–139, May 18, 2014, URL: http://www.nasa.gov/press/2014/may/spacex-dragon-spacecraft-returns-critical-nasa-science-from-space-station/#.U31_FnbwUZM

1863) Ames’ Involvement in the SpaceX–3 Resupply Launch,” NASA, April 10, 2014, URL: <http://www.nasa.gov/ames/spacex-3/#.U0eHm6KegkA>

1864) http://www.nasa.gov/sites/default/files/files/SpaceX3cargo_Apr7_508.pdf

1865) Linda Herridge, “Veggie Will Expand Fresh Food Production on Space Station,” NASA, April 10, 2014, URL: http://www.nasa.gov/mission_pages/station/research/news/veggie/#.U0eGf6KegkA

1866) “Micro–7 (SpaceX–3),” NASA, URL: <http://www.nasa.gov/ames/research/space-biosciences/micro-7-spacex-3/#.U0ekwKKegkA>

1867) “T–Cell Activation in Aging (SpaceX–3),” NASA, URL: <http://www.nasa.gov/ames/research/space-biosciences/t-cell-activation-in-aging-spacex-3/#.U0eieaKegkA>

1868) “HEART FLIES (SpaceX–3),” NASA, URL: <http://www.nasa.gov/ames/research/space-biosciences/heart-flies-spacex-3/#.U0els6KegkA>

1869) “Project MERCCURI “Crowdsourced” Space Station Samples Take Flight,” NASA, March 12, 2014, URL: http://www.nasa.gov/mission_pages/station/research/news/merccuri/#.U0eoMqKegkA

1870) “NASA’s Robonaut Legs Headed for International Space Station,” NASA, March 12, 2014, URL: <http://www.nasa.gov/content/nasas-robotaut-legs-headed-for-international-space-station/#.U0d33aKegkA>

1.18.2 Cygnus program of OSC and NASA

The Cygnus spacecraft is a commercial unmanned resupply spacecraft, developed by OSC (Orbital Sciences Corporation) and TAS (Thales Alenia Space) as part of NASA's COTS (Commercial Orbital Transportation Services) demonstration program. It is designed to transport supplies to the ISS (International Space Station) after the retirement of the Space Shuttle program.



Figure 138: Artist's rendition of a Cygnus spacecraft approach to the ISS (image credit: Orbital)

- The Cygnus–1 spacecraft, also known as COTS–1 (Commercial Orbital Transportation Services) to the ISS, was launched on September 18, 2013 from MARS (Mid–Atlantic Regional Spaceport) at Wallops Island, VA, USA. This logistics/test flight mission involved the maiden flight of Cygnus and the final test flight of the OSC Antares–110 launch vehicle. 1871) 1872)

The history making launch marks the first time that a spacecraft launched from Virginia to the ISS. Cygnus separated from the rocket's second stage about 10 minutes after blast–off to reach Earth's orbit, marking the success of the launch. It later deployed both of its solar arrays to supply power to the spacecraft.

On Sept. 29, 2013, astronauts aboard the ISS used a robotic arm to capture and attach Cygnus–1 to the Stations's Harmony node. The maiden flight of Cygnus included a number of systems tests prior to rendezvous with the station. The capsule remained attached to Har-

1871) Trent J. Perrotto, Josh Byerly, "NASA Partner Orbital Sciences Launches Demonstration Mission to Space Station," NASA, Sept. 18, 2013, Release 13–284, URL: <http://www.nasa.gov/press/2013/september/nasa-partner-orbital-sciences-launches-demonstration-mission-to-space-station/#.Ujplj3-JrWI>

1872) "Orbital Successfully Launches Cygnus Spacecraft Aboard Antares Rocket on COTS Demonstration Mission to the International Space Station," Orbital Press Release, Sept. 18, 2013, URL: <http://www.orbital.com/NewsInfo/release.asp?prid=870>

mony until unberthing on Oct. 22, 2013. Prior to its departure from the ISS, Cygnus was loaded with items no longer needed aboard the station. On Oct. 23, 2013, Orbital's Cygnus spacecraft reentered Earth's atmosphere, marking the end of the highly successful cargo resupply demonstration mission Orbital conducted with its NASA partner. The end of the mission also marked the end of the five-year COTS (Commercial Orbital Transportation Services) joint Orbital/NASA development program.^{1873) 1874) 1875)}

After successful completion of the COTS demonstration mission to the station, Orbital will begin conducting eight planned cargo resupply flights to the ISS.

- **Cygnus CRS-1 (Cargo Resupply Mission-1):** Launch on January 9, 2014 (18:07:05 UTC) on an Antares-120 Vehicle of OSC from MARS (Mid-Atlantic Regional Spaceport), Wallops Island, VA.¹⁸⁷⁶⁾

Cygnus CRS Orb-1, also known as Orbital Sciences CRS Flight 1, is the second flight of the Orbital Sciences' unmanned resupply spacecraft Cygnus, its second flight to the ISS (International Space Station) and the third launch of the company's Antares launch vehicle. The flight is the first of 8 under the CRS (Commercial Resupply Services) contract to NASA and is also referred to as COTS (Commercial Orbital Transportation Services).

The cargo craft was loaded with 1261 kg supplies for the station, including vital science experiments to expand the research capability of the Expedition 38 crew members aboard the orbiting laboratory, crew provisions, spare parts and experiment hardware. – Also aboard the flight are 23 student experiments that will involve more than 10,000 students on the ground. These experiments will involve life sciences topics ranging from amoeba reproduction to calcium in the bones to salamanders.

The secondary payloads (34 CubeSats, commercial payloads of Orbital Sciences) on the Cygnus CRS-1 mission were:

- ArduSat-2, a 2U CubeSat (2 kg), a crowd-funded project of NanoSatisfi LLC.
- LituanicaSAT-1, a CubeSat of KTU (Kaunas University of Technology), Kaunas, Lithuania.
- LitSat-1, a 1U CubeSat of LSF (Lithuanian Space Federation).
- SkyCube, a 1U CubeSat, a crowd-funded project of Southern Stars Group LLC, San Francisco, CA, USA.
- UAPSat-1, a 1U CubeSat of UAP (Universidad Alas Peruanas), built by INRAS-PUCP (Institute for Radio Astronomy of the Pontificia Universidad Católica del Perú), Lima, Peru.
- Flock-1 fleet of 28 satellites (all 3U CubeSats) of Planet Labs Inc. of San Francisco, CA. Flock 1 is designed to deliver frequent, low-cost and high-resolution imagery of the planet that could help monitor deforestation, track natural disasters and benefit humanity in a number of other ways. All Flock-1 nanosatellites provide imagery with a resolution of 3–5 m.

All CubeSats will be using the NanoRacks deployer system on the ISS. They are deployed using the J-SSOD (JEM Small Satellite Orbital Deployer).

1873) "Cygnus Reenters Earth's Atmosphere; COTS Demonstration Mission Successfully Completed," Orbital, Oct. 23, 2013, URL: <http://www.orbital.com/antares-cygnus/>

1874) Trent J. Perrotto, Josh Byerly, "NASA Partner Orbital Sciences Completes First Flight to Space Station as Astronauts Capture Cygnus Spacecraft," NASA, News Release 13-292, Sept. 29, 2013, URL: <http://www.nasa.gov/press/2013/september/nasa-partner-orbital-sciences-completes-first-flight-to-space-station-as/#.Ukj0Kn-JrWI>

1875) Chris Bergen, "Orbital's Cygnus successfully berthed on the ISS," NASA Spaceflight.com, Sept. 28, 2013, URL: <http://www.nasaspaceflight.com/2013/09/cygnus-second-attempt-berth-iss/>

1876) Trent J. Perrotto, Josh Byerly, "New Science, NASA Cargo Launches to Space Station Aboard Orbital-1 Mission," NASA, Release 14-009, URL: http://www.nasa.gov/press/2014/january/new-science-nasa-cargo-launches-to-space-station-aboard-orbital-1-mission/#.Us98i_uFf_o

The Cygnus CRS Orb–1 spacecraft arrived at the ISS on Jan. 12, 2013 when astronauts captured the Cygnus supply craft using a robotic arm. The arrival capped the first successful contracted cargo delivery by Orbital Sciences Corp. of Dulles, VA, for NASA. ¹⁸⁷⁷⁾

The Cygnus CRS Orb–1 spacecraft remained attached to Harmony until the planned unberthing on February 18, 2014. The spacecraft experienced a destructive reentry into Earth's atmosphere on Feb. 19, 2014.

¹⁸⁷⁷⁾ Trent J. Perrotto, Josh Byerly, "New NASA Science Arrives at Space Station Aboard Orbital Sciences Cygnus Spacecraft," NASA Release, 14–013, Jan. 12, 2013, URL: http://www.nasa.gov/press/2014/january/new-nasa-science-arrives-at-space-station-aboard-orbital-sciences-cygnus/#.UtKhuvuFf_o

1.19 Small satellites in spaceflight/remote sensing

Already in the early 1960s, the first spacecraft of a family of tiny communication satellites, referred to as **OSCAR** (Orbiting Satellite Carrying Amateur Radio), was designed and developed by a California-based group of amateur radio enthusiasts. OSCAR-1, the first battery-powered amateur satellite with a mass of 4.5 kg, was launched Dec. 12, 1961 (piggyback to the Discover-36 spacecraft of the USAF) from VAFB (Vandenberg Air Force Base), CA (orbit of 372 km x 211 km, inclination of 81.2°, period of 91.8 min). OSCAR-1 orbited for 22 days, over 570 amateur radio operators in 28 countries reported receiving its simple 'HI-HI' Morse code signals in VHF. ^{1878) 1879)}

In 1969, AMSAT (Radio Amateur Satellite Corporation) was founded in Washington DC as an educational organization to give amateur radio satellites an international base. – Some OSCAR family advancements include the launch of the very first satellite voice transponder (on OSCAR-3, launch March 9, 1965), and the development of highly advanced digital "store-and-forward" (SCAR-9 on UoSAT-1), launch Oct. 6, 1981) messaging transponder techniques.

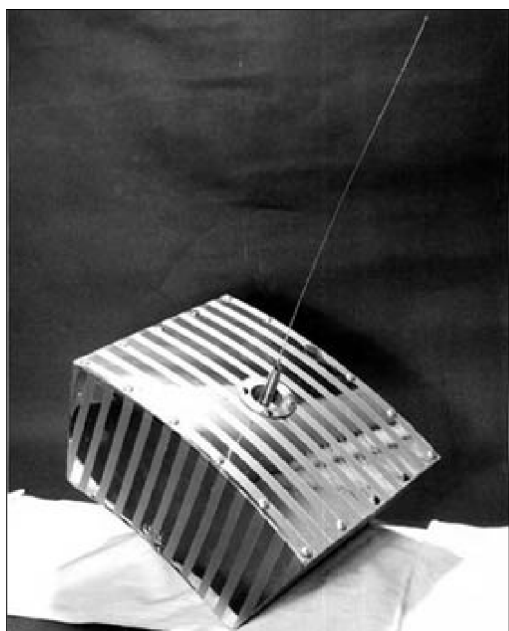


Figure 139: Illustration of OSCAR-1 satellite (image credit: AMSAT)

The first **university satellite** in history was Australis-OSCAR-5 (or simply OSCAR-5), developed by students at the University of Melbourne, Melbourne, Australia. OSCAR-5 had a launch mass of 17.7 kg (9 kg of which was battery mass), a size of 30 cm x 43 cm x 15 cm, and featured a passive magnetic attitude stabilization with 2 bar magnets. OSCAR-5 was launched piggyback to ITOS-1 (TIROS-M weather satellite) of NASA on Jan. 23, 1970 by a Thor Delta vehicle from VAFB, CA, USA. The orbit was 1476 km x 1431 km, inclination of 101.8° and a period of 115 minutes. ^{1880) 1881)}

Like many new developments, the small satellites of the early spaceage were simply overlooked by the established space industry, the space agencies, as well as by the media. There were the many new discoveries of the early missions of the Soviet Union and the USA which caught the attention of the world, as well as the race to the moon in the 1960s.

1878) "A Brief History of Amateur Satellites," URL: <http://www.amsat.org/amsat/sats/n7hpr/history.html>

1879) Frank H. Bauer, "Amateur Radio, NASA, and Small Satellites: An Indelible Link," URL: <http://www.gwu.edu/~spi/assets/docs/111209Bauer.pdf>

1880) <http://www.amsat.org/amsat-new/satellites/satInfo.php?satID=28&retURL=satellites/frequencies.php>

1881) "Australis OSCAR 5," URL: <http://www.users.on.net/~gratclif/amsatvk/oscar5.html>

The international amateur radio satellite community and associated universities must be regarded as the true pioneers of small satellite technology. They were driven by very real constraints, regarding financial support and technical resources, to evolve a highly pragmatic and cost-effective philosophy for small-scale space engineering as the only practicable means to gain access to space.

A rethinking of the situation started with the re-invention of microsatellites in the latter part of the 1970s – spearheaded at the University of Surrey in Guildford, Surrey, UK. In particular, a **design-to-capability approach** was adopted to achieve cost reductions by focusing on available, and existing technologies. Some guidelines of the Surrey design effort were: a) a small project should only have a small set of goals that could be developed by small engineering teams, and b) the new approach favored quick response times of all aspects of satellite manufacturing.

- UoSat-1 of the University of Surrey was launched on 6.10.1981 as a secondary payload to NASA's SME (Solar Mesosphere Explorer) mission.
- UoSat-2 was launched on 01.03.1984 as a secondary payload to NASA's Landsat-5. UoSAT-2 carried the first digital S&F payload (Digitalker speech synthesizer, specifically designed for school demonstrations of satellite telemetry and orbital physics) in orbit using a protocol suite by the name of PACSAT. The microsatellite had a mass of 70 kg. UoSAT-2 was one of the first satellites to prove that commercial grade microprocessors and memory chips, which had only just become readily available, mass produced and cheaper in the early 80s as part of the microcomputer revolution, could be used to build small, cost-effective yet capable satellites.

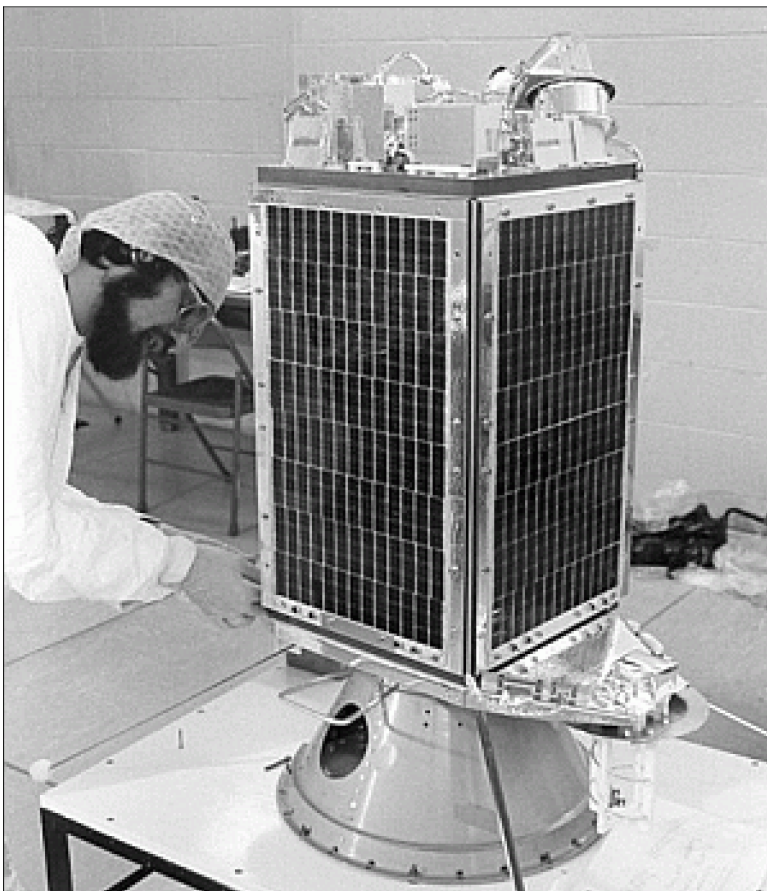


Figure 140: Photo of UoSAT-2 (image credit: SSTL)

On March 1, 2014, UoSAT-2 celebrated 30 years on orbit, still transmitting its VHF telemetry on a regular 11-day cycle and the on-board real-time clock still tells the time –

although running somewhat late! The satellite's batteries are exhausted after some 160,000 charge cycles, and transmissions are now detectable only when it is sunlight, but the telemetry continues to be tracked by amateur radio satellite enthusiasts (AMSAT) worldwide – using the predictable transmissions to help calibrate their equipment.¹⁸⁸²⁾

- UoSAT–3 (launch Jan. 22, 1990) was the first microsatellite developed and built to an innovative **modular bus design** by SSTL (tray structure).

The success of the first two microsatellites by the University of Surrey caused the creation of an early spin–off company, namely **SSTL** (Surrey Satellite Technology Ltd.) in 1985, which is now regarded as the pioneer in microsatellite design, including the introduction of a modular and flexible platform (MicroBus).

The availability of the first **microprocessors** in the 1970s represented a quantum jump in spacecraft capabilities. The first spaceborne microprocessor (Intel 8080) on an Earth observation spacecraft was flown on the SeaSat mission of NASA/JPL in 1978 (S/C mass: 2300 kg). *This technology introduction represented in turn a prime catalyst in the development of microsatellites since it enabled small physical structures in support of sophisticated data handling applications. All microsatellites of SSTL (as well as of other developers) featured a microprocessor as onboard computer.*

Miniaturization techniques of solid–state electronics, sensors, optics, actuators (i.e. miniature mechanisms), etc., are important enabling factors in microsatellite design. Short development times from project approval to S/C launch were the result.

This new approach seems to gain momentum, everywhere. There is also a realization that small–project financing can easier find support in tight budgets, this applies to government sponsorship of research projects as well as to the commercial sector. Calculated risks are being taken again. Many organizations are 're–organizing' to improve the conditions for innovation and creativity. The future seems to have room for microsatellites as well as for larger–class satellites, depending on applications.

The early microsatellites of the 1980s were simple S/C, they were for instance built without a propulsion system, due to the cost and complexity of such a system. Attitude control was typically performed using magnetic torquers and/or gravity stabilization, at a later time reaction or momentum wheels were introduced. Also, propulsion for attitude control using tiny thrusters could be implemented using cold pressurized gas. However, for orbit changes, such a cold gas system remained simply too inefficient. – Small satellite projects have also small budgets. Thus, by their very nature, they depend on launch opportunities as secondary payloads which are offered by larger satellites. As a consequence, a microsatellite project has only the choice of taking the same orbit of the main satellite payload.

In the late 1990s the miniaturization technology is considered viable for **integration of electric propulsion systems onto small satellites** – to obtain orbit maneuverability. Examples: STRV–1a (launch June 17, 1994) a microsatellite of DERA (S/C mass of 52 kg), made flight tests of the xenon gas flow control system, developed for the UK–10 IPS (Ion Propulsion System), with associated solenoid valves, orifices, and valve actuating electronics (M.47.1.1). Deep Space 1 (launch Oct. 24, 1998), a minisatellite of NASA/JPL with a mass of 490 kg, carried IPS (Ion Propulsion System) to demonstrate deep space propulsion. UoSAT–12, a minisatellite of SSTL (launch April 12, 1999, S/C mass of 325 kg) carries an electric propulsion system, a 100 W resistojet, which uses nitrous oxide as its working fluid.

The CAN (Controller Area Network) bus technology, providing a distributed data handling architecture, was first introduced by SSTL on the FaSat–Alfa microsatellite (launch Aug. 31, 1995). In the meantime, this bus standard has been implemented in many small satellite missions.

1882) "UoSAT–2 clocks up an outstanding 30 years of in–orbit operations," SSTL, March 5, 2014, URL: <http://www.sstl.co.uk/News-and-Events/2014-News-Archive/UoSAT-2-clocks-up-an-outstanding-30-years-of-in-orbit>

The SNAP–1 nanosatellite mission of SSTL (Surrey, UK, launch June 28, 2000) is a prime example of miniaturization, offering in parallel a great variety of functional capability within a total S/C mass of 6.5 kg (see D.62.17). SNAP–1 was developed with a VHF uplink (9.6 kbit/s), S–band downlink (38.4 or 76.8 kbit/s), a StrongARM onboard computer (4 MB EDAC memory), a CAN bus for data handling, three–axis attitude determination and control, a GPS receiver (SRG–05), power subsystem (4W/9W average/peak, 6–cell NiCd battery), a CMOS camera that served as its primary payload, and a microthruster of 30 μ N with a Δv capacity of 3 m/s (the micro–propulsion system had the size of a pencil). During in–orbit deployment, SNAP–1 demonstrated immediate functionality by completing a 60 second imaging sequence of its own deployment, commencing two seconds upon separation from the deployer platform.

At the start of the 21st century, the spectrum of microsatellite services is by all means as impressive as that of their bigger brother satellites, but at considerably reduced costs. Overall, microsatellites experienced an impressive evolution from flying gadgets to real and advanced service providers. In fact, microsatellites make it possible to open up new fields of services previously considered too expensive (in particular technological missions are in this category). As a consequence, the space agencies as well as the military establishments of the world are re–evaluating their programs, in favor of smaller systems, to offer a solution for ever tighter budgets. ^{1883) 1884)}

ADCS (Attitude Determination and Control Subsystems). Early microsatellite attitude control subsystems were rather limited in their control capabilities. In the early 1990s, the common attitude stabilization modes were to leave the spacecraft unstabilized, magnetically locked to the Earth’s magnetic field, or gravity–gradient controlled. Only a few experimental systems would use something more advanced. Pointing accuracies in the order of 1° were state of the art.

Generally, attitude was sensed with magnetometers which measured the amplitude and direction of the magnetic field vector relative to the spacecraft coordinate system. This measurement was then compared with that of a model of the geomagnetic field for the specific orbital location and the attitude between the spacecraft axes and the inertial reference frame was evaluated. There were also coarse sun sensors. The prime actuators used were magnetic coils and gravity gradient booms.

In the mid and late 1990s momentum–bias and experimental three–axis systems were deployed as sufficiently small wheels became available on the market, and it was not until after 2005 that agile 3–axis controlled small satellites were becoming commonplace. In particular, the pointing accuracy performance in smallsats has improved considerably – becoming ever more suitable for imaging missions as well as other applications.

- The first microsatellite known to fly a modern momentum exchange device is TUBSAT–B (launch Jan. 25, 1994, mass of 40 kg) of the Technical University of Berlin (TUB). The reaction wheel was based on a modified COTS DC brushless motor. The technology of the reaction wheel was further enhanced on the TUBSAT–N (nanosatellite, launch July 7, 1998, mass 8 kg). A single 659 g reaction wheel was used, along with a magnetic control system.

- A further improved ADCS (Attitude Determination and Control Subsystem) was used on DLR–TUBSAT (launch May 26, 1999, mass 45 kg). The microsatellite used 3 improved reaction wheels. The reaction wheels for all TUBSAT missions were provided by Teldix GmbH of Heidelberg. More recent Teldix wheels (Teldix RSI–01 and –02) are based on the TUBSAT wheel design and have been used on a number of small missions including KITSAT–3 (KAIST, launch May 26, 1999), Inspector (EADS Astrium, launch Oct. 5, 1997 to MIR Station), Orbcomm (microsatellite constellation of Orbcomm), and on PROBA–1 of ESA (launch Oct. 22, 2001).

1883) C. E. Willey, B. Huettl, D. Downen, S. W. Hill, “Miniature Mechanisms Tool Kit for Micro Spacecraft,” JHU/APL Technical Digest, Vol. 22, No 2, 2001, pp. 115–119

1884) A. L. Lew, B. Q. Le, P. D. Schwartz, et al., “Microsatellites: An Enabling Technology for Government and Commercial Aerospace Applications,” JHU/APL Technical Digest, Vol. 22, No 2, 2001, pp. 124–134

- The first set of reaction wheels developed by SSTL was flown on FASat–Alfa (launch Aug. 31, 1995) and FASat–Bravo (launch July 10, 1998) as demonstration introduction. Primary actuation was still provided by gravity gradient control (boom). The UoSat–12 microsatellite (1999) demonstrated also an electric propulsion system (resistojet) for attitude control.
- Microsatellite agility is now enhanced by the use of control moment gyros (CMG), with SSTL's first CMG flown on BilSat–1 (launch 27.09.2003). It is expected that the same level of ADCS capabilities will become available on smaller and smaller satellites in future. MEMS (Micro–Electromechanical System) sensors and actuators are the key enabling technologies for the miniaturization of the ADCS subsystem.
- Satellite attitude control: In the last years an evolution has taken place in the attitude control architecture design of new satellites. The star sensor is becoming the main on-board reference attitude sensor. This evolution is linked with the improvement of onboard autonomy, the angular FOV, the star catalog capacity, and the software treatment of power. – The star sensor can be easily adapted to any type of orbit. A “lost–in–space” attitude of a satellite can easily be fixed by a star sensor within a few seconds.
- Technology demonstration of tiny reaction wheels into the ADCS of nanosatellites and picosatellites:
 - 1) The CanX–2 (Canadian Advanced Nanosatellite eXperiment–2) of UTIAS/SFL (University of Toronto, Institute for Aerospace Studies/Space Flight Laboratory) is flying a reaction wheel, developed by UTIAS/SFL in cooperation with Sinclair Interplanetary. It is a 30 mNm wheel based on a custom (scalable) motor design. The wheel uses a vacuum grease and does not require a pressurized enclosure. The launch of the triple–cube nanosatellite (3.5 kg) took place on April 28, 2008.
 - 2) BeeSat (Berlin Experimental Educational Satellite) of TUB/ILR, Berlin will fly the “microwheel” system in a CubeSat. The 3 microwheels for 3–axis stabilization have a total mass of 150 g including the wheel drive electronics. BeeSat (1 kg) was launched on Sept. 23, 2009.

Table 94: Introduction of ADCS technology into smallsats 1885) 1886) 1887)

Method/System	Accuracy	Axes	Comment
Spin stabilization	0.1–1.0°	2	Passive, simple, cheap, inertially oriented; S/C is spun about an axis with high moment of inertia. Spin must be maintained by another system (thrusters, etc). A spin stabilized spacecraft may be a pure spinner, or it may be dual spun. In a dual–spin S/C the payload, e.g. the antenna, is despun while the other portion of the S/C spins to provide gyroscopic stability.
Gravity Gradient (GG)	1–5°	2	Passive, simple, cheap, central body oriented; to completely determine attitude, another sensor is needed. Often, a sun sensor or magnetometer is being used in combination. GG can provide a stable reference below an orbital altitude of 2000 km. Torque range: 10^{-6} – 10^{-3} Nm.
RCS (Reaction Control System)	0.01–1°	3	Expensive, quick response, consumables; active control using multiple thrusters; torque range: 10^{-2} – 10 Nm. IMUs or accelerometers are being needed to update both position and attitude.
Magnetorquer	1–2°	2	Cheap, slow, lightweight, LEO only; magnetic torquer (coils or rods) use a current through wires that interacts with the Earth's magnetic field to produce a torque. Torque range: 10^{-2} – 10^{-1} Nm.

1885) P. Davies, A. da Silva Curiel, A. Lecuyot, M. Sweeting, J. King, “Silicon Sky Volume II: What has changed in the Last 15 Years?,” Proceedings of the 21st Annual AIAA/USU Conference on Small Satellites, Logan, UT, USA, Aug. 13–16, 2007, SSC07–I–04

1886) A. Borrien, B. Castets, A. Cadiou, “Overview of CNES Research and Technology Activities on Small Platforms,” Proceedings of the 4S Symposium: ‘Small Satellite Systems and Services,’ Chia Laguna Sardinia, Italy, Sept. 25–29, 2006, ESA SP–618

1887) G. Michalareas, S. B. Gabriel, E. Rogers, “Spacecraft Attitude Estimation based on Magnetometer Measurements and the Covariance Intersection Algorithm,” Proceedings of the IEEE Aerospace Conference, Big Sky, MT, March 9–16, 2002

Method/System	Accuracy	Axes	Comment
Momentum wheel (MW)	0.1–1°	2	Expensive, similar to dual spin; momentum wheels operate with a bias momentum, meaning that they run at a steady-state, non-zero speed. There are several MW types: A zero momentum wheel – stabilizes one axis by changing the rotational rate to produce a torque. Momentum and reaction wheels do not exert external torques on a S/C. Instead, they exchange momentum with the vehicle, enabling it to rotate about an axis while the wheels themselves speed up or slow down accordingly.
Reaction wheel	0.001–1°	3	Expensive, precise faster slew; Usually at least three zero momentum wheels aligned with each axis. Reaction wheels usually operate at a nominal speed of zero. They provide control torque by changing their speed of rotation. In this way, angular momentum is exchanged between the wheel and the S/C. Torque range: 10 ⁻¹ – 1 Nm
CMG (Control Moment Gyro)	0.001–1°	3	Expensive, used to be heavy, quick for fast slew, 3-axes; CMG: one or more wheels on gimbals that rotate; CMG, is a high-performance actuator that consists of wheels spinning at constant speed, mounted on one or more gimbals. Torque range: 10 ⁻² – 10 ³ Nm.

Table 95: Common actuation techniques for attitude control

1.19.1 Small satellite classification

The term “**microsatellite**” was very probably coined by members of the AMSAT–NA (North America) community. In the mid–1960s, their tiny communication spacecraft, all well below 10 kg, were indeed “micros” – at least two orders of magnitude smaller, when compared with the established spacecraft missions of the time. Most experts in the field had a smile when asked about the objectives and the future of such toys in space – that became eventually known as “microsatellites.” Could these toys do anything worthwhile? There were many prejudices in the space community when the topic of “microsatellite” was mentioned at space conferences in the 1980s and 1990s.

Martin Sweeting of SSTL wrote in his paper of 1991: “It may come somewhat as a surprise to learn that some 20 microsatellites have been placed into orbit in the amateur satellite service over the last 25 years! Within Europe, the University of Surrey and its technology transfer company Surrey Satellite Technology Ltd. leads research into microsatellite engineering techniques through its UoSat microsatellite programme.”¹⁸⁸⁸⁾

In the same paper, Martin Sweeting proposed also a first known classification of “small satellites” as shown in Table 96. Views on what constitutes a small satellite depend on the perspective of the beholder. A small satellite to NASA or to Roskosmos may be considered as a monster to a university department. Naturally, there are many different ways to classify artificial satellites – by function, type of orbit, cost, size, performance, and so forth. However, a classification by mass turns out to be quite useful because it has a direct bearing on the launch cost of a spacecraft, representing a considerable hurdle for every mission.

Nanosatellite	< 10 kg
Microsatellite	10 – 100 kg
Minisatellite	100 – 500 kg
Small satellite	500 – 1000 kg
Large satellite	> 1000 kg

Table 96: First satellite classification by Martin Sweeting (as of 1991)

Since only the term “microsatellite” was in use in the time frame prior to the 1990s, the author, who had designed several microsatellites at the time, established his satellite classes in

¹⁸⁸⁸⁾ M. N. Sweeting, “Why Satellites are Scaling Down,” Space Technology International, 1991, pp. 55–59 (the journal was generally referred to as “Space Technology” which has since been discontinued – I happen to have a copy of the original paper, courtesy of Martin Sweeting)

the following way: He took the name “microsatellite” for a starter of his class names, and set a mass range to it. Then he selected the other class names by using the magnitude order prefixes of our decimal system to signify the smallness of a satellite in each category by analogy. Hence, the diminutive prefixes (mini, micro, nano, etc. – representing in mathematical terms steps of three orders of magnitude between each other) were chosen for the various small satellite classes – to signify only to a certain extent the corresponding mass classes of small satellites.

In the meantime, two more classes (pico, and femto) were added to the original proposal of Martin Sweeting. Also, a correction to the minisatellite class is appropriate, a change from the 100–500 kg to the 100–1000 kg range, to stick to the logic of magnitude orders. The revised version is given in Table 97. Within this classification, the term “small satellite” class is used to cover all spacecraft with a launch mass of less than 1000 kg.

Satellite Class		Mass
Large satellite (observatory, etc.)		> 1000 kg
Minisatellite	Small Satellite Class (or LightSats)	100 – 1000 kg
Microsatellite		10 – 100 kg
Nanosatellite		1 – 10 kg
Picosatellite		0.1 – 1 kg
Femtosatellite	Satellite–on–a–chip	1 – 100 g

Table 97: Satellite classification by mass criterion

Various authors/organizations have advocated these changes in the recent past. **An upper limit of 1000 kg for “minisatellites”** was for instance adopted at the **UNISPACE III** (Third United Nations Conference on the Exploration and Peaceful Uses of Outer Space), Vienna, Austria, 19–30.07.1999. At this conference, the cost for developing and manufacturing a typical minisatellite was indicated to be in the order of 5–20 million, while the price tag for microsatellites was estimated as between 2–5 million, and for nanosatellites could be below 1 million US \$ (all at 1999 price levels).^{1889) 1890) 1891)}

In particular, the small satellite mission philosophy at UNISPACE III was described to require a design–to–cost approach, within strict cost and schedule constraints, mostly combined with a single mission objective. This focused approach was noted to be supported by the following trends:^{1892) 1893) 1894)}

- Advances in electronic miniaturization and associated performance capability
- The recent appearance on the market of new small launchers (e.g. through the use of modified military missiles to launch small satellites)
- The possibility of “independence” in space (small satellites can provide an affordable way for many countries to achieve Earth Observation and/or defense capability, without relying on inputs from the major spacefaring nations)
- Ongoing reduction in mission complexity as well as in those costs associated with management; with meeting safety regulations etc.

1889) “International Study on Cost–Effective Earth Observation Missions,” Rainer Sandau (editor, et al.), A. A. Balkema Publishers of Taylor & Francis, 2006, ISBN 10: 0–415–39136–9, URL: <http://iaaweb.org/iaa/Studies/earthobservation.pdf>

1890) R. Sandau, J. Esper, L. Paxton, “Outcomes and Visions of the International Study on Cost–effective Earth Observation Missions,” Proceedings of the 57th IAC/IAF/IAA (International Astronautical Congress), Valencia, Spain, Oct. 2–6, 2006, IAC–06–B5.4.04

1891) Herbert J. Kramer, Arthur P. Cracknell, “An overview of small satellites in remote sensing,” International Journal of Remote Sensing Vol. 29, No. 15, Aug. 10, 2008, pp. 4285–4337

1892) D. J. Barnhart, T. Vladimirova, M. Baker, M. N. Sweeting, “A Low–Cost Femtosatellite to enable Distributed Space Missions,” Proceedings of the 57th IAC/IAF/IAA (International Astronautical Congress), Valencia, Spain, Oct. 2–6, 2006, IAC–06–B5.6.06

1893) <http://www.ee.surrey.ac.uk/SSC/CSER/UOSAT/classification.html>

1894) <http://www.unoosa.org/oosa/unisp–3/index.html>

The advantages of small satellite missions were considered as:

- more frequent mission opportunities and therefore faster return of science and for application data
- larger variety of missions and therefore also greater diversification of potential users
- more rapid expansion of the technical and/or scientific knowledge base
- greater involvement of local and small industry.

An early survey¹⁸⁹⁵⁾ ¹⁸⁹⁶⁾ on the phenomenon and rationale of small satellites was also conducted by such organizations as the Committee on Small Satellites of IAA (International Academy of Aeronautics) in the late 1980s.

Naturally, the capabilities and performance of these tiny pioneering monsters of nano– and picosatellites are still very limited and “inferior” to those of their bigger brothers, the micro– and minisatellites (because they have less pointing accuracy, less power, less communication capability, etc.). However, the main advantages of nano– and picosatellites are their very low cost and the speed of designing/building a satellite practically from off–the–shelf components; these are indeed strong arguments, even for a limited set of objectives that can be achieved. In particular, such applications as technology demonstrations are favored within the class of nano– and picosatellites (an example is the introduction of such concepts as spacecraft constellations (networks or clusters) for distributed Earth observations or for communication purposes in LEO orbits). The satellite classification of the Glossary (Table 947), is simply repeated here for better reference to the reader.¹⁸⁹⁷⁾

1.19.2 UoSat family of small satellites:

A new approach to small–satellite design was started in the latter part of the 1970s at the University of Surrey in Guildford, Surrey, UK. An early guiding principle was to make spaceflight affordable to a larger community of interested parties. This required in particular a **design–to–capability approach** to achieve cost reductions by focusing on available, and existing technologies. A small project should only have a small set of goals (requirements) that could be developed by small engineering teams. Each mission under consideration had to adapt to these constraints. Next to low costs, higher risks were taken again with the introduction of more advanced concepts or new technologies into mission designs. More COTS products were used, either to space–qualify these components or subsystems for other missions, or to demonstrate new capabilities on a microsatellite.

The Center of Satellite Engineering (CSER) at the University of Surrey launched its first microsatellite, UoSat–1 on Oct. 6, 1981 as a secondary payload to NASA’s SME (Solar Mesosphere Explorer) mission. This was followed by UoSat–2 with a launch on March 1, 1984 (secondary payload to Landsat–5).¹⁸⁹⁸⁾ Both microsatellites carried experimental communications and technology demonstrations within the amateur satellite service and operated in orbit successfully for more than 8 and 5 years, respectively. As a consequence of these early successes, the University of Surrey created a company, **SSTL** (Surrey Satellite Technology Ltd.) in 1985, dedicated to small satellite research and development looking for new concepts in functionality, services, and in cost reductions.

UoSat–3 (launch Jan. 22, 1990) was the first microsatellite developed and built to an **innovative modular bus design** by SSTL. The introduction of standard hardware and software

1895) “Inexpensive Scientific Satellite Missions,” IAA Position Paper, IAA Workshop: Bordeaux, 18–20.05.1989, and Working Group Meetings of Zürich (10.07.1989), Paris (18.07.1989), Malaga (09.10.1989), published in Acta Astronautica, Vol. 31, 1993, pp. 145–167, URL: <http://iaaweb.org/iaa/Studies/inexsat.pdf>

1896) “The Case for Small Satellites,” IAA Position Paper, Acta Astronautica, Vol. 31, 1993, pp. 103–144

1897) R. Fleeter, “Being Disruptive,” Launchspace Magazine, Volume 3.01, Feb/Mar 1998

1898) <http://www.ee.surrey.ac.uk/SSC/CSER/UOSAT/missions/index.html>

components provided considerably more flexibility to spacecraft and subsystem manufacturing, integration and testing. In particular, the new approach favored quick response times of all aspects of satellite manufacturing. This modular design has since been used successfully on all microsattellites of SSTL and is being widely adopted for microsattellite designs worldwide.

The launch industry reacted to the launch requirements of these new small satellites as secondary payloads by providing newly developed launch structures. For example, **ASAP** (Ariane Structure for Auxiliary Payloads) by ArianeSpace was ready for launch in 1989 offering launch opportunities for multiple small satellites. The ASAP–5 ring structure can accommodate up to 8 microsattellites with a volume restriction of 60 cm x 60 cm x 80 cm. UoSats–3 and UoSats–4 were the first microsattellites, plus 3 nanosatellites of AMSAT (PACSat, DOVE, LUSat), launched into LEO with ASAP (22.01.1990), along with the primary payload SPOT–2.

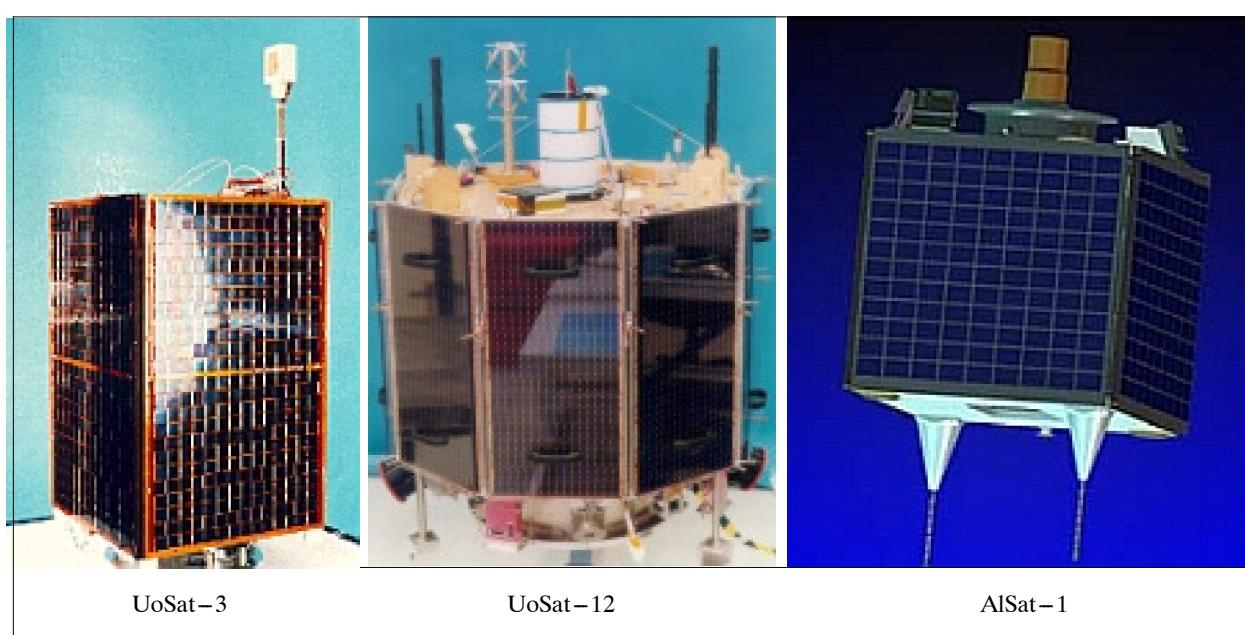


Figure 141: Typical satellites of the SSTL family (image credit: SSTL)

Today, SSTL is regarded the pioneer of microsattellite design, including a modular and flexible platform (MicroBus), and the development suitable instruments. Miniaturization techniques of solid–state electronics, sensors, optics, actuators (i.e., miniature mechanisms), etc., are important enabling factors in microsattellite design. Short development times from project approval to spacecraft launch were the result. This new approach seems to gain momentum, everywhere. There is also a realization that small–project financing can easier find support in tight budgets, this applies to government sponsorship of research projects as well as to the commercial sector. Calculated risks are being taken again. Many organizations are ‘re–organizing’ to improve the conditions for innovation and creativity. The future seems to have room for microsattellites as well as for larger–class satellites, depending on applications and required performance.

Spacecraft	Launch (end mission)	Payload, objectives, comments	Mass Power
The first UoSats spacecraft had in particular S&F (Store & Forward) payloads			
UoSats–1 (Oscar–9)	06.10.1981	MicroSat bus, proof of S&F concept, data downlink in VHF (plus S–band and X–band beacons), amateur radio communications; payload: CCD camera, space dust detectors. After 8 years of service, UoSats–1 reentered in Oct. 1989.	52 kg 30 W

Spacecraft	Launch (end mission)	Payload, objectives, comments	Mass Power
UoSat-2 (Oscar-11)	01.03.1984	MicroSat bus, technology demonstration mission: First digital S&F mission using the PACSAT protocol suite, 1200 baud AFSK, 128 kByte memory. Amateur radio service	60 kg, 30 W
UoSat-3 (Oscar-14)	22.01.1990	MicroSat-70 bus, S&F, 4 MByte file store, FSK digitally filtered, HealthNet/VITA. Payload: CREDO of DRA,	50 kg 35 W
UoSat-4 (Oscar-15)	22.01.1990	MicroSat-70 bus: Technology demonstrations for ESA and DRA; however communications were lost after 2 days in orbit (electrical failure)	45 kg 30 W
UoSat-5 (Oscar-17)	17.07.1991	MicroSat-70 bus: S&F, 13 MByte file store, 9600 baud, FSK digitally filtered. payload: TDE, EIS (Earth Imaging System), SCTE. <i>UoSat-5 was the first microsatellite to demonstrate reliable, predictable and repeatable Earth observation.</i>	50 kg 35 W
S-80/T Matra-Espace, CNES	11.08.1992	MicroSat-70 bus; S&F, 16 MByte file store, 9600 baud, FSK digitally filtered, transparent measurement transponder. – This represented the first fully commercial application of the UoSAT bus technology (turnkey system).	50 kg 35 W
KITSat-1 (Oscar-23) Korea	11.08.1992	MicroSat-70 bus; S&F, 16 MByte file store, 9600 baud, FSK digitally filtered, DSP experiment using TMS320C25/C30, capability for adaptive modulation. Payloads: EIS, DSPE, PACSAT, CRE,	49 kg 30 W
PoSat-1 Oscar-28) Portugal	26.09.1993	MicroSat-70 bus; S&F, 16 MByte file store, 9600/38400 baud, FSK digitally filtered, DSP experiment includes MSK downlink option and adaptive modulation. Payload: EIS, SIS, <i>first COTS-based GPS receiver on a microsatellite</i> (Trimble TANS-II receiver), CRE (Cosmic Ray Experiment), TDE, DSPE, first data onboard data compression on a microsatellite	49 kg 30 W
HealthSat-2	26.09.1993	MicroSat-70 bus (turnkey): S&F, 3x16 MByte file store, 9600/38400 baud, FSK digitally filtered, adaptive transmitter power under onboard computer control	48 kg 30 W
CERISE (DGA, France)	07.07.1995	MicroSat-70 bus (turnkey); French military, S&F, 9600/38400 baud, FSK digitally filtered; Sensor complement: topside sounder and intelligence payload,	50 kg 40 W
FASat-Alpha Chile	31.08.1995	MicroSat-70 bus; S&F, 9.6/76.8 kbaud, FSK digitally filtered, DSP communications payload. CAN bus first introduction on a S/C, first SSTL developed reaction wheels flown; Sensor complement: EIS, OLME (Ozone Layer Monitoring Experiment), SSDRE (Solid-State Data Recorder Experiment) with 256 MByte of RAM memory	50 kg 35 W
FASat-Bravo Chile	10.07.1998	MicroSat-70 bus; Reflight of FASat-Alpha sensor complement – due to the fact that the FASat-Alpha S/C couldn't be released from Sich-1 spacecraft.	50 kg 35 W
TMSat-1 (Oscar-31) Thai-Paht-1	10.07.1998	MicroSat-70 bus; S&F “email” comms, 9600 baud, FSK digitally filtered; PACSAT, DSPE (Digital Signal Processing Experiment), GPS receiver, EIS, OBC-186+OBC-386, CMOS video camera,	49 kg 35 W
Advanced missions			
UoSat-12	21.04.1999 (21.09.2003)	Technology mission: Introduction of MiniSat-400 bus in minisatellite design, CAN bus, electric propulsion system (resistojet, nitrous oxide as working fluid), in June 2000 first Internet access demonstration with IP protocols to flying a LEO S/C (UoSat-12 was assigned an IP address), in Jan. 2001, UoSat-12 became the first webserver in space (demo by OMNI lab of NASA/GSFC). UoSat operations ended in Sept. 2003	325 kg 150 W
Clementine Alcatel Space	03.12.1999	MicroSat-70 bus (turnkey); French military (DGA) electronic intelligence research payload on MicroSat-70 platform	50 kg 35 W

Spacecraft	Launch (end mission)	Payload, objectives, comments	Mass Power
SNAP-1	28.06.2000	Technology mission with nanosatellite, 3-axis stabilized with momentum wheel and magnetorquers, GPS receiver for orbit determination, APS camera to function as remote inspector, MPS (Micro Propulsion System), rendezvous demo with Tsinghua-1, controlled orbital maneuvers,	6.5 kg 2.5 W
Tsinghua-1 Tsinghua University, China	28.06.2000	MicroSat-70 bus; MEIS (Multispectral Earth Imaging System) x 2, 50 m resolution, 400 km swath First 3-axis controlled microsatellite	50 kg 35 W
TiungSat-1 ATSB Malaysia	26.09.2000	MicroSat-70 bus; S&F, MSEIS - a narrow angle system of 3 cameras, MEIS - a wide angle camera in NIR, DSPE (Digital Signal Processing Experiment), CEDEX (Cosmic Ray Energy Deposition Experiment),	50 kg 35 W
PICOSat STP (USAF)	30.09.2001 (31.12.2004)	US military S/C on MicroSat-70 bus (turnkey); technology demonstration (new procurement approach); payload: (PBEX, IOX, CERTO, SUITE)	67 kg 40 W
TopSat QinetiQ, UK	27.10.2005 (ops in 2008)	MicroSat-150 bus (turnkey); technology demonstration for high-resolution imaging; RALCam1 with 2.8 m GSD (Pan), 5.6 m GSD (MS)	115 kg
GIOVE-A (ESA)	28.12.2005 (ops in 2008)	Use of newly developed minisatellite bus, GMP, representing the first element in space for Europe's Galileo Program in MEO (low-cost rapid response approach).	600 kg
CFESat LANL (DOE),	09.03.2007	US research/technology mission on MicroSat-100 bus (turnkey): Radio for VHF/UHF spectrum monitoring for ionospheric and lightning studies, reprogrammable FPGA payloads,	160 kg
RapidEye MDA, (5 S/C)	29.08.2008	MicroSat-150 bus (turnkey); 5 S/C constellation, commercial MS imaging system in 5 bands at 6.5 m GSD, swath of 78 km;	175 kg 100 W
DMC (Disaster Monitoring Constellation) – initially proposed in 1996			
AlSat-1 CNTS, Algeria	28.11.2002 (ops in 2008)	SSTL-100 bus; ESIS (Extended Swath Imaging System) with 32 m resolution MS, 600 km swath;	98 kg
BILSAT-1 TUBITAK, Turkey	27.09.2003 (Aug. 2006)	SSTL-100 bus; Pan camera: resolution of 12 m, swath of 25 km, FOR: 300 km; MS system: resolution=26 m, snapshots of 55 km, FOR: 300 km; Coban: 4-band camera with a resolution of 120 m	110 kg
NigeriaSat-1 NASRDA	27.09.2003 (ops in 2008)	SSTL-100 bus; ESIS with 32 m resolution MS, 600 km swath;	98 kg
UK-DMC-1 BNSC, UK	27.09.2003 (ops in 2008)	SSTL-100 bus; ESIS with 32 m resolution MS, 600 km swath; technology demonstrations: commercial internet router,	110 kg
Beijing-1 MoST, China	27.10.2005 (ops in 2008)	SSTL-150: ESIS with 32 m resolution MS, 600 km swath; CMT (China Mapping Telescope): 4 m resolution, 24 km swath, X-band downlink of 40 Mbit/s	168 kg
Second generation of DMC with advanced payloads (DMC 2nd Generation)			
Deimos-1, Spain	July 29, 2009	SSTL-100 bus (turnkey); Provision of MS imagery (3 bands) for commercial applications (650 km swath, 22 m GSD), X-band downlink	88 kg
UK-DMC-2 BNSC, UK	July 29, 2009	SSTL-100 bus (turnkey); Provision of MS imagery (3 bands) for commercial applications (650 km swath, 22 m GSD), X-band downlink	96 kg
NigeriaSat-2 NASRDA	Aug. 17, 2011	SSTL-300 bus, minisatellite; Provision of high-resolution imagery (2.5 m Pan+5 m MS) in a swath of 20 km: plus 32 m MS imagery (4 bands) in a swath of 300 km. Note: with regard to the medium resolution imagery, Nigeria requested the 32 m resolution (and not the 22 m resolution) to be compliant with the imagery of NigeriaSat-1.	300 kg

Table 98: Overview of small satellite missions built by SSTL

1.19.3 Small satellite technology transfer programs – opening the era of global participation in space missions

There are many ways and means and forms of “technology transfer programs” in the field of space programs and missions. For instance, space agencies generally transfer newly validated technology obtained in space to their national industries to increase/promote the applications base of this newly found knowledge. NASA and ESA have practised this type of transfer for a number of years.

However, this chapter deals simply with “small satellite technology transfer programs” provided by a company or an institution or an agency to a customer – generally an institution of a foreign country, in providing project partnerships on a cooperative and affordable basis involving in particular **on–the–job training of engineers** (generally in–house) for a space mission of the customer’s choice. The key objective is to facilitate activities that substantially enhance international education and training in Earth observation techniques; thus, ensuring mission success.

Following is a sample list of rather successful on–the job training arrangements:

- **SSTL** (Surrey Satellite Technology Ltd.) – In 1990, very early in its microsatellite–development history, SSTL at the University of Surrey, UK started the first microsatellite technology transfer program, providing partnerships and on–the–job training of engineers and scientists of foreign national organizations in cooperative programs – in particular to those who weren’t in a position to start or afford their own space projects – to participate in the development of their own microsatellite. ¹⁸⁹⁹⁾

The basic idea was to use the modular UoSat bus (also referred to as MicroBus) for each project and to select/develop payloads that were most suitable to the interest of the customer. On–site training of technical teams of the customer was provided by SSTL to achieve expertise in many aspects of spacecraft and instrument design as well as in spacecraft operations.

A number of rather fruitful SSTL cooperative projects with effective knowhow transfer were started in this way, known as the **KHTT** (Know How Training and Transfer) program at SSTL. ¹⁹⁰⁰⁾

– **KitSat–1** (Korea Institute of Technology Satellite) of KAIST (Korean Advanced Institute of Science and Technology), Daejeon, Korea (launch: 26.09.1993). As a consequence, KitSat–2 was already built entirely by KAIST engineers in Korea and launched on Sept. 26, 1993.

– **PoSat–1** (Portuguese Satellite–1) of the Portuguese consortium LNETI (Laboratorio Nacional de Engenharia e Tecnologia Industrial). Four engineers were sent to Surrey to participate in on–the–job training and produce the first Portuguese satellite. Launch of PoSat–1 on Sept. 26, 1993.

– **FASat–Alfa** (Fuerza Aerea Satellite – Alfa) and **FaSat–Bravo**, a program between the Chilean Air Force (FACH = Fuerza Aerea de Chile) and SSTL. Launch of FASat–Alfa on Aug. 31, 1995.

– **TMSAT** (Thai Microsatellite), TMSAT was renamed to **Thai–Paht–1**. An SSTL project between TSC (Thai Satellite Communication) and MUT (Mahanakorn University of Technology), both of Bangkok, Thailand. Launch of TMSAT on July 10, 1998.

¹⁸⁹⁹⁾ H. J. Kramer, “An Overview of Small Satellites in Remote Sensing,” Proceedings of the International Workshop on Earth Observation Small Satellites for Remote Sensing Applications (EOSS 2007), Kuala Lumpur, Malaysia, Nov. 20–23, 2007

¹⁹⁰⁰⁾ Andy Bradford, “Small Satellite Programmes to Enable National Space Capability,” ISU, Graz, Austria, July 2011, URL: <http://www.oosa.unvienna.org/pdf/bst/ISU-SSP2011/TP1AndyBradfordPresentation.pdf>

– Tsinghua–1, a microsatellite of Tsinghua University, Beijing was developed and integrated at SSTL with on–the job training of Tsinghua engineers. Launch of Tsinghua–1 on June 28, 2000.

– TiungSat–1, a cooperative project of SSTL and eight Malaysian engineers from ATSB (Astronautic Technology SB) of Kuala Lumpur, Malaysia. Launch of TiungSat–1 on Sept. 26, 2000.

In 1996, SSTL proposed initially a **DMC** (Disaster Monitoring Constellation) to the remote–sensing community. The idea was to provide a daily global imaging capability at medium resolution (32 m), in 3–4 spectral bands, for rapid–response disaster monitoring and mitigation. By 1999, five customers or subscribers to the DMC idea had signed agreements with SSTL to share observational data of their spacecraft with every other member in the consortium in case of a disaster event. This innovative proposal provided opportunities, especially to developing countries. The DMC consortium comprises a partnership between organizations in Algeria, China, Nigeria, Turkey and the United Kingdom. Again, cooperative projects with effective knowhow transfer to the customer were realized by SSTL:

– AlSat–1 of CNTS (Centre National des Techniques Spatiales), Arzew, Algeria. Launch on Nov. 28, 2002

– NigeriaSat–1 was built in partnership with NASRDA (National Space Research & Development Agency) and funded by the Government of Nigeria. Launch on Sept. 27, 2003.

– BILSAT–1 is an Earth observation and technology demonstration mission of BILTEN TUBITAK–ODTU (Science Board of Scientific and Technical Research Council) of Ankara, Turkey. Launch on Sept. 27, 2003.

– Beijing–1 was built at SSTL in partnership with MOST (Ministry of Science and Technology) of China. Launch on Oct. 27, 2005.

– NigeriaSat–2, a minisatellite of 300 kg of the DMC–2 series, is under development at SSTL as of 2007/8. The NASRDA contract with SSTL specifies to develop and build NigeriaSat–2, including the related ground infrastructure, and a training program to further develop an indigenous space capability in the Federal Republic of Nigeria. The spacecraft was launched on Aug. 17, 2011.

DMC is in fact the first operational Earth imaging constellation providing pushbroom imagery in a wide swath. All DMC spacecraft are flown in a single orbital plane providing a cumulative swath. It represents the first application of microsatellites using propulsion for orbit maneuvers and constellation maintenance.

The practise of customer–team training service has been adopted by other space companies/institutes in the form of cooperative agreements:

- **EADS Astrium** – formerly MMS (Matra Marconi Space) ^{1901) 1902) 1903)} of Toulouse, France – started its partnership program of foreign national organizations already in 1992 with NSPO (National Space Organization) of Taiwan as its first customer – offering training courses on various levels of knowhow transfer. This was followed by the following cooperative projects:

1901) Guy Limouzin, Ian Encke, “Earth Observation programs Cooperation with ASTRIUM,” Proceedings of the International Workshop on Earth Observation Small Satellites for Remote Sensing Applications (EOSS 2007), Kuala Lumpur, Malaysia, Nov. 20–23, 2007

1902) H. Lambert, G. Limouzin, “The EADS Astrium Experience of International Cooperation,” Proceedings of the Asian Space Conference 2007, Singapore, March 21–23, 2007

1903) H. Lambert, D. Pawlak, G. Limuzin, J.–P. Gardelle, “The EADS Astrium Experience of International Cooperation,” Proceedings of the 58th IAC (International Astronautical Congress), International Space Expo, Hyderabad, India, Sept. 24–28, 2007, IAC–07–B1.1.04

- The FormoSat–2 spacecraft of NSPO (launch May 20, 2004) was built at EADS Astrium, SAS, France. In this project, the design of the **RSI** (Remote Sensing Instrument) sensor involved training of the NSPO team by EADS Astrium.
- In 2000, the EADS Astrium joint project team in Korea for the development of KOMP-SAT–2 involved 10 German and French engineers within the development team of KARI (Korea Aerospace Research Institute), Daejon. The support covered the design phase to AIT (Assembly, Integration and Test), launch and early orbit operations.
- In 1997–8, EADS Astrium trained 40 Korean engineers of ADD in Earth observation design. The engineers were staying at the Astrium facilities for two years in the UK (SAR) and France (EO). The training involved the design of an optical and a SAR payload.
- In July 2004, EADS Astrium SAS signed a cooperative agreement for delivery of the THEOS–1 spacecraft with GISTDA (Geo–Informatics and Space Technology Development Agency) of Bangkok, Thailand. The contract also specifies on–the–job training of Thai engineers as part of the EADS Astrium development team. The joint project team for a full system design, development & production (satellite, ground segment and launch) consists of 20 Thai engineers over 30 months in France and 20 Thai operators trained in Thailand. The launch of THEOS–1 took place on Oct. 1, 2008. ¹⁹⁰⁴⁾
- In May 2005, EADS Astrium SAS received a contract award from KARI, Korea to design and manufacture the first Korean multifunctional geostationary satellite, COMS–1 (Communication, Ocean and Meteorological Satellite–1) as well as the MI and GOCI payloads (prime contractor). The cooperative agreement calls for the training of over 40 Korean engineers by the Astrium design team. COMS–1 was launched on June 26, 2010.
- In 2006, EADS Astrium received a contract from KARI to provide instrument engineering support (training) and instrument manufacture for the KOMPSAT–3 spacecraft. Launch of KOMPSAT–3 on May 17, 2012.
- AlSat–2 (Algeria Satellite–2) is an optical Earth observation project of CNTS (Algerian National Space Technology Centre). In Feb. 2006, CNTS signed an agreement with EADS Astrium SAS to design and built two satellites. The first of these, AlSat–2A, has been integrated and tested in France at EADS Astrium, whereas the second one, AlSat–2B, will be integrated in Algeria within the small satellite development center (UDPS) in Oran. The cooperation agreement makes provision for 20 Algerian engineers to work side–by–side with the EADS Astrium development team, with intensive training given in space technology over a period of two years.
- In August 2008, the government of Chile signed a contract with EADS Astrium SAS for the development of the SSOT (Sistema Satelital para la Observación de la Tierra – Satellite for Earth Observation) system. The cooperation agreement makes provision for Chilean engineers to work alongside the Astrium development team. They will be given intensive training in space technology and will participate directly in SSOT project development. SSOT was launched on Dec. 17, 2011. ¹⁹⁰⁵⁾
- In August 2010, the government of Vietnam awarded a contract to EADS Astrium of France for the development of VNREDSat–1A (Vietnam Natural Resources, Environment and Disaster–monitoring Satellite), including the space and ground segments. This follows from an intergovernmental agreement on space cooperation between France and Vietnam in November 2009, in which the French government affirmed its commitment to building a closer partnership with Vietnam in the domain of science and technology. The satellite will be built in Toulouse by an Astrium team including 15 Vietnamese engineers.

1904) T. Charupatt, "THEOS – The First Earth Observation Satellite of Thailand," URL: http://www.aprsaf.org/data/p_saprsaf_data/repo_ap11cd/ss_info/5_SS_THEOS.pdf

1905) "Astrium wins Chilean optical Earth observation system," August 7, 2008, URL: http://www.eads.com/1024/es/investor/News_and_Events/news_ir/2008/20080807_atrium_chile_SSOT.html

The goal of the trainee program is to develop an indigenous capability to build future small satellites in Vietnam. VNREDSat–1A was launched on May 7, 2013.¹⁹⁰⁶⁾

Customer	Country	Type of training	Year
NSPO	Taiwan	Academic training courses	1992
NSPO	Taiwan	Design of the RSI (Remote Sensing Instrument) for FormoSat–2 (formerly known as ROCSat–2)	1993
KARI	Korea	Design of KARISat	1995
MOTC/MOSTE	Thailand	Academic courses/ remote sensing project engineering	1996–7
NileSat MOD	Egypt	Operator training & academic training	1997–7
ADD	Korea	KEOpS & ROKSAR (phase 1) design	1997–8
KARI	Korea	KOMPSAT–2 engineering; support to equipment procurement	2000–04
NSPO	Taiwan	FormoSat–2 development (integrated team)	2000–04
MOTC,GISTDA	Thailand	THEOS–1 development (integrated team)	2004–08
KARI	Korea	COMS–1 development (integrated team)	2005–08
ASAL/CNTS	Algeria	AlSat–2A & AlSat–2B development (integrated team)	2006–09
KARI	Korea	KOMPSAT–3 payload development	2006–09
ACE	Chile	SSOT development (integrated team)	2009–11
STI–VAST	Vietnam	VNREDSAT–1A development (integrated team)	2011–13
KGS	Kazakhstan	KazEOSat–2 development (integrated team)	2011–13

Table 99: EADS Astrium partnerships with institutions of foreign countries

- **TUB (Technical University of Berlin)** – In 1995, a collaborative agreement was signed between CRTS (Centre Royal Teledetection Spatiales) of Rabat, Morocco, and the Institute of Aeronautics and Astronautics (IRS) at the TUB, Berlin, Germany. The contract called for on–the–job training of Moroccan engineers along with the design and development of Maroc–TUBSAT (launch: 10.12.2001).
 - In 2003, the TUB (Technical University of Berlin) signed a MOU with LAPAN, the Indonesian National Institute of Aeronautics and Space of Jakarta, Indonesia involving a training program of LAPAN engineers at TUB and at DLR, along with all the development stages of the spacecraft and its instruments. LAPAN–TUBSAT, a microsatellite of 56 kg, was launched successfully on Jan. 10, 2007 on a PSLV vehicle of ISRO.
- **TRW** – The FormoSat–1 spacecraft development of NSPO (formerly ROCSat–1), Taiwan (launch Jan. 26, 1999) was realized as a cooperative development project between TRW of Redondo Beach, CA (USA) and NSPO (National Space Organization) of Taiwan offering training capabilities and participation for NSPO engineers in spacecraft design, testing, and spacecraft operation/control. The joint development effort started in June 1994 at the TRW facilities. In May 1997, the S/C was returned to NSPO for integration and testing. The launch of FormoSat–1 took place on Jan. 26, 1999.¹⁹⁰⁷⁾
- **SI (Satrec Initiative Co. Ltd.)** is a spin–off company of Daejeon, Korea which was established in January, 2000 by former SaTReC (KAIST) engineers, Daejeon, Korea. In the 1990s, these engineers were themselves trainees at SSTL for the Korean KITSat program. Since 2000, SI is providing training courses for its customers.
 - The X–Sat project of NTU (Nanyang Technological University), Singapore signed a contract with SI in 2000 to build the IRIS imager for X–Sat and to train its engineers in the development of the instrument. Another contract followed in 2003. X–Sat was launched on April 20, 2011.

1906) “Astrium signs development contract with Vietnam for an Earth observation satellite – VNREDSat–1,” Aug. 2, 2010, URL: http://www.astrium.eads.net/en/press_centre/astrium-signs-development-contract-with-vietnam-for-an-earth-observation.html

1907) <http://www.nspo.org.tw/2005e/projects/project1/intro.htm>

- In 2000, SI provided training for the TiungSat–1 team of ATSB Sdn (Malaysia) in spacecraft operations used for the LEOP (Launch and Early Operations Phase) of the mission. TiungSat–1 was launched Sept. 26, 2000.
- The RazakSat project of ATSB, Malaysia. In 2001, ATSB signed a cooperative agreement with SI of Daejeon, Korea. The contract included on–the–job training of ATSB engineers. RazakSat was launched on July 14, 2009.
- In 2005, SI provided some training (concept design) for the THEOS project of GISTDA engineers, Thailand.
- DubaiSat–1 is an initiative of EIAST (Emirates Institution for Advanced Science and Technology), a UAE (United Arab Emirates) government entity to build and operate a remote sensing imaging satellite. To this effect, a cooperative agreement was signed with SI of Daejeon, Korea in April 2006 which includes an on–the–job training program of a team of UAE engineers in Korea at SI. DubaiSat–1 was launched on July 29, 2009.
- **Yuzhnoye** – In 2001, the EgyptSat–1 project was signed between NARSS (National Authority for Remote Sensing and Space Science) of Egypt and the State Design Office “Yuzhnoye”, Dnepropetrovsk, Ukraine. Yuzhnoye designed and developed the spacecraft. The contract included also technical expertise and on–the–job training to Egyptian engineers as well as technology transfer (launch: 17.04.2007).

1.19.4 Small satellite initiatives in the USA

The **SMEX** (Small Explorer) program of NASA started in 1988 to provide frequent opportunities for highly focused and relatively inexpensive space science missions on minisatellites (SAMPEX, FAST, SWAS, TRACE, and WIRE). The basic approach was to use a modular design for multiple missions (or a class of missions). Modular designs became possible because the satellite industry reached a state of maturity and has a large heritage of past satellite designs to learn from and build upon.¹⁹⁰⁸⁾

- **SAMPEX** (Solar Anomalous and Magnetospheric Particle Explorer) to monitor the magnetospheric particle populations which occasionally plunge into the middle atmosphere of the Earth. S/C mass of 161 kg, launch July 3, 1992. It was the first mission in USA to implement the CCSDS communication standards.
- **FAST** (Fast Auroral Snapshot Explorer) with the goal to measure and to study the rapidly varying electric and magnetic fields and the flow of electrons and ions in the aurora regions of the Earth. S/C mass of 190 kg, launch Aug. 21, 1996.
- **TRACE** (Transition Region and Coronal Explorer) a solar minisatellite of NASA (250 kg). The S/C carries a single instrument, a high–resolution multispectral spectrometer in EUV and UV. TRACE was launched on Apr. 2, 1998 and is operational as of 2007 (design life of 1 year).
- **SWAS** (Submillimeter Wave Astronomy Satellite), a SMEX mission of NASA with a launch on Dec. 5, 1998. An astronomy mission with a S/C mass of 288 kg. The minisatellite provides a pointing accuracy of 38 arcseconds and jitter < 19 arcseconds. The main instrument is a complete radio telescope in space.
- **WIRE** (Wide–Field Infrared Explorer) of NASA with a launch March 4, 1999. WIRE is also an astronomy mission to study the evolution of galaxies. Launch mass of 259 kg. The

1908) W. M. Reid, W. Hansell, T. Phillips, “The Implementation of Satellite Attitude Control System Software Using Object Oriented Design,” Proceedings of the 12th Small Satellite Conference of AIAA/USU, Logan, UT, USA, Aug. 31 – Sept. 11, 1998, SSC98–I–7, URL: <http://microsat.sm.bmstu.ru/e–library/ccdh/Soft/ssci7.pdf>

main instrument, WIRE, consists of a cryogenically-cooled, 30 cm imaging telescope. However, WIRE was unable to carry out its primary science mission due to attitude problems.

NASA started also a Small Spacecraft Technology Initiative (SSTI) program in 1994 with the objective to demonstrate technologies and new approaches for reducing the cost and time of getting civil and commercial space missions from the drawing board to orbit. The program permitted the spacecraft builder to incorporate commercial standards in the design and qualification process. The first SSTI projects were the spacecraft “Lewis” and “Clark” named after the leaders of the early 19th century US expedition to the Pacific northwest.¹⁹⁰⁹⁾

- The Lewis minisatellite was designed and built by the team led by TRW, Redondo Beach, CA. The spacecraft had a launch mass of 288 kg (launch Aug. 23, 1997) carrying a sensor complement of three instruments: HSI (Hyperspectral Imager), LEISA (Linear Etalon Imaging Spectrometer Array), and UCB (Extreme Ultraviolet Cosmic Background Explorer). The S/C was lost after 3 days due to an attitude control failure.
- The Clark minisatellite was built by a team led by CTA Space Systems of McLean, VA. The S/C had a launch mass of 305 kg, representing a demonstration of 36 advanced technologies. However, at the end of Feb. 1998, NASA cancelled the Clark mission due to severe cost overruns and launch delays.
- The TOMS-EP (Total Ozone Mapping Spectrometer-Earth Probe) mission of NASA was built by TRW. The spacecraft was launched on July 2, 1996 (S/C mass of 294 kg, design life of 2 years) and provided ozone monitoring for > 10 years. The spacecraft had been operating on the backup transmitter since the primary transmitter failed in April 1998.
- OCO (Orbiting Carbon Observatory) is a minisatellite mission of NASA (S/C mass of 407 kg using the LeoStar-2 bus of OSC) to provide global measurements of atmospheric carbon dioxide. OCO was launched on 24.02.2009 – but the launch vehicle experienced a failure.

DoD and DARPA (Defense Advanced Research Projects Agency), USA, started a “LightSat initiative” in the mid-1980s with the goal to reduce the costs and development time of small spacecraft in the 50 to 1000 kg range. The first microsatellite developed under this program within less than a year was GLOMR (Global Low-Orbit Message Relay), a digital store-and-forward un-stabilized communications satellite (mass of 62 kg) with a launch on Space Shuttle (STS-61-A, Oct. 30 1985). GLOMR collected sensor data from the ground segment and reentered the atmosphere after 14 months in orbit.

The MightySat program of AFRL (Air Force Research Laboratory) started in 1994 with the objective to provide an environment for frequent, inexpensive, on-orbit demonstrations of emerging space system technologies and to accelerate their transition into operational use.

- MightySat-1 was a spin-stabilized microsatellite of 63 kg launched on Dec. 14, 1998 on the Space Shuttle and ejected. The spacecraft carried several advanced experiments to demonstrate the new technologies. MightySat-1 reentered the atmosphere on Nov. 16, 1999 due to its relatively low orbital altitude. All objectives were accomplished.
- MightySat-2 was a technology demonstration mission US Defense Space Test Program (test of high-risk, high-payoff space system technologies), initiated in 1996. The 3-axis stabilized small satellite had a mass of 121 kg (payload mass of 37 kg) and was launched July 19, 2000. The main sensor was FTHSI (Fourier Transform HyperSpectral Imager). The S-band downlink permitted only a low duty cycle of the instrument. The S/C reentered the atmosphere in Nov. 2002.

¹⁹⁰⁹⁾ <http://www.sti.nasa.gov/tto/spinoff1996/17.html>

Starting in 2003, the DoD has gradually developed a new space operations concept, called Operationally Responsive Space (ORS), which calls for the rapid development and launch of spacecraft to augment or partially replace existing spacecraft. Major partners in the program are AFRL, NRL and industry. The objective is to develop new small launch vehicles, standardized buses and “plug-and-play” architectures for small satellites, and the TacSat series of technology demonstration satellites. The goal is to dramatically shorten the development time required for small satellites. The first spacecraft in the program, **TacSat-2** with a mass of 370 kg, was launched on Dec. 16, 2006. Finally, small satellites have found their place as part of a balanced diet of spacecraft types needed to carry out DoD missions.

- In July 2007, DARPA issued a broad agency announcement for a program it calls **System F6** (“F6” is derived from a number of terms used to describe the program: future, fast, flexible, fractionated, and free flying). The objective is to create a “self-forming network of spacecraft nodes” that together act like a single satellite. In its solicitation, DARPA has identified a number of key technologies needed for an F6 system to be successful. These include networking and wireless communications capabilities among the spacecraft nodes, distributed computing, wireless power transfer, cluster flight operations, and the development of a spacecraft “black box” for each node to diagnose and recover from failures. DARPA is looking for innovative proposals for the performance of research, development, design, and testing to support the agency’s System F6 concept. ¹⁹¹⁰⁾

The System F6 Program, which is envisioned to culminate in an on-orbit demonstration in 2015–2016, is designed to validate a new space mission concept in which a cluster of smaller, wirelessly connected spacecraft replaces the typical single spacecraft carrying numerous instruments and payloads. ^{1911) 1912)}

The following table provides an (incomplete) overview of small satellite missions over the last three decades launched in the USA.

Mission	Sponsor	S/C contractor	Launch mass (kg)	Launch date (end mission)	Comments
IMP-8 (Explorer 50)	NASA	NASA/GSFC	410	26.10.1973 (ops in 2007)	Studies of the magnetotail, cosmic rays, solar wind
MagSat (AEM-3)	NASA	JHU/APL	182	30.10.1978 (11.06.1980)	First precise measurements of the global magnetic field
REX	STP (USAF)	OSC (CTA)	77	29.06.1991	Radiation environment
SAMPEX	NASA	NASA/GSFC	161	03.07.1992	Science experiments
ALEXIS	DOE LANL	AeroAstro	115	25.04.1993 (29.04.2005)	Technology demonstration (ALEXIS, BlackBeard)
RADCAL	STP (USAF)	OSC (CTA)	95 kg	25.06.1993	Radar calibration satellite
STEP-0	STP (USAF)	TRW	489	13.03.1994	Autonomy experiments
OrbView-1 MicroLab	NASA/OSC	OSC	74	03.04.1995 (April 2000)	Lightning (OTD), GPS/Met, proof of concept
TOMS-EP	NASA	TRW	295	02.07.1996 (ops in 2007)	Ozone mapping (TOMS)
REX-II	STP (USAF)	OSC	113	09.03.1996	Radiation environment (REX, ADACS)
FAST	NASA	NASA/GSFC	191	21.08.1996	Auroral mapping (ESA, TEAMS, EFLPI, MFI)
HETE	NASA	MIT, AeroAstro	128	04.11.1996	High energy experiments (launch failure)
SAC-B	CONAE, NASA	CONAE	191	04.11.1996	Study of solar physics (launch failure)

1910) http://www.darpa.mil/TTO/solicit/BAA07-31/F6_BAA_Final_07-16-07.doc

1911) “DARPA selects SwRI’s K-band space crosslink radio for flight development as part of System F6 Program,” Space Daily, Jan. 7, 2013, URL: http://www.spacedaily.com/reports/DARPA_selects_SwRIs_K_band_space_crosslink_radio_for_flight_development_as_part_of_System_F6_Program_999.html

1912) http://www.darpa.mil/Our_Work/tto/Programs/System_F6.aspx

Mission	Sponsor	S/C contractor	Launch mass (kg)	Launch date (end mission)	Comments
OrbView–2 Sea STAR	NASA	OSC	390	01.08.1997 (ops in 2007)	Ocean color (SeaWiFS)
Lewis	NASA	TRW	385	23.08.1997 (28.09.1997)	Hyperspectral imaging (no operations possible), LEISA (study of aurorae)
ACE	NASA	JHU/APL	785	25.08.1997 (ops in 2007)	Space weather (SWIMS, SWICS, ULEIS, SEPICA, SIS, CRIS, EPAM, etc.)
FORTE	DOE	LANL, SNL	236	29.08.1997 (ops in 2006)	Monitoring of lightning (EC, RF, OLS)
SNOE	NASA	LASP	132	26.02.1998 (Dec. 2003)	Atmospheric physics (UVS, AP, SXP, BGSR)
GFO	US Navy	BATC (Boulder)	357	10.02.1998 (ops in 2007)	Altimetry (GFO–RA, WVR, TRSR, LRA)
TRACE	NASA	NASA/GSFC	250	02.04.1998 (ops in 2007)	Solar physics (TRACE)
STEX/ATEX	NRO/NRL	Lockheed Martin	691	03.10.1998 (June 2000)	Tether deployment experiment
SWAS	NASA	NASA/GSFC	288	05.12.1998	Astronomy mission
DS1	NASA	JPL, Spec- trum Astro	486	24.10.1998 Dec. 2001)	Technology demonstration (IPS, AutoNav, PEPE, etc.)
MightySat–I	STP (USAF)	OSC	69	14.12.1998 (Nov. 1999)	Technology (ACS, ASCE, Maple–1, SMARD, MPID)
WIRE	NASA	NASA/GSFC	259	04.03.1999	
Terriers	NASA, Bos- ton Universi- ty	AeroAstro	288	18.05.1999	Space physics (S/C could not be operated)
QuikSCAT	NASA, NOAA	JPL, BACT	970	19.01.1999 (ops in 2007)	Ocean wind measure (SeaWinds)
Ikonos–2	GeoEye (Space Imag- ing)	Lockheed Martin	817	24.09.1999 (ops in 2008)	High resolution Pan+ MS imagery
AcrimSat	NASA, JPL	OSC	115	20.12.1999 (ops in 2008)	Earth's radiation budget (ACRIM–III)
MTI	DOE (SNL, LANL)	BATC	587	12.03.2000 (ops in 2007)	MTI (Multispectral Thermal Imager), HXRS
IMAGE	NASA	LMMS	496	25.03.2000 (Dec. 2005)	Magnetosphere (LENA, MENA, HENA, EUV, FUV, WIC, SI, GEO, RPI)
TSX–5	STP, BMDO, DERA (UK)	OSC	250	07.06.2000	Technology demonstration (STRV–2, CEASE)
MightySat– II.1	STP (USAF)	Spectrum Astro	121	19.07. 2000 (Aug. 2002)	Demonstration of hyper- spectral imaging (FTHSI), Picosat1.1 release Sep. 2002
EO–1	NASA	Swales	572	21.11.2000 (ops in 2008)	Tech. demonstration (ALI, Hyperion, LAC, AutoCon)
Genesis	NASA	Lockheed Martin	636	08.08.2001 08.09.2004	Solar wind sample return mission to L1
QuickBird–2	DigitalGlobe	BATC	931	18.10.2001 (ops in 2008)	High resolution Pan + MS imagery
TIMED	NASA	JHU/APL	660	07.12.2001 (ops in 2008)	Study of energetics of meso- sphere/ionosphere
XSS–10	AFRL, NASA, NRL	Boeing Rock- etdyne	31	29.01.2002 (24h mission)	Demonstration of servicing capability
RHESSI	NASA UCB/SSL	Spectrum Astro	290	05.02.2002 (ops in 2008)	Physics of particle accelera- tion and energy release in solar flares
Coriolis	STP, ONR, NRL	Spectrum Astro	827	06.01.2003 (ops in 2008)	Tech demo (WindSat, SMEI)
ICESat	NASA	BATC	970	13.01.2003 (ops in 2008)	GLAS, GPS receiver, RRA)

Mission	Sponsor	S/C contractor	Launch mass (kg)	Launch date (end mission)	Comments
CHIPSat	NASA, UCB	SpaceDev	85	13.01.2003 (Apr. 2008)	Tech demo mission of UCB/SSL; EUV spectra of sun
SORCE	NASA, LASP	OSC	290	25.01.2003 (ops in 2008)	Earth radiation budget (TIM, SOLSTICE, SIM, XPS)
OrbView-3	GeoEye	OSC	360	26.06.2003 (0403.2007)	High resolution PAN+ MS imagery
XSS-11	AFRL	Lockheed Martin	145	11.04.2005	Rendezvous with inactive S/C (on-orbit servicing)
ST5 (Space Technology 5)	NASA	NASA/GSFC	25 / S/C	22.03.2006 (30.06.2006)	Technology verification of 3 S/C constellation (3 months)
CloudSat	NASA/CSA	BATC	700	28.04.2006 (ops in 2008)	EO: CPR (Cloud Profiling Radar)
CALIPSO	NASA/CNES	Alcatel Alenia Space	635	28.04.2006 (ops in 2008)	EO: (CALIOP, IIR, WFC)
STEREO	NASA	JHU/APL	620 /S/C	26.10.2006 (ops in 2008)	2 S/C mission in Sun-Earth connection program
TacSat-2	DoD/AFRL	MicroSat Systems	370	16.12.2006 (Dec. 2007)	Technology demonstration + EO payload
GeneSat-1 (triple Cube-Sat)	NASA/ARC	SCU, Stanford	4.6	16.12.2006 (Feb. 2007) (ops in 2009)	Study the effects of the microgravity environment on biological cultures
THEMIS	NASA	Swales (UCB)	128 / S/C	17.02.2007 (ops in 2010)	Constellation of 5 Probes in HEO to study magnetospheric substorms
MidSTAR-1	USNA	USNA	120	09.03.2007	Tech demo (ICSat, CFTP)
FalconSat-3	USAFA	SpaceQuest	54	09.03.2007	Tech demo boom deployment
STPSat-1	STP (USAF) AFRL	AeroAstro	170	09.03.2007 (ops in 2008)	EO: SHIMMER, CITRIS, MEPSI
AIM (SMEX mission)	NASA, Hampton University	OSC	210	25.04.2007 (ops in 2011)	Study the causes of Earth's highest-altitude clouds
OCO	NASA/JPL	OSC	407	24.02.2009 launch failure	Global measurements of atmospheric carbon dioxide
TacSat-3	NRL, AFRL	ATK	< 400	10.05.2009	Hyperspectral imaging mission (VNIR, SWIR)
Glory	NASA	OSC	550	04.03.2011 launch failure	Climate research mission: APS, CC, TIM
ST8	NASA	OSC	194	2011 ?	Tech demos: NGU, Sail-MAST, MLHP, DM)

Table 100: Small satellites of the USA (chronological order of missions)

A fairly recent development in the USA to increase multiple secondary launch opportunities at affordable costs was provided with the **ESPA** (EELV Secondary Payload Adapter) fixture of AFRL. The ESPA standard interface consists of a ring that is installed between the rocket's upper stage and the primary payload. Up to six small (≤ 180 kg each) secondary payloads may be carried with the ESPA configuration.

The first demonstration flight with ESPA capability, namely STP-1 (Space Test Program-1) of DARPA, took place on March 9, 2007 from Cape Canaveral, FLA. The STP-1 rideshare mission consisted of a six-vehicle payload: Orbital Express (OE) consisting of ASTRO and NextSat, MidSTAR-1, STPSat-1, CFESat, and FalconSat-3. The six spacecraft were successfully deployed into two orbital planes at two different altitudes.

1.19.5 Small satellite development in the rest of the world:

The EXOS (Exospheric Observation Satellite) series was developed by ISAS (Institute for Space and Astronomical Science) of the University of Tokyo, Japan. EXOS–A (launch: 04.02.1978, mass of 126 kg) and EXOS–B (launch: 16.09.1978, mass of 92 kg), the Japanese contribution of the International Magnetospheric Study.

EXOS–B carried out coordinated observations with Exos–A – investigations of correlated mechanisms between particles and fields and plasma turbulence were made with in–situ measurement techniques using electrostatic particle analyzers. The EXOS series spacecraft are in effect good examples in the class of “small satellites” of their time period. Each one of them represented a **custom design** as well as a corresponding manufacturing process.

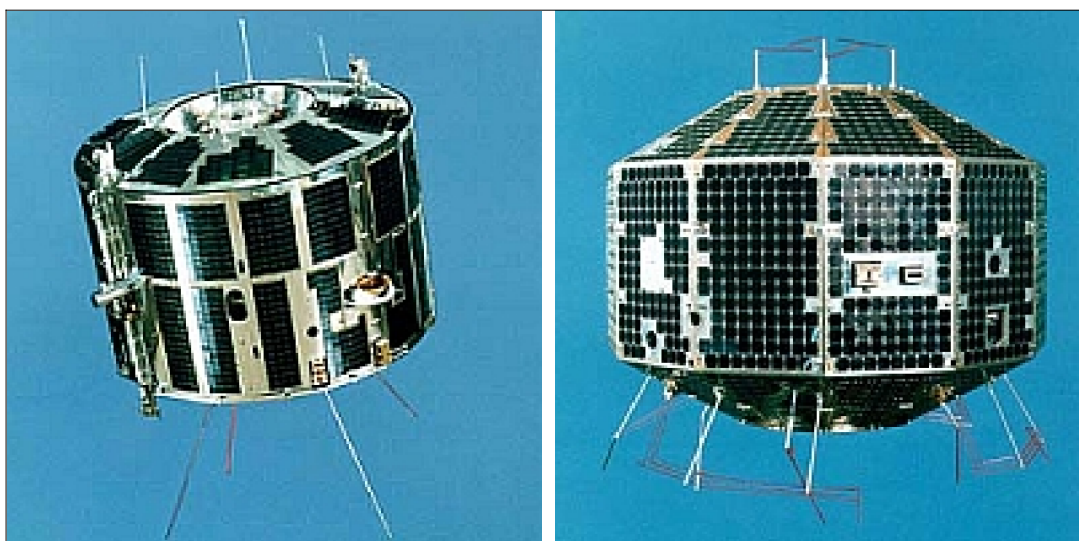


Figure 142: View of the EXOS–A (left) and EXOS–B spacecraft (image credit: ISAS)

The following table provides an (incomplete) overview of small satellite missions over the last three decades launched by the rest of the world.

Mission	Sponsor	S/C contractor	Launch mass (kg)	Launch date (end mission)	Comments
EXOS–A (Kyokko)	Japan	ISAS Japan	126	04.02.1978	Study of the magnetosphere (auroral activity, plasma)
EXOS–B (Jikiken)	Japan	ISAS Japan	92	16.09.1978	First observation across the plasma pause (part of international magnetospheric study)
Rohini–3	ISRO, India	ISRO	41.5	17.04.1983 (24.09.1984)	Launch from Sriharikota, a sphere of 65 cm diameter, 2 cameras provided over 50,000 images, L–band downlink
EXOS–C (Ohzora)	Japan	ISAS Japan	208	14.02.1984 (1987)	Study of tracers in the atmosphere & wave–particle interactions in the ionosphere
AMPTE with IRM S/C, UKS S/C, CCE S/C	Germany, UK, USA, NASA	MPE, RAL, JHU/APL	705, 78, 240	16.08.1984 (12.08.1986), (16.01.1985), (10.01.1989)	3 S/C mission, studies of solar–terrestrial interactions, release of tracers to study the magnetosphere
Viking	SNSB Sweden	SSC Sweden	246 kg	22.02.1986 (12.05.1987)	Interaction of solar wind with Earth’s atmosphere
IRS–1A	ISRO	ISRO	975	17.03.1988 (2003)	EO (LISS–1, LISS–2)
EXOS–D (Akebono)	Japan	ISAS Japan	294	22.02.1989	Study the mechanism of auroral charged particle precipitation in the polar cusp region

Mission	Sponsor	S/C contractor	Launch mass (kg)	Launch date (end mission)	Comments
Ulysses (ISPM)	ESA/NASA	Dornier System Germany	370	06.10.1990 (01.07.2007))	Solar polar mission with a payload of 11 instruments
TUBSAT-A	TU Berlin	TU Berlin	35	17.07.1991 (Spring 2007)	S&F communications, Technology demonstrations
Solar-A (Yohkoh)	JAXA (ISAS)	ISAS	390	30.08.1991 (15.12.2001)	Solar physics mission of Japan (HXT, SXT, BCS, WBS)
STRV-1a, STRV-1b	MoD (UK)	QinetiQ (DERA)	52 54	17.06.1992 (March 1998)	Technology demonstrations into GTO
GEOTAIL	JAXA/NASA	JAXA/ISAS	970	14.07.1992 (ops in 2007)	Study the dynamics of the Earth's magnetotail
Freja	SNSB Sweden	SSC MPE Garching	256	06.10.1992	Study of auroral phenomena in ionosphere, magnetosphere
SCD-1	INPE Brazil	INPE	115	09.02.1993 (ops in 2007)	Data collection satellite
KitSat-2	Korea	KAIST Korea	50	26.09.1993	EIS camera with WAC (2 km) + NAC (200 m resolution)
TUBSAT-B	TU Berlin	TU Berlin	45	25.01.1994 (05.03.1994)	First microsat to fly a modern reaction wheel; Video camera for snapshots
IRS-P2	ISRO	ISRO	870	15.10.1994 (Sep. 1997)	EO (LISS-2M)
Astrid-1	SNSB Sweden	SSC, IRF-K	27	24.01.1995 (Sept. 1995)	Spin-stabilized S/C, study of the Earth's near space plasma
IRS-P3	ISRO	ISRO	922	21.03.1996 (late 2003)	EO (WiFS, MOS, XRAP)
Equator-S	DARA Germany	MPE Garching	235	02.12.1997	Solar-terrestrial energy transport mission, study of plasma
TUBSAT-N, +N1	TU Berlin	TU Berlin	8 3	07.07.1998 (2000, 2002)	Submarine launch, S&F communications, bidirectional data transfer with buoys, etc.
TechSat (Gurwin-II)	Technion Israel	Technion	48	10.07.1998 (ops in 2008)	Tech demos: (OM, ERIP, SOREQ, SUPEX, XDEX,)
SCD-2	INPE Brazil	INPE	117	23.10.1998 (ops in 2007)	Data collection satellite
Astrid-2	SNSB Sweden	SSC	30	10.12.1998	High-resolution E-field and B-field measurements in the auroral region, ASC of DTU
FormoSat-1 (ROCSat-1)	NSPO Taiwan	TRW	402	26.01.1999 (June 2004)	EO (OCI, IPEI, ECP) formerly ROCSat-1
SUNSAT South Africa	Stellenbosch University	Stellenbosch	64	23.02.1999 (19.01.2001)	EO payload: HRI, TRSR, MIS, Magnetometer, LRA
Ørsted (Oersted)	Denmark	Terma A/S	60.7	23.02.1999 (ops in 2008)	Geomagnetic research (Magnetometers, CPD, ASC, TRSR)
SJ-5	China	CAST Beijing	298	10.05.1999 (Feb. 2000)	Science & technology demonstration (new bus: CAST968)
DLR-TUBSAT	DLR	TU Berlin	45	26.05.1999 (ops in 2008)	Introduction of hibernation mode operations in ACS,
KitSat-3	KAIST Korea	KAIST	110	26.05.1999 (Dec. 2003)	EO demonstration mission (MEIS, REME, HEPT, ETP)
KompSat-1 (Arirang-1)	KARI Korea	TRW, KARI	510	20.12.1999 (30.12.2007)	EO (EOC, OSMI, SPS)
OPAL	SSDL Stanford	SSDL Stanford	25	27.01.2000	Deployment of picosatellites
JAWSAT	USAF Weber State	USAF Weber State	192	27.01.2000	Technology demonstration of S/C deployments
CHAMP	GFZ, DLR Germany	EADS Astrium	522	15.07.2000 (ops in 2008)	Geo (TRSR-2, STAR, LRR, MIAS, ASC, DIDM)

Mission	Sponsor	S/C contractor	Launch mass (kg)	Launch date (end mission)	Comments
MITA	ASI Italy	Carlo Gavazzi Space	170	15.07.2000 (15.08.2001)	Technology demonstration of platform and payloads
UniSat-1	University of Rome	La Sapienza GAUSS	12	26.09.2000	Technology demonstrations, spin-stabilized S/C
STRV-1c STRV-1d	MoD (UK)	QinetiQ (DERA)	100 100	16.11.2000 (2001)	Technology demonstrations into GTO
SAC-C	CONAE, NASA,	INVAP	485	21.11.2000 (ops in 2008)	EO (MMRS, HRTC, HSC, Ørsted-2, IST, INES, GOLPE, ICARE, WTE)
EROS-A	ImageSat Cyprus	IAI Israel	250	05.12.2000 (ops in 2008)	High resolution Pan imagery
Odin	SNSB Sweden	SSC	250	20.02.2001 (ops in 2008)	Aeronomy/astronomy mission (SMR, OSIRIS)
PROBA	ESA	Verhaert, Belgium	149	22.10.2001 (ops in 2008)	EO (CHRIS, SREM, DEBIE), Autonomy demo,
BIRD	DLR	DLR	94	22.10.2001	EO (HSRS, WAOSS-B, HORUS)
Munin	IRF Sweden	IRF, Umeå University	6	21.11.2001 (02.12.2001)	Study of auroral activity (MEDUSA, DINA)
Kolibri-2000	Russia Australia	IKI	25.5	26.11.2001 (03.03.2002)	Student technology demonstration
Jason-1	CNES/ NASA	Alcatel Alenia Space	500	07.12.2001 (ops in 2008)	Altimetry (Poseidon-2, JMR, TRSR, LRA))
MAROC-TUBSAT	CRTS Morocco	TU Berlin	47	10.12.2001 (ops in 2008)	ACS hibernation mode, star sensor for ACS, EIC (Earth Imaging Camera)
GRACE	USA-Ger- many	EADS Astrium	432 / S/C	17.03.2002 (ops in 2008)	Geodetic SST mission (dual satellites, gravity field)
HY-1A	SOA Beijing	CAST China	365	15.05.2002 (April 2004)	Survey of ocean resources (COCTS, CZI)
MicroLabSat (μ LabSat)	JAXA	JAXA, NICT	54	14.12.2002 (27.09.2006)	Technology demonstrations, test of new satellite separation mechanism
FedSat	CRCSS Australia	SIL (SSTL)	58	14.12.2002 (June 2006)	EO: CPE, ADAM, NewMag, BlackJack, AIM
UniSat-2	University of Rome	La Sapienza GAUSS	10	20.12.2002	Spin-stabilized S/C, AMI (Aerosol Monitoring Instrument), DIS (Debris Sensor), CGM (Cold Gas μ thruster)
MIMOSA	ASU/CAS Czech Re- public	Space De- vices, Prague	55	30.06.2003	Density distribution of the upper ionosphere (MACEK)
SciSat-1	CSA Canada	Bristol Aero- space	152	13.08.2003 (ops in 2008)	Atmospheric research (ACE-FTS, MAESTRO)
SMART-1	ESA	SSC Sweden	367	23.09.2003 (03.09.2006)	Moon mission using electric propulsion
STSat-1 (Uribyol-4)	MOST Korea	KAIST SaTReC	120	27.09.2003 (Oct. 2005)	Tech demo (FIMS, SPP, DCS/ADAM)
SERVIS-1	NEDO, METI	USEF Japan	840	30.10.2003 (01.11.2005)	Tech demo/validation of COTS components
DSP-1	CNSA (Chi- na) / ESA	DFHSat Beijing	330	29.12.2003 (14.10.2007)	Study of magnetosphere in geospace
FormoSat-2 ROCSat-2)	NSPO Taiwan	EADS Astrium	746	20.05.2004 (ops in 2008))	EO (RSI, ISUAL)
DEMETER	CNES FRance	CNES	129	29.06.2004 (ops in 2008)	Geophysical parameters (IMSC, IPD, ISL, IAP)
UniSat-3	University of Rome	La Sapienza GAUSS	12	29.06.2004 (ops in 2008)	Technology demonstrations with solar cells
DSP-2	CNSA (Chi- na) / ESA	DFHSat Beijing	330	25.07.2004 (ops in 2008)	Study of magnetosphere in geospace

Mission	Sponsor	S/C contractor	Launch mass (kg)	Launch date (end mission)	Comments
PARASOL	CNES France	CNES	120	18.12.2004 (ops in 2008)	EO mission in A-Train of NASA
NanoSat-1	INTA Spain	INTA	19	18.12.2004 (ops in 2008)	Tech demo: OWLS (Optical Wireless Links for intra-Satellite) communications
INDEX (Reimei)	JAXA	JAXA	72	23.08.2005 (ops in 2007)	Tech demo, auroral emissions (EISA, MAC, CRM)
OICETS (Kirari)	JAXA	NEC Tokyo	570	23.08.2005 (16.10.2006)	Inter-orbit laser communication experiments
Monitor-E	KhSC Russia	KhSC	750	26.08.2005 (ops in 2007)	Imaging mission with Pan+MS imagery
CryoSat-1	ESA	EADS Astrium	670	08.10.2005	EO (SIRAL, DORIS, LRR) Launch failure
TopSat	QinetiQ, RAL, UK	SSTL	115	27.10.2005 (ops in 2008)	High resolution Pan + MS imagery
SSETI Express	ESA	European Universities	62	27.10.2005	Deployment of 3 CubeSats: UWE-1, NCube-2, XI-V
GIOVE-A	ESA	SSTL	602	28.12.2005 (ops in 2008)	First S/C of Galileo In-Orbit Validation, secured frequency
CUTE-1.7	Tokyo Inst. Technology	LSS	6	21.02.2006 (16.03.2006)	Technology demonstrations
FormoSat-3 (ROCSat-3, COSMIC)	NSPO UCAR	OSC	69 / S/C	15.04.2006 (ops in 2008)	6 S/C constellation Meteorology (IGOR, TIP, CERTO/TBB)
EROS-B	ImageSat Cyprus	IAI Israel	350	25.04.2006 (ops in 2008)	High resolution Pan imagery (commercial)
COMPASS-2	Roskosmos Russia	IZMIRAN Troitsk	85	26.05.2006 (July 2007)	Demonstration of topside sounding techniques
UniSat-4	University of Rome	La Sapienza GAUSS	10	26.07.2006	Technology experiments launch failure of Dnepr
KompSat-2 (Arirang-2)	KARI Korea	EADS Astrium	800	28.07.2006 (ops in 2008)	EO (MSC) high resolution Pan + MS imagery
Solar-B (Hinode)	JAXA NASA, SAO	MELCO	900	23.09.2006 (ops in 2008)	Solar physics mission of Japan, USA, & UK (SOT, XRT, EIS)
HIT-Sat	Hokkaido Institute of Technology	HIT Japan	3	23.09.2006	Technology demonstration
SAR-Lupe-1	BMVg Germany	OHB-System	770 / S/C	19.12.2006 (ops in 2008)	X-band SAR constellation (5 S/C) of the German Defense Ministry
CartoSat-2	ISRO, India	ISRO	680	10.01.2007 (ops in 2010)	High resolution Pan imagery
LAPAN-TUBSAT	LAPAN Indonesia	TU Berlin	56	10.01.2007 (ops in 2008)	Camera with 5 m resolution Camera with 200 m resolution
HY-1B	SOA Beijing	DFHSat (CAST)	360	11.04.2007	Survey of ocean resources
EgyptSat-1	NARSS Egypt	Yuzhnoye Ukraine	100	17.04.2007	High-resolution MS imager, + S&F communications
SAR-Lupe-2	BMVg Germany	OHB-System	770 / S/C	02.07.2007 (ops in 2008)	X-band SAR constellation (5 S/C) of the German Defense Ministry
TecSAR	MoD Israel	IAI/MBT Israel	300	21.01.2008	SAR payload (X-band) on a minisatellite
CanX-2	UTIAS/SFL Toronto	UTIAS/SFL	3.5	28.04.2008	Tech demo: NanoPS, CMOS/APS imager, Argus, GOE
Delfi-C3	TU Delft	TU Delft	3	28.04.2008	Triple CubeSat demo mission
Jason-2 (OSTM)	CNES/NASA	Thales Alenia Space (TAS)	553	20.06.2008	Altimetry (Poseidon-3, AMR, DORIS, TRSR-2, LRA)

Mission	Sponsor	S/C contractor	Launch mass (kg)	Launch date (end mission)	Comments
RapidEye	RapidEye Germany	MDA, SSTL	175 / S/C	29.08.2008	5 S/C constellation imaging mission (REIS)
THEOS	GISTDA Thailand	EADS Astrium	750	01.10.2008	High resolution Pan+MS im- agery
Chandrayaan	ISRO, India	ISRO	650	22.10.2008	Moon mission of ISRO
SDS-1	JAXA Japan	JAXA	100	23.01.2009	Technology demonstration mission
PRISM	University of Tokyo	ISSL (UT)	5	23.01.2009	Technology pathfinder: use of extensible boom optics system
SPRITESat	Tohoku University	Tohoku Uni- versity, Japan	50	23.01.2009	Monitoring of luminous emis- sions (sprites), in atmosphere
RazakSat (MACSat)	ATSB Malaysia	SI Korea/ ATSB	190	14.07.2009	High resolution Pan+ MS im- agery
DubaiSat-1	EIAST, Dubai	SI (Satrec Ini- tiative), Korea	< 200	29.07.2009	High-resolution imaging in Pan and MS
STSat-2	MOST Korea	KAIST SaTReC	< 100	25.08.2009	Science mission: first launch with Korean-built launcher. Unfortunately a failure oc- curred
ZASat-002	South Africa	SunSpace	82 kg	17.09.2009	SumbandilaSat with imager
Tatiana-2	Mosow State Univ.	VNIIEM	120 kg	17.09.2009	Science mission to observe TLE and NVU emissions
Sterkh-2		PO Polyot	171 kg	17.09.2009	COSPAS-S&RSAT mission
UGATUSat	UGATU	PO Polyot	30 kg	17.09.2009	University microsatellite
OceanSat-2	ISRO, India	ISRO	950	23.09.2009	Ocean surface physics (color, winds, etc.) & atmosphere
SMOS	ESA	Alcatel Alenia Space	670	02.11.2009	Tech demo in soil moisture & ocean salinity (MIRAS)
PROBA-2	ESA	QinetiQ/Ver- haert Belgium	130	02.11.2009	Science payload for sun moni- toring (SWAP, LYRA, TPMU, DSLP), tech. demos
SERVIS-2	NEDO, METI	USEF Japan	740	02.06.2010	Tech demo/validation of COTS components
CryoSat-2	ESA	EADS Astrium	670	08.04.2010	EO (SIRAL, DORIS, LRR)
Picard	CNES	CNES	155	15.06.2010	Monitoring of solar diameter
PRISMA (2 S/C)	SNSB Sweden	SSC	150 50	15.06.2010	GNC demonstrations: auton- omous formation, rendez- vous, proximity operations
AlSat-2A	ASAL, Algeria	EADS Astrium	116	12.07.2010	High resolution Pan + MS imagery
X-Sat	NTU Singapore	DSO Singapore	120	20.04.2011	EO, Iris, PPU
YouthSat	ISRO		92 kg	20.04.2011	Hyperspectral imager
RASAT	Government Turkey	TUBITAK- Uzay	113	17.08.2011	First imaging mission devel- oped in Turkey
Chibis-M	Roskosmos Russia	IKI	40	02.11.2011	Monitoring of transient events TLEs and TGFs
ALMASat-1	U. of Bolo- gna, Italy	U. of Bologna	25	13.02.2012	Technology demonstration
CASSIOPE	CSA Canada	MDA, Bristol Aerospace	500	29.09.2013	Ionospheric research (ePOP), Mail delivery service (CX)
Swarm	ESA	EADS Astrium	500 / S/C	22.11.2013	Constellation of 3 S/C to sur- vey the geomagnetic field
ASNARO	NEC, USEF Japan	NEC	450	2014	High resolution imaging mis- sion in VNIR
PRISMA	ASI Italy	Carlo Gavazzi Space	560 kg	2014	Hyperspectral imaging mis- sion in VNIR & SWIR

Mission	Sponsor	S/C contractor	Launch mass (kg)	Launch date (end mission)	Comments
Flying Lap-top	University of Stuttgart	IRS	< 100	2014	Technology demonstration, EO (MICS, TICS)
VEN μ S	ISA, CNES Israel, France	IAI/MBT Israel	~ 260 kg	2014	High resolution imaging mission in VNIR
TARANIS	CNES France	CNES	152	2015	Study of transient event energetic mechanisms (transient luminous emissions)
Microscope	CNES/ESA	CNES/ ONERA	200	2016	Test of equivalence principle, SAGE, DFACS
EnMAP	DLR, GFZ Germany	OHB System	850	2017	Hyperspectral imaging mission (VNIR, SWIR)

Table 101: Small satellites of rest of the world (chronological order of missions)

Major development of smallsat programs, aside from SSTL, are provided by the following institutions/companies:

- The Institute of Aeronautics and Astronautics (ILR) at the Technical University of Berlin (TUB), Germany, started with its TUBSAT program in 1985. A major objective was to explore technical capabilities in microsatellite design in particular in the field of attitude determination and space-related applications. The DLR-TUBSAT and subsequent missions introduced hibernation mode operations.

Satellite	Payload Class	S/C Mass	Launcher	Launch Date	Operational status
TUBSAT-A	S&F communications	35 kg	Ariane-4	17.07.1991	Ops as of 2007
TUBSAT-B	Earth observation	45 kg	Tsyklon	25.01.1994	Mission ended
TUBSAT-N, N1	S&F communications	8 kg, 3 kg	SHTIL	07.07.1998	Mission ended
DLR-TUBSAT	Earth observation	45 kg	PSLV	26.05.1999	Ops as of 2008
MAROC-TUBSAT	Earth observation	47 kg	Zenit	10.12.2001	Ops as of 2008
LAPAN-TUBSAT	Earth observation	56 kg	PSLV-C7	10.01.2007	Ops in 2008
BeeSat (CubeSat)	Technology test of "microwheels"	1 kg		23.09.2009	Ops in 2010
DST 8	DST (Dobson Space Telescope) test of foldable optics	1 kg		2008?	
DST 35		~ 70 kg		2010	
DST 50		~ 100 kg		2012	

Table 102: Overview of the TUBSAT program

- SSC (Swedish Space Corporation), Solna, Sweden.

Satellite	Observations	S/C Mass	Launch Date	Operational status
Viking	Interaction of solar wind with Earth's atmosphere	246 kg	22.02.1986	12.05.1987 (end)
Freja	Study of auroral phenomena in ionosphere, magnetosphere	256 kg	06.10.1992	
Astrid-1	Study of the Earth's near space plasma	27 kg	24.01.1995	Sept. 1995 (end)
Astrid-2	High-resolution E-field and B-field measurements in the auroral region	30 kg	10.12.1998	
Odin	Aeronomy/astronomy mission (SMR, OSIRIS)	250 kg	20.02.2001	ops in 2007
Smart-1	Moon mission of ESA using electric propulsion (built by)	367 kg	23.09.2003	03.09.2006 (moon impact)
PRISMA	GNC demonstrations: autonomous formation, rendezvous, proximity operations	150 kg 50 kg	15.06.2010	

Table 103: Smallsat missions developed at SSC, Sweden

- KAIST and SaTReC (Satellite Technology Research Center) of Daejeon, Korea started with the development of their own smallsat programs in 1992 (after gaining their experience in a technology transfer program at SSTL, Surrey, UK – followed with the launch of KitSat–1 in 1991).
 - KitSat–2, developed by KAIST and SaTReC in Korea, was launched on Ariane-4 (along with PoSAT-1 and HealthSAT-2), September 26, 1993 as an auxiliary payload on the SPOT-3 launch from Kourou.
 - KitSat–3 (110 kg, launch 26.05.1999), developed by KAIST and SaTReC, carried MEIS (Multispectral Earth Imaging System) developed by SaTReC in cooperation with Stellenbosch University, South Africa. Mission operations were terminated in Dec. 2003 after 4 1/2 years of mission service (battery had reached a very low level). In addition, there were 4 other instruments onboard.
 - STSat–1 (106 kg, launch 27.09.2003), is a technology demonstration mission developed by KAIST and SaTReC (based on the KitSat series). The regular observation mission lasted until October 2005 – when some abnormal attitude behavior of the spacecraft was detected.
 - STSat–2 (~ 100 kg, launch Aug. 25, 2009, a launch failure occurred) is being developed by SaTReC. It carries a payload of: DREAM (Dual–channel Radiometers for Earth and Atmosphere Monitoring), LRA (Laser Retroreflector Array), DHST (Dual Head Star Tracker), PPT (Pulsed Plasma Thruster), and FDSS (Fine Digital Sun Sensor), a technology demonstration experiment.

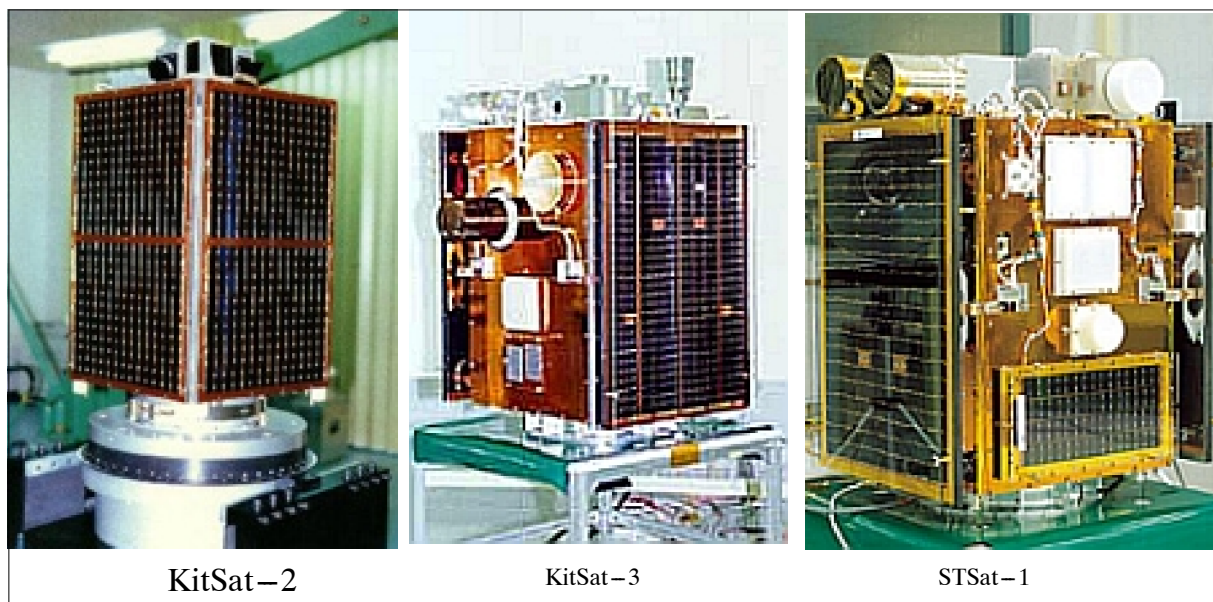


Figure 143: Illustration of small Korean satellites (image credit: SaTReC)

- CNES (French Space Agency) started with the development of a small satellite series family, called Myriade, in 1999. Satellite AIT (Assembly, Integration and Test) is performed by CNES or French industry. There is a partnership between CNES, Thales Alenia Space (TAS, formerly Alcatel Alenia Space), and EADS/Astrium SAS.. The partnership agreement permits TAS and EADS to use the Myriade bus design and products for their own applications/missions.

Satellite	Observations	S/C Mass	Launch Date	Operational status
DEMETER	Geophysical parameters	129 kg	29.06.2004	Ops as of 2010
PARASOL	EO mission in A-Train of NASA	120 kg	18.12.2004	Ops as of 2010
Picard	Monitoring of solar diameter	155 kg	15.06.2010	
AlSat-2A	High resolution imaging S/C of Algeria built by EADS Astrium. Astrium calls its Myriade bus version AstroSat-100	116 kg	12.07.2010	
Microscope	Test of equivalence principle	200 kg	2012	

Table 104: Some smallsats of the Myriade family of CNES

- SI (Satrec Initiative) of Daejeon, Korea was established in January, 2000 by former SaTReC engineers, Daejeon, Korea. SI is the developer of small satellites like: RazakSat, DubaiSat-1, DubaiSat-2, X-SAT, RASAT, etc. SI is the developer of various optical imaging instruments. In 2012, SI was appointed as the exclusive global data distributor of KOMPSAT imagery (KOMPSAT-2, KOMPSAT-3, and KOMPSAT-5).¹⁹¹³⁾

¹⁹¹³⁾ http://www.satreci.com/eng/ds1_1.html?tno=5#a32

1.19.6 University/Student–Developed Satellites & Payloads

During the 1990s, satellite and payload development projects became the program of choice for challenging (multi–year) training courses in quite a few engineering departments at universities throughout the world. The intent was (and is) always to enrich the student training program, to stimulate interest in a problem–solving multi–disciplinary technical environment, to be imaginative and resourceful, and to take some risks – with ample and essential help from mentors and partners (industry, institutional, or otherwise). Cooperation on many levels and active participation/publication within the international space science community are important ingredients in the overall objectives of research and development. In some instances, project–sharing among engineering departments of several universities is being practiced in order to handle the demanding and complex project goals in a certain time frame. In general, a good amount of enthusiasm and lots of volunteer work by all parties involved are needed to bring such low–cost program activities to maturity – an invaluable amount of professionalism is gained for all students in such programs.

The luxury of failure: The advantages universities bring to spacecraft development can be summed in one word: failure. Students have the “luxury” to fail (i.e., failure is an option), something that most in professional space industry must avoid. In fact, failing and learning from failure are some of the most important parts of a student’s education. Students in a university setting are encouraged to seek out innovative (and therefore often risky) approaches to solving problems. By taking risks and comparing their results with standard methods, the students gain insight into the underlying phenomena and have a better appreciation for accepted practice.¹⁹¹⁴⁾

One of the most difficult problems of small satellite building is to get a launch opportunity as a secondary payload with some primary payload. Many things have to be considered for such a piggyback flight, including the orbit, the price tag, and in particular the long waiting periods.

The following table provides an (incomplete) overview of small satellite missions over the last 2 1/2 decades launched by various universities.

Spacecraft	Launch	Comments
UoSat–1 (University of Surrey), UK	06.10.1981	First microsatellite of CSER (Center of Satellite Engineering) of the University of Surrey, mass of 52 kg (Oscar–9), various beacons in VHF, UHF & microwave, S–band telemetry, onboard camera with one of the earliest CCD detectors providing snapshot imagery of 2 km resolution
UoSat–2 (University of Surrey), UK	01.03.1984	Technology demonstration mission: First digital S&F (Store & Forward) mission using the PACSAT protocol suite, 1200 baud AFSK, 128 kByte memory. Amateur radio service (Oscar–11), imaging camera
NUSAT (Weber State College), Ogden, UT, USA	29.04.1985	Northern Utah Satellite, mass of 54 kg, NUSAT was deployed from a GAS canister on Shuttle (STS–51B). NUSAT–1 was designed to study high–altitude radar field patterns for FAA (Federal Aviation Agency). After 595 days in orbit, NUSAT reentered on Dec. 15, 1986.
WeberSat (Weber State College), Ogden, UT, USA	21.01.1990	WeberSat is a joint project of CAST (Center for Aerospace Technology) at Weber State University with AMSAT–NA. AMSAT–NA asked CAST to participate in the fabrication of 4 microsatellites. For their contribution, CAST received ownership one of the 4 microsatellites which was named WeberSat. Payload: color video camera, visual light spectrometer, micrometeorite impact detector.
TUBSAT–A (Technical University Berlin)	17.07.1991	S/C mass of 35 kg, the objectives are to study S&F techniques and to test an attitude control system, TUBSAT–A is fully operational as of 2007 (15 years)
TUBSAT–B (Berlin, Germany)	25.01.1994	S/C mass of 45 kg, Payload: a video camera system in the VNIR spectral range capable of taking snapshots of the ground. Contact was lost on 05.03.1994 after 39 days of successful operations.

1914) M. A. Swartwout, “The Role of Universities in Small Satellite Research,” Aug. 1997, URL: <http://ssdl.stanford.edu/ssdl/images/stories/papers/1997/ssdl9705.pdf>

Spacecraft	Launch	Comments
BremSat-1 (University of Bremen)	09.02.1994 (STS-60)	S/C mass of 63 kg (spin stabilized), deployed from Shuttle; payload of 6 experiments; the S/C was operated for over a year
SURFSat (Cal-Tech, Pasadena, CA + others)	04.11.1995	S/C mass of 55 kg, The satellite is designed to mimic signals from planetary S/C, and radiates milliwatt level RF signals in X-, Ku-, & Ka-band. The signals support research and development experiments supporting future implementation of Ka-band communications. Test for NASA's Deep Space Network.
Sputnik-II (France & Russia)	03.11.1997	S/C mass of 3 kg (1/3 scale), a commemorative functioning replica of the original Sputnik (40th anniversary), deployed from MIR station, decay in atmosphere on 21.05.1998
TUBSAT-N/N1	07.07.1998	Tandem launch July 7, 1998 on a Russian SS-N-23 military launch vehicle from the Barents Sea. S/C mass of 8.5 kg and 3 kg, respectively. Use of UHF/VHF communications to collect sensor data from the ground segment. TUBSAT-N1 reentered on 20.10.2000, TUBSAT-N reentered on 22.04.2002 - due to low perigees
TechSat/Gurwin-II (Technion, Israel)	10.07.1998	S/C mass of 48 kg (3-axis stabilized), design life of 1 year. Payload: OM-2 (Ozone Meter-2), ERIP (Earth Remote-Sensing Imaging Package) a CCD video camera with image size of 52 km and 52 m resolution, SOREQ (Single Event Monitor for Detecting Protons and Heavy Ions in Space), SUPLEX (Superconductivity Experiment), XDEX (X-ray Detector Experiment), SLRRE (Satellite Laser Ranging Retroreflector Experiment), TechSat/Gurwin-II is operating nominally as of 2007.
SEDSat-1 (University of Alabama)	24.10.1998	S/C mass of 36 kg, technology demonstration, payload: digital video camera with a PAL system pointed at horizon (used for attitude determination), telephoto camera pointed to nadir
PanSat (Naval Postgraduate School) Monterey	29.10.1998 (STS-95)	S/C mass of 57 kg, demonstration of digital communications using direct-sequence spread-spectrum and store-and-forward packet radio technology. Status: the S/C operated for more than 3 years.
SUNSAT (Stellenbosch University, South Africa)	23.02.1999	S/C mass of 64 kg, tray-based design, gravity-gradient boom and 3-axis stabilized, payload: HRI (High Resolution Imager) with 15 m resolution on a swath of 51 km. TRSR (TurboRogue Space Receiver) of JPL, MIS (Meteoroid Impact Sensor) + LRR of NASA, Last contact after on 19.01.2001 after nearly 2 years of operations.
TERRIERS (Boston University + others)	18.05.1999	S/C mass of 122 kg, The primary goal was to obtain individual 2-D (altitude-latitude) profiles of ionospheric electron density using EUV (Extreme Ultraviolet), visible and radio instruments. After orbit injection the TERRIERS S/C failed to orientate itself to allow the solar panels to work fully and its battery lost power after launch. Failure.
DLR-TUBSAT (TUB+DLR)	26.05.1999	S/C mass of 45 kg, test of an attitude control system which permits hibernation during inactivity periods, most of the time the S/C is in hibernation mode to save power, in case of an event the attitude is resort within a few minutes. A commercial camera provides video imagery. The S/C is operational as of 2007.
STARSHINE-1 (NRL/NCST)	27.05.1999 (STS-96)	S/C mass of 39 kg, students built hundreds of tiny mirrors which covered the outer surface of the sphere of 47.5 cm. The twinkling satellite was visible to the naked eye against the star background. Reentry on 19.02.2000.
ASUSat-1, (ASU, Tempe, AZ, USA)	27.01.2000	S/C mass of 5.9 kg, power of 8.14 W; multiple launch as a secondary payload to JAWSAT, OPAL, FalconSat-1 and OSCE) on a Minotaur vehicle; Status: only a very short period of telemetry data could be received from ASUSat-1 after deployment
FalconSat-1 (USFAA Colorado)	27.01.2000	S/C mass of 50 kg; secondary payload on JAWSAT, the FalconSat-1 S/C failed soon after deployment, apparently due to a power failure
UniSat-1 (University of Rome, Italy)	26.09.2000	S/C mass of 12 kg, a technology demonstration satellite of GAUSS (Gruppo di Astrodinamica dell' Universita degli Studi "la Sapienza")
PCSat (USNA, Annapolis, MD)	30.09.2001	S/C mass of 11 kg (launch from Kodiak, AK), demonstration of mobile vehicle tracking and communications for GPS-equipped remote travelers. It uses the APRS (Automatic Position Reporting System) protocols of AMSAT.

Spacecraft	Launch	Comments
SAPPHIRE (Stanford University)	30.09.2001	S/C mass of 19.6 kg (launch from Kodiak, AK), payload of THD (Tunneling Horizon Detector), Digital Camera, Voice Synthesizer, Telemetry Experiment
STARSHINE-3	30.09.2001	S/C mass of 91 kg, sphere of 94 cm (launch from Kodiak, AK), covered with 1500 student-polished mirrors plus 20 laser retroreflectors,
STARSHINE-2 (NRL, Washington)	05.12.2001 (STS-108)	Same mass and size as STARSHINE-1, The 846 mirrors that cover the outside surface of this S/C have been polished by students in 26 countries. Reentry of S/C on May 5, 2002
Maroc-TUBSAT (TUB+CRTS, Morocco)	10.12.2001	S/C mass of 47 kg, Payload: EIC (Earth Imaging Camera) of RAL. The FOV is $\pm 8.5^\circ \times \pm 8^\circ$, providing an image size of about 190 km x 144 km at a resolution of 250 m (snapshot imagery). Maroc-TUBSAT is operational as of 2007.
UniSat-2 (University of Rome, Italy)	20.12.2002	S/C mass of 10 kg (multiple S/C launch on Dnepr-1 vehicle), the objective of this mission is to develop, and demonstrate an onboard micro-propulsion system, CGM (Cold Gas Microthruster). A variable thrust of up to 560 μN is generated. CGM has a total mass of 0.835 kg.
UniSat-3 (University of Rome, Italy)	29.06.2004	S/C mass of 12 kg, (multiple S/C launch on Dnepr-1 vehicle), UniSat-3 is operational as of 2007 (3 years after launch). Payload: technology experiments (solar cell, magnetometer, etc.)
FalconSat-2 (USAFA Colorado)	24.03.2006	S/C mass of 19.5 kg, a launch failure on Falcon-1 (SpaceX) was experienced, the S/C was 3-axis stabilized combination of solar-pressure spin tapes and hysteresis rods, communications in S-band and VHF
UniSat-4 (University of Rome, Italy)	26.07.2006	S/C mass of 10 kg (multiple S/C launch on Dnepr-1 vehicle). A launch failure occurred after 2 minutes of flight representing a great setback and disappointment to all institutions involved (22 small satellites). - UniSat-4 payload: MPPT (Maximum Peak Power Tracking), COTS cameras, GPS receiver, magnetometers, SIRDARIA (Spacecraft Integrated Reentry Device Aero Resistant Increasing Area), TPS,
LAPAN-TUBSAT TUB+LAPAN (Indonesia)	10.01.2007	S/C mass of 56 kg, Payload: commercial high-resolution video camera with a detector of 752 x 582 pixels. The spatial ground resolution is 5 m on a swath width of 3.5 km. A second wide-angle CCD video camera has a resolution of 200 m on a swath of 81 km. Interactive S/C pointing for event monitoring.
FalconSat-3 (USAFA Colorado)	09.03.2007	S/C mass of 54 kg, multiple launch on STP-1 flight; demonstration of boom deployment technology; payload: MPACS (Micro Propulsion Attitude Control System), FLAPS (Flat Plasma Spectrometer), and PLANE (Plasma Local Anomalous Noise Environment)
PRISM (ISSL, University of Tokyo)	23.01.2009	PRISM (Picosatellite for Remote-sensing and Innovative Space Missions) S/C mass of 5 kg (3-axis stabilized), An extensible boom concept is being used in the optics system to provide sufficient focal length for the imaging task.
Flying Laptop (University of Stuttgart, IRS, Germany)	2013	S/C mass of ~ 100 kg with the objective to demonstrate and qualify new small-satellite technologies for future projects. 3-axis stabilization (micro star tracker) for high-accuracy pointing. Use of an FPGA-based OBC. Payload: MICS (Multispectral Imaging Camera System), TICS (Thermal Infrared Camera System), BRDF (Bi-directional Reflectance Distribution Function) measurements; Demonstration of precipitation measurements in Ka-band, etc. Panoramic camera to provide context color video imagery of Earth.

Table 105: Overview of small satellites developed by universities (chronological order)

1.19.7 CubeSats

CubeSats – represent a first attempt to standardize the bus structure and deployment of picosatellites for low-cost experiments and applications (see N.37), in particular for student-built satellites at universities. CubeSat is the name given a cube-shaped **picosatellite design** of 10 cm side length and a mass of ≤ 1 kg. ^{1915) 1916) 1917) 1918)}

The CubeSat idea, concept and program began in 1999 at SSDL (Space Systems Development Laboratory) of Stanford University under the leadership of Robert J. Twiggs. The overall objective of the CubeSat program is to provide an effective framework (including specifications and guidelines) for the design, construction and launch of picosatellites. All CubeSats feature a standard form factor and share launches by using standard launch tubes, referred to as P-PODs (Poly Picosatellite Orbital Deployers), provided by the Stanford/CalPoly CubeSat program.

In the meantime (starting in 2006) the CubeSat volume has been enlarged into one direction (length) by doubling (2U) or tripling (3U) the original unit size of 10 cm. Hence the 2U (2 unit) CubeSat form factor has a nominal size of 10 cm x 10 cm x 20 cm and a mass of 2 kg, while the 3U version has a size of 10 cm x 10 cm x 30 cm with a mass of 3 kg. – From a launch perspective, coexistence of the three options (1U, 2U, 3U) of CubeSats are possible because each P-POD deployer system can nominally accommodate either 3 (1U) CubeSats (stacked one behind the other), or a load of 1U+2U CubeSats, or a single 3U CubeSat.

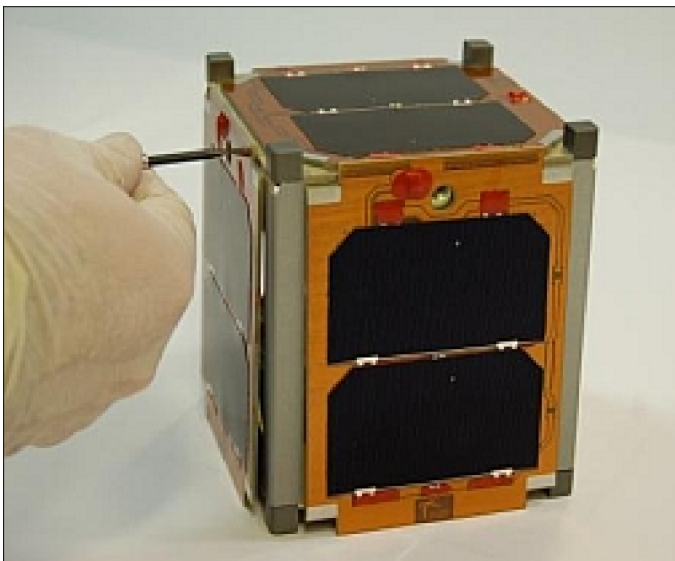


Figure 144: Illustration of a 1U CubeSat

The 2U and 3U form factor CubeSats, which are now **nanosatellites** on account of their increased mass ($1 \text{ kg} \leq \text{nanosatellite} \leq 10 \text{ kg}$), offer of course the double or triple volume for the spacecraft designer/developer – leading to a better integration of instruments and spacecraft subsystems. In particular, a better chance for a tiny 3-axis attitude control system is given. And proper attitude knowledge is a prerequisite for any imaging mission as well as many science missions.

1915) Note: Stanford University and California Polytechnic State University in San Luis Obispo, CA (referred to as CalPoly) have combined efforts to develop a means of launching small standard picosatellites called CubeSats.

1916) F. M. Pranajaya, R. E. Zee, P. Lundahl Thomsen, M. Blanke, R. Wisniewski, L. Franklin, J. Puig – Suari, “An Affordable, Low – Risk Approach to Launching Research Spacecraft as Tertiary Payloads,” Proceedings of AIAA/USU Conference on Small Satellites, Logan, UT, Aug. 11 – 14, 2003, SSC03 – VI – 1

1917) Francois Visser, “CubeSats – An Introduction,” URL: http://www.space.gov.za/eee5024f/presentations/Visser_CubeSats.pdf

1918) Kirk Woellert, “The value of CubeSats to national innovation systems,” UN – ISU SSP 2011 TP Small Satellites TP2, URL: <http://www.oosa.unvienna.org/pdf/bst/ISU-SSP2011/TP2KirkWoellert.pdf>

- The first CubeSat mission, involving half a dozen picosatellites as secondary payloads, took place on June 30, 2003 on a Rockot KS vehicle of Eurockot from Plesetsk, Russia. The CubeSat S/C are: XI (University of Tokyo), CUTE–I (Tokyo Institute of Technology), CanX–1 of UTIAS/SFL (University of Toronto Institute for Aerospace Studies/ Space Flight Laboratory), AAUSat (Aalborg University of Denmark), [Note: AAUSat is also referred to as AAU–CubeSat], DTUSat (Technical University of Denmark), QuakeSat (Stanford University, Stanford, CA).
- The second multiple spacecraft launch, involving 3 CubeSats (UWE–1, XI–V, and nCube–2), was released/deployed from SSETI–Express, a microsatellite of European students, and itself a secondary payload on a multiple S/C mission. The launch of this S/C mission took place on Oct. 27, 2005 (Cosmos–3M launch vehicle of AKO Polyot from the Plesetsk Cosmodrome, Russia) involving the following S/C: TopSat of QinetiQ (UK), and China–DMC+4 (Beijing–1) of SSTL (UK) as primary payloads. – The other secondary payloads on this multi–satellite flight were: SSETI Express (European Students), Mozhayets 5 (Russia), Sinah–1 (Iran), and Rubin–5 (OHB, Bremen, Germany).
- On July 26, 2006, a launch of multiple smallsats on a Dnepr–1 launch vehicle from Baikonur, Kazakhstan (launch provider: ISC Kosmotras), **ended in a total launch failure after about 2 minutes of flight.** The following CubeSats were on this flight: ION (University of Illinois), Sacred (University of Arizona), KUTESat (Kansas University), ICEcube–1, –2 (Cornell University), Rincon (University of Arizona), SEEDS–1 (Nihon University), HAUSat–1 (Hankuk Aviation University), nCube–1 (Norsk Romsenter), Merope (Montana St. University), AeroCube–1 (The Aerospace Corporation), PolySat–1, –2 (CalPoly), and Voyager (University of Hawaii); Additional smallsats on the flight were: Belka (RKK Energia) 250 kg, the first remote sensing satellite of Belarus, Baumanets (NPO Mash) 80 kg, UniSat–4 (University of Rome, Italy) 12 kg, and PicPot (University of Torino, Italy) 3 kg. **This launch failure represented a great setback and disappointment to all involved, in particular to the members of the 14 CubeSat projects.** All the work and effort of years from many student satellite teams from around the world was lost in a single instant. The launch failure was due to a malfunctioning hydraulic drive unit in a combustion chamber on the booster’s first stage. – Unfortunately, occasional launch failures are simply part of spaceflight – in spite of careful launch preparations. ¹⁹¹⁹⁾
- A single CubeSat, GeneSat–1 (a triple cube or 3U) of NASA/ARC was launched on Dec. 16, 2006 as a secondary payload to TacSat–2 of AFRL. The launch site was NASA’s Wallops Flight Facility, Wallops Island, VA, USA.
- On April 17, 2007, seven CubeSats were launched on a Dnepr vehicle from Baikonur, Kazakhstan (EgyptSat as primary payload). These were: PolySat–3 (CP–3) and PolySat–4 (CP–4) of CalPoly; AeroCube–2 of The Aerospace Corporation; CSTB1 (CubeSat TestBed 1) of the Boeing Company; CAPE–1 (Cajun Advanced Picosatellite Experiment 1) of the University of Louisiana; MAST (Multi–Application Survivable Tether) of Stanford and TUI; and Libertad–1 of the University of Sergio Arboleda, Columbia.
- On April 28, 2008, the PSLV launch vehicle of ISRO launched a total of ten satellites with CartoSat–2A as the primary payload. The secondary payloads on this flight were a microsatellite, IMS–1 (Indian Microsatellite–1) of ISRO as well as 8 nanosatellites. These were: CanX–2 of UTIAS/SFL, University of Toronto, Canada; AAUSat–2 of Aalborg University, Denmark; COMPASS–1 of the University of Applied Science, Aachen, Germany; Delfi–C3 of the Technical University of Delft, The Netherlands; SEEDS–2 of Nihon University, Tokyo, Japan; CUTE–1.7+APD–2 of of the Tokio Institue of Technology, Japan; NTS (Nanosatellite Tracking of Ships) of COM DEV / UTIAS/SFL, Toronto,

¹⁹¹⁹⁾ L. David, “Recent CubeSat Losses Spur Renewed Development,” Space News, Sep. 4, 2006, p. 14

Canada; and Rubin–8–AIS, an experimental space technology mission of OHB–System, Bremen, Germany.

– The TacSat–3 spacecraft of AFRL was launched on May 19, 2009 on a Minotaur–1 vehicle of OSC (Orbital Sciences Corporation) from the commercial MARS (Mid–Atlantic Regional Spaceport) facility at Wallops Island, VA, USA. Secondary payloads on this flight were the CubeSats: PharmaSat–1 (~ 5 kg) a nanosat of NASA/ARC, AeroCube–3 of the Aerospace Corporation of El Segundo, CA, HawkSat–1 of the Hawk Institute for Space Sciences (HISS), Pocomoke City, MD, and CP–6 (CalPoly–6) of California Polytechnic State University, San Luis Obispo, CA.

– On Sept. 23, 2009, the PSLV launch vehicle of ISRO launched a total of 7 satellites, OceanSat–2 (960 kg) being the primary payload. The secondary payloads on this flight were 4 CubeSats (BeeSat, ITUpSat–1, SwissCube–1, UWE–2) and 2 nanosatellites (Rubin–9.1 and Rubin–9.2) of OHB Bremen with AIS receivers.

• CubeSat Kit: As of 2004, Pumpkin Inc. of San Francisco, CA is providing a CubeSat Kit™, consisting of hardware, software and software tools, combined with other third–party development tools, is a turnkey solution for developing CubeSat satellites. ^{1920) 1921)}

The professional service, such as a CubeSat structure, is considered a good entry for university teams into their own design projects. Several CubeSat projects have used this option:

– MAST (Multi–Application Survivable Tether), a 3U CubeSat of Stanford University and TUI (Tethers Unlimited Inc.); Launch April 17, 2007

– Libertad–1, a 1U CubeSat of the University of Sergio Arboleda, Columbia. Launch April 17, 2007

– Delfi–C3, a 3U CubeSat of Delft University of Technology, Delft, The Netherlands. Launch April 28, 2008

– HawkSat–1 of HISS (Hawk Institute for Space Sciences), Pocomoke City, MD, USA; Launch May 19, 2009.

Launch date	Launch vehicle	Nr of CubeSats	1U (single cube)	2U (double cube)	3U (triple cube)
30.06.2003	Rockot	6	5	0	1
27.10.2005	Cosmos–3M	3	3	0	0
21.02.2206	M–V–8	1	0	1	0
26.07.2006	Dnepr–1 (launch failure)	14	13	1	0
16.12.2006	Minotaur	1	0	0	1
17.04.2007	Dnepr–1	7	6	0	1
28.04.2008	PSLV–C9	6	3	1	2
03.08.2008	Falcon–1 (launch failure)	2	0	0	2
19.05.2009	Minotaur	4	3	0	1
23.09.2009	PSLV–C14	4	4	0	0
20.05.2010	H–IIA	3	3	0	0
12.07.2010	PSLV–C15	1	1	0	0

Table 106: Overview of some CubeSat launches ¹⁹²²⁾

• Most existing lightsats (or “litesats”), in particular nanosatellites, feature one of two types of primary bus structures: 1) a load–bearing shell structure, or 2) a stack of compo-

1920) <http://www.pumpkininc.com/content/doc/brief/npb-1.pdf>

1921) <http://www.cubesatkit.com/>

1922) Bryan E. Bingham, Quinn Young, “The Road to a Three–Axis Stabilized CubeSat,” Proceedings of the 32nd AAS Guidance and Control Conference, Breckenridge, CO, USA, Jan. 31.– Feb. 4, 2009, AAS 09–086

ment trays with stiffeners. The designs use either a sandwich construction, stiffened plates, or thin-walled trays (also referred to as cast design). The materials chosen are either fiber-reinforced composites or aluminum as primary structures. Sandwich structures are usually composed of two face sheets bonded to a core.¹⁹²³⁾ The most common core type material is aluminum honeycomb, constructed of bonded strips of aluminum foil which are expanded to create hexagonal cells. Both metals and fiber-reinforced composites can be used in honeycomb panels.

In the early 21st century, the sandwich design approach seems to be the most efficient S/C structure design technique, offering compact and modular choices with minimal mass. On the other hand, the cast structure design approach seems to be particularly suitable for mass production of nanosatellites that are needed for larger constellations. The cast design is based on different modules attached to the main structure. Some advantages of the cast or tray structure are: modular design, flexibility, each assembly can be handled independently, minimum assembly time, less number of parts.

On a historical note: The very limited space available inside and outside of a standard 1U CubeSat and the availability of $\sim 1-2$ W of power on average, has naturally provided great challenges to all development teams in dealing with all the limitations. – The following items are considered recurrent problem areas for all developers, even in 2010, more than 10 years after the introduction of the CubeSat concept by Robert J. Twiggs.

- Low processing power
- Inaccurate pointing capability, in particular for imaging purposes
- Power consumption constraints
- Limited data downlink
- Poor support for interconnectivity
- Very few resources available for the payload.

Launch Date	Nanosatellite	Comment
03.11.1997	Sputnik-II, built by French students from the l'Aeroclub of France and staff from the Russian Aeronautical Federation	A S/C of only 3 kg deployed from the MIR space station (with VHF-FM beacon transmitter)
07.07.1998	TUBSAT-N and -N1 of TU Berlin, Germany	A dual underwater/space launch of data collection satellites
27.01.2000	ASUSat-1 (Arizona State University)	S/C mass of 5.9 kg (launch on JAWSAT)
28.06.2000	SNAP-1 of SSTL (UK) and an academic team of Surrey University	S/C mass of 6.5 kg. SNAP-1 was deployed from the Nadezhda mother ship.
26.09.2000	UniSat-1 of University of Rome, Italy	S/C mass of 12 kg (educational program)
21.11.2000	Munin of IRF Sweden (S/C mass of 6 kg)	Space science and space weather activity,
20.12.2002	UniSat-2 of University of Rome	S/C mass of 10 kg (educational program)
Launch Date	Picosatellite	Comment
27.01.2000	All picosats were ejected from OPAL of Stanford University (as mother ship) StenSat, of amateur enthusiasts Artemis, of Santa Clara University PICOSAT1.0, a tethered 2 S/C system from the Aerospace Corporation	No ground communication with StenSat No ground communication with Artemis Communication established with ground and in crosslink

1923) B. Shirgur, D. Shannon, "The Design and Feasibility Study of Nanosatellite Structures for Current and Future FSI Micro-missions," 14th Annual AIAA/USU Conference on Small Satellites, Logan, UT, Aug. 21-24, 2000, SSC00-VII-5

Launch Date	Nanosatellite	Comment
19.07.2000	PICOSAT1.1, a tethered system from the Aerospace Corporation was launched and flown on MightySat II.1 (as mother ship)	Each PICOSAT has a mass of 0.275 kg. The system was ejected successfully from MightySat II.1 13 months after launch.
06.12.2002	Release of MEPSI (MEMS–based PICO-SAT Inspector), 2 tethered picosats of AFRL from STS–113	Each picosat has a mass of about 1 kg. Demonstration of a launch system and communication with ground station.

Table 107: Chronology of early nanosatellite and picosatellite launches

• *In the timeframe 2008/2010, payload developers around the world are becoming increasingly aware of the potential benefits that very small spacecraft, such as CubeSats, can offer for fast turn–around, low–cost missions.* ¹⁹²⁴⁾ ¹⁹²⁵⁾ *This increased interest in CubeSats for commercial, military and scientific missions is resulting in some exciting and challenging applications for this miniature satellite platform. The challenges include the ability to realize fine attitude control, the need to overcome the physical challenge of payload accommodation, but most consistently, is the capacity to generate and store enough power on–board the spacecraft to fulfill the mission requirements.*

In particular, the 2U and 3U form factor CubeSat versions (nanosatellites) are being considered as popular candidates for a number of challenging payload missions of the prospective CubeSat user community. The power generation capability on the most popular CubeSat platform size, the 3U, can be significantly improved through the use of deployed solar panels (achieving power level of up to ~ 10 W). The technology is available for these CubeSat upgrades. The increased volume and power generation of these form factors provide in turn the capability for better processing, pointing control (3–axis stabilization), and higher rate communications, all of which are necessary functions for relevant scientific or military missions. In addition, the 3U CubeSats, equipped with deployable solar arrays, antennas and cold gas propulsion systems – can take advantage of the full volume of the standard P–POD deployer system.

As a consequence of these maturing technical CubeSat capabilities, and the realization of the potential operational usefulness of CubeSat constellations, some interesting developments are taking place in the CubeSat scene:

– PEARL, an initiative for an advanced CubeSat bus standard, is being developed by SDL (Space Dynamics Laboratory) of USU (Utah State University) and funded by AFRL (Air Force Research Laboratory) at Kirtland AFB, NM. The PEARL bus is focused in particular on the 3U CubeSat form factor which incorporates the top–of–the–line in CubeSat subsystem technologies. The bus features four deployable solar arrays as well as four fixed, body–mounted panels. SDL has developed mini–reaction wheels for pointing that take up only 0.5U. In conjunction with the miniature reaction wheels is a miniature sun–sensor which has a targeted accuracy of 0.01°. The avionics chassis takes up 1.5U which leaves 1U available for the CubeSat payload. The goal of the PEARL initiative is to migrate eventually to an all space–grade components capability. ¹⁹²⁶⁾ ¹⁹²⁷⁾ ¹⁹²⁸⁾

– Coral (just a name / not an acronym) is a subsequent 3U CubeSat bus initiative to PEARL which is being developed in partnership by Comtech AeroAstro Corporation and

¹⁹²⁴⁾ Craig Clark, “Huge Power Demand...Itsy–Bitsy Satellite: Solving the CubeSat Power Paradox,” Proceedings of the 24th Annual AIAA/USU Conference on Small Satellites, Logan, UT, USA, Aug. 9–12, 2010, SSC10–III–5

¹⁹²⁵⁾ Kirk Woellert, Pascale Ehrenfreund, Antonio J. Ricco, Henry Hertzfeld, “CubeSats: Cost–effective science and technology platforms for emerging and developing nations,” Advances in Space Research, Vol. 47, 2011, pp. 663–684, URL: http://www.gwu.edu/~spi/assets/docs/Woellert_cubesats.pdf

¹⁹²⁶⁾ “PEARL (Picosatellite Exo–Atmospheric Research Laboratory) Fact Sheet of SDL, URL: <http://www.sdl.usu.edu/programs/pearl.pdf>

¹⁹²⁷⁾ Quinn Young, Robert Burt, Mike Watson, Lorin Zollinger, “PEARL CubeSat Bus Building Toward Operational Missions,” CubeSat Summer Workshop –8–9 August 2009, URL: http://mstl.atl.calpoly.edu/~jfoley/Summer2009/Sat_1245_PEARL_Young_Final.pdf

¹⁹²⁸⁾ Charlie L. Galliard, “Study of the Small: Potential for Operational Military Use of CubeSats,” Proceedings of the 24th Annual AIAA/USU Conference on Small Satellites, Logan, UT, USA, Aug. 9–12, 2010, SSC10–III–2

SDL (Space Dynamics Laboratory) of USU. The name “Coral” was given to this project to differentiate between the two busses. ¹⁹²⁹⁾

– QB50 CubeSat constellation: QB50 is an international cooperative CubeSat initiative of the VKI (Von Karman Institute for Fluid Dynamics) in Brussels, Belgium which started in 2009. The initiative aims at launching a network of 50 CubeSats to orbit in the lower thermosphere region for three months and perform in-situ measurements. The QB50 project has the scientific objective of studying multi-point in-situ the temporal and spatial variations of a number of key parameters in the lower thermosphere (between 330 and 90 km altitude) with a network of about 50 CubeSats, separated by a few hundred km, all spacecraft are carrying an identical sensor complement.

The QB50 project uses the 2U form factor of CubeSats; it has support from NASA and ESA. A total of 36 CubeSats are envisaged to be provided by European universities in 21 countries, 10 by universities in the U.S., two by universities in Canada and two by Japanese universities. A launch of the QB50 constellation is planned for June 2013. The QB50 project is quite an endeavor, and if successful; it will prove the increased utility of flying multiple CubeSats over a single CubeSat and help demonstrate that CubeSats aren't just “anything more than toys” or “some form of space debris”. ^{1930) 1931)}

– In February 2010, the US NRO (National Reconnaissance Office)¹⁹³²⁾ contracted with Boeing Phantom Works division (HQ in St. Louis, Missouri) for as many as 50 triple-unit (3U) Cubesats for use in technology demonstrations. The current (2010) NRO Colony program is set to build 10 CubeSats/year. ¹⁹³³⁾

This is a good indication of the state of maturity and potential that the CubeSat development has gained within the last decade. The inexpensive satellite platforms will be used for the follow-on to an NRO research program called “Colony”, a space weather nanosatellite constellation, managed by NRL.

The first two space weather Colony-I demonstration 3U CubeSats, also known as the QbX-1 and QbX-2 (CubeSat Experiment-1 and -2), were launched on Dec. 8, 2010. Both CubeSats featured the MAI-100 (Maryland Aerospace Inc.-100), a 3-axis ADCS (Attitude Determination and Control Subsystem) with a mass of 0.865 kg. The pointing systems performed flawlessly for 29 and 39 days, respectively, before reentering Earth's atmosphere in January 2011. – The primary payload on the flight was the Dragon C1 spacecraft module developed by SpaceX (launch vehicle: Falcon-9) and sponsored by NASA's COTS (Commercial Orbital Transportation Services) program. ^{1934) 1935)}

NRO is planning two separate multiple CubeSat missions: Colony-I and Colony-II. These missions are set up to leverage multiple CubeSats which will carry various SEM

1929) Steven W. Schenk, Robert Burt, “Coral: A High Performance Design Expanding CubeSat Mission Options,” Proceedings of the 24th Annual AIAA/USU Conference on Small Satellites, Logan, UT, USA, Aug. 9–12, 2010, SSC10–III–4

1930) Jean Muylaert, Ruedeger Reinhard, Cem Ozan Asma, “QB50: An International Network of 50 CubeSats for Multi-Point, In-Situ Measurements in the Lower Thermosphere and Re-Entry Research,” Proceedings of the Symposium on Small Satellite Systems and Services (4S), Funchal, Madeira, Portugal, May 31–June 4, 2010

1931) J. Muylaert, R. Reinhard, C. Asma, “QB50 An international network of 50 double CubeSats for multi-point, in-situ, long-duration measurements in the lower thermosphere and for re-entry research,” Proceedings of the 7th Annual CubeSat Developers' Workshop, CalPoly, San Luis Obispo, CA, USA, April 21–23, 2010, URL: http://cubesat.calpoly.edu/images/cubesat/presentations/DevelopersWorkshop2010/2_1020_qb50_vki_muylaert_apr2010_calpoly.pdf

1932) Turner Brinton, “NRO Taps Boeing for Next Batch of Cubesats,” April 12, 2010, p. 16, URL: <http://www.space-news.com/military/100408-nro-taps-boeing-next-cubesats.html>

1933) Daniel Edwards, “NRO Weather Colony Program,” Space Sentinel, Vol. 2, No 2, 2010, URL: http://www.nro.gov/spacesentinel/Unclassified_SS_-_Weather_Colony_-_single.pdf

1934) David Shultz, Rebecca Unruh, David Williamson, John Anttonen, “Colony: A New Business Model for Research and Development,” Proceedings of the 24th Annual AIAA/USU Conference on Small Satellites, Logan, UT, USA, Aug. 9–12, 2010, SSC10–IV–2

1935) Andrew E. Kalman, Robert S. Call, “Lessons Learned from the First Wave of Common-architecture CubeSats,” 8th Annual CubeSat Developers' Workshop, CalPoly, San Luis Obispo, CA, USA, April 20–22, 2011, URL: http://www.cubesat.org/images/2011_Spring_Workshop/thur_p3.00_kalman_pumpkin_csdwslo_2011.pdf

(Space Environmental Monitoring) payloads.¹⁹³⁶⁾ The idea is that a cluster of CubeSats with various sensors orbiting at the same time will build a more complete picture of the space weather environment. This is important to the NRO because the information gathered may be added to current space weather outage prediction models. These models, in turn, provide valuable data for the prediction of space weather events which may adversely impact the large national assets under control of the NRO. Although CubeSats are out of the normal purview of the NRO, the decision to pursue these missions shows that the NRO leadership has identified the great operational potential that they offer.

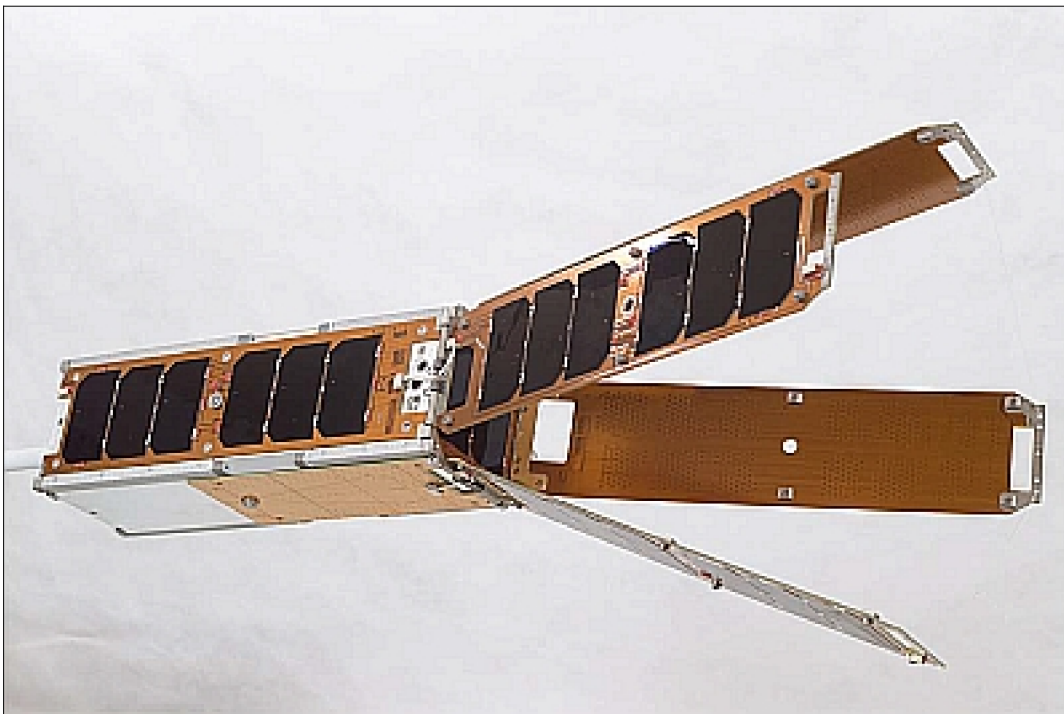


Figure 145: Illustration of a Colony–I nanosatellite with a 3U Pumpkin Kit (image credit: Pumpkin Inc.)

- In 2011, the CubeSat deployer system standard of 1U, 2U and 3U form factor is being extended over the existing P–POD standard. The new specification currently governs CubeSats larger than the 3U size. This includes deployer systems which are referred to as **CSDs** (Canisterized Satellite Dispensers) with the following physical parameters:

- 6U (mass of 12 kg, size of 12 cm x 24 cm x 36 cm)
- 12U (mass of 24 kg, size of 23 cm x 24 cm x 36 cm)
- 27U (mass of 54 kg, size of 34 cm x 35 cm x 36 cm).

Expanding upon the success of the 1U and 3U, a larger family of payloads will enable even greater scientific and military capabilities. These 6U, 12 and 27U payloads feature advanced technologies that streamline integration and ensure mission success.

These specifications were arrived at after extensive consultations with the main players of the existing CubeSat standards (Jordi Puig–Suari, Bob Twiggs, PSC (Planetary Systems Corporation) of Silver Spring, MD, and the US CubeSat community, including the military organizations of STP and AFLR). The CSDs are boxes that small payloads (CubeSats) are housed in during launch and dispensed from once in space. These dispensers reduce the risk

¹⁹³⁶⁾ Charlie L. Galliard, “Study of the Small: Potential for Operational Military Use of CubeSats,” Proceedings of the 24th Annual AIAA/USU Conference on Small Satellites, Logan, UT, USA, Aug. 9–12, 2010, SSC10–III–2

that small secondary or tertiary payloads in the dispenser can damage the primary or be damaged by the primary. ^{1937) 1938) 1939)}

- **ELaNa** (Education Launch of Nanosatellite) program of NASA. In 2010, NASA started with the ELaNa initiative to foster CubeSat launch opportunities. One of NASA's missions is to attract and retain students in the science, technology, engineering and mathematics, or STEM disciplines. Creating missions or programs to achieve this important goal helps to strengthen NASA and the nation's future work force as well as engage and inspire Americans and the rest of the world. ^{1940) 1941)}

NASA announced in 2010 that it would sponsor the flight of a dozen university and government CubeSats under the ELaNa program. It followed up that announcement with the selection of twenty more CubeSat missions in 2011 and thirty–three more in 2012. Of those 65 missions, 49 are led by universities. By design, ELaNa provides launch support, not mission assurance.

– The ELaNa–1 mission was comprised of three 1U CubeSats: E1P–1 (Explorer–1 Prime) of Montana State University, HERMES of the University of Colorado, Boulder, and KySat–1 of Kentucky Space. The CubeSats were integrated in CalPoly's P–POD and were secondary payloads to NASA's Glory mission (launch on March 4, 2011 on a Taurus–XL vehicle from VAFB). Unfortunately, the launch of the Glory spacecraft, along with the secondary payloads, **failed to reach orbit** and ended in the Pacific Ocean.

– The ELaNa–3 mission was launched on Oct. 28, 2011 from VAFB, a secondary payload to the NASA/NOAA NPP (NPOESS Preparatory Payload) mission. The ELaNa–3 payload consisted of the following CubeSats or nanosatellites: AubieSat–1 of Auburn University, DICE (2 nanosatellites) of Utah State University, E1P–2 of Montana State University, RAX–2 and M–Cubed of the University of Michigan. All secondary payloads were deployed into an elliptical orbit. ¹⁹⁴²⁾

The DICE nanosatellites carried the first publically–acknowledged high–speed radio, the L3 Cadet–U radio at a frequency of 465 MHz with a downlink data rate of 3 Mbit/s using the 18 m UHF dish of Wallops.

– The ELaNa–6 mission was launched on Sept. 13, 2012 from VAFB, secondary payloads to the NROL–36 primary mission. The ELaNa–6 payload consisted of the following CubeSats or nanosatellites: SMDC–ONE 2.1, SMDC–ONE 2.2, AeroCube–4.0, AeroCube–4.5, Aeneas, CSSWE, CP5, CXBN, CINEMA–1, and Re (STARE–A).

– The ORS–3/ELaNa–4 launch on Nov. 20, 2013 is a collaboration between the ORS (Operationally Responsive Space) office and the ELaNa (Educational Launch of Nanosatellite) program. It is the first launch of the CubeStack Adapter, commonly called the “wafer.” The CubeStack Adapter is built by Moog CSA Engineering, mounts between the upper stage of the rocket and the primary payload, and holds up to eight 3U CubeSat dis-

1937) Ryan Hevner, Walter Holemans, Jordi Puig–Suari, Robert Twiggs, “An Advanced Standard for CubeSats,” Proceedings of the 25th Annual AIAA/USU Conference on Small Satellites, Logan, UT, USA, Aug. 8–11, 2011, paper: SSC11–II–3

1938) <http://www.planetarysystemscorp.com/>

1939) Ryan Hevner, Walter Holmans, Jordi Puig–Suari, Robert Twiggs, “Payload for Canisterized Satellite Dispenser (CSD) Specification Sheet,” PSC, 2002206 Rev A Payload Specification for 6U, 12U and 27U, June 13, 2011,, URL: http://media.wix.com/ugd/1c8e8f_1a22469e04cc02cebd01afe852c06bde.pdf?dn=2002206+Rev+A+Payload+Specification+for+6U,+12U+and+27U.pdf

1940) Garrett Lee Skrobot, “ELaNa – Educational Launch of Nanosatellite Enhance Education through Space Flight,” Proceedings of the 25th Annual AIAA/USU Conference on Small Satellites, Logan, UT, USA, Aug. 8–11, 2011, paper: SSC11–II–2, URL: http://ntrs.nasa.gov/archive/nasa/casi.ntrs.nasa.gov/20110014498_2011015126.pdf

1941) Mason Peck, “Space Technology: Investments in Our Future,” iCubeSat 2012, 1st Interplanetary CubeSat Workshop, Cambridge, MA, USA, May 29–30, 2012, URL: http://icubesat.files.wordpress.com/2012/06/icubesat-org-2012-k-1-presentation_peck.pdf

1942) “CubeSat ELaNa III Launch on NPP Mission,” NASA, October 2011, URL: http://www.nasa.gov/pdf/598567main_65121-2011-CA000-NPP_CubeSat_Factsheet_FINAL.pdf

pensers. The ELaNa-4 CubeSats are: Black Night-1, TetherSat, NPS-SCAT, Ho'pono-pono, COPPER, ChargerSat-1, SPA-1 Trailblazer, Vermont Lunar CubeSat, SwampSat-1, CAPE-2, DragonSat-1, KYSat-2, PhoneSat-2.4, and TJ³Sat.

In addition, there are the government sponsored nanosatellites (all 3U CubeSats): ORS-1, ORS-2, ORS-3, Prometheus-1, -2, -3, and -4, SENSE-A, SENSE-B, Firefly, and STARE-B (HORUS). – This is the first CubeSat launch for which the FCC encouraged all non-government CubeSats to obtain experimental licenses. ¹⁹⁴³⁾

- On Feb. 13, 2012, seven CubeSats and a microsatellite (AlmaSat, University of Bologna, Italy) were launched by ESA's Education Office on the maiden flight of the Vega launch vehicle from Kourou. The primary payload on this flight was **LARES**, a geodynamic satellite (400 kg) of Italy. The CubeSats were: Xatcobeo (a collaboration of the University of Vigo and INTA, Spain); Robusta (University of Montpellier 2, France); e-st@r (Politecnico di Torino, Italy); Goliat (University of Bucharest, Romania); PW-Sat (Warsaw University of Technology, Poland), MaSat-1 (Budapest University of Technology and Economics, Hungary); and UniCubeSat GG (Università di Roma 'La Sapienza', Italy).
- On Feb. 25, 2013, the STRaND-1 (Surrey Training, Research and Nanosatellite Demonstrator), a 3U CubeSat (nanosatellite) of SSTL (Surrey Satellite Technology Limited) and the USSC (University of Surrey Space Centre), Guildford, UK was launched on the PSLV-C20 flight of ISRO. STRaND-1 represents the world's first **smartphone** (Nexus-One) on a nanosatellite. The smartphone will be used as the operating system of the nanosatellite. ¹⁹⁴⁴⁾

1.19.8 CubeLab modules and NanoRacks platforms – research on ISS

The CubeLab standard, based on the CubeSat form-factor (10 cm cube), was developed to expand the research capabilities in microgravity on the ISS (International Space Station) to a broader and more diverse collection of researchers. The CubeLab standard leverages several well known, well defined, and well supported standards to simplify access to space for those developers; these include the CubeSat standard for the physical form-factor and the USB (Universal Serial Bus) standard for power and data connection.

The NanoRacks platform serves as the interface between individual CubeLab modules and the ISS, providing mechanical mounting points and electrical connections for power and data connectivity. Each of these platforms are installed in an EXPRESS rack locker within an EXPRESS rack located in the JEM of the ISS. In the fall of 2010 two NanoRack platforms have been installed and are operational aboard the ISS.

NanoRacks is a commercially operated research facility onboard the ISS, designed and developed by NanoRacks LLC of Houston, TX, and of Laguna Woods, CA, USA. Each platform provides room for up to 16 customer payloads to plug effortlessly into a standard USB connector, which provides both power and data connectivity. Its PnP (Plug-n-Play) system uses a simple, standardized interface that reduces payload integration cost and schedule for nano-scale research on the orbiting laboratory. ¹⁹⁴⁵⁾

NanoRacks LLC is working under a Space Act Agreement awarded by NASA from a competitive announcement of opportunity for the use of the National Laboratory on the International Space Station. NanoRacks LLC signed the Space Act Agreement in September

¹⁹⁴³⁾ Bryan Klofas, "Upcoming CubeSat Launches: The Flood Has Arrived," AMSAT-NA Symposium Houston, TX, USA, 1 November 2013, URL: http://www.klofas.com/papers/klofas_upcoming_cubesat_launches.pdf

¹⁹⁴⁴⁾ "Science & Exploration – STRaND-1 Smartphone Nanosatellite," URL: <http://www.sstl.co.uk/divisions/earth-observation-science/science-missions/strand-nanosatellite>

¹⁹⁴⁵⁾ "Commercial Facility Activated on U.S. National Laboratory Onboard International Space Station," NASA, July 23, 2010, URL: http://www.nasa.gov/mission_pages/station/research/nanoracks.html

2009 and partnered with Kentucky Space and the Space Systems Laboratory (SSL) at the University of Kentucky (UK). The funding to build and certify the rack inserts has come exclusively from NanoRacks and their customers.

The NanoRacks platform and the CubeLab standard ¹⁹⁴⁶⁾ ¹⁹⁴⁷⁾ provide a unique new opportunity for inexpensive repeatable access to the ISS for small payloads. ¹⁹⁴⁸⁾ ¹⁹⁴⁹⁾ ¹⁹⁵⁰⁾ ¹⁹⁵¹⁾ The NanoRacks platform serves as the interface between CubeLab modules and the ISS while providing mechanical attachment, power, and data transfer to each module. The CubeLab standard defines mechanical and electrical requirements for CubeLab modules. CubeLabs can be flown to and from the ISS on a variety of manned and unmanned vehicles to support a wide variety of microgravity experiments. Once aboard the ISS CubeLabs are installed in the NanoRacks platforms.

Note: NanoRacks is described on the eoPortal in a separate file under ISS Utilization.

Size of 1U CubeLab module	10 cm x 10 cm x 10 cm
Mass, power	≤ 1 kg, 2 W (max)
Voltage, current	5 VDC (max), 400 mA (max)
Cooling requirements	2 W (max)
Data	Intermittent USB (Universal Serial Bus) connectivity
Crew time	Negotiated as needed
Timeframe of experiment delivery	L-6 to L-3 months
Return mass	Negotiated as needed

Table 108: Overview of a CubeLab unit performance characteristics/requirements (Ref. 1950)

Larger CubeLab modules are possible with 2U (10 cm x 10 cm x 20 cm), 4U (10 cm x 10 cm x 40 cm), and up to 2U x 4U (10 cm x 20 cm x 40 cm) configurations, Figure 146 shows the various CubeLab form-factor layouts to accommodate larger payloads. CubeLab modules are physically attached to the NanoRacks platform using USB type B connectors.

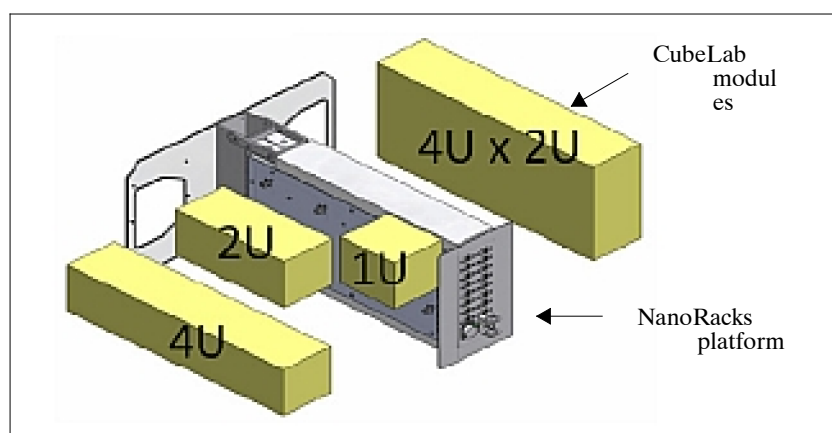


Figure 146: Illustration of possible CubeLab module configurations and a NanoRack (image credit: Kentucky Space, NanoRacks LLC)

1946) James E. Lumpp, Jr., Daniel M. Erb, Twyman S. Clements, Jason T. Rexroat, Michael D. Johnson, “The CubeLab Standard for Improved Access to the International Space Station,” 011 IEEE Aerospace Conference, Big Sky, MT, USA, March 5–12, 2011

1947) “Interface Control Document Between CubeLab Modules and the NanoRacks Platform,” Kentucky Space, Document: 8400–NRP–ICD–1, January 11, 2011, Rev. 1, URL: <http://ssl.engineering.uky.edu/files/2011/01/8400-NRP-ICD-1.pdf>

1948) <http://www.nanorackslc.com/>

1949) “NanoRack & CubeLabs,” SSL (Space Systems Laboratory), University of Kentucky, URL: <http://ssl.engineering.uky.edu/missions/international-space-station/nanorack-cubelabs/>

1950) “NanoRacks Experiment Overview,” April 20, 2010, URL: <http://www.nanorackslc.com/wp-content/uploads/2010/12/NanoRacks-Experiment-Overview.pdf>

1951) Jason Crusan, “Innovation and Technology,” NASA Space Operations Mission Directorate, April 22, 2010, URL: http://erc.ivv.nasa.gov/pdf/471898main_Crusan_SOMD_Innovation_Overvietee_4_22.pdf

CubeLab operations: NanoRacks LLC, working with its partner Kentucky Space, has a turnkey operational system that can handle all aspects of customer requirements, from payload development, to NASA integration to mission operations, all in a customer friendly environment.

The plug-and-play nature of the NanoRacks–CubeLab modules allows for interested parties, such as universities or commercial companies, to fly small and relatively inexpensive payloads aboard the station. This enables microgravity research for those who may not otherwise have had the opportunity.

Real-time operations aboard the ISS, including installation, activation, data transfer, and deactivation of CubeLab modules, are coordinated by the NanoRacks Operations Center in the SSL (Space Systems Laboratory) at the University of Kentucky through the HOSC (Huntsville Operations Support Center) at MSFC. The NanoRacks/SSL Operations Center consists of a secure operation console tied into NASA voice loops, real-time astronaut and ground systems scheduling systems, procedure development and viewing tools, real-time telemetry feeds, and live high-definition video feeds from the ISS.

Initial installation on ISS: In July and August 2010, the ISS was outfitted with the first two NanoRack platforms, flown to orbit on STS–131 (19A) on April 5, 2010 and STS–132 (ULF4) on May 14, 2010, giving the ISS the capacity to support up to 32 1U CubeLab modules. The NanoRack–1 and NanoRack–2 were installed in EXPRESS Rack–4 which is accommodated in JEM (Japanese Experiment Module) of ISS.

- In 2010, four CubeLab modules were flown to the ISS. Two modules, CubeLab1 and CubeLab–2, were flown with each NanoRacks platform. Each of the four modules was designed to test the effects of ionizing radiation on commercial flash memory devices inside the EXPRESS Rack locker. The motivation of this testing was that COTS (Commercial Off-the-Shelf) electronic components can suffer from SEEs (Single Event Effects) in the presence of radiation in LEO (Low Earth Orbit) and baseline testing of these components should provide valuable guidance for future CubeLab module development (Ref. 1946).
- On Jan. 22, 2011, HTV–2 of JAXA was launched from TNSC, Japan. In its payload was also a 2U CubeLab experiment of a student team from Valley Christian High School, San Jose, CA, USA. The experiment used a student-designed, self-contained plant-seed growth chamber (COTS products) that plugged into the NanoRacks–CubeLab platform inside the Japanese JEM/Kibo module onboard the ISS. An internal camera provided snapshots of the stages of growth during the experiment, which crew members then downlinked to the school as data for analysis. The experiment remained in orbit for 53 days, a total of 3005 photos were downloaded. The 2U CubeLab was returned to Earth on a Soyuz vehicle on March 16, 2011. An analysis of the experiment revealed that all system performed as designed. ¹⁹⁵²⁾ [1953\)](#)

1952) Dan Saldana, “The Sky is No Longer the Limit,” 2U CubeLab presentation of Valley Christian High School Students, 8th Annual CubeSat Developers’ Workshop, Calpoly San Luis Obispo, CA, April 20–22, 2011, URL: http://www.cubesat.org/images/2011_Spring_Workshop/wed_p2.30_saldana_cal%20polyws.pdf

1953) Jessica Nimon, “Students Blaze a Trail Using NanoRacks–CubeLabs for Space Station Research, NASA, Dec. 22, 2010, URL: http://www.nasa.gov/mission_pages/station/research/news/nanoracks.html

1.19.9 Current status and outlook in the smallsat service spectrum

In the early 21st century, the spectrum of microsatellite services is by all means as impressive as that of their bigger brother satellites, but at considerably reduced costs. Overall, microsatellites experienced an impressive evolution from flying gadgets to real and advanced service providers. In fact, microsatellites make it possible to open up new fields of services previously considered too expensive (in particular technological missions are in this category). As a consequence, all space agencies as well as the military establishments of the world have been (or are) re-evaluating their programs, in favor of smaller systems, to offer a solution for ever tighter budgets. It meant in fact an entirely new approach of project management and procurement techniques by the agencies to keep costs in bounds. In particular, the academic world realized its chance in bringing in new ideas and in getting involved in affordable missions of their own. ^{1954) 1955)}

As of 2008, there are **SAR (Synthetic Aperture Radar) as well as hyperspectral imaging missions on minisatellites** – in operation and in planning. A major challenge for high-resolution imaging missions or for hyperspectral missions on small S/C is the thermal stability on the imaging instrument and bus – to provide sharp imagery.

- The SAR–Lupe constellation (observations in X–band), consisting of five minisatellites for the German Defense Ministry, developed by OHB–System of Bremen, has all minisatellites in orbit (770 kg/satellite) as of July 22, 2008.
- The TecSAR mission of the Israel Defense Ministry (300 kg, launch Jan. 21, 2008) is designed and built by IAI/MBT (Israel Aerospace Industries Ltd.). Observations are being done in X–band at spatial resolutions of 8–1 m depending on mode of operations.
- An example of planned civil minisatellite SAR missions is the “AstroSAR–Lite” initiative of Astrium Ltd. and SSTL. The goal is to provide low–cost mission solutions with innovative designs to customers in the field of SAR (Synthetic Aperture Radar) observations.
 - The PROBA mission of ESA (launch 22.10. 2001) is flying CHRIS (Compact High Resolution Imaging Spectrometer), a UK hyperspectral imager developed by SSTL. The spectral range of 400–1050 nm provides a 34 m spatial resolution at full swath (62 bands, plus 1 band for calibration). PROBA is operational as of 2009.
 - TacSat–3 is a DoD (USA) technology demonstration minisatellite with a launch on May 19, 2009. It carries ARTEMIS (Advanced Responsive Tactically Effective Military Imaging Spectrometer), a hyperspectral imager of AFRL and the US Army. – An equally important aspect of TacSat–3 represents a first implementation of *a demonstration of emerging avionics and interface standards as well as of modular spacecraft bus standards*.
 - ZASat–003 (South African Satellite–003) of SunSpace Ltd. employs a multi–sensor imager for hyperspectral imagery in the region of 400–2350 nm. A launch of the minisatellite is expected in 2012.
 - PRISMA (Hyperspectral Precursor and Application Mission) of ASI, Italy is a minisatellite mission (400 kg) under development with a planned launch in 2012. Observations will be conducted in VNIR (400–1010 nm), 92 bands, and in SWIR (920–2505 nm) in 157 bands. The GSD = 30 m on a swath of 30 km.
 - The EnMAP mission of DLR (Germany) is a small satellite hyperspectral mission (850 kg) under development with a planned launch in 2017. Observations will be conducted in the spectral range of 420–2450 nm in continuous bands of 10–40 nm width, sampled at 5 to 20 nm intervals. The GSD (Ground Sampling Distance) will be 30 m.

1954) R. Sandau, “Potential and shortcoming of small satellite for topographic mapping,” Proceedings of ISPRS Workshop, Ankara, Turkey, Feb. 14–16, 2006, http://www.isprs.org/commission1/ankara06/makaleler/Sandau_Small_Satellite.pdf

1955) A. L. Lew, B. Q. Le, P. D. Schwartz, et al., “Microsatellites: An Enabling Technology for Government and Commercial Aerospace Applications,” JHU/APL Technical Digest, Vol. 22, No 2, 2001, pp. 124–134

In their modern reincarnation, a worldwide community of innovators has chosen to leverage the technological advances in electronics, materials, and sensors to create satellites that are physically smaller, technically simpler, and much more affordable to acquire, launch and operate. In particular, the technology of component/instrument miniaturization is making considerable progress in the field of **integrated microsystems** – the introduction of micro– and nano– technologies into space applications. The vision is to build modular microsystems, platforms on a chip, that integrate the domains of electronics, photonics, MEMS (Micro–Electro–Mechanical Systems), architectures, and algorithms into an intelligent set of tools. The future lies in reconfigurable and adaptable microsystems. ¹⁹⁵⁶⁾ [1957\)](#) ¹⁹⁵⁸⁾

With these developments in mind, there is definitely an exciting future ahead for small satellite missions in many fields of spaceflight. ¹⁹⁵⁹⁾ For instance, small satellites represent the only affordable and meaningful solution for the development of future cooperative distributed space systems – constellations and formations – to provide a new observational dimension in the field remote sensing.

In general, distributed satellite constellations offer a number of advantages over monolithic systems such as:

- Distributed constellations do generally have a smaller mass and cost less to launch
- Distributed satellites may perform better during deployment
- Distributed satellite constellations provide a means for graceful degradation
- Distributed constellations offer new observation options (such as stereo imaging, improvement of the revisit time, etc.).

Table 109 gives some overview of such constellations in operation as well as in planning or under development. However, in the vast field of Sun–Earth research, there are mission requirements that call for hundreds of near–simultaneous measurements at widely distributed locations within the Earth’s magnetosphere. Obviously, these new constellations require a high degree of operational autonomy as well as new concepts in spacecraft deployment and manufacturing.

Mission	Launch	Description
GRACE (USA, Germany)	17.03.2002	Constellation of two minisatellites (432 kg each) in co–planar orbit to measure the Earth’s gravity field. GRACE is operational as of 2008.
DMC (SSTL)	2002–2005	Constellation of five microsatellites providing daily global medium–resolution imagery of 32 m (co–planar orbit with cumulative swath)
ST5 (NASA)	22.03.2006	Technology verification of a three microsatellites constellation for the duration of 3 months (after all mission objectives were completed).
FormoSat–3/ COSMIC (NSPO, UCAR)	14.04.2006	Constellation of 6 microsatellites in 3 orbital planes (Taiwan/USA). Collection of radio occultation data of Earth’s atmosphere for operational weather prediction, climate, ionospheric and gravity research
STEREO (NASA)	26.10.2006	A two satellite constellation (620 kg each) in NASA’s Sun–Earth connection program (heliocentric orbit in the ecliptic plane) to observe the sun in stereo

1956) J. C. Zolper, “Integrated Microsystems: A Revolution on Five Frontiers,” Proceedings of DARPAtech 2005, 09–11.08.2005, Anaheim, CA, USA, URL: <http://192.5.18.102/darpatech2005/presentations/mto/zolper.pdf>

1957) S. Echtersley, J. Schalk, M. Kluge, O. Coumar, K. Haria, “The EADS micropack project A novel, modular approach to packaging integrated microsystems for exciting future mission applications in space,” 5th ESA Round Table on Micro/Nano Technologies for Space, 03–05.10.2005, Noordwijk, The Netherlands, URL: <https://escies.org/GetFile?rsrcid=1638>

1958) C. E. Willey, B. Huettl, D. Downen, S. W. Hill, “Miniature Mechanisms Tool Kit for Micro Spacecraft,” JHU/APL Technical Digest, Vol. 22, No 2, 2001, pp. 115–119

1959) W. W. Saylor, K. Smaagard, N. Nordby, D. J. Barnhart, “New Scientific Capabilities Enabled by Autonomous Constellations of Smallsats,” Proceedings of the 21st Annual AIAA/USU Conference on Small Satellites, Logan, UT, USA, Aug. 13–16, 2007, SSC07–II–7

Mission	Launch	Description
THEMIS (NASA)	17.02.2007	Constellation of five Probes in HEO to study magnetospheric substorms, each S/C has a mass of 128 kg
SAR–Lupe (Germany)	19.12.2006 02.07.2007 01.11.2007 27.03.2008 22.07.2008	Constellation of 5 minisatellites in 3 orbital planes providing high–resolution SAR data in X–band. Each S/C has a mass of 770 kg. Five S/C in orbit as of July 22, 2008.
A–Train (NASA,CNES)	2002–2008	The A–Train, a “loose formation” of NASA and CNES, consists of a mix of large spacecraft (Aura and Aqua) and small spacecraft (PARASOL, CloudSat, CALIPSO, and OCO) in one orbital plane.
RapidEye (Black-Bridge)	29.08.2008	Constellation of five minisatellites (175 kg) in a co–planar orbit to provide high–resolution multispectral imagery (6.5 m) on a daily basis
HJ–1A, –1B, –1C (NDRCC/SEPA), China	05.09.2008	Constellation HJ–1 (Environmental Protection & Disaster Monitoring Constellation). In the first phase, HJ–1 consists of two optical and one SAR minisatellite (HJ–1C) in S–band.
HJ–1C	18.11.2012	HJ–1C, a SAR satellite, will join the HJ–1A and HJ–1B satellites
DMC–2nd generation (SSTL)	29.07.2009 17.08.2011	Constellation of 2 minisatellites in one orbital plane (Deimos–1, UK–DMC–2 NigeriaSat–2 providing wide–swath medium and high–resolution imagery. NigeriaSat–X
Prisma (SSC, DLR, CNES)	15.06.2010	Constellation of 2 microsattellites (145 kg and 50 kg) to demonstrate formation flying and rendezvous technologies.
Pleiades (CNES)	17.12.2011 (first S/C) 02.12.2012	Pleiades–HR1A. Constellation of two high–resolution minisatellites (980 kg) in one orbital plane (launch within one year). GSD = 0.7 m for Pan and 2.8 m for MS on a swath of 20 km. Pleiades–HR1B
Swarm (ESA)	22.11.2013	Minisatellite constellation of 3 S/C to provide the best ever survey of the geomagnetic field (multi–point measurements in 3 orbital planes)
MMS or MagCon (NASA)	2015	The Magnetospheric MultiScale constellation consists of 4 S/C (in development)
FormoSat–7/ COSMIC–2 (USA, Taiwan)	2016, 2018	Constellation of 12 minisatellites in 2 orbital planes (Taiwan/USA), a successor to FormoSat–3/COSMIC constellation. Two launches of 6 satellites each in 2016 and 2018.

Table 109: Overview of small satellite constellation missions in remote sensing

1.20 Overview of Operational Meteorological Missions

Meteorology is the study of the interplay between atmospheric temperature, pressure, humidity, and winds. Spaceborne operational meteorological services, namely the measurement of short-term weather variations in the lower regions of the atmosphere (in particular the troposphere as well as the Earth's surface), are provided by two types of satellite constellations: LEO (Low Earth Orbit) and GEO (Geostationary Orbit).

The era of meteorological satellites started with the launch of TIROS-1, a LEO S/C of NASA, on April 1, 1960 (a small spin-stabilized S/C with a mass of 122 kg). The first generation of meteorological spacecraft were de-facto research satellites which played a major role in defining future operational systems. The first operational satellites, ESSA-1 (Environmental Science and Services Administration, launch Feb. 3, 1966 of ESSA-1) and ESSA-2 (launch Feb. 28, 1966), were 2nd generation spacecraft, in morning and afternoon orbits, respectively. They provided operational direct readout with ATP (Automatic Picture Transmission) on even-numbered ESSAs, and global imagery with stored Vidicon imagery, odd numbered. It is important to realize that forerunner experimental TIROS-8 (launch Dec. 21, 1963) and Nimbus-1 (1964) satellites provided the first APT broadcast service for worldwide users (see 1.28).

Technologically, spaceborne meteorological instruments and data analysis/interpretation have progressed considerably in quality and quantity over the last 40+ year period, from the era of "pictures" to high-resolution digital renderings from a variety of spectral bands, providing information about the atmosphere, clouds, and land and sea surface properties. Today's data products are being utilized for a variety of applications that span scales from now-casting to long-term climate studies, and include land, ocean, atmosphere and ecological applications. Indeed it would be difficult to find an area of operational meteorology that had not come under satellite "influence."

At the start of the 21st century, meteorological information from GEO and LEO satellites is a key factor to the art of local forecasting, across scales from synoptic scale (1000s to 100s km) to mesoscales (100 to 10s km). New observation schemes and sources of meteorological parameter fields are being opened with GPS signal applications: a) in ground-based meteorology (see 1.20.5), b) in radio occultation monitoring (see 1.20.4), and c) in bistatic reflection measurements (see 1.20.6). Note: As of 2002, all of the GPS meteorological signal applications are still in an experimental or demonstration state, but they have the potential to augment considerably the data of the conventional GEO and LEO meteorological satellites – at low cost.

"Today we can make 3-5-day weather forecasts with nearly 80% accuracy. That's fantastic. In 10 year's time, with all we can learn from our upcoming missions, we intend to push that out to 7 to 10 days with the same accuracy [Note: The improvement in forecast skill at six days is equivalent to gaining an extension of forecast capability of several hours. This magnitude of improvement is quite significant when compared with the rate of general forecast improvement over the last decade]. With the right investments in observations and computational modeling, we might even push that out to 14 days perhaps 20 years from now." (Daniel Goldin, NASA Administrator, at JHU/APL address, Oct. 10, 2000, Ref. 20).

Meteorological research has transformed the way society thinks about weather and climate in its relatively short lifetime.¹⁹⁶⁰⁾ At the beginning of the 20th century, most people assumed that the assimilative capacity of the atmosphere was infinite, climate was relatively constant, and most weather events were unpredictable. In the early 21st century, thanks in large part to meteorological research, most educated people know that the assimilative ca-

1960) R. E. Morss, W. H. Hooke, "The Outlook for U.S. Meteorological Research in a Commercializing World: Fair Early, but Clouds Moving in?," BAMS (Bulletin of the American Meteorological Society), Vol. 86, No 7, July 2005, pp. 921-936

capacity of the atmosphere is finite, even on global scales; climate is variable, sometimes abruptly so; and weather is considerably more predictable than previously thought.

The global nature of weather systems and satellite observations places satellite data at the very heart of NWP (Numerical Weather Prediction) needs, especially as forecasts extend out to ranges of several days. Indeed, weather and climate forecasts have been revolutionized during the past 40 years. This is in part due to: a) availability of almost global observations, b) improved computer systems and algorithms, and c) considerable advances in modeling and data assimilation (in particular for tropospheric models).¹⁹⁶¹⁾

Surveys from NCEP (National Centers for Environmental Prediction) and ECMWF (European Center for Medium–Range Weather Forecasts) indicate that available meteorological data are under–utilized. The main reasons for this under–utilization include: insufficient communications capability, computer power, and the immaturity of operational models and data assimilation systems that link the S/C data to the numerical model.

- General definition of “hindcast”, “nowcast”, and “forecast” service functions in the context of meteorological weather.¹⁹⁶²⁾

- A **hindcast** incorporates past or historical observational data for diagnostic purposes (assessment and/or verification strategy of available data sets of a defined period to evaluate a particular feature or a behavior). Hindcast activities are employed for such functions as: climate research, demonstration of predictive model performance, algorithm verification, improvement tests of forecast products, trend analysis studies of particular phenomena, demonstration of integrated forecast sequence characteristics including control. A hindcast may also be made as an inverse calculation, fitting a forward simulation model to observations.

- A **nowcast** incorporates recent (and often near real–time) observed meteorological, oceanographic, and/or river flow rate data; covers the period of time from the recent past to the present; and makes predictions for locations where observational data are not available. The present is the time at which the nowcast is made, and at which the most recent observations are from a few minutes to an hour old. A nowcast is used to convey information regarding weather events in the next few (generally 1–6) hours.

- A **forecast** incorporates meteorological, oceanographic, and/or river flow rate forecasts; makes predictions for locations where observational data will not be available; and is usually initialized by the results of a nowcast. Medium range in forecasting (with periodic update intervals) refers generally to information 3–7 days in advance.

- **Nowcasting in operational meteorology refers to a chain of processes to be conducted in very short time periods** – including spaceborne (airborne and/or ground–based network) event monitoring of mesoscale weather patterns (generally of active convective systems causing local thunderstorms, high winds, flash floods, fog, or other hazardous events), the quick provision of the data for analysis (short delay times), and the nowcast prediction, reflecting the conditions as they currently exist. The nature of current nowcasting capabilities require a concerted and coordinated (i.e., automated) service approach by all parties involved to be able to broadcast warnings of hazardous events. The technique of nowcasting is increasingly becoming a basic service demand by the various end user communities to be able to react to events causing property damage and in particular to be able to protect life. – At the start of the 21st century, most nowcasting definitions/services call for a short–range prediction capability within a timeframe of < 3 hours, the conventional approach is to use mostly local detail for initial conditions. More advanced nowcasting methods have expand-

1961) Z. Boybeyi, D. P. Bacon, M. L. Kaplan, “The Use of Adaptive (Targeted) Observations of Operational Numerical Weather Forecasting,” Pecora 15/Land Satellite Information IV Conference, ISPRS Commission I Mid–term Symposium/FIEOS (Future Intelligent Earth Observing Satellites), Nov. 10–14, 2002, Denver, CO

1962) “NOS Procedures for Developing and Implementing Operational Nowcast and Forecast Systems for PORTS,” NOAA Technical Report NOS CO–OPS 0020, Jan. 1999, <http://chartmaker.nco.noaa.gov/csdl/op/techrpt.pdf>

ed to include the blending of extrapolation techniques, statistical techniques, heuristic techniques, and NWP (Numerical Weather Prediction).¹⁹⁶³⁾¹⁹⁶⁴⁾ The accuracy of local weather forecasting depends very much on the availability of the nowcasting data, and the quick processing capability of large amounts of complementary data sets for identification of severe weather systems. – Note: For weather forecasting the WMO (World Meteorological Organisation) defines nowcasting as within one hour, with short term forecasting falling between one hour and a day.

While observations from polar orbiting LEO weather satellites often detect mesoscale phenomena at the needed spatial resolutions, they lack the temporal resolution required for many nowcasting applications. GEO satellites are in fact the natural candidates for nowcasting applications – if the spatial and spectral resolution requirements can be met. With regard to repeat observations (i.e. temporal resolution), instrument technology and transmission performance is now available to provide this latter requirement on GEO weather satellites. The spectrum of nowcasting data will also include sensor data from a greater variety of sources such as lightning mappers and SAR instruments next to the conventional radiometric and imaging weather data. Examples of emerging service capabilities for nowcasting are:

- MSG–1 of EUMETSAT (launch Aug. 28, 2002) offers a full disk image every 15 minutes, twice the previous imaging rate (however, the spatial resolution of the IR data is still in the order of 3 km)
- CMC (Canadian Meteorological Center) has developed SCRIBE, an expert system capable of generating automatically or interactively any type of weather products for a region or a specific locality in Canada. As of 2003/4, the system is being upgraded to include the latest local observations and nowcasting data on a continuous basis.¹⁹⁶⁵⁾
- The era of GOES–R (NOAA 3rd generation geostationary satellite, launch 2014) instrument technology, ABI (Advanced Baseline Imager) and HES (Hyperspectral Environmental Suite) sounder, will be able to provide data at resolutions (spatial, spectral, temporal, even simultaneous multiresolution) fully amenable to nowcasting. The nowcasting function support capability is a prime objective of GOES–R.

Note: As of fall 2006, it looks like the HES instrument has been cancelled due to cost overruns.¹⁹⁶⁶⁾

Background: Nowcasting methods based on satellite and ground–based Doppler radar data are a topic since the 1980s.¹⁹⁶⁷⁾ However, first nowcasting products from satellite data became available in the 1990s by various weather agencies and institutions. The service hinges very much on the timely availability of sufficient observable data at the needed resolutions (initial state specification is fundamental to nowcasting) to provide quantitative estimates. General warnings of hazardous events have become possible with the availability of mass communications. – Future nowcasting services and products will not only come from weather satellites, but also from other spacecraft observations such as from altimetry and radar missions. For instance, an objective of the Jason–1 (and Jason–2) altimeter missions is to provide a near real–time data and product service for operational activities such as marine nowcasting, and numerical prediction of sea state, ocean circulation, and weather.

1963) B. J. Conway, et al., (eds), “COST 78 Meteorology. Nowcasting, a survey of current knowledge, techniques and practice, Project–1: Understanding of phenomena,” 1996, Luxembourg.

1964) T. Keenan, S. S en esi, S. Yamada, J. Wilson, P. Joe, J. Koestinen, et al., “Nowcasting and the WWRP: Report of WWRP Ad Hoc Nowcast Working Group,” July 9, 2003

1965) C. Landry¹, M. Ouellet, R. Parent, J–F Deschenes, R. Verret, “Observations and Nowcasting in SCRIBE,” 20th International Conference on Interactive Information and Processing Systems (IIPS) for Meteorology, Oceanography, and Hydrology, Seattle, WA, Jan. 11–15, 2004

1966) J. Singer, “NOAA Tells Congress GOES–R Cost Nearly Double Previous Estimate,” Space News, Vol. 17, Issue 38, Oct. 2, 2006, pp. 1 & 12

1967) B. W. Golding, S. S en esi, K. Browning, B. Bizzarri, W. Benesch, D. Rosenfeld, V. Levizzani, H. Roesli, et al., “EUMETSAT Position Paper on Observation Requirements for Nowcasting and Very Short Range Forecasting in 2015–2025,” Feb. 28, 2003

The dominant forecasting method in the time frame 2015–2025 is expected to be provided by NWP algorithms and techniques, which by then will be able to resolve the scales of interest in very short–range forecasting.

1.20.1 Contributions of Environmental Satellite Data to Meteorology

Operational meteorology has generally two major sources of satellite data: a) operational meteorological satellites in LEO and GEO, and b) environmental satellites/instruments [availability/integration of R&D (Research & Development) data for operational meteorology (study of complex interactions between the Earth's atmosphere, oceans and land surfaces, also study of long–term and large–scale effects of the Earth system)]. It should be pointed out that the field of operational spaceborne meteorology has particularly benefited from complementary data of environmental/demonstration instruments flown on several research missions (designed primarily to study specific processes of scientific interest or to test new observing technologies). Of particular importance is wind (tropospheric and ocean surface) data on a global basis in this context (the ocean surface wind vector is a key parameter in understanding the weather due to its dominant role in the energy exchange at the air–sea interface). A few example missions/instruments in this category are [only short recounts are provided, see also chapter 1.4.7 (Sounding of the Atmosphere)]: 1968) 1969) 1970)

- The ERS–1 (launch July 17, 1991) and ERS–2 (launch Apr. 21, 1995) missions of ESA flew the instruments AMI–SCAT and RA–1 (Radar Altimeter–1). The data of both instruments permitted estimation of ocean surface wind speed, AMI–SCAT also of wind direction. In parallel, ATSR provided SST. See D.17.

The ERS program demonstrated among other things that satellite altimetry data is a new and valuable tool to monitor land and ocean surfaces with important applications to such fields as hydrology and regional climate variability (by monitoring slight changes in sea level, ocean currents and polar ice).

- The same findings were provided by the TOPEX/Poseidon mission (launch Aug. 10, 1992) of NASA and CNES. See chapter 1.21.2 (Satellite Altimetry). TOPEX/Poseidon is best known for its ability to monitor the progress of large–scale ocean phenomena like El Niño, La Niña and a long–term ocean feature called the Pacific Decadal Oscillation that waxes and wanes every 20 to 30 years. In 2002, after ten years of operations, TOPEX/Poseidon continues to provide its data for long–term climate forecasting and prediction models. TOPEX/Poseidon produced the first global views of seasonal current changes. It maps year–to–year changes in upper–ocean heat storage. The satellite has improved our understanding of tides, producing the world's most precise global tidal maps and demystifying deep–ocean tides and their effect on ocean circulation. It monitors global mean sea–level changes, an effective indicator of the consequence of global temperature change. Its data are input into atmospheric models for forecasting hurricane seasons and individual storm severity.
- The ADEOS mission of NASDA (launch Aug. 17, 1996) carried the NASA NSCAT instrument for surface wind speed and direction estimation. See D.1.
- The TRMM cooperative mission of NASA/NASDA (launch Nov. 27, 1997) is carrying PR (Precipitation Radar) of NASDA with the objective to measure 3–D rainfall distribution (from surface to about 20 km). Rain rates down to about 0.7 mm/h can be detected. The normalized radar cross–section of PR offers also the capability to extract ocean surface

1968) J. F. W. Purdom, "Environmental Satellite Remote Sensing In The 21st Century," International Symposium on Remote Sensing of Environment (ISRSE), Buenos Aires, Argentina, April 8–12, 2002

1969) G. R. Asrar, "Contribution of environmental satellites to WMO programs: past and present," WMO Bulletin, Vol. 51, No 2, April 2002, pp. 120–129

1970) S. Briggs, E. Oriol–Pibernet, "The European Space Agency's contribution to environmental surveillance," WMO Bulletin, Vol. 51, No 2, April 2002, pp. 130–136

winds.¹⁹⁷¹⁾ In parallel, there is TMI (TRMM Microwave Imager) of NASA to measure SST, wind speed, columnar water vapor, cloud liquid water, and rain rate. The CERES demonstration instrument of NASA measures the radiation from the top of the clouds as well as from the Earth's surface. TRMM focuses on the intensity of tropical rainfall, which is indicative of whether a cyclone is weakening or strengthening.

- The IRS–P4 (OceanSat–1) mission of ISRO (launch May 26, 1999) carries MSMR (Multifrequency Scanning Microwave Radiometer) to measure sea surface temperature (SST), sea surface wind speed (SSW), atmospheric water vapor (WV), and cloud liquid water content (CLW). See D.24.7.
- The QuikSCAT mission of NASA (launch June 19, 1999) with SeaWinds (wind speed and direction on a swath of 1800 km in width making about 400,000 measurements and covering 90% of the Earth's surface in one day). See A.25.
- The Terra (launch Dec. 18, 1999) mission of NASA is flying the MODIS instrument providing a number of environmental parameters, in particular SST.
- The Envisat mission of ESA (launch Mar. 1, 2002, see D.13) is with 8,300 kg the largest environmental satellite ever built. It flies a total of 10 instruments, among them RA–2 to estimate the wind speed and significant wave height (besides altimetry). In addition, there are the atmospheric instruments onboard with GOMOS, MIPAS and SCIAMACHY. AATSR (Advanced Along Track Scanning Radiometer) provides SST (with an accuracy of 0.3°C) and TOA (Top–of–Atmosphere) brightness temperature at 1 km resolution. The MERIS instrument provides operational products relevant for global climate and climate change studies. The most important parameters are the cloud optical thickness, albedo, top pressure, cloud type and reflectance. This set of parameters coupled with the MERIS global and long–term observation strategy should lead to a better understanding of the role of clouds in the global energy budget and their impact on the Earth's climate.
- The Aqua mission of NASA (launch May 4, 2002) is dedicated to the study of the Earth's interrelated processes (atmosphere, oceans, and land surface) and their relationship to the Earth system climate changes. The MODIS instrument provides a number of environmental parameters, in particular SST. The AMSR–E provides sea surface wind fields, precipitation rate, water vapor content and surface moisture content. AIRS provides hyperspectral measurements of global temperature/humidity profiles in the atmosphere (among other measurements). AMSU/HSB provides in parallel temperature and humidity soundings of the atmosphere. See D.15.2.¹⁹⁷²⁾
- The ADEOS–II mission of JAXA (launch Dec. 14, 2002) flies SeaWinds (wind speed and direction) a NASA scatterometer. The ADEOS–II instruments provide information in water and energy cycling. AMSR acquires water vapor, precipitation, SST, sea surface wind, sea ice, etc. See D.2.
- The Coriolis mission of NRL (launch Jan. 6, 2003) carries WindSat (Wind Microwave Radiometer) as its prime instrument. The objective of the polarimetric WindSat is to conduct an operational demonstration of the WindSat system (demonstrator to MIS on NPOESS) and to measure the ocean surface wind vector (speed and direction) for a number of practical applications (secondary measurements are sea surface temperature, rain rate and water vapor). See A.12.
- The CryoSat mission of ESA (launch Oct. 8, 2005 – but launch failure) with SIRAL (SAR Interferometer Radar Altimeter) has the prime objective to observe ice sheet interiors, the ice sheet margins, for sea ice and other topography (variations in the thickness of the

1971) L. Li, E. Im, L. N. Connor, P. S. Chang, "Detecting Ocean Surface Winds Using TRMM Precipitation Radar," Proceedings of IGARSS 2002, Toronto, Canada, June 24–28, 2002

1972) M. Mecham, "With Aqua, NASA Shifts Climate Studies to Water," Aviation Week & Space Technology, Apr. 1, 2002, pp. 50–52

Earth's continental ice sheets and marine ice cover). Sea ice plays a central role in Arctic climate. See E.2.

- The EO-3 (Earth Observing-3, GIFTS-IOMI Mission) GEO satellite, a joint NASA, Navy, and NOAA mission (launch 2010 ???), carries the instrument GIFTS (Geostationary Imaging Fourier Transform Spectrometer) to demonstrate the requirements on NOAA's future HES (Hyperspectral Environment Suite)¹⁹⁷³ capabilities of the GOES-R program. HES is planned to fly on GOES-R (launch in 2014) and beyond. GIFTS on EO-3, a multi-channel imager and sounding interferometer, is well suited to analyze a variety of atmospheric and surface phenomena (see M.13).
- The SMOS (Soil Moisture and Ocean Salinity Mission) of ESA (launch Nov. 2, 2009) will demonstrate synthetic aperture radiometry with MIRAS (Microwave Imaging Radiometer using Aperture Synthesis). The objectives are to obtain multi-incidence observations of two crucial variables, namely soil moisture (SM) over land and ocean salinity (OS) over the sea, with sufficient spatial resolution and revisit time for modeling weather and climate. MIRAS also monitors the vegetation water content, snow cover and ice structure. Both variables, SM and OS, are used in predictive atmospheric, oceanographic and hydrologic models and may be important for extreme event forecasting.
- The NPP (NPOESS Preparatory Project) of NASA/IPO (launch Oct. 28, 2011). The objective is to demonstrate the performance of four advanced instruments: VIIRS (Visible/Infrared Imager and Radiometer Suite), CrIS (Cross-Track Infrared Sounder), OMPS (Ozone Mapping and Profiler Suite), and ATMS (Advanced Technology Microwave Sounder). See G.9.
- ADM-Aeolus (Atmospheric Dynamics Mission), the 2nd Earth Explorer core mission of ESA, is planned for launch in 2011. It carries ALADIN (Atmospheric Laser Doppler Instrument), a Doppler wind lidar. The primary objective is to provide highly accurate wind profile measurements over the altitude range 0-20 km, for an improved analysis of the global three-dimensional wind field. Such knowledge is crucial to the understanding of the atmospheric dynamics, including the global transport of energy, water, aerosols, chemicals and other airborne materials – to be able to deal with many aspects of climate research and climate and weather prediction. See A.3.
- The GCOM (Global Change Observation Mission) program of JAXA (successor to ADEOS, ADEOS-II) and partners is dedicated to the study of global change phenomena by studying transport processes in the atmosphere of the carbon cycle and the energy cycle. Carbon plays many roles in the Earth system. It forms our food and acts as our primary energy source, but is also a major contributor to the planetary greenhouse effect and the potential for climate change. Carbon GCOM aims at estimating the primary production as well as to monitor the carbon flux; in addition, measurement of greenhouse gases such as CO₂, CH₄, and O₃. The GCOM program consists of three elements:¹⁹⁷⁴
 - GOSAT (Greenhouse gas Observing Satellite). The emphasis is on atmospheric monitoring (clarify sources and sinks of CO₂ on a continental scale). GOSAT carries TANSO-FTS (Thermal And Near infrared Sensor for carbon Observation – Fourier Transform Spectrometer) and TANSO-CAI (Thermal And Near infrared Sensor for carbon Observation – Cloud and Aerosol Imager). The launch of GOSAT took place on Jan. 23, 2009.
 - GCOM-W1 (Water), a sea observation mission. The primary goal is to contribute to observations related to global water and energy circulation. The payload consists of an AMSR2 (Advanced Microwave Scanning Radiometer-2) instrument. GCOM-W1 was launched on May 17, 2012.

1973) Note: The previous name of HES was ABS (Advanced Baseline Sounder) in the NOAA program

1974) H. Shimoda, "Present Status of GCOM Mission," Proceedings of IEEE/IGARSS, Toulouse, France, July 21-25, 2003

– GCOM–C1 (Climate). The primary goal of the GCOM–C mission is to contribute to surface and atmospheric measurements related to the **climate change** with emphasis on the carbon cycle and the radiation budget. The payload consists of a second–generation GLI (SGLI) instrument. The high resolution global observation of ocean color by SGLI/GCOM–C is expected to play an important role of the study of interaction between climate change and marine ecosystem.

– GPM (Global Precipitation Measurement) research mission of NASA and JAXA with advanced rain measuring instruments. The DPR (Dual–frequency Precipitation Radar) is provided by JAXA/ CRL on the core satellite. GPM is a follow–up mission to TRMM encompassing eventually a constellation of a core S/C plus data from contributing missions. The GPM core satellite was launched on Feb. 27, 2014.

- OCO (Orbiting Carbon Observatory) is a NASA/JPL minisatellite science mission within ESSP.¹⁹⁷⁵⁾ The OCO objective is to provide global measurements of atmospheric carbon dioxide (CO₂) needed to describe the geographic distribution and variability of carbon dioxide sources and sinks to address the complex nature of the carbon cycle. The OCO spacecraft was launched on Feb. 24, 2009 – unfortunately the Taurus–XL vehicle experienced a launch failure. – OCO will become part of the “A–Train” to correlate the OCO data with data acquired by other instruments (AIRS) on Earth observing spacecraft.

Note: CO₂ is the principal atmospheric component of the global carbon cycle. The overwhelming scientific consensus predicts that human emissions of carbon dioxide will warm the planet over the coming decades and centuries. By how much and how quickly is still up for dispute, but most agree it’s time to take action. Reducing carbon dioxide emissions is the key to counteract global warming.

- SPECTRA (Surface Processes and Ecosystem Changes Through Response Analysis) is an Earth Explorer candidate mission in ESA’s Living Planet Program. A major objective is to provide detailed and precise measurements of vegetation amounts and conditions with a spatial resolution sufficient to characterize individual vegetation types and to assess the role of the terrestrial component of the global carbon cycle.¹⁹⁷⁶⁾ A launch is expected in 2009.

- The availability of hyperspectral infrared sounding data on Aqua, MetOp, Suomi–NPP, and JPSS will improve the temperature and moisture profiling in meteorology.

¹⁹⁷⁵⁾ C. Johnson, D. Crisp, “The Orbiting Carbon Observatory Mission,” 4th IAA Symposium on Small Satellites for Earth Observation, Berlin, Germany, April 7–11, 2003

¹⁹⁷⁶⁾ http://www.esa.int/esaLP/ASE12YNW9SC_spectra_0.html

1.20.2 LEO (Low Earth Orbit) Meteorological Satellite Missions

LEO S/C in polar sun–synchronous orbits provide wide–swath repeat observations (same sun illumination angles) of a given Earth surface region at the same time of the day (due to same latitudinal crossings).

- The first meteorological LEO services started with NASA’s launch of TIROS–1 (Television Infrared Observation Satellite) on April 1, 1960, the first true weather satellite. Since then, five generations of polar–orbiting meteorological S/C were developed by NASA and flown by NOAA as outlined in Table 110. – The NOAA 4th–generation polar program (ATN), which started in 1978 with the launch of TIROS–N, is based on the services of two operational satellites flying in complementary sun–synchronous orbits, one in a “morning or AM” orbit, and the second in an “afternoon or PM” orbit.

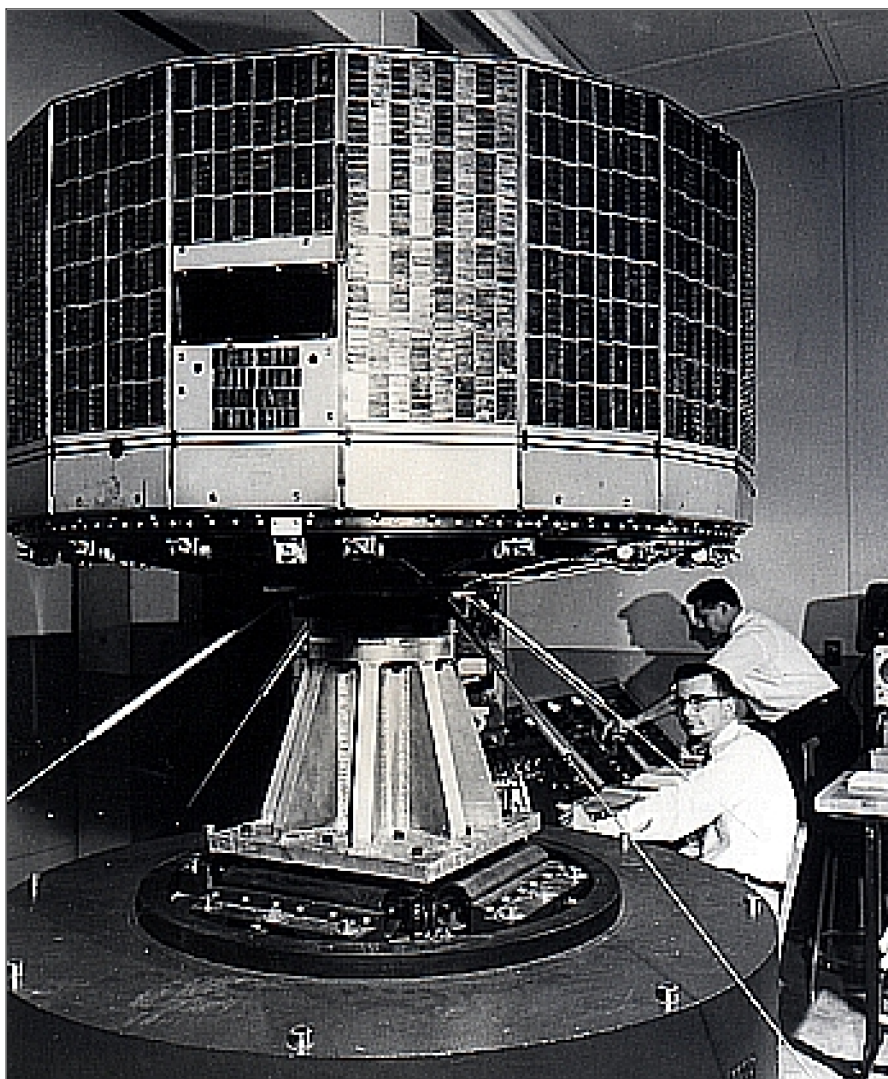


Figure 147: Photo of the TIROS–1 spacecraft (image credit: NASA)

- The US military services of DoD built their own polar–orbiting meteorological satellite series in parallel to the civil system of NASA/NOAA, referred to as DMSP (Defense Meteorological Satellite Program). The first generation of DMSP S/C started with the launch of a Block 4 series satellite on Jan. 19, 1965 and ended with the launch of a Block 5C S/C on Feb 19, 1976. The various generations of DMSP satellites are listed in Table 558. The OLS (Operational Linescan System) instrument on DMSP provides in addition to its normal daytime (visible) imagery also nighttime imagery with its IR channels.
- The Meteor–1 series of the former USSR started with the launch of Meteor–1–1 on March 23, 1969; the 1st generation series lasted until 1978 with the launch of

Meteor-1-28. This was succeeded by the Meteor 2 series from 1975 to 1990 (Meteor-2-1 to 2-21), and further by the Meteor-3 series from 1985 to the present time (see Table 614).

- The Chinese polar-orbiting meteorological program started in 1977 followed by the launch of the FY-1A (Feng-Yun-1) satellite of CMA (China Meteorological Administration) on Sept. 7, 1988 and FY-1B on Sept. 3, 1990, etc.

The 2nd generation polar orbiting program starts with FY-3A (launch May 27, 2008) featuring a global imaging and sounding capability, and a DCS (Data Collection System) capability. The imaging instruments are: VIRR (Visible and Infrared Radiometer), MERIS (Medium Resolution Spectral Imager), and MWRI (Microwave Radiation Imager). The sounding instruments are: IRAS (Infrared Atmospheric Sounder), ASI (Atmospheric Sounding Interferometer), MWTS (Microwave Temperature Sounder), and MWS (Microwave Humidity Sounder). FY-3B was launched on Nov. 4, 2010 (same payload as FY-3A).¹⁹⁷⁷⁾

1st generation 1960 – 1965	TIROS series [TIROS-1 (1960) to TIROS-10 (1965)]
2nd generation 1966 – 1969	TOS (TIROS Operational System) series as pre-launch designation. The in-orbit satellite designation was ESSA [ESSA-1 (1966) to ESSA-9 (1969)], after the S/C operating agency.
3rd generation 1970 – 1976	ITOS (Improved TIROS Operational System) series as pre-launch designation. The in-orbit satellite designation was NOAA [NOAA-1 (1970) to NOAA-5 (1976)]
4th generation 1978 – 1994	ATN [Advanced TIROS-N] series. After TIROS-N (1978) the pre-launch designation changed to NOAA-A (the corresponding inflight name was NOAA-6). The pre-launch letter designation was kept throughout. NOAA-8 through NOAA-14 were designated ATN (Advanced TIROS-N) spacecraft, equipped for S&R (Search and Rescue) and growth instruments.
5th generation 1998 – 2007	NOAA-15 (pre-launch NOAA-K), NOAA-L, -M, -N, and -N' incorporate advanced instrumentation and are designated "NOAA next."

Table 110: Overview of the US civilian polar meteorological programs

- EUMETSAT, the European meteorological service provider, was planning on a polar-orbiting satellite series since the mid 1980s. Since the early 1990s, NOAA and EUMETSAT have been discussing/planning future polar cooperation with increased European responsibility for the "morning orbit" to ensure continuity of the POES (Polar-orbiting Operational Environmental Satellites) services. The basic intent is to join the space segment of the emerging MetOp program of EUMETSAT with the existing POES program of NOAA into a fully coordinated service, thus sharing the costs of a program for synergistic reasons. The plans came to a common baseline and agreement, referred to as IJPS (Initial Joint Polar System), in 1998. IJPS comprises two series of independent, but fully coordinated polar satellite systems, namely POES and MetOp, to provide for the continuous and timely collection and exchange of environmental data from space.

EUMETSAT plans to include its satellites MetOp-A, -B, -C and -D for the morning orbit, while NOAA is starting with its NOAA-N and N' spacecraft for the afternoon orbit of the coordinated system (launch of NOAA-N on May 20, 2005). MetOp-A was launched on Oct. 19, 2006. – In this context, Europe (i.e. ESA, EUMETSAT) refers to its application-oriented missions (this includes operational meteorological and climate monitoring missions) in LEO and GEO as "Earth Watch Missions" (MetOp, MSG). The Earth Watch concept was introduced in 1994/5, dealing in particular with prototype operational missions and serving applications-oriented needs in partnership of industry and/or public agencies.

¹⁹⁷⁷⁾ C. Dong, W. Zhang, "The Sounding Instruments on Second Generation of Chinese Meteorological Satellite FY-3," 13th ITSC (International TOVS Study Conference), Sainte Adèle, Quebec, Canada, Oct 28 – Nov. 4, 2003, http://cimss.ssec.wisc.edu/itwg/itsc/itsc13/session6/6_1_chaohua.pdf

Long-term operational service provision is the ultimate aim of the ESA Earth Watch program.

- Suomi–NPP (National Polar-orbiting Partnership Mission). NASA developed the NPP mission (launch Oct. 28, 2011) with the objective to demonstrate/validate the operation of advanced instruments (VIIRS, CrIS, ATMS, OMPS, CERES) scheduled to fly on JPSS (Joint Polar Satellite System). ATMS (Advanced Technology Microwave Sounder) is a NASA-provided instrument with the objective to combine the passive-microwave observation capabilities of three heritage instruments, namely AMSU–A1/A2 and MHS, into a single instrument with a correspondingly reduced mass and power consumption and with advanced microwave-receiver electronics technologies. NASA is also providing the NPP spacecraft and the launch. NPP is considered to bridge the gap between NASA's EOS spacecraft (Terra, Aqua, and Aura) and the operational JPSS missions.

Satellite Series (Agency)	Launch	Major Instruments	Comment
NOAA–2 to –5 (NOAA)	21.10. 1971, 29.7. 1976	VHRR	2580 km swath
TIROS–N (NOAA– POES) NOAA–15 to –L, M, N, N'	13.10.1978 13.5.1998 – 2007	AVHRR AVHRR/3	>2600 km swath >2600 km swath
DMSP Block 5D–1 (DoD) DMSP Block 5D–2 (DoD) DMSP Block 5D–3 (DoD)	11.9.1976 – 14.7.1980 18.6.1987 12.12.1999	OLS OLS, SSM/I OLS, SSM/I,	3000 km swath SSMIS replaces SSM/I starting with F–16 (2003)
Meteor–3 series of Russia	24.10.1985	MR–2000M, MR–900B	3100 km, 2600 km swath
Meteor–3M–1 of Russia Meteor–3M–2 of Russia	10.12.2001 2004	MTVZA, SAGE–III	2200 km swath Rosaviakosmos
FY–1A, 1B, 1C (CMA, China) FY–3A, FY–3B, FY–3C	7.9.1988, 3.9.1990, 10.5. 2000 27.05.2008, 04.11.2010 23.09.2013	MVISR VIRR, IRAS, etc. MWS–2, etc.	2800 km swath 1st generation 2nd gen.experimental 2nd gen.experimental 2nd gen. operational
MetOp/EPS (EUMETSAT)	19.10.2006, MetOp–A 17.09.2012, MetOp–B	AVHRR/3, MHS, IASI (8000 channels)	PM complement to NOAA–POES series
Suomi–NPP, (NASA, NOAA)	28.10.2011	VIIRS, CrIS, ATMS, OMPS, CERES	(NPOESS Preparatory Project)
JPSS (NASA)	2016	VIIRS, CrIS, ATMS, OMPS, CERES	Next generation of NOAA–POES series

Table 111: Overview of polar-orbiting meteorological satellite series

- JPSS, formerly NPOESS (National Polar-orbiting Operational Environmental Satellite System), represents the future US civil meteorological polar-orbiting system with the objective to provide a single national remote-sensing capability for meteorological, oceanographic, climatic and space environmental data. The JPSS data sets will contain a number of variables that are currently not included in operational measurements (such as: radiation budget, total ozone, wind speed and direction, ocean topography, and ocean color) and will offer improved quality for some variables now being measured (such as: atmospheric moisture and temperature profiles, all-weather SST, and vegetation indices).

The launch of JPSS–1 is planned for 2016. Initial plans for the merger of the two services started in 1993. The following NPOESS sensor payloads are under development: MIS (Microwave Imager/Sounder) of SSM/I (Special Sensor Microwave Imager), SSMIS (Special Sensor Microwave Imager Sounder) and TMI (TRMM Microwave Imager) heritage, CrIS (Cross-Track Infrared Sounder) of HIRS/4, AIRS and IASI heritage, OMPS (Ozone Mapping and Profiler Suite) of SBUV/2, TOMS and GOME heritage, VIIRS (Visible/Infrared Imager and Radiometer Suite) of OLS, AVHRR/3, MODIS, and SeaWiFS heritage, and SESS (Space Environment Sensor Suite) of SEM–2 heritage. – When operational, the NPOESS system will provide global three-hour repeat coverage.

In the fall of 2002, NGST (Northrop Grumman Space Technology)¹⁹⁷⁸⁾ [formerly TRW Inc. of Redondo Beach, CA], was awarded a single prime contract, referred to as A&O (Acquisition and Operations), by IPO (for Shared System Performance Responsibility) to build and deploy the NPOESS spacecraft series. NGST, with its teammate Raytheon, is responsible for developing, integrating, deploying, and operating NPOESS satellites to meet the tri-agency requirements for NPOESS over the 10-year operational life of the program.

In Feb. 2010, the **NPOESS** (National Polar-orbiting Environmental Satellite System) tri-agency program was terminated by the US government due to severe cost overruns and program delays. The NPOESS program was a joint DoD/NOAA/NASA endeavor that tried to integrate the capabilities and infrastructure of the NOAA POES (Polar-Orbiting Environmental Satellite) program, the DoD DMSP (Defense Meteorological Satellite Program), and NASA's long-term continuous climate record collection.

The major challenge of NPOESS was jointly executing the program between three agencies of different size with divergent objectives and different acquisition procedures.^{1979) 1980) 1981)}

In 2009, an IRT (Independent Review Team) concluded that the current NPOESS program, in the absence of managerial and funding adjustments, has a low probability of success and data continuity is at extreme risk. The Office of Science and Technology, with the Office of Management and Budget and the National Security Council, as well as representatives from each agency, examined various options to increase the probability of success and reduce the risk to data continuity.

NOAA's restructured satellite program, the civilian **JPSS**, was created in the aftermath of the White House's Feb. 2010 decision to cancel NPOESS. The development of the new JPSS will be managed by NASA/GSFC while the spacecraft will be owned and operated by NOAA. The launch of JPSS-1 is planned for 2016.

- The JPSS (formerly NPOESS) system, together with the MetOp/EPS system, will constitute the polar component of the next generation meteorological observing system.

Some LEO meteorological instruments: An overview cannot be complete without giving credit to at least one workhorse instrument, AVHRR (Advanced Very High Resolution Radiometer).

- AVHRR (Advanced Very High Resolution Radiometer) of the NOAA-POES satellite series is the spaceborne instrument with the longest service period, the widest data distribution and data analysis in the history of operational meteorology, oceanography, climatology, vegetation monitoring, and land and sea ice observation. The instrument provides wide-swath (>2600 km, $FOV = \pm 56^\circ$) multispectral imagery of about 1.1 km spatial resolution from LEO polar orbits (nominal altitude of 833 km). The resolution of 1.1 km is still quite high for the wide-swath measurement of large-scale meteorological phenomena. The imagery is used in a great variety of applications, such as: investigation of clouds, land-water boundaries, snow and ice extent, sea surface temperature, day and night cloud distribution, vegetation index, etc.

The benefit of AVHRR data lies in its high temporal frequency of daily global coverage. The AVHRR instrument was initially designed for meteorological applications. — It is of inter-

1978) J. D. Cunningham, C. S. Nelson, "The National Polar-orbiting Operational Environmental Satellite System Next Generation U.S. Earth Observation System," Proceedings of ISRSE (International Symposium of Remote sensing of Environment), Honolulu, HI, Nov. 101-14, 2003

1979) "Joint Polar Satellite System," NOAA/NESDIS Newsletter 4, 2010, URL: <http://www.nesdis.noaa.gov/pdf/jpss.pdf>

1980) "Restructuring the National Polar-orbiting Operational Environmental Satellite System," earthzine, Feb. 23, 2010, URL: <http://www.earthzine.org/2010/02/23/restructuring-the-national-polar-orbiting-operational-environmental-satellite-system/>

1981) Turner Brinton, "White House Dissolves NPOESS Partnership in Blow to Northrop," Space News, Feb. 2, 2010, URL: <http://www.spacenews.com/civil/100202-white-house-dissolves-npoess-satellite-partnership.html>

est to note that initial objectives of AVHRR were to develop a system that would provide a more efficient way to track clouds, estimate snow cover extent, and estimate sea surface temperature. It wasn't until a few years after the launch of the first AVHRR instrument that its usefulness in monitoring global vegetation became obvious.

Channel No.	TIROS-N	NOAA-6, -8, -10	NOAA-7, -9, -11, -12, -14	IFOV (mrad)	Principal use of channel
1	0.550 – 0.90	0.550 – 0.68	0.550 – 0.68	1.39	Day cloud and surface mapping
2	0.725 – 1.10	0.725 – 1.10	0.725 – 1.10	1.41	Surface water delineation, vegetation mapping
3	3.550 – 3.93	3.550 – 3.93	3.550 – 3.93	1.51	SST and fire detection
4	10.50 – 11.50	10.50 – 11.50	10.30 – 11.30	1.41	SST and night time cloud mapping
5	repeat of Channel 4	repeat of Channel 4	11.50 – 12.50	1.30	Surface temperature and day/night cloud mapping
AVHRR/1			AVHRR/2		Instrument configuration/designation

Table 112: Spectral channels of AVHRR

Channel	Center wavelength (μm)	Spectral Range FWHM (μm)	Channel Noise	Detector Type
1	0.630	0.58 – 0.68	SNR \geq 9:1 @ 0.5% albedo	Silicon
2	0.862	0.725 – 1.00	SNR \geq 9:1 @ 0.5% albedo	Silicon
3a	1.61	1.58 – 1.64	SNR \geq 20:1 @ 0.5% albedo	InGaAs
3b	3.74	3.55 – 3.93	NEAT \leq 0.12 K @ 300 K	InSb
4	10.80	10.30 – 11.30	NEAT \leq 0.12 K @ 300 K	HgCdTe
5	12.00	11.50 – 12.50	NEAT \leq 0.12 K @ 300 K	HgCdTe

Table 113: Spectral parameters of AVHRR/3 (starting with NOAA-15)

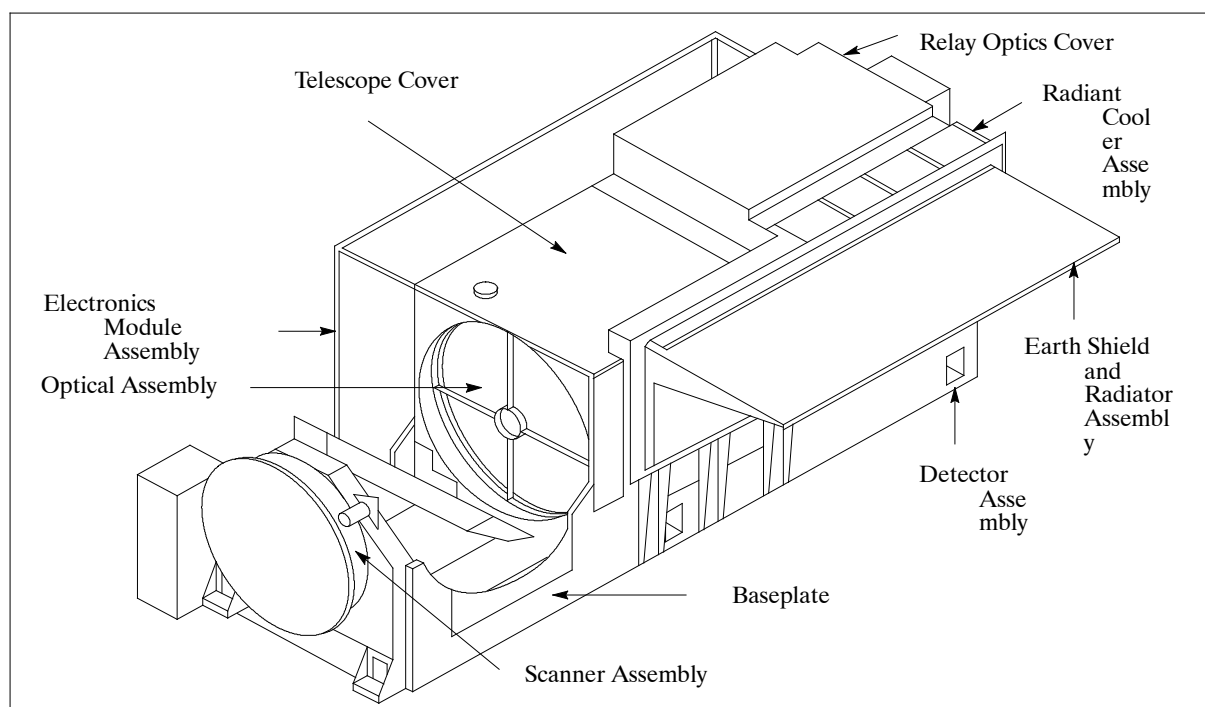


Figure 148: Illustration of the AVHRR instrument

Three generations of AVHRR whiskbroom scanning instruments (built by ITT Aerospace of Fort Wayne, IN) provided daily global coverage starting from 1978 (TIROS-N) to the

turn of the millennium and beyond. The first 3rd generation instrument (AVHRR/3) with six channels was launched on May 13, 1998 as part of the NOAA–15 sensor complement. Although described in G.14.1, G.14.11, and G.15.1, it is worthwhile to repeat some tables of this remarkable instrument.

AVHRR is of VHRR (Very High Resolution Radiometer) heritage, a two–channel instrument flown on the ITOS (Improved TIROS Operational System) series, starting with NOAA–2 (ITOS–D), launch of ITOS–D on Oct. 15, 1972. The last one of the series flying the VHRR instrument was NOAA–5 (ITOS–H) with a launch July 29, 1976.

Spacecraft	Launch Date	Ascending Node	Descending Node	S/C Service Period	
TIROS–N	Oct. 13, 1978	15:00	03:00	Oct. 19, 1978	Jan. 30, 1980
NOAA–6	Jun. 27, 1979	19:30	07:30	Jun. 27, 1979	Nov. 16, 1986
NOAA–7	Jun. 23, 1981	14:30	02:30	Aug. 24, 1981	Jun. 7, 1986
NOAA–8	Mar. 28, 1983	19:30	07:30	May 3, 1983	Oct. 31, 1985
NOAA–9	Dec. 12, 1984	14:20	02:20	Feb. 25, 1985	Aug. 3, 1995
NOAA–10	Sep. 17, 1986	19:30	07:30	Nov. 17, 1986	March 1995
NOAA–11	Sep. 24, 1988	13:30	01:40	Nov. 8, 1988	Sep. 9, 1994
NOAA–12	May 14, 1991	19:30	07:30	May 14, 1991	present
NOAA–13	Aug. 9, 1993	Failure 12 days after launch, NOAA lost contact with the S/C			
NOAA–14	Dec. 30, 1994	13:40	01:40	Dec. 30, 1994	present
NOAA–15	May 13, 1998	19:26	07:26	Dec. 15, 1998	present
NOAA–16	Sep. 21, 2000	14:00	02:00	Sept. 21, 2000	present
NOAA–17	June 24, 2002		10:00		
NOAA–17 is the last NOAA S/C in morning orbit; the future morning service is rendered by MetOp					

Table 114: Temporal AVHRR coverage of NOAA POES series satellites

1.20.2.1 Sea Surface Temperature (SST) measurements from LEO satellites

- SST is a physical parameter derived from microwave radiometer data as well as from infrared imagery (best retrieval of infrared SST observations in cloudless regions). The analysis of SST observations is an important indicator of the coupling between the ocean surface and the atmosphere – used in climate modeling and in many other fields (meteorology/oceanography). In general, observations at two or three wavelengths (in atmospheric windows) are combined in order to correct for atmospheric attenuation due to water vapor and aerosols. ¹⁹⁸²⁾ The ability to monitor global and regional surface temperature has improved considerably; it is now possible to use SST observations as indicators of regional – to basin–scale change, as well as for forecasting stress on the natural flora and faunal assemblages. SST is also very sensitive to changes in the ocean circulation, as demonstrated time and again by the ENSO cycle. – The longest data set of in–situ SST observations is based on observations initially made from ships (capturing buckets of seawater from over the sides of ships and measuring the temperature with a thermometer). From about 1870 onwards the ship observations were sufficiently frequent (very limited spatial coverage) to permit a global SST analysis.

First spaceborne infrared SST data was provided by the VHRR (Very High Resolution Radiometer) instrument flown on NOAA–2 (launch Oct. 15, 1972). Better spaceborne SST retrievals became available from channels 3 and 4 of the AVHRR/1 instrument flown on the TIROS–N S/C (launch Oct. 13, 1978). More accurate SST retrievals became available with the introduction of AVHRR/2, first flown on NOAA–7 (launch June 23, 1981) and subsequent NOAA/POES missions. The AVHRR/3 instrument generation (with 6 bands) was

¹⁹⁸²⁾ E. P. McClain, W. G. Pichel, C. C. Walton, Z. Ahmad, J. Sutton (1983) "Multichannel improvements to satellite derived global sea surface temperatures," *Advances in Space Research*, Vol. 2, 1983, pp.43–47.

first flown on NOAA–15 (launch May 13, 1998). SST observations are made from AVHRR using statistically derived retrievals schemes, to an accuracy of 0.4 to 0.6 K. The NOAA/NASA Pathfinder AVHRR/SST product is a high quality dataset derived from the NOAA/POES series of satellites that start with the NOAA–9 in 1985. This dataset represents a historical reprocessing of the entire AVHRR time series using consistent SST algorithms, improved satellite and intersatellite calibration, quality control and cloud detection.

The ATSR (Along Track Scanning Radiometer) instrument of ESA is flown on ERS–1/2 missions since July 1991 measuring infrared radiances (3 channels) from the Earth's surface at spatial resolutions of 1 km. ¹⁹⁸³⁾ ¹⁹⁸⁴⁾ ¹⁹⁸⁵⁾ AATSR of ESA (Advanced ATSR), flown on Envisat, provides a radiometric resolution of 0.1 K, an SST accuracy <0.5 K, and a spatial resolution of 1 km. A unique feature of all ATSR/AATSR instruments is their dual–observation geometry (forward and nadir scanning), doubling their retrieval capability. AASTR provides significantly improved calibration and noise parameters as compared to AVHRR/3. However, continuity of AASTR data beyond the Envisat era is not assured unless introduced into an operational system.

Mission	Instrument	Comment
NOAA/POES series starting with VHRR on NOAA–2 (launch Oct. 15, 1972)	VHRR, AVHRR/1, AVHRR/2, and AVHRR/3 (first /3 flight on NOAA–15 (launch May 13, 1998)	Operational series Operational series
Meteor–2 series starting with Meteor–2–4 (launch Oct. 25, 89)	Klimat	Pre–operational instrument of PLANETA, Russia
ERS–1 (launch July 17, 1991) ERS–2 (launch Apr. 21, 1995)	ATSR ATSR–2	Pre–operational instrument Pre–operational instrument
TRMM (launch Nov. 27, 1997)	TMI	Pre–operational instrument
IRS–P4 (launch May 26, 1999)	MSMR of ISRO	Pre–operational instrument
FY–1B (launch Sept. 3, 1990) FY–1C (launch May 10, 1999)	MVISR (Multichannel Visible and IR Scanning Radiometer)	Pre–operational instrument of CMA, China
Okean–O–1 (launch Jul. 16, 1999)	Delta–2D (Conical Scanning Microwave Radiometer)	Okean–O–1 operations lasted until fall 2000
Terra (launch Dec. 18, 1999) Aqua (launch May 4, 2002)	MODIS MODIS, AMSR–E	Pre–operational instrument Pre–operational instruments
Meteor–3M–1 (launch Dec. 10, 2001), Russia	MTVZA (Microwave Imaging/Sounding Radiometer)	Pre–operational instrument
Envisat (launch Mar. 1, 2002)	AATSR	Pre–operational instrument
HY–1A (Haiyang–1, launch May 15, 2002)	COCTS (Chinese Ocean Color and Temperature Scanner)	Pre–operational instrument
ADEOS–II (launch Dec. 14, 2002), JAXA	AMSR (Advanced Microwave Scanning Radiometer), GLI	Pre–operational instrument
Coriolis (launch Jan. 6, 2003)	WindSat	Demonstration for CMIS
Sich–1M (launch Dec. 24, 2004) Russia, Ukraine	MTVZA–OK (Combined Microwave–Optical Imaging/Sounding Radiometer)	Pre–operational instrument
EPS–MetOp series (starting with MetOp–A, launch Oct. 19, 2006)	AVHRR/3, IASI	Operational series
SMOS of ESA (launch Nov. 2, 2009)	MIRAS (for SSS and SST retrieval)	Demonstration instrument

1983) R. W. Reynolds, “Specific Contributions to the Observing System: Sea Surface Temperature,” Proceedings of OCEANOBS 99, Oct. 18–22, 1999, Saint Raphael, France

1984) C. J. Merchant, “Sea Surface Temperature – A Dynamic Field: Developments in Research and Operations,” The 2003 EUMETSAT Meteorological Satellite Conference, Weimar, Germany, Sept. 29 – Oct. 3, 2003

1985) http://www.met-office.gov.uk/research/nwp/satellite/infrared/sst/sst_climate.html

Mission	Instrument	Comment
GCOM-B1, JAXA (2008)	SGLI (Second-generation Global Imager) and AMSR-2	Pre-operational instruments
NPP (NPOESS Preparatory Project), launch Oct. 28, 2011	VIIRS (Visible/Infrared Imager and Radiometer Suite)	Pre-operational instrument
MetOp-B, launch Sept. 17, 2012	AVHRR/3, IASI	Operational series
JPSS (launch in 2016)	VIIRS, CMIS (Conical-scanning Microwave Imager/Sounder)	Operational series

Table 115: Overview of spaceborne LEO instruments suitable for SST retrieval

The accuracy of SST data is of great importance for climate modeling and climate change detection/prediction [numerical climate modeling with GCMs (Global Climate Models)]. The energy (gas) transfer between the ocean surface and the atmosphere is highly dependent on the “skin temperature” of the surface waters (surface winds are another important factor). For illustration: An error of 0.1 K in SST knowledge corresponds to an error in the global flux of CO₂ of 15%, while an error of 0.5 K leads to an error of 75% in CO₂ flux. – The algorithms for SST retrieval include the MCSST (Multichannel SST) and NLSST (Non-Linear SST) algorithms, and the newly implemented experimental ACSST (Aerosol-Corrected SST) scheme. 1986) 1987) 1988) 1989) 1990)

Passive microwave radiometers offer an all-weather observation capability for measuring SST (some atmospheric attenuation is experienced). The challenge with microwave instruments is to increase the spatial resolution of the data (which are in the ranges of 20–100 km depending on channel frequency). The first such instruments are: TMI (TRMM Microwave Imager) on TRMM, MSMR (Multifrequency Scanning Microwave Radiometer) on IRS-P4 (ISRO), MODIS and AMSR-E on Aqua (NASA) and AMSR on ADEOS-II (JAXA). MODIS is also flown on the Terra spacecraft of NASA. The MIS (Microwave Imager/Sounder) of the planned NPOESS series, an advanced instrument of SSM/I and SSMIS heritage of the DMSP (US/DoD) ¹⁹⁹¹⁾ satellite series, is a single look passive polarimetric microwave radiometer. SST is going to be one of the MIS data products with a medium-scale spatial resolution of about 25 km.

Note: Microwave SSTs cannot be obtained within about 100 km of the coast with current sensors because of contamination in the 5% sidelobes, and can be biased by islands of scale 1 km within the main field of view. But nonetheless, for non-coastal, lower resolution applications, MW SSTs are an excellent addition to the infrared SST observing system.

- 1986) C. C. Walton, W. G. Pichel, J. F. Sapper, D. A. May, “The development and operational application of nonlinear algorithms for the measurement of sea surface temperatures with the NOAA polarorbiting environmental satellites,” *Journal of Geophysical Research*, Vol, 103(C12), 1998, pp. 27,999–28,012.
- 1987) N. R. Nalli, F. Arzayus, E. Bayler, et al., “Satellite Sea Surface Temperature (SST) Research at NOAA/NESDIS,” <http://ams.confex.com/ams/pdfpapers/72091.pdf>
- 1988) E. P. McClain W. G. Pichel, C. C. Walton, “Comparative performance of AVHRR-based multichannel sea surface temperatures,” *Journal of Geophysical Research*, Vol, 90, 1985, p.11,587
- 1989) P. Schluessel, W. J. Emery, H. Grassl, T. Mammen, “On the bulk-skin temperature difference and its impact on satellite-remote sensing of sea surface temperature,” *Journal of Geophysical Research*, Vol. 95, 1990, p. 13,341
- 1990) C. C. Walton, “Nonlinear multichannel algorithms for estimating sea surface temperature with AVHRR satellite data,” *Journal of Applied Meteorology*, Vol. 27, 1988, p. 115
- 1991) Note: Earlier microwave radiometers like SMMR on SeaSat and Nimbus-7 (both launches in 1978) were poorly calibrated for for SST retrieval. The SSM/I instrument, flown on the DMSP series, did not have the low frequency channels needed for accurate SST retrieval algorithms.

1.20.3 GEO (Geostationary Orbit) Weather Satellites

The geostationary orbit provides new observation concepts, a synoptic view of Earth's disk. Satellites in geostationary orbits exhibit a fixed—position, constant—signal and a **continuous—coverage relationship** with large area coverage between the satellite and its ground segment. Conventional observation data, provided by the S/C instruments from GEO locations (about 45 times further away than LEO systems at altitude of 800 km), are generally of coarse resolution (in the order of kilometers). However, the data are ideal to monitor large—scale weather phenomena. — Since the mid 1960s a global network of geostationary meteorological satellites has been built up continuously around the equator orbital plane by the various national agencies of the world to provide an ever—increasing service to its user community. The data of the various satellite series also contribute to GARP (Global Atmospheric Research Program) of WMO.

- The NASA ATS (Application Technology Satellite) series set the stage for demonstrations (in particular communication experiments, first meteorological observations, etc.) in geostationary orbits. ATS—1 (launch Dec. 6, 1966, with a mass of 414 kg) flew SSCC (Spin—Scan Cloudcover Camera) to provide continuous cloudcover patterns of the full—disk Earth view. The telescope photomultiplier assembly could be tilted in discrete steps to $\pm 7.5^\circ$ to a north—south scan (equivalent to $\pm 52^\circ$ latitude). The east—west scan was provided by the S/C spin of 100 rpm. A ground resolution of about 4 km was obtained. SSCC operated on ATS—1 until Oct. 16, 1972.

ATS—1 (Applications Technology Satellite), a spin—stabilized S/C (mass of 352 kg), built by Hughes Aircraft Company, was the first experimental near—geostationary weather satellite (position at 150° W longitude) with the ability to “**see weather systems**” with SSCC, an instrument built by Hughes SBRC.^{1992) 1993)} The optical system consisted of a two—element Cassegrain—type telescopes. SSCC provided imagery of the Earth in the visible spectrum. Within the first month of the availability of ATS—1 imagery, a time—sequence movie of mesoscale cloud patterns in motion was shown on TV (the animated imagery revealed atmospheric motion and their potential use for research and operations). By the early 1970s ATS imagery was being used in US operational forecast centers. ATS—1 also served as a platform for several communication experiments:

- C—band communications experiment (also used for international TV broadcasts)
- VHF communications package. The VHF experiment tested the ability to act as a link between ground stations and aircraft, demonstrated collection of meteorological data from remote terminals, and evaluated the feasibility of using VHF signals for navigation.
- A WEFAX (Weather Facsimile) system experiment was flown for the first time with the intention to test satellite retransmissions of meteorological data products to participating ground stations.

The ATS—3 S/C (launched Nov. 5, 1967, positioned at 70° W, spin stabilized, mass = 365 kg, equipped with a mechanically despun antenna)¹⁹⁹⁴⁾ flew for the first time the **MSSCC** (Multicolor Spin—Scan Cloud Camera) instrument (built by SBRC) providing full—disk Earth—cloud images in color. A cartwheel mounting configuration was realized with MSSCC (the concept was first introduced on TIROS—9), i. e., the instrument was mounted with its optical axis perpendicular to the S/C spin axis, permitting to view the Earth through a special aperture in the S/C cylindrical wall.

1992) W. P. Menzel, “Cloud Tracking with Satellite Imagery: From the Pioneering Work of Ted Fujita to the Present,” *Bulletin of the American Meteorological Society*, Vol. 82, No 1, Jan. 2001, pp. 33–47

1993) T. Fujita, W. A. Bohan, “Detailed Views of Mesoscale Cloud Patterns Filmed from ATS—1 Pictures,” a 16 mm film of 9 minute length is available from Walter A. Bohan Co., P. O. Box 736, Park Ridge, IL 60068–0736, USA

1994) J. R. Greaves, W. E. Shenk, “The Development of the Geosynchronous Weather Satellite System,” *Monitoring Earth's Ocean, Land, and Atmosphere from Space – Sensors, Systems, and Applications*, Progress in Astronautics and Aeronautics, AIAA, Volume 97, 1985, pp. 150–181

• NASA's demonstration of two Synchronous Meteorological Satellites (SMS) began with the launch of SMS-1 on May 17, 1974. NOAA's operation of the GOES series followed with the launch of GOES-1 in October 1975. The SMS satellites carried VISSR (Visible Infrared Spin-Scan Radiometer) as prime instruments. VISSR provided high-quality day/night cloudcover data and made radiance temperature measurements of the Earth-atmosphere system. – The evolution of ATS into SMS and eventually into the GOES series permitted new services like the routine tracking of clouds with infrared imagery available for cloud height determination and nighttime tracking capabilities.

S/C Series (Agency)	Launch	Major Instruments	Comment
ATS-1 to ATS-6 (NASA) GOES-1 to -7 (NOAA) GOES-8 to -12 (NOAA) GOES-R series (planning)	6.12.1966, 12.8.1969 16.10.1975, 26.2.1987 13.4.1994, 23.7. 2001 for 2014-2029 period	SSCC (MSSCC ATS-3) VISSR GOES-Imager, Sounder ABI,, HES,	Tech. Demonstration 1st generation 2nd gener. (GOES-P) 3rd Generation
GMS-1 to -5 (JMA) MTSAT-1 (JMA, et al.) MTSAT-1R (JMA) MTSAT-2 (JMA)	14.7.1977, 18.3.1995 Nov. 15, 1999 (launch failure of H-2 vehicle) Launch Feb. 26, 2005 Launch Feb. 18, 2006	VISSR Imager (GOES heritage) JAMI JAMI	1st generation 2nd generation
Meteosat-1 to -7 (Eumetsat) Meteosat-8 [(MSG-1) to MSG-4] MTG series (in planning)	23.11.1977, 3.9.1997 28.8.2002 for period after 2015	MVIRI SEVIRI, GERB	1st generation 2nd generation 3rd generation
INSAT-1B to -1D (ISRO) INSAT-2A to -2E (ISRO) INSAT-3B (ISRO) INSAT-3A (ISRO) MetSat-1/Kalpana-1 (ISRO) INSAT-3D	30.8.1983 - 12.6.1990 9.7.1992 - 2.4.1999 21.3.2000 9.4.2003 12.9.2002 2006 25.07.2013	VHRR VHRR/2 VHRR/2 VHRR/2 Imager+sounder Imager+sounder	Starting with -2E Communications only Weather satellite only Weather satellite only
GOMS-1 (Russia/Planeta) GOMS-2 (Electro-L, Russia)	31.10.1994 20.01.2011	STR MSU-GS, GGAK-E	1st generation 2nd generation
FY-2A to -2B (CMA), China FY-2C, FY-2D, FY-2E FY-4 series (in planning)	10.6.1997, 26.6.2000, 19.10.2004, 8.12.2006, 2009 for period after 2010	S-VISSR	1st generation 2nd generation
COMS-1 (KARI) Korea	26.06.2010	MI (Meteorological Imager), GOCI (Geostationary Ocean Color Imager)	1st generation <i>GOCI is the first ocean color imager from GEO</i>

Table 116: Overview of geostationary meteorological satellites

• The current 2nd generation GOES system of NOAA (GOES-8 to -12 and -N to -P series) consists of two operational satellites covering the East and West portions of the Americas. The constellation consists of environmental sensors, auxiliary payload services and rebroadcast capabilities. GOES auxiliary payload services consist of DCS (Direct Communication Services), EMWIN (EMergency Weather Information Network), LRIT (Low Rate Information Transfer), and S&RSat (Search And Rescue Satellite Aided Tracking). Initial LRIT operations were started in Aug. 2003, the transition will be complete in 2005. LRIT is a digital communications transmission system, a broadcast service with increased capabilities (data compression, larger volumes, etc.), provided by the GOES satellites, replacing the current analog WEFAX (Weather Facsimile) transmission system.

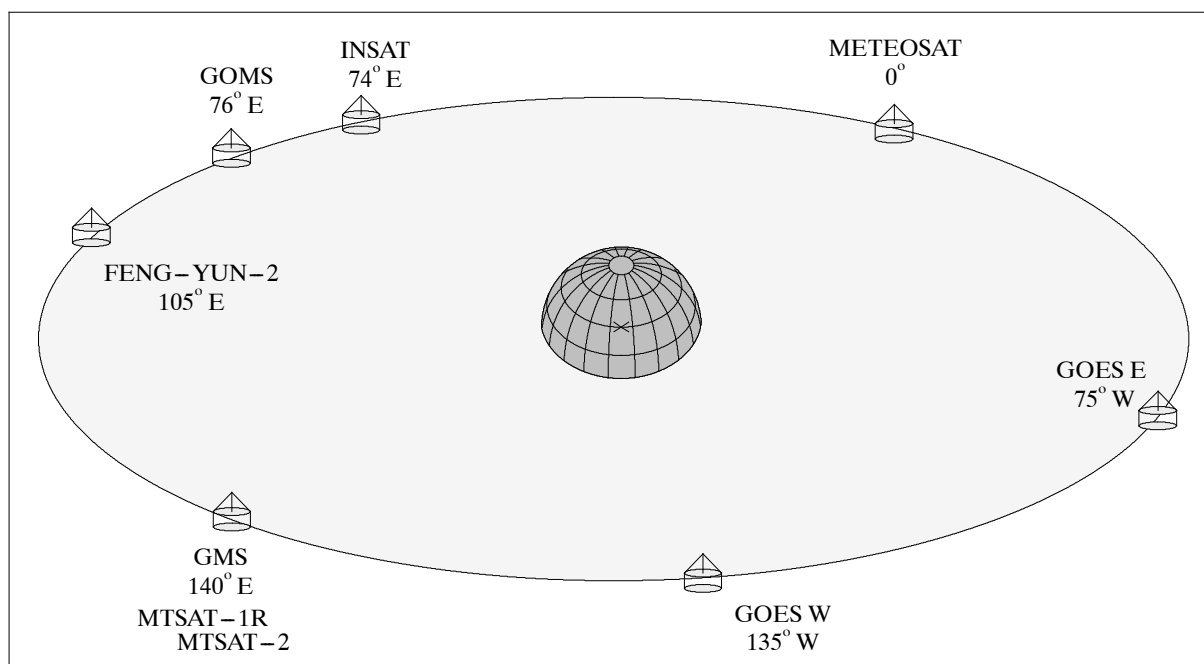


Figure 149: The geostationary meteorological satellite families

- Japan started its geostationary meteorological program with the launch of GMS-1 (Geostationary Meteorological Satellite-1, referred to as Himawari-1 in Japan) of JMA (Japan Meteorological Agency) and JAXA (formerly NASDA) on July 7, 1977 (see F.3). The newest entry into the ring, MTSAT-1 (Multifunctional Transport Satellite-1) with a launch Nov. 15, 1999 (however, a launch failure of the H-2 vehicle occurred), provides the double service of an “aeronautical mission” (providing navigation data to air-traffic control services in the Asia-Pacific region) and a “meteorological mission.” In the latter function, MTSAT is a successor program to the GMS series. A replacement satellite, MTSAT-1R, was launched Feb. 26, 2005. The prime instrument of the meteorology mission on MTSAT-1R is JAMI (Japanese Advanced Meteorological Imager), see F.10.1.2. MTSAT-2 was launched on Feb. 18, 2006.
- The METEOSAT program of Europe was initiated by ESA in 1972 followed by a launch of METEOSAT-1 (a demonstration satellite) on Nov. 23, 1977. The EUMETSAT convention was signed on May 24, 1983 by 16 countries. On January 1, 1987, responsibility for the operation of the METEOSAT spacecraft was transferred from ESA to EUMETSAT (F.8). The MSG (METEOSAT Second Generation) series with a launch of MSG-1 on Aug. 28, 2002 provides considerable improvements (location at 10° W).
- India started planning of the INSAT series in the 1970s with a launch of INSAT-1B on April 30, 1983 (see F.6). INSAT is a multipurpose operational satellite system series (geostationary) employed for meteorological observation over India and the Indian Ocean, as well as for domestic telecommunications (nationwide direct TV broadcasting, TV program distribution, meteorological data distribution, etc.). The ISRO-developed prime instrument VHRR (Very High-Resolution Radiometer) was enhanced several times providing high-quality data of 2 km spatial resolution in the visible and SWIR bands, and 8 km resolution in the IR and TIR bands. VHRR/2 was introduced with INSAT-2E (including a water vapor band at 5.7–7.1 μm). The last satellite of INSAT-1 series, namely INSAT-1D, was deactivated on May 14, 2002 after providing useful services for about 12 years.
- In 2000, the Government of India approved a dedicated GEO weather satellite program named **MetSat** (Meteorological Satellite). The launch of MetSat-1 into GTO took place on Sept. 12, 2002 with ISRO’s PSLV (Polar Satellite Launch Vehicle) from SHAR (Sriharikota High Altitude Range), India (launch mass of 1055 kg including 560 kg of pro-

pellant; S/C position at 74° E). MetSat–1, equipped with VHRR, is expected to fill the void caused by two important meteorological payloads, namely VHRR/2 on INSAT–2E which failed already in 1999. On Nov. 4, 2000, ISRO was forced to retire INSAT–2B, after it ran out of station—keeping fuel (in July 2000, INSAT–2B completed its design life of seven years of operation). This action stopped of course also the VHRR instrument on INSAT–2B, used for operational meteorology. Note: In a commemorative ceremony on Feb. 6, 2003, the MetSat–1 satellite of ISRO was renamed to **Kalpana–1** by Indian Prime Minister Atal Bihari Vajpayee. This is to honor Kalpana Chawla, born in Karnal (1961), India, who died as a NASA astronaut on Feb. 1, 2003 over the southern USA when Space Shuttle Columbia (flight STS–107, Jan. 16 – Feb. 1, 2003) and her crew perished during reentry.

- Russia launched GOMS–1 (Geostationary Operational Meteorological Satellite–1) on October 31, 1994. STR (Scanning TV Radiometer) is the prime instrument to observe clouds and underlying surface in VIS and IR bands. GOMS–1, also referred to as Electro–1, ended operations in Nov. 2000. Russia launched Electro–L / GOMS–2 spacecraft on January 20, 2011. Until that time, the Russian weather service is dependent on the services provided by Meteosat of EUMETSAT with regard to GEO data.

- China joined the geostationary meteorological club in 1997 with the launch of FY–2A (Feng–Yun–2A) on June 10, 1997. The prime sensor, S–VISSR (Stretched – Visible and Infrared Spin–Scan Radiometer) is an optomechanical system, providing observations in three bands (at resolutions of: 1.25 km in VIS, 5 km in IR and water vapor). Upgrade of VISSR on FY–2C, –2D, –2E (5 channels). – The 2nd generation satellites in GEO, FY–4 series, is expected to be launched beyond the time frame of 2010.

- Definition of GOES–R (start in 2000). The next–generation (3rd) geostationary weather satellite family of NOAA, under definition/development at NOAA, NASA as well as at other institutions, begins with the GOES–R spacecraft and its newly defined sensor complement (launch of GOES–R is planned for 2014). The GOES–R objectives are to overcome some of the shortcomings of the current system by providing: mission continuity [with the current system data losses occur for several hours each day during the weeks around the spring and fall equinoxes (eclipse)], simultaneous hemispheric, synoptic, and mesoscale imaging, and data timeliness (considerable improvements in data latency). The new series will provide greatly enhanced observation capabilities with two prime instruments: ABI (Advanced Baseline Imager), and HES (Hyperspectral Environmental Suite), an infrared sounder.

The key enabling technology introduced by both instruments is the provision of multiple simultaneous observation scenes (multiresolution data of three pointable target regions of different size and resolution – spatial and temporal), permitting new and better data interpretation capabilities. ABI offers imaging of three area sectors, referred to as: FD (Full Disk), CONUS (Contiguous USA), and Mesoscale, each with a different coverage size. Temporal coverage of: 1 FD, 3 CONUS and 30 Mesoscale images, every 15 minutes; the spatial coverage is 0.5 km for VIS and 2 km for IR. The HES operational concept consists also of three regional observation functions on different scales (can be performed simultaneously): high–resolution hemispheric DS (Disk Sounding), SW/M (Severe Weather/Mesoscale) soundings, and CW (Coastal Water) imaging. HES will feature about 1500 narrow spectral bands in IR for much improved vertical sounding, and a 4 km ground spatial resolution on the sounder.¹⁹⁹⁵⁾ Considering both spatial and spectral performance, the HES specifications require about a two order of magnitude performance increase over the currently used GOES–I to –P atmospheric sounder. Synergistic use of ABI and HES data provide products with better accuracy than that from either system alone. GOES–R will provide partial global repeat coverage every 15 minutes or less – – representing a contributing ele-

1995) J. Li, F. Sun, T. J. Schmit, W. P. Menzel, J. Gurka, “Study of the Hyperspectral Environmental Suite (HES) on GOES–R,” 20th International Conference on Interactive Information and Processing Systems (IIPS) for Meteorology, Oceanography, and Hydrology, Seattle, WA, Jan. 11–15, 2004

ment in the USA to an IEOS (Integrated Earth Observation System), together with NPOESS. A GMS (Geostationary Microwave Sounder) is also considered to be part of the payload on the GOES-R (-S, -T, -U) series to demonstrate observations in the microwave region. 1996) 1997) 1998)

- Preparatory activities for the MTG (Meteosat Third Generation) series planning (user mission consultation process and requirements, and pre-phase A concept studies) were initiated by EUMETSAT and ESA at the end of 2000. The development and test phase of the MTG system is planned for the time frame 2009–2014.

1.20.3.1 Sea Surface Temperature (SST) from GEO satellites

SST products are also being generated from multi-channel infrared brightness temperatures, referred to as MCSST (Multi-Channel SST) of instruments on weather satellites in GEO – complementing the SST products from LEO. 1999) 2000) A newer SST retrieval scheme is based on RTM (Radiative Transfer Modeling) algorithms. SST observations from GEO permit high temporal resolutions in particular of the oceans up to moderate latitudes. There is now the capability to determine the diurnal cycle of SST throughout most of the world's oceans [in regions of persistent cloud cover, observations from GEO increase the likelihood of obtaining a clear-sky observation and thus allow the possibility of resolving the diurnal cycle of SST]. This represents also an important step in the production of a global high-resolution SST analysis that combines polar and geostationary observations. SST data products from GEO represent a more recent development. Some examples of missions are: 2001) 2002) 2003) 2004) 2005)

- NOAA/NESDIS is providing SST products from the GOES Imager of its GOES-9 (on an experimental basis), -10, and -12 satellites, located at longitudes 154.5° E, 135° W and 75° W, respectively. This service began in 2000 by offering the first operational products.
- SEVIRI (Spinning Enhanced Visible and Infrared Imager) of EUMETSAT is flown on MSG-1 (launch Aug. 28, 2002). The MSG-1 processing chains of SST products (SEVIRI brightness temperatures at 3.9, 11 and 12 μm) started in mid-2003.
- CMA of China is also readying its algorithms for SST product generation from its FY-2 (launch June 10, 1997) spacecraft in GEO.

- 1996) E. Miller, M. Madden, B. Nelson, "National Oceanic And Atmospheric Administration's (NOAA) – Next Generation Geostationary Satellite (GOES R)," ISRSE, Honolulu, HI, Nov. 10–14, 2003
- 1997) J. F. W. Purdom, "Geostationary Hyperspectral Imaging from 0.4 to 1 Microns A Potent Tool for Analysis and Now-casting," The 2003 EUMETSAT Meteorological Satellite Conference, Weimar, Germany, Sept. 29 – Oct. 3, 2003
- 1998) J. J. Gurka, T. J. Schmit, R. R. Reynolds, "Highlights from the second GOES Users' Conference: Recommendations for the GOES-R Series," 20th International Conference on Interactive Information and Processing Systems (IIPS) for Meteorology, Oceanography, and Hydrology, Seattle, WA, Jan. 11–15, 2004
- 1999) E. Maturi, A. Harris, N. Nalli, C. Merchant, S. McCullum, R. Meiggs, R. Potash, "NOAA's Operational Geostationary Sea Surface Temperature Products," 84th AMS Annual Meeting, Seattle WA, January 11–15, 2004
- 2000) P. Le Borgne, G. Legendre, A. Marsouin, "Ocean and Sea Ice SAF Products from MSG Data," The 2003 EUMETSAT Meteorological Satellite Conference, Weimar, Germany, Sept. 29 – Oct. 3, 2003
- 2001) N. R. Nalli, F. Arzayus, E. Bayler, P. Chang, P. Clemente-Colón, A. Harris, A. Ignatov, R. Legeckis, et al., "Satellite Sea Surface Temperature (SST) Research at NOAA/NESDIS," 84th AMS Annual Meeting, Seattle WA, Jan. 11–15, 2004
- 2002) X. Wu, W. P. Menzel, G. Wade, "Estimation of sea surface temperatures using GOES 8/9 radiance measurements," Bulletin of the American Meteorological Society, Vol. 80, 1999, pp. 1127–1138.
- 2003) C. J. Merchant, A. R. Harris, M. J. Murray, A. M. Zavody, "Toward the elimination of bias in satellite retrievals of sea surface temperature, 1, Theory, modeling and interalgorithm comparison. Journal of Geophysical Research, Vol. 104(C10), 1999 pp. 23565–23,578
- 2004) C. J. Merchant, A. R. Harris, "Toward the elimination of bias in satellite retrievals of sea surface temperature, 2, Comparison with in situ measurements," Journal of Geophysical Research, Vol. 104(C10), 1999 pp. 23,579 – 23,590.
- 2005) <http://www.gisdevelopment.net/aars/acrs/1999/ts8/ts8205.shtml>

- The MTSAT – 1R (Multifunction Transport Satellite) of JMA (launch Feb. 26, 2005) is equipped with JAMI (Japanese Advanced Meteorological Imager) on its meteorological mission. JAMI features four infrared bands, two of them (TIR1 and TIR2) are providing SST and water vapor retrievals.
- The MI (Meteorological Imager), flown on the COMS – 1 (Communication, Ocean and Meteorological Satellite – 1) spacecraft of Korea (launch June 26, 2010) is providing SST data in the TIR bands (10.3 – 11.3 μm and 11.5 – 12.5 μm) of the instrument.

In addition, the COMS – 1 spacecraft is flying **GOCI** (Geostationary Ocean Color Imager), the world's 1st geostationary ocean color imager with the objective to provide multispectral (8 – band) VIS/NIR data.

1.20.4 GPS/GNSS meteorology – RF (Radio Frequency) occultation monitoring

Refractive occultation monitoring, also referred to as **RF occultation monitoring** (Earth–observation applications of navigation systems and use of GPS receivers as science instruments in meteorology applications). In 1995, retrievals of Earth’s atmospheric limb soundings (moisture and temperature distributions) were first demonstrated by GPS receiver sounding techniques referred to as “refractive occultation monitoring.” The measurement technique makes use of occulting navigation signals of the GPS constellation satellites (rising or setting behind the Earth’s limb) as they pass through the atmosphere and are intercepted by a GPS receiver located either on a LEO S/C, or anywhere on the surface of Earth (the signal refraction angle and/or retardation is measured with the GPS receivers). The highly accurate measurements, obtained with these special–function GPS receivers, permit the derivation of vertical profiles of the temperature [temperature profiles with an high vertical resolution (≤ 1 km) and accuracy (≤ 1 K)], pressure and humidity in the atmosphere, as well as profiles of electron content in the ionosphere. ^{2006) 2007) 2008)}

GPS occultation measurements from LEO S/C represent a valuable and economic data source in addition to the traditional meteorological measurements (e.g., radiosonde, nadir–viewing satellite based radiometers) and ground–based GPS networks (antenna zenith delays).

Background: The RO (Radio Occultation) technique was proposed/invented in the early 1960s by a team of NASA/JPL and Stanford University (the first relevant proposal came from Stanford University Center for Radar Astronomy in 1962). It was first successfully demonstrated in NASA’s planetary exploration program to Mars (Mariner–IV launch in 1964, flyby in July 1965). Since then nearly every US planetary mission has included a radio occultation instrument. ²⁰⁰⁹⁾ The occultation technique was applied to Earth’s ionosphere in 1974–1975 using the radio link between the GEOS–3 and ATS–6 satellites. Applying this technique to the Earth’s atmosphere and using the GPS constellation as a source and a GPS receiver in LEO was first suggested in the late 1980s in two papers: ²⁰¹⁰⁾

– A. S. Gurvich, T. G. Krasilnikova, “Navigation Satellites for Radio Sounding of the Earth’s Atmosphere,” Issled. Zemli Kosmosa, Vol. 6, 1986 (in English: Soviet Journal of Remote Sensing, 6, 1990),

– T. P. Yunck et al. “The role of GPS in precise Earth observation, Proceedings of the IEEE Position, Location, and Navigation Symposium, Orlando, FLA, 1988.

Also in 1988, JPL submitted a proposal for the development of GGI (GPS Geosciences Instrument) to be flown on NASA’s EOS (Earth Observing System) spacecraft. Unfortunately, GGI was never flown, but the development effort enabled eventually the development of GPS/MET. – The deployment of GNSS (Global Navigation Satellite Systems) constellations such as GPS and GLONASS with their network of navigation signals made radio occultation techniques possible in the Earth’s atmosphere for applications of weather and climate studies. Prior to GPS, there was a general lack of radio sources suited to meet the performance requirements of refractive radio occultation.

• The **GPS/MET** instrument of UCAR/JPL on OrbView–1/Microlab–1 (launch April 3, 1995, B.11) introduced this alternate sounding technique to Earth observation, starting a

2006) T. P. Yunck, C. H. Liu, R. Ware, “A History of GPS Sounding,” Special issue of TAO (Terrestrial, Atmospheric and Oceanic Science, Vol. 11, No 1, March 2000, pp. 1–20

2007) W. G. Melbourne, et al., “The Application of Spaceborne GPS to Atmospheric Limb Sounding and Global Change Monitoring, JPL Pub. 94–18, Pasadena, CA, 147 pp., 1994

2008) W. Bertiger, Y. Bar–Sever, S. Desai, et al., “Precise Orbit Determination for the Shuttle Radar Topography Mission using a New Generation of GPS Receiver,” ION GPS–2000, Sept. 19–22, 2000, Salt Lake City, UT, pp.1646–1654

2009) R. E. Kursinski, G. A. Hajj, S. S. Leroy, B. Herman, “The GPS Radio Occultation Technique, TAO, Vol.11, No 1, March 2000, pp. 53–114, see also: <http://tao.gcc.ntu.edu.tw/pdf/v11-1/v111pi.pdf>

2010) <http://www.geooptics.com/GeoOptics/Frames.html>

new era of atmospheric profiling technology. GPS/MET temperature retrieval accuracies of better than 1K have been demonstrated in the altitude range of 10–30 km during the proof-of-concept phase of the mission with vertical resolutions of better than 1 km. This all-weather sounding technique promises to greatly contribute to global atmospheric monitoring, offering an abundance of data for operational meteorology and climatology. TEC (Total Electron Content) profiles of the ionosphere may be obtained by means of the Abel inversion technique which assumes spherical symmetry. The TRSR (TurboRogue Space Receiver) instruments of GFO (GEOSAT Follow-On, launch Feb. 10, 1998), SUNSAT and Ørsted (both were launched Feb. 23, 1999) missions are a further development of the GPS/MET instrument on OrbView-1/Microlab-1. The TRSR instruments of NASA/JPL were manufactured by Allen Osborne Associates Inc. of Westlake Village, CA. 2011) 2012) 2013) 2014)

- The following missions use the **BlackJack** configuration (built by SpectrumAstro of Gilbert, AZ, for JPL – AstroNav is the SpectrumAstro product name for BlackJack) a new generation of GPS flight receiver and a TRSR successor: SRTM (Feb. 11–22, 2000), CHAMP (launch July 15, 2000), SAC-C (launch Nov. 21, 2000), Jason-1 (launch Dec. 7, 2001), GRACE (launch March 17, 2002), ICESat (use of two BlackJack units, launch Jan. 13, 2003). 2015) 2016) 2017) As an integrated service system (offering the functions of tracking mode, occultation mode, and altimetry mode support), the full BlackJack configuration is using a multiple antenna design.

Other missions using refractive radio occultation techniques are: a) MetOp-A (launch Oct. 19, 2006) with GRAS (GNSS Receiver for Atmospheric Sounding), and b) FormoSat-3/COSMIC (Constellation Observing System for Meteorology, Ionosphere and Climate), a collaborative US/Taiwanese six-microsatellite constellation, a launch took place on April 14, 2006. FormoSat-3/COSMIC with its **IGOR** (Integrated GPS Occultation Receiver) GPS receiver [of BlackJack heritage, IGOR was built by BRE (Broad Reach Engineering) Company of Tempe, AZ, under JPL license] demonstrates – for the first time – the usefulness of microsatellite constellations in obtaining global atmospheric “snapshots” in near-real time. The system has the potential to furnish valuable data for weather prediction, global climate-change analysis and research, and ionospheric research and prediction. The IGOR receivers are fully software compatible with the BlackJack device.

The basic functions of the radio occultation technique include: a) reception of signals that have crossed the atmosphere at varying altitudes by means of two antenna arrays; b) acquisition of such signals, also during the rise (ascending) of occultation events, when a signal first appears after crossing dense tropospheric layers causing large dynamics in amplitude and phase; c) signal tracking to provide precise amplitude and phase measurements; d) onboard processing to support occultation-event predictions, also to aid the tracking.

- As of 2002, preliminary evaluations of BlackJack data from CHAMP and SAC-C indicate this technology will be applicable to fields as diverse as weather prediction and climate

- 2011) G. A. Hajj, L. J. Romans, “Ionospheric electron density profiles obtained with the Global Positioning System: Results from the GPS/MET experiment,”. *Radio Science*, Vol 33, No 1, pp.175–190, January–February 1998
- 2012) M. García-Fernández, M. Hernández-Pajares, J. M. Juan, J. Sanz, R. Orús, “Improving the determination of electron density profiles combining ground and LEO GPS data,” NAVITEC 2001, 1st ESA Workshop on Satellite Navigation User Equipment Technologies, Dec. 10–12, 2001, ESA/ESTEC
- 2013) G. Hajj, E. R. Kursinski, et. al., “Sensing the Atmosphere From a Low-Earth Orbiter Tracking GPS: Early Results and Lessons From the GPS/MET Experiment,” *Proceedings of ION GPS-95*, Sept. 12–15, 1995, pp. 1167–1174
- 2014) E. R. Kursinski, G. A. Hajj, J. T. Schofield, R. P. Linfield, K. R. Hardy, “Observing Earth’s Atmosphere with Radio Occultation Measurements using the Global Positioning System,” *Journal of Geophysical Research* Vol. 102, 1997
- 2015) P. Silvestrin, P. J. Baptista, P. Hoeg, “Radio Occultation Data Analysis: From Planetary Atmosphere Sounding to Operational Meteorology,” *Proceedings of 32nd ESLAB Symposium on Remote Sensing Methodology for Earth Observation and Planetary Exploration*, ESA/ESTEC, Sept. 15–18, 1998 (SP-423 Dec. 1998), pp.179–187
- 2016) P. Silvestrin, “Earth-Observation Applications of Navigation Satellites,” *ESA Bulletin*, No 102, May 2000, pp. 101–106
- 2017) P. Silvestrin, R. Bagge, M. Bonnedal, et al., “Spaceborne GNSS Radio Occultation Instrumentation for Operational Applications,” *ION GPS 2000*, Sept. 19–22, 2000, Salt Lake City, UT, pp. 872–880

research, Sun–Earth interaction research, solid Earth dynamics and oceanography. It may also be used to create the first 3–D images of Earth’s ionosphere, a turbulent and mysterious shroud of charged particles that, when stimulated by solar flares, can disrupt communications around the world.

- ROSA (Radio Occultation Sounder for Atmospheric studies) is a new GPS occultation receiver provided by ASI (Italian Space Agency) and a first flight on the OceanSat–2 mission of ISRO (launch Sept. 23, 2009). The ROSA instrument has been developed by TAS–I (Thales Alenia Space–Italia) formerly Laben. The ROSA payload is a dual channel GPS receiver with two antennae and a receiver package. The radio–occultation antenna, looking along the satellite velocity vector, receives signals from the ‘rising’ GPS satellites near the Earth horizon. These signals get refracted by the atmosphere and from the bending angle, the temperature and humidity profiles are derived. The POD (Precise Orbit Determination) antenna, looking at the zenith of the satellite, gives precise position of the receiver.

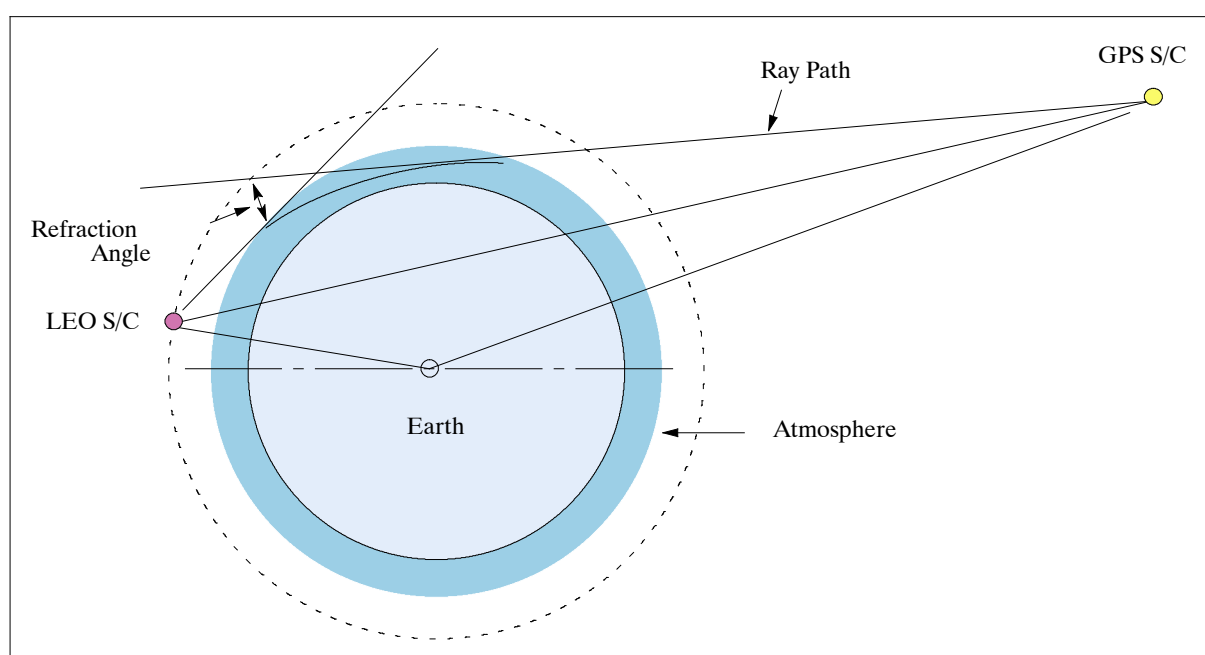


Figure 150: Schematic occultation monitoring configuration for a S/C in LEO

- TriG (GPS+Galileo+GLONASS) receiver of NASA/JPL. The objective is to provide GRO (GNSS Radio Occultation) measurements in the stratosphere and troposphere that contribute to two major societal benefits: monitoring climate and climate variability; and improving operational weather prediction. In 2009, TriG is a proposed development intended for the support of the follow–on constellation of the current Taiwanese/US FormoSat–3/COSMIC mission, which is expected to continue operations through 2011. The follow–on mission will be a new constellation of 12 to 18 satellites equipped with the GNSS RO payload (i.e. TriG receiver) and collect over 9000 soundings per day. This higher density of sounding profiles will be useful for global and mesoscale models, and also severe weather forecasting. (2018) (2019)

The TriG receiver will inherit the POD (Precise Orbit Determination) and RO (Radio Occultation) algorithms from the BlackJack/IGOR implementation. The hardware can be upgraded to high–rel CPU, logic and RF components to provide higher TID, SEU and SEE

2018) T. K. Meehan, “The TriG Digital Beam Steered Sounder,” Proceedings of the 2009 IEEE Aerospace Conference, Big Sky, MT, USA, March 7–14, 2009

2019) Chen–Joe Fong, Nick L. Yen, Chung–Huei Chu, Chun–Chieh Hsiao, Shan–Kuo Yang, Yao–Chang Lin, Shao–Shing Chen, Yuei–An Liou, Sien Chi, “In Quest of Global Radio Occultation Mission for Meteorology beyond 2011,” Proceedings of the 2009 IEEE Aerospace Conference, Big Sky, MT, USA, March 7–14, 2009

tolerance. The new hardware will add a third frequency, L5 and increase the number of channels from 16 to 36. The tracking specific hardware is reconfigurable FPGA logic which can be remotely programmed (even post-launch) to track new signal modulations anticipated for GLONASS (CDMA) and Galileo. – Producing precise measurements at three RF frequencies from multiple antennas will require a new RF signal processing development. The solution proposed for TriG is a high-rel, rad-hard RF-ASIC chip that can amplify, downconvert, filter and digitize separate L1, L2 and L5 analog RF streams in a thumbnail sized package.

Mission	Instrument	Comment
OrbView-1/Microlab (launch Apr. 3, 1995)	GPS/MET	NASA/UCAR
GFO (launch Feb. 10, 1998)	TRSR (JPL)	US Navy
SUNSAT (launch Feb. 23, 1999) Ørsted (launch Feb. 23, 1999)	TRSR TRSR	University of Stellenbosch, South Africa Danish geomagnetic mission
SRTM (Feb. 11–22, 2000) Shuttle mission	BlackJack (JPL)	NASA, DLR, ASI
CHAMP (launch Jul. 15, 2000)	IGOR	GFZ, DLR
TiungSat (launch Sept. 26, 2000), D.62.19	Experimental GPS	ATSB (Malaysia) S/C built by SSTL. Refractive sounding of the ionosphere
SAC-C (launch Nov. 21, 2000)	IGOR/GOLPE; INES	CONAE, NASA/JPL Laben/ASI (INES prototype instrument)
PICOSat (launch Sept. 30, 2001) of USAF/SSP	IOX (SMC)	Ionospheric Sounding Experiment measures electron profiles (TEC) with GPS, IOX is of TRSR heritage
Jason-1 (launch Dec. 7, 2001)	TRSR-2/IGOR	NASA/CNES mission, RO measurements, instrument provided by JPL/BRE
FedSat (launch Dec. 14, 2002), TEC (Total Electron Content)	BlackJack (AstroNav)	Australian mission (CRCSS), single antenna configuration, TEC monitoring
GRACE (launch March 17, 2002)	IGOR	US-German Earth gravity mission
ICESat (launch Jan. 13, 2003)	BlackJack	NASA (2 BJ instruments)
COSMO/SkyMed constellation of ASI (launch of first S/C on June 8, 2007)	LAGRANGE	Demonstration model of Laben S.p.A. for GNSS occultation monitoring
FormoSat-3/COSMIC (launch Apr. 14, 2006) Constellation of six microsatellites	IGOR	Taiwanese-US mission. Note: The mission is also referred to as FormoSat-3
MetOp-A (launch Oct. 19, 2006)	GRAS	EUMETSAT mission
TacSat-2 (launch Dec. 16, 2006)	IGOR	AFRL demonstration mission with IGOR provided by BRE
TerraSAR-X (launch June 15, 2007)	TOR/IGOR	DLR/EADS Astrium mission, TOR provided by GFZ and UTA/CSR
Jason-2 (launch June 20, 2008), operated by NOAA and EUMETSAT	TRSR-2/IGOR	NASA/CNES mission, RO measurements, instrument provided by JPL/BRE
OceanSat-2 (launch Sept. 23, 2009)	ROSA	ISRO mission, ROSA is provided by ASI of Italy
TanDEM-X (launch June 21, 2010)	TOR/IGOR	DLR/EADS Astrium mission, TOR provided by GFZ and UTA/CSR
SAC-D/Aquarius (launch June 10, 2011)	ROSA	CONAE (Argentina)/NASA mission, ROSA is provided by ASI of Italy
Megha/Tropiques (launch Oct. 12, 2011)	GPS-ROS	ISRO/CNES mission, GPS-ROS provided by ASI of Italy
MetOp-B (launch Sept. 17, 2012)	GRAS	EUMETSAT/ESA mission
KOMPSAT-5 (launch Aug. 22, 2013)	AOPOD	KARI mission (Korea with AOPOD of KASI)
CICERO (first launch 2013, planned)	Pyxis	US constellation, Pyxis GPS receiver from BroadReach (IGOR follow-up)
FormoSat-7/COSMIC-2 (2015, 2017)	TriG-RO	Taiwan-US constellation of 12 S/C (follow-up mission FormoSat-3/COSMIC)
IridiumNext (launch 2015–2017)	CTECS	A sensor of the GEOScan assembly

Mission	Instrument	Comment
GEMSS (India, launch 2014)	Pyxis	Proposal
MetOp-C (launch 2016)	GRAS	EUMETSAT/ESA mission

Table 117: Overview of missions with refractive occultation measurements

1.20.5 GPS/GNSS meteorology – ground–based networks

Atmospheric GPS–signal monitoring can be done by ground–based as well as space–based distributed network receivers from LEO spacecraft. 2020) 2021) 2022) 2023) Ground–based GPS meteorology refers simply to permanently installed GPS receiver networks, whose data is used for estimates of atmospheric conditions, in particular of the total column **IWV (Integrated Water Vapor) content of the atmosphere**. [Note: In some publications reference is made to **IPW (Integrated Precipitable Water– Vapor)** which is of course the same as total column IWV]. Water vapor, not evenly distributed in the Earth’s atmosphere, is a significant component of the dynamics of the atmosphere, its interaction with other atmospheric constituents correlates strongly with daily weather patterns. IWP refers to the amount of water (in mm of height) that would result from condensing all of the water vapor in a column of air, extending from the Earth’s surface to the top of the atmosphere. Generally, the ground–based measurements include barometric pressure, temperature, and humidity necessary to determine the precipitable water vapor, or IWV. 2024) 2025)

The technique is based on the estimation of the tropospheric delay time of GPS signals. The delay, regarded as a nuisance parameter by some signal users (like geodesists), can be directly related to the amount of water vapor in the atmospheric column; hence, it is a product of considerable value for meteorologists in NWP (Numerical Weather Prediction) and climate models. – The new GPS application of IWV measurement has been developed starting in the mid–1990s. Such GPS signal measurements can be obtained under all weather conditions; they have an accuracy comparable to IWV data derived from radiosonde and water vapor radiometers measurements.

Accurate, frequent, and dense sampling of IWV is needed for operational weather forecasting as well as for weather and climate research. Given the present operational weather data systems, inadequate resolution of the temporal and spatial variability of water vapor has been cited as the single greatest obstacle to improved short–range precipitation forecasts. The field of GPS meteorology has made great strides over the past few years. Numerous groups have demonstrated the ability to use GPS receiver networks to estimate IWV over a regional area. Some examples of early ground–based refractive occultation monitoring networks are:

– A demonstration network of ground–based GPS receivers 2026) has been established by NOAA/FSL (Forecast Systems Laboratory) in Boulder, Colorado to test the new weather observing and climate monitoring system for NOAA (in Feb. 1999 the demonstration network contained 40 active sites; it contained 200 sites by 2002).

2020) D. A. Garay, J. F. Raquet, M. M. Miller, “Algorithm Considerations for GPS Meteorology in a Military Environment,” ION–GPS 2002, Portland OR, Sept. 24–27, 2002

2021) B. G. Bevis, S. Businger, T. A. Herring, C. Rocken, R. A. Anthes, R. H. Ware, “GPS Meteorology: Remote Sensing of Atmospheric Water Vapor Using the Global Positioning System,” *Journal of Geophysical Research*, Vol. 97, 1992, pp. 15787–15801.

2022) S. Businger, S. R. Chiswell, M. Bevis, J. Duan, R. A. Anthes, C. Rocken, et al., “The Promise of GPS in Atmospheric Monitoring,” *Bulletin of the American Meteorological Society*, Vol. 77, 1996, pp. 5–18.

2023) <http://gpsmet.fsl.noaa.gov/jsp/background/background.jsp>

2024) <http://www.paroscientific.com/gpsmet.htm>

2025) L. Cucurull, A. Rius, F. Vandenberghe, M. de Ponte, “4D–VAR assimilation of GPS–derived ZTD: a Case Study,” ION GPS 2001, 11–14 September 2001, Salt Lake City, UT

2026) S. I. Gutman, K. L. Holub, “Ground–based GPS Meteorology at the NOAA Forecast Systems Laboratory,” 4th Symposium on Integrated Observing Systems, 1999, Long Beach, CA, Jan. 10–14, 2000

- Other demonstration networks are reported by AGRS.NL (Active GPS Reference System Netherlands). Three Dutch institutes executed a two-year project (September 1996–October 1998) on GPS Water Vapor Meteorology. ²⁰²⁷⁾
- AGNES (Automated GPS Network for Switzerland). The network was started in 1998; at the end of 2001 it consisted of 29 permanently operating GPS tracking stations. AGNES is a multipurpose network which serves as reference for surveying, real-time positioning services and for scientific applications. Since Dec. 2001, the GPS data are additionally processed on an hourly basis. So-called ZTD (Zenith Total Delay) estimates are derived every hour. With known surface pressure and temperature these values are converted to integrated water vapor (IWV).
- EUREF (European Reference Frame) started out in the 1990s for geodetic applications (Earth reference frame). Over 100 GPS stations were part of the EUREF network in 2000. Interdisciplinary monitoring/investigations including geodynamics, sea level monitoring and GPS meteorology were started in the late 1990s. Within the EU COST (Cooperation in the Field of Scientific and Technical Research) program, a number of processing centers were set up (COST Action 716, starting in early 2001) for the “Exploitation of Ground Based GPS for Climate and NWP” in near-real time (NRT). As of mid-2003, there are seven analysis in Europe each serving a number of GPS stations: ASI (Agenzia Spaziale Italiana), Matera, Italy, 38 stations; GOP (Geodetic Observatory Pecny), Czech Republic, 45 stations; GFZ (GeoForschungsZentrum) Potsdam, Germany, 71 stations; IEEC (Institut d’Estudis Espacials de Catalunya), Barcelona, Spain, 13 stations; LPT (Federal Office of Topography), Wabern, Switzerland, 62 stations; NKG (Nordic Geodetic Commission, Statens Kartverk, Norway), Onsala, Sweden, 25 stations; NKGS (Nordic Geodetic Commission, Onsala Space Observatory), Sweden, 44 stations. ²⁰²⁸⁾
- In 2000, the Institute of Engineering Surveying and Space Geodesy of the University of Nottingham, UK, received a three year contract from the EC (European Commission) to assess the feasibility and accuracy of producing GPS IPW estimates for both meteorological and climatological applications.
- A GASP (GPS Atmosphere Sounding Project) initiative was started in 2000 at GFZ (Potsdam, Germany) with the establishment of a NRT (Near-Real-Time) GPS network service. GASP consists of two parts: a) ground-based monitoring of IWV, using mostly SAPOS (Satellite Positioning Service), a ground-based DGPS network of over 200 sites of DGPS reference stations in Germany, and b) GPS radio occultation measurements of the CHAMP satellite mission. GASP assimilates the inputs from both information sources into atmospheric and ionospheric modeling and analysis, exploring the impact of these new products for such applications as numerical weather prediction (NWP), climate variability studies, and space weather monitoring. The GASP NRT service provides its IWV data within 40 minutes of reception. ^{2029) 2030)}

Obviously, the GPS–IWV measurement technique is more advantageous than conventional water vapor observing systems because of its relatively low-cost, high-measurement accuracy, all-weather operability, and long-term measurement stability. Furthermore a ground-based GPS receiver network can operate autonomously providing nearly real-time data to the meteorologists. Since ground-based GPS–IWV data are compatible with spaceborne IWV data retrievals, they provide an independent method for calibrating and validating global satellite observations. – A disadvantage of the GPS–IWV data retrieval

2027) <http://www.knmi.nl/onderzk/atmoond/GPS/>

2028) G. Elgered, et al., “Ground-Based GPS for Climate and Numerical Weather Prediction Applications,” EGU Newsletter – the eggs, issue 4, June 2003, pp. 22–24

2029) Ch. Reigber, G. Gendt, G. Dick, M. Tomassini, “Near-Real-Time Water Vapor Monitoring for Weather Forecasts,” GPS World, Jan. 2002, pp. 18–26

2030) “Exploitation of Ground-Based GPS for Meteorology,” COST Action 716 Workshop GeoForschungsZentrum (GFZ) Potsdam, January 28–29, 2002

method is that so far no direct information is provided as to the actual vertical distribution of water vapor in the atmosphere (what is known is the total column content of water vapor).²⁰³¹⁾

1.20.6 GPS/GNSS bistatic ocean reflection measurements

Ocean surface reflection measurements of GNSS signals (GNSS–R) are being used in a bistatic radar configuration as sources of opportunity (a passive bistatic/multistatic remote sensing technique to obtain altimetric as well as other information, surface wind parameters).^{2032) 2033) 2034) 2035) 2036) 2037) 2038) 2039) 2040)} The underlying principle in GNSS–R is the use of reflected signals to infer properties of the reflecting surfaces. The sea surface provides the ocean–atmosphere link, regulating momentum, energy and gas exchange, and several fundamental ocean circulation features are directly related to wind–wave induced turbulent transports in the oceanic mixed layer. In particular, eddies and gyres are fundamental agents for mixing, heat transport and feedback to general circulation, as well as transport of nutrients, chemicals and biota for biochemical processes.

Note: A multistatic altimeter can be regarded as a multistatic radar for which the transmitters and the receivers belong to different systems.

The idea to use satellite radionavigation system satellites as signal sources of opportunity is of great interest to the Earth observation community. Satellite radionavigation systems are closely related to radar systems in that they are also based on the spread–spectrum principle. They operate in L–band, which is almost free of rain attenuation. With current GNSS signal bandwidths in the range of 2–20 MHz, they rank at the lower end of state–of–the–art spaceborne radar instruments; however, the GNSS signals are emitted with exclusive timing accuracy and the position of the transmitting satellites is precisely known. The current existence of two GNSS constellations, GPS/NAVSTAR and GLONASS, and one in development, GALILEO, are providing a continuous pool of signals of opportunity which may be used for wide–area spaceborne reflectometry measurements (GNSS–R).²⁰⁴¹⁾

Background: The detection of bistatic GPS signals scattered and reflected off the ocean surface were obtained experimentally on an aircraft platform in 1991 and reported by a French team (Dassault Electronique) in 1994. Earlier work by Boeing had revealed the existence of such signals in connection with multipath effects (Boeing Co. report FAA–RD–73–57–V of 1973). In 1993, Manuel Martin–Neira of ESA/ESTEC proposed and presented a multistatic sea surface altimeter concept, referred to as **PARIS** (Passive Reflectometry and Interference System), based on an interferometric approach which combines the direct and

- 2031) E. Fragner, R. Weber, “The impact of precise orbit information on ZTD and IWV estimates using ground based GNSS data,” GNSS 2003, Graz, Austria, April 22–25, 2003
- 2032) G. A. Hajj, C. Zuffada, “Theoretical description of a bistatic system for ocean altimetry using the GPS signal,” *Radio Science*, Vol. 38, No. 5, 2003, pp. 10–1 to 10–18
- 2033) S. T. Lowe, J. L. LaBrecque, C. Zuffada, et al., “First Spaceborne Observation of an Earth–reflected GPS Signal,” *Radio Science*, Vol. 37, No 1, Jan.–Feb. 2002
- 2034) J.–C. Auber, A. Bibaut, J.–M. Rigal, “Characterizations of Multipath on Land and Sea at GPS Frequencies,” *Proceedings of ION GPS–94*, Vol. 2, pp. 1155–1171
- 2035) J. L. Garrison, S. J. Katzberg, M. I. Hill, “Effect of Sea Roughness on Bistatically Scattered Range Coded Signals from the Global Positioning System,” *Geophysical Research Letters*, Vol. 25, No 13, 1998, pp. 2257–2260
- 2036) D. Masters, P. Axelrad, V. Zavorotny, S. J. Katzberg, F. Lalezari, “A Passive GPS Bistatic Radar Altimeter for Aircraft Navigation,” *Proceedings of the ION–GPS*, Salt Lake City, UT, Sept. 11–14, 2001
- 2037) J. Garrison, S. Katzberg, “The application of reflected GPS signals to ocean and wetland remote sensing,” *Proceedings of the 5th International Conference on Remote Sensing for Marine and Coastal Environments*, San Diego, CA, October 5–7, 1998, Vol. 1, pp. 522–529
- 2038) J. L. Garrison, S. J. Katzberg, C. T. Howell, “Detection of Ocean Reflected GPS Signals: Theory and Experiment,” *Proceedings of IEEE Southeastcon’97*, Blacksburg, VA, April 12–14, 1997, pp. 290–294
- 2039) Information provided by T. P. Yunck of NASA/JPL
- 2040) J. S. LaBrecque, L. Loewe, L. Young, E. Caro, S. Wu, L. Romans, “Recent Advances in the study of GPS Earth surface reflections from orbiting receivers,” UNAVACO Community Meeting, 1998
- 2041) G. A. Hajj, C. Zuffada, “Theoretical description of a bistatic system for ocean altimetry using the GPS signal,” *Radio Science*, Vol. 38 No 5, 1089, doi:10.1029/2002RS002787, Oct. 15, 2003

ocean—reflected GNSS signals.²⁰⁴²⁾ That work included accuracy analysis and discussions of alternative altimetry constellations. With 24 satellites (transmitters) in the GPS constellation, a single GPS receiver on a spacecraft represents a multistatic system (in combination with the GPS constellation), capable of intercepting reflections from several ocean regions simultaneously. Then, in 1994, French engineers reported the accidental acquisition of ocean reflected GPS signals by an aircraft—mounted GPS receiver.²⁰⁴³⁾ Stephen J. Katzberg and James L. Garrison of NASA/LaRC first analytically predicted the change in GPS signal structure following an ocean reflection.²⁰⁴⁴⁾ They then demonstrated the tracking of reflected GPS signals with airborne off—the—shelf GPS receivers [three aircraft flights over the Chesapeake Bay and the Eastern Shore of Virginia were conducted in Aug. 1996 using a **DDMR** (Delay Doppler Mapping Receiver)].²⁰⁴⁵⁾ ²⁰⁴⁶⁾

On the spaceborne side, GNSS signal reflections (referred to as GNSS—R or as GPS—R) were first observed by a JPL team after the SRL—02 (Shuttle Radar Laboratory—02) mission (STS—68, Sept 30 — Oct. 11, 1994).²⁰⁴⁷⁾ On hindsight, GNSS—R signals were also discovered for the SRL—01 mission (SIR—C/X—SAR on flight STS—59, Apr. 9—20, 1994). In 1998, Stephen T. Lowe et al., conducted a search of possible GPS—R data in the SRL—01 mission data and discovered 4 seconds worth of GPS—R signals (with the expected temporal shape and coherence properties), reflected of the ocean and embedded in recordings of calibration data.

The concept of GPS (or better: GNSS) signal reflection measurements (as a source for bistatic surface scattering) is based on ocean surface roughness which results in multipath signal reflections emanating from the GPS and GLONASS satellite constellations.²⁰⁴⁸⁾ ²⁰⁴⁹⁾ ²⁰⁵⁰⁾ ²⁰⁵¹⁾ ²⁰⁵²⁾ ²⁰⁵³⁾ In this measurement configuration, each point of the reflected surface introduces various kinds of modulation to the signal, concerning amplitude, delay, phase and its derivatives. This modulation is partially due to the measurement geometry, i.e. the geometry between transmitter, reflecting surface and receiver, and partially due to the surface and its variability in time, in particular the sea—surface motion, but also due to atmospheric effects. If the geometry is well known, the geometric modulation of delay and phase cannot only be removed but it can be used to separate the signals reflected from different areas of the surface by combined frequency—domain filtering and time—domain gating, which is referred to as **DDMR** (Delay Doppler Mapping Receiver) system. The signals filtered in this way contain only the modulation due to the surface and the atmosphere. Essen-

- 2042) M. Martin—Neira, “A Passive Reflectometry and Interferometry System (PARIS): Application to Ocean Altimetry,” *ESA Journal*, Vol.17, No.4, 1993, pp. 331—355
- 2043) J. C. Auber, A. Bibaut, J. M. Rigal, “Characterization of multipath on land and sea at GPS frequencies,” *Proceedings of ION GPS—94*, Salt Lake City, UT, 1994, pp. 1155—1171
- 2044) S. J. Katzberg, J. L. Garrison, “Utilizing GPS to determine ionospheric delay over the ocean,” *Technical Memo*, TM—4750, NASA/LaRC, Hampton, VA, 1966, pp. 13
- 2045) E. Cardellach, J. M. Aparicio, D. Pino, J. Torrobella, A. Rius, “Coastal Sea State Measurements Using GPS Reflected Signals from an Airborne Platform,” *ION—GPS 2002*, Portland, OR, Sept. 24—27, 2002
- 2046) D. Mickler, P. Axelrad, G. Born, “Using GPS reflections for satellite remote sensing,” *Acta Astronautica*, Vol. 55, 2004, pp. 39—49
- 2047) S. T. Lowe, J. L. LaBrecque, C. Zuffada, L. J. Romans, L. E. Young, G. A. Hajj, “First spaceborne observations of an earth—reflected GPS signal,” submitted to *Radio Science*, July 2000, published in *Radio Science*, Vol. 37, No 1, Jan.—Feb. 2002, pp. 7—1 to 7—28
- 2048) M. Martin—Neira, “A Passive Reflectometry and Interferometry System (PARIS): Application to Ocean Altimetry,” *ESA Journal*, 17 (4), 1993, pp. 331—355
- 2049) M. Martin—Neira, et al., “ESA’s activities on GPS reflected signals for Earth observation,” *Proceedings of Ionospheric Determination and Specification for Ocean Altimetry and GPS Surface Reflections Workshop*, JPL, Pasadena, Dec. 1997
- 2050) A. Komjathy, J. L. Garrison, V. Zavorotny, “GPS: A New Tool for Ocean Science,” *GPS World*, Apr. 1999, pp. 50—56
- 2051) C. B. Erol, F. Arýkan, O. Arýkan, “A New Technique for TEC Estimation,” *Proceedings of IGARSS 2002*, Toronto, Canada, June 24—28, 2002
- 2052) J. L. Garrison, A. Komjathy, V. U. Zavorotny, S. L. Katzberg, “Wind speed measurement using forward scattered GPS signals,” *Transaction of Geoscience and Remote Sensing*, Vol. 40, No.1, 2002, pp. 50—65
- 2053) M. Sust, H. Reichinger, “Architectural Design of a Global Navigation Satellite Systems Receiver for the Processing of Sea—Surface Signal Reflections,” *NAVITEC 2001*, 1st Workshop on Satellite Navigation User Equipment Technologies, Dec. 10—12, 2001, ESA/ESTEC, Noordwijk, The Netherlands

tially, this is a multipath channel characterization setup. In contrast to nadir-looking instruments the bistatic concept allows for measurements under grazing angles. On the one hand this allows to achieve better spatial resolution for a given number of orbiting instruments and on the other hand, certain surface features, invisible to nadir-looking instruments, can be observed.

The measurements picked up by a DDM receiver system may be used to determine such parameters as wave height, wind speed, and wind direction. The strength of the reflected signals (normally regarded as surface clutter or simply as noise) is also a discriminator between wet and dry surface areas and, therefore, can be applied to coastal and wetland mapping. In this concept, high spatial resolutions are obtained with wide-beam and low-gain receiving antennas by using the GPS carrier-phase and its PRN code modulation. This is similar to the SAR (Synthetic Aperture Radar) technique in which the Doppler frequency shifts and pulsed-signal time delays are used to create a small footprint on the mapped surface. – By combining code-range and Doppler measurements, a receiver can distinguish particular patches of the ocean surface illuminated by GPS signals. – In some ways, the above GPS ocean surface reflection discovery is similar to that of using GPS to map the ionosphere's TEC (Total Electron Content) by measuring propagation delay differences between the L1/L2 frequencies.

The GNSS-based concept of altimetry with reflective pseudorange noise (PRN) operates in a bistatic/multistatic geometry (i.e., the transmitted and received signals travel two different paths) with the following features:

- Up to 20 ocean height measurements are possible simultaneously with a single LEO receiver for the measurement of reflected GNSS signals. In comparison, traditional altimetry is limited to looking in the nadir direction and obtaining one height observation at a time below the altimeter.
- GNSS reflection coverage is very dense but random, while in traditional altimetry, the coverage is regular according to a certain repeat pattern. However, the reflected signal retrieval produces only modest SNRs with low-gain antennas.²⁰⁵⁴⁾ Hence, exploitation of GNSS reflections observed from space is still rather speculative at the start of the 21st century. It will require high gain antennas (preferably >26 dB gain) with multiple independently steerable beams. A single platform might typically see 10–12 reflections at once over the oceans. Measurement precision will be modest; hence, massive averaging is required to get to the 5-cm level that will be needed for mesoscale ocean circulation. Recent ESA studies show that a GNSS-R mission should allow mapping of the mesoscale variability in high eddy variability regions better than Jason-1 + Envisat together.
- When the GNSS signal impinges on the ocean surface, it is scattered randomly with maximum power in the direction of the specular reflection. Since the ocean reflectance depends on the surface temperature and salinity, in principle, measuring the return power with sufficient accuracy could eventually be used to infer these parameters.
- The GNSS reflection relies on detecting the amount of energy return of the GNSS signal by correlating the pseudo-random code of the reflected signal and a delayed model of the same code generated in the receiver. By examining the power return at different delays and Doppler shifts, different parts of the ocean are sensed. The footprint of GNSS reflection is determined by the intersection of iso-Doppler and iso-range contours.
- The BlackJack GPS receiver configurations/implementations of the missions CHAMP (launch July 15, 2000; see BlackJack description under E.1) and SAC-C (launch Nov. 21, 2000) have the added capability of bistatic ocean reflection measurements, originating from the GPS and GLONASS constellations (besides refractive atmospheric occultation moni-

2054) G. Ruffini, O. Germain, F. Soulat, M. Taani, M. Caparrini, "GNSS-R: Operational Applications," Proceedings of the 2003 Workshop on Oceanography with GNSS Reflections, Barcelona, Spain, July 2003

toring). This relatively new technique of “GNSS reflected pseudorange altimetry” recovery with onboard GPS (or GNSS) receivers will eventually permit applications such as oceanic circulation sensing (particularly eddy–scale currents that are missed by today’s altimetry missions), and scatterometry (measuring the shape of the reflected pulse) for determining wind speeds. The CHAMP and SAC–C GNSS reflection experiments are considered simple engineering tests of opportunity with antenna gains of only 6–9 dB. Thus, long averaging times are needed just to detect the signals. – Essential to the success of GNSS–recovered altimetry and scatterometry is the ability to see multiple reflected signals simultaneously. Note: The Blackjack instrument on SAC–C is also referred to as GOLPE (GPS Occultation and Passive reflection Experiment) provided by JPL.

The UK–DMC microsatellite (launch Sept. 27, 2003)²⁰⁵⁵⁾²⁰⁵⁶⁾ is carrying a GPS Reflection Experiment by using the SGR–10 (Space GPS Receiver–10) along with 3 antennas. As of 2005, the instrumentation collected over 30 data sets, mostly from the ocean but also from land and ice surfaces.²⁰⁵⁷⁾²⁰⁵⁸⁾

A general limitation of the current GNSS signals for ocean altimetry is their relatively narrow bandwidth, about 20 MHz, which limits the achievable ranging precision to 1 m, using the civil C/A code pseudorange. – The modernized GPS signal, however, and the future Galileo system will provide more satellites (thus more observations) and more frequencies for civilian use (each system up to three), featuring also more power and more bandwidth. These GNSS enhancements will contribute decisively to the improvement of the return when used as a remote sensing tool. One particular characteristic, offered by future GNSS signals, is the possibility of performing combined carrier–phase measurements from different carrier frequencies. The reflected signals have a Doppler spread inherent to the geometry of the measurement system, such as a LEO spacecraft flying over the rough ocean surface illuminated by the constellation of GNSS transmitters.²⁰⁵⁹⁾

The proposed concept by ESA/ESTEC (Martin–Neira, et al.) employs the PIP (PARIS Interferometric Processing) technique, using several carrier frequencies as transmitted by the GPS and the future Galileo GNSS systems, to obtain a phase observable out of the complex cross–correlation between the fields. In this concept, the PIP technique handles the reflected signals from the ocean surface as a “typical radar return produced by a distributed target” – the signals remain coherent over a short time and have large amplitude variations. Several PIP validation experiments/campaigns have been done or are in progress. All indications are that using the technique of “wide–lane processing,” that is, the combination of the phases from the different carriers, a more coherent observable is obtained which is quite powerful for ocean remote sensing. In addition to altimetry, the measurement of the GNSS multi–carrier reflected signals can potentially provide accurate surface wind speed estimations based on the analysis of statistical fluctuations over the carrier phases.

An inspection of Figure 151 leads to the conclusion that a spaceborne scatterometer for reflected GNSS signals could be designed, a passive or “parasitic” scatterometer configura-

-
- 2055) S. Gleason et al., “Detection and Processing of Bistatically Reflected GPS Signals From Low Earth Orbit for the Purposes of Ocean Remote Sensing,” *IEEE Transactions on Geoscience and Remote Sensing*, Vol. 43, No. 6, pp. 1229–1241, June 2005.
- 2056) S. Gleason, M. Adjrak, “An Attempt to Sense Ocean Winds and Waves Empirically Using Bistatic GNSS Reflections in Low Earth Orbit,” *Proceedings of IGARSS (International Geoscience and Remote Sensing Symposium)*, Seoul, Korea, July 25–29, 2005.
- 2057) S. Gleason, A. da Silva Curiel, S. Makin, M. Sweeting, “A Global System for Detecting Dangerous Seas Using GNSS Bistatic Radar Technology,” *Proceedings of the 56th IAC 2005*, Fukuoda, Japan, Oct. 17–21, 2005, IAC–05–B2.1.07
- 2058) S. Gleason, M. Adjrak, M. J. Unwin, “Sensing Ocean, Ice and Land Reflected Signals From Space: Results from the UK–DMC GPS Reflectometry Experiment,” *Proceedings of ION GNSS 2005*, Long Beach, CA, Sept. 13–16, 2005
- 2059) M. Martin–Neira, P. Colmenarejo, G. Ruffini, C. Serra, “Altimetry precision of 1 cm over a pond using the wide–lane carrier phase of GPS reflected signals,” *Canadian Journal of Remote Sensing*, Vol. 28, No 3, 2002, pp. 394–403

tion so to speak, monitoring all signals of opportunity. Obviously, further research and demonstrations are needed to develop this technique. ²⁰⁶⁰⁾

As of 2003, a first spaceborne PARIS demonstration is being planned/designed for the L-SAR instrument of the TerraSAR-L mission of ESA (launch 2010?). In this setup, the L-SAR instrument antenna is passively listening for the GNSS-R (Reflected GNSS signal) observables from the ocean surface.

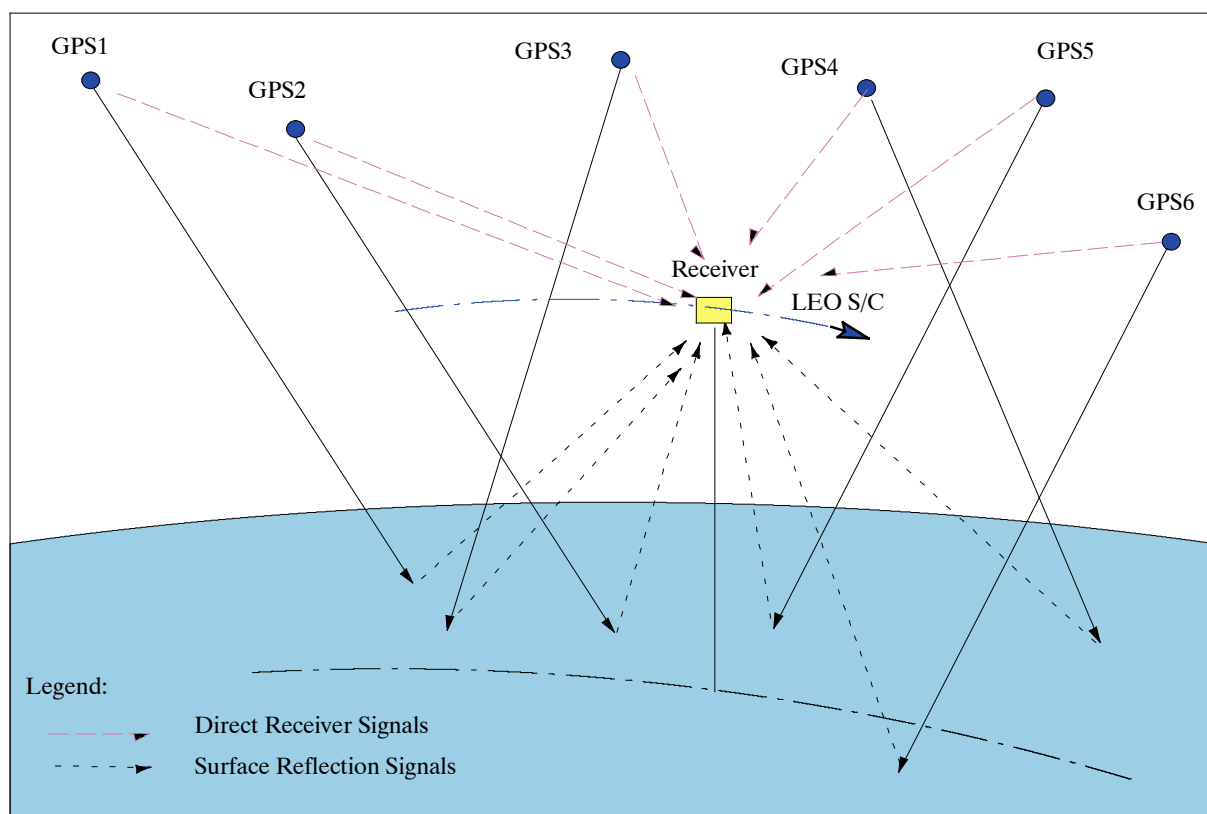


Figure 151: Schematic illustration of GPS multistatic ocean reflection

Today's GNSS constellations represent a continuous pool of RF signal sources that are transmitted toward Earth (through the atmosphere), thus providing numerous signals of opportunity that are reflected by the Earth's surface (ocean or land) and may be acquired by an airborne or spaceborne antenna and receiver (bistatic altimetry application, etc.). Unlike monostatic radar altimetry with rather narrow sub-trajectory coverage capability (a line of discrete small-area measurement points is provided), the method of ocean-reflected GNSS signal monitoring promises to offer eventually much wider coverage swaths, which will to a better extent enable the study of large-area phenomena such as ocean eddies and in particular ocean currents.

A further use of GNSS-R ^{2061) 2062)} data is anticipated in ionospheric tomography monitoring applications by extracting information about the ionospheric electron density distribution. The GNSS-R approach offers the means to provide a high number of bistatic TEC (Total Electron Content) measurements over the oceans.

2060) V. U. Zavorotny, "Bistatic GPS Signal Scattering from an Ocean Surface: Theoretical Modeling and Wind Speed Retrieval from Aircraft Measurements," Workshop on Meteorological and Oceanographic Applications of GNSS Surface Reflections: From Modeling to User Requirements July 6th 1999, De Bilt, The Netherlands, URL: <http://www.etl.noaa.gov/~vzavorotny/#intro>

2061) J. Marco, G. Ruffini, L. Ruffini, "Ionospheric (H-atom) Tomography: a Feasibility Study using GNSS Reflections," ESA, Dec. 2002, <http://arxiv.org/ftp/physics/papers/0212/0212087.pdf>

2062) G. Ruffini, E. Cardellach, A. Flores, L. Cucurull, A. Rius, "Ionospheric Calibration of Radar Altimeters Using GPS Tomography," Geophysical Research Letters, Vol 25, No 20, pp. 3771–3774, 1998.

1.21 Oceanography – A growing demand in Earth Observation

Oceanography is the study of Earth's oceans comprising three major interdisciplinary fields of investigation:

- 1) Physical oceanography: the study of all the physical properties of the ocean – e.g. currents and waves, marine geodesy, etc.
- 2) Chemical oceanography: the study of its chemistry
- 3) Marine biology and marine ecology: the study of the organisms that live in the oceans.

The scope of this chapter is mostly limited to the various topics of physical oceanography which is by itself a very large interdisciplinary field of study, requiring effective international cooperation in many programs.

Oceans cover 71% of the Earth's surface. The total ocean volume (salt water) is estimated to be $1.35 \times 10^9 \text{ km}^3$, representing a gigantic reservoir of energy and resources. The mass of the oceans is about 300 times larger than the mass of the atmosphere; the heat storage capacity of the oceans is 1200 times the heat capacity of the atmosphere; the oceans provide 70 times the carbon storage capacity of the atmosphere. The oceans play indeed a decisive role in the evolution of the world's climate. Through irradiation of the sun and exchanges with the atmosphere, they receive considerable quantities of heat, in particular at the intertropical latitudes, which they store due to their high thermal capacity, and which the ocean currents redistribute from the equatorial regions to the polar regions. Thus, the world's oceans represent a major regulating factor in our climatic system. Their circulation and evolution must be understood (via satellite observations and other means of observation) to account for the climate variability.

Status quo in 2006: The age of global satellite observations, in particular the introduction of continuous spaceborne altimetry missions since the early 1990s, have revolutionized the concepts of conventional oceanography. The availability of precise altimetric data required great initial efforts in modeling techniques for numerical data analysis, which in turn resulted in greatly improved GMCs (General Circulation Models) on various scales (regional or mesoscale, global scale). The ocean is seen to be time varying on all space and time scales – something we must live with. The designers of the altimetric missions anticipated many of the major results, including the very strong El Nino signals, the ability to determine the mesoscale variability everywhere, the estimation of frequency–wavenumber spectra and the considerable, if still limited, capability of determining the absolute circulation.

The very high accuracies and precisions of the altimetry missions produced some results which were not anticipated. These include, especially, the very strong high latitude barotropic fluctuations, and the internal tide results.²⁰⁶³⁾ The latter in particular triggered a huge new interest in the role of tides in controlling the ocean circulation and more generally in the question of the energetics of the circulation. – Another major surprise, of widespread interest, was that the measurements proved accurate enough to detect **global sea – level rise** at an accuracy of about 1mm/year. For the first time, the spatial complexity of the sea level rise patterns could be seen. The observations have stimulated a major, and continuing, effort to partition the rise between heating, cooling and net evaporation and precipitation.²⁰⁶⁴⁾

The key observables from space today are the measurement of:

- a) Altimetric height (sea level) to infer sea surface topography, wave heights and wind patterns, and ocean currents

²⁰⁶³⁾ Note: The term “barotropic” refers to a state in a water mass in which the surfaces of constant pressure are parallel to the surfaces of constant density.

²⁰⁶⁴⁾ C. Wunsch, “Altimetry Since 1980,” Symposium: 15 Years of Progress in Radar Altimetry, Venice, Italy, March 13–18, 2006

- b) SST (Sea Surface Temperature)
- c) Ocean color.

These variables are the backbone prognostic indicators in operational oceanography. The near future will add a further key observable, namely:

- SSS (Sea Surface Salinity), to study the links between ocean circulation and global water cycles – to be demonstrated in the SMOS mission of ESA and the SAC–D/Aquarius mission of NASA/CONAE. ²⁰⁶⁵⁾

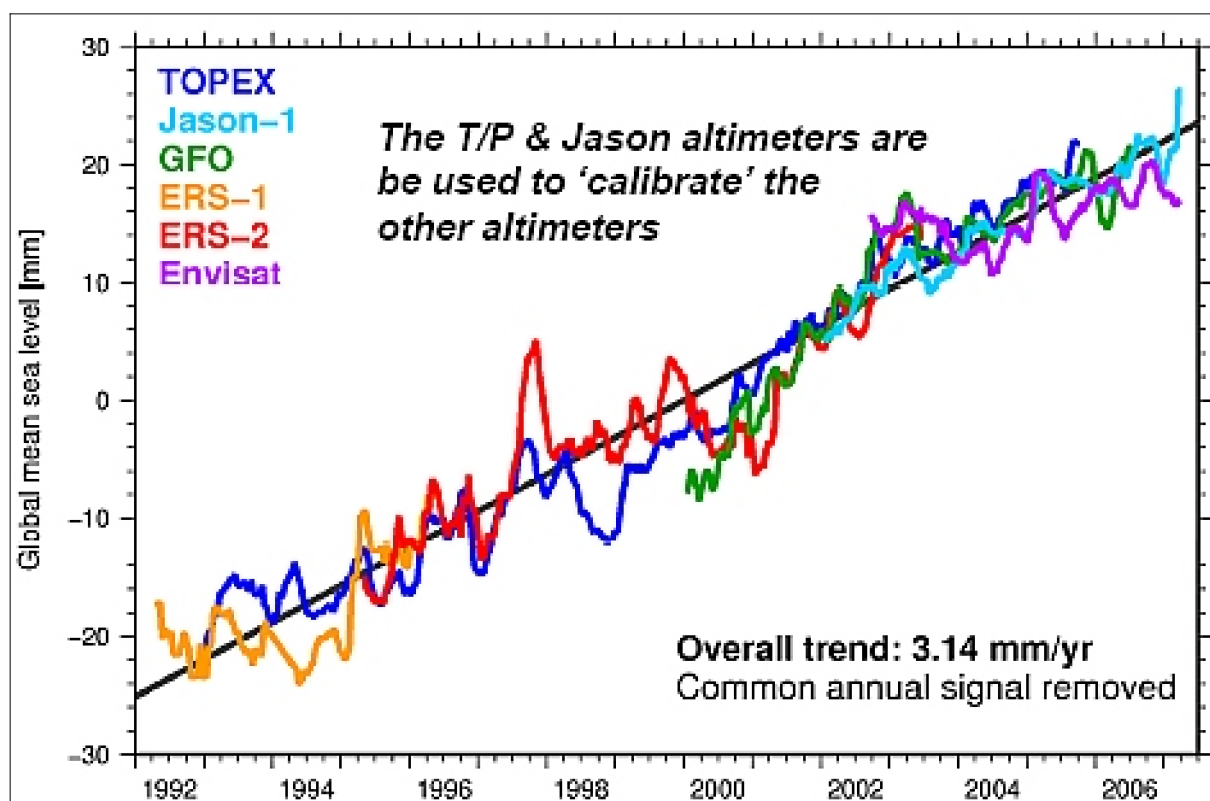


Figure 152: Long-term global sea level rise observations of altimetric missions (image credit: NOAA)

Legend to Figure 152: The data record built by the missions T/P, Jason–1, GFO, ERS–1 & –2, Envisat, and Jason–2 represents the first multi–decadal global record for addressing the issue of sea level rise – which has been identified by the 2007 IPCC (Inter–Governmental Panel for Climate Change) assessment as one of the most important consequences and indicators of global climate change.

The Jason–2/OSTM mission of CNES/NASA (launch June 20, 2008) is considered to be the first “**operational altimetry mission**” representing a switch of service support from ‘research institutions’ to ‘operational institutions’ (NOAA and EUMETSAT). The objective is to foster near real–time operational applications in the fields of oceanography, marine meteorology, seasonal prediction and climate monitoring.

The long–term goals of oceanography are to understand the processes and their interactions at the various time and space scales, to simulate these processes (modeling), and to make predictions, if possible. In particular, this requires sustainability of service provision

2065) Anny Cazenave, D. P. Chambers, P. Cipollini, L. L. Fu, J. W. Hurrell, M. Merrifield, R. S. Nerem, H. P. Plag, C. K. Shum, J. Willis, “Plenary Paper on ‘SEA LEVEL RISE: Regional and global trends’,” Proceedings of OceanObs’09, Venice, Italy, Sept. 21–25, 2009, URL: http://www.oceanobs09.net/plenary/files/Cazenave_Sea_Level_PLENARY_Paper.pdf

on a long-term basis in the future. ²⁰⁶⁶⁾

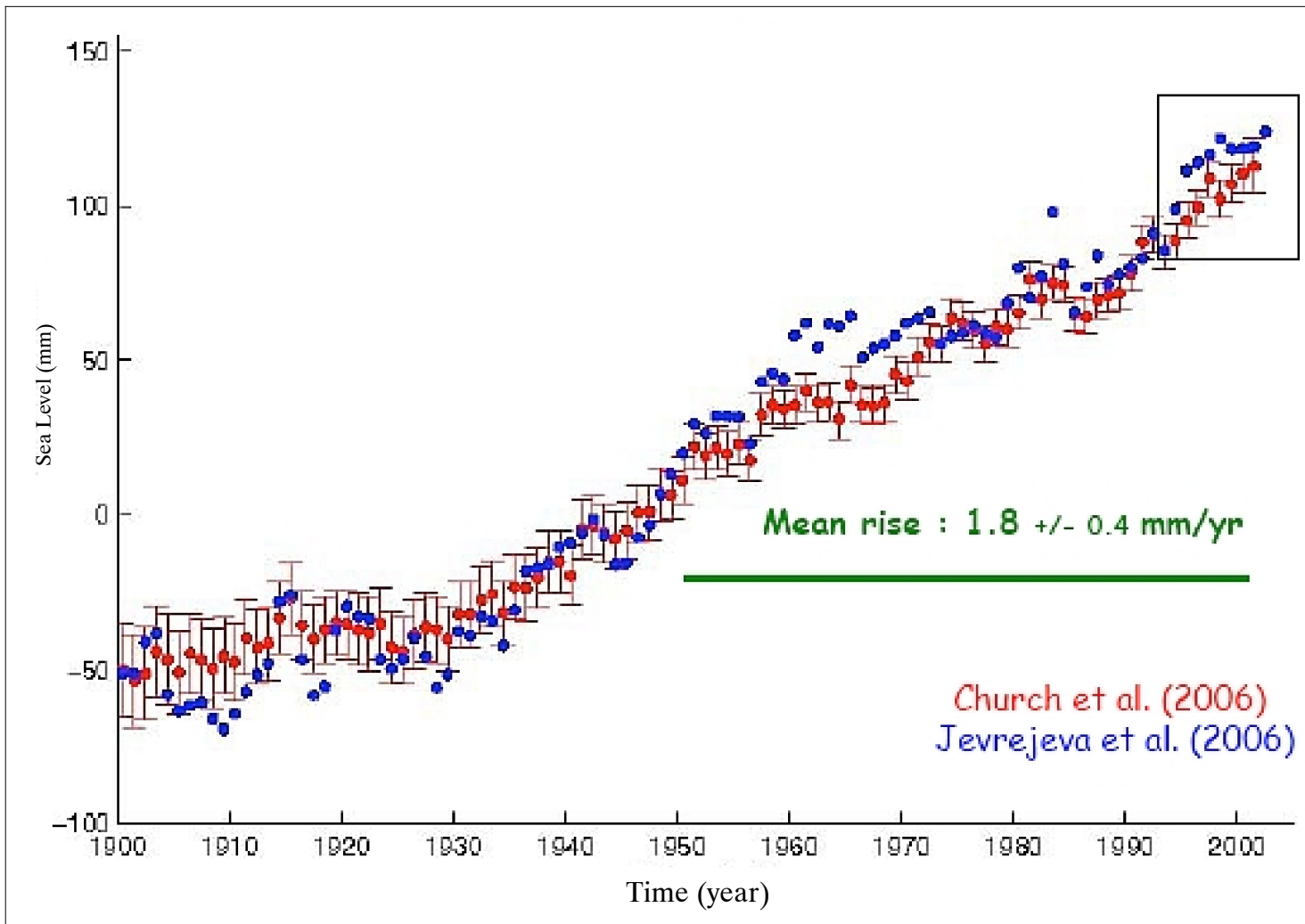


Figure 153: Mean sea level from tide gauges, 20th century (image credit: LEGOS/CNES, NOAA, NASA)

Some historical background: Man's earliest attempts to master the 'great waters' (oceanography) required him to know something more than just the performance of his ship. History has shown repeatedly that some understanding of the sea and atmospheric conditions was helpful, if not vital. Knowledge, for example, of prevailing winds aided the success of the seafarers from early times on. The primary concern of any seafarer was – and is – navigation and safe passage in foreign, as well as domestic, waters. ²⁰⁶⁷⁾

The formal gathering of ocean knowledge as a science discipline (oceanography) started in the early to mid 19th century. It provided new insights and understanding of the phenomena and turned up a number of innovations to aid navigation. Some examples are:

- Development of the mechanical gyroscope in the early 1800s
- Development of more accurate chronometers
- Charts of wind and current patterns were developed (including first charts of the Gulf Stream)
- The British “Challenger Expedition” (1872–1876, on the corvette H.M.S. Challenger II), sponsored by the Royal Society and Royal Navy, was the first modern, deep-ocean,

²⁰⁶⁶⁾ Y. Baillion, T. Huiban, “Present and Future Oceanography Missions,” Proceedings of the 57th IAC/IAF/IAA (International Astronautical Congress), Valencia, Spain, Oct. 2–6, 2006, IAC-06-B1.6.05

²⁰⁶⁷⁾ <http://inventors.about.com/library/inventors/bloceanography.htm>

global sampling expedition and was one of the most important voyages of the 19th century. Challenger visited all of the world oceans covering a total distance of 127,000 km. Scientists on board studied the physical conditions of the deep ocean, the chemical composition of seawater, physical and chemical characteristics of seafloor deposits, and the distribution of organic life at all water depths. The depth of the Mariana Trench (about 11° N, 142° E) just east of the Mariana Islands in the Pacific was measured at 8185 m. The “Report of the Scientific Results of the Exploring Voyage of H.M.S. Challenger” covered 50 volumes (practically the foundation of oceanography, published between 1885 and 1895), analyzed by over 100 scientists.

- In 1893, the Norwegian Explorer Fridtjof Nansen (1861–1930) led a voyage to the Arctic to test his theories about surface circulation in Arctic waters. This was the beginning of the exploration of Polar Seas that continued into the early 20th century.
- At the start of the 20th century, lead line soundings still remained the best method for plumbing the depth of the ocean bottom.

As technological advances of the 20th century were made in engineering and later also in electronics, the ability to explore the ocean in greater detail became increasingly sophisticated. Advances during the two world wars were also important as the sea became an important “battle field”. Use of sonar (echo location), developed during WW–I and WW–II, has proved crucial to our increased understanding of the morphology of the ocean basins.

- Study of underwater acoustics
- The sonar technique was developed during WW–I (based on reflected sound waves) to detect submerged targets
- Measurement of water body depths in ocean basins, referred to as bathymetry (sonic depth finder – which determines depth by measuring the elapsed time of an echo). The ocean floor had distinctive features (ridges, mountains, etc.).
- etc.
- Ocean mass change from the GRACE (Gravity Recovery and Climate Experiment) mission: Net water flux into and out of the ocean causes its mass to change. Such changes in ocean mass give rise to gravitational variations that are detectable by the GRACE mission (launch March 17, 2002). This has allowed, for the first time, direct estimates of the global ocean mass contribution to sea level change. ²⁰⁶⁸⁾

1.21.1 Physical oceanography

Physical oceanography is the study of the fluid motions of the ocean environment, e.g. surface and internal waves, air–sea exchanges, turbulence and mixing, acoustics, heating and cooling, wave and wind–induced currents, tides, tsunamis, storm surges, large–scale waves affected by Earth’s rotation, large–scale eddies, general circulation and its changes, coupled ocean–atmosphere dynamics for weather and climate.

As illustrated in Figure 154, the timescales of ocean physical processes extend from seconds to years, and the spatial scales range from mm to 1000 km to cover the various phenomena. Imagery from SAR (Synthetic Aperture Radar) missions provides key data on ocean swell, internal waves, mesoscale circulation including fronts and eddies, and a wide range of atmospheric processes. Data on atmospheric processes include measurements of wind speed and direction, detection of atmospheric roll vortices and turbulence, and identification of the extent and structure of storms and rain cells. Even the processes with relatively longer time-

²⁰⁶⁸⁾ D. P. Chambers, J. Wahr, R. S. Nerem, “Preliminary observations of global ocean mass variations with GRACE,” *Geophysical Research Letters*, Vol. 31, 2004, L13310, doi:10.1029/2004GL020461

scales, such as fronts, eddies, and gyre circulations, may fluctuate over a period of a few days or even less. In terms of operational interests, service monitoring of ship traffic, detection of natural and anthropogenic slicks, identification of icebergs, and sea ice navigation are perhaps best done with SAR imagery. 2069) 2070) 2071)

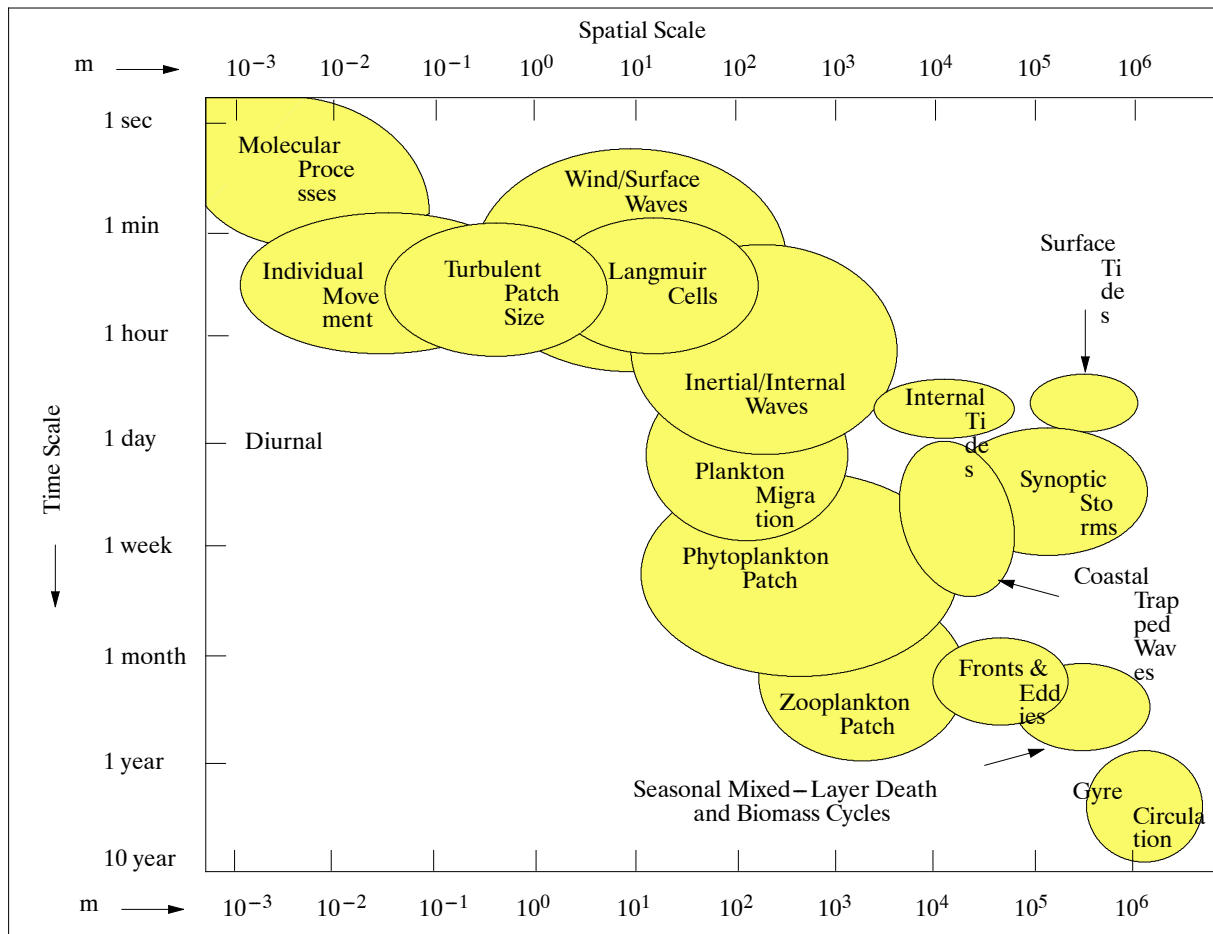


Figure 154: Temporal and spatial scales of key physical and biological processes in the ocean 2072)

How is the ocean sampled from satellites? In general terms (and not including altimetry, which is dedicated to gyre circulation), the primary satellite ocean sensors enable routine monitoring of nearly the entire global ocean every 12 h to 2 days. These include sensors (radiometers) for SST (Sea Surface Temperature) and ocean color, some instruments have about 3000 km swath widths with 1 km resolution and provide twice-daily global coverage. **Scatterometers** for measuring ocean surface winds (see 1.4.3.5) have swath widths varying between 500 and 1800 km with resolutions from 25 to 50 km.

2069) T. D. Dickey, "The Emergence of Concurrent High-Resolution Physical and Bio-Optical Measurements in the Upper Ocean and Their Applications," *Review of Geophysics*, Vol. 29, No 3, 1991, pp. 383-412

2070) G. C. Chang, T. D. Dickey, "Optical and physical variability on timescales from minutes to the seasonal cycle on the New England shelf: July 1996 - June 1997," *Journal of Geophysical Research*, Vol. 106, pp. 9435-9453, 2001

2071) B. Holt, J. Hilland, "Rapid-Repeat SAR Imaging of the Ocean Surface: Are Daily Observations Possible?" *JHU/APL Technical Digest*, Vol. 21, No 1, 2000, pp. 7-14

2072) Note: The illustration was originally presented in Ref. 7479) and kindly provided by Benjamin Holt of NASA/JPL.

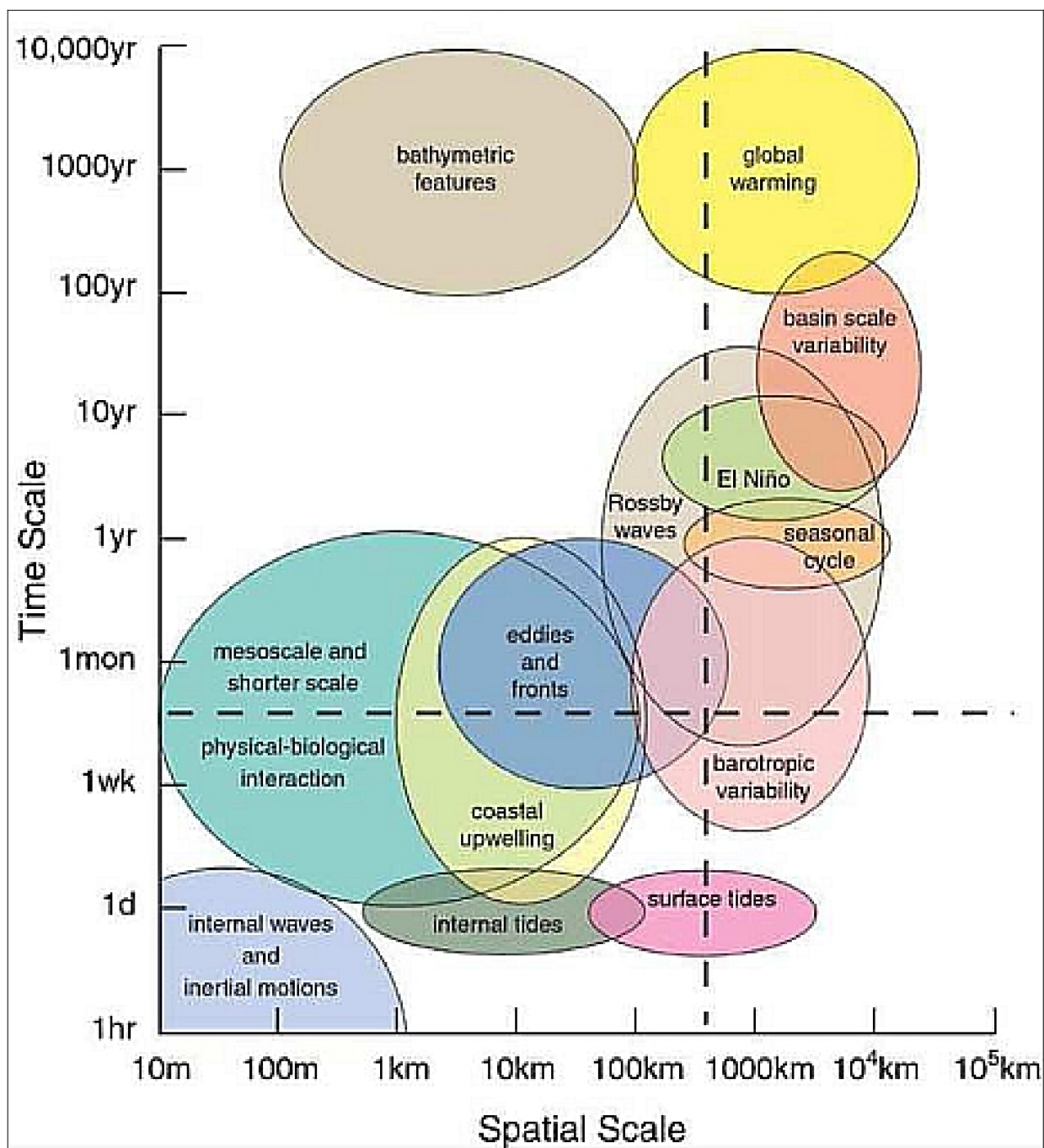


Figure 155: Alternate view of temporal and spatial scales of oceanography events and phenomena (image credit: Carrère, 2010)

The SAR and altimeter instruments are capable of making wave measurements. The altimeter provides estimates of sea surface height, wind speed, significant wave height and wave period, but only in a very narrow swath of spot measurements directly beneath the track of the satellite). The SAR data with sufficient resolution provides good detail of the ocean's short wave field as it responds to interactions with the atmosphere, longer waves, and currents. Passive microwave imagers have viewing parameters similar to those of scatterometers. In addition, DCS (Data Collection Systems), such as the **Argos** system on a number of spaceborne meteorological platforms, and the **Argo network** (or Argo array) of freely-drifting ocean profiling floats at various ocean depths, gather environmental in-situ data from autonomous platforms in the ground segment (on and in the ocean) and deliver their data via satellite to a worldwide user community. Argo is an international effort of collecting high-quality temperature and salinity profiles from the upper 2000 m of the ice-free

global ocean and currents intermediate depths. The Argo data come from battery-powered autonomous floats that drift mostly at depth, where they are stabilized at a constant pressure level by being less compressible than sea water. The Argo network is capable of monitoring effectively the pulse of the global heat balance, because over 90% of the observed increase in heat content of the air/land/sea climate system over the past 50 years occurred in the ocean. Initial deployment of Argo floats began in 1999/2000. ^{2073) 2074) 2075)}

In Dec. 2003, the Argo network consisted of 1000 deployed profiling floats. When fully deployed (global array of 3000 floats), Argo will provide a quantitative description of the evolving state of the upper ocean and the patterns of ocean climate variability, including heat and freshwater storage and transport. Given the national commitments of Argo–float–provision, the full Argo array should be reached by 2006. The target array represents one float at every 3° latitude and longitude. – In 2009, the Argo network consists of 3300 floats. ²⁰⁷⁶⁾

The Argo data are of vital importance for two global projects that were Argo’s originators/sponsors, **GODAE** (Global Ocean Data Assimilation Experiment) and **CLIVAR** (Climate Variability and Predictability) in which the ocean’s role is crucial.. Argo is also a pilot project of **GOOS** (Global Ocean Observing System).

Since early 2005, the ocean observing system has included global elements of subsurface and satellite data. Hence, there have been a number of applications that combine the Argo array, altimetry, as well as other datasets in the “**integrated approach**.” The global sea level makes a good example of this type of application. Changes in global average sea level are due to both – to volume expansion by warming (thermosteric sea level), and to changes in the oceans’ mass (eustatic sea level) through exchange with continental sources from ice and stored water. Each of these is observed individually: total sea level by satellite altimetry, thermosteric sea level by Argo, and the eustatic sea level by the satellite gravity mission (GRACE). ²⁰⁷⁷⁾

The major external forces acting on the ocean are those of **wind** (generating waves, turbulence, large scale waves, circulation), heating due to the sun and geothermal energy, cooling, evaporation due to sun and wind, precipitation, tidal potential of the moon and the sun, earthquakes, gravity, friction. Internal forces acting on the ocean are those of pressure gradients, viscosity and/or friction, etc.

The available capabilities for climate change predictions are still decades away at the start of the 21st century due to insufficient knowledge of the processes involved and the interactions between the different components of the climate system. There are also difficulties in understanding and representing some of the processes in numerical models. Further long–term ocean observations (spaceborne, in–situ, etc.) are needed to cover the various time– and space scales and to improve the fidelity of **GCMs** (Global Climate Models). ²⁰⁷⁸⁾

2073) J. Gould, D. Roemmich, S. Wijffels, H. Freeland, et al., “Argo Profiling Floats Bring New Era of In Situ Ocean Observations,” AGU EOS Transactions, Vol. 85, No 19, May 11, 2004, pp. 185, 190, 191

2074) S. Levitus, J. I. Antonov, J. Wang, T. L. Delworth, K. W. Dixon, A. J. Broccoli, “Anthropogenic warming of Earth’s climate system,” Science, Vol. 292, April 13, 2001, pp. 267–270

2075) <http://www.argo.ucsd.edu/>

2076) Dean Roemmich, Lars Boehme, Hervé Claustre, Howard Freeland, Masao Fukasawa, Gustavo Goni6, W. John Gould, Niki Gruber, Maria Hood, Elizabeth Kent, Rick Lumpkin, Shawn Smith, Pierre Testor, “Integrating the ocean observing system: mobile platforms,” Proceedings of OceanObs’09, Venice, Italy, Sept. 21–25, 2009, URL: http://www.oceanobs09.net/plenary/files/Roemmich_mobile_platforms_PLENARY_Paper_v2.pdf

2077) D. Roemmich, J. Gould, “Argo: The Integrated Approach,” Symposium: 15 Years of Progress in Radar Altimetry, Venice, Italy, March 13–18, 2006

2078) C. Simionato, ““Geosciences: The Future, Chapter 4, International Association of the Physical Sciences of the Oceans,” Final Report of the IUGG Working Group Geosciences: The Future, July 7, 2003

1.21.2 Satellite Altimetry

Satellite measurements of the global surface topography of the ocean in recent years have revealed the critical role of the ocean in disasters, weather, climate, water resources, marine ecosystems, and human health. These measurements, coming from a simultaneous series or constellation of satellites carrying altimeters, are a fundamental part of any global Earth observing system.

Shaped by currents, winds and Earth's gravity, the surface of the ocean tells a larger story about its most basic functions; how it stores vast amounts of energy from the sun, how it moves that energy around the globe and how it works together with the atmosphere to create climate and weather. Just as forecasting atmospheric changes requires both surface pressure and atmospheric density, so does forecasting ocean circulation require the surface pressure field from the ocean surface topography as well as density profiles in the ocean. Sampling is key: scientists have learned that one altimeter is not enough. At least one precision altimeter in an inclined reference orbit must be joined with at least two complementary altimeters in polar orbits to observe the full range of scales from global to mesoscale. In addition, for scientific understanding and operational forecasts, the altimetry data must be combined with in situ information that comes from various sources including the global Argo float array, moored buoys, and coastal sea level gages. When fully operational, the constellation and in situ measurements will provide valuable societal information. ²⁰⁷⁹⁾

Surface topography (sea level) measurements are the most essential observable required for global operational oceanography as it is a strong constraint to infer the 4D ocean circulation. This observable is obtained thanks to altimeter systems allowing global, real-time and all-weather measurements with high space/time resolution. Altimeters also measure significant wave height and winds, which are essential for operational wave forecasting.

Satellite altimetry offers the capability to observe Earth (the sea surface) in a time frame of several days, providing data products on a grid-scale (the small footprint of the measurement itself and the sampling frequency along the orbital path offer only a limited coverage). Due to the favorable reflective properties of water, the method of altimetry is especially suitable for measurements over the ocean. The spaceborne height measurement technique of the sea surface provides in effect not only the height measurement, but an integrated information set along the measurement path, from the sea surface to the spacecraft. The analysis of this altimetry data is being used in a great variety of applications involving such fields as meteorology (sea surface winds), climate, ocean topography, ocean currents, oceanography, geoid modeling, plate tectonics, etc. Altimetry itself needs in turn good reference frames – to be able to relate its monitoring data reliably to all these services and functions.

- Altimeters are active microwave instruments for the accurate measurement of vertical distances (between the spacecraft and the altimeter footprint on the ocean surface). *It is important to note that all altimeters are profiling instruments and do not yield an image. Thus, they essentially provide only spot measurements of water surface elevations.* ²⁰⁸⁰⁾

The technology determines the two-way delay of the radar pulse echo from the Earth's surface to a very high precision (in the 1990s to less than a nanosecond). The concept has also the capability to measure the power and the shape of the reflected radar pulses. The data provide in particular information on ocean topography [the gravity grids reveal also all of the major structures of the ocean floor. The "equipotential surface" of the ocean bulges outward and inward mimicking closely the topography of the ocean floor. – The actual ocean

2079) "Establishment of a U.S. National Land Imaging Program," URL: http://earthobservations.org/documents/sbas/cl/64_Establishment%20of%20a%20US%20National%20Land%20Imaging%20Program.pdf

2080) Note: Due to this feature of ocean-floor mimicry, first attempts have been made to use sea surface topography measurements to derive data for mapping structure, geology and topography of the sea floor. This is done through conversion of sea surface topography to gravity and then to sea floor topography through a series of mathematical calculations and modeling. Features greater than approximately 15 km wide can be identified and structures beneath sediment cover are "exposed" on gravity maps

surface deviates by up to 100 m from the ideal ellipsoid. The bumps and dips (troughs) in geoid height are caused by minute variations in the Earth's gravitational field].²⁰⁸¹⁾

Background: Spaceage altimetry got really started in August 1969 with the NASA–sponsored Williamstown Conference (Williamstown, MA, USA) – – where it was decided to use space systems to learn more about the Earth and the oceans.^{2082) 2083)} Specifically, the conference recommended that:

- Satellite geodesy to measure the Earth's gravity field
- Ocean altimetry for physical oceanography and studies of the rheology of the oceanic lithosphere
- Space techniques such as Satellite Laser Ranging (SLR), Very Long Baseline Interferometry (VLBI), and Lunar Laser Ranging (LLR) to measure plate motion and deformation, and Earth orientation.

These recommendations were incorporated into a NASA plan which led to the establishment in 1972 of the Earth and Ocean Dynamics Applications Program. First among the recommendations was the development of satellites with “10 cm accuracy altimeters ... to measure the geopotential and mean sea level accurately enough to ... determine the general circulation of the oceans (and) to resolve the spatial variations in the gravity field to 100 km half wavelength.”

First spaceborne monostatic altimetry measurements (demonstrations) of ocean surface heights started in 1973 with S–193 (Passive Microwave Radiometer/Active Scatterometer and Radar Altimeter) instrument on NASA's Skylab missions SL–2, SL–3 and SL–4 (1973–1974) at an altitude of 435 km (see L.5). Using a pulse width of 0.1 microsecond this system was able to get a resolution of 15 m. The availability of the S–193 altimeter data opened the way to a direct comparison of the altimeter heights with a computed gravimetric geoid.²⁰⁸⁴⁾

In altimetry the variation of the return signal strength (as the cube power of height) and the footprint area with the altitude requires the use of the pulse compression for higher altitudes.²⁰⁸⁵⁾ Since GEOS–3 (launch Apr. 9, 1975), flying at an average altitude of 840 km, all altimeters have used pulse compression – the resolution due to this compression has been improved. GEOS–3 offered significant improvements over the Skylab altimeter (S–193), including improved performance as well as greater global coverage.

The SeaSat (launch June 27, 1978) ALT instrument, designed and built by JHU/APL, is regarded the first high performance altimeter (first use of the full–deramp technique; introduction of the capability of waveform sampling). In contrast with previous designs, the samples are now an integral part of the altitude tracking process and are used in such a way that the system adapts as a function of wave height to tracker performances. Despite the premature demise of the SeaSat S/C after only 100 days in orbit, the altimeter performance clearly demonstrated the significance of the signal processing innovation, it was adopted as the standard approach for new radar altimeters. GEOSAT (1985 – 1990) altimetry introduced also measurements of sea–state and ocean surface winds. GEOSAT performed two separate missions: a) the primary geodetic mission, and b) the ERM (Exact Repeat

2081) D. T. Sandwell, W. H. F. Smith, “Exploring the Ocean Basins with Satellite Altimeter Data,” at URL: <http://www.ngdc.noaa.gov/mgg/bathymetry/predicted/explore.HTML>

2082) W. M. Kaula, Williamstown Report, “The Terrestrial Environment, Solid–Earth and Ocean Physics: Application of Space and Astronomic Techniques,” Report of a Study at Williamstown, MA, NASA Contractor Report, CR–1599, April 1970

2083) D. McAdoo, “Marine geoid, gravity and bathymetry: an increasingly clear view with satellite altimetry,” Symposium: 15 Years of Progress in Radar Altimetry, Venice, Italy, March 13–18, 2006

2084) J. T. McGoogan, L.S. Miller, G. S. Brown, G. S. Hayne, “The S–193 Radar Altimeter Experiment, Satellite Altimetry Applications, IEEE Transactions, June, 1974.

2085) R. F. Gasparovic, R. K. Raney, R. C. Beal, “Ocean Remote Sensing Research and Applications at ALP,” JHU/APL Technical Digest, Vol. 20, No 4, pp. 600–610, 1999

Mission, Nov. 8, 1986 to Jan. 5, 1990), in which it retraced the SeaSat ground tracks, provided the first long-term high-quality altimeter measurements to the scientific community.

The modern age of satellite altimetric studies of ocean surface topography began in the early 1990s: The RA-1 altimeter on ERS-1 (launch 1991) and on ERS-2 of ESA (since 1995) was designed to optimize its performance over all types of surfaces. RA-1 provided high-accuracy (3 cm precision) elevation measurements of the ocean surface topography, wave height and wind speed from a sun-synchronous orbit (the first polar-orbiting satellite with an altimeter on-board). ERS-1 was in ERM (Exact Repeat Mission), a 35-day repeat orbit from April 1992 to December 1994 and from mid-1995 to 1999 (mission end). The geodetic mission (GM) of ERS-1 started in April 1994 and included two, successive 168-day repeat periods whose tracks were offset by 8 km producing a 366-day super-cycle. The ERS/GM observations are considered the “most important marine geological and geophysical data set collected in the past (15 years)” and enabled mapping of virtually the entire global marine gravity field to a two-dimensional, full-wavelength spatial resolution of 20 km or better. ²⁰⁸⁶⁾ ²⁰⁸⁷⁾

The NRA (NASA Radar Altimeter) instrument on TOPEX/Poseidon (launch Aug. 10, 1992), designed to optimize performances over ocean surfaces, is regarded the first dual-frequency altimeter, permitting the estimation of ionospheric range delay. The TOPEX/Poseidon mission has demonstrated that the time variation of ocean topography (dynamic and thermodynamic) can be determined with an accuracy and precision of a few centimeters. For the first time, the seasonal cycle and other temporal variabilities of the ocean have been determined globally with high accuracy, yielding fundamentally important information for testing ocean circulation models. *TOPEX/Poseidon was the first mission specifically designed to measure sea-surface topography for the determination of ocean circulation.* The missions ERS-1/2 and TOPEX/Poseidon are part of international oceanographic and meteorological programs, such as WOCE (World Ocean Circulation Experiment) and TOGA (Tropical Ocean and Global Atmosphere), both linked to WCRP (World Climate Research Programme). Major observations/phenomena of the TOPEX/Poseidon mission data analysis are: (see Ref. 1969)

- Oceanic circulation, including the movement of Rossby and Kelvin waves ²⁰⁸⁸⁾ ²⁰⁸⁹⁾
- Oceanic and coastal tides
- El Nino, La Nina, and the Pacific Decadal Oscillation
- El Nino-like circulation in the Atlantic Ocean
- Oceanic seasons in the Mediterranean
- Ocean floor topography from surface data used to refine the geoid model.

Historical background: The **Rossby waves** are named after Carl-Gustav Rossby (1898 – 1957)] of Stockholm, Sweden (Swedish-US meteorologist). In 1928, he organized the first university level meteorological program in the United States at the Massachusetts Institute of Technology (MIT). In 1939, he became the assistant chief of research at the US Weather Bureau, and in 1940 the chairman of the Department of Meteorology at the University of Chicago.

2086) D. T. Sandwell, W. H. F. Smith, “Marine gravity anomaly from Geosat and ERS-1 satellite altimetry,” *Journal of Geophysical Research*, Vol. 102, No B5, 1997, pp. 10039–10054

2087) J. Benveniste, Y. Menard, “Taking the Measure of Earth, Fifteen Years of Progress in Radar Altimetry,” *ESA Bulletin*, No. 128, Nov. 2006, pp. 42–51

2088) J. P. Angell, T. R. Robinson, S. P. Lawrence, “TOPEX Observations of Kelvin, Rossby and Tropical Instability Waves in the Pacific Ocean,” http://ion.le.ac.uk/remote_sensing/COSPAR_Rossby_jpa.pdf

2089) Carl Gustav Rossby (1898 – 1957) was born in Stockholm, Sweden. In the 1930s he became a US citizen and worked for the US Weather Bureau. He became a pioneer in the field of large-scale circulations.

Rossby waves owe their existence to the rotation of the Earth. They are easily observed in the atmosphere (i.e. as large-scale meanders of the mid-latitude jet stream). Their existence in the oceans was first theorized by Rossby in the 1930s. Rossby waves couldn't be detected until the advent of radar altimetry because they occur internally and are very small on the ocean surface, about 10 cm high, making them impossible to detect from onboard an oceanographic research vessel.

Rossby waves are also known as **planetary waves**, they are solutions of simplified forms of the equations governing the dynamics of the atmosphere and oceans (large-scale ocean dynamics phenomena). They serve as archetypes for the sinuous large-scale motions of the mid-latitude troposphere. They are horizontal transverse waves with large values of vorticity and with divergence which is negligible by comparison. Their most characteristic feature is that they move westward relative to the zonal atmospheric flow. This strange lopsidedness is a result of the Earth's rotation, which breaks the symmetry of east-west reflection. Rossby waves of very long wavelength are important in communicating changes in the large-scale circulation to the gyre interior. Kelvin waves can run around the boundaries of an ocean and transmit information about changes in large-scale forcing or boundary conditions eastward along the equator. ^{2090) 2091)}

- Ocean-surface topography measurements beyond the TOPEX/Poseidon era. The successor altimetry missions (Jason-1, Envisat, Jason-2, etc.) have broadened the list of science objectives. Data analysis of these missions is expected to:
 - Measure global sea-height change and provide a continuous view of changing global ocean surface topography
 - Calculate the transport of heat, water mass, nutrients, and salt by the oceans
 - Increase understanding of ocean circulation and seasonal changes and how the general ocean circulation changes through time
 - Provide estimates of significant wave height and wind speeds over the ocean.

Ocean reflection measurements of GNSS signals as sources of opportunity (a passive altimetry technique). See chapter 1.20.6.

- Starting in the 1990s, altimetry missions were more and more integrated into international oceanographic and meteorological programs such as WOCE (World Ocean Circulation Experiment) and TOGA (Tropical Ocean and Global Atmosphere), both are linked to the WCRP (World Climate Research Program).

Systematic monitoring of the sea level ²⁰⁹²⁾ (as well as of large lakes and rivers) is the prime objective of spaceborne altimetry applications. Covering about 70% of the Earth's surface, the oceans are the best guardians of the delicate balances controlling our planet. There are three main reasons for the rise and fall in sea level throughout the Earth's geological history:

- 1) Changes in the shape and volume of ocean basins due to plate motions
- 2) Movements of water masses between the polar ice caps and the oceans through ice formation and melting
- 3) Variations in water density with changes in temperature and salinity.

The first of these phenomena is rather slow, while the other two may be quick, they are closely tied to climate change. However, while a rise in sea level due to an inflow of water

2090) C. G. Rossby, et al., "Relations between variations in the intensity of the zonal circulation of the atmosphere and the displacements of the semipermanent centers of action," *Journal of Marine Research*, Vol. 2, 1939, pp. 38–55

2091) <http://www.soc.soton.ac.uk/JRD/SAT/Rossby/Rossbyintro.html>

2092) J.-F. Minster, "Rising sea level under close surveillance," *CNES Magazine* No 19, May, 2003, p. 36

masses is rapid and uniform, it takes in the order of 1000 years for a rise in temperature to spread throughout the oceans. This is why sea level changes due to warming are spatially very unequal.

Aside from sea level monitoring, ²⁰⁹³⁾ altimeter data has also proved invaluable for a suite of practical applications including:

- Ocean forecasting systems
 - Ship routing
 - Precision marine operations such as cable–laying and oil production
 - Ocean acoustics for Navy operations
 - Fisheries management
 - Marine mammal habitat monitoring
 - Hurricane forecasting and tracking
 - Debris tracking.
- Spaceborne radar altimeters have been profiling the ocean surface continuously since 1991, through the ERS–1, TOPEX/Poseidon, ERS–2, GFO (GEOSAT Follow–On), Jason–1, and Envisat missions. Their observations have afforded the geoscience community a revolutionary and dramatically–improving view of the global marine gravity field – and geoid. These altimetric marine gravity fields have led directly to a greatly improved understanding of global bathymetry, marine tectonics, ocean circulation and climate variability. Planetary waves can certainly be considered a success story for altimetry, given the quantum leap in the quality of the observational evidence made possible by the availability of high–quality SSH (Sea Surface Height) fields, and the substantial revision of our theoretical understanding of planetary waves sparked by those observations. The global altimetry observations highlighted significantly faster waves with respect to the classical theory of planetary wave propagation, calling for a revision of the theory. ^{2094) 2095)}
 - The altimeters of ICESat and CryoSat, GLAS (Geoscience Laser Altimeter System) and SIRAL (SAR Interferometer Radar Altimeter), respectively, are considered primarily as research instruments to measure such parameters as: ice sheet topography, cloud heights, planetary boundary layer heights, and aerosol vertical structure. Sea ice plays a central role in arctic climate.

Mission/ Sensor	Launch Date	Range Preci- sion (cm)	Fre- quency (GHz)	Uncom- pressed Pulse Width (μ s)	Com- pressed Pulse Width (μ s)	Peak Power (W)	Beam Limited Foot- print (km)	Pulse Limited Foot- print (km)	Orbit altitude, inclina- tion (km/ $^{\circ}$)
Skylab, S–193	14.5.73	90	13.9			2000		8	435, 50
GEOS–3, ALT	9.4.75	50	13.9	1	12.5	2000	38	3.5	843,115
SeaSat, ALT	27.6.78	10	13.5	3.2	3.1	2000	22	1.7	800,108
GEOSAT, Radar Alt	12.3.85	5	13.5	102.4	3.1	20	29	1.7	800,108

2093) M. Srinivasan, R. Leben, L.–L. Fu, Y. Menard, E. Dombrowsky, F. Blanc, “Satellite Altimetry Applications: Operational Oceanography from Space,” Proceedings of the Weikko A. Heiskanen Symposium in Geodesy, Ohio State University, Columbus, OH, USA, Oct. 1–4, 2002

2094) P. D. Cotton, Y. Menard, “The Future Role of Satellite Altimetry – Early Recommendations From the GAMBLE Project,” The 2003 EUMETSAT Meteorological Satellite Conference, Weimar, Germany, Sept. 29 – Oct. 3, 2003

2095) P. Cipollini, P. G. Challenor, D. Cromwell, I. S. Robinson, G. D. Quartly, “How satellites have improved our knowledge of extratropical planetary waves in the ocean,” Symposium: 15 Years of Progress in Radar Altimetry, Venice, Italy, March 13–18, 2006

Mission/ Sensor	Launch Date	Range Precision (cm)	Fre- quency (GHz)	Uncom- pressed Pulse Width (μ s)	Com- pressed Pulse Width (μ s)	Peak Power (W)	Beam Limited Foot- print (km)	Pulse Limited Foot- print (km)	Orbit altitude, inclina- tion (km/ $^{\circ}$)
ERS-1, RA-1	17.7.91	5-7	13.8	20	3	55	18	1.7	785,98.5
Topex/Pos NRA Posei- don-1	10.8.92	2.4 2.5	13.6/5.3 13.65	102.4	3.1	20 5	26/65	2.2	1334, 63.5
ERS-2, RA-1	21.4.95	5-7	13.8	20	3	55	18	1.7	785,98.5
Priroda (Geben)	23.4.96	10	13.76	1.7	12.5	40	13	2.3	400, 52
GFO-1, RA	10.2. 98	3.5	13.5					2	800, 108
Jason-1 Posei- don-2	7.12.01		13.575/ 5.3	105		58			1336, 66
Envisat RA-2	1.3.2002	<4.5	13.575 3.2	20		60 60		1.7	800, 98.55
ICESat-1 GLAS	13.01. 2003	<10						0.7	705, 94
CryoSat SIRAL	08.10. 2005		13.6	51		25	Launch failure		720, 92
Jason-2 Posei- don-3	20.06. 2008		13.575/ 5.3	20					1336, 66
CryoSat-2 SIRAL	08.04. 2010		13.6	51		25			720, 92
HY-2A ALT	15.08. 2011		13.58 5.25	102.4		20	16		963, 99.3
SARAL/ AltiKa	25.02. 2013		35.75	107			8		800, 98.55
Senti- nel-3A SRAL	2013		13.575 5.41						815, 98.6

Table 118: Chronological survey of spaceborne radar altimeters

- **Altimetry calibration in the period 1992–2012:** Altimetry calibration has evolved from an engineering-oriented discipline in the early 1990s to a multidisciplinary scientific endeavor at present. Early efforts focused on the determination of constant measurement bias at a few dedicated sites equipped with multiple sensors including a tide gauge. Evaluations of the geophysical data products were undertaken, but mainly with the intent of verifying compliance with mission requirements. ²⁰⁹⁶⁾

- With the launch of T/P (TOPEX/Poseidon), calibration efforts grew significantly more diverse and rigorous as they attempted to address the most scientifically challenging problems. One important advance was the use of globally distributed tide gauge of opportunity to reduce errors in monitoring the stability of the altimeter measurement system. This development provided a robust verification on the capability of altimetry to measure the global mean sea level change. This new objective has motivated more thorough studies of the entire measurement system, including errors in altimeter, radiometer, orbit determination, etc. The challenges include the need for more robust radiometer calibration by perhaps flipping the instrument periodically for “cold-sky” calibration in future missions.

- The cross-calibration between T/P and Jason-1 and between Jason-1 and Jason-2 has created an unprecedented opportunity for evaluation of the uncertainty of altimetry

²⁰⁹⁶⁾ Lee-Lueng Fu, Bruce J. Haines, “Evolution of Altimetry Calibration and Future Challenges,” Proceedings of the Symposium ‘20 years of Progress in Radar Altimetry’, Venice, Italy, Sept. 24–29, 2012, (ESA SP-710, Feb. 2013)

measurements globally and over various spatial scales. The comparison of measurements over the same ground tracks with time separation about 1 minute reveals the relative measurement errors from all sources. This is an ideal way to cross–calibrate successive missions.

– The accuracy and precision of T/P were utilized to cross–calibrate other simultaneously flying satellite altimeters to minimize large–scale errors in their measurements. This approach to merging T/P and ERS–1 data increased significantly the spatial and temporal resolution of the merged data products with optimal accuracy. – Such efforts have led to a record of uniformly gridded global SSH (Sea Surface Height) products spanning the past two decades, using data from T/P and its succeeding missions of Jason–1 and Jason–2, in combination with all other altimetry missions, including ERS–1, ERS–2, Envisat, and GFO (GEOSAT Follow–On). – With progressively improved geoid models available from the GRACE and GOCE missions as well as modeling efforts, the absolute ocean surface topography has also become available. The two–decade long altimetry data record has fundamentally advanced global oceanography to an unprecedented level. Satellite altimetry has become a standard resource in the tool bag of both research oceanographers and practitioners needing routine oceanic information.

– Dedicated calibration sites provide the foundation of the 20–yr calibration program underpinning the success of the combined T/P and Jason missions. Located along the 10–day repeat ground track shared by these missions, these sites are carefully instrumented to provide an independent (in–situ) determination of SSH relative to the geocenter. The absolute (geocentric) in–situ observations provide the basis for calibrating the altimetric SSH measurements made by the satellite as it overflies each location every 10 days. ²⁰⁹⁷⁾

• **Sea level change:** In the last 20 years, a great leap forward has occurred in sea level change science, largely due to the influx of satellite altimeter and gravity measurements. Satellite altimetry has observed an average increase in sea level of 3.2 ± 0.4 mm/year over 1993–2012, which is greater than the 20th century rate (~ 1.8 mm/year), but the cause of this is still being investigated. Depending on the time period considered, roughly a third of the current rise may be attributed to thermal expansion, and twothirds to the combination of melting mountain glaciers and polar ice sheets (Figure 156).

Excellent agreement has been found between satellite altimeter measurements, GRACE ocean mass estimates, and thermosteric measurements from the Argo floats. Interannual variations in GMSL (Global Mean Sea Level) are largely ENSO–driven. One of the big advances in our understanding over the last 20 years is that these interannual changes in GMSL are largely driven by interannual changes in land water storage via changes in precipitation and subsequent water storage. While there are decadal sea level variations, it is not clear to what level these map into GMSL variations. The presence of these interannual and decadal variations in GMSL makes the detection of anthropogenic contributions difficult. ²⁰⁹⁸⁾

When satellite altimetry is coupled with satellite gravity measurements, sea level change can be understood as an expansion of the ocean water due to increasing heat content coupled with changes in the amount of water stored on land – both in ice and liquid form. Satellite altimetry critically provides the regional changes in sea level in addition to the global mean.

2097) P. Bonnefond, J.–D. Desjonqueres, B. Haines, S. Mertikas, C. Watson, “Absolute Calibration of the TOPEX/Poseidon and Jason Measurement Systems: Twenty Years of Monitoring from Dedicated Sites,” Proceedings of the Symposium ‘20 years of Progress in Radar Altimetry’, Venice, Italy, Sept. 24–29, 2012, (ESA SP–710, Feb. 2013)

2098) R. S. Nerem, D. P. Chambers, M. Merrifield, G. Mitchum, D. Masters, “A 20 Year Climate Data Record of Sea Level Change: What have we learned?” Proceedings of the Symposium ‘20 years of Progress in Radar Altimetry’, Venice, Italy, Sept. 24–29, 2012, (ESA SP–710, Feb. 2013)

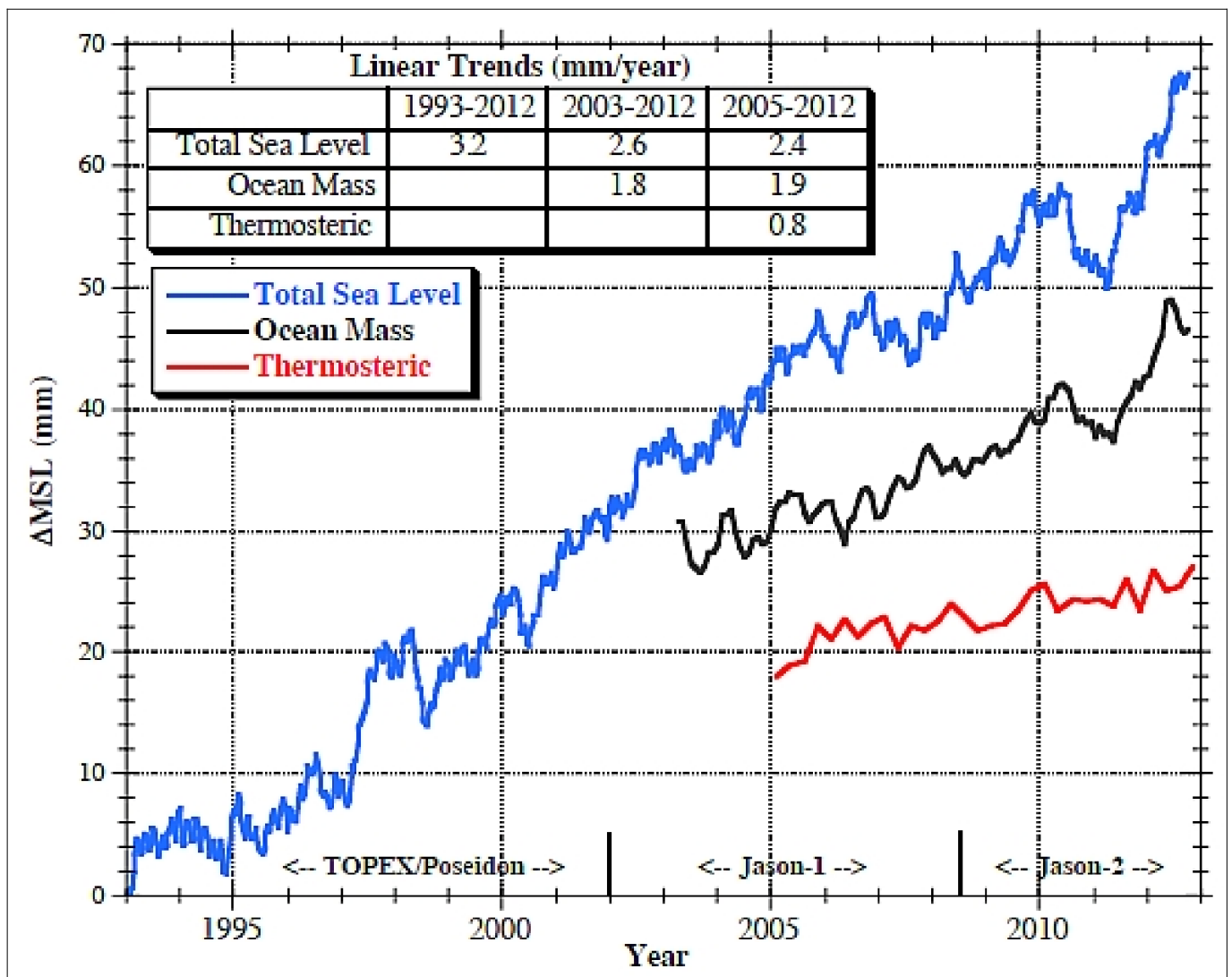


Figure 156: Time series of global mean sea level (GMSL) since 1993 obtained from the TOPEX/Poseidon, Jason-1, and Jason-2 satellite altimeters. Seasonal signals have been removed from the data and the inverse barometer and global isostatic adjustment corrections have been applied. (image credit: U. of Colorado, U. of South Florida, U. of Hawaii)

- **Operational altimetry** is becoming more and more a reality at the start of the 21st century – because it has demonstrated interdisciplinary applications across many fields such as: oceanography, geodesy, hydrology, glaciology, and geophysics. It qualifies itself as an essential component of global Earth observing systems. There is a generally accepted need for long, accurate time series of multi-mission altimeter data, which requires standards on formats, geophysical corrections and reference frames, as well as the knowledge of the long-term stability of altimeter and its ancillary sensors. The latter implies cross-calibration between past, present, and future altimeter missions as well as between different altimeter technologies (pulse limited, laser, lidar, wide swath, Delay Doppler, etc).²⁰⁹⁹⁾

Operational altimetry refers to a sufficient infrastructure to make data products available in a timely and continuous manner to the needs of a larger operational oceanography community.²¹⁰⁰⁾ In particular, this is a main objective of **GODAE** (Global Ocean Data Assimilation Experiment), an international framework to eventually obtain an integrated and com-

2099) W. Bosch, C. K. Shum, P. Woodworth, G. Mitchum, “An International Altimetry Service – focussing altimetry for global Earth observing systems,” Symposium: 15 Years of Progress in Radar Altimetry, Venice, Italy, March 13–18, 2006

2100) <http://www.bom.gov.au/bmrc/ocean/GODAE/>

prehensive ocean observing system. Several pioneering research programs (international multi-year campaigns) have already contributed or are contributing to the GODAE goal.

- WOCE (World Ocean Circulation Experiment). The WOCE program is a cooperative international effort (WCRP initiative of 1983) involving scientists from 40 nations.
- TOGA/COARE (Tropical Oceans and Global Atmosphere Experiment / Coupled Ocean Atmosphere Response Experiment). TOGA was initiated in 1985 by WMO.
- CLIVAR (Climate Variability and Predictability). A major WCRP (World Climate Research Program) initiative since 1993.
- Argo (Array for Geostrophic Oceanography). Argo represents a global network of sea-going floats for a better understanding of the world's oceans. Argo is an international ocean program, part of GCOS/GOOS and CLIVAR – eventually it will consist of an array of 3000 free-drifting (Lagrangian) profiling floats, at various depths, that measure the temperature and salinity of the upper 2000 m of the ocean; start of deployment in 2000, more than 3000 floats are expected by 2006. Argo provides data complementary to remote sensing data to initialize and constrain ocean models.

To perform **operational oceanography**, spaceborne and in-situ measurements of the ocean state (of as many missions as possible and of many buoys in the ocean) must be merged with physical models of the oceans (assimilation process) to deliver regional and global analysis of the ocean state, to be able to make forecasts of its future state. Oceanic variability especially affects major oceanic currents, has a significant effect on climatic changes. Obviously, operational altimetry data products are an important ingredient in this operational oceanography effort. ²¹⁰¹⁾ ²¹⁰²⁾

With regard to spacecraft operations of future altimetry missions, the following changes are being implemented. While mission operations of Jason-1 are still being conducted by NASA and CNES, the operational function of Jason-2 (launch June 20, 2008) will be carried out by NOAA and EUMETSAT, respectively (the operators of US and European weather satellites). This switch of service support from research institutions to operational institutions is a definite sign of a service mature enough to become operational.

- Plans for the Jason-2 mission (NASA, CNES, launch June 20, 2008) called for a conventional core mission, based on the Jason-1 follow-on instrumentation, and in parallel a demonstration mission of NASA/JPL involving the new concept of an interferometric radar configuration, referred to as **WSOA** (Wide Swath Ocean Altimeter). The objective of the experimental WSOA was to demonstrate for the first time ocean topography observations (using cross-track interferometry) from a single platform over swaths of 200 km. The design of the WSOA configuration uses two antennas separated by a 7 m mast and the interferometric technique to map directly under the satellite and over a 200 km swath the dynamic sea surface topography.

Note: As of March 2005, NASA has decided to cease further development of the Ocean Surface Topography Mission (OSTM) WSOA instrument (Wide-Swath Ocean Altimeter). – In the meantime, new plans for a wide-swath altimetry capability are being studied under the name of **SWOT** (Surface Water Ocean Topography), see chapter 1.21.2.4.

- **Coastal altimetry:** The coastal zone can be defined, as a rule of thumb, as 0–50 km from coastline, but in practice it is any place where standard altimetry gets into trouble as waveforms are non-Brown and/or corrections become inaccurate. Traditionally, data in the coastal zone are flagged as bad and left unused. Starting in the early 21st century, a vibrant

2101) P. Escudier, "Ocean Altimetry Status after Jason1 and Envisat Launch," Proceedings of the 54th IAC, Bremen, Germany, Sept. 29 – Oct. 3, 2003, IAC-03-B1.05

2102) P. Y. Le Traon, "From Satellite Altimetry to Operational Oceanography: A Historical Perspective," Proceedings of the Symposium '20 years of Progress in Radar Altimetry', Venice, Italy, Sept. 24–29, 2012, (ESA SP-710, Feb. 2013)

community of researchers has started to believe that most of those coastal data can be recovered and that coastal altimetry can be a legitimate component of coastal observing systems. This is also important for SAR and Ka-band altimetry, which have intrinsically better coastal performance than conventional altimetry. ²¹⁰³⁾

Coastal altimetry improves the retrieval of sea surface height and significant wave height in the coastal strip essentially by two means: specialized retracking and improved corrections. Specialized retracking is achieved by using better waveform models, which account for the change of echo shape in the coastal environment, or by innovative (2-D or sequential) retracking techniques. As far as corrections are concerned, the most crucial is the correction of path delay due to water vapor (“wet tropospheric” correction).

The recent availability of delay-Doppler (SAR altimeter) data allows a much better characterization of short scales. When the track approaches the coast almost orthogonally, the waveforms conform well to the delay-Doppler Altimetry model (and give sensible results when retracked), up to 500 m from the coast or even closer.

- Radar altimetry from space started in the context of WOCE (World Ocean Circulation Experiment). Since its inception, the altimetry community has expanded in size and scope from a few handful of ocean scientists and a couple of countries to a worldwide concerted effort involving both R&D and operational space agencies from Europe, USA, China and India, benefiting from the expertise of several hundreds of scientists and engineers, serving the needs of thousands of data users, and covering a variety of disciplines, from large-scale to mesoscale oceanography, through to coastal studies, ice sheets and ice cap survey, marine geodesy, hydrology and limnology. One crucial achievement of radar altimetry has been the 20 year record of sea level rise and its geographic pattern and variability, a key climate indicator of global warming, made possible by the incredible accuracy of the combined technique of sea surface height measurement and precise orbit determination. ²¹⁰⁴⁾

Radar altimetry is a key component of GEOSS (Global Earth Observation System of Systems), and over the last 20 years has provided the principal global data source enabling the development of operational oceanography. Radar altimetry contributes to a large number of societal needs, from climate monitoring to weather forecasting, with subsequent applications in a range of activities of socioeconomic importance, including agriculture, health, energy, water, maritime safety, etc.

1.21.2.1 Altimetry principles

Conventional altimetry can be described as run-of-time distance measurements taken from a vertically tracking satellite to the geoid. A spaceborne radar altimeter maps the sea surface, which is complex, but which largely conforms to the equipotential surface known as the geoid. The ocean surface departs significantly (at the meter level) from the geoid – this departure is of great interest to the science community (oceanographers, meteorologists, geophysicists, etc.) for it reflects the global circulation patterns and also, in the form of tides and changes in sea level, fundamental climatic and solid Earth phenomena. Furthermore, altimetry provides approximate estimates of the geoid itself, in the form of a mean surface obtained by averaging measurements taken over many satellite passes over the same locations. More detailed explanations on altimetry are given below.

²¹⁰³⁾ Paolo Cipollini, Jérôme Benveniste, Laury Miller, Nicolas Picot, Remko Scharroo, Ted Strub, Doug Vandemark, Stefano Vignudelli, Simona Zoffoli, Ole Andersen, Lifeng Bao, Florence Birol, Emanuel Coelho, Xiaoli Deng, William Emery, Luciana Fenoglio, Joana Fernandes, Jesus Gomez-Enri, David Griffin, Guoqi Han, Jessica Hausman, Kaoru Ichikawa, Andrey Kostianoy, Villy Kourafalou, Sylvie Labroue, Richard Ray, Martin Saraceno, Walter Smith, Pierre Thibaut, John Wilkin, Somayajulu Yenamandra, “Conquering the Coastal Zone: A New Frontier for Satellite Altimetry,” Proceedings of the Symposium ‘20 years of Progress in Radar Altimetry’, Venice, Italy, Sept. 24–29, 2012, (ESA SP–710, Feb. 2013)

²¹⁰⁴⁾ Jérôme Benveniste, Rosemary Morrow, Jean-Louis Fellous, Albert Fischer, “Summary and Recommendations from the ‘20 Years of Progress in Radar Altimetry’ Symposium,” Proceedings of the Symposium ‘20 years of Progress in Radar Altimetry’, Venice, Italy, Sept. 24–29, 2012, (ESA SP–710, Feb. 2013)

- A radar altimeter onboard a satellite permanently transmits signals at high frequency to the Earth's surface, and receives the echo from the sea surface. This is analyzed to derive a precise measurement of the round-trip time between the satellite and the sea surface. By averaging the estimates, say, over a second, this produces a very accurate measurement of the satellite-to-ocean range. However, as electromagnetic waves travel through the atmosphere, they can be decelerated by water vapor or by free electron ionization effects in the ionosphere. Once these phenomena are corrected for, the final range R is estimated within 2 cm.
- The pulse-limited footprint of an altimeter is defined as the radius of the leading edge of the pulse when the trailing edge of the pulse first hits the ocean surface.²¹⁰⁵⁾
- Until 2011, almost all altimetry missions have been based on standard pulse-limited Ku-band altimetry. The notable exceptions so far are: IceSat-1 and CryoSat-2.
- Satellite orbit: The ultimate aim is to measure sea level relative to a terrestrial reference frame. This requires independent measurements (accurate tracking) of the satellite orbital trajectory, i.e. exact latitude, longitude and altitude coordinates. The critical orbital parameters for satellite altimetry are altitude, inclination and period.
- Sea surface height (SSH): SSH is the range at a given instant from the sea surface to a reference ellipsoid. SSH is simply the difference between the satellite height (S) and the altimetric range (R): $SSH = S - R$. The SSH value takes account of such effects as:
 - The sea surface height which would exist without any disturbances (wind, currents, tides, etc.). This surface, called the **geoid**, is due to gravity variations around the world, which are in turn due to major mass and density differences on the sea-floor. For example, a denser rock zone on the sea-floor may deform the sea level in the order of tens of meters; this is visible as a hill on the geoid.
 - The ocean circulation, or dynamic topography. The ocean circulation, which comprises a permanent stationary component (permanent circulation linked to Earth's rotation, permanent winds, etc.) and a highly variable component (due to wind, tides, seasonal variations, etc.). The mean effect is on the order of one meter.

Conventional altimeter payloads on such missions as TOPEX/Poseidon, ERS-1/2, Envisat, and Jason-1 are looking for dynamic topographic signals. These may be only a few cm in height, against a background of height variations of the geoid that run as large as ± 150 m the globally-averaged geoid. Further, the topographic signals may have large-scale resolutions of 1000 km and more. The consequence of these requirements is that the altimeter should follow a repeating track (to an accuracy of ± 1 km or better) so that after many cycles, the geoid can be determined. Once that is in hand, then the cm-level signals can be extracted. Dynamic topographic objectives carry other implications as well. The sea surface height must be measured absolutely. It should be recalled that a radar (altimeter) does not measure distance, it measures time delay, which if the speed of propagation is known, can be converted to distance. When accuracies of ~ 1 cm over a range of ~ 1000 km are required, even very small variations in the speed of light can generate unacceptable errors. Hence, all sources of path delay, etc., have to be estimated and compensated. Thus, a state-of-the-art ocean topographic altimeter uses two frequencies (to measure and remove delays from free electrons in the ionosphere), and requires a bore-sighted two- or three-frequency radiometer (to estimate and remove delays from atmospheric moisture).

- **Altimetry over inland water heights.** The most well established use of altimetry over land is the measurement of inland water heights. This field has evolved rapidly over the past two decades (since the mid 1980s). Initial work over a handful of large targets has expanded to the current capability to monitor thousands of river and lake heights worldwide. Two fac-

²¹⁰⁵⁾ David T. Sandwell, "Radar Altimetry," 2011, URL: <http://topex.ucsd.edu/rs/altimetry.pdf>

tors have been critical to the advances made in inland water monitoring. The first is the inclusion of a designed capability to track rapidly varying land surfaces, deployed on the ERS RA-1 and RA-2 on Envisat. The second is in the analysis of inland water echoes, with the ability to identify and re-track to that part of a complex return corresponding to the underlying water surface. In particular, TOPEX/Poseidon and ERS-2 have obtained long-time series of data, now being continued by Envisat and Jason-1. The unique multi-mission dataset already gathered, with its varied temporal sampling, frequencies of operation, and differing instrument characteristics has provided a vast database of echoes over more than a decade and sampling many thousands of rivers and lakes worldwide. ²¹⁰⁶⁾

This decadal global dataset holds a vast amount of climate related information; one conclusion from all researchers in this field is that this valuable monitoring capability must be continued by future altimeter missions. The comparatively recent area of research in inland water height applications is evolving rapidly, and the potential of this technique is only now being realized.

The next generation of altimeters [SRAL (SAR Radar Altimeter) of Sentinel-3A, launch in 2014] with higher PRF and along-track delay-Doppler processing will increase the monitoring capability by several orders of magnitude. In terms of resolution as well as accuracy, the SAR mode is a revolution for small size inhomogeneous targets such as small rivers. ²¹⁰⁷⁾

1.21.2.2 Geodetic altimetry

Geodetic altimetry is fundamentally different from “conventional” oceanographic altimetry. In contrast, geodesy (according to the Sandwell and Smith algorithm) requires only that mean sea surface slopes be measured, over scales of < 200 km. Absolute sea surface height is not needed. Hence, a “simple” single-frequency altimeter is sufficient. Sea surface slope estimation down to scales as small as 6 km (half wavelength), however, can only be obtained if: ^{2108) 2109) 2110)}

- 1) The instrument precision (height variance) is very small, and
- 2) The average spacing between neighboring tracks is 6 km or less.

These two requirements dictate: 1) a delay-Doppler instrument, and 2) a non-repeating orbit, respectively. The delay-Doppler approach increases the degrees-of-freedom in the height waveform; hence, its inherent precision is better (by nearly a factor of two) than that of a conventional altimeter. In spaceborne altimetry all measurements are made at nadir. A cross-track resolution is the result of a non-repeating orbit, so that, after a year or so, the density of surface tracks accumulates; hence, their average proximity decreases with time. An example of a non-repeating orbit altimetry mission is the so-called geodetic mission of GEOSAT (March 1985 to Sept. 1986), the phase during the first 18 months of the mission.

²¹⁰⁶⁾ P. A. M. Berry, “Two decades of inland water monitoring using satellite radar altimetry,” Symposium: 15 Years of Progress in Radar Altimetry, Venice, Italy, March 13–18, 2006

²¹⁰⁷⁾ P. A. M. Berry, R. G. Smith, M. K. Salloway, M. Quessou, J. Benveniste, “20 Years of River and Lake Monitoring from Multi-Mission Satellite Radar Altimetry,” Proceedings of the Symposium ‘20 years of Progress in Radar Altimetry’, Venice, Italy, Sept. 24–29, 2012, (ESA SP-710, Feb. 2013)

²¹⁰⁸⁾ Courtesy of R. Keith Raney of JHU/APL, Laurel, MD

²¹⁰⁹⁾ W. H. F. Smith, D. T. Sandwell, “Bathymetric prediction from dense satellite altimetry and sparse shipboard bathymetry,” Journal of Geophysical Research, Vol 99, 1994, pp. 21803–21824.

²¹¹⁰⁾ D. T. Sandwell, W. H. F. Smith, S. Gille, S. Jayne, K. Soofi, B. Coakley, “Bathymetry from Space: White paper in support of a high-resolution, ocean altimeter mission,” Version 1.5, June 28, 2001, URL: http://topex.ucsd.edu/marine_grav/white_paper.pdf

1.21.2.3 Delay–Doppler altimeter concept

The delay–Doppler altimeter (DDA) differs from a conventional radar altimeter concept in that it exploits coherent processing of groups of transmitted pulses and the full Doppler bandwidth is exploited to make the most efficient use of the power reflected from Earth's surface. While the conventional altimeter technique is to measure the distance between the satellite and the mean ocean surface, the delay/Doppler method differs from those instruments in two ways:

- Pulse–to–pulse coherence and full Doppler processing to allow for measurement of the along–track position of the range measurement
- Use of two antennas and two receiver channels that allow for measurement of the across–track angle of the range measurement.

This is a significant improvement over conventional Doppler beam sharpening.^{2111) 2112)} In order to exploit this full bandwidth, the range variation that exists across the Doppler bins is removed as part of the data processing. The reflected pulses from a given area of the observed surface are integrated over the entire time that the target area is within the radar beamwidth. As a result, much more of the reflected energy is captured and a smaller transmitted power is required to obtain a given level of performance.

The central innovation of the delay/Doppler technology is that the returns from a group of transmissions along–track are coherently processed together, rather than incoherently as is customary. The coherent along–track processing allows much more of the instrument's radiated power to be converted into height measurement data. – The phase between two otherwise identical coherent signals is a direct measure of the time shift between them (referred to as phase–monopulse technique). If the geometry of the observation space is known, then the observed phase shift can be inverted to an angular offset. The phase–monopulse technique uses this principle to estimate the angle of arrival between two signals collected through separated antennas.

- An airborne instrument named **D2P** (Delay–Doppler Phase–monopulse Radar) was developed and built by JHU/APL which demonstrated the technology in various test flights in the spring and summer of 2000 (P.63). In addition, S/C missions (WITTEX, ABYSS) with the objective of altimetric bathymetry recovery from sea surface slopes have been proposed based on delay–Doppler technology.
- **SIRAL** (SAR Interferometer Radar Altimeter), the CryoSat mission altimeter of ESA (launch on Oct. 8, 2005 – but launch failure), employs the DDA concepts that have been demonstrated with the D2P radar. – The **CryoSat–2** mission of ESA with SIRAL onboard was launched on April 8, 2010.^{2113) 2114) 2115)}

The Cryosat–2 mission is the first altimeter mission to operate the **SARM** (SAR mode), next to the conventional **LRM** (Low Resolution Mode), in the SIRAL (SAT Interferometer Radar Altimeter) instrument.

- **SRAL** (SAR Radar Altimeter), a dual–band (C+Ku–band) altimeter operating in conventional radar–altimeter mode as on Poseidon–3 (Jason–2), and in advanced SAR

2111) R. K. Raney, "The Delay/Doppler Radar Altimeter," IEEE Transactions on Geoscience and Remote Sensing, Vol. 36, No 5, Sept. 1998, pp. 1578–1588; also URL: www.lpi.usra.edu/meetings/outerplanets2001/pdf/4045.pdf

2112) R. K. Raney, W. H. F. Smith, "The Delay–Doppler Altimeter: More Precision and a Smaller Footprint," 4th Weikko A. Heiskanen Symposium in Geodesy, The Ohio State University, Columbus, OH, USA, Oct. 1–4, 2002

2113) R. K. Raney, D. L. Porter, "WITTEX: An Innovative Three–Satellite Radar Altimeter Concept," IEEE Transactions on Geoscience and Remote Sensing, Vol. 39, No 11, Nov. 2001, pp. 2387–2391

2114) W. H. F. Smith, R. K. Raney, "Altimetric Bathymetry from Surface Slopes (ABYSS): Seafloor Geophysics from Space for Ocean Climate," Proceedings of the Weikko A. Heiskanen Symposium in Geodesy, Ohio State University, Columbus, OH, USA, Oct. 1–4, 2002

2115) R. K. Raney, "The Delay/Doppler Radar Altimeter," IEEE Transactions on Geoscience and Remote Sensing, Vol. 36, No 5, Sept. 1998, pp. 1578–1588

mode (burst mode), or SARM, over sea ice and coastal regions. The instrument is being developed for the Sentinel-3 mission (launch 2014) of the European Copernicus (formerly GMES) program. The SRAL concept is of Poseidon-3 and SIRAL instrument heritage.

1.21.2.4 Wide-swath altimetry:

To be able to map ocean mesoscale phenomena adequately, it is necessary to resolve phenomena which are on the order of the Rossby radius of deformation (a conservative value would be on the order of 30 km) and have a typical lifetime on the order of a month. It is not possible to reconcile both of these requirements with a single nadir-looking altimeter.

So far, the coarse cross-track sampling and measurement precision of nadir-looking altimeters have prevented resolving scales shorter than 100 km, the sub-mesoscales that are important for understanding the dynamics of the ocean kinetic energy and the vertical transfer processes in the ocean that account for 50% of the exchange of water properties (nutrients, dissolved CO₂, heat) between the upper and the deep ocean. These processes are critical to the understanding of the role of the ocean in regulating global climate change.

SWOT (Surface Water Ocean Topography) is a wide-swath altimeter mission concept – a proposal under study/definition in 2009 by NASA and CNES – for accurate future monitoring of local sea level changes at the land-sea interface. The SWOT mission has been recommended in 2007 by the NRC (National Research Council) decadal survey “Earth Science and Applications from Space: National Imperatives for the Next Decade and Beyond” for implementation by NASA. – In June 2010, NASA has released a plan for “Responding to the Challenge of Climate and Environmental Change” in which NASA requests a budget that allows SWOT to be launched in 2020. ^{2116) 2117) 2118) 2119) 2120)}

The overall scientific objectives and goals of SWOT, in particular by the water resources and hydrologic community, are to contribute to a fundamental understanding of the Earth system by providing global measurements of continental surface water storage changes and discharge, which are critical for water and climate cycle models.

The main mission goals of the demonstration mission are:

- The primary oceanographic objectives of the SWOT mission are to characterize the ocean mesoscale and sub-mesoscale circulation at spatial resolutions of 10 km and larger.
- The hydrologic science objectives of the SWOT mission are:
 - To provide a global inventory of all terrestrial surface water bodies whose surface area exceeds 250 m² (lakes, reservoirs, wetlands) and rivers whose width exceeds 100 m (requirement) (50 m goal)
 - To measure the global storage change in terrestrial surface water bodies (for man-made reservoirs, total storage) at sub-monthly, seasonal, and annual time scales.

2116) http://science.nasa.gov/media/medialibrary/2010/07/01/Climate_Architecture_Final.pdf

2117) <http://swot.jpl.nasa.gov/>

2118) Ernesto Rodríguez, “Surface Water and Ocean Topography Mission (SWOT),” NASA/JPL, March 19, 2009, URL: http://swot.jpl.nasa.gov/files/SWOT_science_reqs_final.pdf

2119) Lee-Lueng Fu, Douglas Alsdorf, Ernesto Rodriguez, Rosemary Morrow, Nelly Mognard, Juliette Lambin, Parag Vaze, Thierry Lafon, “The SWOT (Surface Water and Ocean Topography) Mission: Spaceborne Radar Interferometry for Oceanographic and Hydrological Applications,” Proceedings of OceanObs’09, Venice, Italy, Sept. 21–25, 2009, URL: https://abstracts.congrex.com/scripts/jmevent/abstracts/FCXNL-09A02a-1655721-1-SWOT_OceanObs09_paper_revised_final.doc

2120) Douglas Alsdorf, Nelly Mognard, Ernesto Rodriguez, “Transforming Surface Water Hydrology through SWOT Altimetry,” Proceedings of the Symposium ‘20 years of Progress in Radar Altimetry’, Venice, Italy, Sept. 24–29, 2012, (ESA SP-710, Feb. 2013)

– To estimate the global change in river discharge at sub-monthly, seasonal, and annual time scales.

The core SWOT payload is **KaRIN** (Ka-band Radar Interferometer), consisting of two radar antennas at either end of a 10 m mast, allowing it to measure the elevation of the surface along a 120 km wide swath (Figure 157).

Obviously, quite a few technological challenges have to be resolved to provide the observations in the precision and resolution required. A mission life of three years (min) is required to sample seasonal and inter-annual variability for both the ocean and surface water height changes appropriately.

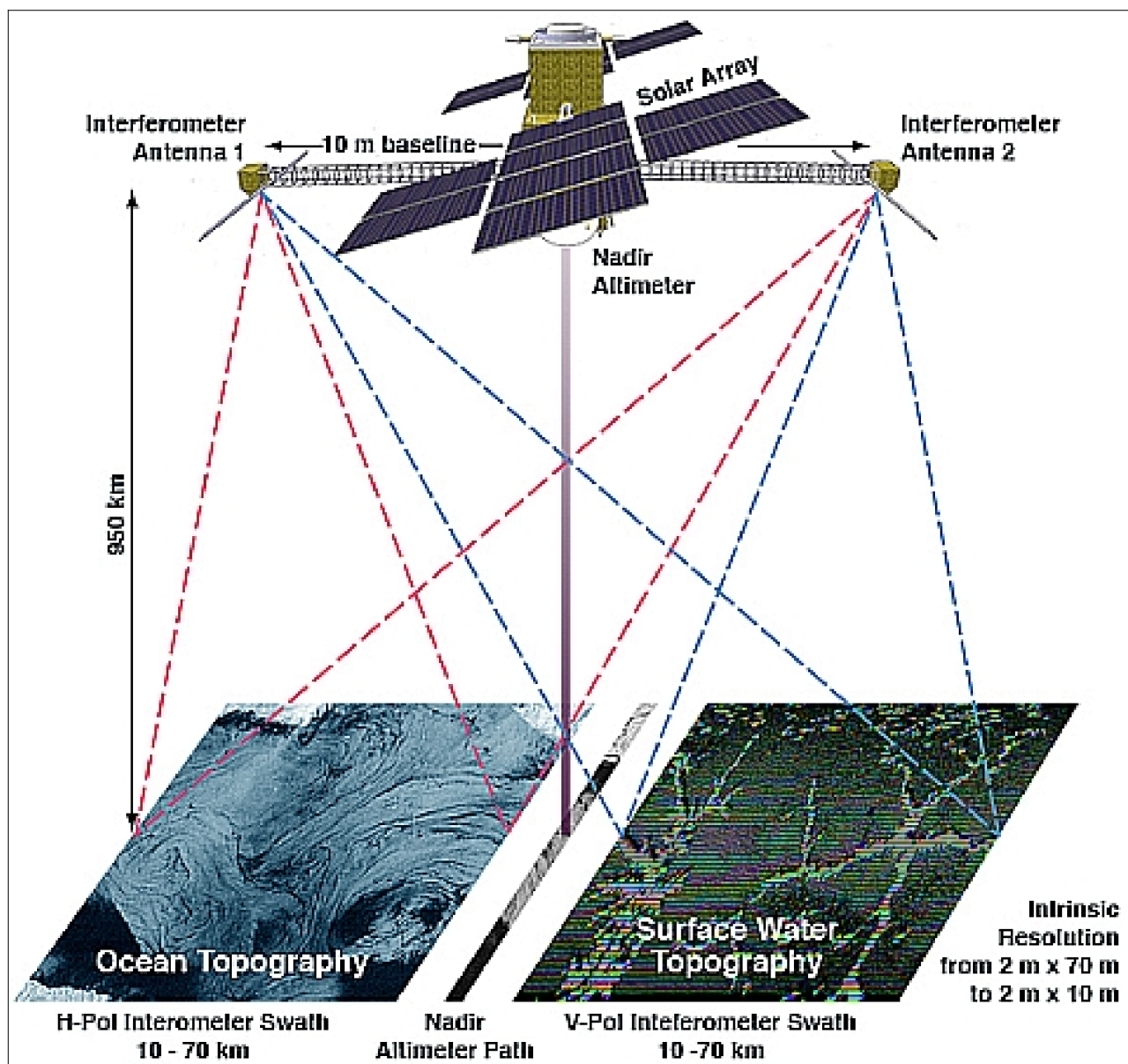


Figure 157: Illustration of the SWOT mission observation concept (image credit: NASA, CNES)

1.21.3 SST (Sea Surface Temperature)

The topics of spaceborne SST measurements from LEO and from GEO are covered in chapters 1.20.2.1 and 1.20.3.1, respectively. The SST variable has a strong influence on the exchange of heat, momentum, water and gases between the ocean surface and the atmosphere. Its knowledge is essential for predicting the dynamic behavior of the atmosphere and

the ocean. SST is also an important indicator of climate and climate change, so to speak a finger on the pulse of the planet itself.

1.21.4 Ocean color observations

The spectra retrieved with an imaging spectrometer show absorption features that are matter specific and depend on quantum mechanical interactions as well as molecular structure and scattering properties of the observed material. Observing reflected solar illumination (thermal emissions) with such detailed spectral resolution enables direct identification of virtually all diagnostic absorption features in minerals and soils, the examination of physical and biological components in marine and inland waters, and the study of biochemical processes in vegetation.

“Ocean color” is a shorthand term for a specific set of optical measurements from airborne or spaceborne instruments used to determine the radiance backscattered from water and across the air–sea interface at some or many spectral bands. Ocean color is determined by the interactions of incident light (reflected sunlight) with substances or particles present in the water. The most significant constituents are free–floating photosynthetic organisms (phytoplankton) and inorganic particulates.

The value of ocean–color data lies in the long–term monitoring of the marine environment, thereby providing a better understanding of the role of oceans in the global carbon cycle [the carbon cycle ²¹²¹) feedback has a very important influence on climate research; the ocean has a significant role in the carbon cycle due to the dissolution of CO₂ in water and the release of dimethyl sulfide (DMS) gas by phytoplankton (ocean algae)]. The prime observables of ocean–color instruments are basically the chlorophyll and gelbstoff concentrations in the surface layer of the ocean. The concentration of chlorophyll is used to estimate the abundance of phytoplankton in ocean waters, and hence the abundance of ocean biota. The observations permit also concentration estimations of algae over large ocean regions and the study of near–surface phytoplankton “blooms” and ocean pollution.

- A spaceborne spectroradiometer (multi–channel scanning radiometer) by the name of CZCS (Coastal Zone Color Scanner), launched on Nimbus–7 (Oct. 24, 1978) provided first images of **ocean color** (chlorophyll and gelbstoff concentration) distribution. CZCS measured in five optical and one TIR band at a spatial resolution of 825 m on a swath of 1600 km. The measurements were optimized for use over water. The CZCS instrument operated for seven years. The data of this first–generation ocean color instrument contributed greatly to our understanding of the marine environment and its biological, biochemical, and physical processes. Monitoring of marine phytoplankton is of great importance because it accounts for nearly half of the world’s total primary productivity. Biomass turnover rates for plankton ecosystems are 100 times faster than those for terrestrial systems, leading to a close relationship between upper–ocean ecology and physical forcing.

Sensor, Sensor Provider	Platform	Launch/Introduction
CZCS, NASA, USA	Nimbus–7	Oct. 24, 1978 – June 22, 1986
OCE, NASA/GSFC, USA	Shuttle (SIR–A mission), STS–2	Nov. 12–14, 1981
MOS, DLR, Germany	IRS–P3 (ISRO, India) Priroda (MIR module, Russia)	March 21, 1996 April 26, 1996
OCTS, NASDA, Japan POLDER, CNES, France	ADEOS	Aug. 17, 1996 – June 30, 1997 (some ocean color products)
SeaWiFS, OSC/Orbimage, USA	OrbView–2/SeaStar (previous name)	Aug. 1, 1997
OCI, NSPO, Taiwan	ROCSAT–1 (FormoSat–1)	Jan. 26, 1999
OCM, ISRO, India	IRS–P4 (OceanSat–1)	May 26, 1999

2121) R. J. Charlson, J. Lovelock, M. O. Andreae, Stephen Warren, “Oceanic phytoplankton, atmospheric sulphur, cloud albedo and climate, *Nature*, Vol. 326, 1987, pp. 655–661

Sensor, Sensor Provider	Platform	Launch/Introduction
MODIS, NASA/GSFC, USA	Terra (previous name: EOS/AM-1)	Dec. 18, 1999
OSMI, KARI, Korea	KOMPSAT-1	Dec. 20, 1999
MERIS, ESA, Europe	Envisat	Mar. 1, 2002
MODIS, NASA/GSFC, USA	Aqua (formerly EOS/PM-1)	May 4, 2002
COCTS, SITP, China	HY-1A (Haiyang-1)	May 15, 2002
GLI, JAXA, Japan Polder-2, CNES, France	ADEOS-II (Midori-II)	Dec. 14, 2002 (mission failed on Oct. 25, 2003)
Polder-3, CNES, France	PARASOL	Dec. 18, 2004
COCTS & CZI, CNSA, China	HY-1B	April 11, 2007
HICO, ONR & NRL, USA	JEM-EF (Japan) of ISS	Sept. 18, 2009
OCM-2, ISRO, India	OceanSat-2	Sept. 23, 2009
GOCI, KARI/KORDI, Korea	COMS-1 (first ocean color sensor in GEO)	June 26, 2010
VIIRS, IPO, USA	NPP	Oct. 28, 2011
VIIRS, IPO, USA	JPSS	planned for 2016

Table 119: Overview of spaceborne sensors for ocean color detection

Sensor	Ground Resolution (km)	Swath Width (km)	Spectral Bands (range nm)	Data Repetivity (days)	Sensor Tilt Capability	Absolute Radiomet. Accuracy	Polarization Sensitivity
CZCS	0.825	1600	5 bands 443–800+TIR	2			
OCE	0.90	180	8 bands 464 – 773				
MOS-A MOS-B MOS-C	1.57 x 1.40 0.52 x 0.52 0.52 x 0.64	195 200 192	4 (755–768) 13 (408–1011) 1 (1600)				
OCTS	0.70	1400	8 bands 402 – 885 + 4 IR	2	±20°	<10%	<2–5%
SeaWiFS	1.1 LAC 4.5 GAC	2800 LAC 1500 GAC	8 bands 402 – 885	2	±20°	<5%	<2%
MODIS	1	2330	9 bands 405 – 877	2	none	<3%	<2% (<5% at 412 nm)
OCM	0.36	1420	8 bands 402 – 885	2	±20°	<10%	<2%
OCI	0.80	691	6 bands 433 – 885				
COCTS	1.1	1400	8 bands 402–885 +2 TIR	2		10–40%	
OSMI	1 0.85 nadir	800	8 bands 400 – 885		±45°		
MERIS	0.3 and 1.2	1150	15 bands 390 – 1040	3		<2%	<0.5%
GLI	1/0.25	1600	36 bands 375 – 2250	2			<2%

Table 120: Some performance parameters of ocean color sensors (multispectral radiometers)

ECCO (Estimating the Circulation and Climate of the Ocean). ECCO is a joint project between the Massachusetts Institute of Technology and NASA's Jet Propulsion Laboratory in Pasadena, CA. The objective is to visualize observed ocean current data over longer periods of time (June 2005–December 2007). ECCO uses advanced mathematical tools to

combine observations with the MIT numerical ocean model to obtain realistic descriptions of how ocean circulation evolves over time. 2122) 2123) 2124)

These model–data syntheses are among the largest computations of their kind ever undertaken. They are made possible by high–end computing resources provided by NASA/ARC (Ames Research Center) in Moffett Field, CA.

ECCO model–data syntheses are being used to quantify the ocean’s role in the global carbon cycle, to understand the recent evolution of the polar oceans, to monitor time–evolving heat, water, and chemical exchanges within and between different components of the Earth system, and for many other science applications. In the particular model–data synthesis used for this visualization, only the larger, ocean basin–wide scales have been adjusted to fit observations. Smaller–scale ocean currents are free to evolve on their own according to the computer model’s equations.

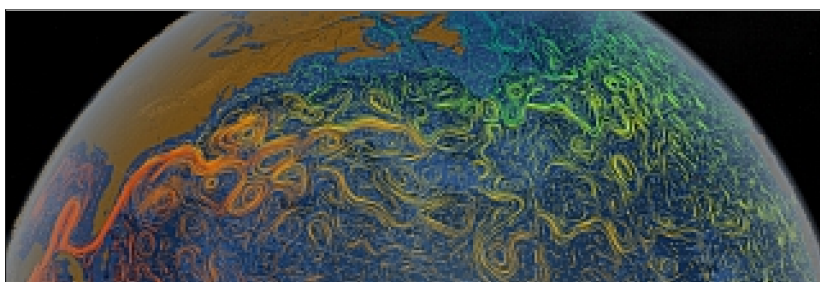


Figure 158: Visualization of the Gulf Stream stretching from the Gulf of Mexico all the way over towards Western Europe (image credit: NASA/GSFC, MIT, JPL)

Data used by the ECCO project include: sea surface height from NASA’s TOPEX/Poseidon, Jason–1, and Jason–2/OSTM mission altimeters; gravity from the NASA/DLR GRACE (Gravity Recovery and Climate Experiment) mission; surface wind stress from NASA’s QuikScat mission; sea surface temperature from JAXA’s AMRSE (Advanced Microwave Scanning Radiometer–EOS) instrument on NASA’s Aqua mission; sea ice concentration and velocity data from passive microwave radiometers; and temperature and salinity profiles from shipborne casts, moorings and the international Argo ocean observation system.

1.21.5 SSS (Sea Surface Salinity)

SSS (Sea Surface Salinity) and its variation across the oceans is an important parameter in physical oceanography. Even small variations in SSS can have dramatic effects on the water cycle and ocean circulation. SSS is a measure of concentration, in particular the concentration of dissolved salts in the upper layer (a few cm) of the ocean surface. Throughout Earth’s history, certain processes have served to make the ocean salty. The weathering of rocks delivers minerals, including salt, into the ocean. Evaporation of ocean water and formation of sea ice both increase the salinity of the ocean. However these “salinity raising” factors are continually counterbalanced by processes that decrease salinity such as the continuous input of fresh water from rivers, precipitation of rain and snow, and melting of ice.

Seawater, on the average, contains 35 g of salt per 1 kg of seawater. The salts in seawater affect the structure and properties of the water in seawater. The salts in seawater are really

2122) “Perpetual Ocean,” URL: <http://svs.gsfc.nasa.gov/vis/a000000/a003800/a003827/>

2123) Aries Keck, “NASA Views Our Perpetual Ocean,” Space Daily, April 11, 2012, URL: http://www.spacedaily.com/reports/NASA_Views_Our_Perpetual_Ocean_999.html

2124) Aries Keck, “NASA Views Our Perpetual Ocean,” NASA/JPL, April 9, 2012, URL: <http://www.nasa.gov/topics/earth/features/perpetual-ocean.html>

ions. Ions, in turn, affect the physical properties of water. The density of seawater is greater than the density of pure water. Hence, changes in salt concentration at the ocean surface affect the weight of surface waters. Fresh water is light (lower density) and floats on the surface, while salty water is more dense and sinks.

Together, salinity and temperature determine seawater density and buoyancy, driving the extent of ocean stratification, mixing, and water mass formation. Greater salinity, like colder temperatures, results in an increase in ocean density with a corresponding depression of the sea surface height. In warmer, fresher waters, the density is lower resulting in an elevation of the sea surface. These height differences are related to the circulation of the ocean. The changes in density bring warm water poleward on the surface to replace the sinking water driving the global thermohaline (heat & salt) circulation within the ocean called the Global Conveyor Belt.²¹²⁵⁾

As of 2006, two radiometric research missions are under development with the objective to demonstrate the measure the SSS distributions over the oceans. Both missions are using L-band radiometry to observe ocean surface brightness temperature.

- 1) The **SMOS** (Soil Moisture and Ocean Salinity) mission in LEO (Low Earth Orbit) of ESA (launch Nov. 2, 2009) employs the synthetic aperture radiometer concept with MIRAS (Microwave Imaging Radiometer using Aperture Synthesis).
- 2) The **SAC-D/Aquarius** mission, a cooperative project of NASA and CONAE (launch June 10, 2011), employs the pushbroom radiometer concept with a large antenna.

SSS is one of the fundamentals variables for which global sustained observations are needed in CLIVAR, the international program on CLimate VARIability and predictability, and GOOS, the Global Ocean Observing System.

1.21.6 Oversight of ocean programs by global organizations

The global effects of the oceans on climate and the environment is of concern to all of civilization. The fostering and coordination of ocean programs is provided by **GOOS** (Global Ocean Observing System), a joint program of **IOC** (Intergovernmental Oceanographic Commission), **WMO** (World Meteorological Organization), **UNEP** (United Nations Environmental Program), and **ICSU** (International Council of Scientific Unions). The GOOS structure integrates real-time in-situ and satellite observations with numerical models to form model-based information products for a variety of applications. The initial GOOS was formed in 1991. European GOOS (EuroGOOS) was formed in 1994 as one of several regional GOOS activities. Operational programs such as GODAE (Global Ocean Data Assimilation Experiment), MERCATOR (a program of French institutions for GODAE, since 1996) and Argo (Array for Geostrophic Oceanography) are GOOS pilot projects.

WOCE (World Ocean Circulation Experiment) is an unprecedented effort during the period 1990–1997 by scientists from more than 30 nations to study the large-scale circulation of the ocean (use of data from satellites, many ships, in-situ data from thousands of instruments, and campaigns (like TOGA/WOCE) – to obtain a basic description of the physical properties and circulation of the global ocean). JGOFS (Joint Global Ocean Flux Study) is an international and multi-disciplinary program with participants from more than 20 nations that was initiated in 1987 by ICSU. The objectives of JGOFS are to assess more accurately, and to understand better the processes controlling, regional to global and seasonal to interannual fluxes of carbon between the atmosphere, ocean surface and ocean interior, and their sensitivity to climate changes.

²¹²⁵⁾ <http://science.hq.nasa.gov/oceans/physical/SSS.html>

IGOS (Integrated Global Observation Strategy) was initiated in 1998, an international effort aimed to globally monitor quantitative information on carbon sources. Long-term observations are required to improve the understanding of the present state and future behavior of the global carbon cycle, particularly the factors that control the global atmospheric CO₂ (carbon dioxide) level. The buildup of atmospheric CO₂, driven by the combustion of fossil fuels along with deforestation and other changes in land use, is the largest contributor to the global increase in the greenhouse effect. The concentrations of CO₂ and CH₄ in the atmosphere are the highest they have been in the past 25 million years. In fact, the CO₂ level has increased by over 30% since the start of the industrial age. The recent climate history indicates that there has been a global warming of about 0.5 °C over the past 100 years which is generally attributed to increasing concentrations of the greenhouse gas CO₂.^{2126) 2127)}

2126) The development and implementation of the IGOS is through a partnership, IGOS-P, among space agencies, as represented by CEOS (Committee on Earth Observation Satellites); GOOS (Global Ocean Observing System), GTOS (Global Terrestrial Observing System), and GCOS (Global Climate Observing System), and the research community, as represented by two major international research programs, IGBP (International Geosphere-Biosphere Program) and WCRP (World Climate Research Program).

2127) Ph. Cias, B. Moore, W. Steffen, et al., "Integrated Global Carbon Observation Theme," IGCO, Nov. 17, 2003, IGOS International Workshop, Tokyo, Feb. 4-6, 2004

1.22 Solar–Terrestrial Connection

The sun as the central star in the solar system plays a fundamental role to all planets in our constellation, in particular to all life on Earth. Hence, the interactions of all kinds (magnetic fields, radiative energy, solar wind, energetic particles, etc.) between the sun and the Earth are of vital interest to humankind. The term “heliophysics” is used to describe the science of the sun–Earth system, the field of study has expanded significantly in the early 21st century. Predicting solar activity is an extremely complicated task, and being able to forecast the sun’s behavior solves only half of the equation. Equally important is being able to understand how the Earth’s magnetic field and atmosphere respond to any given solar storm. – The United Nations declared 2007 the “International Heliophysical Year” in hopes of stimulating global involvement.

The scope of documentation includes also missions with direct observations of the sun itself and its variability over time. In the context of solar–terrestrial connection, the following topics are of particular interest:

- Interaction of solar radiation with Earth’s atmosphere,
- Earth’s radiation budget,
- The solar wind,
- Earth’s magnetosphere
- Space weather
- X–ray imaging. The mixed payload complement of a number of missions is the reason why the topic of X–ray imaging is part of this document. ²¹²⁸⁾

The sun is the source for almost all radiation (i.e. energy) that Earth is intercepting from the universe, consisting of a large portion of the EMS (Electromagnetic Spectrum). For most solar observations, the relevant physical phenomena of interest require an observation coverage over extremely broad temporal, spatial, and spectral ranges, generally covering a span of 8–10 orders of magnitude for each range. **As it turns out, the entire breadth of the EMS radiation is only available and observable from an orbital vantage point** (i.e., a spaceborne instrument in Earth orbit or further out). In particular, accurate measurements of solar radiation can only be made from space, due to the variable (and incompletely known) transmission of the Earth’s atmosphere. The possibility that these changes can induce sufficiently large changes in the troposphere to affect Earth’s climate is a subject of active research. Hence, by placing observing instruments into orbit (instead of on the ground) provides the following advantages: ²¹²⁹⁾

- Extended wavelength coverage. The terrestrial atmosphere is effectively opaque to UV, EUV, X–ray and gamma–ray radiation; in the IR spectrum, only a few narrow transmission windows are available. Hence, most of the EMS does not reach the ground.

Fortunately for us, all of the high energy X–rays and most UV is filtered out long before it reaches the ground. Much of the infrared radiation is also absorbed by our atmosphere far above our heads. Most radio waves do make it to the ground, along with a narrow “window” of IR, UV, and visible light frequencies (Figure 159). ²¹³⁰⁾

- Extended or continuous temporal coverage. Studies of solar phenomena often require many hours, days or weeks of continuous coverage. For some studies a network of ground–

2128) M. A. Calabrese, K. A. Potocki, D. Carson, J. Robinson, J. Ayon, J. Oberright, J. T. VanSant, “NASA’s Sun–Earth Connection Program Strategic Planning, Missions & Technology Needs (2003–2028),” Proceedings of IEEE Aerospace Conference, Big. Sky, MT, USA, March 8–15, 2003

2129) L. Golub, “Solar observation from space,” review article, Review of Scientific Instruments, Vol. 74, No 11, Nov. 2003, pp. 4583–4600

2130) Randy Russell, “Solar Energy in Earth’s Atmosphere,” 2007, http://www.windows.ucar.edu/tour/link=/earth/Atmosphere/earth_atmosph_radiation_budget.html

based observations around the world can provide the continuity, but this is not possible at wavelengths that do not reach the ground.

In addition to solar radiation variability, celestial mechanics impose quasi-cyclical variations in the parameters of the Earth orbit and rotation, thereby inducing major changes in the distribution of solar radiation incident upon the Earth surface and the timing of seasons, with still poorly understood consequences for the succession of glacial and interglacial climates.²¹³¹⁾

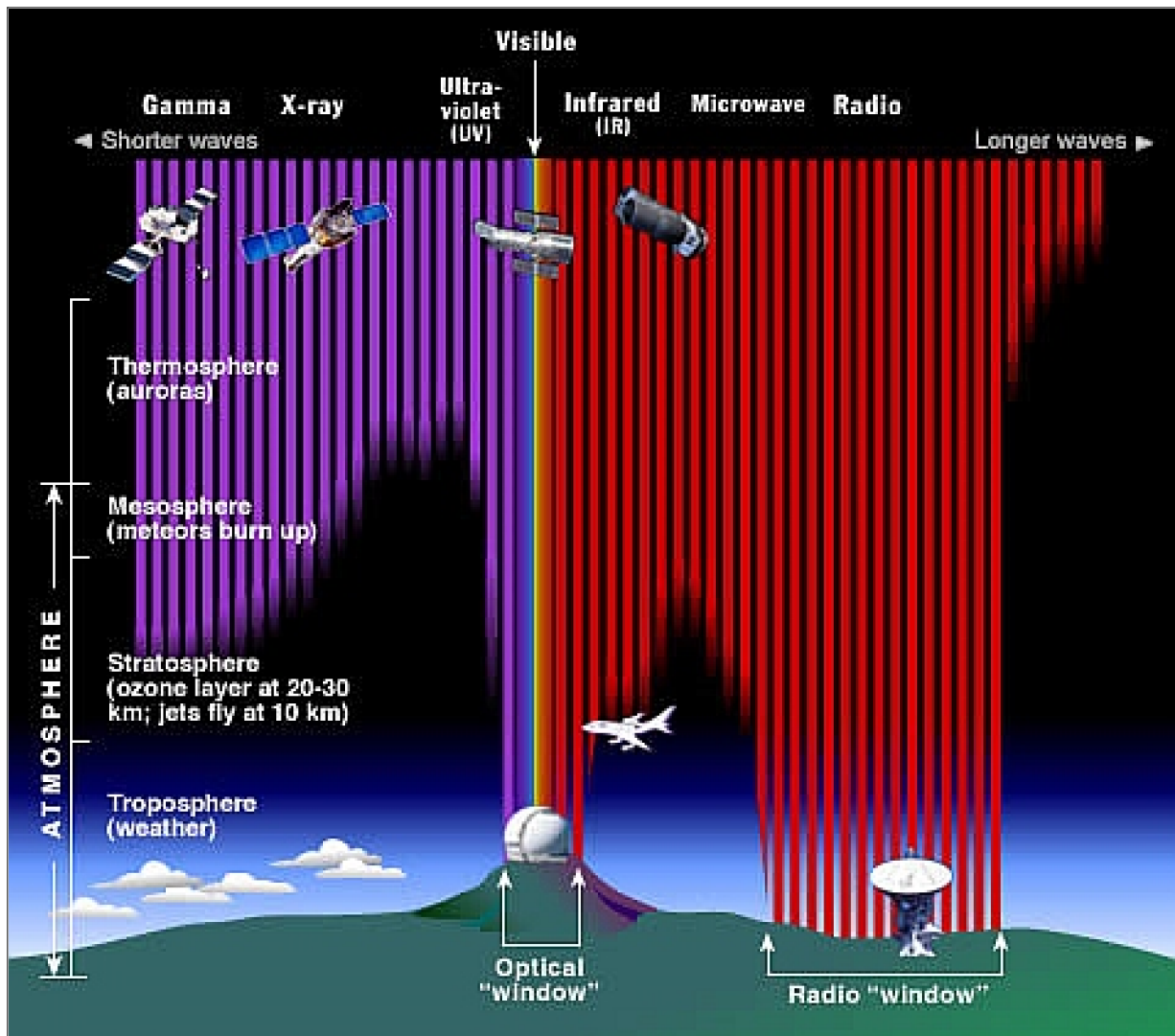


Figure 159: Illustration of EM radiation penetration through Earth's atmosphere (image credit: STCI/JHU/NASA)

1.22.1 Solar radiation and Earth's atmosphere

- **Atmospheric effects:** Not all of the solar radiation received at the periphery of the atmosphere reaches the surfaces of the Earth. This is because the Earth's atmosphere plays an important role in selectively controlling the passage towards the Earth's surface of the various components of solar radiation.²¹³²⁾

A considerable portion of solar radiation is reflected back into outer space upon striking the uppermost layers of the atmosphere, and also from the tops of clouds. The fraction of solar

2131) "Understanding Earth System Change," NASA's Earth Science Enterprise Research Strategy for 2000–2010," Dec. 2000, http://www.earth.nasa.gov/visions/researchstrat/Chap1_Research_Strategy.doc

2132) <http://almashriq.hiof.no/lebanon/600/610/614/solar-water/unesco/21-23.html>

irradiation reflected back into space is termed the "albedo" and is highly variable depending on the surface type and intervening atmosphere (e.g. clouds). In the course of penetration through the atmosphere, some of the incoming radiation is either absorbed or scattered in all directions by atmospheric gases, vapors, and dust particles (aerosols). In fact, there are two processes known to be involved in atmospheric scattering of solar radiation. These are termed selective scattering and non-selective scattering. These two processes are determined by the different sizes of particles in the atmosphere.

– Selective scattering is so named because radiations with shorter wavelengths are selectively scattered much more extensively than those with longer wavelengths. It is caused by atmospheric gases or particles that are smaller in dimension than the wavelength of a particular radiation. Such scattering is caused by gas molecules, smoke, fumes, and haze. Under clear atmospheric conditions, therefore, selective scattering turns out to be much less severe than when the atmosphere is extensively polluted from anthropogenic sources.

Selective atmospheric scattering is, broadly speaking, inversely proportional to the wavelength of radiation and, therefore, decreases in the following order of magnitude: gamma-ray, X-ray, far UV > near UV > violet > blue > green > yellow > orange > red > infrared. Accordingly, the most severely scattered radiation is that which falls in the ultraviolet, violet, and blue bands of the spectrum. The scattering effect on radiation in these three bands is roughly ten times as great as on the red rays of sunlight. – It is interesting to note that the selective scattering of violet and blue light by the atmosphere causes the blue colour of the sky.

– Non-selective scattering occurring in the lower atmosphere is caused by dust, fog, and clouds with particle sizes more than ten times the wavelength of the components of solar radiation. Since the amount of scattering is equal for all wavelengths, clouds and fog appear white although their water particles are colourless. Atmospheric gases also absorb solar energy at certain wavelength intervals called absorption bands, in contrast to the wavelength regions characterized by high transmittance of solar radiation called atmospheric transmission bands, or atmospheric windows.

• The Earth's atmosphere and oceans are components of a vast heat engine which governs our weather and climate. The heat source for this engine is the solar radiation which is absorbed by the Earth atmosphere/ocean/land/cryosphere system and the heat sink is the radiation emitted by this system. This system is extremely complex and has a number of modes of response ranging from microscale in time and space to planetary scale interdecadal variations. – The components of the Earth's radiation field, i.e. the absorbed solar radiation and the emitted radiation are dynamic quantities which vary in space and time. The radiation components are both, cause and effect, due to their interactions with the other parts of the weather/climate system. The radiation energy from the sun drives many biological, geophysical and biogeochemical processes that may ultimately influence climate itself.

– Clouds play a major role in Earth's radiation budget. They are extremely variable in space and time and can either heat or cool the Earth, depending on their height. With their high albedo, clouds reflect sunlight, tending to cool the Earth. Low clouds also serve to reflect radiation from the surface, thereby retaining heat within the system. Absorption of sunlight causes clouds to dissipate. Radiation from cloud tops increases the turbulence and mixing near the cloud top, and absorption of radiation from the lower ground increases turbulence near the bottom of the cloud, except in inversion situations, such as the polar winters, where radiation from the cloud bottom tends to suppress turbulence and mixing. The interaction of clouds with the surface can be important to the cloud's lifetime. A cold ocean for example can maintain a cloud cover over it as a feedback system.

– Most solar radiation which is absorbed by the Earth system is absorbed at the surface. Radiation absorbed at the surface provides sensible and latent heat, which evaporates surface water and melts snow and ice. Because of the small heat capacity of land, most of this

sensible heat is transferred to the air. For the ocean, the sensible heat raises the sea surface temperature (SST). It has been shown that the surface radiation of a region is so intimately related to the various processes that its climate classification can be determined from the annual mean and ranges of the net shortwave and longwave fluxes at the surface. Snow cover is important in interseasonal variations because the high albedo of snow causes a positive feedback so that the presence/absence of snow tends to extend itself. This change of energy balance at the surface will affect the flow of air, possibly creating effects at a distance.

– The oceans are driven by friction of wind, by temperature gradients and by salinity gradients, which are created by rain and melting of ice. The SST is a major factor in climate variability, as its large thermal inertia causes it to have response times of months and greater. The sea surface temperature SST is driven largely by radiation and air/sea interactions. The radiation is in turn modulated by cloud cover, which is highly variable. The coupling of cloud cover to the ocean is an area of active research, as this interaction affects both the ocean temperatures and the clouds, leading to climate variations which are not yet understood.

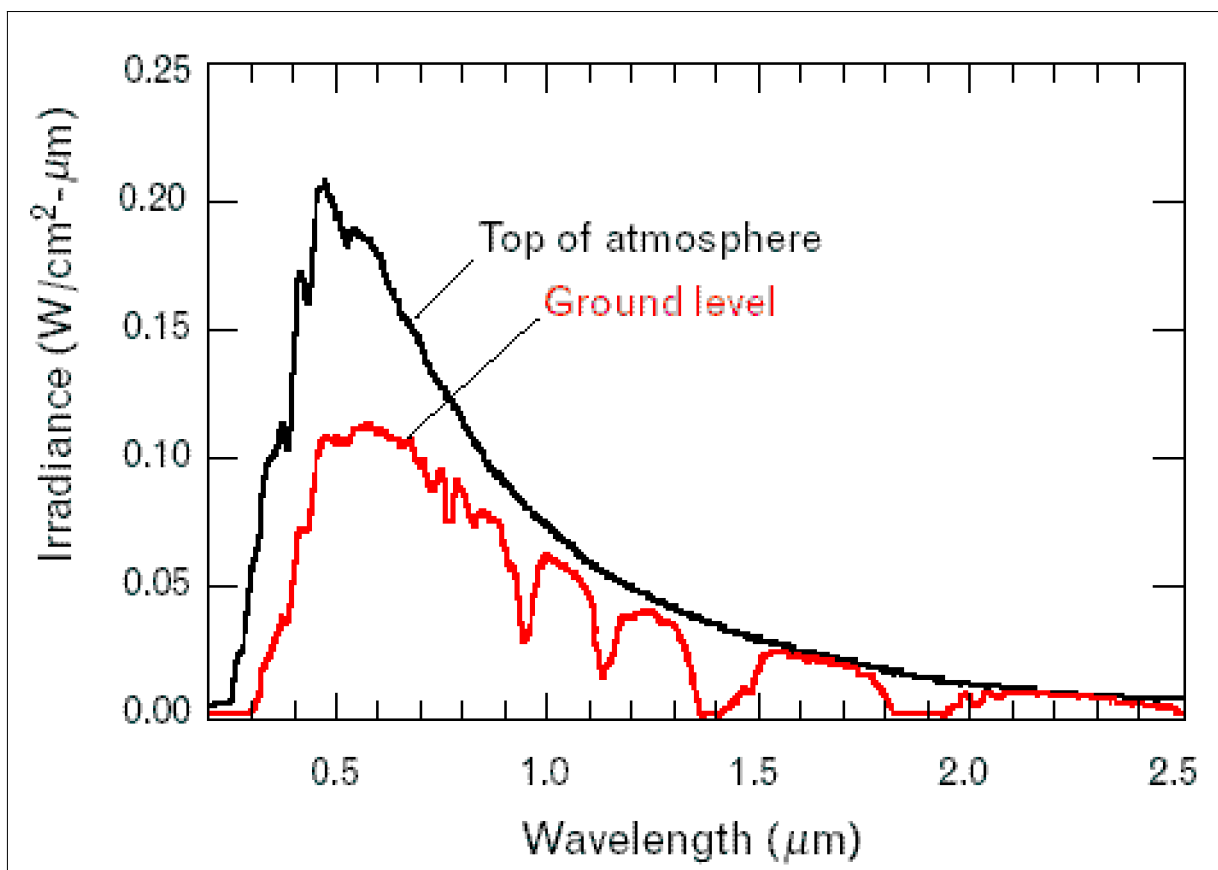


Figure 160: Solar irradiance curves at top of the atmosphere and at ground level

- Estimation of the Earth's radiation energy distribution at the **Earth's surface** – also referred to as SSI (Surface Solar Irradiance). All of the energy available at the Earth's surface for heating and cooling of the air (sensible heat), evaporating water from the soil and vegetation (latent heat), and heating or cooling of the soil (soil conduction) is a response to the fluxes of solar and thermal radiation within the Earth–atmosphere system. Solar radiation causes a response in TIR (Thermal Infrared) reradiation at the Earth's surface with important consequences for local and global energy balances. The monitoring and modeling of the solar energy balance at the Earth's surface has applications in many disciplines (e.g. agriculture, water resources, climate change research). While land surface fluxes can be measured with in–situ techniques, there has been a steady progress in estimating the

components of the land (as well as the ocean) surface energy balance from orbit since the first meteorological satellites were launched in the 1960s. Researches on the estimation of SSI were made using the data in particular from geostationary meteorological satellites, since GEO satellites have an advantage to observe solar radiation that is reflected by the Earth's surface and clouds (reradiation), or diffused by the atmosphere in the visible channel of the satellite instruments. ^{2133) 2134)}

Albedo is defined as the fraction of incident radiation that is reflected by a surface. While reflectance is defined as this same fraction for a single incidence angle, albedo is the directional integration of reflectance over all sun–view geometries. Albedo is therefore dependent on the bidirectional reflectance distribution function (BRDF). It turns out that small increases or decreases in surface albedo can significantly impact regional and global climate. Remote sensing instruments do not directly measure surface albedo. As a result, albedo must be inferred through analysis, i.e. a series of manipulations to the measured data.

At the start of the 21st century, satellite data can already provide a data quality similar to ground–based measurements and at very high spatial resolution, taking into account the physical and optical properties of clouds (clouds have a high albedo, causing much of the solar irradiation to be reflected back to space before it can ever reach the Earth's surface). For the oceans, the amount and intensity of light reaching the ocean surface is a crucial variable affecting the production of carbon by phytoplankton (primary production).

1.22.2 Earth's Radiation Budget and Solar Constant

Historically mankind has long recognized the importance of understanding the sun as the Earth's energy source. The development of the telescope in the early seventeenth century brought the sun under close scrutiny and discoveries rapidly followed – sunspots, filaments, prominences, faculae, etc. Developments and improvements in spectroscopy were applied to the sun, and likewise led to discoveries of new atomic species and unexpected high states of ionization. Coronagraphs and other specialized instruments also have had great success in unraveling the mysteries of the sun. Naturally as the science of radiometry progressed, attempts were made to record the **radiative output from the sun and to determine the amount of solar variability.** ^{2135) 2136) 2137) 2138) 2139)}

Since the 1880s, routine solar irradiance measurements were made from the ground to detect an eventual variability. The irradiance was referred to as the “**solar constant**” because atmospheric transmittance variability, of the order of several percent, prevented the detection of any systematic irradiance changes from the Earth's surface in those early measurements.

[The observation of the sun's radiation budget from a ground–based reference is difficult at best, because this measurement must be corrected for atmospheric absorption and scattering. Rayleigh scattering, aerosol scattering, and molecular and atomic absorption all attenuate the solar radiation. In order to recover the TOA (Top of Atmosphere) TOA) irradiance, the ground–based observations had to be extrapolated, but the necessary adjust-

2133) J. D. Tarpley, 1979: Estimating incident solar radiation at the earth's surface from geostationary satellite data,” *Journal of Applied Meteorology*, Vol 18, 1979, pp. 1172–1181

2134) G. R. Diak, J. R. Mecikalski, M. C. Anderson, J. M. Norman, W. P. Kustas, R. D. Torn, R. L. DeWolf, “Estimating Land Surface Energy Budgets from Space,” *BAMS*, January 2004, pp. 65–78

2135) G. Rottman, “The SORCE Mission,” *Solar Physics*, Vol. 230/1–2 (Special Issue SORCE), 2005, pp. 7–25

2136) D. Crommelynck, S. Dewitte, “Metrology of Total Solar Irradiance Monitoring,” *Advances in Space Research*, Vol. 24, No 2, 1999, pp. 195–204

2137) R. B. Lee III, M. A. Gibson, R. S. Wilson, S. Thomas, “Long–term total solar irradiance variability during sunspot cycle 22,” *Journal of Geophysical Research*, Vol. 100, No A2, pp. 1667–1675, Feb. 1, 1995

2138) E. N. Parker, “The Physics of the Sun and the Gateway to the Stars,” *Physics Today*, June 2000, pp. 26–31

2139) Tony Phillips, “Solar Variability and Terrestrial Climate,” *NASA Science News*, Jan. 8, 2012, URL: http://science.nasa.gov/science–news/science–at–nasa/2013/08jan_sunclimate/

ments were large. In the final analysis the estimated TSI values were deemed valid to only the order of a couple of percent. In the final analysis, there was general consensus that long-term variations of the sun were probably less than the measurement error of a couple percent, and at this level the solar irradiance could be considered “constant” – and this was referred to as the “**solar constant**” up for the most part of the 20th century – a persistent misnomer as we know today.]

The space age permitted for the first time a more accurate measurement and assessment of the Earth’s radiation energy budget from orbit (i.e. the incoming solar radiation measured from outside the atmosphere). The “solar constant,” nowadays more accurately referred to as **TSI** (Total Solar Irradiance), is the radiative power received normally onto a unit area at the mean Earth/Sun distance. Along with Earth’s global average albedo and the emitted longwave radiation, it determines Earth’s global average equilibrium temperature. Solar radiation is the primary power source driving our climate system. Hence, knowledge of the long-term **TSI variability is essential in understanding the past and future climate changes.**

Although the sun looks constant to the human observer, the sun turns out to be a variable star. The solar activity waxes and wanes with a complex rhythm that researchers are still sorting out. The most famous “beat” is the 11-year sunspot cycle – actually, the solar cycle may range in length from 9–12 years.²¹⁴⁰⁾

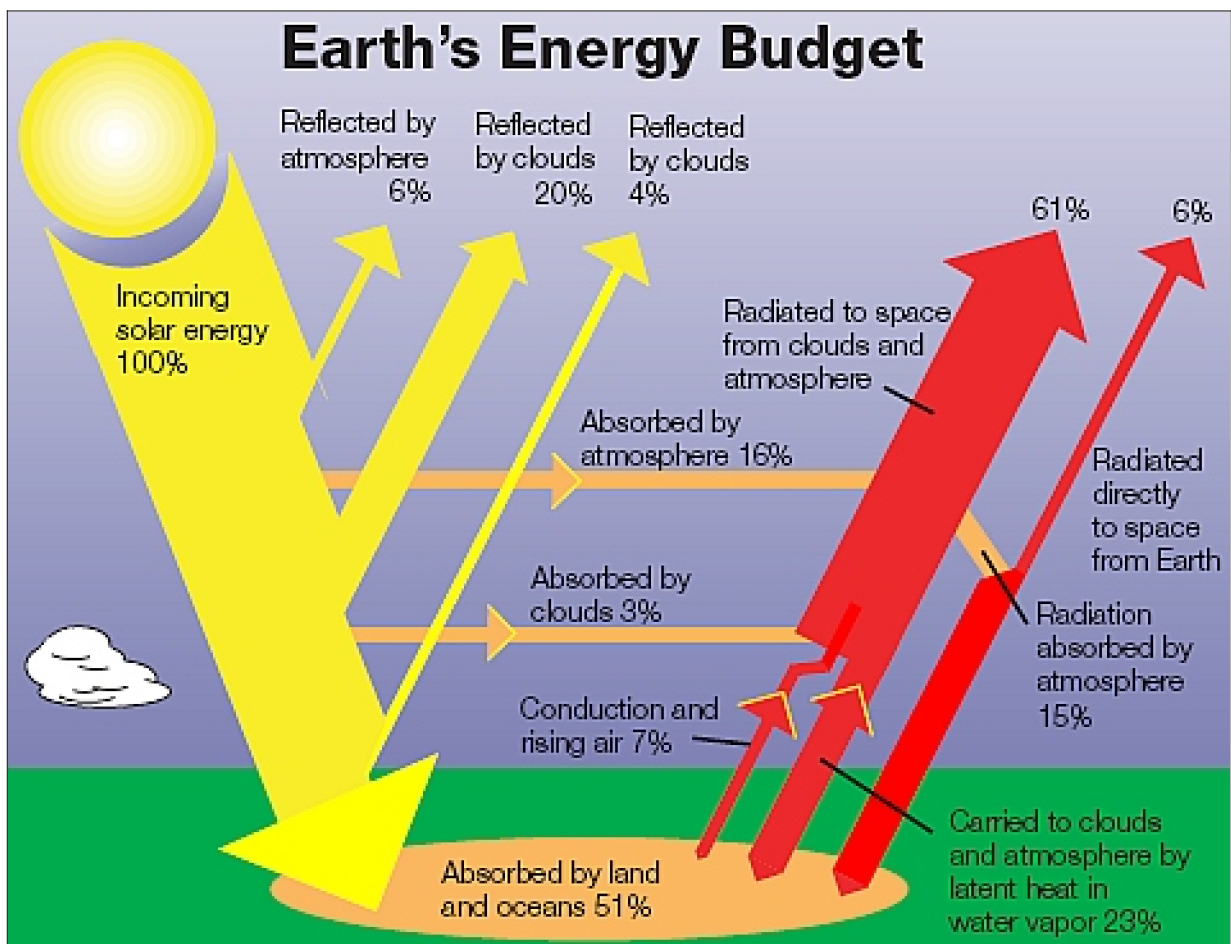


Figure 161: Schematic view of the various components affecting the Earth’s energy budget (image credit: NASA, IRMB)

The solar irradiance (and consequently its luminosity) varies slightly over an 11-year cycle (about 0.1%). The larger portion of variability in solar radiation at short wavelengths (UV

²¹⁴⁰⁾ Tony Phillips, “Solar Dynamics Observatory: The ‘Variable Sun’ Mission,” NASA, Feb. 5, 2010, URL: http://science.nasa.gov/headlines/y2010/05feb_sdo.htm?list1291671

and below) is known to affect the chemistry and composition of the stratosphere, with the magnitude of the effect increasing with altitude through the mesosphere and thermosphere. The variations occur over time scales from a day up to and exceeding the 11–year solar cycle. This cycle of the sun’s magnetic activity alters its energy output, as well as the occurrence of sunspots, solar flares, and/or CMEs (Coronal Mass Ejections), the latter represents a huge eruption of material (magnetized plasma) from the solar atmosphere into interplanetary space. While solar flares affect the ionosphere, CMEs occur when the magnetosphere is disturbed by plasma that propagates through interplanetary space to the Earth after sudden disruptions in the solar magnetic field. Fortunately, Earth’s magnetosphere prevents charged particles from reaching us. ²¹⁴¹⁾

Solar Flares: Solar flares are giant explosions on the sun that send energy, light and high speed particles into space. These flares are often associated with solar magnetic storms known as CMEs (Coronal Mass Ejections).

Solar flares happen when the powerful magnetic fields in and around the sun reconnect. They’re usually associated with active regions, often seen as sun spots, where the magnetic fields are strongest. CME events produce Geomagnetic Disturbances (GMD) which produce Ground Induced Currents (GIC) on Earth.

Flares are classified according to their strength (X–ray brightness temperature in the wavelength range of 1 – 8 Å or 0.1–0.8 nm). The smallest ones are B–class, followed by C, M and X, the largest. Similar to the Richter scale for earthquakes, each letter represents a ten–fold increase in energy output. So an X is 10 times an M and 100 times a C. Within each letter class, there is a finer scale from 1 to 9. ²¹⁴²⁾

Class	Peak Intensity (W/m ²) in the spectral range 1–8 Å
B	$I < 10^{-6}$
C	$10^{-6} < I < 10^{-5}$
M	$10^{-5} < I < 10^{-4}$
X	$I > 10^{-4}$

Table 121: Overview of solar flare classification

A multiplier is used to indicate the level within each class. For example: M6 = 6 x 10⁻⁵ W/m².

C–class flares are too weak to noticeably affect Earth. M–class flares can cause brief radio blackouts at the poles and minor radiation storms that might endanger astronauts. It’s the X–class flares that are the real juggernauts. Although X is the last letter, there are flares more than 10 times the power of an X1, so X–class flares can go higher than 9.

- The most powerful flare on record in the space age occurred on Nov. 4, 2003 (the flare started on October 29, 2003 and is also referred to as the Halloween storm), during the last solar maximum. It was so powerful that it saturated the detectors of the GOES spacecraft. They cut–out at X17, and the flare was later estimated to be about X45. A powerful X–class flare like that can create long lasting radiation storms, which can harm satellites, and even give airline passengers flying near the poles small radiation doses. X flares also have the potential to create global transmission problems and world–wide blackouts. The seriousness of an X–class flare pointed at Earth is why NASA and NOAA constantly monitor the sun.

Extensive satellite problems were reported due to the Halloween storm, including the loss of the ADEOS–2 spacecraft of JAXA (launch Dec. 14, 2002).

2141) Iliia I. Roussev, Klaus Galsgaard, Cooper Downs, Noé Lugaz, Igor V. Sokolov, Elena Moise, Jun Lin, “Explaining fast ejections of plasma and exotic X–ray emission from the solar corona,” *Nature Physics*, Sept. 23, 2012, doi:10.1038/nphys2427

2142) “X–Class: A Guide to Solar Flares,” NASA/GSFC, URL: <http://svs.gsfc.nasa.gov/vis/a010000/a010100/a010109/>

- The most powerful solar flare of the last 500 years was the first flare to be observed, on September 1, 1859, and was reported by British astronomer Richard Carrington. The event is named the **Solar storm of 1859**, or the "Carrington event". A flare was visible to the naked-eye and produced stunning auroras down to tropical latitudes such as Cuba or Hawaii, and set telegraph systems on fire. The flare left a trace in the Greenland ice in the form of nitrates and beryllium-10, which allow its strength to be measured today. ²¹⁴³⁾ ²¹⁴⁴⁾
- On July 23, 2012, a plasma cloud or "CME" rocketed away from the sun as fast as 3000 km/s, more than four times faster than a typical eruption. The storm tore through Earth orbit, but fortunately Earth wasn't there. Instead it hit the STEREO-A spacecraft. Researchers have been analyzing the data ever since, and they have concluded that the storm was one of the strongest in recorded history. ²¹⁴⁵⁾ ²¹⁴⁶⁾

STEREO-A sensors detected the CME arrival only about 19 h later and made in situ measurements of the solar wind and interplanetary magnetic field. Using a well-proven geomagnetic storm forecast model, the researchers found that the 23–24 July event would certainly have produced a geomagnetic storm that was comparable to the largest events of the twentieth century ($D_{st} \sim -500$ nT). Using plausible assumptions about seasonal and time-of-day orientation of the Earth's magnetic dipole, the most extreme modeled value of storm-time disturbance would have been $D_{st} = -1182$ nT. This is considerably larger than estimates for the famous Carrington storm of 1859. This is considerably larger than estimates for the famous Carrington storm of 1859. This finding has far reaching implications because it demonstrates that extreme space weather conditions such as those during March of 1989 or September of 1859 can happen even during a modest solar activity cycle such as the one presently underway. ²¹⁴⁷⁾ ²¹⁴⁸⁾

Note: The D_{st} index measures the globally averaged change (geomagnetic disturbance) in the magnetic field near Earth's equator.

The solar constant and ERB (Earth Radiation Budget):

The solar constant, as defined for planet Earth, is the amount of radiative energy per unit time per unit area (i.e., energy flux or radiative power at normal incidence) intercepted by Earth at the average distance from the sun (1 AU) – on top of Earth's atmosphere.

In 2010/2011, the most probable value of total solar irradiance (TSI) ²¹⁴⁹⁾ representative of solar minimum is: $TSI = 1360.8 \pm 0.5 \text{ W m}^{-2}$, lower than the canonical value of $1365.4 \pm 1.3 \text{ W m}^{-2}$ recommended a decade ago. This new value, measured by SORCE/TIM, is validated by irradiance comparisons to a NIST-calibrated cryogenic radiometer in the new TSI Radiometer Facility. Uncorrected scattering and diffraction are shown to cause erroneously high readings in non-TIM instruments.

2143) Trudy E. Bell, Tony Phillips, "A Super Solar Flare," NASA, May 6, 2008, URL: http://science.nasa.gov/science--news/science--at--nasa/2008/06may_carringtonflare/

2144) <http://www.solarstorms.org/SRefStorms.html>

2145) Karen C. Fox, "NASA STEREO Observes One of the Fastest CMEs On Record," NASA, Aug. 13, 2012, URL: http://www.nasa.gov/mission_pages/stereo/news/fast-cme.html

2146) Daniel N. Baker, "A Major Solar Eruptive Event in July 2012: Defining Extreme Space Weather Scenarios," Space Weather Workshop 2014, Boulder, CO, USA, April 8–11, 2014

2147) D. N. Baker, X. Li, A. Pulkkinen, C. M. Ngwira, M. L. Mays, A. B. Galvin, K. D. C. Simunac, "A major solar eruptive event in July 2012: Defining extreme space weather scenarios," Space Weather, VOL. 11, 585–591, doi:10.1002/swe.20097, 2013, URL: <http://onlinelibrary.wiley.com/doi/10.1002/swe.20097/pdf>

2148) Chigomezyo M. Ngwira, Antti Pulkkinen, M. Leila Mays, Maria M. Kuznetsova, A. B. Galvin, Kristin Simunac, Daniel N. Baker, Xinlin Li, Yihua Zheng, Alex Gloer, "Simulation of the 23 July 2012 extreme space weather event: What if this extremely rare CME was Earth directed?," Space Weather, VOL. 11, 671–679, doi:10.1002/2013SW000990, 2013, URL: <http://onlinelibrary.wiley.com/doi/10.1002/2013SW000990/pdf>

2149) Greg Kopp, Judith L. Lean, "A new, lower value of total solar irradiance: Evidence and climate significance," Geophysical Research Letters, Vol. 38, L01706, doi:10.1029/2010GL045777, 2011, URL: http://www.atmos.physic.utoronto.ca/~jclub/journalclub_files/kopp_lean_2011.pdf

The continuous observation of the solar irradiance at the highest possible precision and accuracy is an important objective of the Earth climate change program. It requires high quality metrology in the space environment linked to ground solar radiometric comparisons supported by laboratory characterization activities.

The Earth radiation budget (ERB) is the difference between the Earth's absorbed solar radiation and the longwave radiation emitted by the Earth and its atmosphere. The concept applies globally to the whole Earth and locally to any place, with important consequences due to its gradients. Similarly, the net radiation at TOA (Top of the Atmosphere) is derived as a function of the planetary albedo and the longwave radiation emitted by Earth into space. ERB measurements seek to contribute to two key scientific goals: 1) the determination of how long- and shortwave fluxes are distributed in the atmosphere and how they vary in time, and 2) the development of a quantitative understanding of the links between the radiation budget and the properties of the atmosphere and the surface related to the energy budget and its processes. Accurate solar irradiance data are not only of particular importance for the assessment of the radiative forcing of the climate system, but also necessary for an efficient planning and operation of solar energy systems.



Figure 162: Photo of the full-scale recreation of the Explorer-7 satellite (image credit: UW-SECC)

Legend to Figure 162: The recreation of the Explorer-7 was on display at the 2009 UW-SSEC (University of Wisconsin - Space Science and Engineering Center) celebration of the 50th anniversary of the satellite's successful launch and operation (GOES Users' Conference at CIMSS/SSEC, Madison WI, Nov. 3-5, 2009).

First Earth radiation budget measurements of the space age go back to the late 1950s, with instruments flown on Soviet and US satellites. - NASA launched **Explorer-7** on Oct. 13, 1959. The "Thermal Radiation Experiment" of Explorer-7 was designed to measure incident and reflected solar UV radiation and terrestrial IR radiation in order to obtain a better understanding of the driving forces of the Earth-atmosphere system. The primary instrumentation consisted of five bolometers (detectors) in the form of hollow silver hemispheres that were thermally insulated from, but in close proximity to specially aluminized mirrors.

The hemispheres thereby behaved very much like isolated spheres in space.^{2150) 2151)} Two of the hemispheres had black coatings and responded about equally to solar and terrestrial radiation. A third hemisphere, coated white, was more sensitive to terrestrial radiation than to solar radiation. A complete set of four temperature observations and one reference sample required 30 s. Thus, in each orbit, about 180 temperature measurements could be obtained. The experiment was a success, and usable data were obtained from launch until February 28, 1961. Although the measurement method was rather crude by today's standards, it provided the first valuable data on the basic radiation energy balance of the planet. Maps of radiation (reflected and emitted) were mapped for the first time from LEO.

In the early 1970s, the importance of improving knowledge on the Earth's radiation budget was recognized [i.e., the balance between incoming energy from the sun and the outgoing thermal (longwave) and reflected (shortwave) energy from the Earth] and its relationship with the Earth's climate. NASA built a multichannel absolute radiometer instrument (blackbody calibrated) by the name of ERB (Earth Radiation Budget) which was flown for the first time on Nimbus-6 (launch June 12, 1975, M.29.6). However, the analysis of the ERB data failed to detect any irradiance variability due to degraded responses of the ERB radiometer.

An improved version of **ERB was subsequently flown on Nimbus-7** (launch Oct. 24, 1978, M.29.7; TSI broadband data from ERB on Nimbus-7 were available until the end of 1993). *This radiometer was stable enough to detect short-term and long-term solar irradiance variability. ERB was the first long term solar monitor utilizing the ESCC (Electrically Self Calibrating Cavity) technique.*^{2152) 2153)}

The modern ESCC radiometer technique introduced two operational features: the so-called '**active cavity**' operational mode and the **differential measurement** approach. The active cavity operational mode is one in which the same thermodynamic state is maintained for the cavity sensor in both the solar observation (shutter open) and reference (shutter closed) phases of a measurement. The differential measurement approach utilizes only the differences between solar observation and reference values, eliminating measurement dependence on the International Practical Temperature Scale. – The active cavity operation is achieved by using an electronic servosystem to provide electrical heating power for the cavity detector during both shutter open and closed phases of measurement. The power is controlled at the amount required to sustain constant relative, internal instrument temperatures in the two measurement phases. The measurement then reduces to relating the cavity heating power in the shutter open and closed phases and several other key sensor parameters to the International System of units (SI). Operation does not depend on the International Practical Temperature Scale and the observational uncertainties are reduced to differences between small terms in the two measurement phases. The combination of these techniques greatly decreases the overall measurement uncertainty.²¹⁵⁴⁾

The design of the absolute cavity radiometer technique is based on **the principle of substitution of electrical power for radiative power** (the idea of the cavity design is to come as close as possible to a "perfect absorber" of solar radiation). The function of the cavity is to provide a physical enclosure for the trapping (absorption) of all incoming (broadband) solar radiation. All of these substitution radiometers are of the type "broadband", i.e. they are

2150) Note: The Thermal Radiation Experiment was developed by Verner Edward Suomi (1915–1995) and his colleagues at the University of Wisconsin, Madison, WI. V. E. Suomi is regarded the father of satellite meteorology.

2151) V. E. Suomi, "The radiation balance of the earth from a satellite," *Annals of the IGY*, Vol. 1, 1958, pp. 331–340

2152) J. R. Hickey, et al., "Total solar irradiance measurements by ERB/Nimbus-7, a review of nine years," *Space Science Review*, Vol. 48, 1988, pp. 321–342

2153) Note: The prototype ESCC pyrhelimeter with many of the essential features in use today was developed by Charles Abbot of the Smithsonian Astrophysical Observatory (SAO, Cambridge, MA, USA) in the first decade of the 20th century.

2154) R. C. Willson, J. Hansen, A. Mordvinov, H. H. Hudson, "Algorithm Theoretical Basis Document (ATBD) for the Third Active Cavity Radiometer Irradiance Monitor Experiment (ACRIM-III)," 1999, http://eospsoc.gsfc.nasa.gov/eos_homepage/for_scientists/atbd/docs/ACRIM/atbd-acrim.pdf

using all or a major portion of the spectrum (in two steps or so) for a hemispherical flux measurement, as opposed to “spectrally resolved” instruments.

The success of ERB on Nimbus–7 resulted in the development of a number of TSI instruments for various missions. Since the solar constant is one of the prime determining factors of the Earth’s climate (together with the cloud cover and the Earth’s thermal emission), the data obtained is used in such applications as climate change, solar physics studies, and Earth radiation budget estimates. Solar–constant instruments are generally very sensitive and accurate radiometers for the measurement of solar radiation. Most sensor designs employ the method of “active cavity detector geometry” pyrheliometers (detector in equilibrium with incident solar radiation) and variations thereof.²¹⁵⁵⁾ Following is a survey of “Earth radiation budget missions,” most of them with absolute or active cavity radiometers for the measurement of TSI; there are also instruments (such as HCMM, ScaRaB and GERB) that are not of the absolute radiometer type.

- A first comprehensive thermal survey of the Earth’s surface was provided by HCMM (Heat Capacity Mapping Mission, launch April 26, 1978, end of mission Sept. 30, 1980) of NASA. The satellite featured a Heat Capacity Mapping Radiometer (HCRM) for the measurement of the heat budget, in particular the thermal inertia of the land surface for geological studies.
- SMM (Solar Maximum Mission, launch Feb. 14, 1980, ACRIM data until 1989) flew ACRIM–I (Active Cavity Radiometer Irradiance Monitor) of NASA/JPL and provided data until 1989. The ACRIM–I and ERB/Nimbus–7 instruments detected a short–term (less than 27–day solar rotational period) irradiance variability of as much as 0.2% and a long–term variability of about 0.1%.²¹⁵⁶⁾
- A new generation instrument was realized with ERBE (Earth Radiation Budget Experiment) of NASA/LaRC, first flown on ERBS (Earth Radiation Budget Satellite, launch Oct. 5, 1984), then on NOAA–9 (launch Dec. 12, 1984), and NOAA–10 (launch Sept. 17, 1986). ERBE was able to provide more accurate and systematic parameters for estimating the Earth’s radiation budget. ERBE flew both wide–field–of–view, flat–plate radiometers and the narrow–field–of–view scanning radiometric telescopes measuring with three channels the “short wave”, the “long wave” and the “total” radiances. The improved spatial resolution of flux data achieved with this scanner, by taking into account the bidirectional reflection functions at the TOA, is perhaps the most important advance offered by ERBE, because it led to better estimates of the difference between cloudy and clear–sky fluxes and thus a better estimate of the effect of clouds on Earth’s radiation budget.^{2157) 2158) 2159) 2160)}
- The instruments ACRIM–II, SOLSTICE (Solar/Stellar Irradiance Comparison Experiment) and SUSIM (Solar Ultraviolet Spectral Irradiance Monitor), all with the objective to measure solar radiation, are flown on NASA’s UARS (Upper Atmosphere Research Satellite) mission. Launch Sept. 12, 1991, the S/C is operational as of 2001 (UARS standby mode as of Sept. 30, 2001 – seven of the ten instruments are still functional).

2155) C. Fröhlich, “Observations of Irradiance Variations,” pp. 15–24 in *Solar Variability and Climate*, Editors: E. Friis–Christensen, C. Fröhlich, J. D. Haigh, M. Schüssler and R. von Steiger, Kluwer Academic Publishers, ISBN 0–7923–6741–3, 2000

2156) D. V. Hoyt, H. L. Kyle, J. R. Hickey, R. H. Maschhoff, “The Nimbus–7 solar total irradiance: A new algorithm for its derivation,” *Journal of Geophysical Research*, Vol. 97, 1992, pp. 51–63

2157) K. A. Bush, G. L. Smith, R. B. Lee III, D. F. Young, “The Earth Radiation Budget Experiment (ERBE) 15–year data set,” *Proceedings of SPIE*, Vol. 4881, 9th International Symposium on Remote Sensing, Aghia Pelagia, Crete, Greece, Sept. 23–27, 2002

2158) E. F. Harrison, P. Minnis, B. R. Barkstrom, et al., “Seasonal variation of cloud radiative forcing derived from tire ERBE,” *Journal of Geophysical Research*, Vol. 95: 1990, pp. 18667–18703

2159) B. R. Barkstrom, E. F. Harrison, R. B. Lee, “Earth Radiation Budget Experiment,” *.EOS (AGU)*, Vol. 7, No. 9, Feb. 1990, pp. 297–304

2160) R. B. Lee III, B. R. Barkstrom, R. D. Cess, “Characteristics of the earth radiation budget experiment solar monitors,” *Applied Optics*, Vol. 26, pp 3090–3096, 1987

- EURECA–1 (European Retrievable Carrier). An ESA long–term free–flyer platform (J.5.1) launched on Shuttle flight STS–46 on July 31, 1992 and retrieved with STS–57 on July 1, 1993. Two instruments aboard EURECA were dedicated to solar observations, namely SOVA (Solar Constant and Variability Instrument) with D. Crommelynck as PI, and SOSP (Solar Spectrum Instrument) with G.Thuillier as PI.
- The ScaRaB (Scanner for Radiation Budget) program of CNES (France, Russia and Germany are program partners), started in 1987 with the objective to measure the terms of the Earth’s radiation budget. Two of three instruments, built by CNRS/LMD and operated by CNES, were flown already on Meteor–3–7 (launch Jan. 25, 1994, ScaRaB stopped operating March 5, 1995) and Resurs–O1–4 (launch July 10, 1998 – failure of the backup downlink on Apr. 8, 1999 causing a termination of ScaRaB operations), respectively. The third instrument is planned to be flown on a future mission (currently a CNES/ISRO climate mission in the tropics is considered the most likely candidate, namely Megha–Tropiques). ²¹⁶¹⁾ Note: ScaRaB performs no measurements of TSI. However, the overall radiation budget analysis of ScaRaB uses solar constant values from other sources (such as ISP–2).
- VIRGO (Variability of Solar Irradiance and Gravity Oscillations), an ESA AO instrument package flown on SOHO (launch Dec. 2, 1995, operational as of 2007). The subunits DIARAD (Differential Absolute Radiometer) and PMO6–V are the absolute radiometers in this assembly. Regularly updated observations of the solar constant can be found at the following reference: ²¹⁶²⁾
- ISP–2 (Izmeritel Solnechnoy Postoyannoy–2 – a Solar Constant Instrument) flown on Russia’s RESURS–O1–4 (launch July 10, 1998). The intention is to complement the ScaRaB measurements.
- CERES (Clouds and the Earth’s Radiant Energy System), a scanning thermistor–bolometer instrument of ERBE heritage of NASA/LaRC, is flown on TRMM (Tropical Rainfall Measuring Mission), launch Nov. 27, 1997, as a single cross–track radiance sensor of short (0.3–5 μm), long– (8–12 μm) and total wave (0.3–100 μm ; prototype flight model flown on TRMM) TRMM CERES data was provided from Dec. 1997 to Sept. 1998. – Two further advanced CERES instruments are also being flown on NASA’s Terra mission (launch Dec. 18, 1999) as a dual–track scanner (two radiometers) in XT (Cross–Track) support or in a RAPS (Rotational Azimuth Plane Scan) support mode. Another CERES instrument system (two radiometers) are being flown on Aqua (formerly EOS/PM1) of NASA (launch May 4, 2002).
- ACRIM–III on ACRIMSAT (NASA), launch Dec. 20, 1999 (see A.2)
- **First Earth radiation budget measurements from GEO.** GERB (Geostationary Earth Radiation Budget) is an ESA–developed instrument of the EUMETSAT MSG–1 (Meteosat Second Generation) mission, a two–channel broadband radiometer, provided by a consortium led by the UK (NERC), Belgium (SSTC) and Italy (ASI). The launch of MSG–1 (Meteosat–8) took place on Aug. 28, 2002. *The instrument measures the radiances leaving the Earth at TOA (Top of the Atmosphere); it provides an image of the reflected sunlight and infrared radiation at a five–minute sampling rate, covering the shortwave (0.32 – 4.0 μm) and longwave (4.0 > 100 μm) regions of the spectrum.* A full Earth view period of GERB detectors require 250 revolutions of the spin–stabilized S/C (150 s). Hence, a full disk measurement plus calibration of one channel is obtained in 2.5 minutes. – The overall radiation budget analysis of GERB uses solar–constant values from other sources. GERB data analysis is a joint effort between RAL (UK) and RMIB (Royal Meteorological Institute of Belgium), Belgium. Since the evaluation of the TOA Earth radiation balance terms (conversion of radiances to TOA fluxes) are being made available to within three hours after

²¹⁶¹⁾ Information provided by M. Rouzé of CNES

²¹⁶²⁾ <http://remotesensing.oma.be/solarconstant/solar.html>

observation, the GERB observations can make a unique contribution to the understanding of the Earth's climate balance (diurnal sampling), since such measurements have never been carried out before from geostationary orbit (see F.9).^{2163) 2164)}

GERB instruments are also planned to be flown on the follow-up MSG missions. Note: The imaging data of GERB are acquired by EUMETSAT, sent to RAL for pre-processing and then forwarded to RMIB for further processing and distributing to the community. GERB data are also being compared with CERES data in LEO on the Terra S/C of NASA. The GERB FOV (Field of View) from GEO is a particularly good test bed for studying the interaction between aerosols and the climate system.

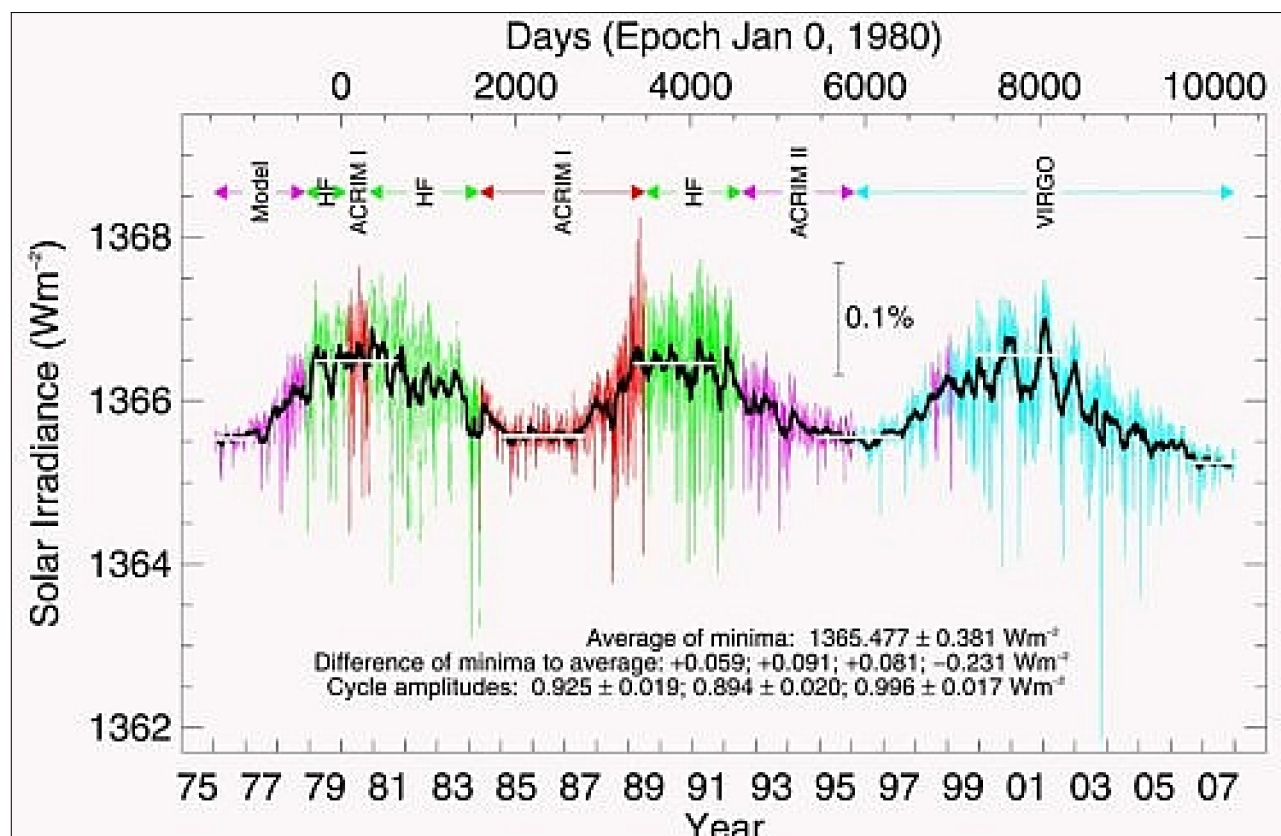


Figure 163: Spaceage measurements of the total solar irradiance (image credit: C. Fröhlich)²¹⁶⁵⁾

- NASA funded TIM (Total Irradiance Monitor), developed at LASP (Laboratory for Atmospheric and Space Physics) of the University of Colorado, flown on SORCE (Solar Radiation and Climate Experiment). SORCE is part of NASA's ESE (Earth Science Enterprise) program with a launch Jan. 25, 2003. Besides very precise and accurate solar irradiance measurements with TIM, the other instruments of SORCE, namely SOLSTICE (Solar/Stellar Irradiance Comparison Experiment), SIM (Spectral Irradiance Monitor), and XPS (XUV Photometer System), complement the solar spectral irradiance measurements at wavelengths extending from the far ultraviolet to the near infrared.

- The Glory mission of NASA (launch March 4, 2011, launch failure) will fly the TIM instrument of LASP to continue the solar irradiation measurements of the SORCE mission.

- A TIM instrument, referred to by the name of TSIS (Total Solar Irradiance Sensor), is also planned to fly on NASA's NPP (NPOESS Preparatory Project) with a launch on Oct. 28,

2163) J. E. Russell, J. E. Harries, J. Hanafin, H. Brindley, J. M. Fytan, R. P. Allan, A. Slingo, M. A. Ringer, "The Geostationary Earth Radiation Budget (GERB) Experiment: Science and Applications," The EUMETSAT Meteorological Satellite Conference, Weimar, Germany, Sept. 29 – Oct. 3, 2003

2164) <http://gerb.oma.be/>

2165) "Deep Solar Minimum," NASA, April 1, 2009, URL: http://science.nasa.gov/headlines/v2009/01apr_deepsolarminimum.htm?list1291671

2011 and on NPOESS (National Polar-orbiting Operational Environmental Satellite System) of IPO (Integrated Program Office) with a first launch projected for 2014.

- NISTAR (National Institute of Standards and Technology Advanced Radiometer) is a three-channel cavity radiometer of the NASA mission Triana (currently no planned launch, the entire payload is in mothball) which measures the Earth's "irradiance" in the small angle as seen from a halo orbit at L1 (Lagrangian point 1), about 1.5 million km from Earth in the direction of the sun. The NISTAR TSI measurements offer a great opportunity to compare its radiances with instruments in LEO (Low Earth Orbit) and in GEO (GERB). Note: NASA has terminated the Triana mission as of Jan. 2006.²¹⁶⁶⁾

- SOLAR (Solar Monitoring Observatory) is an ESA experiment package on ISS consisting of three instruments, namely SOVIM (Solar Variability and Irradiance Monitor) covers the near-UV, VIS and TIR, developed by the Observatory of Davos, Switzerland; SOLSPEC (Solar Spectral Irradiance Measurements) covers the range 180–3000 nm, developed by CNRS of France; and SolACES (Solar Auto-Calibrating EUV/UV Spectrophotometers) with a coverage of 17–220 nm, developed by the Fraunhofer Institute, Germany. SOVIM and SOLSPEC are the upgraded versions of instruments that have already accomplished several orbital flights without failure.²¹⁶⁷⁾ The overall objective is to measure the solar spectral irradiance with unprecedented accuracy. The three instruments cover the combined wavelength range from 17–3080 nm. The SOLAR package is located on CEPF (Columbus External Payload Facility), part of COF (Columbus Orbital Facility), the ESA module of ISS. A launch of Columbus along with the SOLAR payload took place on Shuttle flight STS-122 (Feb. 7–20, 2008).

- Picard is a CNES solar-terrestrial microsatellite mission (launch June 15, 2010), named after Jean Picard (1620–1682), a French astronomer. Two instruments measure the solar constant: SOVAP (Solar Constant Variability, Picard) of RMIB (Royal Meteorological Institute of Belgium) in Brussels, and PREMOS (Precision Monitoring of Solar variability) photometric spectral band measurements of WRC (World Radiation Center) of Davos, Switzerland. The measurement of the solar diameter is done by SODISM (Solar Diameter Imager and Surface Mapper), a CNRS/SA (Verrières-le-Buisson, France) instrument in collaboration with ESA/ESTEC.

- PREMOS is the first and so far only radiometer in space with a SI-traceable irradiance calibration in vacuum. PREMOS is traceable to the irradiance calibration facility at LASP in Boulder (TRF).²¹⁶⁸⁾

- The US NPOESS satellite series (with a first launch in 2014) will be flying two radiation budget instruments:

- ERBS (Earth Radiation Budget Sensor). The objective is to measure Earth radiation budget parameters and atmospheric radiation from the top of the atmosphere to the surface. ERBS is allocated to fly on the LTAN 13:30 S/C series.

- TSIS (Total Solar Irradiance Sensor) instrument of TIM (Total Irradiance Monitor) heritage, flown on SORCE (Solar Radiation and Climate Experiment). TSIS is a total solar irradiance monitor plus a 0.2–2 μm solar spectral irradiance monitor. The objective is to measure the variability in the sun's radiative output. TSIS is allocated to fly on the LTAN 17:30 NPOESS S/C series.

- Periodic (short-term) measurements were conducted in particular with SOLCON (Solar Constant Sensor) on a number of Shuttle flights. The SOLCON-1 instrument is a

2166) A. Lawler, "NASA Terminates Gore's Eye on Earth," *Science*, Jan. 6, 2006, Vol. 311

2167) http://esapub.esrin.esa.it/sp/sp1270/chapter3_sp1270.pdf

2168) Werner Schmutz, "Long term monitoring of Total Solar Irradiance: Results and Challenges," Proceedings of the 49th Session of UNCOUOS-STSC (UN Committee on the Peaceful Uses of Outer Space – Scientific and Technical Subcommittee), Vienna, Austria, Feb. 6–17, 2012, URL: <http://www.oosa.unvienna.org/pdf/pres/stsc2012/tech-20E.pdf>

cooperative effort of RMIB (Belgium), Space Science Dept. of ESA, and NASA/LaRC. The **SOLCON radiometer is the first differential absolute solar radiometer in space** based on a full symmetrical metrological design (two side by side cavities) and operation (successive opened and closed state of the measurement cavity). During Shuttle flights, SOLCON is used to determine the **SARR** (Space Absolute Radiometric Reference) adjustment coefficients of other satellite solar constant instruments that are active at the same time (the objective of SARR is to relate all existing total solar irradiance measurements with each other).²¹⁶⁹⁾

The first such SARR measurements were conducted on the STS–56 mission of ATLAS–2 in 1993, determining the adjustment coefficients of ACRIM–II flown on UARS and on ERBS (Earth Radiation Budget Satellite), and those of SOVA (Solar Constant and Variability Instrument) on EURECA–1 [SOLCON–2 was of the same design as SOVA with the SOVA1 Dual Differential Absolute Radiometer (DIARAD) composed of two independently characterized channels and the SOVA 2 set of two mono–channel active and backup radiometers]. Further SARR measurements of SOLCON were conducted with the following radiometers:²¹⁷⁰⁾

- STS–95 (1998) flight. VIRGO (Variability of Solar Irradiance and Gravity Oscillations) radiometers flown on SOHO, and ACRIM–II flown on UARS and on ERBS.
- On flight STS–107 SOLCON–3 has been used to determine the SARR coefficients of ACRIM–III on ACRIMSAT and to verify the VIRGO coefficients on SOHO.

Launch Vehicle	Date	Mission	Instrument
STS–9 (Shuttle)	Nov. 28 – Dec. 8, 1983	Spacelab–1 (ESA)	SOLCON–1
STS–45	March 24 – April 2, 1992	ATLAS–1 (NASA)	SOLCON–2, ACRIM–II
STS–46/57	Jul. 31, 1992 – Jun. 21, 1993	EURECA (ESA)	SOVA–1, SOVA
STS–56	April 8–17, 1993	ATLAS–2 (NASA)	SOLCON–2, ACRIM–II
STS–66	Nov. 3–14, 1994	ATLAS–3 (NASA)	SOLCON–2, ACRIM–II
STS–85	Aug. 7–19, 1997	Hitchhiker (NASA)	SOVA–1
STS–95	Oct. 29 – Nov. 7, 1998	Hitchhiker (NASA)	SOLCON–2
STS–107	Jan. 16–Feb. 1, 2003	FREESTAR (NASA)	SOLCON–3

Table 122: Chronology of Shuttle–based solar–constant measurements with absolute radiometers

Use of solar energy in deep space missions: The main criterion for deciding on whether to use solar or nuclear power is distance from or orientation with respect to the Sun. Figure 164 shows the variation of solar energy flux with distance from the Sun, which follows Planck’s inverse square law with distance. For most applications, nuclear makes best sense for missions beyond Mars orbit, although improvements in array technology continue to push this limit further out.

In spite of these disadvantages, there are two recent deep space missions that use solar cell power – without the use of RTG (Radioisotope Thermoelectric Generator) technology. These missions are:

- The Rosetta mission of ESA (launch March 2, 2004), rendezvous with Comet 67P/Churyumov–Gerasimenko in 2014 at a distance of 4.4 AU from Earth.

2169) D. Crommelynck, A. Fichot, R. B. LEE III, J. Romero, “First realization of the space absolute radiometric reference (SARR) during the ATLAS 2 flight period,” *Advances in Space Research*, Vol. 16, No 8, pp (8)17–(8)23, 1995

2170) S. Dewitte, A. Joukoff, D. Crommelynck, R. B. Lee III, R. Helizon, R. S. Wilson, “Contribution of the Solar Constant (SOLCON) Program to the Long Term Total Solar Irradiance Observations,” *Space Scientific Research in Belgium/Vol. 2, Space Science Part 1, Chapter 2, Solar Physics*, pp. 183–191

- The Dawn spacecraft of NASA (launch Sept. 28, 2007) an 8 year mission on its way to the Asteroid Belt (between Mars and Jupiter).

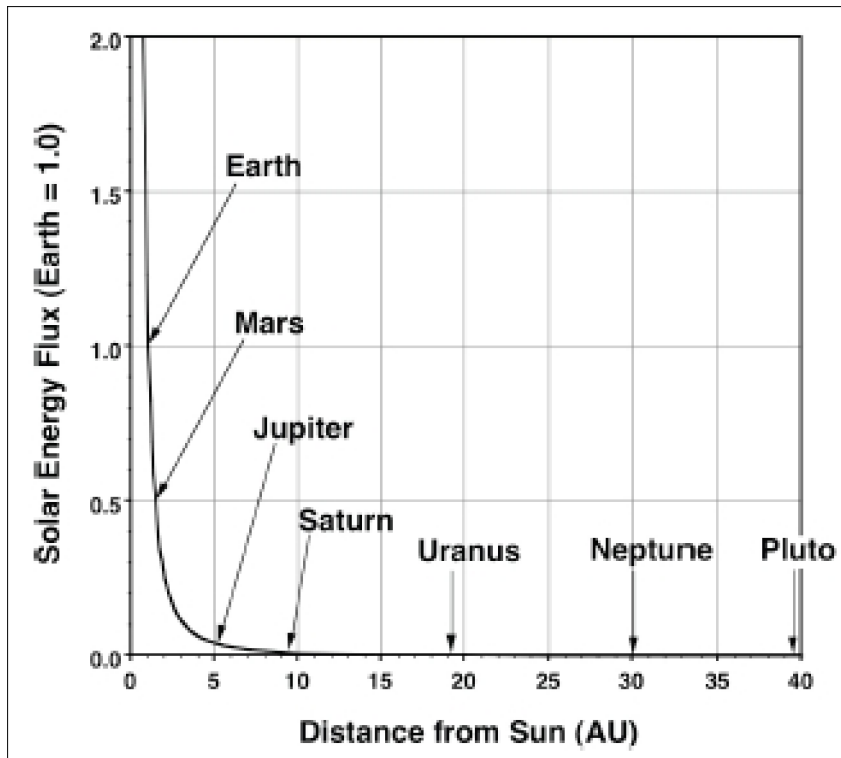


Figure 164: Solar energy flux versus distance from the Sun (image credit: NASA)

1.22.3 Solar Wind Observation

The solar wind is a thin blast of electrified gas – a plasma or “particle radiation” consisting of protons, alpha particles (two-fold ionized helium), heavy ions and electrons – emitted by the surface of the sun, which blows radially from the sun into all directions, naturally also toward and past the Earth at speeds ranging from 300 – 1000 km/s (or about 1–3.3 million km/h) – it represents a mass loss from the sun of $\sim 10^{15}$ kg/year.^{2171) 2172)} The solar wind provides the medium through which the sun interacts directly with the Earth; it shapes the Earth’s magnetosphere and supplies energy to its many processes. Earth itself possesses a strong internal magnetic field that prevents the solar wind from hitting the upper atmosphere. Instead, the solar wind becomes diverted around the Earth’s magnetic obstacle, called the magnetosphere.

The presence of the perpetual solar wind is directly indicated by the continuing fluctuations of the geomagnetic field at the surface of Earth, particularly at high latitudes, the continuing aurora activity at high latitudes, the varying intensity of the galactic cosmic ray radiation, and the antisolar orientation of the gaseous tails of comets. However, these effects, known individually for decades and centuries, are evidence only of some form of external disturbance, and the scientific challenge over the last century has been to work out precisely what that disturbance really is.

The existence proof of the solar wind is a discovery of the space age by data analysis first conducted from the Soviet Luna spacecraft series [Luna–1 (launch Jan. 2, 1959), Luna–2 (launch Sept. 12, 1959), and Luna–3 (Oct. 14, 1959)] on their flight to the moon.^{2173) 2174)} The first tentative evidence of the solar wind was observed with an experiment of Konstantin I. Gringauz (1918–1993, USSR) and his team onboard the Luna–2 and Luna–3 spacecraft. The total electric charge of arriving ions was measured in the “ion trap experiment” (4 ion traps in the voltage range of –10 V to +15 V on Luna–2) Gringauz noted that the signal fluctuated as the spacecraft spun around its axis, suggesting an ion flow was entering the instrument whenever it faced the sun.

In 1961, James Dungey (UK) proposed a mechanism for transmitting solar wind energy to the magnetosphere by direct magnetic linkage between the two. The magnetopause, the boundary between magnetosphere and the solar wind, was observed for the first time by NASA’s Explorer–10 in 1961 (launch March 25, 1961). The S/C featured an elaborate ion trap, called Modulated Faraday Cup, built by a team of MIT (Herbert Bridge, Bruno Rossi). The first variations in the speed of the solar wind (27 days intervals) were observed in 1962 from the Mariner–II spacecraft of NASA/JPL (launch Aug. 27, 1962) on its way to Venus with an instrument called CPA (Curved Plate Analyzer). CPA measured 113 days of data (continuous radial flow of high and low solar wind streams), the general properties of the solar wind (speed, temperature, and helium content) were surveyed. The data analysis of the IMP–1 (Interplanetary Monitoring Platform 1, launch Nov. 27, 1963, the mission is also known as Explorer–18) revealed a large bow shock formed in the solar wind ahead of the magnetosphere, and a long magnetic tail on the night side of the Earth. In 1983, the ISEE–3 (International Sun–Earth Explorer 3) mission explored the distant magnetotail, before heading for comet Giacobini–Zinner. The Ulysses S/C (launch Oct. 6, 1990), a joint ESA/NASA solar mission (365 kg of launch mass, the total instruments mass is 55 kg), passed above the sun’s south pole in Sept. 1994, and above the north pole in 1995 (the second set of polar passes took place from Sept. 2000 to Jan. 2001 (south) and Sept. to Dec. 2001 (north). This first mission with an out–of–ecliptic orbit confirmed that the polar regions of the sun

2171) E. N. Parker, “A history of the solar wind concept,” [The Century of Space Science, Vol. I., Eds. M Huber, J. Geiss, and J. Bleeker \(Kluwer Academic Publishers, 2002\).](#)

2172) <http://www.magazine.noaa.gov/stories/mag93.htm>

2173) T. I. Gombosi, “Modeling Gringauz’s legacy from the solar wind to weakly magnetized solar system bodies,” International Symposium on Space Plasma Studies by In–Situ and Remote Measurements (Gringauz Symposium), Moscow, Russia, June 1–5, 1998.

2174) <http://www-spf.gsfc.nasa.gov/Education/whsolwi.html>

also have such outwards-directed field lines, as evidenced by the “polar plumes” seen in the corona during a total eclipse of the sun. The existence of a steady fast-flowing solar wind above the solar poles was observed along with many associated phenomena.^{2175) 2176)}

Characteristics: The solar wind plasma consists of primarily of hot electrons and protons with a minor fraction of He^{2+} ions and some other heavier ions (typically at high charge states). The solar wind originating from the streamers (closed field lines of the sun) is slow, while that originating from the coronal holes is fast. This creates the so-called “corotating interaction regions” (CIR) in the interplanetary space. As the solar wind moves away from the sun, tangential discontinuities and interplanetary (fast) shocks are formed, creating pressure variations. Typical periodicities in the solar wind can be divided into those that reflect the time scales of the solar processes themselves, those that reflect the rotation of the Sun, and those that reflect the orientation of Earth (the most typical observation point) with respect to the Sun. The first include the 11- and 22-year solar cycles and the 1.3 year and 154 day cycles. The scale sizes of solar wind/IMF structures are typically smaller than the extent of the Earth’s magnetosphere (about $40 R_E$).²¹⁷⁷⁾

Parameter	Minimum	Average	Maximum
Flux ($\text{cm}^{-2} \text{s}^{-1}$)	1	3	100
Velocity (km s^{-1})	200	400	900
Density (particles/ cm^3)	0.4	6.5	100
Helium (%)	0	5	25
B (nT)	0.2	6	80

Table 123: Some characteristics of the solar wind

Effect on Earth and planets: All planets of the solar system are surrounded by the hot, magnetized, supersonic collisionless solar wind plasma capable of conducting electrical current and carrying a large amount of kinetic and electrical energy. Due to the supersonic nature of the solar wind, shock waves are formed in front of the planets (see bow shock). Some of the solar wind energy finds its way into the Earth’s magnetosphere, ionosphere and atmosphere, and

- Drives the magnetospheric convection system and energizes much of the plasma on the Earth’s magnetic field lines
- Drives field line resonances and other geomagnetic pulsations
- Creates geomagnetic activity
- Heats the polar upper atmosphere
- Drives large neutral atmospheric winds.

Because of these effects, the changes in the solar wind plasma parameters (density, velocity, etc.) and IMF (especially direction in relation to Earth’s own field) are very important for magnetospheric and ionospheric physics, and the scientific community tries to have continuous monitoring of these parameters via satellites. Also, interactions between the solar wind and the Earth’s magnetic field lead to creation of the auroral oval – a high latitude region of the Earth’s ionosphere. In the auroral zone, irregular precipitation of energetic electrons occurs during substorm events – resulting in optical and UV emissions (Northern/Southern Lights). During such events, structured depletions/enhancements of total electron content (TEC) can occur in the auroral ionosphere (at E-region altitudes of 110

2175) Marcia Neugebauer, “Pioneers of space physics: A career in the solar wind,” *Journal of Geophysical Research*, Vol. 102, No A12, Dec. 1, 1997, pp. 26,887–26,894.

2176) B. Rossi, “Interplanetary plasma,” *Space Research, Proceedings of 3rd International Space Science Symposium*, Washington, 1962, p. 529, North-Holland, New York, 1962.

2177) <http://www oulu.fi/~spaceweb/textbook/solarwind.html>

km). Auroral activity is a major concern for reliable operation of GPS positioning applications at high latitudes. Auroral substorms are characterized by increased spatial and temporal decorrelations of ionospheric range delay, and loss of signal availability can occur during periods of ionospheric scintillations.²¹⁷⁸⁾

Background on the early history of the solar wind:^{2179) 2180) 2181) 2182) 2183)} The first indication that the sun might be emitting a “wind” came from comet tails, observed to point away from the sun, whether the comet was approaching the sun or whether it was moving away. Johannes Kepler (1571–1630, German astronomer) in the early 1600s guessed that those tails were driven by the pressure of sunlight, and his guess still holds true for the many comet tails which consist of dust.

The phenomenon and mechanism of so-called “particle bursts” from the sun was first discussed by S. Chapman and V. Ferraro in 1931. These particle bursts would cause a compression of the geomagnetic field. According to their model (now known to be erroneous) a solar wind would only occur temporarily in connection with flares or other specific solar phenomena. — In 1951, Ludwig F. Biermann (1907–1986, of the Max–Planck–Institut für Physik and Astrophysik at Göttingen, Germany) studied tails of comets as they passed near the sun and showed that the pressure of solar radiation alone can not explain his observations.

As a consequence, he suggested the concept of a continuous solar wind that exists always and essentially affects (bends) the formation of cometary tails (he explained that the motion of the ions was due to their being entrained in a flow of particles being given off by the sun and moving radially outwards). Biermann also estimated the velocity of the solar wind to be in the range 500–1500 km/s. However, the name “**solar wind**” was coined by **Eugene N. Parker** at the Enrico Fermi Institute of the University of Chicago in 1958, when developing the theory of the (continuous) solar wind. He predicted that the solar corona must expand (due to the fact that the corona emits a supersonic flow of plasma); he called the outward streaming coronal gas “solar wind.”

- The ISEE–3 (International Sun–Earth Explorer–3) mission, with a launch in 1978, was first placed into a halo orbit at L1 (Lagrangian point L1, located ~ 1.5 million km toward to sun) for nearly four years. It was then directed to study the geomagnetic tail for a first–ever exploration of that region. This resulted in the discovery of gigantic plasmoids that were ejected from the near–Earth magnetosphere. After exploring the nature of the geomagnetic tail, ISEE–3 was sent off for the first spacecraft encounter with a comet in September 1985. When ISEE–3 was near Comet Giacobini–Zinner, first measurements of the solar wind’s interaction with a comet were obtained.

- The Ulysses S/C (launch Oct. 6, 1990, K.32) of ESA/NASA is the **first S/C having left the ecliptic plane to observe the polar regions of the sun** using a slingshot past Jupiter (a gravity assist maneuver) to obtain such a **sun–centered, out–of–ecliptic orbit**.²¹⁸⁴⁾ — With a period of 6.2 years, the orbit is inclined at 80.2° to the solar equator. The perihelion (point of closest approach to the sun) is at 1.3 AU, and the aphelion at 5.4 AU (the most distant point in the orbit). The three major objectives are to study the sun, the solar wind characteristics (speed, temperature and composition), and interstellar space. Although Ulysses is the first S/C to probe the sun’s polar regions, it does not travel near the sun. The

2178) M. El–Gizawy, S. Skone, “A Canadian Ionospheric Warning and Alert System,” ION–GPS 2002, Portland, OR, Sept. 24–27, 2002

2179) S. Chapman, V. C. A. Ferraro, “A new theory of magnetic storms,” *Terrestrial Magnetism and Atmospheric Electricity*, Vol. 36, 1931, pp. 77–97

2180) L. Biermann, “Kometenschweife und solare Korpuskularstrahlung,” *Zeitschrift für Astrophysik.*, Vol. 29, p. 274, 1951

2181) <http://www-istp.gsfc.nasa.gov/Education/wsolwind.html>

2182) E. N. Parker, “Dynamics of the interplanetary gas and magnetic fields,” *Astrophysical Journal*, Vol. 128, p. 664, 1958

2183) E. N. Parker, “Extension of the solar corona into interplanetary space,” *Journal of Geophysical Research.*, Vol. 64, p. 1675, 1959

2184) R. G. Marsden, E. S. Smith, “News from the Sun’s Poles – Courtesy of Ulysses,” *ESA Bulletin* 114, May 2003, pp. 60–67

long duration of the Ulysses mission enabled comprehensive observations to be made over the sun's poles at both solar maximum and solar minimum. In 1994, it was reported that near the south pole the solar wind is flowing away from the sun at nearly twice the speed that is typically observed near the sun's equator (great variability of the solar wind configuration during solar maximum and solar minimum).

Mission	Instruments	Comment
ACE, launch Aug. 25, 1997 positioned at L1	SWIMS, SWICS, SWEPAM	Focus on solar wind composition and acceleration
AMPTE, launch Aug. 16, 84		Release of trace gases into the solar wind
Cluster-2, launch Jul. 16, 00	CIS, HIA, STAFF	Study of solar wind bow shock
DS1, launch Oct 24, 1998	PEPE	Solar wind energy spectrum
DSP (Double Star Project), launch in 2003, China, ESA	HIA, LEID, LFEWD, PEACE	Study of solar wind with magnetosphere
Equator-S, launch Dec. 2, 1997		Solar wind measurements with WIND and SOHO
Genesis, launch Aug. 8, 2001	Collector Array, Solar Wind Concentrator	Solar wind measurement, collection and return of solar wind samples. Halo orbit at L1, Return to Earth on Sept. 8, 2004
GEOTAIL, launch Jul. 24, 1992	LEP, CPI	Measurement of fluctuations in the solar wind
IMAGE, launch March 25, 2000	LENA, MENA, HENA	Response of magnetosphere with solar wind
IMP-8, launch Oct. 26, 1973	GAF, MAP	Plasma field environment for magnetospheric studies
INTERBALL, launch Aug. 3, 1995 and Aug. 29, 1996	Monitor-3, etc.	Solar wind energy and interaction with the Earth's magnetosphere
ISEE-1, -2, launch Oct. 2, 77	SWE, EGD, OGM, SHM,	Study of Earth's bow shock
ISEE-3, launch Aug. 12, 78	BAH, OGH, SBH	Measurement of solar wind/plasma fields First ever cometary encounter 7800 km tailward of comet Giacobini-Zinner.
NOAA-15, launch May 13, 1998	SEM-2 package	An operational space weather warning system
POLAR, launch Feb. 24, 1996	MFE, TIMAS,	Coupling of the solar wind and magnetosphere, study of particle populations
SOHO, launch Dec. 2, 1995	UVCS, SWAN, CELIAS,	Study of solar wind and energetic particles, interaction with the Earth. First tracing of the slow-speed solar wind
STEREO, launch Oct. 26, 2006	IMPACT, SWEA, PLASTIC, SWAVES,	Measurements of solar wind in a helio-centric elliptical orbit in the ecliptic plane at 1 AU
TIMED, launch Dec. 7, 2001	TIDI	Solar wind structure in MLTI (Mesosphere and Lower-Thermosphere/Ionosphere) region
TIROS-N, launch 1978 and on all S/C of NOAA POES	SEM (NOAA/SEC package)	Measurement of solar wind particle flux
Triana (the mission was cancelled as of 2006)	PlasMag	Study of solar wind in halo orbit at L1
Ulysses, launch Oct. 6, 1990	SWICS, SWOOPS, UARP,	Study of the solar wind
USA-184, launch June 28, 2006, NRO mission	TWINS-1	Response of magnetosphere with solar wind
USA-200, launch March 13, 2008, NRO mission	TWINS-2	Response of magnetosphere with solar wind
Viking, launch Feb. 22, 1986	V1, V2, V3, V4L	Solar wind interaction with the magnetosphere
WIND, launch Nov. 1, 1994	MFI, WAVES, SWE, SMS, EPACT, PLASMA,	Study of solar wind mass momentum and energy. Halo orbit at L1

Table 124: Some solar wind experiments/studies (alphabetic order of missions)

Using data from an aging WIND spacecraft of NASA, **researchers have found signs of an energy source in the solar wind that has caught the attention of fusion researchers.** NASA will be able to test the theory later this decade when it sends a new probe into the sun for a closer look. ²¹⁸⁵⁾

The discovery was made by a group of astronomers trying to solve a decades–old mystery: **What heats and accelerates the solar wind?**

The solar wind is a hot and fast flow of magnetized gas that streams away from the sun’s upper atmosphere. It is made of hydrogen and helium ions with a sprinkling of heavier elements. Researchers liken it to the steam from a pot of water boiling on a stove; the sun is literally boiling itself away.

But the solar wind does something that steam in the kitchen never does. As steam rises from a pot, it slows and cools. As solar wind leaves the sun, it accelerates, tripling in speed as it passes through the corona. Furthermore, something inside the solar wind continues to add heat even as it blows into the cold of space.

Finding that “something” has been a goal of researchers for decades. In the 1970s and 80s, observations by two German/US Helios spacecraft set the stage for early theories, which usually included some mixture of plasma instabilities, magnetohydrodynamic waves, and turbulent heating. Narrowing down the possibilities was a challenge. The answer, it turns out, has been hiding in a dataset from one of NASA’s oldest active spacecraft, a solar probe named Wind.

The source of the heating in the solar wind is ion cyclotron waves. Ion cyclotron waves are made of protons that circle in wavelike – rhythms around the sun’s Hampshire) and expanded by Vitaly Galinsky and Valentin Shevchenko (UC San Diego), ion cyclotron waves emanate from the sun; coursing through the solar wind, they heat the gas to millions of degrees and accelerate its flow to millions of miles per hour. – Justin Kasper of the Harvard–Smithsonian Center for Astrophysics, Massachusetts, and collaborators present a model that demonstrates how certain plasma waves, called ion cyclotron waves, will preferentially heat heavier ions travelling below a threshold velocity. Kasper’s findings confirm that ion cyclotron waves are indeed active, at least in the vicinity of Earth where the WIND spacecraft operates. ^{2186) 2187)}

Plasma carrying a spectrum of counterpropagating field–aligned ion–cyclotron waves, can strongly and preferentially heat ions through a stochastic Fermi mechanism. Such a process has been proposed to explain the extreme temperatures, temperature anisotropies, and speeds of ions in the solar corona and solar wind. The team of researchers quantified, how differential flow between ion species results in a Doppler shift in the wave spectrum, that can prevent this strong heating. Two critical values of differential flow were derived for strong heating of the core and tail of a given ion distribution function. The comparison of these predictions to observations from the Wind spacecraft reveals excellent agreement. Solar wind helium, that meets the condition for strong core heating, is nearly 7 times hotter than hydrogen on average. Ion–cyclotron resonance contributes to heating in the solar wind, and there is a close link between heating, differential flow, and temperature anisotropy (Ref. 2187).

Table 125: First plausible explanations for solar corona wind heating in 2013 ^{2185) 2186) 2187)}

2185) Tony Pillips, “Solar Wind Energy Source Discovered,” NASA Science News, March 8, 20143, URL: http://science.nasa.gov/science–news/science–at–nasa/2013/08mar_solarwind/

2186) Justin C. Kasper, Bennett A. Maruca, Michael L. Stevens, Arnaud Zaslavsky, “Sensitive Test for Ion–Cyclotron Resonant Heating in the Solar Wind,” Physical Review Letters, Vol. 110, Issue 9, 091102, Feb. 28, 2013, URL: <http://prl.aps.org/abstract/PRL/v110/i9/e091102>

2187) Justin C. Kasper, Bennett A. Maruca, Michael L. Stevens, Arnaud Zaslavsky, “Sensitive Test for Ion–Cyclotron Resonant Heating in the Solar Wind,” Physical Review Letters, Vol. 110, Issue 9, 091102, Feb. 28, 2013, URL: <http://prl.aps.org/abstract/PRL/v110/i9/e091102>

- Monitoring of the solar wind (i.e. of space weather parameters) is being conducted from several spacecraft located at the Lagrangian point L1 in the Earth–Sun system, about 1.5 million km from Earth. The solar wind reaches L1 about one hour prior to reaching Earth; this vantage position is being used to provide early warning in space weather monitoring services (geomagnetic storms, etc.). Some spacecraft with solar wind instruments at L1 are: ²¹⁸⁸⁾

- WIND of NASA/GSFC (launch Nov. 4, 1994; orbiting L1 since 2004 continuously)

- ACE (Advanced Composition Explorer) of NASA (launch Aug. 25, 1997; orbiting L1 since 1997). The ACE mission is operating nominally in 2012 – providing continuous, real–time space weather data.

- SOHO (Solar and Heliospheric Observatory) of ESA/NASA (launch Dec. 2, 1995; orbiting L1 since 1996). – The SOHO spacecraft is a major contributor to space weather forecasts, by observing solar flares and CMEs (both are aspects of the same event).

- Genesis of NASA (launch Aug. 8, 2001). ²¹⁸⁹⁾ The Genesis mission has the objective to collect solar wind particles at L1 (outside the Earth’s magnetosphere) for at least 22 months and return these particles to Earth (by a sample return capsule) after mission completion in Sept. 2004. The L1 location was reached May 22, 2002. The sample collection period ended on April 1, 2004. This has been followed by a 5 month return mission to Earth. On Sept. 8, 2004, the sample return capsule of Genesis crashed into the desert of Utah (at an estimated speed of 310 km/h) due to the failure of a parachute deployment (its drogue and parafoil systems failed to deploy – a design flaw in the reentry system has been identified as the most likely cause of the spacecraft’s free fall onto the surface of Earth). After inspection of the damage, NASA is optimistic that a portion of the solar wind samples can still be salvaged from the Genesis capsule. ²¹⁹⁰⁾ Preliminary findings point to an incorrectly installed accelerometer, which was unable to sense the deceleration upon reentry and initiate the parachute deployment sequence. ²¹⁹¹⁾

- The IMAGE S/C (launch March 25, 2000, K.18) of NASA carries three ENA (Energetic Neutral Atom) imagers (LENA, MENA, and HENA) whose combined energy coverage permits the detection of ENAs with energies ranging from 1 eV to 500 keV per atomic mass unit (amu). Each neutral atom instrument generates images showing the intensity and spatial distribution of ENA radiation emissions produced in the inner magnetosphere through charge–exchange reactions between geocoronal neutral hydrogen and various magnetospheric ion populations. Neutral atom imaging of the ionosphere and magnetosphere is possible because the Earth’s geocorona acts like an imaging screen for magnetospheric and ionospheric ions. ²¹⁹²⁾ [The neutral atoms in the space environment are measured against the large and ubiquitous UV background which can produce high noise count rates in MCP detectors]. To date, four different techniques have been developed to allow neutral atom detection and imaging against the UV background:

- A thick foil which blocks the UV

- An ultra thin charge conversion foil to ionize ENAs (which are then passed through an electrostatic analyzer)

- A charge exchange surface from which ENAs can reflect as ions which are then analyzed

²¹⁸⁸⁾ Craig E. Roberts, “Long term missions at the Sun–Earth Libration Point L1: ACE, SOHO and Wind,” Proceedings of the AAS/AIAA Astrodynamics Specialist Conference, Girdwood, Alaska, USA, July 31– Aug. 4, 2011

²¹⁸⁹⁾ N. G. Smith, K. E. Williams, R. C. Wiens, C. E. Rasbach, “Genesis – The Middle Years,” Proceedings of IEEE Aerospace Conference, Big Sky, MT, USA, March 8–15, 2003

²¹⁹⁰⁾ B. Berger, “NASA Optimistic Genesis will Yield Useful Samples,” Space News, Sept. 13, 2004, p. 18

²¹⁹¹⁾ R. C. Wiens, “Genesis Capsule Yields Solar Wind Samples,” EOS Transactions of AGU, Vol. 85, No 47, Nov. 23, 2004, pp. 497–498

²¹⁹²⁾ D. J. McComas, “Two Wide–Angle Imaging Neutral–Atom Spectrometers,”

- Transmission gratings which block UV but allow ENAs to pass.

The IMAGE spacecraft and its sensor complement represent a new era of magnetospheric observation capability. While traditional instruments provide in-situ observations of the magnetospheric plasma environment, the new ENA devices are able to image the plasma motions by detecting the particles and their traveling directions (the imaging is done using “electromagnetic wave sounding”).

Data of the IMAGE sensors made space storms visible for the first time [HENA has provided the first-ever images (2-min cadence) of geomagnetic storm ring current growth, main phase, and recovery with full particle energy resolution, finally capturing the dynamics of Earth’s reaction to solar and solar wind storms]. Regarding the solar wind, the IMAGE data show that the Earth atmosphere plays an active but ever-changing role in diverting and absorbing the solar wind. The ionosphere dissipates great amounts of energy flung at Earth by ejecting about 100 tons of hydrogen and oxygen into space during each solar storm. ²¹⁹³⁾

Background: Energetic neutral atoms (ENAs) are produced when energetic magnetospheric ions undergo charge-exchange collisions with the thermal neutral atoms (hydrogen, helium, oxygen) that make up the Earth’s extended atmosphere (the geocorona). This type of interaction can take place in the “ring current”, the mid and auroral latitude energetic particle precipitation zones, and within the low altitude equatorial ion belt that is itself formed by ionization of earthward directed ENAs via collisions in the low altitude equatorial atmosphere. Since ENAs are unaffected by the Earth’s magnetic field, these energetic neutrals travel away in straight line trajectories from the points of charge exchange. The remote detection of these particles provides a powerful means through which the global distribution and properties of the geocorona and ring current can be inferred.

The first suggestion that ENAs emitted from the radiation belts and ring current could be used to remotely sense the magnetospheric energetic ion population was made by D. Hovestadt et al., ²¹⁹⁴⁾ in 1972, and the first global image of ENA emissions was produced by E. C. Roelof in 1987 from data acquired by the ISEE-1 (International Sun-Earth Explorer-1) spacecraft of NASA/ESA (launch Oct. 2, 1977). ^{2195) 2196)}

Mission	ENA Instruments
ATLAS-1 of NASA on STS-45 (launch Mar. 24, 1992)	ENAP (Energetic Neutral Atom Precipitation), of the University of Texas, Dallas
Astrid-1 of IRF-K, Kiruna, Sweden (launch Jan. 24, 1995)	PIPPI (Prelude in Planetary Particle Imaging), a neutral particle imager
POLAR of NASA, (launch Feb. 24, 1996)	CEPPAD/SEPS (Comprehensive Energetic-Particle Pitch Angle Distribution / Source Loss Cone Energetic Particle Spectrometer)
SAC-B of CONAE (launch Nov. 4, 1996), the 3rd stage failed to separate from the S/C	ISENA (Imaging Spectrometer for Energetic Neutral Atoms) of CNR/IFSI, Italy
IMAGE of NASA (launch March 25, 2000)	LENA, MENA, HENA
Mars Express (launch June 2, 2003) of ESA	ASPERA (Analyzer of Space Plasmas and Energetic Neutral Atoms), of NASA built by SwRI
USA-184 of NRO, launch June 28, 2006	TWINS-1 of NASA

2193) L. J. Zanetti, “Atmospheric, Oceanic, and Space Environment Research at APL,” Johns Hopkins APL Technical Digest, Vol. 24, No 1, 2003, pp. 31-40

2194) D. Hovestadt, B. Hausler, M. Scholer, “Observation of energetic particles at very low altitudes near the geomagnetic equator,” Physical Review Letters, Vol. 28, p. 1340, 1972.

2195) E. C. Roelof, “Energetic neutral atom image of a storm-time ring current,” Geophysical Research. Letters, Vol. 14, p. 652, 1987

2196) E. C. Roelof, D. G. Mitchell, D. J. Williams, “Energetic Neutral Atoms (E Greater than 50 keV) from the Ring Current: IMP 7/8 and ISEE 1,” Journal of Geophysical Research, Vol. 90, No 10, 1985, p.991

Mission	ENA Instruments
IBEX of NASA, SwRI, launch Oct. 19, 2008	IBEX–Lo and IBEX–Hi
USA–200 of NRO, launch March 13, 2008	TWINS–2 (Two Wide–angle Imaging Neutral–atom Spectrometers) of NASA

Table 126: Overview of some early ENA instruments flown on various missions

Mission	Instrument	Objective or Measurement
AE–C (NASA), Launch Dec. 16, 1973	VAE (Visible Airglow Experiment)	Measurement of airglow and aurora features
APEX (Active Plasma Experiment), launch Dec. 18, 1991	Suite of sensors	Study of auroral–ionospheric relationships
ARGOS (DoD), launch Feb. 23, 1999	EUVIP, HIRAAS, LORAAS, GIMI	Characterization of the aurora
Astrid–1 (IRF–K), Sweden, launch Jan. 24, 1995 Astrid–2, launch Dec. 10, 1998	MIO (Miniature Imaging Optics) PIA of MPAe	Auroral emissions Auroral imaging
ATLAS–1 (NASA) STS–45, launch March 24, 1992	AEPI (Atmospheric Emissions Photometric Imaging)	Images of natural and induced aurorae and airglow
DE–1 (Dynamic Explorer) of NASA, launch Aug. 3, 1981	EICS (Energetic Ion Mass Spectrometer), SAI (Spin–Scan Auroral Imager)	Coupling of magnetosphere/ionosphere, auroral images in UV and VIS
DMSP series of DoD	OLS (Operational Linescan System), SSULI (Special Sensor Ultraviolet Limb Imager), SSUSI (Special Sensor Ultraviolet Spectrographic Imager)	OLS auroral images (nighttime) since the mid–1970s, SSULI and SSUSI starting with F–16 in 2003
DODGE (DoD) launch July 1, 1967	Dual Vidicon Cameras	Some measurement of airglow and aurorae
EXOS–A (ISAS, Japan) launch Feb. 4, 1978 EXOS–D, launch Feb. 22, 1989	UV–TV camera, UV Glow Spectrophotometer ATV (Auroral TV)	Measurement of auroral activity, with ATV auroral imagery in UV and VIS
FREJA (Sweden), Oct. 6, 1992	F5 (Auroral UV Imager)	Study of aurorae
GEOTAIL (ISAS/NASA), launch July 24, 1992	CPI (Comprehensive Plasma Investigation)	Auroral imaging for magnetotail plasma dynamics
HILAT (DoD) or P83–1, launch Jun. 27, 1983	AIM (Auroral Ionospheric Mapper) built by APL	Imaging of the sunlit aurora
IMAGE (NASA), launch May, 25, 2000	WIC (Wideband Imaging Camera), SI (Spectrographic Imager), MENA (Medium–Energy Neutral Atom Imager), HENA, EUV	Broadband auroral imaging, different types of aurorae, etc. Imaging of ENAs, substorms, and ion populations of the cusp
INTERBALL (Russia, etc.), launch of Auroral Probe Aug. 29, 1996	UFSIPS, UVAI	Study of aurorae
Lewis (NASA) launch Aug. 23, 1997, contact to Lewis was lost on Aug. 26, 1997	LEISA	Study of nightglow aurorae
MSX (DoD), launch Apr. 24, 1996	UVISI with 4 cameras and 5 imaging spectrometers	Study of aurorae in FUV–VIS, tomographic imagery
POLAR (NASA), launch Feb. 24, 1996	UVI (UV Imager), VIS (Visible Imaging System)	Study of dayside and nightside aurorae
ROCSat–2 (NSPO), launch May 20, 2004	ISUAL (Imager of Sprite Upper Atmospheric Lightning)	Study of aurorae and airglow
SNOE (U. of Colorado) launch Feb. 26, 1998	AP (Auroral Photometer)	Study of auroral emissions
STS–39, launch Apr. 28, 1991	CIRRIS (DoD)	Study of aurorae and airglow
TIMED (NASA), launch Dec. 7, 2001	GUVI (Global UV Imager)	Horizon–to–horizon imagery in five bands with coverage of one limb (away from the sun)
Viking (Sweden), launch Feb. 22, 1986	V5 (Auroral Imaging Experiment)	Study of dynamic behavior of aurorae

Table 127: Some space science missions/instruments relating to auroral imaging

- In the spring of 2009, ESA's Cluster mission revealed, for the first time, how turbulence develops in space just outside the Earth's magnetic environment. This result improves the understanding of turbulence, a key physical process by which energy throughout the Universe is transported from large scales at which it is input, to small scales where it is dissipated. ²¹⁹⁷⁾

The solar wind, when it reaches a magnetized planet, is first decelerated from supersonic to subsonic speed by a shock wave (called the bow shock), located in front of the magnetopause. The region between the bow shock and the magnetopause is called the magnetosheath. This region is one of the most turbulent environments of near-Earth space, making it an excellent laboratory in which to study turbulence. Characterizing the properties of the magnetic turbulence in this region is of prime importance to understand its role in fundamental processes such as energy dissipation or the acceleration of particles to high-energies.

The Cluster mission showed that extreme solar activity drastically compresses the magnetosphere and modifies the composition of ions in the near-Earth environment. A new model is needed to take these flare changes into consideration and to deduct how these changes affect orbiting satellites, including the GPS system. – Under normal solar conditions, satellites orbit within the magnetosphere — the protective magnetic bubble carved out by Earth's magnetic field. But when solar activity increases, the picture changes significantly: the magnetosphere gets compressed and particles get energized, exposing satellites to higher doses of radiation that can perturb signal reception. This is why monitoring and forecasting its impact on near-Earth space is becoming increasingly critical to safeguard daily life on Earth. ²¹⁹⁸⁾

- **Extend of the solar wind in the solar system:** The NASA spacecraft, Voyager 1 (launch Sept. 5, 1977), and Voyager 2 (launch Aug. 20, 1977), continue both on their grand tour of the solar system. Both spacecraft observe also the solar wind. – In December 2010, NASA is reporting that the Voyager 1 spacecraft has reached interstellar space, a distant point at the edge of the solar system where there is **no outward motion of the solar wind**. After a 33 year voyage, the Voyager 1 spacecraft is some 17.4 billion km (17.4×10^9 km) away from the sun and has crossed into an area where the velocity of the hot ionized gas, or plasma, emanating directly outward from the sun has slowed to zero. ^{2199) 2200)}

The event is a major milestone in Voyager 1's passage through the heliosheath (start in 2004), the turbulent outer shell of the sun's sphere of influence, and the spacecraft's upcoming departure from our solar system. Voyager 1 is travelling at a speed of ~ 17 km/s and Voyager 2 at ~ 15 km/s. In the next few years, scientists expect Voyager 2 to encounter the same kind of phenomenon as Voyager 1.

– On March 7, 2011, Voyager 1 performed a spacecraft maneuver to enable the Voyager 1's LECPC (Low Energy Charged Particle) instrument to gather the sun's stream of charged particles. The project wants to find out in which direction is the sun's stream of charged particles banking when it nears the edge of the solar system. The spacecraft hadn't done such a maneuver for the last 21 years. ²²⁰¹⁾

Since the direction of the solar wind has changed and its radial speed has dropped to zero, The project had to change the orientation of Voyager 1 so the Low Energy Charged Particle

2197) "Cluster's insight into space turbulence," ESA, March 25, 2009, URL: <http://sci.esa.int/science-e/www/object/index.cfm?fobjectid=44480>

2198) Philippe Escoubet, "Watching solar activity muddle Earth's magnetic field," April 29, 2009, ESA, URL: http://www.esa.int/esaCP/SEM75BNJTF_index_0.html

2199) "NASA Probe Sees Solar Wind Decline," NASA, Dec. 13, 2010, URL: http://www.nasa.gov/mission_pages/voyager/voyager20101213.html

2200) "Voyager 1 Has Outdistanced the Solar Wind," Universe Today, Dec. 13, 2010, URL: <http://www.universetoday.com/81662/voyager-1-has-outdistanced-the-solar-wind/>

2201) "Voyager Seeks the Answer Blowin' in the Wind," NASA/JPL, March 8, 2011, URL: <http://www.jpl.nasa.gov/news/news.cfm?release=2011-069>

instrument can act like a kind of weather vane to see which way the wind is now blowing. Knowing the strength and direction of the wind is critical to understanding the shape of the solar bubble and estimating how much farther it is to the edge of interstellar space.

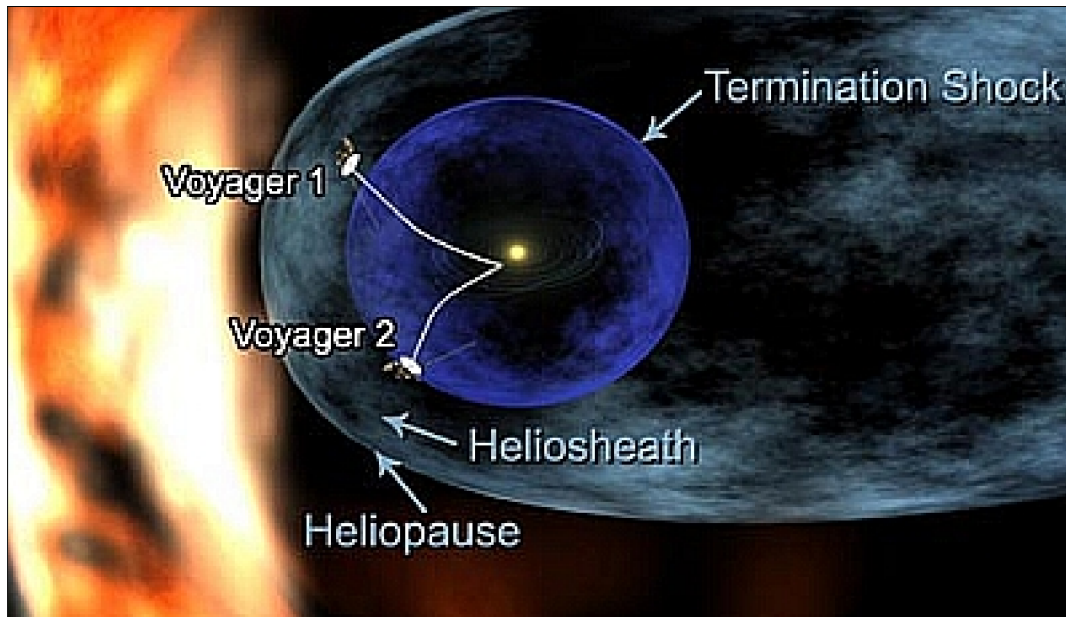


Figure 165: Artist concept of the two Voyager spacecraft as they approach interstellar space (image credit: NASA/JPL)

– Sept. 5, 2012 marked the 35th anniversary of Voyager–1 on–orbit operations. The planetary probe is now an interstellar traveler, having traveled farther from Earth than any manmade object in history (18.21 billion km from home as of Sept. 5, 2012 – or 121 times the distance from the Earth to the Sun). Light takes 33 hours and 44 minutes to travel the distance from Voyager–1 to Earth. ²²⁰²⁾

– December 2012: NASA’s Voyager 1 spacecraft has entered a new region at the far reaches of our solar system that scientists feel is the final area the spacecraft has to cross before reaching interstellar space. Scientists refer to this new region as a magnetic highway for charged particles because our sun’s magnetic field lines are connected to interstellar magnetic field lines. This connection allows lower–energy charged particles that originate from inside our heliosphere — or the bubble of charged particles the sun blows around itself — to zoom out and allows higher–energy particles from outside to stream in. Before entering this region, the charged particles bounced around in all directions, as if trapped on local roads inside the heliosphere. ²²⁰³⁾

The Voyager team infers, this region is still inside our solar bubble because the direction of the magnetic field lines has not changed. The direction of these magnetic field lines is predicted to change when Voyager breaks through to interstellar space.

– June 27, 2013: ²²⁰⁴⁾Data from Voyager–1 suggest the spacecraft is closer to becoming the first human–made object to reach interstellar space. Scientists do not know exactly how far Voyager–1 has to go to reach interstellar space. They estimate it could take several more months, or even years, to get there. The heliosphere is dominated by the sun’s magnetic field and an ionized wind expanding outward from the sun. Outside the heliosphere, interstellar space is filled with matter from other stars and the magnetic field present in the nearby region of the Milky Way.

²²⁰²⁾ “A Voyager Far From Home,” NASA, Sept. 5, 2012, URL: <http://earthobservatory.nasa.gov/IOTD/view.php?id=79091>

²²⁰³⁾ “NASA Voyager 1 Encounters New Region in Deep Space,” NASA/JPL, Dec. 03, 2012, URL: <http://www.jpl.nasa.gov/news/news.php?release=2012-381#5>

²²⁰⁴⁾ Jia–Rui C. Cook, Steve Cole, “NASA’s Voyager 1 explores final frontier of our ‘solar bubble’, NASA, June 27, 2013, URL: http://voyager.jpl.nasa.gov/news/voyager_final_frontier.html

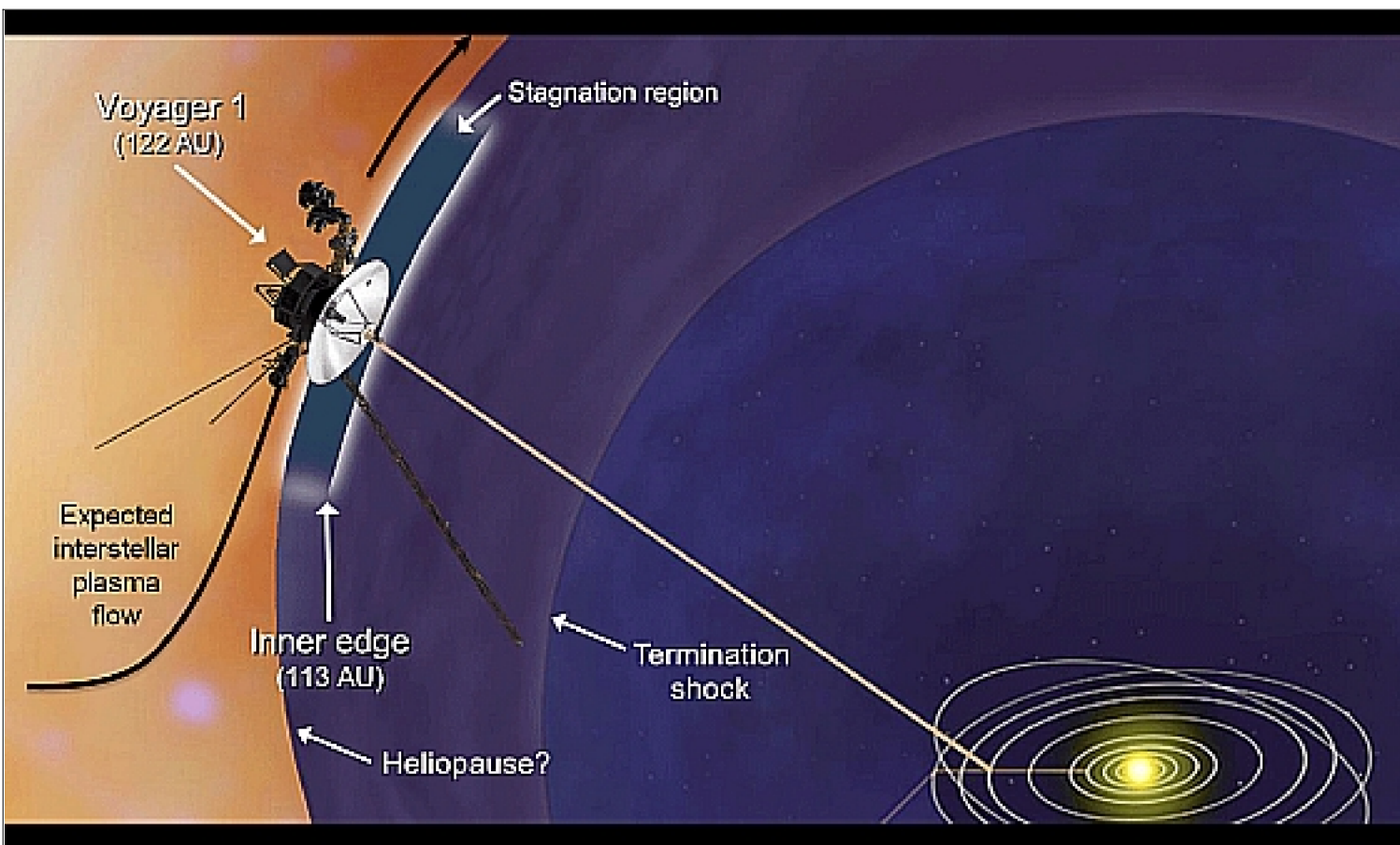


Figure 166: This artist's concept shows plasma flows around NASA's Voyager 1 spacecraft as it approaches interstellar space (image credit: NASA/JPL)

– Sept. 12, 2013: NASA's **Voyager-1 spacecraft officially is the first human-made object to venture into interstellar space.** The 36-year-old probe is about 19 billion km from our sun. New and unexpected data indicate Voyager-1 has been traveling for about one year through plasma, or ionized gas, present in the space between stars. Voyager is in a transitional region immediately outside the solar bubble, where some effects from our sun are still evident. ^{2205) 2206)}

Voyager-1 does not have a working plasma sensor, so scientists needed a different way to measure the spacecraft's plasma environment to make a definitive determination of its location. A coronal mass ejection, or a massive burst of solar wind and magnetic fields, that erupted from the sun in March 2012 provided scientists the data they needed. When this unexpected gift from the sun eventually arrived at Voyager-1's location 13 months later, in April 2013, the plasma around the spacecraft began to vibrate like a violin string. On April 9, Voyager-1's plasma wave instrument detected the movement. The pitch of the oscillations helped scientists determine the density of the plasma. The particular oscillations meant the spacecraft was bathed in plasma more than 40 times denser than what they had encountered in the outer layer of the heliosphere. Density of this sort is to be expected in interstellar space.

The plasma wave science team reviewed its data and found an earlier, fainter set of oscillations in October and November 2012. Through extrapolation of measured plasma densities

2205) Dwayne Brown, Jia-Rui C. Cook, "NASA Spacecraft Embarks on Historic Journey into Interstellar Space," NASA, Release 13-280, URL: <http://www.nasa.gov/press/2013/september/nasa-spacecraft-embarks-on-historic-journey-into-interstellar-space/#.UjK-N3-JrWI>

2206) Tony Phillips, "Voyager 1 has left the Solar System," NASA Science News, Sept. 12, 2013, URL: http://science.nasa.gov/science-news/science-at-nasa/2013/12sep_voyager1/

from both events, the team determined Voyager – 1 first entered interstellar space in August 2012.

- **Solar wind interaction with the interstellar medium.** IBEX (Interstellar Boundary Explorer) is a NASA technology demonstration mission which was launched on Oct. 19, 2008.

- In June 2009, the IBEX team reported that the IBEX–Hi instrument has made the first observations of very fast hydrogen atoms coming from the moon, following decades of speculation and searching for their existence. ²²⁰⁷⁾ The IBEX team estimates that only about 10% of the solar wind ions reflect off the sunward side of the moon as neutral atoms, while the remaining 90% are embedded in the lunar surface. The characteristics of the lunar surface, such as dust, craters and rocks, play a role in determining the percentage of particles that become embedded and the percentage of neutral particles, as well as their direction of travel, that scatter.

- In January 2010, the IBEX researchers presented an explanation of the giant ribbon. The ribbon is a reflection – – it is where solar wind particles heading out into interstellar space are reflected back into the solar system by a galactic magnetic field. ²²⁰⁸⁾ ²²⁰⁹⁾

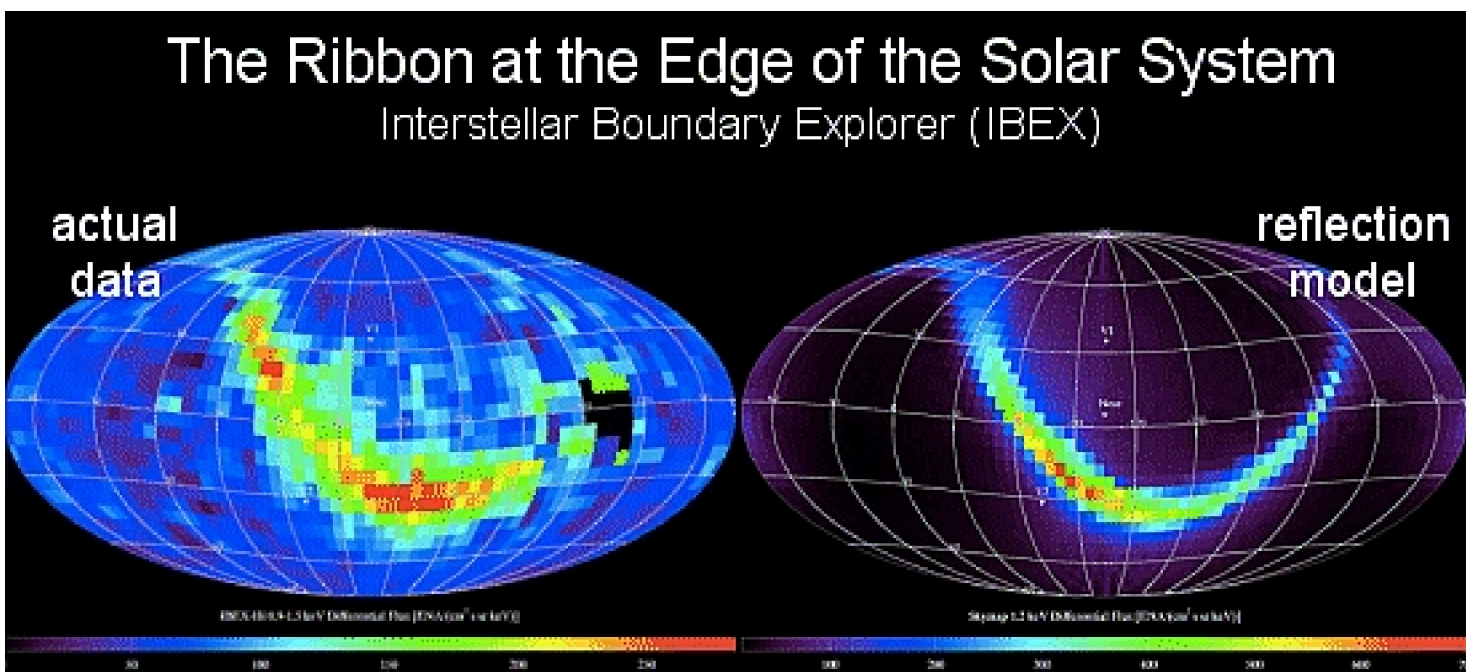


Figure 167: A comparison of the IBEX ENA observations (left) with a 3D magnetic reflection model (image credit: NASA)

- The IBEX Ribbon of energy is of course a major discovery of the mission requiring scientific interpretation. This was done by the IBEX science team in a publication of the *Astrophysical Journal* in April 2011.

The finding, which overturns 40 years of theory, provides insight into the fundamental structure of the heliosphere, which in turn helps scientists understand similar structures or “astrospheres” that surround other star systems throughout the cosmos. Isolating and separating the ribbon from the IBEX maps was like pulling the drapes from our window to discover

²²⁰⁷⁾ “IBEX spacecraft detects fast neutral hydrogen coming from the moon, gives insight to particle “recycling” processes in space,” June 18, 2009, URL: <http://www.swri.org/9what/releases/2009/IBEX-Hi.htm>

²²⁰⁸⁾ Tony Phillips, “Giant Ribbon at the Edge of the Solar System: Mystery Solved?,” NASA, Jan. 15, 2010, URL: http://science.nasa.gov/headlines/y2010/15jan_ibex2.htm?list1291671

²²⁰⁹⁾ J. Heerikhuisen, N.V. Pogorelov, G.P. Zank, G.B. Crew, P.C. Frisch, H.O. Funsten, P.H. Janzen, D.J. McComas, D.B. Reisenfeld, N.A. Schwadron, “Pick–Up Ions in the Outer Heliosheath: A Possible Mechanism for the Interstellar Boundary EXplorer Ribbon,” *Astrophysical Journal*, Vol. 708, Jan. 10, 2010, L126–L130 doi: 10.1088/2041–8205/708/2/L126

the landscape at the edge of the solar system. The IBEX maps are very rich scientifically and are critical in helping scientists understand how our space environment is controlled by the galactic medium. They provide the first images of our solar system's boundaries, which control the access to potentially harmful galactic cosmic rays as well as all other matter from deep space. — The most energetic galactic cosmic rays penetrate even the powerful magnetic fields closest to Earth and eventually collide and interact with Earth's atmosphere. The direct or indirect effects of these cosmic rays on the Earth system, including our biosphere, remain poorly understood and are often highly controversial. ²²¹⁰⁾

Prior to IBEX, most scientists believed that the global boundaries of our solar system were controlled mainly by the motion of our solar system through the galaxy and the solar wind, an extremely fast flow of electrically charged matter that flows out from the Sun. The IBEX maps reveal the galactic magnetic field is also a critical part of the Sun's interaction with the galaxy. ²²¹¹⁾

-
- 2210) N. A. Schwadron, F. Allegrini, M. Bzowski, E. R. Christian, G. B. Crew, M. Dayeh, R. DeMajistre, P. Frisch, H. O. Funsten, S. A. Fuselier, K. Goodrich, M. Gruntman, P. Janzen, H. Kucharek, G. Livadiotis, D. J. McComas, E. Moebius, C. Prested, D. Reisenfeld, M. Reno, E. Roelof, J. Siegel, R. Vanderspek, "Separation of the Interstellar Boundary Explorer Ribbon from Globally Distributed Energetic Neutral Atom Flux," *The Astrophysical Journal*, Vol. 731, No 1, April 12, 2011, doi: 10.1088/0004-637X/731/1/56, Online version of the article is at: URL: <http://iopscience.iop.org/0004-637X/731/1/56>
- 2211) "IBEX Scientists Isolate Mysterious "Ribbon" of Energy and Particles that Wraps Around Solar System Boundary," University of New Hampshire, March 30, 2011, URL: http://www.unh.edu/news/cj_nr/2011/mar/ds30ribbon.cfm

1.22.4 Earth's Magnetosphere

The Earth is a huge magnet, and its magnetic influence extends far into space. Magnetic fields play an important role in many of the physical processes throughout the Universe. The Earth in particular has a large and complicated magnetic field, the major part of which is produced by a self-sustaining dynamo, operating in the fluid outer-core. It turns out that measurements, taken at or near the surface of the Earth, are the superposition of magnetic fields originating from the outer core as well as the fields caused by magnetized rocks in the Earth's crust, electric currents flowing in the ionosphere, magnetosphere and oceans, and by currents induced in the Earth by time-varying external fields. **On Earth, the magnetosphere acts as an invisible shield, we're protected by our planet's magnetic field from harmful radiation** (cosmic rays, solar wind), but out in space, it gets a lot more dangerous. ²²¹²⁾

A particular dangerous region is Earth's Van Allen radiation belt, a torus of energetic charged particles (plasma) around Earth, which is held in place by Earth's magnetic field. The inner belt, the one discovered by Van Allen's Geiger counter, occupies a compact region above the equator. It is a region of high-energy charged particles result from cosmic rays. The outer radiation belt is seen as part of the plasma trapped in the magnetosphere. The name "radiation belt" is usually applied to the more energetic part of that plasma population, e.g. ions of about 1 MeV of energy. The more numerous lower-energy particles are known as the "ring current", since they carry the current responsible for magnetic storms.

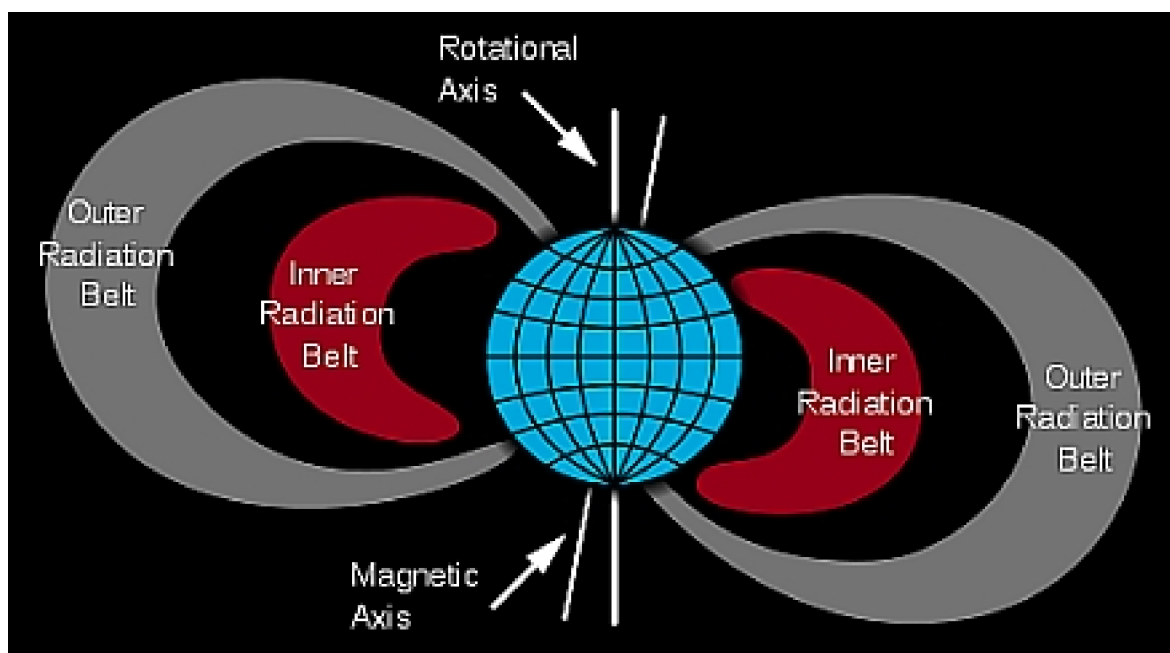


Figure 168: Schematic view of the Van Allen radiation belts (image credit: NASA)

The magnetosphere is the region of space to which the Earth's magnetic field is confined by the solar wind plasma blowing outward from the sun, extending to distances in excess of 60,000 km from Earth in the so-called magnetotail.

Close to Earth, the magnetic field is roughly a magnetic dipole that is tilted 11.5° from Earth's rotational axis and offset from the center of the planet. For most purposes, the dipole approximation is poor, and there are more sophisticated models that account for the steady changes of the central field as well as the dynamic outer boundaries.

The Earth's magnetosphere is formed from two essential ingredients. The first is the Earth's magnetic field (or geomagnetic field), generated by currents flowing in the Earth's core.

²²¹²⁾ D. P. Stern, "The Exploration of the Earth's Magnetosphere," <http://www-istp.gsfc.nasa.gov/Education/Intro.html>

More than 90% of the geomagnetic field is generated in Earth's outer core.²²¹³⁾ ²²¹⁴⁾ ²²¹⁵⁾ Outside the Earth this field has the same form as that of a bar magnet, a dipole field, aligned approximately with the Earth's spin axis. The second ingredient of the geomagnetic field is the solar wind, a fully ionized hydrogen/helium plasma that streams continuously outward from the sun into the solar system at speeds of about 300–800 km/s [the average speed is 1.5 million km/h – with a distance of 150 million km away from Earth this translates to about 100 hours of travel time]. There is a third ingredient that also plays an important role: the Earth's ionosphere. The upper atmosphere is partially ionized by far-ultraviolet (FUV) and X rays from the sun above altitudes of about 100 km. The resulting ionosphere forms a second source of plasma for the magnetosphere, mainly of protons, singly charged helium and oxygen, and the requisite number of electrons for electric charge neutrality.

Chapman–Ferraro magnetosphere. The basic nature of the interaction between the solar wind and the Earth's magnetic field, leading to the concept of the Earth's magnetosphere, was first deduced by Sydney Chapman (English scientist, 1888–1970) and his student Vincenzo C. A. Ferraro in the early 1930s. It is based on two theoretical principles. The first concerns the way in which plasmas and magnetic fields interact; they behave, approximately, as if they are "frozen" together. As a result of this freezing together, magnetic fields are transported by flowing plasmas; the field lines are bent and twisted as the flow bends and twists. An important example is the interplanetary magnetic field. It is wound into a large spiral structure by the sun's rotation, and near the Earth it has a strength of about 5 nanotesla (nT). This is a rather weak field, about one ten thousandth of the field at the Earth's surface, but nevertheless, it plays a crucial role in the Earth's interaction with the solar wind. The second principle concerns the force that the magnetic field exerts on the plasma, which usually opposes the bending and twisting of the field, or its compression, in the frozen–in flow.

Between Earth's magnetosphere and the upper atmosphere at high latitudes, there is a continuous flow and exchange of energy and momentum, carried by energetic particles, currents, and waves, towards and away from Earth, guided by Earth's magnetic field. As part of this process, intense quasistatic electric fields and associated potential drops aligned with Earth's magnetic field are formed, governed by the requirements of charge neutrality and current continuity in the space plasma. The term quasistatic is used to describe that the structures are stable on a time scale long compared to the time needed for a charged particle to pass the structure. The region where such parallel electric fields are formed is known as the AAR (Auroral Acceleration Region), typically located between 4000 and 12 000 km above the polar atmosphere.²²¹⁶⁾

Aurora and the associated acceleration processes are ubiquitous space plasma processes, occurring throughout the solar system, such as around Jupiter and Saturn. The suggestion that electric fields, aligned with Earth's magnetic field lines, accelerate particles producing aurora was first made by Hannes Alfvén. Since then it has been well confirmed experimentally by satellite and rocket measurements. The parallel electric fields occur together with converging or diverging electric fields perpendicular to the magnetic field, in U-shaped potential structures, or together with monopolar (one-directional) electric fields in S-shaped potential structures.

2213) Note: The name "magnetosphere" was first proposed in 1959 by Thomas Gold of Cornell University (Ithaca, NY), defining the magnetic environment around Earth. Eventually, the meaning of "magnetosphere" encompassed all phenomena affected by the interaction of Earth's magnetic field with the solar wind and the cosmic plasma flux.

2214) http://www.agu.org/sci_soc/cowley.html

2215) R. B. Langley, "Getting Your Bearings: The Magnetic Compass and GPS," *GPS World*, Sept. 2003, pp. 70–81

2216) Göran T. Marklund, Soheil Sadeghi, Tomas Karlsson, Per–Arne Lindqvist, Hans Nilsson, Colin Forsyth, Andrew Fazakerley, Elizabeth A. Lucek, Jolene Pickett, "Altitude Distribution of the Auroral Acceleration Potential Determined from Cluster Satellite Data at Different Heights," *Physical Review Letters*, Vol. 106, 055002, Feb. 4, 2011

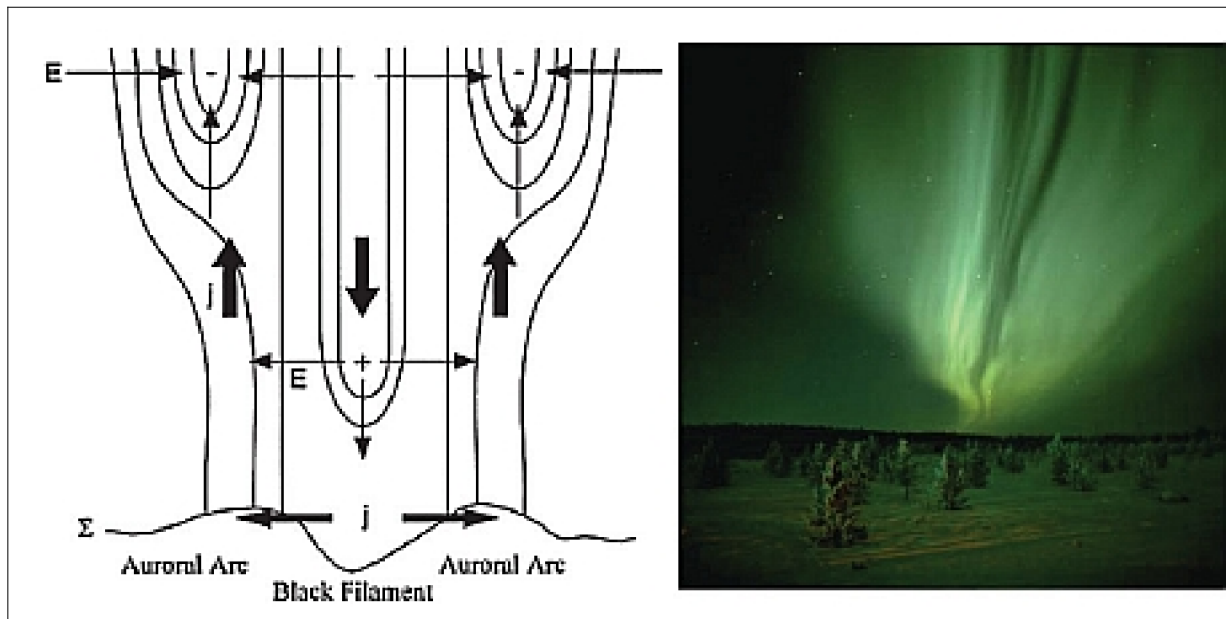


Figure 169: Schematic of the electric field and current system (left) representative of 2 parallel arcs (right) in upward current regions, separated by dark bands in regions of downward current (image credit: KTH)

Legend to Figure 169: The arcs are produced by high-energy electrons colliding with the upper atmosphere, after being accelerated by an upward directed parallel electric field at altitudes around one Earth radius. Above the dark areas, a downward directed electric field accelerates electrons away from Earth, corresponding to a downward current.

Although the aurora phenomena were studied by many past satellite missions, the Cluster mission of ESA is the first to explore the auroral acceleration region with multiprobes. The Cluster orbits were lowered in late 2008, enabling frequent crossings of the AAR (Ref. 2216).

One of the most important processes for transferring energy and momentum from the solar environment to Earth's magnetosphere is the concept of **magnetic reconnection**.²²¹⁷⁾ The Earth's magnetosphere is actually controlled by reconnection; it is electromagnetically coupled to the solar wind and reconnects in the tail (multiscale coupling phenomenon). This process changes magnetic energy into particle (plasma) energy; it changes the topology of magnetic fields by breaking magnetic lines of force and reconnecting them in a different way. Reconnection plays a role in three distinct regions in Earth's magnetosphere: on the dayside magnetopause at low latitudes, near the polar cusp, and in the magnetotail.

Background: The complex phenomenon/process of magnetic reconnection has its origins in the 1940s. R. G. Giovanelli proposed a theory of solar flares according to which electrons accelerated by induction electric fields near magnetic neutral points excite the optical emissions of chromospheric atoms.^{2218) 2219) 2220)} He suggested that magnetic X-type null points can serve as locations for plasma heating and acceleration in solar flares and magnetic substorms. In 1961, James W. Dungey (Cambridge University, UK) was instrumental in proposing the idea of an open reconnecting model and mechanism for transmitting solar wind energy to the magnetosphere by direct magnetic linkage between the two. Dungey proposed that an X-type neutral point (or line) at the front of the magnetosphere enabled

2217) C. T. Russell, R. L. McPherron, "The magnetotail and substorms, *Space Science Reviews*, Vol. 15, 1973, p. 205

2218) R. G. Giovanelli, "A Theory of chromospheric flares," *Nature*, Vol. 158, 1946, p. 81

2219) J. W. Dungey, "Interplanetary magnetic field and the auroral zones," *Physical Review Letters*, Vol. 93, 1961., pp. 47–48

2220) J. W. Dungey, "Conditions for the occurrence of electrical discharges in astrophysical systems," *Philosophical Magazine*, Vol. 44, 1953, pp. 725–738

terrestrial field lines to link up with interplanetary ones and produce “open” field lines, with one end on earth and the other in distant space. ²²²¹⁾

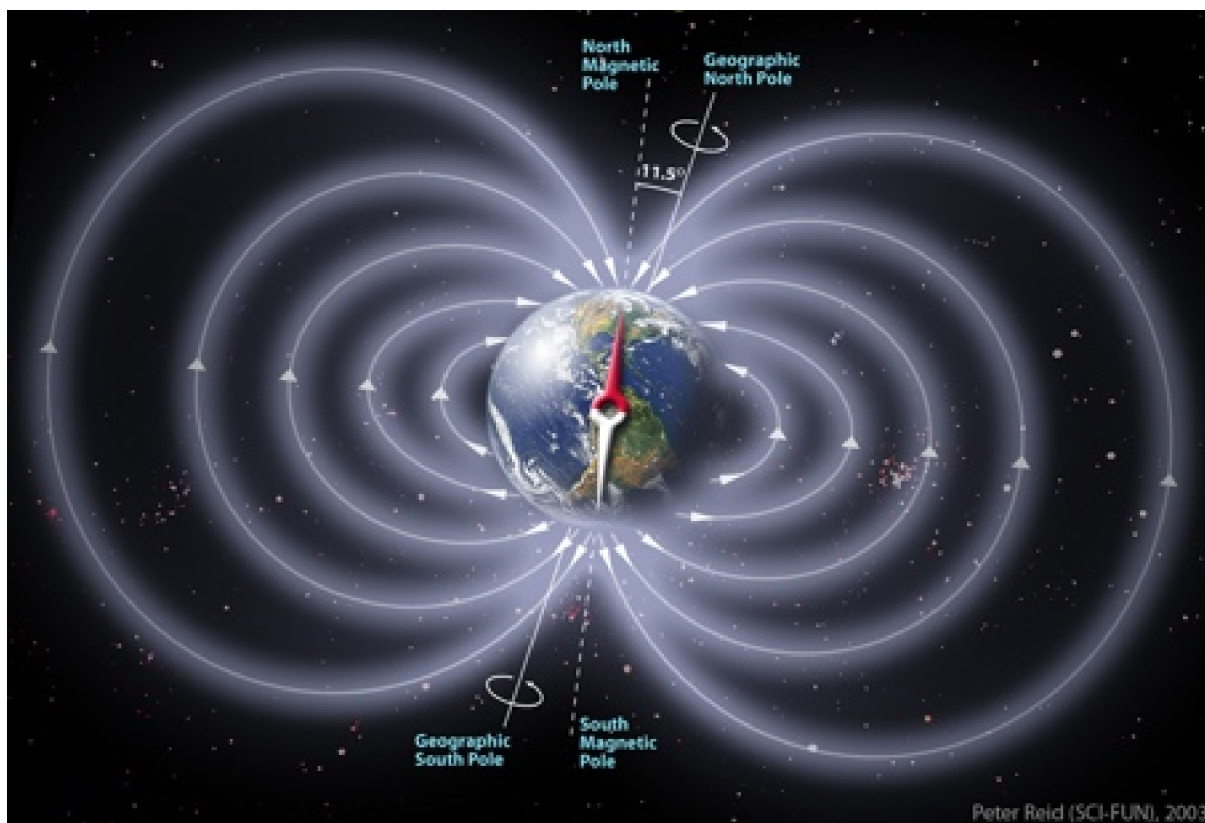


Figure 170: The Earth's magnetic field (image credit: P. Reid)

The search for reconnection continues at the start of the 21st century, the overall model of the geomagnetosphere is known, but the specific understanding of the reconnection process and its complex features (of how the magnetosphere interacts with the solar environment, substorms in the magnetosphere, coronal mass ejections) require continued research into the Earth–space environment.

Note: In June 2007, ESA is reporting that scientists have **obtained for the first time ever a 3–D picture of magnetic reconnection events with data of the Cluster mission** analyzing an event in Oct. 2001 when the four Cluster spacecraft were flying in formation at approximately 110 000 km from Earth in the magnetotail. The satellites meandered around a reconnection region over a period of nearly 15 minutes. During reconnection, the geometry of the magnetic field forms an X–shape, also called a ‘magnetic null’. Analyzed in 2–D, the magnetic field, plasma density and flow velocity data collected during this event showed that only one reconnection region with an X–shape, or a magnetic null, was seen by the satellites. – By analyzing a subset of the same data in 3–D with a higher temporal resolution, the scientists found what they were looking for. Two magnetic reconnection sites jumped out, along with the null–null line which connects two magnetic nulls, a previously unobserved phenomenon. ²²²²⁾

The magnetosphere has a complicated internal structure, consisting of the Van Allen belts, the plasma sheet, and the magnetotail. Chapman and Ferraro predicted the outer boundary of the Earth's magnetosphere being compressed on the sunward side by solar radiation, and they predicted also that there would be radiation belts (the Van Allen belts were discovered with Explorer–1, launch Jan. 31, 1958).

2221) http://www-istp.gsfc.nasa.gov/Education/bh2_5.html

2222) “Pioneering 3D view of near–Earth magnetic ‘dance’,” June 29, 2007, URL: http://www.esa.int/esaSC/SEM_UOH9OY2F_index_0.html

The geomagnetic main field can be modeled mathematically. Two such models are:

- IGRF (International Geomagnetic Reference Field). IGRF models the field and its secular variation using a set of harmonic coefficients in a truncated series expansion of a geomagnetic potential function and its time derivative. The magnetic field is the gradient of this potential. The current model is known as IGRF2000. Updates occur generally every 5 years.
- WMM (World Magnetic Model). The WMM model, produced by the British Geological Survey and by USGS (United States Geological Survey), is similar to that of IGRF.

Satellites observing magnetic forces in space have found that lines from most points on Earth are confined inside a fairly well-defined cavity, the magnetosphere of the Earth. The space outside it is dominated by the sun, and by the fast “solar wind” of free ions and electrons emitted by the sun. The solar wind pushes back the Earth’s field somewhat, but ultimately is forced to detour, leaving the Earth’s lines enclosed in a bullet shaped cavity, which on the night side continues as a long cylinder, like the tail of a comet. The boundary surface between interplanetary field lines and those of the Earth is called the magnetopause.

The offset of Earth’s magnetic dipole from the geometric center of the planet causes a weaker field region over the South Atlantic Ocean and an opposing region of stronger field over northern Asia. As the trapped inner-zone particles execute their bounce motion along field lines, they can reach lower altitudes at a region known as the “South Atlantic Anomaly”. All spacecraft in low Earth orbit penetrate the inner zone in the South Atlantic Anomaly even if their altitude is below the belt at other positions in the orbit.

While relative stability is one key property of the inner zone, variability is the outstanding characteristic of the outer radiation belt. The solar wind and interplanetary magnetic field affect this weaker field region of the magnetosphere more than the inner zone, leading to shorter lifetimes of trapped particles and more dynamics. Details of how the magnetosphere accelerates electrons to millions of electron volts in a few seconds have been recently glimpsed; however, the mechanism that accelerates the electrons more routinely in geomagnetic storms has not been established even after 40 years of research. Observations over many years with well understood space environment instruments will be needed before researchers can understand the outer zone’s variability and its extreme behavior. ²²²³⁾

The magnetic field is also of importance for the Earth’s external environment. While it is known that the air density in the thermosphere is related to geomagnetic activity, recent results from the German CHAMP mission have indicated that air density is locally affected by geomagnetic activity in a specific way that is still to be explored and understood.

Background: Most early spaceage magnetosphere discoveries are reported in chapters 1.22.3 (Solar Wind Observations) and O.17. Newer missions in this context are:

- The Ørsted microsatellite mission of Denmark was launched Feb. 23, 1999, providing highly accurate and sensitive measurements of the geomagnetic field. The Ørsted observations opened a decade of geopotential field research by an international team (the first satellite to measure the three components of the Earth’s magnetic field since MagSat). The Ørsted data are a major source to update the IGRF (International Geomagnetic Reference Field) model. For instance, the IGRF2000 field model was based entirely on Oersted data. The Ørsted mission is operational as of 2010.
- IMAGE (Imager for Magnetopause-to-Aurora Global Exploration) of NASA (launch March 25, 2000). IMAGE is the first satellite mission dedicated to imaging the Earth’s magnetosphere (investigating the response of the magnetosphere with the solar wind).

²²²³⁾ J. E. Mazur, “An Overview of the Space Radiation Environment,” Crosslink, Vol. 4, No 2, 2003, <http://www.aero.org/publications/crosslink/summer2003/02.html>

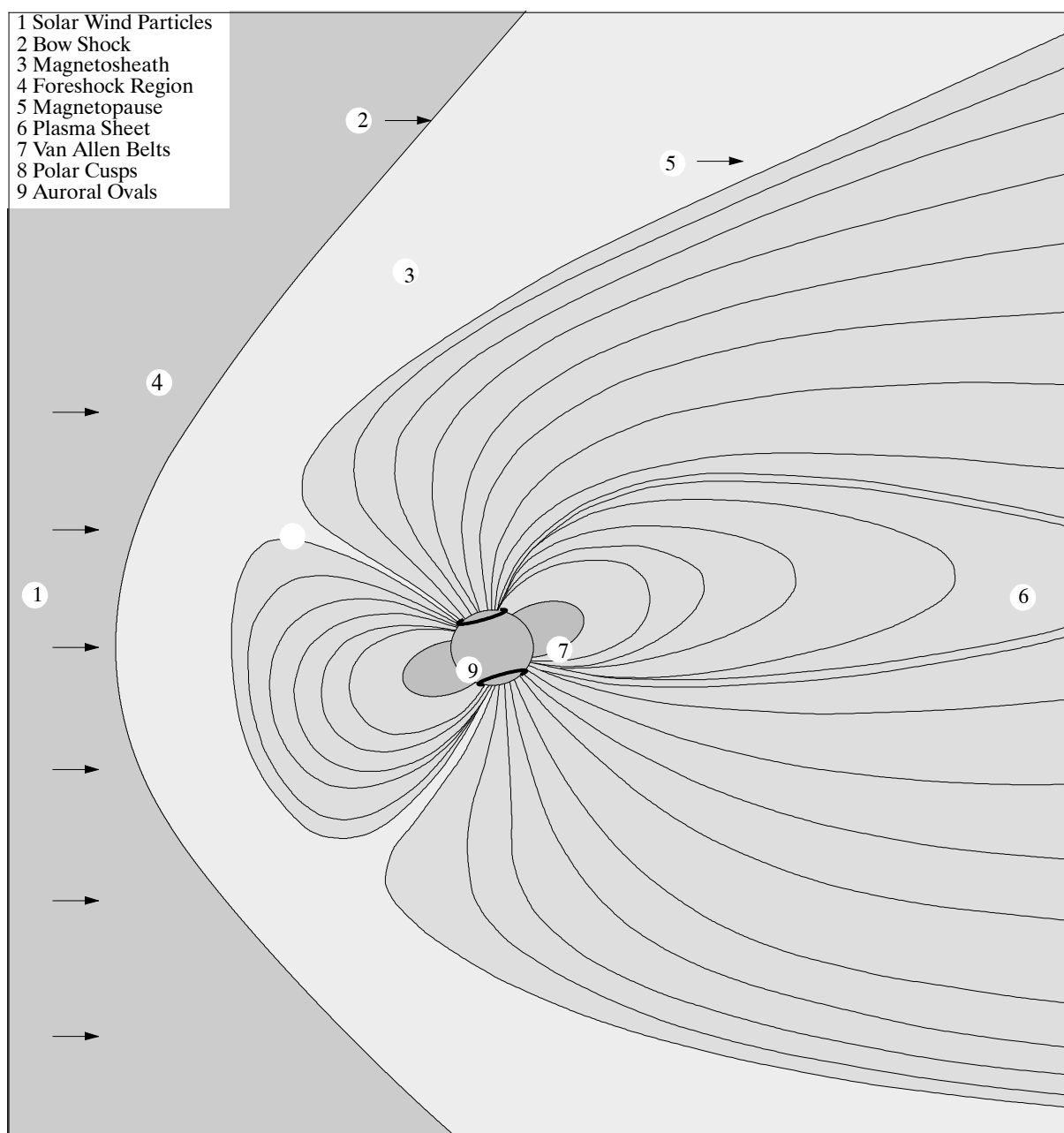


Figure 171: Characteristic model of the Earth's magnetosphere

- DSP (Double Star Project), a cooperative mission of CNSA (Chinese National Space Administration) of Beijing and ESA (launch of DSP-1 Dec. 29, 2003, launch of DSP-2, July 25, 2004). The overall objective is to explore the Earth's magnetosphere. The two spacecraft are called TC-1 and TC-2, where TC stands for 'Tan Ce' which means 'Explorer'. The DSP payload includes 8 ESA instruments (identical to those on the Cluster mission) and some Chinese instruments.
- THEMIS (Time History of Events and Macroscale Interactions during Substorms) is a five microsatellite constellation of NASA (launch Feb 17, 2007, launch mass of 126 kg / S/C). The objective is to provide answers to critical questions about the magnetosphere (tail region) and related space weather to determine the causes of the global reconfigurations of the Earth's magnetosphere that are evidenced in auroral activity. Auroral eruptions are a manifestation of the magnetospheric substorms. THEMIS is considered a complementary program to NASA's MMS mission.

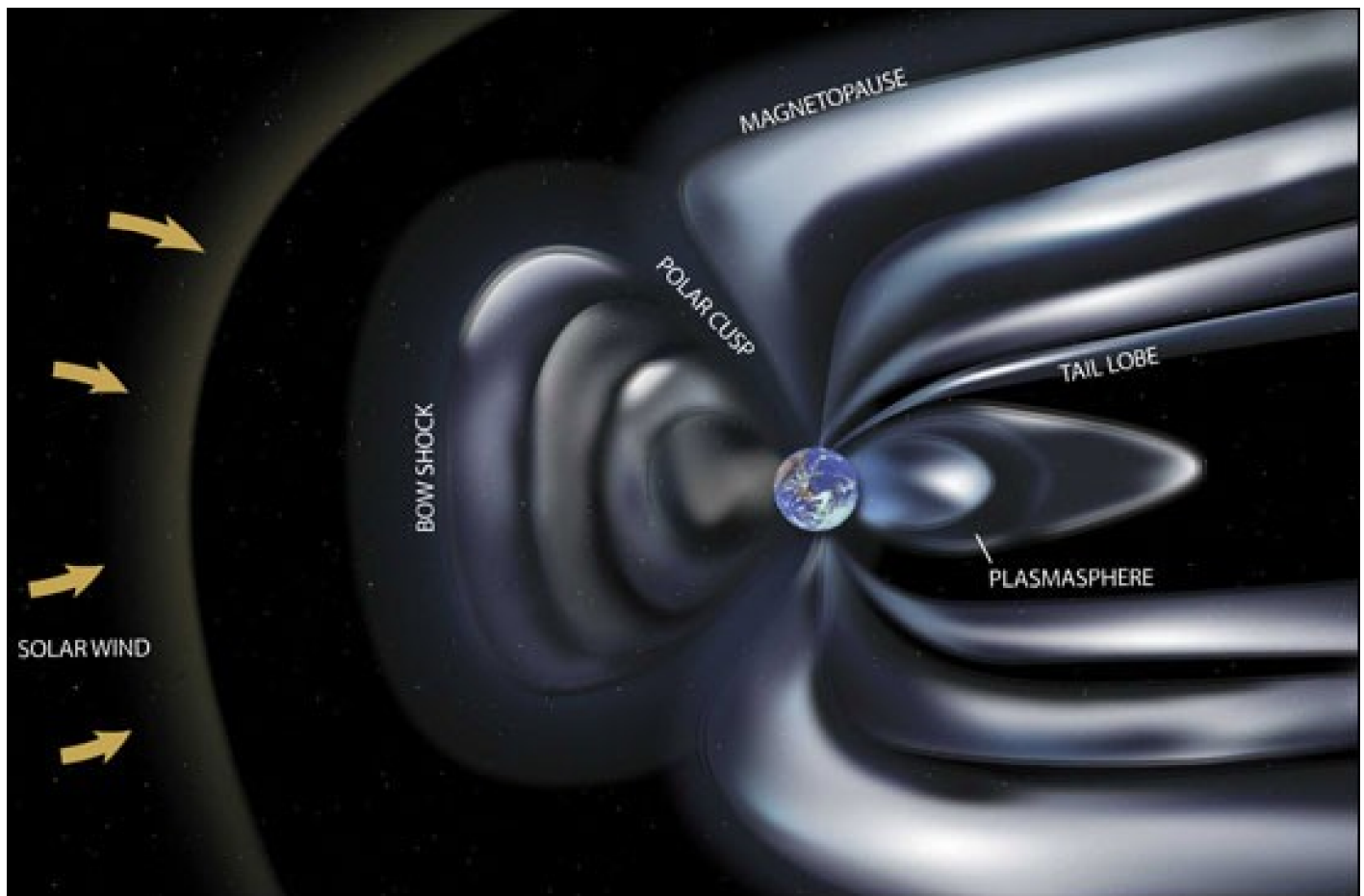


Figure 172: Artist's rendition of Earth's magnetosphere (image credit: NASA)

In the timeframe 2008/9, the THEMIS mission was able to answer longstanding fundamental questions concerning the nature of the substorm instabilities that abruptly and explosively release solar wind energy stored within the Earth's magnetotail. – A network of ASIs (All-Sky Cameras) deployed around the Alaskan/Canadian Arctic region in support of NASA's THEMIS mission has made a startling discovery about the Northern Lights. **Sometimes, vast curtains of aurora borealis collide, producing spectacular outbursts of light.** The 20 ASIs photographed auroras from below while the spacecraft sampled charged particles and electromagnetic fields from above. Together, the on-ground cameras and spacecraft could see the action from both sides and were able to piece together cause and effect. In 2009, Toshi Nishimura of UCLA assembled continent-wide movies from the observations of the individual ASI cameras. ^{2224) 2225) 2226)}

- Swarm, a geomagnetic LEO constellation of ESA (launch of 3 minisatellites Nov. 22, 2013). The overall objective is to provide the best ever survey (multi-point observations) of the geomagnetic field and its temporal evolution, to gain new insights into the Earth system by improving our understanding of the Earth's interior and climate. – As it turns out, accurate measurements of the geomagnetic field are one of the very few ways by which the Earth's interior properties, especially concerning dynamic processes in the core and the mantle, can be deduced. In addition, the geomagnetic field and its interaction with the solar wind plays an important role in forming the external environment of the Earth in a way that also affects space weather and atmospheric processes related to climate and weather.

²²²⁴⁾ Michael Carlowicz, "Colliding auroras produce an explosion of light," NASA, Dec. 17, 2009, URL: http://www.eurekalert.org/pub_releases/2009-12/nsfc-cap121709.php

²²²⁵⁾ "Colliding Auroras Create Explosions," Universe Today, Dec. 17, 2009, URL: <http://www.universetoday.com/2009/12/17/colliding-auroras-create-explosions/>

²²²⁶⁾ "Colliding Auroras Produce Explosions Of Light," Space Daily, Dec. 18, 2009, URL: http://www.spacedaily.com/reports/Colliding_Auroras_Produce_Explosions_Of_Light_999.html

- MMS (Magnetospheric MultiScale) mission of NASA (planned launch in 2013). The objective is the study of magnetic reconnection, charged particle acceleration, and turbulence in regions of the Earth's magnetosphere.
- The Cluster mission of ESA – a constellation of 4 spacecraft along with the two Chinese/ESA DSP (Double Star Satellites) – observed two large CME events on January 21, 2005 and on December 13, 2006. Fortunately, the spacecraft were favorably positioned to observe the events at a large scale. The satellites carried out coordinated measurements of the response of the magnetosphere to these events. ^{2227) 2228)}

During both events, the velocity of positively charged particles in the solar wind was found to be higher than 900 km/s, more than twice their normal speed. In addition, the density of charged particles around Earth was recorded as five times higher than normal. The measurements taken in January 2005 also showed a drastic change in ion composition.

These factors together **caused the magnetosphere to be compressed**. Data show that the 'nose' of the dayside magnetopause (the outer boundary of the magnetosphere), usually located about 60,000 km from Earth, was only 25,000 km away.

The second explosion in December 2006 released extremely powerful high-energy X-rays followed by a huge amount of mass from the solar atmosphere (called a coronal mass ejection). During the event, GPS signal reception on ground was lost.

- **Earth's magnetic field provides vital protection:** A chance alignment of planets during a passing gust of the solar wind has allowed scientists to compare the protective effects of Earth's magnetic field with that of Mars' naked atmosphere. The result is clear: Earth's magnetic field is vital for keeping our atmosphere in place. ²²²⁹⁾

The alignment took place on January 6, 2008. Using ESA's Cluster and Mars Express missions to provide data from Earth and Mars, respectively, scientists compared the loss of oxygen from the two planets' atmospheres as the same stream of solar wind hit them. This allowed a direct evaluation of the effectiveness of Earth's magnetic field in protecting our atmosphere.

They found that while the pressure of the solar wind increased at each planet by similar amounts, the increase in the rate of loss of martian oxygen was ten times that of Earth's increase. Such a difference would have a dramatic impact over billions of years, leading to large losses of the martian atmosphere, perhaps explaining or at least contributing to its current tenuous state. – The result proves the efficacy of Earth's magnetic field in deflecting the solar wind and protecting our atmosphere.

- **Cluster observes a 'porous' magnetopause:** A new study (2012), based on data from ESA's Cluster mission, shows that it is easier for the solar wind to penetrate Earth's magnetosphere than had previously been thought. ^{2230) 2231)}

Previous discoveries derived from Cluster measurements have shown that the magnetopause is weakened by the KHWs (Kelvin–Helmholtz Waves). These are huge swirls of plasma, up to 40,000 km across, which develop along the outer edge of the magnetosphere. Kelvin–Helmholtz instabilities can occur when two adjacent flows are travelling with different speeds, so one is slipping past the other. The same phenomenon also occurs in the atmosphere when two air layers lying close to each other move at different speed.

2227) http://www.esa.int/esaSC/SEMF75BNJTF_index_0.html

2228) I. S. Dandouras, H. Rème, J. Cao, P. Escoubet, "Magnetosphere response to the 2005 and 2006 extreme solar events as observed by the Cluster and Double Star spacecraft," *Advances in Space Research*. Vol.43, 2009, pp. 618–623.

2229) "Earth's magnetic field provides vital protection," ESA, March 8, 2012, URL: http://www.esa.int/esaSC/SEMXXW7YBZG_index_0.html

2230) "Cluster observes a 'porous' magnetopause," ESA, Oct. 24, 2012, URL: <http://sci.esa.int/science-e/www/object/index.cfm?fobjectid=50977>

2231) Kyoung-Joo Hwang, Melvyn L. Goldstein, Maria M. Kuznetsova, Yongli Wang, Adolfo F. Viñas, David Gary Sibeck, "The first in-situ observation of Kelvin–Helmholtz waves at high latitude magnetopause during strongly dawnward interplanetary magnetic field conditions," *Journal of Geophysical Research*, Vol. 117, A08233, 2012, doi:10.1029/2011JA017256

One consequence of the presence of KHWs is that they result in a sudden, dramatic reconfiguration of the magnetic field lines – known as magnetic reconnection. This process of breaking and reconnecting field lines enables charged particles from the solar wind to enter the magnetosphere.

One key factor in the magnetosphere/solar wind interaction is the magnetic alignment of the IMFs (Interplanetary Magnetic Fields). It is generally thought that the most important process by which the solar wind enters Earth's magnetosphere is reconnection on Earth's dayside. This is most efficient when the IMF is aligned southward – the opposite to the northward alignment of Earth's magnetic field. The temporary tangling of the field lines creates ideal conditions for magnetic reconnection, allowing large amounts of plasma and magnetic energy to be transferred from the solar wind to the magnetosphere.

Magnetic reconnection also occurs with a northward orientation of the IMF, but it is more localized to higher latitudes. Spacecraft observations have indicated that Kelvin–Helmholtz waves may also play an important role in the transfer of solar wind material into the magnetosphere during a northward IMF.

A team of US scientists has now (2012) used Cluster data to show that KHW can form at high–latitudes, on the dawn/dusk flanks of the magnetopause, under other orientations of the IMF. The data were obtained between 12:00 and 17:00 UT on 12 January 2003, when the four Cluster spacecraft were in tetrahedral formation, about 4000 km apart, and flying close to the northern duskward cusp region of Earth's magnetosphere. The quartet was outbound, heading toward the evening side magnetopause.

Whilst the magnitude of the magnetic field components generally declined until about 15:10 UT, the data were also punctuated by repeated short, but well defined, drops in the magnetic field. During those intervals, the data indicated the presence of more low–energy particles, as well as high density and low temperature. These conditions were typical of the outer region of the magnetopause.

After each encounter with this outer part of this boundary layer, Cluster returned to a region of the magnetosphere which was characterised by low density and high temperature and populated largely with higher energy particles. This pattern of change represented rapid compression and expansion of the dayside magnetosphere, associated with dynamic pressure variations in the solar wind and the passage of a discontinuity in the IMF. The spacecraft then remained in the magnetosphere before re–encountering the magnetopause at 16:23 UT.

The fluctuations mostly propagated tailward, passing along the magnetopause. However, by comparing the boundary conditions before and after the passage of the IMF discontinuity, the team found that the KH instabilities were more frequent after the discontinuity passed by. Their conclusions were supported by computer simulations of the conditions along the Cluster trajectory, which showed the expansion of the magnetosphere after the discontinuity passed.

This was the first time that the presence of KHWs (Kelvin–Helmholtz Waves) at the magnetopause had been demonstrated at high latitude for a dawnward orientation of the IMF (Ref. 2230).

Magnetospheric substorms: A new study based on data from ESA's Cluster mission has revealed the importance of bursty bulk flows (BBFs) – fast streams of plasma that are launched towards Earth during the magnetic substorms that give rise to bright aurorae. By modelling these fast plasma streams using a kinetic approach, scientists have discovered that earlier studies based on magnetohydrodynamics tended to underestimate their role in the energy transfer during magnetic substorms. The new, more accurate description suggests that BBFs can carry up to one third of the total energy transferred during a substorm; in such cases, BBFs represent a major contributor to the brightening of aurorae. ²²³²⁾

Bright aurorae arise during magnetic substorms, violent events in Earth's magnetic environment, the magnetosphere. Substorms result from variations in the solar wind, the stream of electrically charged particles released by the Sun. When the solar wind changes in such a way as to invert the orientation of the interplanetary magnetic field, the tail of the magnetosphere gets compressed and blows powerful streams of highly – energetic plasma both towards Earth and in the opposite direction. As a consequence, plasma particles can infiltrate the upper layer of Earth's atmosphere – the ionosphere – producing breath – taking aurorae but also disturbing telecommunication networks and GPS.

While the overall picture underlying magnetic substorms and aurorae is understood quite well, the science community is still far from the detailed understanding that would allow to predict phenomena in Earth's magnetosphere. In the study presented, the international team tried to achieve a more accurate description of the magnetospheric plasma by applying an alternative approach to the analysis of BBFs, which are very fast streams of particles launched towards Earth during a substorm.

One of the vexed questions in the study of magnetic substorms concerns how exactly energy is transported across the magnetosphere, and in particular to Earth, during these events. Exploiting data from ESA's Cluster mission, Jinbin Cao and his collaborators have revealed the importance of BBFs, a previously neglected mechanism. Surprisingly, BBFs turned out to be a major player in the energy transfer during the magnetic substorm that was analyzed in this study.

The ESA study is based on data gathered with the CIS (Cluster Ion Spectrometry) experiment on board one of the four Cluster spacecraft (C1) on 30 July 2002. The results are described in the paper by Jinbin Cao of the Space Science Institute, Beihang University, Beijing, China as lead author. ²²³²⁾

The energy transport of BBFs is very important to the understanding of substorm energy transport. Previous studies all used the MHD (Magnetohydrodynamics) bulk parameters to calculate the energy flux density of BBFs. BBFs are short – lived phenomena, lasting typically ten to twenty minutes, and previous studies considered their contribution to the total energy transferred in a substorm to be marginal, adding up to only 5%. – In this approach, the team used the kinetic approach, i.e., the ion velocity distribution function to study the energy transport of an earthward bursty bulk flow observed by Cluster C1 on 30 July 2002.

Studying the dynamics of plasma is notoriously complex, and even more so in the magnetic environment of our planet. Collision dominated plasmas, such as those in planetary ionospheres, are usually modelled in terms of MHD, an approach which treats all particles in the plasma as part of a single fluid. In Earth's magnetosphere, however, the experimental constraints coming from in situ measurements are so precise that they reveal that the MHD approximation is not always applicable.

Table 128: The Cluster mission of ESA finds the source of the aurora energy boost ^{2232) 2233)}

²²³²⁾ Jinbin Cao, Yudian Ma, George Parks, Henri Reme, Iannis Dandouras, Tielong Zhang, "Kinetic analysis of the energy transport of bursty bulk flows in the plasma sheet", *Journal of Geophysical Research: Space Physics*, Vol. 118, Issue 1, Jan. 2013, pp. 313–320, doi: 10.1029/2012JA018351

²²³³⁾ Jinbin Cao, Geore Parks, Iannis Dandouras, Matt Taylor, "Cluster finds source of aurora energy boost," ESA, April 10, 2013, URL: <http://sci.esa.int/science-e/www/object/index.cfm?fobjectid=51651>

1.22.5 Space Weather

The time–variable response of the Earth’s space environment to the solar wind (including solar eruptions and flares) is termed ‘**space weather**.’ Space weather is a consequence of sun behavior (solar activity), the nature of Earth’s magnetic field and atmosphere (in particular the ionosphere and magnetosphere), and Earth’s location in the solar system. The solar wind, propagating against the Earth’s magnetic field and interacting with it, shapes the near–Earth space environment.

When energetic electrons and protons from the sun reach Earth, they interact with components of the upper atmosphere. In addition to producing the luminescent aurora borealis, this interaction can generate winds and push atmospheric constituents to higher altitudes, where they can increase the drag on satellites. The energetic particles can also ionize the molecular nitrogen and atomic oxygen in the upper atmosphere, which can radically alter the ionosphere and interfere with satellite–based communications.

Space weather can influence the performance and reliability of basic services like spaceborne/airborne electronic systems as well as of groundbased systems (communication systems, the grid infrastructure of electric power utility companies, commercial airlines, navigation systems like GPS and LORAN, satellite launches and operations, etc.) and can endanger human life and health (spacewalks of astronauts). The effects of a sudden ionospheric disturbance are an increase in the local electron concentration in the ionosphere, which can cause a total radiocommunication blackout. The more we depend upon space systems for our everyday lives, such as when we use mobile phones and GPS navigation, the more susceptible we become to space weather. – Other effects of space weather are: aurorae (beautiful atmospheric displays in the polar regions caused by high–energy electrons and protons striking the upper atmosphere) and changes of climate. The space environment hazards that spacecraft and mission designers and operators need to be concerned with are: 2234) 2235) 2236)

- Solar environment. The solar environment, directly or indirectly, effects all the other hazard environments. The solar activity level, which follows an 11–year cycle, is a directly contributing factor which interacts to the radiation, thermal and plasma environments. The increased energy output from the sun during its active periods heats the Earth’s atmosphere and causes it to expand, which can effect the impact and neutral atmosphere environments, as well.

- Magnetic environment. The fields generated by the magnetic environment can directly interact with spacecraft. This is often taken advantage of in the attitude control subsystems, which can employ magnetometers and magnetic torque rods. The magnetic environment is also a major factor in determining the radiation and plasma environments around the Earth. There are two classic uses of magnetic torque rods in attitude control. One is for momentum management of wheel–based systems. The other is for angular momentum and nutation control of spinning, momentum–biased, and dual–spin spacecraft.

- Radiation environment. The radiation environment is principally composed of naturally occurring charged particles trapped in the Earth’s magnetic field (also known as the Van Allen belts). Energetic solar particles and galactic cosmic rays also contribute to the natural radiation environment.

- Thermal environment. The thermal environment consists of thermal energy flux from the sun, the solar energy reflected back into space (and towards the spacecraft) from the

2234) M. Enoch, et al., “An Integrated Space Environment Analysis Tool (SEAT),” Proceedings of the 13th AIAA/USU Conference on Small Satellites, Aug. 23–26, 1999, Logan UT, SSC99–IIa–6

2235) Note: The first journal dedicated to the theme of space weather is: “Space Weather – The International Journal of Research and Applications,” published by AGU as of fall 2003, URL: <http://www.agu.org/journals/sw/>

2236) Keith Strong, Julia Saba, Therese Kucera, “Understanding Space Weather: The Sun as a variable Star,” BAMS, Sept. 2012, pp: 1327–1335, URL: <http://journals.ametsoc.org/doi/pdf/10.1175/BAMS-D-11-00179.1>

Earth, referred to as albedo and the direct longwave thermal emission of the Earth due to its temperature, sometimes referred to as Earthshine.

- Impact environment. The impact environment consists of material from natural occurring micrometeoroids and from man-made debris flux. Due to the high relative velocities, even tiny particles can cause direct physical damage to the satellite structure and solar panels and can also induce damaging electrostatic discharges.
- Plasma environment. The plasma environment is mostly composed of charged particles (electrons) with energies too low to be a radiation hazard. However, these particles can strike and deposit themselves on external surfaces of the spacecraft or penetrate through the surface and deposit on internal components, causing electrostatic charge build-up. This charge can build up to high enough levels to create electrostatic discharge hazards that can damage spacecraft electronic components.
- Neutral atmosphere environment. The neutral atmospheric environment is the residual atmosphere remaining at spacecraft altitudes. The neutral atmosphere can contain atomic oxygen, which can damage the materials used on spacecraft in LEO. Other residual atmospheric chemicals can also react with materials or be a source of contamination for optical systems.

Some examples of important near-Earth space environment parameters are: ²²³⁷⁾

- 1) The number, flux, and energy of energetic particles in the auroral region and/or the radiation belts
- 2) The number, density, temperature, and composition of neutrals and ions in the upper atmosphere (the thermosphere and ionosphere, respectively)
- 3) The wind speed in the upper atmosphere (above 200 km)
- 4) The ion drift velocity and/or DC component of the electric field
- 5) Small scale fluctuations in the ionosphere that lead to radio scintillation.

The development and introduction of suitable instruments and systematic space weather observations started in the 1970s from spacecraft.

- SEM (Space Environment Monitor). SEM is an operational NOAA instrument package with the objective to provide “**space weather**” on a regular basis to the user community by measuring the solar wind particle flux and its variations. The package is provided by NOAA/SEC (Space Environment Center) in Boulder, CO. SEM-1 instruments were initially introduced on satellites in geostationary orbit starting in 1974. SMS-1 (launch May 17, 1974), a predecessor of the NOAA-GOES series, was the first satellite to carry SEM. NOAA introduced SEM on the POES series (G.14.1) as well starting with TIROS-N in 1978. An upgraded instrument package, SEM-2, was introduced into the POES series spacecraft with the launch of NOAA-K (NOAA-15) on May, 13, 1998 (G.15.2).

The SEM package of the GOES series was upgraded with the introduction of SXI (Solar X-ray Imager) instrument on GOES-12 (launch July 23, 2001) and the follow-up spacecraft of the series (see GOES-12 under 1.22.6). SXI obtains a continuous sequence of corona X-ray images from the sun to monitor solar activity for its effects on the Earth’s upper atmosphere. NOAA/SEC is planning in addition a new SEM suite for the next-generation GOES series, starting with GOES-R (projected launch in 2014).

- As of 2002, analysis of the IMAGE satellite data ²²³⁸⁾ (NASA S/C, launch Mar. 25, 2000) revealed that a layer in the Earth’s outer atmosphere acts like a heat shield by absorb-

²²³⁷⁾ Larry Payton, Jeanne Holm, Michele Weiss, Robert Schaefer, Aaron Rogers, Ann Darrin, “Space Weather and Virtual Organizations,” Proceedings of the 60th IAC (International Astronautical Congress), Daejeon, Korea, Oct. 12–16, 2009, IAC-09.B5.1.7

ing energy from space storms, which reduces their ability to heat the lower atmosphere. However, it imposes a heavy toll for its services by creating a billion-degree cloud of electrified gas, or plasma, that surrounds our planet.

- The DMSP–F16 weather satellite of DoD (launch Oct. 18, 2003) is flying the SSUSI (Special Sensor Ultraviolet Spectrographic Imager) instrument that measures UV radiation from the Earth’s atmosphere and ionosphere, it also measures visible radiation (airglow and terrestrial albedo). The instrument provides the NOAA–5D–3 satellite series with the ability to obtain photometric observations of the nightglow and nightside aurora. 2239)
- The TIMED (Thermosphere, Ionosphere, Mesosphere Energetics and Dynamics) mission of NASA (launch Dec. 7, 2001) is flying the GUVI (Global Ultraviolet Imager) instrument, actually of SSUSI heritage (flown on the DMSP F–16) and a joint collaboration between JHU/APL and The Aerospace Corporation, El Segundo, CA. The objective is to monitor three general regions: the daytime low– to mid–latitude thermosphere, the nighttime low– to mid–latitude ionosphere, and the high–latitude auroral zone. The goal is to obtain a detailed quantitative and predictive understanding of auroral phenomena.

Space Weather Forecast Capabilities:

Space weather forecasting has improved dramatically over the past three decades. There have been numerous recent advancements in space weather, particularly in the arena of international efforts to collaborate on research and the development of policies and programs to mitigate risks to society and technology. 2240)

- In January 2011, NOAA announced the transition from research to operations of the first magnetohydrodynamic physics–based space weather prediction model named ENLIL. These models provide forecasters with a 1–4 day advance warning of solar plasma and CMEs directed at Earth. 2241)
- In October 2006, the U.S. Air Force Weather Agency implemented the first physics–based global heliospheric forecast model, Hakamada–Akasofu–Fry Version 2 (HAFv2), into operations. 2242)
- Since August 2006, the European Digital Upper Atmosphere Server (DIAS), co–funded by the EU (European Union) has regularly provided space weather forecasts of the solar wind and geomagnetic activity. 2243)
- NOAA/SEC in partnership with the USAF 2244) 2245) 2246) is providing a comprehensive online (near real–time) space weather monitoring service offering a spectrum of parameters and forecasts of solar and geophysical events to all parties of interest. In addition, a lot of background information is provided. SEC is the national and world warning center for disturbances in the space environment that can affect people and equipment. Note: The SEC web server began in December 1993, the Gopher/FTP servers in July 1994.

2238) Earth’s Space Storm Shield Offers Protection at a Price,” <http://www.gsfc.nasa.gov/topstory/20020509images-su.html>

2239) J. Hecht, “Space Weather and the Upper Atmosphere,” Crosslink, Vol. 6, No 1, 2005, <http://www.aero.org/publications/crosslink/winter2005/05.html>

2240) Emma Kiele Fry, “Global Socio–Economic Risks, Impacts, and Recommendations for Space Weather Policies and Initiatives,” Proceedings of IAC 2011 (62nd International Astronautical Congress), Cape Town, South Africa, Oct. 3–7, 2011, paper: IAC–11–E3.4.5

2241) “First Large–Scale, Physics–Based Space Weather Model Transitions Into Operation,” NSF Press release, Jan. 16, 2011, URL: http://www.nsf.gov/news/news_summ.jsp?cntn_id=118395

2242) C. D. Fry, T. R. Detman, M. Dryer, Z. Smith, W. Sun, C. S. Deehr, S.–I. Akasofu, C.–C. Wu, S. McKenna–Lawlo, “Real–time solar wind forecasting: Capabilities and challenges,” Journal of Atmospheric and Solar–Terrestrial Physics, Vol. 69, Issues 1–2, Feb. 2007, pp. 109–115

2243) I. Tsagouri, A. Mikhailov, L. Perrone, A. Belehaki, “Evaluation of the performance of DIAS ionospheric forecasting models,” EGU General Assembly 2010, 2–7 May, 2010. Vienna, Austria

2244) <http://www.sec.noaa.gov/SWN/>

2245) <http://www.windows.ucar.edu/spaceweather/>

2246) <http://www.spaceweather.com/>

- At the start of the 21st century, ESA is also considering a space weather applications service program (network) of its own, complementing the NOAA/SEC–provided service with emphasis on European applications. ^{2247) 2248)}
- In the spring of 2006, ESA started the pilot operation of SWENET (Space Weather European Network), a centralized Website, to provide SSA (Space Situational Awareness) online services to a European user community. The SWE Data Center is located at the ESA station in Redu, Belgium, and is hosting this SSA SWE web portal and the following applications:
 - EDID (European Debris Impact Database)
 - IONMON (Ionosphere Monitoring Facility (IONMON))
 - ODI (Open Data Interface)
 - SEDAT (Space Environment Data System)
 - SEISOP (Space Environment System for Mission Operations)
 - SPENVIS (Space Environment Information System)
 - SWENET (Space Weather European Network) of Services.

- **SOHO** (Solar Heliospheric Observatory) of ESA and NASA, launch Dec. 2, 1995 and operational in 2013. SOHO has already followed the Sun through more than one complete solar cycle. ESA extended the mission to the end of 2016.
- **STEREO–A and –B** (Solar–Terrestrial Relations Observatory) of NASA, launch on Oct. 26, 2006. Orbit: Heliocentric elliptical orbit in the ecliptic plane drifting at about 22° per year from the Sun–Earth line (at nearly 1 AU). The STEREO mission observes the entire Sun.
- **SOLAR–B/Hinode** of JAXA/ISIS, launch on Sept. 23, 2006. Multidimensional observations of the Sun in the optical, EUV and X–ray regions. The current mission extension is up to the end of 2014.
- **PROBA–2** (Project for On–Board Autonomy–2) of ESA with a scientific payload dedicated to sun observations and monitoring. Launch on Nov. 2, 2009. Mission extension to the end of 2016.
- **SDO** (Solar Dynamics Observatory) of NASA, launch on Feb. 11, 2010. Orbit: Inclined geosynchronous circular orbit (GSO), altitude ~ 35,756 km, inclination = 28.5°, the spacecraft is positioned at a longitude of 102° W. The emphasis is on the study of the Sun’s magnetic field and the solar outer atmosphere.
- **IRIS** (Interface Region Imaging Spectrograph) of NASA, launch on June 28, 2013. The objective is to obtain UV spectra and images with high resolution in space (1/3 arcsec) and time (1s) focused on the chromosphere and the transition region of the Sun.

Table 129: Overview of Solar missions operational in 2013

2247) A. Glover, A. Hilgers, E. Daly, R. Marsden, “Tomorrow’s Space Weather Forecast,” ESA Bulletin 114, May, 2003, pp. 28–37

2248) R. B. Horne, et al., “Space Weather Parameters Required by the Users, Synthesis of User Requirements,” ESA Study by Alcatel Consortium, Feb. 2001

1.22.6 X-ray imaging

X-rays are the natural signatures of the high-energy universe, a high-frequency electromagnetic radiation. Any object heated to more than a million degrees Kelvin begins to give off significant quantities of X-rays (electromagnetic radiation is produced whenever high-speed collisions between electrons and protons occur). This is around the temperature of the sun's outer atmosphere, known as the corona. It is therefore no surprise that X-ray astronomy began with studies of the sun before detections of other X-ray objects elsewhere in the universe were made. ²²⁴⁹⁾ ²²⁵⁰⁾

The sun appears completely different in the X-ray region of the spectrum than in the visible region. X-rays are emitted by very hot gases in the outer solar atmosphere, the corona, where the temperature reaches a few million degrees; the much cooler surface of the Sun, at $\sim 6,000$ K, is not hot enough to emit X-rays. As a result, an X-ray image reveals a bright glow for the corona and a black disk for the surface of the sun. The EUV (Extreme Ultra-Violet) and X-ray regions of the spectrum have been especially significant in solar studies from space because these wavelengths are produced directly by solar activity. At the end of the 20th century it became known that nearly every astronomical object, from nearby comets to stars and distant quasars, emits X-rays.

Since X-rays are being absorbed by Earth's atmosphere, the discovery and detection of this high-energy celestial radiation had to wait until the dawn of the spaceage. The following list (incomplete) provides some background on the missions and instruments flown on such astrophysics missions.

- **The field of X-ray astronomy began in 1962** with a sounding rocket flight carrying a Geiger counter that discovered the first X-rays from an astronomical object outside the Solar System. The Sun was known to be a bright X-ray source, but because it is so much closer than other stars, no other stars were expected to be detectable in the X-ray spectrum. The purpose of the 1962 rocket flight (US Aerobee 150 rocket launched in June 1962 from the White Sands Missile Range (NM) with ~ 10 minute observation flight above the atmosphere) was to investigate X-rays from the moon. – Instead, this flight discovered both **Scorpius X-1** (Sco X-1), the brightest X-ray source in the constellation of Scorpius (located in the direction of the center of the Milky Way), and a completely unexpected diffuse glow of X-rays known as the “**cosmic X-ray background**.” Later it was found that the X-ray emission of this source (Scorpius X-1) was 10,000 times greater than its optical emission. Based on these discoveries, Riccardo Giacconi (American astrophysicist – born in Genoa, Italy in 1931) received the Nobel Prize in Physics in 2002. ²²⁵¹⁾
- The first satellite to make observations of the X-ray sky was OSO-3 (Orbiting Solar Observatory-3) of NASA launched on March 8, 1963. OSO-3 produced an all-sky map of the diffuse X-ray background in the energy range of 10–40 keV.
- The US Vela satellites (spin-stabilized) of DoD and AEC (Atomic Energy Commission) provided X-ray observations as a byproduct (primary objective was the detection of nuclear blasts). Vela-5A and -5B were launched on May 23, 1969. Vela-5A flew the scintillation X-ray detector ASM (All Sky Monitor; energy range: 3–12 keV, operational life of 1 year). Vela-5B carried also ASM as well as 6 gamma ray detectors (energy range of 150–750 keV, operational life until June 19, 1979). They were among the first satellites to detect gamma ray bursts.
- Uhuru (Swahili word for “freedom”), also known as SAS-1 (Small Astronomical Satellite 1) was the first Earth-orbiting mission dedicated entirely to celestial X-ray astrono-

²²⁴⁹⁾ http://www.esa.int/export/esaSC/SEMTA2T1VED_index_0.html

²²⁵⁰⁾ <http://heasarc.gsfc.nasa.gov/docs/corp/observatories.html>

²²⁵¹⁾ Riccardo Giacconi, “The Dawn of X-Ray Astronomy,” Nobel Lecture, Dec. 8, 2002, URL: http://nobelprize.org/nobel_prizes/physics/laureates/2002/giacconi-lecture.pdf

my. Uhuru of NASA was launched on 12 December 1970 from the San Marco platform in Kenya (energy range: 2–20 keV).

- HEAO–1 (High Energy Astronomy Observatory) of NASA with a launch Aug. 12, 1977 (energy range: 0.2 keV – 10 MeV)
 - HEAO–2 (or Einstein Observatory) of NASA with a launch Nov. 12, 1978 (energy range: 0.2 – 20 keV); the first X–ray telescope in space imaging cosmic sources. *The Einstein Observatory started the realm of focussing X–ray astronomy, with a big improvement both in sensitivity and angular resolution.*
 - EXOSAT (ESA X–ray Observatory) with a launch May 26, 1983 (energy range: 0.05 – 50 keV). S/C in HEO orbit of 90 hour period (2,919 km x 189,000 km, 71.4°). EXOSAT provided detailed observations of celestial X–ray sources. S/C reentered on May 26, 1986.
 - ASTRO–C (Ginga) of Japan with a launch Feb. 5, 1987 (energy range: 1 – 500 keV)
 - Granat a Russian X–ray/gamma–ray astronomy mission in collaboration with other European countries. Launch Dec. 1, 1989 (energy range: 2 keV – 100 MeV).
 - ROSAT (Röntgen Satellite), a collaboration of Germany, USA, and UK with a launch June 1, 1990 (energy range: X–ray 0.1 – 2.5 keV, EUV 62–206 eV); all sky–survey in the soft X–ray band. The ROSAT X–ray imaging telescope detected about 150,000 new X–ray sources during its lifetime. The instrument had the capability to locate these sources with an accuracy of < 10 arcsec while operating in pointing mode.²²⁵²⁾ The ROSAT spacecraft reentered Earth’s atmosphere on October 23, 2011 over the Bay of Bengal. It is not known whether any parts of the satellite reached Earth’s surface.²²⁵³⁾
 - ASCA (Advanced Satellite for Cosmology and Astrophysics) of Japan with a launch Feb. 20, 1993 (energy range: 0.4 – 10 keV). First X–ray mission to combine imaging capability with broad passband, good spectral resolution, and a large effective area.
 - RXTE (Rossi X–ray Timing Explorer) of NASA with a launch Dec. 30, 1995 (energy range: 2 – 250 keV); Very large collecting area and all–sky monitoring of bright sources. RXTE had 3 instruments: 1) PCA (Proportional Counter Array) to detect the lower part of the X–ray energy range, 2) HEXTE (High Energy X–ray Timing Experiment) to observe the upper energy range, and 3) ASM (All Sky Monitor). HEXTE demonstrated the capability to time tag X–ray photons (15– 250 keV) with an accuracy of 8 μ s (which enabled the discoveries of millisecond pulsations that reveal the spin rates of neutron stars).
 - Chandra of NASA with a launch July 23, 1999 (energy range: 0.1 – 10 keV); highly–eccentric Earth orbit of 64 hour period. Spatial resolution < 1 arcsec.
 - SWIFT observatory, a multi–wavelength spacecraft of NASA/GSFC with a launch on Nov. 20, 2004. SWIFT carries 3 instruments: BAT (Burst Alert Telescope) to detect GRBs (Gamma Ray Bursts) in the energy range 15–150 keV; XRT (X–Ray Telescope) in the energy range 0.2–10 keV, it can take images and perform spectral analyses of the GRB afterglow; UVOT (Ultraviolet/Optical Telescope) used to detect an optical afterglow.²²⁵⁴⁾
- On June 21, 2010, a record–breaking GRB (named GRB 100621A) blinded temporarily the XRT instrument on SWIFT — the brightest light source ever seen in X–ray wavelengths at cosmological distances (arriving from 5 billion light years away). The burst was so bright when it first erupted that the data–analysis software shut down. The scientists then were able to measure the blast’s X–ray brightness at 143,000 X–ray photons per

2252) <http://www.mpe.mpg.de/xray/research/profile.php>

2253) “ROSAT re–entered atmosphere over Bay of Bengal,” DRL, October 25, 2011, URL: http://www.dlr.de/dlr/en/desktopdefault.aspx/tabid-10081/151_read-1779/year-2011/

2254) “The Swift Gamma–Ray Burst Mission,” NASA, URL: <http://swift.gsfc.nasa.gov/docs/swift/swiftsc.html>

second during its fleeting period of greatest brightness, which is more than 140 times brighter than the brightest continuous X-ray source in the sky. ²²⁵⁵⁾

– In January 2011, an international team of scientists using data from NASA's Swift satellite confirms the existence of a largely unseen population of black-hole-powered galaxies. Their X-ray emissions are so heavily absorbed that little more than a dozen are known. Yet astronomers say that despite the deeply dimmed X-rays, the sources may represent the tip of the iceberg, accounting for at least one-fifth of all active galaxies. ²²⁵⁶⁾

- XMM-Newton (X-ray Multi-Mirror Mission) of ESA with a launch Dec. 10, 1999 (energy range: 0.1 – 15 keV). Very large collecting area; simultaneous X-ray and optical (170–650 nm of UV, VIS) observations. HEO (Highly Elliptical Orbit) of 19,200 km x 101,900 km, inclination of 52.97°.

The XMM-Newton mission is using the X-ray detector design technology that was developed in Europe for the JET-X (Joint European X-Ray Telescope) instrument, a 3.5 m focal length X-ray telescope built by a consortium of groups from Italy and Russia and scientific groups from the UK; from the University of Leicester, the University of Birmingham, the Mullard Space Science Laboratory and the Rutherford Appleton Laboratory. JET-X was one of a six instruments provided by the international scientific community for Russian Spectrum-Röntgen-Gamma (Spectrum X-Gamma) high energy astrophysics mission, whose launch was originally planned for 1992/3, but severe delays to the program occurred in the wake of the collapse of the Soviet Union and the severe economic crisis in Russia that followed. Eventually, the Spectrum X-Gamma mission was simply cancelled.

Thanks to the Chandra and XMM-Newton spacecraft missions, spectacular images of the X-ray sky can now be obtained with the detection of hundred of thousands of sources of all kinds. Unfortunately this leap step forward has been possible only below ~ 10 keV. Above this value, i.e. in the so called hard X-ray band, so far only passive collimators could be used, as those on board of the BeppoSAX and RossiXTE satellites, or coded masks as those on board of the InteGRAL and Swift spacecraft. As a result, only a few hundred sources are known in the whole sky in the 10–100 keV band.

The Simbol-X formation-flying mission ²²⁵⁷⁾, a new X-ray joint project under study/definition by CNES (France) and ASI (Italy), will have the capability to obtain X-ray images in the energy range of 0.5–80 keV (covering the entire X-ray range) with very good sensitivity and spatial resolution. A launch of Simbol-X is planned for the timeframe 2014.

In Sept. 2007, ESA released ²²⁵⁸⁾ the largest catalog of X-ray sources ever, referred to as **2XMM**, compiled from 6 years of observations of the XMM-Newton mission. The catalog contains 247,000 X-ray source detections which relate to 192,000 unique X-ray sources, making it the largest collection of objects ever observed in the X-ray spectrum. The mission is expected to provide observations for at least a decade. In the fall of 2007, the ESA Science Program Committee approved a mission extension until the end of 2012.

XMM-Newton has, for the first time, detected signals from both stars of a binary pulsar system in X-rays, unveiling a scientific goldmine. Each star of the closely-packed system is a dense neutron star, spinning extremely fast, radiating X-rays in pulses. The binary pulsar

2255) "Record-Breaking X-ray Blast Briefly Blinds Space Observatory," URL: <http://www.science.psu.edu/news-and-events/2010-news/Burrows7-2010>

2256) Francis Reddy, "Swift Survey Finds 'Missing' Active Galaxies," NASA, Jan. 20, 2011, URL: http://www.nasa.gov/mission_pages/swift/bursts/active-galactic-nucleus.html

2257) G. Tagliaferri, P. Ferrando, J.-M. Le Duigou, G. Pareschi, P. Laurent, G. Malaguti, R. Clédassou, M. Piermaria, O. La Marle, F. Fiore, P. Giommi, "Simbol-X: A Formation Flight Mission with an unprecedented Imaging Capability in the 0.5–80 keV Band," Proceedings of the 7th ICSO (International Conference on Space Optics) 2008, Toulouse, France, Oct. 14–17, 2008, URL: <http://www.icsconference2008.com/cd/pdf/S10%20-%20X-Ray%20-%20Tagliaferri.pdf>

2258) http://www.esa.int/esaSC/SEMEVLMPO5F_index_0.html

PSR J0737–3039 was first spotted by astronomers in 2003 in radio wavelengths. XMM–Newton discovered X–ray emission from both pulsars in October 2006. ²²⁵⁹⁾ ²²⁶⁰⁾

Dec. 10, 2009 marks a decade of remarkable discoveries, outstanding achievements and extraordinary scientific insights with XMM–Newton. The payload comprises 3 co–aligned Wolter type I grazing incidence (reflective) gold–coated imaging X–ray telescopes each with an effective area of $\sim 1500 \text{ cm}^2$ @ 1 keV, the largest by far of any X–ray observatory. – The XMM–Newton spacecraft and instruments are in excellent condition and able to continue to operate for another decade. ²²⁶¹⁾ ²²⁶²⁾

In April 2010, the 2XMM catalog has been extended by an additional 42,000 X–ray sources. This cosmic X–ray library is a valuable resource allowing astronomers to explore the extreme universe. ²²⁶³⁾

In July 2013, ESA released a new catalog from the XMM–Newton space telescope which provides an unprecedented cosmic X–ray library for the exploration of the extreme Universe. The third XMM–Newton Serendipitous Source Catalog (3XMM–DR4) contains more than half a million sources, all of which are provided to a better quality than ever before. Improved data processing means that source identification is more reliable, and fainter objects are detected. ²²⁶⁴⁾

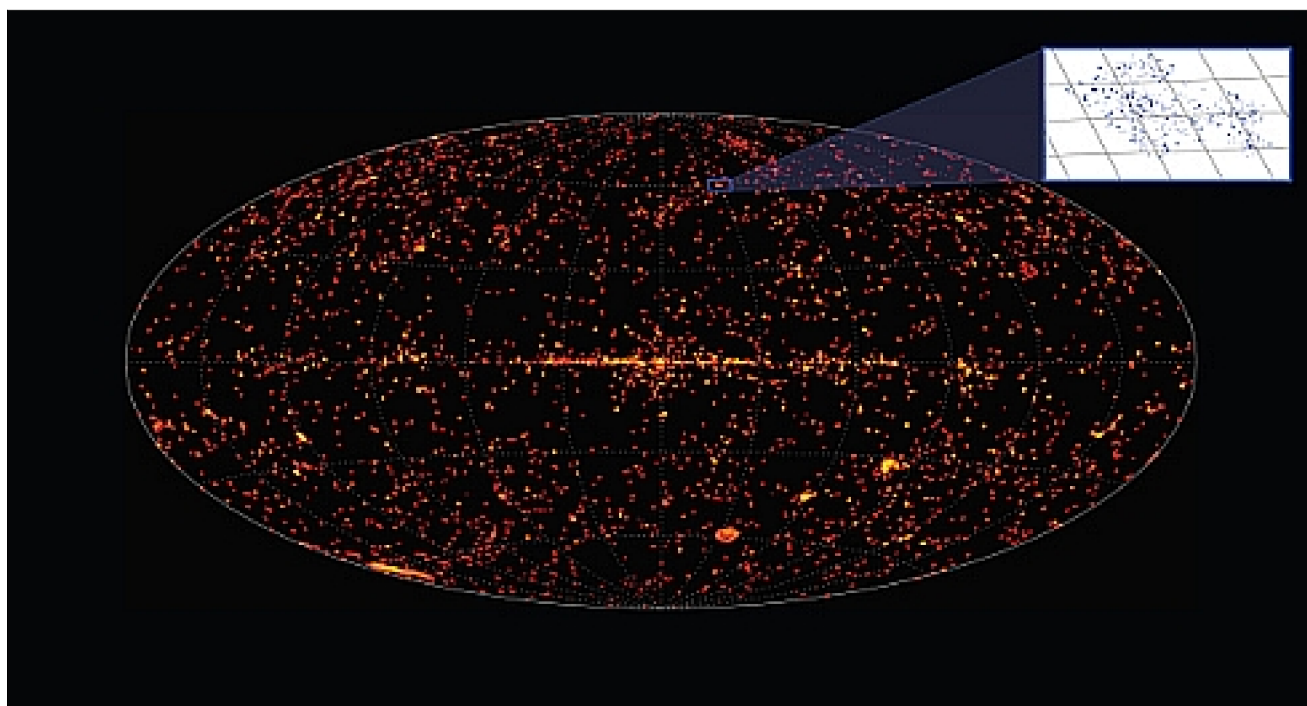


Figure 173: All–sky map of the third XMM–Newton Serendipitous Source Catalog (image credit: ESA/XMM–Newton/EPIC/Mike Watson)

Legend to Figure 173: The sources in the 3XMM catalog are identified and isolated from serendipitous data recorded by XMM–Newton’s EPIC X–ray cameras. In each of the

²²⁵⁹⁾ http://www.esa.int/esaSC/SEMAKORHKHF_index_0.html

²²⁶⁰⁾ A. Pellizzoni, A. Tiengo, A. De Luca, P. Esposito, and S. Mereghetti, “PSRJ0737–3039: Interacting pulsars in X–rays,” *Astrophysical Journal*, May 2008.

²²⁶¹⁾ “XMM–Newton celebrates a golden decade of X–ray astrophysics,” ESA, Dec. 10, 2009, URL: <http://sci.esa.int/science-e/www/object/index.cfm?fobjectid=46071>

²²⁶²⁾ Norbert Schartel, María Santos–Lleo, Arvind Parmar, Jean Clavel, “10 Years of Discovery, Commemorating XMM–Newton’s first decade,” *ESA Bulletin* Nr. 141, Feb. 2010, pp. 2–9

²²⁶³⁾ “XMM–Newton releases new edition of cosmic catalogue,” April 28, 2010, URL: <http://sci.esa.int/science-e/www/object/index.cfm?fobjectid=46958>

²²⁶⁴⁾ “Latest XMM–Newton Catalog offers new X–ray Vision,” ESA, July 23, 2013, URL: <http://sci.esa.int/xmm-newton/52082-latest-xmm-newton-catalogue-offers-new-x-ray-vision/>

600–700 observations made each year, around 70 extra sources are captured in addition to the target object which usually only takes up a small fraction of the field of view. Covering observations between February 2000 and December 2012, the catalog contains some 531 261 X–ray source detections relating to 372 728 unique X–ray sources. — The inset shows an expanded view of the small region indicated where the individual sources can be seen.

– In the spring of 2014, the XMM–Newton mission is planned to be operated long into this decade (and beyond) since spacecraft and instruments are performing admirably without major degradation. The only life limiting item being the hydrazine reserves on board has been extended by various measures from 2019 to 2027 with a potential improvement to 2030 currently under investigation. ²²⁶⁵⁾

- The introduction of X–ray interferometry technology represents the next step in providing a high–angular–resolution imaging capability of celestial X–ray sources. Proposals in this direction are: the NASA MAXIM Pathfinder and the follow–up MAXIM (Micro–Arcsecond X–ray Imaging Mission) satellite concepts. The goal is to achieve μ arcsec pointing accuracies in the X–ray spectrum. ²²⁶⁶⁾

Within Earth’s environment, X–rays are also being generated by precipitating energetic electrons (energetic electrons precipitating into the Earth’s upper atmosphere cause the auroral emissions from excited atoms and molecules, but X–ray bremsstrahlung is also generated when the electrons are decelerated). The bremsstrahlung is emitted by charged particles slowing down in the spacecraft material by scattering of atomic nuclei. The primary particle is ultimately absorbed while the bremsstrahlung can be highly penetrating.

– In the context of spaceflight, X–ray radiation causes considerable damage to the performance of electronic spacecraft components. This applies for instance to imaging detectors, such as CCDs. ²²⁶⁷⁾

- X–ray sensor applications. Devices measuring in the X–ray spectrum are being used in a variety of applications. Examples are: to observe X–ray sources in the universe (astronomy, study of particle transport mechanisms in the interplanetary medium), to measure the sun’s X–ray radiation (study of solar flares, warning services of solar flares for possible S/C damage, etc.), to diagnose the chemistry of a planet’s surface, to monitor the Earth’s atmosphere for nuclear explosions in support of the Nuclear Non–proliferation Treaty and the Atomic Test Ban, and to monitor the morphology and spectra of energetic electron precipitation and its effect on the Earth’s atmosphere.

- NASA’s Fermi Gamma–ray Space Telescope (launch June 11, 2008) discovered in October 2008 the first pulsar that beams only in **gamma rays** – representing the first example of a new class of pulsars. The gamma–ray–only pulsar lies within a supernova remnant known as CTA 1, which is located about 4,600 light years away in the constellation Cepheus. Its lighthouse–like beam sweeps Earth’s way every 316.86 milliseconds. Scientists speculate that CTA 1 is only the first of a large population of similar objects. ²²⁶⁸⁾

– In August 2010, the LAT (Large Area Telescope) instrument of the Fermi Gamma–ray Space Telescope mission ²²⁶⁹⁾ detected gamma rays from a nova for the first time, a finding that surprises both observers and theorists. The discovery dispels the long–held idea that nova explosions are not powerful enough to produce such high–energy radiation.

2265) Marcus G. F. Kirsch, Jim Martin, Andreas Rudolph, Alastair McDonald, Rainer Kresken, Anders Elfving, Mauro Pantaleoni, Thomas Godard, Norbert Pfeil, Timothy Finn, Frederic Schmidt, Detlef Webert, Uwe Weissmann, Andre Vasconcelos, “Extending the lifetime of ESA’s X–ray observatory XMM–Newton,” SpaceOps 2014, 13th International Conference on Space Operations, Pasadena, CA, USA, May 5–9, 2014, paper: AIAA 2014–1608

2266) MAXIM Pathfinder, <http://maxim.gsfc.nasa.gov/pathfinder.html>

2267) J. Stadsnes, K. Aarsnes, J. Bjordal, “X–ray Imaging of the Aurora,” <http://www-ssc.igpp.ucla.edu/IASTP/55/>

2268) Nancy Atkinson, “Fermi Telescope Makes First Big Discovery: Gamma Ray Pulsar,” URL: <http://www.universetoday.com/2008/10/17/fermi-telescope-makes-first-big-discovery-gamma-ray-pulsar/>

2269) “Fermi Detects Gamma–Rays From Exploding Nova,” Aug. 24, 2010, URL: http://www.spacedaily.com/reports/Fermi_Detects_Gamma_Rays_From_Exploding_Nova_999.html

– On March 7, 2012, the LAT instrument of the Fermi Gamma-ray Space Telescope mission detected gamma rays from the strongest solar eruption so far observed by LAT.²²⁷⁰⁾ At the flare’s peak, the LAT detected gamma rays with two billion times the energy of visible light, or about 4 GeV, easily setting a record for the highest-energy light ever detected during or immediately after a solar flare. The flare lasted for about 20 hours. Additionally, the event marks the first time a > 100 MeV gamma-ray source has been localized to the sun’s disk, thanks to the LAT’s keen angular resolution.

- NuSTAR (Nuclear Spectroscopic Telescope Array), a NASA Explorer Program mission (launch on June 13, 2012), will provide a greater capability for using high-energy X-rays to detect black holes than any currently existing instrument. NuSTAR has been designed to answer fundamental questions about the universe. NuSTAR is the first focusing hard X-ray telescope (5–80 keV) to orbit Earth and is expected to greatly exceed the performance of the largest ground-based observatories that have observed this region of the electromagnetic spectrum. NuSTAR will also complement astrophysics missions that explore the cosmos in other regions of the spectrum.

- AstroSat (Astronomy Satellite) is India’s first astronomy mission with a planned launch in late 2012. AstroSat carries four coaligned astronomy payloads for simultaneous multi-band observations and one ultraviolet instrument with two telescopes. The LAXPC instrument provides an energy range of 3–80 keV, the CZTI instrument detects energy in the range of 10–150 keV.

- The IXO (International X-ray Observatory) mission is a next-generation facility and a collaboration between NASA, ESA, and JAXA^{2271) 2272) 2273) 2274) 2275) 2276)} which is planned to launch in 2021. It combines elements from NASA’s prior Constellation X program and ESA’s XEUS program (in July 2008, the IXO program agreement was announced to the astronomical community). IXO will be a Great Observatory-class mission which builds upon the legacies of the Chandra and XMM-Newton X-ray observatories. IXO will address fundamental and timely questions in astrophysics and cosmology:

What happens close to a black hole?

How did supermassive black holes grow?

How does large scale structure form?

What is the connection between these processes?

IXO will have a mass of around 6600 kg and will be approximately 23 m long and 4 m in diameter. The Wolter-I X-ray telescope optical design requires about 14,000 0.4 mm thick glass mirror segments to be densely packed into a 3.2 m diameter FMA (Flight Mirror Assembly) and supported with micron level accuracy and stability. Key challenges addressed by the FMA design concept include bonding the mirrors into the module without distortion, designing the segment support for glass survivability, keeping the structure light enough to launch, providing a large effective area, and preventing unacceptable thermal distortion.

Background: X-rays were discovered in Nov. 1895 by the German physicist Wilhelm Conrad Röntgen (1845–1923). His experiments at the University of Würzburg focused on light

2270) “NASA’s Fermi detects the highest-energy light from a solar flare,” NASA, June 11, 2012, URL: http://www.nasa.gov/mission_pages/GLAST/news/highest-energy.html

2271) Ryan S. McClelland, David W. Robinson, “Design Concept for the International X-Ray Observatory Flight Mirror Assembly,” Proceedings of the 2009 IEEE Aerospace Conference, Big Sky, MT, USA, March 7–14, 2009

2272) Jay Bookbinder, “The International X-ray Observatory,” URL: http://ixo.gsfc.nasa.gov/decadal_references/IXOAstro2010DecadalDocument.pdf

2273) <http://ixo.gsfc.nasa.gov/>

2274) <http://sci.esa.int/science-e/www/object/index.cfm?fobjectid=44091>

2275) Didier Barret, “The ESA/NASA/JAXA International X-ray Observatory (IXO),” URL: <http://www.iap.fr/seminaires/SeminairesIAP/2009/presentations/barret/Barret.pdf>

2276) David Robinson, “Current Technology Development Efforts on the International X-Ray Observatory,” 2011 IEEE Aerospace Conference, Big Sky, MT, USA, March 5–12, 2011

phenomena and other emissions generated by discharging an electric current in a cathode ray glass tube (he evacuated the tube of all air, filled it with a special gas, and passed a high electric voltage through it). In the experimental setup, Röntgen's attention was drawn to a glowing fluorescent screen on a nearby table. He realized that the fluorescence was caused by invisible rays originating from the tube. The new type of radiation had the ability to penetrate matter, like human tissue; Röntgen saw the bones of his hand clearly displayed in an outline of flesh. The mysterious radiation was soon referred to as "X-ray radiation" because "X" stood for the "unknown" (however, in Germany, the new radiation was called "Röntgenstrahlung" in honor of the discoverer). The first ever Nobel Prize for physics was awarded to Wilhelm Röntgen in 1901 for his discovery of X-rays.

Radiation spectrum	Photon energy range	Spectral range	Frequency range
EUV	0.02 – 0.2 keV	60 – 6 nm	5×10^{16} – 5×10^{18} Hz
Low-energy (soft) X-rays	0.2 – 2 keV	6 – 0.6 nm	5×10^{18} – 5×10^{19} Hz
Medium-energy X-rays	2 – 10 keV	0.6 – 0.1 nm	5×10^{19} – 3×10^{19} Hz
High-energy (hard) X-rays	10 – 400 keV	0.1 – 0.003 nm	3×10^{19} – 1×10^{22} Hz
Gamma-rays	> 400 keV	< 0.003 nm (< 3 pm)	> 1×10^{22} Hz

Table 130: Overview of high-energy spectral ranges

Some basic characteristics of X-ray radiation: ²²⁷⁷⁾

- The X-ray spectrum is generally considered from 60 nm (EUV) to about 3 pm in wavelengths (see Table 130).
- X-ray radiation penetrates solid matter. The degree of penetration is least in materials containing elements of high density and high atomic number. A sheet of lead (Pb) absorbs X-ray radiation completely.
- **The Earth's atmosphere is completely opaque to X-ray radiation**, i.e. to photons with energy levels above ~ 100 eV [Note: the Earth's atmosphere absorbs radiation over a large portion of the electromagnetic spectrum]. **Hence, observations of incoming X-ray radiation can only be done on a long-term basis by instruments on satellites.** This is the reason why the field of spaceborne X-ray (as well as UV and gamma-ray) astronomy is relatively young, starting in the early 1970s.
- X-ray radiation interacts with matter by ejecting electrons from matter by the photoelectric effect and other mechanisms. In photo-electric absorption, a photon is absorbed in the process of removing an electron from an atom. The high energy of the X-ray is necessary for it to take place.
- X-ray radiation ionizes a gas – permitting it to conduct. This effect may for instance be used to measure the energy of X-ray radiation.
- X-ray radiation causes certain substances to fluoresce (e.g. barium). In X-ray fluorescence of trace elements, the filter deposit is irradiated by high energy X-rays that eject inner shell electrons from the atoms of each element in the sample. When a higher energy electron drops into the vacant lower energy orbital, a fluorescent X-ray photon is released. The energy of this photon is unique to each element, and the number of photons is proportional to the concentration of the element.
- X-ray radiation exhibits also diffraction characteristics. ^{2278) 2279)} In 1912, the physicists Max von Laue, Walter Friedrich and Paul Knipping (all at the University of Munich) succeeded in the first demonstration of X-ray diffraction in crystal structures, thus render-

²²⁷⁷⁾ P. Ferrando, "SIMBOL-X: a new generation X-ray telescope in the 0.5–70 keV range," Proceedings of International Symposium Formation Flying Mission & Technologies, Oct. 29–31, 2002, Toulouse, France

ing proof of the wave-like nature of X-ray radiation (phenomenon of constructive interference).²²⁸⁰⁾

- X-ray detection technology: High-energy radiation (X-ray, gamma-ray) observations require in general special detection techniques. These are due to the difference in the way high-energy electromagnetic radiation interacts with matter compared to wavelengths longer than the ultraviolet. In the optical and microwave wavelength regions the methods and instruments are basically similar to those in ground-based astronomy.
- X-rays are capable to expose photographic film (integrating detector)
- X-ray sources generally emit fewer high-energy photons (as compared to photons of the optical spectrum) so that X-ray detectors can detect and measure individual X-ray photons, and accumulate enough photons to make an accurate picture of the total source. – A flux of one photon/(cm² s) in the 1–10 keV range observed at Earth constitutes a bright cosmic X-ray source.

The interpretation of X-ray emissions from astrophysical objects relies on the detailed spectral information, and on the morphology of the emission. The emission lines carry information on the physical state of the emitting plasma (density, temperature, state of ionization, thermal versus non-thermal emission process), whereas the morphology of the emission allows deep insights into the physics of the objects studied.

Some background on X-ray instrumentation:

The design of an X-ray imaging system (optics) poses some difficulties due to the constraints imposed by the interaction of X-rays with matter.^{2281) 2282) 2283)} First, X-rays impinging at normal incidence on any material are largely absorbed rather than reflected. Secondly, the index of refraction, n , is about 1 at X-ray wavelengths for all materials. Any refracting system (i.e., lens) sufficiently thin to transmit X-rays must therefore possess a long focal length. For most materials, however, the index of refraction is slightly less than unity at X-ray wavelengths. This property offers the possibility of using “**total external reflection**” of X-rays incident on a surface **near grazing incidence**. As long as the grazing angles are very shallow, about one degree, the X-rays do not penetrate the surface but are reflected, just like visible light.

Prior to the introduction of imaging optics into X-ray astronomy, the most sensitive X-ray instruments consisted of collimated detectors with large collecting areas. A large collecting area was required in order to obtain a sufficiently strong signal from the relatively weak X-ray sources, in the presence of a large background signal. Placing a collimator in front of a large-area detector restricted the size of the sky from which a signal was collected at any time, and thus reduced the background signal when the detector was pointed at a source. For very bright X-ray sources, this approach is still adequate.

A complete spaceborne X-ray imaging instrument consists of the following elements: telescope, dispersing element, detector, a processing and telemetry unit, and a background rejection system.

2278) W. Friedrich, P. Knipping, M. Laue, “Interferenz-Erscheinungen bei Röntgenstrahlen,” Proceedings (Sitzungsberichte) of the Bavarian Academy of Sciences, June 8, 1912, pp. 303–322

2279) M. Laue, “Eine quantitative Prüfung der Theorie für die Interferenzerscheinungen bei Röntgenstrahlen,” Proceedings (Sitzungsberichte) of the Bavarian Academy of Sciences, June 8, 1912, pp. 363–373

2280) “Laue’s Discovery of X-ray Diffraction by Crystals,” Chapter 4, <http://www.iucr.org/iucr-top/publ/50YearsOfX-rayDiffraction/chap4.pdf>

2281) http://imagine.gsfc.nasa.gov/docs/science/how_12/xray_telescopes.html

2282) Note: A very useful formula which helps converting from wavelengths to energies, and vice versa, is the following: Energy (keV) = 1.24 / Wavelength (nm)

2283) R. Hudec, V. Maršíková, L. Pína, A. Inneman, M. Skulinová, “New Trends in Space X-ray Optics,” ICSO 2010 (International Conference on Space Optics), Rhodes Island, Greece, Oct. 4–8, 2010, URL: <http://congrex.nl/ICSO/Papers/Session%2014a/Hudec.pdf>

Telescope: A concept for increasing the ability to detect weaker sources is the use of an X-ray telescope to create an image of a portion of the X-ray sky. – The instrument system can either be with or without the capability to sense the direction of incoming radiation. There are all-sky monitors and active radiation shields which haven't any or have only very rough directional sensitivity, but the majority of systems include a telescope or at least a collimator. The structure of a focusing telescope is determined by the ability of effectively reflecting the incoming radiation. In modern astronomical telescopes lenses (refracting systems) are hardly ever used as the main focusing elements. This is due to the fact that high-energy photons (X-ray, gamma-ray) are effectively absorbed in mirror surfaces, and therefore large incidence angles and designs similar to optical telescopes cannot be applied.

The utilization of X-ray mirrors for extra-solar X-ray astronomy had to await the development of electronic detectors with both high quantum efficiency and the ability to determine the location of the arrival of an X-ray photon in two dimensions. The first such detectors were the Imaging Proportional Counter (IPC) and the MCP (Microchannel Plate) detector. Subsequently, more sensitive detectors including CCD spectrometers and imaging gas scintillation proportional counters have been employed.

Metal surfaces are capable of reflecting high energy photons if very small reflection angles (a few degrees or less) are used. Telescope designs of this type are called grazing incidence telescopes, and they have been used in XUV to X-ray astronomy (up to photon energies of a few tens of keV) starting from the 1970's.

X-ray imaging techniques below 10 keV (soft X-ray imaging): One difficulty of X-ray instrumentation is that X-ray photons cannot be focussed as lower wavelength ones, since they are absorbed by matter under normal incidence conditions. Reflection on a surface can occur only under grazing incidence angles, the cut-off angle decreasing when the energy increases. This has been the major problem in building X-ray telescopes, and is the reason why X-ray instruments imaging characteristics look poor compared to optical astronomy. Below ~ 10 keV, astrophysics missions are flying with focussing X-ray mirrors built on this grazing incidence reflection property. The X-ray instruments of the Chandra mission of NASA (launch Jul. 23, 1999) and of the XMM-Newton mission of ESA (launch Dec. 10, 1999) operate on this principle.

[At about 0.5 arcsecond resolution, Chandra cannot quite achieve the clarity of Hubble. But Chandra is seeing a huge slice of the universe that Hubble cannot see due to the limitations of optical light. In fact, after just six months in space, Chandra was detecting new types of galaxies and black hole activity so distant and faint that Hubble couldn't even follow-up with optical observations.]

X-ray imaging techniques above 10 keV: Hard X-ray imaging instrumentation relies on the following techniques:

- Use of a simple collimator to select a part of the sky, with photons detected by a non imaging detector system. First applications to guide X-ray and gamma-ray photons were actually pure collimator systems, which do not apply any focusing, but merely block out the radiation from unwanted directions. These have very limited imaging capability, and require large detectors if large effective areas are desired. Pure collimator systems were used in e.g. the first astronomical X-ray observations in 1970's. The first spaceborne focussing X-ray telescope flew on Skylab in 1973 (launch May 14, 1973) and recorded over 35,000 full-disk images of the sun over a 9-month period (see L.5).

- The modern technique of hard X-ray imaging employs a coded mask, which for each point source in the sky projects an unambiguous pattern onto an imaging detector system. The sky image is reconstructed by unfolding the mask motives from the image measured by the detector. This technique, which allows to reach angular resolutions of about 5–15 arcminutes, is employed in ESA's **InteGRAL** (International Gamma-Ray Astrophysics Laboratory) mission launched Oct. 17, 2002.

Note: A coded mask is placed in front of the detector usually together with a mechanical collimator. The mask is basically a plate with a well defined pattern of equally sized holes (normally thousands) in the plate. The holes pass a radiation pattern to the position-sensitive focal plane detector, and the pattern can be decoded to produce a unique solution of the original image of the sky.

On Oct. 17, 2012, ESA's *InteGRAL* mission was 10 years on orbit – observing rare breeds of stars to the feeding habits of black holes, the mission has been uncovering the secrets of the most energetic phenomena in the Universe. Highlights of the mission so far have included the study of the emission from electron-positron annihilation across the sky, the discovery of two previously unknown classes of X-ray binaries, the characterization of the cosmic X-ray background and the first detection of polarization in gamma-ray sources. (2284) (2285)

Two notable types of X-ray telescopes:

1) For X-ray imaging with very good angular resolution, **Wolter telescopes** (Hans Wolter, German Physicist, University of Kiel) are being used which have a *FOV* (*Field of View*) of only about 1° . In the timeframe 1951–1952, Wolter outlined ways of building such aplanatic telescope systems of grazing incidence mirror configurations that satisfied the Abbe sine condition (i.e. free of both spherical aberration and coma). (2286)

Such Wolter telescopes were used on *Skylab* (1973/4) to investigate the corona of the sun. These were followed in 1978 by NASA's *Einstein Observatory*, and in 1983 by ESA's *EXOSAT*, both equipped with Wolter telescopes having aperture openings of 56 cm and 17 cm, respectively.

Further example missions with an imaging Wolter X-ray telescope are:

- *ROSAT* (launch June 1, 1990)
- *Chandra* (launch June 23, 1999) mission of NASA (focal length of 10 m and four nested Wolter telescopes, a spatial resolving power of 0.5 arcsec). However, *Chandra* sacrifices effective area (i.e. throughput) to achieve the optical stability necessary to provide the sub-arc second resolution.

2284) “Integral: a decade revealing the high-energy sky,” ESA, Oct. 17, 2012, URL: http://www.esa.int/esaSC/SEMV8W3S18H_index_0.html

2285) “INTEGRAL celebrates a decade of discoveries,” ESA Science and Technology, Oct. 17, 2012, URL: <http://sci.esa.int/science-e/www/object/index.cfm?fobjectid=50938>

2286) Hans Wolter, “Glancing Incidence Mirror Systems as Imaging Optics for X-rays (Spiegelsysteme Streifenden Einfalls als Abbildende Optiken für Röntgenstrahlen)”, *Annalen der Physik*, Vol. 10:, No 1–2, 1952, pp. 94–114.

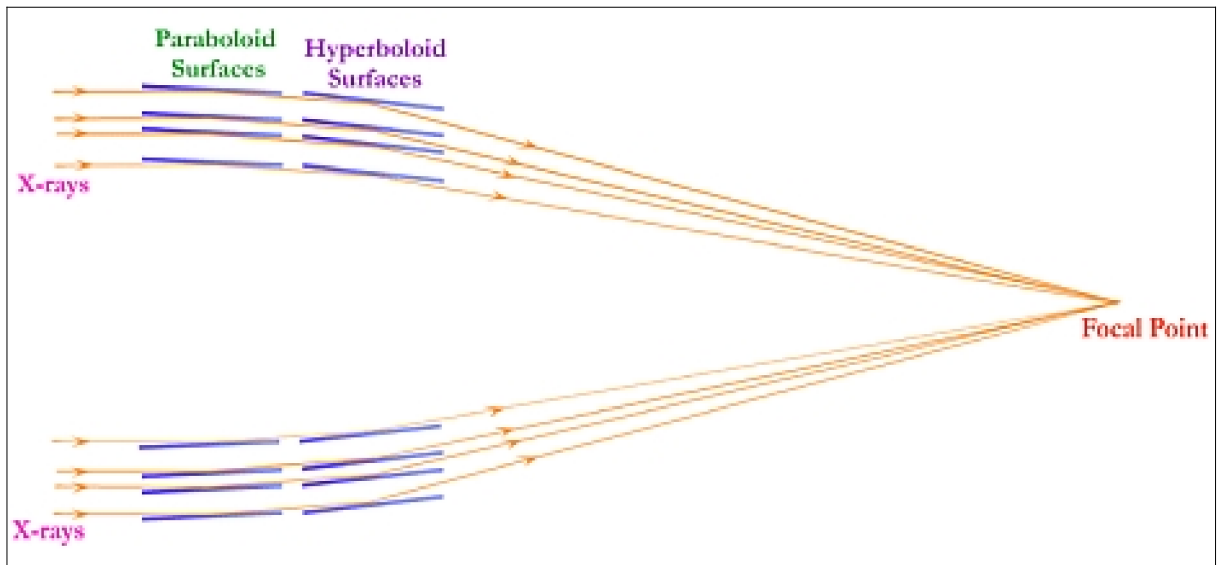


Figure 174: Schematic of a near-grazing incidence Wolter configuration of the Chandra mission (image credit: Harvard University)

– XMM–Newton of ESA (launch Dec. 10, 1999)²²⁸⁷) with three large Wolter mirror systems, each consisting of 58 nested mirror shells with a focal length of 7.50 m (a modest angular resolution of ~ 10 arcsec is provided but large effective area). The total telescope optical surface area is more than 120 m^2 – bigger than a tennis court. In 2011 the mission is fully operational, operations are approved until the end of 2012. Further extensions will be reviewed in 2 year time slots.



Figure 175: Curved mirrors stacked within one of three optical modules of the XMM–Newton telescope. Each one contains 58 mirrors with a total telescope optical surface of more than 120 m^2 (image credit: ESA)

– The NuSTAR (Nuclear Spectroscopic Telescope Array) minisatellite mission of NASA (launch June 13, 2012) is the first focusing hard X-ray telescope consisting of two co–

²²⁸⁷) Norbert Schartel, “10 Years Of XMM XMM–Newton:Scientific Achievements And Future Prospects,” X–Ray Astronomy 2009 Conference, Bologna, Sept. 7–11, 2009, URL: http://www.iasfbo.inaf.it/events/xray2009/pdf/schartel_n.pdf

aligned grazing angle incidence x-ray mirrors, coated with depth-graded multilayers, focusing onto two cadmium-zinc-telluride pixel detectors that are separated from the mirrors by 10 m. The long focal length required by the hard X-ray optics demands the use of a 10 m extendable mast.

– ASTRO-H is a JAXA mission with a planned launch in 2014. The payload features two identical mirror-detector pairs: HXT (Hard X-ray Telescope) and HXI (Hard X-ray Imager). The HXT has conical-foil mirrors with graded multilayer reflection surfaces that provide a 5–80 keV energy range.²²⁸⁸⁾

– XEUS (X-ray Evolving Universe Spectroscopy mission) of ESA (launch planned for 2015) will make use of a single Wolter I module having a diameter of 9.9 m (focal length of 50 m). – Note: In 2008, ESA cancelled the XEUS project in favor of the new collaborative IXO (International X-ray Observatory) candidate mission to be developed with NASA and JAXA. A launch of IXO is planned for the timeframe 2020.

For IXO, the aim is to boost XMM's collecting area 20-fold, while delivering three times the resolution. Achieving this demands new technology: while NASA is investigating an alternative called 'slumped glass', ESA is focusing on silicon pore optics, based around commercial silicon wafers. A major science driver for the design of IXO is a long focal length (20 m), since this allows a greater photon-collecting capability at higher photon energies. – IXO will have a launch mass of ~ 6600 kg and will be ~ 10 m long and 4 m in diameter in its launch configuration. The spacecraft will be about 23 m long in its deployed configuration. The nominal mission lifetime is five years, with consumables sized for 10 years of operations.

2) In the 21st century, the **Lobster Eye optics telescope** geometry for WFOV (Wide Field of View) imaging of soft X-rays (up to several keV) represents an alternate approach to X-ray imaging in particular with respect to ASM (All Sky Monitor) applications.

The wide-field X-ray telescope configurations may be used for ASM (All Sky Monitor) applications; they are expected to contribute essentially to the study of various astrophysical objects such as AGN (Active Galactic Nuclei), SNe (Supernovae), GRBs (Gamma-ray Bursts), XRFs (X-ray Flashes), galactic binary sources, stars, CVs (Cataclysmic Variables), X-ray novae, various transient sources, etc.

The LWFT (Lobster-Eye Wide Field Telescope) experiment was initially proposed in 1999 as the "Lobster-ISS" technology experiment by the University of Leicester led consortium in response to the ESA call for two 'flexi-missions' (F2 and F3) for the ISS (Lobster-ISS).^{2289) 2290)}

As of fall 2005, LWFT is an ASM payload planned to be flown on the SRG (Spectrum Röntgen Gamma) mission of Roskosmos of Moscow (planned launch in 2013). SRG is an international cooperative space research and technology demonstration mission with the partners: Roskosmos (Russian Space Agency); ESA (European Space Agency), IKI (Space Research Institute), Moscow; MPE (Max-Planck-Institute for extraterrestrial Physics), Garching, Germany; and the Space Research Center of the University of Leicester, Leicester, UK.

2288) http://astro-h.isas.jaxa.jp/si/index_e.html

2289) G. W. Fraser, A. N. Brunton, N. P. Bannister, J. F. Pearson, M. J. Ward, T. Stevenson, D. J. Watson, B. Warwick, et al., "Lobster-ISS: An Imaging X-ray All-sky Monitor for the International Space Station," Proceedings of SPIE, Vol. 4497, 2001, pp. 115–126, 'X-Ray and Gamma-Ray Instrumentation for Astronomy XII,' Kathryn A. Flanagan; Oswald H. Siegmund; Eds., URL: http://www.src.le.ac.uk/projects/lobster/Repository/spie_13_07_01.pdf

2290) <http://www.src.le.ac.uk/projects/lobster/home.htm>

The unique design of the lobster eye has been intensely studied to help understand how it allows some crustaceans (shrimps, prawns, crayfish and lobsters) to see in low light and murky waters. Unlike the more common compound eyes of insects, which have hexagonal facets, the lobster eye design incorporates square facets that are arranged radially to form an optic array with a 180° WFOV. Lobster eyes consist of thousands of tiny square facets which gather the light by **reflection** rather than refraction as human eyes and most animal eyes do.

The Lobster Eye technology was first proposed by W. K. H. Schmidt in 1975 (MPAe Lindau, Germany). The innovative telescope design consists of one or two sets of plane mirrors used in a grazing incidence configuration. The plane reflectors are arranged in an uniform radial pattern around the perimeter of a cylinder of radius R . X-rays from a given direction are focussed to a line on the surface of a cylinder of radius $R/2$.²²⁹¹⁾

In 1977, Roger Angel of the University of Arizona proposed an alternate X-ray instrument design based on slightly different arrangement, sometimes referred as two-dimensional lobster eye optics. The full lobster-eye optical grazing incidence X-ray objective consists of numerous tiny square cells located on the sphere and is similar to the reflective eyes of macruran crustaceans such as lobsters. The field of view can be made as large as desired, and good efficiency can be obtained for photon energies up to 10 keV.²²⁹²⁾

Table 131: Some background on WFOV X-ray imaging history ^{2291) 2292) 2293)}

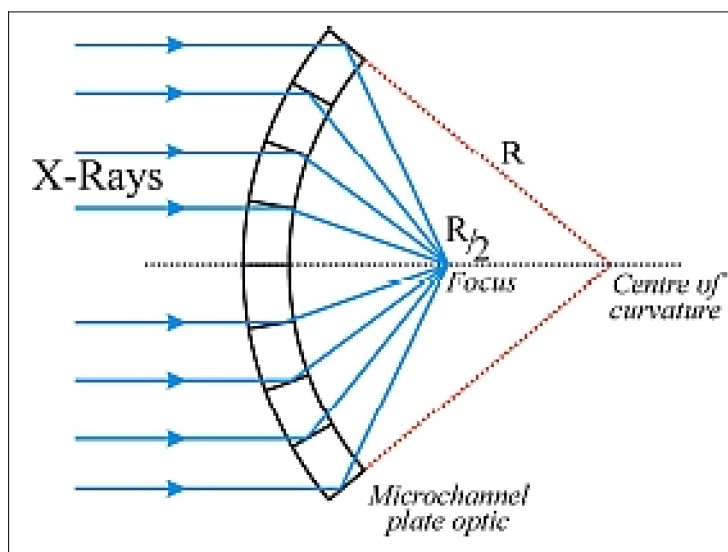


Figure 176: Focal plane diagram showing lobster-eye geometry (image credit: UL)

The goal of LWFT (Lobster) is to approach the limit of “all the sky, all the time.” The instrument consists of 5 “lobster eye” MCP (Microchannel Plate) telescope modules. Each module has a FOV of $\sim 30^\circ \times 30^\circ$ providing an instantaneous coverage of approximately 10% of the sky. When the satellite is in all-sky survey mode up to 80% of the accessible sky will be monitored once every orbit (~ 95 min) over a time-line extending up to 4 years (dependent on the final mission operations plan). LWFT provides a very impressive capability for studying time-variable phenomena and surveying the entire sky in the soft X-ray band.

Note: In 2008, the **LWFT instrumentation was removed from the SRG** (Spectrum Röntgen Gamma) mission due to budgetary problems in the UK.

2291) W. K. H. Schmidt, “A proposed X-ray focusing device with wide field of view for use in X-ray astronomy,” *Nuclear Instruments and Methods*, Vol. 127, 1975, pp. 285–292

2292) J. Roger. P. Angel, “Lobster eyes as X-ray telescopes,” *Astrophysical Journal*, Part 1, Vol. 233, Oct. 1, 1979, pp. 364–373

2293) Chris Ashcraft, “New design innovations from biomimetics,” URL: <http://creation.com/lobster-eye-design>

In 2012, NASA/GSFC is developing a “Lobster Transient X–ray Detector” consisting of a microchannel plate, a thin, curved slab of material dotted with tiny tubes across the surface. The instrument is planned to be installed on the ISS in the timeframe 2014/15. ²²⁹⁴⁾

Dispersive element filters in X–ray observations:

There can be a dispersive element and/or filters which determine the spectral interval passing further. The dispersive element may be a prism, a diffraction grating, or a crystal, whichever is suitable for the wavelength region and the desired spectral resolution.

Detectors: Imaging spectroscopy of ionizing radiation in the **X–ray range** targets the simultaneous detection of energy and interaction point of an X–ray photon with the detector material. Typical application is the field of X–ray astronomy, where spaceborne observatories carrying an X–ray optical system, e.g. Wolter Type X–ray telescopes, are combined with a dedicated focal plane instrumentation featuring varying kinds of X–ray detectors.

The detector collects the incoming X–ray radiation and responds in an accurately determined manner, the output being some physically measurable signal (e.g., electric charge, current or voltage). In some cases, the energy of the X–ray radiation (photons) is so high that it interacts with solids and liquids via the photoelectric effect.

X–ray imaging detectors are being used from astronomy to material science and to clinical radiology applications. The first X–ray detector used was photographic film; it was found that silver halide crystallites would darken when exposed to X–ray radiation. The majority of conventional X–ray detection techniques rely on film and phosphor storage screens. Commercially available systems generally utilize secondary detection media, such as phosphor plates or scintillator conversion layers. All of the above methods have some shortcomings, such as in resolution, radiation collection efficiency, or in the provision of multispectral (color) imagery. The semiconductor approach offers better detection solutions; hence, they are extensively being used in X–ray detection schemes. ²²⁹⁵⁾

State-of-the-art astronomical X-ray imagers all include silicon charge-coupled device (CCD) detectors. In 2009, APS (Active Pixel Sensors) under development for scientific applications use one of two architectures. a) A monolithic sensor is fabricated from a single wafer of semiconductor material which contains both the photosensitive volume and the readout circuitry of each pixel. b) A hybrid sensor is comprised of two (or more) wafers which are fabricated separately and then bonded together. One wafer of a hybrid contains the photosensitive volume (the detector layer or tier) and another wafer contains the readout circuitry.

- Semiconductor detectors based on silicon (CCDs) are suitable for soft X–ray energies <10 keV (spectral range of 0.1 nm to 60 nm). In the soft X–ray range, energy resolutions of <1keV are obtained. Germanium detectors are more suitable for the hard X–ray region with energies between 10 keV and about 1000 keV (or 1 MeV).
- Low–temperature bolometers are also used as high–resolution X–ray detectors. In these designs, X–rays are detected by semiconductors and cooled to very low temperatures (about 0.1 K) for high energy resolutions.
- MCP (Microchannel Plate), coupled with a scintillator, a film, or a CCD array, can provide X–ray imaging (suitable from UV to X–ray to γ –ray range). MCPs are used for plasma particle, ion, photon, and/or electron counting applications (measurement of ionospheric fluxes in the solar wind, etc.).

2294) Lori Keeseey, “Measuring Transient X–rays with Lobster Eyes,” NASA, May 21, 2012, URL: <http://www.nasa.gov/topics/technology/features/lobster-eyes.html>

2295) A. Owens, T. Peacock, P. Underwood, S. Nenonen, et al., “A New Generation of Space X–Ray Imagers that Could Help Fight Cancer,” ESA Bulletin, No. 108, Nov. 2001, pp. 32–38

• The XMM–Newton cornerstone mission (launch Dec. 10, 1999) of ESA was the first to introduce the **pnCCD** detector technology (also spelling of: pn–CCD) for the focal plane of a camera, EPIC (European Photon Imaging Camera), in the field of X–ray observations. A pnCCD (i.e., pn–junction CCD), and different from MOS–CCD implementations, developed for spectroscopy and imaging of X–rays with high time resolution and quantum efficiency. The excellent performance of the focal plane camera has been maintained so far. The energy resolution in particular has shown hardly any degradation since launch. ^{2296) 2297)}

Future missions and other applications require pnCCDs with smaller pixels and even faster readout. A potential application is the Russian/German SRG (Spectrum Röntgen Gamma) mission (launch 2012) with the eROSITA (extended Roentgen Survey with an Imaging Telescope Array) instrument of MPE Garching. As in conventional CCDs, pnCCDs equally can be designed in a frame store format. This optimizes the ratio of exposure to transfer time, but requires more space on a chip because the store area does not serve as an active area but as an analog storage region.



Figure 177: Prototype of the eROSITA pnCCD detector module with 2 cm x 2 cm large pnCCD (image credit: MPI–HLL)

- At the start of the 21 century, X–ray detection can probably be best served with a compound semiconductor, in particular of the type GaAs (gallium arsenide), according to the ESA GaAS sensor development program. It offers the following system requirements:
 - High density to provide a high detection efficiency
 - A wide enough bandgap to ensure room–temperature operation
 - A time response matched to the expected photon fluxes
 - A uniformity in spatial response in excess of 99.99%

The band–gap of GaAs detectors is high enough that it does not need cryogenic cooling, and low enough that sub–keV spectral resolution is achievable at hard X–ray energies. Room–temperature operation is an important consideration for X–ray systems.

²²⁹⁶⁾ “Frame Store pnCCD for eROSITA,” URL: http://www.hll.mpg.de/graphics/PDF_BrochArticle/MPI-HLL-brochure_7_2.pdf

²²⁹⁷⁾ Norbert Meidinger, Stefan Bonerz, Rouven Eckhardt, Jakob Englhauser, Robert Hartmann, Günther Hasinger, Peter Holl, Norbert Krause, Gerhard Lutz, Rainer Richter, Heike Soltau, Lothar Strüder, Joachim Trümper, “First measurements with a frame store PN–CCD X–ray detector,” Nuclear Instruments and Methods in Physics Research Section A: Accelerators, Spectrometers, Detectors and Associated Equipment, Vol. 512, Issues 1–2, 11 Oct. 2003, Pages 341–349

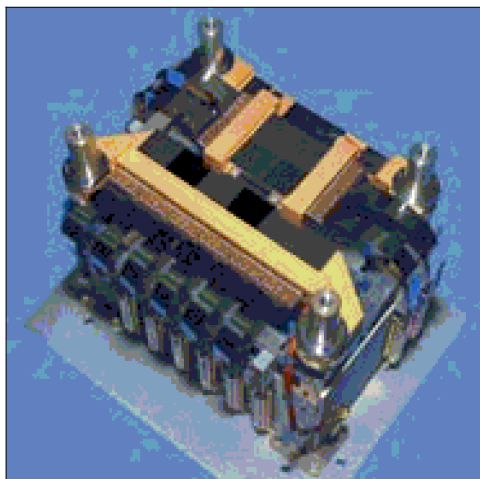


Figure 178: ACIS detector array (image credit: MIT/LL)

Example of an X-ray CCD detector: The ACIS (AXAF CCD Imaging Spectrometer) X-ray instrument of NASA's Chandra spacecraft features high-sensitivity CCDs with excellent charge-transfer characteristics. The flight assembly (Figure 178) shows two distinct arrays: a square imaging array and a linear spectrometer array. The angular resolution of the detectors is better than 0.5 arcseconds, a factor of 10 greater than other X-ray observatories. The energy resolution is a factor of 10 greater, and the sensitivity is a factor of 20 greater than that of any other X-ray detectors in orbit. ²²⁹⁸⁾

The ACIS CCD instruments were constructed jointly by the MIT Center for Space Research and the Department of Astronomy at the Pennsylvania State University.

Background rejection system: There are several other aspects which have to be accounted for in the high-energy detector system design. Perhaps the most important is the external and internal background radiation of the system. External background is of profound importance in space environment where the system is exposed to primary cosmic radiation. Internal background may be a problem especially for the infrared detectors, where some parts of the system may radiate in the same wavelength band as observed by the detector. Radiation shields, either passive which just block off the unwanted radiation, or active which also measure the radiation when it is absorbed by or passing through the shield, are used in spaceborne instruments.

- Solar observations in the high-energy spectrum are performed by a number of dedicated satellite missions, normally with strong international cooperation. Prominent examples in this class are SOHO of ESA/NASA (launch Dec. 2, 1995) and the STEREO mission of NASA with a launch on Oct. 26, 2006 (K.30) with the objective to study CMEs (Coronal Mass Ejections) of the sun.

The twin STEREO spacecraft witnessed a huge CME of the sun in February 2009 when sunspot 11012 unexpectedly erupted. ^{2299) 2300)} The angular position of STEREO-B was directly over the blast site while STEREO-A was stationed at right angles — a perfect geometry for cracking the phenomenon on the sun known as the "solar tsunami." The scale of a solar tsunami is so staggering that solar physicists doubted their senses in the past when observing such an event. It rose up higher than Earth itself and rippled out from a central point in a circular pattern millions of kilometers in circumference. Skeptical observers suggested it might be a shadow of some kind—a trick of the eye—but surely not a real wave.

2298) <http://acis.mit.edu/acis/>

2299) Tony Phillips, "Monster Waves on the Sun are Real," NASA, Nov. 24, 2009, URL: http://science.nasa.gov/headlines/y2009/24nov_solartsunami.htm?list1291671

2300) <http://stereo.gsfc.nasa.gov/news/SolarTsunami.shtml>

• There are also some Earth–observation missions with instruments dedicated for sun observations. Examples:

– Coriolis of NRL with SMEI (Solar Mass Ejection Imager), launch Jan. 6, 2003 (see A.12).

– GOES–12 of NOAA (launch July 23, 2001). It is the first GOES–series satellite to carry a solar X–ray imager in addition to its standard imager. The instrument is called SXI (Solar X–ray Imager). It images the solar atmosphere once per minute, giving virtually continuous updates on solar flare occurrences, which can disrupt communications on Earth (see F.4.2). The SXI instrument is providing space weather forecasters with near real–time imagery of the sun’s explosive atmosphere, helping them issue timely warnings when solar activity might harm spaceborne and/or ground–based assets (see also 1.22.5). The SXI employs a small telescope that makes use of advanced technology and grazing incidence optics to allow it to see the sun’s outer atmosphere or corona in X–rays.

S/C Mission	X–Ray Instruments	Comment
AGILE (launch Apr. 23, 2007)	GRID (Gamma Ray Imaging Detector), Super–AGILE, Mini–Calorimeter	Gamma rays in 30 MeV – 50 GeV range Hard X–rays in 10–40 keV range 250 keV – 100 MeV range
ALEXIS (launch Apr. 25, 1993)	ALEXIS	Soft X–ray monitor (6 telescopes)
ARGOS (launch Feb. 23, 1999), DoD	USA (Unconventional Stellar Aspect)	X–ray timing, time–resolved spectroscopy, Feasibility tests of X–ray S/C navigation
Astro–E2/Suzaku (launch July 10, 2005)	XRS (X–ray Spectrometer), 4 XIS (X–ray Imaging Spectrometer), HXD (Hard X–ray Detector)	JAXA astronomy mission in collaboration with NASA. Astro–E2 covers the energy range 0.2–600 keV with 3 instruments. Note: In Aug. 2005, JAXA discovered that all liquid helium had evaporated making the XRS observations useless.
Bhaskara (launch Nov. 20, 1981)	X–ray monitor experiment	Study of transient and long–term X–ray sources (ISRO)
Chandra X–ray Observatory of NASA, formerly AXAF (launch July 23, 1999 on STS–93)	ACIS, HRC, HETGS, LETGS	The telescope features 4 nested pairs of grazing incidence paraboloid and hyperboloid mirrors, diameter 1.2 m, focal length of 10 m, collecting area of 400 cm ² at 1 keV
CORONAS–I (Mar. 2, 1994) CORONAS–F (Jul. 31, 2001)	TEREK–C, RES–C, DIOGENESS, HELICON, IRIS,	Study of the solar atmosphere structure
DMSP series	SSB, SSB/X–2,	Array–based systems for the detection of X–rays emitted by the atmosphere
GOMS (launch Oct. 31, 1994)	RMS	Study of solar X–ray radiation
GPS/Navstar (Block–II satellites)	IONDS, CXD is follow–up sensor	Monitoring of nuclear explosions, CXD (Combined X–ray detector and Dosimeter)
RHESSI (launch Feb. 5, 2002) initially referred to as “HESSI”	RHESSI	Study of solar flares in X–ray and gamma–ray region (3 keV to 20 MeV) covering soft and hard X–rays
IMP–8 (launch Oct. 26, 1973)	CPME, EPE	Solar X–rays
Integral (launch Oct. 17, 2002), ESA	JEM–X (Joint European X–ray Monitor) SPI (Spectrometer on INTEGRAL)	Study of X–ray sources in the energy range 3–35 keV, angular resolution of 1 arcmin Gamma–ray sources in the energy range 20 keV–8 MeV
Interball (launch Aug. 3, 1995)	SKA–2, DOK–2X, RF–15, SOSNA–2	Tail Probe instruments
IRS–P3 (launch March 21, 1996)	XRAP (X–Ray Astronomy Payload)	Study of X–ray sources
ISEE–3 (launch Aug. 12, 1978)	ANH,	Study of solar flares
JEM/Kibo, the JAXA module on ISS, launch Sept. 10, 2009	MAXI (Monitor of All–sky X–ray Image)	MAXI monitors the X–ray spectrum of extra–galactic objects

S/C Mission	X-Ray Instruments	Comment
MTI (launch March 12, 2000)	HXRS	Measures solar X-ray emissions in 8 bands
NOAA-GOES series (launch of GOES-M on July 23, 2001)	SEM package, XRS, SXI (GOES-12)	Monitoring of the solar-terrestrial environment
NuSTAR (launch on June 13, 2012)	NuSTAR	Detection of hard X-rays in the energy range of 5-80 keV
POLAR (launch Feb 24, 1996)	PIXIE (pinhole camera concept)	Study of energetic electron precipitation on and its effect on the atmosphere
Skylab (launch May 14, 1973)	S-054 and S-056	First study of the sun in X-ray range
SMART-1 (launch Sept. 27, 2003)	D-CIXS, XSM	Moon surface chemistry, swept charge detector design, instrument mass of 3 kg
SMM (launch Feb 14, 1980)	GRS, HXBRS (study of electron acceleration of solar flares), HXIS, XRP	GRS made important contributions to the international study of Supernova 87A, which in Feb. 1987 provided astronomers with their first opportunity to study such an explosion
SNOE (launch Feb. 26, 1998)	SXP	Monitoring of soft X-ray flux from the sun
SOHO (launch Dec. 2, 1995)	CDS, EIT, UVCS, LASCO	Study of the composition of the solar corona, etc.
Solar-A (launch Aug. 30, 1991)	HXT, SXT,	Study of high-energy solar phenomena
Solar-B (launch Sept. 23, 2006)	XRT	Study of high-energy solar phenomena
SORCE (Jan. 25, 2003)	XPS (SXP heritage)	Solar EUV measurement
STS-35 (Dec. 2-11, 1990), Shuttle mission of NASA	BBXRT (Broad Band X-ray Telescope)	BBXRT (first focusing X-ray telescope) was part of the ASTRO-1 payload operating in the energy range 0.3-12 keV
TRACE (launch Apr. 2, 1998)	TRACE	Study of coronal mass ejections, etc.
UARS (launch Sept 12, 1991)	AXIS,	Measurement of Bremsstrahlung X-rays from Earth
Ulysses (launch Oct. 6, 1990, end of mission: July 1, 2008)	GRB	X-ray and gamma-ray measurement of solar and cosmic origin
XMM-Newton (launch Dec. 10, 1999)	EPIC (European Photon Imaging Camera) (3), RGS (2)	EPIC can register extremely weak X-ray radiation

Table 132: Overview of some missions flying X-ray instruments (alphabetical order) ²³⁰¹

²³⁰¹ Note: The NASA mission HESSI was formally renamed in April 2002 to RHESSI (Reuven Ramaty High Energy Solar Spectroscopic Imager). This renaming is in recognition of the enormous contribution that Reuven Ramaty made to gamma-ray astronomy in general and to the HESSI program in particular. Reuven Ramaty died in 2001, after a long and distinguished career in the Laboratory for High Energy Astrophysics at NASA/GSFC.

1.23 Navigation – Geodesy in Action

Navigation is the art of establishing position and direction (orientation and heading) of an object in space (or elsewhere), generally involving distances, angles and time to known references – all based on geodetic principles. The object (platform) attitude is also of fundamental importance, since it serves in general as a reference for most sensor observations. Of particular interest are the ground–based and onboard instruments which provide inputs for orbit and/or attitude determination. In general, orbit determination is an iterative process, building upon the results of previous solutions, and on tracking data inputs from various sources over significant time periods. In spite of these obstacles, orbit determination is becoming an increasingly automated process due to better real–time computing capabilities and ever–improving algorithms (and filters) in the latter 1990s.

The functions of satellite orbit and attitude determination have traditionally been performed on the ground. Commands were then uplinked to the satellite to relay the pre-computed information. Historically, the lack of onboard processing power and the complexity of required algorithms have precluded the application of onboard orbit and attitude determination. – However, at the start of the 21st century, there is a trend to automate the orbit and attitude determination functions and to move them onboard the spacecraft. The benefits are savings in operational manpower as well as improved functionalities (ability to locate targets of opportunity, etc.). An onboard automation process is also a natural consequence of constellation and formation flight requirements, to coordinate all real–time functions in support of the planned constellation and formation–flying projects.²³⁰²⁾

In spaceflight, the term “navigation” is often a synonym for **GNC (Guidance Navigation & Control) or GN&C**, involving a) the knowledge and prediction of spacecraft position and velocity, referred to as orbit determination, and b) the execution of orbit maneuvers (station keeping, orbit raising, etc.), referred to as flight path control. In addition, the attitude of a vehicle is of importance as it performs its observation mission. A short definition of each function is:²³⁰³⁾

- Navigation is the subject of computing the position and orientation of the spacecraft platform with respect to either some inertial coordinate system (such as a star or several stars) or a rotating reference system (such as the Earth).
- Guidance is the process of propagating the current state of the spacecraft forward in time to predict the future behavior of the spacecraft and to compare it to the desired profile.
- Control is the process of orienting and moving the spacecraft platform in the desired direction required by the guidance. This includes attitude stabilization (maintaining the attitude in a desired state), attitude maneuver control (changing the attitude from one orientation, or the old state, to another orientation, the new state), and firing engines to move the spacecraft to the desired trajectory.
- Precision timekeeping is one of the bedrock technologies of modern science and technology. It underpins precise navigation on Earth and in deep space, synchronization of broadband data streams, precision measurements of motion, forces and fields, and tests of the constancy of the laws of nature over time.

Some background: The history of navigation, of finding the way, is as old as humankind. The Latin roots of “navis” (ship) and “agere” (to move or direct) indicate that navigation was mainly used in the past to guide ships across the seas. In the modern world, the term navigation encompasses the guidance generally: on the seas, on land, in the air, as well as in inner and outer space.

2302) T. C. Esposito, “Multiple Autonomous Discrete Event Controllers for Constellations,” Proceedings of IEEE Aerospace Conference, Big Sky, MT, USA, March 8–15, 2003

2303) C. Schrodinger, “GNC,” <http://www.tsgc.utexas.edu/archive/subsystems/ngc.pdf>

Some records indicate that the Chinese were using the magnetic compass (a heading or bearing device) around AD 1000, western Europeans by 1187, Arabs by 1220, and Scandinavians by 1300. This represented a first technological breakthrough.

Of particular interest to all navigators are navigation aids. Conventional “way finding methods” included the observation of landmarks on the Earth’s surface (lighthouses, beacons, buoys, prominent rocks and cliffs, sounding of water depths, shorelines, etc.), and of celestial navigation, finding position and heading (keeping course) by observation of the stars, the sun, and the moon.

The “longitude problem”: The art of celestial navigation was in particular in need of an accurate time standard. Even two centuries after Columbus, no clock could keep time well enough to aid in fixing longitude. For more than two centuries the issue of longitude determination on the high seas enticed the most enlightened minds in Europe and became such a major concern that in 1713 Britain, with the “Longitude Act”, formed a group of famous scientists (the “Longitude Board”) to find a possible solution. Twenty thousand pounds were offered to anyone who proved to be able to determine the longitude of a ship in open water with an accuracy of 30 nautical miles (about 55 km).

The problem of fixing longitude was solved, when John Harrison in England produced several chronometers between 1730 and 1763. In 1761, Harrison’s chronometer lost or gained only about one second a day – incredibly accurate for the time. For the next two centuries, sextants and chronometers were used in combination to provide latitude and longitude information.



Figure 179: Illustration of a sextant (image credit: ESA) ²³⁰⁴

The sextant, invented around 1731/32 independently by Thomas Godfrey (American Colonies) and by John Hadley (Great Britain), uses a system of mirrors to measure the exact

²³⁰⁴) Marco Lisi, “A Short History of Navigation Technologies: from Ulysses to GNSS’s,” Proceedings of the ENC–GNSS 2009 (European Navigation Conference–Global Navigation Satellite Systems), Naples, Italy, May 3–6, 2009

angle of stars, the moon and the sun above the horizon. Initially, however, the sextant could only determine latitudes (i.e. the position on Earth measured north or south of the equator). Seamen were still unable to calculate their longitude (i.e. the position on Earth east or west of a reference meridian). Then in 1757, John Campbell of the the Royal Navy (Great Britain) invented a sextant that could measure both longitude and latitude. Over the 18th and 19th centuries, sextants and chronometers were used in combination to obtain information on latitude and longitude. It was only at the beginning of the 20th century that, with the advent of radio waves, various radio navigation systems were developed, which were then widely used during the Second World War (Ref. 2304).

It took a while until humankind obtained a proper perception of Earth as a planet in the solar system and later on of its true dimensions and shape (Earth observation from space was a great help in this venture). Within the last century there have also been great strides in the observation and discovery of the surrounding universe. The early space age permitted also the first excursions into our solar system by unmanned probes with truly great achievements in navigation. However, the vastness and true greatness of the universe has been and remains to be observed by astronomy (ground-based and spaceborne).

Geodesy is the discipline of measuring and mapping the dynamic shape (and size) of the Earth's surface (the geoid representation), including the Earth's gravity field and its rotation – and the establishment of general reference systems. ²³⁰⁵⁾

This definition includes the orientation of the Earth in space, and temporal variations of the Earth's orientation, its surface and its gravity field. **Space geodesy** (also referred to as satellite geodesy) is an interdisciplinary science which uses spaceborne and airborne remotely sensed, and ground-based measurements to study the shape and size of the Earth, the planets and their satellites, and their changes; to precisely determine position and velocity of points or objects at the surface or orbiting the planet, within a realized terrestrial reference system. Positioning (or point position determination) is a subdiscipline of geodesy. In short, the three pillars of geodesy are: ²³⁰⁶⁾

- Geometry and kinematics
- Earth orientation and rotation
- Gravity field and dynamics.

Modern geodetic tools such as GPS signals, radar and laser altimetry, interferometric SAR observations, and SST (Satellite-to-Satellite Tracking) techniques are accurate enough to monitor time variations in the Earth related to plate tectonics, post-glacial, ocean circulation and atmospheric circulation. Geodesy attempts to solve geophysical problems by assimilating observable phenomena (such as variations in the Earth's rotation, gravity, geocenter, and surface deformations) into models. Today, these observations come from a variety of sources including SLR (Satellite Laser Ranging), VLBI (Very Long Baseline Interferometry), GPS, DORIS (Doppler Orbitography and Radiopositioning Integrated by Satellite) and PRARE (Precision Rate and Range-Rate Equipment).

Note: Actually, the discipline of **geodynamics** is studying the processes involved in the rotation and deformation (plate tectonics, crustal motion and deformation of the surface and sea level caused by glacial loading and unloading, etc.) of the Earth. In this context, geodesy is being used to monitor these effects. Geodesy has, in a real way, been reinvented to meet the extraordinary accuracy requirements of geodynamics.

²³⁰⁵⁾ In general relativity the terms geodesic (noun) and geodetic (adjective) refer to paths followed by massive bodies ("geodesics") and light rays ("null geodesics") in curved four dimensional space-time. This usage is an outcome of the history of tensor analysis, the mathematical machinery applied in Einstein's theory.

²³⁰⁶⁾ F. Barlier, M. Lefebvre, "A new look at planet Earth: Satellite geodesy and geosciences," The Century of Space Science, 2001, pp. 1623–1651, Kluwer Academic Publishers, URL: <http://www.ipgp.jussieu.fr/~tarantola/Files/Professional/Teaching/Seminar/Texts/Barlier-Lefebvre.pdf>

In the early 21st century, the author Benjamin F. Chao (NASA/GSFC) states: “After three decades and three orders of magnitude of advances, *space geodesy* is poised for prime time in observing the integrated mass transports that take place in the Earth system, from high atmosphere to the deep interior of the core. As such, space geodesy has become a new remote sensing tool, in monitoring climatic and geophysical changes with ever increasing sensitivity and resolution.

*The transports of mass and energy are key processes that determine the dynamics of our Earth system. The Earth system can be conveniently viewed through its components, so-called geophysical fluids – the atmosphere, hydrosphere, cryosphere, biosphere, lithosphere, and the deep interior of mantle and cores. All geophysical fluids undergo a host of mass transports for various reasons, external as well as internal. Studying these processes is undoubtedly a most interdisciplinary field in all of Earth sciences.”*²³⁰⁷⁾

1.23.1 Some background on datums and reference systems

Today’s Earth navigation is based on a geodetic coordinate system (providing a dense global coverage by using latitude and longitude to fix position) and on commonly used datums (standards) to permit proper referencing of locations in various coordinate systems, to support a multitude of map projections, to determine distances between any two points, as well as for a multitude of other functions and services. Central to almost all navigation and positioning tasks is the notion that a map coordinate is of little value without reference to recognizable features on the surface of the Earth.

- So-called ecliptic coordinates were already used by Hipparchos and Ptolemy in their star catalogs, and were the standard of celestial measurement until the Renaissance, when they were replaced by the equatorial coordinate system of the Earth. The equatorial coordinate system is identical to the ecliptic system, except that it uses the celestial equator for horizontal measurement instead of the ecliptic.
- Celestial coordinates. The celestial sphere has a north and south celestial pole as well as a celestial equator which are projected reference points to the same positions on the Earth surface. Right ascension and declination serve as an absolute coordinate system fixed on the sky, rather than a relative system like the zenith/horizon system. Right ascension is the equivalent of longitude, only measured in hours, minutes and seconds (since the Earth rotates in the same units). Declination is the equivalent of latitude measured in degrees from the celestial equator (0 to 90°). Any point of the celestial (i.e. the position of a star or planet) can be referenced with a unique right ascension and declination.
- Historically, horizontal positioning of a point on the Earth’s surface (such as latitude and longitude) evolved from calculations based on celestial observations from that location. Distinct points – or stations – could be linked by measured networks, forming the geodetic basis for mapping systems. Mapping systems in the western tradition were terrestrially based, and were referenced to specific models of the shape and size of the Earth, called reference ellipsoids. These systems were generally called “datums” (from the singular of “data”) in reference to the single specific point where the mapping system was “tied to the ground,” i.e. linked to the reference ellipsoid.²³⁰⁸⁾

Determining a vertical position was and is substantially harder than finding a horizontal position. This is because vertical positions, usually height above sea-level, are expressed relative to an equipotential gravitational surface. This can be imagined by mentally extending the plane of the ocean’s surface at the seashore inland running underneath mountains at

2307) B. F. Chao, “Geodesy Is Not Just for Static Measurements Any More,” EOS Transactions, AGU, Vol. 84, No. 16, April 22, 2003, pp. 145–156, URL: http://ncu.npotech.org.tw/Uploads/%7BDFBDD00A-27AC-45A3-B4B0-B4A565094E87%7D_2003_EOSarticle.pdf

2308) John Cloud, “Crossing the Olentangy River: The Figure of the Earth and the Military-Industrial-Academic-Complex, 1947–1972,” http://geodesy.ceegs.ohio-state.edu/50_years/Olentangy.pdf

a height corresponding to the gravitational level of the sea surface. This hypothetical sea level at rest is called the **geoid**. However, the Earth's mass is distributed unevenly, and the oceanic crust is denser than the continental crust. The result is that the real geoid undulates in comparison to the smooth and symmetrical figure of the imaginary reference ellipsoid. ²³⁰⁹⁾

- An important datum in the history of navigation is the **“International Meridian Conference of 1884”** which took place in Washington D.C. in October 1884 (attended by 41 delegates from 25 nations) on invitation of the President of the United States, Chester A. Arthur. The conference formally adopted the **Prime Meridian line (0° longitude) passing through the Greenwich Observatory near London, England**. This action of a single world meridian was highly desirable to replace the numerous one's already in existence by various seafaring nations. It was further established that: ²³¹⁰⁾

- All longitude would be calculated both east and west from this meridian up to 180°
- All countries would adopt a universal day
- The universal day would be a Mean Solar Day, beginning at the Mean Midnight at Greenwich and counted on a 24 hour clock.
- Nautical and astronomical days everywhere would begin at mean midnight
- All technical studies to regulate and extend the application of the decimal system to the division of time and space would be supported.

The International Date Line is lying along the 180° line of longitude (actually a zigzag line in the Pacific), thus establishing two simultaneous dates on Earth – to the west of this imaginary line is the location of the new day, while to the east of the 180° line there is still the date of the previous day. An explanation: A day lasts 24 hours, but a date lasts 48 hours (going through all time zones)! Two parallel dates of 48 hours each, divided by 2, provides us again our 24 hour day. The introduction of a date line solved also the problem of the circumnavigator's paradox.

The Greenwich meridian also serves as the basis for the world's standard time zone system. The mean solar time at Greenwich is now called Universal Time (UT) and was formerly called Greenwich Mean Time (GMT). The introduction of a GMT/UT meant, it is for instance 12 o'clock UT when the sun passes the meridian at Greenwich. The division into 24 time zones was suggested by the Canadian engineer Sandford Fleming in 1883. It is easy to calculate and to project onto Earth. There are 360° of longitude and the Earth takes 24 hours to rotate around its axis thus creating day and night. The time in each zone (15°) differs by one hour from the time in the next, and it differs by a multitude of an hour from the Universal Time. All places within the same zone use the same time. It is up to the individual countries whether they keep to the time zones into which they fall or not.

In this worldwide adopted coordinate system, the baseline for latitude measurement is the equator plane and the baseline for longitude measurements is half of a great circle passing through Greenwich, England. ²³¹¹⁾ Geodetic latitude and longitude are measured as angles with the origin of the angular measurements at the center of the Earth. The latitude value indicates the angular measurement above or below the equator plane, with a latitude at the equator being zero degrees. Longitude lines (meridians) are the intersection of the Earth's surface and a plane going through the Earth's north–south (rotational) axis and the point of interest on the Earth's surface. Zero degrees longitude is the longitude line passing through Greenwich, England (prime meridian plane).

²³⁰⁹⁾ Note: The geoid is a surface along which the gravity potential is everywhere equal and to which the direction of gravity is always perpendicular.

²³¹⁰⁾ <http://millennium-dome.com/info/conference.htm>

²³¹¹⁾ Note: A great circle is an imaginary circle on the surface of a sphere whose center is the center of the sphere. Great circles that pass through both the north and south poles are called meridians, or lines of longitude.

Geodetic satellites up to 1970

Geodetic accuracy increased rapidly in the decade after the launch of Sputnik (Oct. 4, 1957). Multiple satellites tested three different types of tracking systems (see 1.23.3).

- **Optical tracking** by cameras on the ground observing a series of bright ECHO satellites. These balloon satellites of 30 m diameter (ECHO – 1A launch Aug. 12, 1960) were deployed using inflation gas. ECHO (1960) and PAGEOS (Passive Geodetic Earth Orbiting Satellite) of NASA (1966) led to the first models of Earth's gravity field and of the upper atmosphere density, improving global geodetic accuracy from 200 m to 10–15 m.
- **Radio tracking** using one-way Doppler. The Transit/Tranet (1960 to 1988, US Navy), Diapason ('waveband') of CNES (19 kg, launch Feb. 17, 1966) and Diademe – 1 and – 2 (Feb. 1967, CNES) led to all-weather global positioning systems.

Transit allowed oceanographic ships to navigate with 1 km accuracy, a vast improvement over 10–20 km accuracy of celestial-navigation techniques.

- **Satellite Laser Ranging (SLR)**, a corner cube reflector experiment on satellites was first demonstrated on BE – B (Beacon Explorer – B/ or Explorer – 22) of NASA/GSFC (Oct. 10, 1964), then on GEOS – 1, (launch Nov. 6, 1965), Diademe – 1 and – 2 (Feb. 1967) of CNES. This led to measurements of a satellites position with ~ 3 m accuracy (eventually to a few cm accuracy). The measurements produced much new information about Earth's gravity field.

Geodetic satellites in the decade 1970–1980

At the same time oceanographers were perfecting altimeters, geodesists were busy refining knowledge of Earth's gravity field, an Earth reference system, and tracking station locations.

- Starlette of CNES (launch Feb. 6, 1975) was the first satellite with high mass relative to its surface area (the entire S/C surface consisted of corner cube reflectors), making it ideal for geodetic studies and mapping of earth's gravity field. The satellite was 25 cm in diameter with a mass of 52 kg. It was accurately tracked by SLR techniques.
- Lageos – 1 of NASA (launch May 4, 1976) was similar to Starlette, but operated at a higher altitude of 5950 km. It is ideal for studying polar motion and Earth's rotation. The satellite is 60 cm in diameter with a mass of 405 kg. It too is accurately tracked by laser tracking systems.

Geodetic satellites in the decade 1980–1990

- **DORIS** (Doppler Orbitography and Radiopositioning Integrated by Satellite). This is a one-way, two-frequency, ground-to-satellite Doppler tracking system developed by CNES, GRGS (Groupe de Recherches de Géodésie Spatiale), and IGN (Institut Géographique National) beginning in 1983. It was flown successfully on SPOT – 2 (launch Jan. 22, 1990) and on many later satellites, including Topex/Poseidon. DORIS was designed to produce orbits with 1 cm accuracy when used with the improved gravity fields. The system is based on the ARGOS widely used in oceanography for tracking drifters.
- **PRARE** (Precision Range and Range Rate Equipment) is a compact, spaceborne, two-way, two-frequency microwave satellite tracking system developed by the German GFZ (GeoForschungsZentrum) beginning in 1982. PRARE was initially installed on ERS – 1 (launch July 17, 1991), but could not be operated. Further PRARE uses: Meteor – 3 – 7 (launch Jan. 25, 1994, PRARE demonstration operations until March 1995), ERS – 2 (launch April 21, 1995).

Figure 180: Overview of early geodetic satellites/experiments ²³¹²⁾

²³¹²⁾ M. Lefebvre, R. Stewart, "History of Altimetry," Symposium: 15 Years of Progress in Radar Altimetry, Venice, Italy, March 13–18, 2006, http://earth.esa.int/workshops/venice06/participants/129/paper_129_stewart.pdf

More recent geodetic satellite missions are:

- Lageos-2 of ASI and NASA (deployment from space shuttle Columbia on Oct. 22, 1992, STS-52) laser ranging mission in MEO.
- Stella laser ranging mission of CNES (launch Sept. 26, 1993).
- CHAMP (Challenging Multisatellite Payload) of GFZ and DLR, Germany, launch July 15, 2000. CHAMP provides global long- to medium- wavelength recovery of the static and time variable Earth gravity field from orbit perturbation analyses for use in geophysics.
- GRACE (Gravity Recovery And Climate Experiment), a US-German dual-minisatellite SST (Satellite-to-Satellite Tracking) geodetic mission with the overall objective to obtain long-term data with unprecedented accuracy for global (high-resolution) models of the mean and the time-variable components of the Earth's gravity field. Launch of mission on March 17, 2002.
- GP-B (Gravity Probe-B) of NASA (launch April 20, 2004). The data from the GP-B gyroscopes clearly confirm Einstein's predicted geodetic effect to a precision of better than 1%. However, the frame-dragging effect is (so far) much smaller than predicted.
- GOCE (Gravity field and steady-state Ocean Circulation Explorer), an ESA mission with a launch on March 17, 2009. The mission objectives are to determine the stationary gravity field – geoid and gravity anomalies with high accuracy (1 cm of geoid heights, and 1 mgal) at spatial grid resolutions of 100 km or less over the Earth's surface.
- LARES (LAsER RELativity Satellite), an Italian laser ranging mission (launch Feb. 13, 2012). The objective is to measure in particular the effect of frame-dragging.

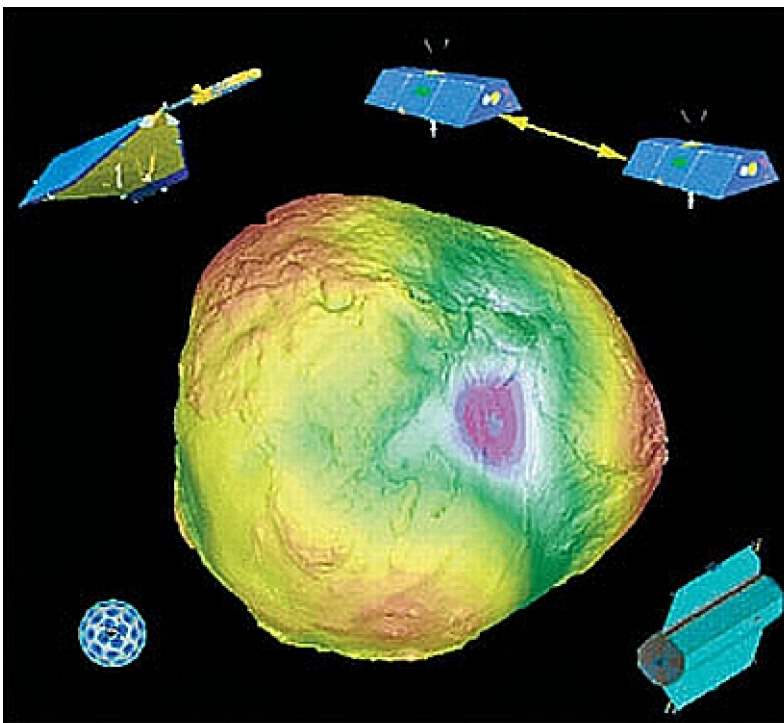


Figure 181: Animation of Earth's gravity field derived from Lageos, CHAMP, GRACE, and GOCE observations (image credit: GFZ, ESA, CEOS) ²³¹³⁾ ²³¹⁴⁾

²³¹³⁾ <http://www-app2.gfz-potsdam.de/sec13/animated-potato-e-cms.html>

²³¹⁴⁾ http://www.eohandbook.com/eohb2009/earth_gravity.html

1.23.1.1 Geodetic reference frames

While the international latitude–longitude reference frame is very suitable for navigation purposes, other geodetic (i.e. terrestrial or surface) reference frames were needed for such applications as cadastral, surveying, map making, and many other practical functions of everyday life. National geodetic reference frames were created in the past (19th century) to suit these needs. At the start of the space age, most of the national reference frames were not identical/compatible for historical reasons. In particular, large existing geodetic systems such as NAD (North American Datum), ED (European Datum) and TD (Tokyo Datum) were quite incompatible to provide a basis for inter–continental geodetic information systems. ^{2315) 2316)}

Soon after the first satellites were in orbit, geodesists, by observing the perturbing effect on satellite motion, began to evaluate the Earth’s gravitational field. The photography of satellites with respect to stars was the first type of precise measurements of the angular positions of satellites. These determinations were followed by a rapid succession of more extensive and accurate descriptions of the Earth’s gravity field. Early space geodesy was conducted primarily using optical instruments (photographic processes) adapted from earlier stellar systems.

The visual tracking of the ECHO satellites in the early 1960s put several geodetic institutes in a position, to establish for the first time geodetic intercontinental links. For example, one of the most successful tracking campaigns in this era provided the geodetic connection between Europe and Africa. The PAGEOS (Passive Geodetic Earth Orbiting Satellite) mission of NASA (launch June 24, 1966), represented a more stable balloon satellite in orbit at a higher altitude (2953 km x 5207 km). The existing Wild BC4 cameras from the US Coast Guard and USGS (United States Geological Survey) were deployed in networks occupying some 40 sites – well distributed around the Earth. The geocentric positions of the 40 stations were published and were considered at the time as making one of the first homogeneous global Earth reference systems. However, the best accuracy of these new positions (reference points) was no better than ~ 2 arcsec which translated to about 10–20 m on Earth. ²³¹⁷⁾

The first satellite equipped with laser corner cube reflectors was BE–B (Beacon Explorer–B –also referred to as Explorer–22 mission) of NASA, with a launch Oct. 10, 1964 (see chapter 1.23.3.6). The new technique of round–trip signal measurements between a ground station and the satellite permitted to calculate more precise orbits with accuracies in the 1–1.5 m range.

Radio frequency tracking: ^{2318) 2319) 2320) 2321) 2322)} With the development of the US Navy Navigation Satellite System (TRANSIT), Doppler satellite geodesy became a cheaper, more rapid technique for space geodesy. One of the striking characteristics of space geodesy in the 1960s and 1970s was the almost complete separation between the optical school and the Doppler school.

2315) Note: A geodetic coordinate system is correctly defined by describing the following: a) reference ellipsoid, b) system origin, and c) axis orientation.

2316) <http://www.nima.mil/GandG/geolav/TR80003E.HTM#ZZ11>

2317) F. Barlier, M. Lefebvre, “A new look at planet Earth: Satellite geodesy and geosciences,” The Century of Space Science, 2001, Kluwer Academic Publishers, URL: http://lareg.ensg.ign.fr/AGRET/doc/ML+FB_sci_siecle.pdf

2318) J. A. O’Keefe, A. Eckels, R. K. Squires, “The Gravitational Field of the Earth,” The Astronomical Journal, Vol. 64, No. 7, Sept. 1959, pp. 245–253

2319) H. F. Mickielsen, “Fifth Harmonic of the Earth’s Gravitational Field,” American Rocket Society Journal, p. 976, Oct. 1960.

2320) D. G. King–Hele, “Evaluation of the Second, Fourth and Sixth Harmonics in the Earth’s Gravitational Potential,” Nature, Vol. 187, p. 490, August 6, 1960

2321) W. H. Guier, G. C. Weiffenbach, “A Satellite Doppler Navigation System,” Proceedings of the Institute of Radio Engineers, Vol. 48, No. 4, pp. 507–516, April 1960

2322) A. G. Evans, R. W. Hill, G. Blewitt, E. R. Swift, T. P. Yunck, R. Hatch, S. M. Lichten, S. Malys, J. Bossler, J. P. Cunningham, “The Global Positioning System Geodesy Odyssey,” Navigation, Journal. of the Institute of Navigation, Vol. 49 No 1, pp. 7–34, Spring 2002

The TRANSIT system had a significant impact on the development of space geodesy. It proved that a system based on the measurement of the Doppler shift of signals generated by stable oscillators on board satellites could be used for positioning with a remarkable accuracy (0.1–0.5 m relative, about 1 m absolute). The satellites transmitted information on two carrier frequencies (400 MHz and 150 MHz) near the microwave band. The two frequencies allowed for a compensation of ionospheric refraction. Rather small receivers connected to omnidirectional antennas made the technique well suited to establish regional and global geodetic networks. Observation periods of a few days were required to obtain the above stated accuracy.

Satellite navigation systems such as Transit (for Doppler), GPS and GLONASS (for positioning) and other space-based measurement techniques (SLR) require a single global geodetic datum to fix position. Hence, considerable efforts in global geodetic reference frame standardization were initiated during the last four decades of the 20th century to suit the fundamental requirements on global datum definition and use. It became also apparent to extend the definitions to include more physical models, including, for instance, spherical harmonic models for the Earth's gravity field. Some of these geodetic coordinate frame efforts are (all with an Earth-centered datum):

- **WGS60** (World Geodetic System 1960).^{2323) 2324)} In 1960, research efforts of the US Army, Navy, and Air Force were combined to create the World Geodetic System of 1960, based on a combination of surface gravity data, astro-geodetic data, and Shoran (Short Range Aid to Navigation) and Hiran (an improved version of Shoran) geo-positioning surveys to obtain a best-fitting ellipsoid for the most significant datum areas.

- **WGS66** (World Geodetic System 1966). In 1966, DoD formed a World Geodetic System Committee to develop an improved WGS, based on greater surface data and increasing volumes of satellite data. The satellite data came from the Navy's TRANSIT Doppler navigation system and from four different programs of optical geodetic satellites, referred to as ANNA (Army-Navy-NASA-Air Force). The first geodetic satellite was ANNA-1B, launched in 1962. ANNA systems included geodetic cameras, electronic ranging and Doppler. These early systems have made it possible to perform various geodetic measurements to relate known or unknown positions to the Earth's center, to relate unknown positions to existing triangulation networks, and to relate the triangulation networks to each other. – The defining parameters of the WGS66 ellipsoid were the Earth flattening factor (1/298.25), determined from satellite data and the semimajor axis (6,378,145 m), determined from a combination of Doppler satellite and astro-geodetic data. A worldwide 5° x 5° mean free air gravity anomaly field provided the basic data for producing the WGS66 gravimetric geoid.

- **WGS72** (World Geodetic System 1972). A principal objective of WGS is to allow referencing of local geodetic systems to a single geocentric system. WGS72 is the result of an extensive effort (extending over 3 years) to collect satellite, surface gravity, and astrogeodetic data available throughout 1972 [a major data source were Doppler data from DoD (CORONA program) and non-DoD satellites]. These data were combined using a unified WGS solution (a large-scale least squares adjustment). The value for the semimajor axis of the WGS72 ellipsoid is 6,378,135 m (10 m shorter than the one of WGS66, based on several calculations and indicators including a combination of satellite and surface gravity data for position and gravitational field determinations). An Earth flattening factor of 1/298.26 was adopted.

Note: WGS 72, considered to be the standard for about a decade, contained a gravity field represented by about 450 coefficients and could demonstrate a system consistency of about 1 m, while the overall accuracy for tracking station locations was estimated at about 3 m.

2323) M. Hooijberg, "Practical Geodesy," Amsterdam: Springer, 1999, p. 44

2324) Note: The Shoran and Hiran systems provided a means for early electronic surveys from an airborne vehicle or a platform.

– **WGS84** (World Geodetic System 1984). WGS84 was also developed by DoD and is an improvement and a replacement for WGS72. Radar altimeter data from GEOSAT was used to deduce geoid heights from oceanic regions of latitude $\pm 70^\circ$. Geoid heights were also deduced from a large number of ground–based Doppler stations and ground–based laser satellite–tracking data, as well as surface gravity data [at the time of WGS 84 development, its reference frame realization was defined by TRANSIT tracking stations; however, to define the most accurate TRANSIT coordinates, external calibration was necessary]. **The GPS system uses the WGS84 as coordinate reference frame.** The GPS satellites send their positions in WGS84 as part of the broadcast signal recorded by the receivers, all calculations internal to receivers are also performed in WGS84. ^{2325) 2326)}

Definition: WGS84 is a set of parameters for determining geometric and physical geodetic relationships on a global scale. ²³²⁷⁾ The system includes a geocentric reference ellipsoid, a coordinate system, and a gravity field model. The ellipsoid is essentially that of the International Union of Geodesy and Geophysics Geodetic Reference System 1980 (GRS80). The coordinate system is a realization of the conventional terrestrial system, as established by the International Earth Rotation Service.

In 1983 the WGS 84 development committee adopted the BTS (Bureau International de l'Heure Terrestrial System) as the external comparison standard for the WGS 84. The BTS, based on very long baseline interferometry (VLBI) and other observations, was globally distributed and very accurate. The WGS 84 TRANSIT tracking station coordinates were adjusted to match the BTS as well as possible.

Note: In WGS 84, several thousand gravity coefficients were determined, and the separation between “Optical” and “Doppler” satellite measurements was somewhat reduced; however, most major datum parameters were greatly influenced by Doppler satellite measurements. Space geodesy computations performed with WGS 84 demonstrate internal consistency of several tens of centimeters, with an estimated accuracy of about 1 m.

- Parallel to the US efforts of DoD and other organizations, the following framework was defined within the standardization bodies of the international community: ²³²⁸⁾

GRS (Geodetic Reference System). In geodesy, two distinct reference systems are to be noted:

- An Earth–fixed coordinate system called CTS (Conventional Terrestrial System)
- A space–fixed (quasi) inertial system called CIS (Conventional Inertial System)

Both systems share the Earth's center of gravity (geocenter) as their origin, and the Earth's rotational axis as a coordinate axis. The reciprocal connection is through precession and nutation, as well as Earth–rotation (polar motion and time). The ellipsoid called GRS67 (Geodetic Reference System 1967) was recommended by IAG (International Association of Geodesy), one of seven associations within IUGG (International Union of Geodesy and Geophysics) at the Lucerne, Switzerland meeting. ²³²⁹⁾ – The ellipsoid called **GRS80** was approved and adopted at the 1979 meeting of the IUGG held in Canberra, Australia. GRS80 is based on the theory of the geocentric equipotential ellipsoid. In this system the equatorial radius of the Earth is 6,378,137 m [ellipsoid flattening factor: 1/298.257; angular velocity of the Earth: 7292115×10^{-11} rad/s; the Earth's gravitational constant (atmosphere

2325) “World Geodetic System 1984,” DoD DMA TR 8350.2, September 1987

2326) R. B. Langley, “A GPS Glossary,” GPS World, October 1995, pp. 61–63

2327) A coordinate reference frame has to be accomplished by an Earth's gravity model. For example, the WGS84 uses a spherical harmonic expansion of the gravity potential up to the order and degree 360. For Galileo a similar model must be considered. In that context, the European satellite gravity missions GOCE and CHAMP as well as the US/German mission GRACE are of importance.

2328) W. Torge, “More than 130 years of International Cooperation,” <http://www.gfy.ku.dk/~iag/handbook/his.htm>

2329) “Geodetic Reference System 1967,” International Association of Geodesy, IAG Special Publication, No 3, Paris, 1971

included): $3986005 \times 10^{-8} \text{ m}^3/\text{s}^2$]. The ellipsoidal parameters of the WGS84 standard are identical with the corresponding values of GRS80. The CIS reference is now realized by extragalactic radio sources, in connection with a limited number of fixed stars. By including the satellites' orbits into the models, geocentric station coordinates can be determined now with cm accuracy, thus realizing the CIS.

Background: 2330) 2331) 2332) 2333) 2334) 2335) In 1899 the ILS (International Latitude Service) was established to coordinate the observations of the Earth's rotation pole. These motions are caused by the gravitational forces of sun and moon as well as by geophysical processes within the atmosphere, the oceans and the interior of the Earth. In 1962 the ILS was superseded by the IPMS (International Polar Motion Service). Until 1984 the rotation of the Earth was monitored using a rigid Earth model, by IPMS and BIH (Bureau International de l'Heure) the International Bureau for Time Measurements (Paris), with latitude and time observations from a number of observatories. In 1987, IUGG decided, in cooperation with IAU (International Astronomical Union), to combine the services of IPMS and BIH into the newly established organization called IERS (International Earth Rotation Service), with the Central Bureau at the Paris Observatory. Since January 1, 1988, the Central Bureau of IERS monitors and maintains the international reference frame, referred to as **ITRF** (International Terrestrial Reference Frame). The ITRF is a set of points with their 3-D Cartesian coordinates which realize an ideal reference system, the **ITRS** (International Terrestrial Reference System). 2336)

In 1991 at the 20th General Assembly in Vienna, Austria, IUGG (and IAU) defined and adopted a new **CTRS** (Conventional Terrestrial Reference System), with consideration of relativistic effects and of Earth deformation (i.e. long-term geodynamics of plate motions). CTRS replaces the older CTS. In addition, the ITRS, as defined by the IUGG resolution No. 2, was adopted in agreement with IAU. The CTRS characteristics are:

- CTRS is defined from a geocentric non-rotating system by a spatial rotation leading to a quasi-Cartesian system
- The geocentric non-rotating system is identical to the Geocentric Reference System (GRS80) as defined in the IAU resolutions
- The coordinate time of CTRS as well as of GRS is **TCG** (Geocentric Coordinate Time)
- The origin of the system is at the geocenter of the Earth's masses including oceans and atmosphere
- The system has no global residual rotation with respect to horizontal motions at the Earth's surface.

CTRS assumes a spherical Earth, it does not take any flattening factors into account. The pole of this system is known as the CIO (Conventional International Origin). The Z-axis is coincident with the Earth's principal rotational axis, with the positive direction toward the CIO. The X-axis passes through the intersection of the CTRS reference equatorial plane and the CTRS reference meridian. The positive X-axis is in the direction of the CTRS ref-

2330) <http://www.iers.org/iers/products/itrf/>

2331) M. J. Merrigan, E. R. Swift, R. F. Wong, J. T. Saffel, "A Refinement to the World Geodetic System 1984 Reference Frame, Proceedings of ION-GPS 2002, Portland, OR, Sept. 24-27, 2002, URL: <http://www.nima.mil/GandG/sathtml/IONReport8-20-02.pdf>

2332) E. R. Swift, "Improved WGS84 Coordinates for the DMA and Air Force GPS Tracking Sites," Proceedings of ION GPS-1994, Salt Lake City, Utah, USA, Sept. 20-23, 1994

2333) R. Snay, G. Adams, M. Chin, S. Frakes, T. Soler, N. Weston, "The Synergistic CORS Program Continues to Evolve," Proceedings of ION GPS-1994, Salt Lake City, Utah, USA, Sept. 20-23, 1994

2334) C. Boucher, Z. Altamimi, "International Terrestrial Reference Frame," GPS World, September 1996

2335) Z. Altamimi, P. Sillard, C. Boucher (eds), (2001). "The 2000 International Terrestrial Reference Frame (ITRF2000), IERS Technical Note 31, Observatoire de Paris, Aug. 2001.

2336) Dennis D. McCarthy, G. Gerard Petit (eds.), "IERS Conventions (2003), International Earth Rotation and Reference Systems Service (IERS)," IERS Technical Note ; No. 32, URL: <ftp://tai.bipm.org/iers/conv2003/tn32.pdf>

erence meridian. The positive Y – axis completes the rotating right – handed Cartesian system.

An important underlying concept is that reference system definitions are purely definitions and must be realized through some defined process. Particularly relevant realizations of CTRS are:

– WGS84 as used for GPS. WGS84 is practically also a realization of the ITRS, realized and maintained by the coordinates of the GPS control station network on a global scale. The network is in fact an international collaborative activity (routine activities commenced at the beginning of 1994). The first GPS derivation of WGS 84 coordinates used data collected in 1992 from the ten USAF (United States Air Force) and DMA (Defense Mapping Agency) stations and from a set of globally distributed civilian stations defined in the ITRF. The GPS Time standard is referred to as **GPST**. GPST is the internal GPS navigation time scale, which is not adjusted for leap seconds, and which is very gently steered to UTC (USNO) modulo 1 second. GPS Time is specified to be maintained to within 1 μ m modulo integral seconds; and for the past ten years it has been maintained to within (± 25 ns) of this goal. ^{2337) 2338)}

– PZ90 (Parametri Zemli 1990 – or in English: Parameters of the Earth System 1990) as used for GLONASS since 1993. PZ90 is an Earth – centered and Earth – fixed terrestrial reference frame. PZ90 (also referred to as PZ – 90) is realized through a network of geodetic reference stations in Russia. ^{2339) 2340)}

The Russian geocentric coordinate system “The Parameters of the Earth – 1990” (PZ – 90) is used for the purposes of the geodetic provision of the orbital flights and solving the navigation problems. – The improved version of the state geocentric coordinate system “The Parameters of the Earth – 1990” (PZ – 90.02) is used for the purposes of increasing the performance specifications of the GLONASS, improving the geodetic provision of the orbital flights and solving the navigation problems. ²³⁴¹⁾

– **ITRF** (International Terrestrial Reference Frame). ²³⁴²⁾ ITRF is the realization of the ITRS through space – based measurements at specific sites (fundamental stations) around the globe and is affected by factors in the observation and processing of both the station and satellite positions and their motions. Ground – based networks of co – located space geodetic techniques at each fundamental station (VLBI, SLR, GNSS, and DORIS) are the basis for the development and maintenance of the ITRF.

The ITRF is the metric of reference for measurements of global change. ²³⁴³⁾ GGOS (Global Geodetic Observing System) of IAG (International Association of Geodesy) has established a task to develop a strategy to design, integrate and maintain the fundamental geodetic network and supporting infrastructure in a sustainable way to satisfy the long – term requirements for the reference frame.

The ITRF is used for ground navigation and for tracking spacecraft in Earth orbit. It is also used to monitor many aspects of global climate change, including sea level rise and its

2337) E. Swift, “Improved WGS 84 Coordinates for the DMA and Air Force GPS Tracking Sites,” Proceedings of ION GPS – 94, Salt Lake City, UT, Sept. 20 – 23, 1994

2338) Jörg H. Hahn, Edward D. Powers, “A Report on GPS and Galileo Time Offset Coordination Efforts,” URL: http://www.giove.esa.int/images/userpage/HAHN_GGTOSStatusPID428033.pdf

2339) J. – H. Keong, “GPS/GLONASS Attitude Determination with a Common Clock using a Single Difference Approach,” Proceedings of ION – GPS99, Nashville, TN, Sept. 14 – 17, 1999

2340) http://aviadocs.net/AIP/aic/aic-2008-03_eng.pdf

2341) Anatoly Lipin, “Application GBAS GNSS in the Russian Federation,” Paris, June 9 – 11, 2009, URL: http://www-paris.icao.int/documents_open_meetings/download.php?maincategory=84&subcategory=86&file=Day3_9_GNSS_in_RF_ALipin.pdf

2342) Z. Yang, “Regional geometric changes of the Earth Observed by VLBI, GPS and SLR,” Proceedings of the Weikko A. Heiskanen Symposium in Geodesy, Ohio State University, Columbus, OH, USA, Oct. 1 – 4, 2002

2343) Michael Pearlman, Erricos Pavlis, Chopa Ma, Zuheir Altamini, Carey Noll, David Stowers, “The Global Geodetic Observing System: Space Geodesy Networks for the Future,” 17th International Workshop on Laser Ranging Bad Koetzing, Germany, May 16 – 20, 2011, URL: http://cddis.gsfc.nasa.gov/lw17/docs/papers/session1/07-Networks1_Pearlman.pdf

sources; imbalances in ice mass at Earth's poles; and the continuing rebound of Earth's surface following the retreat of the massive ice sheets that blanketed much of Earth during the last Ice Age.

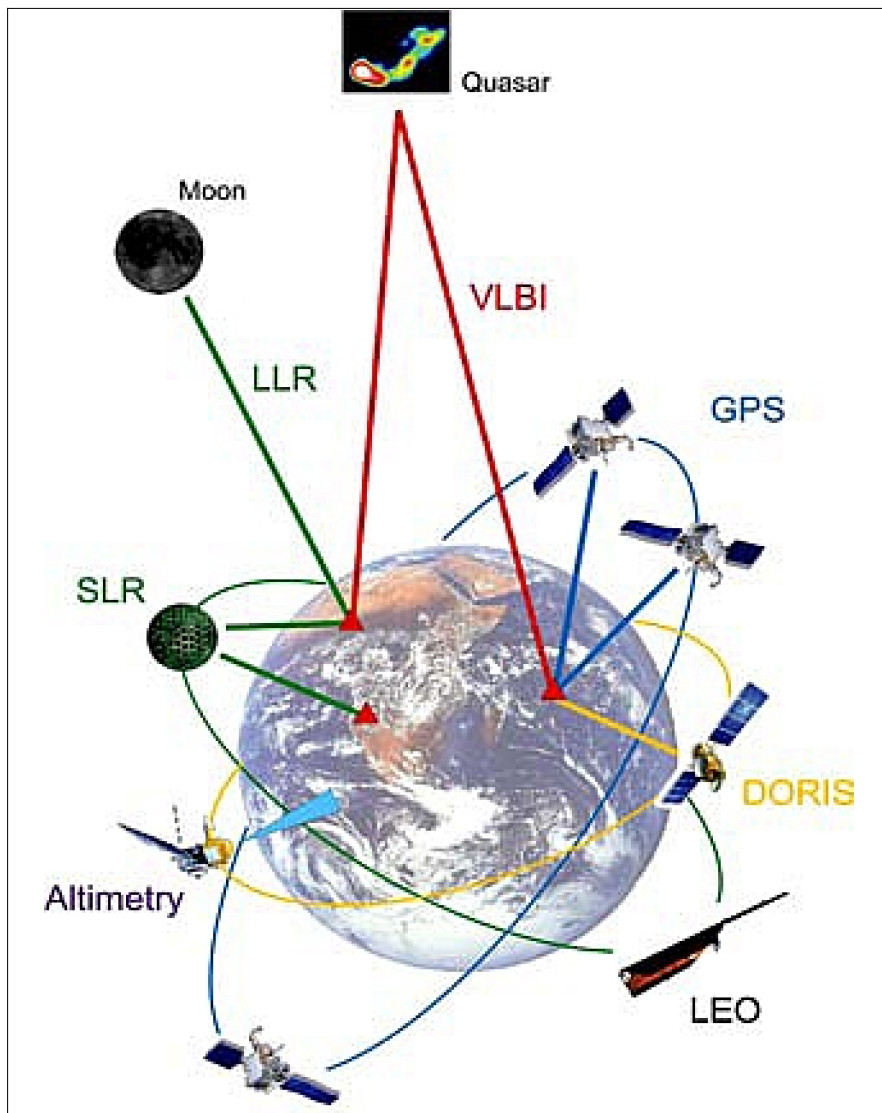


Figure 182: Integrating existing geodetic capabilities provide an improved reference frame ²³⁴⁴⁾

Some ITRF realizations are: ITRF96, ITRF97, ITRF2000, based on a combination of geodetic techniques including SLR, VLBI, GPS, DORIS (Figure 182).

- GTRF (Galileo Terrestrial Reference Frame). The European Galileo radionavigation system opted for UTC/TAI (International Atomic Time) and ITRF as its time and coordinate references. In practical terms, the GTRF will be an independent realization of ITRS (International Terrestrial Reference System). The GST (Galileo System Time) as realized in the infrastructure will be kept to within 50 ns to UTC. The GST start epoch is defined as 00:00 UT on Sunday August 22, 1999 (midnight between August 21st and 22nd). ²³⁴⁵⁾

- CGS2000 (China Geodetic System). This coordinate system is being used for the Compass/BeiDou-2 navigation constellation (full service is planned for 2015). The CGS2000 coincides with the ITRF system closely (within a few cm); hence, for most applications the

²³⁴⁴⁾ Summary Statement from the World Climate Research Program Workshop, 'Understanding Sea-Level Rise and Variability,' Intergovernmental Oceanographic Commission of UNESCO, Paris, France, June 6–9, 2006. URL: http://wcrp.wmo.int/pdf/summary%20statement%202006-1004_low-res.pdf

²³⁴⁵⁾ G. W. Hein, J. Godet, J.–L. Issler, J.–C. Martin, P. Erhard, R. Lucas–Rodriguez, T. Pratt, "Status of Galileo Frequency and Signal Design," Proceedings of ION–GPS 2002, Portland, OR, Sept. 24–27, 2002

difference between CGS2000 and ITRF can be neglected. The Compass/BeiDou–2 time reference is referred to as **BDT** (Bei Dou system Time), traced to UTC, and will be synchronized with UTC within 100 ns. The epoch time of BDT is UTC 00d 2006. Similar to the GPS time, the Compass time is a continuous time scale which does not introduce any leap seconds. BDT is derived from the atomic clock ensemble in the Compass ground control center and can be traced to UTC. ²³⁴⁶⁾

The WGS84 and ITRF reference frames are consistent. The differences between WGS84 (G1150) and ITRF2000 are in the centimeter range, worldwide. This implies for the interoperability of both GNSS systems that the WGS84 and GTRF will be identical within the accuracy of both realizations (i.e. coordinate reference frames are compatible).

IERS publishes revised ITRF positions and velocities every few years for a worldwide network of geodetic stations (some 150 sites in 2002). Each IERS solution for these positions and velocities uses observations obtained from various geodetic techniques including GPS, VLBI (Very Long Baseline Interferometry), DORIS, and SLR (Satellite Laser Ranging). New solutions not only incorporate at least an additional year of data, but also the most current understanding of the Earth's dynamics.

With regard to GPS reference stations, there are a number of national initiatives underway providing services to their user communities. These networks of reference stations serve also for an ever increasing number of applications. One of these involves crustal movements. Some examples:

- NGS (National Geodetic Survey) of NOAA/NOS created a cooperative national network called CORS (Continuously Operating Reference Station), to make data from hundreds of such GPS base stations, located in the United States, freely available to the public via the Internet. In April 2002, CORS comprised over 600 stations in USA with a growth rate of several stations per month. CORS is a composite network of GPS tracking stations or regional sub-networks established by a wide variety of agencies (over 60), institutions and private companies; it provides a reliable flow of GPS data from precisely known positions that can be used to easily access the National Spatial Reference System. CORS is also providing a number of value-added services. ^{2347) 2348) 2349)}
- In the past decade, geodetic measurements (GPS, GNSS) have been widely used to monitor crustal motions ranging from tectonic plates to local surveys of active faults, with precision levels on the order of 2–3 mm/yr (horizontally). Starting in the late 1990s, the increasing accuracy and density of space geodetic measurements has also permitted to test plate rigidity at a 2 mm/yr level. ²³⁵⁰⁾
- Japan created GEONET (GPS Earth Observation Network) ²³⁵¹⁾ in 1993 which produced a large amount of crustal movement data (secular, transient, and periodic crustal movements) over the past decade. The GEONET data clarified also various new aspects of crustal dynamics and earthquake physics.

2346) Shaowu Dong, Haitao Wu, Xiaohui Li, Shuren Guo, Qiangwen Yang, "The Compass and its time reference system," *Metrologia*, Vol. 45, December 5, 2008, pp. 47–50, URL: http://www.iop.org/EJ/article/0026-1394/45/6/S08/met8_6_S08.pdf?request-id=9dacd747-430a-42f7-9737-da72ab426f93

2347) R. Snay, G. Adams, M. Chin, et al., "The National and Cooperative CORS Program," Proceedings of the Weikko A. Heiskanen Symposium in Geodesy, Ohio State University, Columbus, OH, USA, Oct. 1–4, 2002

2348) G. L. Mader, "National CORS Network Design: Station Spacing and Data Rates," Proceedings of the Weikko A. Heiskanen Symposium in Geodesy, Ohio State University, Columbus, OH, USA, Oct. 1–4, 2002

2349) S. Hilla, M. Cline, "Evaluating Pseudorange Multipath Effects at Stations in the National CORS Network," Weikko A. Heiskanen Symposium in Geodesy, Ohio State University, Columbus, OH, USA, Oct. 1–4, 2002

2350) J.-M. Nocquet, E. Calais, "Crustal Velocity Field of Western Europe from Permanent GPS Array Solutions, 1996–2001," Proceedings of the Weikko A. Heiskanen Symposium in Geodesy, Ohio State University, Columbus, OH, USA, Oct. 1–4, 2002

2351) K. Heki, "Secular, Transient and Periodic Crustal Deformation Observed in the Japanese Nationwide GPS Array," Proceedings of the Weikko A. Heiskanen Symposium in Geodesy, Ohio State University, Columbus, OH, USA, Oct. 1–4, 2002

- The accuracy for dynamic geodesy and — to a large extent — all space geodesy, is dependent on accurate positioning of the satellite. In turn, satellite orbit computation accuracy (and satellite ephemeris accuracy) is dependent on the accuracy of the space geodesy. Satellite observations made from the ground can be used accurately only if the ground station locations are known accurately, while the orbit itself can be computed accurately only if all of the forces governing the satellite motion are known. The early dynamic geodesists observed satellite prediction errors and made bootstrap corrections to the gravity models. GPS benefited greatly from the existing WGS gravity model. Techniques that eliminate common-mode errors among ground locations provide improved accuracy over limited distances, but they still depend on satellite position accuracy. GPS geodesy, like GPS navigation, relies on the accuracy, quality, and timeliness of the orbit computation and prediction (Ref. 2322).

- The arsenal of geodetic measurement methods has increased considerably in number and accuracy since the early days of space flight. It includes some of the following techniques (besides the conventional satellite imaging, Doppler satellite surveying, and ground-based triangulation surveys):

- SLR (Satellite Laser Ranging), see chapter 1.23.3.6. There is now the **ILRS** (International Laser Ranging Service) providing high-accuracy data sets.²³⁵²⁾

- LLR (Lunar Laser Ranging). The first men on the moon on July 20, 1969 (Apollo-11 flight) deployed a rack structure (July 21) with an array of 100 fused silica retroreflectors designed to return some of the light of a pulsed laser beam to the telescope to which the laser equipment is coupled. The Apollo-11 retroreflector equipment is referred to as **LURE** (Lunar Laser Ranging Experiment). On Aug. 1, 1969, the Lick Observatory of the University of California at Santa Cruz (on Mt. Hamilton east of San Jose, CA) succeeded in obtaining strong return signals from LURE and in measuring the difference between the observed and predicted range with an accuracy of 7 m.²³⁵³⁾

Since Apollo deployed laser retroreflectors, astronomers have routinely used them track how the moon is slowly moving away from the Earth. This helps scientists develop a better understanding of the processes that are causing this motion, including what's occurring inside the moon's core and the tidal motions on the Earth.

- CEMERLL (Compensated Earth-Moon-Earth Retroreflector Laser Link), an experiment jointly performed by the U.S. Air Force Phillips Laboratory's SOR (Starfire Optical Range) and the Jet Propulsion Laboratory. The experiment was conducted at the SOR facility, Kirtland Air Force Base, New Mexico, from March through September 1994.²³⁵⁴⁾ CEMERLL was the first atmosphere-compensated laser beam propagation to the Apollo lunar retroreflectors. A Q-switched Nd:YAG beam was compensated for atmospheric turbulence and transmitted from the 1.5 m telescope at the SOR to the Apollo 15 corner-cube array near Hadley Rille on the Moon. The location of the Apollo 15 lunar reflectors is shown in Figure 183 along with the Russian Lunakhods and the Apollo 11 and Apollo 14 reflectors. The retroreflected laser pulse was collected at the 3.5 m telescope, also located at SOR. The experiment was conducted during either the first or last quarter phases of the Moon when the retroreflectors were in the dark area of the lunar landscape. The objective of the experiment was to evaluate the benefits of adaptive optics to free-space laser com-

2352) Michael Pearlman, "International Laser Ranging Service," February 12, 2009, URL: http://www.stimson.org/space/pdf/MP_Laser_Ranging_2_2009.pdf

2353) P. L. Bender, D. G. Currie, R. H. Dicke, D. H. Eckhardt, J. E. Faller, W. M. Kaula, J. D. Mulholland, H. H. Plotkin, S. K. Poultney, E. C. Silverberg, D. T. Wilkinson, J. G. Williams, C. O. Alley, "The Lure Laser Ranging Experiment," *Science*, Volume 182, Issue 4109, pp. 229–238, 1973, URL: <http://www.physics.ucsd.edu/~tmurphy/apollo/doc/Bender.pdf>

2354) K. E. Wilson, P. R. Leatherman, R. Cleis, J. Spinhirne, R. Q. Fugate, "Results of the Compensated Earth-Moon-Earth Retroreflector Laser Link (CEMERLL) Experiment," TDA Progress Report 42–131, Nov. 15, 1997, URL: http://ntrs.nasa.gov/archive/nasa/casi.ntrs.nasa.gov/20040191393_2004178891.pdf

munications by comparing the statistics of uncompensated and compensated laser beam propagation. The experiment proved the value of adaptive optics on the uplink laser. ²³⁵⁵⁾

– The Russian Lunokhod 1 retroreflector was sent aboard the unmanned Luna 17 mission, which landed on the moon November 17, 1970, releasing a robotic rover that roamed the lunar surface. The exact location of the retroreflector was somehow lost for quite some time. However, in the spring of 2010, using information of NASA's LRO instrument teams, researchers at the University of California San Diego have successfully pinpointed the location of a long lost light reflector left on the lunar surface by bouncing laser signals from Earth to the Russian Lunokhod 1 retroreflector. ²³⁵⁶⁾

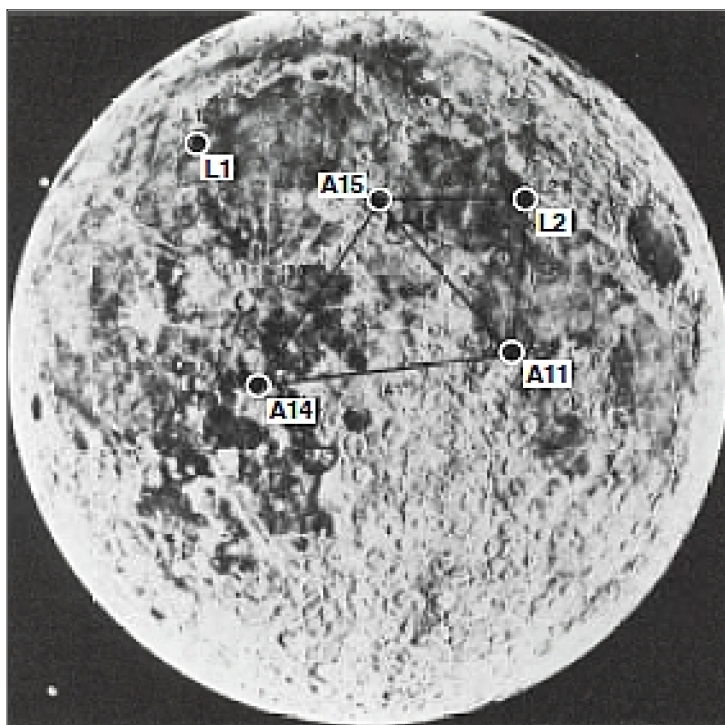


Figure 183: Locations of Apollo and Lunakod reflector packages on the Moon (image credit: AFRL)

– VLBI (Very Long Baseline Interferometry), see 1.23.3.3. Observations of extragalactic radio sources provide the geodetic information to determine the vector separations between the antennas of two widely separated radio telescopes on Earth. A major goal of VLBI is to reduce the uncertainty in intercontinental baselines to the centimeter level. IVS (International VLBI Service) is used for data set access and for coordination of activities.

– Satellite altimetry, see 1.21.2.

– The GNSS constellations of NAVSTAR/GPS, GLONASS, (and the future Galileo system), see 1.27.6. An IGS (International GPS Service) was established in 1991 to provide GPS measurements from a global network of reference stations. The official IGS service provision by IAG (International Association of Geodesy) was launched in January 1994. At the start of the 21st century, the IGS network IGS) consists of more than 200 stations and was originally set up for geodynamic applications, as determination of tectonic plate motions.

The IGS service provides a first order geometric reference worldwide; it employs, maintains and contributes to the ITRF (International Terrestrial Reference Frame). The IGS

²³⁵⁵⁾ R.J. Cesarone, D.S. Abraham, S. Shambayati, J. Rush, "Deep-Space Optical Communications, Visions, Trends, and Prospects," IEEE International Conference on Space Optical Systems and Applications (ICSOS), Pasadena, CA, USA, May 10–12, 2011, URL: <http://trs-new.jpl.nasa.gov/dspace/bitstream/2014/42088/1/11-1326.pdf>

²³⁵⁶⁾ "LRO Team Helps Track Laser Signals To Russian Rover Mirror," Space Travel, April 27, 2010, URL: http://www.space-travel.com/reports/LRO_Team_Helps_Track_Laser_Signals_To_Russian_Rover_Mirror_999.html

infrastructure (and regional and local densifications) forms the backbone for GNSS positioning and mapping activities all over the world, and not just only for the class of highest accuracy! The European densification of the IGS is EPN (EUREF Permanent Network). The IGS and EPN infrastructure are considered to play a crucial role in the implementation of the reference system for Galileo.

- SST (Satellite-to-Satellite Tracking), see 1.23.3.2. The GRACE constellation is an example of SST measurements.
- Systems such as: DORIS (Determination Orbite Radiopositionnement Integres Satellite) and PRARE (Precise Range And Range-rate Equipment).
- Inertial surveying (gradiometry and accelerometry), see 1.23.3.8. This refers to inertial navigation by determining the position and velocity of a vehicle solely by means of sensing that vehicle's accelerations and performing the necessary integrations to determine the position and velocity on a real-time basis. [Note that the technique of inertial surveying does not require inter-station visibility, and does not rely on measurements of external signals, but which can still determine relative position to a high accuracy.] Example of drag-free missions are CHAMP and GRACE.

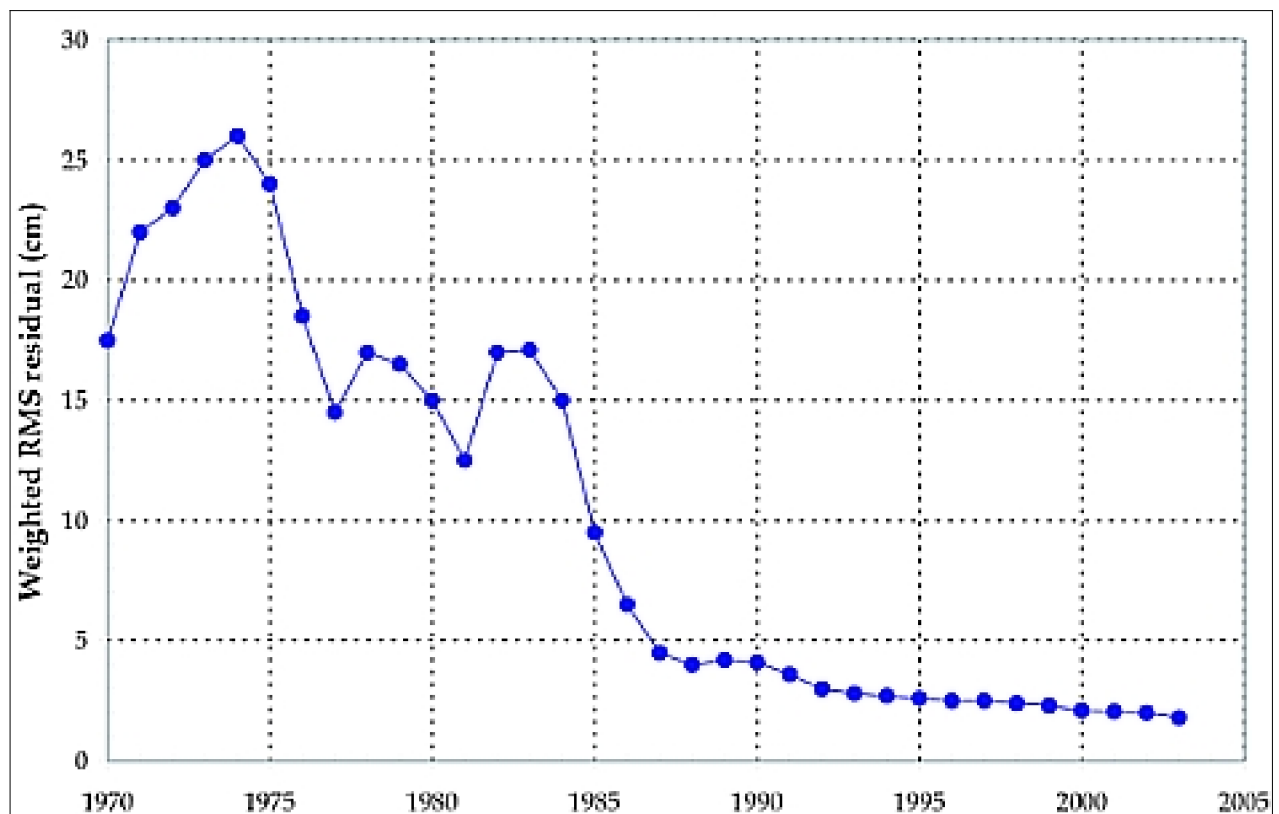


Figure 184: Historical accuracy of LLR data (image credit: INFN, NASA)²³⁵⁷⁾

- Earth rotation. The services of SLR, LLR, VLBI and DORIS are being used by IERS (International Earth Rotation Service) to monitor the Earth's polar motion and rotation time. Polar motion consists of two main signal components: the Chandler wobble with a period of 14 months, and the annual oscillation. The Chandler wobble is characterized by a time-varying energy behavior, i.e. the amplitude and the frequency are time-dependent functions. The wobble has diurnal and semi-diurnal variations with amplitudes of a fraction of a milliarcsecond (marsec) that are due to a combination of oceanic tides and atmo-

²³⁵⁷⁾ Simone Dell'Agnello, Douglas G. Currie, Giovanni O. Delle Monache, Claudio Cantone, Marina Ruggieri, Alessandro Boni, Roberto Vittori, Giuseppe Bianco, Bradford Behr, David W. Carrier, Gia Dvali, Arsen Hajian, Tom Murphy, Ken Nordtvedt, David Rubincam, "Next Generation Lunar Laser Ranging and Its GNSS Applications," Proceedings of the 2010 IEEE Aerospace Conference, Big Sky, MT, USA, March 6–13, 2010

spheric mass fluctuations; the rate of rotation fluctuates by up to a millisecond per day.²³⁵⁸⁾
2359)

Accurate knowledge of the motions of the pole is important for maintenance of reference frames and understanding of planetary physics. For instance, the causes of temporal variations in the Earth's gravity field arise in response to changes in the mass distribution both on and beneath the Earth's surface. It turns out that water movement (both of surface water and groundwater) is one of the major causes of fluctuations in mass on the Earth's surface. Other causes for Earth's gravity variations are being attributed to mass changes in the atmosphere, the oceans, postglacier rebound (from the enormous mass of the glaciers), and melting ice in the polar regions.

- Establishment and maintenance of the (four-dimensional) geometric reference frame. This task is primarily solved by the geometry-related IAG (International Association of Geodesy) services, namely IERS (International Earth Rotation Service), IGS (International GPS Service), IVS (International VLBI Service) and ILRS (International Laser Ranging Service). The geometric reference frame is (must be) used for all high-accuracy applications (e. g., precise orbits for LEOs (Low Earth Orbiting satellites).

- WRS (World Reference System).²³⁶⁰⁾ WRS is simply a global notation system for data of the Landsat program (Note: it should be understood that WRS has nothing to do with a geodetic frame, it is placed here simply for convenience). WRS enables a user to inquire about satellite imagery (ground coverage in any repeat cycle) over any portion of the world by specifying a nominal scene center designated by PATH and ROW numbers. The WRS has proven valuable for the cataloging, referencing, and day-to-day use of imagery transmitted from the sensors of the Landsat program.

- WRS-1 is being used for the Landsat-1 to -3 mission data. The 18-day ground coverage cycle for Landsat 1-3 is accomplished in 251 orbits. WRS-1 assigns sequential path numbers from east to west to 251 nominal satellite orbital tracks, starting with number 001 for the first track which crosses the equator at 65.48° west longitude.

- WRS-2 is being used for Landsat-4, -5 and -7 mission data (extension to WRS-1). WRS-2 defines Landsat scenes as 185 km x 180 km rectangular areas on the Earth's surface designated by path and row coordinates. The 16-day ground coverage cycle for Landsat 4-7 is accomplished in 233 orbits. Hence, the WRS-2 system is made up of 233 paths numbered 001 to 233, east to west, with Path 001 crossing the equator at 64.60° west longitude.

- All members of the "A-train" (afternoon constellation of NASA: Aqua, PARASOL and Aura) are also using the WRS-2 frame; except CALIPSO and CloudSat.

- Positioning (Ref. 2322): The term **absolute positioning**, when used in the discipline of geodetic surveying, generally refers to a process that establishes the Earth-centered, Earth-fixed coordinates of a solitary station on the Earth's surface. Unlike relative positioning (differential positioning), the absolute positioning process does not depend on use of a previously determined reference station position. Instead, a set of satellite positions and clock states are obtained from an existing satellite ephemeris. A position estimation algorithm is employed that uses data collected at the solitary station over some period of time, typically at least a few hours or more.

2358) Note: The wobbling motion of the Earth was first detected by Seth C. Chandler (US astronomer, 1846-1913) in 1891 and has been under observation ever since. The Earth pole motion phenomenon is also referred to as the "Chandler Wobble." The pole motion, due to the dynamic flattening of the Earth, appears when the rotation axis does not coincide anymore with the polar main axes of inertia.

2359) B. F. Chao, C. Bruyning, "Forcing of Polar Motion in the Chandler Frequency Band: An Opportunity to Evaluate Interannual Climate Variations," AGU EOS Transactions, Vol. 86, No 3, Jan. 18, 2005, p.26

2360) <http://landsat.gsfc.nasa.gov/about/wrs.html>

1.23.1.2 Gravity datums and some measurement concepts

The gravity field of the Earth is variable in both space and time, and is an integral constraint on the mean and time variable mass distribution in the Earth. The study of the Earth's gravity field leads to the determination of the geoid. The geoid is by definition the main **equipotential surface** (an ellipsoid) of the Earth's gravity field – it would coincide with the ocean surface without ocean currents, winds, and other disturbances, i. e., with the hypothetical sea surface. The geoid is used as a datum for gravity surveys (a hypothetical ocean surface at rest). **The gravity field is in effect the natural reference to define the vertical position: the height.** It is also defined as the physical (or gravimetric) reference system. With its determination, the representation of 70% of the Earth's surface (the oceans) is achieved. The Earth's gravity field (high resolution and precision) is needed for many applications in the geosciences. In geodesy, for example, the gravity field is needed for levelling with GPS, in oceanography it is important for studying ocean circulation, in geophysics a better knowledge of the Earth's gravity field provides also better boundary conditions in the study of the Earth's interior. Also, a precise ocean geoid model is essential to recover dynamic sea – surface topography, and thus ocean circulation, by satellite altimetry.

- **Historical background** on gravity reference systems (gravity models). Traditionally, scientists constructed gravity maps using a combination of land measurements and ship records. However, those measurements weren't accurate enough to capture the slight changes in water movement that cause gravity to change over time.

In 1900, the so – called “Vienna Gravity System” was adopted by IAG (International Association of Geodesy). A strategy was devised of establishing a global gravity standard by connection with relative measurements to the most accurate possible absolute station. A much improved “gravity datum” was the so – called “Potsdam Gravity System” in 1906. Reversible pendulums were used to measure absolute gravity at Potsdam, Germany. The value measured at this time was later adopted as the initial point for the “Potsdam gravity reference system.” Using relative measurements, several points on each continent were connected to Potsdam, and these served as the fundamental base stations for many relative gravity surveys.

The Potsdam system, however, was found to be in error and, in 1971, was replaced by the **IGSN – 71** (International Gravity Standardization Net 1971). The IGSN contains 1854 re – occupiable stations distributed worldwide. The acceleration of gravity at each point was determined by a least squares adjustment that included a number of absolute gravity measurements and a multitude of relative gravity measurements that interconnected all stations. The IGSN – 71 established the basic “gravity datum” for today's relative gravity surveys. – Since there are variations in the densities of the Earth's crustal materials as well as terrain variations, the observed gravity of the earth varies irregularly from point to point. As a result the surface known as the geoid is an irregular figure.

- The first spaceborne gravity field of Earth was produced in 1983 derived from altimetric measurements. The necessity of a high – resolution satellite – borne gravity field mission was already defined in 1969 in the so – called “**Williamstown Report**” by the leading geoscientists at that time. The idea was to derive the gravity field and positions at the Earth's surface and in space consistently at the same level of precision. But somehow, such a mission could not be realized due to a lack of funding. ²³⁶¹⁾

At the start of the 21 century, survey methods for EGMs (Earth Gravity Models) can be obtained from satellite altimetry with spatial resolutions of 2' x 2' (arcsec), and an accuracy of 2 – 10 mgal. The accuracy is limited by tide models, troposphere, editing, etc. Many gravity field models (regional and global scale) have been developed since the availability of alti-

²³⁶¹⁾ Williamstown Report:: “The Terrestrial Environment: Solid – Earth and Ocean Physics: Application of Space and Astronomic Techniques,” Report of a Study at Williamstown, MA., to NASA, William M. Kaula (ed.); NASA Contractor Report CR – 1599, 1970

metry data, only a few global models are being listed here for reference. The interested reader is referred to the following reference. ²³⁶²⁾

- EGM96 (Earth Gravity Model 1996). Developed in 1996–1998 as a collaborative effort of NASA/GSFC, NIMA and OSU (Ohio State University). It is based on surface gravity data, altimeter–derived gravity anomalies from ERS–1 and from GEOSAT, extensive satellite tracking data (GPS, TDRSS, DORIS, TRANET), and direct altimeter ranges from TOPEX/POSEIDON, ERS–1, and GEOSAT. ²³⁶³⁾ ²³⁶⁴⁾ [2365\)](#)
- IFE88E2 (Institut für Erdmessung 1988) University of Hannover, Germany in cooperation with the Kort–og–Matrikelstirelsen, Denmark and the Statens Kartverk, Norway. IFE88E2 is a tailored model, complete to degree and order 360. ²³⁶⁶⁾ IFE88E2 is based on the OSU86F (Ohio State University 1988) coefficients set, which was used as a start model. The low degree coefficients of the OSU86F were not modified due to the limited data collection area and due to the fact that these coefficients are well determined from the analysis of the satellite orbit perturbations.
- OSU91A (Ohio State University 1991 A). ²³⁶⁷⁾ The OSU91A potential coefficients model was obtained as a merger of two potential coefficients data sets:
 - A potential coefficients model up to degree 50, selected on the basis of a combination of the GEM–T2 (Goddard Earth Model–T2) potential coefficients, surface gravity normal equations and one year of GEOSAT altimeter data
 - A potential coefficients model from degree 51 to degree 360, calculated using a global set of adjusted anomalies (combination solution with the GEM–T2 potential coefficients and a recent 30° x 30° mean gravity anomaly data set).
- GEM–T3 (Goddard Earth Model–T3). ²³⁶⁸⁾ This model was developed by NASA/GSFC in the early 1990s from tracking data acquired on 31 satellite orbits in combination with surface gravimetry and satellite altimetry (GEOS–3, SeaSat, GEOSAT). It describes the gravity field up to degree and order 50.
- GGM01 (GRACE Gravity Model 01) of 2003. ²³⁶⁹⁾ ²³⁷⁰⁾ GGM01 has been computed from 111 days of GRACE K–band ranging data (spanning April to Nov. 2002); it is differenced from a global mean sea surface (MSS) computed from a decade of satellite altimetry to determine a mean dynamic ocean topography (DOT). For the first time, all major current systems are clearly observed in the DOT from spaceborne measurements. At wavelengths of 500 km or longer, GGM01 produces a better marine geoid than any previous gravity model. The accuracy of final GRACE geoids is expected to be a few out to a degree/order of 70.

2362) http://www-app2.gfz-potsdam.de/pb1/op/grace/index_GRACE.html

2363) F. G. Lemoine et al. "The Development of the Joint NASA GSFC and the National Imagery and Mapping Agency (NIMA) geopotential Model Egm96," NASA/TP–1998–206861. NASA/GSFC, July 1998.

2364) <http://164.214.2.59/GandG/wgs-84/egm96.html>

2365) "EGM96: The NASA GSFC and NIMA Joint Geopotential Model," URL: <http://cddis.gsfc.nasa.gov/926/egm96/egm96.html>

2366) T. Basic, H. Denker, P. Knudsen, D. Solheim, W. Torge, "A new geopotential model tailored to gravity data in Europe," Gravity, Gradiometry and Gravimetry, International Association of Geodesy Symposia, Symposium n. 103, R. Rummel and R. G. Hipkin Eds., Springer–Verlag, pp. 109–118, 1990.

2367) R. H. Rapp, Y. M. Wang, N. K. Pavlis, "The Ohio State 1991 geopotential and sea surface topography harmonic coefficient models," Report n. 410, Department of Geodetic Science and Surveying, The Ohio State University, Columbus, Ohio, 1991.

2368) F. J. Lerch, R. S. Nerem, et al., "Geopotential models from satellite tracking, altimeter and surface gravity data GEM–T3 and GEM–T3S," Journal of Geophysical Research, Vol. 99, n. 82, pp. 2815–2839, Feb. 10, 1994.

2369) B. D. Tapley, D. P. Chambers, S. Bettadpur, J. C. Ries, "Large scale ocean circulation from the GRACE GGM01 Geoid," Geophysical Research Letters, Vol. 30 No 22, 2163, doi:10.1029/2003GL018622, Nov. 15, 2003.

2370) http://www.csr.utexas.edu/grace/gravity/ggm01/GGM01_Notes.pdf

- Earth Gravity Model “EIGEN–GRACE_02S” (from GRACE data only, released Feb. 13, 2004): An Earth gravity field model complete to degree and order 150 from GRACE.²³⁷¹⁾
- GGM02 (GRACE Gravity Model 02) is based on the analysis of 363 days of GRACE in–flight data, spread between April 4, 2002 and Dec 31, 2003. GGM02 was released Oct. 29, 2004. GGM02 is an improved Earth gravity field model.²³⁷²⁾

GRACE (Gravity Recovery and Climate Recovery) is a cooperative US–German dual–minisatellite mission with a launch March 17, 2002 – and the reason for the greatly improved gravity models. The mission concept makes use of measurements of the inter–satellite range and its derivatives between two co–planar satellites (in low–altitude and polar orbits), using a K–band microwave tracking system (with ultrastable quartz oscillators) and a GPS receiver system (BlackJack) for precision orbit determination to enable accurate orbit determination. The tiny relative orbital changes of the two GRACE spacecraft permit to deduce the Earth’s minute gravity field changes from one month to the next mostly due to the mass changes of water on Earth’s surface. Since water in all its forms has mass, the ocean can actually be weighted as it moves around (changes in polar ice caps or local rainfall may also be determined). – Hence, GRACE observes the hydrologic cycle of Earth, allowing the analyst to track water as it evaporates into the atmosphere, falls on land in the form of rainfall or snow, or runs off into the ocean. The biggest freshwater hydrologic events that GRACE detects are the rainfall runoff in the larger river basins, like the Amazon, and the monsoon cycle in India. In addition to gauging changes in water mass on Earth’s surface, GRACE can detect large–scale water (or moisture) changes underground.²³⁷³⁾

- Some background on differential gravity (“g”) measurements:²³⁷⁴⁾ Instrumental capabilities for both relative and absolute gravity measurements have evolved over the last 40 years of the 20th century to the point, where today measurements can be made at the parts in 10^9 level of precision ($1 \mu\text{gal} \cong 10^{-9} \text{ g}$). Conventional instruments which measure gravity differences are basically the pendulum and the gravimeter (which is in essence a spring balance). A gravimeter consists of a measured weight on a spring scale.²³⁷⁵⁾

By the mid 19th century, measurement capabilities (pendulum method) for g had reached a precision of 1 in 10^6 ($1 \text{ mgal} \cong 10^{-6} \text{ g}$) and an accuracy of 1 in 10^5 . In the 20th century, two principle gravimeter methods have been employed (both can be used to measure the vertical gravity differences at the $10 \mu\text{gal}$ level of precision):

- The LaCoste & Romberg gravimeter that uses a “zero length” spring to create a stable mechanical configuration with the result that a small change in gravity results in a large position change of the supported mass.
- The Scintrex gravimeter that uses a simple (fused silica) spring with a (necessarily) high degree of temperature control (to avoid temperature induced changes in the length of the spring masquerading as gravity changes) and a sensitive sensor to detect the minute gravity–induced length changes of its spring.

The 2nd half of the 20th century saw also the development of free–fall and free–fall interferometric methods for absolute gravity measurement (1980). As a consequence, JILA, an interdisciplinary institute for research at the University of Colorado and NIST, developed

2371) C. Reigber, R. Schmidt, F. Flechtner, R. König, U. Meyer, K.–H. Neumayer, P. Schwintzer, S. Yuan Zhu, “An Earth gravity field model complete to degree and order 150 from GRACE: EIGEN–GRACE02S,” *Journal of Geodynamics* Vol. 39, No 1, 2005, pp. 1–10

2372) <http://www.csr.utexas.edu/grace/gravity/>

2373) Laura Naranjo, “Matter in Motion: Earth’s Changing Gravity,” *The Earth Observer* (NASA), Vol. 17, Issue 5, Sept.–Oct. 2005, pp. 4–6

2374) J. E. Faller, “The Measurement of the Acceleration due to Gravity,” *Proceedings of the Weikko A. Heiskanen Symposium in Geodesy*, Ohio State University, Columbus, OH, USA, Oct. 1–4, 2002

2375) Note: Gravity may be observed by an absolute technique (e.g. in a free fall experiment) or relatively (as a difference) by a spring gravimeter.

the “JILAg” instrument in the 1990s, capable of measuring absolute gravity at the parts in 10^9 level of accuracy. JILAg was commercialized in 1998 as the FG-5 (tradename) via a government-to-industry technology transfer. As of 2001, FG-5 is a transportable absolute gravimeter apparatus of Micro-g Solutions, Inc. of Erie, CO. The instrument measures the gravity gradient by tracking the differential free-fall of two simultaneously falling objects with a laser interferometer. ²³⁷⁶⁾

The technique of airborne gravimetry has advanced considerably over the last decade. Beginning with Greenland (1995) and extending to other regions of the world lacking in terrestrial gravity observations, airborne gravity surveys have proven to be accurate and cost effective. Airborne gravimetry has made a significant contribution to the Arctic Gravity Project, an initiative under IGGC (International Gravity and Geoid Commission) of IAG (International Association of Geodesy), where the gravity anomaly field of the entire Arctic region north of 64° N has been compiled on a $5' \times 5'$ grid. The goal of airborne gravimetry is to achieve a 1 mgal precision with a spatial resolution of 1 km. Airborne gravimetry has contributed to the development of EGM96 and will play a significant role in future Earth Gravity Models (EGM200X). ²³⁷⁷⁾

Conventionally, the gravity field has been treated as a static field because it is dominated by the internal mass distribution of the solid Earth, which was created on time scales from millions to billions of years. With the new satellite gravity missions, complemented by airborne gravity, it is possible to observe variations caused by dynamic processes (mass redistribution) that vary on time scales from hours to thousands years.

Current plans call for the development of a gravitational model ²³⁷⁸⁾ complete to degree and order 720 by 2005/6 (suitable for CHAMP, GRACE and GOCE). From about 2008 onwards, it is expected that the computation of a 1 cm geoid accuracy with 100 km half wavelength will become possible.

- On the spaceborne side, the Earth’s gravity field is being measured with the use of three techniques:

- 1) Gravity measurements using GPS signals have been demonstrated in the 2nd half of the 1990s in combination with INS (Inertial Navigation System) devices. High-performance GPS/INS navigation systems, flown on aircraft, have proven to be suitable for vector gravimetry determination by a number of analyses and tests with actual data. In this configuration, the gravity vector can be determined with a precision of 3–6 mgal and a spatial resolution of about 10 km. This translates into a geoid profiling capability with a precision of better than 10 cm. ²³⁷⁹⁾

A variation of this technique is to track the orbit of a low-altitude satellite precisely with a system like GPS in combination with an accelerometer. The measurement by the accelerometer onboard the satellite, at its center of mass, is then used to determine the non-gravitational surface forces (solar radiation, aerodynamic drag, and so forth) to which the satellite is subjected, in order to find the trajectory deviations induced by the Earth’s gravitational anomalies alone. The US/German CHAMP mission (launch July 15, 2000) employs such a system.

- 2) Satellite-to-satellite tracking (SST) technique. This involves the measurement of relative speed variations of two low-altitude satellites induced by gravitational anomalies.

2376) J. P. Schwarz, D. S. Robertson, T. M. Niebauer, J. E. Faller, “A Free-Fall Determination of the Newtonian Constant of Gravity,” *Science*, Vol. 282, 2230–2234, 1998

2377) S. C. Kenyon, R. Forsberg, J. Brozena, N. K. Pavlis, “The Contribution of Airborne Gravimetry to the Arctic Gravity Project and Future Earth Gravity Models,” *Proceedings of the Weikko A. Heiskanen Symposium in Geodesy*, Ohio State University, Columbus, OH, USA, Oct. 1–4, 2002

2378) N. K. Pavlis, “Some Design Considerations for the Development of a New Earth Gravitational Model,” *Proceedings of the Weikko A. Heiskanen Symposium in Geodesy*, Ohio State University, Columbus, OH, Oct. 1–4, 2002

2379) C. Jekeli, J. Serpas, “Geoid Profiling Using Airborne GPS/INS Vector Gravimetry,” *Proceedings of the Weikko A. Heiskanen Symposium in Geodesy*, Ohio State University, Columbus, OH, USA, Oct. 1–4, 2002

This concept is being practiced in the US/German GRACE mission (launch Mar. 17, 2002). See also chapters 1.23.3.2 and 1.23.3.8 for more information.

3) Use of two accelerometers onboard a satellite and determination of the difference between the accelerations measured by each instrument. The difference is representative of the gravity gradient along the axis of the two accelerometers. This is a one-axis gradiometer. The GOCE mission of ESA (launch March 17, 2009) employs such a concept.

- **GGMplus** (Global Gravity Model plus): GGMplus provides maps and data of Earth's gravity at 200 m resolution for all land and near-coastal areas of our planet between $\pm 60^\circ$ latitude.

In August 2013, a new ultrahigh resolution picture of Earth's gravity was provided over all continents and numerous islands within $\pm 60^\circ$ latitude. This was achieved through augmentation of new satellite and terrestrial gravity with topography data and use of massive parallel computation techniques, delivering local detail at ~ 200 m spatial resolution. The new picture of Earth's gravity encompasses a suite of gridded estimates of gravity accelerations, radial and horizontal field components, and quasi-geoid heights at over 3 billion points covering 80% of Earth's land masses. The new models are beneficial for a wide range of scientific and engineering applications and freely available to the public. ²³⁸⁰⁾

The new high-resolution maps of Earth's gravity field were created by a joint Australian-German research team, led by Christian Hirt of Curtin University in Western Australia, and the Technical University of Munich, show gravitational variations up to 40% larger than previously assumed. ^{2381) 2382)}

GGMplus describes the Earth's gravity field in terms of frequently used functionals (i) gravity accelerations, (ii) gravity disturbances, (iii) North-South and East-West deflections of the vertical, and (iv) quasigeoid heights at 3,062,677,383 points at 7.2 arcsec spatial resolution. ²³⁸³⁾

GGMplus is a composite gravity field model that is based on GRACE and GOCE information (providing the spatial scales of 10000 down to ~ 100 km), EGM2008 (scales of 100 km to ~ 10 km) and topographic gravity effects from RTM-forward-modelling (~ 10 km to ~ 250 m). In particular, GGMplus incorporates:

- 7 years of GRACE satellite data (ITG2010s by University of Bonn,) ²³⁸⁴⁾
- 2 years of GOCE satellite data (4th-generation TIM-4 release by European Space Agency) ^{2385) 2386)}

²³⁸⁰⁾ Christian Hirt, Sten J. Claessens, Thomas Fecher, Michael Kuhn, Roland Pail, Moritz Rexer, "New ultra-high resolution picture of Earth's gravity field," *Geophysical Research Letters*, 2013, Article first published online: 28 Aug. 2013, DOI: 10.1002/grl.50838, URL of abstract: <http://onlinelibrary.wiley.com/doi/10.1002/grl.50838/abstract>

²³⁸¹⁾ "Gravity Variations Over Earth Much Bigger Than Previously Thought," *Science Daily*, Sept. 4, 2013, URL: <http://www.sciencedaily.com/releases/2013/09/130904105345.htm>

²³⁸²⁾ Megan Meates, "Gravity variations much bigger than previously thought," Curtin University, Sept. 4, 2013, URL: http://www.eurekalert.org/pub_releases/2013-09/cu-gvm090413.php

²³⁸³⁾ "GGMplus 200m-resolution maps of Earth's gravity field," Western Australian Centre for Geodesy, Aug. 13, 2013, URL: <http://geodesy.curtin.edu.au/research/models/GGMplus/index.cfm>

²³⁸⁴⁾ Torsten Mayer-Gurr, Enrico Kurtenbach, Anette Eicker, "The ITG GRACE 2010 model," University of Bonn, Germany, 2010, URL: <http://www.igg.uni-bonn.de/apmg/index.php?id=itg-grace2010>

²³⁸⁵⁾ Roland Pail, Sean Bruinsma, Federica Migliaccio, Christoph Förste, Helmut Goiginger, Wolf-Dieter Schuh, Eduard Höck, Mirko Reguzzoni, Jan Martin Brockmann, Oleg Abrikosov, Martin Veicherts, Thomas Fecher, Reinhard Mayrhofer, Ina Krasbutter, Fernando Sansò, Carl Christian Tscherning, "First GOCE gravity field models derived by three different approaches," *Journal of Geodesy*, Vol. 85, 2011, pp: 819-843, DOI 10.1007/s00190-011-0467-x,

²³⁸⁶⁾ Roland Pail, Helmut Goiginger, Wolf-Dieter Schuh, Eduard Höck, Jan Martin Brockmann, Thomas Fecher, Reinhard Mayrhofer, Ina Krasbutter, Torsten Mayer-Gurr, "GOCE-only Gravity Field Model derived from 8 months of GOCE data," *Proceedings of '4th International GOCE User Workshop', Munich, Germany, 31 March - 1 April 2011, (ESA SP-696, July 2011),* URL: http://www.iapg.bv.tum.de/mediadb/1733001/1733002/p11_pail.pdf

- The EGM2008 global gravity model (by the US NGA (National Geospatial Intelligence Agency), ²³⁸⁷)
- 7.5 arcsec SRTM topography data (V4.1 release, 2008) ²³⁸⁸)
- 30 arcsec SRTM30_PLUS bathymetry data (V7.0 release) over near–coastal areas. ²³⁸⁹)

The Earth’s gravitational pull is smallest on the top of the Huascaran mountain in the South American Andes, and largest near the North Pole.

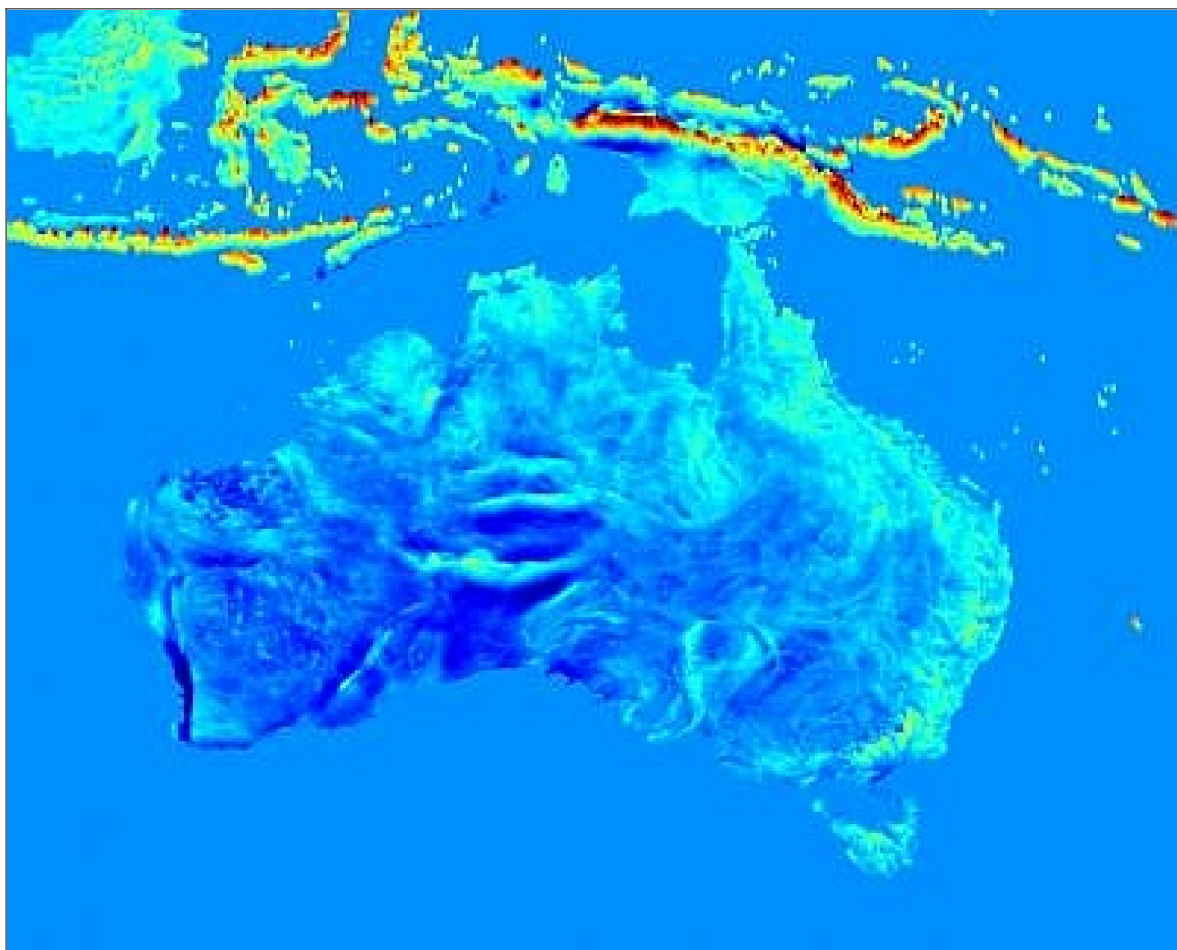


Figure 185: New high–resolution gravity map (an extract) over Australia and South–East Asia (image credit: Christian Hirt, Curtin University)

2387) Nikolaos K. Pavlis, Simon A. Holmes, Steve Kenyon, John K. Factor, “The Development and Evaluation of the Earth Gravitational Model 2008 (EGM2008),” *Journal of Geophysical Research*, 2012, doi:10.1029/2011JB008916

2388) A. Jarvis, H. I. Reuter, A. Nelson, E. Guevara, “Hole–filled SRTM for the globe Version 4, “ 2008, available from the CGIAR–CSI SRTM 90m Database, URL: <http://srtm.csi.cgiar.org>

2389) J. J. Becker, D. T. Sandwell, W. H. F. Smith, J. Braud, B. Binder, J. Depner, D. Fabre, J. Factor, S. Ingalls, S–H. Kim, R. Ladner, K. Marks, S. Nelson, A. Pharaoh, R. Trimmer, J. Von Rosenberg, G. Wallace, P. Weatherall, “Global Bathymetry and Elevation Data at 30 Arc Seconds Resolution: SRTM30_PLUS,” *Marine Geodesy*, Vol. 32, Issue 4, 2009, pp: 355–371, DOI: 10.1080/01490410903297766

1.23.2 Attitude sensing and actuation instruments

Spacecraft attitude refers to the angular orientation of the spacecraft body vector with respect to an external reference frame. Generally, an AOCS (Attitude Orbit Control Subsystem) or simply an ADCS (Attitude Determination and Control Subsystem) consists of a set of **sensors** (to measure attitude and position of the S/C), and a set of **actuators** to impart control functions (torques and forces) to the attitude and orbit of a S/C. An AOCS periodically acquires measurements (on the satellite attitude and orbital position) from a set of sensors and uses them to compute control signals that are sent to a set of actuators. A constraint imposed by all instrument design are physical characteristics involving size, mass, and power requirements of the device. The major performance characteristics are generally: accuracy, stability, FOV, modulation transfer function, resolution and reliability.

The most common types of attitude sensors are:

- Sun sensor: to measure the direction of the sun line in the sensor's reference frame. The FOV of a sun sensor is nearly hemispherical.
- Earth horizon sensor: measures the Earth's horizon direction in the sensor's FOV (Field of View).
- Magnetometer (magnetic compass): measures the direction (and strength) of the Earth's magnetic field in the sensor's FOV. Their accuracy is generally low and varies widely from system to system. The fluxgate magnetometer is the most common type utilized in space flight (heading device).
- Gyroscope: measures the inertial angular rate of the satellite. Gyroscopes can have one or two sensitive axes. They give the projection of the satellite angular rate on the sensitive axes. Gyroscopes are often combined in packages to give measurements along up to six axes.
- Star sensor: measures the positions of several stars in its field of view. It also performs pattern recognition on the stars it sees to identify the portion of sky at which it is looking.
- GPS receiver: primarily used for position determination; it can also provide an inertial measurement of the host satellite attitude.
- A very uncommon but rather effective attitude sensor is CESS (Coarse Earth–Sun Sensor) of CHAMP and GRACE heritage (a patented design of EADS Astrium GmbH). CESS will also be flown on CryoSat (launch Oct. 8, 2005 – but **launch failure**) and TerraSAR–X (launch June 15, 2007). CESS provides attitude measurements ($< 6^\circ$) with respect to the Earth and sun for initial acquisition and coarse pointing. The FOV of CESS is a full spherical one, i.e. no special search maneuvers are necessary to find the Earth or the sun. The concept is based on temperature differences measured by 6 omnidirectional arranged sensor heads (PT1000 thermistors) about the S/C surface. Three of these sensors are covered with a black paint coat, while the other three are covered with an OSR (Oil Stain Remover) coated sense area. Hence, each of the two equally sized sensor segments provide well known absorption properties in infrared (as same as possible) and visible spectral ranges (as different as possible). Subsequent computation in the software part yields the direction of the Earth and the sun vector (when visible). At spacecraft rates $< 0.5^\circ/\text{s}$, the mean error (rms over one orbit) is $< 6^\circ$ for the Earth and sun vector at a 1σ noise of 1° (0.5°) for the Earth (sun) vector.

The most common types of actuators are:

- Reaction wheels (RW) and momentum wheels (MW): a set of rotating wheels that can be accelerated or braked. The action of accelerating or braking causes a torque to be applied to the satellite by reaction. The primary difference between RW and MW systems is in the nominal spin rate of the flywheels. Reaction wheels typically have zero nominal angular velocity, which slowly changes in response to small environmental torques. Once the maxi-

imum operating speed is reached, external torques must be applied to the spacecraft in a “momentum unloading” maneuver. These torques are typically applied using thrusters or magnetic torquer rods. Momentum wheels typically have a momentum bias, and spin at a large angular velocity, which slowly changes to absorb small environmental torques. Momentum unloading maneuvers are also required. Examples: All SPOT satellites of CNES use magnetically suspended momentum wheels, as does the AMSAT AO40 satellite, launched on November 15, 2000.

- **Magnetorquers:** devices that interact with the Earth’s magnetic field to generate a control torque. This function may be used for S/C attitude adjustment or for momentum unloading (see also 1.23.2.4 on magnetometry).
- **Thrusters:** generally, a gas jet is emitted which imparts a force to the spacecraft. If the direction of the gas jet does not go through the satellite center of gravity, then a torque on the satellite results. By combining jets from suitably located thrusters, it is possible to apply either pure forces or pure torques to the satellite. A thruster system or RCS (Reaction Control System) may also be used for reaction wheel unloading.

The gravity gradient stabilization is considered a passive technique. All early satellites were spin–stabilized to maintain inertial orientation.²³⁹⁰ The spinning motion creates a stiff angular momentum vector which tends to resist external disturbance torques. However, spinners usually require a supplementary active control system to initiate and adjust the spacecraft’s spin rate and attitude and to counteract disturbances. Spin stabilization typically provides pointing accuracies between about $0.3 - 1^\circ$, depending on the spin rate.

Satellites with three–axis stabilization employ a multisensor attitude control assembly; however, this was not available technology in the early days of spaceflight. The three–axis concept is the most accurate method of stabilization, and the spacecraft may be pointed, in principle, into any direction, with accuracy limited only by the sophistication of the control system. At the turn of the 21st century, there is a tendency to replace conventional Earth horizon sensors and also sun sensors of the attitude control system by star trackers. Stars provide a much finer reference (point source) thus keeping the satellite pointing more accurately (in fact, stars provide an inertial reference).

The image formed of a star by focussing through a lens is actually not a point but a blurred spot. Thus point sources emit light which is processed by the optical system, because of diffraction (and the possible presence of aberration), this light is smeared out into some sort of blur spot over a finite area on the image plane rather than focus to a point. When this patch is scanned the distribution of intensities can be described by a mathematical function. This function is known as the **point spread function (PSF)** of the lens. It is the impulse response of the system whether it is optically perfect or not. In a well corrected system, the PSF is the Airy irradiance distribution function centered in the Gaussian image point.²³⁹¹

IMU (Inertial Measurement Unit). For S/C that use onboard guidance and undergo multi–axis propulsion, IMUs are necessary to provide the information needed to update the spacecraft’s position and velocity. IMUs may also provide attitude updates for these S/C.

Sensing method	Accuracy	Axes	Comment
Sun sensor	0.1°	2	Cheap, simple, reliable, intermittent use only during orbit; determines direction/vector to the sun; provides accurate two–axis pointing knowledge
Earth horizon sensor	0.05°	2	Expensive, orbit dependant, poor in yaw; distinguishes Earth’s horizon, usually by its IR transition or horizon; there are multiple types of horizon sensors.

2390) Note: The development of early satellite stabilization technology is closely related to the study of spinning objects. The so–called “major–axis–rule” states that a spacecraft can only be spin–stabilized about its major axis, due to the internal energy dissipation which is present in any physical system.

2391) C. Fosu, G W. Hein, B. Eissfeller, “Determination of Centroid of CCD Star Images,” Proceedings of ISPRS 2004, Istanbul, Turkey, July 12–23, 2004

Sensing method	Accuracy	Axes	Comment
Magnetometer	1°	2–3	Cheap, low altitude only, continuous coverage; measures direction of Earth's magnetic field
Star Tracker	0.001°	3	Expensive, heavy, complex, very accurate; conventional employ CCD imager, newer types use APS technology; inertial reference
Gyroscope	0.001°/hr	3	Expensive, drifts with time; senses rotation rate, not attitude; three gyros for three-axis measurements; rate is integrated over time to determine changes in attitude; inertial reference

Table 133: Common attitude sensing techniques/devices

- The first spaceborne horizon sensor was flown on TIROS–2 (launch Nov. 23, 1960). A further new feature on this S/C was the introduction of magnetic attitude control, i.e., adjustment of spin axis orientation along the orbital path. The attitude device consisted of 250 cores of wire wound around the outer surface of the spacecraft. The interaction between the induced magnetic field in the spacecraft and the Earth's magnetic field provided the necessary torque for attitude control.

Method/System	Accuracy	Axes	Comment
Spin stabilization	0.1 – 1.0°	2	Passive, simple, cheap, inertially oriented; S/C is spun about an axis with high moment of inertia. Spin must be maintained by another system (thrusters, etc). A spin stabilized spacecraft may be a pure spinner, or it may be dual spun. In a dual-spin S/C the payload, e.g. the antenna, is despun while the other portion of the S/C spins to provide gyroscopic stability.
Gravity Gradient (GG)	1 – 5°	2	Passive, simple, cheap, central body oriented; to completely determine attitude, another sensor is needed. Often, a sun sensor or magnetometer is being used in combination. GG can provide a stable reference below an orbital altitude of 2000 km. Torque range: 10^{-6} – 10^{-3} Nm.
RCS (Reaction Control System)	0.01 – 1°	3	Expensive, quick response, consumables; active control using multiple thrusters; torque range: 10^{-2} – 10 Nm. IMUs or accelerometers are being needed to update both position and attitude.
Magnetorquer	1 – 2°	2	Cheap, slow, lightweight, LEO only; magnetic torquer (coils or rods) use a current through wires that interacts with the Earth's magnetic field to produce a torque. Torque range: 10^{-2} – 10^{-1} Nm.
Momentum wheel (MW)	0.1 – 1°	2	Expensive, similar to dual spin; momentum wheels operate with a bias momentum, meaning that they run at a steady-state, non-zero speed. There are several MW types: A zero momentum wheel – stabilizes one axis by changing the rotational rate to produce a torque. Momentum and reaction wheels do not exert external torques on a S/C. Instead, they exchange momentum with the vehicle, enabling it to rotate about an axis while the wheels themselves speed up or slow down accordingly.
Reaction wheel	0.001 – 1°	3	Expensive, precise faster slew; Usually at least three zero momentum wheels aligned with each axis. Reaction wheels usually operate at a nominal speed of zero. They provide control torque by changing their speed of rotation. In this way, angular momentum is exchanged between the wheel and the S/C. Torque range: 10^{-1} – 1 Nm
CMG (Control Moment Gyro)	0.001 – 1°	3	Expensive, used to be heavy, quick for fast slew, 3-axes; CMG: one or more wheels on gimbals that rotate; CMG, is a high-performance actuator that consists of wheels spinning at constant speed, mounted on one or more gimbals. Torque range: 10^{-2} – 10^3 Nm.

Table 134: Common actuation techniques for attitude control

Passive Control	Semi-passive Control	Active Control
Gravity Gradient (GG)	Momentum bias with magnetics	Propellant
Spinner with nutation damping	Reaction wheels with magnetics for momentum dumping	Reaction wheels with propellant for momentum dumping
Dual spinner with nutation damper	CMGs with magnetics for momentum dumping	CMGs with propellant for momentum dumping

Table 135: Overview of various attitude control concepts

- The first microsatellite known to fly a modern momentum exchange device is TUBSAT-B (launch Jan. 25, 1994, mass of 40 kg) of the Technical University of Berlin. The reaction wheel is based on a modified COTS DC brushless motor. The technology of the reaction wheel was further enhanced on the TUBSAT-N nanosatellite (launch July 7, 1998, mass 8 kg). A single 659 g reaction wheel was used, along with a magnetic control system. A further improved ADCS (Attitude Determination and Control Subsystem) was used on DLR-TUBSAT (launch May 26, 1999, mass 45 kg). The microsatellite used 3 improved reaction wheels. The reaction wheels for all TUBSAT missions were provided by Teldix GmbH of Heidelberg. More recent Teldix wheels (Teldix RSI-01 and -02) are based on the TUBSAT wheel design and have been used on a number of small missions including KITSAT-3 (KAIST, launch May 26, 1999), Inspector (EADS Astrium, launch Oct. 5, 1997 to MIR Station), Orbcomm (microsatellite constellation of Orbcomm), and on PROBA-1 (DLR, launch Oct. 22, 2001). The first reaction wheel developed by SSTL was flown on FASat-Alfa (launch Aug. 31, 1995) and FASat-Bravo (launch July 10, 1998).
- Programmed yaw steering of the S/C. The ERS-1 S/C (launch July 17, 1991) of ESA introduced the concept of yaw steering (a form of dynamic attitude control) to compensate for Earth rotation (about 4° per orbit). The vertical axis of the S/C is pointed towards the geodetic nadir to optimize the observation performance of its payload instruments. This involves a carefully controlled rotation about the yaw axis over the course of each orbit. As a result, the natural coordinate system of the radar instrument (AMI) remains orthogonal to the ground track of the S/C. In addition, ERS-1 introduced a roll-tilt mode in which the entire S/C can be rotated about its horizontal axis. This permits radar imaging at different incidence angles over limited periods of time.

1.23.2.1 Sun sensors

Historically, the first sun sensors were employed in the early 1950s for the guidance of ground-based solar telescopes as well as in automatic sextants. They entered the space age on rocket flights in the late 1950s. The development of solar cells for spacecraft power generation provided indirect benefits to the sun sensor technology. Silicon solar cells suitably modified, photodiodes, and light-activated semiconductor controlled rectifiers were rapidly incorporated into solar sensor designs. ²³⁹²⁾

The sun was used as the first natural reference in space flight for attitude determination of the spacecraft and/or sensor orientation (attitude calculated from sun angle measurements), usually in combination with an Earth horizon sensor and/or other sensors (magnetometers, gyroscopes, etc.). A multitude of sun sensor designs have been developed throughout the space age for a great variety of applications and performance characteristics (coarse and fine pointing combinations, etc.). ²³⁹³⁾

Two categories of conventional sun sensors exist: digital and analog types. ²³⁹⁴⁾ The digital sun sensor illuminates different geometric patterns on the detector plane. The presence or absence of light imaged on the plane defines a digital signal that can be translated into the

2392) J. Bebris, et al., "Spacecraft Sun Sensors," NASA Space Vehicle Design Criteria (Guidance and Control), NASA SP-8047, June 1970, URL: <http://www.aoe.vt.edu/~cdhall/courses/aoe4065/NASADesignSPs/sp8047.pdf>

2393) Note: For spinning spacecraft, a sun sensor provides the solar aspect angle, referring to the angle between the spin axis and the spacecraft - sun vector

sun angle. In comparison, an analog sun sensor outputs analog currents, from which the sun angles can be derived directly.

– **Digital Sun Attitude Detector (DSAD).** The apparent position of the sun is an important spacecraft attitude measurement that is used by virtually all attitude determination and control subsystems. This measurement is commonly made with a sensor called a digital solar attitude detector (DSAD). DSAD is a sensor assembly and technology that computes the 2-D position of a bright spot (sun) within its FOV. All DSAD detectors are comprised of an optical system, (often a pinhole, or an array of slits), a position-sensitive detector (sometimes constructed from an array of discrete photodetectors), and an electronic signal processing system to provide an interface to the spacecraft. JHU/APL is a principal developer of the DSAD technology sponsored by NASA's ATP (Advanced Technology Program). A DSAD imaging system is planned to fly in NASA's STEREO mission (launch Oct. 26, 2006) to demonstrate the feasibility of autonomous solar navigation.

The next step in the program was the development of a **μDSAD** (Micro DSAD), capable of incorporating the entire sensor and its interface on a single chip. Such a sensor is of great utility in microsatellites in support of formation flying as well as many other applications. The patented μDSAD design combines a centroiding position-sensitive active-pixel architecture (on CMOS basis, 0.5 μm process, 200 x 200 pixels) with standard imaging capability for providing optional "engineering channel" images (for use in monitoring solar panel, boom, and antenna deployments or for sighting stars or other items of interest). The chip includes all analog support circuitry. An external FPGA is used to implement digital control and an I²C interface (4 wires including power and ground). The entire system (μDSAD chip and FPGA controller) dissipates less than 20 mW with nominal illumination conditions.^{2395) 2396)} The first two prototype μDSAD sensors are being flown on NASA's CONTOUR (Comet Nucleus Tour) mission with a launch on July 3, 2002.

– **Micro sun sensor.** As of 2002, NASA/JPL developed a micro sun sensor based on MEMS technology. The design employs a tiny gold and chrome-plated silicon wafer placed at a distance of 0.9 mm from an APS (Active Pixel Sensor) chip. The APS chip contains all camera functions on the chip. The mask consists of hundreds of pinholes. The sun angle can be determined based on the position of the aperture centroids, just like a sundial. The centroid of the apertures is calculated with algorithms similar to those utilized in star trackers. The packaged micro sun sensor has a mass of 11 grams, a volume of 4.2 cm³ and a power consumption of 30 mW. The accuracy of the micro sun sensor is better than 1 arcminute and the maximum field of view is 160°. The micro sun sensor is essentially a pinhole camera with an f/No of about 30 and multiple pinholes. It consists of two key components: 1) a MEMS based mask and 2) a "camera on a chip" APS image detector. The high-resolution multi aperture mask is placed close to the image detector.²³⁹⁷⁾

– **DSS (Digital Sun Sensor).**²³⁹⁸⁾ In 2002, a low-cost DSS was developed within the framework of ESA's ARTES-5 program (built by TNO-TPD, EADS-SODERN, and FillFactory). The sensor employs APS detector technology (512 x 512 pixels) with on-chip AD conversion. A FOV of 120° x 120° is provided with a target accuracy of 0.02° and a resolution of 0.01°. The sensor incorporates a maximum of operational autonomy.

2394) [5] James R. Wertz: "Spacecraft Attitude Determination and Control," D. Reidel Publishing Company, Dordrecht, Holland, 1978, pp. 858 (13th printing of the book as of 2001).

2395) M. N. Martin, K. Strohbehn, S. E. Jaskulek, "Micro Digital Solar Attitude Detector Chip," Proceedings of IEEE Aerospace Conference, Big Sky, MT, March 8-15, 2003

2396) S. E. Jaskulek, K. Strohbehn, M. N. Martin, "Micro Digital Solar Attitude Detector and Imager," AIAA/USU Conference on Small Satellites, Logan UT, Aug. 13-16, 2001, SSC01-IX-2

2397) C. C. Liebe, S. Mobasser, Y. Bae, et al., Micro Sun Sensor, "Proceedings of the IEEE Aerospace Conference, Big Sky, MT, March 9-16, 2002

2398) N. van der Heiden, C. W. de Boom, R. Robin, M. Pochard, H. Meier, "Design, Production and Test of a low cost Digital Sun Sensor (DSS) by TNO-TPD, SODERN, and FillFactory," 5th ESA Conference on Guidance Navigation and Control Systems, Oct. 22-25, 2002, Frascati, Italy, ESA SP-516

- Autonomy in attitude and orbit determination in an Earth–sun based system. An inherent disadvantage of conventional Earth–sun based attitude sensing functionality of an AOCS (Attitude and Orbit Control Subsystem) are occasional singularities (for instance: occasional or periodic collinear positions of Earth and sun references), during which a direct three–axis attitude determination is no longer possible. Instead of using ground–based measurements, onboard GPS attitude measurements in combination with various attitude sensors, e.g. star sensors, are used in a semi–autonomous AOCS. The nomenclature “semi–autonomous” is used since the solution relies on the presence of GPS satellites for orbit determination.

1.23.2.2 Sextant–type attitude and position determination in spaceborne missions

The idea of a sextant–type optical navigation capability in space is as old as spaceflight itself. Robert J. Magee of MIT (Massachusetts Institute of Technology) began his studies and experimentation of a space sextant concept in 1959. The design employed two telescopes, a reference (fixed) telescope, and an adjustable acquisition telescope, both mounted in the same plane of sight.²³⁹⁹⁾ The operation of the sextant required in addition a pair of sun finders, a general–purpose computer, and a reaction system to make corrections to the vehicle’s flight path. This was indeed a very bold and courageous undertaking in the very early space age, considering the non–existence of any space infrastructure with regard to instrumentation, algorithms, and processors to handle such a monumental task.

The traditional sextant is an observation instrument with double–reflecting mirrors, which combines the locations of dual objects into a single image for the determination of angles between reference surfaces and/or celestial bodies. In all Earth–based applications, use is made of “local vertical” or “local horizontal” references to obtain a location determination. However, the realization of a generalized sextant concept in space turned out to be rather demanding. Position and attitude determination by a single instrument in orbit around a central body requires multiple references to determine a) the instantaneous state vector to the center of the body, and b) angular references to celestial bodies. For an Earth–orbiting spacecraft, this implies the simultaneous and continuous knowledge of the Earth center vector, as well as angle references to celestial bodies for an unambiguous triangulation analysis (free of singularities). Obviously, the most accurate celestial references in this observation scheme are provided by the stars as inertial references and point sources.

A modern optical multi–target (or multi–object) sensor design approach, such as an Earth–Star based imaging system in an AOCS (Attitude and Orbit Control Subsystem)²⁴⁰⁰⁾ of a spacecraft, offers the means to mimic the sextant design concept and to provide sufficient processing power. It has the potential to provide a fully autonomous attitude and position determination service, including the function of a planning tool (navigation aid) in space flight. In fact, such a space sextant system is capable to provide a rather generalized solution, regardless of orbit type (LEO, GEO, etc.), including satellite observations in orbits around other planets.

Following are some examples of sextant–concept introduction/demonstration in spaceborne missions.

- The first spaceborne sextant experiments (with a hand–held device) were conducted aboard Gemini–4 (June 4–7, 1965) and in the follow–up Apollo missions. The instrument was designed to measure the angle between the edges of the Earth, or the angle between celestial bodies. The astronauts took angular readings on stars, the planets, the moon, and other visible objects to derive the spacecraft’s position along its trajectory.

2399) R. J. Magee, “An Automatic Space Sextant for Space Navigation,” American Rocket Society (ARS), Space Flight Report to the Nation, New York, Oct. 9–15, 1961, ARS–2250–61

2400) C. Kuehl, M. Melf, H. Diehl, E. Gottzein, “Micro Tech Sensor for Attitude and Orbit Determination,” Proceedings of the 26th AAS Conference on Guidance and Control, Breckenridge, CO, Feb. 5–9, 2003, Vol. 113 Advances in the Astronautical Sciences, Edited by I. J. Gravseth and R. D. Culp

– SS–ANARS (Space Sextant–Autonomous Navigation and Attitude Reference System). SS–ANARS, a USAF instrument within STP (Space Test Program), built by Martin Marietta Aerospace, Denver, CO, was flown on Shuttle flight STS–4 (June 27–July 4, 1982), as part of a DoD payload (the SS–ANARS project definition started in 1973). Obviously, this new sextant design was strongly influenced by Magee’s earlier design. SS–ANARS was a gimballed two–telescope system, consisting of a lunar– and a star telescope, azimuth prism, elevation collimation mirror, and a gyro package. The objective was to provide an onboard angle determination capability with the use of an onboard computer by measuring the angles between celestial bodies to an accuracy of 1 arcsec. Observations of stars and lunar limb angles from a nadir reference gyro were measured. The Earth horizon azimuth and elevation were separately referenced. The total mass of the SS–ANARS instrument was about 112 kg. – The major drawbacks of this sextant implementation were: a) the relative motion of the two telescope FOVs (Field of View) to each other, and b) only two lines of sight were used (in a single acquisition), resulting in an ambiguity/unobservability of the complete state (position and attitude), as is the case for a Sun–Earth–sensor combination. From hindsight, the SS–ANARS development was indeed a very complex and challenging design, a bold and daring attempt by all parties involved.²⁴⁰¹⁾

– A more advanced scheme of an onboard sextant–mode implementation into a single instrument (Earth/star optical imaging system) of an AOCS was flown on MITA.^{2402) 2403) 2404) 2405) 2406)} The MITA (Microsatellite Italiano a Tecnologia Avanza) mission of ASI, Italy (launch July 15, 2000; end of mission Aug. 15, 2001, LEO orbit of 450 km altitude), carried a technology sensor package by the name of **MTS–AOMS** (Micro Tech Sensor–Attitude and Orbit Measurement System), developed and funded by EADS Astrium GmbH (see M.26) and consisting of three elements: an APS (Active Pixel Sensor) Camera with beamsplitter–optic, a Magnetic Field Sensor, and an Angular Rate Sensor (ESA provided the flight opportunity for this package in its Technology Flight Opportunity Program). A major objective was to obtain combined attitude and orbit measurements in the optical AOCS experiment by referencing Earth’s horizon and star images. The camera with beamsplitter optics and APS detector (size of 386 x 290 pixels), was used in this experiment in a so–called **‘sextant–mode’ configuration**. This arrangement permitted the simultaneous imaging of the star field and the Earth horizon onto the detector via the beamsplitter. The MTS–AOMS flight experiment was an experimental prototype with no onboard processing capability. *Although this new dual–object camera observation concept was challenging from the standpoint of image processing (algorithms for Earth horizon and center determination) – it represented in effect a first–step result to a “true autonomous attitude and orbit determination capability” by means of a single optical AOCS instrument.*

– The next logical step in the space sextant development process is obviously the provision of real–time onboard algorithms (in form of an ASIC or a microprocessor implementation), supporting the sextant orbit and attitude determination; and of course a flight opportunity for a full demonstration of the autonomous sextant capability.

2401) A. D. Mikelson, “Integrated Orbit/Attitude Determination,” AGARD Spacecraft Pointing and Position Control 13 p (N82–20208 11–12)}, Nov. 1981, URL of Abstract: http://adsabs.harvard.edu/cgi-bin/nph-bib_query?bibcode=1981sppc.agar.....M

2402) C. Kuehl, M. Melf, H. Diehl, E. Gottzein, “Experimental Evaluation of the Micro–Tech–Sensor for Attitude and Orbit Determination,” 16th IFAC Symposium on Automatic Control in Aerospace, Volume 2, Session 9, June 14–18, 2004, Saint Petersburg, Russia

2403) Considerable information and background to this chapter was kindly provided by Christopher Kuhl of EADS Astrium GmbH, Munich, Germany

2404) C. T. F. Kuhl; M. Melf; H. Diehl; E. Gottzein, “Flight Test Results of the Micro–Tech–Sensor for Attitude and Orbit Determination,” ESA/ESTEC, Fourth Round Table on Micro/ Nano Technologies for Space, May 2003

2405) M. Melf, S. Manhart, “Micro–Tech.–Sensor for Attitude and Orbit Determination,” ESA/ESTEC, Third Round Table on Micro/Nano Technologies for Space, May 2000

2406) H. Diehl, W. Platz, H. Zinner, E. Gottzein, “Kombinierter Erd–Sternsensor für gleichzeitige Bahn– und Lagebestimmung,” Patent: DE 198 46 690 A1, 1998

1.23.2.3 Gyroscopes

Some gyroscope history: The mechanical gyroscope (gyros=rotation in Greek) has been around since the early 1800s. The first known modern prototype gyroscope apparatus was built in 1810 by Johann G. F. von Bohnenberger (1765–1831) of Tübingen, Germany. It was made using a heavy ball instead of a wheel, but since it had no scientific application, it faded into history.

In 1851, the French physicist J. B. Leon Foucault (1819–1868) first conceived of the gyro as an inertial reference (he also named the instrument “**gyroscope**” consisting of a rotor wheel mounted in gimbal rings to permit free turning in any direction— Foucault detected the Earth’s rotation in his pendulum experiment). Foucault subsequently showed that a gyroscope could detect the rotation of the Earth (a gyroscope employs the principle of conservation of angular momentum). The better-known demonstration of the **Foucault pendulum** (a purely mechanical system) showed that the plane of rotation of a freely-swinging pendulum rotated with a period that depends on the latitude of its location. In 1852, on the basis of this experiment, Foucault invented the first spinning gyroscope in which the inertia of the rotor’s axis of rotation is substituted for that of the plane of vibration.

The availability of electricity set the stage of the first electrically driven gyroscope by G. M. Hopkins in 1890. In 1908, the German inventor H. Anschütz-Kaempfe patented the first gyroscopic compass that aimed in the north direction. In the same year, the American entrepreneur Elmer A. Sperry (1860–1930) patented his version of a gyroscopic compass (the first automatic pilot) into a usable technology which found immediate applications in early aircraft and later in maritime navigation. The first automatic pilot for ships was produced by the Anschütz Company in Kiel, Germany, and installed in a Danish passenger ship in 1916. Also in 1916, a three-frame gyro was used in the design of the first artificial horizon for aircraft. This instrument indicates roll (side to side) and pitch (fore and aft) attitude to the pilot and is especially useful in the absence of a visible horizon.

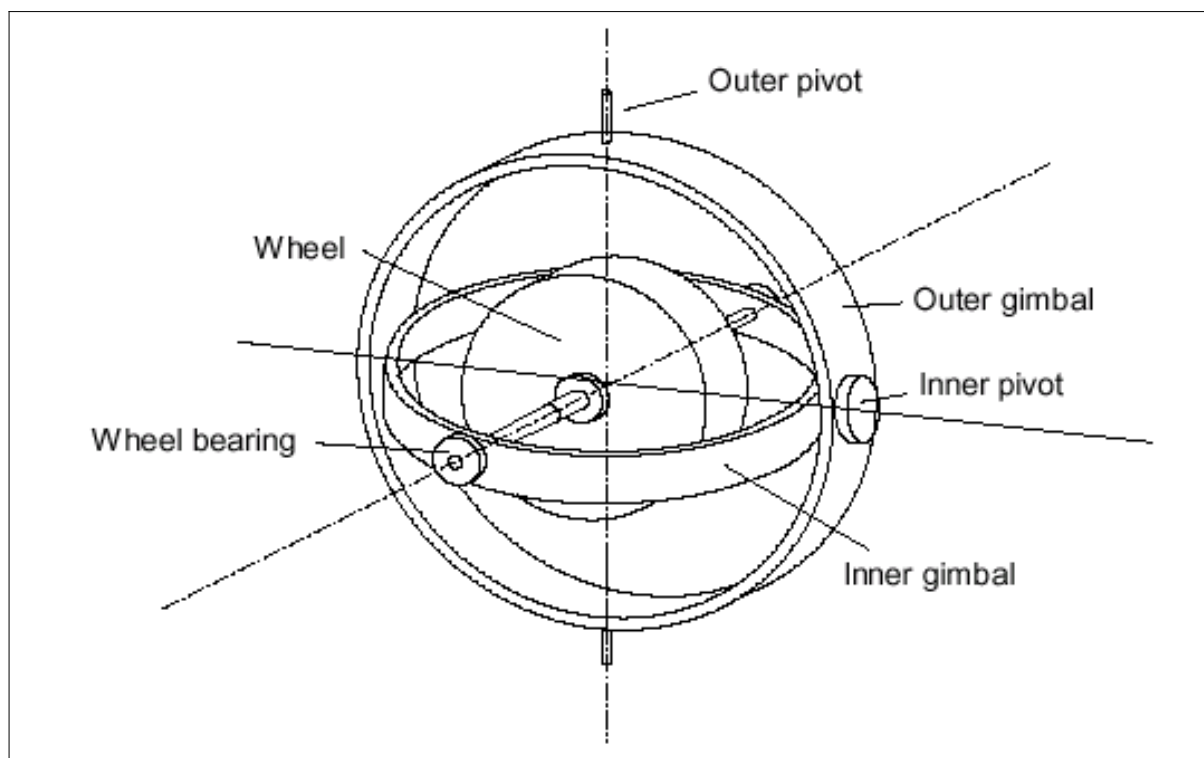


Figure 186: Typical two-axis mechanical gyroscope configuration

Gyroscopes, accelerometers and star trackers are inertial sensors to obtain information on orientation (attitude) and accelerations relative to an inertial reference frame. Attitude

measurements of a gyroscope provide angular information, while acceleration measurements (which are corrected for gravity and, integrated twice for distance) provide linear information.

The classical gyroscope is a mechanical device with a rapidly spinning mass (solid body or rotor of substantial moment of inertia), supported on a mount (e.g. a gimbal structure) that allows freedom of tilt of the spin axis relative to the base on which it is mounted. The momentum of such a rotor causes the gyro to retain its attitude when the mount is tilted. The ability of the gyro to maintain its orientation (due to the stored energy, namely the angular momentum) is employed in a number of applications (compass, direction finder, steering mechanisms, inertial guidance systems, etc.). – A practical gyroscope suffers from a phenomenon known as drift due to undesired torques resulting from imperfections in machining, bearing and lubrication frictional torques, material impurities, etc.

Since the early 1960s, new generations of gyroscopes were developed (in particular through research funded by the military), working on different principles than the conventional mechanical gyroscope. The Ring Laser Gyro (RLG) and the Fiber–Optic Gyro (FOG) are such new developments based on optical (interferometric) principles.

- **RLG (Ring Laser Gyroscope).** RLG is a Sagnac effect optical gyro which uses an active HeNe lasing medium in a mirror–defined ring cavity. Two contra–rotating beams of coherent (laser) light circulate within the quartz ring cavity. The RLG technique was first demonstrated in 1960 at Bell Labs, it took another 20 years of testing for operational use of the system in commercial aircraft (RLGs of the Sperry Corporation were introduced in the early 1980s in such aircraft as the Boeing 757 and 767). The RLG objective is the measurement of angular rate. The concept is based on the principles of general relativity, which predict that the distance around a closed optical path in a rotating frame of reference depends on the direction the path is traversed. A beam of light traveling around the path in the direction of rotation has to travel farther than one traveling in the opposite direction of rotation. The pathlength difference (and frequency change) is used as a measure of angular rotation.

Ring laser gyroscopes rely on laser beams propagating in opposite directions along the same closed loop or "ring." The beams interfere with one another forming a stable pattern, but that pattern shifts in direct proportion to the rotation rate of the whole laser–ring system (called the "Sagnac effect").

Some characteristics of an RLG are: 1) it offers long–term stability and it is insensitive to the environment; 2) it can operate continuously and has no start–up time; 3) it can withstand large angular rates ($800^\circ/\text{s}$); 4) it has a digital output; 5) it has no moving parts as the conventional gyro (however, in practice it is kept in motion to minimize some error sources); 6) it requires very little power for operation.

- **FOG (Fiber–Optic Gyro).** A solid–state device with no moving parts for the measurement of angular rate (first demonstrated in 1976).^{2407) 2408) 2409) 2410) 2411)} In a FOG, the two light beams rotate in a spool of optical fiber. The measurement concept is based on the Sagnac effect, which defines an optical phase shift between counter–propagating beams in a rotating coil of fiber. This phase shift is proportional to the rotation rate about the axis of the coil, with a scale factor related to the coil geometry and the optical wavelength. Examples of implementations: NASDA's TR1–A rocket (a microgravity mission, Japan),

2407) W. K. Burns, "Fiber Optic Gyroscopes – Light is Better," *Optics & Photonics News*, May 1998, pp. 28–32

2408) K. Hotate, "Fiber Optic Gyros Put in New Spin on Navigation," *Photonics Spectra*, April 1997, pp. 108–112

2409) P. J. Klass, "Fiber–Optic Gyros Now Challenging Laser Gyros," *Aviation Week & Space Technology*, July 1, 1996, pp. 62–64

2410) E. Boussarie, "Pleiades high–resolution system – innovative technologies," *CNES Magazine* No 17, Nov. 2000, pp.20–21

2411) Note: After launch the MUSES–B satellite (the initial name of MUSES–B was VSOP) was renamed to HALCA (Highly Advanced Laboratory for Communications and Astronomy). The SVLBI measurements provide baseline lengths of up to 3 Earth diameters.

launched in 1991, marked the first spaceborne experimental application of a FOG instrument. The Japanese MUSES–B (Mu Space Engineering Satellite – VLBI measurements in astronomy) mission of ISAS, launch Feb. 12, 1997, uses a hybrid FOG/radio–wave guidance system as well as an open–loop FOG for rate control (providing a drift rate of $0.05^\circ/\text{h}$). – In the late 1990s, performance range sensitivities (drift rates) of FOG devices vary from $0.001^\circ/\text{hr}$ to $100^\circ/\text{hr}$ with dynamic ranges (usable measuring range) of 10^4 to 10^5 . – The Planck S/C of ESA (launch May 14, 2009), the CNES Pleiades spacecraft series (launch of Pleiades–HR1 on Dec. 17, 2011) employ FOG technology [Astrix family of FOGs of EADS Astrium with ESA funding] to deliver the required pointing performance in terms of image geolocation and geometric quality.



Figure 187: Astrix 200 FOG: coil size: 5 km, angular random walk: $0.0002^\circ/\text{hr}$, scale factor stability: 30 ppm, 20 W, 7 kg, lifetime 5 years (image credit: ESA)

- LTP (LISA Technology Package) of ESA flown on the LISA Pathfinder mission (there are two minisatellites flying to L1). The key technology to be demonstrated by the LISA Pathfinder mission (launch in 2011) is 'inertial sensor performance' – the inertial sensor makes sure that the proof mass is really flying 'disturbance–free', and also measures the position of the satellite with respect to the proof mass, and 'disturbance–free flight control' – which uses mN (micro–Newton) thrusters to control the spacecraft position with an accuracy at the level of microns (μm). The inertial sensor works by detecting changes in the electrical field created by the proof mass itself, with electrodes mounted on the housing around the proof mass. The LTP core instrument includes two inertial sensors. Each inertial sensor is located in a cube of 10 cm side length that surrounds the proof mass (the proof mass floats inside this cube without touching its walls). – Note: The LISA Pathfinder mission does not aim to make measurements of separation between proof masses in distant satellites, as LISA will do, but at testing the performance of the inertial sensor (and two proof masses in the same satellite are enough for that).

- **Piezoelectric microgyroscope.** Piezoelectric vibrating gyroscopes use Coriolis forces to measure rate of rotation. Starting in 1997, a new generation of microgyroscopes, based on MEMS principles, was developed out of a technology cooperation agreement between NASA/JPL, UCLA, and HSC (Hughes Space and Communications Company). The instrument (1999), an all–silicon chip, has a size of 4 mm x 4 mm and a mass of less than one gram

(the mass of the entire 3-axis microgyroscope is < 30 gram, power of about 1 W, size of 1.5 cm x 1.5 cm x 3 cm, rate of > 360°/s, etc.). The new microgyroscope is lighter, cheaper, higher-performing and less complex than its conventional counterparts, while uniquely designed for continuous and long-term space operation. The instrument concept is based on a cloverleaf design that is tied down and vibrates at a very high speed. The gyroscope senses the Coriolis acceleration, which results from the vibratory motion in a rotating reference frame, to detect rotation. The design represents a qualitative step forward in gyroscope development.

The applications of angular rate gyros include navigation of manned and unmanned platforms, location of fleet vehicles, and attitude heading measurements. Fiber-optic gyros can also provide antenna pointing and tracking. Following are some typical classes of gyro applications:

- General low-precision navigation (such as for automobiles) is done with gyros providing drift rates of 10°/hr – 100°/hr
- Attitude and heading references for airplanes use gyros with drift rates of 1°/hr
- Precision inertial navigation as used in commercial airplanes and on some space platforms use gyros with drift rates of 0.01°/hr – 0.001°/hr.
- High-precision inertial navigation with a drift rate of <0.001°/hr is used for satellite pointing and tracking applications.

Three parameters define the performance of optical gyroscopes:

- Bias drift (a shift in the instrument zero point in the absence of rotation)
- Optical scale factor (a proportionality constant between applied rate and instrument output)
- Output noise (due to signal processing electronics, noise in the optical detection process, and thermal fluctuations in the optical fiber).
- **HRG** (Hemispherical Resonant Gyroscope). Among the vibration gyroscopes, the HRG is the only one of the inertial class. The HRG technology was first developed in the United States (research work started in the mid-1960s – and first patented in 1979) by the Delco company [now Northrop Grumman (Litton)], which demonstrated the high performance potential of the technology.

The HRG technique is based on a high-performance vibratory gyro whose inertially sensitive element is a fused silica hemispherical shell covered with a thin film of metallization. Electrostatic forcers surrounding the shell establish a standing resonant wave on the rim of the shell. As the gyro is rotated about its axis, the standing wave pattern does not rotate with the peripheral rotation of the shell, but counter-rotates by a constant fraction (0.3) of the input angle. Thus, the change in position of the standing wave, detected by capacitive pick-offs, is directly proportional to the angular movement of the resonator. In this mode of operation, termed whole angle mode, the HRG is an integrating sensor. The HRG can also be caged in a force rebalance mode to restrain the standing wave to a particular location, and acts as a rate sensor. The whole angle mode is useful when an excellent scale factor stability and linearity are required over a wide dynamic range. The force rebalance mode offers excellent angle resolution for pointing operations.

The advantages of the HRG concept is that it is lightweight, very compact, operates in a vacuum, and has no moving parts, so that life expectancy limited only by the electronics, which are provided redundantly for expected lifetimes of more than 15 years. Since its debut in space in the mid-1990s, the HRG technique has been used on many spacecraft, including the NEAR/Shoemaker (Near Earth Asteroid Rendezvous) spacecraft (launch Feb. 17, 1996) and the Cassini mission (both missions of NASA).

1.23.2.4 Magnetometry and magnetometers

Magnetic fields are omnipresent in nature; just about every body in the solar system has magnetic fields associated with it, either of interior origin, induced, or remanent. The IMF (Interplanetary Magnetic Field) is the extension into space of the sun's magnetic field carried outwards by the supersonic flow of the solar wind. Space magnetometry can be traced back to measurements of the Earth's magnetic field with instruments flown on balloons and rockets in the early 1950s. The early space probes made significant discoveries: the Earth's magnetosphere, the comet–tail–like geometry of the anti–sunward Earth magnetic field, the IMF, and the many boundaries associated with the interaction of the Earth's magnetic field with the solar wind. ²⁴¹²⁾

Magnetic field measurements are essential to organize and understand energetic charged particle and plasma flows and to derive fundamental information about the environment surrounding different bodies in the solar system. Magnetic field measurements represent also one of the few remote–sensing tools used by spacecraft (gravity being the other) that provide information about the deep interior of a planet rather than just its surface and/or atmosphere (dynamic processes in the core and mantle). Planetary magnetic fields like those of the Earth, Jupiter, and Saturn are generated by currents circulating their liquid metallic cores or perhaps the core–mantle interface. – Magnetic field measurements are being used in many Earth–orbiting spacecraft for engineering applications; these include attitude determination and control, spacecraft momentum management, and scientific instrument pointing. Earth's magnetic frame provides a convenient “natural” frame of reference, which can be modeled with good accuracy and be used by onboard instruments to establish their orientation and by active control systems.

At the start of the 21st century, geomagnetic mapping missions are the most demanding in terms of absolute accuracy and resolution, approaching < 1 part in 100,000 in magnitude and a few arcsec in direction. – Magnetic instruments provide significant cost, simplicity, and reliability advantages over inertial–based sensor systems, whenever absolute angular measurement accuracies of $1–2^\circ$ are acceptable. A common application of magnetometers in LEO spacecraft is the control of electromagnets which, when energized, apply a torque to the spacecraft by interacting with the geomagnetic field. This technique is utilized either to desaturate momentum wheels or to re–orient the S/C along a desired direction. – A more recent application of magnetometer data is in the field of “space weather” prediction and the quantitative assessment of solar–terrestrial events.

The Earth's magnetic field at the surface near the equator has an approximate strength of 31,000 nT (nano–tesla) or 0.31 G (Gauss). In SI units, the magnetic induction is measured in tesla which corresponds to 10^4 G ($1 \text{ T} = 10^4 \text{ G} = 10^9$ gamma, the latter two are alternate units to the SI unit of Tesla). The following examples illustrate the large dynamic ranges of magnetic field intensities encountered in the solar system: Solar magnetic fields associated with coronal loops and prominences can reach values as high as several thousand Gauss. The IMF at Earth's orbit (at 1 AU) is typically in the order of 5–10 nT. At the orbit of Uranus and Neptune, the IMF is as low as 0.05 nT.

The design and implementation of magnetically “clean” spacecraft is a demanding task. Since it is practically impossible to reduce the stray S/C magnetic field for sensitive measurements, magnetometers are commonly boom–mounted. This technique exploits the fact that the magnetic fields produced by finite sources decrease rapidly with distance (proportional to r^{-3} where r is the distance to the source). Many missions use long, deployable booms which must be rigid (typically a truss–like boom) to preserve the alignment of the measurements. However, the high cost of deployable booms and their potential effects on spacecraft dynamics limit the affordable boom length. Hence, a so–called “dual mag-

2412) M. H. Acuna, “Space–based magnetometers,” Review of Scientific Instruments, Vol. 73, No 11, Nov. 2002, pp. 3717–3736

netometer” technique was proposed and later introduced by Norman F. Ness et al. at NASA in 1971 to ease the problem of making sensitive magnetic field measurements in the presence of a significant S/C field. The method is based on the experimental observation that beyond a certain distance most spacecraft-generated magnetic fields decrease proportional to r^{-3} . Hence, when two magnetometers are used in parallel, mounted along a radial boom at distances r_1 and r_2 (of a moderately long boom), respectively, it is possible to separate the spacecraft-generated magnetic field from the external ambient magnetic field.²⁴¹³⁾ A particular advantage of the dual magnetometer method is that it allows unambiguous real-time identification and monitoring of the time variation of the spacecraft-generated field. In addition, the use of two magnetometers provides full measurement redundancy. The Pioneer-10 and -11 spacecraft, launched in 1973 to explore Jupiter and Saturn, were able to achieve a residual static field of <0.01 nT with the principal magnetometer located at the end of a 3 m boom.

- Magnetometers measure the strength and direction of the magnetic field. There are two generic classes of instruments:
 - Scalar magnetometers capable of measuring the magnitude of the magnetic field
 - Vector magnetometers which measure the strength and direction of the magnetic field.

Both classes of instruments are being used in space. However, vector magnetometers are far more common due to their capability of providing directional information. This “heading” information is a very significant navigation parameter.

- A simple scalar magnetometer was devised by C. F. Gauss in 1832, consisting of a permanent bar magnet suspended horizontally by a gold fiber. Measuring the period of oscillation of the magnet in the Earth’s magnetic field gives a measure of the field’s strength.
- The fluxgate magnetometer, a vector-type device, is the most common type of magnetic instrument used in spacecraft. The technique was invented in the late 1920s and published in 1936 in Germany by H. Aschenbrenner and G. Goubau.²⁴¹⁴⁾²⁴¹⁵⁾ This was followed by rapid developments during and after World War II when fluxgate systems were installed in aircraft to search for submarines, to aid in making navigation charts and for geophysical exploration. The fluxgate sensor, as the name implies, is a device used to “gate” the ambient magnetic flux threading a coil, converting it from a time stationary field into a time varying field. The latter gives rise to induced voltage in a sensing coil proportional to the strength and direction of the field. A variation of the same principle introduced by Aschenbrenner and Goubau uses a continuous ring core in place of the two inductors.
- Magnetometers are flown to measure the attitude of the S/C relative to the Earth’s magnetic field.²⁴¹⁶⁾ As such, they are normally part of the onboard attitude system. Magnetometers, in particular triaxial fluxgate instruments, are also flown as a science instrument to measure the geomagnetic field. The first ring core fluxgate magnetometers used in space were in the Lunar Surface Magnetometer package left on the surface of the moon by the Aug. 10, 1992) of NASA astronauts of Apollo 16 in April 1972. Table 136 represents a chronology of fluxgate magnetometers flown as science instruments on various missions.
- Magnetic damping. In a satellite, magnetic damping can be realized with hysteresis rods (nickel-iron rods which are easily magnetized, even by the Earth’s weak magnetic field. Such rods, rotated in a magnetic field, dissipate a fixed amount of energy for every

2413) N. F. Ness, K. W. Behannon, R. P. Lepping, K. H. Schatten, “Use of Two Magnetometers for Magnetic Field Measurements on a Spacecraft,” *Journal of Geophysical Research*, Vol. 76, No 16, June 1971, pp. 3564–35773

2414) H. Aschenbrenner, G. Goubau, “Eine Anordnung zur Registrierung rascher magnetischer Störungen,” *Hochfrequenztechnik und Elektroakustik*, Vol. 47, No 6, pp. 177–181, 1936.

2415) R. C. Snare, “A History of Vector Magnetometry in Space,” <http://www-ssc.igpp.ucla.edu/personnel/russell/ESS265/History.html>

2416) <http://www-ssc.igpp.ucla.edu/personnel/russell/ESS265/History.html>

revolution). The concept was invented by R. E. Fischell of JHU/APL and first flown on Transit–5A–3 in 1963. Such a rod produces a constant retarding torque which opposes any rotation. Since this opposing torque remains constant, even for a small rotation, hysteresis damping is effective even at low angular velocities.

Mission	Launch	Instrument	Comment
DODGE (DoD)	July 1, 1967	Triaxial magnetometer	S/C was operational for over 3 years
GEOS–2 (NASA)	Jan. 11, 1968	Uniaxial fluxgate	
TRIAD–1 (US Navy)	Sept. 2, 1972	Triaxial magnetometer	
TRIAD–2	Oct. 11, 1975		
TRIAD–3	Sept. 1, 1976		
IMP–8 (NASA)	Oct. 26, 1973	GNF (triaxial fluxgate)	S/C was operational in 1997
GEOS–1 (ESA)	Apr. 20, 1977	S–331 (triaxial fluxgate)	S/C was operated until Apr. 1980
GEOS–2 (ESA)	July 14, 1978	S–331 (triaxial fluxgate)	S/C operated until Oct. 1985
MAGSAT (APL, NASA, USGS)	Oct. 30, 1979	Scalar and vector magnetometers	MAGSAT employed a scissor boom of 6 m length
DE–1/DE–2 (NASA)	Aug. 3, 1981	MAG–1 (triaxial)	Combined launch of S/C
IRM (Germany)	Aug. 16, 1984	Triaxial magnetometer	AMPTE mission with 3 subsatellites
UKS (UK)	Aug. 16, 1984	Triaxial magnetometer	
CCE (USA)	Aug. 16, 1984	Triaxial magnetometer	
Viking (Sweden)	Feb. 22, 1986	V2 (triaxial)	End of mission May 12, 1987
EXOS–D (ISAS)	Feb. 22, 1989	MFG (triaxial)	Akebono mission (Japan)
Magion–2 (Czech)	Sept. 28, 1989	SGR–7 (triaxial)	Magion is subsatellite of ACTIVE
Ulysses (ESA/NASA)	Oct. 6, 1990	FGM/VHM	Boom–mounted magnetometers
UARS (NASA)	Sept. 13, 1991	VMAG part of PEM	
APEX (USSR)	Dec. 18, 1991	SGR–5 (triaxial)	Magion–3 is subsatellite of APEX
Magion–3 (Czech)		SGR–7 (triaxial)	
GEOTAIL (ISAS/NASA)	Jul. 24, 1992	MGF	Boom–mounted. Study of magnetotail over a wide range of distances
FREJA (Sweden)	Oct. 6, 1992	F2 (triaxial)	Boom–mounted
WIND (NASA)	Nov. 1, 1994	MFI	Astro–mast boom of 12 m length
POLAR (NASA)	Feb. 24, 1996	MFE (triaxial)	Two instruments, 6 m boom
FAST (NASA)	Aug. 21, 1996	MFE (triaxial)	
ACE (NASA)	Aug. 25, 1997	Magnetic Field Monitor	Triaxial fluxgate
DMSP/F7 (DoD)	Dec. 18, 1983	SSM (triaxial)	NASA instrument
DMSP/F12 (DoD)	Aug. 29, 1994	SSM (triaxial)	
DMSP/F13 (DoD)	Mar. 24, 1995	SSM (triaxial)	
DMSP/F15 (DoD)	Dec. 12, 1999	SSM (triaxial)	
Equator–S (MPI)	Dec. 2, 1997	MAM (triaxial)	Boom–mounted
ASTRID–2 (Sweden)	Dec. 10, 1998	EMMA	
Ørsted (Denmark)	Feb. 23, 1999	Vector+scalar magnetometer	Both instruments are boom–mounted. Precise mapping of the geomagnetic field.
SACI–1 (INPE)	Oct. 14, 1999	MAGNEX (triaxial)	Boom–mounted
OPAL (Stanford)	Jan. 27, 2000		
CHAMP (GFZ)	July 15, 2000	MIAS (scalar+triaxial)	Boom–mounted package of OVM and FGM
Cluster–2 (ESA)	July 16, 2000 Aug. 9, 2000	FGM	Boom–mounted (2) on all S/C. FGM measures the 3–D ambient magnetic field.
SAC–C (CONAE)	Nov. 21, 2000	Ørsted–2	Boom–mounted
FedSat (CSIRO)	Dec. 14, 2002	NewMag	Boom–mounted

Table 136: Chronology of some fluxgate magnetometers flown on geomagnetic field missions

- Magnetometers traditionally have been used on spacecraft for sensing of coarse attitudes (in the order of 1°) and for input to the momentum control logic (magnetic torquers). However, in combination with accurate calibration and the availability of accurate gyro-

scope data, attitude accuracies of better than 0.1° can be obtained using only magnetometer data and rate data. This was done at GSFC with UARS data (launch of UARS, Sept. 13, 1991).

- A new magnetometer technology, referred to as SQUID (Superconducting Quantum Interference Device), offers significantly increased sensitivity over conventional magnetometers. A first spaceborne implementation of this technology is flown on the DoD ARGOS satellite (launch Feb. 23, 1999). The SQUID instrument is called HTSSE–II (High Temperature Superconducting Space Experiment II), designed and developed at NRL to demonstrate the performance of superconducting (semiconductors and RF) components at cryogenic temperatures of 70–80 K (see M.3).
- A SQUID magnetometer is also flown on Gravity Probe–B (launch April 20, 2004).
- While fluxgate magnetometers are expected to remain the mainstay of magnetometry, there have been considerable improvements in the field of magnetoresistance technology. New miniature magnetoresistive devices may eventually replace conventional fluxgate magnetometers. The advantages of magnetoresistive sensors include high sensitivity, wide bandwidth, large dynamic range and easy incorporation into payloads of many small networked spacecraft.

1.23.2.5 Star sensors

The stars in the sky have been used as guideposts throughout the long history of human navigation. By their very nature, all stars represent an **inertial reference as well as an excellent point source** (in comparison, the apparent sun disk angle as seen from Earth is on average about 32 arcmin). Hence, space navigation by stars is a very attractive solution for high–accuracy pointing applications. The determination of attitude of a spacecraft by triangulation of stars in an image is therefore a rather desirable input for an AOCS (Attitude and Orbit Control Subsystem). However, the very faint energy level of starlight in the presence of extraneous light sources and noise has provided considerable design challenges in the detection and tracking process of these minute references (stars) throughout the history of spaceflight.

Background: The first attempt to operate a star tracker ²⁴¹⁷⁾ in the upper atmosphere was made in 1959 by JHU/APL in connection with a balloon–borne Venus experiment by the name of Stratolab High (demonstration of a planet–oriented fine pointing system). Later, ²⁴¹⁸⁾ star trackers for extended operation periods in space were developed for such programs as Mariner, Surveyor (launches 1966–68 to the moon), Lunar Orbiter (launch of Lunar Orbiter–1 Aug. 10, 1966), OAO (Orbiting Astronomical Observatory) with OAO–1 launch April 8, 1966, Voyager (Voyager–1 launch Sept. 5, 1977), etc.

All these star tracker implementations employed the following basic principle: a) optics for energy collection of a target star, b) a scanning or mechanical modulation mechanism to focus the star light, c) a photodetector to detect the signal and to convert it into an electrical signal (information on star brightness and the angle of the star direction relative to the optical axis). ²⁴¹⁹⁾ In the tracking systems on Mariner and Lunar Orbiter, electronic deflection served to null the track signal anywhere in the field of view (FOV). Surveyor, with its photomultiplier system, achieved null tracking by roll motion of the spacecraft. In the OAO star tracker, nulling was done with a photomultiplier by means of torque–driven gimbals. – The unique location of the bright star Canopus near the southern pole of the ecliptic plane (14°) has been used by many of these missions as the reference star.

²⁴¹⁷⁾ A star tracker is basically a camera and pattern matching system that uses constellations and stars to determine the direction in which a satellite is pointing.

²⁴¹⁸⁾ Note: The Mariner–1 and –2 missions to Venus had launches July 22 and August 27, 1962; Mariner–3 and –4 missions to Mars with launches Nov. 5 and 28, 1964; there were a total of 10 Mariner mission, the last one was launched Nov. 3, 1973 to Venus and Mercury.

²⁴¹⁹⁾ J. Bebris, et al., “Spacecraft Star Trackers,” NASA Space Vehicle Design Criteria (Guidance and Control, NASA SP–8026, July 1970, URL: <http://www.aoe.vt.edu/~cdhall/courses/aoe4065/NASADesignSPs/sp8026.pdf>)

Early attitude sensors in EO missions as well as in commercial communication missions (LEO, GEO) didn't use the stars as reference due to a lack of sensitivity of early CCDs and APS detectors (first CCD detectors for imagery were only available starting with the 1970s and they were initially used in spaceflight for solar radiation applications, with an energy source several orders of magnitude larger than a star; first APS detectors showed up in the 1990s). Also, the period of early space flight didn't enjoy today's infrastructure of affordable microelectronics, storage capacity for star catalogs and extensive algorithms, to develop star sensors in the first place. While the early star sensors were only able to track a single star (mostly in an on-off support mode), modern star sensors (21st century) are capable to identify and track multiple stars of various brightness levels and to provide continuous highly-accurate pointing data to the AOCS of a spacecraft.

Star sensors trackers are onboard cameras that scan areas in space and digitally record the position and brightness of stars. Using a sensed image of a portion of the sky, stars are located and identified. An onboard computer compares the images with star maps in memory to determine the spacecraft's exact 3-D attitude. The second step (after identification) is to "track" (follow) the star(s) and to control the orientation of the platform (input information to onboard control subsystems to more precisely orient the satellite for maximum pointing accuracy). The term "star sensor" is used to refer generically to any sensor using star measurements to derive its output.

Star sensors trackers have traditionally occupied the 'top-tier' in the attitude estimation system, providing high precision attitude estimates once other sensors and actuators have brought the satellite's dynamics under tight control. No sensor system can match the precision of star tracking, but this elevated performance often comes at the cost of a relatively small operational envelope.

The first star sensors with CCD detector technology for improved attitude control were developed in the 1980s. Some early instruments are:

- The Giotto S/C of ESA (launch Mar. 14, 1986) carried "Star Mapper," a solid-state star sensor of TNO/TPD (Delft), which relayed stellar coordinates to ESA/ESOC to enable the reconstitution of the S/C attitude during its interplanetary journey.
- All spacecraft in the IRS imaging satellites series of ISRO employ a star sensor as part of the attitude sensing devices in AOCS, starting with IRS-1A (launch March 17, 1988).
- ASTRO-1, developed by Jena-Optronik GmbH between 1984-1987 (as VEB Carl Zeiss Jena). The ASTRO-1 has been operating successfully aboard the Russian MIR station since 1989. ASTRO-1 consists of three optical heads each including a CCD-chip (520 x 580 pixels), 3 processors and an attitude determination processor (mass: 41.5 kg, power: 90 W).
- ASTRA (Advanced Star Tracker), developed in 1990 by Hughes Danbury Optical Systems, Inc., Danbury, CT (later Raytheon Optical Systems; now Goodrich Electro-Optical Systems), was flown on TOPEX/Poseidon (launch Aug. 10, 1992) of NASA and CNES. ASTRA uses a CCD detector with the processing capability of a 16-bit microprocessor, FOV = 8.8° x 9.6°. The T/P mission employs two units, ASTRA-1A and -1B, each has a mass of 2.6 kg. Tracking of a single star. ASTRA was furnished with a TEC (Thermoelectric Cooler) to maintain the CCD at -2°C. ASTRA has a pointing accuracy of 17 arcsec (1σ) @ 10 Hz. An ASTRA-1A failure occurred in April 1998 when the backup ASTRA-1B took over.²⁴²⁰⁾
- In the 1990s, more demanding pointing requirements resulted in the development of new star sensors for many missions. The minimum capabilities for an autonomous star

2420) P. Sanneman, B. Lee, P. Vanderham, "TOPEX/Poseidon: Controlling the Attitude of a 10-Year Old," Proceedings of the 26th AAS Conference on Guidance and Control, Breckenridge, CO, Feb. 5-9, 2003, Vol. 113 Advances in the Astronautical Sciences, Edited by I. J. Gravseth and R. D. Culp, AAS 03-077, pp. 597-618

tracker are: a) autonomous attitude determination (lost-in-space solution) and autonomously recognizes the inertial orientation of its boresight axis, and b) autonomous attitude tracking, all to a prescribed reference system. Today, star trackers are a key attitude-measuring component in most new attitude control systems. Some examples of advanced star sensor systems are:

- **ASC** (Advanced Stellar Compass), a pioneering star tracker developed by DTU (Technical University of Denmark) at Lyngby, and flown on the Danish satellite Ørsted (launch Feb. 23, 1999, see E.18) with an attitude precision of a few arcseconds. Redundant ASCs are also flown on the SAC-C mission of CONAE (launch Nov. 21, 2000). In addition, the CHAMP mission of GFZ/DLR is flying ASC (launch July 15, 2000, see E.1) as well as GRACE (launch Mar. 17, 2002), CONTOUR (launch July 3, 2002), ADEOS-II (launch Dec. 14, 2002), SMART-1 (launch Sept. 27, 2003), and GOCE (launch March 17, 2009). ASC (Advanced Stellar Compass) of DTU and PASS (Payload Autonomous Star Sensor), the latter developed and built in collaboration by Sira Electro-Optics Ltd and MMS (UK), are both flown on ESA's PROBA (launch Oct. 22, 2001, see M.33) mission. PASS has a wide FOV ($19.3^\circ \times 14.4^\circ$) and about 3 arcseconds of pointing accuracy in pitch and yaw.

Some background on resolution history: As imagers, star sensors depend of course on the resolving power of their optical system. The unaided human eye is capable to see detail as fine as approximately 100 arcseconds. When Galileo turned his optical telescope toward the sky in 1609/1610, he was able to resolve features of about 10 arcseconds. This mere 10-fold increase in optical resolution allowed Galileo to see moons around Jupiter and craters on our own moon.

The reflecting telescope of HST (Hubble Space Telescope), launched April 24, 1990, has a resolving power of about 0.1 arcseconds, representing a 100-fold improvement over Galileo's telescope.

The MUSES-B satellite of ISAS (Japan), launched Feb. 12, 1997 and renamed to HALCA (Highly Advanced Laboratory for Communications and Astronomy), employs SVLBI (Space Very Long Baseline Interferometry) techniques in combination with Japanese ground telescopes and other telescopes around the world (international project cooperation), achieving a maximum resolving power of about 90 microarcseconds (μarcsec) with observations at microwave wavelengths. This is about 100 times better than that of the HST. The HALCA mission was retired in 2005.

At the start of the 21st century, NASA is in the process of defining a future mission called MAXIM (Micro-Arcsecond X-ray Imaging Mission). The goal is to achieve a resolving power of $1 \mu\text{arcsec}$ – to be able to investigate eventually black holes! Again, interferometry (i.e., SVLBI technique) is the answer to achieve such extreme resolutions.

First flights of the ASC series instruments were on TEAMSAT (launch Oct. 30, 1997), on ASTRID-2 (launch Dec. 10, 1998), and on Oersted (launch Feb. 23, 1999). ASC is flying on all these missions in slightly varying configurations; the full autonomy support of the ASC includes, among other things such functions as: fast solving of the lost-in-space problem, outlier rejection, performance tuning, SEL/SEU (Single Event Latch-up/Single Event Upset) detection, and recovery. ²⁴²¹⁾

As of 2002/3, a μASC (Micro Advanced Stellar Compass) is under development at DTU whose performance parameters are given in Table 137 alongside with those of ASC. There are additional features of μASC such as:

²⁴²¹⁾ J. L. Jørgensen, "In Orbit Performance of a fully Autonomous Star Tracker," 4th ESA International Conference on Spacecraft Guidance, Navigation and Control Systems, Oct. 18–21, 1999, pp. 103–110, ESA/ESTEC, Noordwijk, The Netherlands, (ESA SP-425, Feb. 2000)

- The μ ASC consists of a fully hot/cold redundant μ DPU (micro Data Processing Unit) that drives up to four CHU (Camera Head Units).²⁴²²⁾
- Improved radiation tolerance [in particular to radiation environment increases such as SAA (South Atlantic Anomaly)] for longer life times
- The μ ASC has a considerable amount of computing power that can be used to support other applications or devices that can be triggered or implemented depending on the mission (external devices may be sun sensors, magnetometers, etc.)
- DSN (Deep Space Navigation) module. Enabled by telecommand, this function computes the instantaneous heliocentric inertial position of the S/C relying solely on the knowledge of the Julian date and the observed right ascension and declination of at least one planet. The accuracy of this attitude determination is sufficient to autonomously point the high gain antenna toward Earth from anywhere in the solar system, should the ground link be lost for any reason.
- IVM (Inertial Velocity Measurement). The μ ASC is also the first and only instrument capable of determining autonomously and instantaneously the inertial velocity of the S/C (measurements available for earthbound and Deep Space missions)
- TDI (Time Delay Integration) at user control. The main advantages of this application are: 1) to increase the accuracy of the attitude determination at high speed; 2) to improve the maximum rate at which the attitude can reliably be measured; and 3) to have a better accuracy in the tracking of faint objects.
- AST (Autonomous Star Tracker) of the DoD/NRO STEX (Space Technology Experiment, P59) satellite (launch Oct. 3, 1998), developed by LMMS (Lockheed Martin Missile & Space Company). AST provides attitude information to an accuracy of 0.005° . AST is also flown on the following missions: DS1 of NASA (launch Jul. 29, 1999); SRTM (Shuttle Radar Topography Mission of NASA, launch Feb. 11–22, 2000); IMAGE of NASA (launch Mar. 25, 2000), EO–1 of NASA (launch Nov. 21, 2000); TIMED of NASA (launch Dec. 7, 2001), and WMAP (Wilkinson Microwave Anisotropy Probe) of NASA/GSFC with a launch June 30, 2001). AST identifies up to 50 stars in the field–of–view and then computes and outputs the satellite attitude. – Following attitude acquisition, AST returns to its track mode, where it provides three–axis attitude and rate at a customer–selectable frequency up to 5 Hz. The AST comprises athermalized, radiation–hardened refractive optics, a frame–transfer CCD, camera electronics, a compact single board computer with a 32–bit RISC processor, and an all–sky guide star database.
- The attitude control and navigation system of DLR’s BIRD mission²⁴²³⁾ (launch Oct. 22, 2001) employs redundant ASTRO–5 star sensors (plus a three–axis gyro+ sun sensors, etc.). Each ASTRO–5 has a mass of 1.5 kg. The two star sensors have different lines of sight for measurement of the attitude with a high precision in all axes. The BIRD mission is the first spaceborne realization of the ASTRO–5 star sensor of Jena–Optronik.
- ASTRO–15 is a new–generation autonomous CCD star sensor of Jena–Optronik GmbH (Jena, Germany) with a FOV of $13.8^\circ \times 13.8^\circ$, up to 8 stars per frame can be recognized. It is providing a LOS pointing accuracy of ≤ 1 arcsec in pitch/yaw and ≤ 10 arcsec in roll (1σ). The ASTRO–15 system may be used a) as autonomous star sensor (with its own processor for attitude determination), or b) as a star tracker (only sensor head, no processor). A first application of ASTRO–15 is realized on a classified communications mission of the USAF, namely DSCS–III–A3 (Defense Satellite Communications System), a LM

2422) J. L. Jørgensen, T. Denver, M. Betto, P. S. Jørgensen, “MicroASC A Miniature Star Tracker,” 4th IAA Symposium on Small Satellites for Earth Observation, Berlin, Germany, April 7–11, 2003

2423) K. Briess, W. Bärwald, M. Hartmann, et al., “Orbit Experience and First Results of the BIRD–Mission,” Proceedings of 53rd IAC and World Space Congress, Oct. 10–19, 2002, Houston, TX, IAA.11.2.01

(Lockheed Martin) built satellite series with a launch March 11, 2003. As of 2004, ASTRO-15 became the standard star sensor flown on the BSS 702 platform.²⁴²⁴⁾

- SED16/26 (EADS–Sodern) is a product line of CCD–based autonomous star trackers, with the SED26 being the ITAR (International Traffic in Arms Regulation) free version. As of 2008, up to 52 SED16 or SED26 are successfully operating in orbit, since the first launch in May 2002 on–board the SPOT–5 spacecraft of CNES.²⁴²⁵⁾



Figure 188: Photo of the SED26 star trackers (image credit: EADS–Sodern)

- PASS (Payload Autonomous Star Tracker), developed by Sira Electro–Optics and EADS Astrium Ltd., UK, is being flown on ESA’s PROBA mission (launch Oct. 22, 2001). PASS is of AST (Autonomous Star Tracker) heritage flown on XMM–Newton (launch Dec. 10, 1999) of ESA. PASS has a mass of 2.4 kg and a FOV of $19^\circ \times 14^\circ$ with pointing accuracies of a few arcseconds at 5 Hz update rate. Other features: a) PASS uses a miniature optical head with a radiation–hardened lens and a CCD qualified for space missions, radiatively cooled; b) radiation tolerant DSP–based processor system; c) patented EADS Astrium/Quine algorithms with an efficient star pattern matching against the onboard star catalogue leading to a low processor load. The commercial name of PASS is AST20 (Autonomous Star Tracker).

2424) M. Mittnacht, W. Fichter, E. Gottzein, et al., “Multi–Sensor Navigation and Attitude Determination System for Space Applications,” ION–GPS 2002, Portland, OR, Sept. 24–27, 2002

2425) J. Ouaknine, P. Jacob, L. Blarre, Y. Kocher, “In–flight results synthesis of up to 52 SED16/26 Star Trackers,” Proceedings of the 7th ICSO (International Conference on Space Optics) 2008, Toulouse, France, Oct. 14–17, 2008, URL: <http://www.icsconference2008.com/cd/pdf/Poster–Auxillary%20Sensors%20–%20Ouaknine.pdf>

Star Tracker Class	Requirement	ASC	μASC (dual redundant, *)
Initial acquisition (solve lost-in-space problem)	< 1 minute	300 ms	80 ms
Pointing accuracy (EOL)	30 arcsec (3 σ)	3 arcsec (3 σ)	2 arcsec (3 σ)
Attitude rate	Up to 1°/s	Up to 7°/s	Up to 20°/s
Update rate	Up to 4 Hz	Up to 4 Hz	Up to 32 Hz
Operational availability	99.9%	99.995%	99.995%
Instrument mass, power	< 2 kg, <10 W	1 kg, 7.8 W	0.425 kg (*), 1.9 W
Instrument size	10x10x10 cm, proc. unit 5x5x5 cm, camera head	DPU: 10x10x10 cm CHU: 5x5x5 cm	μDPU: 10x10x4.5 cm (*) μCHU: 5x5x5 cm (up to 4)
Lifetime	3–5 years	11 years	30+ years
Reliability	99.995%	99.95%	99.999%

Table 137: Typical performance requirements for autonomous star trackers

- CALTRAC^R is a wide-angle star tracker system developed by EMS Technologies Inc. Ottawa, Canada. The sensor employs CCD imaging technology (tracking of up to 8 optical samples/s of the portion of the sky in view and calculation of the quaternion) for autonomous attitude determination; a pointing accuracy of $< \pm 0.005^\circ$ in pitch & yaw and $< \pm 0.01^\circ$ in roll is provided. The engineering model was space-qualified on STS-101 (May 19–29, 2000) and on STS-106 (Sept. 8–20, 2000). CALTRAC is being also being flown on NASA's Genesis mission (launch Aug. 8, 2001) and on Jason-1 of NASA/CNES (launch Dec. 7, 2001), as well as on other missions.

- MAST (Micro APS-based Star Tracker) of NASA/JPL.²⁴²⁶⁾ The MAST concept uses advanced CMOS/APS imaging technology with a low-mass and low-power instrument design, consisting of only two chips, one is used to image the stars and an ASIC chip. MAST has an attitude accuracy of 7.5 arcseconds, an APS of 1024 x 1024 pixels, the instrument mass is 42 gram, and the total radiation dose is 30 krad. The first fabrication of the APS chip at the end of 2002. The following features are provided:

- Wide FOV (Field of View) of $20^\circ \times 20^\circ$
- The imaging detector is a single chip device that incorporates the imaging array, timing and control, programming registers, 10 bit A/D converter and operates from a single power supply. The instrument power consumption is 69 mW in tracking mode.
- The APS tracks multiple windows simultaneously (up to 8 with programmable window size). This capability greatly simplifies the interface, enabling system miniaturization.
- A single ASIC chip includes all star tracker functions. The ASIC contains an I²C interface, fast logic for initial centroid acquisition, 8051 microcontroller, memory
- MAST outputs only the raw pixel data in predefined small windows. The spacecraft computer includes the star catalog, does the initial attitude acquisition and calculates the attitude quaternion.

Generally, star sensors in the time-frame 1997–2000 are designed to image only a portion of the sky and report the location of any stars that are tracked. Among other factors, the accuracy of these devices is historically limited by three design parameters: 1) A small FOV in the order of $8^\circ \times 8^\circ$, 2) The capability to track 5 stars simultaneously, and 3) A CCD detector array with a 512 pixel square imaging area. These choices have led to a limiting measurement accuracy of about 5 arcseconds per star and per frame.

UniNav (Universal Navigator). UniNav is a complete, integrated attitude sensing package developed by EADS Astrium Ltd. and partners, UK (the UniNav design is of PASS heritage

2426) C. C. Liebe, L. Alkalai, G. Domingo, et al., "Micro APS Based Star Tracker," Proceedings of the IEEE Aerospace Conference, Big Sky, MT, March 9–16, 2002

flown on PROBA). It comprises a miniaturized autonomous star sensor based on APS (Active Pixel Sensor) technology and three MEMS rate gyros. The software, situated in its own optional miniaturized processor or in the spacecraft avionics system, uses the patented Quine star recognition algorithm and Kalman filter data fusion of star and rate measurements to produce a nine element state vector that is highly reliable across a wide dynamic range.^{2427) 2428)} – The overall objective is to provide generalized AOCS (Attitude Orbit Control System) functions, ranging from launch vehicle separation through coarse or fine pointing to anomaly (lost-in-space) recovery, as a single-sensor solution. UniNav can be used as the primary attitude sensing system for mini- and microsatellites or as a highly capable, but cost-effective, fault detection and correction system for large spacecraft. The demonstration model is based on a commercial lens, providing a FOV of 20° x 20° with a STAT-250 APS. UniNav was completed and tested in 2003. The instrument has a mass of 0.5 kg, power consumption of 3 W average and 9 W max, size = 140mm x 70mm x 70mm, interface = SpaceWire (IEEE 1355), accurate 3-axis measurement of rate range: up to ±25°/s. The UK mission EarthSHINE (Earth Sun-Heliosphere INteractions Experiment – a launch expected in 2009 to L1) uses the UniNav package.

1.23.2.6 Advanced actuators –CMG (Control Moment Gyroscope)

A CMG represents a new actuator class for an agile attitude control system – consisting of a spinning rotor and one or more motorized gimbals that tilt the rotor's angular momentum.²⁴²⁹⁾ As the rotor tilts, the changing angular momentum causes a gyroscopic torque that rotates the spacecraft. CMGs are inertial actuators capable of generating a very high torque, in particular with respect to conventional reaction wheel or momentum wheel performance characteristics (which provide typical torques in the range 0.01 Nm to a few Nm). CMGs convert electrical power into angular momentum (a gimbal motor controls the spin, while a wheel motor controls the rate of wheel rotation).

Since electric power is a renewable energy source on a spacecraft, this makes CMGs an attractive alternative to propulsive control on long-duration missions.²⁴³⁰⁾ CMGs are momentum exchange/storage devices (a recoverable energy source), offering gyroscopic stability inherent in flywheels to control attitude; hence, they represent an attractive actuator solution for an AOCS (Attitude Orbit Control System) of a spacecraft. CMG devices provide generally an actuator/sensor function, i.e. a control/measurement combination. A CMG is an actuator consisting of a wheel spinning at constant speed (flywheel), mounted on one, two or a four-gimbal assembly, providing one-degree, two-degree, or three-degree of freedom attitude control, respectively. Note: The use of a flywheel is to store energy. Conceptually, a flywheel is a “mechanical battery” providing the potential to combine the energy-storage and the attitude-control functions into a single device.²⁴³¹⁾

Principle of operation:^{2432) 2433)} A CMG attitude control systems use flywheels mounted in gimbal frames that can be rotated about the gimbal axis. The spin rate is held constant relative to the gimbal frame, and the gimbal axis is perpendicular to the spin axis. The attitude control is effected by changing the gimbal angles to absorb external torques or to produce a

2427) UniNav is part of the UK AMSTAP (Aerospace Microsystems Technology Applications Partnership) initiative (started in 2000), a team comprising EADS Astrium Ltd., University of Cranfield and Sira Electro-Optics, with the support of BNSC (British National Space Center), are developing the concept of an attitude sensor that exploits MST (Micro System Technology) gyros and the rapidly evolving star tracking technology.

2428) Information provided by David J. Purll of Sira Electro-Optics, Chislehurst, UK

2429) C. Salenc, X. Roser, “AOCS for Agile Scientific Spacecraft with Mini-CMGs,” 4th ESA International Conference on Spacecraft Guidance, Navigation and Control Systems, Oct. 18–21, 1999, pp. 379–384, ESA/ESTEC, Noordwijk, The Netherlands, (ESA SP-425, Feb. 2000)

2430) J. R. Wertz, “Spacecraft Attitude Determination and Control,” Reidel, Dordrecht, 1984.

2431) H. Yoon, P. Tsiotras, “Spacecraft Adaptive Attitude and Power Tracking with Variable Speed Control Moment Gyroscopes,” Journal of Guidance, Control and Dynamics, Vol. 25, No. 6, November–December 2002

2432) C. D. Hall, “Integrated Spacecraft Power and Attitude Control Systems Using Flywheels,” <http://www.aoe.vt.edu/~cdhall/courses/aoe4065/litrev.pdf>

large-angle rotational maneuver. Two types of CMGs have been used: single-gimbal CMGs and double-gimbal CMGs. The double-gimbal variety may experience gimbal lock.

When a torque is applied about the input axis of a CMG, the angular momentum vector of the wheel precesses in order to align itself with the input torque. This causes a change in the CMG's momentum vector. Since the total angular momentum vector of the spacecraft is conserved, the entire spacecraft then rotates in such a way as to maintain the total angular momentum at a constant value. – A CMG or gyrotorquer is used in the opposite sense of a rate gyro. A commanded displacement of the gimbal output axis, with a resultant change in the angular momentum vector, causes a control torque to be applied to the spacecraft at the gyro input axis.

CMGs can generate large torques up to 5000 Nm normal to the rotor axis and to the gimbal rotation axis.^{2434) 2435)} The efficiency of the CMG system is greatly improved over the reaction wheel system since the rotor operates at a constant speed for which the efficiency can be optimized. A Single Gimbal CMG (SGCMG) is an actuator (flywheel and motor) with a constant speed momentum wheel, gimballed in one axis only. For full three-axis control of a spacecraft, a cluster of four CMGs is normally used. Conventional designs including four or more CMGs do not suppress singularities, but there is then an infinity of paths of the precession angles (i.e. tilting angles) which generate the required kinetic or dynamic moment, and this redundancy is used to avoid singular configurations.

CMG history in space: Fairly large CMG designs have already some history in spaceflight, the first application of CMGs was mainly momentum management onboard large space structures, all of them space stations (Skylab, MIR, ISS).

– Three CMGs (each with a rotor diameter of 53 cm, and a mass of 65.5 kg) were installed on NASA's Skylab to provide attitude control for the ATM (Apollo Telescope Mount) Solar Observatory of the US Skylab (launch May 14, 1973) during solar observations.^{2436) 2437)} The instrument had to be pointed within 2.5 arcseconds of the desired direction and held there without drifting more than 2.5 arcseconds in 15 minutes' time. Each CMG was a double-gimbal-mounted unit, electrically driven with a nominal spin of 9100 rpm, and capable of providing an angular momentum of 315 Nms. This CMG system maintained the Skylab orientation to within 3 arcmin. An order of magnitude more stable pointing was needed for the Solar Observatory. This was accomplished with a solar pointing control system (PCS). Since mechanical constraints limited the travel of the CMG gimbals, saturation was experienced. This required desaturation (momentum dumping) of the gyroscopes using the thrusters of the attitude control system.

– The CMG concept of gyro-stabilization has also been employed on the Russian MIR station, referred to as ROS (Gyrodyne Flywheel Orientation System). The Kvant 1/2 modules each carried six gyrodyne CMGs (launch of Kvant-1 module on March 30, 1987; launch of Kvant-2 module on Nov. 26, 1989). They were being used to provide attitude stabilization for MIR (provision of 10 arcsec orientation during astronomical observations). A gyrodyne replacement was installed on the MIR complex on Shuttle flight STS-76 (Atlantis, March 22–31, 1996) to MIR.

2433) B. Hamilton, B. Underhill, "Modern Momentum Systems for Spacecraft Attitude Control," Proceedings of the 29th Annual AAS GNC 2006 (Guidance & Navigation Conference), Breckenridge, CO, USA, Feb. 4–8, 2006, AAS 06–028

2434) G. Carron de la Morinais, C. Salenc, M. Privat, "Mini CMG Development for Future European Agile Satellite," 5th ESA Conference on Guidance Navigation and Control Systems, Oct. 22–25, 2002, Frascati, Italy, ESA SP-516

2435) A. Defendini, P. Faucheux, P. Guay; J. Morand, "A Compact CMG Product for Agile satellites," 5th ESA Conference on Guidance Navigation and Control Systems, Oct. 22–25, 2002, Frascati, Italy, ESA SP-516

2436) M. H. Kaplan, "Modern Spacecraft Dynamics and Control," Wiley, New York, 1976

2437) <http://history.nasa.gov/SP-4208/ch9.htm#170>

— Four CMGs were installed on ISS (International Space Station) as the primary attitude control system, along with an RCS (Reaction Control System) for CMG desaturation with RCS [STS-92 flight of Discovery (Oct. 11–24, 2000, ISS-05-3A flight) provided: ITS (Integrated Truss Structure) Z1 and the CMGs which were attached to the Z1 truss]. Their objective is to keep the ISS (International Space Station) complex oriented. The four CMGs operate as momentum storage devices that exchange momentum with the ISS through induced gyroscopic torques created by a motor-driven constant-speed momentum wheel mounted in two orthogonal gimbals. Both gimbals have torquer motors and position resolvers mounted on the rotational axis and move by use of a gear train system. The momentum wheel is mounted inside the inner gimbal and is supported by bearings on both sides of the spin axis. Each CMG has a diameter of 1.22 m, a mass of 227 kg, a nominal spin rate of 6,600 rpm, and is capable of producing a torque of up to 257 Nm. Each CMG consists of a large flat wheel that develops an angular momentum of 4880 Nms (newton meter second) about its spin axis. The total momentum storage capacity of the CMG cluster is about 19,000 Nms.



Figure 189: Photo of one CMG prepared by Boeing technicians at NASA/KSC prior to ISS installation in July 1998 (image credit: NASA)

The gimbal rotational velocity is $0.2^\circ/\text{s}$ (average) and $3.1^\circ/\text{s}$ (max).²⁴³⁸⁾ Each rotating wheel is mounted in a two-degree-of-freedom gimbal system that can point the spin axis (momentum vector) of the wheel in any direction. Only the operation of two CMGs is needed to keep the ISS stabilized. The CMGs are also needed for momentum desaturation, in particular during robotic payload operations. One of the stabilizing CMGs (CMG-1) suffered a failure on June 8, 2002 (a replacement of CMG-1 occurred on flight STS-114, July 26–Aug. 9, 2005).

²⁴³⁸⁾ R. R. Burt, "International Space Station Control Moment Gyro Failure," Proceedings of the 26th AAS Conference on Guidance and Control, Breckenridge, CO, Feb. 5–9, 2003, Vol. 113 Advances in the Astronautical Sciences, Edited by I. J. Gravseth and R. D. Culp, AAS 03-072, pp. 543–556

Note: Initial attitude control of ISS was provided by the Zarya (or FGB) module of Roskosmos, until the CMGs of NASA were attached with the Z1 truss assembly, and activated during the 5A flight (STS-98 flight of Atlantis, Feb. 7–20, 2001).

Operation of the ISS CMG system:

- The flywheels spin at constant speed of 6,600 rpm
- The onboard control software uses the actual angular position and momentum data to calculate the torque needed to rotate the station in the desired direction
- Electric motors apply a torque to the gimbals, speeding up or slowing down their rotation
- If the flywheel axis aligns with the axis about which the station rotates, it is unable to apply a useful torque. This is referred to as gimbal lock.
- If the torque required to rotate the station to a desired position is more than the CMGs can supply, then the system is said to be saturated and the station thrusters must be used to rotate the station. In general, a CMG saturation may occur during orbiter rendezvous and docking periods.
- **New-generation small-scale CMG technology development.** Agility considerably increases the operational envelope and efficiency of spacecraft and substantially increases the return potential of observational data. In the time frame 1996–97, an ESA-funded study at EADS Astrium SAS (formerly MMS, France) provided a first proof that a small CMG with a few Nms (newton meter second) of angular momentum could fulfill the pointing needs of a number of future EO missions based on small platforms (simple and cost-effective CMG designs based on conventional components). A design breakthrough was achieved in 1998 when a **singularity-free steering method was defined**. This ensured singularity-free maneuvers within the complete capacity envelope of the CMG cluster.

The algorithms developed make it possible to operate with only three CMGs in case of a reduced cluster (failure case or nominal case for some missions), making the concept particularly attractive for reliability aspects. Once the feasibility of an agile normal mode was demonstrated in 1999, the operations during the other phases were analyzed. Then the fine-pointing performance during imaging sequences was assessed, in coordination with microvibration analyses. The other ACMS (Attitude Control and Measurement Subsystem) modes were redefined for CMG-based attitude control; in particular, the orbit control and safe-hold modes of new LEO platforms was adapted to CMGs. In the time frame 2001–02, the new CMG technology was considered a mature enough solution to be chosen as the baseline for the new-generation Pleiades imaging satellite series of CNES. The new CMG design is patented by EADS Astrium SAS. ^{2439) 2440)}

At the start of the 21st century, the new small CMG technology (small mass, small volume, and small power requirements as well as new control algorithms and advances in bearings and lubricants) is just beginning to be used for demanding attitude control applications in small spacecraft (the angular momentum range of 5–20 Nms is of particular interest). These CMGs rely on the gyroscopic effect to produce large output torques. In particular, the potential of spacecraft agility considerably increases the operational envelope and efficiency of the observation process (larger field of regard) and substantially increases the return of Earth and science data. Agile scenarios in Earth observation include multi-strip

2439) A. Defendini, K. Lagadec, P. Guay, T. Blais, G. Griseri, “Low Cost CMG-Based AOCS Designs,” 4th ESA International Conference on Spacecraft Guidance, Navigation and Control Systems, Oct. 18–21, 1999, pp. 393–398, ESA/ESTEC

2440) X. Roser, M. Sghedoni, “Control Moment Gyroscopes (CMGs) and their application in future scientific missions,” Third ESA International Conference on Spacecraft Guidance, Navigation & Control Systems, Noordwijk, NL, Nov. 25–28, 1997, ESA SP-381, pp. 523–528

mosaics or dense successions of images, with combined roll (cross–track coverage), pitch (along–track motion) and yaw (image strips orientation) maneuvers. ²⁴⁴¹⁾

- Some examples of **small–scale CMG implementations** with spacecraft body–pointing capabilities are:

- GyroWheel™ is a CMG development of Bristol Aerospace Ltd of Winnipeg, Manitoba, Canada (a subsidiary of Magellan Aerospace Corporation). GyroWheel is being flown on the SciSat–1/ACE mission of CSA (launch Aug. 13, 2003) as an actuator/sensor demonstration experiment. The design is based on a spinning flex–gimbal system as opposed to the conventional non–spinning motor–driven gimbals. This innovation allows for maintaining the same three–axis momentum steering capability as a CMG. ^{2442) 2443)}

Parameter	Value	Parameter	Value
Instrument mass	5.5 kg @ 4 Nms torque 6.75 kg @ 16 Nms	Instrument power	15.5 W @ 1500 rpm 101 W @ 6000 rpm
Min reaction torque – Spin axis – Tilt axis	76 mNm (at 1200 rpm) 122 mNm (at 0° tilt)	Command & data I/F	Serial RS–422, or MIL–STD–155B
Gyro bias stability	< 1°/hr	Design life	> 10 years
Max rotor tilt angle	±7°	Speed range	1200–6000 rpm
Radiation tolerance	100 krad (Si) total dose	Onboard processing	16 MIPS total
Instrument size	23.5 cm dia x 13.5 cm	Input voltage	28±6 V
		Static balance	< 1 gm–cm

Table 138: Characteristics of the GyroWheel



Figure 190: Photo of the MicroWheel (image credit: Bristol Aerospace Ltd.)

- The BilSat–1 microsatellite of TUBITAK–BILTEN, Turkey, part of SSTL’s (Surrey, UK) DMC (Disaster Monitoring Constellation) mission, features an experimental CMG system with a total mass of 1.17 kg including all electronics (power = 1.7–6.5 W, output torque = 52.5 mNm, average slew rate of 3°/s). The three–axis control mode provides the satellite the ability to slew about any defined axis of nominally up to ±40° permitting ob-

2441) Note: In a body–pointing configuration the imaging instrument has a coaligned orientation with regard to the S/C. Hence, the entire system is tilted into a particular line–of–sight to image a target region.

2442) G. Tyc, D. A. Staley, W. R. Whitehead, S. Pradhan, S. Ower, J. Cain, M. Wiktowy “GyroWheel™ – An Innovative new Actuator/Sensor for Spacecraft Attitude Control,” 13th AIAA/USU Conference for Small Satellites, Aug. 23–26, 1999, Logan UT, SSC99–XI–8, URL: <http://microsat.sm.bmstu.ru/e-library/Algorithms/Hardware/wheels/ts-xi-8.pdf>

2443) M. Senez, N. Pokrupa, B. Taylor, D. Staley, M. Vinnins, “The GyroWheel™ Testing and Flight Qualification Program,” AAS Guidance and Control Conference 2002, Breckenridge, CO, Feb. 6–10, 2002

servation capabilities within a wide FOR (Field of Regard), even wider slews are possible. The body–pointing feature and slewing capability enables also stereoscopic imaging as well as target tracking within the operational scenario of BilSat–1. The CMGs are placed in a 2–CMG parallel arrangement where the gimbal axes are perpendicular to the x–y plane and are parallel to each other. A launch of BilSat–1, along with NigeriaSat–1 and UK–DMC, took place Sept. 27, 2003. ^{2444) 2445) 2446) 2447) 2448) 2449)}

Parameter	Value	Parameter	Value
Instrument mass	2.2 kg	Instrument size	135 mm x 155 x 190
Power (max)	12 W	Torque	95 mNm
Angular momentum	0.28 Nms	Gimbal rate	9°/s

Table 139: General performance characteristics of SSTL CMG system design

– The Pleiades satellite series of CNES (launch of Pleiades–HR1 on Dec. 17, 2011, S/C mass of 980 kg) ²⁴⁵⁰⁾ features a CMG cluster design system, developed by EADS Astrium SAS (with CNES support), on a LEOSTAR platform in support of spacecraft pointing agility (slew rate support), and the use of FOGs (Fiber Optic Gyroscope) for high–accuracy attitude measurements. ²⁴⁵¹⁾

The CMG system is being used in support of very demanding maneuvering requirements: rapid slewing (i.e. body pointing of the S/C within $\pm 60^\circ$). A cluster of four CMG actuators is being used, positioned in a pyramid configuration. The system is referred to as **CMG 15–45S** (15 Nms, 45 Nm, standard): it delivers a torque up to 45 Nm with a wheel of 15 Nms (angular momentum), sufficient to point a satellite in the 1000 kg class at more than 3°/s of slew rate within < 2 s; the compact architecture can be used for satellites from 1000 kg down to mini– and microsatellites. For Pleiades program applications, the requirements call for CMG fatigue failure modes in excess of 1.8×10^6 cycles under an average output torque of 19 Nm. ²⁴⁵²⁾

Parameter	Value	Parameter	Value
Output torque	45 Nm	CMG mass; volume	15 kg; diameter = 270 mm, height = 350 mm
Angular momentum	15 Nms	Stiffness	120 Hz
Data bus interface	MIL–STD–1553 (or RS–422)	Electronics mass (1 box for 4 CMGs)	1.7 kg per channel
Power use per CMG (including electronics)	23 W at max speed	Electronics volume (1 box for 4 CMGs)	270 mm x 200 mm x 160 mm

Table 140: Characteristics of the CMG 15–45S (for S/C in the 1000 kg class)

- ²⁴⁴⁴⁾ V. J. Lappas, P. Oosthuizen, P. Madle, L. P. Cowie, G. Yuksel, D. Ferin, “Design, Analysis and In–orbit Performance of the BILSAT–1 Microsatellite Twin Control Moment Gyroscope Experimental Cluster,” Proceedings of IAC 2004, Vancouver, Canada, Oct. 4–8, 2004, IAC–04–A.4.08
- ²⁴⁴⁵⁾ V. J. Lappas, W. H. Steyn, C. I. Underwood, “Practical Results on the Development of a Control Moment Gyro Based Attitude Control System for Agile Small Satellites,” AIAA/USU Small Satellite Conference, Logan, Utah, August 12–15, 2002
- ²⁴⁴⁶⁾ V. J. Lappas, W. H. Steyn, C. I. Underwood, “Attitude Control of Small Satellites using Control Moment Gyros,” 52nd IAF Congress, Toulouse, France, Oct. 1–5, 2001
- ²⁴⁴⁷⁾ V. J. Lappas, W. H. Steyn, C. I. Underwood, “Laboratory Experiments of a Control Moment Gyroscope Cluster for Agile Small Satellites,” 5th International ESA Conference on Guidance Navigation and Control Systems, Frascati, Italy, Oct. 22–25, 2002, ESA SP–516
- ²⁴⁴⁸⁾ L. M. Gomes, G. Yuksel, V. Lappas, A. da Silva Curiel, A. Bradford, C. Ozkaptan, M. Sweeting, “BilSat: Advancing Smallsat Capabilities,” AIAA/USU Conference on Small Satellites, Logan, UT, Aug. 11–14, 2003
- ²⁴⁴⁹⁾ V. J. Lappas, “Control Techniques for Aerospace Systems,” May, 7, 2003, URL: <http://www.ae.metu.edu.tr/~ozan/control/cmgaero.pdf>
- ²⁴⁵⁰⁾ A. Defendini, P. Fauchaux, P. Guay, J. Morand, H. Heimerl, “A Compact CMG product for agile satellites,” 5th International ESA Conference on Guidance Navigation and Control Systems, Frascati, Italy, Oct. 22–25, 2002
- ²⁴⁵¹⁾ B. Girouart, I. Sebbag, J.–M. Lachiver, “Performances of the Pleiades–HR Agile Attitude Control System,” 5th International ESA Conference on Guidance Navigation and Control Systems” Frascati, Italy, Oct. 22–25, 2002
- ²⁴⁵²⁾ P. Damilano, Pleiades High Resolution Satellite: a Solution for Military and Civilian Needs in Metric–Class Optical Observation,” AIAA/USU Conference on Small Satellites, Aug. 13–16, 2001, SSC01–1–5

Parameter	μ CMG (SSTL)	15–45S (Astrium)	M–50 (Honeywell)
Momentum (Nms)	0.28	15	75
Torque, peak (Nm)	0.074	45	75
Mass of 1 gyro (kg)		16.7	28
Assembly total mass (kg)	2.2	84	< 100
Power (Q/P, W)	8.5, 12	25, 92 (4)	35, 95
Rotor speed (rpm)	20,000	< 6,000	6,000
Design life (year)	–	–	> 7
Rotation (degrees)	180	360	360

Table 141: Comparison of some small CMG systems ²⁴⁵³⁾



Figure 191: Illustration of one CMG 15–45S actuator (image credit: EADS Astrium SAS, CNES)

– DigitalGlobe of Longmont, CO is flying its next–generation commercial high–resolution imaging satellite, WorldView–1 (launch Sept. 18, 2007), with CMG actuator technology (of Honeywell Defense & Space Electronic Systems, Phoenix, AZ) for precise and highly responsive pointing control and considerably increased spacecraft agility (slew maneuver support). WorldView–1 is the successor mission to QuickBird–2.

The Honeywell M–50 CMG capitalizes on the wide range and experience of Honeywell on large CMGs that have flown on a number of military related missions. The M50 CMG has an angular momentum range of 25–75 Nms, an output torque of 0.075–75 Nm, power of 11–95 W, rotor speeds of 4500–6500 rpm, and a mass of 28 kg (1 gyro). The M–50 CMG assembly has a mass of \sim 100 kg. ^{2454) 2455) 2456)}

- Coupled energy storage and attitude control capability in flywheels. NASA/GRC is developing the IPACS (Integrated Power and Attitude Control System) concept (and a long–term program), *combining existing reaction wheel technology with flywheel energy storage con-*

2453) F. B. Abbott, B. Hamilton, T. Kreider, P. Di Leonardo, D. Smith, “MCS (Momentum Control System) Revolution,” Proceedings of the 29th Annual AAS GNC 2006 (Guidance & Navigation Conference), Breckenridge, CO, USA, Feb. 4–8, 2006, AAS 06–032

2454) J. Bates, “NGA Plans Second NextView Award by End of September,” Space News, March 29, 2004, p. 8

2455) M. A. Peck, “Low–Power, High–Agility Space Robotics,” <http://www.mae.cornell.edu/mpeck/documents/Papers/PeckCMGRobotics.pdf>

2456) <http://www.honeywell.com/sites/aero/Pointing–Momentum–Control.htm>

cepts (CMGs) to combine attitude control and electrical power components (i.e. the function of onboard storage batteries).

The use of flywheels instead of batteries to store energy on spacecraft was suggested as early as 1961 in a paper by J. B. Roes. Power tracking for charging and discharging the wheels is added to complete the IPACS functional framework. An IPACS must perform two functions – attitude control and power tracking – simultaneously.^{2457) 2458)} It must provide commanded torques for attitude control and generate power, accumulate energy, and store energy. A flywheel produces or absorbs power by changing its wheel speed. Attitude control torques are produced by changes in the net angular momentum vector. – The torques applied by the energy/momentum wheels (CMGs) are decomposed into two spaces that are orthogonal to each other, with the attitude – control torques and power – tracking torques in each space. – Future NASA missions like GEC (Geospace Electrodynamic Connections) and many others (NPOESS series) are planning on this technology. Some examples of IPACS demonstrations are:^{2459) 2460) 2461) 2462) 2463)}

- An IPACS laboratory demonstration unit, called COMET (Coordinated Momentum and Energy Transfer), is being developed at Lockheed Martin with NASA/GRC funding.
- The objective of the NASA FESS (Flywheel Energy Storage System) project is to develop a prototype flywheel battery system for possible use as replacements for the ISS electro – chemical batteries.
- The FACETS (Flywheel Attitude Control Energy Transmission and Storage) program of AFRL was initiated with Honeywell Engines, Systems & Services Division, Tempe, AZ.

1.23.2.7 Spacecraft/platform and instrument pointing

- Spacecraft/platform and instrument pointing is an important aspect of navigation (see also same heading in Appendix A). The ability to locate a sensor measurement with the required accuracy on the Earth’s surface (or to point at a faint celestial body from an orbiting platform) has made great strides in four decades of spaceflight.

Precision pointing is also a function of platform stability through suitable attitude sensing and control mechanisms. Early spacecraft had pointing accuracies of about $\pm 1^\circ$ which is in the same order of magnitude as spacecraft with gravity – gradient boom stabilization in the 1990s. Three – axis stabilized spacecraft, such as the NOAA/POES series (starting with TIROS – N) and the early SPOT series (SPOT – 1, – 2, – 3) offer pointing accuracies of 0.1° . IPS (Instrument Pointing System) of ESA (built by Dornier, Friedrichshafen), first flown on Shuttle flight STS – 51 – F as Spacelab – 2 in July/Aug. 1985, then on STS – 35 as Astro – 1 (Dec. 2 – 10, 1990), and again on STS – 67 as Astro – 2 (March 2 – 18, 1995), is providing a pointing stability within ± 1.2 arcseconds for all sensors on the platform (see J.7).

2457) T. Michaelis, “Integrated Power and Attitude Control System (IPACS),” AIAA/USU Conference on Small Satellites, Logan, UT, Aug. 31 – Sept. 3, 1998, SSC98 – IX – 6

2458) P. Tsiotras, H. Shen, C. Hall, “Satellite Attitude Control and Power Tracking with Energy/Momentum Wheels,” Journal of Guidance, Control, and Dynamics, Vol. 24, No. 1, January – February 2001, pp. 23 – 34; URL: <http://www.ae.gatech.edu/~ptsiotra/Papers/jgcd99.pdf>

2459) V. Babushka, S. M. Beatty, B. J. deBlonk, J. L. Fausz, “A Review of Technology Developments in Flywheel Attitude Control and Energy Transmission Systems,” Proceedings of the IEEE Aerospace Conference, Big Sky, MT, March 6 – 13, 2004

2460) K. L. McLallin, J. Fausz, R. H. Jansen, R. D. Bauer, “Aerospace Flywheel Technology Development for IPACS Applications, Proceedings of IECCEC’01:36th Intersociety Energy Conversion Engineering Conference, July 29 – August 2, 2001, Savannah, Georgia

2461) B. H. Kenny, R. Jansen, P. Kascak, T. Dever, W. Santiago, “Demonstration of Single Axis Combined Attitude Control and Energy Storage Using Two Flywheels,” Proceedings of the IEEE Aerospace Conference, Big Sky, MT, March 6 – 13, 2004

2462) J. B. Roes, “An Electro – Mechanical Energy Storage System for Space Application,” Progress in Astronautics and Rocketry, Vol. 3, Academic, New York, 1961, pp. 613 – 622.

2463) C. D. Hall, “High – Speed Flywheels for Integrated Energy Storage and Attitude Control,” Proceedings of the American Control Conference, Albuquerque, NM, June 4 – 6, 1997, pp. 1894 – 1898

- The imaging sensor OSA (Optical Sensor Assembly) on Ikonos–2 (launch Sept. 24, 1999) is providing an absolute ground location accuracy of 12 m (without the use of ground control points), the relative accuracy is 2 m. The imagery of such a sensor may certainly be used for cartographic applications (see Table 950).
- The HST (Hubble Space Telescope) is the most precisely pointed instrument in spaceborne astronomy. The pointing requirements call for a continuous 24 hour target lock maintenance of 0.007 arcseconds (2 millionth degree).
- High–accuracy pointing for intersatellite links is needed for a number of acquisition applications, in particular for the support optical free–space communication (optical terminals at end points). The technology involves: a) the acquisition of signals, b) the tracking of the signal sources, and c) the pointing of transmitters and receivers; all functions require high speed and high–accuracy pointing support (without the ability to return a beam along the line–of–sight towards the companion terminal, communications cannot take place). Conventional ATP (Acquisition, Tracking & Pointing) systems generally employ large angle tracking and scan capability with fine–tracking mode and acquisition step stability. The SILEX (Semiconductor Intersatellite Link Experiment) design of ESA, with a LEO terminal on SPOT–4 and a GEO terminal on ARTEMIS, required pointing errors of $< 10 \mu\text{rad}$ (or $< 0.0005^\circ$). This pointing accuracy is several orders of magnitude smaller (better) than open–loop pointing of a typical platform.²⁴⁶⁴
- A separate class of pointing accuracy, namely < 1 milliarcsecond (marcsec), is required of Gravity Probe–B (Relativity Mission, launch April 20, 2004), a spin–stabilized spacecraft. This is four orders of magnitude higher than IPS or close to six orders of magnitude higher than normal three–axis stabilized spacecraft. The GP–B spacecraft contains two star trackers to perform the “spotting function” for the telescope – one wide FOV (Field of View) and one narrow FOV (called the star sensor). The wide FOV star tracker is used to locate the general region of the heavens containing the guide star, and then the narrow FOV star tracker helps align the space vehicle with the guide star (< 20 marcsec). – The onboard telescope basically performs the same function as the star trackers, but it uses a different technique, and it is orders of magnitude more precise and more accurate. The narrow FOV star tracker has a field of view on the order of 1° (60 arcminutes), and it can focus to a position within perhaps one arcminute – about the same as the entire FOV of the onboard telescope, which can pinpoint the guide star’s position to within a milliarcsecond (in fact 0.1 marcsec).
- The ARGOS mission of DoD (launch Feb. 23, 1999) is flying an instrument by the name of USA (Unconventional Stellar Aspect) also referred to as NRL–801 experiment. USA conducts feasibility tests of X–ray satellite navigation and new computational approaches to autonomous parameter estimation that includes GPS inputs and a variety of redundant truth measures. There are reasons why X–ray navigation might prove to be attractive in the future. The advantages are associated mainly with drawbacks of optical methods or with potential advantages of X–ray characteristics that have no exact analogs in the optical wavelengths (M.3).
- Hexapod and CPD (Coarse Pointing Device) systems of ISS (International Space Station), developed and provided by ESA. – One of the many ISS services is the accommodation of scientific/technological payloads and observing instruments on a standard carrier, the ExPS (Express Pallet System), located on the Integrated Truss Assembly. Up to six payload sites can be grouped on one Pallet by means of ExPA (Express Pallet Adapter).²⁴⁶⁵ Depending on the location of the ExPA (nadir and zenith facing), both Earth and universe

²⁴⁶⁴) N. Aversa, L. Vaillon, G. Feusier, C. Canudas de Witt, et al., “Design of Advanced Solutions for High Precision Acquisition & Tracking Systems,” 5th ESA Conference on Guidance Navigation and Control Systems, Oct. 22–25, 2002, Frascati, Italy, ESA SP–516, pp. 507–515

²⁴⁶⁵) B. Musetti, B. Cibrario, F. Pepe, “Hexapod and CPD Pointing Control Systems,” 4th ESA International Conference on Spacecraft Guidance, Navigation and Control Systems, Oct. 18–21, 1999, pp. 459–466, ESA/ESTEC

observations are possible. However, accurate instrument pointing requires a pointing system if mounted on the Pallet directly. This is due to several disturbance effects such as orbital motion, orbital plane precession, seasonal sun apparent motion, and ISS deviation from nominal attitude resulting from gravity and drag forces.

1) Hexapod is a Steward platform for small range accurate pointing based on a six–degree–of freedom concept. The objective is to support such instruments as SAGE–III of NASA/LaRC (see L.2.13). Hexapod pointing requirements call for a pointing accuracy of ± 90 arcseconds, a pointing stability of $0.0025^\circ/\text{s}$, a pointing range of $\pm 8^\circ$, and a pointing rate of $1.2^\circ/\text{s}$.

2) The CPD is a two–axes cardanic platform for coarse pointing and larger rotational capabilities; it is devoted to accommodate sun pointing instruments and radiation and biology experiments requiring sun pointing. CDP is a tracking system, the objective is to compensate the ISS attitude variation. CDP supports the payloads: a) Expose Payload a multi–user facility accommodating photo–processing, photo–biology and exo–biology experiments. b) SIA (Sun Instrument Assembly) for the study of solar irradiance. CDP pointing requirements call for a pointing accuracy of $\pm 1.0^\circ$, a pointing stability of 0.3° , a pointing range of $\pm 40^\circ$, and a pointing rate of $4^\circ/\text{min}$.

Technique	Instrument	Mission	Pointing accuracy (angular resolution)
Star tracker (based on CCD detectors)	ASC (Advanced Stellar Compass)	Ørsted (launch Feb 23, 1999)	3–4 arcsec
	ASC + PASS (Payload Autonomous Star Sensor)	PROBA (launch Oct. 22, 2001)	3–4 arcsec (ASC) 3–4 arcsec (PASS)
	AST (Autonomous Star Tracker), built at LMMS	DS1, NASA (launch Jul. 19, 1999) EO–1, (launch Nov. 21, 2000) TIMED (launch Dec. 7, 2001) WMAP (launch Jun. 30, 2001)	0.005°
	CALTRAC (of EMS Technologies)	Genesis (launch Aug. 8, 2001) Jason–1 (launch Dec. 7, 2001)	$< \pm 0.005^\circ$ in pitch & yaw, $< \pm 0.01^\circ$ in roll
	STR (Star Tracker) of Selex Galileo	Herschel (launch May 14, 2009)	< 0.8 arcsec(1σ) APE (Absolute Pointing Error) in 2012
Star tracker (APS detectors)	ISC (Inertial Stellar Compass), Draper Lab	TacSat–2 of DoD (launch Dec. 16, 2006)	0.1° (1σ) in each axis
	MAST (Micro APS–based Star Tracker), JPL		7.5 arcsec
VLBI	VLBI system (Earth–based system)		0.1–0.2 marcsec (milli–arcsecond level)
SVLBI (Space–Very Long Baseline Interferometry)	SVLBI system (first mission of its kind)	HALCA (Highly Advanced Laboratory for Communications and Astronomy), launch Feb. 12, 1997	90 μarcsec
	SVLBI system	ARISE (Advanced Radio Interferometry between Space and Earth), launch in 2005	10–20 μarcsec
	SVLBI system	JWST (James Webb Space Telescope) launch 2015 to L2	(milli–arcsecond level)

Table 142: Comparison of some instrument/system pointing accuracies

- DMC (Dynamic Motion Compensation). The GOES–N spacecraft of NOAA (launch May 24, 2006) carries a newly developed AOCs instrument, SIAD (Stellar Inertial Attitude Determination), designed by BSS (see F.4.4). SIAD provides a real–time dynamic compensation environment of S/C jitters to an accuracy of $10 \mu\text{rad}$, 3σ . This technology is referred to as DMC (Dynamic Motion Compensation), permitting a high precision “virtual platform” for scanning observations of imaging instruments flown in GEO.
- Very high pointing requirements and platform stability constraints are in particular needed for the GOES–R next–generation satellites series of NOAA with an initial launch

planned for 2014. The current plan of GOES–R calls for the support of three Earth–scanning instruments, namely ABI (Advanced Baseline Imager) and two HES (Hyperspectral Environmental Suite) imagers. The HES instruments will perform full Disk Soundings (DS) and Coastal Water (CW) imaging. The spacecraft disturbance sources include reaction wheels, solar array tracking, and the Earth–scanning instruments themselves. The optical performance requirements of these Earth–scanning instruments drive their instrument line of sight (LOS) stability requirements.²⁴⁶⁶⁾

- “SmartScan” is an intelligent imaging correction technique under development at ESA solving the problem of image correction for satellite pushbroom cameras which are disturbed by satellite attitude instability effects [satellite cameras with linear sensors are particularly sensitive to attitude errors, which cause considerable image distortions]. The SmartScan concept uses in–situ measurements of the image motion with additional CCD sensors in the focal plane and real–time image processing of these measurements by an onboard Joint Transform Optical Correlator. The system has been successfully demonstrated by laboratory tests and by an airborne flight demonstration in July 2002 (Do–228 aircraft of DLR). The errors of the image motion record (corresponding to the residual image distortions after correction) were generally within ≤ 0.25 pixels (1 sigma). The application of the SmartScan system allows high quality imaging with a pushbroom image sensor from satellites with only moderate attitude stability, including satellites, which are not specially designed for imaging missions.^{2467) 2468) 2469)}

2466) D. A. Early, A. D. Reth, O. I. Rodriguez–Alvarez, “Spacecraft pointing stability constraints and instrument disturbance limits for optical remote sensing satellites,” Proceedings of SPIE, Vol. 5234–62, Sensors, Systems, and Next–Generation Satellites II, Sept. 8–12, 2003, Barcelona, Spain

2467) V. Tcherykh, S. Dyblenko, K. Janschek, K. Seifart, B. Harnisch, “Airborne test results for a smart pushbroom imaging system with optoelectronic image correction,” Proceedings of SPIE, Vol. 5234–61, Sensors, Systems, and Next–Generation Satellites II, Sept. 8–12, 2003, Barcelona, Spain

2468) V. Tcherykh, S. Dyblenko K. Janschek, K. Seifart, B. Harnisch, “Clever Imaging with SmartScan,” ESA Bulletin No 123, Aug. 2005, pp. 40–45

2469) K. Janschek, V. Tcherykh, S. Dyblenko, “SmartScan – Smart Pushbroom Imaging System for Shaky Space Platforms,” Proceedings of the 20th Annual AIAA/USU Conference on Small Satellites, Logan, UT, Aug. 14–17, 2006, paper: SSC06–VI–3

1.23.3 Tracking Techniques

The term “tracking” has many meanings and connotations in the context of navigation. In general, it refers to:

- The process of measuring position (range, angles, round–trip signal time) by following a moving object
- Orbit determination: using the measured data determining and predicting its position and velocity over time (real–time by a GPS receiver). Unlike conventional land–based tracking techniques, onboard GPS tracking methods are not limited by the time that a spacecraft is in the line–of–sight of a tracking station. GPS tracking also has the advantage that it provides measurements throughout any orbital arc and requires additional reference data from only relatively inexpensive terrestrial GPS receivers. Finally, the three dimensional nature of GPS measurements allows for superior 3–D positioning. An onboard GPS receiver can thus provide a real–time orbit solution.
- The ability of measuring/determining relative position between several objects in orbit (this may for instance be used for rendezvous monitoring using a range finder in form of a laser range finder and a vision sensor)²⁴⁷⁰)
- The function or ability of “pointing” an instrument, an antenna (following a ground station while transmitting data), an array of instruments (possibly in various orbits), a spacecraft, a beam – – in the prescribed direction with varying degrees of required pointing accuracy and speed.
- The parameter of acceleration (range rate) plays also an important role next to position and velocity of an object, in particular in geodetic applications (gravity) involving drag–free orbits.
- Onboard attitude sensing is also a tracking function (of horizon sensors, sun sensors, star trackers, magnetometers, etc.), finding attitude by triangulation against known references.
- Event monitoring, either by an onboard instrument (searching its imagery for particular events), or of an onboard DCS (Data Collection System) searching the ground segment for possible data–transmission contacts, represents also a tracking function in a wider sense. This applies also to S&RSAT (Search and Rescue Satellite Aided Tracking) by tracking emergency beacons like PLB (Personal Locator Beam).
- ATP (Acquisition, Tracking & Pointing) system in support of optical intersatellite communications.
- etc.

Over the years, a multitude of tracking techniques and concepts have been developed; often several techniques are being used in parallel (onboard, on–ground, from other sources, continuously, intermittently, in real–time, offline, in combination with attitude, absolute or relative positioning, etc.), depending on the requirements of orbital accuracy. The time (epoch) is the fundamental parameter to all measurements.²⁴⁷¹)

Tracking measurements (data) may originate from such measurement sources/devices as: Doppler, onboard GPS receiver (at the start of the 21st century, onboard GPS receivers

2470) Note: A laser range finder is a device that measures the distance to a target, but the beam orientation is fixed. This is different from a laser radar, where the orientation of the beam can be changed (navigation and guidance device). Laser range finders have been demonstrated on a number of missions. The Apollo–15 mission in 1971 was probably the first to use a range finder.

2471) Note: By convention, the epoch in use today is called J2000.0, which refers to the mean equator and equinox of year 2000, nominally January 1st 12:00 hours Universal Time (UT). The “J” means Julian year, which is 365.25 days long.

have advanced to such a state, where they are considered the primary tracking source for orbit determination of many LEO missions), ground-based SLR (Satellite Laser Ranging); SST (Satellite-to-Satellite) microwave tracking; altimetry, radio tracking systems such as: PRARE (Precise Range And Range-rate Equipment), and DORIS (Determination Orbite Radiopositionnement Integres Satellite); radio tracking by interferometry such as VLBI (Very Long Baseline Interferometry), and SVLBI (Space VLBI); etc. – Modern satellites that require precise positioning are equipped with several independent tracking devices. Starting from the 1970s, most satellite tracking techniques improved by several orders of magnitude, both in terms of quality (measurement precision and accuracy) and quantity (number and rapid availability of data, and spatial and temporal coverage).²⁴⁷²⁾

Note: The field of “tracking” is so large that its theme is spread over virtually all chapters of navigation and not just dealt with under “tracking techniques.”

The two-way support of the communication function requires the satellite to carry a simple transceiver (i.e., a dedicated transmitter and receiver). In order to also accomplish the tracking function, the satellite must carry a transponder which, in addition to providing two-way communications, also returns the tracking antenna’s transmitted **ranging signal**, thus, permitting the quick determination of the distance between the ground antenna and the spacecraft.

Ground-based navigation is with us from the very beginning of the space age. The conventional tracking methods are “ranging,” “Doppler velocity,” and “angle-only” (when no transponder is onboard) determination along the line of sight.²⁴⁷³⁾ Ranging (radial distance) is derived from transit time, namely the round-trip light time of ranging signals from the spacecraft transponder, while the ground antenna pointing direction provides angular information. More precise angle measuring methods are those of “differenced Doppler” and VLBI. The Doppler shift is a measure of object velocity. A two-way coherent transmission mode permits the measurement of the induced Doppler shift to within 1 Hz, since the uplink frequency is known with great precision. The Doppler shift is directly proportional to the radial component of the spacecraft’s velocity. – The measurement accuracy is dependent on the frequency band selected. Conventional ranging and Doppler measurement capabilities are in the microwave region, such as S-band with typical accuracies in the order of about 0.5 m. Satellite laser ranging (SLR) techniques between a ground-based laser station and a satellite use the much shorter wavelengths of visible light, resulting in a single-shot precision of <2 cm.

1.23.3.1 Doppler tracking techniques

The Doppler shift is the phenomenon of how an object’s relative motion changes the apparent frequency of its radiation source. The Austrian physicist Christian Doppler (1803–1853) first described it in 1842, in relation to stars. By definition, the Doppler shift denotes the difference between the frequency of the radiation received at a point and the frequency of the radiation at its source, when observer and source are moving with respect to each other. The concept of Doppler tracking (one-way or two-way) employs the Doppler shift (Doppler ranging) to determine the orbit (angular information is provided by the antenna direction). Doppler tracking is a well established tracking technique.

- Background: The concept of Doppler tracking is to determine a satellite’s orbit and the inverse problem of locating transmitters on Earth using satellites. Soon after the launch of Sputnik-1 (Oct. 4, 1957), JHU/APL (Johns Hopkins University/Applied Physics Laboratory) researchers W. H. Guier and G. C. Weiffenbach discovered that they could **determine**

²⁴⁷²⁾ P. Exertier, P. Bonnefond, Y. Ménard, “Contribution of Space Techniques to Jason-1 Altimeter Calibration,” Newsletter No 8, http://www-aviso.cnes.fr:8090/HTML/information/publication/news/news8/exertier_fr.html

²⁴⁷³⁾ Note: In the very early period of space flight, the technique of optical tracking was employed by the use of the Baker-Nunn camera.

a satellite's orbit solely from RF Doppler shift measurements made on a single pass over their laboratory. Their technique was based on the following premises: if one knew the geodetic position from which the signal was recorded, and made certain assumptions about the Earth's mass, the Doppler shift could be used to derive the characteristics of the satellite's orbit – and permitting to calculate the satellite's Keplerian elements. ^{2474) 2475) 2476)}

The Sputnik satellite transmitted a continuous 20.001 MHz tone. The Soviets had chosen this frequency so that anyone with a 20 MHz reference could pick up the difference signal as an audible tone, varying roughly between 500 and 1500 Hz (from about C above middle C to G an octave and a half higher). The variation, of course, was Doppler. Using a ground-based receiver, APL engineers W. H. Guier and G. C. Weiffenbach captured and processed this signal. – From the pattern of the Doppler shift, the time of a spacecraft's closest approach to the receiver could be determined, and with some refinement, Guier and Weiffenbach were quickly achieving better orbit knowledge (measured by ability to predict subsequent passes) than anyone else. ²⁴⁷⁷⁾

The Doppler technique is to observe the effect of a transmitter and a receiver in motion. This is a relative velocity measurement. In satellite geodesy, the Doppler effect is only observed with radio techniques (taking into account the dry and wet tropospheric signal delay). The DORIS system of CNES is based on Doppler measurements. The DORIS configuration consists of about 40 Doppler beacons in the ground segment and a receiver on a LEO satellite (space segment).

Spacecraft	Launch Date	Innovation
Sputnik-1	Oct. 4, 1957	Satellite Doppler tracking
Transit-1A	Sept. 17, 1959	Yo-Yo spin/despin mechanism
Transit-1B	Apr. 13, 1960	Dual-frequency Doppler tracking for correcting ionospheric error First attitude-controlled S/C using permanent magnets First solar attitude detectors
Transit-2A	June 22, 1960	First rideshare dual-payload launch (Transit-2A and Solrad-1 of NRL) and the first piggyback separation, demonstrated before on Transit-1B
Transit-3B	Feb. 21, 1961	First satellite electronic memory in space (384 bit of magnetic core register – required to store its own orbit ephemeris)
Transit-4A	June 29, 1961	First nuclear power generator tested in a spacecraft (RTG)
TRAAC	Nov. 15, 1961	Damping of satellite vibration by lossy spring-and-mass technique. (TRAAC= Transit Research And Attitude Control) satellite
ANNA-1B	Oct. 31, 1962	First geodetic satellite (ANNA = Army Navy, NASA, Air Force) which also flew the first gallium arsenide cell in space.
Transit-5A-1	Dec. 19, 1962	First uplink authentication system
Transit-5A-3	June 16, 1963	First successful gravity-gradient stabilization (plus spring-and-mass damping) to maintain Earth pointing for one side of the S/C. – Automatic temperature S/C control
Transit-5C-1	June 4, 1964	Demonstration that hysteresis rods, used previously for damping magnetic stabilization, were also effective for gravity-gradient stabilization
DME-A	Nov. 29, 1965	Magnetic spin/despin system (DME=Direct Measurement Explorer)
SAS-1	Dec. 12, 1970	Dual-spin control of satellite pointing (Small Astronomy Explorer-1)

2474) W. H. Guier, G. C. Weiffenbach; "A Satellite Doppler Navigational System," Proceedings of the IRE; Vol. 48, No. 4; April 1960; p. 507

2475) Note: The very concept of being able to compute a location on Earth by observing the change in frequency of a spaceborne transmitter during a single pass was initially ridiculed by a number of reputable scientists.

2476) William H. Guier, George C. Weiffenbach, "Genesis of Satellite Navigation," Johns Hopkins APL Technical Digest, Vol. 18, No 2, 1007, pp. 178–181, URL: <http://www.jhuapl.edu/techdigest/TD/td1802/guier.pdf>

2477) Robert L. Henderson, William S. Devereux, Thomas Thompson, "Navigation at APL: A Historical Perspective and a Look Forward," Johns Hopkins Technical Digest, Vol. 29, No 3, 2010, pp. 201–217, URL: <http://www.jhuapl.edu/techdigest/TD/td2903/Henderson.pdf>

Spacecraft	Launch Date	Innovation
Triad (Transit–improved DISCOS)	Sept. 2, 1972	First satellite compensated for drag and radiation pressure. The drag–free concept was realized with DISCOS (Disturbance Compensation Device). First demonstration of single–frequency refraction–free satellite navigation using pseudonoise modulation.
DODGE	July 1, 1967	First yaw stabilization of a satellite using a ‘pitch axis wheel’ [constant–speed ‘momentum wheel’] DODGE = DoD Gravity Experiment, M.10
GEOS–3	April 9, 1975	Demonstration of first satellite–to–satellite tracking. By closed–loop tracking with a S–band transponder, the position of GEOS–3 was measured relative to that of ATS–6 of known position.
TIP–II	Oct. 12, 1975	Crystal oscillator as onboard timing system with all drift removed by a programmable synthesizer. TIP = Transit Improvement Program
SeaSat SAR downlink	Jun. 27, 1978	Quadrifilar helix antenna with beam shaping to compensate for slant range
Magsat	Oct 30, 1979	First attitude and command systems using microprocessors
Landsat–4	Jul. 16, 1982	GPSPAC (see 1.27.5) the first spaceborne GPS receiver in history
GEOSAT–A	Mar. 12, 1985	Bifilar helix antenna
MSX	April 24, 1996	First spaceborne hyperspectral imager, UVISI (Ultraviolet/Visible Imaging and Spectrographic Imaging)

Table 143: Some technology innovations introduced by JHU/APL ²⁴⁷⁸⁾ ²⁴⁷⁹⁾

In early 1958, F. T. McClure of JHU/APL inverted the problem: **if the position of the satellite were accurately known, then Doppler data could tell an observer on the ground his unknown position** (Note: the inverse problem became later known as the “navigation problem”). The implications of this discovery were enormous. It opened the world, particularly the world’s oceans, to electronic positioning. This realization led eventually to the conceptual design of the first satellite Doppler navigation system, namely “**Transit**” for the US Navy (H.7, and 1.27.2). Other names of Transit were NAVSAT and NNSS (Navy Navigation Satellite System). The accuracy of the positioning was critically dependent on the accuracy of the determination of the satellites’ positions. ²⁴⁸⁰⁾

All satellites that transmit continuously on stable frequencies can be used for Doppler measurements. When the Doppler principle is to be used for orbit analysis, i.e. for the establishment of a precise global navigation system with real–time capability, the satellite system must meet at least the following requirements:

- Global distribution of satellite orbits, and
- Real–time transfer of information about satellite position and time to users.
- S/C tracking techniques, tracking system behavior and geodetic studies were the objective of three dedicated NASA missions, namely GEOS–1 (launch Nov. 6, 1965, E.6.1), GEOS–2 (launch Jan. 11, 1968) and GEOS–3 (launch April 9, 1975). Doppler instruments onboard and on–ground were employed for systematic range and range–rate measurements. Doppler shift measurements of a spaceborne Doppler instrument were also used to establish the structure of the Earth’s gravity field to a fairly good accuracy.

Note: In the early spaceage, the SECOR (Sequential Collation of Ranges) technique was developed particularly for geodetic applications (two–way ranging). One of the first SECOR transponders was flown on the US satellite ANNA–1B (launch Oct. 31, 1962). A total of 16 satellites with SECOR transponders were launched in the period 1964–1979, among them GEOS–1 and GEOS–2. The basic idea of SECOR tracking is forming a group of 4 ground stations and one satellite. Three of the four ground stations were considered to be at known positions while the fourth one had to be “located” using the method of triangulation.

²⁴⁷⁸⁾ E. J. Hoffman, “Spacecraft Design Innovations in the APL Space Department,” Johns Hopkins APL Technical Digest, Vol. 13, No. 1, 1992, pp. 167–181

²⁴⁷⁹⁾ R. B. Kershner, “Technical Innovations in the APL Space Department,” Johns Hopkins APL Technical Digest, Vol. 1, No. 4, 1980, pp. 264–278

²⁴⁸⁰⁾ The Legacy of Transit, Special issue of Johns Hopkins APL Technical Digest, Jan.–March 1998, Vol. 19, No. 1

- Noncoherent Doppler in-flight tracking. Noncoherent Doppler tracking has been devised as a means to achieve highly accurate, two-way Doppler measurements with a simple, transceiver-based communications system. This technique has been flown as an experiment on NASA's TIMED spacecraft (launch Dec. 7, 2001, see A.31), as the operational technique for Doppler tracking on CONTOUR, and is baselined on several future deep space missions at JHU/APL. The JHU/APL-developed technique obviates the need for coherency between the uplink's carrier tracking oscillator and the downlink carrier. In this technique, the uplink carrier signal is received and compared with the receiver's onboard reference oscillator. This operation results in a set of phase comparison counts, placed in the telemetry and transmitted to the ground. The challenge to making Doppler velocity measurements with a transceiver is that the downlink carrier frequency is determined solely by the onboard frequency reference. The bias and drift of the reference oscillator frequency will obscure the Doppler velocity if no provision is made to remove their effects. ²⁴⁸¹⁾
- Australia's FedSat (launch Dec. 14, 2002) Ka-band Earth station for the downlink of the onboard DCS (Data Collection System) data (see M.15), is regarded the world's first implementation of the Doppler principle as a Ka-band tracking technique with a single dish, located at the UTS (University of Technology Sydney), Kuringai Campus. The tracking technique is called FAST (Frequency Assisted Spatial Tracking). ²⁴⁸²⁾²⁴⁸³⁾ The FAST concept states that assuming the orbit is known, then the Doppler and Doppler rate are sufficient to specify the satellite position. The derived position can then be fused with other spatial data and used to track the satellite. Fairly stable microsatellite pointing accuracies are required for this type of tracking technique. The Ka-band system is mainly used as a demonstration and research tool (properties of low-power Ka-band signals on small satellites, etc.). In the meantime, a second Ka-band station was set up at the University of South Australia in Adelaide for FedSat tracking/research.

1.23.3.2 Satellite-to-satellite tracking technique (SST)

SST is an indirect gravity field mapping technique, using satellites as test masses to measure the effect of gravity through the precise monitoring of the motion of the satellites.

The concept is based on tracking the "relative motion" between two satellites (high-low measurement concept based on the GPS constellation and a spacecraft in LEO). SST is employed in particular in geodetic applications (gravity missions) to obtain highly accurate orbits for LEO satellites, and from these, by applying orbit perturbation analysis, the structure of the Earth's gravity field. The lack of sufficient coverage in ground station tracking capability requires such measures. SST was demonstrated for the first time ever in 1968, mapping the near side gravity field of the moon (with Earth being considered a satellite of the moon). ^{2484) 2485) 2486)} With regard to the Earth's gravity field, SST was first demonstrated between GEOS-3 (in LEO) and ATS-6 (Applied Technology Satellite), a geostationary S/C of NASA in April 1975 (closed-loop tracking with a S-band transponder, the position of GEOS-3 was measured relative to that of ATS-6 of known position). Howev-

2481) C. C. DeBoy, J. R. Jensen, M. S. Asher, "Noncoherent Doppler Tracking: First Flight Results," 4th IAA Symposium on Small Satellites for Earth Observation, April 7-11, 2003, Berlin, Germany

2482) E. Aboutanios, S. Reisenfeld, "Analysis Of Frequency Assisted Spatial Tracking For Low Earth Orbit Satellites," Sixth Ka-band Utilization Conference, Cleveland, OH, May 31 - June 2, 2000, pp 397-403

2483) E. Aboutanios, "Error Analysis of Frequency Assisted Spatial Tracking (Fast) Concept for FedSat Low Earth Orbit Satellite," Proceedings of the 3rd CRCSS Conference, Newcastle NSW, Australia, Feb. 13-16, 2001

2484) J. Rush, "Current Issues in the Use of the Global Positioning System Aboard Satellites," *Acta Astronautica*, Vol. 47, No 2-9, 2000, pp. 377-387

2485) W. Bertiger, P. Abusali, et al., "The First Low Earth Orbiter with Precise GPS Positioning: TOPEX/Poseidon," ION Proceedings, Sept. 1993

2486) P. Argentiero, et al., "Results of GEOS 3/ATS-6 Satellite-to-Satellite Tracking Orbit Determination Experiment," *Journal of Geophysical Research*, Vol. 84, No. B8, pp. 3921-3925, 1979.

er, few results were obtained due to the relatively high altitude of the lower satellite (E.7.3, GEOS-3 perigee of 818 km, apogee of 858 km).²⁴⁸⁷⁾

Later in 1975, there were SST measurements between the Apollo-18 S/C (launch of Apollo-18 ASTP on July 15, 1975) in LEO and ATS-6. A further SST demonstration was conducted between the GPS constellation (in MEO) and the TOPEX/Poseidon altimeter satellite in LEO [the GPS receiver (6 channels, two frequencies, code and phase) aboard TOPEX/Poseidon is providing GPS-SST data since Dec. 1992; there exists an almost continuous data set for 1993. In addition to the GPS receiver, TOPEX/Poseidon was tracked with TDRS (Tracking Data Relay Satellite), DORIS (onboard the S/C) and SLR (Satellite Laser Ranging). Comparison of the tracking information from the four sources has demonstrated a satellite position determination capability in the <5 cm range. This level of accuracy is achieved through post-pass processing of the GPS data obtained from the satellite's GPS receiver. Unfortunately, the artificial anti-spoofing GPS signal degradation switched on again in 1994/5, permitted only occasional GPS observations, not advantageous for routine precise orbit determination]. The contribution of TOPEX/Poseidon GPS-SST data to existing gravity-field models were not very significant, due to the relative high altitude of the TOPEX/Poseidon (1334 km) orbit. But whenever anti-spoofing-off periods were available, then GPS observations provided an orbit restitution with centimeter-level accuracy, an essential requirement for the quality of an altimeter mission.

Note: SST methods for applications in gravity field recovery favor low-altitude orbits (referred to as low-low SST or SST-II), in which two orbiters flying close-proximity circular trajectories, perform relative velocity or range measurements of high accuracy, at the lowest possible altitude (in the co-orbiting satellite approach, the basic observed quantity can be a distance or a Doppler frequency shift, or both). – The other viable approach (at the end of the 1990s) is continuous onboard GPS position measurements with high-quality receivers, providing a second and independent satellite-to-satellite tracking method, in combination with low-low SST-II. The global long-wave gravity field recovery by GPS is based primarily on the combined carrier-phase measurement onboard the LEO S/C, and a network of ground receivers which allow the recovery of the GPS trajectories. High-low GPS SST-hl is also applied for onboard navigation purposes.

- CHAMP mission of GFZ/DLR (launch July 15, 2000). The LEO CHAMP S/C and the MEO GPS satellite-constellation establish a so called high-low satellite-to-satellite (SST) link for the BlackJack instrument.
- The SST technique is extensively being employed on the dual-minisatellite GRACE mission (launch March 17, 2002, see E.13) separated about 200 km in a near-polar, near-co-planar orbits. This involves continuous ranging measurements between the two spacecraft. Variations in the gravity field cause the range between the two satellites to vary. The objective is to obtain long-term data with unprecedented accuracy for global (high-resolution) models of the mean and the time-variable components of the Earth's gravity field. In fact, GRACE software products provide monthly estimates of the time-varying gravity field, which are largely due to the redistribution of water mass in the Earth system, with a spatial resolution of ~ 500 km and an accuracy of 1 cm equivalent water.
- The GOCE (Gravity field and steady-state Ocean Circulation Explorer) mission of ESA (launch March 17, 2009) is a combined SGG (Satellite Gravity Gradiometry) and SST (Satellite-to-Satellite Tracking) mission using SSTI (Satellite to Satellite Tracking Instrument). The objective is to provide the SST-hl (Satellite-to-Satellite Tracking – high/low) contribution to the gravity field recovery, by the simultaneous tracking of up to 12 GNSS signals. In addition, SSTI provides data for precise orbit determination; it is also used for real-time on-board navigation and attitude-reference-frame determination.

²⁴⁸⁷⁾ Information provided by P. Schwintzer of GFZ Potsdam

- GRAIL (Gravity Recovery and Interior Laboratory) is an SST lunar–orbiting mission of two co–orbiting minisatellites in NASA’s Discovery Program with the objective to measure the moon’s gravity field in unprecedented detail. The GRAIL mission concept for the moon (with circular lunar orbits of 55 km in altitude) is based on the same technologies introduced by the GRACE mission in Earth orbit. The GRAIL mission was launched on Sept. 10, 2011. The twin spacecraft achieved lunar orbit on January 1, 2012.

1.23.3.3 VLBI (Very Long Baseline Interferometry) and SVLBI (Space VLBI)

VLBI is an Earth–based geometric observation technique, originally pioneered and introduced in the field of radio astronomy, measuring simultaneously the time difference between the arrival of radio signals, emitted from a distant source (such as quasars), at two or more widely–separated antennas (up to an Earth diameter) of the global radio–astronomy network. The electronic linkage of a network of radio telescopes creates in effect a **virtual interferometer** array geometry, permitting the simultaneous view of the same target from widely–separated locations on Earth, where all antennas in the network form an **effective synthetic aperture** (a sparse synthetic aperture of enormous size, as large as the largest separation of the individual antennas, all of known positions). Obviously, such a powerful measurement technique is capable to observe astrophysical objects in better detail (sensitivity) and with a much greater **angular resolution** than any other astronomical technique. However, Earth–based VLBI is limited by the physical dimensions of Earth.^{2488) 2489) 2490)}

While VLBI was originally conceived to produce ultra–high resolution images of those distant radio objects, the technique was extended in the late 1960s to make also ultra–high precision geodetic (triangulation) and geodynamic measurements. VLBI is unique in its ability to define an inertial reference frame and to measure the Earth’s orientation in this frame. Since the antennas of the global radio astronomy network are fixed to the Earth, their locations track the instantaneous orientation of the Earth in the inertial reference frame. Relative changes in the antenna locations (the measurement precision at the centimeter level) from a series of measurements indicate tectonic plate motion, regional deformation, and local uplift or subsidence. Hence, VLBI has also become an effective tool for geodetic observations.

VLBI applications are based on international cooperation. The current average accuracy of quasar positions observed by VLBI radiosystems is about 0.1–0.2 milliarcseconds (1 milliarcsecond = 0.00000028° or 2.8×10^{-7}). In comparison, a single large optical telescope achieves average star position accuracies of about 10 milliarcseconds.

Deep space tracking of S/C with VLBI: The VLBI technique, also referred to as the **delta–DOR** (delta–Differential One–way Ranging) or Δ VLBI, is also available for space navigation (location of an interplanetary or deep space probe) thanks to pioneering work by NASA/JPL. In these applications, the ground antennas at two different locations on Earth record sequentially the signal from a spacecraft and a nearby extragalactic radio source of known celestial coordinates (generally a quasar) to produce two different time delays. The time delay of the quasar signal is used for clock synchronization at the two ground tracking stations. What matters for orbit determination is the difference between the spacecraft and quasar delays, hence the name Δ VLBI or Δ DOR for this type of observables. The Δ DOR techniques provides very accurate plane–of–sky measurements of spacecraft position

2488) Note: Radio astronomy refers to the spectral range of microwaves, generally considered to be in the wavelength range from 1 mm to 1 m (<300 GHz frequencies < 300 MHz)

2489) <http://web.mit.edu/newsoffice/tt/1994/nov16/38584.html>

2490) <http://lupus.gsfc.nasa.gov/brochure/bintro.html>

which complement existing line-of-sight ranging and Doppler measurements.²⁴⁹¹⁾

Until the early 1990s interplanetary navigation relied almost exclusively upon range and range rate measurements exploiting two-way, coherent radio links at S-band or X-band. These radiometric observables were routinely generated at ground stations equipped with suitable electronics and highly stable frequency standards (such as hydrogen masers). Single dish observations are operationally simple, but unfortunately do not provide an immediate determination of the angular position of interplanetary probes (the angle observables obtained from conical scanning are so poor to be useless for the navigational needs of current interplanetary missions).²⁴⁹²⁾

VLBI determines the relative angular position of a spacecraft with respect to a compact calibration radio source (normally a quasar).²⁴⁹³⁾ Using VLBI, current precision techniques in measurements of spacecraft angular position, based on group delay measurements, achieve an accuracy of a few (2–5) nanoradian. This requires making measurements with 10–15 minute integration time on a calibration source with a flux density typically at least a few hundred milli-Jansky (mJy). Therefore, a calibrator is generally 5–10° away from the direction of the spacecraft.

Following is some historic background on VLBI introduction:

- In 1957,²⁴⁹⁴⁾ two large steerable dishes at Owens Valley Radio Observatory (OVRO is a Caltech facility) near Big Pine, CA, were linked together to form a microwave interferometer.
- In 1964, Cambridge University (Cambridge, UK) demonstrated the operation of the “One Mile Array.” This system introduced a new technique called “**aperture synthesis**” which processed data from each element in the system and constructed an image as if it had been made by a single telescope.²⁴⁹⁵⁾
- In the late 1970s, the Very Large Array (VLA), an aperture synthesis array, was built by the National Radio Astronomy Observatory (NRAO) near Socorro, New Mexico (USA) in a Y-shape consisting of 27 antennas. The data collected from all antennas combined in VLA was comparable to the resolving power of a single antenna of 36 km in diameter. The US VLBI Consortium was formed in 1981.
- In 1980, EVN (European VLBI Network) was formed by five European institutions: MPIfR (Max Planck Institut für Radioastronomie), Bonn, Germany; IRA (Istituto di Radio Astronomia), Bologna, Italy; ASTRON, Dwingeloo, The Netherlands; OSO (Onsala Space Observatory), Onsala, Sweden; and the Merlin/VLBI National Facility at the University of Manchester, UK. EVN is administered by the European Consortium for VLBI. As of 2000, it includes a total of 14 major institutes, including JIVE (Joint Institute for VLBI in Europe). The EVN is a collaboration of the major Radio Astronomical Institutes in Europe, Asia and South Africa and performs high angular resolution observations of cosmic radio sources.

2491) L. Iess, R. B. Puyuelo, A. Ardito, G. Comoretto, M. Lanucara, R. Maddè, M. Mercolino, G. Rapino, M. Sensi, P. Tortora, “The European ΔDOR Correlator,” Proceedings of the 57th IAC/IAF/IAA (International Astronautical Congress), Valencia, Spain, Oct. 2–6, 2006, IAC–06–C1.6.04

2492) N. James, R. Abello, M. Lanucara, M. Mercolino, R. Maddè, “Implementation of an ESA delta-DOR Capability,” Proceedings of the 57th IAC/IAF/IAA (International Astronautical Congress), Valencia, Spain, Oct. 2–6, 2006, IAC–06–B.3.1.06

2493) Walid A. Majid, “Compact Radio Source Density and Precision Spacecraft Tracking,” Proceedings of the 2009 IEEE Aerospace Conference, Big Sky, MT, USA, March 7–14, 2009

2494) J. Yang, “The Future of Radio Astronomy Interferometry,” 1999, http://worldnetva.pwnet.org/russia/vang/Jiaying_paper.doc

2495) Note: The technique of “mosaicking”, or aperture-synthesis interferometry, combines images of different parts of the sky (generated by each telescope of an array) to produce a large field of view, in effect, simulating one large telescope from an array.

- In 1985, the VLBA (Very Long Baseline Array) initiative ²⁴⁹⁶⁾ was started by NRAO and the Haystack Observatory of MIT, Cambridge, MA. VLBA consists of a system of 10 radio telescopes from Hawaii to the Virgin Islands, controlled from Socorro, New Mexico (VLBA was dedicated in 1993). In May 1997, VLBA and VLA made combined observations with the HALCA spacecraft of ISAS in an SVLBI configuration.
- Geodetic VLBI observations provided the first direct confirmation of tectonic plate motion at the end of the 1980's [CDP (Crustal Dynamics Project) of NASA/GSFC which lasted until 1991]. At the start of the 21st century, VLBI observations measure the motions with an accuracy less than 1 mm/year jointly with other space geodetic techniques such as GPS and SLR [international cooperation within a SGP (Space Geodesy Program)].
- In Sept. 2004, European and US astronomers linked up their radio telescopes for the first time in real-time, through the Internet, thereby creating the world's biggest virtual radio telescope by merging observations from instruments in the UK, Sweden, the Netherlands, Poland, and Puerto Rico. ²⁴⁹⁷⁾ The virtual instrument had a maximum separation of the antennas of 8200 km, giving a resolution of at least 20 milliarcseconds (mas); this is about 5 times better than the Hubble Space Telescope (HST). Note: HST provides resolutions of about 0.1 arcsec. – In the past, the VLBI technique was severely hampered because the data had to be recorded onto tape and then shipped to a central processing facility for analysis. The solution, to link the telescopes electronically in real-time, enables astronomers to analyze the data as it happens. The technique, referred to e-VLBI, is only possible now that high-bandwidth network connectivity is a reality. The emerging technology of e-VLBI is set to revolutionize radio astronomy. As network bandwidths increase, so too will the sensitivity of e-VLBI arrays, allowing clearer views of the furthest and faintest regions of space.
- In the spring of 2006, ESA completed the implementation of its ΔDOR (delta-Differential One-way Ranging) deep space ground station network in New Norcia (Australia) and Cebreros (Spain). The new capability provides tracking services for such deep space missions as Rosetta, Mars Express, Venus Express and SMART-1.
- **SVLBI (Space Very Long Baseline Interferometry)** is an extension of the VLBI concept by linking a spaceborne radio telescope with an array of Earth-based telescopes. Such configurations increase the effective synthetic aperture generally by an order of magnitude as compared to purely VLBI observations. A number of scenarios are possible such as: a) spaceborne telescope in LEO or GEO with a corresponding Earth VLBI segment; b) a purely spaceborne configuration of two or more satellites, each equipped with a telescope, in widely-spaced orbits; c) a spaceborne configuration with one satellite at L1 or L2, another one in GEO, as well as a corresponding Earth VLBI segment; d) etc. The following items give a short overview of initial SVLBI activities.
 - The first ever SVLBI (Space Very Long Baseline Interferometry) technical feasibility experiments were carried out on Aug. 2, 1986 by Levy et al. Use of the TDRSE (TDRS-1) 4.9 m antenna as a spaceborne radio telescope (in GEO) operating at 2.3 GHz for the observation of three quasars. ²⁴⁹⁸⁾ ²⁴⁹⁹⁾ In the setup, the received signals were transmitted over an analog data link to a Mark 3 terminal at White Sands, NM. Baselines from TDRSE to Earth-based 64 m telescopes at Tidbinbilla (a NASA DSN station, built in 1964), Australia, and at Usuda (25 m telescope of ISAS), Japan, ranged up to 17,800 km, about 1.4 earth diameters. A total of four successful 800 second scans were obtained in that session. After the event, the data from all three antennas were successfully cross-correlated.

2496) D. G. Finley, "Astronomers Make First Images With Space Radio Telescope," July 2, 1997, URL: <http://www.nrao.edu/pr/1997/halca/>

2497) http://www.universetoday.com/am/publish/radio_telescopes_around_world_realtime.html?8102004

2498) G. S. Levy, R. P. Linfield, J. S. Ulvestad, et al., "Very Long Baseline Interferometric Observations Made with an Orbiting Radio Telescope," *Science*, Vol 234, 1986, p. 187–189

2499) J. S. Ulvestad, "Space Radio Astronomy," *Proceedings of Space Technology and Applications International Forum (STAI-97)*, Albuquerque, NM, Jan. 26–30, 1997

Deep-space missions require precise navigation, in particular when approaching bodies such as Mars, Venus or a comet. How precise?

It's necessary to pinpoint a spacecraft 100 million km from Earth to within 1 km. To achieve this level of accuracy, ESA experts use 'quasars' – the most luminous objects known in the Universe – as beacons in a technique known as delta-DOR (Delta-Differential One-Way Ranging).

Quasars are fascinating objects that can emit 1000 times the energy of our entire Milky Way galaxy. This prodigious luminosity originates from a region only about the size of our Solar System. Quasars are fuelled by supermassive black holes – which might be billions of times as massive as our Sun – feeding on matter at the center of their host galaxies.

Since quasars are extremely bright and distant, they can be used as reference points for spacecraft navigation. In the delta-DOR technique, radio signals from a spacecraft are received by two separate ground stations, one, say, in New Norcia, Australia and one in Cebreros, Spain, and the difference in the times of arrival is precisely measured.

Next, errors due to the radio signals passing through Earth's atmosphere are corrected by simultaneously tracking a quasar – the coordinates of which are precisely known. For delta-DOR to work, the quasar and the spacecraft should be within 10° as seen from Earth. There are around 200 000 quasars known in the Sloan Digital Sky Survey, and almost any of them are potential candidates to be used in delta-DOR tracking.

Once the location of the spacecraft derived from the ground stations is compared to the known location of the quasar, engineers can apply corrections, delivering a significantly more accurate fix on its position. Quasar locations define a reference system. They enable engineers to improve the precision of the measurements taken by ground stations and improve the accuracy of the direction to the spacecraft to an order of a millionth of a degree.

Using the results of the delta-DOR processing together with the range and Doppler measurements, which are also derived from the spacecraft signals received on ground, ESA can achieve an accuracy in spacecraft location of just several hundred meters at a distance of 100 000 000 km.

Table 144: Use of quasars and the delta-DOR technique for deep space navigation ²⁵⁰⁰⁾

– ISAS (Institute for Space and Astronomical Science) of the University of Tokyo, Japan, launched the MUSES-B satellite on Feb. 12, 1997 which was renamed to **HALCA** (Highly Advanced Laboratory for Communications and Astronomy) after launch. ²⁵⁰¹⁾ The HALCA spacecraft carries a telescope for SVLBI observations. Elliptical orbit: apogee of 21,400 km, perigee of 560 km, 31° inclination and a period of about 6.3 hours. HALCA is considered a 1st generation SVLBI mission (deployable parabolic mesh antenna of 8 m aperture diameter, total antenna mass of 200 kg). Observations are made at the following frequencies: 1.6 GHz (18 cm), 5 GHz (6 cm), and 22 GHz (1.3 cm). The SVLBI measurements provide baseline lengths of up to about 3 Earth diameters (32,000 km) in combination with Japanese ground telescopes and other telescopes around the world (international project cooperation), achieving a maximum resolving power of about 90 microarcseconds at microwave wavelengths (about 100 times better than that of the Hubble Space Telescope). ²⁵⁰²⁾ ²⁵⁰³⁾

2500) "Brightest Beacons," ESA, October 01, 2013, URL: http://www.esa.int/Our_Activities/Operations/Highlights/Brightest_beacons

2501) Note: Japan started in 1979 with a five year plan of VLBI development which included VSOP (VLBI Space Observatory Program). An official proposal was made by ISAS 1987. Later, VSOP was renamed to MUSES-B, which was again renamed to HALCA, after launch.

2502) <http://www.vsop.isas.ac.jp/index.html>

2503) <http://www.drao- ofr.hia- iha.nrc- cnrc.gc.ca/science/vlbi/vsop/index.shtml>

- VSOP–2 (VLBI Space Observatory Project–2) is a further SVLBI project of JAXA (formerly ISAS), a follow–up mission to HALCA considered for launch in 2012. After launch the VSOP–2 mission will be referred to as ASTRO–G.
- ARISE (Advanced Radio Interferometry between Space and Earth). A NASA/JPL SVLBI astronomy satellite mission in planning consisting of a 25 m diameter radio telescope (an inflatable structure with a very thin reflecting surface that does all the work in collecting light from the cosmos) in a highly elliptical Earth orbit (HEO). The nominal orbit has a perigee height of 5,000 km and an apogee of 40,000–50,000 km. ARISE provides SVLBI observations in with combination with a network of ground telescopes (resolutions up to 10–20 microarcseconds. A launch is now considered for 2015.

1.23.3.4 PaCoRa (Passive Correlation Ranging) for geostationary satellites

PaCoRa is a project tested and realized in the timeframe 2010–2013 by SES Techcom Services (prime) and Fraunhofer IIS, supported by the ESA ARTES 3–4 program. The goals of the project were: ²⁵⁰⁴⁾

- 3) Provide highly accurate orbit predictions of geostationary satellites that allow dense collocation (up to 8 satellites) in one orbital box.
- 4) Minimize the impact of ranging operations on the satellite by avoiding the use of transponder invasive techniques. The system shall be payload signal independent.
- 5) Respond to a global demand of geostationary satellite’s tracking and orbit data.
- 6) Minimize the cost of ranging operations by automating measurements.

PaCoRa is a non–invasive ranging method which can be used for multiple downlink signal types. Due to its passive nature there is no need to transmit a tracking signal to the satellite, minimizing the potential impact on spacecraft and ground operations. Additionally, the ground stations do not require large antennas, which helps to keep down the cost of the system.

²⁵⁰⁴⁾“Passive Correlation Ranging (PaCoRa),” ESA, March 13, 2013, URL: <http://telecom.esa.int/telecom/www/object/index.cfm?fobjectid=32323>

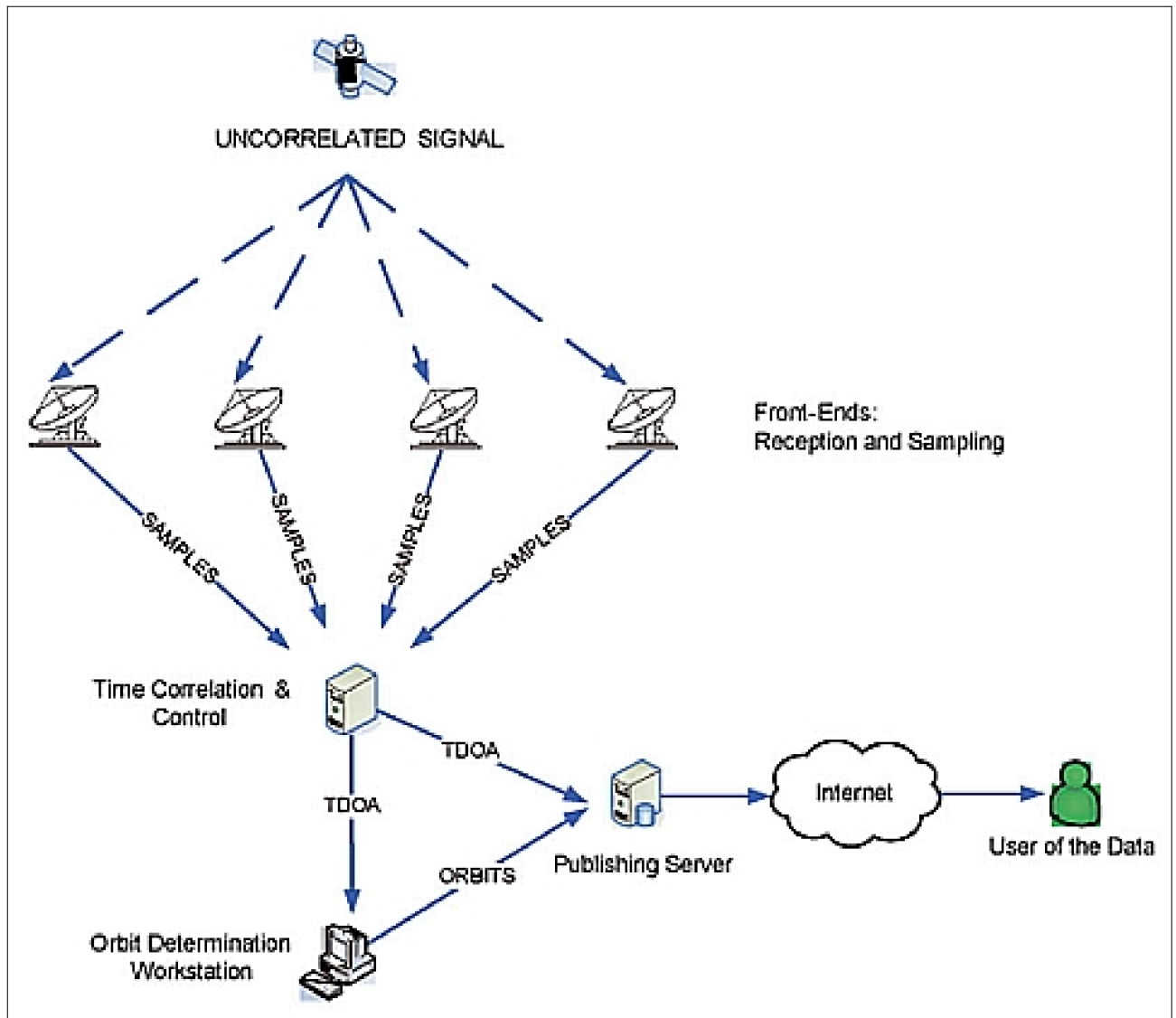


Figure 192: Schematic view of the PaCoRa elements (image credit: PaCoRa project team)

The system is composed of a tracking subsystem, an orbit determination subsystem and a back–end.

Tracking system: Is formed of small size terminals (i.e.1.2 m dish) that receive a regular satellite payload signal, sample the signal, timestamp it and transfer it via land lines to the central station. In order to achieve the best orbit calculations, 4 terminals are needed that have to be geographically spread within the satellite footprint. The Central station collects the sampled data and performs a time correlation that produces the TDOA (Time Difference of Arrival). It is also in charge of automating and synchronizing the measurements of the distributed system.

Orbit Determination system: The tracking data are fed into the orbit determination system that periodically triggers an orbit calculation. By knowing the precise location of the front–ends and using highly accurate models, the software computes the orbit.

Back–end: The satellite tracking data (TDOA) and the orbit data (orbital elements) are stored in a safe database. The data which have to be published are pushed to the Publishing Server which allows data requests coming from the Internet.

In its first implementation, PaCoRa used 5 front–end receiving stations, 4 main and 1 back up. The initial implementation system has been designed, built and tested for Ku–band

signals, but it can easily be upgraded to other frequency bands by means of a simple adaptation of the RF components on the antenna front end. ²⁵⁰⁵⁾

Automated functions enable the operator to configure a schedule from which the system can run autonomously. Centralized monitoring and control software enable a new satellite to be added to an existing schedule by the ground operator. – The PaCoRa system will be available for commercialization as a complete turn–key system.

1.23.3.5 Nulling interferometry

Nulling interferometry refers to a new multi–aperture (large baseline) technique at the start of the 21st century for direct optical imaging of planets circling nearby stars (used by astronomers). Nulling interferometry works by creating at least two subapertures, both looking at the same target (a bright star), but positioned so starlight from each subaperture travels in slightly different paths before being sensed by the detector. When properly aligned, crests of lightwaves from one subaperture will line up with the troughs of the lightwaves from the other, thereby cancelling the light of the bright star (the star signal is roughly 10^6 times stronger than the planet signal orbiting the star).

Nulling interferometry is a promising technique for reducing the apparent brightness of a star relative to its surroundings. As such, nulling interferometry has the potential to enable direct detection of extrasolar planets (also referred to as **exoplanets**) and zodiacal light (see O.9.3).

The idea of nulling interferometry was first proposed in 1978 by Ronald N. Bracewell of Stanford University. ²⁵⁰⁶⁾ The first exoplanet in the vicinity of a “live star” was detected indirectly on Oct. 6, 1995 (around the star 51 Pegasi – discovered by Michael Mayor and Didier Queloz of the Observatoire de Genève, Switzerland) by the so–called “transit survey” using the method of photometric observations, i.e. periodic dimming of starlight (using radial velocity measurements – tiny Doppler shifts) as a planet moves across a star. ²⁵⁰⁷⁾ ²⁵⁰⁸⁾

The reference to a “live star” is made, as opposed to an old neutron star (or “pulsar”) that is at the end of its life. In fact, the very first extrasolar planet, one of the size of Earth, was discovered by Alexander Wolszczan (Pennsylvania State University) in 1991 by means of extremely accurate radio observations, in orbit around a neutron star, known as PSR 1257+12. This star rotates at the incredible speed of 161 revolutions per second (the period is 6.21 milliseconds) and is a pulsar, i.e., a dead star, the extremely compact remains of a sun bigger than ours that exploded as a huge supernova many millions of years ago. ²⁵⁰⁹⁾

November 19, 2010 marked the date that more than 500 exoplanets have been confirmed found by various groups of researchers. ²⁵¹⁰⁾

Examples of proposed/planned nulling interferometry satellite missions were: SIM Lite (Space Interferometer Mission) and TPF (Terrestrial Planet Finder), both of NASA. – Note: In 2007, NASA cancelled the SIM as well as the TPF missions due to budgetary problems.

²⁵⁰⁵⁾ “A new way to track geostationary orbiting satellites,” ESA, May 22, 2013, URL: <http://telecom.esa.int/telecom/www/object/index.cfm?fobjectid=32417>

²⁵⁰⁶⁾ M. Mayor, D. Queloz. “A Jupiter–mass companion to a solar–type star”. *Nature*, Vol. 378 (6555), pp.355–9, November 23, 1995

²⁵⁰⁷⁾ “Exoplanet History – From Intuition to Discovery,” URL: <http://planetquest.jpl.nasa.gov/page/history>

²⁵⁰⁸⁾ Malcom Curtis, “Mayor’s Exoplanet Discovery Transforms Astronomy,” URL: <http://michelmayor.ch/first-discovery/>

²⁵⁰⁹⁾ “The Discovery of Exoplanets,” URL: <http://www.lifeinuniverse.org/noflash/History-08-01.html>

²⁵¹⁰⁾ “Exoplanet Discovery Lists top 500,” *Universe Today*, Nov. 30, 2010, URL: <http://www.universetoday.com/80671/exoplanet-discovery-lists-top-500/>

From ESA there is DARWIN (Detection and Analysis of Remote Worlds by Interferometric Nulling) with a planned launch for 2015. ²⁵¹¹⁾ ²⁵¹²⁾ ²⁵¹³⁾

Recent studies on a two-aperture nulling interferometry instrument designs at NASA/GSFC suggest that instrument angular resolution can be better than conventionally assumed, namely by an order of magnitude. The reasons: a) the interferometer response decreases quadratically inside the null while the number of signal photons increases exponentially as the planet gets closer to the star; and b) use of the new “ratio-of-two-wavelength” technique. ²⁵¹⁴⁾ Simulations were conducted with FSKI (Fourier–Kelvin Stellar Interferometer), consisting of two 0.5 m apertures on a 12.5 m baseline. The results indicate that a significant number of known extrasolar planets will be detectable when using the FSKI technique.

- The first **optical snapshot of an exoplanet**, orbiting a star outside our solar system, was taken with the Hubble Space Telescope’s ACS (Advanced Camera for Surveys) – and published in Nov. 2008. The photo of the exoplanet Fomalhaut b, orbiting the star Fomalhaut at a distance about four times that between Neptune and the sun, was taken by Paul Kalas and James R. Graham of UCB (University of California at Berkeley). Fomalhaut is 25 light years from our solar system in the southern constellation Piscus Austrinus (southern fish). ²⁵¹⁵⁾ – Kalas has two photos of the exoplanet Fomalhaut b, taken in 2004 and 2006, which show that its movement over a 21-month period exactly fits what would be expected from a planet orbiting Fomalhaut every 872 years at a distance of 119 au (astronomical units).

- On the same day, Hubble publicised strikingly sharp images of an exoplanet orbiting the star Fomalhaut – the ground-based Keck–Gemini campaign (Keck Observatory, Hawaii) made the first direct observations in 2008 of a multi-exoplanet system around a star called HR8799.

- A few days later, yet another image came in from another research group at the European Southern Observatory (ESO), spotting the very compact orbit of an exoplanet around the star Beta Pictorus.

Considering there have never been any direct observations ²⁵¹⁶⁾ of exoplanets before November 2008 – although we have known about the presence of worlds orbiting other stars for many years via indirect methods – this has been a revolutionary year for exoplanet hunters.

- In 2010, astronomers using ESO’s HARPS (High Accuracy Radial velocity Planet Searcher) instrument at the ESO La Silla 3.6 m telescope in Chile, have discovered a planetary system containing at least five planets, orbiting the Sun-like star HD 10180. The researchers also have tantalizing evidence that two other planets may be present, one of which would have the lowest mass ever found. The five strongest signals correspond to planets with Neptune-like masses – between 13 and 25 Earth masses – which orbit the star with

2511) A. Nordt, D. Schaechter, L. Ames, J. Oseas, “Picometer Knowledge Transfer Testbed of the Space Interferometry Mission: Overview and Status,” Proceedings of IEEE Aerospace Conference, Big Sky, MT, March 8–15, 2003

2512) C. Noecker, R. Linfield, D. Miller, D. Osterman, S. Kilston, M. Lieber, W. Babb, A. Cavender, J. Jacobs, “Cold Interferometric Nulling Demonstration In Space (CINDIS),” Proceedings of IEEE Aerospace Conference, Big Sky, MT, USA, March 8–15, 2003

2513) E. Serabyn, “Faint Near-Neighbor Detection with a Fiber Nuller,” NSTC2007 (NASA Science and Technology Conference 2007), June 19–20, 2007, College Park, MD, USA, URL: http://esto.nasa.gov/conferences/nstc2007/papers/Serabyn_Gene_C1P1_NSTC-07-0006.pdf

2514) W. C. Danchi, D. Deming, M. J. Kuchner, S. Seager, “Detection of Close-In Extrasolar Giant Planets Using the Fourier–Kelvin Stellar Interferometer,” *Astrophysical Journal Letters*, Vol. 597, No 1, L57–60, Nov. 1, 2003

2515) “First Optical Photo Of Exoplanet Orbiting Nearby Star,” Spacedaily Nov. 14, 2008, URL: http://www.spacedaily.com/reports/First_Optical_Photo_Of_Exoplanet_Orbiting_Nearby_Star_999.html

2516) Ian O’Neill, “Time Magazine Top 10 Scientific Discoveries of 2008: Space and Physics Dominate,” Dec. 11, 2008, URL: <http://www.universetoday.com/2008/12/11/time-magazine-top-10-scientific-discoveries-of-2008-space-and-physics-dominate/>

periods ranging from about 6 to 600 days. These planets are located between 0.06 and 1.4 times the Earth–Sun distance from their central star. ²⁵¹⁷⁾

– In November 2010, astronomers discovered the first exoplanet that originated in another galaxy. The planet’s host star belongs to a dwarf galaxy which was swallowed up by our home galaxy, the Milky Way, billions of years ago. The planet, which has been designated HIP 13044 b, has a minimum mass of 1.25 times the mass of Jupiter. The star system is located about 2000 light–years from Earth in the southern constellation Fornax (“the chemical furnace”).

The planet was discovered with the radial velocity method, which measures tiny wobbles of a star caused by a planet’s gravitational pull. HIP 13044’s wobbles were detected with the high–resolution spectrograph FEROS at the 2.2 m MPG/ESO telescope at ESO’s La Silla observatory in Chile. ²⁵¹⁸⁾

– In Dec. 2011, NASA announced that its Kepler spacecraft discovered the first Earth–size planets orbiting a sun–like star outside our solar system. The planets, called Kepler–20e and Kepler–20f, are too close to their star to be in the so–called habitable zone where liquid water could exist on a planet’s surface, but they are the smallest exoplanets ever confirmed around a star like our sun. ^{2519) 2520)}

The discovery marks the next important milestone in the ultimate search for planets like Earth. The new planets are thought to be rocky. Kepler–20e is slightly smaller than Venus, measuring 0.87 times the radius of Earth. Kepler–20f is a bit larger than Earth, measuring 1.03 times its radius. Both planets reside in a five–planet system called Kepler–20, approximately 1,000 light–years away in the constellation Lyra.

• At the end of 2011, there were a total of 716 confirmed exoplanets and 2,326 planetary candidates, found by both orbiting space telescopes like Kepler and ground–based observatories.

Most currently known exoplanets were found either by detecting the effect of the gravitational pull of the planet on its host star or by catching the planet as it passes in front of its star and slightly dims it. Both of these techniques are much more sensitive to planets that are either massive or close to their stars, or both, and many planets will be missed.

An international team of astronomers has searched for exoplanets using a totally different method – gravitational microlensing – that can detect planets over a wide range of mass and those that lie much further from their stars. ²⁵²¹⁾ – In January 2012, after a six–year search that surveyed millions of stars in the MilkyWay, the international team concluded that planets around stars are the rule rather than the exception. ²⁵²²⁾

• In July 2012, astronomers using NASA’s Spitzer Space Telescope have detected what they believe is a planet two–thirds the size of Earth. The exoplanet candidate, called

2517) “Seven–Planet System Discovered,” Space Daily, Aug. 27, 2010, URL: http://www.spacedaily.com/reports/Seven_Planet_System_Discovered_999.html

2518) “An exoplanet from another galaxy,” MPIA (Max Planck Institute for Astronomy) Science Release 2010–11–18, URL: http://www.mpia.de/Public/menu_q2.php?Aktuelles/PR/2010/PR101118/PR_101118_en-hidden.html

2519) Tony Phillips, “Kepler Discovers Earth–size Exoplanets,” NASA, Dec. 20, 2011, URL: http://science.nasa.gov/science-news/science-at-nasa/2011/20dec_earth-sized/

2520) http://www.nasa.gov/mission_pages/kepler/main/index.html

2521) A. Cassan, D. Kubas, J. – P. Beaulieu, M. Dominik, K. Horne, J. Greenhill, J. Wambsganss, J. Menzies, A. Williams, U. G. Jørgensen, A. Udalski, D. P. Bennett, M. D. Albrow, V. Batista, S. Brillant, J. A. R. Caldwell, A. Cole, Ch. Coutures, K. H. Cook, S. Dieters, D. Dominis Prester, J. Donatowicz, P. Fouqué, K. Hill, et. al., “One or more bound planets per Milky Way star from microlensing observations,” *Nature*, Vol. 481, Jan. 12, 2012, pp. 167–169

2522) “Planet Population is Plentiful,” Space Daily, Jan. 12, 2012, URL: http://www.spacedaily.com/reports/Planet_Population_is_Plentiful_999.html

UCF–1.01, is located a mere 33 light–years away, making it possibly the nearest world to our solar system that is smaller than our home planet. ^{2523) 2524)}

The hot new planet candidate was found unexpectedly in Spitzer observations. Kevin Stevenson (University of Central Florida) and his colleagues were studying the Neptune–sized exoplanet GJ 436b, already known to exist around the red–dwarf star GJ 436. In the Spitzer data, the astronomers noticed slight dips in the amount of infrared light streaming from the star, separate from the dips caused by GJ 436b. A review of Spitzer archival data showed the dips were periodic, suggesting a second planet might be blocking out a small fraction of the star’s light.

- In October 2012, ESO (European Southern Observatory) astronomers at the La Silla observatory in Chile have discovered an enticing new planet that could be considered our next–door neighbor. The planet is orbiting a star in the Alpha Centauri system — the closest system to our own, just 4.3 light years away — and the planet has a mass about the same as Earth. It is also the lightest exoplanet ever discovered around a sun–like star. The planet is called Alpha Centauri Bb and it whips around its star every 3.2 days, orbiting at a distance of just 6 million km, closer than Mercury’s orbit around the Sun. ^{2525) 2526)}

High–precision measurements have been obtained for Alpha Centauri B between February 2008 and July 2011 using the HARPS (High Accuracy Radial velocity Planet Searcher) spectrograph, a high–resolution (R = 110,000) cross–dispersed echelle spectrograph installed on the 3.6 m telescope at LaSilla.

Note: The first exoplanet around a Sun–like star was found by the same team back in 1995 and there are now 843 Exoplanets with the addition of Alpha Centauri Bb. Most are much bigger than Earth, and many are as big as Jupiter.

- April 2013: An international team of scientists analyzing data from NASA’s Kepler mission has found a planetary system with two small, potentially rocky planets that lie within the habitable zone of their star. The star, Kepler–62, is a bit smaller and cooler than our Sun, and is home to a five–planet system. Two of the worlds, Kepler–62e and Kepler–62f are the smallest exoplanets yet found in a habitable zone, and they might both be covered in water or ice, depending on what kind of atmosphere they might have.

The Kepler–62 system has five planets; 62b, 62c, 62d, 62e and 62f. The Kepler–69 system has two planets; 69b and 69c. Kepler–62e, 62f and 69c are the super–Earth–sized planets. – The new planets brings the number of confirmed exoplanets to 861. ^{2527) 2528)}

Two of the newly discovered planets orbit a star smaller and cooler than the sun. Kepler–62f is only 40 % larger than Earth, making it the exoplanet closest to the size of our planet known in the habitable zone of another star. Kepler–62f is likely to have a rocky composition. Kepler–62e, orbits on the inner edge of the habitable zone and is roughly 60 percent larger than Earth.

2523) J.D. Harrington, Whitney Clavin, “NASA’S Spitzer Finds Evidence for an Exoplanet Smaller than Earth,” NASA release 12–238, July 18, 2012, URL: http://www.nasa.gov/home/hqnews/2012/jul/HQ_12-238_Spitzer_Small_Exoplanet.html

2524) Kevin B. Stevenson, Joseph Harrington, Nate B. Lust, Nikole K. Lewis, Guillaume Montagnier, Julianne I. Moses, Channon Visscher, Jasmina Blečić, Ryan A. Hardy, Patricio Cubillos, Christopher J. Campo, “Two nearby sub–Earth–sized exoplanet candidates in the GJ 436 system,” *Astrophysics Journal*, 2012

2525) Xavier Dumusque, Francesco Pepe, Christophe Lovis, Damien Ségransan, Johannes Sahlmann, Willy Benz, François Bouchy, Michel Mayor, Didier Queloz, Nuno Santos, Stéphane Udry, “An Earth mass planet orbiting Alpha Centauri B,” URL: <http://www.eso.org/public/archives/releases/sciencepapers/eso1241/eso1241a.pdf>

2526) Nancy Aktinson, “Next Door Neighbors? Earth–Sized Planet Discovered in Nearest Star System to Us,” *Universe Today*, Oct. 16, 2012, URL: <http://www.universetoday.com/98031/next-door-neighbors-earth-sized-planet-discovered-in-nearest-star-system-to-us/>

2527) Michele Johnson, J. D. Harrington, “NASA’s Kepler Discovers Its Smallest ‘Habitable Zone’ Planets to Date,” NASA release 13–112, April 18, 2013, URL: http://www.nasa.gov/mission_pages/kepler/news/kepler-62-kepler-69.html

2528) Tony Phillips, “Kepler Discovers Smallest ‘Habitable Zone’ Planets,” NASA, April 18, 2013, URL: http://science.nasa.gov/science-news/science-at-nasa/2013/18apr_habitablezone/

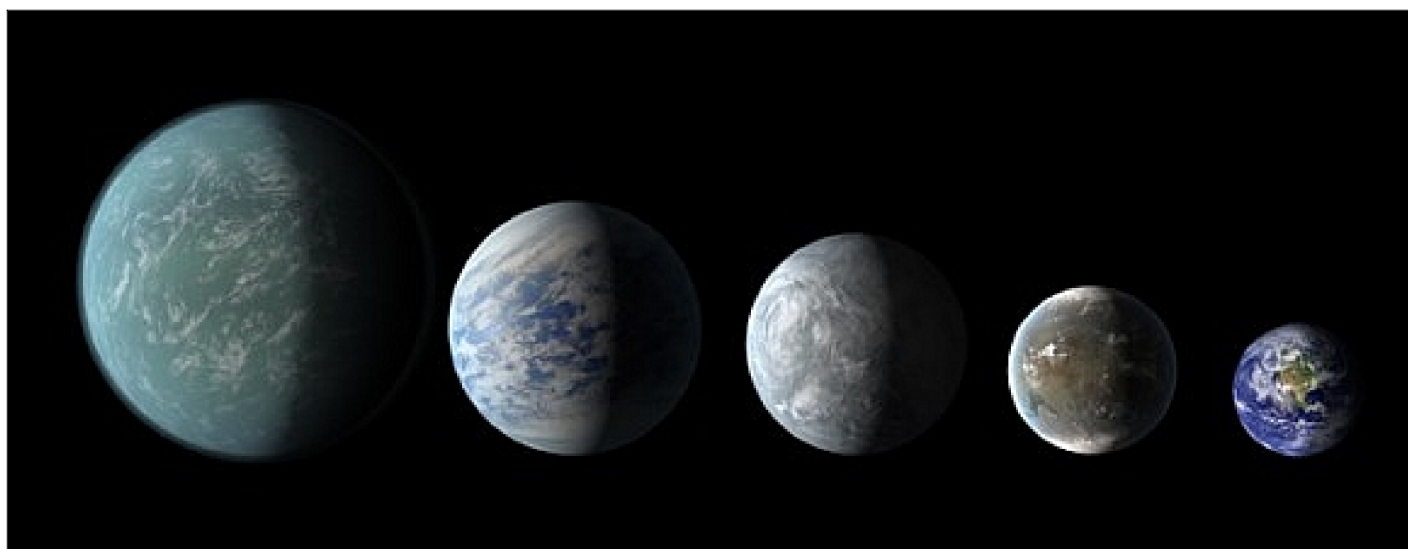


Figure 193: Relative sizes of Kepler habitable zone planets discovered in April, 2013 (image credit: NASA(ARC, JPL–Caltech)

Legend to Figure 193: Left to right: Kepler–22b, Kepler–69c, Kepler–62e, Kepler–62f and Earth (except for Earth, these are artists’ renditions).

The third planet, Kepler–69c, is 70 % larger than the size of Earth, and orbits in the habitable zone of a star similar to our sun. Astronomers are uncertain about the composition of Kepler–69c, but its orbit of 242 days around a sun–like star resembles that of our neighboring planet Venus.

Scientists do not know whether life could exist on the newfound planets, but their discovery signals we are another step closer to finding a world similar to Earth around a star like our sun.

- In May 2013, NASA’s Kepler telescope has lost its ability to precisely point toward stars, putting its exoplanet search in jeopardy. One of the reaction wheels – devices which enable the spacecraft to aim in different directions without firing thrusters – has failed. This is of grave concern because last year reaction wheel #2 failed, and now #4 has failed. With the failure of a second reaction wheel, it’s unlikely that the spacecraft will be able to return to the high pointing accuracy that enables its high–precision photometry. However, no decision has been made to end data collection. ²⁵²⁹⁾
- July 2013: Astronomers working with NASA’s Hubble Space Telescope have deduced the actual color of a planet orbiting another star 63 light years away. The planet is HD 189733b, one of the closest exoplanets that can be seen crossing the face of its star, and its color is cobalt blue. If seen directly, this planet would look like a deep blue dot, reminiscent of Earth’s color as seen from space. Although the planet resembles Earth in terms of color, it is not an Earth–like world. ²⁵³⁰⁾
- Oct. 22, 2013: The count of exoplanets circling distant stars has passed a benchmark figure, astronomers said, as the 1,000th was added to a European database. With the help of the Super Wide Angle Search for Planets (SuperWASP) collaboration, the number jumped from 999 to 1,010 overnight, Discovery.com reported. ²⁵³¹⁾
- With exoplanet discoveries coming at us several times a month, finding these worlds is a hot field of research. Once the planets are found and confirmed, however, there’s a lot more

2529) “Kepler Mission Manager Update,” NASA, May 15, 2013, URL: http://www.nasa.gov/mission_pages/kepler/news/keplerm-20130515.html

2530) Tony Phillips, “Hubble finds a cobalt blue planet,” NASA, July 11, 2013, URL: http://science.nasa.gov/science-news/science-at-nasa/2013/11jul_cobaltblue/

2531) “Count of discovered exoplanets passes the 1,000 mark,” Space Daily, Oct. 22, 2013, URL: http://www.spacedaily.com/reports/Count_of_discovered_exoplanets_passes_the_1000_mark_999.html

that has to be done to understand them. What are they made of? How habitable are they? What are their atmospheres like? These are questions we are only beginning to understand.

- In Feb. 2014, ESA's Science Program Committee selected the PLATO (Planetary Transits and Oscillations of stars) mission for implementation as part of its Cosmic Vision 2015–2025 Program. The mission will address two key themes of Cosmic Vision: what are the conditions for planet formation and the emergence of life, and how does the Solar System work? PLATO will monitor relatively nearby stars, searching for tiny, regular dips in brightness as their planets transit in front of them, temporarily blocking out a small fraction of the starlight. A launch of PLATO is planned for 2024. ²⁵³²⁾
- On Feb. 26, 2014, NASA's Kepler mission announced the discovery of 715 new planets. These newly-verified worlds orbit 305 stars, revealing multiple-planet systems much like our own solar system. Nearly 95% of these planets are smaller than Neptune, which is almost four times the size of Earth. This discovery marks a significant increase in the number of known small-sized planets more akin to Earth than previously identified exoplanets, which are planets outside our solar system. ^{2533) 2534) 2535)}

Since the discovery of the first planets outside our solar system roughly two decades ago, verification has been a laborious planet-by-planet process. Now, scientists have a statistical technique that can be applied to many planets at once when they are found in systems that harbor more than one planet around the same star.

The research team used a technique called verification by multiplicity, which relies in part on the logic of probability. Kepler observes 150,000 stars, and has found a few thousand of those to have planet candidates. If the candidates were randomly distributed among Kepler's stars, only a handful would have more than one planet candidate. However, Kepler observed hundreds of stars that have multiple planet candidates. Through a careful study of this sample, these 715 new planets were verified.

- On April 17, 2014, NASA announced that astronomers have discovered the first Earth-size planet orbiting a star in the "habitable zone", using the Kepler Space Telescope. The discovery of Kepler-186f is a significant step toward finding worlds like our planet Earth. While planets have previously been found in the habitable zone, they are all at least 40% larger in size than Earth and understanding their makeup is challenging. Kepler-186f is more reminiscent of Earth. – Kepler-186f resides in the Kepler-186 system about 500 light-years from Earth in the constellation Cygnus. The system is also home to four inner planets, seen lined up in orbit around a host star that is half the size and mass of the sun. ²⁵³⁶⁾

2532) "ESA selects planet-hunting PLATO mission," ESA, Feb. 19, 2014, URL: <http://sci.esa.int/plato/53707-esa-selects-planet-hunting-plato-mission/>

2533) Michele Johnson, J. D. Harrington, "NASA's Kepler Mission Announces a Planet Bonanza, 715 New Worlds," NASA Release 14-059, February 26, 2014, URL: http://www.nasa.gov/ames/kepler/nasa-kepler-mission-announces-a-planet-bonanza/#.Uw6_LM7ihqM

2534) Jack J. Lissauer, Geoffrey W. Marcy, Stephen T. Bryson, Jason F. Rowe, Daniel Jontof-Hutter, Eric Agol, William J. Borucki, Joshua A. Carter, Eric B. Ford, Ronald L. Gilliland, Rea Kolbl, Kimberly M. Star, Jason H. Steffen, Guillermo Torres, "Validation of Kepler's Multiple Planet Candidates. II: Refined Statistical Framework and Descriptions of Systems of Special Interest," *Astrophysical Journal*, 25 Feb. 2014, URL: <http://www.nasa.gov/sites/default/files/files/arXivValidationMultisII.pdf>

2535) Jason F. Rowe, Stephen T. Bryson, Geoffrey W. Marcy, Jack J. Lissauer, Daniel Jontof-Hutter, Fergal Mullally, Ronald L. Gilliland, Howard Isaacson, Eric Ford, Steve B. Howell, William J. Borucki, Michael Haas, Daniel Huber, Jason H. Steffen, Susan E. Thompson, Elisa Quintana, Thomas Barclay, Martin Still, Jonathan Fortney, T. N. Gautier III, Roger Hunter, Douglas A. Caldwell, David R. Ciardi, Edna Devore, William Cochran, Jon Jenkins, Eric Agol, Joshua A. Carter, John Geary, "Validation of Kepler's Multiple Planet Candidates. III: Light Curve Analysis & Announcement of Hundreds of New Multi-planet Systems," *Astrophysical Journal*, 25 Feb. 2014, URL: <http://www.nasa.gov/sites/default/files/files/arXivValidationMultisIII.pdf>

2536) J. D. Harrington, Michele Johnson, Karen Randall, "NASA's Kepler Telescope Discovers First Earth-Size Planet in 'Habitable Zone'," NASA, April 17, 2014, URL: <https://navigator.gmx.net/navigator/show?sid=b502659f6952b760f2d9129874ed-ba7e4c9b19f332fbf36b27473ec7bb64f54e92f001976b2e4f2a72d4ca96f53a7823#mail>

1.23.3.6 Satellite Laser Ranging (SLR)

SLR provides a direct and unambiguous observation of the distance between a laser station on the surface of the Earth and a spacecraft equipped with a passive laser retroreflector (LRR). The concept of SLR is based on measuring the round-trip signal time of a laser beam between a ground station and retroreflectors onboard a spacecraft (see Glossary). The “range” or distance between the satellite and the observing site, is approximately equal to one half of the two-way travel time multiplied by the speed of light.²⁵³⁷⁾ SLR is a highly accurate measuring technique providing, among others, the mm-level terrestrial reference frame and the product of the universal gravitational constant G (SLR data, collected from a variety of satellites, is the dominant contributor to modern gravity field models). SLR is also sensitive to the location of the Earth’s center of mass; the time history of its motion with respect to the origin of the terrestrial reference frame has been obtained since 1987 with an accuracy of a few millimeters.^{2538) 2539)}

In particular, SLR is often used to calibrate other measurement techniques such as radar altimeters. SLR techniques are also a strong contributor to advances in precision orbit determination. The SLR measurement precision has improved from a few meters in the mid-1960s to the cm level (even several mm) at the start of the 21st century. The statistical treatment of a large number of measurements helps to improve the precision. The main drawbacks of SLR are its reliance on weather conditions (atmospheric refraction models), the treatment of systematic errors in the measurement apparatus, and the need of trained personnel on the ground.

The passive SLR technique was first successfully demonstrated with a ‘laser tracking reflector experiment’ flown on the following spacecraft: BE-B (Beacon Explorer-B/ or Explorer-22) of NASA, launch Oct. 10, 1964; GEOS-1 of NASA (launch Nov. 6, 1965); Diademe-1 and -2 (Feb. 1967) of CNES, GEOS-2 of NASA (launch Jan. 11, 1968) also referred to as Explorer-36, GEOS-3 (launch Apr. 9, 1975) and SeaSat of NASA/JPL (launch June 27, 1978). International cooperation and participation of many agencies has successively led to a global network of SLR ground stations (see H.5.3.6). – SLR measurements are applied to such fields as: global tectonic plate motion, regional crustal deformation near plate boundaries, Earth’s gravity field and the orientation of its polar axis and its rate of spin. – A passive satellite laser-ranging measurement capability (entire S/C consists of laser corner reflectors) from ground to space was first provided with the CNES Starlette satellite (launch, Feb. 6, 1975).

In the early 1980s, the SLR and Lunar Laser Ranging (LLR) communities participated in MERIT (Monitoring Earth Rotation and Intercomparison of Techniques) to demonstrate the utility of modern space geodesy techniques in determining Earth rotation parameters. Earth rotation solutions, based on laser ranging to LAGEOS, have been delivered weekly since 1981, and represent the longest, continuous Earth rotation series obtained using modern space techniques.

S/C or Mission (instrument)	Launch	Comment
BE-B (Beacon Explorer-B/ or Explorer-22)	Oct. 10, 1964	First corner cube experiment on a S/C
GEOS-1 (Laser Tracking Reflector), NASA	Nov. 6, 1965	322 cubes were mounted on fiberglass panels on the bottom rim of the S/C

2537) Note: An optical retroreflector is a device that reflects light back to the light source, regardless of the angle of incidence on its path of incidence. This behavior is unlike a mirror which does that only if the mirror is exactly perpendicular to the light beam. The retroreflector effect can be commonly obtained in two ways: with a set of three perpendicular mirrors (a corner cube reflector) and with a transparent sphere of material with refractive index 2. Typically, a retroreflector has fairly wide field of view (FOV), so it does not need to be pointed precisely to operate.

2538) P. Bonnefond, P. Exertier, P. Schaeffer, S. Bruinsma, F. Barlier, “Satellite Altimetry From a Short-Arc Orbit Technique: Application to the Mediterranean,” *Journal of Geophysics and Remote Sensing*, Vol. 100 (C12), pp. 25365–25382, 1995

2539) Michael Pearlman, “Satellite Laser Ranging (SLR) and the International Laser Ranging Service (ILRS),” International Technical Laser Workshop on SLR Tracking of GNSS Constellations, Metsovo, Greece, Sept. 14–19, 2009, URL: http://cdsis.gsfc.nasa.gov/metsovo/docs/PPPEARLMAN_ILRS_andSLRStatus.pdf

Diademe-1 of CNES Diademe-2 of CNES	Feb. 8, 1967 Feb. 15, 1967	Payload: USO (Ultra Stable Oscillator) to test one-way Doppler, and laser reflectors (SLR pilot experiment with 3 ground stations)
GEOS-2 (Laser Tracking Reflector), NASA	Jan. 11, 1968	Identical system as flown on GEOS-1
GEOS-3 (Laser Tracking Reflector), NASA and JHU/APL	Apr. 9, 1975	264 quartz cube corner reflectors mounted on a 45° conic frustum
Starlette, CNES	Feb. 6, 1976	First mission where the entire S/C consists of laser corner reflectors
LAGEOS-I, NASA, MEO orbit	May 4, 1976	
SeaSat (Laser Tracking Reflector), NASA/JPL	June 27, 1978	96 fused silica 3.75 cm hexagonal corner cube retroreflectors
EGS (Ajisai), NASDA, Japan	Aug. 12, 1986	318 mirrors and 120 laser reflector assemblies (1436 corner cube reflectors)
GEO-IK, NPO PM, Krasnojarsk, USSR The series of GEO-IK S/C is incomplete due to lacking information	May 30, 1988 Aug. 28, 1989 1990 Nov. 24, 1994	Orbit:1500 km altitude, inclin. =73.6° Orbit:1500 km altitude, inclin.=73.6°
ETALON-1, (RRA), USSR, MEO orbit ETALON-2, (RRA), USSR, MEO orbit	Jan. 10, 1989 May 31, 1989	2140 laser reflectors on RRA
ERS-1 (LRR), ESA	July 17, 1991	
TOPEX/Poseidon (LRA), NASA/CNES	Aug. 10, 1992	
LAGEOS-II of ASI and NASA, MEO orbit	Oct. 22, 1992	
Stella, CNES	Sept. 26, 1993	Stella is an exact twin of Starlette
MSTI-2 (RRA), BMDO/SMC	May 8, 1994	
GFZ-1 of GFZ, Potsdam, Germany	April 9, 1995	Low-altitude and slowly decaying orbit
ERS-2 (LRR), ESA	April 21, 1995	
Meteor-2-22, Russia	Aug. 31, 1993	Fizeau retroreflector array
RESURS-01-3 (RRA), Russia	Nov. 4, 1994	Fizeau retroreflector array
TiPS (Tether Physics and Survivability), DoD/NRL, see M.53	June 20, 1996	Retroreflectors are mounted on the exterior surfaces Ralph and Norton
ADEOS (RIS), NASDA, JEA	Aug. 17, 1996	Design of a hollow and flat cube-corner retroreflector
WESTPAC, EOS Australia (RESURS-01-4)	July 10, 1998	Fizeau retroreflector array
Techsat/Gurwin-II (SLRRE), Technion Israel Institute of Technology, launched with RESURS-01-4 satellite, see N.30	July 10, 1998	Array of laser retroreflectors, corner-cube mounted on the Earth-viewing panel
STEX/ATEX, DoD/NRL	Oct. 3, 1998	
SUNSAT, Stellenbosch University, SA	Feb. 23, 1999	Eight retroreflectors
CHAMP (LRR), GFZ, Germany	July 15, 2000	
Jason-1 (LRA), CNES/NASA	Dec. 7, 2001	
REFLECTOR, Russian S/C with a mass of 7 kg and gravity-boom stabilization	Dec. 10, 2001	Nanosatellite on Meteor-3M-1 launch, retroreflector array of 32 corner cubes
Meteor-3M-1 (RRA)	Dec. 10, 2001	Meteor-3M-1 has also its own RRA
Envisat (LRR), ESA	Mar. 1, 2002	
GRACE (LRA), NASA/DLR/GFZ	Mar. 17, 2002	
ADEOS-II, JAXA	Dec. 14, 2002	Loss of power forced JAXA to terminate the mission
ICESat (GLAS), NASA/GSFC	Jan. 13, 2003	
Gravity Probe-B, NASA, Stanford University	Apr. 20, 2004	
ALOS, JAXA (formerly NASDA)	Jan. 24, 2006	

Table 145: Chronology of some SLR (Satellite Laser Ranging) systems

- An extension of the SLR ²⁵⁴⁰ (ground to satellite) technique inverts the traditional SLR system with the ranging hardware being placed onboard a satellite to range to the ground. This technique is being introduced with the GLAS (Geoscience Laser Altimeter

System) instrument of the EOS program on ICESat (launch Jan. 13, 2003) for high-resolution ice and land topography mapping (realized already in the Mars Explorer Mission).

- Modulation of retroreflectors. The state of the art of modulating retroreflectors has progressed considerably in the 1990s. The advent of ferro-electric liquid crystals (FLCs) and the technology to produce MEMS (Micro-Electro-Mechanical Systems) make new optoelectronic systems available. The most significant development has been the increase in the switching speeds that now allow data to be sent at tens of kilohertz up to multi-megahertz with very low power consumption. The technologies used for these devices are:
 - Ferro-electric liquid crystal (FLC) – Switches the polarization by reversing the polarity of the bias voltage
 - Multiple Quantum Well Device (MQW)²⁵⁴¹ – Switches resonance to pass or reject optical beam by electro-absorption. Solid-state MQW retromodulators may be utilized to provide spacecraft-to-spacecraft laser communication (interrogation) and navigation (relative position and orientation). MQW modulators have very high switching speeds.
 - Atomic Absorption Cell (AAC) – Quantum electronic filter
 - MEMS Spoiled Corner Cube – Diffuse or specular surface reflection on one surface of the retroreflector
 - Switchable Gratings (PLZT) – Uses piezo-electric transducers to momentarily create diffracting surface on one surface of the retroreflector.
- Double-Difference (DD) Approach of Space Geodesy – SLR/LLR/GNSS/VLBI: Double-differences have been widely used in the processing of global GPS measurements, forming so-called GPS baselines, or vectors between IGS stations. When ETALON and LAGEOS satellites are observed by SLR, any orbit error propagates directly into station coordinates. However, by forming differences between two satellites and two ground stations this orbit error can be eliminated or to a great extent reduced. Both satellites need to be observed quasi-simultaneously in the same tracking sessions in order that station range bias and common reflector signature effect are removed by differencing. By forming single-difference of SLR measurements between two stations and a common satellite, range biases are not eliminated, thus singledifference to another satellite in a common view is needed. In this way, double-difference SLR measurements of utmost precision and accuracy are obtained.²⁵⁴²

1.23.3.7 Active laser tracking systems

At the start of the 21st century, there is great interest and considerable demand for space surveillance applications, in particular in risk mitigation and debris avoidance for satellites. There is also a need to provide accurate flight information from a single observation point on a moving platform or on a cluster of spacecraft (maintenance and control of these cluster configurations require accurate position sensing and actuation). Hence, the requirements (goal) call for automated tracking capabilities of spaceborne objects (in LEO, MEO, GEO) from the ground, including high-resolution information on the spatial features of such space objects for identification purposes. The desired parameters are object orientation,

2540) B. E. Schulz, "Spaceborne Laser Altimetry," Proceedings of the Weikko A. Heiskanen Symposium in Geodesy, Ohio State University, Columbus, OH, USA, Oct. 1-4, 2002

2541) N. G. Creamer, G. C. Gilbreath, T. J. Meehan, et al., "Multiple Quantum Well Retromodulators for Spacecraft-To-Spacecraft Laser Interrogation, Communication, and Navigation," AIAA/USU Conference on Small Satellites, Logan UT, Aug. 13-16, 2001, SSC01-VI-6

2542) Drazen Svehla, Rune Floberghagen, Roger Haagmans, Ulf Klein, Bernd Sierk, Luigi Cacciapuoti, "SLR Measurements of the Forthcoming ESA Earth Observation and Fundamental Physics Missions and Their Applications in the Reference Frames Realization," 2012, URL: http://www.lnf.infn.it/conference/laser2012/3wednesday/12_svehla/svehla_1.pdf

precision orbit track (position and velocity), and size and shape of the object. In addition, temporal variations of these spatial parameters are needed to characterize and assess the nature and intent of a specific space object being tracked. – Generally, none of these objects have laser retroreflectors (as in conventional SLR applications) that could be used for tracking. Passive SLR systems measure the position (range) of a spacecraft, but do not provide velocity and other needed parameters of the object to be tracked.

A possible solution may be found in active laser tracking systems. In such a concept, a laser is being used to illuminate distant objects; light reflected by the object(s) is then detected and analyzed by a surveillance system to identify and track them.^{2543) 2544)} The laser beam is locked onto the target surface in an active tracking configuration. This permits for retrieving complete information on the target's spatial/angular position and the velocity component that is normal to the measuring platform. A promising technique to realize such laser tracking concepts is to use the non-linear Optical Phase Conjugation (OPC) scheme; it allows for compensation of spatial intra-cavity non-uniformities, as well as atmospheric turbulence on the laser pass. In this detection scheme, a PCM (Phase Conjugate Mirror) in a laser coupled-cavity uses OPC to eliminate the imperfections and aberrations of the lasing media and the intra-cavity optical elements, and to generate a diffraction-limited laser.

The technology introduced so far has only been on a demonstration level.²⁵⁴⁵⁾ Obviously, the military is very interested in such tracking systems for its surveillance needs, but there are also demands for civil tracking applications to analyze potential debris problems and more. An example of an early experimental system is ATLAS (Active Tracker Laser) of the US AFRL (Air Force Research Laboratory) which was developed by Northrop Grumman in 1996. ATLAS employs a solid-state, diode-array-pumped laser with an average output power of 500 W in the infrared region and a pulse repetition rate of 2.5 kHz.

- MRR (Modulating Retroreflector), a communication device using a corner cube reflector (CCR) array at one node of the link. An optical modulating retroreflector is a device that couples an optical retroreflector with a modulator, which provides the ability to turn the retro-reflected beam on or off as a method of encoding data.²⁵⁴⁶⁾ Using an MRR device allows a node to send data without having its own active laser, provided that the recipient of the data supplies the optical energy. An MRR-based optical link consists of two nodes: an interrogator node, equipped with an active laser, and an MRR node, equipped with an MRR device. Typically an MRR-based link operates in half-duplex mode. – MRR components can be very small and operate at extremely low power level, which significantly extends the operational lifetime. A distinct advantage of using MRR technology is the much relaxed pointing requirement. The typical field of view (FOV) of an MRR device can be as large as several ten's degrees. Using an array of MRR, a very large field of regard (FOR) can be achieved. Using a space-division receiver, an MRR-based optical system can be channelized to receive multiple modulated beams simultaneously.

1.23.3.8 Gradiometry, accelerometry, drag-free satellites

Gradiometry is the measurement and study of the gradient of the gravitational field of the Earth (or some other body).²⁵⁴⁷⁾ Gradiometric techniques are used in remote sensing applications because a gravitational sensor cannot discriminate between the local gravity vec-

2543) V. Markov, A. Khizhnyak, E. Scott, B. Zel'dovich, T. Martinez, Shiang Liu, "System concept and some characteristics of the coupled-cavity laser system for active target tracking," SPIE Annual Meeting 2002: Remote Sensing and Space Technology, High-Resolution Wavefront Control: Methods, Devices, and Applications IV, Seattle, WA, July 7-11, 2002, SPIE Vol. 4825

2544) J. McGarry, J. Degnan, P. Titterton, H. Sweeney, B. Conklin, P. Dunn, "Automated tracking for advanced satellite laser ranging systems," Proceedings of SPIE Aerosense Conference, Vol.2739, Apr. 8-12, 1996, pp.89-103

2545) <http://www.eos-aus.com/corporatedetails.htm>

2546) J. L. Gao, "Optical Retroreflector-based Sensor Networks for In-Situ Science Applications," Proceedings of IEEE Aerospace Conference, Big Sky, MT, March 8-15, 2003

2547) Note: The gravity vector is, by definition, normal to a surface of gravitational equipotential.

tor and instrumental accelerations (the Equivalence Principle). To distinguish gravity from platform accelerations (vibrations, drag, etc.), the Equivalence Principle requires a differential measurement. A gravity gradiometer detects the spatial derivative of the gravitational field and ideally is immune to the vibrations of the platform. However, the gradient technique measures only the effects of gravity and does not respond (at least not in principle) to instrumental accelerations. Gravity gradiometry is strongly sensitive to the gravity field induced by the topographic and isostatic masses of the Earth.

Gradiometry and accelerometry are important measurement techniques in the field of geodetic and geodynamic applications (i.e., tracking). The measurement principle of gravity gradiometry is based on differential accelerometry (gravity gradients are the second order derivatives of the gravitational potential). The overall objective is the determination of Earth's gravity field to a sufficient degree of accuracy and resolution (grid size) to permit such functions as gravity field modeling, high-resolution geoid modeling (the geoid is defined purely by the Earth's gravity field), and a number of other evaluations including inputs for plate tectonics and crustal dynamics. A better knowledge of the Earth's gravity field and its temporal changes may improve our understanding of the physics of the interior of the Earth; it may also explain a number of mechanisms leading to the building of the Earth's crust, the evolution of the green house effect, the ocean dynamics and its currents, and of the interaction of continents. ^{2548) 2549)}

The Earth's gravity field is the response to the mass density distribution of the Earth and its rotation. While the rotational contribution to gravity is represented by a mathematically very simple model, the gravitational part is extremely difficult to model and not known with sufficient accuracy and resolution on a global scale. ²⁵⁵⁰⁾ The gravitational field is harmonic outside the Earth's surface and can be conveniently represented by a series of solid spherical harmonics. The modeling all of its irregularities (which are due to the irregularities of the Earth's mass density distribution), requires, strictly speaking, an infinite number of parameters (e.g., harmonic coefficients). The estimation of these parameters requires data which are sensitive with respect to these parameters. Naturally, a finite data set can only provide an approximation to reality.

- Gradiometry measurement of the Earth's gravity field from space. Two basic and complementary approaches are in use:
 - SST (Satellite-to-Satellite Tracking Technique), see 1.23.3.2
 - SGG (Satellite Gravity Gradiometry)

SGG measures second derivatives of the gravity vector, called gravity gradients, onboard a S/C in various directions with the use of a gradiometer, consisting of several accelerometers operated in differential mode. Gravity gradients are highly sensitive to the local features of the gravity field in the proximity of the measurement location. ²⁵⁵¹⁾ SST is best at providing the long and medium wavelength of the geopotential, while SGG performs best at the shorter wavelengths as a result of the measurement bandwidth characteristics of the accelerometers. Both approaches favor low-altitude orbits (providing a greater sensitivity to gravity variations) in which air drag modeling is critical, because the non-gravitational orbit perturbations have to be separated from the purely gravitational ones.

2548) Note: The conventional gravimeter measures a single component (the vertical component) of the gravity field vector. In contrast, a gravity gradiometer can measure up to five of the nine terms in the gravity field's gradient tensor which completely describes the anomalous gravity field gradient. A very appealing advantage of the gradiometer method is its greater immunity to the large translational accelerations which adversely affect conventional gravimeters in dynamic environments (e.g., ships and aircraft).

2549) R. Rummel, G. Balmino, J. Johannessen, P. Visser, P. Woodworth, "Dedicated gravity field missions – principles and aims," *Journal of Geodynamics*, Vol. 33, 2002, pp. 3–20

2550) Austrian Report to COSPAR XXXIV. Plenary Meeting of Cospar, Houston, TX, Oct. 10–19, 2002, pp. 12
<http://www.asaspac.at/topics/download/Austrian%20COSPAR%20Report%202002.pdf>

2551) K.-H. Ilk, "Gravity Field Determination by Satellite Gravity Gradiometry," IAG Special Commission SC7,
http://www.gfy.ku.dk/~iag/Travaux_99/sc7.htm

- Synergies of gravity missions. The three satellite missions designed for gravity field recovery, CHAMP (launch July 15, 2000), GRACE (launch March 17, 2002) and GOCE (launch March 17, 2009) are complementary in observation technique, sequence, coverage, spatial and time resolution. While CHAMP and specifically GRACE have global coverage (with orbit inclinations of 87.28° for CHAMP and 89° for GRACE), GOCE will have to fly in a sun–synchronous orbit (inclination 96.5°) due to solar power constraints. This means on one hand that CHAMP and GRACE will help to fill the polar gap for GOCE, and on the other hand that GRACE and GOCE will complement each other with their expected error characteristics in their measurement bandwidths. ^{2552) 2553) 2554)}

One of the main goals of the GRACE mission is to provide monthly global gravity field solutions to determine the time–variable gravity field. The data of the three missions offer indeed a great potential for global geoid model improvements. The GRACE twin mission by itself is expected to improve knowledge of the Earth’s geoid height from the current meter level to the centimeter level. If the mission meets all of its goals, the knowledge of the gravitational field will be improved by a factor 100, and the changes in the field will be determined on a monthly basis.

- **Drag–free satellite.** A drag–free satellite, free falling along a space–time geodesic, is the ideal test bench for some of the most advanced gravitation theories, from the general relativity validation to the search for experimental evidence of the existence of gravitational waves. The objective of all drag–free systems is to compensate all non–gravitational disturbances acting on an orbiting satellite. In addition to the primary scientific data, the analysis of the thrust history and the orbit–tracking data yields highly valuable information about the residual atmosphere density and the higher harmonics of the gravity field of the Earth.

Note: For S/C operated in LEO, gravitational forces due to the non–uniform mass distribution of the Earth are dominating the orbit and attitude perturbation spectra. Non–gravitational forces are mainly caused by momentum exchange with the spacecraft surface, they are mostly of second order. The most prominent of these forces originate from the interaction of the S/C surface with molecules and ions of the thermosphere, and from the solar photon pressure (photons are reflected as albedo from the illuminated Earth hemisphere, or which are reemitted by the whole Earth as delayed IR reradiation). In contrast with gravitational perturbations, the aerodynamic and radiation pressure effects are difficult to model since they require a good knowledge of the S/C geometry and surface properties, and they also require reliable estimates of the molecule and photon particle flux.

In general, the elements of a drag–free system consist of high–precision accelerometers (using free–floating proof masses), micro–Newton (μN) thrusters (using technologies like FEEP, cold gas, etc.), and a corresponding control system, referred to as DFC (Drag–Free Control) system. When combined with the attitude control system of the S/C, the system is mostly referred to as DFACS (Drag–Free and Attitude Control System), to compensate for the non–gravitational influences.

The original drag–free concept involves centering a free–floating test mass located inside a satellite. ²⁵⁵⁵⁾ *As the test mass is free of external disturbances, it follows a purely gravitational orbit. Since the satellite is forced to follow the test mass, it too follows the same gravitational orbit. The schematic is illustrated in Figure 194. The external disturbance forces F_{dist} will move the satellite (housing) relative to the test mass (TM). The change in the relative position is measured and then used to derive the appropriate control force F_{control} which has to be ap-*

2552) T. Gruber, “Gravity Field Models beyond CHAMP, GRACE and GOCE: A Synergetic View of Global Gravity Field Computation,” Proceedings of the Weikko A. Heiskanen Symposium in Geodesy, Ohio State University, Columbus, OH, USA, Oct. 1–4, 2002

2553) Note: The GRACE observable is the intersatellite range or range–rate. This component is similar to a gradiometric along–track inline component (V_{xx}), which is known to be one of the weaker components.

2554) C. Dunn, W. Bertiger, Y. Bar–Sever, S. Bettadpur, J. Kim, et al., “Instrument of GRACE – GPS Augments Gravity Measurements,” GPS World, Feb. 2003, pp. 16–28

2555) S. Scheithauer, A. Schleicher, S. Theil, “Overview on High Accuracy Acceleration Sensors for Scientific Space Missions,” Proceedings of 54th IAC, Bremen, Germany, Sept. 29 – Oct. 3, 2003

plied in order to drive the displacement to zero. As the relative displacement of the test mass has to be measured (electrostatically, magnetically or otherwise) there will be a coupling between the test mass and the satellite/sensor housing. This coupling is depicted as springs in Figure 194.

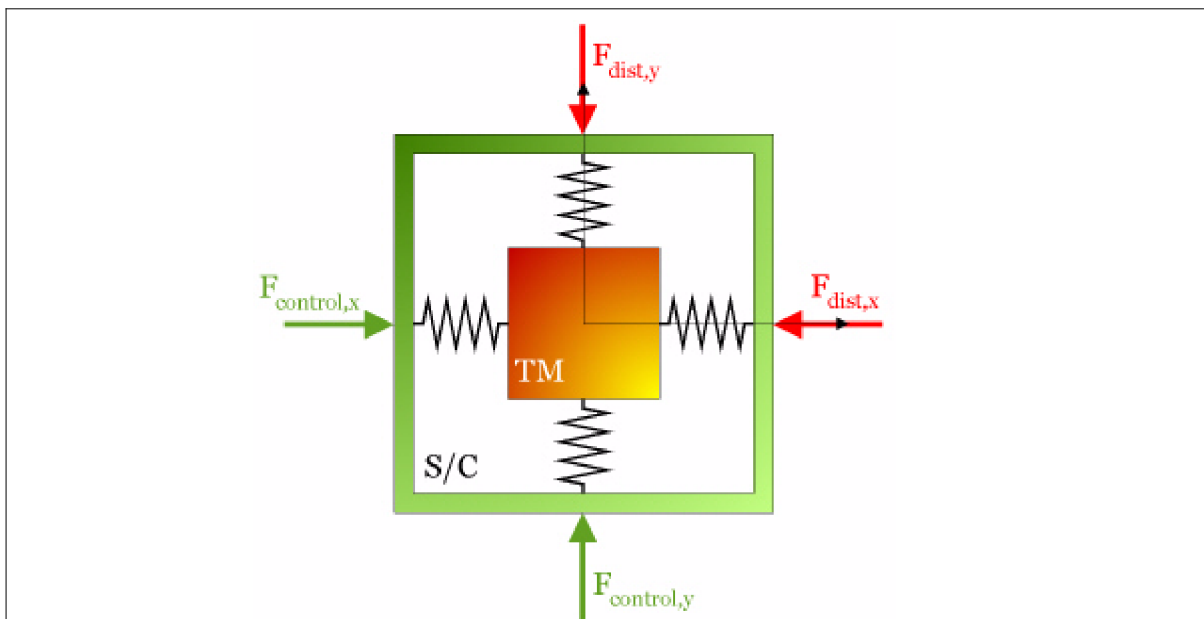


Figure 194: Schematic illustration of the drag-free concept

Operational modes in drag-free sensors: In general one can distinguish between two different operating modes, the so called Accelerometer Mode (AM), and the Displacement Mode (DM).

- The DM concept uses a “free-floating” test mass. The displacement of this test mass relative to the housing is measured by the sensor. This sensor signal is used to control the satellite to follow the test mass in order to drive the relative displacement to zero. In doing so the external disturbances on the test mass are minimized and the test mass – and thereby the satellite – will follow a free-fall orbit. The advantage of the DM concept is that the sensor accuracy is very high since no or very little force is needed to suspend the test mass which means there is very little sensor actuation noise. A disadvantage of DM is that the sensor is not inherently stable.
- In the AM concept, the test mass is forced to follow the satellite. The relative distance between test mass and satellite is driven to zero by the internal control system. The force needed to control the test mass is a measure for the acceleration acting on the satellite. The advantage of the AM concept is that the sensor is inherently stable. The disadvantages of AM is that the internal control loop limits the bandwidth of the drag-free control loop. Also, the sensor accuracy is lower due to the higher sensor actuation noise.
- The selection of an operational mode concept depends strongly on the scientific goal of the satellite. If the only purpose of the drag-free sensor is the measurement of the accelerations acting on a specific point inside the satellite (to minimize these accelerations by a drag-free control system), AM preferable. If, on the other hand, the relative displacement is needed for scientific issues, or if a very high accuracy demand forbids the use of AM, then DM should be chosen.

Examples of drag-free satellites are: Triad-1 of the US Navy and built by JHU/APL (launched Sept. 2, 1972) is considered the first satellite to fly a completely gravitational orbit (free-floating proof mass), free from all surface forces such as drag and radiation pressure. The orbit could in fact be predicted for up to 60 days (see also Table 143 and H.7).

Triad–2 (launch Oct. 11, 1975) and Triad–3 (launch Sept. 1, 1976) were follow–up drag–free missions to Triad–1. The GP–B (Gravity Probe–B) mission of NASA (launch April 20, 2004), and the ESA GOCE (Gravity Field and Steady–State Ocean Circulation Explorer) mission with a launch on March 17, 2009, are further satellites employing the drag–free concept. – For illustration, the stringent DFC requirements for the LISA mission are shown in Table 147.²⁵⁵⁶⁾

- Accelerometer mode (AM) concept. The measurement of spacecraft surface forces requires ingenious designs due to various forces (drag, solar and Earth radiation pressure) and orientation knowledge needed for proper results.^{2557) 2558)} An accelerometer at the S/C center of mass can measure these forces that cause non–gravitational orbit perturbations. A large accelerometer class employs the concept of force balance: a frame contains a moving proof–mass, the servo control detects its position and exerts a force to maintain the proof–mass motionless with respect to this frame. The combination of position sensing and force actuating results in accelerometer designs based on the following principles: piezoelectric, piezoresistive, acoustic, capacitive (electrostatic), and magnetic. The most commonly used measurement principles are a) electrostatic, and b) magnetic.
- Electrostatic measurement principle (Ref. 2555): In this concept, electrodes are distributed around the test mass. An electrode and the opposing test mass area are forming a condenser. These condensers act as capacitive detectors. Two different principles can be applied in order to measure the relative displacement and attitude of the test mass relative to the housing: “gap sensing” or “slide sensing.”

Mission	Comment
Triad series of US Navy (Triad–1 launch Sept. 2, 1972); Triad–2 launch Oct. 11, 1975	DISCOS obtained a residual acceleration of $5 \times 10^{-11} \text{ ms}^{-2}$. Triad–2 was equipped with a redundant pulsed–plasma thruster (PPT)
CHAMP of Germany, launch July 15, 2000	STAR of ONERA
GRACE, a dual minisatellite mission, launch March 17, 2002	SuperSTAR of ONERA to measure non–gravitational accelerations. Note, GRACE measures drag forces, but does not compensate for them.
GP–B (Gravity Probe–B) of NASA/Stanford, launch April 20, 2004	Drag–free control with proportional helium thrusters and a drag–free proof mass ($< 10^{-12} \text{ g}$).
GOCE of ESA, launch March 17, 2009	DFACS (Drag–Free and Attitude Control System) compensates drag with thrusters
LISA Pathfinder of ESA (launch 2011); Note: ST7 (Space Technology–7) NMP mission of NASA, originally a separate mission, is planned to fly on SMART–2 with its DRS (Disturbance Reduction System)	A technology demonstrator for LISA. LISA Pathfinder will carry two drag–free sensors operated in displacement mode (in addition, an accelerator mode is foreseen)
Microscope of CNES (launch in 2012/13)	Drag–free S/C (DFACS) for a test of EP (Equivalence Principle) with an accuracy of one in 10^{15}
HYPHER (High–Precision Cold Atom Interferometry in Space), proposed ESA mission	DFACS is used to keep the measurement devices ASU (Atomic Sagnac Unit) and PST (Precise Star Tracker) within their operational envelope
LISA (Laser Interferometry Space Antenna) a joint mission of ESA and NASA with a launch in 2017	The LISA formation of 3 S/C represents a giant interferometer to be used to detect gravitational waves. Each S/C contains a proof mass and a DFACS (Drag–Free Attitude Control System)

Table 146: Overview of some drag–free missions

- Magnetic measurement principle: A relatively new concept to measure the relative displacement and attitude of a test mass is the use of the SQUID (Superconducting Quantum

²⁵⁵⁶⁾ R. Leach, “Development of a μ –Newton Thruster for use with a Drag–Free Control System and Formation Flying Satellites,” Proceedings of International Symposium Formation Flying Mission & Technologies, Oct. 29–31, 2002, Toulouse, France

²⁵⁵⁷⁾ P. Touboul, B. Foulon, E. Willemonot, “Electrostatic Space Accelerometers for Present and Future Missions,” Acta Astronautica, Vol. 45, No. 10, 1999, pp. 605–617

²⁵⁵⁸⁾ V. Josselin, P. Touboul, R. Kielbasa, “Capacitive detection scheme for space accelerometer applications,” Sensors and Actuators, Vol. 78, 1999, pp. 92–98

Interference Device) technique. This method provides measurement sensitivities in the order of a femto meter (10^{-15} m) with high stability made possible in a cryogenic environment at about 2 K. In their simplest form, the SQUIDS comprise a superconducting ring broken by two very narrow insulating gaps. The resistance of a SQUID to the passage of a supercurrent depends on quantum interference.

At the beginning of the 21st century, sensitivity requirements of accelerometers for space applications generally call for acceleration measurements below the pico-g (10^{-12} g) level.

The following instruments are examples of linear micro-accelerometers on various missions (past and future):

- CACTUS. A first version of an electrostatic accelerometer (measuring differential accelerations between the external surface and a small ball placed at the center of mass), referred to as CACTUS (Capteur Accélérométrique Capacitif Triaxial Ultra Sensible), developed and built by ONERA (Office National d'Etudes et de Recherches Aérospatiales) of Chatillon, France, was flown on the CASTOR D-5B S/C (of CNES, launch May 17, 1975, with nominal S/C operations until 1979) for atmospheric density studies. The measured precision was 10^{-10} m/s² (or 10^{-11} g). Note: The CACTUS accelerometer used a spherical proof mass inside a spherical cavity and capacitive position sensing. However, electrical forces were applied to the proof mass to keep it centered in the cavity, rather than servo-controlling the spacecraft to follow the proof mass. The strength of the electrical forces required on the proof mass determined the acceleration of the spacecraft due to non-gravitational forces.^{2559) 2560)}

- SAMS (Space Acceleration Measurement System).²⁵⁶¹⁾ SAMS is an operational space flight experiment developed by NASA/GRC (see also 1.8.2.3). The objective is to measure and record acceleration (vibrations and quasi-constant accelerations) in low-gravity settings, including facilities on Earth, the space shuttle, and the International Space Station. SAMS has already been used on more than 20 shuttle missions and the Mir Space Station. SAMS was also used on STS-107. Initial flight of SAMS on STS-43 /Aug. 2-11, 1991).

- The inertial sensor GRADIO was developed by ONERA in the early 1990s for use in a proposed joint ESA-NASA mission called ARISTOTELES. The differences in acceleration between four GRADIO accelerometers on the spacecraft were to be used to measure the gradients in the Earth's gravitational field, and thus determine the field. However, the mission ARISTOTELES was cancelled in 1994/5 due to budget reasons. The GRADIO accelerometer used a rectangular proof mass 4 cm x 4 cm x 1 cm in size, rather than a sphere.

- Another ONERA accelerometer by the name of ASTRE (Accéléromètre Spatial Triaxial Electrostatique), was part of the ESA Microgravity Measurement Assembly (MMA), and flown on STS-55 (Apr. 26 - May 6, 1993), STS-83 (Apr. 4-8, 1997) and on STS-94 (Jul. 1-17, 1997).^{2562) 2563)} The objective was the characterization of the Shuttle's microvibratory environment. The resolution achieved by ASTRE was 10^{-9} g in the measurement bandwidth DC to 1 Hz (monitoring of the low-frequency acceleration environment). The ASTRE working principle is based on keeping a proof mass motionless in its nominal position and attitude by means of electrostatic suspension, such that the required electrostatic forces are a direct measure of the three acceleration components.

2559) A. Bernard, "Super-Cactus: project of 10^{-11} g three axis accelerometer," *Acta Astronautica*, Vol.7, 1980, pp. 401-416

2560) C. J. Koblinsky, P. Gaspar, and G. Lagerloef, editors, "The Future of Spaceborne Altimetry: Oceans and Climate Change," Joint Oceanographic Institutions Inc., Washington, DC, 1992, pp. 72-73

2561) http://microgravity.grc.nasa.gov/MSD/MSD_htmls/sams.html

2562) <http://esapub.esrin.esa.it/microgra/micrv8n2/natv8n2.htm>

2563) M. Nati, A. Bernard, B. Foulon, P. Touboul, "ASTRE, a highly performant accelerometer for the low frequency range of the microgravity environment," Proceedings of the 24th Symposium on space environmental control systems, Friedrichshafen Germany, pp.9, 1994

Parameter	Value	Comment or function
Precision thrust range	0.1 – 25 μN	Oppose solar radiation pressure
Precision thrust control	$\pm 0.1 \mu\text{N}$	Spacecraft control to 10 nm
Coarse thrust range	25 – 100 μN	Spacecraft tip-off recovery
Coarse thrust control	$\pm 1 \mu\text{N}$	Spacecraft tip-off recovery
Thrust noise	$< 0.1 \mu\text{N} (\text{Hz})^{1/2}$	
Specific impulse	$> 500 \text{ s}$	Keep fuel within mass margin
Design life @ 25 μN	$> 3 \text{ years}$	10 year goal
Mass of instrument	$< 10 \text{ kg}$	4 thrusters + electronics
Steady-state power	$< 5 \text{ W}$	1 thruster @ 25 μN
Volume of instrument	$< 1000 \text{ cm}^3$	4 thrusters + electronics

Table 147: DFC system requirements for the LISA mission

– STAR (Space Three-axis Accelerometer for Research mission) is a CNES-provided accelerometer system developed by ONERA and flown on the CHAMP mission (launch July 15, 2000). The objective is to measure all non-gravitational accelerations of the satellite (drag, solar and Earth radiation pressure) in order to determine the Earth's gravity field from purely gravitational orbit perturbations. The accelerometer measurement principle is based on electrostatic suspension of a proof-mass in a cage. Instantaneous position of the proof-mass is measured by three capacitive sensors which permit a determination of the acceleration vector. The instrument has a dynamic range of $\pm 10^{-4} \text{ ms}^{-2}$, a resolution of better than $\pm 3 \times 10^{-9} \text{ ms}^{-2}$, and a frequency range of 10^{-1} to 10^{-4} Hz . ²⁵⁶⁴⁾

– In 1996, a Czech micro-accelerometer by the name of MACEK (Mikroakcelerometr), designed and developed at the Institute of Astronomy of the Academy of Sciences of the Czech Republic at Ondrejov, was flown as a technology experiment on Shuttle flight STS-79 (Sept. 16 – 26, 1996). MACEK was placed inside of Spacehab, about 2 m away from the center of gravity of the Shuttle (measurement of Shuttle vibrations during the orbital flight phase, performance tests of MACEK). MACEK employs the concept of an electrostatically compensated proof-mass with a measurement accuracy of 10^{-9} m/s^2 . The first version of MACEK has been flown on the Russian satellite Resurs-F1 in 1992 (launch June 23, 1992, proof of concept flight for MACEK). – An upgraded version of the MACEK (10^{-10} m/s^2) instrument is flying on the Czech MIMOSA (Microaccelerometric Measurements of Satellite Accelerations) satellite mission (launch June 30, 2003, see E.17). ²⁵⁶⁵⁾

– The GOCE (Gravity field and steady-state Ocean Circulation Explorer) mission of ESA with a launch on March 17, 2009, is flying EGG (Electrostatic Gravity Gradiometer), developed by ONERA, in an SGG (Satellite Gravity Gradiometer) configuration, combined with an SSTI (Satellite-to-Satellite Tracking Instrument) configuration. See E.11. The EGG will provide the medium- and short-wavelength terms of the Earth's gravity field. The GOCE objective is to provide accurate models of the Earth's gravity field (1–2 mgal) and its geoid (1–2 cm) at fairly high spatial resolutions of 100 km. This is in particular required for research in solid Earth physics, geodesy, oceanography and of the ice sheets.

Gravity field/ Field of application	Complementary data
Proof-of-concept of SST-hl combined with 3-D accelerometry	CHAMP
Temporal variations of Earth gravity field	Available models (tides, atmospheric pressure, ocean variability) and results from GRACE
Gravity field at polar caps and small-scale gravity information in some regions	Available and planned airborne and terrestrial gravimetry data

²⁵⁶⁴⁾ P. Touboul, B. Foulon, G. – M. Le Clerc, "STAR, the accelerometer of the geodesic mission CHAMP," 49th International Astronautical Congress, Melbourne (Australia), Sept. 28 – Oct. 2, 1998, TP 1998–224

²⁵⁶⁵⁾ L. Sehnal, R. Peresty, L. Pospisilova, A. Kohlhase, "Dynamical Microaccelerometric Measurements on board Space Shuttle," Acta Astronautica, Vol. 47, No 1, 2000, pp. 27–34

Gravity field/ Field of application	Complementary data
Solid–Earth physics	Topographic models (DTMs) and seismic tomography as primary data sets, lithospheric magnetic field from ØRSTED and CHAMP and planned magnetometry satellite missions
Oceanography	Data sets from past, current and future ocean altimetry (GEOSAT, T/P, ERS–1 & 2, Envisat, Jason etc.)
Ice research	Ice altimetry (ICESat, CryoSat) and INSAR
Geodesy	Current and future global satellite positioning and navigation systems (SLR, VLBI, DORIS, GPS, GLONASS, GNSS–2)
Sea–level	GLOSS (Global tide–gauge network), GPS/DORIS, satellite ocean and ice altimetry and GPS

Table 148: Overview of complementary data in combination with GOCE data

Note: GOCE and GRACE (Gravity Recovery and Climate Recovery) are complementary missions with GRACE focusing in particular on the temporal variations of the gravity field and GOCE on attaining maximum spatial resolution of the gravity field. These various complementary satellite gravity field concepts as well as those from other satellite mission and airborne observations are summarized in Table 148. – It turns out that a global gravity field map, created from just two weeks of data in the early mission of GRACE, is proving to be substantially more accurate than the combined results of more than three decades of satellite and surface measurements collected before GRACE (GRACE is providing a global gravity field once every thirty days).

– For LISA (Laser Interferometry Space Antenna) a joint mission of ESA and NASA with a launch in 2013, the optical measurements are made between the proof masses in different spacecraft rather than between the spacecraft themselves. Thus the acceleration of the proof mass with respect to its cavity does not have to be measured (nevertheless, the displacement between proof mass and cavity has to be measured). The main objective of the LISA inertial sensor is to provide a reference mass that moves inertially to a high accuracy, except for the effects of slowly varying bias forces outside the gravitational wave frequency band.

Gravity/Mag.–field missions	Description
Cosmos–26 (Soviet Union)	Launch March 18, 1964. The USSR Cosmos–26 satellite provided the first global magnetic mapping of the Earth’s surface.
Prognoz–6 (Soviet Union) Magnetic field measurements	Prognoz–6 (launch Sept. 26, 1977), IZMIRAN (data provider) Prognoz–7 (launch Nov. 11, 1978), IZMIRAN Prognoz–9 (launch July. 1, 1983), IZMIRAN
ISEE–1/2 (NASA/ESA)	ISEE–1/2 (launch Oct. 2, 1977). The RUM/RUD magnetometer experiment of UCLA studied the dynamic plasma field of the Earth
GEOS–2 (ESA)	GEOS–2 (launch July 24, 1978, E.6.2) into a near GEO. Objective: Measurement of fluctuations in the Earth’s magnetic field and waves and particles. Two years of data.
MAGSAT (APL, NASA, USGS)	MAGSAT (launch Oct. 30, 1979, operated to June 1980) was the first mission to systematically measure the Earth’s magnetic field. It provided the first IGRF (International Geomagnetic Reference Field) model based on global scalar and vector data of high accuracy, determining the core radius and mapping fluid motions at the core mantle boundary.
Interball (IKI, Russia)	Interball (launch Aug. 3, 1995) constellation of 4 S/C carries the FM–3I fluxgate magnetometers (solar wind interaction with the magnetosphere).
POLAR (NASA)	POLAR (launch Feb. 24, 1996) flies MFE (Magnetic Fields Experiment of UCLA to study the coupling of the solar wind and the magnetosphere
FAST (NASA)	FAST (launch Aug. 21, 1996) flies MFI (Magnetic Fields Instrument) of UCLA to measure the vector DC and AC magnetic fields.
ASTRID–2 (SSC, IRF–K, Sweden)	ASTRID–2 (launch Dec. 10, 1998) with the objective to perform high–resolution E–field and B–field measurements in the auroral region
Ørsted (TUD, Denmark)	Ørsted (launch Feb. 23, 1999) with the objective to perform highly accurate and sensitive measurements of the geomagnetic field

Gravity/Mag.–field missions	Description
SACI–1 (INPE, Brazil)	SACI–1 (launch Oct. 14, 1999). The MAGNEX instrument investigates the phenomena related to current alignment with the trans–equatorial field and the plasma electrodynamics involving the Earth, specifically in the region of the South Atlantic Anomaly.
SAC–C (CONAE, NASA, DSRI, etc.)	SAC–C launch Nov. 21, 2000. The objective of Ørsted–2 (Magnetic Mapping Payload) instrument suite is to map the Earth’s magnetic field.
IMAGE (NASA, SwRI)	IMAGE launch on Mar. 25, 2000. The objective is to study the global response of the Earth’s magnetosphere to changes in the solar wind. NASA’s first S/C for making ENA measurements of the terrestrial magnetosphere.
CHAMP (GFZ, DLR, Germany)	CHAMP launch July 15, 2000. Gravity field and magnetic field mapping (MIAS and DIDM). Use of SST/GPS + laser for orbit restitution and accelerometry for non–gravitational force measurements
GRACE (NASA/DLR)	A dual minisatellite mission (launch March 17, 2002) with accelerometers and GPS receivers for SST (+laser), like CHAMP plus ultra–precise low–low SST. The measured gravity field is about 10 times more accurate for large–scale features than any pre–GRACE gravity model of Earth.
FEDSAT (CSIRO) Australia	FEDSAT (launch Dec. 14, 2002). The objectives of the NewMag instrument are to measure electrical currents and perturbations in the Earth’s magnetic field.
GOCE (ESA)	A gravity field mission (launch March 17, 2009) with three–axis satellite gravity gradiometry (SGG) provided by EGG (Electrostatic Gravity Gradiometer) and SSTI (Satellite to Satellite Tracking Instrument) for SST. The GOCE version gradiometry is considered to be two orders of magnitude more sensitive (and also more challenging) than that of CHAMP and GRACE.
Microscope (CNES, ONERA)	A microsatellite mission (2012) with the objective to measure EP (Equivalence Principle) to an accuracy of one part in 10^{15}
Planned but not flown missions	
Gravity/Mag.–field missions	Description (the listing of the following missions is kept for historical reasons). All the gravity objectives, concepts and goals which were elaborated for them are still valid.
GRAVSAT (NASA)	A mission defined in the 1980s and cancelled in 1987 due to technical difficulties and budget constraints
GGM (Gravity Gradiometer Mission), NASA also known as SGGM	Objective: to map the Earth’s gravity and magnetic fields using two drag–free S/C orbiting in polar orbit at a very low altitude. The project was cancelled in 1987.
GRADIO (CNES) (a gradiometer instrument – not a mission)	Under study by CNES and terminated in the 1980s. GRADIO was a satellite gravity gradiometer experiment aimed at measuring the full set of gravity gradients (and separating it from the spacecraft attitude disturbances) by means of eight three–axis micro–accelerometers of a new generation.
ARISTOTELES (ESA/NASA)	Mission studies started in 1989 with the objective to fly a high–low SST mission using GPS and satellite gravity gradient measurements (GRADIO). ARISTOTELES was terminated in 1994/5 due to budget constraints
GAMES (NASA/CNES)	A two (co–orbiting) S/C mission was designed with laser measurements between S/C. A GPS receiver on one S/C was planned for LEO orbit determination. Also measurement of the magnetic field. GAMES was cancelled in the 1990s due to budget constraints.

Table 149: Overview of gravity/magnetic field missions flown (and not flown)

1.23.3.9 Precise Orbit Determination (POD)

POD principle: ²⁵⁶⁶⁾ ²⁵⁶⁷⁾ Position and velocity of a satellite for given instants of time can precisely and continuously be determined by numerical integration of the orbit dynamics within a differential improvement process. Starting from an initial orbital motion model a set of parameters for the adjustment of the initial conditions and the perturbing forces is solved iteratively in order to eventually arrive at an integrated orbit fitting the measurements best in the least squares sense. The foundations of this technique were laid down by William M. Kaula, an American physicist of Australian descent (1926–2000), considered to be the father of space–based geodesy.

Background on classical dynamic orbit determination: Conventional ground–based tracking systems seldom provide coverage from more than one direction at a time, and often provide no coverage. To supply the missing information for orbit determination, an orbit model must be fit to the tracking data. The most precise orbit estimation strategies employ orbit models derived from detailed models of the forces acting on the satellite, a technique known as dynamic orbit determination. – The technique begins with a set of tracking measurements [e.g., GPS, SLR, Doppler, DORIS (along with a global network), VLBI, SST, SAR interferometry, altimetry measurements] along with models of the forces and satellite mass. Those models yield a model of satellite acceleration over time, from which, by double integration, a nominal or a priori trajectory is formed. To produce the orbit solution (state vector), the two constants of integration – the initial position and velocity – also known as the epoch state, are estimated (Ref. 2322).

In a simple and conventional approach, using only one tracking method, GPS receiver data may for instance be used to obtain a fast onboard navigation solution with moderate accuracy. An improved but more complex solution would be to use GPS code and/or carrier measurements. In addition, various tracking intervals may be used in either approach, like batch processing or continuous tracking. This example demonstrates that the choice of orbit determination is depending on the accuracy requirements and the amount of effort to be invested.

Satellite tracking and orbit determination are essential elements of practically all satellite missions. Knowledge of the spacecraft position at any time is a requirement for all operational planning activities. There are several application areas in EO (geodesy, geodynamics, atmospheric sciences, constellation navigation, etc.) with accuracy requirements for the Precise Orbit Determination (POD). Examples are:

- For altimetry satellites, the orbit determination results are an essential part of the scientific data – by providing the link between the range observation made by the altimeter instrument and the terrestrial reference frame. ²⁵⁶⁸⁾ The accuracy requirements for the Precise Orbit Determination (POD) of altimeter satellites, such as TOPEX/Poseidon, Jason–1, Envisat, and ICESat are therefore several orders of magnitude higher than for most other satellites. Any errors in the orbit determination also directly affect the accuracy of their scientific products. All altimeter–carrying satellites have therefore been equipped with high–precision tracking capabilities, such as SLR, DORIS and GPS (combinations).
- Radio occultation instruments flown on LEO spacecraft. For precision analysis of GNSS radio occultation data, especially at altitudes between 30–60 km, LEO and GPS satellite velocities have to be known to about 0.1 mm/s or better. This requires POD techniques. An example is the MetOp (Meteorological Operational Satellite) mission of EU-METSAT which carries the GRAS ((GNSS Receiver for Atmospheric Sounding) instru-

²⁵⁶⁶⁾ W. M. Kaula, “Theory of satellite geodesy: applications of satellites to geodesy,” Blaisdell Publishing Company, Waltham, MA, 1966.

²⁵⁶⁷⁾ W. M. Kaula, “Analysis of Satellite Observations for Longitudinal Variations of the Gravitational Field,” Space Research, Vol. 2, 1961 pp. 360–372

²⁵⁶⁸⁾ E. Doornbos, M. Naeije, R. Scharroo, “Final Report for GAMBLE WP 4: Orbit Determination and Satellite Tracking Workshop,” aPR. 1, 2003, http://www.deos.tudelft.nl/gamble/docs/GAMBLE_finalreport_theme3.pdf

ment. In GRAS POD, the target accuracy for orbit (10cm) and clock offset (1ns) has to be obtained based on 10–minute datasets and within a few minutes of processing time. Only a sequential algorithm can achieve this.

Tracking system	TRA-NET	SLR	DORIS	PRARE	GPS	Orbit error	Launch Date
Measurement precision	RR 2–10 mm/s	Range 0.5 – 5 cm	RR (RangeRate) 0.35–0.5 mm/s	Range+RR 2.5 cm, 0.25 mm/s	Phase 0.2–0.5 cm	cm	
Seasat	yes	yes	no	no	no	30	27.6.78
GEOSAT	yes	no	no	no	no	10	12.3.85
ERS–1	no	yes	no	failed	no	5	17.7.91
Topex/Poseidon	no	yes	yes	no	yes	2	10.8.92
ERS–2	no	yes	no	yes	no	4	21.4.95
GFO	no	yes	no	no	failed	5	10.2.98
Jason–1	no	yes	yes	no	yes	2	7.12.2001
Envisat	no	yes	yes	no	no	3	1.3.2002
ICESat	no	yes	no	no	yes	5	1.13.2003
CryoSat	no	yes	yes	no	no	3	8.10.2005 launch failure
Jason–2	no	yes	yes	no	yes	2	20.6.2008

Table 150: Tracking methods used for various altimeter missions (Ref 2568)

- POD techniques are being required for constellation maintenance services such as COSMO/SkyMed, ROCSat–3/COSMIC, etc.

Gravity field models: Satellite laser ranging (SLR) data has been an integral part of Earth gravity model development since the days of the earliest GEM (Goddard Earth Models) in the 1970s. SLR data have contributed both directly in the form of tracking of the multiplicity of satellites that have made up these solutions, and indirectly in the definition and stabilization of the terrestrial reference frame. The evolution of the SLR technology required improvements in modeling and yielded ever–refined models. ^{2569) 2570) 2571)}

The launch of the Lageos–1 (launch May 4, 1976) satellite contributed greatly to early SLR technology by providing an unambiguous measurement of range, with well–calibrated system biases. This SLR data formed the core of state–of–the–art gravity models developed at NASA/GSFC – starting with GEM–5 (Goddard Earth Model–5) in 1983, GEM–9, and GEM–L2.

Note: At the time of the Lageos launch, lasers with a precision of 40 cm provided the bulk of the tracking support. The next generation of lasers, using pulse–choppers, delivered data at the precision of 2–5 cm.

Uncertainties in the Earth’s gravity field have long been the major error source in orbit determination of altimetry satellites. A great improvement in gravity field modeling was made possible by past altimeter missions, with their high accuracy satellite tracking and altimeter measurements. This has reduced the radial orbit error from meters in the 1980’s to a few cm nowadays. The effect of the Earth’s gravity perturbations decreases rapidly with the orbit altitude. The effects on TOPEX/Poseidon and Jason–1 at 1336 km, are therefore much smaller than on GEOSAT, GFO, ERS and Envisat, at roughly 800 km.

²⁵⁶⁹⁾ F. G. Lemoine, S. M. Klosko, D. S. Chinn, C. M. Cox, “The Development of NASA Gravity Models and their Dependence on SLR,” Proceedings of the 13th International Workshop on Laser Ranging: (Science Session), Oct. 7–12, 2002, Washington D:C., USA, URL: cddis.nasa.gov/lw13/docs/papers/sci_lemoine_1m.pdf

²⁵⁷⁰⁾ F. J. Lerch, S. M. Klosko, G. B. Patel, “A Refined Gravity Model from Lageos (GEM–L2),” Geophysical Research Letters, Vol. 9, No 11, Nov. 1982, pp. 1263–1266

²⁵⁷¹⁾ F. J. Lerch, S. M. Klosko, R. E. Laubscher, C. A. Wagner, Journal of Geophysical Research, Vol. 84, (138), 1979, pp. 3897–3915

Gravity field models are generally generated using tracking data from a variety of satellites at different inclinations and altitudes, combined with surface gravity and altimeter measurements. For this reason, the gravity-induced orbit error of a certain satellite for a certain model, depends heavily on how much tracking data of this satellite (or other satellites in the same or similar orbit), have been used in the generation of this model. Therefore, so-called tailored models have been generated to push the orbit accuracy to its limits. Examples of these are (see also 1.23.1.2 for gravity field models):

- JGM-1 (Joint Gravity Model) effort, developed by NASA/GSFC started in 1982.²⁵⁷²⁾ This model, along with other model and tracking system improvements, resulted in a pre-launch radial orbit accuracy of T/P on the order of 13 cm. The JGM-1 model was developed before the launch of TOPEX/POSEIDON (T/P) and was the result of a multi-year effort to improve the Earth's gravity model by a new inversion of tracking data on over 30 satellites, altimeter data from Seasat and GEOSAT, and direct gravity measurements on the Earth's surface (land and marine gravimetry).
- JGM-2 of NASA/GSFC. A post-launch tuning/adjustment of the JGM-1 gravity model (after the launch of TOPEX/POSEIDON) resulted in JGM-2.
- JGM-3. An update to the JGM-1 and JGM-2 models developed at NASA/GSFC and the University of Texas (inclusion of more tracking data on T/P, and especially the inclusion of about 40 days of GPS tracking). Combined with improved tide models based on the T/P altimeter data, and some additional refinements of the orbit determination strategy, the current orbit accuracy of approximately 2 cm was achieved.^{2573) 2574)} [Marshall et al., 1995].
- DGM-E04 for ERS-1/2. DGM stands for DUT/DEOS Gravity Model, with DUT (Delft University of Technology) and DEOS (Delft Institute for Earth-Oriented Space Research), Delft, Netherlands. DGM-E04 is based on precise, preliminary, or near-real-time orbits using SLR and crossover tracking data.²⁵⁷⁵⁾
- The GRIM5-C1 model [developed in a joint GFZ (GeoForschungsZentrum) and GRGS (Groupe de Recherches de Géodésie Spatiale) effort] represents the current state of the art in long wavelength gravity field modelling for POD, providing improvements over earlier models for both the TOPEX/Poseidon and ERS orbits.²⁵⁷⁶⁾

During the last decade (1990s) orbit errors of altimeter satellites have come down by more than an order of magnitude, and more advances are expected when new gravity models based on CHAMP, GRACE and GOCE data have been produced.

The conventional POD technique is a ground-based offline batch process in which the various tracking elements are collected and analyzed a posteriori. The CHAMP project provides RSO (Rapid Science Orbit) on an operational day-by-day basis with position accuracies of < 10 cm. As of 2003, USO (Ultra-rapid Science Orbit) products (i.e. atmospheric soundings) of CHAMP are delivered with a time delay slightly above 3 hours after reception.

Precise GPS tracking of a LEO spacecraft requires at least one onboard GPS receiver as well as processing of both GPS observables, namely the carrier phase and pseudorange

2572) R. S. Nerem, F. J. Lerch, J. A. Marshall, et al., "Gravity model development for TOPEX/POSEIDON: joint gravity models 1 and 2", *Journal of Geophysical Research*, Vol. 99, No C12, Dec. 15, 1994, pp. 24421-24447

2573) B. Tapley, M. Watkins, J. Ries, G. Davis, R. Eanes, S. Poole, et al., "The JGM-3 Geopotential Model," *Journal of Geophysical Research*, Vol. 101, 1996, pp. 28029-28049

2574) J. A. Marshall, N. P. Zelensky, S. M. Klosko, D. S. Chinn, et al., "The temporal and spatial characteristics of the TOPEX/POSEIDON radial orbit error," *Journal of Geophysical Research*, Vol. 100(C12), 1995, pp. 25331-25352

2575) R. Scharroo, P. Visser, "Precise orbit determination and gravity field improvement for the ERS satellites," *Journal of Geophysical Research*, Vol. 103(C4), April 1998, pp. 8113ñ-8127

2576) T. Gruber, A. Bode, C. Reigber, P. Schwintzer, R. Biancale, J.-M. Lemoine, "Grim5-c1: Combination solution of the global gravity field to degree and order 120," *Geophysical Research Letters*, Vol. 27, 2000

measurements in a relative positioning approach. In this setup, parallel GPS measurements are being required simultaneously at terrestrial GPS observing sites. The terrestrial receiver-to-spaceborne receiver measurements are then incorporated into a classical orbit determination estimation algorithm (a posteriori analysis). For both carrier phase and pseudorange observables, there are offsets of the receiver and GPS (transmitter) satellite clocks from GPS Time and there are further delays due to the troposphere and ionosphere as well as smaller effects due to multipath and receiver noise. Measurement combination and differencing can almost entirely remove the timing offsets and the ionospheric and tropospheric delays but increases the noise of the resultant observables and also reduces the measurement strength. In the phase measurements, the initial phase is unknown by an integer number of cycles. This can be determined by the carrier phase triple difference. ²⁵⁷⁷⁾ ²⁵⁷⁸⁾ ²⁵⁷⁹⁾

Three basic strategies are in use at the start of the 21st century to determine precise orbits using GPS. These are 1) dynamic, 2) kinematic, and 3) hybrid strategies:

1) In the dynamic strategy, a mathematical model for the forces acting on the LEO are used to produce a nominal trajectory using a nominal spacecraft state vector. A more accurate trajectory is then found by selecting the LEO state that best fits the GPS tracking measurements in a least squares sense. – As long as the dynamic models are adequate, the effect of noisy instantaneous tracking measurements on the solution are reduced for longer data arcs.

2) In the kinematic strategy, the rationale is that the actual path of the LEO may be closer to the precise GPS position estimates than the trajectory determined by a dynamic model. The LEO dynamic and spacecraft models are completely removed, thus explaining why the kinematic strategy is otherwise known as a non-dynamic strategy. The spacecraft state and a process noise vector representing three force corrections can be estimated at each measurement time in a Kalman filter formulation. Theoretically, a radial position of about 3 cm may be achieved with this approach from one day's worth of data. – The method relies on the precision of the GPS observations and the relative location of the LEO and terrestrial receivers with respect to the GPS constellation and the continuous GPS satellite tracking from the spaceborne GPS receiver. ²⁵⁸⁰⁾

3) The hybrid strategy combines the strengths of dynamic and kinematic approaches. The idea is to combine tracking observables from several high-precision measurement techniques such as GPS, SLR, DORIS, etc. The T/P (TOPEX/Poseidon, launch Aug. 10, 1992) spacecraft of NASA pioneered this concept. In addition to its GPS receiver, the T/P spacecraft has been tracked with TDRS (Tracking Data Relay Satellite), DORIS (onboard the S/C) and SLR (Satellite Laser Ranging). A posteriori analysis of the tracking information from the four sources has demonstrated a satellite position determination capability in the < 5 cm range. Many other projects followed this hybrid POD approach.

Future orbit determination developments are heading towards a real-time POD service. However, this requires to install the differential orbit improvement process onboard the spacecraft (i.e., migration from batch mode to filter mode). The RADARSAT-2 satellite of MDA/CSA (launch on Dec. 14, 2007, chapter D.42.4) is probably the first mission to employ

²⁵⁷⁷⁾ The conventional ground-based POD technique has been or will be implemented for many missions such as: TOPEX/Poseidon (launch Aug. 10, 1992), Jason-1 (launch Dec. 7, 2001), CHAMP (launch July 15, 2000), GRACE (launch Mar. 17, 2002), CryoSat (launch Oct. 8, 2005 – but launch failure), ROCSat-3/COSMIC (launch Apr. 14, 2006), GOCE (launch March 17, 2009), and TerraSAR-X (launch June 15, 2007)

²⁵⁷⁸⁾ G. Michalak, G. Baustert, R. Koenig, C. Reigber, "CHAMP Rapid Science Orbit Determination – Status and Future Prospects," in C. Reigber, H. Lühr, P. Schwintzer, (Eds.), *First CHAMP Mission Results for Gravity, Magnetic and Atmospheric Studies*, Springer-Verlag, Berlin, Heidelberg, 2003

²⁵⁷⁹⁾ Preliminary Design of a PARIS Mode in a SAR Mission, Final Report of EADS Astrium Ltd. to ESA, 2002, The title of Chapter 7 is: "Precision Orbit Determination," pp. 35–36

²⁵⁸⁰⁾ D. Svehla, M. Rothacher, "Kinematic and Dynamic Precise Orbit Determination of Low Earth Orbiters," 2nd International GOCE User Workshop, ESA/ESRIN, Frascati, Italy, March 8–10, 2004, URL: http://earth.esa.int/workshops/goce04/participants/222/poster_GOCE_POD_Svehla_Rothacher.pdf

a real-time onboard POD software package in combination with its dual-frequency LAGRANGE GPS receiver (a 12-channel instrument which produces pseudorange and Doppler phase measurements). An orbital filter is used to combine the GPS measurements with high fidelity orbit models.

1.23.3.10 Gravitomagnetism, frame dragging and gravitational lensing

Gravitomagnetism describes the general relativistic curvature of space-time around massive bodies, like Earth. By its very nature, gravitomagnetism refers to the hypothetical analog of magnetism predicted for a moving mass that would cause geodetic spin precession (i.e., a change in the orientation of a spinning mass's axis). The gravitomagnetic field is one of the most important predictions of Einstein's Theory of General Relativity, which has no Newtonian counterpart, it emerges as a consequence of mass-energy currents. Gravitomagnetism is the tendency for a massive spinning body to apply a torque to nearby objects. The fundamental principle of general relativity asserts that accelerated reference frames and reference frames in gravitation fields are equivalent. General relativity states that clocks run slower in strong gravitational fields (or highly accelerated frames), predicting a gravitational redshift. It also predicts the existence of gravitational lensing,²⁵⁸¹⁾ gravitational waves, and gravitomagnetism.

There are three main effects of gravitomagnetism:²⁵⁸²⁾

1) Precession of a gyroscope. In the field of a body rotating with angular momentum, a gyroscope at a distance r precesses with an angular velocity. A gyroscope orbiting Earth tends to tilt away from the plane of its orbit because the Earth is dragging it. Einstein referred to this effect as **frame dragging** in which the orbit of a small body orbiting around a rotating massive one is slightly perturbed by the rotation.

2) Precession of orbital planes (**nodal precession of a spinning top**, also referred to as **geodetic effect**). According to Einstein's Theory of General Relativity, a large body like Earth warps local space and time (spacetime) much like a marble would dent a bed sheet it is lying on. This is known as the geodetic effect (a consequence of the geodetic effect is that it gradually changes the spin direction of a gyroscope). For a gyroscope orbiting near the Earth, this distortion leads to a tilting of the gyroscope's spin axis in the plane of the orbit. This effect is predicted by general relativity theory to be 150 times larger than the frame dragging.²⁵⁸³⁾ Examples of nodal precision: 1) The whole orbital plane of a satellite is itself a kind of enormous gyroscope dragged by the gravitomagnetic field; 2) Earth itself is a perturbed spinning gyroscope, each spin around the sun lasts one year, and each gyration around the nutation cone (cone angle of 23.45°) takes 26,000 years.

3) Precession of the pericenter. This is known as the **Lense-Thirring effect**, first predicted by two Austrian physicists Josef Lense (1890–1985) and Hans Thirring (1888–1976) in 1918.²⁵⁸⁴⁾ They calculated the advance of the pericenter and line of nodes of a particle orbiting a rotating mass – due to frame dragging. They proposed that the rotation of planets and stars or any rotating mass twists the structure of spacetime near that mass. Not only is local spacetime curved near the sun, it is twisted by the sun's rotation.

2581) Note: Gravitational lensing is an important tool for the study of the distribution of dark matter in the universe. Gravitational lenses produce multiple images of single astronomical objects.

2582) C. Will, "The Search for Frame-Dragging," <http://www.phys.lsu.edu/mog/mog10/node9.html>

2583) <http://funphysics.jpl.nasa.gov/technical/grp/grav-probeb.html>

2584) Josef Lense, Hans Thirring, "Über den Einfluß der Eigenrotation der Zentralkörper auf die Bewegung der Planeten und Monde nach der Einsteinschen Gravitationstheorie," *Physikalische Zeitschrift* 19, 156, 1918 [On the Influence of the Proper Rotation of Central Bodies on the Motions of Planets and Moons According to Einstein's Theory of Gravitation].

Background: In Einstein's Theory of General Relativity (gravity), the concept of inertial frame has only a local meaning, and a local inertial frame is "rotationally dragged" by mass–energy currents. In other words, moving masses influence and change the orientation of the axes of a local inertial frame (e.g., a gyroscope). Hence, an external current of mass, such as the spinning Earth, "drags" and changes the orientation of gyroscopes. This is the "rotational dragging of inertial frames," or "frame dragging" as Einstein referred to it – – the spin of a body must change the geometry of the universe by generating space–time curvature. Simply stated the phenomenon says that all celestial bodies that rotate, such as the sun, or the Earth, create a force that pulls space towards them (also referred to as gravitomagnetic orbital perturbation). The theory implies that Earth's rotation should influence the motion of its orbiting satellites. Obviously, the effect of frame dragging is most pronounced near massive, fast spinning objects in the universe.

Since Albert Einstein published his Theory of General Relativity in 1916, several experiments have been discussed and proposed to measure the rotational dragging of an inertial frame by a spinning body. The first examples of direct measurements are:

- In the 1990s, an Italian team (CNR/IFSI, University of Rome, University of Pisa, etc.) performed an analysis of the orbits of Lageos–1 (launch May 4, 1976) and Lageos–II (launch Oct. 22, 1992), using existing laser ranging observations (3.1 years of measurement data) along with a highly accurate modeling technique (JGM–3 and EGM–96 gravity models) and the 1994 version of GEODYN II (an orbit determination program of NASA/GSFC). The result of the analysis was that the gravitomagnetic field has changed the point of perigee of the satellite Lageos–II by about 11 m during the observation period of 3.1 years (the plane of the orbits of LAGEOS I and II were shifted by about 2 m/year in the direction of the Earth's rotation). Both Lageos satellites are in MEO orbits (Lageos–II altitude of 5900 km, inclination = 52.65, period of 3.758 hours).²⁵⁸⁵⁾
- In November 1997, astronomers using NASA's RXTE (Rossi X–ray Timing Explorer) spacecraft observations made a startling discovery: evidence that supports this effect known as frame dragging. The astronomers found evidence to support frame dragging by observing a binary star system in which a normal star feeds the disk of accreting matter spiraling into the event horizon of a black hole.^{2586) 2587)}
- **First direct measurement of the frame dragging and geodetic effects and their magnitudes is being provided by GP–B (Gravity Probe–B).**²⁵⁸⁸⁾ The objective of GP–B mission of NASA (launch Apr. 20, 2004, flying at an altitude of 640 km and an inclination of 90°) is to measure with great accuracy the phenomenon on orientation of the axes of spin in orbiting gyroscopes (four superconducting gyroscopes are flown on GP–B, see E.12). GP–B monitors any drift in the gyroscopes' spin axis alignment in relation to its guide star, IM Pegasi (HR 8703). GP–B provides a drag–free environment to compensate for all non–gravitational disturbances acting on the spacecraft. SQUIDs (Superconducting Quantum Interference Device), which are very sensitive magnetometers, provide the gyroscopic readouts. A SQUID has the capability to detect a field change of 5×10^{-14} Gauss within a few days, which corresponds to a gyro tilt of 0.1 milliarcseconds.

In 1959, the theoretical concept of a frame dragging experiment was independently conceived and formulated by Leonard Schiff of Stanford University and George W. Pugh of the Pentagon. According to calculations by L. Schiff, the frame–dragging effect (rotation of space–time) should turn the gyroscope with the Earth through an angle of 41 milliarcseconds.

2585) I. Ciufolini, E. C. Pavlis, F. Chiappa, et al., "Test of General Relativity and Measurement of the Lense–Thirring Effect with Two Earth Satellites," *Science*, Vol. 279, March 27, 1998, pp. 2100–2103

2586) K. C. Cole, "MIT Scientists Find Evidence Of Long–Sought Space Warping," <http://www.rdrop.com/users/green/school/framdrag.htm>

2587) <http://www-tech.mit.edu/V117/N57/warping.57w.html>

2588) Note: Gravity Probe A was a relativity experiment relating to the equivalence of gravitational and inertial mass, performed in 1976 by NASA and the Smithsonian Astrophysical Observatory (suborbital flight).

conds in a time period of one year (corresponding to $1.17^\circ \times 10^{-5}$). According to Einstein, a second, much larger change in spin direction, the geodetic effect, follows from the gyroscope's motion through this spacetime curvature. The predicted effect for a gyroscope is a rotation in the orbit–plane of 6,600 milliarcseconds per year – quite a large angle by relativistic standards.

- ESA is defining a fundamental physics mission (under assessment as of 2003) called HYPHER (Hyper–Precision Cold Atom Interferometry in Space). In the time frame 2008/10, HYPHER will make the first map of the spatial contours of the gravitomagnetic effect close to Earth (the aim is to measure whether any rotation is associated with the Earth's gravitational field).^{2589) 2590)} It will achieve about 1% precision over a one–year measurement time. As they move in their orbit, atom gyroscopes (also referred to as quantum gyroscopes) with high sensitivity for rotation rates (10^{-12} rad/s at 1 Hz) will trace the latitudinal variation of the Earth's drag with respect to an inertial reference provided by a guide star monitored by a high–performance star tracker PST (Precision Star Tracker). The mission will provide the first test of the prediction, which flows from Einstein's general theory, that nearby space should be dragged round by the Earth's spin.

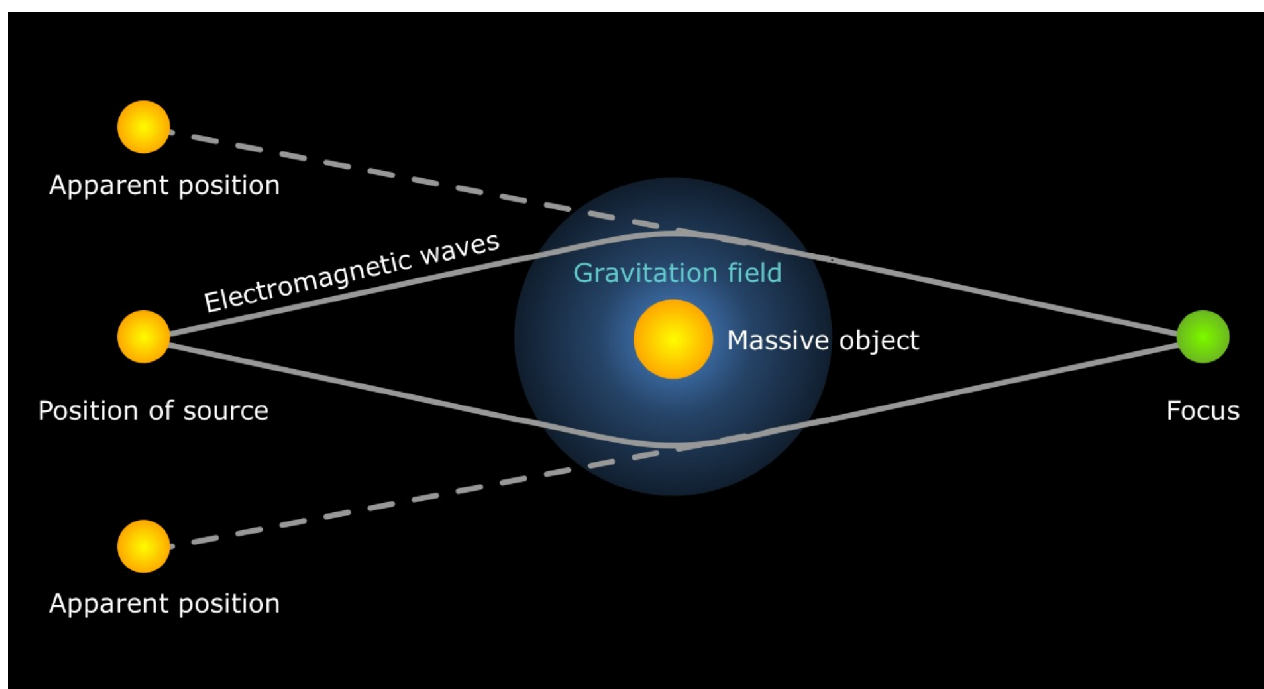


Figure 195: Illustration of the gravitational lens principle (image credit: DLR)

Gravitational lensing:

According to Einstein, space–time is a structure in itself, in which all cosmic objects — planets, stars, galaxies — reside. Every object with mass puts a “dent” in this structure in all dimensions; the more massive an object, the “deeper” the dent. Light energy travels in a straight line, but when it encounters these dents it can dip in and veer off–course, an effect we see from Earth as gravitational lensing.²⁵⁹¹⁾

Einstein also predicted that exceptionally massive, rapidly rotating objects — such as a white dwarf binary pair — would create outwardly–expanding ripples in space–time that

2589) http://maxim.gsfc.nasa.gov/documents/Mission_Concept_Work/ISAL_January_2002_SST/Astrometry/hyper-atomic-gyro.pdf

2590) W. Fichter, U. Johann, G. Bagnasco, P. Airey, “Spacecraft Design for Cold Atom Interferometry in Space,” Proceedings of IAC, Bremen, Germany, Sept. 29 – Oct. 3, 2003

2591) Jason Major, “Effects of Einstein’s Elusive Gravity Waves Observed,” Universe Today, Aug. 29, 2012, URL: <http://www.universetoday.com/97107/effects-of-einsteins-elusive-gravity-waves-observed/#ixzz250ovjBbx>

would ultimately “steal” kinetic energy from the objects themselves. These gravitational waves would be very subtle, yet in theory, observable.

A gravitational lens is formed when the light from a very distant, bright source (such as a quasar) is “bent” around a massive object (such as a massive galaxy) between the source object and the observer. This process is known as gravitational lensing, and was one of the predictions made by Einstein’s general relativity.

There are three classes of gravitational lensing:

- 1) Strong lensing: where there are easily visible distortions such as the formation of Einstein rings, arcs, and multiple images.
- 2) Weak lensing: where the distortions of background objects are much smaller and can only be detected by analyzing large numbers of objects to find distortions of only a few percent.
- 3) Microlensing: where no distortion in shape can be seen but the amount of light received from a background object changes in time. Typically, both the background source and the lens are stars in the Milky Way.

Gravitational microlensing is an astronomical observation technique taking advantage of the gravitational lensing effect of a foreground compact mass, such as a planet or star, as it passes very close to the line of sight to a more distant source, such as a star or a quasar. As light from the source star streams toward Earth, the gravity of the intervening lensing star bends the light rays. This creates a significant increase in brightness during the weeks or months that the two stars are in close proximity. – The distinguishing characteristic between microlensing and other cases of gravitational lensing is that the multiple distorted images of the source which the lens may induce are not individually resolvable by optical telescopes. Instead, with microlensing a single apparent image is observed with a brightness given by the combined brightness of the individual images.²⁵⁹²⁾ Astronomers who constantly monitor dense star clusters have recorded several hundred microlensing events each year since the early 1990’s.

– A first test of gravitational light–bending was confirmed in 1919 during a solar eclipse (May 29, 1919), when the English astronomer Arthur S. Eddington (1882–1944) observed the light from stars passing close to the sun was slightly bent, so that stars appeared slightly out of position. The measurement involved an expedition to Principe Island in West Africa.

– In 1979, the first gravitational lens was discovered accidentally by Dennis Walsh, Bob Carswell, and Ray Weymann using the Kitt Peak National Observatory 2.1 m telescope (AZ, USA). The object became known as the “Twin Quasar” since it initially looked like two identical quasars (but was actually only one object); it is officially named Q0957+561.

– In 2005, astronomers (an international team of 73 collaborators from 32 institutions) used the technique of microlensing with a network of telescopes – thereby discovering an extrasolar planet (exoplanet), named OGLE–2005–BLG –390Lb, only 5.5 times larger than the Earth, orbiting a star in the Sagittarius constellation (20,000 light years away close to the center of the Milky Way). The OGLE (Optical Gravitational Lensing Experiment) project telescopes first observed the lensing event of the exoplanet on July 11, 2005 (it is the smallest and the most Earth–like exoplanet discovered to date).²⁵⁹³⁾

OGLE is a long–term (NSF and NASA funded) research project that began sky searches for stellar variability in 1997.

²⁵⁹²⁾ http://en.wikipedia.org/wiki/Gravitational_microlensing

²⁵⁹³⁾ J. – P. Beaulieu, D. P. Bennett, P. Fouque, A. Williams, M. Dominik, U. G. Joergensen, D. Kubas, A. Cassan, C. Couatres, J. Greenhill, K. Hill, J. Menzies, P. D. Sackett, A. Albrow, et al., “Discovery of a cool planet of 5.5 Earth masses through gravitational microlensing,” *Nature*, Vol. 439, Jan. 26, 2006, pp. 437–440

– In February 2008, the COSMOS project announced the compilation of a large catalog of gravitational lenses in the distant universe, finding 67 galaxies lensed by massive elliptical and lenticular–shaped galaxies. If this is representative, there might be nearly 500 000 similar gravitational lenses in total over the whole sky. ²⁵⁹⁴⁾

The detailed survey of small region of the sky (about the same as 9 times the area of the full moon) was conducted by astronomers of the COSMOS project, led by Nick Scoville at the California Institute of Technology. Observations from several observatories were used including the Hubble Space Telescope (HST), the Spitzer Space Telescope, the XMM–Newton spacecraft, the Chandra X–ray Observatory, the Very Large Telescope (VLT), and the Subaru Telescope. – Out of these 67 lenses, the most impressive ones show the distorted and warped light of one or two background galaxies. At least four of the lenses give rise to Einstein rings, a complete circular image of a background galaxy. Such a ring is formed when the background galaxy, a massive foreground galaxy and the Hubble Space Telescope are all aligned perfectly.

– In 2010, the HSO (Herschel Space Observatory) mission of ESA (launch May 14, 2009) is providing a gravitational lens Bonanza. The first results from the Herschel–ATLAS survey, taken with SPIRE (Spectral and Photometric Imaging Receiver), have shown that far–infrared surveys provide a remarkably efficient method of finding gravitational lenses, which allow astronomers to zoom in on much more distant galaxies than they would otherwise be able to. ²⁵⁹⁵⁾

The Herschel–ATLAS images contain thousands of galaxies, most so far away that the light has taken billions of years to reach us. The Herschel–ATLAS team investigated five surprisingly bright objects in a small patch of the sky. Looking at the positions of these bright objects with optical telescopes on the Earth, they found galaxies that would not normally be bright at the far–infrared wavelengths observed by Herschel. This led them to suspect that the galaxies seen in visible light might be gravitational lenses magnifying much more distant galaxies seen by Herschel in the infrared region.

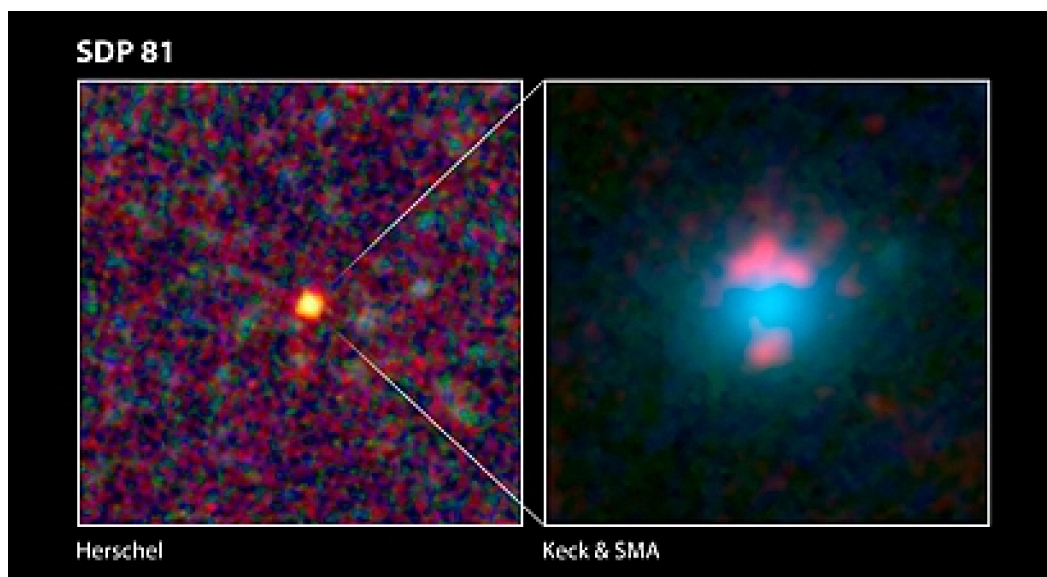


Figure 196: A gravitational lens system discovered by Herschel (image credit: ESA)

The magnification provided by these cosmic zoom lenses allows astronomers to study much fainter galaxies, and in more detail than would otherwise be possible. They are the key to

2594) “Hubble discovers 67 gravitationally–lensed galaxies in the distant universe,” Feb. 19, 2008, URL: http://www.esa.int/esaSC/SEMVGVMVHJCF_index_0.html

2595) Herschel–ATLAS Gravitational Lenses,” URL: <http://herschel.cf.ac.uk/results/herschel-atlas-gravitational-lenses>

understanding how the building blocks of the Universe have changed since they were in their infancy.

The galaxy SDP 81 is one of five distant submillimeter galaxies that were identified by HSO as being peculiar by virtue of appearing as particularly bright objects at sub–millimeter wavelengths. Closer observation at higher resolution using ground–based telescopes (Keck & SMA at right) revealed that Herschel had found a submillimeter galaxy being gravitationally lensed by another, foreground galaxy. ²⁵⁹⁶⁾

The right image of Figure 196 shows the foreground galaxy (blue) is seen at optical wavelengths by the W. M. Keck Observatory in Hawaii. The background galaxy (pink) shines brightly at much longer wavelengths, and was imaged using the submillimeter observations of the Smithsonian Astrophysical Observatory’s Submillimeter Array (SMA), also in Hawaii.

- An international team of astronomers, using NASA’s Fermi observatory, has made the first–ever gamma–ray measurements of a gravitational lens. In September 2012, Fermi’s LAT (Large Area Telescope) detected a series of bright gamma–ray flares from a source known as B0218+357, located some 4.35 billion light–years from Earth in the direction of a constellation called Triangulum. These powerful flares, in a known gravitational lens system, provided the key to making the lens measurement. ^{2597) 2598)}

The research team identified three episodes of flares showing playback delays of 11.46 days, with the strongest evidence found in a sequence of flares captured during the week–long LAT observations. – Intriguingly, the gamma–ray delay is about a day longer than radio observations report for this system. And while the flares and their playback show similar gamma–ray brightness, in radio wavelengths one blazar image is about four times brighter than the other.

The scientists say that comparing radio and gamma–ray observations of additional lens systems could help provide new insights into the workings of powerful black–hole jets and establish new constraints on important cosmological quantities like the Hubble constant, which describes the universe’s rate of expansion.

2596) “New method reveals gravitationally lensed galaxies in Herschel–ATLAS first survey,” ESA, Nov. 4, 2010, URL: <http://sci.esa.int/science–e/www/object/index.cfm?fobjectid=47888>

2597) J. D. Harrington, Lynn Chandler, “NASA’s Fermi Makes First Gamma–ray Study of a Gravitational Lens,” NASA, Release 14–005, Jan. 06, 2014, URL: http://www.nasa.gov/press/2014/january/nasas–fermi–makes–first–gamma–ray–study–of–a–gravitational–lens/#.Us43b_uFf_o

2598) C. C. Cheung, S. Larsson, J. D. Scargle, M. A. Amin, R. D. Blandford, D. Bulmash, J. Chiang, S. Ciprini, R. H. D. Corbet, E. E. Falco, P. J. Marshall, D. L. Wood, M. Ajello, D. Bastieri, A. Chekhtman, F. D’Ammando, M. Giroletti, J. E. Grove, B. Lott, R. Ojha, M. Orienti, J. S. Perkins, M. Razzano, A. W. Smith, D. J. Thompson, K. S. Wood, “Fermi–LAT Detection of Gravitational Lens Delayed Gamma–ray Flares from Blazar B0218+357,” Submitted to *Astrophysical Journal Letters*, Jan. 02. 2014

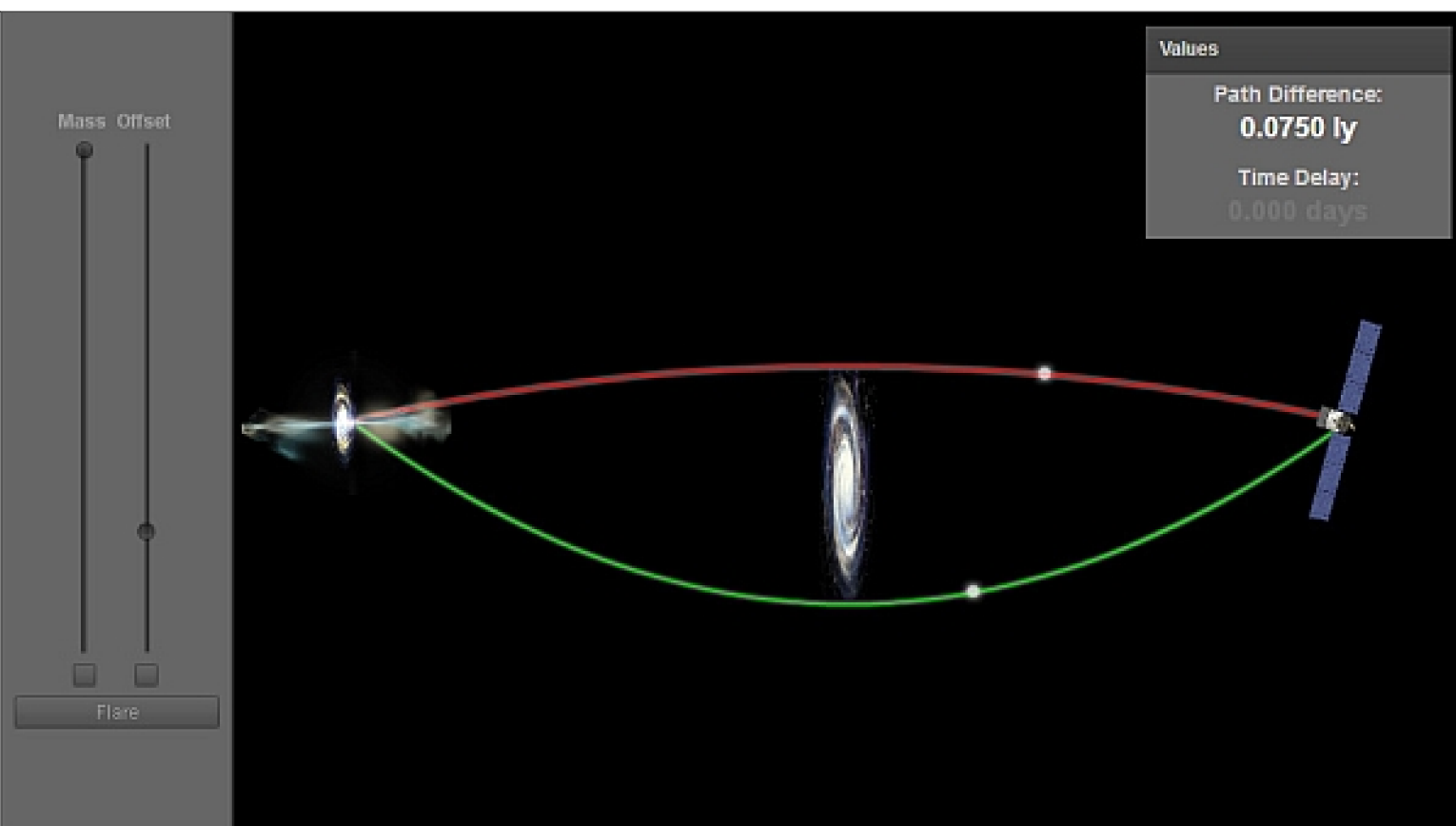


Figure 197: Gravitational lensing scheme as observed by the Fermi LAT (image credit: NASA/GSFC)

1.23.4 Introduction of quantum technology applications in spaceflight

At the start of the 21st century, a new class of enabling technologies promises to offer services for real applications which are based on quantum mechanic principles – a theory originally conceived by Max Planck in 1900 – with measurement dimensions on the atomic scale. Obviously, these applications have the potential to increase the measurement capabilities of new devices (with regard to accuracy, precision, and interpretation) by many orders of magnitude. Only fairly recent technology developments (since the 1980s) permitted the introduction of some spaceborne components, sensors, and experiments that utilize the new quantum technologies. In parallel, quantum technology applications are also being introduced into such fields as: quantum information technology (quantum computers, quantum cryptography, and communications), and nanotechnology in general. All these developments have propelled quantum mechanics into a multidisciplinary frontier research topic.

Some examples of quantum technology developments relating to new sensors or components in space applications are: ²⁵⁹⁹⁾ ²⁶⁰⁰⁾

- **QWIP (Quantum Well Infrared Photodetector)**

The field of quantum optoelectronics deals with electrically induced optical properties of nanometer–scale structures such as **quantum dots, superlattices and quantum wells.**

²⁵⁹⁹⁾ http://www.esa.int/SPECIALS/GSP/SEMU42ZO4HD_2.html

²⁶⁰⁰⁾ Josep Perdigues–Armengol, Zoran Sodnik, Clovis De Matos, “Leap ahead in space communications – Quantum technologies for space systems,” ESA Bulletin No 137, February 2009, pp. 32–38, URL: http://www.esa.int/es-apidoc/bulletin/bulletin137/bul137e_perdigues_armengol.pdf

When the dimensions of these structures become comparable to the wavelength of the electrons, or the photons they generate, their optical and electrical properties are modified. – The use of QWIP arrays to detect infrared radiation can be explained by using the basic principles of quantum mechanics. The quantum well is equivalent to the well-known “particle in a box problem” in quantum mechanics. QWIPs utilize the photoexcitation of electrons (hole) between the ground state and the first excited state in the conduction (valance) band quantum well. The quantum well structure is designed so that these photo-excited carriers can escape from the quantum well and be collected as photocurrent. QWIPs are being used as intrinsic infrared detectors in the spectral range 6–20 μm .

The QWIP technology was developed in the 1980s by Barry F. Levine and his colleagues at Lucent’s Bell Labs (formerly AT&T Bell Labs) in close cooperation with NASA (GSFC and JPL).²⁶⁰¹⁾ In the meantime, the QWIP infrared imaging detection technology has been and is being introduced into many observation applications such as in: fire fighting, volcanology, medicine, military surveillance and reconnaissance, astronomy, and general Earth observation applications; hyperspectral imaging is among them. In 2001, the QWIP technology was one of the new developments inducted into the US Space Technology Hall of Fame.

– In Feb. 2003, a NASA/GSFC team fabricated and tested the first large-format QWIP detector array of one million pixels, a GaAs semiconductor chip.^{2602) 2603)}

– In 2008, NASA/GSFC revised the design of the infrared detector concept of the TIRS (Thermal Infrared Sensor) imager for the LDCM (Landsat Data Continuity Mission), launch on Feb. 11, 2013. The initially considered HgCdTe-based detector design was changed to a QWIP design due to the emergence of broadband QWIP capabilities in the MWIR and TIR regions of the spectrum. The introduction of QWIP technology for an operational EO mission represents a breakthrough made possible through collaborative efforts of GSFC, the Army Research Lab and industry.²⁶⁰⁴⁾

An important advantage of the GaAs QWIP technology is the ability to fabricate arrays in a fashion similar to and compatible with the silicon IC technology. The designer’s ability to easily select the spectral response of the material in the spectral range from 3 μm to beyond 15 μm is the result of the success of band-gap engineering.²⁶⁰⁵⁾

- **QGG (Quantum Gravity Gradiometry)**

The experimental developments of laser cooling and manipulation of atoms, first introduced in the 1990s, have lead to an entirely new class of gravity sensors: namely the **quantum gravity gradiometer (QGG)** based on atom interferometry. Unlike any previously known gravity sensors, the quantum gravity gradiometer uses atoms themselves as drag-free test masses. At the same time, the quantum wave-like nature of atoms is utilized to carry out interferometric measurement of the effect of gravity on the atoms. The exquisite sensitivity potentially achievable with atom-wave interferometry holds great promise for

2601) S. D. Gunapala, S. V. Bandara, “Quantum Well Infrared Photodetector (QWIP) Focal Plane Arrays,” Published in “Semiconductors and Semimetals” series, Vol. 62, 1999

2602) M. Jhabvala, K. Choi, A. Goldberg, A. La, S. Gunapala, “Development of a 1 k x 1 k GaAs QWIP far IR imaging array,” Proceedings of NASA’s ESTC, Palo Alto, CA June 22–24, 2004

2603) <http://www.gsfc.nasa.gov/topstory/2003/0123qwip.html>

2604) M. Jhabvala, D. Reuter, K. Choi, C. Jhabvala, M. Sundaram, “QWIP-Based Thermal Infrared Sensor for the Landsat Data Continuity Mission,” Proceedings of the QSIP (Quantum Structure Infrared Photodetector) 2009 International Conference, January 18–23, 2009, Yosemite, CA, URL: <http://qsip.jpl.nasa.gov/presentations/Murzy%20Jhabvala%20QWIP%20Based%20Thermal%20Infrared%20Sensor%20for%20Landsat%20Data%20Continuity%20Mission.pdf>

2605) M. Jhabvala, K. K. Choi, C. Monroy, A. La, “Development of a 1 k x 1 k, 8–12 μm QWIP array,” Infrared Physics & Technology, Volume 50, Issues 2–3, April 2007, pp. 234–239

new gravity mapping and monitoring capabilities – higher measurement sensitivity, finer spatial resolution, and temporal monitoring. ²⁶⁰⁶⁾ ²⁶⁰⁷⁾

As of 2003/4, the goal of a NASA/JPL research team is to construct a viable laboratory instrument based on these principles to be used eventually in a spaceborne mission in support of geodesy applications.

As of 2006, NASA/JPL completed the development of a laboratory–based quantum gravity gradiometer based on atom interferometer technology (dual light–pulse concept). ²⁶⁰⁸⁾ This represents a first step towards a new spaceborne gradiometer instrument, which can significantly contribute to global gravity mapping and monitoring important in the understanding of the solid earth, ice and oceans, and dynamic processes.

Background: Light–pulse interferometers work on the principle of quantum–mechanical particle–wave duality that when an atom absorbs or emits a photon, momentum must be conserved between the atom and the light field. The wave–like nature of atoms is exploited to construct an atom interferometer analogous to laser interferometers. John F. Clauser of LLNL (Lawrence Livermore National Laboratory), Livermore, CA, first proposed using an atom interferometer as a gravity sensor in 1988. ²⁶⁰⁹⁾ In his conclusion he states: *Practical scientific applications of the proposed interferometer include measurements of the Lense–Thirring and de Sitter precessions, measurements of the composition–dependent “fifth force,” observation of time delays of the gravitational fields of the sun and moon (and thus the speed of gravitational waves), measurement of gravitational gradients, tests of the Equivalence Principle, and measurements of energy shifts of the total energy of a free atom (such as those due to symmetry breaking effects). Important practical applications of such devices occur in the fields of navigation, geology, surveying and the analysis of structures.* – However, his idea could not be fully realized until subsequent advances in laser cooling and manipulation of atoms were available. S. Chu and M. Kasevich of Stanford University first demonstrated the measurement of “g” using a light–pulse atom interferometer in 1992. ²⁶¹⁰⁾

In the 1990s and later on, matter–wave interferometry has shown its potential to be an extremely sensitive probe for inertial forces. Photons carry momentum, when an atom absorbs/emits a photon, its momentum changes accordingly. *In a quantum gravity gradiometer, the atoms themselves are being used as test masses. At the same time, the quantum nature of atom as matter–wave is utilized to carry out interferometric measurement of the effect of gravity on the atoms.*

- **Quantum gyroscopes**

The quantum gyroscope is a concept proposed at NASA/JPL (Jon Dowling) in 1997. Calculations suggest that the two–input port optical quantum gyroscope ought to be about 10^8 times more sensitive to rotations than a one–input port optical gyroscope. ²⁶¹¹⁾

The measurement of rotation (or spin) is closely tied to gyroscopic measurements since the principle is based on the conservation of angular momentum. SQUID (Superconducting

2606) N. Yu, J. M. Kohel, J. Ramerez–Serrano, J. R. Kellogg, L. Lim, L. Maleki, “Progress towards a space–borne quantum gravity gradiometer,” Proceedings of NASA ESTC (Earth Science Technology Conference), Palo Alto, CA, June 22–24, 2004, <http://esto.gsfc.nasa.gov/conferences/estc2004/papers/b4p1.pdf>

2607) N. Yu, J. M. Kohel, L. Romans, L. Maleki, “Quantum Gravity Gradiometer Sensor for Earth Science Applications,” Proceedings of NASA ESTC (Earth Science Technology Conference), Pasadena, CA, June 11–13, 2002, URL: [http://esto.nasa.gov/conferences/estc-2002/Papers/B3P5\(Yu\).pdf](http://esto.nasa.gov/conferences/estc-2002/Papers/B3P5(Yu).pdf)

2608) J. M. Kohel, N. Yu, J. R. Kellogg, R. J. Thompson, D. C. Aveline, L. Maleki, “Quantum Gravity Gradiometer Development for Space,” Proceedings of the Sixth Annual NASA Earth Science Technology Conference (ESTC 2006), College Park, MD, USA, June 27–29, 2006, URL: <http://www.esto.nasa.gov/conferences/ESTC2006/papers/b4p1.pdf>

2609) J. F. Clauser, “Ultra–high sensitivity accelerometers and gyroscopes using neutral atom matter–wave interferometry,” *Physica B* (North Holland, Amsterdam), Vol. 151, 1988, pp. 262–272, Elsevier Science Publishers B.V.

2610) M. Kasevich, S. Chu, “Measurement of the gravitational acceleration of an atom with a lightpulsed atom interferometer,” *Applied Physics B*, Vol. 54, 1992., pp. 321–332

2611) <http://cs.jpl.nasa.gov/qct/qGyro.htm>

Quantum Interference Device), is a fairly new detector type most sensitive for magnetic field detection, in particular with superconducting technology. A solid–state magnetometer formed by the parallel circuit of two Josephson junctions is called a direct current or a DC–SQUID. In practical SQUID measuring instruments, by means of a negative feedback with an additional coil, the flux through the SQUID loop is held constant. The strength of the feedback current necessary for this is then a measure of the magnetic field to be measured.

In 2001, the phenomenon of quantum interference was also demonstrated in a liquid state experiment, namely in a **superfluid SQUID** at UCB (University of California, Berkeley). *The double–path experiment demonstrated that quantum interference is identical to the interference between light waves, electrons, atomic beams and electrical currents in solid superconductors.*^{2612) 2613)} In the experimental setup, the superfluid SQUID geometry, analogous to the superconducting DC–SQUID configuration, provided the rotation detection (analogous to a gyroscopic detection) in the superfluid; the quantum phase shift was controlled by using the rotation of the Earth. Hence, a superfluid SQUID couples to rotation measuring minute changes in rotation; the technology may for instance be used as a detector of absolute rotation measurement. The sensitivity of the superfluid SQUID technology gives rise to the development of a quantum gyroscope. This is of vital interest for future missions in geodesy (detecting minute gravitational deviations, etc.). The ESA mission HYPER (Hyper–Precision Cold Atom Interferometry in Space), under definition in 2004, may be able to use this new technology.

Rotation measurements are also being considered in spin electronics applications to enable manipulations of the electron charge and spin. The ability to manage electron spin is expected to lead to improvements in electronic systems and devices used in photonics, data processing and communications applications.

- **Applications of improved atomic clocks:**

ACES (Atomic Clock Ensemble in Space) is an ESA–selected nadir–oriented instrument to be flown on ISS (launch expected in the 2015–16 time frame). ACES is a laser–cooled cesium atomic clock, exploiting the microgravity conditions onboard ISS to reach unprecedented precision not achievable on Earth. In fact, a cold atomic clock works more accurately under weightlessness than under Earth’s gravity. The laser cooling is used to reduce the thermal velocity of atoms to a few cm/s, corresponding to a temperature of about 1 K.

Background on laser cooling. The technology of laser cooling began with the development of a set of tools using laser beams to slow atoms down, cooling them to within a millionth of a degree above absolute zero (the atoms actually relinquish their heat energy to laser light and thus reach lower and lower temperatures). At these cold temperatures, cesium atoms are left with a residual velocity of only 1 cm/s. This slowing of atoms allows longer observation times to study the atoms’ behavior. When a laser–cooled vapor (like cesium) is taken to microgravity, the observation time is increased considerably because the cold and slow atoms will not fall out of the observer’s view as quickly as they do under the influence of the Earth’s gravity. The small residual velocity makes for instance cesium atoms attractive candidates for precision spectroscopy in atomic clocks.

Laser cooling techniques have also been used to cause a cloud of atoms to condense into the Bose–Einstein state, a new state of matter similar to superfluid helium. The BEC (Bose–Einstein Condensate) occurs when atoms at a particular temperature and pressure, on the removal of some energy, fall into lock–step with one another.

2612) R. W. Simmonds, A. Marchenkov, E. Hoskinson, J. C. Davis, R. E. Packard, “Quantum Interference of superfluid ³He,” *Nature*, Vol. 412, July 5, 2001, pp. 55–58

2613) R. Sanders, “Quantum interference demonstrated for first time in liquids as physicists make superfluid analog of super–conducting SQUID, a potential ultrasensitive gyroscope,” July 5, 2001, URL: http://www.berkeley.edu/news/media/releases/2001/07/05_SQUID.html

Background on BEC: The Bose–Einstein condensate is a purely quantum form of matter, first predicted by Albert Einstein and the Indian physicist Satyendra Nath Bose in 1924. Normally, light appears to heat things up (through absorption of light by the material). However, it is possible, in some cases, to use light to cause materials to give up more energy than they absorb, causing them to cool. Basic research with laser cooling of atoms was first done in the 1980s by Steven Chu of Stanford University, Claude Cohen–Tannoudji of College de France, and William D. Phillips of NIST (National Institute of Standards and Technology), Gaithersburg, MD. However, it took until 1995 when the first BEC was created and observed by the three scientists in a laboratory at the University of Colorado. For this work the physicists listed above were awarded the 1997 Nobel Prize in Physics.

- **Free–space quantum cryptography:** Quantum cryptography is an enabling technology that uses the laws of physics to transmit information securely. In such systems, the vehicle to transfer quantum information is a single photon. However, the Earth–bound transmission distance is limited by the absorption of photons in an optical fiber in which the maximum demonstrated range is about 100 km. The distance for quantum key distribution (QKD) using optical fibers is limited by the background level in the optical fiber at around 100 km, and the fact that optical fibers have non–linearity in polarization.

Free–space quantum cryptography between a ground station and a satellite is a way of sending the quantum information further distances than that with optical fibers since there is no birefringence effect in the atmosphere. The free–space quantum cryptography concept offers an ideal medium for transmitting photon–based quantum information. It is suitable as the fundamental functional architecture for future computer processing and communications – ensuring absolute security and quantum teleportation between distant terminals. Photon–based quantum schemes make use of entangled photons that cannot be cloned; hence, cannot be amplified. ²⁶¹⁴⁾

History: Quantum cryptography was first demonstrated by C. H. Bennett and G. Brassard (USA) in 1984 with the transmission distance of 30 cm. Diurnal 10 km QKD (Quantum Key Distribution) was conducted by LANL (Los Alamos National Laboratory) in 2002. Recently, successful laser communication experiments between satellites including ground stations have been demonstrated. ²⁶¹⁵⁾

- A first optical free–space data transmission test, using the laser link between ARTEMIS (ESA) and SPOT–4 (CNES), was realized on Nov. 21, 2001 on four consecutive SPOT–4 orbits for contact periods between four and 20 minutes each. The **SILEX** terminal onboard ARTEMIS, in a parking orbit of 31,000 km, activated its optical beacon to scan the area where SPOT was expected to be (LEO at 830 km). ^{2616) 2617) 2618)}

- The first bi–directional optical link (data and command transmission) between OICETS/Kirari and ESA's ARTEMIS spacecraft (LEO–GEO) was made on Dec. 9, 2005. This represented the world's first bidirectional optical interorbit communication. ²⁶¹⁹⁾

- JAXA/NICT carried out optical communication experiments between March 22–31, 2006 using laser beams between OICETS and the optical ground station (referred to as

2614) M. Toyoshima, Y. Takayama, W. Klaus, H. Kunimori, M. Fujiwara, M. Sasaki, "Free–space quantum cryptography with quantum and telecom communications channels," 58th IAC (International Astronautical Congress), International Space Expo, Hyderabad, India, Sept. 24–28, 2007, IAC–07–B2.3.07

2615) C. H. Bennett, G. Brassard, "Quantum Cryptography: Public Key Distribution and Coin Tossing," Proceedings of International Conference on Computers, Systems & Signal Processing, Bangalore, India, 1984

2616) "ARTEMIS and SPOT–4 chat with laser light," ESA Bulletin, No 108, Nov. 2001, p. 114

2617) I. Gaudel, L. Moliner, B. Romeo, S. Teodomante, "Operational Use of PASTEL Passenger on SPOT–4 Satellite," Proceedings of 54th IAC (International Astronautical Congress), Bremen, Germany, Sept. 29 – Oct. 3, 2003

2618) T. T. Nielsen, G. Oppenhaeuser, B. Laurent, G. Planche, "In–orbit test results of the optical intersatellite link, SILEX. A milestone in satellite communication," Proceedings of the 53rd International Astronautical Congress, Houston, TX, USA, Oct. 2002, IAC–02–M.2.01

2619) Y. Fujiwara, M. Mokuno, T. Jono, T. Yamawaki, K. Arai, M. Toyoshima, H. Kunimori, Z. Sodnik, A. Bird, B. Deme- lenne, "Optical Interorbit Communications Engineering Test Satellite (OICETS)," Proceedings of the 57th IAC/ IAF/IAA (International Astronautical Congress), Valencia, Spain, Oct. 2–6, 2006, IAC–06–B3.5.10

KODEN) of NICT in Koganei, Tokyo. The experiments were successfully performed on March 31 (LEO–ground station) as well as in May 2006. This required a highly sophisticated pointing technology because the satellite had to keep sending laser beams accurately to the ground station while moving at orbital speed. ²⁶²⁰⁾

– Quantum key distributions over a 23 km distance between buildings and mountains were achieved by Weinfurter et al. of LMU (Ludwig–Maximilian University, Munich, Germany. ²⁶²¹⁾

– Space–QUEST (QUantum Entanglement for Space ExperimenTs) is an ESA technology demonstration project with the overall objective to demonstrate a **quantum communications space–to–ground experiment from the International Space Station (ISS)**. ²⁶²²⁾ A European research consortium led by Vienna University (Austria) submitted in 2004 the Space–QUEST proposal. The objectives of the Space–QUEST experiment are to demonstrate, for the first time: a) Unconditional secure global distribution of cryptographic keys from space, based on novel quantum communication techniques like QKD (Quantum Key Distribution), and b) Research of fundamental quantum physics principles beyond the capabilities of Earth–bound laboratories by utilizing the added value of the space environment. A launch of Space–QUEST is planned for the end of 2014. The duration of the Space–QUEST experiment is estimated to be 1 year. ²⁶²³⁾

²⁶²⁰⁾ M. Toyoshima, K. Takizawa, T. Kuri, W. Klaus, M. Toyoda, H. Kunimori, T. Jono, Y. Takayama, K. Arai, “Development of the Optical Ground Station for the OICETS Satellite and Experimental Results,” Proceedings of the 57th IAC/IAF/IAA (International Astronautical Congress), Valencia, Spain, Oct. 2–6, 2006, IAC–06–B3.4.04

²⁶²¹⁾ C. Kurtsiefer, P. Zarda, M. Halder, H. Weinfurter, P. M. Gorman, P. R. Tapster, J. G. Rarity, “A step towards global key distribution,” *Nature*, Vol. 419, 2002, p. 450

²⁶²²⁾ J. M. Perdignes Armengol, B. Furch, C. Jacinto de Matos, O. Minster, L. Cacciapuoti, M. Pfennigbauer, M. Aspelmeyer, T. Jennewein, R. Ursin, T. Schmitt–Manderbach, G. Baister, J. Rarity, W. Leeb, C. Barbieri, H. Weinfurter, A. Zeilinger, “Quantum Communications at ESA: Towards a Space Experiment on the ISS,” 58th IAC (International Astronautical Congress), International Space Expo, Hyderabad, India, Sept. 24–28, 2007, IAC–07–B2.3.05

²⁶²³⁾ R. Ursin, T. Jennewein, J. Kofler, J. M. Perdignes, L. Cacciapuoti, C. J. de Matos, M. Aspelmeyer, A. Valencia, T. Scheidl, A. Fedrizzi, A. Acin, C. Barbieri, G. Bianco, C. Brukner, J. Capmany, S. Cova, D. Gigenbach, W. Leeb, R. H. Hadfield, R. Laflamme, N. Lütkenhaus, G. Milburn, M. Peev, T. Ralph, J. Rarity, R. Renner, E. Samain, N. Solomos, W. Tittel, J. P. Torres, M. Toyoshima, A. Ortigosa–Blanch, V. Pruneri, P. Villoresi, I. Walmsley, G. Weihs, H. Weinfurter, M. Zukowski, A. Zeilinger, “Space–QUEST: Experiments with quantum entanglement in space,” Proceedings of the 59th IAC (International Astronautical Congress), Glasgow, Scotland, UK, Sept. 29 to Oct. 3, 2008, IAC–08.A2.1.3

1.24 Satellite Orbits

Newton's laws of motion provide the basis for orbital mechanics. A satellite's orbit is generally defined by six independent parameters (see Table 151). For remote sensing satellites the most important parameters are: a) mean radial distance with regard to the Earth's center of mass, referred to as semi-major axis [the radial extremes are designated by **perigee** (min) and **apogee** (max) above the Earth's surface]; b) **inclination** (angle between the Earth's equatorial plane and the spacecraft's orbital plane (major axis)); and c) by the time, or **period**, it takes to complete one orbit about a central body like Earth. The orbital period increases with the mean altitude of the orbit, so a satellite in LEO moves faster than a satellite in MEO, and still faster than a satellite in GEO.

In general, Earth orbits are elliptical; circular orbits are a special case of elliptical orbits (providing on average a constant-altitude observation geometry, a constant orbital speed, as well as a constant signal strength). Satellites in non-circular orbits (i.e., eccentricity > 0) move faster when they are closer to the Earth (i.e. at perigee), and slower when they are farther away (i.e. closer to apogee).

Parameter	Description
R_E	6378 km, the average Earth equatorial radius
T_{GEO}, T_{GSO}	Earth rotation period = 24 h (in mean solar time)
n_{sun}	Mean motion of the fictitious mean sun, $n_{sun} = 0.9856^\circ/\text{day}$
$d\theta/dt$ (theta-dot)	Theta-dot is the sidereal rotational rate of the Earth = $360.9856^\circ/\text{day}$; consequently the Earth sidereal rotation period is 23 h 56 m 4 s.
Orbital revolution	A revolution or period is defined as the time from one perigee to the next
Keplerian Elements	
a	Semi-major axis (or mean orbital radius)
e	Eccentricity: defines the shape of the orbital ellipse, if $e=0$ the orbit is circular
i	Inclination of orbital plane to equatorial plane. The orbital plane always goes through the center of the Earth; $i=0^\circ$ (equatorial orbit), $i = 90^\circ$ (polar orbit)
Ω (Omega = RAAN)	Right ascension of ascending node; the longitude of the ascending node at which the orbit crosses the equator northbound; RAAN is an angle, measured at the center of the Earth, from the vernal equinox to the ascending node. For some orbits the right ascension of the ascending node (Ω) may move as much as $6^\circ/\text{day}$.
ω (omega)	Argument of perigee: the angle between the ascending node and the perigee; for some orbits the argument of perigee (ω) may move as much as $12^\circ/\text{day}$.
T_0	Epoch, time at which the orbital elements are defined
Special Orbits	
SSO (Sun-synchronous Orbit)	$\Omega\text{-dot} = n_{sun}$; most near-Earth SSOs have inclinations between 97° and 103° . SSO is characterized by synchronizing the rate of change of ascending node ascension to the rate of the Earth rotation around the sun
GEO (Geostationary Orbit)	$n = \text{theta-dot}$ (where n is the mean motion of the satellite), and in addition: i (inclination) = 0, and e (eccentricity) = 0
GSO (Geosynchronous Orbit)	$n = \text{theta-dot}$ (where n is the mean motion of the satellite)
Molniya-type orbit	ω (omega-dot) = 0 (i.e., no secular drift of the perigee), with $i = 63.43^\circ$ (generally orbits of 12 hour periods with very long times in apogee. The ground track for the northern hemisphere loops back on itself in a narrow pattern that enables multiple observing opportunities per orbit

Table 151: Overview of some orbital parameters/definitions and special type orbits

Obviously, an infinite number of possible orbits can be defined for a spacecraft in Earth orbit. However, a number of special Earth orbit types (or classes) evolved since the early spaceage to cover particular observational and/or operational characteristics such as: LEO (polar, SSO, etc.), MEO, GEO (GTO, GSO), HEO (Molniya, etc.), and Halo orbits (these are briefly covered in the following chapters). Generally, the observation coverage of a geo-

graphical area increases with increasing observation distance from Earth (but the spatial resolution decreases with increasing distance).

In general, the LEO–type observation provides high spatial resolution with low temporal resolution – while GEO–type observation provides for low spatial resolution, but high temporal resolution. Note: The GEO observation occurs at a distance of about 45 times farther away than the LEO observation (considering an average LEO altitude of 800 km).

From a legal/management point of view, all orbits represent a natural space resource to be shared by all participants, with some orbits of rather limited capacity. The ITU (International Telecommunications Union) is the entity which regulates for instance the use of GEO (Geostationary Orbit) traffic of satellites (allocation of GEO position – only 360° of orbital arc are available in the equator plane) as well as of the radio frequency spectrum for all orbits of airborne and spaceborne vehicles (another natural space resource of very limited capacity to be shared by all).²⁶²⁴⁾

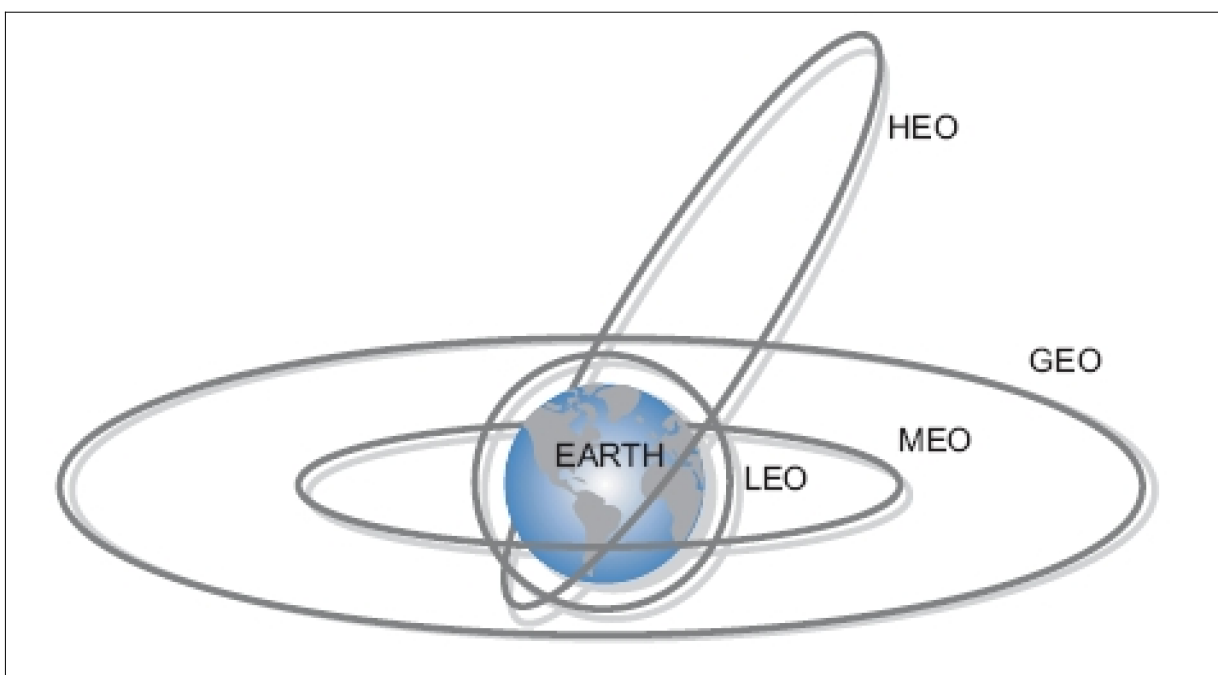


Figure 198: Overview of some Earth orbit types

1.24.1 LEO (Low Earth Orbit)

The general altitude range of LEOs is < 2000 km above the Earth's surface with orbital periods of about 90–120 minutes (in general all inclinations are possible). The orbital velocity of a LEO spacecraft with regard to an observer on Earth is generally in the order of 7–8 km/s (requiring fast observation schemes; this involves also coping with large Doppler shifts for communication needs and other measurement services).²⁶²⁵⁾²⁶²⁶⁾ The circular LEO is the most common and natural orbit for Earth observation, in particular in the altitude range of about 200–900 km with orbital periods of about 90–105 minutes. The polar orbit, and in particular the sun–synchronous orbit, are special LEO subclasses.

²⁶²⁴⁾ Note: ITU is an UN agency since 1947 to cover standards for a wide range of telecommunication services

²⁶²⁵⁾ Note: From a viewpoint of orbital mechanics, circular orbits are only on average “circular,” referring to average conditions over long–term periods (1000 years or so). No satellite is in reality orbiting in a circular orbit. The nature of Keplerian elements is variable; this means the semi–major axis on a circular orbit ($e=0.0$) is actually varying by about 20 km for satellites in LEO. Naturally, this affects to some extent the observation geometries with the additional effect of polar oblateness.

²⁶²⁶⁾ Note: Satellites [Ofeq series of IAI (Israel Aircraft Industries)] launched from Israel (Palmachim Air Force Base south of Tel Aviv) orbit from **east to west**, as opposed to the traditional west to east direction, as Israel can only safely launch rockets westbound, over the Mediterranean Sea.

The very first satellites, like Sputnik–1 and most successors, had LEO orbits and were launched in an eastward direction (thereby gaining a boost with the Earth’s rotation), and obtaining an inclination of the launch site’s latitude. – To achieve a polar orbit requires more energy, thus more propellant, than does an orbit of low inclination. A polar orbit cannot take advantage of the “free ride” provided by the Earth’s rotation, and thus the launch vehicle must provide all of the energy for attaining orbital speed.²⁶²⁷⁾

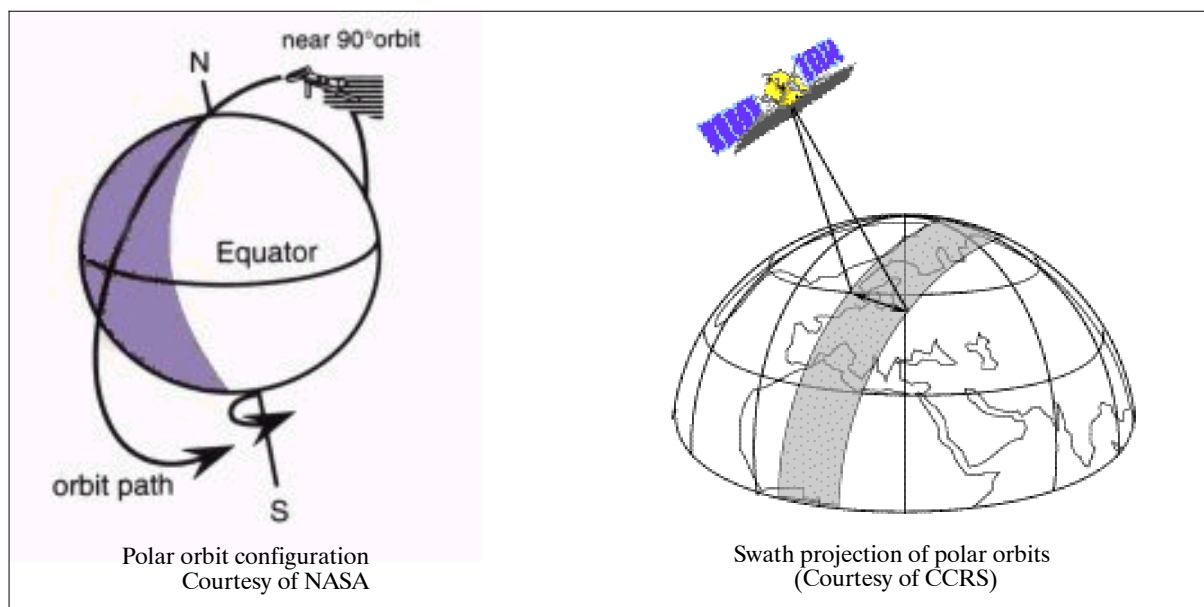


Figure 199: Schematic illustration of polar orbits and swath projections

The vast majority of LEO spacecraft, orbit at altitudes of ≤ 1000 km. The 1000 km altitude limit represents a ceiling of a region, in which the **atmospheric drag** is still being felt for a long–term decaying orbit (the decay may actually last for centuries for spacecraft in orbits close to the limit). All spacecraft in orbits with perigee altitudes > 1000 km, and without any onboard deorbiting means, must be considered as “eternal debris” at EOL (End of Life). In most space applications, drag is considered an unwanted disturbance related to atmospheric density changes. These changes are induced by solar extreme ultraviolet irradiance (EUV) variations, i.e., one of the effects of space weather.

The class of LEO satellites can only provide **intermittent coverage** of a geographical area (considering a single spacecraft). The observation coverage from LEOs is limited by the FOV (Field of View) of the satellite’s observation instruments. A nadir–viewing spacecraft with its payload FOV (Field of View) can only see a small portion of the Earth’s surface instantaneously, namely the footprint, resulting in a coverage geometry of observation swaths (normally the width of the imagery on Earth’s surface) by the various instruments in a continuous observation support mode (and provided by the spacecraft’s orbital motion). This scenario results in a periodic observation coverage of a rotating Earth. Satellite contact periods with ground stations are generally limited to about 8–12 minutes, depending on the orbital geometry relation to a particular station.

Global LEO observation coverage was an early requirement in spaceflight. This led to new strategies in mission design concepts – in particular with regard to orbital plane inclinations and to orbital altitudes. Obviously Earth observation coverage is much more effective by a LEO spacecraft with a high inclination (say 90° , a polar orbit) than one with a low or even 0° inclination (i.e. an equatorial orbit). In a **polar orbit** (in which the satellite passes over or fairly close to the vicinity of both poles), the entire Earth is rotating underneath the orbital path of the satellite, thus permitting a global coverage in a minimum time of 12 hours

²⁶²⁷⁾ <http://www.geo-orbit.org/sizepgs/geodef.html#anchor1302357>

(if slightly overlapping observation swaths can be provided). In this setup, the satellite's orbit and the rotation of the Earth work together to allow complete coverage of the Earth's surface, after it has completed one complete cycle of orbits. – In an inclined orbit of 60° , for instance, observation coverage can only be provided ranging from the equator up to the latitudes of $\pm 60^\circ$. Hence, polar orbits (with inclinations close to 90°) turn out to be particularly useful for global mapping and surveillance functions.

The study of these general coverage schemes was of particular interest in the early phase of the space age and far beyond, opening up new vistas for various kinds of mission applications and service configurations.

- **Observation coverage** considerations in polar orbits, including SSOs (Sun–Synchronous Orbits) which are near–polar orbits: A spacecraft in a LEO polar or near–polar orbit (within an altitude range of about 200–2000 km) provides on average 16 to about 10 orbits per day (dictated by orbital mechanics). This corresponds to 25.7° of longitudinal separation between successive orbits related to the equator (Earth circumference of 360° divided by an average of 14 orbits at about 800 km altitude). In a single orbit, two swath widths should be added to the coverage, accounting for the northward (ascending) orbital path on one side of Earth and for the southward (descending) orbital path on the other side of the pole – all in one orbital revolution. However, if the orbit is also sun–synchronous, the ascending pass is most likely on the shadowed side of the Earth, while the descending pass is on the sunlit side.²⁶²⁸) Hence, sensors recording reflected solar energy only, image the Earth's surface on a descending pass of the orbit only, i.e. when solar illumination is available. In general, each polar orbit experiences about 70% of sunlight exposure and about 30% of darkness or shadowing (in an average 100 minute orbit, this amounts to 70 minutes sunlight and 30 minute shade).

- Contiguous repeat coverage. Obviously, the observation geometry in a polar orbit is such as to provide contiguous repeat coverage on every orbital path at the poles as well as at high latitudes (in the polar regions). However, the sunlit swath projection requirements (of 25.7° longitude) widen constantly along the orbital path of a spacecraft flying over a rotating Earth, reaching twice per orbit a maximum in the equator plane with about 2860 km between adjacent orbits (Earth equatorial circumference of 40,000 km divided by 14 orbits). **This implies an observation swath width of at least 2860 km if a daily global overlapping coverage of the sunlit portion of the orbit is required.**

Active sensors which provide their own illumination, or passive sensors that record emitted (e.g. thermal) radiation, can also image the Earth's surface on nighttime passes of the orbit.

In Earth observation there are not many imaging instruments providing swath widths around 2900 km or more (they all deal with weather or environmental parameter observations). Some examples of sensors with a daily global coverage capability in polar orbits are:

- AVHRR (Advanced Very High Resolution Radiometer) of the NOAA/POES series and on the future MetOp series of EUMETSAT (MetOp–A launch Oct. 19, 2006), provides a swath width of 2900 km (FOV of $\pm 55.37^\circ$)

- OLS (Operational Linescan System) of the DMSP series has a swath of 2960 km (FOV = $\pm 56.25^\circ$)

- SeaWiFS (Sea–Viewing Wide Field–of–View Sensor) of the OrbView–2 mission of ORBIMAGE (launch Aug. 1, 1997) provides a swath width of 2800 km in LAC (Local Area Coverage) mode; FOV = $\pm 58.3^\circ$.

- MSU–MR (Low Resolution Multispectral Scanner), flown on the Meteor–3M series of Russia (launch of Meteor–3M–1 on Dec. 10, 2001), provides a swath width of 3000 km

²⁶²⁸) In general, SSOs may have any defined local time (equator crossing time) in either of their ascending or descending nodes. There is no rule that the ascending pass of an SSO has to be in the sun's shadow.

- VIIRS (Visible/Infrared Imager and Radiometer Suite) of the future US NPOESS series provides a swath width of 3000 km (corresponding to a FOV of $\pm 55.84^\circ$)
- OMPS (Ozone Mapping and Profiler Suite) instrument of NPOESS provides also global daily maps of the amount of ozone in the vertical column of the atmosphere (in UV range).

All of the above instruments provide a global daily overlapping coverage in their VNIR bands of reflected solar energy (imagery of visible bands); in addition, the instruments provide a twice-daily global overlapping coverage in their respective SWIR/MWIR/TIR bands of emitted radiation (OMPS is excepted which has only a UV/VNIR spectral range).

In general, the swath widths of observation instruments do not add up easily to exact integral parts of orbital coverage cycles. It means, there are coverage gaps between two adjacent orbits. In these cases, the interval of time required for the satellite to complete its orbit cycle is not the same as the “**revisit or repeat period.**” The revisit period is defined for a specific site and represents the minimal time interval (in days) between two imaging opportunities of this specific site. The ground track repeatability is defined by the time period (in days) between the satellite revolutions having the same ground track.

Quick revisit times of a particular area (with preference to “daily” and not something like 16 days) are often a much wanted requirement of an imaging mission. However, a more frequent coverage of a given area can only be provided from LEO orbits at higher altitudes (say 3000 km) providing considerably wider ground swaths (or from a constellation of spacecraft). On the other hand, a higher orbit for a given instrument means also a coarser resolution of the imagery. Current technology requires a compromise for an optimal solution. But the not so far future will also permit these higher orbits at fairly good resolutions of the imagery.

- Another development, namely that of directional instrument pointing or spacecraft pointing (also referred to as “body pointing”), must be considered for event coverage or for commissioned imaging coverage of particular surface regions. The pointing agility of a spacecraft, introduced mostly since the 1990s with increasing capabilities, led to the introduction of FOR (Field of Regard) coverage. FOR designates the angular coverage capability beyond (and including) the swath – it allows the imaging of nearby events of interest that happen to be just outside the regular (generally nadir-centered) swath.

Background on the introduction of some observation schemes:

- The US satellite Discoverer-1 (launch on a Thor vehicle from VAFB on Feb. 28, 1959, apogee = 968 km, perigee = 163 km, inclination = 89.7° , period = 96 min) was the first spacecraft in **polar orbit**. It flew a military payload. This was followed by the “Transit” navigation satellite series of the US Navy. Starting with the launch of Transit-5A-1 (and follow-up satellites of the series) on a Scout vehicle from VAFB, CA, on Dec. 18, 1962.
- In the field of Earth observation, the orbital strategy of **polar orbit** was introduced with Nimbus-1 (launch Aug. 28, 1964), then with TIROS-9 (launch Jan. 22, 1965). The polar orbit enabled the provision of full repetitive global coverage. Depending on sufficient swath width, some sensors (such as AVHRR of the NOAA POES series with a swath > 2900 km and OLS of the DMSP series with a swath of 3000 km) were able to provide daily global coverage, while other sensors needed several days for a repeat cycle.
- **Coverage from a LEO constellation** of spacecraft in the same orbital plane. This technique is being employed in some EO missions for quick revisit times on a global scale. In this context, “revisit” refers to the capability to fly again over a given geographic site and to image the site under different conditions (e.g., with a varying incidence angle). In general, all S/C of a constellation (of 4–5 S/C) are being positioned in the same orbital plane and phased in equal distances around the orbit. The S/C fly actually in the same orbital arc in an

Earth frame, which means that the successive observation swaths are generally overlapping (due to Earth rotation) and adding to the overall swath width of the constellation. Some examples of constellation observation coverage are:

- The US–German GRACE constellation (launch March 17, 2002) consists of two S/C in a polar co–planar orbit at distances of 170–270 km apart. The intersatellite range is measured very accurately between the freely moving S/C to derive high–resolution models of Earth’s gravity field.
- As of 2004, the international DMC (Disaster Monitoring Constellation), built and managed by SSTL, consists of four microsatellites from various countries [AlSat–1 (Algeria), BILSAT–1 (Turkey), NigeriaSat–1 (Nigeria), and UK–DMCSat–1 (UK)] in the same orbital plane. All S/C fly an optical sensor payload of medium resolution and a fairly wide swath providing rapid coverage (daily revisits are possible).
- The ROCSat–3/COSMIC constellation is a joint project of NSPO (Taiwan) and UCAR (USA), consisting of 6 microsatellites all in a single orbital plane. A launch took place on April 14, 2006. The objective is to collect atmospheric remote sensing (occultation data from GPS signals) for operational weather prediction, climate, ionospheric (space weather monitoring), and geodesy research.
- The COSMO–SkyMed mission of ASI consists of a total of 4 spacecraft in the same orbital plane (launch of the first S/C on June 8, 2007, launch of COSMO–SkyMed–2 on Dec. 9, 2007, launch of COSMO–SkyMed–3 on Oct. 25, 2008, launch of COSMO–SkyMed–4 on Nov. 6, 2010 – carrying SAR instruments (observations in the microwave region).
- The RapidEye constellation of BlackBridge employs 5 S/C in the same orbital plane (launch Aug. 29, 2008) to perform observations in the optical region.

1.24.1.1 Sun–Synchronous Orbit (SSO), a LEO subgroup

In general, a near–Earth SSO (also referred to as heliosynchronous orbit) is a special case of the near–polar orbit. Sun–synchronous orbits are made possible by the fact that the Earth is not a perfect sphere. In an SSO, the daily rotation of the orbital satellite plane (with respect to the equatorial plane) is identical to the mean motion of the fictitious sun around the Earth – which in turn is identical to the mean motion of the Earth around the sun. The effect of the rotation of the orbital satellite plane is due to the oblateness of the Earth [i.e., the SSO orbit design is such that the Earth’s mass inhomogeneities cause the slight orbit precession of about 0.9856° per day (Ω) to the east, equivalent to the daily revolution rate of Earth around the sun]. Hence, SSO observations are locked into a fixed (solar) time of the day. Note: All satellite orbits, at any inclination other than exactly 90° , are affected gravitationally by the fact that the Earth is not a perfect sphere.

Some characteristics of SSOs are:

- The most important characteristic of a sun–synchronous orbit is the provision of **repeat observations (same sun illumination angles and viewing geometry)** of a given Earth surface region at the same time of the day (due to same latitudinal crossings), improving considerably the conditions for data analysis. The orbital plane of an SSO always presents the same aspect with respect to the sun.
- An SSO provides also a good power provision for the spacecraft; the nearly constant sunlight ratio of the satellite on each orbit implies a near constant solar energy supply for the satellite platform. As near–polar orbits, SSOs permit also global observation coverage.
- All sun–synchronous orbits are retrograde orbits ²⁶²⁹ (i.e., they have inclinations in the range $90^\circ \leq i \leq 180^\circ$). In retrograde orbits, the projection of the satellite’s position onto

the equatorial plane revolves in the direction opposite to Earth's rotation (i.e. a retrograde orbit has a westward motion or precession on consecutive orbits).

Note: Orbital mechanics permits to define high–altitude SSOs with maximum inclinations of 180° (the latter orbital plane is of course in the equator plane). However, these orbits are of little observational interest due to their very limited range of coverage in the equator plane only. ²⁶³⁰⁾

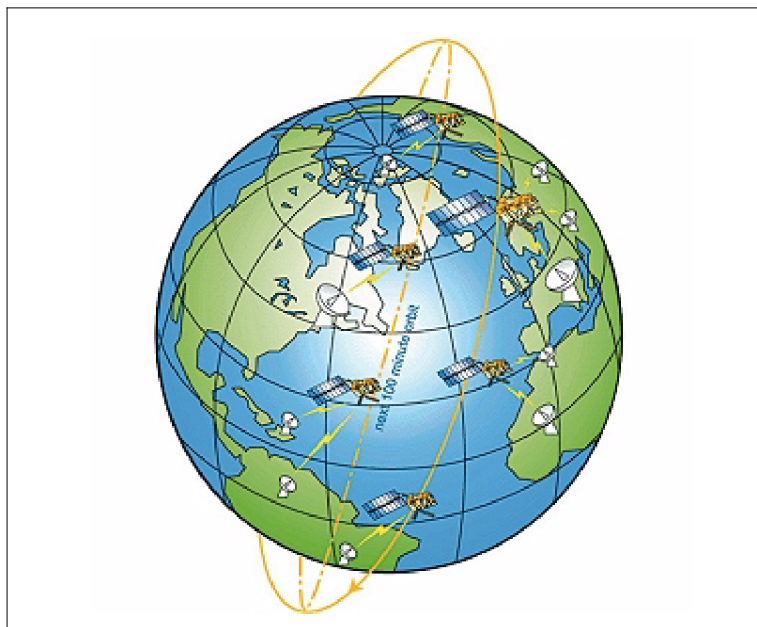


Figure 200: Schematic of two successive sun–synchronous orbits of a S/C ²⁶³¹⁾

- Assuming that orbital altitudes of ≤ 1000 km are considered to produce too much residual drag, the minimum inclination available for SSOs will be about 100° . Lower inclinations, which are closer to polar orbits, would lead to SSOs at altitudes below 1000 km. SSOs with inclinations between 90° and 96° are not possible because they would require negative orbital altitudes.
- The closer a circular SSO approaches a polar orbit, the lower will be the orbital altitude. **The SSO has indeed become the most widely used orbit for Earth monitoring applications due to its special observation characteristics.** An SSO for observational imagery is generally circular within an altitude range of about 300–900 km (most SSOs have 700–800 km circular orbits), a radial distance permitting fairly good ground resolutions for optical as well as microwave instruments. The time of nodal equator crossing may of course be defined for any time of the day; however, most missions usually select this time between mid–morning and mid–afternoon on the sunlit side of the orbit.

Some examples of the sun–synchronous orbit are:

- **The first SSO in a military program** was realized on the early classified DMSP (Defense Meteorological Satellite Program) series of DoD. The code name of the spacecraft was P35–2 with a launch on Aug. 23, 1962. The orbit of P35–2 was: perigee of 578 km, apogee of 752 km, inclination of 98.5° , period of 98.1 min, spacecraft mass of 91 kg. The COSPAR designation of P35–2 was: 1962–A–Omicron–1 (also known as Ops–3502 and FTV–3502).

2629) http://www.ae.utexas.edu/design/mission_planning/mission_resources/orbital_mechanics/Sun_Synchronous_Orbits.pdf

2630) Information on the topic of orbital mechanics for the various orbit types was kindly provided by Friedrich E. Jochim of DLR/GSOC.

2631) Courtesy of EUMETSAT

- **The first SSO in a civilian program was realized on TIROS–9** of NASA (launch Jan. 22, 1965), using an elliptical orbit with an apogee of 2582 km, a perigee of 705 km, an inclination of 96.4° , and a period of 119.2 minutes. This was followed by TIROS–10 (launch July 2, 1965). TIROS–10 had already a near–circular SSO with an apogee of 837 km, a perigee of 751 km, an inclination of 98.65° , and a period of 100.76 minutes. The SSO retrograde orbit drifted westward at about $1^\circ/\text{day}$.
- All Landsat missions (launch of LS–1 on July 23, 1973) featured SSOs with an average nominal orbital altitude of 905 km for LS–1, LS–2, and LS–3. The follow–up missions had nominal altitudes of 705 km and a sun–synchronous orbit.
- The SPOT satellite series of CNES (in continuous operation since 1986) uses SSOs, so do all commercial imaging missions as well as many other missions in Earth observation.
- A fairly uncommon SSO is the one selected for the ST5 (Space Technology 5) mission of NASA, a launch took place on March 22, 2006. ST5 has an elliptical orbit with a perigee at about 300 km and an apogee of about 4500 km, the inclination is 105.6° (period of 136 minutes). The objective is to measure the effect of the sun’s activity on Earth’s magnetic field.
- The **dawn–orbit** (or **dawn–dusk orbit**)²⁶³² is a special case of the sun–synchronous orbit (normally at local equator crossing times of 6 AM or at 6 PM) where the satellite trails the Earth’s shadow. When the sun shines on one side of the Earth, it casts a shadow on the opposite side of the Earth – this shadow is nighttime. The dawn–dusk plane represents an orbit 90° to the noon–midnight plane – thus, the sun vector is nearly perpendicular to the orbit plane during the entire mission.

Because the satellite never moves into this shadow, the sun’s light is always on it, i.e. like perpetual daytime. Since the satellite is close to the shadow, the part of the Earth the satellite is directly above is always at sunset or at sunrise; that is why this kind of orbit is called a dawn–dusk orbit.

A dawn–dusk orbit allows a satellite to always have its solar panels in the sun, obviously a great advantage for a power–hungry spacecraft with active instruments like SARs, lidars, or scatterometers. In addition, a dawn–dusk orbit simplifies the satellite design since no solar panel steering mechanism is needed to maintain normal incidence to the sun; also the solar array utilization efficiency increases, and the battery size decreases. Besides, a satellite in dawn–dusk orbit experiences a very stable thermal condition, one side of the satellite being permanently illuminated by the sun, the opposite side always facing deep space.

[Note: Spacecraft with sun–synchronous orbits using other nodal crossing times than dawn–dusk (say at 10:00 hours) experience an **ecliptic phase** once per orbit (moving into the shadow of the sun); during this period the spacecraft must rely on its battery power to maintain operations].

Some examples of spacecraft placed into sun–synchronous dawn–dusk orbits are:

- The MAGSAT spacecraft (also referred to as Explorer 61) of NASA (launch Oct. 30, 1979, the satellite remained in its orbit for seven and a half months until June 11, 1980) was probably the first satellite in a dawn–dusk orbit for observational reasons. Since magnetic fields from the magnetosphere are a disturbing factor in such a mission, a factor that strongly depends on the orientation of the orbit relative to the sun’s direction, a dawn–dusk orbit was selected which kept the orbit’s orientation relative to the sun stable. The effect was that observational disturbances also stayed more or less the same throughout the mission.²⁶³³

²⁶³²) Note: The path of the dawn–dusk orbit along the terminator is somewhat “theoretical.” Throughout a year, portions of the orbit will be at times in the sun’s shadow due to ecliptic effects of the sun’s motion and the eccentricity of Earth’s orbit.

²⁶³³) <http://www-istp.gsfc.nasa.gov/Education/wlopolar.html>

- The Astrid–1 microsatellite of IRF–K (Swedish Institute of Space Physics in Kiruna) with a launch Jan. 24, 1995 employed a dawn–dusk orbit during the initial phase of its mission.
- The RADARSAT missions of Canada (launch Apr. 11, 1995, and the follow–up RADARSAT–2 with a launch Dec. 14, 2007)
- The QuikSCAT mission of NASA (launch June 19, 1999) with the SeaWinds scatterometer aboard uses a dawn orbit with a nodal crossing time at 6:00 hours.
- The COSMO–SkyMed constellation of ASI, Italy (launch of first satellite on June 8, 2007, launch of COSMO–SkyMed–2 on Dec. 9, 2007, COSMO–SkyMed–3 on Oct. 25, 2008), COSMO–SkyMed–4 on Nov. 6, 2010
- The GOCE (Gravity field and steady–state Ocean Circulation Explorer) mission of ESA (launch March 17, 2009)
- The TerraSAR–X1 mission of DLR/EADS–Astrium (launch June 15, 2007)
- The ADM–Aeolus mission of ESA (launch 2011).
- Starting in the mid–1990s, the LEO space region is also heavily being used by the communications industry, providing the services of the “Big LEO” and “Little LEO” constellations.

1.24.1.2 Exact repeat orbits (a LEO subgroup)

Orbits designed with repeating (or subrecurrent) ground tracks follow specific objectives in some types of missions (Earth observation missions or rendezvous and docking missions). The exact repeat orbit concept covers identical groundtracks at a given repeat cycle, representing a tradeoff between duration of repeat cycle and track spacing.²⁶³⁴⁾ In Earth observation, the limited observation capability of single LEO missions, in particular for geodetic applications (objective: provision of large–scale high–resolution measurements of ocean topography), has led to exact repeat pass designs to obtain surface grids for measurement correlations (i.e., cross–track sampling is pre–determined by the exact repeat orbit pattern). Measurements of ocean topography by radar altimetry inevitably *involve a tradeoff between spatial resolution and temporal resolution*; improvement of one results in degradation of the other. In single–pass interferometric SAR applications, the nearly exact repeat orbit allows formation of an interferometric baseline. Exact repeat orbit missions play also an important role in Earth gravity model studies.²⁶³⁵⁾ A future approach to this coverage–limited problem may be the use of a satellite formation with coordinated orbits.

Some application examples of exact repeat pass missions in Earth observation are:

1) Altimetry missions. In altimetry missions, the exact repeat orbit represents an excellent reference to relate measurements from various altimeter missions (on space–time scales). In fact, all altimeter missions, maintained in a repeating orbit configuration, facilitate the separation of sea height variations from the geoid. Exact repeat orbit altimeter measurements provide a grid of crossover points for the estimation of the ocean current velocity vector (the finer the grid – the better). – A crossover is defined as the intersection of the satellite ground track with itself.²⁶³⁶⁾ At this location, the two crossing passes (one ascending and one descending) provide independent sea level measurements at the same place but at different times. Crossover differences contain information about uncertainties

2634) D. B. Chelton, “Report of the High–Resolution Ocean Topography Science Working Group Meeting,” March 28–29, 2001

2635) Note: A subrecurrent orbit means that after a certain number of days, the satellite repeats its original orbit. This orbit enables the satellite to observe the same area at regular intervals.

2636) <http://www.nodc.noaa.gov/General/CDR–detdesc/crossover.html>

in the satellite ephemeris and therefore enable correction of radial orbit error. Orbit–corrected crossover differences form the basis for studies of sea level variability, both in a statistical sense and for computation of sea level time series. Tide model studies represent another type of crossover difference application.

Altimeter data makes ocean currents detectable as slopes in the sea surface. Hence, the ocean currents can be detected and monitored. Small–scale features are visible as well, like eddies, which are generated by the large–scale currents such as the Gulf Stream. Satellite tracking and altimeter data are also being used to improve the long wavelength component (>1000 km) of the global geoid models. – In general, perturbations in the satellite orbit result in excursions from the “exact repeat” groundtrack in the order of ± 1 km about the nominal repeat path. This misalignment leads to an error in the estimates of sea surface height variations because of the local slope in the geoid.

Some examples of exact repeat pass altimeter missions are:

- The GEOSAT (Geodetic Satellite) altimeter mission of the US Navy (launch March 12, 1985, built by JHU/APL) consisted of two mission phases.²⁶³⁷⁾ The first one was the classified Geodetic Mission (GM); mission duration = 18 months (until Sept. 1986). GM was based on a 23–day near–repeat orbit which was permitted to drift, ultimately producing a tightly spaced ground track pattern. The second mission phase is known as the ‘Exact Repeat Mission’ (ERM), which was unclassified; it started Oct. 1, 1986 and ended in January 1990. In ERM, the orbit was changed to an exact repeat cycle of 17.05 days for the observation of geodetic parameters of the oceans (dense map of marine geoid, surface height data for assimilation into numerical models and mapping the progression of El Niño in the equatorial Pacific).
- The GFO (GEOSAT Follow–On) satellite (launch Feb. 10, 1998)²⁶³⁸⁾ retraces the orbit of the GEOSAT altimeter ERM (Exact Repeat Mission) mission phase at 800 km altitude, 108° inclination, 0.001 eccentricity, 101.4 min period, latitudinal coverage of $\pm 72^\circ$. The objective is to obtain a dense global grid of altimeter data (crossover points) for use in the areas of geodesy (Earth’s gravitational models), the study of fronts and eddies, winds, waves and ice topography, physical oceanography in the ERM. The 17.05–day exact repeat orbit of GFO retraces the ERM ground track within ± 1 km.
- The TOPEX/Poseidon (T/P) altimeter mission of NASA/CNES (launch Aug. 12, 1992) uses a circular non–sun–synchronous orbit; 1334 km altitude, 2 hour period, an inclination of 66° , 10–day exact repeat orbits. T/P represents the first dedicated satellite radar altimeter mission optimally designed for scientific study of the ocean.²⁶³⁹⁾ The instrument measurement accuracy of the dual–frequency altimeter onboard T/P improved by more than a factor of two and the orbit accuracy improved by more than an order of magnitude, resulting in an overall measurement accuracy of about 4 cm. The T/P orbit configuration was chosen specifically for measuring the large–scale SSH (Sea Surface Height) field for studies of ocean variability on monthly and longer time scales. This dictates an orbit with approximately a 10–day repeat period in order to minimize temporal aliasing of mesoscale variability at the measurement.
- Jason–1 mission of NASA/CNES (launch Dec. 1, 2001). The Jason–1 operational orbit follows an “exact repeat ground track” (or a frozen orbit) every 127 revolutions in ten days with the same characteristics as those of T/P (identical orbital tracks (about a minute apart) to perform cross calibration). In this tandem setup, Jason–1 is located one minute ahead of T/P. Both missions are providing high–resolution topography measurement data sets.

2637) B. J. Haines, G. H. Born, G. W. Rosborough, J. G. Marsh, R. G. Williamson, “Precise orbit computation for the GEOSAT exact repeat mission,” *Journal of Geophysical Research*, Vol. 95, No C3, 1990

2638) http://enterprise.spawar.navy.mil/UploadedFiles/gfo_fs.pdf

2639) D. B. Chelton, J. C. Ries, B. J. Haines, L.–L. Fu, P.S. Callahan, 2001: “Satellite altimetry,” in *Satellite Altimetry and the Earth Sciences: A Handbook for Techniques and Applications*, L.–L. Fu and A. Cazenave, Eds., Academic Press 2001, pp. 1–131.

Note: A “**frozen orbit**” is characterized by keeping (or trying to keep) constant the argument of perigee and eccentricity of the orbit, in such way that, to a given latitude, the satellite always passes at the same altitude, benefiting the data users due to this regularity (by making the measurements more consistent). With a frozen orbit, the variation in geodetic height over the same location on successive orbits can be held to a minimum.

- The altimeter crossover data of the ESA missions ERS–1 (35–day repeat and 168–day repeat interleave mission phases), and ERS–2 (35–day repeat) may also be used (in combination with satellite tracking data) for Earth gravity model studies.
- The ICESat (Ice, Cloud and land Elevation Satellite) mission of NASA (launch Jan. 13, 2003) features an exact repeat orbit with a repeat cycle of 183 days to enable uniform sampling of the surface with high resolution. The sensor complement consists of a) GLAS (Geoscience Laser Altimeter System) to measure ice sheet topography, cloud heights, planetary boundary layer heights, and aerosol vertical structure; b) two GPS BlackJack receivers; c) a laser reflector array for ground–based SLR measurements.

2) Interferometric repeat pass missions (InSAR). In the general repeat pass interferometry concept, the scenes are acquired at different times, so there is a time difference as well as viewing geometry to consider (baseline).²⁶⁴⁰ The passes must have rather similar viewing geometry in order to allow extraction of the relative phase difference. This usually requires that the satellite be on an exact repeat orbit. The small difference in viewing geometry allows the extraction of topographic information, in the same way as with a single pass interferometric system (such as SRTM). The superposition of repeat pass imagery provides interference fringes representing the effects of topography and/or motion.

Temporal decorrelation and atmospheric distortions limit the performance of conventional repeat pass interferometry. Repeat pass observations imply significant time lags of several days up to several weeks between the acquisitions of the two interferometric channels. Hence, temporal decorrelation is expected to become a major issue, especially at shorter wavelengths. Hence, a general problem in LEO SAR observations is to minimize the InSAR repeat periods. Wide instantaneous accessibility does not necessarily minimize the repeat time; rather, extensive cumulative (orbit–averaged) accessibility is desired to reduce the orbit repeat period required for global coverage.

Some examples of interferometric repeat pass missions are:

- The SRL–1/2 missions of NASA/DLR/ASI in 1994 (April 9–20 for SRL–1 (STS–59), Sept. 30 – Oct. 11 for SRL–2 (STS–68), also referred to as SIR–C/X–SAR missions, see J.23) employed two–pass (and repeat pass) interferometry for topographic mapping (detection of topographic surface change in SRL–1 and SRL–2). The SRL–2 11–day mission had an orbit with a nominal altitude of 215 km and an inclination of 57°. This resulted in a slightly drifting orbit for the first 6 days, almost exactly duplicating the SRL–1 orbit for one day (at times to within 10 m). For days 7–11, the orbit was lowered to a 1–day exact repeat orbit (200 km). The SRL–2 mission permitted for instance the analysis of active lava flow (surface change imagery) on the Kilauea volcano in Hawaii.
- ESA’s ERS–1/2 tandem mission (start in Aug. 1995, end in May 1996). The prime objectives were focused on the collection of SAR data pairs for exploitation in interferometry, together with the synergistic use of instruments on the two platforms. The configuration was that of two–pass measurements of a single–antenna SAR platform (the same SAR instrument on both satellites observing the same area on the ground), permitting the superposition technique of imagery (in data processing) of fairly close repeat tracks. The C–band SAR instruments of the ERS–1/2 and RADARSAT–1 (launch Nov 4, 1995, 24–day exact repeat orbit) missions demonstrated the ability to detect cm–scale surface strain over large

²⁶⁴⁰ P. A. Rosen, S. Hensley, G. Peltzer, M. Simons, “Updated Repeat Orbit Interferometry Package Released,” EOS Transactions, AGU, Vol. 85, No.5, Feb. 3, 2004, URL: http://www.agu.org/eos_elec/000487e.html

contiguous areas. In this context, RADARSAT–1 provides large–scale coverage of the Arctic sea ice cover on a 3–day basis with its wide–swath ScanSAR mode (460 km).

- ESA’s Envisat mission (launch Mar. 1, 2002) operates in a 35 day exact repeat pass cycle of 501 orbits with an inclination of 98.5° (sun–synchronous orbit of 800 km). Envisat has the same ground track as ERS–2 (within ± 1 km) with its orbit 30 minutes ahead of ERS–2. This orbital configuration permits repeat pass observation studies for its active sensor complement [RA–2 (Radar Altimeter–2), ASAR (Advanced SAR)]: a) as a single mission, and b) as a tandem mission with ERS–2. This orbit pattern has sub–cycles of 3 and 17 days, providing global coverage, with correspondingly coarser sampling, at these intervals.²⁶⁴¹⁾

Parameter	TerraSAR–L	ALOS	RADARSAT–2	TerraSAR–X
Wavelength	23.8 cm (L–band)	23.6 cm (L–band)	5.55 cm (C–band)	3.1 cm (X–band)
Chirp bandwidth	80 MHz	14 MHz (full pol.)	30 (100) MHz	150 MHz
Peak power (rad.)	4740 W	2000 W	1650 W	2260 W
Duty cycle	3.5% (7%/2)	3.5% (7%/2)	3% (6%/2)	9% (18%/2)
Rx noise figure	2.5 dB	4 dB	4 dB	4.5 dB
Losses (atmosphere, swath,)	<5 dB (for 40 km swath)	<5 dB (for 40 km swath)	3 dB (for 25 km swath)	6 dB (split antenna!)
Antenna size	11 m x 2.86 m	8.9 m x 3.1 m	15 m x 1.5 m	4.8 m x 0.7 m
Co–registration	1/10 pixel	1/10 pixel	1/10 pixel	1/10 pixel
Quantization (BAQ)	4 bit	4 bit	4 bit	4 bit
Orbital height	629 km	691 km	798 km	514 km
Repeat cycle	14 days	46 days	24 days	11 days

Table 152: System parameters of some LEO repeat pass missions (see Ref. 539)

3) Tracking missions in geodesy.

- The objective of ESA’s GOCE (Gravity field and steady–state Ocean Circulation Explorer) mission (launch March 17, 2009) is to obtain a high–accuracy, high–resolution model of the Earth’s static gravity field, represented by spherical harmonic coefficients complete up to degree and order 300, which corresponds to a shortest spatial half–wavelength of < 70 km. The GOCE mission requirements call for an SSO (Sun–Synchronous Orbit) circular exact repeat orbit.²⁶⁴²⁾ The GOCE measurement system is based on a sensor fusion concept: satellite–to–satellite (SST) tracking in the high–low mode (hl–SST) using GPS, plus onboard satellite gravity gradiometry (SGG). This data contains abundant information about the gravity field of the Earth on a near–global scale (except for the polar gaps due to the sun–synchronous orbit configuration), from very low (derived mostly from hl–SST) to high (derived mostly from SGG) frequencies.

²⁶⁴¹⁾ <http://envisat.esa.int/dataproducts/ra2-mwr/CNTR1-1-4.htm>

²⁶⁴²⁾ R. Pail, M. Wermuth, “GOCE SGG and SST quicklook gravity field analysis,” *Advances in Geosciences (EGU)*, Vol. 1, No 1, 2003, pp. 5–9

1.24.2 GEO (Geostationary Earth Orbit)

A geostationary orbit is a circular orbit in the equatorial plane (inclination = 0°) revolving about the Earth in the same direction and with the same period as the Earth's rotation. A satellite in GEO remains fixed with respect to an observer on Earth. A geostationary orbit is a special case of the geosynchronous orbit (GSO), both have a period equal to the Earth's rotational period, namely the **sidereal day** which is 23 h 56 m 4 s in length or 1436.1 minutes (the sidereal day refers to the rotation of Earth in inertial space). However, the synodic rotation rate of a satellite in GEO or GSO (i.e. the rotation rate with respect to the sun) is exactly 24 hours. GEO refers to a special orbit in which a satellite appears to be stationary over a point on the Earth's surface i.e., the actual geocentric longitude of the S/C remains constant. The orbital velocity of the spacecraft is 3.075 km/s to match the rotation speed of the Earth at GEO altitude. To ensure that a satellite remains over a particular point on the Earth's surface, the geostationary orbit must also be **circular** (zero eccentricity) and have zero inclination, i.e. the orbital plane must be coincident with the equator plane. In general, all geostationary orbits are geosynchronous, but not all geosynchronous orbits are geostationary.²⁶⁴³⁾

The radial distance of GEO is approximately **35,786 km** above the Earth's surface.²⁶⁴⁴⁾ The orbital radius of GEO is $6.6107 R_E$ (with $R_E = 6378$ km) or about 42,164 km from the Earth's center of mass. This is consequently the altitude at which the 'centrifugal force' caused by the rotation of the Earth is equal to its 'gravitational attraction.' A spacecraft in GEO requires **stationkeeping services** (N–S as well as E–W) caused by the following influences or perturbations:

- Lunar and solar gravitational perturbations. The gravitational attractions of the sun and the moon, the solar radiation pressure and the slight misalignment between the centrifugal force and the Earth's gravitational force disturb the sought–after 'equilibrium.'
- The GEO plane is not identical with the Earth's orbit plane in the ecliptic. The Earth's orbital plane has an inclination of about 23.45° to the ecliptic.
- The noncircular shape of the Earth's equator causes satellites to be slowly drawn to one of two stable equilibrium points along the equator, resulting in an east–west libration (drifting back and forth) about these points.

The daily orbital motions (pendulum–like swings) of a GEO spacecraft are in the order of about 0.05 arcsec in N–S as well as E–W. Stationkeeping implies periodic orbital maintenance maneuvers, involving energy consumption. – The GEO concept is quite extensively utilized by meteorological and communication satellites (as well as by broadcasting satellites). It is indeed the most crowded orbit of all due to the fact that only one geostationary plane is available, namely the equator plane.

- The GEO geometry provides some special features and capabilities for Earth observation, for communication as well as for other applications:
 - GEO offers a fixed–position relation between the satellite and the ground; hence, a **continuous viewing/service capability of the same large footprint is given**, the entire viewable Earth disk subtends an angle of 17.4° , representing 42% of the Earth's surface (however, the polar regions of the Earth are not accessible from GEO). Obviously, the best coverage of GEO satellites is given in the equatorial regions.
 - Three evenly spaced S/C in GEO can provide a continuous **global coverage with the polar regions excepted** (coverage to about $\pm 70^\circ$ of latitude max is possible with distortions

²⁶⁴³⁾ Note: The terms "geosynchronous" and "geostationary" are not synonymous: geosynchronous specifies only the orbit period, while geostationary also specifies the shape and orientation of the orbit. Historically, the geostationary orbit was simply abbreviated with "GEO." I stick to this abbreviation. This leaves the acronym GSO to the more general type orbit designation of "Geosynchronous Orbit." It so happens that these two terms are often interchanged in the literature.

²⁶⁴⁴⁾ T. S. Kelso, "Basics of the Geostationary Orbit," <http://celestrak.com/columns/v04n07/>

increasing with latitudes). The useful imaging disc for a GEO satellite reaches up to about 60° of latitude in either hemisphere, but only at the sub-satellite longitude.

- GEO provides in particular a synoptic view [or the “big picture”], a different perspective in scale and quality of Earth observations distinct from coverage-limited LEO observations. Certain large-scale phenomena and/or features (weather patterns, circulations, etc.) can best be observed from GEO due to its panoramic viewing capability of Earth; i.e., coverage of entire large-scale processes (cyclones) embedded within neighboring structures.

- The observation distance from GEO to Earth’s surface, about 36,000 km, is 45 times farther away than from LEO (considering an average LEO orbit of 800 km). This **large distance ratio remains a challenge for remote sensing applications in terms of proper spatial resolutions for Earth surface imagery** (implying tougher design constraints on imaging instruments). In the field of meteorology, this “GEO resolution deficiency” has led to a combined approach of LEO and GEO observations to obtain a more “global view.”

- For communications, the large distance causes in particular signal roundtrip delay times. Another advantage of GEO location is that antennas in the ground segment need no apparent motion to follow the S/C.

- GEO offers a continuous view of the diurnal cycle. It supports also frequent observations of highly variable parameters like precipitation

- Time-lapse imaging is possible (due to constant position) for repetitive measurements, permitting the capture of weather pattern imagery, etc.

- The GEO position supports the use of long integration times (making possible faint signal acquisition)

- For weather forecasting, the observations from a GEO location offers a short-notice warning capability – while the observations from LEO weather satellites (polar orbiting) are being used for longer-term forecasting.

- A spacecraft in GEO is not eclipsed by the Earth but is in sunlight continuously, 24 hours a day, due to its high orbit of 36,000 km altitude (the apparent sun traverses an angle of $\pm 23^\circ$ perpendicular to the Earth’s equator, the spacecraft’s orbital plane). The only exceptions are several days around the **seasonal equinoxes**, March 21 and September 22, when the satellite will be eclipsed briefly around midnight (i.e., Earth is between the sun and the spacecraft), for up to an hour and 12 minutes.

Example of equinox observation consequence: The viewing geometry design of the current GOES satellite series of NOAA (GOES-I-M and N-P) is such that sunlight may directly impinge on the optical path of its observation instruments which may lead to a degradation of radiometric accuracies. To avoid such damage, data is neither sensed nor provided during these periods – termed the “keep out zones” by NOAA. The combined impact on the current GOES series is a 3–4 hour loss of data for 10 to 12 days before and after each equinox.

- The periodic GEO position maintenance function is referred to as “**station-keeping**” to adjust the drift and orbit of a GEO spacecraft. Orbital perturbations are introduced by the solar radiation pressure as well as by the gravitational effects of the sun and moon.

- *It should also be noted that a spacecraft launch into GEO is generally much costlier than a launch of the same spacecraft into LEO. Simply stated, it takes considerably more energy to transport a satellite into GEO, requiring a much larger launch vehicle.*

Two basic launch techniques are available to reach GEO:

- 1) direct injection into GEO

2) launch into GEO via GTO (Geosynchronous Transfer Orbit); in this case the spacecraft is responsible for boosting itself into GEO.

These two launch approaches have a substantial impact on both, the availability of launch opportunities as well as on the complexity of the spacecraft bus design. In general, most spacecraft reach GEO via GTO.

Historical background: The concept of a geostationary orbit seems to have several independent authors – men of vision and imagination:

a) The Russian school teacher and visionary, Konstantin E. Tsiolkovsky of Kaluga, Russia (1857–1935, referred to as the father of astronautics), suggested around 1895 of putting a “celestial castle” at the end of a spindle–shaped cable, with the “castle” orbiting the Earth in a geosynchronous orbit (i.e. the castle would remain over the same spot on Earth). In Tsiolkovsky’s tower (also referred to as “space tower”), an elevator would ride up the cable to the “castle.” Konstantin Tsiolkovsky wrote numerous science and science–fiction articles on space travel at the turn of the century (19th to 20th).

b) Hermann Potocnic [Dec. 22, 1892 – Aug. 27, 1929, born in Pola (Pulj), Moravia, Austrian–Hungarian Empire, an engineer (Vienna) and retired captain of the army] published his concepts of future space travel in a book with the title: “Das Problem der Befahrung des Weltraums – Der Raketen–Motor,” Richard Carl Schmidt & Co., Berlin W62, 2. Auflage, 1929. He used the pseudonym of Hermann Noordung for the publication, since he was afraid to be ridiculed by his peers.²⁶⁴⁵ In the book (page 98), Noordung proposed a stationary orbit of a space station (referred to as “Raumwarte” for astronomical observations) at radius 42,300 km from Earth center (or about 35,900 km above the surface), in the equator plane, with a chosen orbital speed of about 3080 m/s – resulting in a free orbit with an angular velocity equal to that of Earth rotation. An orbiting body would seem to be stationary over a certain point at the equator.

c) Arthur C. Clarke (born Dec. 16, 1917 in Somerset, England; he died on March 19, 2008 in his adopted home in Colombo, Sri Lanka) published an article in 1945 with the title: “Extra–terrestrial Relays: Can Rocket Stations Give World–wide Radio Coverage?” (Wireless World, Oct. 1945) where he described the principles of satellite communication in geostationary orbit. Clarke suggested that if a satellite were placed above Earth’s equator at just the right height – 35,888 km – it would orbit Earth exactly once in 24 hours – and seem to stay put in the sky above some point on the ground.

In 1947, Arthur C. Clarke proposed how three satellites, suspended in orbits 35,888 km above the equator, could serve as relay platforms for the entire Earth. He cautioned that the concept was based on the theory that microwave radio signals would not bounce off the atmosphere like shortwave signals, something that wasn’t known for certain in 1947.

- Syncom–2 (launch July 26, 1963 on a Thor Delta vehicle, built by Hughes Aircraft Corp., now Boeing Satellite Systems, Inc.) of NASA, was the first successful experimental communication satellite to achieve geostationary orbit (S/C mass of 35 kg, power = 28 W).²⁶⁴⁶ Positioned over the Atlantic, it demonstrated the feasibility of geostationary satellite communications. Syncom–2, designed for 1 year lifetime, remained operational through 1966 (decommissioned in April 1969). Note: Syncom–1 (launched Feb. 14, 1963) achieved GEO orbit but contact was lost after it was placed in orbit (electronics failure).

- Intelsat–2 (commonly called “Early Bird”) was the world’s first commercial communications satellite in GEO (launch April 6, 1965, the S/C was built and operated by Comsat an international government–chartered organization). The spacecraft (mass of 39 kg) provided the first scheduled transoceanic TV service and was operational for 3.5 years (mostly

²⁶⁴⁵) Note: A 1st edition of the book could not be located anywhere. The reprint of “Das Problem der Befahrung des Weltraums,” Ausgabe von 1929, is available at Turia + Kant Verlag: ISBN: 3–85132–060–3

²⁶⁴⁶) <http://www.boeing.com/defense-space/space/bss/factsheets/376/syncom/syncom.html>

demonstration of technology). IntelSat–2 supported 240 telephone links or one television channel. In 1969, Intelsat completed the first global GEO communication network deployment consisting of three spacecraft.

- The objective of ATS (Applications Technology Satellite) program, a series of six NASA S/C, was to explore and test new technologies and concepts for communications, meteorological and navigation satellites (investigation of the geostationary orbit environment). Note: ATS–2 and ATS–4 were MEO satellites, the rest of the ATS program were GEO satellites.

- In the 1990s the geostationary orbit (GEO) has indeed become the most densely populated orbit of satellites. This is due in particular to the needs of the communication industry as well as to some GEO weather satellites [USA (NOAA), Europe (EUMETSAT), Japan (JMA), Russia (Planeta/HYDROMET), India (ISRO/IMD), China (NSMC/CMA), etc.]. Over the years, spacecraft removal from GEO has become a necessity at EOL (End of Orbital Life) to avoid havoc with neighboring operational spacecraft. A common spacecraft retirement practice from GEO is to boost it into a slightly higher orbit. Occasionally, retired communication satellites are also moved into inclined orbits. However, this practice involves again a twice daily crossing of the equator plane.

1.24.2.1 GSO (Geosynchronous Orbit)

A geosynchronous orbit is one with an orbital period matching the rotation rate of the Earth (sidereal day). However, the definition of a geosynchronous orbit says nothing about the shape of the orbit, or the orientation of the orbital plane with respect to the equator. Hence, the orbit can be highly elliptical, and/or it can be inclined with respect to the equator, and still be synchronous with the Earth's rotation. This general nature of a GSO implies there is no fixed position relationship relative to an observer on Earth. Several GSO configurations are possible:

- Circular GSO with an inclination. A GSO satellite with an eccentricity of zero and an inclination different from zero is not stationary when observed from the Earth. This particular orbit has the property of remaining stationary over a particular meridian (there is no longitudinal precession for successive orbits but variable latitudinal motion along the meridian). An inclined circular orbit provides a ground track describing the slim figure 8 (see Figure 201). An inclination of 50° causes a latitudinal displacement of $\pm 50^\circ$ during one orbital period (one sidereal day). The subsatellite velocity of this orbit varies from 2600 m/s at the equator to about 1100 m/s at the inclination maxima ($\pm 50^\circ$ latitude). This GSO subgroup is also sometimes referred to as IGSO (Inclined Geosynchronous Orbit). In an IGSO, the subsatellite track crosses the equator plane in either the ascending or descending node in exactly 24 hours of mean solar time.

- Non–circular GSO within the equator plane. This orbit provides a daily E–W ground track.

- Non–circular GSO with an inclination. A more general ground track is provided.

So far, there has not been much use of satellite observations or operations in GSO. Nonetheless, there are plenty of potential applications from GSO for the future. Some early examples of S/C in GSO are:

- IUE (International Ultraviolet Explorer), a joint astronomical mission of NASA, ESA, and PPARC (Particle Physics and Astronomy Research Council) UK, was launched Jan. 26,

1978.²⁶⁴⁷⁾²⁶⁴⁸⁾ IUE featured an elliptical inclined GSO over the Atlantic Ocean as its nominal operating orbit: the initial orbit was at 32,050 km x 52,254 km with an inclination of 28.6° and a period of 23.927 h; at mission end the orbit was: 36,360 km x 48,003 km with an inclination of 35.9°. IUE remained operational until its hydrazine was deliberately vented, its batteries drained and its transmitter turned off on Sept. 30, 1996.

- The US DoD communication minisatellite pair LES-8 [Lincoln (Laboratory) Experimental Satellite-8] and LES-9 (tandem launch of both S/C on Mar. 15, 1976) were placed into inclined GSOs with 14° inclination. Their respective inclined GSO longitudinal positions were at 94.5° W, and at 103° W, respectively (end of operation in Jan. 1996). LES-8/-9 were the first cross-linked military satellites. A Ka-band ISL (Intersatellite Link) utilized tracking antennas to maintain the link with the other spacecraft as it moved through its figure-eight track.

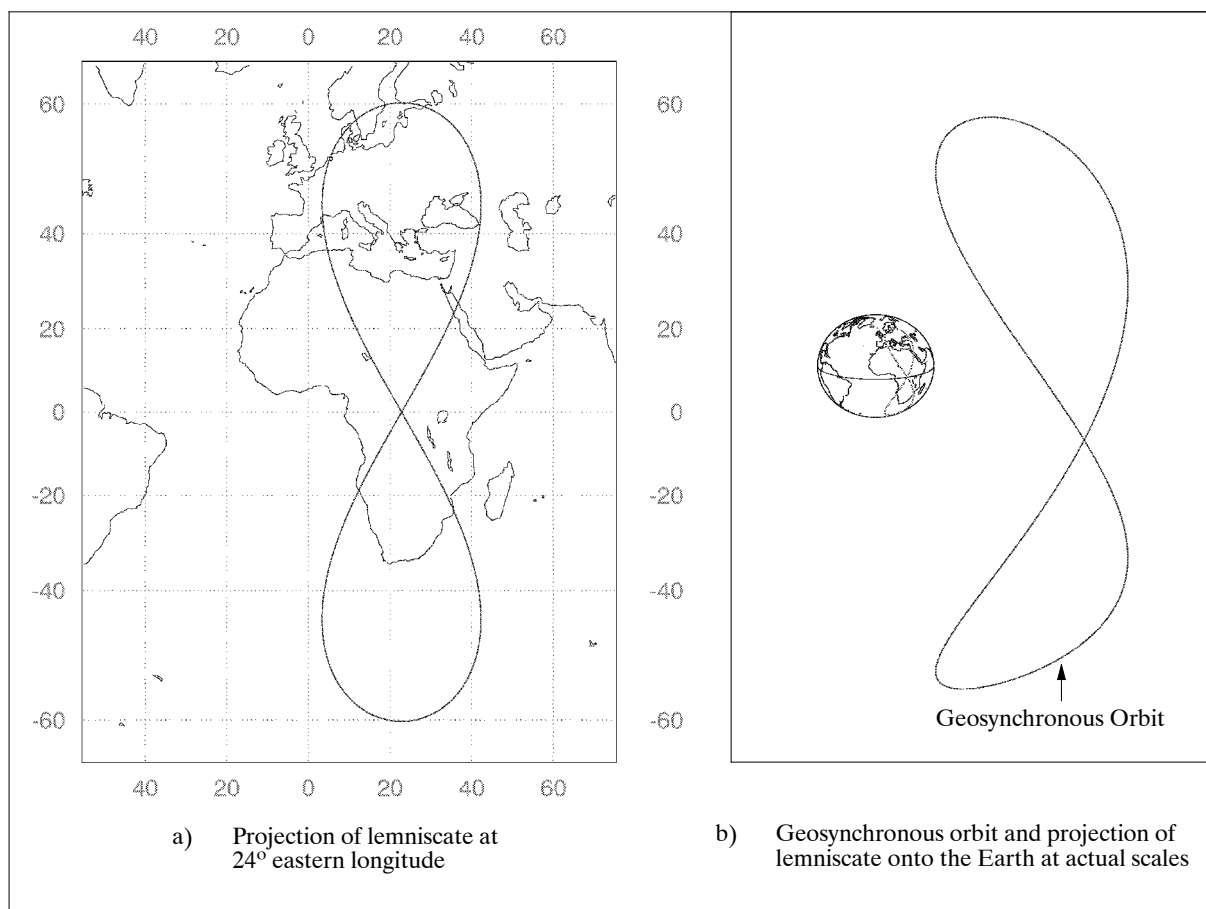


Figure 201: A lemniscate of a geosynchronous orbit with an inclination of 60° (image credit: F. Jochim, DLR)

²⁶⁴⁷⁾ <http://sci.esa.int/science-e/www/area/index.cfm?fareaid=22>

²⁶⁴⁸⁾ <http://satobs.org/seesat/Mar-1999/0311.html>

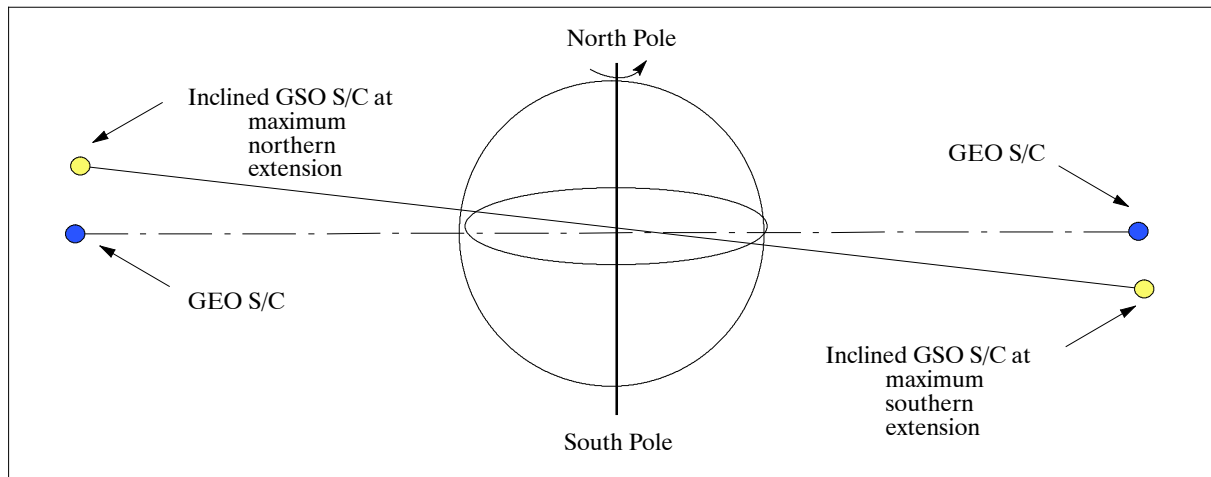


Figure 202: Orientation of GEO and inclined GEO in space (at maxima)

- The ACTS (Advanced Communications Technology Satellite) mission of NASA (launch Sept. 1993) was maintained as a GEO satellite until 1998 (far exceeding its planned demonstration period of 2 years). After 5 years of successful demonstrations, the satellite's north–south stationkeeping was discontinued in Aug. 1998. The system is now operating in an inclined orbit that increases at a rate of $0.8^\circ/\text{year}$.²⁶⁴⁹⁾
- The commercial S–DARS (Satellite Digital Audio Radio Services) constellation of Sirius XM Radio Inc., New York (3 spacecraft) has been operating over North America since 2000 (launch of first S/C on July 1 2000, launch of third S/C on Dec. 1, 2000). The constellation is providing its broadcasting services in highly inclined elliptical geosynchronous orbits (seamless broadcast coverage to mobile users in the contiguous US). S–DARS is operating flawlessly as of 2009.^{2650) 2651)}
- The Milstar–2 communication satellite constellation of DoD (in orbit by 2003) employs a low inclination GSO (Geosynchronous Orbit) configuration. The constellation features jam–proof communications between fixed–site, mobile, and portable terminals. Launch of Milstar–2–4 on April 8, 2003 from Cape Canaveral, FL, USA.
- The SDO (Solar Dynamics Observatory) research mission of NASA (launch Feb. 11, 2010) employs a circular GSO of 28.5° inclination.
- The QZSS (Quasi Zenith Satellite System), a navigation constellation of three spacecraft, will use inclined, elliptical geosynchronous orbits at an inclination of 45° . A launch of the first spacecraft, QZS–1 is planned for 2010.
- Galileo constellation of Europe. In addition to a MEO constellation, a circular inclined GSO overlay was considered in the early planning phase of GalileoSat (Europe's space segment of a navigation constellation), but this option was eventually dropped for economic reasons.
- GSO may, for instance, be used in the future for SAR observations from geosynchronous altitudes. Initial proposals of a SAR mission concept from an inclined circular geosynchronous orbit, referred to as “GEOSAR,” were already published by Kiyu Tomiyasu in 1978 and 1983. An advantage of the GSO concept is that it provides relative observation

2649) R. A. Bauer, “Advanced Communications Technology Satellite (ACTS) Used for Inclined Orbit Operations,” <http://www.grc.nasa.gov/WWW/RT1999/6000/6100bauer.html>

2650) R. D. Briskman, R. J. Prevaux, “S–DARS broadcast from inclined, elliptical orbits,” *Acta Astronautica*, Vol. 54, Issue 7, April 2004, pp. 503–518, Paper IAF–01–M.S.04 presented at the 52nd International Astronautical Congress, 1–5 October 2001, Toulouse, France

2651) R. D. Briskman, J. V. Foust, “An improved satellite digital audio radio services orbital constellation,” 58th IAC (International Astronautical Congress), International Space Expo, Hyderabad, India, Sept. 24–28, 2007, IAC–07–B2.4.01

velocities of the target area with respect to the SAR instrument, required for SAR imaging. 2652) 2653) 2654)

1.24.2.2 GTO (Geosynchronous Transfer Orbit)

GTO is an elliptical orbit with perigees usually between 300 – 600 km, an apogee of about 36,000 km and an initial period of about 11 hours. A standard GTO is an orbit which requires the minimum energy to reach geostationary altitude. In the normal case, GTO is the short-term initial orbit (or parking orbit) of a S/C after launch to be placed into GEO by a sequence of orbit raising maneuvers that are executed by the satellite's own propulsion system to circularize the elliptical orbit eventually into GEO. Orbit raising maneuver: At GTO apogee, the payload usually fires an onboard motor (commonly referred to as "apogee boost motor") to circularize the orbit and adjust the inclination to zero. Most GEO satellites (weather and/or communication) go through this procedure.

Secondly, GTO may be used as a long-term observation orbit, usually selected by S/C with payloads that measure the harsh solar radiation environment. GTO implies that a S/C passes through the Van Allen radiation belts [these are regions located at about 1.4–1.5 R_E (inner) and 4.5–6 R_E (outer) where many energetically charged particles from the solar wind are trapped in the Earth's magnetic field] four times per day, causing them to be exposed, in a twelve month period, to levels of radiation equivalent to about 8–10 years in GEO or in LEO. GTO gives also exposure to other environmental effects such as atomic oxygen erosion at perigee and electrostatic charging at apogee. – The accelerated life testing of radiation effects provided by GTO is a unique opportunity to evaluate for instance new technology solar panels quickly and cost-effectively.

- Examples of S/C in long-term GTO are: CRRES of NASA/DoD (launch July 25, 1990, A.13); STRV-1a and -1b of DERA, UK (launch June 17, 1994, M.47); STRV-1c/1d of DERA (launch Nov. 16, 2000); MDS-1 of JAXA (launch Feb. 4, 2002; the MDS-1 operations were terminated on Sept. 27, 2003, after 18 months of operations that were planned for a mission life of 1 year).
- The GTO turns out to be a very frequented initial orbit due to the many launches of communication satellites – for further advancement into GEO. This frequent "access to space" offers of course many opportunities for small secondary payloads. However, for most of these potential secondary missions, GTO or GEO orbits are not acceptable or "non-ideal" for their mission requirements. Hence, solutions must be found for the secondary payloads to transfer from a GTO into an SSO (Sun-synchronous Orbit) or into something in-between that turns out to be more acceptable to the secondary mission.

2652) K. Tomiyasu, "Synthetic aperture radar in geosynchronous orbit," Digest on the International IEEE Antennas and Propagation Symposium, College Park, MD, May 1978, pp. 42–45

2653) K. Tomiyasu, J. L. Pacelli, "Synthetic Aperture Radar Imaging from an Inclined Geosynchronous Orbit," IEEE Transaction on Geoscience and Remote Sensing, Vol. GE-21, No 3, pp. 324–328, 1983

2654) S. N. Madsen, W. Edelstein, L. D. DiDomenico, J. LaBrecque "A Geosynchronous Synthetic Aperture Radar for Tectonic Mapping, Disaster Management, Measurement of Vegetation and Soil Moisture," IGARSS 2001, Sydney, Australia, July 9–13, 2001, <http://esto.nasa.gov/conferences/igarss-2002/01Presnt/07101030.ppt>

1.24.3 MEO (Medium Earth Orbit)

MEOs are defined for an altitude range of about 3000 km to about 25,000 km above the Earth's surface. MEO orbits provide considerably longer contact times with the user on Earth's surface, as well as much larger footprints than spacecraft in LEO (the nadir velocity decreases with altitude and the swath width increases). Spacecraft in MEO may offer higher ground resolutions in imagery than those from GEO (due to its lower altitude).

A MEO disadvantage is the long-term exposure to the Van Allen radiation belts (requiring proper shielding). MEO orbits are mostly circular and may be designed for any inclination. The orbital periods of MEO satellites range from about 3 to 15 hours and more. The spacecraft with orbits of 12 hours are also referred to as semi-synchronous. In the communication industry, MEOs are also referred to as **ICO** (Intermediate Circular Orbit); the service of these satellites is being used in communications because of shorter signal propagation delay times than those from GEO. Examples of typical MEO S/C are:

- Some laser ranging satellites (passive systems) such as: LAGEOS-1 of NASA (launch May 4, 1976, altitude 5900 km). ETALON-1 of USSR (launch Jan. 10, 1989, altitude about 19,000 km).
- **Navigation satellite constellations** of GPS (GPS-1 launch Feb. 22, 1978, altitudes of about 20,000 km, period of about 12 hours) and GLONASS (GLONASS-1, -2, -3 launch, Oct. 12, 1982; altitudes of about 19,000 km, period of about 11.25 hours). Prior to the GPS constellation, the launch of NTS-2 (June 23, 1977) had a MEO orbit of 13900 km. The Galileo navigation constellation of ESA will also be deployed into MEO (launch 2013) at near-circular orbital altitudes of about 23,600 km. In case of the GPS constellation, the selected 12 hour period of MEO is resonant with the Earth's rotation rate (2 orbits/day), so the orbit track repeats itself each day. Full and continuous Earth coverage of a MEO constellation is given by positioning the various spacecraft into several orbital planes. Examples:
 - The GLONASS constellation of nominally 24 S/C has three orbital planes (8 satellites are equally spaced in each plane with a 45° argument of latitude displacement)
 - The GPS constellation of nominally 24 S/C has six orbital planes (24/6 constellation) with a 60° separation within a plane
 - The Galileo constellation will feature 27 S/C (nominally) in three orbital planes (symmetrical 27/3/1 Walker constellation).
- Some communication satellites in MEO: Telstar-1 (launch July 10, 1962) and Telstar-2 (launch May 7, 1963) of AT&T (American Telephone & Telegraph) company are considered the first experimental communication satellites in MEO. Telstar-1 delivered the first television transmission across the Atlantic in 1962. Because Telstar-1 was placed into an elliptical MEO that varied from low to medium altitudes, the satellite was visible contemporaneously to Earth stations on both sides of the Atlantic for only about 30 minutes at a time. – A much more recent entry into MEO communications is the Inmarsat-P constellation (provision of a hand-held telephone system), consisting of 12 satellites in two MEO planes of 10,335 km altitude.
- The introduction of new and improved observation (instrument) technology offers the potential to provide eventually also high spatial, temporal and spectral resolution environmental data from MEO orbits. At the start of the 21st century, the MEO orbit is being studied and considered by NOAA and other agencies (EUMETSAT) for future integrated concepts of environmental satellite missions. For instance, a MEO constellation of 4 S/C (circular altitude of 10,400 km, 6 hour orbit) would be capable of viewing Earth's polar regions on a continuous basis, 24 hours a day, seven days a week. – An obvious advantage of

MEO (over GEO) is the fact that it allows a range of observations configurations with sufficient coverage and spatial resolution for passive microwave radiometry.^{2655) 2656) 2657) 2658)}

– The DSX (Demonstration and Science Experiments) spacecraft of the U.S. AFRL (Air Force Research Laboratory) is an exploratory mission into MEO (orbit of 6,000 km x 12,000 km, inclination = 120°) to measure the harsh space environment in this region. A launch is planned for the fall of 2012.²⁶⁵⁹⁾

– The RBSP (Radiation Belt Storm Probes) dual-spacecraft mission of NASA has the goal to understand the sun's influence on the Earth and near-Earth space by studying the planet's radiation belts on various scales of space and time. The selected orbit is 620 km x 30540 km with an inclination of 10° (almost GTO). The RBSP mission seeks to resolve decades-old scientific mysteries of how the particles in MEO become energized to such high levels, and how the radiation belts vary so dramatically with changing conditions on the sun. The RBSP spacecraft were launched on August, 30, 2012.

• O3b Networks constellation of O3b Networks Ltd. The O3b constellation, designed and developed by Thales Alenia Space, is in MEO with an orbital altitude of 8063 km with an inclination of < 0.1° and a period of 6 hours. The first cluster of the constellation (4 satellites) was launched from Kourou on June 25, 2013. A total of 12 O3b Networks satellites are to be orbited by Arianespace in groups of four. The objective of O3b Networks is to provide broadband connectivity everywhere on Earth within ±45° of the equator. The vast coverage area includes emerging and insufficiently connected markets in Latin America, Africa, the Middle East, Asia and Australia, with a collective population of over 3 billion people (provision of Internet services to consumers and businesses in nearly 180 countries with low-cost, high-speed, low latency Internet and mobile connectivity).^{2660) 2661)}

2655) G. J. Dittberner, S. N. Bajpai, A. J. Gerber, R. Baron, F. Rogez, "A Medium Earth Orbit Constellation for Polar Wind Measurements," Proceedings of the 2006 EUMETSAT Meteorological Satellite Conference, Helsinki, Finland, June 12–16, 2006

2656) A. J. Gerber, R. L. Baron, D. M. Tralli, M. Crison, S. Bajpai, G. Dittberner, "Medium Earth Orbit Architecture for an Integrated Environmental Satellite System," EOM (Earth Observation Magazine), Vol. 13, No 6, Oct. 2004

2657) G. J. Dittberner, A. J. Gerber, D. M. Tralli, S. Bajpai, "Medium Earth Orbit (MEO) as a Venue for Future NOAA Satellite Missions," Proceedings of the 2005 EUMETSAT Meteorological Conference, Dubrovnik, Croatia, Sept. 19–23, 2005, EUMETSAT P46, ISBN 92–9110–073–0, pp. 31–38

2658) J. E. Charlton, R. K. Child, C. Milner, N. Atkinson, U. Klein, "Future Passive Microwave Radiometry Missions," Proceedings of the 2005 EUMETSAT Meteorological Conference, Dubrovnik, Croatia, Sept. 19–23, 2005, EUMETSAT P46, ISBN 92–9110–073–0, pp. 56–64

2659) Mark Scherbarth, Durand Smith, Aaron Adler, Greg Ginet, "AFRL's Demonstration and Science Experiments (DSX) Mission," Proceedings of SPIE, Vol. 7438, 'Solar Physics and Space Weather Instrumentation III,' Ed. Silvano Fineschi & Judy A. Fennelly, San Diego, CA, USA: SPIE, August 4, 2009, URL: <http://dspace.mit.edu/open-access-disseminate/1721.1/52739>

2660) "Arianespace Soyuz Puts Four O3b Networks' Birds Into Orbit," June 25, 2013, URL: http://www.space-travel.com/reports/Arianespace_Soyuz_Puts_Four_O3b_Networks_Birds_Into_Orbit_999.html

2661) <http://www.o3bnetworks.com/welcome-to-o3b>

1.24.4 HEO (Highly–elliptical Earth Orbit)

A HEO is greater than a GEO. If the HEO period turns out to be greater than a day, it is referred to as “supersynchronous.” A typical HEO is highly inclined, has a perigee of about 500 km and an apogee of 5–10 R_E and more. The observation objectives in HEO orbits involve mainly investigations of the energy transport between the sun and the Earth in the interplanetary plasma (energetic particle fluxes, etc.), solar–terrestrial interactions (in particular in the auroral regions), as well as magnetic field studies. Some examples of satellites in HEO are:

The IMP–4, –5, –6, –7 and –8 (Interplanetary Monitoring Platform series of NASA – also referred to as Explorers 34, 41, 43, 47, and 50, respectively). IMP–4 was launched on May 24, 1967 (apogee of 34 R_E , perigee of 250 km). IMP–8 was launched Oct. 26, 1973. HEOS–1A (Highly Eccentric Orbit Satellite) of ESRO Launch Dec. 5, 1968. HEOS–1A orbit of 424 km x 223 428 km, 28.3°. A number of the Prognoz spacecraft series of the USSR (magnetospheric research, etc.) had apogees ranging from 200,000 – 800,000 km (or about 30–125 R_E) such as Prognoz–6 (launch Sept. 26, 1977, Prognoz–7 (launch Nov. 11, 1978), and Prognoz–9 (launch July 1, 1983). Onboard the Prognoz–9 spacecraft was also the Relict–1 experiment to investigate the large–scale anisotropy of relict radiation.. The ISEE–1 and –2 satellites (K.21) had a joint launch on Oct. 2, 1977 (apogee at 23 R_E). The AMPTE satellites (IRM, UKS, CCE, see K.4) were launched on Aug. 16, 1984. GEOTAIL, launch July 24, 1992. WIND, launch Nov. 1, 1994. INTERBALL (launch of Tail probe Aug. 3, 1995, Auroral Probe launch Aug. 29, 1996). POLAR, launch Feb. 24, 1996.

Equator–S, launch Dec. 2, 1997. The Chandra X–ray Observatory of NASA, launch on Shuttle flight STS–93 on July 23, 1999. The Chandra HEO is 16,000 km x 133,000 km, inclination of 28.4° and a period of 3809 minutes (63.5 h orbit). The XMM (X–Ray Multi–Mirror Mission – Note: XMM was officially renamed to “Newton” in Feb. 2000) of ESA, launch Dec. 10, 1999 with an Ariane–5 vehicle from Kourou, has an operational orbit of: perigee = 7000 km, apogee = 114,000 km, an inclination of 40° and a period of 47.86 hours.²⁶⁶²⁾ The IMAGE (Imager for Magnetopause–to–Aurora Global Exploration) mission of NASA/GSFC (launch Mar. 25, 2000), has a polar orbit of: perigee = 1000 km, apogee = 7 R_E (44,647 km). The location of the apogee changes during the course of the two–year mission, both in latitude and, because of the Earth’s revolution about the sun, in local time. The Cluster–II mission of ESA (launch Aug. 9, 2000, 4 satellites) features polar HEOs with perigees of 19,000 km and apogees of 119,000 km (period of 57 hours). The DSP (Double Star Project) of CNSA (China) and ESA (launch of DSP–1 on Dec. 29, 2003) has an equatorial orbit with a perigee of 570 km and an apogee of 78,970 km (~ 12 R_E), inclination = 28.5°, Kepler period of 20.91 hours. The DSP–1 objective is to study Earth’s magnetic tail. DSP–2 (launch July 25, 2004) has a polar orbit with a perigee of 700 km, an apogee of 39,000 km, and an inclination of 90°.

1.24.4.1 Molniya–type orbits (a HEO subgroup)

Molniya–type (also Molnya spelling) orbits represent a special HEO class used for communication as well as observation services. These HEO orbits are chosen in such a fashion that maximum service provision (coverage and viewing time) can be provided to a particular high–latitude region of the Earth (including the polar regions).

Note: Molniya means “lightning” in Russian. The Molniya–type orbit is named after the first launch vehicles, Molniya, that were capable of transporting a satellite into this particu-

²⁶⁶²⁾ The Chandra X–ray Observatory is named in honor of the late India–American Nobel Laureate Subrahmanyan Chandrasekhar (born Oct. 19, 1910 in Lahore, India (now Pakistan), died Aug. 21, 1995 in Chicago, IL). In the 1930’s, Chandra, as he was known then, showed that stars whose mass was 1.4 times greater than the sun would eventually collapse into objects which we now know as black holes. In 1983, Chandra was awarded the Nobel prize in physics for his studies of the physical processes important to the structure and evolution of stars.

lar HEO orbit. There is also a series of Soviet/Russian spacecraft, named Molniya, flying in Molniya orbits.

Prominent examples are the numerous Molniya – type orbits (apogee of 39950 km, perigee about 500–800 km); they are characterized by long orbital periods (12 hours, making them semisynchronous), a high eccentricity (0.7 – 0.75) and an **inclination of approximately 63.4°** – whose apogee (in excess of 8 hours by far the longest duration period of the orbit) occurs always in the intended region, namely the northern hemisphere for extended – period communication coverage services (a quasi zenithal system over the region to be covered).

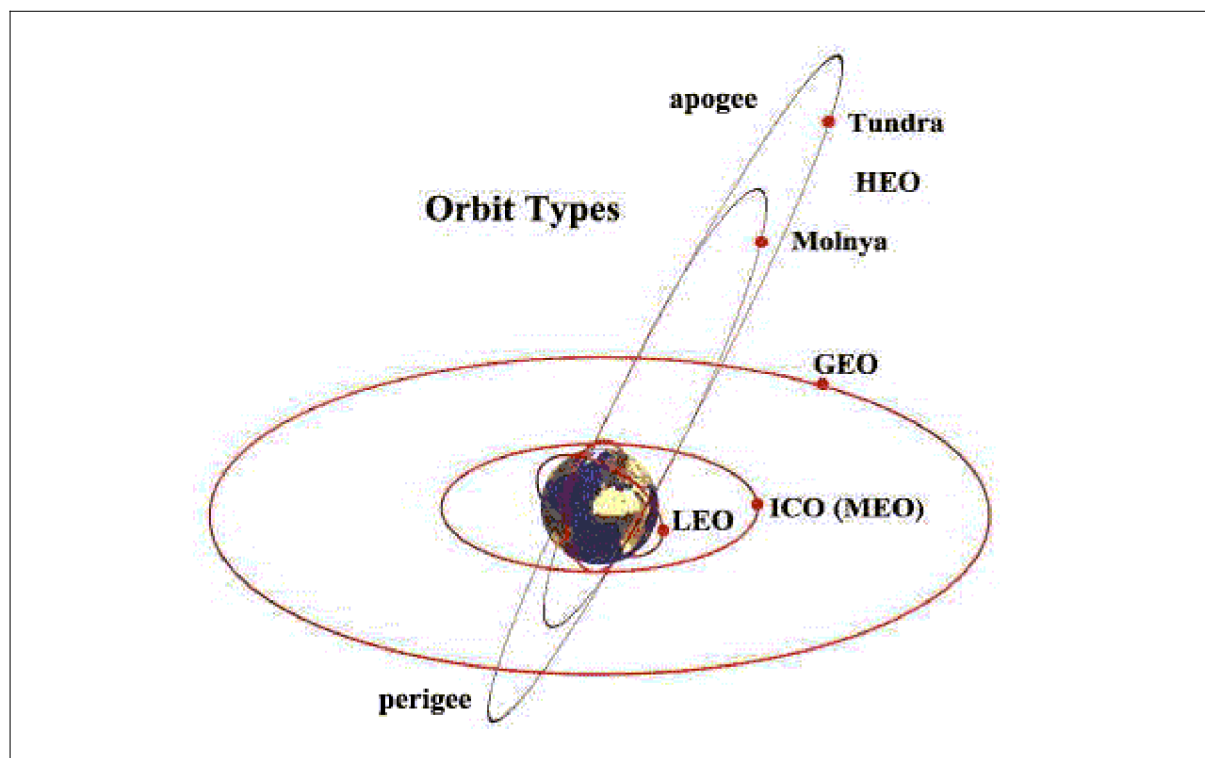


Figure 203: Illustration of various Earth orbit type concepts ²⁶⁶³⁾

Compared to LEO systems, a smaller number of satellites is required for limited areas or regions, which is one of the principle merits of this system. – The orbital period of half a sidereal day enables a Molniya – type spacecraft to follow the same ground track (repeating ground tracks) on each orbit. This represents an important criteria for high – latitude service provision. The spacecraft thus appears in the same relative position in the sky during each pass. Since the orbital period is half a day, apogee occurs twice per day, typically once over Russia and once over Canada. ^{2664) 2665)} The 63.4° inclination is essential to the stability of the Molniya orbit, keeping the argument of perigee fixed. And because ω is fixed, the apogee stays at a given latitude. Due to the equatorial bulge of the Earth, this inclination results in no rotation of the line of apsides and maintains the apogee high above the northern hemisphere (and the perigee always in the southern hemisphere). – All HEOs, including Molniya – type orbits, experience large Doppler shifts, due to the relatively large movement of a satellite in HEO with respect to an observer on the Earth. Hence, satellite systems using this type of orbit need to be able to cope with large Doppler shifts.

²⁶⁶³⁾ <http://www.geo-orbit.org/sizepgs/geodef.html>

²⁶⁶⁴⁾ J. E. Draim, R. Inciardi, P. Cefola, R. Proulx, D. Carter, "Demonstration of the COBRA Teardrop Concept Using Two Smallsats in 8 – Hour Elliptic Orbits," AIAA/USU Conference on Small Satellites, Aug. 13 – 16, 2001, Logan, UT, SSC – 01 – II – 3

²⁶⁶⁵⁾ T. J. Racey, P. W. Somers, "Tracking Molniya Satellites – A Surveillance of Space Program at the Royal Military College," http://www.rmc.ca/academic/physics/castor/tracking97_e.html

The first prototype Molniya spacecraft was launched in 1964. The launch of the Molniya – 1 satellite series occurred April 23, 1965 (over 20 spacecraft of the series were launched until 1974), followed by the Molniya – 2 series with first launches in 1972 and countless S/C of the Molniya – 3 series (first launch in 1974). The Russian Tundra satellite system fits also into this class. Tundra employs 2 satellites in two 24 hour orbits separated by 180° around the Earth, with an apogee distance at 53,622 km and a perigee at 17,951 km. The Molniya series represents also the first communication satellites of the former USSR. Until 1983, the Soviet Union maintained a Molniya (“lighting”) constellation of four Molniya – 3 communication satellites. The operational constellation was eventually increased to 16 satellites. ²⁶⁶⁶⁾

Background: The original design of the Molniya – type HEO orbits in the early 1960s is considered to be a remarkable accomplishment in orbital mechanics pioneered by Russian engineers to deliver satellite services to high – latitude locations. Most Molniya orbits have orbital inclinations of about 63.4° in order to reduce or eliminate rotation of the line of apsides (major axis of the ellipse) due to gravitational perturbations. This prevents their apogees from drifting away from their initial latitude. [Note: The perigee of the orbit literally moves along the plane of the orbit at a rate dependent on the inclination. This condition is known as the “rotation of the apsides.” It turns out that at two special inclinations, the apsidal rotation rate is zero. *These inclinations are either at 63.4° or at 116.6° (complementary angle).* If a satellite is at 63.4° inclination, and the perigee is in the southern hemisphere, the perigee will remain in the southern hemisphere.]

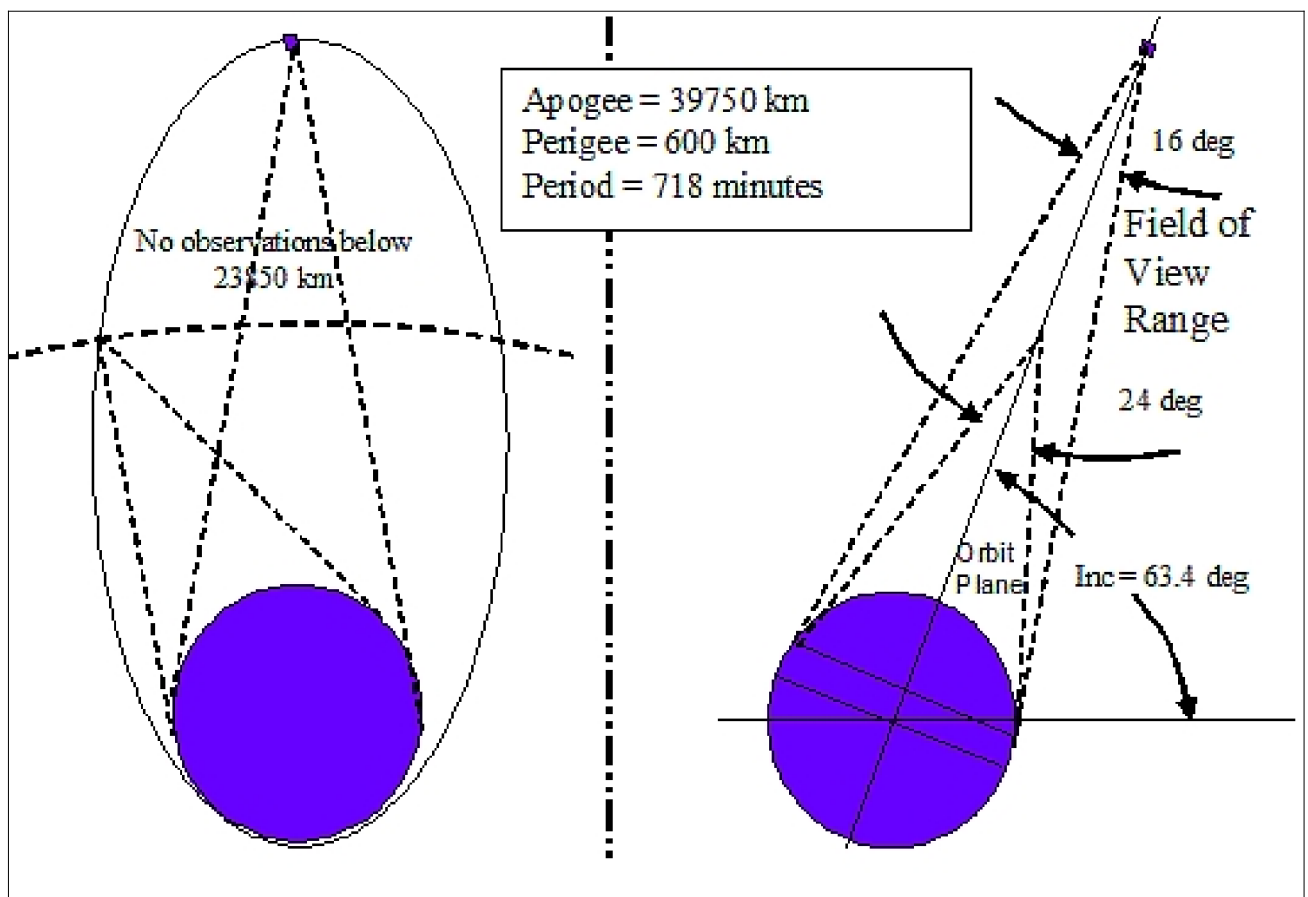


Figure 204: Overview of Molniya orbit parameters (image credit: NASA/GSFC)

A spacecraft in a Molniya orbit lingers for instance over Russia for about 8 hours per day. This implies that an orbital configuration of at least three satellites in sequence can provide a continuous coverage of Russia (or any other large land mass). The Russian Molniya orbits

²⁶⁶⁶⁾ <http://www.fas.org/spp/guide/russia/comm/elliptical/molniya.htm>

have arguments of perigee (ω) at or near 270° so that the resulting observation coverage was highly biased toward the northern hemisphere. Spacecraft in Molniya orbits also have repeating ground tracks, thus providing steady coverage with some station-keeping requirements. The Molniya orbits are in general less stable than geostationary orbits.²⁶⁶⁷⁾

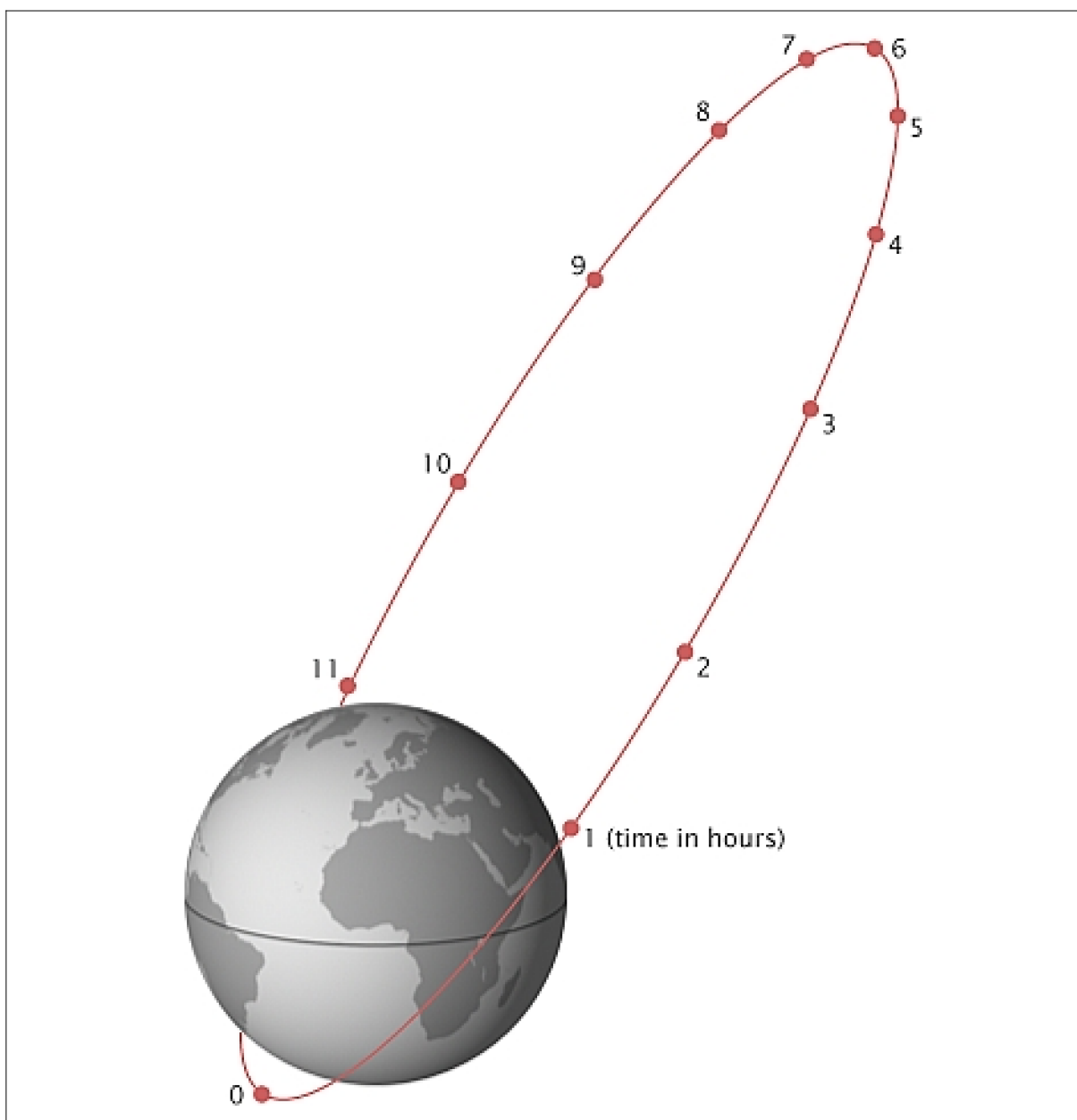


Figure 205: The Molniya orbit. Usually the period from perigee + 2 hours to perigee + 10 hours is used to transmit to the northern hemisphere (image credit: Wikipedia)

Other examples: The Chinese mission SJ-4 (launch Feb. 8, 1994) used a Molniya orbit of 210 km x 36,125 km. The US military has been using Molniya-type orbits for some of its classified surveillance satellites since the early 1970s. For instance, six first generation SDS (Satellite Data System) data relay satellites of DoD were launched from 1976 to 1987 (the SDS are being used for real-time data relay from reconnaissance gathering satellites which are out of range from US tracking stations). The AMSAT-Oscar-40 spacecraft, also referred to as AMSAT-3D (launch Nov. 16, 2000, Kourou), was initially inserted into GTO and then into a Molniya orbit (1000 km x 47000 km) with an inclination of 63.4° to provide

²⁶⁶⁷⁾ M. S. Konstantinov, V. A. Obukhov, V. G. Petukhov, G. A. Popov, G. G. Tchernobelsky, "Spacecraft Station-keeping on the Molniya Orbit Using Electric Propulsion," Proceedings of the 56th IAC 2005, Fukuoda, Japan, Oct. 17-21, 2005, IAC-05-C1.1.01

long communication times for its users in the northern hemisphere. — The long-term use of Molniya-type orbits has also generated its share of debris in these orbits; still, at the start of the 21st century there is an undiminished demand for Molniya-type orbits in communication and reconnaissance applications.

Naturally, HEO constellation designs with other orbital periods than 12 hours (Molniya type) are possible (say, 8 hour period, etc.). Consequently, they provide other observation characteristics. — Molniya-type orbits (as well as all HEOs) experience the same harsh space environment as GTOs with daily passes through the Van Allen radiation belts.

It turns out that the **8 hour Molniya orbit** is much more suitable for Earth observation than the 12 hour orbit (used for communications), providing a lower apogee (27,263 km at apogee for an 8 hour Molniya orbit versus 39,950 km for a 12 hour Molniya orbit). Hence, the 8 hour orbit is not as technically demanding on the EO instruments. A constellation of 3–4 satellites in an 8 hour Molniya orbit (which is actually an elliptical MEO) could provide 24 hour real-time high latitude coverage of critical areas of the northern hemisphere.

- NASA/GSFC is considering the semisynchronous Molniya orbit for polar region observations since 2004. A single satellite in a Molniya orbit would allow to extend GEO-type imaging (i.e. over extended periods) all the way to the north pole for a total of 16 hours per day. Two satellites would ensure 24 hour coverage of the entire northern hemisphere, and four satellites would extend the continuous coverage to the entire globe.

The MOI (Molniya Orbit Imager) of GSFC ²⁶⁶⁸ is a concept for a high-latitude quasi-geostationary mission that would be ideally suited for multitemporal imaging e.g. for satellite winds purposes without most of the disadvantages of the LEO (Low Earth Orbit) imagers. In the Molniya orbit, imaging is performed during the roughly 500 minute apogee dwell period (67% of the total duration of the orbit) when the satellite is above the curved line in the left panel of Figure 204.

Since the Molniya orbit is longitudinally “blind” — i.e. all regions of the high northern latitudes are imaged about equally well regardless of where exactly the apogee points are located — a mission in this orbit is an excellent candidate for international collaboration.

- **Arctica** (also spelling of Arktika) is a Russian polar meteorological mission proposal of Roskosmos and Roshydromet (Moscow). The project definition phase started in 2007. The scenario involves two satellites in HEO (Highly Elliptical Orbit — i.e., Molniya-type orbits) with an inclination of 63.4°, and an orbital period of 12 hours. This configuration would allow a quasi permanent coverage of high-latitude areas for weather, ice and snow monitoring as well as for telecommunications and data collection. — A launch of Arctica is planned from 2015 onwards. ²⁶⁶⁹
- Canada agencies of CSA, Environment Canada, and DND are planning **PCW** (Polar Communications and Weather), a 2 satellite mission, using Molniya orbits with a 12 hour period. ²⁶⁷⁰ The objective is to improve weather forecasting, and environmental and climate change monitoring, as well as, provide continuous broadband communications capabilities throughout all of the Arctic. — In July 2009, CSA and its Government partners awarded a contract to the Canadian industrial consortium led by MDA (MacDonald Dettwiler and Associates, Ltd.) of Richmond, BC to conduct a Mission Concept Definition (Phase A) study. A launch of the 2 PCW spacecraft is planned for the timeframe 2017.

2668) Lars Peter Riishojgaard, “The Molniya Orbit Imager,” Proceedings of the 2006 EUMETSAT Meteorological Satellite Conference, Helsinki, Finland, June 12–16, 2006, URL: http://www.eumetsat.int/HOME/Main/AboutEUMETSAT/Publications/ConferenceandWorkshopProceedings/2006/groups/cps/documents/document/pdf_conf_p48_sl_10_riishojg_v.pdf

2669) “Russia proposes launch of Arktika space monitoring project in 2014,” RiaNovosti, Aug. 16, 2010, URL: <http://en.rian.ru/russia/20100816/160223630.html>

2670) Guennadi Kroupnik, “Polar Communications & Weather (PCW) Mission,” Space and the Arctic Workshop, Stockholm, Sweden, Oct. 20–21, 2009, URL: <http://earth.eo.esa.int/workshops/spaceandthearctic09/kroupnik.pdf>

1.24.5 Lagrangian Points

Lagrangian points (also referred to as “libration points”) in space are defined as points where the gravitational and centrifugal forces cancel out or balance – due to two or more bodies (the sun, or planets) – and thus where a spacecraft can be positioned in equilibrium at zero velocity (the gravitational pull of the two large masses precisely equals the centripetal force required to rotate with them). The description of “libration points” results from the fact that a body (or a spacecraft) will oscillate or “**librate**” at these points, retaining the same average position relative to the two large bodies they orbit with.

The Italian born (Turin, 1736) mathematician **Joseph – Louis Lagrange** (later French mathematician, he died in Paris in 1813) showed, that there were five equilibrium solutions to the “three body problem” where one massless body is submitted to the gravitational field of two massive bodies. They are called Lagrangian points or libration points. In 1772, Lagrange received the prize of the Paris Academy of Sciences for proving mathematically that five positions of net zero–force exist in a rotating two–body gravity field [he shared the prize of the “three –body –problem” solution with **Leonard Euler** (1707–1783) of Switzerland].

The Lagrangian points are particular solutions of the equations of motion applied to the “Problem of Three Bodies” in an orbital plane of two massive bodies in circular orbits around a common center of gravity and a third body of negligible mass. The equilibrium or libration points represent singularities in the equations of motion where velocity and acceleration components are zero and the gravitational forces are balanced. *Lagrange deduced that any object, such as a satellite, placed in the vicinity of such a libration point (Lagrange point), will be stationary with respect to the reference frame in which the two large bodies are rotating.*

The equations of motion always yield **five points** at which the third body can remain at equilibrium. Three of the points are on the line passing through the centers of mass of the two massive bodies – L3 beyond the most massive body, L2 beyond the less massive body, and L1 (the point through which the mass transfer occurs) between the two bodies. The points L1, L2, and L3 are also known as the **collinear libration points** (on the same axis of the mutually rotating system such as the Sun – Earth line). The other two points, L4 and L5, are located at the two points in the orbit of the less massive component which are equidistant (equilateral triangle) from the two main components, as illustrated in Figure 207.^{2671) 2672) 2673) 2674)}

1.24.5.1 Sun – Earth system

Sun – Earth system (actually the Sun – Earth/Moon barycenter system): The L1 and L2 locations are just about **1.5 million km** from Earth (in the direction Earth – sun), in which the sun/Earth gravitational forces are balanced (the L1 distance from Earth corresponds 1/100 the distance Earth – Sun).

The L1 point is located towards the sun and provides a continuous full – disk view of the sunlit half of the Earth as well as of the sun; the L2 point is away from the sun (on the opposite side of Earth, i.e., in the direction of the universe) and provides a complementary continuous view of the night side of the Earth. The first three Lagrangian points of the sun/Earth system, namely L1, L2 and L3, lie along an axis with Earth and the sun, with L3 on the oppo-

2671) Fred P. J. Rimrott, “Introductory Orbit Dynamics,” Vieweg, Braunschweig/Wiesbaden, 1989, pp. 156–158

2672) Karl Stumpff, “Himmelsmechanik,” Band II, VEB Deutscher Verlag der Wissenschaften, Berlin 1965

2673) O. Trivailo, “Spacecraft Stability, Dynamics and Control Near the Triangular Lagrange Points Influenced by Multiple Trojan Asteroids,” Proceedings of IAC 2004, Vancouver, Canada, Oct. 4–8, 2004, IAC–04–W.2.01

2674) J. – Y. Prado, E. Hinglais, “A Communication Hub in Lagrange L1 for Opening the Area to Small Satellites,” Proceedings of the IAA Symposium on Small Satellite Systems and Services (4S), Rhodes, Greece, May 26–30, 2008, ESA SP – 660, August 2008

site side of the sun from Earth. The other Lagrangian points, L4 and L5, are in the same orbit plane around the sun as Earth; however, L4 is 60° ahead of Earth while L5 is trailing Earth by 60° .²⁶⁷⁵⁾

The stability of L1 and L2 orbital position (saddle points in the orbital computation) can be maintained for a duration of about 23 days, while L3 maintains stability for about 150 days. The triangular libration points L4 and L5, forming an equilateral triangle with one large mass, are the most stable points of the system. Whenever the mass ratio of the two large bodies exceeds 24.96, then these points remain permanently quasi-stable. The stability properties of L4 and L5 makes these locations in the Sun–Earth system as collectors of cosmic debris (also referred to as “Trojans”).^{2676) 2677)}

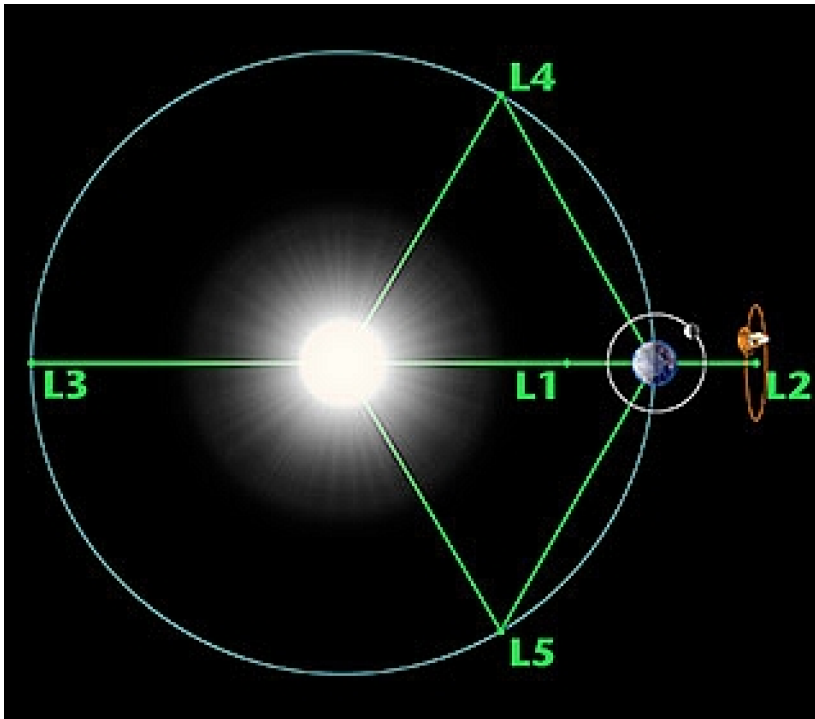


Figure 206: Lagrangian points of the Sun–Earth system (image credit: NASA)^{2678) 2679)}

Lissajous and halo orbits about the Lagrangian points:

Lissajous orbits are named after the French physicist Jules–Antoine Lissajous (1822–1880) who studied the behavior of vibrations. He found that the curved lines on the screen would combine to make a figure eight pattern (Lissajous curves).

Lissajous orbits are the natural motion of a satellite around a collinear libration point in a two–body system and require less momentum change to be expended for station keeping than halo orbits, where the satellite follows a simple circular or elliptical path about the libration point.

A spacecraft may orbit around any of the libration points (quasi periodic orbit) which, using a simplified motion theory (circular restricted three body problem), can be depicted as a Lissajous curve. Lissajous orbits, typically involve displacements from the Sun–Earth line ranging from thousands to hundreds of thousands of km.

²⁶⁷⁵⁾ W. Wiscombe, J. Herman, F. Valero, “L–1 and L–2 Observatories for Earth Science in the Post–2010 Era,” Proceedings of IGARSS 2002, Toronto, Canada, June 24–28, 2002

²⁶⁷⁶⁾ J. E. Howard, H. R. Dullin, M. Horanyi, “Stability of Halo Orbits,” Physical Review Letters, Vol. 84, No. 15, April 10, 2000, pp. 3244–3247

²⁶⁷⁷⁾ http://map.gsfc.nasa.gov/m_mm/ob_techorbit1.html

²⁶⁷⁸⁾ http://map.gsfc.nasa.gov/mission/observatory_l2.html

²⁶⁷⁹⁾ <http://www.physics.montana.edu/faculty/cornish/lagrange.html>

The **halo orbit family** is a special case of the Lissajous orbit where the period of motion along the three directions of space is equal. These solutions exist only for large excursions from the Sun–Earth line ($> 650,000$ km), the corresponding period is about 6 months.. A spacecraft in a halo orbit around a Lagrangian point (say L1 of Sun–Earth system) describes huge loops around this L1 point such that its orbits resemble a so–called “halo” (i.e., a ring around an imaginary center, namely L1). Lissajous orbits are the natural motion of a satellite around a collinear libration point in a two–body system and require less momentum change to be expended for station keeping than halo orbits, where the satellite follows a simple circular or elliptical path about the libration point.

The L1 and L2 librations points of the Sun–Earth system offer the particular quality of providing stable thermal as well as illumination environments. Hence, both vicinities of L1 and L2 are considered as very attractive regions for solving problems of solar–terrestrial physics. Spacecraft flown to either L1 or to L2 are generally considered to be in the class of “deep–space” missions.

The use of Lagrangian points as possible orbital locations for space missions was first recognized and studied by Guiseppe (Beppi) Colombo (Italy) and Robert F. Farquhar (USA) in the early 1960s. 2680) 2681) 2682) 2683) 2684) 2685)

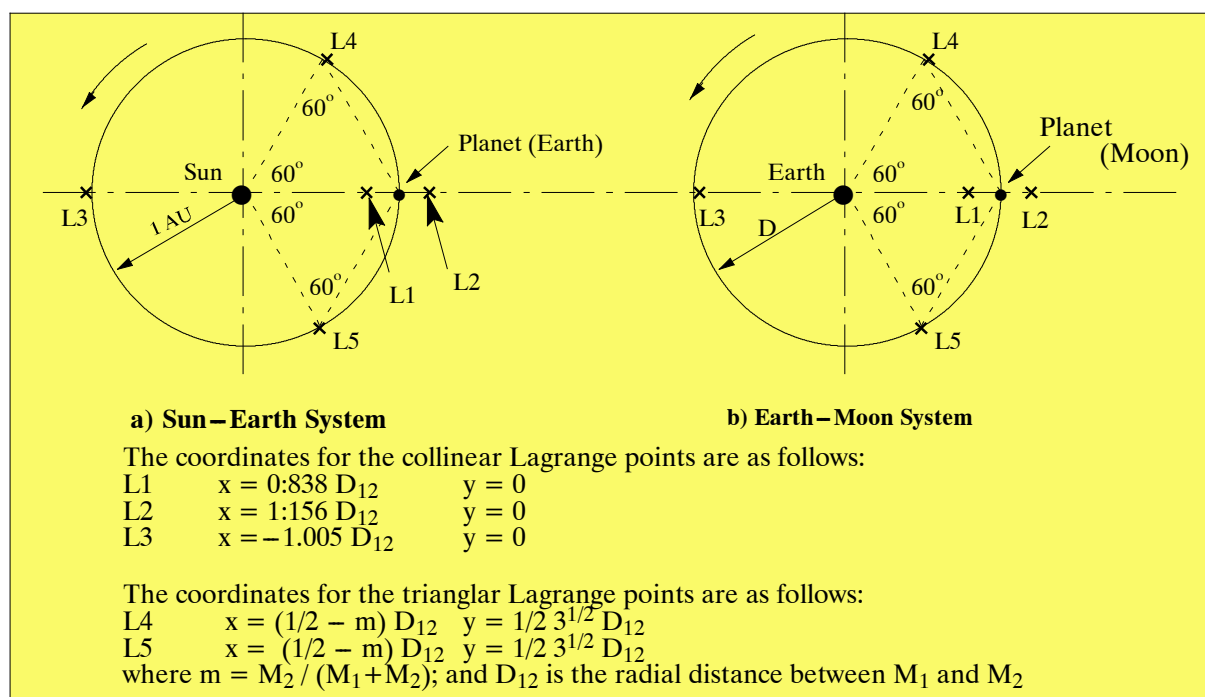


Figure 207: Lagrangian points of the Sun–Earth and Earth–Moon systems

- **Observation characteristics from L1 in the Sun–Earth system:** L1 is an ideal outlook point for Earth observations (in UV, VIS and up to TIR are all within current technological capabilities) as well as for monitoring of “space weather” parameters (the supersonic solar wind reaches L1 about one hour prior to reaching Earth). L1 is located outside the Earth’s

2680) G. Colombo, “On the Satellites of the Earth–Moon System,” Atti dell’Accademia Nazionale dei Lincei. Rendiconti, Series 8, Vol. 28, pp. 169–172, 1960, in Italian

2681) R. W. Farquhar, “Preliminary Considerations for the Establishment of a Satellite in the Neighborhood of Centers of Libration,” MS. Thesis, UCLA, Dec. 1960; see also: <http://highorbits.jhuapl.edu/ntrr346.htm>

2682) G. Colombo, “The Stabilization of an Artificial Satellite at the Inferior Conjunction Point of the Earth–Moon–System,” Smithsonian Astrophysics Observatory Special Report, No. 80, Nov. 1961

2683) R. Farquhar, “Halo Orbits and Lunar Swing–by Missions of the 1990’s,” Acta Astronautica, Vol 24, 1991, pp. 227–234

2684) M. Hechler, A. Yanez, “Orbits around L2 with Non–Gravitational Perturbations,” Proceedings of IAC, 2004, Vancouver, Canada, Oct. 4–8, 2004, IAC–04–A.7.01

2685) <http://highorbits.jhuapl.edu/>

magnetosphere (see Figure 208). L1 allows an uninterrupted view of the sun and requires infrequent spacecraft maneuvers to stay in orbit (low Δv for maintaining the spacecraft near one of the L1/L2 points, station keeping needs about 10 m/s per year). Also, the thermal environment of the spacecraft is very stable and smooth as the sun is always seen in the same direction. There is no eclipse in L1. The L1 perspective is also of particular value for studies of cloud properties at solar wavelengths, since there are no shadows from this vantage point. Another advantage of the L1 location is the existence of a very small gravitational force environment. This has implications for missions with extremely high performance requirements in disturbance forces.

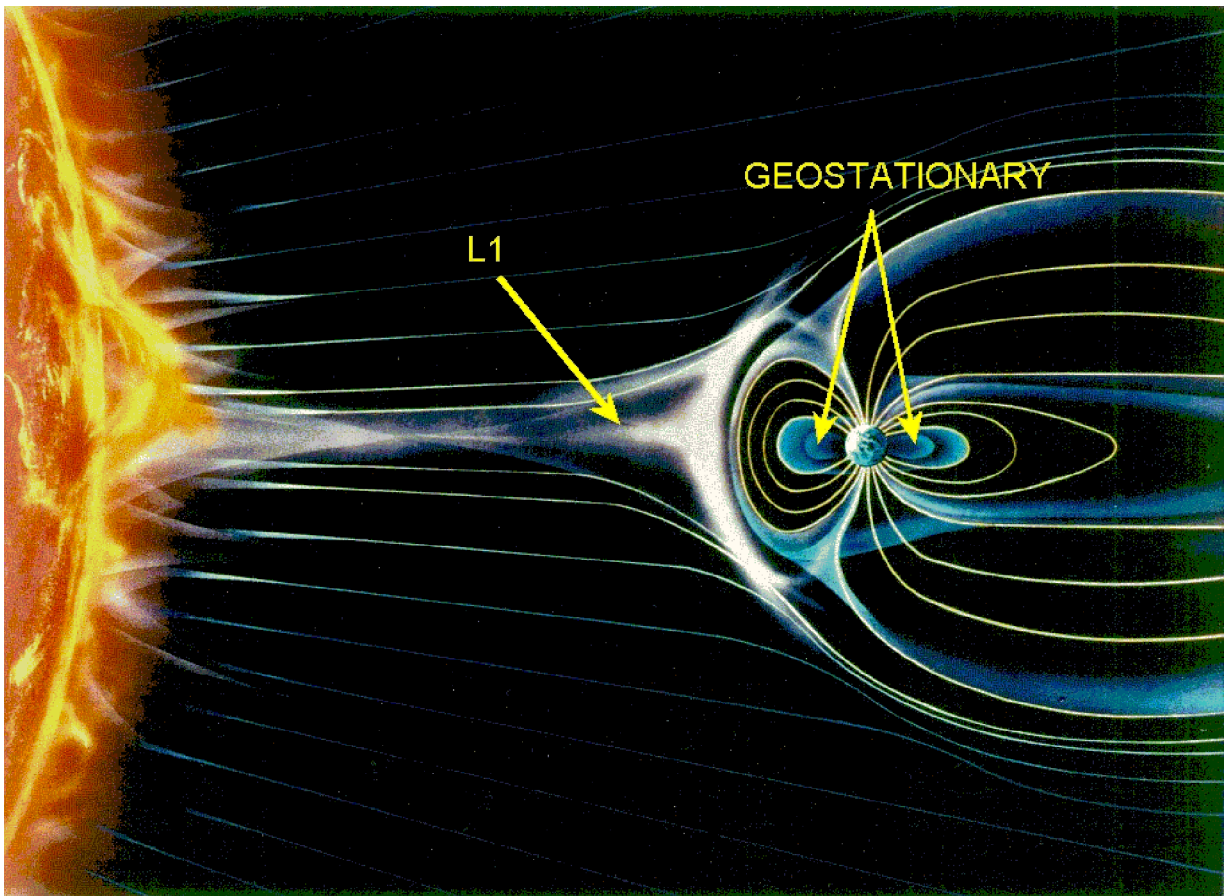


Figure 208: L1 location in Sun–Earth system relative to the magnetosphere (not to scale)

- **Observation characteristics from L2 in the Sun–Earth system:** Views of the nighttime hemisphere from L2 can be of value for monitoring lightening on Earth. Objects at or near L1 and L2 experience the same gravitational force as the Earth itself, and thus become new “planets” with the same orbital period as Earth around the sun. In fact, a satellite at L1 or L2 executes a three dimensional elliptical orbit about the Lagrange point as the Earth, the moon, and satellite system orbit the sun. From L1 or L2, the Earth occupies almost the same 0.5° FOV (Field of View) as the sun does from Earth – although slightly smaller since the rim of the sun is visible from L2 (an advantage for limb scanning!). Twin observatories at L1 and L2 can observe every point on Earth continuously – a true synoptic coverage and a new way to look at Earth.

Note: In the Sun–Earth system the L2 point is about the same distance away as L1 but at the opposite side of the Earth (in the anti–sun direction). This implies that a spacecraft positioned at L2 is always located in the Earth’s shadow. An advantage of L2 is astronomical viewing (looking toward the universe) due to constant lighting conditions. L2 is also advantageous for microwave radiation reception (radio signals) from the universe (encounter of much lower radio frequency interference levels than with observations made from Earth).

- **Observation characteristics from L3 in the Sun_Earth system:** From an Earth perspective, the L3 points remains hidden behind the sun at all times. A spacecraft at L3 would encounter communication problems with Earth since the sun is always positioned in between. Hence, it is quite unlikely that a spacecraft will ever be sent to L3.

The L4 and L5 points are home to stable orbits so long as the mass ratio between the two large masses exceeds 24.96. This condition is satisfied for both the Earth–Sun and Earth–Moon systems, and for many other pairs of bodies in the solar system. Objects found orbiting at the L4 and L5 points are often called Trojans after the three large asteroids Agamemnon, Achilles and Hector that orbit in the L4 and L5 points of the Jupiter–Sun system. (According to Homer, Hector was the Trojan champion slain by Achilles during King Agamemnon’s siege of Troy). There are hundreds of Trojan Asteroids in the solar system. Most orbit with Jupiter, but others orbit with Mars. In addition, several of Saturn’s moons have Trojan companions. No large asteroids have been found at the Trojan points of the Earth–Moon or Earth–Sun systems. However, in 1956 the Polish astronomer Kordylewski discovered large concentrations of dust at the Trojan points of the Earth–Moon system.

Researchers Jack Lissauera, and John Chambers noticed that more than 2200 cataloged asteroids are located about the L4 and L5 points of the Sun–Jupiter system, and five bodies have been discovered around the L4 point of the Sun–Neptune system. ²⁶⁸⁶⁾ [2687\)](#)

Examples of satellites in L1 halo orbits of the Sun–Earth system are:

- ISEE–3 (International Sun–Earth Explorer), NASA/GSFC, launch Aug. 12, 1978; ISEE–3 remained at L1 for 4 years, requiring less than 10 m/s difference in velocity to adhere to its orbit. ISEE–3 was the pioneering mission to a libration point, demonstrating that such orbits could be used as prime locations for solar observations.
- RELICT–2, an astrophysics mission of Russia. In 1990, this was the first mission concept that planned to use a lunar swingby to achieve a mission orbit solely around a libration point L2. Unfortunately, the RELICT–2 mission was never launched.
- WIND (NASA, launch Nov. 1, 1994; WIND was placed into a halo orbit in Nov. 1996). WIND made a considerable loop around L1 repeating this several times.
- SOHO (Solar and Heliospheric Observatory), of ESA/NASA, launch Dec. 2, 1995. L1 was reached in 1996. SOHO has set an unprecedented standard for solar observations.
- ACE (Advanced Composition Explorer), NASA/GSFC, launch Aug. 25, 1997.
- Genesis of NASA/JPL with a launch Aug. 8, 2001; Genesis went into the halo orbit on November 16, 2001. In 2004, Genesis returned to Earth (sample return mission). ²⁶⁸⁸⁾
- Another planned mission into a halo orbit at L1 is the LISA Pathfinder mission of ESA (launch 2011), to operate in an L1–Lissajous orbit [advanced instruments: LTP (LISA Test Package), and DRS (Disturbance Reduction System)].

Examples of spacecraft missions to L2 in the Sun–Earth system are: (see Figure 207): ²⁶⁸⁹⁾

- WMAP (Wilkinson Microwave Anisotropy Probe) of NASA/GSFC with a launch June 30, 2001, L2–Lissajous orbit; the objective is to probe conditions in the early universe by

²⁶⁸⁶⁾ <http://www.universetoday.com/2008/05/06/did-earth-have-more-than-one-moon/>

²⁶⁸⁷⁾ J. L. Lissauera, J. E. Chambers, “Solar and planetary destabilization of the Earth–Moon triangular Lagrangian points,” *Icarus*, Vol. 195, Issue 1, May 2008, pp. 16–27

²⁶⁸⁸⁾ D. W. Dunham, R. W. Farquhar, “Libration Point Missions, 1978–2002,” 7th Libration Point Orbits and Applications, Girona, Spain, June 10–14, 2002

²⁶⁸⁹⁾ J.–Y. Prado, L. Torres, J. Benoist, E. Hinglais, I. Gibek, “A Communication Hub in Lagrange Points for Opening the Aerea to Small Satellites,” Proceedings of IAC 2004, Vancouver, Canada, Oct. 4–8, 2004, IAC–04–M.5.06

measuring the properties of the cosmic microwave background (CMB anisotropy) radiation over the full sky.²⁶⁹⁰⁾

Note: WMAP concluded its mission in August 2010 after 9 years of observations. The spacecraft has not only given scientists their best look at this remnant glow, but also established the scientific model that describes the history and structure of the universe.²⁶⁹¹⁾

– HSO (Herschel Space Observatory) of ESA (collaboration with NASA) and the Planck spacecraft of ESA, both missions were launched on May 14, 2009.

Note: The Planck spacecraft worked perfectly for 30 months. It ran out of coolant on January 14, 2012 (as expected), ending the HFI (High Frequency Instrument) observations. The spacecraft completed five full-sky surveys with both instruments. The LFI (Low Frequency Instrument), which does not need to be super-cold (but is still at 18 K), will continue taking data for another year.²⁶⁹²⁾

On Oct. 19, 2013, the LFI was switched off, having completed its science operations on October 3, 2013. ESA's Planck space telescope has provided new insight into the history of our Universe. Although science observations are now complete, the legacy of the Planck mission lives on.²⁶⁹³⁾

On Oct. 23, 2013, ESA's Planck space telescope has been turned off after nearly 4.5 years soaking up the relic radiation from the Big Bang and studying the evolution of stars and galaxies throughout the Universe's history. This marks the end of an extraordinary cosmology mission.²⁶⁹⁴⁾

– JWST (James Webb Space Telescope) of NASA, ESA and CSA with a planned launch in 2015.

– The DARWIN mission of ESA (launch 2015) uses a Lissajous orbit around L2.

Mission	Agency	Launch date	Main mission objective	Location (H for Halo)	Lissajous size (x 1000 km)
ISEE-3	NASA	1978	Solar wind	L1/H	670 x 120
WIND	NASA	1994	Solar wind	L1/H	(short stay @ L1 only)
SOHO	ESA	1995	Solar physics	L1/H	650 x 120
ACE	NASA	1997	Solar wind	L1	260 x 160
WMAP	NASA	2001	Astrophysics	L2	200 x 200
Genesis	NASA	2001	Solar wind sample return	L1/H	650 x 120
HSO (Herschel Space Observatory)	ESA	2009	IR astronomy	L2/L	500 x 800
Planck	ESA	2009	Cosmology	L2/H	
Eddington	ESA	2010	Search of exoplanets	L2	
LISA Pathfinder	ESA	2011	Technology demonstration	L1	500 x 800
Gaia	ESA	2013	Astrometry	L2	100 x 100
JASMINE	JAXA	>2014	IR Astrometry	L2	
JWST	NASA	>2015	Astronomy	L2	
DARWIN	ESA	>2015	Search of exoplanets	L2	

Table 153: Overview of missions to L1/L2 Lagrangian points

²⁶⁹⁰⁾ Note: In Feb. 2003, NASA renamed the MAP (Microwave Anisotropy Probe) mission in honor of David Wilkinson to WMAP (Wilkinson Microwave Anisotropy Probe).

²⁶⁹¹⁾ <http://map.gsfc.nasa.gov/mission/>

²⁶⁹²⁾ "Planck's HFI completes its survey of early Universe," ESA, Jan. 16, 2012, URL: http://www.esa.int/esaSC/SEMxWNMXDXG_index_0.html

²⁶⁹³⁾ "Celebrating the legacy of ESA's Planck mission," ESA, October 18, 2013, URL: <http://sci.esa.int/planck/53106-celebrating-the-legacy-of-planck/>

²⁶⁹⁴⁾ "Last command sent to ESA's Planck Space Telescope," ESA, Oct. 23, 2013, URL: <http://sci.esa.int/planck/53116-last-command-sent-to-esa-planck-space-telescope/>

1.24.5.2 Earth–Moon system

The distance from the moon center of mass to L1 is 61,350.3 km (Figure 207). The distance from the moon center of mass to L2 is 61,347.5 km. The distance from Earth’s center of mass to L3 is 381,666.3 km (L3 lies on the opposite side of Earth in the Earth–Moon system; L3 has the distinction that the moon can never be seen from its position).

For the Earth–Moon system, the ratio between the mass of the Moon and Earth is about 1:81. For such large mass ratios, the L4 and L5 points can probably be considered as fairly “stable” – an error in position results not in an unstable orbit, but in a stable “libration orbit” around the actual point.²⁶⁹⁵⁾ – However, from safety considerations, it should be pointed out that the colinear points (L1, L2) of the Earth–Moon system are much less suitable and stable for spacecraft positioning than those of the Earth–Sun system. Small deviations from the Lagrangian points would require immediate station–keeping maneuvers. The configuration of the lunar libration points rotates around the Earth once each month.²⁶⁹⁶⁾

Examples of spacecraft missions to L1 and L2 in the Earth–Moon system:

The THEMIS (Time History of Events and Macroscale Interactions during Substorms) mission of NASA (launch Feb. 17, 2007), a constellation of five microsatellites in five different HEO (Highly Elliptical Orbits), completed its primary mission in 2009.

- Probe 1: Orbital period of 4 days, perigee 1.500 R_E, apogee 31.645 R_E, inclination 7.0°
- Probe 2: Orbital period of 2 days, perigee 1.168 R_E, apogee 19.770 R_E, inclination 7.0°

Since all spacecraft are very healthy and operating nominally, the project began planning in 2008 for an extended THEMIS mission – split into two parts. THEMIS–low consists of the 3 inner probes and continues to study Earth’s environment. The two outer probes, P1 and P2, will explore the space environment of the moon. – This new mission was renamed to **ARTEMIS** (Acceleration Reconnection Turbulence, and Electrodynamics of Moon Interaction with the Sun). The goal is to maneuver the two spacecraft into the Earth–Moon Lagrangian points and eventually into lunar orbit – to observe the same phenomena as before but from a different perspective.^{2697) 2698)}

2695) C. Maccone, “NASA Gateways at L1 and L2 and the Radio–Quiet Moon Farside Imperative,” Proceedings of IAC 2004, Vancouver, Canada, Oct. 4–8, 2004, IAA.1.1.1.08

2696) <http://www.oasis-nss.org/articles/2001/08/lagrange.html>

2697) “Road Cleared for ARTEMIS Mission Implementation,” UCB/SSL, Feb. 27, 2009, URL: <http://themis.ssl.berkeley.edu/news.shtml>

2698) Mark Woodard, David Folta, Dennis Woodfork, “ARTEMIS: The First Mission to the Lunar Libration Orbits,” URL: <http://www.mediatec-dif.com/issfd/IntMiDeI/Woodard.pdf>

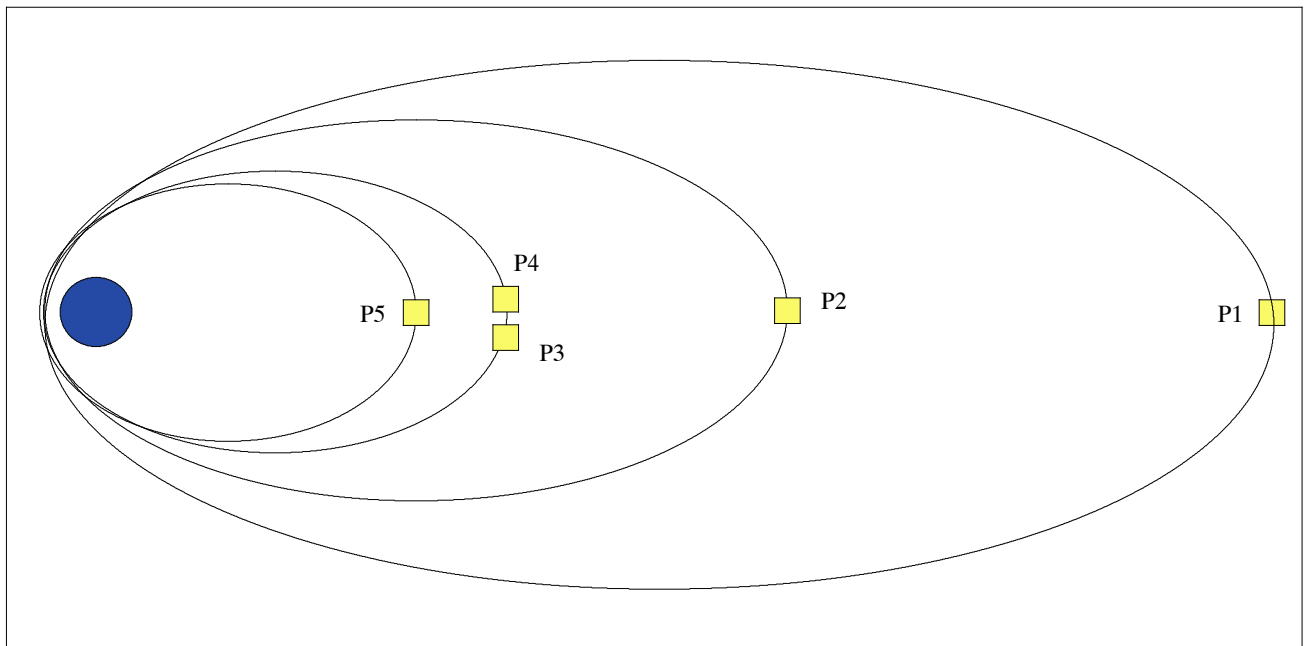


Figure 209: Illustration of deployed constellation in HEO (image credit: UCB)

The translunar orbit injections for P1 and P2 occurred in January and March 2010, respectively, with lunar libration point (L2) orbit captures in August and October 2010. After collecting science data in the Lissajous orbits for several months, the two spacecraft will be maneuvered into selenocentric orbits.

The ARTEMIS–P1 spacecraft arrived in its Lissajous orbit in August 2010. ²⁶⁹⁹⁾ In late March 2011, both spacecraft will be maneuvered into elliptical lunar orbits where they will continue to observe magnetospheric dynamics, solar wind and the space environment over the course of several years.

ARTEMIS is the first mission to navigate to and perform stationkeeping operations around the Earth–Moon L1 and L2 Lagrangian points.

The ARTEMIS science mission begins once both spacecraft are inserted into their Lissajous orbits. Since L1 and L2 are unstable Lagrangian points, the operations team must perform frequent stationkeeping maneuvers to maintain each spacecraft in the Lissajous orbits for several months.

Lunar phase: At the completion of the Lissajous orbit phase, the ARTEMIS satellites will perform large orbit maneuvers to depart the lunar libration point orbits and be captured into selenocentric orbits.

1.24.6 Observation coverage of constellations

The general objective of a satellite constellation is to provide either a global coverage configuration on a continuous basis, or to improve the partial coverage situation (increased temporal coverage of the target area), as can be offered by a single spacecraft. Such constellation designs consist of a group of satellites with coordinated coverage, operating together under shared control, synchronized so that they overlap well in coverage and reinforce rather than interfere with one another.

Satellite constellation coverage and geometry – determining the minimum number of satellites needed to provide a service, and their orbits – is a field in itself and beyond the scope

²⁶⁹⁹⁾ David Folta, Mark Woodard, “ARTEMIS – The First Earth–Moon Libration Orbiter,” NASA, Sept. 13, 2010, URL: http://www.nasa.gov/mission_pages/themis/news/artemis-orbit.html

of this text. However, an interesting classical coverage concept is use of the **Walker constellation** for applications in remote sensing, navigation, and in the wide field of communication services.

The Walker constellation^{2700) 2701) 2702)} is named after John G. Walker of RAE [Royal Aircraft Establishment at Farnborough, UK – later renamed to DERA (Defence Evaluation and Research Agency); as of July 2, 2001 DERA was renamed to QinetiQ]. Walker was a pioneer in studying Earth–coverage problems (in particular equal–area distributions) with various satellite constellation configurations.^{2703) 2704)}

In the early 1970s, Walker systematized and simplified the definition of orbital constellation design for the case of circular orbits by specifying the key parameters as T/P/F. The value 'T' is the total number of satellites; 'P' is the number of planes; and, 'F' is a phasing angle by which satellites in an adjacent plane lead their twin in the previous plane. The phasing angle 'F' is defined as $360^\circ/T$. The planes are equally spaced around, and equally inclined to, the equatorial plane. In a symmetrical constellation of T satellites, T/P satellites are evenly spaced on each orbital plane, and P orbital planes are evenly spaced through 360° of ascending node. The advantage of inclined Walker constellations is the permanent network topology in the space segment.

Walker introduced a measure, referred to as PU (Pattern Unit) = $360^\circ/T$, to calculate the phase angle (phase angle = $F \times \text{PU}$). Example: T/P/F = 54/9/3; then PU = 6.667° ; and the phase angle = 20° .²⁷⁰⁵⁾

- Example 1 of a Walker constellation 27/3/1: In this case 27 satellites are in a symmetrical Walker configuration (in three orbital planes).
- Example 2: 18/6/1. In this case 18 satellites are distributed in six planes ($\Delta=60^\circ$), the phasing $\phi=20^\circ$ (see Figure 210).

In the early phase of the GPS constellation development, Walker proposed a six–plane, 18 satellite constellation²⁷⁰⁶⁾ (with all planes inclined to the equator and satellites equally spaced within a plane) – a classic Walker constellation: 18/6/2 which was eventually selected and accepted by the US Air Force. Later on, this 18/6/2 concept was changed to 24/6/2 when technical studies showed that no 18 satellite constellation could avoid intermittent outages, as well as periods of large navigational errors. The six additional spacecraft in the constellation were simply referred to as “operating in–orbit spares.”

2700) J. G. Walker, “Circular Orbit Patterns Providing Continuous Whole Earth Coverage”, Royal Aircraft Establishment, Technical Report 70211, Nov. 1970

2701) J. G. Walker, “Continuous Whole–Earth Coverage by Circular–Orbit Satellites,” IEE Conference publication No. 95, 1973, in Satellite Systems for Mobile Communications and Surveillance, pp. 35–38.

2702) J. G. Walker, “Continuous Whole–Earth Coverage by Circular–Orbit Satellite Patterns,” Technical Report 77044, Royal Aircraft Establishment, Farnborough, UK, March 24, 1977 (full report of 80 pages)

2703) J. G. Walker, “Some Circular Orbit Patterns Providing Continuous Whole Earth Coverage, Journal of the British Interplanetary Society, Vol. 24, 1971, pp. 369–384

2704) J. G. Walker, “Satellite Constellations,” Journal of the British Interplanetary Society, Vol. 37, 1984, pp. 559–571

2705) Information provided by Friedrich Jochim of DLR/GSOC.

2706) J. E. Draim, “Satellite Constellations,” Proceedings of IAC 2004, Vancouver Canada, Oct. 4–8, 2004, IAC–04–A.5.01

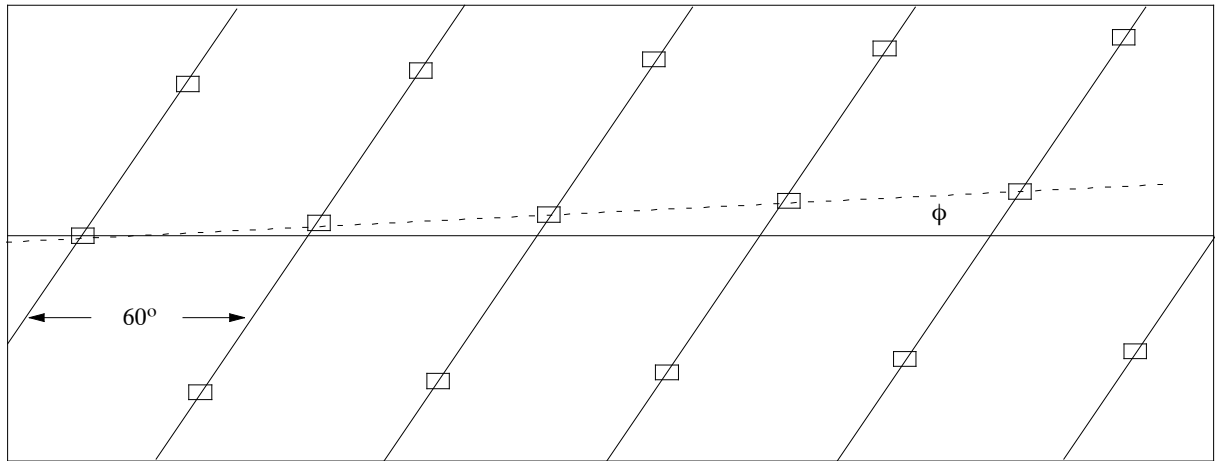


Figure 210: Equal distribution of a Walker constellation 18/6/1

Although the coverage concept of Walker was first implemented with the GPS constellation in MEO, the general concept is valid in LEO, MEO or in GEO satellite constellations. The GPS constellation of 24 MEO satellites is a Walker type constellation: 24/6/2, a semisynchronous orbit with an inclination (early phase of the program) of 63° – however, the inclination decreased to 55° due to launch vehicle constraints. Examples are:

- The Galileo constellation of 30 MEO satellites (European navigation system under development, start of operations in 2016) is a Walker type constellation: 27/3/1, plus three active spares. This adds up to 10 satellites per orbital plane. The three plane approach offers an easier replenishment of satellites.
- The communication industry employs a number of LEO Walker constellations such as: M-Star (proposed by Motorola), Iridium (66 satellites in 6 planes), OrbcComm, etc.

1.25 Orbital maneuvering and encounters

Orbital maneuvering encompasses all orbital changes after insertion required to place a satellite in the intended orbit. The first satellite maneuvers most likely occurred on January 2, 1959, with the Soviet Luna–1 mission to the moon – requiring countless maneuvers, including circularizing to initial launch orbit, doing midcourse corrections, and so on. Although Luna–1 missed the moon by about 5000 km, the feat of orbital maneuvering was remarkable at this early stage of spaceflight. Later, on Sept. 12, 1959 (launch), the Soviet Union corrected some of their difficulties and crashed Luna–2 into the lunar surface, near the crater Archimedes. The crash (on Sept. 14, 1959) was intentional because retro–rocket technology for a soft landing hadn't matured enough to be installed on a satellite. ²⁷⁰⁷⁾

Close encounters/rendezvous of satellites with celestial bodies. The art of satellite navigation has evolved steadily over the years, resulting occasionally in close flyby maneuvers. Examples are:

- The Giotto mission of ESA encountered Halley's Comet 1986. The S/C encountered Halley on March 13, 1986, at a distance of 0.89 AU from the sun and 0.98 AU from the Earth and an angle of 107° from the comet–sun line. The actual closest approach of the S/C to Halley was measured at 596 km. During the Giotto extended mission, the spacecraft successfully encountered Comet P/Grigg–Skjellerup on July 10, 1992. The closest approach was approximately 200 km. ²⁷⁰⁸⁾
- On July 29, 1999, the DS1 spacecraft of NASA/JPL successfully performed a close flyby of asteroid 9969 Braille using the AutoNav system. At about 27 km separation, it was by far the closest flyby of an asteroid so far attempted. On Sept. 22, 2001, DS–1 encountered and flew by the comet Borrelly at a speed of 16.5 km/s. DS1 came within 2200 km of Borrelly's 10km long core, transmitting 30 black–and–white images of the coma.
- The NEAR (Near Earth Asteroid Rendezvous S/C)/Shoemaker satellite of NASA, in orbit around asteroid 433 Eros since Feb. 14, 2000, experienced its closest encounter with Eros on Oct. 26, 2000. ²⁷⁰⁹⁾ ²⁷¹⁰⁾ The flyby, with corresponding surface observation, occurred at an elevation of about 5 km, planned and supervised by the mission control center at JHU/APL. The NEAR/Shoemaker S/C then performed year–long observations of Eros (322 million km from Earth). **On Feb 12, 2001, it was commanded by JHU/APL to land on the asteroid** (the S/C was not built for landing). The final touchdown speed of the craft was about 1.7 m/s after some descent maneuvers. Six high–resolution MSI images (<10 cm) of the asteroid were acquired during the descent at altitudes of <500 m. All S/C instruments kept operating after touchdown. The GRS (Gamma Ray Spectrometer) was detecting key chemical signatures of a “planetesimal” – one of the original building blocks of planets – up to two weeks after touchdown when the mission was ended. NEAR/Shoemaker thus became the first spacecraft ever to land on an asteroid. Launched Feb. 17, 1996, the NEAR S/C was the first mission in NASA's Discovery Program of low–cost planetary missions.
- The Stardust sample return mission of NASA (launch Feb. 7, 1999) encountered Comet Wild 2 on Jan. 2, 2004 (the closest distance to the comet was about 250 km at a relative speed of about 21,960 km/h, Wild 2 has a nucleus of about 5 km in diameter). Return of interstellar as well as cometary dust particle samples to Earth in January 2006 (dust particles from the comet's dust coma were collected in a pad of low–density aerogel capable of preserving the particles). **The Stardust capsule of 46 kg landed safely on a parachute in the**

2707) D. V. Vallado, “Fundamentals of Astrodynamics and Applications,” Second Edition, Published jointly by Microcosm Press (El Segundo, CA), Kluwer Academic Publishers (Dordrecht, The Netherlands), 2001, pp. 303–304

2708) <http://nssdc.gsfc.nasa.gov/planetary/giotto.html>

2709) R. L. Nelson, K. E. Whittenburg, M. E. Holdridge, “433 Eros Landing – Development of NEAR Shoemaker's Controlled Descent Sequence,” AIAA/USU Conference on Small Satellites, Logan, UT, Aug. 13–16, 2001, SSC01–I–1

2710) A. Heyler, J. C. Ray, T. E. Strikwerda, D. R. Haley, “Performance of the NEAR G&C System During Cruise, Eros Orbit, and Controlled Descent,” AAS Guidance and Control Conference, Breckenridge, CO, Feb. 6–10, 2002

Utah desert on Jan. 15, 2006. Scientists believe these precious samples will help provide answers to fundamental questions about comets and the origins of the solar system.

The dust collection task (tiny specks of solid matter, called interstellar dust grains, that permeate the galaxy) started on Aug. 5, 2002. On Nov. 1, 2002, Stardust completed a close flyby of asteroid Annefrank (within 3,300 km, Annefrank is about 4 km in diameter) as an opportunity for a full dress rehearsal of procedures the spacecraft used during its Jan. 2, 2004 encounter with its primary science target, comet Wild 2. Comet Wild 2 was discovered in 1978, it has an orbit of 6.39 years somewhere between Mars and Jupiter.

NASA's **Stardust–NExT** (New Exploration of Tempel–1) is a follow–on mission for Stardust on its trajectory to comet Temple 1 (which was previously visited by the Deep Impact Probe on July 4, 2005). Stardust–NExT encountered comet Temple–1 on Feb. 14, 2011 and returned 72 images of great detail from Tempel 1 taken during closest approach. The high resolution images are amazingly sharp and clearly show a pockmarked and crater rich terrain of both new and previously unseen territory on the icy comets' surface.²⁷¹¹⁾

An analysis of the Stardust–NExT imagery showed clearly the craters on Temple 1 which resulted from the visit of the Deep Impact Probe on July 4, 2005.²⁷¹²⁾

The Stardust–NexT spacecraft sent its last transmission to Earth on March 24, 2011 shortly after depleting fuel and ceasing operations. During an 11–year period, the venerable spacecraft collected and returned comet material to Earth and was reused after the end of its prime mission in 2006 to observe and study another comet during February 2011.

- The **CONTOUR** (Comet Nucleus Tour) mission of NASA (launch July 3, 2002). The CONTOUR mission is scheduled to visit 3 comets within five years. The first planned stop is with comet Encke in Nov. 2003; in June 2006 (after repeated flybys of Earth to change trajectory) comet Schwassmann–Wachmann 3 is being visited; if the fuel supply permits, comet d'Arrest will be visited in Aug. 2008.

Note: The CONTOUR S/C went silent on Aug. 15, 2002 as it fired an onboard rocket to leave Earth orbit. Ground controllers at JHU/APL had expected to establish radio contact with the S/C shortly after the engine fired, but so far they never received a signal. – An investigation board came to the conclusion that a possible cause for this accident was structural failure of the spacecraft due to plume heating during the embedded solid–rocket motor burn.

- The Rosetta mission of ESA (launch March 2, 2004).²⁷¹³⁾ After a series of flybys, one of Mars and three of Earth (to gain enough speed), and encounters with at least one asteroid, Rosetta will rendezvous with comet Comet 67P/Churyumov–Gerasimenko in May 2014 (at a distance of about 675 million km from Earth, corresponding to 4.5 AU). For 18 months, the satellite will then orbit the comet's tiny nucleus (about 4 km in diameter) as it gets closer to the sun. During this period, the Rosetta orbiter will deploy a lander, named Philae, for a touchdown and study of the comet's surface in Nov. 2014. The Rosetta orbiter has 11 observing instruments, while Philae has 10 instruments.

- On Sept. 5, 2008, Rosetta experienced a planned close flyby of asteroid “Steins 2867” at a distance of 800 km, a space rock of ~ 10 km in size in the asteroid belt, to carry out its first scientific work in a decade–long trek into the Solar System. The encounter took place at a distance of 360 million km from Earth. Its goal was to get rare, close–up photographs and surface scanning of an asteroid, part of the intriguing debris left over from the building of

2711) Ken Kremer, “Stardust–NExT Unveils Astoundingly Detailed and Crater–rich Photos of Comet Tempel 1,” Universe Today, Feb. 15, 2011, URL: <http://www.universetoday.com/83319/stardust-next-unveils-astoundingly-detailed-and-crater-rich-photos-of-comet-tempel-1/>

2712) Ken Kremer, “NASA's Stardust Discovers Human made Deep Impact Crater on Comet Tempel 1,” Universe Today, Feb. 16, 2011, URL: <http://www.universetoday.com/83335/nasa%E2%80%99s-stardust-discovers-human-made-deep-impact-crater-on-comet-tempel-1/>

2713) G. Schilling, “Comet Chasers Get Serious,” Science, Vol. 297, July 5, 2002, pp. 44–45

the Solar System. – The Rosetta spacecraft had been roused from hibernation for the meeting with asteroid Steins. ^{2714) 2715) 2716)}

Launch	March 2, 2004	
1st Earth swingby	March 4, 2005	distance from Earth: 1955 km
Mars swingby	Feb. 25, 2007	distance from Mars: 250 km
2nd Earth swingby	Nov. 13, 2007	distance from Earth: 5301 km
Steins flyby	Sept. 5, 2008	distance from Steins: 800 km
3rd Earth swingby	Nov. 13, 2009	distance from Earth: 2500 km
Lutetia flyby	June 10, 2010	distance from Lutetia: 3162 km
Comet rendezvous maneuvers	May 22, 2014	distance from comet: 600,000–100,000 km
Lander delivery	Nov. 10, 2014	distance from comet: 1–2 km
End of mission	December 2015	

Table 154: Overview of Rosetta mission timeline

– On July 10, 2010 Rosetta headed for a flyby of asteroid Lutetia. The close pass allowed around 2 hours of good imaging. The spacecraft has returned the first close-up images of the asteroid showing it is most probably a primitive survivor from the violent birth of the Solar System. The images show that Lutetia is heavily cratered, having suffered many impacts during its 4.5 billion years of existence. As Rosetta drew close, a giant bowl-shaped depression stretching across much of the asteroid rotated into view. The images confirm that Lutetia is an elongated body, with its longest side around 130 km. ²⁷¹⁷⁾

The flyby marks the attainment of one of Rosetta’s main scientific objectives. The spacecraft will now continue to its primary target, comet Churyumov – Gerasimenko. It will rendezvous with the comet in 2014, mapping it and studying it. It will then accompany the comet for months, from near the orbit of Jupiter down to its closest approach to the Sun. In November 2014, Rosetta will deploy Philae to land on the comet nucleus.

- The Deep Impact mission of NASA (launch Jan. 12, 2005). A mother–daughter dual spacecraft carries an impactor with a mass of 370 kg (flyby of mother S/C and observation of the impactor’s collision with the comet). The objective was to hit the nucleus of Comet 9P/Tempel 1 in July 2005. The fairly large comet Tempel 1 (of size 5 km wide and about 12 km in length) won’t be destroyed or deflected by the impactor.

– **On July 4, 2005, the impactor spacecraft of Deep Impact crashed into Comet 9P/Tempel 1.** The two objects collided at a speed of 10 km/s. The force of this collision generated a tremendous amount of heat and light which served to illuminate the whole area for the Deep Impact flyby spacecraft. The impactor spacecraft was able to capture images of Tempel 1 as it approached, and the last image was taken at an altitude of only 30 km. Data from Deep Impact’s flyby spacecraft instruments indicate an immense cloud of fine powdery material was released when the probe slammed into the nucleus of comet Tempel 1. – The collision encounter of Deep Impact with Comet 9P/Tempel 1 has been watched by a large number of spacecraft instruments (Hubble, XMM–Newton, Rosetta, etc.) as well as by many ground–based observatories around the world. ²⁷¹⁸⁾

Deep Impact’s crash did indirectly reveal the overall compositional nature of Tempel’s sun-warmed outer surface layering, by allowing us to observe the timing with which different types of vaporized ices erupted out of the surface during the first few seconds after the crash.

2714) http://www.esa.int/esaCP/SEMUOWO4KKF_index_0.html

2715) <http://sci.esa.int/science-e/www/object/index.cfm?fobjectid=43369>

2716) Sylvain Lodirot, Andrea Accomazzo, Mathias Lauer, Trevor Morley, Paolo Ferri, Gerhard Schwehm, “The First European Asteroid Flyby – Rosetta operations for the flyby of asteroid 2867 Steins,” ESA Bulletin No 137, Feb. 2009, pp. 68–74, URL: http://www.esa.int/esapub/bulletin/bulletin137/bul137i_lodirot.pdf

2717) “Rosetta triumphs at asteroid Lutetia,” ESA, July 10, 2010, URL: http://www.esa.int/SPECIALS/Rosetta/SEM44DZOFBG_0.html

2718) http://www.nasa.gov/mission_pages/deepimpact/main/index.html

1.26 On–Orbit Servicing (OOS) missions

Space logistics, the ability of on–orbit service provision, is a natural consequence of high–value assets in space (like HST and ISS) as well as of ever increasing satellite fleets in all fields of space endeavors. Without any logistics, satellites have severe limitations affecting their operational life and functional capabilities. The conventional practice in spacecraft and instrument building puts very high demands on reliability resulting in redundant and expensive satellites. With this approach, a spacecraft may still be lost even if the majority of its components are operational. Redundancy in turn produces heavy spacecraft which require extra lift capacity for launch services. ^{2719) 2720) 2721)}

Since the 1970s, several challenging projects around the world have already dealt with OSS supported either by astronauts (Hubble repair missions) or simply by automation and robotics concepts. The emerging technologies of the 21st century may change the conventional practices of the past (at least to some degree) with the introduction of on–orbit servicing technologies and capabilities, in particular with regard to unmanned autonomous satellite missions. The solutions offered by the space industry must be affordable in order to be accepted.

Limitations: There are many physical limitations associated with servicing satellites. The foremost constraint is related to energy needs to achieve orbit. In order to simply achieve LEO (Low Earth Orbit), the required energy, in terms of velocity change, is roughly 9,650 m/s. To achieve MEO (Medium Earth Orbit) this is in excess of 10,000 m/s. Finally, GEO (Geostationary Earth Orbit) requires at least 13,580 m/s. These figures assume launch from a ground–based launch facility with direct injection into the respective orbit. The next largest energy constraint is associated with on–orbit maneuvering. In those cases where orbit–raising, deorbit, or life extension is involved, large amounts of propellant may be required to complete a mission. ²⁷²²⁾

Some examples of servicing or repair missions are:

- On NASA's various Skylab missions (1973–1974), astronauts installed some new equipment (deployment of sunshades and a solar array) and repaired instruments and/or science experiments as well. The early experiences with OOS required space suited humans performing the servicing tasks through EVA (Extra Vehicular Activity) missions.
- Shuttle repair/servicing missions. The first Shuttle repair mission took place in April 1984 (STS–41C). The SMM (Solar Maximum Mission) S/C became the first satellite to be retrieved, repaired, and redeployed in orbit by a Shuttle crew (with the help of Canadarm1). The STS–51A mission (Nov. 8–16, 1984) retrieved two commercial satellites Palapa B2 and Westar–6 (Palapa B2 and Westar–6 were launched on STS–41B on Feb. 4, 1984 and had failed to reach proper orbit). A further Shuttle repair mission occurred on the Discovery flight STS–51–I (Aug. 27–Sept. 3, 1985). The primary mission of the crew was to deploy three commercial communications satellites and to retrieve and repair SYNCOM IV–3 which was deployed during the STS 51–D mission in April 1985 and had malfunctioned. In addition, a middeck materials processing experiment was flown. A rendezvous maneuver was successful in meeting the ailing SYNCOM IV–3 spacecraft; the malfunction was repaired – permitting commands from the ground to activate the spacecraft's systems

²⁷¹⁹⁾ G. Leisman, "Analysis of onboard Servicing Architectures using Microsatellites, Advanced Propulsion, Secondary Opportunities and the Military Spaceplane Concept," Proceedings of the AIAA 2000 Space Conference and Exhibition, Long Beach, CA, Sept. 19–21, 2000

²⁷²⁰⁾ A. Tatsch, N. Fitz–Coy, S. Gladun, "On–orbit Servicing: A Brief Survey," PerMIS 2006 (Performance Metrics for Intelligent Systems), Gaithersburg, MD, Aug. 21–23, 2006, URL: http://www.isd.mel.nist.gov/PerMIS_2006/proceedings/PerMIS_papers/PerMIS06.Final_Tatsch.pdf

²⁷²¹⁾ D. C. Woffinden, D. K. Geller, "The Road to Autonomous Orbital Rendezvous," http://www.mae.usu.edu/aerospace/publications/JDSC_RoadToAutonomy.pdf

²⁷²²⁾ M. H. Kaplan, "The Road to OOS: Enabling Architecture," 2002, http://www.on-orbit-servicing.com/workshop_2002/OOS-Docs-ST6-1/3-3a.pdf

and eventually sending it into its proper geosynchronous orbit. The repair activity involved the first manual grapple and manual deployment of a satellite by a crew member.



Figure 211: NASA astronaut Dale Gardner captured in a daring EVA the malfunctioning WESTAR-6 satellite in Nov. 1984 (image credit: NASA)

Hubble servicing missions:

HST (Hubble Space Telescope) was launched April 24, 1990 on Shuttle flight STS-31. However, after Hubble's deployment, scientist realized that the telescope's primary mirror had a flaw called "spherical aberration." The outer edge of the mirror was ground too flat by a depth of $4\ \mu\text{m}$. This aberration resulted in images that were fuzzy because some of the light from the objects being studied was being scattered. After the amount of aberration was understood, scientists and engineers developed **WFPC2** (Wide Field/Planetary Camera 2) and

COSTAR (Corrective Optics Space Telescope Axial Replacement), which were installed in Hubble during the first space shuttle servicing mission in 1993. – Without periodic onboard servicing, HST would have been a disaster and would not have produced all of the great science it has. ^{2723) 2724)}

- **SM–1** (Servicing Mission–1). The first Hubble repair mission was launched Dec. 2, 1993 on STS–61. Installation of COSTAR. COSTAR deployed corrective optics in front of three of Hubble’s first–generation instruments – the Faint Object Camera, the Goddard High Resolution Spectrometer, and the Faint Object Spectrograph. In addition, SM–1 included the installation and replacement of other components including: solar arrays, solar array drive electronics, magnetometers, two rate sensor units, two gyroscope electronic control units, etc.

After SM–1, Hubble became operational transmitting stupefying images of supernovas, gigantic explosions that marked the death of a star and revealed mysterious black holes in the center of virtually all galaxies. Thanks to these observations, delivered with 10 times the clarity of the most powerful telescopes on Earth, astronomers have been able to confirm that the universe is expanding at an accelerating rate and to calculate its age with greater precision as an estimated 13.7 billion years.

- **SM–2**. The second Hubble service flight was on STS–82 (Feb. 11–21, 1997). The installation of new instruments extended Hubble’s wavelength range into the near infrared for imaging and spectroscopy, allowing to probe the most distant reaches of the universe. The replacement of failed or degraded spacecraft components increased efficiency and performance. The newly installed instruments were: **STIS** (Space Telescope Imaging Spectrograph), **NICMOS** (Near Infrared Camera and Multi–Object Spectrometer).

- **SM–3**. **HOST** (Hubble Orbital System Test). The third Hubble service flight was on STS–95 (Oct. 29 – Nov. 7, 1998). This Shuttle mission provided a unique opportunity to test key pieces of new Hubble hardware before they would be installed in the telescope. By flying in an orbit similar to Hubble’s, the Shuttle allowed engineers to determine how the new equipment on HOST would perform on the telescope. HOST engineers monitored the effects of radiation on Hubble’s new hardware, including an advanced computer, digital data recorder, and cryogenic cooling system. All the new technologies on the HOST platform performed up to expectation.

- **SM–3A**. The fourth Hubble service flight on STS–103 took place Dec. 19–27, 1999. Objective: replacement of gyroscopes (after the third of Hubble’s six gyroscopes failed), a fine guidance sensor and a S/C computer. Installation of six voltage/temperature kits for the S/C batteries. Installation of a new transmitter, solid–state recorder (12 Gbit), and thermal insulation blankets.

- **SM–3B**. A routine servicing mission to HST took place Mar. 1– 11, 2002 on STS–109. Installation of **ACS** (Advanced Camera for Surveys), built by Ball Aerospace for NASA and consisting of three cameras in the spectral range of 0.12–1.0 μm . The WFC (Wide Field Camera) uses a CCD area array of 16 Mpixel (4096 x 4096). The second is a HRC (High Resolution Camera) using a 1024 x 1024 CCD array and a high sensitivity in the UV. The third camera, the SBC (Solar–Blind Camera), is a far–ultraviolet, pulse–counting array that has a relatively high throughput at 121 nm. **SA–3** (Solar Array–3) installation and

²⁷²³⁾ Edwin P. Hubble (Nov. 20, 1889–Sept. 28, 1953) was an American astronomer. He profoundly changed astronomers’ understanding of the nature of the universe by demonstrating the existence of other galaxies besides the Milky Way. He also discovered that the degree of redshift observed in light coming from a galaxy increased in proportion to the distance of that galaxy from the Milky Way. This became known as Hubble’s law, and would help establish that the universe is expanding.

²⁷²⁴⁾ Note: When originally planned in 1979, the Large Space Telescope program called for return to Earth, refurbishment, and re–launch every 5 years, with on–orbit servicing every 2.5 years. Hardware lifetime and reliability requirements were based on that 2.5 year interval between servicing missions. In 1985, contamination and structural loading concerns associated with return to Earth aboard the Shuttle eliminated the concept of ground return from the program. NASA decided that on–orbit servicing might be adequate to maintain HST for its 15 year design life.

PCU (Power Control Unit). Installation of a new experimental cryocooler for NICMOS (70 K cooling to revive its IR vision, and extend its life by several years).

- **SM-4.** The launch **SM-4** (Servicing Mission-4), or flight STS-125 on Space Shuttle Atlantis, took place on May 11, 2009 (landing on May 24, 2009) with seven astronauts aboard (RMS capture, repair and upgrade of the 11,000 kg HST spacecraft at an orbital altitude of 560 km). Five spacewalks are required to refurbish Hubble with state-of-the-art science instruments designed to improve the telescope's discovery capabilities. The goal of the long overdue service mission is to extend the star-gazer's life by at least five years (the 2003 Columbia disaster that saw the shuttle disintegrate as it re-entered Earth's atmosphere, killing all seven crew members was the main reason for the long delay).



Figure 212: STS-125 astronauts navigate the exterior of the Hubble Space Telescope on the end of the remote manipulator system arm, controlled from inside Atlantis' crew cabin (image credit: NASA)

The priorities of the servicing mission are: ²⁷²⁵⁾

- Three Rate Sensor Unit (gyroscope) removal and replacement (only two of the six gyros are currently in operation)
- **WFC3** (Wide Field Camera 3). WFC3 replaces WFPC2 (Wide Field Planetary Camera 2). Use of 4 k x 2 k CCD e2v detector array providing full-frame imaging. – The WFPC2 was originally installed in the first Hubble servicing mission in 1993, and was nicknamed “the camera that saved Hubble” because its special optics were able to overcome the spherical aberration in the telescope's main mirror. ²⁷²⁶⁾
- Science instrument C&DH (Command & Data Handling) system swap out (replacement of a unit that failed in Sept. 2008)

²⁷²⁵⁾ “Space Shuttle Mission STS-125, The Final Visit to Hubble,” NASA Press Kit, URL: http://www.nasa.gov/pdf/331922main_STS-125_Shuttle_Press_Kit.pdf

²⁷²⁶⁾ Nancy Atkinson, “Camera That Saved Hubble is Replaced,” Universe Today, May 14, 2009, URL: <http://www.universetoday.com/2009/05/14/camera-that-saved-hubble-is-replaced/>

- **COS** (Cosmic Origins Spectrograph) installation and replacement of COSTAR of SM–1. COS is a medium resolution spectrograph specifically designed to observe in the near and mid ultraviolet spectral range.
- Battery module replacement installation (Bays 2 and 3). This is the first battery replacement in 19 years.
- Fine Guidance Sensor 2 removal and replacement (it is one of three sensors that help point and lock the telescope on targets)
- Repair of **ACS** (Advanced Camera for Surveys): ACS has been inoperable since January 2007, when its backup power supply system failed. Replacement of the entire electronics box, which will be powered by a separate low-voltage power supply. One piece of new technology is an ASIC, that enables an entire circuit board's worth of electronics to be condensed into a very small package. It will be a part of the new CCD in the CEB (CCD Electronics Box) that will be installed to repair the failed ACS instrument. – The ASIC design is the same as the one already developed and tested for the JWST (James Webb Space Telescope) mission. However, the electronics packaging for Hubble is different because of the different operating conditions such as temperature and electronics environments. ^{2727) 2728)}
- New Outer Blanket Layer installation (Bays 8, 5 & 7)
- Reboost of the HST spacecraft altitude.

On May 18, 2009, the astronauts successfully completed all the EVAs for the Hubble Servicing Mission, accomplishing all the mission goals. ^{2729) 2730)}

The refurbished and upgraded telescope will undergo 3–4 months of re-commissioning, a period during which each of the four cameras and spectrographs either installed or repaired by the Atlantis astronauts will be checked and re-calibrated before scientists resume their observations. – Hubble's upgrade is expected to extend the telescope's life until 2014. In that same year, the NASA/ESA/CSA James Webb Space Telescope (JWST) will launch.

On Sept. 9, 2009, astronomers declared the Hubble Space telescope as recommissioned and operational; it is now a fully rejuvenated observatory with the release of spectacular new images and data from four of its six operating science instruments. ²⁷³¹⁾

On April 24, 2010, the Hubble mission partners (NASA, ESA, CSA) celebrated the 20th anniversary of the spacecraft in orbit – and a mandate to continue its excellent observation services until 2013.

Background: NASA cancelled the next servicing mission (SM–4) of the Shuttle and all follow-up flights to Hubble as of mid-January 2004 due to budgetary problems and to safety concerns. It means that Hubble will remain in orbit as long as it can fulfill its duties, then be brought back into Earth's atmosphere, with reentry expected in 2011. The JWST (James Webb Space Telescope) mission is considered to be the successor of Hubble with a planned launch in 2015.

In May/June 2004, NASA was reconsidering its decision on the SM–4 mission to Hubble due to mounting pressure from the Hubble community and from Congress – to keep the

2727) "Hubble to Receive High-Tech JWST Technology," May 8, 2009, URL: <http://www.spaceref.com/news/view-pr.html?pid=28167>

2728) Timothy J. Cole, "On-Orbit Repair of Satellites using Fastener Capture Plates to Eliminate Debris," 2011 IEEE Aerospace Conference, Big Sky, MT, USA, March 5–12, 2011

2729) Nancy Atkinson, "Hubble Servicing Mission 4 in Pictures, Part 1," Universe Today, May 17, 2009, URL: <http://www.universetoday.com/2009/05/17/hubble-servicing-mission-4-in-pictures-part-1/>

2730) Nancy Atkinson, "uper-Tools Essential to Hubble Mission Success," Universe Today, May 18, 2009, URL: <http://www.universetoday.com/2009/05/18/super-tools-essential-to-hubble-mission-success/>

2731) "Spectacular First Images from the Rejuvenated Hubble Space Telescope," Sept. 9, 2009, URL: http://science.nasa.gov/headlines/y2009/09sep_hubbleimages.htm?list1291671

Hubble mission alive until JWST is definitively in orbit. – A possible robotic mission scenario is considered referred to as **HRSDM** (HST Robotic Servicing and Deorbit Mission). To extend the scientific mission of HST, the robotic mission must launch by the end of 2007 to be of any use. This timing constraint represents a great challenge for the readiness of HRV (HST Robotic Vehicle).^{2732) 2733)} – In Jan. 2005, NASA awarded a contract to MDA (MacDonald Dettwiler and Associates Ltd.) to investigate a potential solution for a robotic servicing mission to rescue HST.

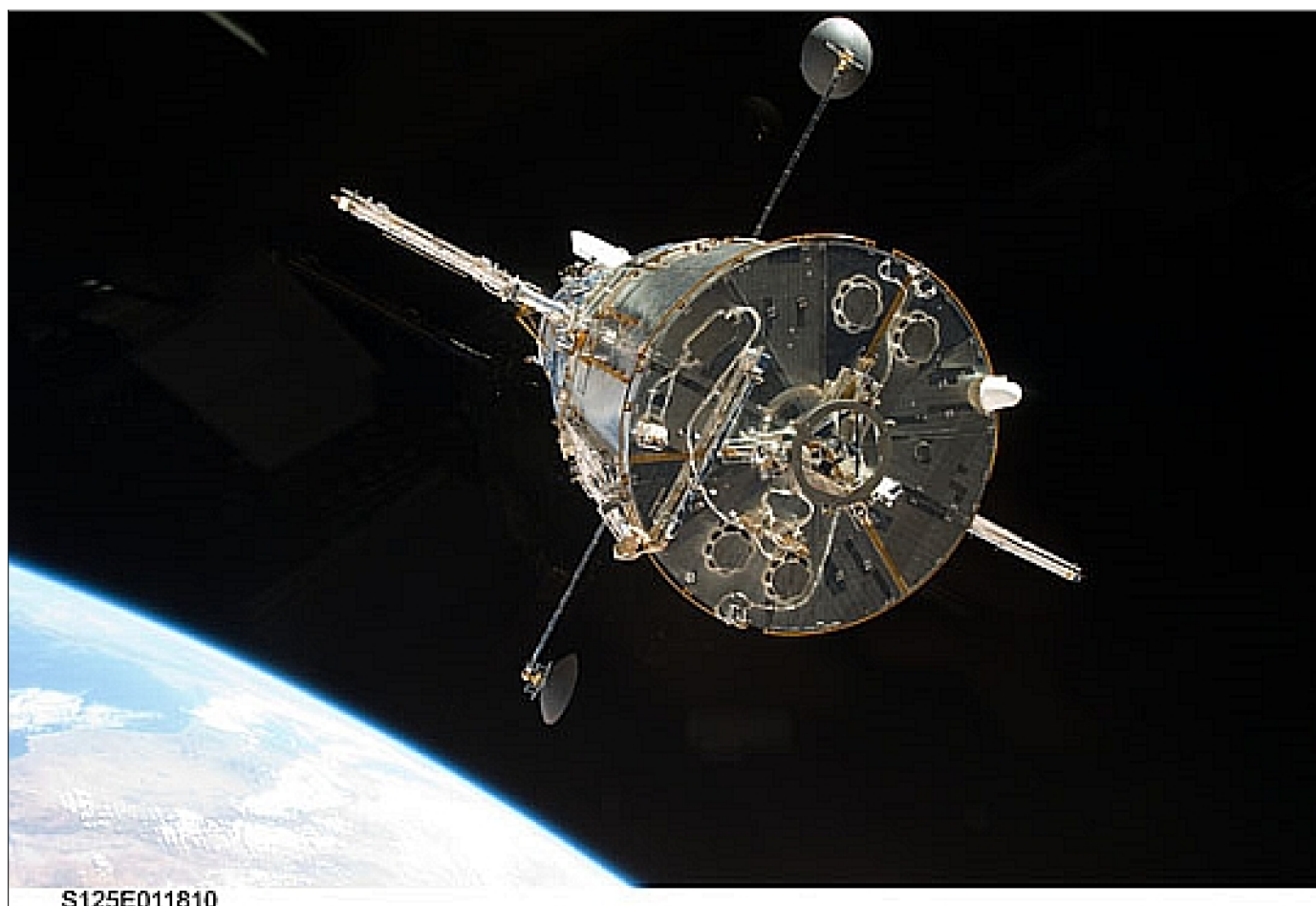


Figure 213: Hubble floats in space after being released by the Shuttle RMS on SM–4 (image credit: NASA)

On Oct. 31, 2006, NASA Administrator Mike Griffin announced new plans for a Hubble repair mission, SM–4 (Servicing Mission–4), for the spring of 2009.²⁷³⁴⁾ The 11–day Hubble flight is designated as STS–125 and slated to launch aboard the Discovery orbiter. The concept adopted is **an astronaut–led Shuttle mission** to Hubble (which voids the robotic servicing mission concept that was studied earlier). The overall objective of SM–4 is to extend the operational life of Hubble at least until 2014.

2732) L. David, “Canadian Company Grapples With Hubble Servicing,” Space News, June 21, 2004, p. 9

2733) D. King, “Saving Hubble,” Proceedings of IAC 2004, Vancouver, Canada, Oct. 4–8, 2004, IAC–04–IAA.4.9.1.05

2734) “NASA Completes Two Important Reviews for Upcoming Hubble Mission,” Spacedaily, April 23, 2007, URL: http://www.spacedaily.com/reports/NASA_Completes_Two_Important_Reviews_for_Upcoming_Hubble_Mission_999.html

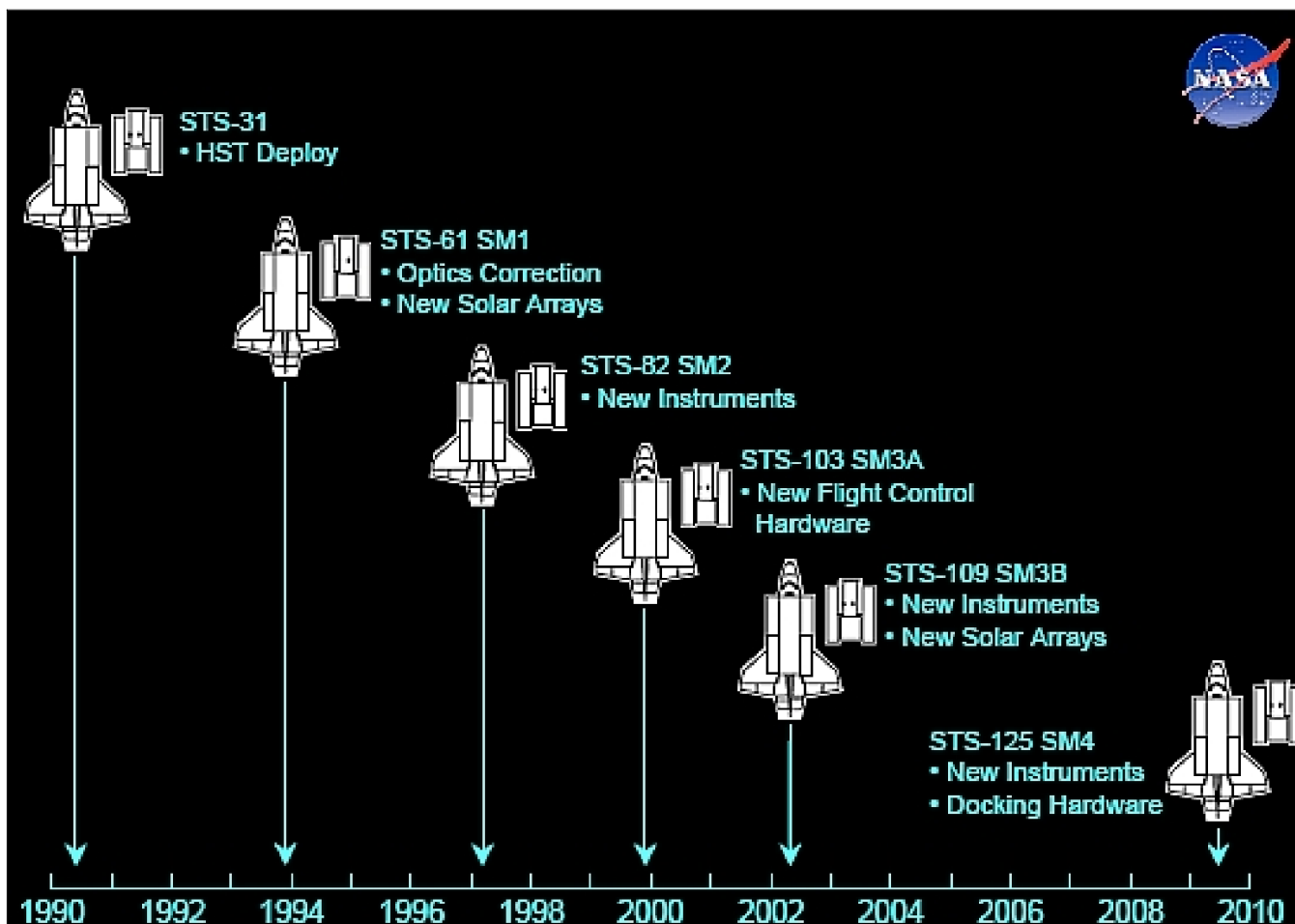


Figure 214: Overview of of Hubble servicing missions (image credit: NASA, USA) ²⁷³⁵⁾

- On March 17, 2014, the HST (Hubble Space Telescope) celebrated its 24th anniversary on orbit. The HST mission is a project of international cooperation between NASA and ESA. ²⁷³⁶⁾
- The various service flights (1987 to 2000) to the Russian MIR Station were used to service/repair some onboard hardware.
- Servicing of a stranded commercial communications satellite (Intelsat 603) by Shuttle flight STS-49 (May 7–16, 1992, inaugural voyage of Shuttle Endeavour). The task required crew EVA (Extra Vehicular Activity) capturing capturing Intelsat 603 and hauling it into the cargo bay (it took a couple of days of troubleshooting to complete the capture task). The crew then attached a new booster to its base and Intelsat 603 was redeployed into GEO. Intelsat 603 continued its operational service life until 2002 when it was replaced by Intelsat 905 (launch June 5, 2002 on Ariane-44L).

Background: Intelsat 603 was launched on Mar. 14, 1990 by a Titan-3 vehicle. Human error led to a mis-wiring of the Titan 3's second stage and the satellite so the two would not separate. The only way to save Intelsat 603 was to separate the S/C from its attached upper stage. Unable to reach its intended orbit, Intelsat 603 was left stranded in a useless orbit for two years.

²⁷³⁵⁾ John L. Goodman, Stephen R. Walker, "Hubble Servicing Challenges Drive Innovation of Shuttle Rendezvous Techniques," AAS 09-013, Proceedings of the AAS Guidance and Control Conference, Breckenridge, CO, USA, Jan. 31.- Feb. 4, 2009

²⁷³⁶⁾ J. D. Harrington, Ray Villard, "Hubble Celebrates 24th Anniversary with Infrared Image of Nearby Star Factory," NASA, March 17, 2014, URL: <http://www.nasa.gov/press/2014/march/hubble-celebrates-24th-anniversary-with-infrared-image-of-nearby-star-factory/#.UycMLs52H5o>

• **The ISS (International Space Station)** build-up era in LEO began in 1998. Service flights to ISS are being provided by the USA and by Russia on a continual basis. The total fleet of vehicles, which will perform RVD/B (Rendezvous and Docking/Berthing) maneuvers with the ISS includes:

- US Space Shuttle (manned missions)
- Russian Soyuz spacecraft (manned missions)
- Russian Progress spacecraft (unmanned autonomous resupply vehicle). See description of Progress below.
- ATV (Automated Transfer Vehicle). ATV is an ESA unmanned autonomous cargo resupply vehicle, put into orbit by the Ariane-5 launcher. The ES ATV version of the Ariane 5 has been designed to place ATV into a 300 km circular low Earth orbit (LEO) inclined to 51.6°. The first launch of AVT (called Jules Verne) took place on March 9, 2008. Jules Verne docked at the ISS on April 3, 2008 (the long wait in orbit was due to the fact that the Space Shuttle flight STS-123 was visiting ISS at the same time).

On Sept. 8, 2008, the ATV automatically undocked on schedule from ISS, loaded with waste and dispensable items from the Station, and ended with a controlled destructive atmospheric reentry in the Pacific Ocean on Sept. 29, 2008.

- HTV (H-II Transfer Vehicle) of JAXA, Japan (unmanned autonomous vehicles).

All unmanned autonomous vehicles have the capability for resupply, to remove waste from the station and re-boost the station to a higher altitude to compensate for atmospheric drag. Hence, the ISS turns out to be the most important application of RVD/B technology introduction in the first two decades of the 21st century.

The capability of on-orbit servicing is of course not limited to Shuttle or Soyuz flights (based on manned servicing techniques developed in the 1980s) resulting in very high service bills for a single mission. Neither is OOS limited to the current (Progress) and future generation (ATV, HTV) of unmanned autonomous spacecraft.

Examples: Small robotic spacecraft in combination with new technologies may in fact be the answer to potential future servicing mission capabilities in such fields as: a) mission repair, b) maintenance and scheduled repair, c) replenishment of consumables, and d) preplanned product improvements and upgrades. The OOS mission architecture will consist of a set of required hardware elements, software programs, protocols, and operational procedures. First experiments with on-orbit servicing have already been conducted.

• **SVS (Space Vision System)**. SVS is a Canadian-built camera system, sponsored by CSA and NASA with its maiden flight (prototype) on Shuttle STS-52 (Oct. 22 – Nov. 1, 1992). Since then, SVS has completed four Shuttle flights. The Shuttle mission STS-88 (Dec. 4 – 15, 1998), an assembly flight with the module Unity to ISS, marked the first operational use of SVS. The primary objective of SVS is to help astronauts perform so-called blind mates of the space station modules. SVS is a computer-aided vision system that works in conjunction with four stationary cameras located inside the Shuttle's cargo bay and two cameras attached to the robotic arm itself. ²⁷³⁷⁾

• **AERCam (Autonomous EVA Robotic Camera)**, a free-flying space camera (of NASA/MSFC). The first demonstration occurred on STS-87 (November 19 to December 5, 1997). The free-flyer, a spherical vehicle of 33 cm in diameter and a mass of 16 kg, has a self contained cold gas propulsion system giving it the capability to be propelled with a 6

²⁷³⁷⁾ B. Berger, "Astronauts Use Space Vision to Assemble Station," Space News, Feb. 1, 1999, p. 10

degrees of freedom control system.²⁷³⁸⁾ Onboard the free – flyer are rate sensors to provide data for an automatic attitude hold capability. The AERCam “Sprint” version, also referred to as AERCam – I, is flown under remote control (teleoperation with hand controllers by a crew member). AERCam employs a pair of stereo cameras for vision feedback to the operator (and ground). AERCam is powered by lithium batteries. Its electrical supply and nitrogen supply (propulsion) are designed to last at least seven hours, the maximum length of a normal spacewalk.

- MiniAERCam (Miniature Autonomous EVA Robotic Camera).^{2739) 2740)} A spherical – shaped free – flying space camera of about 19 cm diameter (NASA/MSFC) using dense packaging and miniaturized components. Two digital cameras are aligned with the + X direction of the vehicle. One of these cameras provides NTSC – standard color video, while the other camera may be used for high – resolution still images. A third color video camera is positioned in the + Y direction for an orthogonal view. MiniAERCam features two custom GPS antennas, one on top and one on the bottom.

The avionics system includes a processor board, a video compression and imaging system, a wireless ethernet (IEEE 802.11b), and a LED array for illumination. A communications antenna is located near the top GPS antenna. Data buses include: RS – 232, I²C, for instrumentation, and LVDS (Low Voltage Differential Signaling) device interfaces. The vision subsystem consists of three CMOS/APS imagers, an onboard video compression system, and an off – board video decompression and display system. The propulsion system employs Xenon. The MiniAERCam program was initiated in 2000, a functional prototype had been designed, developed, integrated and tested by 2002. The functional spectrum of MiniAERCam offers a) visual inspection of space vehicles (ISS), b) to serve as a test platform for evaluating algorithms and relative navigation for autonomous proximity operations, or c) to evaluate candidate sensors and technology. MiniAERCam has a mass of 4.7 kg and a power consumption of 18.2 W.

- Inspector platform family of EADS Astrium GmbH (formerly DASA). The program started in 1993 as a joint project of DASA/Space Infrastructure, RSC Energia, and The Boeing Company. The objective was to monitor events in space (docking maneuvers, etc.) and to extend the inspection capabilities for MIR as well as for ISS. At the start of the 21st century the Inspector family consists of X – MIR and three more service structures (ISS Inspector, Visitor, and Operator) in varying phases of development:²⁷⁴¹⁾

- X – MIR Inspector was launched on its first demonstration flight to the Mir station on Oct. 5, 1997. The prime objectives were to verify the video navigation system and the visual inspection capabilities of X – MIR in the neighborhood of MIR. On Dec. 17, 1997, X – MIR started its demonstration flight as a free – flying observer service module, by orbiting MIR. The successful X – MIR demonstration lasted from 1997 to 1998 providing high – quality video imagery of MIR as well as of the docking sequences of the service vehicle Progress. X – MIR consists of: a) space vehicle, b) monitoring and control station, and c) transport launch container. X – MIR was remotely controlled from MCS (Monitoring and Control Station) onboard the MIR station. MCS consisted of a laptop PC, a video display, a video recorder and an electronic module for radio communications, power distribution and navigation.²⁷⁴²⁾

The prime objective of the ISS Inspector is the inspection of the surfaces of the ISS or visit-

²⁷³⁸⁾ <http://spaceflight.nasa.gov/station/assembly/sprint/>

²⁷³⁹⁾ L. Abbott, “MiniAERCam Avionics,” Proceedings of IEEE Aerospace Conference, Big Sky, MT, Aug. 11 – 14, 2003

²⁷⁴⁰⁾ J. Wagenknecht, S. Fredrickson, T. Manning, B. Jones, “Design, Development and Testing of the Miniature Autonomous Extravehicular Robotic Camera (MiniAERCam) Guidance, Navigation and Control System,” Proceedings of the 26th AAS Conference on Guidance and Control, Breckenridge, CO, Feb. 5 – 9, 2003, Vol. 113 Advances in the Astronautical Sciences, Edited by I. J. Gravseth and R. D. Culp, AAS – 03 – 015, pp. 187 – 205

²⁷⁴¹⁾ “The Inspector Product Family,” brochure provided by F. Steinsiek of DASA/Space Infrastructure, Bremen

²⁷⁴²⁾ H. Günther, “From MIR to ISS – The Inspector Mission,” Proceedings of the 4th International Symposium on Small Satellites Systems and Services, Sept. 14 – 18, 1998, Antibes Juan les Pins, France

ing transportation vehicles (US Space Shuttle, Proton vehicle, etc.). In 1997 NASA selected the Inspector for the AETD (Advanced Engineering and Technology) program. The prime objective of the Inspector for ISS services is the inspection of space vehicle surfaces (video and infrared observations), this includes the ISS and visiting spacecraft. The Inspector payload performs also leakage, contamination and radiation environment monitoring of the ISS.

The Visitor concept is a co-orbiting multi-purpose platform of ISS to be used for various payload operations in the fields of science observations, technology or commercial applications. Visitor is able to carry various kinds of payloads under very low gravity conditions. The payloads are mounted onto standard payload modules, referred to as ORU (Orbital Replaceable Unit) or onto ExPA (Express Pallet Adapter).

- SRMS (Shuttle Remote Manipulator System) of CSA, also known as **Canadarm1** on Shuttle, has enabled on-orbit servicing missions such as payload/satellite deployment, maneuvering, servicing and retrieval, Extra-Vehicular Activity (EVA) astronaut assist, Shuttle inspection and servicing, Orbit Replaceable Unit (ORU) manipulation, as well as on-orbit construction and assembly. In addition to the Palapa B2, Westar-6 and Hubble servicing missions, Canadarm has been involved in the International Space Station (ISS) assembly missions.

SRMS, built by MD Robotics of Spar Aerospace of Canada, is in service since 1981 in the Shuttle program of NASA. A total of five Canadarms have been built and delivered to NASA with delivery dates of: April 1981, January 1983, Dec. 1983, March 1985, and Aug. 1993. Canadarm1, developed by SPAR Aerospace Ltd. of Canada as prime contractor to NRCC (National Research Council of Canada), was first flown and successfully operated on Columbia's second mission, STS-2 (Nov. 12-14, 1981). Canadarm1, with an arm length of 15 m, has performed flawlessly for over 20 years although originally, it was designed for "only" a life of ten years. – Note: In 1999, MD Robotics of Spar Aerospace was acquired by MDA (MacDonald, Dettwiler and Associates) of Richmond, B.C, Canada.

- ROTEX (Robot Technology Experiment), an experimental robotic arm of DLR (Germany), was flown on STS-55 (Apr. 26- May 6, 1993) to demonstrate on-orbit assembly of subsystems. ROTEX successfully completed multiple tasks that include replacement of a simulated Orbital Replacement Unit (ORU) and capture of a free-flying object via on-board and ground teleoperation and autonomous scripts. By accomplishing tasks from autonomous scripts during the experiment, ROTEX became the first autonomous space robotic system.

- SPSR (Space Portable SpectroReflectometer) of NASA (see J.26.5). SPSR is a small battery-powered instrument (16.7 kg) providing solar absorptance measurements on S/C surfaces. The instrument was flown to MIR during the Shuttle STS-86 mission (Sept 27 – Oct. 6, 1997). In early 1998, the SPSR was utilized during various EVA operations to check spacecraft surfaces for optical performance. SPSR was returned to Earth at the conclusion of the STS-89 mission (Jan. 22-31, 1998).

- ETS-VII, a Japanese technology demonstration satellite (launch Nov. 27, 1997) of JAXA (former NASDA). ETS-VII conducted a series of rendezvous, docking, and space robotic technology experiments. For instance, it conducted the first successful release, tracking, and capture of a subsatellite without help from the ground on Sept. 1, 1999. The ETS-VII system consists of two spacecraft: a chaser satellite (Hikoboshi), and a target satellite (Orihime). Some of the key experiments executed during the ETS-VII mission include: ²⁷⁴³

- Visual inspection of onboard equipment by a robotic vision system
- ORU (Orbital Replaceable Unit) handling and simulated fuel supply experiments

²⁷⁴³ P. Malaviarachchi, T. J. Reedman, A. C. M. Allen, D. Sinclair, "A Small Satellite Concept for On-Orbit Servicing of Spacecraft," AIAA/USU Small Satellite Conference, Logan, UT, Aug. 11-14, 2003

- Handling of small equipment by ETS–VII small robot arm including the use of a task-board handling tool
- Handling of truss structures
- An antenna assembly experiment
- Ground teleoperation of the ETS–VII robot
- Handling and berthing of the 410kg ETS–VII target satellite (Orihime) with ETS–VII robot on chaser satellite (Hikoboshi)
- Rendezvous and docking by the ETS–VII Orihime with Hikoboshi.

Engineers commanded the Orihime to float about 200 mm away from the Hikoboshi main satellite body. Then, using a robotic arm and grapple attached to the larger craft, Orihime was retrieved and held firmly in place. The entire capture procedure, including the activation of the robotic arm and extension, was conducted automatically without help from ground control computers.

- Joint NASDA–DLR teleoperation experiments of the onboard robotic arm on ETS–VII were conducted in the time frame April 19–21, 1999. The GETEX (German Teleoperation Experiment) ground control system of DLR was installed at the Tsukuba Space Center and linked to NASDA’s robot experiment system. The following experiments were conducted:

- Evaluating the motion of the satellite attitude during onboard robot arm operations
- World model update for onboard robot operations
- Tele–manipulating the onboard robot using virtual reality technology.²⁷⁴⁴⁾

Previous automatic docking activities, such as those conducted with the Russian Soyuz and Progress S/C, have used either operator assistance or ground control computers. On Oct. 30, 1967, the USSR accomplished the first docking of two unmanned satellites in LEO (Cosmos–186 and Cosmos–188).

- **MSS** (Mobile Servicing System) of ISS was provided by CSA Canada. MSS is a robotics system, developed by MDA (MacDonald Dettwiler and Associates Ltd) Space Systems of Brampton, Ontario, Canada. MSS consists of the following elements:²⁷⁴⁵⁾

- **SSRMS** (Space Station Remote Manipulator System) also known as **Canadarm2**. In April 2001, SSRMS was flown and installed on ISS. The main purpose of Canadarm2 is to assist in the assembly and maintenance of the ISS infrastructure.

- **MBS** (Mobile Base System). With the installation of MBS was in June 2002 (STS–111), SSRMS was able to slide along the main truss of the station (lateral mobility), providing an additional functional capability with four Power Data Grapple Fixtures.

- **SPDM** (Special Purpose Dexterous Manipulator), also known as **Dextre**, was launched onboard Space Shuttle Endeavour (STS–123) in March 2008. Dextre was designed to perform ISS maintenance and servicing tasks with command and control performed by on–orbit crew, using the RWS (Robotics Workstation).

However, after after SPDM’s launch, NASA directed that all SPDM on–orbit activities shall be performed through ground control. The need for SPDM ground control is driven by

²⁷⁴⁴⁾ G. Hirzinger, K. Landzettel, B. Brunner, M. Fischer, C. Preusche, D. Reintsema, A. Albu–Schäffer, G. Schreiber, B.–M. Steinmetz, “DLR’s robotics technologies for on–orbit servicing,” *Advanced Robotics*, Vol. 18, No 2, March 1, 2004, pp. 139–174

²⁷⁴⁵⁾ Mustafa Mirza, Kyle Lee, Aaron Kratt, Richard Rembala, “Enhanced ISS Maintenance and Servicing Through SPDM Ground Control,” *Proceedings of the 60th IAC (International Astronautical Congress)*, Daejeon, Korea, Oct. 12–16, 2009, IAC–09.B3.3.4

the desire to offload robotic tasks from the on-orbit ISS crew. This, in turn, allows more efficient use of the limited on-orbit crew time, and maximizes flexibility in meeting program, engineering, and science objectives. The major challenges of ISS maintenance operations require removing and installing various ORUs (Orbital Replaceable Units). – In 2008, a maintenance task was identified for Dextre that involved the swapping two RPCMs (Remote Power Controller Modules) on the ISS.

- MEPSI (MEMS-based PicoSat Inspector), a technology validation flight (one of six precursor flights) of AFRL on STS-113 (Nov. 23 to Dec. 4, 2002, see M.46). MEPSI, built by The Aerospace Corporation and JPL, contains a pair of MEMS-based picosats (each with a mass of about 1 kg) in a launcher that ejects the two tethered picosats from the spacecraft (16 m tether). The launch system is mounted to a standard Shuttle-provided APC (Adaptive Payload Carrier). The total assembly is called PLA (Payload Launcher Assembly) with a mass of 8 kg. After release, the picosats operate on battery power for several days to complete mission objectives (demonstrate the launch system, establish communications between the two picosats and the ground system). The long-term goal is to establish an autonomous inspection capability.

The launch of the second MEPSI mission, along with MEPSI-2A and -2B, took place on Shuttle flight STS-121 (July 4, 2006). The mission goals include: 1) to demonstrate a MEMS Inertial Rate Measurement Unit (IRMU), and 2) to demonstrate a MEMS Transmit/Receive (T/R) switch.

- XSS-10 (Experimental Spacecraft System-10), a demonstrator microsatellite (31 kg) of the US AFRL (Air Force Research Laboratory), was launched on Jan. 29, 2003 as a secondary payload to the GPS satellite (2R-8) on a Delta-2 launch vehicle from KSC.²⁷⁴⁶ Demonstration of inspection (live video) of the second stage of the Delta-2 launcher (total operation of a day, see M.59.1). Shortly after reaching orbit, the XSS-10 maneuvered about 200 m away from the second stage vehicle, and then approached it taking live video of the target vehicle. XSS-10 featured its own propulsion system, however, no re-docking was involved. The XSS-10 operations were successful and fulfilled all primary mission objectives.

- XSS-11 (Experimental Spacecraft System-11) is a further development of AFRL (launch April 11, 2005). The minisatellite of about 145 kg launch mass is envisioned to explore, demonstrate and flight-qualify some microsatellite technologies. Emphasis is being placed on autonomous on-orbit operations. One of the future mission goals is to collect samples of rocks and soil from Mars and return them to Earth for analysis.

Note: After launch (April 11, 2005), the spacecraft underwent an extended checkout period to verify all functions of components and subsystems. The spacecraft accomplished significant mission milestones by rendezvousing three to four times with the upper stage of the Minotaur launch vehicle at distances between 1.5 km and 500 m. So far, XSS-11 has already completed more than 75 natural motion circumnavigations of the expended rocket body. The fuel consumption and efficiency is good, and the spacecraft is expected to be operational for another year.

- Inspection services during launch and early-orbit phases are already practiced with onboard miniature cameras providing visible proof to the mission operators of such functions as stage separation, antenna deployment, secondary vehicle deployment, and many other onboard activities and events. An example of inspection services is TEAMSAT (M.52), an ESA/ESTEC low-cost satellite demonstrator mission (launch Oct 30, 1997) with VTS (Visual Telemetry System).

- The SNAP-1 nanosatellite mission of SSTL (Surrey Satellite Technology Ltd), UK, with a launch on June 28, 2000 (along with Tsinghua-1 of China) is quipped with MVS (Machine Vision System) permitting SNAP-1 to function as a remote inspector.

²⁷⁴⁶ G. Budris, "Integrating Secondaries on Delta II (Overview of XSS-10)," Proceedings of the IEEE Aerospace Conference, Big Sky, MT, March 6-13, 2004

- Most work on autonomous on-orbit assembly and servicing has been confined to very high-value assets such as ISS. Servicing spacecraft developments considered for ISS are: a) CTV (Cargo Transfer Vehicle) of NASA; b) ATV (Automated Transfer Vehicle) of ESA, a cargo resupply vehicle for ISS to be launched by Ariane-5; and c) HOPE of JAXA.
- OOS (On-Orbit Servicing) upgrade/refurbishment of a spacecraft configuration within the ISS Utilization Program. XEUS (X-ray Evolving Universe Spectroscopy) is an ESA long-term astronomy observatory in study/planning as of 1999–2003 and a potential successor to XMM-Newton (launch Dec. 10, 1999). XEUS will consist of two separate S/C, the MSC (Mirror S/C) and the DSC (Detector S/C), both in LEO and separated at a distance of 50 m (representing the telescope focal length) in FTO (Fellow Traveller Orbit). The mission profile of XEUS foresees several phases: ²⁷⁴⁷⁾
 - An initial LEO observation mission slightly higher than that of ISS for a duration of 4–6 years. The initial configuration (XEUS-1) consists of an X-ray mirror S/C with a 1 keV effective area of 6 m² (diameter of 4.5 m²).
 - Rendezvous and refurbishment of XEUS at ISS. After a period of operations XEUS-1 will visit the ISS to assemble/attach additional mirror elements that have already been transported to the ISS. ²⁷⁴⁸⁾ In this way the initial mirror area of 6 m² will grow to 30 m² (10 m diameter at 1 keV). This will involve the use of ISS robotics such as ERA (European Robotics Arm) for the X-ray mirror assembly. The large aperture mirror required for XEUS is achieved through a new concept: the mirror is made up of segments, known as petals (each of these petals will be aligned using an active system). The assembly approach of XEUS at ISS makes it possible to accommodate an antenna of considerably larger mass, and therefore larger diameter and better surface accuracy.
 - After the refurbishment and upgrade at the ISS, XEUS-2 will return to its FTO where it will continue its astrophysics program, but now with a much enhanced capability (XEUS-2 will be around 200 times more sensitive than XMM-Newton).
- Generally, all OOS activities will be driven by the needs of the satellite owners/operators and the promise of resulting benefits. The overall service concept for OOS missions covers the following spectrum of applications: ²⁷⁴⁹⁾
 - Re-orbiting: move of target to/in its target orbit
 - Deorbiting: move of target to a graveyard orbit or initiation of a destructive reentry
 - Salvage: refers to a salvage of a target (e.g., orbital station or non-destructive reentry)
 - Maintenance: refueling or other resupply of the target
 - Repair: diagnosis and correction or repair of failures or faulty units of a target
 - Retrofit: upgrade and/or assembly of orbital replacement units of the target
 - Docked inspection: system and fault diagnosis of the target using physical connectors
 - Remote inspection: remote system and fault diagnosis of the target.
- A European consortium of companies is developing OLEV (Orbit Life Extension Vehicle) to provide a commercial on-orbit service capability with the objective to extend the

²⁷⁴⁷⁾ R. Licata, M. Parisch, I. J. Ruiz Urien, M. De Bartolomei, G. Grisoni, F. Didot, "Robotic Assembly of Large Space Structures: Application to XEUS, Proceedings of ASTRA (Advanced Space Technology for Robotics and Automation), Workshop, ASTRA 2002, Nov. 19–21–2002 at ESA/ESTEC, Noordwijk, The Netherlands, pp. 133–145

²⁷⁴⁸⁾ P. Laryssa, E. Lindsay, O. Layi, O. Marius, K. Nara, L. Aris, T. Ed, "International Space Station Robotics: A Comparative Study of ERA, JEMRMS, and MSS," Proceedings of ASTRA (Advanced Space Technology for Robotics and Automation), Workshop, ASTRA 2002, Nov. 19–21–2002 at ESA/ESTEC, Noordwijk, The Netherlands

²⁷⁴⁹⁾ J. Kreisel, "On-Orbit Servicing of Satellites (OOS): Its Potential Market and Impact," Proceedings of ASTRA (Advanced Space Technology for Robotics and Automation), Workshop, ASTRA 2002, Nov. 19–21–2002 at ESA/ESTEC, Noordwijk, The Netherlands

operational lifetime of geostationary (communication) satellites. The industrial consortium of SSC (Solna, Sweden), Kayser–Threde GmbH (Munich, Germany) and SENER Ingeniería y Sistemas S. A. (Madrid, Spain) is in charge to develop and industrialize the space and ground segment, while OSSL (Orbital Satellite Services Ltd.) of London, UK is the customer agent for operations support. The OLEV system is building on the SMART–1 (Small Mission for Advanced Research in Technology) platform developed by SSC (Swedish Space Corporation) for ESA (moon mission, launch in 2003).

SMART–OLEV is a further development of the former CX–OLEVTM (ConeXpress–Orbital Life Extension Vehicle) spacecraft concept using a flight proven platform technology to limit the development cost (project reorganization in 2007).^{2750) 2751)} The OLEV tug–based concept employs the cone–shaped payload adapter design of EADS–CASA used on every mission of Ariane–5. Electric propulsion is used both for orbit transfer of OLEV (from GTO to GEO) and stationkeeping. The goal of the SMART–OLEV project is to provide docking services in space to the first GEO client in the timeframe 2010.²⁷⁵²⁾

- The VGS (Video Guidance Sensor) flight demonstrations were flown on Shuttle flights STS–87 (Nov. 19 to Dec. 5, 1997) and STS–95 (Oct. 29 to Nov. 7, 1998)). The VGS system consisted of a video camera (CCD with 484 x 770 pixels) and dual–frequency lasers at 808 and 850 nm. The VGS package was mounted in the cargo bay of the Shuttle, it used the SPARTAN spacecraft, in close proximity of the Shuttle, as its optical target (SPARTAN was equipped with retroreflectors). The lasers illuminated the retroreflectors of the target, the reflected video images provided position information of the target and its distance from the Shuttle. The laser–video system offered improved accuracy over the use of radio frequency control systems for future docking maneuvers. VGS used five VME cards and two power supplies to drive and cool the lasers and camera and to capture and process the video frames into reflected spot coordinated. The VGS locked on when the Shuttle approached SPARTAN within a distance of 150 m. VGS was developed by NASA/MSFC as part of the future AR&C (Automated Rendezvous and Capture) system.

- **Progress cargo ship.** The Space Agency of Russia, Roskosmos, is providing an autonomous unmanned docking capability with its Progress spacecraft – servicing space stations. The Progress support concept is based on single–use cargo freighters (modified Soyuz capsules) – that fly **unmanned as automatic, robot ships under remote control.** The first Progress M cargo ship was launched in August 1989 toward the Mir space station.

Background: The Progress concept of resupply and disintegration on return into Earth’s atmosphere was developed by NPO Energia. It’s roots go back to the Salyut–6 space station era with a first servicing flight in January 1978. A total of 43 Progress flights of the original modification were launched toward Salyut–6 and Salyut7 space stations, and all successfully completed their missions.

Model Progress M1: A so–called “propellant” modification of the spacecraft was developed specifically for ISS (International Space Station), starting in 1998. RKK Energia “repackaged” the middle (refueling) section of the spacecraft to allow the delivery of more fuel to the ISS. The first M1 version of the Progress spacecraft was launched on Feb. 1, 2000 toward the Mir space station. On August 6, 2000, the first Progress spacecraft (M1–3) was launched toward the ISS.²⁷⁵³⁾

Resupply flights to the ISS are scheduled on an average period of 8 weeks, taking about 2500 kg of goods to the station – food, fuel, water, clothing, office supplies, scientific experi-

2750) Clemens Kaiser, Fredrik Sjöberg, Juan Manuel Delcurac, Baard Eilertsen, “SMART–OLEV—An orbital life extension vehicle for servicing commercial spacecrafts in GEO” *Acta Astronautica*, Vol. 63, Issues 1–4, July–August 2008, pp. 400–410

2751) J. M. Del Cura, G. Saavedra, R. Sánchez–Maestro, A. Sebastián, G. Ortega, J.–P. Lejault, “ConeXpress Orbital Life Extension Vehicle (CX–OLEV) GNC,” *Proceedings of the 57th IAC/IAF/IAA (International Astronautical Congress)*, Valencia, Spain, Oct. 2–6, 2006, IAC–06–C1.8.08

2752) M. Leipold, A. Daton–Lovett, “Highly compact deployable and retrievable boom,” *Proceedings of the 57th IAC/IAF/IAA (International Astronautical Congress)*, Valencia, Spain, Oct. 2–6, 2006, IAC–06–C2.2.03

2753) <http://www.russianspaceweb.com/progress.html>

ments to be conducted, replacement parts, newspapers and mail from home, and other necessities.

The day after the disastrous loss of Shuttle Columbia (Feb. 1, 2003), Russia's Progress M-47 flight completed its 100th launch in the series of unmanned automatic cargo carriers when it was blasted to space on Feb. 2, 2003, on a Soyuz-U rocket from the Baikonur Cosmodrome in Kazakhstan. At the ISS on Feb. 4, 2003, Progress M-47 docked automatically with the Zvezda module. The previously docked Progress M1-9 had been undocked on Feb. 1 2003, and deorbited to burn up in Earth's atmosphere. ²⁷⁵⁴⁾

- ROKVISS (Robotic Components Verification on ISS) is a German (DLR) technology experiment, a light-weight manipulator system (the DLR industry partners were Kayser-Threde of Munich and EADS Space Transportation of Bremen). The objective is in-flight demonstration and verification of the ROKVISS functionality, a highly integrated modular robotic structure. ROKVISS is installed on the outside of the Zvezda Service Module of Russia at ISS. The verification includes the demonstration of the joint-elements, as well as the applicability of new robotic control modes for automatic operations for online closed-loop control by the human operator (tele-presence operational mode). ²⁷⁵⁵⁾

A flight of ROKVISS on a Progress service flight M-51 took place on Dec. 23, 2004. ²⁷⁵⁶⁾ The ROKVISS functions and services are planned to be used on future manned and unmanned space missions for handling tasks such as maintenance, repair, assembly, etc.. The experiment basically consists of a robot, an attached pointer, a stereo video and a mono camera system. Since Feb. 2005, ROKVISS is operated by DLR using the Weilheim station (supported by ZUP, Moscow). ²⁷⁵⁷⁾

On Nov. 15, 2010, ROKVISS completed its 5 year mission on ISS. The instrument (7 kg) will be returned to DLR in April 2011 on a Soyuz flight. ²⁷⁵⁸⁾

- DART (Demonstration of Autonomous Rendezvous Technology) is a rendezvous demonstration mission of NASA (launch April 15, 2005). The objective is to test enabling (autonomous) technologies required to locate and rendezvous with other target spacecraft (client) – in particular, to perform and validate close proximity operations and its control between the DART vehicle and a passive target satellite in orbit. The DART spacecraft has been designed and built by OSC (Orbital Sciences Corporation) of Dulles, VA. Once in orbit, DART will rendezvous with the target satellite MUBLCOM (Multiple Paths, Beyond-Line-of-Site Communications) of DARPA, a microsatellite launched May 18, 1999 and equipped with retroreflectors. Over a period of 24 hours, DART will perform several autonomous, close proximity operations with MUBLCOM, including station keeping, docking approaches, and collision avoidance maneuvers. DART employs AVGS (Advanced Video Guidance Sensor), a laser-based optical system (that works with cooperative retroreflectors on the target satellite) incorporating advanced optics and electronics. In addition, it receives a continuous GPS information stream broadcasted from the MUBLCOM satellite to track the satellite within a range of about 100 m.

Note: The DART maneuvers ended prematurely. A NASA investigation after the mishap found that DART had used up its pressurized nitrogen gas maneuvering fuel before it could complete the rendezvous. The investigation board determined that excessive thruster fir-

²⁷⁵⁴⁾ <http://www.spacetoday.org/SpcStns/Progress100thFlight.html>

²⁷⁵⁵⁾ R. Dittmann, M. Turk, W. Paetsch, K. Landzettel, W. Naumann, J. Dalcolmo, "Robotic Components Verification on ISS (ROKVISS)," Proceedings of IAC 2004, Vancouver, Canada, Oct. 4-8, 2004, IAC-04-1.7.01

²⁷⁵⁶⁾ W. Griethe, S. Erb, S. Remus, "Space Communication Concepts for Remotely Operated Systems," Proceedings of the 57th IAC/IAF/IAA (International Astronautical Congress), Valencia, Spain, Oct. 2-6, 2006, IAC-06-B3.1.02

²⁷⁵⁷⁾ B. Rebele, B. Schaefer, A. Albu-Schaeffer, W. Bertleff, K. Landzettel, "Robotic Joints and Contact Dynamics Experiments: Lessons Learned from ROKVISS," Proceedings of the 9th ESA Workshop on Advanced Space Technologies for Robotics and Automation (ASTRA 2006), Noordwijk, The Netherlands, Nov. 28-30, 2006

²⁷⁵⁸⁾ "German Robotic Arm Completes Its Five-Year ISS Mission," Nov. 17, 2010, URL: http://www.space-travel.com/reports/German_Robotic_Arm_Completes_Its_Five_Year_ISS_Mission_999.html

ings in response to incorrect navigational data caused the spacecraft to run out of thruster fuel during its approach, so it could not avoid the low-velocity collision with MUBLCOM. A DART design deficiency was that it couldn't to receive commands from the ground. ²⁷⁵⁹⁾

- A DARPA-funded unmanned rendezvous and docking program is **OE (Orbital Express)**. The overall objective of OE is to demonstrate autonomous on-orbit servicing in the time frame spring 2007 (launch March 9, 2007 of OE) using a system called ARCSS (Autonomous Rendezvous and Capture Sensor System). ²⁷⁶⁰⁾ The mission scenario employs two spacecraft, the ASTRO (Autonomous Space Transfer and Robotic Orbiter) servicing spacecraft (under development at Boeing), and NEXTSat, the S/C to be serviced (under development at BATC). The basic requirement of ARCSS is to provide the parameters of: relative angle, range, position and attitude between the chaser (ASTRO) and client (NEXTSat) to the ASTRO GN&C (Guidance Navigation & Control) system. ²⁷⁶¹⁾ ²⁷⁶²⁾ ASTRO and NextSat were part of a multiple satellite launch, referred to as the Air Force's Space Test Program (STP-1). To line up with NextSat for docking, ASTRO will use a laser sensor system, as well as the AVGS (Advanced Video Guidance Sensor) first flown on DART. – As part of the technology demonstration, requirements called also for development of "industry standard servicing interfaces and protocols" that can be utilized by future spacecraft developers. The OE demonstration is also viewed under the aspect to provide eventually an alternate access capability for ISS logistic serving by commercial providers.

The OE mission servicing demonstration lasted from March to July 2007 – meeting or exceeding all test objectives to become the world's first spacecraft capable of performing autonomous on-orbit servicing functions. ²⁷⁶³⁾

- **BX-1 (BanXing-1)** is a companion (inspection) demonstration spacecraft of the **SZ-7 (Shenzhou-7)** mission, China's third manned spaceship, which was launched on Sept. 25, 2008. The BX-1 spacecraft (40 kg) was built by the Shanghai Engineering Center for Microsatellites / Chinese Academy of Sciences (SECM/CAS), Shanghai, China. BX-1 was deployed in-orbit on Sept. 27, 2008 – by ejecting it from the nose of the SZ-7 orbital spacecraft. The objectives of BX-1 were to demonstrate: ²⁷⁶⁴⁾

- In-orbit ejection from the SZ-7 spaceship
- Image capture demonstration with the on-board cameras of the SZ-7 spaceship from a nearby orbit
- Use of the AOCS and propulsion subsystems of BX-1 to realize companion (formation) flying.

During the first 20 minutes after ejection, BX-1 took videos and imagery of the spaceship, and kept pointing to the spaceship during the imaging phase. In late December 2008, BX-1 was still orbiting in space, free of any problems. On January 6, 2009, the BACC (Beijing Aerospace Control Center) reported that the BX-1 microsatellite finished its mission after 100 days in space.

²⁷⁵⁹⁾ P. Berardelli, "Lots Of Little Errors Caused DART Spacecraft Mishap," Spacedaily, May 17, 2006, URL: http://www.spacedaily.com/reports/Lots_Of_Little_Errors_Caused_DART_Spacecraft_Mishap.html

²⁷⁶⁰⁾ J. Shoemaker, M. Wright, S. Sivapiragasam, "Orbital Express Space Operations Architecture Program," Proceedings of AIAA/USU Conference on Small Satellites, Logan, UT, USA, Aug. 11–14, 2003, SSC03-IV-2

²⁷⁶¹⁾ C. Crumbly, M. Bailey, "NASA's Alternate Access to Station Concept," Proceedings 53rd IAC, Houston, TX, Oct. 10–19, 2002, URL: <http://www.nasawatch.com/iss/10.15.02.sli.alt.access.ppt>

²⁷⁶²⁾ Boeing Orbital Express to Demonstrate New On-Orbit Servicing Capability, March 11, 2007, URL: http://www.spacemart.com/reports/Boeing_Orbital_Express_to_Demonstrate_New_On_Orbit_Servicing_Capability_999.html

²⁷⁶³⁾ "Boeing Demonstrates Future On-Orbit Servicing Capability With Orbital Express," SpaceMart, Aug. 31, 2007, http://www.spacemart.com/reports/Boeing_Demonstrates_Future_On_Orbit_Servicing_Capability_With_Orbital_Express_999.html

²⁷⁶⁴⁾ Zhencai Zhu, Hongyu Chen, Wen Chen, Yilin Zhou, Yong Yu, Caixia Cao, "BX-1: the Companion Microsatellite in Shenzhou-7 Mission," Proceedings of the 23rd Annual AIAA/USU Conference on Small Satellites, Logan, UT, USA, Aug. 10–13, 2009, SSC09-IV-4

- **TriDAR** (Triangulation + LIDAR) is autonomous vision-based relative navigation system developed by Neptec Design Group (Ottawa, Canada) and funded by the Canadian Space Agency (CSA) and NASA. It provides guidance information that can be used to guide an unmanned vehicle during rendezvous and docking operations in space. TriDAR does not rely on any reference markers positioned on the target spacecraft. – Instead, TriDAR relies on a laser based 3D sensor and a thermal imager. TriDAR’s proprietary software uses the geometric information contained in successive 3D images to match against the known shape of the target object and calculate its position and orientation.

The combination of this TriDAR hardware and software create a dynamic, powerful and resourceful system which will enable efficient and reliable docking without the need for traditional target arrays. The AR&D (Autonomous Rendezvous & Docking) system combines a short range, high precision autosynchronous triangulation sensor with a mid- to long-range time-of-flight LIDAR sensor in the same unit. The two sensors share the same optical path and control electronics resulting in a compact package with a multi-range, multi-role capability. ²⁷⁶⁵⁾

NASA tested the TriDAR system on the STS-128 Discovery mission to ISS (Aug. 25. to Sept. 7, 2009). TriDAR provided the astronauts with real-time guidance information during rendezvous and docking with the ISS. It automatically acquired and tracked the ISS using only knowledge about its shape. This event marked the first time a 3D sensor based “targetless” tracking vision system was used in space. Overall the TriDAR systems considered state-of-the-art technology and one of the most advanced vision systems to fly in space. ^{2766) 2767) 2768)}

- **DEOS** (Deutsche Orbitale Servicing Mission): The DEOS (German Orbital Servicing) mission is an in-orbit technology demonstration mission of DLR. The DEOS mission will focus on guidance and navigation, capturing of non-cooperative as well as cooperative client satellites, performing orbital maneuvers with the coupled system and the controlled deorbiting of the two coupled satellites. Various scenarios in the area of rendezvous and docking as well as reentry capabilities will be considered. The goal of DEOS is to demonstrate and validate maintenance and repair technology for space systems and OOS (On-Orbit-Servicing) by the means of robotics technology for many years. A launch of the DEOS satellites is planned for the timeframe 2015 or beyond. ^{2769) 2770)}

²⁷⁶⁵⁾ http://www.neptec.com/pdf/Neptec_TriDAR.pdf

²⁷⁶⁶⁾ “NASA Tests Neptec Vision System on STS-128 for Unmanned Docking Operations,” URL: http://www.neptec.com/News2009/24Aug09_TriDAR_STS128.html

²⁷⁶⁷⁾ “NASA to test Neptec’s TriDAR sensor on the STS-128 Space Shuttle Mission,” URL: http://www.neptec.com/Neptec_TriDAR_WP0809.html

²⁷⁶⁸⁾ Tim Luu, Stephane Ruel, Martin Labrie, “TriDAR Test Results Onboard Final Shuttle Mission, Applications for Future of Non-Cooperative Autonomous Rendezvous & Docking,” Proceedings of i-SAIRAS (International Symposium on Artificial Intelligence, Robotics and Automation in Space), Turin, Italy, Sept. 4-6, 2012, URL: http://robotics.estec.esa.int/i-SAIRAS/isairas2012/Papers/Session%204B/04B_04_luu.pdf

²⁷⁶⁹⁾ D. Reintsema, B. Sommer, T. Wolf, J. Theater, A. Radthke, J. Sommer, W. Naumann, P. Rank, “DEOS – In-flight Technology Demonstration of German’s Robotics Approach to Dispose Malfunctioned Satellites,” Proceedings of ASTRA 2011 (11th Symposium on Advanced Space Technologies in Robotics and Automation), ESA/ESTEC, Noordwijk, the Netherlands, April 12-14, 2011, URL: <http://robotics.estec.esa.int/ASTRA/Astra2011/Papers/00/FCXNL-11A06-2145230-1-2145230wolf.pdf>

²⁷⁷⁰⁾ F. Sellmaier, M. Plura, M. Stelzer, A. Ohndorf, H. Müller, K. Landzettel, “Mission Operations Concepts for Robotic Missions,” Proceedings of IAC 2011 (62nd International Astronautical Congress), Cape Town, South Africa, Oct. 3-7, 2011, paper: IAC-11-B6.2.7

1.27 Satellite Radionavigation Systems

Radionavigation refers to the determination of position, velocity and/or other characteristics of an object, or to obtaining information relating to these parameters, by means of the propagation properties of radio waves.

Radionavigation systems employ the concept of triangulation with line-of-sight radio signals from different satellites to find position – in the same fashion that angular measurements of distant stars were made (and are still being made) throughout the maritime navigation history to find position. Instead of angular measurements to natural stars, **the new systems (GPS and GLONASS) introduced the concept of radio-ranging measurements (pseudorange) as observables.** In this triangulation scheme, the user's receiver determines the distance from the user to each of several satellites. Since the positions of the satellites are known, either through previous publication or as part of the satellite's broadcast information, the user's position can be determined (only the satellite signals are needed).

The currently operational second generation of satellite radionavigation systems (GPS in particular, GLONASS), dual-use service systems for the military and civil communities, started nothing less but a revolution in navigation applications, permeating all facets of society, i.e., providing global services to those traditionally involved with navigation (aviation, shipping, space flight) as well as the ever-increasing segment of classical non-navigators [utility networks (gas, electricity, water, mobile phones, financial transactions, travel support, assistance for disabled people, road and railway transport services, etc.), steering of assembly lines in manufacturing, tracking and location-based services (farming, hazard tracking, emergency response, security services, information on points of interest, etc.), timing standard, etc.]. At the start of the 21st century, civil GPS applications far outnumber the military applications, both are beginning to play an increasing role in national economies.

Since neither the current GPS nor the GLONASS (nor the future Galileo) constellations are able to provide all aviation positioning requirements, so-called wide area augmentation systems are being developed to provide enhanced performance services of integrity, availability, and continuity monitoring on a regional scale. The topic of network service security (protection against unintentional signal interference and potential jamming threats or actions) is also an important upgrade aspect. The US WAAS (Wide Area Augmentation System) is expected to provide an initial operational service capability in 2003.

1.27.1 LORAN (Long-Range Navigation) and other pre-GPS systems

Land-based radionavigation came into existence with the development of the Decca Navigator system of Decca Radio and Television Ltd. of London, UK; it was initially used for guiding the leading minesweepers and landing craft in the Allied invasion of Normandy during World War II. The system was originally conceived by W. J. O'Brien (USA) in the time frame 1936–39 as a method of measuring the ground speed of aircraft for trial purposes, and was indeed originally called an "Aircraft Position Indicator." The Decca system was one of the first to give the user a position, rather than a series of bearings. Decca is based around a chain of master transmitting stations, each one backed up by a trio of slave stations (low-frequency hyperbolic navigation system, it worked by comparing the phase difference of radio signals emitted by several radio stations). DECCA services covered much of western Europe, parts of Canada, the Persian Gulf and the Bay of Bengal.

- LORAN is a ground-based hyperbolic radionavigation system (the term 'hyperbolic' refers to the reflected ionospheric transmissions) which uses the difference in the time of arrival of signals from individual transmitters to establish position. Historically, LORAN was developed at MIT (DoD funded) during World War II as a navigation aid, known as LORAN-A. The operation of LORAN-A was in the 1850–1950 kHz radio band.

LORAN–A had a range of 1000 km. Later **LORAN–B** was developed to improve the accuracy of **LORAN–A**. The USCG (US Coast Guard) Coast Guard, a participant in the development of **LORAN**, took overall responsibilities for **LORAN** in the 1960's. In 1958 **LORAN–C** became operational; it was also used commercially for marine navigation. **LORAN–C** was designated as an approved navigation system for the coastal modes of maritime navigation. It provided excellent coverage and enjoyed widespread use along all US Coasts and the Great Lakes. In 1974, the **LORAN–C** system was transferred to civil authority (DOT). Later, FAA extended **LORAN–C** coverage to include the continental USA because **LORAN** applications are not limited to marine users. It can and has been developed and used by all modes of transportation as well as non–transportation applications such as radiosondes for weather balloons. Before the widespread use of GPS, **LORAN–C** attracted considerable attention from civil aviation users because of its Area Navigation (RNAV) capability. RNAV systems are aircraft navigation systems that can, at a minimum, calculate the aircraft position at any point in the service area.

LORAN–C is a long–range (in excess of 1850 km), low–frequency (90 – 110 kHz) radio–navigation system comprising transmitters, control stations, and SAM (System Area Monitors). The basic element of a **LORAN** navigation system is the **LORAN** chain, consisting of one master and two to six transmitter stations. A **LORAN–C** user receiver measures the time difference (TD) between the arrival of a pulse from the master transmitter and a secondary transmitter of a particular chain. Like any radionavigation system, **LORAN–C** depends fundamentally on precise time and frequency to deliver its services. **LORAN–C** transmissions consist of groups of eight or nine accurately timed and phase–coded pulses at a carrier frequency between 90 and 110 kHz. Each chain consists of a master and a number of slave transmitters.²⁷⁷¹ – In the mid 1960's **LORAN–D** (a low power transportable system with a range of 1100 km) was developed by the USAF. – **LORAN** signals propagate as a ground wave, but sky waves reflected from the ionosphere are also received. – In the early 1990s, DoD declared that by the end of 1994, there would be no further military requirement for the system and authorized the transfer of **LORAN–C** assets to host nations for civil use. The USA planed to terminate **LORAN–C** operations on Dec. 31, 2000.

A rebirth of **LORAN–C** in Europe was initiated in 1992 as a result of an international agreement between the US and six European countries (Denmark, France, Germany, Ireland, the Netherlands, and Norway), known as NELS (Northwest European **LORAN–C** System). The NELS network, consisting of nine stations with a control center at Brest (France), started operations in 1999. In Europe the timing of all NELS stations, Master and Secondaries, are synchronized to UTC to allow “rho–rho” position finding. This way of timing also eases integrating Loran–C and GPS pseudorange in a single position estimation algorithm. The performance characteristics of the NELS network are: absolute location accuracy of 100–460 m; repeatable accuracy of 20–100 m; availability per station of 99.9%; and availability per chain of 99.7%. A policy recommendation of IALA (International Association of Marine Aids and Lighthouse Authorities) states that the future use of radionavigation be based on complementary satellite and terrestrial systems.^{2772) 2773)}

In 2000, the EC (European Commission) initiated a project called GLORIA (GNSS and **LORAN–C** in Road and Rail Applications) in the framework of the European IST (Information Society Technologies) program. The objective is to analyze the combination of **LORAN–C**/GNSS also with other systems, e.g., dead reckoning components. with respect to possible improvements of the reliability and availability of the position determination. This combination is expected to strengthen the reliability and availability of position deter-

2771) Note: The **LORAN** system was important to the development of GPS because it was the first system to employ time difference of arrival of radio signals in a navigation system, a technique later extended to the NAVSTAR satellite navigation system.

2772) G. M. Hermes, “NELS Status – Operational and political status,” GNSS 2003, Graz, Austria, April 22–25, 2003

2773) U. Klinge, “A European Approach for an Integrated System – **LORAN–C**/Eurofix,” Galileo's World, Vol. 1, No 1, Winter 2000

mination and opens the door to new applications and to major improvements in the redesign of existing road and rail applications.²⁷⁷⁴⁾

Lately, LORAN–C receives new attention due to the vulnerability of GNSS to all kinds of interferences.²⁷⁷⁵⁾ There are five significant breakthroughs that brought LORAN–C into the current high–tech century: improved transmitter time–of–emission control accuracy, autonomous integrity messaging by the stations (blink), gained knowledge of the ASF (Additional Secondary Factor), the capability to broadcast data via LORAN–C and, finally, the development of high–performance receivers that process all signals in view, irrespective in which chain these stations operate.

Eurofix (developed in the 1990s at Delft University of Technology) is an integrated Navigation system, which combines GPS and LORAN–C. The LORAN–C signals are additionally modulated to broadcast differential GPS and especially integrity information.²⁷⁷⁶⁾ A Eurofix user can correct and validate GPS observations and calculate his position. The accurate GPS position is then used to calibrate the LORAN–C ranges to determine the unknown ASF. In case GPS becomes unavailable, for instance due to shadowing or interference, calibrated LORAN–C can be used to continue positioning. The dissimilarity of the Loran and GPS signals decreases the probability that they both will be unavailable at the same time.

In 2002 the USA revised its LORAN–C plans. The FPR (Federal Radionavigation Plan) of DOT and DoD, reasserts the DOT policy to continue to operate LORAN–C “in the short term while evaluating the long–term need for the system.” Recently, there has also been research in modulating data onto LORAN–C for DGPS (Differential Global Position System) corrections and WAAS (Wide Area Augmentation System) broadcasts. LORAN–C may also be used to aid GPS in cases of weak signal availability. In the end, LORAN–C might become a redundant navigation system for GPS if all FAA performance requirements can be satisfied.^{2777) 2778)}

There are other radionavigation systems aside from LORAN: The US Omega [a global VLF (Very Low Frequency) band radionavigation system, developed in the post WW–II era], uses phase differences of continuous–wave radio signals (see Glossary on Omega). Further systems in the same class are: VOR/DME (VHF Omnidirectional Range/Distance Measuring Equipment), and TACAN (Tactical Air Communication and Navigation).

eLORAN (enhanced LORAN): eLORAN is an internationally–standardized PNT (Positioning, Navigation, and Timing) service for use by many modes of transport and in other applications. It is the latest in the longstanding and proven series of low–frequency, LORAN (LONg–RANGE Navigation) systems, one that takes full advantage of 21st century technology.

- eLORAN meets the accuracy, availability, integrity, and continuity performance requirements for aviation non–precision instrument approaches, maritime harbor entrance and approach maneuvers, land–mobile vehicle navigation, and location–based services, and is a precise source of time and frequency for applications such as telecommunications.

2774) M. Maurer, “The GLORIA Project Integration of GNSS Receivers with LORAN–C/Eurofix,” NAVITEC 2001, 1st Workshop on Satellite Navigation User Equipment Technologies, Dec. 10–12, 2001, ESA/ESTEC, Noordwijk, The Netherlands

2775) W. J. Pelgrum, D. van Willigen, “Loran–C Challenges GNSS: From a Quarter Nautical Mile Down to Meter–Level Accuracy,” GNSS 2003, Graz, Austria, April 22–25, 2003

2776) A. W. S. Helwig, G. W. A. Offermans, W. J. Pelgrum, R. Kellenbach, D. van Willigen, “The Best of Two Worlds: GPS+Loran–C Snugly Together in a PocketPC–sized Device,” GNSS 2003, Graz, Austria, April 22–25, 2003

2777) S. Lo, P. Enge, L. Boyce, B. Peterson, T. Gunther, B. Wenzel, Booz Allen Hamilton; K. Carroll, K. Bridges, M. Narins, “The LORAN Integrity Performance Panel,” ION–GPS 2002, Portland, OR, Sept. 24–27, 2002

2778) B. Peterson, “The Development and Deployment of Receiver Technology to Evaluate eLoran Performance,” GNSS 2003, Graz, Austria, April 22–25, 2003

- eLORAN is an independent, dissimilar, complement to Global Navigation Satellite Systems (GNSS). It allows GNSS users to retain the safety, security, and economic benefits of GNSS, even when their satellite services are disrupted.

The eLORAN system meets a set of worldwide standards and operates wholly independently of GPS, GLONASS, Galileo, or any future GNSS. Each user's eLORAN receiver will be operable in all regions where an eLORAN service is provided. eLORAN receivers shall work automatically, with minimal user input.

The core eLORAN system comprises modernized control centers, transmitting stations and monitoring sites. eLORAN transmissions are synchronized to an identifiable, publicly-certified, source of UTC (Coordinated Universal Time) by a method wholly independent of GNSS. This allows the eLORAN Service Provider to operate on a time scale that is synchronized with but operates independently of GNSS time scales. Synchronizing to a common time source will also allow receivers to employ a mixture of eLORAN and satellite signals.

Background on eLORAN: In September 2001, almost simultaneously with the “9/11” act of terrorism, the US Government published its “Volpe Report”⁴. This spelled out the degree to which the US, like other nations worldwide, was starting to base its critical infrastructures on GPS. The Report explained the vulnerability of GPS (and similar GNSS systems) to disruption by intentional or unintentional interference. It identified Loran as a potential solution to this important problem. This attracted interest worldwide, and provided an impetus to modernize the Loran system in the USA.²⁷⁷⁹⁾

– A team representing 40 international government agencies, companies, and universities and led by the U.S. FAA (Federal Aviation Administration), developed eLORAN technology in response to the 2001 Volpe Report on GPS vulnerability. The team showed that existing Loran-C assets modernized to radiate eLORAN, plus high-performance digital receivers, could meet a wide range of U.S. national and international requirements. These included harbor entrance maneuvering by ships, nonprecision instrument approaches by aircraft, and the Stratum 1 frequency standard and UTC timing required by the telecommunications industry.

– In 2008, the Department of Homeland Security announced that the U.S. was adopting eLORAN as its national GPS backup. The 2008 U.S. announcement to proceed with eLORAN led to an upsurge of interest in converting stations and operations from LORAN-C to eLORAN.

– The United Kingdom, stating that “robust, reliable and high-performance PNT (Positioning, Navigation and Timing) service is the lifeblood of modern society's critical infrastructure,” deployed a new station for eLORAN. Together with LORAN-C stations in France, Germany, Norway and the Faroe Islands, the UK now provides a prototype eLORAN service around the clock.

– While the USA selected eLORAN as backup to GPS in 2008 – the eLORAN service was dropped in 2010 by the US government (no budget available).²⁷⁸⁰⁾

²⁷⁷⁹⁾ “Enhanced Loran (eLoran) Definition Document,” Report Version: 1.0, 16 October 2007, URL: <http://www.loran.org/ILAArchive/eLoran%20Definition%20Document/eLoran%20Definition%20Document-1.0.pdf>

²⁷⁸⁰⁾ Phillip W. Ward, “GNSS Robustness: The Interface Challenge,” Proceedings of ION GNSS 2010, Portland, OR, USA, Sept. 21–24, 2010

1.27.2 The Transit System

The first generation spaceborne operational radionavigation systems, **Transit** (Navy Navigation Satellite System, USA) and **Tsyklon** (USSR), were mostly reserved for military use; however, they were of pivotal importance due to the insights gained in the nature of navigation and the considerable advances in early space–age technology. The Transit constellation employed the concept of Doppler measurements. Unlike the purely geometry satellite triangulation, the “new dynamic satellite orbits” were computed by using Kepler’s laws of celestial mechanics and the gravity field of the Earth. These led to a trail of 3–D satellite coordinates, as a function of time, with Transit–Doppler measurements providing the observations. Together, they produced relatively quickly (i.e., within 30 minutes) geodetic positions of ground points, without the need for an extensive network of satellite triangulation. However, due to the substantial uncertainties in the values of the parameters of the gravity field, and the other complex models affecting the motion of these satellites in the 1970s, these results were less accurate than those obtained by satellite triangulation. ²⁷⁸¹⁾ ²⁷⁸²⁾ ²⁷⁸³⁾

The Transit and Tsyklon constellations were eventually followed by second generation navigation systems, namely **GPS** and **GLONASS**, which were again developed, built and operated by the military services; but their use was so revolutionary and universal, that the civil community was permitted to use this new utility as well.

- Transit navigation program (US Navy, see H.7). ²⁷⁸⁴⁾ The first operational US navigation satellite was Transit–1B (designed and built at JHU/APL), launched April 13, 1960 aboard a Thor–Able rocket from Cape Canaveral. Starting with Transit–5A–3 (launch June 16, 1963), each satellite in the series featured a gravity–gradient boom for stabilization and had a total mass of about 55 kg (polar circular orbits at altitudes of about 1100 km). Transit is generally credited with demonstrating the feasibility of using artificial satellites as navigational aids. By the end of 1962, a first position fix could be performed by a Polaris vessel. The Transit system was used by the US Navy in 1964, it became fully operational in 1966 (12 S/C constellation with seven operational and five stored S/C in orbit). ²⁷⁸⁵⁾ ²⁴⁷⁸⁾ ²⁷⁸⁶⁾ The satellites broadcast their signals on two frequencies: 150 and 400 MHz. The dual–frequency method was introduced for the first time (on Transit–1B) to correct for ionospheric refraction effects (the 2nd frequency enabled the distortion to be cancelled out). – The Navy’s Transit (2–D) navigation system allowed the user to determine position by measuring the Doppler shift of the received signal (constant tone broadcast – the frequency of 150 MHz was transmitted to correct for ionospheric delay). The 2–D system did not permit velocity determination.

In 1967 the Transit system was released for non–military purposes, a benefit to broad ocean navigation. The Transit series reached a peak utilization of about 100,000 commercial and military users in the late 1980s. The Transit system was decommissioned on Dec. 31, 1996. For over three decades the experience and use of the Transit system influenced considerably the field of geodetic positioning techniques, in particular the development of the emerging GPS (Global Positioning System).

One of the technologies required to make Transit possible was a considerable improvement on time and frequency standards. To realize the fixed site survey accuracy of 1 m, the satel-

²⁷⁸¹⁾ V. Ashkenazi, “GNSS: A Global Enterprise?,” Proceedings of GNSS 2003, Graz, Austria, April 22–25, 2003, Plenary Opening Session: Keynote Presentation

²⁷⁸²⁾ B. W. Parkinson, T. Stansell, R. Beard, K. Gromov, “A History of Satellite Navigation,” Navigation, ION, Vol. 42, No. 1, Special Issue, Spring 1995, pp. 109–164

²⁷⁸³⁾ B. W. Parkinson, “GPS Eyewitness: The Early Years,” GPS World, September 1994, pp. 32–45

²⁷⁸⁴⁾ R. J. Danchik, “An Overview of Transit Development,” JHU/APL Technical Digest, Vol. 19, No 1, 1998, pp. 18–26

²⁷⁸⁵⁾ Note: Some benefits of satellite navigation are: precise, all–weather, worldwide availability, timekeeping capability, and unified reference coordinates.

²⁷⁸⁶⁾ Note: To achieve the required accuracy of the Transit system position measurement, APL had to develop a time standard several orders of magnitude more precise than existing devices (time frame of 1958/59).

lite Doppler signal at 400 MHz must be measured to 0.0005 Hz (a resolution of 5×10^{-12}). In 1960, the best standards of frequency were only good to resolve 5×10^{-10} and could only measure the 400 MHz carrier to 0.2 Hz. APL established a precision time and frequency facility to support the necessary development of various equipment needed for Transit.

- Timation (Time Navigation) program. A US Navy satellite navigation system, initiated in 1964, designed by NRL (Naval Research Laboratory), with the objective to explore the idea of continuous navigation – of providing both accurate position and precise time to passive terrestrial observers (passive ranging). Timation–1, a small (39 kg) gravity–gradient stabilized satellite, was launched May 31, 1967 (VAFB, Thor Agena–D) into a 810 km polar orbit (as a secondary payload, along with GGSE–4, –5, Calsphere–3, –4, NRL–PL–153, –154, and –159). Timation–2 was launched Sept. 30, 1969; both S/C flew with stable quartz oscillators. The STR (Side Tone Ranging) signals were transmitted with a continuous Doppler tracking beacon at about 400 MHz. The experience with the new time system of Timation was a technology demonstrator for future missions.

- In 1964, SAMSO (Space and Missile System Organization) of the USAF in El Segundo, CA initiated a parallel navigation system program to that of the Navy, referred to as ‘**Project 621 B**’, with the objective to use a constellation of satellites for navigation signal transmission from highly eccentric orbits of 24–hours periods. First signal propagation tests were conducted in 1969 using ATS–5 of NASA. Then in 1972, a four–channel airborne receiver was tested with signals transmitted from the ground (satellite signal simulation) at Holloman AFB, NM. The demonstration used a new type of signal, modulated with a PRN (Pseudo Random Noise) code, to provide ranging and timing data. The signal modulation technique used a repeated digital sequence of random bits – that permitted a navigation user device to detect a start (“phase”) of the repeated sequence. Recognition of the repeat sequence allowed to determine the range to the signal emitter (satellite). The PRN (spread spectrum) technology turned out to be a key ingredient for GPS signal ranging (see Glossary).

1.27.3 NAVSTAR/GPS (Global Positioning System)

GPS is the operational global navigation system of the US. The nominal space segment consists of the GPS satellites with an operational constellation of 24 satellites: 21 operational satellites plus three active spares. The GPS constellation is deployed at MEO (Medium Earth Orbit) altitudes of about 20,000 km, in six orbital planes (orbital plane separation of 60°), providing periods of about 12 hours (2 orbits/day). A ground repeat track of a GPS satellite is achieved in 1 sidereal day. See also chapter H.5 for a description of GPS.

Background: Start of the NAVSTAR/GPS program took place in April 1973 (a joint-services program on DoD direction) by merging of the Timation and 621 B programs. The proposed new system concept integrated the basic concept of Timation, employing passive ranging precision clocks (time-of-propagation measurements by the user), and the PRN signal technology of Project 621 B – for an eventual constellation of multiple satellites in circular orbits for global coverage. The new GPS measurement technique employs the “time difference-of-arrival” concept (requiring the simultaneous view of four satellites) rather than the Doppler shift of its predecessor system, Transit, to determine position.

- The first spaceborne atomic clocks were flown in the GPS pre-series concept validation program of NRL, referred to as NTS (Navigation Technology Program – previous name was ‘Timation’). NTS-1 (a renamed and modified Timation-2A satellite), a three-axis stabilized S/C, was launched on July 14, 1974 into a 13900 km orbit, the payload included two modified commercial rubidium oscillators (Efratom, Munich). The navigation signals were transmitted in L-band. NTS-2 was launched June 23, 1977 from VAFB and placed into a 12 hour (semisynchronous) orbit – later used by the GPS satellites. The NTS-2 payload included two cesium clocks (Frequency and Time Inc.) and the PRN code generator. The signals were in L-band and modulated with a PRN code. NTS-2 was actually the first test satellite that contained the basic system features of the soon-to-follow GPS satellites. ²⁷⁸⁷⁾
- Launch of the first GPS-series navigation satellite, called NAVSTAR-1 (built by Rockwell International), on February 22, 1978 and declared operational March 29, 1978 (see Table 674 of GPS launches). The first full GPS constellation with 21 operational satellites was reached in 1994. On February 17, 1995, the FAA announced that GPS is now operational and is an integral part of US air traffic control system. The US Air Force Space Command declared the **GPS system operational as of July 17, 1995** for the international user community. The year 1995 is certainly a historic navigation event; for the first time in history, military and civil users could access an all-weather, day-night, global positioning and timing system. – *At the end of the 1990s, GPS rapidly became an integral component of an emerging global information resource and infrastructure. GPS is probably the best example of a technology which started its life as a military tool and then developed into a global multi-faceted civilian utility. The beneficial applications and influence of GPS are comparable to those of the PC, the mobile phone, internet, and electricity. GPS is a generous gift of the American people, without any service charge, to the whole world.* ^{2788) 2789) 2790)}
- All GPS satellite signal radiation of the GPS constellation (at 20,000 km altitude) is directed toward Earth, providing coverage in particular for “Earth-bound” users, this includes also S/C in the envelope of LEO and MEO orbits. Naturally, coverage will decrease with altitudes approaching those of the GPS constellation and beyond (GEO, etc.).
- With the deployment of the GPS constellation, the SA (Selective Availability) service has been used to degrade the GPS signal (L1) for the civil community while retaining the

2787) Hugo Fruehauf, “GPS Basics to GNSS Future,” October 2008, URL: http://www.frequelec.com/gps_gnss/gps_basics-gnss_future_10-08.pdf

2788) M. Shaw, P. Levin, J. Martel, “The DoD: Stewards of a Global Information Resource, The NAVSTAR Global Positioning System (GPS),” Proceedings of ION GPS-97, Sept. 16–19, 1997, Kansas City, MO, pp. 1237–1243

2789) V. Ashkenazi, “Directions 2002,” GPS World, Dec. 2001, p. 11

2790) G. Seeber, “Directions 2002,” GPS World, Dec. 2001, pp.20

higher – accuracy signals for US and allied military forces (as well as for approved receivers of NASA satellite projects).

S/C Generation & (No of S/C)	Period of launches	Comment	Manufacturer
Block I (11)	1978–1985	S/C were able to sustain on–board operations for up to 3.5 days between navigation message uploads from the ground.	Rockwell International, Seal Beach, CA
Block II (9)	Feb. 1989 – Aug. 1990	Incorporation of radiation–hardening capabilities is a significant improvement of the block–II design	Rockwell International, Seal Beach, CA
Block IIA (20)	Nov. 1990 – Nov. 1996	Normal operations were performed on a daily basis to account for orbital perturbations and to provide accurate ephemeris data	Rockwell International, Seal Beach, CA
Block IIR (21)	Jan. 1997 – GPS– IIR–9, 3.3.2003	Enhanced autonomous S/C operations (AutoNav) for up to six months; improved navigation accuracy	Lockheed Martin, Valley Forge, PA
Block IIR–M	GPS IIR–M1, 2004	Modernized Block IIR for 8 out of 21 in the series; M–code for military use, new civil L2 transmitters	Lockheed Martin, Valley Forge, PA
Block IIF (33)	GPS IIF–SV1 May 28, 2010	Crosslink communications within constellation, L5 signal capability, 12 years design life	Boeing Company, formerly Rockwell
Block III (or GPS III)	2014 (next generation SV)	First 8 S/C were authorized in 2008. Capabilities: New L1C signal, higher GPS signal power, longer SV lifetime, higher signal availability.	Based on Lockheed–Martin A2100A bus ²⁷⁹¹⁾

Table 155: Overview of GPS satellite generations ²⁷⁹¹⁾

- **Removal of the SA (Selective Availability) feature** for the GPS constellation signal on May 2, 2000 (the SA levels were set to zero at 0400 UT). ^{2792) 2793)} The Presidential Directive (of US President Bill Clinton) permits civil users worldwide general access to the highest–possible accuracy of GPS signals. Ionospheric effects are now the major source of signal error.

Background on GPS policy: A March 26, 1996 Presidential Directive (PD) promised to review the SA issue every year starting in 2000, and to remove SA in 2007 at the latest. The PD of Bill Clinton provided a strategic vision for the management and use of GPS, introducing the system to be for “dual–use” purposes and to have Selective Availability (SA, also spelled S/A), an intentional degradation of public GPS signals, set to zero.

- Economic benefits of dual use: With the change in GPS policy, the technology quickly became adopted into people’s lives, while it is mainly known for car navigation. GPS equipment revenues averaged \$33.5 billion USD annually during the 2005–2010 period, with commercial GPS revenue taking 25%, and consumer GPS dominating with 59% of the sales. – For example, farmers use GPS technology for precision agricultural farming for greater efficiency. The technology is integrated into the various farm management phases, from sowing to harvest.

- The modernized GPS frequency plan contemplates a civilian three–carrier signal structure at frequencies L1, L2, and L5. The multi–carrier nature of these signals and the expected increase in power over present transmitter levels will facilitate the use of “wide–lane” techniques to provide accurate ionospheric correction, precise delta–height observations, and potentially accurate wind speed estimations. Future upgrades of GPS include an increase in the emitted power and the addition of two new civilian signals, one at L2 (to

²⁷⁹¹⁾ Willard Marquis, Michael Shaw, “GPS III Bring New Capabilities to the Global Community,” Inside GNSS, Sept./Oct. 2011, URL: <http://www.insidegnss.com/auto/sepoct11–Marquis.pdf>

²⁷⁹²⁾ R. E. Neilan, A. Moore, T. Springer, J. Kouba, J. Ray, Ch. Reigber, “International GPS Service 2000: Life without SA,” ION GPS 2000, Slat Lake City, UT, Sept. 19–22, 2000, pp. 438–446

²⁷⁹³⁾ P. B. de Selding, “Europe Cheers While Questioning End of GPS Selective Availability,” Space News, May 15, 2000, pp. 4 and 26

measure ionospheric delay), and an entirely new L5 signal centered at 1176.45 MHz for aeronautical use (see H.5.1.5). The first upgrade will allow the correction of meter–level ionospheric errors down to the cm–level. In addition, a 5 dB increase in transmitted power at both L1 and L2 over the current specified values is expected. ^{2794) 2795) 2796)}

The new L5 signal is announced with 6 dB higher power than the current L1 signal, split into in–phase and quadrature components, to improve resistance and interference, especially from other pulse–emitting systems in the same band, as DME (Distance Measurement Equipment). Two other very attractive features of L5 are its high chip rate (10.23 MHz) and bandwidth (at least 20 MHz) and the fact that no data will be transmitted on the quadrature signal, thus allowing for easier processing and improved performance when used for remote sensing.

Performance feature	Block II & IIA	Block IIR	Block IIF (requirements)
Nr. of navigation signals	3 signals	3 signals	up to 5 signals
Signal power to user (combined L1 and L2)	– 158.2 dBW L1 – 166 dBW L2	– 158.2 dBW L1 – 166 dBW L2	– 156.4 L1 C/A, – 155.7 L1 P (dBW) – 152.6 dBW L2
Space & ground URE	2–3 m	1–2 m (Auto-Nav)	0.75 – 1 m crosslink navigation
Civil performance (2 dRMS)	100 m with SA 25 m w/o SA	100 m with SA 25 m w/o SA	< 10 m w/o SA (Selective Availability) and with ionospheric correction
Design life	7.5 years	10 years	15 years
Design flexibility	N/A	Auxiliary payload 45 kg, 90W	Auxiliary payload capacity up to 180 kg and 275 – 1000 W of power

Table 156: Performance parameter comparison of GPS satellite generations

- On June 21, 2010, the GPS operations center (Missile Systems Center’s Global Positioning Systems Wing) announced that the first GPS IIF–1 satellite, launched on May 27, 2010, has begun test transmissions of the new safety–of–life (L5) navigation signal. ²⁷⁹⁷⁾

GPS IIF satellites offer new and enhanced capabilities, including a jam–resistant military signal, greater accuracy through improved atomic clock technology, and a protected civilian L5 signal to aid commercial aviation and safety–of–life applications. – Operational service of the GPS IIF–1 spacecraft started in late August 2010. ²⁷⁹⁸⁾

The GPS IIF spacecraft series are providing greater navigational accuracy through improvements in atomic clock technology, a more resilient signal for commercial aviation and safety–of–life applications, a longer design life of 12 years and a mass of ~ 1630 kg.

- In March 2013, ^{2799) 2800)} the U.S. Air Force Space Command announced plans to begin formal testing of the new **CNAV** (Civilian Navigation Message) capability on the operational GPS constellation during the summer of 2013. – These tests will ensure enterprise–level readiness to operate, broadcast and receive modernized civil navigation messages using L2C and L5 signals prior to the expected deployment of the Next Generation Operational Control System (OCX) in mid–2016.

2794) M. Shaw, K. Sandhoo, D. Turner, “Modernization of the global positioning system,” GPS World, Sept. 2000, pp. 36–44

2795) A. J. Van Dierendonck, C. Hegarty, “The new L5 civil GPS signal,” GPS World, Sept. 2000, pp. 64–71

2796) W. Marquis, “M is for modernization: block IIR–M satellites improve on a classic,” GPS World, Sept. 2001, pp. 36–42

2797) “Officials Announces Initial Test Transmissions From GPS Satellite,” Space Daily, June 21, 2010, URL: http://www.spacedaily.com/reports/Officials_Announces_Initial_Test_Transmissions_From_GPS_Satellite_999.html

2798) “First Boeing–Built GPS IIF Satellite Enters Service With USAF,” Space Daily, Aug. 31, 2010, URL: http://www.spacedaily.com/reports/First_Boeing_Built_GPS_IIF_Satellite_Enters_Service_With_USAF_999.html

2799) “Lockheed Martin GPS Satellites To Help Test New L2C Signal Civil Navigation Capability to Improve GPS Navigation,” GPS Daily, April 17, 2013, URL: http://www.gpsdaily.com/reports/Lockheed_Martin_GPS_Satellites_To_Help_Test_New_L2C_Signal_Civil_Navigation_Capability_to_Improve_GPS_Navigation_999.html

2800) Stephanie Wan, A. J. Oria, “GNSS Civilian/Military Dual–Use Policy Issues,” Proceedings of the 64th International Astronautical Congress (IAC 2013), Beijing, China, Sept. 23–27, 2013, paper: IAC–13–B2.7.1

CNAV messages may include navigation information such as the GPS Almanac, clock ephemeris, and other SV parameters. The CNAV message types contain higher precision representations of the quasi-Keplerian parameters than those contained in the Legacy Navigation Message, and more accurate GPS space vehicle position estimates.

Since June 2013, the GPS-Directorate has been conducting Live-Sky CNAV testing in preparation for the deployment of the OCX to ensure enterprise-level readiness to operate, broadcast and receive the modernized civil navigation messages on L2C and L5. The test program will span several years and will evolve to support modernized civil navigation performance objectives.

- **Modernized civil GPS signals:** The GPS 2nd and 3rd GPS civil signals, respectively L2C and L5, were developed to work with the GPS L1 Coarse Acquisition (L1 C/A) and meet commercial and scientific needs (L2C) as well as support “safety of life” applications such as aviation (L5). The 4th civil signal, known as L1C, was developed for interoperability with the Galileo Open Service (OS). These new signals enable civil users to utilize the maximum benefit for GPS and provide interoperability with international GNSS partners. The benefits of civil signals also include the improvement of mobile GPS reception in cities, and areas with ‘urban canyon’ environments. While L1C was originally developed for GPS and Galileo, now other GNSS Providers such as the Japanese QZSS (Quasi-Zenith Satellite System) and Indian Regional Navigation Satellite System (IRNSS), and China’s Compass/Beidou system, are adopting L1C as a standard for international interoperability (Ref. 2800).
- **GPS-SAR (GPS Search and Rescue):** The GPS III SAR (Search & Rescue) payload began as the proof-of-concept DASS (Distress Alerting Satellite System), it uses an S-band downlink and was developed by the NASA SAR Mission Office in partnership with the DoD and SNL (Sandia National Laboratory) in support of the NSARC (National SAR Committee) and successfully implemented on GPS –IIR(M), and –IIF space vehicles (Figure 4). NASA has invested about \$35M to develop the POC DASS. The operational version of DASS, renamed GPS-SAR (GPS Search and Rescue), is planned for the GPS III constellation starting with Space Vehicle 9 for launch in the 2019 timeframe. Canada is funding and providing the search-and-rescue repeaters for GPS III. GPS-SAR will provide: 406 MHz ‘bent pipe’ repeaters on future GPS satellites; full compatibility with existing and future 406 MHz beacons; and global near-instantaneous detection and location (Ref. 2800).

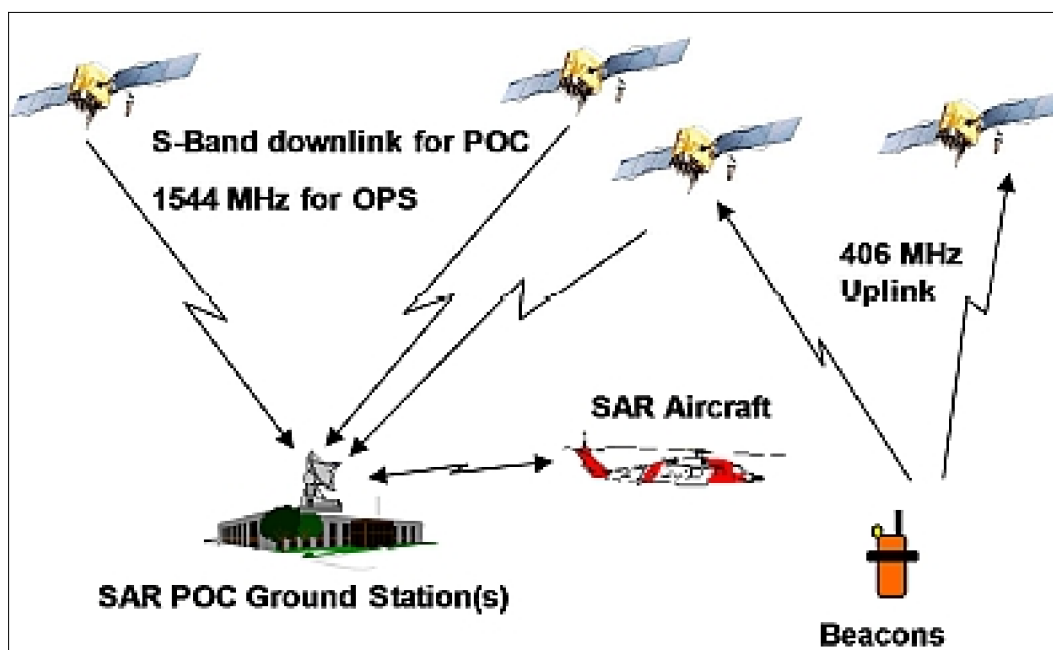


Figure 215: Proof-of-concept DASS (image credit: NASA)

1.27.4 GLONASS (Global Orbiting and Navigation Satellite System)

The Soviet/Russian GLONASS was initially designed mainly for military purposes. It consists of a nominal constellation of 24 satellites in three orbital planes (8 S/C per plane) with MEO orbital altitudes of 19,100 km (circular). The ascending nodes of the constellation are 120° apart. The period of a S/C is 11 hours and 15 minutes. A ground track repeat is achieved in 8 sidereal days. GLONASS observation data are available with the L1 signal of the standard accuracy without any selective availability. See also chapter H.4 for a GLONASS description.

- Launch of the first three GLONASS-series navigation satellites, called GLONASS-1, 2 and -3 (Cosmos 1413, 1414 and 1415 deployed), on October 12, 1982 (see chapter H.4 and Table 672).²⁸⁰¹⁾

Note: The first USSR navigation satellite, **Tsyklon**, was launched into a circular orbit of 750 km, on Cosmos flight 192, November 23, 1967. Tsyklon navigation was based on Doppler shift techniques. Tsyklon was followed by a six-satellite constellation with the name of Parus (also Tsikada-M). A virtually identical civilian navigation network with the name of Tsikada began deployments in 1976 with Kosmos 883, the constellation employs four orbital planes separated by 45°.

- The GLONASS constellation with 24 satellites was fully deployed in December 1995. But after 1995 to the end of 1998, the GLONASS constellation has been degraded due to lack of the federal budget funding. In 1999, GLONASS became a dual-use system by Presidential Decree, with two agencies responsible for the system: namely the Ministry of Defense for the military side, and the Russian Aviation and Space Agency (Rosaviakosmos) for the civil side. In addition, GLONASS is open for international cooperation.

- In Aug. 2001, the Russian Government adopted and approved a long-term federal program of GLONASS sustainment and modernization, ensuring also the user equipment development as well as serial production. This governmental action represents in fact a first in Russian (and Soviet) history, namely that a specific space program experiences the phases of development, operational sustainment, and modernization in the framework of a dedicated federal program (with a budget and a 10 year planning horizon). Coordinator of all activities in the framework of the GLONASS Program now is Rosaviakosmos. The State Budget money dedicated for GLONASS flows through Rosaviakosmos and Ministry of Defense as equal partners.²⁸⁰²⁾ – The Federal GLONASS Program involves six entities (agencies, ministries, institutions): Rosaviakosmos, Ministry of Defense, Russian Agency of the Control Systems (RACS), Ministry of Transport, Ministry of Industry, Science and Technologies (MIST), Russian Mapping and Geodesy Agency (RMGA) – with the program coordination at Rosaviakosmos. The Ministry of Defence has been assigned responsibility for GLONASS operation and maintenance. All the actions recognize the importance of a full functional navigation capability for a national economy.

- As of April 2003, the GLONASS constellation consists of 12 satellites, 8 of which are operational and one is completing the flight tests. The current degraded constellation may experience signal outages in the order of 3–4 hours. However, In combination with GPS even now GLONASS use is improving the navigation quality. – The nearest launch of another three GLONASS satellites is scheduled for the second half of 2003. One of the three satellites will be GLONASS-M with extended lifetime to 7 years. Up to 11 GLONASS-M type satellites are expected to be deployed by 2006. A second signal (in frequency band F2) will be implemented in the M-series for improved location performance. – From 2005 onwards, plans call for a new generation of GLONASS-K satellites with extended performances, transmitting the third civil signal in the F3 frequency band (27 GLONASS-

²⁸⁰¹⁾ N. L. Johnson, "GLONASS Spacecraft," GPS World, November 1994, pp. 51–58

²⁸⁰²⁾ S. Revniviykh, G. Polischuk, V. Kozlov, V. Klimov, N. Anfimov, V. Bartenev, V. Kossenko, Y. Urlichich, N. Ivanov, A. Tyulyakov, "Status and Development of GLONASS," GNSS 2003, Graz, Austria, April, 22–25, 2003

K in the time frame 2005–2012). Generally, the full (24 satellites) GLONASS constellation transmitting two civil signals will be available from 2010 onwards.

- The Russian Federal Program for GLONASS Sustainment, Development and Use for 2012 – 2020 was approved on March 3, 2012. GLONASS Program is one of the priority programs of the Russian Government. The program goals are: ²⁸⁰³⁾
 - Maintaining the GLONASS performance at a level comparable to other GNSS.
 - Further development of GLONASS aimed at: a) improving performance to be competitive with other GNSS; b) pursuing leadership in satellite navigation; c) consolidating evolution of system’s components.
 - Promotion of GLONASS global use.

Key quality indicator of the program: guaranteed provision of announced GLONASS performance characteristics.

Total satellites in the constellation	29 spacecraft
Operational	23 spacecraft
In commissioning phase	–
In maintenance	3 spacecraft
Spares	2 spacecraft
In flight test phase	1 spacecraft

Table 157: GLONASS constellation status in February 2013

The solutions for performance improvement are:

- Space segment modernization (new signals, new clocks, more accurate attitude control, cross links, predictable SV behavior)
- Ground control segment modernization (new OD&TS software, expanded monitoring stations and up–link network, more stable system time scale steered to UTC (SU), more accurate Geodesy Reference PZ–90.11 adjusted to ITRF within cm level)
- Space–based and ground–based augmentations
- Advanced user receivers
- Real–time system performance monitoring system.
- On July 02, 2013, a Proton vehicle with 3 GLONASS–M spacecraft onboard (Serial No 48, 49 and 50) exploded right after launch (17 seconds) from the Baikonur Cosmodrome in Kazakhstan (first stage failure, rocket crashed near the launch pad). Roscosmos said that a preliminary assessment has found no fatalities or major injuries, nor any damage to the launch installations. ²⁸⁰⁴⁾
- On March 23, 2014 (UTC 22:54) a GLONASS–M type spacecraft was launched on a Soyuz–2.1b vehicle from the Plesetsk Launch Complex (GLONASS serial No 53). As of March 23, 2014, the Glonass constellation includes 24 functioning satellites with three additional satellites in reserve and one undergoing flight tests. ²⁸⁰⁵⁾
- On June 14, 2014, (17:16:48 UTC) a GLONASS–M type spacecraft (1414 kg) was launched on a Soyuz–2.1b vehicle from the Plesetsk Launch Complex.

2803) A. Terekhov, “GLONASS Government Policy, Status and Modernization,” Roscosmos, Proceedings of the 50th Session of Scientific & Technical Subcommittee of UNCOPUOS, Vienna, Austria, Feb. 11–22, 2013, URL: <http://www.oosa.unvienna.org/pdf/pres/stsc2013/tech-32E.pdf>

2804) Sayora Mashanlo, “Russian Proton M Rocket Explodes Just After Blast Off,” Space Travel, July 02, 2013, URL: <http://www.space-travel.com/reports/Unmanned-Russian-rocket-explodes-on-takeoff-999.html>

2805) Patrick Blau, “Soyuz successfully delivers Glonass–M Navigation Satellite to Orbit,” Spaceflight 101, March 23, 2014, URL: <http://www.spaceflight101.com/soyuz-2-1b-glonass-754-launch-updates.html>

1.27.5 GPS and GLONASS, applications in space

- Position and time measurements with ground–based GPS and GLONASS receivers have been made with partial GPS and GLONASS constellations since the first launch in each constellation (first institutionally, then by the civil community as commercial receivers became available). The evolution of the GPS receiver: In 1978, Texas Instruments decided to make available one of the first GPS receivers for civil use. Its price tag was \$153,000. In 1988, Magellan offered the first hand–held GPS receiver. Its cost was \$3,500. In 1997, Magellan offered the first GPS receiver to break the \$100 price barrier. Called the GPS Pioneer, it is a 12–channel, 7–ounce mobile unit powered by two AA batteries. The global GPS receiver market produced over 1 million units in 1997.
- Demonstration of GPS receiver position and velocity measurements from LEO satellites. The Landsat–4 (launch July 16, 1982) and Landsat–5 (launch March 1, 1984) spacecraft are flying the first experimental GPS receivers referred to as **GPSPAC** [GPS receiver and processor Package (the first onboard GPS receivers in history had to cope with a partial constellation of GPS satellites)]. GPSPAC (designed at JHU/APL, NASA as co–sponsor, built by Magnavox) is an integrated GPS receiver/processor assembly (R/PA), whose tracking data is used for spacecraft time system synchronization and for post–event (on–ground) orbit determination. Despite the sparse GPS constellation in orbit, GPSPAC demonstrated navigational accuracy of better than 50 m over 10– to 30–minute arcs on 88% of the revolutions. Two more GPSPAC instruments were flown on two DoD host satellites with launches in 1983 and 1984, respectively. Since those early days, many GPS receivers have been installed on all types of satellites. ^{2806) 2807)}
- **Introduction of the GPS carrier–frequency phase measurement technique.** In the pre–operational period of GPS service provision [Initial Operating Capability (IOC) of the GPS system was declared in December 1993], the civil user community had to live with measurement accuracies in the 50–100 m range provided by the SPS (Standard Positioning Service) signals. The pseudorange measurement technique (the intentional downgrading of GPS signal quality) for positioning services, introduced the errors caused by atmospheric effects and SA (Selective Availability). ^{2808) 2809)}

In the early 1980s, two MIT radio astronomers (Counselman and Shapiro) suggested to the GPS user community, to use the **carrier frequency to make phase measurements**, instead of using the prescribed pseudorange modulation technique. This change in measurement technique opened up a window of greatly increased accuracies – namely centimeter–range GPS – provided one could resolve the so–called integer ambiguity (integer number of whole wavelengths). In response to this new opportunity, a number of commercial receiver manufacturers developed high–precision geodetic GPS receivers capable of relative positioning accuracies of a few centimeters. As a consequence, new applications became possible in such fields as geodesy, oceanography, land surveying, astronomy and many others. By 1987 it was known (within a small community) that unclassified “quasi–codeless” receivers with broad–beam antennas could recover dual–frequency GPS phase with the requisite millimeter precision, and that a strategy of concurrent observing from multiple sites would permit “double differencing” and related techniques to eliminate selective availability and other clock errors. Thus, in the 1990s, the technique of carrier–phase tracking of

2806) E. J. Hoffman, W. P. Birmingham, “GPSPAC – A spaceborne GPS navigation set,” IEEE PLANS (Position Location and Navigation Symposium), San Diego, CA, Nov. 6–9, 1978

2807) W. H. Wooden, J. Teles, “Landsat–D/Global Positioning System Experiment,” AIAA Astrodynamics Conference, Danvers, MA, USA., Aug 11–13, 1980.

2808) V. Ashkenazi, “Galileo – Challenge and Opportunity,” Galileo’s World, Vol. 1, No 1, Winter 2000, pp. 42–44

2809) Note: The pseudorange measurement technique is also referred to as “**code–based GPS**.” Code–based DGPS techniques use the GPS “pseudorange” measurement. Code–based DGPS removes certain errors from the pseudorange measurements to provide an accurate position solution. The pseudorange measurement is obtained by the GPS receiver locking onto a GPS satellite’s pseudorandom code. The GPS pseudorange measurement is essentially the difference between the time of transmission of the GPS signal from the satellite and the time of reception by the GPS receiver. The pseudorange measurement is an absolute range measurement between the receiver and the satellite, and therefore DGPS systems are relatively easy to implement.

GPS signals has resulted in a revolution in land surveying as well as in other fields such as refractive occultation monitoring.²⁸¹⁰⁾

With regard to occultation monitoring, it was then a small step to see that analog techniques could be applied directly to occultation processing to remove clock errors.²⁸¹¹⁾ It thus emerged that the one-way GPS observing constraint, which at first seemed to demand stable clocks everywhere in the system, could be artfully adapted through concurrent observations to eliminate stable clocks altogether. This enabled both accurate retrievals and a reduction in instrument cost. Moreover, it was becoming clear that the basic techniques of GPS geodesy could be extended to provide orbit determination on the level of a few centimeters for LEO spacecraft, adequate for occultation analysis.

- **Introduction of DGPS (Differential GPS) services.**²⁸¹²⁾ DGPS is a further approach by the civilian GPS user community to overcome the large errors provided by pseudorange signal measurements. DGPS is fundamentally a relative positioning measurement approach, the GPS receiver may be on a moving platform (vehicle, ship, airplane or satellite). The DGPS concept is based on the principle that a user is affected by satellite ephemeris, atmospheric propagation, SA, and clock synchronization errors to the same extent as a relatively nearby reference station. By predicting the reference receiver's position to a high degree of accuracy, one can set up a system that can be used to calculate corrections to the pseudoranges measured to the various GPS satellites and to transmit these corrections to a multitude of users in the vicinity (100 km radius and more) of the reference station. The use of the DGPS technique (as well of RTK) provide relative positioning accuracies with respect to a reference system.

- Over the last decade (1990s) systems for DGPS started to expand from one reference station into integrated networks of reference stations. The distance between reference stations typically lies in the order of 50–70 km. Also, using the IGS (International GPS Service) ephemeris products rather than a broadcast navigation message to interpolate a higher accuracy satellite position and clock (<5 cm/0.1 ns) can improve the accuracy of position determination.

- Further advances by the civilian user community led to the development of **RTK (Real-Time Kinematic) GPS tracking**, enabling the receiver to make **precise carrier-frequency phase measurements** while in motion. The complication introduced with these measurements is the unknown cycle ambiguity, which needs to be resolved in order to exploit the millimeter carrier phase precision to the full extent for relative positioning. See also H.5.3, H.5.4.

The accuracy of RTK positioning is limited by the distance dependent errors from orbit, ionosphere and troposphere as well as station dependent influences like multipath and antenna phase center variations. In survey-type RTK applications with centimeter accuracy requirements, permanent reference station networks are being employed more frequently at the start of the 21st century. The advantages provided by these reference station arrays include improved modeling of the remaining tropospheric, ionospheric and orbit biases. Methods and concepts reflect the improvements in performance and reliability in some kind of closed system approaches. Standardization discussions underway within RTCM (Radio Technical Commission for Maritime Services) target the interoperability between the reference station systems and roving receivers from various manufacturers. Two exam-

2810) J. T. Wu, "Elimination of clock errors in a GPS based tracking system," AIAA-84-2052, AIAA/AAS Astrodynamics Conference, Seattle, WA, August. 1984

2811) T. P. Yunck, C. H. Liu, R. Ware, "A History of GPS Sounding," Special issue of TAO (Terrestrial, Atmospheric and Oceanic Science, Vol. 11, No 1, March 2000, pp. 1–20

2812) Note: The adjective "differential" refers to the fact that the user receiver is positioned with respect to the nearby reference or base station at a known location.

ples of commercially available network–based RTK–positioning error correction techniques to roving users are: ²⁸¹³⁾ ²⁸¹⁴⁾ ²⁸¹⁵⁾

– FKP (Flächenkorrekturparameter – or area correction parameter), developed at the University of Hannover. In this concept, FKP coefficients are computed for every satellite covering ionospheric, tropospheric and orbit effects (with regard to a specific network area and at specific time intervals, at least every 10 s). The measurement corrections, reduced by the station–satellite slope distances of the reference stations, are then transmitted via RTCM messages Type 20/21 as well as the FKPs for interpolation via a customized RTCM type 59 message.

– VRS (Virtual Reference Stations) concept of Trimble (the VRS software consists of a network of Trimble GPS receivers communicating with a control center to calculate GPS error corrections that are applicable over a wide area). In this concept, the rovers also receive network information but additionally transmit, via NMEA (National Marine Electronics Association) messages, their approximate positions to a central computing facility. This facility calculates the station–satellite slope distances for the approximate positions and then, from the reference station observations, interpolates the corrections corresponding to a virtual reference station near the rover. These virtual measurements are unique to each rover and transmitted to them via RTCM messages of type 20/21 or 18/19. The concept of “virtual reference stations” allows to eliminate/reduce systematic errors in reference station data, i.e. allows to increase the distance to the reference station for RTK positioning while increasing the reliability of the system and reducing the initialization time.

Mode	Autonomous SPP (Single Point Positioning)		Differential or Relative Mode			
	SPS (Standard Position Service)	PPS (Precise Positioning Service)	WAAS (Wide Area Augmentation System)	DGPS	RTK	Static survey and geodesy
Measurement technique	Code	Code	Code	Code with carrier smoothing	Carrier	Carrier
Accuracy	8–10 m	6–10 m	5–10 m	1–7 m	0.1 –0.3 m	0.01 m

Table 158: GPS horizontal positioning accuracies in different modes

- Determination of water level with an RTK GPS buoy. ²⁸¹⁶⁾ An RTK–equipped buoy can potentially be used to accurately measure water level height above the WGS84 ellipsoid. The goal is to use this method eventually for such applications as: a) determination of water level to establish the separation between tidal datum and GPS datum; b) determination of water level for calibration of altimetric sensors on aircraft or spacecraft. Experiments with a RTK–equipped buoy of the US NAVOCEANO (Naval Oceanographic Office) over a period 2001–2003 provide encouraging results.
- Demonstration of GPS high–precision orbit determination. The GPSDR (GPS Demonstration Receiver) of Motorola was flown on two missions: EUVE (Extreme Ultraviolet Explorer, launch June 7, 1992, of NASA/GSFC) and TOPEX/Poseidon (launch Aug. 10,

2813) H.–J. Euler, C. R. Keenan, B. E. Zebhauser, G. Wübbena, “Study of a Simplified Approach in Utilizing Information from Permanent Reference Station Arrays,” ION GPS 2001, Sept. 11–14, 2001, Salt Lake City, UT

2814) G. Fotopoulos, M. E. Cannon, “An overview of multi–reference station methods for cm–level positioning,” GPS Solutions (John Wiley&Sons Inc.), Vol. 4, No 3, 2001, pp. 1–10

2815) B. Eissfeller, Ch. Tiberius, T. Pany, R. Biberger, T. Schueler, G. Heinrichs, “Real–Time Kinematic in the Light of GPS Modernization and Galileo,” ION GPS 2001, Sept. 11–14, 2001, Salt Lake City, UT

2816) S. Bisnath, D. Wells, S. Howden, D. Dodd, D. Wiesenbug, “Development of an Operational RTK GPS–Equipped Buoy for Water Level Recovery,” ION GPS/GNSS 2003, Portland, OR, Sept. 9–12, 2003

1992) to demonstrate/validate accurate orbit determination with GPS data.^{2817) 2818)} Two GPSDR instruments (dual-frequency receivers producing long cycle-slip free carrier-phase passes as well as pseudorange measurements) on TOPEX/Poseidon were the first spaceborne receivers obtaining high-accuracy range measurements and demonstrated DGPS techniques with a set of IGS (International GPS Service) ground reference stations. A comparison of orbit parameters from three independent techniques (retroreflectors for SLR, DORIS and GPS), all available on TOPEX/Poseidon, obtained GPS orbit differences <25 cm (3D rms). These results of GPS orbit reconstitution are indeed impressive in terms of accuracy.

- Spaceborne orbit determination with a GPS receiver (initial validation flight tests). The goal is the provision of a real-time service of autonomous onboard functions (orbit, etc.). The provision of mean orbital elements is a first step toward operational autonomy. The orbital elements are being used on the ground for ground station operations and other support functions; they are also being used onboard for S/C operations. In general, however, there are further functional services needed for autonomous onboard S/C operations, such as: position, velocity and time; GPS receiver data logging; S/C clock synchronization; data logging; instrument triggering by position; status monitoring, and more. – The introduction of onboard autonomy has certainly great potential of reducing operating costs of future missions.

Background: Orbit determination is generally based on two models, namely the dynamic model (describing the forces acting on the satellite), and the observation model (providing the relationship between the measurements of the tracking system). This requires considerable onboard processing and storage capability. A recursive Kalman filter algorithm provides a sequential approach to combine the inputs of both models, namely the satellite's motion (in the dynamic Earth model) with the GPS measurements (observation model) as they become available, resulting in best estimates of position and velocity (continuous comparison and update of actual with estimated values).²⁸¹⁹⁾

– PoSAT-1 (launch Sept. 26, 1993, built at SSTL, UK) is the first microsatellite to make use of a GPS receiver in orbit, and to autonomously determine its orbit through the processing of GPS data into orbital elements.^{2820) 2821)} The GNU (GPS Navigation Unit) consists of a TANS Vector-II 6-channel C/A code receiver of Trimble and is operated with a software package run on a Transputer Data Processing Unit (a T800 32-bit RISC microprocessor). The GNU is operated intermittently to conserve power. Some services demonstrated on PoSAT-1 are: a) orbital elements: they provide a prediction accuracy of 1–10 km for two weeks, and b) the variables of position, velocity and time can be requested at any time. While basic attitude determination on PoSAT-1 was performed with magnetometers and sun sensors, there was in addition a demonstration of attitude determination using the single GPS antenna of GNU.

– Since 1993 NASA/JSC was conducting different GPS experiments to validate concepts required to fly GPS as an in-line avionics component on Shuttle missions. The reason: an anticipated beginning of TACAN ground-station phase out in 2000 prompted the Shuttle program to reexamine the use of GPS as a TACAN (Tactical Air Communication and Navi-

2817) R. Muellerschoen, S. Lichten, U. Lindqwister, W. Bertiger, "Results of an Automated GPS Tracking System in Support of Topex/Poseidon and GPS/MET," Proceedings of ION GPS-95, Sept. 12–15, 1995, pp. 183–193

2818) W. Bertiger, et al., "The First Low Earth Orbiter with precise GPS Positioning: Topex/Poseidon," Proceedings of ION GPS-93, Salt Lake City, Utah, Sept. 22–24, 1993

2819) V. Ashkenazi, W. Chen, et al., "Real-Time Autonomous Orbit Determination of LEO Satellites using GPS," Proceedings of ION GPS-97, Sept. 16–19, 1997, Kansas City, MO, pp. 755–761

2820) M. Unwin, M. Sweeting, "A Practical Demonstration of Low Cost Autonomous Orbit Determination Using GPS," Proceedings of ION GPS-95, Sept. 12–15, 1995, Palm Springs, CA, pp. 579–587

2821) P. J. Buist, Y. Hashida, M. Unwin, M. Schroeder, "Full Attitude From a Single GPS Antenna: Demonstration of Concept with Orbital Data from PoSAT-1," 4th ESA International Conference on Spacecraft Guidance, Navigation and Control Systems, Oct. 18–21, 1999, pp. 493–498 ESA/ESTEC

gation) replacement.^{2822) 2823)} A series of seven flights were conducted on Endeavour which started with STS–56 (April 1993) using a Rockwell Collins 3M receiver operating in SPS mode. The next phase of Shuttle/GPS operations used a PPS (Precise Positioning Service) receiver as a single string navigation device [Rockwell Collins MAGR/S (Miniaturized Airborne GPS Receiver/Shuttle)]. The first flight was on STS–79 (Sept. 16–26, 1996). During flight the navigation data was downlinked in real–time for display. During landing, the GPS system performance was compared to TACAN, the primary Shuttle navigation device. In the summer of 2002, the Shuttle program successfully completed an integration, ground test, and flight test effort to certify a GPS receiver for use on the Shuttle orbiters. The certification led to use of a single GPS receiver on each orbiter along with three existing TACAN units. Eventually, NASA will replace the TACAN units with a GPS receiver on each orbiter.

- The REX–II satellite of USAF (see below, launch March 9, 1996) provides GPS–generated orbital elements in the downlink.
- The ORFEUS–SPAS–II free–flyer payload on Shuttle flight STS 80 (November 19–December 7, 1996) flew the first GPS Tensor receiver system (SS/L and LABEN) capable of providing onboard orbit parameters with an adapted Kalman filter algorithm along with Earth model software.
- The DORIS system of CNES, with a prototype payload first flown on SPOT–2 (launch Jan. 22, 1990) and later on TOPEX/Poseidon (launch Aug. 10, 1992), is a microwave tracking system (with the use of a global ground network). Successful long–term onboard orbit determination has been demonstrated with DIODE (Doris Immediate Orbit Determination), a DORIS software package first flown on SPOT–4 (Mar. 24, 1998, see H.8.1). Further DORIS/DIODE systems fly on Envisat, Jason–1, SPOT–5, etc.
- **GDGPS** (Global Differential GPS) system of NASA, and a subset of NASA’s Global GPS Network (GGN – some 40 reference stations), consisting of geodetic quality dual–frequency receivers. The GDGPS system, developed and operated by JPL (since 2001), combines innovative software and hardware components with advanced Internet technology to provide end–to–end capabilities for autonomous, real–time orbit determination, time transfer, and positioning, with an unprecedented level of accuracy (10 cm horizontal and 20 cm vertical for kinetic applications anywhere on Earth) and availability (at any time).^{2824) 2825) 2826) 2827) 2828)}

This feature is particularly valuable in support of event monitoring functions and kinematic applications of equipment on Earth–orbiting satellites (also on airplanes and terrestrial vehicles) with positional accuracy requirements of centimeters to decimeters. The GDGPS analysis concept employs a state–space approach, where the orbits of the GPS satellites are precisely modeled, and the primary estimated parameters are the satellite epoch states. This approach guarantees that the corrections will be globally and uniformly valid. The system is geared toward users carrying dual–frequency receivers. The ground segment consists of the ground network of reference GPS receivers, the operations centers, and the In-

2822) F. H. Bauer, J. R. O’Donnell, “Space–Based GPS 1996 Mission Overview,” Proceedings of ION GPS–96, Sept. 17–20, 1996, Kansas City MO, pp. 1293–1302

2823) J. L. Goodman, “Parallel Processing GPS Augments TACAN in the Space Shuttle,” GPS World, Oct. 2002, pp. 20–28

2824) Y. Bar–Sever, R. Muellerschoen, “The NASA’s Global Differential GPS System – Present and Future,” Proceedings of ESTC (Earth Science Technology Conference), College Park, MD, June 24–26, 2003

2825) Y. Bar–Sever, R. Muellerschoen, A. Reichert, “The Development and Demonstration of NASA’s Global Differential System,” Earth Science Technology Conference, Pasadena, CA, June 11–13, 2002

2826) Y. Bar–Sever, R. Muellerschoen, A. Reichert, M. Vozoff, L. Young, “NASA’s Internet–Based Global Differential GPS System,” NAVITEC 2001, 1st Workshop on Satellite Navigation User Equipment Technologies, Dec. 10–12, 2001, ESA/ESTEC, Noordwijk, The Netherlands

2827) Note: The GDGPS system is also known under the name of **IGDG** (Internet–based Global Differential GPS)

2828) M. O. Kechine, C. C. J. M. Tiberius, H. van der Marel, “Experimental verification of Internet–based Global Differential GPS,” ION GPS/GNSS 2003, Portland, OR, Sept. 9–12, 2003

ternet, which serves as the data communication channel between the reference network and the operations centers. – Note: One of the major advantages that dual–frequency receivers have over single frequency ones is that an on–the–fly (OTF) search can be performed quickly, due to the combination of L1 and L2 data resulting in the wide lane phase observable.

At the heart of the operations center is the GPS orbit determination process, where the Real Time GIPSY (RTG) software ingests the streaming GPS data and generates real–time estimates of the dynamic GPS orbits, one–second GPS clocks, and tropospheric delay estimates for each reference site. The estimated GPS orbits and clocks are differenced with the GPS broadcast ephemerides to form the global differential corrections. These differential corrections are then optimally packed to allow for efficient relay to the users. The correction data stream is made available to authorized users via several communication channels. The first is the open internet, where a user can connect to a TCP or UDP server running at the processing center. Remote users can establish such a connection through a broadband hookup (e.g. Ethernet), or through telephony, including wireless telephones such as provided by the Iridium system.

As of 2003, the GDGPS system processes real–time GPS data from a global network of more than 40 dual–frequency GPS ground sites. The utility has in particular been demonstrated in precise airborne navigation applications (support of InSAR, etc. with accuracies of 10 cm horizontally and 20 cm vertically for users anywhere in the world). In addition, the RTG flight software will be demonstrated on orbit and is being projected for a number of spaceborne missions. NASA is also considering TDRS broadcasts of the differential correction message.

After the magnitude 8.8 Chilean earthquake on Feb. 27, 2010 a team led by Y. Tony Song of NASA/JPL used real–time data from the *GDGPS network to successfully predict the size of the resulting tsunami. The network combines global and regional real–time data from hundreds of GPS sites and estimates their positions every second. It can detect ground motions as small as a few centimeters.* – *Song's team concluded that the Chilean earthquake, the fifth largest ever recorded by instruments, would generate a moderate, or local, tsunami unlikely to cause significant destruction in the Pacific. The tsunami's effect was relatively small outside of Chile.* – Song's GPS–based prediction was later confirmed using sea surface height measurements from the joint NASA/CNES Jason–1 and Jason–2 altimetry satellites.²⁸²⁹⁾

- The first GPS attitude determination systems²⁸³⁰⁾ – proof–of–concept demonstrations – were conducted on research aircraft, and on a commercial airliner.

- Three GPS attitude measurement flight tests were conducted in April/May 1991 on a DC–3 aircraft of Ohio University by using an Ashtech–3DF (Three–dimensional Direction Finding) 24–channel receiver configured in four 6–channel sections, and four microstrip patch antennas (fuselage and wing–tip mounted). Attitude data were computed, stored and displayed in realtime by two PCs.

- A Stanford University attitude demonstration was conducted with a Trimble TANS Vector GPS receiver on a Piper Dakota aircraft in 1991. Four strip–mounted antennas were used for attitude sensing. A 486 laptop computer provided both real–time display and data recording for post–flight analysis.²⁸³¹⁾

2829) Dwayne Brown, Alan Buis, “NASA Demonstrates Tsunami Prediction System,” NASA Media Services, June 14, 2010

2830) F. van Graas, M. Braasch, “GPS Interferometric Attitude and Heading Determination: Initial Flight Test Results,” Navigation ION, Vol. 38, No. 4, Winter 1991–92, pp. 297–316

2831) C. E. Cohen, B. W. Parkinson, “Aircraft Applications of GPS–based Attitude Determination,” Proceedings of ION GPS–92, Albuquerque, NM, Sept. 1992, pp. 775–782

- On January 12, 1993, a flight experiment was conducted on a NASA/Ames King Air 200 aircraft²⁸³²) with the objective to evaluate the dynamic response of a GPS attitude system. The attitude equipment consisted of two independent systems: INU (inertial Navigation Unit) and a six-channel C/A code GPS receiver (TANS Vector) and four microstrip patch antennas (fuselage and wing-tip mounted). Attitude data from both systems were recorded for post-flight analysis.
- On Dec. 10, 1994, a test flight of a TANS Vector receiver on board a DC-10 commercial airliner (United Airlines) demonstrated the potential for SATCOM antenna pointing, by providing aircraft attitude measurements (Note: Proper antenna pointing requires knowledge of aircraft position, satellite position and aircraft attitude).²⁸³³) The aircraft used a Honeywell SATCOM system beam-steering antenna, two INS (Delco Carousel IV – the Carousel is a free azimuth INU which contains four-gimbal IRUs), a vertical gyro and a compass. In addition to the TANS Vector receiver, the aircraft was equipped with two modified TNL-8100 GPS receivers. The TANS Vector receiver exhibited expected performance during all phases of the test flight when compared to the reference measurements.
- Demonstration of spaceborne GPS orbit and attitude measurements. A number of tests for attitude determination with “prototype GPS receivers” have been carried out (or are planned) on Shuttle and on various commercial and military satellites. Table 159 lists a chronology of these instruments (see also chapter H.5.3.4).
- The RADCAL spacecraft of the USAF (launch June 25, 1993)²⁸³⁴ 4594) performed the first known attitude determination experiment using GPS carrier-phase measurements with two TANS Quadrex GPS receivers (see D.43). The CRISTA-SPAS-1 mission of DARA/NASA on Shuttle flight STS-56 (Nov. 3-14, 1994) provided the “first demonstration of real-time attitude determination” on the SPAS free-flyer platform of DASA (one day receiver operation). See also chapter J.1.2.
- The REX-II satellite of USAF (launch March 9, 1996), with a GPS experiment by the name of ADACS, can be regarded the first successful demonstration of closed-loop attitude control application using real-time GPS carrier-phase-based attitude measurement as sensor input (first time on March 29, 1996). It is also the first mission to provide orbital elements in the downlink.
- The first spaceborne flight demonstration of **SIGI** (Space Integrated GPS/INS) took place on Shuttle flight STS-101 (May 19-29, 2000) under the name of SOAR (SIGI Operational Attitude Readiness). A reflight of SOAR occurred on STS-106 (Sept. 8-20, 2000). SIGI became fully operational on ISS in May 2002. It is now determining the attitude, position and speed of ISS on a continuous basis. Prior orbit determination of ISS required ground tracking (once per day) and other techniques. The GPS antennas, brought to ISS with STS-110 (Apr. 8-19, 2002), were the final piece of the system (installed on the truss). The antennas feed their information to two GPS receivers, located in the US Lab Destiny. Another unit of SIGI is planned on CRV (Crew Return Vehicle). CRV is scheduled to become an operational part of the station in 2004/5 (CRV is designed to be used as a life-boat in case of an emergency evacuation from ISS). See also H.5.3.4. – SIGI is a NASA instrument based on the Honeywell model H-764G EGI (Embedded GPS/INS); Honeywell Space Systems is also the prime contractor of SIGI on ISS. Honeywell’s COTS baseline H-764G SIGI design is a modular system which is integrated (tightly coupled) with either an embedded Collins or Trimble GPS receiver [either P(Y) and C/A code]. Over 9000 SIGI

2832) C. E. Cohen, B. W. Parkinson, D. McNally, “Flight Tests of Attitude Determination Using GPS Compared Against an Inertial Navigation Unit,” *Navigation ION*, Vol. 41, No. 1, Spring 1994, pp. 83-97

2833) L. Kruczynski, J. Delucchi, T. Iacobacci, “Results of DC-10 Tests using GPS Attitude Determination,” *Proceedings of ION GPS-95*,

2834) A. K. Reichert, P. Axelrad, “Carrier-Phase Multipath Corrections for GPS-based Satellite Attitude Determination,” *Navigation*, Vol. 48, no 2, Summer 2001, pp. 77-88

and EGI systems have been delivered worldwide as of early 2003 (widely used in military applications such as fighter jets).^{2835) 2836) 2837)}

At the beginning of the 21st century it is expected that lightweight spaceborne GPS receiver systems, providing the functions of: position, velocity, attitude, attitude rate and time, are going to replace a number of conventional attitude measurement devices such as horizon sensors and sun trackers. The GPS orbit/attitude receiver in combination with a control scheme (actuator) offers sound technical and economical attitude–control solutions. Previous experiments with GPS attitude determination have demonstrated a potential for coarse attitude determination in the 0.1° range. Also spaceborne GPS receivers have demonstrated a time transfer capability of <100 ns, thus making very precise, coordinated time available to spacecraft systems.

Launch Date	Mission	GPS Receiver	Comment
June 25, 1993	RADCAL (USAF)	TANS Quadrex (Trimble)	2 cross–strapped receivers, attitude solutions in post–processing
Sept. 12–22, 1993	ORFEUS–SPAS–1 (DARA)	Alcatel/SEL receiver,	Shuttle STS–51, free flyer C/A code +L1 carrier–phase
Aug. 3, 1994	APEX (USAF)	TANS Vector	Trimble Navigation instrument
Nov. 3–14, 1994	CRISTA–SPAS–1 (DARA/NASA)	Alcatel/SEL Rx+ TANS Vector + IRU	Shuttle STS–66, SPAS free–flyer
Jan. 11–20, 1996	GADACS (NASA)	TANS Vector (2)	Shuttle STS–72, on SPARTAN
March 9, 1996	REX–II (USAF)	TANS Vector (2) named ADACS	First long–term mission with GPS orbit/attitude determination
May 19–29, 1996	GANE (NASA)	TANS Vector + IRU	Shuttle STS–77
Nov.19–Dec 7, 96	ORFEUS–SPAS–2 (DARA/NASA)	Alcatel/SEL Rx+ GPS Tensor (Laben) TANS Quadrex	Shuttle STS–80, SPAS free–flyer; also relative navigation experiment ARP of ESA/ESTEC
May15–24, 1997 Sep. 25–Oct. 6, 97	ARP (ESA) Shuttle/MIR ARP (ESA) Shuttle/MIR	GPS Tensor (Laben) GPS Tensor (Laben)	STS–84 Shuttle – MIR rendezvous STS–86 Shuttle – MIR rendezvous
Aug. 23, 1997	SSTI–Lewis (NASA)	GPS Tensor (2) named GADFLY	Lewis could not be operated and reentered Sept. 28, 1997
Aug.7–19, 1997	CRISTA–SPAS–2	Alcatel/SEL Rx+ GPS Tensor	Shuttle STS–85, SPAS free–flyer
Dec. 24, 1997	EarlyBird–1 (Earth-watch)	Vector and Viceroy	S/C lost contact with ground
Feb. 14, 98 (1st four satellites)	Globalstar (constellation of 48 satellites)	GPS Tensor on SS/L LS–400 platform	Big LEO communication system of Globalstar L. P., San Jose, CA
1998	SSTI–Clark (NASA)	TANS Vector (2) named GADFLY	NASA cancelled the Clark mission in Feb. 1998
Feb. 23, 1999	ARGOS (USAF)	Embedded receiver	
Nov. 15, 2000	AMSAT–3D (AMSAT)	TANS Vector (2)	AMSAT OSCAR–40 Spacecraft
Apr. 20, 2004	Gravity Probe B (NASA)	GPS Tensor	
1998–2003	ISS (NASA, ESA, CSA, JAXA, and RKA)	SIGI (Space Integrated GPS/INS)	Start of SIGI operation on ISS is planned for 2002

Table 159: Overview of early spaceborne GPS attitude receivers flown on various missions

2835) Z. Zubkow, “Honeywell SIGI (Space Integrated GPS/INS) H–764G System,” Proceedings of the 26th AAS Conference on Guidance and Control, Breckenridge, CO, Feb. 5–9, 2003, Vol. 113 Advances in the Astronautical Sciences, Edited by I. J. Gravseth and R. D. Culp, AAS 03–037, pp. 337–337

2836) J. Um, E. G. Lightsey, “Space Flight Test Results for the SOAR Experiment,” ION–2000, Salt Lake City, UT, Sept. 19–22, 2000, pp. 2243–2251

2837) J. Um, E. G. Lightsey, “GPS Attitude Determination for the SOAR Experiment,” Navigation, Vol. 48, No 3, Fall 2001, pp. 181–194

The following two tables, Table 160 and Table 161, provide an (incomplete) overview and some characteristics of present and planned GPS receivers (as of 2007) for space applications for single- and dual-frequency receivers, respectively. ²⁸³⁸⁾

Manufacturer	Receiver	Channels	Antennas	Power, Mass	TID (krad)	Sample Missions
Thales Alenia Space (F, I)	TopStar 3000	12–16 C/A	1–4	1.5 W 1.5 kg	> 30	DEMETER, KOMPSAT–2
EADS Astrium GmbH (Germany)	MosaicGNSS	6–8 C/A	1	10 W 1 kg	> 30	SAR–Lupe, TerraSAR–X, ADM/Aeolus
General Dynamics, USA	Viceroy	12 C/A	1–2	4.7 W 1.2 kg	15	MSTI–3, SeaStar, MIR, ORBVIEW, KOMPSAT–1
SSTL (UK)	SRG–05	12 C/A	1	0.8 W 20 g	> 10	SNAP–1,
SSTL (UK)	SRG–20	4x6 C/A	4	6.3 W 1 kg	> 10	UoSat–12, PROBA–1, BILSAT,
DLR (Germany)	Phoenix–S	12 C/A	1	0.9 kg 20 g	15	PROBA–2, X_SAT, Flying LapTop, ARGO, PRISMA
Accord (India)	NAV2000HDGP	8 C/A	1	2.5 W 50 g		X–SAT

Table 160: Single-frequency GPS receivers for space applications

Manufacturer	Receiver	Channels	Antennas	Power, Mass	TID (krad)	Sample Missions
SAAB (Sweden)	GRAS	12 C/A, P1/2	3	30 W 30 kg		MetOp–A
Laben (Italy)	Lagrange	16x3 C/A, P1/2	1	30 W 5.2 kg	20	SAC–C, RADAR–SAT–2, GOCE,
General Dynamics, USA	Monarch	6–24 C/A, P1/2	1–4	25 W 4 kg	100	
JPL/Broad Reach Engineering	BlackJack/IGOR	16x3 C/A, P1/2	4	10 W 3.2/4.6 kg	20	SAC–C, CHAMP, GRACE, Jason–1, FormoSat–3 COSMIC, ICESat, TerraSAR–X,
Thales Alenia Space	TopStar 3000G2	6x2 C/A, L2C	1			PROBA–2
Austrian Aerospace	GNSS Navigation Receiver	Up to 36 C/A, P1/2	2		> 20	Under development
Broad Reach Engineering, USA	Pyxis Nautica	16–64 C/A, P1/2	1–4	20 W 2.5 kg		Under development
NovAtel (Canada)	OEM4–G2L	12x2 C/A, P2	1	1.5 W 50 g	6	CanX–2, CASSIOPE,
Septentrio (Belgium)	PolaRx2	16x3 C/A, P1/2	1 (3)	5 W 120 g	9	TET

Table 161: Dual-frequency GPS receivers for space applications

- Flight demonstrations of relative navigation using GPS observables. ESA, in cooperation with NASA, DARA, and RKA (now Roskosmos), conducted three flight demonstrations in its ARP (ATV Rendezvous Pre–development) program with proximity navigation approaches [ATV is the Automated Transfer Vehicle, the ESA resupply vehicle for ISS (International Space Station)].

- Deployment and retrieval maneuvers of SPAS release/approach with Shuttle. The ORFEUS–SPAS–2 free–flyer on Shuttle flight STS–80 (Nov. 19 – Dec. 7, 1996) carried,

²⁸³⁸⁾ O. Montenbruck, M. Markgraf, M. Garcia–Fernandez, A. Helm, “GPS for Microsatellites – Status and Perspectives,” Proceedings of the 6th IAA Symposium on Small Satellites for Earth Observation, Berlin, Germany, April 23–26, 2007

in addition to its prime payload, an ARP secondary payload of ESA/ESTEC, consisting of a GPS Tensor receiver and R-GPS (Relative-GPS) navigation algorithms (developed by MMS). The Shuttle orbiter carried also a GPS receiver (TANS Quadrex), implemented on the fixed part of WSF (Wake Shield Facility) within the cargo bay, and an optical sensor TCS (Trajectory Control Sensor). TCS (of NASA, a laser based sensor) verified the R-GPS measurements by tracking a retro-reflector mounted on the x-face of ORFEUS-SPAS. 2839) 2840)

- Shuttle - MIR flight approach and departure phases. ARP proximity navigation approaches were demonstrated with an instrument package of GPS Tensor (Laben) in combination with the R-GPS algorithm, and a close-range laser sensor, referred to as RVS (Rendezvous Sensor), built by DASA Jena Optronik - on Shuttle flights STS-84 (May 15-24, 1997) and STS-86 (Sep. 25-Oct. 6, 97). The GPS receiver of the MOMS-NAV payload (DARA) on MIR/Priroda provided GPS measurements from the other direction. The Shuttle RVS used three retro-reflectors installed on MIR.

- Integrated GPS+GLONASS receiver technology. 2841) The combination of GPS and GLONASS signals enhances the overall navigation solution in three ways: availability, integrity and accuracy. The GLONASS constellation has no deliberate signal degradation; hence, the GPS+GLONASS horizontal accuracy is 15-20m compared to 100m for GPS-only (with SA on).

- In 1996/7 first GPS+GLONASS receivers 2842) came onto the market. Some models: GG24 (Ashtech, Sunnyvale, CA), GePOS RG24 (Carl Zeiss Geodetic Systems, Jena, Germany), ASN-22 (DASA, Ulm Germany), GSR2400 (Sokkia Corp., Overland Park, KS), GNSS-300 (3S Navigation, Laguna Hills, CA).

- The private company Soft Nav Ltd. of St. Petersburg, Russia [established in early 1998; mainly of former employees of RIRT (Russian Institute of Radionavigation and Time), St. Petersburg, was instrumental in developing a combined GPS/GLONASS avionics software package which was used in a number of receivers such as ASN-22 of former DASA, now EADS Astrium GmbH [which features 18 parallel signal channels (10 GPS/6 GLONASS/2 EGNOS)]. The same experts were also key participants in the development of the world's first GLONASS receivers: ASN-16 (developed in the early 1990s), ASN-21 and SNS-85, mainly flown on Russian military aircraft such as MIG-31, TU-160, IL-96, IL-114, and TU-204.

- Soft Nav Ltd. is also a contributor to the EADS Astrium GmbH developed receiver called MosaicGNSS. The backbone of this receiver is the software correlator developed by Soft Nav. All signal processing and navigation processing functions are being performed in software. The single board MosaicGNSS receiver is embedded in an AOCS (Attitude and Orbit Control System), providing precise autonomous orbit determination for spaceborne applications from LEO to HEO, MEO and GEO. The MosaicAODS (Attitude and Orbit Determination System) is based on the MosaicGNSS receiver and complemented by a star sensor (ASTRO-15 of Jena Optronik GmbH) and optional gyros. Thus, the MosaicAODS makes the full state information continuously available. It can be used as integral part of a spacecraft ICDS (Integrated Control and Data Handling System) or as a stand-alone unit. Extensive simulator tests of MosaicAODS were successful. MosaicGNSS (along with MosaicAODS and ASTRO-15), a radiation-hardened receiver (100 krad), will be flown on

2839) M. Cislighi, U. Thomas, M. Lellouch, J. M. Pairo, "Development and Verification of Automated Rendezvous for ATV," Proceedings IAF-96-T.2.08, Oct. 7-11, 1996, Beijing

2840) M. Cislighi, U. Thomas, M. Lellouch, G. Limouzin, "ATV - Pre-development Program - Flight Demonstrations," IAF-97.T.2.03

2841) Note: Prior to measurement integration of GPS and GLONASS into one receiver, proper transformations must be established between the two time scales [UTC(USNO) and UTC(SU)], and the two coordinate systems [WGS84 and PE90 respectively]

2842) GPS World Receiver Survey, GPS World, January 1998, pp. 46-59

the German TerraSAR–X satellite (launch June 15, 2007); it will be an integral part of the new OBC in a redundant configuration. ^{2843) 2844) 2845) 2846) 2847) 2848)}

– En–route navigation in civil aviation. Airborne testing against a proven flight truth source (Z–12 dual–frequency GPS + ground–based reference station). In September 1996, Ashtech Inc. and Universal Avionics made the world’s first transoceanic flight with GPS+GLONASS technology, using an Ashtech GG24 receiver for an overseas flight (from Shannon, Ireland to Teterboro, NJ, USA). During the flight the 24–channel receiver computed positions using up to 17 satellites. Horizontal positions within an accuracy of 16 m were achieved 95% of the time. The potential benefits to civil aviation (navigation and positioning operations) in general have become increasingly obvious. ²⁸⁴⁹⁾

Some background of AGGA (Advanced GPS/GLONASS ASIC) receiver development
AGGA was predominantly developed within the ESA–funded EOPP (Earth Observation Development Program). AGGA experienced several redesigns, functional enhancements, miniaturization, and demonstrations. AGGA–2 represents the 2nd generation version of AGGA.
<ul style="list-style-type: none"> • The first GPS/GLONASS receiver breadboard model was developed in the timeframe 1993–95 at ISN (Institute of Navigation) of the University of Nottingham, UK. This system featured eight dual–frequency channels with 20 FPGAs and power of 50 W.
<ul style="list-style-type: none"> • In the period 1994–96, IMEC (Belgium) studied miniaturization of the ISN device.
<ul style="list-style-type: none"> • In the period 1996–98, IMEC performed a redesign of the ISN receiver with functional enhancements into a highly integrated ASIC (also part of ARTES–5 program).
<ul style="list-style-type: none"> • A full validation of AGGA–0 was done by Austrian Aerospace and ESA in 1998
<ul style="list-style-type: none"> • Design/development of a flight–worthy AGGA–2 device within the period 1998–99, with validation by Austrian Aerospace and ESA in 1999
<ul style="list-style-type: none"> • P–code bug fix in AGGA–2 by Saab–Ericsson Space (Sweden) in 2000 and subsequent validation by Austrian Aerospace
<ul style="list-style-type: none"> • AGGA–2 functionality and features: <ul style="list-style-type: none"> – 12 single frequency channels (36 complex correlators) each capable of tracking any GNSS C/A code signals – 4 P–code units for dual–frequency operation and semi–codeless tracking (ESA–ISN patent) – Supports IF sampling, R2C (real–to–complex) conversion, final down conversion – Highly configurable and programmable – Either 8 real inputs or 4 complex inputs, each 2 bits, support of different input formats – Signal level detector, clock and time–base generator and antenna switch controller – 32–bit microprocessor interface with interrupt controller and basic I/O port – Features for multipath mitigation and adequate semi–codeless tracking of GPS Y code <p>2004 version: AGGA–2a is available to industry as an application–specific standard product (T7905E component from ATMEL)</p>

2843) A. V. Botchkovski, M. Chistyakov, N. Golubev, et al., “Softflex: An Advanced Approach to Design of GNSS Receiver with Software Correlator,” Proceedings of ION GPS’99, Nashville, TN, Sept. 14–17, 1999.

2844) Note: In MosaicAODS, the ASTRO–15 system is being used as a star tracker. All attitude algorithms, commanding, mode logic, etc. are being performed on the common platform MosaicGNSS. MosaicAODS can operate with various star sensors, it is not tied in any way to ASTRO–15..

2845) Information provided by Michael Mittnacht of EADS Astrium GmbH

2846) M. Mittnacht, W. Fichter, E. Gottzein, M. Hartrampf, A. Konrad, P. A. Krauss, et al., ”Multi–Sensor Navigation and Attitude Determination System for Space Applications,” ION–GPS 2002, Portland, OR, Sept. 24–27, 2002

2847) M. Mittnacht, E. Gottzein, M. Hartrampf, A. Konrad, “Closed Loop Test Environment for Space Applications using GPS Signals,” Proceedings of the 26th AAS Conference on Guidance and Control, Breckenridge, CO, Feb. 5–9, 2003, Vol. 113 Advances in the Astronautical Sciences, Edited by I. J. Gravseth and R. D. Culp, AAS–03–039

2848) A. Botchkovski., N. Mikhailov, S. Pospelov, “GNSS Software Receivers: Recent Developments,” Proceedings of 7th St. Petersburg International Conference on Integrated Navigation Systems, St. Petersburg, Russia, May 29–31, 2000

2849) J. G. Murphy, W. V. Cottrell, “Airborne Testing of GPS+GLONASS Positioning Sensor Against A Proven Test Truth Source,” Proceedings of ION GPS–97, Sept. 16–19, 1997, Kansas City, MO, pp. 1047–1054

Some background of AGGA (Advanced GPS/GLONASS ASIC) receiver development
<ul style="list-style-type: none"> • Applications supported by AGGA–2: <ul style="list-style-type: none"> – Spacecraft control: onboard determination of spacecraft position, attitude and time in real–time – POD (Precise Orbit Determination): onboard receiver, L1 and L2 carrier phase tracking, in combination with ground reference stations and with post–processing on ground (cm accuracy) – POD (Precise Orbit Determination): onboard receiver, L1 and L2 carrier phase tracking, in combination with ground reference stations and with post–processing on ground (cm accuracy) – Atmospheric sounding: refractive limb sounding technique, onboard receiver with on–ground post–processing, to determine temperature and humidity profiles up to 50 km – Reference stations: ground–based receiver with real–time processing, to compensate for errors – AGGA receivers are supporting the following navigation systems: GPS, GLONASS, EGNOS (Europe), WAAS (USA), MTSAT (Japan). – AGGA instruments on spaceborne missions: Several receiver designs employ the AGGA–2 chip of ATMEL Wireless & Microcontrollers, including GRAS on MetOp, SSTI on GOCE (E.11), Lagrange on RADARSAT–2 and on COSMO/SkyMed.
<ul style="list-style-type: none"> • The AGGA–3 development was built on the specifications and design of AGGA–2. <ul style="list-style-type: none"> – AGGA–3 is adding functionality to process new Galileo public signals (E1b, E1c, L5a, L5b) and new optimized GPS (L1 C/A, L2C, L5) signals – AGGA–3 provides enhanced high speed digital signal processing functionality, a powerful onboard microprocessor, LEON–FT (AT697E by Atmel), and versatile interfaces for a wide range of GNSS applications. integration of more functionality on–chip (e.g. among others, digital down–conversion from IF (Intermediate Frequency), the LEON2–FT microprocessor IP core, high–speed SpaceWire interfaces, more baseband channels, tracking aids, etc);
<ul style="list-style-type: none"> • The AGGA–4 development will include several improvements due to the changes in the specifications of Galileo and modernized GPS signals <ul style="list-style-type: none"> – AGGA–4 provides enhancement of flexibility (EADS Astrium, Austrian Aerospace) to process both memory–based codes, mainly for E1b, E1c, while keeping long LFSR generated codes for GPS L2C – improvement of the design methodology, optimising the device scalability and reducing the gate count, so that a larger number of GNSS channel can be fitted in the chip.

Table 162: Overview of ESA’s AGGA receiver development ^{2850) 2851)}

– Spaceborne testing. a) A GPS+GLONASS receiver [LAGRANGE™ (Laben GNSS Receiver for Advanced Navigation, Geodesy and Experiments) of Laben S.p.A., Vimodrone, Italy] is part of the SAC–C satellite payload with a launch Nov. 21, 2000. The design employs the AGGA–2 (Advanced GPS/GLONASS ASIC) chip device providing an integrated AODS (Attitude and Orbit Determination System) using a hybrid parallel multiplex scheme for attitude determination, b) an ESA GPS+GLONASS receiver by the name of GRAS (GNSS Receiver for Atmospheric Sounding) is part of the MetOp–A satellite (see G.2.2). LAGRANGE processes the received GPS and GLONASS signals in both the L1 and L2 frequency bands, allowing compensation of ionospheric delays. A special codeless adaptive tracking scheme is implemented in order to process the encrypted P(Y) signals transmitted in the GPS L2 frequency band when Anti–Spoofing is on. ^{2852) 2853)}

As of 2009, AGGA–2 is a space–qualified digital integrated circuit providing all the high–speed digital signal processing functionality for EO applications such as atmospheric sounding with RO (Radio Occultation) and POD (Precise Orbit Determination) of LEO spacecraft for gravity field determination, altimetry, SAR interferometry, etc.

2850) P. Silvestrin, P. Sinander, “An Integrated Circuit for Spaceborne Instruments Employing Navigation Satellite Signals,” ESA, Vol. 10, No. 1 March 2000, URL: <http://esapub.esrin.esa.it/pff/pffv10n1/pffsilve.pdf>

2851) S. Fischer, P. Rastetter, M. Mittnacht, F. Griesauer, P. Silvestrin, “AGGA–3 in an Avionic System,” ESA Workshop on Spacecraft Data Systems and Software (SDSS 2005), ESA/ESTEC, Noordwijk, Oct. 17–20, 2005

2852) P. A. Kraus, S. Berberich, A. Konrad, A. Jaupitre, L. Vaillon, “Attitude Determination Using the AGGA–2,” 5th ESA Conference on Guidance Navigation and Control Systems, Oct. 22–25, 2002, Frascati, Italy, ESA SP–516

2853) L. Marradi, E. Banfi, A. Mambretti, “The LAGRANGE™ Receiver: Design and In–Flight Demonstration,” NAVITEC 2001, 1st Workshop on Satellite Navigation User Equipment Technologies, Dec. 10–12, 2001, ESA/ESTEC, Noordwijk, The Netherlands

The AGGA-4 (of ESA funding) should be commercially available in late 2010 for the European space industry. ²⁸⁵⁴⁾

- Starting in about 1994/5, spaceborne/airborne GPS/GLONASS receiver applications developed into two major functional directions:
 - Use of the receiver as a navigation sensor – to determine relative and absolute spacecraft attitude, orbit and time. The receiver is expected to provide an engineering environment of real-time, autonomous onboard support to the spacecraft (mission-critical functions).
 - Use of the (GPS/GLONASS) receiver as a science instrument in Earth observation – to perform atmospheric sounding measurements, gravity measurements, ionospheric sounding measurements, etc. These science applications require extensive postprocessing of the data to achieve the desired results. – Receivers are included on virtually all new Earth-observation missions. Parallel to orbit determination, the technology opened new applications in atmospheric profiling (GPS/MET on OrbView-1/Microlab-1, launch April 3, 1995) and possibly in ocean altimetry (SAC-C). NASA/JPL-provided dual-frequency GPS receivers are part of four geomagnetic missions: Ørsted (launch Feb. 23, 1999), SUNSAT (launch Feb. 23, 1999), CHAMP (launch July 15, 2000), and SAC-C, launch Nov. 21, 2000) – and also of such missions as: SRTM (Shuttle Radar Topography Mission, launch Feb. 11–22, 2000), Jason (launch Dec. 7, 2001), GRACE (Gravity Recovery and Climate Experiment) with a launch Mar. 17, 2002.
- Demonstration of GPS receiver measurements in satellite orbits outside of the MEO GPS constellation of 20,000 km altitudes.
 - The TEAMSAT/YES (Young Engineers' Satellite) spacecraft (ESA technology demonstrator payload on Ariane-5 test flight with a launch Oct. 30, 1997) made GPS measurements in its HEO orbit at an altitude of 25,000 km.
 - The Motorola GPS Viceroy receiver ²⁸⁵⁵⁾ of the Equator-S (launch Dec. 2, 1997) satellite – with a near-equatorial HEO orbit of 10 R_E distance apogee and low perigee at 500 km – was able to measure carrier phase and/or C/A code of up to three GPS satellites at altitudes of 34,000 km (Dec. 3, 1997 while in transfer orbit). The GPS receiver measurements were considered for post-event (on-ground) orbit determination at GSOC. In addition, GPS side-lobe measurements were verified.
 - AMSAT-3D (launch Nov. 15, 2000, also referred to as AMSAT OSCAR-40) in a HEO (Molniya) orbit of 1000 x 58,800 km, inclination = 63.4°. ²⁸⁵⁶⁾ The AMSAT-GPS experiment is to demonstrate real-time GPS attitude and orbit determination above the GPS constellation (two Trimble TANS Vector (6-channel, L1, C/A code) GPS receivers along with two sets of four GPS antennas, GEC Plessey front-end chipset and AMD 29200 embedded RISC processor board). An additional experiment is to map the GPS signal patterns outside the GPS constellation. GPS signals from all around the orbit were measured. SNR levels up to 48 db-Hz were measured near apogee.
 - GPS measurements in GEO. ²⁸⁵⁷⁾ In general, GPS receivers in GEO cope with unfavorable conditions which are: 1) poor visibility and geometrical distribution of GPS signals, and 2) weak GPS signal power (low SNR). In spite of these handicaps, GPS pseudorange

2854) J. Roselló Guasch, R. Weigand, G. Lopez Risueño, P. Silvestrin, "AGGA-4 – Core device for GNSS space-receivers of the next decade," Proceedings of NAVITEC 2008, 4th ESA Workshop on Satellite Navigation User Equipment Technologies GNSS User Technologies in the Sensor Fusion Era, Dec. 10–12, 2008, Noordwijk, The Netherlands

2855) O. Balbach, et al., "Tracking of GPS Above GPS Satellite Altitude: Results of the GPS Experiment on the HEO Mission Equator-S," Proceedings of ION GPS 1998 Conference, Nashville, TN, 1998

2856) M. C. Moreau, E. P. Davis, J. Russell Carpenter, D. Kelbel, G. W. Davis, P. Axelrad, "Results from the GPS Flight Experiment on the High Earth Orbit AMSAT OSCAR-40 Spacecraft," ION-GPS 2002, Portland, OR, Sept. 24–27, 2002

measurements were already demonstrated in GEO for orbit determination in US military applications. Since geostationary orbit determination is a very attractive option for commercial GEO satellite operations, solutions are being introduced to a new generation of GPS receivers for any satellites in GEO. Two examples:

- EADS Astrium GmbH offers an instrument, MosaicGNSS,²⁸⁵⁸ a GNSS receiver using a software and hardware correlation (applications in LEO, GEO, MEO, HEO) and capable of tracking up to 8 GPS satellites. The so-called MosaicAODS is a spaceborne Attitude & Orbit Determination System, extended by a star sensor and an optional INS. The system provides the full state vector information (position, velocity, attitude, and time) permitting a good degree of onboard autonomy. MosaicAODS is planned to fly on TerraSAR-X (launch June 15, 2007).
- The TOPSTAR 3000 GPS receiver of TAS (Thales Alenia Space, ESA and CNES sponsored)²⁸⁵⁹ employs a filter and integration techniques to analyze weak GPS signals. TOPSTAR 3000 (a 4-antenna 24-channel C/A code GPS receiver) is part of the Stentor spacecraft (Note: a launch of Stentor took place on Dec. 11, 2002; however, a launch failure of Ariane 5 ECA occurred, destroying the Stentor S/C) to be used as a navigation tool for GEO spacecraft.
- Second frequency for civil GPS users (Block IIF series). Uninterrupted access to “carrier phase” of the L2 frequency will be provided as a second civil frequency. This agreement was announced Feb. 27, 1997, by DoT and DoD. The goal of the second civil frequency is to enhance GPS civil capabilities by: 1.) providing a redundant signal for civil use in the event that the GPS L1 were to become unavailable (due to jamming or interference), and 2.) enhancing civil GPS performance by providing a second civil frequency for ionospheric delay calculations, a critical design requirement for the FAA’s Wide Area Augmentation System (WAAS). The first Block-IIR-M GPS satellite launch is planned for 2003, ushering into operation the new L2 civil and L1/L2 military signals, and IOC (Initial Operational Capability) for WAAS and initial operations of LAAS (Local Area Augmentation System).
- CDGPS (Carrier-phase Differential GPS), see H.5.3. CDGPS sensing techniques provide very precise measures of relative position (1–2 cm level) and attitude between vehicles in formation (CDGPS is demonstrated to be useful in relative positioning and orbit determination in indoor and outdoor experimental settings). Given GPS measurements at two nearby antennas, relative position between these antennas can be estimated to a high degree of accuracy based on tracking the relative phase. Sample implementations: 1) CDGPS is flown on the Orion microsatellite of Stanford University (planned launch at the end of 2001).^{2860) 2861)}

The Orion CDGPS receiver (total instrument mass of 1.07 kg, including processors) consists of a single 6-antenna attitude and relative navigation receiver using carrier-differential GPS. 2) As of 2001, AeroAstro Inc. of Herndon, VA is developing “Star Ranger” (initially intended for the TechSat-21 mission of AFRL). The Star Ranger design concept utilizes Ku-band for its operation (intersatellite communication), DSSS (Direct Sequence Spread Spectrum) for precise ranging, a two-PN code technique for multiple access within the three-satellite formation, and CDGPS for the determination of relative position and atti-

2857) J. D. Kronman, “Experience Using GPS for Orbit Determination of a Geosynchronous Satellite,” Proceedings of ION GPS-2000, Sept. 19–22, 2000, Salt Lake City, UT, pp. 1622–1626

2858) M. Mitnacht, W. Fichter, “Real-Time Onboard Orbit Determination of GEO Satellites using Software and Hardware Correlation,” Proceedings of ION GPS-2000, Sept. 19–22, 2000, Salt Lake City, UT, pp. 1976–1984

2859) Ch. Mehlen, D. Laurichesse, “Real-time GEO orbit determination using TOPSTAR 3000 GPS Receiver,” Proceedings of ION GPS-2000, Sept. 19–22, 2000, Salt Lake City, UT, pp. 1985–1994

2860) R. Zaenick, K. Kohlhepp, “GPS Micro Navigation and Communication System for Clusters of Micro and Nanosatellites,” Proceedings of the 14th AIAA/USU Conference on Small Satellites, Logan, UT, Aug. 21–24, 2000, SSC00-VI-8

2861) F. D. Busse, J. P. How, J. Simpson, “Demonstration of Adaptive Extended Kalman Filter for Low Earth Orbit Formation Estimation Using CDGPS,” ION-GPS 2002, Portland, OR, Sept. 24–27, 2002

tude between the formation flying satellites. The mass of Star Ranger is expected to be < 2 kg.

- **Integration of GPS and INS (Inertial Navigation System) to GPS/INS.** GPS and INS are two different, but very complementary, positioning systems. GPS is, essentially, a geometry–based system, with navigation determined by distances a receiver is from the different GPS satellites. It has the advantage of long–term position accuracy; errors from one observation time do not propagate to the next observation. – Unlike GPS, an INS system is based on the laws of Newtonian physics and initialization errors propagate throughout the trajectory. Although the long–term accuracy of a stand–alone INS cannot compare to that of GPS, its navigation solution is still necessary during times of GPS loss.²⁸⁶²⁾

The integration of GPS with INS devices improves the quality and integrity of each navigation system due to synergistic effects of the tight sensor combination and data fusion: use of GPS permits calibration of inertial instrument biases, and the INS can be used to improve the tracking and re–acquisition performance of the GPS receiver.^{2863) 2864)} Traditionally, INS devices provide positioning and attitude information for the guidance (and perhaps control) of a wide range of moving platforms in space, the air, at sea, or on the ground. A concern in INS applications is the time–dependent growth of systematic errors. It turns out that precise GPS satellite measurements are ideally suited for the calibration of INS systematic errors. Therefore, integrated INS and GPS (and/or Glonass) systems, i.e. GPS/INS devices, have been developed, which can provide high–rate precise positioning and attitude information. Many applications have benefited from GPS/INS integration. Some advantages of integrating these very complementary navigation systems are:

- Cycle slips in GPS data can be detected and eliminated in real–time by using the high short–term accuracy of the INS velocity
- The excellent positioning accuracy of differential GPS (DGPS) can be used to provide frequent updates to the inertial system which allows in–flight calibration and thus a major reduction of INS orientation errors. In general, the fact that nine independent measurements are available for the determination of the six required trajectory parameters greatly enhances the reliability of the system. Usually, a Kalman filter is used to handle both types of signals for optimal measurement performance.
- The DGPS/INS²⁸⁶⁵⁾ performance permits for direct georeferencing of source data from imaging instruments. In fact, GPS/INS platform orientation systems have emerged as core components of modern imaging platforms – in particular in airborne photogrammetric mapping applications.²⁸⁶⁶⁾
- GPS/INS technology can be used for over–the–horizon intelligence gathering, reconnaissance, and targeting.

Most of the early GPS/INS²⁸⁶⁷⁾ applications have been developed for military purposes and have focused on improved accuracy of anti–jam performance. For most civil aviation applications, accuracy is not the primary issue. The primary shortcoming of GPS for civil avi-

2862) D. A. Grejner–Brzezinska, Y. Yi, C. Toth, R. Anderson, J. Davenport, D. Kopcha, R. Salman “Enhanced Gravity Compensation for Improved Inertial Navigation Accuracy,” ION GPS/GNSS 2003, Sept. 9–12, 2003, Portland, OR, USA

2863) J. Wang, L. Dai, T. Tsujii, C. Rizos, D. Grejner–Brzezinska, C. Toth, “GPS/INS/Pseudolite Integration: Concepts, Simulation and Testing,” ION GPS 2001, Sept. 11–14, 2001, Salt Lake City, UT, pp. 2708–2715

2864) M. Harigae, T. Nishizawa, H. Tomita, “Development of GPS Aided Inertial Navigation System for High Speed Flight Demonstrator,” ION GPS 2001, Sept. 11–14, 2001, Salt Lake City, UT, pp. 2665–2675

2865) M. M. R. Mostafa, “Calibration In Multi–Sensor Environment,” ION GPS 2001, Sept. 11–14, 2001, Salt Lake City, UT, pp. 2693–2699

2866) N. Haala, D. Fritsch, D. Stallmann, M. Cramer, “On the Performance of Digital Airborne Pushbroom Cameras for Photogrammetric Data Processing – A Case Study,” Proceedings of ISPRS Congress, Amsterdam, The Netherlands, July 16–23, 2000 Vol. XXXIII

2867) T. Murphy, M. Harris, M. Braasch, “Availability of GPS/INS Integration Methods,” ION GPS 2001, Sept. 11–14, 2001, Salt Lake City, UT, pp. 600–609

ation is the availability of service with integrity (civil aviation). So far (2001), very few GPS/INS applications have been focused on enhancing the availability of GPS with integrity.

- Joint GPS/LEO navigation receiver. As of 2000/1 new dual–use tracking concepts of GPS and LEO constellation signals are being considered by the communications industry. Commercial LEO satellite systems, such as Orbcmm, Iridium, and Globalstar, provide a global coverage of their data and/or voice services. In addition to these prime services, the LEO constellations may also serve as “guide posts in space” to complement and enhance the GPS navigation performance.^{2868) 2869)} The combined use of positioning and two–way communication in LEOs may eventually lead to such applications ranging from emergency roadside assistance to location–based merchandising. The overall objective is to achieve precision (cm–level) navigation performance using pre–existent LEO transceiver hardware. In this concept, the LEOs provide additional ranging signals, which improves GDOP, availability of navigation solutions, and availability of RAIM (Receiver Autonomous Integrity Monitoring) geometry. The geometric diversity, achieved mainly by the motion of the LEOs, enables the GPS/LEO receiver to resolve the integer cycle ambiguities on the GPS constellation signals as well as parameters related to the cycle ambiguities on the LEO signals. First experimental tests have been conducted with the Orbcmm constellation in conjunction with GPS.
- At the start of the 21st century, well over two decades since the launch of NAVSTAR–1 (Feb. 22, 1978), GPS has exploded onto the scene, introducing itself into our society in ways never before conceived. Essentially providing anytime, anywhere positioning and timing, GPS is now integrated into nearly all major commercial and infrastructure components, including transportation, communications, energy, and commerce. The maritime industry has largely adopted it, and the aviation industry is establishing the groundwork for its use in nearly every phase of flight.²⁸⁷⁰⁾
- Hybrid navigation concepts (i.e. digital multi–sensor systems) with considerable performance improvements are achieved with the functional integration of GPS receivers with other attitude measurement devices such as: a) GPS + star sensor, b) GPS + magnetometer, c) GPS/INS + magnetometer, d) CDGPS/INS (Carrier–phase Differential GPS/INS). Each design takes the particular instrument advantages and disadvantages into account, reaching a hybrid navigation solution that is superior in its performance (quality and integrity) to that of various a single–instrument implementations.^{2871) 2872)}
- At the end of the first decade of 21st century, GPS has become the indispensable tool for precision navigation. A wide range of terrestrial applications has been developed, which includes such diverse areas as precision farming, open pit mining, surveying, bridge deflection monitoring, race car tracking and Earth crustal motion measurements. In aeronautics, the GPS nowadays supports the control of unmanned aerial vehicles, en–route, approach and landing navigation of airplanes and even enables the precision landing of fighter aircraft on carriers.

Common to all high precision applications is the use of so–called carrier phase measurements which measure the beat–phase of the received signal relative to a reference signal at the nominal frequency. Carrier phase measurements offer an extremely low measurement noise of typically 1 mm, which is two to three orders of magnitude lower than that of pseudo-

2868) M. Rabinowitz, B. W. Parkinson, K. Gromov, C. H. Cohen, “Architectures for Joint GPS/LEO Satellite Carrier Phase Receivers Designed for Rapid Robust Resolution of Carrier Cycle Ambiguities on Mobile Platforms,” ION GPS 2000, Slat Lake City, UT, Sept. 19–22, 2000, pp. 881–890

2869) M. Rabinowitz, B. W. Parkinson, J. J. Spilker, “Some Capabilities of a Joint GPS–LEO Navigation System,” ION GPS 2000, Slat Lake City, UT, Sept. 19–22, 2000, pp. 225–265

2870) J. W. Lavrakas, “A Systems Approach to a National Position, Navigation and Timing Service,” ION GPS 2001, Sept. 11–14, 2001, Salt Lake City, UT

2871) Ch. Arbinger, W. Enderle, O. Wagner, “GPS Based Star Sensor Aiding for Attitude Determination in High Dynamics,” ION GPS 2001, Sept. 11–14, 2001, Salt Lake City, UT, pp. 2952–2959

2872) J. D. Thienel, R. R. Haman, “GPS/Magnetometer Based Satellite Navigation and Attitude Determination,” ION GPS 2001, Sept. 11–14, 2001, Salt Lake City, UT, pp. 2946–2951

range measurements employed in more simple positioning techniques. The full strength of carrier phase based navigation is revealed in differential applications, which benefit from a high level of common error cancellation and enable a resolution of the unknown carrier phase ambiguity. This enables mm to cm positioning accuracies in post–processing and even real–time applications.²⁸⁷³⁾

- PRARE and DORIS are microwave tracking systems requiring a host satellite (for the space segment instrument) and global ground–based tracking networks for precise orbit determination. Both systems (PRARE and DORIS) require an orbit determination process using conventional dynamic techniques (with physical models) whose accuracies depend on the quality of the models.

PRARE (H.8.2) was initially installed on ERS–1 (launch July 17, 1991), but could not be operated. Further PRARE uses: Meteor–3–7 (launch Jan. 25, 1994, PRARE demonstration operations until March 1995), ERS–2 (April 21, 1995). PRARE is a two–way tracking system, broadcasting dual–frequency signals (2200 and 8500 MHz) from a transmitter on-board the host satellite to receiver–transponders on the ground. The signals are modulated by pseudonoise ranging codes to permit both range and range–rate measurements. The 8500 MHz signal is coherently transponded back to the host satellite (at 7200 MHz) for on-board range and range rate extraction. The 2200 MHz signal is received and tracked on the ground to provide an ionospheric correction. As of 2004, PRARE is operational on ERS–2.

DORIS was a prototype payload on SPOT–2 (launch Jan. 22, 1990) and SPOT–3 (launch Sept. 26, 1993); then flown on: TOPEX/Poseidon (launch Aug. 10, 1992). DORIS was initially a one–way Doppler system which broadcasts continuously at two frequencies: 401 and 2036 MHz. A two–way upgrade is planned for use on Envisat (launch Mar. 1, 2002). The DORIS instrument on the host satellite observes individual ground beacons in sequence and measures the Doppler frequency of the received signals.

- December 2013: The GPS Directorate celebrated the 20th anniversary of achieving Initial Operational Capability (IOC) for GPS on Dec. 8, 2013.²⁸⁷⁴⁾

In the 20 years since IOC, GPS has never failed to deliver on the global PNT (Positioning, Navigation and Timing) service commitments made by the DoD (Department of Defense) in the PPS (Precise Positioning Service) Performance Standard (PPS PS) and in the SPS Performance Standard (SPS PS) – both of which trace directly back to the original Global Positioning System (GPS) Standard Positioning Service Signal Specification (SPS SS) which was officially promulgated on Dec. 8, 1993 by the Assistant Secretary of Defense for Command, Control, Communication and Intelligence (C3I) as the formal document which defined IOC.

2873) Simone D’Amico, Oliver Montenbruck, “Differential GPS: An Enabling Technology for Formation Flying Satellites,” Proceedings of the 7th IAA Symposium on Small Satellites for Earth Observation, Berlin, Germany, May 4–7, 2009, IAA–B7–1403

2874) “20th Anniversary of Initial Operational Capability of the GPS Constellation,” GPS Daily, January 20, 2014, URL: http://www.gpsdaily.com/reports/20th_Anniversary_of_Initial_Operational_Capability_of_the_GPS_Constellation_999.html

1.27.6 GNSS (Global Navigation Satellite System) Augmentation Systems

GNSS is a concept to circumvent the limitations of current navigation system service provision. The limitations of current/future radionavigation systems (GPS, GLONASS, Galileo) are evident in particular in the area of aviation requirements to achieve a level of performance critical for civil aviation applications. Specific requirements are in the areas of: **accuracy, availability, integrity and continuity of service.**

Some of these risks could be attenuated by a receiver interoperability mode (GPS, GLONASS, Galileo), providing substantial improvements in redundancy (multiple navigation systems), accuracy as well as better coverage and integrity. However, this situation does still not provide sufficiently enough performance in safety–critical transportation applications (aviation and shipping). A workable solution can only be provided by complementary regional Wide Area Augmentation Systems (WAAS) which are being developed and deployed in USA, Europe, and Asia (see H.3). International cooperation is required to provide system interoperability.

The first generation GNSS–1 comprises the following elements: GPS, GLONASS as prime navigation constellations and their augmentation systems [WAAS (Wide Area Augmentation System) of the US, EGNOS (European Geostationary Navigation Overlay System) of Europe, and MSAS (Multi–Transport Satellite Augmentation System) of Japan].²⁸⁷⁵⁾ The three augmentation segments of GNSS–1 are expected to provide their IOC (Initial Operational Capability) in the time frame 2003/5. In fact, the formal completion of the technical qualification of EGNOS and the acceptance of the EGNOS system was delivered to ESA on June 16, 2005 by the European industry.

- Enhanced performance of GPS and GLONASS constellation service provision (of integrity, availability, accuracy, and continuity monitoring) for civil aviation applications. This type of service requires so–called augmentation systems, since neither the current GPS nor the GLONASS constellation are able to provide the needed functions. Augmentation systems are referred to by their generic name as SBAS (Satellite–Based Augmentation System) and GBAS (Ground–Based Augmentation System). An SBAS consists of a network of ground stations that monitor the navigation signals of the primary constellations (GPS and GLONASS). The ground stations send their observations to one or more master control stations, which generate the augmentation message. This in turn is sent to uplink stations for transmission to GEO satellites (Inmarsat). The GEO satellites broadcast their **SBAS message** to the user community, modulated onto a GPS look–alike signal at L1 (1575.42 MHz) GPS frequency (see H.3).

Starting in the 1990s with the WAAS (USA) and EGNOS (Europe) initiatives, several other countries have started their own initiatives to develop and implement regional augmentation systems in addition to the primary constellations. In 2002, these initiatives are at various stages of planning/development or initial service provision.

- WAAS (Wide Area Augmentation System) of USA (FAA)
- EGNOS (European Geostationary Navigation Overlay System) of Europe (European Tripartite Group; coverage of ECAC region)
- MSAS (Multi–Transport Satellite Augmentation System) of Japan (JCAB)
- CWAAS (Canadian WAAS) of Canada (NavCanada)
- SNAS (Satellite Navigation Augmentation System) of China

²⁸⁷⁵⁾ “EGNOS system delivered to ESA by industry,” http://www.esa.int/esaNA/SEM2VV1DU8E_index_0.html

- GRAS (Ground-based Regional Augmentation System) of Australia ²⁸⁷⁶ ²⁸⁷⁷)
- GAGAN (GPS And Geostationary Augmented Navigation) of India (ISRO).
- SDCM (System of Differential Correction and Monitoring), SBAS of GLONASS in planning as of 2009 by Roskosmos. ²⁸⁷⁸)

The following GEO satellite service providers are involved in the regional broadcast of SBAS messages to the user community.

- Inmarsat. The service started with the Inmarsat-3 (third generation) constellation in 1996. The Inmarsat-3 navigation transponders form an integral part of two SBAS systems, WAAS and EGNOS. – Each of the new Inmarsat-4 satellite series (launch of Inmarsat-4F1 on March 11, 2005, launch of Inmarsat-4F2 on Nov. 8, 2005, launch of Inmarsat-4F3 on Aug. 18, 2008) incorporates a navigation transponder for L1 and L5 frequency SBAS operations [service in bent-pipe mode, support of the same functions (with enhanced features) as the Inmarsat-3 navigation transponder]. Starting with the Inmarsat-4F1 service, an L5 frequency navigation signal (2nd civil GPS signal) is being broadcast for the first time from space, paving the way for the introduction of the second civil frequency for SBAS systems. ²⁸⁷⁹ ²⁸⁸⁰)

- WAAS achieved its IOC (Initial Operating Capability) in January 2003, providing a location accuracy of 2–3 m (horizontal and vertical). It was commissioned on July 10, 2003 as part of the US NAS (National Airspace System). The FOC (Full Operating Capability) is expected in the late 2007 time frame.

- BNTS-1 (BeiDou Navigation Test Satellite-1) of China (launch Oct. 31, 2000). BNTS-1 is the space segment to SNAS of China. BeiDou means “Northern Dipper.”

- BNTS-1B (launch Dec. 21, 2000). The Space Technology Research Institute, one of the five major research institutions of CASC (China Aerospace Science and Technology Corporation), built the BNTS satellites. BNTS provides navigation services for highway traffic, railway transport and ocean operations in China. Note: The final BeiDou constellation will consist of 4 GEO satellites.

- ARTEMIS (Advanced Relay and Technology Mission Satellite) of ESA, launch July 12, 2001 (see M.4). ARTEMIS complements the required constellation of three GEO satellites (2 Inmarsats+ ARTEMIS) in the ECAC (European Civil Aviation Conference) region.

- MTSAT (Multifunctional Transport Satellite) of Japan (JMA and JCAB), launch of MTSAT-1R on Feb. 26, 2005 (MTSAT-1 experienced a launch failure Nov. 15, 1999). MTSAT is the space segment to MSAS of Japan. MTSAT-2 was launched on Feb. 18, 2006.

- Generally there are two types of integrity concepts and methods in use for GNSS (GPS) integrity monitoring, i.e. RAIM and SBAS (Satellite-Based Augmentation System) integrity concepts. RAIM (Receiver Autonomous Integrity Monitoring) is based on redundant measurements.

- EGNOS operations. As of July 2005, ESSP (European Satellite Services Provider) – a consortium of AENA (Spain), DFS (Germany), DSNA (France), ENAV (Italy), NATS

²⁸⁷⁶) K. W. McPherson, W. S. Ely, G. K. Crosby, et al., “New Test Results with a Ground-based Regional Augmentation System (GRAS) in Australia,” ION GPS 2001, 11–14 September 2001, Salt Lake City, UT

²⁸⁷⁷) G. K. Crosby, W. S. Ely, K. W. McPherson, et al., “A Ground-based Regional Augmentation System (GRAS) – The Australian Proposal,” ION-2000, Salt Lake City, UT, Sept. 19–22, 2000, pp. 713–721

²⁸⁷⁸) “Russia Building Out GLONASS Monitoring Network, Augmentation System,” Inside GNSS, Aug. 19, 2009, URL: <http://www.insidegnss.com/node/1631>

²⁸⁷⁹) R. Pinto, “Inmarsat: an Approach for Integration of EGNOS and Galileo,” Proceedings of 8th International Symposium of Satellite Navigation Systems, Mat 26–28, 2003, Strasbourg, France

²⁸⁸⁰) C. Soddu, A. J. Van Dierendonck, H. Secretan, J. Ventura-Traveset, P.-Y. Dusseauze, R. Pasquali, “Inmarsat-4 First L1/L5 Satellite: Preparing for SBAS L5 Services,” ION GNSS 2005, Long Beach, CA, Sept. 13–16, 2005

(United Kingdom), NAV (Portugal), and Skyguide (Switzerland) – started the “initial operations phase” of EGNOS, a joint project of ESA, EC, and Eurocontrol. ^{2881) 2882) 2883)}

As of the end of 2005, the EGNOS ground infrastructure consists of 4 MCC (Mission Control Centers), 6 NLES (Navigation Land Earth Stations), and 31 RIMS (Ranging and Integrity Monitoring Station). Since December 2003, when the first transmissions were made, 3 geostationary satellites (Inmarsat–3, AOR–E, Inmarsat–3 IND–W), and ESA’s ARTEMIS have been transmitting successfully EGNOS signals.

- Technology demonstration of precision GPS–assisted aircraft landings. A US government–industry team accomplished the first precision approach by a civil aircraft, using the military **JPALS** (Joint Precision Approach and Landing System) at Holloman AFB, NM. A Boeing 727–200F aircraft (of FedEx Express Inc.), equipped with MMR (Multi–Mode Receiver) of Rockwell–Collins (GNLU–930), successfully conducted category–I (200 foot ceiling and 0.5 visibility) approaches and autolandings using the JPALS DGPS (Differential GPS) ground station, designed and developed by Raytheon Company for the USAF. The military test flight activities took place from June to Aug. 2001 using JPALS of the USAF. Over 280 military aircraft approaches were conducted at Holloman AFB using the USAF C–12J test aircraft. The JPALS equipment was also used for the military/civil interoperability demonstrations of JPALS/LAAS. On Aug. 25, 2001, a series of 16 approaches were conducted with the FedEx aircraft using the civil LAAS equipment (MMR). ^{2884) 2885) 2886)}

Precision approaches were conducted using precision guidance formed from C/A and Y–code differential solutions; Y–code solutions were used in both benign and hostile EMI environments to investigate the performance of operational and next–generation techniques for the mitigation of electronic interference in the GPS frequency band. Basically, the aircraft were guided by DGPS signals, integrity information, and precision approach path points transmitted from the JPALS ground station. The JPALS demonstration system is a test platform hosting multiple antenna, antenna electronics, and GPS receiver technologies integrated to provide a differential GPS precision approach capability based primarily on the civil LAAS (Local Area Augmentation System). The demonstration system consisted of a ground segment and an airborne segment and implemented core functionality envisioned in the proposed JPALS LDGPS (Local Area Differential Global Positioning System) program. – JPALS is the military version of the civilian LAAS (Local–Area Augmentation System) of FAA; JPALS and LAAS are similar and interoperable systems (both programs started in 1999, JPALS initial DoD program approval in May 1996).

Similarly, a civilian LAAS prototype station installed at Salt Lake City International Airport [Raytheon’s RAYNAV–4100 LGF (LAAS Ground Facility)] guided 16 precision landings there by the FedEx aircraft on Aug. 26, 2001 (demonstration of civil onboard GPS equipment with a civil LASS).

In the same context, on April 23, 2001, an FA–18A Hornet aircraft of the US Navy touched down on deck of the USS Theodore Roosevelt aircraft carrier performing the “first ever” fully automated landing at sea using GPS. The SRGPS (Shipboard Relative GPS), the Navy version of JPALS, achieved a touchdown dispersion of 5.6 m horizontal and a vertical accu-

2881) X. Berenguer, C. Ruf, J. C. Levy, D. Flament, J. Ventura–Traveset, D. Brocard, “EGNOS Performance at System ORR,” ION GNSS 2005, Long Beach, CA, Sept. 13–16, 2005

2882) http://www.esa.int/esaNA/SEMFOA808BE_index_0.html

2883) L. Gauthier, J. Ventura–Traveset, F. Toran, c. de Lesthievant, J.–Y. Bedu, “EGNOS Operations and their planned Evolution,” ESA Bulletin, No 124, Nov. 2005, pp. 56–61

2884) T. Katanik, S. Simon, C. Bett, B. Driscoll, D. Tsamis, J. Flemming, R. Norwood, J. Barry, “Interoperability Between Civil LAAS and Military JPALS Precision Approach and Landing Systems,” ION GPS 2001, Sept. 11–14, 2001, Salt Lake City, UT

2885) “Civil–Military Interoperability For GPS Assisted Aircraft Landings Demonstrated,” <http://www.spacedaily.com/news/gps-01k.html>

2886) Ch. J. Bett, S. A. Simon, B. J. Farnworth, R. W. Boyd, J. J. Brewer, “Flight Test of the JPALS LDGPS Demonstration System,” ION GPS 2001, Sept. 11–14, 2001, Salt Lake City, UT

racy of 12 cm. The aircraft carrier was equipped with SRGPS, providing 3–D coverage for up to 100 aircraft at a range of as much as 200 nautical miles.

JPALS key performance requirements call for: a) landing minima / guidance quality, b) system transportability and short set–up time, c) shipboard compatibility, d) non–vulnerability to signal disruption/spoofing, e) standardization, interoperability, and commonality to other LDGPS (compliance with RTCA messages), f) information exchange capability.

- In March 2002, plans of the US government (Federal Radionavigation Plan) call for a transition commitment from land–based to space–based radionavigation systems (GNSS–1) for **civilian aircraft navigation** in 2010 (originally planned for 2008). This implies primary reliance on the GPS constellation with its augmentation systems starting from 2010 onwards. ²⁸⁸⁷⁾

- GNSS–2 (Global Navigation Satellite System–2). The second generation GNSS comprises all elements of GNSS–1 plus Galileo plus Compass. GNSS–2 is planned to be operational by 2015.

- EGNOS flight trials. In March 2007, a test plane of the Direction Générale de l’Aviation Civile (DGAC – French Civil Aviation Authority) was specially equipped to make tests using EGNOS. At Limoges airport the ATR42 aircraft made a number of approaches and landings using the new procedures, in each case aligning itself with the runway’s axis and then following a descent path to touchdown. Inside the aircraft, the method of analyzing the quality of the EGNOS signals was by comparing the landing phases guided by satellite with landings using traditional means such as the ILS (Instrument Landing System). The results of these trials show again that EGNOS signals allow approaches and landings that meet the safety standards that govern international air traffic.

One of the main advantages of EGNOS in this application is that it is available everywhere in Europe without the need for ground infrastructure and it provides vertical guidance procedures for every runway. Furthermore, the cockpit data display is the same as that for ILS, so there are no familiarization problems for the pilots and no additional training costs. Currently in pre–operational service, EGNOS will be certified in 2009 for safety–of–life applications such as air traffic control. ²⁸⁸⁸⁾

- The **EGNOS ‘Open Service’ operations started on Oct. 1, 2009**. This represents a major milestone for the project: its primary service is now available to all users equipped with EGNOS–compatible receivers. Most mass–market satellite navigation receivers being sold today in Europe are ready for EGNOS. EGNOS significantly improves the accuracy of GPS signals, typically from 5–10 m to 1–3 m, while offering a service guarantee by means of integrity signal, and providing additional ranging signals. EGNOS operates at the GPS L1 frequency, and its signal is receivable with standard GPS frontends. ^{2889) 2890)}

The EC (European Commission) now owns and manages the EGNOS system. ESA is the design and procurement agent through a delegation agreement with the EC. The ESSP (European Satellite Services Provider), founded by seven air navigation services providers and based in Toulouse, France, manages EGNOS operations.

- In early September 2007, a GNSS “**Providers Forum**” was established at the second meeting of the International Committee on Global Navigation Satellite Systems (ICG) in Bangalore, India, with the aim to promote greater compatibility and interoperability among current and future providers of the Global Navigation Satellite Systems (GNSS) services. The members of the forum and their current and future systems include: China (CNSS,

2887) J. Bates, “Vulnerability Issue Delays GPS–Based Aircraft Navigation,” Space News, Apr. 1, 2002, p. 6

2888) http://www.esa.int/esaNA/SEMTHVLJC0F_index_0.html

2889) “EGNOS ‘Open Service’ available: a new era for European navigation begins today,” ESA, Oct. 1, 2009, URL: http://www.esa.int/esaCP/SEM2HGF280G_index_0.html

2890) Pieter De Smet, “The European GNSS Programme EGNOS and Galileo,” Sept. 8, 2009, URL: <http://www.turbocontent.files/IGLOSpace.ppt>

SNAS), EU (Galileo, EGNOS), India (IRNSS, GAGAN), Japan (QZSS, MSAS), Russia (GLONASS), and the USA (GPS, WAAS).^{2891) 2892)}

The United Nations Office for Outer Space Affairs (UNOOSA, Vienna, Austria) functions as the Executive Secretariat of the ICG (International Committee on GNSS) and the Providers Forum. The ICG was established on a voluntary basis as an informal body to promote cooperation, as appropriate, on matters of mutual interest related to civil satellite-based positioning, navigation, timing and value-added services, as well as the compatibility and interoperability of global navigation satellite systems, while increasing their use to support sustainable development, particularly in developing countries, and held its first meeting in Vienna in 2005, and its second meeting in Bangalore, India, in 2007.

Parameter	GPS	GLONASS	Galileo	Compass (CNSS)	QZSS (GSO)	IRNSS (GSO)
Country	USA	Russia	Europe	China	Japan	India
First launch	Feb. 22, 1978	Oct. 12, 1982	Dec. 28, 2005 GIOVE-A	April 14, 2007	Sept. 11, 2010	2013/14
FOC (Full Operational Capability)	July 17, 1995	Jan. 18, 1996	2014	2015	2016	2015
Service provision	Global	Global	Global	Global	Regional	Regional
Services: D-dual use, C-civilian	D	D	C (D PRS)	D	D	D
Commercial service	No	No	Yes	Yes	Yes	
No of S/C	21+3 nominal 28 (27.12.05) 31 (01.06.08)	24 nominal 13 (27.12.05) 17 (14.11.08)	27+3 nominal	27+3+5 (MEO, GSO, GEO)	3	7
S/C design life	10 years GPS-IIR	G: 3 yr G-M: 7 yr G-K: 10-12	> 12 years	8 years	12 years	9.4 yr GEO 11 yr GSO
S/C mass	~ 2000 kg GPS-IIR	1415 kg 850 kg (G-K)	~ 730 kg	~ 2300 kg	4100 kg 1800 kg (dry)	1330 kg
Orbital planes	6	3	3	3	3	3 S/C in GEO 4 S/C in GSO
Inclinations	55°	64.8°	56°	55.5°	39° – 47°	0°, 29°
Orbital altitude	~ 20,200 km	~ 19,100 km	~ 23,200 km	~ 21,400 km	35,786 km	35,786 km
Semimajor axis	26,560 km	25,508 km	29,601 km	27,840 km	42,164 km	
Orbital period	11 h 58 m	11 h 15 m	14h 22 min	12 h 50 m	23 h 56 m	23 h 56 m
Coordinate frame	WGS84	PZ90	GTRF	CGS2000	JGS	
Time system	GPST	UTC Moscow	GST	BDT	QZSST	
Signal access	CDMA	FDMA	CDMA	CDMA	CDMA	CDMA
Frequencies (MHz)	L1: 1575.42 L2: 1227.60 L5: 1176.45	G1: 1602 G2: 1246 G3: TBD	E1: 1575.42 E5a: 1176.45 E5b: 1207.14 E6: 1278.75	B1-2: 1589.74 (E1) B-1: 1561.1 (E2) B2: 1207.14 (E5b) B3: 1268.52 (E6)	L1C: 1575.42 L2C: 1227.60 L5: 1176.45 Lex: 1278.75	L5: 1176.45 S: 2492.08 a) standard b) authorized
Intersatellite links	Yes	G-M, K, Yes	No	No	No	
Integrity monitoring	No GPS III Yes	No G-K: Yes	Yes	Yes	Yes	

Table 163: Overview of current and future GNSS constellations

According to Table 163, the future GNSS is expected to provide more frequencies with more than 120 GNSS satellites when all the systems become fully operational. The increasing

2891) "International Committee on GNS Forms New Providers Forum," ION Newsletter, Fall 2007, pp.8-9, URL: <http://www.ion.org/newsletter/v17n3.pdf>

2892) Homepage of Providers Forum, URL: <http://www.oosa.unvienna.org/oosa/SAP/gnss/icg/providersforum.html>

number of spacecraft and constellations will provide a tighter network of observations. The interoperability and compatibility of signals and services from the various constellations is of utmost importance for the global user communities. ^{2893) 2894) 2895) 2896) 2897)}

Satellite	Inmarsat 3F2	ARTEMIS	Inmarsat 4F2
Launch date	Sept. 6, 1996	July 12, 2001	Nov. 8, 2005
Orbit slot	15.4° E	21.5° E	25° E
PRN	120	124	126
Channels	L1	L1	L1
Service provided	EGNOS	EGNOS	ESTB (EGNOS System Test Bed)

Table 164: Current EGNOS signals in space (SIS) from GEO spacecraft

- In March 2009, SES ASTRA contracted a hosted payload with the EC (European Commission) for the EGNOS (European Geostationary Navigation Overlay Service). The SES–5 ASTRA–4B (formerly SIRIUS–5) new commercial satellite (launch on July 9, 2012) hosts a 100 kg L–band tailor–made payload dedicated to EGNOS services. The orbit slot of ASTRA–4B is 5° E. ²⁸⁹⁸⁾

In January 2010, the EC awarded SES a second contract to provide a second EGNOS payload on its ASTRA–5B satellite, to be located at 31.5° East longitude.

Note: The ASTRA–5B spacecraft was launched on March 22, 2014.

Channel	L1	E5
Center frequency	1575.42 MHz	1191.795 MHz
Bandwidth	20 MHz	51 MHz
Polarization	RHCP	RHCP
Transmit power (EIRP)	≥ 31 dBW	≥ 33 dBW
Coverage	Global	Global
Carrier Frequency Stability	1 x 10 ⁻¹¹ over 1–100 s	1 x 10 ⁻¹¹ over 1–100 s

Table 165: ASTRA–4B EGNOS payload requirements summary

EGNOS supplements the primary GPS – and in the future also the GLONASS and GALILEO – navigation systems by reporting and improving the reliability and accuracy of the signals. It will also provide European navigation services ahead of the deployment of GALILEO. The EGNOS service is available over Europe and northern Africa and will be fully compatible with GALILEO.

On March 2, 2011, the **EGNOS Safety–of–Life signal was formally declared available to aviation**. For the first time, space–based navigation signals have become officially usable

2893) Meng–Lun Tsai, Yu–Sheng Huang, Kai–Wei Chiang, Ming Yang, “The Impact of Compass/BeiDou–2 on Future GNSS: A Perspective from Asia,” 4th Asian Space Conference 2008, Oct. 13–3, 2008, Taipei, Taiwan, URL: <http://www2.nspo.org.tw/ASC2008/4th%20Asian%20Space%20Conference%202008/oral/S22–03.pdf>

2894) “Report on the Third Meeting of the International Committee on Global Navigation Satellite Systems (ICG),” ICG–3 (Third Meeting of the International Committee on GNSS), Dec. 8–12, 2008, Pasadena, CA, USA, URL: http://www.fig.net/news/news_2008/icg_3_pasadena_december_2008.pdf

2895) Brad Parkinson, “The Future of Satellite Navigation (PNT),” Stanford University, Stanford, CA, USA June 11, 2007, URL: http://scpnt.stanford.edu/downloads/3.%20Parkinson_%20PNT–Symposium_The%20Future%20of%20Satellite%20Navigationv11.pdf

2896) Ken Alexander, “U.S. Programs & Policy,” CNS/ATM 2008, Tampa, FLA, June 26, 2008, URL: <http://pnt.gov/pub-lic/2008/2008–06–CNSATM/alexander.ppt>

2897) S. V. Kibe, “GAGAN & IRNSS,” ICG–3 (Third Meeting of the International Committee on GNSS), Dec. 8–12, 2008, Pasadena, CA, USA, URL: <http://www.oosa.unvienna.org/pdf/icg/2008/icg3/07.pdf>

2898) “European Commission Selects SES ASTRA For Navigation Service EGNOS,” March 16, 2009, URL: <http://www.ses–astra.com/business/en/news–events/news–latest/index.php?pressRelease=/pressReleases/pressReleaseList/09–03–16/index.php>

for the critical task of vertically guiding aircraft during landing approaches.²⁸⁹⁹⁾

By using three satellites and a 40–strong network of ground stations, the European Geostationary Navigation Overlay System (EGNOS) sharpens the accuracy of GPS satnav signals across Europe.

The signals are guaranteed to the extremely high reliability set out by the International Civil Aviation Organisation standard, adapted for Europe by Eurocontrol, the European Organisation for the Safety of Air Navigation.

- **SPEED** (Support Platform for EGNOS Evolution and Demonstration). SPEED is an ESA developed complete Test Bed environment in support of the EGNOS platform for evolutions and demonstrations. SPEED has been developed as the natural successor of ESTB (EGNOS System Test Bed) both for rationalizing EGNOS releases qualification and for performing innovative SBAS experiments and demonstrations. SPEED is fully representative of EGNOS when fitted with EGNOS operational algorithms. It is also designed for SBAS experiments thanks to its flexibility, allowing adjusting the platform to the users' needs. It allows easy algorithms update and tuning during experimentation phases. SPEED has a “Fast Replay” capability allowing processing a one–week data scenario in a single day.²⁹⁰⁰⁾

After 18 months of exploitation in the fall of 2012, SPEED has proven its ability to cover a wide range of services to study and assess SBAS performances, from EGNOS release qualification & support to operations, to lead SBAS experiments like HISTB (High Integrity Test Bed). The SPEED capacity of full representativeness will largely contribute to maintain the EGNOS V2 service in the coming years. The future of the SBAS services shall also take benefit of SPEED's already integrated features, like the handling of Multi–constellation & Multi–frequencies navigation data and the connection to IGS (International GNSS Service) stations.

- GNSS has become a part of our lives in such a way that if it was no longer available, the world economy would suffer. In the dual–use capacity, military GNSS systems (GPS) needed to consider civil users, and thereby dedicating signals for civilian use. As such, these signals have enabled safety of life capabilities, as well as widespread commercial use. With the growing need for international cooperation, multilateral forums such as the ICG (International Committee on GNSS) has allowed GNSS providers to be engaged in discussions on how to improve the civil aspect of GNSS. As a result, with GPS taking the lead in establishing policies that continue to provide universal positioning, navigation, and timing capabilities to all users free of charge, provider nations other than the USA have followed in the footsteps to ensure that navigation systems, albeit many built for military purposes, will also have the public benefit from their system.

- In February 2014, the **GAGAN** (GPS–Aided Geo Augmented Navigation) system of India, jointly developed by Airports Authority of India, ISRO (Indian Space Research Organization) and Raytheon, has achieved certification level Required Navigation Performance (RNP) 0.1.²⁹⁰¹⁾

Civil aircraft in Indian airspace will now have access to more precision navigation data than ever before. The GAGAN system is a Satellite Based Augmentation System (SBAS) equipped with the most advanced air navigation technology available.

The GAGAN system includes 15 reference stations strategically placed in India to optimize signal availability, uplink stations, master control stations, communication network and as-

2899) “EGNOS navigation system begins serving Europe's aircraft,” ESA, March 2, 2011, URL: http://www.esa.int/esaCP/SEM98MUTLKG_index_0.html

2900) H. Delfour, J. A. Gicquel, P. Larhantec, D. Joly, D. Lekaim, M. Jeannot, J. M. Melinotte, “Support Platform for EGNOS Evolution and Demonstration (SPEED),” Proceedings of NAVITEC 2012, 6th ESA Workshop on Satellite Navigation Technologies, ESA/ESTEC, Noordwijk, The Netherlands, Dec. 5–7, 2012

2901) “GAGAN System reaches certification milestone in India,” GPS Daily, Feb. 11, 2014, URL: http://www.gpsdaily.com/reports/GAGAN_System_reaches_certification_milestone_in_India_999.html

sociated software, all integrated to two Geostationary Earth Orbit satellites transmitting GPS corrections in C- and L-bands.

GAGAN is the fourth SBAS system certified for operational use. The system provides coverage for the entire Indian Flight Information Region via broadcast signals from the Indian built GSAT-8 and GSAT-10 satellites. Raytheon has co-developed three of the four world's SBAS systems in concert with national aviation and transportation authorities.

1.27.7 Galileo

Galileo is Europe's planned civilian–managed GNSS (Global Navigation Satellite System) program under design and development by ESA and the EC (European Commission). The overall system architecture includes the space segment, the ground control segment, the ground mission segment and the user segment. The planned space segment architecture consists of a MEO constellation of 30 satellites placed in three orbital planes with an inclination of 56° and a mean altitude of 23616 km. 27 The satellites are organized to give a 27/3/1 Walker constellation. One satellite per plane will act as an active spare for the other 9 MEO satellites in the same plane (quick recovery in case of failure). The orbital period is 5/3 revolutions/day. Each satellite in the constellation will broadcast precise time signals, together with clock synchronization, orbit ephemeris and other data. The Galileo system will provide eight open and two PRS (Public Regulated Service) signals per satellite. See also chapter H.2 for a Galileo system description.

In July 2003, ESA awarded two contracts, one to SSTL (Guildford, UK) and one to Galileo Industries SA of Brussels, each one is to build a Galileo test satellite for the Galileo satellite navigation system. The purpose is to transmit test signals at the frequencies reserved for Galileo so that the project secures those frequencies with ITU. Both test satellites are regarded as forerunners of the system's in–orbit validation phase (risk mitigation). The satellites will also test various critical technologies. Also, an initial performance demonstration capability and in–orbit system validation of two further Galileo spacecraft is planned for 2006. 2902) 2903) 2904) 2905)

- GIOVE–A (Galileo In–Orbit Validation Element–A), built by SSTL for ESA, was launched successfully on Dec. 28, 2005 from Baikonur, Kazakhstan, on a Soyuz–Fregat launcher into MEO (Medium Earth Orbit)
- GIOVE–B, built by Galileo Industries for ESA, was launched on April 27, 2008 from Baikonur. GIOVE–B is the first navigation satellite to carry a maser clock known as **PHM** (Passive Hydrogen Maser), with a stability better than 1 ns per day. It also provides a signal first with **MBOC** (Multiplexed Binary Offset Carrier). The new signal supports efforts towards Galileo–GPS cooperation.

Background: In early 1999 the EU proposed a strategy with the goal to design, implement and operate its own (civil) constellation of navigation satellites with the appropriate terrestrial infrastructure within a program by the name of Galileo. The space segment of the overall Galileo program is referred to as GalileoSat. Galileo is considered an element in a future GNSS–2 (Global Navigation Satellite System–2) – currently comprising GPS, GLONASS and their future augmentation systems. The rationale for Galileo is the provision of a service with a certifiable service performance level, which neither GPS nor GLONASS can presently do. The goal is the support of safety–critical civilian applications, especially in civil aviation, marine navigation, and road transport. Formal approval and funding of the Galileo program was given by the European Council of Transport Ministers on March 26, 2002. The goal is to complete implementation of the Galileo system by 2011. Although Galileo is a civil system, it doesn't mean it doesn't have military applications and implications in its service provision.

Successful deployment of Galileo will more than double the number of GNSS signals in space available to the user community. This large increase in satellites will benefit not only

2902) Note: Galileo Industries SA is a European joint venture of the following companies (to define and build the Galileo System): Alenia Spazio of Rome, Alcatel Space of Paris, EADS Astrium Ltd. of Stevenage, UK, and EADS Astrium GmbH of Friedrichshafen, Germany.

2903) K. Strodl, G. Naddeo, J. Samson, P. Dieleman, M. Ferraguto, H.–J. von der Hardt, F. Gottifredi, "Galileo System Verification: Approach, Methods, and Tools," GNSS 2003, Graz, Austria, April 22–25, 2003

2904) N. Mjøs, P. Robert, "Galileo System Certification – An Expert View," GNSS 2003, Graz, Austria, April 22–25, 2003

2905) A. Hornbostel, A. Schroth, U. Grunert, et al., "The DLR Project GalileoNAV: An Overview," GNSS 2003, Graz, Austria, April 22–25, 2003

single–point accuracy but also position reliability and the ability of GNSS user equipment to resolve integer ambiguities when using carrier–phase tracking techniques.

Agreements on GPS and Galileo navigation signal standards:

- On June 2004, the United States and the European Union (EU) have completed negotiations on an agreement to harmonize their respective satellite navigation systems: the existing U.S. Global Positioning Satellite (GPS) system and the planned European Galileo system. The US–EU agreement was signed on June 26, 2004, in Shannon, Ireland by the Secretary of State Colin Powell and the European Commission Vice President, Loyola de Palacio. ^{2906) 2907) 2908)}

The essence of the agreement was to switch to a range of frequencies and modulations known as BOC 1.1 (Binary Offset Carrier 1.1), allowing both the EU and the US forces to block each other’s signals in the battlefield without disabling the entire system. The European Union also agreed to address the “mutual concerns related to the protection of allied and US national security capabilities.”

As a result of achieving harmonization, the signals emitted by the two systems’ open services “are going to become the de–facto world standard in civilian satellite radio navigation” and will permit users to use either system – or both at the same time – with a single receiver. The civil user level interoperability of the GPS and Galileo signals consists of:

- Geodesy nearly identical ~ 2 cm
- Timing different but each system will transmit timing offsets
- Radio frequency compatible.

This allows manufacturers to build “dual system” civil receivers where the civil users can choose to use GPS, Galileo, or a combination of signals based on their needs.

- On July 26, 2007, the United States and the European Union announced an agreement for a common GPS–Galileo signal, called **MBOC** (Multiplexed Binary Offset Carrier) for civilian use. In the future, this will allow receivers to track the GPS and/or Galileo signals with higher accuracy, even in challenging environments. These signals will be implemented on the Galileo Open Service and the GPS–IIIA new civil signal. ²⁹⁰⁹⁾

Building on the historic cooperative agreement on GPS and Galileo signed between the two parties in June 2004, a joint compatibility and interoperability working group overcame technical challenges to design interoperable optimized civil signals that will also protect common security interests.

The resulting GPS L1C signal and Galileo L1F signal have been optimized to use the MBOC waveform. Future receivers using the MBOC signal should be able to track the GPS and/or Galileo signals with higher accuracy in challenging environments that include multipath, noise, and interference.

- Oct. 21, 2011: Launch of the first two **IOV** (In–Orbit Validation) navigation satellites of the operational Galileo series from Kourou, Europe’s Spaceport in French Guiana. This represented the first launch of a Soyuz launch vehicle from Kourou (Soyuz–STB/Fregat–

2906) “U.S., EU to Sign Landmark GPS–Galileo Agreement,” June 24, 2004, URL: <http://useu.usmission.gov/Article.asp?ID=E671D95A-FC0B-4AC5-BDCD-7F89291D2670>

2907) “Agreement on the Promotion, Provision and Use of Galileo and GPS Satellite–based Navigation Systems and Related Applications,” June 2004, URL: <http://pnt.gov/public/docs/2004-US-EC-agreement.pdf>

2908) R. Braibanti, “GPS – Galileo Cooperation Agreement,” Aug. 24, 2004, Washington, DC, URL: http://www.ion.org/sections/washington/august_2004_briefing.ppt

2909) “U.S., EU Announce Final Design for GPS–Galileo Civil Signal,” July 26, 2007, URL: http://useu.usmission.gov/Dossiers/Galileo_GPS/Jul2607_Civil_Signal_Accord.asp

MT).²⁹¹⁰⁾ — *Note: The documentation of the Galileo program is classified; hence, there will be no description of the spacecraft and their payloads on the eoPortal.*

- The flight tests of the first two IOV satellites (IOV–1 and IOV–2), built by Astrium and launched on Oct. 21, 2011, were officially completed in late March 2012. Thus, the two satellites became the first working components of the Galileo system. — It is planned, that by 2014/15, 14 satellites will be orbiting the Earth, and they will be able to provide the users with navigation services.^{2911) 2912)}
- Oct. 12, 2012: Launch of the second pair (IOV–3 and IOV–4) of Europe’s Galileo navigation satellites from Kourou by the Soyuz ST–B launcher, operated by Arianespace.
 - The third Galileo Flight Model, known as FM3 (IOV–3), transmitted its first test navigation signal in the E1 band on Dec. 1, 2012, the band being used for Galileo’s freely available Open Service interoperable with GPS. Then, on the morning of Dec. 4, 2012, the satellite broadcast signals across all three Galileo bands – E1, E5 and E6.²⁹¹³⁾
- Once all 14 are in orbit, the 18–strong Galileo constellation will achieve ‘Initial Operational Capability’ and will be able to provide initial navigation services – the full range of services will be available once all 30 satellites are in place in 2018.²⁹¹⁴⁾
- **First Galileo position fix:** The first position fix of longitude, latitude and altitude took place at the Navigation Laboratory at ESA’s technical heart ESTEC, in Noordwijk, the Netherlands on the morning of 12 March, 2013, with an accuracy between 10 –15 m — which is expected taking into account the limited infrastructure deployed so far. — This is considered a historic milestone for the Galileo navigation system, the very first determination of a ground location using the four Galileo satellites currently in orbit together with their ground facilities.²⁹¹⁵⁾

This fix relies on an entirely new European infrastructure, from the satellites in space to the two control centers in Italy and Germany, linked to a global network of ground stations on European territory.

Once testing of the latest two satellites (IOV–3 and IOV–4) was complete, in recent weeks the project efforts focused on the generation of navigation messages and their dissemination to receivers on the ground.

With only four satellites for the time being, the present Galileo constellation is visible at the same time for a maximum two to three hours daily. This frequency will increase as more satellites join them, along with extra ground stations coming online, for Galileo’s early services to start at the end of 2014.

- On May 15, 2013, the first Galileo **FOC** (Full Operational Capability) satellite was delivered to ESA/ESTEC for rigorous testing. Like all the other 21 FOC satellites so far procured by ESA, the satellite’s prime contractor is OHB in Bremen, Germany and the navigation payload was produced by SSTL (Surrey Satellite Technology Ltd) in Guildford, UK.. A

2910) “One Soyuz launcher, two Galileo satellites, three successes for Europe,” ESA, Oct. 21, 2011, URL: http://www.esa.int/esaCP/SEM167GURTG_index_0.html

2911) Olga Zakutnyaya, “Galileo satellites intensify competition on the market of navigation,” April 10, 2012, URL: http://www.spacedaily.com/reports/Galileo_satellites_intensify_competition_on_the_market_of_navigation_999.html

2912) Christina Wagner, Veit Lechner, “Galileo Payload In–orbit Test Preparation and Execution,” Proceedings of SpaceOps 2012, The 12th International Conference on Space Operations, Stockholm, Sweden, June 11–15, 2012

2913) “Third Galileo satellite begins transmitting navigation signal,” ESA, Dec. 4, 2012, URL: http://www.esa.int/esaCP/SEM2R5F16AH_index_0.html

2914) “First payload ready for next batch of Galileo satellites,” ESA, April 19, 2012, URL: http://www.esa.int/esaCP/SEM1Z7KWZ0H_index_0.html

2915) “Galileo fixes Europe’s position in space,” ESA, March 13, 2013, URL: http://www.esa.int/Our_Activities/Navigation/Galileo_fixes_Europe_s_position_in_history

second Galileo FOC satellite is due to join its predecessor at ESTEC later this summer, preparing for a launch scheduled for later this year. ²⁹¹⁶⁾

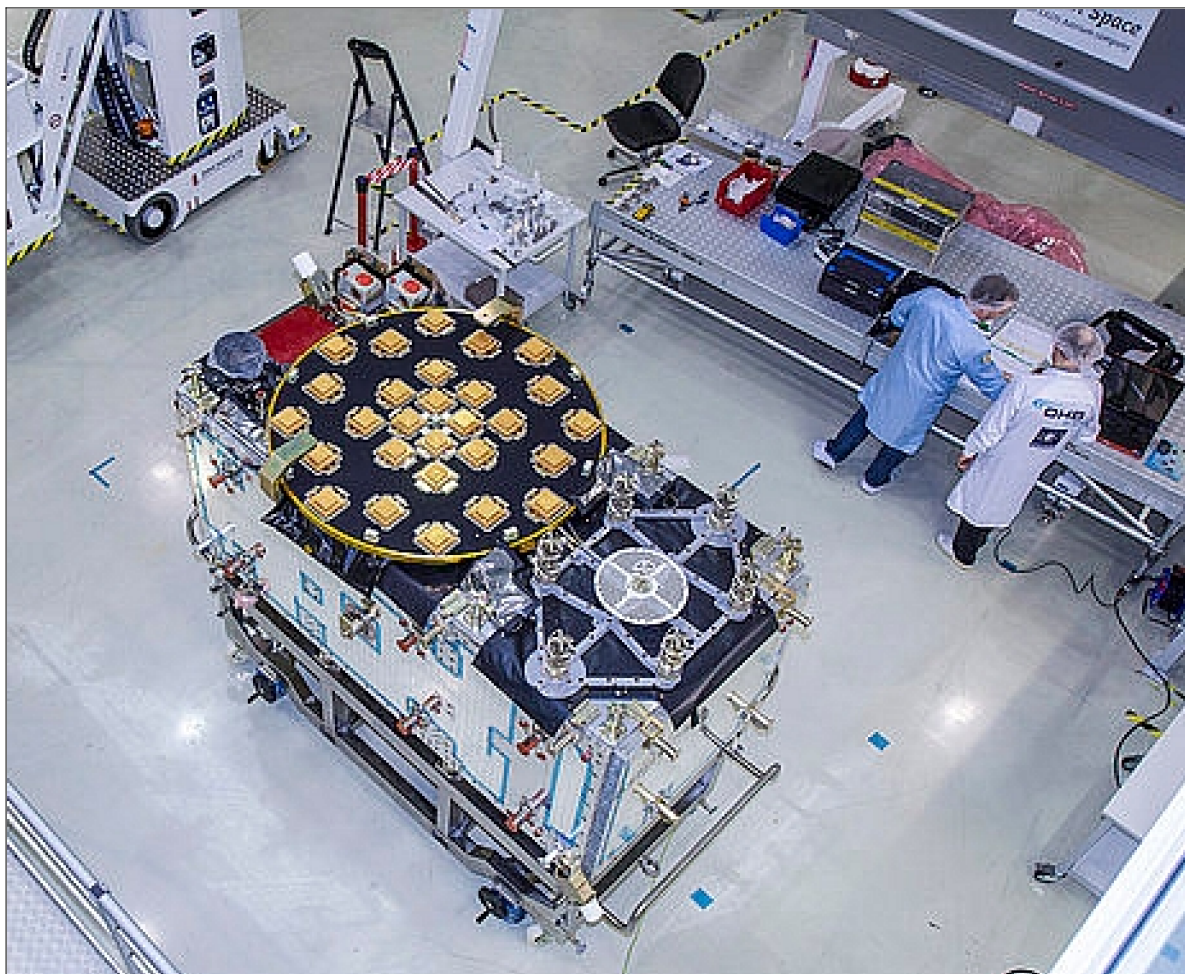


Figure 216: Photo of the first Galileo FOC satellite released on June 24, 2013 (image credit: OHB)

- Dec. 12, 2013: ESA's Galileo satellites have achieved their very first aerial fix of longitude, latitude and altitude, enabling the inflight tracking of a test aircraft. ESA's four Galileo satellites in orbit have supported months of positioning tests on the ground across Europe since the very first fix back in March. – Now the first aerial tracking using Galileo has taken place, marking the first time ever that Europe has been able to determine the position of an aircraft using only its own independent navigation system. ²⁹¹⁷⁾

This milestone took place on a Fairchild Metro–II above Gilze–Rijen Air Force Base in the Netherlands at 12:38 GMT on 12 November, 2013. The tests were scheduled during periods when all four Galileo satellites were visible in the sky – four being the minimum needed for positioning fixes.

The receivers fixed the plane's position and, as well as determining key variables such as the 'position, velocity and timing' accuracy, time to first fix, signal to noise ratio, range error and range-rate error. The testing covered both Galileo's publicly available Open Service and the more precise, encrypted Public Regulated Service, whose availability is limited to governmental entities.

- **IOV (In–Orbit Validation):** On February 10, 2014, ESA is reporting that the in–orbit validation of Galileo has been achieved: Europe now has the operational nucleus of its own

2916) http://www.esa.int/Our_Activities/Navigation/Highlights/New_breed

2917) "Galileo achieves its first airborne tracking," ESA, Dec. 12, 2013, URL: http://www.esa.int/Our_Activities/Navigation/Galileo_achieves_its_first_airborne_tracking

satellite navigation constellation in place – the world’s first civil–owned and operated sat-nav system.²⁹¹⁸⁾

In 2011 and 2012 the first four satellites were launched into orbit. Four is the minimum number needed to perform navigation fixes. In the following year, these satellites were combined with a growing global ground infrastructure to allow the project to undergo its crucial In–Orbit Validation phase: IOV. IOV was required to demonstrate that the future performance of the constellation can be met. The entire self–sufficient system has been shown as capable of performing positioning fixes across the planet.

1.27.8 CNSS (Compass/BeiDou Navigation Satellite System)

CNSS is an independent global navigation satellite system under development by China. Although the program was initiated by China’s military forces, China established an agency, namely CSNPC (China Satellite Navigation Project Center) in the timeframe 2006/7, to take charge of the research, building, and management of CNSS.

The BeiDou–2 program, the global navigation satellite system, was officially started in 2005 and announced by China in October 2006 (which was later renamed to Compass). The new system will be a constellation of 35 satellites, which include 5 geostationary orbit (GEO) satellites and 30 medium Earth orbit (MEO) satellites, that will offer complete coverage of the globe.

Launch date	Satellite	Orbit, position	Comment
BeiDou–1 (1st generation)			
Oct. 31, 2000	BeiDou–1A	GEO, 140° E	BeiDou–1A, BeiDou–1B, and BeiDou–1C belong to the original BeiDou–1 system
Dec. 21, 2000	BeiDou–1B	GEO, 80° E	
May 25, 2003	BeiDou–1C	GEO, 110.5° E	
Feb. 3, 2007	BeiDou–1D	GEO, 58.75° E	BeiDou–1D and BeiDou–1E are considered as the additional satellites for the BeiDou–2 system.
TBD	BeiDou–1E	GEO, 160° E	
April 14, 2007	Compass–M1	MEO, altitude = 21,150 km, inclination = 55.5°	Launch from Xichang on a Long March–3A vehicle
BeiDou–2 (2nd generation)			
April 14, 2009	BeiDou–2 (Compass–G2)	GEO1, drifting	Non–operational
Jan. 17, 2010	BeiDou–2 (Compass–G1)	GEO2, 144.5° E	Launch from Xichang on a Long March–3C vehicle
June 2, 2010	BeiDou–2 (Compass–G3)	GEO3, 84.7° E	Launch from Xichang on a Long March–3C vehicle
August 1, 2010 (UTC)	BeiDou–2 (Compass–IGSO1)	IGSO1 (Inclined GeoSynchronous Orbit), 118°E, 55° inclination	Launch from Xichang on a Long March–3A vehicle
Nov. 1, 2010	BeiDou–2 (Compass–G4)	GEO4, 160° E	Launch from Xichang on a Long March–3C vehicle
Dec. 18, 2010	BeiDou–2 (Compass–IGSO2)	IGSO2, 118° E, 55° inclination	Launch from Xichang on a Long March–3C vehicle
April 10, 2011	BeiDou–2 (Compass–IGSO3)	IGSO3, 118° E, 55° inclination	Launch from the Xichang Satellite Launch Center
July 26, 2011	BeiDou–2 (Compass–IGSO4)	IGSO4, 120° E, 55° inclination	Launch from the Xichang Satellite Launch Center

²⁹¹⁸⁾ “Galileo works, and works well,” ESA, Feb. 10, 2014, URL: http://www.esa.int/Our_Activities/Navigation/Galileo_works_and_works_well

Launch date	Satellite	Orbit, position	Comment
Dec. 02, 2011	BeiDou-2 (Compass-IGSO5)	IGSO5, 55° inclination	Launch from the Xichang on a Long March-3A vehicle
Feb. 24, 2012	BeiDou-2 (Compass-G5)	GEO5, 58.82° E	Launch from Xichang on a Long March-3C vehicle
April 29, 2012	BeiDou-2 Compass-M3 Compass-M4	Two MEO spacecraft deployed in 21,500 km orbits, 55° inclination, period = 12 hours	Launch from Xichang on a Long March-3B vehicle
Sept. 18, 2012	BeiDou-2 Compass-M5 Compass-M6	Two MEO spacecraft deployed in 21,500 km orbits, 55° inclination, period = 12 hours	Launch from Xichang on a Long March-3B/E vehicle
Oct. 25, 2012	BeiDou-2 (Compass-G6)	GEO6, 110.5° E	Launch from Xichang on a Long March-3C vehicle

Table 166: Chronology of BeiDou satellite launches ²⁹¹⁹⁾

The concept of the of BeiDou-1 program, the first generation demonstration system, was originally designed to be a regional navigation satellite system servicing China. Unlike the GPS, GLONASS, and Galileo systems, which use MEO (Medium Earth Orbit) satellites, BeiDou-1 uses satellites in geostationary orbit. This means that the system does not require a large constellation of satellites, but it also limits the coverage to areas on Earth where the satellites are visible. The area that can be serviced with BeiDou-1 is from 70°E to 140°E, and from 5°N to 55°N.

Each BeiDou-1 spacecraft has a launch mass of about 2200 kg, developed by DFH of CAST (China Academy of Space Technology) and of CASC (China Aerospace Science and Technology Corporation), Beijing. The spacecraft bus of the BeiDou-2 series is referred to as DFH-3.

The objective of Compass/BeiDou-2 is to provide two levels of service: a) an open service free to the global user community, and b) an authorized (licensed) service. ^{2920) 2921) 2922)}

- The open service will provide a positioning accuracy of 10 m, a timing accuracy of 20 ns, and a velocity accuracy of 0.2 m/s.
- The authorized service will ensure a highly reliable use to the community on a commercial basis (also for the military).

Compass /BeiDou-2 signal characteristics:

- Frequencies: B1, B2, B3
 - B1: 1561.098 ± 2.046 MHz
 - B1-2: 1589.742 ± 2.046 MHz
 - B2: 1207.14 ± 12 MHz
 - B3: 1268.52 ± 12 MHz
- Signals and modulation:

2919) "Compass (Beidou-II)," Dragon in Space, URL: <http://www.dragoninspace.com/navigation/compass-beidou2.aspx>

2920) Jun Lu, "COMPASS/BeiDou Navigation Satellite System Development," ICG-3 (Third Meeting of the International Committee on GNSS), Dec. 8-12, 2008, Pasadena, CA, USA, URL: <http://www.oosa.unvienna.org/pdf/icg/2008/icg3/06.pdf>

2921) T. Grelier, A. Ghion, J. Dantepal, L. Ries, A. DeLatour, J.-L. Issler, J. A. Avila-Rodriguez, S. Wallner, G. W. Hein, "Compass Signal Structure and First Measurements," ION GNSS 20th International Technical Meeting of the Satellite Division, Sept. 25-28, 2007, Fort Worth, TX, USA

2922) T. Grelier, J. Dantepal, A. Delatour, A. Ghion, L. Ries, "Initial observation and analysis of Compass MEO satellite signals," Inside GNSS, May/June 2007, pp. 39-43, URL: http://www.insidegnss.com/auto/IG0607_CompassFinal.pdf

- B1 (QPSK), B1–MBOC (Multiplexed Binary Offset Carrier), B1–2 (QPSK)
- B2 (QPSK), B2–BOC (Binary Offset Carrier)
- B3 (QPSK), B3–BOC
- L5 (QPSK).

CNSS coordinate system:

- Compass/BeiDou coordinate system is referred to as CGS2000 (China Geodetic System 2000)
- It coincides with ITRF within a few cm; hence, for most applications the difference between CGS2000 and ITRF can be neglected.
- The Compass/BeiDou–2 time reference is referred to as **BDT** (Bei Dou system Time), traced to UTC, and will be synchronized with UTC within 100 ns.

Coordinating Compass/BeiDou–2 with other GNSS constellations:²⁹²³⁾ Interoperability is one of the most important aspects in the design of the Compass timing system; the time differences of BDT – GPST and BDT – GST (Galileo System Time) are measured in the Compass central control station and will later be broadcast as part of the navigation messages of the GNSS systems.

The BeiDou system started to provide services on a trial basis on Dec. 27, 2011. The system has been used in transportation, weather forecasting, marine fisheries, hydrological monitoring, and mapping.

- In late December 2012, the BeiDou system began providing services to users in the Asian–Pacific region. The services include positioning, navigation, timing and short messages for China and surrounding areas. The open service will be provided with positioning accuracy of 10 m, velocity accuracy of 0.2 m/s and one–way timing accuracy of 50 ns.^{2924) 2925)}

1.27.9 QZSS (Quasi–Zenith Satellite System)

QZSS is a Japanese regional satellite navigation system under development at JAXA. The navigation system objective is to broadcast GPS–interoperable and augmentation signals as well as original Japanese (QZSS) signals from a three–spacecraft constellation in inclined, elliptical geosynchronous orbits. With this system concept, users in and around Japan and Oceania/Australia can use seamless positioning, navigation, and timing services, even in urban canyons and mountainous areas.

QZSS occupies a unique location within the spectrum of satellite navigation systems in that it is designed to augment another satellite navigation system (in this case, GPS) but is not limited to a “bent–pipe” transposition of ground–generated ranging signals through a GEO communications satellite. Instead, QZSS satellites will occupy inclined elliptical geosynchronous orbits for optimal high–elevation visibility in the area of coverage. The QZSS constellation (when completed) will operate more like independently–operating GPS or Galileo navigation satellites rather than in the restricted ground–controlled manner com-

²⁹²³⁾ Shaowu Dong, Xiaohui Li, Haitao Wu, “About Compass Time and its Coordination with other GNSS,” 39th Annual Precise Time and Time Interval (PTTI) Meeting, Long Beach, CA, USA, Nov. 27–29, 2007, URL: <http://tycho.usno.navy.mil/ptti/ptti2007/paper3.pdf>

²⁹²⁴⁾ “China’s Beidou system starts service in Asian–Pacific,” Space Daily, Dec. 28, 2012, URL: http://www.spacedaily.com/reports/Chinas_Beidou_system_starts_service_in_Asian_Pacific_999.html

²⁹²⁵⁾ J. Lu, “BeiDou Navigation Satellite System and International Activities,” Proceedings of the 50th Session of Scientific & Technical Subcommittee of UNCOPUOS, Vienna, Austria, Feb. 11–22, 2013, URL: <http://www.oosa.unvienna.org/pdf/pres/stsc2013/tech-37E.pdf>

mon to SBAS GEO augmentation satellites.²⁹²⁶⁾

QZSS architecture: The QZSS system consists of a space segment and a ground segment. The space segment consists initially of a single QZS (Quasi–Zenith Navigation Satellite). The ground segment mainly comprises a Master Control Station (MCS), a Monitoring Station (MS), Tracking and Control Stations (TCS), and systems of other national research institutes. About 10 MSs will be placed around Japan and overseas to estimate and predict the QZS orbit and clock more precisely.

Orbit of the QZSS: Semi–major axis = 42,164 km (± 10 km), eccentricity = < 0.099 , inclination = $39^\circ \sim 47^\circ$, argument of perigee = $270^\circ \pm 1^\circ$, central longitudinal ground track = $135^\circ \pm 5^\circ$ East, period = 23 hours 56 minutes.

The QZSS constellation in the final operational stage consists of three satellites in inclined, elliptical geosynchronous orbits whose planes are 120° apart.²⁹²⁷⁾

The QZS–1 spacecraft (nickname Michibiki) was launched successfully on Sept. 11, 2010 on an H–IIA vehicle from the Tanegashima Space Center, Japan.

- After launch, the first step of the QZSS program foresees technical validation followed by application demonstrations of the QZSS concepts and features.
- The 2nd and 3rd QZSS satellites will be launched several years later. Full system operation will be demonstrated.

QZSS signals: The QZS will transmit six signals on four frequencies; it has GPS interoperable and GPS augmentation capabilities. There are L1C, L1–C/A, and L1–SAIF (Sub–meter class Augmentation with Integrity Function) signals on the L1–band, the L2C signal on the L2–band, the L5 signal on the L5–band, and the LEX (L experimental) signal on the E6–band. The GPS interoperable signals are L1C, L1–C/A, L2C, and L5 signals. These signals are designed to have interoperability with GPS.

The deployment of Galileo, QZSS, and the modernization of GPS (Global Positioning System) will provide additional signals with increasingly complex modulations and multiplexing schemes, enabling performance enhancements in terms of availability, accuracy, and robustness. The GPS L5 capability will reach 24 satellites in 2018. Additionally, 4 QZSSs will be deployed by 2020. Pseudo–range observables stemming from L5 in both GPS and QZS have higher accuracy than the conventional signals such as L1. The Galileo E5 AltBOC (Alternate Binary Offset Carrier) has a more accurate range measurement to the centimeter level.²⁹²⁸⁾

2926) S. Pullen, “Worldwide Trends in GNSS Development and their Implications for Civil User Performance and Safety,” URL: <http://waas.stanford.edu/~www/papers/gps/PDF/PullenJapanGNSS07.pdf>

2927) H. Miyamoto, M. Kishimoto, H. Hase, M. Sawabe, K. Terada, “Design of Quasi–Zenith Satellite Navigation System and ground segment,” Proceedings of the 26th ISTS (International Symposium on Space Technology and Science), Hamamatsu City, Japan, June 1–8, 2008, paper: 2008–f–03, URL: <http://www.senkyo.co.jp/ists2008/pdf/2008–f–03.pdf>

2928) Hiroko Tokura, Taro Suzuki, Tomoji Takasu, Nobuaki Kubo, “The Possibility of Precise Automobile Navigation using GPS/QZS L5 and Galileo E5 Pseudo–ranges,” Proceedings of ITM 2013 (International Technical Meeting) of The Institute of Navigation, San Diego, Ca, USA, January 28–30, 2013

1.27.10 IRNSS (Indian Regional Navigational Satellite System)

IRNSS is an autonomous and independent regional navigation system being developed by India. It is designed to provide an accurate position information service to users in India as well as in the region extending up to 1500 km from its boundary, which is the primary service area of IRNSS. The Extended Service Area lies between primary service area and area enclosed by the rectangle from latitude 30° S to 50° N, and in longitude from 30° E to 130° E.

IRNSS will provide two types of services, namely, SPS (Standard Positioning Service) which is provided to all the users, and RS (Restricted Service), which is an encrypted service provided only to the authorized users. The IRNSS system is expected to provide a position accuracy of better than 20 m in the primary service area.

IRNSS is comprised of a space segment and a ground segment. The IRNSS space segment consists of seven satellites, with three satellites in GEO (Geostationary Orbit) and four satellites in inclined GSO (Geosynchronous Orbit). Such a constellation configuration will provide continuous radio visibility with the Indian control stations.

IRNSS is designed to be compatible with the US GPS (Global Positioning System) and Europe's upcoming Galileo constellation using navigation signals in S-band and at L5.

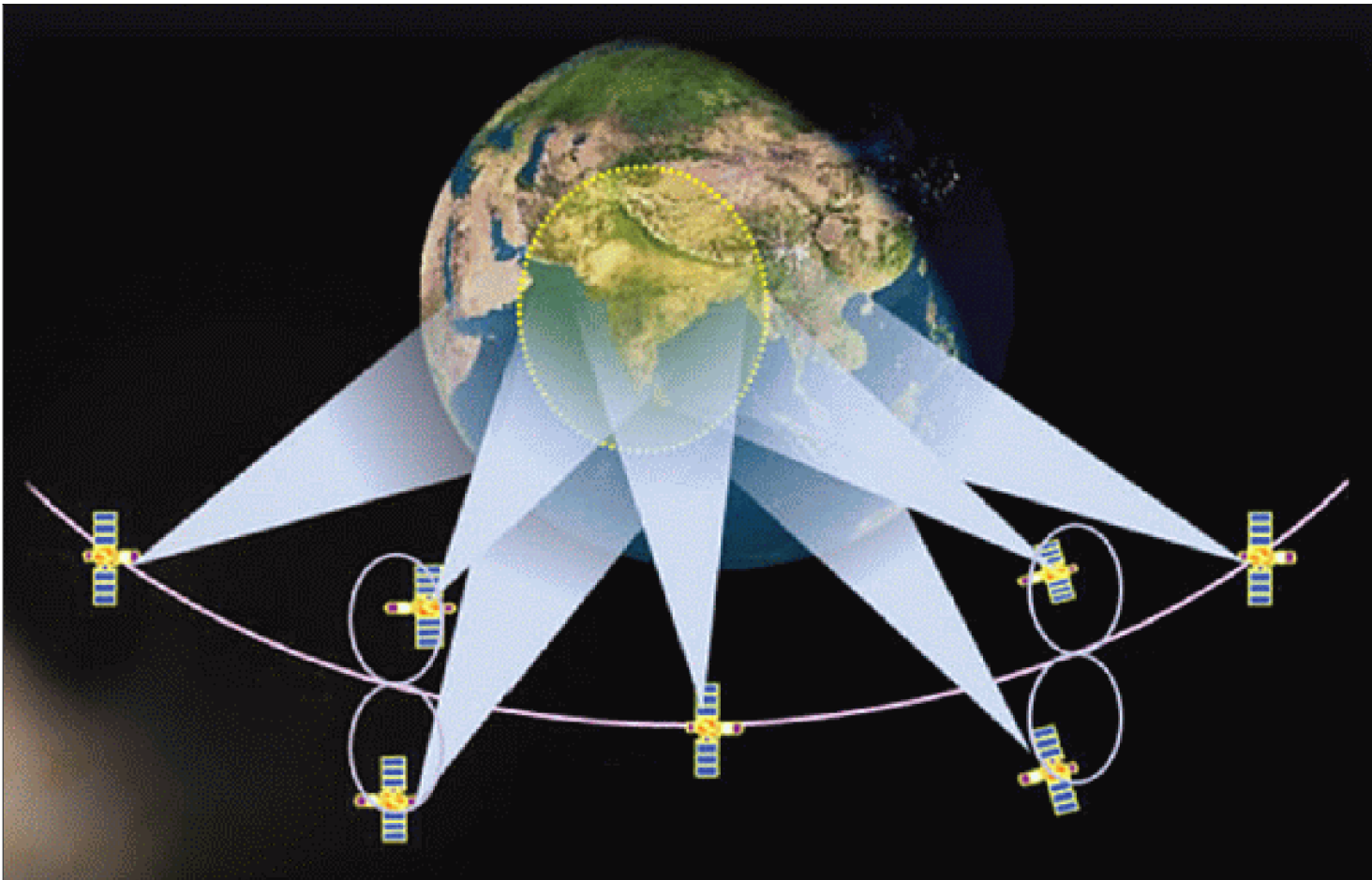


Figure 217: The IRNSS space segment coverage region consisting of seven satellites when completed (image credit: ISRO)

The IRNSS constellation architecture consists of the following elements:

- **Space segment:** The IRNSS satellites carry a navigation payload in a redundant configuration. A separate C-band transponder for precise CDMA ranging is included in the payload configuration. The important functions of the IRNSS payload are: Transmission of the

navigational timing information in the L5 bands; transmission of navigation, timing information in S–band; generation of navigation data on–board, CDMA ranging transponder for precise ranging.

The navigation payload will have the following subsystems: NSGU (Navigation Signal Generation Unit), Atomic clock unit, comprising of Rubidium atomic clocks, clock management and control unit, frequency generation unit, modulation unit, high power amplifier unit, power combining unit and navigation antenna.

The IRNSS spacecraft are dedicated for navigation services and they are configured to be of a class that can be launched by the Indian launcher PSLV. The design incorporates most of the proven subsystems available indigenously tailoring it specifically for the navigation.

The space segment distribution of satellites is as follows:

- 3 satellites in GEO (Geostationary Orbit) at the longitudes 32.5°, 83° and 131.5° East.
- 4 satellites in GSO (Geosynchronous Orbit) placed at inclination of 29° with longitude crossing at 55° and 111.75° East
- Two spare satellites are also planned. The satellites are specially configured for the navigation. Same configuration for GEO and GSO which is desirable for the production of the satellites.
- Plans call for the IRNSS satellites to be launched by the Indian launcher PSLV.
- **Ground segment:** The ground segment is responsible for the maintenance and operation of the IRNSS constellation. It contains a whole complement of the elements required for a basic constellation and is mainly comprised of:
 - Master Control Center for spacecraft control and navigation, IRNSS tracking and integrity monitoring stations, CDMA ranging stations, uplinking and telemetry stations, communication links and network timing center.
- **User segment:** Specially designed receivers and antennas are needed to receive the IRNSS signals. The receivers are also planned for receiving multi–constellation signals inclusive of GPS, GLONASS, Galileo and IRNSS. It is planned to broadcast the time difference between the IRNSS time and the time of the other constellations to enable the users to take advantage of the signals available to them.

The user segment consists of IRNSS receivers operating in:

- Single frequency (L5 at 1176.45 MHz or S–band at 2492.028 MHz)
- Dual frequency (L5 and S–band).

- Launch of IRNSS–1A on July 1, 2013 on the PSLV–C22 vehicle from SDSC (Satish Dhawan Space Center) SHAR on the east coast of India.
 - IRNSS–1A (GSO at 55° E), has already started functioning after extensive on orbit test and evaluation to confirm its satisfactory performance.
- Launch of IRNSS–1B on April 4, 2014 on the PSLV–C22 vehicle from SDSC . The spacecraft will also be positined at GSO at 55° E.

Table 167: Overview of IRNSS spacecraft launches

1.28 Services

Earth observation is a valuable information source. The rendering of any sustained or long-term service implies the provision of an operational capability. The early introduction of the NASA/NOAA broadcast service policy of free access to polar-orbit weather satellite data reception generated a totally new participative/cooperative research and application environment for a global user community (laboratories and research institutes in particular). Real-time data reception of AVHRR data became affordable to many with the installation of a simple receiving station. Eventually a network of thousands of small ground stations was realized, and the AVHRR sensor became the best known sensor in the world. The most important service aspect was probably the provision of a timely, reliable and repetitive data stream to the user community which in turn accelerated the pace of exploration and of technological development in the various fields of applications.

- TIROS-1 (launch April 1, 1960) is regarded the first true weather satellite.
- Starting with TIROS-8 (launch Dec. 21, 1963), real-time observational data were transmitted (broadcast) continuously in APT (Automatic Picture Transmission) mode to ground stations. Eventually, APT pictures could be received on fairly simple ground stations anywhere in the world.

Introduction of **APT and HRPT** (High Resolution Picture Transmission) broadcast modes (VHF link for ATP and L-band link for HRPT) in parallel with TIROS-N (launch Oct. 13, 1978). Further broadcast services of 'weather data' followed:

- The Terra satellite (launch Dec. 18, 1999) of NASA's EOS (Earth Observing System) program introduced a direct broadcast in X-band for instrument data (MODIS) to the user community.
- The Aqua (formerly EOS/PM-1) S/C of NASA (launch May 4, 2002) provides a direct broadcast in X-band for all its instrument data, including MODIS
- MetOp-A of EUMETSAT (launch Oct. 19, 2006) supports a real-time broadcast of instrument data to local users by means of LRPT (72 kbit/s in VHF for selected instruments) links and HRPT (3.5 Mbit/s in L-band) links.
- Suomi-NPP (NPOESS Preparatory Project) of NASA/IPO (launch Oct. 28, 2011) provides X-band broadcasts of instrument data at 15 Mbit/s.
- JPSS (planned launch in 2016) features a broadcast services of two data streams:
 - LRD (Low Rate Data) in L-band (1706.5 MHz) at a data rate of 3.88 Mbit/s (4 Mbit/s nominally) with full CCSDS convolutional coding, Viterbi decoding, and Reed Solomon encoding/decoding into a tracking receive antenna aperture of 1 m diameter. This data stream supports the retrieval of 23 EDRs (out of a total of 55). The LDR broadcast is a subset of the full NPOESS sensor data set and is intended for the global user community. The LRD format is compatible with the AHRPT (Advanced High Resolution Picture Transmission) format, accepted and approved by CGMS (Coordinating Group on Meteorological Satellites); it will also be used on the MetOp spacecraft.
 - HRD (High Rate Data) in X-band (7.75–785 GHz) at a rate of 20 Mbit/s (required receiver antenna diameter of 2 m with a bandwidth of 30 MHz). This data stream supports the retrieval of 51 EDRs, a complete full-resolution data set containing all sensor data and auxiliary/ancillary data necessary to generate all NPOESS EDRs (except some Earth Radiation EDRs); it is intended to support users at fixed, regional hubs.
- WEFAX (Weather Facsimile) services. The first installation of WEFAX on ATS-1 (launch Dec. 6 1966) worked well until 1972. It demonstrated that WEFAX transmissions were practical. The original transponder received on 149.22 MHz and transmitted on 135.6

MHz. Due to technological design improvements and interference with the aeronautical band, these frequencies were re-allocated to the S-band frequencies. The most pertinent one of these to date is the 1691 MHz WEFAX frequency.

- Presumably, NOAA-6 (launch June 27, 1979) is regarded as the first **operational** satellite of the TIROS-N series.
- The onboard store & forward data concept (with a data recorder and a data dump during a station pass) was introduced fairly early in the game (TIROS-1 with a launch in 1960 had a tape recorder). The lack of world-wide coverage (ground stations) for data downlinks dictated this strategy.
- Global coverage once per day was first provided by AVHRR on TIROS-N (launch Oct. 13, 1978)
- Introduction of **search and rescue services (COSPAS-S&RSAT)** on polar-orbiting satellites with the launch of COSPAS-1 on June 29, 1982 (Soviet Union) and with the S&RSAT payload flown on NOAA-8, March 28, 1983. The polar-orbiting satellites with the S&RSAT payload are also referred to as **LEOS&R**. The LEOS&R system calculates the location of distress events using Doppler processing techniques.²⁹²⁹⁾
The complementary **GEOS&R** (Geostationary Search and Rescue) system has been developed for GEO satellites. The GEOS&R system consists of 406 MHz repeaters carried on board various geostationary satellites (the Doppler effect technique cannot be used on a GEO system). The first GEOS&R (demonstration) system was flown on GOES-7 (launch Feb. 26, 1987). ISRO introduced the COSPAS-S&RSAT service over the Indian Ocean in 1992 with its **SAS&R** (Satellite Aided Search and Rescue) payload flown on the GEO INSAT-2 series, starting with INSAT-2A (launch July 9, 1992). GEOS&R is also flown on the MSG series of EUMETSAT (launch of MSG-1 Aug. 28, 2002, renamed to Meteosat-8 as of Jan. 29, 2004 when the operational service officially started).

– As of 2002 (20th anniversary of service), the COSPAS/S&RSAT system comprises six LEOS&R payloads (launch period of 2000–2004 to orbit the last in the current generation of instruments that began in 1998) and three GEO satellite payloads, dedicated for search & rescue services.^{2930) 2931)} In addition, there is a worldwide network of 48 ground stations for receiving and processing distress alert signals and 24 MCCs (Mission Control Centers) for relaying distress alerts. This infrastructure has moved far beyond the program's initial goals, since in 1982 none of the founding partners (USA, Canada, France, and the Soviet Union) had yet formed a clear idea of the international cooperation structures needed to operate the system successfully.

– Starting with the launch of MetOp-A satellite of EUMETSAT (launch Oct. 19, 2006), the next generation of CNES S&RSAT instruments with new digital technologies for improved receiver sensitivity (developed by Thales and Alcatel Space) are being flown on the MetOp series as well as on the NOAA-POES series.

– **MEOS&R** (Medium-Earth Orbit Search-and-Rescue): The planning in 2002 calls for S&RSAT systems to be deployed on the MEO Navigation Satellite Constellations of GPS (USA), GLONASS (Russia), and Galileo (Europe, ESA, EC). The intent is to provide a search and rescue service alongside the established COSPAS/S&RSAT service and infrastructure. The payload on the GPS constellation is referred to as **DASS** (Distress Alerting Satellite System), the payload on GLONASS will be **S&R/GLONASS**, while the name of the Galileo payload is **S&R/Galileo**.

MEOS&R (or MEOSAR) overcomes the limitations of the current COSPAS-S&RSAT system based on satellites that are either in GEO or in LEO. MEOS&R provides visibility

²⁹²⁹⁾ <http://www.sarsat.noaa.gov/>

²⁹³⁰⁾ D. Levesque, "Cospas-Sarsat – Looking to the future," CNES Magazine, No 16, July 2002, pp. 23–24

²⁹³¹⁾ C. Gal, "2000–2010 – A decade of technical achievement," CNES Magazine, No 16, July 2002, pp. 25–27

of a large portion of Earth's surface and, because of the large number of satellites in each constellation, will be able to provide near-instantaneous detection, identification, receipt of encoded position, and independent localization of distress beacons. Moreover, since the MEOS&R allows handling of multiple signal paths, the detection and tracking of beacons should become more efficient. Distress calls being located almost instantaneously should allow tracking moving vessels or airplanes in distress.

For the MEOS&R constellations, there is also the capability that the system will be able to return information back to the distress radiobeacon initiator via the MEOS&R downlink. Confirmation to the person in distress – that their distress alert has been received – might improve their morale, thus enhancing their chances for survival. – MEOS&R operational alerts could be available (i.e. start their service) in the timeframe 2014–2016.

In October 2013, ESA completed a pair of dedicated ground stations at opposite ends of Europe. This enabled the first Galileo satellites in MEO to participate in global testing of the COSPAS–SARSAT (S&RSAT) search and rescue system. – The Maspalomas station, at the southern end of the largest island of the Canary Islands, at the southern fringe of European waters, was activated in June 2013. And this last month has seen the Svalbard site on Spitsbergen in the Norwegian Arctic come on line — the two sites can already communicate and willsoon be performing joint tests. ²⁹³²⁾

Founded by Canada, France, Russia and the US, COSPAS–S&RSat has assisted in the rescue of tens of thousands of souls in its three decades of service. Distress signals from across the globe are detected by satellites, then swiftly relayed to the nearest search and rescue (SAR) authorities.



Figure 218: Photo of the MEOLUT (MEO Local User Terminal) at the Maspalomas station (image credit: ESA)

The Galileo satellites, tested in combination with the same S&R (SAR) payloads on Russian Glonass satellites as well as compatible repeaters on a pair of US GPS satellites, showed

²⁹³²⁾ “European Ground Stations enable Galileo Search and Rescue Testing,” ESA, Oct. 8, 2013, URL: http://www.esa.int/Our_Activities/Navigation/European_ground_stations_enable_Galileo_search_and_rescue_testing

an ability to pinpoint simulated emergency beacons down to an accuracy of 2–5 km in a matter of minutes. Maspalomas and Spitsbergen will combine with a third station at Larnaca in Cyprus, currently approaching completion. These three sites are monitored and controlled from the SAR Ground Segment Data Service Provider site, based at Toulouse in France.

Each site is equipped with four antennas to track four satellites. The stations are networked to share raw data, effectively acting as a single huge 12–antenna station, achieving unprecedented detection time and localisation accuracy.

- Introduction of spaceborne data collection systems (**DCS**) in LEO. The first DCS anywhere was IRLS (Interrogation, Recording, and Location System) flown on Nimbus–3 (launch April 14, 1969, see M.29.3). DCS were also flown on the first three Landsat S/C, LS–1, LS–2, and LS–3 (LS–1 launch July 23, 1972). The first Argos DCS in LEO (polar orbit) was flown on TIROS–N (launch Oct. 13, 1978). The first DCS in GEO orbit was flown on SMS–1 (launch May 17, 1974). In the meantime all geostationary meteorological satellites series (METEOSAT, NOAA–GOES, GMS (JMA), etc. use DCS or variations thereof (see Table 279 for DCS). The following Argos upgrades are realized or planned:

- Starting with NOAA–15 (launch May 13, 1998), a modified Argos data collection system is flown referred to as Argos DCS–2. The data transmission rate for DCS–2 changed from 1200 bit/s to 2560 bit/s. The PTT capacity was increased from four to eight, this means eight DRU (Data Recovery Unit) onboard. The data are formatted and stored, then dumped each time the satellites moves within visibility of one of the three ground stations (Wallops, Gilmore Creek, or CMS). VHF and S–band transmitters also perform real–time relay (broadcast) for any user station within visibility.

- The first Argos–Next instrument is being flown on ADEOS–II (launch Dec. 14, 2002) providing **two–way messaging services** (demonstration for Argos/ADCS).

- The first 3rd generation Argos system, also referred to as Argos/ADCS (Advanced Data Collection System), is scheduled to fly on MetOp–A (launch Oct. 19, 2006) of EUMETSAT, and of course on the POES series S/C of NOAA starting with NOAA–N' (launch Feb. 6, 2009). Argos/ADCS features two–way messaging services, data reception at 401.65 MHz, data transmission at 466 MHz, and higher data rates.

- Satellite navigation data, such as position, velocity, and time, of GPS (GPS–1 launch in 1978) and GLONASS (first GLONASS launch in 1982) systems. The GPS constellation became operationally available in 1994 (officially in 1995). The real–time global availability of navigation data has spawned numerous positioning and navigation applications that have surpassed initial expectations. They are fast becoming an indispensable part of people's everyday lives. The navigation services on all levels (civil and military aviation, coastal and ocean ship navigation, automobile navigation, surveying, etc.) are becoming increasingly essential to the world's infrastructure. As a consequence, a large commercial market of equipment and service providers is unfolding, responding to the new needs of society.

- GPS time is being utilized as a cost–effective standard time source by many operators. Networks like Internet and many TTPs are being synchronized by GPS time. The GPS time service is provided by USNO (US Naval Observatory). GPS provides two types of time:

- GPS time. Defined by its 'composite clock.' It consists of an ensemble of more than 20 GPS space and ground–based atomic frequency standards. GPS time is referenced to UTC (Universal Time Coordinated) as maintained by USNO. Time updates are maintained to within 1 μ s of UTC by the operators of the GPS Master Control Station at Falcon Air Force Base, Colorado Springs. Note: GPS time differs from UTC by the number of leap seconds accumulated since January 1980.

– UTC. To obtain UTC from GPS, users must apply the GPS–UTC (USNO) correction, available in the navigation message, to transition from GPS time to an estimate of UTC (USNO). The estimate of UTC (USNO) is called UTC (GPS).²⁹³³⁾

Starting in the mid 1980s a number of commercial services have come into the Earth observation arena to complement (or replace) the institutional services.

- Spacecraft operators and data distributors like Eosat (Landsat–4, –5)
- In 1990, SSTL of Surrey (UK) started a unique microsatellite technology transfer program, providing on–the–job training of engineers and scientists of foreign national organizations in cooperative programs [KAIST (Korea), LNETI (Portugal), FACH (Chile), TMSC (Thailand), etc.]. Affordable access to space is the overall theme of the service. – The design, building and operating experience of their own microsatellites gave these organizations a means to start/continue their own involvement in national space programs. The ‘Surrey Space Centre’ of SSTL (since 1992) is a European center of excellence, a facility which accommodates the activities for the technology transfer service of academic and post–graduate research.
- Distributors of imaging data products from a particular spacecraft and sensor (SPOT Image, Eurimage, etc.)
- The RADARSAT–1 satellite of CSA, Canada, is an Earth observation mission for SAR data, operated on a commercial basis by RSI.
- Real–time ERS altimetry data are distributed via Internet.²⁹³⁴⁾ The NOAA/NODC Laboratory for Satellite Altimetry (LSA) receives ERS altimetry data and generates RGDRs (Real–time Geophysical Data Records). These RGDRs are distributed via Internet and may be used in oceanographic analysis and model assimilation studies.

Mission	Data Availability	Sensor	Band	Spatial Resolution
Landsat–4, –5	1982	TM	0.45 – 2.35 μm (MS)	30 m
Landsat–7	1999	ETM+	0.50 – 0.90 μm (Pan)	15 m
SPOT–1, –2, –3	1986	HRV	0.51 – 0.73 μm (Pan)	10 m
Resurs–O1–1, 2, 3	1985	MSU–E	0.50 – 0.90 μm (MS)	45 m x 33 m
JERS–1	1992	OPS	0.52 – 2.40 μm (MS)	18 m x 24 m
IRS–1C, IRS–1D	1996, 1997	PAN	0.50 – 0.75 μm (Pan)	6 m

Table 168: Availability of long–term high–resolution imaging data of major Earth surface missions

- A multitude of commercial enterprises provide their services in the airborne arena, most with a full service (aircraft, sensor(s), data recording and processing, etc.).
- NOAA GOES program direct broadcast services:²⁹³⁵⁾ Current GOES satellites (GOES–I/M and GOES–N/P) provide direct broadcast of meteorological data to users through the **GVAR** (GOES Variable) broadcast link, a transponded service at L–band rebroadcast through the GOES satellites. – GOES–R (launch in 2015), the next (3rd) generation GEO S/C series, will support mission operations of the system and generation and distribution of data and products in near–real time to the user community through **GRB** (GOES Rebroadcast) services.

2933) F. Vannicola, “The Time Is Now,” GPS World Showcase, Dec. 1997, p. 40

2934) J. Lillibridge, “Real–time ERS altimetry at NOAA,” Earth System Monitor, Vol. 9, No. 3, March 1999, pp. 6–9

2935) Andrew W. Royle, William M. Callicott, “GOES Direct Broadcast Service History and Future,” Proceedings of the 2009 IEEE Aerospace Conference, Big Sky, MT, USA, March 7–14, 2009

A 2003 analysis by NOAA indicated that over 150 GVAR sites were in operation ranging from New Zealand in the Far East to Spain and France in Western Europe. A significant user presence outside of the U.S. also exists in the Caribbean, Canada, and Latin America. Mobile GVAR capabilities in use by the U.S. Navy and U.S. Air Force account for additional GVAR receive stations.

Parameter	GVAR (GOES I–P)	GRB (GOES–R)
Start of broadcast service	GOES–8 (I) launch Apr. 13, 1994	GOES–R launch 2015
Full disk image	30 minutes	5 minutes (Mode 4) 15 minutes (Mode 3)
Other modes	Rapid Scan, Super Rapid Scan	3000 km x 5000 km, CONUS: 5 min, Multiple concurrent 1000 km x 1000 km, Mesoscale: one every 30 sec
Polarization	Linear	Dual circular polarized
Receive frequency	1685.7 MHz, (L–band)	1690 MHz, (L–band)
Packetization	GVAR blocks (0–11)	CCSDS 133.0–B–1
Data compression	None	Lossless
Data rate	2.11 Mbit/s	~ 30 Mbit/s
Antenna coverage	Earth coverage to 5° above horizon	Earth coverage to 5° above horizon
Data sources	Imager and Sounder	ABI (16 bands), GLM, SEISS, EXIS, SUVI, MAG
Space weather	~ 100 kbit/s (separate link)	~ 2 Mbit/s
Lightning data	None	~ 0.5 Mbit/s

Table 169: GOES direct broadcast service capabilities

- **Shuttle Small Payload Program (SSPP).** A flight service package offered by NASA for payload masses in the range between 23 kg to about 2270 kg. SSPP is for “small, self–contained payloads” with the objective to ensure diverse user groups (educational, commercial, government, foreign experimenters, etc.) to have access to space at reasonable costs. Payloads are accommodated by providing various carrier systems [GAS, Hitchhiker, Hitchhiker Jr., and SEM (Space Experiment Module)] in the Shuttle’s unpressurized payload bay. SSPP started in 1984.

Note: In general a S/C launch from Shuttle has advantages and disadvantages. Typically the low orbit implies a relatively short lifetime for the mission. This may be of interest in itself, as the orbital decay can be studied. But the Shuttle is the only launcher that really allows a payload to be viewed being released into space. In addition the g–loads are modest compared with other launchers.

- **GAS (Get Away Special).** GAS is a carrier system concept with standards and conditions relating to GAS payloads (they must fit in a standard container of 0.14 m³ in volume with a payload mass not exceeding 90 kg, two or more experiments may be included in a single container). In addition, GAS payloads must be self–powered and be easy to handle for the payload crew. The GAS container is made of aluminum with circular end plates. It can be pressurized (or evacuated) to suit experiment requirements.

GAS payloads are mounted during flight in the Shuttle payload bay, on the sidewall, or on a cross–bay truss structure (referred to as “getaway bridge”). The aluminum bridge fits across the payload bay of the orbiter and offers a convenient and economical way of flying several GAS canisters. The getaway bridge, capable of holding up to 12 canisters, made its maiden flight on STS–61–C (Jan. 12–18, 1986).

The service was initially announced by NASA in 1976, five years prior to the first Shuttle flight in 1981. The first GAS demonstration payload, FVP (Flight Verification Payload), was flown in 1982 on STS–3 (Mar. 22–30, 1982). The first customer GAS payload, G–001 of Utah State University, flew on STS–4 (June 27 – July 4, 1982). STS–95 (Oct. 29 – Nov. 7, 1998) is the 33rd Shuttle mission with the GAS payload service. Almost 200 individual GAS canisters have been flown in these 33 missions for a very diverse user community.

– **Hitchhiker carrier system.** The Hitchhiker concept is based on a modular and expandable carrier with the provision of extended functional features (standard power, data, and command services for customer equipment). The structure can carry equipment mounted in canisters but also has mounting plates of various sizes for user equipment (provision of options). The carrier provides electrical power (28 VDC), command signals (1200 baud), and downlink data interfaces (various data rates: 1200 baud asynchronous low-rate, 1–1400 kbit/s medium rate). Hitchhiker customers are able to operate their payloads from the ground segment (GSFC) using their own ground support equipment (usually a PC) to send commands and display data. The ACE (Advanced Carrier Equipment) package provides such standard services devices as: power distribution unit, remote interfaces unit, Hitchhiker central unit, digital storage unit, Hitchhiker video interface unit, and lightweight avionics plate. NASA initiated the service in 1984. The first flight was on STS–61–C (Jan. 12–18, 1986) with the Hitchhiker–G1 payload [consisting of IEH–1 (International Extreme Ultraviolet Hitchhiker, CAPL–2 (Combined Pumped Loop–2), TES (Thermal Energy Storage), etc.]. The SLA–1 (Shuttle Laser Altimeter) experiment on STS–72 (Jan. 11–20, 1996) was also a Hitchhiker payload.

– **Hitchhiker Jr. carrier system.** A limited Hitchhiker version, designed for payloads which do not need the functions of command and telemetry interfaces from the experiment to the ground (GSFC). The CONCAP–IV–3 payload on STS–69 (Sept. 7–18, 1995) was the first to use the Hitchhiker Jr. service package. The experiment was activated and de-activated by the Shuttle crew via a laptop computer. This requires autonomous payload operations for the duration of the experiment. The SOLSE/LORE (Shuttle Ozone Limb Sounding Experiment/Limb Ozone Retrieval Experiment), a NASA instrument package flown on STS–87 (Nov. 19 – Dec. 5, 1997), used also the Hitchhiker Jr. service version.

– **SEM (Space Experiment Module) carrier system.** The SEM program is an upgrade version of the GAS program. It uses GAS canisters with the added feature of installed power provision and more. On behalf of frequent student requests, NASA funded in 1995 the SEM program and designed a standard power supply. As a result, the standard SEM consists of subsystems which function together to provide containment, structural support, power, experiment command and data storage capabilities for experiment support. This new functional capability/availability of the carrier system permitted the students to focus their energies on creating their own experiments. The very first flight of the SEM system, SEM–1, took place on STS–80 (Nov. 19 – Dec. 7, 1996) with many experiments, built by students in cooperation with their mentors of various High Schools and Universities across the USA.

- Commercial spaceborne imaging missions with high-resolution data (1 m) have been introduced in the latter nineties (1998) by several companies and/or consortia (Space Imaging EOSAT, Earthwatch, Resource 21, OrbView, etc.). The consortia provide also a full ground segment with corresponding archives and services. Their imaging products are being offered to anyone who pays for the service.

The provision of commercial imaging is considered a major shift in Earth observation policies – from government-sponsored research institutes toward private enterprise.

- Underwater/space launch. July 7, 1998, a Russian nuclear submarine of the Northern Fleet launched two environmental nanosatellites, TUBSAT–N and –N1 of the Technical University of Berlin, into Earth orbit (launch site of western Barents Sea). The launch represents the world's first underwater/space launch of a satellite into Earth orbit on the basis of a commercial service.

- First commercial satellite constellations in LEO (Low Earth Orbit). In 1998, the first two major satellite telephone systems, so-called “Big LEO Systems” of global handheld telephone service as well as mobile fax and data services, were launched. Iridium, a network developed by Motorola, completed its planned 66-spacecraft constellation in LEO, and started service. Globalstar, created by Loral, successfully launched its first 8 satellites.

However, 12 other spacecraft were lost in a failure of Ukraine's Zenit rocket. In all, Iridium featured 10 launches and Globalstar had three.

On the "Little LEO Systems" front of non-voice messaging and data relay (i.e. store & forward) services, ORBCOMM of Dulles VA, had the complete constellation of 35 satellites in orbit (with altitudes of 825 km) on Dec. 4, 1999. The initial launch of this constellation started on April 3, 1995. The ORBCOMM System is a wide area, packet switched, two-way data communication system. Communications to and from Subscriber Communicators (SCs) and the geographically distributed ORBCOMM Gateways are accomplished via the LEO constellation of microsattellites (43 kg).

1.29 Start of International Cooperation

The space age in general and Earth observation in particular turned out to be a natural field for all types of national and international cooperations/participations – unmatched in history. Initial cooperation (with NASA) started with permissions to operate ground stations in various countries. Later on, foreign ground station operators contributed to NASA missions through tracking and data receiving services. International cooperation in the early 1960s manifested itself also in such policies of flying sensors (experiments) of non-US scientists on NASA missions or in providing launches for foreign satellites. This evolved eventually in the common design and construction of spacecraft and instruments. In January 1970, NASA had official cooperations with agencies/institutes of 35 foreign countries (agreements of ground stations, exchange of personnel, etc. brought the total cooperations to 74 countries). Some of the first cooperations involving research satellites are listed below: ²⁹³⁶⁾

- Ariel–1, a product of USA/UK cooperation, was launched April 26, 1962 on a Thor–Delta vehicle from Cape Canaveral (60 kg S/C, 389 km x 1214 km inclined orbit at 54°) with the objective to measure parameters of the ionosphere and of the sun.
- Alouette–1, a Canada/USA cooperative venture, was launched September 29, 1962 from VAFB, CA aboard a Thor–Agena B launch vehicle (Alouette–1 mass = 145 kg) with the objective to investigate the ionosphere.
- San Marco–1 (mass of 254 kg), an Italian satellite, was launched Dec. 15, 1964 with a US launcher, a Scout–X4 launch vehicle of NASA from Wallops Island, VA, to investigate atmospheric densities. Orbit: 200 km x 842 km, inclination of 37.8°. – The San Marco project was a cooperative effort of NASA and the Centro Ricerche Aerospaziali at the University of Rome (Italy), with NASA providing launch vehicles, use of its facilities, and training of Italian personnel. All succeeding “San Marco” spacecraft were launched from Italy’s near-equatorial San Marco off-shore station near Malindi in Kenya. The project was initially proposed to NASA by the Italian Space Commission in 1961.
- Asterix–1, the first French satellite launched on November 26, 1965 on a French launch vehicle, Diamant, from Hammaguir, Algeria (Elliptical orbit, apogee of 1736 km, perigee of 530 km, inclination of 34.3°). The 41.7kg satellite transmitted for two days. FR–1, the first operational French satellite, was launched into a 780 km orbit on Dec. 6, 1965 on a Scout launcher from Vandenberg AFB. The satellite was used to study the ionosphere.
- WRESAT (Weapons Research Establishment Satellite), an Australian/US S/C involved the development and launch from Woomera, Australia, of a small scientific satellite (mass of 50 kg) on Nov. 29, 1967 (reentry Jan. 10, 1968). The satellite was placed in a near-polar orbit (perigee = 198 km, apogee = 1252 km, inclination = 83.3°, period = 99.3 min) by a US Redstone rocket. The objective was to monitor solar radiation in the upper atmosphere and to demonstrate an Australian capability for developing a satellite. WRE was the agency that managed the Woomera Rocket Range. ²⁹³⁷⁾
- ESRO–1/Aurora, an ESRO (Europe)/NASA cooperative venture (86 kg S/C mass), was launched Oct. 3, 1968 from VAFB to investigate auroras and the ionosphere. Prior to this, ESRO–2B (a 75 kg S/C) was launched on May 17, 1968 on a Scout launcher from VAFB with a payload measuring cosmic rays and solar X-rays. – ESRO–1/Boreas, almost identical to ESRO–1/Aurora, was launched Oct. 1, 1969 from VAFB and performed similar measurements simultaneously with its sister spacecraft Aurora.
- Azur–1, a German satellite (71 kg), was launched Nov. 11, 1969 on a Scout vehicle from VAFB (387 km x 3150 km sun-synchronous orbit inclined at 103°), to investigate radiation belts, solar particles and polar lights.

²⁹³⁶⁾ W. Buedeler, “Geschichte der Raumfahrt,” Sigloch Edition, Künzelsau, 1979,

²⁹³⁷⁾ K. Dougherty, “Wresat: Australia’s First Satellite,” Proceedings of the 59th IAC (International Astronautical Congress), Glasgow, Scotland, UK, Sept. 29 to Oct. 3, 2008, IAC–08–E4.3.5

- ANS-1, Netherlands satellite (129 kg), launched August 30, 1974 on a Scout vehicle from VAFB, CA (258 km x 1173km inclined orbit at 98°). ANS-1 studied UV spectra of young stars, and hard and soft X-rays from cosmic sources.
- Intasat, Spain/USA satellite, was launched November 15, 1974.
- COS-B, the first ESA/NASA satellite, was launched August 9, 1975 to investigate stellar X-ray and gamma-ray radiation.
- India conducted the world's largest sociological experiment, in the mid-1970s (1975-1976), using space technology through the experimental project called SITE (Satellite Instructional Television Experiment) for which NASA provided its ATS-6 (Application Technology Satellite), a communications satellite positioned over the Indian Ocean. This enabled the direct broadcast of educational programs on agriculture, family planning, health, hygiene, etc. - to TV sets in about 2400 villages across six states of rural India. This experiment was the precursor to the establishment of the multipurpose INSAT system in the 1980s. At that time, India procured all the four satellites under the INSAT-1 series from a US company (Ford Aerospace Corporation) and three of them namely INSAT-1A, INSAT-1B, INSAT-1D were also launched by US launch vehicles.
- Meteosat-1, the first geostationary ESA weather satellite, was NASA-launched on November 23, 1977.
- APPLE (Ariane Passenger Payload Experiment). ISRO developed the passenger payload APPLE in 1980, a indigenously a 672 kg state-of-the-art three-axis stabilized GEO communication satellite APPLE. ESA offered to ISRO a free flight on one of Ariane's demonstration flights in June 1981. The APPLE satellite had only one communication transponder, but the entire exercise of building a large three-axis stabilized satellite to operate in the geostationary orbit resulted in ISRO acquiring the necessary expertise that was to prove invaluable to build the indigenous second generation INSAT-2 series of satellites in the 1990s.²⁹³⁸⁾
- In the USSR, the program **Intercosmos** was created in 1967 with the objective to invite cooperation/participation of Soviet-affiliated countries in the Soviet space program with their own national contributions. An important area of participation was in remote sensing, building sensors for specific missions, dissemination and scientific interpretation of data, etc. The new policy fostered a number of collaborative science projects among its nine members as well as with other nations. The Intercosmos satellite series began with the launch of Intercosmos-1 on October 14, 1969. The payload featured, beside Soviet, also Czech and East-German instruments for the measurement of UV and X-ray radiation in the upper atmosphere. Up to 1991, there were a total of 25 Intercosmos satellites.
- The first foreign-built satellites launched from a Russian launch site, were from France.
 - Aureole-1 was launched from Plesetsk by an SL-8 vehicle on Dec. 27, 1971 into an orbit of 410 km x 2500 km, inclination of 74°. S/C mass of 300 kg. Objective: study of the aurora borealis and ionosphere.
 - SRET-1 was launched from Plesetsk on Apr. 4, 1972 along with the Molniya-1 spacecraft. The French satellite was placed in a 460 km x 39248km orbit and was used to study radiation effects on solar cells.
 - Aureole-2 was launched from Plesetsk by an SL-8 vehicle on Dec. 26, 1973. S/C mass of 400 kg. Orbit: 400 km x 1975 km, inclination of 74°.
 - April 19, 1975. Launch of the first Indian satellite, Aryabhata of ISRO, by a Cosmos launch vehicle.

²⁹³⁸⁾ K. S. Jayaraman, "India Plans New Insat Design Around Private Sector Needs," Space News, Dec. 18, 2000, pp. 4, 44

– SRET–2, a technological research and study satellite, was launched piggyback on a Molniya satellite from Plesetsk on June 5, 1975. The 29.6kg satellite was used to test the passive cryogenic radiation system for Meteosat cooling, and to study of the aging of thermal casings and plastic films.

- International partnerships have also been very successful in solar and space physics. NASA is the lead agency for the GGS (Global Geospace Science) program which includes the WIND and POLAR satellites, both of which have important international components. Conversely, ESA is the lead agency for Ulysses, SOHO (Solar and Heliospheric Observatory) and Cluster, while ISAS of Japan is the lead for Yohkoh (Solar–A), and Geotail. Within STP (Solar Terrestrial Probes) program, NASA has the lead with TIMED and STEREO while JAXA (formerly ISAS) has the lead of Solar–B.

- In the latter part of the 1990s, the cooperations between partners in the Earth observation community have reached new dimensions. They are truly global in nature – a network of interrelations – they are so numerous and on so many levels (permeating many facets of society and affecting our every–day lives) – too complex for the scope of this writing.

- SEA Launch is a spacecraft launch service that uses a mobile sea platform for equatorial launches of commercial payloads on special rockets (Sea Launch was formed in 1995, first launch in 1999). It has assembled and launched 24 rockets (as of 2007). Partners in the joint Sea Launch venture are the Boeing Commercial Space Company (United States), RSC Energia (Russia), SDO Yuzhnoye/PO Yuzhmash (Ukraine) and Aker ASA (Norway).

As of 2004, the Sea Launch Company, based in Long Beach, CA (USA), provides also contracting and management services for Land Launch. Space International Services in Moscow provides hardware and services originating in Russia, Ukraine and Kazakhstan, in a subcontracting arrangement with Sea Launch.

- Public/private partnerships are vital for the continued growth and commercialization of the space sector. Historically, spaceborne systems have become a business only after the high–risk technologies and markets have been developed, most often through government initiatives and with public funding. First government/industrial project partnerships in the area of Earth observation were being introduced as early as 1985. The overall objective is cost–sharing of ever tighter government space budgets with commercial companies in projects that require new technology introduction. The investing companies are given some incentives (commercial data rights and/or ownership of the S/C, etc.) to recover their investments and to make a profit. An effective framework in such partnerships includes benefits to all partners. Some examples in satellite development are: ²⁹³⁹⁾ ²⁹⁴⁰⁾

- In Sept. 1985 the US company Eosat was selected by NOAA (government) to operate the Landsat system (LS–4 and LS–5), to market LS data, and to build and launch LS–6.

- SPIN–2 venture of Russia (since 1992). SPIN–2 is a joint venture (company), located in Washington DC, of Interbranch Association SOVINFORMSPUTNIK (Moscow, Russia), Aerial Images, Inc. (Raleigh, NC), and Central Trading Systems, Inc., (Huntington Bay, NY). The objective is to market high–resolution panchromatic imagery data (2 m) of past Russian missions, in particular data from the Resurs–F series.

- RADARSAT–1 (launch Apr. 11, 1995) and RADARSAT–2 (launch Dec. 14, 2007) are jointly–funded SAR missions of CSA (Canadian Space Agency) and MDA (MacDonald Dettwiler and Associates Ltd. of Richmond, BC). CSA is providing approximately 75% of the funding for the development of the satellites and MDA is investing the difference. MDA owns and operates the satellites. CSA's investment will be recovered through the supply of imagery to a number of Canadian government agencies during the mission lifetime.

²⁹³⁹⁾ D. L. Glackin, "International Earth remote sensing: overview 1980–2010," Proceedings of the SPIE International Symposium on Optical Science and Technology, San Diego, July 2000

²⁹⁴⁰⁾ "International Space Cooperation: Solving Global Problems," Report of an AIAA, UN/OOSA, CEAS, CASI Workshop, April 1999 (printed and distributed by AIAA)

– OrbView–1/Microlab–1 and OrbView–2/SeaStar are commercially built and operated small satellites of OSC (Dulles, VA) flying government–sponsored instruments, OTD of NASA/MSFC and GPS/MET of UCAR in the case of OrbView–1, and SeaWiFS of GSFC on OrbView–2. Data of these instruments is provided to government agencies as well as commercially sold (SeaWiFS).

– In Europe, CNES is introducing cost–sharing programs with commercial S/C builders. The SPOT–5 satellite development is such a joint venture of CNES with French industry, namely MMS (Matra Marconi Space), now EADS Astrium SAS. Earlier S/C in the SPOT series of CNES (government) started data distribution arrangements with private companies like Spot Image. [Note: the CNES contract with EADS Astrium SAS is referred to as: Public–Private Partnership (PPP) program in which EADS Astrium SAS has a share of 47%]²⁹⁴¹⁾

– The LightSAR project of NASA was conceived as a public/industry partnership.²⁹⁴²⁾ However, in July 1999, NASA cancelled the project due to lack of interest from industry. Industry officials could not see a sufficiently large commercial market for L–band imagery (a NASA requirement) to justify the required investments.

– ISRO of Bangalore, India, announced in Nov. 2000 a new policy by inviting private sector investments with corresponding customer equipment and service–sharing arrangements on its GEO program of INSAT satellites. User demand is mostly expected in the field of communications.

• TerraSAR PPP alliance. As of 2001, Infoterra/TerraSAR was a proposed cooperative Public–Private Partnership (PPP) program between the Infoterra Company (EADS Astrium) and ESA. The fundamental objective of the Infoterra/TerraSAR initiative is to establish a self–sustaining geo–information business built on European strengths in SAR satellite technology, in SAR applications expertise and in the provision of services based on Earth observation data sources. TerraSAR is planned to be an element of the ESA Earth Watch program. The initial program calls for two satellites, featuring high–resolution X–band and L–band SAR imagery, respectively.

The TerraSAR–X project drew from EADS Astrium’s experience, as well as Germany’s national EO experience with the SIR–C and SRTM satellites, and various economic feasibility studies.

TerraSAR–X is also the first German PPP space project in the field of remote sensing, established between the German Aerospace Center (DLR) and the industrial space company EADS Astrium GmbH. The PPP cooperation agreement of March 2002 is the “charter” of the PPP and defines DLR’S obligations, the most important ones being:²⁹⁴³⁾ ²⁹⁴⁴⁾

- DLR awards the TerraSAR–X manufacturing R&D contract to EADS Astrium
- DLR creates and operates for 5 years the TerraSAR–X ground segment
- DLR obtains 50% of the data for scientific use (“scientific” being well defined)

The Astrium obligations are defined as:

- Astrium contributes financially to the manufacturing costs of TerraSAR–X

2941) Note: In a general PPP scheme the business aspect of a mission becomes a critical element of the entire program, including the space segment, the ground segment, as well as the service sector.

2942) W. Ferster, “Weak Industry Response Brings End to LightSAR,” Space News, Aug. 9, 1999, p. 3

2943) Mathias Spude, Max Grimard, “The Astrium Experience – A Large Space System Prime Contractor Point Of View Towards PPP Space Projects,” Proceedings of the 59th IAC (International Astronautical Congress), Glasgow, Scotland, UK, Sept. 29 to Oct. 3, 2008, IAC–08–E3.3.3

2944) Gérardine Meishan Goh, Bernhard Schmidt–Tedd, “Public–Private–Partnerships in Space Programmes: The German Experience,” Proceedings of the 59th IAC (International Astronautical Congress), Glasgow, Scotland, UK, Sept. 29 to Oct. 3, 2008, IAC–08–E3.3.6

- Astrium obtains 50% of the data for commercial use / exploitation
- Astrium contributes financially to the costs of the ground operations
- Astrium creates at its own expenses an industrial structure for commercializing the TerraSAR–X data.
- In case of a commercial success, Astrium finances a second TerraSAR–X 2 out of the profit made by commercializing the data. TerraSAR–X 2 would be a purely commercial satellite in Astrium ownership. All data would exclusively be with Astrium. DLR could get data at cost basis (“Herstellpreis”). Manufacturing, launch and operations of TerraSAR–X 2 are estimated at some € 200 million.

Since the launch of TerraSAR–X in 2007, the spacecraft and its payload work excellently delivering the data expected by its designers. After the commissioning phase, Infoterra makes extensive use of the TerraSAR–X data. Infoterra provides new–quality radar data as well as a variety of radar based geo–information products. Moreover, Infoterra has been creating a substantial portfolio of image products, geo–information products, and data access services, as well as numerous applications using TerraSAR–X data.

Both facts – satellite in orbit and services operative – indicate that the PPP scenario has proven its validity. If there was not the PPP scenario, TerraSAR–X would not be in orbit and delivering the data.

The upcoming twin satellite of TerraSAR–X, namely TanDEM–X (launch June 21, 2010) within the same PPP framework with DLR, will allow the generation of global digital elevation models (DEMs) by 2012.

- The commercial RapidEye minisatellite constellation (launch of 5 S/C on Aug. 29, 2008) of RapidEye AG, Brandenburg, Germany, became a cooperative PPP on May 16, 2001 when the German government passed legislation of a new national space program. The German PPP program is managed by DLR (German Aerospace Center).
- COSMO–SkyMed (Italy) and Pleiades (France) program alliance. France and Italy signed an agreement (MOU) on Jan. 29, 2001 to jointly develop four radar satellites and two optical satellites. The first COSMO–SkyMed high–resolution radar satellite was launched on June 8, 2007; COSMO–SkyMed–2 was launched on Dec. 9, 2007, COSMO–SkyMed–3 on Oct. 25, 2008, COSMO–SkyMed–4 on Nov. 6, 2010. – Pleiades is the SPOT successor program of CNES. The first Pleiades–HR1 high–resolution optical satellite was launched on Dec. 17, 2011. COSMO–SkyMed as well as Pleiades are also PPP programs within ESA’s Earth Watch and Copernicus (formerly GMES) initiatives.
- *The “US Commercial Remote Sensing Policy Initiative” of 2003 created in effect a government partnership with the US commercial satellite industry* (Presidential Directive of April 25, 2003). Sponsored by NGA (National Geospatial–Intelligence Agency, formerly known as NIMA) which provides mapping and related services for the US military and intelligence community, the **NextView** program is designed to assure the availability of high–resolution imagery from the next series of US commercial satellites. NGA is sponsoring the construction and launch of these satellites to fill imagery and geospatial needs for military, intelligence, foreign policy, homeland security and civil users.
 - In September 2003, NGA awarded the first NextView agreement to DigitalGlobe, Inc., Longmont, CO. The two NextView acquisitions provide NGA with sources to mitigate a potential gap in availability of commercial imagery to support the geospatial mission and implement the US Commercial Remote Sensing Space Policy. The WorldView–1 spacecraft of DigitalGlobe, providing imagery of 0.5 m resolution, was launched on Sept. 18, 2007. WorldView–2 was launched on Oct. 8, 2009, providing Pan data of 0.46 m and MS data of 1.8 m GSD.
 - In September 2004, NGA awarded a second vendor agreement with Orbimage of Dulles, VA (GeoEye Inc. as of Jan. 2006) within the NexView program. The contract

provided Orbimage with both long-term revenue commitments, as well as capital for the development of OrbView-5, Orbimage's next-generation high-resolution imaging satellite which was renamed to GeoEye-1 and launched on Sept. 6, 2008. GeoEye-1 provided imagery at a spatial resolution of 0.41 m.

The two NextView contracts, a cost-sharing in a sort of public-private partnership (PPP), represented NGA's commitment to forging long lasting partnerships between the US Federal Government and the US commercial remote sensing industry. One of NGA's key transformation initiatives is seamless integration of commercial imagery into all operations.

Already in January 2003, NGA had issued first contracts in the so-called "**ClearView Program**" to buy imagery from the then-three US commercial owner/operators: DigitalGlobe, Space Imaging of Thornton, CO, and Orbimage. The ClearView contracts represent a long-term commitment to the industry by guaranteeing a minimum amount of purchases to the providers of high-resolution imagery for three years, with two additional one-year options.

- Not all PPP arrangements are working to plan – as experienced by the European Satellite **Navigation Program Galileo**. The original plan had been to transfer the funding of and the responsibility over Galileo to a private industry consortium in a PPP program arrangement which would build and run the system. However, the consortium finally refused to take full responsibility and assume all risks without certain financial guarantees from the EU. – On hindsight, the underlying reason for the failure of PPP was the lack of a clear business plan to generate direct revenues from Galileo. Undoubtedly, there is a huge indirect value through job and value creation but no direct revenues for the consortium.

The failure of the PPP initiative meant Galileo had to be fully funded with European Union budgets. Ever since, Galileo has been the constant subject of political disagreements about its financing. From which EU budgets (e.g. agriculture) and how quickly money should be made available to Galileo has never been off the agenda. The official EU point of view was and is that Galileo is needed to guarantee independent satellite-based positioning in Europe under all circumstances.²⁹⁴⁵⁾

The conversion process from the initial PPP concept to a publicly funded Galileo program occurred in the time frame 2006–2008 and caused considerable delays in the procurement of the program. – A 2009 audit report of the European Court of Auditors comes to the conclusion that the Galileo program has been poorly managed. The Galileo Joint Undertaking — a body set up in 2003 and scrapped in 2006 — was given the task of supervising Galileo's technological development activities but "was seriously constrained by governance issues, an incomplete budget, delays and the industrial organization of the development and validation phase."²⁹⁴⁶⁾

- At the start of the 21 century, success of international cooperation among and between the world's space agencies is based on the following principles, according to William Barry of NASA (formulated at the IAF Specialists' Symposium, Paris, France, Dec. 3–5, 2001):
 - Mutual efforts to understand each other and keep an eye on the common objectives
 - A willingness to invest in each other – it is not only money, it is also an investment in human capital and relationships crucial to successful cooperation
 - An openness, understanding and patience that leads to higher levels of mutual trust and shared success.

2945) Dominique Bonte, "Europe's Galileo Satellite Project Remains Boggled Down by Political and Funding Disagreements," Nov. 16, 2007, URL: http://www.abiresearch.com/Blog/Telematics_Blog/450

2946) "EU satnav project ill-conceived: auditors court," GPS Daily, June 29, 2009, URL: http://www.gpsdaily.com/reports/EU_satnav_project_ill-conceived_auditors_court_999.html

- NOAA weather satellite on loan to JMA (Japan Meteorological Agency).²⁹⁴⁷⁾ In May 2002, NOAA announced that the US has agreed to lend Japan a geostationary environmental satellite to ensure weather data from the Western Pacific are available continuously should a weakening Japanese satellite fail. GOES-9 could be placed in an orbit over the Western Pacific region. The GOES-9 backup service is needed for JMA's GMS-5 which is past its expected operational life (GMS-5 was launched in 1995). GOES-9 started its backup service in April 2003. The replacement follow-on S/C, MTSAT-1R (Multifunctional Transportation Satellite-1 Replacement), was launched Feb. 26, 2005. GOES-9, also launched in 1995, does not meet US weather forecasting requirements, but does have sounding and limited imaging capabilities which supplying data comparable to that of the GMS-5. The loan of this satellite set the stage for long-term mutual backup arrangements between the United States and Japan.
- The India-US Joint Working Group (JWG) on Civil Space Cooperation held its first meeting at Antariksh Bhavan, the Headquarters of ISRO at Bangalore during June 29-30, 2005. This Joint Working Group was constituted as a follow up to the India-United States Conference on Space Science, Applications and Commerce held in Bangalore during June 21-25, 2004. The JWG explored the potential and possibility of cooperation in Earth observation, satellite communication, satellite navigation and its application, space science, natural hazards research and disaster management support, and education and training in space. These topics were identified based upon the vision document on strengthening India-US cooperation issued at the end of the June 2004 Bangalore Conference.
- The DMC (Disaster Monitoring Constellation) program of SSTL (Surrey Satellite Technology Ltd), UK, is a showcase of international collaboration success with a number of countries participating in the constellation: Algeria, China, Nigeria, Thailand, Turkey and the United Kingdom. The first launch of the DMC series started on Nov. 28, 2002 with Al-Sat-1. As of fall 2005, the DMC contains 5 microsattellites in one orbital plane observing the entire Earth on a daily basis with wide-swath medium-resolution imagery (32 m). The program gave several of the participating countries a chance to establish a first immediate national asset in space. The DMC satellites were developed as cooperative projects at SSTL and included technology transfer and on-the-job training. The well-trained staff of engineers of each country was able to operate their new microsattellite, to participate in a network of spacecraft, and to go on with further projects of their own. DMC represents a novel form of international collaboration - a satellite constellation where each satellite is owned by a different country. By purchasing a single satellite, the owning country has the added benefit of being part of a constellation. Not only does this provide benefits such as vastly improved data timeliness (daily revisits of medium-resolution optical imagery on a global scale), it also allows the costs of the operational and exploitation systems to be shared amongst the participating countries.
- The **International Charter "Space and Major Disasters"** was founded in July 1999 by ESA and CNES, followed by CSA (Canadian Space Agency) in Oct. 1999. In Sept. 2001, NOAA and ISRO (Indian Space Research Organization) also became members of the Charter. The Argentine Space Agency (CONAE) joined in July 2003.²⁹⁴⁸⁾ The Japan Aerospace Exploration Agency (JAXA) became a member in February 2005. The United States Geological Survey (USGS) has also joined the Charter as part of the U.S. team. BNSC/DMC became a member in November 2005. - In April 2007, GeoEye and DigitalGlobe two American commercial satellite imagery firms, joined forces with the USGS. In May 2007, CNSA (China National Space Administration) became a member of the joint initiative. On July 7, 2011, KARI (Korea Aerospace Research Institute) became a member of the International Charter. INPE (National Institute for Space Research) of Brazil became a member on Nov. 8, 2011. Roscosmos of Russia became a member on August 28, 2013.

²⁹⁴⁷⁾ <http://www.publicaffairs.noaa.gov/releases2002/may02/noaa02056.html>

²⁹⁴⁸⁾ <http://www.disasterscharter.org/home>

The objective of the International Charter is to provide a unified system of space data acquisition and delivery to those affected by natural or man-made disasters through Authorized Users. Each member agency has committed resources to support the provisions of the Charter and thus is helping to mitigate the effects of disasters on human life and property. 2949) 2950)

The International Charter was declared formally operational on November 1, 2000. An Authorized User can now call a single number to request the mobilization of the space and associated ground resources (RADARSAT, ERS, ENVISAT, SPOT, IRS, SAC-C, NOAA satellites, LANDSAT, ALOS, DMC satellites and others) of the member agencies to obtain data and information on a disaster occurrence.

- **Sentinal Asia:** The Sentinel Asia initiative is the international cooperation led by **APR-SAF** (Asia-Pacific Regional Space Agency Forum) to assist disaster management by Remote Sensing and Web-GIS technologies in the Asia-Pacific region. According to UN statistics, the Asia and Oceania region has the largest proportion of natural disasters in the world. Sentinel Asia was proposed in 2004 by APRSAF to showcase the value and impact of earth observation technologies, combined with near real-time internet dissemination methods and Web-GIS mapping tools. 2951)

Sentinel Asia is organized by JPT (Joint Project Team); JPT consists of 65 organizations including 56 agencies from 22 countries and 9 international organizations.

- In July 2010, JAXA established the KUOA (Kibo Utilization Office for Asia) to further facilitate cooperative activities among Asia Pacific nations. A SEU WG (Space Environment Utilization Working Group) was set up under APRSAF to explore the possibility of joint utilization in 2005, and has been studying joint activity plans to be performed on board the ISS and its Japanese Experiment Module “Kibo”. The SEU WG is open to all APRSAF member organizations who intend to promote space environment utilization. 2952)

The first multilateral joint mission was planned by the Asian Kibo Mission Planning Task Force. Plant seeds from Indonesia, Malaysia, Thailand and Vietnam, along with those from Japan, were delivered to Kibo by “Kounotori”, the HTV Transfer Vehicle, launched from Tanegashima, Japan on January 24th, 2011.

- **EXPReS** (Express Production Real-time e-VLBI Service). 2953) The Arecibo Observatory in Puerto Rico has joined forces with telescopes located in North America, South America, Europe and Africa to create the observing power of a radio telescope nearly 11,000 km in diameter. The system, called EXPReS, went “live” for the first time on May 22, 2008 with all antennae observing the same part of the sky. This is an historic project where international collaboration has resulted in the most powerful radio telescope system available to date. The term e-VLBI stands for “electronic Very Long Baseline Interferometry”. Data from the EXPReS project is transmitted to the central signal processor at the Joint Institute for VLBI in Europe (JIVE) in Holland, where speeds of data-streaming have exceeded Arecibo’s previous record four times over.

- **Secondary EO payloads on commercial constellations:** The commercial global coverage communications provider Iridium Communications Inc. is developing an Iridium

2949) http://www.esa.int/esaEO/SEMCG59RR1F_environment_0.html

2950) Atsuyo Ito, “Issues of International Charter on Space and Major Disasters : Haiti Earthquake,” ISPRS/ESPI/IAA/ IISL Conference “Current legal issues for satellite Earth observation”, Vienna, Austria, April 8–9, 2010, URL: <http://www.espi.or.at/images/stories/dokumente/conference2010/ito.pdf>

2951) <http://dmss.tksc.jaxa.jp/sentinel/contents/SA-intro.html>

2952) Muneo Takaoki, Nobuyoshi Fujimoto, Shiho Ogawa, Masataka Yamamoto, Yoshinori Fujimori, Naoki Nagai, Kazuhiro Miyazaki, Shigeki Kamigaichi, “Kibo Utilization Cooperation with Asian countries,” Proceedings of the 28th ISTS (International Symposium on Space Technology and Science), Okinawa, Japan, June 5–12, 2011, paper: 2011-h-20

2953) I. O’Neill, “Arecibo Joins Forces with Global Antennae to Simulate 6,800 Mile Telescope,” June 10, 2008, Universe Today, URL: <http://www.universetoday.com/2008/06/10/arecibo-joins-forces-with-global-antennae-to-simulate-6800-mile-telescope/>

NEXT generation LEO communications constellation (66 satellites at 780 km orbiting altitude in 6 orbital planes of 11 S/C per plane, inclination = 86.4°) to be launched in the time-frame 2015–17 (seamless replacement of the current constellation to ensure mission and service continuity). *The NEXT spacecraft definition, which started in 2006, is such that it offers next to the Iridium communication payload also a multiple secondary payload allocation of about 125 kg (total) to be used for partnerships of other customers. In particular, the Iridium management has invited to host "bolt and go" secondary payloads from the Earth—observation community. This constellation—based EO system opportunity has the potential of providing a comprehensive synergistic data set until 2030 and beyond.* ^{2954) 2955) 2956)}

The EO community is definitely interested in this offer. It requires immediate action on possible observation scenarios (instrument selections, collaboration of various partners, etc.) and on the funding profiles (long-term commitments) to coordinate a common strategy. Potential observation interest from a constellation is seen in the following fields:

- Radiation budget monitoring
- Altimetry
- GNSS occultation monitoring
- Ocean color and wind monitoring.
- **Air traffic service of Iridium NEXT as hosted payload:** In parallel to the EO hosted payloads, Iridium through its new joint venture Aireon LLC, will be putting **ADS–B** (Automatic Dependent Surveillance–Broadcast) receivers on its next-generation satellite constellation as hosted payloads, aimed at bringing global, real-time aircraft surveillance for ANSPs (Air Navigation Service Providers).

In November 2012, Iridium Communications Inc. announced that it has finalized an agreement with NAV Canada regarding Aireon LLC, a joint venture that will allow air traffic management agencies around the globe to continuously track aircraft anywhere in the world. For the first time ever, ANSPs around the world will be able to track aircraft from pole-to-pole, including oceanic airspace and remote regions. The new capability will provide significant benefits to the aviation industry, including substantial fuel savings, a reduction in greenhouse gas emissions and enhanced safety and efficiency for passengers. The venture will be operated under a PPP (Public Private Partnership) between the U.S. FAA (Federal Aviation Administration), industry and the world's major ANSPs. ^{2957) 2958)}

Note: The PROBA–V mission of ESA (launch May 7, 2013) carries the first spaceborne ADS–B receiver. As of October 2013, a wealth of data has been received.

– In March 2014, Aireon LLC announced that the ADS–B receiver payload for the system has successfully completed qualification testing for operation in the harsh environment of space. This achievement is a key building block in the deployment of Aireon and represents a significant milestone in validating that the payload and system design will provide robust reception of ADS–B signals from space. The company will now begin production of 81 ADS–B 1090 Extended Squitter (ES) receiver payloads, designed by Harris Corporation,

2954) Don Thoma, "Iridium NEXT Partnership in Earth Observation: Hosting Radio Occultation Sensors on Commercial Communications Satellite Constellations," Second Formosat–3/COSMIC Data Users Workshop, Boulder, CO, USA, Oct. 22–24, 2007, URL: http://www.cosmic.ucar.edu/oct2007workshop/pdf/thoma_24.pdf

2955) Don Thoma, "Iridium NEXT Partnership in Earth Observation: Costs and Schedules," Royal Society, London, January 22, 2008, URL: <http://www.tridentsensors.com/pdf/Thoma.pdf>

2956) Lars Peter Riishojgaard, Dennis Chesters, "The 'BOREAS' Concept for Imaging Polar Winds from the Iridium NEXT Constellation," Proceedings of the SPIE, Volume 7087, pp. 70870P–70870P–8 (2008), URL: http://www.eumetsat.int/groups/cps/documents/document/pdf_conf_p_s1_03_riishojg_p.pdf

2957) "Iridium Completes Formal Agreement for Global Air Traffic Joint Venture With NAV CANADA," Iridium, Nov. 19, 2012, URL: <http://investor.iridium.com/releasedetail.cfm?ReleaseID=722252>

2958) "Public Private Partnerships," Aviation and Climate Change Seminar, ICAO Headquarters, Montreal, Canada, October 23–24, 2012, URL: http://www.icao.int/Meetings/acli/Documents/NEXA_24October-am.pdf

that will be hosted on the Iridium NEXT satellite constellation, launching in 2015. The receiver payloads will complement ground-based air traffic surveillance systems currently in use by seamlessly relaying position and status information of aircraft flying over oceans, poles and remote regions to air traffic controllers on the ground. ²⁹⁵⁹⁾

- NASA/JAXA collaboration: In a unique collaboration between national space agencies, the United States and Japan began combining elements of their satellite resources April 2010 to increase a critical type of Earth observation data. The partnership will more than double the quantity of this data that is used to explore earthquake hazards, forest declines, and changing water resources in the Americas.

This new partnership between NASA and JAXA uses NASA's TDRSS (Tracking and Data Relay Satellite System) to download observations over North and South America taken by instruments on JAXA's ALOS spacecraft. By combining NASA and JAXA data—relay satellite resources, coverage of North and South America nearly doubles. Observations will be made about twice as often. In particular, L-band SAR imagery from the PALSAR instrument on ALOS are being made available.

The NASA—JAXA agreement continues a long and productive partnership between the nations in satellite observation of Earth. Japanese instruments are flying on NASA's Terra and Aqua satellites, and NASA sensors have flown on previous Japanese Earth—observation missions. The NASA—JAXA GPM (Global Precipitation Measurement) mission (launch Feb. 27, 2014) includes both NASA— and JAXA—supplied sensors on a NASA satellite launched on a JAXA rocket. ²⁹⁶⁰⁾

The space cooperation between Canada and ESA (European Space Agency) is unique — dating back to the beginning of the European space program in the early 1970s. ESA is the only international space agency in the world and, to this day, Canada is the only non-European country to be so closely associated with ESA. ²⁹⁶¹⁾

- The first cooperation agreement between the Government of Canada and ESA was signed on 9 December 1978, and entered into force on 1 January 1979. It was renewed in 1984 and again in 1989, the second time for a period of ten years, expiring on 31 December 1998.

These agreements, which were part of a broader strategy of the Canadian government to strengthen cooperation with Europe in critical areas of science and technology, made it possible for Canada to participate directly in ESA programs, activities and deliberations. Canadian industry has the ability to bid for, and receive, contracts for work in programs of interest. Canada also obtained the right to participate in ESA's deliberative bodies, and to take part in decision making.

The year 1998 marked the 20th anniversary of the signing of the first Cooperation Agreement between Canada and the European Space Agency (ESA), which has resulted in numerous benefits on both sides of the Atlantic. These include the development of strategic technologies for Canadian and European space programs, the creation of alliances between Canadian and European space companies, and a 'rapprochement' between Canada and Europe in space science and technology.

2959) "Aireon Completes Successful Space Qualification Test of Hosted Payload;" Aireon LLC, March 5, 2014, URL: <http://globenewswire.com/news-release/2014/03/05/615749/10071273/en/Aireon-Completes-Successful-Space-Qualification-Test-of-Hosted-Payload.html>

2960) Steve Cole, "Innovative NASA—JAXA Partnership Benefits Global Earth Science," April 12, 2010, URL: http://www.nasa.gov/home/hqnews/2010/apr/HQ_10-079_NASA-JAXA.html

- On Dec. 15, 2010, ESA and CSA (Canadian Space Agency) signed a new cooperation agreement in Paris that will extend their partnership for a further 10 years, until 2020. ²⁹⁶²⁾

It enables the creation of teaming arrangements between Canadian and European industries, thereby fostering competitiveness and the opening of new markets for Canadian industry. Academia and the Government of Canada rely on the ESA data, science and technologies to support science as well as operational needs. Areas of investment include Earth Observation, Satellite Communications, Navigation, and Space Exploration – all fields in which Canadian industry has a competitive and recognized expertise. ²⁹⁶³⁾

ESA and Canada have enjoyed a 30–year partnership that has led to many successful space projects. They will now continue to build on their shared interests. Their focus will continue to be on space applications.

ESA and Canada have joined forces in telecommunications, including Olympus, Artemis and Advanced Research in Telecommunications Systems (ARTES); Earth observation, including ERS, Envisat and Global Monitoring for Environment & Security (Copernicus, formerly GMES); navigation, including Galileo; and related technologies, such as the GSTP (General Support Technology Program).

The benefits of the ESA–Canada relationship extend beyond good cooperation between the two space agencies. European and Canadian companies have forged strong alliances, creating teaming arrangements and opportunities for new markets.

Table 170: Cooperation agreements between Canada and Europe ^{2961) 2962) 2963)}

- In a declaration adopted on June 1, 2011, the UN Committee on the Peaceful Uses of Outer Space (UNCOPUOS), ²⁹⁶⁴⁾ which is also marking 50 years since its first session in 1961, voiced its conviction that space science and technology and their applications, including satellite communications, Earth observation systems and satellite navigation technologies, provide indispensable tools for sustainable development.

The UNCOPUOS declaration called upon States to take measures at the national, regional and global levels to engage in common efforts to use space science and technology and their applications to preserve Earth and its space environment for future generations.

- The EDRS (European Data Relay Satellite) constellation is being implemented in a PPP (Public–Private Partnership) arrangement between ESA and Astrium Services, ²⁹⁶⁵⁾ an innovative structure in which ESA leads the creation of the initial system and infrastructure that is later taken over for full exploitation and further development by a commercial partner. EDRS will boost European–developed technology and make use of a cutting–edge intersatellite laser communication system as well as new data dissemination infrastructure on the ground.

- The retirement plans of the Space Shuttle for 2010, announced by the Bush Administration in 2004, provided an entirely new servicing situation for the ISS (International Space Station) program in the first decade of the new century. NASA was responsible for providing resupply and return cargo services to the ISS under international agreements. NASA originally intended to meet this requirement through Space Shuttle flights as well as

2961) G. Leclerc, S. Lessard, “Canada and ESA: 20 Years of Cooperation,” ESA Bulletin No 96, Nov. 1998 URL: <http://www.esa.int/esapub/bulletin/bullet96/LECLERC.pdf>

2962) “ESA and Canada renew partnership in space science and technology,” ESA, Dec. 15, 2010, URL: http://www.esa.int/esaCP/SEM8C8SRJHG_index_0.html

2963) “Europe and Canada: Partners in Space – A Model of International Co–Operation,” CSA, Dec. 15, 2010, URL: http://www.asc-csa.gc.ca/eng/media/news_releases/2010/1215.asp

2964) “UN stresses need for global cooperation on using outer space,” June 1, 2011, URL: <http://www.un.org/apps/news/story.asp?NewsID=38579&Cr=general+assembly&Cr1>

2965) “Announcement of Opportunity for Hosted Payload on board EDRS–C Satellite,” ESA, Sept. 22, 2011, URL: <http://telecom.esa.int/telecom/media/document/2011%2009%2022%20EDRS%20AO%20workshop%20presentation%20-%20full%20set%20-%20final.pdf>

through bartering with the international partners for transportation services on their vehicles. However, the announcement of the Bush Administration did not relieve NASA from its obligations for the ISS cargo transportation services. Hence, NASA and FAA (Federal Aviation Administration) developed a strategy to partner with private industry to assist in the development of private industry transportation services, and then to directly contract for resupply and return transportation services after these designs have proven reliable.²⁹⁶⁶⁾

The objective of the initiative was to procure critical resupply services for the ISS from the end of the Space Shuttle program to the end of the ISS Program (the period of performance for the then current ISS acquisition was seven years, from January 1, 2009 through December 31, 2015). The fundamental purpose of the CRS contract was that NASA would procure services and not hardware. In contrast to the Space Shuttle Program, NASA will not own or operate the launch vehicles and spacecraft that are used to deliver and return cargo. Since the U.S. Government does not own or operate these CRS launch vehicles or spacecraft, the launch and reentry of the cargo vehicles is treated as a commercial activity that must be licensed by the FAA to ensure that public safety is maintained (Ref. 2966).

NASA established a two–phased approach to initiate the commercial space transportation industry’s ability to fulfill its needs through the Commercial Crew & Cargo Program Office (C3PO) at NASA/JSFC.

1) Development and demonstration in the so–called **COTS** (Commercial Orbital Transportation Services) phase. Under COTS, NASA helps industry develop and demonstrate its own cargo space transportation capabilities. Industry leads and directs its own efforts with NASA providing technical and financial assistance. NASA is investing approximately \$800M from 2006 through 2012 toward cargo space transportation flight demonstrations which are planned for completion in 2012. NASA payments are made only upon completion of progress milestones by its industry partners.

2) ISS Commercial Resupply Services (CRS): Phase 2 is a competitive procurement for cargo services to support the ISS. NASA awarded two contracts for transportation services in December 2008 to SpaceX and Orbital. The CRS contracts procured a total of 20 cargo transportation missions to the ISS through 2015.²⁹⁶⁷⁾

The COTS program was announced on January 18, 2006. Two COTS commercial partners were selected: SpaceX (Space Exploration Technologies) and RpK (Rocketplane–Kistler). The agreement with RpK was later terminated after it failed to complete financial and technical milestones. A second competition was held to select a new funded commercial partner which resulted in selection of Orbital (Orbital Sciences Corporation) in February 2008.

Space Act Agreements: C3PO uses NASA’s Space Act authority to establish industry agreements and provide the legal flexibility necessary for the program. These agreements are known as SAAs (Space Act Agreements). The winners of the COTS competitions received funded SAAs. Companies with SAAs are not contractors; they are known as **Commercial Partners (CPs)**.

The COTS commercial partners are responsible for the overall design, development, manufacturing, testing, and operation of their COTS system. In order to receive NASA financial assistance, the COTS partners must conduct the COTS demonstrations according to the terms and conditions in their SAAs and consistent with the COTS ISS Service Requirements Document (ISRD) and the ISS–to–COTS Interface Requirements Document (IRD).

2966) “NASA and Federal Aviation Administration Joint Program Management Plan (PMP) for the Commercial Resupply Services Contracts,” April 2011, URL: http://www.faa.gov/about/office_org/headquarters_offices/ast/media/Joint%20Program%20Management%20Plan%20for%20FAA–NASA%20Partnership%20on%20CRS–Signed%20and%20Final%20April%202011.pdf

2967) “NASA Commercial Orbital Transportation Services,” NASA, March 2, 2012, URL: <http://www.nasa.gov/offices/c3po/about/c3po.html>

- On July 25, 2013, the European AlphaSat/Inmarsat–XL was launched successfully from Kourou on Ariane–5 ECA. This is the first flight and in–orbit verification of the Alphabus platform, the new multi–purpose platform for the high–power payload communications satellite market, developed through a PPP (Public–Private Partnership) of ESA, Inmarsat Global Ltd. and EADS Astrium, and supported by the ARTES program.²⁹⁶⁸⁾

The ARTES program has supported not only the development of the Alphabus platform, on which Alphasat is based, but also developed the innovative embarked technologies. There are four technology demonstration payloads embarked on the satellite. The four hosted payloads include an advanced laser terminal, the precursor to the EDRS (European Data Relay System), a Q–V Band communication and propagation experiment, an Advanced startracker, and an environment effects facility to monitor the GEO radiation environment and its effects on electronic components and sensors.

The Alphasat project is a great example of a public, private partnership building technology which is needed by customers. Its payload has been developed with both the technology and services downstream markets in mind.

- On August 28, 2013, NOAA and EUMETSAT signed a long–term cooperative agreement ensuring continued spaceborne weather, water and climate monitoring. The contract was signed in a ceremony at the European Union Delegation in Washington, D.C., by Kathryn D. Sullivan, NOAA Acting Administrator, and Alan Ratier, Director General of EUMETSAT. The partnership between EUMETSAT and NOAA has continuously developed over the last 30 years and taken a strategic dimension, bringing substantial benefits to Europe, the USA and the worldwide user communities. EUMETSAT and NOAA are planning to expand their cooperation into the next decades, with the implementation of the Joint Polar System combining the EUMETSAT Metop–Second Generation and the NOAA JPSS satellites, and of the planned Jason–CS (Jason–Continuity of Service) program, also involving ESA and the European Commission.^{2969) 2970)}
- In October 2013, a PPP contract was signed between SES of Luxembourg and ESA in a program called **Electra**. The objective is to develop an innovative small and medium sized, fully electric geostationary platform, that utilizes electric propulsion instead of conventional chemical propulsion for the transfer into the geostationary orbit as well as on orbit station keeping. The satellite platform can thus take advantage of smaller launch vehicles or dual launch capabilities, while carrying payload capabilities equivalent to current mid–sized satellites in terms of power consumption and number of active transponders. SES is the prime contractor to ESA for the first phase of the program and is working with OHB System AG of Bremen as a subcontractor for the corresponding manufacturing design of the Electra platform. – Electra represents three partnerships in one: between SES and OHB, to develop the best solution for SES and the future needs of other satellite operators; between SES and ESA, to offer the best possible validation in orbit of a new technology; and between ESA and DLR to capitalize on previous investments.²⁹⁷¹⁾

Electra is the first partnership project established under ESA’s ARTES–33 program,²⁹⁷²⁾ which supports market–driven innovations from industry that require flight heritage and in–orbit validation – proof that they work in space – so that they are more readily embraced by the marketplace.

2968) “Alphasat launches successfully,” ESA, July 26, 2013, URL: <http://telecom.esa.int/telecom/www/object/index.cfm?fobjectid=32512>

2969) EUMETSAT and NOAA sign long–term agreement for weather and climate monitoring from space,” EUMETSAT, August 28, 2013, URL: http://www.eumetsat.int/website/home/News/DAT_2077973.html

2970) “NOAA, EUMETSAT sign long–term agreement for weather, climate monitoring,” NOAA, August 28, 2013, URL: http://www.noaa.gov/stories/2013/20130828_EUMETSAT.html

2971) SES Partners With ESA To Develop Innovative Satellite Platform Electra,” Space Daily, Oct. 17, 2013, URL: http://www.spacedaily.com/reports/SES_Partners_With_ESA_To_Develop_Innovative_Satellite_Platform_Electra_999.html

2972) “ESA drives forward with all–electric telecom satellites,” ESA Press Release No 32–2013, Oct. 17, 2013, URL: http://www.esa.int/For_Media/Press_Releases/ESA_drives_forward_with_all-electric_telecom_satellites

- On Jan. 31, 2014, the UKSA (UK Space Agency) and CNES of France signed an agreement for closer cooperation in space activities. The deal includes an initial UK investment of £15 million in key instruments for the next generation of European weather satellites and will enable UK scientists to conduct the most comprehensive global survey of Earth's surface water. The agreement paved the way for joint work on Earth observation, telecommunications, space weather and research and technologies in the space field.²⁹⁷³⁾

Projects for immediate collaboration include an instrument for EUMETSAT – the next generation of European weather satellites, and the CNES/NASA project on global fresh water distribution.

- The UK will make an industrial contribution to the French IASI instrument for EUMETSAT – the next generation of European weather satellites. This Franco–British collaboration will help increase forecasting accuracy and enhance the value of weather forecasting services to society and business.
- Following the signature of the new framework agreement, the UK will gain involvement in a CNES/NASA project on global fresh water distribution. The mission will conduct the most comprehensive global survey of Earth's surface water ever, using the SWOT (Surface Water and Ocean Topography) satellite. SWOT will measure how water bodies on Earth change over time, helping us improve ocean circulation models, weather and climate predictions, and freshwater management around the world.

1.29.1 Realization of international cooperation in manned space programs

On May 24, 1972, the Soviet Union (Alexei N. Kosygin) and the USA (Richard M. Nixon) signed in Moscow formal bilateral agreements of cooperation in peaceful space research and utilization. Initial talks on mutual cooperation had already started in 1969.²⁹⁷⁴⁾²⁹⁷⁵⁾

- The first project to be realized was the Apollo–Soyuz Test Project (ASTP), leading to a common spaceflight (docking of both spacecraft, Apollo 18 and Soyuz–19) on July 17, 1975 (the flight was from July 15 – 24, 1975). This represented the first international meeting of men in orbit. The main objects were to test the compatibility of rendezvous and docking systems for American and Soviet spacecraft, to open the way for international space rescue as well as future joint manned flights. The Apollo spacecraft was nearly identical to the one that orbited the Moon and later carried astronauts to Skylab. The Soyuz craft was the primary Soviet spacecraft used for manned flight since its introduction in 1967. A docking module was designed and constructed by NASA to serve as an airlock and transfer corridor between the two craft.
- The Spacelab program of NASA, with over 25 missions over a period of 16 years (1983–1999) has probably generated the greatest amount of cooperation in any space program so far. Over 500 PI (Principal Investigators) were involved in the program. Their investigations have included major scientific efforts in such fields as astrophysics, atmospheric science, the life sciences, space plasma physics, and Earth observations. The Spacelab program represents the longest duration, the most multi–disciplinary and the most international of any space programs conducted so far. Until 1994, in addition to the 242 students who had completed masters or Ph.D. degrees within the Spacelab program, a few hundred government and university institutions and other organizations, had been involved at the PI level, with the degree of international participation being valued higher than on any other

2973) “£15 million investment seals UK/ France space collaboration,” UKSA, Jan. 31, 2014, URL: <http://www.bis.gov.uk/ukspaceagency/news-and-events/2014/Jan/uk-france-agreement>

2974) http://www.gctc.ru/eng/direct/exter_coop_e.htm

2975) http://www.nasa.gov/50th/50th_magazine/coldWarCoOp.html

space program. Obviously, the number of Co-Investigators, team members and contractors was up in the thousands. Also, a number of research centers were started by a role in the Spacelab program. ²⁹⁷⁶⁾

- In 1985, General Secretary Mikhail S. Gorbachev and President Ronald W. Reagan met in Geneva, Switzerland. They had just received the report of the tenth meeting of USA–USSR Joint Committee on Cooperation in the Field of Environmental Protection, held the prior week in Moscow. Acknowledging the usefulness of those meetings, their joint statement concluding the summit meeting observed that “both sides agreed to contribute to the preservation of the environment – a global task through joint research and practical measure.”

- The Priroda module project of the Mir Space Station (Mir Core Module launch on Feb. 20, 1986) was originally an all–Soviet remote sensing project for combined civilian and military surveillance of the Earth. – Then in 1985, the Priroda project took on an international aspect when experiments scheduled for launch aboard smaller satellites within the Interkosmos program were moved to Priroda. However, throughout the planning and development phases, the Priroda project was plagued by many reconfigurations, setbacks and delays. The Priroda module was originally scheduled for delivery in the late 1980s, then the launch was scheduled for 1990; but by 1990 this had been pushed back to 1992. ^{2977) 2978)}

In this timeframe, NASA was developing its own space station program and was looking for international partners, in particular a cooperation with the Mir station program, because a lot of invaluable experience could be gained on both sides, the USA and the USSR. Already in 1983, NASA and its partners in Europe, Japan, and Canada were discussing the possibility of a joint space station. On January 25, 1984, President Reagan gave his approval for the development of a permanently manned space station. The first launch of ISS module was planned for 1992, the 500th anniversary of the discovery of America by Christopher Columbus. However, it took until 1998 when this goal could be realized. ²⁹⁷⁹⁾

- ISS Treaties: In 1988 a treaty was formulated to document agreements regarding the development of a new orbiting Space Station. The treaty was updated in 1998 with the addition of Russian participation in the program. ²⁹⁸⁰⁾ Fifteen national governments signed the treaty thus establishing a framework for cooperation on the International Space Station program. This intergovernmental agreement (IGA) provided the basis for how the contributing partners would develop and operate the ISS. Fundamental issues such as program funding, cross waivers for liability, data rights and intellectual property are all addressed by the IGA.

- With the end of the Cold War in early 1990s and the collapse of the former USSR, the Russian space program declined considerably due to a lack of funding. – Already in 1990, the US and the USSR began a joint program of scientific and manned space flight studies in response to agreements reached by the Bush Administration. Initial activities included the conduct of medical experiments studying the effects of long–duration space flight on board Mir. Provisions were made for the flight of a Russian cosmonaut on Space Shuttle, and of an American astronaut on board Mir.

In April 1993, General Secretary Boris Yeltsin met President Bill Clinton in Vancouver, Canada. The summit resulted in an agreement to establish a US–Russian commission on

²⁹⁷⁶⁾ Marsha R. Torr, “Scientific achievements of 10 years of Spacelab – An overview of the missions,” AIAA–1994–4646, Space Programs and Technologies Conference, Huntsville, AL, Sept. 27–29, 1994

²⁹⁷⁷⁾ <http://www.astronautix.com/craft/mirplex.htm>

²⁹⁷⁸⁾ <http://www.astronautix.com/craft/priroda.htm>

²⁹⁷⁹⁾ “From Cold War to international cooperation – the story of the ISS,” http://www.dlr.de/iss/en/desktopdefault.aspx/tabid-1945/2746_read-4182/

²⁹⁸⁰⁾ Michael Raftery, Gordon R. Woodcock, “International Space Station as a platform for Exploration beyond Low Earth Orbit,” Proceedings of the 61st IAC (International Astronautical Congress), Prague, Czech Republic, Sept. 27–Oct. 1, 2010, IAC–10.B6.6.–B3.4.1

technological cooperation in the fields of energy and space, chaired by Russian Prime Minister Viktor Chernomyrdin and Vice President Al Gore.

On Dec. 16, 1993, a cooperative Shuttle/Mir agreement was signed between the newly established Russian Space Agency (Rosaviakosmos at the time, Roskosmos since 2004) and NASA involving a series of Shuttle flights to the Mir station complex in the timeframe 1994–1998. NASA agreed also to provide funds to complete the Spektr and Priroda modules for the Mir station using US funds, providing 600 to 700 kg of US experiments to be installed.

The joint cooperative space program of the United States and the Russian Federation, involving the Space Shuttle and the Mir station, spelled out the following goals: ²⁹⁸¹⁾

- First, the program permits NASA to develop, maintain, and enhance capabilities and operations to allow humans to live and work continuously in space.
- Second, by establishing a relationship with Russia as an international partner for the human exploration and exploitation of space, the United States can reduce the cost of future U.S. space initiatives by applying Russian–developed technology.
- Third, by flying Space Shuttle missions to the Russian Mir, the United States can enhance its understanding of long–duration operations, and gain life sciences and microgravity research benefits from long–duration experimentation.
- Fourth, early cooperation with the Russian partners permits NASA to develop common systems and operating procedures which will increase the probability of success and mitigate risks in the design, assembly, and operation of the International Space Station (ISS) in which Russia is a full partner.
- Fifth, by engaging Russia in constructive space work, the United States can advance its foreign policy initiatives.
- Finally, this relationship between the U.S. and Russian space agencies advances U.S. national space programs as well as U.S. aerospace industry.

The Shuttle–Mir Joint Program, February 1995 to June 1998, included 11 space shuttle flights and seven US astronaut residencies, called increments, on the Russian space station Mir. Space shuttles also conducted crew exchanges and delivered supplies and equipment. These activities definitely opened a new era of international cooperation in space.

- The first Shuttle docking at the MIR space station began on June 30, 1995 with the docking of both S/C. The event occurred on Shuttle flight STS–71 (Atlantis, June 27 – July 7, 1995).
- At the Dec. 16, 1993 meeting (Mir/Shuttle agreement between Russia and USA), the USA invited Russia to join the international space station program.
- In 1995, the ESA Council of Ministers (Toulouse, France) integrated the European automated transfer vehicle (ATV), intended to transport payloads to the ISS, into the program. The first flight of the ATV to the ISS took place in March 2008.
- *The newly established US–Russian partnership paid huge dividends when the Space Shuttle fleet was grounded after the Columbia accident in early February 2003. The Russian Soyuz spacecraft was the only remaining means of reaching the ISS, and so it rescued the stranded American and Russian astronauts, and provided transport of people and supplies to the ISS until the US was able to resume the shuttle program. In fact, the resumption of Shuttle flights started again with STS–114 (July 26–Aug. 9, 2005) after 2 1/2 years of Shuttle grounding.*
- Competition and cooperation: In Feb. 2007, a commemoration took place in Washington, DC, entitled: “Space Cooperation Highlights 200 Years of U.S.–Russia Relations”

²⁹⁸¹⁾ http://www.hq.nasa.gov/office/budget/fy96/hsf_2.html

where the U.S. Department of State celebrated 200 years of U.S. – Russian diplomatic relations, while NASA commemorated the 45th anniversary of John Glenn’s orbits of Earth in Friendship 7 in 1962. “In exploring outer space,” said Yuri Ushakov, Russia’s ambassador to the United States, “we are not only partners but rivals as well. That rivalry, that competition, however, produced brilliant results. ... A half a century ago, in 1957, the Soviet Union launched the first man–made satellite, and America [responded] by establishing NASA and the launch of their own space vessels.”²⁹⁸²)

- The International Space Station (ISS) has shattered numerous world records in space but one of its most enduring legacies will be the development and use of a new management model for large, extremely complex engineering projects. This new model, which is based on international cooperation at the program level still allows for and encourages competition at the level of technology, thus providing a stable platform for the testing of new ideas in the harsh environment of space (Ref. 2980).

- Programmatic cooperation: Stability in the political support for any program is crucial and often difficult to maintain over long periods of time. All complex programs struggle during the development phase to overcome technical, cost and schedule problems and ISS was certainly no exception. However, what ISS had that most programs do not have is a treaty signed by fifteen nations committed to stay the course. This treaty provides an extra measure of stability that is essential on the most difficult projects because each partner nation must weigh the political consequences of breaking its commitment to all the other partner nations.

- International experience during construction and operations of the ISS has fundamentally changed the way future large – scale civil space programs should be conducted. It is now clear that a management model based on international collaboration at the program level and competition at the technology level can provide both long term program stability as well as flexible evolution of capability. It has also been shown that both commercial and government sponsored technology developments are well supported in this management model (Ref. 2980).

- **AMS–02** (Alpha Magnetic Spectrometer) is one of the most complex space scientific instruments ever built. AMS–02 was flown on the next–to–last Shuttle flight (STS–134, launch on May 16, 2011) to the ISS. AMS–02 is not only the largest scientific instrument installed on the ISS (7,500 kg), but it also considered the result of the largest international collaboration for a single experiment in space.

Construction, integration, and testing of the AMS–02 Experiment, representing more than a decade of work (actually 17 years), was carried out by an international team, referred to as the **AMS Collaboration**, composed of about 600 physicists and 56 institutes and organizations from 16 countries: USA, Asia (China, Korea, Taiwan), Europe, including nine ESA Member States and Russia, and organized under an agreement between NASA and the U.S. Department of Energy (DOE). The AMS program is led by Samuel S. Ting of MIT.

After the extension of ISS operations and utilization in March 2010 from 2015 to 2020 and beyond (2028), the AMS Collaboration decided to continue AMS–02 operations for the total period of the ISS operational life, if possible to 2028 to achieve the best results.

²⁹⁸²) <http://www.america.gov/st/washfile–english/2007/February/200702211314591cniirellep0.7167169.html>

1.30 Regional Initiatives of Spacefaring Nations

In the last decade of the 20th century and in the early 21st century, emerging spacefaring nations in particular are realizing the benefits of Earth observation and space technology to socio–economic development. However, involvement in this field is rather challenging in view of available resources, manpower, and education standard. A possible way to achieve a country’s goal is to establish international cooperation on a long–term basis.

International cooperation agreements on space–related activities started with the early spaceage, since the other industrialized nations between the two rivals of the Cold War era, USA and USSR, could not afford to set their sights immediately on the development of their own complete space programs. But the global nature of space flight simply required international cooperations to cover the space missions. – Nowadays, there are hundreds of international cooperation agreements and partnerships in place. And the experiences of the industrialized nations have shown that national space programs, as well as international cooperations, have contributed to the development of commercial products and services in all fields of scientific and economic endeavors. ²⁹⁸³⁾

Two regional initiatives of emerging spacefaring nations (among several) are presented to show their striving goals and activities in capacity building in space science and technology (producing highly trained scientists, engineers and technicians, and transfer the knowledge gained to other sectors of the economy), and in sharing their resources.

1.30.1 APRSAF (Asia–Pacific Regional Space Agency Forum)

APRSAF was established in 1993 in response to the declaration adopted by the Asia–Pacific International Space Year Conference (APIC) in 1992. The leadership of Japan with MEXT (Ministry of Education, Culture, Sports, Science and Technology) and JAXA were decisive for the start of APRSAF. A major objective of APRSAF is to coordinate the Asia–Pacific nations activities in space to leverage the capabilities of its members for purposes that could otherwise not be accomplished individually. ²⁹⁸⁴⁾

As of December 2011, the participants of APRSAF come from 325 organizations of 35 countries (inside and outside of the Asia–Pacific region) and 24 international organizations (e.g. the United States, Canada, France, and several United Nations offices).

APRSAF supports the establishment of international projects as solutions for common issues such as disasters and environmental protection so that the participating parties can realize cooperation.

- **Sentinel Asia (SA):** The Sentinel Asia initiative is a voluntary collaboration between space agencies and disaster management agencies, applying remote sensing and Web–GIS technologies to support disaster management in the Asia–Pacific region. Sentinel Asia is promoted by APRSAF and the international community (UN ESCAP, UN OOSA, ASEAN, the Asian Institute of Technology (AIT), etc.), and the disaster reduction community, ADRC (Asian Disaster Reduction Center) and its member organizations. ^{2985) 2986)}

Asia has been seriously damaged by natural disasters over the last 30 years. The region sustained 57% of global fatalities and 89 % of the total victims associated with such disasters.

²⁹⁸³⁾ M. Ansdell, L. Delgado, D. Hendrickson. “Analyzing the Development Paths of Emerging Spacefaring Nations – Opportunities or Challenges for Space Sustainability?,” April 2011, IAFF 6159: Capstone Research, URL: http://www.gwu.edu/~cistp/assets/docs/capstone/2011/Ansdell%20Delgado%20Hendrickson_Final.pdf

²⁹⁸⁴⁾ <http://www.aprsaf.org/>

²⁹⁸⁵⁾ http://www.aprsaf.org/initiatives/sentinel_asia/

²⁹⁸⁶⁾ Hiroki Kai, “Sentinel Asia – Voluntary Initiatives for establishing a Disaster Management Support System in the Asia–Pacific Region,” Sept. 2006, URL: <http://www.a-a-r-s.org/ws-eowm/download/Plenary4/Sentinel%20Aisa.pdf>

Under these circumstances, the APRSAF proposed Sentinel Asia in 2005 to showcase the value and impact of earth observation technologies, combined with near real-time Internet dissemination methods and Web-GIS mapping tools for disaster management support in the Asia-Pacific region.

The main activities of Sentinel Asia are as follows:

- Emergency observation by Earth observation satellites upon requests in case of major disasters
- Wildfire monitoring, flood monitoring, and glacier lake outburst flood (GLOF) monitoring
- Capacity building and human resources development for more effective disaster management.

In Step 1 of emergency observations,²⁹⁸⁷⁾ the ALOS (Advanced Land Observing Satellite) of JAXA and the IRS (Indian Remote Sensing Satellites) of ISRO have carried out emergency observations in the case of major disasters in the Asia-Pacific region. SA Step 1 (2006–2007) has served as a good demonstrator project to share disaster-related information obtained by several Earth observation satellites.

The SA Step 2 project was initiated in June 2008 at the JPT (Joint Project Team) meeting in Kobe, Japan. In addition to Step 1's Earth observation satellites such as ALOS of JAXA, MTSAT-1R of JMA, and IRS of ISRO, new Earth observation satellites such as KOMP-SAT (Korean Multi-purpose Satellite) of KARI, THEOS (Thai Earth Observation System) of GISTDA of Thailand, FORMOSAT of NARL (National Applied Research Laboratories) of Taiwan, and communications satellites such as WINDS (Wideband Internet-working Engineering Test and Demonstration Satellite) of JAXA) have joined. These organizations are called DPN (Data Provider Node) of Sentinel Asia, and these satellites are called "Sentinel Asia Constellation."

There is a success story in SAFE prototyping in Vietnam for forest monitoring and water resources managements from 2008 to 2010.

- FPD/MARD (Vietnamese Forest Protection Department, Ministry of Agriculture and Rural Development) is the agency having responsibility for Forest Management in Vietnam. FPD has a MODIS receiving station and provides wildfire Hotspot information to the rural branch. As the next step, FPD is trying to strengthen the forest management by the use of MODIS data.

- **SAFE** (Space Applications For Environment), since 2008: Climate change and human activities accelerate hazards, such as deforestation, landslides, droughts, and floods in Asia-Pacific countries. To mitigate these hazards, environmental monitoring has become important. SAFE aims to encourage environmental monitoring for climate change mitigation and adaptation studies, as well as studies on other forms of practical application, using space applications.^{2988) 2989)}

- **STAR** (Satellite Technology for the Asia-Pacific Region), since 2009: The STAR program is an international initiative to develop small satellites in collaboration with engineers

2987) K. Kaku, A. Ono, M. Kawai, "Sentinel Asia Step 2 – The Overview and Evolution from Step 1," International Archives of the Photogrammetry, Remote Sensing and Spatial Information Science, Volume XXXVIII, Part 8, Kyoto Japan 2010, URL: http://www.isprs.org/proceedings/XXXVIII/part8/pdf/JTS35_20100301164014.pdf

2988) <http://www.aprsaf.org/initiatives/safe/>

2989) Shin-ichi Sobue, Toru Fukuda, Toshio Koike, Wataru Takeuchi, Tsugito Nagano, Tomoyuki Nukui, "The Overview of Space Applications for Environment Initiates," International Archives of the Photogrammetry, Remote Sensing and Spatial Information Science, Volume XXXVIII, Part 8, Kyoto Japan 2010, URL: http://www.isprs.org/proceedings/XXXVIII/part8/pdf/JTS11_20100205112948.pdf

and researchers from the Asia–Pacific region. The objectives are to:²⁹⁹⁰⁾

- Provide opportunities to build capacity for Space Agency staff in the Asia–Pacific region in satellite development
- Increase the number of earth observation satellites that can be used in the Asia–Pacific Region to satisfy the future needs of the region.

Participants in the STAR program are; India (ISRO), Indonesia (LAPAN), Japan (JAXA), Korea (KARI), Malaysia (ANGKASA), Thailand (GISTDA), and VietNam (VAST/STI).

The APRSAF organization conducts annual meetings initiated jointly by MEXT/JAXA of Japan, and a co–host country. Some examples of meetings are:

APRSAF–11 took place Nov. 3–5, 2004, Canberra, Australia
 APRSAF–12 took place Oct. 11–13, 2005, Kitakyushu, Japan
 APRSAF–13 took place in Dec. 2006 in Jakarta, Indonesia
 APRSAF–14 took place in Nov. 2007 in Bangalore, India
 APRSAF–15 took place in Dec. 2008 in Hanoi, Vietnam
 APRSAF–16, took place in January 2010, Bangkok, Thailand
 APRSAF–17, took place Nov. 23–26, 2010, Melbourne, Australia
 APRSAF–18, took place December 6–9, 2011, Singapore
 APRSAF–19, took place December 11–14, 2012, Kuala Lumpur, Malaysia
 APRSAT–20, took place December 03–06, 2013, Hanoi, Vietnam
 AORSAT–21 will take place Decmber 2–5, 2014, Tokyo, Japan.²⁹⁹¹⁾

1.30.2 ALC (African Leadership Conference on Space Science and Technology for Sustainable Development)

The establishment of the ALC (African Leadership Conference on Space Science and Technology for Sustainable Development) was a regional initiative of the African member states of UN COPUOS (United Nations Committee on The Peaceful Uses of Outer Space) in 2005. During the UN COPUOS session in 2004, Algeria, Nigeria and South Africa agreed to organize the ALC as a forum to enhance high–level cooperation among African countries in space affairs.

The aim is the raise the profile of space in the African political leadership and to emphasize the importance of space science & technology for the durable socioeconomic development of Africa. The ALC convenes every second year. The main objectives of ALC are:²⁹⁹²⁾

- To provide a forum for exchange of ideas on the impact which space technology could have in addressing Africa’s development challenges and in contributing to its development agenda
- To identify opportunities for cooperation in the utilization of space technology for the development and benefit of Africa
- To identify common capacity–building requirements and the cooperative means to address such needs
- To promote cooperation with inter–governmental and international non–governmental entities, such as UNOOSA, IAF, IAA, etc.

²⁹⁹⁰⁾http://APRSAF/initiatives/star_program/

²⁹⁹¹⁾ Akiko Suzuki, “Asia–Pacific Reginal Space Agency Forum in 2013 & 2014 – Renovating for New Era,” Proceedings of the 51st Session of Scientific & Technical Subcommittee of UNCOUOS, Vienna, Austria, Feb. 11–22, 2014, URL: <http://www.unoosa.org/pdf/pres/stsc2014/tech–30E.pdf>

²⁹⁹²⁾A. Kedjar, “3rd African Leadership Conference on Space Science and Technology for Sustainable Development,” 2009, URL: <http://www.oosa.unvienna.org/pdf/pres/copuos2009/tech–39.pdf>

- To identify a series of concrete follow-up actions and projects to be conducted during the intersessional periods of the Conference. ²⁹⁹³⁾ ²⁹⁹⁴⁾

1) The first ALC conference took place in Abuja, Nigeria, November 23–25, 2005 at NASRDA (National Space Research and Development Agency). One of its recommendations was that a standing series of conferences should be arranged where African leaders and space professionals could meet on a biannual basis to exchange information and to make plans for the development of Africa's capabilities to harness space science and technology.

2) The 2nd ALC was held in Pretoria, South Africa, from 2–4 October 2007. The conference brought together 113 space professionals, government officials, industry representatives, scientists, engineers and academics from 11 African countries for discussions in a wide range of topics spanning from basic space science to space applications and the role of space science and technology in Africa's development.

3) The 3rd ALC was organized by the Algerian Space Agency (ASAL) and UNOOSA (United Nations Office for Outer Space Affairs), and was held in Algiers, Algeria from Dec. 7–9, 2009. The conference was attended by 142 experts from 10 countries with 6 African countries (Algeria, Kenya, Niger, South Africa, Tunisia) and the following international and regional organizations: UNOOSA, UNESCO, FAO [Food and Agriculture Organization (of the UN)], ACMAD (African Centre of Meteorological Application for Development), OSS, CRASTE-LF (African Regional Centre for Space Science and Technology Education), IAF (International Astronautical Federation). ²⁹⁹⁵⁾ ²⁹⁹⁶⁾

Signing of agreements : In parallel of the meeting of Algiers, the Algerian Space Agency signed two agreements:

- The first agreement, with UNOOSA on the establishment of a Regional Support Office in Algeria, for the use of Space-based Information for Disaster Management and Emergency Response (SPIDER Program), which will be in charge of coordination in North Africa.

- The second agreement — signed by the Space Agencies of: Algeria, South Africa, Nigeria and Kenya — is about the implementation of **ARMC** (African Resource and environmental Management satellite Constellation).

The four nations (Algeria, South Africa, Nigeria and Kenya) have the goal to develop African-made satellites to address regional needs and build up regional capabilities. Although no hardware exists so far (2012), ARMC has brought together key African space nations with top-down support from the highest levels of government, critical for program sustainability.

Note: The so-called ARM (African Resource Management) concept was initially proposed at the Addis-Ababa (Ethiopia) UN Workshop of Space Technology for Disaster Management, July 1–5, 2002. The idea was to introduce resource management as an alternative to disaster management on the continent of Africa. In particular, to create a geo-information system focused on African priorities.

²⁹⁹³⁾ P. Martinez, "The 2nd African Leadership Conference on Space Science and Technology for Sustainable Development," African Skies/CIEUX Africans, No 12, October 2008, URL: <http://www.sao.ac.za/~wgssa/archive/as12/PMartinez2.pdf>

²⁹⁹⁴⁾ S. Mostert, "Impact of SumbandilaSat on Sustainable Development in context of African Resource Management Constellation," UN Workshop 'Use of Space Technology for Sustainable Development,' April 25–27, 2007, Rabat, Morocco, URL: <http://www.unoosa.org/pdf/sap/2007/morocco/presentations/4-12.pdf>

²⁹⁹⁵⁾ A. Kedjar, "3rd African Leadership Conference on Space Science and Technology for Sustainable Development," COPUOS, Scientific and Technical Subcommittee 47th session, Vienna, Austria, Feb. 8–19, 2010, URL: <http://www.osa.unvienna.org/pdf/pres/stsc2010/tech-52.pdf>

²⁹⁹⁶⁾ Margaret W. Maimba, "Outcome of the 4th African Leadership Conference 2011," Proceedings of the 49 Session of UN COPUOS (Committee on the Peaceful Uses of Outer Space), STSC (Scientific and Technological Subcommittee), Vienna, Austria, Feb. 6–17, 2012, URL: <http://www.osa.unvienna.org/pdf/pres/stsc2012/tech-29E.pdf>

4) The 4th ALC was hosted by the Government of Kenya and held in Mombasa, Kenya, from 26 to 29 September 2011. UNOOSA (UN Office for Outer Space Affairs) provided funding support to the conference and organized sessions on capacity building in space technology development and space law. 2997) 2998) 2999)

The conference concluded with the promulgation of the "**Mombasa Declaration**" 3000) which contains observations and recommendations for activities in space science and technology for Africa. The BSTI (Basic Space Technology Initiative) will in particular aim to contribute to the following recommendations:

For the development of Africa's human capital resources in space science and technology, action should be taken to:

- A. To improve access to high–level education and training in space science and technology on the continent
- B. To acknowledge and harness the expertise already present on the African continent through the development of a comprehensive database of African space science and technology experts
- C. To align with existing human capital development initiatives of the African Union
- D. To utilize existing training centers in Africa and to promote greater cooperation among education and training institutions to develop appropriate training programs in space science and technology that respond to Africa's needs
- E. To encourage African countries to increase their utilization of and support for the Regional Centres for Space Science and Technology Education, affiliated to the United Nations, located in Morocco and Nigeria
- F. To promote knowledge sharing through regional space conferences and through scholarly interaction among African institutions
- G. To support the existing networks and associations of space professionals in Africa
- H. To encourage the development and implementation of university curricula in space science and technology in Africa.

The ALCs are open to other African countries willing to join the initiative.

The **ARMC** (African Resource and Environmental Management Satellite Constellation) initiative of Algeria, Kenya, Nigeria and South African has the objectives to pool resources and launch at least one medium to high–resolution satellite into space every two years starting with a launch in 2013.

AfriGEOSS: An initiative to reinforce Earth observation in Africa: 3001)

In 2012, GEO (Group on Earth Observations) has launched the AfriGEOSS initiative, which aims to coordinate the implementation of the Global Earth Observation System of Systems (GEOSS) and related Earth observation activities in Africa.

Supported by the GEO Secretariat and recognized by the Executive Committee, this initiative seeks to identify the challenges and then put in place measures to enhance Africa's participation in, and contribution to, GEOSS. This participation will contribute to the contin-

2997) "Fourth African Leadership Conference on Space Science and Technology for Sustainable Development," UNOOSA, Oct. 25, 2011, URL: <http://www.unoosa.org/oosa/en/SAP/bsti/alc2011.html>

2998) M. Ansdell, L. Delgado, D. Hendrickson. "Analyzing the Development Paths of Emerging Spacefaring Nations – Opportunities or Challenges for Space Sustainability?," April 2011, IAFF 6159: Capstone Research, URL: http://www.gwu.edu/~cistp/assets/docs/capstone/2011/Ansdell%20Delgado%20Hendrickson_Final.pdf

2999) Olufemi A. Agboola, "Space System and Engineering in Africa: Nigeria as a Case Study," The 4th African Leadership Conference on Space Science and Technology for Sustainable Development – ALC 2011, Mombasa, Kenya, Sept. 26 – 28, 2011, URL: http://www.oosa.unvienna.org/pdf/bst/ALC2010/10_NIGERIA-ALC-2011-ESS-V1.pdf

3000) "The Mombasa Declaration on Space and Africa's Development," URL: http://www.unoosa.org/pdf/bst/ALC2010/Mombasa_Declaration_Final_final_28-10-2011.pdf

3001) "AfriGEOSS: An initiative to reinforce Earth observation in Africa," GEO News, Issue #9, May 25, 2012, URL: http://www.earthobservations.org/art_019_002.shtml

ent's efforts to bridge the digital divide and to build a knowledge-based economy using GEO networks and the GEOSS infrastructure.

The proposed priorities of AfriGEOSS are ground stations to support a coordinated data acquisition strategy for Africa, the African Resources and Environmental Management Constellation (ARMC), and AfricaGeoSat-1, among others.

The first step will be to engage the ground stations in Kenya (Malindi), Egypt (NARSS), South Africa (SANSA), Nigeria (NASRDA), Gabon and Algeria (ASAL). Implementing this strategy will complement the data policy of ARMC (African Resources and Environmental Management Constellation).

The ARMC initiative will provide Africa with timely, free, open and unrestricted access to medium to high resolution data over Africa for natural resources management applications.

1.31 A brief overview of the EMS (Electromagnetic Spectrum)

Virtually our entire knowledge about the Universe is based upon the observation of electromagnetic waves, such as visible light, infrared, ultraviolet, radio, X-rays and gamma rays.

Spectral regions. The EMS (Electromagnetic Spectrum) is a continuum extending over a wide range of energies and wavelengths: from about 10^{11} m (ULF waves) and 10^7 m (very long radio waves) to about 10^{-15} m (very short gamma rays). High-energy cosmic rays are even shorter.

For convenience, the EMS is subdivided into a number of spectral regions and subregions to suit the needs of particular applications, or for use in various fields of science. In general, there are no hard boundaries to each spectral region or subregion; they just blend into a continuum of smoothly changing wavelengths. This leads to many overlapping definitions in the literature (on all levels). The best accepted boundaries for any spectral region are probably those of visible light ($0.4 - 0.7 \mu\text{m}$), a narrow interval that can be detected by the human eye. The so-called superregions are a convenient shortcut for coverage of certain phenomena and/or use of similar instrument classes. The general boundaries of the superregions are:

- The so-called **“high-energy spectrum”** consists of the X-ray, gamma-ray, and cosmic-ray regions, all of which are overlapping depending on application or research objective. The high-energy radiation is mostly of the non-thermal type.
- The so-called **optical spectrum** extends from $0.01 \mu\text{m}$ to $1000 \mu\text{m}$ in wavelength, i.e., from the UV to the FIR regions inclusively. The infrared region ($0.7 - 1000 \mu\text{m}$) itself represents by far the greatest portion of the optical spectrum and is generally divided into a number of subregions (NIR, SWIR, MWIR, TIR, VLWIR, FIR). The atmospheric reflected infrared (IR, $0.7 - 3 \mu\text{m}$) subregion, in turn, consists of the subregions NIR+SWIR. A telescope generally serves as the radiation collection aperture in an optical instrument.
- The so-called **microwave region** extends roughly from 1 mm to 1 m in wavelength ($\leq 300 \text{ GHz}$ frequencies $\leq 300 \text{ MHz}$)
- The so-called **“radio region”** or **“radio frequency (RF) spectrum,”** as defined by ITU (International Telecommunication Union), extends from 0.1 mm to 10^4 km in wavelength, covering the frequency range from SMMW [Submillimeter Wave: 0.1 mm to 1 mm in wavelength] over EHF [Extremely High Frequency ($30 \leq 300 \text{ GHz}$)] to ELF [Extremely Low Frequency ($30 \leq 300 \text{ Hz}$)]. An inspection of Table 171 shows that the entire microwave region, and a portion of the optical region, are actually part of the upper-most radio region (overlap). Often, the terms “microwave region” and “radio region” are being used interchangeably (see Table 172). The reason is that most emphasis, in particular in communications, is placed into the 1 mm to 1 m wavelength range (covering the bands UHF, SHF and EHF, i.e., the microwave region). The infringement into the optical region (with SMMW) from the radio and microwave sides demonstrates only the increasing technological capabilities that are being conquered by these communities.

An antenna is generally the collecting aperture for microwave or RF instruments.

- The so-called **ULF waves** occur virtually everywhere within the magnetosphere and at any time. They are a response to changes in the magnetosphere, and are thus evidence of its dynamic behavior. The designation ULF usually refers to waves with frequencies $< 1 \text{ Hz}$. Waves with frequencies in the mHz range have scale sizes comparable to the size of the magnetosphere and are therefore strongly affected by the magnetospheric structure.

Super region	Region or Subregion	Comment
High energy	Cosmic rays	Radiation of galactic origin. Energy spectrum: from about $10^{11} \text{ eV} - 10^{21} \text{ eV}$
	γ -rays	Gamma-rays: photon energy: $> 400 \text{ keV}$; spectral range: $\leq 3 \text{ pm}$ (0.003 nm)
	X-rays	Soft X-rays: photon energy: $0.1 - 10 \text{ keV}$; spectral range: $6 - 0.1 \text{ nm}$ Hard X-rays: photon energy: $10 - 400 \text{ keV}$; spectral range: $0.1 - 0.003 \text{ nm}$

Super region	Region or Subregion	Comment
Optical	UV NUV FUV EUV	Ultraviolet: 6 – 400 nm Near Ultraviolet: 125 – 400 nm Far Ultraviolet: 60 – 125 nm Extreme Ultraviolet: 6 – 60 nm (EUV, also abbreviated as XUV) The term VUV (Vacuum UV) is also used for the range: $10 < \lambda < 200$ nm
	VIS	Visible: 0.4 – 0.7 μm
	NIR	Near infrared: 0.7 – 1.3 μm
	VNIR	Visible/Near infrared: 0.4 – 1.3 μm , – the predominant mode of energy detection is that of reflected sunlight
	SWIR	Short–Wave infrared: 1.3 – 3 μm – the predominant mode of energy detection is that of reflected sunlight
	MWIR (also referred to as MIR)	Mid–Wave infrared: 3 – 6 μm – the detected energy is a mixture of solar reflected and thermally emitted radiation. MWIR offers nearly 100% atmospheric transmission, with the added benefit of lower, ambient, background noise.
	TIR	Thermal infrared: 6 – 14 μm [also referred to as LWIR (Long wavelength infrared)] – practically all energy received (detected) is attributed to thermal emission. LWIR actually spans from 8–14 μm . The atmosphere provides nearly 100% transmission on the 9–12 μm band (window).
	VLWIR	Very Long–Wavelength Infrared (14 – 30 μm), emissive detection
	FIR	Far infrared: 30 – 1000 μm (note: 1000 μm = 1 mm). FIR radiation can be measured remotely by the thermal emission technique. A problem with this technique is instrument self–emission.
	Radio	SMMW
MW		Microwave region: 1 mm – 1 m (frequency range ≤ 300 GHz to ≥ 300 MHz) – the detected energy is of microwave (thermal) emissions. Since microwave sensors do not depend on solar illumination the observations are virtually independent of aerosols and also much less affected by clouds (cirrus) than sensors operating in IR or VIS.
RF		Radio frequency spectrum: 10 ⁴ km to 0.1 mm (30 Hz to 3000 GHz)
ULF (Ultra Low Frequency)		The ULF wave region (geomagnetic pulsations) covers roughly the frequency range from 1 mHz to 1 Hz (with corresponding periods of 1000 s to 1 s and wavelengths of the order to about 10 R _E and much more), i.e., from the lowest the Earth's magnetic cavity can support up to the various ion gyro–frequencies. – ULF waves are a permanent feature in the region called the magnetosphere, where the behavior of charged particles is influenced by the Earth's intrinsic magnetic field. These waves transport momentum and energy from the solar wind to the magnetosphere and farther down to the ionosphere. In addition, the waves interact with the charged particles in the magnetosphere and modify their energy and direction of motion with important consequences for the dynamic processes such as geomagnetic storms and the formation of auroral arcs.

Table 171: Overview of spectral regions of the EMS

ITU Designation	Name of Frequency Band	Frequency Band	Wavelength (λ)	Remarks/Use
ELF	Extremely Low Frequency (Megametric waves)	30 < 300 Hz	10 ⁴ – 100 km	Alternating current (50 – 60 Hz)
VF	Voice Frequency	300 Hz < 3 kHz	10 ³ – 100 km	Voice (telephony)
VLF	Very–low Frequency (Myriametric waves)	10 < 30 kHz	30 – 10 km	Radiotelegraphy

ITU Designation	Name of Frequency Band	Frequency Band	Wavelength (λ)	Remarks/Use
LF	Low Frequency (Kilometric waves)	30 < 300 kHz	10 – 1 km	Radiotelegraphy, radio
MF	Medium Frequency (Hectometric waves)	300 < 3000 kHz	1000 – 100 m	Radio, (AM radio)
HF	High Frequency (Decametric waves)	3 < 30 MHz	100 – 10 m	Radiotelephony, radio navigation, amateur radio
VHF	Very–High Frequency (Metric waves)	30 < 300 MHz	10 – 1 m	Radio, TV, radio navigation, radiobeacon, (FM radio)
UHF	Ultra–High Frequency (Decimetric waves)	300 < 3000 MHz	1 m – 0.1 m	broadcast, laser, MW heating
SHF	Super–High Frequency (Centimetric waves)	3 < 30 GHz	10 – 1 cm	
EHF	Extremely–High Frequency (Millimetric waves)	30 < 300 GHz	10 – 1 mm (millimeter waves)	Safe communications
SMMW	Submillimeter Waves (Decimillimetric waves)	300 < 3000 GHz (or 0.3 < 3 THz)	1 – 0.1 mm	



 ← ITU Radio Spectrum
  ← Microwave Spectrum

Table 172: Overview of ITU radio spectrum designations

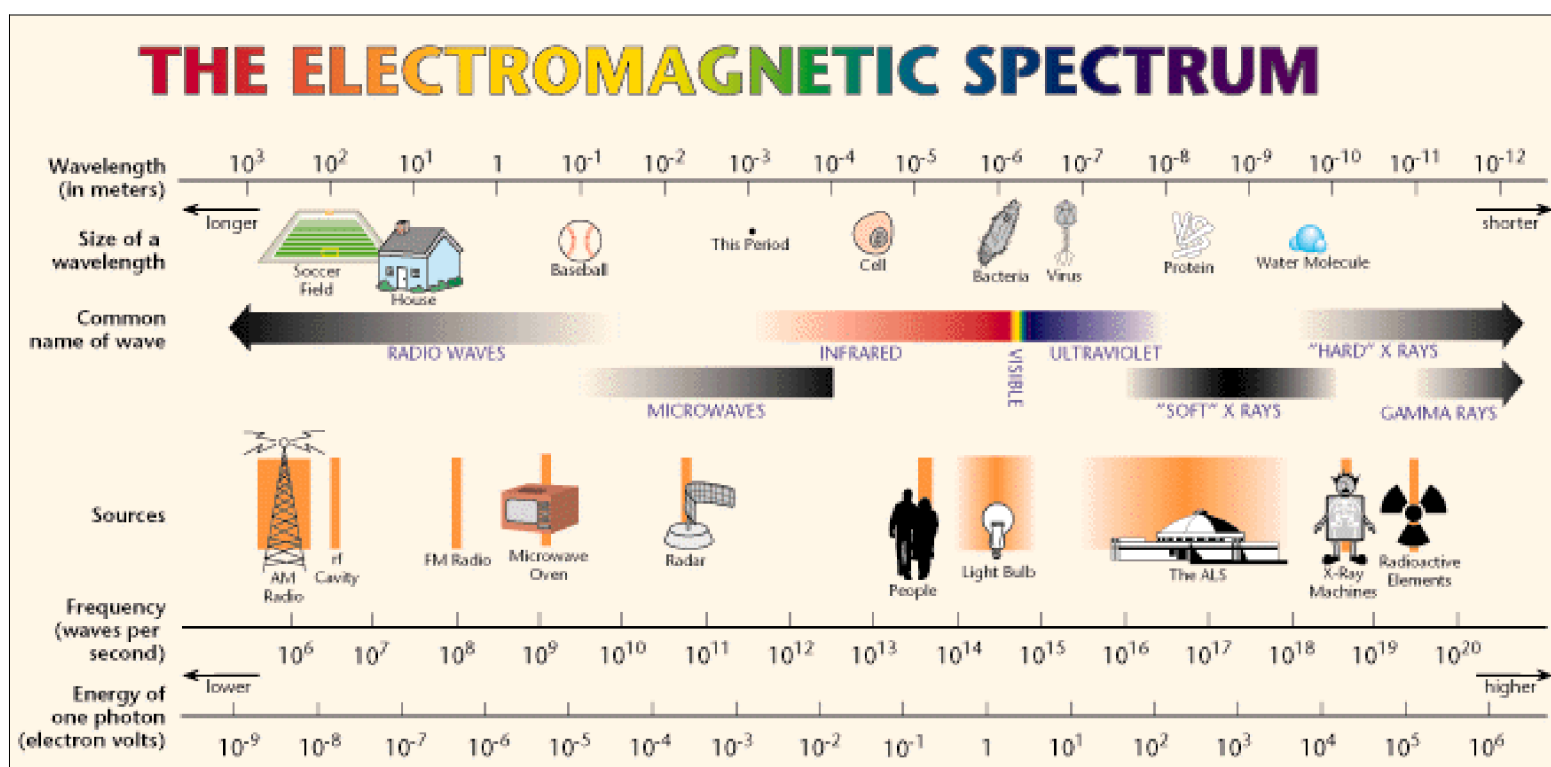


Figure 219: Illustration of the EMS ³⁰⁰²⁾

Allocation of frequency bands in the microwave region:

The frequency bands used for space radiocommunications and SAR applications are often denoted by various letters such as C–band, L–band, S–Band, etc. This practice of denoting frequency bands by letters has its origin in early radar (radio detecting and ranging) applications. Table 173 shows the standard letter designations for radar frequency bands of

3002) <http://www.jbl.gov/MicroWorlds/ALSTool/EMSpec/EMSpec2.html>

ASPRS (American Society for Photogrammetry and Remote Sensing) and of IEEE (Institute of Electrical and Electronic Engineers). There are many more definitions around, depending on author or institute.

The following comments pertain to Table 173:

- The official ITU designation for UHF extends from 300 to 3,000 MHz. In radar practice, however, the upper limit is usually taken as 1,000 MHz with the L– and S–band being used to describe the higher UHF region.
- The radar UHF band is sometimes called the P–band. Note: The WRC–03 (World Radio Conference 2003) provided a new allocation for **P–band SAR applications in the 432–438 MHz frequency range**.
- The designation “mm–band” is derived from “millimeter wave radar”, and is also used to refer to V– and W–bands, when general information relating to the region above 40 GHz is to be conveyed.
- The sub–mm band designation of 0.1 mm – 1 mm (radar) is almost identical to the FIR (Far Infrared) region of 30 μm – 1000 μm (telescope) in the optical spectrum. This is because for some people the FIR region ends at 100 μm , and the region between 100 μm and 1 mm (1000 μm) is referred to as the ‘sub–millimeter’ region.

The ASPRS radar band designations can also be found in the following reference: “Principles & Applications of Imaging Radar,” 1998, edited by Floyd M. Henderson & Anthony J. Lewis, published by ASPRS in cooperation with John Wiley & Sons, Inc., p. 138, ISBN: 0–471–29406–3. The book is volume 2 of the 3rd edition (series): Manual of Remote Sensing.

Radar Band	Wavelength Range	Frequency Range			
P–band	136 – 77 cm	220 – 390 MHz			
UHF	100 – 30 cm	300 – 1 GHz	Radar Band	Wavelength Range	Frequency Range
L–band	30 – 15 cm	1 – 2 GHz	L–band	30 – 15 cm	1 – 2 GHz
S–band	15 – 7.5 cm	2 – 4 GHz	S–band	15 – 7.5 cm	2 – 4 GHz
C–band	7.5 – 3.75 cm	4 – 8 GHz	C	7.5 – 3.75 cm	4 – 8 GHz
X–band	3.75 – 2.4 cm	8 – 12.5 GHz	X	3.75 – 2.5 cm	8 – 12 GHz
Ku–band	2.4 – 1.67 cm	12.5 – 18 GHz	Ku	2.5 – 1.67 cm	12 – 18 GHz
K–band	1.67 – 1.18 cm	18 – 26.5 GHz	K	1.67 – 1.11 cm	18 – 27 GHz
Ka–band	1.18 – 0.75 cm	26.5 – 40 GHz	Ka	1.11 – 0.75 cm	27 – 40 GHz
V–band		40 – 75 GHz	V	0.75 – 0.40 cm	40 – 75 GHz
W–band		75 – 110 GHz	W	0.40 – 0.275 cm	75 – 110 GHz
			mm–band	2.75 – 1.0 mm	110 – 300 GHz
			Sub–mm–band	1.0 – 0.1 mm	300 – 3000 GHz
ASPRS Definitions			IEEE Definitions		

Table 173: Radar band letter designations of ASPRS and IEEE

Radio Wave Propagation: Electromagnetic waves propagate in space at the speed of light (c), approximately 300,000 km/s. The wave amplitude varies periodically in time with frequency (f) measured in periods per second (Hz). The distance from crest to crest is the wavelength (λ), measured in meters. The relationship between these three parameters is: $f = c/\lambda$

Radio waves with frequencies of the order of 1 megahertz (MHz) can be reflected by the ionized atmosphere, or refracted when entering or coming out of these ionospheric layers,

or even attenuated when crossing them. These effects, which influence the ray path, depend on the wavelength (or frequency), and the angle of incidence. Thus, radio messages can be sent to considerable distances, over the horizon and to the antipodes. Yet, some frequency limitations remain; the highest frequencies are not reflected at all. This last property makes space telecommunication possible. However, at the higher frequencies, radiation is affected by the atmospheric particles and molecules encountered, such as ice, rain drops, water vapor, and oxygen.

Relevance of spaceflight:

What makes satellite observation missions so valuable and powerful is the absence of the atmosphere in orbit, and consequently the **availability of the entire electromagnetic spectrum (EMS)** into the observation direction toward outer space. This fact is making spaceborne spectroscopy a very powerful tool for all astronomic observations. Naturally, the entire EMS is also available into the direction toward Earth, but only to the top of the atmosphere in its entirety.³⁰⁰³⁾

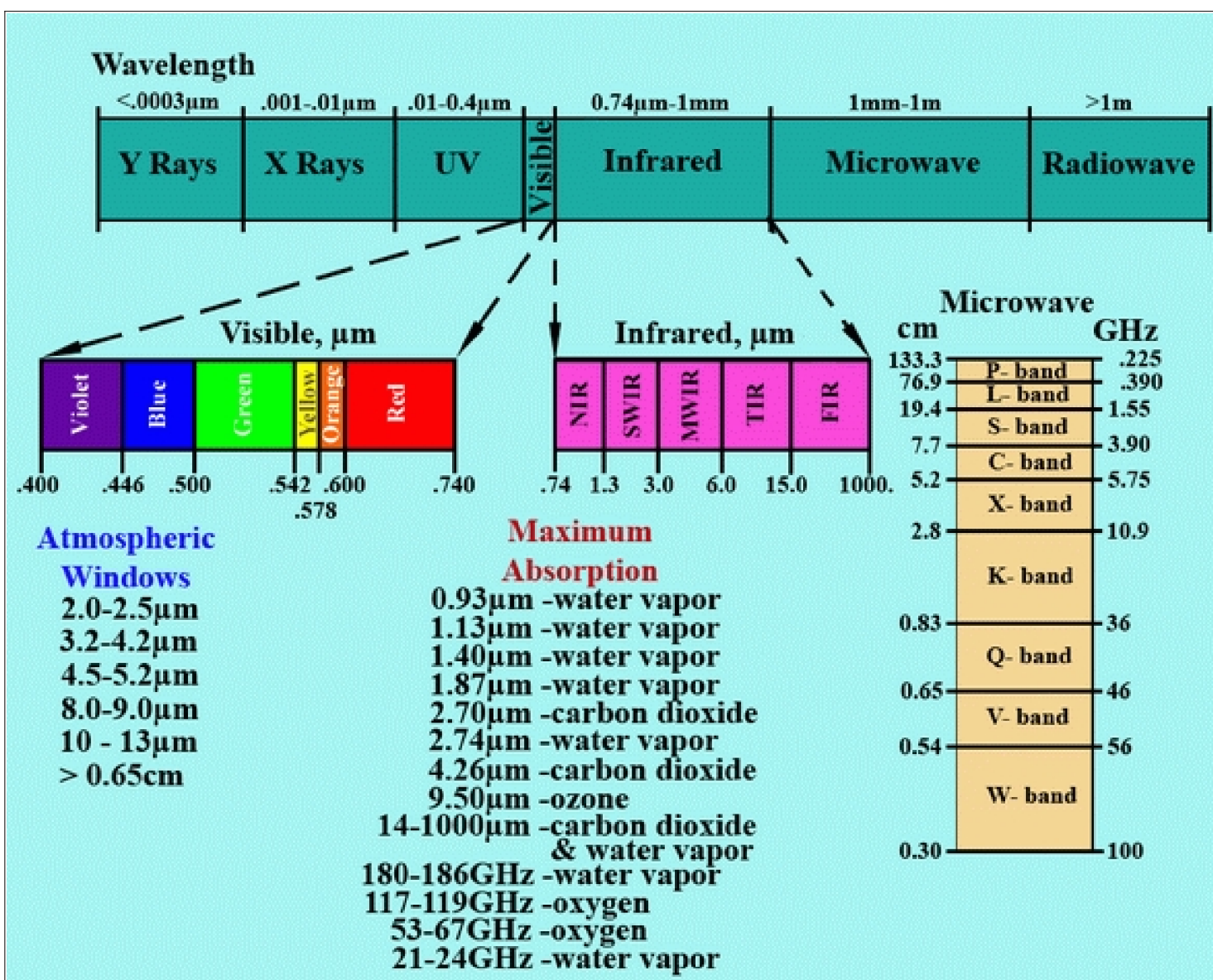


Figure 220: EMS, atmospheric windows and wavelengths of maximum absorption in the atmosphere³⁰⁰⁴⁾

3003) <http://www.astro.uiuc.edu/~jkaler/sow/spectra.html#visual>

3004) <http://cearac.poi.dvo.ru/en/services/support/>

The Earth's atmosphere plays an important filter role for all incoming radiation, selectively controlling the passage towards the Earth's surface of the various components of solar radiation. In the course of penetration through the atmosphere, some of the incoming radiation is either absorbed or scattered in all directions by atmospheric gases, vapors, and dust particles (aerosols).

In Earth observation missions, emission/absorption lines are being used to monitor the terrestrial atmosphere. Spectral regions of high transmittance in the EMS are referred to as atmospheric transmission bands or as **atmospheric windows**. The visible spectrum, a very tiny portion of the EMS, is the dominant band for surface imagery. But atmospheric windows are of great importance for passive surface observations in the infrared region as well as in the microwave region.

Figure 221 provides a general overview of the EMS penetration into Earth's atmosphere. The range of radio and microwave radiation, representing the low energy radiation as well as visible light and some infrared radiation, penetrate the atmosphere almost in total. This is not the case for high energy radiation in the UV, X-ray and gamma-ray ranges which are being absorbed by the higher layers of the atmosphere.

However, due to some atmospheric absorption, radio astronomy has gone from ground to space, especially in the millimeter and sub-millimeter wave radio astronomy. An example is the SWAS (Submillimeter Wave Astronomy Satellite) mission of NASA with a launch on Dec. 5, 1998

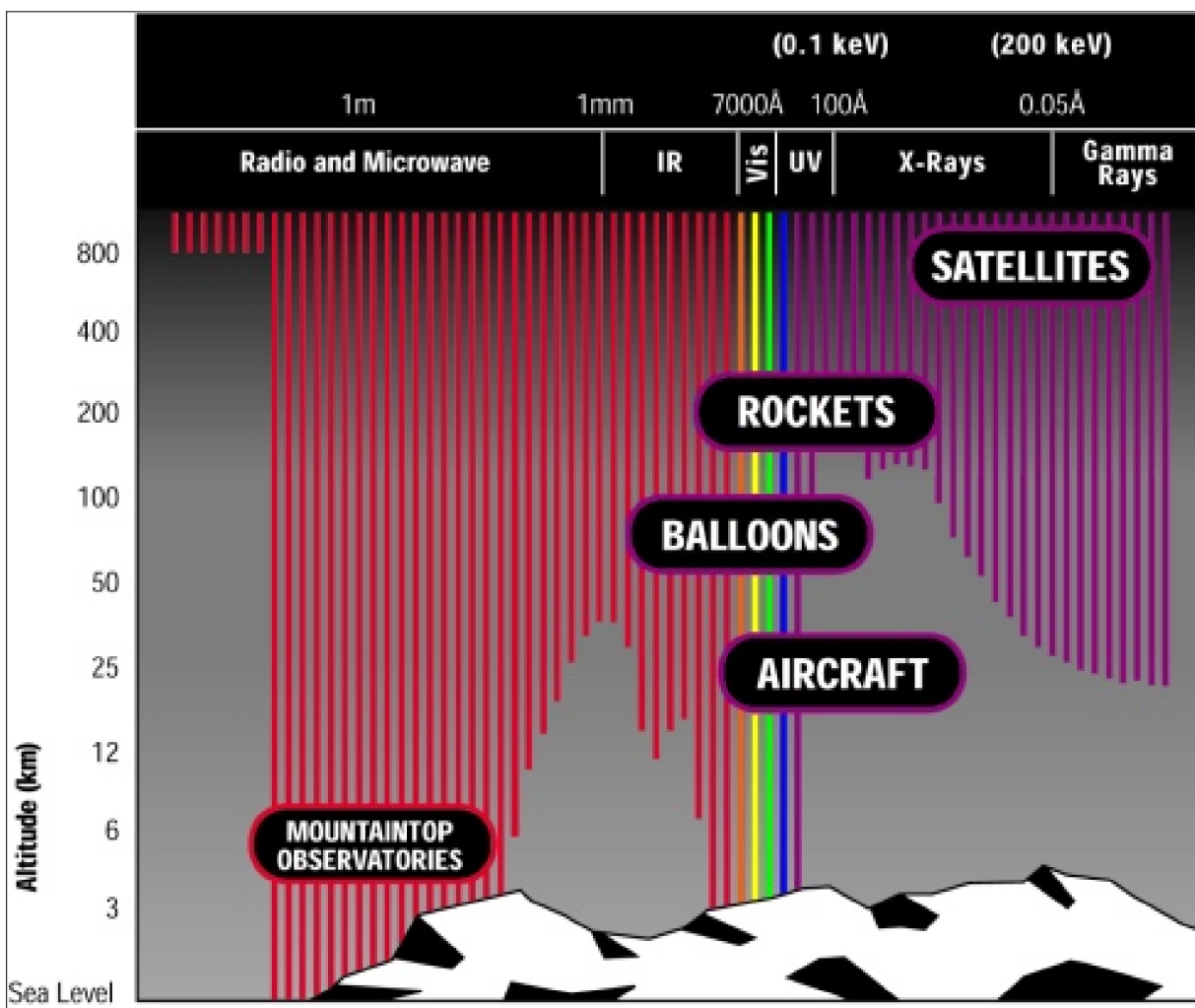


Figure 221: Penetration pattern of incoming EMS radiation into Earth's atmosphere (image credit: Harvard University)

1.32 Launch table of EO missions

The following table contains the “EO” missions (in alphabetical order according to mission acronym) that were launched after the 3rd edition was published in early 1996. Excepted are Shuttle launches and GPS/GLONASS launches, each of these series has its own launch table in this volume. There is no claim for completeness.

Note: EO missions were added gradually that took place prior to 1996 to obtain a better overview of various satellite series.

Mission	Launch Date	Comment
ACE	Aug. 25, 1997	Advanced Composition Explorer, NASA/GSFC
ACRIMSAT	Dec. 21, 1999	NASA minisatellite to monitor the amount of total solar energy
ACTS	Sept. 12, 1993	ACTS (Advanced Communications Technology Satellite) of NASA, launch on STS-51 mission. The objective was to demonstrate Ka-band communications. Deactivation on Apr. 28, 2004
ADEOS	Aug. 17, 1996	Advanced Earth Observing Satellite, JAXA (formerly NASDA)
ADEOS-II, FedSat, μ LabSat WEOS	Dec. 14, 2002	JAXA satellite on H-IIA launcher from TNSC; Secondary payloads: FedSat of Australia, μ-LabSat of JAXA, Japan and WEOS (Whale Ecology Observation Satellite) of the Chiba Institute of Technology, Japan
AEHF-1	Aug. 14, 2010	Launch of USA-214 or AEHF-1 [Advanced EHF (Extremely-High Frequency)] communication satellite of USAF from Cape Canaveral FL on Atlas-5-531 vehicle (launch mass of 6168 kg)
AEHF-2	May 04, 2012	Launch of USA-246 (AEHF-3), a communication satellite of the USAF from Cape Canaveral, FL, on Atlas-5-531 vehicle into GEO
AEHF-3	Sept. 18, 2013	Launch of USA-235 (AEHF-2), a communication satellite of the USAF from Cape Canaveral, FL, on Atlas-5-531 vehicle into GEO (launch mass of 6168 kg). Use of A2100 spacecraft bus of Lockheed Martin.
AGILE (ASI) AAM (Advanced Avionics Module)	Apr. 23, 2007	Launch of an Italian astronomical satellite, 352 kg S/C, (detection of gamma ray bursts) into LEO by the PSVL vehicle of ISRO (first commercial launch of ISRO)
AIM (Aeronomy of Ice in the Mesosphere)	Apr. 25, 2007	Launch of a NASA minisatellite (210 kg) on a Pegasus-XL vehicle from VAFB, CA
ALEXIS	Apr. 25, 1993	A minisatellite technology demonstration mission of LANL, USA, Pegasus air launch
ALOS/Daichi	Jan. 24, 2006	JAXA L-SAR satellite on H-IIA launcher from TNSC, Japan
ALOS-2/Daichi-2 Secondary payloads: Rising-2 UNIFORM-1 SOCRATES SPROUT	May 24, 2014	JAXA L-SAR satellite on a H-IIA F24 launcher from TNSC, Japan Microsatellite of Tohoku University and Hokkaido University Microsatellite of Wakahaya University Microsatellite of NICT Nanosatellite of Nihon University
AlphaSat/InmarsatI-XL Secondary payload: INSAT-3D	July 25, 2013	Launch AlphaSat/InmarsatI-XL a technology/communication satellite of ESA/Inmarsat Plc. London on Ariane-5 ECA from Kourou (first Alphabus of Europe). A GEO weather satellite of ISRO (mass of 2100 kg)
AlSAT-1 (SSTL/CNTS) Mozhayets (Russia) Rubin-3-DSI (OHB Bremen)	Nov. 28, 2002	Algerian Satellite-1 (of CNTS cooperative venture SSTL, UK, first S/C of the DMC (Disaster Monitoring Constellation) series, launch from Plesetsk, Russia on a Cosmos-3M vehicle. AlSat-1 is a secondary payload to Mozhaetz (or Mozhayets), a geodesy microsatellite mission designed by students of the Mozhaiskiy Military Space Engineering Academy, St. Petersburg, and built by NPO-PM. The payload contains a GLONASS/GPS receiver, a particle detector, and an amateur radio payload.
AMSAT-3D	Nov. 15, 2000	AMSAT-3D is an amateur satellite (AO-40), launched aboard an Ariane vehicle from Kourou, French Guiana

Mission	Launch Date	Comment
Antares maiden flight Secondary payloads: PhoneSat-1.0 (2) PhoneSat-2.0 Dove-1	Apr. 21, 2013	Launch of OSCs new Antares vehicle with a Cygnus capsule mass simulator (~ 3800 kg) from the Wallops Flight Facility, Wallops Island, VA (NASA COTS program). Two 1U CubeSats, technology demonstrations of NASA/ARC A 1U CubeSat, technology demonstration of NASA/ARC A nanosatellite (5.5 kg) of Cosmogia Inc. Sunnyvale, CA
Aqua (EOS/PM-1)	May 04, 2002	NASA satellite on Delta-2 launcher from VAFB
ARGOS	Feb. 23, 1999	DoD technology satellite, launch from VAFB
Arkon-2 (Kosmos 2344)	July 25, 2002	Russian military high-resolution (1 m) optoelectronic reconnaissance mission. Launch from Baikonur on a Proton launch vehicle. Mass: 2,600 kg. orbit: 1,506 km x 1,774 km, inclination = 63.5°
ARTEMIS	July 12, 2001	ESA communication/technology spacecraft, Ariane-5 launch
ASTRID-2	Dec. 10, 1998	Swedish solar-terrestrial energy transport mission (IRF-K)
Astro-E	Feb. 10, 2000	ISAS astronomy X-ray mission with XRS of NASA as prime instrument, launch on M-5 vehicle from Kagoshima island, Japan (launch failure of first stage)
Astro-E2 (Suzaku) TSD	July 10, 2005	JAXA astronomy X-ray mission, launch on M-5 vehicle from Kagoshima island, Japan (launch mass of 1,680 kg) Secondary payload (Tokyo Tech Separation system Demonstration), a CubeSat deployer, of Tokyo Institute of Technology
Astro-F (Akari, meaning 'light') CUTE-1.7	Feb. 21, 2006	JAXA/ISAS infrared astronomy satellite with a cooled telescope of 67 cm aperture diameter; launch site: Uchinoura Space Center, Japan. - The CUTE-1.7 CubeSat of the Tokyo Institute of Technology, Tokyo was a secondary payload on this flight. SSO (Sun-synchronous orbit) of Astro-F at 745 km altitude.
ATV-1 (Jules Verne)	Mar. 09, 2008	Launch of the ESA ATV-1 (Automated Transfer Vehicle-1) on an Ariane-5 launch vehicle from Kourou - destination: ISS
ATV-2 (Johannes Kepler)	Feb. 16, 2011	Launch of ESA vehicle ATV-2 from Kourou on Ariane-5 to ISS, cargo mass ~ 20,000 kg - destination: ISS (service flight)
ATV-3 (Edoardo Amaldi)	Mar. 23, 2012	Launch of ESA vehicle ATV-3 from Kourou on Ariane-5ES to ISS, cargo mass 20,000 kg - destination: ISS (service flight)
ATV-4 (Albert Einstein)	June 5, 2013	Launch of ESA vehicle ATV-4 from Kourou on Ariane-5ES to ISS, cargo mass 20,190 kg - destination: ISS (service flight)
Aura	July 15, 2004	NASA mission (EOS-Chem) on Delta-2 7920 vehicle from VAFB
Bion-M1 Secondary payloads: BEESAT-2 and -3 SOMP OSSI-1 Dove-2 AIST-2(Aist means 'stork' in Russian)	Apr. 19, 2013	Russian spacecraft with biological and medical payloads of Russia and an international community. Launch on Soyuz-2.1b vehicle from Baikonur, Kazakhstan. Two 1U CubeSats of TU Berlin, Germany A 1U CubeSat of TU Dresden, Germany An amateur radio CubeSat by the Korean artist Song Hojun A 3U CubeSat of Cosmogia Inc., Sunnyvale, CA, USA A microsatellite (39 kg) designed by the Samara Aerospace University and built by TsSKB-Progress, Samara, Russia.
BNTS-1	Oct. 31, 2000	BeiDou Navigation Test Satellite-1, experimental navigation S/C of China, in GEO at location of 140° E
BNTS-1B	Dec. 21, 2000	Launch of 2nd spacecraft with a Long March 3A from Xichang
CALIPSO CloudSat	Apr. 28, 2006	NASA/CNES mission. Launch on a Delta-2 vehicle from VAFB, CA. The co-passenger payload was CloudSat.
CartoSat-1 (IRS-P5)	May 05, 2005	ISRO, PSLV launcher from SHAR, along with HamSat (VUSat) of AmSat India as secondary payload
CartoSat-2	Jan. 10, 2007	ISRO high-resolution imaging mission, Launch on PSLV-7 vehicle from SDSC Sriharikota Range, India, along with SRE-1, LAPAN-TUBSAT, and PehuenSat-1 (Argentina).

Mission	Launch Date	Comment
CartoSat-2A IMS-1 CanX-2, AAUSat-2, Cute-1.7+APD-2 Compass-1, Delfi-C3, SEEDS-2 NTS Rubin-8-AIS	April 28, 2008	Indian military high-resolution imaging mission, built by ISRO Indian Microsatellite-1 of ISRO (83 kg) Triple CubeSat of UTIAS/SFL, Toronto, Canada (3.5 kg) CubeSat of Aalborg University, Denmark Double CubeSat, Tokyo Institute of Technology, Tokyo, Japan CubeSat of the University of Aachen, Germany Triple CubeSat, Technical University of Delft, The Netherlands CubeSat (3 kg) of Nihon University, Japan Nanosatellite of Com Dev / UTIAS/SFL, Toronto, Canada Nanosatellite of OHB-System, Bremen, Germany
CartoSat-2B AISat-2A AISSat-1 StudSat TISat-1	July 12, 2010	ISRO high-resolution imaging mission, Launch on PSLV-7 vehicle from SDSC Sriharikota Range, India, Secondary payloads: High-resolution imaging mission of Algeria (116 kg) Nanosatellite of Norway (6.5 kg) built by UTIAS/SSL, Toronto Student Satellite, nanosatellite built by several Indian Universities CubeSat developed by SUPSI (University of Applied Sciences of Southern Switzerland), Lugano-Manno
CASSIOPE Secondary payloads: CUSat-1, CUSat-2 DANDE POPACS	Sept. 29, 2013	Launch of CASSIOPE minisatellite of CSA on a Falcon-9 V1.1 from VAFB, CA, orbit of 320 km x 1500 km, inclination = 80° Microsatellites (each 41 kg) of Cornell University, Ithacy, N.Y. Microsatellite (~ 50 kg) of the University of Colorado, Boulder Three passive spheres, collaborative nanosatellite project of universities (Drexel, MSU, Univ. of Arkansas, Morehead, etc.)
CBERS-1 (ZY-1 FM1) SACI-1	Oct. 14, 1999	First Chinese/Brazil imaging mission. Launch on a CZ-4B vehicle from the Taiyuan Satellite Launch Center, China SACI-1 (Satélite de Aplicações Científicas) is a secondary payload (microsatellite, 80 kg) of Brazil to study near Earth plasma.
CBERS-2 (ZY-1 FM2)	Oct. 21, 2003	China (CAST)/Brazil (INPE) mission, ZY-1B (Resource), also called CBERS-2, launch from Taiyuan on a CZ-4B vehicle, along with CX-1 (Chuang Xin-1)
CBERS-2B (ZY-1-FM2B)	Sept. 19, 2007	China (CAST)/Brazil (INPE) mission on a CZ-4B vehicle from the Taiyuan Satellite Launch Center in China
CBERS-3	Dec. 09, 2013	China (CNSA)/Brazil (INPE) mission on a CZ-4B vehicle from the Taiyuan Satellite Launch Center in China, launch failure
CGRO (NASA)	Apr. 05, 1991	The Compton Gamma Ray Observatory was launched on Atlantis STS-37 from KSC. With 17, 000 kg, it was the heaviest astrophysical payload flown so far.
CHAMP	July 15, 2000	Challenging Minisatellite Payload (GFZ/DLR)
Chandra X-ray Observatory	July 23, 1999	The NASA Chandra X-ray Observatory was launched on shuttle flight STS-93 (Columbia) from Cape Canaveral, FLA
Chandrayaan-1	Oct. 22, 2008	Moon mission of ISRO. Launch on the PSLV-C11 vehicle from the Satish Dhawan Space Centre (SHAR) in Sriharikota, India
Chang'e-1	Oct. 24, 2007	Launch of the Chinese moon mission of CNSA, Chang'e, on a Long March 3A launch vehicle from the XSLC (Xichang Satellite Launch Center), Sichuan Province, China. Note: Chang'e-1 successfully concluded its mission on March 1, 2009 when it impacted on the surface of the moon.
Chang'e-2	Oct. 01, 2010	Launch of the Chinese moon mission of CNSA, Chang'e-2, on a Long March 3C launch vehicle from XSLC, Sichuan, China.
Chang'e-3	Dec. 01, 2013	Launch of the Chinese moon mission of CNSA, Chang'e-3, on a Long March 3B launch vehicle from XSLC, Sichuan, China. First Chinese soft-landing mission of the moon.
Chibis-M	Oct. 30, 2011	Microsatellite of IKI (Moscow) to study space weather. Launch on Progress-M-13M resupply vehicle to ISS. In late Jan. 2012, lift and deployment of Chibis-M into an orbit of 480 km during the return flight of Progress-M.

Mission	Launch Date	Comment
China DMC+4 TopSat SSETI Mozahayets-5 Sinah-1 UWE-1 NCube-2 Xi-V Rubin-5	Oct. 27, 2005	Multiple launch of micro- and picosatellites on a Cosmos-3M vehicle from Plesetsk, Russia Referred to as Beijing-1 , 140 kg EO satellite for DMC of SSTL EO satellite (108 kg) of QinetiQ, UK European student satellite (80 kg, coordinated at ESA) Russian Geodesy, Education, Amateur Radio S/C (64 kg) Iranian Research Organization for Science & Technology (20 kg) CubeSat of U. of Würzburg, released from SSETI (1 kg) CubeSat of Norsk Romsenter, Norway, released from SSETI CubeSat of U. of Tokyo, Japan, released from SSETI Messaging and Science S/C of OHB, Bremen, Germany
CloudSat CALIPSO	Apr. 28, 2006	A NASA/CSA mission. Launch on a Delta-2 from VAFB, CA; The co-passenger payload was CALIPSO.
Clementine	Apr. 25, 1994	DoD/NASA joint lunar mission. Launch on a Titan-2G from VAFB, CA
Cluster-1	June 04, 1996	ESA, launch failure (4 spacecraft)
Cluster-2	July 16, 2000 Aug. 09, 2000	ESA, two S/C were launched at a time ESA, two S/C were launched at a time
C/NOFS	April 16, 2008	Launch of a US minisatellite mission undertaken within the Space Test Program (STP) of DoD on a Pegasus-XL vehicle from the Kwajalein Atoll, Republic of the Marshall Islands. C/NOFS is designed to demonstrate the monitoring and forecasting of the ionospheric scintillation in real-time and on a global scale.
COMPASS-1	Dec. 10, 2001	Microsatellite of IZMIRAN, Russia; Secondary payload to Meteor-3M-1; COMPASS-1 experienced uncontrolled behavior
COMPASS-2	May 26, 2006	IZMIRAN microsatellite, Russia, Launch on a nuclear-powered submarine in the Barents Sea
COMS-1 ArabSat-5A	June 26, 2010	Launch of KARI's (Korea's) Communications, oceanography and meteorological satellite from Kourou on Ariane-5 ECA, (GEO) Launch of Saudi Arabian communication satellite (primary payload) into GEO. Ttotal payload mass of 8393 kg (both S/C).
CONTOUR	July 03, 2002	NASA S/C on a Delta 7425 launcher from KSC
Coriolis (P98-2)	Jan. 06, 2003	NRL-IPO satellite (with WindSat payload), launch with Titan-2 from VAFB
Coronas-I	Mar. 02, 1994	Russian and NKAU (Ukraine) solar physics mission
Coronas-F	July 31, 2001	Russian and NKAU (Ukraine) solar physics mission
CoRoT	Dec. 27, 2006	CNES-led astronomy mission, launch on a Soyuz-Fregat vehicle from Baikonur, Kazakhstan (detection of exoplanets). Note: On Nov. 2, 2012, the CoRoT mission experienced a computer failure. CNES announced in June 2013 that the mission has been retired.
COSMO-SkyMed-1	June 08, 2007	Italian SAR mission of ASI and the Italian Ministry of Defense. Launch from VAFB, CA, on a Delta-2 vehicle. This represents the launch of the first S/C of a four S/C constellation.
COSMO-SkyMed-2	Dec. 09, 2007	Launch from VAFB, CA, on a Delta-2 vehicle of ULA
COSMO-SkyMed-3	Oct. 25, 2008	Launch from VAFB, CA, on a Delta-2 vehicle of ULA
COSMO-SkyMed-4	Nov. 6, 2010	Launch from VAFB, CA, on a Delta-2 vehicle of ULA
CRISTA-SPAS-2	Aug. 07-19, 1997	STS-85
CryoSat	Oct. 08, 2005	ESA Earth Explorer Opportunity Mission-1 from Plesetsk, Russia, launch failure of Rockot-KM due separation problems between 2nd and 3rd stages
CryoSat-2	Apr. 08, 2010	ESA follow-on mission of CryoSat from Baikonur, Kazakhstan on a Dnepr vehicle.

Mission	Launch Date	Comment
CubeSats (14) Belka (250 kg), Baumanets (80 kg), UniSat-4 (12 kg) PicPot (3 kg)	July 26, 2006	Launch of smallsats on a Dnepr-1 launch vehicle from Baikonur, Kazakhstan, launch failure after 2 minutes of flight . The following CubeSats were flown: ION (U. of Illinois), Sacred (U. of Arizona), KUTESat (Kansas U.), ICEcube-1, -2 (Cornell U.), Rincon (U. of Arizona), SEEDS-1 (Nihon U.), HAUSat-1 (Hankuk Av. U.), nCube-1 (Norsk Romsenter), Merope (Montana St. U.), AeroCube-1 (Aerospace Corp.), PolySat-1, -2 (CalPoly), and Voyager (U. of Hawaii); additional smallsats on the flight were: Belka (RKK Energia), Baumanets (NPO Mash), UniSat-4 (U. of Rome), and PicPot (U. of Torino)
CubeSats (7) EgyptSat-1 SaudiSat-2 SaudiComsat-3, -4, -5, -6, and -7	April 17, 2007	Launch of 14 smallsats on a Dnepr-1 launch vehicle from Baikonur, Kazakhstan. Seven CubeSats were flown: PolySat-3 and PolySat-4 of CalPoly; AeroCube-2 of The Aerospace Corporation; CSTB1 of the Boeing Company; CAPE-1 of the University of Louisiana; MAST of Stanford and TUI; and Libertad-1 of the University of Sergio Arboleda, Columbia
CUTE-1.7	Feb. 21, 2006	CUTE-1.7 is a secondary payload (CubeSat) of the Tokyo Institute of Technology, Tokyo, Japan; launched on an M-5 vehicle from the Uchinoura Space Center, Japan. The prime payload on this flight was Astro-F (960 kg) of JAXA/ISAS
Cygnus-1	Sept. 18, 2013	Launch of OSC/NASA maiden flight of Cygnus-1, COTS demonstration flight on Antares 110 vehicle - from MARS (Mid-Atlantic Regional Spaceport) on Wallops Island, VA.
Cygnus CRS Orb-1 Secondary payloads: ArduSat-2 LituanicaSat-1 LitSat-1 SkyCube UAPSat-1 Flock-1 constellation	Jan. 09, 2014	Launch of OSC CRS-1 (Cargo Resupply Mission-1), contracted by NASA, to the ISS. CRS-1 is loaded with 1261 kg of supplies for the ISS. Also 23 students experiments. 34 CubeSats, commercially transported payloads by OSC: 2U CubeSat (2 kg), a crowd-funded project of NanoSatisfi LLC 1U CubeSat of KTU (Kaunas University of Technology), Kaunas 1U CubeSat of LSF (Lithuanian Space Federation) 1U CubeSat, a crowd-funded project of Southern Stars Group 1U CubeSat of UAP, Lima, Peru 28 3U CubeSats of Planet Labs, San Francisco. All Flock-1 nanosatellites provide imagery with a resolution of 3-5 m.
Dawn (NASA)	Sept. 27, 2007	NASA mission to the asteroid belt (study of Ceres and Vesta), launch on a Delta-2925 vehicle from Cape Canaveral, FLA
DMC microsatellite constellation, SSTL STSat-1 Mozhayets-4 Rubin-4-DSI Larets (Russia)	Sept. 27, 2003	Multi-satellite launch on a Cosmos-3M vehicle from Plesetsk, Russia; Three S/C of SSTL's DMC constellation, consisting of BilSat-1 (Turkey), NigeriaSat-1 and UK-DMC; STSat-1 (formerly KAISTSat-4) of KAIST, Korea; Mozhayets-4 of Russia, Rubin-4-DSI of OHB-System, Germany, and Larets of Russia
DMC-2G constell. UK-DMC-2 Deimos-1 DubaiSat-1 AprizeSat-3, -4 NanoSat-1B	July 29, 2009	Multi-satellite launch on a Dnepr vehicle from Baikonur, Kazakhstan, Two S/C of SSTL's DMC 2nd generation constellation consisting of UK-DMC-2 and Deimos-1 (each 96 kg). DubaiSat-1 (EIAST) of UAE (United Arab Emirates), 190 kg AprizeSat-3, -4 of Aprize Satellite Inc (Argentina), 12 kg each NanoSat-1B of INTA, Spain (23.5 kg)
Deep Impact	Jan. 12, 2005	NASA comet mission. Launch of 601 kg S/C from Cape Canaveral on a Delta-2 vehicle. An Impactor of 371 kg slammed onto comet Temple-1 on July 4, 2005. - The Deep Impact mission ended in Sept. 2013 after JPL was unable to communicate with the spacecraft anymore.
Deep Space1 (DS1)	Oct. 24, 1998	DS1 is the first mission with ion propulsion, NASA/JPL
DEMETER SaudiSat-2 AMSat OE (Echo) LatinSat-C LatinSat-D SaudiComsat1 SaudiComsat2 UniSat-3	Jun. 29, 2004	Multiple launch of micro- and nanosatellites on Dnepr-LV vehicle from Baikonur CNES microsatellite (first of Myriade series); 125 kg (France) Science microsatellite of Riyadh Space Research Institute Amateur Radio nanosatellite of AmSat-NA (North America) Nanosatellite of Arize Satellite Argentina (12 kg) Nanosatellite of Arize Satellite Argentina (12 kg) Nanosatellite of Riyadh Space Research Institute (KACST) Nanosatellite of Riyadh Space Research Institute (KACST) Science nanosatellite of University of Rome, Italy (12 kg)
DMSP, 5D-2 F-12	Aug. 29, 1994	DoD/USAF meteorology satellite, launch from VAFB
DMSP, 5D-2 F-13	Mar. 24, 1995	DoD/USAF meteorology satellite, launch from VAFB

Mission	Launch Date	Comment
DMSP, 5D-2 F-14	Apr. 04, 1997	DoD/USAF meteorology satellite, launch from VAFB
DMSP, 5D-3 F-15	Dec. 12, 1999	launch aboard a Titan 2 rocket from VAFB, CA
DMSP, 5D-3, F-16	Oct. 18, 2003	DoD/USAF meteorology satellite, launch aboard a Titan 2 rocket from VAFB (launch mass of 1154 kg)
DMSP, 5D-3, F-17	Nov. 04, 2006	DoD/USAF meteorology satellite, launch aboard a Delta-4 (EELV) rocket from VAFB (launch mass of 1154 kg)
DMSP, 5D-3, F-18	Oct. 18, 2009	DoD/USAF meteorology satellite, launch aboard an Atlas-5 rocket of ULA from VAFB (launch mass of 1154 kg)
DMSP, 5D-3, F-19	Apr. 03, 2014	DoD/USAF meteorology satellite, launch aboard an Atlas-5 rocket of ULA from VAFB (launch mass of 1230 kg)
Dragon spacecraft	June 04, 2010	Dragon is a demonstration/qualification unit on the maiden flight of the Falcon-9 rocket of SpaceX from Cape Canaveral, FLA. This represents a milestone in the SpaceX commercial transportation effort (future launch service provision to the ISS).
Dragon C1 spacecraft (COTS 1 demonstration flight) Secondary payloads: SMDC-ONE Caerus/Mayflower QbX-1 (CubeSat Experiment-1) QbX-2 (CubeSat Experiment-2)	Dec. 08, 2010	SpaceX launched the Dragon space capsule into orbit (~ 300 km, I = 34.5°) and retrieved the capsule successfully after two orbits in the Pacific Ocean (launch site: Cape Canaveral, Falcon-9 launcher). For NASA, the PPP mission was of great significance for future flights to ISS. – Space and Missile Defense Command-Operational Nanosatellite Effect (nanosatellite of ~ 4.5 kg of US Army) – 1U CubeSat technology mission of USC+ 2U CubeSat of Northrop Grumman and Novaworks – 3U CubeSat Colony I bus of Pumpkin Inc. for NRO (National Reconnaissance Office) – 3U CubeSat, Colony I bus of Pumpkin Inc. for NRO, both CubeSats are technology missions
Dragon C2/C3	May 22, 2012	Launch of COTS 2 flight of Dragon of SpaceX from Cape Canaveral on a Falcon-9 vehicle. First visit of the Dragon capsule to the ISS on May 25 and delivery of supplies. Recovery of the capsule in the Pacific Ocean on May 31, 2012.
Dragon CRS-1	Oct. 08, 2012	Launch of SpaceX CRS-1 (Cargo Resupply Services-1) mission to the ISS. Launch site: Cape Canaveral. Splashdown in the Pacific on Oct. 28, 2012 (and recovery).
Dragon CRS-2	Mar. 01, 2013	Launch of the SpaceX CRS-2 mission to the ISS from Cape Canaveral, FL on Falcon-9 vehicle.
Dragon CRS-3 Secondary payloads: KickSat All-Star SporeSat TSAT PhoneSat-2.5	Apr. 18, 2014	Launch of the SpaceX CRS-3 mission to the ISS from Cape Canaveral, FL on Falcon-9v.1.1 vehicle. 3U CubeSat of Cornell University, deployment of 250 femtosats 3U CubeSat of COSGC (Colorado Space Grant Consortium) 3U CubeSat of NASA/ARC 2U CubeSat of Taylor University, Upland, Indiana 1U CubeSat of NASA/ARC
DRTS (Kodama)	Sept. 10, 2002	JAXA Data Relay Test Satellite-(90° E) from Tanegashima with H-IIA-F3 vehicle. The secondary payload was USERS (Unmanned Space Experiment Recovery System), a separate S/C
DS1 (Deep Space1)	Oct. 24, 1998	NASA technology demonstration mission, launch from Cape Canaveral on a Delta launcher. SEDSAT-1 as secondary payload
DSP-1 (TC-1)	Dec. 29, 2003	Launch of Double Star Project-1 of CNSA/ESA from Xichang
DSP-2 (TC-2)	July 26, 2004	Launch of Double Star Project-2 of CNSA/ESA from Taiyuan, China

Mission	Launch Date	Comment
DubaiSat-2, STSat-3 Secondary payloads: SkySat-1 WNISat-1 BRITE-PL-1 AprizeSat-7 & -8 UniSat-5 ICUBE-1 HumSat-D PUCPSat-1 Eagle-1, Eagle-2 Wren QBSout-1S Dove-3, Dove-4 Delfi-n3Xt Triton-1 CINEMA-2 & -3 CubeBug-2 GOMX-1 NEE-02 Krysaor FUNCube-1 HiNCube-1 ZACUBE-1 UWE-3 First-MOVE Velox-P2 OPTOS BPA-3	Nov. 21, 2013	Launch of Dnepr Cluster mission from Yasnıy Cosmodrome, Russia with the primary payloads DubaiSat-2 of EIAST and STSat-3 of KARI, Korea. A commercial imaging S/C (100 kg) of Skybox Imaging, CA, A nanosatellite (10 kg) of Axelspace, Tokyo, Japan A nanosatellite (7 kg) of SRC/PAS, Warsaw, Poland Two nanosatellites of AprizeSat, Argentina (SpaceQuest) A microsatellite (28 kg) of the University of Rome, Italy A CubeSat of PIST (Pakistan Institute of Space Technology) A CubeSat of the University of Vigo, Spain A 1U CubeSat of INRAS, Lima, Peru + Pocket-PUCP Two PocketQubs of Morehead State Uni. & Kentucky Space FemoSat (1U PocketQub) of StaDoKo UG, Aachen, Germany A 2.5U PocketQub of the University of Maryland Two 3U CubeSats of Cosmogia Inc., Sunnyvale, CA, USA A 3U CubeSat of TU Delft, The Netherlands A 3U CubeSat of ISIS-BV, The Netherlands 2 3U CubeSats of KHU (Kyung Hee University), Seoul, Korea A 2U CubeSat of Argentina A 2U CubeSat of GomSpace ApS of Aalborg, Denmark A 1U CubeSat of EXA (Ecuadorian Civilian Space Agency) A 1U CubeSat of AMSAT UK A 1U CubeSat of Narvik University College, Narvik, Norway A 1U CubeSat of CPUT, Cape Town, South Africa A 1U CubeSat of the University of Würzburg, Germany A 1U CubeSat of Technische Universität München, Germany A CubeSat of Nanyang Technological University, Singapore A 3U CubeSat of INTA, Madrid, Spain A S/C (Advanced Avionics Unit) of Hartron-Arkos, Ukraine
EarlyBird	Dec. 24, 1997	EarthWatch controllers lost contact with the S/C on Dec. 28, '97
EGS (Ajisai) JAS-1 (FUJI-1)	Aug. 12, 1986	Launch on the H-1 vehicle from TNSC, Japan (Geodetic S/C) Japan Amateur radio Satellite as secondary payload (50 kg)
EgyptSat-2	Apr. 16, 2014	Launch of high-resolution EgyptSat-2 (MisrSat-2) satellite (1050 kg) of NARSS (built by RSC Energia) on a Soyuz-U vehicle from Baikonur, Kazakhstan. Orbit of 700 km at 51.6°.
Electro-L / GOMS-2	Jan. 20, 2011	Geostationary weather satellite of Russia. Launch on a Zenith-2 vehicle from Baikonur, Kazakhstan, launch mass of ~1620 kg
ENVISAT	Mar. 01, 2002	ESA, Ariane-5 launch from Kourou (direct SSO launch)
EO-1	Nov. 21, 2000	Earth Observing-1 of NASA
Equator-S	Dec. 02, 1997	MPI Garching, DLR
EROS-A	Jan. 22, 1998	West Indian Space Ltd., Cayman Islands, Shavit launcher failure from Palmachim, Israel
EROS-A	Dec. 05, 2000	Commercial imagery of ImageSat International from Svobodny, Russia, on a Start-1 launch vehicle.
EROS-B	Apr. 25, 2006	Launch of commercial imaging satellite of ImageSat International on Start-1 launcher (350 kg) from Svobodny, Russia
ERS-1	July 17, 1991	ESA mission (launch mass of 2300 kg), Ariane-4, Kourou
ERS-2	Apr. 21, 1995	ESA mission (launch mass of 2300 kg), Ariane-4, Kourou
Etalon-1	Jan. 10, 1989	Geodetic mission of Russia (1415 kg). Launch from Baikonur along with two GLONASS spacecraft
Etalon-2	May 31, 1989	Geodetic mission of Russia (1415 kg). Launch from Baikonur along with two GLONASS spacecraft
ETS-VII	Nov. 27, 1997	Technology mission of JAXA (formerly NASDA), along with TRMM of NASA from Tanegashima, Japan
ETS-VIII	Dec. 18, 2006	Technology mission of JAXA. Launch on a H-2A vehicle from Tanegashima, Japan
FAISAT-2V	Sept. 24, 1997	Data collection, communication
FalconSat-1	Jan. 27, 2000	Microsatellite of US Air Force Academy. Launch on a Pegasus vehicle from VAFB, CA. FalconSat-1 experienced a power failure shortly after deployment
FalconSat-2	Mar. 24, 2006	Microsatellite of US Air Force Academy. Launch on Falcon-1 launch vehicle of SpaceX. Launch failure on maiden flight of Falcon-1 from the Kwajalein Atoll (Marshall Islands, Pacific)

Mission	Launch Date	Comment
FASat-Bravo	July 10, 1998	Microsatellite of Chile built by SSTL (secondary payload to RE-SURS-O-4)
FAST	Aug. 21, 1996	NASA/GSFC mission within SMEX
FedSat	Dec. 14, 2002	Australian satellite of CSIRO, secondary payload to ADEOS-II
Foton-M3	Sept. 14, 2007	ESA payload/experiments (400 kg, including YES2) on a Russian S/C. Launch from Baikonur, Kazakhstan (12 day mission).
FORTE	Aug. 29, 1997	Fast On-Orbit Recording of Transient Events, LANL, SNL
FY-1C	May 10, 1999	Feng-Yun-1C, China (along with SJ-5)
FY-1D, HY-1A	May 15, 2002	CAST (China), both S/C were launched from Taiyuan. FY-1 is a meteorological S/C in LEO. HY-1A (Haiyang-1/Ocean-1) is an ocean observation satellite.
FY-2A	June 10, 1997	Launch of GEO weather satellite of China (CASC)
FY-2B	June 26, 2000	Launch of GEO weather satellite of China (CASC)
FY-2C (Feng Yun-2C)	Oct. 19, 2004	Launch of GEO weather satellite of China on a CZ-3A vehicle from Xichang Launch Site, China
FY-2D	Dec. 8, 2006	Launch of GEO weather satellite of China on a CZ-3A vehicle from Xichang Launch Site, China
FY-2E	Dec. 23, 2008	Launch of GEO weather satellite of China on a CZ-3A vehicle from Xichang Launch Site, China (replacement for FY-2C)
FY-2F	Jan. 13, 2012	Launch of GEO weather satellite of China on a CZ-3A vehicle from Xichang Launch Site, China (replacement for FY-2C)
FY-3A	May 27, 2008	Launch of a LEO weather satellite of China (CNSA) on a LM-4C launch vehicle from the Taiyuan Launch Center
FY-3B	Nov. 04, 2010	Launch of a LEO weather satellite of China (CNSA) on a LM-4C launch vehicle from the Taiyuan Launch Center
FY-3C	Sept. 23, 2013	Launch of a LEO weather satellite of China (CNSA) on a LM-4C launch vehicle from the Taiyuan Launch Center
Gaia	Dec. 19, 2013	Launch of ESA space astrometry satellite on Soyuz-STB with Fregat upper stage from Kourou. Lissajous orbit to L2. The FPA of the camera has ~ 1 Gpixel (largest developed so far).
GCOM-W1 Secondary payloads: KOMPSAT-3 SDS-4 HORYU-2	May 17, 2012 (UTC)	Launch of GCOM-W1 (Shizuku) of JAXA from TNSC, Japan on the H-IIA vehicle Co-payload (980 kg) of KARI (Korea), high-resolution imaging Small Demonstration Satellite of JAXA (50 kg) Nanosatellite (7 kg) of KIT, Japan
Genesis-1	July 12, 2006	Technology demonstration flight of an inflatable S/C of Bigelow Aerospace. Launch on a Dnepr-1 vehicle from Yasny, Russia
Genesis-2	June 28, 2007	Technology demonstration flight of an inflatable S/C of Bigelow Aerospace. Launch on a Dnepr-1 vehicle from Yasny, Russia
GeneSat-1	Dec. 16, 2006	A CubeSat of NASA/ARC and various universities (a secondary payload to TacSat-2). Minotaur launch from Wallops Island, VA
Genesis	Aug. 08, 2001	NASA, Solar wind sample return mission
Genesis PFD-1	July 12, 2006	A privately built and financed habitable structure of Bigelow Aerospace (entrepreneur Robert Bigelow). It is intended to be available for research, manufacturing and other uses, including lodging for future space tourists. Launch on a Dnepr-1 vehicle from Dombrovsky Missile Site, Yasny (Siberia), Russia.
GF-1 (Gaofen-1) Secondary payloads: TurkSat-3USat NEE-01 Pegasus CubeBug-1	Apr. 26, 2013	Launch of the first high-resolution EO mission of China on a CZ-2D vehicle from the Jiuquan Launch Center. A 3U CubeSat (4 kg) of ITU (Istanbul Technical University) A 1U CubeSat of EXA (Ecuadorian Civilian Space Agency) A 2U CubeSat of INVAP, Argentina
GeoEye-1	Sept. 06, 2008	Launch of high-resolution imaging S/C of GeoEye (Dulles, VA) from VAFB, CA on a Delta-2 vehicle
GeoLITE	May 18, 2001	NRO technology demonstration mission (LaserCom, UHF communication payload), launch from Cape Canaveral on Delta-2
GEOS-1, Explorer 29	Nov. 06, 1965	NASA Geodetic S/C, launch from Cape Canaveral, FLA
GEOS-2, Explorer 36	Jan. 11, 1968	NASA Geodetic S/C, launch from VAFB, CA

Mission	Launch Date	Comment
GEOS-3	April 09, 1975	NASA Geodynamics Experimental Ocean Satellite, VAFB, CA
GEOS-1	April 20, 1977	ESA Geostationary Scientific Satellite, launch from Cape Canaveral, FLA
GEOS-2	July 14, 1978	ESA Geostationary Scientific Satellite, launch from Cape Canaveral, FLA
GEOSAT	Mar. 12, 1985	USN mission. Launch on Atlas-E vehicle from VAFB, CA
GFO-1	Feb. 10, 1998	GEOSAT follow-on Satellite, US Navy
GIOVE-A (GSTB-V2/A)	Dec. 28, 2005	Successful launch of the first European navigation satellite (Galileo In-Orbit Validation Element-A) from Baikonur, Kazakhstan, into MEO (Medium Earth Orbit), built by SSTL for ESA
GIOVE-B	April 27, 2008	Launch of the second experimental European navigation satellite from Baikonur, built by the ESNI consortium
GLAST (Fermi Gamma-Ray Telescope)	June 11, 2008	NASA astrophysics mission to study gamma rays. Launch on a Delta-2 vehicle from Cape Canaveral, FLA - Note: NASA renamed the GLAST mission to Fermi Gamma-ray Space Telescope as of August 26, 2008.
Glory Secondary Cube-Sats: Explorer 1 (PRIME) KySat-1 HERMES	Mar. 04, 2011	NASA Earth Climate and atmospheric mission, Launch on a Taurus-XL vehicle from VAFB, launch failure CubeSat of Montana State University CubeSat of Kentucky Space CubeSat of the University of Colorado at Boulder.
GOCE	Mar. 17, 2008	ESA geodynamics and geodetic mission. Launch on a Rocket vehicle from Plesetsk, Russia.
GOES-8 (I)	Apr. 13, 1994	GOES-8 was at 75° W, working nearly 9 years; as of Jan. 2004, GOES-8 is on standby in an inclined orbit, still potentially useful GOES-8 was deactivated in May 2004 and placed into a disposal orbit 350 km above its GEO position
GOES-9 (J)	May 23, 1995	GOES-I to -M S/C were built by SS/L; Deactivated in Aug. 1998, due to failing bearings in the momentum wheels. Since Apr. 2003, GOES-9 is providing backup service for GMS-5 of Japan
GOES-10 (K)	Apr. 25, 1997	NASA launch on Atlas-1 vehicle from Cape Canaveral
GOES-11 (-L)	May 03, 2000	NASA launch of NOAA weather satellite
GOES-12 (M)	July 23, 2001	NASA launch of NOAA weather satellite on Atlas-II vehicle from Cape Canaveral, FLA
GOES-13 (N)	May 24, 2006	NASA launch of NOAA weather satellite on a Delta-4 vehicle from Cape Canaveral Air Force Station, FLA
GOES-14 (O)	June 27, 2009	NASA launch of NOAA weather satellite on a Delta-4 vehicle from Cape Canaveral Air Force Station, FLA
GOES-15 (P)	Mar. 04, 2010	NASA launch of NOAA weather satellite on a Delta-4 vehicle from Cape Canaveral Air Force Station, FLA
Göktürk-2	Dec. 18, 2012	EO satellite (dual-use, civil, defense) of Turkey designed by TUBITAK and built by Turkish Aerospace Industries (TUSAS) for the Turkish Ministry of National Defense. Launch from Jiuquan Launch Center of China, Long March-2D vehicle. SSO of 686 km, Pan=2.5 m, MS=10 m, SWIR=20 m, Swath=20 km.
GOMS-1	Oct. 31, 1994	Geostationary weather satellite of Russia. Launch on a Proton vehicle from Baikonur, Kazakhstan, launch mass of 2400 kg
GOMS-2 / Electro-L	Jan. 20, 2011	Geostationary weather satellite of Russia. Launch on a Zenith-2 vehicle from Baikonur, Kazakhstan, launch mass of ~1620 kg

Mission	Launch Date	Comment
GPM Secondary payloads ShindaiSat STARS-2 TeikyoSat-3 ITF-1 OPUSat INVADER KSat-2	Feb. 27, 2014	Launch of a cooperative NASA-JAXA GPM (Global Precipitation Measurement) mission on a H2A launch vehicle from the Tanegashima Space Center, Japan. A microsatellite (35 kg) of Shinshu University to demonstrate LED light as an optical communications link over large distance. Nanosatellite of Kagawa University, Takamatsu, Kagawa, Japan A bioscience microsatellite (~ 20 kg) of Teikyo University A 1U CubeSat of the University of Tsukuba, Tsukuba, Japan. OPUSat (Osaka Prefecture University Satellite), a 1U CubeSat A 1U CubeSat of Tama Art University A CubeSat of Kagoshima University with a mass of ~ 1.5 kg
GOSAT /Ibuki Secondary payloads: SDS-1 (JAXA) SOHLA-1 SpriteSat PRISM Kagakaki KKS-1 STARS-1	Jan. 23, 2009	Greenhouse gases Observing Satellite of JAXA. Launch on H-IIA vehicle from TNSC, Japan, 1750 kg Small Demonstration Satellite-1 of JAXA, ~ 100 kg Space Oriented Higashiosaka Leading Association-1), 50kg Tohoku University, Japan (microsatellite of ~ 50 kg) Technology satellite of ISSL of the University of Tokyo, 5 kg SORUNSat-1, Japan, 20 kg Kouku Kosen Satellite-1 of Tokyo Metropolitan College, 3 kg Space Tethered autonomous Robotic Satellite-1 of Kagawa University, Japan, ~ 10 kg
GPS IIF-1	May 28, 2010	Launch on Delta-4 vehicle from Cape Canaveral, FL. The GPS IIF SV-1 S/C is the first of 12 GPS IIF S/C, built by Boeing. First to broadcast operational L5 signal. SVN 62.
GPS IIF-2	July 16, 2011	Launch on Delta-4 vehicle from Cape Canaveral, FL. SVN 63.
GPS IIF-3	Oct. 04, 2012	Launch on Delta-4 vehicle from Cape Canaveral, FL. SVN 65
GPS IIF-4	May 15, 2013	Launch on Delta-5 vehicle from Cape Canaveral, FL. SVN 66
GPS IIF-5	Feb. 21, 2014	Launch on Delta-5 vehicle from Cape Canaveral, FL. SVN 64
GPS IIF-6	May 17, 2014	Launch on Delta-4 vehicle from Cape Canaveral, FL. SVN 67
GRACE	Mar. 17, 2002	US-German dual-minisatellite mission (launch from Plesetsk)
GRAIL	Sept. 10, 2011	NASA dual-spacecraft mission to the moon, launch from Cape Canaveral, FLA on a Delta-2 vehicle.
Gravity Probe-A (GP-A)	June 18, 1976	Scout-D launch vehicle from Wallops Island, VA. The probe attained a ballistic (sub-orbital) flight path with an apogee of 10,000 km (measurement time of 1 hour 55 minutes).
Gravity Probe-B (GP-B)	April 20, 2004	GP-B is a NASA and Stanford University fundamental science mission, launch on a Delta-2 vehicle from VAFB, CA
GSAT-4	April 15, 2010	ISRO satellite with a Ka-band transponder and payload for a GPS-aided navigation system. Launch failure of the GSLV (Geostationary Satellite Launch Vehicle) on the maiden flight with the nation's first home-built cryogenic upper stage.
GSAT-14	Jan. 05, 2014	Launch of ISRO GSAT-14 communication satellite from Sriharikota into GTO by a GSLV Mk.II D5 rocket. <i>First successful flight of ISRO developed cryogenic engine.</i>
Helios-1A UPMSat-1	July 07, 1995	Military reconnaissance S/C of France, Italy and Spain, Ariane-4 Secondary payload (microsatellite, 47 kg) of UPM (Universidad Politécnica de Madrid), Spain
Helios-1B Clementine	Dec. 03, 1999	Military reconnaissance S/C of France, Italy and Spain, Ariane-4 launch, Clementine (built by SSTL) was a secondary S/C
Helios-2A, PARASOL (1) Essaim (4, "swarm" in French) NanoSat-01	Dec. 18, 2004	Launch of French (DGA) Helios-2A optical reconnaissance S/C as primary payload on Ariane-5 ECA from Kourou. Secondary payloads are five microsatellites using the Myriade bus: PARASOL of CNES + 4 Essaim eavesdropping S/C of DGA Experimental microsatellite (20 kg) of INTA, Spain
Helios-2B	Dec. 18, 2009	Launch of French (DGA) Helios-2B optical reconnaissance S/C on Ariane-5 ECA from Kourou. The S/C was produced by EADS Astrium with a mass of ~ 4200 kg. The imaging payload was built by TAS-I. The partner countries of France are: Belgium, Spain, Italy and Greece.

Mission	Launch Date	Comment
HEO-1 (SBIRS)	June 25, 2006	Launch of the 1st USAF SBIRS (Space-Based Infrared System) payload into a highly elliptical Molniya orbit (launch site: VAFB). Use: infrared event detection and reporting of ballistic missile launches. On Aug. 5, 2008, Lockheed Martin announced the successful on-orbit handover of HEO-1 to the USAF.
HEO-2 (SBIRS)	Mar. 13, 2008	Launch of the 2nd USAF SBIRS payload into a Molniya orbit (1112 km x 35,780 km) with an inclination of 63.6°.
Herschel (HSO) and Planck	May 14, 2009	Launch of two ESA spacecraft on Ariane-5 ECA (6000 kg total launch mass) from Kourou. Both spacecraft are on their way to L2 to operate from independent orbits (Lissajous and Halo, respectively)
HESSI (RHESSI)	Feb. 05, 2002	NASA solar physics mission, Pegasus XL launch
HJ-1A (Huan Jing) HJ-1B	Sept. 05, 2008	Launch of the first 2 S/C of the Environmental Protection & Disaster Monitoring Constellation (optical payloads) from TSLC (Taiyuan Satellite Launch Center), China
HJ-1C (Huan Jing-1C) NewTech-1, XY-1 HummerSat-1 HummerSat-1A	Nov. 18, 2012 Sec. payloads	Launch of HJ-1C (Environment-1C, 890 kg, CNSA) with SAR payload from TSLC on a CZ-2C vehicle New Technology Demonstration Satellite of CASC, also known as XY-1 (Xin Yan-1) A minisatellite (160 kg) of CAST, also known as Fengniao-1 A microsatellite (30 kg) of CAST, also known as Fengniao-1A
HST (Hubble Space Telescope)	April 24, 1990	NASA/ESA astronomy mission, launch on Space Shuttle Discovery (STS-31). Deployed into LEO, average altitude of 600 km, inclination of 28.5°
Inaugural flight of heavy lift launcher. HLVOLSDP 3CSat-1 (Sparkie) 3CSat-2 (Ralphie)	Dec. 21, 2004	Multiple launch of microsatellites on a Delta 4H/4050H vehicle (maiden flight) of Boeing from Cape Canaveral, FLA Demosat (dummy payload) of US Air Force (5993 kg) Technology demonstration of New Mexico State University Technology demonstration of University of Colorado, Boulder The 3CSat microsatellites did not reach the orbit. Demosat did not reach its intended geostationary orbit.
HTV-1 (Kounotori)	Sept. 10, 2009	Launch of H-II Transfer Vehicle-1 of JAXA to ISS. Reentry of HTV-1 in Nov. 2009
HTV-2	Jan. 22, 2011	Launch of HTV-2 of JAXA to ISS, cargo mass = 5300 kg
HTV-3 Secondary payloads: RAIKO FITSat-1 (Niwaka) We-Wish F-1 TechEdSat	July 21, 2012	Launch of HTV-3 of JAXA to ISS (on the H-IIB launch vehicle from Tanegashima, Japan), cargo mass of ~ 4,600 kg - A 2 kg CubeSat of Tohoku and Wakayama Universities, Japan - A 1U CubeSat of FIT (Fukuoka Institute of Technology) - A 1U CubeSat of Meisei Electric Company, Japan - A 1U CubeSat of FTP University, Hanoi, Vietnam - A 1U CubeSat of San Jose State University, CA, USA
HTV-4 Secondary payloads: TechEdSat-3 PicoDragon ArduSat-1 ArduSat-X	Aug. 3, 2013	Launch of HTV-4 of JAXA to ISS (on the H-IIB launch vehicle from Tanegashima, Japan), cargo mass of ~ 3,600 kg - A 3U CubeSat of NASA/ARC (Ames Research Center) - A 1U CubeSat of VNSC (Vietnam National Center) - A 1U CubeSat of NanoSatisfi Inc., San Francisco, CA, USA - A 1U CubeSat of NanoSatisfi Inc., San Francisco, CA, USA
HY-1A	May 15, 2002	China, HY-1A (Haiyang-1/Ocean-1) is an ocean observation S/C, launch from Taiyuan launch site in China
HY-1B	April 11, 2007	China, HY-1B was developed by DFH of CAST, launch from Taiyuan on an LM-2C vehicle
HY-2A (Haiyang-2A)	Aug. 15, 2011	CNSA of China, HY-2A was developed by DFH of CAST, launch from Taiyuan on a Long March-4B vehicle
HYLAS-1	Nov. 26, 2010	Communications Ka-band demonstration S/C of Avanti Communications and ESA (PPP project). Launch of Ariane-5 (along with Intelsat-17)
HYLAS-2	Aug. 02.2012	Launch of a communications Ka-band satellite of Avanti Communications Group PLC with Ariane-5 from Kourou. The co-passenger on this flight was the Intelsat-20 satellite.
IBEX	Oct. 19, 2008	Launch of NASA S/C from the Kwajalein Atoll in the Pacific Ocean. IBEX (Interstellar Boundary Explorer) will image & map the dynamic interactions taking place in the outer solar system

Mission	Launch Date	Comment
ICESat/CHIPSat	Jan. 13, 2003	NASA launch on Delta-2 from VAFB, CHIPSat is a secondary microsatellite of UCB/SSL, built by SpaceDev Inc., Poway, CA
IGS-1a (radar) IGS-1b (optical)	Mar. 28, 2003	JAXA launch of first Japanese military reconnaissance mission (optical and SAR), H2A vehicle from Tanegashima, Japan, both S/C have an orbit of about 492 km in altitude
IGS-2a (radar) IGS-2b (optical)	Nov. 29, 2003	Japanese military reconnaissance missions (optical and SAR), H2A vehicle from Tanegashima (launch failure)
IGS-3a (radar)	Sept. 11, 2006	Japanese military reconnaissance mission (850 kg, Information Gathering Satellite-3a) with about 1 m resolution. Launch provided by JAXA on the H2A/2002 vehicle from Tanegashima. Operator: JIDF (Japanese Information Defense Force).
IGS-3b (radar) IGS-3v (optical)	Feb. 24, 2007	Japanese military reconnaissance missions (optical and SAR), H2A vehicle from Tanegashima (to make up for the launch failure on Nov. 23, 2003)
IGS-5a (optical)	Nov. 28, 2009	Japanese military S/C IGS-4 (Information Gathering Satellite), an imager with a resolution of ~ 60 cm. Launch on an H-2A rocket from TNSC, Japan.
IGS-4a (optical)	Sept. 23, 2011	Japanese military S/C IGS-4 (Information Gathering Satellite), an imager with a resolution of ~ 60 cm. Launch on an H-2A rocket from TNSC, Japan.
IGS (radar)	Dec. 12, 2011	Japanese military radar satellite, launch on the H2A vehicle from TNSC, Japan
IGS (radar 4) IGS-5v (optical)	Jan. 27, 2013	Two Japanese reconnaissance satellites. Launch on the H2A vehicle from TNSC, Japan
Ikonos-1	Apr. 27, 1999	Space Imaging, launch failure
Ikonos-2	Sept. 24, 1999	A remote sensing mission of Space Imaging, Thornton, CO; launch on an Athena vehicle from VAFB, CA
IMAGE	Mar. 25, 1999	DOE S/C launch from VAFB
INDEX	Aug. 23, 2005	JAXA technology mission. Launch on Dnepr-1 from Baikonur
Inmarsat-5F1	Dec. 08, 2013	Launch of Inmarsat-5F1 with first Global Xpress Service S/C into GEO on a Proton M/Breeze M vehicle from Baikonur.
INSAT-2B	July 22, 1993	GEO meteorological/communication satellite of ISRO
INSAT-2D	June 03, 1997	GEO meteorological/communication satellite of ISRO
INSAT-2E	April 02, 1999	GEO meteorological/communication satellite of ISRO
INSAT-3A	April 09, 2003	ISRO communication & meteorology S/C, launch on Ariane-5G along with Galaxy-12 of PanAmSat Corp. (communications)
INSAT-3C	Feb. 03, 2002	ISRO communications satellite into GEO, Ariane-4 launch
INSAT-3E	Sept. 27, 2003	ISRO communications satellite into GEO, Ariane-5G
InteGRAL	Oct. 17, 2002	ESA astrophysics mission, launch from Baikonur Cosmodrome into HEO (150,000 km x 9,000 km, inclination 51.6°). InteGRAL (International Gamma-Ray Astrophysics Laboratory) is equipped with 2 gamma-ray telescopes, an X-ray monitor and an optical camera.
IntelSat-14 (IS-14)	Nov. 23, 2009	Launch of IS-14 communication satellite on an Atlas-V-431 vehicle from Cape Canaveral, FLA. In addition to the commercial payload, IS-14 carries the IRIS-NGGS technology payload to perform IP routing.
Interball-2	Aug. 29, 1996	Auroral Probe of Interball (Molniya-M launch from Plesetsk) Magion-5 as subsatellite
IOV-1, IOV-2, (In-Orbit Validation, Galileo)	Oct. 21, 2011	Launch of first pair of Europe's Galileo navigation satellites from Kourou by the first launch of the Russian Soyuz vehicle from Europe's spaceport in Kourou, French Guiana.
IOV-3, IOV-4 (In-Orbit Validation, Galileo)	Oct. 12, 2012	Launch of the second pair of Europe's Galileo navigation satellites from Kourou by the Soyuz ST-B launcher, operated by Arianespace. These satellites were built by a consortium led by Astrium as prime contractor.
IRIS Observatory	June 28, 2013	Launch of the NASA IRIS spacecraft (solar mission) on Pegasus XL vehicle of OSC from VAFB, CA

Mission	Launch Date	Comment
IRNSS-1A	July 01, 2013	Launch of first ISRO navigational satellite on PSLV-C22 XL vehicle from SDSC (Satish Dhawan Space Center SHAR). Launch mass of 1425 kg.
IRNSS-1B	Apr. 04, 2014	Launch of first ISRO navigational satellite on PSLV-C24 XL vehicle from SDSC (Satish Dhawan Space Center SHAR).
IRS-1A	Mar. 17, 1988	ISRO EO S/C, India, on a Vostok launch vehicle from Baikonur
IRS-1B	Aug. 29, 1991	ISRO EO S/C, on a Vostok launch vehicle from Baikonur
IRS-1E (P1)	Sept. 20, 1993	ISRO EO S/C, PSLV launcher from SHAR (launch failure)
IRS-P2	Oct. 15, 1994	ISRO EO S/C on a PSLV launcher from SHAR
IRS-1C	Dec. 28, 1995	ISRO EO S/C on a Molniya launcher from Baikonur
IRS-1D	Sept. 29, 1997	ISRO EO S/C on a PSLV launcher from SHAR
IRS-P3	Mar. 21, 1996	ISRO, EO S/C on a PSLV launcher from SHAR
IRS-P4 (OceanSat-1)	May 26, 1999	ISRO, PSLV launcher from SHAR, along with KITSAT-3 and DLR-TUBSAT
IRS-P5 (CartoSat-1)	May 05, 2005	ISRO, PSLV launcher from SHAR, along with HamSat (VUSat) of AmSat India as secondary payload
IRS-P6 (ResourceSat-1)	Oct. 17, 2003	ISRO imaging satellite (also called ResourceSat-1) on PSLV from SHAR, India; Launch mass of 1360 kg
ISEE-1, -2	Oct. 22, 1977	A joint launch was provided by NASA into HEO of the NASA/ESA cooperative mission in the ISEE (International Sun-Earth Explorer) program.
ISEE-3	Aug. 12, 1978	ISEE-3 of NASA was the first S/C in history which was placed into a halo orbit of L1, 1.5 million km from Earth into the sun direction
Jason-1	Dec. 07, 2001	NASA launch (Delta-2-7925) from VAFB, CA
Jason-2/OSTM	June 20, 2008	NASA/CNES mission, NASA launch on Delta-2 from VAFB, CA
JAWSAT	Jan. 26, 2000	Weber University, secondary payloads: FalconSat-1, ASU-Sat-1, OPAL, StenSat, PICOSAT-1, -2, Artemis
JERS-1	Feb. 11, 1992	NASDA SAR satellite from Tanegashima Space Center, (H-I)
Jumpstart mission of Falcon-1 with: Trailblazer, NanoSail-D, PRESat,	Aug. 03, 2008	Falcon-1 launch vehicle of SpaceX. Launch failure on third flight attempt of Falcon-1 from the Kwajalein Atoll (Marshall Islands, Pacific). Payloads aboard: Trailblazer of DoD (Space-Dev), PRESat of NASA/ARC, and NanoSail-D (NASA/MSFC)
Jumpstart-2, payload mass simulator with a mass of 165 kg	Sept. 28, 2008	On flight 4, the Falcon-1 launch vehicle achieved Earth orbit – representing the first privately developed liquid fuel rocket to orbit the Earth. Launch site: Kwajalein Atoll (Marshall Islands, Pacific).
Juno (New Frontier)	Aug. 05, 2011	NASA mission of solar-powered S/C to Jupiter from Cape Canaveral, FLA (Atlas-V launch vehicle). Arrival at Jupiter in July 2016. Study of the early solar system.
Kanopus-V-N1 Secondary payloads: Belka-2 TET-1 Zond-PP exactView-1	July 22, 2012	Launch of Roskosmos and Roshhydromet/Planeta mission on Soyuz FG/Fregat vehicle from the Baikonur Cosmodrome. – Minisatellite of Belarus (NASRB) with a mass of ~ 400 kg. – A technology probe of DLR, Germany with a mass of 120 kg – A microsatellite of IRE, Moscow – A microsatellite (100 kg) of exactEarth (COM DEV), Canada
KazEOSat-1	Apr. 30, 2014	Launch of high-resolution spacecraft (830 kg) of Kazcosmos, Kazakhstan on Vega vehicle (VV03) from Kourou.

Mission	Launch Date	Comment
KazEOSat-2 + Deimos-2 (primary S/C) Secondary payloads: UNISat-6 Lemur-1 TigriSat ANTELSAT AeroCube-6 SaudiSat-4 AprizeSat-9 & -10 Hodoyoshi-3 & -4 BRITE-CA-1, -2 TabletSat-Aurora BugSat-1 Perseus-M1 & M2 QB50P1, QB50P2 NanoSatC-Br1 DTUSat-2 POPSat-HIP-1 PolyITAN-1 PACE Duchifat-1 11 Flock-1C	June 19, 2014	Launch of a two primary S/C. KazEOSat-2 (185 kg) of Kazcosmos, Kazakhstan on a Dnepr-1 vehicle (cluster launch of 37 S/C) from the Yasný Cosmodrome, Russia. Deimos-2 (310 kg) is a high-resolution minisatellite of Deimos Elecnor, Spain. A microsatellite of La Sapienza of Rome, releasing 4 S/C: - A 3U CubeSat of NanoSatisfi, San Francisco, CA - A 3U CubeSat of La Sapienza of Rome, Italy - A 2U CubeSat of UdelaR, San Marino, Uruguay - A 1/2U CubeSat of The Aerospace Corporation, El Segundo. Microsatellite (112 kg) of KACST, Saudi Arabia Nanosatellites (each 12 kg) of SpaceQuest, USA Microsatellites (60 and 65 kg) of the University of Tokyo, Japan Two nanosatellites (7 kg each) of UTIAS/SFL, Toronto, Canada Microsatellite (25 kg) of SPUTNIX, Russia Microsatellite (22 kg) of Satellogic S.A., Argentina Two 6U CubeSats of Canopus Systems US / Dauria Aerospace Two 2U CubeSats (2 kg each) of Von Karman Institute, Brussels A 1U CubeSat of universities in Brazil and INPE, Brazil A 1U CubeSat of DTU (Technical University of Denmark) A 3U CubeSat of Microspace Rapid Pte Ltd., Singapore A CubeSat of KPI (Kiev Polytechnic Institute), Kiev, Ukraine 2U CubeSat, NCKU (National Cheng Kung University), Taiwan A 1U CubeSat of HSC (Herzliya Science Center), Israel 11 3U CubeSats (5 kg each) of Planet Labs, San Francisco, CA.
Kepler	March 6, 2009	NASA launch (Cape Canaveral, Delta-2) of a mission (0.95 m space telescope) to find Earth-like planetary systems in the Milky Way. Kepler is in an Earth-trailing heliocentric orbit. The telescope is designed to find Earth-size planets in the habitable zone of sun-like stars.
KITSat-1	Aug. 11, 1992	KAIST (Korea) piggyback launch on Ariane-4 ASAP (V.52), along with Topex/Poseidon S/C as the primary payload.
KitSat-2	Sept. 26, 1993	KAIST (Korea) piggyback launch on Ariane-4 ASAP as an auxiliary payload on the SPOT-3 launch from Kourou
KitSat-3	May 26, 1999	KAIST (Korea) secondary payload to IRS-P4 of ISRO
KOMPSAT-1 (Arirang-1)	Dec. 21, 1999	Cooperative minisatellite technology-training program of KARI with TRW, EOC (Electro-Optical Camera) and OSMI (Ocean Scanning Multispectral Imager) instruments
KOMPSAT-2 (Arirang-2)	July 28, 2006	Remote sensing satellite of KARI, Korea, launch on a Rockot KM vehicle of Eurockot from Plesetsk, Russia
KOMPSAT-3 Secondary payloads: SDS-4 HORUYU-2	May 17, 2012	Optical high-resolution satellite of KARI, Korea, launch on a H-IIA vehicle of JAXA (co-payload with GCOM-W1, JAXA) A minisatellite of JAXA with a mass of 48 kg A nanosatellite (7 kg) of KIT (Kyushu Institute of Technology)
KOMPSAT-5 (Arirang-5)	Aug. 22, 2013	X-band SAR satellite of KARI, Korea, launch on a Dnepr-1 vehicle of ISC Kosmotras, Russia, from the Dombarovsky Launch Site, Yasný, Russia.
Kondor-E1	June 27, 2013	S-band SAR satellite of NPOMash, Moscow, Russia; launch on a Strela vehicle from the Baikonur Cosmodrome, Kazakhstan.
Lacrosse-1 (Onyx)	Dec. 02, 1988	DoD/NRO radar imaging satellite. Launch on Shuttle flight STS-27 from KSC. The S/C was deorbited in 1997.
Lacrosse-2 (Onyx)	Mar. 08, 1991	DoD/NRO radar imaging satellite. Launch from VAFB on a Titan-4A vehicle
Lacrosse-3 (Onyx)	Oct. 24, 1997	DoD/NRO radar imaging satellite. Launch from VAFB on a Titan-4A vehicle
Lacrosse-4 (Onyx)	Aug. 17, 2000	DoD/NRO radar imaging satellite (mass= 14500 kg). Launch from VAFB on a Titan-4B vehicle
Lacrosse-5 (Onyx)	Apr. 30, 2005	DoD/NRO radar imaging satellite, mass= 16000 kg. Launch from VAFB on a Titan-4B vehicle. Orbit= 718 km x 712 km, inclination = 57°
Lageos-1	May 04, 1976	NASA and ASI geodetic satellite (laser ranging) in MEO (Medium Earth Orbit), launch on Delta-2913 vehicle from VAFB, CA
Lageos-2	Oct. 22, 1992	NASA-ASI geodetic satellite (laser ranging) in MEO, deployment from space shuttle Columbia (STS-52)
LADEE	Sept. 07, 2013	NASA lunar mission, launch on the Minotaur-V vehicle from MARS (Mid-Atlantic Regional Spaceport), Wallops Island, VA

Mission	Launch Date	Comment
Landsat-1 (ERTS)	July 23, 1972	NASA S/C, launch of first Earth observation satellite with MSS and RBV payload from VAFB, CA
Landsat-2	Jan. 22, 1975	NASA S/C, launch from VAFB, CA on a Delta 2914 vehicle
Landsat-3	Mar. 05, 1978	NASA S/C, launch from VAFB, CA on a Delta 2914 vehicle
Landsat-4	July 16, 1982	NASA S/C, first S/C operated by NOAA, first use of TM
Landsat-5	Mar. 01, 1984	NASA S/C, launch on a Delta vehicle from VAFB, CA
Landsat-6	Oct. 5, 1993	NASA S/C, launch failure (contact lost during launch)
Landsat-7	Apr. 15, 1999	NASA S/C with ETM+ imaging instrument
Landsat-8 (LDCM)	Feb. 11, 2013	NASA S/C, launch on an Atlas-V-401 vehicle from VAFB, CA
LARES Secondary payloads AlmaSat (μ Satellite) Xatcobeo Robusta e-st@r Goliat PW-Sat MaSat-1 (CubeSat) UniCubeSat GG	Feb. 13, 2012	Italian geodynamic satellite (400 kg 36.7 cm dia.) to test frame dragging. Launch on maiden flight of the Vega launcher from Kourou, French Guiana by Arianespace. University of Bologna, Italy (total mass of 20.5 kg with adapter) University of Vigo and INTA, Spain (1 kg CubeSat) University of Montpellier 2, France (1 kg CubeSat) Politecnico di Torino, Italy (1 kg CubeSat) University of Bucharest, Romania (1 kg CubeSat) Warsaw University of Technology, Poland, (1 kg CubeSat) Budapest University of Technology and Economics, Hungary Universit� di Roma 'La Sapienza', Italy, (1 kg CubeSat)
Lewis	Aug. 23, 1997	NASA, The Lewis S/C reentered the atmosphere Sept. 28, 1997. The Clark mission was cancelled in Feb 1998 due to cost overruns and launch delays
LRO (Lunar Reconnaissance Orbiter)	June 18, 2009	Launch of LRO+LCROSS (moon missions) on an Atlas V 401 launch vehicle from KSC (Kennedy Space Center), Cape Canaveral, FLA.
Mangalyaan (Mars craft in Hindi)	Nov. 05.2013	Launch of the first ISRO MOM (Mars Orbiter Mission) from SDSC SHAR on the PSLV-C25 vehicle. The 1350 kg spacecraft is on a 10 month cruise phase to Mars to study the Martian atmosphere.
Mars Express	June 02, 2003	ESA science mission to Mars, launch on a Soyuz-Fregat launch vehicle from Baikonur, Kazakhstan
MAVEN	Nov. 18, 2013	NASA space probe to Mars to study the Martian atmosphere while orbiting Mars. Launch on Atlas-5-401 vehicle from Cape Canaveral, FL.
MDS-1 (Tsubasa)	Feb. 04, 2002	NASDA H-2A vehicle test launch with two payloads: NASDA's MDS-1 technology mission in GTO; and an ISAS vehicle
Megha-Tropiques Secondary payloads: SRMSat Jugnu VesselSat-1	Oct. 12, 2011	Launch of ISRO/CNES meteorological mission on PSLV-C18 from SDSC-SHAR, India Satellite (10 kg) of SRM (Sri Ramaswamy Memorial) University Satellite (3 kg) of IIT (Indian Institute of Technology), Kanpur Satellite (29 kg) of LuxSpace with AIS payload
MegSat-0	April 28, 1999	Italian data collection satellite
Meteor-3M-1	Dec. 10, 2001	Russian weather satellite along with four secondary payloads: BADR-B, Compass-1, Maroc-TUBSAT, Reflector
Meteor-M-1 Tatiana-2 Sterkh-2 UGATUSat ZASat/Sumbandila BLITS IRIS	Sept. 17, 2009	Russian weather satellite along with six secondary payloads: - Universitetskii, 120 kg of Lomonosov Moscow State University - COSPAS-S&RSat (171 kg) - Ufa State Aviation Technical University (UGATU), 30 kg - Microsatellite (imaging, 82 kg) of SunSpace, South Africa - A nanosatellite (7.53 kg, sphere reflector) - An experimental unit attached to the Fregat upper stage
Meteosat-1	Nov. 23, 1977	ESA, launch on a Thor-Delta vehicle from Cape Canaveral
Meteosat-2	June 19, 1981	ESA, launch on Ariane from Kourou
Meteosat-3	June 15, 1988	ESA/EUMETSAT, launch on Ariane from Kourou
Meteosat-4	Mar. 06, 1989	ESA/EUMETSAT, launch on Ariane from Kourou
Meteosat-5	Mar. 02, 1991	In 1998 repositioning to 65° East for INDOEX campaign support. As of 2002, Meteosat-5 continues the Indian Ocean Data Coverage Service at 63° E.
Meteosat-6	Nov. 20, 1993	ESA/EUMETSAT, Standby satellite at 10°W since June 1998
Meteosat-7	Sept. 03, 1997	ESA/EUMETSAT, operational as of 2004

Mission	Launch Date	Comment
Meteosat-8 (MSG-1)	Aug. 28, 2002	Launched as MSG-1; it became Meteosat-8 in Jan. 2004 when declared to be operational (after the commissioning phase)
Meteosat-9	Dec. 22, 2005	Launched as MSG-2 of EUMETSAT;
MetOp-A	Oct. 19, 2006	Launch of the first polar orbiting meteorological S/C of EU-METSAT from Baikonur, Kazakhstan on a Soyuz-2.1A/Fregat vehicle
MetOp-B	Sept. 17, 2012	Launch of second polar orbiting EUMETSAT S/C from Baikonur, Kazakhstan on a Soyuz-2.1A/Fregat vehicle
MetSat-1	Sept. 12, 2002	ISRO (India) from SHAR (replacement of INSAT-2E), PSLV launch into GTO
MightySAT-1	Dec. 04, 1998	AFRL technology S/C, launched as HH payload on STS-88, Dec. 14, 1998
MightySat II.1	July 19, 2000	AFRL technology S/C with ten technologies and FTHSI
MIMOSA, MOST, CubeSats (6)	June 30, 2003	MIMOSA (Czech Republic), MOST of CSA; all S/C have been launched on Rockot KS of Eurockot from Plesetsk, Russia; the CubeSats are: -XI (Uni. of Tokyo), CUTE-I (Tokyo Institute of Technology), CanX-1 (U. of Toronto), AAUSat (Aalborg U. Denmark), DTUSat (Technical U. of Denmark), QuakeSat (Stanford U.), Monitor E mock-up (GKNPT Khrunichev)
MINISAT-01	April 21, 1997	INTA of Spain, air-launch on a Pegasus-XL vehicle from the Canary Islands, Spain
MITA	July 15, 2000	MITA (Minisatellite Italiano di Tecnologia Avanzata)
Monitor-E	June 30, 2003	Launch on a Rockot KS vehicle of Eurockot from Plesetsk, Russia (along with MIMOSA, MOST, and 6 CubeSats). Monitor-E was a mock-up spacecraft of GKNPT Khrunichev Space Center, Moscow, Russia with a mass of 700 kg. The payload Monitor-E remained on the upper stage of the launch vehicle.
Monitor-E1	Aug. 26, 2005	An Earth observation mission of Roskosmos, built by GKNPT of Moscow. Launch from Plesetsk, Russia on a Rockot-KM vehicle
MSG-1, Meteosat Second Generation	Aug. 28, 2002	EUMETSAT mission, Ariane-5 launch from Kourou along with the Eutelsat communications satellite Atlantic Bird 1
MSG-2 (Meteosat-09)	Dec. 22, 2005	EUMETSAT mission (2034 kg), Ariane-5 ECA launch from Kourou along with INSat-4A (3081 kg) of ISRO
MSG-3 (Meteosat-10)	July 05, 2012	EUMETSAT mission (2000 kg), Ariane-5 ECA launch from Kourou along with EchoStar-XVII (6100 kg), a broadband Ka-band S/C for the American operator Hughes Network Systems.
MSL (Mars Science Laboratory)	Nov. 26, 2011	Launch of NASA/JPL Curiosity rover on an Atlas-5 vehicle from the Cape Canaveral Air Force Station, FL. Destination: Mars. Curiosity landed on Mars on August 5, 2012.
MSX	April 24, 1996	DoD satellite launch from VAFB
MTI	Mar. 12, 2000	DOE satellite launch from VAFB (Taurus vehicle of OSC)
MTSAT	Nov. 15, 1999	NASDA, launch failure
MTSAT-1R	Feb. 26, 2005	Japanese Meteorology and Transport satellite (in GEO), launch on H-2A vehicle from Tanegashima, Japan (into GTO)
MTSAT-2	Feb. 18, 2006	Japanese Meteorology and Transport satellite (in GEO), launch on H-2A vehicle from Tanegashima, Japan (into GTO)
Munin	Nov. 21, 2000	IRF (Sweden) nanosatellite, secondary payload to EO-1 and SAC-C
MUOS-1 (Mobile User Objective System)	Feb. 24, 2012	Launch of MUOS-1, US Navy next generation communications satellite into GEO; launch from Cape Canaveral on Atlas V 551. MUOS is an UHF (300 MHz to 3 GHz frequency range) system.
MUOS-2	July 19, 2012	Launch of MUOS-2, US Navy next generation communications satellite into GEO; launch from Cape Canaveral on Atlas V 551. Launch mass of ~ 7000 kg (S/C built by Lockheed Martin).
MUSES-B/HALCA	Feb. 12, 1997	ISAS (Japan) SVLBI satellite launch on M-V rocket of ISAS from the Kagoshima Space Center, Japan. After launch MUSES-B was renamed to HALCA. HALCA is a 1st generation SVLBI mission (deployable mesh antenna of 8 m aperture).

Mission	Launch Date	Comment
MUSES-C (Hayabusa)	May 09, 2003	JAXA (formerly ISAS) asteroid sample return mission (to asteroid 1998 SF36), launch with M-5 vehicle from Kagoshima, Japan. In June 2010, the S/C was recovered after a 7-year journey in the desert (Woomera) of Australia.
Nadezhda-7	Sep. 26, 2002	Launch from Plesetsk launch site, COSPAS-S&RSAT series
Nadezhda-6, Tsinghua-1, SNAP-1,	June 28, 2000	Launch from Plesetsk launch site, with Nadezhda-6 as prime payload (S&RSat, COSPAS), SSTL technology S/C,
Nadezhda-5	Dec. 10, 1998	Launch from Plesetsk, Russian search and rescue satellite in COSPAS-S&RSAT series
NEAR	Feb. 17, 1996	NASA S/C launch on a Delta vehicle from Cape Canaveral. Flyby of asteroid 433 EROS on Dec. 23, 1998. Next rendezvous with EROS in mid-Feb. 2000
NFIRE	April 24, 2007	NFIRE (Near Field Infrared Experiment) spacecraft of MDA, launch on Minotaur vehicle of OSC from Wallops Island, VA First LCT (Laser Communication Terminal) of Tesat onboard
Nimbus-1	Aug. 28, 1964	NASA, launch on a Thor-Agena-B vehicle from VAFB, CA
Nimbus-2	May 15, 1966	NASA, launch on a Thor-Agena-D vehicle from VAFB, CA
Nimbus-3	Apr. 14, 1969	NASA, launch on a Thor-Agena-D vehicle from VAFB, CA
Nimbus-4	Apr. 8, 1970	NASA, launch on a Thor-Agena-D vehicle from VAFB, CA
Nimbus-5	Dec. 11, 1972	NASA, launch on a Thor-Agena-D vehicle from VAFB, CA
Nimbus-6	June 12, 1975	NASA, launch on a Thor-Agena vehicle from VAFB, CA
Nimbus-7	Oct. 24, 1978	NASA, launch on a Thor-Agena-D vehicle from VAFB, CA; payload: CZCS, ERB, SBUV/TOMS, SAM-II, SAMS, SMMR
NOAA-6 (-B)	June 27, 1979	NOAA weather satellite, launch on Atlas E/F from VAFB
NOAA-7 (-C)	June 23, 1981	NOAA weather satellite, launch on Atlas E/F from VAFB
NOAA-8 (-E)	Mar. 28, 1983	NOAA weather satellite, launch on Atlas E/F from VAFB, first S/C of ATN (Advanced TIROS-N) series (1st of 4th generation)
NOAA-9 (-F)	Dec. 12, 1984	NOAA weather satellite,
NOAA-10 (-G)	Sept. 17, 1986	NOAA weather satellite (POES)
NOAA-11 (-H)	Sept. 24, 1988	NOAA weather satellite (POES)
NOAA-12 (-D)	May 14, 1991	NOAA weather satellite (POES)
NOAA-13 (-I)	Aug. 09, 1993	NOAA weather satellite (POES), a S/C failure (power loss) occurred on Aug. 21, 1993, NOAA lost contact with the S/C
NOAA-14 (-J)	Dec. 30, 1994	NOAA weather satellite (POES series), last S/C of 4th generation
NOAA-15 (-K)	May 13, 1998	NOAA weather satellite (POES), 1st S/C of 5th generation
NOAA-16 (-L)	Sept. 21, 2000	NOAA weather satellite
NOAA-17 (-M)	June 24, 2002	NASA/NOAA POES series S/C, launch with Titan-2 from VAFB
NOAA-18 (-N)	May 20, 2005	NASA/NOAA POES series S/C, launch with Delta-2-7320 vehicle from VAFB (launch mass of 1420 kg)
NOAA-19 (-N') i.e. NOAA-N prime	Feb. 06, 2009	NASA/NOAA POES series S/C, launch with Delta-2-7320 vehicle from VAFB. This is the last S/C of the 5th generation.
NPP (NPOESS Preparatory Project) Secondary payloads: AubieSat-1 DICE E1P-2 RAX-2 M-Cubed	Oct. 28, 2011	NASA/NOAA mission, launch on a Delta-7920 vehicle from VAFB (new generation weather satellite mission). Launch sponsored by the NASA's ElaNa-3 initiative. 1U CubeSat of Auburn University, Auburn, AL Two 1.U CubeSats of Utah State University, Logan, UT CubeSat mission of Montana State University, Bozeman, MT 3U CubeSat of the University of Michigan, Ann Arbor, MI 1U CubeSat of the University of Michigan, Ann Arbor, MI In Jan. 2012, NASA renamed the NPP mission to Suomi-NPP
NROL-41	Sept. 21, 2010	Launch of NRO reconnaissance mission (FIA Radar-1 payload) from VAFB on an Atlas-5-501 vehicle of ULA into LEO
NROL-25	Apr. 03, 2012	Launch of NRO reconnaissance mission (FIA Radar-2 payload) from VAFB on an Atlas-5-501 vehicle of ULA into LEO
NROL-15	June 29, 2012	Launch of NRO reconnaissance satellite (Mentor class) from the Space Launch Complex-37, Cape Canaveral Air Force Station, FLA on an Atlas-IV vehicle; launch provider: ULA. GEO orbit.

Mission	Launch Date	Comment
NROL-38	June 20, 2012	Launch of NRO reconnaissance satellite from the Space Launch Complex-41, Cape Canaveral Air Force Station, FLA on an Atlas-V vehicle; launch provider: ULA (United Launch Alliance).
NROL-36 Secondary payloads: SMDC-ONE 2.1 SMDC-ONE 2.2 AeroCube-4.5 AeroCube-4.0 Aeneas Re (STARE-A) CSSWE CXBN CP5 CINEMA-1	Sept. 13, 2012	Launch of NRO reconnaissance satellites NOSS-36A and NOSS-36B from VAFB, CA on Atlas-5-411 vehicle of ULA. ELaNa-6 payloads of NASA: CINEMA, CSSWE, CP5, CXBN. 3U CubeSat of US Army SMDC/ARSTRAT, 4.1 kg 3U CubeSat of US Army SMDC/ARSTRAT, 4.1 kg 2 x 1U CubeSats of The Aerospace Corporation, each 1.3 kg 1U CubeSat of The Aerospace Corporation, each 1.1 kg 3U CubeSat of USC, Marina Del Ray, CA, 3.7 kg 3U CubeSat of LLNL, Livermore, CA, 4 kg 3U CubeSat of the University of Colorado, Boulder, 3.5 kg 2U CubeSat of Morehead State University, 2.6 kg 1U CubeSat of CalPoly, San Luis Obispo, CA, 1.1 kg 3U CubeSat of USB/SSL Berkeley, CA, 2.8 kg
NROL-65 (USA-245)	Aug. 28, 2013	Launch of NRO reconnaissance satellite (optical imaging) from VAFB on a Delta-4 Heavy vehicle of ULA into LEO. It is the last KH-11 reconnaissance satellite, and the last spacecraft to be launched in the Keyhole program.
NROL-39 Secondary payloads AeroCube-5a, -5b ALICE CUNYSAT-1 FIREBIRD-A, -B MCubed/COVE-2 SMDC-ONE-2.3 SMDC-ONE-2.4 SNaP TacSat-6	Dec. 06, 2013	Launch of NRO reconnaissance mission (FIA Radar-3 payload) from VAFB on an Atlas-5-501 vehicle of ULA into LEO Two 1.5U CubeSats of The Aerospace Corporation A 3U CubeSat of AFIT (Air Force Institute of Technology) 1U CubeSat of the Medgar Evers College, Brooklyn, N.Y., City University of New York. Two 1.5U CubeSats of MSU (Montana State University) A 1U CubeSat of the University of Michigan and NASA/JPL Two 3U CubeSats of the U.S. Army SMDC/ARSTRAT of Huntsville AL (Redstone Arsenal) A 3U CubeSat of the U.S. Army SMDC/ARSTRAT A 3U CubeSat of the U.S. Army SMDC/ARSTRAT and ORS.
NROL-67	Apr. 10, 2014	Launch of NRO reconnaissance mission (radar tracking) from Cape Canaveral, FL, on an Atlas-5 vehicle of ULA
NROL-33	May 22, 2014	Launch of NRO reconnaissance mission from Cape Canaveral, FL, on an Atlas-5-401 vehicle of ULA, USA-252, (most likely payload: Quasar, GEO communications)
NuSTAR	June 13, 2012	Launch of a NASA X-ray astronomy mission on a Pegasus-XL vehicle from the Kwajalein Atoll (Pacific Ocean)
O3b Networks Ltd. MEO constellation	June 25, 2013	Launch of 4 O3b satellites (O3b-1, O3b-2, O3b-4) into MEO (8063 km) with Soyuz-STB/Fregat-MT of Arianespace from Kourou (flight VS05). The network will combine the ubiquitous reach of satellite communication with the speed of fiber to deliver satellite Internet services and mobile backhaul services to emerging markets. Total payload mass of 3,204 kg.
OceanSat-1 (IRS-P4)	May 26, 1999	ISRO, PSLV launcher from SHAR, along with KITSAT-3 and DLR-TUBSAT
OceanSat-2 BeeSat ITUpSat-1 SwissCube UWE-2 Rubin-9.1, Rubin-9.2	Sept. 23, 2009	ISRO, PSLV launcher from SHAR, along with 6 small satellites CubeSat of TUB (Technical University of Berlin), Germany Istanbul Technical University PicoSatellite-1, Turkey CubeSat of Ecole Polytechnique Federale de Lausanne CubeSat University of Würzburg), Würzburg, Germany Nanosatellites of ÖHB-System, Bremen, Germany. Both nanosatellites carry AIS receivers
OCO (Orbiting Carbon Observatory)	Feb. 24, 2009	NASA spacecraft with a launch on a Taurus-XL vehicle from VAFB, CA. Unfortunately, the OCO satellite failed to reach orbit. A mishap investigation board is to investigate the failure.
OCO-2	July 02, 2014	NASA spacecraft with a launch on a Delta-2 vehicle from VAFB, CA, USA. (Orbiting Carbon Observatory-2)
Odin	Feb. 20, 2001	Swedish satellite for astronomic and atmospheric research
Oersted	Feb. 23, 1999	DTU of Denmark S/C, Earth's magnetic field measurements

Mission	Launch Date	Comment
Ofeq-1 (Horizon-1)	Sept. 19, 1988	First EO experimental satellite of Israel, launched on Shavit from the Palmachim Space Centre (south of Tel-Aviv) and placed in a low elliptical (250 km x 1150 km) orbit at the unusual inclination of 143° (westwards, providing about 6 passes/day over Israel). S/C mass of 155 kg (no imager payload).
Ofeq-2	April 03, 1990	Israel military experimental satellite built by IAI (Shavit launch). S/C mass of 160 kg, power of 246 W, S-band communications. No imager. Reentry into the atmosphere on July 9, 1990.
Ofeq-3 (Horizon-3)	April 05, 1995	Israel military optical imaging satellite of IAI (launch in westward direction). Orbit: 370-750 km. Seven years of operational life. First imaging satellite of Israel.
Ofeq-4	Jan. 22, 1998	Israel military optical imaging satellite of IAI, launch failure
Ofeq-5 (use of OptSat 2000 bus)	May 28, 2002	Israel military optical imaging satellite of IAI (2nd generation reconnaissance). Ofeq-5 was launched on a Shavit vehicle from the Palmachim air force base (launch in westbound direction, 143.5°). From an altitude of 500 km, Pan resolution = 0.5 m, MS= 1 m. The S/C mass is 300 kg, the orbit is 369 km x 771 km.
Ofeq-6	Sept. 06, 2004	Israel military optical imaging satellite of IAI, launch failure . Malfunction in the third stage of its Shavit carrier rocket.
Ofeq-7 (use of OptSat 2000 bus)	June 11, 2007	Israel military optical imaging satellite of IAI (reconnaissance with advanced imaging capability, military and civil use of data). Launch on a Shavit vehicle from Palmachim
Ofeq-9 (use of OptSat 2000 bus)	June 22, 2010	Israel military optical imaging satellite of IAI (reconnaissance with advanced imaging capability). Launch with the Shavit launch vehicle from the Palmachim base, Israel. High resolution imagery (70 cm resolution) on a swath of 7 km. Pointing accuracy within 20 m. Orbital altitude is ~ 500 km.
Ofeq-10	Apr. 09, 2014	Israel military SAR satellite built by IAI/MBT and Elta Systems for the Israel Defense Forces. Launch on a Shavit vehicle from Palmachim, Israel. The first two examples of this satellite (Tec-SAR, also referred to as Ofeq-8, and RISAT-2) were launched on the Indian PSLV rockets. Ofeq-10 carries a more advanced version of the EL/M-2070 SAR payload.
OICETS	Aug. 23, 2005	A JAXA technology S/C to test laser communications. Launch on a Dnepr-1 vehicle from Baikonur. Launch mass of 530 kg
Okean-E, (Cosmos-1076)	Feb. 12, 1979	USSR remote sensing satellite, launch from Plesetsk on Tsyklon-3 launch vehicle
Okean-E, (Cosmos-1151)	Jan. 23, 1980	USSR remote sensing satellite, launch from Plesetsk on Tsyklon-3 launch vehicle
Okean-OE-N1	Oct. 28, 1983	USSR remote sensing satellite, launch from Plesetsk
Okean-OE-N2	Oct. 28, 1984	USSR remote sensing satellite, launch from Plesetsk
Okean-O1-N1	July 29, 1986	USSR remote sensing satellite, launch from Plesetsk
Okean-O1-N2	July 16, 1987	USSR remote sensing satellite, launch from Plesetsk
Okean-O1-N3	July 5, 1988	USSR remote sensing satellite, launch from Plesetsk
Okean-O1-N4	June 9, 1989	USSR remote sensing satellite, launch from Plesetsk
Okean-O1-N5	Feb. 28, 1990	USSR remote sensing satellite, launch from Plesetsk
Okean-O1-N6	June 4, 1991	USSR remote sensing satellite, launch from Plesetsk
Okean-O1-N7	Oct. 11, 1994	USSR remote sensing satellite, launch from Plesetsk, Russia
Okean-O1-N8 (renamed Sich-1)	Aug. 31, 1995	Ukrainian/Russian remote sensing satellite, launch on a Tsyklon-3 vehicle from Plesetsk, Russia
Okean-O-1	July 17, 1999	Ukrainian/Russian remote sensing satellite, launch from Baikonur on a Zenit-2 vehicle
OrbView-1 (Microlab-1)	April 03, 1995	Orbimage of OSC, Dulles, VA with a NASA payload; launch on a Pegasus vehicle from VAFB, CA (launched as Microlab-1). In addition, the commercial satellites Orbcomm FM1 and FM2 were launched.
Orbview-2 (SeaStar)	Aug. 01, 1997	Orbimage of OSC, Dulles, VA; SeaWiFS sensor for ocean color data
OrbView-3	June 26, 2003	ORBIMAGE commercial imaging satellite (launch mass of 304 kg); launch on a Pegasus-XL vehicle from VAFB, CA
OrbView-4/ QuikTOMS	Sept. 21 2001	OrbImage and NASA S/C on Taurus launch vehicle from VAFB. launch failure

Mission	Launch Date	Comment
ORFEUS-SPAS-2	Nov. 19, 1996	Payload on Shuttle flight STS-80, landing on Dec. 7, 1996
ORS-1 (or ORS Sat-1)	June 30, 2011	Launch of the ORS-1 (Operational Responsive Space-1) spacecraft, a prototype S/C of the USAF on a Minotaur vehicle of OSC from MARS, Wallops Island, VA, USA (a classified mission of DoD). Orbit: Circular orbit of 400 km, inclination=40°, period=90 min.
ORS-3/STPSat-3 Secondary payloads: ORS-1 ORSES ORS-2 ORS-3 Prometheus-1 Prometheus-2 Prometheus-3 Prometheus-4 SENSE-A SENSE-B Firefly STARE-B HORUS Black Knight-1 TetherSat NPS-SCAT Ho'ponopono COPPER ChargerSat-1 SPA-1 Trailblazer Lunar CubeSat SwampSat CAPE-2 DragonSat-1 KYSat-2 PhoneSat-2.4 TJ ³ Sat	Nov. 20, 2013 (28 payloads)	Launch of ORS-3/STPSat-3 on Minotaur-1 vehicle of OSC from MARS, VA. 3U CubeSat of ORS (Operationally Responsive Space) Office ORS Tech 1, a 3U CubeSat of ORS ORS Tech 2, a 3U CubeSat of ORS 3U CubeSat of LANL (Los Alamos National Laboratory) 3U CubeSat of LANL 3U CubeSat of LANL 3U CubeSat of LANL 3U CubeSat of SMC/XR 3U CubeSat of SMC/XR 3U CubeSat of NASA/NRO/NSF 3U CubeSat, LLNL (Lawrence Livermore National Laboratory) 1U CubeSat of USMA (US Military Academy) 3U CubeSat of USNA (US Naval Academy) 1U CubeSat of NPS (Naval Postgraduate School) 3U CubeSat of the University of Hawaii, Manoa, HI 1U CubeSat of St Louis University, St. Louis, MO 1U CubeSat of the University of Alabama, Huntsville 1U CubeSat of the University of New Mexico 1U CubeSat of the Vermont Technical College, Burlington, VT 1U CubeSat of the University of Florida, Gainesville, FL 1U CubeSat of the University of Louisiana, Lafayette, LA 1U CubeSat of Drexel University, Philadelphia, PA 1U CubeSat of Kentucky Space, University of Kentucky 1U CubeSat of NASA/ARC, Moffett Field, CA 1U CubeSat of Thomas Jefferson High School, Alexandria, VA
PANSAT	Oct. 29, 1998	launch on STS-95, PANSAT was built by NPS (Naval Postgraduate School) in Monterey, CA (see N.19)
PARASOL (1) Helios-IIA Essaim (4, "swarm") NanoSat-1	Dec. 18, 2004	Launch of PARASOL of CNES as secondary payload to Helios-IIA (DGA) optical reconnaissance S/C as primary payload on Ariane-5 G+ from Kourou. Other payloads are 4 microsattelites Essaim eavesdropping S/C of DGA, +NanoSat-1 of INTA
Parus, Universitet-sky Tatiana-1 (Tatyana)	Jan. 20, 2005	Launch of Cosmos-2414 (2005-002A) with the Parus navigation satellite (820 kg) + Tatiana-1 (30 kg) on a Kosmos-3M vehicle from Plesetsk, Russia.
Picard PRISMA	June 15, 2010	CNES solar-terrestrial satellite, launch on a Dnepr vehicle of ISC Kosmostras from Yasný/Dombrovsky, Russia Swedish-led (SSC) technology mission of two microsattelites (secondary payload)
PICOSat/Starshine-3, etc.	Sept. 30, 2001	PICOSat of US AFRL (Technology S/C). Launch on Athena-1 vehicle from Kodiak Island, AK - including Sapphire of Stanford University and PCSat of USNA
Pleiades-HR1A Secondary payloads ELISA-1, 2, 3, 4 SSOT	Dec. 17, 2011	Launch of CNES High-resolution commercial imaging satellite from Kourou on a Soyuz-STA/Fregat launcher. Microsatellite imaging constellation (120 kg each), CNES/DGA High-resolution imaging microsatellite (117 kg) of ACE, Chile
Pleiades-HR1B	Dec. 02, 2012	Launch of CNES High-resolution commercial imaging satellite from Kourou on a Soyuz-STA/Fregat launcher.
POLAR	Feb. 24, 1996	NASA/GSFC solar-terrestrial mission
PoSat-1	Sept. 26, 1993	Launch as secondary payload to SPOT-3 from Kourou. PoSat-1 (Portuguese Satellite-1), built by SSTL is operational as of Sept. 2004.
Priroda	April 23, 1996	Russia, module of MIR station
PROBA	Oct. 21, 2001	ESA technology minisatellite, launch on PSLV from SHAR, India, secondary payload to TES of ISRO and BIRD of DLR
PROBA-2	Nov. 02, 2009	ESA technology minisatellite. Launch as secondary payload to SMOS on Rockot vehicle from Plesetsk, Russia

Mission	Launch Date	Comment
PROBA-V Secondary payloads VNREDSat-1A ESTCube-1	May 07, 2013	ESA/CNES minisatellite (140 kg), launch on Vega vehicle (VV02) from Kourou with the VTG (Vegetation) payload. Microsatellite of VAST (Vietnam Academy of Science and Technology) Estonian Student Satellite-1 CubeSat of the University of Turtu
QuickBird-1	Nov. 20, 2000	Earthwatch, commercial imaging, launch failure
QuickBird-2	Oct. 18, 2001	DigitalGlobe of Longmont, CO (former EarthWatch Inc.) commercial imaging satellite, Delta-2 launch from VAFB
QuikSCAT	June 19, 1999	NASA/JPL, wind measurements
QZS-1 (Michibiki)	Sept. 11, 2010	
RADARSAT-1	Nov. 24, 1995	CSA, Canada, NASA launch on a Delta II vehicle from Vandenberg AFB, CA
RADARSAT-2	Dec. 14, 2007	CSA & MDA Canada; launch on a Soyuz vehicle (launch provider: Starsem) from Baikonur, Kazakhstan.
RADCAL (P92-1)	June 25, 1993	The microsatellite (95 kg) of the USAF was launched from VAFB on a Scout vehicle into an orbit of 753 km x 882 km, inclination of 89.5°. Objective: calibration of US C-band radar installations around the world.
RapidEye	Aug. 29, 2008	Single launch of 5 RapidEye imaging minisatellites on a Dnepr vehicle from Baikonur, Kazakhstan, launch provider: ISC Kosmotras. The S/C are owned and operated by BlackBridge, Berlin, Germany
RazakSat	July 14, 2009	Launch of a Malaysian imaging minisatellite on a Falcon 1 vehicle of SpaceX. Launch site: Kwajalein Atoll, Marshall Islands
RBSP	Aug. 30, 2012	Launch of 2 minisatellites (Radiation Belt Storm Probes) of NASA from Cape Canaveral on an Atlas-v 401 launch vehicle.
ResourceSat-2 Secondary payloads: - XSat (X-Sat) - YouthSat	April 20, 2011	Launch of an ISRO RS mission on PSLV-C16 from SDSC (Satish Dhawan Space Centre), India (common orbit with IRS-P6) Microsatellite (106 kg) of NTU, Singapore Microsatellite of ISRO (92 kg) with LiVHySI (Limb Viewing Hyperspectral Imager)
Resurs-DK1	June 15, 2006	A commercial EO imaging satellite (6650 kg) of TsSKB Progress, Samara, Russia. Launch on a Soyuz-FG rocket from Baikonur
Resurs-F	Nov. 18, 1997	launch from Plesetsk
Resurs-F-1M	Sept. 28, 1999	RKA
Resurs-O1-1	Oct. 03, 1985	USSR remote sensing satellite from Baikonur on Zenit-2 vehicle
Resurs-O1-2	April 20, 1988	USSR remote sensing satellite from Baikonur on Zenit-2 vehicle
Resurs-O1-3	Nov. 04, 1994	RKA remote sensing satellite from Baikonur on Zenit-2 vehicle
Resurs-O1-4	July 10, 1998	RKA RS satellite launched from Baikonur on a Zenit-2 vehicle Secondary payloads: LLMS/IRIS, TMSat (Thailand), TechSat/Gurwin-II (Israel), FASat-Bravo (Chile), SAFIR-2 (OHB), WESTPAC (Australia)
Resurs-P1	June 25, 2013	A commercial EO imaging satellite (launch mass of <7000 kg) of TsSKB Progress, Samara, Russia. Launch on a Soyuz-2-1b vehicle from Baikonur, Kazakhstan.
REX-2	March 9, 1996	DoD S/C launch on a Pegasus vehicle from VAFB
RHESSI (HESSI)	Feb. 05, 2002	NASA solar physics mission, Pegasus XL launch
RISAT-1	Apr. 04, 2012	ISRO C-band SAR satellite. Launch on PSVL-19 from SDSC.
RISAT-2 ANUSat	April 20, 2009	ISRO reconnaissance minisatellite of 300 kg (C-band SAR payload) built by IAI/MBT, Israel. Launch on a PSLV vehicle from SDSC SHAR, India. ANUSat (40 kg) of Anna University was the secondary payload.
ROCSAT-1	Jan. 27, 1999	First S/C of Taiwan with an ocean color sensor
ROCSat-2 (re-named FormoSat-2)	May 20, 2004	NSPO (Taiwan) remote sensing mission. Launch on Taurus XL vehicle of OSC from VAFB, CA
ROCSat-3 (re-named FormoSat-3)	April 14, 2006	NSPO (Taiwan) remote sensing constellation of 6 S/C. Launch on Minotaur vehicle of OSC from VAFB, CA

Mission	Launch Date	Comment
ROSAT	June 01, 1990	German (DLR) X-ray spacecraft, launch on a Delta-2 vehicle from Cape Canaveral, FLA. ROSAT operated for over 8 years until Feb. 12, 1999. Reentry of ROSAT on Oct. 23, 2011.
Rosetta	Mar. 02, 2004	ESA science/astronomy mission (study of the origins of comets), Launch on Ariane-5G launcher (with Comet Lander "Roland")
RXTE	Dec. 05, 1995	NASA (Rossi X-ray Timing Explorer) astronomy mission (3200 kg). Launch from Cape Canaveral on a Delta vehicle. The S/C was decommissioned on Jan. 5, 2012.
SAC-A	Dec. 04, 1998	CONAE, Argentina, launched as HH payload on STS-88
SAC-B	Nov. 04, 1996	CONAE, Argentina, Pegasus XL launch failure
SAC-C	Nov. 21, 2000	CONAE, NASA, launched as secondary payload to EO-1
SAC-D/Aquarius	June 10, 2010	CONAE, NASA, launch on Delta-2 vehicle from VAFB, CA
SACI-1	Oct. 14, 1999	INPE, secondary payload to ZY-1 of CASC
SAMPEX	July 03, 1992	NASA mission in the SMEX program
SAR-Lupe-1	Dec. 19, 2006	German military S/C. Launch of the 1st S/C in a 5 S/C constellation from Plesetsk, Russia, on a Cosmos-3M vehicle
SAR-Lupe-2	July 02, 2007	German military S/C. Launch from Plesetsk, Russia, on a Cosmos-3M vehicle
SAR-Lupe-3	Nov. 01, 2007	German military S/C. Launch from Plesetsk, Russia, on a Cosmos-3M vehicle. Rubin-7-AIS of OHB, Bremen was a secondary test payload which remained attached to the upper stage.
SAR-Lupe-4	Mar. 27, 2008	German military S/C. Launch from Plesetsk, Russia, on a Cosmos-3M vehicle
SAR-Lupe-5	July 22, 2008	German military S/C. Launch from Plesetsk, Russia, on a Cosmos-3M vehicle. The SAR-Lupe constellation is complete.
SARAL Secondary payloads: BRITE- Austria UniBRITE Sapphire NEOSSat AAUSat3 STRaND-1	Feb. 25, 2013	Launch of Indo-French Ka-band altimeter mission on PSLC-C20 vehicle from SDSC-SHAR, India A nanosatellite of TU Graz with a mass of 6.5 kg A nanosatellite of University of Vienna with a mass of 6.5 kg A Space Surveillance Mission of Canada with a mass of 148 kg A microsatellite of Canada with a mass of 74 kg CubeSat of Aalborg University, Denmark A nanosatellite of SSTL, UK with a mass of 4.3 kg
SBIRS-GEO-1	May 06, 2011	Launch of the first SBIRS (Space Based Infrared System) GEO-1 spacecraft of the US Air Force from Cape Canaveral on an Atlas-5 vehicle.
SBIRS-GEO-2 (USA-241)	Mar. 19, 2013	Launch of SBIRS-GEO-2 of the USAF on Atlas-5 401 from Cape Canaveral, FL. (infrared surveillance from GEO)
SBIRS-HEO-1	June 28, 2006	HEO-1 is a hosted payload onboard of NROL-22. Launched from VAFB on a Delta4M vehicle.
SBIRS-HEO-2	Mar. 13, 2008	HEO-1 is a hosted payload onboard of NROL-28. Launched from VAFB on an Atlas-5 vehicle.
SBSS-1	Sept. 26, 2010	Launch of the first SBSS (Space-Based Surveillance System) S/C of the U.S. AFSPC from VAFB, CA. The objective is to track space debris to accomplish SSA (Space Situational Awareness).
SCD-2	Oct. 23, 1998	Data collection satellite of INPE
SCD-2A	Nov. 02, 1997	INPE, VLS launch vehicle failure from Alcantara
SDO (Solar Dynamics Observatory)	Feb. 11, 2010	NASA solar science mission, launch on Atlas-V vehicle from KSC, FLA
SciSat-1	Aug.13, 2003	A CSA (Canada) S/C to study atmospheric ozone depletion, Pegasus-XL launch provided by NASA, from VAFB, CA
SeaSat	June 27, 1978	NASA S/C with first spaceborne SAR payload in history. Launch from VAFB, CA. Mission duration of 105 days due to an abrupt electrical power failure (end of mission on Oct. 10, 1978).
SEDSAT-1	Oct. 24, 1998	Secondary payload to DS-1, S/C of Univ. of Alabama
SELENE (Kaguya)	Sept. 14, 2007	Lunar mission of JAXA, Japan. Launch on H-IIA vehicle from TNSC (S/C mass of 3000 kg).
Sentinel-1A	Apr. 03, 2014	An ESA SAR satellite in the Copernicus program. Launch on a Soyuz-STB Fregat vehicle from Kourou.
SERVIS-1	Oct. 30, 2003	Technology mission of USEF, Japan; launch on a Rocket-KM of Eurockot from Plesetsk, Russia, launch mass of 840 kg

Mission	Launch Date	Comment
SERVIS-2	June 2, 2010	Technology mission of USEF, Japan; launch on a Rockot-KM of Eurokot from Plesetsk, Russia, launch mass of 740 kg
SES-8	Dec. 03.2013	Communication satellite of SES (3138 kg) launched from Cape Canaveral, FL. This was the first launch of a Falcon-9 V1.1 vehicle of SpaceX into GEO.
Shenzhou-5 (SZ-5)	Oct. 15, 2003	First Chinese manned flight on a CZ-2F launcher from the Jiuquan Satellite Launch Center in China (14 orbits prior to re-entry on Oct. 16). Shenzhou means "magic vessel or divine vessel" Yang Liwei became the first Chinese taikonaut
Shenzhou-6 (SZ-6)	Oct. 12, 2005	Second Chinese manned flight from the Jiuquan Satellite Launch Center in China. Two taikonauts were for 5 days in orbit.
Shenzhou-7 (SZ-7) BX-1	Sept. 25, 2008	Chinese manned flight of 3 days during with 3 taikonauts on board and the first successful EVA of a taikonaut during orbits 27-29 . Successful landing on Sept. 28, 2008. Ejection of an inspection microsatellite, BX-1 , on Sept. 27, 2008 from the nose of the SZ-7 orbital module - flying in formation with the mother spacecraft and taking imagery of SZ-7.
Shenzhou-8 (SZ-8)	Oct. 31, 2011	Launch from JSLC on a Long March 2F vehicle. The Shenzhou-8 spacecraft was automatically docked (China's first) with the Tiangong-1 space module in Nov. 2011. Shenzhou-8 landing on Nov. 17, 2011.
Shenzhou-9 (SZ-9)	June 16, 2012	SZ-9 was launched on a Long March 2F vehicle. SZ-9 is the second spacecraft and first manned Chinese spacecraft to have docked with the Tiangong-1 space station, which took place on June 18, 2012. The mission's crew of 3 taikonauts includes the first Chinese female astronaut, Liu Yang. Launch from the Jiuquan Satellite Launch Center. The taikonauts entered the Tiangong-1 station on June 18, 2012. The Shenzhou-9 spacecraft and the 3 taikonauts returned to Earth (Inner Mongolia landing) on June 29, 2012 (13 day mission).
Shenzhou-10	June 11, 2013	A third and final mission to Tiangong-1, the manned Shenzhou-10 vehicle, docked automatically on June 13, 2013. This was China's second manned spaceflight mission (2 men, 1 woman astronaut) to the Tiangong-1 space module. China aims to complete the space station by 2020. - The Shenzhou-10 spacecraft and the 3 taikonauts returned to Earth (Inner Mongolia landing) on June 26, 2013 (15 day mission).
Shiyao-1 (Tansuo-1) Naxing-1	April 18, 2004	Minisatellite (stereo imager) technology mission of Harbin Institute of Technology (China) with a CZ-2C vehicle from Xichang, China, S/C mass of 204 kg, orbit of 600 km, inclination 97.7° Naxing-1 a microsatellite (25 kg) of Tsinghua University, China
Shiyao-3 Chuangxin 1-02	Nov. 05, 2008	Technology demonstration satellite of Harbin Institute of Technology (China). Launch with CZ-2D from Jiuquan. EO satellite of CAS to collect hydrological and meteorological data.
Shiyao-4 Chuangxin 1-03	Nov. 20, 2011	Technology demonstration satellite of CNSA. Launch with CZ-2D from Jiuquan. EO satellite of CAS to collect hydrological and meteorological data.
Sich-1 (Okean-O1-N8)	Aug. 31, 1995	Ukrainian/Russian Earth and ocean monitoring mission, launch on a Tsyklon-3 vehicle from Plesetsk, Russia
Sich-2 Secondary payloads: NigeriaSat-2 NigeriaSat-X EduSat RASAT AprizeSat-5 and -6 BPA-2	Aug. 17, 2011	Ukrainian EO mission of NSAU. Dnepr launch from Yasny/Dombrowsky launch site, Russia High-resolution EO mission of NARSDA, Nigeria Medium-resolution EO mission of NARSDA Microsatellite of the University of Rome, Italy Microsatellite of Tubitak Uzay, of Ankara, Turkey Microsatellites with AIS payload of Aprize Satellite Inc Advanced Avionics Unit-2 of Hartron-Arkos, Ukraine (remained attached to upper stage)

Mission	Launch Date	Comment
Sich-1M (Modified) MS-1TK (Mikron)	Dec. 24, 2004	Ukrainian/Russian (NKAU) Earth and ocean monitoring mission in the optical, infrared and the SHF bands. Launch on a Tsyklon-3 vehicle from Plesetsk, Russia (2263 kg mass of Sich-1M). Microsatellite (65 kg) of NKAU, technology demonstration
SIRTF (renamed to "Spitzer Space Telescope")	Aug. 25, 2003	A NASA astronomy observatory, launch on a Delta-2 from Cape Canaveral, FLA; SIRTF (Space Infrared Telescope Facility). Spitzer is in an Earth-trailing heliocentric orbit. The primary mirror is 85 cm in diameter.
SJ-1 (Shi Jian-1) China	Mar. 03, 1971	Chinese minisatellite of 221 kg for particle measurements. Launch on CZ-1 vehicle from Jiuquan launch complex, China
SJ-2, China SJ-2A SJ-2B	Sept. 20, 1981	Chinese minisatellites (science missions). Launch of first multiple spacecraft from China on FB-1 (Feng Bao-1) launcher from Jiuquan launch complex, China
SJ-4, China	Feb. 08, 1994	Chinese minisatellite of 397 kg. Launch on LM-3A vehicle from the Xichang launch complex, China
SJ-5, China	May 10, 1999	A CAST technology demonstration mission, launch on LM-4B vehicle from the Taiyuan launch site. SJ-5 was a secondary payload to FY-1C (meteorological payload of China)
SJ-6A, China SJ-6B	Sept. 08, 2004	Launch from the Taiyuan launch site on a CZ-4B launch vehicle
SJ-7	July 06, 2005	Launch from the Jiuquan launch site on CZ-2D launch vehicle
SJ-6C, China SJ-6D	Oct. 23, 2006	Launch from the Taiyuan launch site on a CZ-4B launch vehicle
SJ-6E, China SJ-6F	Oct. 25, 2008	Launch from the Taiyuan launch site on a CZ-4B launch vehicle
SJ-6G, China SJ-6H	Oct. 06, 2010	Launch from the Taiyuan launch site on a CZ-4B launch vehicle
SJ-11-01, CNSA	Nov. 12, 2009	Launch from the Jiuquan launch site on CZ-2C launch vehicle
SJ-12-01	June 15, 2010	Launch from the Jiuquan launch site on CZ-2D launch vehicle
SJ-11-03	July 06, 2011	Launch from the Jiuquan launch site on CZ-2C launch vehicle
SJ-11-02	July 29, 2011	Launch from the Jiuquan launch site on CZ-2C launch vehicle
SJ-11-04	Aug. 18, 2011	Launch failure: Jiuquan launch site, CZ-2C launch vehicle
SJ-11-05	July 15, 2013	Launch from the Jiuquan launch site on CZ-2C launch vehicle
SJ-11-06	Mar. 31, 2014	Launch from the Jiuquan launch site on CZ-2C launch vehicle
SJ-9A (Shi Jian9A) SJ-9B (Shi Jian 9B)	Oct. 14, 2012	Launch of technology demonstration missions into LEO. Launch from Taiyuan launch site on CZ-2C/SMA. This is the first formation flying mission of CNSA, China.
SJ-11-05	July 15, 2013	Launch from the Jiuquan launch site on CZ-2C launch vehicle
SJ-15 Shiyan-7 Chuang Xin-3	July 19, 2013	Launch from Taiyuan launch site on Long March4C vehicle. Technology demonstration missions of China into LEO
Skylab-1 (SL-1)	May 14, 1973	NASA station was launched by a Saturn V booster (unmanned)
Skylab-2 (SL-2) Landing	May 25, 1973 June 22, 1973	First manned Skylab mission. The crew conducted solar astronomy and Earth resources experiments, medical studies, and five student experiments
Skylab-3 (SL-3) Landing	July 28, 1973 Sept. 25, 1973	Second manned Skylab mission. Continued maintenance of the space station and extensive scientific and medical experiments.
Skylab-4 (SL-4) Landing	Nov. 16, 1973 Feb. 08, 1974	Last manned Skylab mission.
SloshSat-FLEVO	Feb. 12, 2005	A technology payload of ESA and NIVR. Launch on Ariane-5 ECA qualification flight from Kourou. Primary payloads of XTAR-EUR and MaqSat-B2 into GTO
SMART-1 (ESA) INSAT-3E e-Bird-1	Sept. 27, 2003	ESA microsatellite technology mission to the moon; launch on Ariane 5G along with INSAT-3E (ISRO) and e-Bird-1 (communication satellite of Eutelsat)
SMEX/FAST	Aug. 21, 1996	NASA/GSFC, (Fast Auroral Snapshot Explorer)
SMEX/TRACE	Apr. 02, 1998	NASA/GSFC, (Transition Region and Coronal Explorer)
SMOS	Nov. 02, 2009	ESA technology demonstration mission. Launch on Rocket vehicle from Plesetsk, Russia
PROBA-2		ESA technology demonstration mission (secondary payload)

Mission	Launch Date	Comment
SNOE	Feb. 25, 1998	University of Colorado at Boulder (LASP); SNOE reentered the atmosphere on Dec. 13, 2003
SOHO	Dec. 02, 1995	ESA/NASA mission, launch from Cape Canaveral on Atlas-2
Solar-A (Yohkoh)	Aug. 30, 1991	JAXA physics mission (formerly ISAS). Launch by an M-3SII-6 launch vehicle from the Kagoshima Space Center, Japan
Solar-B (Hinode) HIT-SAT	Sept. 23, 2006	JAXA spacecraft, on a JAXA M-V-7 launch vehicle from USC (Uchinoura Space Center), Japan Secondary payload (3 kg) of Hokkaido Institute of Technology)
SORCE	Jan. 25, 2003	NASA satellite on a Pegasus XL launcher from KSC
SpaceX CRS-1	Oct. 8, 2012 (UTC)	Launch of the first SpaceX operational mission under their Commercial Resupply Services (CRS-1) contract with NASA. Use of Falcon-9 vehicle with Dragon cargo spacecraft to ISS. CRS-1 carried also the OG2-1 (Orbcomm Second Generation-1) prototype communications satellite, which was deployed prior to station arrival into a lower orbit than planned.
SPEKTR-R	July 18, 2011	Launch of an international VLBI mission of Roskosmos, Russia, from Baikonur on a Zenith-3F vehicle. Study of radio sources in the Milky Way with a 10 m radio telescope of Lebedev Physical Institute. Launch mass of ~ 3600 kg, HEO orbit of ~ 1000 km x 340,000 km, inclination = 51.6°, period ~ 193 hours.
Spirale-A and -B	Feb. 12, 2009	A reconnaissance constellation of DGA (France) with 2 satellites in GTO, S/C mass of 120 kg (each). Launch from Kourou on Ariane-5 as auxiliary payloads to Hot Bird 10 and NSS-9.
SPOT-1	Feb. 22, 1986	CNES, launch on Ariane from Kourou
SPOT-2	Jan. 22, 1990	CNES, launch on Ariane from Kourou
SPOT-3	Sept. 26, 1993	CNES, launch on Ariane from Kourou
SPOT-4	March 23, 1998	CNES, a new instrument "VEGETATION" is flown
SPOT-5	May 04, 2002	CNES Earth imaging mission, Ariane-4 launch from Kourou, two picosatellites, IDEFIX of AMSAT-France are secondary payloads
SPOT-6 Secondary payload: PROITERES	Sept. 09, 2012	EADS Astrium commercial imaging mission, PSLV-C21 launch of ISRO from SDSC-SHAR, India (S/C mass 712 kg) Nanosatellite of Osaka Institute of Technology, Osaka, Japan
SPOT-7 Secondary payloads CanX-4, CanX-5 AISat VELOX-1	June 30, 2014	Airbus Space and Defence commercial imaging mission, PSLV-C23, launch of ISRO from SDSC-SHAR, (S/C mass 714 kg). Nanosatellites (each 15 kg) of UTIAS/SFL, Toronto, Canada A technology demonstration satellite (14 kg) of DLR, Germany A 3U CubeSat (4.5 kg) of NTU, Singapore
SPRINT-A Nickname: Hisaki	Sept. 14, 2013	JAXA launched the first Epsilon-1 vehicle from the Uchinoura Space Center, Japan with the SPRINT-A (Spectroscopic Planet Observatory for Recognition of Interaction of Atmosphere) payload. SPRINT-A mass = 348 kg, orbit: 950 km x 1150 km, 31°.
SRTM	Feb. 11-22, 2000	NASA/DLR/ASI mission (Shuttle Radar Topography Mission)
ST5	Mar. 22, 2006	NASA microsatellite constellation (launch from VAFB)
Starlette	Feb. 06, 1975	CNES geodetic satellite (laser ranging), launch from Kourou on a Diamant BP4 launch vehicle
STARSHINE-1	May 27, 1999	Student satellite on STS-96 (reentry of S/C Feb. 18, 2000)
STEDI/SNOE	Feb. 26, 1998	(Student Nitric Oxide Explorer), NASA, Univ. of Colorado on a Pegasus XL vehicle from VAFB, CA
Stella	Sept. 26, 1993	CNES geodetic satellite (copy of Starlette, laser ranging, mass of 48 kg), launch from Kourou on an Ariane-4 launcher
Stentor	Dec. 11, 2002	CNES communication technology S/C (2210 kg) on Ariane 5 vehicle (launch failure). HotBird-7 was co-passenger on launch
STEREO	Oct. 26, 2006 (UTC)	NASA Sun-Earth mission of twin S/C in heliocentric orbits, launch on Delta-2 vehicle from Cape Canaveral, FLA
STEX/ATEX	Oct. 03, 1998	NRO technology mission launched from VAFB with tether experiment (of NRL) and many enabling technologies

Mission	Launch Date	Comment
STP-1 Payloads: (6 S/C) OE MidStar-1 STPSat-1 CFESat FalconSat-3	Mar. 09, 2007	First DoD technology demonstration mission with ESPA on an Atlas-V launch vehicle from Cape Canaveral, FLA. Orbital Express (primary) consisting of ASTRO and NextSat MidStar-1 of USNA STPSat-1 of AFRL CFESat of LANL FalconSat-3 of USNPS
STP-S26 Payloads: STPSat-2 RAX O/OREOS FASTSat-HSV FalconSat-5 FASTRAC-1, -2	Nov. 20, 2010 (UTC)	DoD (USAF) technology demonstration mission with ESPA on a Minotaur-IV vehicle (with HAPS) from KLC (Kodiak Launch Complex), AK (circular orbit of 650 km, 72° inclination) Primary payload (also STP-SIV) with a mass of 137 kg A 3U CubeSat mission of the University of Michigan (3 kg) A 3U CubeSat mission of NASA/ARC (5.5 kg) A minisatellite of NASA/MSFC (150 kg) including NanoSail-D2 A minisatellite mission of USAFA (161 kg) A nanosatellite pair of the University of Texas (54 kg total mass)
STRV-1c/d	Nov. 16, 2000	DERA satellites – Note: Only the first two weeks of both missions were successful. Then, telemetry from both spacecraft (STRV-1c and -1d) indicated a serious problem. The unrecoverable problem with the spacecraft receivers caused the end of the mission.
STSat-1	Sept. 27, 2003	Science and Technology Satellite-1 of KAIST (formerly known as KAISTSat-4) was launched on a Cosmos-3M from Plesetsk
STSat-2	Aug. 25, 2009	Science and Technology Satellite-2 of KAIST, Korea. Launch with KSLV-1 from the Naro space Center in Korea. Unfortunately, a launch failure occurred on the maiden flight of KSLV-1
STSat-2B	June 10, 2010	Science and Technology Satellite-2B of KARI, Korea. Launch with KSLV-1 (now referred to as Naro-1) from the Naro space Center in Korea. Unfortunately, a launch failure occurred after 2 minutes of flight. The Naro-1 rocket uses a Russian liquid-fueled first stage and a Korean solid-fueled upper stage. An investigation of the failure is being conducted.
STSat-2C	Jan. 30, 2013	Science and Technology Satellite-2C of KARI, Korea. Launch with Naro-1 (Korea developed launcher) from the Naro Space Center in Korea.
SUNSAT	Feb. 23, 1999	Student-built satellite of Stellenbosch University, SA
Swarm constellation	Nov. 22, 2013	Launch of 3 Swarm minisatellites of ESA on a Rockot vehicle from Plesetsk, Russia. The objective is to provide the best ever survey of the Earth's magnetic field.
SWIFT	Nov. 20, 2004	NASA astrophysics mission to observe gamma rays. Launch on a Delta-2 vehicle from Cape Canaveral, FLA
SZ-1 (Shenzhou-1)	Nov. 20, 1999	First Chinese test launch for manned space flight (but without Taikonauts). After 14 orbits, the recovery capsule touched down in the Inner-Mongolia region of north China on Nov. 21, 1999
SZ-2 (China)	Jan. 9, 2001	Second Chinese unmanned test launch from JSLC (Jiuquan Satellite Launch Center). Capsule landing on Jan. 16, 2001.
SZ-3 (China)	Mar. 25, 2002	The SZ-3 spacecraft flew CMODIS (Chinese Medium Resolution Spectral Imager), among other EO sensors. Reentry of SZ-3 on Nov. 12, 2002 over the southern hemisphere: impact at 22° S, 109° E (first long-duration unmanned flight; the orbital module disintegrated on reentry after nearly 232 days in orbit).
SZ-4 (China)	Dec. 29, 2002	The SZ-4 spacecraft flew MMSS (Multimode Microwave Sensor System) consisting of a radar altimeter, a microwave scatterometer and a microwave radiometer. Seven day mission with a capsule landing on Jan. 5, 2003.
SZ-5 (China)	Oct. 15, 2003	SZ-5 carried the first Chinese Taikonaut into space. After 14 orbits the SZ-5 capsule launched successfully on Oct. 16, 2003

Mission	Launch Date	Comment
SZ-8 (China)	Oct. 31, 2011	Shenzhou-8 was launched on board a Long March vehicle from the Jiuquan Satellite Launch Center. On Nov. 2, 2011 SZ-8 docked with Tiangong-1. – A 2 nd successful docking was performed on Nov. 14, 2011 (after separation of 140 m of the two spacecraft). On board is the SIMBOX (Science in Microgravity Box) experimental facility of DLR containing 17 experiments from the fields of biology and medicine, which will be conducted by German researchers together with their Chinese colleagues. On Nov. 17, 2011, Shenzhou-8 landed in north China's Inner Mongolia Autonomous Region.
TacSat-2 GeneSat-1	Dec. 16, 2006	Technology demonstration S/C of AFRL. Launch on a Minotaur vehicle from NASA's Wallops Flight Facility, Wallops Island, VA. A CubeSat of NASA/ARC and various universities (secondary payload to TacSat-2)
TacSat-3 + Secondary payloads:	May 19, 2009	Technology demonstration S/C of AFRL. Launch on a Minotaur vehicle from MARS (Mid-Atlantic Regional Spaceport) facility, Wallops Island, VA. Secondary payloads (CubeSats): PharmaSat-1, AeroCube-3, HawkSat-1, and CP-6.
TanDEM-X	June 21, 2010	The TanDEM-X mission of DLR was launched on a Dnepr-1 vehicle of ISC Kosmotras from Baikonur, Kazakhstan.
TDRS-H	June 30, 2000	NASA Data Relay satellite
TDRS-I (TDRS-9)	Mar. 08, 2002	NASA Tracking and Data Relay Satellite
TDRS-J (TDRS-10)	Dec. 05, 2002	NASA Tracking and Data Relay Satellite, launch on Atlas-2A from Cape Canaveral
TDRS-K (TDRS-11)	Jan. 31, 2013	NASA Tracking and Data Relay Satellite, launch on Atlas-V 401 vehicle from Cape Canaveral, FL, launch provider: ULA.
TDRS-L (TDRS-12)	Jan. 24, 2014 (02:33 UTC)	NASA Tracking and Data Relay Satellite, launch on Atlas-V 401 vehicle from Cape Canaveral, FL, launch provider: ULA.
TEAMSAT, YES	Oct. 30, 1997	ESA technology demonstrator payload on Ariane-5 test flight
TechSat/Gurwin-II	July 10, 1998	Technion Israel Institute of Technology, Haifa, Israel
TecSAR	Jan. 21, 2008	ISRO launch of an IAI (Israel Aerospace Industries) SAR satellite from SDSC (Satish Dhawan Space Center), India
Terra (EOS/AM1)	Dec. 19, 1999	NASA S/C with MODIS, ASTER, etc.
TERRIERS	May 18, 1999	Boston University/NASA. Note: the S/C got lost and could not be operated
TES, PROBA, BIRD	Oct. 22, 2001	ISRO prime payload TES (Technology Experiment Satellite), a classified S/C of ISRO (military surveillance); secondary payloads are: PROBA of ESA and BIRD of DLR; Launch from SHAR on a PSLV-C3 vehicle, orbit of 560 km, inclination of 98.7°
TerraSAR-X	June 08, 2007	German SAR mission (DLR). Launch on a Dnepr-1 vehicle from Baikonur, Kazakhstan
TH-1 (Tian Hui-1)	Aug. 24, 2010	Launch of a CNSA EO satellite (stereo imagery) from the Jiuquan Satellite Launch Center) in China.
THEOS	Oct. 01, 2008	Launch of THEOS (Thailand Earth Observation System) of GISTA on a Dnepr vehicle from Yasny/Dombrovsky, Russia
Tiangong-1 (TG-1) Heavenly Palace-1	Sept. 29, 2011	China launched its first space station module into orbit on a Long March 2F/G vehicle from the Jiuquan Satellite Launch Center, China. It is part of a space station program with the goal to place a full-size, semi-permanent crewed space station into orbit by 2020. The 8,500 kg TG-1 (length = 10.4 m, diameter = 3.35 m) was designed to stay in space for at least 2 years and support crews of up to three astronauts for short duration stays. The TG-1 module orbits at an altitude of ~ 350 km, inclination = 42°. It will be the target of at least three upcoming space missions – Shenzhou 8, 9 and 10.
Tianlian I-01	April 25, 2008	Launch of China's first data tracking and relay satellite on a March-3C vehicle from Xichang SLC (Satellite Launch Center)
Tianlian I-02	July 12, 2011	Launch of China's 3rd data tracking and relay satellite on a March-3C vehicle from the Xichang SLC

Mission	Launch Date	Comment
Tianlian I-03	July 25, 2012	Launch of China's 2nd data tracking and relay satellite on a March-3C vehicle from the Xichang SLC
TIMED	Dec. 07, 2001	NASA launch (Delta-2-7925) from VAFB
TiungSat-1	Sept. 26, 2000	Microsatellite of ATSB, Kuala Lumpur, Malaysia (built by SSTL)
TMSat / Thai-Paht-1	July 10, 1998	Microsatellite of Thailand built at SSTL by a Thai engineering team, the new name of the spacecraft is Thai-Paht-1 . Launch as secondary payload on a Zenit-2 vehicle from Baikonur.
TOMS-EP	July 02, 1996	NASA S/C, Ozone measurements
TOPEX/Poseidon	Aug. 11, 1992	NASA/CNES mission with a launch from Kourou on Ariane-4, French Guiana (CNES paid for the launch). The KitSat-1 microsatellite of KAIST (Korea) was on this flight as a piggyback payload, use of ASAP (V.52).
TRACE	April 02, 1998	NASA/GSFC mission in the SMEX (Small Explorer) program
TRMM	Nov. 27, 1997	NASDA/NASA (Tropical Rainfall Measuring Mission) on H-II launcher from Tanegashima, Japan (along with ETS-VII)
Tsinghua-1	June 28, 2000	Tsinghua University, Beijing - Imaging Demonstrator Mission Three S/C in Cosmos launch from Plesetsk (SNAP-1, Nadezhda-6 (Hope) and Tsinghua-1
TSX-5	June 06, 2000	DoD with STRV-2 payload package and CEASE
TUBSAT-A	July 17, 1991	Technical University Berlin (TUB); launch from Kourou on Ariane-4 (secondary payload to ERS-1 of ESA)
TUBSAT-B	Jan. 25, 1994	TUB S/C, launch on a Tsyklon vehicle from Plesetsk, Russia, as a secondary payload to Meteor-3-7
TUBSAT-N+N-1	July 07, 1998	Data collection satellites of TU Berlin, Russian submarine tandem launch from the western Barents Sea
DLR-TUBSAT	May 26, 1999	Earth observation, TU Berlin (TUB)
Maroc-TUBSAT	Dec. 10, 2001	TUB and CRTS (Morocco) S/C, launch on a Zenit-2 vehicle from Baikonur as secondary payload to Meteor-3M-1
LAPAN-TUBSAT	Jan. 10, 2007	LAPAN (Indonesia). Launch on PSLV-7 vehicle from SHAR, India. CartoSat-2 was the primary payload.
TWINS-1	June 28, 2006	Hosted NASA payload TWINS (Two Wide-angle Imaging Neutral-atom Spectrometers) on NROL-22 flight (spacecraft USA-184). Delta-4M launcher from VAFB, CA
TWINS-2	Mar. 13, 2008	Hosted NASA payload on NROL-28 flight (spacecraft USA-200). Atlas-5-411 launcher from VAFB, CA
UARS	Sept. 12, 1991	NASA mission with a launch on STS-48 (deployed on Sept. 15, 1991). UARS (Upper Atmosphere Research Satellite).
UoSat-1	Oct. 6, 1981	First microsatellite of SSTL, Surrey, UK; launch as secondary payload on a Thor Delta from VAFB. Reentry on Oct. 13, 1989
UoSat-2	Mar. 1, 1984	Launch as secondary payload to Landsat-5. UoSat-2 is still operational as of Sept. 2004.
UoSat-3 also known as HealthSat-1	Jan. 22, 1990	Launch as secondary payload to SPOT-2 from Kourou. The mission ended in May 1997 due to OBC failure. First use of ASAP ring on an Ariane launch vehicle.
UoSat-4	Jan. 22, 1990	Launch alongside UoSat-3 as secondary payload to SPOT-2. Communications were lost shortly after launch.
UoSat-5	July 17, 1991	Launch as secondary payload to ERS-1 from Kourou. UoSat-5 is operational as of Sept. 2004.
UoSat-12	Apr. 21, 1999	First minisatellite of SSTL. Operations ended in Sept. 2003.
UniSat-1	Sept. 26, 2000	Dnepr launch from Baikonur with SaudiSat-1A/1B (SISR), UniSat (University of Rome, Italy), MegSat-1 (MegSat SPA, Italy), and TiungSat 1 of ATSB, Malaysia
UniSat-2 LatinSat-1/2 Rubin-2 SaudiSat-2 Trailblazer	Dec. 20, 2002	Launch of nanosatellites (Dnepr 1 launch from Baikonur) into 650 km circular orbit at 65° inclination. UniSat-2 of the University of Rome, Italy. LatinSat-1, -2 of Aprize Satellite Inc., Argentina (S&F communication, S/C built by SpaceQuest Ltd., Fairfax, VA, each S/C of 11 kg), Rubin-2 of OHB-System, Germany (technology), SaudiSat-2 (1c) of KACST, Saudi Arabia (technology), and Trailblazer (dummy payload of 110 kg), TransOrbital Inc., La Jolla, CA, USA

Mission	Launch Date	Comment
UniSat-3	June 29, 2004	Multisatellite launch on a Dnepr launch vehicle from Baikonur
VCO (Planet-C) IKAROS UNITEC-1 Negai-Star Waseda-Sat-2 KSAT	May 20, 2010	JAXA launched VCO (Venus Climate Orbiter), nickname: Akatsuki, ~ 500 kg, from TNSC on the H-IIA F17 vehicle. Secondary payloads are: A minisatellite of JAXA (~ 315 kg) to demonstrate solar sails A microsatellite (21 kg) of UNISEC, Japan flying toward Venus A CubeSat of Soka University, Japan A CubeSat of Waseda University, Tokyo, Japan A CubeSat of Kagoshima University, Japan
VRSS-1	Sept. 29, 2012	VRSS-1 (Venezuela Remote Sensing Satellite) was launched by a Long March 2D vehicle from the Jiuquan Launch Center, China. In 2012, VRSS-1 was renamed to Francisco Miranda .
WESTPAC	July 10, 1998	Australian research S/C of Electro Optic Systems Pty Ltd (EOS)
WISE	Dec. 14, 2009	WISE (Wide-field Infrared Survey Explorer) of NASA was launched on a Delta-2 vehicle from VAFB, CA.
WMAP	June 30, 2001	Launch of NASA astronomy probe on a Delta-II vehicle into L2 orbit
WorldView-1	Sept. 18, 2007	Launch of a commercial imaging satellite of Digital Globe on a Delta-2920 vehicle from VAFB, CA
WorldView-2	Oct. 08, 2009	Launch of a commercial imaging satellite of Digital Globe on a Delta-2920 vehicle from VAFB, CA
X-37-B OTV-1	April 22, 2010	Launch of an unpiloted robotic demonstration spaceplane, OTV (Orbital Test Vehicle), a classified project of DARPA, from CCAFS, FLA (use of an Atlas-5 vehicle of ULA). The objective of the USAF OTV-1 is to demonstrate autonomous orbital flight, reentry and landing. OTV-1, built by Boeing, is 9 m in length and 4.5 m wide and a total mass of 5400 kg. It has a payload bay size of 2.1 m x 1.2 m (a mini space shuttle in shape) with a max. payload capability of 226 kg. OTV has the capability to remain in orbit for 270 days.
XMM-Newton	Dec. 10, 1999	ESA astronomy mission, launch on Ariane-5 from Kourou into HEO (113,083 km x 8,062 km, inclination=36.86°)
XSS-10	Jan. 29, 2003	Experimental Spacecraft System-11 of AFRL (USA), launch as a secondary payload to a GPS spacecraft (2R-8) on a Delta-2 vehicle from KSC, FLA
XSS-11	April 11, 2005	Experimental Spacecraft System-11 of AFRL (USA), launch on a Minotaur vehicle from VAFB, CA; Demonstration of autonomous rendezvous technology
Yaogan-1	April 27, 2006	A remote sensing satellite of China with a mass of 2700 kg (first spaceborne SAR payload of China) built by CAST (China Academy of Space Technology), launch from the TSLC (Taiyuan Satellite Launch Center)
Yaogan-2	May 25, 2007	A remote sensing satellite of China (electro-optical payload built by CAST) was launched from JSLC (Jiuquan Satellite Launch Center), China
Yaogan-3	Nov. 12, 2007	China launched a remote sensing satellite (SAR payload) from TSLC
Yaogan-4	Dec. 01, 2008	A remote sensing satellite of China (electro-optical payload built by CAST) was launched from JSLC, China (Long March -2D)
Yaogan-5	Dec. 15, 2008	A remote sensing satellite of China (SAR payload built by CAST) was launched from the TSLC, China (Long March -4B)
Yaogan-6	April 22, 2009	China launched a remote sensing satellite (SAR payload) from TSLC
Yaogan-7	Dec. 10, 2009	China launched a remote sensing satellite (optical reconnaissance) from the Jiuquan Satellite Launch Center (JSLC) in the northwestern Gansu Province.
Yaogan-8	Dec. 15, 2009	China launched a remote sensing satellite from the Taiyuan Launch Center on a Long March 4C vehicle. HOPE-1 was a secondary payload (minisatellite)
Yaogan-9	Mar. 04. 2010	China launched a remote sensing satellite (optical and radar reconnaissance) from JSLC on a Long March 4C vehicle.
Yaogan-10	Aug. 09, 2010	China (CNSA), Long March-4C launch of a satellite from TSLC

Mission	Launch Date	Comment
Yaogan-11 Secondary payloads: Zheda Pixing-1A1 Zheda Pixing-1A2	Sept. 22, 2010	China (CNSA), Long March-2D launch of a remote sensing satellite from JSLC (Jiuquan Satellite Launch Center), Launch of two technology demonstration picosatellites of Zhejiang University (ZDPS-1A-1 and ZDPS-1A-2), with a total mass of 3.5 kg.
Yaogan-12 TianXun-1	Nov. 09.2011	China launched a remote sensing satellite from the Taiyuan Launch Center on a Long March 4B vehicle. Secondary payload (microsatellite, 35 kg) for technology demonstrations, Nanjing University of Aeronautics and Astronautics
Yaogan-13	Nov. 29, 2011	China (CNSA) remote sensing satellite, Long March-2C vehicle, launch from TSLC
Yaogan-14 Tiantuo-1 (TT-1)	May 10, 2012	China (CNSA), Long March-4B launch of a satellite from TSLC China, a nanosatellite (9.3 kg) as secondary payload. TT-1 was built by NUDT (National University of Defense Technology)
Yaogan-15	May 29, 2012	China (CNSA), Long March-4C launch of a satellite from TSLC
Yaogan-16A Yaogan-16B Yaogan-16C	Nov. 25, 2012	China (CNSA), Long March-4C launch of a satellite from JSLC (Jiuquan Satellite Launch Center)
Yaogan-19	Nov. 20, 2013	China (CNSA), Long March-4C launch of a satellite from TSLC (Taiyuan Satellite Launch Center), reconnaissance
Yubileiny (RS-30)	May 23, 2008	Russian microsatellite (45 kg) a technology demonstration mission, built by ISS-ISS-Reshetnev Company (the former NPO PM), launch on a Rockot vehicle from Plesetsk, Russia. Yubileiny was a secondary payload to a cluster of three Gonet satellites.
Yubileiny-2 Primary payloads: Gonets-M-3 & -4 Strela-3/Rodnik	July 28, 2012	Russian microsatellite (65 kg), a technology demonstration mission and a secondary payload. Rockot vehicle from Plesetsk. Communication satellites of Roscosmos Military reconnaissance satellite.
ZY-1A FM1 (Zi Yuan-1 FM1) see also CBERS-1	Oct. 14, 1999	ZY-1A (Resource) was launched on a Long March 4B vehicle from the Taiyuan Satellite Launch Center.
ZY-1B FM2 (CBERS-2	Oct. 21, 2003	China/Brazil mission, ZY-1B (Resource), also called CBERS-2, launch from Taiyuan on a CZ-4B vehicle, along with CX-1 (Chuang Xin-1)
ZY-2 FMA (Zi Yuan-2 FMA) ZY-2 is 2 nd generation series FM=Flight Model	Sept. 01, 2000	Chinese CZ-4B launch vehicle with the Zi Yuan 2 remote sensing satellite from the Taiyuan launch facility (altitude of 492 km, inclination of 97.4°). ZY-2 is a classified mission also code-named Jianbing-3 and is considered China's first high-resolution military optical reconnaissance satellite (< 5 m resolution). The S/C remained operational until 2004. ³⁰⁰⁵⁾
ZY-2 FMB (Zi Yuan-2 FMB)	Oct. 27, 2002	Launch of the Chinese reconnaissance mission ZY-2B from the Taiyuan launch facility. SSO of 477.5 km x 505.4 km, inclination of 97.4°, period of 94.4 min. ZY-2B operates in tandem with ZY-2A. Image resolution of 3 m Pan.
ZY-2 FMC (Zi Yuan-2 FMC)	Nov. 06, 2004	Launch of the remote sensing satellite ZY-2C of CAST, China, from the Taiyuan launch facility.
ZY-1-02C (Zi Yuan-1 FMC)	Dec. 22, 2011	Launch of the remote sensing satellite ZY 1-02C of CAST, China (CNSA), from the Taiyuan launch facility (Long March 4B). Ziyuan 1-02C was the third satellite in the CBERS-2 series, but was developed as a Chinese only project with no Brazilian participation. ³⁰⁰⁶⁾
ZY-3A (Zi Yuan-3A) VesselSat-2 (secondary payload)	Jan. 09, 2012	Launch of the remote sensing satellite ZY-3A of CNSA from Taiyuan (Long March 4B). Orbit of 506 km. Launch mass = 2600 kg. VesselSat-2 of Luxspace (OHB) with an AIS payload is a secondary payload (microsatellite mass = 29 kg).

Table 174: EO satellite launches since submission of 3rd edition to the publisher (Feb. 1996) ^{3005) 3006)}

3005) "Ziyuan 2," URL: <http://www.sinodefence.com/satellites/ziyuan2.asp>

3006) "Ziyuan 1-02C," URL: <http://www.sinodefence.com/satellites/cbers-ziyuan.asp>

1.33 Space Shuttle Mission Chronology

The following table contains brief information on all Shuttle flights with regard to orbits, launch/landing dates, orbiter type, and payload complement. ³⁰⁰⁷⁾ ³⁰⁰⁸⁾ ³⁰⁰⁹⁾ ³⁰¹⁰⁾ All payload abbreviations are defined in Appendix: “Acronyms and Abbreviations”; however, no descriptions are given for these Shuttle payloads (which is beyond the scope). The interested reader may consult the corresponding NASA homepages on internet.

Note: Following STS–9 (Space Transport System) the flight numbering system was changed. Thus, the next flight, instead of being designated STS–10, became STS 41–B. The new numbering system was supposed to be more specific; the first numeral stood for the fiscal year of the launch, the “4” for 1984. The second numeral represented the launch site, 1 for KSC, and 2 for VAFB. The letter “B” designated the launch in the fiscal year. Following the Challenger accident (Jan. 28, 1986) NASA reestablished the original numbering system.

Mission Incl., Alt.(km)	Launch/ Landing Date	Orbiter	Mission Highlights / Payload Complement
Legend: I = Inclination (°) A = Nominal Flight Altitude (km)			
STS–1 I:40.3°, A:307	12. April 1981 14. April 1981	Columbia	Major systems tested, orbiter sustained tile damage
STS–2 I:38°, A:290	12. Nov. 1981 14. Nov. 1981	Columbia	OSTA–1 payload (including SIR–A, MAPS, OCE, SMIRR, Canadarm1), see chapter J.21
STS–3 I:38°, A:272	22. Mar. 1982 30. Mar. 1982	Columbia	Get Away Special (GAS), Spacelab pallet mounted, OSS–1 payload, MLR, EEVT, HBT, SSIP
STS–4 I:28.5°, A:364	27. June 1982 4. July 1982	Columbia	DoD Payload (CIRRIS, HUP, SS–ANARS, SEPS, SWC, etc.), Get Away Special (GAS), CFES, MLR, IECM, SSIP
STS–5 I:28.5°, A:340	11. Nov. 1982 16. Nov. 1982	Columbia	ANIK C–3 and SBS C satellites, Get Away Special, SSIP
STS–6 I:28.5°, A:330	4. April 1983 9. April 1983	Challenger	1 st EVA, TDRS–1, CFES, MLR, RME, NOSL, Get Away Specials
STS–7 I:28.5°, A:360 km	18. June 1983 24. June 1983	Challenger	ANIK–C2 and PALAPA–B1 satellites, Get Away Specials, 10 experiments mounted on SPAS–01 (MOMS–01), OSTA–2 payload, CFES, MLR, SSIP
STS–8 I:28.5°, A:353	30. Aug. 1983 5. Sept. 1983	Challenger	INSAT–1B satellite, CFES, SSIP, ICAT, RME, Get Away Specials
STS–9 I:57°, A:287	28. Nov. 1983 8. Dec. 1983	Columbia	Spacelab–1 mission (ESA), see J.24
STS–41–B I:28.5°, A:300 km	3. Feb. 1984 11. Feb. 1984	Challenger	WESTAR–6 and PALAPA–B2 satellites, GAS, SPAS–2, MOMS–01, Cinema–360 camera, ACES, MLR, RME, IEF
STS–41–C I:28.5°, A: 580	6. April 1984 13. April 1984	Challenger	SMM satellite repair in orbit, LDEF deployment (57 experiments), IMAX camera, RME, Cinema–360, SSIP
STS–41–D I:28.5°, A:340 km	30. Aug. 1984 5. Sept. 1984	Discovery	3 satellites (SBS–D, SYNCOM IV–2, TELSTAR), OAST–1, CFES III, RME, SSIP, IMAX camera, CLOUDS
STS–41–G I:57°, A:352	5. Oct. 1984 13. Oct. 1984	Challenger	ERBS satellite,OSTA–3, LFC, IMAX camera, CANEX, APE, RME, TLD, MAPS, SIR–B, Get Away Specials
STS–51–A I:28.5°, A:342	8. Nov. 1984 16. Nov. 1984	Discovery	TELESAT–H (ANIK) and SYNCOM IV–1, retrieval of PALAPA–B–2 and WESTAR–VI, DMOS, RME
STS–51–C I:28.5°, A:407	24. Jan. 1985 27. Jan. 1985	Discovery	DoD payload
STS–51–D I:28.5, A:527	12. April 1985 19. April 1985	Discovery	TELSAT–I (ANIK C–1) and SYNCOM IV–3 satellites, CFES III, SSIP, AFE, Get Away Specials, PPE
STS–51–B I:57°, A: 411 km	29. April 1985 6. May 1985	Challenger	Spacelab–3 mission ESA, see J.25 [material sciences, life sciences, fluid mechanics, atmospheric physics (AT-MOS), and astronomy], Get Away Specials (NUSAT)

3007) Information taken from NASA publication: “Space Shuttle Mission Chronology 1981–1992,” and from Internet

3008) The acronyms of Shuttle payload complements are listed in Appendix C “Acronyms and Abbreviations”

3009) Shuttle orbits provided by J. Gass of NASA/GSFC

3010) “NASA Long–Term Plan For Shuttle Missions Details Station Timing,” Space News March 7–13, p. 26, 1994

Mission Incl., Alt.(km)	Launch/ Landing Date	Orbiter	Mission Highlights / Payload Complement
STS-51-G I:28.5°, A:405	17. June 1985 24. June 1985	Discovery	MORELOS-A, ARABSAT-A and TELSTAR-3D satellites, SPARTAN-1, Get Away Specials, HPTE, ADSF
STS-51-F I:49.5° A:383 km+	29. July 1985 6. Aug. 1985	Challenger	Spacelab-2 mission, [life sciences, plasma physics (PDP), astronomy (XRT, IRT), high-energy astro-physics, solar physics (SUSIM, HRTS, CHASE, SOUP), atmospheric physics, and technology research IPS]
STS-51-I I:28.5°, A:514	27. Aug. 1985 3. Sept. 1985	Discovery	ASC-1, AUSSAT-1, and SYNCOM IV-4 satellites, PVTOS
STS-52-J I:28.5°, A:590	3. Oct. 1985 7. Oct. 1985	Atlantis	DoD mission
STS-61-A I:57°, A:383	30. Oct. 1985 6. Nov. 1985	Challenger	Spacelab D1 (German mission), GLOMR satellite of DARPA deployed from Get Away Special canister
STS-61-B I:28.5° A:416 km	26. Nov. 1985 3. Dec. 1985	Atlantis	MORELOS-B, AUSSAT-2, and SATCOM satellites, EASE, ACCESS, CFES, DMOS, MPSE, OEX, Get Away Special, IMAX cargo bay camera (ICBC)
STS-61-C I:28.5°, A:392	12. Jan. 1986 18. Jan. 1986	Columbia	SATCOM KU-1 satellite, CHAMP, MSL-2, Hitchhiker-G1, IR-IE, IBSE, HPCG, SSIP, Get Away Specials
STS-51-L	28. Jan. 1986	Challenger	Accident !!!! (catastrophic failure) TDRS-B, SPARTAN-Halley
STS-26 I:28.5°, A:376	29. Sept. 1988 3. Oct. 1988	Discovery	TDRS-3 satellite, PVTOS, PCG, IRCFE, ARC, IFE, MLE, PPE, ELRAD, ADSF, SSIP, OASIS-1
STS-27 I:57°, A:460	2. Dec. 1988 6. Dec. 1988	Atlantis	DoD payload, deployment of USA-34, this code name designates the first high-resolution imaging radar S/C of the US military (also known under the name Lacrosse-1). Orbit of Lacrosse-1 was raised to 668 km x 703 km.
STS-29 I:28.5°, A:340	13. Mar. 1989 18. Mar. 1989	Discovery	TDRS-4 satellite, OASIS-1, SHARE, PCG, CHROMEX, SSIP, AMOS, IMAX camera
STS-30 I:28.8°, A:340	4. May 1989 8. May 1989	Atlantis	Magellan/Venus radar mapper S/C, MLE, FEA, AMOS
STS-28 I:57°, A:	8. Aug. 1989 13. Aug. 1989	Columbia	DoD payload
STS-34 I:34.3°, A:342	18. Oct. 1989 23. Oct. 1989	Atlantis	Galileo S/C to Jupiter, SSBUV, GHCD, PM, STEX, MLE, IMAX camera, AMOS, SSIP
STS-33 I:28.5°, A:	22. Nov. 1989 27. Nov. 1989	Discovery	DoD payload
STS-32 I:28.5°, A:389	9. Jan. 1990 20. Jan. 1990	Columbia	SYNCOM IV-F5 satellite (DoD), retrieval of LDEF, CNCR, PCG, FEA, AFE, L3, MLE, IMAX, AMOS
STS-36,A:811 I:62-65°	28. Feb. 1990 4. Mar. 1990	Atlantis	DoD payload (AFP-731)
STS-31 I:28.5°, A:703	24. April 1990 29. April 1990	Discovery	HST satellite, IMAX (ICBC), APM, PCG, RME III, IPMP, SSIP, AMOS
STS-41 I:28.5°, A:340	6. Oct. 1990 10. Oct. 1990	Discovery	Ulysses spacecraft (ESA/NASA), SSBUV, ISAC, CHROMEX, VCS, SSCE, IPMP, PSE, RME III, SSIP, AMOS
STS-38	15. Nov. 1990 20. Nov. 1990	Atlantis	DoD payload
STS-35 I:28.5°, A:520	2. Dec. 1990 10. Dec. 1990	Columbia	ASTRO-1 observatory (consisting of HUT, WUPPE, UIT, BBXRT, and IPS), SAREX-2, AMOS
STS-37 I:28.5°, A:518	5. April 1991 11. April 1991	Atlantis	CGRO (Compton Gamma Ray Observatory), CETA, APM, SAREX II, PCG, BIMDA, RME III, AMOS
STS-39 I:57°, A:298	28. April 1991 6. May 1991	Discovery	DoD classified mission including unclassified payload: AFP-675, IBSS, CIV, CRO, SPAS-II, STP-1, RME III, CLOUDS-1
STS-40 I:28.5°, A:340	5. June 1991 14. June 1991	Columbia	SLS-1 (Spacelab Life Sciences-1), Get Away Specials, MODE, OEX, GBA-2
STS-43 I:28.5° A:340 km	2. Aug. 1991 11. Aug. 1991	Atlantis	TDRS-5 satellite, SHARE II, SSBUV, TPCE, OCTW, APE-B, PCG III, BIMDA, IPMP, SAMS, SSCE, UVPI, AMOS

Mission Incl., Alt.(km)	Launch/ Landing Date	Orbiter	Mission Highlights / Payload Complement
STS-48 I:57°, A:657	12. Sept. 1991 18. Sept. 1991	Discovery	UARS satellite, APM, MODE, SAM, CREAM, PARE, PCG II-2, IPMP, AMOS
STS-44 I:28.5° A:416 km	24. Nov. 1991 1. Dec. 1991	Atlantis	DoD mission, DSP (Defense Support Satellite), plus unclassified payloads: IOCM, AMOS, CREAM, SAM, RME III, VFT-1, UVPI
STS-42 I:57° A:348 km	22. Jan. 1992 30. Jan. 1992	Discovery	IML-1 (International Microgravity Laboratory-1), Get Away Specials, GOSAMR-1, IMAX, IPMP, RME III, SSIP, GBA-3
STS-45 I:57°, A:340	24. Mar. 1992 2. April 1992	Atlantis	ATLAS-1 payload (ATMOS, MAS, SSBUV, ACRIM, SOLCON, SOLSPEC, SUSIM), Get Away Special, IPMP, STL-01, RME III, VFT-2, CLOUDS, SAREX II
STS-49 I:28.4°, A:390	7. May 1992 16. May 1992	Endeavour	EVA, Intelsat-VI capture and redeployment, ASEM, CPCG, UVPI, AMOS
STS-50 I:28.5°, A:350	25. June 1992 9. July 1992	Columbia	USML-1 (US Microgravity Lab-1), IPMP, SAREX II, UVPI
STS-46 I:28.5° A:502 km	31. July 1992 8. Aug. 1992	Atlantis	EURECA-1 satellite, TSS-1 (Tethered Satellite System), EOIM-III/TEMP, CONCAP II and III, ICBC, LDCE, AMOS, PHCF, UVPI
STS-47 I:57°, A:346	12. Sept. 1992 20. Sept. 1992	Endeavour	Spacelab-J (Japan), Get Away Specials, ISIAH, SSCE, SAREX II, AMOS, UVPI, GBA-4
STS-52 I:28.5° A:302 km	22. Oct. 1992 1. Nov. 1992	Columbia	LAGEOS-II, USMP-1, CANEX-2, SVS, MELEO, QUELD, PARLIQ, OGLW-2, SATO, CTA, CMIX, CPCG, CVTE, HPP, PSE, SPIE, UVPI, TPCE, ASP
STS-53 I:57° A:370 km	2. Dec. 1992 9. Dec. 1992	Discovery	DoD payload GCP, Get Away Specials, CRYOHP, ODERACS, BLAST, CLOUDS, CREAM, FARE, HERCULES, MIS-1, RME III, STL, VFT-2
STS-54 I:28.5°, A:296	13. Jan. 1993 19. Jan. 1993	Endeavour	TDRS-6 satellite, DXS, CGBA, CHROMEX, PARE, SAMS, SSCE
STS-56 I:57°, A:296	8. April 1993 17. April 1993	Discovery	ATLAS-2 payload (ATMOS, MAS, SSBUV, ACRIM, SOLCON, SOLSPEC, SUSIM), SPARTAN-201, SUVE, CMIX, PARE, STL-1, CREAM, HERCULES, RME III, AMOS
STS-55 I:28.5°, A:296	26. April 1993 6. May 1993	Columbia	Spacelab D2 (MOMS-02, MEDEA, WL, HOLOP, USS, MAUS, AOET, AR, BB, BA, ROTEX, MMA), SAREX
STS-57 I:28.5° A:474 km	21. June 1993 1. July 1993	Endeavour	SPACEHAB-1 (22 experiments), EURECA-1 retrieval, Get Away Specials, CONCAP IV, SHOOT, FARE, SAREX-II, AMOS
STS-51 I:28.5° A:296 km	12. Sept. 1993 22. Sept. 1993	Discovery	ACTS satellite, ASTRO-SPAS deployment of ORFEUS, IMAX, LDCE, CPCG, CHROMEX-04, HRSGS-A, APE-B, IPMP, RME III, AMOS
STS-58 I:39°, A:283	18. Oct. 1993 1. Nov. 1993	Columbia	SLS-2 (Spacelab Life Sciences-2), DEEFD, OARE, SAREX-II, PILOT
STS-61 I:28.5°, A:594	2. Dec. 1993 13. Dec. 1993	Endeavour	Hubble Space Telescope (HST) repair mission (optical correction), IMAX
STS-60 I:57°, A:404	3. Feb. 1994 11. Feb. 1994	Discovery	WSF-01, Spacehab-2, COB/GBA, SAREX-2, APE-B, ODERACS, BREMSAT, CPL
STS-62, I:39°, A:260	4. Mar. 1994 18. Mar. 1994	Columbia	USMP-2, OAST-2, DEE, SSBUV/A, LDCE, APCG, PSE, CPCG, CGBA, BDS, MODE, AMOS, BSTC, EDO
STS-59, I:57°, A:222	9. Apr. 1994 20. Apr. 1994	Endeavour	SRL-01 (Space Radar Laboratory, also referred to as SIR-C/X-SAR, see J.23), MAPS (J.13), CONCAP-4, SAREX-2, STL, TUFI, VFT-4, GAS (x3)
STS-65 I:28.5°, A:260	8. July 1994 23 July 1994	Columbia	IML-2, APCF, CPCG, AMOS, OARE, SAREX-2, EDO, MAST
STS-64 I:57°, A:258	9. Sept. 1994 20. Sept. 1994	Discovery	LITE-1 (see J.11), ROMPS, SPARTAN-201, TCS, SPIFEX, GAS, SAFER, SSCE, BRIC, RME, MAST, SAREX-II, AMOS, GBA-7
STS-68 I:57°, A:222	30. Sept. 1994 11. Oct. 1994	Endeavour	SRL-02 (SLR02 is comprised of: SIR-C/X-SAR, see J.23), MAPS (J.13)), CPCG, BRIC, Chromex, CREAM, MAST, GAS (5)

Mission Incl., Alt.(km)	Launch/ Landing Date	Orbiter	Mission Highlights / Payload Complement
STS-66, I:57°, A:305	3. Nov. 1994 14. Nov. 1994	Atlantis	ATLAS-03 (ATMOS, MAS, SSBUV, ACRIM, SOLCON, SOLSPEC, SUSIM), CRISTA-SPAS (MAHR-SI), ESCAPE-II, PCG, SAMS, HPP
STS-63 I:51.6°, A:310	3. Feb. 1995 11. Feb. 1995	Discovery	Shuttle-MIR rendezvous and fly-around; IMAX, Payloads: Spacehab-3, SPARTAN-204 (IN-STEP), CGP/ODERACS, SSCE, AMOS, CONCAP-II, ICBC, CGP
STS-67, I:28.5°, A:400	2. Mar. 1995 18. Mar. 1995	Endeavour	Astro-2 observatory (consisting of HUT, UIT, WUPPE and IPS), GAS, CMIX, PCG, MACE
STS-71, I:51.6° A:395	27 June 1995 7 July 1995	Atlantis	MIR Docking, Spacelab-MIR, SAREX-II, IMAX
STS-70, I:28.4° A:295	13. July 1995 21 July 1995	Discovery	TDRS-7, MAST, RME-III, STL-B, WINDEX, VFT-4, BRIC, CPCG, HERCULES, MIS-B, NIH-R
STS-69, I:28.5° A:370	7. Sept. 1995 18 Sept. 1995	Endeavour	WSF-2, deployment of SPARTAN-201-3, CAPL-2, TES-2, GAS, GBA, IEH-1, CONCAP-IV-3
STS-73, I:39° A:271	20. Oct. 1995 5. Nov. 1995	Columbia	Microgravity Laboratory 2 (USML-2), OARE-06, SAMS, 3DMA, STABLE
STS-74 I:51.6°, A:395	12. Nov. 1995 20. Nov. 1995	Atlantis	MIR flight 2, ICBC-05, IMAX, GLO-4, PASDE-1, MCSA, SAREX, GAS
STS-72 I:28.5°, A:455	11. Jan. 1996 20. Jan. 1996	Endeavour	Space Flyer Unit (SFU) retrieval, SSBUV-8, SLA-1, GAS, SPARTAN-206 (with REFLEX, GADACS, SELODE, SPRE), NIH-R3, NIH-C5, PCG,
STS-75 I:28.5°, A:298	22. Feb. 1996 9. Mar. 1996	Columbia	TSS-1R, USMP-3
STS-76 I:51.6°, A:292	22. Mar. 1996 31. Mar. 1996	Atlantis	MIR flight 3 (MEEP), Spacehab-SM, GAS, (Earth-KAM)
STS-77 I:39°, A:284	19. May 1996 29. May 1996	Endeavour	Spacehab-4, Spartan-207 (IAE), TEAMS (GANE, PAMS, VRTE), GBA-9 (11 GAS)
STS-78 I:39°, A:278	20. June 1996 7. July 1996	Columbia	Spacelab/LMS, SAMS-D, OARE, BDPU (TMIBD, SIE), SAREX-II
STS-79 I:51.6°, A:360	16. Sept. 1996 26. Sept. 1996	Atlantis	MIR flight 4, IMAX, Spacehab (MACEK), SAREX-II
STS-80 I:28.5°, A:470	19. Nov. 1996 7. Dec. 1996	Columbia	ORFEUS-SPAS II, WSF-3, SEM-1
STS-81 I:51.6°, A:440	12. Jan. 1997 22. Jan. 1997	Atlantis	MIR flight 5, Spacehab, SAREX-II, KidSat (Earth-KAM)
STS-82 I:28.45°, A:592	11 Feb. 1997 21 Feb. 1997	Discovery	Hubble Servicing Mission 2 (installation of two new instruments, STIS and NICMOS)
STS-83 I:28:45°, A:297	4 Apr. 1997 8. Apr. 1997	Columbia	MSL-1 (mission was terminated due to electrical power problems) MMA was part of MSL-1
STS-84 I:51.6°, A:	15. May 1997 24. May 1997	Atlantis	MIR flight 6, Spacehab-5,
STS-94 I:28.45°, A:295	1 Jul. 1997 17 Jul. 1997	Columbia	MSL-1 reflight, CRYOFD, OARE, SAREX, MSX
STS-85 I:57°, A:290	7. Aug. 1997 19. Aug. 1997	Discovery	CRISTA-SPAS-2, MAHRSI, TAS-1 (SOLCON, ISIR, SLA-2, CVX, SEM-2, TPF, CFE, SAAMD/WBSAAMD), MFD (TPFLEX, ESEM), IEH (UV-STAR, SEH, DATA-CHASER, GLO), PCG-STES, MSX-8, GAS (2), BDS-03, SIMPLEX, SWUIS, BRIC-10, SSCE-7
STS-86 I:51.6°, A:296, A:395 dock	25. Sept. 1997 6. Oct. 1997	Atlantis	MIR flight 7, Spacehab, MEEP, SEEDS-II, RME's, KidSat, CPCG, CREAM, CCM-A, MSX, SIMPLEX
STS-87 I:28.45°, A:276	19. Nov. 1997 5. Dec. 1997	Columbia	USMP-4, Spartan-201-4, OARE, SOLSE/LORE, LHP, TGDF, NaSBE, GAS, MGBX, CUE, MSX, CUE, SIMPLEX, AERCam/Sprint
STS-89 I:51.6°, A:296 A:395 dock	22. Jan. 1998 31. Jan. 1988	Endeavour	MIR flight 8, Spacehab-DM (ADV XDT, ADV CGBA, EORE, MGM, RME, SAMS), MPNE, SIMPLEX, CE-BAS TMIP, GPS DTO, OSVS, BIO3D, EarthKAM
STS:90 I:39°, A:280	17. Apr. 1998 3. May 1998	Columbia	Neurolab (Spacelab module), GAS (G-722), SVFE
STS-91 I:51.6°, A:385	2. June 1998 12. June 1998	Discovery	MIR flight 9, AMS, Spacehab-SM, GAS, SEM-3,

Mission Incl., Alt.(km)	Launch/ Landing Date	Orbiter	Mission Highlights / Payload Complement
STS-95 I:28.4°, A:555	29. Oct. 1998 7. Nov. 1998	Discovery	Spacehab, HOST, IEH-03 (UVSTAR, SEH, SOLCON, STAR-LITE, PANSAT, CODAG), SPARTAN-201-5, SEM-4, GAS, IVHM-1,
STS-88 I:51.6°, A:390	4. Dec. 1998 15. Dec. 1998	Endeavour	ISS-1 (1st Space Station Assembly Flight) element called Unity, MightySat I, SAC-A, AMTEC, AWCS, ICBC, GAS (G-093), SEM-07
STS-96 I:51.66°, A:390	27. May 1999 6. June 1999	Discovery	ISS-2 flight, IVHM-2, Starshine (educational satellite), ICC, SVFE (GAS), SPACEHAB
STS-93 I:28.4°, A:290	23 July 1999 28 July 1999	Columbia	Chandra/AXAF-1 (deployment of X-Ray Observatory, a S/C with its own integral propulsion system), MSX, SIMPLEX, SWUIS, SAREX-II, GOSAMR, BRIC, MEMS, CGBA, MEMS, PGIM, LFSAH
STS-103 I:28.4°, A:590	17 Dec. 1999 26 Dec. 1999	Discovery	Hubble Servicing Mission 3 (replacement of all six gyroscopes, a guidance sensor, and a S/C computer). Installation of a voltage/temperature kit for the S/C batteries. Installation of a new transmitter, solid state recorder (12 Gbit), and thermal insulation blankets.
STS-99 I:57°, A:233	11 Feb. 2000 22. Feb. 2000	Endeavour	SRTM (Shuttle Radar Topography Mission), EarthKAM
STS-101 I:51.6°, A:340	19. May 2000 29. May 2000	Atlantis	ISS-2A.2a assembly/maintenance flight Payloads: ICC (Integrated Cargo Carrier), MARS (Mission to America's Remarkable Schools), SEM-6 (Space Experiment Module-6), SPACEHAB/DM (Double Module), Bio-Tube Precursor Experiment. - The current orbit of ISS is 368 km x 342 km. The average orbit decay of ISS is about 1.5 to 2 km/week. Atlantis raises the ISS orbit by about 30 km.
STS-106 I:51.6°, A:320	8 Sept. 2000 20. Sept. 2000	Atlantis	ISS-2A.2b assembly flight. Payloads: ICC, SPACEHAB/DM (including MACE-II),
STS-92 I:51.6°, A:320	11. Oct. 2000 24. Oct. 2000	Discovery	ISS-05-3A assembly flight. Payloads: Z-1 Truss/SLP, CMG (Control Moment Gyros), Ku/S-Band, PMA-3/SLP, DDCU (heat pipes), IMAX
STS-97 I:51.6°, A:310	30. Nov. 2000 11. Dec. 2000	Endeavour	ISS-04-4A flight. PV Module P6 (solar arrays and batteries)
STS-98 I:51.6°, A:310	07. Feb. 2001 20. Feb. 2001	Atlantis	ISS-07-5A assembly flight. Payloads: US Lab Destiny, ORU, PDGF, also EarthKAM
STS-102 I:51.6°, A:340	08. Mar. 2001 21. Mar. 2001	Discovery	ISS-07-5A1 assembly flight. Payload: Leonardo Multi-purpose Logistics Module (MPLM)
STS-100 I:51.6°, A:315	19. Apr. 2001 01. May 2001	Endeavour	ISS-09-6A assembly flight. Payload: Raffaello MPLM-1, Racks/SLP, SSRMS (Canadarm2), LCA,RU, UHF Antenna
STS-104 I:51.6°, A:440	12. July 2001 24. July 2001	Atlantis	ISS-7A assembly flight. Payload: Airlock and support systems
STS-105 I:51.6°, A:440	10. Aug. 2001 22. Aug. 2001	Discovery	ISS-7A.1 logistics flight. Payload: Donatello (MPLM-3), HEAT (Hitchhiker Experiments Advanced Technology), a collection of GAS canisters, consisting of ACE (Advanced Carrier Equipment), SimpleSat, SEM-10 (Student Experiment Module), G-774, and G-780. MISSE (Materials International Space Station Experiment)
STS-108 I:51.6°, A:340	05. Dec. 2001 16. Dec. 2001	Endeavour	ISS-UF-1 (Utilization Flight 1). Payloads: Raffaello MPLM (with resupplies for Destiny), LMC with 4 GAS and MACH-1 [with STARSHINE-2 (deployed into a 387 km orbit), Hitchhiker Jr., 2 SEMs, COLLIDE-2, CPL-3]
STS-109 I:28.5°, A:570	01. Mar. 2002 11. Mar. 2002	Columbia	HST servicing mission 3B . ACS, SA-3 (Solar Array-3), NICMOS cryocooler, PCU, Reaction Wheel Assembly,
STS-110 I:51.6°, A:340	08. Apr. 2002 19. Apr. 2002	Atlantis	ISS-8A assembly flight. Payload includes S0 (S-Zero) truss segment and MT (Mobile Transporter). In addition, 5 powered payloads were transferred to ISS.

Mission Incl., Alt.(km)	Launch/ Landing Date	Orbiter	Mission Highlights / Payload Complement
STS-111 I:51.6°, A:340	05. Jun. 2002 19. Jun. 2002	Endeavour	ISS-UF-2 (Utilization Flight 2). Payload: MPLM with payload racks, MBS (Mobile Base System) installed on MT to complete MSS (Mobile Servicing System) of Canada.
STS-112 I:51.6°, A:375	07. Oct. 2002 18. Oct. 2002	Atlantis	ISS-9A assembly flight. Payload includes first starboard truss segment, S1, attached to the S0 truss. Backup S-band communication; CETA (Equipment Translation Aid). Secondary payloads: SHIMMER (see J.18), RAM-BO
STS-113 I:51.6°, A:370	24. Nov. 2002 07 Dec. 2002	Endeavour	ISS-11A, Payload: ITS-P1 (Integrated Truss Structure-Port1), MEPSI as secondary payload, etc.
STS-107 I:39°, A:290	16. Jan. 2003 01. Feb. 2003	Columbia	Space research mission; Payload: FREESTAR (consisting of 6 experiments: MEIDEX, SOLSE-2, CVX-2, SOLCON-3, SEM-14, LPT/CANDOS), SIMPLEX, Spacehab (363 kg payload including STARNAV), -- Reentry catastrophe of Shuttle Columbia on Feb. 1, 2003 disintegrating over Texas - resulting in the tragic loss of the crew of 7 astronauts
There were no Shuttle flights for 2 1/2 years after the tragedy of Feb. 1, 2003			
STS-114 I:51.6°, A:340	26. July 2005 05. Aug. 2005	Discovery	ISS-LF1; Payload: MPLM (Raffaello), ESP-2 (External Platform Stowage), removal and replacement of CMG-1 (Control Moment Gyro) on ISS,
STS-121 I:51.6°, A:340	04.Jul. 2006 17.Jul. 2006	Discovery	ISS-ULF1.1; Payload: MPLM (Leonardo), ICC (Integrated Cargo Carrier), LMC (Lightweight Multi-Purpose Experiment Support Structure Carrier)
STS-115 I:51.6°, A:340	09. Sept. 2006 21.Sept. 2006	Atlantis	ISS-12A; Payload: Second port truss segment (ITS P3/P4), Second set of solar arrays and batteries
STS-116 I:51.6°, A:350	10 Dec. 2006 22 Dec. 2006	Discovery	ISS-12.A.1; Payload: Third port truss segment, ICC (Integrated Cargo Carrier), SPHERES, Deployment of ANDE, MEPSI and RAFT
STS-117 I:51.6°, A:340	08 June 2007 22 June 2007	Atlantis	ISS-13A; Payload: ITS (Integrated Truss Segment) S3/S4
STS-118 I:51.6°, A:340	08 Aug. 2007 21 Aug. 2007	Endeavour	ISS-13A.1; Payload: Starboard 5 (S5) segment; ESP-3
STS-120 I:51.6°, A:340	23. Oct. 2007 07.Nov. 2007	Discovery	ISS-10A; Payload: Node 2 (Harmony)
STS-122 I:51.6°, A:340	07.Feb. 2008 20. Feb. 2008	Atlantis	ISS-1E; Payload: Columbus Laboratory of ESA
STS-123 I:51.6°, A:340	11. Mar. 2008 26. Mar. 2008	Endeavour	ISS-1J/A; Payload: ELM-PS (Experiment Logistics Module-Pressurized Section) of JAXA, SPDM (Dextre)
STS-124 I:51.6°, A:340	31. May 2008 11. June 2008	Discovery	ISS-1J/B; Payload: JEM-PM (Japanese Experiment Module-Pressurized Module) of JAXA, JEM-RMS (Japanese Remote Manipulator System) to the ISS.
STS-126 I:51.5°, A: 350	14. Nov. 2008 30. Nov. 2008	Endeavour	ISS-ULF2; The objective is to provide additional capability for the ISS to house astronauts and to increase the station crew size from three to the desired six crew members by spring 2009.
STS-119 I:51.6°, A:340	15. Mar. 2009 28. Mar. 2009	Discovery	ISS-15A; Payload: Starboard Integrated Truss Segment (S6)
STS-125 I:28.5°, A: 570 km	11. May 2009 24. May 2009	Atlantis	Hubble SM-4 (Servicing Mission-4). Five spacewalks were needed to refurbish Hubble with state-of-the-art science instruments.
STS-127 I:51.6°, A:340	15. July 2009 31. July 2009	Endeavour	ISS-2J/A; Payload: MAXI, SEDAAP and ICS of the JEM/Kibo; ICC-VLD, DragonSat of NASA, ANDE-2 of NRL
STS-128 I:51.6°, A:350	29 Aug. 2009 11. Sept. 2009	Discovery	ISS-17A; Payload: MPLM and LMC (Lightweight Multi-Purpose Experiment Support Structure Carrier), GLACIER (a freezer for samples) and other supplies on middeck
STS-129 I:51.6°, A:360	16. Nov. 2009 27. Nov. 2009	Atlantis	ISS-ULF-3; Payload: ELC (ExPRESS Logistics Carrier) 1 & 2, GLACIER, SASA (S-band Antenna and Support Assembly), MISSE-7,

Mission Incl., Alt.(km)	Launch/ Landing Date	Orbiter	Mission Highlights / Payload Complement
STS–130 I:51.6°, A:350	08. Feb. 2010 22. Feb. 2010	Endeavour	ISS assembly flight 20A. Payload: Tranquility module (formerly Node–3) and the Cupola, a robotic control station with six windows around its sides and another in the center that provides a 360° view around the station.
STS–131 I:51.6°, A:350	05. Apr. 2010 20. Apr. 2010	Discovery	ISS flight 19A. Payload: Middeck and MPLM (Multi–Purpose Logistics Module) cargo transfers. The following racks were installed: MAREs, WORF, MELFI–3, EXPRESS–7, CQ–2 (Crew Quarters–No 2), 2 ZSR (Zero–g Stowage Racks).
STS–132 I:51.6°, A:350	14. May 2010 26. May 2010	Atlantis	ISS ULF–4 flight. Payload: MRM1 (Mini–Research Module) of Roskosmos also known as Rasset. ERA (European Robotic Arm) of ESA. Six battery ORUs (Orbital Replacement Units) for Port 6. SGANT (Space–to–Ground Antenna) for Ku–band communications between ISS and TRDS.
STS–133 I:51.6°, A:350	24. Feb. 2011 09. Mar. 2011	Discovery	ISS ULF–5 flight. Payload: PMM (Permanent Multipurpose Module), ELC4 (Express Logistics Carrier 4), Robonaut–2 (R2), NPBX (Nucleate Pool Boiling Experiment).
STS–134 I:51.6°, A:350	16. May 2011 01. June 2011	Endeavour	ISS ULF6 flight. Payload: AMS–02 (Alpha Magnetic Spectrometer), ExPRESS, MHTEX. Delivery of spare arm for Dextre.
STS–135 I:51.6°, A:350	08. July 2011 21. July 2011	Atlantis	ISS ULF7 flight: Payload: MPLM, LMC, GLACIER, iPhone, ARFTA, RRM, TriDAR, PSSC–2

The Shuttle Remote Manipulator System (SRMS), also known as Canadarm (or Canadarm1), is a series of robotic arms that were used on the Space Shuttle orbiters to deploy, maneuver and capture payloads.

In 1975, NASA and NRC (Canadian National Research Council) signed a memorandum of understanding that Canada would develop and construct the SRMS. NRC awarded the SRMS contract to an industrial team led by SPAR Aerospace, Ltd. Later, the SPAR robotics division, located in Brampton, Ontario was acquired by MDA (MacDonald Dettwiler) and was renamed to MD Robotics.

The first SRMS, developed by SPAR, was delivered to NASA in February 1981. It was first flown on STS–2 (Columbia) on November 12, 1981. The original Canadarm was capable of deploying or retrieving payloads with a mass of up to 332.5 kg in space. In the mid–1990s, the arm control system was redesigned to increase the payload capability to 3,293 kg in order to support space station assembly operations.

The basic Canadarm configuration consists of a manipulator arm; a Canadarm display and control panel, including rotational and translational hand controllers at the orbiter aft flight deck flight crew station; and a manipulator controller interface unit that interfaces with the orbiter computer. Most of the time, the arm operators see what they are doing by looking at the Advanced Space Vision System screen next to the controllers.

The Canadarm is 15.2 m long, and 38 cm in diameter with six degrees of freedom. It has a mass of 410 kg by itself, and 450 kg as part of the total system. Canadarm has six joints that correspond roughly to the joints of the human arm, with shoulder yaw and pitch joints; an elbow pitch joint; and wrist pitch, yaw, and roll joints. The end effector is the unit at the end of the wrist that grapples the payload's grapple fixture.

Five Canadarms were built and flown on NASA's orbiters. They worked flawlessly on 90 Shuttle missions and together spent a total of 944 days in space.

Table 175: Short background on the history of Canadarm1 ³⁰¹¹⁾

³⁰¹¹⁾ “Canadarm,” Wikipedia, URL: <http://en.wikipedia.org/wiki/Canadarm>

1.34 Coordinates of satellite launch sites around the world

Name of Launch Site	Resp. Organization (Country)	Location	Remarks
Baikonur Cosmodrome (Tyuratam Leninsk)	Kazakhstan	45.6° N, 63.4° E	since 1957, launch of manned S/C, interplanetary S/C and geostationary S/C
Plesetsk (northern Cosmodrome)	Russia	62.8° N, 40.1° E	since 1966, launch of polar orbiting satellites
Kapustin Yar (Volgograd Cosmodrome)	Russia	48.4° N, 45.8° E	since 1962, launch of small satellites and interplanetary space probes
Cape Canaveral Air Force Station (CCAFS), FL	USAF/NASA (USA)	28.5° N, 80.0° W	since 1958, launch of manned S/C, interplanetary S/C, GEO satellites, etc.
Kennedy Space Center, FL	NASA (USA)	28.5° N, 80.0° W	since 1967, Complex 39 (launch of Saturn V vehicle, adapted to launch the Shuttle)
Vandenberg AFB, CA	USAF/NASA (USA)	34.4° N, 120.35° W	since 1959, launches of S/C into polar orbit
Vandenberg AFB, CA Commercial spaceport	Spaceport Systems International L.P.	34.4° N, 120.35° W	since 1998 (a joint venture of ITT Industries and CA Commercial Spaceport Inc.) launches of S/C into polar orbit
Wallops Island, VA referred to as MARS (Mid-Atlantic Regional Spaceport)	NASA/GSFC WFF (USA)	37.8° N, 75.5° W	since 1961, launch of sounding rockets and Scout launcher for small satellites, commercial launches since 1997
Edwards AFB, CA	USAF (USA)	35.0° N 118.0° W	Space Shuttle returns since 1981
Tanegashima Kagoshima Space Center	ISAS, U. of Tokyo, (Japan)	31.2° N, 131.1° E	since 1970, launch of scientific satellites
Tanegashima Space Center (TNSC)	JAXA (Japan)	30.4° N, 131.0° E	since 1975, launch site for scientific and commercial satellites
SHAR Sriharikota (Satish Dhawan Space Center)	ISRO (India)	13.9° N, 80.4° E	since 1980, launch of ISRO satellites
San Marco Platform (off the coast of Kenya)	CRA, U. of Rome (Italy)	2.9° S, 40.3° E	since 1967, launch of Scout rockets for NASA/ASI
Guiana Space Centre Kourou (Fr. Guiana)	CNES/ESA	5.2° N, 52.8° W	since 1970, launch of scientific and commercial satellites, in particular into GEO using Ariane vehicles. Starting in 2010 also launches of Soyuz-ST vehicles built by TsSKB-Progress Vega launches started in Feb. 2012
Woomera Range	WRE (Australia)	31.1° S, 136.8° E	since 1967, launch of sounding rockets since 1999, launch of LEO S/C (Kistler)
Jiuquan Satellite Launch Center (JSLC)	China	40.6° N, 99.9° E	since 1970, launch of experimental satellites
Xichang Satellite Launch Center (XSLC)	China	28.25° N, 102.0° E	since 1984, launch of satellites into geost. and polar orbits
Taiyuan Satellite Launch Center (TSLC)	China	37.5° N, 112.6° E	since 1988, launches of CZ-4A and -4B into polar orbits for remote sensing
Esrang, Kiruna	SSC (Sweden)	67.9° N, 21.0° E	launch of sounding rockets and balloons
Alcantara Launch Center (CLA)	CTA/INPE (Brazil)	2.3° S, 44.4° W	in preparation for satellite launches
Palmachim/Yavne	Israel	31.5° N 34.5° E	since 1989, launch of LEO satellites into westward direction (Ofeq series of IAI)
Svobodny Cosmodrome	Russia	51.4° N, 128.3° E	since 1996, Start-1 launcher (Zeya, etc. EarlyBird)
Sea Launch	Partnership of Boeing Co. USA, Yuzhnoye, Ukraine RKK Energia, Russia, and Kvaerner Maritima A.S. Oslo, Norway	Pacific Ocean	since March 27, 1999, inaugural launch of two-stage Zenit (Zenit-3SL and Zenit-2) rockets of the Yuzhnoye Design Bureau. The first commercial launch was on Oct. 9, 1999. The Sea Launch home port is Long Beach, CA for the command ship and launch platform

Name of Launch Site	Resp. Organization (Country)	Location	Remarks
Poker Flat Research Range (PFRR), AK	University of Alaska (USA)	65.117° N 147.60° W	since 1968 sounding rocket launch facility (auroral and meteorological research), located about 50 km north of Fairbanks
Kodiak Launch Complex (KLC) on Kodiak Island, AK	AADC (Alaska Aerospace Development Corporation)	57.445° N 152.34° W	The first satellite launch took place on Sept. 30 2001, with PICOSat of AFRL, Athena-1 vehicle (along with Starshine-3 and PCSat).
“Reagan Test Site” on the Kwajalein Atoll, part of the Republic of the Marshall Islands – also referred to as USAKA (US Army Kwajalein Atoll)	US Military Range run by the Army	9.99° N 167.6° E	Launch site (since World War II) for missiles and, occasionally, Pegasus and Falcon-1 launched small satellites
Yasny Launch Base (a Russian strategic missile facility) Alternate names: Dombrovsky, Kapustin Yar	ISC Kosmotras, Russia	51.0° N 58.0° E	Yasny Launch Base is a new Russian space launch base dedicated to Dnepr launch vehicles. First launch of a Dnepr occurred on April 21, 1999 (launch of UoSat-12 of SSTL, UK, Also launch of Genesis-1 and -2 of Bigelow Aerospace
Naro Space Center, Koheung (Goheung), Korea	KARI (Korea)	34.43° N 127.54° E	First launch of STSat-2 on Aug. 25, 2009 (a launch failure occurred). – First successful launch on January 30, 2013 with STSat-2C.
Uchinoura Space Center (USC), Kagoshima Prefecture, Japan	JAXA (Japan)	31.25° N 131.08° E	since 1962, launch of sounding rockets and satellites. – The first launch of the Epsilon rocket with SPRINT-A minisatellite on Sept. 14, 2013
PMRF (Pacific Missile Range Facility), Kauai, HI	US Naval Facility and Airport on Kauai Island, HI	22.02° N 159.78° W	Existing facility of the US Navy. A launch of the ORS-4 mission is planned in 2014 on the Super Strypi launcher.
Vostochny (meaning “eastern”) Cosmodrome	Roscosmos (Russia)	51.81° N 128.25° E	A new Russian Far East launch base in development. Commissioning is planned for 2015 and launch of first Angara rocket. First manned launch to start in 2018.